

Health.
Technology.
Humanity.

June 7-12, 2015
Toronto, Canada



JUNE 7 - 12 • 2015 • TORONTO
WORLD CONGRESS
ON MEDICAL PHYSICS & BIOMEDICAL ENGINEERING

Onsite Program

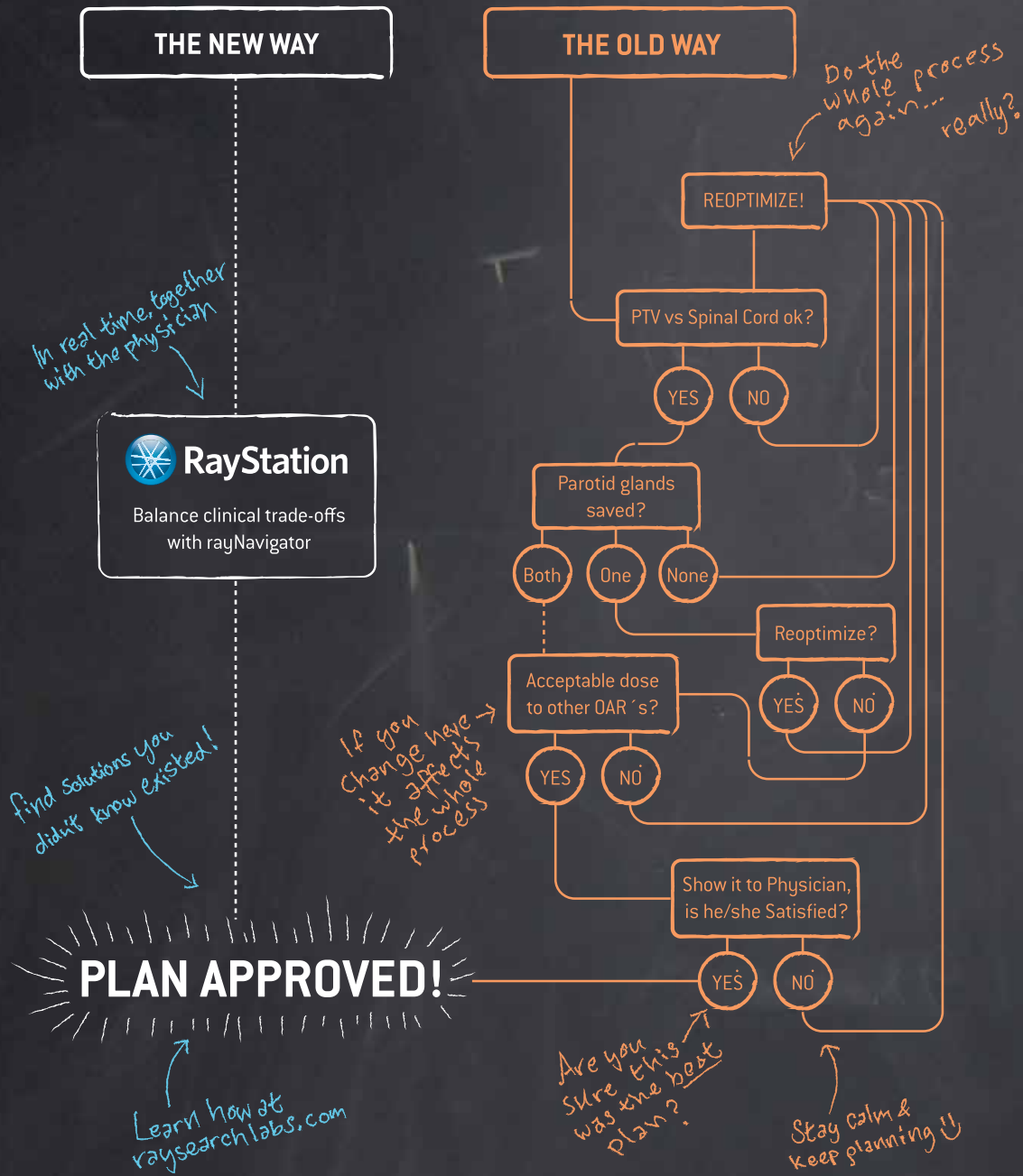
World Congress on Medical Physics and Biomedical Engineering



WWW.WC2015.ORG

ISBN: 978-1-988006-00-0

MULTI-CRITERIA OPTIMIZATION WILL CHANGE THE WAY YOU PLAN



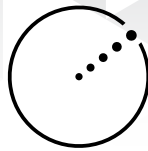
**ADVANCING
CANCER
TREATMENT**

*Visit us at booth
1219 and get
a demonstration*



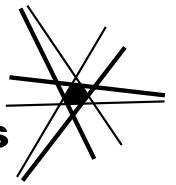
The 2015 IUPESM
World Congress
on Medical Physics
and Biomedical
Engineering wishes
to thank the following
sponsors, supporters
and partners:

► GOLD SPONSORS



ELEKTA

RaySearch
Laboratories



► SILVER SPONSOR

VARIAN
medical systems

► BRONZE SPONSORS



► SUPPORTERS

SIEMENS



► ACADEMIC PARTNERS



► MEDIA PARTNER

IOP Publishing

SPONSORS

TABLE OF CONTENTS



Health.
Technology.
Humanity.

Welcome Messages	3	Industry Supported Symposia	37
Hosts & Committees	10	Program at a Glance	38
Congress Venue	12	Plenary Sessions	40
Adopt a Delegate	14	Special Sessions	44
Science Fair Youth Outreach	14	Continuing Education Sessions	52
Flat Albert	15	Monday, June 8 2015	52
Registration Information	16	Tuesday, June 9 2015	54
Information for Speakers & Presenters	17	Wednesday, June 10 2015	56
Onsite Services & General Information	18	Thursday, June 11 2015	58
Social Events	19	Friday, June 12 2015	60
Social Tours	20	Scientific Program by Track	62
Exhibit Information	21	Scientific Program by Day	70
Exhibitors	22	Monday, June 8 2015	70
Exhibit Floor Plan	24	Tuesday, June 9 2015	80
Exhibitor Biographies	25	Wednesday, June 10 2015	94
Scientific Program	37	Thursday, June 11 2015	105
		Friday, June 12 2015	120
		Posters	126
		Author Index	139



Congress Secretariat

International Conference Services, Ltd.
2101 – 1177 West Hastings St.
Vancouver, BC, Canada, V6E 2K3

Tel +1 604 681 2153
Fax +1 604 681 1049

vancouver@icsevents.com
www.icsevents.com

WELCOME MESSAGES

Dear Colleagues,



As Co-chairs of the 2015 World Congress on Medical Physics and Biomedical Engineering, it is our great pleasure to welcome you to Toronto.

The World Congress is co-hosted by IUPESM (International Union for Physical and Engineering Sciences in Medicine), IOMP (international Organization for Medical Physics), IFMBE (International Federation for Medical and Biological Engineering), and here in Canada by COMP (Canadian Organization of Medical Physicists) and CMBES (Canadian Medical and Biological Engineering Society). These five organizations have collaborated to ensure that this Congress features exciting scientific sessions on a wide range of topics in medical physics and biomedical engineering, presented by scientists and engineers from around the world.

The Congress Organizing Committee and its sub-committees have worked hard to develop a rich and stimulating scientific program, with time set aside for mingling with colleagues and celebrating our successes. We are also proud of the range of plenary sessions, ancillary meetings and continuing education events being offered, along with an excellent range of exhibits. We encourage you to explore and participate in the various offerings of the congress. We also thank our congress planning partners, International Congress Services Ltd., whose people have worked tirelessly to ensure that this Congress is a rewarding and pleasurable experience for all.

We encourage you to reconnect with colleagues you may not have seen for a while, and to take the opportunity to meet new colleagues and form new connections around the world. Also, do take some time to explore our city. Here in Toronto, we are proud to be one of the most multicultural cities in the world, and of our rating as the safest large metropolitan area in North America. There are many exciting cultural sites nearby and a wonderful variety of restaurants serving many different cuisines, so don't hesitate to explore our city and enjoy its warmth and diversity.

Thank you for attending the 2015 World Congress, and welcome to Toronto!



David Jaffray, PhD



Tony Easty, PhD, PEng, CCE

WELCOME MESSAGES

Welcome to the 2015 World Congress on Medical Physics and Biomedical Engineering

We have created a World Congress—Why? What possesses us to work for three years to create this triennial event? Are we crazy? What has compelled David and Tony to take a chunk of their lives and of those many, many other people who contributed on the Congress Organizing Committee and all of the other WC 2015 committees and donate it to a World Congress on Medical Physics and Biomedical Engineering? This is among the greatest non-deductible, charitable contributions of which I am aware! It must be pretty important to them and to us. Thank you David Jaffrey and thank you Tony Easty—I don't know how many times you will hear this during the coming week, but I can assure you that it will not be enough times!

Anticipation for this World Congress has been building slowly since our last gathering in Beijing, but recently that anticipation has been crescendoing. We have collected an international snapshot of advances in medical physics and biomedical engineering. This is an excellent opportunity to share best practices and theories, strengthen and create new global relationships, mentor young engineers and physicists and begin new projects at home and abroad. Thank you all present for your support and assistance in making WC 2015 a success! We could not have done it without you.

The five themes of the World Congress are:

- 1) Global Health Challenges,
- 2) Evidence and Health Informatics,
- 3) Women in Biomedical Engineering and Medical Physics,
- 4) Urban Health and Future Earth, and
- 5) Next Generation Medicine.

These are broad themes that capture some of the most important issues we face today.

We have the privilege of celebrating the lives and work of several IUPESM, IFMBE and IOMP Award winners, who will be introduced at the Opening Ceremony and will each give us a “kort verslag” or precis of their work. We will have the additional pleasure of recognizing the achievements of early-career medical and biological engineers and medical physicists who have won one of several young investigator awards here in Toronto.

You, the people here, will have the opportunity to discuss the future of clinical engineering, medical physics and biomedical engineering. You have the chance to attend many special sessions within the 5 themes and 19 tracks of the World Congress. You can help shape policies for both developed and developing nations.

The delegates to the IUPESM General Assembly and the IOMP and IFMBE General Assemblies will be able to select their leaders for the immediate future; they will also select the location of the 2021 World Congress. Please delegates - vote intelligently and secure a good realization of our future.

Since I first read these words of T.S. Eliot in LITTLE GIDDING (No. 4 of 'Four Quartets') I have been strangely calmed by them; I thought I would share them with you as I wish you a successful WC 2015:

We shall not cease from exploration

And the end of all our exploring

Will be to arrive where we started

And know the place for the first time.

Best wishes,



Herbert F. Voigt, PhD
IUPESM President

WELCOME MESSAGES



INTERNATIONAL ORGANIZATION FOR MEDICAL PHYSICS

Member of the International Union of Physical and Engineering Sciences in Medicine
(Union Member of the International Council for Science)

Welcome to World Congress on Medical Physics & Biomedical Engineering 2015, Toronto, Canada

Kin-Yin Cheung, President of IOMP

On behalf of the International Organization for Medical Physics (IOMP), it is my great pleasure and honour extending my warmest welcome to all participants in this 13th World Congress on Medical Physics & Biomedical Engineering being held in the wonderful city of Toronto, Canada during June 6-12, 2015.

I wish to convey my gratitude to the Canadian Organization of Medical Physicists (COMP) and Canadian Medical and Biological Engineering Society (CMBES) for hosting this great event and to congratulate them for the huge success in this special occasion. The event provides a unique opportunity and a multi-disciplinary scientific platform for medical physicists, biomedical engineers, and other professionals from related fields from all over the world to exchange ideas and share their knowledge, experience, and research findings for the purpose of promoting human health through advances in science and technology in healthcare.

I would also like to congratulate the Congress Co-Chairs, Professor David Jaffray and Dr. Tony Easty, and their team members for putting up an outstanding congress with such an excellent scientific program. May I convey my appreciation to them for all their efforts and contributions in making this congress a most memorable one.

Last but not least, I wish all participants a very fruitful congress and an enjoyable stay in the beautiful city of Toronto.

Kin-Yin Cheung, PhD
President

WELCOME MESSAGES



IFMBE Welcome to the World Congress on Medical Physics and Biomedical Engineering 2015!

Each and every World Congress on Medical Physics and Biomedical Engineering is a chance for delegates from numerous countries from all over the world to review their own achievements and to have a closer look into the future of medical physics and biomedical engineering: which are the hottest topics in research, what can be expected from research results and from development, which are the new emerging technologies and what impact may be expected from them in medicine and health care, what are the highest needs for current care givers, how to make the education in medical physics and biomedical engineering better and more efficient. The World Congress is a platform for medical physicists and biomedical engineers to build a common policy for further improvement of health care and for planning common action under the umbrella of the International Union for Physical and Engineering Sciences in Medicine (IUPESM).

International Federation of Medical and Biological Engineering (IFMBE) is proud to be a sponsor of the World Congress this June, in Toronto, Canada. Biomedical engineers from most of more than 60 IFMBE affiliated Biomedical Engineering Societies will gather to exchange their knowledge and experience between themselves and also with colleagues who have their primary interest in medical physics, medicine and other professions linked with biomedical engineering. Contacts made at previous World Congresses enabled building of international research team which were successful gaining project in the field and where collaboration lasted for a long time. The Federation makes the most of the World Congress to reward distinguished scientists in biomedical engineering who have devoted their research for many years to biomedical engineering but at the same line, rewards early stage scientists and young investigators. There is more that 50 years since the Federation was founded (in 1959) and from the first World Congress in 1982, so that a whole crosssection of careers in biomedical engineering can be identified and appropriately evaluated.

I sincerely hope that all delegates of the Congress will gain from the scientific sessions and also that you all will enjoy the social activities of and around the Congress and of the appealing city of Toronto!



Ratko Magjarević, PhD
President, IFMBE

WELCOME MESSAGES



Premier of Ontario - Première ministre de l'Ontario

June 7–12, 2015

A PERSONAL MESSAGE FROM THE PREMIER

On behalf of the Government of Ontario, I am delighted to extend warm greetings to everyone attending the IUPESM World Congress on Medical Physics and Biomedical Engineering in Toronto.

I would like to take this opportunity to commend the IUPESM for its commitment to supporting biomedical engineers and physicists in the ongoing advancement of these vital fields.

As Premier, I am proud that Ontario has the opportunity to host an event that facilitates fruitful discourse between clinicians, researchers, educators and practitioners with the noble aim to improve global health outcomes. With an impressive array of lectures, educational sessions and workshops, this conference is sure to both enlighten and inform.

I would also like to thank IUPESM for choosing our province to host this wonderful event. I am confident that all the delegates and guests will enjoy their time in Toronto, our vibrant and diverse capital city.

Please accept my best wishes for an informative and memorable congress.

A handwritten signature in black ink that reads "Kathleen Wynne".

Kathleen Wynne
Premier

WELCOME MESSAGES



CMBES/SCGB

Welcome / Bienvenue

On behalf of the Canadian Medical and Biological Engineering Society, I would like to welcome each of you to Toronto for the World Congress on Medical Physics and Biomedical Engineering.

The committee organizers and countless volunteers have worked hard to put forward a great program including an impressive line-up of educational courses.

I would like to extend my appreciation for the support of the Sponsors and Exhibitors who will be on hand Sunday evening through Thursday to market their latest products and services. Please spend some time at the Exhibit Hall to see what's new and improved.

Note that CMBES is celebrating its 50th anniversary this year. We have an amazing and rich history founded by innovators, scientists, and biomedical/clinical engineers, who uniquely served patients, the medical community, and Canadian Healthcare.

Please enjoy the learning and sharing with colleagues from the international community over the next few days and don't forget to join us for the Gala dinner on Wednesday night and the AGM on Thursday evening. I also hope you have a little bit of spare time to enjoy some of the sights around Toronto.

Au nom de la Société Canadienne de Génie Biomédical, j'aimerais souhaiter la bienvenue à chacun de vous à Toronto pour le Congrès Mondial sur la physique médicale et le génie biomédical.

Les organisateurs du comité et les innombrables bénévoles ont travaillé très fort pour mettre de l'avant un excellent programme qui inclut également un nombre impressionnant de cours de formation continue.

Je tiens à exprimer ma gratitude pour le soutien des commanditaires et des exposants qui seront sur place du dimanche soir au jeudi pour présenter leurs plus récents produits et services. N'oubliez pas, s'il vous plaît d'en profiter pour prendre quelques minutes pour aller au salon des exposants afin de découvrir les dernières nouveautés et améliorations.

Notez que le CMBES célèbre son 50^e anniversaire cette année. Nous avons une histoire étonnante et riche fondée par les innovateurs, les scientifiques et les ingénieurs cliniques et biomédicaux, qui ont concentré leurs efforts pour apporter des bénéfices pour la santé les patients, la communauté médicale et le système de santé canadien.

Je vous souhaite une bonne conférence et j'espère que vous profiterez de cette occasion d'apprendre et de partager avec les collègues de la communauté internationale au cours des prochains jours. N'oubliez pas de nous rejoindre pour le dîner de gala du mercredi soir et l'Assemblée Générale du jeudi soir. Enfin, j'espère aussi que vous trouverez un peu de temps libre pour profiter de certains des attraits touristiques de Toronto et sa région.

Sincerely,

A handwritten signature in black ink, appearing to read 'M. Poulin'.

Martin Poulin, M.Eng., P.Eng.
President, CMBES/SCGB

WELCOME MESSAGES

Dear Delegates of the 2015 World Congress on Medical Physics and Biomedical Engineering,



On behalf of the Canadian Organisation of Medical Physicists and the Medical Physics community in Canada, Welcome to Toronto!

The theme for this year's World Congress is "Health * Technology * Humanity". I believe this captures the spirit of this meeting, and explains why it is so important that Medical Physicists and Biomedical Engineers meet together, and on a world scale. Medical technology is increasingly central in patient care; we as Physicists and Engineers are uniquely trained and able to improve human health through technology. The World Congress is the most comprehensive medical technology meeting in the world; this year we are welcoming delegates from 89 countries from all corners of the world to come to Toronto and share our knowledge and ideas to help improve human health for everyone.

COMP is very pleased to be able to contribute to improving global health through our contributions to this meeting. The planning for this meeting has been underway in earnest for about 20 months now, and we are grateful for the many volunteers who have committed much time and effort to plan this meeting for you. COMP is also grateful to our partner organisation in this event, the Canadian Medical and Biological Engineering Society, for co-organising the event with us. I believe that both societies are benefited tremendously through the interactions and planning with our partners. We are also grateful to the World Organisations, the IUPESM, IOMP and IFMBE, for giving us the opportunity to plan the premier Medical Physics and Biological Engineering conference in the world. It has been a privilege to host this event, and we are proud to be able to bring it to you.

I would like to reserve my greatest thanks to you, the delegates attending this meeting. This meeting will offer a world class program of talks and education sessions, covering 19 different tracks that could not be possible without your contributions. Without your hard work, commitment and enthusiasm for medical technology, this meeting would not be possible.

Thank you for making the trip to Toronto, and enjoy the meeting!



Marco Carlone, PhD
President, COMP

HOSTS & COMMITTEES

► HOSTS

International Union for Physical and Engineering Sciences in Medicine (IUPESM)



The IUPESM represents the combined efforts of more than 40,000 medical physicists and biomedical engineers working on the physical and engineering science of medicine. The principal objectives of IUPESM are: (a) to contribute to the advancement of physical and engineering science in medicine for the benefit and wellbeing of humanity; (b) to organize international cooperation and promote communication among those engaged in health-care science and technology; (c) to coordinate activities of mutual interest to engineering and physical science within the health care field, including international and regional scientific congresses, seminars, working groups, regional support programs and scientific and technical publications; (d) to represent the professional interests and views of engineers and physical scientists in the health-care community.

International Organization for Medical Physics (IOMP)



The IOMP represents over 18,000 medical physicists worldwide, 80 adhering national member organizations and 6 regional organizations. The mission of IOMP is to advance medical physics practice worldwide by disseminating scientific and technical information, fostering the educational and professional development of medical physicists, and promoting the highest quality medical services for patients.

International Federation of Medical and Biological Engineering (IFMBE)



IFMBE is primarily a federation of national and transnational organizations. These organizations represent national interests in medical and biological engineering. The objectives of the IFMBE are scientific, technological, literary, and educational. Within the field of medical, biological and clinical engineering IFMBE's aims are to encourage research and the application of knowledge, and to disseminate information and promote collaboration.

Canadian Organization of Medical Physicists (COMP)



COMP is the main professional body for medical physicists practicing in Canada. The membership is composed of graduate students, professional physicists, scientists, and academics located at universities, hospitals, cancer centers, and government research facilities. Every member has an educational or professional background in physics or engineering as it applies to medicine. COMP's vision is to be the recognized leader and primary resource for medical physics in Canada. COMP's mission is to champion medical physicists' efforts for patient care excellence through education, knowledge transfer, advocacy and partnerships.

Canadian Medical and Biological Engineering Society (CMBES)



CMBES is Canada's principal society for engineering in medicine and biology. The Society's aims are twofold: scientific and educational: directed toward the advancement of the theory and practice of medical device technology; and professional: directed toward the advancement of all individuals in Canada who are engaged in interdisciplinary work involving engineering, the life sciences and medicine.

HOSTS & COMMITTEES

► COMMITTEES

Congress Coordinating Committee

Herbert F. Voigt, USA
Kin Yin Cheung, China
Ratko Magjarevic, Croatia
James Goh, Singapore
Madan M. Rehani, Austria
Shankar M. Krishnan, USA

Congress Organizing Committee

Co-Chair: David Jaffray, Canada
Co-Chair: Tony Easty, Canada
Secretary: Jean-Pierre Bissonnette, Canada

Finance Committee

Michael J. Capuano, Canada
Crystal Plume Angers, Canada
Kyle Eckhardt, Canada
Anchali Krisanachinda, Thailand
Shankar M. Krishnan, USA
Marc Nyssen, Belgium
Horacio Patrocinio, Canada
Peter Smith, UK

International Advisory Committee

Monique Frize, Canada (Co-Chair)
Jacob Van Dyk, Canada (Co-Chair)
Herbert F. Voight, USA (Co-Chair)
Kin Yin Cheung, China (Co-Chair)
Ratko Magjarevic, Croatia (Co-Chair)
Muthana Al-Ghazi, USA
Rodolfo Alfonso-Laguardía, Cuba
Pedro Andreo, Sweden
Michael Balderson, Canada
Gilda Barabino, USA
Eva Bezak, Australia
Marin Bodale, Romania
Caridad Borrás, USA
Saide Calil, Brazil
Amanda Cherpak, Canada
Stelios Christofides, Cyprus
Luca Cozzi, Switzerland

Sarah G. Cuddy-Walsh, Canada
Carlos E. de Almeida, Brazil
Andre Dekker, Netherlands
Olga M. Dona Lemus, Canada
Ibrahim Duhaini, Lebanon
Yubo Fan, China
Dietmar Georg, Austria
Eduard Gershkevitch, Estonia
Birgit Glasmacher, Germany
Wassim Jalbout, Lebanon
Eleni Kaldoudi, Greece
Valeriy Kostylev, Russia
Shankar M. Krishnan, USA
Tomas Kron, Australia
Andrel Linnenbank, Netherlands
Susana B. Llanusa Ruiz, Cuba
Nigel Lovell, Australia
Loredana Marcu, Romania
Hasmik Martirosyan, Canada
Brendan McClean, Ireland
Kwan-Hoong Ng, Malaysia
Azam Niroomand-Rad, USA
Fridtjof Nuesslin, Germany
Marc Nyssen, Belgium
Nicolas Pallikarakis, Greece
Laura Poole-Warren, Australia
John Puentes, France
Paul B. Ravindran, India
Madan M. Rehani, Austria
Laura M. Roa, Spain
David Rogers, Canada
Howell Round, New Zealand
Otto Sauer, Germany
Slavik Tabakov, UK
Peck Ha Tan, Singapore
Nitish Thakor, Singapore
Virginia Tsapaki, Greece
Max Valentinuzzi, Argentina
Min Wang, China
Karin Wårdell, Sweden
Habib Zaidi, Switzerland

Publicity Committee

Marco Carlone, Canada
Jean Ngoie, Canada
Parminder Basran, Canada
Denis Derome, Canada
Young Lee, Canada
Marc MacKenzie, Alberta
Doug Moseley, Canada
Nadia Octave, Canada
Conrad Yuen, Canada

Sponsorship Committee

Murray Rice, Canada
Michael Sharpe, Canada
Michael J. Capuano, Canada
Marco Carlone, Canada
Nancy Barrett, Canada
Ibrahim Duhaini, Lebanon

Scientific Committee

David Jaffray, Canada
Tony Easty, Canada
Monique Frize, Canada
Luc Beaulieu, Canada
John Rowlands, Canada
Christopher Yip, Canada

Professional Standards Committee

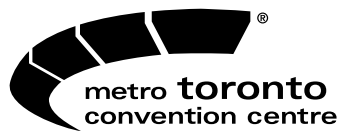
Jerry Battista, Canada
Dave Gretzinger, Canada

Education Committee

Anthony Chan, Canada
Jean-Pierre Bissonnette, Canada
Andrew Ibey, Canada
Ervin Podgorsak, Canada
David Falagario, Canada
Jacob Van Dyk, Canada
Eric Tam, Hong Kong
Beatriz Sánchez, Chile
Mohcine El Garch, Canada
Gnahoua Zoabli, Canada
Antonio Hernandez, USA

CONGRESS VENUE

The IUPESM World Congress 2015 will take place in the South Building of the Metro Toronto Convention Centre. The Convention Centre is located in the heart of downtown Toronto. The South Building is accessible via Bremner Boulevard as well as from the North Building via Front Street.



Metro Toronto Convention Centre

South Building
222 Bremner Boulevard,
Toronto, Ontario, Canada M5V 3L9



Toronto, Ontario, Canada

One of Canada's best kept secrets, Toronto is on par with New York City, San Francisco and Chicago when it comes to cultural attractions and urban sophistication.

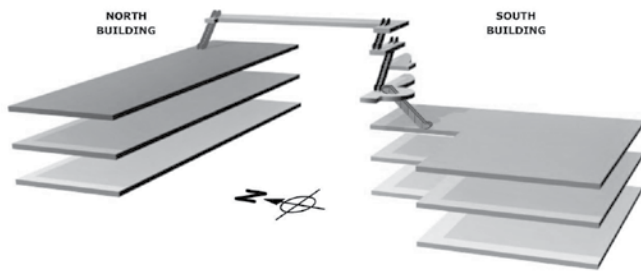
The landmark CN Tower is the tallest freestanding structure in the world. Take the elevator to the top for a breathtaking view of the city, Lake Ontario and more. Stroll next door and experience Ripley's Aquarium as you explore the wonders of the sea or a catch a Blue Jays Baseball game at Rogers Centre or just walk around the massive engineering marvel. Check out the Royal Ontario Museum, the largest in Canada with its fascinating archaeology and natural history exhibits, and the Art Gallery of Ontario, with a fine collection of European and Canadian works. You won't want to miss the electric shops and restaurants on Queen Street West or the elegant boutiques and fine restaurants in Yorkville.

And there's more: harbour front is a complex of unique shops and restaurants right on beautiful Lake Ontario. From harbour front you can hop on a ferry to the Toronto Islands for a picnic and outdoor recreation such as beach volleyball.

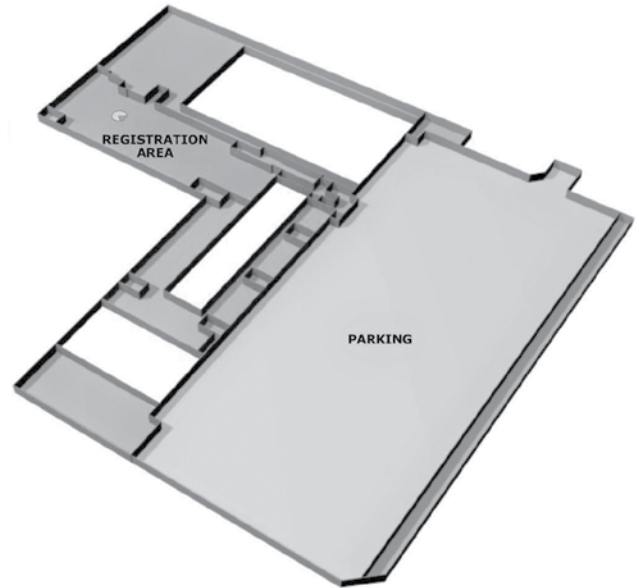
Explore the area and take a day trip to another wonder of the world and experience Niagara Falls or take a break right next door and experience Ontario's wine country. Toronto and the surrounding areas are a great family destination and most attractions are child-friendly. The city itself is clean, safe and easy to explore either on foot or by public transportation.

CONGRESS VENUE

South Building

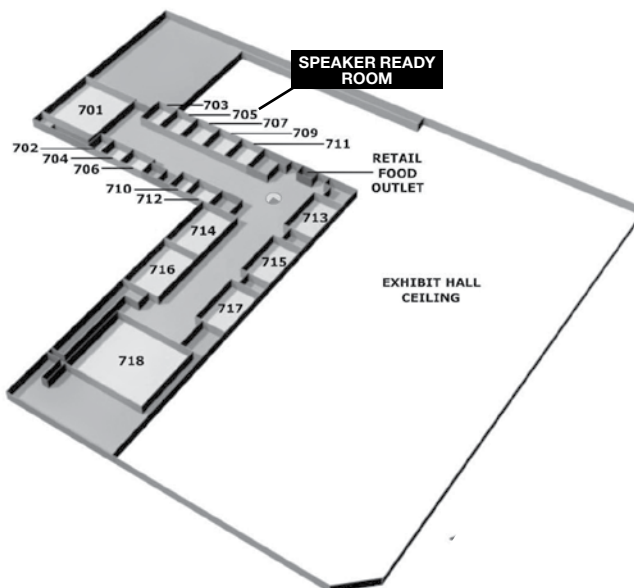


Level 600

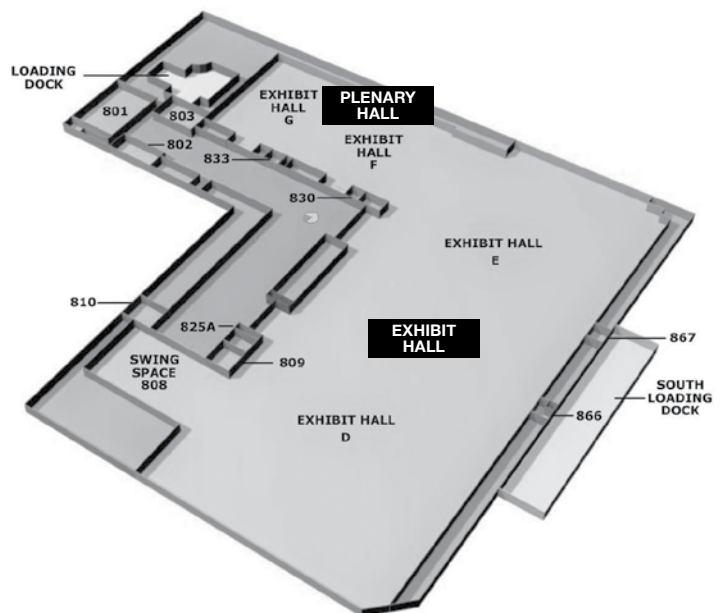


CONGRESS VENUE

Level 700



Level 800



ADOPT A DELEGATE

The IUPESM 2015 World Congress is proud to support the 'Adopt a Delegate/Student' initiative, giving prospective delegates from a developed world setting the opportunity to adopt or part finance the registration and accommodation costs of a peer from an emerging economy.

► We would like to thank the following people for their consideration and support:

Herbert F. Voigt

David Rogers

David Jaffray

Modus Medical Devices Inc.

Murray Rice

Grace Zeng

William Gentles

Raymond Wu

Ichiro Sakuma

David Spencer

Vincent Lam

Joyce Shen

Tony Easty

SCIENCE FAIR YOUTH OUTREACH

Winners of a local science fair have been invited to participate in the IUPESM 2015 Youth Outreach Program. 26 youths between the ages of 15–18 will present their 18 Science Fair projects on Wednesday, June 10.

They will start their day by listening to the Key Note Session by Gordon MCBear and Mary Gospodarowicz, followed by attending the session on "What is a medical physicist? What is a biomedical engineer?" After, they are taken on a guided tour of selected posters and the exhibit floor by a Professor. After lunch, their day concludes by presenting their Science Fair projects in the Exhibit Hall, interacting with congress delegates.

FOLLOW US ON SOCIAL MEDIA:

 **TWITTER @IUPESMWC2015**
www.twitter.com/IUPESMWC2015

 **FACEBOOK**
www.facebook.com/groups/WCon2015/

DOWNLOAD THE MOBILE APP:

Abstracts Online/ Personal Itinerary Builder

Attendees are invited to utilize the World Congress 2015 App, which is available for download on the Congress Website at WC2015.org

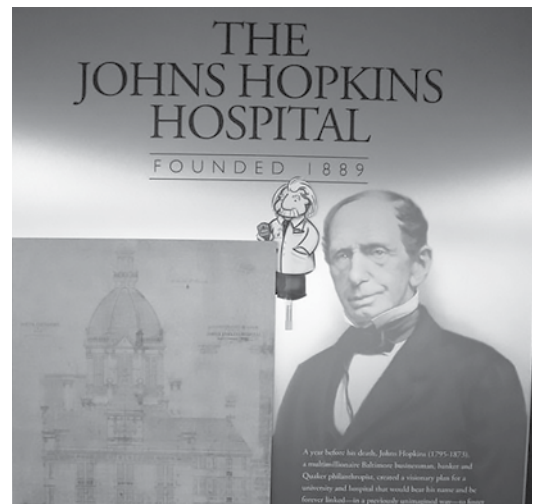
This app allows you to view abstracts, presenters, the program schedule and sessions, selecting abstracts and sessions of interest to build your own personal itinerary builder.

FLAT ALBERT

Flat Albert is a flat version of very well known Albert Einstein.

We encouraged you to take a picture of Flat Albert in an interesting place and post it to our Facebook and Twitter pages #wc2015yyz.

Here are some of our favourites:



FLAT ALBERT

REGISTRATION INFORMATION

Registration Counter Hours

Registration is located on Level 600, South Building of Metro Toronto Convention Centre.

Sunday, June 7	11:00 – 20:00
Monday, June 8	07:00 – 17:30
Tuesday, June 9	07:00 – 17:30
Wednesday, June 10	07:00 – 17:30
Thursday, June 11	07:00 – 17:30
Friday, June 12	07:00 – 13:00

The Toronto Information Desk is located in the Registration area on Level 600, South Building of Metro Toronto Convention Centre. Staff will provide local information and assist with:

- ▶ Ground Transportation
- ▶ Airport Transfers
- ▶ Sightseeing Tours
- ▶ Pre- and Post Tours
- ▶ Restaurant recommendations and booking
- ▶ Local PA and Personal Concierge Services

Delegate Help Desk

Delegate Help Desk is located on Level 600, South Building of Metro Toronto Convention Centre.

SUPPORTED BY

**RaySearch
Laboratories**



Sunday, June 7	11:00 – 20:00
Monday, June 8	07:00 – 17:30
Tuesday, June 9	07:00 – 17:30
Wednesday, June 10	07:00 – 17:30
Thursday, June 11	07:00 – 17:30
Friday, June 12	07:00 – 13:00

If you require assistance or any information regarding the Congress, please see the staff at the Delegate Information

Counter located in the registration area, on Level 600, South Building of Metro Toronto Convention Centre.

Registration Materials

Registration Materials include:

- ▶ Name Badge
- ▶ Delegate Bag Voucher
(not included in Accompanying Person Registration)
- ▶ Onsite Program Book Voucher

Delegate Bag Booth

Delegate Help Desk is located on level 600, South Building of Metro Toronto Convention Centre

Sunday, June 7	11:00 – 20:00
Monday, June 8	07:00 – 17:30
Tuesday, June 9	07:00 – 17:30

Delegate Bags include:

- ▶ Invitation Flyers for Industry Supported Symposia
- ▶ Additional Promotional Flyers from Sponsors and Exhibitors

SUPPORTED BY



Name Badges

Delegates and guests are requested to wear their name badge at all times in order to participate in the Scientific Sessions, Social Events and Exhibition.

Lost Badge/Name Changes:

A 50 CAD fee applies for any reprints due to onsite name changes or lost badges.

Badge Color Identification

▶ Delegate – Blue

- ▶ Access to all Scientific Program & Continuing Education Sessions (except any specially ticketed sessions)
- ▶ Access to Exhibit Hall
- ▶ Congress Bag
- ▶ Onsite Program and Congress Handouts
- ▶ Welcome Reception
- ▶ Networking Breaks
- ▶ Discounted Gala Dinner Ticket

▶ Single Day – Red

- ▶ Access to all Scientific Program & Continuing Education Sessions (except any specially ticketed sessions) on day of attendance
- ▶ Access to Exhibit Hall on day of attendance
- ▶ Congress Bag
- ▶ Onsite Program and Congress Handouts
- ▶ Networking Breaks on day of attendance

▶ Exhibitor – Green

- ▶ Access to Exhibit Hall
- ▶ Onsite Program and Congress Handouts
- ▶ Welcome Reception
- ▶ Networking Breaks
- ▶ Option to Purchase Gala Dinner Tickets

▶ Accompanying Person - Yellow

- ▶ Access to Exhibit Hall
- ▶ Welcome Reception
- ▶ Networking Breaks
- ▶ Discounted Gala Dinner Ticket Rate

LEAD RETRIEVAL

By allowing to have your badge scanned, you are indicating your consent to receive e-mail marketing

INFORMATION FOR SPEAKERS & PRESENTERS

Speaker Ready Room

SUPPORTED BY



All invited speakers as well as oral abstract presenters are required to report to the Speaker Ready Room at least 24 hours prior to their scheduled presentation in order to upload their presentation slides or to check their previously uploaded slides. Computers are available to preview and upload presentations. Presenters should make sure all fonts appear as expected. No file submissions will be accepted in the session rooms.

The Speaker Ready Room is located in Room 705 on Level 700.

Sunday, June 7	11:00 – 20:00
Monday, June 8	07:00 – 17:30
Tuesday, June 9	07:00 – 17:30
Wednesday, June 11	07:00 – 17:30
Thursday, June 12	07:00 – 17:30
Friday, June 12	07:00 – 13:00

Invited Speakers and Oral / Abstract Presenters

All speakers are asked to be in the session room at least 10 minutes prior to the start of their session.

Poster Presenters

All Poster Presentations/Boards are located in Hall E on Level 800, South Building of Metro Toronto Convention Centre.

Each Poster Board will be shared by two posters on each side. The Poster Boards are identified with Poster Numbers that correspond with the pre-assigned Poster Numbers for each poster presentation. The Poster Numbers are also published in this program book and in the Online Abstract Book.

Poster set up time:	Sunday, June 7	15:00 – 17:45
Poster take down:	Thursday, June 11	17:00 – 19:00
<small>(any posters not removed by 19:00 will be discarded by management)</small>		

Poster Sessions

Posters will be displayed at all times during the Exhibit Opening Hours each day starting Sunday June 7. Presenters are asked to stand by their poster during the following times to informally answer questions from Congress delegates:

- ▶ **Morning & afternoon Networking Breaks:**
10:00 – 10:30 AND 16:30 – 17:00 Monday, June 8 to Thursday, June 11.
- ▶ **During the Welcome Reception:**
18:00 – 20:00 on Sunday, June 7.

ONSITE SERVICES & GENERAL INFORMATION

Abstracts

All accepted and confirmed abstracts are published in the IUPESM World Congress Onsite Program and Abstract Book. This will be available on the Congress website.

All Full Papers accepted by the World Congress will be published by Springer in the IFMBE Proceedings 2015.

Delegate Lounges

SUPPORTED BY



The delegate lounges are located in the Exhibit Hall, see floorplan page 35.

Internet Café

SUPPORTED BY



The internet café is located in the Exhibit Hall.

Wireless Internet

SUPPORTED BY



Wireless internet is available in the public areas of the venue but not the meeting rooms or the Exhibit Hall.

Charging Station & Lounge

SUPPORTED BY



The charging station & lounge is located in the Exhibit Hall.

Congress Signage

SUPPORTED BY



Water Stations

SUPPORTED BY



Welcome Reception

SUPPORTED BY



All delegates are invited to attend the Welcome Reception on Sunday June 9 at 18:00 in the Exhibit Hall.

Lost and Found

Lost and found items should be returned/claimed at the registration desk.

Lunch

Lunch will not be provided by the Congress. However, there are plenty of restaurant choices in the area. A café, a convenience store and vending machines are all located within the Centre and there are also numerous restaurant options within a few minutes walk of the Convention Centre:

► **SOCO Kitchen + Bar**

Located within the Delta Hotel offers laid back style of eating, with the opportunity to look over Bremner Street on their patio.

► **Pita & Grill**

For a lighter meal head to Pita & Grill for a grab and go option.

► **360 Restaurant**

Upmarket Dining with sky high view in the world famous CN Tower.

Networking Breaks

Networking Breaks (hot beverages and snacks) are served on Level 700 at the following times:

► **Monday, June 8** 10:00 – 10:30
and 16:30 – 17:00

SUPPORTED BY



► **Tuesday, June 9** 10:00 – 10:30
and 16:30 – 17:00

SUPPORTED BY



► **Wednesday, June 10** 10:00 – 10:30
and 16:30 – 17:00

SUPPORTED BY



► **Thursday, June 11** 10:00 – 10:30

SUPPORTED BY



SUPPORTED BY



► **Friday, June 12** 10:00 – 10:30

SUPPORTED BY



CAMPEP Accreditation

For Medical Physicists:

The IUPESM 2015 World Congress Continuing Education Program is CAMPEP Accredited for up to 82 MPCEC credits. If you will be applying to CAMPEP for your MPCEC credits following the Congress and have not already paid the \$11(CAD) CAMPEP fee then you will be able to pay this fee at the registration desk during registration hours. After the Congress you will be contacted by CAMPEP regarding Accreditation.

For Biomedical Engineers:

The IUPESM 2015 World Congress Continuing Education Program can be used for points towards Clinical Engineering Certification Renewal.

SOCIAL EVENTS



SOCIAL EVENTS

Be sure to join us for these events during the week:

► Welcome Reception

SUPPORTED BY



ELEKTA

Sunday, June 7, 2015 18:00 – 20:00
Exhibit Hall E

Enjoy some light hors d'oeuvres and a beverage, along with a subdued jazz trio, as you connect with exhibitors. This is your opportunity to network and connect with industry colleagues.

► Opening Ceremony & President's Welcome Address

Monday, June 8, 2015 10:30 – 12:00
Exhibit Hall F/G

Your opening ceremony and president's welcome address will be greeted by Canadian inspired entertainment, followed by the formalities of any President's Welcome Address. You will hear all about what you can expect to experience throughout the congress and Toronto as your host city!

► Gala Dinner

Wednesday, June 10, 2015 19:00 – 23:00
Exhibit Hall F/G

After a busy week at the congress, tonight you will enjoy a delicious meal with fellow colleagues and new friends. Roaming entertainment will emerge throughout the evening and an upbeat band will perform top hits after dinner so you can show off your dancing moves.

► Closing Ceremony & Awards Presentation

Friday, June 12, 2015 15:00 – 16:00
Exhibit Hall F/G

Final remarks from the President, the organizing committees and your incoming officers will be announced here! Be sure to attend to hear where the next congress location will take place!

SOCIAL TOURS



Explore the area and take a day trip to experience one of the world wonders Niagara Falls or take the half day, fun and informative Toronto City Tour.

Niagara Falls Tour

The premium full-day tour of the Falls starts with your hotel pickup in the morning. On our first stop we'll have time to explore Niagara-on-the-Lake.

www.niagarafallstourism.com/about/niagara-on-the-lake/

"NOTL" Niagara-on-the-Lake is a picturesque town just a few minutes drive outside of Niagara Falls. You'll enjoy 40 minutes taking pictures and exploring some of the unique shops. Before you actually reach the Falls, we'll also see the Floral Clock, Niagara River and whirl pool, Sir Adam Beck Power Station, Queenston Heights, and the Spanish Aero Car. During the day, we will make a stop at one of Niagara Falls' famous wineries. There you will have an opportunity to sample wine before continuing our Niagara Falls adventure. The tour is structured to give you 2-3 hours of free time at the Falls. This gives you plenty of time to add in additional activities you want to do, plus stop for lunch, which is on your own time and budget. Recant the day's memories on the bus ride back until you're dropped back at your hotel doorstep.



Toronto City Tour

The half day, fun and informative Toronto City Tour will transport you to some of the city's most popular sights as you relax aboard our new air-conditioned bus. We will show you over 17 attractions. Our stops include the St. Lawrence Market where you can buy lunch and a stroll through the pedestrian friendly Distillery District.



Shopping Tour

www.premiumoutlets.com/outlets/outlet.asp?id=109

Toronto Premium Outlets features a high end collection of the finest brands for you, your family and your home. Our Tour bus will pick you up from your hotel lobby between and take you the Outlets just 45 minutes outside of Toronto. Once we arrive you will receive a VIP Coupon book plus a special gift just for you from Toronto Premium Outlets management team.

**Please go to our website for more details or to book a tour:
wc2015.org/events-tours/pre-post-tours/**

EXHIBIT INFORMATION

Location

Hall E on Level 800, South Building
of Metro Toronto Convention Centre.

Exhibit Hours

Sunday, June 7	18:00 – 20:00
Monday, June 8	09:30 – 17:00
Tuesday, June 9	09:30 – 17:00
Wednesday, June 10	09:30 – 17:00
Thursday, June 11	09:30 – 17:00



EXHIBIT INFORMATION

Exhibit Features

- ▶ Exhibit Information Booth
- ▶ Show Service Provider Desk
- ▶ Internet Café
- ▶ Food & Beverage Stations
- ▶ Delegate Lounges

SUPPORTED BY

**RaySearch
Laboratories**



- ▶ Charging Station & Lounge

SUPPORTED BY

**RaySearch
Laboratories**



SUPPORTED BY



Canadian Nuclear Safety Commission
Commission canadienne de sûreté nucléaire

VARIAN
medical systems

EXHIBITORS

Alphabetical

Accuray Inc.	3104
American Association of Physicists in Medicine (AAPM)	1212
ANDA Medical	3604
ArjoHuntleigh Canada Inc.	3213
Bayer HealthCare	3503
Best Theratronics	3303
Biomedical Engineering Society (BMES)	2709TT
BRACCO IMAGING Canada	2301
Brainlab	1102
Canadian Medical and Biological Engineering Society (CMBES)	2305
Canadian Nuclear Safety Commission	1228
Canadian Organization of Medical Physicists (COMP)	1115
CareFusion	2202
Carleton University	3406
CDR Systems	1127
Centre for Imaging Technology Commercialization (CIMTEC)	2211
CIRS	1224
Covidien	2203
CRC Press/Taylor & Francis	1107
Department of Radiation Oncology, University of Toronto	1114
Dräger	2110
Dunlee	2204
ECRI Institute	2711TT
Elekta	1202
Engineering World Health	2713TT
Fibertech Canada	2503
Fluke Biomedical/RaySafe	3112
GCX Corporation	2505
GE Healthcare	2302
Getinge Group	3114
Harpell Associates Inc.	3305
Heidelberg University	1111
IBA	1331
IEEE, Engineering in Medicine & Biology Society	2104
Institution of Engineering and Technology	2715TT
International Federation of Medical and Biological Engineering (IFMBE)	2309
International Organization for Medical Physics (IOMP)	1119
International Union for Physical and Engineering Sciences in Medicine (IUPESM)	3214
IOP Publishing	1103
IPEM	3606
iRT Systems	1124
LAP Laser	1214
Maquet-Dynamed	3211

MedTech Hub	3203, 3206
MedView Technologies	2213
MIM Software Inc.	2205
Mobius Medical Systems	1323
Modus Medical Devices Inc.	1309
Naf Sacs	1120
NELCO	1205
Olympus Canada Inc.	2112
Oncology Systems Limited Inc.	1230
Orfit Industries America	1211
Pacific Medical LLC	2106
PartsSource	2209
Philips Healthcare	1201
Physio-Control	2306
Precision X-Ray	1210
PTW	1220
Qfix	1327
Radcal Corporation	3204
Radiological Imaging Technology Inc.	1213
RaySearch	1219
RTI - From Radiation to Information	1125
Shimifrez	2214
Southwest Medical Resources	2210
Spacelabs Healthcare	2114
Spectrum Technologies, Inc.	2412
Springer	2311
Standard Imaging	1110
Sun Nuclear Corporation	1329
Synaptive	3404
Technical Prospects	2102
The Phantom Lab/Image Owl	1209
Tropical Health & Education Trust (THET)	2511
University of Waterloo, Engineering	2414
USOC Medical	2201
Varian Medical Systems	1234
Western Medical Biophysics and BME	3507
World Congress 2018, Prague	3311
World Congress 2021, Candidate City – Singapore	3614
World Congress 2021, Candidate City – Taipei	3212
World Congress 2021, Candidate City – Mexico City	3307
World Health Organization	3313
Xoft, a subsidiary of iCAD, Inc.	1129
Zimmer Canada	2303

EXHIBITORS

Numerical

Brainlab	1102	PartsSource	2209
IOP Publishing	1103	Southwest Medical Resources	2210
CRC Press/Taylor & Francis	1107	Centre for Imaging Technology Commercialization (CIMTEC)	2211
Standard Imaging	1110	MedView Technologies	2213
Heidelberg University	1111	Shimifrez	2214
Department of Radiation Oncology, University of Toronto	1114	BRACCO IMAGING Canada	2301
Canadian Organization of Medical Physicists (COMP)	1115	GE Healthcare	2302
International Organization for Medical Physics (IOMP)	1119	Zimmer Canada	2303
Naf Sacs	1120	Canadian Medical and Biological Engineering Society (CMBES)	2305
iRT Systems	1124	Physio-Control	2306
RTI - From Radiation to Information	1125	International Federation of Medical and Biological Engineering (IFMBE)	2309
CDR Systems	1127	Springer	2311
Xoft, a subsidiary of iCAD, Inc.	1129	Spectrum Technologies, Inc.	2412
Philips Healthcare	1201	University of Waterloo, Engineering	2414
Elekta	1202	Fibertech Canada	2503
NELCO	1205	GCX Corporation	2505
The Phantom Lab/Image Owl	1209	Tropical Health & Education Trust (THET)	2511
Precision X-Ray	1210	Biomedical Engineering Society (BMES)	2709TT
Orfit Industries America	1211	ECRI Institute	2711TT
American Association of Physicists in Medicine (AAPM)	1212	Engineering World Health	2713TT
Radiological Imaging Technology Inc.	1213	Institution of Engineering and Technology	2715TT
LAP Laser	1214	Accuray Inc.	3104
RaySearch	1219	Fluke Biomedical/RaySafe	3112
PTW	1220	Getinge Group	3114
CIRS	1224	MedTech Hub	3203, 3206
Canadian Nuclear Safety Commission	1228	Radcal Corporation	3204
Oncology Systems Limited Inc.	1230	Maquet-Dynamed	3211
Varian Medical Systems	1234	World Congress 2021, Candidate City – Taipei	3212
Modus Medical Devices Inc.	1309	ArjoHuntleigh Canada Inc.	3213
Mobius Medical Systems	1323	International Union for Physical and Engineering Sciences in Medicine (IUPESM)	3214
Qfix	1327	Best Theratronics	3303
Sun Nuclear Corporation	1329	Harpell Associates Inc.	3305
IBA	1331	World Congress 2021, Candidate City – Mexico City	3307
Technical Prospects	2102	World Congress 2018, Prague	3311
IEEE, Engineering in Medicine & Biology Society	2104	World Health Organization	3313
Pacific Medical LLC	2106	Synaptive	3404
Dräger	2110	Carleton University	3406
Olympus Canada Inc.	2112	Bayer HealthCare	3503
Spacelabs Healthcare	2114	Western Medical Biophysics and BME	3507
USOC Medical	2201	ANDA Medical	3604
CareFusion	2202	IPEM	3606
Covidien	2203	World Congress 2021, Candidate City – Singapore	3614
Dunlee	2204		
MIM Software Inc.	2205		

EXHIBITOR BIOGRAPHIES

Accuray | Booth # 3104



Accuray Incorporated is a radiation oncology company that develops, manufactures and sells precise, innovative tumor treatment solutions that set the standard of care with the aim of helping patients live longer, better lives. The company's leading-edge technologies deliver the full range of radiation therapy and radiosurgery treatments.

American Association of Physicists in Medicine (AAPM) | Booth # 1212



The mission of AAPM, a professional organization of 8,400+ members, is to advance the science, education and professional practice of medical physics. Visit booth #1212 for information on AAPM programs, to see a demonstration of the Virtual Library and to pick up complimentary copies of the Medical Physics journal.

ANDA Medical | Booth # 3604



ANDA Medical provides new and refurbished medical equipment to the global community. By locating medical products from the finest health facilities around the world, we maintain strong relationships with hospitals, medical suppliers, and OEMs. With consistent access to high-quality medical equipment we provide our customers with products at a fraction of the cost. This is our top priority.

ArjoHuntleigh Canada Inc. | Booth # 3213

ARJOHUNTLEIGH
GETINGE GROUP
A medical device company offering innovative solutions in Patient Handling, Therapeutic Surfaces, Medical Beds, Hygiene and Disinfection. ArjoHuntleigh offers programs to ensure facilities meet their needs while providing safe and efficient care.

Bayer Healthcare | Booth # 3503



Bayer HealthCare

Bayer's Radimetrics™ Enterprise Platform is an integrated radiation dose and contrast dose* management solution. Platform tools can help customers drive compliance, efficiency and reproducible quality. Customizable dashboards facilitate enterprise-wide analytics and protocol management. With industry-leading repair capabilities, quality, and customer care, Multi Vendor Service provides the best value in third-party service.

*Requires Medrad® Stellant® CT Injection System/Certegra® Workstation

Best Theratronics | Booth # 3303

**Best
Theratronics**

Best Theratronics Ltd. is a Canadian component of TeamBest™. We manufacture external beam therapy units (Equinox®, GammaBeam® 100-80, and the new GammaBeam® 500 Total Body Irradiator), blood and research irradiators (Gammacell® 1000 & 3000, Raycell® Mk2, Gammacell® 40E, GammaBeam® X200), and variable energy cyclotrons for radioisotope production and research.

Biomedical Engineering Society (BMES) | Booth # 2709TT



BMES
BIOMEDICAL ENGINEERING SOCIETY

The Mission of the BMES is to build and support the biomedical engineering community, locally, nationally and internationally, with activities designed to communicate recent advances, discoveries, and inventions; promote education and professional development; and integrate the perspectives of the academic, medical, governmental, and business sectors.

BRACCO® IMAGING Canada | Booth # 2301

LIFE FROM INSIDE

BRACCO® IMAGING Canada, world leader in medical imaging presents the latest contrast injection technologies in Radiology and Cardiac CathLab with ACISTCVi™, CTEmpres3D™ syringeless injector, and EmpowerCTA+™, with Nexo™ Contrast management and NexoDose™ Radiation Dose softwares. BIC distributes Invivo Corporation technologies (MR compatible patient monitoring, DynaCAD Breast and Prostate, UroNav fusion biopsy system, etc)

Canadian Organization of Medical Physicists | Booth # 1115

The Canadian Organization of Medical Physicists is the professional body for medical physicists in Canada. The membership is composed of physicists, scientists and academics located at universities, hospitals, cancer centres and government research facilities as well as graduate students and post-doctoral fellows. Members have an educational or professional background in physics or engineering as it applies to medicine.

The Canadian Organization of Medical Physicists is the

Brainlab Technology | Booth # 1102

Brainlab technology powers treatments in radiosurgery as well as numerous surgical fields including neurosurgery, orthopedic, ENT, CMF, spine and trauma. Founded in Munich in 1989, Brainlab has over 8,900 systems installed in about 100 countries.

Brainlab technology powers treatments in radiosurgery as well as

CareFusion | Booth # 2202**CareFusion***has joined BD*

At CareFusion, we serve the healthcare industry with products and services that support infection prevention, medication management, operating room efficiency, respiratory care and healthcare analytics products and services. As of March 2015, CareFusion has joined BD to become one of the largest global leaders in the medical technology industry.

At CareFusion, we serve the healthcare industry with products and

Canadian Medical and Biological Engineering Society | Booth # 2305**CMBES/SCGB**

The Canadian Medical and Biological Engineering Society is Canada's principal society for engineering in medicine and biology. The Society's mission is to advance and promote the theory and practice of engineering sciences and technology to medicine and biology, serving as a forum for information exchange between healthcare professionals, scientists, and the general public.

The Canadian Medical and Biological Engineering Society is Canada's principal society for engineering in medicine and biology. The Society's mission is to advance and promote the

Please stop by the CMBES booth # 2513 to find out more about our role, programs, networking opportunities and the 2016 Congress in May, 2016 in Calgary, Alberta.

Carleton University | Booth # 3406**Carleton UNIVERSITY****Canada's Capital University**

Carleton University, located in Canada's beautiful capital city Ottawa, offers an MASc in biomedical engineering, and MSc and PhD Physics with specialization in medical physics (the PhD is CAMPEP accredited). Our programs are networked with world-class clinical facilities and national laboratories making Carleton a stimulating academic and research environment.

Carleton University, located in Canada's beautiful capital city Ottawa, offers an MASc in biomedical engineering, and MSc and PhD Physics with

Carleton University, located in Canada's beautiful capital city Ottawa, offers an MASc in biomedical engineering, and MSc and PhD Physics with specialization in medical physics (the PhD is CAMPEP accredited). Our programs are networked with world-class clinical facilities and national laboratories making Carleton a stimulating academic and research environment. carleton.ca

Canadian Nuclear Safety Commission | Booth # 1228

Canadian Nuclear Safety Commission
Commission canadienne de sûreté nucléaire

The Canadian Nuclear Safety Commission, Canada's independent nuclear regulator, regulates the use of nuclear energy and materials to protect health, safety, security and the environment and to implement Canada's international commitments on the peaceful use of nuclear energy; and to disseminate objective scientific, technical and regulatory information to the public.

The Canadian Nuclear Safety Commission, Canada's independent nuclear regulator, regulates the use of nuclear energy and materials to protect health, safety,

CDR Systems | Booth # 1127

A global company CDR Systems offers proven next generation Frameless SRS, SRT, IMRT, IGRT, SBRT, Breast, Pelvis and H&N precision patient positioning and Immobilization products used by leading organizations worldwide. See why at our booth or email to arrange a demo. You can also keep in touch with the latest advancements in patient immobilization at: twitter.com/CDRSystems and online www.cdrrsys.ca

A global company CDR Systems offers proven next generation Frameless SRS, SRT, IMRT,

Centre for Imaging Technology Commercialization (CIMTEC) | Booth # 2211



CIMTEC builds and tests clinical prototypes in the broad areas of 3D visualization, image analysis and mecha-

tronics design with specific expertise in image-guided interventions and digital pathology. Through technology development, business advice, and clinical testing, CIMTEC helps researchers, startups and small to medium-sized companies commercialize their medical imaging innovations.

CIRS | Booth # 1224



Tissue Simulation & Phantom Technology

CIRS is recognized world wide for tissue simulation technology

and is the leader in the manufacture of phantoms and simulators for radiation therapy QA and dosimetry, diagnostic imaging and quality assurance as well as training and demonstration phantoms for CT, mammography, ultrasound, MRI, radiation therapy, fluoroscopy, radiography and emerging modalities.

Covidien | Booth # 2203



COVIDIEN

Covidien is a leading global healthcare products company

that creates innovative medical solutions for better patient outcomes and delivers value through clinical leadership and excellence. Please visit www.covidien.com to learn more about our business.

CRC Press | Booth # 1107



CRC Press
Taylor & Francis Group

CRC Press/Taylor and Francis is a leading international publisher of references, textbooks and

professional handbooks in medical physics and biomedical engineering. Visit our booth to browse and enter to receive special prizes and discounts on new and bestselling titles. Editors Francesca McGowan (francesca.mcgowan@tandf.co.uk) and Michael Slaughter (Michael.Slaughter@taylorandfrancis.com) will be available to discuss new project ideas.

Department of Radiation Oncology, University of Toronto | Booth # 1114



Radiation Oncology
UNIVERSITY OF TORONTO

The Accelerated Education Program is putting innovation to work through

education dedicated to promoting essential aspects of clinical care. Learning environments are engaging, creative and interactive, putting the focus on interprofessional activities that enhance team work. The goal of AEP is to deliver relevant, excellent programming for all radiation medicine professionals.

Dräger | Booth # 2110



As an international leader in medical and safety technology, Dräger develops innovative equipment and solutions that

people the world over trust. No matter where Dräger products are used, it's always about life. Whether for use in the OR, ICU or Neonatal Care, Dräger products protect, support and save lives.

Dunlee | Booth # 2204



For over 65 years, Dunlee has remained at the forefront of medical imaging as an interna-

tional leader in research, design, and manufacturing of high-performance replacement tubes for CT and general radiography. We also offer Technical Webinars and the Dunlee App, which features the Dunlee Academy, a virtual tube installation guide.

ECRI Institute | Booth # 2711TT



ECRI Institute is an independent nonprofit with more than 40 years of experience

researching the best approaches to improving patient care. Our unbiased, evidence-based research, information, and advice help you address patient safety, quality and risk management challenges, procure cost-effective technology, and align capital investments with strategic technology needs.

Elekta | Booth # 1202**ELEKTA**

Elekta is a human care company pioneering significant innovations and clinical solutions for treating cancer

and brain disorders. The company develops sophisticated, state-of-the-art tools and treatment planning systems for radiation therapy, radiosurgery and brachytherapy, as well as workflow enhancing software systems across the spectrum of cancer care.

GE Healthcare | Booth # 2302

GE (NYSE: GE) imagines things others don't, builds things others can't and delivers outcomes that

make the world work better. GE brings together the physical and digital worlds in ways no other company can. In its labs and factories and on the ground with customers, GE is inventing the next industrial era to move, power, build and cure the world. www.ge.com

Engineering World Health | Booth # 2713TT

engineeringworldhealth
www.ewh.org

Engineering World Health works with students and the BME community to improve healthcare delivery in developing world hospitals. We build local capacity to maintain medical equipment, make repairs, and develop

low-cost technologies. Visit us to learn about our Summer Institute and making a lasting impact on developing world health care!

Getinge Group | Booth # 3114**GETINGE
GETINGE GROUP**

Getinge is a leading global medical technology company with operations in the areas of surgery, intensive care, infection control, care ergonomics and wound care. Getinge provides equipment, systems and solutions that aims to contribute to quality enhancements and cost efficiency within healthcare and the life sciences.

Fibertech | Booth # 2503**FIBERTECH**

Since 1994, Fibertech continues to be the number #1 hospital

equipment service facility in Canada. Specializing in repair of flexible and rigid endoscopes, rigid instrumentation, power tools and phaco hand pieces. Training and education programs provide a complete experience for our customer.

Harpell Associates | Booth # 3305**HARPELL ASSOCIATES**

Harpell Associates is a company dedicated to selling high quality healthcare care

products, and services to Radiation Oncology, Nuclear and Radiological imaging centers throughout Canada. With over 35 years of experience in the Canadian health care industry we have developed a reputation of providing outstanding customer service throughout the industry.

Fluke Biomedical / Unfors RaySafe | Booth # 3112**FLUKE****Biomedical**

Together Fluke Biomedical and Unfors RaySafe strive to improve the quality of global health, one measurement at a

time. We provide most reliable quality assurance solutions to make medical equipment safer to use. We serve biomedical engineers, quality-assurance technicians, medical physicists, oncologists, and radiation-safety professionals. For more information, visit www.flukebiomedical.com.

Heidelberg University | Booth # 1111

Heidelberg University, founded in 1386, is the oldest University in Germany with a strong

international orientation. In 2010 the first postgraduate distance learning Master program the "Master Online Advanced Physical Methods in Radiotherapy (APMR)" was launched. Since then additional distance learning programs in the field of Medical Physics have topped off the offer.

GCX Corporation | Booth # 2505**GCX[®]
Mounting Solutions**

GCX Corporation - the world-wide leader in medical instrument mounting solutions. Over

forty years of industry experience has given us a unique understanding of the interaction between medical devices, users, and healthcare environments. We partner with you to create mounting products that enable caregivers to deliver improved patient care.

IBA | Booth # 1331

IBA is a global medical technology company focused on bringing integrated and innovative solutions for the diagnosis and treatment of cancer. The Company is the worldwide technology

leader in the field of proton therapy. IBA also has a radiation dosimetry business and develops particle accelerators for the medical world and industry.

IEEE Engineering in Medicine and Biology Society
| Booth # 2104



IEEE Engineering in Medicine and Biology Society is the world's largest society of biomedical engineers. We provide access to people, practices, information, ideas and opinions shaping one of

the fastest growing, technical fields. EMBS focuses on development and application of engineering concepts/ methods to provide solutions to medical and healthcare problems.

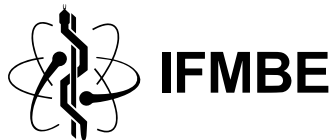
Institution of Engineering and Technology
| Booth # 2715TT



The IET journals portfolio offers high quality research in a number of topic areas including medical and biomedical research.

Healthcare Technology Letters, IET Image Processing, IET Nanobiotechnology and IET Systems Biology are all key journals in this fast-paced field and considered an invaluable source for researchers and practitioners. Find out more at www.ietdl.org/journals.

International Federation for Medical and Biological Engineering (IFMBE) | Booth # 2309



The International Federation for Medical and Biological Engineering (IFMBE) is primarily a federation of national and transnational

societies. These professional organizations represent interests in medical and biological engineering. The IFMBE is also a Non-Governmental Organization (NGO) for the United Nations and the World Health Organization (WHO), where we are uniquely positioned to influence the delivery of health care to the world through Biomedical and Clinical Engineering.

International Organization for Medical Physics (IOMP)
| Booth # 1119



International Organization for Medical Physics (IOMP) represents over 18,000 medical physicists worldwide and 80 national member organisations.

The mission of IOMP is to advance medical physics practice worldwide by disseminating scientific and technical information, fostering the educational and professional development of medical physicists, and promoting the highest quality medical services for patients.

International Union for Physical and Engineering Sciences in Medicine (IUPESM) | Booth # 3214



IUPESM is a non-profit scientific NGO. The founding constituent organizations are IFMBE and IOMP. The objective is to contribute to the advancement of physical and engineering science in medicine for the well-being of humanity. IUPESM is the custodian of the triennial World Congress for Medical Physics and Biomedical Engineering.

IOP Publishing | Booth # 1103



IOP Publishing (iopublishing.org) provides a range of journals, books, websites,

magazines, congress proceedings and services through which leading-edge scientific research is distributed worldwide. Visit our stand to find out more about IOP Biosciences - our journals publishing in a number of fields, including medical physics, biomedical engineering and biophysics.

IPEM | Booth # 3606



IPEM Institute of Physics and Engineering in Medicine

The Institute of Physics and Engineering in

Medicine (IPEM) is dedicated to bringing together physical science, engineering and clinical professionals in academia, and healthcare to share knowledge, advance science / technology and inform / educate the public with the purpose of improving the understanding, and treatment of disease and management of patients.

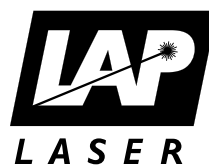
iRT Systems | Booth # 1124



iRT is a new company founded in 2013 to introduce innovative new products into the radiation therapy market with the goal to improve patient safety and the overall quality of treatment.

Our first project is the development and certification of the Integral Quality Monitor (IQM) System, a revolutionary new device for real-time quality assurance.

LAP Laser | Booth # 1214



LAP of America Laser Applications, L.L.C has been delivering state of the art patient alignment laser systems for radiation therapy, nuclear medicine, and diagnostic radiology since 1997.

Building on a strong tradition of excellence in the medical industry LAP has become the world leader in patient alignment laser systems.

Maquet-Dynamed | Booth # 3211

MAQUET-DYNAMED

MAQUET is a subsidiary of the publicly listed

Swedish Group of companies GETINGE AB. The MAQUET brand represents the Medical Systems Business area and together with two other Business Areas ARJO Extended Care and GETINGE Infection Control, the entire GETINGE group of companies focuses on forward-looking medical technology.



MedTech Hub
| Booth # 3203, 3206

ACMIT | Booth # 3203, 3206



ACMIT is a translational research center focused on technology for minimally invasive surgery that combines multidisciplinary know-how with that of international experts. The organizational

structure of ACMIT reflects the quest for scientific excellence and successful technology development. ACMIT's goal is to bring developments to their real use in clinical context within reasonable time.

CTMH | Booth # 3203, 3206



CTMH is collaboration between Karolinska

Institutet, Royal Institute of Technology and Stockholm County Council to help develop the region as a world-class medical technology center. CTMH creates venues and activities that stimulate and develop exchanges between industry, academia and health care in the boundaries between technology, health, research and application.

Hong Kong Science & Technology Parks Corporation (HKSTP) | Booth # 3203, 3206



Comprising Hong Kong Science Park, InnoCentre and Industrial Estates, Hong Kong Science & Technology Parks Corporation

(HKSTP) is a statutory body dedicated to building a vibrant innovation and technology ecosystem to connect stakeholders, nurture technology talents, facilitate collaboration, and catalyse innovations to deliver social and economic benefits to Hong Kong and the region.

Institute of Biomedical Engineering | Booth # 3203, 3206



The Institute of Biomedical Engineering is a leading university-based deliverer of medtech R&D and innovation.

The IBME brings together businesses, clinicians and academics to establish the technical feasibility, clinical desirability and commercial viability of cutting edge medical technology. We're pioneering this engagement through both our MedTech Accelerator Programme and our PhD training scheme.

Medical Valley EMN | Booth # 3203, 3206



The Medical Valley EMN (e.V.) association assumes key tasks in the medical technology cluster and supports all members with comprehensive

services. The association facilitates knowledge exchange, promotes the cluster internationally, and supports start-up companies. The overall goal is to develop the EMN area into a model region for optimal healthcare.

Morgridge Institute for Research | Booth # 3203, 3206



The Morgridge Institute for Research is a private, nonprofit biomedical research institute in Madison, Wis., affiliated with the University

of Wisconsin-Madison. The institute works to improve human health by conducting, enabling and translating interdisciplinary biomedical research. Current research includes regenerative biology, virology, medical engineering and core computational technology.

Ontario Brain Institute | Booth # 3203, 3206



The Ontario Brain Institute is a provincially-funded, not-for-profit research centre seeking to maximize the impact of neuroscience and establish Ontario as a world leader in brain research, commercialization and care.

We create partnerships between researchers, clinicians, industry, patients, and their advocates to foster discovery and deliver innovative products and service.

Sunnybrook Research Institute | Booth # 3203, 3206



Sunnybrook Research Institute (SRI) is the research enterprise of Sunnybrook Health

Sciences Centre and is affiliated with the University of Toronto. Scientists at SRI strive to understand and prevent disease, and to develop treatments that enhance and extend life. They are renowned for excellence in the biological, physical and evaluative clinical sciences.

Techna | Booth # 3203, 3206



Techna is an institute of University Health Network, in collaboration with the

University of Toronto, focused on the accelerated development and exploitation of technology for improved health. Techna is designed to shorten the time interval from technology discovery to application through a continuum of clinically driven innovation, technology & process development.

Thunder Bay Regional Research Institute (TBRI) | Booth # 3203, 3206

Thunder Bay Regional Research Institute

In partnership with
Thunder Bay Regional Health Sciences Centre
Affiliated with Lakehead University

Established in 2007 as Canada's newest molecular imaging and advanced diagnostics research institute, TBRI is now the research arm of the

Thunder Bay Regional Health Sciences Centre. Currently Scientists, Physician Researchers and Clinicians are engaged in research which contributes to innovative treatments and improved diagnostic tools.

MedView Technologies | Booth # 2213



MedView was founded in 2013 to commercialize a highly innovative & proprietary technology

based on Spatially Resolved Diffusive Reflectance Spectroscopy, with potential applications in the medical diagnostics, pharmaceutical manufacturing, and food/material inspection fields. We are currently developing a vein detection medical device, with potential market size of up to \$4B.

MIM Software Inc. | Booth # 2205



MIM Software Inc. provides practical imaging solutions in the fields of radiation oncology, radiology, nuclear medicine, urology, neuroimaging, and cardiac imaging. MIM offers solutions for computer workstations, as well as mobile and cloud-based platforms. MIM products are sold globally to imaging centers, hospitals, specialty clinics, research organizations, and pharmaceutical companies.

Mobius Medical Systems | Booth # 1323



Mobius Medical Systems provides the radiation oncology community with

innovative software to streamline quality assurance. Mobius3D and MobiusFX are the first solutions for full 3D verification of both patient plan and delivery. Reclaim your nights and weekends! MobiusFX provides comprehensive patient specific QA in as little as one minute.

Modus Medical Devices Inc. | Booth # 1309



For 15 years, QUASAR™ has inspired physicists worldwide to seek the highest quality assurance

standards in the field of medical imaging and radiotherapy. With 3,000 phantoms in over 1,800 treatment centres, Modus products are built to provide you with confidence that every patient is receiving the best possible treatment.

NELCO | Booth # 1205



NELCO is the worldwide leader in the design, manufacturing and construction of radiation shielding products and

facilities for radiation therapy and diagnostic imaging. NELCO's 80 year dedication to customer service, quality, and innovative products has resulted in over 4000 radiation therapy doors installed worldwide and over 5000 customers.

Olympus Canada Inc. | Booth # 2112



Olympus develops leading edge technology for healthcare

professionals that help improve outcomes and enhance quality of life for patients. Visit us at Booth #2112 in the exhibit hall or on-line at www.olympuscanada.com

Oncology Systems Limited Inc. | Booth # 1230

ONCOLOGY SYSTEMS LIMITED

ImSimQA software is a complete toolkit for performing QA on Deformable Image Registration algorithms. OnQ RTS is an automated clinical system for performing Adaptive Planning functions including Deformable Image Registration. Add function without adding process to your department. Canadian distributors of MacroMedics immobilization and patient positioning devices.

Orfit Industries America | Booth # 1211

Orfit supplies High Precision Immobilization Systems including Adult /Pediatric Head/Neck systems using Frameless full and open face masks. MammoRx Breast Boards, SBRT Systems, Prone Breast Solutions, Extremities, Pelvis/Abdomen, Proton and MR Compatible systems are available.

Precision, reproducibility, ease of use, high patient comfort are hallmarks of the systems

Pacific Medical LLC | Booth # 2106

ONE SOLUTION FOR ALL YOUR PATIENT MONITORING NEEDS

Pacific Medical LLC specializes with providing PARTS and REPAIR SERVICES for

Patient Monitors, Modules, Telemetry, Infusion Pumps, Suction Regulators, Fetal Transducers, SpO2/ECG/TEMP/ NIBP Cables, O2 Blenders, Endoscopes and Gas Analyzers. Pacific Medical carries the largest patient monitoring inventory in our industry and is recognized for its customer service response team.

For more information visit: www.pacificmedicalsupply.com.

PartsSource | Booth # 2209

PARTSOURCE® PartsSource is a leading provider of supply chain solutions for medical replacement parts for providers, Independent Services Organizations and OEMs in the healthcare industry who need to innovate their procurement process to reduce their overall sourcing costs.

Phillips Healthcare | Booth # 1201

Philips is dedicated to creating the future of healthcare and saving lives. We develop innovative solutions across the continuum of care in partnership with clinicians and our customers to improve patient outcomes, provide better value, and expand access to care. www.philips.com

Physio-Control | Booth # 2306

LIFEPAK® defibrillator/monitors and automated external defibrillators from Physio-Control set the standard for quality and reliability and are used by more physicians, hospitals and emergency medical services than any other brand.

Physio-Control continues to lead the industry through innovation and advanced technology. For more information, visit our website at www.physio-control.com.

Precision X-Ray | Booth # 1210

Precision X-Ray is the leading provider of safe, high output X-Ray irradiators used in modern translational cancer research. It's our mission to continually develop X-ray systems that help researchers globally to better understand radiation induced effects in the sciences of molecular biology and cancer research.

PTW | Booth # 1220

Knowing what responsibility means

Since 1922 PTW has been a dosimetry pioneer, growing into a global market leader for high-tech dosimetry solutions, well-known for their product excellence and innovative strength.

Today, PTW dosimetry products are the first choice by healthcare professionals in radiotherapy, diagnostic radiology, nuclear medicine and health physics. For more information, visit www.ptwny.com.

Qfix | Booth # 1327

Qfix provides state-of-the-art patient positioning and immobilization devices to optimize patient outcomes.

The Qfix kVue™ IGRT Couch Top design allows customization for individual patient needs through the most advanced array of treatment solutions for head and neck, breast, lung, prostate and other disease sites. Please visit www.Qfix.com for more information.

Radcal Corporation | Booth # 3204

Radcal is synonymous with quality non-invasive diagnostic x-ray meters and ion chambers. The Accu-Gold Family of meters utilizes Radcal ion chambers and solid-state Multisensors for all your parameter measurements in all modalities. The newest addition to the Family is the Accu-Dose+ and WiFi data transmission.

Providing Better Solutions for You. www.Radcal.com

Radiological Imaging Technology Inc. | Booth # 1213



RIT manufacturers RIT113 Radiation Therapy Dosimetry software, and RADIA software for automated QC phantom analysis. RIT software

packages are designed to enable QA on all aspects of modern radiation therapy and diagnostic imaging, including TG-142 for linear accelerators, TG-148 for helical tomotherapy, and ACR CT and MRI testing.

Raysearch Laboratories | Booth # 1219



RaySearch is a medical technology company that develops advanced software solutions for improved

radiation therapy of cancer. RaySearch markets the RayStation® treatment planning system to clinics all over the world. In addition, RaySearch's products are distributed through licensing agreements with leading medical technology companies. RaySearch's software is used by over 2,500 clinics in more than 65 countries.

RTI (From Radiation to Information) | Booth # 1125



From Radiation to Information

RTI provides complete quality assurance solutions for all X-ray modalities and facilities. We have "click &

go" solutions for X-ray quality assurance of X-ray modalities and facilities. Everything between basic service to specialists.

Our X-ray multimeter scan "do it all in one shot" – kV, time, dose, dose rate, HVL, pulsed fluoroscopy and total filtration.

Shimifrez | Booth # 2214



Shimifrez is the world's most trusted name in micro, thin metal

manufacturing, utilizing precision photo chemical machining (PCM). PCM produces highly accurate and identical thin metal components for small & large batches. PCM eliminates the cost of hard tooling, improves design flexibility and shortens lead times (72 hours) while eliminating burring and stress problems.

Southwest Medical Resources | Booth # 2210



Southwest Medical Resources is a world class independent service organization offering complete sales, service and

rental solutions for Diagnostic Imaging Equipment. Our leadership in the industry is driven by a team of experts and unmatched resources. We exist to bring quality and value to our customers.

Spacelabs Healthcare | Booth # 2114



Spacelabs Healthcare's philosophy is to develop innovative medical devices to

provide the best care experience for not only the patient and the clinician, but also the patients' families. Providing devices that help reduce stress can help enhance the experience for both patient and visitor alike.

Spectrum Technologies, Inc. | Booth # 2412



Test Instrument Calibration and Repair
800-342-7748
www.goSTI.cc

Spectrum Technologies, Inc. provides test instrument calibration and repair for the biomedical, commercial, and industrial

markets. On-site services are available regionally and depot services are available worldwide. Our main office is in Pennsylvania with branch offices strategically located across the USA and two in Canada. Our website: www.goSTI.cc Email: info@goSTI.cc

Springer | Booth # 2311



Looking to publish your research? Discover Springer's print and electronic publication

services, including Open Access! Get high-quality review, maximum readership and rapid distribution. Visit our booth or springer.com/authors. You can also browse key titles in your field and buy (e)books at discount prices. With Springer you are in good company.

Standard Imaging | Booth # 1110



Dedication to customer service, forging partnerships

and fostering innovation helps Standard Imaging pave an intuitive path to superior QA. Beginning with the HDR 1000 Well Chamber to the W1 Scintillator and PIPSPRO Software today, Standard Imaging provides its customers with practical, precise products for their QA needs.

Sun Nuclear Corporation (SNC) | Booth # 1329

Sun Nuclear Corporation (SNC) is the worldwide market share

leader in QA and Dosimetry solutions for Radiation Oncology. While others speak of innovation, we live it. Our mission is to provide you with better outcomes that save time. SNC supports FFF Beams, VMAT, IMRT, SRS, TomoTherapy, CyberKnife, and Conventional external beam treatments.

Synaptive Medical | Booth # 3404

Synaptive Medical has dedicated more than 50 engineers and scientists specifically to the development of neurosurgical technologies. The result? Our BrightMatter™ Neurosurgery Products provide advanced tools and information for surgeons and hospitals to focus on patient outcomes.

Technical Prospects | Booth # 2102

EXPERTS IN SIEMENS MEDICAL IMAGING

Technical Prospects has been in business

over 18 years, providing quality Siemens parts and service to nearly 500 customers worldwide. As a well-known medical imaging parts reseller, our main objective is to provide quality parts and service, technical support, maintenance services and training to medical facilities and health care providers.

The Phantom Lab/Image Owl | Booth # 1209

The Phantom Laboratory (www.phantomlab.com) manufactures medical imaging and radiation therapy phantoms. In addition to our standard

products we offer custom and OEM phantoms. We also work with Image Owl (www.imageowl.com) to provide fully automated, cloud-based, CT, MR and DBT image quality measurement and database services.

Tropical Health & Education Trust (THET) | Booth # 2511

THET is a specialist global health organisation that educates, trains and supports health workers through partnerships; enabling people

in low and middle-income countries to access essential healthcare. THET helped develop the first Biomedical Engineering training course in Zambia and are working with Government to improve medical equipment management and maintenance.

University of Waterloo, Engineering | Booth # 2414

Waterloo Engineering is home to 60+ researchers focused in biomedical engineering and biotech-

nology, who produce advancements in pharmaceutical delivery systems, affordable imaging systems, software solutions for healthcare and more. With strong partnerships in industry, healthcare and government, our researchers create next-generation technology to tackle the world's toughest biomedical problems.

USOC Medical | Booth # 2201

USOC Medical provides biomedical equipment repair solutions to healthcare

facilities, clinics and medical companies of all types and sizes. We are committed to providing high-quality, cost-effective equipment and services to all of our clients. Each member of our organization is dedicated to excellence and continual organization and professional improvement.

Varian Medical Systems | Booth # 1234

Varian Medical Systems is a leading manufacturer of medical devices for treating cancer and other conditions

with radiotherapy, radiosurgery, proton therapy, and brachytherapy. The company also produces informatics software for managing comprehensive cancer clinics. Varian is a premier supplier of tubes, digital detectors, and image processing workstations for X-ray imaging. www.varian.com

Western Medical Biophysics and BME | Booth # 3507



Welcome to Canada's first Biophysics Department – home to 90 researchers and 100 graduate students. Working closely with research institutes and

hospitals, we offer unique training opportunities in biomedical imaging, cardiovascular studies (microcirculation & hemodynamics), biomechanics, and cancer diagnosis & therapy, using a wide range of experimental and computational techniques.

World Congress 2018, Prague | Booth # 3311



The IUPESM World Congress 2018 will be held in Prague, Czech Republic on June 3 - 8, 2018. For constant updates please visit www.iupesm2018.org.

We invite you to visit our booth No. 3311 to try to win a FREE REGISTRATION for IUPESM 2018.

World Congress 2021, Candidate City - Mexico City | Booth # 3307



promote and enhance knowledge and education in biomedical engineering nationwide and its utilization for human health and well-being. www.somib.org.mx

The Mexican Society of Biomedical Engineering (SOMIB) serves as the lead society and professional home for biomedical engineering. Our main mission is to

World Congress 2021, Candidate City – Singapore | Booth # 3614



time it will be held in South East Asia. We are ready to welcome the global community of medical physicists and biomedical engineers to our multi-cultural city.

Choose Singapore for 2021 World Congress - Singapore is excited to put forth a bid to host the IUPESM World Congress in 2021, the first

World Congress 2021, Candidate City – Taipei | Booth # 3212



supports from local hospitals and related industrial companies will be offered for this important meeting. We believe that Taipei will be the optimum choice for this worldwide event in 2021.

The IUPESM 2021 World Congress (WC-2021) has proposed to be hosted in Taipei, an international city with convenient and well-equipped facilities, by the Chinese Society of Medical Physics, Taipei and Taiwanese Society of Biomedical Engineering together. Many

World Health Organization | Booth # 3313



World Health Organization

The World Health Organization is a U.N. specialized agency with a mandate as the directing and coordinating authority of international public health work. Through its 6 regional offices, 147 country offices, 8000+ staff, and collaborators the WHO strives towards: "Attainment by all peoples of the highest possible level of health." The World Health Organization is a U.N. specialized agency with a mandate as the directing and coordinating authority of international public health work. Through its 6 regional offices, 147 country offices, 8000+ staff, and collaborators the WHO strives towards: "Attainment by all peoples of the highest possible level of health."

The World Health Organization is a U.N. specialized agency with a mandate as the directing and coordinating authority of international public health work. Through its 6 regional offices, 147 country offices, 8000+ staff, and collaborators the WHO strives towards: "Attainment by all peoples of the highest possible level of health."

Xoft, a subsidiary of iCAD, Inc. | Booth # 1129



iCAD delivers innovative cancer detection and radiation therapy solutions and services that enable clinicians to find and treat cancers earlier and while enhancing patient care. iCAD's Xoft® Axxent® Electronic Brachytherapy (eBx®) System® delivers high dose rate, low energy radiation, which targets cancer while minimizing exposure to surrounding healthy tissue. For more information, visit www.icadmed.com.

Zimmer Canada | Booth # 2303



Founded in 1927 and headquartered in Indiana, Zimmer designs, develops, manufactures and markets orthopaedic reconstructive, spinal, trauma and dental implants, plus related surgical products. Zimmer has operations in more than 25 countries and sells products in more than 100 countries. The Company is supported by more than 8,500 employees worldwide.

Founded in 1927 and headquartered in Indiana, Zimmer designs, develops, manufactures and markets

CONNECTED CARE

Because the future is collaborative



Visit Elekta at the World Congress of Medical Physics and Biomedical Engineering 2015 in Toronto Canada and discover how we are bringing information-guided cancer™ care to you.

Stop by our **booth # 1202** to learn more about the latest innovations in:

- Monaco® - Complete treatment planning system
- MOSAIQ® - Oncology information system
- AQUA - Machine quality management
- Oncentra® brachy planning (v4.5) - Comprehensive treatment planning for brachytherapy
- Flexitron® treatment delivery - Afterloading platform

Also, please join us for lunch where Stanley Benedict of University California Davis will discuss:
“New Technology Developments to Improve Patient Safety in Radiation Therapy”

Learn how a better focus on safety in technology can deliver better precision, better reliability and better outcomes. This is an important guidance for Elekta and consistent with the stated goals of ASTRO, ACR and more.

Presenter:

Stanley H. Benedict, Ph.D., DABR, FAAPM

Professor & Vice Chair of Clinical Physics

Department of Radiation Oncology

University of California at Davis Comprehensive Cancer Center

June 9th, 2015

12:15 - 1:15 pm EST

Metro Toronto Convention

Center Room 718A

Please register at: <http://www.elekta.com/wc2015symposium>



INDUSTRY SUPPORTED SYMPOSIA

Monday, June 8, 2015 | 12:15 – 13:15

► Room 718A

SYMPOSIUM SUPPORTED BY



Advancing Radiation Therapy through Software Innovation

Delegates are welcome to attend RaySearch's Lunch Symposium. It will show how software will be the driving force of innovation in radiation therapy and notably in adaptive therapy.

Tuesday, June 9, 2015 | 12:15 – 13:15

► Room 718A

SYMPOSIUM SUPPORTED BY



New Technology Developments to Improve Patient Safety in Radiation Therapy

Learn how a better focus on safety in technology can deliver better precision, better reliability and better outcomes. This is an important guidance for Elekta and consistent with the stated goals of ASTRO, ACR and more.

Wednesday, June 10, 2015 | 12:15 – 13:15

► Room 716B

SYMPOSIUM SUPPORTED BY



Improving Medication Safety through Infusion Pump Auto-Programming and EMR System Interoperability

Interoperability between infusion systems and a hospital EMR presents new opportunities for improving IV infusion safety, patient care and clinical workflow. At this event, attendees will have the opportunity to learn about experiences with system integration and the benefits it brings to patients, clinicians, IT, BioMed and Informatics.

Thursday, June 11, 2015 | 12:15 – 13:15

► Room 714B

SYMPOSIUM SUPPORTED BY



Accuray's Innovative Radiation Therapy and Clinical Benefits

Through close collaboration with our customers, we have developed premier oncology tools that meet the needs of clinicians and the demands of any oncology department. Our portfolio of products allows clinicians to treat tumors of all sizes, regardless of their location in the body. Please join us to learn more about Accuray's offerings in the radiation therapy field.

PROGRAM AT A GLANCE

	SAT. ► JUNE 6	SUNDAY ► JUNE 7	MONDAY ► JUNE 8	TUESDAY ► JUNE 9		
8:00	CANADIAN COLLEGE OF PHYSICISTS IN MEDICINE (CCPM) EXAMS	CANADIAN COLLEGE OF PHYSICISTS IN MEDICINE (CCPM) EXAMS USE OF AAPM TASK GROUP 100 RECOMMENDED RISK ASSESSMENT APPROACH TO DEVELOP A RISK BASED QUALITY MANAGEMENT PROGRAM IN RADIATION THERAPY RT RESEARCH SYSTEM DEVELOPMENT ON OPEN SOURCE SLICERRT PLATFORM (SLICERRT HANDS ON TUTORIAL) AUTOSEG 2015 JOINT YOUNG INVESTIGATOR SYMPOSIUM (IOMP AND IFMBE)	SCIENTIFIC SESSIONS INCLUDING PRESIDENT'S CALL	SCIENTIFIC SESSIONS INCLUDING PRESIDENT'S CALL		
8:30			CONTINUING EDUCATION SESSIONS (ENGLISH, FRENCH, SPANISH)	CONTINUING EDUCATION SESSIONS (FRENCH, ENGLISH, SPANISH)		
9:00					IFMBE AWARDEES PRESENTATIONS	
9:30					IOMP GENERAL ASSEMBLY	
10:00				NETWORKING BREAK		NETWORKING BREAK
10:30						
11:00					OPENING CEREMONY & PRESIDENT'S WELCOME ADDRESS	THE FUTURE OF CLINICAL ENGINEERING
11:30						INNOVATIVE BIOMEDICAL ENGINEERING RESEARCH IN ASIA
12:00						SCIENTIFIC SESSIONS INCLUDING PRESIDENT'S CALL
12:30					INDUSTRY SYMPOSIUM SUPPORTED BY RAYSEARCH	CONTINUING EDUCATION SESSIONS (ENGLISH, FRENCH, SPANISH)
13:00						INDUSTRY SYMPOSIUM SUPPORTED BY ELEKTA
13:30						
14:00					THEME PLENARY KEYNOTE SESSION - MONIQUE FRIZE & LONDA SCHIEBINGER	THEME PLENARY KEYNOTE SESSION - JEFF IMMELT
14:30						(JOINED BY A DISCUSSION PANEL OF DEPUTY MINISTER BOB BELL & MARY GOSPODAROWICZ)
15:00					SCIENTIFIC SESSIONS INCLUDING PRESIDENT'S CALL	SCIENTIFIC SESSIONS INCLUDING PRESIDENT'S CALL
15:30					CONTINUING EDUCATION SESSIONS (ENGLISH, FRENCH)	CONTINUING EDUCATION SESSIONS (ENGLISH, FRENCH, SPANISH)
16:00						IOMP AWARDEES PRESENTATIONS
16:30					NETWORKING BREAK	NETWORKING BREAK
17:00						PRESENTATION OF WC 2021 BIDS
17:30					SCIENTIFIC SESSIONS INCLUDING PRESIDENT'S CALL	SCIENTIFIC SESSIONS INCLUDING PRESIDENT'S CALL
18:00					CONTINUING EDUCATION SESSIONS (ENGLISH, FRENCH, SPANISH)	CONTINUING EDUCATION SESSIONS (ENGLISH, FRENCH, SPANISH)
18:30						IUPESM AWARDEES PRESENTATION
19:00		WELCOME RECEPTION				
19:30						
20:00				IFME & IOMP PRESIDENTIAL RECEPTION (BY INVITATION ONLY)		
20:30						
21:00						
21:30						
22:00						
22:30	EXHIBIT & POSTER HALL HOURS 18:00 – 20:00	EXHIBIT & POSTER HALL HOURS 09:30 – 17:00	EXHIBIT & POSTER HALL HOURS 09:30 – 17:00	EXHIBIT & POSTER HALL HOURS 09:30 – 17:00		

WEDNESDAY ► JUNE 10

THURSDAY ► JUNE 11

FRIDAY ► JUNE 12

THEME PLENARY KEYNOTE SESSION - GORDON MCBEAN & MARY GOSPODAROWICZ					SCIENTIFIC SESSIONS INCLUDING PRESIDENT'S CALL			CONTINUING EDUCATION SESSIONS (ENGLISH)		IFMBE STUDENT DESIGN COMPETITION PRESENTATIONS		SCIENTIFIC SESSIONS INCLUDING PRESIDENT'S CALL		CONTINUING EDUCATION SESSIONS (ENGLISH)	
NETWORKING BREAK					NETWORKING BREAK							NETWORKING BREAK			
ICSU BIOUNIONS CLUSTER SESSION	WORLD SUMMIT ON THE SUPPORTABILITY OF MEDICAL DEVICES	CONTINUING EDUCATION SESSIONS (ENGLISH, FRENCH, SPANISH)	SCIENTIFIC SESSIONS INCLUDING PRESIDENT'S CALL		IAMBE GENERAL ASSEMBLY	SCIENTIFIC SESSIONS INCLUDING PRESIDENT'S CALL		CONTINUING EDUCATION SESSIONS (ENGLISH)		ADDRESSING GLOBAL CHANGES			SCIENTIFIC SESSIONS INCLUDING PRESIDENT'S CALL	CONTINUING EDUCATION SESSIONS (ENGLISH)	
HTA ROUND TABLE	INDUSTRY SYMPOSIUM SUPPORTED BY CAREFUSION				INDUSTRY SYMPOSIUM SUPPORTED BY ACCURAY	SPREADING & INTEGRATING HUMAN FACTORS EXPERTISE IN HEALTHCARE	SOCIAL IMPLICATIONS OF TECHNOLOGY WORKSHOP	MEDICAL PHYSICISTS WITHOUT BORDERS	EMBEDDED SENSOR SYSTEMS FOR HEALTH WORKSHOP	CHALLENGES & BENEFITS OF CLINICAL ENGINEERING PEER REVIEW	CLOSING CEREMONY & YOUNG INVESTIGATORS AWARDS PRESENTATION				
HTA FOR BIOMEDICAL ENGINEERS WORKSHOP	MEDICAL PHYSICS & BIOMEDICAL ENGINEERING RESPONSE TO CANCER CONTROL: A GLOBAL HEALTH CHALLENGE	CONTINUING EDUCATION SESSIONS (ENGLISH, FRENCH, SPANISH)	SCIENTIFIC SESSIONS INCLUDING PRESIDENT'S CALL		IFMBE GENERAL ASSEMBLY	THEME PLENARY KEYNOTE SESSION - EDWARD SHORTLIFFE & VIMLA PATEL									
NETWORKING BREAK					SCIENTIFIC SESSIONS INCLUDING PRESIDENT'S CALL		CONTINUING EDUCATION SESSIONS (ENGLISH)		WC2015 LEADERS' SUMMIT		IUPESM - HTTG WORKSHOP ON INNOVATIONS IN THE USE OF MOBILE DEVICES IN HEALTHCARE				
CONTINUING EDUCATION SESSIONS (ENGLISH, FRENCH, SPANISH)			SCIENTIFIC SESSIONS INCLUDING PRESIDENT'S CALL		IUPESM GENERAL ASSEMBLY	SCIENTIFIC SESSIONS INCLUDING PRESIDENT'S CALL	CONTINUING EDUCATION SESSIONS (ENGLISH)	CCPM AGM	QC IN RADIO-THERAPY: DEFINING THE NEXT STEPS	MEDTECH INSTITUTES RECEPTION (BY INVITATION ONLY)					
GALA DINNER					CMBES AGM			COMP AGM							
EXHIBIT & POSTER HALL HOURS 09:30 - 17:00					EXHIBIT & POSTER HALL HOURS 09:30 - 17:00										

8:00
8:30
9:00
9:30
10:00
10:30
11:00
11:30
12:00
12:30
13:00
13:30
14:00
14:30
15:00
15:30
16:00
16:30
17:00
17:30
18:00
18:30
19:00
19:30
20:00
20:30
21:00
21:30
22:00
22:30

PROGRAM AT A GLANCE

PLENARY SESSIONS

Monday, June 8 2015

SESSION DATE: MONDAY, JUNE 8 2015
 SESSION TIME: 13:30 - 15:00
 SESSION ROOM: PLENARY HALL (HALLS F&G)
 SESSION TITLE: PL01 - WOMEN IN BIOMEDICAL ENGINEERING AND MEDICAL PHYSICS
 SPEAKER(S): MONIQUE FRIZE & LONDA SCHIEBINGER

PL01.1 Engaging Women and Men for a Better Future Worldwide

Speaker(s): **Monique Frize**

Systems and Computer Engineering, Carleton University, Ottawa/ON/CANADA



From the three approaches suggested by Londa Schiebinger to harness the power of gender analysis, this part of the presentation deals with the first two: "Fixing the number of women" and "fixing the institutions". Women and men can generate and participate in activities that lead to an increased participation of women in biomedical engineering and

medical physics. Evidence also exists, demonstrating that there are economic benefits and more complete solutions created by gender balanced design teams and an increased number of women in decision-making bodies such as corporate boards, management teams in industry, government, and universities. It is critical to collect sex disaggregated data on undergraduate post-secondary enrolments and graduations in science and engineering, as well as to understand the gender participation in the workplace in these fields. Examining the issues that limit women's participation at all levels is a first step, which can then be followed by the development and implementation of strategies that help eliminate gender bias and provide the necessary support for women to have a successful career in these fields.

PL01.2 Gendered Innovations in Health & Technology

Speaker(s): Londa Schiebinger

Stanford University, Stanford, United States of America



How can we harness the power of gender analysis to discover new things? Schiebinger identified three major approaches to gender in science research, policy, and practice: 1) "Fix the Numbers of Women" focuses on increasing women's participation; 2) "Fix the Institutions" promotes gender equality in careers through structural change in research

organizations; and 3) "Fix the Knowledge" or "gendered innovations" stimulates excellence in science and technology by integrating sex and gender analysis into research. This talk focuses on the third approach. Gendered Innovations: 1) develops state-of-the-art methods of sex and gender analysis for scientists and engineers; and 2) provides 24 case studies as concrete illustrations of how sex and gender analysis leads to new ideas and excellence in research. Several case studies will be discussed, including stem cells, assistive technologies for the elderly, and osteoporosis in men. All case studies can be found at: <http://genderedinnovations.stanford.edu/>. To match the global reach of science and technology, this project was developed through a collaboration of over sixty experts from across the United States, Europe, and Canada (and has now extended to Asia). Gendered Innovations was funded by the National Science Foundation, the European Commission, and Stanford University.

Tuesday, June 9 2015

SESSION DATE: **TUESDAY, JUNE 9 2015**
SESSION TIME: **13:30 - 14:30**
SESSION ROOM: **PLENARY HALL (HALLS F&G)**
SESSION TITLE: **PL02 - NEXT GENERATION MEDICINE**
SPEAKER(S): **JEFF IMMELT**

PL02.1 Innovation, Healthcare and the Future

Speaker(s): **Jeff Immelt**

Chairman and CEO of GE, Fairfield/CT/UNITED STATES OF AMERICA



Jeff Immelt, Chairman & CEO of GE, will talk about healthcare innovation and how GE has been repositioning its business to succeed in a market that is demanding more technology, more flexibility and more tailored solutions.

Wednesday, June 10 2015

SESSION DATE: **WEDNESDAY, JUNE 10 2015**
SESSION TIME: **8:00 - 10:00**
SESSION ROOM: **PLENARY HALL (HALLS F&G)**
SESSION TITLE: **PL03 - URBAN HEALTH AND FUTURE EARTH / GLOBAL HEALTH CHALLENGES**
SPEAKER(S): **GORDON MCBEAN & MARY GOSPODAROWICZ**

PL03.1 The Changing Urban Environment and Health in a Future Earth

Speaker(s): **Gordon Mcbean**

Western University, London/ON/CANADA



Around our planet there have been increasing numbers of disasters due to floods, storms, earthquakes and other natural hazards. Although earthquakes are most horrific when they happen, climate-related events cause about three-quarters of all disasters and as the climate warms, these hazards are increasing. There is also the migration to people to major

cities, often on coasts of the oceans or major rivers. The result is the intersection of the effects of the major issues of climate change, disaster risk reduction and sustainable development. In all cases we need to look to the future and takes actions now to reduce losses in the future.

In 2015, nations will negotiate a revised framework on action on disaster risk reduction, a possible Paris-protocol on climate change and Sustainable Development Goals to be attained by all countries by 2030. The draft list of SDGs includes: end poverty and hunger; attain healthy life for all at all ages; secure water and sanitation; and build inclusive, safe and sustainable cities and human settlements. For the global science community, the challenge is providing the scientific basis for definitions and approaches, including how to achieve these goals and the criteria for measurement of progress.

This presentation will bring together these issues in the context of the new international research programs Future Earth: Research for Global Sustainability; Integrated Research on Disaster Risk; and Health and Wellbeing in the Changing Urban Environment: a Systems Analysis Approach; with a Canadian-funded project, Coastal Cities at Risk: Building Adaptive Capacity for Managing Climate Change in Coastal Megacities. The Future Earth program is adopting an approach to involve the stakeholder community in the research program from the beginning to co-design and co-produce the research based on the logic that this will make the research most directly relevant to societies needs to address these issues. The Coastal Cities research project is integrating across social-natural-economic-engineering and health sciences to develop a systems approach to quantifying urban resilience and then undertake “what if” experiments to identify the most effective approaches to improving resilience and reducing impacts, recognizing the complex interactions across these elements of society.

The International Council for Science is leading the Science and Technology Major Groups to input to these UN processes and will endeavour to bring these scientific principles to the negotiations. Working with UN agencies such as UNESCO, UNU and WMO, and non-governmental partners such as the Inter-Academy Medical Panel, the Council will continue in the coming decades to assert the importance of scientific bases for these international agreements and national actions. We need to have the full support of medical physicists and biomedical engineers engaged in supporting health care in diverse environments in order to achieve these societal objectives, consistent with the Council's Mission to strengthen international science for the benefit of society - all societies and all people.

PL03.2 Cancer: The Global Health Challenge

Speaker(s): **Mary Gospodarowicz**



Professor of Radiation Oncology, University of Toronto, Canada. Medical Director, Princess Margaret Cancer Centre, and Regional Vice President, Cancer Care Ontario

Thursday, June 11 2015

SESSION DATE: **THURSDAY, JUNE 11 2015**
 SESSION TIME: **13:30 - 15:00**
 SESSION ROOM: **PLENARY HALL (HALLS F&G)**
 SESSION TITLE: **PL04 - EVIDENCE AND HEALTH INFORMATICS**
 SPEAKER(S): **EDWARD SHORTLIFFE & VIMLA PATEL**

PL04.1 Academic Biomedical Informatics: Synergies and Challenges at the Interface with Industry

Speaker(s): **Edward Shortliffe**

College of Health Solutions, Arizona State University, Phoenix/ UNITED STATES OF AMERICA



Academic biomedical informatics has achieved great successes through research contributions and education of professional informaticians over several decades, now reflected in a thriving commercial marketplace for electronic health records and other informatics tools. That very success, coupled with changes in the ability of governments to support research at past levels,

is forcing a reconsideration of the directions and emphases for faculty members in informatics academic units. In this presentation Dr. Shortliffe will discuss those forces and propose areas of emphasis that will strengthen the academic discipline as it continues to evolve. He will distinguish the roles of academic informaticians as practitioners of informatics, as researchers, and as educators. He will also stress the necessary synergies between academic informatics and the health information technology industry, arguing that both will be strengthened by more fertile relationships and joint efforts.

PL04.2 Cognitive Challenges for Safe Human Computer Interaction

Speaker(s): **Vimla Patel**

*The New York Academy of Medicine and Columbia University,
New York/UNITED STATES OF AMERICA*



Given the complexities of modern medicine, delivery of safe and timely care is an ongoing and recognized challenge. Errors, misunderstandings, and inaccuracies—large and small—are routine occurrences in healthcare delivery. Health information technology (IT) has undoubtedly reduced the risk of serious injury for patients.

However, its true potential for preventing medical errors remains only partially realized. Unfortunately, such systems may even give rise to hazards of their own. There is a growing recognition that many errors are attributable neither solely to lapses in human performance nor to flawed technology. Rather they develop as a product of the interaction between human beings and technology. In our view, errors are the product of cognitive activity in human adaptation

to complex physical, social, and cultural environments. How well the design of health IT complements its intended setting and purpose is critically important for safe and effective performance. In this presentation, I will discuss the cognitive challenges we face in understanding human-computer interaction (HCI) that make the integration of computing and clinical practice a difficult task that, improperly addressed, can lead to threats to patient safety.

THURSDAY JUNE 11 2015

PLENARY SESSIONS



SHARPEN YOUR EDGE AGAINST CANCER.

Edge Radiosurgery: Making radiosurgery an option for more patients.

Deliver accurate radiosurgery treatments quickly and efficiently with the Edge™ radiosurgery system. Edge's advanced technology enables you to offer powerful, non-invasive radiosurgery treatments anywhere in the body where radiation is indicated. Expand treatment options for patients and gain a competitive edge with the system as dedicated as you are.

Visit us at IUPESM World
Congress 2015. Booth #1234.
Learn more about Edge Radiosurgery
at varian.com/Edge

VARIAN
medical systems
A partner for **life**

Radiation treatments may cause side effects that can vary depending on the part of the body being treated. The most frequent ones are typically temporary and may include, but are not limited to, irritation to the respiratory, digestive, urinary or reproductive systems, fatigue, nausea, skin irritation, and hair loss. In some patients, they can be severe. Radiation treatment is not appropriate for all cancers. See varian.com/use-and-safety for more information.

© 2015 Varian Medical Systems, Inc. Varian and Varian Medical Systems are registered trademarks, and Edge is a trademark of Varian Medical Systems, Inc.

SPECIAL SESSIONS

Sunday, June 7 2015

SESSION DATE: **SUNDAY, JUNE 7 2015**
 SESSION TIME: **08:00 - 17:15**
 SESSION ROOM: **716**
 SESSION TITLE: **SS01 - USE OF AAPM TASK GROUP 100 RECOMMENDED RISK ASSESSMENT APPROACH TO DEVELOP A RISK BASED QUALITY MANAGEMENT PROGRAM IN RADIATION THERAPY**

SESSION ORGANIZER(S): **SAIFUL HUQ**

AGENDA:

TG-100 overview and introduction	Saiful Huq
Safety Guidance for Radiotherapy	Peter Dunscombe
Incident learning systems: Structure, terminology and taxonomies	Peter Dunscombe
Exercise 1: Event Classification	
Process mapping	Saiful Huq
Exercise 2: Process Mapping	
Systems and Culture	Jean-Pierre Bissonnette
LUNCH	
Fault Trees	Peter Dunscombe
Exercise 3: Fault Tree Analysis	
Design of QM from the Risk Assessment	Ellen Yorke
Exercise 4: QM Layout	
Change Management	Jean-Pierre Bissonnette
Wrap and final questions	Saiful Huq

SESSION DATE: **SUNDAY, JUNE 7 2015**
 SESSION TIME: **08:00 - 13:30**
 SESSION ROOM: **715B**
 SESSION TITLE: **SS02 - AUTOSEG 2015**
 SESSION ORGANIZER(S): **STEPHEN BREEN & VLADIMIR PEKAR**

Introduction to Session:

This program will focus on automated methods for medical image segmentation. Topics will include: clinical applications, algorithms, and computational implementation.

Medical physicists, biomedical engineers, imaging scientists, computer scientists and healthcare professionals who use autosegmentation methods will enhance their knowledge and skills by attending this one-day event.

Ten leaders in autosegmentation will be presenting their latest methods and results.

After this event, attendees will be able to describe several autosegmentation algorithms; compare and evaluate different autosegmentation techniques; and select amongst different algorithms for varied imaging modalities and tasks.

SESSION DATE: **SUNDAY, JUNE 7 2015**
 SESSION TIME: **08:00 - 13:30**
 SESSION ROOM: **715A**
 SESSION TITLE: **SS03 - RT RESEARCH SYSTEM DEVELOPMENT ON OPEN-SOURCE SLICERRT PLATFORM**
 SESSION ORGANIZER(S): **GABOR FICHTINGER AND CSABA PINTER**

SESSION DATE: **SUNDAY, JUNE 7 2015**
 SESSION TIME: **13:30 - 18:00**
 SESSION ROOM: **718A**
 SESSION TITLE: **SS04 - YIS PRESENTATIONS – JOINT IOMP & IFMBE**

Monday, June 8 2015

SESSION DATE: **MONDAY, JUNE 8 2015**
SESSION TIME: **15:00 - 16:30**
SESSION ROOM: **714B**
SESSION TITLE: **SS05 - EUROPEAN INITIATIVES IN MEDICAL RADIATION PROTECTION**
SESSION ORGANIZER(S): **EUGENE LIEF AND JOHN DAMILAKIS**

AGENDA:

PIDRL: A European Commission project on Paediatric DRLs	Professor John Damilakis, EFOMP President.
Overview of EFOMP projects on Radiation Protection	Professor Virginia Tsapaki, EFOMP
Collaboration of AAPM and EFOMP on Radiation Protection Projects	Dr. Eugene Lief, AAPM
Question and Answer time	

SESSION DATE: **MONDAY, JUNE 8 2015**
SESSION TIME: **15:00 - 16:00**
SESSION ROOM: **PLENARY HALL (HALLS F&G)**
SESSION TITLE: **SS06 - IOMP AWARDEES PRESENTATIONS**

The Awardees will include:

- ▶ Marie Sklodowska-Curie Award: **Colin Orton**
- ▶ Harold Johns Medal: **William Hendee**

SESSION DATE: **MONDAY, JUNE 8 2015**
SESSION TIME: **16:00 - 18:00**
SESSION ROOM: **PLENARY HALL (HALLS F&G)**
SESSION TITLE: **SS07.1 - PRESENTATION OF 2021 BIDS**

SESSION DATE: **MONDAY, JUNE 8 2015**
SESSION TIME: **18:00 - 19:00**
SESSION ROOM: **PLENARY HALL (HALLS F&G)**
SESSION TITLE: **SS07.2 - IUPESM AWARDEES PRESENTATIONS**

The Awardees will include:

- ▶ IUPESM Award of Merit - IFMBE recipient: **Fumihiko Kajiya**
- ▶ IUPESM Award of Merit - Medical Physics: **Peter Smith**

Tuesday, June 9 2015

SESSION DATE: **TUESDAY, JUNE 9 2015**
SESSION TIME: **08:00 - 10:00**
SESSION ROOM: **PLENARY HALL (HALLS F&G)**
SESSION TITLE: **SS10 - IFMBE AWARDEES PRESENTATIONS**

The Awardees will include:

- ▶ IFMBE Laura M.C. Bassi Award: **Alison Noble**
- ▶ IFMBE Otto Schmidt Award: **Karin Wardell**
- ▶ IFMBE Vladimir Zworykin Award: **Chwee Teck Lim**
- ▶ IFMBE John A. Hopps Distinguished Service Award: **Robert M. Nerem**

SESSION DATE: **TUESDAY, JUNE 9 2015**
SESSION TIME: **10:30 - 12:00**
SESSION ROOM: **713A**
SESSION TITLE: **SS08 - THE FUTURE OF CLINICAL ENGINEERING EDUCATION**
SESSION ORGANIZER(S): **HERBERT F. VOIGT**

SESSION DATE: **TUESDAY, JUNE 9 2015**
SESSION TIME: **10:30 - 12:00**
SESSION ROOM: **714B**
SESSION TITLE: **SS09 - INNOVATIVE BIOMEDICAL ENGINEERING RESEARCH IN ASIA**
SESSION ORGANIZER(S): **TOH SIEW-LOK AND JAMES GOH**

Wednesday, June 10 2015

SESSION DATE: **WEDNESDAY, JUNE 10 2015**
 SESSION TIME: **10:30 - 12:00**
 SESSION ROOM: **714A**
 SESSION TITLE: **SS11 - ICSU BIO-UNIONS CLUSTER SESSION**
 SESSION ORGANIZER(S): **HERBERT F. VOIGT**

SESSION DATE: **WEDNESDAY, JUNE 10 2015**
 SESSION TIME: **10:30 - 12:00**
 SESSION ROOM: **713A**
 SESSION TITLE: **SS12 - WORLD SUMMIT ON THE SUPPORTABILITY OF MEDICAL DEVICES**
 SESSION ORGANIZER(S): **MIKE CAPUANO AND JEAN NGOIE**

Introduction to Session:

For years, in-house clinical engineering (CE) departments and independent service organizations have faced several challenges. These relate to obtaining the supports required to service and maintain medical equipment in the field. To the CE community, providing safe, cost-effective, and expedient service depends on ability to obtain spare parts, service manuals, technical training, software, and access pass codes. It is becoming increasingly difficult to obtain these items. Manufactures are placing conditions on servicing their products. Either no supports are provided or they charge very high prices to acquire them. Some companies will not allow servicing in the field unless expensive training is acquired. They create proprietary manuals and information separately for OEM eyes only and may charge even more to acquire this. Manufacturers contribute to the issue citing risks to the reliable support of their product. Purchasing agents are easily swayed by vendor claims of complexity that they and only they can service it (not field serviceable) and various other unfounded risks like 'FDA won't allow it.' Manufacturers and CE need to develop an understanding and common ground that will serve both sides so only the patient benefits.

Objectives

To discuss with Biomedical and Clinical Engineers, Physicists, Scientists, Academics, Healthcare Technology Managers, Healthcare Institutions, Manufacturers, Vendors, Independent Service, Organizations, Regulatory Agencies, Independent Research Organizations the issue of serviceability of Medical Devices.

The summit focus will be on questions below:

1. Is there a problem?
2. If so, how do we articulate it?
3. Define 'Supportability'
4. Provide perspective from both sides

5. Listen to comments, questions, and answers
6. List proposals, measures, and recommendations
7. Summarize
8. Publish summit outcome

Impact on the Medical Device Industry

Medical equipment manufacturers may find a competitive edge when they fully support service of equipment in the field. When customers compare a vendor's product, field supportability can be grounds for decision-making. Today's devices and systems are becoming more and more similar from both hardware and software perspectives. The level of distinction among competing products and vendors is shrinking. Correspondingly, characteristics around the purchasing aspect have become increasingly apparent. From an in-house clinical engineering perspective, the vendor's support for field supportability could make acquisition more efficient for in-house CE departments (less haggling). In-house service is known to reduce equipment cost of ownership in hospitals. This apply to all patient related technologies.

Supportability Defined

The level of ease to which a specific medical device or system is serviced by entities other than representatives or direct agents of the original equipment manufacturer (OEM).

SESSION DATE: **WEDNESDAY, JUNE 10 2015**
 SESSION TIME: **12:00 - 13:30**
 SESSION ROOM: **713A**
 SESSION TITLE: **SS13 - HTA OF MEDICAL DEVICES: PREMARKET CHALLENGES (ROUNDTABLE ON HEALTH TECHNOLOGY ASSESSMENT)**
 SESSION ORGANIZER(S): **NICOLAS PALLIKARAKIS AND LEANDRO PECCHIA**

AGENDA:

Regulation of MDs, the EU prospective	<i>Nicolas PalliKarakis, University of Patras, Greece, and Chair HTA Division of IFMBE</i>
Pre-market HTA of Medical Devices: an overview	<i>Leandro Pecchia, University of Warwick, UK, and Treasurer of HTA Division of the IFMBE</i>
From Monitoring the European Innovation Partnership on Active and Healthy Ageing (EIP on AHA) to early technology assessment	<i>Christian Boehler, Joint Research Centre, European Commission, Seville, Spain</i>
Multi-criteria decision analysis as a tool for medical devices assessment: a case study on R&D portfolio decision for new robotics in healthcare	<i>Marjan Hummel, University of Twente, The Netherlands</i>

SESSION DATE: **WEDNESDAY, JUNE 10 2015**
 SESSION TIME: **13:30 - 16:30**
 SESSION ROOM: **714**
 SESSION TITLE: **SS14 - MEDICAL PHYSICS & BIOMEDICAL ENGINEERING RESPONSE TO CANCER CONTROL: A GLOBAL HEALTH CHALLENGE (A SYMPOSIUM SPONSORED BY IUPESM-HTTG & UICC-GTFRC)**
 SESSION ORGANIZER(S): **JAKE VAN DYK AND CARI BORRAS**

SESSION DATE: **WEDNESDAY, JUNE 10 2015**
 SESSION TIME: **13:30 - 15:00**
 SESSION ROOM: **713A**
 SESSION TITLE: **SS15 - METHODS AND TOOLS FOR PRE-MARKET HTA OF MEDICAL DEVICES (HEALTH TECHNOLOGY ASSESSMENT FOR BIOMEDICAL ENGINEERS WORKSHOP)**
 SESSION ORGANIZER(S): **NICOLAS PALLIKARAKIS AND LEANDRO PECCHIA**

AGENDA:

13:30-13:35	Introduction	Cari Borrás, Chair, IUPESM-Health Technology Task Group (HTTG), Washington DC, United States
13:35-14:00	The Global Cancer Burden and WHO's Response	Adriana Velazquez, World Health Organization (WHO), Geneva, Switzerland
14:00-14:25	Biomedical Engineering Research for Cancer Diagnostics and Therapeutics	Ratko Magjarević, University of Zagreb, Zagreb, Croatia
14:25-14:50	Appropriate Technologies for Cancer Diagnostics and Therapeutics	Cari Borrás, HTTG, Washington DC, United States
14:50-15:15	IAEA Activities in Support of Radiation Therapy Services	Joanna Izewska, International Atomic Energy Agency (IAEA), Vienna, Austria
15:15-15:40	Initiatives of Expertise Mobilization	Jacob Van Dyk, Western University, London, Ontario, Canada
15:40-16:05	Equal Access to Radiation Therapy by 2035	David Jaffray, Global Task Force on Radiotherapy for Cancer Control (GTFRC), Ontario Cancer Institute, Toronto, Canada
16:05-16:30	Discussion and Summary	Jacob Van Dyk, Western University, London, Ontario, Canada

AGENDA:

Multi-criteria decision analysis for medical devices assessment	Marjan Hummel, University of Twente, the Nederland
A tool to monitor the European Innovation Partnership on Active and Healthy Ageing: development, implementation and potential use for pre-market HTA	Christian Boehler, Joint Research Centre, European Commission, Seville, Spain
AHP for user need elicitation: method and available tools	Leandro Pecchia, University of Warwick and Treasurer of HTA Division of the IFMBE

SESSION DATE: **THURSDAY, JUNE 11 2015**
 SESSION TIME: **10:30 - 12:00**
 SESSION ROOM: **713A**
 SESSION TITLE: **SS16 - ADDRESSING GLOBAL CHALLENGES**
 SESSION ORGANIZER(S): **ROGER KAMM**

Introduction to Session:

This Special Session “Addressing Global Challenges” will be presented by the past and current Chairs of the International Academy of Medical and Biological Engineering of the IFMBE.

The Opening Presentation by Robert Nerem is on “Bioengineering in the 21st Century”, followed by presentations on a variety of topics addressing global challenges from different perspectives including device technologies, information technologies, and innovative uses of physiological modeling.

AGENDA:

Bioengineering in the 21st Century	Robert Nerem (Georgia Technological Institute, USA)
Contribution of medical and biological engineering to medical care in coming super-aging society -collaboration among academia, industry and government	Ueno Shoogo (Dept of Applied Quantum Physics, Graduate School of Engineering, Kyushu University, Japan) Fumihiko Kajiya (Kawasaki University of Medical Welfare and Kawasaki Medical School, Japan)
ICT for Prevention of Non-Communicable Diseases	Niilo Saranummi (VTT Technical Research Centre of Finland, Finland)
The Future Potential for Living, Multicellular Machines	Roger Kamm (Massachusetts Institute of Technology, USA)

SESSION DATE: **THURSDAY, JUNE 11 2015**
 SESSION TIME: **12:00 - 13:30**
 SESSION ROOM: **715B**
 SESSION TITLE: **SS17 - SPREADING AND INTEGRATING HUMAN FACTORS EXPERTISE IN HEALTHCARE AN INTERNATIONAL PANEL DISCUSSION**
 SESSION ORGANIZER(S): **SONIA PINKNEY AND TONY EASTY**

Introduction to Session:

Over the past decade, improving patient safety has been a priority for many healthcare organizations, but progress in the reduction of preventable patient harm has been slow. Human factors (HF) is recognized as an important scientific approach to improve health technology safety when applied to both pre-market (e.g., improved technology design), and post-market (e.g., improved practices, training and technology configuration/ implementation) activities. HF is a discipline focused on improving safety by recognizing that humans are fallible, despite good intentions and hard work. It aims to build system resilience by focusing on the conditions under which people work and building defenses to minimize errors and their impacts.

While the potential for HF to improve healthcare safety is well established, it is not integrated and embedded in most safety initiatives. A possible explanation for this unfulfilled potential is that there are limited HF experts working in healthcare. Most HF-related work to date is done at a few organizations in a few countries (i.e., organizational silos). In addition, there has been a lack of formal professional collaboration between HF experts, patient safety leaders, regulators, clinicians, and health technology managers and designers, resulting in disparate expertise (i.e., professional/expertise silos). As such, there is a need to spread HF expertise internationally and across healthcare-related professions (e.g., clinical engineers, biomedical technicians, designers) so they can be empowered to take more active roles in initiating and leading safety projects that incorporate HF.

HumanEra, an HF team based at the University Health Network in Toronto, Canada, has been teaching HF to various healthcare sectors and stakeholders for almost 10 years. Teaching tactics have included:

- ▶ Introductory HF workshops
- ▶ HF method courses
- ▶ Partnering with healthcare organizations to build in-house HF teams/expertise (multi-year contracts focused on project-based collaborations)
- ▶ An introductory HF book (expected publication late 2015)

This session will consist of a panel of HumanEra teachers and past international students to share our combined experiences in teaching, learning, and applying HF for the first time to a safety initiative. The panel will include representatives from different sectors (e.g., academics, clinical engineers, regulators, designers/vendors) and countries (e.g., Canada, Brazil, Spain).

By attending this session you will:

- ▶ Discover how HF can improve healthcare safety
- ▶ Learn from the panel's experience about applying HF in their different roles/professions, organizations, and/or jurisdictions
- ▶ Contribute to meaningful discussions about how you can become an HF champion and help to accelerate the adoption of HF in your organization
- ▶ Meet international professionals interested in HF collaboration to contribute to the cross-fertilization of this important field

AGENDA:

Overview:	A brief introduction to HF will be provided (e.g., define HF for the healthcare context)
Presentations:	Each panel member will present a short summary of their experience in promoting and applying HF to healthcare, focusing on their successes and barriers.
Interactive discussion:	The presentations will serve as a springboard for an interactive discussion between panel members and the audience. Moderated by Dr. Patricia Trbovich

SESSION DATE: **THURSDAY, JUNE 11 2015**
 SESSION TIME: **12:00 - 13:30**
 SESSION ROOM: **713B**
 SESSION TITLE: **SS18 - MEDICAL PHYSICISTS WITHOUT BORDERS**
 SESSION ORGANIZER(S): **JAKE VAN DYK**

SESSION DATE: **THURSDAY, JUNE 11 2015**
 SESSION TIME: **12:00 - 13:30**
 SESSION ROOM: **717B**
 SESSION TITLE: **SS19 - SOCIAL IMPLICATIONS OF TECHNOLOGY WORKSHOP (IN HONOR OF OUR FRIEND & COLLEAGUE; DR LODEWIJK BOS)**
 SESSION ORGANIZER(S): **LUIS KUN**

AGENDA:

Introductory Words from the President of IUPESM	Dr. Herbert F. Voigt (USA)
A Homage to Rene Favaloro's Life: Upgrading Biomedical Engineering Curricula Through Medical Humanism	Dr. Ricardo Armentano (Argentina)
Social Implications of Technology Reuse for a Sustainable Growth	Dr. Laura Roa (Spain)
Realizing and Preserving Privacy and Security for Self, in Interoperable Global Healthcare Venues	Dr. Robert Mathews (USA)
Ethical Issues in Public Health Epidemiology	Dr. Rajaram Lakshminarayan (USA)
A 2015 Moral and Ethical version of the Internet Neutrality Debate: The Digital Divide and Homecare Delivery for the less fortunate	Dr. Luis Kun (USA)

SESSION DATE: **THURSDAY, JUNE 11 2015**
 SESSION TIME: **12:00 - 13:30**
 SESSION ROOM: **716B**
 SESSION TITLE: **SS20 - EMBEDDED SENSOR SYSTEMS FOR HEALTH WORKSHOP**
 SESSION ORGANIZER(S): **MARIA LINDEN**

AGENDA:

12:00-12:05	Introduction	Maria Lindén, Mälardalen University
12:05-12:20	Embedded Sensor Systems with the Prospect of Monitoring, Promoting and Rehabilitating Health	Maria Lindén, Mälardalen University
12:20-12:35	A Four-Wheeled Rollator with Automated Walking Aid	Olof Lindahl, Umeå University Hospital
12:35-12:50	Towards Implementing More Intelligent Healthcare	Hamid Gholamhosseini, Auckland University, New Zealand
12:50-13:05	Early Stroke Detection by Microwaves	Magnus Otterskog, Mälardalen University
13:05-13:20	Current Developments and the Future of ECG Devices	Ivan Tomasic, Mälardalen University
13:20-13:30	Discussion	

SESSION DATE: **THURSDAY, JUNE 11 2015**
 SESSION TIME: **12:00 - 13:30**
 SESSION ROOM: **713A**
 SESSION TITLE: **SS25 - CHALLENGES AND BENEFITS OF CLINICAL ENGINEERING PEER REVIEW**
 SESSION ORGANIZER(S): **MICHAEL J. CAPUANO & JEAN NGOIE**

AGENDA:

13:00 pm	Introduction
13:05pm	Setting the Stage
13:15pm	Panelist Commentary
13:45pm	Panel Discussion
14:15pm	Last Word
14:25pm	Closing Comments

SESSION DATE: **THURSDAY, JUNE 11 2015**
 SESSION TIME: **15:00 - 17:00**
 SESSION ROOM: **PLENARY HALL (HALLS F&G)**
 SESSION TITLE: **SS21 - LEADERS SUMMIT**
 SESSION ORGANIZER(S): **DR. HERB VOIGT, DR. TONY EASTY AND DR. DAVID JAFFRAY**

Introduction to Session:

The World Biomedical Engineering and Medical Physics Leaders' Summit is the inaugural tri-annual high-level policy meeting dedicated exclusively to furthering the role of biomedical engineering and medical physics in medicine. This unique event brings together key decision makers, academics, and practicing engineers and physicists from around the globe and encourages timely debate on emerging issues related to the development and sustainability of the role and impact of medical physicists and biomedical engineers in medicine and healthcare. The Summit provides a unique and important forum to secure a coordinated, multileveled global response to the need, demand, and importance of creating and supporting strong academic and clinical teams of biomedical engineers and medical physicists for the benefit of human health.

Key Objectives of the Leaders' Summit:

- ▶ Raising awareness among leading decision makers to ensure the role of biomedical engineering and medical physics is recognized as a local, regional, and global health priority.
- ▶ Providing a forum to exchange information and innovative ideas on how to create and sustain academic and clinical programs in medical physics and biomedical engineering.
- ▶ Creating a force that galvanizes the leadership and decision-makers in academia, industry, and medicine to assure the role of these two translational and impactful disciplines expand their impact on human health.
- ▶ Defining compelling messages to support the critical role that biomedical engineers and medical physics play in supporting and advancing human health.

SESSION DATE: **THURSDAY, JUNE 11 2015**
 SESSION TIME: **15:00 - 19:00**
 SESSION ROOM: **714A**
 SESSION TITLE: **SS22 - IUPESM-HTTG WORKSHOP ON INNOVATIONS IN THE USE OF MOBILE DEVICES IN HEALTHCARE**
 SESSION ORGANIZER(S): **CARI BORRAS**

SESSION DATE: **THURSDAY, JUNE 11 2015**
 SESSION TIME: **17:00 - 19:00**
 SESSION ROOM: **802B**
 SESSION TITLE: **SS23 - QC IN RADIOTHERAPY: DEFINING THE NEXT STEPS**
 SESSION ORGANIZER(S): **JEAN-PIERRE BISSONNETTE**

AGENDA:

15.00-15.15	Welcome Remarks; Objectives of the Workshop	Cari Borrás, IUPESM-HTTG Chair, Washington DC, USA
15.15-16.00	General Overview (The state of TeleHealth, TeleMedicine, and mHealth)	Kwan-Hoong Ng, Department of Biomedical Imaging, University of Malaya, Kuala Lumpur, Malaysia
	Implementation, Barriers and Policy Issues:	
16.00-16.25	Industrialized Areas	Yadin David, Biomedical Engineering Consultants, LLC., Houston, USA
16.25-16.50	Resource-limited Regions	K. Siddique-e Rabbani, Department of Biomedical Physics & Technology, University of Dhaka, Bangladesh
16.50-17.05	Development of Healthcare Applications using Facilities and Functions available in Modern Mobile Devices	Marlen Perez-Diaz, Center for Studies on Electronic and Information Technologies. Central University of Las Villas, Santa Clara, Villa Clara, Cuba
17.05-17.20	Quality of Service Assessment, Maintenance and Sustainability Issues	J. Tobey Clark, Instrumentation and Technical Services, University of Vermont, Burlington, Vermont, USA
	Point of Care Solutions:	
17.20-17.55	Demonstration	K. Siddique-e Rabbani, Department of Biomedical Physics & Technology, University of Dhaka, Bangladesh
17.55-18.30	Demonstration	Kwan Hoong Ng, Department of Biomedical Imaging, University of Malaya, Kuala Lumpur, Malaysia
18.30-18.50	Discussion	
18.50-19.00	Summary and Recommendations	Colin Orton, Wayne University, Detroit, Michigan, USA

SESSION DATE: **THURSDAY, JUNE 11 2015**
 SESSION TIME: **08:00 - 10:00**
 SESSION ROOM: **714A**
 SESSION TITLE: **SS24 - IFMBE "STUDENT DESIGN COMPETITION" PRESENTATIONS**
 SESSION ORGANIZER(S): **IFMBE**

SESSION TITLE: **MEDTECH SESSIONS**

MedTech
 INSTITUTES

SESSION #1: TUESDAY, JUNE 9 2015, 15:00 – 16:30; IN ROOM 803A

SESSION #2: WEDNESDAY, JUNE 10 2015, 17:00 – 19:00; IN ROOM 713A

SESSION #3: THURSDAY, JUNE 11 2015, 15:00 – 16:30; IN ROOM 802B

CONTINUING EDUCATION SESSIONS

Monday, June 8 2015

SESSION TIME: 08:00 – 10:00
SESSION ROOM: 802A
SESSION NAME: **BMEE01 - GENERAL BME EDUCATION**

- 08:00** BMEE01.1 Biomaterials - Cell-Material Interactions: Biochemistry & Physics
Dennis Discher, United States
- 09:00** BMEE01.2: Radiology 101: Intro to X-Ray tubes / BME Technical/Service Courses (manufacture & maintenance)
Phillip Bogolub, United States

SESSION TIME: 08:00 – 10:00
SESSION ROOM: 801A + 801B
SESSION NAME: **JT01 - IMAGING**

- 08:00** JT01.1: SPECT and Gamma Camera State-Of-The-Art Technology and Current Research
R Glenn Wells
- 09:00** JT01.2: Magnetic Resonance Imaging State-Of-The-Art Technology and Current Research
Richard Frayne, Canada

SESSION TIME: 08:00 – 10:00
SESSION ROOM: 802B
SESSION NAME: **MPS01 - RADIATION THERAPY**

- 08:00** MPS01.1: Radiobiology applications for clinicians - Isoeffective dose calculations, Hypofractionation, TCP/NTCP
Beatriz Sánchez, Chile

SESSION TIME: 08:00 – 10:00
SESSION ROOM: 803A
SESSION NAME: **MPF01 - IMAGERIE**

- 08:00** MPF01.1: Tomodensitométrie: les nouveaux développements et avenues de recherche
Philippe Després, Canada
- 09:00** MPF01.2: Résonance magnétique: les nouveaux développements et avenues de recherche
Martin Lepage, Canada

SESSION TIME: 08:00 – 10:00
SESSION ROOM: 802B
SESSION NAME: **MPS01 - RADIATION THERAPY**

- 08:00** MPF01.1: Tomodensitométrie: les nouveaux développements et avenues de recherche
Beatriz Sánchez, Chile

SESSION TIME: 08:00 – 10:00
SESSION ROOM: 803B
SESSION NAME: **BMEF01 - GENERAL BME EDUCATION/ BME TECHNICAL/SERVICE COURSES**

- 08:00** BMEF01.1: Exemples de Donnes Pratiques en Génie Clinique et Indicateurs
Mochine El Garch, Canada

SESSION TIME: 15:00 – 16:00
SESSION ROOM: 801A
SESSION NAME: **BMEE02 - MEDICAL DEVICE DEVELOPMENT AND COMMERCIALIZATION**

- 15:00** BMEE02.1: Med-Tech Commercialization – A Research Hospital's Perspective
Mark Taylor, Canada

SESSION TIME: 15:00 – 16:30
SESSION ROOM: 801B
SESSION NAME: MPE01 - MEDICAL PHYSICS EDUCATION & PROFESSIONAL ISSUES

- 15:00 MPE01.1: Workforce Models for Medical Physicists
Julian Malicki, Poland
- 15:30 MPE01.2: International Educational Standards: Can We Define a Common Medical Physics Curriculum?
Colin Orton, United States
Raymond Wu, United States
Tomas Kron, Australia

SESSION TIME: 15:00 – 16:30
SESSION ROOM: 803B
SESSION NAME: MPF02 - SYSTÈMES INFORMATISÉS

- 15:00 MPF02.1: Éléments de base: réseaux informatiques, serveurs, et standards de communication
Stefan Michalowski, Canada

SESSION TIME: 15:00 – 16:00
SESSION ROOM: 802B
SESSION NAME: MPE02 - RADIATION THERAPY

- 15:00 MPE02.1: Adaptive Radiotherapy
Jan-Jakob Sonke, The Netherlands

SESSION TIME: 15:00 – 16:00
SESSION ROOM: 803B
SESSION NAME: BMEF02 - GESTION EN GÉNIE BIOMÉDICAL/ CLINIQUE

- 15:00 BMEF02.1: Clinical Engineering Standards of Practice – Normes de pratique en génie clinique- Nouvelle édition canadienne en français
Mochine El Garch, Canada
Bill Gentles, Canada

SESSION TIME: 18:00 – 19:00
SESSION ROOM: 801A
SESSION NAME: BMEE03 - BIOINFORMATICS, TELEMEDICINE AND HOSPITAL

- 18:00 BMEE03.1: DICOM & PACS: Managing Digital Imaging Networks Information Systems
Marvin Mitchell, Canada

SESSION TIME: 17:00 – 19:00
SESSION ROOM: 801B
SESSION NAME: MPE03 - RADIATION THERAPY

- 17:00 MPE03.1: Image-Guided Radiotherapy, Including Commissioning, QC, and Imaging Dose
Douglas Moseley, Canada
- 18:00 MPE03.2: In Vivo Dosimetry
Ben Mijnheer, The Netherlands

SESSION TIME: 17:00 – 19:00
SESSION ROOM: 802B
SESSION NAME: MPS02 - COMPUTERIZED SYSTEMS

- 17:00 MPS02.1: Radiation Treatment Planning Systems and Dose Computation Algorithms (including Monte Carlo)
Antonio Leal Plaza, Spain

SESSION TIME: 17:00 – 19:00
SESSION ROOM: 803A
SESSION NAME: MPF03 - RADIOTHÉRAPIE

- 17:00 MPF03.1: Appareils spécialisés: Tomotherapy, CyberKnife, Brainlab, Gamma Knife
Veronique Vallet
- 18:00 MPF03.2: Curiethérapie guidée par l'image
Luc Beaulieu, Canada

SESSION TIME: 17:00 – 19:00
SESSION ROOM: 803B
SESSION NAME: BMEF03 - GESTION EN GÉNIE BIOMÉDICAL/ CLINIQUE

- 17:00 BMEF03.1: Impacts de la Technologie Médicale sur la Santé de la Mère et de l'Enfant
Gnahoua Zoabli, Canada

Tuesday, June 9 2015

TUESDAY JUNE 9 2015

CONTINUING EDUCATION

SESSION TIME: 08:00 – 10:00

SESSION ROOM: 801A + 801B

SESSION NAME: JT02 - PROCUREMENT & EQUIPMENT SELECTION

08:00 JT02.1: UNICEF's Approach to Medical Device Selection and Procurement for Low-Resource Setting
Shauna Mullally, Denmark

09:00 JT02.2: Equipment Donation and Disposal - Goodwill vs. Risk
Mario Ramirez, Canada

SESSION TIME: 08:00 – 09:00

SESSION ROOM: 802B

SESSION NAME: MPF04 - LA FORMATION ET LE CHEMINEMENT DE CARRIÈRE DES PHYSICIENS MÉDICAUX

08:00 MPF04.1: Les Standards Professionnels et la Certification des Physiciens Médecins
Clément Arsenault, Canada

SESSION TIME: 08:00 – 10:00

SESSION ROOM: 802B

SESSION NAME: MPS03 - RADIATION THERAPY

08:00 MPS03.1: Protontherapy
Alejandro Mazal

09:00 MPS03.2: Nanoparticles and Radiotherapy
Yolanda Prezado, France

SESSION TIME: 08:00 – 10:00

SESSION ROOM: 803A

SESSION NAME: MPF05 - QUALITÉ ET SÉCURITÉ

08:00 MPF05.1: Le Partenariat Canadien pour la Qualité en Radiothérapie
Normand Frenière, Canada

09:00 MPF05.2: L'ingénierie des facteurs humains
Jean-Yves Fiset, Canada

SESSION TIME: 08:00 – 10:00

SESSION ROOM: 803B

SESSION NAME: BMEF04 - GESTION EN GÉNIE BIOMÉDICAL/ CLINIQUEN

08:00 BMEF04.1: La Gestion de Projets et de Portefeuille de Projets en Technologies de la Santé
Mochine El Garch, Canada

SESSION TIME: 10:30 – 12:00

SESSION ROOM: 801A + 801B

SESSION NAME: JT03 - IMAGING

10:30 JT03.1: CT State-Of-The-Art Technology and Current Research Topics
Ting Lee, Canada

11:30 JT03.2: Review of PET State-Of-The-Art Technology and Current Research Topics, Including PET/CT and PET/MR
Roger Lecomte, Canada

SESSION TIME: 10:30 – 11:30

SESSION ROOM: 803B

SESSION NAME: BMEF04 - GESTION EN GÉNIE BIOMÉDICAL/ CLINIQUEN

10:30 BMEF04.1: La Gestion de Projets et de Portefeuille de Projets en Technologies de la Santé
Mochine El Garch, Canada

SESSION TIME: 10:30 – 12:00

SESSION ROOM: 802A

SESSION NAME: BMES01 - INTEROPERABILITY IN HEALTH TECHNOLOGY

10:30 BMES01.1: Healthcare Continuum
Vladimir Quintero, Columbia

SESSION TIME: 10:30 – 11:30

SESSION ROOM: 802B

SESSION NAME: MPS04 - IMAGING

10:30 MPS04.1: CT Basics
Caridad Borràs, United States

SESSION TIME: 10:30 – 12:00

SESSION ROOM: 803A

SESSION NAME: MPF06 - IMAGERIE

10:30 MPF06.1: La Boîte à Outils du Physicien Moderne: Instruments de Contrôle de Qualité
Alain Gauvin, Canada

10:30 MPF06.2: La Radiologie Interventionnelle, Incluant un Survol des Nouvelles Technologies et Approches
Cécile Salvat, France

SESSION TIME: 15:00 – 16:30

SESSION ROOM: 801B

SESSION NAME: MPF03 - RADIOTHÉRAPIE

15:00 MPE04.1: Quality Framework: The Canadian Partnership for Quality Radiotherapy
Michael Milosevic, Canada

16:00 MPE04.2: Radiation Oncology Practice Accreditation in the United States
Steve de Boer, United States

SESSION TIME: 15:00 – 16:30
SESSION ROOM: 802A
SESSION NAME: **BMES02 - INTEROPERABILITY IN HEALTH TECHNOLOGY**

15:00 BMES02.1: Business Opportunities
Mario Castañeda, United States

SESSION TIME: 15:00 – 16:30
SESSION ROOM: 802B
SESSION NAME: **MPS05 - COMPUTERIZED SYSTEM**

15:00 MPS05.1: Managing Respiratory Motion, Including 4D and Gating Techniques; QC
Miguel A. de la Casa, Spain

16:00 MPS05.2: Computerized Systems Basics: Servers, Data Standards (DICOM, HL7), Virtual Machines, Portable Devices
Armando Alaminos Bouza, Brazil

SESSION TIME: 15:00 – 16:30
SESSION ROOM: 801A
SESSION NAME: **BMEE04 - GENERAL BME EDUCATION**

15:00 BMEE04.1: Biomaterials - Polymer/Organic Coatings
Min Wang, People's Republic of China

SESSION TIME: 15:00 – 18:30
SESSION ROOM: 803B
SESSION NAME: **BMEF05 - GESTION EN GÉNIE BIOMÉDICAL/ CLINIQUE**

15:00 BMEF05.1: Implantation du Guide des Bonnes Pratiques de L'ingénierie Biomédicale en Etablissement de Santé
Fabienne Debiais, Canada
Christine Lafontaine, Canada

SESSION TIME: 17:00 – 18:30
SESSION ROOM: 801B
SESSION NAME: **MPE05 - COMPUTERIZED SYSTEMS**

17:00 MPE05.1: Database Rudiments and Clinical Use
John Kildea, Canada

17:30 MPE05.2: Modern Radiotherapy Treatment Planning: Capabilities, Commissioning, and Clinical Use
Benedick Fraass, United States

SESSION TIME: 17:00 – 19:00
SESSION ROOM: 803B
SESSION NAME: **BMEF05 - GESTION EN GÉNIE BIOMÉDICAL/ CLINIQUE**

17:00 BMEF05.1: Implantation du Guide des Bonnes Pratiques de L'ingénierie Biomédicale en Etablissement de Santé
Fabienne Debiais, Canada
Christine Lafontaine, Canada

SESSION TIME: 17:00 – 19:00
SESSION ROOM: 801A
SESSION NAME: **BMEE05 - CLINICAL ENGINEERING/ TECHNOLOGY MANAGEMENT**

17:00 BMEE05.1: Introduction to Medical Technology Management (Clinical Engineering Practice)
Calill Saide, Brazil

SESSION TIME: 17:00 – 19:00
SESSION ROOM: 803A
SESSION NAME: **MPF07 - RADIOTHÉRAPIE**

17:00 MPF07.1: Nouvelles Technologies et Approches en Curiethérapie
Luc Beaulieu, Canada

18:00 MPF07.2: Protontherapy
Alejandro Mazal, France

SESSION TIME: 17:00 – 18:30
SESSION ROOM: 802A
SESSION NAME: **MPS06 - COMPUTERIZED SYSTEM**

17:00 MPS06.1: Optimization: IMRT and VMAT
Antonio Leal Plaza, Spain

18:00 MPS06.2: Automated Contouring
Armando Alaminos Bouza, Brazil

SESSION TIME: 17:00 – 19:10
SESSION ROOM: 802B
SESSION NAME: **MPS07 - RADIATION THERAPY**

17:00 MPS07.1: Image-Guided Radiotherapy, Including QC and Imaging Dose; Adaptative Radiotherapy
Daniel Venencia, Argentina

Wednesday, June 10 2015

WEDNESDAY JUNE 10 2015

CONTINUING EDUCATION

SESSION TIME: 10:30 – 12:00
SESSION ROOM: 801A + 801B
SESSION NAME: JT04 - ETHICS

10:30 JT04.1: Ethics for Biomedical Engineers and Medical Physicists Workshop
Jean-Pierre Bissonnette, Canada
Monique Frize, Canada

SESSION TIME: 10:30 – 11:30
SESSION ROOM: 802B
SESSION NAME: MPS09 - RADIATION THERAPY

10:30 MPS09.1: Peripheral Neutron and Photon Doses
Beatriz Sanchez Nieto, Chile

SESSION TIME: 10:30 – 11:30
SESSION ROOM: 802A
SESSION NAME: MPS08 - MEDICAL PHYSICS EDUCATION AND PROFESSIONAL ISSUES

10:30 MPS08.1: Curriculum Design: How to Train the Next Generation of Physicists?
Maria Ester Brandan, Mexico

SESSION TIME: 10:30 – 11:30
SESSION ROOM: 803B
SESSION NAME: BMEE06 - MEDICAL DEVICE DEVELOPMENT AND COMMERCIALIZATION

10:30 BMEE06.1: Regulatory Issues in Biocompatibility
Paul Santerre, Canada

SESSION TIME: 10:30 – 12:30
SESSION ROOM: 803A
SESSION NAME: MPF08 - SYSTÈMES INFORMATISÉS / QUALITÉ ET SÉCURITÉ

10:30 MPF08.1: Algorithmes de Calcul de Dose, Incluant Monte Carlo
Raphaël Moeckli, Switzerland

11:30 MPF08.2: Utilisation de la Maîtrise Statistique des Processus en Milieu Hospitalier
Karine Herlevin (Gérard), France

SESSION TIME: 13:30 – 14:30
SESSION ROOM: 801A
SESSION NAME: BMEE07 - BIOINFORMATICS, TELEMEDICINE AND HOSPITAL INFORMATION SYSTEMS

13:30 BMEE07.1: E-medicine and Remote Medical Consultations
Gilad Epstein, Canada

SESSION TIME: 13:30 – 15:00
SESSION ROOM: 801B
SESSION NAME: MPE06 - IMAGING

13:30 MPE06.1: 4D Imaging/ 460
Stewart Gaede, Canada

14:30 MPE06.2: Dose from X-Ray Imaging Procedures
John Boone, United States

SESSION TIME: 13:30 – 14:30
SESSION ROOM: 802B
SESSION NAME: MPS10 - RADIATION THERAPY

13:30 MPS10.1: The Modern Physicist Tool Box: How to Choose Between Current Dosimeters
Faustino Gómez, Spain

SESSION TIME: 13:30 – 15:00
SESSION ROOM: 803A
SESSION NAME: MPF09 - IMAGERIE

13:30 MPF09.1: TEP: Les Nouveaux Développements et Avenues de Recherche
Roger Lecomte, Canada

14:30 MPF09.2: Dosimétrie et Radioprotection en Radiologie
Sylvain Deschênes, Canada

SESSION TIME: 15:00 – 16:00
SESSION ROOM: 803A
SESSION NAME: BMEE08 - GENERAL BME EDUCATION

15:00 BMEE08.1: Biomechanics - Implant design
Cheng-Kung (Richard) Cheng, Chinese Taipei

SESSION TIME: 13:30 – 16:00
SESSION ROOM: 802A
SESSION NAME: MPE07 - RADIATION SAFETY

13:30 MPE07.1: What can IAEA do for the Clinical Medical Physicist?
Joanna Izewska, Austria

14:20 MPE07.2: Safety Learning and Safety Management to Prevent Radiotherapy Incidents
Ola Holmberg, Austria

15:20 MPE07.3: Equipment Standards and Performance Measurements for Radiotherapy
Jean Moran, United States

SESSION TIME: 15:00 – 16:30
SESSION ROOM: 801A
SESSION NAME: **BMEE09 - BIOINFORMATICS, TELEMEDICINE AND HOSPITAL**

15:00 BMEE09.1: Medical Device Network Connectivity
Ryan Forde, United States

SESSION TIME: 15:00 – 16:30
SESSION ROOM: 801B
SESSION NAME: **MPE08 - QUALITY & SAFETY**

15:00 MPE08.1: Quality Systems in Radiotherapy
Mary Coffey, Ireland

16:00 MPE08.2: Cost and Resource Management of Radiotherapy
Peter Dunscombe, Canada

SESSION TIME: 15:00 – 16:00
SESSION ROOM: 802B
SESSION NAME: **MPS11 - RADIATION THERAPY**

15:00 MPS11.1: Dosimetry Under Non-Reference Conditions
Faustino Gómez, Spain

SESSION TIME: 15:00 – 16:30
SESSION ROOM: 803A
SESSION NAME: **MPF10 - RADIOTHÉRAPIE**

15:00 MPF10.1: La Radiothérapie Guidée par L'image, Incluant Doses et CQ
Myriam Ayadi-Zahra, France

16:00 MPF10.2: Dosimétrie in Vivo
Louis Archambault, Canada

SESSION TIME: 15:00 – 16:00
SESSION ROOM: 803B
SESSION NAME: **BMEE10 - GENERAL BME EDUCATION**

15:00 BMEE10.1: Multiscale Biomechanics in Deep Tissue Injuries
Arthur Mak, Hong Kong

SESSION TIME: 17:00 – 19:00
SESSION ROOM: 801A
SESSION NAME: **BMEE11 - CLINICAL ENGINEERING/ TECHNOLOGY MANAGEMENT**

17:00 BMEE11.1: Trends in Medical Device Certification and Improving Patient Safety through Evolving Standards
Dale Morgan, Canada

18:00 BMEE11.2: Quantitative Musculoskeletal Ultrasound
Yongping Zheng, China

SESSION TIME: 17:00 – 19:00
SESSION ROOM: 802B
SESSION NAME: **MPS12 - IMAGING**

17:00 MPS12.1: PET State-of-the Art and Current Research Topics (Including CT-PET and CT-MRI)
Josep Martí-Climent, Spain

18:00 MPS12.2: 4D Imaging
Manuel Llorente Manso, Spain

SESSION TIME: 17:00 – 19:00
SESSION ROOM: 803A
SESSION NAME: **MPF11 - RADIOTHÉRAPIE**

17:00 MPF11.1: Stéréotaxie Extra-Crânienne: Techniques et CQ
Myriam Ayadi-Zahra, France

18:00 MPF11.2: La Radiothérapie Adaptative
Bernard Lachance, Canada

SESSION TIME: 17:00 – 19:00
SESSION ROOM: 803B
SESSION NAME: **BMEE12 - GENERAL BME EDUCATION**

17:00 BMEE12.1: Clinical Engineers & Biomedical Engineering Technologists Certification - International Perspective
Larry Boyce, Canada
Petr Kresta, Canada

SESSION TIME: 17:00 – 18:30
SESSION ROOM: 801B
SESSION NAME: **MPE09 - RADIATION THERAPY**

17:00 MPE09.1: The Modern Physicist Tool Box: How to Choose Between Current Dosimeters
Jan Seuntjens, Canada

17:30 MPE09.2: Radiobiology Applications for Clinical Physicists: Isoeffective dose calculations; Hypofractionation; TCP/NTCP; Peripheral doses and secondary cancers
Michael Joiner, United States

SESSION TIME: 16:00 – 19:00
SESSION ROOM: 802A
SESSION NAME: **BMES03 - INTEROPERABILITY IN HEALTH TECHNOLOGY**

16:00 BMES03.1: Trends on IT and Health Technology
Antono Hernandez, United States

17:30 BMES03.2: Interoperability - Profiles - IHE
Vladimir Quintero, Columbia

Thursday, June 11 2015

THURSDAY JUNE 11 2015

CONTINUING EDUCATION

SESSION TIME: 08:00 – 10:00
SESSION ROOM: 801A + 801B
SESSION NAME: JT05 - LEADERSHIP

- 08:00** JT05.1: What is Leadership?
A Roundtable from Recognized Leaders
Kin-Yin Cheung, Hong Kong
Tony Easty, Canada
David Jaffray, Canada
Ratko Magjarevic, Croatia
Herbert F. Voigt, United States
- 09:30** JT05.2: Meet the Leaders
Kin-Yin Cheung, Hong Kong
Tony Easty, Canada
David Jaffray, Canada
Ratko Magjarevic, Croatia
Herbert F. Voigt, United States

SESSION TIME: 08:00 – 10:00
SESSION ROOM: 803A
SESSION NAME: BMEE13 - CLINICAL ENGINEERING

- 08:00** BMEE13.1: Patient safety and Optimal Performance:
A Holistic Framework for Medical Devices
Saleh Altayyar, Saudi Arabia
Michael Cheng, Canada
Hal Hilfi, Canada
Julie Polisen, Canada

SESSION TIME: 08:00 – 10:00
SESSION ROOM: 802B
SESSION NAME: MPE10 - COMPUTERIZED SYSTEMS

- 08:00** MPE10.1: Dose Computation Algorithms, Including
Monte Carlo
Tommy Knoos, Sweden
- 09:00** MPE10.2: Treatment Planning Optimization:
IMRT and VMAT
Jan Unkelbach, United States

SESSION TIME: 08:00 – 10:00
SESSION ROOM: 803B
SESSION NAME: MPE11 - RADIATION THERAPY

- 08:00** MPE11.1: Linear Accelerator Technology
Malcolm McEwen, Canada
- 09:00** MPE11.2: Reference Dosimetry and its Uncertainties
Malcolm McEwen, Canada
David Rogers, Canada

SESSION TIME: 10:30 – 12:00
SESSION ROOM: 802B
SESSION NAME: MPE12 - COMPUTERIZED SYSTEMS

- 10:30** MPE12.1: Image Registration
Mike Velec, Canada
- 11:30** MPE12.2: Automated Segmentation of Images for
Treatment Planning Purposes
Greg Sharp, United States

SESSION TIME: 10:30 – 11:30
SESSION ROOM: 802A
SESSION NAME: BMEE14 - NEURAL & REHABILITATION
ENGINEERING

- 10:30** BMEE14.1: Neuro-robotics – Neurally Interfaced and
Inspired Prosthesis
Nitish Thakor, Singapore

SESSION TIME: 10:30 – 11:30
SESSION ROOM: 803B
SESSION NAME: MPE13 - MEDICAL PHYSICS EDUCATION AND
PROFESSIONAL ISSUES

- 10:30** MPE13.1: Advocacy for Physicists and How to Deal
with Government, Unions, Regulators, and Employers
Jerry Battista, Canada
Wayne Beckham, Canada

SESSION TIME: 10:30 – 12:00
SESSION ROOM: 801A + 801B
SESSION NAME: JT06 - LEADERSHIP

- 10:30** JT06.1: Hosting and Organizing an International
Meeting
Mathias Posch, Canada
- 11:15** JT06.2: Social Media in Science and Medicine
Parminder Basran, Canada

SESSION TIME: 10:30 – 12:30
SESSION ROOM: 803A
SESSION NAME: BMEE15 - CLINICAL ENGINEERING/TECHNOLOGY
MANAGEMENT/ GENERAL BME EDUCATION

- 10:30** BMEE15.1: Introduction to Root Cause Analysis (RCA)
and Failure Modes and Effects Analysis (FMEA) to
Support Medication Safety Initiatives
Julie Greenall, Canada
- 11:30** BMEE15.2: Biomechanics - Computational Modeling
and Analysis
Yubo Fan, People's Republic of China

SESSION TIME: 15:00 – 16:30
SESSION ROOM: 8031B
SESSION NAME: MPE14 - RADIATION THERAPY

- 15:00 MPE14.1: Radiotherapy Units: Cobalt-60 Units and Gamma Knife Units
Steve Goetsch, United States
- 15:30 MPE14.2: Brachytherapy: Overview of State-Of-The-Art and New Developments
Nicole Nesvacil, Austria

SESSION TIME: 15:00 – 16:30
SESSION ROOM: 803B
SESSION NAME: MPE15 - COMPUTERIZED SYSTEMS

- 15:00 MPE15.1: Managing Respiratory Motion in Radiation Oncology
Paul Keall, Australia
- 16:00 MPE15.2: RadOnc Treatment Management Systems and the Paperless Treatment Process
Benedick Fraass, United States

SESSION TIME: 15:00 – 16:30
SESSION ROOM: 801A
SESSION NAME: BMEE16 - BME TECHNICAL/SERVICE COURSES

- 15:00 BMEE16.1: Surgical Laser: Technology and Safety Issues
Murray Greenwood, Canada

SESSION TIME: 15:00 – 16:00
SESSION ROOM: 802A
SESSION NAME: BMEE17 - MEDICAL DEVICE DEVELOPMENT & COMMERCIALIZATION

- 15:00 BMEE17.1: Technology Commercialization - Road Map and Precautions
Thomas Rock Mackie, United States

SESSION TIME: 15:00 – 16:00
SESSION ROOM: 803A
SESSION NAME: BMEE18 - GENERAL BME EDUCATION

- 15:00 BMEE18.1: BioMEMS - Microsensors; Microactuators; Microfluidics; Micro-Total Analysis Systems (e.g., Genomics and Proteomics)
David Weitz, Canada

SESSION TIME: 17:00 – 19:00
SESSION ROOM: 801A
SESSION NAME: BMEE19 - BME TECHNICAL/SERVICE COURSES

- 17:00 BMEE19.1: Rechargeable Batteries: Characteristics, Performance, and Maintenance
Isidor Buchmann, Canada

SESSION TIME: 17:00 – 19:00
SESSION ROOM: 801B
SESSION NAME: MPE16 - RADIATION THERAPY

- 17:00 MPE16.1: Specialized Units: Tomotherapy and CyberKnife Systems
Martina Descovich, United States
Robert Staton, United States
- 18:00 MPE16.2: Heavy Particle / Light Ion Therapy
Oliver Jäkel, Germany

SESSION TIME: 17:00 – 19:00
SESSION ROOM: 803A
SESSION NAME: BMEE21 - GENERAL BME EDUCATION

- 17:00 BMEE21.1: Biomaterials - Cell-surface Interaction
Caroline Loy, Canada
- 18:00 BMEE21.2: Biomaterials - Plasma Medicine
Michael Keidar, United States

SESSION TIME: 17:00 – 19:00
SESSION ROOM: 803B
SESSION NAME: MPE17 - RADIATION THERAPY

- 17:00 MPE17.1: Chemotherapy and its Influence on Radiotherapy: Basics for Clinical Physicists
Eva Bezak, Australia
- 18:00 MPE17.2: Models of Delivery of Radiation Therapy (Private, Public, BCCA/CCO, etc)
Thomas McGowan, The Bahamas
Michael Sherar, Canada

SESSION TIME: 17:00 – 18:00
SESSION ROOM: 802A
SESSION NAME: BMEE20 - HUMAN FACTORS & MEDICAL DEVICE SAFETY

- 17:00 BMEE20.1: Clinical Alarms Management (incl. IHE Alarm Communication Mgt)
Tobey Clark, United States
Yadin David, United States
Marjorie Funk, Germany

Friday, June 12 2015

FRIDAY JUNE 12 2015

CONTINUING EDUCATION

SESSION TIME: 08:00 – 10:00
SESSION ROOM: 801A + 801B
SESSION NAME: JT07 - HUMAN FACTORS & MEDICAL DEVICE SAFETY

- 08:00 JT07.1: FMEA and Root Cause Analysis
Eric Ford, United States
- 09:00 JT07.2: Human Factors and United States Ability Assessment
Patricia Trbovich, Canada

SESSION TIME: 08:00 – 10:00
SESSION ROOM: 802A
SESSION NAME: BMEE22 - GENERAL BME EDUCATION

- 08:00 BMEE22.1: Biosensors and Signal Processing - Signal Analysis and Processing
Sri Krishnan, Canada
- 09:00 BMEE22.2: Cellular and Biomolecular Engineering - Nanoparticles in Diagnostic Therapy
Mukesh Harisinghani, United States

SESSION TIME: 08:00 – 10:00
SESSION ROOM: 802B
SESSION NAME: MPE18 - MEDICAL PHYSICS EDUCATION AND PROFESSIONAL ISSUES

- 08:00 MPE18.1: Curriculum Design: How to Train the Next Generation of Physicists?
John Damilakis, Greece
- 09:00 MPE18.2: Professional Standards and Certification of Qualified Individuals
Geoff Ibbott, United States
Matthew Schmid, Canada

SESSION TIME: 08:00 – 10:00
SESSION ROOM: 803A
SESSION NAME: BMEE23 - CLINICAL ENGINEERING/ TECHNOLOGY MANAGEMENT

- 08:00 BMEE23.1: Clinical Engineering Standards of Practice - Canadian New Edition and Other Countries
Anthony Chan, Canada
Bill Gentles, Canada
- 09:00 BMEE23.2: Emerging Medical Technologies - What to Expect, How to Prepare for it
Jim Keller, United States

SESSION TIME: 08:00 – 10:00
SESSION ROOM: 803B
SESSION NAME: MPE19 - RADIATION THERAPY

- 08:00 MPE19.1: Commissioning, Clinical Implementation and Quality Assurance for Stereotactic Body Radiation Therapy
Timothy Solberg, United States

SESSION TIME: 10:30 – 12:00
SESSION ROOM: 802A
SESSION NAME: BMEE24 - MEDICAL DEVICE DEVELOPMENT AND COMMERCIALIZATION

- 10:30 BMEE24.1: The Product Development Cycle
Lahav Gill, Canada

SESSION TIME: 10:30 – 12:00
SESSION ROOM: 801A + 801B
SESSION NAME: JT08 - SCIENCES & RESEARCH

- 10:30 JT08.1: How to get Grants: Tips for Success
Aaron Foster, United Kingdom
- 11:30 JT08.2: How to Write and Review Research Articles
David Rogers, Canada
David Thwaites, Australia

SESSION TIME: 10:30 – 12:00
SESSION ROOM: 803A
SESSION NAME: BMEE25 - CLINICAL ENGINEERING/ TECHNOLOGY MANAGEMENT

- 10:30 BMEE25.1: Clinical Engineering Best Practice and Bench-marking
Binseng Wang, China

SESSION TIME: 10:30 – 12:00
SESSION ROOM: 802B
SESSION NAME: BMEE26 - CLINICAL ENGINEERING

- 10:30 BMEE26.1: Collaboration on Health Care Decision-Making
Michael Cheng, Canada
Julie Polisen, Canada
Hal Hilfi, Canada

WORLD CONGRESS ON MEDICAL PHYSICS & BIOMEDICAL ENGINEERING

INVITATION TO RAYSEARCH'S LUNCH SYMPOSIUM

ADVANCING RADIATION THERAPY THROUGH SOFTWARE INNOVATION

Monday, June 8, 2015

At 12:15 to 13:15

Metro Toronto Convention Centre, South Building

Room 718A

Lunch will be provided

12:15 - 12:35



Considerations for implementing adaptive therapy using RayStation

Bon Mzenda, Chief Physicist

Auckland Radiation Oncology, Auckland, New Zealand

12:35 - 12:55



Deformable Image Registration and Dose Accumulation

Jean-Pierre Bissonnette & Vicky Kong

Radiation Medicine Program

Princess Margaret Cancer Center, Toronto Canada

12:55 - 13:15



Advancing radiation therapy through software innovation

Johan Löf, CEO

RaySearch Laboratories AB, Stockholm, Sweden

Moderator: Marc Mlyn, CEO, *RaySearch Americas Inc.*

**ADVANCING
CANCER
TREATMENT**



www.raysearchlabs.com

SCIENTIFIC PROGRAM BY TRACK

TRACK 01: IMAGING				
SESSION DATE	TIME	ROOM		SESSION TITLE
MONDAY, JUNE 8, 2015	08:00 – 09:30	718A	SP001	Image Processing and Visualization: Part 1
	15:00 – 16:00	718A	SP013	MRI: Methods
	17:00 – 18:00	718A	SP023	Quantitative Imaging: Part 1
	17:00 – 18:45	701A	SP024	Breast CAD and New Breast Imaging Techniques
TUESDAY, JUNE 9, 2015	08:00 – 10:00	718A	SP034	CT: New Techniques
	08:00 – 09:30	701B	SP035	Imaging Detector Technology
	10:30 – 12:00	701B	SP044	Bio-Impedance and Imaging (Other)
	17:00 – 18:45	718A	SP065	Conebeam CT
	17:00 – 18:45	701B	SP070	Molecular Imaging PET/SPECT: Part 2
WEDNESDAY, JUNE 10, 2015	13:30 – 14:45	718A	SP088	Computer Aided Diagnosis
	15:00 – 16:15	718A	SP096	Optical Imaging: Applications
	15:00 – 17:00	701B	SP097	Quantitative Imaging: Part 2
	17:00 – 18:00	701B	SP104	Phantoms
	17:00 – 19:00	718A	SP105	MRI: Novel Approaches and Molecular Imaging & Applications
THURSDAY, JUNE 11, 2015	10:30 – 11:45	718A	SP128	Multimodality Imaging
	08:00 – 10:00	718A	SP115	CT Image Quality and Dose Optimization
	08:00 – 10:00	701B	SP116	Image Processing and Visualization: Part 2
	10:30 – 12:00	701B	SP129	Image Quality Assessment (Mammography and Other)
	15:00 – 16:30	718A	SP139	Optical Imaging: Methods
	17:00 – 18:45	718A	SP149	Iterative Reconstruction
	17:00 – 18:45	701B	SP150	X-Ray Phase Contrast & Scatter Imaging
FRIDAY, JUNE 12, 2015	08:00 – 09:45	718A	SP161	Angiography / X-ray Imaging
	08:00 – 10:00	701B	SP162	Ultrasound and OCT: Applications
	10:30 – 12:00	718A	SP172	Mammography and Tomosynthesis
	10:30 – 11:45	701B	SP173	Ultrasound and OCT: Methods

TRACK 02: BIOMATERIALS AND REGENERATIVE MEDICINE

SESSION DATE	TIME	ROOM		SESSION TITLE
MONDAY, JUNE 8, 2015	08:00 – 09:45	717B	SP002	Stem Cells in Tissue Engineering and Regeneration
TUESDAY, JUNE 9, 2015	17:00 – 18:45	717B	SP071	Scaffolds in Tissue Engineering
WEDNESDAY, JUNE 10, 2015	15:00 – 16:45	717B	SP098	Biomaterials and Regenerative Medicine

TRACK 03: BIOMECHANICS AND ARTIFICIAL ORGANS

SESSION DATE	TIME	ROOM		SESSION TITLE
MONDAY, JUNE 8, 2015	15:00 – 16:15	701B	SP014	Bone Mechanics
TUESDAY, JUNE 9, 2015	15:00 – 16:30	715A	SP055	Cellular & Molecular Mechanics
	17:00 – 18:15	714B	SP066	Human Movement
WEDNESDAY, JUNE 10, 2015	13:30 – 14:45	701B	SP089	Tissue Modelling
THURSDAY, JUNE 11, 2015	17:00 – 19:00	714B	SP151	Cardio Mechanics & Organs

TRACK 04: RADIATION ONCOLOGY

SESSION DATE	TIME	ROOM		SESSION TITLE
MONDAY, JUNE 8, 2015	08:00 – 09:45	701A	SP003	Brachy Therapy: Part 1
	08:00 – 09:15	718B	SP004	Quality Assurance: Part 1
	15:00 – 16:15	701A	SP015	Other Radiation Oncology: Part 1
	15:00 – 16:30	718B	SP016	Image Guided RT: Part 1
	17:00 – 19:00	718B	SP025	Dose Calculation: Part 1
TUESDAY, JUNE 9, 2015	08:00 – 10:00	718B	SP036	Treatment Planning – Motion and Robustness
	10:30 – 12:00	718B	SP046	Assessment of Radiotherapy Response
	10:30 – 12:00	701A	SP047	Dose Calculation: Part 2
	15:00 – 16:15	701A	SP056	Image Guided RT: Part 2
	15:00 – 16:45	718B	SP057	Quality Assurance: Part 2
	17:00 – 18:45	718B	SP072	Imaging
WEDNESDAY, JUNE 10, 2015	17:00 – 18:45	701A	SP106	PR: Proton Therapy
	17:00 – 18:45	718B	SP107	Beam Delivery
	10:30 – 12:00	701A	SP078	Brachy Therapy: Part 2
	10:30 – 12:00	718B	SP079	Motion Management: Part 1
	10:30 – 11:45	701B	SP080	Other Radiation Oncology: Part 2
THURSDAY, JUNE 11, 2015	08:00 – 19:15	718B	SP117	Treatment Planning – Knowledge Based
	10:30 – 12:00	718B	SP130	Treatment Planning
	10:30 – 12:15	701A	SP131	Quality Assurance: Part 3
	15:00 – 16:15	718B	SP140	Special Treatment Techniques: Part 1
	17:00 – 18:30	718B	SP152	Special Treatment Techniques: Part 2
	17:00 – 18:45	701A	SP153	Quality Assurance: Part 4
FRIDAY, JUNE 12, 2015	10:30 – 11:45	701A	SP174	Motion Management: Part 2
	10:30 – 11:45	718B	SP175	Treatment Planning – Biology & Fractionation

TRACK 05: DOSIMETRY AND RADIATION PROTECTION

SESSION DATE	TIME	ROOM		SESSION TITLE
MONDAY, JUNE 8, 2015	08:00 – 09:15	715B	SP005	Patient Specific QA
	08:00 – 09:15	716A	SP006	Dosimetry in CT
	15:00 – 16:30	716A	SP017	Calculational Techniques in Therapy Dosimetry
	17:00 – 19:00	716A	SP026	Reference Dosimetry – Developments and Monitoring
	17:00 – 18:45	715B	SP027	Development and Application of Phantoms in Clinical Dosimetry
TUESDAY, JUNE 9, 2015	08:00 – 09:45	716A	SP037	Dosimetry in Nuclear Medicine
	08:00 – 09:15	715B	SP038	Dosimetry of Non-Standard Fields
	10:30 – 12:00	716A	SP048	Dosimetry of Protons and Heavy Ions
	15:00 – 16:15	716A	SP058	Characterization of Detector Systems for Therapy Dosimetry: Part 1
	17:00 – 18:30	716A	SP067	Characterization of Detector Systems for Therapy Dosimetry: Part 2
	17:00 – 18:30	715B	SP068	Development of New Methods in Therapy Dosimetry
WEDNESDAY, JUNE 10, 2015	10:30 – 12:00	716A	SP081	Validation and Verification of Therapy Dose Delivery: Part 1
	13:30 – 15:00	716A	SP090	QA Measurements for Therapy Dosimetry
	15:00 – 16:30	716A	SP099	Special Session: Current situation of dosimetry in radiology and radiation protection
	15:00 – 16:00	716B	SP100	Dose Optimization: Focus on DRLs
	17:00 – 18:00	716A	SP108	Patient and Occupational Dose Assessment
	17:00 – 18:30	717A	SP109	Micro- and Nano-Dosimetry
THURSDAY, JUNE 11, 2015	08:00 – 09:30	715B	SP118	Diagnostic Radiology: Dosimetry and Quality Control
	08:00 – 10:00	716A	SP119	Dose Surveys in CT and Interventional Radiology
	10:30-11:30	715B	SP132	Special Session: Implementation of the new BSS including radiation safety culture in medicine
	10:30-11:30	716A	SP133	Validation and Verification of Therapy Dose Delivery: Part 2
	15:00 – 16:15	716A	SP141	Development of New Methods in Therapy Dosimetry: Part 3
	17:00 – 18:00	716A	SP154	Developments in Radiation Protection
	17:00 – 19:00	715B	SP155	Characterization of Detector Systems for Therapy Dosimetry: Part 3
FRIDAY, JUNE 12, 2015	08:00 – 10:00	716A	SP163	Primary Dosimetry Standards
	10:30 – 11:30	716A	SP176	Characterization of Detector Systems for Therapy Dosimetry: Part 4
	10:30 – 11:45	716B	SP177	Radiation Shielding – Design and Outcomes

TRACK 06: NEW TECHNOLOGIES IN CANCER RESEARCH AND TREATMENT

SESSION DATE	TIME	ROOM		SESSION TITLE
MONDAY, JUNE 8, 2015	15:00 – 16:30	717A	SP018	Small Animal Research Technologies
	17:00 – 18:45	717A	SP028	HIFU Therapy, Microwave Ablation, Radiofrequency Ablation, Cryotherapy
TUESDAY, JUNE 9, 2015	10:30 – 12:00	717B	SP049	Nanotechnology in Radiation Therapy and Imaging: Part 1
	17:00 – 18:30	701A	SP069	Novel Detectors, Phantoms and Software, Diagnostic Techniques
WEDNESDAY, JUNE 10, 2015	13:30 – 14:30	717B	SP091	Nanotechnology in Radiation Therapy and Imaging: Part 2
THURSDAY, JUNE 11, 2015	15:00 – 16:15	701B	SP142	Light Ion Radiotherapy
FRIDAY, JUNE 12, 2015	08:00 – 09:45	718B	SP164	Adaptive Radiation Therapy (ART)

TRACK 07: SURGERY, COMPUTER AIDED SURGERY, MINIMAL INVASIVE INTERVENTIONS, ENDOSCOPY AND IMAGE-GUIDED THERAPY, MODELLING AND SIMULATION

SESSION DATE	TIME	ROOM		SESSION TITLE
MONDAY, JUNE 8, 2015	17:00 – 18:45	715A	SP029	Surgical Navigation: Part 1
TUESDAY, JUNE 9, 2015	17:00 – 19:00	715A	SP073	Robotics and Virtual Reality in Surgery
WEDNESDAY, JUNE 10, 2015	17:00 – 18:45	715B	SP110	Surgical Navigation: Part 2
THURSDAY, JUNE 11, 2015	15:00 – 16:00	701A	SP143	Radiotherapy and Guidance
	17:00 – 18:45	715A	SP156	Patient-Specific Modeling and Simulation in Surgery

TRACK 08: BIOSENSOR, NANOTECHNOLOGY, BIOMEMS AND BIOPHOTONICS

SESSION DATE	TIME	ROOM		SESSION TITLE
MONDAY, JUNE 8, 2015	15:00 – 16:30	717B	SP019	Nanobiosensors and Nanotheranostics
	17:00 – 19:00	717B	SP030	Lab-on-chip, BioMEMS and Microfluidics
TUESDAY, JUNE 9, 2015	15:00 – 16:15	717B	SP059	Drug Delivery and Control Release
THURSDAY, JUNE 11, 2015	10:30 – 11:45	717B	SP134	Biosignal Sensing and Body Sensor Networks
	17:00 – 18:15	717B	SP157	Biochips and Blood Analysis

TRACK 09: BIOSIGNAL PROCESSING

SESSION DATE	TIME	ROOM		SESSION TITLE
MONDAY, JUNE 8, 2015	08:00 – 10:00	716B	SP007	Biomedical Signal Quality Analysis
	15:00 – 16:15	716B	SP020	Biomedical Modeling
	17:00 – 18:15	716B	SP031	Pattern Classification
TUESDAY, JUNE 9, 2015	08:00 – 09:45	716B	SP039	ECG
	10:30 – 12:15	716B	SP050	Time-Frequency Analysis
	17:00 – 19:00	716B	SP074	Biomedical Monitoring & Bioelectromagnetism
WEDNESDAY, JUNE 10, 2015	10:30 – 11:45	716B	SP082	Nonlinear Dynamic Analysis
THURSDAY, JUNE 11, 2015	08:00 – 09:30	716B	SP120	Biomedical Diagnosis & Prediction
	15:00 – 16:30	716B	SP144	EMG/MMG
FRIDAY, JUNE 12, 2015	08:00 – 09:15	716B	SP165	EEG

TRACK 10: REHABILITATION MEDICINE, SPORTS MEDICINE, REHABILITATION ENGINEERING AND PROSTHETICS

SESSION DATE	TIME	ROOM		SESSION TITLE
MONDAY, JUNE 8, 2015	08:00 – 10:00	715A	SP008	Spinal Cord / Brain Injury & Upper Limb Measurement and Treatments
TUESDAY, JUNE 9, 2015	08:00 – 09:30	715A	SP040	Ergonomics, Wearable Sensors and Virtual Reality
	10:30 – 11:30	715A	SP051	Rehabilitation Robotics
WEDNESDAY, JUNE 10, 2015	10:30 – 11:30	715B	SP083	Lower Limb Injury Assessment and Treatment & Prosthetics and Assistive Devices
THURSDAY, JUNE 11, 2015	15:00 – 17:00	715A	SP145	Developing Tools for Successful Aging: Independent Mobility & Visual Impairment

TRACK 11: NEUROENGINEERING, NEURAL SYSTEMS

SESSION DATE	TIME	ROOM		SESSION TITLE
MONDAY, JUNE 8, 2015	17:00 – 18:30	701B	SP032	Neural Interfaces and Regeneration
TUESDAY, JUNE 9, 2015	08:00 – 09:45	714A	SP041	Brain Computer/Machine Interfaces
	10:30 – 11:45	714A	SP052	Functional Neuroimaging and Neuronavigation
WEDNESDAY, JUNE 10, 2015	13:30 – 14:45	717A	SP092	Neural Signal Processing: Part 1
	15:00 – 16:45	717A	SP101	Stimulation and Monitoring
THURSDAY, JUNE 11, 2015	08:00 – 09:45	714B	SP121	Deep Brain Stimulation
	10:30 – 12:00	714B	SP135	Neural Signal Processing: Part 2
FRIDAY, JUNE 12, 2015	08:00 – 09:45	714B	SP166	NeuroProstheses
	10:30 – 12:00	715B	SP178	Neuroimaging, Neuronavigation and Neurological Disorders

TRACK 12: MEDICAL DEVICES				
SESSION DATE	TIME	ROOM		SESSION TITLE
MONDAY, JUNE 8, 2015	15:00 – 16:45	715B	SP021	Public Health, Active and Healthy Aging
TUESDAY, JUNE 9, 2015	10:30 – 11:45	715B	SP053	Cardiovascular Instrumentation
	15:00 – 16:30	714B	SP060	Special Session: UNESCO International Year of Light
	15:00 – 16:45	715B	SP061	Improvement of Diagnosis and Therapies
WEDNESDAY, JUNE 10, 2015	10:30 – 12:00	717B	SP084	New Designing Ideas
	15:00 – 17:00	715A	SP102	Clinical Information Systems and Decision Support
	17:00 – 18:45	716B	SP111	Cardiovascular
	17:00 – 18:45	717B	SP112	Instrumentation
	10:30 – 11:30	716B	SP136	Brain, Head/Neck, Spine: Part 1
THURSDAY, JUNE 11, 2015	15:00 – 16:15	717B	SP146	MSK
FRIDAY, JUNE 12, 2015	08:00 – 10:00	715B	SP167	GI and GU
	08:00 – 09:45	717B	SP168	Health Challenges in Resource-Poor Nations
	08:00 – 09:45	701A	SP169	Self Engagement, Patient Empowerment and mHealth
	10:30 – 11:30	715B	SP179	Medical Devices: Miscellaneous

TRACK 14: INFORMATION TECHNOLOGIES IN HEALTHCARE DELIVERY AND MANAGEMENT				
SESSION DATE	TIME	ROOM		SESSION TITLE
WEDNESDAY, JUNE 10, 2015	17:00 – 19:00	715A	SP113	Information Technologies in Healthcare Delivery and Management: Part 1
THURSDAY, JUNE 11, 2015	15:00 – 16:30	715B	SP147	Information Technologies in Healthcare Delivery and Management: Part 2
FRIDAY, JUNE 12, 2015	08:00 – 09:30	715A	SP170	Information Technologies in Healthcare Delivery and Management: Part 3
	10:30 – 11:30	715A	SP180	Information Technologies in Healthcare Delivery and Management: Part 4

TRACK 15: BIOINFORMATICS				
SESSION DATE	TIME	ROOM		SESSION TITLE
THURSDAY, JUNE 11, 2015	08:00 – 10:00	717B	SP122	Bioinformatics

TRACK 16: CLINICAL ENGINEERING, CLINICAL PHYSICS, AND PATIENT SAFETY

SESSION DATE	TIME	ROOM		SESSION TITLE
MONDAY, JUNE 8, 2015	07:00 – 09:00	701B	SP009	Patient Safety, Medical Errors and Adverse Events Prevention Related to Health Technologies and Incident Analysis and Management
TUESDAY, JUNE 9, 2015	08:00 – 09:45	701A	SP042	Technology Management Programmes and Equipment Management Systems
	15:00 – 16:45	701B	SP062	Clinical Process Analysis, Optimization, Productivity and Benchmarking
WEDNESDAY, JUNE 10, 2015	13:30 – 14:45	701A	SP093	Health Technology Assessment and Cost Effective Technologies for Developing Countries and Usability and Human Factors Engineering for Medical Devices and System Design: Part 1
	15:00 – 16:15	701A	SP103	Health Technology Assessment and Cost Effective Technologies for Developing Countries and Usability and Human Factors Engineering for Medical Devices and System Design: Part 2
THURSDAY, JUNE 11, 2015	08:00 – 09:45	701A	SP123	Patient Safety, Medical Errors and Adverse Events Prevention Related to Health Technologies

TRACK 17: EDUCATIONAL AND PROFESSIONAL ACTIVITIES

SESSION DATE	TIME	ROOM		SESSION TITLE
MONDAY, JUNE 8, 2015	08:00 – 09:45	715A	SP010	Education and Training in Biomedical Engineering
TUESDAY, JUNE 9, 2015	15:00-17:00	717A	SP063	Accreditation, Certification and Licensure Issues
	17:00 – 19:00	713A	SP075	Special Session: Appropriate Technology in Imaging and Radiotherapy – Functionality and Safety Aspects
THURSDAY, JUNE 11, 2015	17:00 – 19:00	717A	SP158	Educational Activities and Training in Medical Physics
	08:00 – 09:30	717A	SP124	Medical Physics in Developing Countries
	08:00 – 10:00	713A	SP125	Technology Enhanced Education
	10:30 – 12:00	714A	SP137	Special Session: Building Medical Physics Capacity in Developing Countries

TRACK 18: GENDER, SCIENCE AND TECHNOLOGY

SESSION DATE	TIME	ROOM		SESSION TITLE
MONDAY, JUNE 8, 2015	08:00 – 09:30	717A	SP011	Overview of Gender Roles in Medical Physics in North America
TUESDAY, JUNE 9, 2015	08:00 – 09:30	717A	SP043	Women in BioMedical Engineering
	10:30 – 12:00	717A	SP054	Women in Medical Physics: Current Status
WEDNESDAY, JUNE 10, 2015	10:30 – 11:45	717A	SP085	Women in Medical Physics: Current Status

TRACK 19: BIOPHYSICS AND MODELLING

SESSION DATE	TIME	ROOM		SESSION TITLE
TUESDAY, JUNE 9, 2015	17:15 – 19:00	717A	SP076	Radiobiological Modelling
WEDNESDAY, JUNE 10, 2015	10:30 – 11:45	715A	SP086	Biological Effects of Ionizing Radiation
	13:30 – 14:15	715A	SP094	Biological Modelling
THURSDAY, JUNE 11, 2015	08:00 – 09:45	715A	SP126	Computational Biology & Hemodynamics
	17:00 – 18:15	716B	SP159	Transport and Physiological Modelling

PRESIDENT'S CALL

SESSION DATE	TIME	ROOM		SESSION TITLE
MONDAY, JUNE 8, 2015	15:00 – 16:30	713B	SP022	Educational and Professional Activities: Part 1
	17:00 – 18:15	713B	SP033	Imaging: Part 1
TUESDAY, JUNE 9, 2015	15:00 – 16:15	713B	SP064	Biomechanics and Artificial Organs
	17:00 – 18:45	713B	SP077	Radiation Oncology
WEDNESDAY, JUNE 10, 2015	10:30 – 12:15	713B	SP087	Educational and Professional Activities: Part 2
	13:30 – 15:15	713B	SP095	Biosignal Processing & Pulmonary & Respiratory
	17:00 – 18:00	713B	SP114	Dosimetry and Radiation Protection
THURSDAY, JUNE 11, 2015	08:00 – 09:30	713B	SP127	Informatics In Health Care And Public Health / Biosensor, Nanotechnology, Biomems And Biophotonics
	10:30 – 11:45	713B	SP138	Biosensor, Nanotechnology, Biomems And Biophotonics / New Technologies In Cancer Research And Treatment
	15:00 – 16:30	713B	SP148	Medical Devices / Surgery, Computer Aided Surgery, Minimal Invasive Interventions, Endoscopy And Image-Guided Therapy, Modeling And Simulation
	17:00 – 18:15	713B	SP160	Neuroengineering, Neural Systems / Biophysics And Modelling
FRIDAY, JUNE 12, 2015	08:00 – 10:00	714A	SP171	Clinical Engineering / Physics, Patient Safety & Imaging

SCIENTIFIC PROGRAM BY DAY

► **Monday, June 8 2015**

Monday, June 8 2015

SESSION TIME: 08:00 - 09:30
 SESSION ROOM: 718A
 SESSION TRACK: TRACK 01: IMAGING
 SESSION NAME: SP001 - IMAGE PROCESSING AND VISUALIZATION: PART 1
 SESSION CHAIR(S): MARLEN PEREZ-DIAZ, CUBA

- 08:00** SP001.1 - The Use of Wavelet Filters for Reducing Noise in Posterior Fossa Computed Tomography Images
Marlen Perez-Diaz, Cuba
- 08:15** SP001.2 - Automatic Liver Localization based on Classification Random Forest with KNN for Prediction
Fucang Jia, People's Republic of China
- 08:30** SP001.3 - Brain Tumor Target Volume Segmentation: Local Region Based Approach
Hossein Aslian, Italy
- 08:45** SP001.4 - A Novel Automatic White Balance Algorithm for the 3D Image of Stereoscopic Endoscopy
Ling Li, People's Republic of China
- 09:00** SP001.5 - A new log-compression rule for B-mode ultrasound imaging adjusted to the human visual system
Ramon Fernandes, Brazil
- 09:15** SP001.6 - Comparison of Independent Component Analysis (ICA) Algorithm for Heart Rate Measurement Based on Facial Imaging
Irina Septiana, Indonesia

SESSION TIME: 08:00 - 09:45
 SESSION ROOM: 717B
 SESSION TRACK: TRACK 02: BIOMATERIALS AND REGENERATIVE MEDICINE
 SESSION NAME: SP002 - STEM CELLS IN TISSUE ENGINEERING AND REGENERATION
 SESSION CHAIR(S): GILDA BARABINO, UNITED STATES
 ALICIA EL HAJ, UNITED KINGDOM

- 08:00** SP002.1 - **KEYNOTE:** Biomaterials and Regenerative Medicine: Micro-environmental Modulation for Controlled Cell Differentiation and Tissue Development
Gilda Barabino, United States
- 08:30** SP002.2 - **KEYNOTE:** Defining the regulatory metrics for regenerative medicine using novel biomaterial tagging strategies
Alicia El Haj, United Kingdom
- 09:00** SP002.3 - The role of electric fields in promoting precursor cell migration to enhance wound repair
Stephanie Iwasa, Canada
- 09:15** SP002.4 - The role of niche architecture on muscle stem cell division orientation
Richard Cheng, Canada
- 09:30** SP002.5 - Mapping the Stem Cell's Mechanome using Paired Live Cell Multiplexed Imaging and Modeling
Melissa Knothe Tate, Australia

SESSION TIME: 08:00 - 09:45
 SESSION ROOM: 701A
 SESSION TRACK: TRACK 04: RADIATION ONCOLOGY
 SESSION NAME: SP003 - BRACHY THERAPY: PART 1
 SESSION CHAIR(S): SIJI PAUL, INDIA
 SOOK KIEN NG, UNITED STATES

- 08:00** SP003.1 - The impact of in-homogeneity corrected dose calculations for various clinical HDR brachytherapy sites.
Siji Paul, India
- 08:15** SP003.2 - A novel QA device for brachytherapy applicator QA
Sook Kien Ng, United States
- 08:30** SP003.3 - Electromagnetic tracking for catheter reconstruction in ultrasound-guided high-dose-rate brachytherapy of the prostate
Alexandru Nicolae, Canada
- 08:45** SP003.4 - Dosimetric and radiobiological comparison of volumetric modulated arc therapy, high-dose-rate brachytherapy and low-dose-rate permanent seeds implant for localized prostate cancer
Ruijie Yang, People's Republic of China
- 09:00** SP003.5 - A novel system for real-time planning and guidance of breast HDR brachytherapy
Eric Poulin, Canada

- 09:15** SP003.6 - Investigation of electromagnetic catheter tracking approach for spatial reconstruction of implant geometry in high dose rate brachytherapy of prostate cancer
Gabor Fichtinger, Canada
- 09:30** SP003.7 - Endoscopic Tracking for improved Applicator Insertion in Esophagus and Lung HDR Brachytherapy
Robert Weersink, Canada

SESSION TIME: 08:00 – 09:15
 SESSION ROOM: 718B
 SESSION TRACK: TRACK 04: RADIATION ONCOLOGY
 SESSION NAME: SP004 – QUALITY ASSURANCE: PART 1
 SESSION CHAIR(S): STEFANO PECA, CANADA
 VELLAIYAN SUBRAMANI, INDIA

- 08:00** SP004.1 - In Vivo EPID Dosimetry Detects Interfraction Errors in 3D-CRT of Rectal Cancer
Stefano Peca, Canada
- 08:15** SP004.2 - Establishing action thresholds for patient anatomy changes and machine errors during complex treatment using EPID and gamma analysis
Ophélie Piron, Canada
- 08:30** SP004.3 - Dosimetrical characteristics of amorphous silicon electronic portal imager for flattening filter free (FFF) photon beam of upgraded C-series Linear accelerator
Vellian Subramani, India
- 08:45** SP004.4 - Radiation field size, junction and MLC QA using amorphous silicon electronic portal imaging device, an efficient approach to improve routine accuracy
Dany Simard, Canada
- 09:00** SP004.6 - Real-time detection of deviations in radiotherapy beam delivery using a head-mounted detector
Richard Canters, Netherlands

SESSION TIME: 08:00 – 09:15
 SESSION ROOM: 715B
 SESSION TRACK: TRACK 05: DOSIMETRY AND RADIATION PROTECTION
 SESSION NAME: SP005 – PATIENT SPECIFIC QA
 SESSION CHAIR(S): DAVID ROGERS, CANADA

- 08:00** SP005.1 - Verifying dynamic planning in gamma knife radiosurgery using gel dosimetry
Gopishankar Natanasabapathi, India

- 08:15** SP005.2 - Influence of Jaw Tracking in Intensity Modulated and Volumetric Modulated Arc Radiotherapy for Head and Neck Cancers? A Dosimetric Study
Kh Anamul Haque, Bangladesh
- 08:30** SP005.3 - Evaluation of the eye lens dose according to patient setup errors in pediatric head CT examination
Rumi Gotanda, Japan
- 08:45** SP005.4 - Multi-Point Sources on Skin to Assess the Annual Effective Dose by Usage of TENORM added Pillow
Do hyeon Yoo, Republic of Korea
- 09:00** SP005.5 - Patient-Specific Quality Assurance of Respiratory-Gated VMAT Using a Programmable Cylindrical Respiratory Motion Insert for the ArcCHECK™ Phantom
Heather Young, Canada

SESSION TIME: 08:00 – 09:30
 SESSION ROOM: 716A
 SESSION TRACK: TRACK 05: DOSIMETRY AND RADIATION PROTECTION
 SESSION NAME: SP006 – DOSIMETRY IN CT
 SESSION CHAIR(S): ÉTIENNE LÉTOURNEAU, CANADA
 JONATHAN BOIVIN, CANADA

- 08:00** SP006.1 - **KEYNOTE:** Dosimetry and Radiation Protection
Virginia Tsapakis, Greece
- 08:30** SP006.2 - Organ dose reduction while using in-house CBCT patient-specific protocols based on OSL dosimetry
Étienne Létourneau, Canada
- 08:45** SP006.3 - A novel tool for in vivo dosimetry in diagnostic and interventional radiology using plastic scintillation detectors
Jonathan Boivin, Canada
- 09:00** SP006.5 - Assessment of patient's eye lens dose using a custom made anthropomorphic head phantom
Kwan Hoong Ng, Malaysia
- 09:15** SP006.6 - Dose Profile and Equilibrium Doses in CT
Ricardo Terini, Brazil

SESSION TIME: 08:00 – 10:00

SESSION ROOM: 716B

SESSION TRACK: TRACK 09: BIOSIGNAL PROCESSING

SESSION NAME: SP007 – BIOMEDICAL SIGNAL QUALITY ANALYSIS

SESSION CHAIR(S): OMAR ESCALONA, UNITED KINGDOM
GEOFFREY CLARKE, CANADA

- 08:00** SP007.1 - **KEYNOTE:** Biosignal Processing
Adrian Chan, Canada
- 08:30** SP007.2 - Adaptive filter for eliminating baseline wander of pulse wave signals
Anna Akulova, Russian Federation
- 08:45** SP007.3 - Efficacy of DWT denoising in the removal of power line interference and the effect on morphological distortion of underlying atrial fibrillatory waves in AF-ECG
Omar Escalona, United Kingdom
- 09:00** SP007.4 - Quantifying Blood-Oxygen Saturation Measurement Error in Motion Contaminated Pulse Oximetry Signals
Geoffrey Clarke, Canada
- 09:15** SP007.5 - Signal Quality Indices for Ambulatory Electrocardiograms used in Myocardial Ischemia Monitoring
Mohamed Abdelazez, Canada
- 09:30** SP007.6 - A simple algorithm for identifying artifact beats in long ECG recordings
Nini Rao, People's Republic of China
- 09:45** SP007.7 - Automatic Detection of Low-Quality Seismocardiogram Cycles Using the Outlier Approach
Vahid Zakeri, Canada

SESSION TIME: 08:00 – 10:15

SESSION ROOM: 715A

SESSION TRACK: TRACK 10: REHABILITATION MEDICINE, SPORTS MEDICINE, REHABILITATION ENGINEERING AND PROSTHETICS

SESSION NAME: SP008 – SPINAL CORD / BRAIN INJURY & UPPER LIMB MEASUREMENT AND TREATMENTS

SESSION CHAIR(S): AUSTIN BERGQUIST, CANADA
JAMES TUNG, CANADA

- 08:00** SP008.1 - A Validation Test of a Simple Method of Stride Length Measurement Only with Inertial Sensors and a Preliminary Test in FES-assisted Hemiplegic Gait
Takashi Watanabe, Japan
- 08:15** SP008.2 - A novel Treadmill Body Weight Support system using Pneumatic Artificial Muscle actuators: a comparison between active Body Weight Support system and counter weight system
Thuc Tran, Japan

08:30 SP008.3 - A Serious Game for Training and Evaluating the Balance of Hemiparetic Stroke Patients
Pedro Bertemes-Filho, Brazil

08:45 SP008.4 - fNIRS-based analysis of brain activation with knee extension induced by functional electrical stimulation
Misato Ohdaira, Japan

09:00 SP008.5 - Muscle fatigability of isometric and isokinetic knee-extension generated by single-electrode- and spatially-distributed-sequential-stimulation
Austin Bergquist, Canada

09:15 SP008.6 - External modulation of electrical stimulated spinal reflexes - a control modality for human lumbosacral networks in injury induced disconnection from brain control
Winfried Mayr, Austria

09:30 SP008.7 - Motor Control Assessment using Leap Motion: Filtering Methods and Performance in Indoor and Outdoor Environments
Jone Kim, Canada

09:45 SP008.8 - Biceps brachii EMG signals: estimation of dipole sources
Peyman Aghajamaliaval, Canada

10:00 SP008.9 - Validating a Solid-Static Single-Armed Male Prototype Tasked to Produce Dynamic Movement from the Shoulder Through the Preparation Phase
Alicia Gal, Canada

SESSION TIME: 08:00 - 09:00

SESSION ROOM: 701B

SESSION TRACK: TRACK 16: CLINICAL ENGINEERING, CLINICAL PHYSICS, AND PATIENT SAFETY

SESSION NAME: SP009 - PATIENT SAFETY, MEDICAL ERRORS AND ADVERSE EVENTS PREVENTION RELATED TO HEALTH TECHNOLOGIES AND INCIDENT ANALYSIS AND MANAGEMENT

SESSION CHAIR(S): MARY COFFEY, IRELAND

08:00 SP009.1 - Technological Surveillance and Integrity Monitoring of Infusion Systems
David Grosse-Wentrup, Germany

08:15 SP009.2 - Evaluating Patient Safety Risks Related to Oral Chemotherapy: Evolution of a Human Factors Informed Failure Mode and Effects Analysis Framework
Melissa Griffin, Canada

08:30 SP009.3 - Alarm Management Study in Pediatric Special Care Unit
Christopher Bzovey, Canada

08:45 SP009.4 - Failure Modes and Effect Analysis for Stereotactic Radiosurgery: a comparison among three radiotherapy centers in Brazil.
Flavia Cristina Teixeira, Brazil

SESSION TIME: 08:00 – 09:45
 SESSION ROOM: 715A
 SESSION TRACK: **TRACK 17: EDUCATIONAL AND PROFESSIONAL ACTIVITIES**
 SESSION NAME: **SP010 – EDUCATION AND TRAINING IN BIOMEDICAL ENGINEERING**
 SESSION CHAIR(S): **SHANKAR KRISHNAN, UNITED STATES
 MLADEN POLUTA, SOUTH AFRICA**

- 08:00** SP010.1 - Biomedical Engineering in Nigeria: A Developmental Overview
Kenneth Nkuma-Udah, Nigeria
- 08:15** SP010.2 - Biomedical Engineering Education in Peru in 2015: A Unique and Innovative Collaboration in Latin America
Rossana Rivas, Peru
- 08:30** SP010.3 - Improving Biomedical Engineering in Uganda through education, benchmarking and mentorship
Robert Ssekitoleko, Uganda
- 08:45** SP010.4 - Designing Biomedical Engineering Programs to Prepare for Medtech Industry
Shankar Krishnan, United States
- 09:00** SP010.5 - BME vs CE vs HTM vs HbHTA vs EAM. What's in a Name and does it matter?
Mladen Poluta, South Africa
- 09:15** SP010.6 - Clinical Engineering Certification Program in the Americas
Frank Painter, United States
- 09:30** SP010.7 - Biomedical Technology Online Courses for the Americas
Tobey Clark, United States

SESSION TIME: 08:00 – 09:30
 SESSION ROOM: 717A
 SESSION TRACK: **TRACK 18: GENDER, SCIENCE AND TECHNOLOGY**
 SESSION NAME: **SP011 – OVERVIEW OF GENDER ROLES IN MEDICAL PHYSICS IN NORTH AMERICA**
 SESSION CHAIR(S): **PATRICIA TRBOVICH, CANADA
 KRISTY BROCK, UNITED STATES**

- 08:00** SP011.1 - **KEYNOTE:** Gender, Science and Technology: The Role of Women in Medical Physics
Kristy Brock, United States
- 08:30** SP011.2 - Biography of Women in Medical Physics: Maryellen Giger, Ph.D.
Maryellen Giger, United States
- 08:45** SP011.3 - My STEM story: from Martinique in the Caribbean to Quebec City, through France and Vietnam
Nadia Octave, Canada

- 09:00** SP011.4 - My strategies for living (and enjoying) academic research
Rebecca Fahrig, United States
- 09:15** SP011.5 - Early exposure to science leads to fulfilling career in medical physics
Renee Larouche, Canada

SESSION TIME: 15:00 – 16:00
 SESSION ROOM: 718A
 SESSION TRACK: **TRACK 01: IMAGING**
 SESSION NAME: **SP013 – MRI: METHODS**
 SESSION CHAIR(S): **ZOFIA DRZAZGA, POLAND
 CHEMSEDDINE FATNASSI, SWITZERLAND**

- 15:00** SP013.1 - Numerical Simpson's Rule for Real Time and Accurate T2* maps generation Using 3D Quantitative GRE
Chemseddine Fatnassi, Switzerland
- 15:15** SP013.2 - Optimization of Pulse-Triggered fMRI Measurement Delay with Acoustic Stimulation
Zofia Drzazga, Poland
- 15:30** SP013.3 - Improvement of Pseudo Multispectral Classification of Brain MR Images
Chemseddine Fatnassi, Switzerland
- 15:45** SP013.4 - Image reconstruction of RF encoded MRI signals in an inhomogeneous B0 field
Somaie Salajeghe, Canada

SESSION TIME: 15:00 – 16:15
 SESSION ROOM: 701B
 SESSION TRACK: **TRACK 03: BIOMECHANICS AND ARTIFICIAL ORGANS**
 SESSION NAME: **SP014 – BONE MECHANICS**
 SESSION CHAIR(S): **JIE YAO, PEOPLE'S REPUBLIC OF CHINA**

- 15:00** SP014.1 - **KEYNOTE:** Biomechanics and Artificial Organs
Yubo Fan, People's Republic of China
- 15:30** SP014.2 - Improved Semi-automated 3D Kinematic Measurement of Total Knee Arthroplasty Using X-ray Fluoroscopic Images
Takaharu Yamazaki, Japan
- 15:45** SP014.3 - The influence of screw length and stiffness on the tibial mechanical environment in ACL reconstruction
Jie Yao, People's Republic of China
- 16:00** SP014.4 - A new method for determining the effect of follower load on the range of motions in the lumbar spine
Cheng-fei Du, People's Republic of China

SESSION TIME: 15:00 – 16:15

SESSION ROOM: 701A

SESSION TRACK: TRACK 04: RADIATION ONCOLOGY

SESSION NAME: SP015 – OTHER RADIATION ONCOLOGY: PART 1

SESSION CHAIR(S): ESTEBAN BOGGIO, ARGENTINA

- 15:00** SP015.1 - Beta Enhancers: towards a local dose enhancer device for Boron Neutron Capture Therapy (BNCT) on superficial tumors
Esteban Boggio, Argentina
- 15:15** SP015.2 - Nanoparticle Enhanced Radiation Therapies: Is There a Synergy with Chemotherapies?
Linda Rogers, Australia
- 15:30** SP015.3 - Change in Hounsfield Units due to lung expansion as a predictor of LAD and heart displacement in patients undergoing deep inspiration breath hold for left sided breast cancer
Peta Lonski, Australia
- 15:45** SP016.4 - Samarium-153 Labeled Microparticles for Targeted Radionuclide Therapy of Liver Tumor
Chai Hong Yeong, Malaysia
- 16:00** SP016.5 - Anatomical Modelling of the Pregnant Radiotherapy Patient
Tanya Kairn, Australia

SESSION TIME: 15:00 – 16:30

SESSION ROOM: 718B

SESSION TRACK: TRACK 04: RADIATION ONCOLOGY

SESSION NAME: SP016 – IMAGE GUIDED RT: PART 1

SESSION CHAIR(S): JIHYUN YUN, CANADA

- 15:00** SP016.1 - 18F-NaF PET/CT-directed dose escalation in stereotactic body radiotherapy for spine oligometastases from prostate cancer
Lili Wu, People's Republic of China
- 15:15** SP016.2 - Evaluation of a lung tumor autocontouring algorithm for intrafractional tumor tracking using 0.5T linac-MR: phantom and in-vivo study
Jihyun Yun, Canada
- 15:30** SP016.3 - Multi-modal image registration for MR-guided radiotherapy workflow based on detection of features in a customized stereotactic body frame
Paul Mercea, Germany
- 15:45** SP016.4 - A phantom study of impact of probe metal artifact in planning dose for ultrasound-guided radiotherapy
Kai Ding, United States
- 16:00** SP016.5 - Software development for image guidance on the magnetic resonance-guided radiation therapy (MRgRTTM) system
Wenyao Xia, Canada

- 16:15** SP016.6 - Ultrasound guided radiotherapy with rotational correction for patient setup: a feasibility study
Sook Kien Ng, United States

SESSION TIME: 15:00 – 16:30

SESSION ROOM: 716A

SESSION TRACK: TRACK 05: DOSIMETRY AND RADIATION PROTECTION

SESSION NAME: SP017 – CALCULATIONAL TECHNIQUES IN THERAPY DOSIMETRY

SESSION CHAIR(S): VICTOR MALKOV, CANADA

- 15:00** SP017.1 - Dosimetric Effect of Beam Angle on the Unflattened and Flattened Photon Beams: A Monte Carlo study
James Chow, Canada
- 15:15** SP017.2 - Monte Carlo calculations and measurements of the TG-43U1 recommended dosimetric parameters for the 125I (Model IR-Seed2) brachytherapy source
Hassan Ali Nedaie, Iran
- 15:30** SP017.3 - Assessment of RayStation treatment planning algorithm to calculate dose in the presence of lung tissue
Manuel Rodriguez, Canada
- 15:45** SP017.4 - Improving the efficiency of charged particle transport in magnetic fields in EGSnrc
Victor Malkov, Canada
- 16:00** SP017.5 - Accurate Monte Carlo dose calculations for permanent implant prostate brachytherapy: first results from a large scale retrospective study
Nelson Miksys, Canada
- 16:15** SP017.6 - Analytic modelling of in-field and out-of-field bremsstrahlung contamination dose in high energy electron beams used in external radiotherapy
Mohamad Mohamad Alabdoaburas, France

SESSION TIME: 15:00 – 16:30

SESSION ROOM: 717A

SESSION TRACK: TRACK 06: NEW TECHNOLOGIES IN CANCER RESEARCH AND TREATMENT

SESSION NAME: SP018 – SMALL ANIMAL RESEARCH TECHNOLOGIES

SESSION CHAIR(S): DONNA MURRELL, CANADA

- 15:00** SP018.1 - **KEYNOTE:** New Technologies in Cancer Research and Treatment
Frank Verhaegen, Netherlands
- 15:30** SP018.2 - Longitudinal MRI evaluation of whole brain radiotherapy on brain metastasis development and dormancy in a mouse model
Donna Murrell, Canada

- 15:45** SP018.3 - Dual energy micro-CT determination of effective atomic number and electron density
Michael Jensen, Canada
- 16:00** SP018.4 - Tissue characterization using dual energy cone beam CT imaging with a dedicated small animal radiotherapy platform
Patrick Granton, Canada
- 16:15** SP018.5 - Low-dose prostate cancer brachytherapy by injections of radioactive gold nanoparticles (103Pd:Pd@Au NPs)
Myriam Laprise-Pelletier, Canada

SESSION TIME: **15:00 – 16:30**
 SESSION ROOM: **717B**
 SESSION TRACK: **TRACK 08: BIOSENSOR, NANOTECHNOLOGY, BIOMEMS AND BIOPHOTONICS**
 SESSION NAME: **SP019 – NANOBIOSENSORS AND NANOTHERANOSTICS**
 SESSION CHAIR(S): **KWANG OH, UNITED STATES
WALTER H. CHANG, CHINESE TAIPEI**

- 15:00** SP019.1 - Synthesis and evaluation of C595 mAb-conjugated SPIONs nanoprob for specific detection of Prostate cancer
Mohammad Abdolahi, Iran
- 15:15** SP019.2 - Magnetic Resonance Nanotheranostics of Guerin's Carcinoma
Valerii Orel, Ukraine
- 15:30** SP019.3 - Effects of Fluorescence Gold Nanoclusters on Anti-oxidation and Anti-aging by Cell Model
Walter H. Chang, Chinese Taipei
- 15:45** SP019.4 - Nanoparticle-aided Radiotherapy for Retinoblastoma and Choroidal Melanoma
Wilfred Ngwa, United States
- 16:00** SP019.5 - Nanoparticle enhancement of radiation dose: experimental confirmation using scintillation dosimetry
Natalka Suchowerska, Australia
- 16:15** SP019.6 - Graphene Plasmonics as Promising Platform for Highly Sensitive Plasmonic Sensing
Dong Ha Kim, Republic of Korea

SESSION TIME: **15:00 – 16:15**
 SESSION ROOM: **716B**
 SESSION TRACK: **TRACK 09: BIOSIGNAL PROCESSING**
 SESSION NAME: **SP020 – BIOMEDICAL MODELING**
 SESSION CHAIR(S): **RUI FONSECA-PINTO, PORTUGAL
KYUICHI NIIZEKI, JAPAN**

- 15:00** SP020.1 - Respiratory parameters have different patterns in imposed-inspiration and imposed-expiration within a closed pneumatic circuit in rats
Fabio Aoki, Brazil
- 15:15** SP020.2 - Autonomic and cardiovascular responses to food ingestion and gum chewing in healthy young subjects
Kyuichi Niizeki, Japan
- 15:30** SP020.3 - Characteristic Analysis and Modeling for Signals of Auditory Propagation Pathway
Qin Gong, People's Republic of China
- 15:45** SP020.4 - Numerical Optimization Performance of a Perfusion Kinetic Modelling Algorithm using Volumetric DCE CT
Igor Svistoun, Canada
- 16:00** SP020.5 - Validation of a Sympathovagal Balance Model to Evaluate Autonomic Function in Rats Using Time-Frequency Analysis
Rui Fonseca-Pinto, Portugal

SESSION TIME: **15:00 – 16:45**
 SESSION ROOM: **715B**
 SESSION TRACK: **TRACK 13: INFORMATICS IN HEALTH CARE AND PUBLIC HEALTH**
 SESSION NAME: **SP021 – PUBLIC HEALTH, ACTIVE AND HEALTHY AGING**
 SESSION CHAIR(S): **ELINA KALDOUDI, GREECE
CHRISTIAN BOEHLER, SPAIN**

- 15:00** SP021.1 - **KEYNOTE:** Informatics in Health Care and Public Health
Leandro Pecchia, United Kingdom
- 15:30** SP021.2 - Monitoring Information System of Aedes Aegypti Reproduction
Lourdes Brasil, Brazil
- 15:45** SP021.3 - Design and Functionality of a Meta-Reporting Tool within a Medical Devices Vigilance System
Aris Dermitzakis, Greece
- 16:00** SP021.4 - Evaluation of the Impact in the Physical Condition of School Age Children Exposed to an Intervention of Exergaming in Montemorelos Mexico
Gerardo Romo-Cardenas, Mexico
- 16:15** SP021.5 - Using the EIP on AHA monitoring tool for the early technology assessment of a planned device to predict in-hospital falls in the elderly
Christian Boehler, Spain
- 16:30** SP021.6 - An innovative Decision Support System (DSS) for patients with Inflammatory Bowel Disease (IBD)
Vasileios Tsianos, Greece

SESSION TIME: 15:00 – 16:30

SESSION ROOM: 713B

SESSION TRACK: PRESIDENT'S CALL

SESSION NAME: SP022 – EDUCATIONAL AND PROFESSIONAL ACTIVITIES: PART 1

SESSION CHAIR(S): KEITH ISON, UNITED KINGDOM
NILS CHR. STENSETH, FRANCE

- 15:00** SP022.1 - Biomedical Engineering in Nigeria: A Developmental Overview
Kenneth Nkuma-Udah, Nigeria
- 15:15** SP022.2 - Modernising Scientific Careers? A new scheme for the education and training of physicists, engineers and other scientific staff in the UK National Health Service
Keith Ison, United Kingdom
- 15:30** SP022.3 - Medical Physics Residency Program in Developing Countries: Lessons, Challenges and Solutions Learned from a Regional Pilot Training Program
Belal Mofteh, Saudi Arabia
- 15:45** SP022.4 - International Union of Biological Sciences
Nils Chr. Stenseth, France
- 16:00** SP022.5 - Promoting the public image of Medical Physicists and Biomedical Engineers
Michael Cheng, Canada
- 16:15** SP022.6 - The Utilization and Design of Doorless Mazes for Medical Linear Accelerator Rooms In Ontario, Canada
Joseph Szabo, Canada

SESSION TIME: 17:00 – 18:00

SESSION ROOM: 718A

SESSION TRACK: TRACK 01: IMAGING

SESSION NAME: SP023 – QUANTITATIVE IMAGING: PART 1

SESSION CHAIR(S): HAI-LING MARGARET CHENG, CANADA

- 17:00** SP023.1 - Improving quantitative functional imaging with dynamic contrast enhanced studies using a linearized Johnson-Wilson model approach
Fiona Li, Canada
- 17:15** SP023.2 - Early tumor Response assessment using volumetric DCE-CT and DCE-MRI in Metastatic Brain Cancer Patients
Catherine Coolens, Canada
- 17:30** SP023.3 - Diffusion tensor imaging is correlated with quantitative histology in surgically-resected hippocampi of epilepsy patients
Terry Peters, Canada

- 17:45** SP023.4 - Evaluation of fully automatic volumetric GBM segmentation in the TCGA-GBM dataset: Prognosis and correlation with VASARI features
Emmanuel Rios Velazquez, United States

SESSION TIME: 17:00 – 18:45

SESSION ROOM: 701A

SESSION TRACK: TRACK 01: IMAGING

SESSION NAME: SP024 – BREAST CAD AND NEW BREAST IMAGING TECHNIQUES

SESSION CHAIR(S): NANCY MCDONALD, CANADA

- 17:00** SP024.1 - Modelling Breast Cancer Tissue via Analysis of WAXS Signatures
Robert Leclair, Canada
- 17:15** SP024.2 - Analysis of 80 kV WAXS Measurements with a CdTe Breast Biopsy Diffractometer
Nancy McDonald, Canada
- 17:45** SP024.3 - AM-FM features for the classification of Regions of Interest towards the Development of a Breast Cancer Density Specific Computer Aided Detection System
Constantinos Pattichis, Cyprus
- 18:00** SP024.4 - Single Scatter Signals during Dual Detector Volume-of-Interest Breast Cone-Beam Computed Tomography: A New Source of Diagnostic Information?
Curtis Laamanen, Canada
- 18:15** SP024.5 - Investigating automatic techniques in segmentation accuracy of masses in digital mammography images
Karem Marcomini, Brazil
- 18:30** SP024.6 - The Automated Marker-Free Longitudinal IR Breast Image Registration Algorithm
Chi-En Lee, Chinese Taipei

SESSION TIME: 17:00 – 19:00

SESSION ROOM: 718B

SESSION TRACK: TRACK 04: RADIATION ONCOLOGY

SESSION NAME: SP025 – DOSE CALCULATION: PART 1

SESSION CHAIR(S): HUGO BOUCHARD, UNITED KINGDOM
VELLIAN SUBRAMANI, INDIA

- 17:00** SP025.1 - Theoretical ground for testing Monte Carlo transport algorithms coupled to magnetic fields
Hugo Bouchard, United Kingdom
- 17:15** SP025.2 - Primary X-ray source spot size modeling for FFF photon beam in VMAT based Stereotactic Radiosurgery? A comparative clinical study using Acuros-XB and AAA dose calculation algorithm
Vellian Subramani, India

- 17:30** SP025.3 - A Geant4 Helical Tomotherapy model as a tool for 3D dose distribution evaluation
Alessandro Esposito, Portugal
- 17:45** SP025.4 - Development of 4D actual delivered dose calculation system for dynamic tumor-tracking irradiation with a gimbaled linac
Yoshitomo Ishihara, Japan
- 18:00** SP025.5 - Organ Doses from Hepatic Radioembolization with Y-90, Sm-153, Ho-166 and Lu-177: A GEANT4 Monte Carlo Simulation Study
Chai Hong Yeong, Malaysia
- 18:15** SP025.6 - Stereotactic Ablative Radiotherapy (SABR) for lung cancer using Volumetric Modulated Arc Therapy (VMAT) with a 10x Flattening Filter Free (FFF) beam: validation of the calculated dose distribution using Monte Carlo
Tony Mestrovic, Canada
- 18:30** SP025.7 - Performance of the ACUROS? dose calculation algorithm for 6 MV FFF beams in inhomogeneous media
Matthew Schmid, Canada
- 18:45** SP025.8 - Ray Tracing Algorithm for Virtual Source Modelling based on Evaluation of Rounded Leaf End Effect of Multileaf Collimator
Dong Zhou, People's Republic of China

SESSION TIME: **17:00 – 19:00**
 SESSION ROOM: **716A**
 SESSION TRACK: **TRACK 05: DOSIMETRY AND RADIATION PROTECTION**
 SESSION NAME: **SP026 – REFERENCE DOSIMETRY – DEVELOPMENTS AND MONITORING**
 SESSION CHAIR(S): **MCEWEN MALCOLM, CANADA
 CLAUDIU COJOCARU, CANADA**

- 17:00** SP026.1 - The Development of a Device for the Fricke Dosimetry for HDR Brachytherapy
Camila Salata, Brazil
- 17:15** SP026.2 - A New Methodology for the Determination of the G-value for Fricke Dosimetry
Camila Salata, Brazil
- 17:30** SP026.3 - The Use of Fricke Dosimetry as a Primary Standard for the Absorbed Dose to Water for 192Ir HDR-BT Sources: Determination of the G-value
Camila Salata, Brazil
- 17:45** SP026.4 - IAEA Dosimetry Laboratory support to the IAEA/WHO SSDL Network
Joanna Izewska, Austria
- 18:00** SP026.5 - Measurement of Wair in high energy electron beams
Claudiu Cojocaru, Canada
- 18:15** SP026.6 - Monte Carlo corrections for a Fricke-based standard of absorbed dose to water for Ir-192 HDR brachytherapy.
Ernesto Mainegra-Hing, Canada

- 18:30** SP026.7 - Changes in absorbed dose to water caused by dose standard shift for ionization chamber calibration in Japan
Hidetoshi Saitoh, Japan
- 18:45** SP026.8 - A calibration system of therapy-level dosimeter in Japan organized by ANTM
Suoh Sakata, Japan

SESSION TIME: **17:00 - 18:45**
 SESSION ROOM: **715B**
 SESSION TRACK: **TRACK 05: DOSIMETRY AND RADIATION PROTECTION**
 SESSION NAME: **SP027 - DEVELOPMENT AND APPLICATION OF PHANTOMS IN CLINICAL DOSIMETRY**
 SESSION CHAIR(S): **BORRAS CARI, UNITED STATES
 STEPHEN INKOOM, GREECE**

- 17:00** SP027.1 - Fabrication of radiotherapy phantoms using 3D printing
Paul Liu, Australia
- 17:15** SP027.2 - The effect of bismuth shielding during pediatric neck multi-detector computed tomography on thyroid dose and image quality
Stephen Inkoom, Greece
- 17:30** SP027.3 - Use of 3D Printed Materials as Tissue-Equivalent Phantoms
Tanya Kairn, Australia
- 17:45** SP027.4 - Development of water-equivalent materials using the Least Squares Method
Leandro Mariano, Brazil
- 18:00** SP027.5 - Development of deformable moving lung phantom to simulate respiratory motion for lung SBRT
Young Nam Kang, Republic of Korea
- 18:15** SP027.6 - Characterization of a MOSFET-based system for skin dose evaluation with bolus material
Anabela Dias, Portugal
- 18:30** SP027.7 - Calibration procedure optimization through PSDesigner, a multipurpose simulation platform for plastic scintillation dosimeters
Cedric Laliberte-Houdeville, Canada

SESSION TIME: 17:00 – 18:45

SESSION ROOM: 717A

SESSION TRACK: **TRACK 06: NEW TECHNOLOGIES IN CANCER RESEARCH AND TREATMENT**

SESSION NAME: **SP028 – HIFU THERAPY, MICROWAVE ABLATION, RADIOFREQUENCY ABLATION, CRYOTHERAPY**

SESSION CHAIR(S): **TIMOTHY E. DOYLE, UNITED STATES**

- 17:00** SP028.1 - On Understanding of the Limiting Factors in Radiofrequency Ablation on Target Tissue Necrosis Volume
Bing Zhang, People's Republic of China
- 17:15** SP028.2 - Thermal Dose Based Monitoring of Thermal Therapy for Prostate Cancer
Joseph Kumaradas, Canada
- 17:30** SP028.3 - Nanodrug Delivery and Anti-tumor Efficacy for Brain Metastasis of Breast Cancer Enhanced by Short-time Low-dose Ultrasound Hyperthermia
Sheng-Kai Wu, Chinese Taipei
- 17:45** SP028.4 - Evaluating breast cancer surgical margins using high-frequency ultrasound: Statistical analysis of a 17-patient pilot study
Robyn Omer, United States
- 18:00** SP028.5 - The Intraoperative Detection of Breast Cancer in Surgical Margins Using High-Frequency Ultrasound: Studies Using Histology Mimicking Phantoms
Zachary Coffman, United States
- 18:15** SP028.6 - Rapid Molecular Subtyping of Breast Cancer Using High-Frequency Ultrasound (10-120 MHz) and Principal Component Analysis
Caitlin Carter, United States
- 18:30** SP028.7 - Inverse treatment planning using radiofrequency ablation in cancer therapy
Shefali Kulkarni-Thaker, Canada

SESSION TIME: 17:00 - 18:45

SESSION ROOM: 715A

SESSION TRACK: **TRACK 07: SURGERY, COMPUTER AIDED SURGERY, MINIMAL INVASIVE INTERVENTIONS, ENDOSCOPY AND IMAGE-GUIDED THERAPY, MODELLING AND SIMULATION**

SESSION NAME: **SP029 – SURGICAL NAVIGATION: PART 1**

SESSION CHAIR(S): **CHRISTIAN LINTE, PETER MARTIN, CANADA**

- 17:00** SP029.1 - Preliminary evaluation of positron emission based 3D tracking system (PeTrack) in image guided interventions
Simin Razavi, Canada

- 17:15** SP029.2 - Seymour Shield? An Operative Adjunct Device for Maintaining Visualization during Laparoscopic Surgery
Karthik Kannan, Singapore
- 17:30** SP029.3 - Optimizing MRI-targeted fusion prostate biopsy: the effect of systematic error and anisotropy on tumour sampling
Peter Martin, Canada
- 17:45** SP029.4 - Is hemolysis influenced by the dynamic calibration method of CPB roller pumps?
Eduardo Costa, Brazil
- 18:00** SP029.5 - A Fiducial Apparatus for 6DOF Pose Estimation of an External Echo Probe from a Single X-ray Projection: Initial Simulation Studies on Design Requirements
Charles Hatt, United States
- 18:15** SP029.6 - Mechanism design a flexible endoscope with USB adaptation to training.
Francisco Perez Reynoso, Mexico
- 18:30** SP029.7 - 3D Quantitative Evaluation System for Integral Photography based 3D Autostereoscopic Medical Display
Zhencheng Fan, People's Republic of China

SESSION TIME: 17:00 – 19:00

SESSION ROOM: 717B

SESSION TRACK: **TRACK 08: BIOSENSOR, NANOTECHNOLOGY, BIOMEMS AND BIOPHOTONICS**

SESSION NAME: **SP030 – LAB-ON-CHIP, BIOMEMS AND MICROFLUIDICS**

SESSION CHAIR(S): **DONG HA KIM, REPUBLIC OF KOREA KWANG OH, UNITED STATES**

- 17:00** SP030.1 - **KEYNOTE:** Drop-based microfluidics for diagnostic applications
David Weitz, United States
- 17:30** SP030.2 - Enhanced multielectrode configurations in miniaturized 3D electrical impedance spectroscopy and tomography? Monitoring the overall process of tissue engineering with spatial sensing for future challenges in microfluidics
Chiara Canali, Denmark
- 17:45** SP030.3 - On-line monitoring of 2D and 3D cell cultures: electrode configurations for impedance based sensors
Chiara Canali, Denmark
- 18:00** SP030.4 - Development of Microfluidic Paper-Based Electrochemical Immunoassays for the Detection of Prostate Cancer
Sean Rawlinson, United Kingdom
- 18:15** SP030.5 - Investigating chip design for a Raman microfluidic system with clinical radiobiological applications.
Samantha Harder, Canada

- 18:30** SP030.6 - A lab-on-a-chip system for hypoxic investigations on single biological cells
Ahmed Alrifay, Sweden
- 18:45** SP030.7 - Gas Sensors with ZnO Quantum Dots Synthesized by Sol-Gel Methods
Lourdes Brasil, Brazil

SESSION TIME: 17:00 – 18:15

SESSION ROOM: 716B

SESSION TRACK: TRACK 09: BIOSIGNAL PROCESSING

SESSION NAME: SP031 – PATTERN CLASSIFICATION

SESSION CHAIR(S): JAMES GREEN, CANADA

- 17:00** SP031.1 - The Recognition of Pinch-to-Zoom Gesture Based on Surface EMG
Jongin Kim, Republic of Korea
- 17:15** SP031.2 - Feature extraction trends for biomedical signals
Yashodhan Athavale, Canada
- 17:30** SP031.3 - A Hybrid Model for Diagnosing Sever Aortic Stenosis in Asymptomatic Patients using Phonocardiogram
Maria Lindén, Sweden
- 17:45** SP031.4 - Classification of Load in Hands Based on Upper Limb SEMG
Illya Seagal, Canada
- 18:00** SP031.5 - An Intelligent Method for Discrimination between Aortic and Pulmonary Stenosis using Phonocardiogram
Amir Sepehri, Belgium

SESSION TIME: 17:00 – 18:30

SESSION ROOM: 701B

SESSION TRACK: TRACK 11: NEUROENGINEERING, NEURAL SYSTEMS

SESSION NAME: SP032 – NEURAL INTERFACES AND REGENERATION

SESSION CHAIR(S): JOSE ZARIFFA, CANADA
MILOS POPOVIC, CANADA

- 17:00** SP032.1 - **KEYNOTE:** Neuroprosthetic Systems for Enhancement of Neuroplasticity Following Stroke and Spinal Cord Injury
Milos Popovic, Canada
- 17:30** SP032.2 - Demonstration of Graphene Microelectrodes as a Bioelectronic Interface
Michael Horn, United States

- 17:45** SP032.3 - Development of a planar microelectrode array offering long-term, high-resolution neuronal recordings
Pierre Wijdenes, Canada
- 18:00** SP032.4 - Morphological changes in photoreceptors due to DC electric field
Juliana Guerra, Brazil
- 18:15** SP032.5 - Accelerating Neurite Outgrowth Through Electric Field Manipulation
Michael Purdy, Canada

SESSION TIME: 17:00 – 18:15

SESSION ROOM: 713B

SESSION TRACK: PRESIDENT'S CALL

SESSION NAME: SP033 – IMAGING: PART 1

SESSION CHAIR(S): SABEE MOLLOI, UNITED STATES

- 17:00** SP033.1 - Quantification of breast density using dual-energy mammography, CT and MRI
Sabee Molloi, United States
- 17:15** SP033.2 - Study on the Main Nonconformities Found in no Mammography Alagoas State
Fernanda Ferreira, Brazil
- 17:30** SP033.3 - Affordable medical x-ray imaging for the developing world: a global vision
Sorin Marcovici, Canada
- 17:45** SP033.4 - Characterization and Analysis of the Physical Parameters in Dental X-Rays Phantom
Fernanda Ferreira, Brazil
- 18:00** SP033.5 - In Vitro and In Vivo Studies Glycosylated Gadolinium Nanomagnetic Particleas (GD-DTPA-DG) as New Potential Metabolic Contrast Agent in MMRI
Nader Riyahi-Alam, Iran

SCIENTIFIC PROGRAM BY DAY

► Tuesday, June 9 2015

Tuesday, June 9 2015

SESSION TIME: 08:00 – 10:00
 SESSION ROOM: 718A
 SESSION TRACK: TRACK 01: IMAGING
 SESSION NAME: SP034 – CT: NEW TECHNIQUES
 SESSION CHAIR(S): MOHAMMAD REZA AY, IRAN

- 08:00** SP034.1 - Design, modeling and performance evaluation of a small animal Micro-CT scanner: A Monte Carlo study
Mohammad Reza Ay, Iran
- 08:15** SP034.2 - An imaging method by using electron mode of linear accelerator for soft tissue emphasis
Atsushi Myojoyama, Japan
- 08:30** SP034.3 - Anatomical noise model for CT head images: preliminary results
Marlen Perez-Diaz, Cuba
- 08:45** SP034.4 - The potential of spectral-CT for material decomposition with gold-nanoparticle and iodine contrast
Byungdu Jo, Republic of Korea
- 09:00** SP034.5 - Spatial Resolution Studies for a Prototype Proton CT Scanner
Tia Plautz, United States
- 09:15** SP034.6 - Influences of object size and tube potential pairing on the accuracy of iodine quantification using dual energy CT
Josh Grimes, United States
- 09:30** SP034.7 - Characterization of Vulnerable Plaque with Dual-Energy during CT Coronary Angiography: A Phantom Study
Ali Ursani, Canada
- 09:45** SP034.8 - The combination of a custom vascular perfusion contrast agent and dual-energy micro-CT to characterize bone-related vasculature
Justin Tse, Canada

SESSION TIME: 08:00 – 09:30
 SESSION ROOM: 701B
 SESSION TRACK: TRACK 01: IMAGING
 SESSION NAME: SP035 – IMAGING DETECTOR TECHNOLOGY
 SESSION CHAIR(S): FRANCIS LOIGNON-HOULE, CANADA
 ÉMILIE GAUDIN, CANADA

- 08:00** SP035.1 - Detectability in SPECT Myocardial Perfusion Imaging: Comparison between a Conventional and a Semiconductor Detector System
Ana Marques Da Silva, Brazil
- 08:15** SP035.6 - An alternate mathematical modeling of image formation, and framework for performance analysis of positioning algorithms in the scintillation camera
Mohammad Reza Ay, Iran
- 08:30** SP035.3 - Apodized-Aperture Pixel Design of an X-Ray Detector with Enhanced High-Frequency DE and Reduced Noise Aliasing
Elina Ismailova, Canada
- 08:45** SP035.4 - Geant4 Simulations of Scintillation Light Collection and Extraction in PET/CT Detectors
Francis Loignon-Houle, Canada
- 09:00** SP035.5 - LabPETII.5: APD-based Detector Characterization for Pre-clinical PET Imaging
Émilie Gaudin, Canada
- 09:15** SP035.2 - The performance of the CMOS APS detector for dual energy contrast enhanced digital mammography
Ilias Billas, United Kingdom

SESSION TIME: 08:00 – 10:00
 SESSION ROOM: 718B
 SESSION TRACK: TRACK 04: RADIATION ONCOLOGY
 SESSION NAME: SP036 – TREATMENT PLANNING – MOTION AND ROBUSTNESS
 SESSION CHAIR(S): JAN UNKELBACH, UNITED STATES
 ALBIN FREDRIKSSON, SWEDEN

- 08:00** SP036.1 - Robust optimization with independent beams produces robustly matched fields for intensity-modulated proton therapy treatments
Albin Fredriksson, Sweden

- 08:15** SP036.2 - Rotational tolerance in lung cancer image-guided radiation therapy
Peter Hoang, Canada
- 08:30** SP036.3 - Robustness Assessment of a Novel 4D Optimization Approach for Lung Cancer Radiotherapy
Shahad Al-Ward, Canada
- 08:45** SP036.4 - The role of VMAT interplay effects for liver stereotactic body radiation therapy
Gillian Ecclestone, Canada
- 09:00** SP036.5 - Interplay of MLC, gantry and respiratory motion during DCAT delivery
Tanya Kairn, Australia
- 09:15** SP036.6 - Impact of deep inspiration breath hold (DIBH) in lymphoma's radiation therapy treatment
Daniel Venencia, Argentina
- 09:30** SP036.7 - Cardiac sparing in left-sided breast IMRT using robust optimization
Houra Mahmoudzadeh, Canada
- 09:45** SP036.8 - Real Time Tumor Position Control During VMAT Hypofractionated Treatment
Chemseddine Fatnassi, Switzerland

SESSION TIME: **08:00 – 09:45**
 SESSION ROOM: **716A**
 SESSION TRACK: **TRACK 05: DOSIMETRY AND RADIATION PROTECTION**
 SESSION NAME: **SP037 – DOSIMETRY IN NUCLEAR MEDICINE**
 SESSION CHAIR(S): **ALEXANDRA ZVEREVA, GERMANY**

- 08:00** SP037.1 - Comparative Evaluation of Radiation Dose Rates in Cancer Thyroid Patients Treated with Variable Doses of Radioiodine
Ajai Kumar Shukla, India
- 08:15** SP037.2 - Estimation of the influence of other organs of the body in the determination of the gamma fraction energy emitted by iodine 131 deposited within the thyroid gland
Abderrahim Betka, DZ
- 08:30** SP037.3 - Personalized compartmental biokinetic modelling and internal dosimetry of two novel radiopharmaceuticals
Alexandra Zvereva, Germany
- 08:45** SP037.4 - TLD Measurement of Absorbed Dose of Workers in PET/CT Department
Pardis Ghafarian, Iran
- 09:00** SP037.5 - Renewing the radiopharmaceutical accuracy check service for Canadian dose calibrators
Malcolm McEwen, Canada
- 09:15** SP037.6 - Radiation Dose Assessment of ^{99m}Tc-labeled Tetrofosmin in Patients Undergoing Rest-Stress Myocardial Perfusion Scintigraphy
Stella Veloza, Colombia

- 09:30** SP037.8 - Biological Excretion and Half - Life of Remnant Radioactive Iodine 131 in Post Treated Hyperthyroidism Patients.
Shuaa Al-Sadoon, Jo

SESSION TIME: **08:00 – 09:15**
 SESSION ROOM: **715B**
 SESSION TRACK: **TRACK 05: DOSIMETRY AND RADIATION PROTECTION**
 SESSION NAME: **SP038 – DOSIMETRY OF NON-STANDARD FIELDS**
 SESSION CHAIR(S): **HUGO BOUCHARD, UNITED KINGDOM
SIJI PAUL, INDIA**

- 08:00** SP038.1 - Determination of small photon field quality correction factors using EBT3 radiochromic film
Ilias Billas, United Kingdom
- 08:15** SP038.2 - On the physics of megavoltage small photon field dosimetry
Hugo Bouchard, United Kingdom
- 08:30** SP038.3 - Comparison of AAPM TG 148 and UK code of practice of Reference dosimetry in Helical Tomotherapy.
Siji Paul, India
- 08:45** SP038.4 - A new facility to support the adaptation of reference dosimetry in the presence of strong magnetic fields
Simon Duane, United Kingdom
- 09:00** SP038.5 - The use of ionization chambers and Gafchromic films to determine the reference absorbed dose rate and output factors in a CyberKnife® unit small radiation fields
Guerda Massillon-JI, Mexico

SESSION TIME: **08:00 – 09:45**
 SESSION ROOM: **716B**
 SESSION TRACK: **TRACK 09: BIOSIGNAL PROCESSING**
 SESSION NAME: **SP039 – ECG**
 SESSION CHAIR(S): **ADRIAN CHAN, CANADA
PHILIP WARRICK, CANADA**

- 08:00** SP039.1 - Improved T-wave Alternans Detection in ECG Signals
Guangyi Chen, Canada
- 08:15** SP039.2 - Electrical Left Atrial Conduction Delay with Focused Transesophageal Electrocardiography in Cardiac Resynchronization Therapy
Matthias Heinke, Germany

- 08:30** SP039.3 - Electrical Interatrial to Interventricular Conduction Delay Ratio with Focused Transesophageal Electrocardiography in Cardiac Resynchronization Therapy
Matthias Heinke, Germany
- 08:45** SP039.4 - Analytical geometry based parameters for studying repolarization variability in patients with myocardial infarction
Muhammad Hasan, Canada
- 09:00** SP039.5 - Acute Mental Stress Detection via Ultra-short term HRV Analysis
Rossana Castaldo, United Kingdom
- 09:15** SP039.6 - Classification of Abdominal Fetal Electrocardiogram Recordings using Karhunen-Loève Decomposition
Philip Warrick, Canada
- 09:30** SP039.7 - Dictionary Learning Algorithms For The Application Of Ventricular Arrhythmia Classification.
Iman Kalaji, Canada

SESSION TIME: 08:00 – 09:30

SESSION ROOM: 715A

SESSION TRACK: **TRACK 10: REHABILITATION MEDICINE, SPORTS MEDICINE, REHABILITATION ENGINEERING AND PROSTHETICS**

SESSION NAME: **SP040 – ERGONOMICS, WEARABLE SENSORS AND VIRTUAL REALITY**

SESSION CHAIR(S): **MICHELE OLIVER, CANADA**

- 08:00** SP040.1 - **KEYNOTE:** Working to live: The use of field studies and simulations to make workplaces safer
Michele Oliver, Canada
- 08:30** SP040.2 - Pitch movement acceleration measures during the practice of virtual games in adolescents with Down syndrome
Paulo Lopes, Brazil
- 08:45** SP040.3 - Movement Training and Assessment with 3D Virtual Reality for Parkinson's Disease Patient
Chien-An Chen, Chinese Taipei
- 09:00** SP040.4 - Arm angle detection in egocentric video of upper extremity tasks
Jirapat Likitlersuang, Canada
- 09:15** SP040.5 - Development of an image-based calibration technique for use with non-ideal postures in the assessment of kinematics using wearable sensors
Monica Gomez, Canada

SESSION TIME: 08:00 – 09:45

SESSION ROOM: 714A

SESSION TRACK: **TRACK 11: NEUROENGINEERING, NEURAL SYSTEMS**

SESSION NAME: **SP041 – BRAIN COMPUTER/MACHINE INTERFACES**

SESSION CHAIR(S): **BAO-LIANG LU, PEOPLE'S REPUBLIC OF CHINA**

- 08:00** SP041.1 - Cross-subject and Cross-gender Emotion Classification from EEG
Bao-Liang Lu, People's Republic of China
- 08:15** SP041.2 - Comparison of Classification Methods for EEG-based Emotion Recognition
Bao-Liang Lu, People's Republic of China
- 08:30** SP041.3 - A Brain Computer Interface (BCI) based on intermittent photic-stimulation using multiple coherence to command detection
Antonio Infantesi, Brazil
- 08:45** SP041.4 - Volitional modulation of neural activity to control a 2 degree-of-freedom brain-machine interface in a rat model
Martha Garcia, Canada
- 09:00** SP041.5 - Electroencephalography-Based Off-Line Prediction of Specific Grasping Actions Performed with the Same Hand: Towards Integration of Brain-Computer Interfaces and Functional Electrical Stimulation Therapy
Cesar Marquez-Chin, Canada
- 09:15** SP041.6 - Wireless Distributed Intracortical Neural Interfacing: A New Approach for Brain Machine Interfaces
Alireza Zabihian, Canada
- 09:30** SP041.7 - Design and construction of a brain-computer interface for applications in neuro?robotics
Alma Méndez Gordillo, Mexico

SESSION TIME: 08:00 – 09:45

SESSION ROOM: 701A

SESSION TRACK: **TRACK 16: CLINICAL ENGINEERING, CLINICAL PHYSICS, AND PATIENT SAFETY**

SESSION NAME: **SP042 – TECHNOLOGY MANAGEMENT PROGRAMMES AND EQUIPMENT MANAGEMENT SYSTEMS**

SESSION CHAIR(S): **JOHN KILDEA, CANADA
TOM JUDD, UNITED STATES**

- 08:00** SP042.1 - **KEYNOTE:** Medical device systems Health Technology Management (HTM) strategies and best practices
Tom Judd, United States

- 08:30** SP042.3 - Development of a scoring system to support medical equipment replacement prioritization using the Analytical Hierarchy Process (AHP)
Paul Prowse, Canada
- 08:45** SP042.4 - Multi-criteria decision analysis to redesign an Italian Clinical Engineering Service under specific needs and regulation requirements
Irene Lasorsa, Italy
- 09:00** SP042.5 - Developing a system to support equipment repair versus replacement decision making
Sarah Kelso, Canada
- 09:15** SP042.6 - An assessment of Preventive and Performance Maintenance Of Theater Equipment In Public Hospitals Kenya: Case study Five Public Hospitals.
Philip Anyango, Kenya
- 09:30** SP042.7 - Mathematical Model for Reliable Maintenance of Medical Equipment
Abdelbaset Khalaf, South Africa

SESSION TIME: **08:00 – 09:30**

SESSION ROOM: **717A**

SESSION TRACK: **TRACK 18: GENDER, SCIENCE AND TECHNOLOGY**

SESSION NAME: **SP043 – WOMEN IN BIOMEDICAL ENGINEERING**

SESSION CHAIR(S): **PATRICIA TRBOVICH, CANADA
KRISTY BROCK, UNITED STATES**

- 08:00** SP043.1 - **KEYNOTE:** One thousand years of women in science
Monique Frize, Canada
- 08:30** SP043.2 - Creating the Memories and Celebrating the Legacy of Women in Science and Engineering
Ruby Heap, Canada
- 08:45** SP043.3 - Women In Bio-Medical Engineering In Kenya
Salome Mwaura, Kenya
- 09:00** SP043.4 - Physics is a waste of your intelligence
Shada Wadi-Ramahi, Saudi Arabia
- 09:15** SP043.5 - Medical physics? or how a change in career path becomes a passion
Loredana Marcu, Ro

SESSION TIME: **10:30 – 12:00**

SESSION ROOM: **701B**

SESSION TRACK: **TRACK 01: IMAGING**

SESSION NAME: **SP044 – BIO-IMPEDANCE AND IMAGING (OTHER)**

SESSION CHAIR(S): **OLAF DOESSEL, GERMANY
ZHIPENG LIU, PEOPLE'S REPUBLIC OF CHINA**

- 10:30** SP044.1 - Personal Time-Varying Magnetic Fields Evaluation During Activities in MRI Sites
Giuseppe Acri, Italy
- 10:45** SP044.2 - ECG Imaging of Ventricular Extrasystoles
Olaf Doessel, Germany
- 11:00** SP044.3 - Experimental Study on Amplitude Frequency of Acoustic Signal Excited by Coupling Magneto-Acoustic Field
Zhipeng Liu, People's Republic of China
- 11:15** SP044.4 - In vivo electric conductivity values of cervical cancer patients reconstructed with a 3T MR system for improved SAR determination
Edmond Balidemaj, Netherlands
- 11:30** SP044.5 - Focus Tunable Gel Lens Using Annular Dielectric Elastomer Actuator
Thanh Giang La, Singapore
- 11:45** SP044.6 - Ultra-low-field MRI for improving spatial accuracy of bioelectric source imaging
Koos Zevenhoven, Finlandia

SESSION TIME: **10:30 – 12:00**

SESSION ROOM: **718A**

SESSION TRACK: **TRACK 01: IMAGING**

SESSION NAME: **SP045 – MOLECULAR IMAGING PET/SPECT: PART 1**

SESSION CHAIR(S): **AMIR POURMOGHADDAS, CANADA
MOHAMMAD REZA AY, IRAN**

- 10:30** SP045.1 - Quantitative accuracy of SPECT imaging with a dedicated cardiac camera: Physical phantom experiments
Amir Pourmoghaddas, Canada
- 10:45** SP045.2 - The Impact of time of flight algorithm and PSF modeling on standard uptake value in clinical PET/CT imaging
Mohammad Reza Ay, Iran
- 11:00** SP045.3 - Can Pacemaker and ICD degrade CT-Based Attenuation Corrected cardiac SPECT images?
Mohammad Reza Ay, Iran
- 11:15** SP045.4 - Impact of Point spread function modeling on tumor quantification in clinical PET/CT imaging
Mohammad Reza Ay, Iran
- 11:30** SP045.5 - Incidental Thyroid Cancer Identified on 18FDG- PET/CT for Ovarian Cancer Evaluation-Case Study.
Shuaa Al-Sadoon, Jo
- 11:45** SP045.6 - Zinc material filter for scatter correction in Tc-99m myocardial SPECT imaging: Heart thorax phantom study
Nazifah Abdullah, Malaysia

SESSION TIME: 10:30 – 12:00

SESSION ROOM: 718B

SESSION TRACK: TRACK 04: RADIATION ONCOLOGY

SESSION NAME: SP046 – ASSESSMENT OF RADIOTHERAPY RESPONSE

SESSION CHAIR(S): ISSAM EL NAQA, CANADA
SARAH MATTONEN, CANADA

- 10:30** SP046.1 - Early prediction of lung cancer recurrence after stereotactic radiotherapy using texture analysis of automatic graph cuts segmentations
Sarah Mattonen, Canada
- 10:45** SP046.2 - Can parametric response maps predict voxel-wise treatment response? Implications for locally adaptive radiotherapy.
Anthony Lausch, Canada
- 11:00** SP046.3 - Using Magnetic Resonance Imaging Radiomics to Personalize Brain Metastases Treatment
Sarah Mattonen, Canada
- 11:15** SP046.4 - Raman spectroscopy for assessment of radiation therapy response: Pre-clinical animal study results for lung cancer
Suneetha Devpura, United States
- 11:30** SP046.5 - Serial 4DCT and 4DPET imaging to monitor response for locally-advanced non-small cell lung cancer patients undergoing combined chemotherapy and radiotherapy
Jean-Pierre Bissonnette, Canada
- 11:45** SP046.6 - Evaluation and Visualization of Radiogenomic Modeling Frameworks for the Prediction of Normal Tissue Toxicities
Issam El Naqa, Canada

SESSION TIME: 10:30 – 12:00

SESSION ROOM: 701A

SESSION TRACK: TRACK 04: RADIATION ONCOLOGY

SESSION NAME: SP047 – DOSE CALCULATION: PART 2

SESSION CHAIR(S): OTTO SAUER, GERMANY
ALESSANDRO ESPOSITO, PORTUGAL

- 10:30** SP047.1 - Non-Standard IOERT Dose Distributions Scenarios by Monte Carlo Studies
Alessandro Esposito, Portugal
- 10:45** SP047.2 - Validation of a Commercial GPU-Based Monte Carlo Dose Calculation Algorithm for use with an Elekta MRI-Linear Accelerator
Moti Paudel, Canada
- 11:00** SP047.3 - A Dosimetric Evaluation of Interface Effects Using Two Commercial Electron Treatment Planning Algorithms
Mark Yudelev, United States

- 11:15** SP047.4 - 4D Monte Carlo simulation for verification of delivered dose to deforming anatomy
Sara Gholampourkashi, Canada
- 11:30** SP047.5 - Clinical implementation of an EPID-based in vivo dose verification system for SBRT-VMAT delivery; catching errors
Peter McCowan, Canada
- 11:45** SP047.6 - pGPUMCD, a GPU-based Monte Carlo proton transport code
Daniel Maneval, Canada

SESSION TIME: 10:30 – 12:00

SESSION ROOM: 716A

SESSION TRACK: TRACK 05: DOSIMETRY AND RADIATION PROTECTION

SESSION NAME: SP048 – DOSIMETRY OF PROTONS AND HEAVY IONS

SESSION CHAIR(S): HEIDI NETTELBECK, GERMANY
GIULIA ARICO, GERMANY

- 10:30** SP048.1 - An Attempt to Predict the Proton Relative Biological Effectiveness using Radical Recombination
Kiyofumi Haneda, Japan
- 10:45** SP048.2 - A correction method for absorbed dose estimation using TEP-TLSD/SR1 in therapeutic carbon beam
Weishan Chang, Japan
- 11:00** SP048.3 - Biologically-weighted dosimetric quantities based on a multiscale approach
Heidi Nettelbeck, Germany
- 11:15** SP048.4 - Studies of Helium and Carbon Ion Fragmentation processes in Water and in PMMA, using versatile Semiconductor Detectors
Giulia Arico, Germany
- 11:30** SP048.5 - Monte Carlo study of secondary neutron dose for multipurpose nozzle in proton therapy
Sungkoo Cho, Republic of Korea
- 11:45** SP048.6 - Investigation of the uncertainties involved in the low energy proton interaction in different MC-codes for proton therapy application
Lalageh Mirzakhani, Canada

SESSION TIME: 10:30 – 12:00

SESSION ROOM: 717B

SESSION TRACK: TRACK 06: NEW TECHNOLOGIES IN CANCER RESEARCH AND TREATMENT

SESSION NAME: SP049 – NANOTECHNOLOGY IN RADIATION THERAPY AND IMAGING: PART 1

SESSION CHAIR(S): LUC BEAULIEU, CANADA
MICHAEL ANTOSH, UNITED STATES

- 10:30** SP049.1 - A plasma electrochemistry reactor enabling the rapid, efficient, automatic and on-site synthesis of radioactive gold nanoparticles for brachytherapy treatments
Mathieu Bouchard, Canada
- 10:45** SP049.2 - Dose Enhancement in Radiotherapy by Novel Application Of Gadolinium Based MRI Contrast Agent Nanomagnetic Particles in Gel Dosimetry
Nader Riyahi Alam, Iran
- 11:00** SP049.3 - Monte Carlo simulation of the radiosensitizing effect by gold nanoparticles: comparison between proton and X-ray irradiation
Jihun Kwon, Japan
- 11:15** SP049.4 - Colloidal quantum dots: radiation resistant nano-scintillators for radiation-based applications
Marie-Ève Delage, Canada
- 11:30** SP049.5 - Use of gold nanoparticles and pHLIP (pH Low Insertion Peptide) to increase radiation effectiveness in cancer cells.
Michael Antosh, United States
- 11:45** SP049.6 - The use of nanoparticles to improve hadrontherapy
Marta Bolsa-Ferruz, France

SESSION TIME: 10:30 – 12:15
SESSION ROOM: 716B
SESSION TRACK: TRACK 09: BIOSIGNAL PROCESSING
SESSION NAME: SP050 – TIME-FREQUENCY ANALYSIS
SESSION CHAIR(S): NITISH THAKOR, SINGAPORE
SRI KRISHNAN, CANADA

- 10:30** SP050.1 - **KEYNOTE: Frontiers of Neuroengineering**
Nitish Thakor, Singapore
- 11:00** SP050.2 - Neural responses to hearing own names comparing with repeated/non-repeated unfamiliar stimuli
Kaori Tamura, Japan
- 11:15** SP050.3 - MRS data deconvolution through KBDM with multiple signal truncation and clustering: circumventing noise effects
Danilo Da Silva, Brazil
- 11:30** SP050.4 - Quantification of Wavelet Band Metrics for Assessing Heart Rate Variability
Mark Wachowiak, Canada
- 11:45** SP050.5 - Effect of Coffee on EEG Spectral Asymmetry
Maie Bachmann, Estonia
- 12:00** SP050.6 - Effects of Changing in the Neck Fluid Volume, Neck Circumference and Upper Airway during Sleep on Snoring Sound Characteristics
Zahra Moussavi, Canada

SESSION TIME: 10:30 – 11:30
SESSION ROOM: 715A
SESSION TRACK: TRACK 10: REHABILITATION MEDICINE, SPORTS MEDICINE, REHABILITATION ENGINEERING AND PROSTHETICS
SESSION NAME: SP051 – REHABILITATION ROBOTICS
SESSION CHAIR(S): YAHIA AL-SMADI, UNITED STATES

- 10:30** SP051.1 - Biomechanical Simulation of Upper Extremities Exoskeleton to Aid Stroke Patients
Yahia Al-Smadi, United States
- 10:45** SP051.2 - Testing a mobile robot toy for children with disabilities
William Rodríguez, Colombia
- 11:00** SP051.3 - Pilot study of a soft metal hydride actuator for a wearable rehabilitation system
Minako Hosono, Japan
- 11:15** SP051.4 - Robotic Spasticity Quantification: Velocity Dependent Component of Biomechanical Resistance
Nitin Seth, Canada

SESSION TIME: 10:30 – 11:45
SESSION ROOM: 714A
SESSION TRACK: TRACK 11: NEUROENGINEERING, NEURAL SYSTEMS
SESSION NAME: SP052 – FUNCTIONAL NEUROIMAGING AND NEURONAVIGATION
SESSION CHAIR(S): ERVIN SEJDIC, UNITED STATES
HOSSEIN ROUHANI, CANADA

- 10:30** SP052.1 - **KEYNOTE: From human neuron to human brain: Neurosurgical contributions to understanding the brain**
Taufik Valiante, Canada
- 11:00** SP052.2 - Modulation of event-related desynchronization and synchronization during right finger flexion in patients with Amyotrophic Lateral Sclerosis
Natasa Bizovicar, Slovenia
- 11:15** SP052.3 - Functional connectivity patterns associated with swallowing of fluids with various viscosity
Ervin Sejdic, United States
- 11:30** SP052.4 - Distribution of F-Latency (DFL) - a new nerve conduction parameter for early detection of radiculomyelopathy
K Siddique Rabbani, Bangladesh

SESSION TIME: 10:30 – 11:45
 SESSION ROOM: 715B
 SESSION TRACK: TRACK 12: MEDICAL DEVICES
 SESSION NAME: SP053 – CARDIOVASCULAR INSTRUMENTATION
 SESSION CHAIR(S): MARIE KEAYS, IRELAND
 JONATHAN WOLFE, SINGAPORE

- 10:30** SP053.1 - A Microfluidic cell culture Instrument for individual testing of therapeutics.
Marie Keays, Ireland
- 10:45** SP053.2 - A Bioinspired Catheter Harnessing Gecko Adhesion and Inchworm?Like Locomotion for Targeted Drug Delivery
Jonathan Wolfe, Singapore
- 11:00** SP053.3 - Covered stent with perforated membrane for treatment of peripheral atheroembolic disease
Foad Kabinejadian, Singapore
- 11:15** SP053.4 - Nanostructuring Carbon Fibre Probes for Use in Central Venous Catheters
Jolene McHugh, United Kingdom
- 11:30** SP053.5 - Denoising RF defibrillator waveforms for intracardiac atrial substrate impedance characterisation using digital filtering techniques
Omar Escalona, United Kingdom

SESSION TIME: 10:30 – 12:00
 SESSION ROOM: 717A
 SESSION TRACK: TRACK 18: GENDER, SCIENCE AND TECHNOLOGY
 SESSION NAME: SP054 – WOMEN IN MEDICAL PHYSICS: CURRENT STATUS
 SESSION CHAIR(S): PATRICIA TRBOVICH, CANADA
 MONIQUE FRIZE, CANADA

- 10:30** SP054.1 - Experiences as a Women in the Biomedical Engineering Field
Molly Shoichet, Canada
- 11:00** SP054.2 - The Historical Role of Women in Medical Physics
Magdalena Stoeva, United Kingdom
- 11:10** SP054.3 - Women in Medical Physics
Simone Kodlulovitch, Brazil
- 11:20** SP054.4 - Women in Medical Physics; current status in Australia and New Zealand.
Eva Bezak, Australia
- 11:30** SP054.5 - Women in medical physics; Current status
Nicole Ranger, United States
- 11:40** SP054.6 - Women in Medical Physics
Jamila Salem Al Suwaidi, United Arab Emirates

SESSION TIME: 15:00 – 16:30
 SESSION ROOM: 715A
 SESSION TRACK: TRACK 03: BIOMECHANICS AND ARTIFICIAL ORGANS
 SESSION NAME: SP055 – CELLULAR & MOLECULAR MECHANICS
 SESSION CHAIR(S): ANDREW QUIGLEY, CANADA
 SAMUEL BALDWIN, CANADA

- 15:00** SP055.1 - Neurite outgrowth induced by shock waves
Youn Kihwan, Japan
- 15:15** SP055.2 - Investigating mechanical behavior and structural response to strain of bovine tendon collagen fibrils using atomic force microscopy
Andrew Quigley, Canada
- 15:30** SP055.3 - Collagen fibrils from overloaded tendons show sites of discrete plasticity and overall perturbation in molecular packing
Samuel Baldwin, Canada
- 15:45** SP055.4 - Mechanobiology of Hepatic Cells and Engineered Construction of Liver
Mian Long, People's Republic of China
- 16:00** SP055.5 - Modelling and Understanding Normal Pressure Hydrocephalus
Christine Goffin, Germany
- 16:15** SP055.6 - Osteolytic tumour involvement modifies characteristics of Collagen-I within the vertebral bone matrix impacting mechanical behaviour
Mikhail Burke, Canada

SESSION TIME: 15:00 – 16:15
 SESSION ROOM: 701A
 SESSION TRACK: TRACK 04: RADIATION ONCOLOGY
 SESSION NAME: SP056 – IMAGE GUIDED RT: PART 2
 SESSION CHAIR(S): LI ZHOU, PEOPLE'S REPUBLIC OF CHINA
 YUDY ASCENCION, CUBA

- 15:00** SP056.1 - Imaging Dose and Dose Pattern in Image-guided Radiotherapy of Cancers
Li Zhou, People's Republic of China
- 15:15** SP056.2 - Residual errors and dosimetric consequences related to the spinal cord in head and neck radiotherapy
Jinkoo Kim, United States
- 15:30** SP056.3 - An automatic dosimetric and geometric tracking system for head and neck adaptive radiotherapy
Jinkoo Kim, United States
- 15:45** SP056.4 - Morphological Analysis of Tumor Regression and Its Impact on Deformable Image Registration for Adaptive Radiotherapy of Lung Cancer Patients
Hualiang Zhong, United States

16:00 SP056.5 - Assessment of a 4D-CBCT system for managing respiratory motion in Radiotherapy
Judy Ascencion, Cuba

SESSION TIME: **15:00 – 16:45**

SESSION ROOM: **718B**

SESSION TRACK: **TRACK 04: RADIATION ONCOLOGY**

SESSION NAME: **SP057 – QUALITY ASSURANCE: PART 2**

SESSION CHAIR(S): **EDUARD GERSHKEVITSH, ESTONIA**

15:00 SP057.1 - Sensitivity of VMAT patient specific QC devices to linac calibration errors
Eduard Gershkevitch, Estonia

15:15 SP057.2 - Clinical implementation of a novel transmission detector for 3D quality assurance during radiation therapy
Greg Sharp, United States

15:30 SP057.3 - Development of a Radiochromic Film Dosimetry Imaging System
Kevin Alexander, Canada

15:45 SP057.4 - Implementation of MOSFET detectors for in-vivo radiotherapy dosimetry.
Yi Wah Eva Cheung, United Kingdom

16:00 SP057.5 - 3D in vivo dose verification at The Netherlands Cancer Institute
Ben Mijnheer, Netherlands

16:15 SP057.6 - Dosimetric commissioning of high end features in Radiotherapy Treatment Planning Systems: a proposed update of the IAEA TECDOC-1583 guidelines
Rodolfo Alfonso, Cuba

16:30 SP057.7 - Implementation of statistical tolerance for patient specific QA and independent monitor unit calculation
Frédéric Girard, Canada

SESSION TIME: **15:00 – 16:15**

SESSION ROOM: **716A**

SESSION TRACK: **TRACK 05: DOSIMETRY AND RADIATION PROTECTION**

SESSION NAME: **SP058 – CHARACTERIZATION OF DETECTOR SYSTEMS FOR THERAPY DOSIMETRY: PART 1**

SESSION CHAIR(S): **THEODOROU KIKI, GREECE
WARREN CAMPBELL, CANADA**

15:00 SP058.1 - Destructive backscatter-based readout of polymer gel dosimeters: proof of principle
Warren Campbell, Canada

15:15 SP058.2 - New Detector Systems for the Dosimetry in Radiation Therapy
Viktor Iakovenko, Ukraine

15:30 SP058.3 - Dose response evaluation of lung equivalent gel dosimeters by use of a new fitting algorithm
Hassan Ali Nedaie, Iran

15:45 SP058.4 - Photoluminescence response of pure LiF crystals to clinical proton and carbon ions: a preliminary assessment for dose to water evaluations
Jose Villarreal-Barajas, Canada

16:00 SP058.5 - Evaluation of Accuracy and Precision in X-ray Computed Tomography Polymer Gel Dosimetry.
Evan Maynard, Canada

SESSION TIME: **15:00 – 16:15**

SESSION ROOM: **717B**

SESSION TRACK: **TRACK 08: BIOSENSOR, NANOTECHNOLOGY, BIOMEMS AND BIOPHOTONICS**

SESSION NAME: **SP059 – DRUG DELIVERY AND CONTROL RELEASE**

SESSION CHAIR(S): **DONG HA KIM, REPUBLIC OF KOREA**

15:00 SP059.1 - Nanotechnology applied in drug delivery
Lourdes Brasil, Brazil

15:15 SP059.2 - Controlled electrochemical dissolution of iron alginate for smart drug release in micro devices
Ashleigh Anderson, United Kingdom

15:30 SP059.3 - Next generation transdermal drug delivery? An electrochemical approach to pH manipulation for controlled release within smart patch technologies
Ashleigh Anderson, United Kingdom

15:45 SP059.4 - Protein nanocages for stabilization of bio-inspired emulsions/gel systems and cutaneous drug delivery
Sierin Lim, Singapore

16:00 SP059.5 - Image-Guided Predictions of Nanoparticle Transport in Solid Tumors
Shawn Stapleton, United States

SESSION TIME: **15:00 – 16:30**

SESSION ROOM: **714B**

SESSION TRACK: **TRACK 12: MEDICAL DEVICES**

SESSION NAME: **SP060 – SPECIAL SESSION: UNESCO INTERNATIONAL YEAR OF LIGHT**

SESSION CHAIR(S): **BRIAN WILSON, CANADA**

15:00 SP060.1 - **KEYNOTE:** UNESCO International Year of Light
Brian Wilson, Canada

15:30 SP060.2 - Design of Wireless Implantable Optogenetics System for Animal Studies
Fu-yu Chen, New Zealand

- 15:45** SP060.3 - A method to determine the variation of irradiance in bilirubin lamps as function of the time of use
Graciela Salum, Ecuador
- 16:00** SP060.4 - Study of the sensibility of induced heat effects in edible oil measured by interferometric techniques
Joel Espinosa-Barrios, Mexico
- 16:15** SP060.5 - Design and study of Infrared-Guard
Shanmugam Senthilkumar, India

SESSION TIME: 15:00 – 16:30

SESSION ROOM: 715B

SESSION TRACK: TRACK 12: MEDICAL DEVICES

SESSION NAME: SP061 – IMPROVEMENT OF DIAGNOSIS AND THERAPIES

SESSION CHAIR(S): FERNANDO INFANTOSI, BRAZIL
ROMAIN ESPAGNET, CANADA

- 15:00** SP061.1 - Development of heart sparing device for Left Breast Radiotherapy with deep breath-holding
Shanmugam Senthilkumar, India
- 15:15** SP061.2 - HTA for Medical Devices: Multiple-Criteria Decision Making as an Outcome Evaluation Tool
Ivana Jurickova, Czech Republic
- 15:45** SP061.3 - Developing Smart Bandage Materials for the Management of Chronic Wounds in Diabetic Patients
Jolene McHugh, United Kingdom
- 16:00** SP061.4 - A CdZnTe-based automated Blood Counter for Quantitative Molecular Imaging
Romain Espagnet, Canada
- 16:15** SP061.5 - A Portable Free-Hand 3D SPECT System
Harley Chan, Canada
- 16:30** SP061.6 - Probing the Biomechanical Properties of Cells using High-Frequency Ultrasound and Acoustic Levitation
Natalie Sullivan, United States

SESSION TIME: 15:00 – 16:30

SESSION ROOM: 701B

SESSION TRACK: TRACK 16: CLINICAL ENGINEERING, CLINICAL PHYSICS, AND PATIENT SAFETY

SESSION NAME: SP062 – CLINICAL PROCESS ANALYSIS, OPTIMIZATION, PRODUCTIVITY AND BENCHMARKING

SESSION CHAIR(S): BETTSY HERNANDEZ-ZACARIAS, MEXICO
GERARDO ROMO-CARDENAS, MEXICO

- 15:00** SP062.1 - Guaranteeing the quality of rigid endoscopes with the ScopeControl
Herke Jan Noordmans, Netherlands

- 15:15** SP062.2 - Low-entry level CT exam times and availability in worldwide markets
Renan Almeida, Brazil
- 15:30** SP062.3 - The critical evaluation of AV control features in modern pacemakers and cardioverters
Tadeusz Palko, Poland
- 15:45** SP062.4 - Assisted Reproductive Technology Center Design with Quality Function Deployment Approach
Alessio Luschi, Italy
- 16:00** SP062.5 - Study of the Sensitivity on the Measurement of the Prevalence of Total Cholesterol in Blood Serum by Interferometric Techniques
Betsy Hernandez-Zacarias, Mexico
- 16:15** SP062.6 - Critical role of sustaining technology and utilities in healthcare institutions facing disaster through development of an international center for information and training of health technology managers on disaster preparedness
Yadin David, United States

SESSION TIME: 15:00 – 17:15

SESSION ROOM: 717A

SESSION TRACK: TRACK 17: EDUCATIONAL AND PROFESSIONAL ACTIVITIES

SESSION NAME: SP063 – ACCREDITATION, CERTIFICATION AND LICENSURE ISSUES

SESSION CHAIR(S): ADRIANA VELAZQUEZ BERUMEN, SWITZERLAND
RAYMUND WU, UNITED STATES

- 15:00** SP063.1 - **KEYNOTE:** The Current State of Clinical Engineering Education and Career
Yadin David, United States
- 15:30** SP063.2 - The Pursuit of Regulated Health Profession Status for Medical Physicists in Alberta
Charles Kirkby, Canada
- 15:45** SP063.3 - The International Medical Physics Certification Board
Colin Orton, United States
- 16:00** SP063.4 - Radiation protection continued training program evaluation: return on a 7-year experience
Nadia Octave, Canada
- 16:15** SP063.5 - Where to find biomedical engineers worldwide? Mapping biomedical engineers around the world
Adriana Velazquez Berumen, Switzerland
- 16:30** SP063.6 - Oh dear medical physicist and biomedical engineer, why is it difficult to pioneer your specialist career?
Mario Medvedec, Croatia
- 16:45** SP063.7 - Biomedical Engineering Education and Training and Accreditation of Bachelor-degree Biomedical Engineering Programmes
Min Wang, Hong Kong
- 17:00** SP063.8 - IOMP initiative for Validation and Accreditation of MSc courses
Slavik Tabakov, United Kingdom

SESSION TIME: 15:00 – 16:15
 SESSION ROOM: 713B
 SESSION TRACK: **PRESIDENT'S CALL**
 SESSION NAME: **SP064 – BIOMECHANICS AND ARTIFICIAL ORGANS**
 SESSION CHAIR(S): **PETER GOSHULAK, CANADA**
MINA AZIZ, CANADA

- 15:00** SP064.1 - Biomechanical Analysis of Optimal Orientation and Stress Shielding for Short and Long Stem Hip Implants
Peter Goshulak, Canada
- 15:15** SP064.2 - Biomechanical Analysis of Acute Total Hip Replacements after Acetabular Fracture: Plate vs Cable Repair
Mina Aziz, Canada
- 15:30** SP064.3 - Biomechanical Validation of the Radiographic Union Score for Tibial fractures (RUST) as a Predictor for Fracture Healing
Sandra Fiset, Canada
- 15:45** SP064.4 - Patient-specific multi-scaling simulation of blood flow and fractional flow reserve in a coronary artery
Kyung Lee, Republic of Korea
- 16:00** SP064.5 - A Modified PID Algorithm with Fuzzy Control for Closed-loop Artificial Pancreas
Jin Hao Yu, People's Republic of China

SESSION TIME: 17:00 – 18:45
 SESSION ROOM: 718A
 SESSION TRACK: **TRACK 01: IMAGING**
 SESSION NAME: **SP065 – CONEBEAM CT**
 SESSION CHAIR(S): **REBECCA FAHRIG, UNITED STATES**
KERSTIN MUELLER, UNITED STATES

- 17:00** SP065.1 - **KEYNOTE:** Towards Functional C-arm CT Imaging in the Interventional Suite: Progress and challenges
Rebecca Fahrig, United States
- 17:30** SP065.2 - 2D/3D Registration for Motion Compensated Reconstruction in Cone-Beam CT of Knees Under Weight-Bearing Condition
Martin Berger, Germany
- 17:45** SP065.3 - Direct Scatter Estimation and Separation for Cone-beam CT Images Utilizing Monte Carlo Simulation
Yu Wang, People's Republic of China
- 18:00** SP065.4 - Automatic Motion Estimation and Compensation Framework for Weight-bearing C-arm CT scans using Fiducial Markers
Kerstin Mueller, United States

- 18:15** SP065.5 - Evaluation of two-pass view aliasing artifact suppression algorithm using clinical data
Kerstin Mueller, United States
- 18:30** SP065.6 - A simple algorithm to remove metal artifacts in frame based radiosurgical treatments
Gopishankar Natanasabapathi, India

SESSION TIME: 17:00 – 18:15
 SESSION ROOM: 714B
 SESSION TRACK: **TRACK 03: BIOMECHANICS AND ARTIFICIAL ORGANS**
 SESSION NAME: **SP066 – HUMAN MOVEMENT**
 SESSION CHAIR(S): **YUBO FAN, PEOPLE'S REPUBLIC OF CHINA**
EMILY SINITSKI, CANADA

- 17:00** SP066.1 - Fingertip touch adjust postural orientation during perturbed stance
Aizreena Azaman, Japan
- 17:15** SP066.2 - Design and Evaluation of a Prosthetic Knee Joint based on Automatic Stance-Phase Lock (ASPL) Technology for Children with Transfemoral Amputations
Calvin Ngan, Canada
- 17:30** SP066.3 - Frontal plane gait during cross-slope walking for able-bodied and transtibial amputees
Emily Sinitski, Canada
- 17:45** SP066.4 - Impact of gait modifications on hip joint loads during level walking
Masaru Higa, Japan
- 18:00** SP066.5 - The influence of the aquatic environment on the control of gait initiation
Andresa Marinho Buzelli, Canada

SESSION TIME: 17:00 – 18:30
 SESSION ROOM: 716A
 SESSION TRACK: **TRACK 05: DOSIMETRY AND RADIATION PROTECTION**
 SESSION NAME: **SP067 – CHARACTERIZATION OF DETECTOR SYSTEMS FOR THERAPY DOSIMETRY: PART 2**
 SESSION CHAIR(S): **MAGDALENA STOEVA, BULGARIA**
MALCOLM MCEWEN, CANADA

- 17:00** SP067.1 - Reaction of three UV exposure to gafchromic EBT-2 and EBT-3
Toshizo Katsuda, Japan
- 17:15** SP067.2 - Characterizing FujiFilm CR Signal Storage Decay Rates
Thorarin Bjarnason, Canada

- 17:30** SP067.3 - Angular dependence of diode detectors and PinPoint ionization chamber in Gamma Knife dosimetry
Hrvoje Hrsak, Croatia
- 17:45** SP067.4 - Determination of a correction factor to mitigate long term reader fluctuation of the Optically Stimulated Luminescence dosimetry system at the International Atomic Energy Agency
Joanna Izewska, Austria
- 18:00** SP067.5 - Reference and relative dosimetry of standard and small photon fields with new commercially available detectors
Bryan Muir, Canada
- 18:15** SP067.6 - Evaluation of detectors response for small field output factor measurement using multichannel film dosimetry
Gunther Rucka, France

SESSION TIME: 17:00 – 18:30
 SESSION ROOM: 715B
 SESSION TRACK: TRACK 05: DOSIMETRY AND RADIATION PROTECTION
 SESSION NAME: SP068 – DEVELOPMENT OF NEW METHODS IN THERAPY DOSIMETRY
 SESSION CHAIR(S): RICARDO TERINI, BRAZIL
 MEHRAN ZAINI, UNITED STATES

- 17:00** SP068.1 - A Farmer ion chamber as reference to the calibration of CT chambers
Ricardo Terini, Brazil
- 17:15** SP068.2 - Determination of the Uncertainty in the Cross-calibration of an Ionization Chamber Used in Radiation Therapy
Pedro Cardoso, Brazil
- 17:30** SP068.3 - A study of uncertainties in the half-value layer measurement of a miniature kV x-ray source
Peter Watson, Canada
- 17:45** SP068.4 - Low Energy Therapeutic X-Ray Calibration Methods
Mehran Zaini, United States
- 18:00** SP068.5 - Energy response of a thimble-type ionization chamber for Ir-192 and Co-60 radiation beams
Cecilia Kessler, France
- 18:15** SP068.6 - Kilo-voltage X-Ray tube dosimetry Correction factors for in-water measurement in TG-61
Nima Sherafati, Canada

SESSION TIME: 17:00 – 18:30
 SESSION ROOM: 701A
 SESSION TRACK: TRACK 06: NEW TECHNOLOGIES IN CANCER RESEARCH AND TREATMENT
 SESSION NAME: SP069 – NOVEL DETECTORS, PHANTOMS AND SOFTWARE, DIAGNOSTIC TECHNIQUES
 SESSION CHAIR(S): NATALKA SUCHOWERSKA, AUSTRALIA
 MICHAEL LERCH, AUSTRALIA

- 17:00** SP069.1 - Synergistic Action of Ionizing Radiation with Platinum-based Chemotherapeutic Drugs: Soft X-rays and Low-Energy Electrons
Elahe Alizadeh, Canada
- 17:15** SP069.2 - Cherenkov emission dosimetry for electron beam radiotherapy: a Monte Carlo feasibility study of absolute dose prediction
Yana Zlateva, Canada
- 17:30** SP069.3 - Detection of melanoma through image recognition and artificial neural networks
Cristofer Marin, Mexico
- 17:45** SP069.4 - Clinical Implementation of an Intraoperative Radiotherapy Program
Muthana Al-Ghazi, United States
- 18:00** SP069.5 - Performance of a Back-etched Silicon Detector Array Designed to Monitor Each Synchrotron Generated X-ray Beam in Microbeam Radiation Therapy
Michael Lerch, Australia
- 18:15** SP069.6 - Dynamic Mechanical Characterization of a Poly(vinyl alcohol) Breast Palpation Phantom
Gabriel Rodriguez, United States

SESSION TIME: 17:00 – 18:45
 SESSION ROOM: 701B
 SESSION TRACK: TRACK 01: IMAGING
 SESSION NAME: SP070 – MOLECULAR IMAGING PET/SPECT: PART 2
 SESSION CHAIR(S): MOHAMMAD REZA AY, IRAN
 HONGYAN SUN, CANADA

- 17:00** SP070.1 - Optimal Pixelated Crystal for a Molecular SPECT Scanner: A GATE Monte Carlo Study
Mohammad Reza Ay, Iran
- 17:15** SP070.2 - Spinning Knife-Edge Slit-Hole: a Novel Collimation for High-Sensitivity Molecular SPECT
Mohammad Reza Ay, Iran
- 17:30** SP070.3 - Simultaneous estimation of the radioactivity distribution and electron density map from scattered coincidences in PET: A project overview
Hongyan Sun, Canada

- 17:45** SP070.4 - Generating a four-class attenuation map for MR-based attenuation correction of PET data in pelvis region using an automatic segmentation protocol
Hamidreza Saligheh Rad, Iran
- 18:00** SP070.5 - Extracting PET activity distribution from scattered coincidences for non-ideal energy resolutions by modeling the probabilities of annihilation positions within a generalized scattering reconstruction algorithm
Hongyan Sun, Canada
- 18:15** SP070.6 - Quantitative Functional Imaging with Hybrid PET-CT Via Improved Kinetics Modeling: Application to 18F-Fluorocholine PET Imaging of Prostate Cancer
Adam Blais, Canada
- 18:30** SP070.7 - Simultaneous Measurement of Perfusion and Hypoxia in Pancreatic Cancers with Dynamic PET-FAZA Imaging
Ivan Yeung, Canada

SESSION TIME: 17:00 – 18:45
SESSION ROOM: 717B
SESSION TRACK: **TRACK 02: BIOMATERIALS AND REGENERATIVE MEDICINE**
SESSION NAME: **SP071 – SCAFFOLDS IN TISSUE ENGINEERING**
SESSION CHAIR(S): **ALICIA EL-HAJ, UNITED KINGDOM
GILDA BARABINO, UNITED STATES**

- 17:00** SP071.1 - Optimization of Crosslinking Parameters for Biosynthetic Poly(vinyl-alcohol)-Tyramine Hydrogels
Penny Martens, Australia
- 17:15** SP071.2 - A synchrotron radiation microtomography study of wettability and swelling of nanocomposite Alginate/Hydroxyapatite scaffolds for bone tissue engineering
Francesco Brun, Italy
- 17:30** SP071.3 - ECM production and distribution in regenerated cartilage tissue cultured under traction loading.
Yoshinori Sawae, Japan
- 17:45** SP071.4 - Alginate encapsulation: a solution for controlled infiltration of cells within artificial fiber constructs
Birgit Glasmacher, Germany
- 18:00** SP071.5 - Biomineralization and In vivo-Compatibility of LnPO4 Nanorods with Enhanced MR and Luminescence Imaging
Zhongbing Huang, People's Republic of China
- 18:15** SP071.6 - Additive Manufacturing for Creating Multifunctional Tissue Engineering Scaffolds
Min Wang, Hong Kong
- 18:30** SP071.7 - Comparison of different dosage of Ion implantation on electrospun collagen fibers to improve aqueous stability
Nisha Sharma, Canada

SESSION TIME: 17:00 – 18:45
SESSION ROOM: 718B
SESSION TRACK: **TRACK 04: RADIATION ONCOLOGY**
SESSION NAME: **SP072 – IMAGING**
SESSION CHAIR(S): **AMY WALKER, AUSTRALIA
MICHAEL VELEC, CANADA**

- 17:00** SP072.1 - Variations in geometric distortion using static and moving table acquisition for radiotherapy treatment planning applications
Amy Walker, Australia
- 17:15** SP072.2 - Translation of biomechanical deformable image registration (MORFEUS) to the RayStation radiotherapy treatment planning system
Michael Velec, Canada
- 17:30** SP072.3 - Phantom Validation of a Point-Set Deformable Registration Method using Pig Bladder
Roja Zakariaee, Canada
- 17:45** SP072.4 - Automatic bone and air segmentation during generation of synthetic CT from MR data in the brain
Joshua Kim, United States
- 18:00** SP072.5 - Effect of Deformable Registration Accuracy Uncertainty on Lung Dose Accumulation
Navid Samavati, Canada
- 18:15** SP072.6 - Development of a Multi-Modality 4D biomechanical Phantom for Evaluation of Simultaneous Registration/Segmentation Algorithms
Daniel Markel, Canada
- 18:30** SP072.7 - Using Magnetic Resonance Image (MRI) alone in Treatment Planning and Treatment Localization
Shupeng Chen, United States

SESSION TIME: 17:00 – 19:00
SESSION ROOM: 715A
SESSION TRACK: **TRACK 07: SURGERY, COMPUTER AIDED SURGERY, MINIMAL INVASIVE INTERVENTIONS, ENDOSCOPY AND IMAGE-GUIDED THERAPY, MODELLING AND SIMULATION**
SESSION NAME: **SP073 – ROBOTICS AND VIRTUAL REALITY IN SURGERY**
SESSION CHAIR(S): **KARIN WARDELL, SWEDEN
TERRY PETERS, CANADA**

- 17:00** SP073.1 - **KEYNOTE:** Augmented Reality in Image-guided Cardiac Interventions.
Terry Peters, Canada
- 17:30** SP073.2 - Assistant Laparoscopic Postural: Kinematic Behavior
Daniel Lorias-Espinoza, Mexico
- 17:45** SP073.3 - Workspace optimization of a surgical instrument for single port access surgery
Bastian Blase, Germany

- 18:00** SP073.4 - High-Dexterity Telemanipulation Robot for Minimally Invasive Surgery
Sebastian Schlegel, Germany
- 18:15** SP073.5 - Integrated Sensors for a Single-Incision Laparoscopic Instrument
Simon Albrecht, Germany
- 18:30** SP073.6 - Development and Evaluation of an Open-Source 3D Virtual Simulator with Integrated Motion-Tracking as a Teaching Tool for Pedicle Screw Insertion
Stewart McLachlin, Canada
- 18:45** SP073.7 - A Robotic System with Ultrasound Imaging for Patient Setup and Monitoring during Fractionated Radiotherapy
Kai Ding, United States

SESSION TIME: 17:00 – 19:00
 SESSION ROOM: 716B
 SESSION TRACK: TRACK 09: BIOSIGNAL PROCESSING
 SESSION NAME: SP074 – BIOMEDICAL MONITORING & BIOELECTROMAGNETISM
 SESSION CHAIR(S): MILOS POPVIC, CANADA
 MALCOLM LATORRE, SWEDEN

- 17:00** SP074.1 - Towards Dual Respiratory and Cardiac Gated Radiotherapy
Kirpal Kohli, Canada
- 17:15** SP074.2 - A mobile terminal to follow-up the evolution of chronic diseases
Hector Torres, Cuba
- 17:30** SP074.3 - Relationship between the tuning characteristics of stimulus frequency otoacoustic emissions and behavioral tests at moderate levels
Qin Gong, People's Republic of China
- 17:45** SP074.4 - An Axon Mimic for Medical Electrode Tests
Malcolm Latorre, Sweden
- 18:00** SP074.5 - Evaluation the Accuracy of Oscillometric Blood Pressure Measurement According to the AAMI SP10
Haiyan Xiang, People's Republic of China
- 18:15** SP074.6 - PEMF effects on chondrocyte cellularity and gene expression of the rat distal femoral metaphyseal articular cartilage.
Fernando Sotelo-Barroso, Mexico
- 18:30** SP074.7 - Classification of responders versus non-responders to tDCS by analyzing voltage between anode and cathode during treatment session
Isar Nejadgholi, Canada
- 18:45** SP074.8 - Matlab toolbox for bioelectric cardiac images analysis
Juan Alberto Cruz, Brazil

SESSION TIME: 17:00 – 19:00
 SESSION ROOM: 713A
 SESSION TRACK: TRACK 17: EDUCATIONAL AND PROFESSIONAL ACTIVITIES
 SESSION NAME: SP075 – SPECIAL SESSION: APPROPRIATE TECHNOLOGY IN IMAGING AND RADIOTHERAPY – FUNCTIONALITY AND SAFETY ASPECTS
 SESSION CHAIR(S): KIN-YIN CHEUNG, HONG KONG
 ADRIANA VELAZQUEZ BERUMEN, SWITZERLAND

- Speakers:**
- SP075.1 - Kin-Yin Cheung, Hong Kong**
 - SP075.2 - Adriana Valazquez Berumen, Switzerland**
 - SP075.3 - Joanna Izewska, Austria**
 - SP075.4 - Simone Kodlulovich, Brazil**
 - SP075.5 - Ahmed Ibn Seddik, Morocco**
 - SP075.6 - Yimin Hu, People's Republic of China**

SESSION TIME: 17:15 – 19:00
 SESSION ROOM: 717A
 SESSION TRACK: TRACK 19: BIOPHYSICS AND MODELLING
 SESSION NAME: SP076 – RADIOBIOLOGICAL MODELLING
 SESSION CHAIR(S): LEYLA MOGHADDASI, AUSTRALIA

- 17:15** SP076.1 - Radiation Pneumonitis and Low Dose Radiation Hypersensitivity
J. James Gordon, United States
- 17:30** SP076.2 - Dose distribution optimization methods based on biological parameters: Impact of the objective function and reoxygenation and proliferation effects
Araceli Gago Arias, Chile
- 17:45** SP076.3 - Healthy Tissues in The Present of Gold Nano Particles against 103Pd and 125I: Monte Carlo study
Somayeh Asadi, Iran
- 18:00** SP076.4 - Monte-Carlo model development for evaluation of current clinical target volume definitions for Glioblastoma using Boron Neutron Capture Therapy
Leyla Moghaddasi, Australia
- 18:15** SP076.5 - Exploring RBE Dependence on Proton Track Angular Incidence
Piotr Pater, Canada
- 18:30** SP076.6 - DNA Damage Induced in Glioblastoma Cells by I-131: A Comparison between Experimental Data and Monte Carlo Simulation
Fereshteh Koosha, Iran

18:45 SP076.7 - The stochastic extension of the Linear Quadratic model: Taking into account the uncertainty of radiobiological parameters.
Moises Saez-Beltran, Spain

SESSION TIME: 17:00 – 19:00
SESSION ROOM: 713B
SESSION TRACK: **PRESIDENT'S CALL**
SESSION NAME: **SP077 – RADIATION ONCOLOGY**
SESSION CHAIR(S): **RYAN SMITH, AUSTRALIA**
PAUL KEALL, AUSTRALIA

17:00 SP077.1 - Assessment of CT to CBCT Non-Rigid Image Registration in Prostate Cancer Radiation Therapy
Pawel Siciarz, Canada

17:15 SP077.2 - Use of flattening filter free photon beams for off-axis targets in conformal arc stereotactic body radiation therapy
Ashley Smith, United States

17:30 SP077.3 - Dosimetric evaluation of the interplay effect for non-gated VMAT treatment of moving targets with high dose rate FFF beams
Ashley Smith, United States

17:45 SP077.4 - In vivo Image Guided Brachytherapy Verification (IGBV) in high dose rate prostate brachytherapy. Initial Clinical Experience
Ryan Smith, Australia

18:00 SP077.5 - Electronic Portal Imaging Device Dosimetry for IMRT: a Review on Commercially Available Solutions
Omemh Bawazeer, Australia

18:15 SP077.6 - The Nano-X Radiotherapy Machine: Lean Innovation Transforming Global Access to Cancer Care
Paul Keall, Australia

18:30 SP077.7 - Development of an MR and CT compatible non-invasive temperature based optical fiber respiration sensor for use in radiotherapy
Ashley Smith, United States

Biomedical Physics & Engineering Express

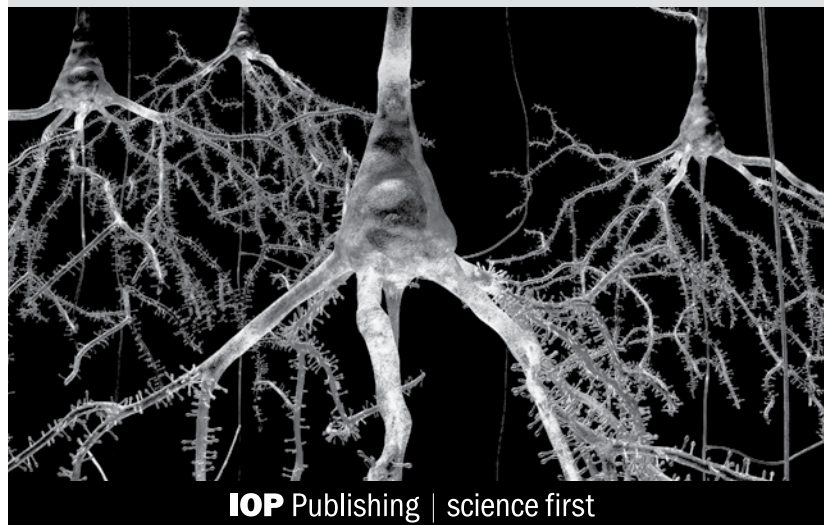
NEW FOR 2015

iopscience.org/bpex

A broad, inclusive, rapid-review journal publishing new research in all areas of biomedical engineering, biophysics and medical physics.



To find out more about publishing your work in BPEX, visit iopscience.org/bpex



IOP Publishing | science first

SCIENTIFIC PROGRAM BY DAY

► **Wednesday, June 10 2015**

Wednesday, June 10 2015

SESSION TIME: 10:30 – 12:00
 SESSION ROOM: 701A
 SESSION TRACK: TRACK 04: RADIATION ONCOLOGY
 SESSION NAME: SP078 – BRACHY THERAPY: PART 2
 SESSION CHAIR(S): JUSTIN SUTHERLAND, CANADA
 MICHELLE HILTS, CANADA

- 10:30** SP078.1 - The Effect of Bladder Preparation on Motion of Organs at Risk in High Dose Rate Gynecological Brachytherapy
Parisa Sadeghi, Canada
- 10:45** SP078.2 - Retrospective Monte Carlo dose calculations for permanent implant prostate brachytherapy using 125I
Justin Sutherland, Canada
- 11:00** SP078.3 - Combining doses for prostate cancer patients receiving external beam radiotherapy and a HDR brachytherapy boost: Dosimetric parameters and dose-surface maps for patients with and without late rectal bleeding
Calyn Moulton, Australia
- 11:15** SP078.4 - Implementation of Permanent Breast Seed Implants in British Columbia: Innovation and Early Results
Michelle Hilts, Canada
- 11:30** SP078.5 - Estimation of α/β for late rectal bleeding via minimum dosimetric differences for prostate cancer patients treated with external beam radiotherapy versus a HDR brachytherapy boost after external beam radiotherapy
Calyn Moulton, Australia
- 11:45** SP078.6 - Failure Mode and Effects Analysis (FMEA) for improving quality assurance for Image-Guided High Dose Rate (HDR) brachytherapy
Shada Wadi-Ramahi, Saudi Arabia

SESSION TIME: 10:30 – 12:00
 SESSION ROOM: 718B
 SESSION TRACK: TRACK 04: RADIATION ONCOLOGY
 SESSION NAME: SP079 – MOTION MANAGEMENT: PART 1
 SESSION CHAIR(S): AMIT SAWANT, UNITED STATES
 TAE SUK SUH, REPUBLIC OF KOREA

- 10:30** SP079.1 - Feasibility of respiratory gated radiotherapy using real-time positron emission tracking
Marc Chamberland, Canada
- 10:45** SP079.2 - The first kilovoltage intrafraction monitoring trial for gated prostate radiotherapy: Accuracy and dosimetric results
Prabhjot Juneja, Australia
- 11:00** SP079.3 - The impact of audio-visual biofeedback with a patient-specific guiding waveform on respiratory motion management: Comparison of two different respiratory management systems
Yujiro Nakajima, Japan
- 11:15** SP079.4 - Tracking Accuracy for Robotic Radiosurgery in the Liver
Jeff Winter, Canada
- 11:30** SP079.5 - Deep Inspiration breath hold lung SBRT- Can Flattening Filter Free beam based VMAT combined with gated CBCT facilitate precise treatment delivery with sufficient dosimetric accuracy?
Vallinayagam shanmuga subramanian, India
- 11:45** SP079.6 - Feasibility of markerless tumor tracking by sequential dual-energy fluoroscopy on a clinical tumor tracking system
Jennifer Dhont, Belgium

SESSION TIME: 10:30 – 11:45
 SESSION ROOM: 701B
 SESSION TRACK: TRACK 04: RADIATION ONCOLOGY
 SESSION NAME: SP080 – OTHER RADIATION ONCOLOGY: PART 2
 SESSION CHAIR(S): KEVIN ALEXANDER, CANADA
 CSABA PINTER, CANADA

- 10:30** SP080.1 - Estimation of the second cancer risk from adjuvant radiation therapy for stage I seminoma of the testis
Michalis Mazonakis, Greece

- 10:45** SP080.2 - 3D Slicer Gel Dosimetry Analysis: Validation of the Calibration Process
Kevin Alexander, Canada
- 11:00** SP080.3 - Whole body interactive 3D visualisation of both the benefits and risks of radiotherapy for common cancers: a tool to guide decision making
David Edmunds, United Kingdom
- 11:15** SP080.4 - A Software App for Radiotherapy with In-situ Dose-painting using high Z nanoparticles
Mohammed Jermoumi, United States
- 11:30** SP080.5 - Performing radiation therapy research using the open-source SlicerRT toolkit
Csaba Pinter, Canada

SESSION TIME: **10:30 – 12:00**
 SESSION ROOM: **716A**
 SESSION TRACK: **TRACK 05: DOSIMETRY AND RADIATION PROTECTION**
 SESSION NAME: **SP081 – VALIDATION AND VERIFICATION OF THERAPY DOSE DELIVERY: PART 1**
 SESSION CHAIR(S): **GEOFFREY IBBOTT, UNITED STATES
 SAADAT ALI, PAKISTAN**

- 10:30** SP081.1 - Validation of Eclipse Treatment planning system Commissioning using Octavius 4D
Paul Ravindran, BN
- 10:45** SP081.2 - Evaluation of Electron Beam Algorithm of Prowess Panther Planning System for Customized Electron Cutouts of different Sizes
Saadat Ali, Pakistan
- 11:00** SP081.3 - Standard Measurements and MU Calibrations for Carbon Beam Therapy of SAGA-HIMAT
Manabu Mizota, Japan
- 11:15** SP081.4 - 3D 'Bridge' Silicon Microdosimeter for RBE Studies in 12C Radiation Therapy
Michael Lerch, Australia
- 11:30** SP081.5 - Characterization of a ZnSe(Te) inorganic scintillator for scintillation dosimetry applications
Patricia Duguay-Drouin, Canada
- 11:45** SP081.6 - Determination of correction factors for the use of ionization chambers in the presence of magnetic fields
Geoffrey Ibbott, United States

SESSION TIME: **10:30 – 11:45**
 SESSION ROOM: **716B**
 SESSION TRACK: **TRACK 09: BIOSIGNAL PROCESSING**
 SESSION NAME: **SP082 – NONLINEAR DYNAMIC ANALYSIS**
 SESSION CHAIR(S): **ZAHRA MOUSSAVI, CANADA
 RICARDO ARMENTANO, ARGENTINA**

- 10:30** SP082.1 - Aging Process: Central Pressure Waveform Loss of Complexity
Ricardo Armentano, Argentina
- 10:45** SP082.2 - Changes in COP scaling behaviour in quiet stance after mTBI
Coren Walters-Stewart, Canada
- 11:00** SP082.3 - Tracking algorithm of spiral wave core in a cardiac tissue using Hilbert transform and phase variance analysis
Naoki Tomii, Japan
- 11:15** SP082.4 - Mapping the Fractal Dimension of Arterial Pressure
Leandro Cymberknop, Argentina
- 11:30** SP082.5 - Moving detrended fluctuation analysis for inspecting time evolution of scale invariant structures in biomedical signals
Hamidreza Saghir, Canada

SESSION TIME: **10:30 – 11:30**
 SESSION ROOM: **715B**
 SESSION TRACK: **TRACK 10: REHABILITATION MEDICINE, SPORTS MEDICINE, REHABILITATION ENGINEERING AND PROSTHETICS**
 SESSION NAME: **SP083 – LOWER LIMB INJURY ASSESSMENT AND TREATMENT & PROSTHETICS AND ASSISTIVE DEVICES**
 SESSION CHAIR(S): **AMY HSIAO, CANADA**

- 10:30** SP083.1 - Design of a braking simulator for the assessment of lower limb fracture recovery
Andrew O'Connell, Canada
- 10:45** SP083.2 - Quantitative measurement of subtalar joint passive stiffness in children with cerebral palsy
Wei Chen, People's Republic of China
- 11:00** SP083.3 - Differences in the parameters of impedance between knees with and without meniscal injury in female athletes
Marysol Garcia-Pérez, Mexico
- 11:15** SP083.4 - Development and evaluation of a mechanical stance controlled orthotic knee joint with stance flexion utilizing a timing based control strategy flexion
Hankyu Lee, Canada

SESSION TIME: 10:30 – 12:00
 SESSION ROOM: 717B
 SESSION TRACK: TRACK 12: MEDICAL DEVICES
 SESSION NAME: SP084 – NEW DESIGNING IDEAS
 SESSION CHAIR(S): ZIWEI HUANG, AUSTRALIA
 FRED HOSEA, UNITED STATES

- 10:30 SP084.1 - Soprano - Nasogastric Tube Insertion Guide
Hwa Liang Leo, Singapore
- 10:45 SP084.2 - High Output Impedance Current-Conveyor Oscillator for Electrical Bioimpedance Applications
Pedro Bertemes-Filho, Brazil
- 11:00 SP084.3 - Healthcare Device for People Affected by Dementia
Sara Velez, Colombia
- 11:15 SP084.4 - Wide Field-of-View Fluorescence Imaging with Curved Sample Chamber for Point-of-Care CD4 Test
Kyunghoon Kim, Republic of Korea
- 11:30 SP084.5 - Moisture effect on antibody longevity on paper substrate and the role of hydroxyl groups in the concept of 'bio-compatible paper'
Ziwei Huang, Australia
- 11:45 SP084.6 - An Interoperability Maturity Roadmap for Medical Device Design and Alignment with IT Systems
Fred Hosea, United States

SESSION TIME: 10:30 – 11:45
 SESSION ROOM: 715A
 SESSION TRACK: TRACK 19: BIOPHYSICS AND MODELLING
 SESSION NAME: SP086 – BIOLOGICAL EFFECTS OF IONIZING RADIATION
 SESSION CHAIR(S): SHIRLEY LEHNERT, CANADA
 WILFRED NGWA, UNITED STATES

- 10:30 SP086.1 - Sensitization of DNA to Ionizing Radiation by Platinum Chemotherapeutic Drugs
Mohammad Rezaee, Canada
- 10:45 SP086.2 - Lymphoma and Choroidal Melanoma cells in the presence of gold nanoparticles: In-Vitro study
Somayeh Asad, Iran
- 11:00 SP086.3 - Multiple Code Comparisons of Proton Interactions in the Presence of Gold Nanoparticles in the Human Eye
Mohammad Faraz Samavat, Iran
- 11:15 SP086.4 - An in-vitro method for calibrating the gamma-H2AX DNA double strand break focus assay in blood lymphocytes for radionuclide therapy
Uta Eberlein, Germany
- 11:30 SP086.5 - Dose enhancement during concomitant chemoradiotherapy using FDA approved concentrations of carboplatin and oxaliplatin nanoparticles
Wilfred Ngwa, United States

SESSION TIME: 10:30 – 11:45
 SESSION ROOM: 717A
 SESSION TRACK: TRACK 18: GENDER, SCIENCE AND TECHNOLOGY
 SESSION NAME: SP085 – WOMEN IN MEDICAL PHYSICS: CURRENT STATUS
 SESSION CHAIR(S): KRISTY BROCK, UNITED STATES
 PAOLO RUSSO, ITALY

- 10:30 SP085.1 - Women in medical physics: Current status Results from IOMP survey
Virginia Tsapakis, Greece
- 10:50 SP085.2 - Is there a 'Leaky Pipeline' for Women in Clinical Medical Physics in Canada?
Wendy Smith, Canada
- 11:10 SP085.3 - Women in Medical field in Brazil: gender equality?
Simone Renha, Brazil
- 11:30 SP085.4 - Women Biomedical Engineers as Consultants in Clinical Engineering Field in Latin American Countries: Case of Study
Claudia Cárdenas Alanís, Mexico

SESSION TIME: 10:30 – 12:15
 SESSION ROOM: 713B
 SESSION TRACK: PRESIDENT'S CALL
 SESSION NAME: SP087 – EDUCATIONAL AND PROFESSIONAL ACTIVITIES: PART 2
 SESSION CHAIR(S): FRANCO SIMINI, URUGUAY

- 10:30 SP087.1 - The potential role of IFMBE in improving the state of medical equipment in developing countries
Andrel Linnenbank, Netherlands
- 10:45 SP087.2 - Biomedical Engineering Education through Outreach Programs in Hospitals
Franco Simini, Uruguay
- 11:00 SP087.3 - Clinical Engineer: a health professional to recognize
Paolo Lago, Italy
- 11:15 SP087.4 - "Rehabilitation Engineering: Designing for Ability" - A summer outreach course for attracting talented high school students to the rehabilitation engineering field
Vicki Komisar, Canada
- 11:30 SP087.5 - A Novel Approach to Train Biomedical Engineers in a Ugandan Setting
Robert Ssekitoleko, Uganda

- 11:45** SP087.6 - A Health Information Technology Management Course for Brazilian Clinical Engineers
Fernando Andrade, Brazil
- 12:00** SP087.7 - A Successful High School Science Mentorship Program: Students on the Beamlines at the Canadian Light Source
Denise Miller, Canada

- 14:15** SP089.4 - 3D numerical investigation of the effects of altered mechanical loading during skeletal growth
Kamel Madi, United Kingdom
- 14:30** SP089.5 - Effects of changing small airway mechanics and inspiratory flow waveforms on pulmonary ventilation: a modeling study
Tianya Liu, People's Republic of China

SESSION TIME: **13:30 – 14:45**
 SESSION ROOM: **718A**
 SESSION TRACK: **TRACK 01: IMAGING**
 SESSION NAME: **SP088 – COMPUTER AIDED DIAGNOSIS**
 SESSION CHAIR(S): **HARINI VEERARAGHAVAN, UNITED STATES
 LUIS VILCAHUAMAN, PERU**

SESSION TIME: **13:30 – 15:00**
 SESSION ROOM: **716A**
 SESSION TRACK: **TRACK 05: DOSIMETRY AND RADIATION PROTECTION**
 SESSION NAME: **SP090 – QA MEASUREMENTS FOR THERAPY DOSIMETRY**
 SESSION CHAIR(S): **EYAD ALHAKEEM, CANADA**

- 13:30** SP088.1 - Automatic Analysis of Plantar Foot Thermal Images in at-Risk Type II Diabetes by Using an Infrared Camera
Luis Vilcahuaman, Peru
- 13:45** SP088.2 - Computer Assisted Diagnosis of Sclerotic Bone Lesions from Dual Energy CT
Harini Veeraraghavan, United States
- 14:00** SP088.3 - Mutual Information Based Template Matching Method for the Computer Aided Diagnosis of Alzheimer Disease
Albert Guvenis, Turkey
- 14:15** SP088.4 - Development of an Anatomical Measurement and Data Analysis Tool Based on the Kinect Sensor for Physical Rehabilitation Applications.
David Duarte-Dyck, Mexico
- 14:30** SP088.5 - Quantitative CT Assessment of Vertebral Fracture Severity
Curtis Caldwell, Canada

- 13:30** SP090.1 - Response Characteristics of a Large-Area Ion Chamber with Various Radiotherapy Beams
Makan Farrokhkish, Canada
- 13:45** SP090.2 - Very small circular fields output factors: Comparison of MC calculations, EBT3 film and micro-diamond measurements
Eyad Alhakeem, Canada
- 14:00** SP090.3 - Investigation of pass rate variability in ArcCheck measurements
Harald Keller, Canada
- 14:15** SP090.4 - Characterization and image quality evaluation for a clinical 2.5 MV in-line portal imaging beam
Jose Villarreal-Barajas, Canada
- 14:30** SP090.5 - Usefulness of the commercialized EPID based dMLC QA tool for Elekta Agility MLC
Samju Cho, Republic of Korea
- 14:45** SP090.6 - In-vivo and pre-treatment quality assurance software validation and verification
Cinzia Talamonti, Italy

SESSION TIME: **13:30 – 14:45**
 SESSION ROOM: **701B**
 SESSION TRACK: **TRACK 03: BIOMECHANICS AND ARTIFICIAL ORGANS**
 SESSION NAME: **SP089 – TISSUE MODELLING**
 SESSION CHAIR(S): **YUBO FAN, PEOPLE'S REPUBLIC OF CHINA
 JOS VANDER SLOTEN, BELGIUM**

SESSION TIME: **13:30 – 14:30**
 SESSION ROOM: **717B**
 SESSION TRACK: **TRACK 06: NEW TECHNOLOGIES IN CANCER RESEARCH AND TREATMENT**
 SESSION NAME: **SP091 – NANOTECHNOLOGY IN RADIATION THERAPY AND IMAGING: PART 2**
 SESSION CHAIR(S): **LOREDANA MARCU, ROMANIA
 MARC ANDRE FORTIN, CANADA**

- 13:30** SP089.1 - The protective effect of the eyelid on ocular injuries in blunt trauma
Xiaoyu Liu, People's Republic of China
- 13:45** SP089.2 - A Tale of Two Tendons: The Tradeoff between Strength and Fatigue Resistance
Samuel Veres, Canada
- 14:00** SP089.3 - Dynamic plantar pressure simulation integrated in case specific multibody gait simulations
Jos Vander Sloten, Belgium

- 13:30** SP091.1 - **KEYNOTE:** New Technologies in Cancer Research and Treatment
Eva Bezak, Australia

- 14:00** SP091.2 - Enhanced uptake of gold nanoparticles coated with polyethylene glycol
Charmaine Cruje, Canada
- 14:15** SP091.3 - Nuclear targeting of gold nanoparticles for improved therapeutics
Celina Yang, Canada

SESSION TIME: 13:30 – 14:45
 SESSION ROOM: 717A
 SESSION TRACK: TRACK 11: NEUROENGINEERING, NEURAL SYSTEMS
 SESSION NAME: SP092 – NEURAL SIGNAL PROCESSING: PART 1
 SESSION CHAIR(S): BERJ BARDAKJIAN, CANADA

- 13:30** SP092.1 - Delta-Modulated High Frequency Oscillations Linked to Pathological Brain in Female Mecp2-Deficient Mice
Sinisa Colic, Canada
- 13:45** SP092.2 - Contrast between Spectral and Connectivity Features for Electroencephalography based Authentication
Chungmin Han, Republic of Korea
- 14:00** SP092.3 - EMG artifact removal using ICA-based dipole distribution from scalp EEG of epileptic patients
Chunsheng Li, Canada
- 14:15** SP092.4 - Power based features of epileptic iEEG rhythms to demarcate brain regions for resection
Joshua Dian, Canada
- 14:30** SP092.5 - The alpha rhythm in a rodent model of epilepsy is enhanced when adenosine receptors are blocked
Vanessa Breton, Canada

SESSION TIME: 13:30 - 14:45
 SESSION ROOM: 701A
 SESSION TRACK: TRACK 16: CLINICAL ENGINEERING, CLINICAL PHYSICS, AND PATIENT SAFETY
 SESSION NAME: SP093 - HEALTH TECHNOLOGY ASSESSMENT AND COST EFFECTIVE TECHNOLOGIES FOR DEVELOPING COUNTRIES AND USABILITY AND HUMAN FACTORS ENGINEERING FOR MEDICAL DEVICES AND SYSTEM DESIGN: PART 1
 SESSION CHAIR(S): ERNESTO IADANZA, ITALY
 STEPHEN BREEN, CANADA

- 13:30** SP093.1 - The maintenance needs of oxygen concentrators in low-resource settings and implications for technician training: Experience from The Gambia
Beverly Bradley, Canada

- 13:45** SP093.2 - Global Medical Devices Pricing Survey
Adriana Velazquez Berumen, Switzerland
- 14:00** SP093.3 - Methodology to evaluate physical environment parameters in healthcare services
Saide Calil, Brazil
- 14:15** SP093.4 - HB-HTA method for the evaluation of exclusive Medical Devices
Paolo Lago, Italy
- 14:30** SP093.5 - Applying Heuristic Evaluation on Medical Devices User Manuals
Fernando Andrade, Brazil

SESSION TIME: 13:30 – 14:15
 SESSION ROOM: 715A
 SESSION TRACK: TRACK 19: BIOPHYSICS AND MODELLING
 SESSION NAME: SP094 – BIOLOGICAL MODELLING
 SESSION CHAIR(S): IULIANA TOMA-DASU, SWEDEN

- 13:30** SP094.1 - Finite Element Analysis of Dynamics of Two Microbubbles Under Ultrasonic Field
Xiao-hui Qiu, People's Republic of China
- 13:45** SP094.2 - The value of individual measurements for tumor control probability predictions in head and neck patients
Iuliana Toma-Dasu, Sweden
- 14:00** SP094.3 - A Novel Technique for Measuring Electrical Permittivity of Biological Tissues at Low Frequencies (100 KHz or lower)
Seyyed Hesabgar, Canada

SESSION TIME: 13:30 – 15:15
 SESSION ROOM: 713B
 SESSION TRACK: PRESIDENT'S CALL
 SESSION NAME: SP095 – BIOSIGNAL PROCESSING & PULMONARY & RESPIRATORY
 SESSION CHAIR(S): VENKATESHWARLA RAJU, INDIA
 NATASA RELJIN, UNITED STATES

- 13:30** SP095.1 - Power Spectral Density Analysis of Tonic Electrodermal Activity for Sympathetic Arousal Assessment
Hugo Posada-Quintero, United States
- 13:45** SP095.2 - Multivariate Analysis Classification Based on Multi-Channel EMG Multisite Microelectrode Recording, Principal Component Analysis, and Hierarchical Clustering
Venkateshwarla Raju, India
- 14:00** SP095.3 - Blanket Fractal Dimension for Estimating Tidal Volume from the Smartphone Acquired Tracheal Sounds: Preliminary Results
Natasa Reljin, United States

- 14:15** SP095.4 - A Robust and Realistic Framework for Clinical Classification of Myocardial Infarction
Yasin Mamatjan, Canada
- 14:30** SP095.5 - A Mother Wavelet Selection Algorithm for Respiratory Rate Estimation from Photoplethysmogram
Dan Guo, People's Republic of China
- 14:45** SP095.6 - Mathematical assessment of variability in respiratory airflow patterns
Saravana Raman, United States
- 15:00** SP095.7 - Spectral Analysis of Respiratory and Cardiac Signals Using Doppler Radar
Philip Tworzydło, Canada

SESSION TIME: **15:00 – 16:15**
 SESSION ROOM: **718A**
 SESSION TRACK: **TRACK 01: IMAGING**
 SESSION NAME: **SP096 – OPTICAL IMAGING: APPLICATIONS**
 SESSION CHAIR(S): **SANTA BOREL, CANADA
 JESSICA PEREZ, CANADA**

- 15:00** SP096.1 - Live-cell Raman microspectroscopy to differentiate between normal and malignant ovarian surface epithelial cells
Santa Borel, Canada
- 15:15** SP096.2 - Quantitative image analysis of fluorescence endomicroscopy video sequences for mesenchymal stem cell tracking in regenerative lung treatment
Jessica Perez, Canada
- 15:30** SP096.3 - Shape-Based Diffuse Optical Tomography for Reconstruction of Photothermal Lesions in Prostate Focal Therapy
Robert Weersink, Canada
- 15:45** SP096.4 - Transrectal diffuse optical tomography to monitor photocoagulation during interstitial photothermal therapy of focal prostate cancer
Robert Weersink, Canada
- 16:00** SP096.5 - The first in vivo, optical images of neuroblasts migrating away from the subventricular zone deep in mouse brain reveal two patterns of migration: implications for future therapeutic use
Teresa Murray, United States

SESSION TIME: **15:00 – 17:00**
 SESSION ROOM: **701B**
 SESSION TRACK: **TRACK 01: IMAGING**
 SESSION NAME: **SP097 – QUANTITATIVE IMAGING: PART 2**
 SESSION CHAIR(S): **HAI-LING MARGARET CHENG, CANADA
 GEOFFREY ZHANG, UNITED STATES**

- 15:00** SP097.1 - Ischemia-time dependent CBF threshold for infarction determined in a porcine model of stroke using CT Perfusion and F-18 FFMZ PET imaging
Eric Wright, Canada
- 15:15** SP097.2 - Characterization of scatter factors in thyroid studies using a pinhole collimator by Monte Carlo Simulation.
Aley Palau, Cuba
- 15:30** SP097.3 - Fluid Quantification Using Temporal Subtraction: Comparing Single to Dual-Energy Digital Chest Radiography
Shailaja Sajja, Canada
- 15:45** SP097.4 - Quantitative low-kVp CT angiography in carotid artery imaging
Tianye Niu, People's Republic of China
- 16:00** SP097.5 - Evaluation of the ΔV Ventilation Calculation Method Using In Vivo XeCT Ventilation Data
Geoffrey Zhang, United States
- 16:15** SP097.6 - Predicting Survival Outcomes of Post-Treatment Glioma Patients by Quantification of Viable Tumour Volume on CMET/FLT PET and MRI.
Christopher Leatherday, Australia
- 16:30** SP097.7 - A Novel Method for Lung's Air Volume Estimation in Exhalation and Inhalation Phases From CT Images
Elham Karami, Canada
- 16:45** SP097.8 - High-resolution micro-CT protocol for assessing lung ventilation and perfusion: image subtraction versus multi-energy analysis
Nancy Ford, Canada

SESSION TIME: **15:00 – 16:45**
 SESSION ROOM: **717B**
 SESSION TRACK: **TRACK 02: BIOMATERIALS AND REGENERATIVE MEDICINE**
 SESSION NAME: **SP098 – BIOMATERIALS AND REGENERATIVE MEDICINE**
 SESSION CHAIR(S): **ALICIA EL-HAJ, UNITED KINGDOM
 GILDA BARABINO, UNITED STATES**

- 15:00** SP098.1 - Finite Element Analysis of Abdominal Aortic Aneurysms to Predict Risk of Rupture - The Role of the Thrombosis Thicknesses.
Omar Altwijri, Saudi Arabia
- 15:15** SP098.2 - High-Frequency Ultrasonic Measurement of Ischemia and Revascularization in Mice with Ligated Femoral Arteries
Andrea Quiroz, United States
- 15:30** SP098.3 - Prevention of Thrombogenesis with a new Silane Based Adlayer on Commonly used Polymers in Medical Equipment Components
Kiril Fedorov, Canada
- 15:45** SP098.4 - Nature's Own 'Smart' Biological Material to Inspire Next-Generation Biomaterials
Joanna Ng, Australia

- 16:00** SP098.5 - Vascular endothelial cell adhesion and hemocompatibility of biochemically- and topographically-modified poly(vinyl alcohol)
Evelyn Yim, Singapore
- 16:15** SP012.1 - Effects of PEMF on Neuroblastoma Cells Previously Exposed to Antidepressants
Teodoro Cordova-Fraga, Mexico
- 16:30** SP012.2 Porous bio-Sic ceramics from wood: approaching new medical implants
Birgit Glasmacher, Germany

SESSION TIME: 15:00 – 16:30
 SESSION ROOM: 716A
 SESSION TRACK: **TRACK 05: DOSIMETRY AND RADIATION PROTECTION**
 SESSION NAME: **SP099 – SPECIAL SESSION: CURRENT SITUATION OF DOSIMETRY IN RADIOLOGY AND RADIATION PROTECTION**
 SESSION CHAIR(S): **MADAN REHANI, UNITED STATES**

- Speakers:**
- SP099.1 - Madan Rehani, United States**
 - SP099.2 - Pablo Jimenez, United States**
 - SP099.3 - Joanna Izewska, Austria**

SESSION TIME: 15:00 – 16:00
 SESSION ROOM: 716B
 SESSION TRACK: **TRACK 05: DOSIMETRY AND RADIATION PROTECTION**
 SESSION NAME: **SP100 – DOSE OPTIMIZATION: FOCUS ON DRLS**
 SESSION CHAIR(S): **GRAEME WARDLAW, CANADA
 JOSEP MARTÍ-CLIMENT, SPAIN**

- 15:00** SP100.1 - A Contribution to the Establishment of Diagnostic Reference Levels in Computed Tomography in Brazil
Ana Marques Da Silva, Brazil
- 15:15** SP100.2 - Canada's Computed Tomography (CT) Survey: Overview and Moving Toward Establishment of DRLs
Graeme Wardlaw, Canada
- 15:30** SP100.3 - Review UAE Dental Radiology Dosimetry Results for National DRLs Establishment
Fatima Al Kaabi, United Arab Emirates
- 15:45** SP100.4 - Should restrictions on the patients' behavior during the radiopharmaceuticals incorporation and after ^{99m}Tc bone scans be imposed?
Josep Martí-Climent, Spain

SESSION TIME: 15:00 – 16:45
 SESSION ROOM: 717A
 SESSION TRACK: **TRACK 11: NEUROENGINEERING, NEURAL SYSTEMS**
 SESSION NAME: **SP101 – STIMULATION AND MONITORING**
 SESSION CHAIR(S): **JOSE ZARIFFA, CANADA**

- 15:00** SP101.1 - Biological Targets of Seizure Therapy in Major Depressive Disorder using EEG Microstate Analysis
Sravya Atluri, Canada
- 15:15** SP101.2 - Magnetic Seizure Therapy for Treatment Resistant Depression: Insights from TMS-EEG Measures
Yinming Sun, Canada
- 15:30** SP101.3 - Deep Transcranial Magnetic Stimulation Using Figure-of-Eight and Halo Coils
Shoogo Ueno, Japan
- 15:45** SP101.4 - Optogenetic Stimulation and Wireless Cortical Recording in Modulating Motor Plasticity and Performance of Free-Moving Rat
Chun-Wei Wu, Chinese Taipei
- 16:00** SP101.5 - Identification of calf muscles response to functional electrical stimulation as linear models
Hossein Rouhani, Canada
- 16:15** SP101.6 - Establishment of Real Human Head Conductivity Model with Ventricular Structure used in TMS Simulation Study
Tao Yin, People's Republic of China
- 16:30** SP101.7 - Study on electric field in real head model induced by H-coil
Tao Yin, People's Republic of China

SESSION TIME: 15:00 – 17:00
 SESSION ROOM: 715A
 SESSION TRACK: **TRACK 13: INFORMATICS IN HEALTH CARE AND PUBLIC HEALTH**
 SESSION NAME: **SP102 – CLINICAL INFORMATION SYSTEMS AND DECISION SUPPORT**
 SESSION CHAIR(S): **LEANDRO PECCHIA, UNITED KINGDOM
 JORGE DOS SANTOS, GREECE**

- 15:00** SP102.1 - A Multi-Attribute Decision Theory Approach to Radiation Dose De-escalation in Oropharyngeal Cancer
Wade Smith, United States
- 15:15** SP102.2 - Large-scale data of basic patient and treatment characteristics significantly improve predictions for post-radiotherapy dyspnea
Andre Dekker, Netherlands

- 15:30** SP102.3 - Substituting human MRI-observed tumor length with automated tumor length calculations for prediction model application
Johan Van Soest, Netherlands
- 15:45** SP102.4 - An Artifact Detection Framework for Clinical Decision Support Systems
Shermeen Nizami, Canada
- 16:00** SP102.5 - Design and implementation of an IT management system for a Medical Physics Department activity workflows
Massimiliano Paolucci, Italy
- 16:15** SP102.6 - Differential Feature Space in Mean Shift Clustering for Automated Melanoma Assessment
Javier Eslava, United States
- 16:30** SP102.7 - Fuzzy-state machine for Triage priority classifier in emergency room
Emmanuel Sánchez Velarde, Mexico
- 16:45** SP102.8 - An Australian mining boom: development of an Australian radiotherapy datamining network for rapid learning from clinical data to support improved clinical decisions
David Thwaites, Australia

SESSION TIME: **15:00 – 16:15**
 SESSION ROOM: **701A**
 SESSION TRACK: **TRACK 16: CLINICAL ENGINEERING, CLINICAL PHYSICS, AND PATIENT SAFETY**
 SESSION NAME: **SP103 - HEALTH TECHNOLOGY ASSESSMENT AND COST EFFECTIVE TECHNOLOGIES FOR DEVELOPING COUNTRIES AND USABILITY AND HUMAN FACTORS ENGINEERING FOR MEDICAL DEVICES AND SYSTEM DESIGN: PART 2**
 SESSION CHAIR(S): **JAMES WEAR, UNITED STATES**

- 15:00** SP103.1 - Novel Medical Device Procurement Tracking Approach
Gleb Donin, Czech Republic
- 15:15** SP103.2 - Influence of shifting patients with off-axis tumor for Tomotherapy
Yingjie Xu, People's Republic of China
- 15:30** SP103.3 - Smart pump user interface evaluation
Carlos Viviani, Brazil
- 15:45** SP103.4 - Studying the human computer interface of a continuous monitoring software by approaching it from both directions
Ying Ling Lin, Canada
- 16:00** SP103.5 - Analysis and experimentation of plantar foot segmentation from thermographic digital images for preventive diagnosis of diabetic foot
Luis Vilcahuaman, Peru

SESSION TIME: **17:00 – 18:00**
 SESSION ROOM: **701B**
 SESSION TRACK: **TRACK 01: IMAGING**
 SESSION NAME: **SP104 – PHANTOMS**
 SESSION CHAIR(S): **DOV MALONEK, ISRAEL
 FERNANDA CAVALCANTE, BRAZIL**

- 17:00** SP104.1 - Monte Carlo simulation of interventional cardiac scenarios using a newborn hybrid phantom and MCNPX code
Fernanda Cavalcante, Brazil
- 17:15** SP104.2 - Computed tomography of a beating heart: High resolution simulator for the assessment of motion artifacts during CT scan of the heart
Dov Malonek, Israel
- 17:30** SP104.3 - Development of Dynamic Anthropomorphic Heart Phantom for Computed tomography
Ali Ursani, Canada
- 17:45** SP104.4 - Development of a PET/MR/CT Compatible Tumour Motion Phantom
John Patrick, Canada

SESSION TIME: **17:00 – 19:00**
 SESSION ROOM: **718A**
 SESSION TRACK: **TRACK 01: IMAGING**
 SESSION NAME: **SP105 – MRI: NOVEL APPROACHES AND MOLECULAR IMAGING & APPLICATIONS**
 SESSION CHAIR(S): **HAI-LING MARGARET CHENG, CANADA
 NADER RIYAHY-ALAM, IRAN**

- 17:00** SP105.1 - **KEYNOTE:** Advancing MRI for Non-invasive Physiological and Cellular Imaging
Hai-Ling Margaret Cheng, Canada
- 17:30** SP105.2 - Detection of Regional Radiation-Induced Lung Injury using Hyperpolarized 129Xe Localized Magnetic Resonance Spectroscopy
Brandon Zanette, Canada
- 17:42** SP105.3 - Conjugate-Mapped Compressed Sensing: a technique to mitigate the side effects of compressed sensing on MTF
Amr Heikal, Canada
- 17:54** SP105.4 - Gadolinium Labeled Glycosylated Nanomagnetic Particles as Metabolic Contrast Agents in Molecular Magnetic Resonance Imaging
Nader Riyahi-Alam, Iran
- 18:06** SP105.5 - Hyperpolarized 129Xe Magnetic Resonance Imaging of a Rat Model of Radiation-Induced Lung Injury Involving Single-Lung Radiation Therapy
Ozkan Doganay, Canada
- 18:18** SP105.6 - Ultra-short Echo Time (UTE) Magnetic Resonance Imaging of Cortical Bone: An Undersampled Acquisition Study
Yanchun Zhu, People's Republic of China

- 18:30 SP105.7 - Brain activation associated with working memory maintenance under anxiety-provoking distracter in patients with obsessive compulsive disorder
Gwang-Woo Jeong, Republic of Korea
- 18:42 SP105.8 - Fractional Anisotropy, Voxel Wise Morphometry and Resting State in Patients with Lateral Amyotrophic Sclerosis
Maria Lopez-Titla, Mexico

SESSION TIME: 17:00 – 18:45
 SESSION ROOM: 701A
 SESSION TRACK: TRACK 04: RADIATION ONCOLOGY
 SESSION NAME: SP106 – PR: PROTON THERAPY
 SESSION CHAIR(S): DANIEL SANCHEZ-PARCERISA, UNITED STATES
 DEREK DOLNEY, UNITED STATES

- 17:00 SP106.1 - **KEYNOTE:** Proton therapy – close to becoming mainstream
Thomas Bortfeld, United States
- 17:30 SP106.2 - Monte Carlo-based Inverse Treatment Plan Optimization for Intensity Modulated Proton Therapy
Yongbao Li, People's Republic of China
- 17:45 SP106.3 - FoCa: a protontherapy treatment planning system written in object-oriented MATLAB
Daniel Sanchez-Parcerisa, United States
- 18:00 SP106.4 - Assessment of the limitations of the dose calculation algorithm of a commercially-available treatment planning system for proton pencil beam scanning
Jessica Scholey, United States
- 18:15 SP106.5 - Impact of the microdosimetric spread on cell survival data analysis
Shirin Enger, Canada
- 18:30 SP106.6 - Magnetically scanned-beam proton radiography using Micromegas detectors
Derek Dolney, United States

SESSION TIME: 17:00 – 18:45
 SESSION ROOM: 718B
 SESSION TRACK: TRACK 04: RADIATION ONCOLOGY
 SESSION NAME: SP107 – BEAM DELIVERY
 SESSION CHAIR(S): NATALKA SUCHOWERSKA, AUSTRALIA
 RACHEL MCCARROLL, UNITED STATES

- 17:00 SP107.1 - A Quantitative Analysis of Teletherapy in Low Resource Settings: Cobalt or Linac?
Rachel McCarroll, United States

- 17:15 SP107.2 - The study of Total Marrow Irradiation Based on Rotational Intensity-modulated techniques
Shouping Xu, People's Republic of China
- 17:30 SP107.3 - IMRT and VMAT comparison for a case of bilateral breast carcinoma
Erick Montenegro, Guatemala
- 17:45 SP107.4 - Measuring the Location and Dynamics of the Beam Spot and Field Centre on a Therapy Linear Accelerator in X-Ray Mode
David Spencer, Canada
- 18:00 SP107.5 - Monte Carlo based optimization of flattening filters for a cobalt-60 total body irradiation unit
Ingrid Lai, Canada
- 18:15 SP107.6 - Monte Carlo study for the design of a novel Gamma-Tomo SBRT system
Grisel Mora, Portugal
- 18:30 SP107.7 - A dosimetric evaluation of flattening filter-free volumetric modulated arc therapy for postoperative treatment of cervical cancer
Fuli Zhang, People's Republic of China

SESSION TIME: 17:00 – 18:00
 SESSION ROOM: 716A
 SESSION TRACK: TRACK 05: DOSIMETRY AND RADIATION PROTECTION
 SESSION NAME: SP108 – PATIENT AND OCCUPATIONAL DOSE ASSESSMENT
 SESSION CHAIR(S): ARUN KUMAR L S, OMAN

- 17:00 SP108.1 - Radiation dose to patients from cardiac interventions performed using image intensifier, flat detector and novel flat detector systems
Roshan Livingstone, India
- 17:15 SP108.2 - First National Occupational Radiation Dose Registry in Ministry of Health and its Validation: An Oman Experience
Arun Kumar L S, Oman
- 17:30 SP108.3 - Assessment of Patient and Staff Doses in Interventional Cerebral Angiography Using OSL
Chryzel Angelica Gonzales, Republic of the Philippines
- 17:45 SP108.4 - A wireless personal dosimeter for Interventional Radiology medical personnel.
Massimiliano Paolucci, Italy

SESSION TIME: 17:00 – 18:15
 SESSION ROOM: 717A
 SESSION TRACK: TRACK 05: DOSIMETRY AND RADIATION PROTECTION
 SESSION NAME: SP109 – MICRO- AND NANO-DOSIMETRY
 SESSION CHAIR(S): ROWAN THOMSON, CANADA
 PATRICIA OLIVER, CANADA

- 17:00** SP109.1 - Development of a Thick Gas Electron Multiplier Based Multi-element Microdosimetric Detector
Soo Hyun Byun, Canada
- 17:15** SP109.2 - Development of a 2-D THGEM Microdosimetric Detector
Sahar Darvish-Molla, Canada
- 17:30** SP109.3 - Quantum versus classical trajectory Monte Carlo simulations of low energy electron transport in condensed media
Rowan Thomson, Canada
- 17:45** SP109.4 - Investigation of the relations between absorbed dose to cellular targets and to bulk tissue for kilovoltage radiation using Monte Carlo simulations and cavity theory
Patricia Oliver, Canada
- 18:00** SP109.5 - Development of transmitted alpha particle microdosimetry using Timepix: Investigation of A549 lung carcinoma cells exposed to alpha particles irradiated from Ra-223
Ruqaya Al Darwish, Australia

SESSION TIME: 17:00 – 18:45
 SESSION ROOM: 715B
 SESSION TRACK: TRACK 07: SURGERY, COMPUTER AIDED SURGERY, MINIMAL INVASIVE INTERVENTIONS, ENDOSCOPY AND IMAGE-GUIDED THERAPY, MODELLING AND SIMULATION
 SESSION NAME: SP110 – SURGICAL NAVIGATION: PART 2
 SESSION CHAIR(S): TERRY PETERS, CANADA
 MICHAEL DALY, CANADA

- 17:00** SP110.1 - **KEYNOTE:** Optical Navigation in Functional Neurosurgery
Karin Wårdell, Sweden
- 17:30** SP110.2 - Endoscopic Electropray: A minimal invasive tool for physical targeted gene delivery
David Hradetzky, Switzerland
- 17:45** SP110.3 - Cone-Beam CT-Guided Fluorescence Tomography for Intraoperative 3D Imaging
Michael Daly, Canada
- 18:00** SP110.4 - An Optimal Motion Profile for a Wireless Endoscopic Capsule Robot
Sina Mahmoudzadeh, Iran

- 18:15** SP110.6 - Orthogonal IR System for Instrumental tracking in Minimally Invasive Spine Procedures for training using Wiimote Technology
Juana Martínez, Mexico
- 18:30** SP110.7 - Use of a Patient-Specific Ventriculostomy Surgical Simulator to Develop a Model for Preoperative Risk Assessment Based on Measures of Anatomical Variation
Ryan Armstrong, Canada

SESSION TIME: 17:00 – 19:00
 SESSION ROOM: 716B
 SESSION TRACK: TRACK 12: MEDICAL DEVICES
 SESSION NAME: SP111 – CARDIOVASCULAR
 SESSION CHAIR(S): OLIVIA COIADO, UNITED STATES
 MICHAEL CHENG, CANADA

- 17:00** SP111.1 - Ultrasound-induced heart rate decrease: Role of age in female rats
Olivia Coiado, United States
- 17:15** SP111.2 - Low cost pulsed wave Doppler ultrasound system for vascular studies
Isabel Arnaiz, Cuba
- 17:30** SP111.3 - Real-Time Three Degree-of-Freedom Measurement of Catheter Motion for Input to a Robotic Catheter Navigation System
Daniel Gelman, Canada
- 17:45** SP111.4 - Pulse Wave Velocity as a Function of Cuff Pressure? Extra Information About the Cardiovascular System
Akos Jobbagy, Hungary
- 18:00** SP111.5 - Cardiac Output estimation through Impedance Cardiography using reconfigurable hardware.
Leidy Alvero González, Cuba
- 18:15** SP111.6 - Microfluorimetry System Instrumentation for Ca²⁺-Associated Fluorescence Imaging of Cardiomyocytes in Response to High Electric Fields
Marcelo Zoccoler, Brazil
- 18:30** SP111.7 - A practical device to warn on impending syncopal episodes
Michael Cheng, Canada
- 18:45** SP111.8 - Robust Blood Pressure Monitoring in Atrial Fibrillation Patients
Saif Ahmad, Canada

SESSION TIME: 17:00 – 18:45
 SESSION ROOM: 717B
 SESSION TRACK: TRACK 12: MEDICAL DEVICES
 SESSION NAME: SP112 – INSTRUMENTATION
 SESSION CHAIR(S): ANTHONY EASTY, CANADA
 GUILLERMO AVENDANO, CHILE

- 17:00 SP112.1 - Adaptation of Surgical Instruments for the Removal of Bladder Tumours
Spencer Barnes, United Kingdom
- 17:15 SP112.2 - A compact gantry based on pulse powered magnets for a laser-based proton radiotherapy
Leonhard Karsch, Germany
- 17:30 SP112.3 - Developing a pH Responsive Mesh as a Smart Skin Wafer in Ostomy Appliances
Anna McLister, United Kingdom
- 17:45 SP112.4 - Development of a smart needle integrated with a micro-structured impedance sensor for the detection of breast cancer
Niall Savage, Ireland
- 18:00 SP112.5 - Towards development of a wearable, miniaturized, bioartificial lung
Esther Novosel, Germany
- 18:15 SP112.6 - Development of a Low Cost Spectrometer for Studies of Diffuse Reflectance with Dermatological Science and Applications
Gerardo Romo-Cardenas, Mexico
- 18:30 SP112.7 - Correctness of bioimpedance data for body composition obtained by BIA approach in various external conditions
Jan Hlubik, Czech Republic

SESSION TIME: 17:00 – 19:00
 SESSION ROOM: 715A
 SESSION TRACK: TRACK 14: INFORMATION TECHNOLOGIES IN HEALTHCARE DELIVERY AND MANAGEMENT
 SESSION NAME: SP113 – INFORMATION TECHNOLOGIES IN HEALTHCARE DELIVERY AND MANAGEMENT: PART 1
 SESSION CHAIR(S): BRUCE CURRAN, UNITED STATES
 JOSEPH CAFAZZO, CANADA

- 17:00 SP113.1 - **KEYNOTE:** Technologies for Patient Self-Care of Chronic Illness: Development and Evidence
Joseph Cafazzo, Canada
- 17:30 SP113.2 - A mobile monitoring tool for the automatic activity recognition and its application for Parkinson's disease rehabilitation
Jorge Cancela, Spain

- 17:45 SP113.3 - My Patient: An Electronic Patient Information Management System
Satish Jaywant, Kuwait
- 18:00 SP113.4 - Hom-e-call? An enhanced fall detection system based on accelerometer and optical sensors applicable in domestic environment
Daniel Wohlrab, Germany
- 18:15 SP113.5 - An Algorithm Based on Voice Description of Meal for Insulin Dose Calculation to Compensate Food Intake
Piotr Foltynski, Poland
- 18:30 SP113.6 - Building neuroscientific evidence and best practices in active and healthy aging
Panagiotis Bamidis, Greece
- 18:45 SP113.7 - Intelligent System for Identification of patients in Healthcare
Giovanni Sagbay, Ecuador

SESSION TIME: 17:00 – 18:00
 SESSION ROOM: 713B
 SESSION TRACK: PRESIDENT'S CALL
 SESSION NAME: SP114 – DOSIMETRY AND RADIATION PROTECTION
 SESSION CHAIR(S): SAMBA RICHARD NDI, CAMEROON
 PANKAJ PARASHAR, INDIA

- 17:00 SP114.1 - Development of Object Simulator for Evaluation Periapical Radiographs
Fernanda Ferreira, Brazil
- 17:15 SP114.2 - Impact Created by Medical Physicist from Regulatory Quality Assurance Controls in Developing Country
Samba Richard Ndi, Cameroon
- 17:30 SP114.3 - Evaluation of Dental X-rays equipment in Sobral-CE, Brazil
Fernanda Ferreira, Brazil
- 17:45 SP114.4 - Effect of static magnetic field exposure on human blood electrolyte levels in vitro
Pankaj Parashar, India

SCIENTIFIC PROGRAM BY DAY

► Thursday, June 11 2015

THURSDAY JUNE 11 2015

Thursday, June 11 2015

SESSION TIME: 08:00 – 10:00
SESSION ROOM: 718A
SESSION TRACK: TRACK 01: IMAGING
SESSION NAME: SP115 – CT IMAGE QUALITY AND DOSE OPTIMIZATION
SESSION CHAIR(S): ANA MARIA MARQUES DA SILVA, BRAZIL

SESSION TIME: 08:00 – 10:00
SESSION ROOM: 701B
SESSION TRACK: TRACK 01: IMAGING
SESSION NAME: SP116 – IMAGE PROCESSING AND VISUALIZATION: PART 2
SESSION CHAIR(S): YIWEN XU, CANADA

- 08:00** SP115.1 - Towards Image Quality Analysis of Small and Full Field of View Dental Cone Beam CT Systems
Ana Maria Marques Da Silva, Brazil
- 08:15** SP115.2 - Rapid non-invasive spatially varying HVL measurements for CT sources
Matthew Randazzo, United States
- 08:30** SP115.3 - Development of a CT protocol management system for automated review of CT scanner protocols
Josh Grimes, United States
- 08:45** SP115.4 - Evaluation of automatic exposure control systems in computed tomography
Paulo Costa, Brazil
- 09:00** SP115.5 - Development of a Software for Image Quality Assessment in Computed Tomography using the Catphan500® Phantom
Paulo Costa, Brazil
- 09:15** SP115.6 - Performance of attenuation-based dynamic CT beam-shaping filtration for elliptical subject geometries in dependence of fan- and projection-angle
Stella Veloza, Colombia
- 09:30** SP115.7 - A software tool for automated artifact detection in scans of the CT daily water phantom
Josh Grimes, United States
- 09:45** SP115.8 - Monte Carlo Simulation of X-ray Spectra in Computed Tomography Scanner using GATE
Mohammad Reza Ay, Iran

- 08:00** SP116.1 - Automated segmentation of whole-slide histology for vessel morphology comparison
Yiwen Xu, Canada
- 08:15** SP116.2 - Using Gamma Maps of Anatomy to Highlight Changes in Anatomy During Image-Guided Adaptive Radiotherapy: Head and neck example
Jeff Kempe, Canada
- 08:30** SP116.3 - Improvement of Ventricle Volumetric Calculation and Visualization in Cardiac MRI
William Rae, South Africa
- 08:45** SP116.4 - Inter-operator variability of 3D prostate magnetic resonance image segmentation using manual and semi-automatic approaches
Maysam Shahedi, Canada
- 09:00** SP116.5 - Derivation of Residual Noise of Filtered Poisson and Gaussian Series
Weiguang Yao, United States
- 09:15** SP116.6 - Fast Registration of Intraoperative Ultrasound and Preoperative MR Images Based on Calibrations of 2D and 3D Ultrasound Probes
Fang Chen, People's Republic of China
- 09:30** SP116.7 - Development of digital subtraction angiography for coronary artery without motion artifacts enabling read-time processing
Megumi Yamamoto, Japan
- 09:45** SP116.8 - Real-time measurement of cardiomyocyte contraction and calcium transients using fast image processing algorithms
Ivo Provazník, Czech Republic

SCIENTIFIC PROGRAM

SESSION TIME: 08:00 – 09:15

SESSION ROOM: 718B

SESSION TRACK: TRACK 04: RADIATION ONCOLOGY

SESSION NAME: SP117 – TREATMENT PLANNING – KNOWLEDGE BASED

SESSION CHAIR(S): ROBERT MACDONALD, CANADA
CHRIS MCINTOSH, CANADA

- 08:00** SP117.1 - **KEYNOTE:** Next Generation Radiotherapy Treatment Planning: Current Status and Future Prospects
Steve Jiang, United States
- 08:30** SP117.2 - Overlap-Guided Fixed-Patient Support Positioning for Cranial SRT
Robert Macdonald, Canada
- 08:45** SP117.3 - Automated Dose Map Prediction Through Radiomics and Regression on the Patient Manifold
Chris McIntosh, Canada
- 09:00** SP117.5 - Models for Predicting Objective Function Weights in Prostate Cancer IMRT
Justin Boutilier, Canada

SESSION TIME: 08:00 – 09:30

SESSION ROOM: 715B

SESSION TRACK: TRACK 05: DOSIMETRY AND RADIATION PROTECTION

SESSION NAME: SP118 – DIAGNOSTIC RADIOLOGY: DOSIMETRY AND QUALITY CONTROL

SESSION CHAIR(S): JAMILA SALEM AL SUWAIDI,
UNITED ARAB EMIRATES
ARUN KUMAR L S, OMAN

- 08:00** SP118.1 - Measuring absorbed-dose to cardiac implantable electronic device using OSL.
Étienne Létourneau, Canada
- 08:15** SP118.2 - Organ dose estimation in computed tomography based on Monte Carlo simulation
Camille Adrien, France
- 08:30** SP118.3 - Comparative study of Average Glandular Doses of three different digital mammography units in three Ministry of Health Hospitals in Oman: An analysis
Arun Kumar L S, Oman
- 08:45** SP118.4 - First Data on Quality Control Test done in Diagnostic X-ray facility at Major Public Hospitals in Kathmandu Valley, Nepal.
Kanchan Adhikari, Nepal
- 09:00** SP118.5 - Estimation of dose distributions in mammography into a tissue equivalent phantom
Josilene Santos, Brazil

- 09:15** SP118.7 - Radiation Dose Assessment for Retrospectively ECG-Gated Coronary Computed Tomography Angiography (CCTA) Examination
C H Yeong, Malaysia

SESSION TIME: 08:00 – 10:00

SESSION ROOM: 716A

SESSION TRACK: TRACK 05: DOSIMETRY AND RADIATION PROTECTION

SESSION NAME: SP119 – DOSE SURVEYS IN CT AND INTERVENTIONAL RADIOLOGY

SESSION CHAIR(S): HAMID KHOSRAVI, CANADA

- 08:00** SP119.1 - CT Dose Optimization: First Results from a Province-Wide Program in Quebec
Manon Rouleau, Canada
- 08:15** SP119.2 - CT overexposure as a consequence of scan length
Mohamed Badawy, Australia
- 08:30** SP119.3 - Regional survey of pediatric patient doses from CT examinations in Tehran, Iran
Hamid Khosravi, Canada
- 08:45** SP119.4 - Dose Reduction Efforts in PET/CT: the Quebec Experience
Manon Rouleau, Canada
- 09:00** SP119.5 - Assessment of high cumulative patient doses of repetitive CT examinations
Cecile Jeukens, Netherlands
- 09:15** SP119.6 - IAEA survey of pediatric computed tomography practice in Pakistan procedures and protocols (2005-2015)
Areesha Zaman, Pakistan
- 09:30** SP119.7 - Occupational Dose Measurement in an Interventional Radiology Facility in Jakarta
Lukmanda Evan Lubis, Indonesia
- 09:45** SP119.8 - Evaluation of the Comparative Effectiveness of Various Jurisdictional Computed Tomography Radiation Dose Reduction Models
Anne Li, Canada

SESSION TIME: 08:00 – 09:30
 SESSION ROOM: 716B
 SESSION TRACK: TRACK 09: BIOSIGNAL PROCESSING
 SESSION NAME: SP120 – BIOMEDICAL DIAGNOSIS & PREDICTION
 SESSION CHAIR(S): JENNIFER HOWCROFT, CANADA
 JAN HAVLÍK, CZECH REPUBLIC

- 08:00 SP120.1 - Desaturation event characteristics and mortality risk in severe sleep apnea
Antti Kulkas, Finlandia
- 08:15 SP120.2 - Static Posturography of Elderly Fallers and Non-Fallers with Eyes Open and Closed
Jennifer Howcroft, Canada
- 08:30 SP120.3 - Quantitative analysis of ventricular ectopic beats evaluated from short-term recordings of heart rate variability before imminent tachyarrhythmia
Marisol Martínez-Alanis, Mexico
- 08:45 SP120.4 - An evaluation of Arterial Stiffness Index in Relation to the State of the Cardiovascular System
Jan Havlík, Czech Republic
- 09:00 SP120.5 - Investigating a Novel Non-invasive Measure to Assess the Upper Airway Narrowing during Sleep
Ying Xuan Zhi, Canada
- 09:15 SP120.6 - Establishing a New Biomarker to Determine Patients at Increased Risk of Developing Obstructive Sleep Apnea Due To Fluid Overloading
Bojan Gavrilovic, Canada

SESSION TIME: 08:00 – 09:45
 SESSION ROOM: 714B
 SESSION TRACK: TRACK 11: NEUROENGINEERING, NEURAL SYSTEMS
 SESSION NAME: SP121 – DEEP BRAIN STIMULATION
 SESSION CHAIR(S): FABIOLA ALONSO, SWEDEN
 VENKATESHWARLA RAJU, INDIA

- 08:00 SP121.1 - A 16-bit High-Voltage Digital Charge-Control Electrical Stimulator
Ulrich Hofmann, Germany
- 08:15 SP121.2 - A method for side effect analysis based on electric field simulations for intraoperative test stimulation in deep brain stimulation surgery
Simone Hemm-Ode, Switzerland
- 08:30 SP121.3 - Comparison of Three Deep Brain Stimulation Lead Designs under Voltage and Current Modes
Fabiola Alonso, Sweden
- 08:45 SP121.4 - Effect of closed-loop and open-loop deep brain stimulation on chronic seizures control
Muhammad Salam, Canada

- 09:00 SP121.5 - Clinical validation of a precise tremor assessment system to aid deep brain stimulation parameter optimisation
Thushara Perera, Australia
- 09:15 SP121.6 - The Role of Microelectrode Recording (MER) in STN DBS Electrode Implantation
Venkateshwarla Raju, India
- 09:30 SP121.7 - Effectiveness of Micro-Electrode-Recording(MER) in Determining Subthalamic-Nuclei Deep Brain Stimulation (STN-DBS) Lead Position in PD Conditions
Venkateshwarla Raju, India

SESSION TIME: 08:00 – 10:00
 SESSION ROOM: 717B
 SESSION TRACK: TRACK 15: BIOINFORMATICS
 SESSION NAME: SP122 – BIOINFORMATICS
 SESSION CHAIR(S): JAMES GREEN, CANADA
 PARVIN MOUSAVI, CANADA

- 08:00 SP122.1 – **KEYNOTE:** Machine learning for bioinformatics in the face of class imbalance
James Green, Canada
- 08:30 SP122.2 - Bioinformatics-based identification of osteoarthritis-associated genes in synovial tissues
Yi-Jiang Song, People's Republic of China
- 08:45 SP122.3 - Dynamic Epistasis Analysis
Aseel Awdeh, Canada
- 09:00 SP122.4 - Transcription factor binding in an expanded epigenetic alphabet
Michael Hoffman, Canada
- 09:15 SP122.5 - Identification of Molecular Phenotypes in Lung Cancer by Integrating Radiomics and Genomics
Patrick Grossmann, United States
- 09:30 SP122.6 - A machine learning method to build multi-SNP predictive models of clinical radiosensitivity
Jung Hun Oh, United States
- 09:45 SP122.7 - Updated Free Energy Parameters Increase MicroRNA Prediction Performance
Robert Peace, Canada

SESSION TIME: 08:00 – 09:45

SESSION ROOM: 701A

SESSION TRACK: **TRACK 16: CLINICAL ENGINEERING, CLINICAL PHYSICS, AND PATIENT SAFETY**

SESSION NAME: **SP123 – PATIENT SAFETY, MEDICAL ERRORS AND ADVERSE EVENTS PREVENTION RELATED TO HEALTH TECHNOLOGIES**

SESSION CHAIR(S): **MARY COFFEY, IRELAND
ANDREW IBEY, CANADA**

- 08:00** SP123.1 - **KEYNOTE:** Incident reporting and learning systems improving quality and safety in radiation oncology
Mary Coffey, Ireland
- 08:30** SP123.2 - Applying an Evidence-based Approach to Managing Alarm Safety: A University Health Network Case Study
Anne Li, Canada
- 08:45** SP123.3 - Using infusion pump logs to recreate a patient safety event: considerations for smart pump improvement
Andrew Ibey, Canada
- 09:00** SP123.4 - Developing an information retrieval engine for medical devices? Vigilance reports
Nicolas Pallikarakis, Greece
- 09:15** SP123.5 - Efficient, all-in-one, Monte Carlo simulations of transit EPID cine-mode dose distributions for patient-specific VMAT quality assurance
Shiqin Su, Canada
- 09:30** SP123.6 - Development of an interactive training tool to help reduce error rate associated with shared infusion volume management tasks
Patricia Trbovich, Canada

SESSION TIME: 08:00 – 09:30

SESSION ROOM: 717A

SESSION TRACK: **TRACK 17: EDUCATIONAL AND PROFESSIONAL ACTIVITIES**

SESSION NAME: **SP124 – MEDICAL PHYSICS IN DEVELOPING COUNTRIES**

SESSION CHAIR(S): **AGNETTE PERALTA,
REPUBLIC OF THE PHILIPPINES
W.H. ROUND, NEW ZEALAND**

- 08:00** SP124.1 - Medical Physics Training Resources for Developing Countries
Muthana Al-Ghazi, United States
- 08:15** SP124.2 - Medical Physics in Indonesia: Current Status and Plans
Supriyanto Ardjo Pawiro, Indonesia
- 08:30** SP124.3 - Surveying Trends in Radiation Oncology Medical Physics in the Asia Pacific Region
Tomas Kron, Australia

08:45 SP124.4 - The Status of Medical Physics in Iraq
Muthana Al-Ghazi, United States

09:00 SP124.5 - Evaluation and Adaptation of Medical Physics Practicum for Nicaraguan Students at a Canadian Cancer Centre
Alana Hudson, Canada

09:15 SP124.6 - Coordination of AAPM Educational Courses for Developing Countries with Major International and Regional Organizations of Medical Physicists
Eugene Lief, United States

SESSION TIME: 08:00 – 10:00

SESSION ROOM: 713A

SESSION TRACK: **TRACK 17: EDUCATIONAL AND PROFESSIONAL ACTIVITIES**

SESSION NAME: **SP125 – TECHNOLOGY ENHANCED EDUCATION**

SESSION CHAIR(S): **JAMES WEAR, UNITED STATES
SLAVIK TABAKOV, UNITED KINGDOM**

- 08:00** SP125.1 - **KEYNOTE:** e-Learning in Medical Physics? pioneering and future trends
Slavik Tabakov, United Kingdom
- 08:30** SP125.2 - A Desk-Top Optical Scanner for Teaching the Principles of Computed Tomography (CT)
Linada Kaci, Canada
- 08:45** SP125.3 - Medical Physics e-Encyclopaedia and Multilingual Dictionary? Upgrade and New Developments
Slavik Tabakov, United Kingdom
- 09:00** SP125.4 - Physics for Medical Students: Technology Enhanced Teaching from the Dipole to the Vectorcardiogram
Ernst Hofer, Austria
- 09:15** SP125.5 - matRad: a multimodality open source treatment planning toolkit
Eduardo Cisternas, Chile
- 09:30** SP125.6 - Creation of a model for online education of clinical engineering and management of medical technologies to reach professionals worldwide
María Moreno Carbajal, Mexico
- 09:45** SP125.7 - Develop of a Mixed, Haptic and Virtual System to Simulate Radiographic Images
Guillermo Avendaño, Chile

SESSION TIME: 08:00 – 09:45

SESSION ROOM: 715A

SESSION TRACK: **TRACK 19: BIOPHYSICS AND MODELLING**

SESSION NAME: **SP126 – COMPUTATIONAL BIOLOGY & HEMODYNAMICS**

SESSION CHAIR(S): **IYAD FAYSSAL, LEBANON**

- 08:00** SP126.1 - Evaluation of Decomposition Analysis on Multi-Models for Digital Volume Pulse Signal
Sheng-Cheng Huang, Chinese Taipei
- 08:15** SP126.2 - Discordant alternans in a one-dimensional cable of ischemic heart tissue.
Yunuen Cervantes Espinosa, Mexico
- 08:30** SP126.3 - A Novel Biomechanical Model of the Left Ventricle for Cardiac Contraction Force Reconstruction Applications
Seyyed Mohammad Hassan Haddad, Canada
- 08:45** SP126.4 - A simulative model approach of cardiopulmonary interaction
Chuong Ngo, Germany
- 09:00** SP126.5 - The Development of SIM to Characterize Blood Volumetric Flow Rate and Hemodynamics in Human Coronary Arteries
Iyad Fayssal, Lebanon
- 09:15** SP126.6 - Determination of Bermang's Minimal Model parameters for diabetic mice treated with Ibervillea sonorae
Rodrigo Sánchez-González, Mexico
- 09:30** SP126.7 - Investigation of flow and turbulence in carotid artery models of varying compliance using particle image velocimetry
Amanda Dicarlo, Canada

SESSION TIME: 08:00 – 09:30

SESSION ROOM: 713B

SESSION TRACK: PRESIDENT'S CALL

SESSION NAME: SP127 – INFORMATICS IN HEALTH CARE AND PUBLIC HEALTH / BIOSENSOR, NANOTECHNOLOGY, BIOMEMS AND BIOPHOTONICS

SESSION CHAIR(S): RICARDO SILVA, ECUADOR
PETER PENNEFATHER, CANADA

- 08:00** SP127.1 - A study on the leading cause of immunisation schedule fall up defaulting and early child hood malnutrition sicknesses in developing countries (uganda in particular) rural areas/villages
Waigonda Saad, Uganda
- 08:15** SP127.2 - From Smart Phones to Smart Health
Ricardo Silva, Ecuador
- 08:30** SP127.3 - Diagnostic Data: a Manifesto
Peter Pennefather, Canada
- 08:45** SP127.4 - Comparative analysis of co-expression networks reveals molecular changes during the cancer progression
Pegah Khosravi, Iran
- 09:00** SP127.5 - Copper Meshed Carbon Black PDMS Electrode for Underwater ECG Monitoring
Justin Bales, United States
- 09:15** SP127.6 - Smartphone-based Monitoring of Tidal Volume and Respiratory Rate
Bersain Reyes, United States

SESSION TIME: 10:30 – 11:45

SESSION ROOM: 718A

SESSION TRACK: TRACK 01: IMAGING

SESSION NAME: SP128 – MULTIMODALITY IMAGING

SESSION CHAIR(S): GANG ZHENG, CANADA
ELISA KALLIONIEMI, FINLANDIA

- 10:30** SP128.1 - Localizing cortical motor representation: A comparative study between navigated transcranial magnetic stimulation, BOLD contrast and arterial spin labeling fMRI
Elisa Kallioniemi, Finlandia
- 10:45** SP128.2 - Evaluation of probable dementia with Lewy bodies using 123I-IMP brain perfusion SPECT, 123I-MIBG myocardial SPECT and voxel-based MRI morphometry
Naoki Kodama, Japan
- 11:00** SP128.3 - Targeted all-organic nanovesicles for multimodal PET/CT and optical fluorescence assessment of lymphatic disseminations in gynaecologic cancers: A radio-pharmaceutical kit to prepare parenteral injections for a 'first-in-woman' clinical study.
Michael Valic, Canada
- 11:15** SP128.4 - Generation of 4-Class Attenuation Map for MRI Based Attenuation Correction of PET Data in the Head Area Using a Novel Combination of STE/DIXON-MRI and FCM Clustering
Hamidreza Saligheh Rad, Iran
- 11:30** SP128.5 - A new low field MRI/gamma detector hybrid system
Andrea Abril, Colombia

SESSION TIME: 10:30 – 12:00

SESSION ROOM: 701B

SESSION TRACK: TRACK 01: IMAGING

SESSION NAME: SP129 – IMAGE QUALITY ASSESSMENT (MAMMOGRAPHY AND OTHER)

SESSION CHAIR(S): JAMES ANNKAH, UNITED KINGDOM
MARÍA-ESTER BRANDAN, MEXICO

- 10:30** SP129.1 - Kilovoltage-CBCT of a Linear Accelerator as a relative imaging device of a spiral CT scanner - dosimetric results
James Annkah, United Kingdom
- 10:45** SP129.2 - Overall performance, image quality and dose in CR mammography systems operating in the Mexico public health sector
María-Ester Brandan, Mexico
- 11:00** SP129.3 - A Catphan attachment for three dimensional measurements of the modulation transfer function
Elsayed Ali, Canada

- 11:15** SP129.4 - Sensitometric analyses of screen-film systems for mammography exams in Brazil
Luis Magalhaes, Brazil
- 11:30** SP129.5 - New Line Contrast Figure of Merit for image quality assessment
Aris Dermitzakis, Greece
- 11:45** SP129.6 - Assessment of Photostimulable Storage Phosphor Imaging Plates Quality in Computed Radiography
Bárbara Friedrich, Brazil

SESSION TIME: 10:30 – 12:00
SESSION ROOM: 718B
SESSION TRACK: TRACK 04: RADIATION ONCOLOGY
SESSION NAME: SP130 – TREATMENT PLANNING
SESSION CHAIR(S): WINNIE LI, CANADA

- 10:30** SP130.1 - Comprehensive Dosimetric Planning Comparison for Early Stage Non-Small Cell Lung Cancer with SABR: Fixed-Beam IMRT versus VMAT versus Tomotherapy
Ilma Xhaferllari, Canada
- 10:45** SP130.2 - Development and Validation of an Open Source Tool for Determining Planning Target Volume Margins in Intracranial Stereotactic Radiotherapy
Winnie Li, Canada
- 11:00** SP130.3 - Dosimetric impact of accurately delineating of the left anterior descending artery in photon and proton radiotherapy
Janid Blanco Kiely, United States
- 11:15** SP130.4 - Objective function surrogates for iterative beam angle selection
Jan Unkelbach, United States
- 11:30** SP130.5 - A preliminary study on the effect of modulated photon radiotherapy (XMRT) optimization for prostate cancer treatment planning
Philip McGeachy, Canada
- 11:45** SP130.6 - Measuring radiation treatment plan similarity in the cloud
Jennifer Andrea, Canada

SESSION TIME: 10:30 – 12:15
SESSION ROOM: 701A
SESSION TRACK: TRACK 04: RADIATION ONCOLOGY
SESSION NAME: SP131 – QUALITY ASSURANCE: PART 3
SESSION CHAIR(S): JIANRONG DAI, PEOPLE'S REPUBLIC OF CHINA
ANDREA MCNIVEN, CANADA

- 10:30** SP131.1 - Sensitivity of Helical Tomotherapy and Elekta Agility VMAT dose distributions to multileaf collimator motion uncertainties for breast radiation treatment with extensive nodal irradiation
Eric Vandervoort, Canada
- 10:45** SP131.2 - Use of Varian Trajectory Log Files for Patient Specific Quality Control of TrueBeam VMAT FFF Treatment Deliveries with Portal Dosimetry and Eclipse
Michael Fan, Canada
- 11:00** SP131.3 - Machine Learning Facilitates Failure Mode Analysis and Virtual QA for IMRT
Gilmer Valdes, United States
- 11:15** SP131.4 - Dosimetric analysis of respiratory-gated RapidArc with varying gating window times
Ju Young Song, Republic of Korea
- 11:30** SP131.5 - Current status of dose-tracking using an integrated commercial system
Stina Svensson, Sweden
- 11:45** SP131.6 - Enabling Continuous Quality Improvement in a Rapidly Changing Clinical Environment through a Multi-Year Multi-Centre IMRT QC Program: 3 Year Experience
Andrea McNiven, Canada
- 12:00** SP131.7 - A new approach to spatial gradient signal encoding for external beam radiotherapy delivery verification
Robert Heaton, Canada

SESSION TIME: 10:30-11:30
SESSION ROOM: 715B
SESSION TRACK: TRACK 05: DOSIMETRY AND RADIATION PROTECTION
SESSION NAME: SP132 – SPECIAL SESSION: IMPLEMENTATION OF THE NEW BSS INCLUDING RADIATION SAFETY CULTURE IN MEDICINE
SESSION CHAIR(S): MADAN REHANI, UNITED STATES

- Speaker: SP132.1 - Madan Rehani, United States**
- Speaker: SP132.2 - Ola Holmberg, Austria**
- Speaker: SP132.3 - Pablo Jimenez, United States**

SESSION TIME: 10:30 – 12:00
SESSION ROOM: 716A
SESSION TRACK: TRACK 05: DOSIMETRY AND RADIATION PROTECTION
SESSION NAME: SP133 – VALIDATION AND VERIFICATION OF THERAPY DOSE DELIVERY: PART 2
SESSION CHAIR(S): SARFEHNIA ARMAN, CANADA
JAMES CHOW, CANADA

Panelists: SP133.1 - *James Chow, Canada*
SP133.2 - *Michel Lalonde, Canada*
SP133.3 - *Kamlesh Passi, India*
SP133.4 - *Nader Moshiri Sedeh, United States*

SESSION TIME: 10:30 – 11:45
SESSION ROOM: 717B
SESSION TRACK: TRACK 08: BIOSENSOR, NANOTECHNOLOGY, BIOMEMS AND BIOPHOTONICS
SESSION NAME: SP134 – BIOSIGNAL SENSING AND BODY SENSOR NETWORKS
SESSION CHAIR(S): KWANG OH, UNITED STATES
JONATHAN LOVELL, UNITED STATES

- 10:30 SP134.1 - Impedance and comfort of dry multipin electrodes for electroencephalography
Patrique Fiedler, Germany
- 10:45 SP134.2 - Wearable Gait Analysis using Vision-aided Inertial Sensor Fusion
Eric Ma, Canada
- 11:00 SP134.3 - Two-Vector Capacitive Electrocardiogram Measurement Using Three Fabric Electrodes for Automobile Application
Shunsuke Takayama, Japan
- 11:15 SP134.5 - Detection of REM Behaviour Disorder Based on Low-Power Compressive Sensing of EMG
Sridhar Krishnan, Canada
- 11:30 SP134.6 - Externally applied pressure on the skin electrode impedance
Bahareh Taji, Canada

SESSION TIME: 10:30 – 12:00
SESSION ROOM: 714B
SESSION TRACK: TRACK 11: NEUROENGINEERING, NEURAL SYSTEMS
SESSION NAME: SP135 – NEURAL SIGNAL PROCESSING: PART 2
SESSION CHAIR(S): MILOS POPOVIC, CANADA
ANGELO ALL, SINGAPORE

- 10:30 SP135.1 - Epileptogenic zone estimation by localizing the generators of delta and high-frequency rhythms extracted from human scalp EEG
Daniel Jacobs, Canada
- 10:45 SP135.2 - Automated Alzheimer's Disease Diagnosis Using a Portable 7-Channel Electroencephalography Device
Raymundo Cassani, Canada
- 11:00 SP135.3 - Transient Propagation of Information Among Cultured Hippocampal Cell Assemblies in a Two-Chamber MEMs Device
Bruce Wheeler, United States
- 11:15 SP135.4 - Investigating the Cortical Dominance in the Pre-Motor Potential during Unilateral Voluntary Task
Antonio Infantsi, Brazil
- 11:30 SP135.5 - A New Dynamic Virtual Stimulation Protocol to Evoke M-VEP and Linear Vection during Orthostatic Posture Control
Antonio Infantsi, Brazil
- 11:45 SP135.6 - Assessment of Bilateral SSEP Signals Enhancement following Transectional Spinal Cord Injury Using Linear Modeling
Angelo All, Singapore

SESSION TIME: 10:30 – 11:30
SESSION ROOM: 716B
SESSION TRACK: TRACK 12: MEDICAL DEVICES
SESSION NAME: SP136 – BRAIN, HEAD/NECK, SPINE: PART 1
SESSION CHAIR(S): ANDREAS SCHMOCKER, SWITZERLAND
FRANCIS BAMBICO, CANADA

- 10:30 SP136.1 - Photopolymerization device for minimally invasive implants: application to nucleus pulposus replacement
Andreas Schmocker, Switzerland
- 10:45 SP136.2 - Design and Technical Evaluation of an Implantable Passive Sensor for Minimally Invasive Wireless Intracranial Pressure Monitoring
Mohammadhossein Behfar, Finlandia
- 11:00 SP136.3 - Investigating the Feasibility of EVestG Assessment for Screening Concussion
Zahra Moussavi, Canada

- 11:15** SP136.4 - Transcranial Direct Current Stimulation of the Rat Medial Prefrontal Cortex: Antidepressant Effects and Regional Brain Changes
Francis Bambico, Canada

SESSION TIME: 10:30 – 12:00
 SESSION ROOM: 714A
 SESSION TRACK: TRACK 17: EDUCATIONAL AND PROFESSIONAL ACTIVITIES
 SESSION NAME: SP137 – SPECIAL SESSION: BUILDING MEDICAL PHYSICS CAPACITY IN DEVELOPING COUNTRIES
 SESSION CHAIR(S): SLAVIK TABAKOV, UNITED KINGDOM
 FRIDTJOF NUESSLIN, GERMANY

- 10:30** Opening Remarks
Slavik Tabakov, United Kingdom
Fridtjof Nuesslin, Germany
- 10:40** SP137.1 - Cost-Effective Provision of Medical Physics and Medical Engineering Services in Healthcare
Peter H S Smith, United Kingdom
- 10:50** SP137.2 - Implementing Training Modules of the Emerald Program in Brazil
Ricardo Terini, Brazil
- 11:00** SP137.3 - Pilot Implementation In The Philippines Of Structured Medical Physics Residency Programs Using The Iaea Training Guides For The Clinical Training Of Medical Physicists
Agnette Peralta, Republic of the Philippines
- 11:10** SP137.4 - Capacity Building of Medical Physics in Bangladesh
Hasin Anupama Azhari, Bangladesh
- 11:20** SP137.5 - Education & Training of Medical Physics in Africa: Challenges & Opportunities
Ahmed IbnSeddick
- 11:30** SP137.6 - Retention of trained medical physicists in African states; Do our Governments have a role to play
Rebecca Nakatudde
- 11:40** SP137.7 - Strengthening Medical Physics Clinical Competencies in a Challenging Environment - Update on the IAEA Supported Nigerian (NIR/6/023) Project
Taofeeq Ige, Nigeria
- 11:50** SP137.8 - Capacity Building of Medical Physics in Ghana and Africa
Stephen Inkoom, Ghana

SESSION TIME: 10:30 - 11:45
 SESSION ROOM: 713B
 SESSION TRACK: PRESIDENT'S CALL
 SESSION NAME: SP138 - BIOSENSOR, NANOTECHNOLOGY, BIOMEMS AND BIOPHOTONICS / NEW TECHNOLOGIES IN CANCER RESEARCH AND TREATMENT
 SESSION CHAIR(S): MOHAMMAD KHOSROSHAHI, CANADA
 NAZANIN MOSAVIAN, UNITED STATES

- 10:30** SP138.1 - Measurement of the Received Power in a Realistic Intrabody Communication Scenario
Zeljka Lucev Vasic, Croatia
- 10:45** SP138.2 - Focused ultrasound-triggered release of Sorafenib from temperature sensitive liposomes for treating renal cell carcinoma
Hakm Murad, United States
- 11:00** SP138.3 - Synthesis and Characterization of SPION Functionalized third Generation dendrimers Conjugated by Gold Nanoparticles and Folic acid for Targeted Breast Cancer Laser Hyperthermia: An In vitro-assay
Mohammad Khosroshahi, Canada
- 11:15** SP138.4 - FIB/SEM Characterization of Microcavity Surface Plasmon Resonance Biosensors
Nazanin Mosavian, United States
- 11:30** SP138.5 - The current status of Microbeam Radiation Therapy at the ESRF and future perspectives
Elke Brauer-Krisch, France

SESSION TIME: 15:00 – 16:30
 SESSION ROOM: 718A
 SESSION TRACK: TRACK 01: IMAGING
 SESSION NAME: SP139 – OPTICAL IMAGING: METHODS
 SESSION CHAIR(S): ARASH DARAFSHEH, UNITED STATES
 HEPING XU, CANADA

- 15:00** SP139.1 - Toward super-resolution imaging of proton radiation-induced DNA double-strand breaks for characterization of -H2AX foci clusters
Arash Darafsheh, United States
- 15:15** SP139.2 - Solution of radiative transport equation in turbid layered media in spatial and frequency domains
Heping Xu, Canada
- 15:30** SP139.3 - Development of a hybrid optical-gamma camera: A new innovation in bedside molecular imaging
Aik Hao Ng, Malaysia
- 15:45** SP139.4 - Sidestream Dark-Field Oximetry with Multicolor LEDs
Tomohiro Kurata, Japan

- 16:00** SP139.5 - Development of Polymer Substrates for Waveguide Evanescent Field Fluorescence Microscopy
Rony Sharon, Canada
- 16:15** SP139.6 - Higher-Order Structural Investigation of Mammalian Septins by Super-Resolution Fluorescence Microscopy
Adriano Vissa, Canada

SESSION TIME: **15:00 – 16:15**
 SESSION ROOM: **718B**
 SESSION TRACK: **TRACK 04: RADIATION ONCOLOGY**
 SESSION NAME: **SP140 – SPECIAL TREATMENT TECHNIQUES: PART 1**
 SESSION CHAIR(S): **WILLIAM Y. SONG, CANADA**

- 15:00** SP140.1 - Credentialing of radiotherapy centres in Australasia for a phase III clinical trial on SABR
Tomas Kron, Australia
- 15:15** SP140.2 - LED-optimized SBRT for Peripheral Early Stage Lung Cancer: A technique to reduce lung dose and potentially allow for re-irradiation
Brandon Disher, Canada
- 15:30** SP140.3 - Delivery of VMAT treatments with nonstandard SAD using dynamic trajectories
Joel Mullins, Canada
- 15:45** SP140.4 - Cone-Beam CT assessment of inter-fraction and intra-fraction motions during lung stereotactic body radiotherapy with and without abdominal compression
Runqing Jiang, Canada
- 16:00** SP140.5 - Initial experience in establishing frameless intra-cranial stereotactic radiosurgery program with Varian TrueBeam STx, 6DoF couch and VisionRT motion control system
Sergei Zavgorodni, Canada

SESSION TIME: **15:00 – 16:15**
 SESSION ROOM: **716A**
 SESSION TRACK: **TRACK 05: DOSIMETRY AND RADIATION PROTECTION**
 SESSION NAME: **SP141 – DEVELOPMENT OF NEW METHODS IN THERAPY DOSIMETRY: PART 3**
 SESSION CHAIR(S): **NICOLE RANGER, UNITED STATES
SIMONE KODLULOVICH, BRAZIL**

- 15:00** SP141.1 - Theoretical description of the saturation correction of ionization chambers in pulsed fields with arbitrary repetition rate
Leonhard Karsch, Germany

- 15:15** SP141.2 - Performance characteristics of Gafchromic EBT3 film in therapeutic electron beams and its practical application as an in-vivo dosimeter in the clinic
Amanda Barry, Ireland
- 15:30** SP141.3 - Photon and electron spectra inside small field detectors for narrow and broad 6 MV photon beams
Hamza Benmakhlouf, Sweden
- 15:45** SP141.4 - Real Time Dose Reconstruction in MV Photon Therapy using a 2D solid state detector array.
Michael Lerch, Australia
- 16:00** SP141.5 - Energy Correction factor for Plane Parallel ion-chamber and its Use in Clinical photon Beam Dosimetry
Kamlesh Passi, India

SESSION TIME: **15:00 – 16:15**
 SESSION ROOM: **701B**
 SESSION TRACK: **TRACK 06: NEW TECHNOLOGIES IN CANCER RESEARCH AND TREATMENT**
 SESSION NAME: **SP142 – LIGHT ION RADIOTHERAPY**
 SESSION CHAIR(S): **ALBIN FREDRIKSSON, SWEDEN
YOLANDA PREZADO, FRANCE**

- 15:00** SP142.1 - Proton Minibeam Radiation Therapy (pMBRT): implementation at a clinical center
Yolanda Prezado, France
- 15:15** SP142.2 - Hadron minibeam radiation therapy: feasibility study at Heidelberg Ion Therapy Center
Yolanda Prezado, France
- 15:30** SP142.3 - Acoustic Range Verification of Proton Beams: Simulation Assessment of the Challenges of Clinical Application
Kevin Jones, United States
- 15:45** SP142.4 - Radiochromic Film Based Dose Calibration and Monitoring for Radiobiological Experiments using Low Energy Proton Beams
Belal Moftah, Saudi Arabia
- 16:00** SP142.5 - Development of 3D measurement device dedicated for range-compensator QA
Shigekazu Fukuda, Japan

SESSION TIME: 15:00 – 16:00

SESSION ROOM: 701A

SESSION TRACK: **TRACK 07: SURGERY, COMPUTER AIDED SURGERY, MINIMAL INVASIVE INTERVENTIONS, ENDOSCOPY AND IMAGE-GUIDED THERAPY, MODELLING AND SIMULATION**SESSION NAME: **SP143 – RADIOTHERAPY AND GUIDANCE**SESSION CHAIR(S): **STEFANIA PALLOTTA, ITALY**

- 15:00** SP143.1 - Sliced Mary: a deformable phantom for the validation of set-up based on surface imaging in radiotherapy treatments
Stefania Pallotta, Italy
- 15:15** SP143.2 - Evaluation of ion chamber response in high dose per pulse electron beams of IORT accelerator using EGSnrc Monte Carlo code
Mostafa Robotjazi, Iran
- 15:30** SP143.3 - Compared QA of APEX Radiosurgery System using ARCHECK Phantom in Dynamic Conformal Arc System and VMAT System
JaeE Hyuk Seo, Republic of Korea
- 15:45** SP143.4 - Head and Neck CT/CBCT Deformable Registration for Image-guided Accurate Radiotherapy System ARTS-IGRT
Xi Pei, People's Republic of China

SESSION TIME: 15:00 – 16:30

SESSION ROOM: 716B

SESSION TRACK: **TRACK 09: BIOSIGNAL PROCESSING**SESSION NAME: **SP144 – EMG/MMG**SESSION CHAIR(S): **GREGG JOHNS, CANADA**

- 15:00** SP144.1 - Estimation of dorsiflexion torque from a mechanomyogram using a Kalman filter
Takanori Uchiyama, Japan
- 15:15** SP144.2 - Upper-Limb Force Modeling using Rotated Ensembles with Fast Orthogonal Search on High-Density Electromyography
Gregg Johns, Canada
- 15:30** SP144.3 - MMG detection of intentional movement in the presence of dyskinetic movements
Marcela Correa Villada, Canada
- 15:45** SP144.4 - Dynamic Noise Reduction in Accelerometer-based Mechanomyography during Pediatric Gait
Katherine Plewa, Canada
- 16:00** SP144.5 - EMG-EMG Coherence in Multisite Writer's Cramp Waveforms - A Study with Advanced Multi-Channel EMG System
Venkateshwarla Raju, India
- 16:15** SP144.6 - An Exploration of the Erector Spinae Muscle for Knee Exoskeleton Control
Teodiano Freire Bastos, Brazil

SESSION TIME: 15:00 – 17:00

SESSION ROOM: 715A

SESSION TRACK: **TRACK 10: REHABILITATION MEDICINE, SPORTS MEDICINE, REHABILITATION ENGINEERING AND PROSTHETICS**SESSION NAME: **SP145 – DEVELOPING TOOLS FOR SUCCESSFUL AGING: INDEPENDENT MOBILITY & VISUAL IMPAIRMENT**SESSION CHAIR(S): **CHARANJIT BAMBRA, CANADA
OLOF LINDAHL, SWEDEN**

- 15:00** SP145.1 - **KEYNOTE:** Aging Successfully at Home: Research and Development to Address the Biggest Challenges Older Adults Face
Tilak Dutta, Canada
- 15:30** SP145.2 - The effect of age and previous exposure to slippery surface on gait adaptation
Yue Li, Canada
- 15:45** SP145.3 - An intelligent rollator for people with mobility impairment
Olof Lindahl, Sweden
- 16:00** SP145.4 - Rehabilitation Engineering: A review of current teaching tools and project based learning
Charanjit Bambra, Canada
- 16:15** SP145.5 - Effects of sloped icy surface on older adults? gait in a simulated winter environment
Yue Li, Canada
- 16:30** SP145.6 - Judging Weight of an Object by a White Cane
Kiyohiko Nunokawa, Japan
- 16:45** SP145.7 - The Effect of Sub chronic Low Dose of DDVP and Sodium Azide on some Bone Biochemical Indices of Albino Rats
Patrick Agbasi, Nigeria

SESSION TIME: 15:00 – 16:15

SESSION ROOM: 717B

SESSION TRACK: **TRACK 12: MEDICAL DEVICES**SESSION NAME: **SP146 – MSK**SESSION CHAIR(S): **RICARDO ARMENTANO, ARGENTINA
ANA TERESA GABRIEL, PORTUGAL**

- 15:00** SP146.1 - Development of Personalized Tourniquet Systems Using a New Technique for Measuring Limb Occlusion Pressure
James McEwen, Canada
- 15:15** SP146.2 - Vertebral Metrics? development of a third and improved prototype
Ana Teresa Gabriel, Portugal
- 15:30** SP146.3 - Does low-intensity pulsed ultrasound stimulation effectively promote bone fracture repair? An overview
Orlando Rey Rúa, Cuba

15:45 SP146.4 - Electrical Stimulation of the Calf Muscle to Reduce Seated Leg Fluid Accumulation and Subsequent Rostral Fluid Shift While Supine
Daniel Vena, Canada

16:00 SP146.5 - Surgical process analysis identifies lack of connectivity between sequential fluoroscopic 2D alignment as a critical impediment in femoral intramedullary nailing
Hamid Ebrahimi, Canada

SESSION TIME: 15:00 – 16:30

SESSION ROOM: 715B

SESSION TRACK: TRACK 14: INFORMATION TECHNOLOGIES IN HEALTHCARE DELIVERY AND MANAGEMENT

SESSION NAME: SP147 – INFORMATION TECHNOLOGIES IN HEALTHCARE DELIVERY AND MANAGEMENT: PART 2

SESSION CHAIR(S): BRUCE CURRAN, UNITED STATES
JOSEPH CAFAZZO, CANADA

15:00 SP147.1 - **KEYNOTE:** The Electronic Medical Record: Can it be integrated with Treatment Delivery and Management?
Bruce Curran, United States

15:30 SP147.2 - AIM Quality Assurance Program Development for CT X-Ray Systems
Douglas McTaggart, Canada

15:45 SP147.3 - Evaluation of Improved Automatic Speech Recognition Prototype for Estonian Language in Radiology Domain
Andrus Paats, Estonia

16:00 SP147.4 - Usability engineering approach towards secure open networks in the integrated operating room of the future
Klaus Radermacher, Germany

16:15 SP147.5 - Whiteboard ESB: Next Generation Data and Workflow Management for Radiation Oncology
John Wolfgang, United States

SESSION TIME: 15:00 – 16:30

SESSION ROOM: 713B

SESSION TRACK: PRESIDENT'S CALL

SESSION NAME: SP148 - MEDICAL DEVICES / SURGERY, COMPUTER AIDED SURGERY, MINIMAL INVASIVE INTERVENTIONS, ENDOSCOPY AND IMAGE-GUIDED THERAPY, MODELING AND SIMULATION

SESSION CHAIR(S): GIDEON NDUBUKA, NIGERIA

15:00 SP148.1 - Oncometer
Priyajit Ghosh, India

15:15 SP148.2 - Ways to outreach medical devices in low resource countries (LRC)
K Siddique Rabbani, Bangladesh

15:30 SP148.3 - South African-Swedish effort on pre-hospital diagnostics of stroke and traumatic injuries
Mikael Persson, Sweden

15:45 SP148.4 - A portable multi-frequency impedance measuring device for biodynamic analysis
Takao Nakamura, Japan

16:00 SP148.5 - A Study of the Challenges of Donating Medical Equipment to Developing Countries
Bill Gentles, Canada

16:15 SP148.6 - The Clinicopathologic Characters and Activity Survey of Sudden Death of Infant in a Depressed Economy: South-Eastern Nigeria Experience.
Gideon Ndubuka, Nigeria

SESSION TIME: 17:00 – 18:45

SESSION ROOM: 718A

SESSION TRACK: TRACK 01: IMAGING

SESSION NAME: SP149 – ITERATIVE RECONSTRUCTION

SESSION CHAIR(S): IDRIS ELBAKRI, CANADA
DMITRI MATENINE, CANADA

17:00 SP149.1 - Preliminary study on reduction of cartoon artifact in the iteratively reconstructed images from sparse projection views
Sunhee Wi, Republic of Korea

17:15 SP149.2 - Evaluation of the OSC-TV Reconstruction Algorithm for Optical Cone-Beam Computed Tomography
Dmitri Matenine, Canada

17:30 SP149.3 - Subjective low contrast performance of four CT scanners with iterative reconstruction
Azeez Omotayo, Canada

17:45 SP149.5 - Sparse-view image reconstruction with compressed sensing and its application in low dose CT myocardial perfusion imaging
Esmail Enjilela, Canada

18:00 SP149.6 - Feasibility study for 3D cone-beam computed tomography reconstruction with few projection data using MLEM algorithm with total variation minimization
Dong Hoon Lee, Republic of Korea

18:15 SP149.7 - A weighted stochastic gradient descent algorithm for image reconstruction in 3D computed tomography
Davood Karimi, Canada

18:30 SP149.8 - Investigation of sparse-angle view in cone beam computed tomography (CBCT) reconstruction algorithm using a sinogram interpolaton method
Dohyeon Kim, Republic of Korea

SESSION TIME: 17:00 – 18:45
 SESSION ROOM: 701B
 SESSION TRACK: TRACK 01: IMAGING
 SESSION NAME: SP150 – X-RAY PHASE CONTRAST & SCATTER IMAGING
 SESSION CHAIR(S): PAUL JOHNS, CANADA
 RHIANNON MURRIE, AUSTRALIA

- 17:00 SP150.1 - Reducing signal extraction artefacts for x-ray scatter imaging with multiple pencil beams
Paul Johns, Canada
- 17:15 SP150.2 - Live animal phase contrast x-ray velocimetry of the lungs: Optimising imaging speed for synchrotron and lab source imaging
Rhiannon Murrie, Australia
- 17:30 SP150.3 - X-ray Phase-Contrast imaging: from mammography to breast tomography using synchrotron radiation
Renata Longo, Italy
- 17:45 SP150.4 - 4 Years of X-ray Imaging at 05B1-1 Beamline at BMIT
Tomasz Wysokinski, Canada
- 18:00 SP150.5 - An energy dispersive bent Laue monochromator for K-edge subtraction imaging
Nazanin Samadi, Canada
- 18:15 SP150.6 - An incoherent implementation of x-ray phase contrast imaging and tomography that maintains high sensitivity at low delivered doses
Alessandro Olivo, United Kingdom
- 18:30 SP150.7 - Indirect measurement of average alveolar size using dynamic phase-contrast imaging
Mercedes Martinson, Canada

SESSION TIME: 17:00 – 19:00
 SESSION ROOM: 714B
 SESSION TRACK: TRACK 03: BIOMECHANICS AND ARTIFICIAL ORGANS
 SESSION NAME: SP151 – CARDIO MECHANICS & ORGANS
 SESSION CHAIR(S): DAVID MACKU, CZECH REPUBLIC

- 17:00 SP151.1 - **KEYNOTE:** Biomechanics and artificial organs
Birgit Glasmacher, Germany
- 17:30 SP151.2 - The Continuous Flow Total Artificial Heart in Clinical Practice
David Macku, Czech Republic
- 17:45 SP151.3 - Power Control Range of Operation for the Left Ventricular Assist Device in Bridge-to-Recovery Treatment
Marwan Simaan, United States

- 18:00 SP151.4 - An quantitative estimation method of peripheral perfusion by using a CCD camera during rotary blood pump support
Yasuyuki Shiraishi, Japan
- 18:15 SP151.5 - Mathematical Modeling of Left Ventricle Stroke Work Following Transcatheter Aortic Valve Replacement Associated With Paravalvular Leaks
Azadeh Saeedi, Canada
- 18:30 SP151.6 - Criteria to study Heart Failure derived from ESPVR
Rachad Shoucri, Canada
- 18:45 SP151.7 - Fluid Dynamics of Transcatheter Aortic Valve Associated with Paravalvular Leak
Azadeh Saeedi, Canada

SESSION TIME: 17:00 – 18:30
 SESSION ROOM: 718B
 SESSION TRACK: TRACK 04: RADIATION ONCOLOGY
 SESSION NAME: SP152 – SPECIAL TREATMENT TECHNIQUES: PART 2
 SESSION CHAIR(S): EMILY HEATH, CANADA
 CHARLES SHANG, UNITED STATES

- 17:00 SP152.1 - Optimal timing in concomitant chemoradiation therapy of colorectal tumors in nude mouse treated with Cisplatin and LipoplatinTM
Thititip Tippayamontri, Canada
- 17:15 SP152.2 - Grid therapy: impact of radiobiological models on calculation of therapeutic ratio
Hassan Ali Nedaie, Iran
- 17:30 SP152.3 - Will CyberKnife M6? Multileaf collimator offer advantages over IRIS? collimator in prostate SBRT?
Charles Shang, United States
- 17:45 SP152.4 - Retrospective analysis of treatment margins for stereotactic ablative lung cancer treatments based on 4D CBCT
Sheeba Thengumpallil, Switzerland
- 18:00 SP152.5 - Using surgical clips in the tracking of liver tumors applied to CyberKnife SBRT treatments
Leonie Petitclerc, Canada
- 18:15 SP152.6 - A Novel Couch-Gantry Trajectory Based Stereotactic Treatment Method
Byron Wilson, Canada

SESSION TIME: 17:00 – 18:45
 SESSION ROOM: 701A
 SESSION TRACK: TRACK 04: RADIATION ONCOLOGY
 SESSION NAME: SP153 – QUALITY ASSURANCE: PART 4
 SESSION CHAIR(S): YOUNG LEE, CANADA
 DAVID THWAITES, AUSTRALIA

- 17:00** SP153.1 - Comparison of AAA and CCC Algorithms for H&N RapidArc pre-patient treatment QA
Thuso Ramaloko, South Africa
- 17:15** SP153.2 - Tuning treatment planning system model parameters for accurate VMAT dose calculation using conformal arc plans
Orest Ostapiak, Canada
- 17:30** SP153.3 - Prostate brachytherapy with Oncentra Seeds: Intra-operative planning and delivery software validation assisted by an FMEA
Renee Larouche, Canada
- 17:45** SP153.4 - Investigation of predictive parameters for pre-treatment measurement pass rates in hypo-fractionated volumetric arc therapy (HF-VMAT) plans of single brain metastasis
Young Lee, Canada
- 18:00** SP153.5 - Inter-centre comparison of dose delivery accuracy for six different linac-planning system combinations for SBRT lung cancer treatment using FFF beams.
David Thwaites, Australia
- 18:15** SP153.6 - A pilot study investigating the impact of treatment delivery uncertainties for lung SABR using step and shoot IMRT and VMAT
David Thwaites, Australia
- 18:30** SP153.7 - Adaptive patient dose assessment using daily 3D cone beam CTs and Monte Carlo simulations
Nevin McVicar, Canada

SESSION TIME: 17:00 – 18:00
 SESSION ROOM: 716A
 SESSION TRACK: TRACK 05: DOSIMETRY AND RADIATION PROTECTION
 SESSION NAME: SP154 – DEVELOPMENTS IN RADIATION PROTECTION
 SESSION CHAIR(S): STEPHEN SAWCHUK, CANADA

- 17:00** SP154.1 - Out-of-field radiation dose to critical organs due to radiotherapy for testicular seminoma with modified dog-leg fields: is there a risk for stochastic effects?
Michalis Mazonakis, Greece
- 17:15** SP154.2 - Peripheral photon dose in organs
Beatriz Sanchez Nieto, Chile

- 17:30** SP154.3 - Gamma Radiation Dose-Response Relationship of Human Thyroid Follicular Cells
Shyamal Chakraborty, Bangladesh
- 17:45** SP154.5 - Aligning the ALARA principle with FFF treatment modalities
Stephen Sawchuk, Canada

SESSION TIME: 17:00 – 19:00
 SESSION ROOM: 715B
 SESSION TRACK: TRACK 05: DOSIMETRY AND RADIATION PROTECTION
 SESSION NAME: SP155 – CHARACTERIZATION OF DETECTOR SYSTEMS FOR THERAPY DOSIMETRY: PART 3
 SESSION CHAIR(S): DIANA ADLIENE, LITHUANIA

- 17:00** SP155.1 - Ferrous - methylthymol blue - gelatin gel dosimeter with improved auto-oxidation stability
Kalin Penev, Canada
- 17:15** SP155.2 - The dosimetric property of TLD2000 thermoluminescent dosimeter
Nan Zhao, People's Republic of China
- 17:30** SP155.3 - Application of 2D thermoluminescent dosimetry in QA test of Cyberknife
Renata Kopec, Poland
- 17:45** SP155.4 - Towards Optical CT scanning of radiochromic 3D dosimeters in mismatched refractive index solutions
Kurtis Dekker, Canada
- 18:00** SP155.5 - Development of a Novel Linear Energy Transfer Detector Using Doped Plastic Scintillators and Monte Carlo Simulation
Humza Nusrat, Canada
- 18:15** SP155.6 - Reduction of residual signal in LiF:Mg, Cu, P thermoluminescent material.
Vinod Nelson, Australia
- 18:30** SP155.7 - Application of dose gels in HDR brachytherapy
Diana Adliene, Lithuania
- 18:45** SP155.8 - Practical 3D QA for Radiation Therapy Based on High-Resolution Laser CT of Reusable Radiochromic Polymer-Gel Dosimeters in Dedicated Phantoms
Stephen Avery, United States

SESSION TIME: 17:00 – 18:45

SESSION ROOM: 715A

SESSION TRACK: **TRACK 07: SURGERY, COMPUTER AIDED SURGERY, MINIMAL INVASIVE INTERVENTIONS, ENDOSCOPY AND IMAGE-GUIDED THERAPY, MODELLING AND SIMULATION**

SESSION NAME: **SP156 – PATIENT-SPECIFIC MODELING AND SIMULATION IN SURGERY**

SESSION CHAIR(S): **KLAUS RADEMACHER, GERMANY
JIN LONG LIU, PEOPLE'S REPUBLIC OF CHINA**

- 17:00** SP156.1 - A Technique for Prostate Registration by Finite Element Modeling
Fangsen Cui, Singapore
- 17:15** SP156.2 - Modeling study of neo-aortic root for arterial switch operation: a structural finite element analysis
Zhaoyong Gu, People's Republic of China
- 17:30** SP156.3 - Preoperative in silico analysis of atherosclerotic calcification vulnerability in carotid artery stenting using Finite Element Analysis by considering Agatston score
Sadegh Riyahi Alam, Italy
- 17:45** SP156.4 - Biomechanical modeling for foot inversion
Junchao Guo, People's Republic of China
- 18:00** SP156.5 - Deformation Method and 3D Modeling of the female body to simulate Core Biopsy procedure
Lourdes Brasil, Brazil
- 18:15** SP156.6 - Effects of Band Position on Hemodynamics of Pulmonary Artery: A Numerical Study of Patient-specific Virtual Procedure
Jin Long Liu, People's Republic of China
- 18:30** SP156.7 - Experimentally validated Biomechanical Model of in vivo Lung under EBRT considering Diaphragm motion hysteresis
Elham Karami, Canada

SESSION TIME: 17:00 – 18:15

SESSION ROOM: 717B

SESSION TRACK: **TRACK 08: BIOSENSOR, NANOTECHNOLOGY, BIOMEMS AND BIOPHOTONICS**

SESSION NAME: **SP157 – BIOCHIPS AND BLOOD ANALYSIS**

SESSION CHAIR(S): **JONATHAN LOVELL, UNITED STATES**

- 17:00** SP157.1 - **KEYNOTE:** On-chip blood Plasma separation using vacuum-assisted micropumping for point-of-care application
Kwang Oh, United States
- 17:30** SP157.2 - Multi-Functional Platform for Blood Group Phenotyping using Surface Plasmon Resonance
Whui Lyn Then, Australia

17:45 SP157.3 - Harmonic generation microscopy investigation of human pathological samples for automated cancer determination
Richard Cisek, Canada

18:00 SP157.4 - Protein Patterning: An investigation on the use of different protein deposition techniques and parameters to transfer proteins onto various surfaces.
Kathryn Clancy, Canada

SESSION TIME: 17:00 – 19:00

SESSION ROOM: 717A

SESSION TRACK: **TRACK 17: EDUCATIONAL AND PROFESSIONAL ACTIVITIES**

SESSION NAME: **SP158 – EDUCATIONAL ACTIVITIES AND TRAINING IN MEDICAL PHYSICS**

SESSION CHAIR(S): **ANCHALI KRISANACHINDA, THAILAND
JOHN DAMILAKIS, GREECE**

- 17:00** SP158.1 - Medical Physics Residencies-101: The What's, Where's, and How's
Jeff Frimeth, Canada
- 17:15** SP158.2 - Education and Clinical Training of Medical Physics in Thailand
Anchali Krisanachinda, Thailand
- 17:30** SP158.3 - Radiation Protection in Medical Imaging and Radiation Oncology
Magdalena Stoeva, Bulgaria
- 17:45** SP158.4 - It's a Medical Physics World! Presenting the Official Bulletin of the International Organization for Medical Physics
Magdalena Stoeva, Bulgaria
- 18:00** SP158.5 - The new IOMP Professional Journal - Medical Physics International - first results
Slavik Tabakov, United Kingdom
- 18:15** SP158.6 - Two First Years of Reuniting, Engaging and Discovering: The Canadian Congress for Undergraduate Women in Physics
Madison Rilling, Canada
- 18:30** SP158.7 - Students' perspective on studying online at Heidelberg University, Germany (UHD)
Marcel Schaefer, Germany
- 18:45** SP158.8 - Launching of the ASEAN College of Medical Physics
Kwan Hoong Ng, Malaysia

SESSION TIME: 17:00 – 18:15
SESSION ROOM: 716B
SESSION TRACK: TRACK 19: BIOPHYSICS AND MODELLING
SESSION NAME: SP159 – TRANSPORT AND PHYSIOLOGICAL MODELLING
SESSION CHAIR(S): CHAI HONG YEONG, MALAYSIA

- 17:00** SP159.1 - **KEYNOTE:** Dwarfing Big Data for Oncology Applications: Necessity and Possibilities
Issam El Naqa, Canada
- 17:30** SP159.2 - Improved temperature monitoring and treatment planning for loco-regional hyperthermia treatments of Non-Muscle Invasive Bladder Cancer (NMIBC)
Gerben Schooneveldt, Netherlands
- 17:45** SP159.3 - A Full 3D CFD Model Coupled with an Outflow Lumped Boundary and Inflow Total Pressure Formulation to Estimate Human Cardiac Perfusion
Iyad Fayssal, Lebanon
- 18:00** SP159.4 - Simulation Model of Image-Guided Percutaneous Thermal Ablation in the Assessment of Optimal Approach for Complete Tumour Ablation
Chai Hong Yeong, Malaysia

SESSION TIME: 17:00 – 18:15
SESSION ROOM: 713B
SESSION TRACK: PRESIDENT'S CALL
SESSION NAME: SP160 – NEUROENGINEERING, NEURAL SYSTEMS / BIOPHYSICS AND MODELLING
SESSION CHAIR(S): VENKATESHWARLA RAJU, INDIA
TEODORO CORDOVA - FRAGA, MEXICO

- 17:00** SP160.1 - From 'Fracking' and 'Macrovoids' to the Onset of Cancer Metastasis: A Mechano-Metabolomics Model of a Plausible Fluid-Solid Network Instability in Tumors
Sai Prakash, United States
- 17:15** SP160.2 - Surface electromyography in quantifying Parkinson's disease and its treatment with deep brain stimulation
Pasi Karjalainen, Finlandia
- 17:30** SP160.3 - A Decade of Experience with Intraoperative Microelectrode Recording in Determining the Subthalamic Nucleus (STN) Deep Brain Stimulation? Lead Positions in 260 Parkinson Diseased Conditions in South India? A Retrospective Study
Venkateshwarla Raju, India
- 17:45** SP160.4 - Vortex of the Magnetic Field on the Growth Rate of Escherichia Coli
Teodoro Cordova - Fraga, Mexico
- 18:00** SP160.5 - Electro Magnetic Therapy and Laser in the Chronic Pain Of The Woman
Manuel Zuniga, Ecuador

SCIENTIFIC PROGRAM BY DAY

► Friday, June 12 2015

Friday, June 12 2015

SESSION TIME: 08:00 – 09:45

SESSION ROOM: 718A

SESSION TRACK: TRACK 01: IMAGING

SESSION NAME: SP161 – ANGIOGRAPHY / X-RAY IMAGING

SESSION CHAIR(S): JOSÉ CARLOS DE LA VEGA, CANADA
JEFF FRIMETH, CANADA

- 08:00 SP161.1 - 5D DSA Using Dual Energy Acquisition
Gabe Shaughnessy, United States
- 08:15 SP161.2 - Investigation of Rhenium-Doped
Microsphere-Based Contrast Agents for Diagnostic
X-Ray Imaging
José Carlos De La Vega, Canada
- 08:45 SP161.3 - Theoretical and experimental comparison
of image signal and noise for dual-energy subtraction
angiography and conventional x-ray angiography
Christiane Burton, Canada
- 09:00 SP161.4 - Some Physical and Clinical Factors
Influencing the Measurement of Precision Error, Least
Significant Change, and Bone Mineral Density in Dual-
Energy X-Ray Absorptiometry
Jeff Frimeth, Canada
- 09:15 SP161.5 - Use of Conventional Regional DXA Scans for
Estimating Whole Body Composition
Mohammad Reza Salamat, Iran
- 09:30 SP161.6 - Multiple Energy Synchrotron Biomedical
Imaging System? Preliminary Results
Bassey Bassey, Canada

SESSION TIME: 08:00 – 10:00

SESSION ROOM: 701B

SESSION TRACK: TRACK 01: IMAGING

SESSION NAME: SP162 – ULTRASOUND AND OCT: APPLICATIONS

SESSION CHAIR(S): DAVID GOERTZ, CANADA
WU QIU, CANADA

- 08:00 SP162.1 - Endoluminal Ultrasound Biomicroscopy for
in vivo detection of caustic esophagitis in rats
João Machado, Brazil

- 08:15 SP162.2 - To tap or not to tap: A comparison of cranial
3D to 2D ultrasound in extremely preterm neonates
with post-hemorrhagic ventricle dilation to predict the
necessity of interventional ventricular tap
Jessica Kishimoto, Canada
- 08:30 SP162.3 - Endoleak and Thrombus Characterization
with Dynamic Elastography after Endoleak
Embolization following Aneurysm Endovascular Repair
Antony Bertrand-Grenier, Canada
- 08:45 SP162.4 - Detecting lipid-rich artery plaque using a
handheld photoacoustic imaging device
Susumu Hirano, Japan
- 09:00 SP162.5 - Intersex differences in posterior eye chamber
by spectral optical coherent tomography
Zofia Drzazga, Poland
- 09:15 SP162.6 - Longitudinal Analysis of 3D Pre-Term
Neonatal Ventricle Ultrasound Images
Wu Qiu, Canada
- 09:30 SP162.7 - Breast Invasive Ductal Carcinoma Assessed
by Conventional Ultrasound and Contrast-Enhanced
Ultrasound in Different T-Stages
Yanchun Zhu, People's Republic of China
- 09:45 SP162.8 - Comparison of ultrasound systems in
scoliosis measurement
Maggie Hess, Canada

SESSION TIME: 08:00 – 10:00

SESSION ROOM: 716A

SESSION TRACK: TRACK 05: DOSIMETRY AND RADIATION
PROTECTION

SESSION NAME: SP163 – PRIMARY DOSIMETRY STANDARDS

SESSION CHAIR(S): NATALKA SUCHOWSKA, AUSTRALIA
RONALD TOSH, UNITED STATES

- 08:00 SP163.1 - **KEYNOTE:** Candidate Technologies for
Next-Generation Dosimetry Standards
Ronald Tosh, United States
- 08:30 SP163.2 - Absorbed dose to water measurements in a
clinical carbon ion beam using water calorimetry
Julia-Maria Osinga, Germany
- 08:45 SP163.3 - Results from the on-going key comparison
BIPM.RI(I)-K6 : What have we learned?
Susanne Picard, France
- 09:00 SP163.4 - Absorbed dose-to-water primary standard
and traceability system for radiotherapy in China
Kun Wang, People's Republic of China

- 09:30** SP163.5 - Design of an MRI-compatible water calorimeter for use in an integrated MRI-Linac and Gamma-Knife
Niloufar Entezari, Canada
- 09:45** SP163.6 - On the practical use of calorimetry for routine absolute dosimetry in the radiotherapy clinic
James Renaud, Canada

SESSION TIME: 08:00 – 09:45
 SESSION ROOM: 718B
 SESSION TRACK: TRACK 06: NEW TECHNOLOGIES IN CANCER RESEARCH AND TREATMENT
 SESSION NAME: SP164 – ADAPTIVE RADIATION THERAPY (ART)
 SESSION CHAIR(S): EVA BEZAK, AUSTRALIA
 DANIEL TAMAGI, CANADA

- 08:00** SP164.1 - Real-time dose reconstruction for adaptive radiation therapy
Martin Fast, United Kingdom
- 08:15** SP164.2 - Evaluation of unified intensity-modulated arc therapy (UIMAT) for the treatment of head-and-neck cancer
Michael Macfarlane, Canada
- 08:30** SP164.3 - A Hybrid IMRT/VMAT Technique for the Treatment of Nasopharyngeal Cancer
Nan Zhao, People's Republic of China
- 08:45** SP164.4 - Interactive real time adaptation of IMRT treatment plans
Cornelis Philippus Kamerling, United Kingdom
- 09:00** SP164.5 - A Hybrid IMRT/VMAT technique for the treatment of non-small cell lung cancer
Nan Zhao, People's Republic of China
- 09:15** SP164.6 - Offline adaptive VMAT - feasibility study using planning CT deformed electron density mapping on daily CBCT to estimate parotid dose volume relationship
Vellian Subramani, India
- 09:30** SP164.7 - Plan Optimization for a Lung Patient on a Parallel Linac-MR System
Daniel Tamagi, Canada

SESSION TIME: 08:00 – 09:15
 SESSION ROOM: 716B
 SESSION TRACK: TRACK 09: BIOSIGNAL PROCESSING
 SESSION NAME: SP165 – EEG
 SESSION CHAIR(S): JENS HAUEISEN, GERMANY
 TEODIANO BASTOS-FILHO, BRAZIL

- 08:00** SP165.1 - A Fully Unsupervised Clustering on Adaptively Segmented Long-term EEG Data
Vaclav Gerla, Czech Republic

- 08:15** SP165.2 - A Real-Time Clustered MUSIC algorithm for the localization of synchronous MEG/EEG source activity
Daniel Baumgarten, Germany
- 08:30** SP165.3 - Spatial harmonics for compressive sensing in electroencephalography
Jens Haueisen, Germany
- 08:45** SP165.4 - An Evaluation of Performance for an Independent SSVEP-BCI Based on Compression Sensing System
Teodiano Bastos-Filho, Brazil
- 09:00** SP165.5 - Multi-way based Source Localization of Multichannel EEG signals Exploiting Hilbert-Huang Transform
Saeed Pouryazdian, Canada

SESSION TIME: 08:00 – 10:00
 SESSION ROOM: 714B
 SESSION TRACK: TRACK 11: NEUROENGINEERING, NEURAL SYSTEMS
 SESSION NAME: SP166 – NEUROPROSTHESES
 SESSION CHAIR(S): PAUL YOO, CANADA

- 08:00** SP166.1 - Enhanced Transcutaneous Electrical Nerve Stimulation (eTENS): A Novel Method of Achieving Posterior Tibial Nerve Stimulation Therapy for Overactive Bladder
Paul Yoo, Canada
- 08:15** SP166.2 - Decreasing Upper Extremity Demands During Sitting Pivot Transfers for Individuals with Spinal Cord Injury by Utilizing Functional Electrical Stimulation
Stephanie Bailey, United States
- 08:30** SP166.3 - Design of Orthotic Mechanisms to Control Stand-to-Sit Maneuver for Individuals with Paraplegia
Ronald Triolo, United States
- 08:45** SP166.4 - Improved Peripheral Nerve Recording with a Small Form-Factor Nerve Cuff Electrode: A Computational Study
Parisa Sabetian, Canada
- 09:00** SP166.5 - Effect of stimulation on non-erect postures with a standing neuroprosthesis
Brooke Odle, United States
- 09:15** SP166.6 - Automatic Detection of Destabilizing Wheelchair Conditions for Modulating Actions of Neuroprostheses to Maintain Seated Posture
Ronald Triolo, United States
- 09:30** SP166.7 - Selecting Upper Extremity Command Signals to Modulate Electrical Stimulation of Trunk Muscles during Manual Wheelchair Propulsion
Stephanie Bailey, United States

SESSION TIME: 08:00 – 10:00
 SESSION ROOM: 715B
 SESSION TRACK: TRACK 12: MEDICAL DEVICES
 SESSION NAME: SP167 – GI AND GU
 SESSION CHAIR(S): FRANCO SIMINI, URUGUAY
 PHILIPPA MAKOBORE, UGANDA

- 08:00 SP167.1 - **KEYNOTE:** Medical Devices
Aaron Fenster, Canada
- 08:30 SP167.2 - Dielectric Properties of Urine for Diabetes Mellitus and Chronic Kidney Disease between 0.2 GHz and 50 GHz
Hua Nong Ting, Malaysia
- 08:45 SP167.3 - Intraoperative Bioelectrical Impedance Measurement for Assisting Segmental Renal Artery Clamping Partial Nephrectomy
Yu Dai, People's Republic of China
- 09:00 SP167.4 - Renal Volume Estimation by Ultrasound Parallel Scanning for Polycystic Kidney Disease Follow-up
Franco Simini, Uruguay
- 09:15 SP167.5 - Can Removal of Middle Molecular Uremic Retention Solutes be Estimated by UV-absorbance Measurements in Spent Dialysate?
Kai Lauri, Estonia
- 09:30 SP167.6 - Discrimination of prostate tissue with a combination of Raman spectroscopy and tactile resonance technology
Olof Lindahl, Sweden
- 09:45 SP167.7 - Appropriate Medical Devices for Low Resource Settings: Electronically Controlled Gravity-Feed Intravenous Infusion Set
Philippa Makobore, Uganda

SESSION TIME: 08:00 – 09:45
 SESSION ROOM: 717B
 SESSION TRACK: TRACK 12: MEDICAL DEVICES
 SESSION NAME: SP168 – HEALTH CHALLENGES IN RESOURCE-POOR NATIONS
 SESSION CHAIR(S): MLADEN POLUTA, SOUTH AFRICA
 KARIM S KARIM, CANADA

- 08:00 SP168.1 - **KEYNOTE:** Medical Devices
Adriana Velazquez Berumen, Switzerland
- 08:30 SP168.2 - Challenges of introducing health technologies to low resource settings in global framework: a case study at WHO
Cai Long, Switzerland
- 08:45 SP168.3 - Portable microwave based stroke and trauma diagnostics
Mikael Persson, Sweden

- 09:00 SP168.4 - Bending the cost curve: Towards a \$1000 diagnostic X-ray imager for scalable and sustainable healthcare
Karim S Karim, Canada
- 09:15 SP168.5 - Creating a Continental Network of Healthcare Innovation Centers: Collaborating across National Boundaries to design Devices and Best Practices
Fred Hosea, United States
- 9:30 SP168.6 - Towards a WHO List of Priority Medical Devices for Cancer Care, targeting low and middle income countries
Miriam Mikhail Lette, Switzerland

SESSION TIME: 08:00 – 09:45
 SESSION ROOM: 701A
 SESSION TRACK: TRACK 13: INFORMATICS IN HEALTH CARE AND PUBLIC HEALTH
 SESSION NAME: SP169 – SELF ENGAGEMENT, PATIENT EMPOWERMENT AND MHEALTH
 SESSION CHAIR(S): GIUSEPPE FICO, SPAIN
 ELENI KALDOUDI, GREECE

- 08:00 SP169.1 - **KEYNOTE:** Empowering patients through information technologies
Eleni Kaldoudi, Greece
- 08:30 SP169.2 - Distributed learning: developing a predictive model for dyspnea in lung cancer patients based on data from multiple hospitals
Johan Van Soest, Netherlands
- 08:45 SP169.3 - User Centered Design to incorporate predictive models for Type 2 Diabetes screening and management into professional decision support tools: preliminary results.
Giuseppe Fico, Spain
- 09:00 SP169.4 - Quantifying Bipolar Disorder for Technology-Assisted Self-Management
James Amor, United Kingdom
- 09:15 SP169.5 - Hippocratic Protocol Design to Improve Security and Privacy in Healthcare Applications for NFC Smartphone
Jose Pirrone Puma, Venezuela
- 09:30 SP169.6 - Extracting Intention from Web Queries? Application in eHealth Personalization
George Drosatos, Greece

SESSION TIME: 08:00 – 09:30

SESSION ROOM: 715A

SESSION TRACK: **TRACK 14: INFORMATION TECHNOLOGIES IN HEALTHCARE DELIVERY AND MANAGEMENT**

SESSION NAME: **SP170 – INFORMATION TECHNOLOGIES IN HEALTHCARE DELIVERY AND MANAGEMENT: PART 3**

SESSION CHAIR(S): **BRUCE CURRAN, UNITED STATES
JOSEPH CAFAZZO, CANADA**

- 08:00** SP170.1 - Wireless equipment localization for medical environments
Daniel Laqua, Germany
- 08:15** SP170.2 - Exploring Approaches to Optimise the Estimation of Preterm Birth Using Machine Learning Techniques
Monique Frize, Canada
- 08:30** SP170.3 - Smartwatch App as the Chest Compression Depth Feedback Device
Yujin Jeong, Republic of Korea
- 08:45** SP170.4 - Diagnosis of the corporal movement in Parkinson's Disease using Kinect Sensors
Jose Pirrone Puma, Venezuela
- 09:00** SP170.5 - A System to Support Regional Screening Programs to Identify School-age Children at Risk of Neurodevelopmental Disorders
Elsa Santos Febles, Cuba
- 09:15** SP170.6 - Support platform to decision making in research and technological development in public health: a brazilian scenario approach
Carlos Rocha, Brazil

SESSION TIME: 08:00 – 10:00

SESSION ROOM: 714A

SESSION TRACK: **PRESIDENT'S CALL**

SESSION NAME: **SP171 – CLINICAL ENGINEERING / PHYSICS, PATIENT SAFETY & IMAGING**

SESSION CHAIR(S): **GORDON CHAN, CANADA
VICTOR MALVAEZ, MEXICO**

- 08:00** SP171.1 - Properties Evaluation of Gd₂O₃-DEG as New Contrast Agent Nanomagnetic Particles Comparing to Gd-DTPA in MRI
Nader Riahi-Alam, Iran
- 08:15** SP171.2 - Imaging the Schlemm's Canal using an ultrahigh resolution spectral-domain optical coherence tomography working at 1.3 micrometer center wavelength
Masreshaw Bayleyegn, Ethiopia
- 08:30** SP171.3 - Technology Trayjectory Hybrid Tomography by Positron Emissions
Victor Malvaez, Mexico

08:45 SP171.4 - Myocardial perfusion imaging by low-dose CT

Sabee Molloy, United States

09:00 SP171.5 - Renal Dynamic Phantom for Use in SPECT
Divanizia Souza, Brazil

09:15 SP171.6 - Physics Plan Checking Practices
Gordon Chan, Canada

09:30 SP171.7 - Commissioning of a Flattening Filter Free
Satya Ranjan Saha, Bangladesh

09:45 SP171.8 - Effects of 24 hour Wakefulness on Tilt Based Targeting Tasks
Jeffrey Bolkhovsky, United States

SESSION TIME: 10:30 – 12:00

SESSION ROOM: 718A

SESSION TRACK: **TRACK 01: IMAGING**

SESSION NAME: **SP172 – MAMMOGRAPHY AND TOMOSYNTHESIS**

SESSION CHAIR(S): **ALESSANDRA TOMAL, BRAZIL
KWAN HOONG NG, MALAYSIA**

- 10:30** SP172.1 - **KEYNOTE:** Evaluation of automatic exposure control in digital mammography
Alessandra Tomal, Brazil
- 11:00** SP172.2 - Comparing the use of force-standardized and pressure-standardized mammographic compression protocols in an Asian context
Kwan Hoong Ng, Malaysia
- 11:15** SP172.3 - Radiation dose of step-and-shoot digital breast tomosynthesis using an anti-scatter grid compared to full field digital mammography in a clinical population
Cecile Jeukens, Netherlands
- 11:45** SP172.4 - Absorbed dose in PMMA and Equivalent Breast Phantom in a Digital Breast Tomosynthesis system: Monte Carlo Assessment
Luis Magalhães, Brazil

SESSION TIME: 10:30 – 11:45

SESSION ROOM: 701B

SESSION TRACK: **TRACK 01: IMAGING**

SESSION NAME: **SP173 – ULTRASOUND AND OCT: METHODS**

SESSION CHAIR(S): **BORNA MARAGHECHI, CANADA
WILLIAM HRINIVICH, CANADA**

- 10:30** SP173.1 - A comparison study on shear wave velocity estimation of thin layered media using shear wave imaging
Jun Keun Jang, Japan

- 10:45** SP173.2 - Temperature Dependence of Nonlinear Acoustic Harmonics in Water: Measurement and Simulation
Borna Maraghechi, Canada
- 11:00** SP173.3 - 3D trans-rectal ultrasound for high-dose-rate prostate brachytherapy: a comparison of sagittally-reconstructed 3D image volumes with sagittally-assisted axial image sets
William Hrinivich, Canada
- 11:15** SP173.4 - Understanding lung ultrasound artifacts using a phantom lung model
Justine Shuhui Loh, United Kingdom
- 11:30** SP173.5 - Accuracy of Tissue Elasticity Measurement using Shear Wave Ultrasound Elastography: A Comparative Phantom Study
Chai Hong Yeong, Malaysia

- 10:45** SP175.2 - Dosimetric and clinical benefits of conformal radiotherapy combined plus volumetric modulated arc therapy in the treatment of non-small cell lung cancer
Xiance Jin, People's Republic of China
- 11:00** SP175.3 - Non-uniform spatiotemporal fractionation schemes in photon radiotherapy
Jan Unkelbach, United States
- 11:15** SP175.4 - Compressed Sensing-Based LDR Brachytherapy Inverse Treatment Planning with Biological Models
Christian Guthier, Germany
- 11:30** SP175.5 - Investigation of Dosimetric and Biological Differences between Flattened and Unflattened Beams from the TrueBeam System
Bhudatt Paliwal, United States

SESSION TIME: **10:30 – 11:45**
SESSION ROOM: **701A**
SESSION TRACK: **TRACK 04: RADIATION ONCOLOGY**
SESSION NAME: **SP174 – MOTION MANAGEMENT: PART 2**
SESSION CHAIR(S): **JOANNA CYGLER, CANADA
PETA LONSKI, AUSTRALIA**

- 10:30** SP174.1 - Assessment of lung dose in patients undergoing deep inspiration breath hold for left sided breast cancer
Peta Lonski, Australia
- 10:45** SP174.2 - Evaluation of 4D dose accumulation in CyberKnife and IMRT treatments
Vincent Cousineau Daoust, Canada
- 11:00** SP174.3 - Application of RADPOS System for Dose and Position Quality Assurance of 4D CyberKnife Treatments
Raanan Marants, Canada
- 11:15** SP174.4 - Derivation of the probabilistic treatment margin for two targets with correlated motion
Marcel Van Herk, Netherlands
- 11:30** SP174.5 - How Truthful Is the 4D Dose Calculation?
Gang Liu, People's Republic of China

SESSION TIME: **10:30 – 11:45**
SESSION ROOM: **718B**
SESSION TRACK: **TRACK 04: RADIATION ONCOLOGY**
SESSION NAME: **SP175 – TREATMENT PLANNING – BIOLOGY & FRACTIONATION**
SESSION CHAIR(S): **JAN UNKELBACH, UNITED STATES**

- 10:30** SP175.1 - Adaptive radiotherapy for bladder cancer using deformable image registration of empty and full bladder
Prabhjot Juneja, Australia

SESSION TIME: **10:30 – 11:30**
SESSION ROOM: **716A**
SESSION TRACK: **TRACK 05: DOSIMETRY AND RADIATION PROTECTION**
SESSION NAME: **SP176 – CHARACTERIZATION OF DETECTOR SYSTEMS FOR THERAPY DOSIMETRY: PART 4**
SESSION CHAIR(S): **GEOFFREY IBBOTT, UNITED STATES
THORARIN BJARNASON, CANADA**

- 10:30** SP176.1 - Evaluation of surface dose distributions using ferrous benzoic xylenol orange translucent PVA cryogel radiochromic dosimeters
Molham Eyadeh, Canada
- 10:45** SP176.2 - Suitability of Diodes for Point Dose Measurements in IMRT/VMAT Beams
Tanya Kairn, Australia
- 11:00** SP176.3 - Development of a boron distribution monitor using prompt gamma-rays for boron neutron capture therapy
Hiroki Tanaka, Japan
- 11:15** SP176.4 - Study of potential effects of a strong magnetic field on radiation dosimeters (TLD, OSLD, EBT3 film, PRESAGE)
Geoffrey Ibbott, United States

SESSION TIME: **10:30 – 11:45**
SESSION ROOM: **716B**
SESSION TRACK: **TRACK 05: DOSIMETRY AND RADIATION PROTECTION**
SESSION NAME: **SP177 – RADIATION SHIELDING – DESIGN AND OUTCOMES**
SESSION CHAIR(S): **BORRAS CARI, UNITED STATES
PAULO COSTA, BRAZIL**

- 10:30** SP177.1 - Simple expression of x-ray doses below 1 MeV grazing incident on shields of concrete and iron backed by lead
Nobuteru Nariyama, Japan
- 10:45** SP177.2 - Evaluation of conversion coefficients from Air Kerma to Ambient Dose Equivalent for secondary barriers in diagnostic radiological facilities
Paulo Costa, Brazil
- 11:00** SP177.3 - Shielding photon beams to account for adjacent, underground building of a radiation therapy facility
Dario Sanz, Argentina
- 11:15** SP177.4 - Vectorization of the time-dependent Boltzmann transport equation for photon beams: applications in radiation shielding
Dario Sanz, Argentina
- 11:30** SP177.5 - The use of FLUKA Monte Code in the re-design of radiotherapy mazes with the use of lead cladding of a few mm thickness
Ihsan Al-Affan, United Kingdom

SESSION TIME: **10:30 – 12:15**
 SESSION ROOM: **714B**
 SESSION TRACK: **TRACK 11: NEUROENGINEERING, NEURAL SYSTEMS**
 SESSION NAME: **SP178 – NEUROIMAGING, NEURONAVIGATION AND NEUROLOGICAL DISORDERS**
 SESSION CHAIR(S): **TAUFIK VALINATE, CANADA**

- 10:30** SP178.1 - Characterization of Single Units in Human Neocortical Slices Maintained In Vitro
Sara Mahallati, Canada
- 10:45** SP178.2 - Astrocytes enhance neuronal long term potentiation in a biophysical model of epilepsy
Vasily Grigorovsky, Canada
- 11:00** SP178.3 - Influence of the 'sympathetic slump' on biomechanics of the sympathetic trunk
Liesbeth Van Hauwermeiren, Belgium
- 11:15** SP178.4 - Superparamagnetic Nanoparticles for Epilepsy Detection
Ebrahim Ghafar-Zadeh, Canada
- 11:30** SP178.5 - Automatic detection of epileptic seizures in scalp EEG
Yasser Pérez, Cuba
- 11:45** SP178.6 - Beta/Theta Neurofeedback Training Effects in Physical Balance of Healthy People
Wenya Nan, People's Republic of China
- 12:00** SP178.7 - Potential Benefits in Comparing the Neural Control Networks Studies Between the Oculomotor and Cardiac Pacing Systems
Michael Cheng, Canada

SESSION TIME: **10:30 – 11:30**
 SESSION ROOM: **715B**
 SESSION TRACK: **TRACK 12: MEDICAL DEVICES**
 SESSION NAME: **SP179 – MEDICAL DEVICES: MISCELLANEOUS**
 SESSION CHAIR(S): **KLAUS RADERMACHER, GERMANY**

- 10:30** SP179.1 - Acceptance Test of the first Hospital Cyclotron for Production of PET tracers in Iran
Pardis Ghafarian, Iran
- 10:45** SP179.2 - HiFEM - An Integrated Approach for Human Centered Risk Management for Medical Devices
Klaus Radermacher, Germany
- 11:00** SP179.3 - Ultrasonic Microscanning for Digital Dental Impressioning
Klaus Radermacher, Germany
- 11:15** SP179.4 - A study on prefrontal blood flow in patients with moderate dementia and severe dementia using near -infraredinfrared
Shingo Takahashi, Japan

SESSION TIME: **10:30 – 11:30**
 SESSION ROOM: **715A**
 SESSION TRACK: **TRACK 14: INFORMATION TECHNOLOGIES IN HEALTHCARE DELIVERY AND MANAGEMENT**
 SESSION NAME: **SP180 – INFORMATION TECHNOLOGIES IN HEALTHCARE DELIVERY AND MANAGEMENT: PART 4**
 SESSION CHAIR(S): **BRUCE CURRAN, UNITED STATES
JOSEPH CAFAZZO, CANADA**

- 10:30** SP180.1 - Increasing efficiency of data transfer in WBANs
Luka Celic, Croatia
- 10:45** SP180.2 - Decision support system for no common emergency in a big city with intelligent routing algorithm and attention quality parameters evaluation.
Lupe Toscano, Peru
- 11:00** SP180.3 - Development of a Multi-Center Clinical Trial Data Archiving and Analysis Platform
Brandon Driscoll, Canada
- 11:15** SP180.4 - Global Health Catalyst: A systematic Space-time compression platform for catalyzing global health collaborations in Radiation Oncology
Wilfred Ngwa, United States

POSTERS

The IUPESM 2015 Posters will be displayed in the Exhibit Hall during open hours.

Presenting Author Stand By Time:

Presenters are request to stand by their posters during the networking breaks scheduled **10:00 - 10:30 and 16:30 - 17:00 Monday, June 8 to Thursday, June 11.**

PS01 – TRACK 01: IMAGING

PS01.001 – A discontinuity artefact at the isocenter of on-board CBCT images

Elsayed Ali, Canada

PS01.002 – Correction of Metal Artefacts Induced from Pacemaker and ICD Leads in CT-Based Attenuation Correction of Cardiac SPECT data

Mohammad Reza Ay, Iran

PS01.003 – Anthropomorphic Phantom of the Pancreas for Scintillation Camera Tests

Lourdes Brasil, Brazil

PS01.004 – Comparing two image processing techniques, Wavelet and Segmentation by threshold, for detecting microcalcifications in an image mammographic.

Lourdes Brasil, Brazil

PS01.005 – Measuring red blood cell velocity in capillary using video and image processing

Surapong Chatpun, Thailand

PS01.006 – Development of a Quantitative PET QA Procedure for Multi-Center Clinical Trials

Brandon Driscoll, Canada

PS01.007 – Unwrapping highly wrapped phase using Nonlinear Multi-Echo phase unwrapping

Chemseddine Fatnassi, Switzerland

PS01.008 – Investigation of optimal display size for viewing MRI images using a digital contrast-detail phantom

Hideki Fujita, Japan

PS01.009 – Investigation of presampled MTF using a slit device with slightly wider aperture

Rumi Gotanda, Japan

PS01.010 – 3D Tumor delineation in Positron Emission Tomography reconstructed images restored by the use of Lucy Richardson blind deconvolution method

Albert Guvenis, Turkey

PS01.011 – Different options for stimulation intensity in mapping cortical motor area in navigated transcranial magnetic stimulation

Petro Julkunen, Finland

PS01.012 – Software Breast Phantom for Phase Contrast Imaging Applications

Nicolas Pallikarakis, Greece

PS01.013 – Actions for Implementation Program of Image Quality of Mammography

Ana Cláudia Patrocínio, Brazil

PS01.014 – Evaluating Techniques of Transformation Intensity for Contrast Enhancement in Mammographic Images

Ana Cláudia Patrocínio, Brazil

PS01.015 – Influence of Contrast Enhancement to Breast Density Classification by Using Sigmoid Function

Ana Cláudia Patrocínio, Brazil

PS01.016 – Evaluation of the difficulties of the learning process of mammographic readings

Ana Cláudia Patrocínio, Brazil

PS01.017 – Non-deterministic optimization using Differential Evolution algorithm to launch seeds for liver segmentation in MDCT

Ana Cláudia Patrocínio, Brazil

PS01.018 – Influence of ROI pattern on segmentation in lung lesions

Ana Cláudia Patrocínio, Brazil

PS01.019 – Comparison between Elliptical and Squared ROI to Launch an Automatic Seed to Region Growing Algorithm on Hepatic Segmentation using CT images

Ana Cláudia Patrocínio, Brazil

PS01.020 – Gd-based Nanoparticles Mediated Magnetic Field Enhancement Inside Homogenous Tissue: Simulation using Finite Element Method

Nader Riyahi-Alama, Iran

PS01.021 – Novel Cylindrical Source Tank for Inserts of Emission Computed Tomography Phantoms

Inayatullah Sayed, Malaysia

PS01.022 – Linear tomosynthesis with flat-panel detector for image guided radiation therapy

Tae-Suk Suh, Republic of Korea

PS01.023 – Evaluation of image quality and dose for digital breast tomosynthesis (DBT) using a semi-analytical model

Alessandra Tomal, Brazil

PS01.024 – Optimization of acquisition parameters of the test of an overall SPECT/CT system performance.

Piotr Tulik, Poland

PS01.025 – Dosimetric Analysis of Patient to a Z-Gradient Coil in Head Magnetic Resonance Imaging

Shoogo Ueno, Japan

PS01.026 – A Novel Optical System for Contrast Enhancement in Histological Plates to Be Processed Digitally

Rubiel Vargas-Canas, Colombia

PS01.027 – Pixel-based dynamic contrast-enhanced CT study with low temporal resolution

Ivan Yeung, Canada

PS01.028 - Method for restoring CT images obtained at low doses

Marlen Perez-Diaz, Cuba

**PS02 – TRACK 02:
BIOMATERIALS AND
REGENERATIVE MEDICINE**

PS02.001 – Chitosan: A Chitinous Biopolymer For The Treatment Of Crude Oil Polluted Water

Eillen Agoha, Nigeria

PS02.002 – Temperature of ice formation affects integrity of alginate 3D constructs after cryopreservation

Birgit Glasmacher, Germany

PS02.003 – Influence of proteins on magnesium in vitro degradation

Birgit Glasmacher, Germany

PS02.004 – Electrospinning of vascular prostheses with anti-kinking properties

Birgit Glasmacher, Germany

PS02.005 – Electrospinning of polycaprolactone/chitosan polymeric fibrous membranes as scaffolds for cardiovascular tissue engineering applications

Birgit Glasmacher, Germany

PS02.006 – Coaxial electrospinning of piezoelectric PVDF/PCL scaffolds for nerve regeneration

Birgit Glasmacher, Germany

PS02.007 – Bio rapid prototyping project: Evaluation of spheroid formation for cells construct

Takeshi Shimoto, Japan

PS02.008 – Scaffold Prototype for Heart Valve Tissue Engineering: Design and Material Analyses

Marcia Simbara, Brazil

PS02.009 – Unidirectionally-frozen silk/gelatin scaffolds for cardiac tissue engineering

Siew-Lok Toh, Singapore

PS02.010 – Engineering Mesenchymal Stromal Cells (MSCs) to be More Immuno-evasive by Altering Cell Culture Conditions

Sowmya Viswanathan, Canada

PS02.011 – Novel zwitterionic polypeptides for improving resistance to non-specific protein adsorption

Xiaojuan Wang, People's Republic of China

PS02.012 – Study on preparation and mechanical properties of polyurethane foam with negative Poisson's ratio

Lizhen Wang, People's Republic of China

PS02.013 – Proliferation of cardiomyocytes in neonatal, future implication in heart regeneration

Lincai Ye, People's Republic of China

PS02.014 – Synergetic effects of released ions from CaO-MgO-SiO₂-based multiphase bioceramics on osteogenic proliferation and differentiation

Meng Zhang, People's Republic of China

PS02.015 – Cooling Rate Effects on the Microstructure Evolutions of Biodegradable Mg2Ca Potential Medical Implant Alloy

Li Li Zhou, People's Republic of China

**PS03 – TRACK 03:
BIOMECHANICS AND
ARTIFICIAL ORGANS**

PS03.001 – Musculoskeletal and Finite Element Simulation of Archery

Yahia Al-Smadi, United States

PS03.002 – Dysfunction Screening in Experimental Arteriovenous Grafts for Hemodialysis Using Inflow and Outflow Hemodynamic Game Analysis

Wei-Ling Chen, Chinese Taipei

PS03.003 – The Effects of Limb Dominance, Sex, and Gait Speed on Multisegment Foot Kinematics During Gait

Victoria Chester, Canada

PS03.004 – Investigation of transfibular locking plate to treat open extra-articular distal tibia fractures

Helena Greene, Canada

PS03.005 – Kinematic analysis after total hip arthroplasty during weight-bearing activities

Satoru Ikebe, Japan

PS03.006 – Estimation of Compressive and Shear Forces on Lumbar Spine during Lifting by Wii Balance Board

Hieyong Jeong, Japan

PS03.007 – A biomechanical evaluation of a novel pedicle screw-based interspinous device used to stabilize the lumbar spine

Yu-Shu Lai, Chinese Taipei

PS03.008 – Hematological, Biochemical, and End-organ effects of the CH-VAD in Ovine Model

Changyan Lin, People's Republic of China

PS03.009 – Novel Low-Profile External Fixator with Simple Locking Mechanism Compared with Commercial Available External Device Could Provide Better Stability in Multicycle Dynamic Loadings

Kang-Ping Lin, Chinese Taipei

PS03.010 – A simple external fixation technique for treating bicondylar tibial plateau fracture: a finite element study

Kang-Ping Lin, Chinese Taipei

PS03.011 – Numerical analysis of the elaborate sound amplification mechanism of the mammalian inner ear

Michio Murakoshi, Japan

**PS04 – TRACK 04
RADIATION ONCOLOGY**

PS04.001 – Image-Guided Intra-arterial Delivery of Yttrium-90 Radioactive Microspheres for the Treatment of Liver Tumors

Muthana Al-Ghazi, United States

PS04.002 – Commissioning of an ASI EPID for patient specific IMRT QA.

David Alonso Fernández, Cuba

PS04.003 – Status of Radiotherapy Treatment in Lebanon

Antar Aly, Qatar

PS04.004 – Verification of VMAT Arc Radiation Therapy Technique for Full Scalp Treatment

Cynthia Araujo, Canada

PS04.005 – Estimating Setup Margins using IGRT Techniques. Preliminary results in Havana

Raul Argota, Cuba

PS04.006 – Uncertainty evaluation of radiation treatment with DIBH for left-sided breast cancer using MV cine imaging

Jae Beom Bae, Republic of Korea

PS04.007 – Evaluation of the Applicability of Pinpoint ion chamber for Dosimetric Quality Assurance of SRS

Jong Geun Baek, Republic of Korea

PS04.008 – Development of a VARIAN 600 C/D Linear Accelerator model using MCNPX 2.6 Monte Carlo code.

Jorge Batista Cancino, Brazil

PS04.009 – A Comparison of Dosimetric Characteristic Between Integrated and Cine Acquisition Modes of a-Si EPID

Omern Bawazeer, Australia

PS04.010 – Predicting clinical outcomes in locally-advanced non-small cell lung cancer using machine learning focusing on tumor and node imaging features

Nathan Becker, Canada

PS04.011 – Risk estimate of second primary cancers after breast radiotherapy

Eva Bezak, Australia

PS04.012 – A beam angle optimization technique for proton pencil beam scanning treatment planning of lower pelvis targets

Janid Blanco Kiely, United States

PS04.013 – Neutron-Photon mixed field dosimetry by TLD700 glow curve analysis and its implementation in dose monitoring for Boron Neutron Capture Therapy (BNCT) treatments

Esteban Boggio, Argentina

PS04.014 – Boron Neutron Capture Therapy (BNCT) neutron beam at RA-6 reactor: Quality Assurance and Quality Control

Esteban Boggio, Argentina

PS04.015 – Improved Pareto navigation using a plan database with segmented plans

Rasmus Bokrantz, Sweden

PS04.016 – Automated measurement of dwell and tandem position in ring HDR applicators

Bruno Carozza, Canada

PS04.017 – eMU Whisperer: An application for assessing patient surface topology and its impact on monitor units in electron beam therapy

Paule Charland, Canada

PS04.018 – Beam modeling of the flattening filter-free beams for VMAT SBRT using the collapsed cone convolution superposition algorithm

Samju Cho, Republic of Korea

PS04.019 – Dependence of Collimator Angle on Prostate VMAT: A Treatment Planning Study

James Chow, Canada

PS04.020 – Dosimetry of Pacemaker in VMAT for Lung SBRT

James Chow, Canada

PS04.021 – Determination of ion chamber correction factors for small composite fields used by the CyberKnife radiosurgery system

Eric Christiansen, Canada

PS04.022 – One-year review of a real-time, ultrasound-based, single-fraction prostate HDR program ? the Halifax experience

Krista Chytyk-Praznik, Canada

PS04.023 – Retrospective evaluation of visually monitored deep inspiration breath hold for breast cancer patients using edge detection

Leigh Conroy, Canada

PS04.024 – DECT Tissue Characterisation and Artefact Suppression Method for Improved Dose Calculations in Brachytherapy Treatments.

Nicolas Cote, Canada

PS04.025 – Radiotherapy Planning using CEER and CADPLAN in a Prostate Cancer Patient

Juan Alberto Cruz, Brazil

PS04.026 – Impact of increasing irradiation time on the treatment of prostate cancers

Alexandru Dasu, Sweden

PS04.027 – Hemi-body Electron irradiation: Development and Verification of this new technique

Panagiotis Delinikolas, Greece

PS04.028 – Deformable image registration and automatic contouring using Cone-Beam CT imaging : A study of volume statistics and similarity measures

Olivier Fillion, Canada

PS04.029 – Acceptance Modulated Radiation Intensity and Enhanced Dynamic Wedge using 2D Ion Chamber Array

Oscar Garcia Contreras, Colombia

PS04.030 – Dose Calculation in Gynecological Brachytherapy using Monte Carlo simulation for intracavitary treatment of Cervical Cancer

Oscar Garcia Contreras, Colombia

PS04.031 – An inverse treatment planning module for Gamma Knife® Perfexion? using 3D Slicer

Kimia Ghobadi, Canada

PS04.032 – Bladder and rectum DVH prediction: a statistical approach for prostate treatment

Frédéric Girard, Canada

PS04.033 – Retrospective evaluation of applicator localization for HDR cervix brachytherapy ? A comparison of MR versus CT

Lisa Glass, Canada

PS04.034 – A general source model for clinical linac heads in photon mode

Wilfredo González, Spain

PS04.035 – Measurement of the beam quality TPR_{20,10} of small radiotherapy fields: Comparison of experimental measurements and Monte Carlo simulations

Eduardo González-Villa, Mexico

PS04.036 – The Effect of Assessment Criteria on Inter-rater Variability in the Evaluation of Skin Reactions following Breast Cancer Radiation Therapy

Riya Goyal, United States

PS04.037 – Two-dimensional probability density function presenting the pre-treatment variability of the rectal wall integrating the variability of the motion of the rectum and the rectal wall thickness

Grigor Grigorov, Canada

PS04.038 – Unbiased Assessment of Detail Detectability in Image Guided Radiation Therapy

Victor Gurvich, United States

PS04.039 – Assessing radiation protection of members living close to patients with implanted 125I seeds in prostate

Takashi Hanada, Japan

PS04.040 – Improvement of MV planar image by elimination of Compton scattered photons and re-projection as primary photons

Masatsugu Hariu, Japan

PS04.041 – Determination of exit fluence by MCNP4 code for IMRT treatment fields and its validation with a conventional EPID system

Benjamin Hernandez Reyes, Mexico

PS04.042 – Accuracy in simulating tumor translation and rotation: Commissioning a motion platform, Hexamotion for tumor motion management QA

Chen-Yu Huang, Australia

PS04.043 – Dosimetric impact of the Acuros XB Algorithm for 25 lung SABR patients treated using the TrueBeam FFF 6MV

Derek Hyde, Canada

PS04.044 – Dynamic resource allocation: Investigating ways to distribute resources in a patient cohort based on plan quality

Elin Hynning, Sweden

PS04.045 – Physical plan evaluation of Head and Neck Cancer at Square Hospital, Bangladesh.

Md. Anwarul Islam, Bangladesh

PS04.046 – IAEA multicentre study of the methodology for advanced dosimetry audit: single IMRT field dose delivery

Joanna Izewska, Austria

PS04.047 – Electron Density Measurements of Metallic Implants with Cobalt-60 Computed Tomography

Christopher Jechel, Canada

PS04.048 – A Systematic Analysis Of The Error Sources Within The CyberKnife M6 Daily AQA Test

Kevin Jordan, United States

PS04.049 – The Use of Boron Neutron Capture Therapy in the Treatment of Cancer Tumours in the Czech Republic

Ivana Jurickova, Czech Republic

PS04.050 – Partial Arc Breast Boost

Tania Karan, Canada

PS04.051 – Determination of the optimal phase for respiratory gated radiotherapy from statistical analysis using a visible guidance system

Sung Kyu Kim, Republic of Korea

PS04.052 – Dosimetric Verifications of the Output Factors in the Small Field less than 3 cm² using the Gafchromic EBT2 films and the Various Detectors

Sung Kyu Kim, Republic of Korea

PS04.053 – Methodology to Evaluate Combined EBRT and HDR Brachytherapy for Cervical Cancer using Equivalent Uniform Dose (EUD) and Tumor Control Probability (TCP)

Yusung Kim, United States

PS04.054 – International Multi-Institutional Bench Mark Study on Dosimetric and Volumetric Modulation using Helical Tomotherapy Treatment Planning for Malignant Pleural Mesothelioma Tumors

Tommy Knöös, United States

PS04.055 – Factors predicting of local relapse in irradiated patients with breast cancer: A Syrian Cohort study

Moussa Krayem, Syria

PS04.056 – Automated Routine Quality Assurance of VMAT

Michael Lamey, Canada

PS04.057 – Evaluation of the clinical usefulness of modulated Arc treatment

Young Kyu Lee, Republic of Korea

PS04.058 – A comparison of linac-based IMRT with helical tomotherapy for craniospinal irradiation

Young Lee, Canada

PS04.059 – A Hardware-Accelerated Software Platform for Adaptive Radiation Therapy

Junghoon Lee, United States

PS04.060 – Predicting the Impact of Surgery on Quality of Life and Risk Management in Patients Afflicted with Glioblastoma Multiforme

Luca Li, Canada

PS04.061 – A memetic algorithm for body gamma knife stereotactic radiotherapy treatment planning

Bin Liang, People's Republic of China

PS04.062 – Gamma evaluation of dose distributions from newly developed dosimetry system for helical tomotherapy

Sangwook Lim, Republic of Korea

PS04.063 – Suitability of a Light Transparent and Electrically Conductive Glass Plate for Construction of a Beam Monitor for Radiation Therapy

Xun Lin, Canada

PS04.064 – Objective assessment of skin erythema caused by radiotherapy

Hiroaki Matsubara, Japan

PS04.065 – Nasopharyngeal carcinoma tumor response to induction chemotherapy followed by concurrent chemo-radiotherapy: A volumetric magnetic resonance imaging study

Nevin McVicar, Canada

PS04.066 – Volumetric Modulated Arc Therapy of Pancreatic Cancer: Dosimetric Advantages as Compared to 3D Conformal Radiation Treatment

Xiangyang Mei, Canada

PS04.067 – Application of ExacTrack BrainLab system for Choroidal melanoma treatments using Stereotactic Radiotherapy and a not invasive immobilization system

Artur Menezes, Brazil

PS04.068 – Dosimetric evaluation of deliverable and navigated Pareto optimal plans generated with Multi-Criteria Optimization

Raphaël Moeckli, Switzerland

PS04.069 – 2D and 3D Approximate Entropy Algorithms for On-line Quantification of Threshold Structure Content in Large Radiotherapy Image Data

Christopher Moore, United Kingdom

PS04.070 – Dosimetric effects of seed positioning uncertainties in ophthalmic plaque brachytherapy

Hali Morrison, Canada

PS04.071 – A Method for Evaluating Deformable Dose Accumulation in RayStation

Joanne Moseley, Canada

PS04.072 – Dosimetric comparison between 3D CRT, full Arc and Partial Arc Vmat techniques in the management of locally advanced lung Cancer using External Beam Radiation Therapy (EBRT).

Samir Mouatassim, Morocco

PS04.073 – Dosimetric and clinical considerations for implementing CBCT based adaptive planning using RayStation

Bongile Mzenda, New Zealand

PS04.074 – A Statistical Study based on comparison between two treatment planning systems while exporting RT structure set

Kamlesh Passi, India

PS04.075 – The Characteristics and Implementation of XR-RV3 Gafchromic Film for Radiotherapy Dosimetry

Supriyanto Ardjo Pawiro, Indonesia

PS04.076 – Weighted comprehensive score evaluation of CBCT image guided positioning accuracy in lung cancer radiation treatment

Yinglin Peng, People's Republic of China

PS04.077 – MCNP Simulation of Leksell Gamma Knife Using Disk Sources for Different Phantom Materials

Ma. Vanessa Francheska Perianes, Philippines

PS04.078 – Dosimetric comparison between RAPIDARC and 3DCRT planning in extremity soft tissue sarcoma

Yannick Poirier, Canada

PS04.079 – Cerebral Functional Alterations Before and After Intensity-Modulated Radiation Therapy in Patients with Nasopharyngeal Carcinoma

Wenting Ren, People's Republic of China

PS04.080 – A Study of Accuracy from Varian Portal Dosimetry for VMAT Patient Specific QA using Monte Carlo

Mohamad Rhani, Singapore

PS04.081 – A study on improvement method of dose distribution using bolus in boron neutron capture therapy for head and neck tumors

Yoshinori Sakurai, Japan

PS04.082 – Peripheral neutron dose estimation: comparison between experimental measurements and TPS estimation

Beatriz Sanchez Nieto, Chile

PS04.083 – Dual Energy X-ray Stereoscopic Image Guidance for Spine SBRT

Mike Sattarivand, Canada

PS04.084 – Comparison between our EPID-IMRT-QA tool and commercial phantom based QA tools

Otto Sauer, Germany

PS04.085 – Dosimetric assessment of a novel metal artifact reduction tool (IMAR)

Andrea Schwahofer, Germany

PS04.086 – An Image quality and dose comparison between Varian OBI and Elekta XVI CBCT systems.

Amani Shaaer, Canada

PS04.087 – An open-source treatment planning system for research in particle therapy: Implementation and dosimetric evaluation

Gregory Sharp, United States

PS04.088 – GMM guided automated Level Set algorithm for PET image segmentation

Chiara Soffientini, Italy

PS04.089 – Impact of the magnitude of MLC radiation leakage in IMRT treatment planning

Jaziel Soto-Muñoz, Mexico

PS04.090 – Modelling multi-leaf collimator defocusing and focal spot partial shielding for TomoTherapy and Elekta accelerators using Monte Carlo methods

Ryan Studinski, Canada

PS04.091 – Can Image-Guided Intensity Modulated Brachytherapy delivery be better than IMRT and classical brachytherapy methods for cervical cancer: A Dosimetric analysis

Vellaiyan Subramani, India

PS04.092 – Analysis on Volumetric and Dosimetric accuracy of Maximum-Intensity Projections based 4DCT for stereotactic body Radiotherapy

Vellaiyan Subramani, India

PS04.093 – 2D/3D registration for compensation of patient positioning error in Korea Heavy Ion Medical Accelerator Center

Tae-Suk Suh, Republic of Korea

PS04.094 – Cardiac movement in deep inspiration breath-hold for left-breast cancer radiotherapy

Tae-Suk Suh, Republic of Korea

PS04.095 – Dosimetric evaluation according to patient set-up errors using biophysical indices in whole breast irradiation

Tae-Suk Suh, Republic of Korea

PS04.096 – Comparison of proton boron fusion therapy with boron neutron capture therapy

Tae-Suk Suh, Republic of Korea

PS04.097 – Verification for prompt gamma ray imaging during proton boron fusion therapy: A Monte Carlo study

Tae-Suk Suh, Republic of Korea

PS04.098 – Feasibility study of flattening filter free beam for stereotactic ablative radiotherapy of localized prostate cancer patients

Tae-Suk Suh, Republic of Korea

PS04.099 – The evaluation of radiobiological and physical impacts based on multi-modality images using in-house software

Tae-Suk Suh, Republic of Korea

PS04.100 – Comparison of Conventional 3D Static Planning and 4D Planning using Dose Warping Technique for Liver SBRT

Tae-Suk Suh, Republic of Korea

PS04.101 – Monte Carlo Design and Simulation of a Grid-type Multi-layer Pixel Collimator for Radiotherapy: Feasibility Study

Tae-Suk Suh, Republic of Korea

PS04.102 – Feasibility study of patient alignment method using tactile array sensors

Tae-Suk Suh, Republic of Korea

PS04.103 – Analysis of motion-induced dose errors according to the tumor motion in helical tomotherapy

Tae-Suk Suh, Republic of Korea

PS04.104 – Drift correction techniques in the tracking of lung tumor motion

Peng Teo, Canada

PS04.105 – Application and Parametric Studies of a Sliding Window Neural Network for Respiratory Motion Predictions of Lung Cancer Patients

Peng Teo, Canada

PS04.106 – VMAT delivery through couch tops: an illustration of loss of dose coverage for prostate plans

Monique Van Prooijen, Canada

PS04.107 – Edge Detection for Automated Biological Tumor Volume Definition Based on FDG-PET/CT-fused Imaging: An Agar Phantom study

Stella Veloza, Colombia

PS04.108 – Comparison between HybridARC and sliding windows IMRT for Spine SBRT tumor

Daniel Venencia, Argentina

PS04.109 – real time dynamic prostate brachytherapy dose calculations using permanent ¹²⁵I implants: technical description and preliminary experience

Daniel Venencia, Argentina

PS04.110 – Design of a simple device for end to end test of IGRT system using ExacTrac

Daniel Venencia, Argentina

PS04.111 – Study on the use of an in-house device to consider the motion effects on absorbed dose determination and measurements using different calculation algorithms in lung SBRT cases

Victor Villamares-Vargas, Mexico

PS04.112 – In-vivo skin dose evaluation for Pd-103 permanent breast radiotherapy implants

Jose Villarreal-Barajas, Canada

PS04.113 – Dosimetric Variations in Permanent Breast Seed Implant (PBSI) Evaluated at Different Arm Positions using Deformable Image Registration

Elizabeth Watt, Canada

PS04.114 – Minimum Planning Target Volume Coverage Necessary for the Delivery of the Prescribed Dose in Lung Radiotherapy

Marcin Wierzbicki, Canada

PS04.115 – A modified methodology to accurately validate CT number constancy for proton therapy

Richard Wu, United States

PS04.116 – Development of a real-time portable applicator monitoring system for gynecologic intracavitary brachytherapy

Junyi Xia, United States

PS04.117 – Quality Assurance of the Radiotherapy Workflow Integrating a Dedicated Wide-bore 3T MRI Simulator

Aitang Xing, Australia

PS04.118 – Evaluation of deformable accumulated parotid doses using different registration algorithms in adaptive head and neck radiotherapy

Shouping Xu, People's Republic of China

PS04.119 – Optimization of brain metastases radiotherapy with TomoHDA

Slav Yartsev, Canada

PS04.120 – A Rapid Learning Approach for the Knowledge Modeling of Radiation Therapy Plan

Lulin Yuan, United States

PS04.121 – Plan comparison and delivery verification for intracranial stereotactic treatments using Varian TrueBeam STx linac

Sergei Zavgorodni, Canada

PS04.122 – A method to convert cone-beam computed tomography (CBCT) image for dose calculation and the phantom evaluation

Guangshun Zhang, People's Republic of China

PS04.123 – Phantom-based evaluations of two binning algorithms for four-dimensional CT reconstruction in lung cancer radiation therapy

Fuli Zhang, People's Republic of China

PS04.124 – Thermoluminescent dosimetry of the model BT-125-1 ¹²⁵I interstitial brachytherapy seed

Nan Zhao, People's Republic of China

PS05 – TRACK 05: DOSIMETRY AND RADIATION PROTECTION

PS05.005 – Dose analysis for paediatric patients under cardiac catheterization at Hamad General Hospital in Qatar. A.E.Aly, H.A. Al-Saloos, H.M. Al Naemi Hamad Medical Corporation, Qatar

Antar Aly, Qatar

PS05.006 – In vivo dosimetry implementation with diodes at the National Radiotherapy Center of the Korle-Bu Teaching Hospital, Ghana

Vivian Della Atuwu-Ampoh, Ghana

PS05.007 – Assessment of radiation dose due to radio frequency emitted from medical high voltage modules

Mohammad Reza Ay, Iran

PS05.008 – Software Assisted Skin Dose Calculation in Fluoroscopically Guided Interventional Procedures

Mohamed Badawy, Australia

PS05.009 – Current Status of a-Si EPID Dosimetry: An Application for Dose Verification in Standard Radiotherapy Techniques

Omemh Bawazeer, Saudi Arabia

PS05.010 – Nanodosimetry of protons in the Bragg peak region based on ionisation cross sections of DNA constituents

Daniel Bennett, Germany

PS05.011 – Micronuclei assessment of Selenium and Vitamin E radioprotective effects in human lymphocytes

Vahid Changizi, Iran

PS05.012 – The Organ and Skin Dose Distribution in Total Body Irradiation

Samju Cho, Republic of Korea

PS05.013 – Comparison of 6MeV and 9MeV Electron Beams for Total Skin Irradiation

Ricardo Contreras, Guatemala

PS05.014 – Analysis of Informal Commerce Sunglasses using Spectroscopy

Juan Alberto Cruz, Brazil

PS05.015 – Dosimetric Evaluation Of Lung Dose Using Indigenously Developed Respiratory motion phantom

G Dheva Shantha Kumari, India

PS05.016 – Activation of Medical Linear Accelerators

Adam Dodd, Canada

PS05.017 – Assessment of Patient Dose in Selected Non-Cardiac Interventional Fluoroscopy Procedures Using OSL Dosimeters

Isabel Elona, PH

PS05.018 – Measurement of Photon and Neutron Dose Distribution in Cyclotron Bunker During F18 and N13 Production

Pardis Ghafarian, Iran

PS05.019 – Energy response of the GAFCHROMIC EBT3 in diagnosis range

Rumi Gotanda, Japan

PS05.020 – Estimation of In Vivo Dosimetry Accuracy with Dose-Volume Histogram

Victor Gurvich, United States

PS05.021 – Evaluation of the dosimetric properties of water equivalent microDiamond detector in high energy photon beam.

Hyun Do Huh, Republic of Korea

PS05.022 – From simple to advanced dosimetry audits in radiotherapy: IAEA coordinated research

Joanna Izewska, Austria

PS05.023 – Noise reduction of radiochromic film: median filter processing of subtraction image

Toshizo Katsuda, Japan

PS05.024 – Proposed Guidelines for Image Quality in Chest PA X-Ray Examinations in Bangladesh

Shahed Khan, United Kingdom

PS05.025 – Evaluation of inhomogeneity correction using monte carlo simulation in stereotactic body radiation therapy (SBRT)

Ji Na Kim, Republic of Korea

PS05.026 – Dosimetric effect of low dose 4D CT by a commercial iterative reconstruction on dose calculation in radiation treatment planning: A phantom study

Hee Jung Kim, Republic of Korea

PS05.027 – An Evaluation of the Use Factor for CyberKnife using Clinical Data

Dong Han Lee, Republic of Korea

PS05.028 – Lung Dose Estimation for a Total Body Computed Tomography Protocol

Juliana Martins, Brazil

PS05.029 – Verification of axial dose distributions with radiochromic films for a translational Total Body Irradiation technique

Ignasi Mendez, Slovenia

PS05.030 – Experimental assessment of out-of-field dose components in high-energy electron beams used in external-beam-radiotherapy

Mohamad Mohamad Alabdoaburas, France

PS05.031 – Dosimetric study for a set iodine-125 seeds using radiochromic films in solid water plates

Arnaldo Mourao Filho, Brazil

PS05.032 – Evaluation of bismuth shielding use in cervical spine CT scans

Arnaldo Mourao Filho, Brazil

PS05.033 – Scanning irradiation of microbeam x-rays in ionization chambers as micro-scale dose analysis tool

Nobuteru Nariyama, Japan

PS05.034 – Dosimetric verification of the scatter integration algorithm of MIRS treatment planning system for photon dose calculations

Hassan Ali Nedaie, Iran

PS05.035 – Characterisation of EPSONV700 flatbed scanner for EBT3 Gafchromic film dosimetry.

Vinod Nelson, Australia

PS05.036 – Nanodosimetric parameters obtained using the Monte Carlo codes PARTRAC, PTra and Geant4-DNA: a comparison study

Heidi Nettelbeck, Germany

PS05.037 – A method to reduce the patient's eye lens dose during cerebral angiography procedures

Kwan Hoong Ng, Malaysia

PS05.038 – Bremsstrahlung generating and shielding by the source of the beta ray

Hiroki Ohtani, Japan

PS05.039 – Angular dependence of absorption spectrum of Gafchromic® EBT2 film

SoAh Park, Republic of Korea

PS05.040 – Patient dose audit in mammography

Grisel Paula, Portugal

PS05.041 – Experience in implementing a dosimetric registry in an oncological facility of a developing country

Sandra Rocha Nava, Mexico

PS05.042 – Effects of irradiation with low and high doses using in vivo rats: analysis of trace elements in blood using SR-TXRF

Camila Salata, Brazil

PS05.043 – Effects of cable extension and photon irradiation on TNRD neutron detector in radiotherapy

Beatriz Sanchez Nieto, Chile

PS05.044 – Thermoluminescence dosimetry (TLD) for in vivo dosimetry in radiation therapy with high single doses

Andrea Schwahofer, Germany

PS05.045 – Study of the response of ionization chambers in photon beams for off-axis point dose

Tetsunori Shimono, Japan

PS05.046 – Analysis of gamma evaluation according to low-dose threshold on VMAT QA

Tae-Suk Suh, Republic of Korea

PS05.047 – Dosimetric accuracy of Acuros XB dose calculation algorithm on an air cavity for EBT3 Gafchromic film

Tae-Suk Suh, Republic of Korea

PS05.048 – Evaluation of Dosimetric Effects on Metal Artifact: Comparison of Dose Distributions Affected by Patient Teeth and Implants

Tae-Suk Suh, Republic of Korea

PS05.049 – Advancement of Dedicated Phantom to demonstrate Dosimetric Effect of Metal Artifact in Head and Neck Cancer

Tae-Suk Suh, Republic of Korea

PS05.050 – Accuracy of radionuclide generation simulation using Antisymmetrized Molecular Dynamics (AMD)

Masaaki Takashina, Japan

PS05.051 – Accurate small field dosimetry requires systematic consistent approaches to measurement, modelling and data reporting.

David Thwaites, Australia

PS05.052 – Determination of Radon/Thoron Concentrations in Some Iraqi Building Materials By Using CR ?39

Abdulredha Younis, Iraq

PS05.053 - Evaluation of Scattered Dose Reduction in Interventional Radiology Using Lead-Free Protection Sheets

Chai Hong Yeong, Malaysia

**PS06 – TRACK 06:
NEW TECHNOLOGIES IN
CANCER RESEARCH AND
TREATMENT**

PS06.001 – GEANT4 versus MCNP5: Monte-Carlo ophthalmic brachytherapy dosimetry in the presence of gold nanoparticles for 125I and 103Pd

Somayeh Asadi, Iran

PS06.002 – Clinical Implementation of an Elekta HexaPOD evo RT Couchtop with kV Cone beam Image Guided Radiation Therapy

Cathy Neath, Canada

PS06.003 – Ex-vivo experimental study with a new cluster-type microwave ablation antenna

Qun Nan, People's Republic of China

PS06.004 – Bio Magnetic Nano Particles (BMNPs) used for cancer treatment via Hyperthermia method

Amirsadegh Rezazadeh Nochehdehi, Iran

PS06.005 – Active control of microbubbles in flow using position and phase variations in three-dimensional acoustic field

Kohji Masuda, Japan

PS06.006 – GATE Monte Carlo Simulation for Dual Head LINAC Modeling

Seungwoo Park, Republic of Korea

PS06.007 – Adaptive radiation therapy of pancreatic cancer patients treated using Tomotherapy: Validation of dose accumulation algorithms using deformable image registration in SlicerRT

Eric Vorauer, Canada

**PS07 – TRACK 07:
SURGERY, COMPUTER AIDED SURGERY, MINIMAL INVASIVE INTERVENTIONS, ENDOSCOPY AND IMAGE-GUIDED THERAPY, MODELLING AND SIMULATION**

PS07.001 – Predictive Fluoroscopy: Minimizing Radiation Dose in Planning Endovascular Therapy for Intracranial Aneurysms

John Baxter, Canada

PS07.002 – Automatically Better Segmentation

John Baxter, Canada

PS07.003 – Utilizing stream feature in GPU Monte Carlo Code to simulate photon Radiotherapy

Yakub Bayhaqi, Indonesia

PS07.004 – The influence of two different drug infusion profiles on the pharmacodynamics model performance

Ana Ferreira, Portugal

PS07.005 – Robotic positioning system of ultrasound transducer for ultrasonic therapy

Shinya Onogi, Japan

PS07.006 – Force Modeling of MRI-Compatible Robot for Pediatric Bone Biopsy

Peyman Shokrollahi, Canada

PS07.007 – Comparing the Effects of Three MRI RF Sequences on Ultrasonic Motors

Peyman Shokrollahi, Canada

**PS08 – TRACK 08:
BIOSENSOR, NANOTECHNOLOGY, BIOMEMS AND BIOPHOTONICS**

PS08.002 – Novel Optical Method to Determine Glass Transition Temperature of Polymers

Yao-Xiong Huang, People's Republic of China

PS08.003 – The Comparison of Temporal Change between Typically Developing Children and Children with ADHD in Rotational Motion Speed of Arms

MIKI Kaneko, Japan

PS09 – TRACK 09: BIOSIGNAL PROCESSING

PS09.001 – Sensitivity of heart rate variability indices for artificially simulated data

Anna Alulova, Russian Federation

PS09.002 – The Smoothness of a signal as a new feature in Signal Averaged Electrocardiogram that can be used in cardiac electrophysiology diagnosis.

Mohammad Reza Ay, Iran

PS09.003 – Comparison of the Three Filter Algorithms for Detection of Electrically-Evoked Short-Latency Responses in Retinal Ganglion Cells.

Myounghwan Choi, Republic of Korea

PS09.004 – Photoacoustic Speckle and Spectral analysis of Vasculature Trees

Muhannad Fadhel, Canada

PS09.005 – The algorithm for the diagnosis of ventricular tachycardias from electrocardiogram

Martin Holub, Czech Republic

PS09.006 – Modelling of Platelet and White Blood Cell in Dengue Patients using Bioelectrical Impedance Analysis technique

Fatimah Ibrahim, Malaysia

PS09.007 – Combination of Multiple Signal Processing Techniques for Multi-class Motor Imagery Detection using Mu Rhythm

Rina Kojima, Japan

PS09.008 – The comparison of severity assessment methods of kinetic tremor in Parkinson's disease using wearable sensors

Hong Ji Lee, Republic of Korea

PS09.009 – Unobstructive blinking detection wearable device utilizing transparent conductive ITO film for smartphone users to prevent of computer vision syndrome

Jeong Su Lee, Republic of Korea

PS09.010 – A Simple, CO₂-Based Method to Reconstruct the Molar Mass of the Dried Respiratory Gas within a New Double-Tracer Single Breath Washout

Johannes Port, Germany

PS09.011 – Mirror Movements in Writer's Cramp? A Study with Multi-Channel EMG

Venkateshwarla Raju, India

**PS10 – TRACK 10:
REHABILITATION MEDICINE, SPORTS MEDICINE, REHABILITATION ENGINEERING AND PROSTHETICS**

PS10.001 – Human Knee Simulation Using CMAC ANN

Lourdes Brasil, Brazil

PS10.002 – Development of New Method to Create In-school Tactile Maps for Visually Impaired Children

Kouki Doi, Japan

PS10.003 – Experimental Study on Usability Evaluation of a Hydraulic Jack Lever

Kouki Doi, Japan

PS10.004 – Neuromuscular Reconnection Methodology By Cap Sense Absorption And Diffusion Signal

Ricardo Jaramillo Diaz, Colombia

PS10.005 – The Development of an Isokinetic Adapter for Prosthesis Users*Usha Kuruganti, Canada***PS10.006 – High Density Electromyography (EMG) for Improved Prosthesis Control***Usha Kuruganti, Canada***PS10.007 – Influence of Spaces between Tactile Dot Patterns and Raised Boundary Line on Tactile Guide Map Line Perceptibility***Harumi Matsumori, Japan***PS10.008 – Influence of Dot Distances on Discrimination of Dot Patterns in Tactile Guide Maps***Harumi Matsumori, Japan***PS10.009 – Statistical Evaluation of Objectivisation of Rehabilitation Process***Iva Novotná, Czech Republic***PS10.010 – Satisfactory Vibrating Conditions of Latissimus Dorsi Tendon to Induce Illusory Horizontal Shoulder Flexion***Yumi Umesawa, Japan***PS10.011 – Satisfactory Vibrating Conditions of Extensor Digitorum Tendon to Induce Illusory Finger Flexion***Yumi Umesawa, Japan***PS10.012 – Prefrontal Brain Activity of Goal Keeper when Penalty Kick***Masaki Yoshida, Japan***PS10.013 – Effect of the moderate high pressure circumstances to metabolism***Masaki Yoshida, Japan*

PS11 – TRACK 11: NEUROENGINEERING, NEURAL SYSTEMS**PS11.001 – Objective Evaluation of Likes and Dislikes by Prefrontal Blood Flows***Miho Asano, Japan***PS11.002 – Robotic Wheelchair Commanded by People with Disabilities Using Low/High-Frequency SSVEP-based BCI***Teodiano Bastos-Filho, Brazil***PS11.003 – Quantifying and overcoming the effect of distractions on cognitive load and brain-computer interface (BCI) performance: Implications for real-world BCI use and cognitive neuroscience***Zahra Emami, Canada***PS11.004 – How Mental Strategy Affects Beta/Theta Neurofeedback Training***Pedro Antonio Mou, Macao***PS11.005 – Stimulations to Basal Ganglia and the Efficiency of Microminiaturized Electrode Recording (MER) to Quantify STN Neurons with Deep Brain Stimulator (DBS)? the Lead Point in Parkinson Diseased Conditions***Venkateshwarla Raju, India***PS11.006 – SCHIZOPHRENIA: Interaction between factors***Bernadete Voichcoski, Brazil*

PS12 – TRACK 12: MEDICAL DEVICES**PS12.001 – Challenges and opportunities in home-based monitoring of cardiac dynamics***Yashodhan Athavale, Canada***PS12.002 – Application of Support Vector Machines in Intelligent Monitoring of Cardiovascular Health on a Mobile Device***Omar Boursalie, Canada***PS12.003 – Design and Implementation of the Software for Multi-parameter Patient's Monitor***Maite Cañizares, Cuba***PS12.004 – Strategy and Tools for Validation of QRS Detection Algorithms in Real Time ECG Monitors***Maite Cañizares, Cuba***PS12.005 – Basic Study on Variability of Measured Data from Touch Test Using Semmes-Weinstein Monofilaments***Manabu Chikai, Japan***PS12.006 – Design and construction of temperature and humidity control channel for a bacteriological incubator***Carlos Duharte, Cuba***PS12.007 – High-Reliability Nerve Stimulator For Aiding Regional Anesthesia Procedures***Carlos Ferri, Brazil***PS12.008 – A study of pressure-volume characteristics of the cuff for hemodynamic parameters measurement***Jan Havlík, Czech Republic***PS12.009 – Format for National Inventory of the Genomic Technology***Beatriz Hernandez, Mexico***PS12.010 – Development of the bedridden person support system using Kinect.***Kouhei Ichimura, Japan***PS12.011 – Quantitative sensory testing using lateral skin stretch at the foot for simple screening of diabetic neuropathy***Shuichi Ino, Japan***PS12.012 – A development of the robot hand for the disability which include sensory feedback.***Tomohiro Iwaki, Japan***PS12.013 – Motor cortical excitability enhanced by paired-pulse transcranial magnetic stimulation with biphasic pulse-form***Petro Julkunen, Finland***PS12.014 – Quality management systems for medical devices in the production of hospital beds***Ivana Jurickova, Czech Republic***PS12.015 – Value of information analysis for use in health technology assessment***Ivana Jurickova, Czech Republic***PS12.016 – Development of a Software Tool for Quick Re-entrainment of the Circadian Pacemaker***Zahra Kazem-Moussavi, Canada***PS12.017 – Which one is better in detecting the speed and quantity of intravenous infusion in the hospital, transmissive or reflective optical method?***Hyun-woo Lee, Republic of Korea***PS12.018 – The effect of stented valve oversizing on hemodynamic flow in the diseased right atrium***Hwa Liang Leo, Singapore*

PS12.019 – Device trial to improve blood flow rate with controlled pressure for blood flow at venous side in single needle dialysis

Yasuyuki Miwa, Japan

PS12.020 – An Embedded Software Solution for Rest ECG Devices

Gisela Montes De Oca, Cuba

PS12.021 – Development of innovative gas phase sterilization technology for nucleolytic degradation

Toshihiko Okazaki, Japan

PS12.022 – Ultrasound Modular Platform: a general purpose open architecture system for medical imaging research

Haroldo Onisto, Brazil

PS12.023 – Design and Preliminary Validation of a Dual Mechanical-Anthropomorphic Breast Phantom with Inclusions

Shigeto Ono, United States

PS12.024 – Evaluation and Analysis of the Results of a prototype Medical Device Vigilance System (MEDEVIPAS)

Nicolas Pallikarakis, Greece

PS12.025 – Medical Device Development – Risk Management

Mayur Patel, United Kingdom

PS12.026 – Analysis of the terminology to name medical devices used in Intensive Care Units – ICUs

Pamela Ribeiro, Brazil

PS12.027 – Determination of Breath Acetone in 298 Type 2 Diabetic Patients using a Ringdown Breath Acetone Analyzer

Meixiu Sun, United States

PS12.028 – A study of the differences between uncompressed sound source and compressed sound source gives EEG of human

Takashi Suzuki, Japan

PS12.029 – Evaluation of the interface pressure characteristics over a temperature regulating air-mattress under different surgical positions

Eric Tam, People's Republic of China

PS12.030 – Continuous cuff-less estimation of systolic blood pressure from pulse wave transit time measured in a chair

Toshiyo Tamura, Japan

PS12.031 – A development of the pressure distribution display which is used in robot hand for the disability

Kenya Tanaka, Japan

PS12.032 – Prototype Development Generating Vacuum for Treating Chronic Wounds Negative Pressure Level Laboratory

Edison Vazquez-Gordillo, Mexico

PS12.033 – Tunable Irradiation System for Corneal Collagen Cross-linking

Liliane Ventura, Brazil

PS12.034 – Electromagnetic high-hydrous gel phantom at a low-frequency band -Improvement in the electrical characteristics by using a carbon microcoil and investigation of its mechanism-

Takahiko Yamamoto, Japan

PS12.035 – Examination of Bisphenol A Elution Concentration in Dialyzers

Yoshihisa Yamashita, Japan

PS12.036 – Automation of a Dispersive Raman Spectrometer Using LabVIEW Aiming In Vivo Diagnosis of Skin Cancer

Renato Zangaro, Brazil

PS12.037 – Effectiveness of Ozone-Liquid Mass Transfer aiming Ozone Therapy

Renato Zangaro, Brazil

PS12.038 - Impedance plethysmograph based on reconfigurable hardware for the study of superficial vessels

Laura Castro Acevedo, Cuba

PS12.039 - The study for bioelectric properties of tissue and organ measured by electrical impedance

Toshiaki Nagakura, Japan

PS13.003 – Becoming of Ubiquitous Sensors for Ubiquitous Healthcare

Sergo Dadunashvili, Georgia

PS13.004 – Design and Implementation of an Application for ECG processing in Mobile Phones

René González-Fernández, Cuba

PS13.005 – A Telemedicine System to follow-up the Evolution of Chronic Diseases in the Community

René González-Fernández, Cuba

PS13.006 – Developing an Appropriate and Affordable Expert System for Medical Diagnosis (ESMD) in Developing Countries

Kenneth Nkuma-Udah, Nigeria

PS13.007 – Assessment of Mobile Health Applications

Nicolas Pallikarakis, Greece

PS13.008 – An Investigation into using Pulse Rate Variability to Predict Clinical Events

Usman Raza, Canada

PS13.009 – A simple device producing electrolyzed water for home care

Koichi Umimoto, Japan

PS13.010 – Developing predictive models using retrospective study of liver cancer patients treated with radiation therapy.

Jason Vickress, Canada

PS13.011 – A Study on the Problems for People to have Colorectal Cancer Screening Tests in Japan?-From the Results of Interviews for 30 Adults-

Naoko Fujiwara, Japan

PS14 – TRACK 14: INFORMATION TECHNOLOGIES IN HEALTHCARE DELIVERY AND MANAGEMENT

PS14.001 – DermApp: an application for Android mobile devices for reception and transmission of skin images

Iván Escalona, Venezuela

PS14.002 – Use of mobile devices for prevention in youngsters of risk factors common to chronic noncommunicable diseases

Iván Escalona, Venezuela

PS13 – TRACK 13: INFORMATICS IN HEALTH CARE and PUBLIC HEALTH

PS13.001 – A Method for Parental Engaged Consent in the Perpetual Secondary Usage of Health Big Data

Yvonne Choi, Canada

PS13.002 – RENEM? Brazilian National List of Equipment and Materials

Murilo Contó, Brazil

PS14.003 – Telemedicine in the Universidad Católica Andrés Bello (UCAB), Venezuela: an academic experience

Iván Escalona, Venezuela

PS14.004 - Passage from analog to digital in radiodiagnostic processes

Paola Freda, Italy

**PS16 – TRACK 16:
CLINICAL ENGINEERING,
CLINICAL PHYSICS, AND
PATIENT SAFETY**

PS16.001 – Increasing the health value per dollar spent: How Human Factors can help inform procurement of healthcare technology

Sandra Ahedo, Spain

PS16.002 – Using Heuristic Analysis to support Usability Evaluation of a low risk medical device under development process

Ana Almeida, Brazil

PS16.003 – First Contact with Human Factors and Usability Evaluation in a Junior Research Project by a Biomedical Engineering Student

Ana Almeida, Brazil

PS16.004 – Non-Contact Measurement of Arterial Compliance (NCMAC)

Delran Anandkumar, United Kingdom

PS16.005 – Developing a Quantitative Performance Assurance Risk Classification Model within a Generalized Risk Scoring System

Vishvek Babbar, Canada

PS16.006 – Project Management for Clinical Engineering? Considerations in the evaluation and acquisition of medical equipment for health services in Brazil

Lourdes Brasil, Brazil

PS16.007 – Human Factors for Health Technology Safety: A new book on incorporating Human Factors into the work of biomedical technology professionals

Andrea Cassano-Piche, Canada

PS16.008 – Politics, value and risk: a system to allocate medical equipment funding

Peter Cook, United Kingdom

PS16.009 – Magnetic Resonance system configuration and editing tools

Danilo Da Silva, Brazil

PS16.010 – The Unintentional Irradiation of a Live Human Fetus During a CT Scan: a case study

Jeff Frimeth, Canada

PS16.011 – Device reconditioning service for home-based assistance. How to choose the right approach.

Ernesto Iadanza, Italy

PS16.012 – Approach to the management of infusion systems in hospitals

Ernesto Iadanza, Italy

PS16.013 – A Basic Study on the Measurement of Electromagnetic Fields in a New University Hospital Building Before and After the Hospital Opened

Kai Ishida, Japan

PS16.014 – IAEA database of national dosimetry audit networks for radiotherapy

Joanna Iżewska, Austria

PS16.015 – Telehealth – Achieving its Promise in 2015

Thomas Judd, United States

PS16.016 – The New Japanese Guidelines for Use of Mobile Phones in Hospitals

Takashi Kano, Japan

PS16.017 – Study on Medical Equipment Location Systems that use RFID Technology

Manabu Kawabe, Japan

PS16.018 – Development of a Regional Prioritization Process for Diagnostic Imaging Equipment Replacements

Petr Kresta, Canada

PS16.019 – Implantable Medical Devices: more Safety with Traceability and Surveillance

Paolo Lago, Italy

PS16.020 – Using standard test methods to ensure quality and maximize supply of personal protective equipment in a time of global emergency response

Ying Ling Lin, Canada

PS16.021 – Creation of a system for the coding of medical devices

Alessio Luschi, Italy

PS16.022 – Establishment of Radiation Qualities for Radiodiagnostics in LCR/ UERJ According to IEC 61267 and TRS 457

Luis Magalhaes, Brazil

PS16.023 – A Healthcare Facilities Qualitative and Multivariate Quantitative Assessment Methodology for Mongolia

Claudio Meirovich, Spain

PS16.024 – Practice of HB-HTA on the Study of HIFU Technology for the Treatment of Prostate Cancer and Uterine Fibroma

Roberto Miniati, Italy

PS16.025 – A Simulation Based Model for Planning Operating Theater Activity in Complex Hospitals: Case Study in Orthopedics

Roberto Miniati, Italy

PS16.028 – Risk management tool in the application HFMEA in purge sector on the Material and Sterilization Centers.

Sérgio Mühlen, Brazil

PS16.029 – Generate health and wealth by innovation

Mayur Patel, United Kingdom

PS16.030 – Validating and comparing Methods for testing Endothelial Function

Ragu Prakash Ratnakumaran, United Kingdom

PS16.031 – Reliability Indicators in the Medical Equipment Management

Renato Garcia Ojeda, Brazil

PS16.032 – Methodology for Safety Movement of Clinical Facilities Focused in Oncology

Sandra Rocha Nava, Mexico

PS16.033 – Design of a remote use ECG with an Optical Communication System (FSO) for Telemedicine Applications

Raul Rodriguez-Aleman, Mexico

PS16.034 – Adverse events and death related to the use of the MRI equipment

Ricardo Sá, Brazil

PS16.035 – Adverse events and injuries related to the use of the MRI equipment

Ricardo Sá, Brazil

PS16.036 – Investigation on solar aging in sunglasses by developing of automated prototype for sun exposure of lenses

Homero Schiabel, Brazil

PS16.037 – Integral clearance of medical rooms based on the type of medical treatment ensures a safe environment upon first use

Casper Smit, Netherlands

PS16.038 – Real-Time Posture Classification and Correction based on a Neuro-Fuzzy Control System

Pedro Vieira, Portugal

PS16.039 – Management of electromagnetic interferences in healthcare facilities – A Review

Gnahoua Zoabli, Canada

PS16.040 – Hospital Mode Design in Smartphones and Tablets for Wireless Security in Healthcare Facilities

Gnahoua Zoabli, Canada

PS17 – TRACK 17: EDUCATIONAL AND PROFESSIONAL ACTIVITIES

PS17.001 – A discipline about Human Factors Engineering and Usability applied to Medical Devices for under graduation courses using Active Learning techniques

Ana Almeida, Brazil

PS17.002 – The medical equipment management inside the accreditation process: a comparison with the Brazilian accredited hospitals

Rodrigo Almeida, Brazil

PS17.003 – The Medical Physics M.Sc. program at the National University of Mexico: Results and lessons learned after 100+ graduates

María-Ester Brandan, Mexico

PS17.004 – An Experience on the dosimetry of HDR Brachytherapy Treatment Planning of Cervical Carcinoma at BPKM Cancer Hospital, Nepal

Surendra Chand, Nepal

PS17.005 – Health IT Education for Clinical Engineers

Thomas Judd, United States

PS17.006 – Professional Development of Medical Physicists in Radiation Oncology for the Commonwealth of Independent States

Marina Kislyakova, Russian Federation

PS17.007 – Assistive Technologies in Biomedical Engineering Education

Lenka Lhotska, Czech Republic

PS17.008 – Future-Proofing Physics and Engineering in Medicine

Kwan Hoong Ng, Malaysia

PS17.009 – Nuclear and Radiological Emergencies – First IAEA Training Course for Medical Physicists

Fridtjof Nuesslin, Germany

PS17.010 – Academic Real Time Digital Medical Image Processing Environment

Ana Cláudia Patrocínio, Brazil

PS17.011 – Detection of Eye Movement; possibility how to control world

Lukas Peter, Czech Republic

PS17.012 – Artificial Neural Network Interactive Activation and Competition Model Service-Oriented Applied to Health

Lourdes Mattos Brasil, Brazil

PS17.013 – Career Progression for Medical Physicists

William Round, New Zealand

PS17.014 – IOMP-W ? the International Organization for Medical Physics Women Subcommittee

Magdalena Stoeva, Bulgaria

PS17.015 – AAPM/IOMP Used Equipment Donation Program

Mohammed Zaidi, United States

PS18 – TRACK 18: GENDER, SCIENCE AND TECHNOLOGY

PS18.001 – Bone density measurements in strontium-rich bone-mimicking phantoms using quantitative ultrasound

Bisma Rizvi, Canada

PS19 – TRACK 19: BIOPHYSICS AND MODELLING

PS19.001 – Numerical Modeling Of The Electrical Impedance Method Of Peripheral Veins Localization

Mugeb Al-Harosh, Russian Federation

PS19.002 – Modeling current density maps in the heart

Mohammadali Beheshti, Canada

PS19.003 – Finite Element Modeling of Gelatin Phantom from Measured Impedance Spectra

Pedro Bertemes-Filho, Brazil

PS19.004 – Prediction of radiation induced direct and indirect cellular damage using a novel ionisation spatial clustering algorithm

Eva Bezak, Australia

PS19.005 – Research on Vibration of Cell Membrane of Plant Seed with Ultrasonic Excitation

Hui Cao, People's Republic of China

PS19.006 – The Effect of Applied Force on Arterial Pulse with a New Flexible Pressure Sensor

WENXUAN Dai, Hong Kong

PS19.007 – The Art of Engineering Medicine: A New Fast Non-Invasive Method to Directly Assess Ischemia in Human Diseased Coronary Arteries

Iyad Fayssal, Lebanon

PS19.008 – Influence of the alteration of the flow topology during the abdominal aortic aneurysm growth

Joly Florian, Canada

PS19.009 – Using the DDST to Train and Test Anthropomorphic Robotic Children

Paul Frenger, United States

PS19.010 – The new low-cost metaphase finder for biological dosimetry

Akira Furukawa, Japan

PS19.011 – Concentrated photoactivation: focusing light through scattering

Pedro Vieira, Portugal

PS19.012 – Steered Molecular Dynamic Simulation Approaches for computing the Blood Brain Barrier (BBB) Diffusion Coefficient

Ebrahim Ghafar Zadeh, Canada

PS19.013 – The study of the relationship between the scatterer particle size of soft tissue in ultrasonic focal region and the frequency offset of backscattered signal

Jianzhong Guo, People's Republic of China

PS19.014 – Dynamic Model for Shear Stress-Dependent NO and Purine Nucleotide Production from Endothelial Cells

Patrick Kirby, United States

PS19.015 – Mechanism of Phospholipase as a Potential Anti-Bacterial Drug Revealed by Nonlinear Spectroscopy

Xiaolin Lu, People's Republic of China

PS19.016 – Cancer stem cells in a hierarchical model of tumour regrowth in five head and neck carcinomas

Loredana Marcu, Australia

PS19.017 – Effects of interaction with electromagnetic field on cell culture of *Saccharomyces cerevisiae*

Aracely Martínez, Mexico

PS19.018 – Obstructive and Sclerotic Disorders affecting Carotid Blood Flow to the Brain

Onaizah Onaizah, Canada

PS19.019 – Estimation of Tissue Temperature in Tumor Hyperthermia Using Ultrasonic Methods

Xiao-jian Wang, People's Republic of China

PS19.020 – Modeling of a Photosensitizer Distribution Relevant to Photodynamic Therapy of Malignant Non-Pigmented and Pigmented Tumors

Marta Wasilewska-Radwanska, Poland

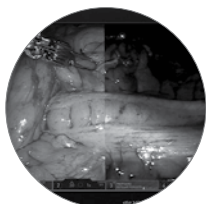
INTUITIVE
SURGICAL®

TECHNOLOGY THAT MATTERS

Advancing Minimally Invasive Surgery



XI STAPLER



XI FIREFLY™



XI VESSEL SEALER



Serious complications may occur in any surgery, including *da Vinci*® Surgery, up to and including death. Examples of serious or life-threatening complications, which may require prolonged and/or unexpected hospitalization and/or reoperation, include but are not limited to, one or more of the following: injury to tissues/organs, bleeding, infection and internal scarring that can cause long-lasting dysfunction/pain. Individual surgical results may vary. For important Safety Information, indications for use, risks, full cautions and warnings, please also refer to www.davincisurgery.com/safety and www.intuitivesurgical.com/safety. © 2015 Intuitive Surgical, Inc. All rights reserved. Product names are trademarks or registered trademarks of their respective holders. PN 1017796 Rev A 3/15

AUTHOR INDEX

Presentation Numbers in Bold =
Author is Presenting Author for this Presentation

A

- Aasia Razzaq.....SP081.2
 Abadie Fabienne..... SP020.5
 Abbas Sajid SP149.1
 Abd Kadir Khairul Azmi BinPS05.037,
 SP006.5
 Abdallah Elsadig O. **PS05.001, PS05.002**
 Abdelazez Mohamed **SP007.5**
 Abdelaziz Mohammed..... **SP019.1**
 Abdoli Mehrsima..... SP131.5
 Abdul Aziz Yang Faridah..... SP118.7, SP172.2
 Abdullah Basri Johan Jeet.....SP015.4,
SP025.5, SP154.4,
 SP159.4, SP173.5
 Abdullah Hussein A. SP051.4
 Abdullah Nazifah **SP045.6**
 Abedi Sajad **PS05.003, PS05.004**
 Abis Giulia.....SP042.4
 Abril Andrea **SP128.5**
 Abshire Caleb SP138.2
 Abuhaimed Abdullah A..... **SP006.4, SP118.6**
 Accardo Agostino P. SP042.4, SP0712
 Acri Giuseppe..... **SP044.1**
 Adame Brooks David..... SP149.4
 Addison Eric K. PS05.006
 Adeyemi Abiodun SP129.1
 Adhikari Kanchan P. **SP118.4**
 Adhikari Tirthraj..... SP118.4
 Adjiri Adouda SP037.2
 Adler Andy..... SP007.4
 Adliene Diana **SP155.7**
 Adrien Camille **SP118.2**
 Aerts Hugo J.W.L. SP023.4, SP122.5
 Aerts Wouter SP089.3
 Afzal M. PS04.019, SP133.1
 Agarwal P SP005.1
 Agbasi Patrick U. **SP145.7**
 Aghajamaliaval Peyman..... **SP008.8**
 Agoha Eillen E.C. **PS02.001**, SP022.1
 Aguilari Marie-Isobel..... SP157.2
 Agulles-Pedros Luis..... SP128.5
 Ahaiwe Josiah PS13.006
 Ahangari Sahar..... SP045.4
 Ahedo Sandra **PS16.001**
 Ahmad Belal SP116.4
 Ahmad Fayyaz..... SP081.2
 Ahmad Saif SP111.8
 Ahmad Syed Bilal SP047.2, SP155.5
 Ahmadzadeh Mohammad Reza..... SP097.7
 Ahn Jungyeol..... PS09.003
 Ahn Seung Do PS04.006
 Ahnesjö Anders..... SP076.5, SP106.5
 Aichert Andre SP065.2
 Aida Nur..... SP119.7
 Ainsley Christopher G..... SP106.4
 Airaksinen Olavi..... SP160.2
 Akagawa Takuya PS05.019, PS05.023,
 SP005.3, SP067.1
 Akbarzadeh Afshin SP128.4
 Akieda Shizuka..... PS02.007
 Akimey Nabilath A. PS16.039
 Akra Mohamed..... PS04.078
 Akulova Anna S. **SP007.2**
 Al Ameri Alfan S.....SP100.3
 Al Darwish Ruqaya **SP109.5**
 Al Halabi Fedaa PS02.005, PS02.006,
 SP151.1
 Al Kaabi Fatima S. **SP100.3**
 Al Suwaidi Jamila..... PS17.014
 Al-Affan Ihsan A.M. **SP177.5**
 Al-Eid Mohammed A. SP037.8
 Al-Ghazi Muthana..... **PS04.001, SP069.4,**
 **SP124.1, SP124.4**
 Al-Hajri Rashid..... SP108.2, SP118.3
 Al-Harosh Mugeb B..... **PS19.001**
 Al-Kalbani Saeed..... SP108.2, SP118.3
 Al-Musawi Taki A. SP037.8
 Al-Najjar Waleed..... SP022.3, SP078.6
 Al-Nashash Hasan SP135.6
 Al-Sadoon Shuaa J. **SP037.8, SP045.5**
 Al-Smadi Yahia M. **PS03.001, SP051.1**
 Al-Ward Shahad **SP036.3**
 Alam Samir PS19.007, SP159.3
 Alaminos-Bouza Armando **MPS05.2,**
 **MPS06.2**
 Alasti Aria..... PS19.012, SP178.4
 Alayoubi Nadia..... PS04.105
 Albrecht Simon..... SP073.3,
 SP073.4, **SP073.5**
 Aldelajlan Saad..... SP142.4
 Aleman Dionne PS04.031, SP028.7
 Aleme Carolina PS05.032
 Alexander Brian SP023.4
 Alexander Kevin M. **SP057.3, SP080.2,**
 SP080.5, SP133.2
 Alfonso Manuel R. SP082.1, SP082.4
 Alfonso Rodolfo PS04.002, SP056.5,
 **SP057.6**
 Alférez Germán H. SP069.3
 Alghamdi Majed..... SP078.1
 Alhakeem Eyad A. **SP090.2**
 Ali Elsayed S.M. **PS01.001, SP129.3**
 Ali Furqan SP081.2
 Ali Saadat **SP081.2**
 Ali Shady..... SP156.3
 Alikarami Fatemeh..... SP086.2
 Alizadeh Elahe **SP069.1**
 Aljadaan Ahmad SP102.1
 All Angelo H. **SP135.6**
 Allen Barry J. SP091.1
 Allen Christine..... SP059.5
 Allen Claudine N. SP049.4
 Almada Maria J. PS04.109, PS04.110
 Almeida Ana P.S.S. **PS16.002, PS16.003,**
 **PS17.001**
 Almeida Ana P.S.S. **PS17.001**
 Almeida Giulia C.M. PS01.019
 Almeida Jefferson J.H. SP040.2
 Almeida Neto Jose R..... SP033.2
 Almeida Renan M. SP062.2, **SP062.2**
 Almeida Rodrigo M.A. .. PS16.002, PS16.003,
 PS17.001, **PS17.002**
 Almeida Rui PS16.038
 Almeida Tássila Catarina S. SP020.2
 Alonso Fabiola..... SP121.2, **SP121.3**
 Alonso Fernández David N. **PS04.002**
 Alonso Sampedro Jose L. PS04.002
 Alpiste Marko..... SP103.5
 Alqahtani Mohammed S.....SP139.3
 Alrifaiy Ahmed..... **SP030.6**
 Alrowaili Ziyad A. SP141.4
 Alsbeih Ghazi..... SP142.4
 Alshamsi Wadha M..... SP100.3
 Alsuwaidi Jamila S..... SP100.3
 Altayyar Saleh..... BMEE13.1
 Altundal Yucel..... SP019.4, SP086.5
 Altuve Miguel A..... SP039.6
 Altwijri Omar **SP098.1**
 Alulova Anna S. **PS09.001**
 Alumäe Tanel SP147.3
 Alvarado Ronald SP127.2
 Alvarez Guillermo D. SP177.4
 Alvarez-Arana Juan SP062.5
 Alvarez-Rivero Aymée..... SP170.5
 Alvero González Leidy M. **SP111.5**
 Alves Cleber PS16.006
 Alves Leandro P..... PS12.037
 Alves Marie-Helene SP071.1
 Aly Antar **PS04.003, PS05.005**
 Alzorkany Faisal..... SP142.4
 Amaya Espinosa Helman Alirio..... PS04.107
 Amirrashedi Bonab Mahsa..... SP049.2
 Amjad Nauman..... SP081.2
 Amor James D. **SP169.4**
 Amorim Pedro PS07.004
 Anand Sneha..... SP114.4
 Anandkumar Delran **PS16.004**, SP16.030
 Anantharaman Ayyalusamy SP164.6
 Anastasiou Athanasios..... PS12.024, SP123.4
 Anastácio Rogério PS01.017, PS01.019
 Andalib Bahram PS05.034
 Anderson Ashleigh **SP059.2, SP059.3**
 Anderson Deirdre E.J. SP098.5
 Ando Takegiro SP055.1
 Andrade Fernando O..... **SP087.6, SP093.5**
 Andrade Thais G. PS16.003
 Andrea Jennifer SP080.2, **SP130.6**
 Andreev Oleg A. SP049.5
 Andreo Pedro SP141.3
 Andres Pablo PS04.013
 Andresen Thomas L. SP030.3
 Andrews Derek SP123.3
 Andrysek Jan SP040.5, SP066.2,
 SP083.4
 Angelo Michele F. PS01.014, PS01.015
 Angelucci Luisa PS14.002
 Anguiano Marta PS04.034
 Anjomani Zahra **SP109.1**, SP109.2
 Ankathi Praveen P..... SP121.7
 Ankerhold Ulrike SP163.2
 Annkah James K. **SP129.1**
 Ansbacher Will..... SP140.5
 Antaki James..... PS12.023
 Antoniadis Athos SP024.3
 Antosh Michael..... **SP049.5**
 Antunes Nilson SP029.4
 Anyango Philip A. **SP042.6**
 Aoki Fabio G. **SP020.1**
 Apitzsch André..... SP113.4
 Arabi Mohamad H. SP070.4
 Aragón-Martínez Nestor..... SP038.5
 Arampatzis Avi..... SP169.6
 Araujo Cynthia **PS04.005**
 Araujo Mariangela..... PS12.026

- Araújo Eduardo C.D..... SP030.7
 Araújo Luiza C.D..... SP030.7
 Arbanil H..... SP088.1
 Arce Rincón Jorge H..... SP126.2
 Archambault Louis **MPF10.2**, PS04.028,
 SP004.2, SP027.7
 Arfelli Fulvia..... SP150.3
 Argota Raul..... **PS04.005**, SP056.5
 Arico Giulia..... **SP048.4**
 Arif Idam PS04.080
 Arilli Chiara..... SP090.6
 Arista M.T..... SP088.1
 Arivarasan Ilamurugu..... SP164.6
 Armentano Ricardo L..... **SP082.1**, SP082.4
 Armour Elwood..... SP003.2
 Armstrong Ryan **SP110.7**
 Armstrong Ryden J..... SP032.3
 Arnaiz Isabel..... **SP111.2**
 Arnold Robert..... SP125.4
 Arora Jaspreet..... SP138.2
 Arora Prabhat SP114.4
 Arredondo Waldmeyer Maria T..... SP113.2
 Arrea Esteban..... SP167.4
 Arsenal Clément..... **MPF04.1**
 Arumugam Sankar PS04.117, SP153.6
 Arun Gandhi SP004.3, SP025.2,
 SP079.5, SP164.6
 Arund Jürgen..... SP167.5
 Arvan Lida M..... SP068.4
 Aryan Arvin SP128.4
 Asa Sylvia..... SP157.3
 Asad Somayeh **SP086.2**
 Asadi Somayeh **SP06.001**, **SP076.3**,
 SP086.3
 Asano Miho PS10.012, PS10.013,
 **PS11.001**
 Ascencion Yudy..... **SP056.5**, **SP057.6**
 Aschenbrenner Katharina P..... SP175.4
 Asgari Mahdi..... SP161.5
 Asgari Vahid..... SP138.3
 Ashraf J..... SP133.1
 Asiev Krum..... SP140.3
 Ask Per..... SP031.3
 Aslian Hossein..... **SP001.3**
 Asnaashari Khadijeh..... SP119.3
 Asquier Nathalie..... SP067.6
 Assi Hisham..... SP028.2
 Åstrand Elaine..... 2507
 Astaraki Mehdi..... SP001.3
 Astrid Astrid..... SP135.6
 Asuncion Maria Christine T..... PS02.009
 Asuni Ganiyu..... SP047.5
 Atarashi Hidenao..... PS16.016
 Athavale Yashodhan..... **PS12.001**, **SP031.2**
 Atkinson Stephanie..... PS03.004
 Atluri Sravya..... **SP101.1**
 Atowa C..... PS02.001
 Atuwu-Ampoh Vivian Della..... **PS05.006**
 Atwal Parmveer..... SP123.5, SP153.7
 Atwell Kathryn..... SP041.5
 Audenino Alberto..... SP156.3
 Audu Musa L..... SP166.5, SP166.6
 Augustin Simo..... SP114.2
 Austman Rebecca..... PS16.018
 Avedaño Guillermo E..... **SP125.7**
 Avery Stephen..... SP142.3, **SP155.8**
 Avezzano Paolo..... PS16.024, PS16.025
 Avila Amy..... SP060.3
 Avila Ramirez Estrella..... SP037.6
 Aviles-Rodriguez Gener..... SP020.4
 Awdeh Aseel..... **SP122.3**
 Ay Mohammad Reza.. **PS01.002**, **PS05.007**,
 PS05.018, **PS09.002**, **SP034.1**,
 **SP035.6**, SP037.4, **SP045.2**,
 **SP045.3**, **SP045.4**, **SP070.1**,
 **SP070.2**, SP070.4, **SP115.8**,
 SP128.4, SP179.1
 Ayadi-Zahra Myriam **MPF10.1**, **MPF11.1**
 Ayala-Dominguez Lizbeth..... SP129.2
 Azaman Aizreena **SP066.1**
 Azbouche Ahmed..... SP037.2
 Azevedo Dario F.G..... SP115.1
 Aziz Mina S.R..... SP064.1, **SP064.2**
 Azuma Masami..... PS13.011
- B**
- Babbar Vishvek **PS16.005**, SP008.5
 Babic Ankica SP031.3
 Babona-Pilipos Robart..... SP002.3
 Babyn Paul..... SP013.4, SP150.7
 Bachmann Maie **SP050.5**
 Badawy Mohamed K..... **PS05.008**,
 **SP119.2**
 Badel Jean-Noel..... MPF11.1
 Bader Gary D..... SP127.4
 Bae Hoonsik..... PS05.039
 Bae Jae Beom..... **PS04.006**
 Baek Jong Geun..... **PS04.007**
 Baeza José Antonio..... MPS02.1, MPS06.1
 Baggarley Shaun P..... PS04.080
 Bai Sen..... SP056.1
 Bailey Michael..... SP102.8, SP153.5
 Bailey Stephanie N..... **SP166.2**, SP166.7
 Bailey Timothy L..... SP122.4
 Bakshshayeshkaram Mehrdad..... SP037.4
 Bakker Akke..... SP045.2, SP045.4, SP070.4
 Balagholi Sahar..... SP059.2
 Balasundaram Krishnanand..... SP086.2
 Balasundaram Krishnanand..... SP039.7
 Baldwin Lesley..... SP063.2
 Baldwin Samuel..... **SP055.3**
 Bales Justin..... **SP127.5**
 Balidemaj Edmond..... **SP044.4**
 Ball David..... SP140.1, SP174.1
 Balleza-Ordaz Marco..... SP083.3
 Balter Peter..... SP107.1
 Bambico Francis R..... **SP136.4**
 Bamba Charanjit **SP145.4**
 Bamidis Panagiotis D..... **SP113.6**
 Banerjee Robyn..... SP078.1
 Bang Hyun Hee..... PS12.017
 Bangert Mark..... SP125.5, SP130.4
 Barabino Gilda..... **SP002.1**
 Barakat M Samir..... SP102.8
 Barbee Kenneth A..... PS19.014
 Barber Jeff..... SP153.5
 Barbosa Gabriela..... SP059.1
 Barbés Benigno..... SP100.41
 Bardakjian Berj L..... SP135.1, SP178.2,
 SPO92.1, SPO92.3,
 SPO92.4, SPO92.5
 Bardella Lucia H..... PS04.067
 Bardsley Katie..... SP002.2
 Barghi Arvand..... SP125.2
 Barciak Erika..... SP170.2
 Barker Kevin..... SP003.5
 Barnes Crispin H.W..... SP019.2
 Barnes Spencer C..... **SP112.1**
 Barnett Erin..... PS04.050
 Barnett Rob..... PS13.010
 Baroni Guido..... PS04.087
 Barrette-Leduc Cécilia..... SP087.7
 Barros Nestor..... SP172.1
 Barroso Regina C..... PS05.042
 Barry Amanda..... **SP141.2**
 Barthold-Beß Simone..... SP158.7
 Bartolac Steve..... SP017.3
 Barton Ken..... SPO46.4, SP076.1
 Barzda Virginijus..... SP157.3
 Basak Cassandra S..... PS04.053
 Baselli Giuseppe..... PS04.088
 Bashkurov Vladimir..... SP034.5
 Basran Parminder..... **JT06.2**
 Bassetti Michael..... SP175.5
 Bassey Bassey..... SP150.5, **SP161.6**
 Basta Dario..... SP150.6
 Bastian-Jordan Matthew..... SP116.4
 Bastos-Filho Teodiano..... **PS11.002**, **SP165.4**
 Batchelar Deidre..... SP078.4
 Batista Cancino Jorge L..... **PS04.008**
 Batista Delano V..... PS04.067
 Batkin Izmil..... SP111.8
 Batle Fernando..... SP037.7
 Battista Jerry J..... **MPE13.1**, SP116.2,
 SP125.2, SP140.2,
 SP155.4, SP164.2
 Bauer Christian..... PS04.116
 Bauer Stefan..... SP023.4
 Bauman Glenn..... SP116.4
 Baumgarten Daniel..... **SP165.2**
 Bawazeer Omemh..... **PS04.009**, **PS05.009**,
 **SP077.5**
 Baxter John S.H..... **PS07.001**, **PS07.002**
 Bay Brian K..... SP089.4
 Bayhaqi Yakub A..... **PS07.003**
 Bayleyegn Masreshaw D..... **SP171.2**
 Beadle Beth..... SP107.1
 Beals Ronald E..... PS04.112
 Beaulieu Luc..... **MPF03.2**, **MPF07.1**,
 SP003.5, SP006.3, SP017.5,
 SP027.7, SP049.4, SP081.5
 Beck Caleb G..... SP068.4
 Becker Nathan..... **PS04.010**, SP046.5
 Beckham Wayne..... MPE13.1
 Beddar Sam..... SP006.3, SP081.5,
 SP176.4
 Bedford James L..... SP164.1
 Bedogni Roberto..... PS04.081, PS05.043
 Bedwani Stephane..... PS04.024, SP174.2
 Beheshti Mohammadali..... **PS19.002**
 Beheshti Soosan..... SP165.5
 Behfar Mohammadhossein..... **SP136.2**
 Beichel Reinhard..... PS04.116
 Beig Mirza..... SP073.6
 Bekaert Laura..... SP178.3
 Belardinelli Andrea..... PS16.025
 Belchior Ana..... PS05.036
 Beldjoudi Guillaume..... MPF11.1
 Belec Jason..... PS04.021, PS04.090,
 SP047.4, SP131.1
 Belev George..... SP087.7, SP150.4,
 SP150.5, SP161.6
 Bellazzini Ronaldo..... SP150.3
 Bellerive Marc..... SP131.3
 Belli Sheila..... PS16.025
 Belyaev Alexander..... SP012.2
 Bencsik Barbara..... PS04.046, PS05.022
 Bendl Rolf..... SP016.3
 Beniagouev Vadim..... SP104.2
 Benitez Erick..... PS05.041
 Benmakhloof Hamza..... **SP141.3**
 Bennett Daniel..... **PS05.010**
 Bentabet Abdelouahab..... SP037.2
 Bera Pranabes..... PS05.022
 Berbeco Ross..... SP019.4, SP086.5
 Berger Martin..... **SP065.2**, SP065.4
 Bergeron Mélanie..... SP035.5
 Bergeron-Savard Marie-Joël..... SP158.6
 Bergh Anders..... SP167.6
 Bergquist Austin J..... **SP008.5**
 Bernardini Marcus Q..... SP128.3
 Bernasconi Andrea..... SP023.3
 Bernasconi Neda..... SP023.3
 Bernhardt Boris..... SP023.3
 Berris Theocharris..... SP080.1, SP154.1
 Bertemes-Filho Pedro..... **PS19.003**,
 **SP008.3**, **SP084.2**
 Berthelet Eric..... PS04.065
 Bertrand Michel..... SP008.8

Bertrand-Grenier Antony..... **SP162.3**
 Bertuzo José E. PS12.022, SP001.5
 Berumen Adriana V..... SP075.1
 Besemann Markus SP066.3
 Betka Abderrahim **SP037.2**
 Betz Michael..... SP036.8
 Beunk Harold..... SP147.5
 Bezak Eva..... **MPE17.1, PS04.011,**
 **PS19.004, SP054.4,** SP076.4,
 **SP091.1,** SP109.5
 Bezak Andrea SP046.5
 Bharat Shyam..... SP003.3
 Bhaskar Sathya Moorthy SP059.4
 Bhatia Sudershan..... PS04.053, PS04.116
 Bhatt Shashank..... PS02.010
 Bhengu John K..... SP153.1
 Bhuiyan Mohammad Anisuzzaman.. SP005.2
 Biasini Maurizio..... SP108.4
 Bichay Tewfik..... PS04.048
 Bielajew Alex..... SP025.1
 Bilda Sebastian..... SP113.4
 Billas Ilias **SP035.2, SP038.1**
 Bisht R K..... SP005.1
 Bisio Angela..... PS08.001
 Bissi Lucia SP108.4
 Bissonnette Jean-Pierre... **JT04.1,** PS04.010,
 PS04.071, SP017.3, **SP046.5**
 Bitarafan-Rajabi Ahmad PS01.002
 Bitaran Rajabi Ahmad..... SP045.3
 Bizovičar Nataša **SP052.2**
 Bjarnason Thorarin A..... **SP067.2**
 Björkman Mats 2507
 Björninen Toni..... SP136.2
 Blackshaw Patricia E. SP139.3
 Blais Adam **SP070.6**
 Blais Craytal..... SP074.7
 Blake Samuel J..... SP153.5, SP153.6
 Blanco Kiely Janid **PS04.012, SP130.3**
 Blank Molly PS12.023
 Blascovi-Assis Silvana Maria..... SP040.2
 Blase Bastian..... **SP073.3,** SP073.4,
 SP073.5
 Blaser Karin F..... SP110.2
 Blaszykowski Christophe SP098.3
 Blinston Charlotte SP023.3
 Bliznakov Zhivko PS12.024
 Bliznakova Kristina..... PS01.012, SP129.5
 Blood Alexander PS04.036
 Blumberger Daniel M..... SP101.1, SP101.2
 Bochud François PS04.068, SP152.4
 Bode Michael..... PS02.004, SP151.1
 Bodey Andrew J..... SP089.4
 Boehler Christian E.H. **SP020.5**
 Boehringer Stephan SP110.2
 Boggio Esteban F. **PS04.013, PS04.014,**
 **SP015.1**
 Bogolub Phillip..... **BMEE01.2**
 Bohoudi Omar..... SP046.3
 Boivin Jonathan..... **SP006.3**
 Bojador Maureen..... SP107.1
 Bokrantz Rasmus..... **PS04.015**
 Bokulic Tomislav SP067.4
 Bold Adiya PS16.023
 Bolic Miodrag SP074.7, SP111.7,
 SP111.8
 Bolkhovskiy Jeffrey..... **SP171.8**
 Bollinger Douglas..... SP106.6
 Bolsa-Ferruz Marta..... **SP049.6**
 Bonakdar Shahin..... SP138.3
 Bonfigli Francesca SP058.4
 Bonillas Antonio..... SP003.3
 Bonomo Pierluigi SP090.6, SP143.1
 Boone John M..... **MPE06.2**
 Booth Jeremy T. PS04.042,
 SP079.2, SP175.1
 Booz Sara M..... SP100.3
 Borchers Kirsten..... SP112.5

Bordy Jean-Marc..... SP118.2
 Borel Santa..... **SP096.1**
 Borges Rodrigo G. PS12.022
 Borggreffe Martin..... SP044.2
 Borgohain Roopam R..... SP144.5
 Borrás Caridad **1351, MPS04.1,** SP062.6
 Borschneck Daniel SP162.8
 Borsio Marcio L. PS13.002
 Bortfeld Thomas..... **SP106.1**
 Bostel Tilmann SP016.3
 Both Stefan..... PS04.012, SP130.3
 Bottigli Ubaldo SP150.3
 Boucenna Rachid..... PS01-007, SP013.1,
 SP013.3, SP036.8
 Bouchard Hugo **SP025.1,**
 SP038.1, **SP038.2,** SP038.4
 Bouchard Mathieu **SP049.1**
 Boudam Karim SP152.5
 Bougherara Habiba SP064.1, SP064.2
 Boughner Derek SP071.7
 Boulanger Marie-Eve..... SP158.6
 Bourbon Pierre-Etienne..... SP136.1
 Bourhis Jean PS04.068, SP152.4
 Boursalie Omar..... **PS12.002**
 Boutilier Justin J. **SP117.5**
 Boutry Sebastien..... SP019.1
 Bouwman Ramona W. SP172.3
 Bowes David PS04.022
 Bowman Wesley..... PS04.083
 Boyce Larry **BMEE12.1**
 Bradley Beverly D. **SP093.1,** SP148.5
 Bradley David A. SP004.5
 Branch Kelley..... SP149.5
 Branco Raquel S. SP135.4
 Brandan Maria-Ester **MPS08.1**
 Brandan Maria-Ester **PS17.003, SP129.2**
 Brasil Lourdes M..... **PS01.003, PS01.004,**
 **PS10.001, PS16.006, SP020.2,**
 **SP030.7,** SP033.2, SP033.4,
 **SP059.1,** SP114.1, **SP156.5**
 Brassard Marie-Eve..... SP087.7
 Brauer-Krisch Elke T. **SP138.5**
 Braz Delson PS05.042
 Breen Stephen L. SP016.5
 Breton Vanessa **SPO92.5**
 Brewer Gregory J. SP135.3
 Brez Alessandro SP150.3
 Brijmohan Yarish..... SP116.3
 Brink Carsten..... SP153.5
 Broadfield Larry SP009.2
 Brock Kristy K. **SP011.1,** SP072.2,
 SP072.5, SP130.2
 Brolo Alexandre G. SP030.5
 Bromley Regina SP153.5
 Brons Stephan SP058.2, SP142.2
 Brown Colin J. SP072.3
 Brown Derek..... PS04.113, SP004.1
 Brown Michael P..... MPE17.1
 Brown Stephen..... SP046.4, SP056.4
 Brualla Luis G. MPS10.1
 Bruce Neil..... PS04.105
 Brun Francesco **SP0712,** SP150.3
 Brunetti Antonio..... SP150.3
 Bryan Richard T..... SP112.1
 Brändal Anna SP145.3
 Bucciolini Marta SP090.6
 Buchheit Isabelle MPF08.2
 Buchmann Isidor **BMEE19.1**
 Buckley Alvan SP083.1
 Budar-Alemán Nayely R. SP102.7, SP126.6
 Budgett David..... SP060.1
 Budillon Patrice..... SP067.6
 Budzanowski Maciej..... SP155.3
 Bueno Marta SP048.3
 Buerk Donald G..... PS19.014
 Bug Marion..... PS05.010, PS05.036,
 SP048.3

Bugby Sarah L..... SP139.3
 Buijsen Jeroen..... SP102.3
 Burianova Veronika..... PS04.049
 Burke Mikhail V. **SP055.6**
 Burneo Jorge G. SP023.3
 Burns David T. SP068.5, SP163.3
 Burns Mark SP140.1
 Burton Christiane..... **SP161.3**
 Busch Vincenz..... SP170.1
 Busoch Carmen PS12.006
 Bynevelt Michael..... SP097.6
 Byun Soo H. SP109.1, SP109.2
 Bzovey Christopher J. **SP009.3**
 Bäcklund Tomas..... SP145.3
 Bäckström Gloria..... SP076.5, SP106.5
 Bär Esther..... PS04.085
 Béliveau-Nadeau Dominic..... SP153.3

C

Cabrales Pedro..... PS01.005
 Cabrera Llanos Agustin I. SP102.7, SP126.6
 Caccavo Francisco..... SP010.7
 Caccia Barbara..... SP025.3
 Cadet Michaelle A. SP098.2
 Cadorette Jules SP035.5
 Cafazo Joseph A. **SP113.1**
 Cagni Elisabetta SP025.3
 Cagy Mauricio SP135.4, SP135.5
 Caine Hannah..... SP175.1
 Calandra Andrea SP108.4
 Caldwell Curtis **SP088.5**
 Calil Saide..... **BMEE05.1,** SP087.6,
 **SP093.3,** SP093.5, SP103.3
 Callorda-Fedeczko Lucas SP088.4
 Campbell Andrew SP097.6
 Campbell Mikki..... SP058.2,
 SP088.5, SP142.2
 Campbell Warren G. **SP058.1**
 Campelo Maria Carolina S..... SP006.6,
 SP068.1
 Campillo Daniel..... SP074.2
 Canali Chiara **SP030.2, SP030.3**
 Canals Raphael SP088.1
 Cancela Jorge **SP113.2**
 Candefjord Stefan SP168.3
 Cansino Naxi SP129.2
 Cantarelli Hoffmann Elias..... SP115.1
 Canters Richard..... **SP004.6**
 Cantor-Rivera Diego SP023.3
 Cao Hui..... **PS19.005,** PS19.013
 Cao Ruifen..... SP065.3, SP143.4
 Capaverde Alexandre S..... SP129.6
 Capuano Michael J..... **SP042.2**
 Carabe Alejandro..... SP106.3, SP139.1
 Carbonari Ronny C..... PS02.008
 Cardan Rex..... SP107.1
 Cardellini Federica PS16.019
 Cardoso Marco F. SP053.4
 Cardoso Leandro X. PS01.003
 Cardoso Paulo F.G. SP020.1
 Cardoso Pedro H.B. **SP068.2**
 Carlen Peter L..... SPO92.3, SPO92.4,
 SPO92.5, SP135.1
 Carnevale Alessandro SP102.5
 Carolan Martin SP102.8, SP141.4
 Carozza Bruno **PS04.016**
 Carrasco Juan-Pablo SP004.6
 Carrier Jean-Francois..... PS04.024, SP152.5,
 SP153.3, SP174.2
 Carrion Daniel..... PS05.008
 Carrogi-Vianna Daniela..... SP040.2
 Carter Caitlin **SP028.6**
 Carter Joseph W.S..... SP150.1
 Carvalho Henrique C. PS12.037
 Carvalho Júnior Albérico B..... SP104.1

- Casado Ana.....PS16.001
 Casal Mariana.....PS04.014
 Casar Bozidar.....SP05.029
 Casas Luis D.....PS04.029
 Casati Marta.....SP090.6
 Cassani Raymundo.....**SP135.2**
 Cassano-Piche Andrea.....**1497**, PS16.001,
**PS16.007**, SP009.2
 Castaldo Rossana.....**SP039.5**
 Castañeda Franxis.....PS14.002
 Castañeda Mario.....**BMES02.1**
 Castañeda William.....PS16.031
 Castellanos Javier.....SP051.2
 Castro Aluisio J.....PS04.067
 Castro Laura L.....**PS12.038**
 Castro-Rodríguez Elena M.....SP074.6
 Catt Benjamin.....SP047.3
 Caudillo-Cisneros Cipriana.....SP074.6
 Causa Lucas.....PS04.108, SP036.6
 Cavalcante Fernanda R.....**SP104.1**
 Caviglia Claudia.....SP030.3
 Cañizares Maite.....**PS12.003**, **PS12.004**,
PS12.020
 Ceballos Ibrain.....PS12.006
 Ceccarelli Lorenzo.....SP030.2
 Ceccherini Vega.....PS16.025
 Celic Luka.....**SP180.1**
 Cerapaitė-Trusinskiene Reda.....SP155.7
 Cerny Martin.....PS17.011
 Cervantes Espinosa Yunuen A.....**SP126.2**
 Chable Ismael.....SP062.5
 Chagnon Frederic.....SP096.2
 Chakraborty Shyamal R.....**SP154.3**
 Chamberland Marc.....SP029.1, **SP079.1**
 Chambers Ann F.....SP018.2
 Chambers Neil C.....SP089.2
 Chan Adrian D.C.....**SP007.1**, SP007.4,
SP007.5, SP008.9, SP074.4,
SP095.7, SP134.6
 Chan Anthony.....**BMEE05.1**, BMEE23.1
 Chan Ariane.....SP172.2
 Chan Biu.....PS04.071
 Chan Gordon.....**SP171.6**
 Chan Harley.....**SP061.5**, SP110.3
 Chan Timothy C.Y.....PS04.010, SP036.7,
SP117.5
 Chan Wen Hsiung.....SP019.3
 Chand Surendra B.....**PS17.004**
 Chander Sanjeev.....**SP111.8**
 Chang Ah Ram.....PS05.026
 Chang Sarah R.....PS12.011, SP166.3
 Chang Ung Kyu.....PS05.027
 Chang Walter H.....**SP019.3**
 Chang Weishan.....**SP048.2**
 Changizi Vahid.....**PS05.011**
 Chapman Dean.....SP150.4, SP150.5,
SP161.6
 Chappell John A.....SP098.2
 Charalambous Christakis.....SP024.3
 Charland Paule M.....**PS04.017**
 Charlebois Serge.....SP035.4
 Charles Paul.....PS05.051
 Chartier Lachlan.....SP081.4
 Chatpun Surapong.....**PS01.005**
 Chau Nguyen Tan.....SP158.8
 Chau Tom.....PS11.003, SP082.5,
SP144.3, SP144.4
 Chaudhary Sahil.....SP096.3
 Chauhan Vijay S.....SP039.1
 Chavandra Jean.....PS05.030, SP017.6
 Chawapun Nisa.....SP158.2
 Checcucci Bruno.....SP102.5, SP108.4
 Chee Justin.....SP087.4
 Chee Youngjoon.....PS09.003, SP170.3
 Chen Albert.....SP090.3
 Chen Chaobin.....SP065.3
 Chen Chien-An.....**SP040.3**
 Chen Chih-Hui.....PS03.009, PS03.010
 Chen Chung-Ming.....SP024.6
 Chen Cui.....PS04.122
 Chen Elvis C.S.....PS07.001
 Chen Fang.....**SP116.6**
 Chen Fu-Yu.....**SP060.1**
 Chen Guangyi.....**SP039.1**
 Chen Guowen.....SP029.7
 Chen Hsin-Chang.....PS03.007
 Chen Huiwen.....PS02.013
 Chen Jeff.....SP046.2
 Chen Jeff Z.....SP018.3, SP164.2
 Chen Jia-Jin.....SP040.3
 Chen Jia-Jin J.....SP101.4
 Chen Jiayun.....PS04.079
 Chen Shupeng.....**SP072.7**
 Chen Wei.....**SP083.2**
 Chen Wei-Ling.....**PS03.002**
 Chen Wen-Chuan.....PS03.009, PS03.010
 Chen Wenxi.....PS12.030
 Chen Xi.....SP020.3
 Chen Xian C.....PS02.014
 Chen Zhuying.....PS12.027
 Cheng Cheng-Kung.....**BMEE08.1**, PS03.007
 Cheng Hai-Ling Margaret.....**SP105.1**
 Cheng Huanhuan.....SP101.6, SP101.7
 Cheng Michael.....**BMEE13.1**, **BMEE26.1**,
**SP022.5**, **SP111.7**, **SP178.7**
 Cheng Richard Y.....**SP002.4**
 Cheng Yu-Ling.....SP093.1
 Cheong Kwang-Ho.....PS05.039
 Cherpak Amanda.....PS04.022, SP17.014
 Chesson Brent.....SP140.1
 Chester Victoria.....**PS03.003**, PS10.005,
PS10.006
 Chettle D.....SP119.3
 Chetty Indrin J.....SP046.4, SP056.2,
SP056.3, SP056.4,
SP072.4, SP076.1
 Chetvertkov Mikhail.....SP056.3
 Cheung Kin-Yin.....**JT05.1**, **JT05.2**,
**SP075.1**, SP158.3, SP158.4
 Cheung Yi Wah Eva.....**SP057.4**
 Chevalier Margarita.....SP129.2
 Chhom Sakborey.....SP158.8
 Chia Joo S.....SP053.2
 Chiang Chi-Feng.....SP028.3
 Chiarizia Roberta.....PS16.011, PS16.012
 Chibani Omar.....SP107.6
 Chikai Manabu.....PS10.003, **PS12.005**,
PS12.011, SP145.6
 Chin Lee.....SP06.007, SP171.6
 Chinvarun Yotin.....SP135.1, SP092.4
 Chiocchini Stefania.....SP108.4
 Chithrani Devika B.....SP091.2, SP091.3
 Cho Byung Chul.....PS04.006
 Cho Dongil.....PS09.003
 Cho Dongrae.....SP031.1
 Cho Gwi.....SP153.5
 Cho Min-Seok.....PS01.022, PS04.100,
PS04.102, PS04.103
 Cho Samju.....**PS04.018**, **PS05.012**,
**SP090.5**
 Cho Seungryong.....SP149.1
 Cho Sungkoo.....**SP048.5**
 Cho Woong.....PS04.093
 Cho Young-Bin.....SP130.2
 Cho Yu Ra.....PS05.027
 Choan E.....SP078.2
 Choi Jang-Hwan.....SP065.2, SP065.4
 Choi Jinho.....PS04.018, SP090.5
 Choi Jonghyun.....SP032.2
 Choi Myounghwan.....**PS09.003**
 Choi Sung Hoon.....SP149.6
 Choi Sunhoon.....PS04.018, PS05.012,
SP090.5
 Choi Young Eun.....PS04.006
 Choi Yvonne.....**PS13.001**
 Chon KiSP095.1, SP095.3, SP127.6, SP171.8
 Chong Tze Tec.....SP053.2
 Chong Yip Boon.....SP167.2
 Chou Chi-Wei.....PS03.007
 Chow James.....**PS04.019**, **PS04.020**,
PS04.037, **SP017.1**, **SP133.1**
 Chow Samantha.....SP093.1
 Chow Tom.....SP079.4
 Chow Yu F.....PS12.029
 Christensen Gary E.....SP097.5
 Christiansen Eric J.....**PS04.021**
 Chrzanowski Wojciech.....SP015.2
 Chrétien Mario.....SP063.4
 Chua Boon.....SP015.3, SP174.1
 Chua Soo Min.....SP135.6
 Chuembou Pekam Fabrice.....SP179.3
 Chukwudebe Gloria A.....PS13.006
 Chung Caroline.....SP023.2
 Chung Hans.....SP06.007
 Chung Jin-Beom.....PS04.098, PS05.047
 Chung Lip Yong.....SP015.4
 Chung Yoonsun.....SP048.5
 Chytyk-Praznik Krista.....**PS04.022**
 Cicioni Roberto.....SP108.4
 Cieza Michael.....SP010.2
 Cifrek Mario.....SP138.1
 Cifter Gizem.....SP080.4, SP086.5
 Ciocca Mario.....SP058.4
 Cisek Oscar.....SP033.3
 Cisek Richard.....**SP157.3**
 Cisternas Eduardo A.....**SP125.5**
 Clancy Kathryn.....**SP157.4**
 Claridge-Mackonis Liz.....SP054.4
 Clark Catharine H.....SP004.5
 Clark J. Tobey.....**1351**, **BMEE20.1**,
SP010.2, **SP010.7**
 Clarke Geoffrey.....**SP007.4**
 Clements Natalie.....SP140.1
 Cleveland Robin O.....SP173.4
 Clotet Roger.....SP113.7, SP170.4
 Cloutier Guy.....SP162.3
 Cloutier Emily.....SP158.6
 Āmiel Vratislav.....SP116.8
 Coates James.....SP046.6
 Cobos Agustin C.....SP177.4
 Cocchi Duccio.....PS16.025
 Cockburn Neil.....SP097.1
 Coelho João.....PS19.011
 Coelli Fernando C.....SP062.2
 Coffey Mary.....**MPE08.1**, **SP123.1**
 Coffman Zachary A.....**SP028.5**
 Cofre Javier.....SP057.6
 Cohen Sarah.....SP104.2
 Coiado Olivia C.....**SP111.1**
 Cojocarau Claudiu D.....SP026.3, **SP026.5**
 Cole Andrew.....SP067.4
 Colic Sinisa.....**SP092.1**
 Colvill Emma.....SP079.2
 Compagnucci Antonella.....SP090.6
 Comsa Daria.....PS04.050, PS04.106
 Conde Silvia V.....SP020.5
 Cong Xiaohu.....SP107.2
 Conroy Leigh.....**PS04.023**, SP085.2
 Constantinou Ioannis.....SP024.3
 Conti Elia.....SP108.4
 Contreras Ricardo.....**PS05.013**, SP107.3
 Contó Murilo.....**PS13.002**
 Cook Peter.....**PS16.008**
 Cool Derek W.....SP029.3, SP116.4
 Coolens Catherine.....SP020.4, **SP023.2**,
SP180.3
 Cooper David M.L.....SP150.4
 Cooper Leon N.....SP049.5
 Cordova - Fraga Teodoro.....**SP012.1**, **SP160.4**
 Corella-Jimenez Francisco.....SP060.3
 Corinthios Mickael.....SP008.8

Correa Villada Marcela **SP144.3**
Cortez Jorge.....PS01.026
Costa Eduardo T..... PS12.022, SP001.5,
..... **SP029.4**
Costa Filipa..... SP047.1
Costa Henrik D'Oark R.....SP156.5
Costa Paulo R..... PS05.028, SP027.4,
..... **SP115.4, SP115.5, SP118.5,**
..... SP137.2, **SP177.2**
Coste Jérôme.....SP121.2
Cote Nicolas **PS04.024**
Cotter Christopher.....SP057.2
Cotua Di Teodoro SP060.2
Court LaurenceSP107.1
Courtney DarlenePS04.078
Cousineau Daoust Vincent..... **SP174.2**
Cowan Nicole SP028.5
Coyle James L..... SP052.3
Craft David.....PS04.015
Craig Tim SP117.5, SP130.2
Crain Melissa SP140.1
Cranmer-Sargison Gavin.....PS05.051
Crawford AnnaSP166.6
Crawford Bruce.....SP057.2
Crezee Johannes SP044.4, SP159.2
Cristancho Mejia Luis F..... PS04.030
Crook JuanitaSP078.4
Crowe Scott SP015.5, SP027.3,
..... SP036.5, SP176.2
Cruje Charmainne **SP091.2**
Cruz Juan Alberto L..... **PS04.025, PS05.014,**
..... **SP074.8**
Cruz Julio..... SP127.2
Cruz-Hernandez Juna Carlos.....SP129.2
Csset Istvan SP026.4
Cugura David..... SP05.029
Cui Fangsen SP053.3, **SP156.1**
Cunha Carneiro Pedro....PS01.015, PS01.016
Cunha Cleidson J.....SP114.1
Cunha Luis T.....SP047.1
Cunningham Ian A..... SP035.3, SP161.3
Curran Bruce **SP147.1**
Cury Fabio.....SP046.6
Custódio Renata A.R.....PS16.002, PS17.001
Cutiongco Marie F..... SP098.5
Cvetkov AsenSP125.3
Cyglar Joanna SP047.4, SP078.2,
..... SP174.3
Cymberknop Leandro J. SP082.1, **SP082.4**
Cymrot Raquel SP040.2
Cyr Bryce..... PS04.056
Cyue Nai Ruei.....SP019.3
Czap Ladislav SP026.4
Czarwinski Renate.....SP158.3
Cárdenas Alanís Claudia D.C. **SP085.4**
Cárdenas Alanís Claudia Del Carmen ...PS16.032
Cândido Murilo R..... PS01.019
Córdova Jency SP069.3
Córdova-Fraga Teodoro.....PS19.017
Côrrea João E.PS16.002, PS17.002
Côté Marie-France.....SP018.5

D

D'Afonseca Netto AluizioSP041.3
D'Esterre Christopher D..... SP097.1
D'Souza DavidSP173.3
Da Cruz Janir Nuno PS11.004
Da Silva Ademir X..... PS04.067
Da Silva Corrêa Vinicius P.....SP156.5
Da Silva Danilo M.D.D. **PS16.009, SP050.3**
Da Silva Paulo José G. SP135.4, SP135.5
Dadunashvili Sergo A. **PS13.003**
Dagrosa Alejandra..... SP015.1
Dahalan Rehir SP015.4
Dahdah N SP151.5

Dai Jianrong PS04.079, SP103.2
Dai Wenxuan **PS19.006**
Dai Xiangkun SP107.2
Dai Yu **SP167.3**
Dajani Hilmi R. SP111.7, SP111.8
Dalla Rosa David SP028.2
Dalton ColinSP032.3, SP032.5
Dalton TaraSP053.1
Daly Michael **SP110.3**
Damilakis John **MPE18.1, SP027.2,**
..... SP063.8, SP080.1,
..... SP125.3, SP154.1
Dannberg Gudrun SP039.2, SP039.3
Darafsheh Arash **SP139.1**
Darko Johnson PS04.037
Darling Gail SP003.7
Dartora Caroline M. SP035.1, SP100.1
Darvish-Molla Sahar.....SP109.1, **SP109.2**
Das Marco SP119.5
Daskalaki AnastasiaPS01.012, SP129.5
Daskalakis Zafiris J. SP101.1, SP101.2
Dasu Alexandru **PS04.026, SP094.2**
Date Hiroyuki SP049.3
Datta Sudip K. SP114.4
David Jakub.....SP120.4
David Marc SP046.6
David Mariano G.SP026.1, SP026.2, **SP026.3**
David Steven..... SP015.3, SP174.1
David Yadin B. **1351, BMEE20.1,**
..... **SP062.6, SP063.1**
Davidson Travis SP074.7
Davis JamesSP030.4, SP053.4,
..... SP059.2, SP059.3,
..... SP061.3, SP112.3
Davydenko George PS04.038
Day Brian SP146.1
De Almeida Carlos Eduardo PS05.042
De Bernardi Elisabetta..... PS04.088
De Boer Peter SP044.4
De Boer Steven **MPE04.2**
De Giobbe Jorge SP087.2
De Groot Friedl SP089.3
De La Fuente Liset.....SP057.6
De La Rocha-Encizo Raul PS12.032
De La Rosette Jean J.M.C.H. SP159.2
De La Vega José Carlos **SP161.2**
De Oliveira M.J.F.....SP180.2
De Pooter Jacco.....SP025.1
De Reijke Theo M.SP159.2
De Ribaupierre Sandrine SP023.3,
..... SP110.7, SP162.2, SP162.6
De Ridder MarkSP079.6
De Roman Mello Marco A. SP125.6
De Ruvo Paquale L.....SP150.3
De Sá Lidia V. SP085.3
De Vathaire Florent PS05.030, SP017.6
Dealmeida Carlos E. SP009.4, SP026.1,
..... SP026.2
Deasy Joseph O. SP088.2, SP122.6
Deb Arun K.....SP154.3
Deb PradipPS04.009, PS05.009, SP077.5
Debiais Fabienne **BMFE05.1**
Deblom FrancoisSP131.2, SP140.3
Debs Cecilia L. PS01.013
Debus JürgenSP158.7
Deepak Kishore K. SP114.4
Dehghan Ehsan SP003.3
Deist Timo M.SP102.2
Dekaban Mark.....SP070.6
Dekker Andre..... **SP102.2, SP102.3,**
..... SP102.8, SP169.2
Dekker Kurtis H.SP125.2, **SP155.4**
Delage Marie-Ève **SP049.4**
Delaney Geoff.....SP102.8
Deligiannakis Antonios SP020.3
Delinikolas Panagiotis G. **PS04.027**
Delis HarrySP099.1

Delogu PasqualeSP150.3
Delong Allison..... PS03.004
Delouya GuilaSP153.3
Delpon Gregory MPF10.1
Deman Pierre.....SP097.8
Demarse Thomas.....SP135.3
Dendale Remi.....MPF07.2, MPS03.1
Deng JunSP056.1
Deng Xiaowu PS04.076, PS04.122
Dengo Erlon C.PS13.002
Denham James W.SP078.3, SP078.5
Dermitzakis Aris..... **SP020.3, SP129.5**
Desai NiralSP106.6
Deschênes Sylvain **MPF07.2**
Descovich Martina MPE16.1
Deshpande Deepak SP003.1, SP038.3
Deshpande Shrikant.....SP153.5
Desplanques Maxime B.J. PS04.087
Després Philippe **MPF01.1, SP047.6,**
..... SP061.4, SP119.1,
..... SP119.4, SP149.2
Dessouki Omar..... SP064.2
Detappe Alexandre.....SP086.5
Devi Konthoujam M. PS04.074
Devi Reena SP003.1, SP038.3
Devic SlobodanSP142.4
Devpura Suneetha..... **SP046.4**
Dezi MirkoPS116.021
Dhani NeeshaSP070.7
Dheva Shantha Kumari G..... **PS05.015**
Dhont Jennifer **SP079.6**
Di Lillo Francesca SP150.3
Di Lorenzo Roberto SP102.5, SP108.4
Diallo Ibrahim PS05.030, SP017.6
Diamond KevinSP176.1
Dian Joshua A. SP178.1, **SP092.4**
Dias Anabela G..... **SP027.6**
Diaz Angelina.....SP097.2
Diaz Moreno Rogelio PS04.002, SP057.6
Dicarlo Amanda **SP126.7**
Diemoz Paul C.SP150.6
Dietrich Jennifer.....SP125.2
Dilvo Maria PS04.027
Dimitrijevic Milan R. SP008.6
Dimofte AndreaSP130.3
Ding HuanjunSP033.1
Ding HuijunSP095.5
Ding Kai **SP016.4, SP016.6,**
..... **SP073.7, SP097.5**
Ding XiaorongPS19.006
Dinh Christoph.....SP165.2
Diogo Lucília N. SP020.5
Dipilato Anna C.....SP108.4
Dirgayussa I G. PS04.080
Dirkse ColineSP124.5
Discher Dennis E. **BMEE01.1**
Disher Brandon **SP140.2**
Disney Gavin.....SP180.3
Distefano GailSP004.5
Djebbari Abdelghani SP151.5
Djoumessi Diane.....SP018.5
Dobashi Suguru.....SP079.3
Dodd Adam C..... **PS05.016**
Doessel Olaf **SP044.2**
Doganay Ozkan..... SP105.2, **SP105.5**
Doi Kouki **PS10.002, PS10.003,**
..... PS10.007, PS10.008, PS10.010,
..... PS10.011, PS12.011, SP145.6
Dolci Diego S. PS04.025
Dolney Derek **SP106.6**
Dominguez-Dominguez Rusbel.....SP112.6
Dominguez-Dominguez Sydney..... SP112.6
Dong NianguoSP156.2
Donin Gleb.....SP061.2, **SP103.1**
Donovan Ellen.....SP080.3
Dori Fabrizio..... PS16.024, PS16.025
Douglass Michael J.J.....PS19.004

- Dowling Jason..... SP072.1
 Doyle Maria..... SP083.1
 Doyle Thomas E..... PS12.002
 Doyle Timothy E..... SP028.4, SP028.5,
 SP028.6, SP061.6, SP098.2
 Drake James M..... PS07.005, PS07.006
 Drangova Maria..... SP034.8, SP104.4,
 SP111.3, SP126.3
 Dreossi Diego..... SP150.3
 Drepps Douglas..... SP062.6
 Dreuil Serge..... SP118.2
 Driscoll Brandon..... **PS01-006**, SP023.2,
 **SP180.3**
 Drosatos George..... SP169.6
 Druzgalski Christopher..... SP095.6, SP102.6
 Drzazga Zofia..... **SP013.2**, **SP162.5**
 Du Cheng-Fei..... **SP014.4**, SP156.4
 Du Jiang..... SP105.6
 Du Jun..... SP167.3
 Du Kaifang..... SP097.5, SP175.5
 Duane Simon..... SP025.1, SP038.2,
 **SP038.4**
 Duarte-Dyck David A..... **SP088.4**
 Dubois Ludwig..... SP018.1
 Dubok Vitalii..... SP012.2
 Duclos Marie..... SP046.6
 Dudek Nancy L..... SP066.3
 Dufva Martin..... SP030.2, SP030.3
 Duguay-Drouin Patricia..... **SP081.5**
 Duhaini Ibrahim..... PS04.003, SP158.4
 Duharte Carlos R..... **PS12.006**
 Dumont Amélie..... SP158.6
 Dunkerley David..... SP161.1
 Dunmore-Buyze Joy..... SP034.8
 Dunn Jr William D..... SP023.4
 Dunscombe Peter..... **MPE08.2**
 Duplan Danny..... SP006.2
 Dutra Douglas..... PS19.003
 Dutta Tilak..... SP087.4, **SP145.1**,
 SP145.2, SP145.5
 Dvořák Jan..... PS12.008, SP120.4
 Dávila Alex E..... SP103.5
 Dávila Torres Hermann..... PS10.004
 Dias Anabela G..... SP047.1
- E**
- Eade Thomas..... SP079.2, SP175.1
 Eagle Anton L..... SP068.4
 Eagleson Roy..... SP110.7
 Easaw Jacob C..... PS04.060
 Easty Tony..... **1497**, **JT05.1**, **JT05.2**,
 PS16.007, SP009.2, SP119.8
 Eberlein Uta..... **SP086.4**
 Ebert Martin A..... SP078.3, SP078.5
 Ebrahimi Hamid..... **SP146.5**
 Ecclestone Gillian..... **SP036.4**
 Echemendía-Montero Adan..... SP170.5
 Echnar Gernot..... SP016.3
 Eckhardt Kyle..... SP042.3
 Edmunds David..... **SP080.3**
 Efstathopoulos Efstathios..... PS04.027
 Eichard Roland..... SP165.3
 Eimil-Suarez Eduardo..... SP170.5
 Ejeta Kennedy O..... PS13.006, SP010.1,
 SP022.1
 Ekman Inger..... SP031.3
 El Alami Omar..... PS04.072
 El Bared Nancy..... SP006.2
 El Far Rodrigo..... SP154.2
 El Gamal Islam..... SP026.3
 El Garch Mohcine..... **BMEF01.1**, **BMEF02.1**,
 **BMEF04.1**
 El Haj Alicia J..... **SP002.2**
 El Naqa Issam..... PS04.088, **SP046.6**,
 SP069.2, SP072.6, SP076.5,
 SP096.2, **SP159.1**
 El-Hachem Nehme..... SP122.5
 Elam Mikael..... SP168.3
 Elbakri Idris..... SP149.3
 Eldib Ahmed..... SP107.6
 Elias Gustavo A..... SP093.3
 Elona Isabel A..... **PS05.017**
 Elpidio Fatima..... PS01.004
 Emami Zahra..... **PS11.003**
 Emnéus Jenny..... SP030.2, SP030.3
 Endo Masahiro..... SP081.3
 Endo Tetsuo..... PS16.013
 Endrizzi Marco..... SP150.6
 Enger Shirin A..... SP048.6, SP076.5, **SP106.5**
 Enjilela Esmaeil..... JT03.1, **SP149.5**
 Entezari Niloufar..... **SP163.5**
 Epstein Gilad..... **BMEE07.1**
 Erazo Mayra..... SP170.4
 Erickson Delnora..... PS05.020
 Erlich Felipe E..... PS04.067
 Escalona Iván..... **PS14.001**, **PS14.002**,
 **PS14.003**
 Escalona Omar J..... **SP007.3**, **SP053.5**
 Escobar Lourdes..... PS16.001
 Eslava Javier..... **SP102.6**
 Eslick Enid..... SP077.6
 Espagnet Romain..... **SP061.4**
 Espino Daniel M..... SP112.1
 Espinosa Medina Marco A..... SP041.7
 Espinosa-Barrios Joel..... **SP060.3**
 Espinoza Ignacio..... SP076.2
 Esposito Alessandro..... **SP025.3**, **SP047.1**
 Esposito Marco..... SP143.1
 Etemadi Zahra..... PS01.002, SP045.3
 Eubanks James H..... SPO92.1
 Evans Andrew H..... SP121.5
 Evans Simon..... SP177.5
 Evertz Florian..... PS02.003
 Eyadeh Molham..... **SP176.1**
 Ezejiofor Tobias I.N..... SP148.6
- F**
- Fabiani Stefania..... SP108.4
 Factor Rachel E..... SP028.4
 Fadhel Muhannad N..... **PS09.004**
 Fahrig Rebecca..... **SP011.4**, **SP065.1**,
 SP065.2, SP065.4, SP065.5
 Fainardi Enrico..... SP046.2
 Fairbrother Amy..... SP028.6
 Falk Tiago H..... SP135.2
 Fallone B Gino..... SP016.2, SP105.3, SP164.7
 Fan Mark..... SP119.8
 Fan Michael..... **SP131.2**
 Fan Zhencheng..... **SP029.7**
 Fanti Viviana..... SP150.3
 Faragallah George..... SP151.3
 Farahani Mohammad Hossien..... SP035.6
 Faria E Sousa Sidney J..... PS12.033
 Faria Sergio..... SP046.6
 Farias Ribeiro Maycon Emely F..... SP074.8
 Farr Jonathan B..... SP116.5
 Farrokhkish Makan..... **SP090.1**
 Farzan Faranak..... SP101.1, SP101.2
 Farias Rubén..... SP015.1
 Fast Martin F..... **SP164.1**
 Fathi Anahita..... SP128.4
 Fatnassi Chemseddine..... **PS01-007**,
 **SP013.1**, **SP013.3**, **SP036.8**
 Fatunde Olumurejiwa..... SP093.2
 Favero Mariana S..... SP035.1
 Fayssal Iyad..... **PS19.007**, **SP126.5**, **SP159.3**
 Feain Ilana..... SP077.6
 Fedon Christian..... SP150.3
 Fedorov Kiril..... **SP098.3**
 Fedotov Aleksandr A..... PS09.001, SP007.2
 Fehr Duc..... SP088.2
 Feld Diana..... PS04.014
 Feltrin Renan..... PS16.031
 Fenineche Nourdine..... SP037.2
 Fennell Lynda..... SP141.2
 Fenster Aaron..... **JT08.1**, SP003.5,
 SP028.7, SP029.3, SP116.4,
 SP162.2, SP162.6,
 **SP167.1**, SP173.3
 Fergiawan Aditya..... PS04.075
 Fernandes Gustavo..... SP066.5
 Fernandes Ramon C..... **SP001.5**
 Fernandez Gonzalez Francisco..... SP076.7
 Fernandez-Letón Pedro..... **MPS05.1**
 Fernando Dayantha..... PS04.001
 Fernie Geoff..... SP145.2, SP145.5
 Fernández María..... SP086.4
 Ferreira Adelaide..... PS16.038
 Ferreira Ana L..... **PS07.004**
 Ferreira Barb..... SP123.3
 Ferreira Ernando S..... PS04.025, PS05.014,
 SP074.8
 Ferreira Fernanda C.L..... PS01.003, **SP033.2**,
 **SP033.4**, **SP114.1**,
 **SP114.3**, SP171.5
 Ferreira Filho José A..... PS12.026, PS16.003,
 PS17.001
 Ferreira Taissa O..... PS01.019
 Ferri Carlos A..... **PS12.007**
 Feygelman Vladimir..... SP097.5
 Fhager Andreas..... SP168.3
 Fiave Prosper A..... SP110.2
 Fichou Denis..... SP053.2
 Fichtinger Gabor..... PS04.087, **SP003.6**,
 SP080.2, SP080.5,
 SP130.6, SP162.8
 Fico Giuseppe..... **SP169.3**
 Fiedler Patrique..... **SP134.1**, SP165.3
 Field G. Colin..... SP063.2, SP164.7
 Field Matthew..... SP102.8
 Filip Sanda M..... PS19.016
 Fillion Olivier..... **PS04.028**
 Fink Simone..... PS04.084
 Finlay Jarod C..... SP139.1
 Fiset Jean-Yves..... **MPF05.2**
 Fiset Sandra..... **SP064.3**
 Fisher Sandra..... SP153.5
 Fleissner Frederik..... SP139.5
 Fletcher John J..... SP027.2
 Flint David..... SP176.4
 Florian Joly..... **PS19.008**
 Foglyano Kevin M..... SP166.2, SP166.3
 Followill David..... SP107.1
 Foltynski Piotr..... **SP113.5**
 Foltz Warren..... SP023.2
 Fonseca Carlos..... SP134.1
 Fonseca-Pinto Rui..... **SP020.5**
 Fontaine Réjean..... SP035.5
 Foormany Farbod H..... PS19.002
 Foos David..... SP097.3
 Footitt Claire..... PS04.054
 Ford Eric..... **JT07.1**
 Ford Nancy L..... **SP097.8**, SP149.7
 Forde Ryan..... **BMEE09.1**
 Forini Nevio..... SP108.4
 Fortin Marc-André..... SP018.5, SP049.1
 Foss Victoria C..... SP107.4
 Foster Paula J..... SP018.2
 Fournier-Bidoz Nathalie..... SP142.1
 Fox David..... SP049.5
 Fraass Benedick A..... **MPE05.2**, **MPE15.2**
 Francis Ros..... SP097.6
 Franco Leo D.O..... SP026.2
 Franco Marcelo L.N..... PS01.018
 Franich Rick D..... SP077.4
 Fraser Correen..... SP056.2

Frayne Richard **JT01.2**
 Freda Paola PS14.004
 Fredriksson Albin **SP036.1**
 Freedman Gary SP130.3
 Freestone Peter S. SP060.1
 Freire Bastos Teodiano..... **SP144.6**
 Freitas Maria Isabel P..... PS16.028
 Frenger Paul **PS19.009**
 Frenière Normand..... **MPF05.1**
 Fridolin Ivo SP147.3, SP167.5
 Friedland Werner PS05.036
 Friedrich Bárbara Q. **SP129.6**
 Friesen Cindy BMEE01.2
 Frimeth Jeff **PS16.010, SP158.1, SP161.4**
 Fritzsche Paul SP170.1
 Frize Monique **JT04.1, PL01.1, SP043.1, SP043.2, SP170.2**
 Froner Ana Paula P. PS01.018
 Frosini Francesco PS16.024, PS16.025
 Fu Wen-Mei SP028.3
 Fujimoto Hiroshi PS10.002, PS10.007, PS10.008, PS10.010, PS10.011
 Fujimoto Nozomi PS04.081
 Fujioka Tomomi PS16.013
 Fujisaki Tetsushi PS16.013
 Fujita Hideki **SP01.008**
 Fujiwara Naoko **PS13.011**
 Fukuda Haruyuki PS01.008
 Fukuda Keisuke SP071.3
 Fukuda Koji SP066.4
 Fukuda Shigekazu SP048.2, **SP142.5**
 Fukumura Akifumi SP026.8
 Fukunaga Kouta PS05.050
 Funk Marjorie **BMEE20.1**
 Funk Richard SP032.4
 Furey Andrew PS03.004, SP083.1
 Furquim Tania A.C. SP118.5, SP172.1
 Furuichi Akihumi SP055.1
 Furukawa Akira **PS19.010**
 Furusawa Yoshiya SP049.6

G

Gaamangwe Tidimogo PS16.005
 Gabos Zsolt SP016.2
 Gabriel Ana Teresa PS16.038, **PS19.011, SP146.2**
 Gabriel Joaquim PS07.004
 Gaede Stewart **MPE06.1**, SP005.5, SP104.4, SP130.1, SP156.7
 Gaede Stuart SP140.2
 Gaeni Shaghayegh SP086.3
 Gagne Isabelle SP140.5
 Gago Araceli A. MPS11.1
 Gago Arias Araceli **SP076.2**
 Gajewski Jan SP155.3
 Gal Alicia M. **SP008.9**
 Galan Sandra SP085.4
 Galea Michael SP119.2
 Galea Raphael SP037.5
 Galiano-Riveros Eduardo PS16.010, SP161.4
 Galvan Hector PS05.041
 Gameil Khalid SP037.5
 Garcia Contreras Oscar J. **PS04.029, PS04.030**
 Garcia Fernando PS04.005
 Garcia Lourdes M. SP06.002
 Garcia Luis G. PS05.013
 Garcia Martha G. **SP041.4**
 Garcia Renato PS16.031
 Garcia-Hernandez Juan Carlos SP118.2
 Garcia-Hernandez Maria Trinitat PS04.081
 Garcia-Liashenko Klaudia SP170.5
 Garcia-Pérez Marysol **SP083.3**

García-García Berta SP100.41
 García-Gómez Sergio MPS02.1, MPS06.1
 Gardi Lori SP003.5
 Garnier Gil SP157.2
 Garranchán Fabiana PS14.001
 Garrigó Edgardo PS04.108, PS04.109, PS04.110, SP036.6
 Gattafoñi Mariano SP102.5
 Gaudin Émilie **SP035.5**
 Gaudreau Chloé SP158.6
 Gaudreault Mathieu SP018.4
 Gautam Prakash D. SP118.4
 Gauvin Alain **MPF06.1**
 Gavrilovic Bojan **SP120.6**
 Gazdhar Amiq SP110.2
 Ge Yaorong PS04.120, SP117.4, SP117.6
 Gebauer-Hötzel Lena SP158.7
 Geijssen E.D. SP159.2
 Geiser Thomas SP110.2
 Gellissen Nicky N. SP172.3
 Gelman Daniel **SP111.3**
 Gemma Corrado PS16.019, SP093.4
 Gennari John SP102.1
 Genov Roman SP121.4
 Gentle David SP006.4, SP118.6
 Gentles Bill **BMEE23.1, BMEF02.1, JT02.2, SP148.5**
 George Paul V. SP108.1
 Gerla Vaclav **SP165.1**
 Germond Jean-François SP152.4
 Gershkevitch Eduard **SP057.1**
 Gershkevitch Mihail SP057.1
 Gete Ermias SP152.6
 Gevaert Thierry SP079.6
 Ghafar Zadeh Ebrahim **PS19.012, SP178.4**
 Ghafarian Pardis PS01.002, **PS05.018, SP037.4, SP045.2, SP045.3, SP045.4, SP070.4, SP128.4, SP179.1**
 Ghahari Alireza SP178.7
 Ghanbarzadeh Sina SP168.4
 Ghandour Sarah PS04.068
 Ghareh Baghi Arash 2507
 Gharehbaghi Arash SP031.3, SP031.5
 Ghenaati Hosein SP033.5, SP171.1
 Ghimire Navagan SP118.4
 Ghobadi Kimia **PS04.031**
 Gholami Somayeh SP152.2
 Gholampourkashi Sara **SP047.4, SP148.1**
 Ghosh Priyajit **SP148.1**
 Giacometti Valentina SP034.5
 Giambattista Joshua PS04.065
 Giani Giuliano SP090.6
 Giannini Barbara PS08.001
 Giatrakos Nikos SP020.3
 Gibson Chris SP022.2
 Gibson Eli SP116.4
 Giger Maryellen L. **SP011.2**
 Gil Lahav **BMEE24.1**
 Gilbert Penney SP002.4
 Gilbert Rachel SP009.2
 Gilchrist Jeff SP170.2
 Gill Bradford SP161.2
 Gillies Robert J. SP122.5
 Gillin Michael PS04.115
 Gilling Dawn PS04.005
 Gingras Luc PS04.028
 Girard Frédéric **PS04.032, SP057.7**
 Giuliani Maximiliano A. SP139.6
 Giusti Valerio SP048.6
 Givhechi Sogol SP159.4
 Glasmacher Birgit **PS02.002, PS02.003, PS02.004, PS02.005, PS02.006, SP012.2, SP071.4, SP151.1**
 Glass Lisa **PS04.033**
 Glenni Robb SP149.5
 Glick Daniel SP06.007

Glide-Hurst Carri SP072.4
 Glowa Christin PS05.044
 Gnirs Regula SP016.3
 Gobbi David G. PS04.060
 Godin Marcelo PS16.010
 Godinez-Tello Richard SP165.4
 Goertzen Andrew SP070.3
 Goetsch Steven **MPE14.1**
 Goffin Christine **SP055.5**
 Goh James Cho-Hong PS02.009
 Golaraei Ahmad SP157.3
 Goldenberg Andrew A. ... PS07.005, PS07.006
 Goldman Stephen SP002.1
 Golosio Bruno SP150.3
 Golovko Tatyana SP019.2
 Golrokh Nodehi Mohammadrasa PS05.018, SP179.1
 Golrokh Rasa PS05.034
 Gomes Leonardo M. PS16.036
 Gomes Marília M.F. PS16.006
 Gomes Ricardo PS19.011
 Gomes Rodrigo D.M. SP162.1
 Gomez Monica D. **SP040.5**
 Gomez-Zepeda Mario SP129.2
 Gomola Igor SP026.4
 Goncalves Victor Hugo L. SP156.5
 Gong Benwei SP001.2
 Gong Hanshun PS04.118
 Gong Qin **SP020.3, SP074.3**
 Gonzales Alejandro H.L. SP177.2
 Gonzales Chryzel Angelica B. **SP108.3**
 Gonzalez Dave A. SP008.7
 Gonzalez Patrick SP057.5
 Gonzalez Rene SP074.2
 Gonzalez Ricardo SP113.7, SP170.4
 Gonzalez Yelina SP057.6
 Gonzalez-Castaño Diego Miguel MPS10.1
 González Sara SP015.1
 González Verence SP069.3
 González Wilfredo **PS04.034**
 González-Fernández René PS12.003, PS12.004, PS12.020, **PS13.004, PS13.005**
 González-Villa Eduardo A. **PS04.035**
 Goo Yongsook PS09.003
 Goodfellow Jonathan SP007.3
 Gozee Gary PS04.117
 Gordon James J. SP056.3, SP056.4, **SP076.1**
 Gorji Ensieh SP033.5, SP105.4
 Gorji Ensiyeh SP049.2, SP171.1
 Goshulak Peter **SP064.1**
 Gospodarowicz Mary **PL03.2**
 Gotanda Rumi **PS01.009, PS05.019, PS05.023, PS05.045, SP005.3, SP067.1**
 Gotanda Tatsuhiro PS01.009, PS05.019, PS05.023, PS05.045, SP067.1
 Gotti Annick MPF06.2
 Goubran Maged SP023.3
 Goudjil Farid MPF07.2, MPS03.1
 Gouldstone Clare SP004.5
 Goussard Yves SP149.2
 Goyal Riya **PS04.036**
 Gracia Federico SP010.7
 Grafe James SP090.4
 Graichen Uwe SP165.3
 Graig Lynne SP054.4
 Granada Talita C. PS01.015
 Grant Charles E. SP122.4
 Grant Jeffrey PS03.003
 Granton Patrick V. SP018.1, **SP018.4**
 Graves David B. **BMEE21.2**
 Green David SP070.7
 Green Garrett PS04.001
 Green James R. SP102.4, **SP122.1,**

- SP122.7
 Green Rylie A..... SP071.1
 Greenall Julie..... **BMEE15.1**
 Greene Helena..... **PS03.004**
 Greenwald Steve..... PS16.004, PS16.030
 Greenwood Murray..... **BMEE16.1**
 Greer Lester L..... PS04.038
 Greilich Steffen..... SP163.2
 Greto Daniela..... SP090.6
 Gretzinger Dave..... SP123.2
 Griebel Stefan..... SP134.1
 Griffin Melissa..... PS16.007, **SP009.2**
 Grigorov Grigor N..... **PS04.037**
 Grigorovsky Vasily..... **SP178.2**
 Grimes Josh..... **SP034.6, SP115.3, SP115.7**
 Grochowska Paulina..... PS04.046, PS05.022, PS16.014, SP067.4
 Grosse-Wentrup David..... **SP009.1**
 Grossmann Patrick..... **SP122.5**
 Grove Olya..... SP122.5
 Groves Elliott..... SP171.4
 Groza Voicu Z..... SP111.8
 Grynberg Sueley E..... PS05.031
 Gryshkov Oleksandr..... PS02.002, SP012.2, SP071.4, SP151.1
 Grzadziel Aleksandra..... SP155.3
 Gsrcia Salvador..... SP105.8
 Gu Hanqing..... PS02.011
 Gu Zhaoyong..... **SP156.2**
 Guardiola Consuelo..... SP139.1
 Guarino Maria P..... SP020.5
 Guatelli Susanna..... SP025.5, SP081.4
 Guedes Pereira Marco A..... SP068.1
 Gueorguiev Gueorgui..... PS04.087, SP057.2
 Guerguerian Anne-Marie..... SP103.4
 Guerra Juliana M..... **SP032.4**
 Guillemette Maxime..... SP006.3
 Guillen-Peralta Alejandra..... PS12.032, SP020.4, SP060.3, SP062.5, SP088.4
 Guo Bin..... SP04.061
 Guo Dan..... **SP095.5**
 Guo Fuxin..... SP164.3
 Guo Jianzhong..... **PS19.013**
 Guo Junchao..... SP014.4, **SP156.4**
 Guo Kaiming..... PS04.105
 Gurvich Victor A..... **PS04.038, PS05.020**
 Guthier Christian V..... **SP175.4**
 Gutierrez Mardemis..... PS14.003
 Gutierrez Sánchez Guadalupe D.J..... PS16.032
 Gutman David A..... SP023.4
 Guvenis Albert..... **PS01.010, SP088.3**
 Gómez Faustino..... **MPS10.1, MPS11.1,** PS05.043
 Gómez Medina Maria F..... SP051.2
 Gómez Miguel..... PS12.003
 Gómez-Muñoz Arnulfo..... SP038.5
- H**
- H. Gazestani Vahid..... SP127.4
 Haasbeek Cornelis J.A..... SP046.1
 Haber Tobias..... SP039.3
 Habib Robert..... PS19.007, SP159.3
 Habor Daniel..... SP179.3
 Haddad Cecília M.K..... SP068.2
 Haddad Seyyed Mohammad Hassan..... **SP126.3**
 Hadway Jennifer..... SP070.6
 Haering Peter..... PS04.085
 Hagen Charlotte..... SP150.6
 Haghgoo Soheila..... SP033.5, SP049.2, SP105.4, SP171.1
 Hai Yuan..... SP001.4
 Haibe-Kains Benjamin..... SP122.5
 Haider Masoom A..... PS01.027
 Haider Raza..... SP081.2
 Hajdok George..... SP140.2
 Hamai Satoshi..... PS03.005
 Hamarneh Ghassan..... SP072.3
 Hamel Louis-André..... SP061.4
 Hammond Alex..... SP164.2
 Hammond Robert R..... SP023.3
 Hamza Sarah..... PS10.005
 Han Chungmin..... **SPO92.2**
 Han Su Chul..... SP06.005
 Han Taejin..... PS05.039
 Han Youngyih..... SP048.5
 Hanada Eisuke..... PS16.016
 Hanada Takashi..... **PS04.039**
 Hanada Kiyofumi..... **SP048.1**
 Haneishi Hideaki..... SP139.4
 Hansen Christian..... SP153.5
 Hanu Andrei R..... SP109.1, SP109.2
 Hao Yao..... SP080.4
 Hao Yu Jin..... **SP064.5**
 Haque Kh Anamul..... **SP005.2**
 Hara Daisuke..... PS03.005
 Haraldsson André..... PS04.054
 Harari Paul..... SP175.5
 Harba Rachid..... SP088.1
 Hardcastle Nick..... SP140.1
 Harder Samantha J..... **SP030.5**
 Hardisty Michael..... SP088.5
 Harisinghani Mukesh..... **BMEE22.2**
 Haritou Maria..... SP123.4
 Hariu Masatsugu..... **PS04.040**
 Harriss-Phillips Wendy..... SP076.4
 Haryanto Freddy..... PS04.080, SP001.6, SP158.8
 Hasan Md.Mahmudul..... PS04.045
 Hasan Muhammad A..... **SP039.4**
 Hasani Mohsen..... SP017.2
 Hashikin Nurul A.A..... SP015.4, SP025.5
 Hashimoto Takayuki..... SP049.3
 Hashizume Makoto..... PS07.007
 Hashtrudi-Zaad Keyvan..... SP144.2
 Hassad Osama..... PS04.054
 Hassan Sabah..... SP087.4
 Hasselbacher Thomas..... SP049.5
 Hatt Charles R..... **SP029.5**
 Hattori Hiroyuki..... PS01.008
 Hau Herman..... SP015.2
 Hauelsen Jens..... SP134.1, SP165.2, **SP165.3**
 Havlik Jiri..... PS12.015
 Havlik Jan..... **PS12.008, SP120.4**
 Haworth Annette..... SP054.4, SP077.4
 Hay Dean C..... SP008.9, SP050.4
 He Baochun..... SP001.2
 He Jiang..... PS08.002
 He Jie..... SP096.3, SP096.4
 He Qichi..... SP069.4
 He Qun..... SP105.6
 Heap Ruby..... **SP043.2**
 Heath Emily..... SP036.3, SP047.4, SP058.5, SP174.2
 Heath Jennifer..... PS13.001
 Heaton Robert K..... PS04.063, PS04.106, SP090.1, **SP131.7**
 Heckman Michael..... SP077.2
 Hedley David..... SP070.7
 Hedman Mattias..... SP094.2
 Hegarty Elaine..... SP105.2, SP105.5
 Heger Stefan..... SP179.3
 Heikal Amr A..... **SP105.3**
 Heinke Matthias..... **SP039.2, SP039.3**
 Heinke Tobias..... SP039.2, SP039.3
 Heinrich Zdravko..... SP067.3
 Heiskanen Arto..... SP030.2, SP030.3
 Hellström Thomas..... SP145.3
 Hemm-Ode Simone..... **SP121.2**
 Herath Sisira..... PS04.009, PS05.009, SP077.5
 Herlevin (Gérard) Karine..... **MPF08.2**
 Hermannsdörfer Thomas..... SP112.2
 Hermosilla Alvaro..... SP057.6
 Hernandez Antono..... **BMES03.1**
 Hernandez Beatriz..... **PS12.009**
 Hernandez Erick E..... PS05.013
 Hernandez Reyes Benjamin..... **PS04.041**
 Hernandez-Zacarias Bettsy..... **SP062.5**
 Hernández-Bojórquez Mariana..... PS04.111
 Hernández-Guzmán Abel..... SP038.5
 Hernández-Oviedo Jorge O..... PS04.111
 Herod Tyler W..... SP089.2
 Herrera Gomez Angel..... PS16.032
 Herrero Laura..... PS16.001
 Hervieux Yannick..... SP105.4, SP153.3
 Hesabgar Seyyed..... **SP094.3**
 Hess Maggie..... **SP162.8**
 Hesser Juergen W..... SP175.4
 Heydarnezhadi Sara..... SP033.5, SP105.4, SP171.1
 Heß Markus..... SP113.4
 Hickey Megan..... SP097.3
 Hidalgo Pilar..... SP030.7
 Hierso Eric..... SP142.1
 Higa Masaru..... **SP066.4**
 Higaki Hidehiko..... PS02.007, PS03.005
 Higby Christine..... PS04.054
 Highnam Ralph..... SP172.2
 Hilfi Hal..... **BMEE13.1, BMEE26.1**
 Hilgers Gerhard..... PS05.010
 Hill Sue..... SP022.2
 Hilton Trevor..... SP135.1, SP092.3
 Hilts Michelle..... SP058.5, **SP078.4**
 Himukai Takeshi..... SP081.3
 Hindocha Naina..... SP129.1
 Hinds Monica T..... SP098.5
 Hinrikus Hiie..... SP050.5
 Hinse Martin..... PS04.032, SP006.2
 Hintenlang David..... SP077.2, SP077.3, SP077.7
 Hintenlang Kathleen..... SP077.2, SP077.3, SP077.7
 Hirano Susumu..... **SP162.4**
 Hiraoka Masahiro..... SP025.4
 Hirayama Ryoichi..... SP049.6
 Hirose Minoru..... PS16.013, PS16.016
 Hirtz Gangolf..... SP113.4
 Hisamoto Miki..... PS01.009
 Hiscock Rochelle..... PS04.073
 Hissoiny Sami..... SP047.2
 Hlubik Jan..... **SP112.7**
 Ho Cheryl..... PS04.065
 Ho Pei..... SP053.3
 Hoang Peter..... **SP036.2**
 Hoelscher Uvo M..... SP009.1
 Hoeschen Christoph..... SP037.3
 Hofer Ernst..... **SP125.4**
 Hoffman Michael M..... **SP122.4**
 Hofmann Nicola S..... PS02.002, SP071.4
 Hofmann Ulrich G..... **SP121.1**
 Hohnloser Peter..... SP145.3
 Holder David..... SP030.2
 Holdsworth David..... SP034.8, SP094.3
 Hollebeek Robert..... SP106.6
 Holloway Lois..... PS04.117, SP072.1, SP102.8, SP153.6
 Holmar Jana..... SP167.5
 Holmberg Ola..... 2849, **MPE07.2**
 Holterhoff Anne..... SP055.5
 Holub Martin..... **PS09.005**
 Homma Dai..... 2955
 Hong Hai Fa..... SP156.6
 Hong Haifa..... PS02.013
 Honjo Haruo..... SP082.3
 Hooper Stuart..... SP150.7
 Hoover Douglas..... SP164.2, SP173.3

Horn Michael R. **SP032.2**
Horta Francisco A. PS19.017
Hosaka Naoto..... SP06.006
Hosea Fred W..... SP062.6, **SP084.6**,
SP168.5
Hosokawa Ren PS16.013
Hosono Minako **SP051.3**
Hosseini Soheil SP035.6
Hoteida Masahiro SP026.8
Hounsell Marcelo D.S. SP008.3
House Michael..... SP078.3, SP078.5
Howcroft Jennifer **SP120.2**
Howie Stephen R. SP093.1
Hoy Carlton..... SP034.7
Hradetzky David **SP110.2**
Hrinivich William T..... **SP173.3**
Hršak Hrvoje..... **SP067.3**
Hsiao Amy..... PS03.004, SP083.1
Hsieh Cho-Han..... SP101.4
Hsieh Jiang SP149.5
Hsu Shu Hui PS04.009
Hsu Yu-Hone SP028.3
Hu Hongjie..... SP097.4
Hu Liqin SP065.3, SP143.4
Hu Qingmao SP001.2
Hu Xiaolei..... SP145.3
Hu Yong PS11.004, SP178.6
Hu Zhihui SP103.2
Huang Botian..... PS04.076
Huang Chen-Yu **PS04.042**
Huang Chih-Chung 2957
Huang J SP127.2
Huang Peng..... PS04.079, SP103.2
Huang Shaomin..... PS04.122
Huang Sheng-Cheng PS03.010, **SP126.1**
Huang Yao X..... SP064.5
Huang Yao-Xiong **PS08.002**
Huang Yun Hu SP049.5
Huang Yun-Peng SP014.4
Huang Zhong B. PS02.014
Huang Zhongbing..... **SP071.5**
Huang Ziwei..... **SP084.5**
Huang Zong-Syuan SP040.3
Hubalewska-Dydejczyk Alicja PS01.024
Hubbard Logan SP171.4
Hudigomo Pamungkas PS04.075
Hudson Alana SP063.2, **SP124.5**
Huerta Monica..... SP113.7, SP169.5, SP170.4
Huerta-Franco María Raquel..... SP083.3
Hugtenburg Richard P. SP177.5
Huh Hyun Do..... **PS05.021**
Huh Yong-Min..... PS05.039
Huizenga Henk SP004.6
Hulshof Maarten C.C.M. SP159.2
Humphries Mark..... PS12.025, PS16.029
Hung Chun-Yu SP131.3
Hunt Peter SP175.1
Hunting Darel..... SP069.1, SP086.1
Huptych Michal..... SP165.1
Huq Mohammed S. 2944, SP009.4
Hur Kwangja PS12.017
Hurley Robert F..... SP034.5
Husain Siraj PS04.113
Husar Peter..... SP170.1
Husssein Khalid I. PS05.001
Hwang Sinchun SP088.2
Hwang Taejin PS05.039
Hyde Derek..... **PS04.043**
Hynning Elin..... **PS04.044**
Häfeli Urs O..... SP161.2
Hämäläinen Matti S. SP165.2
Hårdemark Björn SP072.2, SP131.5

I
ladanza Ernesto..... **PS16.011**, **PS16.012**,
..... PS16.021, PS16.024,
..... PS16.025, SP062.4
Iakovenko V SP142.2
Iakovenko Viktor **SP058.2**
Ibbott Geoffrey S. MPE18.2, **SP081.6**,
..... SP107.1, SP133.1, **SP176.4**
Ibey Andrew..... **SP123.3**
Ibrahim Fatimah..... **PS09.006**
Ibrahim Salma..... SP176.2
Ichimura Kouhei..... **PS12.010**
Ideguchi Tadimitsu PS05.019
Idrobo Pizo Gerardo A..... SP020.2
Ikebe Satoru PS02.007, **PS03.005**
Imagawa David PS04.001
Immelt Jeff **PL02.1**
Inagaki Miki PS13.011
Infante Wilfredo G. PS04.025
Infantosi Antonio F.C. SP041.3, **SP135.4**,
..... **SP135.5**
Ingleby Harry SP070.3
Inkoom Stephen **SP027.2**
Inness Emma..... SP176.2
Ino Shuichi..... PS10.003, PS12.005,
..... **PS12.011**, SP051.3, SP145.6
Iordachita Iulian SP016.4, SP016.6,
..... SP073.7
Iori Mauro SP025.3
Iramina Keiji SP050.2
Irazola Leticia..... MPS09.1, PS04.081,
..... PS05.043, SP154.2
Irish Jonathon..... SP003.7, SP061.5, SP110.3
Isa M PS04.019, SP133.1
Ishida Kai **PS16.013**
Ishihara Yoshitomo **SP025.4**
Ishikawa Atsushi PS02.007
Islam Kashif SP081.2
Islam Md. Anwarul **PS04.045**
Islam Mohammad K. PS04.063, PS04.106,
..... SP090.1, SP131.7
Ismaeel Hussain PS19.007, SP159.3
Ismail Munirah PS12.018
Ismailova Elina **SP035.3**
Ismer Bruno..... SP039.3
Ison Keith..... PS16.008, **SP022.2**
Ivlev Ilya SP061.2, SP103.1
Ivosev Vladimir..... SP049.6
Iwaki Tomohiro **PS12.012**
Iwamoto Yukihide PS02.007, PS03.005
Iwasa Stephanie **SP002.3**
Iwuji Samuel C. SP148.6
Ixquiac Milton E. SP107.3
Izewska Joanna..... **MPE07.1**, **PS04.046**,
..... **PS05.022**, **PS16.014**, **SP026.4**,
..... **SP067.4**, SP075.1, SP099.1

J
Jaberi Ramin SP049.2
Jackson Michael..... SP077.6, SP081.4
Jacobs Daniel..... **SP135.1**, SP092.3
Jafari Amir Homayoun SP128.4
Jafari Shakardokht M. **SP004.5**
Jaffray David A. **JT05.1**, **JT05.2**,
..... PS01.027, PS04.031, PS04.087,
..... PS19.002, SP003.7, SP016.5, SP023.2,
..... SP046.5, SP059.5, SP061.5,
..... SP070.7, SP072.2, SP080.5, SP110.3,
..... SP130.2, SP131.6, SP131.7, SP180.3
Jakstas Karolis SP155.7
Jakubek Jan SP048.4
Jalkanen Ville..... SP167.6
Jamal Norial SP158.8
Jambi Loyal K. SP139.3

Jamema S V SP003.1, SP038.3
James Christopher..... SP169.4
Jan Hao-Yu..... SP126.1
Janaczek Jacek SP100.3
Janerot-Sjoberg Birgitta SP031.3
Jang Hong Seok..... PS05.025, SP027.5
Jang Hyun Soo..... SP04.007
Jang Jun Keun **SP173.1**
Jans Hans-Sonke PS04.070
Janss Armin..... SP147.4, SP179.2
Jaramillo Diaz Ricardo..... **PS10.004**
Jaron Dov PS19.014
Jaseer K SP108.2
Javan Hanna..... SP171.4
Jaywant Satish **SP113.3**
Jean-Pierre Antonella MPF06.2
Jechel Christopher **PS04.047**
Jensen Michael D. SP018.2, **SP018.3**
Jeon Beom Seok..... PS09.008
Jeon Hyo Seon PS09.008
Jeong Gwang-Woo **SP105.7**
Jeong Hieyong **PS03.006**
Jeong Yujin **SP170.3**
Jermoumi Mohammed..... **SP080.4**
Jestrovic Iva..... SP052.3
Jeukens Cecile R..... **SP119.5**, **SP172.3**
Jeyaseelan Asha K. SP046.6
Jeřábková Silvie SP103.1
Jhingran Anuja..... SP107.1
Ji Jing SP089.1
Ji Young Hoon PS05.021, SP06.005
Jia Fucang **SP001.2**
Jia Gu SP001.4
Jia Jing SP143.4
Jia Rongxi..... SP156.2
Jia Xun SP106.2
Jiang Chenyu..... PS12.027
Jiang Chuan PS02.013
Jiang Runqing **SP140.4**
Jiang Steve B..... SP106.2, **SP117.1**
Jiang Wenlei SP128.3
Jiang Yinlai SP008.4
Jiang Yuliang SP164.3
Jimenez Erendira..... SP085.4
Jimenez Moyao Gabriela..... SP085.4
Jimenez Pablo 2849, SP099.1
Jiménez Daniel PS12.003
Jiménez-Ortega Elisa MPS02.1, MPS06.1
Jin Dawei SP103.2
Jin Sunjin SP163.4
Jin Xiance **SP175.2**
Jingu Keiichi SP079.3
Jirasek Andrew..... SP030.5, SP058.1,
..... SP058.5
Jo Byungdu **SP034.4**, SP149.8
Jo Gwang Hwan PS05.021
Jobbagy Akos **SP111.4**
Jochems Arthur T.C..... SP102.2, SP169.2
John Vijay SP138.2
Johns Gregg..... **SP144.2**
Johns Paul C. PS01.001, **SP150.1**
Johnson Carol SP046.3
Johnson Denise..... SP051.4
Johnson James SP122.4
Johnson Michel J. SP050.4
Johnson Peter PS07.001
Johnson Robert P. SP034.5
Joiner Michael **MPE09.2**
Jolly David SP015.3, SP174.1
Jones Ian SP169.4
Jones Kevin C..... **SP142.3**
Jones Mary..... SP121.5
Jonkers Ilse..... SP089.3
Joppek Christoph..... PS09.010
Jordan Kevin J..... SP005.5, SP125.2,
..... SP155.4

- Jordan Kevin T..... **PS04.048**
 Joseph David J..... SP078.3, SP078.5
 Joshi Chandra P..... SP003.6, SP107.5
 Joshi Kishore..... SP003.1, SP038.3
 Joung Sanghyun..... PS12.017
 Judd Thomas M..... **2895, PS16.015, PS17.005**
 Judd Tom..... **SP042.1**
 Julkunen Petro..... **PS01.011, PS12.013,**
 SP128.1
 Juneja Prabhjot..... **SP079.2, SP153.5,**
 **SP175.1**
 Jung Andrew J..... SP090.1
 Jung Haijo..... SP06.005
 Jung Jae-Hong..... SP04.094
 Jung Joo-Young..... PS04.096, PS04.097,
 PS04.101
 Jung Sang Hoon..... SP048.5
 Jung Won Gyun..... PS04.093
 Juresic Ewa..... PS04.117
 Jurickova Ivana..... **PS04.049, PS12.014,**
 **PS12.015, SP061.2**
 Jäger Rudi..... SP170.1
 Jäkel Oliver... **MPE16.2, PS04.085, SP048.4,**
 SP125.5, SP158.7, SP163.2
 Järnefelt Gustaf..... PS12.013
- K**
- Kaabi Nezhadian Mercedeh..... SP053.3
 Kabinejadian Foad..... PS12.018, SP029.2,
 **SP053.3, SP084.1**
 Kaci Linada..... **SP125.2**
 Kadem Lyes..... SP151.5, SP151.7
 Kadoya Noriyuki..... SP079.3
 Kah James C.Y..... 2956
 Kairn Tanya..... **SP015.5, SP027.3,**
 **SP036.5, SP054.4, SP176.2**
 Kakakhail Basim..... SP081.2
 Kalaji Iman..... **SP039.7**
 Kalantzis Georgios..... SP152.3
 Kaldoudi Eleni..... **SP169.1, SP169.6**
 Kale Ss..... SP005.1
 Kalle Sigrid..... SP167.5
 Kallehauge Jesper..... SP175.1
 Kallioniemi Elisa..... PS01.011, **SP128.1**
 Kallon Gibril..... SP150.6
 Kamal Mona..... SP056.3
 Kamali Asi Alireza..... PS05.007, SP070.1,
 SP070.2
 Kamanu Chuks I..... SP148.6
 Kamei Ryogo..... SP014.2
 Kamerling Cornelis Philippus..... SP164.1,
 **SP164.4**
 Kamio Yuji..... SP038.2
 Kamisawa Tomoko..... SP008.4
 Kamm Roger D..... **2869, SP012.3**
 Kan Chung-Dann..... PS03.002
 Kanai Takayuki..... SP079.3
 Kanamori Katsuhiko..... PS10.002
 Kanazawa Mitsutaka..... SP081.3
 Kanda Naveen..... SP133.3
 Kandadai Rukmini M..... SP121.6
 Kaneko Miki..... **PS08.003**
 Kaneko Takeshi..... PS10.002
 Kang Jingbo..... PS04.061
 Kang Sang-Won..... PS04.098, PS05.047,
 PS05.048
 Kang Sei-Kwon..... PS05.039
 Kang Seong-Hee..... PS01.022, PS04.100,
 PS04.102, PS04.103
 Kang Young Nam..... PS04.057, PS05.025,
 **SP027.5, SP143.3**
 Kankaanpää Markku..... SP160.2
 Kannan Karthik..... PS12.018, **SP029.2,**
 SP084.1
- Kano Takashi..... PS12.019, **PS16.016,**
 PS16.017
 Kanyong Prosper..... SP030.4
 Kapur Ajay..... PS04.036
 Karami Elham..... **SP097.7, SP156.7**
 Karan Tania..... **PS04.050**
 Karanfil Cahit..... SP161.6
 Karasawa Kumiko..... PS04.064
 Karger Christian..... SP076.2
 Karhu Jari..... PS12.013
 Karim Karim S..... **SP168.4**
 Karimi Davood..... SP097.8, **SP149.7**
 Karjalainen Pasi A..... **SP160.2**
 Kark Lauren..... SP098.4
 Karlsson Marcus..... SP145.3
 Karotki Alex..... PS04.058
 Karsch Leonhard..... **SP112.2, SP141.1**
 Karube Masataka..... PS04.064
 Karvat Anand..... SP074.1
 Karvounis Evaggelos C..... SP020.6
 Kassae Ali..... SP155.8
 Katano Hiroyuki..... SP156.3
 Katchky Adam..... SP145.2, SP145.5
 Katenka Natalia..... SP049.5
 Kathirvel Murugesan..... SP004.3, SP025.2,
 SP079.5, SP164.6
 Kathriarachchi Vindu..... SP152.3
 Katsuda Toshizo..... PS05.019, **PS05.023,**
 SP005.3, **SP067.1**
 Kauczor Hans-Ulrich..... SP115.6
 Kauffmann Claude..... PS19.008, SP162.3
 Kawabata Fusako..... SP066.4
 Kawabe Manabu..... **PS16.017**
 Kawachi Toru..... SP026.7
 Kawahara Yasuhiro..... PS11.001
 Kawahira Hiroshi..... SP139.4
 Kawaji Yasuyuki..... PS01.009, PS05.019,
 PS05.045, SP005.3
 Kawano Masaru..... PS10.002
 Kawase Yasuhiro..... SP128.2
 Kawrakow Iwan..... SP109.3
 Kazantsev Pavel V..... PS17.006
 Kazantzides Peter..... SP016.4,
 SP016.6, SP073.7
 Kazem-Moussavi Zahra..... **PS12.016**
 Keall Paul..... **MPE15.1, PS04.042,**
 **SP077.6, SP079.2**
 Keating Armand..... SP02.010
 Keays Marie..... **SP053.1**
 Kehler Katherine..... PS04.105
 Keidar Michael..... **BMEE21.2**
 Keller Brian..... SP047.2, SP155.5
 Keller Harald... PS01-006, **SP090.3, SP171.6**
 Keller Jim..... **BMEE23.2**
 Kelso Sarah..... SP042.3, **SP042.5**
 Kemp Arika D..... SP032.2
 Kemp Ben..... SP096.5
 Kempe Jeff..... **SP116.2**
 Kempson Ivan..... SP091.1
 Kennedy Angel..... SP078.5
 Kerns Sarah..... SP122.6
 Kerr Andrew..... PS04.066, SP133.2
 Keshavarz-Motamed Zahra..... SP151.5,
 SP151.7
 Kessar Anastosis..... SP145.4
 Kessler Cecilia..... **SP068.5**
 Keum Ki Chang..... PS04.018, SP090.5
 Keyvanloo Amir..... SP164.7
 Khalaf Abdelbaset..... **SP042.7**
 Khamesi Seyedeh Masoumeh..... PS05.018,
 SP179.1
 Khan Ali R..... SP023.3
 Khan Fazal..... SP057.2
 Khan Rao..... SP058.4, SP090.4, SP130.5
 Khan Shahed..... **PS05.024**
 Khateri Parisa..... SP128.4
 Khismatullin Damir..... SP138.2
- Khobi Mehdi..... SP105.4
 Khosravi Hamid R..... **SP119.3**
 Khosravi Hossein..... SP119.3
 Khosravi Pegah..... **SP127.4**
 Khosroshahi Mohammad... **SP138.3, SP171.1**
 Khosrow-Khavar Farzad..... SP007.7
 Khoushabi Azadeh..... SP136.1
 Kiat Ng T..... SP029.2
 Kida Satoshi..... SP079.3
 Kido Michiko..... PS03.006, PS12.039
 Kiely Patrick A..... SP053.1
 Kihwan Youn..... **SP055.1**
 Kildea John..... **MPE05.1**
 Kim Anthony... PS04.058, SP047.2, SP153.4
 Kim Chan Hyeong..... SP005.4
 Kim Dae-Hyun..... SP048.5
 Kim Dohyeon..... **SP149.8**
 Kim Dong Ha..... **SP019.6**
 Kim Dong-Su..... PS01.022, PS04.100,
 PS04.102, PS04.103
 Kim Eng Chan..... PS04.007
 Kim Gook T..... SP064.4
 Kim Gwang-Won..... SP105.7
 Kim Haeyoung..... PS05.039
 Kim Han Byul..... PS09.008
 Kim Hee Joung..... SP149.6, SP149.8
 Kim Hee Jung..... **PS05.026**
 Kim Hun Jeong..... PS05.021
 Kim Hyemi..... SP149.8
 Kim Jae-Sung..... PS04.098
 Kim Ji Na..... **PS05.025, SP027.5**
 Kim Jin Sung..... SP048.5
 Kim Jinkoo... **SP056.2, SP056.3, SP056.4**
 Kim Jone J..... **SP008.7**
 Kim Jongin..... **SP031.1**
 Kim Joshua..... **SP072.4**
 Kim Jung Kyung..... SP084.4
 Kim Jungheo..... SP048.5
 Kim Juree..... PS04.018, SP090.5
 Kim Kokeun K..... SPO92.2
 Kim Kum Bae..... PS05.021, SP06.005
 Kim Kyeong-Hyeon..... PS01.022, PS04.100,
 PS04.102, PS04.103
 Kim Kyoungju..... PS05.039
 Kim Kyunghoon..... **SP084.4**
 Kim Min Joo..... PS04.093, PS04.094,
 PS04.095, PS04.099, PS05.046
 Kim Moo-Sub..... PS04.096, PS04.097,
 PS04.101
 Kim Peter K..... SP139.6
 Kim Sangkyong K..... SPO92.2
 PS09.008, PS04.093, PS04.094,
 PS05.021
 Kim Seong Hoon..... PS05.021
 Kim Shin-Wook..... SP143.3
 Kim Siyong..... PS01.022, PS04.100,
 PS04.102, SP077.2,
 SP077.3, SP077.7
 Kim Su Ssan..... PS04.006
 Kim Subin..... SP084.4
 Kim Sun Mo..... PS01.027
 Kim Sung Kyu..... PS04.007, **PS04.051,**
 **PS04.052**
 Kim Tae Ho..... PS01.022, PS04.100,
 PS04.102, PS04.103
 Kim Woo Chul..... PS05.021
 Kim Ye Seul..... SP149.6
 Kim Yusung..... **PS04.053, PS04.116**
 Kinashi Yuko..... PS04.081
 King Emily C..... SP087.4
 Kinoshita Hiroshi..... PS01.008
 Kirby Patrick L..... **PS19.014**
 Kirisits Christian..... MPE14.2
 Kirkby Charles J..... **SP063.2**
 Kiselyov Vitalii..... SP012.2
 Kishi Kazuma..... SP079.3
 Kishimoto Jessica..... **SP162.2, SP162.6**
 Kislyakova Marina V..... **PS17.006**

Klein Michael D.....	SP046.4	Król Anita.....	SP013.2	Lasorsa Irene.....	SP042.4
Klose Uwe.....	SP013.2	Kuang Yu.....	SP016.1	Lass Jaanus.....	SP050.5
Kluger Petra.....	SP112.5	Kuchenbecker Stefan.....	PS04.085	Lassmann Michael.....	SP086.4
Klyui Nikolai.....	SP012.2	Kulkarni-Thaker Shefali.....	SP028.7	Lasso Andras.....	PS04.087, SP003.6, SP080.5
Kneebone Andrew.....	SP079.2, SP175.1	Kulkas Antti.....	SP120.1	Latella Benjamin.....	PS16.024
Kneppo Peter.....	SP061.2, SP103.1	Kumar Jyoti.....	SP114.4	Latifi Kujtim.....	SP097.5
Knigge Sara.....	PS02.003, PS02.006	Kumar L S Arun.....	SP108.2, SP118.3	Latorre Malcolm A.....	SP074.4 , SP121.3
Knoos Tommy.....	MPE10.1	Kumaradas Joseph C.....	SP028.2	Lau Gih Keong.....	SP044.5
Knothe Tate Melissa.....	SP098.4	Kumarasiri Akila.....	SP056.2, SP056.3	Lau Jonathan C.....	SP023.3
Knothe Tate Melissa L.....	SP002.5	Kun Luis G.....	2900	Lau Susie.....	SP172.2
Knöös Tommy.....	PS04.054	Kung Cynthia.....	SP003.3	Lau Thuy.....	PS04.054
Ko Hyoungho.....	PS09.003	Kuo Jeffrey.....	PS04.001, SP069.4	Laurent Sophie.....	SP019.1
Koba Yusuke.....	SP048.2	Kurata Tomohiro.....	SP139.4	Lauri Kai.....	SP167.5
Kobayashi Etsuko.....	SP055.1	Kurioka Taishi.....	PS10.012	Laurier Jean.....	SP008.8
Kobayashi Katsumi.....	SP049.6	Kuruganti Usha.....	PS03.003, PS10.005 , PS10.006	Laurikaitiene Jurgita.....	SP155.7
Kobayashi Yoshihiro.....	SP066.4	Kushki Azadeh.....	SP082.5	Lausch Anthony.....	SP046.2
Kobetic Rudi.....	SP166.3	Kusters Martijn.....	SP004.6	Lauterboeck Lothar.....	PS02.002
Koc Alpaslan.....	PS01.010	Kusuhara Toshimasa.....	SP148.4	Lavdas Michael K.....	SP111.3
Kocharian Armen.....	SP031.5	Kuwahata Nao.....	PS01.008	Law Brian.....	SP127.4
Kodama Naoki.....	SP128.2 , SP179.4	Kuwano Tadao.....	PS05.019, PS05.023, SP005.3, SP067.1	Lawrence Shane L.....	PS04.017
Kodlulovich Simone.....	PS17.014, SP054.2	Kwak Jung Won.....	PS04.006	Lazarakis Peter.....	SP077.6
Kodoth Vivek.....	SP007.3, SP053.5	Kwee Sandi A.....	SP016.1	Le Loirec Cindy.....	SP118.2
Kofman Jonathan.....	SP120.2	Kwon Jihun.....	SP049.3	Le Peggy.....	SP06.007
Kohli Kirpal.....	SP074.1	Kyoso Masaki.....	PS09.007	Le Yi.....	SP003.2
Koizumi Masahiko.....	PS05.050	Kyriakidi Kallirroi.....	SP020.6	Leal Plaza Antonio.....	MPS02.1, MPS06.1
Kojima Rina.....	PS09.007	Kyroudi Archontea.....	PS04.068	Leatherday Christopher.....	SP097.6
Kok Henry P.....	SP044.4, SP159.2	Könönen Mervi.....	SP128.1	Leavens Claudia.....	SP046.5
Kokubo Masaki.....	SP025.4	Kühnert Helmut.....	SP039.2, SP039.3	Lecavalier Marie-Ève.....	SP049.4
Kolios Michael C.....	PS09.004, SP173.2	Křiž Jan.....	SP112.7	Leclair Robert J.....	SP024.1 , SP024.4
Komisar Vicki.....	SP087.4			Lecomte Roger.....	JT03.2, MPF09.1 , SP035.4, SP035.5
Kondo Kengo.....	SP162.4, SP173.1			Ledesma Eyglis.....	SP074.2
Kondo Natsuko.....	PS04.081			Ledesma-Valdes Eyglis.....	PS13.005
Kong Youngsun.....	SP127.6			Lediju Bell Muyinatu A.....	SP016.4, SP016.6, SP073.7
Konstantinidis Anastasios C.....	SP035.2			Lee Benajamin.....	SP138.2
Koo Kyo-In.....	PS09.003, SP170.3			Lee Boreom.....	SP031.1
Koosha Fereshteh.....	SP076.6			Lee Chang Yeol.....	PS05.021
Kooy Hanne.....	SP147.5			Lee Chi-En.....	SP024.6
Kopec Renata.....	SP155.3			Lee Choong-Il.....	SP143.3
Kortelainen Jukka.....	SP135.6			Lee Choonsik.....	SP104.1
Koshiji Kohji.....	PS12.034			Lee David S.C.....	SP162.2
Kostylev Dmitriy V.....	PS17.006			Lee Dong Han.....	PS05.027
Kostylev Valeriy A.....	PS17.006			Lee Dong Hoon.....	SP149.6
Kotb Rami.....	SP152.1			Lee Dong-Su.....	PS05.046
Kouloulis Vasilios.....	PS04.027			Lee Eungman.....	PS04.018, PS05.012, SP090.5
Koutsouris Dimitrios.....	SP123.4			Lee Haeng Hwa.....	SP149.6
Koutsouveli Efi.....	PS17.014			Lee Han Yeong.....	PS05.027
Kovacs Michael.....	SP097.1			Lee Hankyu.....	SP083.4
Kovalchuk O.....	SP058.2, SP142.2			Lee Ho.....	PS04.018, PS05.012, SP090.5
Krajca Vladimir.....	SP165.1			Lee Hong Ji.....	PS09.008
Kraus James.....	SP155.8			Lee Hsiao-Yu.....	SP040.3
Krauss Achim.....	SP163.2			Lee Hyun-Woo.....	PS12.017
Krawiec Michele.....	SP078.3, SP078.5			Lee J. Michael.....	SP055.3
Krayem Moussa.....	PS04.055			Lee Jae Kook.....	SP005.4
Kremen Vaclav.....	PS09.005, SP165.1			Lee James Cheow Lei.....	SP158.8
Krenn Matthias.....	SP008.6			Lee Jenny.....	SP036.7
Kreplak Laurent.....	SP055.2, SP055.3			Lee Jeong Su.....	PS09.009
Kresta Petr.....	BMEE12.1 , PS16.005, PS16.018 , SP042.5			Lee Jeong-Woo.....	PS04.098, PS05.047, PS05.048, PS05.049
Kreucker Jochen.....	SP003.3			Lee Jihan.....	PS12.017
Krisanachinda Anchali.....	PS17.014, SP158.2 , SP158.4			Lee Jonny.....	SP004.5
Krisananchinda Anchali.....	SP158.8			Lee Junghoon.....	PS04.059
Krishnan Kalpagam.....	SP074.1			Lee Jungil.....	PS04.018, PS05.012, SP090.5
Krishnan Shankar.....	SP010.4			Lee Kwang Jin.....	SP031.1
Krishnan Sri.....	BMEE22.1			Lee Kyung E.....	SP064.4
Krishnan Sridhar.....	PS12.001, PS19.002, SP031.2, SP039.1, SP039.4, SP134.5 , SP165.4, SP165.5			Lee Me-Yeon.....	PS05.039
Krivoy Agustina.....	PS16.005			Lee Min-Young.....	PS04.095, PS05.046, PS05.048, PS05.049
Krizaj Dejan.....	SP084.2			Lee Peter D.....	SP089.4
Krois Igor.....	SP138.1			Lee Sang Hoon.....	PS04.018, PS05.021, SP090.5
Kroll Florian.....	SP112.2			Lee Sang Wook.....	PS04.006
Kron Tomas.....	MPE01.2, PS04.009, PS05.009, SP015.3, SP063.3, SP124.3, SP140.1 , SP174.1			Lee Seu-Ran.....	PS04.094, PS04.095, PS04.099, PS05.046
Krouglov Serguei.....	SP157.3				
Kruchkov Eugeny.....	SP019.2				

L

La Thanh Giang.....	SP044.5
Laamanen Curtis.....	SP024.4
Labonté Marie-Pier.....	SP158.6
Lachance Bernard.....	MPF11.2
Lacombe Sandrine.....	SP049.6
Lacornerie Thomas.....	PS04.054
Ladzynski Piotr.....	SP113.5
Lafay Frédérique.....	MPF10.1
Lafontaine Christine.....	BMEF05.1
Lagerwaard Frank.....	SP046.3
Lago Paolo.....	PS16.019, SP087.3, SP093.4
Lagueux Jean.....	SP018.5
Lai Ingrid H.....	SP107.5
Lai Yu-Shu.....	PS03.007
Laine Jarmo.....	PS12.013
Laliberte-Houdeville Cedric.....	SP027.7
Lalji Ulrich C.....	SP172.3
Lallena Antonio M.....	PS04.034
Lalonde Michel.....	SP133.2
Lam Karen.....	SP094.3
Lamas Janice.....	PS01.004
Lambin Philippe.....	SP102.2, SP102.3, SP122.5, SP169.2
Lamey Michael.....	PS04.056
Lanconelli Nico.....	SP150.3
Landry Guillaume.....	SP018.4
Lang Min.....	SPO92.1
Langklotz Mandy.....	SP113.4
Lanou Robert.....	SP049.5
Lapointe Claude.....	PS04.005
Laprise-Pelletier Myriam.....	SP018.5
Laqua Daniel.....	SP170.1
Labanoix Lionel.....	SP019.1
Larivière Dominic.....	SP049.4
Larkin John.....	SP072.6
Larocque Matthew.....	SP063.2
Larouche Jeremie.....	SP073.6
Larouche Renee X.....	SP011.5, SP153.3
Larraga-Gutierrez Jose M.....	PS04.035, PS04.089
Larrinaga Eduardo.....	PS04.002, PS04.005, SP057.6

- Lee SukPS04.018, SP090.5
Lee TaewooSP117.5
Lee Thomas M.H.2954
Lee Ting-Yim.....**JT03.1**, SP023.1, SP046.2,
.....SP070.6, SP097.1,
.....SP149.5, SP156.7
Lee Wonkyu K.SPO92.2
Lee Woong Woo.....PS09.008
Lee Yong HeePS04.007
Lee Yong MinPS05.027
Lee Young K.**PS04.058, SP153.4**
Lee Young Kyu.....**PS04.057**
Lees John E.SP139.3
Lefkopoulos Dimitri.....PS05.030, SP017.6
Leger PierreSP072.6
Legnani Walter E.....SP082.1, SP082.4
Lehmann JoergSP153.5
Leijenaar Ralph T.H.SP122.5
Leineweber Matthew J.SP083.4
Lelkes PeterSP112.5
Lemaire Edward D.SP066.3, SP120.2
Lemaire Jean-Jacques.....SP121.2
Lemgruber Alexandre.....SP010.7
Lencart JoanaSP047.1
Leng ShuaiSP034.6, SP115.3, SP115.7
Lengua Rafael E.PS05.013, SP107.3
Leo Hwa Liang**PS12.018, SP053.3**,
.....**SP084.1**
Leon Moloney FernandoSP087.2
Leonhardt SteffenSP055.5, SP126.4
Lepage Martin**MPF01.2**
Leppänen TimoSP120.1
Lerch Michael L.F.....**SP069.5, SP081.4**,
.....**SP141.4**
Lerma ClaudiaSP120.3
Lerouge SophieSP162.3
Lesieutre MariaSP166.3
Lesur OlivierSP096.2
Lesczynski KonradPS04.086
Leventouri TheodoraSP152.3
Levesque Yves R.SP072.6
Lewis CorneliusSP125.3
Lewis CraigSP154.5
Lewis RobSP150.7
Lhotská LenkaPS09.005, PS10.009,
.....**PS17.007**, SP112.7,
.....SP120.4, SP165.1
Li Anne**SP119.8, SP123.2**
Li Bo-HaoPS03.010
Li ChunshengSP135.1, **SPO92.3**
Li Deyu.....SP089.5
Li Fiona**SP023.1**
Li Guiling.....SP122.2
Li Heyse.....PS04.010
Li Jeu-Ying.....PS03.009, PS03.010
Li JianguoPS04.061
Li JinsengSP107.6
Li Ling**SP001.4**
Li Luca Y.**PS04.060**
Li MeiSP016.1
Li MeixianSP053.4
Li MinghuiSP103.2
Li SangPS17.012, SP007.6
Li TaoranSP117.4
Li Wei B.SP037.3
Li Winnie**SP130.2**
Li XiaoSP073.7
Li Xiaolin.....SP020.3
Li Ya Q.SP101.5
Li YingxinPS12.027
Li Yongbao.....**SP106.2**
Li Yue**SP145.2, SP145.5**
Li ZheSP160.2
Li Zhenguang.....SP139.4
Li Zhijian.....SP095.5
Liang Bin.....**PS04.061**
Liang Leo HwaSP029.2
- Liao HongenSP029.7, SP116.6
Liao RuizhiSP116.6
Liao Xiao M.PS02.014
Lief Eugene P.**SP124.6**
Lievens Yolande.....SP102.2
Likitlersuang Jirapat**SP040.4**
Lim Khoon S.SP071.1
Lim SangwookPS04.018, **PS04.062**,
.....PS04.062, SP090.5
Lim Sierin**SP059.4**
Lim-Reinders Stephanie.....SP047.2
Lima Carlos J.D.PS12.037
Lima Nathan W.SP100.1
Lima Raquel J.P.D.PS01.014
Lima Roberto A.PS10.001
Limede Patricia.....SP047.1
Lin Changyan**PS03.008**
Lin Cheng-An J.SP019.3
Lin Chia-HungPS03.002
Lin ErinSP069.4
Lin Kang-Ping.....**PS03.009, PS03.010**,
.....SP001.6, SP126.1
Lin Kao-ChangSP040.3
Lin Kun-JihPS03.009, PS03.010
Lin Lillie.....SP130.3
Lin LiyongSP106.4, SP155.8
Lin Shuyu.....SP19.013
Lin TehPS17.014
Lin Tzu-HungSP028.3
Lin Wen-Chen.....PS03.010, SP126.1
Lin Win-Li.....SP028.3
Lin Xun**PS04.063**, SP131.7
Lin Ying Ling.....PS16.007,
.....**PS16.020, SP103.4**
Lin ZhixiongSP016.1
Linares Haydee M.....SP056.5,
.....SP057.6
Linares Luis A.PS05.013, SP107.3
Linares RafaelMPS02.1, MPS06.1
Lincoln Victor A.C.PS12.033
Lindahl OlofSP030.6, **SP145.3, SP167.6**
Lindén Maria**2507, SP031.3**, SP031.5
Liney GaryPS04.117, SP072.1
Linnenbank Andre**SP087.1**
Liou Houngh-ChiSP028.3
Lipinsky JerrySP171.4
Lisbona AlbertMPF10.1
Lithgow BrianSP136.3
Liu Amy Y.PS04.115
Liu BaochangPS04.017
Liu BoPS04.061, PS04.118
Liu ChangSP056.2, SP056.3
Liu Dingyun.....PS17.012
Liu Feng-Yu.....SP074.1
Liu Gang**SP174.5**
Liu HaixiaPS04.118
Liu Hui.....PS04.076
Liu JamesSP138.2
Liu JianSP071.7
Liu JianfeiSP156.1
Liu Jiuling.....PS12.029
Liu JiminSP156.1
Liu Jin FenSP156.6
Liu Jin Long**SP156.6**
Liu JinfenPS02.013
Liu JingPS19.006
Liu Paul Z.Y.SP019.5, **SP027.1**
Liu SongranPS04.076
Liu Tianya**SP089.5**
Liu WeiPS04.061
Liu Xiaoyu**SP089.1**
Liu YaqiangSP106.2
Liu YifanPS02.012
Liu Zhipeng.....**SP044.3**, SP101.6, SP101.7
Liu ZhuangjianSP156.1
Livi LorenzoSP143.1
Livingstone Roshan S.....**SP108.1**
- Ljungberg BörjeSP167.6
Llopart Xavier.....SP058.2, SP142.2
Llorente Manso Manuel**MPS12.2**
Lo Chao-Chen.....SP040.3
Lobbès Marc B.SP172.3
Lobo JulioSP123.5, SP153.7
Lock MichaelPS13.010, SP116.4
Loh Justine Shuhui.....**SP173.4**
Loh NelsonSP097.6
Loignon-Houle Francis**SP035.4**
Lombardo Lisa M.SP166.2
Long Cai**SP168.2**
Long KarenPS04.113
Long Mian.....**SP055.4**
Longhino Juan.....PS04.013,
.....PS04.014, SP015.1
Longo FrancescoSP152.2
Longo Renata**SP150.3**
Longtin AndreSP082.2
Lonski Peta**SP015.3, SP174.1**
Lopes Maria Carmo.....PS05.040
Lopes Paulo B.**SP040.2**
Lopez Diaz AdlinSP037.7, SP097.2
Lopez Uroza PamelaSP085.4
Lopez-Cardona Juan D.PS13.005
Lopez-Creagh RolandoPS13.005
Lopez-Reyes AlejandroPS13.005
Lopez-Rodriguez RolandoPS13.005
Lopez-Titla Maria M.**SP105.8**
Lorenzo-Ginori Juan V.SP001.1
Lorias-Espinoza Daniel...**SP073.2**, SP029.6,
.....SP110.6
Losier YvesPS10.006
Louie Alexander.....SP140.2
Lourenço Gustavo V.PS16.009
Loy Caroline**BMEE21.1**
Lu Bao-Liang.....**SP041.1, SP041.2**
Lu MaiPS01.025, SP101.3
Lu Xiaolin**PS19.015**
Lubis Lukmanda Evan**SP119.7**, SP124.2
Lucero Juan F.PS05.013, SP107.3
Lucev Vasic Zeljka**SP138.1**
Lum Julian J.SP030.5
Luman Merike.....SP167.5
Luo NingqiPS19.006
Luo YigangSP028.1
Luschi Alessio.....**PS16.021, SP062.4**
Lustberg TimSP102.8
Lustig Robert.....SP106.6
Luz Glécia V.D.S.PS01.003, SP030.7,
.....SP059.1
Luz Renata M.SP129.6
Ly DavisSP163.5
Lye VictoriaSP078.3, SP078.5
Lyrarakis Efrossyni.....SP154.1
Lysenko Mikhail N.....PS17.006
Létourneau DanielSP090.3, SP131.6
Létourneau Étienne**SP006.2, SP118.1**
- ## M
- Ma C.MSP107.6
Ma Eric**SP134.2**
Ma JianSP089.5
Ma LinPS04.118
Ma PanPS04.079, SP103.2
Ma RenSP044.3
Ma Sun YoungPS04.062
Maas BenjaminPS04.065
Macdonald Robert L.**SP117.2**
Macedo Tulio A.A.PS01.017, PS01.019
Macfarlane Michael**SP164.2**
Macgregor StephenSP003.6
Machado JorgeSP19.011
Machado João C.**SP162.1**
Machado Neto Vicente.....PS11.006

- Menon Ravi..... SP094.3
 Mequanint Kibret..... SP155.1
 Mercea Paul..... **SP016.3**
 Mervaala Esa..... SP120.1
 Mesbah Latifa..... PS04.072
 Mestrovic Tony..... **SP025.6**, SP140.5
 Metcalfe Peter..... SP072.1, SP141.4
 Metran-Nascente Cristiane..... SP070.7
 Metser Ur..... SP070.7
 Mettvier Giovanni..... SP150.3
 Metzger Fabian..... SP112.5
 Meyer Tyler S..... PS04.112,
 PS04.113, SP107.4
 Meylan Sylvain..... SP048.3
 Mezzenga Emilio..... SP025.3
 Miao Junjie..... PS04.079
 Michalowski Stefan..... **MPF02.1**
 Midia Mehran..... SP119.3
 Migalska-Musial Karolina..... SP113.5
 Miguel Cruz Antonio..... SP051.2
 Mijnheer Ben..... **MPE03.2**, **SP057.5**
 Mikhail Lette Miriam..... SP075.1
 Miksys Nelson..... **SP017.5**, SP078.2
 Milano Franco..... SP125.3
 Millar Jeremy L..... SP077.4
 Millard Thomas P..... SP150.6
 Miller Andrew..... SP102.8
 Miller Denise..... **SP087.7**, SP150.4
 Miller John..... SP125.2
 Miller-Clemente Rafael A. SP034.3, SP149.4
 Milosevic Michael..... **MPE04.1**, PS01.027,
 SP059.5, SP070.7
 Min Chul Hee..... SP005.4
 Min Chul Kee..... PS05.021
 Ming Xin..... SP056.1
 Miniati Roberto..... PS16.011, PS16.012,
 **PS16.024**, **PS16.025**
 Minor Arturo..... SP110.6
 Minor Martinez Arturo..... SP073.2
 Mintz Adam..... SP008.7
 Minuti Massimo..... SP150.3
 Mir Hasan..... SP135.6
 Miranda De Sa Antonio M.F.L..... **SP041.3**
 Mirandola Alfredo..... SP058.4
 Mirsattari Seyed..... SP023.3
 Mirzakhaniah Lalageh..... **SP048.6**
 Mirzazadeh Shahrzad..... SP148.5
 Misago Ayato..... PS01.009
 Misgeld Berno..... SP126.4
 Mistretta Charles..... SP161.1
 Mitchell Joanne..... SP015.5, SP036.5
 Mitchell Marvin..... **BMEE03.1**
 Mitchell Tracy..... SP140.5
 Mitrelias Thanos..... SP019.2
 Mittler Silvia..... SP139.5
 Miura Hidekazu..... 2955
 Miura Hiromasa..... PS02.007
 Miwa Yasuyuki..... **PS12.019**, PS12.035,
 PS16.017
 Miyabe Yuki..... SP025.4
 Miyazawa Shinya..... SP06.006
 Miyazawa Tasuku..... SP008.1
 Mizota Manabu..... **SP081.3**
 Mizowaki Takashi..... SP025.4
 Mizuno Hideyuki..... SP026.8
 Mneno Stanley..... SP116.3
 Moahmmadzadeh Ali..... SP06.004
 Mochizuki Takashi..... PS07.007, SP06.006
 Modchalingam Mithunan..... SP06.007
 Moeckli Raphaël..... **MPF08.1**, **PS04.068**,
 SP152.4
 Moftah Belal..... PS04.054, **SP022.3**,
 SP078.6, **SP142.4**
 Moghadas Dastjerdi Hadi..... SP097.7
 Moghaddasi Leyla..... **SP076.4**
 Moghe Sachin..... SP034.7
 Mohamad Alabdoaburas Mohamad..... **PS05.030**,
 **SP017.6**
 Mohamed Islam..... PS04.005
 Mohd Paiz Nurhidayah..... PS09.006
 Moineuddin Syed A..... SP129.1
 Mojallali Hamed..... SP110.4
 Molina Velasquez Tatiana..... SP010.7
 Molinari Filippo..... SP156.3
 Moloi Sabee..... **SP033.1**, **SP171.4**
 Mong Kam S..... SP119.2
 Monteiro Emilia C..... SP020.5
 Montenegro Erick O..... PS05.013, **SP107.3**
 Montereali Rosa Maria..... SP058.4
 Montes De Oca Gisela..... **PS12.020**
 Monti Massimiliano..... SP062.4
 Montreuil Jacques..... SP003.5
 Moore Christopher J..... **PS04.069**
 Moore Eric J..... SP112.4
 Moore Eve..... SP087.4
 Moore Michael..... PS16.005
 Mora Grisel M..... **SP107.6**
 Moradi Elham..... SP136.2
 Moradi Mosa..... PS05.007
 Moraes Cecilia R..... PS01.019
 Moraes Heleno S..... SP020.2
 Moran Jean M..... **MPE07.3**
 Morandean Laurence..... SP097.6
 Morbiducci Umberto..... SP156.3
 Moreau Michel..... SP047.2
 Moreau Michele..... SP180.4
 Moreno Carbajal Maria E..... **PS16.026**,
 **PS16.027**, SP093.2, **SP125.6**
 Moreno Eugenio..... SP113.2
 Moreno-Ramirez Adriana..... SP129.2
 Morgan Dale..... **BMEE11.1**
 Morgan Kaye S..... SP150.2
 Morgan Paul S..... SP139.3
 Morin Evelyn..... PS13.008, SP031.4, SP144.2
 Morishita Soichiro..... SP008.4
 Moriya Henrique T..... SP020.1
 Moros Eduardo G..... SP097.5
 Morrier Janelle..... SP063.4
 Morrison Hali..... **PS04.070**
 Morrison Laura..... SP097.1
 Morshead Cindi M..... SP002.3
 Morton Daniel..... SP078.4
 Morán Verónica..... SP100.41
 Mosavian Nazanin..... **SP138.4**
 Moseley Douglas J..... **MPE03.1**
 Moseley Joanne L..... **PS04.071**, SP072.2
 Moser Christophe..... SP136.1
 Moser Michael..... SP028.1
 Moshiri Sedeh Nader..... **SP133.4**
 Mostaar Ahmad..... SP049.2
 Mota Carla L..... PS05.042
 Mottaghi Soheil..... SP121.1
 Mou Pedro..... SP178.6
 Mou Pedro Antonio..... **PS11.004**
 Mouatassim Samir..... **PS04.072**
 Mougél Océane..... MPF08.2
 Moukalled Fadl..... PS19.007,
 SP126.5, SP159.3
 Moulton Calyn R..... **SP078.3**, **SP078.5**
 Moundekar Pooja..... SP003.1, SP038.3
 Mourao Filho Arnaldo P..... **PS05.031**,
 **PS05.032**
 Moussavi Zahra..... **SP050.6**, **SP136.3**
 Mouttet Jean Claude..... SP067.6
 Movahed Allen..... PS04.054
 Movsas Benjamin..... SP056.4
 Mueller Kerstin..... SP065.2, **SP065.4**,
 **SP065.5**
 Mueller Marc..... PS02.004, PS02.005,
 SP151.1
 Mueller Peter P..... PS02.003
 Muhammad Haseena B. SP030.2, SP030.3
 Muhammad Qaiser..... SP113.3
 Muhanna Nidal..... SP110.3
 Muir Bryan R..... PS04.021, **SP067.5**, SP079.1
 Mukhopadhyay Ashok K..... SP114.4
 Mukumoto Nobutaka..... SP025.4
 Mulet-Cartaya Margarita..... PS13.004,
 PS13.005
 Mullally Shauna..... **JT02.1**
 Muller Jr Egon L..... PS16.002
 Mullins Joel..... **SP140.3**
 Mun Peck Shen..... SP167.2
 Murad Hakm..... **SP138.2**
 Murad Sohail..... SP081.2
 Muraja-Murro Anu..... SP120.1
 Murakoshi Michio..... **PS03.011**
 Murdoch Madison..... PS04.114
 Murray Matthew..... SP025.6
 Murray Teresa A..... **SP096.5**
 Murrell Donna H..... **SP018.2**
 Murrie Rhiannon P..... **SP150.2**
 Murugkar Sangeeta..... SP096.1
 Muñoz-Arpaiz Alex..... SP062.5
 Mwaura Salome W..... **SP043.3**
 Myojoyama Atsushi..... PS04.040, **SP034.2**
 Mzenda Bongile..... **PS04.073**
 Mège Jean Pierre..... PS05.030, SP017.6
 Méndez Gordillo Alma R..... **SP041.7**
 Mühle Richard..... SP134.1
 Mühlen Sérgio S..... **PS16.028**, SP032.4
- ## N
- N Muller Robert..... SP019.1
 Nabavi Mansoureh Sadat..... PS05.034
 Nabilath Akimey A..... BMEEF03.1, PS16.040
 Naderi Mansour..... PS05.034
 Nagai Mary K..... SP041.4
 Nagakura Toshiaki..... **PS12.039**
 Nagel Joachim H..... PS09.010
 Nagy Peter..... SP111.4
 Nainggolan Andreas..... PS04.075
 Nakagawa Keiichi..... SP055.1
 Nakagawa Yosuke..... PS04.081
 Nakajima Erika..... SP005.3
 Nakajima Mio..... PS04.064
 Nakajima Yujiro..... **SP079.3**
 Nakamoto Hidetomo..... PS12.035
 Nakamura Mitsuhiko..... SP025.4
 Nakamura Takao..... **SP148.4**
 Nakanishi Yoshitaka..... PS03.005
 Nakashima Yasuharu..... PS03.005
 Nakatani Yukiko..... PS16.020
 Nakayama Koichi..... PS02.007
 Nakayama Shinichi J..... PS01.009
 Nakonechny Keith..... SP171.6
 Nam Sungwoo..... SP032.2
 Nam Yunyoung..... SP127.6
 Nambu Masayuki..... PS10.012, PS11.001
 Namita Takeshi..... SP162.4
 Nan Qun..... **SP06.003**
 Nan Wenya..... PS11.004, **SP178.6**
 Nandor Mark J..... SP166.3
 Nanthakumar Kumaraswamy..... PS19.002
 Narabayashi Masaru..... PS04.081
 Narciso Lucas D.L..... SP100.1
 Narita Katuhisa..... SP026.8
 Nariyama Nobuteru..... **PS05.033**, **SP177.1**
 Nass Michael..... SP170.1
 Nassiri Moulay Ali..... SP119.1, SP119.4
 Natanasabapathi Gopishankar..... **SP005.1**,
 **SP065.6**
 Nataraj Raviraj..... SP166.5
 Natsume Kaoru..... PS07.007
 Nauraye Catherine..... SP142.1
 Ndubuka Gideon I..... PS13.006, SP0110.1,
 SP022.1, **SP148.6**
 Neath Cathy..... PS04.033, **SP06.002**,
 SP171.6

Nedaie Hassan Ali **PS05.034, SP017.2, SP058.3, SP152.2**
 Nederveen A.J. SP044.4
 Nejadgholi Isar **SP074.7**
 Nekolla Stephan SP037.3
 Nelson Vinod K. **PS05.035, SP155.6**
 Neprasova Iveta PS17.011
 Nerem Robert M. **2871**
 Neretti Nicola SP049.5
 Nersissian Denise Y. PS05.028, SP115.4, SP137.2
 Nesvacil Nicole **MPE14.2**
 Neto Tertuliano T. PS05.014
 Nettelbeck Heidi **PS05.036, SP048.3**
 Neumayer Leigh A. SP028.4
 Neves-Junior Wellington F.P. SP068.2
 Newcomer Mitch SP106.6
 Nezhaddehghani Samira SP034.1, SP115.8
 Ng Aik Hao **SP139.3**
 Ng Jin A. PS04.042, SP079.2
 Ng Joanna **SP098.4**
 Ng Kwan Hong ... SP124.3, SP154.4, SP167.2
 Ng Kwan Hoong **1351, PS05.037, PS17.008, SP006.5, SP015.4, SP025.5, SP118.7, SP158.8, SP172.2, SP173.5**
 Ng Sook Kien .. **SP003.2, SP016.4, SP016.6**
 Ngan Calvin **SP066.2**
 Ngo Chuong **SP126.4**
 Ngoepe Malebogo **SP110.5**
 Ngoie Jean SP042.2
 Ngwa Wilfred **SP019.4, SP080.4, SP086.5, SP180.4**
 Ngwogu Kenneth SP148.6
 Nicolae Alexandru M. **SP003.3**
 Nicolau Dan V. SP157.4
 Nie Xiaohui SP06.003
 Niedermaier Ina SP158.7
 Niemöller Sven SP170.1
 Niesen Sandra SP119.5
 Nievas Susana SP015.1
 Nizeki Kyuichi **SP020.2**
 Nikfar Banafshe SP105.4
 Nikfar Banafsheh SP171.1
 Nill Simeon SP164.1, SP164.4
 Nisbet Andrew SP004.5
 Nishimura Takahiro PS10.002, PS10.003
 Niu Carolyn SP157.3
 Niu Tianye **SP097.4**
 Niyitanga Paul SP167.7
 Nizami Shermeen **SP102.4**
 Nkuma-Udah Kenneth I. **PS13.006, SP010.1, SP022.1, SP148.6**
 Noble William S. SP122.4
 Noboa Oscar SP167.4
 Nobrega Jose N. SP136.4
 Noguchi Kazuki SP005.3
 Nogueira Liebert P. PS05.042
 Nogueira Pedro H.D.O. SP030.7
 Nogueira Vladimir F. SP156.5
 Nomura Taishin PS03.006
 Nong Zengxuan SP116.1
 Noordmans Herke Jan **SP062.1**
 Normore Ryan PS03.004
 Norringer Bern PS04.063, SP090.1, SP131.7
 Novaes Leonardo N. SP093.5
 Noveletto Fabricio SP008.3
 Novosel Esther C. **SP112.5**
 Novotná Iva **PS10.009**
 Nowak Anna SP097.6
 Nuesslin Fridtjof **PS17.009**
 Nunes Catarina S. PS07.004
 Nunes Lara M. PS01.018
 Nunokawa Kiyohiko PS10.003, PS12.011, **SP145.6**
 Nusrat Humza **SP155.5**

Nyassi Ebrima SP093.1
 Nyberg Morgan SP167.6
 Nyiri Balazs J. PS01.001, SP129.3
 Nylander Eva SP031.3

O

O'Brien Jr. William D. SP111.1
 O'Connell Andrew **SP083.1**
 O'Donnell Brian D. SP112.4
 O'Neill Eimear SP141.2
 O'Sullivan Martin J. SP112.4
 O'Toole James SP175.1
 Oberije Cary SP102.2
 Ochoa Cesar SP153.6
 Octave Nadia **SP011.3, SP063.4**
 Oda Shigeto SP139.4
 Odle Brooke **SP166.5**
 Odstrčilik Jan SP116.8
 Oeh Uwe SP037.3
 Oelfke Uwe SP164.1, SP164.4
 Oellig Juergen SP004.6
 Oh Jung Hun **SP122.6**
 Oh Kwang W. **SP157.1**
 Oh Se An PS04.051, PS04.052
 Oh Seung Jae PS05.039
 Oh Sungjin PS09.003
 Oh Young Kee PS04.007
 Ohashi Toshio PS04.039
 Ohdaira Misato **SP008.4**
 Ohl Claus D. SP053.2
 Ohnishi Tadasuke PS12.011
 Ohnishi Takashi SP139.4
 Ohno Yuko PS03.006, PS12.039
 Ohtani Hiroki **PS05.038**
 Oinam Arun S. SP141.5
 Okafor Fatima PS02.001
 Okazaki Toshihiko **PS12.021**
 Okuda Hiroshi PS05.045
 Okumura Hiroaki SP026.8
 Okura Yasuhiko SP116.7
 Olaciregui-Ruiz Igor SP057.5
 Olding Tim PS04.066, SP133.2
 Olfat Mostafa SP086.2
 Oliva Piernicola SP150.3
 Oliveira Leticia S. PS01.013
 Oliveira Mamere Leticia PS01.016
 Oliveira Pedro X. SP111.6
 Oliveira Yago PS04.031
 Oliver Michael PS04.086
 Oliver Michele **SP040.1**
 Oliver Patricia **SP109.4**
 Olivo Alessandro **SP150.6**
 Olszanski Arthur SP131.3
 Omata Seiji SP071.3
 Omer Robyn K. **SP028.4, SP028.5**
 Omotayo Azeez **SP149.3**
 Onaizah Onaizah **PS19.018**
 Ong Daphne SP170.2
 Ong Paul J.L. SP053.2
 Ong Teng Aik SP167.2
 Onisto Haroldo J. **PS12.022, SP001.5**
 Ono Akira PS05.050
 Ono Koji PS04.081, SP176.3
 Ono Shigeto **PS12.023**
 Onogi Shinya **SP07.007**
 Ore Valerii E. **SP019.2**
 Ortega Samuel PS14.001
 Ortiz-Seidel Monica PS04.081
 Orton Colin G. **1351, MPE01.2, SP063.3**
 Osei Ernest K. PS04.037
 Osinga Julia-Maria **SP163.2**
 Ostapiak Orest **SP153.2**
 Ostovari Mohsen PS01.020
 Ostrer Harry SP122.6
 Otawova Radka SP061.2

Otsuka Shunichi SP144.1
 Otterskog Magnus 2507
 Otto Karl SP152.6
 Ouyang Han PS04.079
 Owen Daron PS04.033
 Owen Jeniffer SP090.4
 Owen Tim SP133.2
 Owrangi A. SP017.1
 Ozawa Emi PS12.005
 Ozell Benoît SP047.6
 Ozodigwe C.A. PS02.001
 Ozsahin Mahmut PS04.068
 O'Brien Ricky SP079.2

P

Paats Andrus **SP147.3**
 Pacheco Jonathan SP036.6
 Pacheco Marcos T.T. PS12.036
 Pachoud Marc PS04.068
 Pacyniak John M. PS05.020
 Paganin David M. SP150.2
 Paier Fabiola SP143.1
 Painter Frank R. **2897, SP010.6**
 Paiva Fernando F. SP050.3
 Pajonk Iwona SP162.5
 Pak Farideh SP058.3
 Pal Mithilesh K. SP114.4
 Palacios Miguel SP046.3
 Palau Aley **SP037.7, SP097.2**
 Paliwal Bhudatt **SP175.5**
 Palko Tadeusz **SP062.3**
 Pallikarakis Nicolas **PS01.012, PS12.024, PS13.007, SP123.4, SP129.5**
 Pallotta Stefania SP090.6, **SP143.1**
 Palma David A. ... SP046.1, SP116.2, SP164.2
 Palmans Hugo SP038.2, SP048.3
 Pan Youlian SP156.2
 Pandzic Yahir SP103.5
 Pang Geordi SP155.5
 Pankowska Ewa SP113.5
 Pant Jeevan K. SP134.5, SP165.4
 Paoletti Sergio SP071.2
 Paolucci Massimiliano **SP102.5, SP108.4**
 Papadakis Antonios E. SP027.2
 Paquette Benoît SP152.1
 Parameswaran Ash SP074.1
 Parashar Pankaj **SP114.4**
 Pardo Montero Juan MPS11.1, SP076.2
 Park Cheolsoo S. SP092.2
 Park Chul-Woo PS12.017
 Park Hye Young PS09.008
 Park Hye-Jin PS05.048, PS05.049
 Park Hyeonser SP048.5
 Park Hyung Wook SP027.5
 Park Ilhyung PS12.017
 Park Jaeyeong PS12.017
 Park Ji-Yeon PS04.095, PS04.099, PS05.047, PS05.048, PS05.049
 Park Kwang Suk PS09.008, PS09.009, SP092.2
 Park Kwangwoo PS04.018, SP090.5
 Park Kyoung Yong PS12.017
 Park Mun Kyu PS05.027
 Park Seungwoo **SP06.005**
 Park Seyoun PS04.059
 Park So-Hyun PS04.095, PS05.046
 Park Soah **PS05.039**
 Park Su-Jin SP149.8
 Park Sung Yong PS05.026
 Park Yang-Kyun PS04.087
 Parmar Chintan SP122.5
 Parodi Katia SP037.3
 Parrent Andrew G. SP023.3
 Parvathaneni Upendra SP102.1
 Paschoal Cinthia M.M. SP033.2, SP033.4,

-SP114.1, SP114.3
 Passeri Daniele.....SP108.4
 Passi Kamlesh R.**PS04.074, SP133.3, SP141.5**
 Pastorino Matteo.....SP113.2
 Patatoukas Georgios.....PS04.027
 Patchett Brian D.SP061.6
 Patel Daxa.....PS04.033
 Patel Mayur.....**PS12.025, PS16.029**
 Patel Prashant.....SP112.1
 Patel Vimla.....**PL04.2**
 Pater Piotr.....**SP076.5**
 Paterno Aleksander S.....PS19.003
 Patil Nikhilesh.....PS04.022
 Patriarca Annalisa.....SP142.1
 Patrick John C.....**SP104.4**
 Patrocínio Ana Cláudia.....**PS01.013, PS01.014, PS01.015, PS01.016, PS01.017, PS01.018, PS01.019, PS17.010**
 Pattichis Constantinos.....**SP024.3**
 Pattichis Marios.....SP024.3
 Paudel Moti R.....**SP047.2**
 Paul Narinder.....SP034.7, SP097.3, SP104.3
 Paul Siji.....**SP003.1, SP038.3**
 Paula Grisel M.....**PS05.040**
 Paulis Leonie E.....SP172.3
 Pawelke Jörg.....SP112.2
 Pawiro Supriyanto Ardjo.....**PS04.075, PS07.003, SP119.7, SP124.2, SP158.8**
 Paz-Viera Juan E.....SP001.1
 Pazetti Rogerio.....SP020.1
 Peace Robert J.....**SP122.7**
 Peca Stefano.....**SP004.1**
 Pecchia Leandro.....**SP020.1, SP020.5, SP039.5**
 Pezalski Kazimierz.....SP062.3
 Pedram Maysam.....PS19.012, SP178.4
 Peel David.....SP093.1
 Peel Sarah.....SP022.2
 Pei Xi.....**SP143.4**
 Pejovic-Milic Ana.....PS18.001
 Pembroke Alan.....SP141.2
 Penafort Flores Stefany.....SP085.4
 Penev Kalin I.....**SP155.1**
 Penfold Scott.....PS19.004
 Peng Michael.....SP125.2
 Peng Xun.....SP016.1
 Peng Yinglin.....**PS04.076**
 Peng You Lin.....PS02.015
 Pennefather Peter.....**SP127.3**
 Pentiricci Andrea.....SP108.4
 Peper Michel.....SP086.4
 Pepin Catherine M.....SP035.4, SP035.5
 Peppard Richard.....SP121.5
 Peralta Agnette de Perio.....**SP137.3, SP158.8**
 Pereira Barbeiro Rita.....MPS02.1, MPS06.1
 Pereira Claubia.....PS04.008
 Pereira Hugo.....PS16.038
 Pereira Wagner C.....SP062.2
 Perera Thushara.....**SP121.5**
 Perez Jessica R.....**SP096.2**
 Perez Reynoso Francisco D.....**SP029.6**
 Perez Velazquez Jose Luis.....SP121.4
 Perez-Diaz Marlen.....**1351, SP001.1, SP034.3, SP149.4**
 Perianes Ma. Vanessa Francheska P.....**PS04.077**
 Perisinakis Kostas.....SP027.2
 Perkins Alan C.....SP015.4, SP139.3
 Perkins Theodore.....SP122.3
 Perry Gad.....SP078.2
 Persson Mikael.....**SP148.3, SP168.3**
 Perucha Maria.....MPS02.1, MPS06.1
 Pesikan Prdrag.....SP145.4
 Pessana Franco M.....SP082.1, SP082.4
 Petasecca Marco.....SP081.4, SP141.4
 Peter Lukas.....**PS17.011**
 Peters Terry M.....PS07.001, PS07.002, **SP023.3, SP073.1**
 Petersson Kristoffer.....PS04.068
 Petitclerc Leonie.....**SP152.5**
 Petoussi-Henss Nina.....SP037.3
 Petramale Clarice.....PS13.002
 Petroudi Styliani.....SP024.3
 Peucelle Cécile.....SP142.1
 Pfaff Cristina.....SP036.6
 Pfaffenberger Asja.....SP016.3
 Pham Theodore.....SP139.6
 Phan Penny.....SP153.6
 Phan Tien.....PS04.023, SP078.1
 Philips Amanda.....SP015.3, SP174.1
 Philips Damien.....SP015.3, SP174.1
 Phillips Justin.....PS04.087
 Phillips Mark.....SP102.1
 Phoon Justin.....SP029.2
 Pi Kilhwa.....PS09.003
 Piacentini R D.....SP060.2
 Pibarot Philippe.....SP151.7
 Picard Susanne.....**SP163.3**
 Piccinini Massimo.....SP058.4
 Pickering J Geoffrey.....SP116.1
 Pickler Arissa.....PS05.042
 Pierce Greg.....SP036.4
 Pili Graziella.....SP150.3
 Pin Melannie.....SP127.2
 Pinchera Michele.....SP150.3
 Pinkney Sonia.....**1497, SP123.6**
 Pinnell Richard.....SP121.1
 Pinter Csaba.....PS04.087, SP080.2, **SP080.5, SP130.6**
 Pinto Ana M.R.....PS19.003
 Pinto Diana F.D.S.....SP027.6
 Pinto Massimo.....SP048.3
 Pioletti Dominique.....SP136.1
 Pires Andrei L.....SP062.2
 Piron Ophélie.....**SP004.2**
 Pirrone Puma Jose.....PS14.003, SP113.7, **SP169.5, SP170.4**
 Pison Daniela.....SP121.2
 Pistorius Stephen.....PS04.105, PS04.105, SP070.3, SP070.5
 Pita-Machado Reinaldo.....SP001.1
 Pitelka Vasek.....SP034.8
 Pitkänen Minna.....SP128.1
 Pitsillides Andrew A.....SP089.4
 Pizarro P.....SP125.7
 Pizetta Daniel C.....PS16.009
 Piña-Barrera Andres.....SP060.3
 Placidi Pisana.....SP108.4
 Plasencia-Montero Enrique.....SP170.5
 Platoni Kalliopi.....PS04.027
 Platoni Pola.....PS17.014
 Plautz Tia E.....**SP034.5**
 Plewa Katherine.....**SP144.4**
 Plishker William.....PS04.059
 Podda Barbara.....SP042.4
 Poels Kenneth.....SP079.6
 Poepping Tamie L.....PS19.018
 Poirier Jasmine.....SP158.6
 Poirier Yannick.....**PS04.078**
 Polat Esra.....SP088.3
 Poletti Martin E.....PS01.023
 Police Alice.....SP069.4
 Polisena Julie.....BMEE13.1, BMEE26.1
 Polley Brendan.....SP073.6
 Poluta Mladen A.....**SP010.5**
 Poma Ana L.....SP177.4
 Poole-Warren Laura A.....SP071.1
 Pooley Robert.....SP077.7
 Popescu I Antoniu.....SP123.5, SP153.7
 Popovic Marija.....SP068.3
 Popovic Milos.....**SP032.1, SP041.5, SP066.5, SP120.5, SP134.2**
 Popovic Milos R.....SP002.3, SP008.5, SP041.4, SP101.5, SP120.6, SP146.4, SP178.1
 Porcel Erika.....SP049.6
 Port Johannes.....**PS09.010**
 Portieles Miguel.....PS12.003
 Portillo Maria.....SP015.3, SP174.1
 Posada-Quintero Hugo F.....**SP095.1**
 Posch Mathias.....**JT06.1**
 Pospiech Jörg.....SP170.1
 Pospisil S.....SP048.4, SP058.2, SP142.2
 Potters Louis.....PS04.036
 Potyagaylo Danila.....SP044.2
 Poulin Eric.....**SP003.5**
 Pouliot Jean.....SP003.5
 Poulsen Per R.....SP079.2
 Pourmoghaddas Amir.....**SP045.1**
 Pouryazdian Saeed.....**SP165.5**
 Prakash Sai S.....**SP160.1**
 Pratiwi Nurdina G.....SP119.7
 Prato Frank S.....SP104.4
 Praticco Flavio.....SP008.2
 Prestwich William V.....SP109.1, SP109.2
 Prezado Yolanda.....**MPS03.2, SP058.2, SP142.1, SP142.2**
 Prieto Elena.....SP100.4
 Prikryl Emil A.....SP096.1
 Prime Craig.....PS10.006
 Prindis Vit.....PS12.014
 Prokopovich Dale A.....SP081.4
 Provaznik Ivo.....**SP116.8**
 Provenzano Lucas.....SP015.1
 Prowse Paul.....SP009.3, **SP042.3**
 Pu Fang.....SP083.2
 Pu Xi M.....PS02.014
 Pugatch V.....SP058.2, SP142.2
 Pujols-Fariñas Gabriel.....SP170.5
 Purdie Thomas G.....SP036.7, SP046.5, SP117.3
 Purdy Michael T.....**SP032.5**
 Péguret Nicolas.....SP152.4
 Pérez Andrés.....SP076.2
 Pérez Yasser.....**SP178.5**

Q

- Qi Huan.....SP053.2
 Qi, X Sharon.....PS04.054
 Qiao Aike.....SP156.2
 Qin An.....SP072.7
 Qin Michael.....SP171.8
 Qiu Jimmy.....SP003.7
 Qiu Lishen.....SP02.013
 Qiu Wu.....**SP162.6**
 Qiu Xiao-Hui.....PS02.015, PS19.019, **SP094.1**
 Qu Baolin.....PS04.118, SP107.2
 Qu Xiaoting.....PS11.004, SP178.6
 Quan Hong.....SP072.7, SP174.5
 Quaresma Cláudia.....PS16.038, SP146.2
 Quesnel Patrick X.....SP007.5
 Quevedo Antônio A.F.....PS12.007
 Quigley Andrew S.....**SP055.2**
 Quintero Vladimir.....**BMES01.1, BMES03.2**
 Quirk Sarah.....PS04.023, SP124.5
 Quiroga Torres Daniel A.....SP051.2
 Quiroz Andrea N.....**SP098.2**
 Quon Harry.....PS04.059
 Qwarik Ayman A.....SP045.5

R

- Rababah Ali S..... SP053.5
 Rabbani K Siddique..... **1351, SP052.4, SP148.2**
 Rabus Hans..... PS05.010, PS05.036, SP048.3
 Radermacher Klaus..... SP055.5, **SP147.4, SP179.2, SP179.3**
 Rae William I.D..... **SP116.3**
 Rafiei Behrooz SP033.5, SP105.4, SP171.1
 Ragot JérémieMPF06.2
 Rahim Muhammad I. PS02.003
 Rahman Md. M. SP154.3
 Rai Robba..... PS04.117
 Raisali Gholamreza..... SP070.1, SP070.2
 Raissaki Maria SP027.2
 Raj V.Saran SP133.3
 Rajaram Ajay SP057.3
 Raju Venkateshwarla R..... **SP09.011, PS11.005, SP095.2, SP121.6, SP121.7, SP144.5, SP160.3**
 Ralston Anna SP054.4
 Ramaloko Thuso M. **SP153.1**
 Raman Saravana K..... **SP095.6**
 Raman Srinivas..... PS04.010
 Ramaswamy Yougambha SP071.1
 Ramchander Naren SP116.3
 Ramirez Lopez Erika..... PS05.041, PS16.032
 Ramirez Mario **JT02.2**
 Ramos Alexandre C.B. PS17.001
 Ramser Kerstin..... SP030.6, SP167.6
 Ramirez-Sotelo María G. SP102.7, SP126.6
 Randazzo Matthew **SP115.2**
 Ranger Nicole..... PS17.014, **SP054.5**
 Ranjbar Pouya Omid PS12.016
 Rao Nini **PS17.012, SP007.6**
 Rath G K..... SP005.1
 Rath G.K..... PS04.091
 Rathee Satyapal SP016.2
 Ratnakumaran Ragu Prakash PS16.004, **PS16.030**
 Rauch Giuseppe..... PS08.001, SP134.4
 Raval Amish N. SP029.5
 Ravi Ananth SP003.3
 Ravindran Paul B..... **SP081.1**
 Ravindran Sharon..... SP145.2, SP145.5
 Rawlinson Sean P..... **SP030.4**
 Raza Usman **PS13.008**
 Razavi Simin **SP029.1**
 Read Nancy SP164.2
 Real Jéssica V. SP129.6
 Regueiro Angel..... PS12.006
 Rehani Madan M. **2849, SP099.1, SP158.4**
 Rehman J PS04.019, SP133.1
 Reigosa-Crespo Vivian..... SP170.5
 Reina Thamiris R. SP115.4
 Reinhardt Joseph M. SP097.5
 Reis Camila S. **PS16.031**
 Reis Catarina PS19.011
 Reljin Natasa..... **SP095.3, SP127.6**
 Remis R.F. SP044.4
 Remita Hynd..... SP049.6
 Ren Wenting **PS04.079, SP103.2**
 Renaud James SP163.5, **SP163.6**
 Rendon Isguerra Carmen..... SP085.4
 Renha Simone K. **SP085.3**
 Repanas Alexandros ... PS02.005, PS02.006, SP151.1
 Reshetnyak Yana K. SP049.5
 Reversil Luca SP090.6
 Reyes Bersain..... SP095.3, **SP127.6**
 Reyes Mauricio SP023.4
 Reynosa Raysel..... SP037.7
 Rezaeei Mozghan..... SP086.2
- Rezaee Mohammad..... SP017.3, SP069.1, **SP086.1**
 Rezaei Sahar PS01.020
 Rezazadeh Nochehdehi Amirsadegh..... **SP06.004**
 Rhani Mohamad F. **PS04.080**
 Riahi-Alam Nader **SP171.1**
 Ribeiro Bruno PS16.038
 Ribeiro Pamela T..... **PS12.026**
 Ribeiro Rodolfo D.S. PS01.013, PS17.010
 Rice Adam PS04.042
 Rice Murray SP104.3
 Richard Ndi Samba **SP114.2**
 Richard Samuel..... SP097.3
 Richter José A. SP100.41
 Ricketts Kate SP129.1
 Rico-Asención Itzamná O... SP102.7, SP126.6
 Rigon Luigi..... SP150.3
 Rilling Madison **SP158.6**
 Rios Rincón Adriana M. SP051.2
 Rios-Velazquez Emmanuel..... **SP023.4, SP122.5**
 Rishaq Farid Y..... SPO37.8, SP045.5
 Rishaq Mohd Ziad F..... SP045.5
 Rissanen Saara M. SP160.2
 Rivas David SP113.7
 Rivas Rossana..... 2895, **SP010.2**
 Rivest-Henault David..... SP072.1
 Riyahi Alam Sadegh **SP156.3**
 Riyahi-Alam Nader..... **PS01.020, SP033.5, SP105.4, SP049.2**
 Rizvi Bisma **PS18.001**
 Roa Dante..... SP069.4
 Robalrdo Stefano PS08.001
 Robar James PS04.083
 Robotjazi Mostafa..... **SP143.2**
 Robert Carmelle SP158.6
 Robertson Gene E..... SP068.4
 Robinson Adam..... PS04.059
 Rocha Carlos E..... **SP170.6**
 Rocha Mateus A. SP020.2
 Rocha Nava Sandra L. **PS05.041, PS16.032**
 Roda Ana R. PS05.040
 Rodrigues Beatriz A. SP156.5
 Rodrigues George..... SP046.3, SP116.4
 Rodrigues Thiago G. SP020.1
 Rodriguez Denis D..... SP144.6
 Rodriguez Gabriel A. **SP069.6**
 Rodriguez Lilian V. SP137.3
 Rodriguez Manuel **SP017.3**
 Rodriguez Rodriguez Daniela..... SP063.5, SP168.2
 Rodriguez Santiago..... PS12.022
 Rodriguez Sunay SP097.2
 Rodriguez-Aleman Raul..... **PS16.033**
 Rodriguez-Antonio Raul SP020.4
 Rodriguez-Lopez Jaime Aeberto..... SP129.2
 Rodriguez Alberto R. PS12.003, PS12.004
 Rodríguez Fiana PS14.002
 Rodríguez Gemma PS12.003
 Rodríguez William R. **SP051.2**
 Rodríguez-Guadarrama Yael A..... SP093.2
 Rogalewicz Vladimir SP061.2
 Rogers David W.O. JT08.2, **MPE11.2, SP017.4, SP068.6**
 Rogers Linda J. **SP015.2**
 Rohlecke Cora..... SP032.4
 Rojo Elena PS16.001
 Rolfe Peter SP167.7
 Romagnoli Cesare..... SPO29.3, SP116.4
 Romano Walter..... SP162.2
 Romanov Andriy..... SP019.2
 Romero Daniel A. PS12.003
 Romo-Cardenas Gerardo S. PS12.032, PS16.033, **SP020.4, SP060.3, SP062.5, SP088.4, SP112.6**
- Ronzhina Marina..... SP116.8
 Rosa Agostinho..... PS11.004, SP178.6
 Rosa Carla C. SP047.1
 Rosado Carolina..... SP103.5
 Rosado Paulo H. SP026.3
 Rosenberg Ivan SP129.1
 Rosenfeld Anatoly B. SP081.4, SP141.4
 Rosenstein Barry..... SP122.6
 Rosewall Tara SP130.2
 Rosina Jozef SP061.2
 Ross Carl K. SP026.5
 Rostami Aram..... PS05.011
 Rouhani Hossein SPO66.5, **SP101.5**
 Rouleau Manon **SP119.1, SP119.4**
 Round William H. **PS17.013**
 Roy Eric A. SPO08.7
 Royle Gary SP129.1
 Rozendaal Roel SP057.5
 Rozenfeld Anatoly..... SP025.5
 Rucka Gunther **SP067.6**
 Rudek Benedikt..... PS05.010
 Rudie Karen PS13.008
 Ruiz-Gonzalez Yusely SP001.1
 Ruiz-Trejo Cesar SP129.2
 Runz Armin SP016.3
 Ruschin Mark SP153.4
 Rusnac Robert SP056.2
 Russo Cosimino SP093.4
 Russo Paolo SP150.3
 Russo Serenella..... SP143.1
 Ruzgys Paulius SP110.2
 Rykhalskiy Alexander SP019.2
 Rúa Orlando Rey R..... **SP146.3**

S

- Saad Waigonda..... **SP127.1**
 Saatchi Katayoun SP161.2
 Sabetian Parisa **SP166.4**
 Sadeghi Bahman SP171.4
 Sadeghi Mehdi SP127.4
 Sadeghi Parisa **SP078.1**
 Sadeghi-Naini Ali SP097.7
 Sadri Leila SP119.3
 Sadri Minoo SP06.004
 Sadrozinski Hartmut F.- SP034.5
 Saeedi Azadeh **SP151.5, SP151.7**
 Saenz Daniel..... SP175.5
 Saez-Beltran Francisco SP076.7
 Saez-Beltran Moises **SP076.7**
 Safari Mohammad Javad PS05.037, SP006.5
 Sagbay Giovanni **SP113.7, SP170.4**
 Saghir Hamidreza **SP082.5**
 Saha Satya Ranjan **SP171.7**
 Saha Shumit SP050.6
 Sahgal Arjun PS04.058, SP047.2, SP088.5
 Saifudinova Madina SP050.5
 Saifudinova Elizaveta A..... SP165.1
 Saito Shiro PS04.039
 Saitoh Hidetoshi PS04.040, **SP026.7, SP034.2, SP048.2**
 Saitoh Tadashi..... SP020.2
 Sajja Shailaja **SP097.3, SP104.3**
 Sajo Erno SP019.4, SP080.4, SP086.5
 Sakaki Kouji..... SP051.3
 Sakashita Shingo..... SP157.3
 Sakata Suoh **SP026.8**
 Sakellaris Taxiarchis SP047.1
 Sakhaee Saedeeh PS05.034
 Sakuma Ichiro..... SP055.1, SP082.3
 Sakurai Yoshinori..... **PS04.081, SP176.3**
 Sakurai Yusuke..... PS05.050
 Salado Daniela SP049.6
 Salajeghe Somaie..... **SP013.4**
 Salam Muhammad T. **SP121.4**

- Salamat Amir Hossein SP161.5
 Salamat Mohammad Reza **SP161.5**
 Salata Camila **PS05.042, SP026.1, SP026.2, SP026.3**
 Salchow Christina SP165.3
 Saleh Kutaiba SP170.1
 Salerno J SP060.2
 Sales Junior Elias S. SP114.1
 Salgado Rodriguez Paola SP085.4
 Saligheh Rad Hamid SP058.3, **SP070.4, SP128.4**
 Salomons Greg PS04.047, SP171.6
 Salum Graciela M. **SP060.2**
 Salvat Cécile **MPF06.2**
 Samadi Nazanin SP150.4, **SP150.5**
 Samani Abbas SP094.3, SP097.7, SP126.3, SP156.7
 Samavat Mohammad Faraz **SP086.3**
 Samavati Navid **SP072.5**
 Samavi Reza PS12.002
 Same Michael SP101.5
 Samford Glenn PS04.001
 Samiezadeh Saeid SP064.1, SP064.2
 Sanche Leon SP069.1, SP086.1, SP152.1
 Sanchez Carola SP036.6
 Sanchez Nieto Beatriz **MPS09.1, PS04.081, PS05.043, SP076.2, SP154.2**
 Sanchez-Doblado Francisco PS04.081, PS05.043, SP154.2
 Sanchez-Parcerisa Daniel **SP106.3**
 Sancho Lidia SP100.41
 Sankaralingam Marimuthu SP006.4, SP118.6
 Sano Kyosuke SP151.4
 Santana Roberto SP041.2
 Santerre Paul **BMEE06.1**
 Santos Alexandre PS04.011
 Santos Febles Elsa **SP170.5**
 Santos Jhonatan M. SP033.4
 Santos Josilene C. **SP118.5**
 Santos José Paulo PS19.011
 Santos Oziel S. SP020.2
 Santos William S. SP104.1
 Santyr Giles E. SP105.2, SP105.5
 Sanz Dario E. **SP177.3, SP177.4**
 Sapia Glauber E. PS12.022
 Saranummi Niilo **2798**
 Sarasanandarajah Silva PS04.009, PS05.009, SP077.5
 Sarfehnia Arman SP047.2, SP155.5, SP163.5, SP163.6
 Sarkar Saeed SP034.1, SP115.8
 Sarker Mridul SP059.4
 Sarmento Sandra SP047.1
 Sarno Antonio SP150.3
 Sarty Gordon E. SP013.4
 Sasaki David PS04.078
 Sasaki Yosuke SP026.8
 Sathiaraj P SP005.1
 Sato Hiroshi SP081.3
 Sato Hitoshi SP005.3
 Sato Kiyokazu SP079.3
 Sato Yoshinobu SP014.2
 Sattarivand Mike **PS04.083**
 Sauer Otto **PS04.084**
 Savage Niall T.P. **SP112.4**
 Savolainen Petri PS12.013
 Sawacha Zimi SP089.3
 Sawada Akira SP025.4
 Sawada Mayumi PS10.002
 Sawae Yoshinori **SP071.3**
 Sawaguchi Toi SP06.006
 Sawakuchi Gabriel O. SP081.6, SP176.4
 Sawan Mohamad SP041.6
 Sawant Mayur SP003.1, SP038.3
 Sawchuk Stephen **SP154.5**
 Sayed Inayatullah S. **PS01.021**
 Scarpignato Maurizio SP108.4
 Scarso Antonio PS16.019, SP093.4
 Schaefer Marcel **SP158.7**
 Schaly Bryan SP116.2
 Schandar Markus SP112.5
 Schandorf Cyril PS05.006, SP027.2
 Scheerlinck Ludo JT02.1
 Schellenberg Devin SP074.1
 Schemitsch Emil H. SP064.1, SP064.2, SP064.3
 Scherthan Harry SP086.4
 Schettino Giovanni M. PS12.036
 Schettino Giuseppe SP038.4
 Scheurmann Ryan SP131.3
 Schiabel Homero **PS16.036, SP024.5**
 Schiebinger Londa **PL01.2**
 Schimpf Rainer SP044.2
 Schipilow John SP097.8
 Schkommodau Erik SP121.2
 Schlattl Helmut SP037.3
 Schlect David SP015.5
 Schlegel Sebastian SP073.3, **SP073.4, SP073.5**
 Schlegel Wolfgang PS05.044, SP158.7
 Schlözer Robert SP126.4
 Schmid Matthew **MPE18.2, PS04.043, SP025.7**
 Schmittlein Charles R. SP088.2
 Schmocker Andreas **SP136.1**
 Schneider Joerg SP112.5
 Schnerr Roald S. SP119.5
 Schoen Adam R. SP068.4
 Scholey Jessica E. **SP106.4**
 Schooneveldt Gerben SP044.4, **SP159.2**
 Schreiner L John PS04.047, SP003.6, SP057.3, SP080.2, SP107.5
 Schulte Reinhard W. PS05.036, SP034.5
 Schulte Rolf F. SP105.5
 Schulz Henry SP113.4
 Schulze Walther H.W. SP044.2
 Schwahofer Andrea **PS04.085, PS05.044**
 Schwaiger Markus SP037.3
 Schwarzenberger Andreas SP113.4
 Schworer Yaqueline PS04.109, PS04.110
 Schürer Michael SP112.2
 Scoccianti Silvia SP090.6
 Scorzoni Andrea SP108.4
 Seagal Illya **SP031.4**
 Secca Mário SP146.2
 Seema Sharma PS04.091, PS04.092
 Sehgal Chandra M. SP142.3
 Sehgal Varun PS04.001, SP069.4
 Sejdic Ervin **SP052.3**
 Sekine Masaki PS12.030
 Sen Hasan T. SP016.4, SP016.6, SP073.7
 Senan Suresh SP046.1
 Senthilkumar Shanmugam PS05.015, **SP060.4, SP061.1**
 Seo Jae Hyuk **SP143.3**
 Sepehri Amir A. **SP031.5**
 Septiana Lina **SP001.6**
 Serago Christopher SP077.2, SP077.3, SP077.7
 Sermeus Corine SP019.1
 Servoli Leonello SP102.5, SP108.4
 Setayeshi Saeed SP119.3
 Seth Nitin **SP051.4**
 Sethi Seema SP046.4
 Seuntjens Jan **MPE09.1, SP038.2, SP068.3, SP076.5, SP140.3, SP142.4, SP163.6**
 Seyyedi Negisa PS09.002
 Shaer Amani **PS04.086**
 Shabestani Monfared Ali SP037.4
 Shafiei Naser SP070.4
 Shah Ashesh SP121.2
 Shah Syed Inayatullah SP045.6
 Shahedi Maysam **SP116.4**
 Shamloo Amir PS19.012, SP178.4
 Shams Ehsan PS12.016
 Shang Charles **SP152.3**
 Sharafi Ali Akbar SP037.4
 Sharma B S. SP005.1
 Sharma D.N. PS04.091
 Sharma Ishu SP133.3
 Sharma Jitendar K. SP114.4
 Sharma Nisha **SP071.7**
 Sharma Richa PS04.074
 Sharma Suresh C. SP141.5
 Sharon Rony **SP139.5**
 Sharp Gregory C. **MPE12.2, PS04.087, SP057.2, SP080.5**
 Sharp Jonathan C. SP013.4
 Sharpe Michael B. SP117.5
 Sharrock Phillip PS04.069
 Shaughnessy Gabe **SP161.1**
 Shchepotin Igor SP019.2
 Shchukin Sergey I. PS19.001
 Shehadeh Mamoun SP142.4
 Sheikh Sonia SP098.3
 Sheikholeslami Sahar SP017.2
 Sheikhzadeh Peyman PS09.002
 Shekari Mahnaz SP045.2
 Shekhar Raj PS04.059
 Shen Wei SP084.5
 Shenfield Carey SP003.6
 Sheng Yang SP117.6
 Shepherd Duncan E.T. SP112.1
 Sherafati Nima **SP068.6**
 Sherar Michael **MPE17.2**
 Shi Kemei PS02.011
 Shi Shuai SP064.3
 Shigematsu Naoyuki PS04.039
 Shiina Tsuyoshi SP162.4, SP173.1
 Shim Eun B. SP064.4
 Shima Takeshi PS05.038
 Shimada Shigenobu PS10.003
 Shimatani Yuichi PS09.007
 Shimizu Morihito SP026.7
 Shimono Tetsunori PS01.009, PS05.019, **PS05.045, SP005.3**
 Shimoto Takeshi **PS02.007, PS03.005**
 Shin Chae Won PS09.008
 Shin Dong Oh PS05.021
 Shin Eun Hyuk SP048.5
 Shin Han-Back PS04.096, PS04.097, PS04.101
 Shin Hun Joo PS05.025, SP143.3
 Shin Wook-Geun SP005.4
 Shinde Raoji S. SP114.4
 Shinsho Kiyomitsu SP048.2
 Shinya Sachiko PS04.039
 Shiraishi Yasuyuki 2955, **SP151.4**
 Shiraishi Yoshitaka PS03.005
 Shirin Shandiz Mehdi SP070.4
 Shirmohammadi Shervin SP134.6
 Shirvani Pooyan SP130.5
 Shoichet Molly S. **SP054.1**
 Shojae Moghadam Mohsen SP128.4
 Shokrollahi Elnaz PS07.005
 Shokrollahi Mehrnaz SP134.5
 Shokrollahi Peyman **PS07.005, PS07.006**
 Shortliffe Edward **PL04.1**
 Shoucri Rachad M. **SP151.6**
 Shourav M. Mohiuddin K. SP084.4
 Shrestha Samana SP049.5
 Shukla Ajai Kumar **SP037.1**
 Sia Michael PS04.113
 Siciarz Pawel **SP077.1**
 Siddiqui Farzan SP046.4, SP056.2, SP056.3
 Siew Melissa SP150.7
 Silva Ana PS02.003

Silva Catarina.....	PS19.011	Spyrou Nicholas M.	SP004.5	Sveistrup Heidi	SP082.2
Silva Eric D.....	PS18.001	Šrutová Martina	PS09.005	Svensson Cristina.....	SP143.1
Silva Halaine C.M.....	PS01.003	Ssekitoleko Robert T.	SP010.3, SP087.5,	Svensson Stina.....	SP072.2, SP131.5
Silva Lilian F.	SP033.4	SP167.7	Svistoun Igor.....	SP020.4, SP180.3
Silva Marcia D.C.	SP006.6	Ssekitoleko Simon.....	SP167.7	Svobodova Martina	SP169.4
Silva Pedro Augusto F.D.	SP059.1	St Pierre Tim.....	SP078.3, SP078.5	Swaminath Anand	SP079.4
Silva Ricardo.....	SP127.2	St. Aubin Joel.....	SP063.2	Sweeney Lawrence E.....	SP068.4
Silveira Landulfo	PS12.036, PS12.037	Staines Katherine A.....	SP089.4	Sydänheimo Lauri.....	SP136.2
Simaan Marwan A.	SP151.3	Stalpers L.J.	SP044.4	Syed Naweed.....	SP032.3, SP032.5
Simard Dany.....	SP004.4	Stanton Doug.....	SP003.3	Syed Omar Sharifah Faridah	PS09.006
Simbara Marcia M.O.....	PS02.008	Stapleton Shawn	SP059.5	Sykes Jonathan.....	SP153.5
Simira Franco.....	SP087.2, SP167.4	Starreveld Yves P.....	PS04.060	Syme Alasdair.....	SP140.3
Sinitski Emily.....	SP066.3	Staton Robert J.	MPE16.1	Szabo Joseph J.	SP022.6
Sitrin Mauro	SP167.4	Staudacher Alexander H.	SP109.5	Sá Ricardo A.M.	PS16.034, PS16.035
Siva Shankar.....	SP174.1	Stavrianou Kallirroi.....	PS12.024, PS13.007	Sánchez Velarde Emmanuel S.	SP102.7
Slivenka Lubomir	PS04.049	Steenbeke Femke.....	SP079.6	Sánchez-González Rodrigo	SP102.7, SP126.6
Slagowski Jordan.....	SP161.1	Stefancikova Lenka	SP049.6	Sánchez-Nieto Beatriz.....	MPS01.1, MPS09.1
Slezak Cyril.....	SP098.2	Stenseth Nils Chr.....	2856, SP022.4	Sánchez-Velarde Emmanuel	SP126.6
Slezak Paul.....	SP098.2	Sterzing Florian.....	SP016.3		
Slivka Scott W.	SP166.2	Steuten Lotte.....	SP020.5		
Sloane Elliot B.....	PS17.005	Stevanovic Katarina.....	SP087.7		
Sloboda Ron.....	PS04.070	Stevens David A.	SP023.3		
Slosarek Krzysztof.....	SP155.3	Stiller Wolfram.....	PS04.107, SP115.6		
Smit Casper.....	PS16.037	Stoeva Magdalena.....	PS17.014, SP054.2,		
Smith Ashley.....	SP077.2, SP077.3, SP077.7	SP125.3, SP158.3, SP158.4		
Smith Megan M.	SP063.5	Stoll Markus.....	SP016.3		
Smith Ryan L.	SP077.4	Strand Sven-Erik	SP125.3		
Smith Wade P.	SP102.1	Streitenberger Kim	BMEE15.1		
Smith Wendy L.	PS04.023, SP004.1, SP078.1, SP085.2	Strohmeier Daniel.....	SP165.3		
Snyder Karen C.	SP076.1	Studinski Ryan.....	PS04.090		
So Aaron.....	JT03.1, SP149.5	Su Lin	SP016.4, SP016.6, SP073.7		
Soares Alcimar B.....	PS01.017	Su Shiqin	SP123.5		
Soares Antonio V.	SP008.3	Subhash Chander	PS04.091, PS04.092		
Sodagar Amir Massoud	SP041.6	Subramani Vellaiyan	PS04.091, PS04.092		
Soegijono Sugiyantari.....	PS04.075	SP004.3, SP025.2,		
Soejoko Djarwani Soeharso	PS04.075, SP119.7, SP124.2, SP158.8	Subramanian Kala	SP079.5, SP164.6		
Soffientini Chiara D.	PS04.088	Subramanian V.S.....	SP004.3, SP025.2, SP164.6		
Solberg Timothy D.	MPE19.1	Subramanian Vallinayagam Shanmuga.....	SP079.5		
.....	SP106.6, SP131.3, SP139.1	SP019.5		
Soletti Rossana C.....	SP162.1	Suchowerska Natalka	SP015.2, SP019.5,		
Song Han Kyeol.....	SP06.005	SP027.1, SP054.4		
Song Ji-Hye.....	PS05.046	Sugama Atsushi	PS10.003		
Song Ju Young	SP131.4	Sugamoto Kazuomi.....	SP014.2		
Song Ting	SP106.2	Suh Jin-Suck.....	PS05.039		
Song Yeongtak.....	SP170.3	Suh Tae-Suk.....	PS01.022, SP04.093,		
Song Yi-Jiang.....	SP122.2	PS04.094, PS04.095, PS04.096,		
Sonke Jan-Jakob	SP131.5, SP174.4	PS04.097, PS04.098, PS04.099,		
Sood Sandhya.....	PS04.074, SP133.3	PS04.100, PS04.101, PS04.102,		
Soong Hew Choon.....	PS04.054	PS04.103, PS05.046, PS05.047,		
Sorensen Kristina M.	SP028.4	PS05.048, PS05.049, SP143.3		
Sorokin Iurii.....	SP058.2, SP142.2	Suhanic West	SP127.3		
Sosa-Aquino Modesto A.	PS04.041, PS19.017	Suhartanto Heru.....	PS07.003		
Sotelo-Barroso Fernando.....	SP074.6	Sukhovatkin Vlad.....	SP033.3		
Sotelo-De Ávila Alejandro A.....	SP102.7, SP126.6	Sulaiman Saadah	PS09.006		
Soto-Muñoz Jaziel.....	PS04.089	Suleiman Abdelbaset	SP136.3		
Soubiran Paul.....	SP078.2	Sullivan Natalie	SP061.6		
Souhami Luis.....	SP046.6	Sun Alexander.....	SP046.5		
Soulez Gilles.....	PS19.008, SP162.3	Sun Hongyan.....	SP070.3, SP070.5		
Sousa Maria Carmen.....	PS05.040	Sun Meixiu.....	PS12.027		
Sousa Michele C.A.	PS16.028	Sun Shouheng.....	SP049.5		
Souza Divanizia D.N.	SP033.2, SP033.4,	Sun Wenqing.....	PS04.053, PS04.116		
.....	SP171.5	Sun Wenzhao	PS04.076		
Souza Sales Rubens V.	PS01.004	Sun Yinming	SP101.2		
Sowa-Staszczak Anna	PS01.024	Sun Zhen	SP076.1		
Spadinger Ingrid.....	SP072.3	Sun Zhonghua.....	SP118.7		
Spandre Gloria.....	SP150.3	Surry Kathleen.....	SP173.3		
Specht Martin.....	SP170.1	Sushmita Pathy.....	PS04.091		
Speidel Michael A.....	SP029.5, SP161.1	Sutherland Justin.....	SP078.2		
Speller Robert D.	SP035.2	Sutherland Kenneth.....	SP049.3		
Spencer Benjamin.....	SP029.1	Suwanmanee Siwa.....	PS01.005		
Spencer David P.	SP107.4	Suzuki Hiromichi.....	PS12.035		
Sprawls Perry.....	SP125.3, SP158.5	Suzuki Kazumichi	PS04.115		
Spreeuw Hanno	SP057.5	Suzuki Minoru.....	PS04.081, SP176.3		
		Suzuki Takashi.....	PS12.028		
		Suzuki Yasushi.....	PS12.021		

T

Tabakov Slavik.....	SP063.8, SP125.1,				
.....	SP125.3, SP137.2,				
.....	SP158.4, SP158.5				
Tabakova Vassilka	SP125.3				
Tabuchi Akihiko	PS05.019				
Taggar Amandeep.....	SP078.1				
Tagoe Samuel N.A.....	PS05.006				
Taharim Khamizah.....	SP154.4				
Taheri Mahsa.....	SP050.6				
Tailor Ramesh.....	SP176.4				
Taira Yasunori.....	2955				
Tajabadi Maryam	SP138.3				
Taji Bahareh.....	SP134.6				
Takahashi Noriyo.....	PS12.005, PS12.011				
Takahashi Shingo	SP179.4				
Takahashi Wataru.....	PS04.064				
Takase Nobuhiro	SP026.8				
Takashina Masaaki	PS05.050				
Takata Takushi.....	PS04.081, SP176.3				
Takavar Abbas.....	SP058.3, SP143.2				
Takayama Shunsuke	SP134.3				
Takeda Ken.....	SP079.3				
Takeda Yoshihiro	SP005.3				
Takei Masumi.....	PS10.002				
Takeuchi Hiroshi.....	SP128.2				
Talamonti Cinzia	SP090.6, SP143.1				
Tam Cindy	PS04.058				
Tam Eric.....	PS12.029				
Tamagi Daniel.....	SP164.7				
Tamagno Iliezer.....	PS12.022				
Tambasco Mauro	SP115.2				
Tamura Kaori	SP050.2				
Tamura Toshiyo	PS12.030				
Tan Joy L.....	SP121.5				
Tan Samantha	SP097.8				
Tan Sock Keow	SP118.7				
Tanaka Hiroki.....	PS04.081, SP176.3				
Tanaka Kenya	PS12.031				
Tanaka Yoshihiro	PS10.002				
Tang Colin.....	SP077.1, SP078.3, SP078.5				
Tang Qi	PS11.004				
Tang Xiangyang.....	SP097.4				
Tang Zunyi.....	PS12.030				
Tangboonduangjit Puangpen.....	SP158.2				
Tanki Nobuyoshi.....	PS05.019, PS05.023,				
.....	SP005.3, SP067.1				
Tannock Ian F.	SP059.5				
Tannú Alberto	PS16.009				
Tantawiroon Malulee.....	SP158.2				
Tao Jessie.....	SP046.6				
Tapia María S.	PS14.002				
Taussky Daniel.....	SP153.3				
Tavakkoli Jahan	PS18.001, SP173.2				
Tavakolian Kouhyar.....	SP007.7				

- Tavallaei Mohammad A. SP104.4
Tavassoli Hanie SP086.3
Tawfiq Nada PS05.052
Tay Luke SP029.2
Taylor Mark **BMEE02.1**
Taylor Michael L. SP077.4
Tecson Marlon Raul Z. SP158.8
Teichert Katrin PS04.015
Teimoorisichani Mohammadreza SP070.3
Teixeira Flavia Cristina S. **SP009.4**
Teke Tony PS04.043, SP025.7
Teles Pedro SP048.3
Temchenko Volodymyr SP012.2
Ten Haken Randall K. SP076.1
Teo Kevin SP106.6
Teo Peng T. **PS04.105, PS04.105**
Teo Perline SP029.2
Teoh Swee H. SP053.2
Tepe Kyle P. SP166.7
Terini Ricardo A. **SP006.6, SP068.1,**
..... SP068.2, **SP137.2**
Terrón José A. MPS09.1, PS04.081,
..... PS05.043, SP154.2
Testagrossa Barbara SP044.1
Tewari Dheeraj K. SP037.1
Thakor Nitish **BMEE14.1, SP050.1**
Thaung Aung SP081.1
Thebaut Jonathan SP131.2
Then Whui Lyn **SP157.2**
Thengumpalli Sheeba **SP152.4**
Thevathasan Wesley SP121.5
Thiruganasambandamoorthy Venkatesh
..... SP111.7
Thirumalai Swamy Shanmugam SP004.3,
..... SP025.2, SP079.5, SP164.6
Thomas Christopher G. SP117.2
Thomas Steven SP074.1
Thomaz Ricardo L. PS01.017, PS01.019
Thompson Laurel A. SP028.6
Thompson Michael SP098.3
Thompson R T. SP104.4
Thomson Rowan SP017.5, SP078.2,
..... **SP109.3, SP109.4**
Thow Xin Yuan Thow SP135.6
Thwaites David **JT08.2, PS05.051,**
..... **SP102.8, SP153.5,**
..... **SP153.6, SP175.1**
Tian Junfei SP084.5
Tian Suqing SP164.3
Tian Yuan PS04.079
Tian Zhen SP106.2
Tiburzi Mario SP102.5
Tielenburg Rene SP057.5
Tietz Gustavo F. SP068.2
Tiihonen Pekka SP120.1
Tillement Olivier SP049.6
Ting Chu En SP154.4, SP173.5
Ting Hua Nong **SP167.2**
Ting Huong En SP173.5
Tinschert Joachim SP179.3
Tippayamontri Thititip **SP152.1**
Tobal Diego SP167.4
Toh Siew-Lok **PS02.009**
Tokarz Danielle SP157.3
Toma-Dasu Iuliana PS04.026, **SP094.2**
Tomal Alessandra **PS01.023, SP118.5,**
..... **SP172.1**
Tomanová Michaela PS10.009
Tomasic Ivan 2507
Tomaszuc Monika PS01.024
Tomaz Lucas C. PS05.031
Tomii Naoki **SP082.3**
Tomita Tetsuya SP014.2
Tomson Ruth SP167.5
Torres Hector PS12.003,
..... PS13.005, **SP074.2**
Torres Jorge SP036.6
Torres Leonel Alberto SP037.7, SP088.1
Torres Raquel SP170.4
Torres-García Eugenio PS04.111
Torres-Muller Sandra M. SP165.4
Torreyes Mayerith PS14.001
Toscano Lupe N. **SP180.2**
Tosh Ronald **SP163.1**
Toumel Koen PS04.054, SP079.6
Townson Reid SP025.6
Tran Linh T. SP081.4
Tran Thuc V. **SP008.2**
Trapp Jamie PS05.051, SP015.5,
..... SP036.5, SP176.2
Trauernicht Christoph SP107.1
Trbovich Patricia **1497, JT07.2, PS16.001,**
..... PS16.007, SP009.2,
..... SP103.4, **SP123.6**
Tremblay Francois SP074.7
Trimble William S. SP139.6
Triolo Ronald J. SP166.2, **SP166.3,**
..... SP166.5, **SP166.6, SP166.7**
Tromba Giuliana SP150.3
Trono Jade D. PS04.077
Tsai Cheng-Lun PS03.009, PS03.010,
..... SP126.1
Tsang Kyle SP123.6
Tsoo Ming-Sound SP157.3
Tsapakis Virginia PS17.014, **SP006.1,**
..... SP054.2, **SP085.1, SP158.4**
Tse Justin **SP034.8**
Tselepi Marina SP019.2
Tsianos Epameinondas V. SP020.6
Tsianos Vasileios E. **SP020.6**
Tsirmpas Charalampos SP123.4
Tsuboko Yusuke 2955
Tsuji Hiroshi PS04.064
Tsukamoto Akira SP055.1
Tsukamoto Isao PS12.035
Tsunashima Yoshikazu SP081.3
Tuan Muda T S SP118.7
Tulik Piotr **PS01.024**
Tumampus Jonas SP039.2, SP039.3
Tung James Y. SP008.7
Turco Gianluca SP0712
Turcotte Julie SP057.2
Turgeon Stéphane SP049.1
Turrioni João B. PS17.002
Tuček Martin PS12.008
Tworzylko Philip **SP095.7**
Tziakouri Chrysa SP024.3
Töyräs Juha SP120.1
- U**
- U Paul L. SP119.2
Uchiyama Takanori **SP144.1**
Uchôa Maira Mariana C. PS04.025
Uddin Ahmed Mobyen 2507
Uddin Md. M. SP154.3
Udee Nuntawat SP158.2
Ueki Nami SP025.4
Ueno Akinori SP134.3
Ueno Shoogo **PS01.025, SP101.3**
Uhlen Fredrik SP167.5
Ukkonen Leena SP136.2
Ulanov Dmitriy V. PS17.006
Umapathy Karthi PS19.002, SP039.7
Umesawa Yumi PS10.002, **PS10.010,**
..... **PS10.011**
Umetani Keiji PS05.033
Umimoto Koichi **PS13.009**
Ungi Tamas SP162.8
Unkelbach Jan **MPE10.2, SP130.4,**
..... **SP175.3**
Urakabe Eriko SP142.5
Ureba Ana MPS02.1, MPS06.1
- Uriarte-Rivera Héctor J. PS04.111
Urruty Luciana SP167.4
Ursani Ali **SP034.7, SP097.3, SP104.3**
Ursani Fatima SP097.3, SP104.3
Usami Noriko SP049.6
Ushida Takashi SP055.1
- V**
- Vacca Nestor PS04.108
Vacek Jakob SP061.2, SP103.1
Vachon Brigitte SP158.6
Vaez-Zadeh Mehdi SP06.001, SP076.3,
..... SP086.2, SP086.3
Vaezzadeh Vahid SP058.3
Vahidian Mohammad SP06.001, SP076.3
Vahidian Shervin SP06.001
Vai Mang I PS11.004, SP178.6
Vaiciunaite Neringa SP155.7
Valdes Gilmer **SP131.3**
Valenga Marcelo H. SP020.1
Valentini Vincenzo SP102.3
Valiante Taufik **SP052.1, SP178.1**
Valic Michael S. **SP128.3**
Vallejo Fabiola PS04.016, SP006.2
Vallet Veronique **MPF03.1**
Vallieres Isabelle SP140.5
Vallone Ilaria PS16.019, SP093.4
Van Beek Timothy SP047.5
Van Den Berg Bärbel PS16.037
Van Den Berg C.A.T. SP044.4
Van Hauwermeiren Liesbeth **SP178.3**
Van Herk Marcel SP057.5, **SP174.4**
Van Hoof Stefan SP018.1
Van Hoof Tom SP178.3
Van Kranen Simon SP174.4
Van Lieshout Natascha H. PS04.017
Van Ommen Fasco SP159.2
Van Prooijen Monique **PS04.106**
Van Soest Johan SP102.2, **SP102.3,**
..... SP102.8, **SP169.2**
Vandecasteele Katrien SP102.2
Vander Sloten Jos **SP089.3**
Vanderhyden Barbara SP096.1
Vandermeer Aaron PS04.033
Vandervoort Eric PS04.021, **SP131.1,** SP174.3
Vanhove Chris SP018.1
Vanninen Ritva SP128.1
Vanuytven Eric SP047.5
Vanzi Eleonora SP090.6
Varfalvy Nicolas SP004.2
Vargas Verdesoto Milton Xavier PS04.054
Vargas-Canas Rubiel **PS01.026**
Vargas-Luna Miguel SP083.6
Vargas-Perez Hector SP041.4
Varghese Anna SP108.1
Varveris Charalambos SP080.1
Vasquez Alexandra SP113.7
Vasquez-Lopez Jairo A. PS01.026
Vaz Filipe SP134.1
Vaz Yule SP050.3
Vazquez-Gordillo Edison **PS12.032**
Vazquez-Lopez Yair PS16.033
Veeraraghavan Harini **SP088.2**
Veilleux Israel SP096.4
Vellarde Esteban SP003.2
Velazquez Berumen Adriana PS16.020,
..... **SP063.5, SP093.2,**
..... **SP168.1, SP168.2**
Velazquez Santiago MPS02.1, MPS06.1
Velec Michael **MPE12.1, SP072.2,**
..... SP072.5
Velez Sara M. **SP084.3**
Veloza Stella ... **PS04.107, SP037.6, SP115.6**
Vena Daniel **SP146.4**
Venancio Rianne B. PS01.013, PS17.010

Venencia Daniel.....	MPS07.1, PS04.108, PS04.109, PS04.110, SP036.6	Walker Tracy.....	SP087.7	SP146.5
Venkatesan Varagur.....	SP164.2	Wallace Megan.....	SP150.7	Wi Sunhee.....	SP149.1
Venkatraman Subbu.....	SP053.2	Walsh Philip R.....	SP053.5	Wientjes Rens.....	SP062.1
Vennarini Sabina.....	SP130.3	Walsh Sean.....	SP102.8	Wierzbecki Marcin.....	PS04.114, SP036.2,
Ventikos Yiannis.....	SP110.5	Walters-Stewart Coren.....	SP082.2	SP176.1
Ventura Liliane.....	PS12.033, PS16.036	Wan Feng.....	PS11.004, SP178.6	Wiest Roland.....	SP023.4
Venugopal Niranjana.....	SP003.3	Wan Shuying.....	PS04.086	Wigati Kristina Tri.....	SP119.7
Vera-Delgado Karla S.....	SP074.6	Wan Wankei.....	SP071.7	Wijdenes Pierre J.J.....	SP032.3, SP032.5
Verdolin De Sousa Rômulo.....	PS04.008	Wan Yongli.....	SP007.6	Wijesinghe Diluka.....	SP049.5
Verellen Dirk.....	PS04.054, SP079.6	Wang An.....	PS04.087, SP016.5,	Wilches Carlos.....	SP088.1
Veres Atilla.....	PS05.030, SP017.6	SP080.5, SP130.2	Wilches L V.....	SP084.3
Veres Samuel P.....	SP055.2, SP089.2	Wang Binseng.....	BMEE25.1	Wildberger Joachim E.....	SP119.5, SP172.3
Verhaegen Frank.....	SP018.1, SP018.4	Wang Chuji.....	PS12.027	Willett Thomas.....	SP055.6
Vermiglio Giuseppe.....	SP044.1	Wang Gaofeng.....	SP097.4	Wilson Brian C.....	SP096.1, SP096.3,
Verrier Molly.....	SP066.5	Wang Hai.....	SP016.1	SP096.4, SP110.3, SP157.3
Versnick Colin.....	SP125.2	Wang Jian.....	SP160.2	Wilson Byron.....	SP152.6
Vestergaard Anen.....	SP175.1	Wang Junjie.....	PS04.123, SP003.4,	Winter Jeff D.....	SP079.4
Vetter Richard.....	SP158.3	SP155.2, SP164.3, SP164.5	Winter Stefan.....	SP126.4
Vickress Jason R.....	PS13.010	Wang Kai.....	PS04.079	Wither Rob.....	SP092.1
Vidoto Edson L.G.....	PS16.009	Wang Kevin.....	PS04.031	Wohlrab Daniel.....	SP113.4
Vieira Daniel V.....	SP115.5	Wang Kun.....	SP163.4	Wojcik Paulina.....	PS01.024
Vieira Junior Francisco U.....	SP029.4	Wang Li Z.....	SP083.2, SP156.4	Wolffart Stefan.....	SP179.3
Vieira Pedro.....	PS16.038, SP19.011,	Wang Lizhen.....	PS02.012, SP014.3, SP089.1	Wolfe Jonathan.....	SP053.2
.....	SP146.2	Wang Min.....	BMEE04.1, SP063.7,	Wolff Anders.....	SP030.2, SP030.3
Vigneault Eric.....	SP017.5	SP071.6	Wolfgang John.....	SP147.5
Vijlbriet Ron.....	SP057.5	Wang Mingjie.....	PS05.010	Wong Eugene.....	PS13.010, SP018.2,
Vilcahuaman Luis.....	2895, SP010.2, SP010.7,	Wang Rosalie H.....	SP087.4	SP018.3, SP046.2,
.....	SP088.1, SP103.5	Wang Xiao-Jian.....	PS19.019, SP094.1	SP164.2, SP173.3
Villa Parra Ana Cecilia.....	SP144.6	Wang Xiaojuan.....	PS02.011	Wong Jeannie Hsiu Ding.....	PS05.037,
Villagrasa Carmen.....	PS05.036, SP048.3	Wang Yao.....	SP074.3	SP006.5
Villagómez Galindo Miguel.....	SP041.7	Wang Yd.....	PS04.123	Wong John.....	PS04.059, SP003.2,
Villagómez Julio C.....	PS19.017	Wang Yinkun.....	SP090.1	SP016.4, SP016.6, SP073.7
Villamares-Vargas Victor A.....	PS04.111	Wang Yu.....	SP065.3, SP151.3	Wong Raimond.....	SP079.4
Villanueva Doreen Alexis F.....	PS04.077	Wang Yu-Lin.....	SP040.3	Wong Rebecca.....	SP003.7
Villarreal-Barajas Jose E.....	PS04.112,	Wang Yuxing.....	SP089.5	Wong Willy.....	SP101.1, SP101.2
.....	SP058.4, SP090.4,	Wang Zhennan.....	PS12.027	Wood Guilherme A.....	SP093.5
.....	SP124.5, SP130.5	Wang Zhiyuan.....	SP162.7	Worm Anna.....	SP087.1
Villaseñor Navarro Yolanda.....	PS05.041	Wanwilairat Somsak.....	PS04.054	Wright Eric A.....	SP097.1
Villegas-Navarro Fernanda.....	SP076.5,	Ward Aaron D.....	SP029.3, SP046.1,	Wright Philip.....	SP077.1
.....	SP106.5	SP046.3, SP116.1, SP116.4	Wright Trinetta.....	SP088.5
Vinceone Volney C.....	SP084.2	Ward Rabab.....	SP097.8, SP149.7	Wronski Matt.....	SP153.4
Vincenti Maria Aurora.....	SP058.4	Wardlaw Graeme M.....	SP100.2	Wu Chun-Wei.....	SP101.4
Vincenzi Alessandro.....	SP150.3	Warkentin Brad.....	SP063.2, SP164.7	Wu Lili.....	SP016.1
Viner Coby.....	SP122.4	Warner Andrew.....	SP046.3	Wu Meng.....	SP065.5
Vines Doug.....	PS01-006, SP046.5, SP070.7	Warrick Philip A.....	SP039.6	Wu Pengwei.....	SP097.4
Viney Richard.....	SP112.1	Wasilewska-Radwanska Marta.....	PS19.020	Wu Q Jackie.....	PS04.120, SP117.4, SP117.6
Vinod Shalini.....	SP102.8, SP153.6	Watanabe Kouya.....	PS12.039	Wu Qian.....	SP143.4
Vissa Adriano.....	SP139.6	Watanabe Shota.....	SP151.4	Wu Raymond K.....	MPE01.2, SP063.3
Viswanathan Sowmya.....	PS02.010	Watanabe Soichiro.....	PS03.006	Wu Richard Y.....	PS04.115
Vittoria Fabio A.....	SP150.6	Watanabe Takashi.....	SP008.1	Wu Sheng-Kai.....	SP028.3
Vivekanandhan Subbiah.....	SP005.1	Watanabe Tsubasa.....	PS04.081	Wu Zhaoxia.....	SP106.2
Viviani Carlos A.B.....	SP103.3	Watson Peter G.....	SP068.3	Wysokinski Tomasz W.....	SP087.7, SP150.4
Voichcoski Bernadete M.....	PS11.006	Watt Elizabeth.....	PS04.112, PS04.113,	Wårdell Karin.....	SP074.4, SP110.1,
Voigt Herbert F.....	2856, 2883, 2895,	SP085.2	SP121.2, SP121.3
.....	JT05.1, JT05.2, SP010.2	Webb Mark A.....	SP087.7, SP150.4		
Vollborn Thorsten.....	SP179.3	Webster Dave.....	SP161.4		
Vollmar Brigitte.....	SP112.5	Weersink Robert A.....	SP003.7, SP096.3,		
Vollmer Thomas.....	SP126.4	SP096.4		
Vooijs Marc.....	SP018.1	Wei Hung-Wen.....	PS03.009, PS03.010	Xhaferllari Ilma.....	SP130.1
Vorauer Eric.....	SP06.007	Weitz David.....	BMEE18.1, SP030.1	Xia Junyi.....	PS04.116
Vujicic Miro.....	SP047.4	Wells Angela.....	PS04.073	Xia Wenyao.....	SP016.5
Vuong Nhung.....	SP096.1	Wells Derek M.....	SP058.1, SP140.5	Xiang Haiyan.....	SP074.5
		Wells R Glenn.....	JT01.1, SP045.1	Xiao Lylia.....	SP087.7
		Wells Woodrow.....	PS04.050	Xie Chuanbin.....	SP107.2
		Welsch Katrin.....	SP164.4	Xie Congying.....	SP175.2
		Welzer Tatjana.....	PS17.007	Xie Liangxi.....	SP016.1
		Wen Zhifei.....	SP176.4	Xie Yaoqin.....	SP105.6, SP162.7
		Weng Yitong.....	SP029.7	Xing Aitang.....	PS04.117
		Wenz Annika.....	SP112.5	Xu Heping.....	SP139.2
		Wenz Frederik.....	SP175.4	Xu Linfeng.....	SP157.1
		Westendarp Zanartu Mattias.....	SP159.2	Xu Ling B.....	SP107.5
		Wester Per.....	SP145.3	Xu Shouping.....	PS04.118, SP070.2
		Whan Renee.....	SP098.4	Xu Tong.....	SP029.1, SP079.1
		Wheeler Bruce C.....	SP135.3	Xu Wei.....	SP107.2
		White Benjamin M.....	PS04.012, SP130.3	Xu Xuanang.....	PS04.061
		White James A.....	SP126.3	Xu Yingjie.....	SP103.2
		Whyne Cari.....	SP055.6, SP073.6, SP088.5,	Xu Yiwen.....	SP116.1

W

Wachowiak Mark P.....	SP050.4
Wachowicz Keith.....	SP016.2, SP105.3
Wada Hiroshi.....	PS03.011
Wadi-Ramah Shada.....	SP022.3, SP043.4,
.....	SP078.6
Wagner Antoine.....	PS04.054
Wakabayashi Genichiro.....	SP048.2
Walden Andrew P.....	SP173.4
Waldron Timothy.....	PS04.116
Walker Amy.....	SP072.1

X

Xhaferllari Ilma.....	SP130.1
Xia Junyi.....	PS04.116
Xia Wenyao.....	SP016.5
Xiang Haiyan.....	SP074.5
Xiao Lylia.....	SP087.7
Xie Chuanbin.....	SP107.2
Xie Congying.....	SP175.2
Xie Liangxi.....	SP016.1
Xie Yaoqin.....	SP105.6, SP162.7
Xing Aitang.....	PS04.117
Xu Heping.....	SP139.2
Xu Linfeng.....	SP157.1
Xu Ling B.....	SP107.5
Xu Shouping.....	PS04.118, SP070.2
Xu Tong.....	SP029.1, SP079.1
Xu Wei.....	SP107.2
Xu Xuanang.....	PS04.061
Xu Yingjie.....	SP103.2
Xu Yiwen.....	SP116.1

Y

Yabunaka Kouichi..... PS05.023, SP067.1
 Yadollahi Azadeh..... SP050.6, SP120.5,
 SP120.6, SP146.4
 Yahya Atiyah..... SP063.2
 Yahyanejad Sanaz..... SP018.1
 Yamada Akihiro..... **2955**
 Yamada Kenji..... PS03.006, PS12.039
 Yamada Kiyohiro..... SP142.5
 Yamagishi Masaaki..... 2955
 Yamakawa Makoto..... SP162.4, SP173.1
 Yamamoto Kenyu..... PS13.011
 Yamamoto Megumi..... **SP116.7**
 Yamamoto Naoyoshi..... PS04.064
 Yamamoto Shin-Ichiroh..... SP008.2, SP066.1
 Yamamoto Takahiko..... **PS12.034**
 Yamamoto Yoshitake..... SP148.4
 Yamamura Osamu..... SP008.4
 Yamashita Ayako..... PS12.035
 Yamashita Wataru..... SP026.8
 Yamashita Yoshihisa..... PS12.019, **PS12.035**
 Yamazaki Masatoshi..... SP082.3
 Yamazaki Takaharu..... **SP014.2**
 Yambe Tomoyuki..... 2955, SP151.4
 Yan Di..... SP072.7, SP174.5
 Yan Qin..... SP156.6
 Yan Yue..... SP175.5
 Yang C J..... SP067.2
 Yang Celina J..... **SP091.3**
 Yang Homer..... SP007.5
 Yang Jong-Chul..... SP105.7
 Yang Li..... SP122.2
 Yang Limin..... PS11.004, SP178.6
 Yang Meili..... SP097.4
 Yang Qing..... SP167.3
 Yang Ruijie..... PS04.123, **SP003.4**,
 SP155.2, SP164.3, SP164.5
 Yang Yang..... PS02.015, SP007.6,
 SP083.2, SP094.1
 Yang Ying..... SP002.2
 Yang Yueh-Hsun..... SP002.1
 Yani Sitti..... PS04.080
 Yao Jie..... **SP014.3**, SP083.2
 Yao Weiguang..... **SP116.5**
 Yartsev Slav..... **PS04.119**, PS13.010
 Yasumura Yoshio..... PS12.039
 Yazaki Marcos L..... SP040.2
 Yazıcı Yasin..... SP095.4
 Ybarra Norma..... SP046.6, SP096.2
 Ye Feng..... PS04.079
 Ye Lincai..... **PS02.013**
 Ye Peiqing..... SP025.8
 Yea Ji Woon..... PS04.051, PS04.052
 Yee Albert..... SP146.5
 Yeom Yeon Soo..... SP005.4
 Yeong C H..... **SP118.7**
 Yeong Chai Hong..... **SP015.4**, **SP025.5**,
SP154.4, SP158.8,
SP159.4, **SP173.5**
 Yeung Ivan..... PS01-006, **PS01.027**,
SP070.7, SP180.3
 Yeung Rosanna..... PS04.023
 Yeung Timothy Pok Chi..... SP046.2, SP046.3
 Yewondwossen Mammo..... PS04.022
 Yim Evelyn K.F..... **SP098.5**
 Yin Fangfang..... PS04.120, SP117.4, SP117.6
 Yin Guang F..... PS02.014
 Yin Tao..... SP044.3, **SP101.6**, **SP101.7**
 Yip Christopher M..... SP139.6
 Yip Cindy..... PS12.029
 Yip Eugene..... SP016.2
 Yohanandan Shivanthan A.C..... SP121.5
 Yokoi Hiroshi..... SP008.4
 Yokoyama Kiyoko..... SP156.3
 Yokoyama Moe..... PS03.006, PS12.039
 Yoneda Misao..... PS13.011

Yong Keong H..... SP032.2
 Yoo Do Hyeon..... **SP005.4**
 Yoo Paul..... **SP166.1**, SP166.4
 Yoon Do-Kun..... PS04.096, SP04.097,
 PS04.101
 Yoon Heenam N..... SP092.2
 Yoon Jae-Woong..... PS05.039
 Yoon Jeongmin..... PS04.018, PS05.012,
 SP090.5
 Yoon Kyoung Jun..... PS04.006
 Yoon Se-Cheol..... SP143.3
 Yorozu Atsunori..... PS04.039
 Yoshida Ken..... SP032.2
 Yoshida Masaki..... **PS10.012**, **PS10.013**,
 PS11.001, PS12.030
 Yoshikawa Hideki..... SP014.2
 Yoshimura Elisabeth M..... SP137.2
 Yoshino Ryoji..... PS16.013
 Young Heather..... **SP005.5**
 Young Michael..... SP057.2
 Younger Alastair..... SP146.1
 Younis Abdulredha S..... **PS05.052**
 Yousef Bassem..... SP107.1
 Yu Lifeng..... SP034.6, SP115.7
 Yu Mina..... SP143.3
 Yu Suhong..... PS04.001, SP069.4
 Yu Wei..... SP107.2
 Yuan Jing..... SP162.6
 Yuan Lulin..... **PS04.120**, **SP117.4**, **SP117.6**
 Yuan Yuan..... PS12.027
 Yubo Fan..... SP014.3, SP014.4,
 SP083.2, SP156.4
 Yucel Altundal..... SP080.4
 Yudelev Mark..... **SP047.3**
 Yun Jihyun..... **SP016.2**

Z

Zabihian Alireza..... **SP041.6**
 Zadeh Gelareh..... SP023.2
 Zaidi Habib..... PS01-007, SP013.1, SP013.3
 Zaidi Mohammed K..... **PS17.015**
 Zaidi Wali..... SP032.3, SP032.5
 Zaini Mehran M..... **SP068.4**
 Zak Yair..... SP104.2
 Zakaria Ahmad..... SP045.6
 Zakaria Golam Abu..... PS04.045
 Zakariae Roja..... **SP072.3**
 Zakeri Vahid..... **SP007.7**
 Zaki George..... PS04.059
 Zaman Areesha..... SP081.2, **SP119.6**
 Zamir Anna..... SP150.6
 Zamir Mair..... PS19.018
 Zanette Brandon..... **SP105.2**
 Zangaro Renato A..... **PS12.036**, **SP12.037**
 Zankl Maria..... SP037.3
 Zanolow Frank..... SP134.1
 Zaqq Dina Q..... SP045.5
 Zargan Sajedeh..... SP037.4
 Zarghami Niloufar..... SP018.2
 Zariffa José..... SP040.4, SP041.4
 Zatserklyaniy Andriy..... SP034.5
 Zavgorodni Sergei..... **PS04.121**, SP025.6,
 SP090.2, **SP140.5**
 Zdero Radovan..... SP064.1, SP064.2, SP064.3
 Zdora Marie Christine..... SP019.5
 Zehtabi Fatemeh..... SP162.3
 Zelaya Diego..... SP127.2
 Zeng-Harpell Grace..... PS04.056
 Zentner Lena..... SP134.1
 Zequera Martha..... SP088.1
 Zeraatkar Navid..... PS01.002, SP045.3
 Zernetsch Holger..... PS02.004, PS02.005,
 SP071.4, SP151.1
 Zerouali Karim..... SP004.4
 Zevenhoven Koos C.J..... **SP044.6**

Zhai Shu Yi..... SP087.7
 Zhan Lixin..... SP140.4
 Zhang Bing..... **SP028.1**
 Zhang Dandan..... PS04.076, PS04.122
 Zhang Edwin..... SP028.1
 Zhang Fuli..... **PS04.123**, **SP107.7**
 Zhang Geng..... SP070.3
 Zhang Geoffrey G..... **SP097.5**
 Zhang Guangshun..... **PS04.122**
 Zhang Haibo..... PS02.013
 Zhang Hui..... SP025.8
 Zhang Jian..... SP163.4
 Zhang Jianxun..... SP167.3
 Zhang Ke..... SP103.2
 Zhang Liang..... SP092.1
 Zhang Meng J..... **PS02.014**
 Zhang Mengying..... SP140.4
 Zhang Sen..... SP029.7
 Zhang Shunqi..... SP044.3
 Zhang Tao..... SP020.3, SP024.3
 Zhang Wei Min..... SP156.6
 Zhang Wenjun..... SP028.1
 Zhang Xile..... SP164.5
 Zhang Yi..... SP115.3
 Zhang Yibao..... SP056.1
 Zhang Yin..... SP016.4, SP016.6, SP073.7
 Zhang Ying..... SP007.6, SP056.1
 Zhang Yingshu..... SP046.4
 Zhang Yuanqing..... PS19.006
 Zhao Chen..... SP101.6, SP101.7
 Zhao Nan..... **PS04.123**, **SP155.2**,
SP164.3, **SP164.5**
 Zhao Ni..... PS19.006
 Zhao Xiaomeng..... PS12.027
 Zhen Jie..... PS17.012, SP007.6
 Zheng Gang..... SP128.3
 Zheng Wei-Long..... SP041.1, SP041.2
 Zheng Weili..... SP072.4
 Zheng Yong-Ping..... **BME11.2**
 Zhi Ying Xuan..... **SP120.5**
 Zhong Hualiang..... SP056.3, **SP056.4**,
 SP076.1
 Zhou Dong..... **SP025.8**
 Zhou Fugen..... PS04.061, PS04.118
 Zhou Li..... **SP056.1**
 Zhou Li Li..... **PS02.015**, SP094.1
 Zhu Jia-Yi..... SP041.1
 Zhu Ning..... SP087.7, SP150.4
 Zhu Ron..... PS04.115
 Zhu Yanchun..... **SP105.6**, **SP162.7**
 Zhu Ying..... SP150.5
 Zhuang Yu Xin..... SP087.7
 Ziegenhein Peter..... SP125.5, SP164.1,
 SP164.4
 Ziemer Benjamin..... SP171.4
 Zinchenko Yuriy..... SP130.5
 Zlateva Yana..... **SP069.2**
 Zoabli Gnahoua..... **BMEF03.1**, **SP16.039**,
SP16.040
 Zoccoler Marcelo..... **SP111.6**
 Zola Elma..... SP120.5
 Zumpano Romero Maria Fernanda..... SP085.4
 Zuniga Manuel E..... **SP160.5**
 Zvereva Alexandra..... **SP037.3**
 Zór Kinga..... SP030.3

JOIN US IN PRAGUE IN 2018!



www.iupesm2018.org



IUPESM
PRAGUE 2018



SHARPEN YOUR EDGE AGAINST CANCER.

EDGE

Edge Radiosurgery: Making radiosurgery an option for more patients.

Deliver accurate radiosurgery treatments quickly and efficiently with the Edge™ radiosurgery system. Edge's advanced technology enables you to offer powerful, non-invasive radiosurgery treatments anywhere in the body where radiation is indicated. Expand treatment options for patients and gain a competitive edge with the system as dedicated as you are.

Visit us at IUPESM World Congress 2015. Booth #1234.

Learn more about Edge Radiosurgery at varian.com/Edge

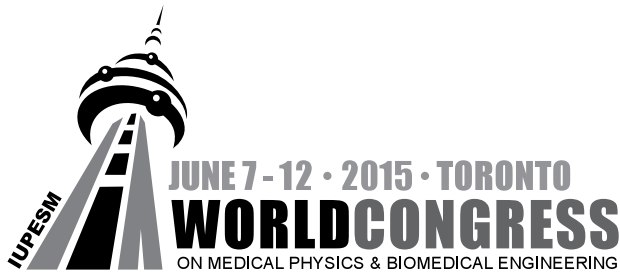
VARIAN
medical systems

A partner for **life**

Radiation treatments may cause side effects that can vary depending on the part of the body being treated. The most frequent ones are typically temporary and may include, but are not limited to, irritation to the respiratory, digestive, urinary or reproductive systems, fatigue, nausea, skin irritation, and hair loss. In some patients, they can be severe. Radiation treatment is not appropriate for all cancers. See varian.com/use-and-safety for more information.

© 2015 Varian Medical Systems, Inc. Varian and Varian Medical Systems are registered trademarks, and Edge is a trademark of Varian Medical Systems, Inc.

TABLE OF CONTENTS



Health.
Technology.
Humanity.

SCIENTIFIC
PROGRAM

PAGE
2

SPECIAL
SESSIONS

PAGE
764

POSTER
ABSTRACTS

PAGE
522

PLENARY
SESSIONS

PAGE
775

CONTINUING
EDUCATION

PAGE
692

SCIENTIFIC PROGRAM

SP001 - Image Processing and Visualization: Part 1

TRACK 01: IMAGING

SP001.1 - The Use of Wavelet Filters for Reducing Noise in Posterior Fossa Computed Tomography Images

Author(s): Reinaldo Pita-Machado¹, Marlen Perez-Diaz², Juan E. Paz-Viera², Juan V. Lorenzo-Ginori², Yusely Ruiz-Gonzalez²
¹Tomography, 1 Centro de Ingeniería Clínica y Electromedicina, Santa Clara/CUBA, ²Study Center On Electronic And Information Technologies, Universidad Central "Marta Abreu" de las Villas, Santa clara/CUBA

This paper describes an experimental search for the best wavelets, to reduce *Poisson* noise in CT.

Five slices containing the posterior fossa from an anthropomorphic phantom and from patients were selected. As their original projections contain noise from the acquisition process, some simulated noise-free lesions were added on the images. After that, the whole images were artificially contaminated with *Poisson* noise over the sinogram-space. The configurations using wavelets drawn from four wavelet families, using various decomposition levels, and different thresholds, were tested in order to determine de-noising performance. The 10 preselected best filters were *Sym4*, *Bior3.5*, *Bior3.7*, *Coif3*, *Coif5*, *dB3*, *dB45*, *db8*, *Sym 20*.

The quality of the resulting images was evaluated using Contrast to Noise Ratio (*CNR*), Human Visual System absolute norm (*H1*), Mean Structural Similarity Index (*MSSIM*) and the *jackknife free-response* methodology. The results were compared with other traditional filters.

The de-noising with wavelet filters improved the image quality of posterior fossa region in terms of an increased *CNR* (see Fig.1), without noticeable structural distortions (see Fig. 2).

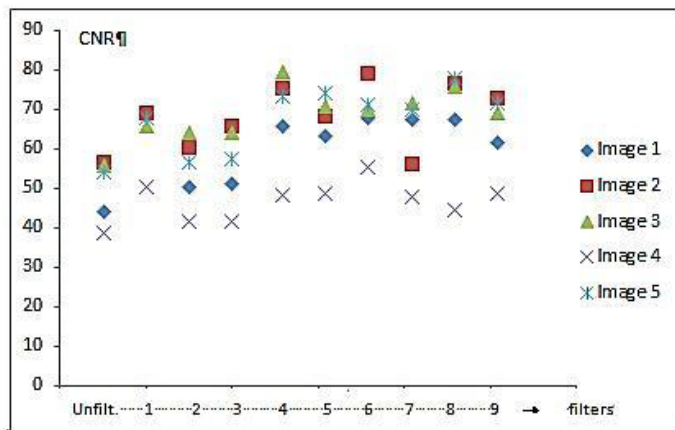


Fig. 1. Contrast to Noise Ratio for filtered and unfiltered images

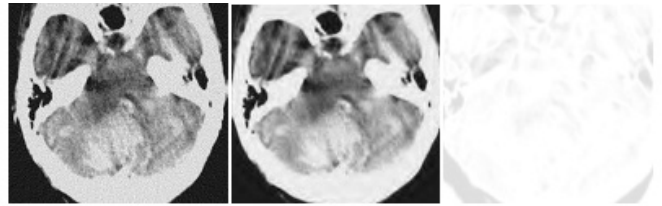


Fig. 2. Region of interest in fossa a) contaminated unfiltered image, b) the corresponding filtered image with *Coif3* and c) *MSSIM* map.

The precision in the observers' reply improved with the filtering procedure in all the cases respect to unfiltered images ($p=0.0003$). The procedure facilitated the localization of small lesions in fossa.

The wavelet filter *Coif 3* ($MSSIM = 0.8152$) had the best performance. It was also better than Median ($MSSIM = 0.7914$) or Wiener filters ($MSSIM = 0.7796$) and similar to Butterworth ($MSSIM = 0.8228$) to remove similar amount of noise with lower spatial resolution lost.

In Conclusion: Wavelet filtering is an alternative to be considered for *Poisson* noise reduction in image processing of posterior fossa head CT images.

SP001.2 - Automatic Liver Localization based on Classification Random Forest with KNN for Prediction

Author(s): Benwei Gong, Baochun He, Qingmao Hu, Fucang Jia
 Shenzhen Institutes of Advanced Technology, Chinese Academy of Sciences, Shenzhen/CHINA

Purpose

Automatic, robust localization of liver in CT images is a prerequisite for robust liver segmentation. Fast, accurate localization of liver is challenging due to the variation in the appearance and shape, and the ambiguous boundaries between the liver and its neighbor organs. Liver segmentation using statistical shape models have shown significant potential, however, wrong localization of the liver region often cause the failure or inaccuracy. By combining and refining the state-of-the-art random forest technique, classification random forest with K Nearest Neighbor (KNN) model was proposed for liver localization.

Methods

In our approach, localization of liver region was taken as the problem of initial segmentation, and the method mainly consisted of two phases: interface localization and K-NN based classification random forest for prediction.

Interface localization: The interface between the abdominal cavity and thoracic area was located as a reference for liver region. Since the intensity features was apparent in lung region (thoracic cavity), a differential model based on such characteristic was used to localize the interface of the right side of the body. Then, the relative spatial coordinates and the relative structural prior with Gaussian kernel function were calculated.

K-NN based Random Forest: To construct an ensemble of independent decision trees without over-fitting, the number of the samples for each class was balanced. A subset of entire datasets as well as feature vectors was randomly chosen for each tree. Besides, the corresponding training samples were stored in each leaf node.

In testing phase, the samples shared similar features will be splitted into the same leaf node. The K-NN based method was used, which relied on the hypothesis that samples from the same structures not only share such features, but are closely localized in image spaces.

Euclidean distance was used in the K-NN model. In the leaf node of each decision tree, testing samples are predicted with a K-NN model using the relative spatial location and the structural prior of the liver.

Results

The performance of our method for liver localization was tested on 19 contrast enhanced CT datasets from Visceral challenge (<http://www.visceral.eu>). We adopted the leave-one-out cross validation using Dice coefficient and Hausdorff distance metric. Compared with AdaBoost and traditional random forest method, our methods had a Dice coefficient of **0.878±0.043** and a Hausdorff distance of **22.13±10.12mm**, while AdaBoost with a Dice coefficient of **0.795±0.075** and a Hausdorff distance of **30.94±9.41mm**; and traditional random forest with a Dice coefficient of **0.829±0.134** and a Hausdorff distance of **30.42±13.42mm**. Paired t-test was used to compare among the three methods, and the difference was statistically significant ($p < 0.001$) except the Dice coefficient of our method and the traditional random forest.

Conclusion

We have proposed a fully automated approach for robust liver localization. As in medical images, anatomy structures are spatially dependent, we applied a spatial KNN model to predict the testing sample from k nearest samples from the same leaf node. Compared with AdaBoost and traditional classification random forest, our method has higher performance.

SP001.3 - Brain Tumor Target Volume Segmentation: Local Region Based Approach

Author(s): Mehdi Astaraki¹, Hossein Aslian²

¹Biomedical Engineering, IAU Science and Research branch, Tehran/IRAN, ²Medical Physics, International Centre for Theoretical Physics (ICTP) and university of Trieste, Trieste/ITALY

In this paper, we comprehensively evaluated clinical application of local robust-region based algorithms to delineate the brain target volumes in radiation therapy treatment planning. Localized region based algorithms can optimize processing time of manual target tumor delineation and have perfect correlation with manual delineation defined by oncologist due to high deformability. Accordingly, they can receive much attention in radiation therapy treatment planning. Firstly, clinical target volumes (CTVs) of 135 slices in 18 patients were manually defined by two oncologists and the average of these contours considered as references in order to compare with semi-automatic results from different four algorithms. Then, four localized region based algorithms named Localizing Region Based Active Contour (LRBAC), Local Chan-Vese Model (LCV), Local Region Chan-Vese Model (LRCV) and Local Gaussian Distribution Fitting (LGDF) were applied to outline CTVs. Finally, comparisons between semi-automatic results and baselines were done according to three different metric criteria: Dice coefficient, Hausdorff distance, and mean absolute distance. Manual delineation processing times of target tumors were also performed. Our result showed that LCV has advantage over other algorithms in terms of the processing time and afterward LRCV is the second fastest method. LRBAC was the second slowest technique; however, we found that processing speed in LRBAC can be almost doubled by replacing the time-consuming re-initialization process with energy penalizing term. Accordingly, due to high accuracy performance of LRBAC algorithm, it can be concluded that the modified version of LRBAC has the best performance in brain target volumes in radiation therapy treatment planning among other localized algorithms in terms of speed and accuracy.

SP001.4 - A Novel Automatic White Balance Algorithm for the 3D Image of Stereoscopic Endoscopy

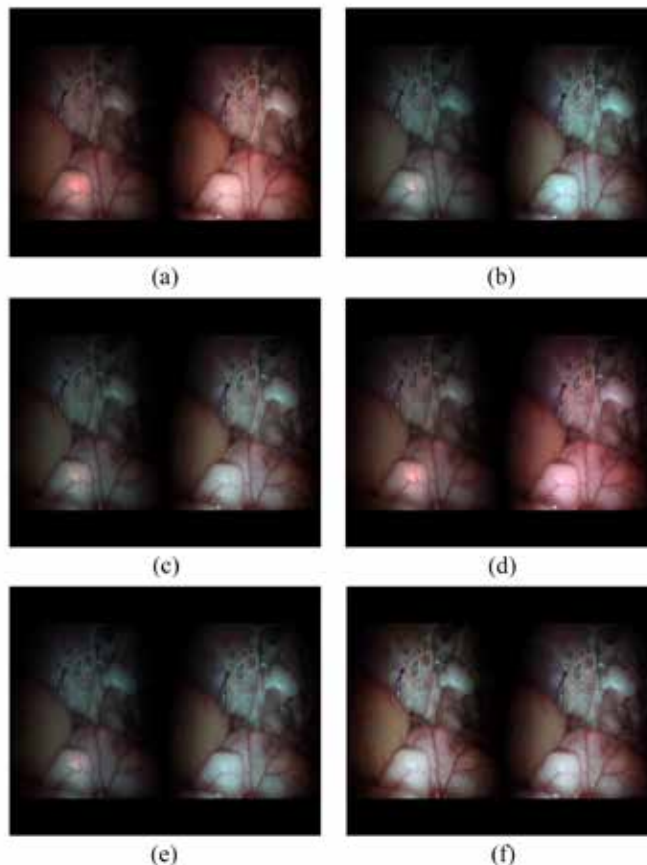
Author(s): Yuan Hai¹, Ling Li², Gu Jia²

¹Shenzhen College Of Advanced Technology, University of Chinese Academy of Sciences, Shenzhen/CHINA, ²Shenzhen Institutes Of Advanced Technology, Chinese Academy of Sciences, Shenzhen/CHINA

Objectives: Automatic white balance is an important function of stereoscopic endoscopy. The 3D image often contains color mismatch and different luminance between two stereo views. It will lead to many problems applying traditional white balance methods for each image of 3D images independently. In order to solve those problems, we proposed a novel automatic white balance algorithm for the 3D image of stereoscopic endoscopy.

Methods: The proposed algorithm consists of three steps: choosing the reference image from two stereo views, adjusting the reference image by the white balance method and color matching. The second step is divided into three parts: the probable white point detection, the white point selection, and the white point adjustment. We use dynamic thresholds to detect white points.

Results: In order to test the effectiveness of the proposed algorithm, the 3D image of stereoscopic endoscopy with color cast is processed by the proposed method, the gray world method (GWM), the robust automatic method (RAWB), the Varsha Chikane's automatic white balance method (VCAWB), and the perfect reflector method (PRM) as illustrated in Fig.1. Further, for making more precise comparisons among the methods, we use the scores of Euclidean Distance(ED) as objective evaluative values. A lower value is expected. At the same time, the values of Bhattacharyya Distance (BD) between two stereo views are calculated to show the similarity degree of two stereo views, the smaller the better. The results are shown in Table 1.



	Original	GW	RAWB	VCAWB	PRM	Proposed method
ED-left	31.403	24.757	28.049	27.005	27.352	12.080
ED-right	18.974	13.610	13.886	16.235	14.913	12.114
ED-average	25.189	19.184	20.968	21.620	21.133	12.097
BD	0.203	0.202	0.205	0.180	0.194	0.005

Conclusions: The experimental results show that the proposed method performs better than others in the effectiveness of white balance and the similarity degree of two stereo views is much improved after applying the proposed method.

SP001.5 - A new log-compression rule for B-mode ultrasound imaging adjusted to the human visual system

Author(s): Ramon C. Fernandes¹, Tiago M. Machado¹, Johannes D. Medeiros Junior¹, Haroldo J. Onisto¹, José E. Bertuzzo¹, Eduardo T. Costa²

¹Department Of Services And Hardware Engineering, Eldorado Research Institute, Campinas/BRAZIL, ²Biomedical Engineering Department, University of Campinas, Campinas/BRAZIL

Introduction: Medical ultrasound imaging has become a major diagnostic technique for searching anatomical and functional pathologies. In B-mode image formation, log compression is the process by which the signal is rendered more suitable for visual analysis. The current ultrasound scanners consider only the image dynamic range, usually understood as the signal range that will be linearly mapped to a grayscale and displayed on a screen. However, human visual system characteristics should be better considered in the image processing as well, requiring understanding of the principles of image formation and their influence on visual perception. Our objective is to present a new log compression rule applied to ultrasound images that also accounts for the characteristics of the human visual system.

Methodology: This new log compression method is not only unique for presenting the whole ultrasonic signal compressed to a certain range and not just part of its dynamic range, but for considering more features, such as contrast and its relation to dynamic range and to brightness perceived by the eyes, or visually distinguishing neighboring tones. Our proposed model for logarithmic compression is divided into three stages: compression, mapping and tonal adjustment. The compression presents, on a logarithmic scale, the signal amplitude compressed to the chosen range; the mapping step relates the intensity of the post-compression with a grayscale level using a sigmoid curve that tends to change the contrast in the central intensity levels giving priority to texture perception and improving contrast. The last step takes into account the tonal differentiation (proposed by Liu and Huang), which determines the distance between tones that make them distinct. The proposed method was tested with phantom images obtained with a commercial B-mode scanner that allows the capture of raw data for image and signal post processing. The results were compared to those of traditional compression methods. We have quantified image information loss for each log compression method using the error relative to the original signal information. All image and data processing were carried out using Matlab®.

Results, Discussion and Conclusions: We noted that for the classical model used in almost all ultrasound systems, there is a signal "clipping", with its amplitude saturated to lower and upper thresholds, producing flat cutoffs. So, just a small part of the total dynamic range is used in the traditional method, leading to possible loss of background information of the image. The proposed method,

however, preserves signal integrity. The proposed log compression is more suitable to human vision, by considering contrast perception and tone differentiation and, since it preserves the echo information, it is better to represent the structures contained in the ultrasonic signal. The proposed method has lead to relative error of less than 0.01% (best case) or 4.5% for the worst case. The proposed method shows potential to reduce compression parameter adjustments for imaging of the anatomical structures of interest.

SP001.6 - Comparison of Independent Component Analysis (ICA) Algorithm for Heart Rate Measurement Based on Facial Imaging

Author(s): Lina Septiana¹, Freddy Haryanto², Kang-Ping Lin³
¹Electrical Engineering, Krida Wacana Christian University, Jakarta/INDONESIA, ²Department Of Physics, Institut Teknologi Bandung, Bandung/INDONESIA, ³Department Of Electrical Engineering, Chung Yuan Christian University, Taoyuan/TAIWAN

This paper deals with the heart rate measurement by performing automatic face tracking and blind source separation of three color channel into independent components. A class of the so-called Independent Component Analysis (ICA) represents a powerful tool for such a detection. Various ICA algorithms have been introduced in the literature; therefore there is a need to compare these methods. In this contribution, two of the most common ICA methods are studied and compared to each other as regarding their ability to recover the independent source signal from normalized RGB of the facial image. These are the Joint Approximate Diagonalization of Eigen matrices (JADE), and the Second Order Blind Identification (SOBI). These two algorithms have been applied to the same data set of RGB traces then compare with commercially calibrated BPV sensor. Both two methods have given approximately consistent results. However SOBI method has shown better accuracy of heart rate measurement over JADE.

SP002 - Stem Cells in Tissue Engineering and Regeneration

TRACK 02: BIOMATERIALS AND REGENERATIVE MEDICINE

SP002.1 - Biomaterials and Regenerative Medicine: Micro-environmental Modulation for Controlled Cell Differentiation and Tissue Development

Author(s): Gilda Barabino¹, Stephen Goldman², Yueh-Hsun Yang³
¹The Grove School Of Engineering, Dean, The City College of New York, New York/NY/UNITED STATES OF AMERICA, ²Army Institute of Surgical Research, San Antonio/TX/UNITED STATES OF AMERICA, ³The City College of New York, New York/NY/UNITED STATES OF AMERICA

The engineering and regeneration of tissues and organs holds great promise for the treatment and prevention of disease and is enabled by natural and synthetic biomaterials that serve as anchors for bioactive molecules and cells. Successful creation of engineered tissues requires a thorough understanding of microenvironments that regulate cellular behavior and tissue formation. Microenvironments define the immediate surroundings of a cell and encompass essential mediators such as soluble factors and extracellular matrix molecules bound to the cell and to adjacent cells. Tissue engineering approaches that aim to manipulate culture parameters and emulate natural microenvironments are sought by combining cells, bioactive agents and biocompatible or biodegradable materials in scalable bioreactors. Among these components, scaffolds or hydrogels made of synthetic or naturally derived polymers are fabricated to meet the requirements for cell survival, matrix biosynthesis, mechanical integrity and integration capacity with host tissues and thus provide appropriate three dimensional substrates for cell growth and tissue development. Bioreactor systems do their part by delivering biophysical and mechanical cues to cultured cells in a tunable, well-defined environment, which greatly improve mass transfer efficiency and tissue quality. Lately, adult stem cells derived from different origins such as bone marrow and adipose tissues have become attractive for repair and regeneration of damaged tissues or organs due to their multi-potency and expandable lifespan, yet achieving controlled stem cell differentiation into a desired cell lineage remains challenging. As an important step toward the fabrication of clinically relevant functional tissue replacements, our laboratory has focused on developing combinatorial methods that endeavor to understand the synergy between cells and micro-environmental factors in order to optimize culture conditions for stem cell differentiation and tissue regeneration. This talk will summarize recent examples of tissue engineering strategies for development of cartilage tissue constructs using stem cells, hydrodynamic bioreactors and microfluidic hydrogels.

SP002.2 - Defining the regulatory metrics for regenerative medicine using novel biomaterial tagging strategies

Author(s): Alicia J. El Haj, Katie Bardsley, Ying Yang
 Institute Of Science And Technology In Medicine, Keele University, Stoke-on-trent/UNITED KINGDOM

Biomaterials can provide a useful platform for controlling the regeneration of tissues with or without the use of different types of stem cells. In order to meet the regulatory needs for clinical use, the standards must be established which enable the complex products to be manufactured in a reproducible way. A non-destructive protocol which can define a biomaterial's degradation and its associated ability to support proliferation and/or promote extracellular matrix deposition or differentiation could be an essential tool for process

manufacturing in regenerative medicine. To achieve this aim, we have designed fluorescent tagged degradable materials which can be monitored on line non-invasively *in vitro* for assessment of tissue engineered products and also *in vivo* for measuring tissue regeneration *in vivo*. Three fluorescently tagged biomaterials, chitosan, fibrin and poly(ethylene glycol) diacrylate-fibrinogen conjugates, were fabricated and the effect of their degradation on cell proliferation and osteogenic protein production was investigated. Alterations observed in fluorescence retention within the biomaterials and the release of fluorescent soluble by-products accurately quantified degradation and was cross-validated by weight loss measurements. Assessment of biomaterial behaviour with and without cells has been measured *in vitro* in bioreactors, *ex vivo* and *in vivo* in rat models. Degradation was shown to have a significant effect on cellular activities, with faster degradation eliciting a decreased cell proliferation and concurrently an increased osteopontin production. A turnover index (TI), which directly describes the effect of biomaterial degradation on cell behaviour, has been defined, with high TIs for matrix production observed on fast degrading biomaterials. This novel TI has the potential to become an essential tool for tissue engineers as it has the ability to highlight biomaterials which are suitable for various applications, such as cell proliferation or differentiation. This ability to predict cellular reactions and pre-select certain biomaterials before clinical studies would be invaluable tool not only for tissue engineering but for regenerative medicine as a whole and may lead to the development of clinically successful therapies.

SP002.3 - The role of electric fields in promoting precursor cell migration to enhance wound repair

Author(s): Stephanie Iwasa¹, Robart Babona-Pilipos², Milos R. Popovic¹, Cindi M. Morshead³

¹Institute Of Biomaterials And Biomedical Engineering, University of Toronto, Toronto/ON/CANADA, ²Toronto Rehabilitation Institute, University Health Network, Toronto/ON/CANADA, ³Department Of Surgery, University of Toronto, Toronto/ON/CANADA

Studies have shown that endogenous electric fields (EFs) are important for directed cell migration and further, externally applied EFs have demonstrated success in promoting wound closure. However, the cellular mechanisms of this therapy remain unclear and limit its potential use. We have previously demonstrated that neural stem and progenitor cells (together termed neural precursor cells, NPCs), undergo rapid and directed cathodal migration in the presence of an EF *in vitro*. Notably, differentiated NPCs do not undergo rapid and directed migration in the presence of an EF. To build on this finding, fluorescent NPCs are plated on ex-vivo spinal cord or brain slices to examine NPC migration in a more biologically relevant environment. Initial results show NPCs migrate in the presence of an EF on spinal cord slices, albeit at a slower speed. We hypothesized that the induced cell migration in the presence of EFs is a generalized feature of precursor cells regardless of their tissue of origin. We tested our hypothesis using skin-derived precursor cells (SKPs), found in the dermal papillae of the skin. SKPs are multipotent and give rise to mesodermal and neural progeny. We examined SKPs colonies isolated *in vitro* and performed the same migration assay as per the NPCs. Interestingly, unlike in NPC migration where >98% of the cells migrated in the EF, the vast majority of SKP cells did not migrate. Of the few cells that displayed directed migration, ~1% migrated to the cathode while another small subpopulation migrated rapidly towards the anode. We have demonstrated through PCR and live-imaging that NPCs express voltage gated calcium channels (VGCCs) that are critical for migration. Indeed, blocking VGCCs leads to a significant reduction in the speed of migration. We predicted the lack of SKP migration might also be the result of the lack of VGCC expression. However, we found that SKPs expressed similar VGCCs to NPCs, suggesting that this was not the reason for the lack of migration. We next proposed that SKPs were differentiating into mature phenotypes in our culture conditions and hence lost their migratory

ability as was seen with differentiated NPC cultures. Our preliminary staining reveals that a small population of plated cells express the neural precursor cell marker Nestin and we hypothesize that it is this neural precursor subpopulation of SKPs that is demonstrating cathodal migration. We are further characterizing the phenotypes of cells migrating towards the anode. Together these findings suggest that cells maintaining a neural precursor phenotype are responsive to EF's, regardless of their tissue of origin.

SP002.4 - The role of niche architecture on muscle stem cell division orientation

Author(s): Richard Y. Cheng¹, Penney Gilbert²

¹Ibbme, University of Toronto, Toronto/ON/CANADA, ²Ibbme, University of Toronto, Toronto/CANADA

Skeletal muscle is comprised of muscle fibres (myofibres) that are embedded within connective tissue. Reconstruction of the adult muscle tissue relies on a pool of resident committed muscle stem cells (MuSCs) situated between the basal lamina and sarcolemma known as "satellite cells" which express the paired-box transcription factor Pax7 necessary for their specification during embryonic development and long-term maintenance during adult life. To maintain tissue homeostasis, MuSCs undergo asymmetric division to produce a committed daughter cell that repairs damage to local fibers and an uncommitted daughter that repopulates the niche. Upon an injury where extensive regeneration is required, MuSCs undergo symmetric divisions in which two uncommitted daughter cells are produced to expand the myogenic progenitor pool. Recent studies indicate that MuSC 'stemness' is contingent on maintaining contact with the basal lamina during division such that asymmetric divisions occur in an apical-basal orientation with respect to the fiber, while symmetric divisions proceed in plane with the fiber (planar). Understanding the molecular mechanisms by which MuSCs undergo cell fate decisions, especially self-renewal, during muscle regeneration is a fundamental goal of modern muscle research.

Using a cyclic compression machine to evaluate the Young's modulus, we found that the bulk stiffness of regenerating muscle is significantly higher compared to healthy control mice. We propose that these changes manifest due to the increased deposition of extracellular matrix (ECM) components in the MuSC niche immediately after injury. We confirmed this using immunohistochemistry and western blotting and observed that the injured MuSC niche contains increased amounts of aligned ECM components such as collagen, fibronectin, and laminin. In addition, atomic force microscopy on isolated individual fibers revealed significant differences between the stiffness of healthy fibers versus injured fibers, indicating that the increased ECM during regeneration is associated with a stiffer niche, which is an aspect capable of modulating MuSC self-renewal in culture as previously showed. To understand if fibrosis alters the niche architecture by physically restricting apical-basal oriented division, we mimicked the healthy and regenerating niche by culturing isolated muscle fibers within soft (12kPa) and stiff (24kPa) agarose gels. Confocal timelapse microscopy allowed us to track cell division orientations over 48 hours of 3D culturing, and here we report that MuSC in a soft environment had a tendency to divide both in the apical-basal (75%) and planar direction (25%), whereas the stiff environment was permissive for mostly planar divisions (84%). Together, this data suggests that changes in the niche architecture due to increased ECM deposition during regeneration play a significant role in supporting MuSC division orientation.

SP002.5 - Mapping the Stem Cell's Mechanome using Paired Live Cell Multiplexed Imaging and Modeling

Author(s): Melissa L. Knothe Tate

Graduate School Of Biomedical Engineering, University of New South Wales, UNSW Sydney/AUSTRALIA

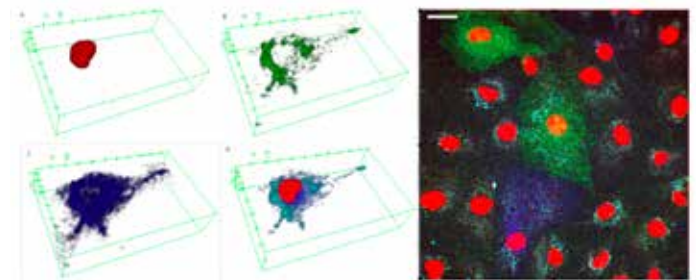
INTRODUCTION

A series of studies using model mesenchymal stem cells [1-5], primary embryonic stem cells [6], and primary adult stem cells [7,8], has established the profound role of mechanoadaptation on lineage commitment and tissue genesis. Here we aimed to develop novel methods to allow for live cell multiplexed fluorescent imaging for the spatiotemporal distribution of the cell nucleus, membrane and cytoskeleton concomitant to delivery of controlled mechanical stresses and measurement of sub-/cellular strains.

METHODS

Cells were cultured *per* previous protocols [1,9] to achieve targeted densities and developmental contexts. Cells were tagged at time zero with Con-A conjugated, microbeads [4]. Actin and tubulin were tagged during transcription using BacMem 2.0 assays (Invitrogen) [3]. Live cell membranes and nuclei were stained using Cyto9, Hoechst, and fluorescence-tagged Wheat Germ Agglutinin [3,10]. Thus, the displacement and spatiotemporal distributions of each cellular constituent could be tracked as a function of controlled mechanical environment (Fig 1). Using a paired multiphysics computational model (Comsol) [5], we then mapped deviatoric and dilatational stresses as a function of stem cell mechanoadaptation.

RESULTS



Live stem cell imaging of the nucleus (red), actin (green), tubulin (blue) and compiled cell structure, followed by multicell image, depicting the same cellular constituents spatially. Scale bar: 20 microns.

DISCUSSION

The novel paired imaging and modeling method allows for live cell multiplexed fluorescent imaging of cell/nucleus shape and volume concomitant to monitoring of spatiotemporal actin and tubulin distribution, as well as *in situ* strain assessment. Akin to mechanical testing of a cell as it evolves and optimizes its structure for prevailing dynamic function, the novel method will enable elucidation of the underlying mechanisms of stem cell mechanoadaptation, potentially paving the way for targeted delivery of physical cues to achieve targeted tissue genesis and healing.

REFERENCES

- [1] S.H. McBride *et al.* *Tissue Engineering*, 2008. [2] M.J. Song *et al.* *PLoS one*, 2010. [3] H. Chang and M.L. Knothe Tate. *Mol Cell Biomechanics*, 2011. [4] M.J. Song *et al.* *PLoS one*, 2012. [5] M.J. Song *et al.* *Biomaterials*, 2013. [6] M.L. Knothe Tate *et al.* *Fields Institute for Mathematics in Biology* 2010. [7] S.F. Evans *et al.*, *Biomaterials*, 2013. [8] H. Chang *et al.*, *Stem Cells Transl Med*, 2014. [9] S.H.

McBride *et al. Tissue Engineering*, 2008. [10] J. Zimmerman and M.L. Knothe Tate. *Mol Cell Biomechanics*, 2011.

ACKNOWLEDGEMENTS

This project has been supported in part through the Paul Trainor and the U.S. National Science Foundations.

SP003 - Brachy Therapy: Part 1

TRACK 04: RADIATION ONCOLOGY

SP003.1 - The impact of in-homogeneity corrected dose calculations for various clinical HDR brachytherapy sites.

Author(s): S V. Jamema, Siji Paul, Reena Devi, Kishore Joshi, Mayur Sawant, Pooja Moundekar, Deepak Deshpande
Medical Physics, Tata Memorial Hospital, Mumbai/INDIA

Purpose: To determine and the impact of in-homogeneity corrected dose calculations for various clinical brachytherapy sites, and to quantify the variation between the two algorithms: TG 43 & Acuros.

Methods: Various clinical sites have been investigated: surface mould of the nose, base of tongue-tonsil implant, soft tissue sarcoma of the chest wall, breast multi catheter APBI, lip, eyelid implant, and gynaecological applications which consisted of two applicators, namely Vienna and ring made up of polymer and stainless steel material respectively. After the implantation, CT scans were obtained, followed by reconstruction of the implant, dose calculation and treatment delivery. The clinical dose calculations were carried out using TG 43 algorithm, which were then re-calculated using Acuros model based dose calculation (Eclipse v 10, VMS). The dose to the target, OARs were evaluated using the DVH parameters, volumes of various isodose levels (V300%, V200%, V100%, V50%) and isodose distribution.

Results: TG 43 overestimated the dose as compared to Acuros for all the implant types. Implants such as eyelid and lip had larger variation >10%, while implants of breast, soft-tissue sarcoma of the chest wall and base of tongue resulted in variation of the order of 5-10%. The gynaecological implants resulted with lowest variation of <5% (Table 1). In surface mould of the nose, the mean dose to the ipsilateral eye resulted in a variation of 11%, while in tongue implant, the dose to the underlying bone resulted in a variation of 9%. In soft tissue sarcoma and breast implant, TG 43 over estimated the dose to the skin by 20 and 35 cGy while the dose to the lung was underestimated by 10cGy per fraction (prescription dose: 4Gy/fraction) (Figure 1). The dose profile at the superficial region was overestimated by 50cGy and 200cGy for lip and eye lid implant.

Conclusion: The impact of in-homogeneity corrected dose calculations for various clinical brachytherapy sites, between the two algorithms, TG 43 & Acuros has been quantified.

Table 1:

Implant	% variation of volumes of isodose levels
Surface mould of the nose	9±7
Base of Tongue and tonsil	8±8
Soft tissue sarcoma of the chest wall	7±2
Breast APBI Multi catheter	8±2
Lip Implant	11±14
Eye Lid Implant	22±37
Gynaecology- Vienna applicator	1±0.2
Gynaecology-ring applicator	4±0.7

SP003.2 - A novel QA device for brachytherapy applicator QA

Author(s): Yi Le, Sook Kien Ng, Esteban Velarde, Elwood Armour, John Wong
 Radiation Oncology, Johns Hopkins University, Baltimore/UNITED STATES OF AMERICA

Purpose/Objective(s):

The commissioning and routine quality assurance (QA) of the source positions for HDR applicators usually requires double exposures of films which is time consuming. The objective of this study is to develop an effective and efficient filmless method for evaluating dwell positions of HDR applicators using a novel QA device.

Materials/Methods:

Material: A device that unifies comprehensive real-time mechanical and dosimetric QA measurements has been developed in our institute for routine external beam QA originally and extended to brachytherapy application. This device comprises an imaging surface for receiving multiple energy sources, a camera for measuring and recording data related and a mirror system for directing the energy sources to a stationary camera. The imaging surface has a resolution of 0.25 mm. Source dwell positions QA for HDR ring and tandem applicator sets was performed using this device as a case study.

Methods: R&T applicator sets were secured to the imaging surface of the QA device (Figure1a). Two sets of images of the applicators were acquired by the QA device. First set of images were acquired using fluoroscopy x-ray with dummy marker in the applicators (Figure 1b). This serves as the reference image and provides the markers' positions for comparison with active source positions. The second set images were acquired using HDR Ir-192 sources (Figure 1c). The images were acquired in integration mode with 20 second integration time. Measurements were repeated five times for each set of applicator and the mean value of the dwell position were determined (Figure 1b). No image registration is necessary since the images were taken by the same device at same location. Data analysis was automated using MATLAB to improve efficiency and eliminate user dependence.

Results:

Tandem applicator measurements indicated all dwell positions were within 1.0 ± 0.4 mm from the dwell positions to the corresponding dummy markers. The most distal dwell position for the ring applicator was found to be within 1.2 ± 0.7 mm from the tip of the dummy mark. Results for symmetric source position analysis are in good agreement with the recommended angle (90°). Using this QA device, the applicator sets only need to be setup once on the imaging surface for repeat measurements.

Conclusions: A method utilizing a novel QA device for HDR applicators QA was demonstrated. The digital high resolution images allow the source dwell positions to be determined quantitatively. Automatic data analysis method significantly reduces time required for repeat measurements.

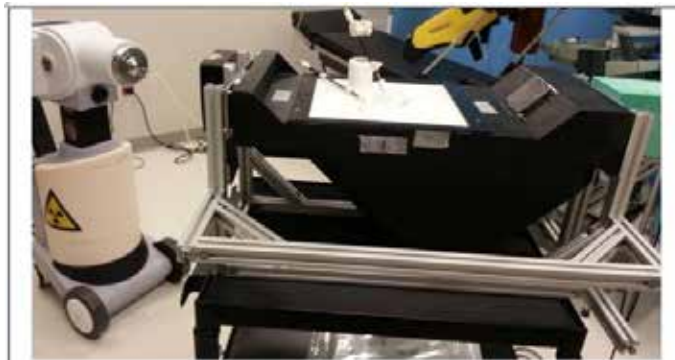


Figure 1a: Ring and tandem applicator sets were secured to the imaging surface of the QA device.

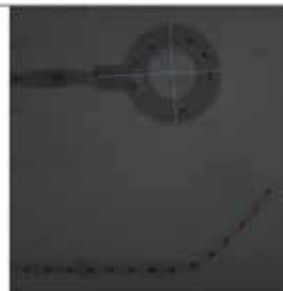


Figure 1b: The reference image was taken using fluoroscopic system. The mean value of the dwell positions (red dots) were plotted on the reference image.



Figure 1c: Illustration of dwell positions used for analysis, produced by irradiation of Ir-192 HDR source.

SP003.3 - Electromagnetic tracking for catheter reconstruction in ultrasound-guided high-dose-rate brachytherapy of the prostate

Author(s): Shyam Bharat¹, Cynthia Kung¹, Ehsan Dehghan¹, Alexandru M. Nicolae², Ananth Ravi², Niranjana Venugopal³, Antonio Bonillas¹, Doug Stanton¹, Jochen Kreucker¹
¹Philips Research North America, New York/UNITED STATES OF AMERICA, ²Medical Physics, Odette Cancer Centre, Toronto/CANADA, ³Saskatoon Cancer Centre, Saskatoon/CANADA

Purpose: The accurate delivery of high-dose-rate (HDR) brachytherapy is dependent on the correct identification of the position and shape of the treatment catheters. In many brachytherapy clinics, transrectal ultrasound (TRUS) imaging is used to identify these catheters. However, manual catheter identification on TRUS can be time consuming, subjective, and operator dependent due to a number of imaging artifacts. We report the use of electromagnetic (EM) tracking technology to determine the position and orientation of catheters inserted in a tissue-equivalent prostate phantom.

METHODS AND MATERIALS: An Aurora EM system (NDI, Waterloo, ON, Canada) was used in this experiment. The accuracy of the EM system was quantified using a three-axis robotic system. In addition, EM tracks acquired from catheters were compared with catheter positions determined from TRUS and CT images, to compare EM system performance to standard clinical imaging modalities. The tracking experiments were performed in a controlled laboratory environment (no EM-signal distorters present), and in a typical brachytherapy operating room (EM-signal distorters present). Additionally, the positional distortion in multiple sensors resulting from the distorting effects of the brachytherapy operating room was characterized.

Results: The robotic validation of the EM system yielded a mean

accuracy of < 0.5 mm for a clinically acceptable field of view in a non-EM-distorting (laboratory) environment. The largest distortion in sensor signal (30s acquisition at 40 Hz), was associated with the brachytherapy equipment cart placed in the proximity of the EM field generator in the brachytherapy operating room. The achievable system accuracy depended largely on the calibration of the TRUS probe, geometry of the tracked devices relative to the EM field generator, and locations of surrounding clinical equipment. To address the issue of variable accuracy, a robust calibration algorithm was developed and integrated into the workflow. The EM-tracked catheter representations were found to have an accuracy of < 1 mm when compared with TRUS- and CT identified positions, both in the laboratory environment and in the brachytherapy operating room, with the addition of the robust calibration. The proposed mapping technique was also found to improve the workflow efficiency of catheter identification.

Conclusions: The high baseline accuracy of the EM system, the consistent agreement between EM-tracked, TRUS- and CT-identified catheters, and the improved workflow efficiency illustrate the potential value of using EM tracking for catheter mapping in high-dose-rate brachytherapy.

SP003.4 - Dosimetric and radiobiological comparison of volumetric modulated arc therapy, high-dose-rate brachytherapy and low-dose-rate permanent seeds implant for localized prostate cancer

Author(s): Ruijie Yang, Junjie Wang
Radiation Oncology, Peking University Third Hospital, Beijing/CHINA

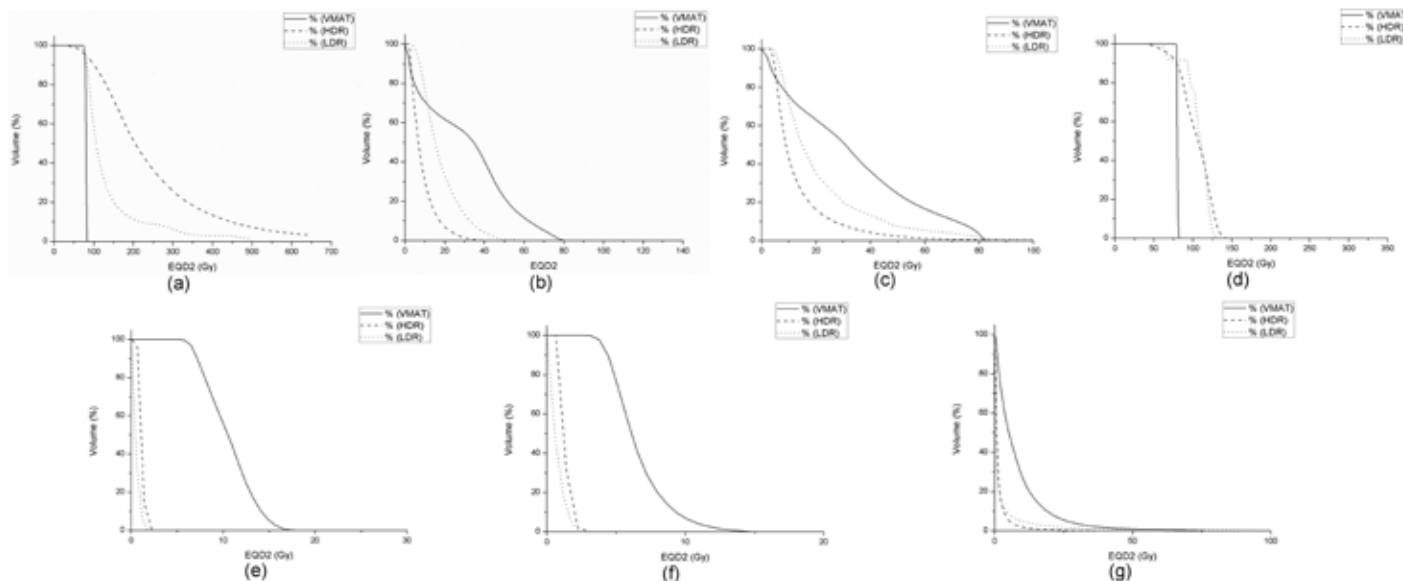
Purpose: To assess the dosimetric and radiobiological differences among volumetric modulated arc therapy (VMAT), high-dose-rate (HDR) brachytherapy, and low-dose-rate (LDR) permanent seeds implant treatment for localized prostate cancer.

was D90 of 34 Gy in 8.5 Gy per fraction for HDR (¹⁹²Ir), and 145 Gy to clinical target volume (CTV) for LDR (¹²⁵I) plans, respectively. The dose and dose volume parameters were evaluated for target, organs at risk and normal tissue. Physical dose were converted to dose based on 2-Gy fractions (equivalent dose in 2 Gy per fraction, EQD2) for comparison of three techniques.

Results: HDR and LDR significantly reduced the dose to rectum and bladder compared with VMAT. The Dmean (EQD2) of rectum decreased 22.36 Gy in HDR and 17.01 Gy in LDR from 30.24 Gy in VMAT, respectively. The Dmean (EQD2) of bladder decreased 6.91 Gy in HDR and 2.53 Gy in LDR from 13.46 Gy in VMAT.

For the femoral heads and normal tissue, the mean doses were also significantly reduced in both HDR and LDR compared with VMAT. For the urethra, the mean dose (EQD2) was 80.26 Gy, 91.23 Gy and 104.91 Gy in VMAT, HDR and LDR, respectively.

Conclusion: For localized prostate cancer, both HDR and LDR brachytherapy were clearly superior in terms of the sparing of rectum, bladder, femoral heads and normal tissue compared with VMAT, with a little higher mean dose to the urethra in LDR. HDR provided the advantage in sparing of urethra compared with LDR



Methods and Materials: Ten patients with localized prostate cancer were selected for this study. Volumetric modulated arc therapy, high-dose-rate brachytherapy and low-dose-rate permanent seeds implant plans were created for each patient. For volumetric modulated arc therapy, planning target volume (PTV) was created by adding a margin of 5 mm to the clinical target volume. Rectum, bladder, urethra and femoral heads were considered as organs at risk. 78 Gy in 39 fractions were prescribed for PTV. The dose prescription

SP003.5 - A novel system for real-time planning and guidance of breast HDR brachytherapy

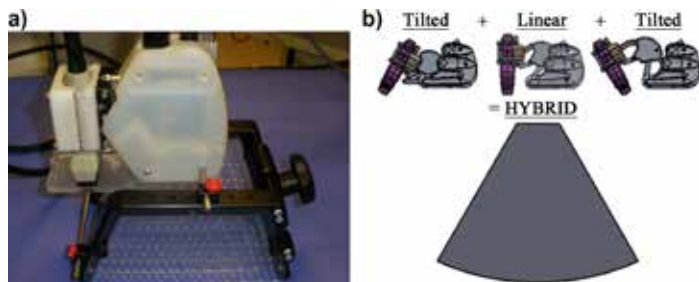
Author(s): Eric Poulin¹, Lori Gardi², Kevin Barker², Jacques Montreuil², Jean Pouliot³, Aaron Fenster², Luc Beaulieu¹
¹Radio-oncologie, CHU de Quebec, Quebec/QC/CANADA, ²Imaging Research Laboratories, Robarts Research Institute, London/ON/CANADA, ³Radiation Oncology, University of California San Francisco, San Francisco/CA/UNITED STATES OF AMERICA

Purpose: In breast interstitial high dose rate (HDR) brachytherapy, the number and positions of the catheters are usually chosen manually using a preimplant CT scan or fixed using 2D ultrasound. Furthermore, there is currently no automated real-time ultrasound guidance system available. In this work, we present a novel system for real-time planning and guidance of breast HDR brachytherapy treatment, using 3DUS.

Methods: A computer controlled robotic 3DUS scanner has been designed to fit on a modified Kuske assembly (Elekta Brachytherapy, Veneendal, The Netherlands). The scanner can be mounted at several positions on the assembly, which allows the user to personalized the position of acquisition, as shown in Fig. 1a. Figure 1b shows the larger field-of-view provided by the hybrid motion of the new 3DUS system. Software modules were developed for the acquisition and reconstruction of ultrasound images. A semi-automatic segmentation algorithm and a needle reconstruction algorithm were integrated into the software to segment the planning target volume and reconstruct the catheters. A tracking module and a catheter optimization algorithm were developed in order to perform real-time planning and guidance of the needle. Linearity, volume and catheter trajectory measurements were performed, using agarose-based phantoms in MRI, CT or 3DUS scanners to validate the new 3DUS system. A new approach, using the template, was used for real-time planning. The method snaps the optimized catheter positions to the available position within the template. The procedure was tested with 14 and 16 catheters, six times each, in an agarose-based phantom with an hypo-echoic mass.

Results: The 3DUS acquisition time requires approximately 20s and the catheter optimization algorithm can obtain 10 complete treatments plans, with the corresponding dosimetric indices, in 90s. There were respectively 3.4 % and 1.4 % difference between MRI/3DUS as well as CT/3DUS volume. Both MRI and CT volume were not statistically significantly different from 3DUS volume (Student *t*-test; *p*>0.05). The 3DUS system was found to measure efficiently the linear dimensions. The mean angular separation distance between catheter trajectories segmented from 3DUS and CT images was $0.42 \pm 0.24^\circ$, while the mean trajectory separation was 0.37 ± 0.17 mm. After the insertion procedure, the real-time approach was shown to enable reduction of the number of catheters without breaking ABS dosimetric recommendations.

Conclusions: A novel system was designed and validated for real-time planning and guidance of breast HDR brachytherapy treatment. A modified system could also be used for permanent breast brachytherapy.



SP003.6 - Investigation of electromagnetic catheter tracking approach for spatial reconstruction of implant geometry in high dose rate brachytherapy of prostate cancer

Author(s): Stephen Macgregor¹, Chandra P. Joshi¹, Andras Lasso², Carey Shenfield¹, Gabor Fichtinger², L John Schreiner¹
¹Departments Of Physics And Oncology, Queen's University, Kingston/ON/CANADA, ²School of Computing, Queen's University, Kingston/ON/CANADA

Introduction: An accurate and rapid spatial reconstruction of implanted catheters in planning image space is vital in the high dose rate (HDR) brachytherapy. This work investigates the accuracy of electromagnetic (EM) catheter tracking for CT-based treatment planning of HDR brachytherapy of prostate cancer.

Methods: A 16-catheter implant was performed under ultrasound guidance on a tissue-equivalent prostate phantom (Model-053G, CIRS, Norfolk, VA) embedded into a pelvic phantom (Figure 1). Seven PinPoint-128 markers (Beekley, Bristol, CT) on the phantom were used to achieve ground-truth registration between the CT image (2mm slices) and EM tracking space. EM tracking was performed with driveBAY magnetic field generator, and Model-600 (reference) and Model-55 (tracking) EM sensors (Ascension Technology, Shelburne, VT). The EM sensor was inserted sequentially into the catheters to obtain location measurements. Data collection was completed using Plus (www.plustoolkit.org) and SlicerIGT (www.SlicerIGT.org) software, and analyzed in MATLAB. EM tracking was performed at field generator-to-surface distances of 5.5cm and 8.0cm for ultrasound probe inside and withdrawn from the rectum. Catheter tracks were reconstructed from locations measured in EM tracking, and catheter reconstruction error was computed as the shortest distance between the EM tracked points and the catheter centrelines reconstructed with spline curve fitting from the CT image space.

Results and Conclusions: Both ground-truth registration and catheter reconstruction were more accurate closer to the field generator, and when the ultrasound probe was withdrawn from the rectum (Table 1). With the probe withdrawn, the sum of RMS errors was less than the catheter diameter and is clinically acceptable. Large range values indicate presence of tracking outliers due to EM tracking inaccuracies in dynamic noise environment (Table 1). These outliers will be eliminated by using extended Kalman filters combining geometric and kinematic constraints; currently a work in progress.

Acknowledgements: RideForDad, Prostate Cancer Research Grant (Kingston-Quinte), and Cancer Care Ontario

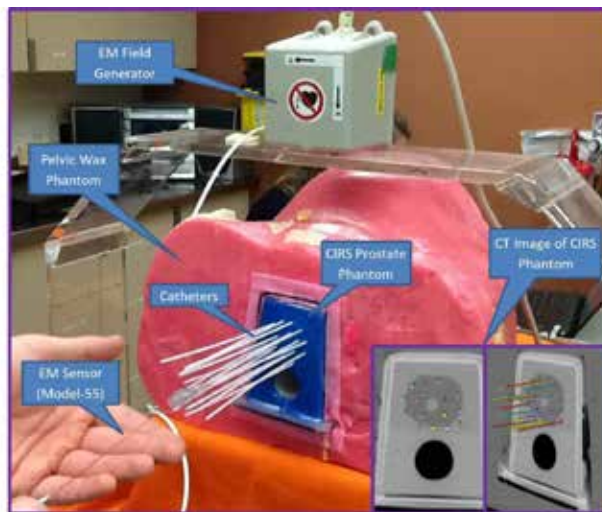


Figure 1: The EM catheter tracking setup. The inset shows catheter points from EM measurements overlaid on CT images of the CIRS prostate phantom.

Table 1: Reconstruction errors in catheter tracks measured in EM tracking space versus the catheter centrelines in CT image space

Distance between EM field generator and the phantom surface	Presence of the ultrasound probe in rectum?	Ground Truth Error (RMS registration error between EM and CT spaces)	Catheter Reconstruction Error (RMS distance of catheter tracks reconstructed from EM and CT)	
			Average	Range
80 mm	YES	1.0 mm	2.2 mm	0.0 – 9.0 mm
	NO	0.8 mm	1.4 mm	0.1 – 3.9 mm
55 mm	YES	1.0 mm	1.7 mm	0.2 – 5.8 mm
	NO	1.1 mm	0.6 mm	0.0 – 3.2 mm

We report our initial clinical testing of this technique on patients with esophageal cancer treated with high dose rate brachytherapy. Feasibility and workflow based on physician and therapist feedback will be presented. A preliminary assessment of the accuracy of the applicator placement when compared to the current standard of care will also be presented.

SP003.7 - Endoscopic Tracking for improved Applicator Insertion in Esophagus and Lung HDR Brachytherapy

Author(s): Robert A. Weersink¹, Jimmy Qiu², Rebecca Wong¹, Gail Darling³, Jonathon Irish³, David A. Jaffray¹

¹Radiation Oncology, University Health Network, Toronto/ON/CANADA, ²Techna Institute, University Health Network, Toronto/CANADA, ³Surgical Oncology, University Health Network, Toronto/CANADA

Intracavitary applicators are used in high dose rate brachytherapy for lung, esophagus and gynecological applications. For lung and esophagus applications, the linear applicators are typically inserted using a combination of endoscopy and fluoroscopy. In the current procedure, endoscopy is used to define the proximal and distal ends of the planned target length. With the endoscope located at these sites, the endoscope and a surface marker are aligned using fluoroscopic imaging. Applicator insertion follows removal of the endoscope, with fluoroscopy guiding placement of the applicator relative to the surface marker. Since visualization is only two-dimensional, applicator placement is prone to error. Furthermore, it exposes staff to unnecessary radiation exposure.

We are developing a new method of applicator insertion that employs tracking and navigation of the endoscope and brachytherapy applicator. The objective is to accurately place the applicator based on direct localization of the endoscopic findings. An electromagnetic tracking device (Aurora, NDI, Waterloo, ON) is fixed inside a standard 8mm diameter flexible endoscope (Olympus). The tracking device measures both position and orientation of the end of the flexible endoscope.

Software developed in-house simultaneously displays and records the coordinates and video stream of the endoscope. If a prior volumetric image has been acquired, the endoscopic recording can be further registered to this image. When the endoscope is at a position of interest, such as the proximal or distal end of the target, the location can be recorded and displayed simultaneously with the position of the endoscope. Multiple points can be recorded. A second tracking device is inserted into the applicator to allow tracking of the coordinates of the applicator. As the applicator is inserted into the esophagus or lung, the previously recorded video is replayed by displaying the closest frame associated with the tracking coordinates of the applicator. The distance of the applicator to the previously recorded points of interest is also displayed as an aid in positioning the applicator. Hence two checks provide confirmation of correct applicator placement: distance to the points of interest and the video frame associated with the location.

SP004 - Quality Assurance: Part 1

TRACK 04: RADIATION ONCOLOGY

SP004.1 - In Vivo EPID Dosimetry Detects Interfraction Errors in 3D-CRT of Rectal Cancer

Author(s): Stefano Peca¹, Derek Brown², Wendy L. Smith¹
¹Department Of Medical Physics, Tom Baker Cancer Centre, Calgary/AB/CANADA, ²Dept Of Radiation Medicine And Applied Sciences, Moores Cancer Center, UC San Diego, La Jolla/CA/UNITED STATES OF AMERICA

BACKGROUND

In vivo dosimetry can record the delivered dose during radiotherapy, which may be used to trigger adaptive radiotherapy or other user intervention. We demonstrate the use of our in-house *in vivo* electronic portal imaging dosimetry in quantifying interfraction dose variability in rectal cancer.

METHODS

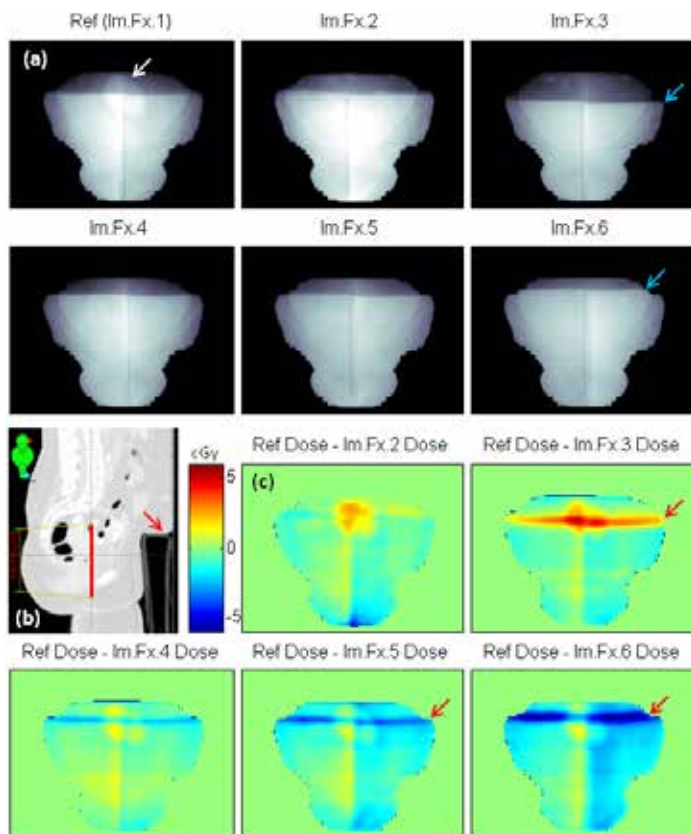
We recorded MV images from nine treatment beams for six patients prone on the belly board, during 4-7 fractions, for a total of 50 measurements. Images were processed with our dosimetry system to produce dose maps. The dose map from the reference fraction was compared to all subsequent ones to determine interfraction delivery variation, yielding 41 dose difference maps.

RESULTS

We identified a number of dose discrepancies. In several patients, persistent gas bubbles may result in cumulative dose deviations large enough to warrant adaptive radiotherapy. In one patient, discrepancies in dose resulted from variability of patient positioning with respect to the belly board (see Figure). In two other patients, dose differences were likely due to variations in compression of the abdomen in the board-couch interface. These issues accumulated significant dose differences throughout treatment and were not readily identified by standard imaging procedures.

CONCLUSION

We are developing an open-source *in vivo* portal dosimetry method to automatically track delivered dose at every fraction. Results can be used to flag unexpected discrepancies, guide adaptive radiotherapy, modify setup technique, or warrant image guidance. Further data is needed to test applicability with other treatment sites and setups.



CAPTION TO FIGURE

Patient F, PA field (GA=0°). (a) Raw EPID images. (b) Lateral view from the TPS showing the imaging plane (red) and the body adapting to the belly board opening. (c) Dose difference maps between the first imaged fraction (Im.Fx.) and five later treatment days. The large horizontal mismatch is located at the edge of the belly board opening (red arrows), indicating inconsistent setup of the patient with respect to the board in the SUP-INF direction. This was verified by visual inspection of the raw images (blue arrows). As well, all dose difference maps are affected by the gas bubble present during the Ref fraction (white arrow).

SP004.2 - Establishing action thresholds for patient anatomy changes and machine errors during complex treatment using EPID and gamma analysis

Author(s): Ophélie Piron¹, Nicolas Varfalvy¹, Louis Archambault²
¹Departement De Radio-oncologie, Hotel-Dieu de Quebec - CHU de Quebec, Quebec/QC/CANADA, ²Departement De Physique, De Genie Physique Et D'optique, Universite Laval, Quebec/QC/CANADA

INTRODUCTION

Our long-term objective is to use *in vivo* data from daily EPID images to identify patients at risk of deviating from their planned treatment. To achieve this, a gamma analysis is performed relative to a reference fraction. The specific objectives of this work are (1) evaluate the sensitivity for different types of error and (2) evaluate the impact of the treatment modality (step-and-shoot IMRT versus VMAT) on the results.

METHODS AND MATERIALS

A homemade head-and-neck phantom was used for all irradiations. A CT scan of the phantom was acquired and clinical treatment plans were applied to it. Errors were introduced and EPID images were acquired. Analysis is performed using the gamma index (3%/3 mm)

relative to a no-error delivery. The fraction of points above certain thresholds and the average gamma value is recorded in every case. Daily reproducibility was also assessed by repeating measurements 5 times.

RESULTS

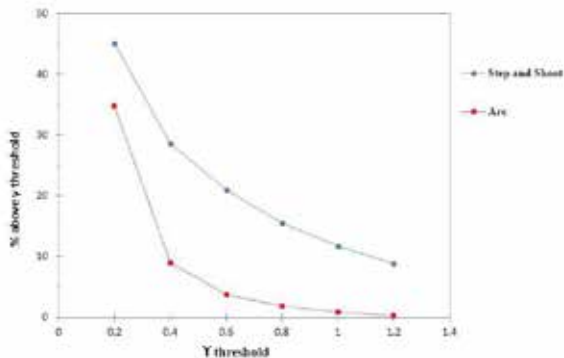


Figure 1: Gamma analysis for using a uniform sheet of 1.5 cm bolus

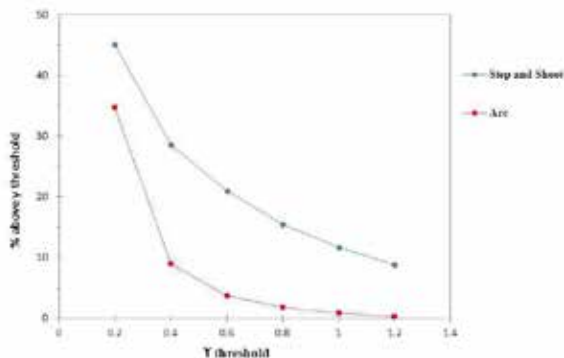


Figure 1: Gamma analysis for using a uniform sheet of 1.5 cm bolus

The errors introduced included: patient positioning, weight losses using a uniform sheet of bolus and leaf errors. Figure 1 and 2 show the fraction of points beyond certain gamma values for patient related errors for both VMAT and IMRT cases. From these figures, it is clear that for similar errors EPID images of arc-based treatments are less perturbed than for step-and-shoot IMRT. Similar results were obtained for errors of different magnitudes. When no error is inserted, 99.4% of pixels have a gamma index below 1 on average using a 1%/1 mm criterion.

CONCLUSION

A wide range of errors was introduced to test the sensitivity of EPID to detect treatment errors. For identical errors, those introduced in IMRT treatments were easier to detect than those introduced in VMAT. This will serve to established personalized action threshold to identify patients at risk of deviating from their planned treatment.

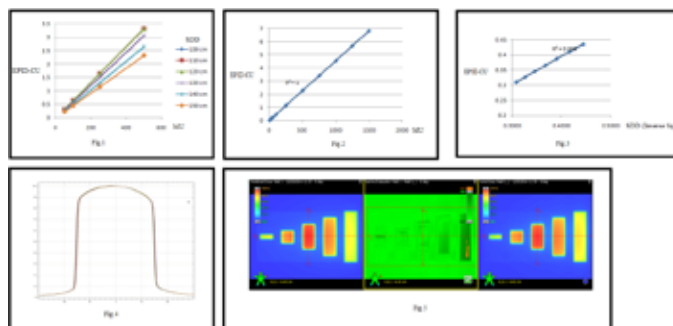
SP004.3 - Dosimetrical characteristics of amorphous silicon electronic portal imager for flattening filter free (FFF) photon beam of upgraded C-series Linear accelerator

Author(s): Gandhi Arun¹, Vellian Subraman², Shanmugam Thirumalai Swamy¹, Murugesan Kathirvel¹, V.S Subramanian¹
¹Radiation Oncology, Yashoda Hospital, Hyderabad/INDIA, ²Radiation Oncology, All India Institute of Medical Sciences, New Delhi/INDIA

Aim: To study the dosimetrical characteristics of amorphous silicon electronic portal imaging system for flattening filter free photon beam of upgraded C-series linear accelerator.

Methods and Materials: Recently our C-series linear accelerator was upgraded to deliver 6MV flattening filter free(FFF) photon beam with the highest dose rate of 1400MU/Min. In this study, we measured and analysed the dosimetrical characteristics of amorphous silicon electronic portal imaging device(aS-EPID) for FFF beam in terms of detector saturation, MU linearity, instantaneous dose rate response, ghosting effect, gantry rotational stability and accuracy of portal dose prediction algorithm. We used indirect method to predict the portal dose images of FFF beam in Eclipse Treatment planning system since the TPS will not allow direct prediction of FFF beam. Pre-treatment quality assurance(QA) using portal dosimetry for IMRT, VMAT and SRS techniques were performed for 30 patients planned with FFF beam. Portal images were acquired at Source to Detector Distance (SDD) of 150cm to evade the saturation issue at high dose rates. Portal dosimetry calibration was done in SRS mode by altering the dose rate to 1400MU/Min at 150cm with the routine beam profile correction and dose normalization. Pre-treatment QA analysis was done using gamma evaluation method.

Results: The aS-EPID saturates at 100cm to 120cm SDD and resolved more than 130cm SDD (Fig.1). The squared correlation coefficient for MU linearity was found $R^2=1$ (Fig.2). Instantaneous dose response for different SDD (corrected for inverse square law) was found $R^2=0.999$ (Fig.3). Short term reproducibility for 10X10cm² field size was measured and found to be within 0.5% (Fig.4). Portal images of different standard test pattern were acquired to analyse the accuracy of portal dose prediction algorithm in TPS and the gamma agreement index (GAI) were (98.7±0.5) (Fig.5) for 3% dose difference(DD) and 3mm distance to agreement(DTA) criteria .The ghosting signal was measured and found to be 0.6% higher than reference signal. The results of pre-treatment QA, GAI for 3% DD and 3mm DTA criteria for IMRT, VMAT, SRS were (98.7±1.2)%, (98.1±1.1)% and (99.1±0.7)% respectively.



Conclusion: The study was performed to analyze the dosimetrical characteristics of aS-EPID and results demonstrates that aS-EPID can be used to measure the portal dose images of FFF beam . For fast, accurate and its high spatial resolution, aS-EPID can be used as a verification tool for FFF beam.

SP004.4 - Radiation field size, junction and MLC QA using amorphous silicon electronic portal imaging device, an efficient approach to improve routine accuracy**Author(s):** Dany Simard, Karim Zerouali

Département De Radio-oncologie, CHUM - Hôpital Notre-Dame, Montréal/CANADA

Introduction: Films have been used for linac QA as a reference 2D detector, but amorphous silicon electronic portal imaging device (EPID) are getting increasingly used for this task even if they offer much lower resolution. EPID is a standard component of modern linacs and it can be used to accelerate QA process. We developed in-house QA tools using EPID to replace films with the objectives of being more efficient, more reproducible, precise, Varian/Elekta compatible and integrated with the QC program database QTrack+.

Method: We designed a phantom to identify beam crosshair on the images with four 5mm diameter truss head screws 4cm apart from the center. The crosshair is marked over 34cm to achieve precise phantom alignment. 10x10cm² and 30x30cm² field limits are also marked with dashed lines to ease jaw projections visualization. Line thickness corresponds to our test tolerances for quick inspection. Our mechanical technician manufactured three high precision copies with a 2D router.

We developed Matlab® EPID image analysis tools to perform fully automatic processing and recording in QTrack+. We implemented functions that allow accuracy beyond the detector resolution for screw and edge detection. Screws are identified using an image correlation with a screw model followed by a circular Hough transform. An oversampling technique is used to enhance edges detections precision. Distances between screws detected are used to evaluate the magnification factor of the phantom on the detector.

Radiation size QA phantom allows light field check (30x30cm²), light/radiation field coincidence (10x10cm²) and radiation field verification (other field sizes).

Junction QA does not require the phantom. Images are integrated over 20MU to remove any effects of beam stabilization on this over-sensitive test (Typical edge gradient of 3% / 0.1mm). Four quarter fields are delivered on the portal imager, by moving the jaws, and then summed to get one junction image. Profiles across the four junctions are analyzed to determine the percentage of local dose variation.

MLC positioning QA consists of portal images acquired for different field sizes collimated with the leaves. To get all MLCs over a 40 cm field at isocenter, two half-blocked images are acquired with opposite EPID lateral translation.

Results: For all phantoms, distances of 80.08±0.07mm between screws have been measured with a digital caliper. Magnification factor accuracy of 0.2% has been attested by comparing EPID and film profiles acquired simultaneously. Radiation size QA with EPID was compared with film QA and an average absolute difference of 0.3mm have been observed on jaws opening. Using EPID, we are able to reproduce measurements within a standard deviation of only 0.2mm, 3 times lower than film. Similar reproducibility gain is observed for monthly clinical measurement. An average absolute difference of 0.3mm has also been observed between MLC positioning QA with EPID and film QA.

Conclusion: We demonstrated that our in-house QA using EPID achieves our **objectives:** efficiency, reproducibility, precision, compatibility and integration. We replaced films for regular QA and we are working to develop new tests using EPID technology to enhance our QA program.

SP004.6 - Real-time detection of deviations in radiotherapy beam delivery using a head-mounted detector**Author(s):** Richard Canters¹, Martijn Kusters¹, Juergen Oellig², Juan-Pablo Carrasco², Henk Huizenga¹¹Radiotherapy, Radboud UMC, Nijmegen/NETHERLANDS, ²iRT Systems GmbH, Koblenz/GERMANY

Purpose: Correct delivery of the planned treatment is of vital importance in radiation therapy. To be able to monitor beam delivery online, the Integral Quality Monitor (IQM, iRT Systems GmbH) was developed. Mounted on the linac head it enables real-time, per-segment evaluation of the delivered beam. In this study we tested the sensitivity for potential errors in a variety of beams on an Elekta linac with MLCi2 head as a beta test in the last development stage.

Methods: We incorporated various forced deviations/errors in four treatment plans (stereotactic lung, lung (VMAT), larynx (VMAT), and head & neck (IMRT)):

An unintentionally performed re-optimization of the beams after plan approval by the radiation oncologist

Incorrect number of monitor units (MU) in two segments of 10, 5, or 2 MU. The beam MU remained the same.

Incorrect leave positioning (retraction of leaves by 1, 0.5, or 0.2 cm) in a single segment.

The clinical beams, without incorporated errors, are used as a reference.

For VMAT beams, we have chosen to smooth the IQM signal over the segments with a Gaussian filter to account for the exact segment timing. Evaluation takes place on the maximum difference in a segment and in the cumulative signal, with respect to the clinical beam. Additionally, the clinical beams were measured repeatedly to take into account machine variations.

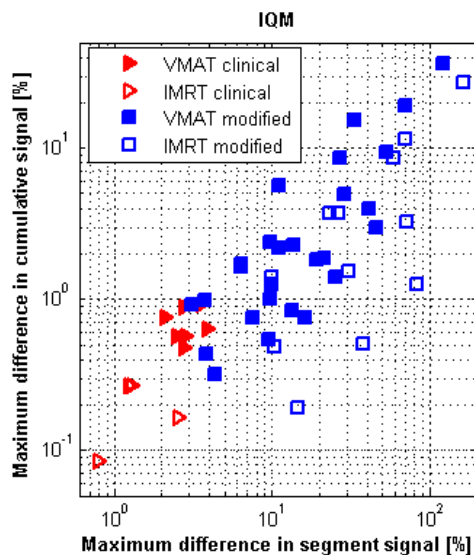
As a comparison, all beams are additionally measured with the Delta⁴ system (Scandidos), the standard QA tool in our department. Analogously to the IQM measurements, the clinical beams are used as references. Median dose difference (DD50) and 95% dose difference (DD95) are assessed as measures of agreement between the beams.

A receiver-operating characteristic (ROC) curve is created by varying the cut-off criterion for error detection to assess the sensitivity and specificity of error detection

Results: In figure 1, the results of the IQM and Delta⁴ system measurements are plotted. The left graph shows the IQM results, where modified beams can be clearly distinguished from reference beams. In the Delta⁴ measurements (middle graph) this effect is less pronounced.

This is confirmed by the ROC-curve (right graph), which shows an improved sensitivity and specificity for error detection by the IQM system compared to the Delta⁴ system.

Conclusions: Our tests of the IQM system on the MLCi2 linac show an excellent sensitivity and specificity in error detection during beam delivery, even for very small deviations in a single segment.



SP005 - Patient Specific QA

TRACK 05: DOSIMETRY AND RADIATION PROTECTION

SP005.1 - Verifying dynamic planning in gamma knife radiosurgery using gel dosimetry

Author(s): Gopishankar Natanasabapathi¹, Subbiah Vivekanandhan², Ss Kale¹, G K. Rath³, R K. Bisht¹, P Agarwal³, P Sathiaraj⁴, B S. Sharma¹

¹Gamma Knife Unit, All India Institute of Medical Sciences, New Delhi/INDIA, ²Neurosciences Centre, All India Institute of Medical Sciences, New Delhi/INDIA, ³Radiation Oncology, All India Institute of Medical Sciences, NEW DELHI/INDIA, ⁴VIT, VELLORE/INDIA

Purpose: To assess dynamic planning based on convolution based algorithm (CABP) in Gamma Knife using gel dosimetry. **Materials and Methods:** PAGAT gel was prepared and filled into cylindrical container of size 8 cm in diameter for verification. An old MRI distortion phantom was modified to accommodate the gel cylinder. Advantage of this modification is that it avoids the use of metal post and pins in the vicinity of the dosimeter which causes artifacts while scanning. A X-ray CT scan was done on the phantom with cylinder positioned in the middle region. CT scanning parameters were: Tube Voltage – 120 KVp., Tube Current – 57 mAs, Slice thickness – 1.0 mm, FOV – 265 x 265 mm². A treatment plan was generated in Leksell Gamma Plan TPS (LGP version 10.1) using CT images of the gel phantom. Using HU values and Electron density information CABP was activated. A single shot plan with third level dynamic planning option was generated using CABPMRI with following parameters were used for scanning: CPMG sequence with 8 TE values, FOV – 256, Matrix size – 256, TR – 5000 ms, slice thickness – 1.2 mm. **Results:** Gamma analysis of the verification showed a pass rate of more than 83 %. This is the first kind of study for three dimensional verification of dynamic planning using convolution algorithm in Gamma Knife Perfexion. **Conclusion:** We propose gel dosimetry as an essential dosimeter for verifying convolution algorithm in Gamma Knife. Further experiments required to validate the verification with close agreement.

SP005.2 - Influence of Jaw Tracking in Intensity Modulated and Volumetric Modulated Arc Radiotherapy for Head and Neck Cancers – A Dosimetric Study

Author(s): Karthick Raj Mani¹, Kh Anamul Haque², Mohammad Anisuzzaman Bhuiyan¹, Koilpillai Joseph Mariadas³

¹Radiation Oncology, United Hospital, Dhaka/BANGLADESH, ²Radiation Oncology Unit, United Hospital, Dhaka/BANGLADESH, ³Department Of Radiotherapy, Sanjay Gandhi Postgraduate Institute of Medical Sciences, Lucknow/INDIA

Aim:

To Study the dosimetric advantage of the Jaw tracking technique in Intensity Modulated Radiotherapy (IMRT) and Volumetric Modulated Arc Therapy (VMAT) for Head and Neck Cancers.

Materials & Methods:

We retrospectively selected ten previously treated Head and Neck cancer patients stage (T1/T2, N1, M0) in this study. All the patients were planned for IMRT and VMAT with Simultaneous Integrated Boost (SIB) technique to deliver a differential dose per fraction to the high, intermediate and low risk volume using a single plan. We intend to deliver 70Gy to the high risk volume, 64Gy to the intermediate risk volume and 56Gy to the low risk volumes in 35 fractions. All

the critical structures were delineated which includes both parotids, spinal cord and both sub mandibular glands. Eclipse treatment planning system, version 11.0 (Varian Medical Systems, Palo Alto, CA), was used in this study. All the plans were planned with 6MV photons using Millennium 120 MLC. Both IMRT and VMAT plans were planned with and without jaw tracking by keeping the same constraints and priorities for the target volumes and critical structures for a particular patient. Plans were normalized at the target mean of the high risk volumes. All the plans were accepted with the criteria of parotid glands mean dose <25Gy and spinal cord maximum point dose <45Gy without compromising the target volumes. Target conformity, dose to the critical structures and low dose volumes were recorded and analyzed for IMRT and VMAT plans with and without jaw tracking for all the patients.

Results & Discussion:

Jaw tracking resulted in decreased dose to critical structures in IMRT and VMAT plans. But significant dose reductions were observed for critical structure in the IMRT Technique with jaw tracking compared to IMRT Technique without jaw tracking. In VMAT with jaw tracking technique the dose reduction to the critical structure were not significant compared to the without jaw tracking technique due to relatively lesser monitor units. Gamma analysis showed greater than 97% of pixels were passed within 3mm distance and 3% dose criteria for all the plans.

SP005.3 - Evaluation of the eye lens dose according to patient setup errors in pediatric head CT examination

Author(s): Rumi Gotanda¹, Toshizo Katsuda², Tatsuhiko Gotanda³, Kazuki Noguchi⁴, Erika Nakajima⁴, Takuya Akagawa⁵, Nobuyoshi Tanki⁵, Tadao Kuwano⁶, Tetsunori Shimono³, Yasuyuki Kawaji³, Hitoshi Sato⁴, Yoshihiro Takeda⁵

¹Department Of Radiological Sciences, Ibaraki Prefectural University of Health Sciences, Inashiki-gun, Ibaraki/JAPAN, ²Department Of Human Relation, Tokai Gakuin University, Gifu/JAPAN, ³Department Of Radiological Science, Faculty Of Health Sciences, Junshin Gakuen University, Fukuoka/JAPAN, ⁴Department Of Radiological Sciences, Ibaraki Prefectural University of Health Sciences, Ibaraki/JAPAN, ⁵Graduate School Of Health Sciences, Okayama University, Okayama/JAPAN, ⁶Osaka Center for Cancer and Cardiovascular Diseases Prevention, Osaka/JAPAN

According to the 2011 ICRP statement, the threshold in absorbed dose for the lens of the eye is now considered to be 0.5 Gy. Therefore, it is important to keep the eye lens doses during head computed tomography examination as low as reasonably achievable. In preliminary study, the surface doses became smaller with decreasing distance from the X-ray tube. Therefore, decreasing the distance from the lens to the X-ray tube (i.e. raising the bed position) is a simple and effective way to reduce the absorbed dose of the lens. However, the occiput doses became higher with increasing distance from the X-ray tube. In this study, the two lenses and the occiput doses associated with patient setup errors and head size were evaluated using phantoms developed for pediatric patients. The phantoms were made using flexible acrylic sheets in a cylindrical shape [diameters of 6 (premature baby), 8 (neonate), 10 (infant), and 12 cm (child)] and placed on the end of the CT bed. The bed position was raised from the center for each phantom size. The two lenses and the occiput doses at each setup were measured using radiochromic film. By raising the bed position, the two lenses doses decreased at all phantom sizes. However, the occiput doses changed in a complex manner according to the phantom size. The absorbed dose ratio of the two lenses and the occiput at ϕ 8 cm phantom are shown in Fig. 1. In this study, raising the bed position is an effective way to reduce the absorbed dose of the lens. However, when the occiput was positioned at the center of the gantry aperture, the occiput dose peaked in all phantom sizes. In addition,

the results indicated a complex dose distribution in pediatric head CT when taking into account the bed position (patient setup errors) and phantom sizes. Furthermore, beam slice width and pitch are important factor in determining the maximum absorbed dose. To keep radiation doses during CT examination as low as reasonably achievable, it is important to clarify the influence of CT scanning settings on CT dose.

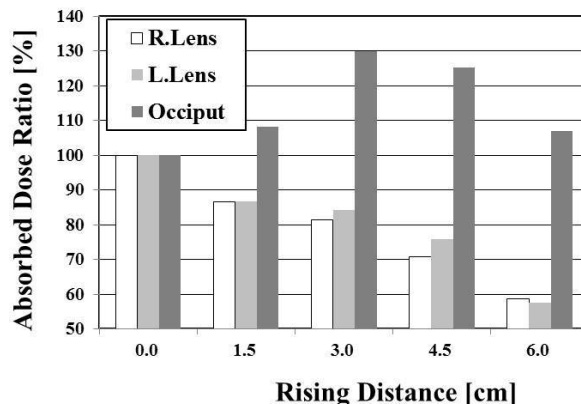


Fig. 1. Absorbed dose ratio at ϕ 8 cm phantom.

SP005.4 - Multi-Point Sources on Skin to Assess the Annual Effective Dose by Usage of TENORM added Pillow

Author(s): Do Hyeon Yoo¹, Wook-Geun Shin¹, Jae Kook Lee², Yeon Soo Yeom³, Chan Hyeong Kim³, Chul Hee Min¹

¹Department Of Radiation Convergence Engineering, Yonsei University, Wonju/KOREA, ²Korea Institute of Nuclear Safety, Daejeon/KOREA, ³Department Of Nuclear Engineering, Hanyang University, Seoul/KOREA

Consumer products containing Technically Enhanced Naturally Occurring Radioactive Material (TENORM) has been distributed in our life. After the accident of Fukushima nuclear power plant, the law called as 'Act on Safety Control of Radioactive Rays around Living Environment' has been implemented to prevent the unnecessary radiation exposure to the public in KOREA. However, the appropriate method to effectively evaluate the exposed dose with TENORM added consumer product was not developed despite the law was into effect from July 2012. The aim of this study is to evaluate the exposed dose with the usage of TENORM added consumer product with Monte Carlo simulation. To assess the annual effective dose, the Monte Carlo method and computational human phantom was employed and the point source on the skin was suggested to effectively determine the various product shape and location.

For the assessment of effective dose with the radionuclide in a consumer product, Polygon-Surface Reference Korean-Man (PSRK-Man) phantom composed of high resolution polygons to represent the organs was developed. To represent the source location of the radioactive material in the product, polygons on skin under the product was selected and the source was generated in the weight center in each polygon. To validate the method defining the point sources on skin later than the realistic source distribution in the product shape and location, organ dose was compared with 1 MeV gammas isotropically emitted in the assumption of the pillow usage with Monte Carlo method using Geant4 tool kits.

Our simulation study shows that the multi-point sources defined on the skin indicate the conservative dose assessment than the sources in the product being modeled because of the close source definition to organs. For bone, skin, and muscle, the organ dose using modeling source was, however, higher than the point source with the increased effective angles. This indicates that increasing the source to organs distributed through the whole body distance could decrease the self-attenuation by other organs. The effective dose with the point source and modeled source was assessed as $5.56E^{-17}$ Sv/particle and $2.97E^{-17}$ Sv/particle, respectively.

The current study shows the potential method for the evaluation of effective dose by the TENORM added products by using the Monte Carlo method. The comparison study also showed that the various shape and usage location of products could be replaced with the point source on the skin. The data based for the exposed dose by whole the point source could enable the effective and convenient assessment of annual effective dose. This technique could also be used for the other field for radiation protection to calculate the effective dose.

Acknowledgment

This research was supported by Korea Institute of Nuclear Safety and Global PH.D fellowship program through the National Research foundation of Korea (NRK) funded by the Ministry of Education (2014021972).

SP005.5 - Patient-Specific Quality Assurance of Respiratory-Gated VMAT Using a Programmable Cylindrical Respiratory Motion Insert for the ArcCHECK™ Phantom

Author(s): Heather Young¹, Kevin J. Jordan², Stewart Gaede²
¹Engineering, University of Waterloo, Waterloo/CANADA, ²Department Of Medical Biophysics, Western University, London/ON/CANADA

Introduction: The ArcCHECK™ phantom is a commonly used four-dimensional detector array for dose delivery verification of IMRT and VMAT. Although the isotropy of this device bodes well for ensuring accuracy for entrance dosimetry per control point, the composite 3D dose distribution may not be accurately represented for tumour sites influenced by respiratory motion. Motion management strategies, such as gating, often requires additional procedures and equipment to ensure accurate delivery. Here, we present a customized programmable moving insert for the ArcCHECK™ phantom that, in a single delivery, can verify both entrance dosimetry, while simultaneously verifying the delivery of respiratory-gated VMAT.

Methods: The QUASAR™ Cylindrical Respiratory Motion Phantom consists of a computer-controlled stepper motor used to move interchangeable cylindrical inserts inside a stationary sleeve placed within the bore of the ArcCHECK™ phantom (Figure 1). To demonstrate its effectiveness for patient specific QA, 4D-CT scans of 8 early-stage lung cancer patients previously treated with gated SBRT were used to characterize the tumour motion and was inputted into the programmable software used to drive an A1SL ion chamber insert. CT images of the ArcCHECK™ with the programmable insert were acquired at multiple static positions in 1mm increments.

Respiratory-gated VMAT plans were recalculated on the phantom scan corresponding to the amplitude of the tumour motion measured with 4D-CT. Each plan was delivered under static, moving (while non-gated), and moving (while gated) conditions. For each patient, standard ArcCHECK™ measurements were compared to the planned dose distributions using SNC Patient 6 software using standard gamma analysis with 5% threshold, 3% dose-difference, and 3mm distance-to-agreement and the measured dose to the A1SL chamber, located at isocentre, was compared to the planned dose.

Results: The pass rate for the static delivery ranged from 98.1% to 99.6%, suggesting a valid phantom setup for entrance dosimetry. The pass rate was not altered for any measurement delivered under motion conditions. A similar result was observed under gated VMAT conditions containing multiple beam holds and dose-rate ramp-up and ramp-down. For six patients, the measured dose to the A1SL ion chamber was within 3% of the planned dose. The maximum dose difference was 5.1% in one patient where the chamber was located in a large dose gradient.

Conclusions: Patient-specific respiratory-gated VMAT verification can be efficiently performed in a single delivery with the ArcCHECK™ phantom containing a moving cylindrical insert.



Figure 1. The QUASAR™ Cylindrical Motion Insert (with A1SL chamber) for the ArcCHECK™ phantom.

SP006 - Dosimetry in CT

TRACK 05: DOSIMETRY AND RADIATION PROTECTION

SP006.1 - Dosimetry and Radiation Protection

Author(s): Virginia Tsapakis

Konstantopoulio General Hospital, Athens/GREECE

It is an actual fact that the primary and most common application of radiation until today is in medicine. Furthermore, medical technology has taken a remarkable boost the last few decades both in patient therapy and medical diagnosis. Not only do we have a big variety of medical equipment but we can access all patient data so much easier than 10 or 20 years ago that is really spectacular. Evolution led us so quickly from soft copy to CD-ROM and now icloud that we sometimes ask ourselves how it was possible to work as we did 5 or 10 years ago. All this has resulted not only on a manifest increase in the number of procedures, but also an expansion into different areas of medicine and the creation of new medical specialties. Presently, complex radiation-based tools and techniques are used in most areas of modern medicine and by specialists who have differing levels of knowledge about radiation, dose and the risks posed to human health by ionising radiation.

Within this context, it is very important to use medical radiation technology with prodigious care due to the presence of ionizing radiation. To put the issue in perspective, the current annual collective dose estimate from medical exposure in the United States has been calculated as roughly equivalent to the total worldwide collective dose generated by the nuclear catastrophe at Chernobyl. Therefore accurate measurement of radiation dose is of utmost importance, not only for patients but also for members of the staff, specially due to the recent International Commission on Radiological Protection reduction in the dose limit for the eye lens of workers (from 150 mSv per year to 20 mSv in a year).

Dosimetry seems to play a fundamental role in the process of developing various radiation protection programs to fit the needs of radiation workers and members of the public, particularly as they relate to mitigating potential health risks from exposure to radiation. Specially due to the fact that there is broad discussion the last years on the possibility that radiation dose received by patients from modern diagnostic examinations can be at a level of significance for the induction of cancer across a population. Moreover, in a number of cases, in the acute damage to particular body organs such as skin and eyes.

The talk will cover the trends in dosimetry and radiation protection focused in diagnostic radiology, image-guided interventional procedures and nuclear medicine studies, illustrated by progress in science and practice of risk communication and changes in societal expectations, and examines challenges that will confront radiation risk communication in the future.

SP006.2 - Organ dose reduction while using in-house CBCT patient-specific protocols based on OSL dosimetry.

Author(s): Étienne Létourneau¹, Fabiola Vallejo¹, Nancy El Bared², Danny Duplan¹, Martin Hinse¹

¹Radio-oncologie, Centre intégré de cancérologie de Laval, Laval/CANADA, ²Université de Montréal, Montréal/CANADA

Purpose/Objectives

In radiation therapy, dose contributions coming from planning and

patient positioning images can seem negligible compared to the treatment dose. However, radiation-induced complications are numerous even at low dose. In order to diminish undesirable effects to the patient, one must concretely apply the ALARA principle and minimize dose to organs at risk (OAR) while not compromising treatment quality. In this study, appropriate adjustments to cone beam computed tomography (CBCT) imaging protocol parameters were performed. This was achieved after measuring the dose to organs in an anthropomorphic phantom filled with optically stimulated luminescent detectors (OSL). All these modifications lead to a significant dose reduction of at least 50% up to a reduction of 90% in comparison with the default protocol doses while still preserving a proper image quality for positioning.

Materials/Methods

Output measurements of the CBCT X-ray tube were performed at 100 kVp and 120 kVp. Measurements were based on the AAPM Task Group 61 protocol using a Farmer-type ionization chamber calibrated for the corresponding beam quality. Once the outputs were determined at the reference point, the correlation between OSL's number of counts and the resultant dose was achieved. An anthropomorphic adult phantom with heterogeneous densities and 271 plugs for OSL detectors covering the whole body was used. Default scan protocols of the head and neck, breast, chest and pelvis were investigated. The mean dose and the maximum dose to the organs were collected over multiple scans to assure the reproducibility of the given method.

Results

The maximum dose to any given organ never exceeded 3.0 cGy for all the default protocols. For the particular head and neck cases, the maximum dose never reached more than 0.4 cGy. Radio-sensitive organs such as lungs, breasts, bone marrow, stomach and intestines received between 1.0 cGy and 2.0 cGy per scan. In the chest and pelvis protocols, the thyroid gland and the testis received more dose than the other organs (2.0 - 3.0 cGy) due to their proximity to the surface and the low attenuation of the beam before reaching the OSLs.

Conclusions

With the new modifications made to the default scan parameters, a considerable organ dose reduction of at least 50% can be achieved for every protocol without compromising image quality for patient positioning. With our in-house protocols, no organ received more than 1.5cGy per scan. These results are therefore in compliance with the ALARA principle. Also, a new ultra-low dose scanning protocol for the chest was introduced giving only 0.1 cGy to the lungs and 0.2 cGy to the heart and thyroid respectively. This significant dose reduction is desirable especially for young lymphoma patients.

SP006.3 - A novel tool for in vivo dosimetry in diagnostic and interventional radiology using plastic scintillation detectors

Author(s): Jonathan Boivin¹, Sam Beddar², Maxime Guillemette³, Luc Beaulieu⁴

¹Département De Radio-oncologie Et Axe Oncologie Du Centre De Recherche Du Chu De Québec, CHU de Québec, Québec/CANADA, ²University of Texas MD Anderson Cancer Center, Houston/TX/UNITED STATES OF AMERICA, ³Genie Biomedical, Institut universitaire de cardiologie et de pneumologie de Québec, Québec/CANADA, ⁴Département De Physique, Génie Physique Et D'optique, Et Centre De Recherche Sur Le Cancer, Université Laval, Québec/CANADA

Plastic scintillation dosimetry is now spreading in multiple areas of clinical practice either for quality assurance or in vivo dose monitor-

ing. While many studies have validated this tool for radiotherapy and brachytherapy, applications in the radiology field are being investigated. Various photodetectors can be part of the plastic scintillation detector (PSD) according to the targeted clinical application. However, no study has compared these detectors in the same conditions to identify the best configuration. Moreover, there is a need for extensive characterization of the low energy response of the scintillator's material for radiology purposes.

The objective of this work is to develop and optimize a PSD for real-time dose rate measurement for low energy beams. The PSD is composed of a scintillating fiber coupled to a clear optical fiber transmitting the scintillator's light to a photodetector.

A spectrometer was used to characterize the scintillator's spectrum under low and high energy exposures. Seven photodetectors were then evaluated to identify their operating range and potential applications. They comprise a photomultiplier tube (PMT), an avalanche photodiode, two passive diodes, and a set of three CCD cameras. The scintillator was exposed to low energy potential beams (120 kVp, 180 kVp, and 220 kVp) of an orthovoltage unit and to linear accelerator 6 MV and 23 MV beams. The source-to-detector distance was varied to explore a broad dose rate range likely to be used in radiology, superficial treatment and radiotherapy. Every detector was able to measure dose rate down to 10 mGy/s while keeping a relative standard deviation below 2 %. The CCD cameras were the less sensitive devices, but they allow multiple fibers to be read simultaneously. Among the photodetectors, the PMT was found to be the most sensitive detector with a relative standard deviation of less than 1 % at the lowest dose rate available.

A second study was performed to observe the scintillator energy dependence to AAPM accredited reference beam qualities of a calibration laboratory. The PMT was included in the PSD design and the scintillator's light signal was characterized for energy levels from 20 kVp to 250 kVp. The PSD's response was then analyzed regarding the reference exposure spectra and the NIST mass energy-absorption coefficients.

The PMT PSD was finally included in an in vivo study for interventional radiology where low dose rate sensitivity is essential. The PSD was located inside a plastic water phantom to measure skin and depth dose from 1 mm down to 24 cm. There was less than a 2 % difference between the PSD measured dose rate and the ion chamber reading located at the same depth.

These results indicate that a broad range of photodetectors can be used for PSD designs, but low dose rate measurements require very sensitive devices such as a PMT.

SP006.5 - Assessment of patient's eye lens dose using a custom made anthropomorphic head phantom

Author(s): Mohammad Javad Safari, Jeannie Hsiu Ding Wong, Kwan Hoong Ng, Khairul Azmi Bin Abd Kadir
Biomedical Imaging, University of Malaya, Kuala Lumpur/MALAYSIA

Purpose: To fabricate an anthropomorphic phantom for patient's radiation dose measurement during diagnostic x-ray procedures.

Materials and Methods: CT images of head of 13 patients were studied and CT number and physical dimensions of the head components were recorded. A head phantom was custom made based on the CT of an adult male using a 3D printer. The phantom's brain was fabricated using polyacrylamide and the eyeballs and skin were fabricated using VytaFlex®40 polyurethane rubber (Figure 1).

The study of the radiation dose distribution over the phantom's eyeball was carried out using a Philips Allura Xper FD20/20 system (80 kV, 3 fps acquisition mode). Gafchromic XR-RV3 film was used to measure absorbed dose at positions corresponding to the surface of the cornea, under the cornea, under the lens, and on the retina of the eyeball.

Result: The custom made phantom has CT numbers that corresponds to the CT numbers of real organs (within 9.0%). The depth dose curve within the eyeball shows a gradual fall off with depth in tissue (Figure 2).

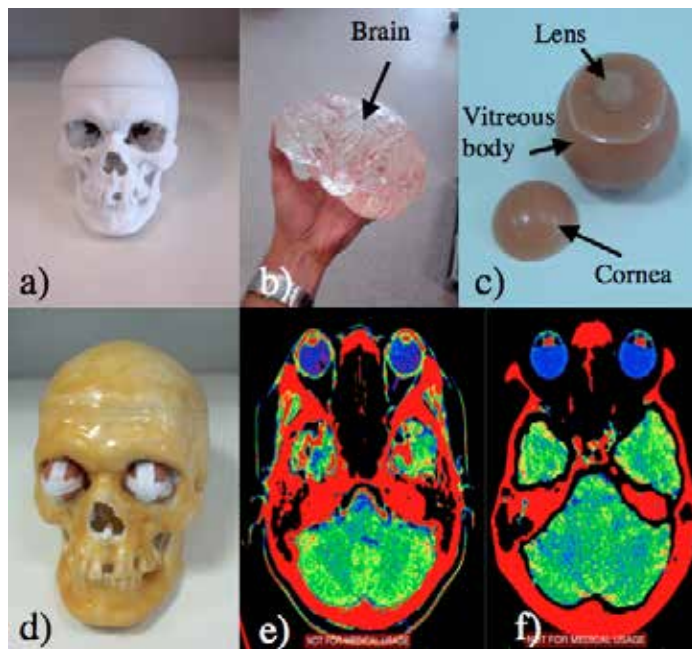


Figure 1 Custom made head phantom, a) 3D printed skull, b) brain, c) eyeball, d) skull covered by polyurethane as skin, e) CT image of patient and f) CT image of the head phantom.

Figure 2 shows the radiation dose at different depths within the phantom eyeballs.

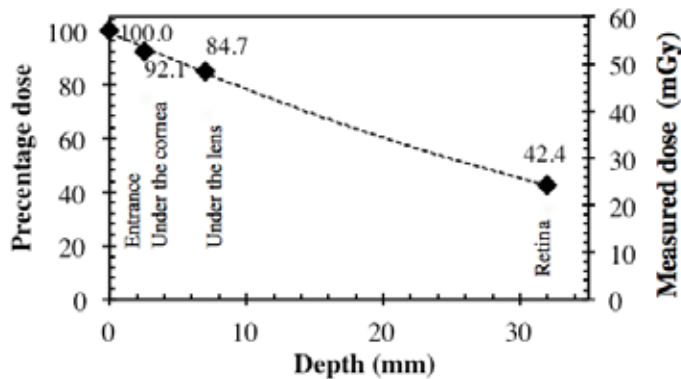


Figure 2 Radiation dose received at different level of the eyeball

Conclusion: A custom made anthropomorphic head phantom was successfully fabricated and used to evaluate eye lens dose during diagnostic fluoroscopy procedures.

SP006.6 - Dose Profile and Equilibrium Doses in CT

Author(s): Ricardo A. Terini¹, Maria Carolina S. Campelo², Marcia D.C. Silva³

¹Depto. De Física, Pontifícia Universidade Católica de São Paulo, São Paulo/BRAZIL, ²Curso De Física, Pontifícia Universidade Católica de São Paulo, São Paulo/BRAZIL, ³Física Médica - Engenharia Clínica, Hospital Israelita Albert Einstein, São Paulo/BRAZIL

Introduction: Absorbed dose in CT exams can be ten times higher than in other common procedures of X-ray imaging and must

be monitored. Dosimetry in CT is still commonly made obtaining CTDI100 values, measured with a “pencil” chamber inside a CT phantom, in a single beam slice and no table movement. In helical and multi-slice tomography with high number of rows, measured values of CTDI100 should underestimate accumulated dose at point $z=0$, as they don't include the contribution of dose profile «tail», caused by scattering in the phantom (or tissue). In this sense, this work aimed to contribute to review the assessment of Dose in CT according to the methodology suggested by AAPM TG 111 [AAPM, Report 111, 2010].

Methodology: Firstly, we have used a Radcal 0.6 cc chamber, previously calibrated in CT standard beam qualities [IAEA, TRS 457, 2007] against a Farmer chamber, to measure dose profiles on a Toshiba Aquilion One scanner (HIAE), through several adjacent slices. Values of Equilibrium Dose free in air, Deq,ar , were obtained for various protocols and pitch values. In the second step, using a large CT phantom (Fig.1), values of central Cumulative Dose ($DL(0)$) were measured for different scan length values (L), for two different abdomen protocols, in order to evaluate the Equilibrium scanning length (Leq) and Equilibrium doses (Deq) (Fig.2). Finally, Planar Average Equilibrium Dose (Deq,p) was evaluated and compared with CTDIvol values displayed in the CT equipment.

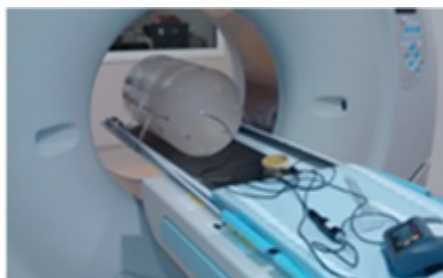


Figure 1 – Setup for the CT clinical measurements using the 0.6 cc chamber and a 450mm phantom.

Results and Discussion: In the survey of dose profiles, slice thickness was evaluated with 19-28% difference compared to the nominal value. It was also observed that Equilibrium Dose free in air increases as the pitch is reduced and that the values of equilibrium dose-pitch product free-in-air ($p.DEQ, air$) are constant. As expected, differences between Planar Average Equilibrium Dose and CTDIvol ranged between 30-37%.

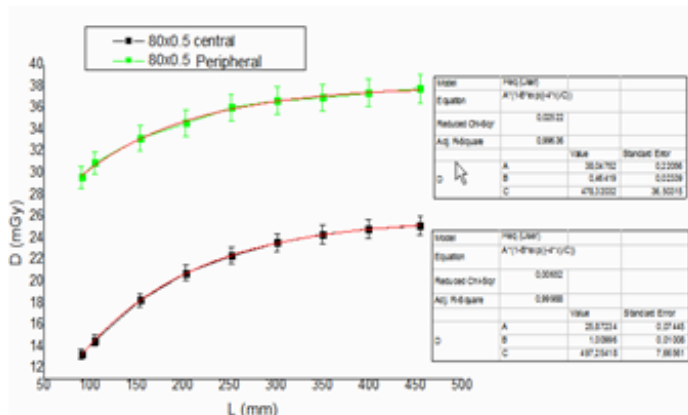


Figure 2 – Approach to equilibrium of central and peripheral axis Cumulative Dose $D_L(0)$, for a beam with 40mm (80x0.5) thickness, in an axial protocol. Red lines are the approximation function to equilibrium.

SP007 - Biomedical Signal Quality Analysis

TRACK 09: BIOSIGNAL PROCESSING

SP007.1 - Biosignal Processing

Author(s): Adrian D.C. Chan

Systems And Computer Engineering, Ottawa-carleton Institute For Biomedical Engineering, Carleton University, Ottawa/ON/CANADA

At the end of this presentation you will be able to:

- 1) explain the need for biomedical signal quality analysis
- 2) discuss the challenges in biomedical signal quality analysis
- 3) describe some of the advances in biomedical signal quality analysis

The democratization of technology is being fueled by technology that is decreasing in size, cost, and power-consumption, while the levels of computing power and interconnectivity are increasing. In healthcare, so called patient-empowering, information-leveraging (PI) technologies are drastically changing the paradigm of biomedical monitoring. Traditionally, biomedical monitoring is performed intermittently by a trained expert, under well-controlled conditions, whereas advances has made it easy for frequent or continuous monitoring; in addition, neither the monitoring environment nor the subject's activity is controlled necessarily (e.g., monitoring can be performed in the home while performing normal activities of daily living). These technologies are not only non-invasive but also non-obtrusive; they can be wearable devices, or integrated into other devices or environments where they may remain unnoticed by the subject. Multi-sensor systems are being increasingly employed, some of which are also multi-modal. These systems may use sensors that are each of lower quality and lower cost, and may not be optimized for a given monitoring application; yet these multi-sensor systems may outperform a higher quality and higher cost individual sensor in terms of accuracy, robustness, and convenience. The rapid increase in biomedical monitoring has resulted in a large focus on “big data” in healthcare.

There has been considerable research and development effort in the acquisition of biomedical data and in data analytics to extract useful information from these data. In many acquisition systems, validation of the data in terms of quality typically requires a human. In data analytics, it is often assumed that data are of adequate quality for processing. When data are not of sufficient quality, this can result in erroneous conclusions including false alarms. For the fourth year in a row, the Emergency Care Research Institute (ECRI) identified alarm hazards as the top health technology hazard.

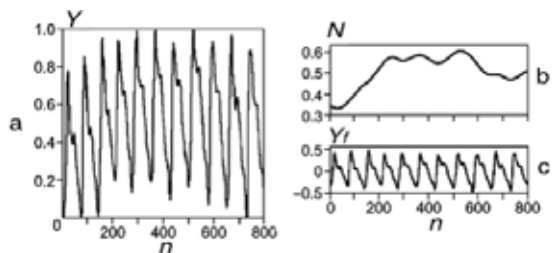
There is a pressing need for increased research on biomedical signal quality analysis. Biomedical signal quality analysis can be organized into four categories: 1) detection, observing the presence of contaminants in the signal, 2) identification, identifying the type of contaminant(s), 3) quantification, estimating the level of contamination, and 4) mitigation, removing or reducing the contamination. In some applications, simple detection may suffice, requiring only the ability to reject poor quality data. For non-expert users, identification of the contaminant type could be useful in providing feedback to remedy the acquisition setup. Biomedical signal quality analysis poses a variety of challenges, including large signal variability (inter- and intra-subject), contaminants that overlap in time and frequency with the signal of interest, and often a low prevalence of clinically significant events.

SP007.2 - Adaptive filter for eliminating baseline wander of pulse wave signals

Author(s): Aleksandr A. Fedotov, Anna S. Akulova
Lasers And Bioengineering Systems, Samara State Aerospace University, Samara/RUSSIAN FEDERATION

Recording and processing of arterial pulse signals are widely used in cardiology instrumental diagnostic systems. The arterial pulse signals are corrupted by physical and physiological interferences. Physiological interferences are happened due to the patient's breathing and the effect of neurohumoral regulation factors and also the presence of low-frequency movement artifacts; these factors lead to the appearance of baseline wander: a nearly periodic low-frequency distortion of random nature. The stochastic nature of baseline drift in biomedical signals and also its broadband nature are the main reasons why new advanced methods should be developed for digital processing of the arterial pulse signal. In this article different baseline wander filtering methods were examined for pulse wave signal. A baseline drift correction method based on generating the reference signal of adaptive filter by using multi-resolution wavelet analysis of the original biosignal was proposed. This approach makes it possible to achieve the least distortions in processing pulse wave compared with other methods of eliminating baseline drifts. The effectiveness of proposed method, as well as other widely used approaches for filtering pulse wave signals such as approximation method, linear frequency filtering was studied.

Fig. 1 shows the fragment of arterial pulse signal with typical baseline wander (a); obtained estimation of the baseline wander (b); the pulse wave signal after application the new method of correction baseline wander proposed in this article (c).



SP007.3 - Efficacy of DWT denoising in the removal of power line interference and the effect on morphological distortion of underlying atrial fibrillatory waves in AF-ECG

Author(s): Jonathan Goodfellow¹, Omar J. Escalona¹, Vivek Kodoth², Ganesh Manoharan²

¹Engineering Research Institute, Ulster University, Newtownabbey/ UNITED KINGDOM, ²The Heart Centre, Royal Victoria Hospital, Belfast/UNITED KINGDOM

Introduction: Power line interference (50Hz) is a corruptive noise source which is commonly encountered when capturing body surface ECG signals. The purpose of this research is to assess the efficacy of Discrete Wavelet Transform (DWT) in removing mains noise by testing over thirty different wavelet functions. The four best performing wavelets were then further analysed to assess their effects on underlying fibrillatory waves which are present in atrial fibrillation patients.

Methods: 18 body surface ECG recordings of 1 kHz sampling frequency, which were corrupted by a range of mains interference levels (-10dB to 10dB) were simulated in MATLAB using an ECGSYN programme from PhysioNet. These signals then underwent a DWT denoising process which included 10-level decomposition, with full band cancellation of coefficients D1-D4, resulting in a significant attenuation of the added mains interference. The efficacy of the DWT denoising performance was assessed across the entire range

of analysing wavelets and also compared to that of notch filtering, a technique which is widely used for mains interference suppression. The results were quantified and compared using three different performance parameters: Signal to Noise Ratio (SNR), Mean Square Error (MSE) and Signal Correlation Value (SCV). Additionally, we wanted to investigate the effect that the top performing wavelets would have on underlying fibrillatory waves which are present in atrial fibrillation electrocardiogram (AF-ECG), as certain key parameters of such waves have been shown to be useful in the characterisation and treatment of the arrhythmia. Five fibrillatory wave signals were extracted from real AF-ECG data using an average template subtraction method and were added to a range of mains corrupted simulated ECG signals. These signals were denoised using the top four performing wavelets and the underlying fibrillatory wave signal was recovered via the subtraction of the original 'clean' simulated ECG signal. Key parameters such as dominant frequency (DF) and total spectral power (TSP) of both the original and recovered fibrillatory wave signals were quantified and compared in order to assess whether or not the DWT denoising process was detrimental to fibrillatory wave characteristics.

Results: 12 out of 32 of the analysing wavelets tested outperformed a traditional notch filtering approach over all three performance indicators: SNR, MSE and SCV when averaged across the sample population. Four of the top performing wavelets were Daubechies 'Db10', Biorthogonal 'Bior6.8', DMeyer 'Dmey' and Symlet 'Sym8', with Db10 providing SNR, MSE and SCV values of 32.50, 5.13x10⁻⁵ and 0.9995 respectively. Fibrillatory waves were minimally affected by DWT processing with a 0% difference in DF and a 0.17% ± 0.25% difference in TSP across the study population.

Conclusions: DWT denoising can be an effective tool in the removal of unwanted 50Hz mains noise, where a range of analysing wavelets provide superior denoising performance when compared to traditional notch filtering. The process of DWT mains noise removal has negligible effects on the morphology or signal characteristics of underlying fibrillatory waves found in AF-ECG signals.

SP007.4 - Quantifying Blood-Oxygen Saturation Measurement Error in Motion Contaminated Pulse Oximetry Signals

Author(s): Geoffrey Clarke, Adrian D.C. Chan, Andy Adler
Systems And Computer Engineering, Carleton University, Ottawa/ CANADA

Oxygen saturation measurements from pulse oximetry (SpO₂) can be unreliable in the presence of motion artifacts. While pulse oximetry is a crucial measurement in controlled environments, such as surgery or intensive care, its vulnerability to motion artifacts has slowed its adoption in wearable continuous monitoring devices. Measurement error can cause errors or delays in clinical decision-making. In remote monitoring applications, pulse oximeters should report measurement confidence along with SpO₂ to help clinicians make decisions about the validity of alarm conditions. This paper seeks to relate signal quality to SpO₂ measurement confidence.

In this study, clean photoplethysmograph (PPG) signals were collected from a pulse oximeter and contaminated with motion artifact. A range of linear combinations of signal and artifact were generated and SpO₂ measurements were calculated. Since true SpO₂ remained constant, measurement variation was caused solely by signal contamination. Unacceptably high measurement error was found below the 15-20 dB signal to noise ratio (SNR) range.

Two models based on Additive White Gaussian Noise (AWGN) were evaluated for their similarity to the motion artifact data. The first had identical noise on both red and infrared PPG signals; the second has uncorrelated noise. Both models successfully predicted negative measurement bias at low SNR, but only the second predicted the observed measurement variance.

SP007.5 - Signal Quality Indices for Ambulatory Electrocardiograms used in Myocardial Ischemia Monitoring

Author(s): Mohamed Abdelazez¹, Adrian D.C. Chan¹, Patrick X. Quesnel¹, Homer Yang²

¹Systems And Computer Engineering, Carleton University, Ottawa/ON/CANADA, ²The Ottawa Hospital, Ottawa/ON/CANADA

Ambulatory electrocardiograms (ECG) can be used to monitor patients for myocardial ischemia. Low ECG signal quality, due to contaminants such as motion artifact, can lead to an increase in false alarms leading to alarm fatigue. The false alarms can be reduced by processing only ECGs of adequate quality, quantified by a signal quality index (SQI); contaminated ECG may be discarded. Four SQIs based on an estimate of the signal-to-noise ratio (SNR) were examined, where the mean, median, 25th percentile and minimum SNR were considered. ECG test data were retrieved from Physionet's Long-Term ST Database; 30 minute segment of ischemic data and 30 minute segment of non-ischemic data were chosen from the record 's20031'. The record is sampled at 250 HZ and has a total of 2 unidentified leads. The SQIs were validated by contaminating 30 second segments of the ECG data with 30 seconds of motion artifact segments scaled at five levels from the record 'em' from the Physionet's Noise Stress Test Database. The result is five copies of each ECG segment each with different calibrated SNR evenly distributed between -10 dB and 10 dB in steps of 5. For each channel of both the non-ischemic and ischemic data of the 's20031' record, 300 segments were created, resulting in a total of 1,200 segments. Four SQIs were then generated for each of these 1,200 segments. The SQIs of each segment were compared to the calibrated SNR of the segment. A Pearson correlation coefficient was calculated between the SQIs and the calibrated SNRs for each of the cases (Fig. 1).

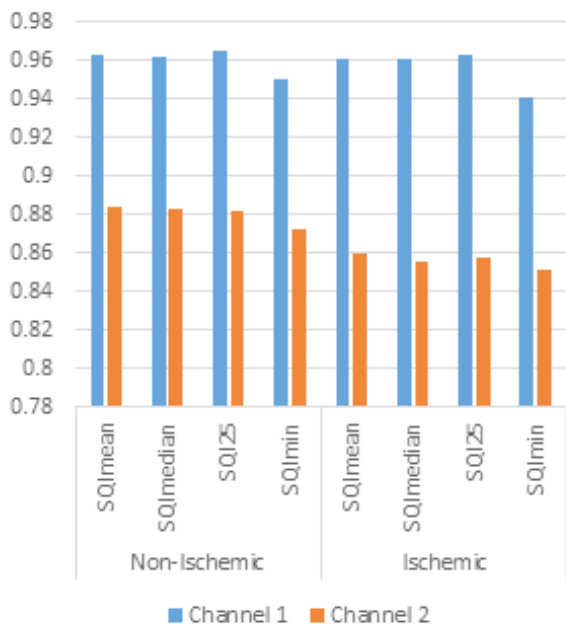


Fig. 1 calculated Pearson correlation coefficient for SQIs and the calibrated SNRs for non-ischemic and ischemic data for channels 1 and 2

It was found that a strong correlation (Pearson correlation coefficient > 0.85) was exhibited between the SQIs and the calibrated SNR for each segment with SQI based on 25th percentile exhibiting highest correlation. The strong correlation indicates that the SQIs are good representatives of signal quality.

SP007.6 - A simple algorithm for identifying artifact beats in long ECG recordings

Author(s): Nini Rao, Yongli Wan, Yang Yang, Ying Zhang, Jie Zhen, Sang Li

Dept. Of Biomedical Engineering, University of Electronic Science and Technology of China, Chengdu/CHINA

Introduction

The artifact beats in ECG recordings make diagnosis and monitoring of heart disease difficult and will increase the misdiagnosis rate. Clinically, it is time-consuming and labor-intensive to identify the artifact beats from long ECG recordings. Thus, there is a great need for developing an algorithm to automatically detect the ECG artifacts.

Data

The simulation data is used to determine the parameters in the algorithm. The independent data is the combinations of real ECGs of normal patients and patients with arrhythmia (such as atrial fibrillation, atrial flutter, ventricular premature beat, etc.) and the measured signals under the case of electrode loss. The sampling frequency is 250Hz and the total length is 2394.58s, in which there are the six segments of artifacts and the eleven segments of ECGs, in total 167.60s and 2226.98s respectively.

Algorithm

For a given ECG segment with the length of L_s , the three steps are carried out to identify its type using the novel algorithm.

Step1: Calculating the standard deviations of R-R interval (RRI) and R-peak amplitude in this ECG segment. If both parameters are synchronously greater than the two given thresholds (denoted by Thr_{RR} and Thr_{RA}), the segment is judged as ECG artifact beats. Otherwise, go to the next step.

Step 2: The ECG segment between $0.3 \cdot RRI$ at each R-peak before and $0.6 \cdot RRI$ at the R-peak after is selected as a template. If the length of a template is less than 100ms, the template is replaced by ECG segment of 700ms starting from $0.3 \cdot RRI$ at this R-peak before. The aim is to ensure each template contains at least three heartbeat cycles for detecting the rhythm.

Step 3: The shift correlation is calculated between the given ECG segment and the template and the correlation function $r(i)$, $i=1,2,3,\dots, L$ is obtained. The periodic wave peaks in the $r(i)$ can be used to reveal the rhythm of the ECG segment. Since the probability that three continuous wave peaks appears in $r(i)$ for the ECG artifacts is very small, the amplitude of the third wave peak of $r(i)$ is selected as the feature parameter discriminating the rhythm of the ECG segment. If this parameter is less than the given threshold (denoted by Thr_{max}), the ECG segment is identified as artifacts.

Results

When the Thr_{RR} , Thr_{RA} and Thr_{max} are set as 20, 10 and 0.75 respectively, the performance of the algorithm reaches optimal on the training data. The accuracy, sensitivity and positive prediction value of the algorithm on the independent data are 97.16%,92.24%,73.76% respectively, which are better than other related methods on the same data.

Conclusions

The logical structure and the computational complexity of the algorithm are simple and low respectively. The algorithm is sensitive to the artifact beats since of high sensitivity. Thus, it is suitable to be applied in the identification of artifact beats in long ECG recordings.

SP007.7 - Automatic Detection of Low-Quality Seismocardiogram Cycles Using the Outlier Approach

Author(s): Vahid Zakeri¹, Farzad Khosrow-Khavar², Kouhyar Tavakolian³

¹Heart Force Medical Inc., Vancouver/BC/CANADA, ²Engineering Science, Simon Fraser University, Burnaby/BC/CANADA, ³Electrical Engineering, University of North Dakota, Grand Forks/ND/UNITED STATES OF AMERICA

In this study, an algorithm was developed to automatically detect the low-quality (LQ) cardiac cycles in seismocardiogram (SCG). The proposed algorithm extracts some features from the SCG signal, which are referred to as signal quality indices (SQIs), and computes the outlier points of each SQI. Our hypothesis was that the identified cycles (outliers) would include the LQ ones. To verify this hypothesis, the algorithm results were compared with the LQ cycles that were labeled manually by an expert in the field. The developed algorithm was tested on total 1697 cardiac cycles, and there was a great overlap between the computed outliers and the LQ cycles (84% of 248 LQ cycles were identified). The proposed algorithm is simple, efficient, and works in an unsupervised manner.

SP008 - Spinal Cord and Brain Injury Treatment

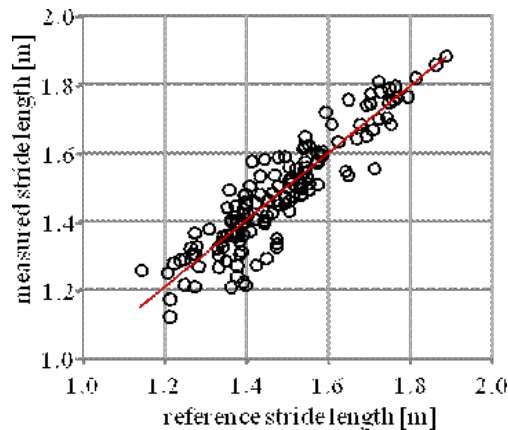
TRACK 10: REHABILITATION MEDICINE, SPORTS MEDICINE, REHABILITATION ENGINEERING AND PROSTHETICS

SP008.1 - A Validation Test of a Simple Method of Stride Length Measurement Only with Inertial Sensors and a Preliminary Test in FES-assisted Hemiplegic Gait

Author(s): Takashi Watanabe¹, Tasuku Miyazawa²

¹Graduate School Of Biomedical Engineering, Tohoku University, Sendai/JAPAN, ²Graduate School of Engineering, Tohoku University, Sendai/JAPAN

This study aimed to realize simplified gait evaluation system only using inertial sensors in order to support motor rehabilitation, healthcare and so on. In this paper, stride length measurement only with inertial sensors for the simple gait evaluation system was tested. First, a calculation method of the stride length was developed, in which acceleration and angular velocity signals of the foot were used. In order to calculate the stride length, the beginning and the ending of the foot movement during walking were detected by acceleration signal for determination of the integration period of motion acceleration of the foot. The motion acceleration was calculated from acceleration and angular velocity signals. The measurement method was evaluated in 10 m walking of 6 neurologically intact subjects attaching inertial sensors using stretchable band on their feet (shoes). Reference data for the stride were measured with portable walkways with embedded, pressure-sensitive sensors. The average values of error and absolute error of measured stride lengths were $0.38 \pm 4.77\%$ and $3.36 \pm 3.04\%$, respectively. Correlation coefficient of the measured length with the reference data was 0.910 and the slope of the regression equation was 0.978. Then, stride lengths of a hemiplegic subject were measured in 10 m walking with and without FES-assisted foot drop correction. Although there was no difference in stride length between with and without the FES-assist, the calculated data from inertial sensor signals supported that the time for 10 m walking measured by therapists decreased when the subject walked with the FES-assist. It was expected that the stride length measurement only with inertial sensor would be practical, and it can be implemented easily.



SP008.2 - A novel Treadmill Body Weight Support system using Pneumatic Artificial Muscle actuators: a comparison between active Body Weight Support system and counter weight system

Author(s): Thuc V. Tran¹, Flavio Prattico², Shin-Ichiroh Yamamoto³
¹Bioscience Engineering, Shibaura Institute of Technology, Saitama-shi/JAPAN, ²Department Of Industrial And Information Engineering And Economics, Università degli Studi dell'Aquila, L'Aquila/ITALY, ³Department Of Bioscience And Engineering, Shibaura Institute of Technology, Saitama City/JAPAN

In recent years, Treadmill Body Weight Support System has been developed and proved the improvement for patients who recover from Spinal Cord Injury. Passive and dynamic systems were shown their capacities to maintain unloading force in the vertical direction, however, there are no system considered that track the moving of the Center of Pressure trajectory during gait training. Our hypothesis is that tracking Center of Pressure trajectory, during gait training, could be more effective than the common system. This paper proposed a new active Body Weight Support system using Pneumatic Artificial Muscle actuators. An active model of new Body Weight Support system with the tracking model of the human center of pressure was developed. The validation tests experiments were implemented with three levels of unloading force 30%, 50% and 70% using new Body Weight Support system and counter weight system for comparison. The speed of the treadmill is set, for all the experiments at 2 km/h. Center of pressure trajectories are recorded for a normal random walk, for the counter weight system and for the Body Weight Support systems. The results showed that the center of pressure trajectory using active system was much fitter with center of pressure pattern of normal gait than counter weight system.

SP008.3 - A Serious Game for Training and Evaluating the Balance of Hemiparetic Stroke Patients

Author(s): Pedro Bertemes-Filho¹, Fabricio Noveletto¹, Antonio V. Soares², Marcelo D.S. Hounsell³
¹Electrical Engineering, Universidade do Estado de Santa Catarina, Joinville/BRAZIL, ²Faculdade Guilherme Guimbala, Associação Catarinense de Ensino, Joinville/BRAZIL, ³Science Computing, Universidade do Estado de Santa Catarina, Joinville/BRAZIL

Stroke is the major cause of disabilities in adults and the second major cause of deaths worldwide. People that survive a stroke present deficits that affect their functional capacities and require rehabilitation for long periods. The use of digital entertaining games has shown to be a helping ally to the rehabilitation process, despite its therapeutic limitations. An alternative to these limitations is the development of games and control interfaces targeted the needs of patients, the so called Serious Games. The aim of this paper is to present the development of a Serious Game for training and evaluation of balance in hemiparetic stroke patients. An integrated biomedical system was, which consists of a balance board with inertial sensors instrumentation and a computer system that runs the game. The aim of the game, called myBalance, is to direct a ball to a target position according to the board signals. Various parameters of the game can be adjusted to comply with patients' limitations. The game has a scoring system that extracts metric information regarding patients' performance during gaming. Preliminary results indicate that the system (board and game) can be easily used for training and evaluation of patients' balance. It was also showed that the game can be used as a metric system for clinical studies. Future works include comparing game scores to standard clinical scales for balance.

SP008.4 - fNIRS-based analysis of brain activation with knee extension induced by functional electrical stimulation

Author(s): Misato Ohdaira¹, Tomoko Kamisawa², Soichiro Morishita³, Yinlai Jiang³, Osamu Yamamura⁴, Hiroshi Yokoi³
¹Mechanical Engineering And Intelligent Systems, yokoi Laboratory, The University Electro-Communications, Chofugaoka, Chofu, Tokyo/JAPAN, ²Fukui-Ken Saiseikai Hospital, Fukui/JAPAN, ³The Brain Science Inspired Life Support Research Center, The University Electro-Communications, Chofugaoka, Chofu, Tokyo/JAPAN, ⁴Second Department of Internal Medicine University of Fukui, Fukui/JAPAN

Patients suffering from paralysis due to aging, accidents, or brain injuries are increasing worldwide. Consequently, there is a compelling need for effective methods for the recovery of motor functions. The involvement of brain plasticity has been suggested effective and previous studies have reported that lost motor function and efficiency due to brain damage can be regained by repeatedly increasing and decreasing brain activation. Functional electrical stimulation (FES) has shown its effectiveness in the recovery of motor function. Brain activity usually decreases with the improvement of muscle control by FES. This study investigated the generality of brain responses during rehabilitation with FES in order to elucidate the recovery mechanism. We monitored the brain activity of one healthy subject with fNIRS over a ten-day period (one experiment per day) during which the knee joint movement was induced by FES with different parameters. The subject was seated in the chair of a leg extension device (Fig.1). The measurement regions covered the primary motor cortex and the somatosensory cortex with transmitters and receivers shown in the right of Fig. 1. Receiver No. 5 in Fig. 1 was positioned on the Cz of the international 10-20 system. We stimulated his left quadriceps muscle with the FES device for 4 seconds. The results suggest that the observed increases and decreases of brain activity induced by FES are common (Fig.2). It is suggested that increasing and decreasing brain activation was evoked by long-term FES stimulation. Further research is needed to examine greater numbers of healthy subjects and patients suffering from paralysis to determine the optimum stimulation parameters for brain activation to involve brain plasticity.

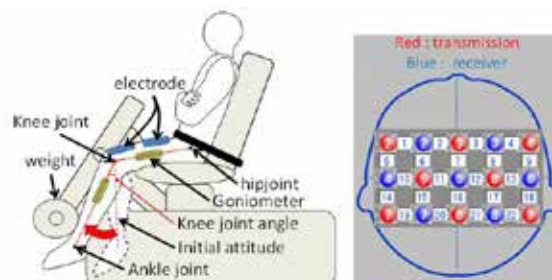


Figure 1. Leg extension experiment and measurement area.

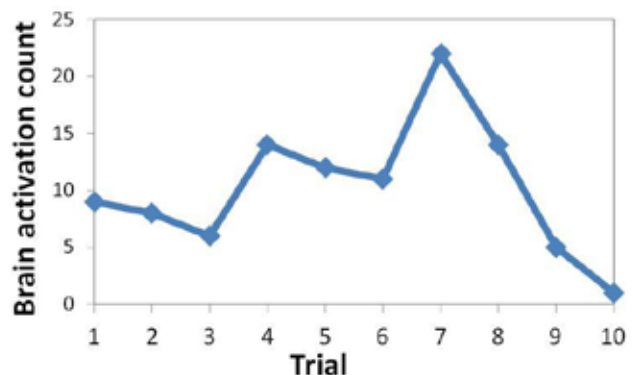


Figure 2. Temporal changes of brain activation counts.

SP008.5 - Muscle fatigability of isometric and isokinetic knee-extension generated by single-electrode- and spatially-distributed-sequential-stimulation.

Author(s): Austin J. Bergquist¹, Vishvek Babbar², Milos R. Popovic², Kei Masani²

¹Toronto Rehabilitation Institute, University Health Network, Toronto/CANADA, ²Institute Of Biomaterials And Biomedical Engineering, University of Toronto, Toronto/CANADA

Background:

Functional electrical stimulation is used in rehabilitation to generate muscle contractions and is conventionally applied using a single active electrode (Single-Electrode-Stimulation; SES; Figure 1A). During SES, muscle fibres are activated in synchrony with each stimulation pulse, resulting in the need of unnaturally high stimulation frequencies to generate functional contractions. High stimulation frequencies result in rapid fatigue, negatively impacting benefits of stimulation rehabilitation. To address this issue, researchers have “spatially distributed” and “sequentially” interleaved stimulation pulses between multiple active electrodes (Spatially-Distributed-Sequential-Stimulation; SDSS; Figure 1A). SDSS allows muscle fibres to be activated in an asynchronous manner, reducing the stimulation frequency at each active electrode, while maintaining activation of the muscle as a whole (Figure 1B). Although SDSS can improve fatigue-resistance of isometric contractions, this method has not been tested during non-isometric conditions.

Purpose:

To reproduce previous findings that SDSS can improve fatigue-resistance of isometric contractions, and to extend this line of inquiry to isokinetic conditions.

Methods:

Two healthy volunteers participated in a 4-hr experiment. Stimulation (40 Hz; 0.3-s-on:0.7-s-off; 120-s total) was delivered to the knee-extensors using SES and SDSS, in separate trials, to generate isometric (0°/s) and isokinetic (180°/s) torque. Isometric and isokinetic contractions were tested on separate legs in separate trials. A rest period of 2-hr was provided between repeated testing of each leg. Protocol order was randomized. Stimulation intensity was set to generate ~40% maximum-voluntary-contraction.

Results:

Fatigue indices were calculated (final torque/initial torque) for isometric (SES=0.37; SDSS=0.57; Figure 1C) and isokinetic (SES=0.36; SDSS=0.39; Figure 1D) contractions.

Conclusion:

Previous findings that SDSS can improve fatigue-resistance of isometric contractions were reproduced. However, the effect of SDSS on improving fatigue-resistance may not be as pronounced during isokinetic, compared with isometric, contractions.

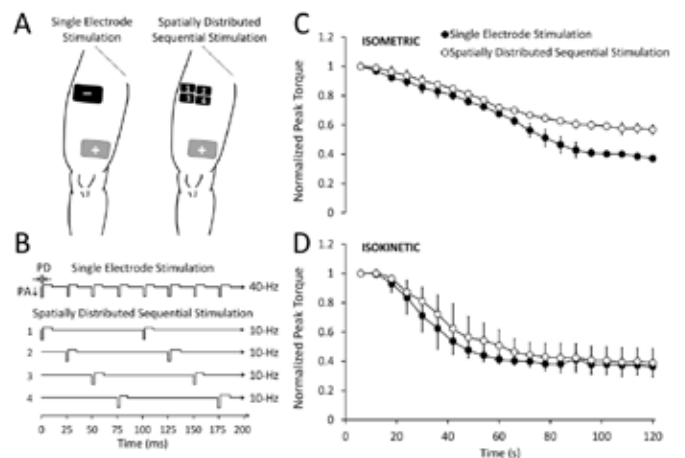


Figure 1. A) Schematic representation of single-electrode- and spatially-distributed-sequential-stimulation (SES and SDSS, respectively). B) Stimulation pulse shape and timing (PD=Pulse Duration; PA=Pulse Amplitude). During SES, pulses were delivered to a single active electrode at 40-Hz. During SDSS, each active electrode (1, 2, 3, 4) was stimulated at 10-Hz, resulting in a 40-Hz stimulation frequency delivered to the knee-extensors as a whole. Normalized isometric (C) and isokinetic (D) peak torque recorded during SES and SDSS (n=2). For each volunteer, peak torque was averaged over 6 contractions to generate 20 data bins. These data were pooled to calculate group means for each bin. Symbols represent group means at each bin. Error bars represent 1 standard deviation.

SP008.6 - External modulation of electrical stimulated spinal reflexes - a control modality for human lumbosacral networks in injury induced disconnection from brain control

Author(s): Winfried Mayr¹, Matthias Krenn¹, Milan R. Dimitrijevic²
¹Center Of Medical Physics And Biomedical Engineering, Medical University of Vienna, Vienna/AUSTRIA, ²Foundation for Movement Recovery, Oslo/NORWAY

Spinal Cord Injury (SCI) can result in various profiles of functional losses in both conducting and processing neural structure in the lesion zone. Sub-lesion structures remain intact, but lose control inputs either directly, due to interrupted efferent pathways or indirectly, by missing reactions due to interrupted afferent pathways, or disturbed processing in damaged higher spinal networks. Identification of artificial control options for this locally altered physiology is an important goal towards improvements in the restoration of movement strategies. Unmasking of functional processes in the present interneuron networks is essential and can be investigated by application of electrical stimulation to afferent nerve structures at lumbar spinal level and recording of reflex reactions from lower extremity muscles. Stimuli can be administered via implanted epidural electrodes or non-invasively via skin attached electrodes. Reactions in the networks reach from monosynaptic, via polysynaptic to complex interneuron processing pathways. Stimulation inputs can induce augmentation and suppression effects resulting in complex motor output patterns that can lead to tonic, rhythmic and even antagonistically coordinated muscle activity. In the current work we show examples how this spectrum of controllable motor outputs can depend on the stimulation parameters frequency and intensity and how the parameter dependent modifications of recorded reflex reactions can support conclusions on underlying neuronal mechanisms, in intact and in altered network structures. Technically this can lead to identification of control characteristics for development of effective support tools, for rehabilitation medicine. We can expect novel treatment options for restoration of movement and a higher potential for regaining functions for persons with SCI.

SP008.7 - Motor Control Assessment using Leap Motion: Filtering Methods and Performance in Indoor and Outdoor Environments

Author(s): Jone J. Kim¹, Dave A. Gonzalez², Adam Mintz², Eric A. Roy², James Y. Tung¹

¹Mechanical And Mechatronics Engineering, University of Waterloo, Waterloo/CANADA, ²Kinesiology, University of Waterloo, Waterloo/CANADA

In this paper, we describe and evaluate a filtering method designed to remove the artifacts from hand/finger kinematics acquired using the Leap Motion controller (or 'Leap'). We report two experiments evaluating this methods: 1) accuracy and precision compared to an established motion-tracking system (Optotrak) and 2) performance in indoor and outdoor environmental conditions. The main findings were that the filtered Leap finger output: i) compared well to motion capture systems in temporal accuracy and precision, ii) moderately well in spatial accuracy and precision, and iii) adequately in indoor settings, but not in outdoor conditions. These advances will inform further development of new tools to assess human motor control

SP008.8 - Biceps brachii EMG signals: estimation of dipole sources

Author(s): Peyman Aghajamaliava¹, Pierre A. Mathieu², Mickael Corinthios¹, Michel Bertrand², Jean Laurier²

¹Génie électrique, École Polytechnique, Montréal/CANADA, ²Physiologie Moléculaire Et Intégrative, Institut de génie biomédical, Montréal/QC/CANADA

The biceps brachii (BB) was shown to be anatomically composed of up to 6 innervated compartments from which as many independent electromyographic (EMG) signal sources could be obtained. Extracting several signals from a single muscle would allow upper-limb amputees to produce several forearm/hand movements with a myoelectric prosthesis. While normal subjects were either sitting or standing-up, we investigated how to activate those compartments by using various right upper limb and hand positions. Five pairs of surface electrodes were put across the short head (SH) and 5 others pairs over the long head (LH) of the BB. Five seconds EMG signals were recorded during isometric contractions produced at a constant level. RMS value of each signal was obtained.

EMG signals were assumed to originate from dipole sources within the arm. A peel-off method served to search for up to 6 dipoles which were used as moving sources in a 3-D finite element forward model study (COMSOL). Arm was modeled either as a single or as 4 concentric cylinders (for skin, subcutaneous fat, muscle and humerus). Comparison was made between amplitude of the simulated and experimental signals.

Results for one seated subject are shown in Fig. 1. In column A, there are significant amplitude differences between some of the experimental signals and model predicted values. Differences were reduced in a second iteration during which dipole parameters are readjusted (column B). With a 4 layers model (column C), differences can be larger and it is also observed that some dipole positions are physiologically incorrect (i.e. in the fat layer). So, while the peel-off method provides a first estimate of the dipoles characteristics, the 4 layers model is necessary to do the proper dipoles readjustments that constrain the position of the dipoles to the muscular tissue.

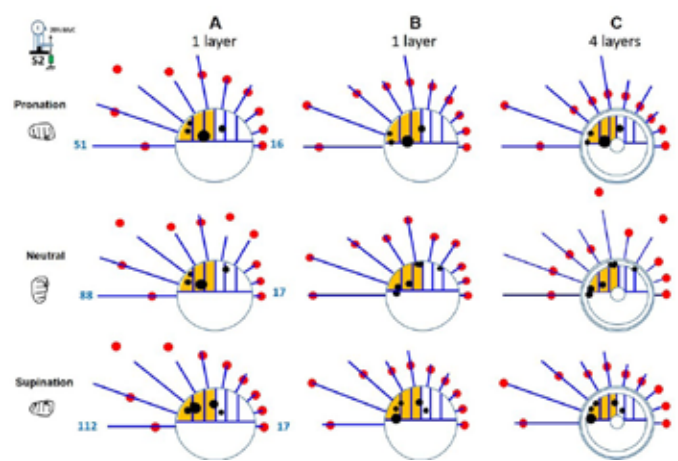


Fig.1. The subject upper-arm is modelled as a single and 4 cylinders geometry within which the 6 compartments of the biceps are hypothetically represented as equal trapezoidal areas (short head region is shaded). The 10 radial line lengths are proportional to the experimental signals RMS values (μV). Position of the outer red bullets is proportional to the simulated results. Within the arm, the amplitude of the dipoles, shown as black bullets, is proportional to their relative intensity. A) Four to five dipoles were obtained with the peel-off method. B) Results obtained following adjustment of those dipoles. C) Same dipole as in B), but using the 4 cylinders model.

SP008.9 - Validating a Solid-Static Single-Armed Male Prototype Tasked to Produce Dynamic Movement from the Shoulder Through the Preparation Phase

Author(s): Alicia M. Gal¹, Adrian D.C. Chan¹, Dean C. Hay²

¹Computer System Engineering, Ottawa Carleton Institute for Biomedical Engineering, Ottawa/CANADA, ²Physical And Health Education, Nipissing University, North Bay/CANADA

The purpose of this study was to design, implement, and validate a methodology to determine baseline measures during the preparation phase (PREP) of seated weight-bearing locomotion. In order to evaluate this methodology this study investigated the external movement produced by the shoulder joint-centre of the upper limb through a seated downward poling motion. A solid-static anatomically correct prototype was designed to produce isolated dynamic movement about a human's shoulder joint-centre; this particular investigation replicated the average male weighing 80kg having fixed elbow (135°) and wrist-stick (45°) angles, and dynamic shoulder start angles (-10° , 0° and $+10^\circ$ to the horizon). The prototype was tasked to produce PREP; a phase identified in seated locomotion produced through a double poling fashion. Trajectory and reaction forces created through PREP were evaluated using a standard Newton-Euler mathematical model in conjunction with a 3-dimensional motion capture system and force plate. Trajectory data concluded that the prototype was of reliable and valid mechanical design producing near identical curves for all trials individually as well as combined averages. Evidence also indicated that all trials displayed similar reaction forces, which produced torque in an anticlockwise direction about the shoulder. Since the prototype is solid and designed to mimic the male upper limb data can be used to describe minimal reaction forces onto the shoulder joint produced from PREP. Understanding external forces at baseline measures allows for valid assumptions to be made or dismissed concerning internal forces within the human body. Dynamic biomechanical analysis requires assumptions involving internal and external parameters when producing a movement. The addition of PREP to the seated propulsion cycle is unclear identifying the need to investigate the biomechanics produced through this phase; full arm extension to pick-plant. This study has developed an improved model of the upper limb during seated double poling.

SP009 - Patient Safety, Medical Errors and Adverse Events Prevention Related to Health Technologies and Incident Analysis and Management

TRACK 16: CLINICAL ENGINEERING, CLINICAL PHYSICS, AND PATIENT SAFETY

SP009.1 - Technological Surveillance and Integrity Monitoring of Infusion Systems

Author(s): David Grosse-Wentrup, Uvo M. Hoelscher
Center For Biomedical Engineering And Ergonomics, Münster University of Applied Sciences, Steinfurt/GERMANY

Infusion therapy is a routine medical procedure. As errors can have potentially fatal consequences, monitoring of infusion systems is mandatory. At present, the technical monitoring of infusions is limited to only a few properties of the infusion system. This passes the demand for vigilance on to the clinical personnel and potentially leaves errors undetected.

By sending small pressure pulses through the interconnected infusion lines, a route map of the infusion system can be created. This map visualizes the connections of infusion lines including line lengths, connection points and connected infusion devices.

This way, errors in the infusion system setup, loosened connections, erroneous stopcock positions and thereby caused under-infusion or reflux can be automatically detected, indicated to clinical personnel, and subsequently corrected before causing harm to the patient.

SP009.2 - Evaluating Patient Safety Risks Related to Oral Chemotherapy: Evolution of a Human Factors Informed Failure Mode and Effects Analysis Framework

Author(s): Melissa Griffin¹, Rachel Gilbert¹, Larry Broadfield², Andrea Cassano-Piche¹, Anthony Easty³, Patricia Trbovich¹
¹Centre For Global Ehealth Innovation, University Health Network, Toronto/ON/CANADA, ²Cancer Care Nova Scotia, Halifax/CANADA, ³Ibbme, University of Toronto, Toronto/CANADA

Chemotherapy is commonly used to treat cancer, which is the leading cause of death in Canada (PHAC, 2012). Chemotherapy treatment involves the use of complicated and flexible drug protocols to care for patients experiencing different types and stages of cancer. A variety of healthcare professionals, who practice in different locations, are involved in the delivery of chemotherapy. Traditionally, most intravenous (IV) chemotherapy is administered to patients in hospital settings, but more recently oral chemotherapy is being delivered in the home and community. Many patients, families, and providers prefer oral to IV chemotherapy for several reasons, including its perceived convenience (Liu, 1997). Manufacturers are facilitating this shift, with an estimated 25% of the 400 new medications currently in development being formulated as oral medications (NCCN, 2008).

IV and oral chemotherapy have comparable toxicity risks and the potential to cause serious harm when not managed properly. However, oral chemotherapy is associated with some unique challenges, such as access, adherence, and safe handling. Many of these challenges stem from a shift in responsibility for administering chemotherapy from healthcare professionals to patients and their families. With increased attention being paid to oral chemotherapy safety (Neuss, 2013), a Canadian provincial cancer agency approached

HumanEra, a team comprised of human factors specialists, to analyze their current practices and identify any risks and opportunities related to oral chemotherapy from a human factors perspective.

Two human factors specialists collected field data using direct observations and semi-structured interviews. Healthcare professionals involved in providing patients with chemotherapy, such as staff in the cancer centre clinics and pharmacy, as well as a number of community pharmacies, were included during data collection. Process maps were created to describe chemotherapy-related processes from when lab work was done through to when chemotherapy was dispensed in the community.

Data were analyzed using a human factors informed failure mode and effects analysis (^{HF}FMEA) framework. This framework was developed iteratively, and is also presented in the upcoming Human Factors for Health Technology Safety book (Cassano-Piché, et al, in preparation). Unlike more traditional FMEA frameworks, the ^{HF}FMEA framework guiding this assessment included three tests: the severity test, the hazard score test, and the single point weakness test; to prioritize which key failure modes to focus on for the remainder of the analysis, making the analysis more efficient. Using this framework, a total of 201 failure modes were identified, with 73% of those being key failure modes requiring further analysis. Although 147 failure modes were still prioritized as key failure modes requiring further attention and analysis (e.g., patient removes the incorrect number of pills from their bottle), the ^{HF}FMEA framework allowed 54 failure modes to be set aside before time was invested identifying causes and recommendations for these lower priority risks (e.g., pharmacy assistant does not pick chemotherapy drug from shelf).

This presentation will provide an overview of the ^{HF}FMEA framework and highlight results from applying this framework to oral chemotherapy processes in a Canadian province, to demonstrate how ^{HF}FMEA can be used to improve healthcare safety.

SP009.3 - Alarm Management Study in Pediatric Special Care Unit

Author(s): Christopher J. Bzovey¹, Paul Prowse²

¹Clinical Engineering, Winnipeg Regional Health Authority, Winnipeg/MB/CANADA, ²Clinical Engineering, Winnipeg Regional Health Authority, Winnipeg/CANADA

There have been a number of critical incidents reported where improperly managed alarms contribute to alarm fatigue in clinicians resulting in patient harm or mortality. Numerous studies have been published in the United States; however there appears to be a lack of publications on alarm management investigation studies conducted within Canada.

The purpose of this work was to investigate the current state of alarm communication and management within the Pediatric Special Care Unit (PSCU). The investigation included an environmental assessment, a staff survey, and a review of the alarm event logs from several medical devices. The staff survey investigated current alarm management practices by analyzing self-reported effects of alarm fatigue experienced in the PSCU. The survey identified ventilators and patient monitors as most heavily contributing to alarm load. Alarm logs were collected from those devices.

The environmental assessment revealed that ventilators within the unit are connected to a latching nurse call system, which requires staff intervention to reset. Within 30-40 seconds after alarming, the alarm increases in volume and pitch resulting in greater distress for the staff and patients within the unit. The staff survey identified that the alarm load they experience has a moderate to high effect on their ability to provide safe patient care (Figure 1). Data collected from the patient monitors demonstrated a significant difference between the number of alarms during the day and night shifts (Figure 2).

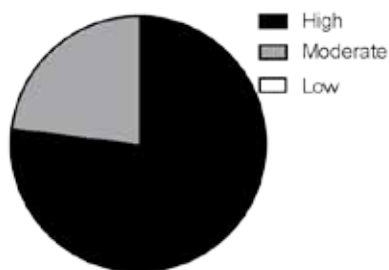


Figure 1: Staff response to the effects of alarm loading experienced in PSCU.

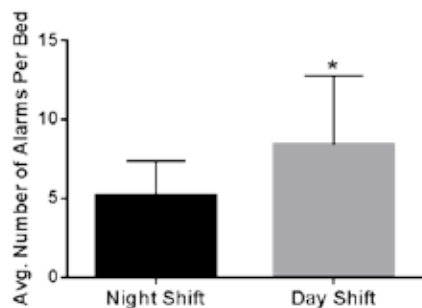


Figure 2: Average number of patient monitor alarms in PSCU per bed during the 12 hour night and day shifts. (*significant difference, $p < 0.05$)

This work demonstrates that alarm load is a problem in the PSCU, and furthermore the intensity is dependent on the time of day. A committee has been established to discuss potential solutions for mitigating the alarm load. The success of this will be discussed during the presentation.

SP009.4 - Failure Modes and Effect Analysis for Stereotactic Radiosurgery: a comparison among three radiotherapy centers in Brazil.

Author(s): Flavia Cristina S. Teixeira, Carlos E. Dealmeida, Mohamed S. Huq
Lcr, LCR/UERJ, Rio de Janeiro/BRAZIL

Task Group 100 of the American Association of Physicists in Medicine recommended the adoption of prospective quality management techniques such as process mapping, failure modes and effects analysis (FMEA) and fault tree analysis (FTA) for analyzing clinical processes and for designing clinic- and site-specific quality management programs that are based on risk assessment. According to this approach, each facility determines the hazards and risks at their own facility based on their own processes and procedures. Appropriate quality control measures are then put in place to mitigate the risks associated with a given process. The goal of the present work was to evaluate the process maps for stereotactic radiosurgery (SRS) treatment at three radiotherapy centers in Brazil and apply the FMEA technique to evaluate similarities and differences, if any, of the hazards and risks associated with these processes. A team, consisting of professionals from different disciplines and involved in the SRS treatment, was formed at each center. Each team was responsible for the development of the process map, and performance of FMEA and FTA. A facilitator knowledgeable in these techniques led the work at each center. The TG100 recommended scales were used for the evaluation of hazard

and severity for each step. Results of the application of FMEA for the major process “treatment planning” are reported here. Hazard index given by the Risk Priority Number (RPN) is found to range from 4 - 270 for various processes and the severity (S) index is found to range from 1 - 10. The RPN values > 100 and severity value ≥ 7 were chosen to flag safety improvement interventions. Number of steps with $RPN > 100$ were found to be 6, 45 and 59 for the three centers. The corresponding values for $S \geq 7$ are 24, 21 and 25 respectively. The range of RPN and S values for each center belong to different process steps and failure modes (see table).

Radiotherapy Center	Process Step	Potential Failure Mode	Potential Causes of Failure	S Min-max	RPN Min-max
Center I	Evaluate DVH	Minimum Dose At Target Not Evaluated	Lack of Standard Procedures	1-10	4-162
Center II	Proceed the Image Fusion	Imaging Not Fused Properly	Software Failures	1-10	7-270
Center III	Insert the Total Dose on TPS	Wrong Dose Inserted	Incorrect Prescription	1-10	4-245

These results show that interventions to improve safety is different for each center and it is associated with the skill level of the professional team as well as the technology used to provide radiosurgery treatment. The present study will very likely be a model for implementation of risk-based prospective quality management program for SRS treatment in Brazil where currently there are 28 radiotherapy centers performing SRS. A complete FMEA for SRS for these three radiotherapy centers is currently under development.

SP010 - Education and Training in Biomedical Engineering

TRACK 17: EDUCATIONAL AND PROFESSIONAL ACTIVITIES

SP010.1 - Biomedical Engineering in Nigeria: A Developmental Overview

Author(s): Kenneth I. Nkuma-Udah, Gideon I. Ndubuka, Kennedy O. Ejeta

Department Of Biomedical Technology, Federal University of Technology, Owerri, Nigeria, Owerri/NIGERIA

Biomedical Engineering (BME) activities in Nigeria can be said to have started in the 1970s during which collaborative efforts were made by engineers, medical doctors, pharmacists, physicists, technicians and other scientist. Although, the pace of development was hitherto slow, most efforts were in the area of training - short courses, continuing education or professional development. However, the coming of NIBE in 1999 has propelled a steady progress of BME activities in Nigeria. This is rightly so, because Nigerian BME professionals from 1999 started addressing issues concerning them as a professional group. BME activities in Nigeria was further given a big boost in 2007, when the first undergraduate programme in BME started in the Federal University of Technology, Owerri, Nigeria with NIBE contributing the foundation members of faculty. NIBE, which stands for Nigerian Institute for Biomedical Engineering, represents the BME profession and its members in Nigeria and in international organisations. Established in 1999 with the vision "to develop and advance the biomedical science, health and human well-being of Nigeria through modern technological approaches comparable to those obtainable in any developed country of the world", NIBE has members largely of the various sciences and classical engineering disciplines from universities and hospitals as well as from other institutions/organisations. It has a membership list of over 2000 members, but financially active membership fluctuates between 100 and 200 depending on the BME activity of each year. NIBE is currently structured in 5 divisions - biological engineering; medical engineering; clinical engineering; rehabilitation engineering; and biomedical physics / allied sciences - to accommodate virtually every field in the sciences. It had its 1st annual BME conference in 2000. Since then it has organised 9 national biomedical engineering conferences and 6 national professional development courses in Nigeria. NIBE has published a newsletter, news@nibe since 2000; a professional journal, Nigerian Journal of Biomedical Engineering since 2001; and electronic mail news, e-nibe since 2003. In 2003, NIBE was admitted as the 50th member of IFMBE. The same year, she co-founded the African Union of Biomedical Engineering and Sciences (AUBES) in Ghana while some members were on a Medical Equipment Training. AUBES was established in order to integrate the effort of various African BME professionals and to expand cooperation on a continental basis. Since 2003, NIBE has made effort with AUBES to pioneer the development of BME in Africa. AUBES's official inauguration and the 1st African Biomedical Conference scheduled to hold in 2005 in Nigeria was cancelled for logistic reasons. However, sustained effort is being geared towards its official inauguration in 2016 in Nigeria. The role of NIBE in developing BME in Nigeria is mainly as a membership group to develop resources for BME by evolving adequate training programmes for members, facilitating accreditation and certification of professionals practicing BME in Nigeria. NIBE is expected to continue to give its members a sense of belonging by becoming the mouth piece of BME professionals in Nigeria. All these development efforts should be a matter of concern for the international BME community.

SP010.2 - Biomedical Engineering Education in Peru in 2015: A Unique and Innovative Collaboration in Latin America

Author(s): Rossana Rivas¹, Luis Vilcahuaman¹, Michael Cieza², J.Tobey Clark³, Herbert F. Voigt⁴

¹Bioengineering Laboratory, Bme Ms Program, Pontifical Catholic University of Peru, Lima/PERU, ²School Of Medicine, Universidad Peruana Cayetano Heredia, Lima/PERU, ³Biomedical Physics & Technology, Instrumentation & Technical Services, University of Vermont, Burlington/VT/UNITED STATES OF AMERICA, ⁴Biomedical Engineering, Boston University, Boston/MA/UNITED STATES OF AMERICA

The Peruvian health sector has a major shortcoming in Latin America because it does not have enough biomedical engineers (BMEs). This situation leads to negative impacts on the quality of a number of outcomes, including: health services, research, management, policies, regulation, etc. Health technology today is engaged in all the key processes: planning, operational, financial, that supports the health organizations. Despite Peruvian health professionals' efforts the lack of an appropriate technological environment and sufficient numbers of BME professionals prevents a good understanding and/or management of the situation, thus affecting the decisions applied to key aspects involved in the sustainability, effectiveness and health disparities in the Peruvian health organizations, both public and private. In addition, the costs due to these inefficiencies jeopardize the governmental investment (public health sector) and the gains of the health enterprises, leading to ineffective, unsafe and inequitable patient care. BME is a discipline devoted to the use of engineering principles and techniques to the study of biological, physiological and medical processes at all length scales. It is a fast growing career in both developed and developing countries, and contributes to the scientific, economic and social development and welfare of society. Its roots are firmly embedded in applying the engineering perspective to health delivery systems and health technology management (clinical engineering). It has been exceptionally successful in applying computational modeling techniques to describe complex biological systems and providing context for experimental approaches to molecular, cellular, tissue and organ system processes. Recently, understanding of biological phenomena has been informing the design of new engineering materials and processes (biomimetic). Most Latin American countries have this specialization at the undergraduate level; model programs exist in Argentina, Brazil, Colombia and Mexico. Two leading Latin American private Peruvian universities, Pontificia Universidad Católica del Peru (PUCP) and Universidad Peruana Cayetano Heredia (UPCH) have agreed to create a joint world-class BME undergraduate program using the institutions' strengths. Peruvian BME status is rising quickly. This academic project between PUCP-UPCH to develop the BME curriculum is a valuable and exciting collaboration. We report here the current situation in Peru with respect to the rise of BME

SP010.3 - Improving Biomedical Engineering in Uganda through education, benchmarking and mentorship

Author(s): Robert T. Ssekitoleko
Physiology, Makerere University, Kampala/UGANDA

Introduction

The field of biomedical engineering is just emerging in many low resource settings. In Uganda, the majority of people looking after and repairing medical equipment have not got appropriate training and skills. In most cases electricians are employed to work mainly as handy men fixing the majority of electrical problems as well as medical devices across the health facilities. Some of these technicians do get some short courses to train them in looking after some specific models of medical equipment. The country has recently accepted that biomedical technicians and engineers are needed for the appropriate management of medical equipment. In some

cases, the biomedical engineers are recruited from abroad to either consult or work as permanent employees. Three training centres in the country have started biomedical engineering training. ECUREI started a biomedical technician diploma before the Ministry of Health initiated a diploma training with Kyambogo University 3.5 years ago. This diploma is supported by the Amalthea trust from the UK. Makerere University started a degree programme 3.5 years ago. With all this training happening, the technicians and engineers job roles have not yet been included in a lot of government hospitals with pay scales a big challenge to many aspiring technicians and engineers in the field.

Methods

A sustainable volunteering project was developed to improve skills of technicians working in seven hospitals. None of the technicians chosen for the project had any formal training in medical equipment management but were routinely involved with the repairs. The main objectives were to improve the process of procurement, repair and disposal of medical equipment by benchmarking with UK and other international standards. A volunteer Biomedical Engineer was recruited from the UK to work as a trainer and provide in-house mentorship to the technician for over 2 years.

The project was in collaboration with the Amalthea trust who provided intensive two weeks training in each year through Kyambogo University. Different parties, including the Ministry of Health, Commercial medical equipment providers and the professional association were always involved throughout the duration of the project. The volunteer also contributed to lecturing and improving the degree programme at Makerere University. Collaboration was formed with the Uganda Industrial Research Institute to replicate the work in other hospitals.

Four technicians were taken to the UK through the commonwealth professional fellowship programme to gain more on job experience.

Results

The technicians showed improved skills, knowledge and confidence about medical equipment management. There has been increased awareness of biomedical engineering profession through workshops and conferences. Inventories were developed using Microsoft Excel and they have been updated yearly since the beginning of the project. There has been increased confidence in the technicians by the clinicians about them handling the medical equipment. The link for the biomedical engineering volunteer between the hospitals and Makerere University means that the students have easy access and can always get feedback from real life scenarios. Some hospitals have set up biomedical engineering workshops and recruited biomedical technicians as a direct result of the project.

SP010.4 - Designing Biomedical Engineering Programs to Prepare for Medtech Industry

Author(s): Shankar Krishnan

Biomedical Engineering, WIT, Boston/MA/UNITED STATES OF AMERICA

The astounding arrays of inventions, innovations and implementations of technologies have resulted in a huge growth in the medical devices and systems worldwide. Medtech industry is instrumental in manufacturing complex medical devices and systems. A vital role is played by Biomedical engineering (BME) in research and development by creating advances in applications of multidisciplinary technologies which ultimately traverse towards improved and efficient health care delivery, which generates consistently increasing demands for biomedical engineers at the international levels. Consequently, the needs for biomedical engineers trigger corre-

sponding requirements for training biomedical engineers, especially for the medtech industry. The responsibility of developing academic programs to train students to gain multidisciplinary knowledge and adequate expertise in research, design, development, manufacturing, operations, compliance and regulatory affairs is bestowed on the academic leaders who face numerous challenges. The objective of this paper is to determine the challenges and present potential solutions in the design of undergraduate biomedical engineering programs to prepare the students for meeting the existing and emerging demands of medtech industry.

The duration of a typical undergraduate BME program is four years in most American Universities. Major challenges are encountered while designing a comprehensive undergraduate BME curriculum within the available duration. Essential factors including the breadth and depth of BME coverage, distribution of relevant theoretical and practical aspects, and, course work, laboratory work, project work knowledge and skillset to fulfill the graduation requirements, in conjunction with appropriate preparation for career paths, are to be considered diligently in the overall design of the BME program. Foundations in mathematics, sciences and engineering are vital prerequisites to the core courses in BME. For achieving superior student outcomes pertaining to conducting experiments and carrying out projects, well-equipped laboratories and faculty mentors with related academic and industrial experience are essential. Additionally, a cluster of elective BME courses catering to the existing and emerging needs of the industry and employers must be incorporated in the curriculum. The aforementioned factors pose strenuous challenges in the BME program design.

A few model designs of BME programs are developed to overcome the challenges cited above. The curricula for the proposed models are formulated employing general structure, track-based structure, and emphasis-based structure. A preferred model is based on emphasis of medical devices and systems in the curriculum coupled with embedded internship or co-operative experiential learning modules to prepare for employment in medtech industry. Real life experiential learning thru placement at a medtech industry or a teaching hospital undoubtedly complements the knowledge and competencies acquired on campus. BME program directors should make special efforts to recruit and retain dedicated faculty and technical staff. Continuing support of resources are necessary for the successful execution of the academic programs. The curricula for the proposed models have been developed in different academic settings and implemented. Extensive experience in designing and directing multiple models for BME undergraduate education lends support to the success of carefully designed site-specific programs to prepare the students for the medtech industry involving medical devices and systems.

SP010.5 - BME vs CE vs HTM vs HbHTA vs EAM. What's in a Name and does it matter?

Author(s): Mladen A. Poluta

Human Biology (bme Division), University of Cape Town, Observatory/SOUTH AFRICA

Background:

Technology is increasingly an essential component of effective healthcare delivery in diverse settings. Ensuring that healthcare technologies are optimally planned, assessed, acquired, implemented, managed and replaced is a complex process involving many stakeholders and players. While the adage "Don't fix what ain't broke" applies in the context of established practices in different jurisdictions, it is nevertheless important to consider where we stand collectively. Greater alignment, clarity of purpose and standardisation - as well as a common future vision - would support stakeholder engagement, demystify guidance to countries (especially those that

are resource-challenged), support capacity building and facilitate both achievement of critical mass in diverse settings and mobilisation of resources for related activities. This paper provides one perspective of the status quo and makes some suggestions for the way forward, with a focus on engineering/technical disciplines related to healthcare technologies.

Issues:

How can we address the lack of uniformity in both nomenclature and practice? For example, BME is often seen as synonymous with CE, but not universally so, and both are referred to by other terms.

What are the generic international classifications pertaining to BME and CE? (Ref: ISCO-08)

How can recognition to be given to the full range of engineering professionals: engineers, technologists and technicians? (Ref: Washington-, Sydney- and Dublin Accords of the International Engineering Alliance)

How different is HTM from Clinical Engineering, and both HTM and CE from the emerging fields of Hospital-based HTA and Engineering Asset Management, respectively?

What are the individual 'value-adds' and focus/impact areas for BME, CE, HTM, HbHTA and EAM, and is there merit in unifying/aligning these disciplines?

Figure 1 below shows how the disciplines/specialities addressed could combine in serving a common purpose, while recognising their specific roles and contributions to the overall process.

Figure 1: Optimised Life-Cycle management of Healthcare technologies, showing the contribution of supporting disciplines, specialities and fields.

SP010.6 - Clinical Engineering Certification Program in the Americas

Author(s): Frank R. Painter

Biomedical Engineering, University of Connecticut, Trumbull/UNITED STATES OF AMERICA

The American College of Clinical Engineering's (ACCE) definition of a clinical engineer is a professional who supports and advances patient care by applying engineering and managerial skills to healthcare technology. One of ACCE's mission statements is to define a body of knowledge on which the profession is based. Using the definition and the information received from a body of knowledge survey sent to over 500 practicing clinical engineers from around the world, in 1990 a clinical engineering certification exam was created.

The Healthcare Technology Certification Commission (HTCC) was formed to oversee the process and a Board of Examiners was formed to create the exam and test the candidates. The financial aspects of the certification process are managed by ACCE on behalf of the HTCC.

After several years it became apparent that the process could be adopted by other countries. In 1995 the Canadian Board of Examiners was formed and the CCE exam became a collaborative process between the Canadian and US Board of Examiners. In the meantime collaboration with several countries in South and Central America as well as the Middle East has been discussed.

The exam process includes of three major components; the application, written exam and oral exam. The application process consists of the simple application, university transcript and three professional references. Through this the candidate must demonstrate they

have sufficient clinical engineering experience to qualify to take the exam. The exam consists of 150 multiple choice questions distributed across CE topics in the same proportion as they appear in the body of knowledge survey results. The oral exam is a structured exam questioning the candidate on three separate real life clinical engineering scenarios.

The Board of Examiners publish an application and a handbook to guide the candidate through the process. These are available on the certification page of the ACCE website (www.accenet.org). This page also includes information on the CCE renewal process, recommended resources for use in preparing for the exam and a list of those currently certified. 221 certified clinical engineers are currently listed.

SP010.7 - Biomedical Technology Online Courses for the Americas

Author(s): Tobey Clark¹, Alexandre Lemgruber², Francisco Caccavo², Tatiana Molina Velasquez³, Federico Gracia⁴, Rossana Rivas⁵, Luis Vilcahuan⁶

¹Instrumentation & Technical Services, University of Vermont, Burlington/UNITED STATES OF AMERICA, ²Health Technologies, Pan American Health Organization, Washington DC/UNITED STATES OF AMERICA, ³Universidad CES, Medellin/COLOMBIA, ⁴Universidad Tecnológica Nacional – Facultad Regional Mendoza, Mendoza/ARGENTINA, ⁵Health Technopole CENGETS PUCP, Lima/PERU, ⁶Bio-engineering Laboratory, Bme Ms Program, Pontifical Catholic University of Peru, Lima/PERU

Latin America and the Caribbean countries are rapidly expanding their healthcare technology usage. Physicians, patients and their families are understanding better the relevant influence of healthcare technology based on clinical, ethical, social, and economic health outcomes. Companies are eager to expand to this growing area, and donations from developed countries of new and used equipment continue.

In general, the regional status of Latin American and Caribbean countries includes: little medical device regulations, a high percentage of devices that are out of service, weak after sale device support with nearly all service from manufacturers or their representatives, a shortage of technical staff in hospitals, very limited maintenance budget, inadequate number of healthcare staff appropriated trained and limited technology management.

What is needed is training and education of staff at the hospital level in the various technologies used in healthcare. Education and training of clinical and technical staff interacting with medical technology enhances the effectiveness and safety of medical care.

Through a grant from the PAHO Foundation (formerly PAHEF), biomedical technology online courses were developed for clinical and technical staff. Online training via the Internet allows 24x7 accesses to training resources in an asynchronous fashion. Extensive use of web resources and simulations enhance the courses. The course topics include anatomy/physiology, engineering concepts, physiological monitors, cardiac therapy devices, ventilators, infusion technology, all imaging modalities, surgical systems, clinical information networks, and therapy devices. The initial English version has been taught in the USA since 2007. The courses were translated to Spanish and adapted for use in Latin America for use in 2008. Over 1000 students from 28 countries have taken the courses at the University of Vermont USA, Universidad CES in Colombia, Universidad Tecnológica Nacional - Facultad Regional Mendoza in Argentina, and Pontificia Universidad Católica del Perú.

In September 2014, the online courses were placed on the PAHO

Virtual Campus for Public Health. The PAHO Virtual Campus for Public Health with over 100 courses offered currently has students from over 140 institutions enrolled from the Americas. The PAHO platform allows a broader range of students from the Americas to enroll in the courses especially those without the funds for university courses. Forty-eight students from twenty-one countries enrolled in the twenty-four week English and Spanish courses – Introduction to Biomedical Technology. Course assessments and evaluation will be available following the end of course on April 24th and will be presented at the WC2015. Future plans are for translation of the courses to Portuguese and adaptation to Brazil, and additional educational offerings on healthcare technology planning and management.

SP011 - Overview of Gender Roles in Medical Physics in North America

TRACK 18: GENDER, SCIENCE AND TECHNOLOGY

SP011.1 - Gender, Science and Technology: The Role of Women in Medical Physics

Author(s): [Kristy K. Brock](#)

Radiation Oncology, University of Michigan, Ann Arbor/MI/UNITED STATES OF AMERICA

The role of women in the field of medical physics has been steadily increasing over time. Data obtained from the AAPM shows that the women comprise an increasing percentage of the overall membership. In the late 1960s, less than 10% of the membership was female, however this has been steadily increasing and in 2014, 21% of the full membership is female and 29% of the overall membership (including student members) is female. If this trend continues at the same rate, by 2044 we would expect equal representation of males and females in the field. It is important to not only evaluate the membership, but also the engagement of women within the active membership and leadership positions within the field and professional society. AAPM staff assisted in mining the membership database for statistics on gender representation in the society membership, engagement in the AAPM, presentations at the annual AAPM meeting, and AAPM leadership. Full membership was used as the gender baseline as student members are not allowed to serve on committees, however they do present at the annual meeting. Engagement in the AAPM was classified as membership on an AAPM committee, which has the structure of 3 councils (Professional, Educational, and Science) under which there are several committees, subcommittees, working groups, and task groups. Presentations at the annual meeting were evaluated based on authorship, first author presenting a poster, first author presenting at the podium (oral), session moderators, invited speakers, and invited speakers in the educational, professional, and scientific track. Presentation data was obtained over the past 5 meetings (2009-2014). Leadership in the AAPM is defined as members of the Board of Directors (nominated by a committee and elected by the full membership or elected from a local chapter), membership on the Executive Committee (nominated by a committee and elected by the full membership), and President (nominated by a committee and elected by the full membership). Gender representation in distinguished awards given by the society was also evaluated.

Of the AAPM membership currently serving on a committee, working group, or task group, 21% are female, the same ratio of women in the AAPM membership. Further evaluation of 'very active' members, defined as membership in 5 or more committees, found that this representation is maintained, with 20% of very active members being female.

Evaluation of the past 10 AAPM annual meeting shows that of the over 60,000 authors of AAPM abstracts, 16% were female. 20% of the 6,794 poster presentations were given by women and 18% of 6,947 oral presentations were given by women. Abstracts acceptance and placement in a poster or oral session (highest scored abstracts) are based on single blind reviews (authors' names are known to the reviewers). Session moderators are selected by the scientific program committee and of the 451 moderators over the past 10 years, 16% were female. The AAPM Meeting Coordination Committee invites speakers for educational, professional and scientific sessions. Over the past 10 years, 17% of the invited speakers in education sessions have been female, 23% in the professional

session, and 12% in the scientific session (however 10% of the scientific session speakers did not have a disclosed gender, likely due to not being a member of the AAPM organization).

The current Board of Directors for AAPM is comprised of 46 individuals, 10 of whom are female (22%). Historically, of the 18 Secretaries of the AAPM, 2 have been women (11%) and 7 of the 15 Treasurers have been women (47%). There have been 57 presidents of the AAPM society, 3 of whom have been women (5%). The first female president of the AAPM was in 1982, the last 2 in 2007 and 2009. Of the 897 awards bestowed by the AAPM, 9% have been awarded to women. The William D. Coolidge Award recognizes 'an AAPM member for an eminent career in medical physics. It is the highest award given by the AAPM' and has only been awarded to one woman, in 1977.

These trends show promising inclusion of women in medical physics. The increase in the number of women pursuing careers in medical physics is evident by the steady increase in the percentage of women making up the membership. It is encouraging to see that this rate of women entering the field is also matched by active engagement in the society (through membership on committees) and emerging in leadership, as seen in membership of the Board of Directors, however not yet matched at the presidential level.

Learning Objectives:

1. Highlight the role of women in Medical Physics.
2. Evaluate the engagement of women in the American Association of Physicists in Medicine.
3. Understand gender related issues in science and technology fields.

SP011.2 - Biography of Women in Medical Physics: Maryellen Giger, Ph.D.

Author(s): Maryellen L. Giger

Radiology/medical Physics, University of Chicago, Chicago/UNITED STATES OF AMERICA

My brothers and I were first-generation college and were raised with the importance of education. Following the completion of my Bachelor's Degree in Mathematics, Physics, and Health Sciences from the Illinois Benedictine College, I studied Physics at the University of Exeter, earning a Master's Degree. This experience led me to the University of Chicago to study Medical Physics, where I earned my PhD in 1985. I continued my tenure at the University of Chicago becoming faculty in 1986 in the Department of Radiology. At the University of Chicago, I have served as Director of the Advanced Imaging Program in the Cancer Research Center, Director of our CAMPEP-accredited Graduate Program in Medical Physics, and Chair of the Committee on Medical Physics. I am currently the A. N. Pritzker Professor of Radiology/Medical Physics and Director of the BSD Imaging Research Institute at the University. My passion for medical physics began while working summers during college at Fermi National Laboratories where I assisted in the beam diagnostic group and the neutron therapy group. I have also served as President (and Chairman of the Board) of the American Association of Physicists in Medicine, Board member of SPIE, and Editor-in-Chief of the SPIE Journal of Medical Imaging. I am a Fellow of AAPM, AIMBE, and SPIE. I was honored to be elected to the National Academy of Engineering and to be named by the International Congress on Medical Physics as one of the 50 medical physicists with the most impact on the field in the last 50 years. I feel that my most significant scientific achievement was providing leading contributions to the field of computer-aided diagnosis. I have more than 170 peer-reviewed publications (over 300 publications), more than 30 patents, and mentored over 100 graduate students, residents, medi-

cal students, and undergraduate students. Also, my husband and I have raised our four children through various trips to AAPM, SPIE, and other scientific meetings. The best part of my "job" is when my student becomes a colleague. I look forward to sharing my experience at the World Congress.

SP011.3 - My STEM story: from Martinique in the Caribbean to Quebec City, through France and Vietnam

Author(s): Nadia Octave

Radiation Oncology, CHU de Québec, Québec/QC/CANADA

It is always a bit intimidating to be asked to come forward to talk about one's personal life, experiences and career path. Someone said stories can move people and inspire them. That is for big stories, I would say. My aim would be just to send seeds in the wind and who knows? May be one will bear fruits? So to start, I am a medical physicist born and raised in Martinique, a French region in the Caribbean. I have a biomedical engineering background with a master in medical technologies from Toulouse Paul Sabatier University, and a specialization in radiation physics and imaging. Two long-term internships in Toronto had a major impact on my following choices and did actually prove to influence all the rest of my career path until my current job position in Quebec City. But that is a long story that I cannot tell in a few words, because I would have to start with the very beginning: my thirst for knowledge of the human body and its biology and my first interest in physics with the moon and astronomy. To this I have to add, the meeting of important role models and mentors to whom I could always refer and who could share their own experiences with me. Also I could tell you about my years of training at the Curie Institute, at the Gustave Roussy Institute and my first position as a junior medical physicist at the Georges Pompidou European Hospital in Paris and also about an experience within the experience working in Vietnam. But more importantly I would like to emphasize on the challenges and obstacles that I overcame. I will also share some strategies that worked for me so that you too can be convinced that the only limits are the ones that we imposed to ourselves. And finally, since stories without actions are meaningless, I will speak about an initiative here today.

SP011.4 - My strategies for living (and enjoying) academic research

Author(s): Rebecca Fahrig

Radiology, Stanford University, Stanford/CA/UNITED STATES OF AMERICA

During the completion of my Bachelor's degree in Physics at the University of Toronto, I became interested in Medical Physics, which led me to pursue a Master's in Medical Biophysics from the University of Toronto. I completed my PhD in Medical Biophysics from the University of Western Ontario, where I focused on novel x-ray imaging techniques. I was awarded a Post-Doctoral Fellowship by the Medical Research Council of Canada, which I completed at Stanford University. Following my fellowship, I joined the faculty at Stanford School of Medicine, where I am currently a Professor (Research) of Radiology. I have had the honor of receiving the Young Investigator's Award from the American Association of Physicists in Medicine, and the Greenfield Award for Best Paper published in Medical Physics. I have published over 100 peer reviewed articles and I am currently the PI on two NIH funded grants. At each stage of my career I have been fortunate to have mentors who have provided sage advice and guidance. I look forward to an exciting World Congress and the opportunity to share my experience in the Gender, Science, and Technology Track.

SP011.5 - Early exposure to science leads to fulfilling career in medical physics**Author(s):** Renee X. Larouche

Radio-oncologie, CHUM - Hôpital Notre-Dame, Montreal/CANADA

I have a happy and fulfilling career working in the field of clinical medical physics for almost 13 years. Although I love my work, finding the perfect balance between work, family life, and volunteering is not an easy task to accomplish. After working in two community radiation oncology clinics, one in Canada and the other in the USA, I finally settled in Montreal. I am now currently employed at the Centre hospitalier de l'Université de Montréal (CHUM- Notre-Dame hospital) in the department of radiation oncology. My general interests are in safety and risk management as well as the implementation of more robust processes in the clinic. Since 2012, I am the Deputy Chief Examiner for the Canadian College of Physicists in Medicine (CCPM). This opportunity allows me to meet a number of young medical physicists from all across Canada.

My life experience in the world of sciences has been very positive. I have received encouragement, worked in nurturing conditions and have had great role models. I was exposed to physics at a very young age when a neighbor who was a physicist recognized my interest in science and nurtured it. In high school, I enrolled in a special science program. This constructive early exposure to science kept me motivated.

We were only three female students majoring in undergraduate physics. The gender issue had never been so obvious. The small number of women did not impact my sense of belonging. Although I felt lonely at times, I wanted to be a physicist just as much as anyone else in that classroom. Fortunately, I met a group of young women enrolled in science or engineering programs and we founded a campus chapter of Women in Science and Engineering (WISE). This was a great time in my life: in fact, a friend I made through WISE is now my daughter's godmother.

As a graduate student in medical physics, I realized that confidence plays a major role when expressing your ideas. Indeed, more importance was given to oral expression during exams than when I was an undergraduate student: I had never experienced the somewhat daunting situation of being questioned by a panel of examiners orally before. I will always remember the stress and fear associated with these exams, but I found that being well prepared and organized was key and is still the solution in my case. I keep this in mind when preparing oral exams for the CCPM.

Fear is often a hurdle for someone to attain his or her potential: fear of not succeeding, fear of ridicule or fear of rejection. The truth is that you are letting yourself down when deciding not to try. Getting out there, pushing yourself is how you are able to develop and, looking back, be proud of what you have accomplished.

SP013 - MRI: Methods**TRACK 01: IMAGING****SP013.1 - Numerical Simpson's Rule for Real Time and Accurate T2* maps generation Using 3D Quantitative GRE****Author(s):** Chemseddine Fatnassi¹, Rachid Boucenna¹, Habib Zaidi²¹Radio-oncology Department, Hirslanden, Lausanne/SWITZERLAND, ²Department Of Nuclear Medicine And Molecular Imaging, Geneva University Hospital, Geneva/SWITZERLAND

Introduction: Quantitative T2* maps can be generated using different approaches, the golden standard being the nonlinear least square (NLLS) exponential signal decay fitting technique. It can be also generated using a logarithmic linear fit (LLf). However, the above mentioned methods based on curve fitting are time consuming and their use in real time challenging. NumART2* approach introduced by Hagberg et al. (2002) computes in real time the T2* but remains echo spacing and signal noise dependent. In this work, we propose an alternative approach relying on Simpson's rule integration that generates in real time accurate T2* maps even in the presence of large echo spacing and high noise value.

Materials and Methods: We propose a method based on Simpson's rule for integrating the temporal signal decay. Instead of a linear approximation (e.g. NumART2*), Simpson's rule combines trapezoidal and midpoint rules to better interpolate the signal decay between echoes. To test our hypothesis, we used simulated brain MRI data (MNI, Canada) and 20 *in vivo* scans performed on a 3T Magnetom Trio (Siemens Healthcare, Erlangen, Germany) using the following parameters: Echoes/GRE/ α /TR/TE1/ Δ TE/size=32/Bipolar/8°/47/ 1.23/1.23ms/136×136×112. An offline generation of T2* was realized using LLf, NLLS (expo) and NumART2*. The maps were evaluated and compared in terms of signal echo spacing and image noise level.

Results and Discussion: In the presence of small echo spacing (Δ TE/T2*) $<$ 0.2), the T2* maps were well generated by all methods, with a slight overestimation when using NumART2*. When Δ TE increases (Δ TE/T2*) $>$ 0.2), NumART2* tends to overestimate the T2* values, although accuracy is well maintained by the other methods. These results can be explained by the quadratic interpolation of signal decay between the echoes that Simpson's rule uses to approximate the area under the signal decay rather than a linear approximation that NumART2* uses. For low noise levels ($<$ 15%), all methods provide highly accuracy results. NumART2* starts to diverge when the noise level becomes significant ($>$ 15%), while Simpson's rule, linear and NLLS fit remain insensitive to added noise. Simpson's rule combines two approximations, namely the midPoint and trapezoidal rules, to compute the signal integral. This combination enables to approximate well the signal decay between two echo points using a smooth quadratic interpolation even in the presence of high noise level, and as such, provides accurate T2* maps.

Conclusion: We proposed an alternative T2* maps generation which relies on Simpson's rule to approximate the geometric area under the signal decay. The method allows rapid whole brain mapping of T2* with a high accuracy even in the presence of large echo spacing or high noise level.

SP013.2 - Optimization of Pulse-Triggered fMRI Measurement Delay with Acoustic Stimulation**Author(s):** Anita Król¹, Zofia Drzazga¹, Uwe Klose²¹Medical Physics, A Chelkowski Institute of Physics, University of Silesia, Katowice/POLAND, ²Diagnostic And Interventional Neuroradiology, University Hospital Tübingen, Tübingen/GERMANY

The purpose of the study was to examine whether improvement of activation maps of auditory cortex and brainstem nuclei is possible when the delay between the cardiac induced pulse signal and the measurements is optimized. Subsequently, the comparison of the height of brain activity obtained for different stimuli - classical and rock music. In five healthy, right-handed volunteers (the mean ages $25,4 \pm 2,8$ years old), musical stimuli were presented binaurally in a block design. Evaluation was performed using 'Matlab' and 'SPM-8new' software with statistical threshold $p < 0.001$ (auditory cortex, AC) and $p < 0.01$ (brainstem). Our results suggest that the manipulation of the trigger delay (TD) time changes the degree of activation in auditory cortex and brainstem nuclei. Detection of auditory cortex was in 16% (TD=0), 30% (TD=200), 8% (TD=400) and 9% (TD=800) higher than without cardiac gating examinations, and correspond to the 41 and 22 Brodmann areas. The 3-selected slices volume included the medial geniculate bodies (MGB), lateral lemniscus nuclei (NLL), superior olivary complex (SOC) and cochlear nuclei (CN). The height of activation depends on duration of trigger delay. Therefore, using various TD time proves that it is possible to increase ability to detect activation in subcortical auditory structures - another method to reduce image signal variability, which was caused by brainstem motion. Examinations with rock type of music bring better than examinations using classical music.

SP013.3 - Improvement of Pseudo Multispectral Classification of Brain MR Images**Author(s):** Chemseddine Fatnassi¹, Rachid Boucenna¹, Habib Zaidi²¹Radio-oncology Department, Hirslanden, Lausanne/SWITZERLAND, ²Department Of Nuclear Medicine And Molecular Imaging, Geneva University Hospital, Geneva/SWITZERLAND

Introduction: Several advanced applications using morphological MRI frequently require segmentation of the imaged volumes. The accurate interpretation of information pertaining to investigation of brain alterations relies on accurate and reproducible brain tissue classification. Different approaches based on thresholding, cluster analysis, a priori information about anatomy and Bayesian classification have been proposed. However, many of them fail when classifying specific regions with low contrast between tissues. In this work, we introduce an enhanced method to classify brain tissue by combining a pseudo-multispectral color transformation (PMC) and improved K-mean clustering. The proposed approach is compared with FSL classification (FMRIB, Oxford, UK).

Materials and Methods: Gray and binary color spaces are commonly used by image processing methods. However, the contrast between brain tissues in some regions is very low e.g. cerebellum(WM and GM interfaces). Consequently, methods fail and wrong classifications might occur. To overcome this problem, the first step consists, after skull stripping, in transforming the T1-MPRAGE data to multispectral data containing 3 different images CIE-XYZ. To better separate neighboring values in WM, GM interfaces, normalized 3-channel data values are weighted by root square function (RSF). RSF minimizes low contrast region brain tissue overlapping. In the second step, an enhanced iterative and non-deterministic K-mean clustering is applied for image classification. The number of K-clusters is initially set to be maximal; the algorithm repeats classification with decreasing K until convergence. Subsequently, gap criterion, used to evaluate the optimal number of clusters, is calculated. Optimal K-cluster is then estimated. In addition, GM, WM and CSF centroid distribution templates are

estimated beforehand using more than 70 human and a couple of simulated data. Based on these parameters, brain tissue classes computed earlier are corrected and reassigned to the new optimal classes. To evaluate our approach, we used 4 numerical brain atlas templates where GM, WM and CSF volumes are known beforehand (ground truth). In addition, 10 clinical MRI studies scanned on a 3T Skyra (Siemens Healthcare, Germany) using T1-MPRAGE sequence with the following parameters: flip/TE/TR/TI=100/4/9.7/20ms. These data sets were classified using PMC and then compared with FSL classification.

Results and Discussion: The numerical brain tissues are classified using the enhanced PMC algorithm with a high accuracy (108% for WM, 101% for GM and 108% for CSF) against FAST-FSL (85% for WM, 119% for GM and 86% for CSF). Silhouette plot indicates that PMC better separates clusters compared to FAST-FSL classification without any tissue misclassification even in presence of low CNR and partial volume effect. The clinical studies show that the proposed approach is faster and more accurate, especially in region with low CNR e.g. cerebellum arbor vitae where the WM and GM are better delineated.

Conclusion: It can be concluded that enhanced PMC classification provides a fast and accurate brain tissue classification. This approach overcomes the low CNR and partial volume effect present in some brain regions, e.g. cerebellum arbor vitae and near the temporal lobe region and seems to be promising for clinical and research applications.

SP013.4 - Image reconstruction of RF encoded MRI signals in an inhomogeneous B0 field**Author(s):** Somaie Salajeghe¹, Paul Babyn², Jonathan C. Sharp³, Gordon E. Sarty¹¹Biomedical Engineering, University of Saskatchewan, Saskatoon/CANADA, ²University of Saskatchewan, Saskatoon/CANADA, ³University of Alberta, Edmonton/CANADA

Introduction: Conventional Magnetic Resonance Imagers (MRI) use a uniform main magnetic field (B0) to polarize the sample being imaged. Non-homogeneity in the B0 field leads to image distortion. In practice it is impossible to have a perfectly homogeneous B0 field so shim coils are used to remove the inhomogeneity of the field. However, shim coils and other B0 homogeneity requirements result in expensive and heavy MRIs. To produce truly portable MRI equipment, the requirements for homogeneity of the B0 field could be removed. When used with TRansmit Array Spatial Encoding (TRASE) [1] to encode information instead of using traditional B0 gradient coils an MRI with an inhomogeneous field could be portable [2]. The TRASE method encodes spatial information through the use of spatially varying B1 transmit phase fields. The feasibility of the reconstruction of TRASE signals under B0 inhomogeneity from a mathematical perspective was investigated.

Method: TRASE signals were simulated for a discrete Shepp and Logan mathematical phantom inside a TRASE RF coil set, composed of a combination of circular Maxwell and Helmholtz coils, in an inhomogeneous B0 field. The field assumed was $B_0(x,y) = Ax^2 + By^2 + C$ where $A = 0.1$, $B = 0.2$ and $C = 0.08$. The simulated TRASE MRI signals were reconstructed using a regularized least squares reconstruction method. The signal from the phantom p may be written in matrix form, with appropriate re-indexing of the collected signal data points, as $S = [T]p$. The image may then be reconstructed using constrained least squares technique. Here a regularized least squares reconstruction was done by adding Tikhonov regularization as $R = \text{argmin} (\|[T]R - S\|^2 + \|\mu [I]R\|^2)$, where μ is a regularization parameter, $[I]$ is the identity matrix and R gives the approximate solution for p .

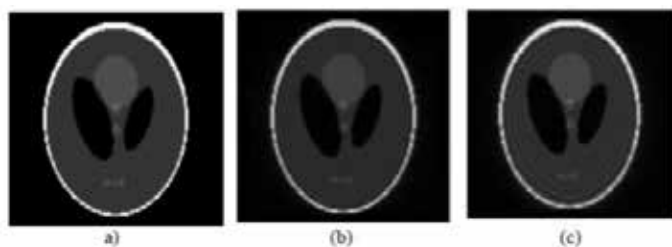


Fig. 1: 128 *128pixel phantom and reconstructions. (a) Phantom. (b) Reconstructed image from a TRASE signal generated in a homogeneous B0 field. (c) Reconstructed image from a TRASE signal in an inhomogeneous B0 field.

Results/Conclusion: Fig. 1 shows regularized least squares inversion of simulated signals from a TRASE coil in an inhomogeneous B0 field. The result is comparable to the reconstruction from a signal generated in a homogeneous B0 field. This is the first step in showing that TRASE in an arbitrary B0 field is possible. The next steps include simulations via the Bloch equations to model the effect of inhomogeneities on the flip angles attained.

References: [1] JC Sharp, SB King. *Magn Reson Med*63:151-161(2010).[2] CZ Cooley et al. *Magn Reson Med*73:872- 883(2014).

SP014 - Bone Mechanics

TRACK 03: BIOMECHANICS AND ARTIFICIAL ORGANS

SP014.2 - Improved Semi-automated 3D Kinematic Measurement of Total Knee Arthroplasty Using X-ray Fluoroscopic Images

Author(s): Takaharu Yamazaki¹, Ryogo Kamei², Tetsuya Tomita³, Yoshinobu Sato⁴, Hideki Yoshikawa⁵, Kazuomi Sugamoto³
¹The Center For Advanced Medical Engineering And Informatics, Osaka University, Osaka/JAPAN, ²Ritsumeikan University, Shiga/JAPAN, ³Orthopaedic Biomaterial Science, Osaka University Graduate School of Medicine, Osaka/JAPAN, ⁴Nara Institute of Science and Technology, Nara/JAPAN, ⁵Orthopaedics, Osaka University Graduate School of Medicine, Osaka/JAPAN

Accurate measurement of 3D dynamic kinematics of total knee arthroplasty (TKA) is very important for evaluating the outcome of surgical procedures and for improving the implants design and clinical outcome. In order to achieve 3D kinematic analysis of TKA, 2D/3D registration techniques, which use X-ray fluoroscopic images and computer aided design (CAD) model of the knee implants, have been applied to clinical cases. However, in previous study, these techniques have needed time-consuming and labor-intensive manual operations in some process, and particularly the process of the manual initial guess poses of the CAD model for each X-ray image was problem for practical clinical applications. In this study, we propose an improved method for semi-automated 3D kinematic measurement of TKA using X-ray fluoroscopic images. The proposed initial pose estimation method of the model is based on the use of a transformation with feature points extracted from each X-ray image using speeded up robust features algorithm. In order to ensure the validity of the proposed method, *in vivo* experiment using X-ray fluoroscopic images of 4 TKA patients during knee motions was performed. As a result of experiment, 3D pose of the model for all X-ray images except for the first frame was automatically stably-estimated, and the success rate (X-ray frame number within error of 1mm / 1 degree relative to all X-ray frame number) for the femoral and tibial component were 83.7 % and 73.5 %, respectively. In addition, the success rate with the proposed method was higher than a conventional method. Consequently, the present method was thought to be very helpful for practical clinical applications.

SP014.3 - The influence of screw length and stiffness on the tibial mechanical environment in ACL reconstruction

Author(s): Jie Yao¹, Lizhen Wang¹, Yubo Fan^{*2}
¹School of Biological Science and Medical Engineering, Key Laboratory for Biomechanics and Mechanobiology of Ministry of Education, National Key Lab of Virtual Reality Technology, Beihang University, Beijing/CHINA, ²National Research Center for Rehabilitation Technical Aids, Beijing/CHINA

Introduction & Objective

Anterior cruciate ligament (ACL) reconstruction is the primary treatment for the ACL injury in orthopedics. However, the post-operative graft laxity has been frequently reported, which would cause knee instability and osteoarthritis in long-term [1]. The interference screw is the popular implant for the graft fixation. It may change the surrounding mechanical environment, induce the undesirable bone remodeling, and lower the graft fixation strength. Therefore, this study aimed to quantify the influence of the screw on the distribution of stress energy density (SED), which correlated with the bone remodeling.

Methods

The finite element model of single-bundle ACL reconstruction was developed. The SED distributions in tibia under the compressive, valgus, and rotational loadings were applied. The influences of the screw length and stiffness on the post-operative SED were calculated.

Results & Discussion

The compressive loading played an predominant role among the three loadings. Under the compressive loading, the SED beneath the screw shaft was decreased, whereas the SED above the screw shaft was increased. Extremely high SED occurred near the screw head and tip.

Increasing the screw length would potentially promote the bone healing at the proximal part of the tunnel, yet aggravate the SED alteration at the distal part. Using a screw modulus approaching to the bone could reduce the undesirable SED alteration.

Conclusion

In ACL reconstruction, using a long screw with the modulus approaching to the bone could provide a beneficial mechanical environment for the post-operative rehabilitation.

Acknowledgment

The present study was supported by grants from National Natural Science Foundation of China (NSFC 11421202, 11120101001), and National Science & Technology Pillar Program of China (2012BAI18B07, 2012BAI22B02).

(* Corresponding author, yubofan@buaa.edu.cn)

Reference

[1] Woo, S.L., et al., Biomechanics of Knee Ligaments: Injury, Healing, and Repair. *Journal of Biomechanics*, 2006. **39**(1): p. 1-20

SP014.4 - A new method for determining the effect of follower load on the range of motions in the lumbar spine

Author(s): Cheng-Fei Du¹, Junchao Guo¹, Yun-Peng Huang², Yubo Fan^{*3}

¹School of Biological Science and Medical Engineering, Bei-hang University, Beijing/CHINA, ²Department Of Orthopaedics, First Affiliated Hospital, FuZhou/CHINA, ³School of Biological Science and Medical Engineering, Key Laboratory for Biomechanics and Mechanobiology of Ministry of Education, National Key Lab of Virtual Reality Technology, Beihang University, Beijing/CHINA

In this study, a new method of applying follower load in finite element (FE) model of lumbar spine was presented. The effect of follower load on the range of motions (ROM) in lumbar spine was also investigated. A three-dimensional nonlinear FE model of lumbar spine (L1-S1) has been developed and validated. Connector elements between each pair of endplates were created to apply follower load. The endpoints of each connector were close to the center of endplate. The follower load of 0N, 500N, 800N, 1200N were respectively applied to explore their influence on the motion response of lumbar spine to the moment of 7.5NM in three principle planes (extension, flexion, right bending, left bending, right torsion, left torsion). The results showed that the direction of follower load was almost along with the curvature of spine and induced very small segmental motion. The follower load made the ROM of lumbar spine slightly increase in extension, while produced the decrease in ROM in other five moments. This stiffening effect became more obvious with an increase in the follower load. The largest percent decrease in motion of lumbar spine due to pre-load was in left torsion (47%), and then right torsion(42%), right lateral bending (21%), left lateral bending(20%), flexion(11%).

SP015 - Other Radiation Oncology: Part 1

TRACK 04: RADIATION ONCOLOGY

SP015.1 - Beta Enhancers: towards a local dose enhancer device for Boron Neutron Capture Therapy (BNCT) on superficial tumors

Author(s): Esteban F. Boggio¹, Juan Longhino¹, Lucas Provenzano², Rubén Farías², Sara González², Susana Nievas³, Alejandra Dagrosa²
¹Reactor And Radiation Physics - Bariloche Atomic Center, Atomic Energy National Commission, San Carlos de Bariloche/ARGENTINA, ²National Council of Scientific and Technical Research, Ciudad Autónoma de Buenos Aires/ARGENTINA, ³Constituyentes Atomic Center, Atomic Energy National Commission, Buenos Aires/ARGENTINA

Introduction. BNCT is a cancerous cells selective, non-conventional radiotherapy modality to treat malignant tumors such as glioblastoma, melanoma and recurrent head and neck cancer. It consists of a two-step procedure: first, the patient is injected with a tumor localizing drug containing a non-radioactive isotope (Boron-10) with high slow neutron capture cross-section. In a second step, the patient is irradiated with neutrons, which are absorbed by the Boron-10 agent with the subsequently nuclear reaction B-10(n, α)Li-7, thereby resulting in dose at cellular level due to the resulting high-LET particles. The Argentine clinical facility for superficial tumors treatment is located at the RA-6 Research Reactor (Bariloche Atomic Center). The neutron beam designed provides a slow neutron flux maximum at approximately 1 cm depth. Due to the penetration of the beam, the total absorbed dose in the first few millimeters of the tissue is lower than in the maximum. Thus, the introduction of a suitable device over the irradiated area to allow a local dose increase without substantially perturbing the primary in-depth dose profile is considered in this work. Some materials for the suggested devices such as Rhodium, Silver and Indium have advantageous properties: a high neutron capture cross-section with fast decay activation products and high energy beta particles emission. As beta radiation has a short penetration range in tissue, it can be used to compensate the superficial dose gradient of the BNCT treatment, or even increase it significantly. These devices are called Beta Enhancers (BE).

Material and Methods. BE are modeled in Monte Carlo (MCNP), with their own characteristic beta emission for each case, to determine those candidates that minimize perturbation effects in the original therapeutic beam and significantly improve the local depth absorbed dose profiles. In order to validate these models, experimental measurements are carried out using radiochromic films and thermoluminescence detectors (TLD) in-depth of a solid phantom with BE positioned on their surface. The validated particle sources are then evaluated in the retrospective treatment planning of selected nodular melanoma treatments of the Argentine BNCT patients. Finally, BE were implemented in a Nude mice cancer model for BNCT that were carried out at the RA-6 facility, in order to preliminarily assess toxicity and efficacy. Nude mice were separated into five groups of 6-9 animals each one: control group, NCT (without boron agent) irradiation, NCT + BE irradiation, BNCT irradiation and BNCT + BE irradiation.

Results. The simulations and its experimental correlations show good agreement, validating thus the computational models of the BE particle sources. Retrospective patient treatment planning and Dose-Volume Histograms show considerably improvement of the local absorbed dose on the treated cancerous tissue. Nude mice cancer model experiment demonstrated the BE efficacy, especially between NCT group and NCT + BE groups. There was no evidence of toxicity.

Conclusions. Beta Enhancers show to be a complementary tool to improve the BNCT of very superficial tumors cases, without significant perturbation of the primary neutron beam used for the treatment.

SP015.2 - Nanoparticle Enhanced Radiation Therapies: Is There a Synergy with Chemotherapies?

Author(s): Linda J. Rogers¹, Herman Hau², Wojciech Chrzanowski², David R. Mckenzie³, Nataka Suchowerska¹

¹Radiation Oncology, Chris O'Brien Lifehouse, Sydney/AUSTRALIA, ²Faculty Of Pharmacy, University of Sydney, Sydney/AUSTRALIA, ³School Of Physics, University of Sydney, Sydney/AUSTRALIA

Introduction

Nanoparticles can enhance the radiation dose, but have exhibited cytotoxicity, which is highly dependent on the ability of nanoparticles to penetrate the cell membrane and accumulate within the cell. Both radiation enhancement and nanoparticle uptake is regulated by the nanoparticle surface characteristics, their size and chemical composition. The goal of this study is to identify the individual and combined synergistic toxicity of radiation therapy and chemotherapy with gold nanoparticles (GNPs). The existence of a synergy would enable the radiation dose and the systemic dose from chemotherapy drugs to be reduced, thereby reducing side effects. Local treatment efficacy, through the synergistic coupling with nanoparticles, would be enhanced.

Method

For the human colon adenocarcinoma (LoVo) cell line, the clonogenic survival response was determined for a 50 kVp beam produced by a Pantak and a 6 MV beam produced by a Varian Novalis linear accelerator, for the chemotherapy drug 5-fluorouracil (5-FU) and for GNPs of diameter 4 nm for a range of concentrations. The GNPs were manufactured using precipitation method and stabilised with PEG. The therapies were combined in pairs to identify individual synergies first, then all three (radiotherapy, nanoparticles and chemotherapeutic) were combined to establish cumulative effects.

Results

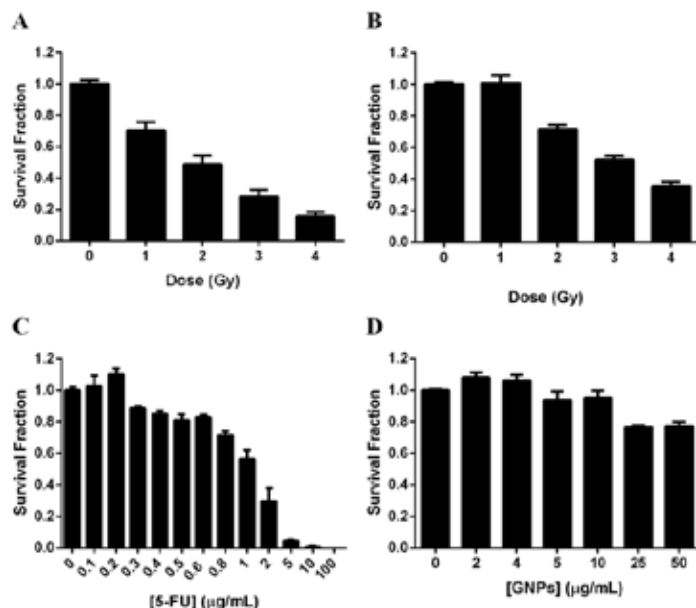


Figure 1: Clonogenic cell survival dose response of LoVo cells to A: 50kVp radiation beam; B: 6MV radiation beam; C: 5-FU; and D: GNPs.

Radiation doses for both energy beams and concentrations of GNPs and 5-FU were chosen such that in combination a paired total loss in cell survival was predicted on the basis of no synergistic effects to be of approximately 50%. The doses used were 1 Gy (kV radiation), 2 Gy (MV radiation), 0.5 µg/mL 5-FU and 50 µg/mL GNPs. It was found that the cells are more sensitive in the kV beam than in the MV beam for the same dose (Figure 1A & 1B), the result of differences in LET. The 5-FU and GNPs at very low doses appear to cause an increase in clonogenic survival however this is not statistically significant.

Conclusion

The nanoparticle toxicity was measurable but small and was concentration dependent. The response to kV radiation produced a greater decrease in survival than MV radiation. The 5-FU response was determined and 50% survival was approximately 1 µg/mL. These results lay the groundwork for synergistic effects. In vivo studies will confirm the translation of our findings.

SP015.3 - Change in Hounsfield Units due to lung expansion as a predictor of LAD and heart displacement in patients undergoing deep inspiration breath hold for left sided breast cancer

Author(s): Peta Lonski¹, David Jolly¹, Boon Chua², Damien Philips³, Maria Portillo³, Steven David², Amanda Philips³, Tomas Kron¹

¹Physical Sciences, Peter MacCallum Cancer Center, Melbourne/AUSTRALIA, ²Department Of Radiation Oncology, Peter MacCallum Cancer Center, Melbourne/AUSTRALIA, ³Radiation Therapy Services, Peter MacCallum Cancer Center, Melbourne/AUSTRALIA

Aim: Deep inspiration breath hold (DIBH) is a cardiac sparing technique for patients with left sided breast cancer undergoing external beam radiotherapy. Little work has been published on patient-specific quality assurance for DIBH. This study aims to assess the relationship between change in lung Hounsfield Units (HU) that occurs between a free breathing (FB) CT scan and deep inspiration breath hold (DIBH) scan and the displacement of the heart and left anterior descending (LAD) coronary artery from the radiation target volume.

Methods: Ten consecutive left sided breast cancer patients underwent a FB and a DIBH CT scan. A single clinician contoured the heart and LAD for all patients. The mean lung HU were sampled over a 2 cm (length) area spanning across the lung on the coronal plane above the diaphragm. For assessment of heart and LAD displacement, a line was drawn on the axial slice using the CT software between the medial and left lateral ball bearings to define a region of interest (reference line), which typically would correspond to a high dose region. The distance of the anterior aspect of the LAD, as well as the amount of heart present from this line was measured on both scans.

Results: The heart and LAD displacement measured from the reference line as a function of the relative change in HU is shown in Figure 1 and 2, respectively. Displacement was found to increase with relative change in HU for the left lung. There was no significant correlation with the right lung.

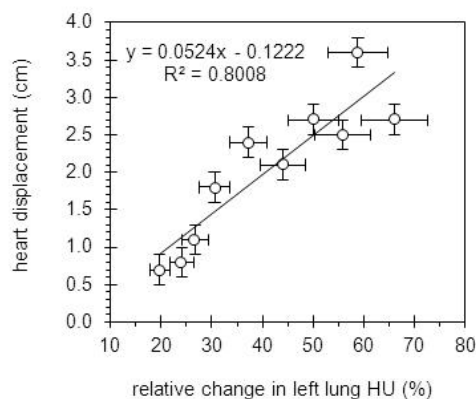


Figure 1 – heart displacement as a function of the relative change in left lung HU

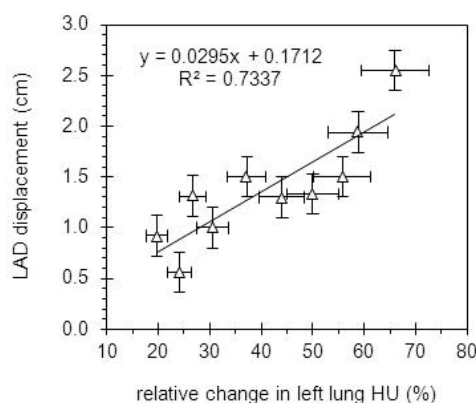


Figure 2 – LAD displacement as a function of the relative change in left lung HU

Conclusion: This study demonstrates that changes in HU of the left lung, which is a surrogate for lung expansion, could potentially be used to predict the heart and LAD displacement achieved in DIBH. Further studies would be required to validate these findings. This may have future implications for patient-specific quality assurance for DIBH.

SP015.4 - Samarium-153 Labeled Microparticles for Targeted Radionuclide Therapy of Liver Tumor

Author(s): Nurul A.A. Hashikin¹, Chai Hong Yeong¹, Basri Johan Jeet Abdullah¹, Kwan Hoong Ng¹, Lip Yong Chung², Rehir Dahalan³, Alan C. Perkins⁴

¹Department Of Biomedical Imaging, Faculty Of Medicine, University of Malaya, Kuala Lumpur/MALAYSIA, ²Department Of Pharmacy, Faculty Of Medicine, University of Malaya, Kuala Lumpur/MALAYSIA, ³Medical Technology Division, Malaysian Nuclear Agency, Bangi/MALAYSIA, ⁴Radiological And Imaging Sciences, University of Nottingham, Nottingham/UNITED KINGDOM

Introduction— Samarium-153 (¹⁵³Sm) is widely used in radiation synovectomy and pain management for patients with bone metastases due to its beta emissions. ¹⁵³Sm also emits gamma radiation of 103 keV which is suitable for imaging, as shown in previous studies. This provides a beneficial alternative for therapy with pure beta emitter, for example in liver radioembolization using Yttrium-90 (⁹⁰Y). This study aimed to explore the theranostics properties of ¹⁵³Sm in targeted radionuclide therapy of unresectable liver cancer.

Materials & Methods— The cation-exchange resin, Amberlite IR-120 H⁺ (Sigma Aldrich, USA) which is commercially available in large beads (620–830 μm), was crushed and sieved into size of 20–40 μm and labelled with 1 g of ¹⁵²SmCl₃ salt prior to neutron activation. Therapeutic activity of 3 GBq ¹⁵³Sm was aimed based on the standard activity used by the ⁹⁰Y SIR-Spheres. The samples were irradiated in 1.494 × 10¹² n.cm⁻².s⁻¹ neutron flux for 6 h. Characterization of the microparticles, gamma spectroscopy, and in-vitro radiolabelling studies were carried out and compared to a commercially available resin readily made in 20–40 μm, Fractogel EMD SO3⁻ (S) (Merck, Germany).

Results— Fourier Transform Infrared (FTIR) spectroscopy of Sm-Amberlite microparticles showed unaffected functional groups within the resin, following size reduction of the beads. However, the microparticles were irregular in shape as shown by the electron microscope. The radioactivity achieved after 6 h of neutron activation was 3.104 ± 0.029 GBq. The specific activity per microparticle for ¹⁵³Sm-Amberlite and ¹⁵³Sm-Fractogel were 55 Bq and 49 Bq, respectively. Gamma spectroscopy data showed that no radioactive impurities were detected in ¹⁵³Sm-Amberlite samples but there was a detectable amount of ²⁴Na in the ¹⁵³Sm-Fractogel samples. Furthermore, Energy Dispersive X-ray (EDX) spectroscopy of Sm-Fractogel showed presence of chlorine impurity but no significant impurities were observed in ¹⁵³Sm-Amberlite samples. Radiolabelling efficiency of ¹⁵³Sm-Amberlite tested in distilled water and blood plasma were excellent (99.9 and 96.9%, respectively) whilst ¹⁵³Sm-Fractogel showed lower labelling efficiency (92.3 and 92.9%, respectively) over a test period of 48 h.

Discussion— Despite the irregular shape due to mechanical grinding of the resin, ¹⁵³Sm-Amberlite formulation showed excellent radiolabelling efficiency and no impurities were detected during the labelling and neutron activation processes. In comparison, the presence of chlorine and ²⁴Na in Sm-Fractogel formulation as well as its lower radiolabelling efficiency make it less suitable to be used for radioembolization of the liver tumour.

Conclusion— ¹⁵³Sm-Amberlite microparticles presented suitable characteristics for liver radioembolization as an alternative to ⁹⁰Y. It has advantage over the ⁹⁰Y for being able to do post-procedure imaging to estimate treatment efficacy. Dosimetric study needs to be carried out to estimate radiation dose contributed by the gamma radiations from the ¹⁵³Sm. Further animal studies are also needed to verify its in-vivo distribution, and biochemical stability.

SP015.5 - Anatomical Modelling of the Pregnant Radiotherapy Patient

Author(s): Tanya Kairn¹, Scott Crowe², Joanne Mitchell¹, David Schlect³, Jamie Trapp⁴

¹Physics, Genesis CancerCare Queensland, Auchenflower/AUSTRALIA, ²Radiation Oncology, Royal Brisbane and Women's Hospital, Herston/QLD/AUSTRALIA, ³Radiation Oncology, Genesis Cancer-Care Queensland, Auchenflower/AUSTRALIA, ⁴Science And Engineering Faculty, Queensland University of Technology, Brisbane/AUSTRALIA

In any case where the use of external beam radiotherapy (EBRT) to treat a pregnant patient is unavoidable, it is important that the radiation dose to the developing fetus is evaluated as accurately as possible. Fetal dose estimates are needed when making treatment planning decisions, when designing personalized radiation shielding and when providing the pregnant patient with an appropriate risk assessment.

Sophisticated models for calculating dose throughout the body have been used for radiation protection and nuclear medicine since the 1960s, however due to the easy availability of patient CT data, the easy availability of patient CT data makes the development of similar

models for EBRT treatment dose calculations obsolete, in most clinical situations. For pregnant patients however, the abdominal anatomy is routinely excluded or shielded, during the acquisition of the treatment planning CT, and therefore cannot be included in out-of-field dose calculations.

This study therefore aimed to take existing anatomical models of pregnant women, currently used for radiation protection and nuclear medicine dose calculations, and adapt them for use in the calculation of fetal dose from external beam radiotherapy (EBRT).

The models investigated were 'KATJA', which was provided as an MCNPX geometry file, and 'RPI-P6', which was provided in a simple, voxelized binary format. In-house code was developed, to convert both models into an 'egsphnt' format, suitable for use with the BEAMnrc and DOSXYZnrc Monte Carlo codes. The geometries and densities of the resulting phantoms were evaluated and found to accurately represent the source data.

As an example of the use of the phantoms, the delivery of a cranial EBRT treatment was simulated using the BEAMnrc and DOSXYZnrc Monte Carlo codes and the likely out-of-field doses to the fetus in each model was calculated. All sources of out-of-field dose (radiation leakage from the linac head, scatter of the primary beam from the linac head and the intervening air, and scatter of the primary beam within the patient) were included in the simulation.

The results of these calculations showed good agreement (within one standard deviation) between the doses calculated in KATJA and RPI-P6, despite substantial anatomical differences between the two models. For a 36 Gy prescription dose to a 233.2 cm³ target in the right brain, the mean doses calculated in a region of interest covering the entire uterus were 1.0 +/- 0.6 mSv for KATJA and 1.3 +/- 0.9 mSv for RPI-P6.

This work is expected to lead to more comprehensive studies of EBRT treatment plan design and its effects on fetal dose in the future. The novel codes developed for this study may also be used to produce EBRT Monte Carlo simulation files from other radiation safety models, including pediatric patients of various ages.

SP016 - Image Guided RT: Part 1

TRACK 04: RADIATION ONCOLOGY

SP016.1 - ¹⁸F-NaF PET/CT-directed dose escalation in stereotactic body radiotherapy for spine oligometastases from prostate cancer

Author(s): Lili Wu¹, Sandi A. Kwee², Mei Li¹, Xun Peng¹, Liangxi Xie¹, Zhixiong Lin¹, Hui Wang³, Yu Kuang³

¹Radiation Oncology, Cancer Hospital of Shantou University Medical College, Shantou/CHINA, ²John A. Burns School Of Medicine, University of Hawaii, Honolulu/HI/UNITED STATES OF AMERICA, ³Department Of Medical Physics, University of Nevada Las Vegas, Las Vegas/NV/UNITED STATES OF AMERICA

Purpose: To investigate the technical feasibility of SBRT dose painting using ¹⁸F-NaF positron emission tomography (PET) scans guidance in patients with spine oligometastases from prostate cancer.

Materials/Methods: Six patients with 15 spine oligometastatic lesions from prostate cancer who had ¹⁸F-fluorine PET/CT scan prior to treatment were retrospectively included. GTVreg was delineated according to the regular tumor boundary shown on PET and/or CT images; and GTVMATV was contoured based on a net metabolically active tumor volume (MATV) defined by 60% of the SUVmax values on ¹⁸F-NaF PET images. The PTVs (PTVreg and PTVMATV) were defined as respective GTVs (plus involved entire vertebral body for PTVreg) with a 3-mm isotropic expansion margin. Three 1-fraction SBRT plans using VMAT technique along with 10 MV flattened filter free (FFF) beams (Plan24Gy, Plan24-27Gy, and Plan24-30Gy) were generated for each patient. All plans included a dose of 24 Gy prescribed to PTVreg. The Plan24-27Gy and Plan24-30Gy also included a simultaneous boost dose of 27 Gy or 30 Gy prescribed to the PTVMATV, respectively. The feasibility of ¹⁸F-NaF PET-guided SBRT dose escalation was evaluated by its ability to achieve 100% of the prescription dose to cover at least 90% of the PTV volume while adhering to organs-at-risk (OARs) dose constraints.

Results: In all 33 SBRT plans generated, the planning objectives and dose constraints were met without exception. Plan24-27Gy and Plan24-30Gy had a significantly higher dose in PTVMATV than Plan24Gy ($p < 0.05$), respectively, while maintaining a similar OARs sparing profile.

Conclusion: Using VMAT with FFF beams to incorporate a simultaneous ¹⁸F-NaF PET-guided radiation boost dose up to 30 Gy into a SBRT plan is technically feasible without violating normal tissue tolerances. The relationship between local control and normal tissue toxicity during ¹⁸F-NaF PET-guided dose escalation in SBRT should be validated in clinical trials.

SP016.2 - Evaluation of a lung tumor autocontouring algorithm for intrafractional tumor tracking using 0.5T linac-MR: phantom and in-vivo study

Author(s): Jihyun Yun, Eugene Yip, Zsolt Gabos, Keith Wachowicz, Satyapal Rathee, B Gino Fallone
Medical Physics, Cross Cancer Institute, Edmonton/CANADA

We developed an autocontouring algorithm for intrafractional lung-tumor tracking using linac-MR, and evaluate its performance with phantom and *in-vivo* MR images.

A pulse-coupled neural network is the main component of the algorithm responsible for tumor contrast improvement from its surrounding anatomy (normal lung, blood vessels). Prior to treatment, an expert user needs to contour the tumor and its maximum anticipated range of motion in pretreatment MR images. During

treatment, however, the algorithm processes each intrafractional MR image and automatically generates a tumor contour without further user input. The algorithm is designed to produce a tumor contour that is the most similar to the expert's one.

To evaluate the algorithm in our linac-MR environment (0.5T MRI), a motion phantom and four lung cancer patients were imaged with 3T MRI at ~4 frames per second, and the images were degraded to reflect the image quality characteristic of lung tumor MR images at 0.5T. During scanning (~3 minutes), the phantom was driven according to four different 1-D motion patterns (sine pattern with 4 cm amplitude, 4 seconds period + three lung tumor motion patterns), and the patients were in free breathing. Each of these pseudo-0.5T images was autocontoured using our algorithm. In each test image, the Dice's coefficient (DCE) and Hausdorff distance (HD) between the expert's manual contour (ROI_{std}) and the algorithm generated contour (ROI_{auto}) were calculated to measure their similarity, and their centroid position difference ($\Delta d_{centroid}$) was calculated.

Our algorithm successfully contoured the shape of a moving tumor from pseudo-0.5T MR images. Example images are shown in Fig. 1, and the autocontouring accuracy is summarized in Table 1. From the *in-vivo* study, we achieved 87–92 % of contouring agreement and centroid tracking accuracy of 1.03–1.35 mm. These results demonstrate the feasibility of lung tumor autocontouring in our laboratory's linac-MR environment.

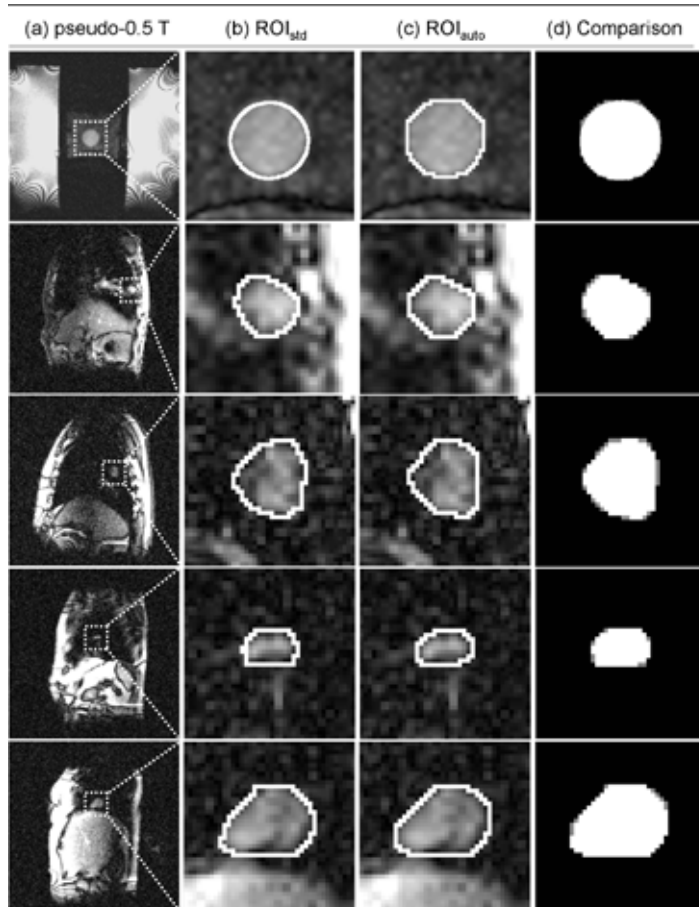


FIG.1. Example images of the phantom (top row) and four patients (bottom three rows). Column (a): pseudo-0.5T images. Column (b) and (c): ROI_{std} and ROI_{auto}. Column (d): comparison between ROI_{std} and ROI_{auto} (overlapping region is shown in white pixels, whereas any deviation is indicated by gray pixels). Each example image (from top to bottom) showed DCE of 0.97, 0.95, 0.97, and 0.98, respectively.

Table 1. Summary of contour shape fidelity and centroid position accuracy							
Mean(SD)		DCE		HD (mm)		$\Delta d_{centroid}$ (mm)	
		Max/Min	Mean(SD)	Max/Min	Mean(SD)	Max/Min	
Phantom	Sine	0.95(0.01)	0.97/0.93	2.82(0.39)	4.02/1.95	0.93(0.29)	2.04/0.23
	1	0.96(0.01)	0.97/0.94	2.61(0.32)	3.60/1.41	0.68(0.24)	1.40/0.04
	2	0.96(0.01)	0.97/0.94	2.61(0.26)	3.60/1.75	0.73(0.24)	1.40/0.03
	3	0.96(0.01)	0.97/0.93	2.68(0.29)	3.60/1.75	0.74(0.24)	1.87/0.05
Patient	1	0.90(0.03)	0.97/0.76	3.38(0.95)	6.43/1.56	1.04(0.53)	3.77/0.05
	2	0.89(0.03)	0.95/0.76	4.35(1.26)	9.49/1.56	1.35(0.71)	4.08/0.02
	3	0.87(0.05)	0.98/0.66	3.13(1.41)	7.95/1.56	1.03(0.63)	3.79/0.01
	4	0.92(0.03)	0.98/0.83	4.11(1.49)	11.03/1.56	1.31(0.70)	4.00/0.06

SP016.3 - Multi-modal image registration for MR-guided radiotherapy workflow based on detection of features in a customized stereotactic body frame

Author(s): Paul Mercea¹, Asja Pfaffenberger¹, Markus Stoll¹, Gernot Echner¹, Armin Runz¹, Regula Gnirs², Florian Sterzing³, Tilmann Bostel³, Rolf Bendl⁴

¹Division Of Medical Physics In Radiation Oncology, German Cancer Research Center (DKFZ), Heidelberg/GERMANY, ²Division Of Radiology, German Cancer Research Center (DKFZ), Heidelberg/GERMANY, ³Department Of Radiation Oncology, University Hospital Heidelberg, Heidelberg/GERMANY, ⁴Faculty Of Medical Informatics, Heilbronn University, Heilbronn/GERMANY

Introduction

Shuttle-based MR-guided radiation therapy with separate MR imaging and treatment devices requires both reproducible patient immobilization and robust multi-modal image registration. In the MR-guidance study [1] currently conducted at our institution a customized stereotactic body frame (CSBF) was developed to facilitate image registration. The aim of this work is to develop an algorithm for fast detection of features in the CSBF in order to support image registration for assessment of patient setup alteration.

Methods

The CSBF is equipped with a long (600mm) and a short (80mm) hose (inner diameter 2mm) filled with contrast agent. The former is bent in its middle at an angle of 28.07° surrounding the latter which is centered horizontally (see Fig.1). Image data of one patient from the MR-guidance study cohort has been selected for evaluation. Besides the treatment planning CT, Cone-Beam CTs (CBCTs) and their corresponding T2 weighted MR images (MRIs) from 16 fractions were used. To identify lines representing the hoses in the images, a probabilistic Hough transform on thresholded gradient image slices is performed in posterior-anterior direction. Detected line pairs oriented towards each other most akin to a notional isosceles triangle formed by a straight line representing the short hose and two lines representing the tapering ends of the long hose are further analyzed. The image data is traversed along the triangle's edges in search of local intensity maximums. Principle component analysis of the detected maximum intensity distribution enables refinement of the detected lines. Eventually, line intersections are re-calculated and used for landmark-based rigid registration.

Results

Evaluation of the algorithm was performed by registration of the detected points from each MRI and CBCT with interactively placed reference points in the planning CT. For the 16 MRIs the mean root mean square registration error (RMSRE) was 0.78mm and for the 16 CBCTs 0.97mm. Additionally, each MRI was matched to its corresponding fraction CBCT resulting in a mean RMSRE of 0.65mm. Registration results were also assessed qualitatively by visual inspection (see Fig.1).

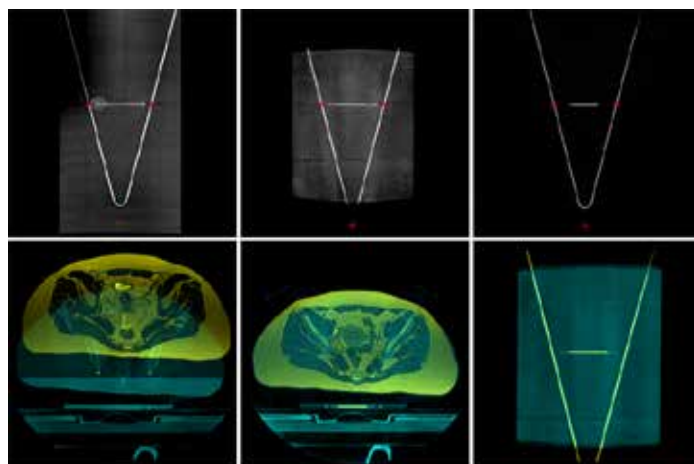


Fig. 1: Top row: Contrast agent filled hoses with detected features (red crosses) in CT (left), CBCT (middle) and T2 weighted MRI (right). Bottom row: Unregistered fusion of fraction CBCT (cyan) and MRI (yellow) (left); Registration result in transversal view (middle) and in coronal view (right). hoses in CBCT and MRI are accurately aligned in both orientations.

Conclusions

An algorithm for multi-modal detection of characteristic features in a CSBF was developed. Accurate results and robust performance on 32 image data sets were achieved. The benefits from incorporating this algorithm, as a preprocessing step, for patient position correction will be evaluated in future research.

Acknowledgements

This research was supported by the German Research Foundation (DFG), SFB/TRR 125.

References

[1] Bostel et al., "MR-guidance—a clinical study ..." Radiation Oncology 2014, 9:12

SP016.4 - A phantom study of impact of probe metal artifact in planning dose for ultrasound-guided radiotherapy

Author(s): Lin Su¹, Sook Kien Ng¹, Yin Zhang¹, Iulian Iordachita², John Wong¹, H T. Sen³, Peter Kazanzides³, Muyinatu A. Lediju Bell³, Kai Ding¹

¹Department Of Radiation Oncology, Johns Hopkins University, Baltimore/UNITED STATES OF AMERICA, ²Department Of Mechanical Engineering, Johns Hopkins University, Baltimore/MD/UNITED STATES OF AMERICA, ³Department Of Computer Science, Johns Hopkins University, Baltimore/MD/UNITED STATES OF AMERICA

Image guided radiotherapy (IGRT) is gaining popularity in radiation oncology. Among different IGRT imaging modalities, ultrasound (US) is portable, affordable, and non-ionizing. To monitor the abdominal organ motion during IGRT, we previously developed a probe holder to reproduce the simulation probe position during treatment. However, the metallic parts inside the probe caused artifacts in the CT images (see Fig. 1). This work quantifies the influence of metal artifacts on the treatment plan.

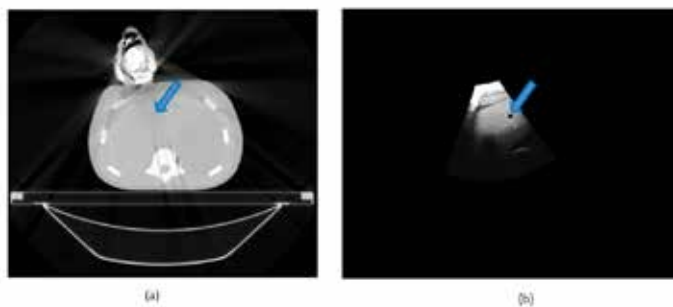
A CIRS Triple Modality 3D Abdominal Phantom (model 057A) including kidneys, lung, and liver, with six tumors inside the liver was scanned using Phillips Brilliance Big Bore CT both with and without the probe in place. A passive arm was used to hold the probe with minimum pressure applied to avoid any phantom deformation. The CT scan without the probe was used for treatment planning in Pinnacle 9.8. Six tumors with distance 60~127 mm to the probe and organs at risk were contoured. Individual plan was made for each tumor. All tumors were prescribed to receive 4000 cGy dose in five fractions. Two VMAT partial arcs avoiding the US probe were

adopted based on the fused CT image. After treatment planning on the CT without US probe, the beams for each tumor were copied to corresponding plan for dose calculation in CT scan with probe and associated metal artifact. The dose difference between two plans due to voxel density variation from CT artifacts was evaluated.

Minimal dose discrepancy was observed between two plans created with and without the probe in place, as shown in Table 1. All six tumors had less than 0.8% mean dose difference due to metal artifact. These results indicate the probe artifacts have minimal impact on treatment planning dose calculation, particularly when the tumor is relatively distant to the probe.

Table 1: The PTV volume, tumor distance to probe, mean PTV dose and PTV dose difference between two plans for six tumors in the liver.

	tumor1	tumor2	tumor3	tumor4	tumor5	tumor6
PTV volume [cm ³]	7.26	2.97	7.84	3.11	2.48	2.30
Tumor distance to probe [mm]	87.2	87.9	61.0	60.4	145.2	127.8
mean PTV dose to plan with probe [cGy]	4126	4182	4134	4093	4153	4240
mean PTV dose to plan without probe [cGy]	4142	4151	4121	4088	4157	4245
mean PTV dose difference [%]	0.39	-0.73	-0.31	-0.10	0.08	0.11



Objectives: This software tool was built to handle reference CT (rCT) and MR (rMR) images from treatment simulation as well as guidance CBCT and MR (gMR) images from daily image guidance. Key design goals include: (i) support various data formats such as DICOM CT, DICOM MR, DICOM spatial registration objects; (ii) provide communication and data flow between different imaging, treatment and storage devices; (iii) perform accurate and robust image registration; (iv) provide a user-friendly graphical interface for users to manipulate data and assess registration quality; and, (v) output couch coordinate shift information to correct patient position for treatment.

Methods: We designed the software to import reference CT and MR images as well as guidance CBCT and MR images from the Mosaic Data Director (MDD), accurately register the guidance MR image to the reference MR, and export couch correction information to the Varian external interface to drive the couch to the correct position. Furthermore, we have developed storage capability to save all patient data, images, and registrations as a DICOM secondary capture, which allows us to re-examine the case and study the MR-guidance performance over time.

Results: All image data from the simulated workflow were successfully loaded into our software tool. Registration of the reference MR to the guidance MR was successful with resulting mean squared errors (MSE) for the four phantom shifts of 0.23 mm, 0.40 mm, 0.11 mm, and 0.10 mm. Registration of the corresponding CT images was also successful with resulting MSE of 0.35mm, 0.21 mm, 0.33mm, and 0.26mm. Couch corrections were generated based on the registration information and exported. Finally, each test case was saved as a DICOM file and stored within the database.

Conclusions: In this study, we demonstrated the successful implementation of a comprehensive image-guidance tool for the MRgRT system in the 3D Slicer platform. We plan to use this tool to study the MRgRT system's performance in guiding patient positioning based on soft tissue contrast and develop novel applications to enhance the clinical value of MR-guidance in radiation therapy.

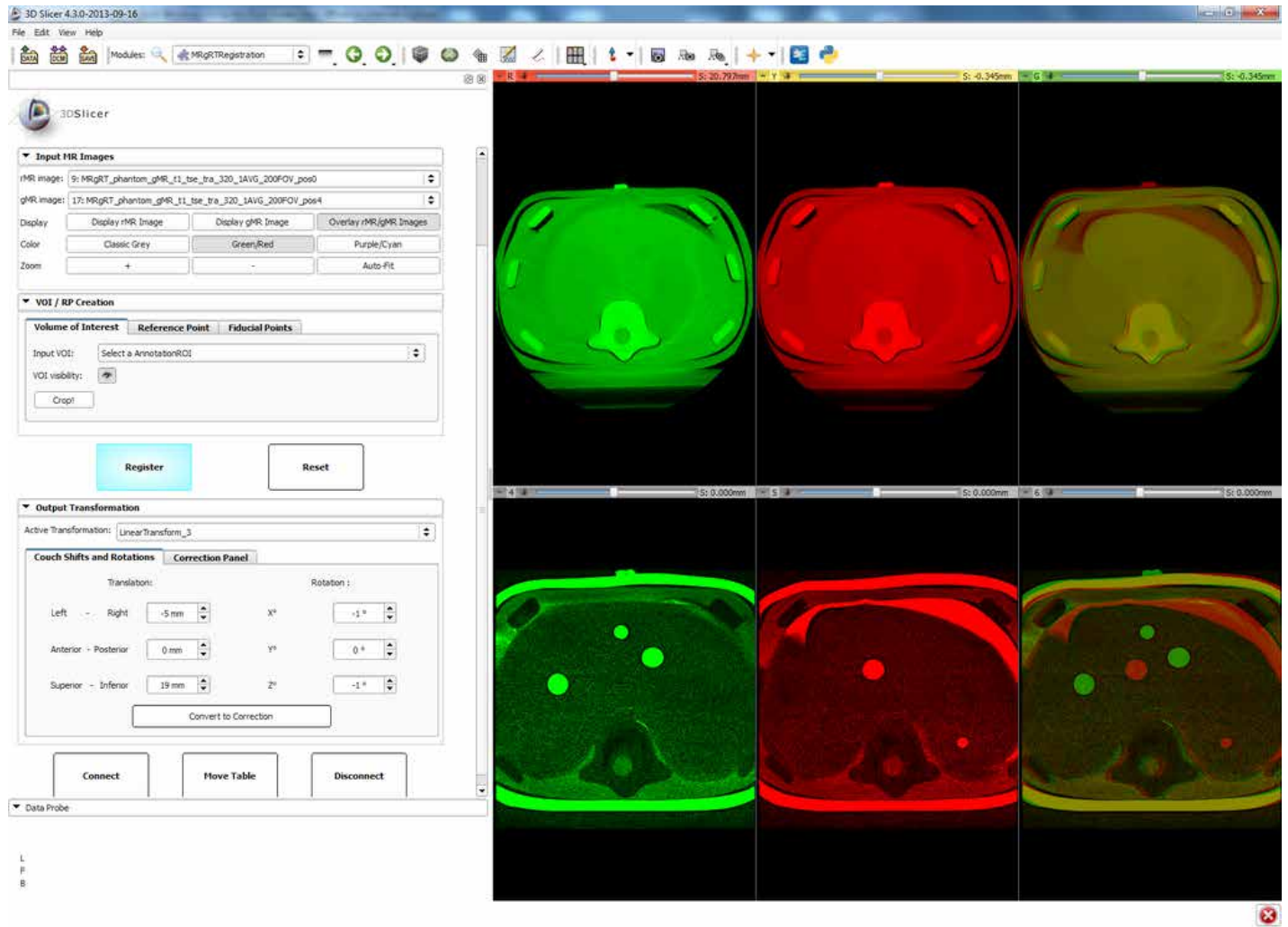
SP016.5 - Software development for image guidance on the magnetic resonance-guided radiation therapy (MRgRT™) system

Author(s): Wenyao Xia¹, Stephen L. Breen², An Wang², David Jaffray²

¹Radiation Physics, Princess Margaret Hospital, Toronto/CANADA, ²Radiation Medicine, Princess Margaret Hospital, Toronto/ON/CANADA

Background: The magnetic resonance-guided radiation therapy (MRgRT™) system utilizes a moveable MRI system to provide image-guidance in a linear accelerator (Linac) vault. By exploiting the superior soft tissue contrast available with MR-guidance, our goal is to provide more accurate patient positioning based on internal soft tissue. To implement cone beam CT (CBCT) and MR guidance effectively, we developed a novel software tool using the 3D Slicer platform.

Figure 1.



SP016.6 - Ultrasound guided radiotherapy with rotational correction for patient setup: a feasibility study

Author(s): Sook Kien Ng¹, Lin Su¹, Yin Zhang¹, Iulian Iordachita², John Wong¹, H T. Sen³, Peter Kazanzides³, Muyinatu A. Lediju Bell³, Kai Ding¹

¹Department Of Radiation Oncology, Johns Hopkins Univesity, Baltimore/MD/UNITED STATES OF AMERICA, ²Department Of Mechanical Engineering, Johns Hopkins University, baltimore/MD/UNITED STATES OF AMERICA, ³Department Of Computer Science, Johns Hopkins University, baltimore/MD/UNITED STATES OF AMERICA

Ultrasound guided radiotherapy is a promising IGRT modality due to its features of no-ionizing and high soft tissue contrast. The Clarity ultrasound system (Elekta, Stockholm, Sweden) has been successfully used in our clinic for real time intra-fraction motion monitoring in prostate SBRT. However, current Clarity system does not have feedback to treatment machine with patient rotational correction. This study aims to investigate the feasibility of applying Clarity system for ultrasound guided patient setup with rotational correction.

In this study, we used a six-degree-freedom robotic patient positioning system, HexaPOD (Elekta, Stockholm, Sweden). Both HexaPOD and Clarity utilize infrared markers and camera for room coordinate positioning. To integrate both systems, the Clarity infrared camera was installed in parallel with HexaPOD camera. A prostate phantom and an ultrasound calibration phantom were secured and aligned to the isocenter. US probe abutting the phantom was fixed via the transperineal ultrasound base plate (Figure 1). A 3D image of the phantom was captured first as patient simulation day ultrasound. Three different rotation levels were used in this study. For the first rotation, we rotated the couch by 1 degree on roll, pitch and yaw. For the second and third levels, 2 and 2.5 degrees were applied. After each rotation, an ultrasound image was acquired as patient treatment day ultrasound. Four ultrasound scans were acquired for each phantom and exported to Velocity (Varian, Palo Alto, CA) for manual image registration analysis (Figure 2).

Minimal rotational discrepancy was found between the actual rotation applied by HexaPod and the analysis from Velocity. The average rotation difference is 0.034 degree for the prostate phantom and 0.026 degree for the calibration phantom. These results show ultrasound images acquired by Clarity system are able to recover rotation correction which can be potentially be sent back to HexaPOD for clinical patient rotation correction.



SP017 - Calculational Techniques in Therapy Dosimetry

TRACK 05: DOSIMETRY AND RADIATION PROTECTION

SP017.1 - Dosimetric Effect of Beam Angle on the Unflattened and Flattened Photon Beams: A Monte Carlo study

Author(s): James Chow¹, A Owrangi²
¹Princess Margaret Cancer Center, Toronto/CANADA, ²University of Michigan Health System, Ann Arbor/UNITED STATES OF AMERICA

This study compared the variations of depth and surface dose on beam angle between the unflattened and flattened photon beams. Monte Carlo simulation based on the EGSnrc code was used in dose calculation. Phase-space files of the 6 MV photon beams (field size = 10 X 10 cm²) were generated with and without the flattening filter based on a Varian TrueBeam linear accelerator. Depth and surface doses were calculated in a water phantom with angles of the photon beams turning from 0° to 15°, 30°, 45°, 60°, 75° and 90°. Our results showed that compared to the flattened photon beam, the unflattened beam had a higher dose in the build-up region but lower dose beyond the depth of maximum dose. With the Monte Carlo beams cross-calibrated to the machine monitor unit in simulations, dose ratios of the unflattened to flattened beams were in the range of 1.6 – 2.6 as shown in Figure 1 with beam angles varying from 0° to 90° in water. In addition, higher surface doses of about 2.5 times were found (Figure 2) with beam angles equal to 0° and 15°. However, surface dose deviation between the unflattened and flattened beam became smaller with an increase of beam angle. Using the photon fluence incorporated to the monitor unit, variations of depth and surface dose on the beam angle were investigated and compared. For the unflattened and flattened photon beams, the surface dose and range of depth dose ratios (unflattened to flattened beam) decreased with an increase of beam angle.

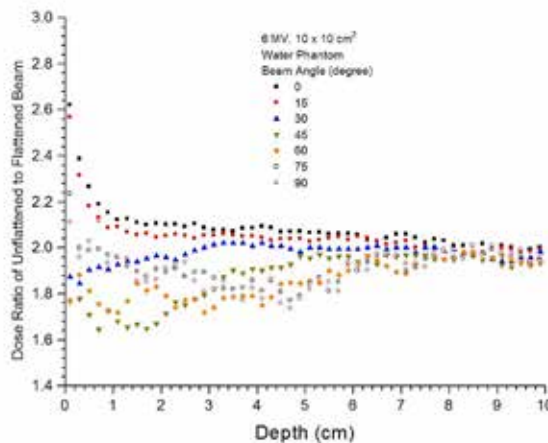


Fig. 1: Relationship between the dose ratio (unflattened to flattened photon beams) and depth.

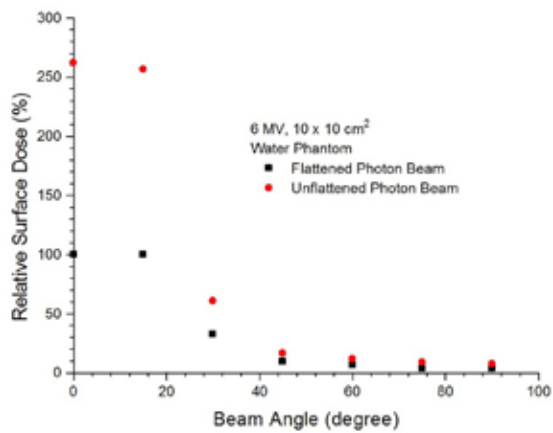


Fig. 2: Relationship between the relative surface dose and beam angle for the 6 MV unflattened and flattened photon beams.

SP017.2 - Monte Carlo calculations and measurements of the TG-43U1 recommended dosimetric parameters for the ^{125}I (Model IR-Seed2) brachytherapy source

Author(s): Hassan Ali Nedaie¹, Sahar Sheikholeslami², Mohsen Hasani², Ali S. Meigooni³

¹Radiotherapy Oncology Department, Cancer Research Centre, Cancer Institute, Tehran University of Medical Sciences, Tehran/IRAN, ²Azad University, Department of Engineering, Science and Research Branch, Islamic Azad University, Tehran/IRAN, ³Comprehensive Cancer Centers of Nevada, Las Vegas/UNITED STATES OF AMERICA

Abstract

Purpose: Recently a new design of the ^{125}I (Model IR-seed2) brachytherapy source has been manufactured for prostate seed implant. Figure 1 show a schematic diagram of this source. The goal of this project is to evaluate the dosimetric characteristics of this source model using experimental and Monte Carlo simulation methods following the recommendation of Task Group 43 of the American Medical Physicist in Medicine (AAPM).

Methods: Dosimetric characteristics of IR-seed2 were determined by using experimental and Monte Carlo simulation methods according to the recommendation by Task Group 43(TG-43U1). The simulations were performed using MCNP5 in water and Plexiglas, and measurements were performed using TLD-GR207A chips dosimeters in Plexiglas Phantom. The Plexiglas data is used for verification of the accuracy of the source and phantom geometry used in the Monte Carlo simulations. The final MC simulated data in water would be recommended for the clinical applications. The experimental setup for measurement of radial dose function and anisotropy function is shown in Fig. 2 and 3.

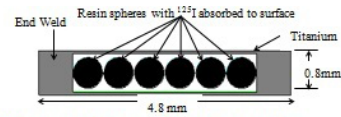


FIG. 1. Schematic diagram of the ^{125}I (Model IR-seed2) brachytherapy source.

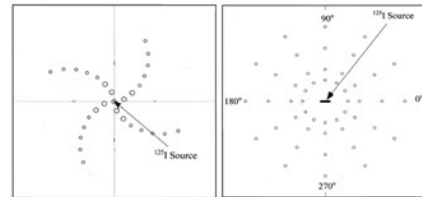


FIG.2. Schematic diagram of the experimental setup for measurement of radial dose function (Left) and 2D anisotropy function (right).

Results: The Monte Carlo calculated dose rate constant Λ of the ^{125}I in water was found to be $0.992 \pm 0.025 \text{ cGyU}^{-1}\text{h}^{-1}$. Radial dose functions of the new source model based on point and line source approximations were calculated at distance ranging from 0.1 to 7 cm. Moreover, $gL(r)$ was measured in Plexiglas phantom material using TLD chips. In addition, the 2D anisotropy function, $F(r,\theta)$, were calculated and measured in both Plexiglas and water phantom.

Conclusions: The results of these investigations show an agreement of about $\pm 7\%$ between the measured and simulated data in Plexiglas. The statistical uncertainty of MC within $\pm 5\%$ relative to the previously published data for different brachytherapy sources.

Based on the results, the Monte Carlo simulated dosimetric parameters of the new ^{125}I source in water are recommended for their clinical applications.

SP017.3 - Assessment of RayStation treatment planning algorithm to calculate dose in the presence of lung tissue

Author(s): Manuel Rodriguez, Mohammad Rezaee, Steve Bartolac, Jean-Pierre Bissonnette
Department Of Radiation Oncology, University of Toronto, Toronto/CANADA

Purpose: To investigate the accuracy of RayStation treatment planning algorithm to calculate absorbed dose when the photon beam is disturbed by attenuation or lateral scatter of lung material.

Materials:

A farmer type ion chamber was placed in the center of $30 \times 30 \times 20 \text{ cm}^3$ water phantom with a 5 cm lung material slab at 3 cm from the chamber when the beam was perpendicular to the lung slab and at 1 cm from the chamber when the beam was parallel to the lung slab. A $\text{SSD}=100\text{cm}$ PDD curve was also measured placing a Gafchromic EBT2 film in the interface of the solidWater-lungSlab with the lung slab parallel to the beam and starting at 10 cm depth. Measurements were taken for 6 and 18 MV photon beams and for 10×10 , 5×5 and $3 \times 3 \text{ cm}^2$ field sizes. The ratio of the dose with and without the lung slab is reported.

Results:

The ratio of the measured dose with and without the lung slab ($D_{\text{lung}}/D_{\text{sw}}$) is within 1% of that ratio calculated by RayStation algorithm for all energies and field sized used when the beams are parallel and perpendicular to the lung slab (table 1). The PDD curves measured with gafchromic film with and without the presence of lung slab agree with those calculated by RayStation algorithm within the uncertainty of the measurements (figure 1), which is within 3%.

Conclusion:

Raystation dose calculation algorithm takes into account inhomogeneity corrections. It models attenuation of the beam and lateral scatter within 1% of points measured with ion chambers. PDD curves in the presence of lung material also agree with gafchromic film measurements within the uncertainty of the measurements. Therefore, RayStation has an acceptable algorithm to correct dose from photon beams perturbed by lung tissue.

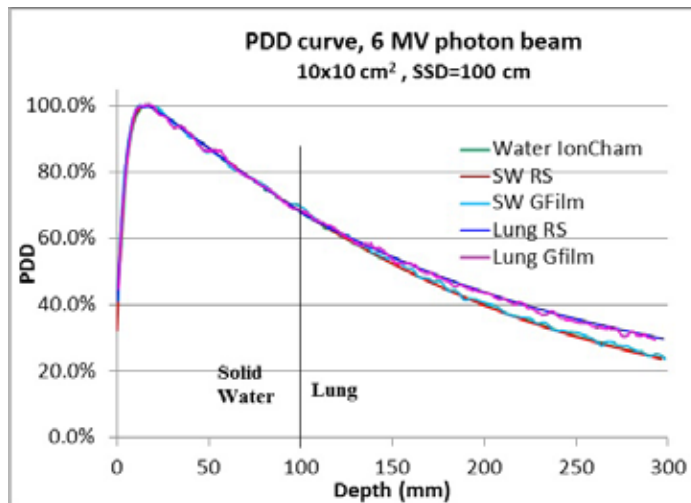


Figure 1.

Table 1. Ratio of the measured dose in solid water with and without the lung slab related to the same ratio calculated by RayStation treatment planning algorithm.

field size	Atten.	Atten.	Lat. scatt	Lat. Scatt
(cm ²)	6 MV	18 MV	6 MV	18MV
10x10	0.9%	0.5%	0.4%	0.4%
5x5	1.0%	0.2%	-0.5%	-0.3%
3x3	1.0%	0.4%	0.6%	0.2%

SP017.4 - Improving the efficiency of charged particle transport in magnetic fields in EGSnrc

Author(s): Victor Malkov, David W.O. Rogers
Department Of Physics, Carleton University, Ottawa/CANADA

Image Guided Radiation Therapy (IGRT) technologies aim to improve the accuracy of the delivery of radiation with the hopes of decreasing damage to healthy tissues and sensitive organs. Synergistic MRI-Radiation therapy machines are a developing technology that can provide improved tumour tracking during treatment to help accommodate for patient motion or unaccounted for bodily changes over the full course of treatment. Porting the advantages of MRI technology into IGRT comes with the cost of introducing a magnetic field around the patient while a radiation beam is present. This

magnetic field (MF) causes curvature in the charged particle trajectory, and can lead to significant variations in dose distributions, particularly at tissue-air interfaces, and lead to changes in the dose response of detectors. Our aim is to evaluate our implementation of the influence of the MF in the EGSnrc Monte Carlo code system, and deliver a detailed study of the increased computational requirements of our code. Monte Carlo (MC) codes have become a staple in radiation treatment planning systems, and are extensively used in radiation dosimetry and Medical Physics research. The EGSnrc code, a popular general purpose MC package used in Medical Physics, previously supported charged particle transport in magnetic fields, but in the transition from EGS4 this feature of the code went untested. Our implementation is based a framework similar to the one originally proposed by Bielajew, but we have introduced a higher order integration algorithm for the condensed history mode and made use of the single scatter algorithm in the EGSnrc code. To properly handle region transitions, additional changes were made related to the boundary crossing algorithm. These alterations lead to a reduction in the total required computational time compared to the previous implementation since larger step sizes can be taken during the simulation. These improvements prove crucial since the original theory required strict step size reduction which can lead to two to 30 fold increases in computation time as compared with the 25% to 50% increases with the current algorithm. The presented results will highlight ion chamber calculations as a function of magnetic field strength and step size constraints to demonstrate the importance of proper selection of system parameters to obtain accurate solutions. These results will be of particular benefit for groups looking to make use of the EGSnrc code or another MC package for calculating dose distributions in the presence of magnetic field. The improved computational efficiency of the presented code reduces the need for large computational facilities, making it a valuable research tool for investigating the effects of magnetic fields on radiotherapy treatments.

SP017.5 - Accurate Monte Carlo dose calculations for permanent implant prostate brachytherapy: first results from a large scale retrospective study

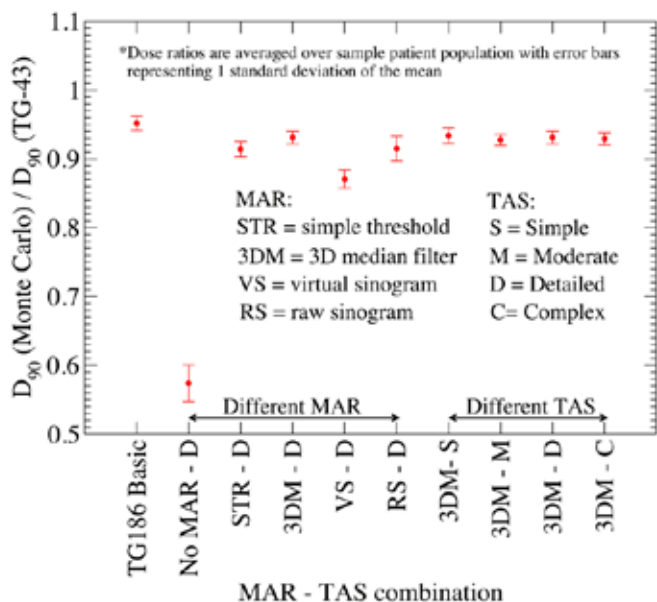
Author(s): Nelson Miksys¹, Eric Vigneault², Luc Beaulieu³, Rowan Thomson¹
¹Department Of Physics, Carleton University, Ottawa/CANADA, ²Université Laval Cancer Research Centre, Quebec City/CANADA, ³Department De Physique Et Centre De Recherche En Cancerologie, Université Laval, Quebec City/CANADA

Recently, the joint AAPM-ESTRO-ABG-ABS TG-186 report endorsed Monte Carlo (MC) dose calculations for brachytherapy as they are more accurate than the traditional TG-43 water-based paradigm. MC dose calculations require accurate patient-specific computational models often derived from post-implant CT images. We have explored issues related to the accurate modelling of the patient geometry by investigating algorithms to mitigate seed artifacts in addition to comparing detailed schemes for mapping image CT numbers to tissue type and mass density in the MC models. Here, we present our advanced MC patient-specific modelling approaches and initial dosimetric results of the first large retrospective MC dose calculation study (of approximately 1000 patients).

The EGSnrc user-code BrachyDose is employed for MC dose calculations of clinical prostate brachytherapy. Seed artifacts are mitigated by applying a metallic artifact reduction (MAR) algorithm to post-implant CT images. Artifact-mitigated images are used to derive MC phantoms by applying one of several tissue assignment schemes (TAS) mapping voxel CT number to tissue composition and mass density. MC-calculated dose distributions and clinical dose metrics for the target and OARs (organs-at-risk) are compared to each other (between different MAR and TAS models) and to TG-43 water-based calculations.

In the target, D90 calculated following the TG-43 approach is about 5% higher than the basic TG-186 MC approach which assigns average soft tissue compositions and uniform mass densities, and up to 15% higher than more accurate MC models that realistically account for calcifications and tissue heterogeneities. Failing to mitigate artifacts and then employing a TAS which assigns calcification results in inaccurate models with seeds encased in calcification and a D90 which is over 40% lower than TG-43 and over 30% lower than more accurate MC models. The application of different MAR methods can change the D90 by over 5%, but typically by only a few percent. Changes in the TAS, including the modelling of calcifications and organ at risk tissues, changes the D90 by a few percent with larger differences in highly calcified patients. OAR doses can vary by tens of percent depending on the assigned tissue compositions.

This work has employed state-of-the-art patient-specific MC models yielding dose calculations that are more accurate than TG-43 and basic TG-186 recommendations. This large-scale retrospective study will enable investigation of correlation between dose and treatment outcome, in addition to assessment of potential changes to prescription dose with the adoption of advanced model-based dose calculations for brachytherapy.



SP017.6 - Analytic modelling of in-field and out-of-field bremsstrahlung contamination dose in high energy electron beams used in external radiotherapy

Author(s): Mohamad Mohamad Alabdoaburas¹, Dimitri Lefkopoulos², Jean Pierre Mège², Jean Chavaudra², Atila Veres³, Florent De Vathaire², Ibrahima Diallo²

¹University of Paris-Sud(11), Orsay/France, ²Medical Physics, Gustave Roussy, Villejuif Cedex/France, ³Equal-Estro laboratory, Villejuif Cedex/France

Introduction

Bremsstrahlung dose component becomes important when scattering dual-foils and scrapers applicators are used, as compared to scanned electron beams and cone applicators. Several studies have been reported on bremsstrahlung dose component inside the irradiation field. The aim of this study is to develop an analytical model for the assessment of the bremsstrahlung dose distribution at any point in the patient in-field and out-of-field.

Materials and methods

The bremsstrahlung dose component in electron beams arises from four main sources considered in our model: scattering dual-foils, collimator jaws, applicator’s scrapers and insert of cerrobend. We have neglected the bremsstrahlung generated in the patient. Our model consists in two main parts: in the first part, we calculate the angular energetic fluence distribution for every bremsstrahlung photon source, using an existing model based on a multi-scattering theorem. In the second part, we calculate the relative number of pixels irradiated by the primary electron beam in every bremsstrahlung photon source. All programmings were executed by Matlab. All detailed information about the geometry, material composition, and size of each component have been provided by the manufacturers. Most of the data on the electrons interactions with matter are based on ICRU-1984 data. Measurements of bremsstrahlung dose component were achieved with TLD-700 powder thermoluminescent dosimeters, from 0 cm to 70 cm from the beam central axis, at a depth of 10 cm in a water phantom for a Varian 2300C/D Linac, operated at 6,9,12 and 18MeV.

Results

We demonstrate that out-of-field bremsstrahlung dose is essentially produced by applicator’s scrapers, while the out-of-field bremsstrahlung dose generated in scattering dual-foils can be neglected. In-field bremsstrahlung dose comes essentially from scattering dual-foils, which represents 70%-80% of total in-field bremsstrahlung dose. Our modelling results show a very good agreement between calculated and measured values, in-field and out-of-field. The average difference between calculated and measured values is less than 10%, which represent a very small difference in absolute dose.

Conclusion/perspective

Our approach can be used to provide a good representation of bremsstrahlung dose distributions in all healthy tissues for any applicator size and type and for any electron beam energy used in high-energy electron beam therapy.

SP018 - Small Animal Research Technologies

TRACK 06: NEW TECHNOLOGIES IN CANCER RESEARCH AND TREATMENT

SP018.1 - New Technologies in Cancer Research and Treatment

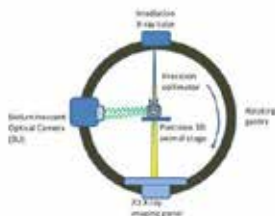
Author(s): Frank Verhaegen¹, Stefan Van Hoof², Patrick V. Granton², Sanaz Yahyanejad³, Marc Vooijs³, Chris Vanhove⁴, Ludwig Dubois³
¹Radiotherapy Physics, Maastricht Clinic, Maastricht/NETHERLANDS, ²Physics, London Regional Cancer Program, London/ON/CANADA, ³Maastricht Lab, University Maastricht, Maastricht/NETHERLANDS, ⁴Medisip, University Ghent, Ghent/BELGIUM

The current state-of-the-art in radiotherapy (RT) is precision fractionated irradiation of tumors, with intended sparing of the surrounding normal tissue. To achieve this, highly accurate methods to aim radiation beams with complex static or dynamic shapes have been developed. In addition, various forms of anatomical and functional imaging (e.g., CT, PET, MR) have been integrated with the irradiation technology to achieve accurate targeting and dose verification. This integration was achieved using complex treatment planning software. These innovations are largely responsible for improved cancer treatment outcomes in recent years, rather than an improved fundamental insight in radiation response of normal and cancer tissues.

To gain more fundamental insight, and also to allow investigating the combination of radiation and other cancer agents, recently much progress was made towards developing advanced small animal combined irradiation/imaging platforms. The recent availability of small animal image-guided precision radiotherapy devices (Fig 1) in a growing number of centers is currently revolutionizing preclinical research. Researchers now can perform SmART (Small Animal RadioTherapy) research with devices that combine precise irradiation with high-resolution imaging in one system; the concept of image guided RT (IGRT). The essential components of a SmART research platform are: precision animal positioning, precision irradiation with small photon beams, onboard CT imaging and onboard bioluminescent imaging, all in the same coordinate system. In addition, an accurate treatment planning software for small animals, SmART-Plan, was developed at our institute. We recently added inverse planning capabilities to SmART-Plan to improve workflow and standardization of preclinical studies.

Several preclinical trials have been initiated at our institute. As an example, we used precision image-guided irradiation of the upper right lung lobes of 76 C57BL/6 adult male mice, with doses of 0-20 Gy. We used image registration and image analysis in this longitudinal study to establish a dose response for radiation-induced lung fibrosis. It was found that the mice were more resistant for high doses of radiation when small beams are used (in the literature, often large field irradiation preclinical studies are reported). This is one of the first studies where accurate irradiation and image analysis are used on such a scale. Many other experiments are being performed or planned now.

The final aim is to identify those combined novel treatments that have the best chance of success for clinical translation. In this work, we will report on the progress of the research in this new field at our institute.



Schematic overview of SmART research platform. At the center of the system the specimen is located on a precision stage. The large ring can rotate around the specimen and holds a precision irradiator, an x-ray imaging panel to acquire a CT scan, and a bioluminescence camera to collect emitted photons from internal markers for biological processes.

SP018.2 - Longitudinal MRI evaluation of whole brain radiotherapy on brain metastasis development and dormancy in a mouse model

Author(s): Donna H. Murrell, Niloufar Zarghami, Michael D. Jensen, Ann F. Chambers, Eugene Wong, Paula J. Foster
 Medical Biophysics, Western University, London/ON/CANADA

A major challenge in breast cancer treatment is its ability to metastasize – commonly to liver, lung, bone, and brain – thereby complicating detection and therapy. When cancer cells arrive at distant sites, they may experience different fates: (1) death, (2) proliferation creating metastases, or (3) dormancy (remaining viable but non-proliferative).

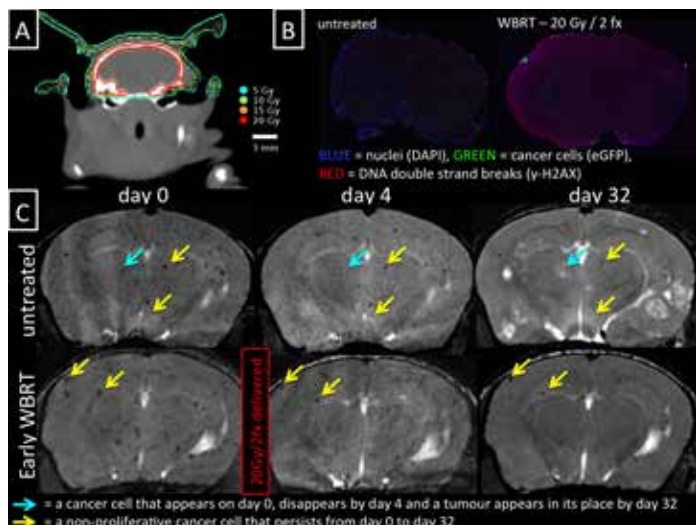
This work uses high-resolution anatomical and iron-labelled cellular MRI techniques developed in the Foster lab (Heyn *et al.*, Magn Reson Med, 2006) to monitor cancer cell fate in the brain during metastasis progression. We combine this with image-guided micro-irradiation techniques developed in the Wong lab (Jensen *et al.*, Med Phys, 2013) to investigate the growth of brain metastatic breast cancer and concurrent responses of metastases and dormant cancer cells to whole brain radiotherapy (WBRT).

The micro-CT/RT system was commissioned for mouse WBRT (20 Gy/2fx) using a collimated field of 10x14 mm and a parallel-opposed beam set-up. A Monte Carlo dose verification calculation was performed to confirm this plan [A]. Tumour morphology and proliferation were assessed by *ex vivo* tissue staining (H&E, Ki67). γ -H2AX staining for DNA double strand breaks confirmed biological damage to the whole brain post-irradiation [B].

Two animal experiments were performed (n=24): (1) 'Late' WBRT delivered when MRI-detectable tumours had developed; this is similar to the case of clinical diagnosis, or (2) 'Early' WBRT given following initial cancer cell arrest in the brain, prior to tumour growth.

'Late' WBRT was able to halt tumour growth. At 11 days post-therapy, the average volume of a treated tumour was significantly smaller than untreated ($p < 0.01$); however, the number of MRI-detectable tumours did not decrease and some tumours continued to grow.

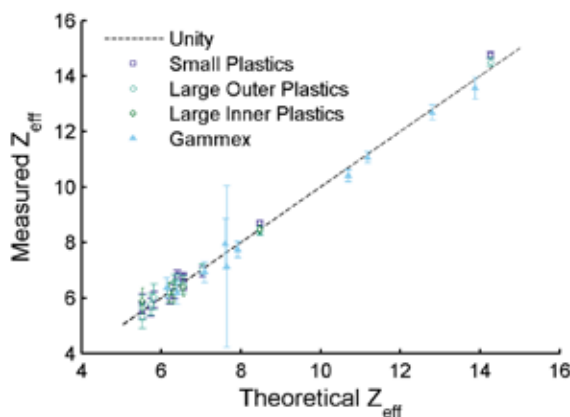
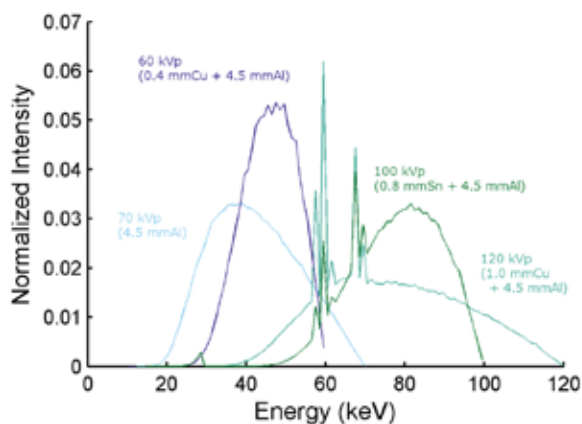
'Early' WBRT was more effective than 'late' and was able to eradicate nearly all tumours [C]. The number of metastases and total tumour volume in treated brains were significantly less than untreated ($p < 0.05$). There was a reduction in the number of MRI signal voids (from solitary iron-labeled cancer cells) over time; however, there was no significant difference between groups at any time point. Signal voids from non-viable cells are cleared from the brain; therefore, residual signal voids observed here are potentially viable dormant cells. This suggests dormant cancer cells can persist and are potentially viable, even if WBRT is delivered very early and has eliminated the tumour burden. Further investigation of the dormant cell population is warranted as these may respond to future proliferation signals and contribute to cancer recurrence.



SP018.3 - Dual energy micro-CT determination of effective atomic number and electron density

Author(s): Michael D. Jensen¹, Jeff Z. Chen², Eugene Wong¹
¹Medical Biophysics, Western University, London/CANADA, ²London Regional Cancer Program, London Health Science Center, London/CANADA

Dual energy micro-CT could improve dose calculation accuracy in small animal image guided radiotherapy by providing the effective atomic number (Z_{eff}) and electron density of tissue. A new CMOS detector with improved detective quantum efficiency has enabled us to narrow the spectrum of the dual energy scans and reduce polyenergetic artefacts in the source images. This allowed us to replace the previous pairing of 70 kVp (4.5 mmAl) and 120 kVp (1.0 mmCu + 4.5 mmAl) by 60 kVp (0.4 mmCu + 4.5 mmAl) and 100 kVp (0.8 mmSn + 4.5 mmAl). We scanned four custom-made micro-CT phantoms of two sizes (three 2.54 cm, one 6.08 cm in diameter) constructed of 11 plastic materials. Twelve electron density inserts from a clinical phantom were also scanned. A previously published image space spectral algorithm for determining Z_{eff} and relative electron density was applied to the micro-CT images. Previous results with the old detector and energy spectrums (70 kVp, 120 kVp) showed beam-hardening artefacts, with the mean percent difference between Z_{eff} theory and measurement of 3.2% for the small phantoms, and 7.8% for the large phantom. With the new detector and aggressively filtered energy spectra (60 kVp, 100 kVp), the mean percent difference between Z_{eff} theory and measurement was 2.2% for the small phantoms and 2.0% for the large phantom. For the clinical electron density inserts, the mean percent difference between theory and measurement improved from 6.0% to 2.9% for Z_{eff} , and 4.5% to 2.8% for relative electron density. The improved performance of the new detector comes at the cost of increased acquisition time, as multiple low dose frame averages are need to reduce photon statistics noise. In conclusion, a new CMOS detector has allowed micro-CT imaging with narrower energy spectra and improved determination of the effective atomic number and relative electron density.



SP018.4 - Tissue characterization using dual energy cone beam CT imaging with a dedicated small animal radiotherapy platform

Author(s): Patrick V. Granton¹, Guillaume Landry², Mathieu Gaudreault³, Frank Verhaegen⁴
¹Physics, London Regional Cancer Program, London/ON/CANADA, ²Department Of Medical Physics, Ludwig-Maximilians-University, Munich/GERMANY, ³Département De Radio-oncologie, CSSS de Chicoutimi, Chicoutimi/CANADA, ⁴Radiotherapy, Maastric Clinic, Maastricht/NETHERLANDS

Purpose

There is a growing number of preclinical image-guided high-precision conformal irradiation devices tailored to small animal geometries. Typically, 225kVp is used as the treatment photon energy. A potential error in the dose prescription lies in the dose calculation phase where there is uncertainty in the tissue composition. Dual-energy CT (DECT) provides estimates of the effective atomic number Z_{eff} and the relative electron density r_e when two CT images are acquired at different energies. As Z_{eff} describes tissue composition; DECT of small animals could yield 1) information on the adequacy of approximating mouse tissues by tabulated human compositions and 2) improved tissue assignment for Monte Carlo-based dose calculation algorithms. The goal of this work was to optimize the selection of kVp-pairs, and investigate a recent DECT algorithm for robustness, accuracy, and precision using a dedicated small animal irradiation platform.

Materials

Two mouse-sized phantoms, one acting as DECT calibration and the other as DECT validation, were custom-made from inserts of the

Gammex (RMI467) and CIRS (062MQA) electron density calibration phantoms, respectively. The phantoms were imaged using a pre-clinical irradiator (XRAD225Cx, PXI) for a series of kVp settings (40-100) in increments of 10 kV. The exposures were adjusted to yield air kerma equivalent imaging dose of 30 cGy for each kVp. Images were decomposed into Zeff and re for each kVp pair and compared against referenced values. The best energy pair was chosen on the basis of accuracy and noise for both Zeff and re . The experimental DECT imaging was compared against simulations using a CT software package (ImaSim) with different amounts of image noise. DECT imaging of a dead mouse, plasticized mouse, and a human heart was performed and assessed.

Results

The 40-80 kVp pair was identified as the optimal DECT protocol, yielding a mean errors of $0.9 \pm 2.6\%$ on Zeff and $0.8 \pm 1.8\%$ on re ; simulation results were similar.

Conclusion

We have implemented DECT for an optimal small animal imaging protocol, enabling tissue characterization for dose calculation of preclinical radiotherapy studies. Using known tissue-like materials for the DECT calibration are important aspects in achieving accurate DECT imaging.

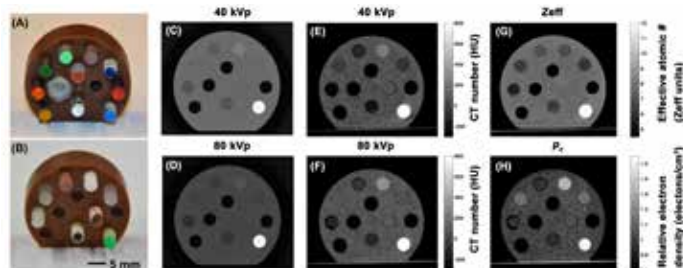


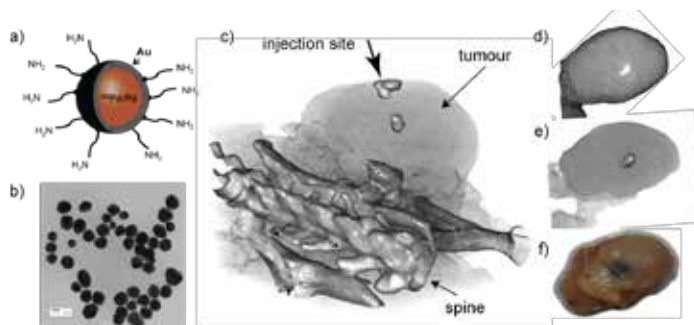
Figure 1 (A,B) Photos of the calibration and validation phantom; (C,D,E,F) Simulated and experimental images of the validation phantom; (G,H) Zeff and re images of the calibration phantom. The average noise within the CT images was 15HU.

SP018.5 - Low-dose prostate cancer brachytherapy by injections of radioactive gold nanoparticles ($^{103}\text{Pd}:\text{Pd}@\text{Au}$ NPs)

Author(s): Myriam Laprise-Pelletier, Diane Djoumessi, Jean Lagueux, Marie-France Côté, Marc-André Fortin
Axe Médecine Régénératrice, Centre de recherche du centre Hospitalier Universitaire de Québec, Québec/CANADA

Here we report on the development of a new approach for low-dose prostate cancer brachytherapy, based on the injection of radioactive $^{103}\text{Pd}:\text{Pd}@\text{Au}$ NPs. Photons emitted by the radioisotope palladium (^{103}Pd ; photon energy : 20.1 and 23.0 keV), interacting with gold distributed in the vicinity of and inside cells, are expected to lead to higher energy deposition compared with conventional low-dose brachytherapy. A rapid (~4h), one-pot procedure was developed to synthesize ultra-small $^{103}\text{Pd}:\text{Pd}$ nanoparticles (radioactive precursor: $^{103}\text{PdCl}_2$, MDS Nordion, Canada), followed by encapsulation with gold (Figure 1a-b; nanoparticle diam.: ~ 40 nm). Thus-obtained core-shell nanoparticles were stabilised with biocompatible polyethylene glycol (NH₂-PEG-SH), purified and concentrated by centrifugation. The tumour retention of $^{103}\text{Pd}:\text{Pd}@\text{Au}$ -PEG NPs was studied in a PC3 prostate cancer xenograft model (n = 11). For this, the NPs were labeled with a moderate (sub-therapeutic) labeling activity level (4 μCi $^{103}\text{Pd}/\text{mmol}$ Au; 2 μL / injection). The animals were CT-scanned immediately after implantation, then at time-points (1 and 8 days). The $^{103}\text{Pd}:\text{Pd}@\text{Au}$ NPs injection sites were clearly

identified and delineated on CT data obtained from each one of the implanted tumours. Volume reconstruction was performed on each injection site (Figure 1c-e), in order to quantify Au NP diffusion. At $t = 2\text{h}$ (n = 3), 1 day (n = 4) and 8 days (n = 8), the tumours were harvested and radioactivity-counted. An organ biodistribution study was also performed (liver, spleen, kidneys, lungs). In 8/11 animals, the total activity retention in the tumours was higher than 80% of the total activity in the animal ($93.2\% \pm 7.7\%$). After 8 days, the % of total activity retained in the tumours, was ($92.0\% \pm 12.1\%$). Liver activities higher than 20% of the total animal activity were found in 3 animals, indicating that, in some injection and tumour conditions (e.g. vascularization of the tumour, interstitial fluid pressure), a fraction of Au NPs is taken up by the vasculature and immune cell processes, ending up in the organs associated to the reticuloendothelial system (liver, spleen). In resume, $^{103}\text{Pd}:\text{Pd}@\text{Au}$ -PEG NPs were efficiently synthesized (rapidity, reaction yield, colloidal stability, NPs concentration, purification), injected in prostate cancer tumours, and efficiently visualised in CT. In the perspective of clinical applications, the liver and spleen Au NP uptake must be adequately controlled by using either a polymeric or a molecular cancer cell targeting strategy to secure the retention of NPs in tumours.



SP019 - Nanobiosensors and Nanotheranostics

TRACK 08: BIOSENSOR, NANOTECHNOLOGY, BIOMEMS AND BIOPHOTONICS

SP019.1 - Synthesis and evaluation of C595 mAb-conjugated SPIONs nanoprobe for specific detection of Prostate cancer

Author(s): Mohammad Abdolahi¹, Sophie Laurent², Lionel Laro-banoix², Corine Sermeus², Sebastien Boutry³, Robert N Muller²
¹Persian Gulf Nuclear Medicine Research Center, Bushehr University of Medical Sciences, Bushehr/IRAN, ²General, Organic And Biomedical Chemistry, University of Mons, Mons/BELGIUM, ³Center for Microscopy and Molecular Imaging, Charleori/BELGIUM

Introduction: Carcinoma of the prostate is the most frequent diagnosed malignant tumor in men and is the second leading cause of cancer-related death in this group. Despite the efficacy of local therapy (surgery or radiation therapy) for treating localized disease, the cure rate is highly dependent on the stage of disease at the diagnosis and early detection of prostate cancer is key to designing effective treatment strategies. However, in its early stages, PC rarely causes symptoms and the majority of men diagnosed with advanced PC at the time of diagnosis. New detection methods are needed for prostate cancer, particularly for metastatic disease, in order to provide patients the best possible staging and treatment. The objective of the present study is to locate primary tumors or distant metastases using MRI with contrast agents targeted specifically to cancer cells. We take advantage of the fact that many types of prostate cancer cells express high levels of mucin 1 (MUC1) oncoprotein on their cell surface. The imaging strategy is to use superparamagnetic iron oxide nanoparticles (SPIONs), attached to an antibody that directly target MUC1, to specifically enhance the contrast of MUC1-expressing prostate cancer cells. The use of antibody-conjugated MRI contrast agents to specifically target cancer cells has been demonstrated previously for some other cancers. Here, we demonstrate an MRI contrast agent targeted specifically to the MUC1-expressing prostate cancer cells.

Methods: A number of cell lines were chosen for MRI experiments: DU-145 cells, which express a high level of MUC1, and LNCaP cells, which do not express MUC1. Conjugation of Mab C595 (anti MUC1) to commercial SPIONs (Micromod, 20 nm diameter) was achieved by using a heterobifunctional linker, sulfo-SMCC. LNCaP and DU-145 cells incubated with conjugated SPIONs. In vitro and in vivo imaging was performed in a 7 T MRI system.

Conclusions: Results of this study showed that through functionalization of SPIONs by C595 monoclonal antibody specific binding of the SPIONs to the MUC1-expressing cells is achievable. With development of this and similar imaging specific vehicles, more effective and detailed diagnosis of prostate cancer through high concentrations of SPIONs at the tumors site is possible.

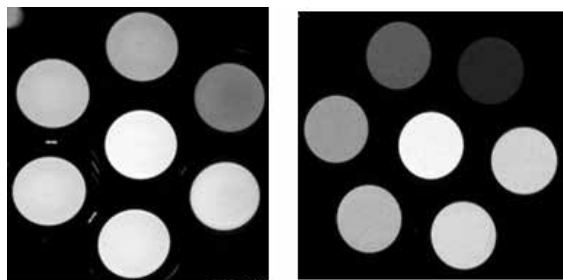


Fig1. T2-weighted imaging of LNCaP cells (3×10^6) after 2h incubation with SPIO-C595 nanoprobe (Left) and DU145 (Right) at Fe concentration of 0, 5, 10, 20, 40, 80 $\mu\text{g/ml}$ (The vial in the middle is PBS alone without any contrast agent).

SP019.2 - Magnetic Resonance Nanotheranostics of Guerin's Carcinoma

Author(s): Valerii E. Orej¹, Thanos Mitrelias², Marina Tselepi², Eugeny Kruchkov¹, Alexander Rykhalskiy¹, Andriy Romanov¹, Tatyana Golovko¹, Crispin H.W. Barnes², Igor Shchepotin¹
¹Medical Physics & Bioengineering Research Laboratory, National Cancer Institute, Kyiv/UKRAINE, ²Cavendish Laboratory, University of Cambridge, Cambridge/UNITED KINGDOM

We proposed a new technology of nanotheranostics that is combination of magnetic resonance therapy and chemotherapy during moderate hyperthermia below 40 °C inside tumor with diagnostics by magnetic resonance imaging. As nanotheranostics agent the multifunctional magnetosensitive nanocomplex consisted of nanoparticles containing Fe₃O₄ with diameters < 50 nm and antitumor drug doxorubicin was used. The synthesis of multifunctional magneto-sensitive nanocomplex was performed in a magnetomechanical reactor. We conducted a detailed imaging study of transplanted Guerin's carcinoma in rats during treatment with magnetic nanotherapy. We showed that treatment with magneto-mechano-chemically synthesized magnetosensitive nanocomplexes based on Fe₃O₄ nanoparticles conjugated with the antitumor agent doxorubicin and followed by irradiation with local electromagnetic irradiation resulted in a better outcome than treatment with conventional doxorubicin or treatment with magnetic nanocomplexes without electromagnetic irradiation. An analysis of magnetic resonance images obtained over time showed that the application of local electromagnetic irradiation did not alter the position of magnetic nanocomplexes in the tumor.

SP019.3 - Effects of Fluorescence Gold Nanoclusters on Anti-oxidation and Anti-aging by Cell Model

Author(s): Walter H. Chang¹, Wen Hsiung Chan², Nai Ruei Cyue¹, Cheng-An J. Lin¹

¹Department Of Biomedical Engineering, Chung Yuan Christian University, Taoyuan/TAIWAN, ²Department Of Biotechnology, Chung Yuan Christian University, Taoyuan/TAIWAN

We have developed gold nanoclusters (Au@DHLA, Diameter = 2nm) with red - NIR fluorescence and excellent biocompatibility as novel bioprobes. Moreover, we further found that Au@DHLA is not only a promising probe for cell labeling but also has the anti-oxidative stress properties and further improved cell viability. These novel findings indicate that Au@DHLA has a potential to reduce senescence and apoptosis. We observed the interaction of Au@DHLA with mouse osteoblasts, fibroblasts, and hepatocytes. Au@DHLA has been found to have rapid and efficient cell uptake into the mouse cells, although the toxicity analysis of mouse osteoblasts, fibroblasts and hepatocytes of the tolerance variation are not the same, but it is confirmed that Au@DHLA for mice cells has a good biocompatibility. In the experiment, we utilized the hydrogen peroxide that induced the increase of the oxidative stress of the mice cells then stained it with the dye (DCF-DA) and flow cytometry is used to observe Au@DHLA. We found the results of the intracellular oxidative stress in mice were reduced and the collagen detected in fibroblasts production in the known Au@DHLA does not affect the production. In detecting the ability of Au@DHLA of calcification experiments, we found that the low concentrations of Au@DHLA do not affect the ability of osteoblast calcification. We also found hepatocytes can generate the cholesterol, however Au@DHLA does not affect the hepatocytes. These study results demonstrated that

Au@DHLA has high potential to be developed as nanomaterials with anti-oxidation, anti-apoptosis and anti-aging properties for the application in medical research, aesthetic medicine, and regeneration medicine.

SP019.4 - Nanoparticle-aided Radiotherapy for Retinoblastoma and Choroidal Melanoma

Author(s): Yucel Altundal¹, Erno Sajo¹, G. M. Makrigrigors², Ross Berbeco², Wilfred Ngwa²

¹Physics & Applied Physics, University of Massachusetts Lowell, Lowell/UNITED STATES OF AMERICA, ²Radiation Oncology, DFCI/BWH/Harvard Medical School, Boston/UNITED STATES OF AMERICA

This work investigates the dosimetric feasibility of employing gold nanoparticles (AuNPs) or carboplatin nanoparticles (CNPs) to enhance radiotherapy (RT) treatment efficacy for ocular cancers: retinoblastoma (Rb) and choroidal melanoma (CM), during kV-energy internal and external beam radiotherapy. The results predict that substantial dose enhancement may be achieved by employing AuNPs or CNPs in conjunction with radiotherapy for ocular cancer using kV-energy photon beams. Brachytherapy sources yield higher dose enhancement than the external beam in kV energy range. However, the external beam has the advantage of being non-invasive.

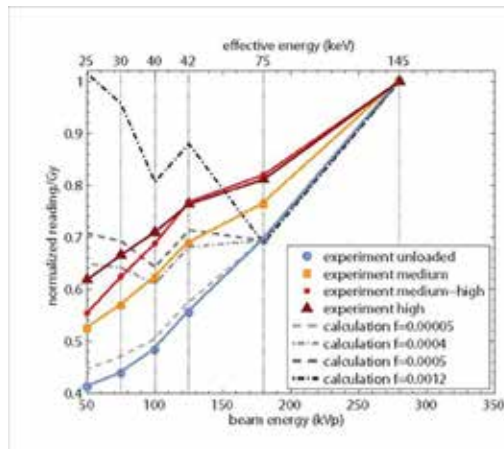
SP019.5 - Nanoparticle enhancement of radiation dose: experimental confirmation using scintillation dosimetry

Author(s): David R. McKenzie¹, Marie Christine Zdora¹, Paul Z.Y. Liu², Natalka Suchowska²

¹School Of Physics, University of Sydney, Sydney/AUSTRALIA, ²Radiation Oncology, Chris O'Brien Lifehouse, Sydney/AUSTRALIA

Nanoparticles of high atomic number enhance the radiation dose delivered and therefore are potentially useful in radiation therapy. The effects of beam energy and nanoparticle size on dose enhancement has been modelled using Monte Carlo and the response of cells has been measured *in-vitro*. However, for different cell-lines a range of responses has been observed, which are not always consistent with the Monte Carlo predictions. The aim of this study is to provide a direct measurement of the dose enhancement that is independent of the cytotoxicity of the particles or the manner in which cells take up the particles.

A composite was made using commercially available liquid scintillator (BC430 or BC 498) and gold nanoparticles (diameter 30nm, Nanopartz Inc). The scintillation light emitted during irradiation was used to evaluate the enhanced dose from the photoelectrons emitted from the nanoparticles. The samples were exposed to radiation beams with a range of energies (50kV, 75kV, 100kV, 125 kV, 180kV and 280kV). Some of the emitted light was absorbed by the nanoparticles and this effect was corrected for. The scintillation light was coupled into a PMMA fibreoptic and transferred to a photo multiplier tube (PMT) for readout. The PMT was calibrated to dose after subtracting the background signal consisting of Cerenkov, fluorescent and stray light. A theory was developed using photon absorption cross sections taken from the NIST XCOM database (Berger et al 1998).



The Figure shows the response of the organic liquid scintillator BC-498 per Gy of delivered dose normalized to 280 kVp for different volume fractions of gold nanoparticles. Theoretical curves (dashed) are the predicted enhancement for different volume fractions of gold nanoparticles and are based on monoenergetic effective energies. The experimental data was obtained with polyenergetic beams. It was found that the scintillator response became less energy dependent for higher nanoparticle loading. However the trend in preferential dose enhancement at lower energies, as predicted by theory, was not well reproduced by experiment. This result suggests that the assumption in the theory, that all photoelectrons are released from the nanoparticles into the surrounding medium is not valid.

We have made a direct measurement of the dose enhancement caused by the presence of gold nanoparticles in a medium under irradiation. The dose was found to be enhanced preferentially at lower photon energies, but not to the extent predicted by a simple theory. This conclusion is independent of the properties of living cells.

SP019.6 - Graphene Plasmonics as Promising Platform for Highly Sensitive Plasmonic Sensing

Author(s): Dong Ha Kim

Chemistry And Nano Science, Ewha Womans University, Seoul/KOREA

Surface plasmon resonance (SPR) is the collectively oscillating charge densities at the interface between thin metal film and dielectrics in resonance with the incident light. SPR-based sensors have emerged as a versatile tool for the label-free and real-time biomolecule sensing during the recent two decades. However, it has been recognized that the sensitivity has yet to be improved to allow for single molecule detection. Incorporation of additional plasmonic nanostructures onto SPR sensor chip is one of the most promising strategies. The use of graphene in conventional plasmonic devices was suggested by several theoretic research studies. Plasmons in graphene were also intensively investigated by some researchers and tight confinement, tunability and long propagation which make graphene as a promising material for SPP-based optical nanodevice applications were reported. It is required to enhance the light-matter interaction for the actual applications despite of relatively high light absorption of single layer graphene. In this regard, the use of graphene in conventional plasmonic devices has been suggested. However, the existing theoretic studies are not consistent with one another and the experimental studies are still at the initial stage. To reveal the role of graphenes on the plasmonic sensors, we deposited graphene oxide (GO) and reduced graphene oxide (rGO) thin films on Au films by layer-by-layer self-assembly method and their refractive index (RI) sensitivity was compared for the first time in SPR-based sensors. The deposition of GO bilayers with number of deposition L from 1 to 5 was carried out by alternative dipping

of Au substrate in positively- and negatively charged GO solutions. The fabrication of layer-by-layer self-assembly of the graphene films was monitored in terms of the SPR angle shift. GO-deposited Au film was treated with hydrazine to reduce the GO. For the rGO-Au sample, 1 bilayer sample showed a higher RI sensitivity than bare Au film, whereas increasing the rGO film from 2 to 5 layers reduced the RI sensitivity. In the case of GO-deposited Au film, the 3 bilayer sample showed the highest sensitivity. The biomolecular sensing was also performed for the graphene multilayer systems using BSA and anti-BSA antibody.

SP020 - Biomedical Modeling

TRACK 09: BIOSIGNAL PROCESSING

SP020.1 - Respiratory parameters have different patterns in imposed-inspiration and imposed-expiration within a closed pneumatic circuit in rats

Author(s): Fabio G. Aoki¹, Marcelo H. Valenga¹, Thiago G. Rodrigues¹, Paulo F.G. Cardoso², Rogerio Pazetti², Henrique T. Moriya¹
¹Escola Politecnica, University of Sao Paulo, Sao Paulo/BRAZIL, ²Instituto Do Coracao, University of Sao Paulo, Sao Paulo/BRAZIL

Computer-controlled research ventilators for small animals (SAV) are often used to assess the respiratory mechanics' parameters such as resistance and elastance of the respiratory system in animal models of disease. In commercially available SAVs, it is common to obtain such parameters with the forced oscillation of a given volume of air into respiratory system with a quasi-sinusoidal pattern in a closed pneumatic circuit (i.e. both the injection and the removal of gas during the piston movement). We hypothesized that obtaining the respiratory mechanical parameters with the linear single-compartment model (LSCM) during the forced inspiration and forced expiration (when calculated together) is not sufficient to explain the physiology of the respiratory system exposed to high doses of bronchial agonist. In order to verify this, male Wistar rats (n = 5) were anesthetized, orotracheally intubated, mechanically ventilated at 90bpm (or 1.5Hz) with a tidal volume of 10mL/kg, and a positive end-expiratory pressure (PEEP) was set at 3cmH₂O. The ventilation was performed in a commercial mechanical ventilator (flexiVent, SCIREQ Inc., Canada) and the animals were infused with a saline solution (PBS), followed by 3 increasing doses (3, 30 and 300mg/mL) of the bronchial agonist methacholine (MCh). Respiratory parameters were calculated by the LSCM. Pressure and volume data, calibrated and corrected by a proprietary software, were analyzed using a computational routine. The full quasi-sinusoidal signal data was compared to inlet and outlet of air from the lungs separately. The data obtained showed that the difference among the three signals (i.e. whole signal, imposed-inspiration, and imposed-expiration) is pronounced at the higher dose (MCh 300mg/mL). Data from imposed-inspiration alone seem to better reflect the respiratory mechanics when a large dose of bronchial agonist is used.

SP020.2 - Autonomic and cardiovascular responses to food ingestion and gum chewing in healthy young subjects

Author(s): Kyuichi Niizeki, Tadashi Saitoh
 Biosystems Engineering, Yamagata University, Yonezawa/JAPAN

Objective: Our previous study has demonstrated that in humans mental stress exerts an influence on the oscillations of respiratory sinus arrhythmia (RSA), inducing incoherent phase lag with respect to breathing in addition to a decrease in the amplitude of RSA¹⁾. It was suggested the enhanced sympathetic nerve activity during stress may modulate the transduction property of cardiac vagal efferent nerve. However, whether coherent oscillations of RSA could be altered by other physiological condition has not been shown. We hypothesized that dietary behavior may induce strong cardio-respiratory synchronization, because that the digestive organs are innervated by parasympathetic nervous system. In this study, we examined cardiovascular responses to eating solid food and chewing a tasteless gum, with special reference to whether the phase coherency of RSA is altered by dietary behavior.

Methods: After 5 min of rest, 14 subjects were asked to eat solid meal [maple flavored Calorie Mate (CM)] at their own pace, which

was followed by 5 min postprandial recording. We also examined the separate effects of mastication on cardiovascular variables by chewing a tasteless gum (GM). We measured ECG by means of wireless electrocardiogram, beat-by-beat blood pressure (BP) by means of Finapres, and breathing activity by inductance plethysmography. The R to R interval (RRI) of ECG wave and respiratory movement signals were sampled with a frequency of 10 Hz. These signals were further band-pass filtered with the frequency range 0.1~0.5 Hz. Instantaneous phases and amplitudes of RSA and respiration were continuously calculated by Hilbert transform, and then phase coherence (λ) between RSA and respiration was computed. Beat-to-beat stroke volume (SV) was determined by the pulse-contour method. Cardiac output (CO) was SV times heart rate (HR) and total peripheral resistance (TPR) was mean BP divided by CO. To assess autonomic activation, the low- and high-frequency components of heart rate variability (HRV) were computed by applying a fast Fourier transform by the Welch method.

Results and Discussion: From rest to CM, transient increase in BP and decrease in RRI were observed. A transient decrease in λ was also observed during CM. At the termination of eating, BP, RRI, and λ gradually returned to the level of resting condition. These responses were slightly blunted in GM. On average, a significant decrease in λ was observed during CM and GM. This was accompanied by increases in BP and CO as well as decrease in RRI under no compensatory reduction in TPR. In contrast to our hypothesis, these cardiovascular responses suggest a shift of sympathovagal balance toward a sympathetic activation. However, HRV indexes did not show any significant changes in response to CM and GM. The λ was positively correlated with normalized amplitude of RSA ($P < 0.01$). We suggest that phase coherence analysis of RSA could provide a sensitive measure for evaluating cardiac autonomic influences on dietary behavior compared to the conventional frequency analysis of HRV.

Reference

1. Niizeki K and Saitoh T. Incoherent oscillations of respiratory sinus arrhythmia during acute mental stress in humans. *Am J Physiol.* 302:H359-H367,2012.

SP020.3 - Characteristic Analysis and Modeling for Signals of Auditory Propagation Pathway

Author(s): Qin Gong¹, Xiaolin Li¹, Tao Zhang², Xi Chen¹

¹Biomedical Engineering, School of Medicine, Tsinghua University, Beijing/CHINA, ²Tsinghua National Laboratory for Information Science and Technology (TNList), Beijing/CHINA

Otoacoustic Emissions (OAE) and Auditory Brainstem Response (ABR) play important roles in the processing information of the auditory perception. Most previous studies only measured one signal simultaneously. When comparing the features between the signals, the testing conditions might be changed, lacking of proofs to ensure the integrity and coherence. Based on the integrated detection system of auditory propagation pathway, the OAEs and ABRs were measured simultaneously in normal subjects under different intensity and frequency of click and tone burst stimulation. The model to simulate the TEOAEs latency-frequency function was built up, and the latencies between OAEs and ABRs were further compared.

SP020.4 - Numerical Optimization Performance of a Perfusion Kinetic Modelling Algorithm using Volumetric DCE CT

Author(s): Igor Svistoun¹, Catherine Coolens²

¹Radiation Physics, Princess Margaret Hospital, Toronto/CANADA, ²Dept Radiation Oncology, University of Toronto, Toronto/ON/CANADA

Introduction: Dynamic-contrast enhanced (DCE) CT imaging is increasingly being used to quantify tissue vascular and functional properties for treatment response assessment by its combination with tracer kinetic modeling. However, clinical kinetic parameter results have been shown to be highly dependent on measurement input and analysis method. Implementing the parameter estimation algorithm involves many design decisions including choice of: data processing sampling rate, continuous-to-discrete system mapping approach and numerical optimization algorithm. As such a simulation framework was designed to investigate the effects of those choices, as well as effects of measured signal aliasing and noise on the accuracy and speed of the parameter estimation.

Methods: A widely-used 2-compartment model (modified Tofts) was chosen which describes the dynamic perfusion properties of a contrast agent using 4 parameters: K_{trans} - transfer from blood plasma into extracellular extra-vascular space, K_{ep} - transfer from extracellular extra-vascular space back to blood plasma, V_b - whole blood volume per unit tissue. To account for separation between injection and measurement site, a time delay τ must be added. The 4parameter estimation from the measured data requires numerical optimization. A test framework was developed where an experimentally derived population-average arterial input function and randomly sampled parameter sets $\{K_{trans}, K_{ep}, V_b, \tau\}$ were used to generate tissue curves. Knowing the ground truth values, 5 numerical optimization algorithms were investigated using multiple starting points from a quasi-random set: sequential quadratic programming (SQP), downhill simplex (Nelder-Mead), pattern search (PS), simulated annealing (SA), and differential evolution (DE). This was repeated for two error function evaluation approaches – finite impulse response (FIR) and infinite impulse response (IIR) approximations of extended Tofts model and the impact of these approaches on speed and accuracy evaluated for sampling rates of 1, 10 and 100 Hz. DE algorithm was implemented in CUDA to run on a GPU for speed improvement testing since processing even a modest area of 128x128x200 voxels would require days on the CPU.

Results: SQP, Nelder-Mead and DE produced good results on clean and noisy input data outperforming SA and PS in terms of speed and accuracy. During calibration, the best 3 algorithms did not exceed absolute error 9.4e-6% for any parameter. When run on typically aliased and noisy ($\sigma=6HU$) data average absolute % errors were: $K_{trans}=11.96\%$, $K_{ep}=8.2\%$, $V_b=25.7\%$, $\tau=3.6\%$. On average SA and PS took 1 and 2 orders of magnitude, respectively, slower to converge. We found IIR to approximate the model much better at sampling rates 10 times lower than those required for FIR approximation i.e. when up sampling same data and processing with FIR at 10Hz the average absolute error drops from $\{4.3\%, 1.7\%, 16.0\%, 1.4\%\}$ to $\{4.3\%, 1.7\%, 6.6\%, 0.3\%\}$ for each parameter. CUDA_DE runtime averaged at 3e-2 sec/voxel – a speed improvement of 199x over CPU_DE.

Conclusion: Evaluation of different optimization algorithms, sampling and noise scenarios indicated a preferred implementation of CUDA_DE. This will be extended to a clinical version with real-time analysis capabilities with ex-vivo kidney perfusion data presented at the meeting.

SP020.5 - Validation of a Sympathovagal Balance Model to Evaluate Autonomic Function in Rats Using Time-Frequency Analysis

Author(s): Rui Fonseca-Pinto¹, Lucília N. Diogo², Sílvia V. Conde², Emilia C. Monteiro², Maria P. Guarino²

¹School Of Technology And Management, Polytechnic Institute of Leiria, Leiria/PORTUGAL, ²Cedoc, Nova Medical School, Faculdade de Ciências Médicas, Lisboa, Portugal, Lisbon/PORTUGAL

The Autonomic Nervous System (ANS) activity can be evaluated in humans by using Heart Rate Variability (HRV) analysis through classical spectral analysis, and more recently by the use of newer techniques by time-frequency analysis. We have previously shown that Blood Pressure (BP) changes felt in HRV spectrum can be assessed and possibly isolated using a hybrid methodology in which HR and BP (in particular diastolic blood pressure) are mixed to produce an instantaneous variation energy plot reflecting the sympathetic and vagal autonomic activity, in other words, the ANS modulation on Heart Rate and Blood Pressure.

In this work we test the same approach in rats with the objective to validate the use of this methodology using continuous Blood Pressure recordings to evaluate the ANS changes.

Data were obtained in 20 rats by using telemetry probes implanted in the abdominal cavity and connected to the abdominal aorta for continuous BP and HR recordings in control situation and also in response to stimuli that change the autonomic response such as chronic intermittent hypoxia and drug administration.

The results showed that this hybrid methodology allows the evaluation of autonomic nervous system balance and can be used in laboratory and eventually in clinical settings to evaluate disautonomies

SP021 - Public Health, Active and Healthy Aging

TRACK 13: INFORMATICS IN HEALTH CARE AND PUBLIC HEALTH

SP021.1 - Informatics in Health Care and Public Health

Author(s): Leandro Pecchia

School Of Engineering, University of Warwick, Coventry/UNITED KINGDOM

Learning objectives:

Attendees non experienced in the study of falls will be introduced to the main challenges of this field and will be able to discriminate, interpret and classify interventions for: risk of falling assessment, fall detection, fall prediction and fall prevention

Attendees will learn how physiological monitoring has been used to assess the risk of falling in the next few months

Attendees will learn how physiological monitoring has been used to predict falls due to postural hypotension in the next few minutes

Abstract

Falls are a major problem of later life, causing loss of independence and quality of life for senior citizen and their families. Falls are difficult to prevent, because caused by complex and dynamic interactions between hundreds of intrinsic (subject specific) and extrinsic (circumstance dependent) risk factors.

Multifactorial interventions seem to be most effective approaches to prevent falls, and includes simultaneously exercises, training, multifactorial home assessments, home safety interventions (i.e. elimination of specific risks) and vitamin supplementations. However, inform these interventions with accurate information about the risk of falling in the next few hours, days or weeks is needed in order to make those interventions more cost-effective and sustainable.

Several technologies have been proposed to support or inform these interventions. Many focused on fall detections using wearable sensors (mainly accelerometers and gyroscopes); unobtrusive sensors (i.e. cameras, Kinect, microphones) or ambient sensors (i.e. infrared or pulse-Doppler radar systems to detect motion or to monitor the ambient response to falls as floor vibrations). Fewer studies aimed to detect falls while happening in order to predict the impact (pre-impact fall prediction) and eventually reduce harms (i.e. inflating airbags). Some studies proposed technologies for the risk of falling assessment, using body-worn kinematic sensors or heel and toe clearance measurements.

However, recent studies proved that there are specific circumstances in which the probability of falling is much higher, especially in-door. For instance, the 30% of indoor falls happen while rising from beds or chairs and the risk of falling in specific hours of the day increases significantly.

This talk will present the preliminary result of two studies investigating for the first time how physiological monitoring and biomedical signal processing can support fall prevention intervention by assessing the risk of falling in the middle term (few weeks) and predicting in the short term (few minutes before) falls due to specific circumstances (i.e. rising from bed or chair). Two case studies will be presented in which Heart Rate Variability (HRV) was used to predict falls or to assess the risk of falling, proving that:

HRV resulted systematically depressed in fallers;

subjects with a depressed HRV showed a significantly increased relative risk of falling in the next few months;

monitoring the HRV in the 5 minutes before standing-up it is possible to predict postural hypotension, which is the main cause of falls happening while rising.

Finally, the preliminary attempts to integrate those predictive modeling in wearable and unobtrusive monitoring applications for falls prevention will be discussed.

SP021.2 - Monitoring Information System of Aedes Aegypti Reproduction

Author(s): Heleno S. Morais¹, Ozziel S. Santos¹, Mateus A. Rocha¹, Tássila Catarina S. Almeida¹, Lourdes M. Brasil², Gerardo A. Idrobo Pizo²

¹College Gamma, University of Brasilia, GAMA/BRAZIL, ²Post-graduate Program In Biomedical Engineering, University of Brasília, Gama/BRAZIL

Aedes aegypti is a mosquito and main transmitter of dengue disease. Dengue is a viral disease that can only be transmitted to Humans by the bite of infected mosquitoes with the virus of the disease. It usually manifests in three clinical types, one of which can lead to death. The classical dengue, is classified as a febrile illness of mild to moderate intensity; dengue hemorrhagic fever, more severe than the last one, it comes to changes in blood clotting of the infected person; and dengue shock syndrome, very rare form, but can be fatal if not treated in time. Furthermore, *Aedes aegypti* transmits diseases like yellow fever, and it also has fully capacity to transmit chikungunya fever. Due to the fact that it is a fatal disease and the eradication of *Aedes Aegypti* is practically impossible, it is very important monitoring and control of *Aedes Aegypti* reproduction. The monitoring and control processes are still precarious when it comes to mosquito eggs counting technology collected through ovitraps vane in breeding sites. Because this processes are performed manually by experts using magnifying glass and tweezers. This paper presents a mechanism to make these processes faster and more efficient, it is a hardware / software interaction mechanism capable of capturing microscopic images of ovitraps vane and from an image processing software automating the counting of eggs contained in the vanes and in the future through geoprocessing inform the locations of higher reproduction of *Aedes aegypti* in a given region.

SP021.3 - Design and Functionality of a Meta-Reporting Tool within a Medical Devices Vigilance System

Author(s): Antonios Deligiannakis¹, Nikos Giatrakos¹, Aris Dermitzakis²

¹Electronic & Computer Engineering, Technical University of Crete, Chania/GREECE, ²Biomedical Technology Unit, Dept. Of Medical Physics, School of Medicine, University of Patras, Rio, Patra/GREECE

Medical Devices (MDs) are an important factor related to the quality of healthcare that patients receive. Although regulations have been applied and standards are imposed on MD manufacturing, faulty behavior incidents (referred to as *adverse events*) are frequently observed and reported by various organizations, such as FDA[1] and EUDAMED[2]. Given these reports, which include information about MD products associated with an adverse event, national healthcare authorities have the duty of examining whether listed products match the equipment of administered institutions and of contacting them with information about the potential risks that admitted patients (or users) may encounter. Subsequently, the individual healthcare institutions should cross-check, appropriately maintain,

or even withdraw the potentially hazardous MD that they own.

To facilitate healthcare authorities promptly notifying institutions under their organizational chart about potentially hazardous devices, we have designed and developed a meta-reporting, web-based tool as a part of the MEDEVIPAS system. Our tool automatically generates meta-reports of *matches* of adverse event reports to inventoried MD equipment and to disseminate these meta-reports to institutions in a user-friendly format, conceivable by non-expert (medical or paramedical) users, such as administrative hospital employees. Our tool receives as input information about MD inventories and crawled reports of adverse events. An entity matching algorithm is executed, matching medical devices in reports with those in MD inventories (and computing a *matching score* in each case) using the manufacturer, model and serial number of a MD, upon the insertion of new reports of adverse events (or of new MDs) in the system. From that point forward, our meta-reporting tool, which is the focus of this paper, provides the necessary functionality to registered users.

Meta-reports are created and made available to registered institutional users via a web application, in a tabular format. The meta-reports display information about potentially affected medical devices of each user, along with data from a related adverse event report, the matching score, etc. This information can also be provided in printable format using the web application. Email alerts are also created and forwarded to their registered accounts automatically upon the detection of a possibly matching device. The alerts are displayed prominently at our web-based tool and remain active until institutional users confirm that they became aware of the cited situations. Our tool also exploits user feedback on the validity of provided meta-reports, which is then incorporated in the entity matching algorithm to increase its accuracy performance (properly modifying the matching score of matched records). Apart from providing meta-reports, analysis capabilities are embodied in our tool in the form of aggregate statistics per MD manufacturer, MD group and registered institution.

Keywords: Medical Device, Vigilance, Adverse event, Reporting Tool

Acknowledgment: *This research has been co-financed by the European Union (European Social Fund – ESF) and Greek national funds through the Operational Program “Education and Lifelong Learning” of the National Strategic Reference Framework (NSRF) - Research Funding Program: Thalis. Investing in knowledge society through the European Social Fund.*

[1] <http://www.fda.gov/Safety/Recalls/EnforcementReports/>

[2] http://ec.europa.eu/health/medical-devices/market-surveillance-vigilance/eudamed/index_en.htm

SP021.4 - Evaluation of the Impact in the Physical Condition of School Age Children Exposed to an Intervention of Exergaming in Montemorelos Mexico

Author(s): Alejandra Guillen-Peralta, Gerardo S. Romo-Cardenas, Raul Rodriguez-Antonio, Gener Aviles-Rodriguez
School Of Engineering, Montemorelos University, Montemorelos/ MEXICO

The current epidemiological situation of overweight and obesity in Mexico has been extensively documented and analyzed. Studies define the situation as a metabolic and inflammatory disease, of chronic course, multifactorial and with high impact on public health.

For the treatment of this multifactorial phenomenon, strategies have been proposed focused in the promotion and health education of the

target audience, seeking at medium- and long term, to prevent and eventually achieve the reduction of this epidemic situation. The school age population is particularly at high risk, with consequences ranging from psychological areas, school performance and organic malfunctioning that could emerge during the lifetime of the individual.

The overweight and obesity appears to be related to environmental factors such as sedentary lifestyle. The improvement of the physical condition through physical activity is a challenge in these new generations.

Considering the sociological features of school age population (6-12 years), their general technological familiarity implied in this age group and their tendency toward virtual interactions, an initiative of using video game platforms was designed performed, in order to promote physical activity (Exergaming). In addition, an evaluation of the impact in the physical condition on the participants through standardized anthropometric and physical performance tests was made, via pre and post testing. Results shows that there is a significant difference in variables related to flexibility, strength and body composition in a such a way, that opens the possibility to consider this type of virtual tools as an option for physical training in school age children.

SP020.5 - Using the EIP on AHA monitoring tool for the early technology assessment of a planned device to predict in-hospital falls in the elderly

Author(s): Christian E.H. Boehler¹, Fabienne Abadie¹, Lotte Steuten², Leandro Pecchia³

¹Joint Research Centre, European Commission, Seville/ SPAIN, ²Panaxea bv, Enschede/NETHERLANDS, ³School Of Engineering, University of Warwick, Coventry/UNITED KINGDOM

In-hospital falls can lead to severe health consequences for the individual and are associated with substantial cost to health and care systems and it is estimated that up to one third of all in-hospital falls happen straight after standing up from a bed or chair. It is possible that a sudden drop in blood pressure shortly after rising is causative for many of these falls and a recent observational study suggested that the blood pressure after standing up can be predicted with high accuracy based on the ECG registered during the five minutes before rising (82.5% accuracy; false positive 10%; false negative 7.5%). This study aims to inform the design of a device that could warn patients about the imminent risk of falling based on a drop in blood pressure after rising in an early assessment of the health and economic outcomes of such a technology. The monitoring and assessment tool for the European Innovation Partnership on Active and Healthy Ageing will be used in order to predict the potential impact of such a device on the number of falls and subsequent health outcomes as well as the impact on healthcare utilisation. The tool rests on a three-state Markov process (including baseline health status, deteriorated health status (i.e. a fall) and death), which allows estimating the probability of patients having a post-fall event with severe health consequences. Health states will be valued using EQ-5D data from the literature and resource use will be estimated based on the documented consequences of falls in a UK hospital setting. The probability of a fall following a sudden drop of blood pressure and the likelihood to prevent a fall through an alarm triggered by such a drop in blood pressure during standing up will be elicited from a group of falls experts with various backgrounds, including participants of the EIP on AHAs Action Group A2 on falls prevention. Key drivers of health and economic outcomes of the planned intervention will be assessed through extensive sensitivity and scenario analyses. With this study we will not just be able to assess the potential impact of a planned warning device for the prevention of in-hospital falls, but also the value of the EIP on AHA monitoring tool for the early evaluation and the pre-market assessment of new and innovative health technologies.

SP021.6 - An innovative Decision Support System (DSS) for patients with Inflammatory Bowel Disease (IBD)

Author(s): Evaggelos C. Karvounis¹, Vasileios E. Tsianos¹, Kallirroi Kyriakidi¹, Epameinondas V. Tsianos²

¹Research Laboratory Of Hepato-gastroenterology, Division Of Gastroenterology, Faculty Of Medicine, School Of Health Sciences, University of Ioannina, Ioannina/GREECE, ²1st Division Of Internal Medicine And Division Of Gastroenterology, Faculty Of Medicine, School Of Health Sciences, University of Ioannina, Ioannina/GREECE

In IBD, investigators have suggested a possible role of various infective agents and recent epidemiological studies and veterinarian reports have reconsidered the pathogenetic role of some microbes and/or related vectors to the potential pathogenesis of some human disease. The etiopathology of IBD still remains unknown. The combined use of lifestyle surveys associated with blood samples and relevant clinical registers seems the best methodology to identify possible links between genetic predisposition, disease occurrence and natural course of the disease.

Such a system will help understand the natural course of the disease, study the predisposing factors and related genes and determine early clinical, genetic and immunological predictors of outcome and response to treatment. We build an efficient personalized web-based platform, in order to manage medical data, using efficient data mining and knowledge extraction techniques. Various variables already defined and determined for which associations are searched within the recorded datasets, discover interesting interrelations and extract new knowledge from multiple and heterogeneous archived data that reflect everyday lifestyle and medical information, examine the results of previous therapeutic regimens and obtain quantitative explanations of the observations and generate efficient reports with intelligent data visualization.

We create an innovative clinical DSS, an efficient web-based platform, which incorporates 2 modules: Data Repository and Knowledge Discovery/Statistics module. The Data Repository module is a centralized data repository for annotation data (clinical, demographic and experimental data), sample source and handling information, processing and quality assurance information, as well as inventory and process flow data. In the front end, it will provide tracking, data query, report generation, process management functions, data handling as well as statistics, data mining and knowledge extraction capability (Knowledge Discovery and Statistics module incorporated in the back-end of the system). Moreover, the module will contain a Data Representation module that will handle the presentation of the extracted knowledge from the patients' data.

For the Data Repository module, a secure database has already been developed. For old patients, medical data from almost 600 patients, using their hard-copy medical records, have already been digitized. Blood sampling has already been achieved in 294 new patients and 234 healthy volunteers, while the results of the genetic (susceptibility gene polymorphisms) and serological (inflammatory and serological prediction markers) study are recorded in the database. Several knowledge discovery techniques have been applied in the Databases, giving more than satisfactory results.

Building such a system, for the first time in Greece, will contribute even more to IBD knowledge and research as the proposed system will create a unique multidisciplinary combined database with combination of clinical, environmental and laboratory data in IBD. In addition, as IBD is regarded to be a multifactorial disease, we hope to better define some factors that clearly predispose to certain IBD phenotypes and IBD disease course. Finally, we hope that the computerized platform will enrich our experience and will contribute towards a better IBD education and training in our medical, nursing and laboratory personnel and serve as a model and a basis for research in other chronic gastrointestinal and/or inflammatory diseases.

SP022 - Educational and Professional Activities: Part 1

PRESIDENTS CALL

SP022.1 - Biomedical Engineering in Nigeria: A Developmental Overview

Author(s): Kenneth I. Nkuma-Udah¹, Eillen E.C. Agoha², Kennedy O. Ejeta³, Gideon I. Ndubuka³

¹Department Of Biomedical Engineering, Federal University of Technology, Owerri, Nigeria, Owerri/NIGERIA, ²Food Sciences And Technology, Abia State University, Uturu,, Uturu/NIGERIA, ³Department Of Biomedical Technology, Federal University of Technology, Owerri, Nigeria, Owerri/NIGERIA

Biomedical Engineering (BME) activities in Nigeria can be said to have started in the 1970s during which collaborative efforts were made by engineers, medical doctors, pharmacists, physicists, technicians and other scientist. Although, the pace of development was hitherto slow, most efforts were in the area of training - short courses, continuing education or professional development. However, the coming of NIBE in 1999 has propelled a steady progress of BME activities in Nigeria. BME activities in Nigeria was further given a big boost in 2007, when the first undergraduate programme in BME started in the Federal University of Technology, Owerri, Nigeria with NIBE contributing the foundation members of faculty. Established in 1999 with the vision "to develop and advance the biomedical science, health and human well-being of Nigeria through modern technological approaches comparable to those obtainable in any developed country of the world". NIBE is currently structured in 5 divisions - biological engineering; medical engineering; clinical engineering; rehabilitation engineering; and biomedical physics / allied sciences - to accommodate virtually every field in the sciences. It had its 1st annual BME conference in 2000. Since then it has organised 9 national biomedical engineering conferences and 6 national professional development courses in Nigeria. In 2003, NIBE was admitted as the 50th member of IFMBE. The same year, she co-founded the African Union of Biomedical Engineering and Sciences (AUBES) in Ghana while some members were on a Medical Equipment Training. The role of NIBE in developing BME in Nigeria is mainly as a membership group to develop resources for BME by evolving adequate training programmes for members, facilitating accreditation and certification of professionals practicing BME in Nigeria.

SP022.2 - Modernising Scientific Careers – a new scheme for the education and training of physicists, engineers and other scientific staff in the UK National Health Service

Author(s): Keith Ison¹, Chris Gibson², Sarah Peel¹, Sue Hill³

¹Medical Physics Department, Guy's and St Thomas' Hospital, London/UNITED KINGDOM, ²National School of Healthcare Science, Birmingham/UNITED KINGDOM, ³NHS England / Health Education England, Leeds/UNITED KINGDOM

Modernising Scientific Careers (MSC) is a UK-wide government initiative to address training and education of the NHS healthcare science workforce (2011). MSC provides a flexible career pathway to meet current and future health system needs via a single coherent training framework across 50,000 healthcare scientists of all disciplines including medical physicists and clinical engineers.

MSC covers all career stages, and the associated training and education programmes incorporate both academic and workplace-based training. Early training is broad based with greater specialisa-

tion in the more advanced programmes. The intent is to develop a skilled yet flexible workforce with sustainable education and training funding. It is already being developed to cover Medical Physics Experts and public health scientists.

The MSC career pathway has four stages and qualifications (2014a):

Assistant and associate training – vocational qualifications for **scientific support roles**

Practitioner Training Programme (PTP) – BSc for healthcare **science practitioners**

Scientist Training Programme (STP) – Masters for **clinical scientists**

Higher Specialist Scientific Training (HSST) – five year doctoral level programme for **consultant clinical scientists** (2014b)

The presentation will outline evidence-based approaches to trainee selection, progress monitoring and assessment and also report initial outcomes. MSC is competency-based and scientists and engineers often approach competencies in a linear fashion, breaking complex real-world scenarios into discrete tasks with defined right answers that do not fully reflect clinical reality or capture all necessary learning. In progressing from academic achievement to professional competence, we propose that trainees should be encouraged to document real workplace processes, acknowledge and reflect on uncertainty, and develop strategies to respond appropriately. These documents would encourage all staff to consider reflective practice as integral to professional competence.

Department of Health (2011) *An overview of Modernising Scientific Careers.*

NHS Employers (2014a) *Modernising Scientific Careers – explaining the facts.*

Health Education England (2014b) *Scaling the Heights: an overview of Higher Specialist Scientific Training (HSST) in Healthcare Science.*

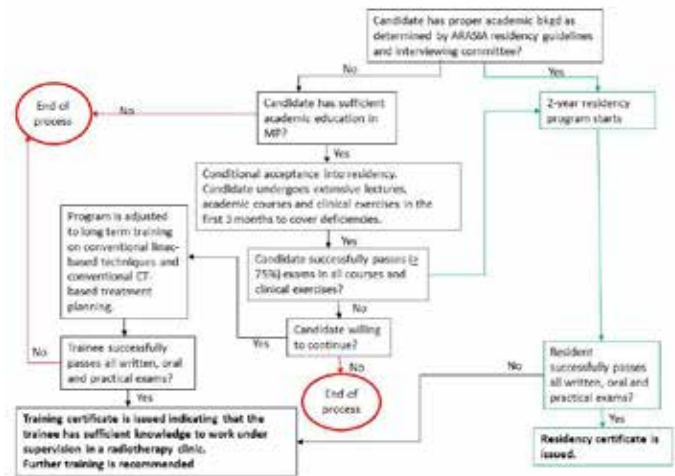


Program				
Education Programme	Duration	Entry requirement	Level	Funding
Assistants, Associates	Up to 3 years	Varies	Varies	Employer
Practitioner Training Programme	3 years	University selection	BSc	Student with NHS placement contribution
Scientist Training Programme	3 years	BSc in relevant area	MSc	Commissioned and funded centrally or in-service funded by employers and fees paid centrally
Higher Specialist Scientist Training	5 years	Clinical Scientist registration	Doctoral level (DClin-Sci / PhD)	Salary supported by employers with external training allowance
Accredited Scientific Practice post registration / regulation	1 - 2 years	Depends on programme	Depends on programme, eg postgraduate Medical Physics Expert-programme, eg post	Academic component employer funded

SP022.3 - Medical Physics Residency Program in Developing Countries: Lessons, Challenges and Solutions Learned from a Regional Pilot Training Program

Author(s): Shada Wadi-Ramahi, Waleed Al-Najjar, Belal Mofthah Biomedical Physics, King Faisal Specialist Hospital and Research Center, Riyadh/SAUDI ARABIA

A regional 2-year structured program in medical physics was established at our institution. The program is supervised by board certified physicists with the objective of graduating clinically qualified medical physicists. The structure of the program is such that all residents undergo the same learning modules during the allotted time. However, we faced many challenges in terms of the competencies and expectations of the candidates, as they came from different countries in the region. MSc level candidates exhibited varying levels of academic competencies, and the clinical expectation varied by country; From conventional treatments using Co-60 to state-of-the-art treatments on linacs. Challenges faced include how to cover various academic deficiencies, which required time-consuming per needed lectures, another major challenge was how to transition Co-60 users into linac users while dealing with other residents who wanted to advance more in linac-based techniques. A third major challenge was how to evaluate the various competencies achieved at the end of the 2 years, given the starting level and background, of course many other challenges presented themselves during the years. In this paper, we present a detailed description of our residency program, the modules it contains and expected competencies, then we discuss in more details the challenges we faced given the heterogeneous mix of the residents and the solutions that evolved, and still is evolving, to overcome these hurdles. Residency programs covering many countries, in which one cannot control education levels, have to evolve and adapt in order to produce useful results. A one-size-fits-all formula found in North America, for example, will fail if copied as is and implemented in developing countries.



SP022.4 - International Union of Biological Sciences

Author(s): Nils Chr. Stenseth Université Paris Sud XI, IUBS, Orsay/France

The International Union of Biological Sciences (IUBS) was established in 1919. IUBS is presently composed of 27 National Members and 80 Scientific Members. The role of IUBS is to promote the study of biological sciences, to initiate, facilitate and coordinate research and other scientific activities necessitating international, interdisciplinary cooperation, to ensure the discussion and dissemination of the results of cooperative research, particularly in connection with IUBS scientific programmes. IUBS sponsors the organization of conferences and also scientific programmes. The current IUBS programmes are dealing with climate change, bionomenclature, Disaster and biodiversity, and also a case study on Bees and Coffee.

The bio-cluster meeting will be a good opportunity to discuss how the different bio-unions programmes and activities could interact for the benefit of our community. On the other hand, it is important to develop our interaction with ICSU and with its programme Future Earth. The bio-cluster of ICSU should discuss and propose ways to improve our participation in this important ICSU programme.

SP022.5 - Promoting the public image of Medical Physicists and Biomedical Engineers

Author(s): Michael Cheng Biomedical Engineer, Ottawa/ON/CANADA

This paper focuses on the alert raised by the IUPESM President that "In many developing countries, there are no physicists or engineers in clinical settings; in developed nations, physicists and engineers are losing their positions in hospitals." The author offers his personal viewpoints derived from the past 30 years in more than 30 developed and developing countries around the world working on medical device regulations and management issues. The conclusion proposed collaborative summit brainstorming.

Despite their technical talent and devotion to their work, most medical physicists (MP) and biomedical/clinical engineers (BME/CE) have less skills in promoting themselves to the public. I think this phenomenon is a weakness that needs to be addressed. We know that industries and some politicians will hardly succeed if they do not make themselves known to the public. The professions must seek ways to promote their public image. I will describe two domains where the merits of the MP and BME/CE are huge but under recognized by the public: 1. MP, BME/CE are principal builders of health-care technology; 2. MP and BME/CE play vital roles in patient safety

with medical devices in healthcare facilities. Then, I will propose outreach to developing countries with references to simple knowledge transfer tools described in two education sessions offered by this Congress WC2015. Lastly, I will suggest examples of opportunities for research to help emerging global health issues, and opportunities to develop personal medical technologies to empower personalized medical care and encourage patient responsibility. A full paper is also submitted with this abstract; the descriptions in the full paper also make references to four other submissions (see below) to this Congress WC2015.

In order to promote the public image of MP and BME/CE, the hurdles to overcome are complex; therefore an appropriate strategy to “market” their huge contributions to global healthcare should be a key topic for collaborative summit brainstorming called by the President.

REFERENCES

Cheng M, Altayyar S, Hilfi H, Polisena J (2015) Patient safety and optimal performance: a holistic framework for medical devices, invited education session, WC2015

Polisena J, Hilfi H, Cheng M, Collaboration in healthcare technology decision making, invited education session, WC2015

Cheng M, Ghahari A, Potential benefits in comparing the neural control networks studies between the oculomotor and cardiac pacing systems, scientific submission, neural system modeling, WC2015

Cheng M, Thiruganasambandamoorthy V, Dajani HR, Bolic M, A practical device to warn on impending syncopal episodes, scientific submission, medical devices, WC2015

SP022.6 - The Utilization and Design of Doorless Mazes for Medical Linear Accelerator Rooms In Ontario, Canada

Author(s): Joseph J. Szabo

Walker Family Cancer Centre Physics, Niagara Health System, St. Catharines/CANADA

Medical linear accelerator rooms in typical cancer centres use mazes for radiation protection, but these are usually short and straight and still require a heavy shielding door at their entrance. Especially for treatment energies higher than 10 MeV the purpose of the door is to attenuate both photons and neutrons that have scattered down the maze, as well as capture gamma rays created by neutrons in the concrete walls, ceiling, floor, and ultimately in the door itself. This radiation must be dealt with to secure the therapy staff working in the control area near the room entrance. Depending on the length of the maze, the door may have to attenuate scattered photons, moderate fast and intermediate neutrons, and finally attenuate capture gamma rays. This requires often massive and cumbersome doors, which usually consist of an initial layer of lead to attenuate the scattered photons and the maze generated capture gamma rays, followed by another layer of quite thick, highly hydrogenous material such as borated polyethylene, to moderate fast and intermediate energy neutrons into low energy thermal neutrons, which then are effectively captured by the boron, while only releasing capture gamma rays of a relatively low energy (0.473 MeV). A final layer of lead at the outside of the door is used to block these capture gamma rays. All this is usually quite heavy, resulting in a door that is 10's of centimeters thick and thousands of kilograms in weight, often requiring tracks and motors to operate, which makes it quite expensive. Also, moving such a heavy door is usually slow and since the door is likely opened and closed more than hundred times a day, it is prone to wear, requiring expensive continuous maintenance. And in the event of a breakdown a manual technique for opening must be available. All this can be avoided if one uses a longer maze. In 1991 the author designed a maze that required no door at all. This maze

was first put into clinical use in the city of Kingston and was the first maze without a door in the province of Ontario. After the successful implementation of this design, it was utilized in all new clinics and many of the older clinics in all of Ontario. In addition, it has been used elsewhere in Canada as well as in parts of the United States. However, in other parts of the world the doorless bunker is still not very well known. This paper is a review of the extent of the use of this design as well as detailed instruction on how to build it to minimally take up real estate by use of multiple bends and strategically placed polyethylene and borated polyethylene panels to reduce the neutron flux well before it reaches the maze entrance. Calculation methods and measurements from the radiation survey for the most recent construction will be shown. In that case the results were so good that the author was actually concerned that his survey meters were not functioning.

SP023 - Quantitative Imaging: Part 1

TRACK 01: IMAGING

SP023.1 - Improving quantitative functional imaging with dynamic contrast enhanced studies using a linearized Johnson-Wilson model approach

Author(s): Fiona Li¹, Ting Yim Lee²

¹Department Of Medical Biophysics, Western University, London/ON/CANADA, ²Lawson Health Research Institute, London/ON/CANADA

Background

The standard two compartment (2-C) model, consisting of vascular and tissue compartments, is frequently used to fit tissue time density curves (TDCs) from dynamic contrast enhanced (DCE) CT or MR studies. However, the compartmental assumption for the vascular space means that the finite vascular transit time is ignored. As image acquisition speed increases beyond 0.5 Hz, parameters estimated by fitting the tissue TDC with the two 2-C model without accounting for the finite vascular transit time could be biased. Also, 2-C model is unable to estimate blood flow (F), it estimates Ktrans instead, which is the flow extraction efficiency product. On the other hand, fitting tissue TDC using the Johnson-Wilson model with the adiabatic approximation (aaJW) will provide estimates of both Ktrans and F that are independently important for investigations of tumor associated angiogenesis. Current applications of the aaJW model use non-linear curve fitting methods to estimate Ktrans and F. These methods are prone to be trapped in local minima while searching for the optimal fit to the tissue TDC resulting in erroneous estimates of model parameters.

Purpose

To develop a method to linearize the fitting of DCE tissue TDC with the aaJW model and compare the method's sensitivity to model parameters and covariances of estimated parameters with non-linear fitting methods

Method

Linearization of 2-C model fitting of tissue TDC has been published before but no attempts to-date have been made for linearization of aaJW model fitting. The method we developed to linearize aaJW model fitting of the tissue TDC is based on time integrals of the arterial TDC (Cp(t)) and the tissue TDC (Q(t)). The stability of the linear and non-linear fitting methods were analyzed using sensitivity analysis which calculated the changes in the fitted tissue TDC with changes in the model parameters or sensitivity functions of both fitting methods. The sensitivity functions were used to estimate the covariances of the estimated parameters for both methods.

Results

The equations for tissue TDC fitting with the aaJW model are:

Non-linear: $Q(t) = F \cdot [D(t-t_0) - D(t-t_0-W)] + K_1 \cdot C_p(t-t_0-W) \cdot \exp(-k_2 \cdot (t-t_0-W))$

Linear: $Q(t) = F \cdot [D(t-t_0) - D(t-t_0-W)] + K_1 \cdot D(t-t_0-W) + F \cdot k_2 \cdot [E(t-t_0) - E(t-t_0-W)] - k_2 \cdot G(t)$

where * is convolution operator, t_0 is the delay between Q(t) and Cp(t), W is the vascular transit time, $K_1 = K_{trans}$, k_2 is backflux rate constant, D(t) is the integral of Cp(t), E(t) is the integral of D(t) and G(t) is the integral of Q(t). The sensitivity functions for the linear fit-

ting method were ~ 5 times larger than those of the non-linear fitting method resulting in the covariances of estimated parameters from the linear fitting method > 1.3 times less than those of the non-linear fitting method.

Conclusions

Unlike the non-linear fitting method, the linear method estimates model parameters at the unique global minimum sum of squared deviations between the fitted and the measured tissue TDC. More importantly, the covariances of the estimated model parameters are significantly less for the linear method than the non-linear method. This would lead to more precise quantitative functional maps from DCE studies and more reliable diagnosis.

SP023.2 - Early tumor Response assessment using volumetric DCE-CT and DCE-MRI in Metastatic Brain Cancer Patients

Author(s): Catherine Coolens¹, Brandon Driscoll¹, Warren Foltz¹, Cynthia Menard¹, Gelareh Zadeh², David Jaffray¹, Caroline Chung¹

¹Radiation Medicine Program, Princess Margaret Cancer Centre, Toronto/CANADA, ²Division Of Neurosurgery, University Health Network, Toronto/CANADA

Introduction: Early change in tumour vascularity following stereotactic radiosurgery (SRS) is a potential biomarker of response. Dynamic contrast enhanced (DCE) MRI is often used to interrogate perfusion but has known limitations to accuracy and precision. Progress in CT technology now allows for volumetric acquisition with 4D temporal dynamic analysis (TDA) of perfusion. As such, DCE-CT presents as a standard for tracer-kinetic validation. This study aims to compare DCE-MRI analysis against DCE-CT supported by a common TDA framework and to evaluate if DCE-MRI and DCE-CT parameters can detect changes in tumor vascular physiology that predict for tumor response to SRS.

Methods: Patients with brain metastases (total of 14 tumours) treated with SRS as part of REB-approved clinical trials underwent volumetric DCE-CT (Toshiba, Aquilion ONE) and DCE-MRI (IMRIS 3T Verio, Siemens) scans at baseline then 7 and 21 days post-SRS. DCE-CT parameters were: 80kV, 100mAs, 1sec interval and 0.468x0.468x1mm. VFA T1 quantification and DCE MRI acquisitions used 3D-FLASH with matching echo times (1.86 msec), repetition times (4.8 msec), and geometric features (1.15x1.15 mm in-plane resolution, 40 slices at 1.5 mm each). DCE-MRI used a 20° flip angle, and 45 frames were acquired every 5.8 sec. Voxel-based whole brain TDA was performed on both DCE-CT and DCE-MR data using in-house software. Perfusion, permeability and Area-under-the-Curve (Ktrans, Ve, AUC) were assessed within each tumour at every time point using the Modified Tofts model and a linear regression was done of temporal changes in these parameters over treatment. Correlation between these vascular parameters and treatment response, evaluated as stable or reduction in tumor volume was assessed.

Results: At Day 21 only one tumor had a volume that remained larger than at baseline while the other tumors showed a decrease in volume of (mean of 53.6 +/- 31%). DCE-CT: 3 of 8 stable or responding tumours revealed a Ktrans reduction of 44.6 +/- 36.6% (p=0.056) at Day 7 post-RS while 10 out of 13 responding tumours had a reduction in Ktrans of 26.0 +/- 16.6 % by Day 20 (p < 0.01). Only one of the non-responding tumours showed a decrease in Ktrans at Day 7 while none did at Day 20. DCE-MRI: 7 of the 8 stable or reducing tumours revealed a Ktrans reduction of 17.4 +/- 16.6% (p<0.05) at Day 7 post-RS while 10 out of 13 responding tumours had a reduction in Ktrans of 24.0 +/- 20.3 % by Day 20 (p < 0.05). MRI results showed weak overall correlations with DCE-CT at either Day 7 (R2=-0.16) or Day 20 (R2 = 0.21) for Ktrans. AUC changes did not correlate significantly with either time point or modality.

Conclusions: This is the first study evaluating perfusion parameters acquired by same-day volumetric DCE CT and DCE MRI in a cohort of metastatic brain patients. The weak correlation between MRI and CT results may reflect issues such as sensitivity to arterial input, tumour type, definition of response, and edema that are under further investigation. These early results show Ktrans reduction at day 20 may predict for eventual tumor response post-SRS.

SP023.3 - Diffusion tensor imaging is correlated with quantitative histology in surgically-resected hippocampi of epilepsy patients

Author(s): Maged Goubran¹, Boris Bernhardt², Charlotte Blinston¹, Diego Cantor-Rivera¹, Jonathan C. Lau³, Robert R. Hammond⁴, Sandrine De Ribaupierre⁵, Jorge G. Burneo³, Seyed Mirsattari³, David A. Stevens³, Andrew G. Parrent³, Andrea Bernasconi², Neda Bernasconi², Terry Peters⁵, Ali R. Khan⁵

¹Imaging, Robarts Research Institute, London/ON/CANADA, ²Mcconnell Brain Imaging Center, Montreal Neurological Institute, Montreal/QC/CANADA, ³Epilepsy Program, Clinical Neurological Sciences, Western University, London/ON/CANADA, ⁴Pathology, Division Of Neuropathology, Western University, London/ON/CANADA, ⁵Medical Biophysics, Western University, London/ON/CANADA

Introduction

Hippocampal sclerosis (HS) is the most common pathology seen in mesial temporal lobe epilepsy (MTLE) patients, and studies have shown a relationship between the pattern of sclerosis and post-surgical outcomes (seizure freedom and memory impairment). Thus, predicting these pathological sub-types pre-operatively can play a significant role in pre-surgical management of TLE patients. Diffusion tensor imaging (DTI) has shown to be a sensitive marker of microstructural changes but the precise relationship of diffusion markers with HS subtypes is not well known. The current study aims to assess these relationships by comparing pre-operative imaging with quantitative markers of neuropathology from histology of the tissue resected after surgery.

Methods

Patients (N=15) undergoing temporal lobectomy were recruited for this study and imaged pre-operatively in a 3T MRI using a research protocol that included diffusion tensor imaging (41+6 directions, 2.5mm isotropic resolution). Tissue was resected en-bloc and prepared for histological processing. Histology slides were cut, stained with H&E, NeuN (neuronal marker) and GFAP (glial marker) for quantitative histology assessment. Hippocampal subfields (CA1, CA2/3, CA4/DG) were manually segmented in the pre-operative MRI and histology slides, and spatial correspondences were found using our validated MRI-histology image registration pipeline. Automated histology image processing was performed to extract maps of neuron density, size, and gliosis, and were correlated against mean diffusivity (MD) and fractional anisotropy (FA) of the corresponding slice.

Results

Histological data for two subjects were discarded due to insufficient tissue to assess delineate the subfields, thus correlations were computed with 13 patients. Mean diffusivity (MD) in the end folium (CA4/DG) was significantly correlated with the number of neurons in CA4 ($r=-0.833$, $p<0.001$) and the size of neurons in CA4 ($r=-0.841$, $p=0.039$). An increase in the extracellular space could explain the significant increase in MD in samples which contained fewer neurons or neurons with smaller average size.

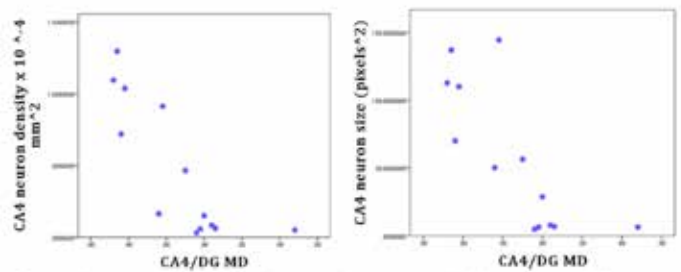


Figure 1: Scatter plots showing significant correlations between diffusion parameters (MD) and quantitative histology (neuron density, neuron size).

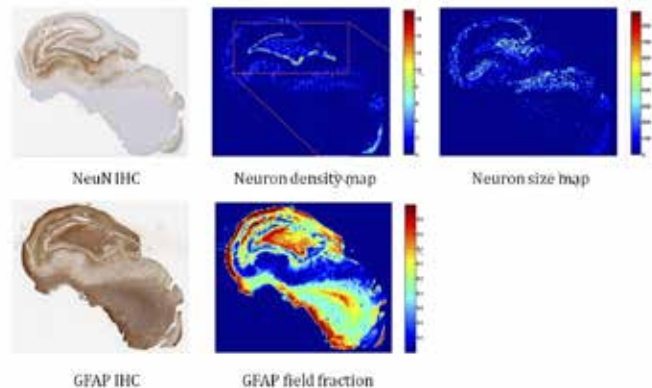


Figure 2: Example of immunohistochemical (IHC) staining of the hippocampus for neuronal markers (NeuN) and glial markers (GFAP), along with quantitative maps derived from these images (neuron density, neuron size, glial field fraction).

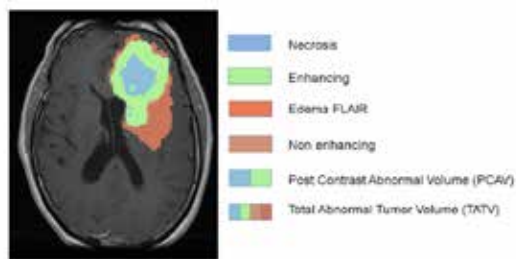
SP023.4 - Evaluation of fully automatic volumetric GBM segmentation in the TCGA-GBM dataset: Prognosis and correlation with VASARI features

Author(s): Emmanuel Rios Velazquez¹, Raphael Meier², William D. Dunn Jr³, Brian Alexander⁴, Roland Wiest⁵, Stefan Bauer², David A. Gutman³, Mauricio Reyes², Hugo J.W.L. Aerts⁴

¹Radiation Oncology, Dana-Farber Cancer Institute | Harvard Medical School, Boston/UNITED STATES OF AMERICA, ²Institute for Surgical Technology and Biomechanics, Bern/SWITZERLAND, ³Department Of Biomedical Informatics, Emory University School of Medicine, Atlanta/GA/UNITED STATES OF AMERICA, ⁴Radiation Oncology, Dana-Farber Cancer Institute, Brigham and Women's Hospital, Harvard Medical School, Boston/UNITED STATES OF AMERICA, ⁵Support Center For Advanced Neuroimaging (scan), Institute for Diagnostic and Interventional Neuroradiology, University Hospital Inselspital and University of Bern, Bern/SWITZERLAND

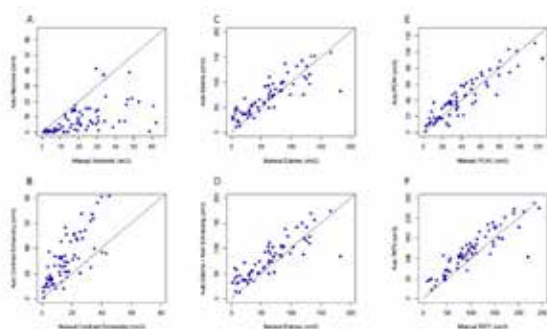
Background: Reproducible definition and quantification of imaging biomarkers is essential. We evaluated a fully automatic MR-based segmentation method by comparing it to manually defined sub-volumes by experienced radiologists in the TCGA-GBM dataset, in terms of sub-volume prognosis and association with VASARI features.

Methods: MRI sets of 67 GBM patients were downloaded from the Cancer Imaging archive. GBM sub-compartments were defined manually and automatically using the Brain Tumor Image Analysis (BraTumIA). Spearman's correlation was used to evaluate the agreement with VASARI features. Prognostic significance was assessed using the C-index.



Tumor sub-compartments as defined by the BraTumIA software. A post contrast abnormal volume (PCAV) was defined as the sum of the necrotic and contrast enhancing volumes. The total abnormal volume (TATV) was defined as the sum of the four sub-compartments: necrosis, enhancing region, non-enhancing region and edema. Note that the non-enhancing tumor region was not manually contoured and therefore the TATV manual was defined as the sum of necrosis, enhancing and edema regions.

Results: The auto segmented sub-volumes showed high agreement with the manually delineated volumes (range r : 0.65 – 0.91). Additionally, auto-segmented volumes showed higher correlation with the VASARI features (auto $r = 0.35, 0.60$ and 0.59 ; manual $r = 0.29, 0.50, 0.43$, for percentages of contrast-enhancing, necrosis and edema, respectively). The relative contrast-enhancing volume and the post contrast abnormal volume (necrotic core + contrast enhancing region) showed the highest C-index (0.73 and 0.72), comparable to manually defined volumes ($p = 0.22$ and $p = 0.07$, respectively). The non-enhancing region defined by BraTumIA showed significantly higher prognostic value ($CI = 0.71$) than the tumor-associated edema ($CI = 0.60$), both of which could not be separated by manual delineation.



Scatter plots showing the correlation between different tumor regions as defined fully automatically or manually drawn. Necrosis showed the weakest correlation (A, $r = 0.65$). Stronger correlations were found for the contrast enhancing and FLAIR envelope regions, (B, $r = 0.79$) and (C, $r = .88$), respectively. PCAV (necrosis + enhancing regions) and the TATV (sum of all sub-compartments), $r = 0.90$ and $r = 0.95$, showed strong correlation as well between automatic and manual segmentation (E + F).

Conclusion: BraTumIA tumor sub-compartments showed higher correlation with VASARI data, and equivalent performance in terms of prognosis compared to manual sub-volumes. This method can enable more reproducible definition and quantification of imaging based biomarkers and has a large potential in high-throughput medical imaging.

SP024 - Breast CAD and New Breast Imaging Techniques

TRACK 01: IMAGING

SP024.1 - Modelling Breast Cancer Tissue via Analysis of WAXS Signatures

Author(s): Robert J. Leclair

Physics, Laurentian University, Sudbury/CANADA

A wide-angle x-ray scatter (WAXS) method to quantify the composition of cancerous tissue is described. The modeling of cancerous tissue is accomplished by analysis of the differential linear scattering coefficients μ_s of fibroglandular (fib) [μ_s, fib], cancerous breast tissue (μ_s, cancer) and water ($\mu_s, \text{h}_2\text{o}$). A model assumed that cancer consisted of fib and a volume of cancerous cells. Most of the scattering properties of the cells can be attributed to water since cells are composed primarily of water. In this work, the volume of cancerous cells was approximated by a volume of water. A two basis function method was used to estimate the μ_s of cancer, namely $\mu_s, \text{cancer}(x) = a_{\text{fib}} \mu_s, \text{fib}(x) + a_{\text{h}_2\text{o}} \mu_s, \text{h}_2\text{o}(x)$ [Eq. 1], where $\mu_s, \text{fib}(x)$ and $\mu_s, \text{h}_2\text{o}(x)$ are the basis functions, a_{fib} and $a_{\text{h}_2\text{o}}$ are coefficients. The variable $x = (1/\lambda) \sin(\theta/2)$ is the momentum transfer which combines dependence of scatter on x-ray wavelength (λ) and scatter angle θ . A system of 78 equations corresponding to x values ranging from 0.80 to 3.2 nm^{-1} was constructed. The coefficients a_{fib} and $a_{\text{h}_2\text{o}}$ of this overdetermined system were calculated via least-squares using the singular value decomposition (svd) method. The coefficients were also used to estimate fractional volumes v of fib (v_{fib}) and h_2o ($v_{\text{h}_2\text{o}}$), namely $v_{\text{fib}} = a_{\text{fib}} / (a_{\text{fib}} + a_{\text{h}_2\text{o}})$ and $v_{\text{h}_2\text{o}} = a_{\text{h}_2\text{o}} / (a_{\text{fib}} + a_{\text{h}_2\text{o}})$. These v values were then used to estimate another more meaningful μ_s estimate of cancer given by $\mu_s, \text{cancer}(x) = v_{\text{fib}} \mu_s, \text{fib}(x) + v_{\text{h}_2\text{o}} \mu_s, \text{h}_2\text{o}(x)$ [Eq. 2]. For one set of diffraction data, $a_{\text{fib}} = 0.23$, $a_{\text{h}_2\text{o}} = 0.73$, $v_{\text{fib}} = 0.24$ and $v_{\text{h}_2\text{o}} = 0.76$ and for the other set $a_{\text{fib}} = 0.83$, $a_{\text{h}_2\text{o}} = 0.31$, $v_{\text{fib}} = 0.73$ and $v_{\text{h}_2\text{o}} = 0.27$. For the first set of data both μ_s estimates (i.e. Eqs. 1 and 2) matched the measured μ_s cancer well whereas for the latter only the μ_s via Eq. 1 provided a reasonable match. The modeling of cancerous tissue via analysis of WAXS signals is an interesting method to learn more about the characteristics of cancer. It was not surprising to see differences in predictions when using different WAXS data for breast tissue since they were different in the first place. The different results obtained justify the needs for more studies on the acquisition of WAXS signals of breast tissue. The presence of fat tissue could have affected the WAXS signals. In a future work, a WAXS fat subtraction protocol will be implemented in order to measure the μ_s coefficients of fib and cancerous tissue without the effects of fat. The measurements of μ_s for cells will also be done. Such data will help in characterizing the make-up of cancer and help determine the potential diagnostic use of WAXS.

SP024.2 - Analysis of 80 kV WAXS Measurements with a CdTe Breast Biopsy Diffractometer

Author(s): Nancy McDonald, Robert J. Leclair

Physics, Laurentian University, Sudbury/CANADA

The wide-angle x-ray scatter (WAXS) signatures of breast tissue may provide an additional source of diagnostic information in the realm of breast diagnostics. Measurements to test the ability of exploring a larger momentum transfer x space with a custom built breast biopsy CdTe diffractometer were performed. 80 kV 3.2 mm diameter beams of 3 min duration interrogated 5 mm diameter, 2 to 5 mm thick samples of polymethyl methacrylate (PMMA) and polycarbonate as well as a 5 mm thick water sample. Scattered spectra $N_s(E)$

were detected at $\theta=6^\circ$ with a $25\text{ mm}^2 \times 1\text{ mm}$ thick CdTe detector. A 3 mm diameter aperture placed 4 cm above the detector yielded a solid angle of detection $\Omega = 4.9 \times 10^{-5}\text{ sr}$ at the sample center. The probed x range was from 0.3 nm^{-1} to 3.38 nm^{-1} . Linear differential scattering coefficients μ_s were calculated via a semianalytical model and compared qualitatively with μ_s calculated using coherent form factors and incoherent scatter functions from the literature. Because of the use of a higher kV beam, the effects associated with fluorescence escape and hole tailing in the CdTe crystal were investigated via the application of a detector response function. The incident spectrum $N_0(E)$ was estimated via application of the scatter model in reverse fashion using measurements of N_s and literature μ_s of plastics. Plastics of varying thicknesses were used to estimate $N_0(E)$. The μ_s of a 5 mm thick water sample matched fairly well with literature between $0.42\text{ nm}^{-1} < x < 1.68\text{ nm}^{-1}$, however, above this region discrepancies occurred. No significant effects were observed when using different sample thicknesses to obtain $N_0(E)$. The same comparisons were performed for a 5 mm thick PMMA sample. These results matched well with literature over the whole range. It is anticipated that some of the pinhole scatter interacted with the Pb holder and then contaminated the N_s spectra. The contamination would be similar for both plastics because of their similar μ values. Regardless, if the μ of the sample being analyzed are similar to those of the sample used to get N_0 , the system is capable of probing a wider x range using an 80kV beam. The detector response function did not have a significant effect on the μ_s curves.

SP024.3 - AM-FM features for the classification of Regions of Interest towards the Development of a Breast Cancer Density Specific Computer Aided Detection System

Author(s): Styliani Petroudi¹, Ioannis Constantinou¹, Chrysa Tziakouri², Athos Antoniadou¹, Christakis Charalambous¹, Marios Pattichis³, Constantinos Pattichis¹

¹University of Cyprus, Nicosia/CYPRUS, ²Nicosia General Hospital, Nicosia/CYPRUS, ³University of New Mexico, Albuquerque/UNITED STATES OF AMERICA

Breast Cancer is the most common cancer in women worldwide. As mammographic double interpretation is not possible everywhere, and with the number of cases rising in addition to time and cost constraints, the development of Computer Aided Detection (CAD) systems with high sensitivity and high specificity is important. Mammographic breast density refers to the prevalence of fibroglandular tissue as it appears on a mammogram and it is an important breast cancer factor risk. Furthermore, breast density may mask abnormalities and/or lower the sensitivity of mammography. The development of density specific CAD systems coupled with automated breast density classification may alleviate the problem by achieving high sensitivity and specificity for certain breast density classes. Women with high breast density may seek supplementary screening – in addition to mammography. Amplitude-Modulation Frequency-Modulation based features have been successfully used to characterize mammographic breast density and to automatically classify mammograms into one of the four Breast Imaging Reporting and Data Systems (BI-RADS) mammographic breast density classes.

This work, presents initial results on the use of multi-scale Instantaneous Amplitude (IA), Instantaneous Phase (IP) and Instantaneous Frequency (IF) information from Amplitude-Modulation Frequency-Modulation (AM-FM) decomposition for the classifications of Regions of Interest (ROIs) from low density mammograms to either normal or cancerous/malignant. A Gabor filter-bank using eight orientations and six different frequency scales is applied for AM-FM demodulation. Dominant component analysis is used for the evaluation of IA, IF and IP at each frequency scale. The IA amplitude reflects local image intensity variations, e.g. edges, with different spatial scale variations reflected in different frequency scales whilst the IF measures local frequency content. First and second order

statistical features are evaluated on each of the normalized histograms of the components across the different scales and are used for characterizing the ROI. Support Vector Machines (SVMs) are used for ROI classification.

All mammograms from the Mammographic Image Analysis Society Database that are classified as fatty are used for the development and the evaluation of the presented CAD system. Regions of different size - segmented using block processing from the mammograms classified as normal-, and the ROIs that hold biopsy proven malignancies (well defined masses, speculated masses, other ill-defined masses, architectural distortion and asymmetry but not calcifications) are used for training the SVM classifier. The SVM with RBF kernel is investigated using tenfold cross validation in order to identify the best parameters. The developed CAD system achieves accuracy over 80%, with sensitivity over 85% and specificity over 75% for all types of masses. The prediction results, achieved using the SVM classifier, are very encouraging. Similar CAD systems using different AM-FM with additional texture features will be developed and evaluated specifically for other mammographic density classes.

Acknowledgements: This work is supported by the Cyprus Research Promotion Foundation's Grant ΤΠΕ/ΟΠΙΖΟ/0311(BIE)/029 and is co-funded by the Republic of Cyprus and the European Regional Development Funds.

SP024.4 - Single Scatter Signals during Dual Detector Volume-of-Interest Breast Cone-Beam Computed Tomography: A New Source of Diagnostic Information?

Author(s): Curtis Laamanen, Robert J. Leclair
Physics, Laurentian University, Sudbury/CANADA

Dual detector breast volume-of-interest (VOI) cone-beam computed tomography (CBCT) is a technique that uses two scans to generate higher quality details of a VOI. A full field scan is acquired at low exposure with a flat panel detector whereas a high resolution scan of the VOI is acquired with a high resolution CMOS detector at higher exposure. The data obtained at lower exposure/resolution is used in conjunction with the higher quality VOI data to reconstruct images. The effects of scattered x rays on details within the VOI are reduced by this technique. In this work it is proposed that during the high resolution scan it could be beneficial to also use the flat panel detector to capture some scattered photons from the VOI for diagnostic purposes. Simulations were performed to assess the potential use of the single scatter that could be captured during the high resolution scan. A 14 cm diameter 10.5 cm long cylinder with an embedded 2 cm diameter spherical lesion was considered. Fibroglandular (fib) and water spheres were chosen to represent benign and cancerous lesions. The following percent mass compositions for the cylinder were considered: 80(fib):20(fat), 60:40, 50:50, 40:60, and 20:80. The distance from the source to isocenter was 58 cm and from the isocenter to detector plane 28 cm. Using a 60 kV beam with an HVL of 3.7 mm Al, energy integrated signals (EIS) were computed for each of the 300×300 1 mm² pixels. In normal full field breast CBCT, a typical mean glandular dose of 6 mGy is used. In this work, the VOI scan had an exposure 4x higher than that of the regular full-field CBCT. The incident cone beam irradiated the smallest VOI which included the spherical lesion. The EIS due to scatter (EISs) from the VOI were calculated for both fib and water lesions embedded in the different cylinder compositions. Since contrast reversal occurred across the detector, the information content was increased by adding pixels selectively. Pixels including signals from primary photons were not included in the summations. The variances in pixel signals were based on the propagation of Poisson noise in ideal energy integrating pixels. The signal-to-noise ratio in terms of EISs for malignant versus benign lesions within cylinders of the same composition were on the order of 20 thereby suggesting potential usefulness of the x-ray scattered photons. A problem

that needs to be addressed, however, is that there were significant variations in signals as a function of cylinder composition for a given lesion type. A study which includes a method to estimate the composition of the main phantom will be conducted.

SP024.5 - Investigating automatic techniques in segmentation accuracy of masses in digital mammography images

Author(s): Karem D. Marcomini, Homero Schiabel
 Dept Of Electrical Engineering, University of São Paulo, São Carlos/ BRAZIL

Many procedures have been developed to aid in the early detection and diagnosis of breast cancer. In this context, Computer-Aided Diagnosis (CAD) schemes were designed to provide to the specialist a reliable second opinion. In such schemes there is a complex step which corresponds to the segmentation since good structures classification is dependent on the features extracted from the segmented images. In this work we propose the use of several methods of automatic segmentation of breast lesions, such as: watershed, fuzzy c-means, k-means, Self-Organizing Map (SOM), Enhanced Independent Component Analysis Mixture Model (EICAMM) and level set. In order to evaluate which of them could provide more accurate results in segmenting breast masses segmented images were compared with those manually delimited by an experienced radiologist. Ten quantitative measures were obtained from the images. These segmentation techniques were applied on different types of lesions, including images corresponding to dense breasts. From the evaluation the level set technique has proved being more effective for the images set used to testing all the methods. It has registered a higher overlap rates in relation to the image segmented by the specialist as well as low rates of under and oversegmentation, reflecting in the high accuracy and low false-positive and error rates.

SP024.6 - The Automated Marker-Free Longitudinal IR Breast Image Registration Algorithm

Author(s): Chi-En Lee, Chung-Ming Chen
 Institute of Biomedical Engineering, National Taiwan University, Taipei/TAIWAN

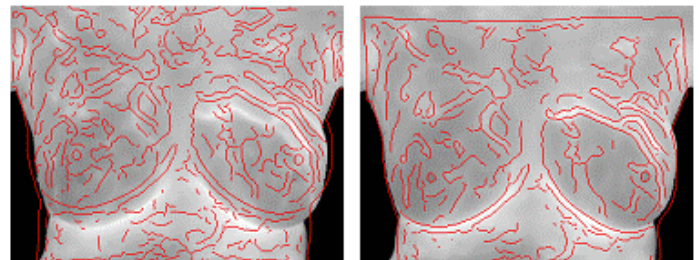
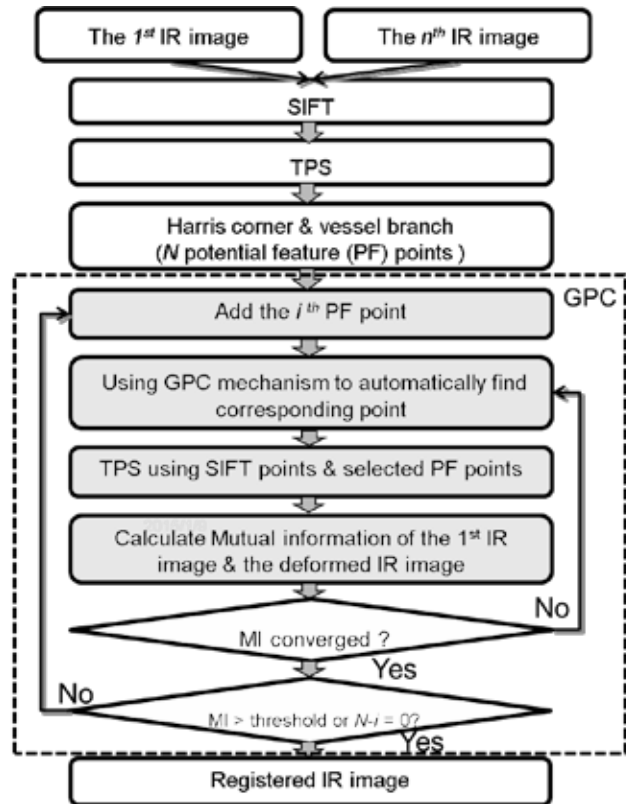
Longitudinal IR image registration is a very difficult task in general because it is impractical and unlikely to keep markers attached on a body surface of a subject for weeks or even longer. To overcome this problem, the new longitudinal IR image registration algorithm (Genetic Particle Competition, GPC), which is the first automated marker-free longitudinal IR image registration algorithm in the world for breast IR images and may be easily extended to other parts of the human body. The algorithm is based on two novel types of fiducial points, which are the corner points of heat patterns and the other is the branch points of the skeletons of heat patterns, and automated determination of corresponding pairs of fiducial points between two images. Suppose two IR images, namely, the 1st IR image and the nth IR image, are registered as depicted on the top of Fig.1. After finding the initial corresponding points by SIFT and deriving the corner points of heat patterns and the branch points of the skeletons of heat patterns, the GPC mechanism operates to find the corresponding point as follows:

Step 1. Randomly generate a set of candidate points around the initial corresponding point, which form the competitors.

Step 2. For each of the competitors on the deformed nth IR image are calculated the mutual information (MI) between the 1st IR image. Define the competitor with the maximal MI as winner, those ranked the top 50% of MIs as the selected competitors, and replace the remaining losers by new randomly generated competitors until the MI of the winner converges.

Step 3. If MI converges, end the registration process for the nth IR image.

Fig. 2 shows the well registration results between the 1st IR image and the nth IR image.



(a)

(b)

SP025 - Dose Calculation: Part 1

TRACK 04: RADIATION ONCOLOGY

SP025.1 - Theoretical ground for testing Monte Carlo transport algorithms coupled to magnetic fields

Author(s): Hugo Bouchard¹, Jacco De Pooter², Simon Duane¹, Alex Bielajew³

¹Radiation Dosimetry, National Physical Laboratory, London/UNITED KINGDOM, ²VSL, Delft/NETHERLANDS, ³Nuclear Engineering And Radiological Sciences, University of Michigan, Ann Arbor/MI/UNITED STATES OF AMERICA

With the advent of MRI-guided radiotherapy, radiation dosimetry in the presence of magnetic fields must be addressed in several ways to assure accurate dose delivery and patient safety. To calculate dose accurately in these conditions, the only known method capable of simulating the transport of charged particles in dense matter in the presence of magnetic fields is Monte Carlo. At the present time, general-purpose codes such as PENELOPE and GEANT4 already offer this option and other codes, such as EGSnrc, remain under development. To assure the accuracy of Monte Carlo results, algorithms must be tested in conditions relevant to radiation dosimetry, such as ionization chamber response to radiation dose. To achieve the same rigorous benchmark as does the Fano cavity test, it is necessary to explore the conditions under which it can be performed in the presence of a magnetic field distribution.

This theoretical study is based on Fano's approach and evaluates the possibility to achieve charged particle equilibrium in heterogeneous media having uniform atomic properties. The Boltzmann radiation transport equation, modified to include the Lorentz force, forms the basis of the theory. Two special conditions for the source and magnetic field distributions are evaluated as potential candidates for new Fano cavity tests. The applicability of Fano's theorem in these conditions is shown and the energy deposition is also derived from first principles.

Using the modified transport equation, it is demonstrated that the two proposed conditions on the source and the magnetic field allow Fano's theorem to apply. Moreover, the energy deposition under these conditions is shown to be identical to the one in the absence of magnetic field, such as in a cavity dose calculation under standard Fano conditions.

This theoretical study demonstrates two possible conditions under which Fano's theorem is applicable in the presence of a magnetic field. While it was previously shown that in general, Fano's theorem cannot hold in the presence of a uniform magnetic field as it does not scale with mass density, this study is a significant improvement towards benchmarking Monte Carlo codes coupling radiation transport with magnetic fields.

SP025.2 - Primary X-ray source spot size modeling for FFF photon beam in VMAT based Stereotactic Radiosurgery – A comparative clinical study using Acuros-XB and AAA dose calculation algorithm

Author(s): Vellian Subramani¹, Murugesan Kathirvel², Gandhi Arun², Shanmugam Thirumalai Swamy³, V.S Subramanian²

¹Radiation Oncology, All India Institute of Medical Sciences, New Delhi/INDIA, ²Research And Development Centre, Bharathiar University, Coimbatore/INDIA, ³Radiation Oncology, YASHODA HOSPITAL, HYDERABAD/INDIA

Aim: Purpose of this study is to find out the appropriate Flatten-

ing Filter Free (FFF) photon beam primary source size for beam modeling in treatment planning system of VMAT based Stereotactic Radiosurgery using Acuros-XB and Analytical Anisotropic Algorithm (AAA) dose calculation algorithm.

Material and Methods: Recently our Clinac-2100CD Varian linear accelerator was upgraded to high dose rate Flattening Filter Free (FFF) 6MV X-rays for Stereotactic Radiosurgery. Beam parameters measured from minimum 2x2cm² to 40x40cm² field. As VMAT/IMRT based Stereotactic Radiosurgery comprises of many small segments, Penumbra modeling play a major role in final dose calculation. Both AAA & Acuros-XB algorithms allow users to fine tune the primary source spot size (SSS) so that computed beam profile penumbra can match with the measured beam penumbra for all the field sizes. SSS were varied from 0 to 2mm in steps of 0.5mm in X&Y direction. For each SSS, dose was calculated for open field sizes of 3x3cm², 5x5cm² & 10x10cm² and was analyzed with measured beam parameters. To evaluate beam modeling a water phantom (size=40x40x40cm³) was created and dose was calculated for different fields & for different SSS. The profiles at dmax and 10cms depth were taken for penumbra analysis with respect to measured profile. For all the SSS & field sizes Distance (in millimeters) to agreement (DTA) were performed between computed & measured 80% and 20% dose point left & right of the central axis (Inflection point method were also utilized). Clinical impact on VMAT based stereotactic treatment analyzed dosimetrically for both algorithms using different SSS beam modeling.

Results: For AAA algorithm, the average DTA at Dmax for SSS of 0, 0.5, 1.0, 1.5, 2.0mm were -0.72±0.57, -0.72±0.57, -0.46±0.56, 0.09±0.40, -0.22±0.42 mm respectively. The average DTA at D10 for SSS of 0, 0.5, 1, 1.5, 2.0 mm were -0.74±0.73, -0.74±0.73, -0.57±0.67, -0.03±0.64, 0.08 ±0.63 mm respectively. Similarly for Acuros-XB algorithm the average DTA at Dmax for SSS of 0, 0.5, 1, 1.5, 2.0 mm were -0.71±0.59, -0.71±0.59, 0.20±0.28, 0.34±0.31, and 0.62±0.38 mm respectively. The average DTA at D10 for SSS of 0, 0.5, 1, 1.5, 2.0mm were -0.52±0.65, -0.52±0.65, -0.15±0.75, -0.09±0.78, 0.11±0.79 mm respectively. Stereotactic treatment plan analysis shows that average PTV mean dose variation with SSS 0.75mm for AAA was found -2.0% compared to 1.0mm default SSS, whereas Acuros-XB SSS 1.2mm variation -1.2% compared to default 1.0mm. Absolute dose measurement results using small volume ion chamber and predicted plan dose variation for VMAT stereotactic plans found very minimal with AAA SSS 0.75mm and Acuros-XB SSS 1.2mm compared to algorithm default SSS.

Conclusion: For AAA algorithm the results shows a good agreement between measured dose and calculated dose for spot sizes of 0.5-1mm. On the other hand for Acuros-XB algorithm, a spot size of 0.5-1mm agrees better for the field size up to 5x5cm² & a spot size of 1-1.5mm agrees better for the field size greater than 5x5cm². Algorithms showed good agreement with measurement for range of fields provided primary source spot configuration has been adequately tuned for precise dose calculation and delivery.

SP025.3 - A Geant4 Helical Tomotherapy model as a tool for 3D dose distribution evaluation

Author(s): Alessandro Esposito¹, Barbara Caccia², Elisabetta Cagni³, Emilio Mezzenga³, Mauro Iori³

¹INESC TEC, Porto/PORTUGAL, ²Technology And Health Department, Istituto Superiore di Sanità, Rome/ITALY, ³Medical Physics Unit, Irccs, Arcispedale Santa Maria Nuova, Reggio Emilia/ITALY

Very high technological level is involved in Helical Tomotherapy (HT). The gantry rotation, couch speed, dose rate and accurate MLC leaf positioning are crucial for accurate dose delivery. For a high quality and safe treatment, a machine Quality Assurance (QA) program and patient-specific dose verifications are requested. The most detailed

and complete description of radiation-matter interaction is taken into account by Monte Carlo (MC) method. Therefore, this approach has become a key issue in patient-specific dose verifications.

In this work, a complete and detailed numerical MC model of a HT unit is developed and commissioned on the basis of experimental data, in order to apply it to QA and treatment plan dose check. The full structure of the simulated HT unit is presented in Figure 1 in both longitudinal and transversal view. After commissioning, the capability of the model unit to well reproduce (or verify) some QA and patients plans has been tested through comparison with the HT treatment planning system (TPS) in terms of 3D dose distribution for a treatment plan on water equivalent specific phantom. In Figure 2 the comparison between HT-TPS and GEANT4 MC calculated dose distributions is shown in transversal view.

The reliability of the simulated system is proven by the very good agreement between simulated and experimental PDD and dose profiles in commissioning. A gamma function test has been applied to the whole data set obtaining 97.5% of gamma point to be less than unity using 2mm and 2% as gamma criteria.

Furthermore, the application can be considered a solid tool to implement and evaluate a patient-specific dose QA for the HT plans given the perfect agreement with the HT-TPS shown by dose profiles in the calculated 3D dose distribution of the treatment plan in water equivalent phantom.

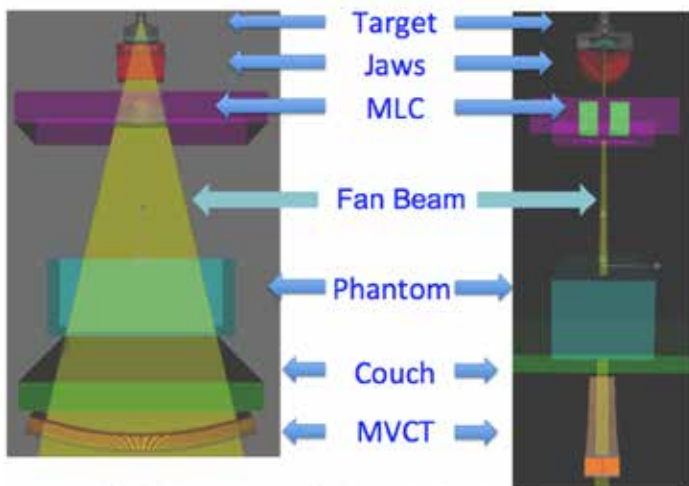


Figure 1. Model of the helical tomotherapy unit (a) in the two sides (longitudinal and transversal)

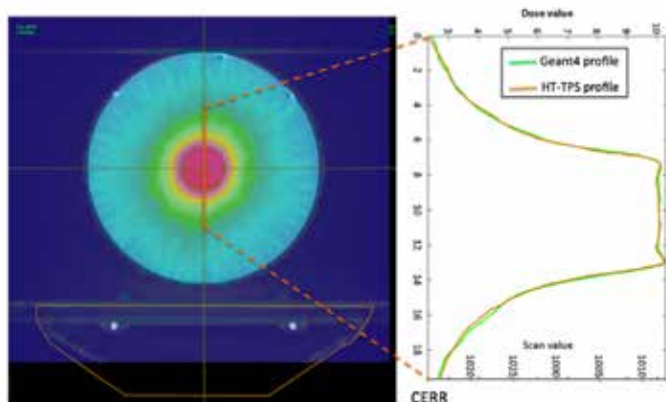


Figure 2 - Comparison of dose distribution obtained by Geant4 simulation with the HT-TPS calculation on cheese phantom in transversal view

SP025.4 - Development of 4D actual delivered dose calculation system for dynamic tumor-tracking irradiation with a gimbaled linac

Author(s): Yoshitomo Ishihara¹, Akira Sawada², Nami Ueki¹, Nobutaka Mukumoto¹, Mitsuhiro Nakamura¹, Yuki Miyabe¹, Yukinori Matsuo¹, Takashi Mizowaki¹, Masaki Kokubo³, Masahiro Hiraoka¹
¹Department Of Radiation Oncology And Image-applied Therapy, Kyoto University Graduate School of Medicine, Kyoto/JAPAN, ²Faculty Of Medical Science, Kyoto College of Medical Science, Kyoto/JAPAN, ³Department Of Radiation Oncology, Kobe City Medical Center General Hospital, Kobe/JAPAN

(1) Purpose

In previous works, we have developed an in-house integrated four-dimensional (4D) Monte Carlo (MC) dose calculation system as a routine verification tool for dynamic tumor-tracking (DTT) irradiation. The purpose of this study was to develop 4D actual delivered dose calculation system for DTT irradiation by gimbals mechanism with Vero4DRRT.

(2) Method

First, plans were created for five patients having lung cancers under the normal protocol for DTT. Furthermore, the modified DTT plans were created in consideration of several errors such as intrafractional mechanical, positional predictive, and overall targeting errors during DTT irradiation. These errors were retrospectively computed from orthogonal fluoroscopy images and the system log files stored during DTT irradiation. Subsequently, 4D MC dose calculation was performed with 6-MV photon beam delivered by the Vero4DRRT using EGSnrc for both the original and the modified DTT plans, respectively. At that time, phase-space data at each respiratory phase was created from the particle data under the MLC with or without the above errors, respectively. Next, 4D dose distribution was created by summing up the dose distribution under the geometrical combination of the target and the MV beam at each respiratory phase. The dose distribution computed with the above errors was regarded as the delivered dose distribution during DTT irradiation while the dose distribution computed without the above errors was regarded as the planned DTT dose distribution. Finally, isodose curves and DVHs were compared between the planned DTT and the delivered DTT dose distribution.

(3)Result

For all cases, 2D gamma passing rate was 93% using criteria of 2% / 2 mm for each dose distribution on the axial, sagittal, and coronal planes at the isocenter, respectively. CTV coverage, mean dose within the lung, and maximum dose within the spinal cord were comparable between the delivered DTT and the planned DTT dose distribution.

(4) Conclusion

We have developed 4D actual delivered dose calculation system for DTT irradiation using the gimbaled x-ray head. The result has demonstrated that DTT irradiation with Vero4DRRT achieves the dose delivery with high accuracy.

SP025.5 - Organ Doses from Hepatic Radioembolization with Y-90, Sm-153, Ho-166 and Lu-177: A GEANT4 Monte Carlo Simulation Study

Author(s): Nurul A.A. Hashikin¹, Chai Hong Yeong¹, Susanna Guatelli², Basri Johan Jeet Abdullah¹, Kwan Hoong Ng¹, Alessandra Malaroda², Anatoly Rozenfeld²

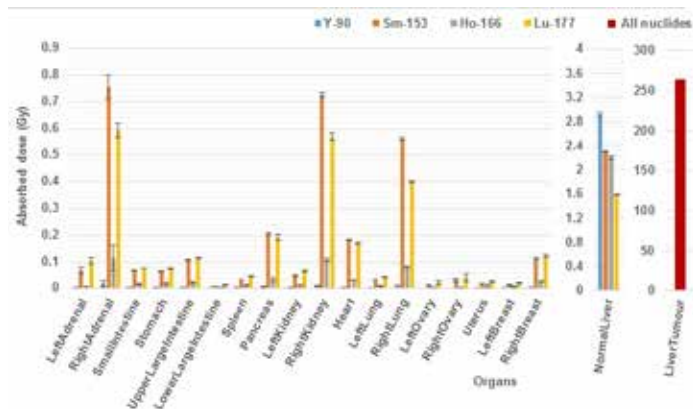
¹Department Of Biomedical Imaging, Faculty Of Medicine, University of Malaya, Kuala Lumpur/MALAYSIA, ²Centre For Medical Radiation Physics, Faculty Of Engineering And Information Sciences, Univer-

sity of Wollongong, Wollongong/NSW/AUSTRALIA

Introduction— Y-90 radioembolization are increasingly used for palliative treatment of advanced liver cancer. Since its physical decay is fully via beta emission, imaging following the treatment is rather challenging. Radionuclides with both beta and gamma emissions have been explored as alternative to Y-90 in liver radioembolization, however little information was available in terms of internal radiation dosimetry.

Materials & Methods— Monte Carlo simulation using GEANT4 source code was carried out. The GEANT4 advanced example human_phantom was used. A mathematical female phantom was adopted with organ geometries as specified in MIRDPamphlet 5. A medium size, spherical hepatic tumor with radius, $r = 4.3$ cm was modelled within the liver volume. Y-90 sources were isotropically distributed within the tumor with total activity of 1.82 GBq determined using Body Surface Area (BSA) method recommended by SIRTex (Sydney, Australia) for the Y-90 therapy. The dose was calculated in all the organs of the human phantom. The simulation was carried out with the assumption of no lung and extrahepatic shunting, with full localization of Y-90 sources within the tumor volume. The resulting tumor dose was validated by comparing it with the dose calculated using partition model. The simulation study was repeated substituting Y-90 with Sm-153, Ho-166 and Lu-177. GEANT4.9.6.p03 was used.

Results— The 333 cm³ tumor volume corresponded to 18% tumor involvement. The tumor and normal liver tissue doses for the Y-90 simulation were (262.9 ± 0.6) Gy and (2.9 ± 0.1) Gy, respectively. In order to deliver tumor dose equivalent to 1.82 GBq Y-90, approximately 8.32, 5.83, and 4.44 GBq were required for Sm-153, Ho-166 and Lu-177, respectively. Doses to other organs were mainly dependent on the gamma energies (Figure 1). All the organ doses did not exceed 1 Gy.



Discussions— Although the organ doses deriving by Sm-153 and Lu-177 were relatively higher compared to Ho-166 and Y-90, the doses were still far below the maximum tolerance limit commonly used in radiotherapy, i.e. 60, 23 and 17.5 Gy for adrenal glands, kidneys and lungs, respectively. Alternative treatment with Sm-153 or Lu-177 is still feasible as long as the organ tolerance limit were not exceeded.

Conclusion— Ho-166, Lu-177 and Sm-153 offer the advantage of emitting useful gammas for post-procedure imaging. They show potentials as Y-90 substitutes for liver radioembolization, delivering a comparable tumor dose, and doses within the maximum tolerance limit to the surrounding organs.

SP025.6 - Stereotactic Ablative Radiotherapy (SABR) for lung cancer using Volumetric Modulated Arc Therapy (VMAT) with a 10x Flattening Filter Free (FFF) beam: validation of the calculated dose distribution using Monte Carlo

Author(s): Tony Mestrovic, Matthew Murray, Reid Townson, Sergei Zavgorodni
 Medical Physics, BC Cancer Agency, Victoria/BC/CANADA

Introduction:

The use of 10xFFF beams for lung SABR treatments has been gaining popularity in the recent years due to the high dose rates (up to 2400 MU/min). The tissue/lung interface in and around the Planning Target Volume (PTV) presents a challenge for dose calculation algorithms to accurately predict the dose to the PTV for 10xFFF beams.

Purpose:

The purpose of this study was to compare the calculated dose distributions using Analytical Anisotropic Algorithm (AAA) and AcurosXB Algorithm in Eclipse™ (Varian) to Monte Carlo (MC) generated dose distributions for 10xFFF VMAT lung SABR treatments.

Method/Materials:

Thirteen lung SABR patients were used in this study with varying PTV locations and sizes (7cc-141cc). Both AAA and AcurosXB were used to calculate the dose distributions for the same treatment plan in Eclipse. The MC system used in this study employed BeamNRC and DoseXYZ codes. The modeling of the MLC leaves was done using the dynamicVarian MLC (DYNVMLC) model. For each patient, the MC system was used to calculate the dose distribution for the same treatment plan that was used in Eclipse. The MC calculated dose was compared to AAA and AcurosXB calculated doses, in terms of: 1) volume of the PTV receiving the prescribed dose (48Gy/4); and 2) PTV mean dose.

Results:

Generally, the dose distributions calculated with AAA and AcurosXB algorithms differed significantly in the peripheral parts of the PTV, near the lung/tissue interface (figure 1). Figure 2 displays the PTV V48Gy and the PTV mean dose for AAA, AcurosXB and MC. The AAA over-estimated the PTV coverage, especially for smaller PTVs. The AcurosXB algorithm showed a significantly better agreement with MC compared to AAA.

Conclusions:

The AcurosXB algorithm agrees significantly better with MC compared to AAA, and therefore it should be used for 10xFFF VMAT lung SABR treatments.

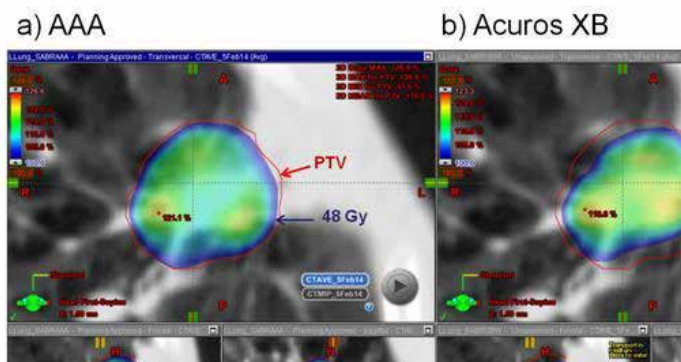


Figure 1

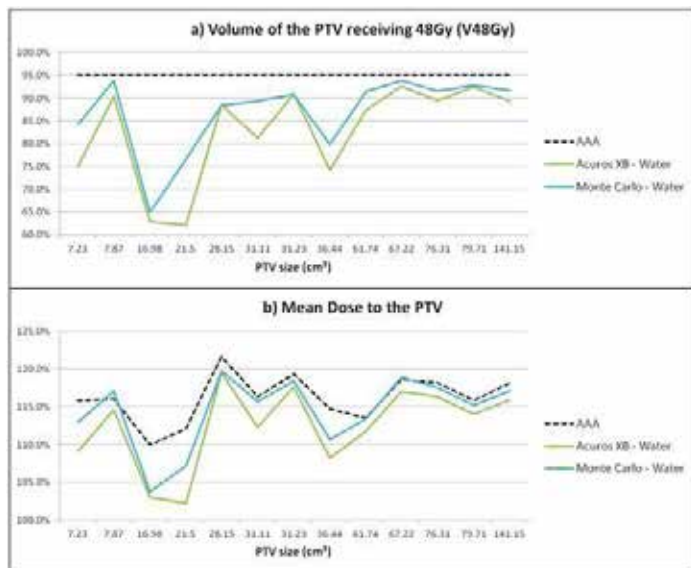


Figure 2

SP025.7 - Performance of the ACUROS™ dose calculation algorithm for 6 MV FFF beams in inhomogeneous media

Author(s): Matthew Schmid¹, Tony Teke²

¹BC Cancer Agency- Centre for Southern Interior, Kelowna/BC/CANADA, ²BC Cancer Agency- Centre for Southern Interior, Kelowna/CANADA

Purpose:

FFF beams are now commonly used in radiation therapy treatment. Because of the high dose rate that these beams typically offer, they are often used for stereotactic body radiotherapy (SBRT) of the lung. Accurate dose calculations are particularly important in these cases due to the high fractional doses delivered. In this study, the accuracy of Varian’s Acuros XB dose calculation algorithm is investigated in inhomogeneous phantoms for both open fields and VMAT treatments.

Methods:

Three series of tests were performed using three different phantoms. ACUROS calculated doses were compared to Monte Carlo (MC) calculations, the anisotropic analytical algorithm (AAA), and film measurements. The phantoms were comprised of water equivalent material, lung equivalent material, and bone equivalent material. In one series of tests, the doses at various depths in slabs of lung and bone material embedded in solid water were evaluated. A second series of tests evaluated the 2D dose distribution in planes containing inhomogeneity boundaries, and a third set of tests used the QUASAR™ phantom (Modus Medical Device Inc.).

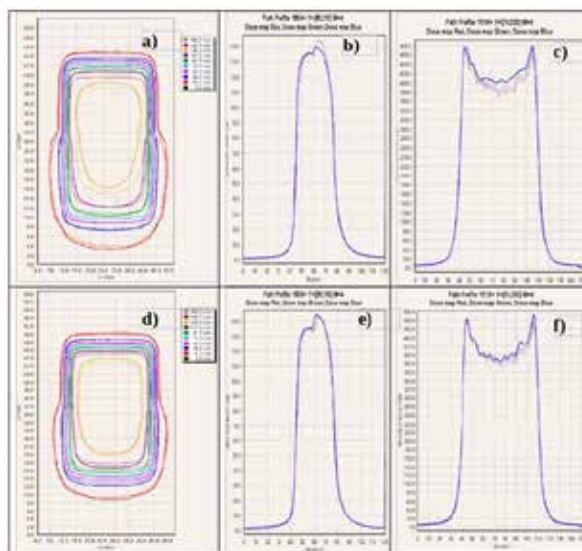
Results:

The depth-dose calculations in a slab of lung material embedded in solid water showed good agreement between the Acuros XB, MC, AAA, and measured values. The calculated depth dose values in a slab of bone embedded in solid water calculated by AAA agreed well with the measured values. Acuros calculated depth doses to medium showed excellent agreement with Monte Carlo calculations (dose to medium) and good agreement with film measurement, but differences above 5% were found in the calculation of dose to water with measurements. Monte Carlo calculations were repeated with the Gachromic film simulated by a thin layer of water and showed excellent agreement with measurements. The 2D dose distributions calculated using the Acuros XB algorithm showed substantially bet-

ter agreement with measurement than the AAA calculations (Figure 1 a,b,d and e). This was also true for the dose calculations in the lung phantom and for VMAT plans on the QUASAR phantom (Figure 1 c and f).

Conclusions:

The Acuros XB algorithm performs well for calculating doses for 6 MV FFF beams in and around lung-like inhomogeneities, and shows better agreement with measurements than the AAA algorithm. In bone-like material, it shows good agreement in calculating the dose to medium, but differences above 5% were found in the calculation of dose to water.



SP025.8 - Ray Tracing Algorithm for Virtual Source Modelling based on Evaluation of Rounded Leaf End Effect of Multileaf Collimator

Author(s): Dong Zhou, Hui Zhang, Peiqing Ye
Department Of Mechanical Engineering, Tsinghua University, Beijing/CHINA

Rounded leaf end effect of multileaf collimator plays a role in penumbra characteristics of dose profile. It strongly influences dose target volume conformity and organ at risk sparing for radiation therapy. Previous studies have shown that parameters in virtual source model could be fitted using dose distribution results obtained from Monte Carlo simulation or dosimetric measurement. However, there is a lack of research in literature reporting on virtual source modeling with the rounded leaf end effect incorporated. In this study, we present an analytical method for virtual source modeling by evaluation of the rounded leaf end effect of multileaf collimator on dose profile. We confine our study to single source modeling, with source energy distribution of Gaussian shaped. Ray Tracing algorithm is introduced and parameter estimation is conducted to revise the source size. Model verification is performed with numerical simulation, which is conducted based on the Monte Carlo codes of EGSnrc/BEAMnrc. It is shown that Ray Tracing algorithm employing the focal spot size of photon source would result in reduced penumbra width, compared with the simulation counterpart. This observation is probably related to the aperture effect of multileaf collimator. In contrast, results of penumbra width and radiation field edge offset using revised source size obtained with parameter estimation agree well with Monte Carlo simulation. In summary, the method we propose could provide insight into virtual source modeling using Ray Tracing algorithm.

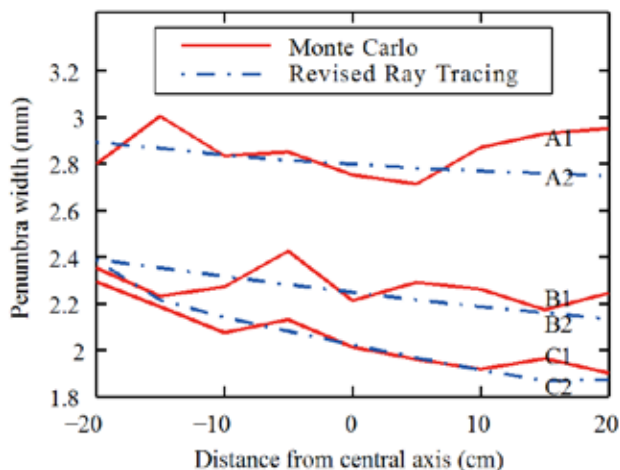


Fig. 1 Penumbra width for Monte Carlo simulation and ray tracing algorithm with source size 2.17 mm FWHM. Curve A, B, and C stand for radius 4, 8 and 15 cm.

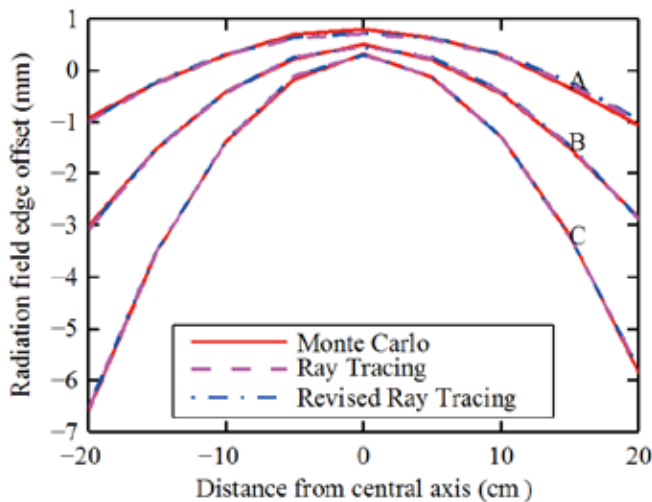


Fig. 2 Radiation field edge offset for Monte Carlo simulation and ray tracing algorithm with source size 2 and 2.17 mm. Curve A, B, and C stand for radius 4, 8 and 15 cm.

SP026 - Reference Dosimetry - Developments and Monitoring

TRACK 05: DOSIMETRY AND RADIATION PROTECTION

SP026.1 - The Development of a Device for the Fricke Dosimetry for HDR Brachytherapy

Author(s): Camila Salata, Mariano G. David, Carlos E. Dealmeida Dbb, Universidade do Estado do Rio de Janeiro, Rio de Janeiro/ BRAZIL

HDR-BT is considered an important option for cancer treatment, but the calibration of the Ir-192 is complex. The Fricke dosimetry has been considered an option to determine the absolute absorbed dose to water. It is composed mainly of water and ferrous sulfate, and the ferric ions in the solution will be converted to ferrous ions by the ionizing radiation, proportionally to the absorbed dose into the solution. The optical density of the solution is measured using a spectrophotometer. As this is a liquid dosimeter it is important to have a device where the solution will be irradiated. Some characteristics of the device should be considered: the wall material should be water equivalent and shouldn't react with the solution; it must be sealed, but easy to vert the solution from the vessel into a cuvette to read it with the spectrophotometer. The main purpose of this study was to develop a device for the irradiation of the Fricke solution, using the HDR-BT Ir-192 sources.

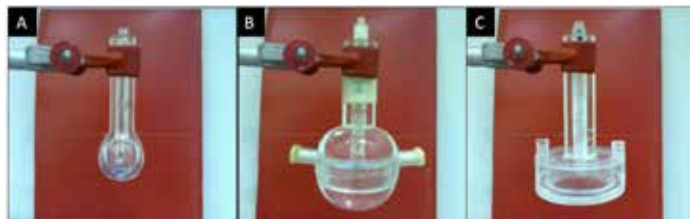


Figure 1: Evolution of the devices created for the Fricke Dosimetry.

The first device created (Figure 1A) consisted of two glass balloons, one inside the other. The solution was disposed in the space between the balloons. The source was positioned in the center, inside a glass tube so it didn't have any contact with the solution. Some measurements were done, and the disadvantages of this device were: the glass material wasn't water equivalent; and the solution wasn't homogeneously irradiated, as the distance from the source wasn't the same on all the irradiated solution. The device was redesigned to improve the measurements (Figure 1B). The main changes were: the wall material was water equivalent, PMMA; the solution volume irradiated was only a central ring, so the solution was homogeneously irradiated. More measurements were done and it was very difficult to fill the device with the solution, and also difficult to vert the solution to the cuvette. The current device (Figure 1C) is a cylinder ring, where the solution is disposed and have corrected those problems. The source position is now calculated to be at the center of the ring. Now it is easier to fill it with the solution, and to vert the solution to the cuvette. Those improvements of the device are very important to the development of the Fricke dosimetry as an option for the Ir-192 sources calibration.

SP026.2 - A New Methodology for the Determination of the G-value for Fricke Dosimetry

Author(s): Camila Salata¹, Leo D.O. Franco², Mariano G. David¹, Carlos E. Dealmeida¹

¹Dbb, Universidade do Estado do Rio de Janeiro, Rio de Janeiro/BRAZIL, ²Dbb, UERJ, Rio de Janeiro/BRAZIL

The Fricke dosimeter is a chemical dosimeter and its base is the ferrous sulfate. It is one of the most widely used chemical dosimeters and has been considered as a possible dosimeter for the determination of the primary standard for the absorbed dose to water of Ir-192 High Dose Rate brachytherapy (HDR-BT) sources. The Fricke dosimeter is mainly composed of water, so its attenuation of radiation is very similar to the water, which turns possible its use as an absolute dosimeter. During the interaction of the radiation with the Fricke solution the ions Fe^{2+} are converted in Fe^{3+} , and this conversion is proportional to the absorbed dose at the solution. One of the parameters used to determine the absorbed dose at the Fricke solution is the chemical yield, known as the *G-value*. The *G-value* can be defined as the number of molecules of Fe^{3+} produced per Joule of energy absorbed in the solution. This parameter has been determined by different authors, for different energies, but those data are old, and the methodology used was based on interpolations. This study proposes a new methodology for the determination of the *G-value* for Ir-192 HDR-BT sources. On the methodology proposed it was used a PMMA phantom (figure 1A) filled with water with three supports of PMMA for the Fricke solution, one for the ion chamber, and one for the Ir-192 source in the center (figure 1B).

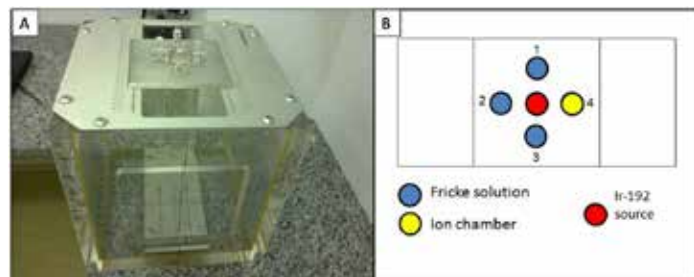


Figure 1: A) PMMA Phantom with the supports for Fricke solution, ion chamber and Ir-192 source. B) The positioning of the supports in detail.

The position of the supports were fixed for each irradiation, and changed clockwise direction, after each irradiation. The source was always fixed in the center of the support. After each irradiation the optical density of the solution was read using a Micronal spectrophotometer. The absorbed dose in the Fricke solution at each position was considered equal to the dose determined by the ion chamber on the same position, the *G-value* was determined for each position. The mean *G-value* found was $1.5786 \times 10^{-6} \pm 0.014 \mu\text{mol}\cdot\text{J}^{-1}$ ($k=1$), which is consistent with the data in the literature. The main advantage of this proposed method is that the *G-value* is measured using the Ir-192 source directly, and not interpolations. Those results will be repeated using a new spectrophotometer recently acquired by the LCR, with better resolution and sensibility. This will improve the uncertainties associated with the measurements.

SP026.3 - The Use of Fricke Dosimetry as a Primary Standard for the Absorbed Dose to Water for 192Ir HDR-BT Sources: Determination of the G-value

Author(s): Camila Salata¹, Mariano G. David¹, Paulo H. Rosado², Islam El Gamal³, Ernesto Mainegra-Hing⁴, Claudiu Cojocaru⁴

¹Dbb, Universidade do Estado do Rio de Janeiro, Rio de Janeiro/BRAZIL, ²Dbb, UERJ, Rio de Janeiro/BRAZIL, ³National Research Council, Ottawa/ON/CANADA, ⁴National Research Council, Ottawa/CANADA

High dose rate brachytherapy (HDR-BT) using ^{192}Ir sources is well accepted as an important treatment option and thus requires an accurate dosimetry standard. However, a dosimetry standard for the direct measurement of the absolute dose to water for this particular source type is currently not available. The Fricke dosimetry is being considered an option as a primary standard for the dose to water for ^{192}Ir sources. This dosimetry technique depends on the oxidation of ferrous ions (Fe^{2+}) to ferric ions (Fe^{3+}) by ionizing radiation. The increased concentration of ferric ions is measured spectrophotometrically at 304 nm. For the determination of the absorbed dose to water, using Fricke dosimetry, it's first necessary to determine the absorbed dose in the Fricke solution. For this purpose some parameters are needed: the difference of the optical density between the control and the irradiated solutions; the pathlength of the cuvette; the density of the solution; the molar linear absorption coefficient of the ferric ions; and the radiation chemical yield of ferric ions, also known as the *G-value*. Among those parameters the *G-value* is one of major concern, as the few literature data on its determination for the ^{192}Ir energy range are old, with large uncertainties and not well described. Previous studies showed different methods for the *G-value* determination: ionometric and calorimetric measurements; estimation of the energy-weighted *G value* from published values, using interpolation; empirically, calculating from empirical equations the radiation yields of the primary products due to solution radiolysis; among others. The *National Research Council* Canada (NRC) developed a promising new method for the *G-value* determination, using the Fricke solution. In this study the NRC method was reproduced at the *Radiological Sciences Laboratory* (LCR), in Rio de Janeiro/Brazil. Briefly, this method consists of interpolating the *G-values* calculated for ^{60}Co and 250 kV x-rays for the average energy of ^{192}Ir (380 keV). The *G-value* for ^{60}Co is calculated using the dose to water determined by a calibrated ion chamber, and making it equivalent of the dose to water in the Fricke solution, also using Monte Carlo calculated factors for this conversion. The same procedure is done for the 250 kV x-rays energy, but the quantity measured with the ion chamber is the air kerma. For the irradiations with the Fricke solution, the NRC developed a device where the polyethylene bags filled with Fricke were later disposed. The irradiations and measurements of this present study were performed at the Brazilian National Laboratory. The result found for the *G-value* for 380 keV is $1.540 \mu\text{mol}\cdot\text{J}^{-1} \pm 1.0\%$. It's important to highlight that this value is different from the ones reported in the literature by at most 3%. For this reason more measurements will be done to confirm this result.

SP026.4 - IAEA Dosimetry Laboratory support to the IAEA/WHO SSDL Network

Author(s): Igor Gomola, Istvan Csete, Ladislav Czap, Joanna Izewska, Ahmed Meghizifene
Nuclear Sciences And Applications, International Atomic Energy Agency, Vienna/AUSTRIA

The IAEA Dosimetry Laboratory (DOL) is the central laboratory of the IAEA/WHO Network of Secondary Standards Dosimetry Laboratories (SSDLs). In 1976, the IAEA in collaboration with the WHO established this Network to provide a forum in which national SSDLs could regularly perform measurement comparisons and thus strengthen confidence in radiation dosimetry coherence worldwide. This Network, through its 84 SSDL members designated by Member States, provides a framework to establish a direct linkage of national dosimetry standards to the international measurement system (SI) of standards and the dissemination of SI quantities and units to end users through the proper calibration of field instruments by the SSDLs.

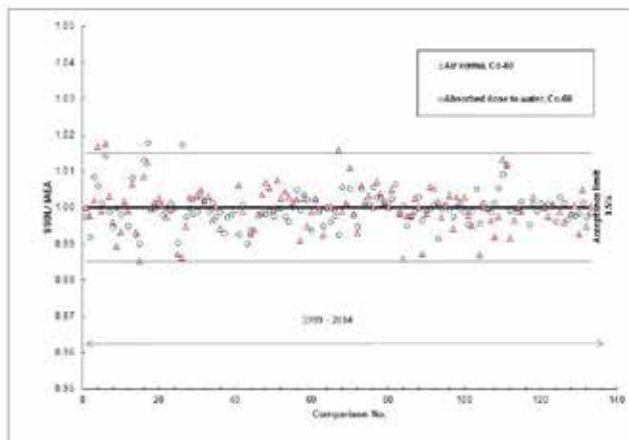
A Quality Management System (QMS) has been established for the DOL following the guidelines of EN ISO/IEC 17025:2005 standard. In 2005, the Joint Committee of the Regional Metrology Organizations (JCRB) and the Bureau International des Poids et Mesures (BIPM)

formally acknowledged that the DOL QMS satisfies the requirements of the Mutual Recognition Arrangement established by the Committee for Weights and Measures (CIPM-MRA). Since that time, the 23 different calibration capabilities of the DOL are peer reviewed regularly; they are internationally accepted, and published in the frame of the CIPM-MRA.

The activities of the IAEA include an inter-laboratory comparison programme (for air kerma, K_{air} , and absorbed dose to water, D_w , in Co-60 beam, and K_{air} for diagnostic X-ray beam qualities) that enables the participating SSDLs to harmonize their calibration practices for measuring instruments used for the determination of different dosimetry quantities in line with the IAEA Codes of Practice TRS-398 and TRS-457. (Figure 2. shows the results for K_{air} and D_w in Co-60 beam)

In addition, the IAEA offers training opportunities in radiation dosimetry, calibration of dosimetry standards dosimetry audits, and quality management for SSDL staff from Member States. The training of SSDL staff contributes to the improvement of measurement capabilities in radiation dosimetry for radiation therapy, diagnostic radiology and radiation protection applications of ionizing radiation in IAEA Member States.

Figure 1. Results of SSDLs in the ongoing therapy level comparison program using participants' transfer chambers. (Participant gets further assistance to perform corrective action(s) if its result is out of the acceptance limit.)



SP026.5 - Measurement of W_{air} in high energy electron beams

Author(s): Claudiu D. Cojocaru, Malcolm R. McEwen, Carl K. Ross
 Ionizing Radiation Standards, National Research Council Canada, Ottawa/ON/CANADA

Ionization chambers are widely used for measuring radiation fields. In the majority of cases, an ion chamber is used as a secondary device (with a calibration against a primary standard of air kerma or absorbed dose) or in a purely relative way (determination of output factors, beam commissioning, etc). For absolute measurements, as in the primary determination of air kerma, a conversion factor is required - W_{air} , the mean energy expended by an energetic electron to create an ion pair in the air of the chamber cavity. A consensus value exists for W_{air} ^{60}Co γ rays, based mainly on comparing the response of a graphite calorimeter with that of a graphite ionization chamber. At higher electron energies (> 5 MeV) the graphite/air stopping power ratio (required to obtain W_{air}) is less dependent on input data such as the mean excitation energy and therefore measurements in the energy range from 5 MeV to 30 MeV will provide

independent information on both the absolute value of W_{air} and its variation with energy.

The Vickers research linac at the National Research Council Canada was used to produce broad beams of electrons with incident energies of 20 MeV and 35 MeV. The ratio of the response of a graphite calorimeter to that of a graphite-walled cavity ionization chamber (with a well-known measuring volume) was determined for each beam. The measurement depth in graphite was varied to yield different mean electron energies at the measurement point and to test the systematics of the measurement procedure (particularly the calorimeter response). The material properties and the geometries were well known and the two devices were well characterized before their use in the experiment. Using the EGSnrc Monte Carlo and its associated user codes, as well as the best available stopping power data for graphite, we calculate the perturbation effects due to the calorimeter and ionization chamber and the effect of extrapolating from scattered to plane-parallel beams. We also used finite element software to model the thermal response of the calorimeter and determine correction factors for heat conduction.

For a single incident energy there was very good consistency for different measurement depths (standard uncertainty ~ 0.2 %) which indicates that there are no significant systematic errors in the measurement procedure or in the determination of correction factors. However, a difference of 1 % was observed between the mean values for W_{air} obtained in the 20 MeV and 35 MeV electron beams. An initial analysis has not indicated a problem with either set of measurements but a calorimeter with a revised design is under construction to further test some of the heat conduction issues, which contribute the largest correction factor. Taking all the measurements obtained as a single data set we arrive at a mean value of $W_{air} = (34.00 \pm 0.15)$ eV. This value agrees within the overall uncertainties with both the ^{60}Co consensus value and electron beams measurements carried out at the US National Institute of Standards and Technology.

SP026.6 - Monte Carlo corrections for a Fricke-based standard of absorbed dose to water for Ir-192 HDR brachytherapy.

Author(s): Ernesto Mainegra-Hing

Measuring Science And Standards, National Research Council of Canada, Ottawa/CANADA

Purpose: Ir-192 HDR Fricke dosimetry requires a conversion factor dose to Fricke to air-kerma to determine the G-value of a 250 kV x-ray beam, and several correction factors to obtain the dose to water at the reference position. These factors can be determined using Monte Carlo (MC) techniques.

Methods: The G-value for an Ir-192 source is determined by interpolation between the G-values of two known beam qualities, Co-60 and 250 kV x-rays. The G-value of the 250 kV x-ray beam is determined by irradiating a bag with Fricke solution of known volume with a 250 kV beam of known air-kerma. A conversion factor dose to Fricke to air-kerma, DF/K_{air} , is calculated using the EGSnrc user-code cavity combined with a BEAMnrc model of the x-ray source. Knowledge of the Ir-192 G-value makes it possible to measure the dose imparted to a Fricke dosimeter placed at the reference position, immersed in a water phantom. The dose to water at the reference position is derived from the dose to Fricke by applying a conversion to dose to water, f^w_F , and several corrections to remove the effects of the holder, catheter, and beaker materials (P_{wall}), and to correct for volume averaging (K_{dd}). These corrections are determined with the EGSnrc user-code cavity by modeling the microSelectron V2 Ir-192 HDR seed used in our lab and the measuring setup in detail.

Results: DF/K_{air} is the largest factor required, with a value of 1.15 [0.06%]. This large value can be explained mostly by the mass

energy absorption coefficient ratio Fricke to air which is about 1.11 [0.02%] as determined using the EGSncr user-code g. An Awall calculation with the user-code cavity shows that the rest of this conversion factor is due to the contribution from secondary particles to the dose to Fricke (Awall=1.036 [0.002%]). Volume averaging contributes the second largest correction, which is about 1.015, while the wall correction and the Fricke to water conversion factor almost cancel out.

Conclusions: MC simulation can be used to determine the corrections required for HDR Fricke dosimetry. The large value of the Fricke to air-kerma conversion factor can be explained by the difference between the mass energy absorption coefficients for the Fricke solution and air. Remaining differences are caused by the contribution from secondary particles. The factor needed to obtain dose to water at the reference position from the dose to a Fricke dosimeter is significantly smaller and mainly due to volume averaging. Future work will focus on the sensitivity of these corrections to systematic uncertainties in the cross sections used for the MC calculations.

SP026.7 - Changes in absorbed dose to water caused by dose standard shift for ionization chamber calibration in Japan

Author(s): Hidetoshi Saitoh¹, Toru Kawachi², Morihiro Shimizu³
¹Graduate School Of Human Health Sciences, Tokyo Metropolitan University, Tokyo/JAPAN, ²Chiba Cancer Center, Chiba/JAPAN, ³National Institute of Advanced Industrial Science and Technology (AIST), Tsukuba/JAPAN

Introduction

The standard of absorbed dose to water in ⁶⁰Co γ rays was established at the National Metrology Institute of Japan (NMIJ) in 2011. Subsequently, ionization chamber calibration service has been provided by the Association for Nuclear Technology in Medicine (ANTM) as a secondary standard dosimetry laboratory and new standard dosimetry protocol by the Japan Society of Medical Physics (JSMP12) has been proposed in 2012. Until 2012, product of the ⁶⁰Co exposure calibration factor N_C and the exposure to absorbed dose conversion coefficient $k_{D,X}$ was substituted for the absorbed dose to water calibration factor ND_w , although previous dosimetry protocol (JSMP01) was based on the IAEA TRS-398. The $k_{D,X}$ was computed using nominal chamber structure and not individual structure. However, ND_w has been computed for individual ionization chamber directly. Accordingly, it was forecasted that uncertainty of absorbed dose to water evaluated by individual user has been reduced by adoption of the ND_w and JSMP12. The third party evaluation of absorbed dose to water has been performed since 2007. In this report, the changes in absorbed dose to water evaluated by the user facilities between the JSMP 01 and 12 is reported.

Method

The third party evaluation of absorbed dose to water has been performed between the Tokyo metropolitan hospitals and the Tokyo metropolitan university (TMU) since 2007. In order to investigate the changes between the JSMP01 and 12, the absorbed dose at calibration depth D_c was evaluated. Absorbed dose measurement was performed separately by the staff of the facilities and the TMU on the same day. Ionization chamber (TN30013, PTW), electrometer (Inovision 35040), digital quartz barometer (745-16B, Paroscientific), digital thermometer (TL1-A, Thermoprobe) and 1D water phantom (WP1D, IBA) was used for the third party evaluation and own equipment was used for the user evaluation.

Results

Before 2011, mean deviation from D_c evaluated by TMU and its standard deviation (1 σ) were from 0.5 % to 0.7 % and from 0.5 %

to 0.7 %, respectively. By the investigation in 2013-2014, ND_w and JSMP12 was adopted in 7 of 11 facilities. By analysis using the result of 7 facilities, mean deviation and its standard deviation was reduced to 0 % and 0.4 %, respectively. As a result, there is significant difference in mean deviation and variance ($p < 0.05$) between JSMP01 and 12.

Conclusion

In this report, it was observed that the deviation and variance between user and third party evaluation of D_c was reduced. Therefore it is confirmed that uncertainty of absorbed dose to water evaluation is reduced by adoption of the ND_w calibration and the new dosimetry protocol JSMP12.

SP026.8 - A calibration system of therapy-level dosimeter in Japan organized by ANTM

Author(s): Suoh Sakata¹, Wataru Yamashita¹, Nobuhiro Takase¹, Masahiro Hoteida¹, Yosuke Sasaki¹, Hiroaki Okumura¹, Hideyuki Mizuno², Katuhisa Narita¹, Akifumi Fukumura²

¹Dose Calibration Center, The Association for Nuclear Technology in Medicine, Chibashi/JAPAN, ²Research Center For Charged Particle Therapy, National Institute of Radiological Sciences, Chibashi/JAPAN

In Japan, the therapy-level dosimeter calibration had been carried out in terms of exposure until 2012. Therefore, the conversion factor $k_{D,X}$ was necessary to convert the calibration factor N_x obtained in air measurement to the water absorbed dose calibration factor ND_w . In 2011, Japanese National Standard Laboratory (National Metrology Institute of Japan, NMIJ) established the national measurement standard of therapy level absorbed dose to water of Co60 and started to deliver this standard. According to the NMIJ activity, the ANTM (Association for Nuclear Technology in Medicine, the SSDL in Japan) has launched a new dosimeter calibration system in terms of absorbed dose to water from October 2012, too. After that, ND_w determined directly in water is delivered to radiotherapy institutions in substitution N_x .

The calibration procedure by ANTM follows Standard Dosimetry 12 published by Japan Society of Medical Physics (JSMP). The concept and formalism of Standard Dosimetry are almost same to IAEA TRS 398. Ionization chambers to be calibrated are fixed at 5cm depth in water phantom. For cylindrical type chambers, appropriate waterproof sleeves are used not only to protect water but also to fix their position in the phantom. The sleeves are made of PMMA with a wall of 1mm in thickness at ionization effective volume of chamber. For flat type chambers that are water proof or have water proof cap are put into water directly.

ANTM is a calibration laboratory certified with the Japan Calibration Service System (JCSS) and can issues certificate with JCSS symbol mark. The JCSS is a standard dissemination system based on Metrological Law. The principles of JCSS are the calibration traceable to national standard and the certification of calibration laboratory. Calibration laboratories certified are proven to have sufficient technical and management competence to carry out calibration. Calibration certificate issued with JCSS symbol mark states both calibration value traceable to the national standard and its uncertainty. Users who use dosimeters calibrated can estimate the uncertainty of their own dose measurements.

During 27 months from October 2012 to December 2014, 5,193 ionization chambers were calibrated in terms of absorbed dose to water. A small differences were seen between calibration factors ND_w and N_x multiplied by $k_{D,X}$ for cylindrical chambers. ND_w are slightly lower than $N_x \times k_{D,X}$ for cylindrical type. The main reason is air gap between chamber wall and water-proofing sleeve. However, there is no difference between calibration factors for flat type chambers. The reason is The standard deviation of calibration factors in consecutive two calibration using absorbed dose to water improved

clearly. For Chambers calibrated with water absorbed dose 2 times or more the changes of calibration factors were small compared to the former calibration system using exposure in air. This shows that the new calibration system of ANTM is well organized and calibration factors are delivered to radiotherapy institutions with less uncertainty.

A new system of doimeter calibration system using absorbed dose to water has started in Japan. The differences of calibration factors are so small that the system is operated stably and satisfactorily.

SP027 - Development and Application of Phantoms in Clinical Dosimetry

TRACK 05: DOSIMETRY AND RADIATION PROTECTION

SP027.1 - Fabrication of radiotherapy phantoms using 3D printing

Author(s): Paul Z.Y. Liu, David R. McKenzie, Natalka Suchowerska
School Of Physics, University of Sydney, Camperdown/NSW/AUSTRALIA

Aim

3D printing is becoming more affordable and accessible. The aim of this work is to demonstrate the feasibility of using this technology to create dosimetric phantoms and customized anatomical phantoms that would otherwise be difficult to manufacture. These phantoms were designed and printed to explore the methodology, advantages and disadvantages of 3D printing techniques.

Method

The cylindrical dosimetric phantom, created in CAD software (*Sketchup*), was customized to hold an array of scintillation dosimeters to validate arc and multi-directional treatments. The anatomical phantom was created using patient CT data, which was converted into a 3D model using *ImageJ*. The open source software *Mesh-labs* was then used to prepare the model for printing.

The phantoms were printed using fused deposition with the UP 3D printer (*3DPP*). Both phantoms were printed as hollow objects and filled with two types of material: dental wax and gel bolus. The resulting phantoms were CT scanned to determine their density and uniformity and irradiated with a therapeutic beam to assess their suitability.

Results

The 3D printed phantoms are shown in Figure 1. CT scans of the printed and filled phantoms showed a uniform electron density with less than 2% variance. Gel bolus yields a uniform phantom that is close to water in mass density ($\rho_{\text{gel}} = 1.07 \text{ g cm}^{-3}$). Dosimetric characterisation of the cylindrical dosimetric phantom filled with gel bolus showed low angular dependence ($< 0.6\%$) indicating that the scintillator was located accurately on the axis.

The anatomical phantom provided an accurate surface representation of the CT image. However, the phantom density does not reflect that of the real anatomy. Other 3D printing techniques, such as selective laser sintering and stereolithography, were found to create solid phantoms of a chosen density without the need to be filled.

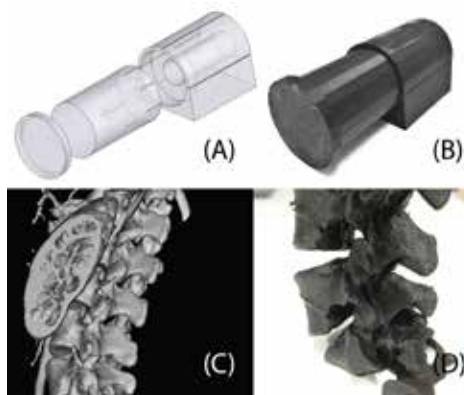


Figure 1. (A) The cylindrical dosimetric phantom in CAD and (B) the 3D printed phantom. (C) A CT scan of the spinal cord and (D) its printed representation.

Conclusion

The fabrication of radiotherapy phantoms using 3D printing is fast and cost effective. Fused deposition is suitable for creating dosimetric phantoms using wax or bolus to fill a hollow model. Customized patient dosimetry can be achieved with 3D printing of anatomical phantoms, however, more sophisticated printing techniques will be required to achieve the desired mass and electron densities.

SP027.2 - The effect of bismuth shielding during pediatric neck multi-detector computed tomography on thyroid dose and image quality

Author(s): Stephen Inkoom¹, Antonios E. Papadakis², Maria Raisaki³, Kostas Perisinakis², Cyril Schandorf⁴, John J. Fletcher⁵, John Damilakis²

¹Department Of Medical Physics, Faculty of Medicine, University of Crete, Iraklion/GREECE, ²Department Of Medical Physics, University Hospital of Heraklion, Iraklion/GREECE, ³Department Of Radiology, Faculty of Medicine, University of Crete, Iraklion/GREECE, ⁴School Of Nuclear And Allied Sciences, University of Ghana, Kwabenya, Accra/GHANA, ⁵Department Of Applied Physics, Faculty of Applied Sciences, University for Development Studies, Navrongo/GHANA

Background: There are no data on the effect of bismuth shielding on absorbed dose to thyroid gland and image quality of pediatric neck multi-detector computed tomography (MDCT) imaging.

Objectives: To investigate and compare the effect of bismuth shielding on thyroid dose, effective dose and image quality in pediatric neck MDCT performed using either fixed tube current or automatic exposure control (AEC) techniques.

Methods: Four pediatric anthropomorphic phantoms that represent the average individual as newborn, 1-year-old, 5-year-old and 10-year-old child underwent routine neck computed tomography (CT) scans using a 16-slice MDCT system. Scans were performed using a) fixed tube current and b) activated-AEC technique. Each scan was performed a) without bismuth shield, b) using a single- and c) using a double-layered bismuth shield placed on the skin surface above the thyroid gland. Scans were repeated following placement of cotton spacers 1, 2 and 3 cm thick between the skin and the shield, to study the effect of skin-to-shielding distance on image noise. Thyroid dose was measured with thermoluminescent dosimeters. The location of the thyroid gland within the phantom slices was determined using a novel approach which employed anthropometric data from CT examinations of patients with body size that closely matched the size of the phantoms. Effective dose (ED) was estimated using the dose length product (DLP) method and specific normalized effective dose per DLP conversion factors for neck, according to the 2007 recommendations of the International Commission on Radiological Protection. Image quality was evaluated on the basis of image noise, which was measured as the standard deviation of the Hounsfield unit (HU) values in selected image regions of interest.

Results: In fixed tube current shielded technique, thyroid dose reduction for single-layered-shield was 17% for newborn and 35% for 10-year-old, and for double-layered-shield was 25% for newborn and 47% for 10-year-old. The dose reduction for AEC-activated unshielded was 27% for newborn and 46% for 10-year-old. The corresponding reduction in AEC-activated scans for single-layered-shield was 40% for newborn and 60% for 10-year-old, and for double-layered-shield was 40% for newborn and 66% for 10-year old. Activation of AEC unshielded compared to fixed tube current unshielded increased the ED by 7% for 1-year-old and decreased

ED by up to 27% for 5-year-old. Image noise was found to be up to 71.5, 112.5, 72.2, and 138.2 HU for fixed tube current single-layered, fixed tube current double-layered, AEC-activated single-layered and AEC-activated double-layered shields, respectively. Elevation of shields by 1, 2 and 3 cm using cotton spacers between shields and phantoms decreased image noise, by 22.0, 9.4 and 5.5 HU respectively for fixed tube current single-layered-shield, while it did not considerably affect thyroid dose. Similar trends were observed for other protocols.

Conclusion: AEC was more effective in thyroid dose reduction compared to in-plane bismuth shields during neck MDCT. The use of fixed tube current with double-layered-shields, and AEC shielded further reduced dose; however, this is associated with higher image noise. Application of cotton spacers had no significant impact on the measured doses, but significantly decreased image noise.

SP027.3 - Use of 3D Printed Materials as Tissue-Equivalent Phantoms

Author(s): Tanya Kairn¹, Tim Markwell², Scott Crowe³

¹Physics, Genesis CancerCare Queensland, Auchenflower/AUSTRALIA, ²Physics, Mater Radiation Oncology, South Brisbane/AUSTRALIA, ³Radiation Oncology, Royal Brisbane and Women's Hospital, Herston/QLD/AUSTRALIA

This study used the example of 3D printing with acrylonitrile butadiene styrene (ABS) as a means to investigate the potential usefulness of benchtop rapid prototyping as a technique for producing patient specific phantoms for radiotherapy dosimetry. Phantom samples were evaluated in terms of their geometric accuracy, tissue equivalence and radiation hardness, when irradiated using a range of clinical radiotherapy beams.

Three small cylinders and one model of a human lung (with tumour) were produced via in-house 3D printing with ABS, using 90%, 50%, 30% and 10% ABS infill densities. Physical measurements were used to test the geometric accuracy of the phantoms. Hounsfield unit values in CT scans of the sample phantoms were used to evaluate the tissue equivalence of the phantoms, in terms of densities and linear attenuation coefficients. The attenuation and scattering effects of the phantoms were also evaluated and compared with the effects of commercial tissue- and lung-equivalent plastics, using film measurements, in five different clinical electron beams and three different photon beams. The radiation sensitivity of the samples was assessed by irradiating the samples for several hours a day for 30 days and then remeasuring the densities and physical dimensions of the samples.

The measured dimensions of the small cylindrical phantoms all matched their planned dimensions, within 1mm. The lung phantom was less accurately matched to the lung geometry on which it was based; the use of manual contours to produce an initial design from the CT images led to some simplification of the shape of the lung and some conservative over-estimation of the size of the tumour.

The cylindrical 3D-printed phantoms with ABS infill densities of 30, 50 and 90% were all found to be relatively homogeneous and to exhibit densities and attenuation coefficients within the range of values identified in the commercial tissue-equivalent materials. Film measurement results confirmed that the attenuation and scattering effects of these samples were similar to the effects of established lung- and tissue-equivalent materials. By contrast, the mesh produced by the 3D printing software, when required to produce a phantom with a 10% ABS infill density was so coarse that an anatomically unrealistic structure consisting of solid ABS walls around relatively large (6 mm diameter) air chambers was clearly resolvable in the CT images of the resulting phantom.

The results of this study suggest that phantoms printed with ABS,

using infill densities of 30% or more, are potentially useful as lung- and tissue-equivalent phantoms for patient-specific radio-therapy dosimetry. A 90% ABS infill density was found to result in a material suitable for modelling tumour, muscle or other soft tissue, while ABS infill densities of 30-50% resulted in phantoms with densities low enough to model lung while also avoiding the course mesh structures that occur when lower infill densities (such as 10% ABS) are used. All cylindrical 3D printed phantom samples were found to be unaffected by prolonged radiation and to accurately match their design specifications. However, care should be taken to avoid over-simplifying anatomical structures when printing more complex phantoms.

SP027.4 - Development of water-equivalent materials using the Least Squares Method

Author(s): Leandro Mariano, Paulo R. Costa
Radiation Dosimetry And Medical Physics Group, Physics Institute, University of São Paulo, São Paulo/BRAZIL

Introduction: The study of water-equivalent materials, which have radiation attenuation and scattering properties similar to the human tissue, is central to the calculation of patient doses in many medical imaging applications. Chemical formulation using thermoplastics as a base and additives for the production of phantoms were developed by the authors for diagnostic imaging energy range (10-150keV).

Methods: The initial composition of the materials was obtained using the Hermann Method. Originally, this method allows the use of three base materials for the manufacture of the water-equivalent materials. In the present work, the Hermann's methodology was generalized to allow the consideration of a generic number of base and additive materials. The Least Square Method was used as well to obtain the composition of the water-equivalent materials. The methodology was to fit the linear attenuation coefficient of the mixture directly on the linear attenuation coefficient of water.

Results and Discussion: The procedure developed in this work has advantages over the Hermann Method since it takes into account the linear attenuation coefficient over the entire energy range of interest. The Figure 1 shows the comparison of the linear attenuation coefficient for two formulations obtained by these methods using the same base materials.

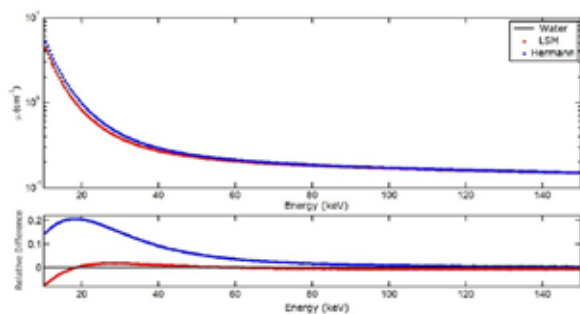


Figure 1 – Linear attenuation coefficient of two water-equivalent materials using the Hermann and the Least Square Methods (LSM).

Moreover, the transmitted and scattered X-ray spectra of some compositions were experimentally measured and simulated using the PENELOPE code.

Conclusions: The results have shown a good agreement with the water attenuation and it has validated this methodology. The Monte Carlo Method can also be very useful to determine the characteris-

tics of transmission and scattering of x-rays of the materials, without requiring its previous manufacture.

Acknowledgments: The authors thank CNPq for financial support under project 167332/2014-7 and CNPq/FAPESP INCT Rad Metrology in Medicine.

References:

F. Salvat, et al, PENELOPE 2011: A code system for Monte Carlo simulation of electron and photon transport, OECD Nuclear Energy Agency, Issy-les-Moulineaux, France, 2011

Hermann K. P. et al; Physics in Medicine and Biology. V. 30: p.1195-1200, 1985

White, D. R Physics in Medicine and Biology. V. 22: p.219-228, 1977

SP027.5 - Development of deformable moving lung phantom to simulate respiratory motion for lung SBRT

Author(s): Young Nam Kang¹, Ji Na Kim², Hyung Wook Park³, Hong Seok Jang¹

¹Department Of Radiation Oncology, Seoul St. Mary's Hospital, College of Medicine, The Catholic University of Korea, Seoul/KOREA, ²Department Of Biomedical Engineering, College of Medicine, The Catholic University of Korea, Seoul/KOREA, ³Department Of Radiation Oncology, Yeouido St. Mary's Hospital, College of Medicine, The Catholic University of Korea, Seoul/KOREA

Stereotactic body radiation therapy (SBRT) requires high accuracy in order to protect healthy organs and destroy the tumor. However, tumors located near the diaphragm are constantly moving during treatment. Respiratory-gated radiotherapy has significant potential for the improvement of the irradiation of tumor sites affected by respiratory motion, such as lung and liver tumors. To measure and minimize the effects of respiratory motion, a realistic deformable phantom is required for use as a gold standard. The purpose of this study was to develop and study the characteristics of a deformable moving lung (DML) phantom, such as simulation, tissue equivalent, and rate of deformation. The rate of change of the lung volume, target deformation, and respiratory signals were measured in this study; they were accurately measured using a realistic deformable phantom. The measured volume difference was 30%, which closely corresponds to the average-difference in human respiration, and the target movement was -30 mm-+30 mm. The measured signals accurately described human respiratory signals. This DML phantom will be useful for the estimation of deformable image registration and in lung SBRT. This study shows that the developed DML phantom can exactly simulate the patient's respiratory signal and it acts as a deformable 4D simulation of a patient's lung with sufficient volume change.

SP027.6 - Characterization of a MOSFET-based system for skin dose evaluation with bolus material

Author(s): Anabela G. Dias¹, Diana F.D.S. Pinto²

¹Física Médica, Instituto Português de Oncologia do Porto Francisco Gentil, Porto/PORTUGAL, ²Radioterapia, Instituto Português de oncologia Francisco Gentil do Porto, Porto/PORTUGAL

Purpose/Objective

Post-surgery radiation therapy is one the treatment steps of locally advanced breast cancer. In vivo skin dose evaluation of the chest wall region is important to ensure sufficient dose in structures near surface and it is a valuable tool during radiation treatment to verify the delivered dose to the target. It is also useful to assess the scattered radiation to the contra-lateral breast. In certain cases, to

increase the skin dose, a bolus material with a specific thickness is frequently placed on the chest wall during the last ten treatment fractions.

The purpose of this work was to characterize a MOSFET-based system for in vivo skin measurements in megavoltage radiation (4 MV and 6 MV) and compare calculated and measured dose with and without bolus material.

Materials/Methods

Full characterization and calibration of the MOSFET-based system was performed regarding reproducibility, linearity, energy, angular, field size and source to surface distance (SSD) dependences for two the photons energies. All measurements with the exception of the angular dependence were performed in a solid water phantom and a Farmer ionization chamber was used for dose comparison. The angular dependence was performed with a Lucy 3D phantom from 0 to 315 degrees in 45 degree increments.

Surface dose on solid water was also assessed in the presence and absence of 1 cm bolus material and compared with calculated dose in the Treatment Planning System (TPS) (only tested with an orthogonal beam).

Results

The detectors presented no energy dependence and a dose linear response for the dose range studied. The measured dose standard deviation varied from 1% to 10% depending on the number of MUs (higher deviation for lower MUs) and the detector. In the therapeutic dose range, the standard deviation for all the detectors is less than 2%. The angular dependence study showed that the deviation is less than 2% over 360°. For SSD response, the system showed linear dependence. Field size dependence was also analyzed and was found to be negligible. Surface dose without bolus is about 50% less than with bolus. The comparison between the TPS calculated and measured doses with and without bolus showed a maximum difference of 5%.

Conclusion

Tests performed on the behavior of the measuring system in reference conditions have results consistent with the manufacturer's specifications for the studied energies. The results show that this system is suitable for in vivo skin dose dosimetry in MV range with and without using bolus material in breast external radiotherapy treatments.

SP027.7 - Calibration procedure optimization through PSDesigner, a multipurpose simulation platform for plastic scintillation dosimeters

Author(s): Cedric Laliberte-Houdeville, Luc Beaulieu, Louis Archambault

Département De Physique, De Génie Physique Et D'optique, Université Laval, Québec/CANADA

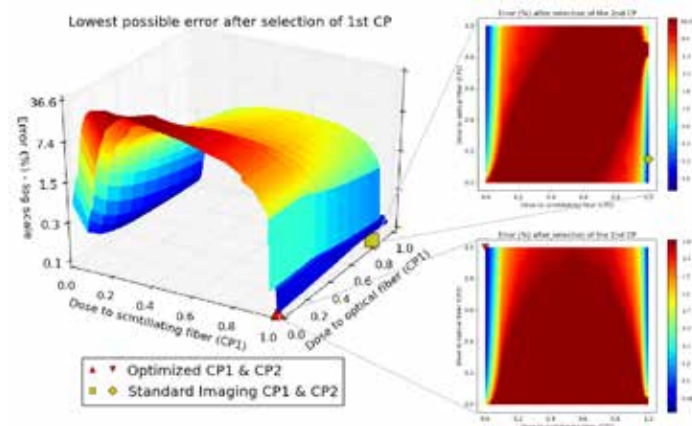
Background The literature offers a wide variety of plastic scintillation dosimeter (PSD) and multipoint PSD proof-of-concept that demonstrate how the use of plastic scintillators can lead to accurate, online and in-vivo dosimeters for radiotherapy and brachytherapy. Nevertheless this accuracy is highly dependent on the calibration procedure and the choice of calibration points (CPs). Due to the lack of clear recommendations, researchers often rely on past experiences and generally accepted consideration to calibrate their specific systems. This study presents a numerical technique to find the optimal CPs of any PSD designs. Designs inspired by the commercially available Exradin W1 and the 2- and 3-points-PSD prototypes recently published by *Therriault-Proulx et al.* are revis-

ited. Their calibration procedures are evaluated and improved to show this technique's capabilities and potential use for future PSD designs of ever-increasing complexity.

Methods This study uses *PSDesigner*, a multi-purpose simulation platform written in Python to generate and evaluate virtual PSDs. With the extensive use of physical data as inputs, this platform can, among others, select optimal CPs. First, virtual PSDs are generated using emissions, attenuation and transmission spectra and response curve of commercially available optical components. Second, calibration procedure involving noisy readings as well as systematic offsets are simulated, generating flawed calibrated PSD. Finally, a stochastic algorithm searches for the best CPs resulting in the most accurate PSD.

Results For the simpler, commercially available Exradin W1-design PSD, Figure 1 shows where optimal CPs ought to be selected. Both the optimal CPs and the ones suggested by Standard Imaging are shown. The latter offers a 0.4% precision on dose measurement; the former improves it down to 0.2%. Figure 1 also shows how intermediate dose to the scintillator, generated in high dose gradient regions, are to be avoided.

The same analysis can be made for a 2-points-PSD inspired system. The optimized CPs, not shown here, result in a 0.6% precision for both measurement points. Work on 3 and more points PSD system is ongoing.



Conclusions The simulation platform developed validates past calibration procedures and shows its useful capabilities for future, more complex PSD design. It goes further, giving the user quantitative insight on how its procedure can be improved and how that will affect dose measurements. The code is versatile and can help researchers optimize complex PSD systems in other ways, notably through the optimal selection of optical components.

SP028 - HIFU Therapy, Microwave Ablation, Radiofrequency Ablation, Cryotherapy

TRACK 06: NEW TECHNOLOGIES IN CANCER RESEARCH AND TREATMENT

SP028.1 - On Understanding of the Limiting Factors in Radiofrequency Ablation on Target Tissue Necrosis Volume

Author(s): Bing Zhang¹, Michael Moser², Edwin Zhang³, Yigang Luo², Wenjun Zhang⁴

¹Complex And Intelligent Systems Research Center, East China University of Science and Technology, Shanghai/CHINA, ²Surgery, University of Saskatchewan, Saskatoon/CANADA, ³Radiology And Diagnostic Imaging, University of Alberta, Saskatoon/CANADA, ⁴Biomedical Engineering, University of Saskatchewan, Saskatoon/CANADA

The aim of this study was to analyze six limiting factors that may be responsible for target tissue necrosis (TTN) generation during the process of radiofrequency ablation (RFA). A comprehensive finite element (FE) model was built to simulate TTN of a liver tissue by using a commercial available RFA system. The model was then served as a test-bed for analysis of factors. Six limiting factors were analyzed using a statistical method. Sixteen RFA experiments were performed, in which the TTN volume was considered as a response variable along with the six control factors. The TTN volumes obtained from the 16 simulations were quite different, ranging from 7.749 to 8433.931 mm³. The applied voltage (V), the frequency (f), the exposure length (L) of the RF electrode, the chilled fluid temperature (T), the large blood vessel (d) in the proximity to target tissue, and the ablation duration (t) account for approximately 78.21%, 9.93%, 2.91%, 0.01%, 4.64%, and 0.08%, respectively, of the effect on the TTN volume. The findings from the present study suggest that the applied voltage (V) and the frequency (f), followed by the large blood vessel (d) in proximity to target tissue, have the highest effect on the TTN volume.

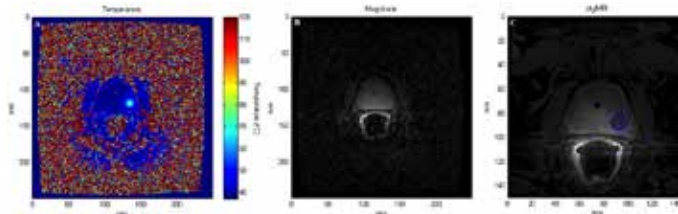
SP028.2 - Thermal Dose Based Monitoring of Thermal Therapy for Prostate Cancer

Author(s): David Dalla Rosa¹, Hisham Assi², Joseph C. Kumaradas³
¹Apotex, Toronto/CANADA, ²Biomedical Engineering, University of Toronto, Toronto/ON/CANADA, ³Physics, Ryerson University, ON/CANADA

Thermal dose is a metric for quantifying the amount of thermal damage taking temperature and exposure time into account. An ideal thermal dose model should produce the same dose for a given amount of damage, regardless of the heating protocol used, or the time-temperature profile that caused the damage. The cumulative-equivalent-minutes at 43 Celsius (CEM43) is the most commonly used thermal dose model. It was originally developed for hyperthermia applications (less than 45 Celsius). The validity and accuracy of this mode for higher temperatures, above 50 Celsius is questionable. A new thermal dose model based on the Arrhenius type Vogel-Tammann-Fulcher equation, known as the improved cumulative equivalent minutes at 43 Celsius (iCEM43), has been developed and fit to publish historic thermal data.

The CEM43 and iCEM43 dose models have been retrospectively used to assess the dose delivered to during laser thermal therapy of low-grade prostate cancer, in order to test the consistency of the two methods. This was done by obtaining MRI thermometry images during treatment and gadolinium enhanced MRI images post-treat-

ment to assess vascular shutdown (as an indicator of acute thermal damage), as shown in the figure below. The iCEM43 dose model was found to be more consistent than the CEM43 dose model in predicting post-treatment vascular shutdown.



SP028.3 - Nanodrug Delivery and Anti-tumor Efficacy for Brain Metastasis of Breast Cancer Enhanced by Short-time Low-dose Ultrasound Hyperthermia

Author(s): Sheng-Kai Wu¹, Chi-Feng Chiang¹, Yu-Hone Hsu¹, Tzu-Hung Lin², Houg-Chi Liou², Wen-Mei Fu², Win-Li Lin³

¹National Taiwan University, Institute of Biomedical Engineering, Taipei/TAIWAN, ²National Taiwan University, Institute of Pharmacology, Taipei/TAIWAN, ³National Health Research Institutes, Institute of Biomedical Engineering and Nanomedicine, Miaoli/TAIWAN

Ultrasound hyperthermia can enhance the delivery of chemotherapeutic agents into tumors, while the blood-brain/tumor barrier inhibits the uptake and accumulation of chemotherapeutic nanodrugs in brain tumors. In this study, we investigated the effects of short-time low-dose (STLD) focused ultrasound (FUS) hyperthermia on the delivery and therapeutic efficacy of pegylated liposomal doxorubicin (PLD) for brain metastasis of breast cancer. Murine breast cancer 4T1-luc2 cells expressing firefly luciferase were injected into female BALB/c mice striatum tissues and used as a brain metastasis model. The mice were intravenously injected with PLD with/without STLD transcranial pulsed/continuous wave FUS hyperthermia on day 6 after tumor implantation. The amounts of doxorubicin accumulated in the normal brain tissues and tumor tissues with/without FUS hyperthermia were measured using fluorometry. The tumor growth for the control, hyperthermia, PLD, and PLD+hyperthermia groups was measured using an IVIS spectrum system every other day starting from day 3. Cell apoptosis and tumor characteristics were assessed using immunohistochemistry. The experimental results showed that STLD transcranial FUS hyperthermia was able to significantly enhance the PLD delivery into brain tumors. The tumor growth was effectively inhibited by a single treatment of PLD+hyperthermia compared with both PLD alone and STLD FUS hyperthermia alone. Immunohistochemical examination further demonstrated the therapeutic efficacy of PLD plus STLD FUS hyperthermia for brain metastasis of breast cancer. The results also showed that with the same STLD, pulsed-wave can even produce a better therapeutic result than continuous-wave FUS hyperthermia. This study indicates that the application of STLD FUS hyperthermia after nanodrug injection may be an effective approach to enhance nanodrug delivery and improve the treatment of metastatic cancers.

SP028.4 - Evaluating breast cancer surgical margins using high-frequency ultrasound: Statistical analysis of a 17-patient pilot study

Author(s): Robyn K. Omer¹, Kristina M. Sorensen², Rachel E. Factor³, Leigh A. Neumayer⁴, Timothy E. Doyle¹

¹Physics, Utah Valley University, Orem/UT/UNITED STATES OF AMERICA, ²Mathematics, Pennsylvania State University, State College/PA/UNITED STATES OF AMERICA, ³Pathology, University of Utah, Salt Lake City/UT/UNITED STATES OF AMERICA, ⁴Surgery, University of Arizona, Tucson/AZ/UNITED STATES OF AMERICA

A critical goal in breast conservation surgery (BCS) is to obtain negative surgical margins to ensure removal of all cancerous tissue. This process usually requires a period of several days to evaluate margin status with conventional pathology, and results in re-excisions for 20-60% of BCS patients due to the lack of a rapid, noninvasive method to evaluate margins in the operating room. Several methods are therefore being investigated for the intraoperative evaluation of margin status. High-frequency (HF) ultrasound (20-80 MHz) was investigated in a 17-patient pilot study for intraoperative margin evaluations during BCS. Through-transmission measurements were acquired from 53 positions on 34 excised specimens at the Huntsman Cancer Institute, Salt Lake City, Utah. Specimens included lymph nodes, surgical margins, tumors, and fibroadenomas. Measurements were acquired with the use of two 50-MHz immersion transducers (Olympus NDT, V358-SU), a HF square-wave pulser/receiver (UTEX, UT340), and a 500-MHz digital oscilloscope (Hewlett-Packard, HP-54522A). Ultrasonic waveforms were averaged in the signal acquisition and downloaded onto a notebook PC using LabVIEW. Parameters acquired from the data included peak density (the number of peaks and valleys in the 20-80 MHz band of the ultrasonic spectra) and attenuation. Peak density is strongly dependent on scattering processes and thus microstructural heterogeneity in the tissue. Statistical analysis of the data for differentiating between malignant and nonmalignant tissue revealed that peak density and attenuation by themselves provided lower accuracy and sensitivity as compared to a multivariate analysis combining the two parameters. Results from the multivariate analysis showed 81.1% accuracy, 76.9% sensitivity, and 85.2% specificity. Table 1 compares the accuracy, sensitivity, and specificity values of HF ultrasound with alternative technologies for intraoperative BCS margin assessments, and shows HF ultrasound is competitive with both small specimen mammography and radio-frequency spectroscopy. Approaches for improving the HF ultrasound method include using additional parameters in the multivariate analysis such as wave speed, calibrating the measurements with phantoms, and conducting larger studies with statistically relevant numbers of patients, specimens, and measurement positions. Such a study at the Huntsman Cancer Institute is currently near completion, and includes 73 patients, 485 specimens, and 1112 measurement positions. Preliminary results are consistent with those from this study.

Table 1. Comparison of results from prospective and clinical trials of margin evaluation methods including small-specimen mammography, radio-frequency spectroscopy, and high-frequency ultrasound.

Method	Small-specimen mammography ¹	Radio-frequency spectroscopy ²	High-frequency ultrasound
Patients	102	298	17
Specimens	102	298	34 (53 positions)
Accuracy	78.4%	62.1%	81.1%
Sensitivity	58.5%	74.8%	76.9%
Specificity	91.8%	46.7%	85.2%

¹ Bathla, *et al.*, Am. J. Surg. **202**, 387-394 (2011).

² Schnabel, *et al.*, Ann. Surg. Oncol. **21**, 1589-1595 (2014).

SP028.5 - The Intraoperative Detection of Breast Cancer in Surgical Margins Using High-Frequency Ultrasound: Studies Using Histology Mimicking Phantoms

Author(s): Zachary A. Coffman¹, Nicole Cowan², Robyn K. Omer³, Timothy E. Doyle⁴

¹Biology, Utah Valley University, Orem/UT/UNITED STATES OF AMERICA, ²Biotechnology, Utah Valley University, Orem/UT/UNITED STATES OF AMERICA, ³Botany, Utah Valley University, Orem/UT/UNITED STATES OF AMERICA, ⁴Physics, Utah Valley University, Orem/UT/UNITED STATES OF AMERICA

Breast cancer is the second most prevalent cancer among women, affecting one out of eight in their lifetime. The ability to differentiate between malignant and normal tissues during breast cancer surgery would enable the surgeon to remove all of the cancer from the affected region in the breast, thereby reducing the risk of recurrence and the need for subsequent surgeries. Two studies conducted at the Huntsman Cancer Institute (Salt Lake City, Utah) showed that high-frequency (HF) ultrasound (20-80 MHz), and in particular the ultrasonic parameters peak density and attenuation, were sensitive to breast tissue pathology. The objective of this study was to determine the effect of tissue microstructure on peak density and attenuation using phantoms that mimic the histology of breast tissue. Phantoms were created from a mixture of distilled water, agarose powder, and 10X TBE stock solution. In order to simulate breast tissue histology and breast density, polyethylene microspheres were embedded into the phantoms in layers, totaling 4 layers per phantom. In one experiment, the volume percent of polyethylene microspheres was kept constant in each phantom while varying microsphere sizes (58-925 μm diameter). In a second experiment, the polyethylene microsphere size (90-106 μm diameter) was kept constant within each phantom while the weight percent concentration of the microspheres varied (0.00g to 0.06g). Pitch-catch measurements were acquired using 50-MHz transducers (Olympus NDT, V358-SU, 0.635-cm diameter active element), a HF pulser-receiver (UTEX, UT340), and a 1-GHz digital oscilloscope (Agilent, DSOX3104A). Glycerol (Genesis Scientific) was used as a coupling agent between the transducers and the phantoms. Spectra were derived from the data, giving peak density (the number of peaks and valleys in the 20-80 MHz range) and attenuation values. The results show that peak density is much more sensitive to the size of the heterogeneity and follows an inverse size (microsphere diameter) relationship, while attenuation is sensitive to the number of heterogeneities present. These results demonstrate that the HF ultrasound parameters, peak density and attenuation, are sensitive to changes in microstructure or heterogeneity observed in malignant breast tissue. Clinical breast cancer studies also showed that, when combined in a multivariate analysis, peak density and attenuation increased the accuracy, specificity, and sensitivity of the measurements for malignant tissue. The high-frequency ultrasound results from the agarose phantoms confirm that peak density and attenuation are complementary parameters for characterizing breast tissue pathology and validate the clinical breast cancer studies conducted at the Huntsman Cancer Institute.

SP028.6 - Rapid Molecular Subtyping of Breast Cancer Using High-Frequency Ultrasound (10-120 MHz) and Principal Component Analysis

Author(s): Caitlin Carter¹, Laurel A. Thompson², Amy Fairbrother¹, Timothy E. Doyle³

¹Biology, Utah Valley University, Orem/UT/UNITED STATES OF AMERICA, ²Chemistry, Utah Valley University, Orem/UT/UNITED STATES OF AMERICA, ³Physics, Utah Valley University, Orem/UT/UNITED STATES OF AMERICA

Introduction: The molecular subtypes of breast cancer correlate more strongly to prognosis and treatment response than traditional classifications based on genetic and protein expression profiles. The mutations found in aggressive subtypes (basal-like and Her2+) alter the expression levels of proteins that regulate the actin cytoskeleton, thereby altering the biomechanical and ultrasonic properties of the cell. Current methods of testing these changes do not easily transfer to real-time diagnostic methods. The ability to determine the subtype of breast tumors during surgery or biopsy would provide physicians with new diagnostic capabilities to screen suspicious lesions, as well as perform high-precision surgery and personalize treatment for patients.

Objective: The hypothesis of this work was to determine the feasibility of using high-frequency ultrasound and principal component analysis (PCA) to characterize and phenotype different molecular subtypes of breast cancer cell lines, and to determine the sensitivity of high-frequency ultrasound to changes in biomechanical properties of the cell.

Methods: Computer simulations were performed to determine if changes in the bulk and shear moduli of the cell cytoplasm would measurably alter high-frequency ultrasonic spectra. To verify these models, ultrasonic measurements of seven breast cancer cell lines with different molecular subtypes were obtained over a period of two years by taking pulse-echo measurements of the cell layer with a 50-MHz transducer immersed directly in the growth media of the cell culture plates. The cell reflections within the waveforms were isolated and spectrally analyzed using computer models and PCA. Heat maps were then generated using relative distances between PCA scores of experimental data and model spectra. These heat maps were used to classify the spectra for subtype profiling. A secondary experiment was performed to validate that the cell reflections isolated from spectral data were in fact the waveforms of the cellular monolayer signal, and to determine if chemical modification of the cytoskeleton could be observed with ultrasound. This was done by treating a cell culture with colchicine which is a known inhibitor of cytoplasmic microtubule formation. Measurements of the treated culture were taken incrementally over a period of 90 minutes to record the effect on the cell signal in real time.

Results: Computer models showed that changes in biomechanical properties of the cell cytoplasm would significantly alter the cell's ultrasonic properties. Experimental results showed that each cell line produced a unique spectral signature while also demonstrating changes due to seeding density. This showed the sensitivity of high-frequency ultrasound to changes in cell microenvironment as well as the molecular subtype of the cells. The colchicine data also verified changes in the cell signal due to the modification of cytoplasmic microtubules. The heat map generated from PCA was able to classify the measured spectra of each cell line based on their individual biomechanical and morphological properties.

Conclusions: The experimental and computational results of this work have demonstrated that high-frequency ultrasound is a feasible method for rapid molecular subtyping of breast cancer. Principal component analysis of the spectral data has additionally demonstrated a prospective approach for the characterization of molecular subtypes.

SP028.7 - Inverse treatment planning using radiofrequency ablation in cancer therapy

Author(s): Shefali Kulkarni-Thaker¹, Dionne Aleman¹, Aaron Fenster²

¹Department Of Mechanical And Industrial Engineering, University of Toronto, Toronto/CANADA, ²Imaging Research Laboratories, Robarts Research Institute, London/CANADA

Radiofrequency ablation (RFA) offers localized and minimally invasive ablation of small-to-medium sized inoperable tumors. In RFA, tissue is ablated due to high temperatures obtained from the current passed through electrodes inserted percutaneously or via open surgery into the target. However RFA can cause incomplete ablation due to several reasons including incorrect needle position. We develop a mathematical framework for pre-operative inverse treatment plans for single and multiple RFA applicators. Borrowing techniques from radiosurgery inverse planning, we design a two stage algorithm where we first identify needle position and orientation, referred to as needle orientation optimization, and then compute the treatment time for optimal thermal dose delivery using thermal dose optimization (TDO). We develop linearly-relaxed TDO models using various thermal damage models including threshold temperature using Pennes Bioheat transfer equation (BHTE) and Arrhenius damage index. We present experimental results on three clinical case studies with 3D patient models.

SP029 - Surgical Navigation: Part 1

TRACK 07: SURGERY, COMPUTER AIDED SURGERY, MINIMAL INVASIVE INTERVENTIONS, ENDOSCOPY AND IMAGE-GUIDED THERAPY, MODELLING AND SIMULATION

SP029.1 - Preliminary evaluation of positron emission based 3D tracking system (PeTrack) in image guided interventions

Author(s): Simin Razavi¹, Benjamin Spencer², Marc Chamberland³, Tong Xu³

¹Department Of Physics, Carleton University, Ottawa/CANADA, ²TIMC-IMAG Laboratory, La Tronche cedex/France, ³Department Of Physics, Carleton University, Ottawa/ON/CANADA

In minimally invasive surgeries, a surgeon needs to precisely locate the surgical tools. The recent advancements in image guided surgeries have enabled monitoring the position of the operative tools in the vicinity of internal organs. We are developing a new real-time three-dimensional (3D) tracking technique for medical procedures called PeTrack (Positron Emission Tracking). PeTrack is designed to track the location of a positron emitting fiducial marker(s) using two pairs of position sensitive gamma ray detectors. The marker can be attached to surgical instruments (e.g. a catheter). PeTrack provides the location of the marker in real-time. PeTrack is co-registered with an x-ray C-arm to enable the navigation (Figure 1).

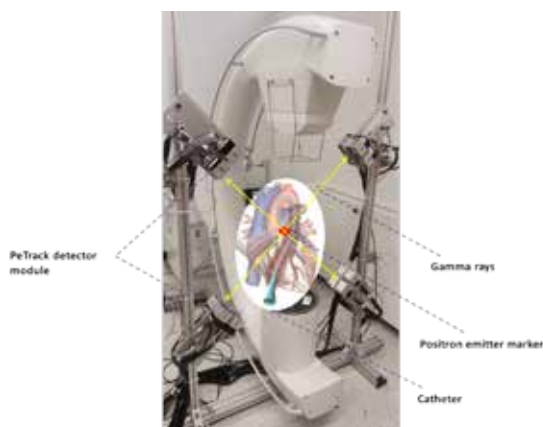


Figure 1

The emitted positron from fiducial marker annihilates with an electron, producing two gamma rays in opposite directions. Gamma rays which belong to single annihilation create coincidence line (COIL). The true location of PeTrack marker is defined to have the minimum root mean square distance to all of the COILs collected in a short time interval (e.g. 100 ms). We studied the sensitivity and distortion of PeTrack by Monte-Carlo simulations and experiments. Results show that the sensitivity fluctuates within the detector field of view and revealed a non-uniform distortion. The distortion can be reduced less than 1 mm by correcting for systematic errors. We also performed a navigation experiment by moving a 13.5 μ Ci marker along a simulated blood vessel and co-registered its positions with an x-ray projection image. Figure 2 shows that PeTrack correctly tracked the locations of the marker.

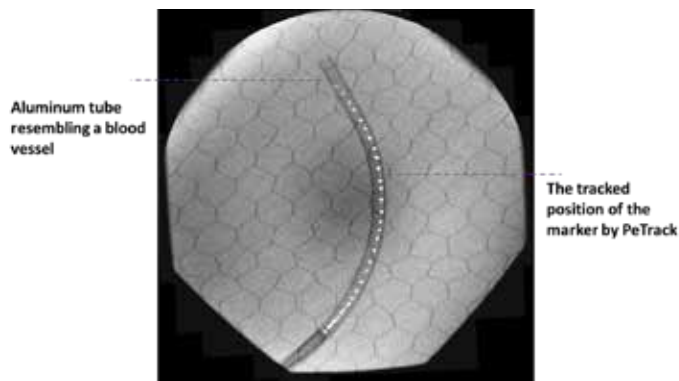


Figure 2

The small dose from the PeTrack marker is offset by the dose reduction when using PeTrack for tracking instead of continuous x-ray fluoroscopy. Therefore, as a wireless tracking technique with sub-millimeter marker and sub-millimeter accuracy, PeTrack has a great potential for 3D navigation during image guided surgery.

SP029.2 - Seymour Shield – An Operative Adjunct Device for Maintaining Visualization during Laparoscopic Surgery

Author(s): Karthik Kannan¹, Foad Kabinejadian², Leo Hwa Liang¹, Justin Phoon³, Perline Teo⁴, Ng T. Kiat⁵, Luke Tay⁶

¹Bio-engineering Department, National University of Singapore, Singapore/SINGAPORE, ²Department Of Surgery, National University of Singapore, Singapore/SINGAPORE, ³QiG Group, Singapore/SINGAPORE, ⁴A*STAR, Singapore/SINGAPORE, ⁵Senior Consultant, Urology, National University Hospital, Singapore/SINGAPORE, ⁶General Surgery, Singapore General Hospital, Singapore/SINGAPORE

During Minimally Invasive Surgery or Laparoscopic Surgery, the surgeon is absolutely dependent on the view from the camera. Yet, the rigid-endoscopic camera lens is prone to getting fouled by smoke, fog, blood and/or vaporized organic debris, all of which obstruct vision and thus necessitates removal of scope from abdomen for cleaning. So when lens fouling happens, surgical workflow halts entirely, which jeopardized patient's safety when visualization is truncated. Hence the scope is removed and the lens is manually cleaned by the nurse with the help of the gauze. Lens is warmed frequently by submerging the tip into a thermos-flask filled with warmed water and it is dried to prevent fogging. Surgeon must then return camera to its previous location and spatially re-ordinate himself in order to resume work. Disruptions in workflow may lead to conversion to open surgery for emergency measures, especially during active bleeding. Currently, conversion rate stands at 10% for most of the laparoscopic surgeries. Time lost contributes to operative duration, which is an independent risk factor for morbidity, as well as cost to the healthcare system. Given that 3.1 million laparoscopic surgeries were performed in USA in 2012 (projected to grow at 5-8%), we estimate a total of 386,000 hours spent cleaning the scope, representing wastage of USD 347 Million in terms of theater time to healthcare system.

At present, laparoscopic sheaths have been devised with fluid irrigation channels that enable lens cleaning without scope removal (EndoScrub 2, Medtronic). However, this still involves loss in visualization and disruption of surgical flow while irrigation is taking place. Recently, a sheath generating air vortex distal to the lens has been developed which disperses smoke produced during electro-cautery dissection (Floshield, MID Surgical). However it is not effective against blood splatter and thus fails to protect the lens during the most critical moments of the surgery.

Hence, to overcome the above defects, we developed a novel

device, the one-stop solution which addresses all the problems encountered. Our product Seymour Shield is a 12mm/14mm sheath that fits over the conventional 10 mm laparoscopic camera with a distal, constantly-rotating, clear, transparent disc (shield). The rotation serves two purposes: firstly, to remove or prevent buildup of excess fluid and particulate debris on the visualization surface by centrifugal force, and secondly to produce an optical illusion of clarity exploiting physiological persistence of vision and the flicker-fusion threshold of human sight. We are using compressed air vacuum which is available readily in Operation Theater as a driver for the whole process. Rotor is designed in such a way that it is propelled by the compressed air and the transparent disk or the shield for the lens is embedded into the rotor. So, as the rotor rotates at high speed, the shield too rotates, thereby shattering all the foreign particles. The compressed air can be used by the doctor whenever required, by just pressing the button in the sheath. Thus Seymour Shield offers easy and instant solution for maintaining clear vision throughout the laparoscopic surgery.

SP029.3 - Optimizing MRI-targeted fusion prostate biopsy: the effect of systematic error and anisotropy on tumour sampling

Author(s): Peter Martin¹, Derek W. Cool², Cesare Romagnoli², Aaron Fenster¹, Aaron D. Ward³

¹Medical Biophysics, Western University, London/ON/CANADA, ²Medical Imaging, Western University, London/CANADA, ³Oncology, Western University, London/ON/CANADA

Background:

Magnetic resonance imaging (MRI)-targeted, 3D transrectal ultrasound (TRUS)-guided “fusion” prostate biopsy intends to reduce the ~23% false negative rate [1] of clinical 2D TRUS-guided sextant biopsy. Although it has been reported to double the positive yield [2], MRI-targeted biopsies still yield false negatives. We propose optimization of biopsy planning, according to the clinician’s desired probability of sampling each tumour. This optimizes needle target positions within tumours, accounting for guidance system errors, image registration errors, and irregular tumour shapes.

Purpose:

Random, systematic and anisotropic biopsy needle delivery errors can arise due to patient and prostate motion, image registration errors, and device-to-image calibration issues. The purpose of this work was to investigate the effect of needle delivery error on tumour sampling probabilities, as a first step toward our over-arching aim of optimizing the number and placement of biopsy targets to obtain an early and accurate characterization of each patient’s cancer.

Methods:

We obtained multiparametric MRI and 3D TRUS images from 49 patients. A radiologist and radiology resident contoured 81 suspicious regions, yielding tumour surfaces that were registered to the TRUS images using an iterative closest point prostate surface-based method. The probability of obtaining a sample of tumour tissue in one attempt was calculated by integrating a 3D Gaussian distribution over each tumour domain, where σ = the needle delivery error. We ran an exhaustive simulation using this error model to investigate how systematic errors and error anisotropy affect tumour sampling probabilities.

Results:

Our experiments indicated that a biopsy system’s lateral and elevational errors have a much greater effect on sampling probabilities, relative to axial error. We have also determined that systematic errors with magnitude <2 mm have a relatively small incremental effect

on sampling probabilities. For a fusion biopsy system with a typical needle delivery error of 3.5 mm, tumours of volume $\leq 1.9 \text{ cm}^3$ may require more than one biopsy attempt to ensure 95% probability of a sample with 50% core involvement, and tumours $\leq 1.0 \text{ cm}^3$ may require more than two attempts (Figure 1).

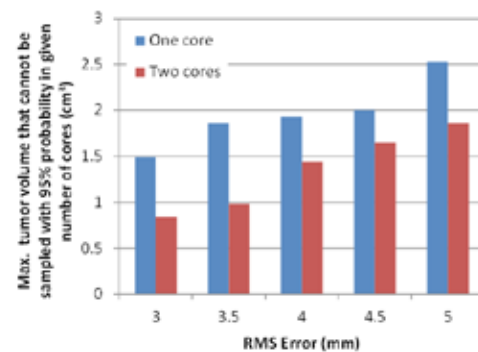


Fig. 1: The upper bound of tumour volume such that there is <95% probability of obtaining a sample with $\geq 50\%$ core involvement, given needle delivery error of the biopsy system.

Impact:

Optimized planning of within-tumour targets for fusion biopsy could support earlier diagnosis of prostate cancer while it remains localized and curable.

[1] Rabbani, F., J Urol 159(4), 1998

[2] Cool, D., LNCS 6963, 2011

SP029.4 - Is hemolysis influenced by the dynamic calibration method of CPB roller pumps?

Author(s): Francisco U. Vieira Junior¹, Nilson Antunes², Eduardo T. Costa³

¹Federal Institute of São Paulo, Campinas/BRAZIL, ²Cardiac, Campinas State University, Campinas/BRAZIL, ³Biomedical Engineering, Campinas State University, Campinas/BRAZIL

Introduction: Roller pumps are widely used in cardiopulmonary bypass (CPB) surgeries due to the easy of their operation, maintenance, safety and cost. Several studies have compared the use of roller pumps with centrifugal pumps but few have evaluate the influence of the different roller pump adjusts on hemolysis. The objective of this work was the in vivo analysis of the influence of roller pump adjustment by the dynamic method on hemolysis prevention.

Methodology: We have measured the hemolysis rate of 87 patients submitted to myocardial revascularization, divided in 4 groups, altering the roller pumps adjustment by the dynamic method. We have used an Auxiliary Calibration Device specially developed for this purpose. The adjustments consisted in the monitoring of the pump output pressure (pump at 10 rpm) with the output tube pinched, the pump rollers were adjusted in order to have mean pressures between 75 and 450 mmHg. The adjustment for each group was as follows: Group 1 (n=20) - 75 mmHg ; Group 2 (n=24) - 150 mmHg; Group 3 (n=22) - 300 mmHg; and Group 4 (n=21) - 450 mmHg. The hemolysis rates were measured before the start of CPB (T0) and 5 minutes after CPB (T1). The blood plasma free hemoglobin (HLP) was calculated using a spectrophotometer and the data related to a measurement at instant “t” was corrected for the hemodilution according to the equation below using Htbase = 27,5%:

$$HPp = HLP(t) \cdot Htbase / Ht(t)$$

The hemolysis rates (Tx) were calculated for each patient for the interval T0-T1 using the following equation:

$$Tx = (HLp1 - HLp0)/(T1 - T0)$$

Results: In Table 1 we show the measurement results for each group. Our results have not shown statistical difference for hemolysis rates between groups (p>0.05).

Table 1 – Registered times during CPB with respective mesasures of free hemoglobin and hemolysis rates. Values are mean ± standard deviation.

	Group 1 (n = 20)	Group 2 (n = 24)	Group 3 (n = 22)	Group 4 (n = 21)	
	Time (min)				pvalue*
T1	0 ± 0	0 ± 0	0 ± 0	0 ± 0	-
T2	95,0±23,2	104,5±22,1	98,7±22,6	104,6±38,2	> 0.55
	HLp (mg/dl)				pvalue*
HLp1	9,3 ± 5,0	6,4 ± 2,0	9,6 ± 7,0	9,3 ± 4,0	<0,0001
HLp2	53,7±18,0	48,1±13,0	52,7±14,6	45,4±11,4	> 0,31
	Hemolysis rates (mg/dl/min)				pvalue*
Tx	0,5 ± 0,2	0,4 ± 0,1	0,5 ± 0,2	0,4 ± 0,1	> 0,05

* Comparison between groups.

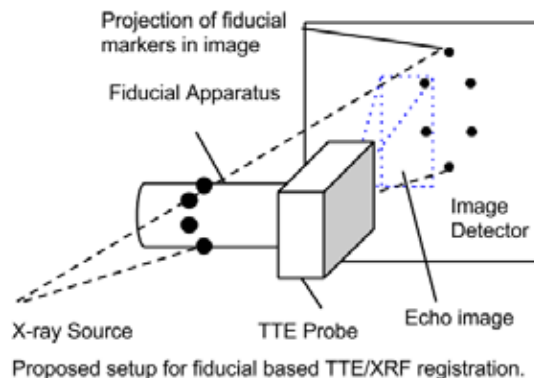
Conclusion: Our results have shown that the calibration of the roller pumps for different adjustments have not influenced the hemolysis rates in the analysed groups. Little occlusive calibrations should be avoided due to possible reflux and errors in flow measurements based on the pump rotation.

SP029.5 - A Fiducial Apparatus for 6DOF Pose Estimation of an External Echo Probe from a Single X-ray Projection: Initial Simulation Studies on Design Requirements

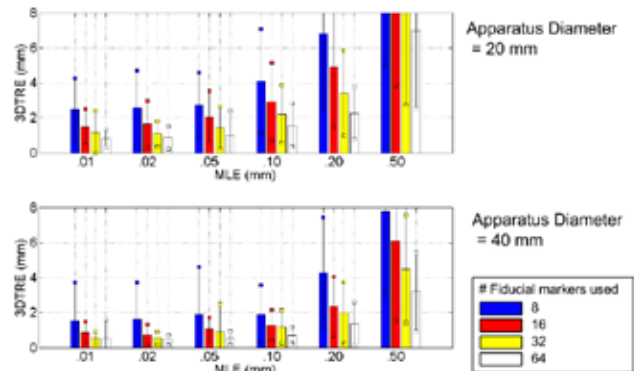
Author(s): Charles R. Hatt¹, Amish N. Raval², Michael A. Speidel³
¹Medical Physics, University of Wisconsin, Madison/UNITED STATES OF AMERICA, ²Cardiovascular Medicine, University of Wisconsin, Madison/WI/UNITED STATES OF AMERICA, ³Medical Physics, University of Wisconsin, Madison/WI/UNITED STATES OF AMERICA

X-ray fluoroscopy (XRF) is considered the primary imaging modality for guidance during cardiac interventions. However, visualization of soft tissue is limited. Image registration between transthoracic echocardiography (TTE) and XRF could potentially be used to fuse soft-tissue imaging with device imaging in minimally sedated patients. We propose a method of XRF/TTE image registration in which a fiducial apparatus is rigidly attached to the TTE probe, and the 3D pose of the fiducial is determined based on its appearance in the XRF image. The fiducial consists of a constellation of radio-opaque markers with known geometry. 3D pose estimation accuracy depends on 1) accurate marker localization in the XRF image, 2) geometric properties of the apparatus such as marker diameter, overall apparatus dimensions, marker count, manufacturing tolerances, and 3) pose estimation method. In this work, we performed simulation studies to examine the effect that each variable had on the 3D target registration error (TRE). In the first experiment, we generated simulated XRF images of a spherical marker with varying levels of peak signal-difference-to-noise ratio (pSDNR) and varying marker diameters, and measured the effect on

marker localization error (MLE). In the second experiment, using a circular constellation of markers, we tested the effect that MLE, manufacturing tolerance, apparatus dimensions, marker count, and shape constraints during optimization had on TRE. Our results showed that MLE was roughly 0.14, 0.05, 0.02 mm for pSDNRs of 10, 20 and 30 using a 2 mm diameter spherical marker. TRE decreased as the marker count and apparatus diameter increased. Manufacturing error increased TRE, but had minor effects for clinically relevant levels of MLE. Results indicate that, for a “medium” level of pSDNR (~15), the optimal fiducial configuration can achieve a 3DTRE of 0.32 ± 0.22 mm, and can achieve a 3DTRE of less than 1.5 mm for noisier images.



3D Target Registration Error For Varying Fiducial Apparatus Design Parameters and Marker Localization Errors (MLE)



SP029.6 - Mechanism design a flexible endoscope with USB adaptation to training.

Author(s): Francisco D. Perez Reynoso¹, Daniel Lorias Espinoza¹, Rigoberto Martínez Méndez²

¹Ingeniería Electrica, Centro de Investigación y de Estudios Avanzados del Instituto Politécnico Nacional, Distrito Federal/MEXICO, ²Ingeniería Electrica, Universidad Autónoma del Estado de México, Toluca México/MEXICO

The aim of this paper is to present a mechanism to adapt a boroscopic camera to the operation of a flexible endoscope and get the vision of a real device, leveraging technology for portable devices to provide surgeons the visualization so important in the training and application of endoscopy, because without this tool is virtually unenforceable.

SP029.7 - 3D Quantitative Evaluation System for Integral Photography based 3D Autostereoscopic Medical Display

Author(s): Zhencheng Fan, Sen Zhang, Yitong Weng, Guowen Chen, Hongen Liao
Biomedical Engineering, School of Medicine, Tsinghua University, China, Beijing/CHINA

3D autostereoscopic display techniques are used in medicine to assist surgeons to have a better knowledge on regions of interest. However, different 3D image generation algorithms and hardware implementations will bring out varied display quality. An objective and quantitative evaluation of clinical display is necessary. To evaluate the quality of 3D displays, we propose a quantitative evaluation system for 3D autostereoscopic medical display in this paper. The proposed evaluation system is composed of a 3D evaluation reference pattern, a 3D image acquisition platform and a quantitative analysis module. Moreover, we apply an integral photography based 3D autostereoscopic medical display to verify the feasibility and availability of the evaluation system. Based on quantification results of the 3D evaluation reference pattern and the 3D medical image, evaluation errors of the viewing angle, imaging depth as well as image quality are acceptable.

SP030 - Lab-on-chip, BioMEMS and Microfluidics**TRACK 08: BIOSENSOR, NANOTECHNOLOGY, BIOMEMS AND BIOPHOTONICS****SP030.1 - Drop-based microfluidics for diagnostic applications**
Author(s):

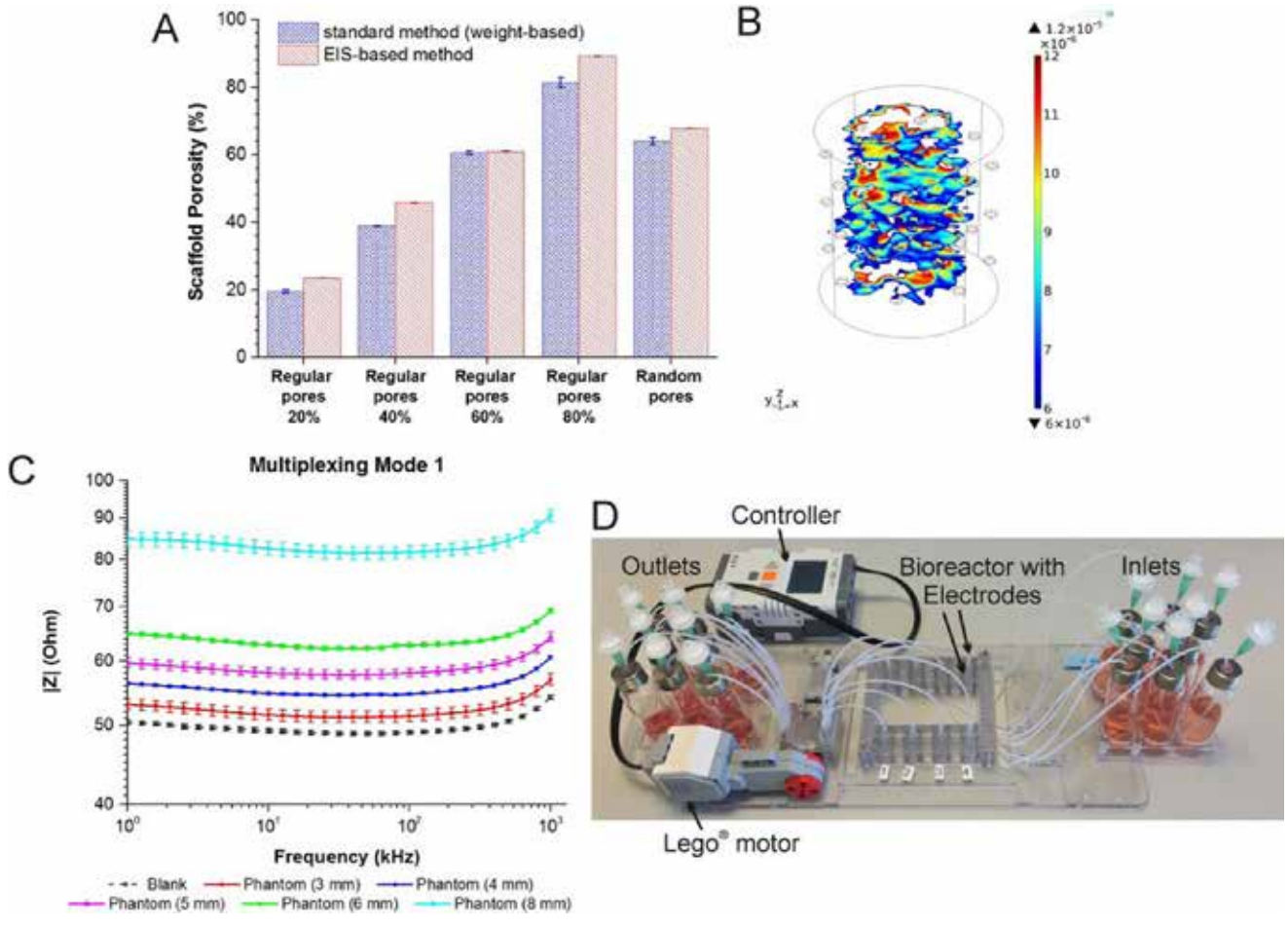
This talk will introduce the use of microfluidics to control very small aqueous drops that can be used as microreactors to perform millions of experiments in very short times and using very small quantities of reagents. These systems have great potential for use in many research and diagnostic applications. Some of these will be described.

SP030.2 - Enhanced multielectrode configurations in miniaturized 3D electrical impedance spectroscopy and tomography - monitoring the overall process of tissue engineering with spatial sensing for future challenges in microfluidics

Author(s): Chiara Canali¹, Haseena B. Muhammad¹, Arto Heiskanen¹, Chiara Mazzoni¹, Lorenzo Ceccarelli¹, Ørjan G. Martinsen², David Holder³, Anders Wolff¹, Martin Dufva¹, Jenny Emnéus¹
¹Micro- And Nanotechnology, Denmark Technical University, Kgs. Lyngby/DENMARK, ²Physics, University of Oslo, Oslo/NORWAY, ³Medical Physics And Bioengineering, University College London, London/UNITED KINGDOM

Over the past two decades, 3D cell culture models have attracted considerable attention to achieve, e.g., in vivo-like structural organization, gene and protein expression, response to stimuli, drug metabolism. A significant challenge in this regard is gaining spatially distributed information when monitoring cell proliferation on a biocompatible scaffold displaying well defined physico-chemical properties. Electrical impedance spectroscopy (EIS) has been shown to be a non-invasive method for biomaterial characterization and monitoring microfluidic cell cultures, gaining an insight on cellular activity and proliferation over time.

We have developed and validated planar and needle-based multi-electrode systems which offer the advantage of switching among different two-, three- and four-electrode configurations to focus impedance-based sensing on specific sub-volumes in a 3D cell culture. Information about scaffold architecture supporting cell organization (e.g. porosity, Fig. 1A), medium conductivity, and 3D spatial distribution of cells can be obtained. Furthermore, four-electrode configurations can also be used for electrical impedance tomography (EIT)-based imaging to map the conductivity distribution within a miniaturized 3D cell culture system (Fig. 1B). Finite element simulations were used to optimize electrode number, spacing and orientation with respect to the bioreactor geometry by maximizing the derived sensitivity field distribution for measurements. Validation with phantom experiments, mimicking cell clusters (Fig. 1C), and cell-based experiments was performed aiming to incorporate spatially enhanced 3D sensing into a 8-channel bioreactor array with integrated microfluidics for real-time monitoring of cell proliferation in porous scaffolds (Fig. 1D). The integration of the developed non-invasive sensing methods enable monitoring of tissue development within otherwise inaccessible areas of a 3D tissue construct, overcoming limitations of more traditional optical techniques.

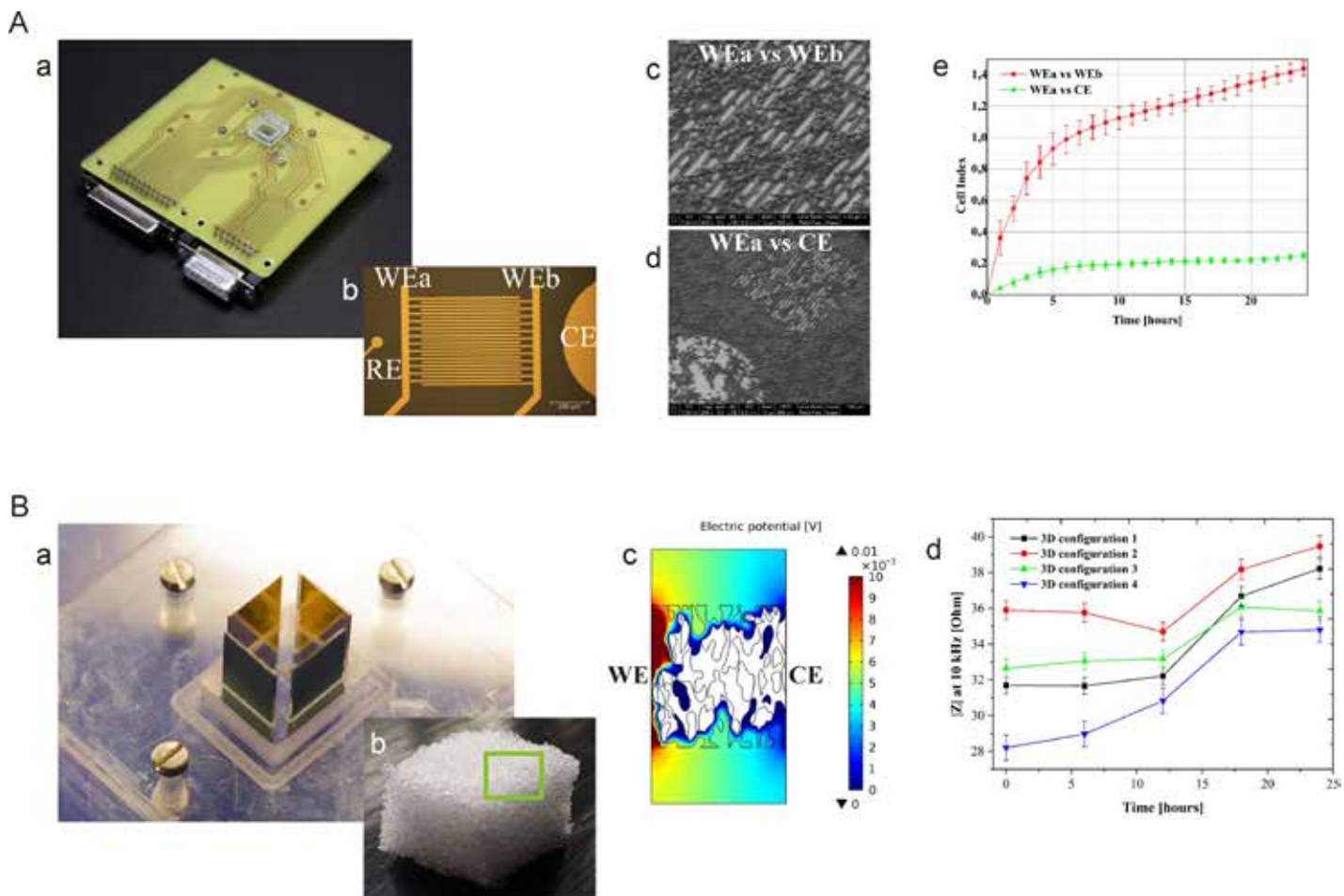


SP030.3 - On-line monitoring of 2D and 3D cell cultures: electrode configurations for impedance based sensors

Author(s): Chiara Canali¹, Claudia Caviglia¹, Kinga Zór¹, Haseena B. Muhammad¹, Arto Heiskanen¹, Ørjan G. Martinsen², Thomas L. Andresen¹, Anders Wolff¹, Martin Dufva¹, Jenny Emnéus¹
¹Micro- And Nanotechnology, Denmark Technical University, Kgs. Lyngby/DENMARK, ²Physics, University of Oslo, Oslo/NORWAY

Electrochemical impedance spectroscopy (EIS) has been proved to be a valuable technique for label-free, real-time and minimal invasive detection of cellular functions in fundamental and applied research. During the last three decades, several two-dimensional (2D) impedance-based systems have been widely used for studying cell adhesion and spreading, proliferation and death. Nowadays, there is an increasing interest towards three-dimensional (3D) cell cultures, which are proposed to create and maintain a more in vivo-like environment. EIS can be applied at different stages when developing a 2D or 3D culture setup, starting from bare scaffold and electrode characterization to monitor cell proliferation and tissue functionality. We present theoretical and experimental comparison of several electrode configurations (or modes) both in 2D (Fig. 1A) and 3D (Fig. 1B) used for following cell growth in real-time. Two different 2D modes were explored measuring between: i) the two combs (working electrode a vs b, WEa vs WEb), interdigitated configuration (Fig. 1Aa,b,c) and ii) WE versus a large counter electrode (CE), conventional "vertical" configuration, and found that the interdigitated configuration provides a higher sensitivity when monitoring HeLa cells adhesion, spreading and growth over 24-h (Fig. 1Ad).

In 3D environment there is a need for adding the third dimension to EIS sensing for spatial resolution to gain information about distribution of cells in the scaffold (Fig. 1Ba,b,c). Moreover, electrode number, geometry and orientation need to be optimized with respect to the deriving sensitivity field distribution. In order to gain information with a good resolution, we show that several two-, three- and four-electrode measurements can be combined to create complementary sensitivity fields which individually focus on specific volumes inside the 3D cell culture and, taken together, cover the whole measurement chamber volume. This approach was tested for growing hepatoblastoma (HepG2) cells embedded within a 5% w/v gelatin scaffold (Fig. 1Bd).



SP030.4 - Development of Microfluidic Paper-Based Electrochemical Immunoassays for the Detection of Prostate Cancer**Author(s):** Sean P. Rawlinson, Prosper Kanyong, James McLaughlin, James Davis

Nibec, School Of Engineering, University of Ulster, Newtownabbey/ UNITED KINGDOM

Prostate cancer or carcinoma of the prostate is one of the most frequently diagnosed malignancies in the world. Prostate cancer is the second leading cause of cancer death in men worldwide and the fourth most common cancer overall, with more than 1.1 million new cases diagnosed in 2012, and more than 307,000 deaths from the disease¹. The prevalence of the condition and mortality will clearly vary from one country to another but tends to be higher in developed countries². Prostate cancer incidence is strongly linked to age with the lowest incidence rates being in younger men. In the UK between 2009 and 2011, only 1% of cases were diagnosed in men under 50 and an average of 36% of cases was diagnosed in men aged 75 years and over¹. In a population with increasing longevity, it is likely that prostate cancer will become even more clinically prevalent in the future. This projected increase is a major concern for the public health sector, especially when there are both problems associated with the detection and the treatment of prostate cancer. Specifically, current practice in prostate cancer and staging leads to inaccurate assessments often resulting in unwanted or even unnecessary treatments that adversely affect the patient's quality of life with little gain. It will also place a considerable burden on the healthcare provider.

The poster presentation details a new approach to the development of microfluidic paper-based electrochemical devices that will be capable of multiparametric detection. Rather than examining single parameter detection, the strategy adopted here involves the laser machining of cellulose based substrates to create an array of microfluidic channels and detection wells as detailed in Figure 1. Screen printed electrodes are positioned within the wells and can be functionalised with a variety of molecular recognition elements (enzyme or antibody) thereby providing a system which is capable of screening a panel of biomarkers relevant to the diagnosis of prostate cancer. The design, development and bioanalytical characterisation of the prototype sensing systems will be presented and the applicability to point of care diagnosis critically assessed.

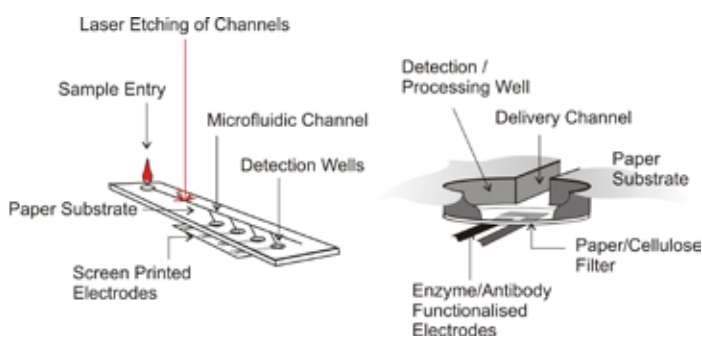


Figure 1. Schematic of the microfluidic array.

References

1. UK, C. R. Prostate cancer mortality statistics. (2014). <http://www.cancerresearchuk.org/cancer-info/cancerstats/types/prostate/mortality/uk-prostate-cancer-mortality-statistics>
2. Ferlay J, Soerjomataram I, Ervik M, Dikshit R, Eser S, Mathers C, Rebelo M, Parkin DM, Forman D, Bray, F. GLOBOCAN 2012 v1.0, Cancer Incidence and Mortality Worldwide: IARC CancerBase No.11 [Internet]. Lyon, France: International Agency for Research on Cancer; 2013.

SP030.5 - Investigating chip design for a Raman microfluidic system with clinical radiobiological applications.**Author(s):** Samantha J. Harder¹, Julian J. Lum², Andrew Jirasek³, Alexandre G. Brolo⁴¹Physics And Astronomy, University of Victoria, Victoria/CANADA, ²Deeley Research Centre, BC Cancer Agency, Victoria/BC/CANADA, ³Physics, University of British Columbia - Okanagan, Kelowna/BC/CANADA, ⁴Chemistry, University of Victoria, Victoria/BC/CANADA

Raman spectroscopy (RS) has been demonstrated as valuable for studying biomolecular responses of human cancer cells to clinically relevant doses of ionizing radiation.¹ Radioresistance in cancer therapy remains a significant problem and recent studies indicate that RS may provide important biological insight into mechanisms of radioresistance.² Raman microfluidic (RMF) systems offer several potential advantages over traditional single cell Raman data acquisition techniques. The precise control of suspended particles in microfluidic environments facilitate automation of data collection, reducing the time required and user dependence of data acquisition. RMF systems facilitate efficient sample use which is favourable when dealing with small or rare samples- as is the case with patient biopsies. RMF systems have the potential to make RS more accessible for applications in the clinic and for wide-spread radiobiological studies. The objective of this work is to investigate microfluidic chip design for single cell Raman spectroscopic studies in radiobiology.

Three different prototype RMF systems have been investigated, to determine an optimal chip substrate and design. The first system is formed from polydimethylsiloxane (PDMS) using soft lithography techniques.³ This system varied slightly from traditional PDMS microfluidic systems by employing a MgF2 coverslip to seal the system instead of glass. MgF2 exhibits a relatively weak Raman spectrum in the spectral region of interest, compared to most glasses, making it ideal as a substrate material for chip design. Second, a novel RMF design was realized by forming the base and top surfaces of the chip using MgF2 with Parafilm forming the channel walls. Lastly, a novel design made entirely out of MgF2 was tested. A channel was laser etched into MgF2 using a Ti:Sapphire laser, and the system was sealed using a MgF2 coverslip. Raman spectra from single cells in each RMF system have been collected, using a Renishaw inVia Raman microscope coupled with a 785 nm laser, in order to determine the optimal chip design for radiobiological Raman studies.

The PDMS based RMF chip yielded cell spectra which were contaminated by Raman peaks characteristic of PDMS. These peaks interfere with cellular Raman signals in spectral regions which are important for assessing radiation-induced responses in cells.^{1,4} The PDMS chip design is, therefore, unsuitable for radiobiological applications. The novel Parafilm-MgF2 and solid MgF2 chip designs yielded suitable cell spectra for studying radiation-induced biomolecular changes in cells, since in both cases there were minimal contributions from the chip material in the Raman spectra.

Both the novel Parafilm-MgF2 and solid MgF2 chip designs are promising for single cell Raman radiobiological studies. Both systems warrant further investigation as potential designs which may facilitate adaptation of Raman spectroscopy for the clinic and for wide-scale biological research.

- References: 1. Harder et al. Applied Spectroscopy, Vol. 69(2), 2015. 2. Matthews et al. Cancer Research (submitted, 2015). 3. Xia et al. Annual Rev. Mat. Sci. Vol. 28(1), 1998. 4. Matthews et al. Phys. Med. Biol. Vol. 56, 2011.

SP030.6 - A lab-on-a-chip system for hypoxic investigations on single biological cells
Author(s): Ahmed Alrifaiy¹, Olof Lindahl², Kerstin Ramser³
¹Neuroscience And Physiology, Gothenburg University - Sahlgrenska Academi, Gothenburg/SWEDEN, ²Centre For Biomedical Engineering And Physics, Umeå University, Umeå/SWEDEN, ³Department Of Engineering Sciences And Mathematics, Luleå University of Technology, Umeå/SWEDEN

Biological investigations during acute and /or long-term hypoxia have become an important key in research that requires extraordinary experimental design. We present a platform of a multifunctional lab-on-a-chip (LOC) system for hypoxic investigation on biological single cells with controlled oxygen content and surroundings. The LOC was combined with the patch clamp technique for electrophysiological investigations, optical tweezers for manipulation of the individual cells in 3D within the closed micro-channel system, absorption spectroscopy to monitor and acquire the spectral response of the cells to different oxygenated states and oxygen sensor to monitor the oxygen level within the chip. All techniques was built on an inverted microscope (IX71, Olympus, Japan), on a vibration free optical table (Figure 1A). The developed gastight LOC in Plexiglas with an integrated patch-clamp micropipette (Figure 1B) is aimed to replace the open system in conventional patch clamp technique to achieve control of the gaseous surroundings of the investigated cells. To test the system, a single red blood cell (RBC) from Chicken (Fitzgerald Industries International, USA) was trapped optically, moved in 3D through the micro-channels of the chip towards the integrated micropipette within the gastight chip. The oxygen levels dissolved in the extracellular solution within the micro-channels was monitored by an oxygen sensor (FOXY, AL3000, Ocean Optics, USA) reached values between 0-18% O₂ which was verified by studying the oxygenation states of the trapped RBC with UV-Vis absorption spectra (Ocean Optics, HR4000, USA) simultaneously, (Figure 1C). The spectral transfer of the investigated cell from the oxygenated state (18% O₂) to the deoxygenated state (0% O₂) happened after about 3,7 minutes while a fully developed deoxygenated spectrum was observed after 4.9 minutes. The gas tightness of the hypoxic chamber to the oxygen diffusion was verified by stopping the flow of deoxygenated solution into the channel system while continuously recording UV-Vis spectra, showing an unchanged deoxygenated state during 90 min. Thereafter, a transfer to the oxygenated absorption spectra was achieved after 7.1min when exposing the cell to normoxic buffer solution. The result above showed the long time viability of the investigated cells as well as the control of the hypoxic conditions within the chip. To verify the system for physiological investigations, successful patch clamp investigations (EPC-7, HEKA, Germany) on a trapped RBC were established and the whole-cell access (R_a) and membrane resistances (R_m) were measured to be 5.1 MΩ and 900 MΩ respectively.

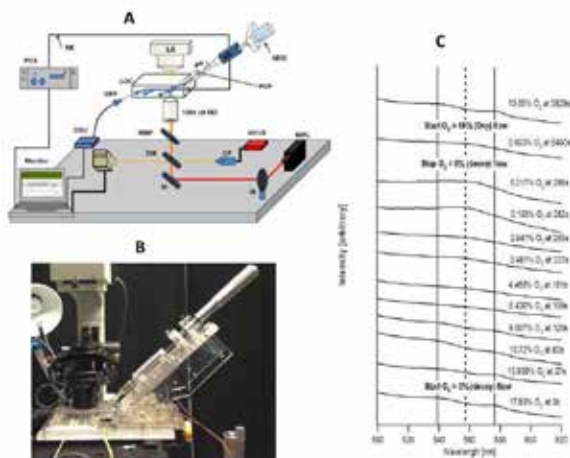


Figure 1: A. Schematic figure of LOC system including all techniques, B. LOC system integrated with patch Clamp technique, C. Absorption spectra of optically trapped chicken RBC with measured oxygen levels and time scale.

SP030.7 - Gas Sensors with ZnO Quantum Dots Synthesized by Sol-Gel Methods
Author(s): Glécia V.D.S. Luz¹, Pedro H.D.O. Nogueira¹, Eduardo C.D.

 Araújo¹, Luiza C.D. Araújo¹, Pilar Hidalgo¹, Lourdes M. Brasil²
¹University Of Brasília At Gama (unb-fga)/nanotechnology Laboratory, University of Brasília, Brasília/BRAZIL, ²Post-graduation Program In Biomedical Engineering, University of Brasília, Gama/BRAZIL

Nanoparticulate semiconductor materials have unique properties and the elucidation of these have led to interesting discoveries in various fields of science and technology. The number of scientific publications has increased in the last decade on ZnO nanostructures and their potential applications. ZnO is used in a number of biomedical applications such as: glucose detection, gas sensors, wound healing and dental filling materials, macrophage adhesion, coating antibodies which identify specific receptors found on cancer cells, improving the dispersion of light in endoscopic techniques, in the formation of electroluminescent and photovoltaic devices, among others. Nanostructures are defined as having at least on dimension between 1 to 100 nm, with peculiar properties and applications, different from their bulk counterparts. ZnO nanostructures and their potential applications has been the focus of many scientific publications in the last decades. ZnO Quantum dots (QDs) are zero-dimensional (0D) structures with great interest of researchers since the 90s and keeping in view the quantization of electron energies in crystals and their transport properties. We studied the effective answers of chemical sensors made from ZnO nanoparticles, synthesized by Sol-Gel Method, for chloroform and ammonium vapors, very present in air conditioner, medical environments and beauty products, for example. These vapors are not toxic at low concentrations, but their increase can cause many health hazards to humans and animals. The results showed that ZnO Sol-Gel QDs sensor demonstrated, apparently, sensitivity to ammonia and no reaction with chloroform vapor. It was evidenced that applicability of nano-sensors consisting of ZnO nanoparticles, specifically ZnO quantum dots, for the detection of ammonia vapors present, for example, in environments that may be harmful to human health. It was noted that the detection process of adsorption/release of ammonia vapors is reversible. Thus, there is a need for further testing with this type of sensor in order to check their behavior when exposed to high gas concentrations, and the change of the thickness of the nanoparticle film applied on the substrate. Furthermore, tests should be conducted including different crystallite sizes and structures, mainly seeking their application in several areas of Biomedical Engineering.

SP031 - Pattern Classification

TRACK 09: BIOSIGNAL PROCESSING

SP031.1 - The Recognition of Pinch-to-Zoom Gesture Based on Surface EMG

Author(s): Jongin Kim¹, Dongrae Cho², Kwang Jin Lee¹, Boreom Lee¹
¹Department Of Medical System Engineering, GIST, Gwangju/KO-REA, ²Mechatronics, gwangju institute of science and technology, Gwangju/KOREA

I. INTRODUCTION

In recent years, a lot of researchers have tried to construct the system to recognize a hand or finger gesture based on the surface electromyogram (sEMG) since it can be used for the human computer interface.

They have only focused on recognizing simple movements such as an extension or flexion of fingers. However, in our present study, we propose a system to recognize a pinch-to-zoom gesture in real-time for practical applications. Pinch-to-zoom is a gesture to change the distance between the thumb and index fingers in order to control the size of images. For inferring the gesture, sEMG was acquired from the first dorsal interosseous muscle and multiclass classification techniques were used.

II. METHODS

A. Experiment and System settings

We recruited six healthy subjects for our experiment. We asked subjects to maintain the distance between thumb and index finger according to the visual cues (0 cm, 4 cm, 8 cm, and 12 cm).

Our system is divided into a sensor interface and computational unit parts. The sensor interface wirelessly transmits the sEMG to computational unit using Bluetooth. We developed graphic user interface (GUI) based on Matlab. The software reduces the noise, extracts the features and provides a visualization of the distance between the thumb and index finger in real time. (See figure1)

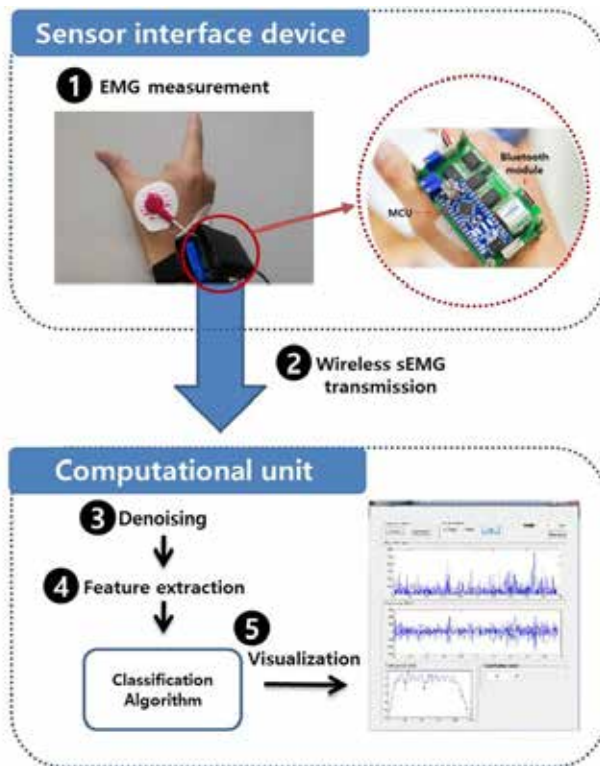
B. Feature extraction and Classification

In order to identify the distinct frequency bands, ANOVA test was conducted between four experimental conditions. Consequently, the powers from 1Hz to 250Hz are statistically significant ($p < 0.01$). Therefore, the powers from 1Hz to 250Hz were used as features for pinch-to-zoom gesture recognition.

The support vector machine (SVM) was used for recognizing the pinch-to-zoom gesture. Several hyperplanes have to be used for solving an N-class problem ($N > 2$) because SVM is based on two-class classification. Therefore, One-versus-One strategy was used for recognizing the pinch-to-zoom gesture.

III. RESULTS

We obtained sEMG data for a total of 400 trials per subject in order to prove the utility of our system, and divided all the data into training and test set. The classifier was constructed using only the training set. In order to accurately estimate the performance of our system, this procedure was repeatedly conducted ten times with different random partitions. As a result, average classification rate over all subjects was about 91.9%. These results prove that our system can be successfully used for recognizing the pinch-to-zoom gesture in real time.



SP031.2 - Feature extraction trends for biomedical signals

Author(s): Yashodhan Athavale¹, Sridhar Krishnan²
¹Electrical & Computer Engineering, Ryerson University, Toronto/ON/CANADA, ²Electrical & Computer Engineering, Ryerson University, Toronto/CANADA

Signal analytics involves identifying signal behavior, extracting linear and non-linear properties, compression or expansion into higher or lower dimensions, and recognizing patterns. Over the last few decades, signal analytics has taken notable evolutionary leaps in terms of measurement – from being simple techniques for analyzing analog/digital signals in time/frequency/joint time-frequency (TF) domain, to being complex techniques for analysis in a higher dimensional sparse domain. The intention behind this is simple – Feature Extraction; i.e. to identify specific signal markers or properties exhibited in one phenomenon, and uses them to distinguish from properties exhibited in another phenomenon [1-9].

One must realize that real world biomedical signals are non-linear, non-stationary and could comprise of multi-modal components. Evolutionary methods such as Autoregressive modeling, Cepstrum modeling, and Fourier and Wavelet analysis can handle non-stationarity through windowing approaches [7, 9], but with certain limitations such as information loss, lower artifact filtering and low signal-to-noise & distortion-ratio (SNDR). We suggest that modern day feature extraction methods must be as intelligent and trainable as the pattern classifier itself. Ideally instead of windowing, it is recommended to handle real-time signals using a streaming or on-the-fly approach, i.e. extract features as the signal propagates through the source. This could be made possible by employing newer sparse and compressive sensing approaches in combination with TF methods such as non-negative matrix factorization; or even a deep learning network constructed using a cascade of wavelet filters. An intelligent feature extractor could possibly eliminate the need for a feature selection technique (such as mRMR - minimum redundancy maximum representation), as this would happen inherently within the feature extractor. Additionally if the features are visually separable between signal classes, then employing a simple linear classifier could reduce system design constraints thus impacting the hardware design positively. Through this study we are attempting to

determine the best combination of signal processing methods which could generate an intelligent feature extractor capable of: [i] robustness to artifacts, [ii] improving SNDR, [iii] handling non-linearity, [iv] handling non-stationarity, [v] assessing signal component variability, [vi] addressing higher dimensionality of feature space by compact or sparse feature generation, and most importantly [vii] generating a feature set which brings out maximum representation of the signal and helps pattern classification. From a hardware perspective we should also include the following criterion: [i] built-in pre-processing and artifact removal, [ii] low power and memory consumption, [iii] real-time signal processing capability and [iv] computationally cost effective.

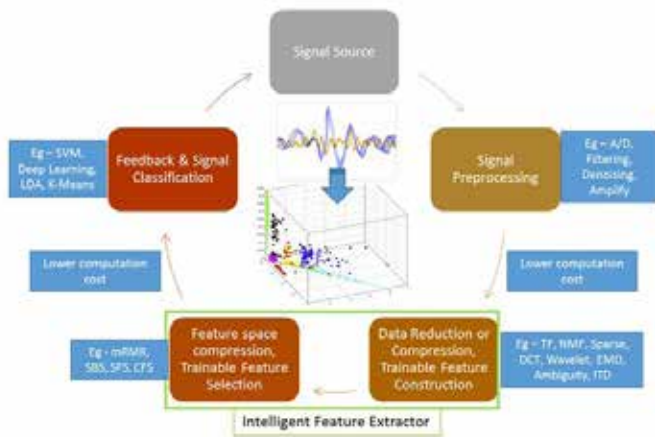


Figure 3. Trends in feature extraction process

SP031.3 - A Hybrid Model for Diagnosing Severe Aortic Stenosis in Asymptomatic Patients using Phonocardiogram

Author(s): Arash Gharehbaghi¹, Per Ask², Eva Nylander³, Birgitta Janerot-Sjoberg⁴, Inger Ekman³, Maria Lindén¹, Anika Babic²
¹Department Of Innovation, Design And Technology, Mälardalen University, Västerås/SWEDEN, ²Department Of Biomedical Engineering, Linköping University, Linköping/SWEDEN, ³Department Of Clinical Physiology, Linköping University, Linköping/SWEDEN, ⁴Department Of Clinical Science, Intervention And Technology, Karolinska Institutet, Stockholm/SWEDEN

This study presents a screening algorithm for severe aortic stenosis (AS), based on a processing method for phonocardiographic (PCG) signal. The processing method employs a hybrid model, constituted of a hidden Markov model and support vector machine. The method benefits from a preprocessing phase for an enhanced learning. The performance of the method is statistically evaluated using PCG signals recorded from 50 individuals who were referred to the echocardiography lab at Linköping University hospital. All the individuals were diagnosed as having a degree of AS, from mild to severe, according to the echocardiographic measurements. The patient group consists of 26 individuals with severe AS, and the rest of the 24 patients comprise the control group. Performance of the method is statistically evaluated using repeated random sub sampling. Results showed a 95% confidence interval of (80.5%-82.8%) / (77.8%- 80.8%) for the accuracy/sensitivity, exhibiting an acceptable performance to be used as decision support system in the primary healthcare center.

SP031.4 - Classification of Load in Hands Based on Upper Limb SEMG

Author(s): Illya Seagal, Evelyn Morin
 Electrical & Computer Engineering, Queen’s University, Kingston/ ON/CANADA

The purpose of this study is to correctly classify load lifted during a pail lift task. Surface EMG (SEMG) data were recorded from six locations on the arm and trunk of 15 subjects. Each subject was asked to lift a pail with one hand onto a platform at waist height in front of him/her. The pail contained masses from 0 kg to 20 kg in increments of 5 kg. Each weight was lifted and set down 5 times.

The down-lift interval of the task was identified from a recording of an electro-mechanical switch and SEMG data from the triceps brachii and brachioradialis were extracted. The data were filtered for noise reduction using a 12th order high pass Type II Chebyshev filter with a cut-off frequency of 25 Hz, and a low pass 1st order Butterworth filter with a cut-off frequency of 490 Hz. The mean absolute value (MAV) and RMS value were computed and used as a feature set. A hierarchical SVM system shown in Figure 1 was used to classify the load lifted.

Overall the mean inter-subject classification success rate for classifiable trials was 0.490 using a train on 1st subject and test on others scheme, and 0.483 using a train on 1st trial and loads of all subjects and test on all other trials scheme. The combined confusion matrix for the former scheme can be seen below. Using simple features and a hierarchical SVM structure, a reasonable inter-subject classification accuracy was achieved. This outcome may be improved in the future by careful selection of additional features.

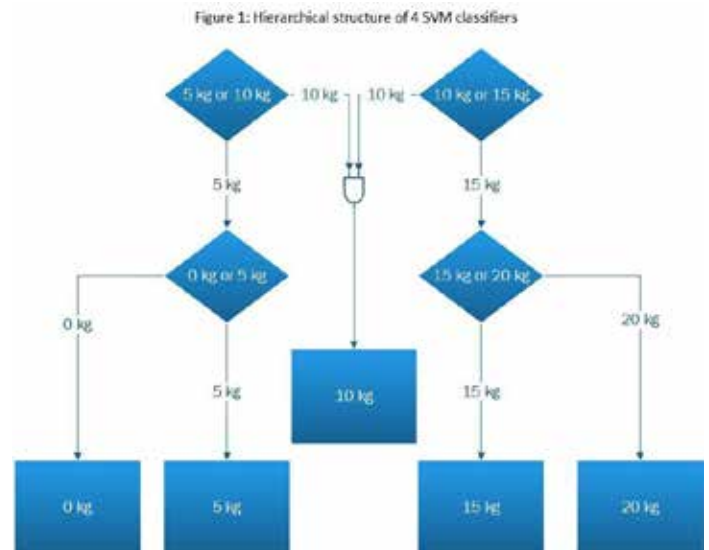


Table 1: Combined confusion matrix for all trials and subjects where the classifier was trained using data from subject 1, and tested on all other subjects. Some trials could not be classified due to poor electro-mechanical switch data.

	predicted 0kg	predicted 5kg	predicted 10kg	predicted 15kg	predicted 20kg	unclassified
known 0kg	43	21	0	0	0	1
known 5kg	11	48	0	0	0	6
known 10kg	15	37	3	4	3	3
known 15kg	0	19	9	9	23	5
known 20kg	0	0	2	5	39	19
unclassified	0	0	0	0	0	0

SP031.5 - An Intelligent Method for Discrimination between Aortic and Pulmonary Stenosis using Phonocardiogram

Author(s): Arash Gharehbaghi¹, Amir A. Sepehri², Armen Kocharian³, Maria Lindén¹

¹Department Of Innovation, Design And Technology, Mälardalen University, Västerås/SWEDEN, ²CAPIS Biomedical Research and Department Center, Mons/BELGIUM, ³Department Of Pediatrics, Tehran University of Medical Sciences, Tehran/IRAN

This study presents an artificial intelligent-based method for processing phonocardiographic (PCG) signal of the patients with ejection murmur to assess the underlying pathology initiating the murmur. The method is based on our unique method for finding disease-related frequency bands in conjunction with a sophisticated statistical classifier. Children with aortic stenosis (AS), and pulmonary stenosis (PS) were the two patient groups subjected to the study, taking the healthy ones (no murmur) as the control group. PCG signals were acquired from 45 referrals to the children University hospital, comprised of 15 individuals of each group; all were diagnosed by the expert pediatric cardiologists according to the echocardiographic measurements together with the complementary tests. The accuracy of the method is evaluated to be 90% and 93.3% using the 5-fold and leave-one-out validation method, respectively. The accuracy is slightly degraded to 86.7% and 93.3% when a Gaussian noise with signal to noise ratio of 20 dB is added to the PCG signals, exhibiting an acceptable immunity against the noise. The method offered promising results to be used as a decision support system in the primary healthcare centers or clinics.

SP032 - Neural Interfaces and Regeneration

TRACK 11: NEUROENGINEERING, NEURAL SYSTEMS

SP032.1 - NEUROPROSTHETIC SYSTEMS FOR ENHANCEMENT OF NEUROPLASTICITY FOLLOWING STROKE AND SPINAL CORD INJURY

Author(s): Milos Popovic

Toronto Rehabilitation Institute, University Health Network, Toronto/
CANADA

In this lecture three neuroprosthetic applications will be presented that do not belong to a typical “garden variety” neuroprostheses that one can commonly find discussed in the literature. The first part of the lecture will showcase a neuroprosthetic application, which is aimed at restoring voluntary hand function after severe stroke. In the lecture the results of a Phase II randomized control trial will be presented, which were pivotal for this technology to become a commercially viable product. The second part of the lecture will discuss a neuroprosthetic system for blood pressure regulation for individuals who suffer from orthostatic hypotension following spinal cord injury. In the lecture the results from a Phase I clinical trial will be presented. The third part of the lecture will showcase use of electrical stimulation technology as means to navigate stem cell migration. In the lecture the proof of principle results will be presented. These three projects have been selected to showcase idea generation, product development and clinical trial validation process commonly practiced at the Rehabilitation Engineering Laboratory. The second objective of this lecture is to stress the importance of system level engineering, as a critical tool in the process of creation, development and validation of neuroprosthetic devices.

SP032.2 - Demonstration of Graphene Microelectrodes as a Bioelectronic Interface

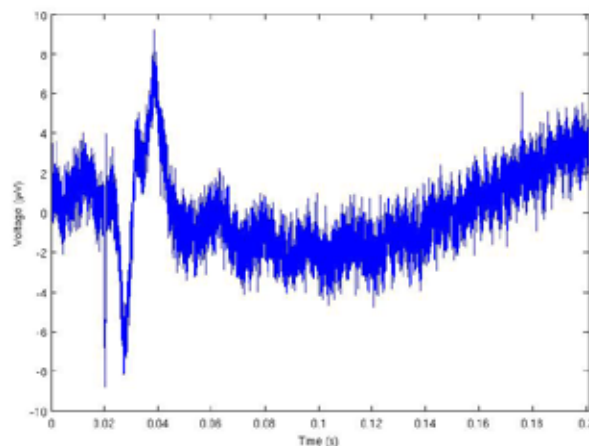
Author(s): Michael R. Horn¹, Arika D. Kemp¹, Keong H. Yong², Jonghyun Choi², Sungwoo Nam², Ken Yoshida¹

¹Biomedical Engineering, Indiana University Purdue University Indianapolis, Indianapolis/IN/UNITED STATES OF AMERICA, ²Mechanical Science And Engineering, University of Illinois at Urbana-Champaign, Urbana/IL/UNITED STATES OF AMERICA

In the past 15 years, our lab has developed intrafascicular microelectrode arrays (MEAs) for use in the peripheral nerve based upon micropatterned polyimide substrates with metal traces and contacts. These were the thin-film Longitudinal Intra-Fascicular Electrode (tLIFE) and the Transversely Implanted Micro-Electrode array (TIME). Acutely, these electrodes provide a high resolution view of the nerve activity within a nerve fascicle as well as a high resolution means to activate subsets of the nerve bundle. In part, the use of polyimide as the substrate material was to reduce the mechanical property mismatch between the neural tissues and the electrode structure as a means to improve the chronic viability of the neural interface. However, chronic implants of tLIFE and TIME structures have shown that despite being several orders of magnitude softer than metal wire electrodes, (~1GPa vs ~150 GPa), the structures became encapsulated in a similar fashion to the metal wire electrodes. It has become clear that the 2 orders of magnitude reduction in modulus was not a sufficiently large enough reduction to show a change in encapsulation of the electrodes in the peripheral nerve, which has a modulus of elasticity of ~100kPa.

We are currently exploring newer softer materials for the substrate, with moduli on the order of 1GPa. However, substrates of softer materials will require traces and contacts that can withstand 10-15% elongation. This pilot study, we explored such a material, graphene.

Analysis of whether a graphene microelectrode array could measure the bioelectrical activity of muscle tissue as a first step towards developing a general purpose ultra-flexible neural or muscular bioelectric interface. A graphene MEA (graMEA) was placed on the surface of an ex vivo rat biceps femoris muscle, and the electrical activity resulting from electrical stimulation of the sciatic nerve was recorded. The resulting twitch activity was simultaneously recorded using conventional intramuscular wire electrodes. It was found that the graMEA was capable of measuring stimulus artifact, compound EMG of the twitch and mechanical movement of the muscle, as shown below. Further advancements to the graphene based electrode include increasing the surface area by crumpling, reducing the contact size to increase spatial resolution of small nerve fibers, and using a field-effect transistor (FET) mode to increase signal to noise ratio. The results of this study provide proof of concept that flexible graphene electrodes can transduce bioelectrical activity of bioelectrically active tissues, opening the way towards developing ultra-small, ultra-flexible bioelectric interfaces.



SP032.3 - Development of a planar microelectrode array offering long-term, high-resolution neuronal recordings

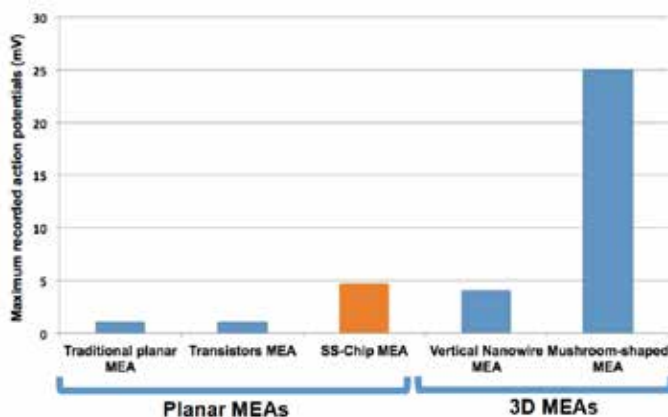
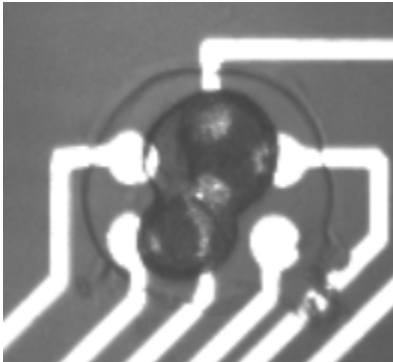
Author(s): Pierre J.J. Wijdenes¹, Colin Dalton², Ryden J. Armstrong³, Wali Zaidi³, Naweed Syed³

¹Biomedical Engineering Program, University of Calgary, Calgary/AB/CANADA, ²Department Of Electrical And Computer Engineering, University of Calgary, Calgary/CANADA, ³Faculty Of Medicine, University Of Calgary, Hotchkiss Brain Institute, Calgary/CANADA

All nervous system functions, ranging from simple reflexes to learning and memory, rely on networks of interconnected brain cells called neurons, which initiate and convey electrical information. Monitoring neuronal activities of a large neuronal ensemble, non-invasively and over an extended time period, is pivotal for understanding all brain functions. A variety of neuro-electronic interfaces now allow monitoring of neuronal and ion channel activities. These neuronal monitoring devices are however limited vis-à-vis their efficacy, fidelity and longer-term recording capabilities. Here we report on a novel microelectrode array that allows the detection and characterization of neural activity from individual cells and networks, over long periods of time with a higher signal-to-noise ratio than commercially available devices.

Our in-house development of planar microelectrode arrays has focused on modifying design parameters and fabrication techniques to improve their performance. One such device, the Soma-Soma Chip (SS-Chip), allows us to record activity from single and paired

cells (pre- and post-synaptic neurons, Figure 1) continuously over extended periods of time with a signal-to-noise ratio higher than similar standard devices (Figure 2). This allows for the analysis of neural activity, which can help to characterize firing patterns of neurons at various developmental-stages. Of particular importance is the precise “signatures” of neuronal firing pattern that offers a unique opportunity to decipher how neuronal activity influences brain network connectivity. Our data underscores the importance of further development of novel planar microelectrode array technologies and suggests that there is still work to be done to improve their signal-to-noise ratio. The ability to conduct long-term recordings should also not be considered optional, as this is critically important for fundamental and clinical neuroscience research. These developments will provide novel tools and open new research opportunities critical for understanding the fundamental cellular and network properties underlying network activity under both normal and disease conditions.



SP032.4 - Morphological changes in photoreceptors due to DC electric field

Author(s): Juliana M. Guerra¹, Cora Rohlecke², Richard Funk², Sérgio S. Mühlen¹

¹Biomedical Engineering Department, UNICAMP, Campinas, SP/BRAZIL, ²Anatomy Department, Technische Universität Dresden, Dresden/GERMANY

Previous studies and experimental evidences suggest an important role for endogenous electric fields in directing cell migration in wound healing, cell development and regeneration. In cultures, applied direct current electric field (dcEF) influences cell division, polarity, shape and motility. Photoreceptors dystrophies are one of the major causes of inherited blindness in the western world; application of EF could be used as a cue to direct photoreceptors cells to growth towards the damaged tissue, apart from the possibility of regeneration of the outer segments. In this study we investigate the

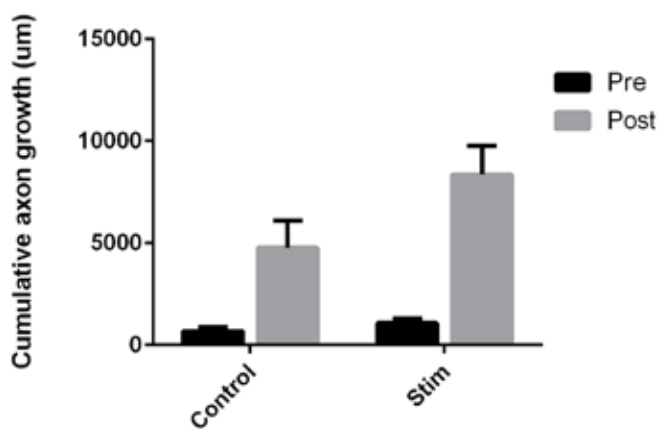
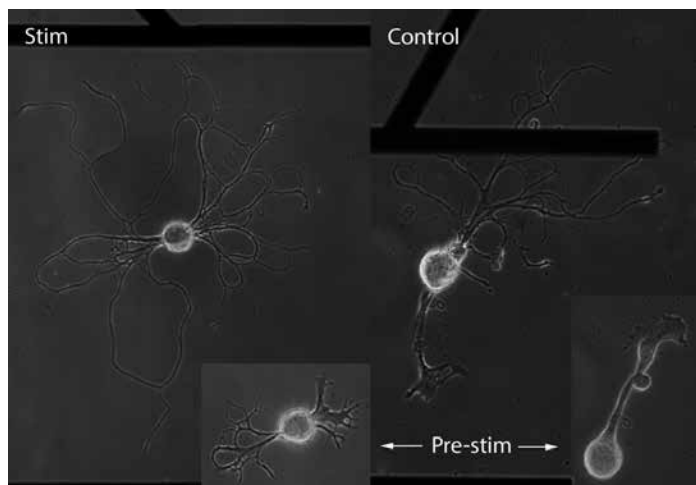
effects of dcEF in the establishment of photoreceptor cell polarity and polarization of intracellular structures, to analyze the special role of an extracellular electrical cue. Using a well established migration assay, photoreceptors cone-like 661W mouse retina cells were stimulated for 5 h with 5 VDC/cm electric field. Using immunofluorescence techniques we have investigated changes in position of important organelles like Microtubules Organizing Center (MTOC), Golgi Apparatus (GA) and nucleus within those cells after the stimulation. In response to the directional stimulus, the cells have extended membrane protrusions towards the cathode; they got elongated perpendicular to the dcEF and have formed a leading edge towards the direction of cues. Directional migration has occurred towards cathode. MTOC and GA were reoriented in the direction of the leading edge of the cells (cathode), while the nucleus was translocated to the back of the cells, in the rear edge. Nuclear positioning is determined by microtubule and actin networks. The Golgi complex was colocalized with the MTOC in order to facilitate polarized secretion and provide membrane and secreted products directly to the most proximate plasma membrane to the leading edge of migrating cells.

SP032.5 - Accelerating Neurite Outgrowth Through Electric Field Manipulation

Author(s): Michael T. Purdy¹, Pierre J.J. Wijdenes¹, Wali Zaidi², Na-weed Syed², Colin Dalton³

¹Biomedical Engineering Program, University of Calgary, Calgary/AB/CANADA, ²Department Of Anatomy And Cell Biology, University of Calgary, Calgary/CANADA, ³Department Of Electrical And Computer Engineering, University of Calgary, Calgary/CANADA

Brief electrical stimulation accelerates neuronal regeneration both in individual cells and in living models. *In vitro* experiments facilitate further understanding of regeneration mechanisms, and stimulation is accomplished through current-injecting micropipettes or commercially available microelectrode arrays. Such stimuli can be approximated as point-sources that emit decaying electric fields with high magnitude field strength near the electrode or micropipette. However, uniform electric fields may be better suited to enhance growth than traditionally used point-source fields. Applied uniform electric fields would allow for long distance stimulation without requiring high voltages that can compromise electrode integrity and cell health. The viability of uniform electric field stimulation was explored in this study through the use of a custom-fabricated planar microelectrode array. Simulation of several electrode configurations resulted in the design of a parallel plate anode-cathode pair. Several electrode pairs were embedded onto a single microelectrode array at various gap widths, to allow for the study of electric field strength on overall growth. With this novel electrode array, individual *Lymnaea* snail cells were stimulated with a 20 Hz, 1 volt pulse train for one hour. Control cells were plated on identical electrode arrays but were not connected to the stimulus generator. The impact of stimulation on growth was measured 24 hours later, and compared to control groups (Fig. 1). Stimulated cells showed an increase in overall neurite length compared to controls (Fig. 2). This effect was seen regardless of stimulus magnitude, within the range of 1000 – 2000 mV/mm. Our preliminary study served as a proof of principal for the application of uniform electric fields as a regenerative technique for nerve regrowth. The designed electrode layout improves upon currently available microelectrode arrays, and will allow for further study of regeneration mechanisms. This layout will be more easily transferred to an implantable design for future clinical use.



SP033 - Imaging: Part 1

PRESIDENTS CALL

SP033.1 - Quantification of breast density using dual-energy mammography, CT and MRI

Author(s): Sabee Molloi, Huanjun Ding
 Radiological Sciences, University of California, Irvine/UNITED STATES OF AMERICA

Breast cancer is the most common cancer and the second leading cause of death from cancer. Mammographic density, which is defined as the ratio of fibroglandular tissue to the total fibroglandular and adipose tissue, is an important risk factor in the development of breast cancer. It has been shown that women with the highest mammographic density (75%–100% fibroglandular volume) have four- to fivefold increased risk of developing breast cancer compared with the lowest density (0%–25% fibroglandular volume). The current standard of care for breast density evaluation involves visual assessment of mammograms. This subjective classification scheme is limited by its considerable intra- and inter-reader variability. Additionally, an important limitation is that an area measurement using mammography ignores the physical 3D character of a real breast. Breasts of different thicknesses can potentially all yield the same measurement of area breast density yet correspond to widely varying volumetric breast density values. Volume-based techniques, which overcome some of the limitations of area-based techniques, include using dual-energy mammography, CT and MRI. Currently, there is no accepted standard for measuring breast density and accuracy of different techniques is not known. Postmortem breast studies were performed to assess the accuracy of breast density measurement for dual-energy mammography, spectral CT, dual-energy cone-beam CT, cone-beam CT and MRI. 40 postmortem breasts were imaged using a dual-energy mammography system. Glandular and adipose equivalent phantoms of uniform thickness were used to calibrate a dual-energy basis decomposition algorithm. Dual-energy decomposition was applied after scatter correction to calculate breast density. Breast density was also estimated using percent volumetric measures described in BI-RADS, standard histogram thresholding and a fuzzy C-mean (FCM) algorithm. The postmortem breasts were also imaged using spectral CT based on CZT photon-counting detectors, dual-energy cone-beam CT and breast MRI. Finally, breasts were chemically decomposed to measure the definitive tissue composition, in terms of water, lipid, and protein. The left-and-right correlations were used to estimate the precision of each technique. The percent fibroglandular volume (%FGV) from chemical analysis was used as the reference standard to assess the accuracy of different techniques to measure breast composition. In the left-and-right comparisons, the standard error estimation (SEE) was calculated to be 9.1%, 9.1%, 9.2% and 4.6% for BI-RADS, standard histogram thresholding, FCM, and dual-energy mammography, respectively. In correlation to %FGV from chemical analysis, SEE was calculated to be 9.9%, 8.6%, 7.2% and 4.7% using quartile volumetric rankings, standard histogram thresholding, FCM, and dual-energy mammography, respectively. The accuracy of breast density measurement for spectral CT, dual-energy cone-beam CT, cone-beam CT and MRI were calculated to be 2.8%, 3.6%, 3.9%, and 6.5%, respectively. In conclusion, the results indicate that dual energy mammography can be used to accurately measure breast density. The variability in breast density estimation using dual energy mammography was substantially lower than quartile volumetric rankings, standard histogram thresholding, FCM and breast MRI. The results also suggested that spectral CT is a very promising technology for breast imaging.

SP033.2 - Study on the Main Nonconformities Found in no Mammography Alagoas State

Author(s): Jose R. Almeida Neto¹, Cinthia M.M. Paschoal², Divanizia D.N. Souza³, Lourdes M. Brasil⁴, Fernanda C.L. Ferreira⁵
¹Phsysics, State University of Health Sciences of Alagoas, Alagoas/BRAZIL, ²Civil Engineering, State University of Vale do Acarau, Sobral/BRAZIL, ³Phsysics, Federal University of Sergipe, São Cristovão/BRAZIL, ⁴University of Brasília, Brasília/BRAZIL, ⁵Federal University of South and Southeast of Pará., Marabá/BRAZIL

Mammography is one of the most important radiological techniques in tracking and control of the breast cancer development; capable to accurately identify the absence or presence of diseases, which can assist in the definition of reliable reports in case of viewing any types of anomaly. In this sense, the aim of this work was to conduct a study of the major non-conformities found in mammograms operating in the State of Alagoas, Brazil, warning the risk of negative and false positive diagnosis. In this work, main non-conformities found in the mammography's equipment of the state are prioritized, such results were classified as compliant and non-compliant according to the guidelines established by the National Agency for Sanitary Vigilance Manual, published in 2005. the tests in mammograms showed that a higher percentage of non-compliance were A1, B2 and B5, as well, may be recommended that the mammography equipment such institutions should undergo maintenance process and rigorous calibration and frequent quality control tests. Mammograms' tests A3, A4 and B1 showed satisfactory results, with compliance above 90% within the parameters established by Decree 453 of National Agency for Sanitary Vigilance. Focusing on all mammograms, it becomes necessary to implement a quality control program

SP033.3 - Affordable medical x-ray imaging for the developing world: a global vision

Author(s): Sorin Marcovici¹, Vlad Sukhovatkin², Oscar Cisek²
¹XLV DIAGNOSTICS INC., Thunder Bay/CANADA, ²XLV DIAGNOSTICS INC, Thunder Bay/ON/CANADA

Imaging technologies, already used routinely for diagnostics, are becoming an essential part of the work flow included in screening, treatment progress monitoring and outcome evaluation. However, various imaging modalities considered standard practice for the medical institutions in the developed world remain today rather inaccessible for the populations at large in the developing countries. One of the limiting factors is the high cost of medical imaging equipment.

To develop and produce low cost, medical imaging systems of good quality requires disruptive innovations and novel approaches to engineering. The sophistication and capabilities of ubiquitous consumer products available today provide a real opportunity to capitalize on their low cost components to drive down significantly the cost of medical imaging equipment.

Following this approach, XLV Diagnostics, a Canadian start-up, is developing a completely new technology, X-ray Light Valve (XLV), for producing very affordable large area, flat panel, x-ray detectors based on which economical medical imaging systems can be built. The first XLV product will be a digital mammography machine for breast cancer screening that will be sold at a fraction of the price asked for presently available machines.

The paper will present the conceptual approach and innovative engineering to create from consumer type components a good quality digital imaging system and will show several of its parametric characteristics.

SP033.4 - Characterization and Analysis of the Physical Parameters in Dental X-Rays Phantom

Author(s): Lilian F. Silva¹, Jhonatan M. Santos¹, Cinthia M.M. Paschoal², Divanizia D.N. Souza³, Lourdes M. Brasil⁴, Fernanda C.L. Ferreira¹
¹Federal University of South and Southeast of Pará., Marabá/BRAZIL, ²Civil Engineering, State University of Vale do Acarau, Sobral/BRAZIL, ³Phsysics, Federal University of Sergipe, São Cristovão/BRAZIL, ⁴University of Brasília, Brasília/BRAZIL

All care related to ionizing radiation exposure to patients, the radiographic image quality and gain time is related to quality control equipment and image. Therefore, it is necessary to be realized by using quality control and intercomparison phantom images with the results of previous tests as well as other types of X-ray equipment, or performing the intercomparison of results of quality control testing. The objective of this study was to characterization, and analysis (intercomparison) results periapical radiographs obtained with phantom and evaluate the high and low contrast in dental radiographs service of Maraba, northern Brazil. For the intercomparison of physical parameter of high and low contrast in the periapical radiographic equipment of the Maraba, a phantom developed in Brazil was used precisely in Aracaju, northeastern. It is worth noting that, the phantom used in this work and the interparameter of the equipment of the images showed satisfactory results bringing out the difference from the standard image. However, tests can be used to switch to other equipment in the surrounding towns of the city of Maraba. Thus allowing the cornerstone for the creation of a database with images obtained with the phantom and can be used in training of students and dental professionals.

SP033.5 - In Vitro and In Vivo Studies Glycosylated Gadolinum Nanomagnetic Particles (GD-DTPA-DG) as New Potential Metabolic Contrast Agent in MMRI

Author(s): Sara -. Heydarnezhadi, Nader Riyahi-Alam, Soheila Haghighi, Ensieh Gorji, Hosein Ghenaati, Behrouz Rafiei
 Tehran university of Medical Science, tehran/IRAN

Early cancer diagnosis using MRI imaging is of high global interest as a noninvasive and powerful modality in molecular imaging. Therefore demand for new MRI contrast agents, with an enhanced sensitivity and advanced functional-ties that improve the targeting to specific tissues or organs, is very high. In this study, D-glucose amine was conjugated to a well-known chelator, diethylenetriamine penta-acetic acid (DTPA), then labeled with Gd to achieve Gd-DTPA-DG, which is a metabolic contrast agent in mMRI. The contrast agent was synthesized and characterized physicochemical using different techniques including dynamic light scattering (DLS), high resolution transmission electron microscopy (HTEM) and inductively coupled plasma atomic emission spectroscopy (ICP-AES). Efficacy of the targeted contrast agent was assessed by measuring relaxation rate in vitro and tumor MR imaging were performed to determine signal intensity (SI) in vivo (0.1 mmol Gd/kg) in female balb/c mice model. According to the results, the nano metabolic contrast agent penetrate into cells and accumulated in tumor, which cause improve the contrast of tumor tissue in comparison with magnetic. The results showed that the novel nano contrast agent could become useful tool in early detection of cancer

SP034 - CT: New Techniques

TRACK 01: IMAGING

SP034.1 - Design, modeling and performance evaluation of a small animal Micro-CT scanner: A Monte Carlo study

Author(s): Samira Nezhaddehghani, Saeed Sarkar, [Mohammad Reza Ay](#)

Department Of Medical Physics And Biomedical Engineering, Tehran University of Medical Sciences, tehran/IRAN

Introduction: Nowadays, by increasing the interest in the use of small animals in biomedical studies, development of small animals imaging systems such as Micro-CT scanners are promoted. Development of the hybrid systems such as SPECT/CT is the other significant factors in development of this kind of scanners. The diagnostic power will be increased by superposition anatomical and functional images in hybrid systems. Furthermore, obtained attenuation map from Micro-CT can be used for attenuation correction of the SPECT data. The purpose of this study was to design and improves the performance of Micro-CT scanner to develop a small animal SPECT/CT system by using the Monte Carlo simulation. The SPECT module called HiReSPECT already fabricated in our Laboratory.

Materials and Methods: In this study the GATE Monte Carlo package was used for accurate modeling of the system, the tube voltage 30-70 kV with focal spot size 30 μm , anode from Tungsten and aluminum filter with thickness of 0.5 mm. The designed detection system has dimension $5.0 \times 18.5 \times 4.7 \text{ cm}^3$ with 100 microns pixels size and an indirect flat-panel scintillator made from CsI(Tl). In this study, the selected distance from the X-ray tube to object 10-12 cm and distance from object to detection system 8-10 cm was considered. These distances were chosen base on the separation length between two detectors and diameter of gantry of HiReSPECT. In analysis and post process the results of the simulation, spatial resolution, noise, contrast and scatter to primary ratio (SPR) was investigated and an optimal design for the scanner detector was presented. The computerized phantom (MOBY) was implemented in simulated scanner and reconstructed images provided by using MATLAB program.

Results Tomographic image of the simulated phantom containing nine cylinders with radial 0.5, 1, 2.5 and 5 mm which were considered filled with tissue equivalent material like skull, lung, ribbon and cartilage were represented the designed system is capable to distinguish soft tissue materials and demonstrate 0.5 mm resolution of the skull (Fig 1-B). The achieved spatial resolution for different materials and dimensions varied in the range of 100 to 150 μm with 0.03% of the noise and 0.0015 of SPR.

Conclusion: In this study, a Micro-CT scanner was simulated with GATE Monte Carlo code by considering geometrical limitation of HiReSPECT. Finally all of mentioned parameters were optimized and were obtained good images of it.

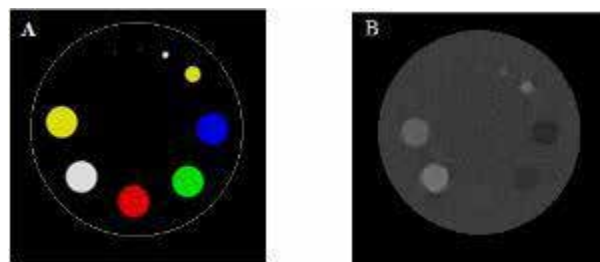


Fig. 1 A) Simulated phantom using GATE code; B) Reconstructed

SP034.2 - An imaging method by using electron mode of linear accelerator for soft tissue emphasis

Author(s): [Atsushi Myojoyama](#), Hidetoshi Saitoh

Radiological Sciences, Tokyo Metropolitan University, Tokyo/JAPAN

Purpose

Megavoltage portal images are used to verify the proper positioning of the patient in image-guided radiation therapy (IGRT). However, the description of low density material reconstructed by MV image doesn't reach kilovoltage one because the flattening filter of linear accelerator causes beam hardening and an increase of scattered photon. To solve this problem, we designed a new image acquisition method by using electron mode of linear accelerator. The low contrast image is acquired by this method because the focus of the target becomes large by attaching to the shadow tray of a linear accelerator, and because Mega-voltage X-rays cause Compton scattering much within human body. To approach those problems, in this study, we propose a 2-pass 3D image reconstruction using simple Monte Carlo method. Feld Kamp, Davis and Kress (FDK) method was used for 3D reconstruction, and BEAMnrc based simple Monte Carlo method was developed to estimate scattering photons.

Method

The portal images were taken by using bremsstrahlung x-ray that was generated by the target newly attached under secondary collimators. To estimate scattering photon, 3D reconstruction was performed in two steps. By the first step, the rough structure was reconstructed by FDK method. In this step, graphic processing unit (GPU) was utilized to reduce the processing time. In this study, a NVIDIA Geforce GTX970 (CUDA) was used for parallel processing. By the next step, the simulation for investigating the relation between the generating position of a scattering photon and EPID data was performed by using the first reconstructed data. Although the most reliable method was Monte Carlo simulation, that was time consuming process and was not practical. Therefore, simple Monte Carlo (SMC) using GPU acceleration was proposed. Although some SMC was proposed, we chose the method of holding and reusing in a memory the result of the full Monte Carlo that was calculated beforehand. In this method, BEAMnrc code system was used for estimating position of scattering photon in an object. Since it was necessary to perform our method for every rotation angle of a gantry, the proposed method needed high-speed processing. This method was accelerated by holding beforehand the full Monte Carlo calculation result to the HU range of primary reconstruction data. Aluminum target were selected for proposed method. This method was simulated and measured on 4, 6 and 9 MeV electron beam.

Result and Conclusion

The calculation time of proposed SMC was about 9 seconds per one projection. The processing time consumed to 180 projections was 27 minutes. The result images emphasized soft tissue than the images acquired by high energy X-ray.

SP034.3 - Anatomical noise model for CT head images: preliminary results

Author(s): [Rafael A. Miller-Clemente](#)¹, [Marlen Perez-Diaz](#)²

¹Group Of Radiation Medical Physics, Biofísica Médica, Santiago de Cuba/CUBA, ²Study Center On Electronic And Information Technologies, Universidad Central "Marta Abreu" de las Villas, Santa clara/CUBA

The availability of an anatomical predictive noise model provides new knowledge about the physical factors tradeoff and the quantitative effect of multiple factors over the diagnostic image quality. Here,

the anatomical noise was defined as the standard deviation of pixel intensities, contained in a region located at the center of an axial CT pediatric head image. Images were obtained by using an Automatic Exposure Control system. The purpose of this work was to determine the association between the noise on diagnostic images and a noise model based on phantom measurements. The model of anatomical noise obtained has an adequate predictive value, with a correlation coefficient of 0.97 (significance level of 95%) and mean square error of 1.9×10^{-6} .

SP034.4 - The potential of spectral-CT for material decomposition with gold-nanoparticle and iodine contrast

Author(s): Byungdu Jo

Department Of Radiological Science, College Of Health Science, Yonsei university, Wonju/KOREA

The objective of this study was to demonstrate feasibility of using gold contrast-agent as a new contrast agent for spectral-computed tomography (CT) system and decompose the iodine and gold materials in the spectral-CT system using K-edge imaging technique. Recently, gold based nanoparticles contrast-agent has been introduced for vulnerable plaque imaging in CT system. The spectral-CT system equipped with Cadmium Zinc Telluride (CZT)-based photon-counting detector has energy-discrimination capabilities and high resolution image acquisition capabilities. We performed a simulation study using the Geant4 Application for Tomographic Emission (GATE) simulation. The CZT detector contained four CZT crystals and total detector length is 51.2 mm with 64 channel array. The results showed that the contrast-to-noise ratios of iodine and gold contrast-agent materials in energy window included K-edge energy of materials (33-49 keV for iodine, 66-81 keV for gold) were increased approximately 1.9 and 1.7 times higher than others. These results also show the possibility of potential of using two contrast-agents at a time to provide the various information of image such as plaque vulnerability assessment.

SP034.5 - Spatial Resolution Studies for a Prototype Proton CT Scanner

Author(s): Tia E. Plautz¹, Robert P. Johnson¹, Hartmut F.-. Sadrozinski¹, Andriy Zatserklyaniy¹, Vladimir Bashkurov², Reinhard W. Schulte², Robert F. Hurley², Valentina Giacometti³
¹Scipp, University of California, Santa Cruz, Santa Cruz/CA/UNITED STATES OF AMERICA, ²Radiation Research Laboratories, Loma Linda University, Loma Linda/UNITED STATES OF AMERICA, ³Centre For Medical Radiation Physics, University of Wollongong, Wollongong/NSW/AUSTRALIA

We report on the simulation and initial beam test results with the pre-clinical (phase II) head scanner developed for proton computed tomography (pCT) by the pCT collaboration. In the future, proton CT may be employed to improve the accuracy of relative stopping power definition in patients treated with proton therapy. The phase II proton CT system consists of two silicon telescopes that track individual protons before and after a phantom, and a novel 5-stage scintillation detector that measures a combination of the residual energy and range of the proton. Residual energy is converted to water equivalent path length (WEPL) of the protons in the scanned object. The set of WEPL values and associated paths of protons passing through the object over a 360° angular scan is processed by an iterative parallelizable reconstruction algorithm that runs on GP-GPU hardware. This report will focus on studies of the spatial resolution of the phase II imaging system, while studies of the achievable accuracy of relative stopping power will be reported elsewhere. A custom edge phantom composed of water-equivalent polymer with 4 body-equivalent material inserts was developed. The phantom was first simulated using Geant4 and then built for experimental

beam tests with 200 MeV protons at the research beam line at the Loma Linda University Medical Center. A modified version of the oversampling method was used in order to construct edge spread functions and modulation transfer functions for materials of varying relative stopping powers located at several radial displacements from the center of the phantom. A combination of angular cuts with the aim to eliminate large-angle scattered protons, the most likely path (MLP) concept, and a superiorization method in iterative image reconstruction are used to improve the spatial resolution of the image reconstruction. These sophisticated and computing-intensive techniques are being compared to simpler and much faster reconstruction methods including filtered back projection along curved paths and cubic-spline path approximation. Reconstructions of pCT data sets obtained with a realistic anatomical head phantom will further complement the analysis of the MTF.

SP034.6 - Influences of object size and tube potential pairing on the accuracy of iodine quantification using dual energy CT

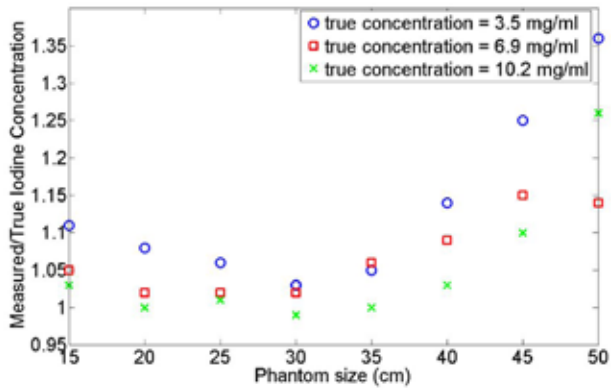
Author(s): Josh Grimes, Lifeng Yu, Shuai Leng, Cynthia Mccollough
Mayo Clinic, Rochester/MN/UNITED STATES OF AMERICA

Purpose: The objective of this study was to evaluate the accuracy of iodine quantification in phantom images acquired on a dual-source dual-energy CT scanner. The influences of phantom size and different tube potential pairs were investigated.

Methods: Three bottles with iodine concentrations of 3.5, 7 and 10.5 mg/mL were placed inside 8 torso-shaped water phantoms ranging from 15 to 50 cm in lateral width. Dual energy scans of each phantom were acquired on a dual-source CT system (Siemens Somatom Force) using 4 different tube potential pairs (low energy: 70, 80, 90, and 100 kV; high energy: 150 kV + 0.6 mm Sn). CTDIvol was matched for all scans of a given phantom size. Images were reconstructed with 1-mm image thickness at 0.8 mm intervals using a medium smooth body kernel. The dual-energy data were post-processed using commercial software (syngo Via Dual Energy, VA30), which generated virtual non-contrast and iodine overlay images. Iodine concentration (in mg/ml) was displayed for regions of interest drawn over the iodine bottles, and compared with the known concentrations for each phantom size and tube potential pairing.

Results: At 70/150Sn, the measured iodine concentration was within 9% of the known concentration for phantom sizes from 15-45 cm. However, images acquired at 70/150Sn were deemed unacceptable for phantom sizes greater than 35 cm due to ring artifacts. At 80/150Sn, 90/150Sn and 100/150Sn, iodine concentrations determined for phantom sizes up to 45 cm agreed with known concentrations within 14%, 25% and 19%, respectively. At 100/150Sn, the iodine concentration in the 50 cm phantom was within 27% of the known value. Iodine quantification was most accurate (within 2% for all tube potential pairs) for the highest iodine concentration (10.5 mg/ml) in the 30 cm phantom. As phantom sizes increased or decreased from 30 cm, iodine concentration was increasingly overestimated.

Conclusion: The accuracy of iodine quantification depends strongly on the phantom size. When selecting the tube potential pairing, both image quality (e.g. artifacts) and accuracy of measured iodine concentration should be considered.



CONTENT ORGANIZATION:

Description of the Dual Energy Coronary Artery Phantom containing arteries with variable degrees of lumen stenosis Specifications for the mass attenuation properties of materials mimicking the spectrum of calcified and non-calcified vulnerable plaque Validation of attenuation properties of phantom based materials compared to biological tissues compared at different energies. Calculation of Dual Energy Index and energy - attenuation plot for iodine and calcium based materials present in the phantom. Use of Dual energy material decomposition software to generate iodine and calcium removed images to improve accuracy of stenosis assessment.


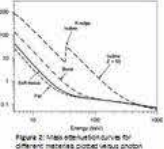


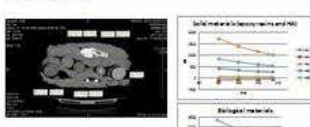
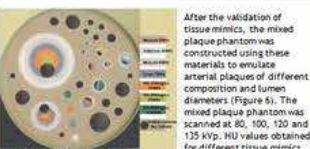
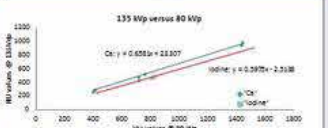
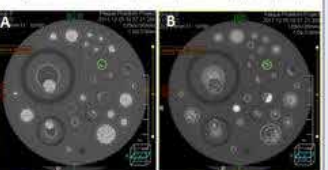

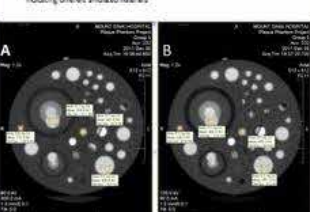
RESULTS SUMMARY:

A tissue equivalent coronary artery phantom is extremely useful in demonstrating significant improvements in accuracy of stenosis measurement and characterization of vulnerable coronary artery plaque with Dual Energy image acquisition and post processing.

SP034.7 - Characterization of Vulnerable Plaque with Dual-Energy during CT Coronary Angiography: A Phantom Study
Author(s): Ali Ursani¹, Sachin Moghe², Carlton Hoy³, Narinder Paul⁴
¹Medical Engineering, University Health Network, Toronto/ON/CANADA, ²Toshiba Medical Research Institute, Toshiba Medical USA, Vernon Hills/IL/UNITED STATES OF AMERICA, ³Mechanical & Industrial Engineering, University of Toronto, Toronto/ON/CANADA, ⁴Medical Imaging, University Health Network, Toronto/CANADA

PURPOSE/AIM:

The aim of this exhibit is to: Demonstrate the utility of Dual Energy image acquisition and post processing to provide high-resolution characterization of mixed arterial plaque in an anthropomorphic coronary artery phantom composed of tissue equivalent materials. Introduce the concept of a Dual Energy index and material decomposition algorithm.

Introduction	Methods	Results	Results
<p>The biological problem</p> <ul style="list-style-type: none"> Cardiovascular disease is the leading cause of mortality For the majority of these cases, the risk is contributed by the vulnerable plaque These lesions are susceptible to shear stress, subsequent rupture and hemorrhage [1]  <p>Limitations of current methodology</p> <ul style="list-style-type: none"> Catheter coronary angiography (CCA) and intra-vascular ultrasound (IVUS) are invasive and expensive procedures [1, 2] <p>Computed tomography as the alternative imaging modality</p> <ul style="list-style-type: none"> Computed tomography (CT) is a non-invasive and fast acquisition modality Current CT technology has several limitations in diagnosing mixed and vulnerable coronary plaque: <ol style="list-style-type: none"> Measured density of tissues is strongly affected by partial volume artifact [3] Low resolution at small vessel diameters [3] 	<p>Aim 1: Construction of arterial phantom</p> <ol style="list-style-type: none"> Select materials that mimics biological tissue in Hounsfield Unit (HU) <p>Commercially available epoxy resin and calcium hydroxyapatite based solid materials with similar atomic characteristics to biological tissues.</p> <ol style="list-style-type: none"> Validation of tissue mimics against biological tissue background <p>The unprocessed materials were inserted into a beef shank with intrinsic biological components (fat, muscle, bone, engorged liver). The composite was scanned using 120 slices CT with 3mm thickness and volume scan. Access to the CT was provided by the courtesy of Medical Engineering department at the University Health Network.</p>  <ol style="list-style-type: none"> Construction of phantom with various orifice diameters and stenosis severity <p>The construction platform consisted of heart tissue mimicking material of 40 HU @ 120 kVp. The cylindrical volumes were generated using lathe machine. The diameter of these cylinders range from 2 mm to 40 mm. The vessel lumen was filled with iodinated contrast media (ICM) diluted to an attenuation of approximately 370 HU.</p> 	<p>Phantom mimic materials were scanned by CT at different tube potentials to validate their similarities to muscle and bone tissues of beef shank (Figure 5).</p>  <p>After the validation of tissue mimics, the mixed plaque phantom was constructed using these materials to emulate arterial plaques of different composition and lumen diameters (Figure 6). The mixed plaque phantom was scanned at 80, 100, 120 and 135 kVp. HU values obtained for different tissue mimics at different tube potentials can be obtained (Figure 7).</p> 	 <p>Figure 9 shows CT images of the mixed plaque phantom which was processed using a Dual Energy Index based algorithm. Pixels identified as calcium were removed from Figure 9A and pixels identified as ICM were removed from Figure 9B. In Figure 9A, it is easy to see where calcium is missing and to a lesser extent, calcium is identifiable in Figure 9B.</p> 
<p>Objective</p> <p>The goal of our project is a proof of concept study to demonstrate whether using single energy measurement at two separate energies (kVp) can resolve high resolution in anthropomorphic coronary phantom arteries carrying mixed material mimicking calcified and non-calcified vulnerable plaque with various degrees of stenosis.</p> <p>Aim 1: Construction of arterial mixed plaque phantom</p> <ol style="list-style-type: none"> Select materials that mimics biological tissue in Hounsfield Unit (HU) Validation of tissue mimics against biological tissue Construction of phantom with various tissue mimics, vessel diameters and stenosis severity. Simulating coronary arteries with calcified and mixed plaque composition.  <p>Aim 2: CT imaging for validation and resolution refinement</p> <p>Refine and distinguish heterogeneous composition of mixed plaque within small diameter (2 to 3.5mm) mimicking coronary arteries.</p>	<p>Aim 2: Refine and distinguish heterogeneous composition within small diameter (2 to 3.5mm) arterial phantom mimic</p> <ul style="list-style-type: none"> The phantom arteries was scanned with CT using variable image acquisition parameters including changing tube potential (80, 100, 120 and 135 kVp) and the current (effective mAs) were varied in order to validate the material's composition and lumen assessment. Axial images were reconstructed with 0.5 and 1 mm slice thickness using cardiac filter kernels (FC02 and FC12). Material validation was carried out by comparing CT attenuation (HU) values obtained at the four kVps for biological tissues and the selected solid materials. CT images were analyzed using Dual Energy material decomposition software (under development). 	 <p>The HU values obtained at 135 kVp for iodine and calcium plugs are plotted against those obtained at 80 kVp, demonstrating an intrinsic difference in dual energy slope between calcium mimics (0.4581) and ICM (0.5975) (Figure 8).</p> <p>Each material can be characterized by its Dual Energy Index.</p> $DEI = \frac{HU(80) - HU(135)}{HU(80) + HU(135) + 2000}$	<p>Significance and Conclusion</p> <p>The creation of an arterial mixed plaque characterization phantom is important because it allows for the comprehensive evaluation of emerging CT scanning technology. We have fabricated our phantom to simulate some of the most challenging situations encountered by clinicians, conditions under which current non-invasive imaging technologies lack resolution and diagnostic power. It is important that engineers and clinicians have the opportunity to understand the efficacy and limitations of CT technology like dual energy scanning so they can formulate methods for improvement[4]. Evaluation of CT scanners often requires repeated scanning at different dose and currents and hence, it is vital that a mixed plaque phantom realistically simulate in vivo arterial conditions.</p> <p>In conclusion, we have developed a mixed plaque arterial phantom that can be used to evaluate and improve CT imaging technology and drive the field of diagnostic medical imaging forward.</p> <p>Acknowledgement</p> <p>Thanks to Toshiba Medical system for providing the CT equipment (Aquilion One CT scanner) and material decomposition software for this thesis.</p> <p>Our special thanks to: Supriya Fouzdar (MEDICAL ENGINEERING TECHNOLOGIST -HU) for helping us use the lathe machine and the milling machine for many long hours.</p> <p>Contacts</p> <p>1. Ursani, Ali, ali.ursani@uhn.on.ca 2. Sachin Moghe, sachin.moghe@tmsi.com</p>

SP034.8 - The combination of a custom vascular perfusion contrast agent and dual-energy micro-CT to characterize bone-related vasculature

Author(s): Justin Tse¹, Vasek Pitelka¹, Joy Dunmore-Buyze², Maria Drangova³, David Holdsworth³

¹Imaging Research Laboratories, University of Western Ontario, Robarts Research Institute, London/CANADA, ²Schulich School Of Medicine And Dentistry, University of Western Ontario, London/CANADA, ³Medical Biophysics, Western University, London/ON/CANADA

Osteoarthritis (OA) is a debilitating chronic joint disease that is becoming a growing concern among the aging population. Due to its complex nature, many questions regarding its initiation and progression remain unanswered. There has been a renewed interest in the bone-associated vasculature, and the role they may play in OA. Thus, having the ability to quantify and characterize the vascular changes (patency, density, and micro-architecture) provide more information into OA's initiation and progression.

Micro-computed tomography (micro-CT) is widely used for its ability to provide well-characterized bone. However, the visualization of associated vasculature is difficult due to their (1) size (5-10 μm for capillaries), (2) poor inherent x-ray contrast, and (3) proximity to highly x-ray attenuating bone. We propose the combination of a custom exogenous vascular perfusion contrast agent, dual-energy micro-CT (DECT), and decomposition algorithms to allow for the distinct and separate visualization of the perfused vasculature and bone.

To demonstrate the capabilities of our combination technique, a lanthanide-based vascular perfusion contrast agent and x-ray filter was developed. We perfused the lower half of a rat with our vascular contrast agent through the aorta and embedded the excised left hindlimb in agar. The sample was then scanned on our GE Vision120 speCZT (GE Healthcare, London, ON) at two energies, with appropriate filtration to tailor the output x-ray spectra, that straddled the absorption edge of our vascular contrast agent.

Figure 1 displays the results of our combination technique. Minimal differences can be observed between the low energy and high energy (Fig. 1) scans. However, once decomposition algorithms are applied, the images can be decomposed into separate and distinct images of bone and perfused vasculature (Fig. 1). 3D Renderings of the bone and its associated vascular supply (Fig. 1 A and B) are presented to further demonstrate the large internal vascular supply of bone. Bone and cartilage degeneration observed in OA may be partially attributed interruptions or changes in their vascular supply.



Fig. 1. Results of DECT, with the Low and High Energy scans decomposed into the distinct and separate images of bone and perfused vasculature. (A-B) 3D renderings displaying the interplay between perfused vasculature (red) and bone (white). Scale bar = 5 mm.

Thus, by applying our combination technique to a well-characterized surgically induced rat hindlimb OA model, we may be able to provide further insight into the role of the joint's vascular supply as OA initiates and progresses.

SP035 - Imaging Detector Technology

TRACK 01: IMAGING

SP035.1 - Detectability in SPECT Myocardial Perfusion Imaging: Comparison between a Conventional and a Semiconductor Detector System

Author(s): Caroline M. Dartora, Mariana S. Favero, Ana M. Marques Da Silva

Faculdade De Física, PUCRS, Porto Alegre/BRAZIL

The aim of this study is to compare cold lesions detectability in myocardium SPECT images acquired by two cameras: a conventional SPECT with scintillation detector (Philips Cardio MD) and a cadmium-zinc-telluride (CZT) semiconductor detector system (GE Discovery NM 530C). The test object is an anthropomorphic torso phantom with cardiac insert, filled with ^{99m}Tc, simulating a SPECT myocardial perfusion acquisition. Images were reconstructed using the standard clinical department protocol, and were analyzed by axial and lateral count profiles and polar distributions. The lateral profile showed that contrast between the lesion region and background in Cardio MD camera is higher (62.2%) than in the CZT camera (42.5%). The axial profile showed a higher contrast (37.0%) in the CZT camera compared to Cardio MD (31.9%). CZT showed a higher contrast between background and maximum activity point along the line (68.2%) than in the Cardio MD (57.5%). Performing the maximum region relative count and the lesion area analysis, it was verified that contrast between these regions are 31.2% and 25.5% to CZT and Cardio MD, respectively. The results showed the cold myocardium lesion detectability is enhanced in the CZT camera. The polar map in the CZT camera displays a better uniformity between the segments' counting, which means the lesion identification is clearer than in the Cardio MD camera, where the distribution is diffuse and the lesion is unclear. In conclusion, the physical performance of CZT camera is higher than conventional camera, but further studies are required to evaluate other parameters, such as spatial resolution, sensitivity and contrast-to-noise ratio.

SP035.2 - The performance of the CMOS APS detector for dual energy contrast enhanced digital mammography

Author(s): Ilias Billas¹, Anastasios C. Konstantinidis², Robert D. Speller³

¹Radiation Dosimetry, National Physical Laboratory, London/UNITED KINGDOM, ²Christie Medical Physics And Engineering, The Christie NHS Foundation Trust, Manchester/UNITED KINGDOM, ³Medical Physics And Bioengineering, University College London, London/UNITED KINGDOM

Dual energy (DE) technique has been used for many years in digital radiography, as it allows significant advantages in image contrast. In mammography, clinical applications have shown that the use of DE contrast enhanced digital mammography (CEDM) can explore angiogenesis in breast carcinoma by tracking the uptake and wash-out of an injected contrast medium, usually iodine, in breast tissue. New digital x-ray detectors, such as complementary metal-oxide-semiconductor (CMOS) active pixel sensor (APS), have the prospective to be combined with this technique for the early detection of breast cancer. They offer an alternative to charge-coupled devices (CCDs) and flat panel detectors (FPDs) due to radiation tolerance, low-cost mass production, low power consumption, very fast image acquisition and low electronic noise. The purpose of this study is to implement the DE CEDM using a CMOS APS based x-ray detector to effectively measure the iodine projected thickness while keeping radiation dose in low levels.

The x-ray performance of the CMOS APS detector is evaluated based on experimentally measured pre-sampling modulation transfer function (pMTF), normalized noise power spectrum (NNPS) and signal-to-noise ratio (SNR). Image simulation is performed modelling the detector characteristics and the x-ray source (Xcomp5r) to estimate optimal dual energy conditions. Breast phantoms are carefully prepared to simulate the properties of real breast tissue and images are acquired using a tungsten anode x-ray source. Inside the phantom, a 2 mm diameter tube, representing the minimum tumor sizes developing angiogenesis, is placed for the injection of the different contrast media concentrations. The mean glandular dose (MGD) is evaluated and kept as low as possible to achieve sufficient image quality. The influence of scatter radiation on DE images is investigated and artefacts are reduced using a scatter-correction algorithm.

The optimum image combination is found to be at 48 kVp for both low- and high-energy x-ray beams with 0.2 mm tin and 0.3 mm copper filtration, respectively. This combination reduces the irradiation time and consequently minimizes patient motion artefacts and radiation dose. For seven image pairs, the total MGD is 1.4 mGy, which does not exceed the equivalent from a typical mammogram. Good agreement is found between the experimental and simulated results (i.e. 0.5% difference), showing that the image simulation tool is accurate to optimize a larger number of parameters and their combinations for good image quality. It is shown that the scatter-correction algorithm yields an improvement of 24% in determining iodine projected thickness, yielding an overall accuracy of the DE CEDM and CMOS APS combination within about 3% compared to the actual iodine projected thickness.

Results show that the iodine projected thickness can be effectively measured from iodinated images, and other applications, such as the measurement of contrast medium kinetics, are expectable. The performance of CMOS APS x-ray detector is within clinically acceptable accuracy and comparable with state-of-the-art technology reported in literature. This indicates that the proposed technology can be successfully combined with the DE CEDM technique for detection of early breast cancer.

SP035.3 - Apodized-Aperture Pixel Design of an X-Ray Detector with Enhanced High-Frequency DQE and Reduced Noise Aliasing

Author(s): [Elina Ismailova](#)¹, [Ian A. Cunningham](#)²

¹Medical Biophysics, University of Western Ontario, London/CANADA, ²Medical Biophysics, University of Western Ontario, London/ON/CANADA

The detective quantum efficiency (DQE) is a characteristic of an imaging system representing its imaging performance relative to an ideal imaging system. While high DQE values are necessary to maximize image quality using low x-ray exposures, typical DQE values are ~0.7 at low spatial frequencies and ~0.3 or less at high frequencies. We describe a CMOS/selenium-based detector using an apodized-aperture pixel (AAP) design that could achieve a new-uniform DQE over all spatial frequencies for mammographic applications. The method uses very small physical sensor elements on the CMOS sensor to synthesis larger image pixels using a novel filter design. A numerical method of optimizing the filter shape to minimize noise aliasing and maximize the DQE is described. A cascaded-systems analysis shows the limiting high-frequency DQE value can be increased from 0.3 to 0.7. The AAP approach is validated on a CMOS/CsI-based laboratory detector where the limiting DQE is increased from 0.2 to 0.4.

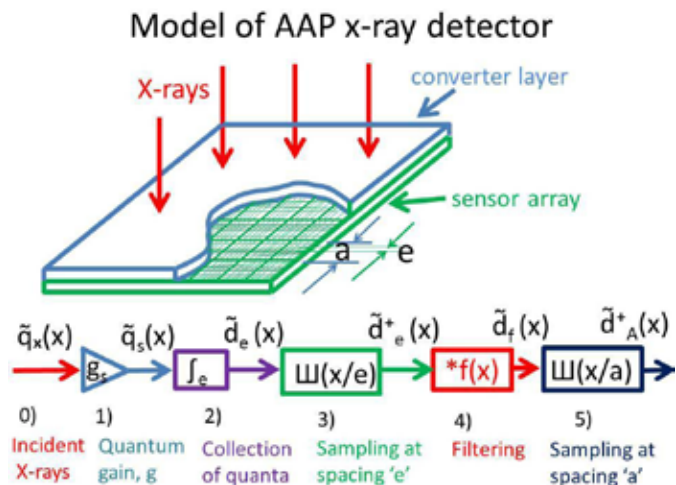


Figure 1 Developed AAP design of an x-ray detector accompanied by the cascaded system analysis.

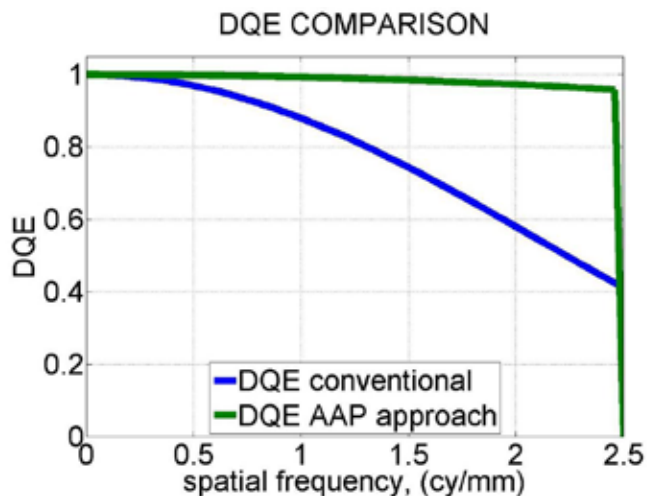


Figure 2 DQE of the conventional versus AAP x-ray detector models.

SP035.4 - Geant4 Simulations of Scintillation Light Collection and Extraction in PET/CT Detectors

Author(s): [Francis Loignon-Houle](#)¹, [Catherine M. Pepin](#)¹, [Serge Charlebois](#)², [Roger Lecomte](#)¹

¹Nuclear Medicine And Radiobiology, Université de Sherbrooke, Sherbrooke/QC/CANADA, ²Electrical And Computer Engineering, Université de Sherbrooke, Sherbrooke/QC/CANADA

Introduction

Scintillation detectors are made of scintillation crystals coupled to photodetectors (photodiode, photomultiplier tube, SiPM, etc.). The performance of these detectors (energy and timing resolution, detection threshold, etc.) strongly depends on the collection and extraction of scintillation light from the crystal to the photodetector. To ensure high spatial resolution and high detection efficiency, scintillators must be arranged in compact arrays with unfavorable shapes for photon transport. In typical polished scintillators ($n=1.8$) with a form factor length/surface > 5 , up to 40% of signal is lost to absorption and trapping within the crystal and attenuation through interfaces to the photodetector. In highly pixelated arrays, this loss is compounded with crosstalk effects, squandering valuable signal to adjacent pixels. The purpose of this study is to uncover processes responsible for light losses in scintillator arrays and investigate ways

of enhancing light transport and extraction from pixelated crystals.

Materials and Methods

The Monte Carlo software Geant4 was used to simulate 511-keV annihilation photon interactions occurring in parallelepiped Lu_{1.9}Y_{0.1}SiO₅ (LYSO) scintillators and to track the propagation of the produced scintillation photons. 4×8 crystal arrays made of 12-mm high pixels at a pitch of 1.2 mm were simulated. All crystal surfaces were defined as polished with reflectors (3M-ESR or silver foil) bonded to the lateral faces using an optical adhesive ($n=1.5$). Each pixel was covered with a diffuse reflector on one end (Lumirror) and read out from the other end by a surface emulating an avalanche photodiode (APD) with quantum efficiency of ~65% @ 420 nm.

Results and Discussion

Simulations revealed four main contributions to crosstalk between scintillators. First, energetic primary electrons generated near pixel lateral surfaces may escape to adjacent crystals, thus losing a fraction of the initial 511-keV energy. Since the maximum mean free path of 511-keV photoelectrons is limited to ~100 μm , this effect was found to be significant for interactions occurring within ~75 μm from the surface (up to 30% signal loss). Second, the 3M-ESR reflectivity severely drops from 98% down to 20% below 400 nm. Signal loss due to photons transmitted through the reflector was estimated to ~10%. This was found to be avoided with metallic reflectors. Third, the manufacturing technique used to assemble scintillator arrays is responsible for some optical leakage at the edges of pixels, resulting in asymmetric optical crosstalk amounting to 3%. Finally, scintillation photon propagation within the optical coupling layer was also found to spread the signal to adjacent crystals.

Scintillation photons escaping through the readout window have to cross multiple interfaces (optical coupling, Si₃N₄ antireflective layer) before reaching the photodetector sensitive area. Simulations reveal a strong dependence of the transmitted light fraction on angular distribution and wavelength of photons reaching each interface. Since most photons impinge on interfaces far from normal incidence, improvements in extracting these photons are feasible by adjusting the thickness and refractive index of the multiple interface layers.

Progress in scintillation light transport and extraction can potentially be achieved by optimizing all factors identified in this simulation study.

SP035.5 - LabPETII.5: APD-based Detector Characterization for Pre-clinical PET Imaging

Author(s): Émilie Gaudin¹, Mélanie Bergeron¹, Catherine M. Pepin¹, Jules Cadorette¹, Réjean Fontaine², Roger Lecomte¹

¹Nuclear Medicine And Radiobiology, Université Sherbrooke, Sherbrooke/CANADA, ²Department Of Electrical And Computer Engineering, Université de Sherbrooke, Sherbrooke/CANADA

Introduction

The LabPETII.5 is an avalanche photodiode (APD) based pixelated detector module designed to achieve submillimetric spatial resolution in pre-clinical positron emission tomography (PET). This technology was also designed to be used as a generic platform for ultra-high resolution PET imaging of small- and medium-size animals and dedicated clinical applications in humans (brain, breast and articulation).

Methods

The detector module is based on a 4×8 array of Lu_{1.9}Y_{0.1}SiO₅ (LYSO) crystals (1.12×1.12×12 mm³) with one-to-one coupling to a 4×8 APD pixel array mounted on a ceramic holder.

Several performance characteristics were measured as a function of bias voltage for a set of 10 prototype modules: dark current (I_D), relative APD gain, noise threshold (converted into keV for 200 cps without source), gain spread (maximum/minimum photopeak position), energy resolution (ΔE) and intrinsic time resolution (ΔT). I_D and APD gain measurements were performed up to breakdown voltage to determine the APD operating range. Other measurements were performed using a LabPET™ multi-channel digital data acquisition system (180 ns peaking time, preamplifier gain=8.4 mV/fC). To estimate the noise level, gain spread and ΔE , a two-minute measurement was acquired with a ⁶⁸Ge source (511 keV) in front of the array, followed by a 30-second background measurement without source to subtract the ¹⁷⁶Lu natural radioactivity present in the LYSO. ΔT measurements were taken in reference to a timing probe consisting of a ¹⁸F-doped liquid scintillation/PMT detector. Results were obtained for bias values from 225 V to a maximum bias where at least 10 channels saturated the electronics.

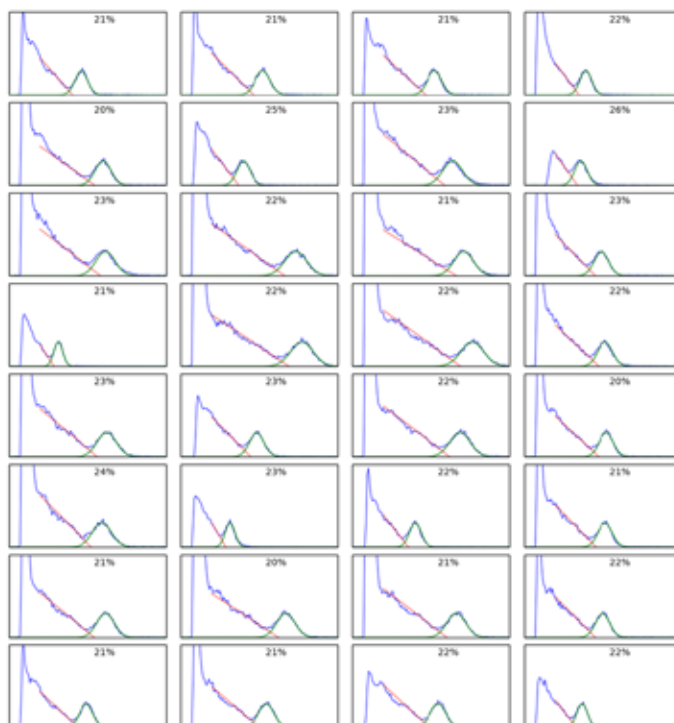
Results

I_D , relative APD gain, and ΔT curves were obtained as a function of bias for all pixels. At the optimum operating bias determined from ΔT measurements, the average I_D , noise, gain spread, ΔE and ΔT results are respectively 18±8 nA, 39±21 keV, 3.2±1, 22±2% and 3.7±0.3 ns (with an energy threshold of 400 keV). Energy spectra with the Compton-corrected energy resolution Gaussian fit are displayed for one typical module in Figure 1.

Conclusion

These results confirm the suitable electronic and physical performance of the detector for annihilation radiation detection. Further investigations are in progress to evaluate the imaging performance of the module for PET.

Figure 1. Energy spectra and resolution (ΔE) for a typical LabPETII.5 module. The ER was measured with a ⁶⁸Ge source (511 keV). The average ΔE is 22 ± 1%. The average noise threshold is 31 ± 7 keV.



SP035.6 - An alternate mathematical modeling of image formation, and framework for performance analysis of positioning algorithms in the scintillation camera

Author(s): Soheil Hosseini, Mohammad Hossien Farahani, Mohammad Reza Ay

Research Center For Molecular And Cellular Imaging, Tehran University of Medical Sciences, Tehran/IRAN

Introduction: Substantive amount of work has been done in modeling the scintillation camera system processes including positioning and image formation. This study presents an alternate mathematical modeling and subsequently framework for performance analysis of different positioning algorithms, followed by experimentation with and comparative study of several of the system parameters.

Methods: Making the assumption that a scintillation occurring in the gamma camera will result in a deterministic number of photons (proportional only to the solid angle at which it sees the detector array), the detector array counts will be found to follow the multinomial distribution with underlying probabilities determined purely through geometrical analysis. The statistical characterizations of mean, variance, and covariance of the counts will therefore be known from statistics. Anger arithmetics being presentable in terms of matrix operations on the counts vector, the mean vector and covariance matrix of the positioning output will therefore be explicitly expressible in terms of statistical characterizations of count values. Maps can moreover be constructed of displacement and blurring intensity corresponding to each point on the detector, characterizing its linearity and resolution performance. This constitutes a framework for performance analysis of different positioning algorithms. In Section I, the model is used to produce comparisons concerning photomultiplier tube (PMT) shape (square-circular-hexagonal), size, non-uniform response, and gain. In Section II, the framework has been used to analyze the performance of two more complex positioning arithmetics, involving nonlinear conditioning and exploitation of row and column sums; to that end, a new matrix formulation of the positioning output is first developed, and statistical characterization of the output are then derived using relations for moments of functions of random vectors. In Section III, the model is extended to include the complete system, including realistic versions of source, collimator and crystal, and maps are constructed for the sample case where the crystal has non-zero thickness.

Results: Figure 1 shows the case where the PMT shape and (equivalent of) size have been studied. Similar figures are created for other parameters.

Discussion: The model is evaluated against Monte Carlo simulation in several scenarios and is found to perfectly match down to any significant digit. This model can be used for in-depth study and analysis of the scintillation camera

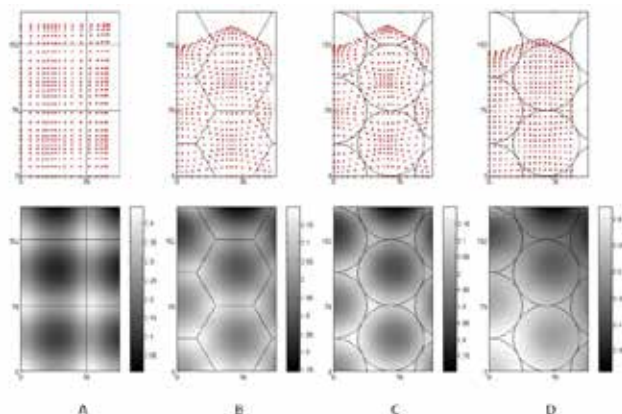


Figure 1 **TOP** Scatter maps showing the positioning output for uniform grid inputs. **BOTTOM** Resolution maps showing the blurring intensity corresponding to each position, in mm FWHM. **LEFT/RIGHT** (A) Square PMTs with source at 3/4 the default value, (B) square replaced by hexagon of equal side-to-side value, (C) hexagon replaced by the inscribing circle, and (D) source moved to 4/3 the default value. Only one quarter of the 4 x 6 detector array and with edges not included are displayed.

SP036 - Treatment Planning - Motion and Robustness

TRACK 04: RADIATION ONCOLOGY

SP036.1 - Robust optimization with independent beams produces robustly matched fields for intensity-modulated proton therapy treatments

Author(s): Albin Fredriksson

Department Of Research, RaySearch Laboratories, Stockholm/SWEDEN

Background

Intensity-modulated proton therapy of the craniospinal axis typically involves matched posterior spinal fields in order to cover the spinal cord. Setup errors separating or bringing the matched fields together can cause respectively under- and overdosage at the field junction. Wedge-shaped matched beam doses, which slowly increase from zero to the prescribed dose, reduce this risk. Beam dose wedges can be achieved by treatment planning using multiple auxiliary planning structures, but such a manual process is often time-consuming. The aim of this work is to give proof-of-concept of how the creation of beam dose wedges can be automated by the use of robust optimization.

Methods

The robust optimization of the RayStation treatment planning system (RaySearch Laboratories, Stockholm, Sweden) was augmented with the ability to let setup uncertainty affect the beams independently. RayStation's robust optimization uses dose distributions for multiple scenarios and aims to minimize the objective value under the worst case scenario. When the setup uncertainty affects the beams independently, a scenario is constituted of a specific setup error for each individual beam. For example, if two beams are used, then the total dose distribution under a given scenario may be the sum of the beam doses resulting when beam 1 is shifted superiorly and beam 2 is shifting inferiorly relative to their isocenters.

Results

Robust optimization with beams independently affected by setup uncertainty was applied to intensity-modulated proton therapy treatment planning for a craniospinal case using two parallel-opposed lateral cranial fields and two matched posterior spinal fields. The independent beam setup uncertainty was set to ± 5 mm along the superoinferior axis. The optimization problem included the planning target volume and the external region without any auxiliary structures. Figure 1 shows line doses of the optimized plan over the spinal field junction. The optimization has resulted in clear beam dose wedges. The nominal total dose is slightly above the prescription of 20 Gy in order to ensure that the total dose resulting when the beams are separated is at the prescription. This provides proof-of-concept that robust optimization is a viable tool for creating robustly matched fields.

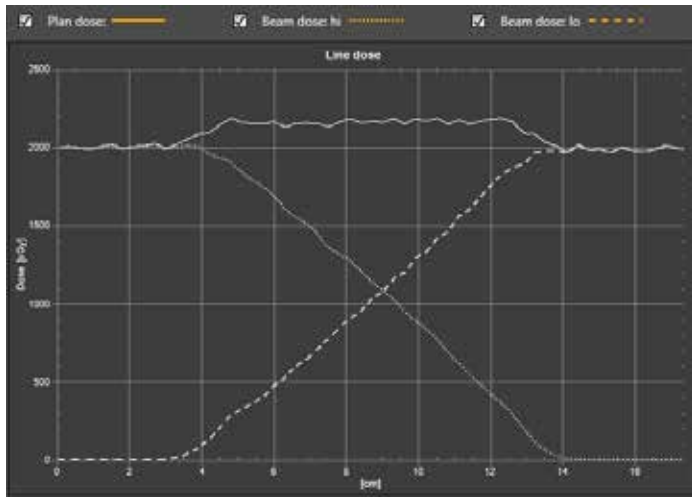


Figure 1: Total dose and beam doses at the junction of the spinal fields resulting from robust optimization with independent beams.

SP036.2 - Rotational tolerance in lung cancer image-guided radiation therapy

Author(s): Peter Hoang¹, Marcin Wierzbicki²
¹McMaster University, Hamilton/ON/CANADA, ²Juravinski Cancer Centre, Hamilton/ON/CANADA

Purpose: Previously, we utilized deformable image registration (DIR) to optimize planning target volume (PTV) margins in lung cancer image-guided radiation therapy (IGRT). In this study, we have developed a method using DIR to assess the tolerance of rotational error for different image matching strategies.

Methods and Materials: 132 cone-beam computed tomography (kV CBCT) images of 8 lung cancer patients were used. Images simulating perfect set-up were created by registering each planning CT image with a CBCT image at each fraction with translations and rotations enabled. These images were rotated in all combinations of the x-,y-, and z-directions (pitch, yaw, roll) by 1,3,5, and 6 degrees around the centre of the spinal cord. Rotated CT images were translated to match the CBCT data nearby the spinal cord/carina or internal target volume (ITV) to obtain a simulated couch correction. Deformable image registration was used to automatically position the planning ITV on each final CBCT. ITV coverage was quantified as the percentage of the ITV surface that fell within generated PTVs.

Results: Each fraction comprised 26 rotation simulations per rotation magnitude, so a total of 3432 simulated images were analyzed per degree rotation. To achieve perfect setup, mean rotations (\pm standard deviation) of 1.3 ± 1.0 , 1.1 ± 0.9 , and 0.6 ± 0.6 degrees about the left-right (LR), anterior-posterior (AP), and superior-inferior (SI) axes were necessary. For our currently employed 6 LR,6 AP,10 SI mm PTV margin with cord/carina matching the mean ITV surface coverage was 99.1 ± 3.8 , 98.7 ± 4.3 , 96.6 ± 6.0 , and $94.5 \pm 7.9\%$ for 1, 3, 5, and 6 degrees of rotation, respectively. Coverage improvement was seen when matching ITV. Alternatively, Table 1 shows the percentage of fractions where at least 99% of the ITV was within the PTV for different PTV margins and image matching strategies.

		Simulated Rotation (degree)																																																					
PTV Margin (LR, AP, SI mm)	Cord/Carina Matching	0*					1					3					5					6																																	
		5,5,5	87.1	86.7	64.1	24.6	13.8	89.4	88.7	79.7	48.9	34.3	91.7	91.2	86.4	61.1	46.1	91.7	91.9	87.9	64.8	49.2	94.7	94.8	92.8	77.5	63.4	91.7	91.4	87.6	58.2	41.1	93.1	94.3	92.3	76.9	61.8	93.9	93.4	91.5	70.8	54.5	97.7	96.7	95.3	86.7	74.4	95.5	95.5	95.5	89.0	77.7	99.2	99.5	99.1

*Based on 132 fractions; represents perfect set-up.

Conclusions: We used deformable image registration to evaluate the effect of rotational error in lung IGRT. Our results show that rotational errors of 3 to 5 degrees have significant effect on target coverage in IGRT protocols where couch corrections are employed to match spinal cord/carina or ITV. These results represent a worst case scenario where the patient is misregistered by the given rotation about at least one axis for all fractions. Future analyses will introduce rotations based on their probability of occurring during a treatment course as measured from previously acquired patient data.

SP036.3 - Robustness Assessment of a Novel 4D Optimization Approach for Lung Cancer Radiotherapy

Author(s): Shahad Al-Ward¹, Emily Heath²
¹Medical Biophysics, Ryerson University, Toronto/CANADA, ²Physics, Carleton University, Ottawa/ON/CANADA

Introduction: Respiratory motion is one of the main challenges in treatment of lung tumours with radiation therapy. A novel approach was developed to generate IMRT treatment plans, which compensate for respiratory motion and its variations, by combining intensity maps from plans optimized on the “worst case” motion variation scenarios. The objective of this work was to test this worst case planning method on both simulated and patient respiratory motion variations.

Methodology: A 4D optimization approach was implemented using the KonRad inverse planning system. Two approaches to combining the 4D optimized intensity maps were investigated: the first approach takes the average of the two intensity maps and the second approach takes the maximum intensity of the two intensity maps. The robustness of these worst case plans was compared with ITV based plans and with 4D plans optimized for the nominal motion only on three different respiratory motion variation scenarios. Study 1 investigated the robustness to simulated amplitude variations. Study 2 investigated the robustness to respiratory motion variations measured from a healthy volunteer who was asked to breathe irregularly. Study 3 investigated the robustness to motion variations of a NSCLC patient. Plans were deemed robust if they met a set of pre-defined clinical criteria for all motion variation scenarios in a given study.

Results: The average intensity worst case method was robust to motion variations in Study 3 only, except that the target volume was slightly over-dosed for the nominal motion case (64.92 Gy). The average intensity approach was not robust to motion variations in Study 1 and 2, which we attribute to the larger variation which occurred in those studies compared to the patient case. The maximum intensity worst case method, the ITV plans and the nominal 4D plans

were not robust to any of the motion variations that were tested for all three studies.

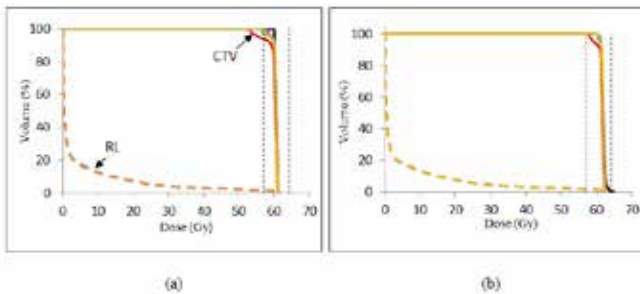


Figure 1: DVHs of (a) Nominal 4D plan and (b) Average intensity worst case plan applied to the patient motion variation scenarios (Study 3). The DVHs of the CTV and the tumour bearing lung (RL) are shown.

Conclusions: A novel approach to create robust IMRT plans has been tested and found to be robust to most patient respiratory motion variations. Further evaluation over a wide range of tumour sizes, motion amplitudes and variability is required to determine the clinical applicability of the worst case planning method.

SP036.4 - The role of VMAT interplay effects for liver stereotactic body radiation therapy

Author(s): Gillian Ecclestone¹, Greg Pierce²

¹Department Of Radiation Therapy, Tom Baker Cancer Centre, Calgary/CANADA, ²Department Of Medical Physics, Tom Baker Cancer Centre, Calgary/CANADA

Stereotactic body radiation therapy (SBRT) is beneficial in the treatment of solid liver cancers as it safely delivers an ablative tumor dose. Volumetric modulated arc therapy (VMAT) is an ideal modality for hypofractionated treatment regimes such as SBRT as it can efficiently deliver a conformal dose. However, treatment accuracy becomes compromised for liver tumors due to their inherent respiratory motion. Clinicians have raised concerns when treating moving targets with VMAT because the tumor motion relative to the dynamically moving MLCs degrades the plan quality; a phenomenon termed interplay. The purpose of this study is to examine if the amount of beam modulation and breathing cycle length elicits interplay effects that influence plan quality for liver SBRT treated with VMAT.

VMAT treatment plans with varying degrees of modulation were constructed using Eclipse treatment planning software, version 11.0 (Varian Medical Systems, Palo Alto, CA). Respiratory motion was modeled using an in house program that shifted the MLC leaves in each plan to simulate the motion of the GTV from the point of view of the radiation beam. IMRT modulation factors (MFs) ranged from 1.5 - 3.5 and respiratory cycle lengths of 3, 5, 10 and 20 seconds were simulated for all plans.

Minor interplay effects were observed and deemed clinically negligible: the 95% dose coverage of the target was not compromised. A slight degradation in the plan quality (size of 95% isodose) was detected and worsened with longer respiratory cycle lengths and low MFs (Fig. 1). This is attributed to the variation in gantry speed that was coupled to the MF. For high MFs (slower gantry speed), more time was available for the tumor motion to average out during each control point and as a result reducing interplay.

We concluded in this limited phantom study that treatment plan quality of liver SBRT is degraded the least by plans with high modulation factors. Plan fidelity was maintained via few partial arcs (to obtain a slow gantry speed) and adequate PTV margins that accounted for respiration.

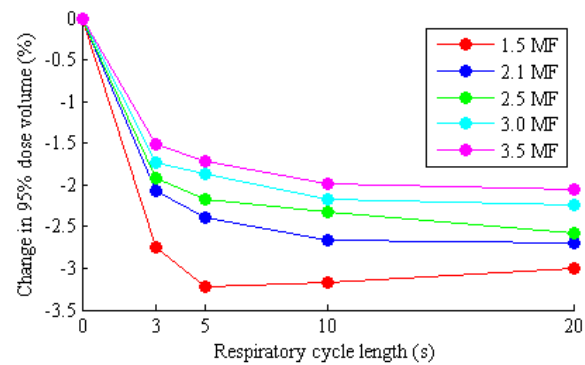


Fig. 1. A plot demonstrating the decrease in plan quality as respiratory cycle length increases and improved plan quality as the MF increases.

SP036.5 - Interplay of MLC, gantry and respiratory motion during DCAT delivery

Author(s): Tanya Kairn¹, Joanne Mitchell¹, Scott Crowe², Jamie Trapp³

¹Physics, Genesis CancerCare Queensland, Auchenflower/AUSTRALIA, ²Radiation Oncology, Royal Brisbane and Women's Hospital, Herston/QLD/AUSTRALIA, ³Science And Engineering Faculty, Queensland University of Technology, Brisbane/AUSTRALIA

This study investigated the possible interplay effects arising from the treatment of moving targets using the dynamic conformal arc therapy (DCAT) technique. Interplay effects are known to arise from the treatment of moving anatomy with dynamic wedges and intensity modulated radiotherapy (IMRT) beams. By contrast, volumetric modulated arc therapy (VMAT) treatment beams are currently regarded as largely immune to the effects of motion interplay. This difference potentially arises from the behaviour of multi-leaf collimator (MLC) leaves during IMRT and VMAT delivery, with MLC leaves that moving from one side of each beam to the other during IMRT delivery and MLC leaves frequently change direction throughout VMAT beam delivery. DCAT treatments of lateral targets, including the peripheral lung, often require the treatment isocenter to be displaced medially to avoid collisions between gantry and couch. In these circumstances, the MLC leaf motions in DCAT beams become similar to MLC motions in IMRT beams, moving in one direction from one side of the beam to the other. This situation leads to the concern that DCAT treatments might be more susceptible to motion interplay effects than an assumed similarity to VMAT treatments would suggest.

To investigate this issue, dose from a modulated test beam was measured, with and without phantom motion and with and without a 30° arc rotation, using a diode array placed on a sinusoidally moving platform. Measurements were repeated at five different collimator angles (0, 22.5, 45, 67.5 and 90°), at two different dose rates (300 and 600 MU/min), allowing the relative effects of leaf direction and leaf speed to be evaluated. When in use, the motion platform provided regular, longitudinal (superior-inferior), sinusoidal motion, with a 40 mm peak-to-peak amplitude and a 4 s period.

Results showed that the phantom's respiratory motion produced blurring of the dose penumbrae and consequent reduction of the area receiving high-doses, as well as dose oscillations throughout the high-dose region, which became more obvious as the MLC motion was aligned with the phantom motion direction. The delivery of the modulated beams as 30° arcs increased the penumbral dose blurring, without reducing the appearance of dose oscillations across the phantom. The dose oscillations arising from interplay

between phantom and MLC motion were found to increase in magnitude when the dose rate was increased from 300 MU/min to 600 MU/min, effectively halving the time taken to deliver each beam.

These results suggest that DCAT treatment beams may be affected by the interplay of MLC motion and patient respiratory motion, to a similar degree as static gantry IMRT treatment beams, rather than being similar to VMAT beams.

For DCAT beams, like IMRT beams, the negative effects of motion interplay may be minimized by aligning the collimator as close to perpendicular to the dominant direction of respiratory motion as possible, by decreasing the dose rate and thereby increasing the total delivery time of each beam, and by including appropriate margins on treatment targets so that dose blurring at the edges of the beam does not compromise tumour control.

SP036.6 - Impact of deep inspiration breath hold (DIBH) in lymphoma's radiation therapy treatment

Author(s): Daniel Venencia, Jorge Torres, Cristina Pfaff, Carola Sanchez, Jonathan Pacheco, Lucas Causa, Edgardo Garrigó
Fisica Medica, Instituto de Radioterapia - Fundacion Marie Curie, Cordoba/ARGENTINA

Purpose: Lymphoma treatments usually require radiation therapy of mediastinum and supraclavicular lymph nodes. Planning target volume (PTV) involves several organs at risk (OAR) such as lungs, heart and esophagus. The percentage of irradiated lung depends on the PTV and total lung volume. Deep inspiration breath hold (DIBH) increase the lung volume. The objective of this work was to evaluate the impact of DIBH in the treatment of lymphoma with radiation therapy.

Methods and Materials: A virtual treatment simulation was performed acquiring two computed tomography (CT) image series of the patient; the first one during DIBH and the second one with free breathing. Fiducials were placed on the patient's anterior torso surface for CT image acquisition and then used for IGRT localization. CT images were exported to treatment planning system (TPS) iPlan v4.5.3 (BrainLAB). PTV and OAR were segmented in the DIBH CT series. Treatment plans were generated using sIMRT or IMRT treatment technique with a 6MV photon beam produced by a Novalis TX linear accelerator equipped with ExacTrac IGRT system with gating capability (BrainLAB). Using iPlan RT Adaptive tool, free breathing's segmentation and plans were generated. Four patients were analyzed (3 sIMRT and one IMRT). All plans were normalized to have the same D95% at the PTVs. Comparison between lung volumes, dose volume histogram for PTV and OAR and monitor unit (MU) were done between DIBH and free breathing plans.

Results: DIBH lung volume increased in average 1997.7cc [1458.7, 2785.7]. Lung DVH comparison between DIBH and free breathing exhibits a decrease of 6.2% [5, 8.8] in V5, 5.5% [4.6, 7.7] in V10, 4.8% [3.1, 8.4] in V20 and 1.4% [-0.9, 3.7] in V30. The heart showed a mean dose reduction by 2.4Gy [-0.5, 8.7] and V10 by 8.6% [3.3, 33.0]. The esophagus did not show any significant dose variations. DIBH and free breathing plans did not show any differences in MU.

Conclusion: Treatment plans for mediastinal lymphoma planned on DIBH showed a dose reduction in lungs and heart. There is no change in the esophagus dose and MU used. Clinical impact of lung and heart dose reduction must be analyzed.

SP036.7 - Cardiac sparing in left-sided breast IMRT using robust optimization

Author(s): Houra Mahmoudzadeh¹, Jenny Lee², Timothy C.Y. Chan¹, Thomas G. Purdie²

¹Mechanical And Industrial Engineering, University of Toronto, Toronto/ON/CANADA, ²Princess Margaret Cancer Centre, Toronto/CANADA

Purpose: Left-sided breast cancer patients are often at a high risk of post-radiation cardiac toxicity, which is evident many years after the treatment. We test the feasibility of a cardiac sparing IMRT treatment planning model for left-sided breast cancer using a robust optimization framework that can be planned and delivered under free breathing.

Methods: Eight patients with stage 0, I or II left-sided breast cancer were included in this study. A 4D-CT scan was acquired, and an average plan based on the pixel-by-pixel averaged 4D-CT was generated for all patients. Six patients were treated using normal free-breathing conditions and the other two under controlled breath-hold using an active breathing control (ABC) device. The robust optimization method was used to generate treatment plans for all patients. The RO method uses the 4D-CT dataset and a model of uncertainty to mathematically ensure that the clinical dose-volume criteria are met under uncertain breathing conditions. A set of 200 simulated breathing patterns was used to compare the outcome of the average and robust methods under free breathing, and deformable registration was used to find the accumulated dose for each plan.

Results: Robust optimized plans dominated the clinical plans in heart sparing without compromising target coverage. Table 1 shows the amplitude of motion for each patient and compares the range of accumulated heart dose of the average and robust methods for the set of simulated breathing patterns. The robust method reduced the dose to the heart by 364cGy on average. For patient 2, who was classified as an ABC patient, the robust method was able to reduce the dose to an acceptable limit, meaning that the patient would not have required an ABC treatment.

Table 1: Comparing the accumulated D10cc of the robust and average methods using a set of simulated breathing patterns. (*patients 2 and 4 were ABC patients)

Patient	Motion (cm)	Heart D10cc (cGy)		Mean RO benefit (cGy)
		Robust	Average	
1	0.31	[347, 376]	[1146, 1183]	801
2*	0.21	[2098, 2367]	[2618, 2780]	465
3	0.36	[235, 735]	[346, 967]	199
4*	0.36	[3934, 3975]	[4113, 4153]	182
5	0.23	[614, 783]	[1276, 1564]	522
6	0.41	[216, 348]	[458, 796]	322
7	0.42	[1304, 2035]	[1729, 2325]	420
8	0.72	[0, 0]	[0, 0]	0

Conclusions: The robust optimization method can improve cardiac sparing in left-sided breast cancer IMRT, and it can potentially reduce the number of patients who need breath-hold treatments.

SP036.8 - Real Time Tumor Position Control During VMAT Hypofractionated Treatment

Author(s): Rachid Boucenna, Chemseddine Fatnassi, Michael Betz
Radio-oncology Department, Hirslanden, Lausanne/SWITZERLAND

Introduction

Hypofractionated treatment requires accurate tumor position control to be effective and safe. We report our initial experience monitoring tumor position during VMAT radiation, using Varian's Motion Intrafraction Review (MIR) system. This system permits real-time target position verification during dose delivery, and incorporates an automatic beam interruption function.

Materials and Methods

We inserted three coils (markers) into the insert of a Lung Dynamic Phantom (LDP®, CIRS). Two image series were acquired with a Big Bore CT (Philips Healthcare).

The first series was acquired without any target motion, and a planning target volume (PTV) was defined using the static target.

The second series was acquired with a 10-mm dynamic sinusoidal shift. Images were synchronized with the breathing curve (RPM, Varian Medical Systems, VMS) in phase mode, and a PTV was created from an internal target volume incorporating target motion. Average reference planning CT images were generated for positioning and treatment plan calculation.

For both PTVs, single-arc VMAT treatment plans were calculated on the Eclipse Treatment Planning System (VMS). Treatment parameters were: beam energy = 6FFF; dose rate = 1200 MU/min; fractional dose = 8 Gy. Treatment was performed with the TrueBeam accelerator version 2.0 (VMS).

For the static target, the phantom was aligned using marker match registration. Marker position on the acquired images was directly matched to the expected position. The LDP® was used to simulate static target volume shifts in the cranial axis. Performance of the system was assessed using two tumor shifts (2 and 4 mm), respectively within and over a predefined spherical tolerance of 3 mm. During treatment, kV images were acquired at each 10° of gantry rotation, and real-time marker positions were automatically checked by the MIR system.

For the dynamic target, a breathing curve was recorded during CBCT acquisition. The phantom was aligned performing registration with the reference CT. During treatment, images were acquired twice per free breathing cycle, and the MIR system used to verify that markers remained within the PTV. An additional test was performed incorporating a right-left shift exceeding the PTV margin without modifying the breathing curve, to assess the MIR system's ability to detect such an error independently of the information provided by the breathing curve.

Results

For the static targets, the 2-mm shift was recognized as within tolerance, and the treatment completed. The 4-mm shift was recognized as unacceptable, triggering beam interruption.

For the dynamic targets, in the absence of an additional left-right shift the MIR system recognized that marker motion remained within the PTV and treatment was completed. In the presence of an additional left-right shift, the system detected markers outside the PTV and the beam was interrupted even in the presence of a "correct" breathing curve.

Conclusion

Real-time automatic marker position verification during VMAT using the MIR system is capable of detecting shifts in both static and dynamic targets, permitting reduced PTV margins for SBRT treatment with a high per-fraction dose. Automatic treatment interruption in the case of sudden excessive shifts can increase both treatment quality and treatment safety.

SP037 - Dosimetry in Nuclear Medicine

TRACK 05: DOSIMETRY AND RADIATION PROTECTION

SP037.1 - Comparative Evaluation of Radiation Dose Rates in Cancer Thyroid Patients Treated with Variable Doses of Radioiodine

Author(s): Ajai Kumar Shukla, Dheeraj K. Tewari
Nuclear Medicine, SGPGIMS, Lucknow/INDIA

Cancer Thyroid patients after near total thyroidectomy are treated at our centre for radioiodine ablation using variable doses of radioiodine ranging from 3700 MBq to 7700 MBq. Initially the regulatory agency had fixed the discharge limits of 400 MBq at a distance of one meter from the patient and it usually involved a minimum isolation of about three days to decline the activity levels in patients to acceptable limits. However recently this discharge limit has now been increased to 1100 MBq and in order to see the effect of this change on the pattern of radiation levels and also on the time of discharge, the present study was undertaken on a total of 27 patients treated with doses of radioiodine I-131 ranging from 3700 MBq to 7400 MBq.

The radiation levels in uSv/hr at one meter in cancer thyroid patients (n=27) were observed to be below 50 uSv/hr on the second day itself which corresponds to about 1100 MBq residual activity. However in patients with metastatic lesions with avid concentration of I-131, the levels could decline below 50 uSv/hr only after three to four days after administration of I-131. The prolonged period taken in decline of the activity was also attributable to the fact that relatively larger amounts of activities upto 5550 MBq and in few patients 7700 MBq were administered. Prior to change of the discharge limits the decline period used to take in some cases as more than seven days particularly in patients with metastatic lesions and administered with larger activities of the order of 5500 MBq to 7700 MBq. The prolonged isolation causes psychological trauma in some patients and therefore it was observed to be a big relief to the patients to have increased discharge limits (which did not cause any significant safety related issues) apart from treating more number of patients within the available infrastructure and number of isolation rooms. In addition it also enabled greater flexibility of dosing the patients with advanced disease conditions thereby reducing the overall cost of treatment.

It could be yet another school of thought to consider fractionation of doses of I-131 in those cases which needed more than seven days of isolation to prevent or minimize the risk of patient landing into extreme level of isolational stress.

SP037.2 - Estimation of the influence of other organs of the body in the determination of the gamma fraction energy emitted by iodine 131 deposited within the thyroid gland

Author(s): Abderrahim Betka¹, Abdelouahab Bentabet², Ahmed Azbouche³, Nourdine Fenineche⁴, Adouda Adjiri¹
¹setif university, setif/ALGERIA, ²BordjBouariridj université, Algeria, BordjBouariridj/ALGERIA, ³centre de recherche nucleaire alger, Alger/ALGERIA, ⁴IRTES-LERMPS/FR FCLAB, UTBM, Belfort, France, Belfort/France

When treating hyperthyroidism using Iodine 131 and to facilitate and accelerate the computation time in the determination of internal dose within the thyroid gland, the shape, composition and volume of the thyroid tissue in this case is the only important factor to take into account.

This study aims to determine the fraction of energy of the gamma

emission of the radioactive isotope iodine 131 in the thyroid gland and the effect of the individual organs constituting the human body with the exception of the thyroid gland by using the geometry and material composition of each organ

To determine the influence of the entire body, and hence its different constituting organs, on the calculation of the fraction of the gamma energy absorbed by the thyroid gland during the treatment of hyperthyroidism using iodine-131, we have performed simulations using the Monte Carlo Penelope code in the following two situations:

- Simulation of the entire body by a mathematical anthropomorphic phantom with simple geometric shapes and for this we used the example included in the Penelope code (male.geo file).

- The second situation involves simulating the thyroid gland alone.

Comparison of the results obtained by simulating the thyroid gland alone to those obtained by simulating the whole body shows a difference of 3% on average. The error in determining the dose by simulating only the geometry of the thyroid gland without involving the geometry of other organs of the body is estimated to 3%.

SP037.3 - Personalized compartmental biokinetic modelling and internal dosimetry of two novel radiopharmaceuticals

Author(s): Alexandra Zvereva¹, Wei B. Li¹, Nina Petoussi-Henss¹, Helmut Schlattl¹, Uwe Oeh¹, Maria Zankl¹, Stephan Nekolla², Christoph Hoeschen¹, Katia Parodi³, Markus Schwaiger²

¹Research Unit Medical Radiation Physics And Diagnostics, Helmholtz Zentrum München, German Research Center for Environmental Health, Neuherberg/GERMANY, ²Department Of Nuclear Medicine, Klinikum rechts der Isar Technische Universität München, Munich/GERMANY, ³Experimental Physics – Medical Physics, Ludwig Maximilians University (LMU) Munich, Garching/GERMANY

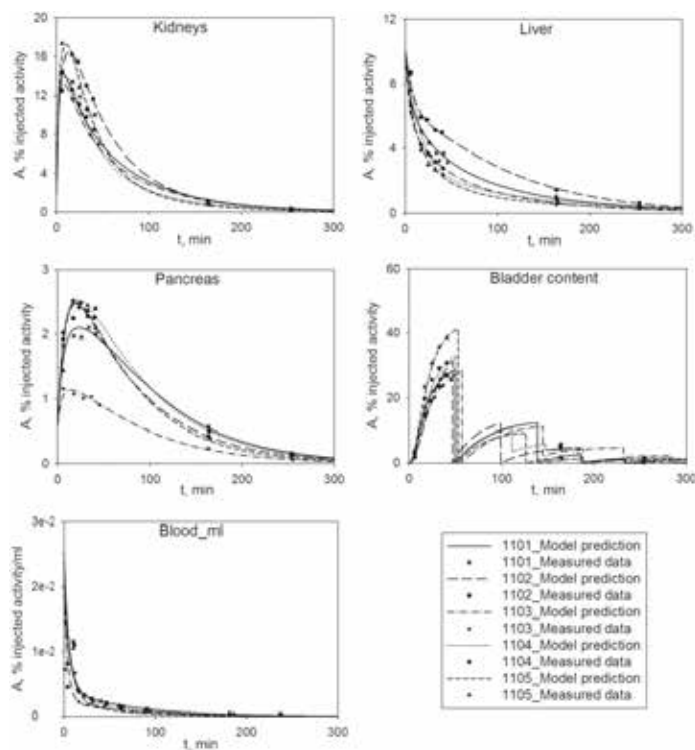
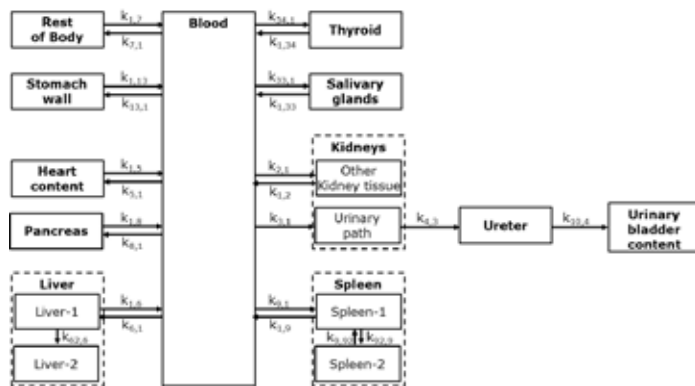
Purpose The objective of this work is to develop personalized compartmental biokinetic models for two novel radiopharmaceuticals BAY85-8050 [1] and BAY94-9392 [2] to predict their distribution in the human body and associated patient-specific organ doses. We also aim to separately consider activities in organ parenchyma and blood in the modelling and dosimetry.

Methods The models are constructed based on clinical PET/CT images, blood and urine samples of 10 healthy volunteers [1,2]. Following an identifiability analysis of the developed models, model parameters were estimated using the commercial program SAAMII. Organ doses were calculated in accordance to the MIRD/ICRP formalism using specific absorbed fractions for photons and electrons previously simulated in the ICRP male and female reference adult computational phantoms.

Results The developed compartmental biokinetic model structure and the subset of the resulting biokinetic model predictions for BAY94-9392 are presented in Figs.1 and 2, respectively. The corresponding figures for BAY85-8050 are not displayed here. The results showed a considerable inter-individual variability between the volunteers with effective dose coefficients of 0.016–0.018 mSv/MBq (BAY85-8050) and 0.011–0.018 mSv/MBq (BAY94-9392). We compared the personalized organ doses for two cases: (a) activities in organ parenchyma and in blood are separately modelled; (b) aggregate activities in perfused organs. For most organs the doses in case (a) were higher. Consequently, the average effective dose coefficients increased by 8.3% and 8.9% in case (a) for BAY85-8050 and BAY94-9392, respectively. Additionally, a strong influence of bladder-voiding intervals on the bladder-wall doses was demonstrated.

Conclusion The developed models can be used to estimate distributions and dose levels of two novel radiopharmaceuticals. The con-

siderable inter-individual variability helps to understand the intrinsic uncertainties when reference models are applied to individuals and justifies the advantage of personalized modelling approaches.



1. Smolarz et al. Eur J Nucl Med Mol Imaging.2013;40(12):1861-8.
2. Smolarz et al. J Nucl Med.2013;54(6):861-6.

SP037.4 - TLD Measurement of Absorbed Dose of Workers in PET/CT Department

Author(s): Pardis Ghafarian¹, Sajedeh Zargan², Ali Shabestani Monfared², Ali Akbar Sharafi³, Mehrdad Bakhshayeshkaram¹, Mohammad Reza Ay⁴

¹Chronic Respiratory Diseases Research Center, National Research Institute Of Tuberculosis And Lung Diseases (nritld), Shahid Beheshti University of Medical Sciences, tehran/IRAN, ²Department Of Medical Physics, Babol University of Medical Sciences, Babol/IRAN, ³Department Of Medical Physics, Iran University of Medical Sciences, Teharn/IRAN, ⁴Department Of Medical Physics And Biomedical Engineering, Tehran University of Medical Sciences, Tehran/IRAN

Introduction: Staff radiation protection is the critical concern in

clinical PET/CT centers due to high gamma energy of F18 using in 18F-FDG PET studies. The aim of this study was to evaluation the staff radiation dose in PET/CT department in Masih Daneshvari hospital.

Material and Method: during complete PET/CT imaging steps (from syringe filling to patient departure) the staff radiation dose was investigated with thermoluminescent dosimeter (TLD). The Hp(3) used for doses to the lens of the eyes and Hp(10) for doses to the whole body and Hp(0.07) for doses to the other part .For increasing the measurement accuracy, three chips of TLD used in each point of measurement.

Result: the staff radiation dose were measured for work load of 53 adult patients who receive 374.28±100.30 MBq (range 127-540 MBq) 18F-FDG activity. The mean±SD total effective doses per unit of activity received by dispensing staff (n=3), imaging staff (n =5) and injection staff (n=2) were 4×10⁻⁴±5.77×10⁻⁵, 8×10⁻⁴± 1×10⁻⁴ and 1×10⁻³±1×10⁻¹ μSv/MBq and received dose in eyes were 1.39×10⁻⁶±5.77×10⁻⁶, 0.87×10⁻⁶±1×10⁻⁴ and 3×10⁻⁴±1×10⁻¹ μSv/MBq as measured with TLD respectively . In this study, the finger radiation dose were higher for injection staff (7×10⁻⁶±1×10⁻¹ μSv/MBq) versus other radiation workers.

Conclusion: staff sensitive organs such as lens of eyes; thyroid and breast were received low dose in our PET/CT and cyclotron Centre. It is observed that the received radiation dose to radiation workers were below the dose limits recommended by the ICRP for all staff working in PET/CT department. This study confirmed that staff’s radiation doses in our PET/CT center were lower than those recommended by the ICRP guideline which can explain using semi-automatic injector, patient video monitoring and strong shielding performed in our center.

SP037.5 - Renewing the radiopharmaceutical accuracy check service for Canadian dose calibrators

Author(s): Raphael Galea, Khalid Gameil, Malcolm R. Mcewen
Measurement Science And Standards, National Research Council, Ottawa/ON/CANADA

For a ten year period from 1986-1996, a small fraction of the Canadian nuclear medicine community participated in a service offered by the National Research Council (NRC) to check the accuracy of administered doses of radiopharmaceuticals. Similar programs exist in many countries and are of particular importance given the advent of new sources of medical isotope production anticipated to begin with the shutdown of the NRU medical isotope production in 2016. This service depends on the Secondary Standard Ionization Chambers Systems (SSIRCS) at NRC which is composed of a TPA and an NPL ion chamber coupled with an electrometer. These chambers were calibrated using radionuclidic artifacts standardized by primary methods.

These chambers have been in operation for several decades but were not operated for several years from 2001-2008 when the radionuclide metrology program ceased operations at NRC. A new data acquisition program (DAQ) was developed and new methods of determining the response of the ion chamber and electrometer were included to add redundancy and added assurance as to the calibration. Comparisons between the original and new DAQs were performed to provide validation to the chambers’ operation as well as continuity with measurements of radionuclidic artifacts still in the NRC inventory.

The original service involved the participant to measure the desired isotope in a syringe and 5 ml serum vial geometries in their dose calibrator and then send the sample to NRC to be measured in the SSIRCS and to permit an impurity check to be performed. In order to attract participation and simplify the process, the NRC is also offering an alternative service in which an ion chamber is sent to the facility, thus not requiring the shipment of isotopes, at the expense

of an impurity check. The NRC conducted a mock service on two commercial dose calibrator models CRC-35R and CRC-ULTRA for Tc99m resulting in serum vial calibration coefficients that were consistent with unity to 1% (1.005 ± 0.006 ($k=2$)). The reference value delivered with the Tc99m dose from the nuclear pharmacy was determined to be 0.977 ± 0.006 ($k=2$) of the calibrated activity. While this is well within the recommended guideline of 10% of the required dosage, in most countries, it is significantly different from unity at the 95% confidence interval to warrant the application of a calibration factor, or to monitor this value on a regular basis to detect potential drift due to mechanical or physical changes to the ion chamber.

This work was important to assure the Canadian nuclear medicine community of the existence, validation and improvements of the SSIRCS at NRC and to provide confidence and encouragement in the participation of this proficiency testing service.

SP037.6 - Radiation Dose Assessment of 99mTc-labeled Tetrofosmin in Patients Undergoing Rest-Stress Myocardial Perfusion Scintigraphy

Author(s): Stella Veloza¹, Estrella Avila Ramirez²
¹Physics, Universidad Nacional de Colombia, Bogota, D.C./COLOMBIA, ²Department Of Nuclear Medicine, DALINDE Medical Centre, Ciudad de Mexico/MEXICO

Purpose: Tetrofosmin labeled with technetium-99m (99mTc) is a myocardial imaging agent. The goal of this research is to evaluate the differences between two methods for assessing radiation dose: internal dosimetry by using a dose calculation program and an analytical model based on patient's weight.

Materials and Methods: A biodistribution of 99mTc-Tetrofosmin as reported in the literature was used in OLINDA/EXM-1.0[®] to estimate patient-specific absorbed and effective radiation doses on 91 adults (33 female, 58 male) who were undergoing 99mTc-Tetrofosmin 8 mCi-rest/ 17 mCi-stress myocardial perfusion imaging. The dosimetry results were compared to the values calculated from scaling by a power function of body weight the values of effective radiation doses for adults from 99mTc-Tetrofosmin rest/stress provided by the International Commission on Radiological Protection (ICRP) publication 106.

Results: The mean effective doses estimated by dosimetry in female patients were 3.46 mSv and 5.91 mSv at rest/stress respectively. In male patients the mean effective dose estimated by dosimetry was 2.87 mGy at rest and 4.86 mGy at stress. For male and female patients of the same weight the dosimetry shows that the women's effective doses are about 17% higher than for men. The effective doses estimated in patients with a weight of 100 kg by the analytical method differed from those based on dosimetry by up to 40% in women and 30% in men at rest and 35% in women and 25% in men at rest.

Conclusions: Even though the standard ICRP dose values are scaled by patients' weight, the effective dose for overweight patients are underestimated, more for female patients than for male patients because ICRP values correspond to an adult male. These underestimations are an important factor to consider if an approach based on differences in patient's weight is used to adjust the amount of activity to be administered.

SP037.8 - Biological Excretion and Half - Life of Remnant Radioactive Iodine 131I in Post Treated Hyperthyroidism Patients.

Author(s): Shuaa J. Al-Sadoon¹, Mohammed A. Al-Eid², Taki A. Al-Musawi³, Farid Y. Risheq⁴

¹Physics In Nuclear Medicine, FARID RISHEQ NUCLEAR MEDICINE PET/CT & BONE DENSITY CENTER, AMMAN/JORDAN, ²Nuclear Medicine, AL-MUSTANSIRIYAH UNIVERSITY, COLLEGE OF MEDICINE, BAGHDAD/IRAQ, ³Medical Physics, ALMUSTANSIRIYA UNIVERSITY, BAGHDAD/IRAQ, ⁴Nuclear Medicine, FARID RISHEQ NUCLEAR MEDICINE PET/CT & BONE DENSITY CENTER, AMMAN/JORDAN

Objective: Following ¹³¹I treatment of hyperthyroidism; remnant activity is depleted by physical decay and bio-excretion. ICRP estimated ¹³¹I biological half-life as (138d-1960), (120d-1979), (80d-1989). This work assesses semi-empirical bio-excretion models and estimates biological half-life of post treated hyperthyroidism patients.

Patients and Method: 17 hyperthyroidism adult patients were treated with ¹³¹I (185-740MBq) depending on hyperthyroidism condition. Thyroid scans were possible by pinhole gamma camera; one and two months post ¹³¹I therapy utilizing remnant activity.

Semi-empirical excretion models developed were:

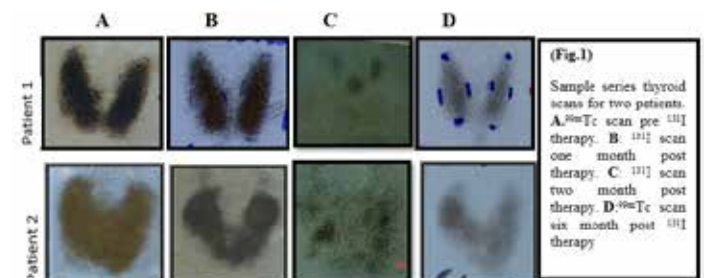
1- fixed amount $\Gamma fa(c/s) = I_0 [e^{-n\lambda_p} - (I_n/I_0)] * [(1 - e^{-\lambda_p}) / (1 - e^{-n\lambda_p})]$

2. fixed fraction $\Gamma ff = e^{-\lambda_p} - (I_n/I_0)^{1/n}$

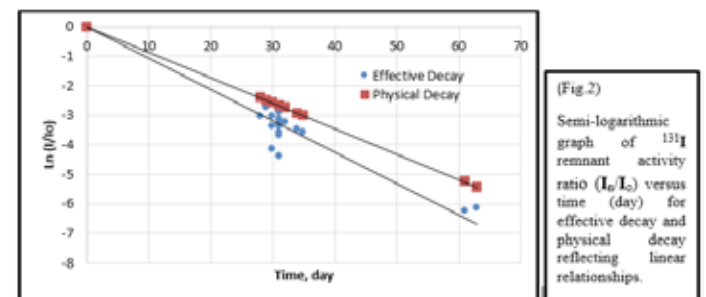
3. exponential $\Gamma e = e^{-\lambda_{be}}$

Bio-excretion/effective decay = $(\ln p - \ln I_n) / (I_0 - I_n)$, $TE = -0.693n(\text{day}) / \ln(I_n/I_0)$, $T_b = T_p TE / (T_p - TE)$, I_0 and I_n are: initial and n^{th} day activity (c/s), decay coefficient $\lambda = 0.693/T$, T =half life(d); subscripts: p, b, E are respectively physical, biological and effective.

Results and Discussion: Sample series of thyroid scans are shown in (Fig.1):(A)^{99m}Tc scan pre-treatment;(B)¹³¹I scan one month post-treatment,(C)¹³¹I scan two month post-treatment;(D)^{99m}Tc scan six months post-treatment.



A semi logarithmic graph of relative (I_n/I_0) versus time (d) showed linear relationship of ¹³¹I remnant activity effective decay and physical decay,(Fig.2), slope=0.693/TE=0.103, $(R^2=0.895)$, and slope=1, $(R^2=1)$ respectively. Accordingly, TE=6.73d, Tb=41.0d. Calculated Tb average value=40.7±21.4d.



Measured bio-excretion of ^{131}I contributes 3.5% of effective decay as compared to 96.5% for physical decay. Fixed amount model predicts ~9.3% bio-excretion contribution; not significant with measured values. Fixed fraction and exponential models predict bio-excretion factor = 0.021 of activity/day (~0.25 physical decay factor = 0.083 of activity/day); significant with measured values.

We conclude that emitted radiation from remnant ^{131}I will destroy thyroid functioning cells, reducing their ability to produce and excrete hormones, and hence increase biological half-life. Thyroid cells will be subjected to radiation hazards (beta and gamma) for 10 physical half-lives = 80 day (remnant activity = 0.1% of initial value). Caution is required with pregnant and breast feeding women.

SP038 - Dosimetry of Non-Standard Fields

TRACK 05: DOSIMETRY AND RADIATION PROTECTION

SP038.1 - Determination of small photon field quality correction factors using EBT3 radiochromic film

Author(s): Ilias Billas, Hugo Bouchard

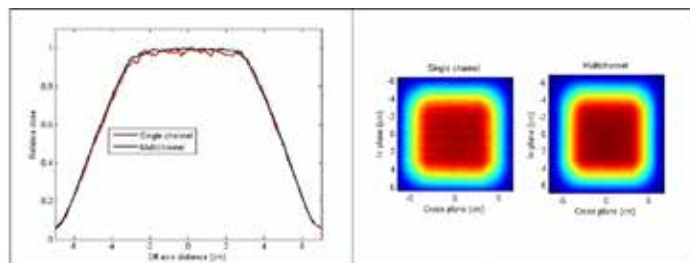
Radiation Dosimetry, National Physical Laboratory, London/UNITED KINGDOM

With the upcoming IAEA-AAPM reference dosimetry protocol on small photon fields, quality correction factor data is needed. To determine these factors accurately, Monte Carlo methods are used but reliable experimental methods remain under investigation. Among the different detectors recommended by IAEA-AAPM for such conditions, radiochromic film remains promising with its high resolution and water-equivalence. However, current methods and film models available commercially (EBT3) focused on clinical applications do not meet the accuracy standards of reference dosimetry, contrary to previous models as shown in literature. The goal of this work is to develop a reliable approach for radiochromic film dosimetry, reaching 0.5% statistical uncertainty on relative pixel dose with EBT3 and reducing systematic errors caused by film thickness inhomogeneity.

An original multichannel method is developed based on a simple 2D model of the film response to dose and thickness and statistical analysis of the calibrated film. Gafchromic EBT3 films are irradiated with cobalt-60 beams homogeneously, allowing obtaining parameters for scanner homogeneity correction, multichannel analysis and dose response calibration. Software is developed for film characterization and analysis. Dose distribution measurements are compared to reference data and an uncertainty budget is made to quantify the performance of the method in correcting systematic errors in film response. Based on the analysis, conditions to achieve 0.5% uncertainty in relative measurements are determined. Systematic errors are compared to the statistical behaviour of pixel dose.

Comparing single and multichannel methods, it is demonstrated that the proposed method reduces systematic errors significantly. The method allows uncertainties in output factors of 1.2% for single measurements and 0.4% for measurements repeated ten times. Comparisons with known dose distributions show systematic errors up to 10% with single channel analysis, while they are on average diminished by a factor up to three and well below statistical uncertainties with the multichannel method. The figure shows a comparison of the methods in measuring a $10 \times 10 \text{ cm}^2$ cobalt-60 beam profile: a beam profile (left) and a dose map (right).

Results suggest that a controlled experimental procedure and proper analysis yield great potential for small photon field dosimetry using radiochromic film, with uncertainties in quality correction factors comparable to previous film models. It is expected that future experiments with small photon fields will validate the theoretical predictions reported herein.



Comparison of the single and multi channel methods in measuring a $10 \times 10 \text{ cm}^2$ cobalt-60 beam profile: a beam profile (left) and a dose map (right).

SP038.2 - On the physics of megavoltage small photon field dosimetry

Author(s): Hugo Bouchard¹, Jan Seuntjens², Yuji Kamio³, Simon Duane¹, Hugo Palmans¹

¹Radiation Dosimetry, National Physical Laboratory, London/ UNITED KINGDOM, ²Medical Physics, McGill University, Montreal/ CANADA, ³CHUM, Montreal/CANADA

The upcoming IAEA-AAPM protocol for dosimetry of small photon fields is expected to improve the calibration of such beams, benefitting patient safety and treatment outcome. As a complement to such procedures, a clear presentation of the main effects responsible for large detector correction factors is highly valuable. The physics of small fields is a rather complex subject and has not yet been treated in the literature in a conceptually sound manner. Hence, confusion over the limitations of dosimetry protocols in small fields still exists. The present study aims to provide a comprehensive explanation why dosimetry of megavoltage small photon fields can require significant quality correction factors.

Several concepts are reviewed from a theoretical point of view. The applicability of cavity theory to small fields is described, and a simpler cavity theory is proposed. The concept of charged particle equilibrium (CPE) and its impact on dosimetry is evaluated in detail. The perturbations caused by the presence of a detector are also analysed thoroughly. Four main effects are identified and related to detector characteristics: 1) the density of the cavity material, 2) the atomic properties of the cavity material, 3) the presence of extra-cameral components and 4) volume averaging effects. The theory is supported by a series of Monte Carlo calculations characterizing detector response to pencil photon beams.

The analysis and results presented here clarify several misconceptions in some of the existing literature on small field dosimetry. Evaluation of the four perturbation effects indicates that significant correction factors arise mainly from the interplay between lack of CPE and cavity density. New Monte Carlo results as well as key publications on the topic strongly support this conclusion. Figure 1 shows simulated detector dose response to a pencil beam under Fano's conditions, and illustrates the interplay between lack of CPE and cavity density.

This study presents an analysis of the physics of small field dosimetry and allows in-depth clarification of the reasons for significant quality correction factors in megavoltage small photon fields. It is expected to be a valuable complement to the upcoming dosimetry protocol which mainly focuses on the technical aspects of small field dosimetry.

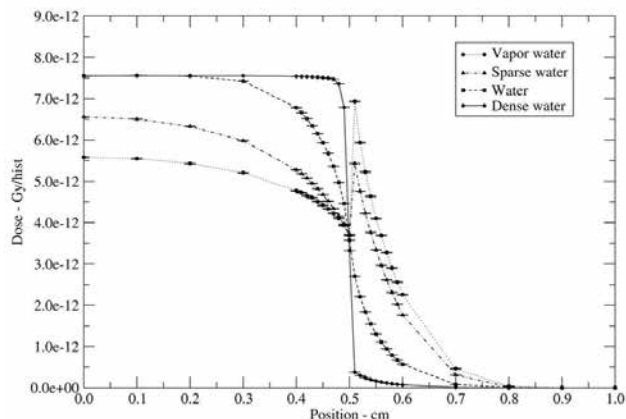


Figure 1. Dose response of a cylindrical cavity, 1 cm diameter, to a 1.25 MeV monoenergetic photon pencil beam, as a function of beam distance from the cavity axis. Calculations are performed using Fano calculations so that the integral of the curve is independent of the cavity density.

SP038.3 - Comparison of AAPM TG 148 and UK code of practice of Reference dosimetry in Helical Tomotherapy.

Author(s): Siji Paul, S.V. Jamema, Reena Devi, Kishore Joshi, Mayur Sawant, Pooja Moundekar, Deepak Deshpande
Medical Physics, Tata Memorial Centre, Mumbai/INDIA

Purpose: To compare AAPM TG 148 and UK code of practice for reference dosimetry of Helical Tomotherapy and to implement and validate a protocol for the beam output measurements.

Methods: Static beam output measurements were carried out using two formalisms AAPM TG 148 and UK code of practice, using two chambers A1SL (Standard imaging) and FC 65G (Scanditronix IBA). According to the UK code of practice, first, tissue phantom ratio TPRTomo for a static 5 × 10 cm² field at an SCD of 85 cm, at depths of 10 cm and 20 cm was measured, followed by conversion of TPRTomo to QITomo using an empirical formula given in the formalism. The absorbed dose to water calibration coefficient for the chamber, ND,w, was determined for QITomo, followed by beam quality correction factor for AISL chamber using this formalism. AAPM TG148 proposed *machine-specific reference (msr)* field, which is nothing but, a static field that uses reference conditions achievable on a helical tomotherapy machine, 5x10 cm² field size at an SSD of 85 cm. In the AAPM TG 148 formalism, PDD10 was measured at 10cm depth for *msr*, which was then converted to PDD10 for TG -51 reference conditions using a polynomial, followed by the determination of absorbed dose to water conversion factor, *kQ,Q0 x kQ, msr,Q (fmsr,fref)* which converts the calibration factor from calibration beam to the machine-specific reference beam.

Results: The difference between the two protocols in the determination of absorbed dose to water(Dw) in the reference conditions was found to be 0.6% and 0.9% for AISL and FC 65G chamber respectively (Table 1). The difference in *kQ, msr* for the reference conditions between the protocols was 0.1 and 0.2% for A1SL and FC65G respectively.

Conclusion: The new code of practice of beam output measurement using reference conditions has been successfully implemented. The choice of ionization chambers, determination of dosimetric corrections, and derivation of absorbed dose to water calibration factors, and the choice of appropriate chamber correction factors described in these formalisms have been found to be practical and implementable.

protocol	Chamber	KQ,msr	ND,w,fmsr(cGy/nC)	Output cGy/min	Ratio
TG148	A1SL	0.998	58.03	848.99	0.994
UK	AISL	0.999	58.03	854.3	
TG148	FC65G	0.9996	48.17	828.3	0.991
UK	FC65G	0.9977	48.17	835.4	

SP038.4 - A new facility to support the adaptation of reference dosimetry in the presence of strong magnetic fields

Author(s): Simon Duane, James Manning, Giuseppe Schettino, Hugo Bouchard
 Radiation Dosimetry, National Physical Laboratory, London/UNITED KINGDOM

Novel technology integrating MRI with the delivery of megavoltage photon radiotherapy promises unique advantages for image guidance. At MRI strengths, magnetic fields can have a significant impact on the dosimetry. To calibrate these new machines, detector dose response must be thoroughly investigated and validated data must be available. However, it remains a challenge to isolate the effect of the magnetic field on dosimeter response. While alanine is a promising nearly water-equivalent detector, its potential as a reference dosimeter in the presence of a strong magnetic field has yet to be demonstrated experimentally.

A new experimental facility, unique among standards laboratories, is set up using a dipole magnet with field strengths up to 2 T in a cobalt-60 beam (see figure). The EPR response of nine 2.4 mm alanine pellets in a $2 \times 2 \times 2$ cm³ mini-phantom, irradiated to 20 Gy in 0 T and 2 T fields, is evaluated repeatedly to assure optimal precision. The effect of the magnetic field on absorbed dose to water is determined using a limit approach combining Monte Carlo data and the magnetic field-independence of kerma.

The uniformity of the pellet dose is consistent with expectations given the stack orientation being parallel to the magnetic field and perpendicular to the beam. Doses are averaged for inner pellets, away from the phantom edges. The dose correction in water and its type B uncertainty are estimated from existing Monte Carlo data. The correction $k_{QB,Q0}$ varies from 0.9897 to 0.9978 over the pellets, with a standard deviation of 0.0030. This gives a mean quality correction factor of 0.9955 with a combined uncertainty of 0.0035 ($k=2$) at 2 T. This result is consistent with the alanine dose response being only slightly affected by the 2 T magnetic field. It is demonstrated alanine has the potential to serve as a reference detector for the experimental determination of magnetic field quality correction factors.

Combined with alanine/EPR dosimetry, the new experimental facility has the capability of validating Monte Carlo data of detector response in strong magnetic fields. This is expected to impact the robustness of future reference dosimetry protocols adapted for use with MRI-guided radiotherapy machines. Future work includes determining the response of alanine in a wide range of field strengths as well as the characterization of this effect on other detectors.

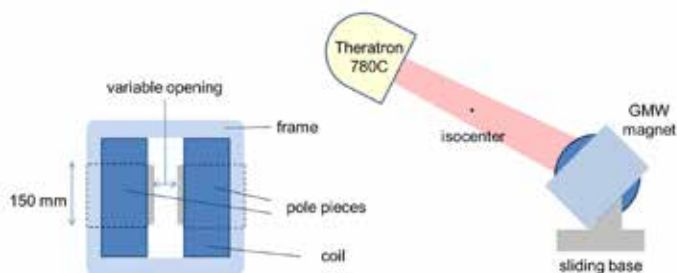


Figure: Experimental setup: a BEV of the magnet, and the configuration in the cobalt-60 vault.

SP038.5 - The use of ionization chambers and Gafchromic films to determine the reference absorbed dose rate and output factors in a CyberKnife® unit small radiation fields

Author(s): Nestor Aragón-Martínez¹, Arnulfo Gómez-Muñoz², Abel Hernández-Guzmán¹, Guerdá Massillon-Jl¹
¹Instituto De Física, Universidad Nacional Autonoma de Mexico, Mexico City/MEXICO, ²Umae Oncología, Centro Médico Nacional Siglo XXI, Mexico City/MEXICO

This work investigated the optimum dosimetric method to measure the absorbed dose to water rate under reference conditions in a CyberKnife® unit using radiochromic film, RCF and three ionization chambers, IC: a) An Exradin A12 associated with a Standard Imaging Supermax 90018 electrometer calibrated at NIST, USA (IC-A12), b) A FC65P Welhöfer Scanditronix (SN2258) coupled with a Dose One (SN17237) electrometer calibrated at IBA, Germany (IC-2258) and c) A FC65P Welhöfer Scanditronix (SN580) connected with a Dose One (SN7969) electrometer calibrated at ININ, Mexico (IC-580). In addition, the output factors for all the fields (12 fields from 5 mm to 60 mm diameter) have been measured using a diode detector NWP484841, Gafchromic film types EBT3 and MD-V3. A Varian® iX linear accelerator was used to measure the correction factor, $k_{fms,refQms,Q}$ needed by the IAEA/AAPM new formalism using IC and films. The measurements in the Varian® iX were carried out in a 10cmx10cm field, 10 cm depth in liquid water at 90 cm and 70 cm SSD and in a 5.4cmx5.4cm field, 10 cm depth at 70 cm SSD to simulate the CyberKnife® conditions. Whereas in the CyberKnife® unit, measurements were performed using ionization chambers and both film types at 70 cm SSD and 10 cm depth in its 6 cm diameter reference field, but for the smallest fields, only Gafchromic films were considered. In the 10cmx10cm field and 90 cm SSD, difference up to 2 % in the absorbed dose to water rate was observed, depending where the IC was calibrated, however within measurement uncertainties, a maximum discrepancy of 0.6% was observed between $k_{fms,refQms,Q}$ measured with different detectors. For the dose rate measured in the CyberKnife® unit, good agreements were observed (variation of 0.75% and 1.35% vs 1.78% and 1.92% uncertainties for EBT3 and MD-V3, respectively) between CI-A12 and films. While, difference about 2% (uncertainty of 1.35%-1.47%) were found between CI-A12 and CI-580. For the output factors, good agreements were obtained for all the dosimeters (variation of 0.1%-1.97% vs 2.4% uncertainty for EBT3 and variation of 0.2%-2.48% vs 2.86% uncertainty for MD-V3, $k=1$). For the smallest field (5 mm), a difference of 7 % was found in the output factor measured with MD-V3 film with respect to others dosimeters, which could possibly be associated to its energy dependence. These results suggest that, the absorbed dose measured at a point within a given field size should be the same, regardless the dosimeter used (CI or RCF) if their dosimetric characteristics are well known. This highlighted the importance of performing dosimetry by controlling all the parameters that could affect the dosimeter response. One can conclude that radiochromic film dosimetry can be considered as an appropriate alternative for measuring absorbed dose to water rate and output factors in small radiation fields and obtain a combined standard uncertainty of less than 2%.

This work was partially supported by Conacyt grant 127409 and PAPIIT-UNAM grant IN105813.

SP039 - ECG

TRACK 09: BIOSIGNAL PROCESSING

SP039.1 - Improved T-wave Alternans Detection in ECG Signals

Author(s): Guangyi Chen¹, Sridhar Krishnan¹, Vijay S. Chauhan²
¹Ryerson University, Toronto/CANADA, ²Toronto General Hospital, Toronto/CANADA

T-wave alternans (TWA) is a pattern in electrocardiogram (ECG) signals characterized by two distinct forms of T-waves appearing in alternation, at a patient's heart rate in the range of 90 to 120 beats per minute. There exists a relation between the amount of TWA, the heart rate at which it appears, and the risk of sudden cardiac death (SCD). Therefore, it is important to develop better methods to detect TWA in ECG signals.

In this paper, we enhance an existing method for detecting TWA in ECG signals. We reduce the noise in the ECG signals adaptively by using dual-tree complex wavelet transform (DTCWT). Our method for detecting TWA is based on the Matlab code of the champion (Jubair Sieed) in the 2008 TWA challenge. We modified his Matlab code in a number of ways as shown in the full paper. We briefly describe the steps of our proposed method for detecting TWA in ECG signals here:

- 1) We perform moderate filtering to the input ECG signal $x_k(t)$, just as the original method.
- 2) Apply wavelet denoising to every ECG signal adaptively.
- 3) We find the R-peaks in the filtered ECG signal.
- 4) We calculate the T-peaks and their amplitude.
- 5) We find the TWA waveform. We use the median instead of the maximum for the T-wave magnitude of each lead.
- 6) We calculate the T-wave magnitude of the whole ECG signal with multiple leads.

In our experiments, we select to use the ECG signals provided by the 2008 TWA challenge, which contains one hundred multi-channel ECG records sampled at 500 Hz with 16-bit resolution over a ± 32 mV ranges. We perform comparisons among our proposed method and three existing methods, developed by Jubair Sieed, Renata Simoliunine, and Mahdi Zarrini. They have posted their Matlab codes on the 2008 TWA website. We select four metrics for measuring the quality of the detected T-waves: Spearman rank correlation coefficient, Kendall rank correlation coefficient, root-mean-square-error (RMSE), and cross correlation (CC). From Table 1, it can be seen that our proposed method performs the best, compared to the three existing methods.

Table 1. A comparison among three existing methods and the proposed method for detecting TWA in ECG signals. The best scores are highlighted in bold font.

Method	Spearman	Kendall	RMSE	CC
Jubair Sieed	0.6496	0.5156	21.7358	0.6580
Renata Simoliunine	0.3836	0.2868	22.6790	0.6187
Mahdi Zarrini	0.5034	0.3495	24.8296	0.5100
Proposed	0.7072	0.5861	20.4036	0.7074

SP039.2 - Electrical Left Atrial Conduction Delay with Focused Transesophageal Electrocardiography in Cardiac Resynchronization Therapy

Author(s): Matthias Heinke¹, Helmut Kühnert², Tobias Heinke³, Jonas Tumamos¹, Gudrun Dannberg²

¹Electrical And Information Technology, Medical Engineering, University of Applied Sciences Offenburg, Offenburg/GERMANY, ²Department Of Internal Medicine I, University of Jena, Jena/GERMANY, ³Healthcare Sector, Siemens AG, Rudolstadt/GERMANY

Cardiac resynchronization therapy (CRT) is an established biventricular pacing therapy in heart failure patients with left bundle branch block and reduced left ventricular ejection fraction, but not all patients improved clinically as CRT responder. Purpose of the study was to evaluate electrical left atrial conduction delay (LACD) with focused transesophageal electrocardiography in CRT responder and CRT non-responder.

Methods: Twenty heart failure patients (age 66.6 ± 8.2 years; 2 females, 18 males) with New York Heart Association functional class 3.0 ± 0.3 and 174.2 ± 40.2 ms QRS duration were analysed using posterior left atrial transesophageal electrocardiography with hemispherical electrodes. Electrical LACD was measured between onset and offset of transesophageal left atrial signal before implantation of CRT devices.

Results: Electrical LACD could be evaluated by bipolar transesophageal left atrial electrocardiography using TO Osypka electrode in all heart failure patients with negative correlation between 54.7 ± 18.1 ms LACD and $24.9 \pm 6.4\%$ left ventricular ejection fraction ($r = -0.65$, $P = 0.002$). There were 16 CRT responders with reduction of New York Heart Association functional class from 3.0 ± 0.29 to 2.1 ± 0.2 ($r = 0.522$, $P = 0.038$) during 9.41 ± 10.96 month biventricular pacing and negative correlation between 49.6 ± 14.2 ms LACD and $26.0 \pm 6.2\%$ left ventricular ejection fraction ($r = -0.533$, $P = 0.034$). There were 4 CRT non-responders with no reduction of New York Heart Association functional class from 3.0 ± 0.4 to 2.8 ± 0.5 ($r = 0.816$, $P = 0.184$) during with 13.88 ± 16.39 month biventricular pacing and no correlation between 75.25 ± 19.17 ms LACD and $20.75 \pm 6.4\%$ left ventricular ejection fraction ($r = -0.831$, $P = 0.169$).

Conclusions: Focused transesophageal left atrial electrocardiography can be utilized to analyse electrical LACD in heart failure patients. LACD correlated negative with left ventricular ejection fraction in CRT responders. LACD may be a useful parameter to evaluate electrical left atrial desynchronization in heart failure patients.

SP039.3 - Electrical Interatrial to Interventricular Conduction Delay Ratio with Focused Transesophageal Electrocardiography in Cardiac Resynchronization Therapy

Author(s): Matthias Heinke¹, Gudrun Dannberg², Tobias Heinke³, Bruno Ismer¹, Tobias Haber¹, Jonas Tumamos¹, Helmut Kühnert²

¹Electrical And Information Technology, Medical Engineering, University of Applied Sciences Offenburg, Offenburg/GERMANY, ²Department Of Internal Medicine I, University of Jena, Jena/GERMANY, ³Healthcare Sector, Siemens AG, Rudolstadt/GERMANY

Cardiac resynchronization therapy (CRT) is an established class I level A biventricular pacing therapy in chronic heart failure patients with left bundle branch block and reduced left ventricular ejection fraction, but not all patients improved clinically. Purpose of the study was to evaluate electrical interatrial conduction delay (IACD) to inter-ventricular conduction delay (IVCD) ratio with focused transesophageal left atrial and left ventricular electrocardiography.

Methods: Thirty eight chronic heart failure patients (age 63.4 ± 10.2 years; 3 females, 35 males) with New York Heart Association (NYHA) functional class 3.0 ± 0.2 and 171.71 ± 36.17 ms QRS duration were analysed using posterior left atrial and left ventricular transesophageal electrocardiography with hemispherical electrodes before CRT. Electrical IACD was measured between onset of P-wave in the surface ECG and onset of left atrial signal. Electrical IVCD was measured between onset of QRS complex in the surface ECG and onset of left ventricular signal.

Results: Electrical IACD and IVCD could be evaluated by transesophageal left atrial and left ventricular electrocardiography in all heart failure patients with correlation to 1.18 ± 0.92 IACD-IVCD-ratio ($r = -0.57$, $P < 0.001$; $r = 0.66$, $P < 0.001$). There were 32 CRT responder with reduction of NYHA class from 3.0 ± 0.22 to 1.97 ± 0.31 ($P < 0.001$) during 16.5 ± 18.9 month CRT with 75.19 ± 33.49 ms IACD, 78.91 ± 24.73 ms IVCD, 1.04 ± 0.66 IACD-IVCD-ratio and correlation between IACD and IACD-IVCD-ratio ($r = 0.84$, $P < 0.001$). There were 6 CRT non-responder with no reduction of NYHA class from 3.0 ± 0.3 to 2.9 ± 0.5 during 14.3 ± 13.7 month biventricular pacing, 50.0 ± 28.26 ms IVCD ($P = 0.014$), 1.92 ± 1.65 IACD-IVCD-ratio ($P = 0.029$) and correlation between 67.0 ± 24.9 ms IACD and IACD-IVCD-ratio ($r = 0.85$, $P = 0.031$).

Conclusions: Focused transesophageal left atrial and left ventricular electrocardiography can be utilized to analyse electrical IACD and IVCD in heart failure patients. IACD-IVCD-ratio may be a useful parameter to evaluate electrical left cardiac desynchronization in heart failure patients.

SP039.4 - Analytical geometry based parameters for studying repolarization variability in patients with myocardial infarction

Author(s): Muhammad A. Hasan, Sridhar Krishnan
Electrical And Computer Engineering, Ryerson University, TORONTO/ON/CANADA

Myocardial infarction (MI) is one of the leading causes of mortality throughout the world [1]. About 69,000 Canadians and 600,000 people in the United States die as a result of heart attack every year [2]. The myocardium cells of the heart are altered in ventricular repolarization after MI. Thus, studying variability in ventricular repolarization on a beat-by-beat basis has gained significant interest from clinicians and basic scientists. Indeed, the T-wave in the ECG signal refers to the ventricular repolarization and is believed to be a predictor for the risk of ventricular arrhythmias [3]. However, the beat-to-beat repolarization variability in MI patients has not been fully understood. Therefore, the purpose of this research is to study the beat-to-beat repolarization variability and to assess the predictive capabilities of geometry based parameters for studying repolarization variability in MI patients (79 patients) compared to healthy subjects (69 subjects). To study the beat-to-beat repolarization variability, we extracted some geometrical based T-wave parameters [T-wave amplitudes (h), distances between Q-wave onset to T-wave max (Q2Tmax), angles between T-wave max and T-wave end with respect to Q-wave (TmaxQTend)] as shown in Figure 1. The detailed methodology have been described in our recent article [3]. We quantified the standard deviation of the extracted parameters as a marker of repolarization variability, respectively for both MI patients and healthy subjects. Beat-to-beat repolarization variability (in all three extracted parameters) was found to be significantly higher in MI patients compared to healthy subjects. In conclusion, this research shows that the geometrical based parameters for repolarization variability may provide markers for separating MI patients and

can be utilized for diagnosis of volunteers with high-risk.

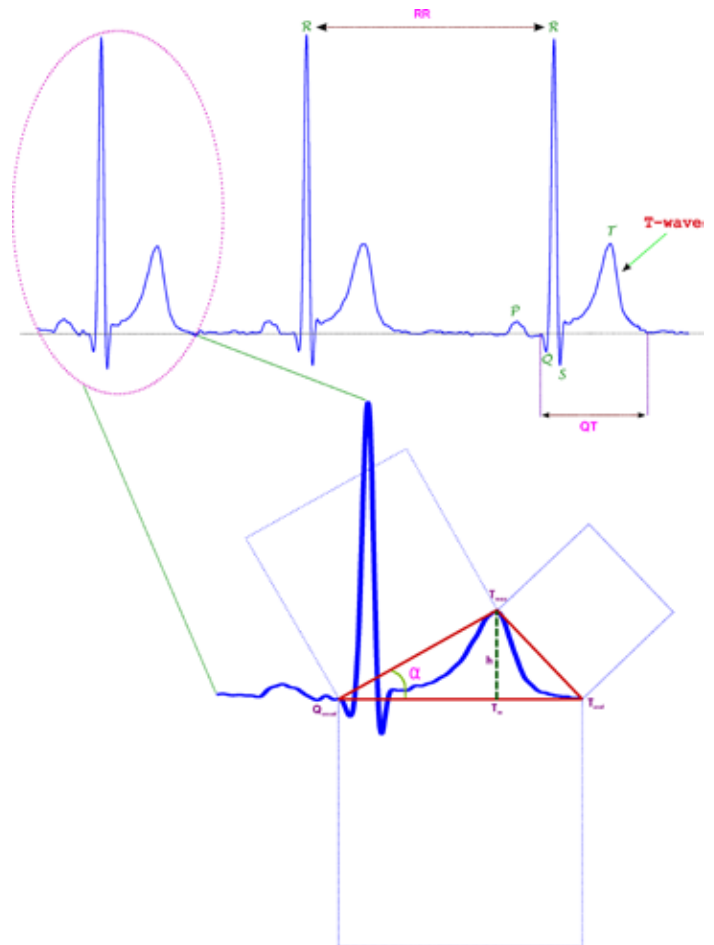


Figure 1: Beat-to-beat ECG. The computation of geometrical based T-wave parameters: T-wave amplitude (h), distances between Q-wave onset to T-wave max (Q2Tmax), angle between T-wave max and T-wave end with respect-to-Q-wave (TmaxQTend)[3].

References:

1. The top 10 causes of death. 2013, World Health Organization.
2. Heart Disease Facts. 2015 12 January]; Available from: <http://www.cdc.gov/heartdisease/facts.htm>.
3. Hasan, M.A., D. Abbott, M. Baumert, and S. Krishnan, Increased beat-to-beat T-wave variability in myocardial infarction patients Physiological Measurement, 2014. (submitted).

SP039.5 - Acute Mental Stress Detection via Ultra-short term HRV Analysis

Author(s): Rossana Castaldo¹, Leandro Pecchia¹, Paolo Melillo²
¹School Of Engineering, University of Warwick, Coventry/UNITED KINGDOM, ²Multidisciplinary Department Of Medical, Surgical And Dental Sciences, Second University of Naples, Naples/ITALY

Background: Acute mental stress reduces working performances and it is one of the first causes of cognitive dysfunctions, cardiovascular disorders and depression. Stress detection via short-term (5 minutes) Heart Rate Variability (HRV) analysis has been widely investigated in the last years. Recent improvements in wearable sensing devices and mobile computing raised a new research question: is ultra-short (2 minutes) HRV analysis as effective as the short-term

analysis to detect mental stress? This study aimed to answer this research question.

Methods: Short and ultra-short HRV analysis were compared in 42 healthy subjects (age 25-38 year) undertaking the widely adopted and highly-effective Stroop Color Word Test (CWT). HRV was extracted by ECG signals recorded during rest and stress session using a chest wearable monitoring device, the BioHarness M3 (ZephyrTech, NZ). According to previous literature on HRV and mental stress, 18 HRV measures were extracted and analyzed using validated software tools. However, among the 18 HRV measures, only those that changed significantly in the short-term were also investigated in the ultra-short term analysis. Variations in HRV measures in short and ultra-short term were compared using the statistical Wilcoxon significance test, because several measures were not normally distributed.

Results: The results of the current study proved that among the 18 HRV measures investigated, 10 HRV measures resulted significantly changed in the short-term analysis during mental stress. Among such 10 HRV measures, only 6 HRV measures presented a consistent behavior in the short and ultra-short registration: Mean RR, Low Frequency power (LF), Sample Entropy (Sampe), Short term and Long term fluctuation slope of Detrended fluctuation analysis (dfa1, dfa2) and Mean line length of Recurrence plot analysis (RPLmean). Particularly, Mean RR and dfa1 significantly increased during stress, while the other significantly decreased. In contrast, the remaining 4 HRV measures, changed significantly in the 5 min analysis but not in the 2 min analysis, although the trends were consistent. In fact, the ratio of LF and High Frequency power (HF) resulted increased during stress, while Correlation dimension (D2), Recurrence rate (REC) and Shannon Entropy (ShanEn) decreased. This can be explained by the fact that in less than 5 minutes the number of RR recorded is too low in order to observe significant changes. This can be verified enrolling more volunteers.

Conclusion: The current study showed that among the 18 HRV measures investigated, 10 resulted significantly changed during mental stress. However among those, only 6 changed consistently both in the short and ultra-short HRV analysis, while 4 resulted to be not significant in ultra-short term. This evidence suggested that in the shift from short to ultra-short HRV analysis, not all the features can be equally used and therefore further studies are needed to prove that HRV measures change significantly even during stress in the ultra-short term.

SP039.6 - Classification of Abdominal Fetal Electrocardiogram Recordings using Karhunen-Loève Decomposition

Author(s): Philip A. Warrick¹, Miguel A. Altuve²

¹Medical Research And Development, PeriGen Inc., Montreal/CANADA, ²Facultad De Ingeniería Electrónica, Universidad Pontificia Bolivariana, Bucaramanga/COLOMBIA

Maternal abdominal ECG acquisition is a non-invasive technique not usually common in clinical practice but with a growing interest since it could provide enough information to explore the cardiovascular condition of the fetus after the 20th week of gestation. Since the maternal and fetal cardiac activities are combined in the ECG signal, several challenges have to be surmounted to obtain a useful fetal ECG signal from the maternal abdominal ECG like the overlapping observed in time and in frequency of both components and the low signal-to-noise ratio of the signal. In the present study, the maternal and fetal activities were exploited through the decomposition of maternal abdominal ECG recordings using the Karhunen-Loève (KL) transform. Then, several feature sets extracted from the KL decomposition and from the ECG signal were combined in support vector machines classifiers to detect the presence and absence of a maternal and/or a fetal QRS complex from ECG segments of

250 ms duration. Results show that a fetal QRS complex was well detected when there was not overlap with a maternal QRS (sensitivity 88.8%, specificity 97.1%) while detection diminished somewhat when overlapping was present (sensitivity 90.7%, specificity 75.9%). Detecting maternal activity using the KL decomposition was a relatively simple task; the main goal of detecting the fetal activity was effectively achieved when the fetus activity occurred in isolation, but was a more difficult task when accompanied by temporally adjacent maternal activity.

SP039.7 - Dictionary Learning Algorithms For The Application Of Ventricular Arrhythmia Classification.

Author(s): Iman Kalaji¹, Krishnanand Balasundaram², Karthi Umapathy²

¹Electrical And Computer Engineering Dept., Ryerson University, Toronto/ON/CANADA, ²Electrical And Computer Engineering Dept., Ryerson University, Toronto/CANADA

Background:

The classification of cardiac arrhythmias such as ventricular tachycardia (VT) and ventricular fibrillation (VF) has been an important research topic in the signal processing field due to its lethal effects. Therefore, it is important to classify arrhythmias to deliver the appropriate treatments and prevent sudden cardiac arrests. Researchers presented an automated algorithm that express non-stationary signals by decomposing them into a linear expansion of different known mathematical functions that are well localized in both time and frequency domains. A family of the mathematical functions (atoms) creates a dictionary; the choice of the dictionary plays an important role in an accurate representation. Hence, researchers developed dictionary learning algorithms to create a learned dictionary using a training data to adapt its content to the given signals such that it provides a better approximation from an over complete redundant dictionary. In this work, due to the non-stationary nature of the electrocardiogram (ECG) signals during an arrhythmic event, these existing algorithms were used to classify between VT and VF signals using the dictionary learning algorithm LC-KSVD. Nine hundred and forty four surface ECG signal segments (four seconds each) from the MIT-BIH database were used for the classification derived from twenty three VF signals and ten VT signals.

Methodology:

The dictionary learning algorithm that is used in this study is called label consistent K-SVD. In the LC-KSVD algorithm, a discriminative dictionary is learned for sparse coding. It uses a class label of a training data as well as it associates label information with each dictionary item to enforce discriminability in sparse codes during the dictionary learning process (same class signals has similar sparse coding). Furthermore, it uses a label consistency constraint called "discriminative sparse-code error" and combines it with the reconstruction error and the classification error to form an objective function. The optimal solution of the objective function is efficiently obtained using the K-SVD Algorithm. This algorithm learns the dictionary, discriminative coding parameters, and classifier parameters for optimal linear classifier simultaneously.

Results and Conclusion:

Based on our analysis using the LC-KSVD algorithm to train an over complete hybrid dictionary consisting of cosine, symlet4, daubechie4 wavelet atoms, we were able to classify the VF and VT signals with an average of accuracy of 70.8% using LDA classifier. The results were validated with four fold cross-validations.

SP040 - Ergonomics, Wearable Sensors and Virtual Reality

TRACK 10: REHABILITATION MEDICINE, SPORTS MEDICINE, REHABILITATION ENGINEERING AND PROSTHETICS

SP040.1 - Working to live: The use of field studies and simulations to make workplaces safer

Author(s): Michele Oliver

School Of Engineering, University of Guelph, Guelph/ON/CANADA

Working to live: The use of field studies and simulations to make workplaces safer

Employers want to reduce accidents and overuse injuries amongst their workers but often they don't possess the required tools and information so they need to turn to research for answers. From a research perspective, first you need to understand the problem and then you can design a solution that will have the greatest impact in reducing or eliminating the problem. This can be accomplished through a combination of field and laboratory studies. To illustrate this I will present results from a series of laboratory and field studies designed to assess and solve occupational problems primarily amongst operators of heavy mobile equipment.

The thought process and studies that went into the design and development of a heavy equipment dynamic armrest will be described. The armrest was designed to translate and rotate in order to mimic natural pendulation of an operator's arm thus minimizing upper limb and neck muscle activity as they operate joystick controls.

Results from a comprehensive field study which concurrently assessed the biomechanical and physiological requirements of overhead crane cab operation in a steel mill will be discussed as will the companion study which utilized the results of the field study to set up a laboratory based simulation in order to determine if a camera based system could reduce musculoskeletal loading in the trunk, arms and neck for crane cab operators by allowing them to maintain a more neutral posture.

The final set of studies I will discuss describe the results of a series of field to lab to field methodologies developed to intelligently retrofit seats used in steel manufacturing mobile equipment in order to minimize operator exposure to whole-body vibration. When companies retrofit machines, seats are usually selected and implemented without an evaluation process based on actual machine and/or terrain specific vibration inputs to assess seat efficacy. In general, operators test and choose seats from a showroom rather than testing them in operating machines. Our research team utilized a person rated hexapod robot simulator to replicate field-based machine specific vibration to evaluate several commercially available seats to identify the best seat for the workplace application. The selected seat was successfully introduced back into the workplace resulting in reduced vibration exposure and improved worker comfort.

Finally, I will talk briefly about some of the ongoing work with our new driving and hexapod robot heavy equipment simulator facilities which bring together a multidisciplinary team of researchers from engineering, computer science and psychology.

SP040.2 - Pitch movement acceleration measures during the practice of virtual games in adolescents with Down syndrome

Author(s): Daniela Carrogi-Vianna¹, Paulo B. Lopes², Raquel Cymrot², Jefferson J.H. Almeida², Marcos L. Yazaki², Silvana Maria Blascovi-Assis³

¹Post Graduation In Developmental Disorders, Universidade Paulista and Universidade Presbiteriana Mackenzie, Sorocaba - São Paulo/BRAZIL, ²School Of Engineering, Universidade Presbiteriana Mackenzie, São Paulo/BRAZIL, ³Post Graduation In Developmental Disorders, Universidade Presbiteriana Mackenzie, São Paulo/BRAZIL

I. INTRODUCTION

Adolescents with Down syndrome (DS) present a range of motor difficulties. Therefore they do not specify a temporal-spatial pattern of muscle contractions, causing major difficulties to perform a task in time.

The Virtual Reality (VR) has been regularly used as a method of physical rehabilitation, which is based on the use of virtual games in order to enable the function of people with several types of disabilities.

The Nintendo® Wii™ console is the most used in the virtual rehabilitation of people with multiple disabilities.

The accelerometry has been used to establish measures of human movement, since it is an inexpensive, effective and feasible method, which has been widely used in scientific researches.

II. OBJECTIVE

Evaluating the characteristics of movement acceleration of upper limbs for adolescents with DS and adolescents with typical development, by playing bowling and golf of Nintendo® Wii™.

III. CASE STUDY AND METHOD

The study evaluated 21 adolescents diagnosed with DS (FDSG and MDSG) and 33 with typical development (FCG and MCG), of both genders (F and M), aged between 10 and 14. The data was gathered by using wireless capacitive triaxial accelerometers.

IV. RESULTS

For the data analysis, four groups were submitted to normality adherence tests, separate by gender.

A. Bowling game

In the significance level of 10%, there was adherence to the normal distribution of the maximum peaks of acceleration obtained by the four groups. The Medium acceleration per group were: FCG 70.51; MCG 70.37; FDSG 37.24; MDSG 45.33.

It was concluded that the groups presented significant statistical differences, with higher peaks of acceleration for MCG and FCG when they are compared with MDSG and FDSG.

B. Golf game

In the significance level of 10%, there was adherence to the normal distribution of the maximum peaks of acceleration, obtained by the three groups (FCG, MCG, FDSG). In the significance level of 10% there was no adherence to the Normal Distribution of the maximum peaks of acceleration for MDSG. The Medium acceleration per group were: FCG 56.80; MCG 74.80; FDSG 30.52; MDSG 45.12.

It was concluded that the groups presented significant statistical differences, with the highest peak of acceleration for the boys groups, which had superior average compared to the girls group, observed in both MCG and FCG, as well as in MDSG and in FDSG.

V. CONCLUSIONS

By efficiently using the accelerometry, it was possible to evaluate

the characteristics of the movement acceleration of the superior limbs of the population diagnosed with DS during the virtual bowling and golf games, using the Nintendo® Wii™ console. It was observed a better performance in every single evaluation for the control group, having lower acceleration in the movement of adolescents with DS. It was concluded that the use of Nintendo® Wii™ associated with the accelerometry technique may be an effective resource to evaluate movement acceleration patterns in population with DS.

SP040.3 - Movement Training and Assessment with 3D Virtual Reality for Parkinson's Disease Patient

Author(s): Chien-An Chen¹, Hsiao-Yu Lee², Zong-Syuan Huang¹, Chao-Chen Lo¹, Jia-Jin Chen¹, Yu-Lin Wang³, Kao-Chang Lin³
¹Biomedical Engineering, National Cheng Kung University, Tainan/TAIWAN, ²Far East University, Tainan/TAIWAN, ³Chi Mei Hospital, Tainan/TAIWAN

Balance problems such as inability to maintain stability and postural transition are common in patients with Parkinson's Disease (PD). In clinical, visual cues are used as rehabilitation program in improving postural stability. Ball catching movement is considered a kind of suitable training program for PD patients because of its characteristics of eye-hand-foot coordination. Furthermore, studies have shown that optical flow could provide motion perceptions and improve movement performance of PD patients. The purpose of this study was to develop a 3D virtual reality (VR) training system for providing optical flow information during catching virtual balls under standing and one-step forward movements for subjects with PD. Fifteen PD participants were recruited from local medical center. The effects of optical flow on postural stability were evaluated by standing and one-step forward task using our 3D VR system providing virtual catching ball with and without optical flow. The arm-trunk movement and trunk movement were utilized as the assessment indices of balance and postural control by inertial sensors attached on waist and bilateral of wrists. Our results showed better arm-trunk coordination and higher similarity of arm symmetry with smoother movement pattern, greater trunk sway, and better postural stability index under the standing task with optical flow. Moreover, PD patients also spent substantially less duration prior to gait initiation and achieved greater inclination angle on one-step forward task. The balance training system accompanied with evaluation system demonstrated that arm-trunk control and balance on ball catching performance of PD patients could be improved with optical flow information.

Keywords: Parkinson's disease, virtual reality, balance, optical flow

SP040.4 - Arm angle detection in egocentric video of upper extremity tasks

Author(s): Jirapat Likitlersuang, José Zariffa
 Institute Of Biomaterials And Biomedical Engineering (ibbme), University of Toronto, Toronto/ON/CANADA

Background: Upper limb function is fundamental to most activities of daily living (ADL), and can be dramatically impaired after neurological injuries, such as spinal cord injury. Currently there is no viable method to assess and monitor hand function once the patient has returned to the community after rehabilitation. Our solution is to track hand use in the community by developing a computer vision (CV)-based wearable sensor using egocentric cameras, in order to capture information about a person's level of independence and reliance on attendant care. Such a system needs to be able to differentiate object manipulations performed by the user from those performed by a caregiver, as well as the user's right and left hands. The angle of the arm in the video is important in this classification. Here we describe and compare three methods for detecting arm angles in egocentric view. **Methods:** Following hand detec-

tion, Method I uses a Haar-like feature to compare the contents of a rectangle extending from the hand to two parallel rectangles on either side, rotating these through 360 degree range. Method II is based on Hough line transforms and attempts to determine which of the detected lines passing through the hand correspond to the edges of the sleeve. Method III detects the contour of the sleeve based on a colour histogram obtained through a calibration step. A least squares fit is then applied to the detected sleeve to determine the angle of the arm. The three methods were tested by comparing their output to manually measured angles, in 120 frames of recorded egocentric video consisting of 4 ADLs from 3 different able-bodied subjects. **Results:** Based on absolute error, Method III was shown to have the best performance with a mean absolute error of 23.70 ± 22.89 degrees. This was followed by Method I with the mean absolute error of 34.79 ± 38.48 degrees and Method II with the mean absolute error of 68.76 ± 58.01 degrees (Fig. 1). **Conclusion:** While Method III had the smallest error, it required a calibration step to determine the colour of the sleeve, and this makes this method less practical compared to Method I, which does not require any calibration and still had a comparable error. We have demonstrated that a Haar-like feature method can easily be integrated with hand detection to determine arm angle in an egocentric CV-based wearable sensor for detecting hand usage at home.

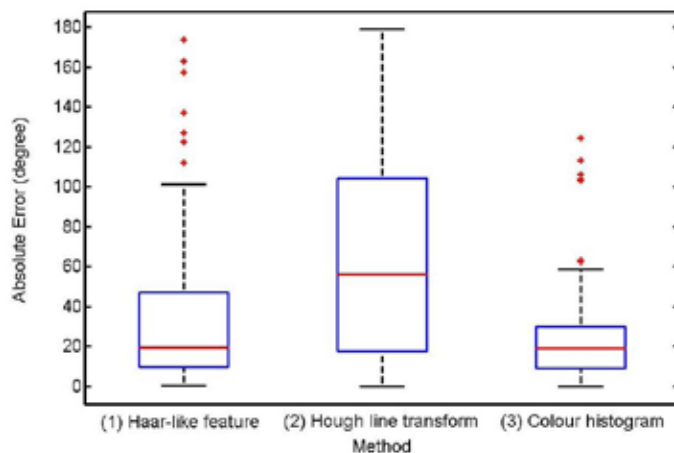


Fig. 1 Absolute error distribution of the three tested methods. Outlier frames are denoted by plus symbols (+).

SP040.5 - Development of an image-based calibration technique for use with non-ideal postures in the assessment of kinematics using wearable sensors

Author(s): Jan Andrysek, Monica D. Gomez
 Institute Of Biomaterials And Biomedical Engineering, University of Toronto, Toronto/ON/CANADA

Introduction

Wearable sensors are emerging low-cost alternatives to expand the current gold-standard camera-based assessment of kinematics, allowing for measurements in real-life conditions and environments. MVN BIOMECH Awinda system is an example of a commercial wearable sensor system used to analyze whole body kinematics. However, to calibrate the device, an ideal upright position known as "Neutral Posture," or "N-Pose," must be attained. Hence, these sensors have limitations in the rehab field where muscle weakness, bone deformity, sensory loss, pain or impaired control hinders or makes it impossible to attain N-Pose. Developing a calibration technique that adjusts the model to account for actual orientation and position of body segments, versus the assumed N-Pose, will improve the estimation of kinematics. Therefore, this study aims to produce calibration parameters which will be used to adjust the "N-

Pose". Here, Kinect sensor is used to extract body segment lengths, knee, hip and ankle angles as the calibration parameters.

Research Objectives

Obj.1 Understand how non-ideal calibration postures affect the accuracy of lower body kinematics estimation.

Obj.2 Develop an image-based calibration technique using Kinect to acquire calibration parameters.

Methods

Obj.1 A pilot study was conducted to assess the accuracy of knee and ankle angles in the sagittal plane of a participant's gait. The MVN BIOMECH Awinda system was used to measure patient's kinematics after calibrating the system with **a**) the N-Pose and two non-ideal calibration postures: **b**) bent knees and **c**) standing on tip-toes.

Obj.2 The depth sensor Kinect for Windows is used to determine the position of optical markers placed on participant's body landmarks. With this information, distance between markers is estimated and then used to find joint centers. Next, joint centers are connected to form lines that will represent the body segments, and from these segment lines angles are calculated using the dot product to find the angle between two vectors. In combination with these positions and angles (calibration parameters), sensor data collected from participant's gait using the MVN BIOMECH's lower body configuration are used to re-estimate gait kinematics.

Preliminary Results

Obj.1 Results showed that for both cases the difference between angles obtained in **(a)** and **(b)** (40.88degrees) and **(a)** and **(c)** (53.88 degrees) is consistent throughout the gait cycle; and the coefficients of multiple correlation [3] represent good level of similarity between **(a)** and **(b)** (0.98) and between **(a)** and **(c)** (0.93). These results show that the inaccuracy of kinematics after calibrating with non-ideal postures is mainly due to the offset between waveforms. This suggests that the proposed calibration technique for Obj. 2, which is in design stage, can provide a good solution for the calibration problem.

Clinical Significance

Improving the calibration process of these wearable systems to account for non-ideal postures makes them suitable for a variety of patient populations. This technique will ultimately provide clinicians and researchers with a valuable tool to analyze the kinematics in real life environments.

SP041 - Brain Computer/Machine Interfaces

TRACK 11: NEUROENGINEERING, NEURAL SYSTEMS

SP041.1 - Cross-subject and Cross-gender Emotion Classification from EEG

Author(s): Jia-Yi Zhu, Wei-Long Zheng, Bao-Liang Lu
Computer Science And Engineering, Shanghai Jiao Tong University, Shanghai/CHINA

Emotion is a general definition for subjective cognition experiences, including psychological and physiological states aroused by one's feeling, thinking, and behaviors. With the development of artificial intelligence, affective computing based on computer systems is considered to make human-machine interaction more friendly and convenient. Recently, progresses of brain-computer technology encourage researches on EEG-based emotion recognition in the field of neuroengineering. Previous studies have indicated that EEG does change with emotional states in specific patterns. To our best knowledge, however, EEG models used in the existing studies were almost subject-dependent. Thus, there is no definite conclusion on whether these patterns are universal across different subjects.

The main goals of this study are to find a subject-independent EEG model for emotion classification and examine gender differences of EEG patterns as one of the major factors affecting the performance of cross-subject models. In this paper, we use movie clips as stimuli to evoke three emotional states: positive, neutral, and negative. We adopt differential entropy as features, and apply linear dynamic system to do feature smoothing. The average in-subject classification accuracy of SVM is 90.97% with five frequency bands on 15 subjects (7 males and 8 females), while the average cross-subject classification accuracy is 64.82% using data from 14 subjects as training set and data from the rest one subject as testing set. This implies that different persons do share similar patterns for EEG changing with emotions, but there are still some individual differences during emotion processing. We also expand the training set from one subject to 14 subjects and find the average accuracy will then continuously increase with some slight ups and downs. Therefore, we can get an observation: A universally applicable EEG model for emotion recognition can be trained using data collected from enough subjects. Moreover, fuzzy-integral-based combination method is used to combine models across frequency bands and get an average improvement of 8%.

We choose data from the same or different genders to do cross-gender emotion classification, seeing Fig. 1. The better performance of using training and testing samples both from female subjects partly implies that there must be gender differences during emotion processing. Also, for female testing subjects, using single female model, or combining male and female models would both improve the performance of cross-subject emotion classification. Moreover, it can be partially illustrated that the universal EEG pattern is likely to behave more obvious among female subjects.

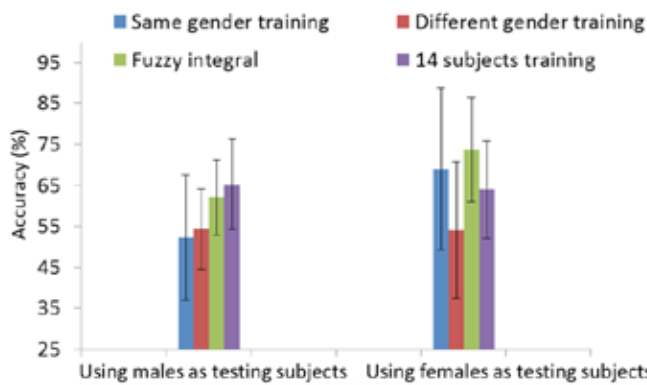


Fig. 1. Average accuracies of cross-gender emotion classification

SP041.2 - Comparison of Classification Methods for EEG-based Emotion Recognition

Author(s): Wei-Long Zheng¹, Roberto Santana², Bao-Liang Lu¹
¹Computer Science And Engineering, Shanghai Jiao Tong University, Shanghai/CHINA, ²University of the Basque Country, San Sebastian/SPAIN

Emotion plays an important role in human communications and decision making. However, the modeling and mechanism of emotions still remain a challenge problem. Besides logical intelligence, emotional intelligence is proposed to narrow down the emotional gap between humans and computers in artificial intelligence. So far, many approaches to emotion recognition have been proposed based on different modalities. Among these approaches, emotion recognition from EEG allows direct assessment of emotional states of users, which has gained more and more attention recently.

In recent years, great progresses in EEG-based emotion recognition have been achieved and various methods have been studied and evaluated. However, a major limitation of these methods is that only a handful of features and classifiers have been compared in each study. Moreover, most studies evaluate their methods on different, usually small datasets, so the results of these studies cannot be compared directly due to different setups of experiments. It is difficult to judge which types of features and classifiers are most suitable for EEG-based emotion recognition. Although recently Jenke et al. performed a systematical comparison of feature extraction and feature selection methods in their work, there is still a lack of detailed comparisons of classification methods for emotion recognition from EEG.

In this paper, we review different classification methods for emotion recognition from EEG and perform a detailed comparison of these methods on a relatively larger dataset of 45 experiments. Since different classifiers could have different discriminative power for emotion classification, we further propose to combine different classifiers using stacking to improve the performance. Experimental results show that the combination of classifiers using stacking can achieve higher accuracies than single classifiers.

To investigate critical brain areas and critical frequency bands for promoting our understanding of emotion processing mechanisms, we perform a contrastive analysis of the weights derived from the classifiers as a way to detect and extract the most relevant features for classification. We find that the relevant features of different classifiers are similar. These results show that most relevant channels locate on the lateral temporal and prefrontal brain areas and the critical frequency bands are beta and gamma bands. Additionally, the weights of Logistic Regression-l2, SVM-linear and SVM-RBF indicate some relevant features in delta bands except for Random Forest.

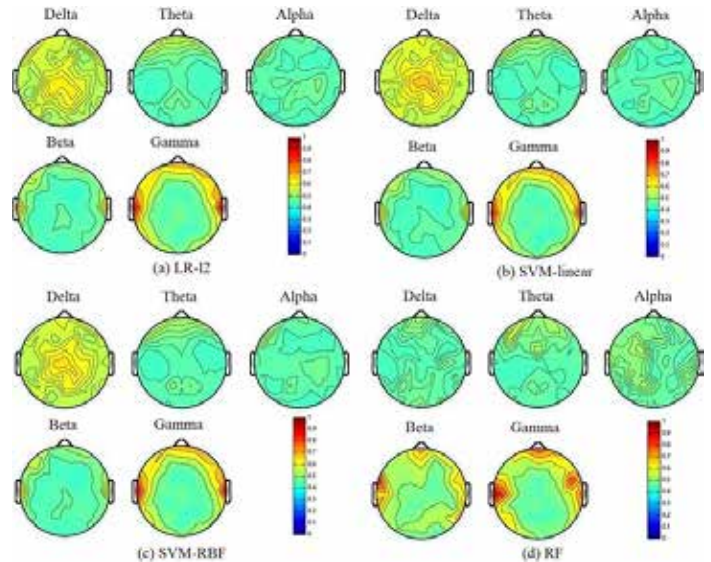


Fig 1. The weight distribution of LR-l2, SVM-linear, SVM-RBF and Random Forest.

SP041.3 - A Brain Computer Interface (BCI) based on intermittent photic-stimulation using multiple coherence to command detection

Author(s): Aluizio D’Affonseca Netto, Antonio M.F.L. Miranda De Sa, Antonio F.C. Infantosi
 Biomedical Engineering, Federal University of Rio de Janeiro, RIO DE JANEIRO/BRAZIL

Brain Computer Interfaces (BCI) are systems that are capable of translating information from the neuronal activity of a subject into controlling signals for devices. BCI may be either passive or active. This latter uses evoked responses to external, sensory stimulation (e.g. intermittent photic stimulation). Active BCIs exhibit reduced complexity and processing time in comparison with passive interfaces. This occurs due to the fact that the evoked responses occur at a known stimulation, which simplifies the detection algorithm. The present work aims at using a modified algorithm for the multiple magnitude-squared coherence (MMSC) estimation for increasing both sensibility and specificity of the decision system, as well as to reduce the response time. The algorithms for multiple coherence calculation were developed using the sweep operator over the augmented spectral matrix. The algorithms for real time calculation and for obtaining BCI controlling signals with lowest latency. EEG from five subjects has been collected using the following monopolar derivations according to the 10-20 International System: O1, O2, P3, P4, C3, C4, Pz and Cz. The hardware was developed specifically for BCI interfaces based on visual stimulation. Each subject was seated in a comfortable armchair with a monitor containing four distinct LEDs each of which flickering at a distinct frequency (24, 28, 32 and 36 Hz). The multiple coherence detector was used to determine to which LED the subject was looking at and this result was used for a BCI that controlled the cursor movement. The MMSC-values were calculated with segments of L = 0.25 s of EEG signal segments. The proposed system is capable of detecting responses within a time lag that is below 4.54 s with average area under the ROC curve equal to 0.91. For a 24 Hz stimulation frequency, the system had sensitivity and specificity equal to, respectively, 88.3 % and 73.2 %. Fig.1 shows a volunteer controlling the cursor position using the BCI system.

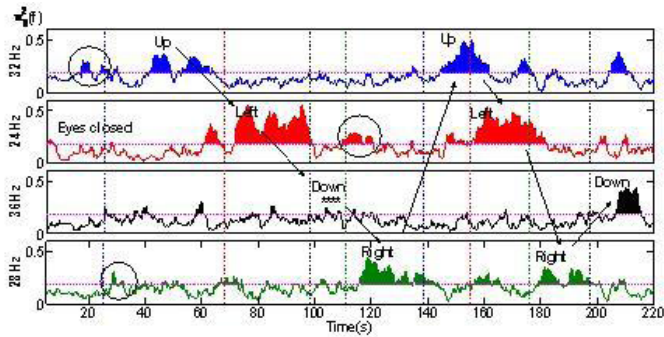


Fig.1: Temporal evolution of the MMSC of a volunteer focusing attention on different stimulus. Horizontal line: detection threshold for a significance level of 5% (0.182). Vertical line indicates the instant of time the volunteer pressed the keyboard indicating the direction of the desired movement to gaze at one of the LEDs (blue for up, red for left, black to green to the right and below). (*) command is not detected, i.e., false negative. The circled is example of false positive. Arrow: sequence of volunteer commands.

SP041.4 - Volitional modulation of neural activity to control a 2 degree-of-freedom brain-machine interface in a rat model

Author(s): Martha G. Garcia¹, Hector Vargas-Perez², Mary K. Nagai³, José Zariffa¹, Milos R. Popovic¹

¹Institute Of Biomaterials And Biomedical Engineering, University of Toronto, Toronto/CANADA, ²Department Of Molecular Genetics, University of Toronto, Toronto/CANADA, ³Toronto Rehabilitation Institute, University Health Network, Toronto/CANADA

Operant conditioning of neural activity is a novel paradigm to control brain-machine interfaces (BMI) that has emerged from the need of creating BMI systems that feel natural and intuitive to the user. The first demonstration of such systems started over 40 years ago with a series of studies in which monkeys volitionally modulated single neuron activity through biofeedback. These systems exploit the volitional drive on cortical neurons that allows them to modify their tuning properties through a process of reward-modulated spike-timing-dependent plasticity. Recent studies have employed this alternative strategy to control motor neuroprosthesis and computer cursors, proving that single neuron activity is a promising signal for BMI control because of its greater simplicity to implement and to use.

The objective of this study was to evaluate a novel paradigm to elicit volitional modulation of neural activity in a rat model to control a two-degree of freedom BMI. In order to do this, we implanted microelectrodes in the motor cortex and trained the rat to modulate the activity from one selected neuron and maintain the firing target rate for up to 3 seconds. When the rat reached a low-rate target a food pellet was dispensed, while sucrose solution was dispensed with a high-rate target. The rat was free to choose whichever reward it wanted to obtain during the conditioning sessions. Biofeedback was provided in real-time through a LED that varied in brightness. We increased the difficulty of the task by incrementing/decrementing the firing rate thresholds or by increasing the hold time every 5-10 minutes.

In a previous study, we showed that the intrinsic spiking properties of cortical neurons determine the performance in a BMI task. We found that fast-spiking neurons are able to quickly adapt to arbitrary rules, while regular-spiking neurons cannot adapt in short periods of time.

In this study, the rat successfully learnt to control two degrees of freedom with fast-spiking neurons. In total, 7 neurons were used to control the BMI. Some interesting observations include: (1) the rat initially preferred to obtain food pellets (low-rate targets) in the first

half of the session and abruptly switched to sucrose solution (high-rate targets) in the second half of the session; (2) the rat successfully suppressed the activity of the neuron and at the same time, was then able to generate bursts of high activity with the same neuron and maintain it for as long as 3 seconds; (3) in the last 3 days of training, the rat no longer showed such marked reward preference during the sessions, but instead learnt to balance the amount of food/sucrose solution rewards obtained in each experiment.

Further work is needed to probe the capabilities and limitations of using operant conditioning of neural activity to develop robust and reliable BMI systems, but we firmly believe this paradigm holds great promise to restore movement after paralysis.

SP041.5 - Electroencephalography-Based Off-Line Prediction of Specific Grasping Actions Performed with the Same Hand: Towards Integration of Brain-Computer Interfaces and Functional Electrical Stimulation Therapy

Author(s): Cesar Marquez-Chin¹, Kathryn Atwell¹, Milos Popovic²

¹Research Department, Toronto Rehabilitation Institute University Health Network, Toronto/CANADA, ²Institute Of Biomaterials And Biomedical Engineering, University of Toronto, Toronto/CANADA

Objectives

There is growing interest in the use of brain-computer interfaces (BCI) for rehabilitation of neurological conditions such as stroke. We have developed functional electrical stimulation (FES) therapies and technologies for almost two decades achieving remarkable restoration of upper limb function. In FES therapy, patients attempt specific functional tasks (e.g., lifting a mug from a table) and, simultaneously, the movement is facilitated with electrical pulses applied to the arm/hand. We are now combining our FES systems with a BCI to assess the efficacy of FES therapy when matching the intended and facilitated movements. The objective of this work was to explore the possibility of identifying specific hand grasps, performed with the same limb, using EEG analysis.

Materials and Methods

Fifteen participants (mean age was 32 and six were women) with no known neurological conditions performed six hand movements in a ready-go-stop sequence while we recorded EEG signals (C1, C2, C3, C4, Cz, F3, F4, and Fz). Four of the movements are commonly trained during stroke rehabilitation (two-finger pinch, palmar and lumbrical grasps, and hand opening — all finger extension). The movements were repeated at least 30 times with the participants' self-identified dominant hand, and four of the subjects repeated the experiment with their non-dominant hand.

The time-resolved spectra (256-sample Hamming window, 128 sample overlap, 256-FFT) between 1 Hz and 50 Hz for all EEG recordings were smoothed and correlated with a hyperbolic tangent function to identify decreases in power (typically associated with the preparation and execution of voluntary movement). The spectral components and time ranges with the largest correlation values resulted in movement-specific maps that were used as features to implement a nearest-neighbour classifier.

Results

For all participants, at least three dominant hand movements were identified correctly with accuracies between 64%-75%, and 67%-85% when the non-dominant hand was used. We found a difference in accuracy for only one of the movements when the analysis was limited to only ipsilateral or contralateral electrodes. Classification of the different intended movements took place 1.2s (+/- 0.8s) to 0.7s (+/- 0.9s) before dominant hand movement onset and 0.7 s (+/- 0.9 s) to 0.4 s (+/- 0.4s) for non-dominant hand movements.

Conclusions

Our results are comparable to other reports describing the prediction and identification of movements performed with the same limb (92% [1] and 45% [2] with 163 and 128 EEG electrodes, respectively). However, the work presented here uses a maximum of eight EEG electrodes increasing its viability for use in a clinical environment. Our next steps will consist of testing the presented procedure with stroke and spinal cord injury patients. To the best of our knowledge, this is the first report on the analysis of EEG activity to predict specific hand movements targeted in stroke and spinal cord injury rehabilitation performed with the same limb, .

1. Zhou J et al. *Comput Biol Med.* 2009 May;39(5):443–52.
2. Xiao R, Ding L. *Comput Math Methods Med.* 2013; Article ID 243257, 10 pages, 2013.

SP041.6 - Wireless Distributed Intracortical Neural Interfacing: A New Approach for Brain Machine Interfaces

Author(s): Alireza Zabihian¹, Amir Massoud Sodagar², Mohamad Sawan¹

¹Electrical Engineering, Polytechnique Montreal, Montreal/CANADA, ²Electrical And Computer Engineering, K.N.Toosi University of Technology, Tehran/IRAN

Brain Machine Interfaces (BMIs), as promising devices for assisting patients with motor disabilities and/or neurological injuries, demand for high-performance recording/simulating capabilities in terms of speed, quality, and quantity, i.e. higher bandwidth, signal-to-noise ratio for neural signal, and interfacing area on cerebral cortex. In this abstract, we present the architecture of a wireless network of implantable microsystems.

There are three major approaches to electrically interface with the brain. They differ in spatial resolution, quality level of signal, and practical area to interface with. Electroencephalography (EEG) is a major approach to record brain activities using multiple surface electrodes on the scalp with poor spatial resolution. Electrocorticography (ECoG) utilizes surface electrodes mounting directly on exposed surface of cerebral cortex. Single-Unit Neural Interfacing is a method to measure single neurons electro-chemical activities (action potentials) using a microelectrode array system. In the last decade, Intracortical Neural Interfacing using wireless implantable microsystems with microelectrode arrays has realized wireless neural prostheses with higher spatial resolution, higher signal quality, and feasibility of freely movement of patient under study. But, in fact, the effective area covered with microelectrode arrays is too limited for most relevant applications.

Here, we propose a novel neural interfacing approach which is as high-performance as intracortical neural interfacing in terms of spatial resolution, quality of signal, and feasibility of freely movement; as well, similar to EEG and ECoG, it covers a significant area of cerebral cortex. The idea is to network several wireless implantable microsystems, which we call it Brain-ASNET: “Brain Area Sensor Network” (Fig. 1). To realize the proposed idea, there are many design aspects to be considered, including network architecture and protocol, and sensor node form factor and power consumption. We choose a star network topology, an ad-hoc TDMA MAC protocol, and OOK modulation in 902-928MHz ISM frequency band. The Custom Integrated Circuit (CIC) is designed and laid-out in an IBM 0.13 μ m CMOS process. The post-layout simulation results show energy efficiency of the designed ad-hoc network protocol and low power dissipation of the CIC. The whole chip, including all functional and peripheral integrated components, consumes 138 μ W and 412 μ W, at 1.2V, configured in a synchronized network as a sensor node and the coordinator, respectively.

At the congress, we will present design and implantation aspects of the proposed network, including proposed network architecture and protocol design, the CIC design, and a conclusion will be presented.

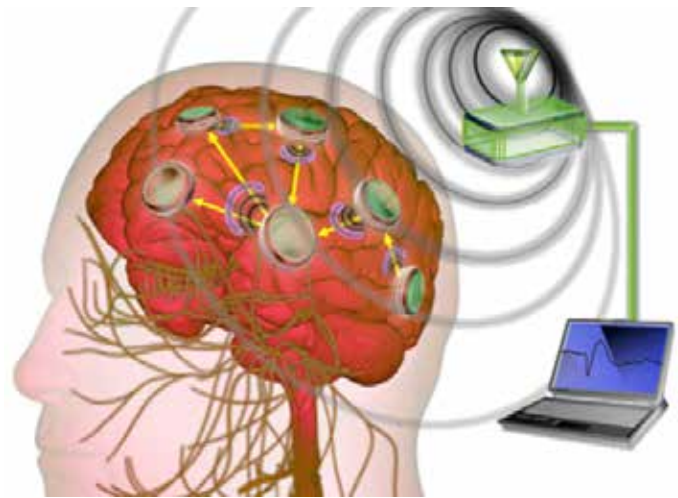


Fig. 1. Illustration of the proposed Brain-ASNET approach

SP041.7 - Design and construction of a brain-computer interface for applications in neuro-robotics

Author(s): Alma R. Méndez Gordillo, Marco A. Espinosa Medina, Miguel Villagómez Galindo
Mechanical Engineering, Universidad Michoacana de San Nicolás de Hidalgo, Morelia/MEXICO

A brain computer interface (BCI) is a device that helps people with motor impairments, to communicate externally using the electrical activity of the brain without the assistance of peripheral nerves or muscle activity, promising further improved quality of life of patients. This investigation presents the design and construction of a neural interface in order to study the signals produced by the brain, using a Mindwave mobile prototype device, which measure spectra power of EEG (Electroencephalography, i.e. alpha waves, beta waves, etc.), NeuroSky eSense meters (attention and meditation) and eye blinks in a safety way. As the main objective is to control 3 axis biomedical devices, particularly a robotic arm Model: K-680 Steren, it is important to highlight the contribution of this work in the control, which will be held through Matlab and ArduinoIO programs.

SP042 - Technology Management Programmes and Equipment Management Systems

TRACK 16: CLINICAL ENGINEERING, CLINICAL PHYSICS, AND PATIENT SAFETY

SP042.1 - Medical device systems Health Technology Management (HTM) strategies and best practices

Author(s): Tom Judd

Kaiser Permanente Clinical Technology, Atlanta/GA/UNITED STATES OF AMERICA

Medical device systems Health Technology Management (HTM) strategies and best practices are now well established in most first world and many developing countries¹. Plans are underway to address identified gaps in HTM, e.g., appropriate equipment selection and lifecycle management. One approach is the 25 years of HTM Seminars provided by WHO-PAHO, IFMBE CED, and ACCE to 70 countries².

There is a new emerging challenge in this space as well, that is the requirement for medical device integration into electronic health records to improve quality and safety of care³.

The Keynote will review this HTM progress, gaps, and new challenges. It will provide a framework to move us forward in collaborative fashion.

¹Health Technology Management in Less-Developed Countries: An Untold Success Story, Authors: Binseng Wang, Thomas Judd, Ismael Cordero, Antonio Hernandez, Adriana Velazquez, unpublished 2011.

²American College of Clinical Engineering (ACCE) International Workshops, see <http://accenet.org/International/Pages/Default.aspx>

³White Paper: New Opportunities for BME/CE Health IT Education, May 2014; Contributors: Elliot Sloane PhD, Joseph P. Welsh JD, and Thomas Judd MS.

SP042.3 - Development of a scoring system to support medical equipment replacement prioritization using the Analytical Hierarchy Process (AHP)

Author(s): Paul Prowse, Kyle Eckhardt, Sarah Kelso

Clinical Engineering, Winnipeg Regional Health Authority, Winnipeg/CANADA

The Winnipeg Regional Health Authority's (WRHA) current approach to medical equipment prioritization is based largely on anecdotal evidence and qualitative information provided by the staff who use the equipment. A group of stakeholders representing clinical programs determines how the equipment is ranked for replacement through a peer-to-peer democratic process. However, the voters have little understanding of the true urgency of equipment replacement for the other clinical programs, so votes are won based on the ability of the program to present a compelling argument. The WRHA's Clinical Engineering Program sought to develop a universal scoring system based on objective criteria to assist in this prioritization process.

A literature review revealed several scoring systems that have been developed utilizing a wide variety of criteria. From these criteria, four were selected for consideration: age, repair cost, reliability, and risk

level. These were selected because they are frequently reported as predictors of replacement priority, and also because they could be universally applied to all equipment based on information available in our in-house Computerized Maintenance Management System (CMMS).

Previous studies have applied relative importance weightings to their chosen criteria based on expert opinion. Few have used a systematic approach, however, to determining the respective weightings. In the newly developed system, the pairwise comparison approach of the Analytical Hierarchy Process (AHP) is employed to determine weights that accurately represent each factor's contribution to a device's replacement urgency. The AHP was completed by several multidisciplinary groups including clinical engineers, nurses, managers, and administrators. The results from each group and the literature review were averaged to establish the final criteria weightings.

With the weightings established, a score from 0 to 100 was applied to each electro-medical asset with a purchase value greater than \$10 000 and recorded in our CMMS. A report of this equipment was distributed to each clinical program to highlight the replacement priority of their equipment as defined by this system. Provided with objective information, decision makers can be better informed about equipment that needs replacement.

Limitations of this system relative to our regional CMMS will be explored alongside the advantages of this process over those developed previously. A summary of the effectiveness of our work in the first year and an outline of our second phase goals will be presented.

SP042.4 - Multi-criteria decision analysis to redesign an Italian Clinical Engineering Service under specific needs and regulation requirements

Author(s): Irene Lasorsa¹, Giulia Abis¹, Barbara Podda², Agostino P. Accardo¹

¹Department Of Engineering And Architecture, University of Trieste, Trieste/ITALY, ²Clinical Engineering Service, ASL 5, Oristano/ITALY

The aim of this study is to fulfill the need of re-engineering the Clinical Engineering Service in an Italian ASL (Local Health Authority) located in Sardinia, in accordance with the Italian regulations for healthcare.

Even if methods for processes redesigning in healthcare organizations are available in the literature, there are no recent evidences of their application in Clinical Engineering Services.

Among the multi-criteria techniques, in this work PAPRIKA was used, since it is an easy-to-use and intuitive method for multi-criteria decision making, based on decision-makers' preferences.

We identified the decision makers' criteria (Table 1) to be fulfilled and four different preference levels for each criterion (Table 2), as inputs of the method. Moreover four different scenarios were identified and, for each scenario and criterion, the decision makers selected the most suitable level. In order to reduce the number of pairwise comparisons among the preference levels associated to the identified criteria, the online software 1000minds, implementing the PAPRIKA method, was used.

After 460 steps, the software allowed to rank the four possible scenarios. The results show that the Alternative A2 (Outsourced management of some of the activities), weighting 68.8%, represents the best solution for the ASL, followed by the Alternative A1 (current situation), weighting 60.8%, and the Alternatives A3 (Compliant to the Italian Ministerial Program SIGAE 4, CONSIP) and A4 (FULL

RISK contract), both weighting 28.2%.

The application of the PAPRIKA method for redesigning the Clinical Engineering Service in compliance with national and regional requirements for hospital accreditation can be considered successful.

Table 1 - Criteria of interest

Criteria	Description
C1	Dimensioning of human resources at CES
C2	Effects on the organization: work processes
C3	Supervisory capacity of the administration
C4	Quality of provided services
C5	Emergency and urgent problems resolution
C6	Annual costs the for biomedical technologies management

Table 2 - Levels of preferences for each Criterion

Criteria	Level	Description
C1	L1	2 engineers, >3 technicians
	L2	1 engineer, 3 technicians
	L3	1 engineer, 2 technicians
	L4	1 engineer, 1 technician
C2	L1	A unique company in charge of all the activities
	L2	A unique company in charge of MP and VSE
	L3	Different companies in charge of the activities
	L4	CES in charge of all the activities
C3, C4	L1	Excellent
	L2	Good
	L3	Sufficient
	L4	Insufficient
C5	L1	Always guaranteed
	L2	Always guaranteed during working hours
	L3	Occasionally guaranteed during working hours
	L4	Never guaranteed
C6	L1	≤2million€
	L2	>2million€, ≤2,25million€
	L3	>2,25million€, ≤2,5million€
	L4	>2,5million€

SP042.5 - Developing a system to support equipment repair versus replacement decision making

Author(s): Sarah Kelso, Petr Kresta
Clinical Engineering Program, Winnipeg Regional Health Authority, Winnipeg/CANADA

Within the Winnipeg Regional Health Authority there is currently no system in place to guide the process of deciding whether a device suffering a major failure should be repaired or replaced. While the question may not arise frequently, it was determined that a consistent, methodical approach would significantly improve the confidence of decision makers and equipment owners, when Clinical Engineering recommends proceeding with a costly repair, or equipment replacement.

The development of a repair versus replace decision making process encompassed three major pieces of work: define a maintenance approach, establish a process for decision making including factors for consideration, and identify the repair cost threshold at which device replacement should be seriously considered.

Thorough analysis of the repair history data for four sample fleets of equipment indicated a general trend of modest increases in repair costs with age over the study period, but no statistically significant relationship between age and repair cost or repair frequency was identified. Therefore, maintenance/replacement approaches based on the assumption that the equivalent annual costs of maintenance will surpass the projected equivalent annual cost of replacement cannot be directly applied.

A two-phase process for repair versus replacement decision making was developed. The first phase relies on a single repair cost limit, set at 50% of the device acquisition cost, to flag the most costly repairs for further review.

The second phase incorporates factors used for equipment replacement planning, determined through an extensive literature review, to evaluate whether a specific case supports repair or replacement. Ten (10) criteria were selected for this evaluation:

- Past repair cost,
- Age,
- Past reliability,
- Present labour effort,
- Manufacturer support,
- Estimated useful life remaining,
- Projected reliability,
- Condition,
- Past usage, and
- Future usage.

The repair cost threshold value of 50% of acquisition cost has been selected as a starting point. This is near the mid-point of the range suggested in the literature. In our case the limit will be applied to parts and external labour costs only (i.e. not in-house labour costs), and is therefore additionally conservative.

A Clinical Engineering standard operating procedure, evaluation worksheet, and communication template were created to support the process. Next steps will include defining applicability to equipment groups/types and limitations therein, clinical stakeholder (equipment owner) education and consultation, implementation across Winnipeg region, and monitoring and improvement.

SP042.6 - An assessment of Preventive and Performance Maintenance Of Theater Equipment In Public Hospitals Kenya: Case study Five Public Hospitals.

Author(s): Philip A. Anyango

Medical Engineering, Kakamega County General Hospital, Kisumu/ KENYA

Medical devices play a key role in health care delivery. They are vital for diagnosis, therapy, monitoring, rehabilitation and care. Effective management of these devices is required to satisfy high quality patient care, clinical and financial governance, including minimising risks of adverse events. Unless medical devices are managed proactively, the same types of adverse incidents happen repeatedly. Good medical device management will greatly assist in reducing their potential for harm.

Cases where life has been lost because of faulty equipment and where patients has been turned away due to non functioning equipment has been captured in both print and electronic media on Kenya. One of the results of the studies done on medical equipment countries cites non functional equipment, as one of the challenges. Lack of maintenance and inadequate funding were found to be the main cause. In the past two decades most countries in Sub Saharan Africa in collaboration with development partners have tried to put in measures to address the challenges including training of technicians, building and equipping workshops. However the challenge still remains. Operation room (theatre) is one of the hospital departments that handle emergency cases and therefore equipment used inside must be in an optimum state all the time.

This paper is about an assessment on preventative and performance assurance maintenance of theatre equipment in five public county referral hospitals in Kenya namely Kisumu, Vihiga, Homa Bay and Kakamega. These hospitals were sampled because of Geographical location and high volume of patients handled.

The assessment focused on four major equipment used in operation room namely, anaesthetic machine, vital signs monitor, suction machine and electrosurgical unit. The main objective was to assess why equipment fail. Areas assessed included; Mode of service and maintenance, compliance to manufacturer's guidelines,, Stick on a dated 'SERVICED' label noting the next date due,, records of the activities carried, by whom, date and signature, availability of service manual, Training and certification of service engineers and possible challenges.

The findings were analyzed and Preliminary results were as follow

On Compliance with manufacturer's guidelines it was found out that; Most maintenance is done by in house staff, Very few equipment are under service contract, Manufactures service and timeline instructions are not followed to the letter. Training and certification of engineers- No evidence of certification of service engineers, Records were not well kept, Major challenges identified included; Insufficient funding'. Inadequate staff and adequate skills

IFrom the results it is evident that the way the equipment is maintained directly affects its performance, lifespan and quality of care to patients and the need for capacity of staff handling the equipment need not be overemphasised.

The paper recommends a comprehensive assessment be carried out in the entire country and should cover entire hospital.

SP042.7 - Mathematical Model for Reliable Maintenance of Medical Equipment

Author(s): Abdelbaset Khalaf

Clinical Engineering, Tshwane University of Technology, Pretoria/ SOUTH AFRICA

This paper proposes a mathematical maintenance model that analyses the effect of maintenance on the survival probability of medical equipment based on maintenance history and age of the equipment. The proposed model is simulated in Scilab using real data extracted from maintenance history of Anaesthesia Machine from Draeger. The analysis using survival approach reveals that conducting preventive maintenance (PM) on the selected medical equipment had a positive impact on survival of equipment. The model is then used to analyse the cost of maintenance scenarios and an appropriate scenario is proposed for Anaesthesia machine. A new failure-cost model is developed which may be used to calculate the number of failures of equipment and the annual maintenance cost. The proposed models may be used as a planning tool for selecting maintenance strategies for various medical equipment.

SP043 - Women in BioMedical Engineering

TRACK 18: GENDER, SCIENCE AND TECHNOLOGY

SP043.1 - One thousand years of women in science

Author(s): Monique Frize

Systems And Computer Engineering, Carleton University, Ottawa/
CANADA

Since the beginning of documented history, in every epoch, women have made significant contributions in science and technology. The challenge, since historians have mainly concentrated on men's work, is to find these women and discover what they have done. A few examples will be presented in this paper, but interested persons can find many books and websites with biographies of women in science and medicine. A few books and websites include women in engineering and technology.

In the 4th century, Hypatia of Alexandria (c.355-415) is said to be the world's leading mathematician and astronomer of her time. She was a popular lecturer on philosophical topics, attracting many students and large audiences. In the middle ages, women became involved in alchemy, herbal medicine, midwifery, and science in its fullest meaning. For example, Hildegard von Bingen (1098-1179) mentioned heliocentricity nearly 400 years before Copernicus and speculated about universal gravitation 500 years before Newton, composed music, and wrote on medicine and natural history. The renaissance counts many women astronomers that include Sophia Brahe (1556-1643), Maria Cunitz (1610-1664), Maria Winkelmann (1670-1720) and Margaret Cavendish (1623-1673) who published extensively on natural philosophy and early modern science, including over a dozen original works. With revised works, this brings her total number of publications to twenty one. Women were also patrons and correspondents of men like Queen Christina of Sweden and Elizabeth von der Platz. The 18th and 19th centuries count numerous women involved in serious science and mathematics such as Laura Bassi, Maria Gaetana Agnesi, Émile du Châtelet, Christina Roccati, Mary Somerville and many others. Only in Bologna and Padua were women granted doctoral degrees in the 18th and early 19th centuries, before women in general were admitted to University starting from the 1870s.

The presentation is meant to stimulate interest in the discovery of women who came before us and especially to demonstrate the importance of collecting papers and archives on women, their life, and their work. The active participation of women in science activities in all epochs, in spite of important obstacles they faced, is a model for girls and women today, since it is much easier now to follow this path than it has been in all past eras. We should be truly inspired by these stories and dream in our own way about the road we wish to follow.

Sources:

The Bold and the Brave: A history of women in science and engineering. Monique Frize, University of Ottawa Press, 2009.

Laura Bassi and Science in 18th Century Europe: The extraordinary life and role of Italy's pioneering female professor. Monique Frize. Springer, July 2013.

SP043.2 - Creating the Memories and Celebrating the Legacy of Women in Science and Engineering

Author(s): Ruby Heap¹, Monique Frize²

¹History, University of Ottawa, Ottawa/ON/CANADA, ²Systems And Computer Engineering, Carleton University, Ottawa/CANADA

For centuries, women around the world have actively participated in science and engineering, both formally and informally. Unfortunately, their contributions as innovators and producers of knowledge in these fields remain, to a large extent, unknown or understated. The history of women scientists and engineers is still in its infancy in a large number of countries. One major reason is their invisibility in traditional and established archives, which collected male records and tended to privilege the life and work of men; but another key obstacle has been these women's inclination to underestimate their own accomplishments, with the result that most did not seek to preserve their papers, and neither did their family, friends, and colleagues. At a time when the call for more women in science and engineering careers resonates strongly within governmental, economic and academic circles, and when there is a strong consensus regarding the benefits of gender equity and increased diversity in these fields, there is a pressing need to provide current and future women scientists with an accurate and inspiring understanding of their past, to learn about the lives and contributions of those who came before them.

This session will discuss an ongoing Canadian initiative which aims to research, recover, and celebrate the lives of women through the creation of an Archives of Women Scientists and Engineers in Canada. Sponsored by the INWES-ERI (International Network of Women Engineers and Scientists-Education and Research Institute), this initiative was launched at a workshop held in September 2014 at the University of Ottawa. Close to 50 participants –engineers, scientists, archivists, librarians, historians, policy makers- discussed the Archives project, along with partners such as the University of Ottawa, IBM Canada, The Canadian Commission for UNESCO, the US Society of Women Engineers (SWE) and a grant from the Social Sciences and Humanities Research Council (SSHRC). An action plan was adopted by the participants and a multidisciplinary Task Force was established to help proceed with its implementation. The main features of the action plan will be discussed in this session: the first steps include building an inventory of existing archives in major local, regional, and national repositories, and in major professional associations and organizations in science and engineering; with the assistance of SWE, we also intend to produce a Best Practices Guide to the discovery, recovery, and preservation of archives (manuscript, printed, audio-visual, digital) on women scientists and engineers.

In this interactive session, participants are invited to exchange with the speakers on approaches, programs and projects that might be developed to document the lives and careers of members of their organisations, document public conferences and exhibitions, books, brochures, oral testimonies, and the preservation of records of scientists and engineers.

SP043.3 - Women In Bio-Medical Engineering In Kenya

Author(s): Salome W. Mwaura

Bio-medical Engineering, MBAGATHI DISTRICT HOSPITAL, NAIROBI/KENYA

Women are often referred to as the weaker sex and in most communities in Kenya, they are regarded as children. It takes a lot of time for male Managers of health facilities to accept them in decision making.

As a primary school going girl, we took my brother to the local district hospital but the Doctors could not fully diagnose his condition due to some equipment in the laboratory and X-ray department

malfunctioning. In my mind, I was wondering what could have been wrong with the equipment and I decided that when I grow up, I must study the course for repair of equipment in hospitals.

After my "O" levels, I got three carrier opportunities in Medical Laboratory, Nursing and Medical Engineering. With my little knowledge about medical engineering, and remembering the incident in hospital earlier, I chose to pursue Medical engineering.

In 1993, I was admitted for a three year Diploma course in medical engineering at Mombasa polytechnic. I joined the civil service in 1997 and I have worked in various hospitals including Kisumu and Nyeri level V and Mbagathi level IV. In 2006, I enrolled for a 2 Year Higher National Diploma course in medical engineering at the Kenya Medical Training College, Nairobi.

In 2006, I was appointed HOD of Bio-medical engineering Department at Mbagathi District hospital heading a team of 8 bio-meds of whom 6 were male. It was an uphill task but today, I can proudly say that my work relation with everybody is very good. I am always involved in decision making as concerns medical engineering in the hospital by the hospital management.

I have attended several trainings. GAME, an American NGO organised one on theatre and ICU equipment in Kisumu, another one by JICA in Nairobi and another in South Africa by SAFHE/CEASA. I have also been to DITEC, USA for an advanced course in X-ray and Imaging.

I am a Member of AMEK which I have served in several capacities, and currently am the Treasurer. I have attended several conferences organised by the International Federation of Hospital Engineering (IFHE). I attend all annual conferences/events organised by AMEK and biennial East African conferences organised by the East African Country associations on rotational basis, the most recent one was in Kigali, Rwanda in December 2014.

Challenges

Biomedical engineering in Kenya is male dominated. Hence, fighting for recognition and appreciation by bosses is a major challenge in the field.

When it comes to factory training, most opportunities are given to men in the ratio of one out of ten.

Working with bosses who come from communities that do not recognise women plays a major role in demotivating women in their day to day operations.

Conclusion

There is need to support these ladies who are doing everything possible to give quality work in medical engineering and give them a chance as they have the capability.

They also need to be empowered academically in order to shine better in the field.

SP043.4 - Physics is a waste of your intelligence

Author(s): Shada Wadi-Ramahi
Biomedical Physics, King Faisal Specialist Hospital and Research Center, Riyadh/SAUDI ARABIA

Going to physics was not an easy road. It was unheard of that students who score high in the Jordanian SAT go to science. My parents were outraged. Graduating first in class in 3.5 years, still did not convince them. I was wasting my time and college was a waste of their money.

Fast forward to 2003, I graduate with a PhD in Medical physics from the US. Time to go home. I land a position in the country's leading cancer center, joining a team of 7 physicists. It was not easy to be the only one with a higher degree in physics, most of the problems though did not come from fellow physicists, but from the chairman who could not handle having a "doctor" female staff. In official communications I was always referred to as "Ms." instead of "Dr.". The excuse was "you are like my daughter". Later the attitude escalated. In one of my earlier meetings with linac vendors in 2004, I challenged the representative of a company on one of his claims. The chairman annoyed that I spoke up, yelled "Hey girl stop this"! It took a good year before attitudes changed to formal behavior At least on paper.

The policies of the institution prevented discrimination, and later I became the head of medical physics. However, harassment came in many forms; it was encouraging male physicists (my subordinates) to side step me and report to the chairman directly, it was over-riding the staff work schedule often after I distribute it (something that never happened to the chief technician ... a male), it was ridiculing my expertise even after I obtained ABR certification, It was stopping warning letters addressed to staff members who yelled at their supervisor (me). Harassment took many forms and shapes. Did I think about leaving? Yes, I wanted to go "back" to the US.

I loved my profession and I was determined not to let a male-dominated culture sway me off track. I am in my country contributing greatly to the treatment of cancer patients, and if I am not part of the force of change then I am a quitter. I endured.

Eleven years later in 2014, when I announced I am leaving to a position in another highly competitive institution in the region, my chairman gave me a counter offer and tried hard to convince me to stay. The offer was generous, and the emotions were real. It was a moment of vindication, my dedication to work and perseverance paid off. Alas, it was time to move on.

Women in science world-wide are a minority, in the Middle East they are a rarity. Women in science in the Middle East who assumes higher positions in par to their male colleagues are a species of their own.

I am proud of my achievements ... I am proud to call myself a medical physicist ... I am proud to call myself an Arab, but above all I am proud to be a woman.

SP043.5 - Medical physics – or how a change in career path becomes a passion

Author(s): Loredana G. Marcu
School Of Chemistry And Physics, University of Adelaide, Adelaide/ SA/AUSTRALIA

I was trained as a physicist in a country under transition after half a century of communism. I enjoyed being a student at the University of Timisoara (Romania) where I studied physics for six years under the guidance of some highly respected professors. After graduation, I was lucky enough to get a teaching position in my hometown at the University of Oradea, where, for the first time, I stood on the other side of the desk. While it was a great teaching experience, I felt that I needed something more for a fulfilled scientific life.

That was the moment of a life-changing decision: moving to Australia. In Adelaide, South Australia, I have been able to continue my scientific education in a specialised branch of physics that I fell in love with. I had the good fortune to be offered a scholarship to attain my PhD in Medical Physics. I got to work with an extraordinary group of people at the Royal Adelaide Hospital where I continued my career for nearly a decade. The people, the facilities and the working conditions all put together offered an optimal learning environment and a

great source of inspiration. Radiobiology became my new passion, a field that I am continuously learning and which never ceases to amaze me.

In life circumstances and priorities change, so after ten years of learning, working and teaching in Adelaide, it was time to give something back to the country where I was raised and educated. I am now back on home soil where I have helped the Physics Department of the Science Faculty within the University of Oradea set up a Medical Physics training programme at both undergraduate and postgraduate levels. It is a wonderful feeling to pass on your own experience and teach students that have the same thirst for knowledge that I had at the beginning of my academic career. Medical Physics is a developing field in Romania and we need enthusiastic and well-trained specialists to raise this branch of science to European standards. The love and passion for this field should start from studenthood, and as the first woman medical physicist has once said "We must have perseverance and above all confidence in ourselves. We must believe that we are gifted for something" (Marie Curie).

SP044 - Bio-Impedance and Imaging (Other)

TRACK 01: IMAGING

SP044.1 - Personal Time-Varying Magnetic Fields Evaluation During Activities in MRI Sites

Author(s): Giuseppe Acri, Barbara Testagrossa, Giuseppe Vermiglio
Dept. Of Sastas, University of Messina, Messina/ITALY

A person moving in and around the MRI site may experience strong time-varying magnetic fields. The physical consequence of the time variation of the magnetic flux density is the induction of currents in body parts. In this paper the time-varying gradient exposure associated with the magnetic flux densities is evaluated and measured. The acquired data, obtained from a personal magnetic dosimeter, represent the magnetic flux density function, $B = B(t)$, related to the operator movement inside the MRI site. Such data have been processed to evaluate the corresponding dB/dt curves, that were estimated by calculating the time derivative. All the measurements were conducted on a 3.0 T MRI site, dedicated to research procedures, in two different conditions: at first during routine patient positioning, and secondly, simulating an emergency. In both the measurement conditions, two dosimeters, with different acquisition times, were simultaneously used. They were positioned the first time on the operator's torso and the second one on his head. The analysis conducted, simulating both normal and emergency conditions, demonstrated that the dB/dt peak values strictly depended on human motion through strong static magnetic fields, and, sometimes, exceeded the recommended limit. This consequence highlighted the necessity of drawing up, as in case of ionizing radiation, behavioural rules to be followed by workers and patients. Therefore it will be necessary to assess risk conditions in a proper manner.

SP044.2 - ECG Imaging of Ventricular Extrasystoles

Author(s): Olaf Doessel¹, Walther H.W. Schulze¹, Danila Potyagaylo¹, Rainer Schimpf², Martin Borggrefe²

¹Institute Of Biomedical Engineering, Karlsruhe Institute of Technology (KIT), Karlsruhe/GERMANY, ²First Department Of Medicine - Cardiology, University Medical Centre Mannheim, Mannheim/GERMANY

Objectives: Frequent ventricular extrasystoles can lead to ventricular tachycardia and ventricular fibrillation and are therefore life threatening. They can be treated with RF ablation, provided the focus of the extrasystole is precisely known. Invasive ablation procedures can be accelerated significantly if the focus of the extrasystole is known beforehand from non-invasive measurements. This project aims at the localization of ventricular extrasystoles from Body Surface Potential Maps (BSPM).

Methods: 9 patients with frequent extrasystoles were selected. BSPM datasets and MRI images were acquired. The MRI data contained an enddiastolic dataset of the heart and a thorax scan. Heart, lungs, liver, spleen, stomach, kidneys and aorta were segmented. Tetrahedral meshes of typically 3000 nodes in the heart and 350000 nodes in the thorax were created for FEM calculations. A thorough localization and registration procedure for the electrodes was implemented. During the invasive procedure stimuli were given at various positions and the BSPM were measured. Finally the foci of the extrasystoles were ablated. Various algorithms of reconstruction of electrophysiological sources in the heart from BSPMs have been implemented and tested, e.g. Tikhonov (with and without bounds), activation times, model based optimization and Maximum-a-Posteriori (MAP) estimates. Thorough validation was carried out

by comparing the reconstructed foci with the ones found during the invasive ablation procedure.

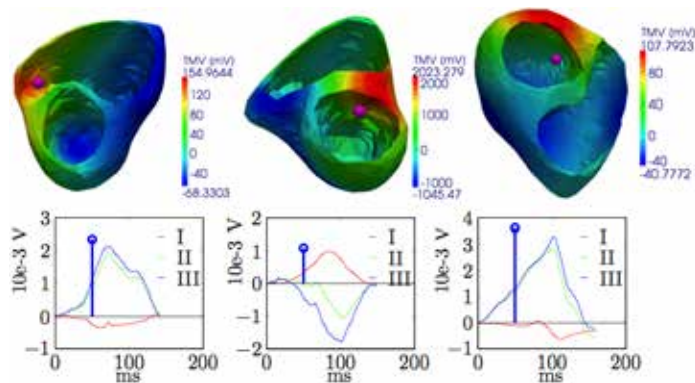


Figure 1: Three examples of reconstructed transmembrane voltages together with the true location of the extrasystole (pink bullet). **Method:** Tikhonov 2nd order. Blue bar indicates the time of reconstruction in the ECG (extracted from the BSPM).

Results: Figure 1 shows three examples. A median error of 20mm was achieved. This is somewhat disappointing but agrees with other publications with thorough validation of ECG imaging. The various reconstruction methods tested in this project deliver good results in one patient and worse results in another – no algorithm is the clear winner for all patients. The model based optimization performs slightly better as compared to the other methods.

Discussion: Despite the fact, that all the reconstruction algorithms mentioned above show very good results in computer simulations, the strict clinical validation uncovers some deficiencies. The results support the hypothesis, that the model assumptions that underlay all reconstruction algorithms are not yet perfect.

SP044.3 - Experimental Study on Amplitude Frequency of Acoustic Signal Excited by Coupling Magneto-Acoustic Field

Author(s): Ren Ma, Shunqi Zhang, Tao Yin, Zhipeng Liu
Institute Of Biomedical Engineering, Chinese Academy of Medical Sciences, Tianjin/CHINA

Object To study the relationship between exciting source characteristic and magneto-acoustic signal, also explore the frequency corresponding relationship between exciting signal and acoustic signal applied on the experimental sample. **Methods** A practical system has been established to detect magneto-acoustic signal. While single period sine pulse current with different amplitude and frequency were loaded in the sample of straight copper wire, acoustic signal was detected synchronously. Amplitude and frequency of exciting current and acoustic signal were analyzed by using time-frequency method, which was adopted by short time Fourier transform STFT and shifted smoothing rectangle window. Then, comparative study was conducted basing on the processed data. **Result** Giving the current same frequency as well as different amplitude, linear relationship is obtained between the output amplitude of acoustic signal and current amplitude. However, giving the current same amplitude as well as different frequency, the corresponding frequency spectrum of acoustic signal show different variation law, and thus, there is great difference among the system functions. **Conclusion** Detecting system is highly sensitive to frequency. In order to acquire more information in the magneto-acoustic signal, both of detecting circuit SNR and acoustic transducer bandwidth should be promoted.

SP044.4 - In vivo electric conductivity values of cervical cancer patients reconstructed with a 3T MR system for improved SAR determination

Author(s): Edmond Balidemaj¹, Peter De Boer¹, Henny P. Kok¹, Gerben Schooneveldt¹, R.F. Remis², C.A.T. Van Den Berg³, A.J. Nederveen¹, L.J. Stalpers¹, Johannes Crezee¹

¹Radiotherapy, Academic Medical Center, Amsterdam/NETHERLANDS, ²Technical University Delft, Delft/NETHERLANDS, ³University Medical Center Utrecht, Utrecht/NETHERLANDS

Introduction: Reliable tissue electrical conductivity (σ) values are required to determine the RF energy absorption for Hyperthermia Treatment Planning (HTP) or for Magnetic Resonance Imaging (MRI) for safety purposes. Currently used σ -values are mostly based on ex vivo measurements, and tumor σ is mostly unknown. Our aim is to acquire in vivo pelvic tissue conductivity for muscle, bladder and cervical tumor using 3T MRI.

Methods: Conductivity values were reconstructed using Electric Properties Tomography (EPT) which is based on the measurable $B1^+$ field. Earlier we have validated this method for the pelvic region using phantom experiments and in vivo simulations. In this study, MR measurements of 12 cervical (squamous cell) carcinoma patients and one uterine adenocarcinoma patient were used to reconstruct σ -values in tumor, muscle and bladder. For a reliable σ -reconstruction the composition of a particular tissue should be relatively homogenous and sufficiently large (>3cm). Thus the σ of 9 tumors and 7 bladder fillings could be reconstructed. Results were compared to literature data.

Results: The reconstructed σ -values of muscle tissue were up to 35% elevated compared to literature values (Figure 1a). Moreover, the reconstructed σ -values of the bladder were up to 10 times higher than values currently used in human models for HTP (Figure 1b). Finally, for 75% of the squamous cell carcinomas the σ -values were 5-12% higher than the σ of muscle tissue found in this study. The reconstructed σ of the adenocarcinoma was 22% higher compared to muscle tissue.

Discussion & Conclusions: This study demonstrated the feasibility to measure the σ of healthy tissue and tumors in vivo. The measured conductivities were higher than reported in literature, which could probably be explained by the higher blood and water content during in vivo conditions. A decrease of σ after death has been reported for (human) liver, (animal) brain and (animal) muscle tissue. The present study showed that the commonly unknown tumor σ is 5-12% higher compared to the σ of muscle. The σ -value reported in the literature for bladder corresponds to bladder wall tissue, the volume percentage of which is lower than that of urine. However, this study shows that urine σ is much higher and shows a large inter-subject variation. Future studies will determine to which extent the reliability of HTP improves when using these patient-specific σ -values. These results are further interesting for applications such as MR safety and RF coil design for MR systems.

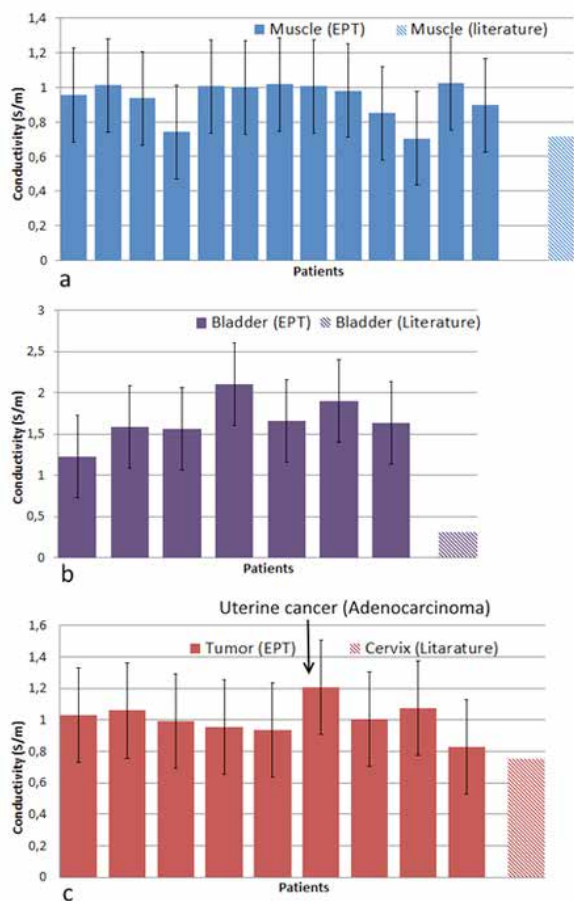


Figure 1. Reconstructed and literature conductivity values of muscle (a), bladder (b) and cervical tumor tissue (c).

SP044.5 - Focus Tunable Gel Lens Using Annular Dielectric Elastomer Actuator

Author(s): Thanh Giang La, Gih Keong Lau
 School Of Mechanical & Aerospace Engineering, Nanyang Technological University, Singapore/SINGAPORE

Liquid lens, which is basically a soft capsule of oil or water, has recently been demonstrated capable of adaptive tunable focus. Its curvature changes can be activated by various means, mechanical, thermal, electrochemical or electrical. In mechanical or pneumatically activated liquid lens, change of liquid pressure or membrane stress can induce the curvature changes and thus the variable focus. Such variable focus liquid lens has a compact and lightweight design with integrated actuator, simpler than hard lenses'. However, it does not have as good shape stability as hard lens. The liquid capsule may sag under gravity if its size is larger than 1cm. In addition, the liquid lens may deform in response to vibration, causing image distortion. In contrary, human crystalline lens, which is made of gel, generally can function robustly despite orientation change and last for a long life time (>40 years).

Inspired by the human crystalline lens, we make use of solid-state silicone gel (Dow Corning Dielectric Gel Kit 3-4170) to build a tunable focus lens, which is electrically activated by an annular dielectric elastomer actuator. The annular dielectric elastomer actuator acts like ciliary muscles that control the eye's lens accommodation. Initially when the actuator is idle, the gel lens is flattened under the membrane pre-tension. Upon activation by the annular actuator that elongates, the gel lens bulges. Our experiment showed that this gel lens can vary focus on the objects between 2.5cm and 30cm when activated under voltages in range of 0-3kV at very small dc current

of <20 μ A. As such, the gel lens consumes low electric power of <60mW to work robustly more than 10,000 cycles. Furthermore, miniaturization of the dielectric elastomer actuators in term of membrane thickness could help reduce the driving voltage requirement. This gel lens showed good potential to be commercially adopted due to its enhanced shape stability.

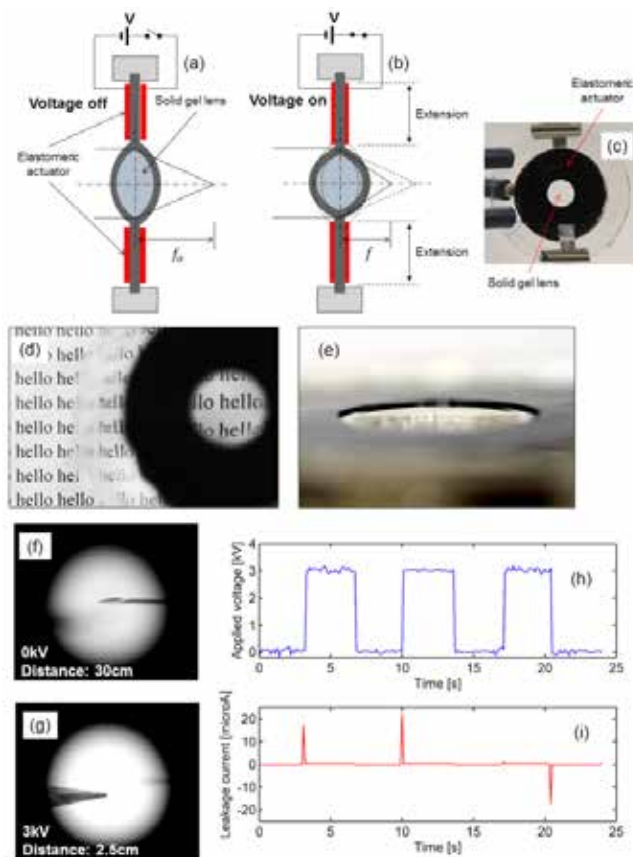


Figure 1. (a) Gel lens is configured with elastomeric actuator (un-activation). (b) The lens is activated by voltage V. (c) The device consists of a gel lens and an actuator. (d) Magnification of the convex gel lens is shown. (e) Photograph of the lens is in angle view. (f) At un-activated state, the lens focused on a far object (a needle) at 30cm-distance from its position. (g) Under 3kV, the lens focused on a near object (pencil) at 2.5cm. (h) External voltage is applied in on-off testing. (i) Dc current through actuator is <20microAmp.

SP044.6 - Ultra-low-field MRI for improving spatial accuracy of bioelectric source imaging

Author(s): Koos C.J. Zevenhoven
 Department Of Neuroscience And Biomedical Engineering, Aalto University, Aalto/Espoo/FINLAND

In magnetoencephalography (MEG), one measures the extremely weak magnetic fields generated by electrical brain activity using an array of highly sensitive, typically superconducting magnetic-field sensors around the head. As a functional brain imaging modality, MEG surpasses functional magnetic resonance imaging (fMRI) in terms of temporal resolution and has a spatial accuracy superior to electroencephalography (EEG). However, the spatial accuracy is limited by coregistration, the procedure of aligning a structural image of the head with the MEG coordinate system. Typically, this is done manually by digitizing anatomical landmarks on the head in the MEG session and separately localizing corresponding points in a structural head MRI.

Besides errors in identifying and digitizing the anatomical landmarks in both modalities, manual coregistration contains errors produced by a number of factors, such as the head-position measurement in MEG, distortions in high-field MRI, skin movements, and small differences between supine and seated positions regarding the geometry of the soft brain and cerebrospinal fluid.

The spatial coregistration accuracy is important not only for the alignment of electrical sources with the anatomy, but also for the reconstruction of the spatial origin of the signals, which depends on the geometry of the head and the changes in electrical conductivity across different tissues. As models for source localization become more detailed, their sensitivity to inaccuracies in geometry and conductivity values increases. The volume currents being particularly important in EEG, an accurate model of the conductivity structure is required especially for full benefit of the complementary information of simultaneous EEG and MEG. A hybrid MEG-MRI system provides natural approaches to addressing these issues.

At Aalto University, Finland, we have built a hybrid MEG-MRI system based on an array of sensors based on Superconducting QUantum Interference Devices (SQUIDS). The MRI is implemented at ultra-low field (ULF), around 50 μ T, and measured inside a magnetically shielded room. The SQUID sensors tailored for ULF MRI can also be used for MEG. Together with the common sensor array, high-precision ULF-MRI electronics, and a stable coil structure, our novel algorithms can transform the largely manual coregistration problem to a fully automatic calibration, thereby eliminating human error and achieving sub-millimeter accuracy.

We describe the current state of our system and present obtained images. We further discuss the unique possibilities, shown recently, of ULF MRI in current-density imaging (CDI), potentially allowing also the imaging of electrical conductivity using the same hybrid device. We describe our methods, computations, and experimental setups for implementing the methods in our hybrid MEG-MRI device, along with preliminary results. If successful, conductivity imaging combined with sub-millimeter automatic coregistration will provide significant improvements to MEG and EEG source localization.

SP045 - Molecular Imaging PET/SPECT: Part 1

TRACK 01: IMAGING

SP045.1 - Quantitative accuracy of SPECT imaging with a dedicated cardiac camera: Physical phantom experiments

Author(s): Amir Pourmoghaddas, R Glenn Wells
Physics, Carleton University, Ottawa/CANADA

Introduction

Recently, there has been increased interest in dedicated cardiac SPECT scanners with multi-pinhole designs and improved detector technology due to their improved count sensitivity and resolution over traditional parallel-hole cameras. However, the pinhole-collimator design introduces position-dependent attenuation, sensitivity and resolution variations. Differences in attenuation patterns and energy-spectrum responses compared to conventional SPECT scanners can also inhibit accurate measurement of activity distributions. Simple correction methods for these effects are easily implemented however their level of accuracy is unclear. In this study, we assess the quantitative accuracy and reproducibility of absolute activity measurements made using easily implemented correction techniques applied to controlled physical phantom experiments.

Materials and Methods

Activity in the cardiac compartment of an Anthropomorphic Torso phantom (Data Spectrum Corporation) was measured through multiple ^{99m}Tc -SPECT acquisitions ($n=10$). The ratio of activity concentrations in organ compartments resembled a clinical ^{99m}Tc -sestamibi scan and was kept consistent across all experiments (6:1 heart to background, 1:1 heart to liver, 6:4 heart to lung ratio). To assess the effect of activity spill-in and increase scatter into the myocardium compartment, experiments were repeated with- and without activity in the soft-tissue torso compartment. The true net activity in each compartment was measured with a dose calibrator (CRC-25R, Capintec Inc). A ten minute SPECT image was acquired using a dedicated multi-pinhole cardiac camera with cadmium-zinc-telluride (CZT) detectors (Discovery NM530c, GE Healthcare), followed by a CT scan for attenuation correction (AC). Data were reconstructed with no corrections (NC), AC and AC with dual energy window (DEW) scatter correction (ACSC), using reconstruction with resolution recovery.

Results

T-tests comparing hot- and cold torso datasets (Table 1) showed no significant mean difference for all three reconstruction methods (NC, AC, ACSC: hot vs cold torso) ($p>0.08$). AC and ACSC significantly reduced the mean error over NC ($p<0.001$). The mean AC and ACSC errors were significantly different for the hot torso ($p=0.04$) but not for the cold torso ($p=0.09$), highlighting the effectiveness of DEW-SC in reducing errors introduced by photon scatter. While DEW-SC seemed to increase measurement uncertainty compared to AC in both cases, the increase was not significant ($p\geq 0.2$). Both AC and ACSC significantly increased uncertainty over NC for the cold torso phantom ($p<0.03$), but not for the hot-torso case ($p>0.1$).

Conclusions

CT-AC and an easily implemented DEW scatter correction significantly improve quantitative measurement of ^{99m}Tc -SPECT myocardial activity with a dedicated cardiac camera producing an error of $\leq 2.2 \pm 6.5\%$.

Table 1. Mean and standard deviation of errors between activity measured using reconstructed images vs true activity inserted into the cardiac compartment of the phantom. † indicates $p < 0.05$ vs NC.

		Measurement error		
		NC	AC	ACSC
Hot Torso (n=5)	Mean (%)	-77.5	5.5	-0.8
	SD (%)	2.0	4.6	5.0
Cold Torso (n=5)	Mean (%)	-76.4	1.6	-2.2
	SD (%)	0.9	3.2†	6.5†

SP045.2 - The Impact of time of flight algorithm and PSF modeling on standard uptake value in clinical PET/CT imaging

Author(s): Mahnaz Shekari¹, Pardis Ghafarian², Mehrdad Bakhshayeshkaram², Mohammad Reza Ay¹

¹Tehran University Of Medical Sciences, Research Center for Molecular and Cellular Imaging, tehran/IRAN, ²Pet/ct And Cyclotron Center, Masih Daneshvari Hospital, Shahid Beheshti University of Medical Sciences, tehran/IRAN

Introduction: Time Of Flight (TOF) and Point Spread Function (PSF) modeling are the most advanced reconstruction algorithms in PET/CT which dramatically improve the image quality. The aim of this study was to evaluate the impact of TOF and PSF modeling on Standard Uptake Value which is commonly used by physicians for staging of metastasis and monitoring response to therapy.

Materials and Methods: In this study, a whole-body ¹⁸F-FDG PET/CT scan performed on 9 patients (BMI=25.4±1.21, 5.02±0.07 MBq per kg) using GE Discovery 690 PET/CT. The scanner was capable to reconstruct images with TOF, and also PSF modeling which is commercially named SharpIR algorithm. All PET data were reconstructed with HD+SharpIR (use for clinical report in this center), TOF, and TOF+SharpIR algorithms. 40 Focal points (short axis diameter of 1.1±0.38cm) were identified, and a semi-quantitative analysis was done by using SUVmean for normal lung tissue, SUVmax, and SUV50 for metastases. Furthermore, impact of lesion size, and location on SUV variation were assessed. We also evaluated noise in liver to analyze quality of clinical PET images.

Results: Our semi-quantitative analysis verify using TOF, and/or SharpIR algorithms significantly enhance SUVmax (15.95±3.38% for TOF, 33.01±3.1% for TOF+SharpIR), and SUV50 (16.37±3.43 for TOF, 34.4±3.23% for TOF+SharpIR) in compare with the image reconstructed using HD+SharpIR. The statistical analysis showed that for smaller lesions, TOF, and TOF+SharpIR lead to more robust changes in SUVmax, and SUV50 (P-value<0.05). Figure.1 shows weak correlation between lesion location and SUV enhancement for both TOF, and TOF+SharpIR algorithms (R²=0.11, R²=0.03 respectively, P-value<0.5). Despite lesions, SUVlung wasn't affected by reconstruction algorithms. Image noise for TOF+SharpIR algorithm was similar to HD+SharpIR, but noise for images reconstructed with TOF algorithm were superior (p-value<0.001).

Conclusion: This study showed that SUVs of metastases are highly affected by reconstruction applied method. Based on our results, it can be concluded that it's vital to consider effects of TOF, and SharpIR algorithms on accuracy of SUV.

SP045.3 - Can Pacemaker and ICD degrade CT-Based Attenuation Corrected cardiac SPECT images?

Author(s): Zahra Etemadi¹, Ahmad Bitaran Rajabi², Hadi Malek³, Pardis Ghafarian⁴, Navid Zeraatkar¹, Mohammad Reza Ay⁵

¹Research Center For Molecular And Cellular Imaging, Tehran University of Medical Sciences, Tehran/IRAN, ²Department Of Nuclear Medicine, Rajaei Cardiovascular, Medical & Research Center, Iran University Of Medical Sciences, Iran, assist.prof, tehran/IRAN, ³Cardiovascular Interventional Research Center, Department of Nuclear Medicine, Rajaei Cardiovascular, Medical, and Research Center, Iran University of Medical Sciences, Tehran, Iran., tehran/IRAN, ⁴Chronic Respiratory Diseases Research Center, National Research Institute Of Tuberculosis And Lung Diseases (nritld), Shahid Beheshti University of Medical Sciences, tehran/IRAN, ⁵Department Of Medical Physics & Biomedical Engineering, Tehran University of Medical Sciences, Tehran/IRAN

Introduction: Quantitative processing of myocardial perfusion is a questionable issue in the SPECT imaging due to the some artifacts such as attenuation. Although it has been demonstrated that CT-based attenuation correction (CTAC) technique can significantly improve the diagnostic accuracy of SPECT imaging, the presence of cardiac Pacemaker and ICD leads in CT imaging will impact the reconstructed myocardial perfusion SPECT image during the CTAC procedure. In this study we investigated and quantified the degradation magnitude of the metallic artifacts due to pacemaker and ICD leads on the CT-based attenuation corrected SPECT images using phantom studies.

Materials and Methods: A cardiac phantom with capability of including pacemaker and ICD leads was scanned in SPECT/CT scanner. Attenuation correction of the SPECT data was performed using the artefactual (metal artifact) CT images (Figure 1). Quantitative evaluation was performed between the actual activity and the measured activity concentration in the myocardial perfusion SPECT images without and with attenuation correction using the volume of interest (VOI)-based analysis on 17 myocardial segments.

Results: Quantitative analysis shows an overestimation of about 9% and 15% and an underestimation of about 6% and 11% in CT-based attenuation corrected SPECT images with pacemaker and ICD leads, respectively.

Conclusion: Since photoelectric interactions are more significant at CT energies and are dependent on atomic number, the metallic composition of pacemaker and ICD leads, especially ICD lead, can induce considerable artifacts on CT images. Despite the influence of cardiac lead-induced artefacts on inaccurate quantification of some segments of the myocardial perfusion SPECT images when using the CT-based attenuation correction process, however it does not induce erroneous clinical interpretation of the SPECT images corrected for attenuation using artefactual CT images. It can be concluded that implementation of down sampling and smoothing on the artefactual CT images for generation of attenuation map reduce the impact of metallic artifact during the CTAC of SPECT data.

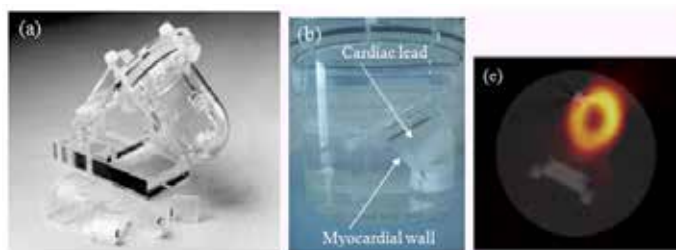


Figure 1. (a) The cardiac Phantom (Cardiac Insert ECT-CAR-1) used for phantom study, (b) the attached ICD lead to the myocardial wall, (c) Fused CT and SPECT image

SP045.4 - Impact of Point spread function modeling on tumor quantification in clinical PET/CT imaging

Author(s): Sahar Ahangari¹, Pardis Ghafarian², Mehrdad Bakhshayeshkaram², Mohammad Reza Ay¹
¹Department Of Medical Physics And Biomedical Engineering, Tehran University of Medical Sciences, tehran/IRAN, ²Pet/ct And Cyclotron Center, Masih Daneshvari Hospital, Shahid Beheshti University of Medical Sciences, tehran/IRAN

Introduction: Quantitative assessment of PET images is increasingly used in cancer staging and therapy monitoring. In PET, partial-volume effects and point-spread function cause inaccuracy in estimation of lesion size and uptake. By regarding PSF-modeling during reconstruction procedure, the spatial resolution of PET images improves and as consequence the partial volume effect reduces. The aim of the present study was to evaluate the impact of PSF reconstruction (HD+SharpIR) compared with conventional OSEM reconstruction (HD) in non TOF PET imaging on quantitative accuracy of the lesions with respect to the lesion contrast.

Materials and Methods: In this study 17 patients (BMI:25.1±0.84) with 100 lesions were scanned using Discovery 690 PET/CT scanner. The patients were scanned 60 minutes after intravenous injection of 370 MBq of FDG (5.25±0.11MBq/kg). Emission data were acquired at 2 min/bed. All images were reconstructed using HD and HD+SharpIR algorithms with 3 iterations, 18 subsets, and 6.4 mm FWHM of post-smoothing filter. Image quality was evaluated by calculating COV (coefficient of variance) for a 3 cm spherical region in liver. The quantitative analysis was performed by measuring relative changes of standardized uptake values (SUV) and lesion size based on lesions location, and contrast with and without PSF-modeling. Contrast was defined as max activity concentration at lesion to mean activity concentration in background.

Results: Average of liver COV for HD and HD+SharpIR were 9.14±0.36 and 7.38%±0.33 respectively. PSF modeling increased SUVmax by 12% compared with HD algorithm. The regression analysis showed that relative differences for SUVmax significantly increased with increasing lesion contrast (figure1, R²=0.41, p<0.001) and lesion distance from the central axis (R²=0.24, p<0.001). For lesions with contrast less than 3, SharpIR algorithm reduced the size of lesion to 4.36%, and for high-contrast lesions (contrast higher than 3) the size decreased up to 17.81%.

Conclusion: Image quality was improved by using of SharpIR algorithm. SharpIR performance was better in lesions with smaller size, further distance from the central axis and higher contrast. So the effectiveness of the algorithm is more in high contrast lesions.

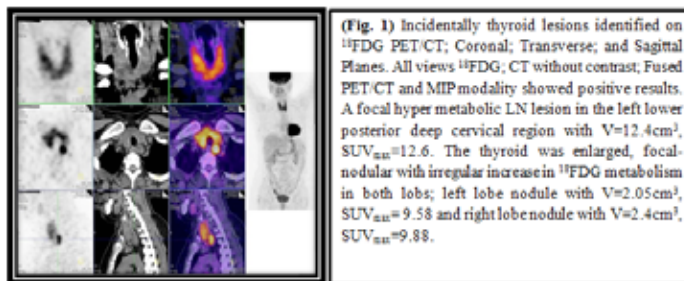
SP045.5 - Incidental Thyroid Cancer Identified on 18FDG- PET/CT for Ovarian Cancer Evaluation-Case Study.

Author(s): Farid Y. Rishq¹, Shuaa J. Al-Sadoon², Mohd Ziad F. Rishq¹, Dina Q. Zaqq³, Ayman A. Qwarik²
¹Nuclear Medicine, FARID RISHEQ NUCLEAR MEDICINE PET/CT & BONE DENSITY CENTER, AMMAN/JORDAN, ²Physics In Nuclear Medicine, FARID RISHEQ NUCLEAR MEDICINE PET/CT & BONE DENSITY CENTER, AMMAN/JORDAN, ³Medicine, PRIVATE PRACTICE ENDOCRINOLOGY & DIABETES, AMMAN/JORDAN

Objective: This study presents the clinical significance of focal increased ¹⁸FDG uptake in the thyroid as incidentally identified on PET/CT for ovarian cancer evaluation. Ovarian cancer is known to metastases to the thyroid resulting in clinical hypothyroidism.

Clinical History and Results: A 54 year-old female with papillary adenocarcinoma of the ovary, underwent ¹⁸FDG-PET/CT post-surgery evaluation. ¹⁸FDG PET/CT was performed 1hr post IV ¹⁸FDG of 370MBq, (Fig. 1). A focal hyper metabolic lymph node lesion was visible in the left lower posterior deep cervical region

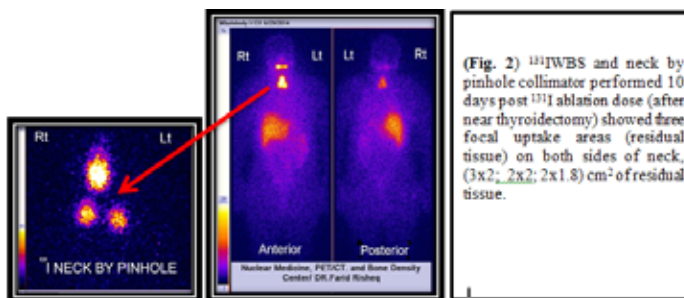
with volume=12.4cm³, SUVmax=12.6. Thyroid was enlarged, focal nodular with irregular hyper metabolic ¹⁸FDG uptake in both lobes. The left and right lobes' nodule volume=(2.05; 2.4)cm³, and SUVmax=(9.58; 9.88) respectfully. The rest of the body showed normal and physiological ¹⁸FDG metabolism. Thyroid Function Test was advised.



(Fig. 1) Incidentally thyroid lesions identified on ¹⁸FDG PET/CT; Coronal; Transverse; and Sagittal Planes. All views ¹⁸FDG; CT without contrast; Fused PET/CT and MIP modality showed positive results. A focal hyper metabolic LN lesion in the left lower posterior deep cervical region with V=12.4cm³, SUV_{max}=12.6. The thyroid was enlarged, focal-nodular with irregular increase in ¹⁸FDG metabolism in both lobes; left lobe nodule with V=2.05cm³, SUV_{max}=9.58 and right lobe nodule with V=2.4cm³, SUV_{max}=9.88.

Results of TSH=7.9 IU/L, Tg=18.9 ng/ml, suggesting diagnosis of lymphocytic thyroiditis or differentiated thyroid cancer. The histopathology of US-guided FNAB samples showed: papillary carcinoma and Hashimoto thyroiditis; classical type. Tumor location: in both lobes with largest diameter: 3.5 cm. Lymph vessel invasion: present.

The patient underwent total thyroidectomy followed by ¹³¹I ablation dose of 3700 MBq. Post therapy ¹³¹I WBS and neck by pinhole showed three focal areas (3x2; 2x2; 2x1.8 cm²) of residual tissue in both sides of neck, (Fig.2).



(Fig. 2) ¹³¹I WBS and neck by pinhole collimator performed 10 days post ¹³¹I ablation dose (after near thyroidectomy) showed three focal uptake areas (residual tissue) on both sides of neck, (3x2; 2x2; 2x1.8 cm²) of residual tissue.

Conclusions: Incidentally found hyper metabolism of ¹⁸FDG PET/CT in thyroid was due to papillary carcinoma, most probably metastases from ovarian cancer. Elevated serum levels of TSH hypothyroid and Tg were significant with incidental finding of focal increased uptake.

We recommend that for patients with ovarian cancer; metastatic disease to thyroid should be considered, especially when PET/CT scan showed focal hyper metabolic lesion in the thyroid or elevated TSH. Further work is needed aiming at assigning a threshold level of SUVmax in thyroid to differentiate benign from malignancy.

SP045.6 - Zinc material filter for scatter correction in Tc-99m myocardial SPECT imaging: Heart thorax phantom study

Author(s): Nazifah Abdullah¹, Syed Inayatullah Shah¹, Ahmad Zakaria², Abdul Rahim Md Shahrir³
¹Allied Health Science, INTERNATIONAL ISLAMIC UNIVERSITY MALAYSIA, KUANTAN, PAHANG/MALAYSIA, ²Health Science, UNIVERSITI SAINS MALAYSIA, KUBANG KERIAN, KELANTAN/MALAYSIA, ³Radiology, INTERNATIONAL ISLAMIC UNIVERSITY MALAYSIA, KUANTAN/MALAYSIA

SPECT is one of the techniques which provide the high diagnostic accuracy for the assessment of myocardial perfusion. However, the limitation in the diagnostic accuracy in the presence of Compton scattered photons in the image data. And the procedure is more

complex in heart thorax phantom compared to homogenous volume.

Thus, this work focuses on the investigations into the effect of Zinc (0.1mm and 0.198mm) material filter on image quality. The anthropomorphic torso phantom was used to perform the experiments. Data acquisition was obtained with the dual head gamma camera (Infinia GE Hawkeye II), equipped with low energy high resolution (LEHR) collimators. The gantry performed a 90° rotation, thus covering 180° (dual-head) with thirty six projections using step and shoot acquisition and with total 2400 kcount. Matrix size 128 x 128 was used with window widths of the energy 20% by using a Tc99m source at 140 keV. The data was reconstructed by a filtered back projection method of Butterworth filter of order 10 and cut off frequency 0.4 cycles/cm was applied. The value of Chang's attenuation correction method was applied by selecting 0.164/cm linear attenuation coefficient. Image quality was analyzed by measuring contrast of lateral, anterior and septal defect using system software Xeleris 2.0. Images tomogram in Short Axis (SA), Vertical Long Axis (VLA) and Horizontal Long Axis (HLA) were also analyzed visually using MATLAB software with and without material filter. Results show that the contrast of the defect-to-healthy myocardium for lateral defect decreased with implantation of material filter compared to without filter, but for anterior defect the results were vice versa. For the septal defect there were slight decrease and increase for Zn 0.1mm and Zn 0.198mm compared to without filter, respectively. For the signal to noise ratio, with usage of Zn 0.1mm, the results show progression for lateral, anterior and septal defect compared to without the filter but is shown decrease for Zn 0.198mm. There was an insignificant decrease for left-ventricle-(LV) to-healthy myocardium contrast with implementation of material filter compared to without a filter. Qualitative analysis shown enhancement image quality for image obtains from Zn filter compared to without a material filter. So the application of the material filter in SPECT imaging has the potential to enhance the quality of the images, so it can increase the accuracy in the interpretation.

SP046 - Assessment of Radiotherapy Response

TRACK 04: RADIATION ONCOLOGY

SP046.1 - Early prediction of lung cancer recurrence after stereotactic radiotherapy using texture analysis of automatic graph cuts segmentations

Author(s): Sarah A. Mattonen¹, David A. Palma², Cornelis J.A. Haasbeek³, Suresh Senan³, Aaron D. Ward¹

¹Department Of Medical Biophysics, The University of Western Ontario, London/CANADA, ²Division Of Radiation Oncology, London Regional Cancer Program, London/CANADA, ³Department Of Radiation Oncology, VU University Medical Center, Amsterdam/NETHERLANDS

Purpose: Stereotactic ablative radiotherapy (SABR) is becoming a standard treatment option for patients with early-stage lung cancer, and can achieve local control rates comparable to surgery. However, following SABR benign radiation induced lung injury (RILI) appears as radiographic changes on computed tomography (CT) imaging. These changes can be tumour-mimicking, making it difficult to distinguish recurrence from benign RILI. Current approaches do not reliably detect recurrence within a year post-SABR. Our previous work has shown the ability of CT texture features calculated within manually delineated regions of interest to predict recurrence post-SABR. The purpose of this study was to evaluate the accuracy CT texture features extracted within automatically derived regions of interest for prediction of eventual tumour recurrence.

Methods: We analyzed 22 patients with 24 lesions (11 recurrence, 13 RILI). Two regions of common post-SABR changes were manually delineated: consolidative and ground-glass opacity (GGO), shown in red and green respectively in Figure 1. The consolidative regions were also automatically delineated using a *OneCut* graph cuts algorithm with the only operator input being the single line segment measuring tumour diameter, normally taken during the clinical workflow. Surrogate GGO regions were approximated by automatic expansion of the consolidative regions. Within the GGO regions, second-order texture features from grey-level co-occurrence matrices were calculated. Classification was performed using a linear Bayes normal classifier and evaluated using cross-validation (CV).

Results: Leave-one-out CV on images taken 2–5 months post-SABR showed robustness of the entropy texture measure, with classification error of 26% and area under the receiver operating characteristic curve (AUC) of 0.77 using the automatic segmentation; the results using a fully manual segmentation were 19% and 0.80 respectively. Using our fully automated approach, AUCs for this feature increased to 0.82 and 0.93 at 8–14 months and 14–20 months post SABR, respectively, suggesting even better performance nearer to the date of clinical diagnosis of recurrence.

Conclusions: Texture features calculated within GGO delineated from a fully automated algorithm using only an input diameter measurement have shown the potential to predict recurrence in individual patients within 6 months of SABR, eliminating the need for any manual delineations. Based on our ongoing validation on a larger sample, we aim to develop a computer-aided diagnosis system which can be integrated into a physician's workstation to improve their assessment of response post-SABR. This could allow for earlier salvage for patients with recurrence, and result in fewer investigations of benign RILI.

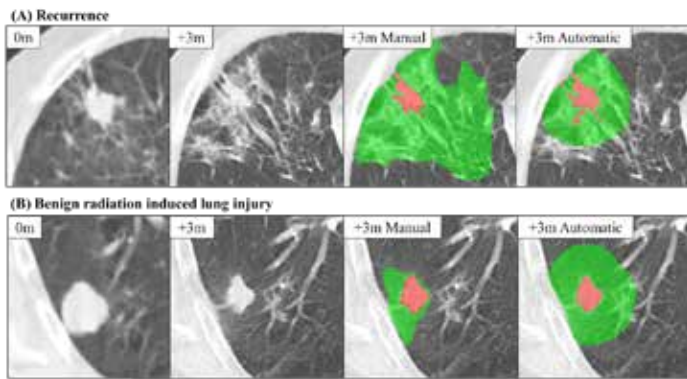
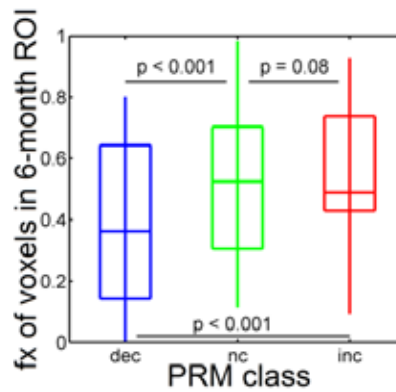


Figure 1: Manual and automatic delineations of post-SABR consolidative (red) and ground-glass opacity (green) findings at 3 months follow-up for a patient with recurrence (A) and radiation-induced lung injury (B). The zero-month (0m) time point indicates the pre-treatment lesion.



In summary, the PRM showed potential for predicting both global and voxel-wise treatment response, however, the relationship between the two could not be directly inferred suggesting that rigorous validation for each target demographic is needed if the PRM is to be used to guide locally adaptive RT.

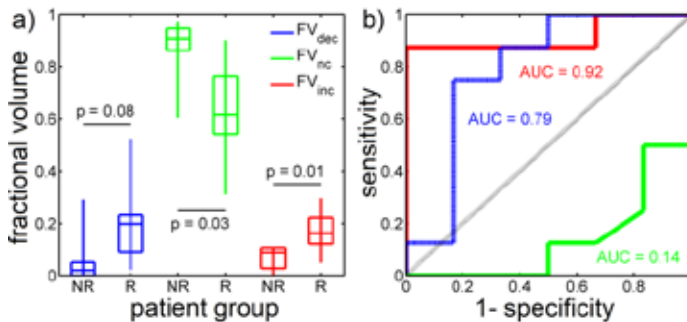
SP046.2 - Can parametric response maps predict voxel-wise treatment response? Implications for locally adaptive radiotherapy.

Author(s): Anthony Lausch¹, Timothy P.C. Yeung¹, Enrico Fainardi², Ting Yim Lee¹, Jeff Chen¹, Eugene Wong¹

¹Medical Biophysics, The University of Western Ontario, London/CANADA, ²Neuroradiology Unit, Department Of Neuroscience And Rehabilitation, Azienda Ospedaliero-Universitaria, Ferrara/ITALY

Parametric response map (PRM) analysis is a voxel-based image analysis method for predicting treatment response which shows promise as a means for guiding locally adaptive radiotherapy (RT) (e.g. sub-volume boosts). However to date, PRM predictive utility has been primarily verified with respect to global outcomes such as overall survival (OS). Here we investigated whether voxel-wise treatment response information can be inferred from a PRM analysis that has been correlated with OS.

PRMs were generated from rigidly registered MRI-derived apparent diffusion coefficient (ADC) maps (1 and 3 months post-RT) for n = 14 patients treated for high-grade glioblastoma. PRMs indicated whether each tumour voxel had undergone a significant increase, decrease, or no significant change in ADC. The fraction of the tumour volume (fractional volume) classified by the PRM as significantly increasing in ADC (FV_{inc}) was the only PRM measure found to be significantly correlated with OS ($\rho = 0.63$, $p = 0.02$, Spearman rank test). FV_{inc} values were then used to classify responding patients (R; OS > 18 months) in a receiver-operating characteristic analysis which produced an area under the curve of 0.92 (Fig. 1).



To investigate voxel-wise treatment response, the fraction of voxels in each PRM class that remained within the tumor boundary at 6 months post-RT was computed for each patient (Fig. 2). Despite the positive correlation with OS, significantly increasing ADC voxels (red) were found to be more likely to remain within the 6-month tumour volume compared to significantly decreasing voxels (blue) within the patient group.

SP046.3 - Using Magnetic Resonance Imaging Radiomics to Personalize Brain Metastases Treatment

Author(s): Sarah A. Mattonen¹, Timothy Pok Chi Yeung¹, George Rodrigues², Andrew Warner¹, Carol Johnson¹, Frank Lagerwaard³, Miguel Palacios³, Omar Bohoudi³, Aaron D. Ward¹

¹London Regional Cancer Program, London/CANADA, ²Department Of Oncology, The University of Western Ontario, London/CANADA, ³Radiation Oncology, VU University Medical Center, Amsterdam/NETHERLANDS

Purpose: For patients with brain metastases, early and accurate treatment selection is critical to maximizing quality of life and potentially extension to life. Prediction of response to stereotactic radiosurgery (SRS) informs personalized treatment selection. The classification of brain metastases as “homogeneous”, “heterogeneous”, and “ring-enhancing” has been shown to be predictive of overall survival (OS) after SRS [1], but is subject to inter-observer variability. Our objective was to improve OS prediction by developing and testing a radiomics software platform for quantitative assessment of brain metastases appearance.

Methods: Thirty-one brain metastasis patients (44 lesions) underwent routine gadolinium-enhanced T1 weighted magnetic resonance (MR) imaging prior to SRS. Each lesion was manually contoured and classified as “homogeneous”, “heterogeneous”, or “ring-enhancing” [1]. Image intensities were normalized using the brain ventricles as a statistical reference. Image features including the first-order image statistics, size and shape-based features, and gray-level co-occurrence (GLCM) textures averaged over 13 three-dimensional offsets were measured. Image features between the three contrast-enhancement groups were measured using the Kruskal-Wallis test followed by the Mann-Whitney U test. Correlations between image features and OS were evaluated using the Spearman correlation.

Results: The median time to compute 335 image features was 0.6 minutes/patient (range: 0.3 – 4.6) using a non-parallel and unoptimized MATLAB implementation. The three contrast-enhancement patterns showed significantly different first-order statistics ($P < 0.0025$) (Figure 1). Size and shape-based features and GLCM-based textures were not significantly different amongst the contrast-enhancement groups. Using the largest lesion in each patient as the index lesion, first-order energy showed a significant correlation with OS ($\rho = -0.61$, $P < 0.001$). Range, 90th percentile, 99th percentile, surface area, normalized radial length entropy, correlation, and cluster prominence showed marginal correlations with OS ($P < 0.05$).

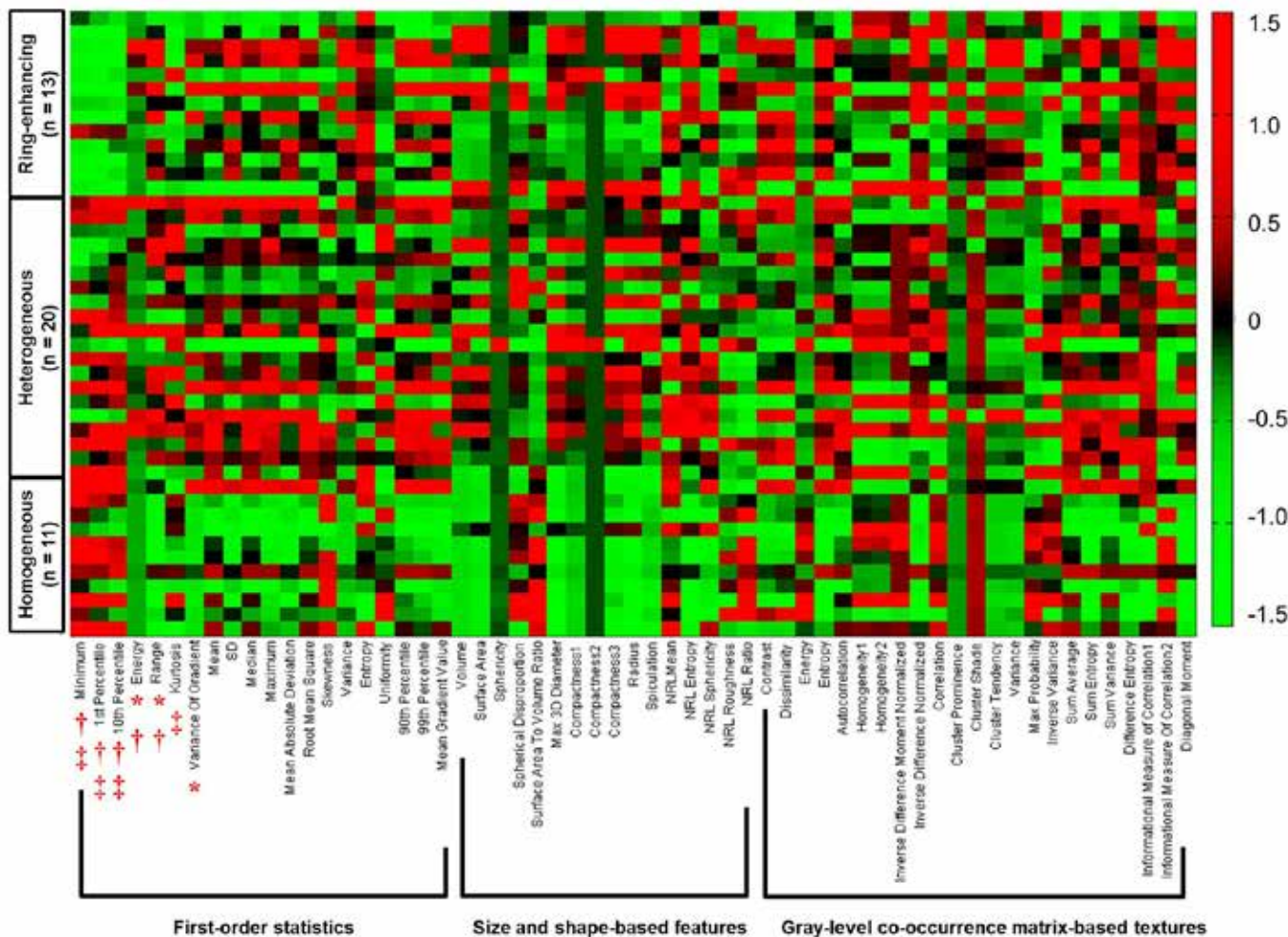


Figure 1. A heat map showing image features (columns) for each lesion (rows). Red and green indicate higher and lower standardized scores, respectively. (*), (†), and (§) represent significant differences between homogeneous vs. heterogeneous lesions, homogeneous vs. ring-enhancing lesions, and heterogeneous vs. ring-enhancing lesions, respectively. A Bonferroni-corrected $P < 0.0025$ was considered significant.

Conclusion: First-order image statistics calculated by our radiomics platform correlated with expert qualitative classification of contrast-enhancement patterns, and first-order energy correlated with OS. Future work includes optimizing the calculation of GLCM-based textures and determining a combination of image features that can accurately predict OS for individual patients.

Reference

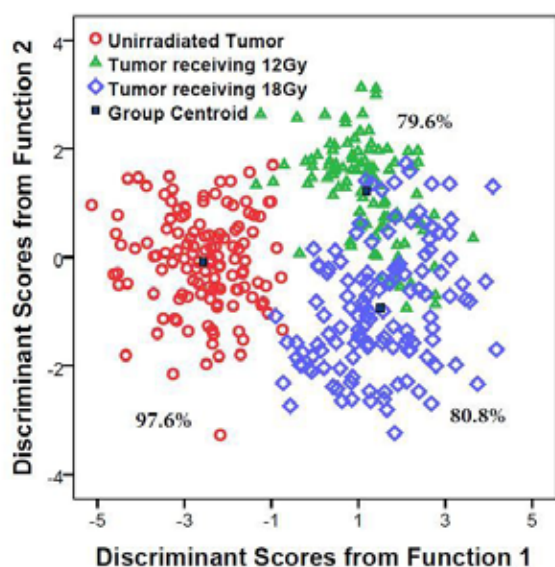
[1] Goodman KA, et al. *Int J Radiat Oncol Biol Phys.* 2001;50:139-46.

SP046.4 - Raman spectroscopy for assessment of radiation therapy response: Pre-clinical animal study results for lung cancer

Author(s): Suneetha Devpura¹, Ken Barton¹, Stephen Brown¹, Yingshu Zhang¹, Seema Sethi², Michael D. Klein³, Farzan Siddiqui¹, Indrin J. Chetty¹

¹Radiation Oncology, Henry Ford Health System, Detroit/MI/UNITED STATES OF AMERICA, ²Pathology, Wayne State University, Detroit/MI/UNITED STATES OF AMERICA, ³Pediatric Surgery, Children's Hospital of Michigan, Detroit/MI/UNITED STATES OF AMERICA

The purpose of this study is to explore whether Raman spectroscopy is able to assess the response of lung tumors and healthy lung tissue in mice following radiation therapy. 4T1 mouse breast cancer cells injected intramuscularly metastasize to the lungs at day 14. These, 4T1 cancer cells were injected subcutaneously into the flanks of 18 Balb/C female mice. Five additional mice were used as "normal lung" controls. After 14 days, cohorts of mice bearing tumors received 6, 12 or 18 Gy to the left lung with 6MV photons. Five mice were treated as "unirradiated tumor" controls. After 24-48 hours, lungs were excised and the specimens were sectioned for Raman measurements and pathologic evaluation using a cryostat-microtome. A total of 775 Raman spectra were collected; 107 from unirradiated normal lung tissues, 126 from unirradiated tumors, and 318 from tumors irradiated with 6, 12 or 18 Gy. Raman spectra were also collected from normal lung tissues of mice with unirradiated tumors (29) as well as irradiated (6, 12 or 18 Gy) tumors (195). Principal component analysis (PCA) and discriminant function analysis (DFA) were performed to analyze and interpret the results. Normal lung tissues and tumors were identified 100% of the time relative to pathologic scoring. Raman spectral data showed prominent results between unirradiated tumor and tumors receiving 12 or 18 Gy. Thus, in a model consisting of unirradiated and irradiated tumors (12 or 18 Gy) classification accuracies were 97.6%, 79.6%, and 80.8%, respectively, relative to pathologic assessment (see Fig.). Overall, 85.4% distinguishability was observed for unirradiated and irradiated (6, 12 or 18 Gy) normal lung tissues. Preliminary results demonstrate the promise for Raman spectroscopy in the prediction of normal vs. lung tumors as well as in the assessment of response of tumor and normal lung tissues following radiation therapy.



DFA plot for unirradiated tumors and irradiated lung tumors with 12 Gy and 18 Gy

SP046.5 - Serial 4DCT and 4DPET imaging to monitor response for locally-advanced non-small cell lung cancer patients undergoing combined chemotherapy and radiotherapy

Author(s): Jean-Pierre Bissonnette¹, Andrea Bezjak², Nathan Becker¹, Claudia Leavens¹, Doug Vines¹, Thomas G. Purdie¹, David Jaffray¹, Alexander Sun²

¹Radiation Physics, Princess Margaret Cancer Centre, Toronto/CANADA, ²Radiation Medicine Program, Princess Margaret Cancer Centre, Toronto/CANADA

Background

Recent research comparing serial PET imaging acquired pre-, post-, and during RT has demonstrated that not only the maximal uptake of 18F-fluoro-2-deoxy-glucose (FDG) within the tumor, but also the heterogeneous patterns of FDG uptake correlate with treatment outcome. We propose to utilize 4DCT with FDG 4DPET scans to monitor the response of patients treated for locally-advanced non-small cell lung cancer (LA-NSCLC) and correlate the observed changes with clinically-relevant endpoints and to point out which patients might require adaptation to improve their chances of successful therapy.

Materials and Methods

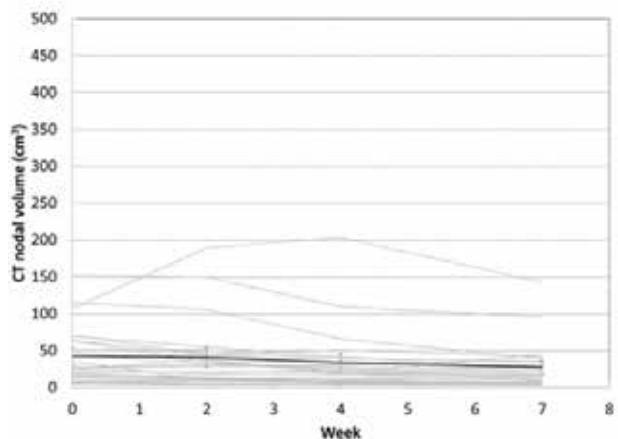
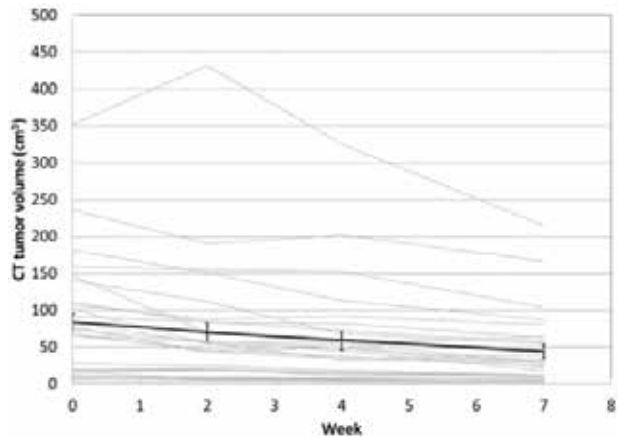
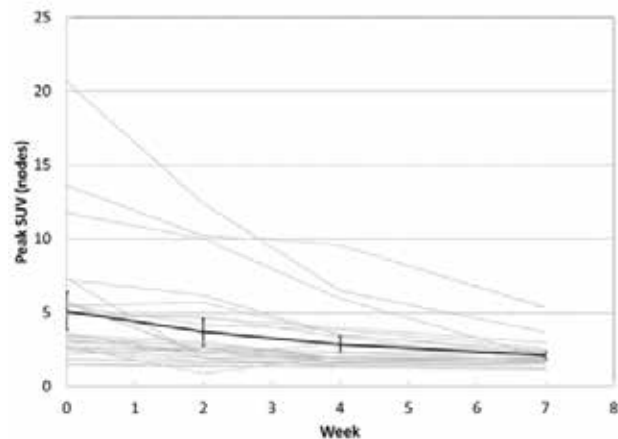
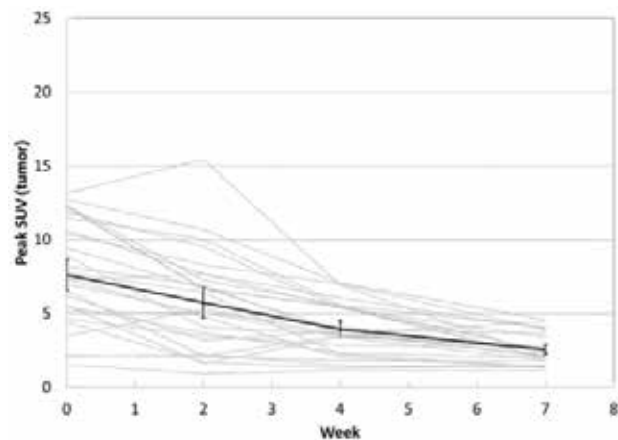
In this ethics-approved prospective study, we enrolled patients with LA-NSCLC receiving curative intent therapy. 4DCT and 4DPET images were acquired prior to (week 0) and during (weeks 2, 4, and 7) therapy. The gross tumor volume was contoured, for both the primary tumor (GTV-T) and for nodal disease (GTV-N) by experienced radiation oncologists on 4DCT datasets. PET image features derived from intensity volume histograms (i.e., SUVpeak, VSUV>3, V50% SUVmax) limited to the internal target volume were derived from matched PET images to identify tumoral (GTVPET-T) and nodal disease (GTVPET-N). Clinical outcomes at two years after treatment were recorded for all patients. All image features and the derivative of these features were tracked as a function of time point.

Results

32 patients were recruited, 27 completing all scans. On average, the GTV-T and GTV-N were reduced, at week 7 to 55±19% and 63±18% of their volume at week 0. Larger reductions were observed for all studied PET image features: on average, the GTVPET-T and GTVPET-N were reduced, at week 7 to 17±8% and 7±3% of their volume at week 0, and the SUVpeak was reduced by 33±4% and 41±8% for tumoral and nodal disease, respectively. On average, the maximum rate of change occurred early in the treatment for all image metrics considered in this study.

Conclusions

In a homogeneous LA-NSCLC population, we have shown, using serial 4DCT and 4DPET images acquired during chemo-radiotherapy, that tumor anatomy and physiology change at different rate, and that the maximal rate of change in image features occurs early into treatment. These results may help determine the optimal time for adaptation of therapy. Correlation of image features and their respective rates of change with clinical outcomes is ongoing.



SP046.6 - Evaluation and Visualization of Radiogenomic Modeling Frameworks for the Prediction of Normal Tissue Toxicities

Author(s): James Coates¹, Asha K. Jeyaseelan¹, Norma Ybarra¹, Jessie Tao¹, Marc David², Sergio Faria², Luis Souhami², Marie Duclos², Issam El Naqa¹, Fabio Cury²

¹Medical Physics Unit, Department Of Oncology, McGill University, Montreal/QC/CANADA, ²Division Of Radiation Oncology, McGill University, Montreal/QC/CANADA

We explore techniques for the evaluation and visualization of radiogenomic data-driven models in an effort to investigate the integration of genetic variations (single nucleotide polymorphisms [SNPs] and copy number variations [CNVs]) with dosimetric and clinical variables in modeling radiation-induced rectal bleeding (RB).

One hundred and twelve (N=112) patients who underwent curative hypofractionated radiotherapy (66 Gy in 22 fractions) between 2002-2010 were retrospectively genotyped for SNPs and CNVs in six genes: XRCC1, XRCC3, VEGFa, TGFβ1, ERCC2 and SOD2. A logistic regression modeling approach was used to assess the risk of severe RB (Grade≥3) using dosimetric, clinical and biological variables. Statistical resampling based on cross-validation was used to evaluate model predictive power and generalizability to unseen data. Principle component analysis (PCA) and vector biplots were used to visualize the quality of model fit.

Biological variable XRCC1 CNV showed good overall fit to RB outcome data (p<0.001). When added to the logistic regression modeling, XRCC1 CNV improved classification performance over standard dosimetric models by 33.5%. No clinical variables were found to adequately fit the data.

As a proof-of-concept, we demonstrated that the combination of genetic and dosimetric variables could provide significant improvement in NTCP prediction using data-driven approaches. Moreover, we have shown that visualization techniques could aid in interpreting multivariate model predictions.

SP047 - Dose Calculation: Part 2

TRACK 04: RADIATION ONCOLOGY

SP047.1 - Non-Standard IOERT Dose Distributions Scenarios by Monte Carlo Studies

Author(s): Alessandro Esposito¹, Taxiarchis Sakellaris¹, Patricia Limeide¹, Filipa Costa², Luís T. Cunha³, Anabela G. Dias³, Joana Lencart³, Sandra Sarmento³, Carla C. Rosa¹

¹INESC TEC, Porto/PORTUGAL, ²Medical Physics, Radiobiology and Radiation Protection Group, Research Centre, Portuguese Institute of Oncology, Porto/PORTUGAL, ³Medical Physics Department, Portuguese Institute of Oncology, Porto/PORTUGAL

In Intra-Operative Electron Radiation Therapy (IOERT) electron beams of high energy are used during surgical interventions, due to their short range and low penetration. This technique allows the direct irradiation of the treatment area, minimizing the dose in adjacent tissues. Due to the complexity of the abdominal and pelvic region sometimes the radiation field includes sensitive and/or uneven tissues.

To study the influence on dose distributions of several factors, such as shielding and irradiation of non-flat surfaces, the Monte Carlo simulation codes BEAMnrc and EGS++ were used to model a Varian Clinac 2100 CD linear accelerator, its hard docking system, IOERT applicators, and water phantom. The simulation model is validated under reference conditions (i.e. dose distributions in a homogeneous water phantom), using the gamma function, with a 2% difference dose and 2mm distance to agreement (DTA) as validation criteria, resulting in 98.3% of concordance between measured and simulated data.

A measurement with a 1cm radiotherapy bolus slab, placed over 16 parallel solid water plaques with gafchromic film in the middle, was also used as validation criterion for a non-standard condition (figure 1), where good agreement was achieved, allowing to use the model for further studies. In figure 2 the dose distribution deformation effect of an irregular surface with respect to the flat condition, is reported, showing a dominant central area of increased absolute dose, linked to distortion of lateral equilibrium. Further studies have been conducted on the effect of shape, dimensions and shielding material, particularly focusing on the case of pelvic region, using a geometrical model of the sacrum bone curvature.

The results obtained will allow a better understanding of dose distributions in pelvic IOERT, which is fundamental both to improve the technique and assess its efficacy, as well as to interpret results from in vivo dose measurements.

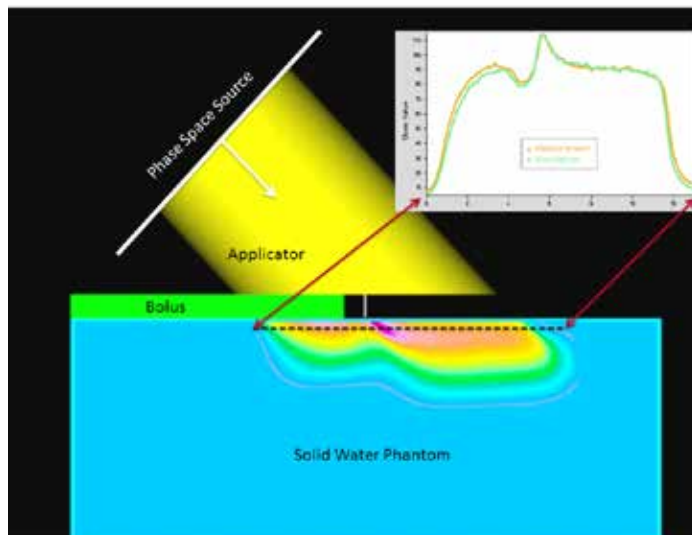


Figure 1 - Non-standard validation condition - dose distribution on tissue equivalent volume, with 1cm thickness of bolus material and 45° beveled applicator of 8cm diameter for a 9MeV beam energy.

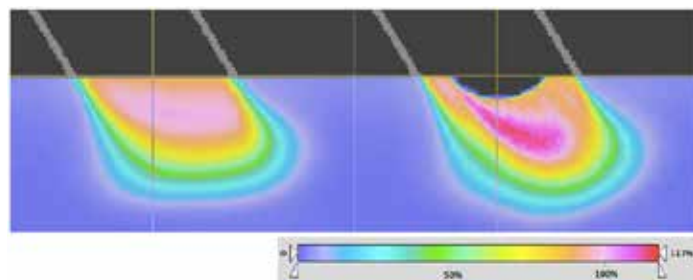


Figure 2 - Dose distribution on tissue equivalent volume, for a 12MeV beam energy, with overlay of 50° beveled applicator of 6cm diameter: flat (left) and curved (right) surface.

SP047.2 - Validation of a Commercial GPU-Based Monte Carlo Dose Calculation Algorithm for use with an Elekta MRI-Linear Accelerator

Author(s): Moti R. Paudel¹, Anthony Kim², Syed Ahmad³, Arman Sarfehnia¹, Stephanie Lim-Reinders⁴, Sami Hissouiny⁵, Michel Moreau⁵, Arjun Sahgal¹, Brian Keller⁶

¹Department Of Radiation Oncology, University of Toronto, Toronto/ON/CANADA, ²Department Of Medical Physics, Sunnybrook Health Sciences Centre, Toronto/ON/CANADA, ³Sunnybrook Research Institute, Toronto/CANADA, ⁴Department Of Physics, University of Toronto, Toronto/ON/CANADA, ⁵Elekta, Maryland Heights/MO/UNITED STATES OF AMERICA, ⁶Institute Of Medical Science, University of Toronto, Toronto/ON/CANADA

Purpose: A treatment planning algorithm from the commercial vendor Elekta™ has been developed to be used with a future MRI-linear accelerator (MRI-LINAC). This is a GPU-based Monte Carlo dose calculation algorithm (GPUMCD) that is capable of modelling the magnetic field (B-field) associated with the MRI-LINAC. The purpose of this work is two-fold 1) to validate the algorithm without the presence of the Bfield as this algorithm can also be used to model a standard linac, and 2) to validate this algorithm, with the B-field activated, against an independent Monte Carlo algorithm (Geant4), as will be the case with the MRI-LINAC.

Methods: The research version of the Monaco TPS version 5.09.05 was used. This version contains the GPUMCD algorithm in addition to the XVMC algorithm that is in current clinical use. For the initial validation of the TPS for a standard linac, a beam model was created for an Elekta Agility linac for 6 MV. A heterogeneous phantom, simulating either bone-in-tissue, lung, tumour-in-lung, or steel-in-tissue, was designed and built to compare radiochromic film

measurements with the ability of the TPS system to model the dose. We compared film measurements with the Monaco GPUMCD and XVMC algorithms and with the Pinnacle collapsed cone algorithm (CCC). In terms of Bfield validation, an independent MC algorithm, Geant4 version 4.10, is being used to compare against Monaco.

Results: For the standard validation (no B-field), film measurements were done in the heterogeneous phantom for field sizes ranging from 1x1 to 10x10 cm², where a tumour in a lung was simulated, and these were compared with Monaco (1x1x1 mm³ dose grid resolution and 0.5% statistical uncertainty) and with Pinnacle. Our preliminary results indicate that Monaco GPUMCD algorithm shows good agreement with measurements for the comparisons done thus far. The largest differences were seen for the 1x1cm² field size, where the measured dose, in the lung region, was higher by 3.5% (compared to GPUMCD), 10% (compared to XVMC) and 14% (compared to CCC). Doses were relative to the depth of dose maximum and uncertainties will be discussed. There was negligible difference between the Monaco GPUMCD and XVMC algorithms for the other field sizes. The results for the B-field modeling are currently being generated and will be presented.

Conclusions: The Monaco GPUMCD algorithm showed good agreement with measurements. The agreement for this algorithm appears better at the small field sizes compared to Monaco XVMC and Pinnacle CCC algorithms.

SP047.3 - A Dosimetric Evaluation of Interface Effects Using Two Commercial Electron Treatment Planning Algorithms

Author(s): Benjamin Catt, Mark Yudelev
Radiation Oncology, McLaren - Macomb, Mt. Clemens/UNITED STATES OF AMERICA

Purpose: In this work, we investigate the accuracy of two commercial Monte Carlo algorithms used for electron treatment planning. In particular, the dose distribution near an interface in a heterogeneous phantom is compared with results obtained from measurements and calculations using EGSnrc.

Methods: Phantoms were constructed and modeled in Eclipse 10.0 (Varian) and Monaco 5.0 (Elekta) treatment planning systems. Slabs of aluminum and bone equivalent material were inserted one at a time into a stack of solid water and situated at 2.9 cm depth, equivalent to dmax for a 12 MeV electron beam. This setup was chosen as an exaggeration of any clinically relevant inconsistencies which may be seen near interfaces. Plans were run on these phantoms and central axis depth doses were compared with results obtained using similar phantoms within EGSnrc. The measurements were performed in a 12 MeV electron beam from a Varian 21 iX linear accelerator using an Exradin A10 parallel plate chamber.

Results: General agreement was observed between calculated and measured dose distributions along the beam's central axis in the regions away from the heterogeneity; however, Varian's eMC algorithm could not properly account for backscatter from higher density materials, instead predicting a decrease in dose just before the interface. This leads to an underestimation of dose by up to 12% near the interface with an aluminum heterogeneity, when compared with ion chamber measurements. Elekta's VMC++ algorithm was able to more accurately account for the presence of the backscatter material, demonstrating an agreement within 1.3% of ion chamber measurements in the region before the interface.

Conclusions: Although Monte Carlo algorithms are widely regarded as the gold standard for accuracy, care must still be taken when using implementations which have been optimized for calculation efficiency, especially within regions lacking electronic equilibrium such as those found near interfaces with bone.

Backscatter factors*		
	Aluminum	Bone
EGSnrc	1.076	1.029
Monaco	1.080	1.055
eMC	0.975	0.988
Measured	1.095	1.042

*Calculated and measured backscatter factors at 1 mm from the heterogeneity of interest.

SP047.4 - 4D Monte Carlo simulation for verification of delivered dose to deforming anatomy

Author(s): Sara Gholampourkashi¹, Miro Vujicic², Raanan Marants¹, Jason Belec², Joanna Cygler³, Emily Heath¹
¹Physics, Carleton University, Ottawa/ON/CANADA, ²Medical Physics, Ottawa Hospital Cancer Center, Ottawa/ON/CANADA, ³Radiation Medicine Program, The Ottawa Hospital Cancer Centre, Ottawa/CANADA

Objective: To develop a dose calculation method using 4D Monte Carlo (MC) simulations that accurately reconstructs and verifies the dose delivered to a moving anatomy during radiotherapy treatments. The method is to be used for accurate dose calculations of dynamic radiation therapy treatment plans such as VMAT (Volumetric Modulated Arc Therapy) and IMRT (Intensity Modulated Radiation Therapy).

Methods: Quasar respiratory motion programmable phantom was used for measurements with an Elekta Agility linac. A square beam of size 4x4 cm² was chosen to cover the tumor (1.5 cm radius) inside the lung insert of the phantom and the source to axis distance (SAD) was 100 cm. The beam was delivered to the phantom in static (no motion) and moving (1.8 cm respiratory amplitude) states. Doses were measured using calibrated EBT3 film and RADPOS 4D dosimetry system.

Treatment planning was performed with XiO Treatment Planning System (TPS). Dose calculated by XiO was compared against results from measurements and MC calculations.

The EGSnrc user code BEAMnrc was used for simulating photon beams from the Elekta Agility linac. The DOSXYZnrc and defDOSXYZnrc user codes were used, respectively, for static and deforming anatomy dose calculations on the phantom file created from 4D CT-scans of the Quasar phantom, using the same beam configurations as in measurements. Dose calculation voxels were 0.25x0.25x0.6 cm³. Varian's Velocity software was used to perform the deformable image registration of the tumor in different respiratory phases to the tumor in the static anatomy. Deformation vectors were then extracted and input to the defDOSXYZnrc code to model the phantom motion during the dose calculation.

Results: Table 1 shows the calculated and measured tumor doses and their uncertainties.

Phantom	Dose (cGy)				%Diff					
	TPS	MC	Measured		MC/TPS	Film/TPS	RADPOS/TPS	Film/MC	RADPOS/MC	Film/RADPOS
			Film	RADPOS						
Static	120.7 ± 1	121.1 ± 0.6	118.9 ± 2.4	116.9 ± 2.4	0.3%	-1.5%	-3.1%	-1.8%	-3.5%	1.7%
Dynamic	-	110.9 ± 0.7	108.5 ± 2.2	112.7 ± 2.3	-	-	-	-2.2%	1.6%	-3.7%

Conclusions: Our work demonstrates that 4D Monte Carlo calculations using the defDOSXYZnrc code is an accurate method to calculate dose delivered in a moving anatomy.

This work was supported by OCAIRO grant.

SP047.5 - Clinical implementation of an EPID-based *in vivo* dose verification system for SBRT-VMAT delivery; catching errors

Author(s): Peter Mccowan¹, Eric Vanuytven², Timothy Van Beek², Ganiyu Asuni², Boyd Mccurdy¹

¹Physics And Astronomy, University of Manitoba, Winnipeg/CANADA, ²Medical Physics, CancerCare Manitoba, Winnipeg/CANADA

Introduction: Most linear accelerators (linacs) used for radiotherapy are equipped with a mega-voltage electronic portal imaging device (EPID). Literature has determined the EPID to be a reliable dosimetric device. The portal dosimetry research group at CancerCare Manitoba has developed a set of physics-based tools which utilize measured EPID data acquired during treatment in order to reconstruct the 3D *in vivo* dose delivered to the patient. Our model can also predict the *in vivo* dose similar to a treatment planning system (TPS). Due to the hypofractionated regimen of stereotactic body radiation therapy (SBRT) treatments, a verification of the inter-fractional dose could provide additional safety for the patient because any error in delivery, when compared to conventional treatments, would have a greater radiobiological impact on the patient. In this study, the results of a one year clinical implementation test of our dose verification system will be presented for lung and spine SBRT-VMAT treatments.

Methods: Our *in vivo* model employs an inverse dose reconstruction method which combines a back-projected measured EPID focal fluence and a predicted linac-head extra-focal fluence. The primary *in vivo* patient dose is calculated by taking the total incident fluence on the patient, converting it to TERMA, and performing a collapsed cone convolution with Monte Carlo derived point-based dose deposition kernels. *In vivo* patient scatter dose is calculated through convolutions of the incident fluence with a library of Monte Carlo derived patient scatter kernels. Heterogeneities are accounted for through radiological scaling of the dose deposition and scatter kernels via electron densities from CT data.

Overall, 43 lung and 13 spine patients were treated over roughly a one year period using a Varian 2300ix model linac operated in 6MV SRS-mode. Continuous EPID images were acquired every 1.25-2.50 seconds. Fractions sizes were between 1 and 8 while doses were in the range of 6 to 24Gy. All per-fraction data were compared to the Eclipse TPS dose calculation. Mean percentage dose differences and 3%/3mm gamma analyses were performed to compare the low dose voxel (LDV) regions (containing 20% of prescribed dose) and the high dose voxel (HDV) regions (containing 80% of prescribed dose).

Results: Three of the lung patients had significant errors in all fractions: mean HDV percentage differences and gamma pass rates were 10-20% and 50% respectively. A review of these three and seven other patient treatment histories (with less significant differences) revealed errors due to anatomical changes, patient setup, planning, as well as disruptions in EPID image acquisition. An average gamma pass rate of 90.6±8.3% and mean percentage dose difference of 4.8±1.9% were determined in the HDV region for the 'other' 40 lung patients. Due to the greater complexity and heterogeneity of the spine treatments slightly less agreeable results were determined.

Conclusion: A robust, EPID-based *in vivo* dose verification system has been employed clinically to test its feasibility in capturing inter-fractional SBRT-VMAT delivery errors. Significant errors were found which should encourage a full clinical implementation.

SP047.6 - pGPUMCD, a GPU-based Monte Carlo proton transport code

Author(s): Daniel Maneval¹, Benoît Ozell², Philippe Després¹

¹Département De Physique, De Génie Physique Et D'optique, Université Laval, Québec/QC/CANADA, ²Département Génie Informatique Et Génie Logiciel, École polytechnique de Montréal, Montréal/QC/CANADA

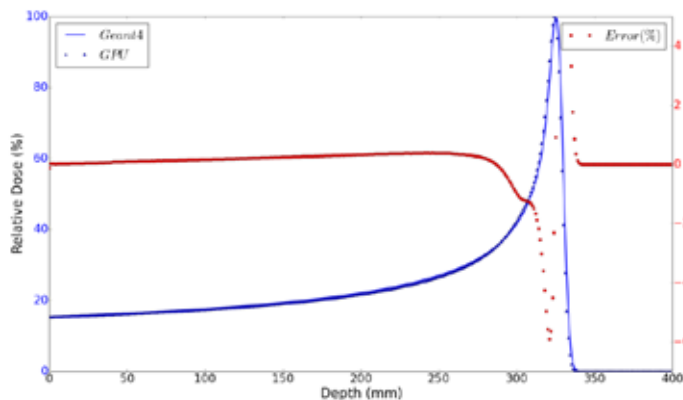
Purpose : The most accurate dose calculations in proton therapy result from Monte Carlo algorithms. However their clinical implementation remains problematic due to long computation times. To accelerate these simulations, a GPU-based Monte Carlo transport code was developed. pGPUMCD is an adaptation for protons of GPUMCD, a validated GPU-based Monte Carlo code for photons and electrons. Implementation strategies and validation results are presented in this work.

Methods : In pGPUMCD, protons are transported in a voxelized geometry by a class II condensed history approach with a continuous slowing down approximation. Energy straggling is considered as well as multiple scattering. Ionizations are modelled and secondary electrons are not transported. Moreover, elastic and non-elastic nuclear interactions in water are considered based on an empirical model. pGPUMCD was benchmarked against Geant4. Simulations consisted in a mono-energetic, mono-directional circular proton beam of radius 1 cm impinging normally homogeneous or heterogeneous phantoms. Relative statistical uncertainties were derived from a history by history scheme and were below 1% in 1 mm³ cubic voxels containing 50% of the maximal dose. A Geforce GTX Titan was used in pGPUMCD while Geant4 simulations were done on a

Xenon-based CPU cluster. The evaluation of GPU/CPU acceleration was carried out without computation of statistical uncertainties and with a single 3.3 GHz Intel Core i3-3220 CPU.

Results : Considering only electromagnetic processes, proton transport with pGPUMCD yielded results within 6% of Geant4 values, with the largest errors in the Bragg peak for a speed-up factor of at least 300 compared to a single-core CPU execution. The transportation of one million protons of 230 MeV took 50 seconds with pGPUMCD and eight hours with Geant4. A complete dose validation is under evaluation with Bragg peaks, dose profiles and gamma studies for several materials and different energies.

Conclusion : GPUMCD now allows proton transport with pGPUMCD. Preliminary results suggest good agreement with Geant4 and significant savings in terms of computation times. Nuclear reactions in water were implemented in pGPUMCD and the validation is under investigation as well as the improvement of efficiency and computation time.



SP048 - Dosimetry of Protons and Heavy Ions

TRACK 05: DOSIMETRY AND RADIATION PROTECTION

SP048.1 - An Attempt to Predict the Proton Relative Biological Effectiveness using Radical Recombination

Author(s): Kiyofumi Haneda

Hiroshima international university, Higashihiroshima/JAPAN

Most proton treatment facilities have adopted a relative biological effectiveness (RBE) of 1.1 for proton therapy. However, most of the in vitro and in vivo studies indicate that the RBE of the spread-out Bragg peak (SOBP) protons increases with depth. The increase in RBE of proton beams on the SOBP is a well-known phenomenon that is difficult to quantify accurately in vivo studies. The reason for this explains that the RBE increases as linear energy transfer (LET) increases within the SOBP. The fact that intra-track radical recombination can indicate to produce fully competent lesions in room. The purpose of this study was to analyze an impact on radical recombination for the RBE in the SOBP proton beams. First, a depth-dose curve for the 210 MeV proton beam measured using a gel dosimeter and an ionization chamber. Second, the spatial distribution of the physical dose was calculated by Monte Carlo code system PHITS; the role of nuclear interaction was taken into account and the geometry of the apparatus was faithfully reproduced. The simulation results were compared with measured the depth-dose distribution and very good agreement was found, and the spatial distribution of an LET-weighted dose with threshold LET value (4.9 keV/μm) was calculated by the same code. Then, the relative distribution of the radical-recombination was calculated from the physical dose and LET-weighted dose. The relative distribution of the radical-recombination was calculated at each depth as the quotient of relative dose obtained using physical and LET-weighted dose. The agreement between the relative distributions of radical-recombination and RBE was good at the SOBP.

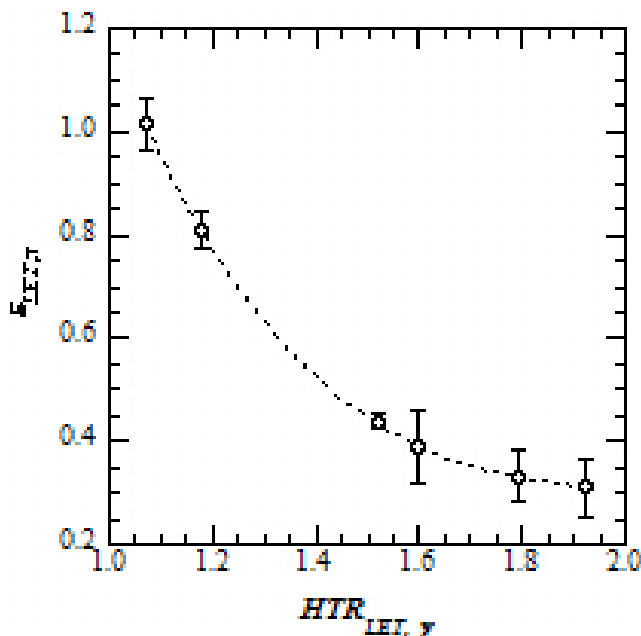
SP048.2 - A correction method for absorbed dose estimation using TEP-TLSD/SR1 in therapeutic carbon beam

Author(s): Weishan Chang¹, Yusuke Koba², Shigekazu Fukuda², Genichiro Wakabayashi³, Hidetoshi Saitoh¹, Kiyomitsu Shinsho¹

¹Radiological Sciences, Tokyo Metropolitan University, Tokyo/JAPAN, ²National Institute of Radiological Sciences, Chiba/JAPAN, ³Kinki University, Osaka/JAPAN

Introduction: TEP-TLSD/SR1, a slab type tissue-equivalent thermoluminescence dosimeter, has the advantage of acquiring 3D dose distribution in a single irradiation. This property is favorable to be a QA tool for radiotherapy. One of the difficulties by means of TLDs in heavy ion dosimetry is the LET dependence of thermoluminescent (TL) efficiency. It has been reported that LET dependence of TEP-TLSD/SR1 can be observed in not only the TL efficiency but also glow curve. The high temperature ratio (HTR) estimated using glow curve is a function of LET. Therefore it is possible to correct TL efficiency without information of LET for therapeutic carbon beam dosimetry. **Purpose:** The relation between HTR and TL efficiency is clarified and the feasibility of TEP-TLSD/SR1 for carbon beam dosimetry is evaluated. **Methods:** An in house TL readout system was used to obtain the glow curve with high accuracy and low uncertainty. Each TLD chip was calibrated individually by absorbed dose to water in ⁶⁰Co γ-rays. The TLD chips were irradiated by a 290 MeV carbon beam to clarify the relationships of HTR vs. LET (*HTR-LET*) and TL efficiency vs. LET (*εLET*). *HTRLET* and *εLET* at ⁶⁰Co γ-ray were normalized to 1. The normalized TL efficiency (*εLET*, Y) as a function of HTR (*HTRLET*, X) was obtained from two relation-

ships HTRLET and ϵ LET. The feasibility of HTR correction for the TEP-TLSD/SR1 was evaluated using a carbon beam. **Results:** The HTR increased with LET, and TL efficiency showed exponential decrease with increasing LET. Dose difference at SOBP region reduced from 20-30% to 10-20% after HTR correction. **Conclusion:** A correction method for determination of absorbed dose in therapeutic carbon beam using TEP-TLSD/SR1 was developed.



The normalized TL efficiency as a function of HTR.

SP048.3 - Biologically-weighted dosimetric quantities based on a multiscale approach

Author(s): Heidi Nettelbeck¹, Hans Rabus¹, Hugo Palmans², Marion Bug¹, Massimo Pinto³, Carmen Villagrasa⁴, Marta Bueno⁴, Sylvain Meylan⁴, Pedro Teles⁵

¹Fundamentals Of Dosimetry, Physikalisch-Technische Bundesanstalt (PTB), Braunschweig/GERMANY, ²Radiation Dosimetry, National Physical Laboratory, London/UNITED KINGDOM, ³Istituto Nazionale di Metrologia delle Radiazioni Ionizzanti (ENEA-INMRI), Santa Maria di Galeria/ITALY, ⁴Institut de Radioprotection et de Sûreté Nucléaire (IRSN), Fontenay-aux-Roses/FRANCE, ⁵Instituto Superior Técnico, Campus Tecnológico e Nuclear (IST-CTN), Sacavém/PORTUGAL

Particle therapy with protons and ions has gained increasing interest and its use has grown worldwide. Due to the different biological dose response of these types of radiation compared to high-energy photon beams, the current approach of treatment prescription is based on the product of the absorbed dose to water and a biological weighting factor. This method, however, is insufficient for quantifying the biological outcome of radiation, hence the need to define new dosimetric quantities that allow a separation of physics and biological processes.

“Biologically-weighted quantities in radiotherapy” (BioQuaRT) [1], a joint research project funded within the European Metrology Research Programme, uses a multiscale approach to lay the foundation for such new dosimetric quantities. This approach involves simulation and experimental techniques to determine the physical properties of ionising particle tracks on different length scales from a few nanometres (diameter of DNA) to micrometres (size of cell

nucleus), which are then correlated with biological effects of radiation.

The present work focuses on the simulation aspect of the project – the development of a comprehensive multiscale simulation tool [2] that incorporates radiation interaction cross sections with DNA and production rates of radical species. This simulation tool is used to relate track structure characteristics at the nano- and micrometre level to biological consequences of radiation interaction, such as DNA strand breaks. This work has led to the development of existing Monte Carlo simulation codes dedicated to radiobiology, in particular PTrA [3] and Geant4-DNA [4], which is used as a base for the simulation tool. The incorporation of interaction cross sections of DNA-substitute materials (rather than the conventional use of water) as well as fragmentation cross sections used to derive DNA strand break probabilities are among the improvements.

This multiscale approach has the potential to underpin the definition of new biologically-weighted dosimetric quantities relating track structure to relative biological effectiveness in proton and ion beam therapy.

References:

- [1] Project website: <http://www.ptb.de/emrp/bioquart.html>.
- [2] H. Palmans, H. Rabus, et al., British J. Radiol. 88: 20140392 (2015)
- [3] B. Grosswendt, Radiat. Prot. Dosim. 110, 789 (2004)
- [4] S. Incerti et al., Med. Phys. 37, 4692-4708 (2010)

Acknowledgements: The EMRP is jointly funded by the participating countries within EURAMET and the European Union.

SP048.4 - Studies of Helium and Carbon Ion Fragmentation processes in Water and in PMMA, using versatile Semiconductor Detectors

Author(s): Giulia Arico¹, Jan Jakubek², S Pospisil², Naruhiro Matsu-fuji³, Oliver Jäkel⁴, Maria Martisikova¹

¹Heidelberg University Hospital, Heidelberg/GERMANY, ²Institute of Experimental Applied Physics (IEAP), Prague/CZECH REPUBLIC, ³National Institute of Radiological Sciences, Chiba/JAPAN, ⁴Heidelberg Ion-Beam Therapy Center (HIT), Heidelberg/GERMANY

Background/Purpose:

Heavy ion radiotherapy enables a more conformed dose distribution to the target than conventional radiotherapy. Moreover, helium and carbon ions have additional advantages when compared to protons, such as a narrower penumbra. However, ions heavier than protons may undergo nuclear fragmentation processes within the patient. The consequence is a spectrum of lighter fragments which affect the delivered biological dose distribution. Currently there is a lack of knowledge regarding ion nuclear fragmentation processes. Our research aims to provide some of the relevant data. The information gained in this study might be used to benchmark Monte Carlo codes and to improve the accuracy of the treatment planning systems.

Materials and Methods:

We use a single particle registration technique to compare the fragments arising from ion beams crossing water and polymethyl methacrylate (PMMA), for different target thicknesses. Solid PMMA is often used in dosimetric measurements to replace water phantoms. The used Timepix detectors [Llopart et al. NIM A 581, 2007], developed by the Medipix collaboration, have a sensitive area of 1.4 cm² (256x256 pixels, 55x55 um pitch) and 300 um or 500 um

thick silicon sensors. The fragmentation processes in water and in PMMA targets are compared, using ion beams with initial energies of 150 MeV/u (helium) and 290 MeV/u (carbon). The detectors are simultaneously placed in front (for beam monitoring) and behind the target. They enable to detect single particles and to measure particle position, arrival time and energy loss in the detector. The characteristics of the registered signal depend on the particle type and energy. Therefore, the signal features are exploited to differentiate between the particle species [Hartmann B. (2013), PhD Thesis, Univ. Heidelberg]. Moreover, particle tracks are reconstructed using several detector layers.

Results:

With the presented experimental setup, we analyse: 1) the percentage of primary ions which undergo fragmentation processes; 2) the number and kind of fragments arising from single primary ions; 3) the relative number of created fragments, for each fragment species; 4) the lateral particle distributions. Comparing the results obtained in water and PMMA targets with same water equivalent thickness, good agreement is achieved in thin targets, while greater differences are obtained above 100 mmw-eq of thickness. Monte Carlo simulations are also performed, for comparison.

Conclusions:

Timepix detectors are small and highly flexible devices, which enable to study fragmentation processes very close to the target. The presented comparison of ion fragmentation processes occurring in water and PMMA phantoms shows some limits in the equivalence of these two materials. The differences become higher with increasing the target thickness and should be carefully taken into account when PMMA is used in place of water for dosimetric purposes.

Acknowledgments:

Measurements are performed at the HIMAC and HIT facilities. This research is funded by the Deutsche Krebshilfe (project 110296) and by the JSPS (project PE14770). This work is carried out as research project 14H339 at NIRS-HIMAC, and in frame of the Medipix collaboration.

SP048.5 - Monte Carlo study of secondary neutron dose for multipurpose nozzle in proton therapy

Author(s): Sungkoo Cho¹, Jin Sung Kim¹, Dae-Hyun Kim¹, Eun Hyuk Shin¹, Youngyih Han¹, Sang Hoon Jung¹, Yoonsun Chung¹, Junggho Kim², Hyeonser Park²

¹Department Of Radiation Oncology, Samsung Medical Center, Seoul/KOREA, ²Center For Ionizing Radiation, Korea Research Institute of Standards and Science, Daejeon/KOREA

Two full rotating gantry with different nozzles (Multipurpose nozzle and Scanning Dedicated nozzle) with conventional cyclotron system is installed and under commissioning for various proton treatment options at Samsung Medical Center in Korea. Currently, an issue in proton therapy is to evaluate the influence of the secondary neutrons produced by nuclear interactions with the modules of nozzle and proton beam. In our proton facility, the multipurpose nozzle was composed of many modules such as scatterer, ridge filter, multi-leaf collimator (MLC), compensator, and aperture. Therefore, the purpose of this study is to investigate neutron dose in multipurpose nozzle for proton beam with Monte Carlo simulation.

A Monte Carlo studies with the Geant4 toolkit were performed based on multipurpose nozzle's geometry (MLC, compensator, aperture, ridge filter, scatterer and etc) given by Sumitomo Heavy Industry and secondary neutron dose was simulated with 230 MeV proton beams and 5 cm SOBP using a 10 x 10 cm² brass aperture

in a 40 x 30 x 30 cm³ water phantom. At first, we calculated the neutron energy spectrum at water phantom surface. Next, we calculated neutron dose at isocenter, 20, 40, 60, 80, 100 cm distance from isocenter and compared with other research groups.

We used the phase space option of Geant4 toolkit to reduce the simulation time for repeated calculations and calculated neutron energy spectrum binned in 30 keV intervals on water phantom surface for wobbling beam at multipurpose nozzle. The portion of neutrons in the total neutron energy spectrum with energies less than 1 MeV and greater than 165 MeV were 53.5% and 43.8%, respectively.

Next, we calculated neutron dose at isocenter, 20, 40, 60, 80, 100 cm from isocenter and 2 different depths (surface and mid-SOBP) for the proton beam with and without water phantom. At a distance of 20 cm from isocenter, the neutron dose rapidly decreased because of the relatively small magnitude of the dose after lateral profile of the proton beam. In the water phantom, low energy neutrons were captured by an absorbing material (water) and high energy neutrons lost energy by inelastic collisions.

Neutron dose to water phantom for multipurpose nozzle under proton treatment conditions was simulated. The results of this showed comparable results with measured or simulated neutron dose of other proton therapy center. In future studies, we plan to investigate experimental measurement of neutron dose and validation of simulation data for treatment beam with additional neutron dose reduction method.

SP048.6 - Investigation of the uncertainties involved in the low energy proton interaction in different MC-codes for proton therapy application

Author(s): Lalageh Mirzakhania¹, Valerio Giusti², Shirin A. Enger¹
¹Medical Physics Unit, McGill University, Montreal/CANADA, ²Dept. Of Civil And Industrial Engineering, University of Pisa, Pisa/ITALY

Background: High precision external radiation therapy can be delivered by protons with a strongly increasing energy deposition that creates a narrow peak of dose, called the Bragg peak at the end of the particle's range and with sharp lateral dose fall-off, allowing to tailor the dose distribution to the target volume. The Monte Carlo (MC) method is an accurate and rigorous tool to simulate radiation transport and score energy deposition in heterogeneous media such as the human body. MC techniques have been implemented clinically for dose calculations in radiotherapy. The electromagnetic processes are well validated in different MC-codes, however there are discrepancies in nuclear models for low energy protons and therefore production of secondary particles such as neutrons. Neutrons contribute to out of field dose and in the long term may cause secondary cancers especially in children and young adults.

Aim: To Implement more accurate physics models and cross section for low energy proton interactions to be able to study secondary cancer induction related to primary protons in a clinical set up.

Method: Depth dose measurements were performed in the Svedberg Laboratory (TSL) proton therapy center at Uppsala University, Sweden, for a Gaussian shaped, mono-energetic beam with an energy of 178.25 ± 0.2 MeV using Scanditronix p-Si diode. The TSL beam setup was modelled and simulated with MC-codes Geant4.10.00 and MCNP6. Calculations were performed with the standard available models and cross section libraries of each code as well as importing new sets of cross sections for proton transport below 200 MeV from the TENDL-2012 library. The primary (proton) and secondary particle fluence (proton, neutron and gamma), proton depth dose and neutron equivalent dose were scored. The secondary particle fluence was filtered by several physics processes to find the process that causes the largest difference.

Results and discussion: The depth dose from protons is in agreement for both codes and measurements. However, there is a significant difference between both versions of Geant4 and MCNP6 in production of secondary particles despite of the use of same cross section library. The default version of Geant4 underestimates the production of secondary neutrons and overestimates the production of gammas compared with the modified version. The main difference between the default and modified version of Geant4 is due to proton inelastic process. The difference between the codes needs further investigation. The calculated neutron fluence must be verified with measurements.

Conclusion: The accuracy of models and cross sections implemented in different MC codes affects the accuracy of the dose calculation for proton beams and estimation of secondary dose calculation.

SP049 - Nanotechnology in Radiation Therapy and Imaging: Part 1

TRACK 06: NEW TECHNOLOGIES IN CANCER RESEARCH AND TREATMENT

SP049.1 - A plasma electrochemistry reactor enabling the rapid, efficient, automatic and on-site synthesis of radioactive gold nanoparticles for brachytherapy treatments

Author(s): [Mathieu Bouchard](#), Stéphane Turgeon, Marc-André Fortin

Centre de recherche du CHU de Québec, Quebec City/CANADA

Gold nanoparticles (Au NPs) are increasingly considered for use as radioactive sources (^{198}Au) for prostate brachytherapy procedures [1], [2]. The range of the ^{198}Au β -particle (0.96 MeV, ~ 11 mm in soft tissue, ~ 1100 cell diameters) is sufficiently long to provide cross-fire effects of a radiation dose delivered to cells within the prostate gland, and short enough to minimize the dose to healthy peripheral tissues. The integration of ^{198}Au NPs into brachytherapy procedures requires the development of more efficient, safer, and more compact Au NP synthesis methods. Indeed, because of their relatively short half-life (2.7 days), ^{198}Au NPs should ideally be synthesized on site (directly in hospitals) and upon request. However, the current NP colloidal synthesis methods invariably rely on the expertise of skilled chemists. The preparation of NPs with current techniques comes with several manipulation steps (ligand exchange, solvent exchange, purification procedures), which represent critical radioprotection challenges. Therefore, novel bench-top technologies must be developed to facilitate the automated production of ^{198}Au NPs. Here we report on the development of a plasma reactor used to synthesize Au NPs based on plasma-liquid electrochemistry (Fig. 1a) [3]. In this reactor, an argon plasma is generated at the surface of an aqueous solution containing gold salts (AuCl_4^-) and surfactant molecules. This method yields a continuous production of stable Au NP suspensions directly in water. Within only 45 minutes, a 50 mL solution containing 1 mM of AuCl_4^- can be reduced into NPs with a reduction yield of $99.3 \pm 0.7\%$. Thus-synthesized Au NPs are readily capped with dextran, a biocompatible molecule widely used in vascular injection media. The diameter of Au NPs can be tuned by varying the initial concentration of dextran in the solution. Finally, an integrated UV-visible spectrometer is used to monitor the Au NPs growth kinetics and their final size (Fig. 1b; plasmon peak: 531 ± 3 nm for 5 nm diameter NPs, 570 ± 4 nm for 120 nm diameter NPs), which is necessary for quality control. Overall, plasma electrochemistry could enable the efficient, on-site and upon request production of ^{198}Au NPs for a next generation of brachytherapy procedures.

References:

- [1] M. K. Khan *et al*, *Nanomedicine Nanotechnol. Biol. Med.*, vol. 4, no. 1, pp. 57–69, 2008.
- [2] R. Shukla *et al*, *Proc. Natl. Acad. Sci.*, vol. 109, no. 31, pp. 12426–12431, 2012.
- [3] M.-A. Fortin *et al*, Patent CA2859694 A1, 2012.

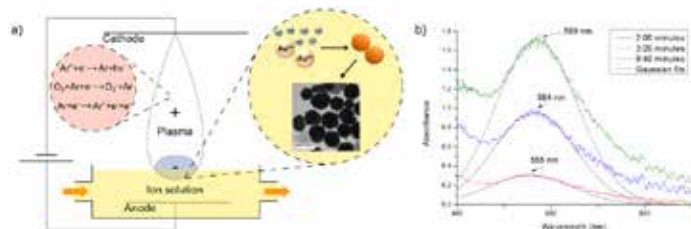


Fig. 1: a) Schematic representation of ^{199}Au NP synthesis by plasma electrochemistry; b) In-situ UV-visible spectroscopic monitoring (plasmon peak; NP size measurement) of plasma-synthesized Au NPs.

SP049.2 - Dose Enhancement in Radiotherapy by Novel Application Of Gadolinium Based MRI Contrast Agent Nanomagnetic Particles in Gel Dosimetry

Author(s): Mahsa Amirrahedi Bonab¹, Nader Riyahi Alam¹, Ahmad Mostaar², Soheila Haghighi³, Ensiyeh Gorji³, Ramin Jaber⁴

¹Medical Physics, tehran university of medical sciences, tehran/IRAN, ²Medical Physics, shahid beheshti university of medical sciences, tehran/IRAN, ³Food And Drug Organization, Pharmaceutical Department, tehran/IRAN, ⁴Cancer Institute, Imam Khomeini hospital, tehran/IRAN

The primary goal of radiotherapy is increasing dose in tumor cells and sparing normal tissues. One of the novel ways to achieve this goal is enhancing tumor dose by high atomic number (z) materials. Using high-z radiosensitizers in tumor cells could increase the effect of radiotherapy treatments through increasing photoelectric cross section and number of auger electrons. Advancements in nanotechnology made it possible to use nanoparticles in cancer imaging and treatments. Although many studies have been done on radiosensitization by different materials, most of them have focused on the dose response in the presence of gold nanoparticles. Of our knowledge there is not any experimental study on the radiosensitizing by gadolinium oxide (Gd_2O_3) nanomagnetic particles in brachytherapy and megavoltage beam radiotherapy. In this study we evaluate dose enhancement properties of gadolinium nanoparticle which is an MRI contrast agent in complex form. Because of increasing relaxation time and high atomic number ($z=64$), Gd_2O_3 can be used in image-guided radiotherapy. In recent studies there was a great interest on MRI guided radiotherapy, so it could be efficient to use an MRI contrast agent simultaneously as radiosensitizer in radiotherapy. Herein, dose enhancement in the presence of gadolinium oxide nanoparticles with 0.1mM concentration in a gel filled phantom was investigated. The results show maximum dose enhancement about $15\% \pm 0.01$ up to $22\% \pm 0.02$ in brachytherapy by Iridium-192, however this value is about $3.8\% \pm 0.002$ in external beam radiotherapy with 6 MV photons. Our study approved radiosensitization property of gadolinium oxide nanoparticles in brachytherapy and external beam radiotherapy.

SP049.3 - Monte Carlo simulation of the radiosensitizing effect by gold nanoparticles: comparison between proton and X-ray irradiation

Author(s): Jihun Kwon, Kenneth Sutherland, Takayuki Hashimoto, Hiroyuki Date
Hokkaido University, Sapporo/JAPAN

Purpose

Radiosensitizer gold nanoparticles (GNPs) have recently drawn attention. GNPs target tumor cells by functionalizing proteins. When GNPs are irradiated, electrons are ejected, causing a dose enhancement effect. Although this effect is usually discussed in the context of X-rays, we have investigated the effectiveness under proton beam irradiation and shown that the dose enhancement occurs in both depth and lateral directions around the GNPs. In this study we compare the characteristics of dose enhancement between protons

and photons.

Methods

The dose distribution around a 20 nm diameter GNP was calculated with the Geant4 Monte Carlo simulation toolkit for a 0.7 MeV proton beam and 6 MV X-rays. For the proton simulation, a GNP was exposed unidirectionally at 0.5 μm depth in a water box ($10 \mu\text{m} \times 1 \mu\text{m} \times 1 \mu\text{m}$) so that the Bragg Peak was formed at the approximate location of the GNP. In the X-ray simulation, two steps were used: (i) 6 MV photons were shot into a water cube (30 cm on a side) and the energy spectra was tallied by 1 nm diameter water spheres at 4 depths, (ii) a GNP inside a water box ($10 \mu\text{m} \times 1 \mu\text{m} \times 1 \mu\text{m}$) was irradiated by four X-ray beams with different spectra. For both types of beams, the incident number of particles was 10^{10} . Five nm width water slabs were positioned at a variety of depths behind the GNP in order to obtain the dose distribution of secondary electrons.

Results

In both proton and X-ray simulations it was confirmed that the dose enhancement effect occurred in both the depth and lateral directions. The effective area in the X-ray beam was shown to be much larger than that in the proton beam. However, the dose enhancement by protons was more intense near the GNP compared to that by X-rays. The results suggest that if GNPs are absorbed into cells or cell nuclei in high concentration, proton beams benefit by higher radiosensitizing effects than X-rays.

Conclusion

The dose enhancement effects of a GNP exposed to proton and X-ray beams was investigated in order to show the difference of dose distributions. A larger effective area was formed by X-rays while a higher enhancement in the vicinity of the GNP was observed in the proton irradiation. The results in this study suggest that the appropriate GNP concentration should be chosen depending on the type of radiation in order to obtain the maximum radiosensitizing effect.

SP049.4 - Colloidal quantum dots: radiation resistant nano-scintillators for radiation-based applications

Author(s): Marie-Ève Delage¹, Marie-Ève Lecavalier², Dominic Larivière², Claudine N. Allen³, Luc Beaulieu⁴

¹Département De Physique, Génie Physique Et D'optique, Et Centre De Recherche Sur Le Cancer, Université Laval, Québec/CANADA, ²Département De Chimie, Université Laval, Québec/CANADA, ³Département De Physique, Génie Physique Et D'optique, Et Centre D'optique Photonique Et Laser, Université Laval, Québec/CANADA, ⁴Radio-oncologie Et Axe Oncologie Du Centre De Recherche Du Chu De Québec, CHU de Québec, Québec/CANADA

Purpose : CdSe quantum dots (QDs) optical properties have been investigated for many years. Their tunable luminescence emission peak, sweeping the visible range, has fed interest in these nanocrystals. Emission wavelengths are directly determined by the size of the QDs, which is well controlled during the nanocrystals synthesis. The choice of the scintillation light color provides flexibility for different applications and allows a predictable match to the best sensitivity range of photodetectors. In this work, we compare a novel CdSe colloidal quantum dots (cQDs) system with multiple layers to an existing CdSe/ZnS commercial sample. This study presents a radio-resistant scintillating quantum-dots formulation for multiple applications in different medical physics fields like dosimetry, imaging as well as other possible applications in nanotheranostics.

Methods: CdSe/CdS/Cd_{0.5}Zn_{0.5}S/ZnS multi-shell cQDs were grown through the successive ionic layer adsorption and reaction (SILAR) synthesis. The nanocrystals, in powder form, were incorporated to a fiber optic-based detector: the cQDs were placed at one extremity of a non-scintillating plastic collecting fiber, with the other extremity free to be coupled to a photodetector. A similar detector

was prepared with commercial CdSe/ZnS (Ocean NanoTech) QDs. Luminescence signal of the QDs was collected with a CCD camera (Apogee U2000C) to measure the integrated signal. Two devices were used to irradiate the QDs: an Xstrahl 200 orthovoltage unit for kV energies (120, 180 and 220 kVp) and a Varian Clinac iX for 6 and 23 MV.

Results: For all beam energies, scintillation intensity decreases as a function of dose cumulated. Damage caused by radiation creates trap states that enhance the proportion of charge carriers experiencing non-radiative recombination, hence decreasing their contribution to the scintillation light. This trend was already reported in the literature but here cQDs demonstrated a better resistance to radiation. For a 220 kVp beam energy, the multi-shell cQDs signal drop of 1.6% per kGy (38% decreases with 23.5 kGy of accumulated dose) compared to a 5% signal loss per kGy measured for the commercial monolayer QDs sample. Literature predicts larger signal drop at MV photon energies, between 500-700%/kGy for monolayer QDs. The commercial CdSe/ZnS QDs shows a similar behavior with a significant drop of 30%/kGy for a 6 MV beam energy, an effect not observed for our cQDs.

Conclusion: Loss of scintillation light production from initial measurement of our cQDs was found to be small and negligible for standard irradiation found in radiation therapy and medical imaging. Therefore, our multi-shell cQDs showed much better resistance to radiation than other commonly used CdSe/ZnS QDs. One could take advantage of this durability in making cQDs part of applications requiring a scintillating material, keeping in mind their particular property of size-tunable emission wavelength.

SP049.5 - Use of gold nanoparticles and pHLIP (pH Low Insertion Peptide) to increase radiation effectiveness in cancer cells.

Author(s): Michael Antosh¹, Diluka Wijesinghe², Samana Shrestha³, Robert Lanou⁴, Yun Hu Huang⁴, Thomas Hasselbacher¹, David Fox¹, Nicola Neretti⁵, Shouheng Sun⁶, Natallia Katenka⁷, Leon N. Cooper⁴, Oleg A. Andreev³, Yana K. Reshetnyak³

¹Institute For Brain And Neural Systems, Brown University, Providence/RI/UNITED STATES OF AMERICA, ²Formerly Of Physics Department, University of Rhode Island, Kingston/RI/UNITED STATES OF AMERICA, ³Physics Department, University of Rhode Island, Kingston/RI/UNITED STATES OF AMERICA, ⁴Department Of Physics, Brown University, Providence/RI/UNITED STATES OF AMERICA, ⁵Department Of Molecular Biology, Cell Biology And Biochemistry, Brown University, Providence/RI/UNITED STATES OF AMERICA, ⁶Department Of Chemistry, Brown University, Providence/RI/UNITED STATES OF AMERICA, ⁷Department Of Computer Science And Statistics, University of Rhode Island, Kingston/RI/UNITED STATES OF AMERICA

Gold nanoparticles have been shown to increase the effectiveness of radiation on cancer. Increased radiation effectiveness would allow for smaller radiation doses to be used on patients, reducing side effects; alternatively, more cancer killing can be achieved using the radiation doses currently in use.

Gold nanoparticles increase radiation effectiveness because they have a higher absorption rate than human tissue at photon energies around 100 keV, and because they release Auger electrons upon irradiation. The effect of these Auger electrons is very localized, which means that proper placement of the gold nanoparticles is crucial in optimizing the effect. In our recent experimental work, we used the cancer-targeting molecule pH Low Insertion Peptide (pHLIP) to target the gold nanoparticles to tumors. pHLIP has been shown to target tumors using the property that tumors are more acidic than normal human tissue.

Our experimental results show that the use of pHLIP with gold nanoparticles causes a statistically significant increase in gold up-

take by cancer cells, and that the gold nanoparticles locate mostly to the cell membrane. In a clonogenic experiment, cells exposed to gold and pHLIP survived less well than control cells as well as cells exposed to gold nanoparticles alone, by a statistically significant amount.

These results suggest that the use of pHLIP significantly improves the impact of gold nanoparticles on improving the effectiveness of radiation. In vivo studies are in preparation. Previous work by members of our research collaboration has shown that pHLIP is capable of significantly increasing the amount of gold that locates to a tumor in a mouse model. Thus, it appears likely that pHLIP will also increase the impact of gold nanoparticles on radiation effectiveness in mice.

SP049.6 - The use of nanoparticles to improve hadrontherapy

Author(s): Marta Bolsa-Ferruz¹, Erika Porcel¹, Noriko Usami², Katsumi Kobayashi², Olivier Tillement³, Hynd Remita⁴, Ryoichi Hirayama⁵, Yoshiya Furusawa⁵, Vladimir Iovsev¹, Daniela Salado¹, Lenka Stefancikova¹, Sandrine Lacombe¹

¹Biophysics, Biophotonics, Institut des Sciences Moleculaires d'Orsay (ISMO), Orsay/France, ²Photon Factory, Institute Of Materials Structure Science, High Energy Accelerator Research Organization, Tsukuba/JAPAN, ³Institut Lumiere-Matiere, Lyon/France, ⁴Laboratoire De Chimie Physique D'orsay, Université Paris Sud 11, Orsay cedex/France, ⁵Research Center For Charged Particle Therapy, National Institute of Radiological Sciences, Chiba/Japan

Radiotherapy, one of the main treatments in cancer, can be improved by the use of heavy atoms, as radiation enhancers. Many investigations are conducted in this area. The challenge is to increase the radiation damage on tumor whilst preserving healthy tissue by improving targeting. Recent developments in nanotechnology brought new perspectives by using nanoparticles, which can be specifically functionalized. We have shown recently that platinum nanoparticles enhance even more than platinum complexes the DNA damage induced as well by fast carbon ions [1], as by gamma rays [2]. This effect is not due to the nature of the incoming radiation but explained by the auto-amplification of electron cascades into the nanoparticles. This result finds strong interest for developing medical protocols such as hadrontherapy and nanomedicine.

Similar results were found with gadolinium based nanoparticles (GBN) which give the possibility to associate RMN imaging to radiotherapy. Furthermore, a decrease of mammalian cell survival was also observed when GBN are associated to ions radiation [3].

This last result allows us to measure how the use of heavy nanoparticles could improve treatments by enhancing efficiency and targeting of radiations into the tumor. The treatment could be simultaneously followed by MRI.

[1] E. Porcel et al., Platinum nanoparticles: a promising material for future cancer therapy?, *Nanotechnology* 21, 85103 (2010)

[2] E. Porcel et al., *Nano-Sensitization under gamma rays and fast ion radiation*, *J. Phys.: Conf. Ser.* 373 (2012)

[3] E. Porcel et al., *The use of theranostic gadolinium-based nanoparticles to improve radiotherapy performances*, *Nanomedicine* (2014)

SP050 - Time-Frequency Analysis

TRACK 09: BIOSIGNAL PROCESSING

SP050.1 - Frontiers of Neuroengineering

Neuroengineering field is seeing an explosive growth thanks to the major brain initiatives worldwide, and the belief that technologies that can push the scientific and clinical frontiers in brain sciences as well as diagnosis and treatment of the nervous system diseases and disorders. Technology is playing a key role from discoveries at cellular to whole brain level. Examples include nano and microprobes are used for recording from neurons, nerves and from many brain regions, and various imaging modalities using high resolution optical neuronal imaging to whole brain functional imaging. Neurotechnology is also playing a key role in diagnostic and therapeutic domains. Among the exciting frontiers are neural interfaces to restore function (limbs and visceral organs), treating brain disorders, neuroprosthetics, and brain machine interfaces. This talk will overview the emerging technologies and key applications and successes driving the field of Neuroengineering as well as lay out several problems and challenges.

SP050.2 - Neural responses to hearing own names comparing with repeated/non-repeated unfamiliar stimuli

Author(s): Kaori Tamura, Toshiki Matsuo, Keiji Iramina
Graduate School Of Systems Life Sciences, Kyushu University, Fukuoka City/JAPAN

Neural responses to self-related stimuli have been investigated to reveal the function of self-recognition. Subject's own name (SON) is the word which closely related to self-recognition process. The present study focused on this own name stimulus and examined neuronal responses to hearing SON by measuring and analyzing electroencephalography (EEG), comparing with hearing unknown names.

Our experimental sequence consisted of calling SON and unfamiliar names (UN) those have no relationship with each participant. However, the habituation caused from stimulus repetition in the experimental design would affect the difference between UNs and SON. Taking this repetition effect into account when we investigate the cognitive function of self-related tasks, we used two kinds of unknown name stimuli conditions. In the one of the conditions, only one UN was selected and presented several times as the same numbers as SON (repeated UN: rUN). In another condition, several types of UNs were presented only at once during an experiment (single presented UN: sUN). By this experimental sequence, we performed EEG measurements and analyzed the collected EEG data by wavelet transform. Then we obtained event-related (de-)synchronization (ERD/ERS) in each condition from wavelet coefficients.

In SON, we found significant beta ERD, while sUN showed beta ERS at the same latency. The mean value of beta power in rUN was midway between those of SON and sUN. This linearity of beta power changes seemed to be related with familiarity levels. SON was the most familiar stimulus among the all stimuli, and stimuli of sUN were completely not because they were presented only once. The familiarity of rUN could be increased by repetition during an experiment, though it was not familiar one before the measurement. Considering these results, we suggest that beta power changes related with the familiarity levels.

SP050.3 - MRS data deconvolution through KBDM with multiple signal truncation and clustering: circumventing noise effects

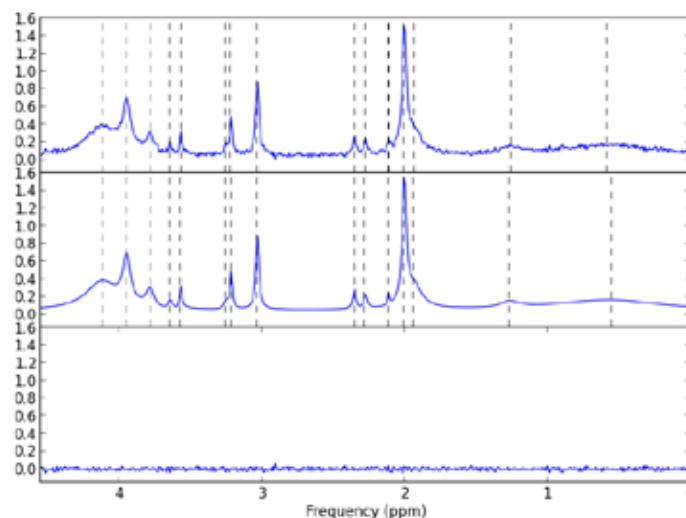
Author(s): Danilo M.D.D. Da Silva¹, Yule Vaz², Fernando F. Paiva¹
¹Departamento De Física E Ciencia Interdisciplinar, Instituto de Física de Sao Carlos, Universidade de Sao Paulo, Sao Carlos/BRAZIL, ²Departamento De Ciencias De Computacao, Instituto de Ciencias Matematicas e de Computacao, Universidade de Sao Paulo, Sao Carlos/BRAZIL

The spectral analysis using Fourier Transform (FT) formalism shown to be very useful in a wide range of MRS applications. However, this technique can be tricky in some cases where peak superposition occurs, a common situation during *in vivo* data quantification process. This work describes an unsupervised deconvolution algorithm using Krylov Basis Diagonalization Method (KBDM) with multiple signal truncation and clustering. The KBDM is a fitting algorithm based on Lorentzian model functions and its mathematical approach is described at [1-4].

Basically, the output of the KBDM is a tuple (T2, frequency, amplitude and phase of each signal component) of M points obtained from a generalized eigenvalue equation of MxM matrices built using M points of the MRS signal. If only K Lorentzian components are present in the signal, the remaining M-K components will vanish for noiseless signal. When noise is present, it will be represented using Lorentzian components, which will lead to spurious components.

We exploited the fact that varying the number of points of the signal (M) used to construct the matrices aforementioned leads to different representations of noise components to minimize its effect in the estimation of each signal component. We applied the method multiple times with different values of M, clustering its results with a density-based algorithm and averaging the values of each cluster. The figure below shows the original noisy signal (top), the estimated signal using our method (middle) and the residual (bottom).

Our results show that using the proposed processing strategy, KBDM-estimated values are highly consistent with simulated values for different sets of spectra and noise level. The effects of the noise in the spectral quantification was not found to be critical, at least for simulated data with signal-to-noise ratio equivalent to that typically found in clinical MRS at 1.5T. In summary, KBDM is a promising tool that can provide complimentary information to the well-established Fourier techniques, especially when overlapping peaks are present. Further studies are in progress in order to validate the proposed method for *in vivo* data processing.



- [1] Mandelshtam VA, Taylor HS. J. Chem. Phys 1997; 107:6756-6769.
[2] Mandelshtam VA, Taylor HS. Phys. Rev. Lett. 1997; 78:3274-3277.

[3] Mandelshtam VA. Prog. Nucl. Mag. Res. Sp. 2001; 38:159-196. [4] Magon CJ et al. J. Magn. Reson. 2012; 222:26-33.

SP050.4 - Quantification of Wavelet Band Metrics for Assessing Heart Rate Variability

Author(s): Mark P. Wachowiak¹, Dean C. Hay², Michel J. Johnson³
¹Computer Science And Mathematics, Nipissing University, North Bay/ON/CANADA, ²Physical And Health Education, Nipissing University, North Bay/ON/CANADA, ³École De Kinésiologie Et De Loisir, Université de Moncton, Moncton/CANADA

Because of its physiological and clinical importance, heart rate variability (HRV) has been investigated with many techniques, including time-frequency methods. In this study, time-varying frequency changes in the lower bands of continuous wavelet transforms directly computed from ECG signals are quantified with statistical and information-theoretic measures. These metrics are compared for resting and lower body negative pressure (LBNP) conditions, and with standard HRV metrics. Although the latter confirm the expected lower variability in the LBNP condition, metrics from the main frequency band in the wavelet transform corresponding to the observed range of heart rate (0.5–1.25 Hz) exhibit statistically significant higher variability than baseline conditions. It is proposed that a more complete HRV analysis can emerge when lower-band variability metrics of ECG in the time-frequency domain is used in conjunction with more traditional time and frequency domain approaches.

SP050.5 - Effect of Coffee on EEG Spectral Asymmetry

Author(s): Madina Saifudinova, Maie Bachmann, Jaanus Lass, Hiie Hinrikus
 Department Of Biomedical Engineering, Technomedicum, Tallinn University of Technology, Tallinn/ESTONIA

This study aims to evaluate the sensitivity of EEG spectral asymmetry index (SASI) for detection of the effect of coffee as a chemical stressor on human EEG. SASI, based on the balance of powers of EEG frequency bands in undisturbed brain, was previously proposed as a novel objective method for evaluation of depression. The experiments were performed on 17 young healthy subjects. The EEG time series were recorded using 9 channels: F3, Fz, F4, C3, C4, P3, P4, O1, O2 (common reference Cz). The coffee intake causes significant decrease of SASI in F3, Fz, F4, C3 and C4 channels. Maximal changes were detected in frontal area, while most significant alterations were observed in parietal brain area in previous depression studies. The results suppose that SASI is a promising measure for evaluating also the effect of chemical stressor on brain bioelectrical activity.

SP050.6 - Effects of Changing in the Neck Fluid Volume, Neck Circumference and Upper Airway during Sleep on Snoring Sound Characteristics

Author(s): Shumit Saha¹, Mahsa Taheri², Zahra Moussavi¹, Azadeh Yadollahi²
¹Biomedical Engineering, University of Manitoba, Winnipeg/CANADA, ²Toronto Rehabilitation Institute-University Health Network, Toronto/ON/CANADA

Introduction: Rostral fluid shift during sleep can increase neck circumference (NC) and narrow the upper airway cross-sectional area (UA-XSA). Such narrowing in UA-XSA may increase turbulence of airflow passing through the upper airway; thus, induce snoring. The objective of this study was to investigate whether acoustic features of snoring change with the increases in NFV, NC and decreases in UA-XSA. We hypothesize that fluid accumulation in the neck changes the snoring sound features in time and frequency domains.

Method: Twelve men (age: 46±13 years, BMI: 26±3, AHI: 39±25) attended the sleep laboratory for a daytime sleep study. Subjects slept in supine position only, and their sleep was assessed by a regular polysomnography. NC and UA-XSA were measured before and after sleep using a measuring tape and acoustic pharyngometry, respectively. During sleep, snoring sounds were recorded with a microphone attached to the neck. Snoring segments were annotated manually by an expert. Snoring features such as duration and occurrence of snoring, average power for seven frequency sub-bands were extracted in various sleep stages as well as the entire sleep duration. Correlations between snoring features and changes in NC and UA-XSA were assessed by Pearson or Spearman's correlations.

Results: Increases in NC after sleep were found to be associated with an increase in average power of the snoring sounds in the frequency range of 100-4000 Hz ($r = 0.76, P=0.011$) and of 150-450 Hz ($r = 0.73, P=0.017$). Furthermore, reductions in UA-XSA increased snoring sounds' average power in the frequency range of 100-4000Hz ($r = -0.70, P=0.025$) and 150-450Hz ($r = -0.64, P=0.044$). Similar strong correlations between snoring sounds' average power and changes in NC (100-4000Hz: $r = 0.72, P= 0.019$; 150-450 Hz: $r = 0.73, P= 0.016$) and UA-XSA (100-4000Hz: $r = -0.71, P= 0.022$; 150-450 Hz: $r = -0.79, P= 0.006$) were achieved in non-REM stage 2 of sleep.

Conclusion: Our findings suggest that an increase in NC and narrowing in the UA-XSA could increase snoring sounds' power in various frequency ranges.

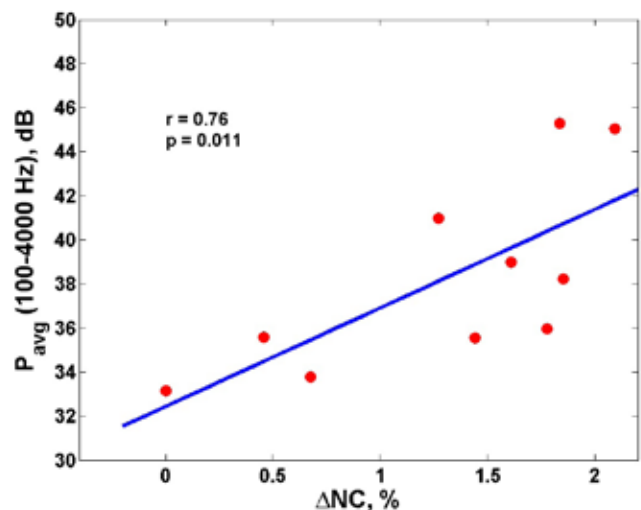


Figure 1. Relationship between percentage change in NC and average power of snoring sounds (calculated over the entire sleep duration) within 100 – 4000 Hz frequency range

SP051 - Rehabilitation Robotics

TRACK 10: REHABILITATION MEDICINE, SPORTS MEDICINE, REHABILITATION ENGINEERING AND PROSTHETICS

SP051.1 - Biomechanical Simulation of Upper Extremities Exoskeleton to Aid Stroke Patients

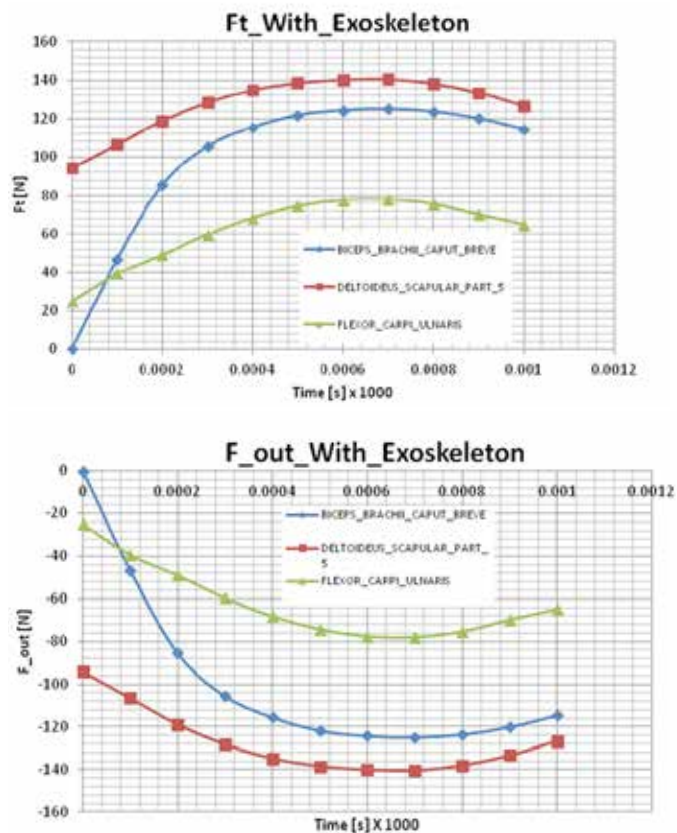
Author(s): Yahia M. Al-Smadi

Mechanical Engineering, Texas A&M University - Kingsville, Kingsville/UNITED STATES OF AMERICA

Recently many efforts are carried out that can help people with restricted arm movement or rehabilitate injuries and disabilities. In this case exoskeleton is the most extensively used equipment to get rid of this restriction. Exoskeleton helps to boost strength and endurance as well as reduce the efforts required to perform various activities in day-to-day life.

In order to manipulate characteristic of the exoskeleton, we carried out two virtual experiments. Initially using Denavit–Hartenberg parameters, we patronized our model with number of degree of freedom. ADAMS and AnyBody simulations were carried out. We computed results of effects over human body with and without exoskeleton.

While studying exoskeleton effect on human arm, we studied several joints, muscles and bones reactions in different load conditions. We studied two different load conditions while concentrating on performance of the exoskeleton. The very first condition was constant load where as the second one is the variable load acting on the arm. In both the case we considered gravity force to get more precise result. Below shown graphs are some of the results which we have explained later.



While doing virtual experiments of an exoskeleton on human arm, we observed significant change in reaction of the muscles, bone and joints movement. We found some muscles reacts same with and without exoskeleton where as at the joints we recorded tremendous output of an exoskeleton and human arm fusion. Selected muscles for our study are Caput breve a short head of biceps brachii muscles, deltoid muscles which responsible for arm movement in scapular plane and the flexor Carpi ulnaris (FCU) muscle which is located in forearm and responsible for flexion and adduction of the hand.

SP051.2 - Testing a mobile robot toy for children with disabilities

Author(s): Adriana M. Rios Rincón, Daniel A. Quiroga Torres, Javier Castellanos, Maria F. Gómez Medina, Antonio Miguel Cruz, William R. Rodríguez

School Of Medicine And Health Sciences, Universidad del Rosario, Bogotá/COLOMBIA

Robots showed a potential to enhance engagement in free play of children with severe motor impairment, however, they are too expensive to be used in low-income settings. The objective of this study is to perform technical assessment of a prototype of a low cost car-like robot that can be operated by head movements for children with motor impairment. We designed a robot that and tested its technical features. We found that the robot power efficiency is low (47%), current peak for both motors were 474.4 mA (right) and 416 mA (left) both of them were below 2 Amp which is the maximum current limit threshold tolerated by the L293B component, as the robots get far away from the control the response time slightly increased. The reaching distance of the remote control was 20.7 meters which is enough for using in therapeutic activities. Regarding the functional features, the robot moved forward in a straight line 86.6% of the tested trials (26/30) and was able to turn 90 degrees left or right 93.3% of the trials (28/30). The robotic prototype met basic technical and functional requirements. Power efficiency, safety and apparel features should be improved for being used by children with using for children with motor impairments.

SP051.3 - Pilot study of a soft metal hydride actuator for a wearable rehabilitation system

Author(s): Minako Hosono¹, Kouji Sakaki², Shuichi Ino²

¹Industrial Research Institute of Shizuoka Prefecture, Shizuoka/JAPAN, ²National Institute of Advanced Industrial Science and Technology, Tsukuba/JAPAN

A prototype actuator for a wearable rehabilitation system was proposed in this study.

A wearable rehabilitation system has a potential to play an important role in remote rehabilitation to free patients from stressful constraints. It is essential for such a rehabilitation system to be reliably safe, compact, and silent. To meet these needs, we have developed a soft metal hydride (MH) actuator utilizing the property of a hydrogen storage alloy for a part of the rehabilitation system.

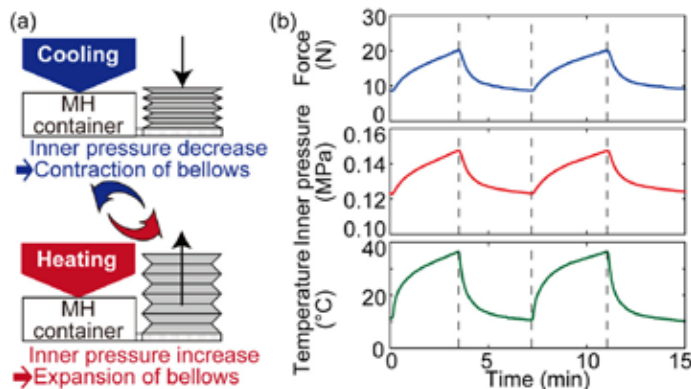
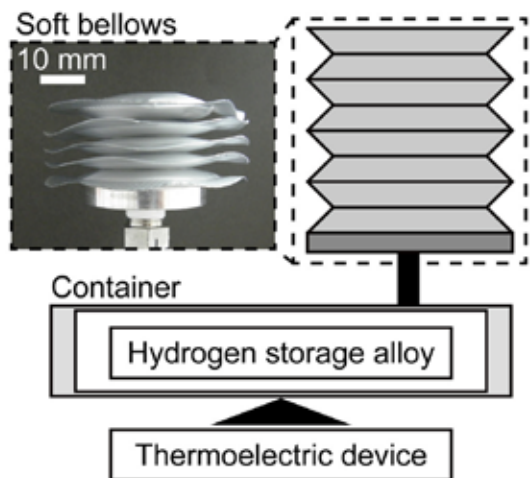
The soft MH actuator consists of a soft bellows made from laminated aluminum film (PE/Al/PET, 0.1 mm in thickness) as an end effector, a container of a hydrogen storage alloy as a source of bellows motion, and a thermoelectric device such as a Peltier device for temperature control (Figure 1). A hydrogen storage alloy can reversibly absorb and release a large amount of hydrogen gas by thermal control, i.e. cooling for absorption of hydrogen and heating for releasing hydrogen from the hydride (Figure 2(a)). By converting this reversible chemical reaction into bellows stroke due to the inner hydrogen pressure change, the soft MH actuator can generate high force by a compact device and realize silent operation and

shock-absorbing function like a cushion¹. In this study, the soft MH actuator, which contained 1 g of alloy (Ti0.5Zr0.5Mn0.8V0.2Ni0.9Al0.1)² and utilized a soft bellows with 50 mm of diameter as the end effector, achieved 20 N cyclic output by controlling the temperature between 284 K to 310 K (Figure 2(b)). From this result, we expect that the soft MH actuator works as a powerful tool in a part of a wearable rehabilitation system.

This work was supported by JSPS KAKENHI Grant Numbers 25560281, 25242057.

¹M. Hosono, et al., Rehabilitation Research and Practice. 2012 (2012) 1-7

²K. Sakaki, et al., Materials Transactions. Vol. 55, No. 8 (2014) 1168-1174



SP051.4 - Robotic Spasticity Quantification: Velocity Dependent Component of Biomechanical Resistance

Author(s): Nitin Seth¹, Denise Johnson², Hussein A. Abdullah³

¹School Of Engineering, University of Guelph, Guelph/CANADA, ²Acquired Brain Injury Program, Regional Rehabilitation Centre, Hamilton Health Sciences, Hamilton/ON/CANADA, ³School Of Engineering, University of Guelph, Guelph/ON/CANADA

Introduction: Spasticity, is commonly referred to as velocity dependent resistance to passive motion arising from upper motor neuron lesions. It is monitored closely and is important for determining stages of recovery. Doctors, physiotherapists and clinicians require more sensitive and quantitative method for spasticity assessment. The most commonly used method is the Modified Ashworth Scale. It has, however, had several studies test its applicability to spasticity assessment and has been deemed reliable for assessment of upper limb flexion/extension.

Methods: Using a robotic system, 5 controlled flexion/extension motions are employed at progressively faster speeds to collect biomechanical resistive force, position, and time data in real time. Motions are performed in the individual’s sagittal plane similar to functional motions of raising an object to their head or face. A linearly separable model quantifies the velocity dependent component of resistance and statistical model demonstrates the effect MAS scores have on the new velocity dependent resistance metric. This study considered healthy controls (n = 44) and individuals with an acquired brain injury receiving treatment for spasticity (n = 39). To determine the best representation, the quantitative spasticity metric was calculated once with flexion data, once with extension data, and a final time with data from both motions.

Results: The MAS, while augmented with an additional value to indicate healthy controls, was found to be significantly effect the metric calculated from both flexion and extension motions. This was true for both MAS bicep and tricep scores. Table 1 lists fixed effects for each of the 4 models.

Effect	F	P
MAS Bicep (Flexion/Extension)	16.25	<0.0001
MAS Tricep (Flexion/Extension)	11.55	<0.0001
Extension Only Data	1.99	0.0987
Flexion Only Data	5.19	0.0008

The metric can also distinguish between the high MAS scores (MAS 2, 3) and low MAS scores (healthy controls, MAS 0, 1) with values that were statistically significantly different.

Discussion/Conclusions: MAS bicep/ tricep scores demonstrated effects on the quantitative spasticity metric. The strongest relationship was determined for metrics calculated from both flexion and extension motions together. Flexion only calculations also found that MAS had a direct effect, whereas it approached significance with extension data. More studies and data is required to determine if a stronger relationship is achievable. The robot’s controlled and varied speed motions allowed for a calculation of a velocity dependent effect to quantify spasticity. These values are determined only from biomechanical data directly relatable to the MAS scale. This data can potentially aid clinicians in making treatment decisions and measuring progress or changes in spasticity.

SP052 - Functional Neuroimaging and Neuronavigation

TRACK 11: NEUROENGINEERING, NEURAL SYSTEMS

SP052.1 - From human neuron to human brain: Neurosurgical contributions to understanding the brain

Author(s): [Taufik Valiante](#)

Director Of The Surgical Epilepsy Program, Krembil Neuroscience Center, Toronto/ON/CANADA

In this talk I will review neurosurgical contributions to understanding the human brain, particularly in the context of surgery for epilepsy and movement disorders. I will review early studies that have led to the understanding of localized cortical function, which formed the basis of initial attempts at understanding information processing within the brain. I will then describe ongoing work using electrocorticography and single unit recordings to elucidate fundamental human brain function including memory, attention, and language. The investigations that I will review will span many levels of investigations, from the activity of single human cortical neurons, to small cortical microcircuits, and then up to large scale integration – largely as a byproduct of the clinical care afforded to people with epilepsy. I will conclude by attempting to outline the limitations of current technologies to record from and control the human brain.

SP052.2 - Modulation of event-related desynchronization and synchronization during right finger flexion in patients with Amyotrophic Lateral Sclerosis

Author(s): [Nataša Bizovičar](#)

University Rehabilitation Institute of Republic of Slovenia, Ljubljana/SLOVENIA

Introduction

Amyotrophic lateral sclerosis (ALS) is a progressive neurodegenerative disorder with signs of upper and lower motor neuron degeneration. Potential electroencephalographic (EEG) methods for studying upper motor neuron and other cortical motor functions during the preparation and execution of volitional movements are so-called event-related desynchronization (ERD) and synchronization (ERS). ERD is a relative EEG power decrease pre- and during motor activity and is described as an electrophysiological correlate of an activated cortical network. ERS is a relative EEG power increase after termination of the movement and is an electrophysiological correlate of cortical areas at rest. The brain has the capacity to change the architecture of the neural networks during learning or as a response to injury. Diseases that affect neuronal networks such as ALS could have an impact on the change in absolute and relative EEG spectral power, its topography and time course. Our aim was to study ERD/ERS related to finger flexion in patients with ALS.

Methods

Twenty-one ALS patients (aged 54-74 years) and nineteen matched controls (aged 48-72 years) were assessed for their hand dexterity and strength, spasticity and functional rating scales. EEGs (10-20 system, 30 channels) were recorded while patients and controls performed self-paced fast right index finger flexion motor task. EEG time-frequency analysis was performed in the alpha (8–12 Hz) and beta (13–30 Hz) bands.

Results

Patients performed significantly worse on all hand function tests and had decreased hand muscle strength compared to control subjects. Latencies of the ERD beginning did not differ between the ALS patients and controls. Patients generated significantly smaller resting alpha spectral power density and lower beta ERD compared to controls. There was a larger difference in ERS between the contra- and ipsilateral brain hemispheres in the ALS group. No significant correlations between ERD/ERS and clinical measures were observed.

Conclusions

There are different morphological and functional changes in the brain of ALS patients described in the literature which could explain some of the changes in ERD and ERS. The reduction of beta ERD could result from the loss of pyramidal cortical neurons and asymmetry of ERS in patients with ALS compared to controls could be the result of interhemispheric corticomotor network degeneration in ALS.

SP052.3 - Functional connectivity patterns associated with swallowing of fluids with various viscosity

Author(s): [Iva Jestrovic](#)¹, [James L. Coyle](#)², [Ervin Sejdic](#)¹

¹Department Of Electrical And Computer Engineering, University of Pittsburgh, Pittsburgh/PA/UNITED STATES OF AMERICA, ²department Of Communications Science And Disorders, University of Pittsburgh, Pittsburgh/PA/UNITED STATES OF AMERICA

Thickened dietary fluids are commonly deployed to prevent ordinary thin liquids from entering the airway of patients with certain swallowing disorders. Their mechanism of action has thus far been attributed to two possible explanations. First, rheological properties of the thicker fluids, may render them less likely to enter a small opening in the poorly-closed airway during swallowing. Alternately, the thicker liquids may adhere to the pharyngeal mucosa thereby reducing their rate of flow. However the possibility that thicker liquids cause perturbations in central sensorimotor processing has not been considered or investigated. Therefore, we investigated the influence of fluid viscosity on associated swallowing brain networks. EEG signals were collected from 55 healthy adults who performed five water, five nectar-thick, and five honey-thick liquid swallows. Standard pre-processing of EEG time-series was utilized and pre-processed signals were filtered in the frequency bands of interest. Brain networks were formed using the time-frequency based synchrony measure. Results showed that increasing fluid viscosity resulted in higher clustering coefficients in all frequency bands ($p < 0.04$) (Figure 1.A), while the characteristic path length tended to be lower in the *Delta*, *Theta*, and *Alpha* frequency bands ($p < 0.03$) (Figure 1.B). Brain networks formed during swallowing of thicker liquids had higher small-world parameters in the *Delta*, *Theta*, and *Alpha* frequency bands ($p < 0.05$) (Figure 1.C). These results provide intriguing possibilities regarding the effects of peripheral manipulations on central processing of swallowing sensorimotor function. Further investigations of the neural basis of dysphagia are warranted to elucidate this and related possibilities.

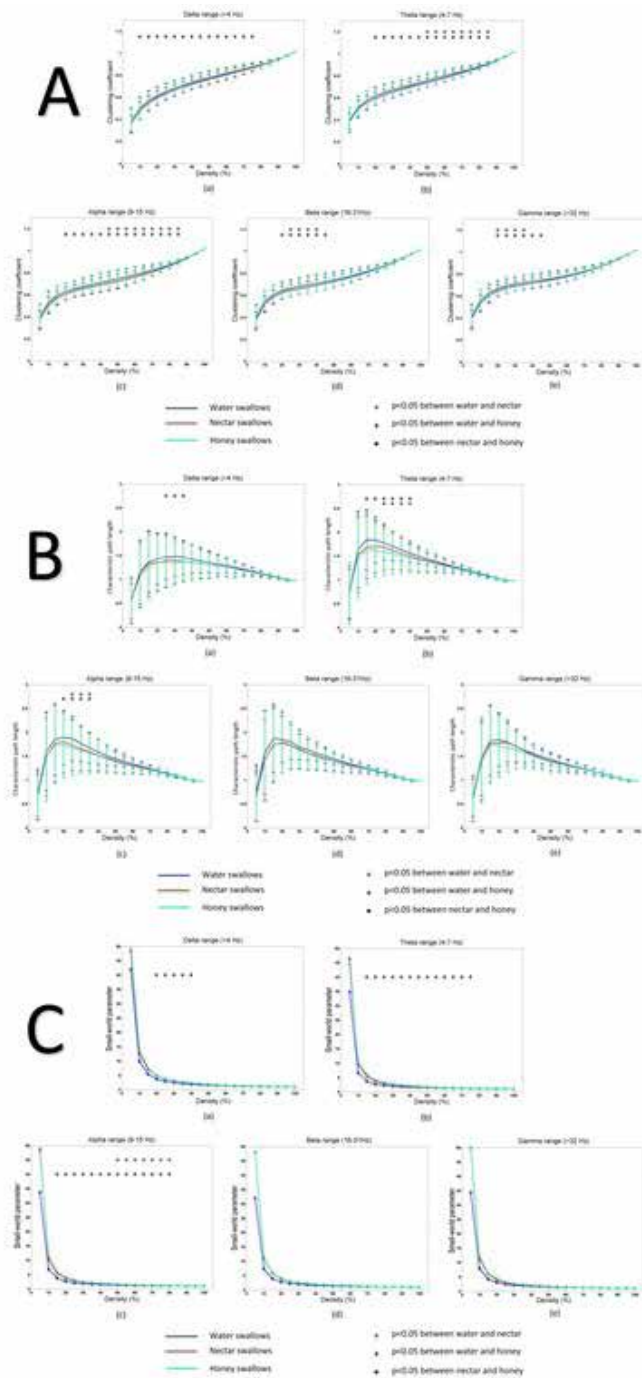


Figure 1: (A) Mean clustering coefficient for a different threshold percentage and for different frequency bands. (B) Mean characteristic path length for a different threshold percentage and for different frequency bands. (C) Small-world parameter for a different threshold percentage and for different frequency bands

SP052.4 - Distribution of F-Latency (DFL) - a new nerve conduction parameter for early detection of radiculo-myelopathy

Author(s): K Siddique Rabbani

Biomedical Physics & Technology, University of Dhaka, Dhaka/BAN-GLADESH

Distribution of F-Latency (DFL) is a new nerve conduction parameter conceived and named by the author several years back and who has led many researchers over the period in improving the understanding of the parameter and its application in early detection of radiculo-myelopathy. The method has been found to work equally for the cervical and the lumbo-sacral regions, however bulk of the systematic work carried out so far is for the former, particularly using the median nerve. Described for the median nerve, DFL is basically a statistical distribution of latencies of F-responses obtained through electrical stimulation of the nerve at the wrist and recording of the evoked muscle responses from the Thenar muscle group at the base of the thumb. F-response is the secondary response occurring due to antidromic conduction of action potentials in the motor nerve fibres from the wrist to the spinal cord, and then through random backfiring in a few percent of cell bodies contributing to action potentials through these backfired nerve fibres. Because of random recruitment of nerve fibres with different conduction velocity values, the F-latencies due to multiple stimulations vary randomly and this has been used to advantage in DFL to get a picture of the distribution of Conduction velocity (DCV) of nerve fibres as an approximate mirror image of DFL, thus contributing to a practical method to measure DCV in a clinical setting, which was not possible earlier. It has been found by groups led by the author that for normal subjects DFL has a single sharp peak while for subjects with cervical radiculopathy (entrapment of the nerve roots near the spinal cord) or myelopathy (compression of the spinal cord due to a vertebral disc bulging or herniation) DFL has double peaks or broad peaks. Hypotheses have been put forward in explaining the causes of the observed patterns which have been verified to a great extent through MRI investigations on the same subjects. Some of the broad peaks are very close to a single peak and a special criterion has been set up, based on a learning process using MRI on the same subjects through a research carried out in Singapore, again led by the author, to identify these subtle broad peaks from single peaks. Recently improved detection has resulted from changing the bin starting values in calculating the statistical frequency distribution that result in the DFL and combining the outcomes of the two distributions. Further work has been carried out in order to assess the minimum number of F-responses needed to differentiate the patterns of DFL in radiculo-myelopathy. It has been found that about 15 F-responses are adequate to distinguish the DFL patterns in the above detection if the bin size is chosen as 2ms. Through the combined procedure, almost 80% correct prediction have been obtained through a double blind study, when evaluated using MRI. It is expected that this method of DFL would become a first line screening test in any peripheral neuropathy in the near future.

SP053 - Cardiovascular Instrumentation

TRACK 12: MEDICAL DEVICES

SP053.1 - A Microfluidic cell culture Instrument for individual testing of therapeutics.

Author(s): Marie Keays¹, Patrick A. Kiely², Tara Dalton¹

¹Stokes Institute, University Of Limerick, Limerick/IRELAND, ²Department Of Life Sciences, And Materials And Surface Science Institute, University Of Limerick, Limerick/IRELAND

The realisation of personalised medicine has been the target of many multidisciplinary scientific teams. A system that can individualise point of care diagnostics has the potential to revolutionise medical treatment. Currently, drug discovery uses 2-dimensional cell culture techniques as a test to monitor the cells reactions to drugs these models have provided the platform for most toxicity and drug testing. However, the requirement of sample containers such as dishes or flasks are a limiting factor and do not lend themselves to automation. With a desire to understand and diagnose disease and infection at a patient specific and cellular level, there is a pressing need to modify procedures to facilitate multi-experimental approaches that are cost effective, automated and use small amounts of patient sample and reagents. This has encouraged us to develop a microfluidic droplet cell culture platform. The proposed system will create droplet cultures and facilitate incubation and imaging of the cultures on one platform. This system facilitates the establishment three-dimensional culture conditions that more accurately mimics natural cell conditions and cell-cell communication. The culture droplets are created in a nano-litre range and multiple unique bioreactor droplets can be prepared and analysed on one system making this a time and cost effective instrument. This system can benefit cancer diagnosis as multiple assays can be mixed with individual culture droplets. This lends itself to drug cocktail testing tested against a specific sample making this a powerful instrument in understanding cells.

SP053.2 - A Bioinspired Catheter Harnessing Gecko Adhesion and Inchworm-Like Locomotion for Targeted Drug Delivery

Author(s): Jonathan Wolfe¹, Huan Qi², Paul J.L. Ong³, Tze Tec Chong⁴, Denis Fichou⁵, Claus D. Ohl⁶, Joo S. Chia⁶, Subbu Venkatraman², Swee H. Teoh⁷

¹Interdisciplinary Graduate School, Nanyang Technological University, Singapore/SINGAPORE, ²Material Science And Engineering, Nanyang Technological University, Singapore/SINGAPORE, ³Cardiology Clinic, Tan Tock Seng Hospital, Singapore/SINGAPORE, ⁴Vascular Surgery, Singapore General Hospital, Singapore/SINGAPORE, ⁵School Of Physical And Mathematical Sciences, Nanyang Technological University, Singapore/SINGAPORE, ⁶Urology & Continence Clinic, Tan Tock Seng Hospital, Singapore/SINGAPORE, ⁷School Of Chemical And Biological Engineering, Nanyang Technological University, Singapore/SINGAPORE

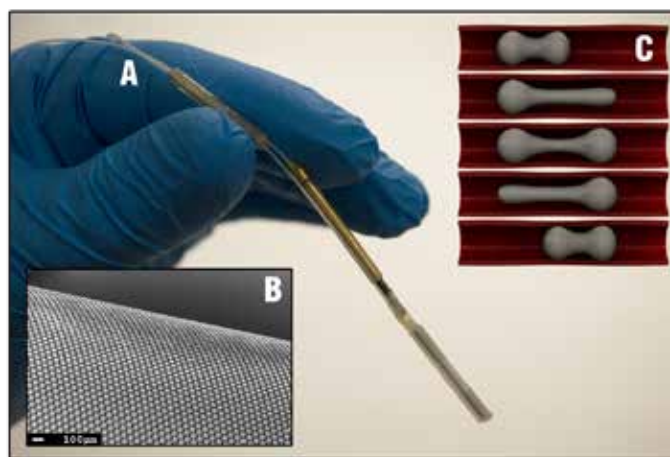
Invented more than 250 years ago, modern catheters have developed into a technological diagnostic/therapeutic medical instruments used in myriad applications such as catheterization, colonoscopy, ureteroscopy, dilating balloon and stenting. Some of the larger devices are capable of carrying sophisticated imaging and sensing modalities with robotic ultra-fine surgical instruments.

In recent years, smart-materials and advanced micro-manufacturing techniques have enabled the construction of millimeter-sized catheters capable of robotic bending and rotation, allowing catheters to maneuver deeper inside the patient's body. However, a fundamen-

tal drawback is that catheters are pushed from the outside by the surgeon. This works well for large diameter vessels but poses many challenging issues for small diameter vessels. As the artery diameter decreases, increasing forces between the catheter and the vessel inner wall causes the catheter to buckle rather than advance. Moreover, the high friction caused by pushing the catheter, especially at curvatures, may result in life-threatening vessel injuries.

To resolve this, we have developed an alternative principle for catheter locomotion, here named *SmartCat*, an inchworm-inspired μ -robotic catheter that is powered by saline pressure. This self-pulling catheter is 2.5 millimeters in diameter, and can autonomously navigate the vessel at a speed of 2 cm/sec. The robots are batch-fabricated, and are thus suitable for mass production.

For safe implementation of the inchworm locomotion, hemocompatible gecko-inspired balloon clampers were developed. This gentle, reusable adhesive enables a dramatic reduction in the force required to achieve adequate vessel grip. In addition, these balloon clampers can also be used to form a close-off region for localized drug delivery.



(A) Prototype of an inchworm-robotic catheter prior to encapsulation within elastic silicone-gecko cloak, shown in (B). (C) Schematic of the inchworm locomotion principle.

SP053.3 - Covered stent with perforated membrane for treatment of peripheral atheroembolic disease

Author(s): Foad Kabinejadian¹, Mercedeh Kaabi Nezhadian², Fangsen Cui³, Pei Ho¹, Hwa Liang Leo²

¹Department Of Surgery, National University of Singapore, Singapore/SINGAPORE, ²Department Of Biomedical Engineering, National University of Singapore, Singapore/SINGAPORE, ³Engineering Mechanics, Institute of High Performance Computing, A*STAR, Singapore/SINGAPORE

We have recently developed a novel stent membrane design for covered stents that prevents emboli while preserving the side-branch flows. Our earlier in vitro studies in models of carotid arteries have shown that this novel design can maintain more than 83% of the original external carotid artery (ECA) branch flow and has the potential to considerably reduce the chance of emboli release as compared to bare metal stents. In the present study, the application of this novel stent membrane design in the treatment of atheroembolic disease in peripheral arteries is investigated. The novel stent design has been tested in a PDMS model of superficial femoral artery (SFA) and its performance has been evaluated in vitro under physiological pulsatile flow condition, utilizing flow visualization (dye injection), and particle image velocimetry (PIV) techniques. These evaluations include the assessment of emboli prevention capability, side-branch flow preservation, and influence on the branch flow pattern and velocity field.

The novel covered stent demonstrated significant emboli prevention capability, and the flow in the side branches was smooth and uniform. This study demonstrated the potential of this novel covered stent design for the treatment of atheroembolic disease in peripheral arteries. However, further in vivo investigations of biological effects and mechanical performance of this covered stent design is warranted.

SP053.4 - Nanostructuring Carbon Fibre Probes for Use in Central Venous Catheters

Author(s): Jolene Mchugh¹, Meixian Li², Marco F. Cardosi³, James Davis¹

¹Nibec, School Of Engineering, University of Ulster, Newtownabbey/ UNITED KINGDOM, ²College Of Chemistry And Molecular Engineering, Peking University, Beijing/CHINA, ³Lifescan Scotland Ltd, Inverness/UNITED KINGDOM

Central venous catheters (CVCs) and peripherally inserted central catheters (PICC) are vital access lines through which to deliver life preserving agents whether nutritional or chemotherapeutic formulations or, as in haemodialysis, allow the removal of toxins that accumulate. It has been estimated that some 5 million central venous access devices are inserted in the US each year but, sadly, the occurrence of catheter-related blood stream infections (CRBSIs) are known to present a considerable challenge for clinicians. This is a long standing problem with some 300,000 cases reported annually which incur considerable costs in terms of additional treatment through increasing the average hospital stay to 7-12 days. The severity of such conditions is highlighted by an unacceptably high mortality rate that can rise as high as 40% for infection by *Candida* species. The subsequent treatment regime is often complicated by the fact that bacteria associated with biofilm formation within the catheter lumen possess an increased resistance to conventional antimicrobial treatments and leads to a prolonged hospital admission which can often necessitate the complete removal of the line to prevent re-infection.

While there has been extensive research into the development of antimicrobial materials to minimise biofilm formation, there are no point of care diagnostics available to provide an early warning for the onset of infection. In most cases, infection is only detected once gross symptoms (typically fever and rigor) appear and has traditionally relied upon the expertise and vigilance of the healthcare staff. As most CVC lines are maintained by outpatients, there can be obvious ambiguity in ascribing a feeling of being unwell. When combined with a reluctance to present a false positive, the conditions can easily progress to the severe detriment of the patient. The present communication has sought to investigate the design of a probe that could, in principle, allow the condition of the line to be autonomously monitored and, ultimately, alert the patient or the healthcare staff to the onset of biofilm formation such more appropriate and effective remedial treatment could be employed that would enhance the lifetime of the line.

The carbon fiber probe described utilizes the oxidation of an endogenous biomarker (Uric Acid) to provide diagnostic information on the condition of intravascular access lines. The probe surface was modified through anodic oxidation to provide a high selectivity towards urate which was used as a redox probe through which the pH could be determined. The sensing rationale relates to the fact that bacterial colonisation and biofilm formation of the line will result in changes to the localised pH at the electrode and thus it could be envisaged that the probe would provide an early warning signal such that remedial treatment could be applied before the film takes hold. A Nernstian response (-60mV/pH) was obtained which was free from the interference of other redox species common to biofluids. The electroanalytical performance of the probe has been optimized and the applicability of the approach demonstrated through testing the responses in whole blood.

SP053.5 - Denoising RF defibrillator waveforms for intracardiac atrial substrate impedance characterisation using digital filtering techniques

Author(s): Omar J. Escalona¹, Philip R. Walsh¹, Ali S. Rababah¹, Vivek Kodoth², Ganesh Manoharan²

¹Engineering Research Institute, Ulster University, Newtownabbey/ UNITED KINGDOM, ²The Heart Centre, Royal Victoria Hospital, Belfast/UNITED KINGDOM

Introduction: Atrial fibrillation (AF) is the most common cardiac arrhythmias and accounts for 30% -40% of all cardiac arrhythmia related hospital admissions. It is also one of the leading causes of stroke. Treatment can be achieved using electrical internal cardioversion, which involves application of an electrical shock to the heart tissue by means of internal electrodes. Recently, novel low-tilt rectilinear waveforms generated by a radiofrequency defibrillator device have shown enhanced efficacy in the treatment of atrial fibrillation in comparison to conventional capacitor based shock waveforms. During defibrillation, intra-cardiac impedance (ICI) is one of the major determinants of success and has been identified as critical to understanding and optimization of therapies. In addition, accurate ICI measurements are thought to provide valuable information about tissue-electrode interface characteristics and may relate to other variables such as voltage amplitude, defibrillation energy threshold and outcome.

Methods: At Royal Victoria Hospital Belfast, voltage and current waveforms were digitally recorded at 250 kHz sampling frequency using a digital oscilloscope (Tektronix TDS 3014B) and a current probe (Fluke 80i-110s) during internal cardioversion of patients with persistent AF using a novel low-tilt rectilinear waveform (generated by a radiofrequency defibrillator device) following a step up energy protocol (50V to 300V in 50V steps). However, typically, the recorded signals are inherently corrupted by electrical noise. The objective of this work was to investigate if it was possible to develop an algorithm, using digital signal processing (DSP) in the MATLAB environment, to denoise the AF defibrillation voltage and current waveforms by applying spectral analysis and digital filtering techniques. Specifically, the MATLAB algorithm was developed to automatically handle the large data files recorded during defibrillation therapy. Patient number and case number were used to automate loading of the associated defibrillation voltage and current waveforms and deduce the sampling frequency; based on a-priori rectilinear pulse width (12ms). The algorithm is designed to then select the desired waveform segment (part of the rectilinear signal at time between 2ms and 10ms) and denoises, generates and plots the filtered waveforms. Finally, the algorithm calculates the dynamic resistance (ICI) and present associated parameters.

Results: Analysing the spectrum of the processed rectilinear waveform signals enabled finding the most appropriate normalized cutoff frequency estimation. The study results provided this being between 0.01 and 0.02 (normalised frequency), which corresponds to 1125Hz - 2250Hz. The evaluation results also indicated that Hanning windowing was more appropriate than Blackman windowing in the spectral analysis preservation of the rectilinear waveform signals. Furthermore, noise reduction of these signals using a 7th order Butterworth filter design was found to be more efficacious in denoising than a 200 order FIR digital filter.

Conclusion: The processing algorithm developed and applied to RF defibrillator waveforms was effective for denoising voltage and current signals. This provides a useful tool for studying large number of patient cases in the characterisation of intra-cardiac impedance and its potential relation to other factors such as the outcome of cardioversion treatment and defibrillation energy threshold.

SP054 - Women in Medical Physics: Current Status

TRACK 18: GENDER, SCIENCE AND TECHNOLOGY

SP054.1 - Experiences as a Women in the Biomedical Engineering Field

Author(s): Molly S. Shoichet

Chemical Engineering And Applied Chemistry, University of Toronto, Toronto/CANADA

Professor Molly Shoichet holds the Tier 1 Canada Research Chair in Tissue Engineering at the University of Toronto. She has published over 480 papers, patents and abstracts and has given over 310 lectures worldwide. She currently leads a laboratory of 25 and has graduated 134 researchers. She founded two spin-off companies, is actively engaged in translational research and science outreach. Dr. Shoichet is the recipient of many prestigious distinctions and the only person to be a Fellow of Canada's 3 National Academies: Canadian Academy of Sciences of the Royal Society of Canada, Canadian Academy of Engineering, and Canadian Academy of Health Sciences. Dr. Shoichet holds the Order of Ontario, Ontario's highest honour and is a Fellow of the American Association for the Advancement of Science. In 2013, her contributions to Canada's innovation agenda and the advancement of knowledge were recognized with the QEII Diamond Jubilee Award. In 2014, she was given the University of Toronto's highest distinction, University Professor, a distinction held by less than 2% of the faculty. Dr. Shoichet received her SB from the Massachusetts Institute of Technology (1987) and her PhD from the University of Massachusetts, Amherst in Polymer Science and Engineering (1992).

SP054.2 - The Historical Role of Women in Medical Physics

Author(s): Magdalena Stoeva¹, Virginia Tsapakis², Simone Kodulovich³

¹IOMP Medical Physics World, York/UNITED KINGDOM, ²Konstantopoulio General Hospital, Athens/GREECE, ³Asociación Latinoamericana de Física Médica (ALFIM), Brazil/BRAZIL

Women have always played a key role in the development of science. The first recorded information for women scientists dates back to over 10-20 centuries BC. Leading women scientists and philosophers during the antiquity have contributed towards the development of various scientific branches - Enheduanna (Sumerian astronomer), Agamede (ancient Greek physician), Merit Ptah (Egyptian physician), Tapputi-Belatekallim (Babylon chemist).

Although for centuries the scientific world was dominated by men, there are many gifted women who made key discoveries, inventions or overall scientific contributions. Whilst discussing the role of women in science, this is indisputably dominated by Marie Skłodowska-Curie – the brilliant physicist and chemist, the first woman to win a Nobel Prize, the first person to win two Nobel Prizes and the only person to win Nobel Prizes in multiple scientific disciplines.

Many other brilliant women have made their contribution to science – some of them with a direct relation to Medical Physics - Irène Joliot-Curie, Goepfert-Mayer, Rosalyn S. Yalow, Harriet Brooks, Chien-Shiung Wu.

To mark the 50th Anniversary of the IOMP, national and regional medical physics organizations nominated medical physicists and other closely related professionals who have made outstanding contribution to the advancement of medical physics and healthcare

through research, clinical developments, education and training activities, service development, and to professional matters over the last 50 years. Women medical physicists have been included in this Outstanding Contributions list as recognition for their devotion and contributions to Medical Physics - Penelope Allisy-Roberts, Carridad Borrás, Maryellen L. Giger, Anchali Krisanachinda.

The trends in the contemporary scientific and working environment and women's dedication to science and practical application of Medical Physics lead to the formation of a number of women scientific and professional societies dedicated to the advancement of Medical Physics.

SP054.4 - Women in Medical Physics; current status in Australia and New Zealand.

Author(s): Eva Bezak

Australasian College of Physical Scientists and Engineers in Medicine (ACPSEM), Adelaide/AUSTRALIA

According to the recent data by Australian Institute of Physics, Australian schoolgirls still prefer life sciences to physical sciences with a 2:1 ratio. This worsens at university to about 4:1. The proportion of women in senior science positions is improving at just 1 per cent per annum, and even going backwards at lower levels.

In the specific case of medical physics, in Australia and New Zealand, there have been some positive developments in enrolment of women into medical physics training and females now account for 30% of trainee medical physicists. This can be considered an achievement considering that 15-20 years ago many departments would not have any or only a few female medical physicists.

However, there is still underrepresentation of women at senior roles and consequently a potential lack of role models for women earlier in their career. There is also a lack of suitable part time positions (especially at senior levels) for women who would like to balance family and work commitments.

Additionally, while the public service is generally accommodating for working mothers, private practice centres can be a different story (long hours, lots of travel). As the ratio of private to public radiation oncology services increases it may result in a more difficult environment for women and there may also be a pronounced gender bias in recruitment.

In conclusion, more work needs to be done mentor and support young women into sustainable careers in the physical sciences and engineering, including medical physics and biomedical engineering. Strategies need to be developed that will allow women successfully balance their family and work commitments both in public and private sectors.

SP055 - Cellular & Molecular Mechanics

TRACK 03: BIOMECHANICS AND ARTIFICIAL ORGANS

SP055.1 - Neurite outgrowth induced by shock waves

Author(s): Youn Kihwan¹, Akira Tsukamoto², Akihumi Furuichi¹, Keiichi Nakagawa³, Takegiro Ando¹, Etsuko Kobayashi¹, Takashi Ushida⁴, Ichiro Sakuma¹

¹Precision Engineering, The University of Tokyo, Tokyo/JAPAN, ²Department Of Applied Physics, National Defense Academy of Japan, Yokosuka/JAPAN, ³Department Of Chemistry, The University of Tokyo, Tokyo/JAPAN, ⁴Department Of Mechanical Engineering, The University of Tokyo, Tokyo/JAPAN

Neurite outgrowth is one of important factors to restore neurodegenerative diseases, such as Parkinson's disease and Alzheimer's disease. One way to stimulate the neurite outgrowth is mechanical stimulation. For example, mechanical stretches were demonstrated to stimulate the neurite outgrowth [1]. Although mechanical stimulations are expected to be superior in treatment targeting, minimally invasive way of mechanical stimulation is required for realizing medical applications. Shock wave is one of the noninvasive ways to introduce mechanical stimulations. In addition with Extracorporeal Shock Wave Therapy (ESWT), recent studies demonstrated that shock wave could stimulate revascularization noninvasively [2]. In this research, we hypothesized that shock wave irradiation could stimulate neurite outgrowth. To verify the hypothesis, PC12 cells, a cell line of pheochromocytoma, were irradiated with shock waves. Before shock wave irradiations, PC12 cells were cultured with DMEM supplemented with 10% FBS, 5% HS, 1% L-glutamine and 30ng/ml NGF for 2days. After that, shock waves were irradiated 10 times/day for 6 days. Peak pressure of shock waves was 3MPa and irradiation frequency was 1Hz. Neurite outgrowth was quantified with NeuronJ (ImageJ add-on software) by measuring the length of selected neurites which were longer than cell bodies. As a result, neurite outgrowth was stimulated with shock wave irradiations on PC12 cells (Fig. 1(a), Fig.1(b)). With the shock wave stimulation, average length of neurites reached $268\mu\text{m} \pm 95\mu\text{m}$ compared to $213\mu\text{m} \pm 88\mu\text{m}$ in control cells without shock wave irradiations (Fig. 1(c), $***p < 0.001$). Through this result, we knew that neurite extension can be promoted by shockwave. Although it was revealed that shock wave could stimulate neurite outgrowth in PC12 cells, further study is required to clarify the mechanical and biological mechanisms by which shock waves promote neurite outgrowth.

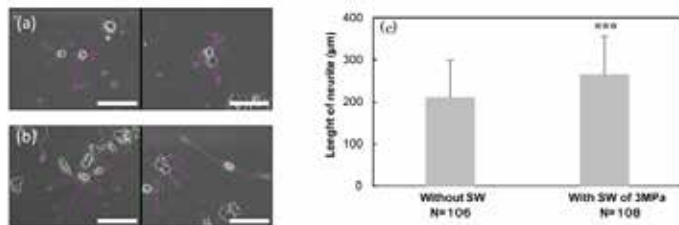


Fig.1 Images of PC12 cells after exposure of NGF without and with Shock Wave (SW) for 6days. Scale bar = 300 μm . (a) Without SW, (b) With SW of 3MPa. (c) The length of neurite after exposure of NGF without and with SW for 6days. A comparison between with and without SW of 3MPa is shown with $***p < 0.001$. 106 neurites without SW and 108 neurites with SW were measured.

REFERENCES

- Higgins S, Lee JS, Ha L, Lim JY. *Biores Open Access*. 2013;2:212-216.
- Nishida T, Shimokawa H, Oi K, Tatewaki H. *Circulation*. 2004; 110: 3055-3061.

SP055.2 - Investigating mechanical behavior and structural response to strain of bovine tendon collagen fibrils using atomic force microscopy

Author(s): Andrew S. Quigley¹, Samuel P. Veres², Laurent Kreplak¹
¹Physics, Dalhousie University, Halifax/NS/CANADA, ²Saint Mary's University, Halifax/CANADA

To fully understand the structure-function properties of tendons and ligaments, it is necessary to understand the mechanical response of their primary load-bearing elements: nanoscale collagen fibrils. The goal of this study is to investigate the mechanical and morphological properties of collagen fibrils as a function of applied strain, and understand the changes in fibril structure caused by tensile load and rupture. Using collagen fibrils extracted from a bovine digital extensor tendon, we developed a technique for mechanically stretching and then quantitatively imaging single, isolated fibrils using an atomic force microscope (AFM). Fibrils were extracted, deposited onto a glass substrate, and then divided into mechanically isolated 50-micron-long segments via evenly spaced epoxy droplets. Using a stiff AFM cantilever, a strain between 0 and 18% (or rupture) was applied to each segment while submerged in phosphate buffered saline (PBS) by displacing the segment's centre laterally at a rate of 1 $\mu\text{m/s}$. The force required to achieve the target strain for each segment was measured with the AFM, and increased with strain. Following the mechanical interventions, each fibril segment was imaged in PBS using the PeakForce Quantitative Nanomechanical Mapping mode of operation to characterize the high-velocity radial modulus, fibril height, and fibril morphology. The high velocity radial modulus is a measurement of molecular density within a fibril, and generally decreased with maximum applied strain. Figure 1 shows the decrease in modulus of a fibril strained to $12.0 \pm 0.5\%$ compared to an unpulled, control segment. Consistent with this modulus trend, the change in height of the fibril generally increased with maximum strain. Fibril swelling is likely associated with water absorption, which would decrease density and high velocity radial modulus. Since the modulus and height of the fibrils changed in regions both with and without evidence of local plastic deformation, we conclude that tensile loading can cause both plastic and non-plastic structural rearrangements within tendon collagen fibrils.

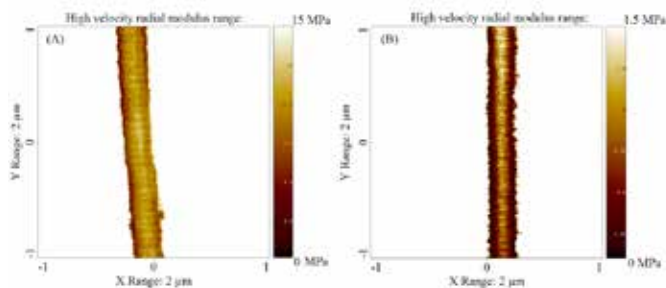


Figure 1 – High velocity radial modulus images of an unloaded control fibril segment (A) compared to a segment loaded in tension to $12.0 \pm 0.5\%$ strain (B). The radial modulus of the loaded segment is lower by an order of magnitude compared to the unpulled control segment.

SP055.3 - Collagen fibrils from overloaded tendons show sites of discrete plasticity and overall perturbation in molecular packing
Author(s): Samuel Baldwin¹, Laurent Kreplak², J. Michael Lee³
¹Physics And Atmospheric Science, Dalhousie University, Halifax/NS/CANADA, ²Physics And Atmospheric Science, Dalhousie University, Halifax/NS/CANADA, ³School Of Biomedical Engineering, Dalhousie University, Halifax/NS/CANADA

Tendons show the ability to resist rupture and to retain partial mechanical function after overload, characteristics which may have evolutionary importance. Understanding the origins of such intrinsic structural toughness, and the mechanisms of cellular response to damage, may provide important insights into tendon trauma and its treatment. Probing the nanoscopic structure of overloaded tendon has revealed an intriguing candidate mechanism. This process, termed discrete plasticity, was revealed by scanning electron microscopy to involve periodic kink deformations along individual collagen fibrils within overloaded tendon [1]. The influence of discrete plasticity on thermal stability of collagen, its enzymatic susceptibility, and its cellular response have been studied; however, the localized, nanoscale mechanical properties of the kinked structure remain unknown [2,3].

Previous work with atomic force microscopy on hydrated collagen fibrils has demonstrated the ability of peak force quantitative nanomechanical mapping as a probe of molecular density, mapping lateral packing variations along individual collagen fibrils by measuring compression modulus at tip velocities above 100 μ m/s [4]. Applying this methodology to fibrils displaying discrete plasticity resulted in high resolution maps of the localized molecular density of kinked structures formed along overloaded collagen fibrils (Figure 1,A). The resulting data demonstrated that the topologically discrete kinks are coupled with a decrease in molecular density along the entire fibril. This decrease can be attributed to an increased uptake of water when compared to control fibrils. High resolution maps of the same fibrils in a dehydrated state clearly demonstrate retention of D-banding axial packing structure throughout the kinked fibril with the exception of periodic fault lines at kink locations (Figure 1, B). This suggests that the axial register of collagen molecules, characteristic of collagen fibrils, is retained in regions spanning the kinked structures of the discrete plasticity phenomenon in collagen.

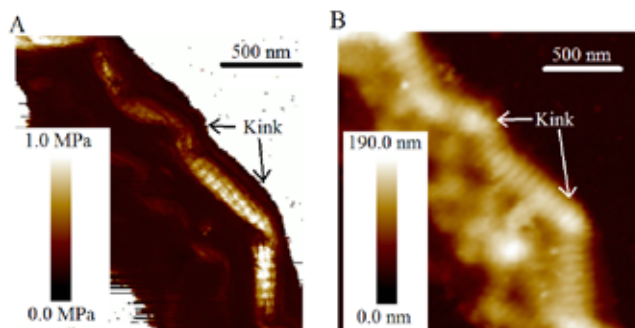


Figure 1: High resolution maps of the same kinked fibril representing (A) its compression modulus in the hydrated state and (B) its height in the dehydrated state.

References:

- [1] Veres, S. P., and J. M. Lee. 2012. *Biophys J* 102:2876-2884.
 [2] Veres, S. P., J. M. Harrison, and J. M. Lee. 2014. *Matrix bio* 33:54-59.
 [3] Veres, S. P., E. P. Brennan-Pierce and J. M. Lee. 2014. *J Biomed Mater Res A* 103:397-408.
 [4] Baldwin S. J., A.S. Quigley, C. Clegg, L. Kreplak. 2014. *Biophys J* 107(8):1794-1801.

SP055.4 - Mechanobiology of Hepatic Cells and Engineered Construction of Liver
Author(s): Mian Long

Center For Biomechanics And Bioengineering, Institute of Mechanics, Chinese Academy of Sciences, Beijing/CHINA

Liver microcirculation is unique due to its complicated structure of sinusoidal nodes, in which multiple types of hepatic and/or hemopoietic cells interact with each other under blood flow in a three-dimensional (3D) environment. Adhesion of flowing leukocytes to liver sinusoidal endothelial cells (LSECs) or Kupffer cells (KCs) is crucial in liver immune responses. While it is known that two β 2 integrins LFA-1 and Mac-1 play distinct roles in the most of organ-specific microcirculations, Mac-1 seems to be predominant in neutrophil (PMN) adhesion and crawling in localized inflammation while the role of LFA-1 is controversial in liver. We first compared the binding kinetics of LFA-1 and Mac-1 to ICAM-1s on mouse LSECs or KCs and found that the binding kinetics between these two integrin molecules is different when ICAM-1s were expressed on distinct cells, supporting that Mac-1 predominantly mediates the adhesion between leukocytes and LSECs and KCs. Next, we tested the flow-induced crawling of mouse PMNs on LSEC monolayer and observed that PMNs tend to migrate along the direction of shear flow and yield high crawling velocity and moving displacement than those under static condition, mainly mediated by LFA-1. Then, we also quantified the impact of substrate stiffness and microtopography on hepatic differentiation of stem cells using 3D in vitro sinusoidal model and engineered liver bioreactor, in which physiologically-mimicking microenvironment is critical for implementing hepatic functions. This work provides an insight for quantifying the intrinsic binding kinetics and the blood flow-induced crawling features of hepatic cells and proposes a novel 3D supporting system for liver function, from a viewpoint of mechanobiology.

This work was supported by National Natural Science Foundation of China grants 31230027 and 31110103918, and Strategic Priority Research Program of Chinese Academy of Sciences grant XDA01030102.

SP055.5 - Modelling and Understanding Normal Pressure Hydrocephalus
Author(s): Christine Goffin¹, Anne Holterhoff¹, Steffen Leonhardt², Klaus Radermacher¹
¹Chair Of Medical Engineering, RWTH Aachen University, Aachen/GERMANY, ²Chair Of Medical Information Technology, RWTH Aachen University, Aachen/GERMANY

Up to 10% of all dementia patients may actually suffer from Normal Pressure Hydrocephalus (NPH), a disease whose pathogenesis is not yet understood. The ventricles enlarge in this particular form of hydrocephalus, although the mean intracranial pressure (ICP) is not elevated. In this paper, the two main biomechanical hypotheses for the formation of NPH are examined by critically reviewing biomechanical models investigating the onset of NPH: 1) A transmante pressure gradient between ventricles and subarachnoid space (SAS) widens the ventricular space mechanically, stresses the ventricular walls and causes edema leading to tissue damage. 2) Disturbed dynamics caused either by reduced compliance, vascular disease, malabsorption or obstructions of cerebrospinal fluid (CSF) pathways cause tissue damage. The different models are analyzed and contrasted with clinical findings in order to summon what could be gained by biomechanical model based analysis. It is the goal of this article to identify open questions that can be answered by biomechanical models.

SP055.6 - Osteolytic tumour involvement modifies characteristics of Collagen-I within the vertebral bone matrix impacting mechanical behaviour

Author(s): Mikhail V. Burke, Cari Whyne, Thomas Willett
University of Toronto, Toronto/CANADA

Vertebral mechanical integrity is diminished in the presence of metastatic disease. Modelling of the biomechanical behaviour of metastatically involved (MI) bones, however, has to date focused on structural changes alone, without accounting for the potential impact of alterations in bone quality (tissue level changes). More specifically, changes in the organic components of the bone matrix. This study aims to characterize vertebral structure, modifications in primary organic constituent of bone: Collagen-I and mechanical consequences due to the presence of osteolytic metastasis.

Osteolytic (n=8) vertebral metastases were generated in an athymic rat model via intracardiac injection of HeLa cancer cells. μ CT imaging was used to quantify the stereologic distribution of mineralized tissue. Transmission electron microscopy (TEM) and high power liquid chromatography (HPLC) were used to assess the organic phase of bone. And finally, mechanical testing of spinal motion segments was conducted through stepwise loading (axial compression) in combination with time-lapsed μ CT imaging.

Osteolytic tumour involvement (TI) caused an increase in trabecular spacing; and a decrease in trabecular number, spacing and tissue & bone mineral density compared to healthy controls. This indicates that osteolytic involvement reduced both the amount of trabecular bone and the mineral density of the remaining bone.

TEM revealed fibril misorientation in osteolytic specimens and a decrease in the fibril diameter of the collagen fibril matrix on the surface of bone adjacent to tumour lesions. HPLC analysis showed no impact of osteolytic disease on the collagen content in bone, but revealed a decrease in specific enzymatic crosslinks (deoxy-pyridinoline) and an increase in non-enzymatic crosslinks (pentosidine) indicative of the operation of reactive oxygen species produced by tumour presence and the resulting oxidative stress.

Osteolytic motion segments when loaded to failure also showed reduced peak failure loads and stiffness with bone failure being focal in nature and not causing major deformation throughout the entire structure with continued loading.

Osteolytic tumour involvement both reduced bone mineral density and caused changes within the organic phase of bone, negatively impacting the mechanical behaviour of bone. Identifying changes in the material phase of (MI) bone and establishing correlations between such changes and the material & mechanical properties/behaviour is critical for the establishment of a fundamental knowledge base needed for modelling and evaluating fracture risk and guiding future treatment options.

SP056 - Image Guided RT: Part 2

TRACK 04: RADIATION ONCOLOGY

SP056.1 - Imaging Dose and Dose Pattern in Image-guided Radiotherapy of Cancers

Author(s): Li Zhou¹, Sen Bai¹, Yibao Zhang², Xin Ming³, Ying Zhang³, Jun Deng⁴

¹Center For Radiation Physics And Technology, Cancer Center, West China Hospital, Sichuan University, Chengdu/CHINA, ²Key Laboratory Of Carcinogenesis And Translational Research (ministry Of Education), Department Of Radiotherapy, Peking University Cancer Hospital & Institute, Beijing/CHINA, ³Department Of Biomedical Engineering, Tianjin University, Tianjin/CHINA, ⁴Department Of Therapeutic Radiology, Yale University, New Haven/CT/UNITED STATES OF AMERICA

Purpose: To systematically evaluate cumulative doses to organs-at-risk from various radiological imaging procedures in image-guided radiotherapy (IGRT) and corresponding dose patterns in a large cohort of cancer patients treated at one institution in past four-and-half years.

Methods and Materials: With IRB approval, 4832 cancer patients treated at our institution during past four-and-half years were collected with their gender, age, circumference as well as all the radiological imaging procedures performed, which may include computed tomography (CT), kilo-voltage portal imaging (kVPI), megavoltage portal imaging (MVPI) and kilovoltage cone-beam computed tomography (kVCBCT). Correlations between patient's size and organ dose were first established via Monte Carlo dose calculations in patient anatomy, and then used for patient-specific organ dose estimation. BEIR VII models were employed for radiation-induced relative risk estimation based on one's gender, age and radiation dose.

Results: There were a total of 5298, 24173, 30605, 35110, 37509 and 9322 procedures performed on 202, 938, 1056, 1117, 1165 and 354 patients in 2009, 2010, 2011, 2012, 2013 and 2014, respectively. Among them, 3.6%, 14.2%, 23.8 and 58.4% were from CT, kVCBCT, MVPI and kVPI, respectively. In total, 92.8%, 90.3% and 68.5% of patients received 30 cGy or less doses to brain, lungs and RBM, respectively. Yet, 80 cGy or more doses were deposited to brain, lungs and RBM in 273 small-sized patients (maximum 136, 278 and 267 cGy, respectively), due largely to repetitive procedures and non-personalized imaging settings.

Conclusions: The cumulative imaging doses and associated cancer risks from multi-imaging procedures were highly patient-specific and lesion-dependent, with much higher doses and risks in pediatric patients. With personalized dose estimation, the impact of radiological imaging procedures can be accounted for effectively for clinical treatment planning and decision-making. This study indicated a pressing need for personalized imaging to maximize its clinical benefits while reducing associated cancer risks.

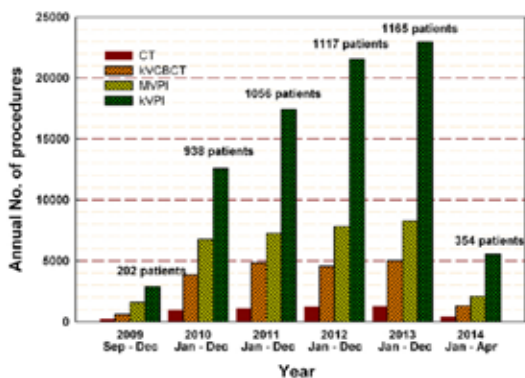


Fig. 1. Comparison of No. of various modalities and new patients each year. CT = computed tomography; kVCBCT = kilovoltage cone-beam computed tomography; MVPI = megavoltage portal imaging; kVPI = kilovoltage portal imaging. This IRB study is approved for the time period of Sep of 2009 to Apr of 2014.

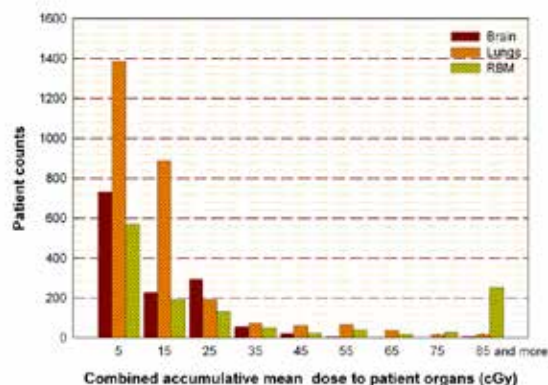


Fig. 2. Comparison among accumulative mean doses to different patient organs from CT, MVPI, kVPI, kVCBCT combined in this study. RBM = red bone marrow.

SP056.2 - Residual errors and dosimetric consequences related to the spinal cord in head and neck radiotherapy

Author(s): Jinkoo Kim, Chang Liu, Akila Kumarasiri, Robert Rusnac, Correen Fraser, Indrin J. Chetty, Farzan Siddiqui
Radiation Oncology, Henry Ford Health System, Detroit/MI/UNITED STATES OF AMERICA

Purpose: To estimate daily setup errors related to the cervical spinal cord and associated dosimetric consequences during head and neck radiotherapy.

Methods and Materials: Ten oropharyngeal cancer patients (stage IV, squamous cell carcinoma) were retrospectively selected. All patients were treated with volumetric modulated arc therapy (VMAT) with two full gantry rotations. A total dose of 60-70 Gy was delivered in 30-35 fractions. The spinal cord dose was constrained to be less than 45 Gy using an expansion margin of 5 mm (PRV). Cone-beam CT (CBCT) imaging was used for daily patient setup, and patients were immobilized with a thermoplastic mask.

In order to measure quantities at each spinal cord level, the spinal cord contours were split into “level” segments (Fig 1a). For the calculation of cumulative dose to cords, 1) dose distributions were calculated on all CBCT images using the original treatment plan, and 2) transferred and accumulated in the corresponding planning CT space using a deformable image registration algorithm. The maximum doses (*Dmax*) in the segmented cord volumes were reported. In addition, the residual setup errors (RSE) were calculated by averaging the deformation vectors in the *level* segments.

Results: The mean RSE for 10 patients are shown in Fig 1b. A minimum error of approximately 1 mm occurred between C3 and C4 and increased for C5-C7. The largest error was observed on Pt #1 (5.6 mm at C7), which was in part due to in-plane rotations, not compensated for during treatment. The estimated cumulative *Dmax* and their relative increase from plan ($\Delta Dmax$) are presented in Fig 1c and Fig 1d respectively. For five patients, the delivered *Dmax* exceeded 45 Gy with a maximum of 47.6 Gy (Fig 1c). The largest increase of 13.4% (5.6Gy) was observed in Pt #1 due to the largest RSE.

Discussions and summary: In regard to the cumulative dose, 5 of 10 patients had the *Dmax* between 45 and 50 Gy, which exceeded the dose constraint of 45 Gy. Structures beyond the C spine were not included in this study due to the limited length of CBCT images. These results indicate that caution must be exercised during daily positioning of patients with head and neck cancers. Proper PRV margins must be developed to ensure that the maximum cord doses from setup errors, such as flexion, are within the maximum dose constraint over the entire course of treatment. Further research in this area is warranted.

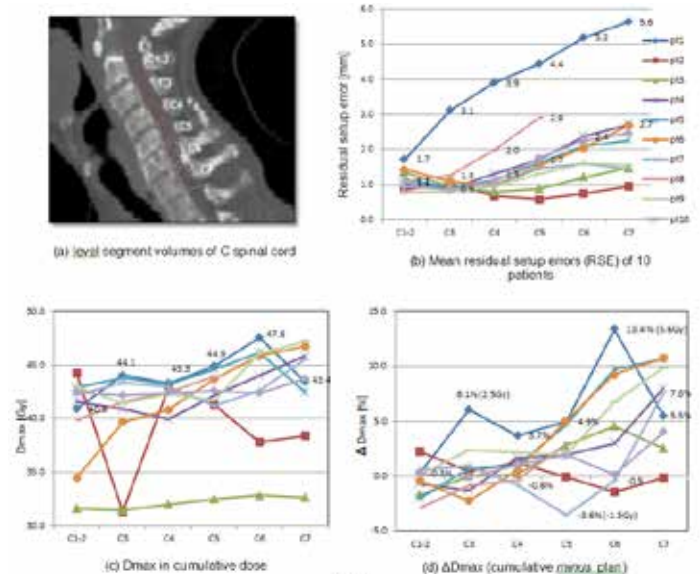


Fig. 1

SP056.3 - An automatic dosimetric and geometric tracking system for head and neck adaptive radiotherapy

Author(s): Chang Liu¹, Akila Kumarasiri¹, Mona Kamal¹, Mikhail Chetvertkov², J. James Gordon¹, Hualiang Zhong¹, Farzan Siddiqui¹, Indrin J. Chetty¹, Jinkoo Kim¹
¹Radiation Oncology, Henry Ford Health System, Detroit/MI/UNITED STATES OF AMERICA, ²Medical Physics, Wayne State University, Detroit/MI/UNITED STATES OF AMERICA

Purpose: The ability to track geometric and dosimetric changes in tumors and organs at risk, over the course of fractionated radiotherapy is essential for proper adaptive radiotherapy (ART). To that end, we have developed an ART engine that integrates clinical processes and groups (Fig1).

Methods: The ART engine is fully autonomous and consists of several modules; data import/export, automatic dose calculation, deformable image registration (DIR), interactive DIR/report review, and messaging. 1) The data import/export module transfers data between the Varian Eclipse TPS and the ART database, implemented via the Varian DICOM DB daemon and the Eclipse Scripting API (ESAPI). 2) The automatic dose calculation module calculates the dose of the day (DoD) on CBCT images. 3) The calculated DoD is then warped via the DIR module to the planning CT for cumula-

tive dose calculation. At the same time, the planning contours are warped to daily CBCT images. 4) The DIR review module allows users to review the quality of registrations in a graphical user interface, and the report review module provides plots of dosimetric/geometric trends, which assists the clinician in evaluating the ongoing treatment quality. Finally, 5) the messaging module notifies clinicians via email for various events.

Results/Discussion: The system has been successfully used for various research projects and is currently being thoroughly tested as part of our institutional software validation and quality assurance process. We have evaluated our DIR algorithm against four commercial DIR algorithms for H&N RT. The estimated accuracy was equivalent or better.

SP056.4 - Morphological Analysis of Tumor Regression and Its Impact on Deformable Image Registration for Adaptive Radiotherapy of Lung Cancer Patients

Author(s): Hualiang Zhong, Jinkoo Kim, James J. Gordon, Stephen Brown, Benjamin Movsas, Indrin J. Chetty
Radiation Oncology, Henry Ford Health System, Detroit/UNITED STATES OF AMERICA

Deformational and mass changes associated with regression of the visible tumor during the course of fractionated radiotherapy have confounded the ability to perform accurate deformable image registration, subsequently limiting the clinical implementation of adaptive radiotherapy. This study sought to investigate the impact of tumor regression on the accuracy of deformable image registrations (DIR) and then to find a solution to improve the performance of DIR for treatment of lung cancer patients. Specifically, daily cone-beam computed tomography (CBCT) images were acquired from three locally advanced NSCLC patients. DIRs were performed from three fractions 1, 10, and 20 to fraction 25 using a B-Spline-based algorithm implemented within the VelocityAI platform. To improve the accuracy of the B-Spline-based registrations in the region of regressing tumors, a hybrid finite element method (FEM) was developed with a mesh defined in a bounding box surrounding the tumor in the target image. The constraints of the FEM model were derived from the displacements generated by the B-Spline registrations. Using the displacement vector fields (DVF) of the B-Spline and hybrid registrations, the source images were warped to their targets. The accuracies of the two registration algorithms were evaluated, using landmark points identified on both the source and target images, as well as quantitative analysis of the generated DVFs. For the three patients, average tumor volumes were reduced by 53% between fraction 1 and fraction 25. Comparison of landmark points showed that the mean errors of the FEM-based hybrid registrations were 1.4, 1.6, and 1.7 mm for the three patients. The average displacement differences between the B-Spline and FEM-hybrid registrations for the three patients were 4.8, 6.2 and 3.9 mm with a maximum of 15 mm for patient 2. Lung tissue does not move consistently with the shrinking tumor. The more the tumor regresses, the larger the B-Spline registration error in the tumor region. The proposed hybrid method that consists of the intensity-based image registration and mechanics-based tissue modeling to correct geometric changes induced by anatomical deformation and tumor regression, respectively, may have the potential to improve the quality of adaptive radiation therapy for lung cancer patients.

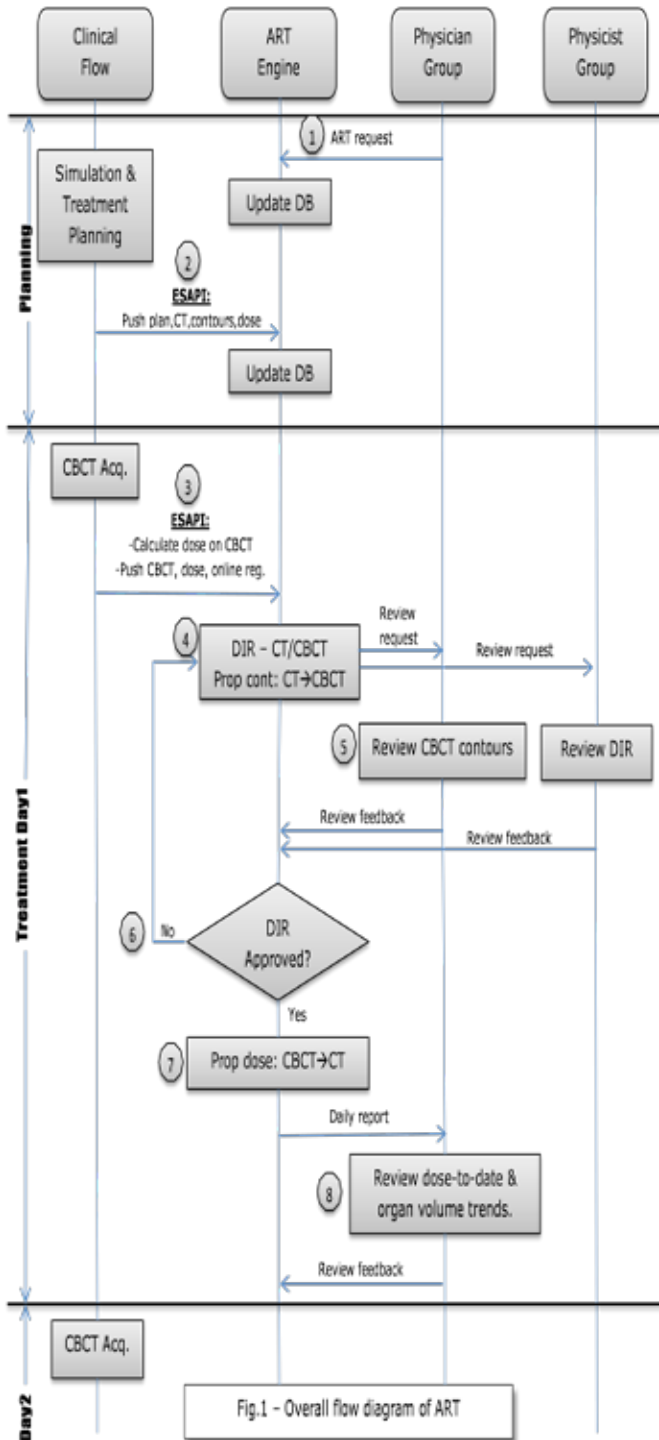


Fig.1 - Overall flow diagram of ART

SP056.5 - Assessment of a 4D-CBCT system for managing respiratory motion in Radiotherapy

Author(s): Yudy Ascencion¹, Rodolfo Alfonso¹, Raul Argota², Haydee Linares¹

¹Nuclear Engineering, High Institute for Applied Technologies and Sciences (InSTEC), Havana/CUBA, ²Radiotherapy, Institute of Oncology and Radiobiology, Havana/CUBA

Setting No.	CBCT Acquisition mode	Tumor motion	PPBC	GS	IR	VRA[mm]			TDA [mm]
						AP	LR	IS	IS
1	3D	No	1	180	med	0.20	0.20	0.20	--
2		Yes	1	180	med	-0.20	-1.15	-8.25	--
3	4D	Yes	10	50	low	0	-1.35	-0.70	0
4				50	med	0.55	-2.15	-1.55	-4
5				100	low	-0.35	-0.80	-1.35	-4
6				100	med	-1.10	0.85	-2.35	-6
7			5	100	low	2.90	-3.05	-4.55	0
8				100	med	-0.50	-3.35	-4.75	-4
9				50	low	-0.85	-2.00	-3.90	0
10				50	med	0.15	-1.45	-5.75	-4

Table 1: Results of evaluated parameters in the *CIRS008A* phantom

Introduction: Four-dimensional image guidance for correcting baseline shifts of tumors, affected by respiratory motion, has become available in the motion management option implemented inside the Elekta’s Cone Beam Computed Tomography (CBCT) system. Using this 4D-CBCT is particularly relevant when the tumor is localized in thorax, allowing reduction of target margins. The aim of this study was to design and test a procedure for appraising the performance of a 4D-CBCT system, intended to improve accuracy in treatment delivery of Stereotactic Body Radiation Therapy (SBRT). **Material and Methods:** Volumetric reconstruction accuracy (VRA), target displacement accuracy (TDA) and patient positioning accuracy (PPA), resulting from the use of the studied 4D-CBCT system (Elekta XVI *VolumeView SymmetryTM*), was evaluated under different acquisition and reconstruction conditions. A *CIRS008A* Dynamic Thorax Phantom was employed, which allows simulation of a breathing human torso, including insertion of «tumors» of different sizes and shapes. Static and dynamic phantom scans were performed with the CBCT system in 3D and 4D (*SymmetryTM*) modes. Resource sparing settings were additionally tested, decreasing the number of reconstructed phases per breathing cycle (PPBC), increasing the gantry speed (GS) or reducing image resolution (IR). The impact on accuracy of these modifications was investigated. **Results:** The acquisition of 3D-CBCT with static phantom was used as baseline for some parameters, as VRA and PPA. The results obtained with the *CIRS008A* phantom (with 2 cm spherical tumor insert) are presented in table 1.

Using the default settings suggested by the manufacturer (No. 3 in table 1), the 4D-CBCT ensures an adequate VRA, compared with the conventional 3D-CBCT (± 1 mm). Reduction of PPBC from 10 to 5 significantly degraded the VRA, emphasized when the GS is increased. An IR increment does not produce substantial benefits in VRA. A preset “shark fin” waveform with known amplitude in the three main axis was used for analysis for the TDA, evidencing that setting 7 guarantees optimal TDA with faster data acquisition and processing and much less data storage requirement. **Conclusions:** The methodology implemented allowed to verify the capability of the *SymmetryTM* tool for optimizing target localization in dynamic conditions, including internal margin assessment, which is not considered in the XVI acceptance testing protocol. It could serve as comprehensive guidance for commissioning and optimizing 4D-CBCT systems intended for IGRT, in low resource environments.

SP057 - Quality Assurance: Part 2

TRACK 04: RADIATION ONCOLOGY

SP057.1 - Sensitivity of VMAT patient specific QC devices to linac calibration errors

Author(s): Eduard Gershkevitch, Mihhail Gershkevitch
Radiotherapy, North Estonia Medical Centre, Tallinn/ESTONIA

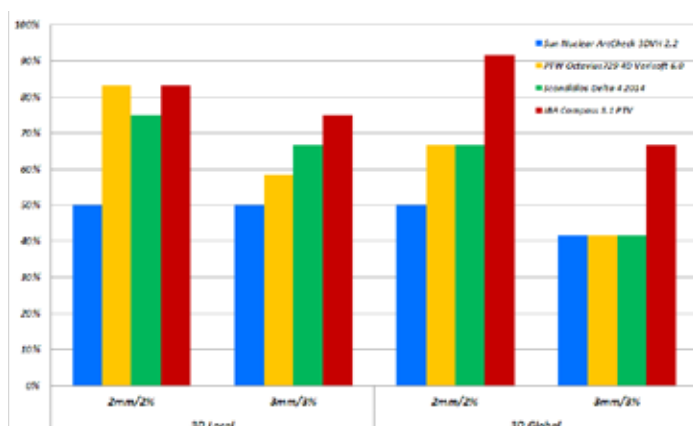
Purpose: The aim of this study was to investigate the impact of linear accelerator calibration (dose and MLC) errors on 3D gamma analyses performed by four different devices for VMAT patient specific QC.

Methods and Material: Different calibration errors were introduced to the Linac and fifteen different VMAT plans (5 prostate, 5 pelvic nodes, 5 head & neck) were measured. The errors include 1) addition of 1.6 mm MLC leaf gap to all leaves; 2) shift of both MLC banks by 1.6 mm in one direction; 3) increasing dose output by 3%, decreasing dose output by 3%. For all conditions the treatment plans were measured with ArcCheck (Sun Nuclear), Octavius 4D (PTW Freiburg), Delta 4 (Scandidos) and Compass (IBA Dosimetry) devices. 3D gamma evaluation using local and global settings were performed. The original measurement (without intentional errors) results were than compared to those with errors and the ability of devices and used metrics to detect the errors were analyzed. Student's T-test was used to evaluate the differences at 0.05 level.

Results: In total 300 measurements were made. The best results for the devices were achieved using 3D gamma index with 2% local dose difference and 2 mm distance to agreement criteria which identified most of the introduced errors (Figure 1). ArcCheck was able to detect 50% of the errors introduced in the present study using 3D gamma metrics while other detectors were able to do so for more than 70%. Compass was able to pick-up the most errors while performing 3D gamma evaluation only on PTV volumes. Octavius 4D was not able to detect the introduced gap to MLC for the pelvic nodes plans, whereas ArcCheck and Compass were not able to do so for the prostate plans.

Conclusion: 3D gamma analyses with 2%/2mm criteria identified more errors than 3%/3mm. Different devices can detect various errors and sensitivity to the introduced errors depends on the anatomical site/modulation complexity. Since not all errors were detected by the tested devices using 3D gamma index the alternative metrics would have to be employed to increase the sensitivity.

Figure 1. Percentage of detected errors with 3D gamma metrics



SP057.2 - Clinical implementation of a novel transmission detector for 3D quality assurance during radiation therapy

Author(s): Gueorgui Gueorguiev¹, Fazal Khan¹, Christopher Cotter¹, Michael Young¹, Bruce Crawford¹, Julie Turcotte¹, Mufeed Mahd², Greg Sharp¹

¹Radiation Oncology, Massachusetts General Hospital, Boston/ UNITED STATES OF AMERICA, ²Electrical & Computer Engineering, University of Massachusetts Lowell, Lowell/UNITED STATES OF AMERICA

Purpose

To investigate the clinical implementation of a novel transmission detector 'Dolphin' for pre-treatment and intra-fractional quality assurance during radiation therapy, and to compare it's performance to that of an another detector - MatriXX.

Materials and Methods

Measurements were performed twice for 34 patients (12 IMRT, 10 VMAT, 1 XSRS and 12 SBRT plans) on Elekta linear accelerator using IBA's COMPASS system, once with MatriXX detector and once with transmission detector. The transmission detector consists of an ion chamber array that measures X-ray fluence, which is then used to reconstruct the 3D radiation dose in the patient image set. Raystation treatment planning system was used to plan all patients. For each measurement and treatment plan structure of interest three statistical parameters in COMPASS system were investigated including, average dose difference, absolute dose difference and 3D gamma test (3mm DTA and 3% dose difference were used as gamma test parameters). Three doses were analyzed, Raystation computed, COMPASS measured with MatriXX detector and COMPASS measured with transmission detector.

Results

For all plans and structures statistical parameter average dose difference showed the biggest difference of an average 3% and maximum of 8% between the three doses investigated. For all plans and structures statistical parameters 3D gamma test and absolute dose difference showed an average of 0.8% and maximum of 3% difference between the three doses investigated. For all plans and structures the average dose difference between the doses acquired with MatriXX and with transmission detector was with an average of 2.5% and maximum of 6% difference. For the same two doses 3D gamma test and absolute dose difference had an average of 0.4% and maximum of 1.8% difference. Both detectors gave satisfactory results with SBRT and XSRS plans, even though the treatment target sizes were small.

Conclusion

IBA's transmission detector measured dose is in good agreement with the dose computed by Raystation and with the dose measured with MatriXX detector. It is a promising device which has the potential to improve the quality assurance process in radiation therapy by allowing to perform pre-treatment and intra-fractional measurements.

SP057.3 - Development of a Radiochromic Film Dosimetry Imaging System

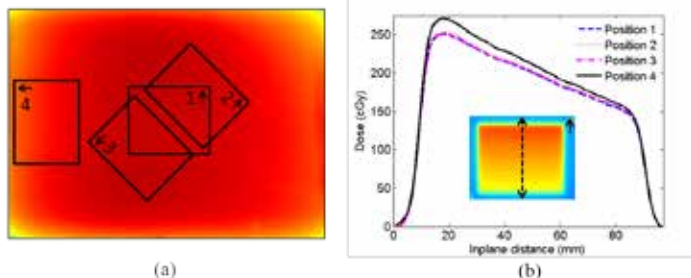
Author(s): Kevin M. Alexander¹, Ajay Rajaram², L John Schreiner²
¹Department Of Physics, Engineering Physics And Astronomy, Queen's University, Kingston/CANADA, ²Department Of Medical Physics, Cancer Centre of Southeastern Ontario, Kingston/ON/CANADA

As radiation therapy treatment modalities advance, dose deliveries for cancer treatments have become more and more complex. Due to their advanced nature, these treatments call for increasingly high spatial resolution dosimetry techniques to verify that a prescribed dose is delivered accurately and precisely. Radiochromic film dosimetry has been adopted in the clinic as a convenient option for quality assurance because it provides high resolution, two-dimensional measurements, is essentially energy independent, and is near tissue equivalent. Unfortunately, it is not always easy to use due to imaging challenges with current readout systems.

Gafchromic EBT3 film (International Specialty Products, Wayne, NJ) is typically read out using an advanced flatbed scanner. However, difficulties overcoming imaging artifacts on these scanners, related to such factors as directional dependence of the dosimetry results with respect to film orientation and non-uniform sensitivity over the scanner area, have prompted the development of strict protocols for film readout and sophisticated image correction techniques. Even with strict protocols, reliable and reproducible dosimetry can be a challenge. To overcome these challenges, a simple readout technique based on components of the Vista optical CT scanner (Modus Medical Devices, London, Canada) was investigated.

In this work, a film readout system consisting of a digital camera and diffuse light box, interfaced with computer image acquisition software has been developed and characterized for the purpose of imaging film. The optical properties of the system, light field flatness and stability, and various calibration techniques were studied and optimized. Films are rapidly read out by averaging 100 images in 7 seconds, producing submillimetre digitized film data with a high signal-to-noise ratio. Single channel and triple channel film readout algorithms have been implemented and applied for dose processing. Validation tests examining simple irradiations as well as more complex dose deliveries (from IMRT, VMAT, and SBRT) showed that film imaging using our imaging system is orientation independent, and that good agreement (< 1.5% dose difference) is found using single channel dosimetry methods with red light illumination in the central region (15 x 20 cm²) of the light field (see Figure). However, when films are imaged near the perimeter of the light box, large dose discrepancies can be produced due to the non-uniformity of the light field (see Figure). Studies are currently underway to improve uniformity.

Overall, this simple imaging technique shows good promise to simplify and improve on existing film dosimetry readout. Further optimization of the system is underway.



(a) Various film imaging positions about the surface of the diffuse red light field.
 (b) Dose profiles for the film irradiated with a 250 MU dynamic wedge, taken along the wedged direction of the dose delivery for each of the imaging positions/orientations shown in (a). The inset shows the dose distribution for the wedge film delivery, and the line along which the profile was measured. The small arrow in the top right corner indicates film orientation in (a). This plot shows that when films are read in the central flat light field area, agreement is better than 1.5% over the entire profile. This agreement fails if one reads a film outside of the central flat light field area, which in this case shows a dose discrepancy of ~8% for imaging at position 4.

SP057.4 - Implementation of MOSFET detectors for in-vivo radiotherapy dosimetry.

Author(s): Yi Wah Eva Cheung
 Medical Engineering & Physics, King's College London, London/ UNITED KINGDOM

Background: In vivo dosimetry is an essential part of radiotherapy (RT) and is recommended by national and international organisations. For patient undergoes radiotherapy for brain tumours or head and neck cancers, lens dose is concerned. Recently, ICRP review the dose to organs at risk (OARs) and reduced the lens dose limit to 50cGy. IAEA suggested that proper eye protection should be used for these patients. For patients undergo total skin electron beam therapy (TSEBT), in vivo dosimetry is important to verify the trunk dose, to ensure appropriate dose is given with sparing effect to the underneath organs. At Guy's and St. Thomas' hospital (GSTT), TLDs were employed for in vivo dosimetry, while It involves complicated pathway. MOSFET is handy and easy to use, it has been widely used in vivo dosimetry in recent years.

Methods. MOSFET characteristics including calibration factor, linearity, post irradiation stability, reproducibility, dose rate, beam angulation, beam energy, field size, temperature and attenuation effect were carried out. Phantom study was performed using MOSFET to measure the lens dose for brain tumour or head and neck cancer and trunk dose for TSEBT. Finally, clinical study was performed for lens dose measurements for two 3D conformal, two IMRT, two VMAT and three tomotherapy patients. Trunk dose measurement was performed for one TSEBT patient.

Results and Discussion. MOSFET sensitivity met the manufacturer's specifications for linearity post irradiation stability and reproducibility. Further study is needed to verify beam angulation and temperature dependence, as our setup used was different from that of the manufacturer's recommendations.

In phantom study, measurements by MOSFET exhibited less variation against treatment planning system (TPS) in both lens dose and trunk dose measurement (max. 2.84cGy and 5cGy respectively) compared to the TLDs (max 5.43cGy to 16.6cGy) respectively.

In real time in vivo lens dose measurement, MOSFET exhibited similar measured dose difference against TPS compared to TLD in most of the cases. It showed higher measured dose difference in a few cases, where technical or patients challenges may be encountered. The measured dose difference in lens dose between TLD and MOSFET were within 4cGy in 78% of cases. For radiotherapy treatment for brain tumour or head and neck cancer, this would contribute no more than 120cGy dose difference over a standard course of 30fractions and is within the acceptance tolerance in GSTT, which is 200cGy dose difference over the whole course of treatment.

Conclusion. The use of MOSFET for in-vivo dosimetry has some advantages and disadvantages. It is physically small and provides accurate real time measurement with simple calibration procedure. Time required for pre and post processing is minimal compared to TLDs. It serves as a good alternative for lens dose measurement in radiotherapy for patients with brain tumour or head and neck cancer. However, practical issues may need to be resolved prior to the application of MOSFET in trunk dose measurement in TSEBT.

SP057.5 - 3D *in vivo* dose verification at The Netherlands Cancer Institute

Author(s): Ben Mijneer, Patrick Gonzalez, Igor Olaciregui-Ruiz, Roel Rozendaal, Hanno Spreeuw, Rene Tielenburg, Ron Vijlbrief, Marcel Van Herk, Anton Mans
Department Of Radiation Oncology, The Netherlands Cancer Institute, Amsterdam/NETHERLANDS

Purpose: 1) To elucidate the clinical implementation of our *offline* 3D *in vivo* dosimetry method for daily patient-specific QA, and 2) to test a method for terminating treatment delivery if the *online* measured 3D dose distribution would result in a strong overdose in the patient.

Methods: Automatic 3D *in vivo* dose verification has been implemented in our department using a-Si EPIDs in combination with a back-projection algorithm, and is applied for almost all IMRT/VMAT and palliative treatments. Comparison of the EPID-based reconstructed and planned 3D dose distribution is done *offline*. In our current clinical workflow we measure the 3D *in vivo* dose distribution during the first fractions of a treatment. When deviations are detected, alerts are raised automatically and actions scheduled. Furthermore, a software package for *online* dose reconstruction has been developed, which processes portal images in real time. Hot spots are then sought in which the average cumulative reconstructed dose exceeds the average total planned dose by at least 20% and 50 cGy. The complete processing of a single portal frame, including hot spot detection, takes about 220 ms, which is faster than the frame rate of about 2.5 frames/s of the portal imager. The software was tested by irradiating an Alderson phantom with two arcs from a head-and-neck VMAT treatment when various types of serious delivery errors were introduced.

Results: 5766 treatment plans were verified in 2013; alerts were raised in 1397 cases (24%). Non-optimal implementation of our method in the clinic, and limitations of the dose reconstruction algorithm are the main sources of alerts. About 50% of the alerts during lung treatments are caused by anatomy changes, while during breast treatments about 50% of the alerts result from patient setup variation. The *online* dose reconstruction tests with the Alderson phantom showed that it was possible to detect hot spots in real time before dose delivery was completed. This information was able to generate a trigger to halt the linac in case of gross errors (see figure). This method would be complemented by *offline* dose verification to detect more subtle errors.

Conclusions: Our automatic *offline* verification method enables large scale clinical implementation of 3D EPID-based *in vivo* dose verification. A prototype *online* 3D dose verification tool using portal images has been successfully tested for various kinds of gross delivery errors, allowing to stop an irradiation in case of serious errors even before a full fraction is given.

SP057.6 - Dosimetric commissioning of high end features in Radiotherapy Treatment Planning Systems: a proposed update of the IAEA TECDOC-1583 guidelines

Author(s): Rodolfo Alfonso¹, Liset De La Fuente², Haydee M. Linares¹, Javier Cofre³, Alvaro Hermosilla³, Yudy Ascencion¹, Yelina Gonzalez⁴, Rogelio Diaz Moreno⁵, Eduardo Larrinaga⁵
¹Nuclear Engineering, High Institute for Applied Technologies and Sciences (InSTEC), Havana/CUBA, ²Radiotherapy, Institute of Oncology and Radiobiology, Havana/CUBA, ³Physics, Universidad de la Frontera, Temuco/CHILE, ⁴Radiotherapy, Hosp. Hnos. Ameijeiras, Havana/CUBA, ⁵Department Of Radiotherapy, Institute of Oncology and Radiobiology, Havana/CUBA

Introduction: The TECDOC-1583 (IAEA, Vienna 2008) proposed a set of test cases for commissioning of dosimetric calculations in Radiotherapy Treatment Planning Systems (RTPS), intended to

preventing severe errors in the treatment planning process in a specific institution. This guideline, however, covered typical treatment techniques only. Linear accelerators with high end capabilities, such as IMRT, SRS, SBRT, IGRT and motion management have been installed in many radiotherapy facilities during recent years in Latin America. A new set of test cases, oriented to assess the accuracy of RTPS dosimetric calculations in such high end applications, not addressed in TECDOC 1583, is proposed.

Methods and Materials: Advanced test cases were conceived based on strategy proposed by TECDOC 1583, for assessing main sources of inaccuracy in dose calculations, provided the RTPS has successfully passed the conventional tests proposed by TECDOC 1583. A total of 6 test cases were designed and tested, employing three phantoms and implemented on two different RTPS .

Test case 1 (IMRT) has the purpose of verifying calculations with intensity modulated static fields. A *CIRS IMRT THORAX phantom, model 002LFC* was employed. Target and avoidance structures, beam arrangement and goals were adapted from the “*CShape (harder)*” test proposed in AAPM TG-119.

Test case 2 (highly conformed arc) is intended to verify calculations with dynamically conformed arcs. The target is a very irregular structure, which demands rapid changes of the dynamic MLC shape with the gantry angle. The same phantom as test case 1 is used.

Test case 3 (SRS-head): is used for checking calculations in small field conditions with stereotactic positioning devices and dynamically conformed arcs. A home-made skull phantom was used.

Test case 4 (SBRT-frame-based) verifies calculations with small fields in low density tissues, including positional accuracy using stereotactic body frames. The same phantom as test case 1 is used.

Test case 5 (SBRT-IGRT): similar to case 4, but using IGRT system.

Test case 6 (4D-SBRT) utilizes a dynamic thorax phantom (CIR-S008A) for evaluating dose calculation features under respiratory motion conditions.

Results and Discussion: Results of test cases are summarized in Table 1. Relative errors are compared with agreement criteria adapted from IAEA TRS-430 and TECDOC-1583, considering complexity of case analyzed.

Table 1. Discrepancies of calculated and measured dose

Test case	RTPS	Points of evaluation	Meas. Dose [cGy]	Calc. Dose [cGy]	Errors [%]	Agreement Criterion [%]
1. IMRT	XiO	Target	209.9	204.4	-2.62%	4
		OAR	70.99	53.97	-8.11%	5
2. Highly Conformed Arc	XiO	Target	218.8	224.0	2.38%	4
		OAR	201.3	201.6	0.14%	5
3. SRS (head)	ERGO++	Target	206.0	200.0	-2.91%	4
4. SBRT (frame-based)	Precise-Plan	Target	288.0	292.0	1.39%	4
5. SBRT (IGRT-based)	XiO	Target	298.0	292.0	-2.01%	4
6. 4D-SBRT	XiO	Target	376.4	354.0	-5.95%	5

$$^a \text{Error [\%]} = 100 * (D_{cal} - D_{meas}) / D_{meas, ref}$$

Conclusions: Proposed test cases demonstrated being very useful not only for assessing RTPS dose calculation accuracy, but as comprehensive end-to-end verification of the overall process.

SP057.7 - Implementation of statistical tolerance for patient specific QA and independent monitor unit calculation

Author(s): Frédéric Girard

Département De Radio-oncologie, Centre intégré de cancérologie de Laval, Laval/QC/CANADA

Purpose: Standard and arbitrary tolerance for patient specific QA and independent monitor unit calculation were replaced by statistical tolerance based on past clinical results. The implementation of these tolerances was evaluated over a period of two years.

Materials and Methods: Patient QA results were collected and analysed statistically. They included ionization chamber dose difference, ArcCHECK (Sun Nuclear Corporation, Melbourne, FL) gamma factor passing rate, and radiochromic film gamma factor passing rate. Gamma factors were calculated with 3% absolute dose and 3 mm distance thresholds. Results from the ionization chamber and the ArcCHECK were divided in different categories based on the treatment plan complexity: 3D conformal (including wedge field), forward planning step and shoot, inverse planning step and shoot and VMAT. Radiochromic film were only used in patient QA when the modulation of the treatment plan was estimated to be very high, therefore the results were not divided into categories. For electron treatment plan, the difference between the measured and calculated depth of the isodose of prescription was also included. In addition, treatment field monitor unit difference calculated by the treatment planification system and the independent system were also included in the analysis and divided into several categories: open, wedge, forward planning step and shoot, inverse planning step and shoot and VMAT. Outliers were removed from each distribution. If the distribution was normal, parametric statistics were used, otherwise non-parametric statistics were used. A first set of tolerances was defined as the 95% confidence interval of the dataset (or the range for 95% of the observation for non-parametric dataset). A second set of tolerances was defined at 99%. Results that were beyond the first tolerances required an investigation but were still deemed acceptable whereas results beyond the second tolerances were unacceptable.

Results: These new tolerances were tested for a period of two years. In most cases, test results that fall beyond tolerances were caused by a preparation error and were easily corrected. In other cases, the errors encountered were real and significant. For example, ionization chamber measurement would sometime fall outside tolerances when a plan was highly modulated. This situation led to the improvement of our QA procedure by using a smaller chamber less prone to this error. In another situation, large differences in the depth of the prescription isodose led to the discovery of a calculation error in our independent monitor unit calculation system in some conditions. In

some rare instances, small calibration errors of the linac were detected using these new tolerances. None of these errors would have been detected with the conventional arbitrary tolerance.

Conclusion: Building new tolerances based on clinic statistical results provides an increased sensitivity of the QA program to errors that may otherwise remain undetected using conventional tolerance.

SP058 - Characterization of Detector Systems for Therapy Dosimetry: Part 1

TRACK 05: DOSIMETRY AND RADIATION PROTECTION

SP058.1 - Destructive backscatter-based readout of polymer gel dosimeters: proof of principle

Author(s): Warren G. Campbell¹, Derek M. Wells², Andrew Jirasek³

¹Physics & Astronomy, University of Victoria, Victoria/BC/CANADA, ²Physics, British Columbia Cancer Agency - Vancouver Island Centre, Victoria/BC/CANADA, ³Physics, University of British Columbia - Okanagan, Kelowna/BC/CANADA

A new method is introduced for evaluating the radiation-induced polymer distributions in polymer gel dosimeters. Destructive backscatter-based readout (DBBR) involves the careful slicing and scanning of dosimeters using dual chromatic scans (e.g., red and blue). Spectral differences in scatter attenuation coefficients cause blue light to be more likely to be scattered by polymers than red light. Comparing the intensities of backscattered red and blue photons allows one to evaluate polymer density.

Two polymer gel dosimeters were irradiated, sliced and scanned using the DBBR method. Scans of central slices in two different irradiation patterns were acquired using a flatbed scanner, and ['blue channel' - 'red channel'] images were used to measure polymer distributions. DBBR scan results were then compared against dose distributions calculated by treatment planning software, and select regions of interest (ROIs) from each scan allowed for quantitative comparison between DBBR values and dose. For comparison, reconstructions were also obtained for the same dosimeters (prior to their destruction) using a fan-beam optical computed tomography (CT) scanner.

Results demonstrate that DBBR is a feasible method for polymer gel dosimeter readout. The new method shows great potential, especially in comparison to optical CT results. The following figures are provided for this short abstract. For more details and discussion, see the full paper abstract.

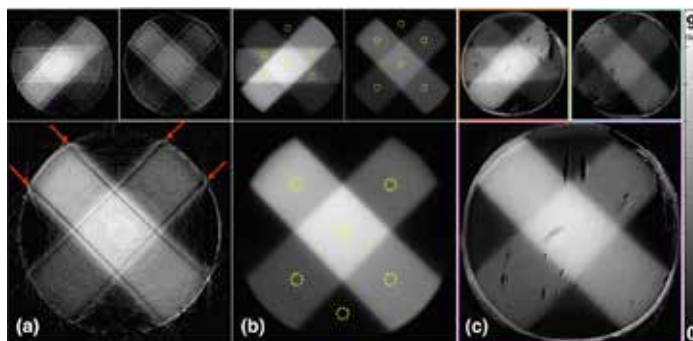


Fig. 1: Dose images for two irradiation patterns – a star pattern and two dosages of a cross pattern – are shown in (a) optical CT reconstructions, (b) TPS-calculated dose distributions, and (c) DBBR scans. Circular ROIs, 5 mm in diameter and indicated in (b), were used for DBBR-to-TPS comparisons and DBBR calibration.

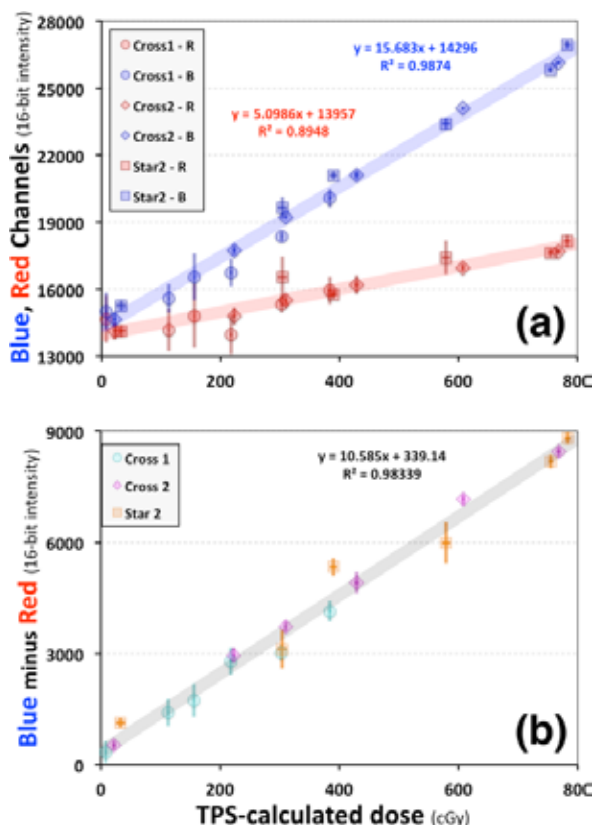


Fig. 2: Plots of ROI comparisons between DBBR and TPS images are shown for (a) blue and red channels, and (b) [blue – red]. Plot points are means and error bars indicate ± 1 standard deviation.

SP058.2 - New Detector Systems for the Dosimetry in Radiation Therapy

Author(s): Viktor Iakovenko¹, Stephan Brons², M Campbell³, O Kovalchuk¹, Xavier Llopart³, Immaculada Martínez-Rovira⁴, S Pospisil⁵, V Pugatch¹, Yolanda Prezado⁴, Iurii Sorokin¹

¹High Energy Physics Department, Kiev Institute for Nuclear Research, Kiev/UKRAINE, ²Heidelberg Ion Beam Therapy Center (HIT), Heidelberg/GERMANY, ³CERN, Geneva/SWITZERLAND, ⁴Laboratoire D'imagerie Et Modélisation En Neurobiologie Et Cancérologie, Centre National de la Recherche Scientifique (CNRS), ORSAY/FRANCE, ⁵Institute of Experimental Applied Physics (IEAP), Prague/CZECH REPUBLIC

The main goal of radiotherapy is to deposit a high dose of ionizing radiation in a tumor while keeping the absorbed dose in the surrounding healthy tissue at a tolerant level. Current developments in radiation therapy require non-destructive beam profile monitoring devices providing dose distribution measurements and imaging in real time. For this purpose a Micro-strip Metal Detector (MMD) has been developed [1]. Physics and techniques of this detector for the dosimetry, measuring and imaging charged particles and synchrotron radiation beams are discussed. An extremely low thickness ($\sim 1 \mu\text{m}$) of the MMD in combination with its high radiation tolerance ($\sim 100 \text{ MGy}$) introduces an opportunity to keep a device in the beam permanently [2]. MMD as well as metal-mode of micropixel detector TimePix have been successfully tested at the Minibeam Radiation Therapy (MBRT) setup (Bio-Medical Beamline ID17, ESRF) [3]. These detectors were explored also in recent studies at Heidelberg Heavy-Ion Therapy Center (HIT) devoted to the evaluation of the prospects of spatially fractionated hadron therapy. Hadron multi-beam structures have been created by the collimators with different shape. Holes or slits were made in aluminum, brass or tungsten (50

mm thick) samples to arrange different multi-beam structure shape ("MATRIX" or "SLIT" structure). Measurements were carried out at HIT with protons (86.72 MeV, 150.95 MeV), carbon ions (100.07 MeV/u and 200.28 MeV/u) and oxygen ion beams (233 MeV/u). MMD and TimePix were applied for the beam intensity and overall beam profile monitoring. For spatially fractionated techniques the peak-to-valley dose ratio (PVDR) is an essential value that defines the efficiency of the MBRT. Both detector types provided PVDR results in excellent agreement with the radiochromic films data.

MMD and TimePix have shown a reliable performance for online beam profile monitoring. Calibrated detector could be used for dose monitoring in real time. The results of our studies suggest the possibility of MMD application in clinical practice. Their implementation will improve beam delivery to tumor tissue, fast imaging and evaluation of data, optimization of treatment regimes.

References:

- [1] Pugatch V. *et al.* Micro-strip metal detector for the beam profile monitoring, Nucl. Instr. Meth. A 581, P. 531 (2007).
- [2] Kovalchuk O. *et al.* Metal micro-detectors for radiation therapy instrumentation, Nuclear Science Symposium and Medical Imaging Conference IEEE, P. 2617-2619 (2011).
- [3] Pugatch V. *et al.* Metal micro-detector TimePix imaging synchrotron radiation beams at the ESRF Bio-Medical Beamline ID17, Nucl. Instr. Meth. A 682, P. 8-11 (2012).

SP058.3 - Dose response evaluation of lung equivalent gel dosimeters by use of a new fitting algorithm

Author(s): Farideh Pak¹, Hassan Ali Nedaie², Abbas Takavar¹, Hamid Saligheh Rad³, Vahid Vaezadeh⁴

¹Medical Physics And Biomedical Engineering, Tehran University of Medical Sciences, Tehran/IRAN, ²Radiotherapy Oncology Department, Cancer Research Centre, Cancer Institute, Tehran University of Medical Sciences, Tehran/IRAN, ³Research Center for Molecular and Cellular Imaging, Tehran University of Medical Sciences, Tehran/IRAN, ⁴Radiotherapy Oncology Department, Cancer Research Centre, Cancer Institute, Tehran University of Medical Sciences, Tehran/IRAN

Low signal to noise ratio (SNR) images of lung equivalent gel dosimeters compare to unit density gels, necessitate use of a different fitting for data analysis. In this study a new fitting method (SQEXP) based on noise correction was introduced and its' feasibility for quantifying absorbed dose in lung equivalent gels was investigated. The effect of new method was studied in term of dose sensitivity, linearity and correlation of calibration curve for both unit and low density gel dosimeter. The results were compared to conventional (Truncation) and a newly introduced method (VAREC).

Dose response of low density gel dosimeter showed wider detectable dose rang (up to 20 Gy) against unit density gel dosimeter (10 Gy). It seems that reaction of excess amount of anti oxidant with hidden oxygen inside of styrofoam beads is responsible for this difference between low and unit density gel dosimeters. Relatively more sensitive calibration curve was obtained by SQEXP method in both type of gel dosimeters. Effect of signal denoising was more significant in low density gel dosimeters when high doses $\geq 10 \text{ Gy}$ were absorbed by the gel. Detectable dynamic dose range of low density did not change by different fitting algorithms but in unit density gel dosimeters it was reduced by VAREC method. Dose sensitivity of low and unit dosimeters was reduced by use of VAREC method.

The SQEXP method seems to be more effective method than conventional algorithms for analysis of low density gel dosimeters especially where steep dose gradients exist such as in intensity-modulated radiation therapy (IMRT) and stereotactic radiosurgery (SRS).

SP058.4 - Photoluminescence response of pure LiF crystals to clinical proton and carbon ions: a preliminary assessment for dose to water evaluations

Author(s): Jose E. Villarreal-Barajas¹, Massimo Piccinini², Mario Ciocca³, Alfredo Miranda³, Maria Aurora Vincenti², Francesca Bonfigli², Rao Khan⁴, Rosa Maria Montecali²

¹Physics And Astronomy, University of Calgary, Calgary/AB/CANADA, ²Photonics, ENEA C.R., Frascati (RM)/ITALY, ³Medical Physics, CNAO, Pavia (PV)/ITALY, ⁴Oncology, University of Calgary, Calgary/CANADA

Visible photoluminescence (PL) of pure LiF crystals irradiated with clinical proton and carbon ion beams has been investigated. The PL response was defined as the PL peak intensity measured at 670 nm when the irradiated pure LiF crystals were excited using the 458 nm line from an Argon laser operated in continuous mode at 25 mW. The emission band centered at 678 nm is due to the formation of F2 colour centres, stable at room temperature. Sets of three commercially available LiF crystals (5x5x0.5 mm³) were simultaneously irradiated. A custom-designed PMMA holder, diameter 30 mm, containing the LiF crystals, was positioned at 2 cm depth (dose plateau) in a PTW horizontal type water tank. The PL vs. dose (absorbed dose to water) was assessed for the intermediate energies of 148 MeV and 278 MeV/u for the proton and carbon ion irradiations, respectively. All irradiations were performed using a scanning beam covering a 6x6 cm² field size. The PL vs. dose in the 2-20 Gy range exhibited a fairly linear behavior for both the proton and carbon ions irradiations, as shown in figure 1. In an independent set of irradiations, a test dose of 5 Gy was given to six sets of three LiF crystals at 62, 148 and 197 MeV for protons and 115, 278 and 380 MeV/u for carbon ions, in order to evaluate the PL signal dependence with beam energy. The response to the 5 Gy test dose for protons was within 3%, while the carbon ions response decreased systematically with increasing beam energy. The PL intensity observed at 115 MeV/u was 30% higher than the one observed at 380 MeV/u. In order to test the dosimetric capabilities of the LiF-PL system, two spread out bragg peaks (SOBP) irradiations were performed at 15 cm depth using beams in the 129-163 MeV and 248-316 MeV/u range for protons and carbon ions, respectively. The proton SOBP dose evaluation was correctly predicted by applying the proton calibration derived at 148 MeV, while the SOBP dose for the carbon ions was overestimated by 7% when using the 278 MeV/u calibration. The PL of LiF can be used for the accurate dose evaluation of clinical proton beams, while a more comprehensive investigation is required to effectively apply the PL of pure LiF crystals to the dose evaluation of clinical carbon ions.

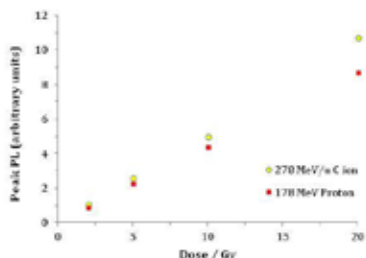


Figure 1. Pure LiF crystals PL peak intensity (measured at 670 nm) for carbon and proton beam irradiations. The carbon irradiations at 278 MeV/u consistently showed a higher PL peak signal of about 20% respect the corresponding proton irradiations at 178 MeV.

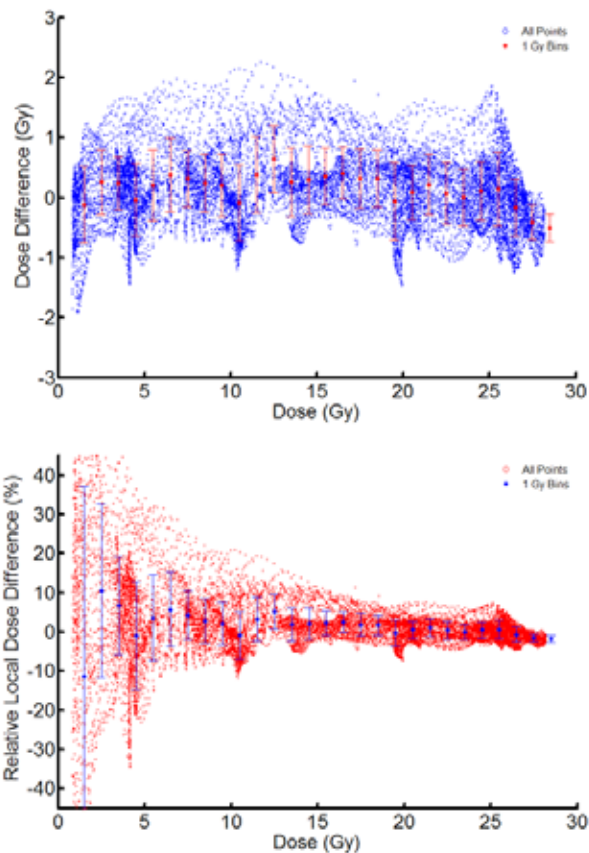
SP058.5 - Evaluation of Accuracy and Precision in X-ray Computed Tomography Polymer Gel Dosimetry.

Author(s): Evan Maynard¹, Andrew Jirasek², Michelle Hilts³, Emily Heath⁴

¹Physics And Astronomy, University of Victoria, Victoria/BC/CANADA, ²Physics, University of British Columbia - Okanagan, Kelowna/BC/CANADA, ³Medical Physics, BC Cancer Agency - Southern Interior, Kelowna/BC/CANADA, ⁴Physics, Carleton University, Ottawa/ON/CANADA

Purpose: To evaluate the accuracy and precision of an x-ray computed tomography (CT) polymer gel dosimetry system.

Methods: A high %T (19.5%T, 23%C) N-isopropylacrylamide (NIPAM) based gel formulation optimized for x-ray CT gel dosimetry was utilized and the results over six different batches of gels were analyzed. All gels were irradiated with three 6 MV beams in a calibration pattern. Post irradiation CT images of the gels were processed using background subtraction, image averaging, adaptive mean filtering and remnant artifact removal. The gel dose distributions were calibrated using a Monte Carlo calculated dose distribution of the calibration pattern and the self-calibrated gel dose was compared to Monte Carlo and a commercial treatment planning system (AAA, Varian, Palo Alto, CA).



Results: Over all gels, the mean local dose difference, which is the difference relative to the dose at the point of interest, was found to be 4.1%. The mean global dose difference, which is the difference relative to the maximum dose, was found to be 1.6%. For these calculations a 10% dose threshold was used and areas of high dose gradient were removed. Results in the higher dose regions produced significantly better local dose difference results than in the low dose regions as can be seen in Table 1. The results in Table 1 also suggest that there is fixed absolute dose accuracy which is not relative to the dose delivered; this effect produces higher local relative dose differences in lower dose regions. This can also be

seen in Figure 1, where the relative dose error decreases as a function of dose delivered.

Table 1: Mean dose differences for six gels in different dose ranges.

Dose Range (Gy)	0-5	5-10	10-15	15-20	20-25	25-30
Mean Dose Difference (σ)	0.40 Gy (0.04)	0.33 Gy (0.03)	0.47 Gy (0.06)	0.55 Gy (0.08)	0.36 Gy (0.02)	0.55 Gy (0.05)
Mean Global Relative Dose Difference (σ)	1.42% (0.14)	1.16% (0.11)	1.67% (0.22)	1.96% (0.28)	1.27% (0.06)	1.96% (0.19)
Mean Local Relative Dose Difference (σ)	9.92% (1.00)	4.19% (0.40)	4.05% (0.53)	2.99% (0.43)	1.61% (0.08)	2.08% (0.20)

Conclusion: The establishment of an overall accuracy and precision of this system provides a framework for potential areas of application such as high dose SABR treatments.

SP059 - Drug Delivery and Control Release

TRACK 08: BIOSENSOR, NANOTECHNOLOGY, BIOMEMS AND BIOPHOTONICS

SP059.1 - Nanotechnology applied in drug delivery

Author(s): Gabriela Barbosa¹, Pedro Augusto F.D. Silva¹, Glécia V.D.S. Luz², Lourdes M. Brasil³

¹Unb At Gama, University of Brasília, Gama/BRAZIL, ²Pos. Engenharia Biomedica, UNIVERSIDADE DE BRASILIA, Brasilia/BRAZIL, ³Fga, UnB, Brasília/BRAZIL

Nanotechnology is a multidisciplinary field that deals with the study, manipulation or rearrangement of particles at the nanoscale, which is equivalent to a billionth of meter, the material at this scale shows unlike physical, chemical and biological properties. This area has impacted a lot in the development of new products in various sectors and has been widely studied for offering effective solutions to several problems, such as pollution, energy rationing and cure of various diseases. What makes the field so promising is that the elements behave differently at the nanoscale, when compared to the macroscale. In this article it will be described how this field can be applied in the biomedical field, especially in controlled drug delivery systems using nanoparticles, nanobots and organometallic compounds, for greater effectiveness in the treatment of diseases. Nanoparticles (NPs) are nanosized particles (3-200 nm), devices or systems that can be made using a variety of materials including polymers, lipids, viruses, and even organometallic compounds. The uses of NP with drug delivery systems have made a remarkable difference in site-specific release of drugs, owing to their physical and chemical characteristics and biological attributes. Various researches in this exciting area have been conducted and several formulations were released in the market and are now routinely used in clinics. In this review will be found a few nanoparticles more used in the medical area, as Solid Lipids Nanoparticles (SLN), Magnetic Nanoparticles, for instance. Nanobots or nanorobots is based on the creation of tiny machines that can do the functions of today's machines, but more exactly, to develop projects that bring benefits in medicine, industry, and others areas. An ideal nanotechnology-based drug delivery system is a pharynx a self-powered, computer-controlled medical nanorobot system capable of digitally precise transport, timing, and targeted delivery of pharmaceutical agents to specific cellular and intracellular destinations within the human body. Some advances with these devices will be described in the review. Organometallic compounds are usually described as components having at least one metal-carbon bond. They also are considered nanoparticles. In the following review, will be discussed the application of Graphene and Carbon Nanotubes in drug delivery systems. Although some researches were not evaluated *in vivo*, there is a high expectation on this field. It is necessary study more about the behavior of nanoparticles at the organism, as well as figure manners to use these devices so that they do not exhibit toxicity to the body.

SP059.2 - Controlled electrochemical dissolution of iron alginate for smart drug release in micro devices

Author(s): Ashleigh Anderson, James Davis
Computing And Engineering, University of Ulster, Newtownabbey/ UNITED KINGDOM

Smart devices that can routinely monitor patient's health with little or no involvement from clinical staff have slowly begun to emerge over recent years and have arisen from significant developments in sensing and communication technologies. In cases where a rapid

response may be required, a much more effective substitute would be the development of a truly smart system that could autonomously act on the information received from the sensing component and, where appropriate, deliver a therapeutic agent in a controlled manner. This presentation details the result of an investigation in to the development of electrochemically initiated transitions of redox gels. The hydrogel structure can be held together through chemical or physical bonds and it is within the resulting network that drugs can be entrapped.

The approach to delivery is highlighted in Figure 1 where there is an electronically controlled layer that separates the drug reservoir from the skin. The core methodology employed in this project will involve electrochemical control to influence the porosity of a redox hydrogel, typically sodium alginate.

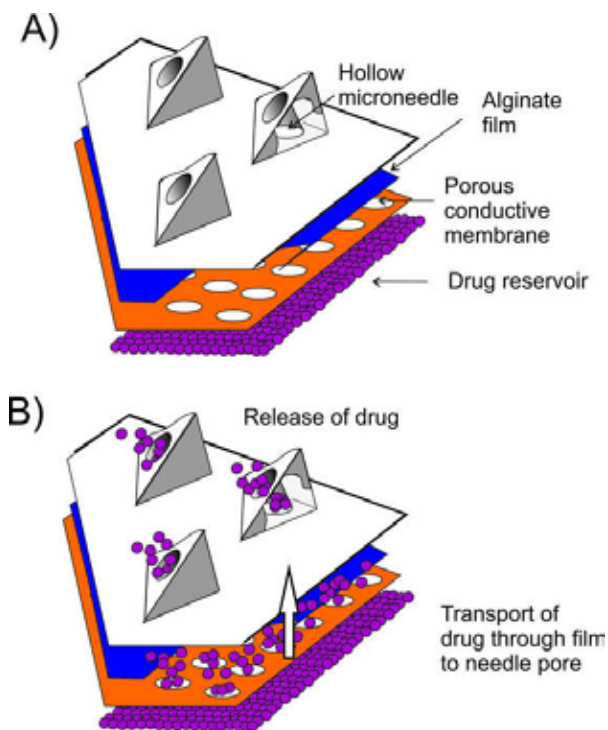


Figure 1. Microneedle patch with alginate release film. A) before release (-1.1V) and B) after release (+0.5V)

The use of the iron as the binding agent is of prime interest in the present context as, in contrast to the other metal ions, it can be electrochemically cycled ($\text{Fe}^{3+}/\text{Fe}^{2+}$). The formation of the film and its dissolution are both controllable through electrochemical means. The oxidation of the Fe^{2+} to Fe^{3+} in the presence of the alginate will activate the crosslinking process and enable site specific deposition at the electrode. While this is similar to the polypyrrole and polythiophene films, there is a crucial difference. The electrochemical reduction of the coordinated Fe^{3+} to Fe^{2+} will result not only in a simple swelling of the film but rather its dissolution. Ordinarily this would be expected to cause significant issues, especially for a film in contact with biofluids, but the alginate-iron system is inherently biocompatible (the alginate is readily hydrolysed under normal physiological conditions) and this may be a critical advantage in the future use of redox films.

SP059.3 - Next generation transdermal drug delivery – An electrochemical approach to pH manipulation for controlled release within smart patch technologies

Author(s): [Ashleigh Anderson](#), James Davis
Computing And Engineering, University of Ulster, Newtownabbey/
UNITED KINGDOM

The majority of conventional controlled release technologies tend to be based around encapsulant systems in which a polymeric binder or gel typically responds to changes in the local environment in which the delivery device has been placed. The contents are typically released when the particle, capsule, film or droplet is exposed to the appropriate physico-chemical trigger (typically a change in pH) with the time-release-dose delivery characteristics controlled through manipulation of the encapsulant formulation. In this communication, the adaptation of this core strategy for use in the next generation of transdermal microdevice or smart patch is explored. A key feature of the approach is the ability to electronically trigger the release of the drug on demand.

The strategy relies on the electrochemical properties of a carbon composite film in which micro-nanoscale pores are created through controlled laser ablation. The porous carbon layer is then combined with the cellulose ester barrier film to complete the prototype patch as indicated in Figure 1. Under normal conditions the enteric coating remains intact with no diffusion of the drug to the bulk of the solution. Upon imposing a reducing potential on the carbon film top layer however, the local pH within the pores is dramatically increased such that hydrolysis of the ester occurs with dissolution of the protective barrier releasing the drug.

The presentation covers three aspects: the design of an innovative microprobe necessary for monitoring the changes in pH within the pores, the structural and electrochemical characterisation of the carbon film and the proof of concept demonstration of a model drug release.

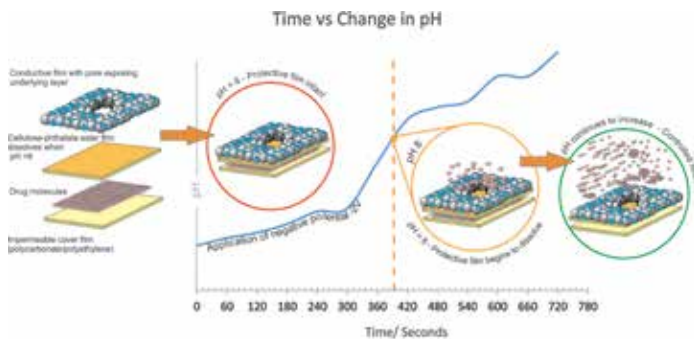


Figure 1. Design of transdermal patch and detail of how drug release is achieved as a result of pH change

SP059.4 - Protein nanocages for stabilization of bio-inspired emulsions/gel systems and cutaneous drug delivery

Author(s): [Sierin Lim](#), Sathya Moorthy Bhaskar, Mridul Sarker
School Of Chemical And Biomedical Engineering, Nanyang Technological University, Singapore/SINGAPORE

Self-assembling protein nanocages forming hollow structures are explored as potential carriers in various nanotechnology applications. The fact that proteins are integral parts of a biological system makes them promising for use as carriers for drug delivery, cosmetics and food emulsifiers. E2 Protein from pyruvate dehydrogenase multienzyme complex of *Geobacillus stearothermophilus* have the capability to self-assemble into a hollow dodecahedral cage of a unique size about 25 nm. The nanocages are extremely thermostable and porous with 12 openings of 5nm each. These inimitable characteristics of E2 protein nanocage are suitable to encapsulate

and carry foreign molecules inside its cavity. E2 protein nanocages are engineered genetically or chemically, to shuttle drugs into the skin cells such as melanocytes (Figure-1) and keratinocytes (Figure-2, protein conjugated to Alex fluor-green, nucleus stain-blue) for the treatment of pigmentary disorders. The existence of both hydrophilic and hydrophobic patches on the surface of E2 protein nanocages molds it to be a surface active bionanoparticle. Our preliminary results show the deposition of E2 protein nanocages at liquid-liquid interface under TIRF microscope (Figure 3). Thus the E2 protein nanocages can also be used as a potential stabilizer of bio-inspired emulsion and gel system. This study can be very functional in designing emulsion-and gel-based pharmaceutical products for topical application, skin care products and food products.

Figure:1

Figure:2

Figure:3

SP059.5 - Image-Guided Predictions of Nanoparticle Transport in Solid Tumors

Author(s): Shawn Stapleton¹, Michael Milosevic¹, Christine Allen², Ian F. Tannock³, David Jaffray⁴

¹Radiation Medicine Program, University Health Network, Toronto/ON/CANADA, ²Leslie Dan Faculty Of Pharmacy, University of Toronto, Toronto/ON/CANADA, ³Medical Biophysics, University of Toronto, Toronto/ON/CANADA, ⁴Techna Institute, University Health Network, Toronto/ON/CANADA

Due to the ability to preferentially accumulate and deliver drug payloads to solid tumours, nanomedicine, including liposomes, has emerged as an exciting therapeutic strategy for cancer therapy. Unfortunately, negligible increases in patient survival following liposome therapy have been observed in the clinical setting. This is due in part to the heterogeneous intra-tumoural transport of cytotoxic drugs, caused by chaotic tumour microcirculation and elevated interstitial fluid pressure (IFP). Here we explored the relationship between tumour microcirculation, IFP, and the intra-tumoural accumulation of liposomes using a combination of quantitative imaging and mathematical modeling. The combination of quantitative imaging and mathematical modeling presents a novel framework to guide nanoparticle drug-delivery in the clinical setting. A biophysical mathematical transport model, termed the intra-tumoural transport model (ITTM), was developed and used in combination with non-invasive imaging methods to predict liposome transport in solid tumours. The ITTM was validated using *in vivo* measurements of accumulation of a computed tomography (CT) liposome contrast agent made in three different tumour models. The ITTM attributed inter-tumoural heterogeneity of liposome accumulation to variations in IFP; however, several limitations were noted, including limitations in the accuracy of intra-tumoural liposome accumulation predictions based solely on IFP. These limitations were mitigated by developing a novel imaging method, termed Volume Fraction Imaging (VFI), to accurately measure additional key transport parameters, including microvascular permeability, perfusion, plasma volume and interstitial volume. VFI is based on the sequential injection of a nanoparticle and freely diffusible CAs. Simulations demonstrated that the VFI method substantially improves the accuracy and precision of plasma and interstitial volume, blood flow, and capillary permeability compared to standard pharmacokinetic modeling. *In vivo* experiments demonstrated that VFI substantially improves quantification of healthy and malignant tissue treated with Sorafenib, radiation, and mild hyperthermia. Using VFI we established that tumour perfusion and plasma volume are also key mediators of the intra-tumoural heterogeneity in liposome accumulation in several tumour models. We probed the relationship between tumour microcirculation using VFI, IFP using a novel image-guided robotic needle positioning

system, and the intra-tumoural distribution of liposomes using volumetric micro-CT imaging where performed. A strong relationship between the radial distribution of IFP, metrics of tumour perfusion, and the intra-tumoural accumulation of liposomes was observed. Therefore, both tumour perfusion and elevated IFP play an integral role in mediating the intra-tumoural accumulation of liposomes, and strengthen the need to account for intra-tumoural heterogeneity in transport properties for guiding the use of nanomedicine in the clinical setting. This work provides a pivotal piece of the image-guided drug delivery schema whereby quantitative imaging can derive patient specific information on drug pharmacokinetics, biodistribution, intra-tumoural transport, biological targets, and mechanisms of resistance. Integrating image-derived information with an established mathematical framework based on the ITTM can conceivably predict drug-transport and treatment response. This represents a major leap forward compared to the convectional chemotherapeutic strategies whereby optimal dosing and scheduling strategies can be prescribed and adapted on a based on validated mathematical models of drug delivery that are informed by quantitative imaging methods.

SP060 - SPECIAL SESSION: UNESCO International Year of Light

TRACK 12: MEDICAL DEVICES

SP060.2 - Design of Wireless Implantable Optogenetics System for Animal Studies

Author(s): Fu-Yu Chen¹, Peter S. Freestone², Simon Malpas¹, Daniel McCormick¹, David Budgett¹

¹Auckland Bioengineering Institute, Auckland/NEW ZEALAND, ²Centre for Brain Research, Auckland/NEW ZEALAND

Optogenetics uses light to manipulate neural activity which has several advantages over conventional electrical stimulation approach including specific cell-type targeting with precise temporal precision, simultaneous stimulation using different wavelengths of light and relatively harmless to targeted tissue. In optogenetics experiments, targeted neurons are transfected with photo-sensitive proteins (opsins) for subsequent exciting or silencing neurons with pulses of visible light.

Optogenetic stimulation offers the prospect of treating lifetime conditions; however, current optogenetics available commercially are mainly connected with wires coming out of head of the animal head which brings a risk of infection and is vulnerable to damage from chewing or scratching. Also, current light stimulation systems are generally not suitable for chronic use due to the risk of infection associated with components located outside the brain. This study aims to investigate the technical feasibility of implementing a fully implantable optogenetics system supporting long-term light stimulation as well as for feasibility of wireless transmission of recorded signals outwards.

A miniature LED die with dimensions of 280µm by 280µm has been sourced with an output wavelength of 470nm which is suitable for exciting the opsin ChR2. The power needed is about 6.4mW to deliver the required optical power for opsin excitation. This is an exciting proof-of-principle outcome showing adequate light from a small package of components consuming a manageable amount of electrical power.

In the experimental setup, the LED die coupled to a 200µm optical fibre is feasible and sufficient to activate ChR2 (>32µW). With 80% of the light transmitted with a bend radius of 2mm, the fibre can be tracked from the brain to the wirelessly powered telemeter located in the abdomen to form a fully implanted optogenetics system. Our results show that LED-fibre optic system is able to generate a cellular response in a ChR2-expressed cell with a short pulse (4ms) of light. The cellular response generated can also be sustained by long duration light stimulation (500ms). The amplitudes of the cellular response can be controlled by changing the light intensity emitted on the targeted cell. This can be achieved by modulating DC voltage supply using Pulse-Width Modulation (PWM) technique. This technique is favorable for implantable device because it is easy to implement using a microcontroller and does not increase the size of the circuit. This experiment motivates the use of the custom-made LED-fibre optic system *in vivo* chronic rodent studies in the future.

Critical questions for technical feasibility include size, optical power, heat generated and physical delivery of the light to the region requiring illumination have been considered.

The proposed module has been validated to measure individual cellular response to optical stimulation of photosensitive rat brain slices performed. This experiment motivates the use of the custom-made LED-fibre optic system for future *in vivo* chronic rat studies includ-

ing animal behavior as well as wireless transmission of recorded brain potentials during various treatment schemes. The implantable wireless optogenetics would have great potential to enhance basic neuroscience research and help develop interventions for various neurological disorders, such as Parkinson's disease.

SP060.3 - A method to determine the variation of irradiance in bilirubin lamps as function of the time of use

Author(s): Graciela M. Salum¹, Di Teodoro Cotua², J Salerno³, E Marino³, R D. Piacentini⁴

¹Yachay Tech, Yachay City Of Knowledge, School of Physics Science and Nanotechnology, Urcuqui/ECUADOR, ²School Of Mathematics, Yachay Tech, Yachay City of Knowledge, Urcuqui/ECUADOR, ³Facultad Regional Rosario, Universidad Tecnológica Nacional, Rosario/ARGENTINA, ⁴Imae, Fac. De Cs Exactas, Ing Y Agrim/unrosario, Laboratorio de Eficiencia Energética, Sustentabilidad Cambio climático, Rosario/ARGENTINA

Hyperbilirubinemia is a pathologic process consisting of the abnormal increase of the amount of bilirubin in the circulating blood, which can cause jaundice. A common treatment is expose the premature newborn to the phototherapy treatment, with lamps that emit in a specific region of the electromagnetic spectrum (mainly 410-550 nm). In the present work we describe one irradiance analysis method to this type of bilirubin lamps (in the case a Phillips TL20W/52), based on the determination of the intensity variation as a mathematical function depends on time (hours) with which we can simulate this behavior. We used the Exhaustive Approximation method combined with the Distinguish region-curve method for the determination of the corresponding function.

Also, we compare the spectral irradiance of the lamp, with the solar spectral irradiance measured with a high quality double monochromator Optronics 756 spectroradiometer, the day October 26 of 2012, at 12:49 local hour, in Rosario, Argentina. As a consequence, it was observed that the lamp intensity is very small compared with the solar one, which means that a careful analysis of the solar radiation incident on a given place needs to be made, if a treatment with natural radiation would be used for bilirubin reduction.

SP060.4 - Study of the sensibility of induced heat effects in edible oil measured by interferometric techniques

Author(s): Joel Espinosa-Barríos¹, Francisco Corella-Jimenez¹, Alejandra Guillen-Peralta², Amy Avila², Gerardo S. Romo-Cardenas¹, Andres Piña-Barrera²

¹School Of Engineering, Montemorelos University, Montemorelos/MEXICO, ²School Of Health Sciences, Montemorelos University, Montemorelos/MEXICO

Currently the use of edible fats and oils in the preparation of fried products has increased, it is known that excessive consumption of foods containing fats, can have a deleterious effect on the health of people, forcing increasingly strict control of oils and fats in fried foods to maintain quality of fried foods and ensure their safety, lack of laboratory facilities in fried food preparation establishments, limit the compliance of existing quality standards requiring new simple alternative methods to be used by the user.[1] Optical interferometers are instruments that can make very precise measurements of objects using the pattern of interference of two waves of light. These devices have been used to characterize materials and study their properties. This paper propose a new prototype of this application in order to reach a characterization protocol of fluids with low differentiation of components. Results in oil samples indicate that it is possible to make characterization using interferometric techniques.

SP060.5 - Design and study of Infrared-Guard**Author(s):** [Shanmugam Senthilkumar](#)

Dept. Of Radiotherapy, Govt. Rajaji Hospital & Madurai Medical College, Madurai/INDIA

Introduction: Gantry - couch collision is a serious concern for cancer patient treatment planning of the radiotherapy machine. The radiotherapy machines moving parts may cause collision between the treatment couch and the treatment head, which affects the accuracy of the machine and sometimes a replacement of parts. If a patient interferes, it results in severe injuries. In this work we have developed Infrared Guard (IRG) to prevent gantry - couch collision in the Radiation Therapy machine.

Material and Methods: The Infrared Guard consists of a distance measuring sensor unit, composed of an integrated combination of PSD (position sensitive detector), infrared sensor and signal processing circuit. The infrared sensor is made up of the emitter (infrared LED) and detector (photodiode). The emitter emits IR light pulse and the receiver detects the corresponding light pulse. The infrared intensity of the emitter influences the detection range. On the IR receiver side, the desired output voltage depends on the detection distance. This output voltage signal connected to an analog amplifier, comparator, or Schmitt-Trigger, to control various functions. IRG device placed in the treatment machine gantry, which is inner side of the gantry and above to the gantry angle indicator. IRG device monitors the region between the collimator face and the treatment table (or) patient. The IRG provides an infrared invisible sensing shield, which covers the entire collimator face. The IRG device sensing area or protection zone distance can be varied according to the requirement with adequate clearance. If the potential collision is detected by the IRG device in the protection zone, the radiotherapy machine will stop the movement and the red LED will glow and also buzzer will produce sound. We have also provided the IRG OFF key in the machine. If you want to override or turn off to the power to the IRG device a blue light will glow and illuminating words Infrared Guard OFF will appear.

Results and Discussion: We have studied this IRG device to monitor the accuracy in the radiotherapy machine using phantoms and patients. Our method correctly confirmed clearance between the patient/treatment table and the gantry. This device is easy to handle, inexpensive and stops the machine movement when the gantry and the couch come nearer to each other. Infrared Guard provides an additional level of safety to automated radiotherapy machine operation. IRG monitors the closeness of the patient treatment couch to the treatment head during remote movements and restrain or stops machine movements prior to a potential collision. IRG provides an additional "set of eye" to monitor and minimize risk. IRG does not require physical contact to detect potential collision. IRG anti-collision device improves the performance of the machine and most importantly reduces the chance of collision.

SP061 - Improvement of Diagnosis and Therapies**TRACK 12: MEDICAL DEVICES****SP061.1 - Development of heart sparing device for Left Breast Radiotherapy with deep breath-holding****Author(s):** [Shanmugam Senthilkumar](#)

Dept. Of Radiotherapy, Govt. Rajaji Hospital & Madurai Medical College, Madurai/INDIA

Introduction

Breast radiotherapy is now part of the routine care of patients with early breast cancer. Adjuvant radiotherapy for post-mastectomy breast cancer patients consists of a pair of tangential photon beams treating the breast tumor bed. In addition, internal mammary chain (IMC) and supraclavicular (SCV) beams are also employed to treat the corresponding lymphatic nodes within the region. Radiotherapy has been shown to reduce recurrence and improve the survival rate for post-mastectomy breast cancer patients. However, the benefits of adjuvant radiotherapy is compromised by the secondary cardiac mortality that occurs 15 to 20 years after the therapy has completed. Therefore, it is critical to develop radiation techniques that retain the benefits but reduce late toxicity to the heart and other organs at risk. Patients with left-sided breast cancer who receive chest wall radiation have increased risk of treatment related cardiovascular morbidity. To reduce the dose to the heart, it has been suggested that electrons be used in the IMC beam. Another strategy to reduce cardiac dose is to employ breathing adapted radiotherapy, including the deep inspiration breath-hold (DIBH) technique. It has been demonstrated that employing the DIBH technique in tangential beams appreciably reduces cardiac dose. However, there has been no study on the effect of utilizing the DIBH technique in IMC electron beams. The aim of this study was to evaluate the effect of decreasing the irradiated cardiac volume in breast-conserving therapy (BCT) with indigenously developed deep inspiration breath-hold device (DIBHD) using breath-adapted radiation therapy (BART).

Materials and Methods

We have developed indigenously deep inspiration breath-hold device (DIBHD), which consist of laser sensor, in-house software, video goggles, a breath hold signal device, alarm and visual indicator. The sensor is used to display the breath-hold position of the chest wall in the computer monitor as graphical signal as well as digital. Patients can able to see their breath hold position while using the video goggles and maintain the uniform level without reducing the lung volume. Once the threshold level reduces, patient starts to exhale the radiation will be stopped, simultaneously alarm will produce sound and visual indicator glows.

Results

DIBHD has been used for the left sided breast cancer patients during the radiotherapy in deep inspiration breath-hold. The tangential fields were planned for each respiratory-gated CT image. The dose-volume histograms (DVHs) of the heart, lung, and breast of each respiratory phase were compared. Patient's position during each breath hold was carefully monitored and make sure the heart is positioned away from the chest wall. Radiation was delivered during these repeated breath holds. A deep breath pulls the diaphragm and heart down and out of the radiation beam path. Delivering radiation treatment during these deep breath holds protects the heart from radiation. We concluded that radiotherapy using DIBHD facilitates a reduction of the irradiated heart volume which enables more complete cardiac sparing without any compromise of PTV coverage.

SP061.2 - HTA for Medical Devices: Multiple-Criteria Decision Making as an Outcome Evaluation Tool

Author(s): Ivana Jurickova¹, Jozef Rosina¹, Vladimir Rogalewicz¹, Ilya Ivlev¹, Gleb Donin², Jakub Vacek¹, Radka Otawova¹, Peter Kneppo¹
¹Department Of Biomedical Technology, Czech Technical University in Prague, Faculty of Biomedical Engineering, Kladno/CZECH REPUBLIC, ²Department Of Biomedical Technology, Czech technical university in Prague, Kladno/CZECH REPUBLIC

Health Technology Assessment (HTA), although having been routinely applied in drugs and surgery for a long time, is still quite challenging in medical devices. The reason is that the main objective of HTA studies for devices is not optimization of the cost-effectiveness ratio, but rather decisions about procurement and/or incorporation of the apparatus. The clinical benefit is not expressed in terms of quality of life, but in the rate of diagnostic yield, comfort of the clinician, or the extent to which the technology makes the therapy shorter and/or more patient-friendly. Utilization of multiple-criteria decision-making methods for evaluation of the aggregated clinical, technical and user's effect (outcome) is recommended as the input to cost-effectiveness analyses. Different methods are derived for strategic and/or operational assessment of new technology.

SP061.3 - Developing Smart Bandage Materials for the Management of Chronic Wounds in Diabetic Patients

Author(s): Jolene Mchugh, Karl Mccreadie, James Davis
 Nibec, School Of Engineering, University of Ulster, Newtownabbey/ UNITED KINGDOM

Bacterial contamination of chronic wounds has long been a major concern for those involved in the management of diabetic foot disease (DFD). The latter is an increasingly common complication of diabetes whose treatment has a profound impact on both patient and health-care resources. In 2013, global healthcare expenditure for diabetes totalled \$548 billion. With the ever increasing population of people with diabetes expected to increase by 55% in 2035, we can expect expenditure to reach \$627 billion and upwards. A study has estimated that a population with diabetes costs three to four times greater than a population without. The majority of these costs are due to the complications that arise from diabetes such as neuropathy, infection and ulceration. It has been estimated that approximately 25% of all diabetes related hospital admissions in the US and the UK are due to such complications and consequent limb threatening infections. Approximately 15% of patients with diabetes will suffer from foot problems and around 7% have a foot ulcer at any given time. Around 56% of foot ulcers become infected, making patients 30 times more likely to have an amputation compared to the general population making it the most common cause of lower limb amputation.

While there has been considerable activity in the development of wound dressings that aim to minimise bacterial contamination and aid the healing process, the majority are passive and possess little or no diagnostic capability. The present communication details the results of an investigation into the use of a smart bandage which can permit electrochemical interrogation of the wound environment and therein proffer the possibility of more timely and effective interventions in the management of the wound.

Carbon loaded polyethylene films were selected as the base substrate for a mechanically flexible and conductive sensing material for use in wound monitoring technologies. The films were processed using laser ablation of the surface to increase the effective surface area of the electrode and were then subject to an oxidative electrochemical etch to improve the electron transfer kinetics. The surface morphology of the resulting film was analyzed and the electrode performance in relation to monitoring uric acid, a key wound biomarker, was optimized. A prototype smart bandage interfaced with a miniaturized potentiostat capable of monitoring the wound condition was developed and the

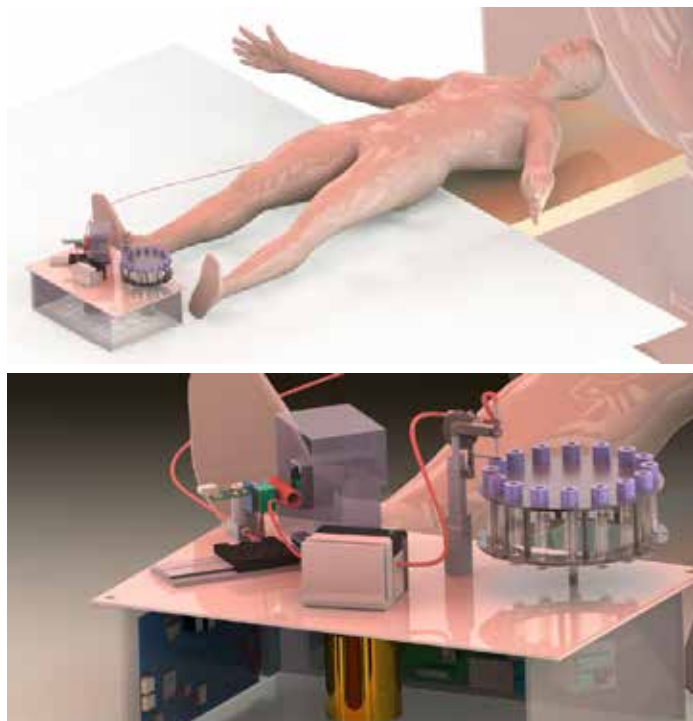
response to urate harnessed to measure both the wound pH and wound severity. The viability of using urate for use in complex fluids was assessed using whole blood and other potential interferences. The mechanical flexibility of the polyethylene film is ideal for incorporation within existing dressing materials and could be produced in bulk at relatively low cost, a pre-requisite given the frequency with which dressings need to be replaced.

SP061.4 - A CdZnTe-based automated Blood Counter for Quantitative Molecular Imaging

Author(s): Romain Espagnet¹, Jean-Pierre Martin², Louis-André Hamel², Philippe Després¹

¹Département De Physique, De Génie Physique Et D'optique, Université Laval, Québec/QC/CANADA, ²Département De Physique, Université de Montréal, Montréal/QC/CANADA

Positron Emission Tomography (PET) and Single-Photon Emission Computed Tomography (SPECT) are well established molecular imaging modalities used in many fields of the biomedical sciences. They allow *in vivo* investigations of biological processes at the molecular level, and provide valuable information on the onset and progression of diseases. The images obtained are based on a measurable number of nuclear disintegrations and, as such, are inherently quantitative. However, the quantitative nature of these modalities is usually dismissed, largely because tools and methods dedicated to quantitative imaging are lacking. Accurate quantification in PET and SPECT typically requires frequent assessments of blood activity through indirect image-based estimations or direct sampling and measurements in a well-counter to obtain a time-activity curve that will feed pharmacokinetic models. These methods however can be inaccurate and error-prone. A new automated tool for the determination of blood activity as a function of time is presented. The device relies on a peristaltic pump for continuous blood withdrawal and can package blood samples in evacuated tubes at specific times for further analysis. The device uses a 20x20x15 mm³ Cadmium Zinc Telluride (CZT) detector, read by a custom-made preamplifier and a FPGA-based signal processing unit. A Graphical User Interface (GUI) offers a user-friendly interface with preselected parameters to perform an acquisition. This paper presents the overall design of the tool as well as preliminary results related to detector performance in terms of linearity, stability and sensitivity. The sensitivity is estimated at 0.9 cps/Bq/ μ L.



SP061.5 - A Portable Free-Hand 3D SPECT System**Author(s):** Jonathon Irish¹, Harley Chan², David Jaffray³¹Surgical Oncology, University Health Network, Toronto/CANADA, ²Radiation Medicine Program, Princess Margaret Cancer Centre / University Health Network, Toronto/CANADA, ³Dept Radiation Oncology, University of Toronto, Toronto/ON/CANADA

We have developed a system that can produce 3-dimensional single photon emission computed tomography (SPECT) images from a handheld gamma camera that can be moved freely by a surgeon around a patient. This system is called FreeSPECT, will better localize lymph nodes for sentinel lymph node biopsies (SNLB). With 3-dimensional image-guidance that can be linked to high-resolution anatomical images from CT or MR, surgeons will be able to more accurately remove lymph nodes and plan around sensitive tissues. The FreeSPECT system we have developed is based upon a lightweight gamma detector (MRG15, Cubresa, Winnipeg, Manitoba) which is small in size and MR compatible. Figure 1 shows the system including the electronics cabinet, gamma detector, and user interface. The silicon photomultiplier (SiPM) detector head has 16 pixels in a square 4x4 pattern, with a 5 mm thick CsI(Tl) scintillator. The detector efficiency is 149.7cps/MBq at 50 mm source distance, and signal multiplexing allows sampling of each pixel every 4 μ s. In-house developed navigation platform "GTxEyes" provide gamma image acquisition, real-time tracking, navigation, visualization, and reality augmentation. This platform is developed based on open-source toolkits and libraries including VTK, ITK, IGSTK, and OpenCV, as well as our own proprietary image reconstruction and co-registration algorithms. Additional capabilities of this platform include critical organ monitoring with visual/audio alerts and image overlay of multi-modality images. Fast deformable Demon image registration algorithm is also available to register pre-operative images (and/or contours) to intra-operative images such as the proposed Free-Hand SPECT image. The prototype FreeSPECT system has integrated optical tracking technology (Spectra, Polaris, NDI), a reference tool affixed to the camera's body for identifying the position and orientation of the gamma camera images in 3D. To precisely locate the gamma camera images in space, the spatial relationship between the tracking tool and camera space is first calibrated. In the localization process, the clinician uses the handheld gamma camera to scan above and around the region of interest. The software records the 6D position and orientation of the camera simultaneously with the gamma image acquisition at every instant. In the prototype system, this recorded information is saved in ASCII text format for subsequent tomographic image reconstruction. The SPECT image reconstruction is based on the ordered subset expectation maximization algorithm as implemented in the NiftyRec open source tomography toolbox. Preliminary results from the FreeSPECT prototype system are shown in Figure 2.



Figure 1: The FreeSPECT prototype system integrates compact gamma camera, optical tracker, and in-house GTxEyes software platform.

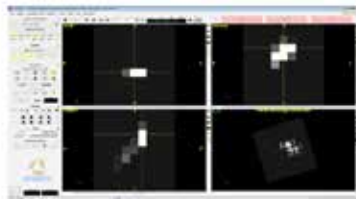


Figure 2: Illustration showing a preliminary result of the FreeSPECT prototype system.

SP061.6 - Probing the Biomechanical Properties of Cells using High-Frequency Ultrasound and Acoustic Levitation**Author(s):** Natalie Sullivan¹, Brian D. Patchett², Timothy E. Doyle²¹Chemistry, Utah Valley University, Orem/UT/UNITED STATES OF AMERICA, ²Physics, Utah Valley University, Orem/UT/UNITED STATES OF AMERICA

Alterations in the biomechanical properties of cells are important in many pathologies including cancer, neurodegenerative diseases, and autoimmune disorders. For example, the more aggressive molecular subtypes of breast cancer may express different biomechanical phenotypes due to subtype-specific mutations which code for proteins that regulate the cytoskeleton. Microtubule destabilization and other cytoskeletal dysfunctions play a pivotal role in neurodegenerative disorders such as Alzheimer's disease. In autoimmune diseases, cytoskeletal changes in T cells are key to signaling, immune recognition, and activation. Our research at Utah Valley University is currently exploring the capabilities of high-frequency ultrasound for detecting variations in the biomechanical properties of cells. To date, high-frequency (10-100 MHz) ultrasonic spectra have been found to be sensitive to breast cancer cell types and chemical modification of the cytoskeleton in cell cultures. The cells are non-invasively probed using a pulse-echo measurement. Time-domain signals acquired from cells are converted into frequency spectra and analyzed for spectral features that correlate to biomechanical properties. Ultrasonic scattering models, experimental data, and data analysis methods such as principal component analysis have confirmed that high-frequency ultrasound can detect changes in the cytoskeleton. However, a critical problem with the current approach is the strong ultrasonic reflection from the well bottom of the cell culture plate, which interferes with the weak ultrasonic signals from the cells adhering to the bottom. The objectives of this study were to develop an approach to eliminate the well-bottom interference from the cell signals, and to provide a capability for probing cells in liquid suspension (thereby expanding application to cells extracted from tissue and blood). The approach uses acoustic levitation to induce free-floating cells into forming a thin, suspended, planar layer which can then be probed by high-frequency ultrasound. Acoustic levitation is accomplished by establishing an acoustic standing wave in the media using a low-frequency ultrasonic transducer. A significant challenge in the acoustic levitation of cells is the random motion of the cells about the node position of the standing wave. This paper reports on a new method for damping cell motion during acoustic levitation. The method uses harmonic modulation of the standing wave to create nodal regions of greater stability and cell localization as compared to a single-frequency standing wave. Numerical simulations indicate that such "acoustic wells" can be created using a multifrequency layered piezoelectric transducer to modulate the standing wave with an optimized set of harmonic frequencies. Breast cancer cells having distinct spectral signatures will be tested to validate the approach. The acoustic levitation system will consist of a 30-MHz function generator, an RF amplifier, and a multifrequency (0.1-1.0 MHz) layered piezoelectric transducer. The high-frequency ultrasound system will consist of a 50-MHz immersion transducer, a high-frequency square-wave pulser/receiver, and a 1-GHz digital storage oscilloscope. Our research group has developed a new method for stabilizing cell motion during acoustic levitation using numerical simulations. This new method promises to not only expand the capabilities of high-frequency ultrasonic testing of the biomechanical properties of cells, but also has applications as a 3D patterning approach in tissue engineering.

SP062 - Clinical Process Analysis, Optimization, Productivity and Benchmarking

TRACK 16: CLINICAL ENGINEERING, CLINICAL PHYSICS, AND PATIENT SAFETY

SP062.1 - Guaranteeing the quality of rigid endoscopes with the ScopeControl

Author(s): Herke Jan Noordmans¹, Rens Wientjes²

¹Fb Medical Technology And Clinical Physics, UMC Utrecht, Utrecht/NETHERLANDS, ²Fb Medical Technology And Clinical Physicist, UMC Utrecht, Utrecht/NETHERLANDS

As rigid endoscopes are re-used after minimal invasive surgery, they degrade over time. To guarantee the optical quality of a rigid endoscope for the next surgery, the ScopeControl has been developed to measure key optical parameters such as light transmission, color correctness, focus, fiber transmission, viewing angle and field of view. The ScopeControl is placed in the reprocessing cycle right after cleaning, before wrapping and sterilizing the endoscope. After a measurement has been performed, all parameter buttons/indicators should turn green. When, however, a parameter button/indicator turns red, its value falls below a pre-defined threshold (acceptation criterion) and the endoscope should be rejected for further processing.

In 2013 a pre-commercial version of the ScopeControl has been tested in six hospitals in the Netherlands. It proves to be stable, and able to measure optical parameters with sufficient precision that it can discriminate between good and bad endoscopes [1]. Since April 2014, the commercial version of the ScopeControl has been in use at the sterilization department of the UMC Utrecht (about 4000 minimally invasive surgeries a year). In this project we want to address several issues when introducing the ScopeControl in the clinical process:

1. What kind of training people of the sterilization department should get in handling and interpreting the results of the ScopeControl.
2. What kind of tracking is needed for endoscopes. Conventional basket tracking systems are often not sufficient as endoscopes are easily swapped between baskets. The ultimate goal is to track on endoscope level (e.g. using a data matrix or RFID).
3. What should be agreed between the departments of sterilization, OR and medical technology about rejecting/accepting endoscopes when reprocessing them or sending them in for repair or replacement. What can be said about the rejection/acceptation levels? Generally a repaired or new endoscope should have a higher quality than an endoscope that is still good enough for surgery. There should be some bandwidth where endoscopes may deteriorate slowly.
4. What kind of reports can be derived from such a system and how can these results be coupled to information from other electronic registration systems in the hospital like basket tracking and OR management systems.
5. Which steps in the reprocessing cycle may damage endoscopes and can we get an idea of their impact? Think of handling, transport, cleaning, disinfection and sterilization.

These issues are illustrated in two examples: The replacement of a large number of rigid endoscopes in a public tendering, and the large fall-out of large number of cystoscopes for children. We look forward to a live discussion to see whether these problems are recognized in other hospitals and which approaches other people have found to address these problems.

Reference

1 Noordmans HJ, et al., Evaluation of the ScopeControl endoscope test system in six hospitals in The Netherlands, *Physica Medica* (2015), <http://dx.doi.org/10.1016/j.ejmp.2014.12.006>

SP062.2 - Low-entry level CT exam times and availability in worldwide markets

Author(s): Renan M. Almeida¹, Fernando C. Coelli², Andrei L. Pires³, Renan M. Almeida⁴, Wagner C. Pereira⁴

¹CEFET "CSF" RJ, Itaguaí/BRAZIL, ²Cefet "CSF" RJ, Itaguaí/BRAZIL, ³UFRJ, Rio de Janeiro/BRAZIL, ⁴Peb/coppe, UFRJ, Rio de Janeiro/BRAZIL

Context and background: Computerized Tomography (CT) is widely used for disease diagnosis, treatment planning, and follow-up. Currently, its state-of-the-art is a 320-slice equipment, but machines with one, two, four and 16 slices are still used in many countries. Exam speed (and, thus, number of exams per period of time) may change among models, but the smallest slice thickness is usually about 1mm regardless of the number of detector rows. However, most of the basic models already had their production discontinued, a situation that makes CT entry level more expensive, and, therefore, decreases its adoption in less developed countries.

Objective: To study the differences in productivity (exams/unit of time under real working conditions) between 1, 2, 4 and 16 slices CTs.

Methods: Four CTs (with one, two, four and 16-slices) were studied relatively to their performance in patient exam time, divided as: *i*) patient arrival; *ii*) patient initial preparation; *iii*) patient positioning in the equipment; *iv*) data scan; *v*) examination time and *vi*) time for patient departure. Times were measured in minutes and seconds by two researchers with an Android Tablet and a timer application. Equipments were located in Rio de Janeiro city or nearby cities in Brazil, 2013-2014. Additionally, an Internet search was performed among equipment producers trying to identify the supplier of the simpler models in the Asian, European and USA markets.

Results: A total of 85 exams were followed, and three had to be discarded, one due to equipment failure at the moment of the exam and two due to patient arrival delays. Average times for the arrival / preparation / positioning / scanning / departure stages did not differ markedly. As for the "scan" stage, the average time for the single slice case was 8'38", as opposed to respectively 2'05"/ 2'31"/ 2'41" for the remaining models.

Concerning model availability, the Internet search identified that few older model options are still available, with the number of slices beginning at "sixteen" among USA and European manufacturers.

Conclusion: Despite their wide variations in technology, average time differences among the studied models were small for the "non-examination" stages, indicating that the general (including ergonomic) characteristics of the equipments did not change markedly. Regarding the "scan" stage, however, 2-16 slices models had a similar and clearly better performance relatively to the single-slice model, and, thus, a similar productivity could be achieved with the former models. This is an important consideration, given that productivity is important both for the public health sector (allowing for attending a larger patient population) and for the private sector. Therefore, these models, if still available, could satisfy the demand of many less developed countries, but the Internet search identified that entry level now refers to 16 slices and over. An alternative for keeping low cost models in production would be the development of "upgradeable platforms" by manufacturers, allowing for the acquisition of more simple alternatives that could be adequately upgraded along time.

SP062.3 - The critical evaluation of AV control features in modern pacemakers and cardioverters**Author(s):** Kazimierz Peczalcki, Tadeusz Palko

Warsaw University of Technology, Warsaw/POLAND

The modern prostheses of different vital systems of human body are equipped in many control features related to the physiological behavior of replaced systems. The critical evaluation of some algorithms for the synchronization of the heart conductive systems that are implemented in modern pacemakers and cardioverters is goal of our evaluation. We describe our clinical evidence that the algorithms should be customized to individual patients. Two of the most important pacing parameters: default atrioventricular interval (AVI) and AVI adapted to heart rate (HR) were evaluated by the authors. The criterion for enrolment to the both study groups was the 80% pacing recorded by the pacemaker holter systems and 100% pacing during the duration of the test.

The goal of the studies was to assess the differences between SV for optimal AVI and SVs for default AVI values proposed by two of the biggest word pacemaker companies and the impact of varying HR on the optimal AVI in two groups of 20 paced patients: first (mean age 74.0 years +/- 7.0 years) consists of 4 females (mean age 75.3 +/- 6.1) and 16 males (mean age 74.3 +/- 4.1) and second treated by DDDR were enrolled the in the study.

The mean value of SV for optimal AVI achieved in the first clinical study is pretty close to SV for default AVI¹ (150 ms) and differ from SV for the second default AVI² (170 ms). Significant changes ($p < 0.05$) were found for SV vs SV². The high SD level of optimal AVI's (mean 148.50 msec., SD 41.07 msec.) shows wide range of its variations assessed for some patients. The estimated default AVI² may be based on a different population of patients for instant North American. All of the facts listed above prove the assumption that the default AVI values preset by companies can lead for nonoptimal settings for some patients. Such wrong settings can be especially important in group of patients with poor condition of cardiac muscle which limits the physiological adaptation of the heart to an intense exercise. The results of the second study of reaction of AVI to increase or decrease of HR lead to similar conclusion. The normal relationships between shorter AVI for faster HR and longer AVI for slower HR simply do not work for some, pretty significant in present study, number of paced patients with impaired systole by atrophy of heart muscles geometry and non physiological systole of paced ventricles (the impulse is propagated from the apex of the heart in opposition to physiological direction of impulse propagation).

Conclusion: The presence of non physiological behavior of the heart conductive system should be taken under consideration during adjustment of parameters of pacing treatment.

SP062.4 - Assisted Reproductive Technology Center Design with Quality Function Deployment Approach**Author(s):** Alessio Luschi¹, Massimiliano Monti², Ernesto Iadanza³¹Information Engineering, University of Florence, FIRENZE/ITALY, ²ESTAV Centro, FIRENZE/ITALY, ³Department Of Information Engineering, University of Florence, Florence/ITALY

Assisted Reproductive Technology (ART) is the technology used to achieve pregnancy in procedures such as fertility medication, artificial insemination, in-vitro fertilization and surrogacy. The paper shows an application of Quality Function Deployment method to Careggi Hospital ART Laboratory of Florence in order to give a prioritization order for ameliorative interventions.

SP062.5 - Study of the Sensitivity on the Measurement of the Prevalence of Total Cholesterol in Blood Serum by Interferometric Techniques**Author(s):** Bettsy Hernandez-Zacarias¹, Gerardo S. Romo-Cardenas¹, Alejandra Guillen-Peralta², Alex Muñoz-Arpaiz¹, Juan Alvarez-Arana², Ismael Chable²¹School Of Engineering, Montemorelos University, Montemorelos/MEXICO, ²School Of Health Sciences, Montemorelos University, Montemorelos/MEXICO

Current blood testing techniques require the use of sensitive equipment and a constant consumption of specific chemical compounds in order to analyze fluid composition and concentration. It is known that optical interferometers are instruments that can make precise measurements of objects using the interference pattern of two light waves. These devices have been used to characterize materials and to study their properties. Interferometric studies results, prove that by this type of optical arrangements combined with image processing, enables a method that applies for fluid characterization. Being this is a non-destructive protocol that could be used for different applications in engineering. This study, propose the use of optical interferometry to analyze blood serum in order to explore the possibility of developing an alternative method for blood sample analysis. The methodology consists of analyzing different blood serum samples previously quantized to determine the effect of the variability of its components in the acquired interferograms. The results show an unexpected behavior of the acquired interferograms in relation of the amount of total cholesterol included in the samples, this in relation with the information generally considered from the medical practice.

The scope of this paper seeks to apply technology and optical engineering also consider the effect of the prevalence of lipid components in blood serum in order to develop a standardized technique that allows the study of concentration information from acquired interferograms and thus validate the option as an alternative to the quantization of such compounds. Helping to complement the knowledge of the biochemistry of the blood and develop novel methods for quantization and analysis of its components by non-destructive techniques and less expensive methods known on the market.

SP062.6 - Critical role of sustaining technology and utilities in healthcare institutions facing disaster through development of an international center for information and training of health technology managers on disaster preparedness**Author(s):** Yadin B. David¹, Caridad Borrás², Fred Hosea³, Douglas Drepps⁴¹Biomedical Engineering Consultnats, LLC, Houston/UNITED STATES OF AMERICA, ²IUPESM, Washington DC/UNITED STATES OF AMERICA, ³Clinical Technology, Kaiser Permanente, San Francisco/CA/UNITED STATES OF AMERICA, ⁴Clinical Engineering, Mercy System, St. Luis/MO/UNITED STATES OF AMERICA**Study/Objective**

Promote awareness of critical role of sustaining technology and utilities in healthcare institutions facing disaster by exploring development and establishment of international center for information and training of health technology managers on disaster preparedness and situation-awareness methodologies.

Background

Review of disasters that affected healthcare institutions suggests a need to make technological systems more robust and better trained users about disaster preparedness. The burden is magnified due to ever growing critical dependency on technology, i.e. central oxygen, vacuum, nuclear, radiological equipment, communication systems.

Methods

The need for a training center based on a case study of the impact

on several hospitals: a flood from tropical storm affected several hospitals and their technological systems in Houston, Texas, 2001. The problems caused by rising water, the immediate response, the recovery efforts and the financial losses will be analyzed. This will also include the transfer of learned lessons to environment of resource-poor countries.

Results

Water caused shutdown of electrical, air, vacuum systems and submerged areas containing radiological equipment. Patients had to be evacuated, unfortunately four patients died, research animals, and years of investigation data lost. The case shows lack of technology-focused plans for triaging healthcare systems and of training programs. There was lack of understanding of systems (including networks) and devices' vulnerability, especially when multiple systems crashed. The possibility of unique hazards like those from radiation-emitting devices and radioactive materials, other biomedical equipment such as mechanical ventilators were considered last. Prioritization of backup and strengthening resilience of technology prior to disaster and during disaster were a last minute approach. The recovery focused on commissioning technologies critical to life. Had the facility been better prepared, lives and financial losses would have been minimized.

Conclusion

Disaster preparedness plans in healthcare institutions must include knowledge of the vulnerabilities they may face and plans to mitigate risk of operations disruption due to technology and utility issues.

SP063 - Accreditation, Certification and Licensure Issues

TRACK 17: EDUCATIONAL AND PROFESSIONAL ACTIVITIES

SP063.1 - The Current State of Clinical Engineering Education and Career

Author(s): [Yadin David](#)

Health Technology Management, Biomedical Engineering Consultants, LLC, Houston/UNITED STATES OF AMERICA

Today's practice of healthcare has grown to depend on the deployment and integration of technological tools for the delivery of its services like never before. Furthermore, these technological tools are being integrated into systems requiring competencies and expertise that challenges conventional training. It is critical, for the practice of safe and effective healthcare services, that these systems and their integrated technological tools are well planned, managed and safely serviced throughout their complete life cycle. Not only the dependence on these systems has grown but even more so, the quality and the volume of the intelligence embedded within these technological tools. Intelligence that guides the management of patients' conditions. As example, the emergence of the utilization of electronic medical records, of health informatics, surgical robots, 3-D medical imaging, smart infusion pumps, bedside telecommunications, wireless accessibility and mobile devices. It is clear, therefore, that clinical engineers for successfully managing their hospital's clinical technology program require new knowledge and additional competencies.

In reviewing the academic preparation of engineers for career in the clinical environment, the clinical engineers, it seems obvious that most if not all are based in the biomedical engineering academic programs. While there are some joint sciences, the training of clinical engineer is different from training of biomedical engineer. The curriculum and the format of the clinical engineering programs must anticipate and train for the specific body-of-knowledge needed for practicing as clinical engineering professional. Therefore, helping its graduate to become successful practitioners that will pursue, after graduation, further professional development and certification supported by lifelong clinically related continuing education. This presentation will provide a review of the healthcare technological tools and their integration into systems. It will further identify how these changes influence the body-of-knowledge that clinical engineers must have. It will summarize some suggestions on how to improve clinical engineering education programs so that their graduates will be successful in their career, happy as professional practitioners, and contributors to best possible care outcomes.

Objectives

1. To describe the relationship between changing healthcare and clinical engineers practice
2. To identify why changes in practice of clinical engineers impact their education and preparation
3. To link specific knowledge that must be part of future clinical engineering education and their career

SP063.2 - The Pursuit of Regulated Health Profession Status for Medical Physicists in Alberta

Author(s): Charles J. Kirkby¹, Joel St. Aubin², Alana Hudson³, Brad Warkentin², Lesley Baldwin², Matthew Larocque², Atiyah Yahya², G. Colin Field²

¹Medical Physics, Jack Ady Cancer Centre, Lethbridge/CANADA, ²Medical Physics, Cross Cancer Institute, Edmonton/CANADA, ³Medical Physics, Tom Baker Cancer Centre, Calgary/CANADA

The purpose of this presentation is to report on the progress towards Medical Physics becoming a regulated health profession in Alberta.

Medical Physicists in Canada have a nationally recognized certification system through membership with the Canadian College of Physicists in Medicine (CCPM). While most Medical Physicist employers desire this membership or its equivalent, it is enforced only voluntarily by hiring institutions and managers. There is no legal requirement for membership with the CCPM to work as a Medical Physicist. Many of the clinical activities performed by Medical Physicists that can have direct clinical consequences for patients in terms of detecting and treating disease can be legally performed by anyone. This lies in contrast with many of our professional peers (physicians, radiation therapists, nurses, etc.), where provincial colleges independently define a scope of clinical practice, regulate those who may conduct that practice, and restrict the practice of certain activities to those registered with the college.

By defining a scope of practice and requiring members of a profession to meet and maintain minimum standards of competence, professional regulation ensures both patient safety and a minimum standard of care. Root cause analysis commonly identifies lack of Medical Physicist involvement, training, or qualifications as a significant contributor to major radiation therapy accidents and near miss situations. This suggests a key link between quality and safety and the regulation of Medical Physics.

In Alberta there are approximately 40 qualified medical physicists. For over five years the Association of Medical Physicists in Alberta (AMPA) has pursued professional regulation under Alberta's Health Professions Act. In 2011, AMPA submitted an application for professional regulation to the Government of Alberta. Government feedback identified small physicist numbers as a primary barrier to regulation: the administrative workload of operating a professional college, and the cost of potential investigations and disciplinary committee hearings (involving legal council) were deemed prohibitive. However, subsequent feedback suggested the potential viability of a joint application with the Alberta Association of Clinical Laboratory Doctoral Scientists (AACLDS), an organization also seeking regulation, but limited by similar membership numbers. AACLDS represents professions including clinical chemists, microbiologists, geneticists, and toxicologists who share several professional similarities with medical physicists. Its members complete PhDs, then do two years of clinical training before writing a national certification exam. In the newly proposed model, Medical Physicists and the professions represented by AACLDS would join and be administrated by the College of Physicians and Surgeons of Alberta. The CPSA is a natural choice because (i) this college is the provincial accreditation body for ionizing radiation devices below energies of 1 MeV and (ii) our groups share common professional ground with physicians and surgeons, including a balance of clinical and academic responsibilities, and the extensive training involved in our professions.

At the time of this abstract submission, AMPA and AACLDS are in the process of submitting this joint application to the Government of Alberta. If successful, Alberta would become the first province in Canada designating Medical Physicists as a regulated health profession.

SP063.3 - The International Medical Physics Certification Board

Author(s): Colin G. Orton¹, Tomas Kron², Raymond K. Wu³

¹Radiation Oncology, Wayne State University, Grosse Pointe/UNITED STATES OF AMERICA, ²Radiation Oncology, Peter MacCallum Cancer Centre, Melbourne/AUSTRALIA, ³Radiation Oncology & Cyberknife Department, University of Arizona Cancer Center, PHOENIX/UNITED STATES OF AMERICA

This talk will present an overview of the objectives of the International Medical Physics Certification Board (IMPCB), progress made since its formation, and the results of recent discussions to assure that the IOMP will play a major role in IMPCB governance in the future. The IMPCB was established in 2010 with the assistance of the Certification Task Group of the IOMP Professional Relations Committee, with the goal of improving the quality of clinical medical physicists and the profession. To achieve this objective, the IMPCB will accredit existing national/regional Medical Physics Certification Boards and encourage and assist those countries/regions that currently have no certification programs to develop them. It also works towards conducting certification examinations for medical physicists practicing where local certification is not currently available. The first tasks of the IMPCB were to develop a model certification program (published in 2011), write the By-Laws (adopted in 2012), and elect the 1st Board of Directors (took office in January, 2014). An Accreditation Committee was established with the initial task of development of the requirements for certification and accreditation (completed in November, 2014). These include requirements for general education (a minimum of a Masters degree), medical physics education (general and specialty), and clinical training. These requirements adhere closely to those published in IOMP Policy Statement No. 2: Basic Requirements for Education and Training of Medical Physicists, and several IAEA documents. Medical physics certification examinations might be in three parts: Part I (a written exam on general medical physics to be taken by all candidates), Part II (a written exam for each specialty), and Part III (an oral exam for each specialty). But the IMPCB recognizes that there are national/regional variations to certification in medical physics based on differences in national/regional legislation and educational traditions, so it gives to national and regional certification bodies considerable freedom to decide on the manner in which a given organization seeking IMPCB accreditation conducts the certification process. The Board decided to initially restrict accreditation of Boards and IMPCB certification examinations for only the three specialties Radiation Oncology Medical Physics, Diagnostic and Interventional Radiological Physics, and Nuclear Medicine Physics, and begin accepting applications for accreditation of national or regional medical physics certification boards in January, 2015. The Board also approved collaboration with the IAEA to work on certification of experienced medical physicists working in countries which currently have no certification Board. For the latter, a Question Bank has been developed for Parts I and II of the IMPCB certification examination.

SP063.4 - Radiation protection continued training program evaluation: return on a 7-year experience

Author(s): Nadia Octave, Janelle Morrier, Mario Chrétien
Radiation Oncology, CHU de Québec - Hôtel-Dieu de Québec, Québec/QC/CANADA

Introduction: As healthcare professionals working with ionizing radiations, radiation safety is of paramount importance. In Canadian regulations (Nuclear Safety and Control Act, NSCA), requirements regarding workers radiation protection (RP) training and training programs are highlighted at different times. We aim to present: (1) our experience of RP training program (RPTP) since its inception in 2007; (2) our RPTP evaluation and (3) how it complies with Canadian regulations.

Materials and Methods: The RPTP implemented is based on 6 educational modalities: (1) oral classroom presentations on general topics, (2) bimonthly bulletin publication distributed both electronically and on paper form, (3) computer-based training, basically interactive modules, with questions and answer to ensure and assess understanding of the notions developed, (4) posters display, (5) practical training on routine tasks and, (6) simulations of emergency situations in working environment. A registration methodology is used to verify the level of knowledge and competence of each worker to safely perform their job. After 5 years of the RPTP implementation, an internal audit was conducted with a 10-question survey designed with Survey Monkey to measure the training effectiveness and perception among users.

Results: Readership of our informative bulletin alone is equal or higher than 70% for the past 4 years with highest rates among technologists. 73 people answered to the satisfaction survey, among them 74% were technologists, 11% were physicists, 11% were physicians and 2.7% and 1.3%, service techs and oncology residents respectively. The preferred educational supports were the interactive modules and the bulletin respectively, while posters are majorly disregarded. Interestingly enough, people are highly attached to classroom format and were very interested in emergency situations simulations. Respondents majorly stated to read the bulletins “always” for 68.5 % and “often” for 13.7%, independently of workers category. The answers are more divergent by work categories when asked about bulletin frequency appropriateness. Technologists are majorly satisfied with the actual bi-monthly rate while radiation oncologists are heavenly distributed between status quo and frequency reduction. Contrariwise, for a majority of the physicists, frequency should be reduced. When asked about perception level of RP knowledge with regards to routine tasks, all physicists and physicians answered “adequate”. Answers were more mitigated among technologists where 68.5% answered “adequate”, 29.6% “basic” and 1.9% “thorough”. Interestingly, the commune highest confidence knowledge in all workers categories was found in RP specific to treatment machines, and the lesser in RP in non-medical related areas. Annual completion of electronic module was majorly accepted.

Conclusion: As stated in the NSCA and other regulations, it is the licensee direct responsibility to ensure that workers receive appropriate training related to their specific jobs. Since its inception, the RPTP was well received and closely monitored. Users’ compliance and feedback helped to better meet their needs while continuously developing a radiation protection culture as proposed by the IRPA. It is possible to conclude that overall department stakeholders feel they have sufficient RP knowledge for their daily duties.

SP063.5 - Where to find biomedical engineers worldwide? Mapping biomedical engineers around the world

Author(s): Daniela Rodriguez Rodriguez, Adriana Velazquez Berumen, Megan M. Smith, Ricardo X. Martinez
His/emp/pau/medical Devices, World Health Organization Headquarters, Geneva/SWITZERLAND

Background

Within health systems around the world trained and qualified biomedical engineering (BME) professionals are required to design, evaluate, regulate, acquire, maintain, manage and train on the safe use of the medical healthcare technologies. Nevertheless the profession is often left out from the health workforce in various countries, and biomedical engineers’ recognition and classification by the International Labour Organization (ILO) is still pending due to lack of statistical information of the current number of biomedical engineers around the world.

Therefore with the intention of: a) promoting the role of biomedical engineering and related disciplines in healthcare, b) disseminating

information about BME educational programmes and societies; and c) acquiring recognition of the profession at country/international level (e.g. International Standard Classification of Occupations (ISCO) by ILO) WHO started efforts to track biomedical engineers’ presence worldwide since 2009 and in four different stages:

- 1- 2009: in collaboration with the University of Campinas, work coordinated by professor S. Caill.
- 2- 2010: C. Long and R. Magjarevik
- 3- 2013-2014: D. Desai, J. Barragan, S. Mullally and N. Jimenez
- 4- 2015: on-going

On January 2015 WHO launched an extensive survey that aims to map biomedical engineers’ presence at a country level. Additionally information on existing professional societies, educational institutions in the field of BME and women’s role within the profession is being collected.

Methodology

2015 survey was sent to over 3200 contacts using WHO medical devices listserv tool. The survey was divided in four parts: country profile, educational institutions, professional societies and international organizations. Each part aimed to collect specific information on the topic and was aimed to be completed by the professionals holding section-specific information.

Additionally a question regarding female presence within the profession was added in each section in order to measure the proportion of women actively working (in different sectors) or recently graduated in BME or related field.

All collected information (including the four stages) is expected to be published in WHO Global Health Observatory (GHO), the World Health Statistics 2015 and ideally in ISCO-18.

Results

Research is ongoing but anticipates disclosing the presence of biomedical engineers by country (country profile), the number of educational institutions per country and the percentage of women actively present in the field. Additionally the presence of biomedical engineers in international organizations (e.g. UN agencies, Red Cross, development agencies, NGOs) and international professional societies is expected to be unveiled.

Conclusion

New information regarding the presence of biomedical engineers is now being collected and is aimed to be publicly available by June 2015. The dissemination and promotion of this information aims to strengthen biomedical engineering recognition in order to improve health care delivery.

SP063.6 - Oh dear medical physicist and biomedical engineer, why is it difficult to pioneer your specialist career?

Author(s): Mario Medvedec

Department Of Nuclear Medicine And Radiation Protection, University Hospital Centre Zagreb, Zagreb/CROATIA

By the end of 2013 Croatia’s health care sector had a permanent work force of about 74,500, around 13,750 medical doctors among whom approximately 9,700 specialists, and about 750 university degree health associates including clinical medical physicists and biomedical engineers. The objective of this paper is to present one national example of medical specialists grandfathering in favor of improved regulation of medical doctor profession, but all in wider context of global efforts towards better perception and regulation of clinical medical physics and biomedical engineering profession worldwide. Equal opportunities of continuing professional education and training, as well as career advancement (internship, residency, subspecialization, postgraduate specialist programs, etc.) should be facilitated and provided to all clinical scientists. Grandfathering is

certainly a usual step to give initial momentum, but grandfathering under the same criteria for all health professionals. For the maximal benefit of the patients, health professionals, health institutions and national health system, it appears that there is an urgent need in Croatia to make decisive actions towards much better perceiving and regulating the status of clinical scientists with background in natural, technical, biotechnical and social sciences.

SP063.7 - Biomedical Engineering Education and Training and Accreditation of Bachelor-degree Biomedical Engineering Programmes

Author(s): Min Wang

Department Of Mechanical Engineering And The Medical Engineering Programme, The University of Hong Kong, Hong Kong/HONG KONG

Hong Kong, like other advanced economies in the Asia-Pacific region, has an aging population and hence high-quality healthcare is required for its citizens. There is therefore an increasing demand for well-educated and well-trained biomedical engineers in Hong Kong. Hong Kong has a well-established system for tertiary education and professional training of engineers. In 2012 in Hong Kong, the British style 3-year university education was changed to the North-American 4-year one, giving local universities various opportunities for reforming their curricula, enhancing teaching and learning, improving student exchange programmes, etc. Biomedical engineering (BME) is a constantly expanding and intrinsically interdisciplinary field. The US and Western Europe as pioneers in the field have provided exemplary BME educational programmes. How to learn from these programmes and then set up their own programmes with distinct features for local students is not an easy task for BME educators in other countries. Hong Kong joined the legion of BME education providers and started BME educational programmes in the mid-1990s. Currently, four universities in Hong Kong provide bachelor-degree level BME education: The Hong Kong Polytechnic University (PolyU), The University of Hong Kong (HKU), The Chinese University of Hong Kong (CUHK), and City University of Hong Kong (CityU). The 3-year curriculum BME programmes (which started in different universities at different times and will all end in 2015) in PolyU, HKU and CUHK have been fully accredited by the Hong Kong Institution of Engineers (HKIE) which is a signatory of the Washington Accord. The accreditation in Hong Kong of 4-year curriculum BME programmes was started in 2013, and in 2014 HKU's 4-year curriculum Medical Engineering Programme became the first BME programme to gain HKIE's provisional accreditation. (A BSc or BEng engineering programme can only gain provisional accreditation, not full accreditation, before it produces its first cohort of graduates.) Another university's BME programme is currently going through the accreditation exercise. All 4-year curriculum engineering programmes put forward for HKIE's accreditation must use the *outcome-based approaches in student learning* and hence the programme's preparation for accreditation and the accreditation itself (criteria, documentation and presentation, process, etc.) are different for those used in the 3-year curriculum accreditation exercises. With these programmes as the foundation, a three-tier BME education is now in place in Hong Kong: the bachelor-degree level education (BSc or BEng), the taught-master degree (MSc), and research degrees (MPhil or PhD). Beyond the university education at these three levels, professional training in BME can be obtained in different organizations in Hong Kong. Government departments and the private sector alike contribute to BME engineer training. This presentation will give an overview of BME education and training in Hong Kong and briefly compare the BME programmes. It will also discuss various aspects of BME programme accreditation, drawing the author's experience as the Programme Director to lead the HKU BME programme through its accreditation and also as the Visiting Team member for HKIE's accreditation of a BME programme in another university.

SP063.8 - IOMP initiative for Validation and Accreditation of MSc courses

Author(s): Slavik Tabakov¹, John Damilakis²

¹Medical Engineering And Physics, King's College London, London/ UNITED KINGDOM, ²Medical Physics, University of Crete, Iraklion/ GREECE

The Education and Training Committee (ETC) of the IOMP guides and supports a number of educational courses, workshops and projects around the world. One of these projects developed a Model Curriculum for post-graduate (MSc level) courses on Medical Physics. It also presented guidance on the organisation of such courses. The next stage of this activity is the initiative of international Validation and Accreditation of MSc courses in Medical Physics. These were briefly described in the book with educational experience from 26 countries (Medical Physics and Engineering Education and Training, available free from: http://www.emerald2.eu/mep/e-book11/ETC_BOOK_2011_ebook_s.pdf).

The Validation and Accreditation of MSc courses will be performed by the IOMP ETC. It will include assessment of the curriculum; assessment of the teaching methods; assessment of the examination process and assessment of the research activities (MSc project). The IOMP Model Curriculum will be used for the purpose and a number of expert medical physicists will be attracted to the validation process. The initial phase of the project will be guided in English and will be based on assessment of an English translation of the MSc Curriculum.

This IOMP activity will allow for a small country with limited expertise to set-up a post-graduate course in Medical Physics. This will boost the profession in many developing countries. The Validation and Accreditation of MSc courses will be used also for supporting step of the future Professional Certification of professionals. It is expected the first MSc courses to be accredited during 2015-16. The paper will present the application form and will discuss the application of the process.

SP064 - Biomechanics and Artificial Organs

PRESIDENTS CALL

SP064.1 - Biomechanical Analysis of Optimal Orientation and Stress Shielding for Short and Long Stem Hip Implants

Author(s): Peter Goshulak¹, Saeid Samiezadeh², Mina S.R. Aziz¹, Habiba Bougherara², Radovan Zdero¹, Emil H. Schemitsch¹

¹Martin Orthopaedic Biomechanics Lab, St. Michael's Hospital, Toronto/CANADA, ²Mechanical & Industrial Engineering, Ryerson University, Toronto/CANADA

Introduction: Short stem hip implants are increasingly common because they conserve bone for future surgeries. They also improve load distribution in the proximal femur. Stress shielding is a problematic effect caused by poor stress distribution, where the bone is understressed and beins to atrophy. The decreased bone density could cause implant loosening and ultimately fracture. The aim of this study was to compare short vs. long stem implants to protect against stress shielding, and to determine if implant orientation has a significant influence.

Methods: Twelve artificial femurs received a short stem modular neck implant or long stem monolithic implant in either neutral or anteverted orientations. Modular neck options – standard, anteverted, and retroverted – were assessed in each short stem. Three additional femurs remained intact as controls. Femurs were mounted in cement blocks in 7 deg adduction and underwent quasistatic axial loading in flexion, neutral, and extension phases of the gait cycle. Strains were collected from surface-mounted strain gauges. A finite element (FE) model employed laser scanned implants and a previously validated femur model. Experimental strains were used to validate the FE model. After validation, the full range of implant types and physiologically possible orientations (i.e. varying anteversion and anterior-posterior offset) were simulated (i.e. n=25 orientations for each implant) under clinical-level loads. Stress was computed in the calcar region and was compared between implants and across each implant's range of orientations. Stress shielding was the overall stress change vs. an intact femur.

Results: FE model strains vs. experimental strains linear graphs showed an excellent fit for no implant (slope=0.898, R=0.943), short stem (slope=0.731, R=0.948) and long stem (slope=0.743, R=0.859). Altering implant orientation had no significant advantage ($\alpha=0.05$, $p>0.05$). Stress shielding existed for short and long stem implants ($p<0.001$), but was higher in the long stem implant (i.e. 63% change from intact femur, $p<0.001$) vs. short stem implants with any of the 3 modular necks (i.e. 39%, 31%, 30% change from intact femur for standard, anteverted, and retroverted necks; $p<0.001$ for difference between all stems except anteverted and retroverted). Long stems showed more distal-dominant stress transfer vs. short stems ($p<0.001$), whilst peak stress was concentrated at the tip of the stem.

Discussion: Implant orientation via anteversion or anterior-posterior offset does not alter stress shielding if the implant is properly inserted into the femoral canal. Short-stem implants reduce stress shielding vs. long-stem implants. Anteverted and retroverted necks further reduce stress shielding. Results indicate some stress shielding in correctly implanted hip stems in patients with realistic activity levels. Implants with shorter stems and longer necks have a greater chance of maintaining calcar bone strength, but these parameters may reduce short-term stability because of increased proximal loading.

SP064.2 - Biomechanical Analysis of Acute Total Hip Replacements after Acetabular Fracture: Plate vs Cable Repair

Author(s): Mina S.R. Aziz¹, Saeid Samiezadeh², Omar Dessouki³, Habiba Bougherara², Emil H. Schemitsch⁴, Radovan Zdero¹

¹Martin Orthopaedic Biomechanics Lab, St. Michael's Hospital, Toronto/CANADA, ²Mechanical & Industrial Engineering, Ryerson University, Toronto/CANADA, ³Department Of Surgery, University of Toronto, Toronto/CANADA, ⁴Institute Of Biomaterials & Biomedical Engineering, University of Toronto, Toronto/CANADA

Introduction

Many techniques widely employed in repairing “complex” type acetabular fractures are not biomechanically validated. This paper analyzed the biomechanical aspects of two main types of repair methods, namely the traditional “plate and screws” method vs a newly introduced “cable” method. for treating complex acetabular fractures in the elderly in the presence of a primary Total Hip Arthroplasty (THA).

Methods

In Phase I, non-destructive experimental and computational analyses were performed on 6 artificial hemipelvis groups, which replicated various repair methods for an acetabular column plus posterior hemitransverse (AHT) acetabular fracture. One group was the intact control, while the other 5 groups were: intact hemipelvis with an acetabular cup of a THA; fractured hemipelvis with an acetabular cup fixed with a posterior column plate and anterior column lag screw; fractured hemipelvis with an acetabular cup fixed with the Mears and Shirahama cable technique; fractured hemipelvis with an acetabular cup fixed with the Kang and Min cable technique; and fractured hemipelvis with an acetabular cup fixed with the Mouhsine et al. cable technique. The groups were experimentally and computationally mounted to rigid supports at the sacro-iliac and symphysis pubis regions. Specimens were subjected to an acetabular non-destructive compressive force of 200 N. Computational model stress maps were directly validated against experimental results from surface strain gage measurements. The computational model was then reanalyzed using a clinical-level load of 2207 N, i.e. 3 x body weight for a 75 kg person. Stress maps were examined using a “highest stiffness” and “lowest peak bone stress” criterion to determine the most biomechanically stable cable fixation method. In Phase II, the plate/screw method (which is a traditional “gold standard” approach) was directly compared to the optimal cable technique from Phase I using experimental destructive loads to obtain stiffness, failure displacement, failure force, failure energy, fracture “sliding”, and fracture “gapping”. Clinical failure was defined as 5 mm displacement in the direction of the loading vector, whilst mechanical failure was defined as the peak force event needed for catastrophic failure of the specimen.

Results

From Phase I, among cable groups the Mouhsine technique provided the best biomechanical stability, yielding the lowest peak bone stress of 181 MPa at 3 x body weight for a 75 kg person. From Phase II, data showed the Plate method's superiority over the Mouhsine method for 2 outcome measurements (i.e. stiffness and failure force at clinical failure), its inferiority for 2 outcomes (i.e. failure displacement and gapping for posterior markers at mechanical failure), and statistical equivalence for the remaining parameters.

Conclusion

This is the first biomechanical investigation on the stability of the conventional Plate technique vs. 3 cable methods for fixing complex acetabular fractures in the presence of a THA. The Plate method was superior for the 2 critical outcomes of stiffness and failure force at clinical failure. However, the Mouhsine cable method is a reasonably effective alternative to the Plate group for repairing complex acetabular fractures in the elderly, as also clinically reported previously in the literature.

SP064.3 - Biomechanical Validation of the Radiographic Union Score for Tibial fractures (RUST) as a Predictor for Fracture Healing**Author(s):** Sandra Fiset¹, Shuai Shi², Radovan Zdero³, Emil H. Schemitsch³¹Institute Of Biomaterials And Biomedical Engineering, University of Toronto, Toronto/ON/CANADA, ²Institute Of Biomaterials & Biomedical Engineering, University of Toronto, Toronto/CANADA, ³Martin Orthopaedic Biomechanics Lab, St. Michael's Hospital, Toronto/CANADA

There is currently no objective parameter to define bone fracture union. This makes it difficult for orthopedic care providers to properly treat fractures in areas that are prone to complications such as the tibial shaft. Additionally, the lack of an objective scale for fracture union complicates the comparison of the endpoints of various clinical studies on novel fracture treatments. The Radiographic Union Score for Tibial fractures (RUST) is gaining popularity as a standard for assessing fracture healing progress via simple orthogonal x-ray images, but it has yet to be biomechanically validated as a predictor of fracture healing.

This study aims to validate RUST as a predictor of biomechanical properties of a fractured bone at different stages during healing using a rat model. A group of 45 male rats will undergo standardized osteotomy of the left tibia and the insertion of an unlocked and unreamed intramedullary nail. Orthogonal radiographs will be taken of the rat's tibia on a weekly basis and each rat will be assigned a RUST score. The first 9 rats to reach RUST scores of 8, 9, 10, 11 and 12 respectfully will be sacrificed and the left tibia will be dissected. A μ -CT scan and bone densitometry will be performed on both the bones. Subsequently, the intramedullary nail will be removed from the left tibia which will undergo biomechanical testing under torsion.

The imaging and mechanical testing results will be compared with the rats' RUST score and a score will be identified as a point when a bone can clinically be considered healed. This will allow for the standardization of an objective parameter to be used in clinical practice and studies.

SP064.4 - Patient-specific multi-scaling simulation of blood flow and fractional flow reserve in a coronary artery**Author(s):** Kyung E. Lee, Gook T. Kim, Eun B. Shim
Mechanical And Biomedical Engineering, Kangwon National University, Kangwondo/KOREA

Fractional flow reserve (FFR) is a well-known gold-standard for stenting decision in a coronary artery. Aim of this study is to present the influences of stenosis on pulsatile flow in multi-scale coronary modelling with virtual narrowing. A further purpose is to better understand the co-relation between fractional flow reserve and biomechanical factors for improving the decision-making strategy of stenting. In the present study, we present a patient-specific 3D coronary arterial modeling by coupled with lumped parameter coronary vascular bed outlet models. The computations of pulsatile flows in coronary artery were performed using a high-speed Navier-Stokes solver based on a finite element method. In this study, we analyse the haemodynamics in terms of various mechanical factors (velocity, pressure, wall shear stress, etc.) with FFR and some other Index. Hybrid FFR-biomechanical factors could play a positive role on decision-making strategy for better diagnosis and prognosis.

SP064.5 - A Modified PID Algorithm with Fuzzy Control for Closed-loop Artificial Pancreas**Author(s):** Jin Hao Yu¹, Yao X. Huang²¹Department Of Medical Devices, Guangdong Food and Drug Vocational College, Guangzhou/CHINA, ²Department Of Biomedical Engineering, Jinan University, Guangzhou/CHINA

Objective: Now, one of the main goals of diabetes treatment research is to develop a set of artificial pancreas incorporating continuous glucose sensors, control algorithm and insulin pumps. The system can completely replace the patient's disability of pancreas, automatically infuse insulin according to the human body blood glucose fluctuations to control blood changes. We intend to study a novel closed-loop control algorithm for insulin infusion system based on the technologies of continuous glucose monitoring system and accurately insulin infusion of insulin pump. The control algorithm can adjust insulin pump dosage instantly, microscale, dynamically, according to the real-time continuous glucose monitoring data of human body.

Methods: We studied the feasibility of a modified proportional-integral-derivative (PID) algorithm which main calculation parameters were optimized in real time by fuzzy control method.

Results: We used the American food and drug administration-approved type 1 diabetes mellitus simulator to evaluate and optimize the modified proportional-integral-derivative controller. The academic version of the simulator includes 10 adults, 10 adolescents and 10 children of virtual type 1 diabetes patients. The control results of 10 adults and 10 adolescents are perfect that the fluctuation range of blood glucose were 100% in the target range. But the results of 10 children were not ideal that the fluctuation range of blood glucose were 60% in the target range.

Conclusion: For adults and adolescents this algorithm can greatly reduce the fluctuation range of blood glucose, control blood glucose level in the target range, greatly improve the accuracy and effectiveness of insulin infusion, make blood glucose levels of diabetic patients close to a normal person. Nevertheless the control effect is not ideal for children, one of the possible reasons maybe more growth hormone in children that lead to larger fluctuation range of blood glucose than adults and adolescents. Although there are lots of work to do, this algorithm can provide better glucose control for adults and adolescents and has very important clinical value.

SP065 - Conebeam CT

TRACK 01: IMAGING

SP065.1 - Towards Functional C-arm CT Imaging in the Interventional Suite: Progress and challenges

Author(s): [Rebecca Fahrig](#)
 Radiology, Stanford University, Stanford/CA/UNITED STATES OF AMERICA

When C-arm CT entered the interventional suite in the late 1990's, the reaction from interventional radiologists ranged from 'we don't need it - we can easily create 3D images in our heads' to 'wow! that's the first time I've been able to see that vessel clearly!' Now, 3D C-arm CT imaging is done routinely during neuro- body- and even cardiac-interventional procedures. Technical advances in system components (faster rotation speeds, digital flat panel detectors with readout rates of 80 frames/s, variable trajectories) have enabled a progression from simple, high-contrast vessel imaging to detection of low-contrast soft-tissue lesions. It is now appropriate to explore what further advances are possible given the rapid evolution of the imaging hardware and software, and what these changes would bring to the interventional suite. We will examine these issues with the goal of providing functional information for intra-procedure and endpoint evaluation.

As a first step towards functional information, significant effort has been expended to improve the quantitative accuracy of C-arm CT reconstructions. The challenge is to improve image quality while providing very short turnaround between data acquisition and volume/data visualization. Corrections for x-ray scatter, view aliasing and patient motion that require no more than 2 iterations keep processing time short while reducing artifact. Additional challenges include detector non-linearity/saturation and restricted field of view.

Fast, multi-sweep acquisitions can be used to image blood flow in the brain and liver, permit assessment of left ventricular function, and visualization of radiofrequency lesions created to treat arrhythmias. Workflows for each imaging goal have been developed and validated against gold standard clinical CT or histology. The challenges, opportunities and limitations of the new functional imaging techniques will be discussed.

SP065.2 - 2D/3D Registration for Motion Compensated Reconstruction in Cone-Beam CT of Knees Under Weight-Bearing Condition

Author(s): [Martin Berger](#)¹, [Kerstin Mueller](#)², [Jang-Hwan Choi](#)², [Andre Aichert](#)¹, [Andreas Maier](#)³, [Rebecca Fahrig](#)²

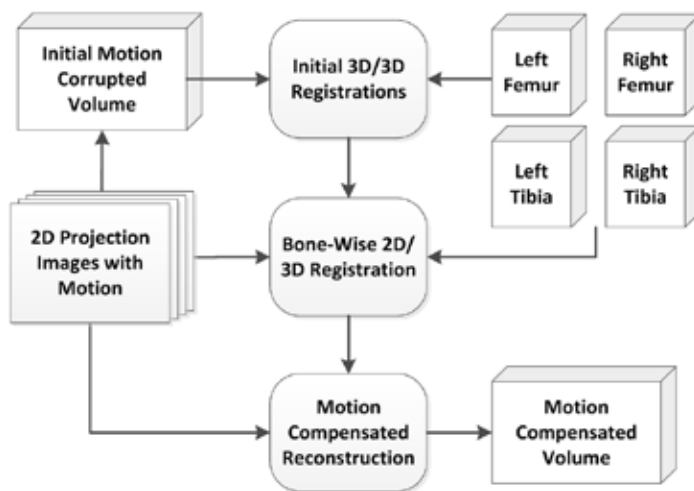
¹Pattern Recognition Lab, Department Of Computer Science, Friedrich-Alexander-University Erlangen-Nuremberg, Erlangen/GERMANY, ²Radiological Sciences Lab, Stanford University, Stanford/UNITED STATES OF AMERICA, ³Research Training Group 1773 "Heterogeneous Image Systems", Erlangen/GERMANY

Introduction: Over the last decade, increased effort has been made to acquire three dimensional images of knee joints under weight-bearing condition. Cone-beam CT systems are popular because of their high flexibility with respect to patient position and scan trajectory. However, scans in a standing or squatting patient position are affected by involuntary patient motion during the acquisition, which results in streaking and blurring artifacts in the reconstructed volumes.

Previous work suggested the use of fiducial markers to estimate and

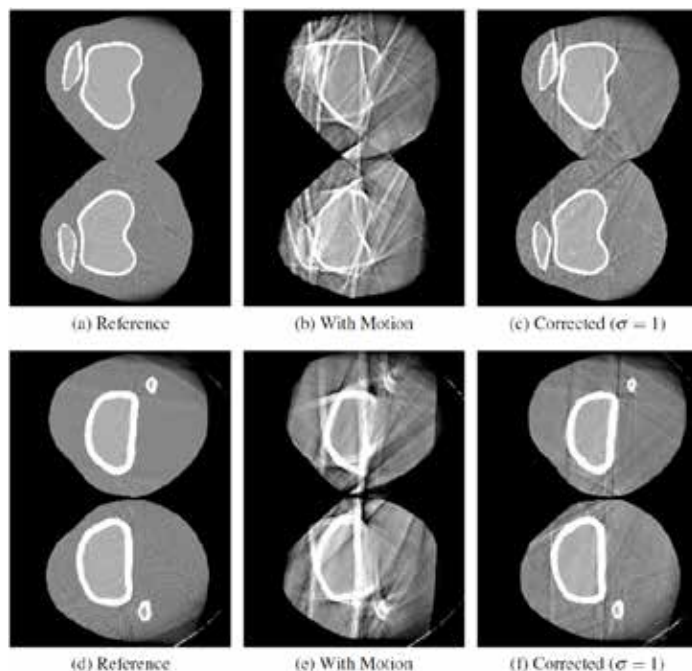
compensate for motion artifacts. However, marker placement on the skin might not accurately reflect the motion at the center of the joint.

Method: We propose a marker-free, data-driven motion compensation method that is based on 2D/3D rigid registrations of segmented bones from a prior, motion-free scan.



The Figure above gives an overview of the pipeline of our method. The segmentations are roughly aligned in 3D with respect to an initial motion corrupted reconstruction. Motion parameters are estimated by 2D/3D registration of each bone to each projection image. After combining the individual bone motions to a global deformation, we can generate a corrected reconstruction.

Results and Discussion: To verify our approach we used a simulated dataset from previous work [1]. Our numeric phantom is based on segmentations of real anatomical structures. Real motion of healthy volunteers was incorporated into the phantom using an optical tracking system.



Our results show great improvement over images without correction. In particular the bones' outlines are accurately restored. This is important because most relevant structures in the knee joint are located close to the bones, e.g., the cartilage. Incorporating smooth-

ness constraints into the registration cost-function further improved the results.

[1] Choi, J.-H. et al.. (2013). Fiducial marker-based correction for involuntary motion in weight-bearing C-arm CT scanning of knees. Part I. Numerical model-based optimization. *Medical Physics*, 40(9), 091905

SP065.3 - Direct Scatter Estimation and Separation for Cone-beam CT Images Utilizing Monte Carlo Simulation

Author(s): Yu Wang, Chaobin Chen, Ruifen Cao, Liqin Hu
University of Science and Technology of China, Hefei/CHINA

Objective: The scatter radiation degrades the reconstructed Cone-beam CT(CBCT) images quality, which limits the application of CBCT images into the re-optimization of treatment plans for Adaptive Radiotherapy (ART). This paper estimated the scatter distribution in the CBCT projections directly utilizing the Monte Carlo simulation. In addition, the scatter separation was taken into account to determine the corresponding scatter fraction introduced by different parts of the system.

Methods and Materials: Using EGSnrc Monte Carlo program, the ELEKTA XVI CBCT system was modeled including the x-ray tube, water phantom with different thickness and flat-panel detector. The LATCH option was adopted to record the particles information, including the fluence, energy, weight, whether a secondary particle and which modules it had interacted with. The model was validated by percentage depth dose (PDD) and lateral profiles measurements. A program based on Visual C++ was developed to extract the primary particles and calculate the total scatter radiation at the scoring plane. At last, the corresponding scatter fractions introduced by different parts of the system were separated.

Results: The calculated PDD and lateral dose profiles were compared against the dose measurements under 1cm water. The dose difference of PDD was better than 1% within the depth of 10cm. More than 85% points of lateral dose profiles was within 2%. For CBCT system, the phantom produced the larger part of the scatter radiation, almost 50% with water thickness of more than 25cm.

Conclusions: The CBCT system has been fully modeled including x-ray tube, phantom and flat-panel detector and the model was validated by the PDD and lateral profiles measurements. The scatter fractions introduced by the phantom with thickness of more than 25cm should be corrected to improve the images quality. This study is expected to be applied to the scatter radiation correction for improving CBCT images quality and optimizing the CBCT modules design.

SP065.4 - Automatic Motion Estimation and Compensation Framework for Weight-bearing C-arm CT scans using Fiducial Markers

Author(s): Kerstin Mueller¹, Martin Berger², Jang-Hwan Choi¹, Andreas Maier², Rebecca Fahrig¹

¹Radiological Sciences Lab, Stanford University, Stanford/CA/UNITED STATES OF AMERICA, ²Research Training Group 1773 "Heterogeneous Image Systems", Erlangen/GERMANY

Cone-beam CT systems are widely used because of their high flexibility with respect to patient position and scan trajectory. In the last years, C-arm CT systems have been used to acquire images in weight-bearing conditions in order to expose, e.g. the knee joint under realistic loads. Straight standing or squatting patient positions lead to involuntary patient motion during the acquisition. In this paper, a fully-automatic motion estimation and compensation framework to mitigate knee-joint motion during weight-bearing C-arm scans is presented. Our framework consists of three major

steps: marker detection with outlier removal, motion estimation and correction, and marker removal. The marker detection is based on an initial estimate of the marker position extracted from the motion-blurred filtered backprojection (FDK) reconstruction and on the fast radial symmetry transformed (FRST) 2-D projection images. The motion is estimated by the alignment of the forward projected 3-D initial marker positions with the actual detected 2-D marker positions. The motion is then corrected in the filtered backprojection step. Finally, the detected markers are removed in the 2-D projection images by simple interpolation. The framework was evaluated on three C-arm CT datasets from one volunteer in a straight standing, moderate squatted and deep squatted position. All 3-D reconstructions show a large improvement in image quality compared to the non-corrected 3-D reconstructions.



Figure 1(a) w/o motion correction



Figure 1(b) with motion correction

SP065.5 - Evaluation of two-pass view aliasing artifact suppression algorithm using clinical data

Author(s): Meng Wu¹, Kerstin Mueller¹, Michael P. Marks², Rebecca Fahrig¹

¹Department Of Radiology, Stanford University, Stanford/UNITED STATES OF AMERICA, ²Department Of Radiology And Neurosurgery, Stanford University, Stanford/UNITED STATES OF AMERICA

Purpose: In brain perfusion CT imaging, state-of-the-art C-arm CT systems can rotate up to 100 degrees / second, which permits CT imaging with high temporal resolution. However, the read-out rate of the flat panel detector often limits the number of projections acquired in the fast scan and causes view aliasing artifacts in the reconstruction. We propose to suppress aliasing artifacts in decomposed projections through feature preserving interpolation.

Methods: The high frequency structures that cause streak artifacts are hidden within the total line integral. Thus, the interpolation-based method for angular up-sampling often fails to correct for these high frequency structures. We propose an FBP-based algorithm using multi-resolution reconstruction to identify the structures in projection space that may cause the artifacts. The adaptive multi-resolution FDK reconstruction adaptively selects the bandwidth of the ramp filter in the FDK method to reconstruct regions of the image at maximal frequency without view aliasing artifacts. A feature preserving interpolation in projection space is used to increase the angular sampling rate. The restored high frequency structures are then added back to the view aliasing-free reconstruction. The proposed method's performance is assessed using real patient C-arm (Artis zee biplane system, Siemens AG, Germany) head scan data. Only 124 out of 248 projections are used for the reconstruction to mimic the sparse-view data in the fast scan. Our results are compared to those with and without linear interpolation method.

Results: As shown in Figure 1, the proposed method can effectively reduce the view aliasing streak artifacts. The structural similarity (SSIM) indices of the brain tissue region using the FDK, linear interpolation, and proposed methods comparing to the ground truth are 0.7428, 0.7686 and 0.8060, respectively. The proposed method also reduces the standard deviation of the brain tissue without contrast (which is assumed to be uniform) from 56.2 HU to 35.7 HU while the linear interpolation method has a standard deviation of 42.5 HU. The proposed method is compatible with a projection-based motion compensation technique to further improve the image quality.

Conclusion: Distinct from other blurring-based and iterative reconstruction methods, our method maximally preserves image spatial resolution with only two iterations. Future investigations will incorporate the technique for noise reduction and compare to sparse view iterative reconstruction.

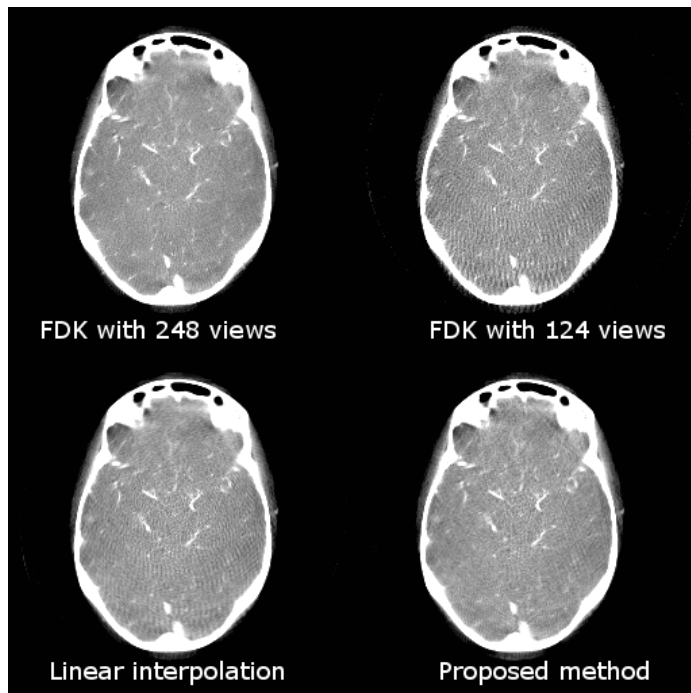


Figure 1, reconstruction results using FDK, linear interpolation and the proposed method. The display window is [-500 500] HU.

SP065.6 - A simple algorithm to remove metal artifacts in frame based radiosurgical treatments

Author(s): Gopishankar Natanasabapathi

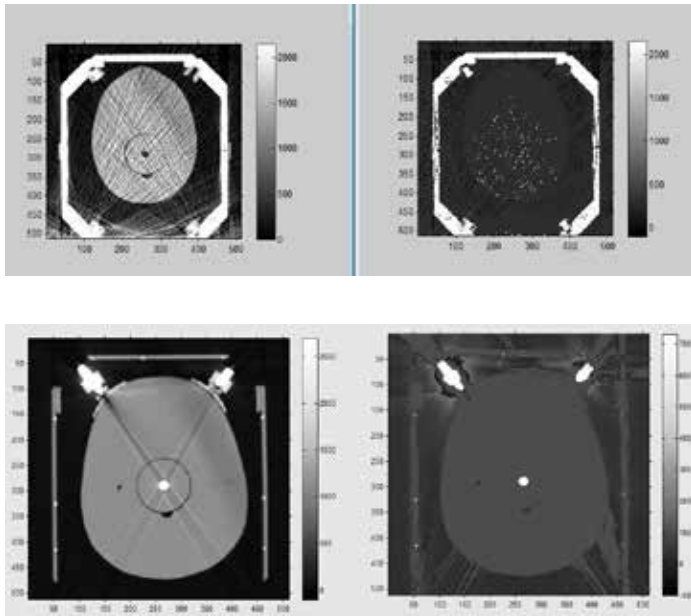
Gamma Knife Unit, All India Institute of Medical Sciences, New Delhi/INDIA

Purpose: To show a simple method to remove metal artifacts generated during imaging for treatment planning purpose. Materials and

Methods: A human head shaped phantom made from acrylic material was fixed to stereotactic Leksell frame for artifact simulation purpose. Four metal screws aided in holding the metal frame to the phantom with carbon fixation posts. An ion chamber positioned in the middle portion of the phantom determines point dose measurement. In this study same ion chamber setup generated artifacts at the phantom center which required artifact removal. CT scans of the phantom were acquired using following scanning parameters: Tube voltage-110 kV, Slice thickness-1 mm and FOV-240 mm. Image slices with severe artifacts were selected for image processing using in-house developed matlab codes. Pixels in the phantom image affected by noise were isolated and digitally post processed by applying threshold value to the hounsfield units (HU).

Results: The images showed more than 95 % improvisation after implementing correction algorithm. Before image correction the HU present in the phantom image due to metal frame and pins was found to be more than 3000 HU. After applying correction algorithm, HU of ion chamber region, metal frame and pin region were restored.

Conclusion: The TPS system of Gamma Knife (GK) performs convolution algorithm based calculation on CT images with HU values range between -1000 to +1024. Any HU values beyond these values are automatically ignored by the TPS during calculation. It means that the TPS ignores the artifact affected region for calculation irrespective of where it is present. This is one of the major limitations of convolution algorithm based planning in GK. The artifact removal method shown in this study is a simple, effective technique which overcomes these limitations and is a valuable tool for GK.



SP066 - Human Movement

TRACK 03: BIOMECHANICS AND ARTIFICIAL ORGANS

SP066.1 - Fingertip touch adjust postural orientation during perturbed stance

Author(s): [Aizreena Azaman](#), Shin-Ichiroh Yamamoto
Department Of Bioscience And Engineering, Shibaura Institute of Technology, Saitama City/JAPAN

Additional sensory information; especially from touch, was suggested to improve stability by reducing body sway. However, it is less known about the effect of touch on the body's joint movement during perturbed standing; which is commonly experienced by public transport users. In this study, subjects were asked to try to maintain their standing position with their fingertips on a rigid surface, while surface perturbation was applied at four different perturbation frequencies (0.2, 0.4, 0.6, and 0.6 Hz) and different vision input. Motion of joint (ankle, hip and head) and relative centre of mass (COM) were recorded and analysed. The results show that fingertip pressure was higher without vision. Furthermore, different fingertip moment directions were recorded between with vision and with no vision. This possibly indicates a preferred fingertip position that can provide better sensory information to replace sensory loss; especially vision. The range of motion of joints also decreased with fingertip touch - except for head motion. Furthermore, even though there were no significant differences observed between with touch and without touch, the relative COM displacement was less with touch. Thus, even with a very light touch, subjects were able to reduce body sway even in a perturbed stance. Further investigation is needed to determine the changes in centre of pressure (COP) and significant position of fingertip, which can enhance stability.

SP066.2 - Design and Evaluation of a Prosthetic Knee Joint based on Automatic Stance-Phase Lock (ASPL) Technology for Children with Transfemoral Amputations

Author(s): [Calvin Ngan](#), Jan Andrysek
Bloorview Research Institute, Holland Bloorview Kids Rehabilitation Hospital, Toronto/ON/CANADA

Introduction: Lower extremity amputation strongly affects an individual's mobility and quality of life, as well as creating a socio-economic burden for society. Studies have shown that amputations in children have a particularly significant impact on their physical and psychological developments. Therefore, it is important to provide child amputees with a well-functioning prosthetic knee joint to restore their mobility function and enable them to partake in physical activities with peers and family.

Problem: Many paediatric prosthetic knee joints in the market incorporate four- or six-bar linkage mechanisms that offer good stance phase control, but their added size and weight make them unsuitable for very small children. Furthermore, to accommodate these size constraints, many designs exclude swing phase control and extension assist mechanisms, negatively impacting user's gait characteristics such as energy expenditure and gait speed. Therefore, the objective of this project is to design and evaluate an original paediatric prosthetic knee that will provide good stance phase stability by incorporating the novel, patented Automatic Stance Phase Lock (ASPL) mechanisms developed in Holland Bloorview Kids Rehabilitation Hospital, and integrating frictional components and extension assist mechanism to offer better swing phase control for the user.

Method: We focus on three major areas: (1) knee design and proto-

type development, (2) structural testing, and (3) functional evaluation via a pilot study. We will use 3D Computer Aided Drawing (CAD) and Finite Element Analysis (FEA) software to develop and structurally optimize the prosthetic knee joint model. A prototype will then be constructed and a series of bench-top structural tests will be performed following the ISO 10328 to test for structural integrity. In the pilot study, a single subject with an unilateral transfemoral amputation will perform six-minute walk tests and gait assessment tests with his/her current prosthetic knee, as well as our prototype. Gait characteristics such as walking velocity, kinetics profiles including knee flexion angle and knee moment, and energy expenditure will be measured and analyzed in both trials. Differences in the key parameters listed above between the prototypes and the conventional knee will be used as an indicator for how functional the prototype is and indicate which design changes may improve areas of concern.

Results: In the current stage of the project, we designed and developed a 3D computer model of the paediatric prosthetic knee. In the model, our prototype is estimated to be 120mm tall and weighs about 355g, which is similar to current commercially available products. It also includes mechanical friction control and extension assist to facilitate the swing phase control for the user. Multiple iterations of FEA on the model were completed, and the results suggested that the design is capable of supporting the specified load listed in the ISO structural test. Therefore we will proceed to fabricating the prototype and performing the structural test imminently. The goal of this project is to prove the feasibility of implementing ASPL technology in a paediatric prosthetic knee, so ultimately it would be possible to provide well-functioning and affordable prostheses for child amputees around the globe.

SP066.3 - Frontal plane gait during cross-slope walking for able-bodied and transtibial amputees

Author(s): Emily Sinitski¹, Edward D. Lemaire¹, Nancy L. Dudek², Markus Besemann³
¹Crrd, The Ottawa Hospital Research Institute, Ottawa/CANADA, ²Faculty Of Medicine, University of Ottawa, Ottawa/CANADA, ³Canadian Forces Health Services Group, Ottawa/CANADA

Cross-slope surfaces are slopes in the frontal plane. Unlike level and inclined surfaces, cross-slope walking requires an asymmetrical gait pattern to keep the body vertical while adapting to different ground heights and angles. Although cross-slopes are a common real-world surface, cross-slope walking literature is predominately on the able-bodied population. For individuals with a lower limb amputation, lack of lower limb musculature may pose a greater challenge for maintaining balance and forward progression on cross-slopes. This research investigated compensatory adaptations in the frontal plane for able-bodied individuals and individuals with a transtibial amputation when walking on moderate cross-slopes.

Fourteen able-bodied (AB) and 14 unilateral transtibial amputees (TTA) participated in this study. Participants walked on a level and $\pm 5^\circ$ cross-slope treadmill at a fixed speed while full body kinematic data were captured within a CAREN-Extended virtual reality environment. Gait outcome measures included, speed, step width, and frontal plane joint angles (ankle, knee, hip, pelvis, and trunk) and sagittal plane joint angles (ankle and knee) at foot contact and during stance. Data were examined using a linear mixed model with a treadmill speed covariate. Post-hoc t-tests with a Holm-Bonferroni correction ($p < 0.05$) were performed to examine differences between groups and walking conditions.

TTA participants walked slower than able-bodied ($AB = 1.29 \pm 0.06$ m/s, $TT = 1.11 \pm 0.15$ m/s; $p < 0.001$). Step width (14.7 ± 0.6 cm) was not significantly different between walking conditions and groups. Compared to level walking (LW), the limb at the top of the cross-slope (TS) had less ankle inversion at foot contact and ankle angle tran-

sitioned to eversion during stance ($p < 0.001$). Conversely, the limb at the bottom of the slope (BS) required more ankle inversion than LW at foot contact and remained inverted during stance ($p < 0.001$). Since the majority of TTA participants wore a prosthetic foot with a split toe, participants were able to achieve ankle in/eversion similar to the AB group for these moderate cross slopes (Table 1). However, during stance, TTA had more lateral trunk motion and smaller pelvis obliquity compared to AB. Prosthetic ankle and knee stance flexion was also smaller for TTA than AB. These findings demonstrated that TTA did not have sufficient prosthetic ankle dorsiflexion to shorten effective prosthetic limb length on the top-cross-slope. As a result, TTA increased lateral trunk motion to compensate for the ground height differences between limbs.

Table 1. Mean and standard deviation of ankle, pelvis, and trunk angles (degrees) during stance. Boldfaced=significantly different from LW and * =significantly different from AB.

		TS	LW	BS
Ankle Angle (+)inversion/(-) eversion	AB	-5.8 (2.3)	-0.4 (2.5)	5.8 (2.5)
	TTA-intact	-6.3 (2.2)	-0.5 (2.3)	5.7 (3.1)
	TTA-pros	-3.3 (3.3)	1.5 (2.8)	6.4 (2.7)
Pelvis Obliquity (+)up/(-)down	AB	3.2 (1.0)	2.5 (0.9)	1.5 (0.8)
	TTA-intact	1.6 (1.4)*	0.3 (1.2)*	-1.5 (1.4)*
	TTA-pros	2.0 (1.7)*	0.6 (1.4)*	-0.5 (2.0)*
Trunk Lateral Tilt (+)up/(-)down	AB	-0.5 (1.3)	-0.8 (1.0)	-1.0 (1.0)
	TTA-intact	-1.9 (1.9)*	-1.5 (1.1)*	-1.5 (1.9)*
	TTA-pros	-2.7 (1.3)*	-2.2 (1.1)*	-2.8 (1.6)*

SP066.4 - Impact of gait modifications on hip joint loads during level walking

Author(s): Masaru Higa¹, Fusako Kawabata¹, Yoshihiro Kobayashi¹, Koji Fukuda²
¹Mechanical Engineering, University of Hyogo, Himeji/JAPAN, ²Human Science And Environment, University of Hyogo, Himeji/JAPAN

A lot of the literature suggests that walking mechanics have an intense impact on the progression of joint diseases such as osteoarthritis (OA). In knee OA, excessive medial tibiofemoral compartment loading is widely believed to contribute to the progression of medial OA. Although the feasibility of gait modifications for reducing knee joint loading has been studied widely, gait modifications have not been investigated to the same extent in people with hip OA. We hypothesized that high loading on the hip joint also contributes to the progression of hip OA. Hence, this study is aimed to show if hip joint forces during walking could be reduced by a slight gait modification. The hip loadings could be measured in vivo with an instrumented hip prosthesis. This method, however, is restricted to a few institutions and patients, and theoretical calculations are difficult. At the same time, the external hip adduction moment during walking is a useful measure for estimating internal hip joint loading. For this reason, we used the hip adduction moment as a quantitative target for gait retraining of hip OA patients. Six healthy adult subjects (mean (SD) age 22 (0.0) years, mean (SD) height 1.68 (0.04) m, mean (SD) weight 60.2 (7.9) kg) took part in this study. A series of normal walking trials at a self-selected speed (step length and cadence) and stride width were performed for each subject. Then the subjects had gait retraining during in which they were asked to alter their stride width by increasing abduction angles without changing any other kinematics. The amount of the modification was limited within a “normal looking” gait. The retraining was also aimed at retaining other motion parameters such as gait speed, step length, cadence, flexion angles and rotation angles of the hip as well as upper body movements. The subjects walked 10 trials for each gait pattern, and a total of 20

trials were performed. Experimental gait data (i.e., joint kinematics and ground reaction forces) and musculoskeletal computer models (OpenSim 2.1) were used to quantify hip joint moments. We also used an inverse dynamics approach to calculate the hip moments during a stance phase. Five of six subjects exhibited an average decreased adduction moment during modified trials ($p < 0.05$). The changes in abduction angles did not have any effect on the shape of the hip adduction moment curve but changed its peak mean magnitude from 3.59 %BW*HT during normal walking to 1.81 %BW*HT during the modified walking at a representative subject. An increase in the peak external rotation of the hip, however, was also observed. This should be eliminated since external rotation could be harmful for patients with high femoral anteversion. In conclusion, we showed that a modified gait pattern can reduce the hip adduction moment. Given the results of this study, we believe that gait retraining may be an acceptable, noninvasive option for the treatment of patients with hip OA.

SP066.5 - The influence of the aquatic environment on the control of gait initiation

Author(s): Andresa Marinho Buzelli¹, Hossein Rouhani¹, Gustavo Fernandes², Kei Masani³, Milos Popovic⁴, Molly Verrier³

¹Rehabilitation Engineering Laboratory, Toronto Rehabilitation Institute - University Health Network, Toronto/CANADA, ²Universidade Federal de Santa Catarina, Florianopolis/BRAZIL, ³Toronto Rehabilitation Institute - University Health Network, Toronto/CANADA, ⁴Institute Of Biomaterials And Biomedical Engineering, University of Toronto, Toronto/CANADA

Background: Gait initiation is a common functional task defined as the transition from stationary standing to steady-state walking. It is vastly investigated in healthy subjects and in individuals with disability. The complex interaction between neuromuscular and biomechanical factors during gait initiation has been investigated mainly in two phases, anticipatory postural adjustments (APAs) and execution of the step. Despite the frequent use of therapy pools for walking training in early stages of locomotor recovery, the effects of immersion on the control of gait initiation have not been reported yet. The objective of the present study is to analyze the center of pressure (COP) trajectories, the vertical and horizontal forces and trunk acceleration (ACC) during APAs, as well as during execution of the first and second steps during gait initiation.

Method: Able-bodied young adults (3 female and 2 male) were requested to initiate gait from a waterproof force plate (AMTI OR6-WP-1000, Watertown) and to continue walking for 5 steps. Individuals performed 10 consecutive trials, on land and in water, on two consecutive days. Subjects initiated gait with the same foot position following a visual cue. Two inertial sensors (Physilog, BioAGM, Lausanne) were attached to L5/S1 vertebrae and to the shank of the initial stance limb. COP landmarks were used to identify APAs and execution of the first step. Shank ACC was used to mark the toe-off and heel strike of the second step. Lower trunk (LT) horizontal ACC (anteroposterior – AP and mediolateral – ML) during APAs and execution phases was computed. The parameters used for evaluation were: peak of anticipatory COP trajectory (APA_Peak); COP length during APAs; length and velocities of COP trajectories during execution of the first step; impulse forces in vertical and AP directions; root mean square (RMS) ACC of trunk during first and second steps. Wilcoxon Matched-Pair Signed-Rank test was used for comparisons between land and water conditions.

Results: Percentage of body mass offloading in water varied between 49% and 57%. COP movements during APA and execution of first step were significantly larger in water compared to land: APA_Peak in ML (5.1±1.7 vs. 3.7±1.5 cm); ML length of COP trajectory when body weight was transferred to the stance limb (22.8±4.2 vs. 18.2±3.5 cm); and ML length of COP during first swing (5.4±1.8

vs. 2.8±1.1 cm). COP velocity in AP during the first swing was slower in water (16.7±4.2 vs. 26.7±4.9 cm/s). The vertical impulse of the stance limb was smaller in water compared to land (340.7±31.1 vs. 425.4±54.2 N.s). LT ACC were smaller in water compared to land with more accentuated change in AP RMS of LT ACC during first step (0.6±0.3 vs. 1.8±0.7 m/s²) and second step (0.7±0.2 vs. 1.6±0.3 m/s²).

Conclusion: Immersion in water increases mediolateral body displacement, and reduces trunk acceleration and vertical impulse force during gait initiation, suggesting potential implications for aquatic rehabilitation.

SP067 - Characterization of Detector Systems for Therapy Dosimetry: Part 2

TRACK 05: DOSIMETRY AND RADIATION PROTECTION

SP067.1 - Reaction of three UV exposure to gafchromic EBT-2 and EBT-3

Author(s): Toshiro Katsuda¹, Rumi Gotanda², Tatsuhiro Gotanda³, Takuya Akagawa⁴, Nobuyoshi Tanki⁵, Tadao Kuwano⁶, Kouichi Yabunaka⁷

¹Department Of Human Relation, Tokai Gakuin University, Kakamigahara/JAPAN, ²Department Of Radiological Sciences, Ibaraki Prefectural University of Health Sciences, Ibaraki/JAPAN, ³Department Of Radiological Science, Faculty Of Health Sciences, Junshin Gakuen University, Fukuoka/JAPAN, ⁴Department Of Radiological Technology, Tokushima Red Cross Hospital, Tokushima/JAPAN, ⁵Center For Life Science Technologies, RIKEN, Kobe/JAPAN, ⁶Graduate School Of Health Sciences, Okayama University, Okayama/JAPAN, ⁷Graduate School Of Medicine, Tokyo University, Bunkyo-ku/JAPAN

Gafchromic films (GAFs) are used for the X-ray dose measurement in the diagnostic examination. It is begun to use for the three-dimensional X-rays dose measurement using the high-resolution characteristic in computed tomography. However, it is necessary to solve a problem of unevenness of active layer of GAFs. It is suggested that the ultraviolet (UV) is substitute as an X-ray. However, wavelength of appropriate UV are unidentified. This study is to decide a wavelength of the UV.

Peak wavelength of 245 nm, 310 nm and 365 nm UV were irradiate to the EBT2 and EBT3. The UV rays were irradiated for 5, 15, 30 and 60 minutes, and irradiation was repeated afterwards until 360 minutes every 60 minutes. The images were split in RGB, and R images were used. ROI of the diameter 1/2 inch was set in the center of subtracted GAF images, and the graph of UV irradiation time and the mean pixel value were made.

There was a reaction in front and back of GAF EBT3 and back of EBT2 in UV-A and B. However, UV-C had few reactions with both aspects of GAF EBT2 and EBT3.

It should be used UV-A for a fact because a wavelength of UV-B may affect the human body.

SP067.2 - Characterizing FujiFilm CR Signal Storage Decay Rates

Author(s): Thorarin A. Bjarnason¹, C J. Yang²

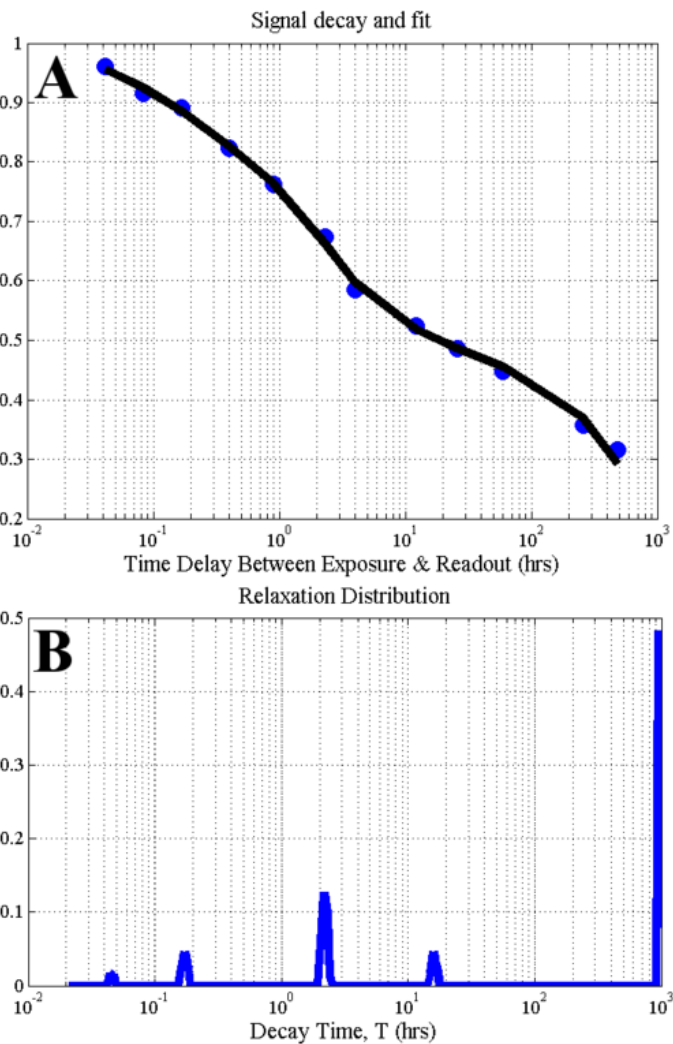
¹Diagnostic Imaging Services, Interior Health, Kelowna/CANADA, ²Sindi Ahluwalia Hawkins Centre For The Southern Interior, British Columbia Cancer Agency, Kelowna/CANADA

Introduction

In this work we outline a method for characterizing x-ray signal retention on Fujifilm CR photostimulable phosphors (PSPs). In order to use CR plates as dosimeters and to ensure the accuracy of image quality and dose indicator metrics, the behavior of x-ray signal storage needs to be characterized. Based on electron-hole storage of PSPs, it is known that in addition to specific frequency light stimulation overcoming the band gap and releasing the stored signal, thermal processes can do likewise, but at slower rates [Rowlands].

Methods/Results

The same FujiFilm CR plate was exposed repeatedly to 700 (± 20) uGy at 120kVp and readouts were spaced out between immediate and 20days, as shown as the blue dots in A. Raw pixel values were extracted from image data and converted to dose as per [Bjarnason1]. When exposures were performed on separate days, all data were normalized using image data scanned immediately on that day. CR plates were sandwiched between 4 mm lead to minimizing background radiation exposure during the measurement time delay. The resulting decay was fit (black line in A) using a sum of exponential decays as per [Bjarnason2], which makes no a priori assumptions as to the number of exponentials present. The resulting relaxation distribution was found (B) and the following decay components were identified: 0.014 @ 2.8min, 0.045 @ 10.3min, 0.126 @ 2.1hr, 0.046 @ 15.9hr, 0.48 @ 40days.



Discussion/Conclusions

In this work we characterized 20 days of CR signal retention. Signal fading of 25% is expected between 10min and 8hr, and then slower after [AAPM 93], but this behavior has not been fully characterized before. We found the signal decay to be multiexponential and can conclude that the first two decay components at 2.8 and 10.3min should minimally affect the CR dose indicator values because even though staff often quickly read the images while signal is being lost due to these decay times, their intensities only account for 5% of the total signal loss occurring after about 1hr. By characterizing the signal loss over longer times, we can use these data to calibrate CR plates for use as area dosimeters. Future work includes testing inter-

plate variability, assessment at different kVps, and assessment of different vendors using different PSP chemical compositions.

References

[Rowlands] Rowlands. *PhysMedBiol* 47:R123-66(2002). [Bjarnason1] Bjarnason&Yang. *COMP-ASM2014:2*. [Bjarnason2] Bjarnason&Mitchell. *JMagnReson*206:200-4(2010). [AAPM93] AAPM report93 (2006).

SP067.3 - Angular dependence of diode detectors and PinPoint ionization chamber in Gamma Knife dosimetry

Author(s): Hrvoje Hršak¹, Marija Majer², Zdravko Heinrich³

¹Department Of Oncology, University Hospital Centre Zagreb, Zagreb/CROATIA, ²Laboratory For Radiation Chemistry And Dosimetry, Institute Ruđer Bošković, Zagreb/CROATIA, ³Department Of Neurosurgery, University Hospital Centre Zagreb, Zagreb/CROATIA

Dosimetry for Gamma-Knife radiosurgery beams requires detectors with high spatial resolution, minimal angular dependence of signal and linear dose response. Angular dependence for shielded (PTW60016 Diode P) and unshielded (PTW60017 Diode E) p-type silicon detectors and PTW31006 PinPoint ionization chamber was measured indirectly with 18, 14, 8 and 4 mm collimator helmet for the Leksell Gamma Knife Model C. Weighted angular dependence correction factors were calculated for each detector and collimator helmet. For Gamma-Knife beams angle range of 84°-54° Diode P detector shows considerable angular dependence of 9% and 8% for the 18 mm and 14, 8, 4 mm collimator, respectively. For Diode E detector this dependence is about 4% for all collimators. Compared to Diode E, Diode P shows stronger angular dependence which may be explained by the increase of electron backscattering from the metal shield of silicon active volume as the angle of incident photon beam decreases, i.e. more photons are entering silicon chip perpendicularly. PinPoint ionization chamber shows angular dependence of less than 3% for 18, 14 and 8 mm helmet and 10% for 4 mm collimator which is probably due to volumetric averaging effect in a small photon beam. Diodes P and E represent good choice for Gamma-Knife dosimetry, while PinPoint ionization chamber is not recommended for dosimetry with the 4 mm collimator helmets. When used for absolute and relative dosimetry of Gamma Knife beams, diodes and PinPoint ionization chamber response should be corrected for angular dependence.

SP067.4 - Determination of a correction factor to mitigate long term reader fluctuation of the Optically Stimulated Luminescence dosimetry system at the International Atomic Energy Agency

Author(s): Andrew Cole, Tomislav Bokulic, Paulina Grochowska, Joanna Izewska
Nuclear Sciences And Applications, International Atomic Energy Agency, Vienna/AUSTRIA

Introduction

The Dosimetry Laboratory at the International Atomic Energy Agency is commissioning an Optically Stimulated Luminescence (OSL) dosimetry system to provide radiotherapy dosimetry audits. The OSL readers' (Microstarⁱⁱ, Landauer) internal mechanism consists of a high powered light emitting diode (LED), optical components and a photo-multiplier tube (PMT). Inbuilt PMT response Quality Assurance checks along with standard measurements from control OSL dosimeters allow the daily performance of the readers to be monitored. Extensive measurements were conducted during a period of 6 weeks. In this time the PMT response showed a fluctuation of 1.7% and the control OSL dosimeters' results exhibited a fluctua-

tion of 1.4%. A correction factor to mitigate this magnitude of reader fluctuation is necessary and was calculated with two separate methods.

Materials/Methods

In the first method, PMT response QA checks were periodically performed directly preceding measurements of a control batch of OSLDs. A linear correlation of the magnitude of control OSLD dose readout to the reader's PMT response was calculated. An inverse of the correlation was calculated and applied as a reader's fluctuation correction factor.

The second method quantified the reader fluctuation in terms of the magnitude of deviation of OSL dosimeter readout values from postulated theoretical values, as demonstrated on an earlier model system [1]. These deviations were deemed attributable to reader fluctuations and the magnitude was correlated to PMT response data to determine a correction factor. In an iterative approach, this method also allowed a more accurate theoretical model to be calculated.

Results

Reader fluctuation correction factors were determined by both methods and applied to daily control OSL readout data. The two methods of determination of reader fluctuation correction factors resulted in reduced long term fluctuation in control OSL readout values to 0.9% and 0.2%, respectively, over the 6 week period. Longer term investigation may allow this to be improved as more data is acquired.

Conclusion

To mitigate the influence of long term reader fluctuation on the determination of OSL dosimetry audit values, a reader correction factor has been determined from two methods. The application of this correction factor has achieved a substantial decrease in the magnitude of reader fluctuations over a period of 6 weeks and will be the basis of protocols to also reduce fluctuation on the short term.

References

[1] Dunn L, Lye J, Kenny J, Lehman J, Williams I, Kron T (2013) Commissioning of optically stimulated luminescence dosimeters for use in radiotherapy. *Radiat. Meas.*, 51:31-39

SP067.5 - Reference and relative dosimetry of standard and small photon fields with new commercially available detectors

Author(s): Bryan R. Muir, Malcolm R. McEwen
Measurement Science And Standards, National Research Council, Ottawa/CANADA

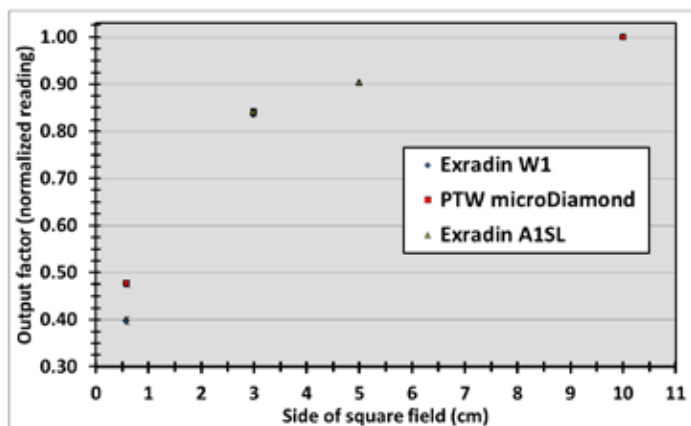
Two new detectors, the PTW microDiamond synthetic diamond detector and the Exradin W1 plastic scintillation detector (PSD), are now available that were designed for the dosimetry of small radiation fields. We investigate the performance of a single version of each detector when used for reference dosimetry of standard fields and relative dosimetry of small fields placing specific emphasis on the determination of associated uncertainties.

Measurements of detector response are made under reference conditions in 6, 10 and 25 MV photon beams from the Elekta *Pre-*

cise linear accelerator in 10x10 cm² field sizes relative to secondary standard reference chambers, calibrated in terms of absorbed dose directly against the National Research Council of Canada (NRC) primary standard water calorimeter. These absolute calibrations are used to derive detector energy dependence as well as short- (hours) and long- (months) term repeatability. Profiles are measured with these detectors in fields as small as 0.6x0.6 cm² shaped by the Elekta photon jaws and used for accurate detector positioning in small fields. Once detectors are properly positioned on the beam axis, small field output factors are measured, keeping the detector position constant and modifying the photon jaw settings. Measurements of output factors are repeated to investigate uncertainties caused by jaw positioning repeatability, detector positioning and the repeatability of the detector response and/or associated noise.

For both detectors, energy dependence is less than 1% comparing calibrations over the range 6-25 MV. The repeatability of the PTW microDiamond response for calibrations under reference conditions is within 0.3% after a period of almost two months. The repeatability of the response of the Exradin W1 PSD is generally also at this level, although sometimes unexpected differences of 1-2% were observed, which require further research for explanation. Profiles measured with the two detectors are in good agreement although the very small signal from the Exradin W1 is much noisier. The attached figure shows small field output factors (i.e., readings normalized to the value obtained in a 10x10 cm² field) with error bars representing type A uncertainties and variations in repeated measurements of output factors. For both detectors, standard uncertainties in reference dosimetry measurements are within 0.4% and are less than 2% for relative dosimetry measurements in very small fields.

Both detectors investigated in this work exhibit very impressive behavior for both reference and relative dosimetry measurements.



SP067.6 - Evaluation of detectors response for small field output factor measurement using multichannel film dosimetry

Author(s): [Gunter Rucka](#), Jean Claude Mouttet, Nathalie Asquier, Patrice Budillon
Centre De Radiothérapie St Louis, Croix-Rouge Française, Toulon/FRANCE

Introduction

Most irradiation technics require dose computing from TPS. Calculation accuracy highly depends on the measurements used for beam modeling. Depending on their characteristics, available detectors may be best suited for specific field sizes when measuring Output Factors (OF). Recent studies compare several active with passive detectors and MonteCarlo calculation.

The goal of our study is to evaluate the response of several active

detectors exposed to 6 MV X-ray beams of different sizes, down to 1x1 cm², while considering EBT3 Gafchromic films as reference.

Materials and methods

Eight EBT3 films were irradiated with field sizes ranging from 1x1 to 10x10 cm². Measurements were done in a home-made RW3 solid water phantom. Multichannel film dosimetry was used for film opacity-to-dose conversion. All films (including background) were irradiated and scanned simultaneously using the efficient protocol described by D. Lewis et al.

Among available active detectors, two ionization chambers and two diodes were studied. Measurements were carried out in a water phantom.

OF measurements were also done by placing both chambers in the solid water phantom, in the same condition as the films. Results were compared to measurements done in water in order to verify scattering components correspondence for all field sizes. This allows active detectors irradiated in water to be compared to the films in RW3 slabs.

Results

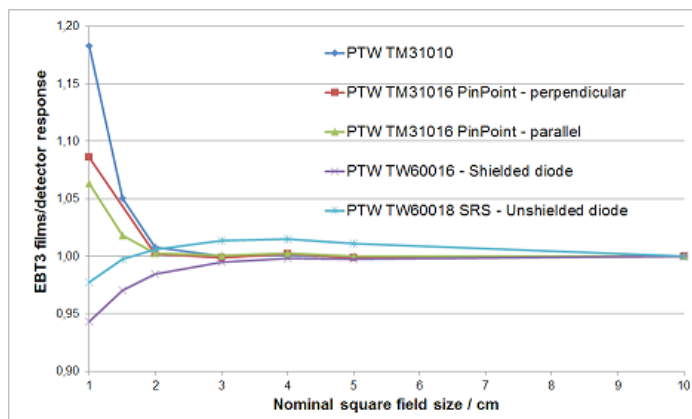


Figure 1

OF obtained with the ionization chambers placed in the water and solid water phantom are identical for field sizes smaller than 15x15cm².

As described in P. Andreo publication, active detector response for each field size was normalized with respect to the reference data. Figure 1 shows results. Concerning ionization chambers, the influence of partial volume averaging is similar to the published results. The three major effects mentioned for the diodes also appear in our results: the charged particles equilibrium between detector material and water, the over-response of the unshielded diode in broad beams and the partial volume averaging.

Conclusion

Our study confirms that partial volume averaging is not the only undesirable effect for OF measurement. Thus, the detector having the best spatial resolution is not systematically the best suited for small fields OF measurements.

SP068 - Development of New Methods in Therapy Dosimetry

TRACK 05: DOSIMETRY AND RADIATION PROTECTION

SP068.1 - A Farmer ion chamber as reference to the calibration of CT chambers

Author(s): Ricardo A. Terini¹, Marco A. Guedes Pereira², Maria Carolina S. Campelo¹

¹Depto. De Física, Pontifícia Universidade Católica de São Paulo, São Paulo/BRAZIL, ²Laboratório De Ensaios Não-destrutivos, Instituto de Energia e Ambiente, Universidade de São Paulo, São Paulo/BRAZIL

Introduction: Computed tomography (CT) is among the largest sources of collective radiation dose. The absorbed dose in CT exams can be ten times higher than in other common procedures of radiographic imaging. To assess the dose of radiation, the necessary meters should be properly calibrated in beams and setups like those measured in field [IAEA, Dosimetry in Radiology: An International Code of Practice, TRS 457, 2007]. AAPM TG111 report [AAPM, Comprehensive methodology for the evaluation of radiation dose in X-ray computed tomography. AAPM report 111, 2010] has proposed improved metrics for CT dosimetry, using a small ion chamber, mainly considering helicoidal and multislice scanning. This study aimed to improve the methodology for CT ion chamber calibration in standard dosimetry laboratories, inspired on IAEA and AAPM recommendations.

Methodology: Initially, CT standard beams (RQT) have been characterized, using a calibrated PTW Farmer chamber as reference. Then, we have investigated some options to the setup to calibrate CT "pencil" type chambers in Air kerma-length product (PKL) by substitution: without any collimator (A) or with a reference collimator of aperture L=2cm (B.2) or L=5cm (B.5) in front of the chamber to be calibrated (Fig.1). Additionally, homogeneity of the pencil chamber response was checked shifting the chamber perpendicularly to the beam, behind the collimator, 1 by 1cm, and repeating the calibration with B.2 setup.

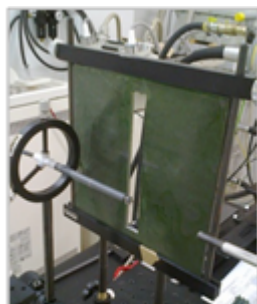


Figure 1 – Setup detail for the CT chamber calibration.

Results and Discussion: Table 1 summarizes the obtained results for 100mm PTW chamber calibration coefficients. Results showed differences up to 2% in the obtained calibration coefficients, depending on the aperture of the used collimator. In the following additional tests, pencil chamber homogeneity just kept up to 3.5cm from the chamber center. Results were very similar for other CT chambers from Radcal Co..

Table 1 – Example of a 100mm CT pencil chamber calibration against the 0.6 cc Farmer reference chamber, for RQT beams, with and without collimation (methods B and A).

Standard beam	PPV (kV)	HVL (mmAl)	NPKL-user (A)	NPKL-user (B.2) (L=2 cm)	NPKL-user (B.5) (L=5 cm)
RQT 8	100.07	6.90	1.003(27)	0.983(20)	0.982(17)
RQT 9	120.03	8.40	1.023(26)	1.001(19)	1.004(16)
RQT 10	149.80	10.10	1.008(27)	0.987(19)	0.992(17)

SP068.2 - Determination of the Uncertainty in the Cross-calibration of an Ionization Chamber Used in Radiation Therapy

Author(s): Pedro H.B. Cardoso¹, Wellington F.P. Neves-Junior¹, Gustavo F. Tietz¹, Cecília M.K. Haddad¹, Ricardo A. Terini²

¹Radioterapia, Sociedade Beneficente de Senhoras Hospital Sírio-Libanês, São Paulo/BRAZIL, ²Depto. De Física, Pontifícia Universidade Católica de São Paulo, São Paulo/BRAZIL

It was performed an analysis of the uncertainties involved in a cross-calibration procedure of an ionization chamber used in Sírio-Libanês Hospital, according to the methodology proposed in IAEA-TEC-DOC-1585, based on ISO GUM. The overall uncertainty obtained was 2,55% (coverage factor k = 2), which meant an increase of 0,04% compared to the reference ionization chamber uncertainty reported by the dosimetry laboratory of LCI-GMR-IPEN/CNEN-SP. In such cases where the uncertainty of the calibration coefficient of the reference instrument is high, this uncertainty dominates the overall uncertainty of the cross-calibration. It was performed an analysis of the uncertainties involved in a cross-calibration procedure of an ionization chamber used in Sírio-Libanês Hospital, according to the methodology proposed in IAEA-TECDOC-1585, based on ISO GUM. The overall uncertainty obtained was 2,55% (coverage factor k = 2), which meant an increase of 0,04% compared to the reference ionization chamber uncertainty reported by the dosimetry laboratory of LCI-GMR-IPEN/CNEN-SP.

Quantity, source of uncertainty	Value of the quantity	Expanded uncertainty U_i	Uncertainty type	Confidence level	Coverage factor k	Standard uncertainty u_i	Sensitivity coefficient c_i	Uncertainty Component $ c_i \cdot u_i $	Degrees of freedom ν_i
Calibration coefficient for the reference instrument									
1. Calibration uncertainty	5.365 cGy/nC	2.51 %	B	95%	2	1.26 %	1.00	1.26	60
2. Stability		0.3 %	B	100%	1.73	0.17 %	1.00	0.17	3
Raw measurements with reference instrument									
3. Repetibility	11.72 nC	0.1 %	A	68%	1	0.06 %	1.00	0.1	9
4. Resolution		0.01 nC	B	100%	1.73	0.05 %	1.00	0.05	100
Raw measurements with user instrument									
5. Repetibility	11.73 nC	0.02 %	A	68%	1	0.02 %	1.00	0.02	9
6. Resolution		0.01 nC	B	100%	1.73	0.05 %	1.00	0.05	100
Temperature during reference readings									
7. Thermometer calibration	21.1 °C	1 %	B	95%	2	0.50 %	0.07	0.04	60
8. Thermometer resolution		0.1 °C	B	100%	1.73	0.27 %	0.07	0.02	100
9. Mean reading uncertainty		0 %	A	68%	1	0.00 %	0.07	0.00	3
Temperature during user readings									
10. Thermometer calibration	21.1 °C	1 %	B	95%	2	0.50 %	0.07	0.04	60
11. Thermometer resolution		0.1 °C	B	100%	1.73	0.27 %	0.07	0.02	100
12. Mean reading uncertainty		0 %	A	68%	1	0.00 %	0.07	0.00	3
Pressure during reference readings									
13. Barometer calibration	928.8 mbar	0 %	B	95%	2	0.00 %	1.00	0.00	60
14. Barometer resolution		0.1 mbar	B	100%	1.73	0.006 %	0.50	0.003	100
15. Mean reading uncertainty		0.03 %	A	68%	1	0.03 %	1.00	0.03	3
Pressure during user readings									
16. Barometer calibration	927.7 mbar	0 %	B	95%	2	0.00 %	1.00	0.00	60
17. Barometer resolution		0.1 mbar	B	100%	1.73	0.006 %	0.50	0.003	100
18. Mean reading uncertainty		0.04 %	A	68%	1	0.04 %	1.00	0.04	3
Positioning of reference instrument									
19. Depth measurement resolution	100 mm	0.1 mm	B	100%	1.73	0.06 mm	0.37 %/mm	0.02	100
20. Deviation from reference depth in phantom		0 mm	B	95%	2	0.00 mm	0.37 %/mm	0.00	3
Positioning of user instrument									
21. Depth measurement resolution	100 mm	0.1 mm	B	100%	1.73	0.06 mm	0.37 %/mm	0.02	100
22. Deviation from reference depth in phantom		0.04 mm	B	100%	1.73	0.02 mm	0.37 %/mm	0.01	10
Calibration coefficient for the user instrument									
Uncertainty of the calibration coefficient	5.350 cGy/nC	2.55 %	Combined	95%	2	1.27 %			63

SP068.3 - A study of uncertainties in the half-value layer measurement of a miniature kV x-ray source

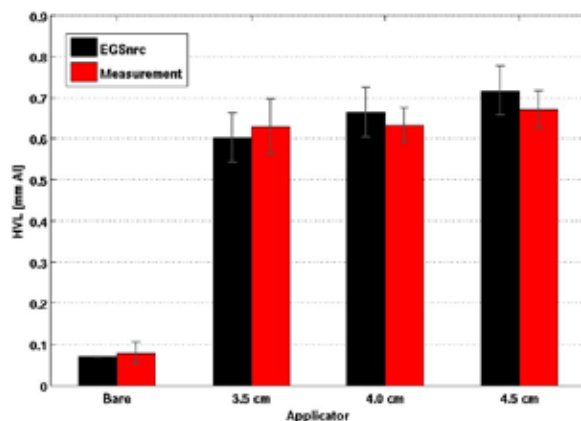
Author(s): Peter G. Watson, Marija Popovic, Jan Seuntjens
 Medical Physics Unit, McGill University, Montreal/CANADA

Air kerma standards for low energy x-ray devices used in electronic brachytherapy or intraoperative radiotherapy critically depend on accurate knowledge of the primary spectrum of the source. A model of a low energy x-ray source (INTRABEAM, Carl Zeiss) using the EGSnrc Monte Carlo (MC) code has been developed. To validate the model in-air, half-value layer (HVL) attenuation measurements were performed and compared with calculated values. For a meaningful comparison, the uncertainties in both the calculated and measured HVL must be well understood. In this work, we discuss the statistical and systematic uncertainties in HVL calculation.

The INTRABEAM source was modeled using the EGSnrc user code cavity. Photon fluence spectra emitted by the source were scored for the bare probe and spherical applicators of 3.5 cm, 4.0 cm, and 4.5 cm diameter. HVL was determined analytically from the simulated spectra by calculating the attenuation of air-kerma for a given thickness of aluminum and source-to-detector air gap. Beam collimation was provided by a lead cylinder surrounding the INTRABEAM source. Foils of high purity aluminum were placed at the exit of the collimator, and attenuation measurements were performed using a PTW 23342 parallel-plate chamber. The measured HVL was determined by curve fitting of the experimentally determined attenuation data. The statistical uncertainty in the MC-calculated HVL was determined by propagating the fluence spectrum uncertainty across the calculation of air-kerma ratio, taking into account photon cross-section uncertainty. The sources of MC systematic uncertainty considered were: the variation in polyetherimide (applicator material) density, collimator positioning error, and source-to-detector positioning error. In the experimental HVL measurement, the uncertainty was estimated by the tolerance

of aluminum attenuator thicknesses and the 95% confidence interval of the fitted attenuation curve. The accuracy of the HVL determination is a critical step in the reference dose calibration of

the INTRABEAM source. Our results indicate that the presence of the lead collimator, due to the emission of fluorescent x-rays, had a non-negligible effect on HVL measurement for the spherical applicators. In the MC calculation of spherical applicator HVLs, the collimator positioning error was found to be one of the dominant contributions to uncertainty ($\Delta HVL = 0.03 \text{ mm Al}$). For the simulated bare probe HVL, statistical errors and source-to-detector positioning contributed equally to the overall uncertainty. Upon comprehensive analysis of sources of experimental errors, we conclude that the simulated HVLs were in good agreement with measurement for the bare probe and spherical applicators.



SP068.4 - Low Energy Therapeutic X-Ray Calibration Methods

Author(s): Mehran M. Zaini, Adam R. Schoen, Lida M. Arvan, Edward I. Marshall, Gene E. Robertson, Caleb G. Beck, Anton L. Eagle, Lawrence E. Sweeney
Northwest Medical Physics Center, Lynnwood/UNITED STATES OF AMERICA

The application of low energy X-rays has recently increased in the dermatology workspace, with the generating tube potential of these radiation beams spanning from 10 to 70kV. Absolute calibration of these low energy radiation units from three different manufacturers has been conducted. Various low-energy calibration protocols were considered for calibrating the low energy beams of the X-ray tubes from three different manufacturers. These protocols included the American Association of Physicists in Medicine (AAPM) Task Group 61 Report (for 40-300 kV beams), the UK Code of Practice from the Institution of Physics and Engineering in Medicine and Biology (IPEMB) for very low-energy X-rays (8-50 kV), International Atomic Energy Agency (IAEA) Technical Reports Series No. 398 (for X-ray up to 100 kV), and Report 10 of the Netherlands Commission on Radiation Dosimetry for low energy X-ray (50-100 kV). Review and comparison of the methodology of these protocols, pertaining to the energy range of Grenz-rays to superficial X-rays, is conducted.

In general, standard calibration laboratories provide an in-air calibration factor, N_k (air-kerma in Gy), and/or an in-water calibration factor, ND_{w,Q_0} (absorbed dose to water in Gy). These factors can in turn be used in air or in a phantom in a clinical setting. The aforementioned protocols allow one or more of such calibration conditions. Because of the wider availability of N_k calibration factors from the US-based standard calibration laboratories and ease of using an in-air calibration technique for low-energy X-ray beams in a clinical setting, the AAPM-TG61 protocol and the data extracted from the British Journal of Radiology Supplement No. 25 were found to be the most practical for the calibration of low energy X-ray units for dermatological applications.

The issues with calibrating such low energies radiation units include having the appropriate equipment, creating a precise physical setup for measurements, and the low SNR when performing HVL measurements. The HVL setup needs to be stable and precise, due to the sensitive nature of these measurements. An air gap between the chamber and the source at these low energy units can change the results significantly. For example, a one millimeter air gap between a specially designed parallel-plate chamber and one of these low-energy X-ray producing units can cause an error in the order of 3%.

SP068.5 - Energy response of a thimble-type ionization chamber for Ir-192 and Co-60 radiation beams

Author(s): Cecilia Kessler, David Burns
BIPM, Sèvres/France

A new international comparison for primary determinations of reference air-kerma rate using Ir-192 brachytherapy sources has been established by the Bureau International des Poids et Mesures (BIPM) and registered in the BIPM Key Comparison Data Base (KCDB) as an ongoing key comparison under the reference BIPM.RI(I)-K7.

The participants in this key comparison, the National Metrology Institutes NMIs, calibrate a thimble-type ionization chamber, model NE 2571, under reference conditions following the corresponding protocol. The comparison result, and thus the degree of equivalence between the NMI and the BIPM, is based on the ratio of the NMI calibration coefficient to that of the BIPM, the latter chosen as the Key Comparison Reference Value (KCRV).

As the BIPM has no primary facility for Ir-192 brachytherapy sources, the reference value is evaluated from the calibration coefficient

of the ionization chamber determined in the BIPM reference Co-60 beam, with a correction factor k_{en} applied to account for the energy dependence of this type of chamber.

This correction factor is calculated using the Monte Carlo code Penelope [1]. The simulation of the chamber (dimensions, shape and materials) was made using the geometry code Pengeom, based on the manufacturer data sheet for the chamber. Using this code, a typical Ir-192 source used for therapy with its encapsulation was simulated.

In the first step the user code simulates the energy spectrum of the Ir-192 source and creates a phase-space file at 5 cm from the source reference point, recording the energy, spatial coordinates and direction of each particle. This file is used in the second step as an input to calculate the calibration coefficient of the ionization chamber at 1 m from the source.

Similarly, the calibration coefficient of the ionization chamber is evaluated for the Co-60 beam, using as input the existing phase-space file corresponding to the BIPM reference beam.

The correction factor k_{en} for the NE 2571 ionization chamber is determined as the ratio of the calibration coefficient evaluated for Ir-192 to that for Co-60. Supporting calculations are made to estimate the uncertainty of k_{en} . The results are compared with published work.

[1] Salvat, F., Fernandez-Varea, J.M., Sempau, J., Penelope – A Code System for Monte Carlo Simulation of Electron and Photon Transport, OECD 2009 NEA No. 6416 (ISBN 978-92-64-99066-1).

SP068.6 - Kilo-voltage X-Ray tube dosimetry Correction factors for in-water measurement in TG-61

Author(s): Nima Sherafati¹, David W.O. Rogers²

¹Physics, Carleton Laboratory for Radiotherapy Physics, Carleton University, Ottawa/ON/CANADA, ²Physics, Carleton Laboratory for Radiotherapy Physics, Carleton University, Ottawa/CANADA

For x-ray tube potentials > 100 kV, the AAPM TG-61 protocol for 40-300 kV x-ray beam dosimetry in radiotherapy recommends an in-water measurement which is based on ionization chambers calibrated in air in terms of air kerma. We studied the variation of the overall correction factor (PQch) and its components (known as corrections for the change in the chamber response due to the change in the spectrum distribution in phantom compared to that used for the calibration in air (kQ), displacement of water by the ionization chamber (Pdis) and displacement of water by the stem (Pstem)) as well as the correction for a waterproofing sleeve (Psheath) with depth and field size for 6 different beam qualities in the orthovoltage x-ray range (100 kV < tube potential < 300 kV). Based on TG-61, the absorbed dose to water at the reference depth (2 cm) is given by : $D_{w,z} = M N_k P_{Qch} P_{sheath} [(\mu_{en}/\rho)_{water}^{air}]_{water}$, where $P_{Qch} = kQ P_{dis} P_{stem}$, M is the fully corrected chamber reading, N_k is the air kerma calibration coefficient for a beam's quality, and $[(\mu_{en}/\rho)_{water}^{air}]_{water}$ is the ratio for water-to-air of the mean mass energy-absorption coefficient, averaged over the photon spectrum at the reference point in water in the absence of the chamber. In contrast with the EGS4 based values used in TG-61, we used the EGSnrc Monte Carlo system, which has a systematic uncertainty of ± 0.1 percent while the values of TG-61 had been calculated using EGS4 which had ± 1 percent systematic uncertainty for ionization chamber calculations. In addition we used the exact geometries of ionization chambers (e.g. NE2571) and better statistics (up to 10^{11} histories for each simulation giving statistical uncertainties of less than ± 0.1 percent) which made an improvement in the correction factor's precision. The results show a maximum 1.5 percent variation of P_{Qch} with depth (2 cm to 8 cm) and field size (20 cm² to 100 cm²) for the NE2571 ionization chamber while the P_{sheath} correction

factor is insignificant. The new values agree well with TG-61 values which demonstrates that the systematic uncertainties in EGS4 cancelled out since the factors are all ratios. Due primarily to its high-z electrode, the variation of PQch with depth and field size for the Exradin A16 ionization chamber is up to 10 percent and the variation with beam quality is up to 40 percent. This suggests ionization chambers with high-z electrodes should not be used for x-ray dosimetry. Depth and field size dependence of the PQch for the Exradin W1 scintillator detector are also being studied.

SP069 - Novel Detectors, Phantoms and Software, Diagnostic Techniques

TRACK 06: NEW TECHNOLOGIES IN CANCER RESEARCH AND TREATMENT

SP069.1 - Synergistic Action of Ionizing Radiation with Platinum-based Chemotherapeutic Drugs: Soft X-rays and Low-Energy Electrons

Author(s): Elahe Alizadeh¹, Mohammad Rezaee², Darel Hunting³, Leon Sanche³

¹Department Of Chemistry And Biochemistry, University of Guelph, Guelph/CANADA, ²Princess Margaret Cancer Centre, Department Of Radiation Oncology, University of Toronto, Toronto/CANADA, ³Département De Médecine Nucléaire Et Radiobiologie, Faculté De Médecine Et Des Sciences De La Santé, Université de Sherbrooke, Sherbrooke/QC/CANADA

The biological impact of ionizing radiation results predominantly from the induction of a variety of lesions in cellular DNA via energy deposition into the DNA itself (direct effect) and its surrounding molecular environment (indirect effect) [1]. The most numerous of intermediate species arising from the direct effect of radiation are non-thermal secondary electrons [2], most of which having energies below 30 eV (i.e., low-energy electrons, LEEs). In the present study, we report results to evaluate the direct effect of ionizing radiation on the formation of both single and cluster lesions in a supercoiled plasmid DNA covalently modified by the platinum anticancer drugs (Pt-drugs) cisplatin, carboplatin and oxaliplatin. Since these Pt-drugs sensitize malignant cells to ionizing radiation, they are currently used in concomitant chemoradiotherapy for cancer treatment; however, the specific mechanisms of the interaction between these Pt-drugs bound to DNA and radiation still remain to be determined [3,4].

Freeze-dried nanoscale films (~10 nm) of either pure DNA or a Pt-drug covalently bound to DNA were prepared onto two different types of substrates, i.e., tantalum and glass surfaces. Samples were exposed to 1.5 keV X-rays, in the presence of dry nitrogen gas and no humidity [5]. The yields of single- and double-strand breaks (SSBs and DSBs) and interduplex cross links (CL) induced in both types of films by X-rays and the spectrum of photo-electrons emitted from tantalum were determined from the initial linear slopes of respective exposure-response curves. In addition, the ratios of the yields from the two different films were determined and referred as an enhancement factor (EF) to represent radiosensitization by the Pt-drugs.

Results presented in Table 1 clearly show that Pt-drugs substantially enhance the formation of DSB and CL in DNA irradiated by X-rays and LEEs, but have virtually no effect on SSB formation. Furthermore, the EFs for DSB and CL are larger for LEEs than X-rays in the presence of Pt-drugs. Since LEEs constitute a major portion of the secondary species generated by high-energy radiation, our finding suggests that in the presence of Pt-adducts, LEEs are the main secondary species responsible for the increase of DSB and CL in the irradiated platinated DNA via the direct effect. According to the linearity of the exposure-response curves, these damages result from a single-event process. Despite similarity between Pt-drugs in the enhancement of the DNA lesions, carboplatin and then oxaliplatin have higher efficiency than cisplatin in the radiosensitization of DNA.

Table 1. Yields of DNA damage ($\times 10^{-8}$ damage/Gy/bp) for soft X-rays and LEEs irradiation of DNA with and without modification by platinum anticancer drugs.

Irradiation	DNA Damage	Pure DNA	Cisplatin-DNA	Carboplatin-DNA	Oxaliplatin-DNA
X-ray	SSB	199.0±25.3	204.0±26.8	237.2±29.7	215.3±37.3
	DSB	ND	4.9±0.8	7.0±1.0	5.4±0.7
	CL	5.1±0.7	6.9±0.8	7.1±0.6	7.0±0.5
LEEs (0-30 eV)	SSB	65.0±6.3	78.2±8.4	84.2±15.1	89.8±14.2
	DSB	ND	19.9±2.8	24.4±2.4	21.5±3.3
	CL	2.2±0.4	5.2±0.5	7.4±2.0	9.0±2.7

• ND: Not Detected

References

- [1] E. Alizadeh and L. Sanche. *Chem. Rev.* **112**: 5578-5602 (2012).
- [2] S. M. Pinblott and J. A. LaVerne. *Radiat Phys Chem* **76**: 1244-1247 (2007).
- [3] Y. Jung, S.J. Lippard. *Chem. Rev.* **107**: 1387-1407 (2007).
- [4] M. Rezaee, D.J. Hunting and L. Sanche. *Int. J. Radiat. Oncol. Biol. Phys.* **87** (4): 847-853 (2013).
- [5] E. Alizadeh, P. Cloutier, D. J. Hunting and L. Sanche. *J. Phys. Chem. B* **115** (15): 4523-4531 (2011).

SP069.2 - Cherenkov emission dosimetry for electron beam radiotherapy: a Monte Carlo feasibility study of absolute dose prediction

Author(s): Yana Zlateva¹, Issam El Naqa²

¹Medical Physics Unit, McGill University, Montreal/CANADA, ²Medical Physics Unit, McGill University, Montreal/QC/CANADA

Current electron beam dosimeters face two major challenges. They are not water/tissue equivalent, and therefore require conversion to dose to water/tissue. Moreover, they must be placed in the radiation beam, which results in beam perturbation and dose averaging. These challenges limit their spatial resolution for intensity-modulated delivery or *in vivo* dosimetry. Yet, Cherenkov radiation by high-energy charged particles is emitted in water and in tissue, can be detected outside the beam, and is inherent to all high-energy radiotherapy beams. Despite these advantages, Cherenkov emission has yet to be implemented for clinical dosimetry. The work presented here investigates via first-principles derivation and Monte Carlo simulation the feasibility of absolute Cherenkov dosimetry for electron beam radiotherapy. A quantitative model for predicting absolute dose from Cherenkov intensity in a phantom was derived from first principles for high-energy charged particles of known incident energy with the assumption that all collisional energy loss is absorbed and all radiative energy loss escapes. The model was validated via simulation of 260 keV - 18 MeV electrons incident on water. Monte Carlo simulations were carried out in Geant4. The absolute Cherenkov dosimetry model presented here was able to predict absolute dose from Cherenkov intensity to within a clinically viable uncertainty of less than 3%.

SP069.3 - Detection of melanoma through image recognition and artificial neural networks

Author(s): Cristofer I. Marín¹, Germán H. Alférez¹, Jency Córdova², Verónica González²

¹Global Software Lab, Universidad de Morelos, Morelos, Mexico, ²Departamento De Apoyo A La Investigación De Ciencias En Salud, Universidad de Morelos, Morelos, Mexico

The incidence of malignant melanoma has significantly increased in the last four decades. Dermatologists are rarely present in rural

or remote areas to perform an early detection of malignant melanoma. Our contribution is a low cost software that automatically and objectively differentiates between a melanoma lesion and a benign nevus in a simple, noninvasive manner. Our approach is based on the "ABCDE" classification of lesions, image processing, and artificial neural networks. The software was developed using images of previously diagnosed malignant melanomas and non-malignant suspicious moles, obtaining a sensibility of 76.56% and a specificity of 87.58%.

SP069.4 - Clinical Implementation of an Intraoperative Radiotherapy Program

Author(s): Muthana Al-Ghazi¹, Varun Sehgal¹, Dante Roa¹, Suhong Yu¹, Qichi He¹, Jeffrey Kuo¹, Erin Lin², Alice Police²

¹Radiation Oncology, University of California, Irvine, Orange/UNITED STATES OF AMERICA, ²Surgery, University of California, Irvine, Orange/CA/UNITED STATES OF AMERICA

Purpose: To outline the process for setting up an intraoperative radiotherapy (IORT) program and its clinical implementation, including dosimetric data, radiation safety aspects and clinical procedures.

Background: IORT has been used in the past for clinical indications such as in the management of localized abdominal tumors. Where applicable, it is efficient and convenient as the radiation treatment is completed at the time of surgery. The modality was almost abandoned except for select large institutions due to the high cost incurred in installing dedicated linear accelerators and orthovoltage units and the requirement for extensive shielding of specially designed operating rooms.

Advances in design of miniaturized x-ray tubes operating at 50 KVP initiated resurgence of interest in this modality. The Zeiss system (Zeiss Inc., Jena, Germany) consists of a portable 50 KVP x-ray tube that is mounted on a robotic arm with 6 degrees of freedom. A sterile applicator is mounted on it and the latter is placed at the tumor bed for dose delivery. Accuracy of applicator position is verified using ultrasound image guidance. A 1 mm sterile tungsten (W) shield is wrapped around the applicator. The shield reduces the radiation levels in the room by a factor of 10³. The procedure can be safely performed in a regular operating room.

Methods: The dosimetric characteristics of the system are confirmed using a parallel plate chamber connected to an electrometer. Measurements are made in a specially designed water phantom. Clinical dose calculations are carried out using these parameters. A check list is developed for quality assurance and safety measures consistent with institutional requirements and manufacturer's recommendations for safe and accurate delivery of radiation treatment following accepted treatment protocols.

Importantly, a radiation survey is carried out around the operating room where IORT procedures take place to ascertain safe levels of exposure to personnel who are not classified as radiation workers. This is easily achieved using the W shield alluded to above.

Results: Dose delivery to patients undergoing IORT using the procedure outlined above can be carried out safely in a regular operating room. The exposure levels in adjacent areas are comparable to background. The procedure is cost effective due to the portability of the system and the low energy of the x-ray emission. Clinically, the system has been used to treat localized early breast tumors and abdominal sites. Detailed dosimetric, radiation safety and clinical data pertaining to the program will be presented.

Conclusion: An IORT program has been implemented at the University of California, Irvine Medical Center for the treatment of breast and abdominal tumors. The approach is convenient to patients as it delivers the radiation treatment at the time of surgery. This is espe-

cially important for patients who have to travel significant distances to radiotherapy centers.

SP069.5 - Performance of a Back-etched Silicon Detector Array Designed to Monitor Each Synchrotron Generated X-ray Beam in Microbeam Radiation Therapy

Author(s): Michael L.F. Lerch

Centre For Medical Radiation Physics, University of Wollongong, Wollongong/AUSTRALIA

Introduction: In Microbeam Radiation Therapy (MRT) the dose rate is ~20,000 Gy/sec. For patient safety, the system must provide real-time feedback to instigate a beam dump if the dose rate moves out of the desirable range.

Purpose: The 3DMiMiC project aims to develop multistrip silicon sensors with parallel readout for use in real-time treatment monitoring of each X-ray microbeam.

Methods and Materials: Silicon array sensors were designed at the Centre for Medical Radiation Physics, University of Wollongong, Australia, simulated using ISE TCAD at the Department of Physics and Technology, University of Bergen, Norway, and fabricated at the SINTEF MiNaLab facility, Norway. Detector tests were carried out at the X-ray Microscopy Beamline, ESRF, France and system testing was done under full MRT conditions at the biomedical beamline, ESRF.

Results:

Figure 1 shows the design (left) optical image (middle) and effective sensitive volume (red/yellow region in right image) when operated at -30 V bias. The central strips are surrounded by a common guard ring structure (clearly visible in the optical and combined fluorescence-charge collection image). The effective volume is extremely well confined to minimise any cross talk between sensor strips (pitch 100 microns).

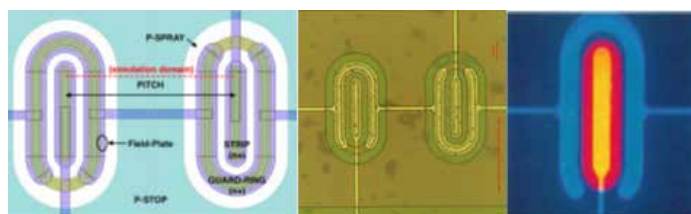


Figure 1.

Figure 2 (left) shows the response of 128 strips when exposed to 32 X-ray microbeams of pitch 102 microns. For every exposed strip, 3 strips are unexposed. The observed roll off in intensity is due to detector-microbeam pitch mismatch. Figure 2 (right) shows the temporal response of a strip in (black) and out (red) of the beam. The signal to noise ratio is excellent (integration time for each point is 14 microseconds).

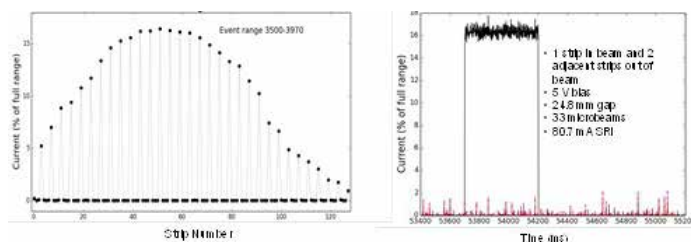


Figure 2.

Conclusion:

A new back-etched silicon detector array has been developed and characterised. Initial testing of the array integrated into a real-time microbeam monitoring system, shows very promising results.

SP069.6 - Dynamic Mechanical Characterization of a Poly(vinyl alcohol) Breast Palpation Phantom

Author(s): Gabriel A. Rodriguez

Carnegie Mellon University, Pittsburgh/UNITED STATES OF AMERICA

Breast phantoms model quantitative and qualitative parameters of bulk tissues to provide a foundation for the calibration and design iteration of different imaging methodologies, particularly for breast cancer screening. Existing breast phantoms can accurately emulate specific properties of tissues for conventional imaging modalities such as MRIs or ultrasound, but are inadequate for the large deformations associated with mechanical palpation. Polyvinyl alcohol (PVA) cryogels provide a unique solution because of stability at large deformations, although current cryogel processing methods suffer from inhomogeneity for large structures such as tissue phantoms. Established cryogel fabrication protocols tune the specific mechanical properties of PVA cryogels by varying concentration of PVA in the solution and the number of freeze-thaw cycles that the cryogel undergoes. Chaotropic salt inclusions in PVA promote amorphous behavior in the cryogels, resulting in an increase in the homogeneity to the bulk mechanical properties of the phantom. This study evaluates the effects of varied salt concentrations on the dynamic mechanical properties of cryogels to improve the stability of mechanical breast tissue phantoms. The elastic and viscoelastic properties of conventional cryogels are compared to cryogels with salt inclusions using dynamic loading. To characterize the tissue analogs for clinical utility, the experimental protocol uses simple compression, large deformations, and strain rates equivalent to those used in clinical palpation. Results are compared with literature values for fatty and fibroglandular breast tissues; the major constituents of the breast. By improving the homogeneity of PVA cryogels with the use of salt inclusions, this work builds on existing tissue analog technologies. The storage and loss moduli from the large deformation, dynamic mechanical analysis of the adapted cryogel technique described here are compared with literature values for both fatty and fibroglandular breast tissues. Further development of mechanically-accurate and multi-modal breast phantoms will provide low-cost and safe alternatives to clinical trials for the validation of developing breast imaging technologies.

SP070 - Molecular Imaging PET/SPECT: Part 2

TRACK 01: IMAGING

SP070.1 - Optimal Pixelated Crystal for a Molecular SPECT

Scanner: A GATE Monte Carlo Study

Author(s): Mohammad Reza Ay¹, Hojat Mahani², Gholamreza Raisali², Alireza Kamali Asl³

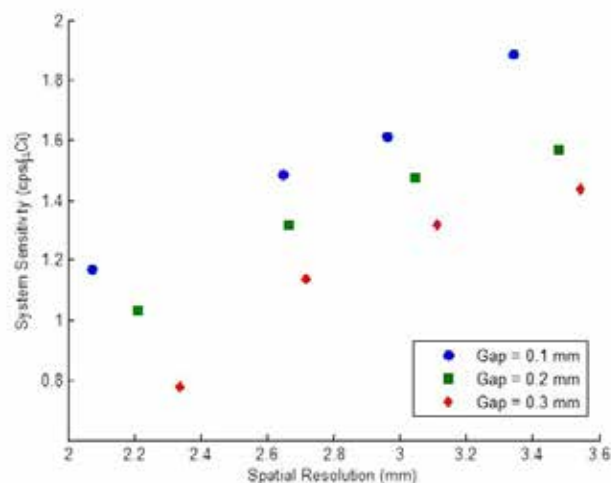
¹Department Of Medical Physics & Biomedical Engineering, Tehran University of Medical Sciences, Tehran/IRAN, ²Radiation Application Research School, Nuclear Science and Technology Research Institute, Tehran/IRAN, ³Shahid Beheshti University, Medical Radiation Faculty, Tehran/IRAN

Objective: It is well-known that resolution-sensitivity tradeoff is the most challenging design consideration in small-animal SPECT. In the present work, we addressed such a compromise from pixelated crystal point-of-view for HiReSPECT system, a high-resolution SPECT camera, developed at Research Center for Molecular and Cellular Imaging.

Materials and Methods: For this purpose, we performed GATE Monte Carlo package to simulate the HiReSPECT scanner and to assess the impact of various crystal configurations on tomographic resolution and system sensitivity, using a ^{99m}Tc point-like source and a flood-filled phantom, respectively. The crystals differed in material, pixel-size, and Epoxy pixel-gap. Point-spread-functions (PSFs) were iteratively reconstructed using a dedicated 3D OSEM algorithm. Equal importance factors were assigned to the two conflicting objectives, and pixelated crystal was then optimized using the weighted-sum method. In addition, the Monte Carlo simulations were validated by means of comparisons with the experimental data.

Results: A good agreement (4.3% difference) between simulated and measured tomographic spatial resolutions at 30 mm radius-of-rotation is observed. Likewise, there is a maximum 9.1% difference, at 120 mm source-to-collimator distance, between our Monte Carlo calculations and the experiments for system sensitivity, all for a 1 × 1 mm² pixel-size and 0.2 mm Epoxy gap CsI(Na) configuration. The results show that CsI(Na) exhibits the highest sensitivity compared to NaI(Tl) and YAP(Ce) as well as a slightly higher spatial resolution, and therefore is the crystal of choice. A sensitivity of 1.61 cps/μCi is achieved for a 1.5 × 1.5 mm² pixel-size and 0.1 mm Epoxy gap CsI(Na)-based camera. Changing pixel-size from 0.5 × 0.5 mm² to 2 × 2 mm² leads to a 35.7% loss in tomographic resolution while sensitivity improves by a factor of 1.52. Based on our Monte Carlo optimization, the 1.5 × 1.5 mm² pixel-size and 0.1 mm Epoxy gap CsI(Na) is the optimal configuration by providing the best tradeoff between spatial resolution and system sensitivity. The crystal-optimized HiReSPECT system also offers a tomographic resolution of 2.98 mm, in terms of FWHM.

Conclusion: Our findings highlighted that performance of a preclinical SPECT imager can be highly affected by the pixelated scintillator configuration, and thereby searching for an optimum configuration is mandatory in order to obtain a more qualified SPECT image.



SP070.2 - Spinning Knife-Edge Slit-Hole: a Novel Collimation for High-Sensitivity Molecular SPECT

Author(s): Hojjat Mahani¹, Gholamreza Raisali², Alireza Kamali Asl³, Mohammad Reza Ay¹

¹Research Center For Molecular And Cellular Imaging, Tehran University of Medical Sciences, Tehran/IRAN, ²Radiation Application Research School, Nuclear Science and Technology Research Institute, Tehran/IRAN, ³Radiation Medicine Engineering Department, Shahid Beheshti University, Tehran/IRAN

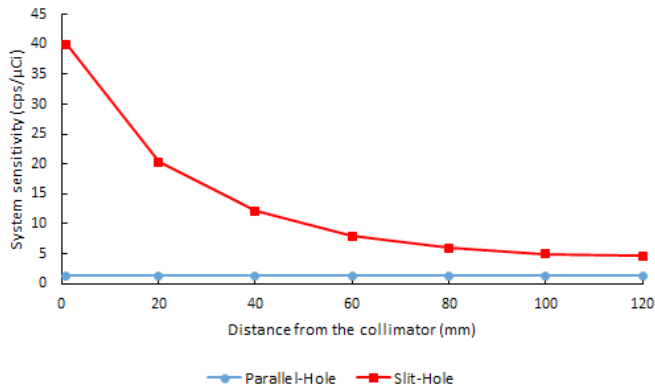
Objective: While conventional collimation systems are widely used in molecular SPECT, such collimators usually limit performance of the camera due to owing a low geometric efficiency. In the present study, we addressed this challenge by proposing a novel collimator offering a high-sensitivity HiReSPECT system, a high-resolution SPECT camera, developed at Research Center for Molecular and Cellular Imaging.

Materials and Methods: For this purpose, we performed GATE Monte Carlo toolkit to design and simulate the collimator for the HiReSPECT scanner. The prototype consists a centered single knife-edge slit-hole of 1.2 mm width extended across long-axis of camera's head, with 30 mm collimator's depth. Planar spatial resolution and in-air sensitivity were assessed at various distances using a ^{99m}Tc point-like source and a flood-field phantom, respectively. At each regular SPECT angle, 16 spin-projections over 180° were then acquired each with 3.75 s time-per-spin. The planar images were iteratively reconstructed using a dedicated MLEM-based algorithm. To speed up our Monte Carlo simulations, a variance reduction technique by ignoring transport of the secondary electrons was also implemented.

Results: Slit-hole geometry give rise to an increased background-subtracted sensitivity of 12.4 times that observed with parallel-hole collimator at 30 mm source-to-collimator distance. System sensitivity with slit-hole collimator falls off as filed-of-view of the camera increases and reaches to a value of 4.6 cps/μCi at 120 mm distance while sensitivity of the system with parallel-hole collimation remains approximately constant over all distances from the collimator and has a value of 1.32 cps/μCi. Slit-hole collimated HiReSPECT scanner provides a magnification factor of 3 and offers a planar spatial resolution, in terms of FWHM, of 3.32 mm compared to 2.91 mm obtained by a parallel-hole collimation, at 10 mm source-to-collimator distance. Implementation of the variance reduction technique in our Monte Carlo simulations results in a 1.51 acceleration factor while imposes no significant effect on spin-projection data.

Conclusion: Our preliminary findings highlighted that the spinning

slit-hole is a promising alternative for parallel-hole collimators with acceptable planar spatial resolution, and therefore the proposed collimator provides a better resolution-sensitivity tradeoff.



Comparison of system sensitivity for the parallel-hole and the slit-hole collimated HiReSPECT scanner. For the slit-hole collimation, the sensitivity is background-subtracted.

SP070.3 - Simultaneous estimation of the radioactivity distribution and electron density map from scattered coincidences in PET: A project overview

Author(s): Hongyan Sun¹, Mohammadreza Teimoorisichani¹, Bryan Mcintosh¹, Geng Zhang¹, Harry Ingleby², Andrew Goertzen¹, Stephen Pistorius¹

¹Physics And Astronomy, University of Manitoba, Winnipeg/CANADA, ²Radiology, University of Manitoba, Winnipeg/MB/CANADA

Quantitatively accurate PET images require correction of measured data for scattered coincidences. Additionally, an anatomical image is required to provide accurate attenuation correction and to facilitate the interpretation of the activity distribution. By taking advantage of accurately measured photon energies and the kinematics of Compton scattering, a 2D surface described by two circular arcs (TCA), which define the possible scattering loci and encompasses the annihilation position, can be identified. In 3D the annihilation is confined to the volume encompassed by the surface obtained by rotating the 2D arc around its axis. Using this premise, we have developed novel iterative reconstruction algorithms which use the scattered coincidences to 1) improve the activity distribution and 2) obtain an electron density map. The results have demonstrated the feasibility and benefits of incorporating scattered coincidences into the image reconstruction process. Incorporating scattered coincidences directly into the radiotracer reconstruction algorithm eliminates the need for scatter correction, and could improve both image quality and system sensitivity. The electron density map reconstructed from scattered coincidences can be directly applied to attenuation correction of the activity distribution, which removes energy scaling and registration problems.

SP070.4 - Generating a four-class attenuation map for MR-based attenuation correction of PET data in pelvis region using an automatic segmentation protocol

Author(s): Hamid Saligheh Rad¹, Mehdi Shirin Shandiz¹, Pardis Ghafarian², Mohamad H. Arabi¹, Mehرداد Bakhshayeshkaram², Naser Shafiei³, Mohammad Reza Ay¹

¹Research Center for Molecular and Cellular Imaging, Tehran University of Medical Sciences, Tehran/IRAN, ²Chronic Respiratory Diseases Research Center, National Research Institute Of Tuberculosis And Lung Diseases (nritld), Shahid Beheshti University of Medical Sciences, tehran/IRAN, ³Imaging Center, Payambaran Hospital, tehran/IRAN

Introduction: It is well known that prostate imaging is one of the killer applications of PET/MRI systems. The main challenge of the current PET/MRI systems in this region field is inaccurate attenuation map (μ map), due to the fact the attenuation coefficients of the tissues are considered as soft tissue or fat in the generated μ maps. This issue leads to overestimation of the tracer uptake in the air cavities of rectum and bowel as well as underestimation of the tracer uptake in bone and adjacent areas to bone in the corrected PET images, especially in regions with thick cortical bones. The aim of this study is to increase the number of tissue classes of μ map in the pelvic area from one class or two classes in currently available PET/MRI scanners to four classes, namely cortical bone, air, soft tissue and fat, by means of a full automatic method. The proposed method consists of a combination of imaging technique, along with an image segmentation protocol.

Material and Methods: The proposed imaging technique was STE (short echo time) that it set on a clinical 1.5T scanner in the pelvis area of two volunteer. The acquisition parameters were 1.31 ms and 60 ms for TE and TR, respectively, with Ernest angle of 15°. The image processing protocol includes five major steps as follows: (I) intensity-inhomogeneity correction; (II) separation of cortical bone and air from other regions using a region-base level set method; (III) separation of cortical bone and air areas using shape analysis method, based on morphological characteristic including level of circularity and symmetry; (IV) separation of soft tissue and fat using thresholding and (V) generation of μ map. The validation of the proposed method was based on comparison with the μ maps generated by CT images as gold standard.

Results: Figure 1, shows acceptable performance the proposed method in segmentation and generation four-class μ map. Quantitative analysis on dice and sensitivity factor are 71% and 65% respectively in cortical bone segmentation as well as 78% and 76% in air segmentation and 82%, 93% respectively, for fat segmentation.

Discussion: The proposed strategy in this study showed that the four-class μ -map can be successfully generated from only one STE-MR image in order to save time, following by the proposed six steps protocol. The proposed method can be a potential alternative to Ultra short echo time (UTE) MR-based attenuation correction, particularly in more common hybrid PET/MRI systems.

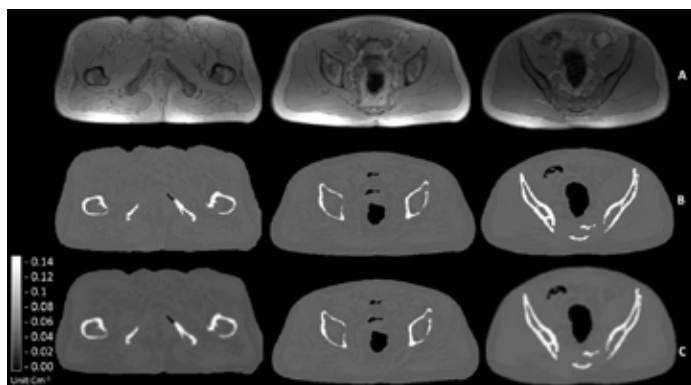


Fig 1. MR image(rowA);segmented image(rowB); μ map(rowC)

SP070.5 - Extracting PET activity distribution from scattered coincidences for non-ideal energy resolutions by modeling the probabilities of annihilation positions within a generalized scattering reconstruction algorithm

Author(s): Hongyan Sun¹, Stephen Pistorius²

¹Physics And Astronomy, University of Manitoba, Winnipeg/MB/CANADA, ²Radiology, University of Manitoba, Winnipeg/MB/CANADA

Scattered coincidences degrade PET images contrast and compromise quantitative accuracy, and corrections for this are required in conventional PET reconstruction algorithms. In contrast to this approach, we have developed an algorithm that extracts the radioactivity distribution by incorporating scattered coincidences into the reconstruction. Using the kinematics of Compton scattering, two circular arcs (TCA), as shown in Fig.1(a), describe the locus of all possible scattering positions and encompass the annihilation position for a scattered coincidence. PET images can be reconstructed from scattered coincidences by projection and backprojection within the area confined by the TCA if the detectors have perfect energy resolution. In our previous work, the varying probability of the annihilation position within TCA is not modeled and a uniform distribution is assumed. In practice, the estimated annihilation position is sensitive to the energy resolution of the detector, which limits the implementation of the proposed algorithm on existing clinical PET scanners. In this work, the probability map of annihilation positions within the TCA is modeled in a normalized coordinate system (See Fig. 1(b)). This map was blurred in the vertical direction to account for the non-ideal energy resolution of the system (see Fig.1(c)), and was incorporated into the generalized scattered (GS) reconstruction algorithm. The results demonstrated that by modelling the probabilities of the annihilation position within the TCA in a normalized coordinate system and by introducing this probability map into the reconstruction, the convergence of the reconstructed activity distribution is improved. The contrast for images generated from scattered events improved by 7% compared to those that did not include the probability distribution in the reconstruction (see Fig.2). For non-ideal energy resolutions of up to 6%, the proposed method improves the contrast and noise properties of the reconstruction.

Results: Simulations showed a k3 bias of 76% with precision of 82.7%, which improved to 9.5% and 23.5%, respectively, when DCE-CT measurements were incorporated into the model (1,000 runs, signal-to-noise ratio = 10). Results from the PC-3 mouse model (below) show that k3 functional maps exhibit significantly higher tumor-to-background ratios compared to SUV maps and distribution volume maps calculated via graphical analysis with the Logan Plot.

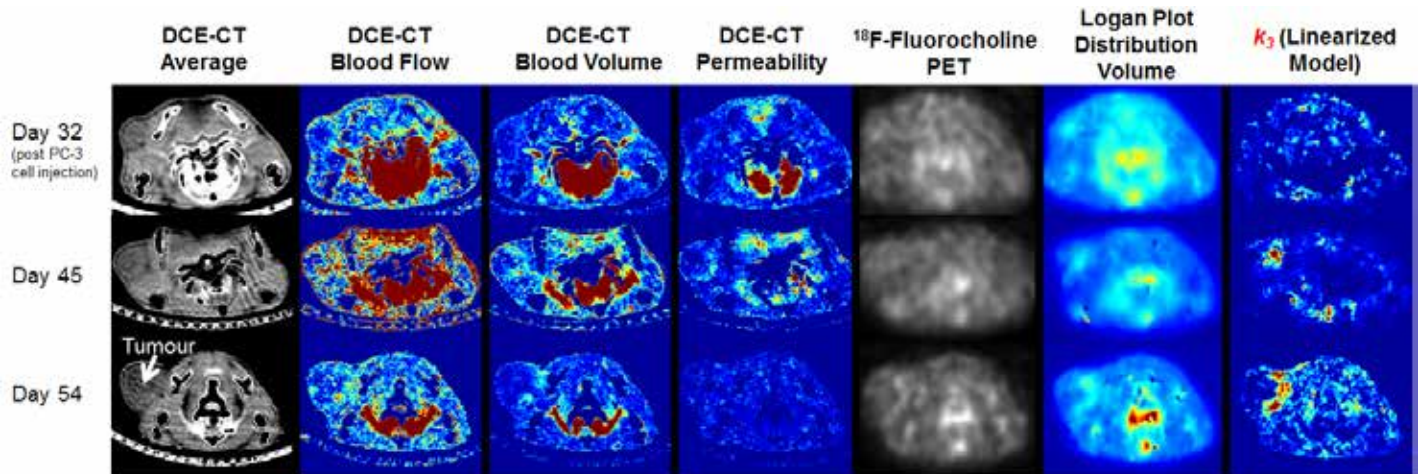
SP070.6 - Quantitative Functional Imaging with Hybrid PET-CT Via Improved Kinetics Modeling: Application to 18F-Fluorocholine PET Imaging of Prostate Cancer

Author(s): Adam Blais, Mark Dekaban, Jennifer Hadway, Ting Yim Lee

Lawson Health Research Institute, London/ON/CANADA

Motivation: ¹⁸F-Fluorocholine (FCH) PET imaging is of interest for the localization of prostate cancer and has the potential to allow more accurate targeting for both biopsy and intra-prostatic radiation dose escalation. However, studies using the standardized uptake value (SUV) have been unable to differentiate prostate cancer from benign prostatic hyperplasia. We hypothesize that this is due to the confounding effects of blood flow and blood volume in the local vasculature, which cannot be discriminated using the SUV. Quantitative kinetic analysis of FCH PET can account for this confounding effect by estimating the k3 parameter, which represents the activity of the choline kinase enzyme, but this is difficult because high parameter covariance reduces the robustness of the k3 estimate.

Methods: We developed a hybrid DCE-CT/PET kinetic model, which uses DCE-CT functional maps to reduce the effect of parameter covariance. Furthermore, this linearized model form is solved with a non-negative least squares algorithm which has only one possible solution and is computationally efficient. Simulations were conducted to investigate the accuracy and precision of k3 estimates and an FCH PET imaging study of a PC-3 mouse model was analyzed to show proof of concept.



Conclusions: In summary, we have developed a computationally efficient technique for accurate estimation of k_3 from noisy dynamic PET data that may be capable of differentiating malignant prostate cancer from benign tissue.

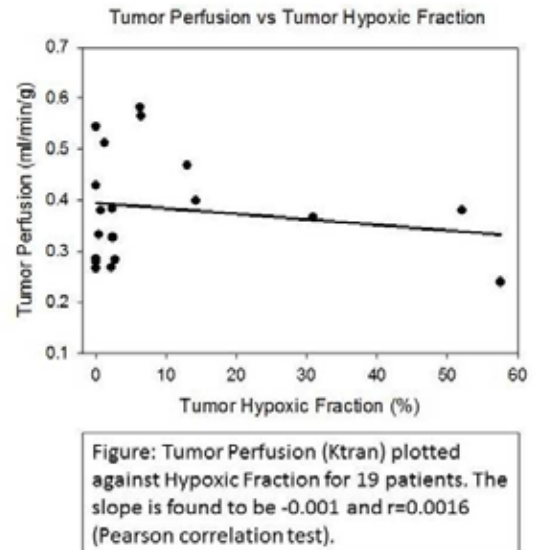
SP070.7 - Simultaneous Measurement of Perfusion and Hypoxia in Pancreatic Cancers with Dynamic PET-FAZA Imaging

Author(s): Ivan Yeung¹, Cristiane Metran-Nascente², Doug Vines¹, Ur Metser³, Neesha Dhani², David Green¹, Michael Milosevic¹, David Jaffray¹, David Hedley²

¹Radiation Medicine Program, Princess Margaret Cancer Centre, Toronto/CANADA, ²Medical Oncology, Princess Margaret Cancer Centre, Toronto/CANADA, ³Medical Imaging, Princess Margaret Cancer Centre, Toronto/CANADA

Background: Pancreatic cancers are believed to be poorly perfusion and hypoxic, and these characteristics have been suggested to explain in part their aggressive biology and poor response to standard treatment. **Method:** We have developed a method to quantify perfusion and hypoxia in pancreatic cancers with dynamic PET imaging post injection of ¹⁸F-fluoroazomycin arabinoside (FAZA). A cohort of 20 patients with pancreatic cancers were scanned with the scanning protocol involving dynamic PET acquisition in the first 60 min followed by a single static scan at 2 hr. The dynamic data were binned for image reconstruction with intervals starting from 10s up to 5 min whereas the static scan was scanned with 2 bed positions of 15 min each. The images were viewed and tumor contoured by a radiologist. To quantify the perfusion component of the tracer kinetics of FAZA, the dynamic data (of 19 patients) were analyzed with a two-compartment model with which, 'Ktran' was calculated as a surrogate of perfusion. Repeated analyses were done on data over 1.5, 5.5 and 15 min to investigate the length of data required to estimate Ktran. The static images were analyzed with the 'Mortensen's method' for hypoxic fraction. The method determines, for each patient, the tumor to mean muscle (skeletal muscle) uptake ratio for each voxel in the tumor; those voxels with uptake ratio higher than unity plus 3 times the standard deviation of the population normalized muscle uptake will be classified as 'hypoxic'. The percentage of 'hypoxic' voxel within the whole tumor will give 'hypoxic fraction'. **Results:** Ktran estimates of 1.5 min data are found to be poorly correlated ($r=0.60, 0.62$) based on the Pearson correlation test with those of 5.5 min and 15 min, whereas the ktran estimates of the latter two are found to be highly correlated ($r=0.98$). The mean Ktran of 5.5 min data is 0.384 ± 0.108 ml/min/g and the hypoxic fraction ranges from 0.0 to 57.6% with median hypoxic fraction of 2.2%. The Pearson correlation between Ktran values and hypoxic fractions gives a negligible slope of -0.001 and $r=0.0016$ as shown in the figure. **Conclusions:** The preliminary results suggested that (i) data of 5.5 min are sufficient to provide robust estimates of Ktran, (ii) The preliminary results do not support the notion that pancreatic

cancers are highly hypoxic, and (iii) there is no significant correlation between perfusion and hypoxia in our cohort of patients.



SP071 - Scaffolds in Tissue Engineering

TRACK 02: BIOMATERIALS AND REGENERATIVE MEDICINE

SP071.1 - Optimization of Crosslinking Parameters for Biosynthetic Poly(vinyl-alcohol)-Tyramine Hydrogels

Author(s): Khoon S. Lim, Yougambha Ramaswamy, Marie-Helene Alves, Rylie A. Green, Laura A. Poole-Warren, Penny Martens
Graduate School Of Biomedical Engineering, UNSW Australia, Sydney/NSW/AUSTRALIA

Photo-polymerizable hydrogels have been widely researched as tissue engineering matrices. When designing a new photocrosslinkable, biosynthetic hydrogel system, a number of parameters need to be optimized, such as the polymerization conditions and amount of biological polymer included. This study aimed to investigate the crosslinking parameters (i.e., choice of initiator, light intensity and irradiation time), as well as the biological polymer (i.e., gelatin) content, for a degradable tyramine functionalized poly(vinyl alcohol) (PVA-Tyr) system. This PVA-Tyr can be photocrosslinked using a visible light initiated process composed of ruthenium (Ru) and persulfate compounds. Comparison of ammonium persulfate (APS) and sodium persulfate (SPS) showed that SPS supported fabrication of higher quality gels at lower concentrations than APS. The initiator concentration and irradiation conditions that were found to produce the best quality PVA-Tyr gels were 2 mM Ru/20 mM SPS and 3 minutes of 15 mW/cm² of visible light. Moreover, incorporation of gelatin into the PVA-Tyr gels successfully facilitated attachment of Schwann cells on the gels. The Schwann cells were able to survive and proliferate over 3 days on the PVA-Tyr/gelatin gels. Overall, this study showed that PVA-Tyr gels have high potential as biomaterials for tissue engineering applications.

SP071.2 - A synchrotron radiation microtomography study of wettability and swelling of nanocomposite Alginate/Hydroxyapatite scaffolds for bone tissue engineering

Author(s): Francesco Brun¹, Gianluca Turco², Sergio Paoletti³, Agostino P. Accardo¹
¹Department Of Engineering And Architecture, University of Trieste, Trieste/ITALY, ²Department Of Medicine, Surgery And Health Sciences, University of Trieste, Trieste/ITALY, ³Department Of Life Sciences, University of Trieste, Trieste/ITALY

Wettability and swelling properties play an important role in a tissue engineering scaffold. An effective methodology for the characterization of these aspects is here presented and applied to nanocomposite Alginate/Hydroxyapatite scaffolds for bone tissue engineering. The methodology exploits synchrotron radiation computed microtomography and image analysis. Wet conditions with both water and simulated body fluid (SBF) were applied to the synthesized 3D constructs and the structure alterations were investigated after 21 days and 60 days of embedding. A quantitative analysis of wettability and swelling behavior through time is also presented and discussed.

SP071.3 - ECM production and distribution in regenerated cartilage tissue cultured under traction loading.

Author(s): Keisuke Fukuda¹, Seiji Omata², Yoshinori Sawae³
¹Graduate School Of Engineering, Kyushu University, Fukuoka/JAPAN, ²Research Center For Advanced Biomechanics, Kyushu University, Fukuoka/JAPAN, ³Faculty Of Engineering, Kyushu University, Fukuoka/JAPAN

An articular cartilage covers sliding surfaces of a diarthrodial joint, and it has important mechanical functions, such as impact absorption, friction reduction, etc. Mechanical stresses and strains exerted in articular cartilage during daily joint movements can stimulate the metabolism of chondrocytes. For the cells embedded in the cartilage, they play an important role to sustain the health and homeostasis of the cartilage tissue. Especially, upregulative effects of the cyclic compression and the hydrostatic pressure on the chondrocytes biosynthesis of extracellular matrix (ECM) have been studied extensively and utilized in the cartilage tissue engineering. However, the regenerated cartilage does not have sufficient dynamic functionalities compared with the normal articular cartilage. The load which arises in a living body is not the simple in fact. The chondrocyte would be exposed to the dynamic and complicated strain field consisting of compression, tension and shear that exerted by both joint loading and friction at the cartilage surface. In this study, the relative motion between cartilage surfaces in a synovial joint is simulated by the rolling-sliding motion of the plastic roller on the cultured chondrocyte-agarose construct and its effects on the formation of regenerated cartilage tissue was investigated.

Chondrocytes isolated from cartilage tissues harvested from metacarpal-phalangeal joints of steers were seeded in agarose gel and cultured 2 or 3 weeks with a traction loading applied to the surface by a roller in the original traction loading machine. This machine consists of upper oscillating plastic roller and lower reciprocating specimen stage. Vertical movement and oscillation of the roller and horizontal reciprocation of the stage were independently driven by three AC servomotors, which were controlled by PC through a control board. The specimen fitted into the culture dish was mounted on the stage and the roller was rolled over its upper surface with a defined slip/roll ratio to apply the traction loading to the construct.

After the culture period, we evaluated the amount of Type II collagen and Glycosaminoglycan (GAG) and also observed the distribution on these ECM molecules in the construct. To identify effects of the traction loading, a control specimen with a same initial cell density and same dimensions was also prepared and cultured simultaneously under the free swelling condition. After the culture experiment, constructs cultured under the traction loading had a clear traction track on the upper surface. Therefore, samples for the analyses were divided into three groups, traction track, outside of the traction track and free swelling condition.

The experiment showed that the traction loading applied to the surface of chondrocyte-agarose constructs could not increase the amount of ECM molecules accumulated in the regenerated cartilage tissue. But, it brought the anisotropic nature in the elaborated cartilaginous tissue and ECM rich layer was formed in the articulating surface of the construct cultured under the traction loading. Therefore, the traction loading on the surface may have a potential to make the structural anisotropy like a natural articular cartilage in regenerated cartilage tissue.

SP071.4 - Alginate encapsulation: a solution for controlled infiltration of cells within artificial fiber constructs

Author(s): Oleksandr Gryshkov, Holger Zernetsch, Nicola S. Hofmann, [Birgit Glasmacher](#)
Leibniz University Hannover, Institute for Multiphase Processes, Hannover/GERMANY

Introduction

Tissue-engineered constructs containing living cells are promising in the field of regenerative medicine and cell-based therapies. The application of tissue engineering presents an engineered polymer-cell construct as an attractive option to treat cardiovascular disorders. A seeded scaffold faces the problem of the growth of cells only on the surface. On the other hand, by combining the encapsulation of cells within alginate beads with scaffold structures, one can develop 3D scaffolds with encapsulated cells [1]. The advantage of this approach, in contrast to direct cell seeding, is in the potential of alginate beads to protect encapsulated cells from shear stress, which occur upon seeding and culture.

Methods

The developed high voltage method was utilized to encapsulate NIH 3T3 cells in 1.5% sterile-filtered alginate solution at concentration of 3×10^6 cells/ml. After encapsulation alginate beads were washed twice with washing solution (WS, 10 mM HEPES, 1.5 mM CaCl₂ at pH = 7.4). Polycaprolactone/poly(lactic acid) fiber mats (PCL-PLA) were generated using electro-spinning. The embedding of alginate beads into PCL scaffold was performed manually at sterile conditions. Afterwards, PCL-PLA fiber mats with entrapped alginate beads containing 3T3 cells were washed twice with WS and cultured in a humidified incubator at 37°C, 5% CO₂ for 24 days. Medium was exchanged every second day with a fresh one. The membrane integrity of 3T3 prior to encapsulation and after dissolution of alginate structure was analyzed using Trypan Blue exclusion method. The viability of encapsulated cells in alginate beads immediately after encapsulation and their presence within the scaffold was assessed using CalceinAM/EthD-1 live-dead viability assay. The presence of embedded alginate beads into fiber mats was confirmed using a scanning electron microscope.

Results

NIH 3T3 cells can be encapsulated into alginate beads (diameter 300 μ m) using high-voltage electro-spraying without significant effect of high voltage on the viability of encapsulated cells post-encapsulation (immediate viability 92% vs. initial 95%). In turn, electro-spinning process allowed generating multi-layered PCL-PLA scaffold with previously incorporated alginate beads containing living cells. Analysis of SEM images proved the presence of alginate beads in the scaffold. Long-term culture of these constructs for 24 days revealed the simultaneous degradation of alginate beads, release of encapsulated 3T3 cells and their attachment to PCL-PLA fiber mat within the scaffold. On the other hand, no viable and adherent cells were observed, if the alginate structure was treated with sodium citrate prior to long-term culture.

Conclusions and outlook

This work shows the perspectives of applying the high-voltage process to generate cell-containing tissue-engineered constructs for regenerative medicine, cell-based therapies and cardio-vascular applications. Further work will be performed to optimize the seeding process including its automatization, as well as to investigate the behavior of such constructs at dynamic conditions.

Acknowledgments

This work is in part supported by the German Research Foundation (DFG) through a scholarship of the cluster of excellence REBIRTH

(EXC 62/1)

References

[1] O. Gryshkov, D. Pogozykh, N. Hofmann *et al.* (2014). Process engineering of high voltage alginate encapsulation of mesenchymal stem cells. *Materials Science and Engineering C* 36, 77-83

SP071.5 - Biomineralization and In vivo-Compatibility of LnPO₄ Nanorods with Enhanced MR and Luminescence Imaging

Author(s): Zhongbing Huang
Sichuan University, Chengdu/CHINA

Introduction: The biocompatibility of nanomaterials with dual-functions is very important for their clinical applications.

Methods: Eu-doped LnPO₄ nanorods (NRs) in the template of silk fibroin (SF) peptides, including GdPO₄, SmPO₄ (named as SF-NRs), are successfully synthesized via a biomineralization process.

Results: lengths of Eu-doped GdPO₄ and SmPO₄ NRs with SF peptides (SF-NRs) are ~150 and 250 nm, respectively, and their diameter is ~10 nm. Compared to pure NRs, SF-NRs have stronger cell luminescence and higher T1 signal-enhancement of *in vitro/in vivo* MRI due to their higher ratio of Eu/Gd (~0.9/5) or Eu/Sm (~1.1/3) and more Eu²⁺/Eu³⁺ in SF-NRs. The images of cell ultrathin sections indicate that endocytosis of SF-NRs into the cytoplasm did not influence mitochondrial architecture at the NR concentrations of 100 mg·mL⁻¹ after 3 d of culture, because PBS/calf serum immersion tests indicate that SF peptide coating could slow metal-ions release and the crystal degradation from NRs. The histological analysis and bio-distributions in tumor-bearing nude mice suggest that, compared to pure NRs, SF-NRs have lower tissue/organ toxicities and could be safely cleared away through renal and fecal excretion in 3 d, especially the existence of more SF-NRs in the tumor field due to SF coating layer in NR surfaces. Furthermore, Eu-doped SF-NRs not only exhibit a higher T1 signal-enhancements (the longitudinal relaxivity *r*₁ value is 1.32 (Gd mM·s)⁻¹ and 0.0145 (Sm mM·s)⁻¹) under a 7.0 T MR imaging system, and a series of *in vivo* T1-weighted MR images between pre- and post-injection in tumor regions in 9 h indicate that average intensity of post-injection of SF-NRs is enhanced 71%, higher the increased value of pure NRs (15.5%), but also show the better luminescence imaging of living cells under the fluorescence microscope.

Conclusions: Our results indicate that Eu-doped SF-NRs have potential as T1 MR imaging contrast agents and optical imaging probe in tumor-detection field.

Acknowledgement: This study was supported by the National Natural Science Foundation of China (No. 51273122).

SP071.6 - Additive Manufacturing for Creating Multifunctional Tissue Engineering Scaffolds

Author(s): Min Wang
Department Of Mechanical Engineering, The University of Hong Kong, Hong Kong/HONG KONG

Tissue engineering has great potential in solving many medical problems that are currently unsolvable or in offering better and long-term solutions as compared to current medical treatments. For human body tissue regeneration, different approaches can be adopted: cell-based, factor-based or scaffold-based tissue engineering. In scaffold-based tissue engineering, cells are encapsulated in the matrices or seeded on the surface of 3D scaffolds, with the scaffolds serving as the extracellular matrix to direct cell adhesion, proliferation and differentiation and thus promote tissue

regeneration. Over the past two decades, many materials and scaffold manufacturing techniques have been investigated by numerous groups around the world for regenerating different body tissues. So far, materials for tissue engineering are predominantly biodegradable polymeric materials, natural or synthetic, and scaffolds are produced using either non-designed manufacturing techniques (solvent casting/particulate leaching, phase separation, gas foaming, electrospinning, etc.) or designed manufacturing techniques. Using designed manufacturing techniques, which include a host of additive manufacturing technologies (the so-called “rapid prototyping (RP) technologies” in previous decades), for making tissue engineering scaffolds has distinctive advantages over some commonly used chemical engineering methods in scaffold fabrication and hence has been attracting increasing attention in the biomedical field. Some additive manufacturing technologies impose stringent requirements for stock materials and studies are thus conducted on preparing stock materials and on evaluating the physical and mechanical properties of scaffolds made of these stock materials. Realizing the shortcomings of common biodegradable polymers as materials for tissue engineering scaffolds with regard to some specific tissues, various research groups now investigate new, more appropriate materials for the regeneration of targeted tissues, which include biodegradable ceramics (including glasses), composites and even metals. Considering the extracellular matrix of bone is a natural nanocomposite comprising nano-sized apatite and collagen fibrils, it is natural to develop polymer-based nanocomposites containing nanoparticles of bioactive and biodegradable ceramics as novel scaffold materials for bone tissue regeneration. Furthermore, mesenchymal stem cells (MSC) are increasingly used in tissue engineering. In this presentation, for illustrating developing biomedical nanocomposites and using additive manufacturing to form multifunctional scaffolds, our research in employing selective laser sintering (SLS), a well-established additive manufacturing technology, for obtaining osteoconductive and osteoinductive scaffolds for bone tissue engineering is introduced. Microspheres of nanocomposites (CHA/PLLA or Ca-P/PHBV) are firstly prepared as raw materials for SLS. Scaffold models of required features can be designed using data from computer-based medical imaging techniques (e.g., MRI). Nanocomposite scaffolds of good quality and consistent quality can be formed via SLS after process optimization. The growth factor rhBMP-2 can be incorporated on surface-modified nanocomposite scaffolds. It can be released from scaffolds in a controlled manner and cause osteogenic differentiation of MSCs *in vitro*. The osteoconductive (owing to the bioceramic nanoparticles) and osteoinductive (due to rhBMP-2) nanocomposite scaffolds formed by SLS stimulate bone tissue regeneration *in vivo*.

SP071.7 - Comparison of different dosage of Ion implantation on electrospun collagen fibers to improve aqueous stability

Author(s): Nisha Sharma¹, Jian Liu², Derek Boughner¹, Wankei Wan¹
¹Biomedical Engineering, University of Western, NAB/CANADA, ²Western, London/CANADA

Comparison of different dosage of Ion implantation on electrospun collagen fibers to improve aqueous stability

Nisha Sharma¹, Jian Liu², Derek Boughner^{1,3}, Wankei Wan^{1,2,3}

¹ Biomedical Engineering Graduate Program, ² Department of Chemical and Biochemical Engineering, ³Department of Medical Biophysics Western University, London, Ontario, Canada

Introduction:

Engineering methods to construct biological tissue substituted has been inspired due to the shortage of donor organ transplantation. Where, the scaffold plays an important role as of assisting, an artificial extracellular matrix to accommodate cells and support three-dimensional tissue regeneration. An ideal scaffold should be

biocompatible, biodegradable, malleable, mechanically strong, and highly porous with a large surface to the volume ratio. Such, ideal scaffolds are highly in demand, for surgical application, regenerative medicine, cell based therapy. An electrospun nanofibrous collagen scaffold is desirable for tissue engineering application, but as prepared, it is unstable in an aqueous environment including cell culture media. Stabilization of these nanofibers has been achieved to varying degrees of success using a chemical crosslinking approach with crosslinking agent such as glutaraldehyde, but they are cytotoxic.

Hypothesis:

Ion beam implantation onto random oriented fibrous scaffold produced by the electrospinning will promote radial artery cells adhesion, migration, differentiation and proliferation. This is the first step towards the successful tissue engineering.

Materials and Methods:

In this study, Collage Rat tail –Type-1 is the material in used to fabricate the electrospinning fibers. These electrospun collagen fibers are crosslinked using a physical approach via ion implantation. Broad energy He⁺ (Helium) and N⁺ (Nitrogen) ion beams are used. Energies of 1.7 MeV and 520 MeV of N⁺ ion and He⁺ ion, respectively were used to surface modify the collagen nanofibrous scaffold. The dose of these ions with similar energies, where varied from (4*10¹⁵ ions /cm² - 1.2 * 10¹⁶ ions/cm²)

Results

These cross-linked scaffolds (nanofibrous) displayed stability in both water and cell culture media with controllable degrees of swelling, where established with two different dosage. The third dosage with the same ions and energy need to be tested.

Discussion and summary

So far, with one of the energy of 1.7 MeV N⁺ of dose of 1.2 * 10¹⁶ ions/cm² and 520 MeV He⁺ of dose of 8 * 10¹⁵ ions /cm² at room temperature. The, X-ray photoelectron spectroscopy (XPS) shows that with nitrogen implantation, two new chemical functional groups, amine and amide, are introduced, which could promote cell adhesion. And, these functional groups were not found in He⁺ implantation.

SP072 - Imaging

TRACK 04: RADIATION ONCOLOGY

SP072.1 - Variations in geometric distortion using static and moving table acquisition for radiotherapy treatment planning applications

Author(s): Amy Walker¹, Gary Liney¹, Lois Holloway², Jason Dowling³, David Rivest-Henault³, Peter Metcalfe²

¹Medical Physics, Liverpool and Macarthur Cancer Therapy Centres and Ingham Institute for Applied Medical Research, Liverpool/AUSTRALIA, ²Centre For Medical Radiation Physics, University of Wollongong, Wollongong/AUSTRALIA, ³Commonwealth Scientific And Industrial Research Organisation, Australian E-Health Research Centre, Brisbane/QLD/AUSTRALIA

Purpose:

Geometric accuracy is essential when imaging patients for radiotherapy treatment planning (RTP). An increased use of MRI for RTP requires consideration of inherent geometric distortions. This study compared variations in geometric distortions observed during image acquisition utilising a continuously moving table, compared to a conventional static table. Continuous moving table acquisition allows for imaging of a longer scan length than static acquisition, a potential benefit for RTP.

Methods:

A new full field of view (FOV) phantom for measuring MRI geometric distortion for the purposes of RTP was designed in-house. Constructed from Dotmar Uniboard, 5830 vitamin E capsules were placed systematically throughout. Phantom dimensions were 500mm x 350mm x 513mm (x,y,z respectively). The phantom was scanned on a Siemens 3 T Skyra with a spoiled gradient echo (GRE) sequence (vendor 3D-correction applied). The phantom was imaged with a static couch and a continuously moving table (TimCT). The MR images were registered to a CT of the phantom to obtain distortion maps.

Results:

Table 1 compares the geometric performance of images acquired with and without a moving table. TimCT enabled imaging of the whole phantom. TimCT acquired with a table speed of 1.1mm/s resulted in the best geometric accuracy. However, the acquisition time was over 9 minutes compared to 2 minutes for the static acquisition. Increasing the table speed to 2mm/s decreased acquisition time, but resulted in increased blurring of the capsules by 170% at the FOV edges. TimCT was limited to 2 possible imaging sequences.

Conclusions:

MRI acquisition utilising TimCT offers a potential alternative for imaging large scan lengths which may be required for RTP, particularly for long FOVs. Both static and moving table image acquisitions are viable scanning options for imaging for RTP. Selection of the acquisition method would depend on the anatomical region under investigation.

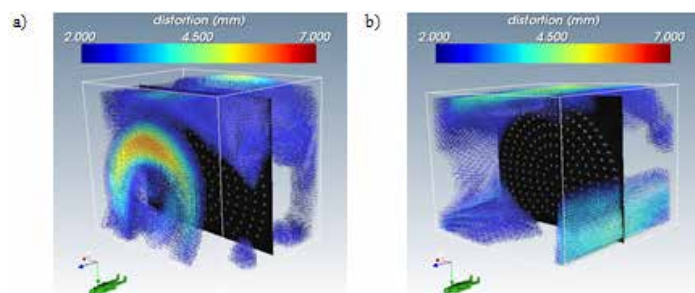


Table 1: Geometric performance of the spoiled GRE acquired with various table speeds

Sequence	Table speed (mm/s)	% phantom imaged	% phantom with distortion < 2 mm	Distance from isocenter where distortion ≤ 2 mm	Maximum distortion (mm)
TimCT	1.1	100	87	147 mm	4.4
TimCT	2	100	61	140 mm	5.8
Non TimCT	0	71	47	55 mm	6.1

SP072.2 - Translation of biomechanical deformable image registration (MORFEUS) to the RayStation radiotherapy treatment planning system

Author(s): Michael Velec¹, Joanne L. Moseley¹, Stina Svensson², Björn Hårdemark², Kristy K. Brock³, David Jaffray¹

¹Radiation Medicine Program, Princess Margaret Cancer Centre, Toronto/ON/CANADA, ²RaySearch Laboratories, Stockholm/SWE-DEN, ³University of Michigan, Ann Arbor/MI/UNITED STATES OF AMERICA

Purpose: Deformable image registration accuracy can vary widely between imaging modalities and even implementations of similar deformation models. Biomechanical model-based deformable registration was implemented in a commercial radiotherapy system and validated on multi-modality imaging.

Materials and Methods: MORFEUS is a MATLAB-based registration algorithm previously developed and validated in-house. A multi-organ tetrahedral mesh model is generated from contours in the reference image, while a subset of additional surfaces is created from body, liver and spleen contours in the target image. These three organs undergo individual surface deformations to align the contours between images and serve as boundary conditions. Finite element analysis (FEA) solves the internal displacements including all of the remaining organs and tumors. Under research collaboration with RaySearch Laboratories, MORFEUS was implemented in a commercial treatment planning system. Results shown are from a pre-clinical release of RayStation (v4.4.100). The organ-specific material properties were optimized separately between implementations. The Poisson's ratios applied in-house (range: 0.4-0.499) differ by <10% from those applied in RayStation-MORFEUS. Variable Young's moduli are applied in-house (range: 1.5-500 kPa), whereas RayStation-MORFEUS effectively applies a uniform stiffness. Boundary conditions are achieved using guided-surface projections for the in-house MORFEUS, whereas RayStation-MORFEUS uses model-based segmentation which adapts a common mesh to corresponding contours. Different third party components are also used for mesh generation and FEA solver, although these function similarly. For 32 patients in total, registration of abdominal images was performed from exhale to inhale 4DCT (or MR), or exhale CT to MR. One patient with 4DCT and MR was previously evaluated in a multi-institution accuracy study, allowing for a comparison to other algorithms. For evaluation between deformed and actual target images, the target registration error (TRE) was quantified as the residual distance between anatomic liver landmarks (median: 5, range: 4-25). For 4DCT and MR-MR, the residual mean distances of the stomach and kidneys surfaces (organs excluded as boundary conditions) were additionally quantified.

Results: The Table demonstrates the registration accuracies of both MORFEUS implementations differ by <1 mm, and both accuracies

are similar to each image resolutions on average. In the multi-institution comparison, for 4DCT both MORFEUS implementations' TRE were within 1 mm of the best-performing algorithm. For CT-MR, the in-house and RayStation-MORFEUS TRE was 1.0 and 1.2 mm lower than the best-performing, non-biomechanical algorithm.

Metric	Data	Region	Mean (maximum) registration accuracy, in mm		
			Baseline rigid	In-house Morfeus	RayStation Morfeus
TRE	4DCT (n=10)	Liver	7.8* (12.7)	2.7 (3.3)	2.7 (3.4)
	CT-MR (n=18)	Liver	6.1* (10.7)	4.0 (5.8)	3.8 (5.6)
	MR-MR (n=5)	Liver	17.9* (23.5)	3.5 (5.9)	2.8 (3.7)
Mean surface distance	4DCT (n=10)	Rt. kidney	2.6* (4.2)	1.6* (2.6)	1.7 (3.0)
		Lt. kidney	2.0* (3.0)	1.1* (1.8)	1.3 (1.8)
		Stomach	2.8 (4.1)	1.9 (3.4)	1.9 (3.6)
	MR-MR (n=5)	Rt. kidney	4.1 (6.6)	1.9 (2.8)	2.3 (3.6)
		Lt. kidney	3.7 (4.9)	1.9 (2.7)	2.1 (3.2)
		Stomach	5.8* (7.2)	3.0 (4.3)	3.5 (4.7)
*p<0.05 versus RayStation-Morfeus					

Conclusions: MORFEUS biomechanical registration was implemented in RayStation. Its registration accuracy and difference from the original implementation are on average within the voxel sizes on multi-modality abdominal imaging.

SP072.3 - Phantom Validation of a Point-Set Deformable Registration Method using Pig Bladder

Author(s): Roja Zakariaee¹, Ghassan Hamarneh², Colin J. Brown², Ingrid Spadinger³

¹Physics, University of British Columbia, Vancouver/BC/CANADA, ²Medical Image Analysis Lab, School Of Computing Science, Simon Fraser University, Burnaby/BC/CANADA, ³Medical Physics, BC Cancer Agency, Vancouver/BC/CANADA

Introduction

Deformable image registration (DIR) is widely used for registering medical images. While the main goal of registering images is to correspond different regions of interest (ROI) within the body, surrounding objects and image artefacts can confuse the DIR algorithm. This occurs, for example, in image-guided multi-fraction gynecological brachytherapy treatment, which uses an intracavitary applicator. Therefore, in applications like dose accumulation for these treatments, an alternative approach is to non-rigidly register delineated ROI contours. However, validating the registration outcomes and accordingly choosing a suitable registration algorithm is challenging, especially for highly deformable ROI with no discriminating features or anatomical landmarks. In this work, a point-set deformable registration technique, called coherent point drift (CPD), is evaluated for registering the bladder surface across treatment fractions.

Methods

A house-made pelvis phantom was used with a freshly harvested pig bladder to model the human anatomy. Multiple plastic and rubber fiducial markers were glued onto the bladder surface at twelve different locations. The bladder was filled with varying amounts (90cc, 180cc, 360cc, and 480 cc) of a water-contrast mixture and CT-scanned each time. The variously filled bladder was contoured manually on each scan using the MIM Maestro software (MIM Software Inc.). In addition, the fiducials were identified on each scan and their positions recorded. The CPD toolbox for MATLAB (Mathworks Inc.) was used to register the contour point-sets of the three smaller bladder sizes to the largest size. The toolbox takes the *target* and moving structure coordinates and outputs the *de-*

formed moving structure coordinates. The fiducial positions were used as landmarks to calculate the target registration errors (TRE) for different points on the bladder surface. Optimized input parameters for CPD registration were found experimentally by searching over the parameter space for values which minimized average TRE over all landmarks.

Results

The appearance of the phantom and the fiducial markers in the CT images was very satisfactory (Fig. 1). The average TRE value obtained for the 480cc-bladder as the *target* structure was 6.4±2.3 mm. TRE values were obtained for alternate target structures, with the 360cc-bladder yielding the lowest TRE value of 5.5±2.1 mm when selected as the target. These TRE values are reasonably small compared to the dimensions of the bladder.

Conclusion

Our validation method shows that the CPD deformable registration technique is a viable method for registering ROI contours, even when lacking distinctive features in the structure.



SP072.4 - Automatic bone and air segmentation during generation of synthetic CT from MR data in the brain

Author(s): Joshua Kim, Weili Zheng, Indrin J. Chetty, Carri Glide-Hurst
 Radiation Oncology, Henry Ford Health System, Detroit/MI/UNITED STATES OF AMERICA

Adequate differentiation of short-T2 tissue types such as bone from air remains a significant challenge for generating accurate electron density maps. This work describes the integration of ultra-short echo time (UTE) datasets and derivative images into our automated brain synthetic CT (synCT) pipeline to generate synCTs for our MR-only radiation treatment planning (RTP) workflow. MR Data from five brain cancer patients were acquired using Philips' 1.0T Panorama open MR-SIM. T1-weighted fast field echo, T2-weighted turbo spin echo, FLAIR, and UTE-DIXON (TE = 0.144/3.4/6.9ms) sequences were acquired for all patients. Affine registrations to the UTE magnitude image (UTE1) were performed. A "bone-enhanced" image was generated from DIXON-water, DIXON-fat, and inverted UTE1 datasets. Images were integrated into an automatic routine using k-means clustering with five clusters and morphological operations to segment combined bone and air voxels. A novel method incorporating post-processed UTE phase maps was introduced, enabling automated segmentation of air voxels from bone via a six-kernel Gaussian Mixture Model. A truth table was constructed based on voxel intensity levels in acquired T1, T2, and FLAIR images to assign non-bone/non-air voxels to three classes: CSF, brain tissue, and fat. A voxel-based weighted summation method incorporating T2,

FLAIR, UTE1, and "bone-enhanced" images was implemented with synCT voxel values calculated by:

$$\text{synCT}_i = \sum_k w_k r(i) M_{k,i}$$

where $M_{k,i}$ is intensity for voxel i of MR image k , $r(i)$ is the voxel's assigned class, and $w_k r(i)$ is a class-dependent weighting factor optimized by minimizing the sum of squares error between simulation CT (simCT) and synCT using a training subset. HU value differences were compared using mean absolute error (MAE). Figure 1 illustrates simCT and synCT images for two patients. Average full field-of-view MAE over all patients was 164.8±23.4 HU, showing close agreement with expected values. UTE phase-derived air maps were compared to threshold-derived simCT air contours, overlapping with 87.2±6.1% of simCT-based volumes. However, phase-derived air maps were often larger than simCT air contours, leading to higher average HU values for simCT versus synCT in air (-695±66 HU vs. -1024 HU). Another consequence was that the enlarged phase-derived contours yielded lower average values in bone (761±86 HU vs. 841±75 HU). Automatic air and bone segmentation methodology was incorporated into a brain cancer synCT pipeline. Calculated HU values demonstrated good agreement with expected simCT values based on MAE, however further refinement of air masks using the phase-based approach is needed.

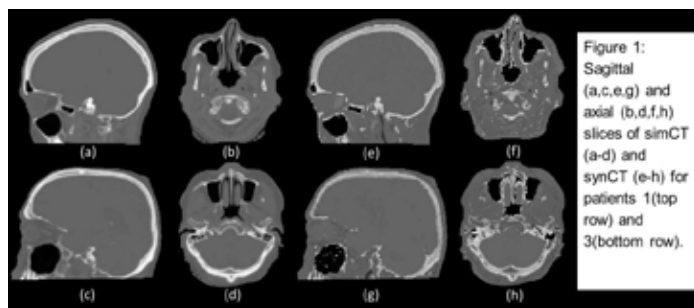


Figure 1: Sagittal (a,c,e,g) and axial (b,d,f,h) slices of simCT (a-d) and synCT (e-h) for patients 1 (top row) and 3 (bottom row).

Supported in part by Philips HealthCare, Best, Netherlands.

SP072.5 - Effect of Deformable Registration Accuracy Uncertainty on Lung Dose Accumulation

Author(s): Navid Samavati¹, Michael Velec², Kristy K. Brock³
¹Ibbme, University of Toronto, Toronto/CANADA, ²Radiation Medicine Program, Princess Margaret Cancer Centre, Toronto/CANADA, ³University of Michigan, Ann Arbor/MI/UNITED STATES OF AMERICA

Objective/Purpose: Deformable image registration (DIR) plays an important role in dose accumulation, such as incorporating breathing motion into the accumulation of the delivered dose based on daily CBCT images. However, it is not yet well understood how the uncertainties associated with DIR methods affect the dose calculations and resulting clinical metrics.

Methods and Materials: In the current study, a biomechanical model based DIR method and a biomechanical-intensity-based hybrid method, which reduced the average registration error by 1.6 mm, were applied to 10 lung cancer patients. Clinically relevant dose parameters were calculated for three dose accumulation scenarios using both algorithms. Dose scenarios included: *static*, *predicted*, and *accumulated*. *Static* dose refers to the clinical plan on the exhale phase of the 4DCT, which accounts for the breathing motion through the use of an asymmetric Planning Target Volume (PTV) margin, but does not account for the normal tissue motion in and out of the PTV during breathing motion. The *predicted dose* calculates the delivered dose based on the breathing motion observed on the 4DCT obtained at the time of treatment planning. The *accumulated dose* calculates the dose delivered based on the

4DCBCT obtained at the start of each treatment fraction. For each dose scenario, the relationship between the dose parameters and a combination of DIR accuracy (Target Registration Error, TRE, and Dice Similarity Coefficient, DSC), tumor volume, and dose heterogeneity of the plan was investigated.

Results: Depending on the dose heterogeneity, measured by Dose Heterogeneity Index (DHI), tumor volume, and DIR accuracy (measured by DSC), in over 30% of the cases differences greater than 1.0 Gy were observed in the minimum dose to 0.5cc (Dmin) of the tumor in the *static* dose calculation. Such differences were due to the errors in propagating the tumor contours from the reference planning 4DCT phase onto a subsequent 4DCT phase using each DIR algorithms and calculating the dose on that phase. The differences were more subtle when breathing motion was modeled explicitly (*predicted* dose) with only one case with over 1.0 Gy Dmin difference. Dmin Differences of up to 2.5 Gy were found in the total *accumulated* dose due to inter-fraction variations. Such dose uncertainties could potentially be clinically significant. Thus, clinical implications of DIR-based dose accumulation outcomes should be interpreted in the context of the geometric uncertainties associated with the DIR algorithm. More specifically, our results suggest that one might expect larger than 1 Gy differences in a specific Dmin (*static, predicted, or accumulated*) due to DIR choice in 10-60% of a patient population if two or more of the following criteria are met: 1) DHI of the plan is larger than 20, 2) DIR induced DSC differences in the tumor exceeds 0.08, and 3) tumor volume (or tumor volume difference) is larger than 10 cc (or 5%).

Conclusion: In summary, reductions in average uncertainty in DIR algorithms by 1.6 mm may have a clinically significant impact on the decision-making metrics used in dose planning and dose accumulation assessment.

SP072.6 - Development of a Multi-Modality 4D biomechanical Phantom for Evaluation of Simultaneous Registration/ Segmentation Algorithms

Author(s): Daniel Markel¹, John Larkin², Pierre Leger³, Yves R. Levesque⁴, Issam El Naqa²

¹Medical Physics Unit, McGill University, Montreal/CANADA, ²Medical Physics, Montreal University Health Centre, Montreal/CANADA, ³Oncology, Montreal University Health Centre, Montreal/QC/CANADA, ⁴Research Institute of the McGill University Health Centre, Montreal/QC/CANADA

Purpose: Simultaneous registration and segmentation, known as regmentation, has the potential to improve both accuracy and efficiency of both procedures when using multimodal images or longitudinally acquired scans. Currently, no gold standard exists for the evaluation of regmentation algorithms, in contrast to existing segmentation or registration algorithms, where several systems have been developed. Presented is a phantom and software package that satisfies several criteria: PET/CT/MRI compatibility, realistic geometric deformations, and reliable ground truths for both segmentation and registration, sequential or simultaneous, with a high degree of consistency.

Method and Materials: The phantom consists of a pair of inflatable swine lungs connected to an in-house built programmable respirator (shown in figure 1) via an 8 meter long vinyl tube. This allows metallic components to stay outside the scan room and thus ensure MRI compatibility. The respirator is able to mimic the breathing traces of patients taken using respiratory bellows. The target was constructed in two compartments from vacuum-sealed sea sponges. The inner and outer compartments simulate a tumor and background respectively. Catheters lead into each compartment allowing for injection of radiotracer. The registration ground truth is determined using a bifurcation-tracking pipeline. The accuracy of the tracking pipeline

was evaluated by applying a known virtual deformation to a CT volume of the swine lungs and comparing the known final locations to the ones detected by the pipeline. The segmentation ground truth was acquired by scanning the inner compartment separately and rigidly registering it to the original scan.

Results: The average bifurcation tracking error was found to be 1.22, 1.26 and 2.26 voxel widths for displacement magnitudes of 2.6, 5.2 and 7.8 cm respectively using a CT scan of a human lung. The tracking error was similarly measured to be 1.36, 1.63 and 2.46 voxel widths for displacements of 1.14, 2.29 and 3.43 cm using the swine lungs. The respirator was able to match breathing traces with a maximum error of 2.2% and an average error of 0.5%.

Conclusion: The 4D biomechanical lung phantom has shown to be a reliable tool for evaluating regmentation algorithms. The bifurcation tracking pipeline's accuracy was measured on the order of a single voxel width up to an acceptable displacement. This is crucial in eliminating the unknown uncertainty with which manual selection of fiducial points may introduce into the evaluation of a registration algorithm.

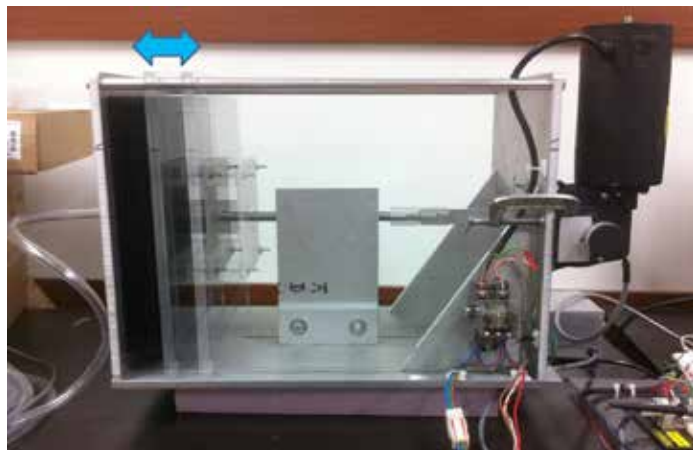


Fig. 1 The computer controlled respirator with its 4 cm range of motion shown.

SP072.7 - Using Magnetic Resonance Image (MRI) alone in Treatment Planning and Treatment Localization

Author(s): Shupeng Chen¹, An Qin¹, Di Yan¹, Hong Quan²

¹Radiation Oncology, Beaumont Health System, Royal Oak/MI/ UNITED STATES OF AMERICA, ²School Of Physics And Technology, Wuhan University, Wuhan/CHINA

Purpose: Using MR image directly for dose calculation and patient treatment position localization has been expected. In this study, a method of creating a synthetic CT image from a MR image was proposed and evaluated using the corresponding CT image numbers, planning dose distribution, and accuracy of daily CBCT image registration.

Method: A pair of MR image and CT image was collected in same day from each of 10 prostate cancer patients. For each patient, the pair of MR and CT images was pre-registered using the deformable image registration (DIR). Then the corresponding CT images were deformed toward MR to create a CT-MR pair. ROIs on the pair of images, including bone, prostate, bladder, rectum and skin, were delineated and used to create ROI masks. 'Leave-one-out' test (9 atlas patients, 1 tested patient) was performed. For each test MR image, auto-segmentation and deformable vector field (DVF) were generated based on inter-patient DIR between the test MR image and the 9 atlas MR images. Synthetic CT was then generated using the paired CT and the corresponding DVF (MR, MR) in the atlas.

The voxel intensity in the synthetic CT was determined based on the paired CT images and the corresponding masks based on the intersection of the masks. The evaluation included the comparison of the CT number, the corresponding calculated dose distribution and the corresponding registration to daily CBCT images between the resulting synthetic CT and the paired CT.

Result: The mean \pm STD of CT number error that calculated on 10 synthetic CT are (2.4 ± 25.23) , (-1.18 ± 39.49) , (-32.46 ± 81.9) and (8.07 ± 146.94) for prostate, bladder, rectum and bone, respectively. The dose discrepancy calculated using the synthetic CT and the actual CT is small, difference of D99 and D95 of target were $< 1\%$, D40 and D5 of rectum and D50 of bladder were $< 1.05\%$. Using the 10 synthetic CT as the reference planning CT for patient daily CBCT (364 fractions) localization achieved the similar results compared to using the actual CT. The translational vector difference were within 1mm with mean \pm STD $(0.37 \pm 0.23\text{mm})$, and the rotational discrepancy was within 1 degree in all 3 directions.

Conclusions: Synthetic CT created using the atlas of pre-registered CT and MR image pairs can be used to be the planning and localization CT image for dose calculation and daily patient position localization and correction.

SP073 - Robotics and Virtual Reality in Surgery

TRACK 07: SURGERY, COMPUTER AIDED SURGERY, MINIMAL INVASIVE INTERVENTIONS, ENDOSCOPY AND IMAGE-GUIDED THERAPY, MODELLING AND SIMULATION

SP073.1 - Augmented Reality in Image-guided Cardiac Interventions.

Author(s):

Many inter-cardiac interventions are performed either via open-heart surgery, or using minimally invasive approaches, where instrumentation is introduced into the cardiac chambers via the vascular system or heart wall. While many of the latter procedures are often employed under x-ray guidance, for some of these, x-ray imaging is not appropriate, and ultrasound is the preferred intra-operative imaging modality.

Two such procedures involves the repair of a mitral-valve leaflet, and the replacement of aortic valves. Both employ instruments introduced into the heart via the apex of the heart. For the mitral procedure, the standard of care for this procedure employs a 3D Trans-esophageal echo (TEE) probe as guidance. In spite of the clinical success of this procedure, many problems are encountered during the navigation of the instrument to the site of the therapy. To overcome these difficulties, we have developed a guidance platform that tracks the US probe and instrument, and augments the US images with virtual elements representing the instrument and target, to optimize the navigation process. Results of using this approach on animal studies have demonstrated increased performance in multiple metrics, and a large reduction in the number of times an instrument intruded into potentially unsafe zones in the heart.

The same platform can be employed to guide Aortic valve replacements. Conventionally, aortic valves are replaced, either using an open procedure, or under X-ray fluoroscopy guidance. The former inflicts unnecessary trauma to the patient, while the latter suffers from the problem of high radiations dose, poor target visibility and potential kidney damage as a result of x-ray contrast administration. To overcome these limitations, we have adapted the above platform to achieve an ultrasound-only solution, again augmented with virtual models of instruments and key targets to guide aortic valve replacement procedures. Preliminary results of this approach on cardiac phantoms indicate that this approach may be as effective as the standard fluoroscopy-guided technique, but without the need for radiation and contrast agents.

SP073.2 - Assistant Laparoscopic Postural: Kinematic Behavior

Author(s): Daniel Lorias-Espinoza, Arturo Minor Martinez Bioelectronics Section, Electrical Department,, CINVESTAV, MEXICO DF/MEXICO

A human laparoscopic assistant can help or hinder the work of the surgeon, so communication between the two must be natural and not cause any cooperation conflict in which the visual or motor perception of the human laparoscopic assistant hampers the optimal vision and concentration of the surgeon. This article shows a new Assistant laparoscopic called PMASS (Postural mechatronics assistant for laparoscopic solo surgery). The objective is to show their dynamic behavior.

SP073.3 - Workspace optimization of a surgical instrument for single port access surgery

Author(s): Bastian Blase, Sebastian Schlegel, Simon Albrecht
Department Of Electromechanical And Optical Systems, Technische Universität Berlin, Berlin/GERMANY

Instruments for laparoscopic single port access surgery have to perform specific movements inside the human abdomen to enable surgeons to perform similar tasks they are familiar with from multi-port minimally invasive surgery. Therefore, these instruments have to move apart before coming together at the surgical site to imitate an anthropomorphic position similar to standard access, thus facilitating handling at the desired target. These movements require additional joints. These joints weaken an instrument's shaft structure and often lead to reduced strength, whereas parallel structures reduce workspace. Hence, instruments with a segmented planar hybrid parallel-serial mechanism have been developed, combining the advantages of both structures. This mechanism is coupled serially with an end-effector. Within a set of several geometric parameters and boundaries, the favored mechanism is optimized by varying the segments' lengths for maximizing a so-called area of dexterity comprising all points that can be reached within an angular range of at least 60°. This area can be described in a cylindrical coordinate system in a phase space composed of the radial tool tip position and its inclination. The different movements of the mechanism and the end-effector are superposed and the phase space is analyzed using image evaluation methods. The optimized dexterous workspace by far exceeds a previously defined area of interest that was determined during in-vivo tests. The instruments based on this optimization proved to be agile in several tests like pick-and-place tasks.

SP073.4 - High-Dexterity Telemanipulation Robot for Minimally Invasive Surgery

Author(s): Sebastian Schlegel, Simon Albrecht, Bastian Blase
Department Of Electromechanical And Optical Systems, Technische Universität Berlin, Berlin/GERMANY

A robotic telemanipulation system for single-port laparoscopy (SPL) is presented, introducing several advantages over known systems. Principally, the system offers great flexibility at the surgical site as the instrument arms are segmented and articulate within the abdominal cavity. The instrument arms were thoroughly designed to ensure stability while maintaining a small cross-section, thus keeping patient trauma to a minimum.

Apart from the arms' solidity, the need for strong actuators is another factor that arises due to the requirement for high manipulation forces during surgery. As, at the same time, available space is extremely limited, extensive research was conducted for finding suitable actuators. Several types of actuators as well as positions within the system were taken into account, prototypes built and tested. Also, as the need arose for some concepts, mechanisms for transporting kinetic energy from the actuators to the joints were examined.

Applying the results of this work, it was possible to build a telemanipulation system consisting of instrument arms, a support base, and a specifically designed user interface. A computer serves to calculate instrument trajectories and respective joint positions from the user input at the interface as well as to facilitate communication between the system's components.

The system exceeds previously defined goals concerning dexterity. Practical tests demonstrated the broad range of movement. At the same time, the extracorporeal components are considerably smaller than their counterparts in telemanipulators on the market, thus improving direct access to the patient during surgery. Furthermore, the complex kinematics of the instrument arms are controlled via an

interface with simplified kinematics modelling the instrument's degrees of freedom (DOF), resulting in intuitive and precise handling.

**SP073.5 - Integrated Sensors for a Single-Incision Laparoscopic Instrument**

Author(s): Simon Albrecht, Bastian Blase, Sebastian Schlegel
Department Of Electromechanical And Optical Systems, Technische Universität Berlin, Berlin/GERMANY

This paper describes different sensor types for integration into a minimally invasive instrument for laparoscopic robotic surgery. A bionic fiber sensor helps to avoid collisions between the instruments' arms and the abdomen during manipulation. Position measurement is included by means of magnetic sensors that deliver feedback signals for the drive mechanism. To provide the surgeon with a haptic feedback, two force sensors are studied to be incorporated into a single incision laparoscopic robotic instrument. Their individual characteristics and impact on haptic feedback are investigated, taking into account the individual sensors' locations.

SP073.6 - Development and Evaluation of an Open-Source 3D Virtual Simulator with Integrated Motion-Tracking as a Teaching Tool for Pedicle Screw Insertion

Author(s): Stewart Mclachlin, Brendan Polley, Mirza Beig, Jeremie Larouche, Cari Whyne
Sunnybrook Research Institute, Toronto/CANADA

Pedicle screw insertion techniques are traditionally taught with limited hands-on training, using artificial or cadaveric models, prior to guided supervision within the operating room. As residency programs move to competency-based curricula, more authentic and accessible teaching tools are required to train next generation spine surgeons. Virtual simulation can provide a valuable tool for practicing challenging surgical procedures; however, its potential depends on effective integration into student learning. The objectives of this work were to develop a freely accessible virtual pedicle screw simulator and to improve the clinical authenticity of the simulator through integration of low-cost motion tracking.

The open-source medical imaging and visualization software, 3D Slicer, was used as the development platform for the virtual simulation. 3D Slicer contains many features for quickly rendering and transforming 3D models of the bony spine anatomy from patient-specific CT scans. The virtual simulation needed to include both pre-operative planning and intra-operative pedicle screw

insertion workflows. Pre-operative planning utilizes CT imaging to identify the vertebral levels requiring instrumentation and take anatomic measurements. The intra-operative screw insertion workflow requires identification of the correct entry point and trajectory to create a safe screw tract with a pedicle probe. This requires skill in complex 3D spatial perception and interpreting 2D images into real-world 3D positioning. To address this required skill development, virtual monitoring of the surgeon's simulated tool was assessed with a low-cost motion tracking sensor in real-time (~\$80, LeapMotion, San Francisco). This allowed a screw surrogate to be tracked as the surgeon defined the virtual screw's insertion point and trajectory on a 3D spine model.

Using a combination of existing and custom-written 3D Slicer Python scripts, an interactive virtual pedicle screw simulator was created. The surgical planning and operative screw insertion were simulated in a six step workflow: (1) identify vertebral levels on CT imaging, (2) choose the surgical region of interest, (3) select screw entry points, (4) take anatomic measurements, (5) define screw trajectory via the LeapMotion, and (6) grade final screw positioning. Initial surgeon feedback of the virtual simulator with integrated motion tracking was positive, with no noticeable lag and high accuracy between the real-world and virtual environments. The software yields high fidelity 3D visualization of the complex geometry and the tracking enabled coordination of motion to small changes in both translational and angular positioning.

The 3D Slicer-based virtual pedicle screw simulation overcomes accessibility issues of previously developed simulators by allowing distribution without the need for expensive commercial software. This will enable trainees to practice instrumentation techniques anywhere they have access to a computer. Further the interactivity provided by the low-cost LeapMotion represents a significant advancement in terms of the simulator's task authenticity. Future work will evaluate the benefit of this simulation platform with use over the course of resident spine rotations to improve planning and surgical competency and in quantitatively evaluating performance.

SP073.7 - A Robotic System with Ultrasound Imaging for Patient Setup and Monitoring during Fractionated Radiotherapy

Author(s): Hasan T. Sen¹, Peter Kazanzides¹, Iulian Iordachita², Muyinatu A. Lediju Bell¹, Xiao Li¹, Lin Su³, Yin Zhang³, Kai Ding³, John Wong³

¹Department Of Computer Science, Johns Hopkins University, Baltimore/UNITED STATES OF AMERICA, ²Department Of Mechanical Engineering, Johns Hopkins University, Baltimore/UNITED STATES OF AMERICA, ³Department Of Radiation Oncology, Johns Hopkins University, Baltimore/UNITED STATES OF AMERICA

We are developing a cooperatively-controlled robot to assist with the application of ultrasound for patient setup and treatment monitoring of abdominal organs during fractionated radiotherapy. The proposed workflow introduces the robot for both simulation and treatment. During simulation, the operator places the 3D ultrasound (US) probe to visualize the target and the probe pose (position and orientation, in room coordinates) is measured by a ceiling-mounted optical tracker. The robot then holds a model probe at this pose during CT acquisition, and also records the probe contact force. The model probe has the same dimensions as the US probe but does not contain any metal parts that would cause CT artifacts. Treatment planning is performed on this CT image with probe-induced deformation. On each treatment day, the robot assists the operator to place the probe at the same pose and contact force as simulation. This cooperative control mode is enabled by a force sensor mounted between the robot end-effector and probe, which measures forces applied on the probe. Virtual springs guide the operator toward the recorded pose, but the operator can pull against the spring to override the recorded pose and replicate the US image

recorded during simulation. This may be necessary to compensate for patient setup errors or anatomical changes. Once the US probe is placed to match the simulation conditions, it can provide real-time monitoring during radiation delivery.

We performed canine experiments using a custom robot that had five active degrees-of-freedom (DOF) and eight passive DOF. In these experiments, three 2.38 mm spherical metal markers were implanted into the kidney of a canine. We followed the proposed workflow for simulation and six fractionated treatments, except that we acquired additional images to measure the markers. Our results showed that placing the US probe at the same pose (in room coordinates) can result in soft-tissue setup errors of up to 35 mm, even after employing conventional setup procedures. The large inter-fraction variation is due primarily to the difficulty in repeatedly repositioning the anesthetized canine. In contrast, the virtual springs enabled the operator to override this pose based on US image feedback and reduce the setup error to within 7 mm. Our experiments also revealed ergonomic challenges, especially because the robot had fewer than six active DOF. We are therefore updating the design to use a commercial 6 DOF robot (UR5, Universal Robots, Odense, Denmark), as shown in Fig. 1.

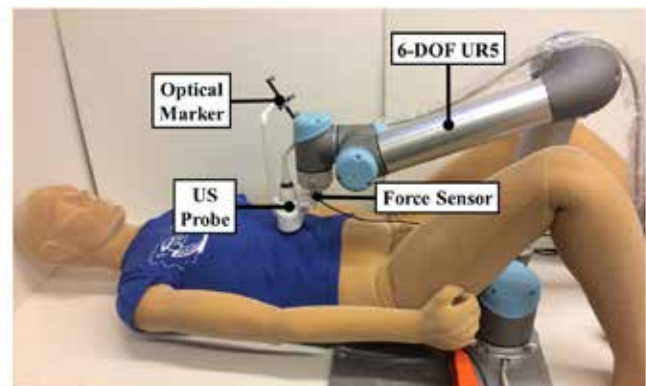


Figure 1: UR5 robot with force sensor for cooperatively-controlled placement of ultrasound (US) probe for patient setup and treatment monitoring during fractionated radiotherapy

SP074 - Biomedical Monitoring and Bioelectromagnetism

TRACK 09: BIOSIGNAL PROCESSING

SP074.1 - Towards Dual Respiratory and Cardiac Gated Radiotherapy

Author(s): Kirpal Kohli¹, Feng-Yu Liu¹, Kalpagam Krishnan¹, Devin Schellenberg², Ash Parameswaran³, Steven Thomas⁴, Anand Karvat²
¹Medical Physics, BC Cancer Agency, Surrey/BC/CANADA, ²Radiation Oncology, BC Cancer Agency, Surrey/CANADA, ³Simon Fraser University, Burnaby/CANADA, ⁴BC Cancer Agency, Vancouver/CANADA

Gating provides a potential solution for managing organ displacement during radiation treatment. In particular, respiratory gating of radiation therapy is an evolving field of study [1,2]. Cardiac gating, meanwhile, remains a largely unexplored area of potential benefit. Electrical impedance measurement has demonstrated its potential application in gating. In the present study, the respiratory and cardiac traces of three healthy human volunteers were recorded by using bioimpedance based simultaneous respiratory and cardiac monitoring circuitry developed in our previous study [3]. Each subject was instructed to maintain a normal breathing rate and hold their breath for a fixed duration. Respiratory motion was also monitored simultaneously using the existing Real-time Position Management™ (RPM) system for validating the impedance trace based on the respiratory motion. Interference caused by the respiratory motion was observed on the recorded cardiac induced bioimpedance change. Comparison of the cardiac traces for both normal breathing and breath holding revealed that the amplitude of the cardiac trace appeared to be modulated by the respiratory pattern. For the signal traces to be potentially applicable for gating purposes, it is desirable that the rendered signal waveform has stable amplitude. The aim of the study is thus to develop a strategy for improving the usability of the cardiac induced bioimpedance trace for radiotherapy gating purposes. A strategy is developed for largely removing the interference in the cardiac signal caused by the respiratory motion based on amplitude demodulation. The following Figure 1 shows a sample bioimpedance trace of recorded respiratory and cardiac motions, together with the amplitude demodulated cardiac trace.

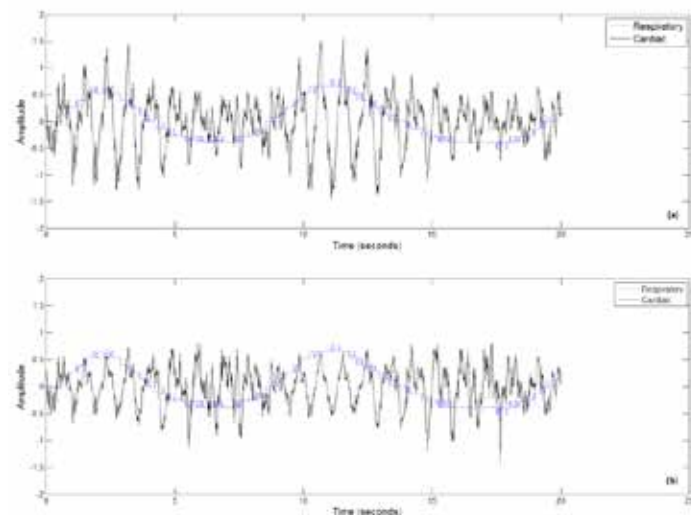


Figure 1: (a) Respiratory trace and cardiac trace of a volunteer subject breathing at a normal rate; (b) the same respiratory trace and the corresponding amplitude-demodulated cardiac trace.

The present study focuses on analyzing the correlation between the cardiac induced and respiratory induced impedance changes recorded and deriving a numerical technique for reducing the fluctuation in the amplitude of the cardiac signal. The technique developed will contribute to the potential application of bioimpedance signal on gating of radiotherapy.

SP074.2 - A mobile terminal to follow-up the evolution of chronic diseases

Author(s): Hector Torres, Rene Gonzalez, Daniel Campillo, Eyglis Ledesma
 Medical Equipment Development, Central Institute of Digital Research, La Habana/CUBA

This paper presents the firmware design of a low cost and consumption portable device intended to collect (Bluetooth) and transmit (GSM/GPRS) biological signals to a website. This solution forms part of an ambulatory monitoring system for patients with related heart diseases like arrhythmia, hypertension and diabetes, giving a more close interaction between patients and doctors. The hardware is based on the MSP430F5419A microcontroller, the CC2540 Bluetooth Low Energy (both from Texas Instruments), and the SIM908 GSM/GPRS/GPS modem from Simcom. The real time operating system FreeRTOS was used in the firmware. QRS complexes are detected and processed in the ECG wave signal; blood pressure and glucose level are processed as well. A robust communication protocol was implemented and an easy graphical user interface also. A total of 50 different samples were uploaded to the website using developed prototypes in a safety way. This is an interesting solution to have into account in this kind of systems due to its low cost.

SP074.3 - Relationship between the tuning characteristics of stimulus otoacoustic emissions and behavioral tests at moderate levels

Author(s): Yao Wang¹, Qin Gong¹, Tao Zhang²
¹Biomedical Engineering, School of Medicine, Tsinghua University, Beijing/CHINA, ²Tsinghua National Laboratory for Information Science and Technology (TNList), Beijing/CHINA

Frequency selectivity, the ability of the auditory system to resolve the frequency components of complex sounds, is typically estimated in humans using a subjective method, the measurement of psychophysical tuning curves (PTCs). Stimulus frequency otoacoustic emission suppression tuning curves (SFOAE STCs) potentially could assess frequency selectivity objectively. We compared PTCs and SFOAE STCs in 24 normal hearing subjects using moderate-level probes with center frequencies near 1, 2, and 4 kHz, showing that both measures of frequency selectivity are similar.

SP074.4 - An Axon Mimic for Medical Electrode Tests

Author(s): Malcolm A. Latorre¹, Adrian D.C. Chan², Karin Wårdell¹
¹Department Of Biomedical Engineering, Linköping University, Linköping/SWEDEN, ²Department Of Systems And Computer Engineering, Carleton University, Ottawa/CANADA

Tissue's heterogeneity makes it ineffective as a test bench and calibration standard for biomedical electrodes. There is a need for an axon mimic that can generate a stable, repeatable, programmable, and physiological A-fiber like action potential (AP). The aim of the project is to assess an electronic A-fiber like system for its potential use as a biomedical electrode test bench.

An equivalent 40 nodes of Ranvier were mimicked using resin embedded gold wire ($\varnothing = 20 \mu\text{m}$). All nodes share one amplitude con-

trol (A) with programmable control for inter-nodal timing (τ), duration (n) and propagation rate from a microcontroller running custom software. Statistically, a 20 μm diameter A-fiber has characteristic inter-nodal spacing of 2 mm and propagation speed of about 120 m/s [1] which results in a 16 μs increment time between activation of successive nodes. LabVIEW and DAQ from National Instruments (Version 8.2, National Instruments Corp. Texas USA) are used for acquisition and control. Custom software implements a simplified behavioral model based on Hodgkin and Huxley's equation [2] with a pulse train ($|P(\tau)|$) propagating along the nodes.

The system was assessed by submerging the nodes in a bath of NaCl 0.9 % solution which acts as the intervening tissue mimic for testing. Data were collected using a pair of standard ECG-electrodes (4831Q, Unomedical a/s, Birkerød, Denmark) with gel removed. The electrode pair was used in a bipolar configuration positioned above the nodes. Fifty repeated measurements ($|P(\tau)|$) = 5, A = 1 V) verified the stability of the system where the time at maximum amplitude was $\text{tpk_max} = 196.4 \pm 0.06$ ms, maximum amplitude was $\text{Vpk_max} = 37.5 \pm 1.3$ μV , and noise floor was $\text{Vnoise} = 0.07 \pm 0.017$ μV .

In conclusion, the system generated a traveling pulse, with programmable amplitudes, durations and times similar to those of a biological AP. The output is stable and repeatable, and most importantly can be coupled to bio-potential electrodes. This platform allows testing and comparisons between surface electrodes and some implantable electrode configurations, as well as general electrode verification, complete systems can also be tested and compared with this stable AP generator.

References

- [1] W. A. H. Rushton, "A theory of the effects of fibre size in medullated nerve," *The Journal of Physiology*, vol. 115, pp. 101-122, 1951.
- [2] A. L. Hodgkin and A. F. Huxley, "A quantitative description of membrane current and its application to conduction and excitation in nerve," *J Physiol*, vol. 117, pp. 500-44, Aug 1952.

SP074.5 - Evaluation the Accuracy of Oscillometric Blood Pressure Measurement According to the AAMI SP10

Author(s): Haiyan Xiang

Institute of Aviation Medicine, Beijing/CHINA

The auscultatory method is regarded as the golden standard in non-invasive arterial blood pressure measurement. The oscillometric method are used widely in most automated blood pressure measurement instruments recently. The limitation of oscillometric method is that both the systolic and the diastolic pressure are estimated using empirical criteria. In fact, there are large variance of the amplitude ratios among population. Therefore, the estimation of the systolic and diastolic blood pressure based on oscillometric technique is not always accurate. In present study, an oscillometric method blood pressure measurement experiment system was established to acquire and analyze the blood pressure measurement data of the subjects with low, medium and high pressure. Eight-five subjects with a wide range of blood pressure were recruited. Each subject was measured three times. The experiment system acquires the cuff pressure and the oscillometric pulse. The manual auscultation measurement was performed on the same-limb simultaneously by two trained observers. The data were analyzed using self-programmed analyzing software based on Matlab. The averages of systolic and diastolic ratios are 0.50 and 0.71 respectively. Both the systolic and diastolic ratios fluctuate in a wide range, especially for the subjects with higher or lower blood pressure. Based on the golden standard, the accuracy of oscillometric method would not be generally accepted for the subjects with a wide range blood pressure.

SP074.6 - PEMF effects on chondrocyte cellularity and gene expression of the rat distal femoral metaphyseal articular cartilage.

Author(s): Fernando Sotelo-Barroso¹, Karla S. Vera-Delgado¹, Elena M. Castro-Rodríguez², Cipriana Caudillo-Cisneros¹, Sergio Marquez Gamino¹

¹Ciencias Aplicadas Al Trabajo, Universidad de Guanajuato, Leon/MEXICO, ²Centro De Investigaciones Biomédicas, Universidad de Colima, Colima/MEXICO

In recent years, interactions between electromagnetic fields and biological systems have increasingly been studied. To date, pulsed electromagnetic fields (PEMF) have a number of well-documented physiological effects on cells and tissues; including the up regulation of gene expression of the transforming growth factor beta super family members, the increase in glycosaminoglycan levels, and anti-inflammatory actions. The purpose of the current study was to determine the effect of PEMF on the rat distal femoral joint cartilage, in terms of chondrocytic gene expression level and cellularity. Twenty female 84 days old Wistar rats, were randomly assigned into two groups: the experimental group received focused PEMF (30 mT/1 Hz/30 min/20 days) on the knee (MS). The control group (Non-MS), was managed similarly, except that PEMF stimulation was simulated. All the animals were euthanized for histological and gene expression evaluation of the knee joint tissues; 6 μm cartilage longitudinal sections were obtained from formalin fixed and paraffin embedded (FFPE) samples, then stained with a hematoxyline-eosine technique. The sections were analyzed in a light clear field microscope in order to quantify the number of chondrocytes per optical field. To determine the expression levels of collagen type XI alpha 2 (col11a2), (sex determining region Y)-box 6 (Sox6), aggrecan (Acan), runt-related transcription factor 2 (Runx2), and alkaline phosphatase liver/bone/kidney (Alpl), total RNA was isolated by a FFPE RNAeasy Kit. For each sample RNA was reverse transcribed using oligo dT as primer. Real time PCR reactions were performed from 50 ng of cDNA. Statistically significant differences were found in joint cartilage cellularity when MS and Non-MS were compared (101.13 ± 26.61 vs 69.66 ± 15.55 cells per optical field, respectively; $p = 0.001$). *Collagen XI*, *Sox6* and *Aggrecan* expression levels were also different in magnetically stimulated tissues relative to control (Differences were evaluated by Student's t test and were considered as significant when $p < 0.05$). On the other hand RUNX2 and *ALPL* expressions showed no significant differences between groups (Student's t test, $p > 0.05$). These results are evidence that *in vivo* PEMF stimulation increases the number of well differentiated knee joint cartilage cells in healthy young adult rats. This finding indicates an *in vivo* trophic effect upon cartilage joint tissue. The action mechanisms could be associated to electrical characteristics of cartilage cells and could be related to new matrix production. The low gene expression of RUNX2 and *ALPL* supports that the chondrocytic response to PEMF do not correspond to a hypertrophic reaction. These results highlight the possible therapeutic future of PEMF in cartilage injuries, and on its ageing.

SP074.7 - Classification of responders versus non-responders to tDCS by analyzing voltage between anode and cathode during treatment session

Author(s): Isar Nejadgholji¹, Travis Davidson², Cryatal Blais³, Francois Tremblay², Miodrag Bolic¹

¹School Of Electrical Engineering And Computer Science, University of Ottawa, Ottawa/CANADA, ²School Of Human Kinetics, University of Ottawa, Ottawa/CANADA, ³Nuraleve Inc., Ottawa/CANADA

Transcranial direct current stimulation (tDCS) has been shown to be beneficial as a potential treatment of several disorders such as depression, addiction and chronic pain. Despite promising results reported in research, there is variability in responsiveness to tDCS among subjects. However, the source of this variability is still

unknown. Creating a mechanism of determining non-responders (vs. responders) is a crucial step in order to either understand the physiology behind tDCS or increase the effectiveness of treatment. This work proposes a versatile method to predict whether a subject responds to tDCS by analyzing the voltage measured between anode and cathode during a tDCS session. Two groups of subjects are determined as responders and non-responders by assessing the effect of tDCS on their motor potential evoked by transcranial magnetic stimulation (TMS). Voltage measurements are modeled by a double Debye model and two relaxation times are extracted for each measurement. A quadratic classifier is trained to recognize responders and non-responders based on these relaxation times. Our classification results show that there is a significant correlation between relaxation times extracted from voltage and responsiveness to tDCS determined through motor evoked potentials. These results suggest that the relative speed of polarization processes occurring in electrodes and tissue may be associated the amount of current delivered to the brain.

SP074.8 - Matlab toolbox for bioelectric cardiac images analysis

Author(s): Juan Alberto L. Cruz, Maycon Emely F. Farias Ribeiro, Ernando S. Ferreira
Department Of Physics, State University of Feira de Santana, FEIRA DE SANTANA/BRAZIL

The heart problems are recognized by the World Health Organization as a major cause of death of human beings. Supported by the concepts of bioelectricity is now possible to better understand the functioning of this organ. In the medical physics research is a priority not to study only new equipment to detect these biosignals, but also new paradigms for processing, allowing the extract improve information of heart activity. We describe isECG (Imaging System for Electrocardiography), a new MATLAB processing toolbox, for bioelectric cardiac image analysis. Using real data (magnetic resonance images and ECG data from 123 bioelectrodes from an anonymous patient) the 3D-realistic heart/thorax geometry, surface ECG-bioelectric potential mapping on torso and myocardium surface potential images were constructed. Specialized routines are available for solution the direct and inverse bioelectric problem, and the results displayed in visualization panels (windows) on the main graphical interface. All ECG bioelectrical potentials signals, are show in new graphical window, and permit it is analysis for an individual ECG signal. Preliminary results demonstrated that isECG is a toolbox that can be used for analysis and visualization of cardiac bioelectric images, and has shown promise for future studies in Bioelectromagnetism.

SP075 - SPECIAL SESSION: Appropriate Technology in Imaging and Radiotherapy - Functionality and Safety Aspects

TRACK 17: EDUCATIONAL AND PROFESSIONAL ACTIVITIES

SP075.1 - Appropriate technology in imaging and radiotherapy - Functionality and Safety aspects

Author(s): Kin-Yin Cheung¹, Adriana V. Berumen², Miriam Mikhail Lette², Joanna IZewska³

¹IOMP, Happy Valley/HONG KONG, ²WHO, Geneva/SWITZERLAND, ³IAEA, Vienna/AUSTRIA

Every country faces resource constraints of some degree insofar as provision of healthcare services, a particularly critical problem in low-resource settings and in view of the rising trend of non-communicable diseases. 70% of cancer-related deaths occur in resource-constrained settings that request access to quality and affordable technologies. In low and middle income (LMI) countries, such medical services for underserved populations are mainly provided by governments. The IAEA/WHO Directory of Radiotherapy Centres (DIRAC) indicates major radiotherapy equipment shortages in these countries. WHO data in the World Health Statistics describe the corresponding census of diagnostic and therapeutic radiation technologies and services. Prioritizing appropriate selection, allocation, use, provision and optimization of cost-effective health technologies and human resources is therefore necessary. Important elements when formulating policy for planning and procurement of healthcare technologies must take into account high cost imaging and radiotherapy equipment, and should be based upon needs assessments and country specific criteria to include compatibility with clinical needs and burden of disease, radiological safety, standard of service and practice, affordability, sustainability, minimum operating requirements, long term functionality in LMI settings in terms of working conditions and infrastructure, and access to maintenance. International guidelines, recommendations, and reports such as produced by the IAEA and WHO can be used in support of planning radiation medicine services. One particular IAEA initiative aims to propose affordable, appropriate and suitable radiotherapy equipment packages and solutions for LMI countries through an IAEA Advisory Group on Increasing Access to Radiotherapy Technologies in Developing Countries (AGaRT), promoting increased access to diagnostic and therapeutic technologies in LMI countries by encouraging the industry to offer complete and integrated solutions that are safe, affordable, highly reliable and effective for low resource settings. WHO has been advising governments for many years in the incorporation of health technologies, including for diagnostic imaging and radiotherapy. For example, the WHO has recently embarked upon a project to list priority medical devices needed for the continuum of clinical management of six highly prevalent cancers, including radiation technologies. WHO is also conducting a Global Initiative on Radiation Safety in Health Care Settings to promote safe and appropriate use of radiation in healthcare. Ten priority actions have been identified in the "Bonn Call for Action" to improve safety and quality in the medical use of radiation for diagnosis and therapy, jointly published by the IAEA and WHO in 2014; engagement of all relevant medical sector stakeholders is warranted to support implementation. The synergies between IOMP, IAEA, WHO and others can enhance the availability of these technologies. Keeping in mind that technology planning criteria are country specific and dynamically change over time as healthcare services and technologies evolve, this joint session provides an excellent forum for global healthcare professionals and experts from international organizations to exchange ideas and experiences, and explore ways of addressing challenges faced during planning and acquisition of appropriate healthcare technologies.

SP076 - Radiobiological Modelling

TRACK 19: BIOPHYSICS AND MODELLING

SP076.1 - Radiation Pneumonitis and Low Dose Radiation Hypersensitivity

Author(s): J. James Gordon¹, Karen C. Snyder¹, Hualiang Zhong¹, Ken Barton¹, Zhen Sun¹, Indrin J. Chetty¹, Martha Matuszak², Randall K. Ten Haken²

¹Radiation Oncology, Henry Ford Health System, Detroit/MI/UNITED STATES OF AMERICA, ²Radiation Oncology, University of Michigan Health System, Ann Arbor/MI/UNITED STATES OF AMERICA

Analysis of a University of Michigan (UMich) clinical trial dose-volume histogram (DVH) dataset is summarized, the goal of which was to improve radiation pneumonitis (RP) prediction. A family of dose-damage profiles featuring low-dose radiation hypersensitivity (RHS) achieved higher predictive accuracy than mean lung dose (MLD), motivating a novel RHS normal tissue complication probability (NTCP) model. Results of this model are summarized. If one makes reasonable assumptions regarding the institution-specific DVH mix, the model can reproduce published MLD – RP risk curves obtained in clinical trials at Duke University, Netherlands Cancer Institute (NKI), Washington University (WU) and the University of Milan (UMilan).

SP076.2 - Dose distribution optimization methods based on biological parameters: Impact of the objective function and reoxygenation and proliferation effects

Author(s): Araceli Gago Arias¹, Andrés Pérez¹, Beatriz Sanchez Nieto¹, Juan Pardo Montero², Christian Karger³, Ignacio Espinoza¹

¹Instituto De Física., Pontificia Universidad Católica de Chile, Santiago/CHILE, ²Servizo De Radiofísica E Protección Radiológica, Complejo Hospital Universitario de Santiago de Compostela, Santiago de Compostela/SPAIN, ³Department Of Medical Physics In Radiation Oncology, German Cancer Research Center (DKFZ), Heidelberg/GERMANY

The non-uniform response of tumors to radiation may compromise radiotherapy treatment outcome when homogeneous dose distributions are used. Responsible for this behavior are mainly the inhomogeneous distributions of oxygen and clonogenic cell density within the tumor. To approach these issues, the delivery of inhomogeneous dose distributions was long ago proposed to increase the efficiency of radiotherapy.

Dose prescription is normally addressed as an optimization problem involving an objective function, OF. Two of the most frequently used OFs aim to: i) maximize the tumor control probability, which is equivalent to minimize the tumor cells survival or ii) seek a uniform density of surviving clonogens.

The published works applying any of these two approaches were implemented using different dose redistribution techniques (subvolume dose boosting, dose painting by numbers) to tumors with distinct radiosensitivity inhomogeneities. Furthermore, they analyzed the impact of different biological factors or employed mathematical tumors modeling these processes in different ways.

This work studies different methods of dose distribution optimization analyzing the above-mentioned OFs under a common methodology. Effects related to the dose heterogeneity allowed in the distribution and the impact of biological processes like reoxygenation and tumor cell proliferation are also studied.

The response of a 2-cm-diameter hypoxic Head-and-Neck virtual tumor to radiotherapy was simulated using a previously published mathematical model [Med Phys. 2015 Jan; 42(1):90]. The model considers the following biological processes: tumor cells proliferation, neo-angiogenesis, diffusion-limited hypoxia, oxygen-dependent cell killing due to radiation, resorption of dead cells, tumor shrinkage and reoxygenation.

A dose painting by numbers approach was chosen to redistribute the dose keeping the average dose delivered to the tumor equal to 2 Gy per fraction.

The impact of the different OFs and dose heterogeneity constraints on treatment outcome was first isolated from other effects. At this stage no tumor cell proliferation was simulated and the tumor oxygenation status was considered to remain constant throughout the treatment. Dose distributions derived for fraction-by-fraction optimizations led to equal treatment outcomes for both OFs. In the dose distributions, the dose modulation was allowed to vary within a 10%, 25%, 35% and a 50% of 2 Gy per fraction. This led to a reduction of 3, 7, 8 and 10, respectively, in the number of fractions needed to achieve tumor control.

Dose distribution optimizations were then performed for a dose heterogeneity limit of 25% of 2 Gy simulating the tumor response considering all the abovementioned biological processes. The effect of changes in the tumor cell proliferation rate was studied for tumor cell doubling-times ranging from 50 to 5 days, including an accelerated repopulation regime arising after two weeks of treatment. The highest therapeutic gain from dose painting was achieved for the simulations with the highest proliferation rate (reduction of 13 fractions compared to the case using uniform dose). When accelerated repopulation is considered, the number of fractions needed to achieve tumor control was lowered from 34, for uniform dose distributions, to 23. The work shows that reoxygenation and tumor cell proliferation play an important role in the simulation of dose-painting.

SP076.3 - Healthy Tissues in The Present of Gold Nano Particles against ¹⁰³Pd and ¹²⁵I: Monte Carlo study

Author(s): Mohammad Vahidian, Somayeh Asadi, Mehdi Vaez-Zadeh, Mahdieh Marghchouei
Physics, K.N.Toosi University of Technology, +/IRAN

The aim of the present Monte Carlo study is to evaluate the method of variation of energy deposition in healthy tissues in the human eye which is irradiated by brachytherapy sources in comparison with the resultant dose increase in the gold nano particle – loaded choroidal melanoma. The effects of GNPs on healthy tissues are compared between ¹⁰³Pd and ¹²⁵I as two ophthalmic brachytherapy sources. To this end, Human eye globe was simulated through the use of MCNP5 code by considering all parts of the eye. Dose distribution in healthy tissues and dosimetry differences in the eye phantom with existing tumor have been taken into account for both mentioned brachytherapy sources. In addition deviances observed in the comparison of simple water phantom and actual simulated eye in present of GNPs are also a matter of interest that has been considered in the present work. Here, both water and eye phantoms were simulated in which the water phantom was the same as the eye phantom with the exception that, water was considered to be the eye composition in all parts of the human eye globe. The previous studies which compared the ophthalmic brachytherapy dosimetry between these two sources reported higher absorbed dose by the tumor for ¹⁰³Pd versus ¹²⁵I for an equivalent radiation time. However, the results of this study show that the calculated dose enhancement factor in the tumor for ¹²⁵I is higher than that of for ¹⁰³Pd. Also, the ratio of the absorbed dose by healthy tissues in the present of GNPs to the absorbed dose by the tumor for ¹⁰³Pd is lower than that

of for ^{125}I . Choose of the optimum size and concentration for GNPs and also the suitable brachytherapy source to achieve the maximum dose in the tumor area and the minimum dose to healthy surrounding tissues need to more practical investigations which is under study and will report in future.

SP076.4 - Monte-Carlo model development for evaluation of current clinical target volume definitions for Glioblastoma using Boron Neutron Capture Therapy

Author(s): Leyla Moghaddasi, Eva Bezak, Wendy Harriss-Phillips
Department Of Medical Physics, Royal Adelaide Hospital, Adelaide/SA/AUSTRALIA

Introduction: Glioblastomas (GBM) are notorious for their extensive diffusion and high fatality rate. Boron Neutron Capture Therapy (BNCT) is a biochemically-targeted type of radiotherapy where thermal neutrons are captured by ^{10}B , resulting in the emission of high LET α -particles and recoiling ^7Li atoms. BNCT has the potential to selectively deliver localized dose to tumour cells diffused into normal brain tissue, with minimal normal tissue toxicity. The aim of the current work is to develop a GBM model, taking into account cellular composition of brain with addition of appropriate ^{10}B concentrations, to determine optimal Clinical Target Volume (CTV) margins for BNCT. It also aims to investigate the effectiveness of GBM cell death (i.e. in the presence of hypoxia and genetic heterogeneity) following BNCT.

Methods: A neutron beam model was developed in GEANT4.9.6.p02 and verified against published data. The neutron beam spectrum was obtained from literature for a cyclotron-produced beam. The calculated percentage depth dose curves (PDDs) in water were compared with measured data to verify the neutron beam in terms of total depth dose and boron dose deposition. The GBM model was structured as follows: firstly, Microscopic Extension Probability (MEP) models were developed using MATLAB-2012a, based on clinical studies reporting on GBM clonogenic spread. Typical ^{10}B concentrations in GBM and normal brain cells were obtained from literature. Each cell was then assigned a ^{10}B concentration depending on its MEP status. Secondly, a Geant4 microdosimetry model was developed to calculate the dose deposited in individual voxels, each representing a GBM/normal cell; the system was defined as a cubic phantom voxelized to 20 μm side voxels (the average size of glioma cells) and irradiated with an epithermal neutron beam. The material of each voxel was set to brain (ICRP-based NIST database) with added boron atoms from the ^{10}B distribution imported from MATLAB. Results from the microdosimetry model and the MEP models were convolved to evaluate survival fractions (SF) for CTV margins of 2.0 & 2.5cm.

Results & Conclusion: Excellent agreement was achieved between the calculated and measured neutron beam PDDs (within 1%) (Figure 1). The resulting boron depth dose deposition was also in agreement with measured data. Ongoing work is focusing on determination of tumour cell SF following BNCT as a function of various MEP models and ^{10}B concentrations.

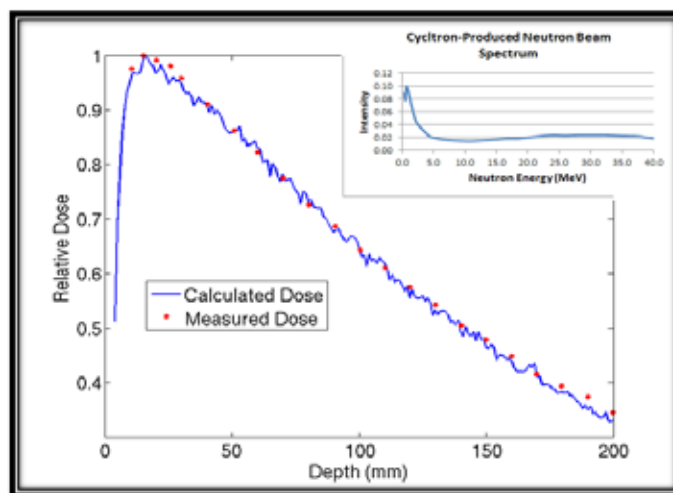


Figure 1 Comparison of calculated and measured total PDDs of a neutron beam in water (Insert: the neutron beam spectrum).

SP076.5 - Exploring RBE Dependence on Proton Track Angular Incidence

Author(s): Piotr Pater¹, Gloria Bäckström¹, Fernanda Villegas-Navarro², Anders Ahnesjö², Shirin A. Enger¹, Jan Seuntjens¹, Issam El Naqa¹

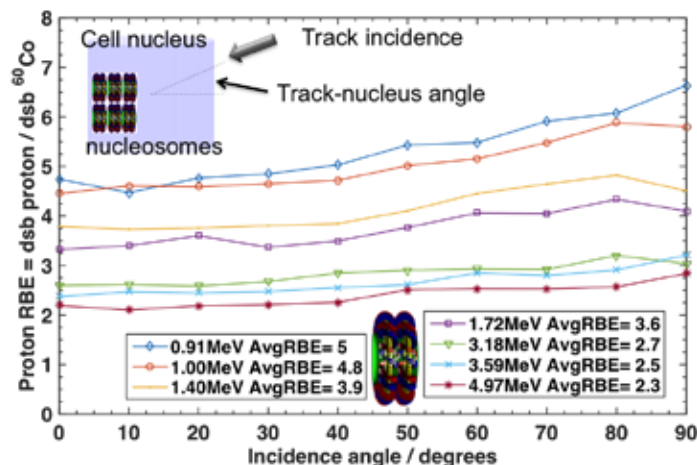
¹McGill University, Montreal/CANADA, ²Uppsala University, Uppsala/SWEDEN

The relative biological effect (RBE) of protons, taken as the ratio of double strand break (dsb) yields for an investigated radiation source to the yields by ^{60}Co , can be computed by overlaying event-by-event Monte Carlo (MC) particle tracks on a cell nucleus model. Strand breaks (sb) occur when energy depositions (ED) sites coincide with the DNA sugar-phosphate backbone. Dsbs are then modelled as arrangements with at least one sb on each strand within 10 base pairs (bp). Human DNA is tightly packed into higher order structures including chromosomes, chromatin fiber, and nucleosomes (beads on a string configuration). This work compares proton RBE for different angular orientations of nucleosomes relative to incident charged particle tracks within a cell nucleus model.

The MC code LlonTrack (Med.Phys.2013;40(6)) was used to generate proton (~1-5 MeV) and ^{60}Co ED tracks, including all secondary electrons (tracking cutoff of 50 eV). ED sites were subsequently overlaid on a simplified cylindrical cell nucleus (~2 μm radius and half-height) at track-nucleus angles from 0 (normal incidence) to 90 degrees (parallel to nucleus axis). Fractions of ~2 Gy were simulated at each angle for each source. A nucleosome, consisting of a 2-turn, double stranded, and circular arrangement of 99 bps, is replicated in an ordered fashion approximately 3×10^7 times in the nucleus and dsbs yields are computed for each fraction.

For ^{60}Co , no angular dependence was detected and the 95% confidence interval on the average angular dsb yield was [2.50 2.65] dsb Gy⁻¹ cell⁻¹, which was used as the reference to calculate RBE for protons. RBE was larger than one at all proton energies and incidence angles, with two significant trends. As expected, the RBE increased with decreasing proton energy. However, RBE also significantly depends on the track-nucleus angle, due to a preferential track alignment with the nucleosomes at higher angles, but also to a higher probability of traversing the nucleus without hitting any DNA targets. For 1 MeV protons, the spherically weighted average RBE is 7 % higher and 22 % lower than the RBE for 0 and 90 degrees respectively. When simulating RBE, angular dependence of the dsb yields due to the nucleus model chosen should be investi-

gated and a spherically weighted average RBE should be reported.



SP076.6 - DNA Damage Induced in Glioblastoma Cells by I-131: A Comparison between Experimental Data and Monte Carlo Simulation

Author(s): Fereshteh Koosha

Medical Physics And Biomedical Engineering, Tehran university of medical sciences, tehran/IRAN

Objective: The passage of ionizing radiation in living cells creates clusters of damaged nucleotides in DNA. In this study, DNA strand breaks induced by the beta particle of iodine-131 (I-131), have been determined experimentally and compared to Monte Carlo simulation results as a theoretical method of determining I-131 damage.

Materials and Methods: For conducting this experimental study, Glioblastoma (GBM) cells were exposed to 10 mCi I-131, at a dose of 2 Gy, in order to create single strand breaks (SSB) and double strand breaks (DSB) in the DNA of irradiated cells. Cells were evaluated quantitatively by the Fast Micromethod assay. The energy spectrum of electrons released in cells were obtained by the macroscopic Monte Carlo code (MCNP4c) and used as an input of the micro Monte Carlo code (MCDS). The percent of damage induced in cells was calculated by Manvitny test.

Results: A significant reduction ($p < 0.05$) in fluorescence intensity in irradiated cells compared to control cells as determined by the Fast Micromethod assay represented induced SSB and DSB damages in the DNA of irradiated cells. By comparing the experimental and theoretical results, the difference between the percent of SSB per Gy was about 7.4% and DSB was about 1% per Gy.

Conclusion: The differences in experimental and theoretical results may be due to the algorithm of applied codes. Since the Fast Micromethod and other experimental techniques do not provide information about the amount of detailed and complex damages of DNA-like base damages, the applied Monte Carlo codes, due to their capability to predict the amount of detailed damages that occur in the DNA of irradiated cells, can be used in *in vitro* experiments and radiation protection areas.

SP076.7 - The stochastic extension of the Linear Quadratic model: Taking into account the uncertainty of radiobiological parameters.

Author(s): Moises Saez-Beltran¹, Francisco Saez-Beltran², Francisco Fernandez Gonzalez³

¹Servicio De Radiofísica Y Protección Radiológica, Complejo Asistencial Universitario de Salamanca, Salamanca/SPAIN, ²Servicio De Radiofísica, Complejo Asistencial de Zamora, Hospital Provincial, Zamora/SPAIN, ³Instituto Universitario Física Fundamental Y Matemáticas, Universidad de Salamanca, Salamanca/SPAIN

Introduction

We show the way to modify the Linear Quadratic model of cell survival used in Radiation Oncology to accommodate uncertainty in the radiobiological parameters (α , β). The objective is, given the probability distribution functions of α and β , find the probability distribution function of the biological equivalent dose, BED, and the probability of cell survival, p . And furthermore, find how this uncertainty propagates through a fractionation scheme. In this paper we show that this can be done in an explicit way without simulation.

Materials and Methods

The stochastic extension of the Linear Quadratic model consist in promoting α , β , p , BED from single value variables to random variables α , β , p , BED. The delivered dose per fraction, d , is considered as a non-random parameter. For a single fraction, there is an analytical relationship between α , β and BED and p , so we can use the rules of probability to get a formula to obtain the probability distribution functions of p and BED from the corresponding probability distribution functions of α , β . For a fractionation scheme of dose, we have to consider sums of stochastic variables, that involves repeated convolutions of probability functions.

Results

If we define equivalent treatments in the mean, for different fractionation schemes, we can recover the formulas of the usual Linear Quadratic model, substituting α , β by the expected value $\langle \alpha \rangle$, $\langle \beta \rangle$. The variance of these treatments can also be shown to be different whenever the variance of α or β is different from zero. For a number of fractions large enough, p can be regarded as a log-normal stochastic variable, due to the central limit theorem.

Discussion

We have described an analytical way to take into account the uncertainty of radiobiological parameters as probability distribution functions into the Linear Quadratic model, without Monte Carlo simulation. This higher level of complexity gives in return better information of the effect of this uncertainty on the treatment outcome. Whether these stochastic extensions may explain data variability better than any more sophisticated "non-stochastic" radiobiological model is yet a matter of experiment.

SP077 - Radiation Oncology

PRESIDENTS CALL

SP077.1 - Assessment of CT to CBCT Non-Rigid Image Registration in Prostate Cancer Radiation Therapy

Author(s): Pawel Siciarz

Medical Physics, CancerCare Manitoba, Winnipeg/CANADA

Purpose: The goal of this project was to investigate the performance of three image registration algorithms implemented in two open source platforms: 3DSlicer and MedInria.

Material and Methods: The study describes CT to CBCT deformable registration by the application of following algorithms: two well known Affine and Fast Symmetric Forces Demons (3DSlicer) as well as Dense Anatomical Block Matching (MedInria) that is based on pyramidal block-matching approach. To the best of author knowledge it is the first study which attempts to investigate the performance of Dense Anatomical Block Matching Algorithm (DABM) for CT to CBCT deformable registration.

Pre-treatment CT (pCT) images of five prostate patients undergoing IMRT were selected for this work. Representative CBCT data sets were acquired in the middle of the radiotherapy treatment to provide the algorithms with realistically challenging registration problem. Deformable registration for each algorithm was followed by the initial Affine alignment of considered images. After registration, structures (GTV, Bladder and Rectum) delineated on pCT were first deformed using obtained vector fields, next propagated to CBCT images and finally compared to the contours delineated on CBCT by experienced Radiation Oncologist. The similarity between deformed CT (dCT) and CBCT images was also analysed.

Accuracy of registration was assessed by the application of the following metrics: Dice Coefficient and Mean Hausdorff Distance for structures comparison as well as voxel-to-voxel absolute intensity difference for dCT-CBCT images comparison. For visualization and better understanding of these numerical values author propose to present differences between considered organ contours as a surface map reflecting surface-to-surface distances for the closest neighbouring points. The map of absolute discrepancies in image intensity between dCT and CBCT for selected image slices are also provided.

Results: Early results clearly indicates very promising performance of Dense Anatomical Block Matching method for challenging non-rigid pCT-to-CBCT registration compared to Affine and Demons algorithms which can be seen at the figure 1. This quick quality assessment is expected to be confirmed by more detailed analysis of proposed similarity metrics. Additionally, smooth and unfolding DVFDABM shows the lack of any unphysical deformations.

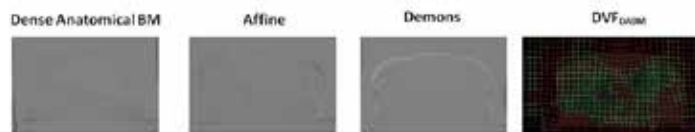


Figure 1. Image Subtraction (CBCT-registered image) for three registration algorithms and deformable vector field for Dense Anatomical Block Matching (DVFDABM).

SP077.2 - Use of flattening filter free photon beams for off-axis targets in conformal arc stereotactic body radiation therapy

Author(s): Ashley Smith¹, Christopher Serago¹, Siyong Kim², Kathleen Hintenlang¹, Michael Heckman³, David Hintenlang⁴

¹Radiation Oncology, Mayo Clinic, Jacksonville/UNITED STATES OF AMERICA, ²Radiation Oncology, College Of Medicine, Virginia Commonwealth University, Richmond/VA/UNITED STATES OF AMERICA, ³Biomedical Statistics And Informatics, Mayo Clinic, Jacksonville/UNITED STATES OF AMERICA, ⁴Biomedical Engineering, University of Florida, Gainesville/UNITED STATES OF AMERICA

Dynamic conformal arc therapy (DCAT) and FFF beams are commonly adopted for efficient conformal dose delivery in SBRT. Off-axis geometry (OAG) may be necessary to obtain full gantry rotation without collision, which has been shown to be beneficial for peripheral targets using flattened beams. We investigated dose distributions in OAG using FFF, and the effect of mechanical rotation induced uncertainty.

Sphere targets (2, 4, and 6 cm diameter) were placed at three locations (central axis, 3 cm, and 6 cm off-axis) in a representative patient CT set. DCAT plans were obtained for 6X, 6FFF, 10X, and 10FFF. Homogeneity index (HI), conformality indices (CI), and beam on time (BOT) were calculated. Mechanical rotation induced uncertainty was evaluated using five SBRT patient plans with laterally located tumors. For each, a plan was generated using FFF beams for OAG and CAG. Each was replanned to account for one degree collimator/couch rotation errors during delivery. Prescription isodose coverage, CI, and lung dose were evaluated.

HI and CI values were similar for flattened and unflattened beams; however, 6FFF provided slightly better values than 10FFF in OAG. For all plans HI and CI were acceptable with the maximum difference between flattened and FFF beams being 0.1. FFF beams showed better conformality for low doses and small targets. Variation due to rotational error for isodose coverage, CI, and lung dose was generally smaller for CAG compared to OAG, with some of these comparisons reaching statistical significance. However, variations in dose distributions for either technique were small and not clinically significant.

FFF beams showed acceptable dose distributions in OAG. 10FFF provides more dramatic BOT reduction, but generally provides less favorable dosimetric indices compared to 6FFF in OAG. Mechanical rotation induced uncertainty had an increased effect for OAG compared to CAG; however, variations for either treatment technique were minimal.

SP077.3 - Dosimetric evaluation of the interplay effect for non-gated VMAT treatment of moving targets with high dose rate FFF beams

Author(s): Ashley Smith¹, Christopher Serago¹, Kathleen Hintenlang¹, Siyong Kim², David Hintenlang³

¹Radiation Oncology, Mayo Clinic, Jacksonville/UNITED STATES OF AMERICA, ²Radiation Oncology, College Of Medicine, Virginia Commonwealth University, Richmond/UNITED STATES OF AMERICA, ³Biomedical Engineering, University of Florida, Gainesville/UNITED STATES OF AMERICA

PURPOSE

Interplay effects exist between multi-leaf collimator movement and tumor motion when treating moving targets with intensity modulated radiation therapy. Dose deviations caused by the interplay effect can be decreased by reducing the dose rate. It is questionable whether flattening filter free (FFF) high dose rate will increase dose deviations caused by the interplay effect for volumetric modulated arc therapy (VMAT). This work evaluates the interplay effect using a moving phantom to simulate respiratory tumor motion for non-respirato-

ry-gated VMAT treatment using FFF beams, and investigates the impact of dose rate.

METHODS

Two VMAT plans were selected from lung patients treated with 6 MV FFF beams. Dose distributions were measured using a 2D ion chamber array placed on a motor-driven motion platform. Respiratory phase was accounted for by dividing the breathing cycle into 8 equally spaced phases and irradiation was initiated at each of the phases. The 8 starting phases were used to simulate the clinical situation of starting the treatment at a random phase in the patient breathing cycle. All fields were delivered in their treatment geometries with and without phantom motion using 3 dose rates: 1400, 600, and 400 MU/min.

Measured dose was compared to planned dose using gamma analysis (3%/3mm), percent of pixels within 5% of pixel dose, and percent of pixels within 10% of pixel dose. Calculations were done for the 8 initial starting phases and repeated for a random sampling of starting phases for 1000 trials. Target coverage was evaluated by the dose difference for four points at the center of the target. Four points at the periphery of the target were used to evaluate planning target volume margin.

RESULTS

Results for 1000 trials of randomly selected motion phases are reported in Table 1. The delivered dose compared to planned dose in the center of the target region was within 5.0% for the static phantom condition and 7.4% for the moving phantom condition. At the periphery of the target the delivered dose differed from planned dose by -0.9% to 13% for the static condition and -28.8% to 39.7% for the moving condition.

CONCLUSION

Our results indicate the interplay effect had an impact on non-gated VMAT when treating a moving target with FFF, however using high FFF dose rate did not increase dose deviations compared to lower dose rates. The impact of the interplay effect on target coverage is acceptable, as long as sufficient margin is given.

Plan	Phantom	Dose Rate (MU/min)	Gamma 3%/3mm	Standard deviation	% of pixels within 5% of dose	Standard deviation	% of pixels within 10% of dose	Standard deviation
1	Static	1400	95.51		92.53		97.06	
1	Moving	1400	86.93	0.84	86.49	0.25	94.06	0.13
1	Moving	600	86.77	0.23	86.55	0.07	94.08	0.04
1	Moving	400	86.64	0.29	86.57	0.04	94.08	0.02
2	Static	1400	97.95		93.80		97.70	
2	Moving	1400	85.86	0.24	85.88	0.24	93.94	0.24
2	Moving	600	86.22	0.36	85.78	0.06	93.89	0.04
2	Moving	400	86.30	0.08	85.84	0.07	93.89	0.05

SP077.4 - In vivo Image Guided Brachytherapy Verification (IGBV) in high dose rate prostate brachytherapy – Initial Clinical Experience

Author(s): Ryan L. Smith¹, Annette Haworth², Jeremy L. Millar¹, Michael L. Taylor³, Rick D. Franich³

¹William Buckland Radiotherapy Centre, The Alfred Hospital, Melbourne/AUSTRALIA, ²Physical Sciences, Peter MacCallum Cancer Centre, East Melbourne/VIC/AUSTRALIA, ³School Of Applied Sciences, RMIT University, Melbourne/VIC/AUSTRALIA

Aim.

High dose rate (HDR) prostate brachytherapy treatment is widely practiced and is a well-established radiotherapy technique. Usually delivered in large dose fractions, poor execution in the delivery of a planned treatment would have significant clinical impact on the patient. The frequency and type of errors that may occur in HDR brachytherapy treatment are mostly unknown as there exist limited options for independent routine monitoring of treatment delivery to identify potential errors and ensure patient safety. We report our initial clinical experience with a novel, non-invasive, source-tracking system based on a flat panel detector (FPD) for treatment verification in HDR prostate brachytherapy: Image Guided Brachytherapy Verification (IGBV).

Materials & Method.

For IGBV, a FPD was mounted in our brachytherapy treatment couch under a customised carbon fibre couch top assembly. Six prostate patients (10 treatment fractions) were included in this clinical study of the IGBV system. At treatment, each patient was aligned on the brachytherapy couch with the target region (prostate) centred over the sensitive imaging area of the FPD. As the HDR treatment proceeded, images of the source position were acquired with the FPD in the form of patient exit radiation. These images were post-processed to determine the position of the source inside the patient and were compared to the treatment plan in order to identify potential errors and verify correct treatment delivery.

Results.

The measured source dwell positions confirmed correct transfer tube connection, afterloader indexer length, source step size and patient/plan selection. The mean linear distance between measured and planned source dwell positions was 2.37 mm (s.d. 0.96mm), after rigid registration with the treatment plan. The average dwell step size across all measured catheters was 2.54 mm (s.d. 0.24mm, n=112). The absolute position of the measured dwells, together with the implanted gold fiducial markers, visible on a pre-treatment radiograph, provided verification of programmed treatment indexer length and therefore delivery to the correct anatomical location. This unique brachytherapy verification process is non-invasive, with the patients virtually unaware of the verification imaging that is occurring during treatment delivery. The total impact on procedure time was less than 15 minutes.

Conclusion.

This novel, non-invasive HDR brachytherapy treatment verification system, IGBV, was implemented clinically, providing confirmation of many treatment parameters by tracking the position of the HDR source as treatment was delivered. An independent treatment monitoring system, such as the one described here, could validate the treatment delivery process in real time, enabling a safety interlock system. The clinical experience with the IGBV system provided confirmation that the treatment was delivered free of potential human related errors. This concept and system will meaningfully improve safety standards by allowing routine treatment verification in HDR brachytherapy across a range of clinical applications.

SP077.5 - Electronic Portal Imaging Device Dosimetry for IMRT: a Review on Commercially Available Solutions

Author(s): Omemh Bawazeer¹, Sisira Herath², Siva Sarasanandara-jah¹, Pradip Deb¹

¹School Of Medical Radiation, RMIT University, Melbourne/AUSTRALIA, ²Radiation Oncology, Peter MacCallum Cancer Centre, Melbourne/AUSTRALIA

Much research has been conducted about the utilization of electronic portal imaging devices (EPID) for dose verification during radiotherapy treatment. Currently a number of commercial solutions are available; Portal Dosimetry, EPIDose, Epiqa, Dosimetry Check, and EPIgray software. Results from separate studies on clinical applications of these solutions are published. The objective of this paper is to review the accuracy of these dosimetry solutions when used for intensity modulated radiotherapy technique (IMRT). Although each solution has a different approach to dose verification, most of the IMRT dosimetry verification results are highly satisfactory. However, performance of one solution is less satisfactory when the patient-couch attenuation occurs. Moreover, none of these solutions correct the back scatter effect resulted from supporting arm. In addition, there are no comparative studies currently available about the accuracy of these solutions except one paper that compared Portal Dosimetry and EPIDose reporting the major differences between these systems. Further studies are needed to compare the accuracy of these commercially available EPID dosimetry solutions.

SP077.6 - The Nano-X Radiotherapy Machine: Lean Innovation Transforming Global Access to Cancer Care

Author(s): Paul Keall¹, Enid Eslick¹, Peter Lazarakis¹, Michael Jackson², Ilana Feain¹

¹Radiation Physics Laboratory, University of Sydney, University of Sydney/AUSTRALIA, ²University of New South Wales, Sydney/AUSTRALIA

There are times in society in which problems with the descriptor “too hard to solve” can no longer be tolerated. The International Cancer Expert Corps, 2014

Time and Place

Radiotherapy is the recommended treatment for half of all cancer patients. Yet, access to radiotherapy is non-existent in 55 countries around the world and limited in most others, especially in regional and rural centres. Epidemiological studies prove an urgent need for 9,000 additional radiotherapy machines to treat a rising global cancer epidemic (International Global TaskForce on Radiotherapy for Cancer Control). Both WHO and IAEA have recently established programs to solve this crisis.

Vision

The Nano-X vision is to level the playing field in global access to radiotherapy. Where cancer patients in low and middle-income countries have access to appropriate treatment and care. Where the machine is designed from the ground up to deliver an affordable and viable solution for the people that need treatment, where they needs treatment, independently of where highly trained workforces live.

The Nano-X Solution

Nano-X, which will enter the international market by 2020, will launch on a wave of global awareness around this epidemic. Nano-X alleviates major obstacles to global radiotherapy utilization with lean innovation and a compact, affordable system for low and middle-income countries with drastically simplified hardware and workflow. A Nano-X schematic is shown: a full clinical prototype is now under construction and the shielded bunker is complete.



Conceptual Innovation: Nano-X will deliver a paradigm shift in radiation oncology by enabling affordable, accessible radiotherapy in resource-limited areas where capital costs and on-site operations are major issues. Nano-X increases patient throughput and decreases on-site staffing using sophisticated algorithms and leveraging telemedicine to enable centralised planning and local treatment with automated decision making. **Methodological Innovation:** Nano-X will treat patients with a fixed vertical beam and a patient rotation couch. This reduces costs enormously by reducing the (i) engineering complexity, (ii) size and radiation shielding requirements of the room (iii) onsite staffing requirements and (iv) time-consuming and inconvenient patient immobilisation procedures and treatment planning. **Technological Innovation:** For Nano-X, tumour motion will be substantial as patients themselves are rotated. The technological innovations in Nano-X are our algorithms for real-time image guidance and dynamic adaptation of the treatment beam to account directly for tumour motion.

SP077.7 - Development of an MR and CT compatible non-invasive temperature based optical fiber respiration sensor for use in radiotherapy

Author(s): Ashley Smith¹, Siyong Kim², Christopher Serago¹, Kathleen Hintenlang¹, Robert Pooley³, David Hintenlang⁴

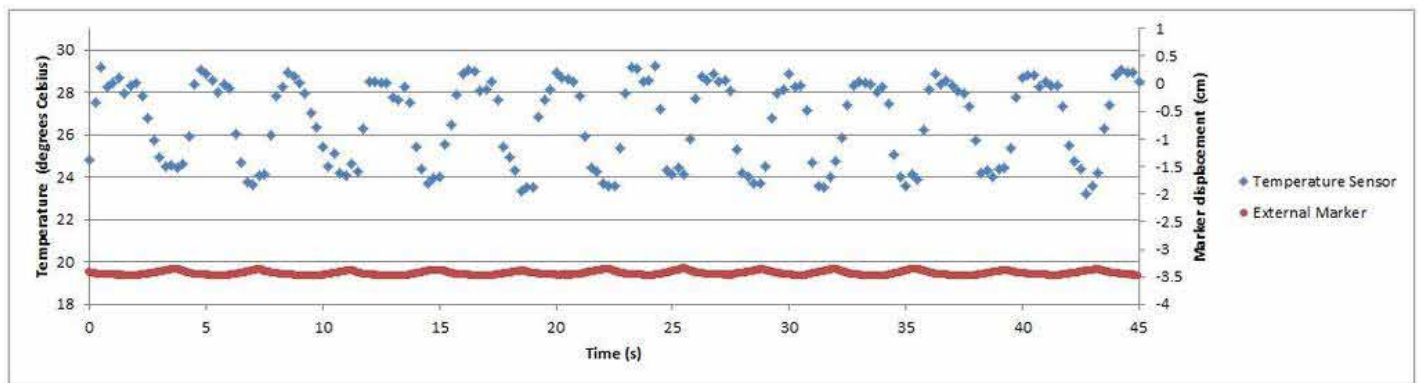
¹Radiation Oncology, Mayo Clinic, Jacksonville/UNITED STATES OF AMERICA, ²Radiation Oncology, College Of Medicine, Virginia Commonwealth University, Richmond/VA/UNITED STATES OF AMERICA, ³Radiology, Mayo Clinic, Jacksonville/UNITED STATES OF AMERICA, ⁴Biomedical Engineering, University of Florida, Gainesville/UNITED STATES OF AMERICA

We have developed a non-invasive temperature based respiration sensor to track the breathing cycle during respiratory gating that is not subject to the limitations of an external marker. The sensor tracks the breathing cycle by measuring the temperature of inspiratory and expiratory air (Figure 1). Because it doesn't rely on movement of the abdomen it can be used with forced shallow breathing (FSB) or thermoplastic body mask immobilization. The sensor is compatible for use in CT, MR, and linear accelerator environments.



Respiration signals were tested with five volunteers using FSB, and compared to simultaneously recorded signals from an external marker. Temperature readings were also tested in a CT, MR, and linear accelerator environment. The sensor's effect on image quality was evaluated for CT and MR.

The temperature sensor successfully recorded the breathing cycle for all volunteers, while the external marker had one failure (Figure 2). Fluctuations in temperature sensor signals were similar to background in both a CT and MR environment. There was greater signal fluctuation when the sensor was placed in a high energy linear accelerator field and given a high dose. The fluctuation was acceptable when the sensor was outside the radiation field. It is recommended that the sensor be placed outside the treatment field during treatment. Image quality was not affected by the temperature sensor for CT or MR.



We have shown that the temperature based respiration sensor can successfully track breathing cycles even when external markers fail. Performance is maintained in MR and ionizing radiation environments; however it is recommended that it not be used in the direct path of a high energy beam. We have verified that respiratory signals can be obtained without deterioration of CT or MR images. It is anticipated that this device would be highly suitable for respiratory gating in radiation therapy.

SP078 - Brachy Therapy: Part 2

TRACK 04: RADIATION ONCOLOGY

SP078.1 - The Effect of Bladder Preparation on Motion of Organs at Risk in High Dose Rate Gynecological Brachytherapy

Author(s): Parisa Sadeghi¹, Robyn Banerjee², Tien Phan², Majed Alghamdi², Amandeep Taggar², Wendy L. Smith¹

¹Physics And Astronomy, University of Calgary, Calgary/CANADA, ²Radiation Oncology, Tom Baker Cancer Centre, Calgary/AB/CANADA

Introduction: High Dose Rate (HDR) brachytherapy is part of the treatment protocol for advanced cervical cancer. The planning process for Magnetic Resonance (MR) guided treatment requires both Computed Tomography (CT) and MR imaging. This combines the high soft tissue contrast of the MR images with the ability of the CT scan to visualize the applicator inside the patient. However, this dual imaging requires multiple patient transfers and increases the overall patient motion. This can lead to changes in both the position and volume of the organs at risk (OARs) in the pelvic region, such as the rectum and bladder.

The purpose of this study is to evaluate the effect of bladder filling (often used to reduce bowel dose) on bladder motion, and quantify the motion of the rectum during HDR brachytherapy of cervical cancer.

Methods: A total of 15 cervical cancer patients were included in this study. Nine patients were treated without introducing bladder filling. Six patients had their bladder contents emptied and re-filled to a specific volume (120 – 200 cc). The change in bladder volume and center of mass (CM) position between the MR and CT imaging sessions, as well as the concordance index (CI) of the contoured bladders on both image sets were calculated using the Eclipse treatment planning system by Varian.

Results and Discussion: It is evident, from the data presented in Table 1 that the prepared bladders display a smaller change in volume compared to the bladders without the filling. In addition, prepared bladders show a mean positional change of 4.2 mm (range: 1.6-8.5 mm), while a positional change of 5.3 mm (range: 1.5-15.4 mm) is observed in the absence of bladder filling. This is interesting because the filling implemented for bowel sparing seems to have the added benefit of reducing bladder mobility. Also the prepared bladders seem to have a higher CI value. The rectum shows an overall positional change of 6.6 ± 4.6 mm over the whole patient population.

Conclusion: Our results clearly display a trend where the bladder preparation leads to a smaller bladder motion, smaller volume change, and higher CI. Although preliminary statistical analysis did not reveal any significant difference between the two bladder preparation protocols, a larger sample size could provide more conclusive results.

	Bladder (Filled) (Mean \pm SD)	Bladder (Not Filled) (Mean \pm SD)	Rectum (Mean \pm SD)
Volume Change (%)	18 \pm 14	40 \pm 55	17 \pm 26
CM motion (mm)	4.2 \pm 2.3	5.3 \pm 4.4	6.6 \pm 4.6
CI	0.74 \pm 0.06	0.59 \pm 0.19	0.51 \pm 0.11
D2cc (cGy)	697 \pm 128	632 \pm 130	460 \pm 87
D1cc (cGy)	766 \pm 143	703 \pm 153	507 \pm 95
D0.1cc (cGy)	930 \pm 170	872 \pm 244	629 \pm 41

Table 1: Preliminary analysis on motion and deformation of the organs at risk between the two imaging sessions of CT and MRI.

SP078.2 - Retrospective Monte Carlo dose calculations for permanent implant prostate brachytherapy using 125I

Author(s): Paul Soubiran¹, Justin Sutherland¹, Nelson Miksys², Ali-Reza Mehan Haidari², Rowan Thomson², E Choan¹, Gad Perry¹, Joanna Cygler¹

¹Radiation Medicine Program, The Ottawa Hospital Cancer Centre, Ottawa/CANADA, ²Physics, Carleton University, Ottawa/ON/CANADA

Clinical dose calculations for low dose-rate (LDR) prostate brachytherapy are currently performed following the protocols defined by the American Association of Physicists in Medicine (AAPM) Task Group no. 43 (TG-43) formalism. Using the TG-43 formalism, absorbed dose is calculated in a homogeneous water environment so the effects of tissue heterogeneities, interseed attenuation, and the finite dimensions of patients are not accounted for. This work retrospectively investigates differences between TG-43 and Monte Carlo (MC) calculated dose distributions for 105 patients treated with LDR prostate brachytherapy at The Ottawa Hospital.

Each of the 105 patients used in this study had a prescribed dose of 145 Gy (Drx) to the prostate through implantation of ¹²⁵I seeds (Model 6711 RAPID Strand™). Treatment planning and seed implantations were performed in real-time using ultrasound images. MC calculations were performed using the EGSnrc user-code Bachy-Dose. Computational phantoms for each patient were generated from CT images acquired 1 month post-implant by a Philips Brilliance CT scanner – Big Bore. Material compositions were assigned to each voxel within image contours based on CT number: prostate and calcification within prostate contours, air and muscle within rectum contours, urinary bladder within bladder contours, and ICRU 46 soft tissue and bone in the remainder of the phantom. CT number thresholds between tissue assignments were assigned consistently between patients and were determined by manual investigation of CT scans for several patients. The mass density of each voxel was derived from a scanner calibration of Hounsfield Units to density. To avoid misassignment of voxels to calcification and since BrachyDose models full seed geometries, seeds and metallic artifacts were removed from scans prior to tissue assignment by over-riding CT numbers above a threshold in the vicinity of the seeds. Dose to medium was calculated with sufficient histories to achieve a statistical uncertainty of less than 2% in prostate volumes.

Dose distributions calculated with BrachyDose differed considerably from those calculated with TG-43. The patient-averaged minimum dose to 90% of the target volume (D90) was 9.5 Gy lower as calculated by BrachyDose compared to TG-43. The average D99 was 52 Gy less than Drx as calculated by BrachyDose compared to 45 Gy less than Drx as calculated by TG-43. Similarly, the patient-averaged percentage volume that received at least 100% of the prescription dose (V100%) was 4% lower as calculated by BrachyDose compared to TG-43. While doses to organs at risk (OAR) also differed

between BrachyDose and TG-43 calculated distributions, the differences were smaller. The patient-averaged highest dose received by 1 cc (D1cc) of the rectum was 103 Gy as calculated by BrachyDose and 110 Gy as calculated by TG-43: a 6.5% difference which may be clinically significant. D1cc for the bladder was 86 Gy for BrachyDose versus 88 Gy for TG-43 calculations, which is not clinically significant.

Retrospective MC calculated dose distributions for 105 Ottawa Hospital patients treated with LDR prostate brachytherapy showed a decrease in average dose coverage of target volumes and OARs as compared with TG-43 calculated dose distributions.

SP078.3 - Combining doses for prostate cancer patients receiving external beam radiotherapy and a HDR brachytherapy boost: Dosimetric parameters and dose-surface maps for patients with and without late rectal bleeding

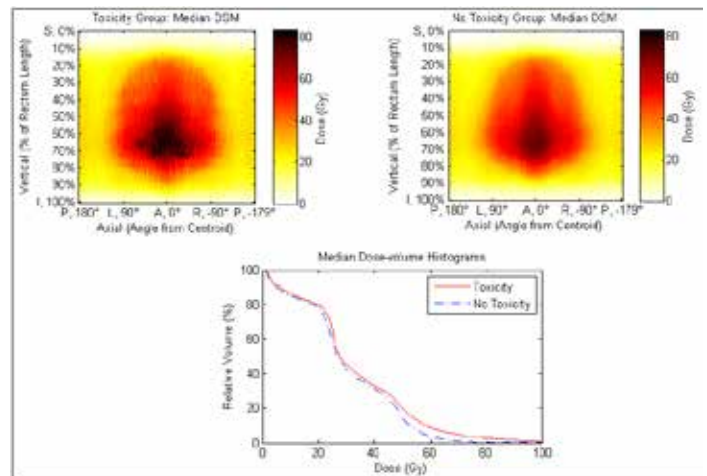
Author(s): Calyn R. Moulton¹, Michael House¹, Victoria Lye², Colin Tang², Michele Krawiec², Tim St Pierre¹, David J. Joseph², James W. Denham³, Martin A. Ebert²

¹School Of Physics, The University of Western Australia, Crawley/WA/AUSTRALIA, ²Radiation Oncology, Sir Charles Gairdner Hospital, Nedlands/WA/AUSTRALIA, ³School Of Medicine And Population Health, The University of Newcastle, Callaghan/NSW/AUSTRALIA

OBJECTIVE: Are post-registration rectum dosimetric parameters and rectum dose-surface maps (DSM) different for groups of patients who did or did not have late bleeding?

Methods: 91 patients received external beam radiotherapy (EBRT) in 23 fractions of 2 Gy and high-dose-rate (HDR) brachytherapy in 3 fractions of 6.5 Gy. The EBRT CT was registered to the HDR CT with a rigid plus deformable multi-pass method (RD) or a rigid plus scale plus deformable multi-pass (RSD) method in Velocity Advanced Imaging. The unregistered EBRT and registered HDR dose distributions were summed after converting to equieffective doses at 2 Gy/fraction ($\alpha/\beta = 3$ and 5.4). The V1Gy to V100Gy (increment=1) and D1% to D100% (increment=1), D1cc, D2cc, D5cc and D10cc were calculated. Rectum DSMs were obtained by virtually unfolding the rectum surface dose slice-by-slice. Patients were classed into toxicity or no toxicity groups if they did or did not have a grade 2 LENT-SOMA rectal bleed from the period 3 months after radiotherapy onwards. The DSMs were spatially analysed by thresholding DSMs from 1 Gy to 100 Gy (increment=1). This analysis included the inferior-superior extent, left-right extent, area, perimeter, compactness, circularity and ellipse fit parameters. Significance ($p < 0.05$) for median comparisons between groups was assessed via two-sided Mann-Whitney U-tests.

Results: The dosimetric and DSM results in the figure are for the RSD registration, HDR dose calculated with the Acuros algorithm and an α/β of 3; however, results were similar for alternatives. The V44Gy, V45Gy, V48Gy to V71Gy, D1% to D28%, D1cc, D2cc, D5cc and D10cc were significantly greater for toxicity (N=18) versus no toxicity (N=73) groups. Patients with toxicity had significantly greater left boundaries, greater right boundaries, greater widths and greater perimeters for various DSM isodose contours (e.g. 51-66 and 83 Gy). The ellipse fits at a number of dose thresholds (e.g. 83 Gy) indicated significantly greater lateral extent, greater eccentricity and greater horizontal orientation for bleeders. The lateral centroid components for some dose thresholds (e.g. 83 Gy) were significantly further to the right for bleeders. The proportions of ellipses filled by various thresholded doses (e.g. 50 Gy) were significantly greater for bleeders.



Conclusion: Multiple dose-volume parameters, derived from registered plans, correlated with bleeding. The lateral coverage of intermediate and high-dose regions was greater and located further to the right for bleeders. For bleeders, the doses in high-dose regions were greater and more contained within fitted ellipses.

ACKNOWLEDGEMENTS: NHMRC (1006447) and University of Western Australia.

SP078.4 - Implementation of Permanent Breast Seed Implants in British Columbia: Innovation and Early Results

Author(s): Michelle Hilts¹, Deidre Batchelar¹, Daniel Morton², Juanita Crook³

¹Medical Physics, BC Cancer Agency - Southern Interior, Kelowna/CANADA, ²Physics And Astronomy, University of Victoria, Victoria/CANADA, ³Radiation Oncology, BC Cancer Agency - Southern Interior, Kelowna/CANADA

Purpose:

Permanent breast seed implant (PBSI) is an attractive option for women with early stage breast cancer as the procedure is completed in a single outpatient session. In 2012 the BC Cancer Agency became only the second institution worldwide to offer this novel technique pioneered in Toronto. In this work we present technique innovations introduced at BCCA as well as preliminary results from our first 15 patients.

MATERIALS AND Methods:

Modelled after the technique introduced by Pignol et al, we use a template and US guided technique to implant needles pre-loaded with Pd-103 into the breast. CT planning (MIM Symphony) is undertaken to deliver 90Gy to a PTV, seroma+1.25cm cropped to skin and chestwall. A pre-treatment simulation step is included to check template position and transfer key landmarks from the treatment plan onto the skin. In the operating room a portable laser is used to confirm positioning and US is used throughout the procedure to monitor needle placement. Post-implant dosimetry is assessed using CTs obtained on day of implant (day0:reported here) and one month post-implant. Deformable image registration is used to define the post-implant seroma from the pre-implant contour. Implant quality is assessed on an evaluative PTV (PTVeval), seroma+0.5cm. In house software was utilized to measure seed displacements (planned to implanted positions) in 10 cases. Patient satisfaction is also reported.

Results:

Pre-implant volumes ranged from 4.1–20.2cc (median 7.0cc) and 31.4–114.2cc (median 47.4cc) for seroma and PTVs respectively. PTVs were well covered with V100 (mean±SD) of 96.1±2.7% using 77±22 seeds in 17±5 needles. Post-implant PTV_{eval} dosimetry (day0) for all patients was (mean±SD): 90.4±9.4%, 86.9±10.8% and 64.4±14.9% for V90, V100 and V150 respectively and 87.1±25.3Gy for D90%. The corresponding PTV_{eval} coverage (mean±SD) for the last 8 implants illustrates rapid convergence to consistently high quality implants: 96.5±2.6%, 93.6±4.6% and 70.9±12.1% for V90, V100 and V150 respectively and 103±16Gy for D90%. Mean seed displacement was 0.9±0.5cm for the 10 patients where seed matching was performed. All patients were very or extremely satisfied with the procedure, citing the single day treatment as a highlight.

Conclusions:

These early results indicate that PBSI is a safe and desirable treatment option for women with low risk breast cancer and technical innovation aimed at increased technique reproducibility has contributed to a rapid learning curve. Our aim, through ongoing technical innovation, is to continue to improve the standardization and reproducibility of PBSI to ultimately enable widespread implementation.



Figure: Pd-103 in seroma

SP078.5 - Estimation of α/β for late rectal bleeding via minimum dosimetric differences for prostate cancer patients treated with external beam radiotherapy versus a HDR brachytherapy boost after external beam radiotherapy

Author(s): Calyn R. Moulton¹, Michael House¹, Victoria Lye², Colin Tang², Michele Krawiec², Angel Kennedy², Tim St Pierre¹, David J. Joseph², James W. Denham³, Martin A. Ebert²

¹School Of Physics, The University of Western Australia, Crawley/WA/AUSTRALIA, ²Radiation Oncology, Sir Charles Gairdner Hospital, Nedlands/WA/AUSTRALIA, ³School Of Medicine And Population Health, The University of Newcastle, Callaghan/NSW/AUSTRALIA

OBJECTIVE: To estimate the α/β for late rectal bleeding via the difference in dosimetric parameters for patients treated with external beam radiotherapy (EBRT) versus a combined treatment of EBRT and high-dose-rate (HDR) brachytherapy.

Methods: In the RADAR trial, 723 patients received 66, 70 or 74 Gy (2 Gy/fraction) of EBRT and 91 patients received 46 Gy (23 fractions) of EBRT and 19.5 Gy (3 fractions) of HDR brachytherapy. HDR dose was calculated with both the Acuros and TG43 algorithms. For combined treatments, the EBRT CT was registered to the HDR CT with a rigid plus scale plus deformable multi-pass (RSD) method

in Velocity Advanced Imaging. The rectum D1cc, D2cc, D5cc and D10cc were calculated for patients receiving EBRT only and patients receiving combined EBRT/HDR. These parameters were correlated with bleeding for patients receiving combined EBRT/HDR. Patients from the two treatments were classed into toxicity groups if they had at least a certain grade (1, 2, or 3) LENT-SOMA rectal bleed from the period 3 months after radiotherapy onwards. The toxicity numbers for the EBRT only/combined treatment groups were 34/374, 18/183 and 5/66 for grades ≥ 1 , ≥ 2 and ≥ 3 . The parameters for patients with toxicity after EBRT only versus after combined EBRT/HDR treatments were compared as follows. (1) The medians of dosimetric parameters for the EBRT only toxicity group were converted to equieffective doses at 2 Gy/fraction with α/β from 0-11 (Increment=0.01). (2) This conversion was also applied to medians of the dosimetric parameters from the unregistered EBRT and registered HDR components for the combined treatment toxicity group. (3) The total median parameters for the combined treatment toxicity group were obtained by summing the converted median dosimetric parameters for the unregistered EBRT and registered HDR components. (4) The α/β with the smallest squared difference between the median converted dosimetric parameters for the two groups was determined and accepted if the squared difference was less than 0.01. (5) Bootstrapped 95% confidence limits (CI) for the α/β were calculated via (1)-(4) after resampling the two groups with replacement (10,000 resamples).

Results: The squared difference criteria for the median dosimetric values were not satisfied for some dosimetric parameters and toxicity criteria. The α/β for the dosimetric parameters, toxicity criteria and TG43/Acurus algorithm options varied from 0.710 to 4.84. The variability was greater across the parameters and toxicity criteria. The α/β (95% CI) for the parameters (toxicity criteria) were 3.98 (0.260-10.1), 0.710 (0.100-6.18), 1.49 (0.0900-10.7) and 3.51 (2.45-8.03) for the D1cc (≥ 1), D2cc (≥ 1), D5cc (≥ 2) and D10cc (≥ 3) options applied with the Acuros algorithm. The mean α/β and mean 95% CI across the parameters, toxicity criteria and TG43/Acurus algorithm options were 2.75 and 0.834-8.94.

Conclusion: The estimated mean α/β was 2.75 for late rectal bleeding. A conclusion on the early/late responding nature of the rectum was not feasible due to variability across parameters and wide confidence intervals. An increased sample size may result in more consistent and precise values across the dosimetric parameters and toxicity criteria.

ACKNOWLEDGEMENTS: NHMRC (1006447) and University of Western Australia.

SP078.6 - Failure Mode and Effects Analysis (FMEA) for improving quality assurance for Image-Guided High Dose Rate (HDR) brachytherapy

Author(s): Shada Wadi-Ramahi, Waleed Al-Najjar, Belal Mofattah Biomedical Physics, King Faisal Specialist Hospital and Research Center, Riyadh/SAUDI ARABIA

Purpose:

To evaluate and develop quality assurance (QA) for image-guided high dose rate (HDR) brachytherapy by applying the failure mode and effects analysis (FMEA).

Method:

We started by mapping the major process tree of HDR brachytherapy, and highlighting the image-dependent steps. "Wrong Treatment Site" was identified as being the ultimate end-point that might result from errors in imaging procedures, and fault tree analysis (FTA) for this error was mapped with all the branches leading to it. The use of conventional imaging (2D) with isocentric and non-isocentric machines was also included for completeness. Potential risk for

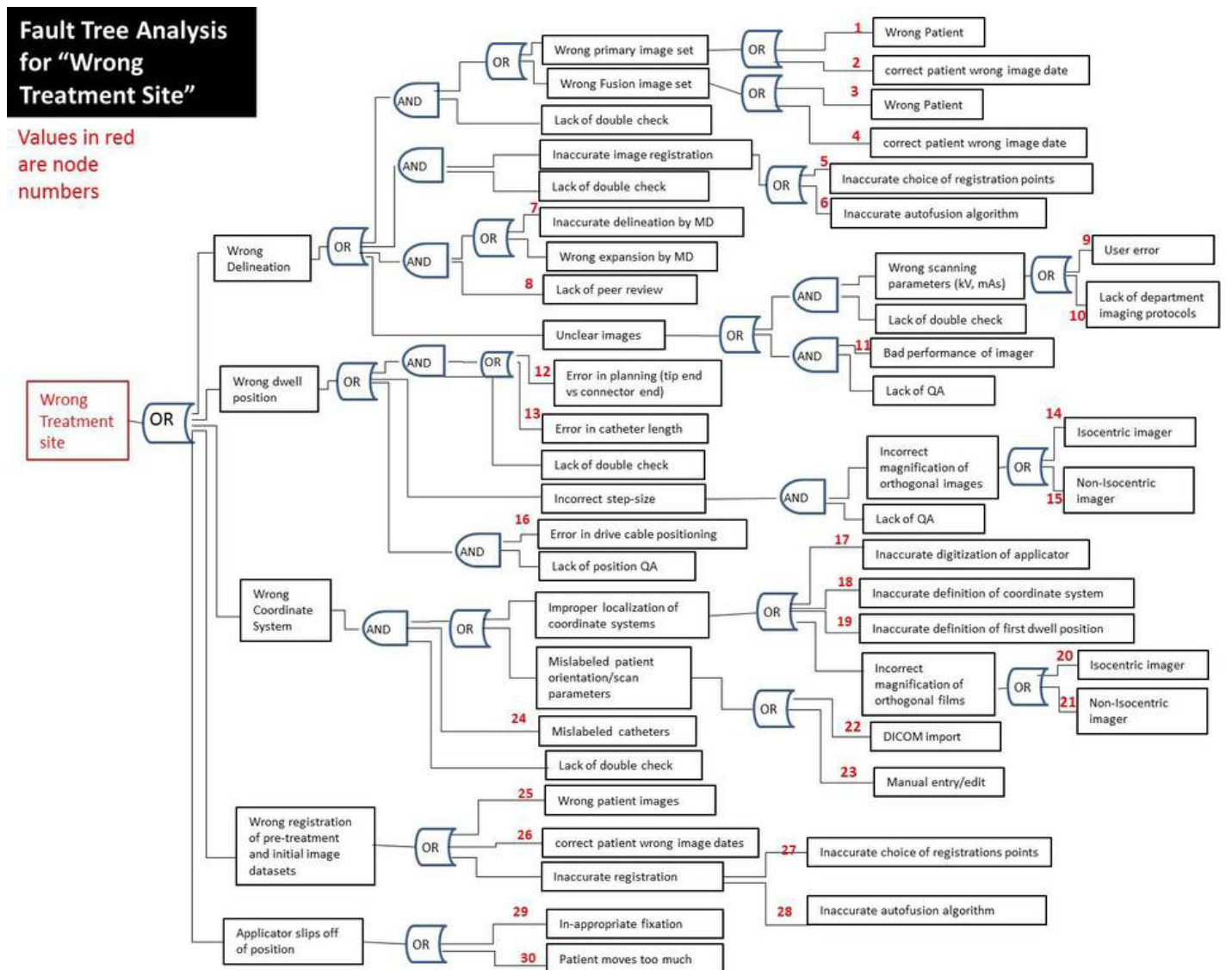
each branch was scored according to the risk priority number (RPN) scoring system (out of 10).

Results:

Fourteen major steps were identified: TPS commissioning, source installation and initial QA, patient diagnosis and selection, applicator insertion, primary image set acquisition, secondary image set acquisition, Image transfer and registration, organ delineation, applicator and coordinate system definition, plan optimization and dose calculation, plan transfer to treatment console station, source connectivity to patient, image verification of applicator position before treatment, and finally treatment delivery. Of these steps, six are image dependent and all leads to one error “Wrong treatment site”. The FTA for “wrong treatment site” identified 30 potential failure nodes (2 are machine related, the rest are human related), see attached figure. Out of the 30, eleven are non-image related. Total RPNs ranged from 11 to 254. RPN for image arm ranged from 11 to 254, whereas for non-images RPN ranged from 45 – 192. RPN higher than 100 was considered potential for high risk. The errors were grouped into three major groups (human, procedural or machine). For each set, we took the analysis further by proposing corrective actions, such as development and implementation of departmental guidelines and QA.

The FTA, revealed a point during the HDR process (nodes 29 and 30) where QA is lacking. Those are non-image related; however, the error can be stopped from propagating by implementing a pre-treatment image verification procedure, which can be achieved by several methods depending on the user’s capabilities.

Conclusion: We have applied FMEA process to image-guided HDR brachytherapy. The fault tree for “wrong treatment site” error identified areas of potential high risk and exposed areas where QA was lacking in the whole procedure. This helped us in re-prioritizing our QA procedures and guidelines.



SP079 - Motion Management: Part 1

TRACK 04: RADIATION ONCOLOGY

SP079.1 - Feasibility of respiratory gated radiotherapy using real-time positron emission tracking

Author(s): Marc Chamberland¹, Malcolm R. Mcewen², Bryan R. Muir², Tong Xu¹

¹Department Of Physics, Carleton University, Ottawa/ON/CAN-ADA, ²Measurement Science And Standards, National Research Council, Ottawa/ON/CANADA

Tumor motion due to respiratory motion can lead to dosimetric errors in the delivery of radiotherapy treatments. Respiratory gating can be used to address this issue but requires external markers or motion surrogates to monitor the breathing motion. However, these are not always well correlated to the true position of the tumor. We present a feasibility study of respiratory gated radiotherapy using a real-time positron emission tracking system.

The tracking system, called PeTrack, uses implanted low activity positron emission markers and position sensitive gamma ray detectors to track breathing motion in real-time. A LabVIEW interface is developed to synchronize gating between the signal from PeTrack and the NRC Elekta *Precise* linac. Prototype PeTrack detectors were mounted on an aluminum frame surrounding a dynamic anthropomorphic thorax phantom (Figure 1). Dose was delivered to the phantom in 500 monitor unit increments with a 3x3 cm² photon beam and with 6 and 10 MV nominal beam energies. Radiochromic films were inserted in the phantom to measure spatial dose distributions. The phantom lung insert was translated in the inferior/superior direction with sinusoidal and real patient breathing motion (± 10 mm amplitude). The motion was tracked using a small ²²Na fiducial marker (0.43 MBq activity) embedded in the lung insert. The beam was turned off when the marker was outside of a 5-mm one dimensional gating window.

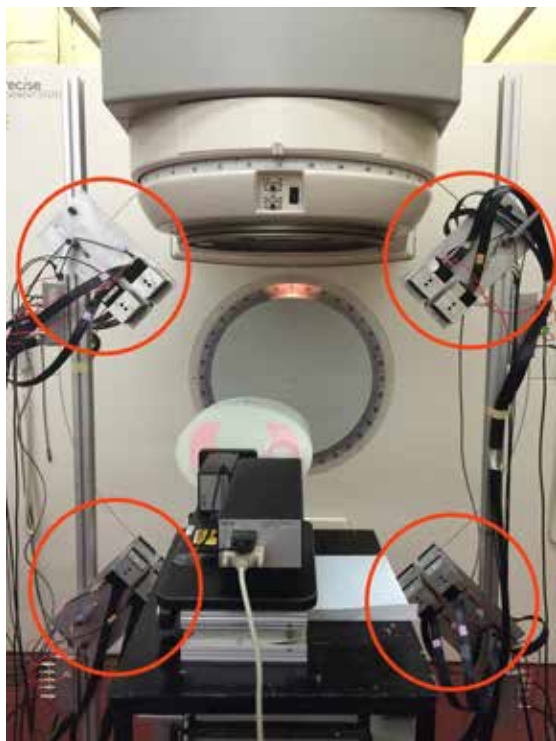


Figure 1: Prototype PeTrack detectors around dynamic phantom.

Clear improvement of the dose distribution is observed between gated and non-gated delivery (Figure 2). Monitoring of the beam on/off times show synchronization with the location of the marker within the latency of the system.

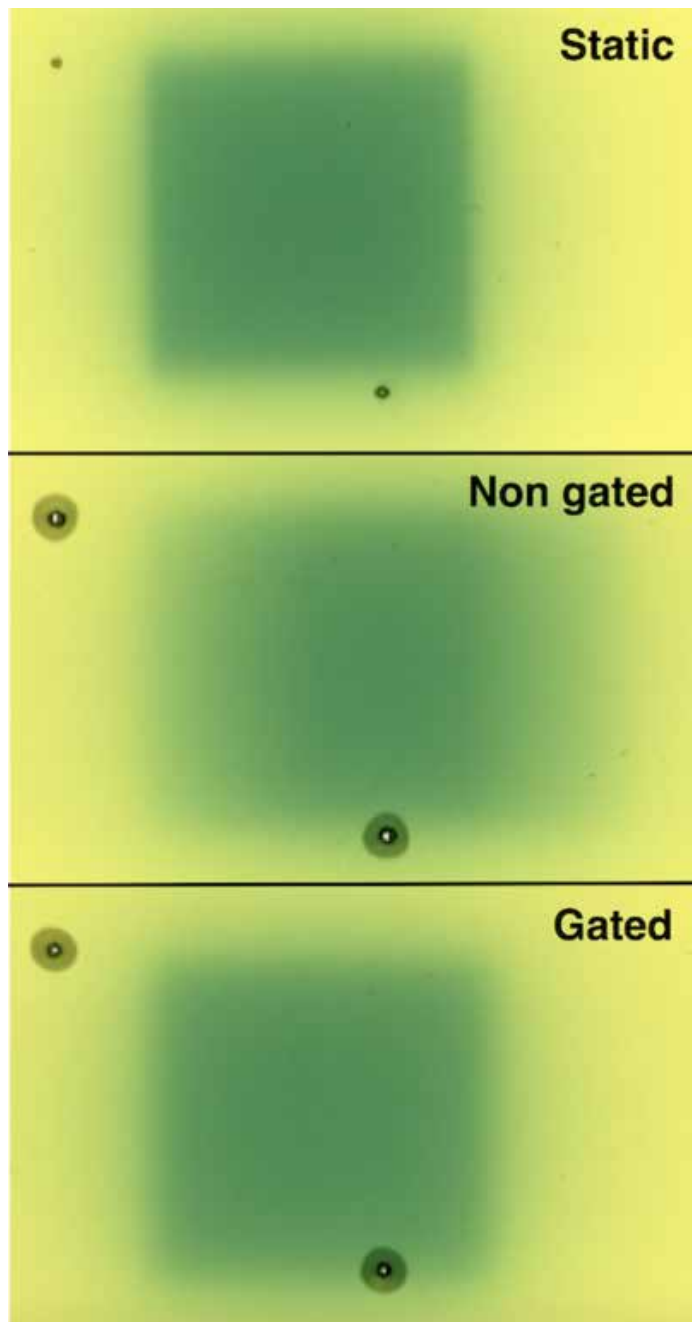


Figure 2: Radiochromic films after exposure.

This study shows the feasibility of using positron emission tracking to improve respiratory gated radiotherapy.

SP079.2 - The first kilovoltage intrafraction monitoring trial for gated prostate radiotherapy: Accuracy and dosimetric results

Author(s): Prabhjot Juneja¹, Jin A. Ng², Emma Colvill², Ricky O'Brien², Thomas Eade³, Andrew Kneebone³, Per R. Poulsen⁴, Jeremy T. Booth¹, Paul Keall²

¹Institute Of Medical Physics, School Of Physics, University of Sydney, Sydney/NSW/AUSTRALIA, ²Radiation Physics Laboratory, Sydney Medical School, University of Sydney, Sydney/AUSTRALIA, ³Northern Sydney Cancer Centre, Royal North Shore Hospital, Sydney/AUSTRALIA, ⁴Department Of Oncology, Aarhus University Hospital, Aarhus/DENMARK

A new real-time IGRT system, kilovoltage intrafraction monitoring (KIM), is undergoing clinical evaluation through a first-in-world prospective clinical trial for prostate cancer patients. KIM uses kV fluoroscopy to monitor, in real-time, the 3D position of radio-opaque markers implanted into the prostate target. The real-time target position is used to guide the treatment: if the prostate moves outside the tolerance (motion exceeding 3mm for 5 seconds) the beam is paused and the patient is repositioned. The goal of this study is to investigate the localisation accuracy and dosimetric impact of the KIM system, in planned 30-patient gated prostate cancer radiotherapy trial.

To date, three patients have completed their 40-fraction treatments. Simultaneous intra-fraction kV and MV images from the 116 fractions were used offline to measure the accuracy of the KIM real-time measurements. The measured triangulated kV-MV marker positions were considered to be ground truth, and were compared to the KIM measurements. For the dosimetry, dose delivered during each fraction with KIM was measured using a motion-synchronized isocenter shift dose reconstruction method. In the fractions with a gating event, dose reconstruction was also carried out for a simulated treatment scenario with no KIM gating correction representing the current standard of care. Target and normal tissue dose volume statistics were compared for the planned treatment delivery, delivery with KIM gating and delivery with no KIM correction (see figure 1). KIM has a finite gating threshold and therefore, in the presence of motion, it will deviate from the planned treatment.

The mean error \pm standard deviation of KIM in the LR, SI and AP directions was 0.14 ± 0.50 , 0.38 ± 0.27 , and -0.48 ± 0.45 mm respectively. In total, 14 fractions had successful KIM gating corrections. Prostate motion with KIM corrections and simulated with no KIM corrections were 1.9 ± 1.2 mm and 3.8 ± 1.4 mm respectively. Mean (range) differences between the planned and KIM corrected doses and the planned and no KIM correction doses were respectively: PTV D95% -1.4 ($-3.4, 0.7$) & -3.1 ($-10.9, -0.7$); CTV D100% -0.8 ($-2.8, 0.7$) & -0.1 ($-7.0, 1.9$); rectum V65% -3.5 ($-9.4, 5.7$) & -4.9 ($-11.2, 18.7$); and bladder V65% 1.58 ($-0.9, 5.8$) & 2.8 ($-1.0, 10.4$).

In conclusion, the results demonstrated that both the accuracy and precision of KIM system are sub-millimetre, and KIM gating improves the agreement between the planned and delivered treatments for prostate radiotherapy. The KIM technology has wide-scale applicability as it is implemented on a standard linear accelerator with little modification.

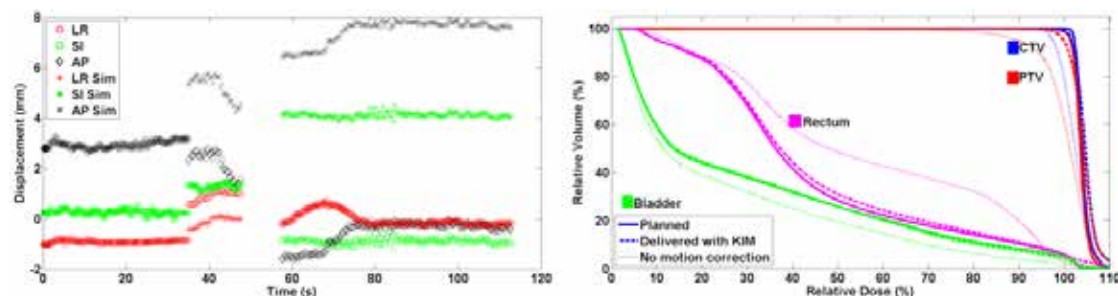


Figure 1. Sample motion (left) during the two VMAT, and corresponding dose volume histograms (right) of the clinical target volume (CTV), planning target volume (PTV), bladder and rectum for the planned, delivered with KIM gating, and simulated delivery without KIM gating correction (no motion correction). This fraction had two gating events.

SP079.3 - The impact of audio-visual biofeedback with a patient-specific guiding waveform on respiratory motion management: Comparison of two different respiratory management systems

Author(s): Yujiro Nakajima¹, Noriyuki Kadoya¹, Satoshi Kida¹, Takayuki Kanai¹, Kazuma Kishi², Kiyokazu Sato², Suguru Dobashi³, Ken Takeda³, Haruo Matsushita¹, Keiichi Jingu¹

¹Radiation Oncology, Tohoku University School of Medicine, Sendai/JAPAN, ²Radiation Technology, Tohoku University Hospital, Sendai/JAPAN, ³Radiological Technology, School Of Health Sciences, Faculty Of Medicine, Tohoku University, Sendai/JAPAN

Purpose: Irregular breathing can influence the outcome of four-dimensional computed tomography imaging for causing artifacts. Audio-visual biofeedback systems associated with patient-specific guiding waveform are known to reduce respiratory irregularities. In Japan, abdomen and chest motion self-control devices (Abches), representing simpler visual coaching techniques without guiding waveform are used instead; however, no studies have compared these two systems to date. Here, we evaluate the effectiveness of respiratory coaching to reduce respiratory irregularities by comparing two respiratory management systems.

Methods: We collected data from eleven healthy volunteers. Bar and wave models were used as audio-visual biofeedback systems. Abches consisted of a respiratory indicator indicating the end of each expiration and inspiration motion (Fig. 1). Respiratory variations were quantified as root mean squared error (RMSE) of displacement and period of breathing cycles.

Results: All coaching techniques improved respiratory variation, compared to free-breathing. A typical case study showing improvements regarding respiratory irregularity is summarized in Fig. 2. Displacement RMSEs were 1.43 ± 0.84 , 1.22 ± 1.13 , 1.21 ± 0.86 , and 0.98 ± 0.47 mm for free-breathing, Abches, bar model, and wave model, respectively. Free-breathing and wave model differed significantly. Period RMSEs were 0.48 ± 0.42 , 0.33 ± 0.31 , 0.23 ± 0.18 , and 0.17 ± 0.05 s for free-breathing, Abches, bar model, and wave model, respectively. For variation in both displacement and period, wave model was superior to free-breathing, bar model, and Abches. The average reduction in displacement and period RMSE compared with wave model were 27% and 47%, respectively.

Conclusions: This study was to evaluate the efficacy of audio-visual biofeedback to reduce respiratory irregularity compared with Abches. Our results showed that audio-visual biofeedback combined with a wave model can potentially provide clinical benefits in respiratory management, although all techniques could reduce respiratory irregularities.

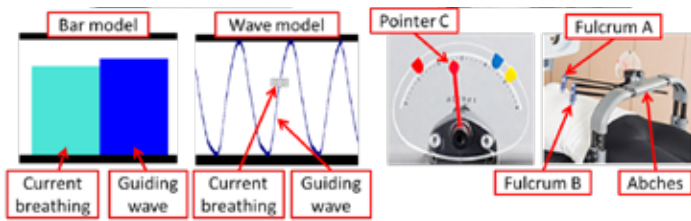


Fig. 1 (a) Audio-visual biofeedback system. (b) Abches system.

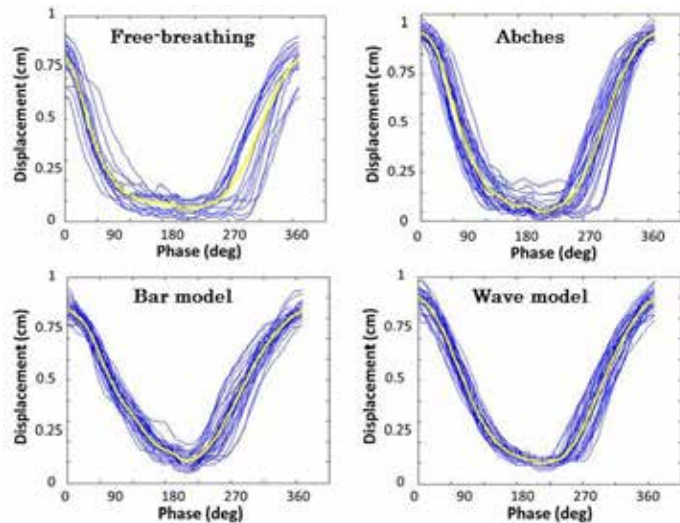


Fig. 2 Example of a respiratory trace with individual breathing cycle (blue line) and average waveform (yellow line).

SP079.4 - Tracking Accuracy for Robotic Radiosurgery in the Liver

Author(s): Jeff D. Winter¹, Raimond Wong², Anand Swaminath², Tom Chow¹

¹Medical Physics, Juravinski Cancer Center, Hamilton/CANADA, ²Oncology, McMaster University, Hamilton/CANADA

Cyberknife® robotic radiosurgical treatment of liver employs an on-line motion management system to track and compensate for target motion during free-breathing. Lesion tracking on the Cyberknife is achieved using a room-mounted orthogonal x-ray system to localize internal fiducial markers as well as an optical camera system to measure the position of the patient’s abdomen during breathing. The system establishes a correlation model linking internal target position to an external optically-tracked surrogate to enable near-real-time robotic adjustments of the linear accelerator. However, inherent system delays (115 ms) require a prediction algorithm to estimate the future position. Throughout treatment, periodic x-ray images are collected to verify and update this internal-external correlation model.

In this study, our aim was to quantify key uncertainties in the targeting of liver lesions on the Cyberknife system. We analyzed the logged Cyberknife tracking information for a total of 28 patient treated over 124 fractions and isolated treatment images collected immediately prior to beam delivery. To assess target amplitude and absolute prediction errors, we isolated 20 s time intervals surrounding each treatment x-ray image. We computed target amplitudes using peak/valley detection and prediction errors using the absolute

difference between the predicted position and the modeled position calculated after 115 ms had elapsed. We computed model correlation errors using the difference between the correlation model’s position estimate and the internal fiducial position from x-ray imaging. To estimate overall uncertainty, we quadratically summed the correlation, prediction and end-to-end targeting error ($\pm 0.5 \text{ mm}^3$) in each direction. We also tested the linear correlation between target amplitude and tracking errors for each direction.

Results showed that the cranio-caudal direction exhibited the greatest correlation and prediction errors, but total radial error was less than 5 mm (Table 1). Significant weak correlations ($r = 0.08 - 0.19$, $p < 0.0001$) existed between target amplitude and correlation errors in all directions except left-right; whereas, strong correlations existed with prediction errors ($r = 0.55 - 0.67$, $p < 0.0001$) for all directions.

Based on the overall 3D radial position errors, results suggest that for 95 % of the beam delivery time the target centroid will be within 4.6 mm of the planned target volume. These results along with consideration for internal fiducial migration, target rotation and liver deformation may help guide planning target volume expansion.

1. Pepin EW et al., Med Phys. 2011 38(7):4036-44

Table 1. Tracking errors for Cyberknife liver treatments. LR = left-right, AP = anterior-posterior, CC = cranial-caudal.

Error	Direction	Mean (mm)	Std Dev. (mm)	95th percentile (mm)
Correlation	LR	0.71	1.01	2.15
	AP	0.64	0.86	1.80
	CC	1.20	1.68	3.50
	Radial	1.74	1.26	4.19
Prediction	LR	0.15	0.09	0.31
	AP	0.09	0.07	0.22
	CC	0.17	0.10	0.36
	Radial	0.26	0.14	0.51
Total	LR	1.24	N/A	2.39
	AP	1.19	N/A	2.07
	CC	1.57	N/A	3.66
	Radial	2.47	N/A	4.56

SP079.5 - Deep Inspiration breath hold lung SBRT- Can Flattening Filter Free beam based VMAT combined with gated CBCT facilitate precise treatment delivery with sufficient dosimetric accuracy?

Author(s): Vallinayagam Shanmuga Subramanian¹, Vellian Subramani², Kala Subramanian¹, Shanmugam Thirumalai Swamy¹, Murugesan Kathirvel³, Gandhi Arun³

¹Radiation Oncology, yashoda hospital, Hyderabad/INDIA, ²Radiation Oncology, All India Institute of Medical Sciences, New Delhi/INDIA, ³Research And Development Centre, Bharathiar University, Coimbatore/INDIA

Objective(s):The combination of VMAT technique using high dose rate FFF beams along with the computer controlled deep inspiration breath hold technique provides opportunity to further reduce treatment margins in lung SBRT over free breathing (FB) approaches. The aim of this study was to investigate the potential benefits of VMAT based DIBH SBRT over FB SBRT. This was performed by conducting a dosimetric comparison of VMAT technique with IMRT

technique using both DIBH & FB approaches.

Materials/Methods: Ten lung SBRT patients treated using 6MVFFF-VMAT based DIBH technique were retrospectively selected for this study. Treatment planning were performed in both DIBH & FB patient data set using IMRT & VMAT techniques. Treated patients dose prescription of 60 Gy in 5 fractions was used as standard dose prescription for the techniques. Plan evaluation was performed with RTOG0813 treatment planning criteria. Paired t test was used for statistical analysis. The dosimetric accuracy of the gated VMAT was assessed using a global gamma index (3% dose difference, 3mm DTA (Distance to agreement) and measured with 2D detector attached to a solid cube phantom. Actual patients number of breath hold cycles and total delivery time with breath hold phases of 20/25s and recovery phases of 25 seconds were also incorporated during QA procedures.

Results: Irrespective of the techniques, DIBH approach could very well satisfy the RTOG0813 treatment planning criteria for the studied patients. As shown in table mean average Dose conformity of 1.03 ± 0.012 for VMAT-DIBH was significantly better as compared with IMRT-FB, VMAT FB & IMRT-DIBH techniques ($p < 0.03$). Mean average Lung V20Gy volume was 4.84 ± 2.4 , 5.22 ± 2.5 , 10.07 ± 2.3 , and $10.27 \pm 2.04\%$ for VMAT-DIBH, IMRT-DIBH, VMAT-BH, and IMRT-BH respectively. In terms of Heart V15cc and Esophagus V5cc maximum dose, VMAT-DIBH plans exhibit the lowest as compared with the other techniques. Both the IMRT & VMAT-DIBH plans could be accurately delivered despite undergoing multiple beam on/off cycles, with mean QA pass rate over 95% (IMRT-DIBH VS VMAT-DIBH - Mean 96.42 ± 1.2 vs 97.8 ± 1.1). Treated DIBH patients gated CBCT analysis showed that average mean setup error was 2.8mm (range 1.5- 4.2mm) in latero- lateral, 3.4mm (range 2.2- 4.8mm) in antero-posterior, 3.2mm (range 2.4- 5.6mm) in cranio-caudal directions.

Table-1

RTOG-0813 treatment planning parameters Mean Average	IMRT – FB	IMRT-BH	VMAT-FB	VMAT-BH	RTOG limit for none deviation
PTV - CI	1.098 ± 0.055	1.068 ± 0.043	1.062 ± 0.038	1.031 ± 0.23	<1.2
P value	0.109		0.083		
Lung V ₂₀ Gy (%)	10.27 ± 5.22	5.22 ± 2.5	10.07 ± 2.3	4.84 ± 2.4	<15%
P value	0.0001		0.0001		
Lung V ₅ Gy (%)	30.11 ± 9.85	19.27 ± 6.88	32.17 ± 9.57	19.19 ± 6.4	-
P value	0.01		0.002		
Heart V ₁₅ cc (cGy)	1157 ± 1034	1013 ± 677	1073 ± 903	947 ± 770	<3200
P value	0.6182		0.8688		
Esophagus V ₅ cc(cGy)	1471 ± 592	1404 ± 667	1362 ± 515	1252 ± 552	<2750
P value	0.812		0.649		

Results:

The results from this study showed that with proper patient coaching FFF beam based DIBH lung SBRT combined with gated CBCT facilitate precise treatment delivery with sufficient clinical dosimetric accuracy.

SP079.6 - Feasibility of markerless tumor tracking by sequential dual-energy fluoroscopy on a clinical tumor tracking system

Author(s): Jennifer Dhont, Kenneth Poels, Dirk Verellen, Koen Tournel, Thierry Gevaert, Femke Steenbeke, Mark De Ridder
Radiotherapy, Universitair Ziekenhuis Brussel, Brussels/BELGIUM

The purpose was to evaluate the feasibility of markerless tumor tracking through the implementation of dual-energy imaging into the current clinical dynamic tracking workflow of the Vero SBRT system. An innovative approach of fast sequential fluoroscopy sequences was implemented omitting the pre-requisite of fast-switching kV-generators.

Two sequential 20s (11Hz) fluoroscopy sequences were acquired at the start of one fraction for 7 patients treated with DT on the Vero system. Sequences were acquired using 2 on-board kV imaging systems located at ±45° from the MV beam axis, at respectively 60kVp (3.2mAs) and 120kVp (2.0mAs). Table 1 shows the kV imager positions that were selected based on marker visibility. Prior to evaluation, the implanted fiducial was removed on all images to be evaluated, to not bias the results. Offline, a normalized cross-correlation algorithm was applied to anatomically match the high (HE) and low-energy (LE) images. Per breathing phase (inhale, exhale, maximum inhale and maximum exhale), the five best matching HE-LE couples were extracted for DE subtraction. A contrast analysis according to gross tumor volume (GTV) was conducted between the DE and HE images based on contrast to noise ratio (CNR). Improved tumor visibility was quantified using an improvement ratio (IR=CNR_{DE}/CNR_{HE}).

DE subtraction through sequential fluoroscopy was incorporated on the Vero system with only minor adjustments to the imaging settings. Removing the implanted fiducial was successful on all images. HE-LE sequence matching was effective for 12 of 14 imaging angles, correlation coefficients per imaging angle can be found in Table 1.

Overlying bony anatomy was removed on all DE images; Figure 2 shows an example. CNR per patient and per imaging angle can be found in Table 1. With the exception of two imaging angles, the DE images showed no significantly improved tumor visibility compared to HE images. Qualitatively, it was observed that for these imaging angles that showed no significantly improved CNR, the tumor tissue could not be reliably visualized on neither HE nor DE images due to a total or partial overlap with other soft tissue.

Dual-energy imaging by sequential fluoroscopy was shown feasible by implementing an additional fluoroscopy sequence into the DT workflow of the Vero system. However, for most imaging angles, DE images did not provide improved tumor visibility over single-energy images, most likely due to an overlap of the tumor with other soft-tissue. Optimizing imager settings and angles is likely to improve the efficacy of dual-energy imaging.

Table 1 Mean correlation coefficient per imager (Im.) between high- (HE) and low-energy (LE) images, contrast-to-noise ratio (CNR) according to gross-tumor-volume for HE and dual-energy (DE) images, and relative improvement ratio (IR=CNR^{DE}/CNR^{HE})

	Correlation coefficient	CNR ± SD		IR
		HE	DE	
patient 1 Im.1 125°	0.954 ± 0.011	0.53±0.15	0.21 ± 0.08	0.41 ± 0.10 p = 0.057
patient 1 Im.2 35°	0.936 ± 0.009	0.23 ± 0.08	0.40 ± 0.11	1.87 ± 0.63 p = 0.323
patient 2 Im.1 315°	0.991 ± 0.001	0.17 ± 0.02	0.12 ± 0.07	0.68 ± 0.42 p = 0.090
patient 2 Im.2 225°	0.980 ± 0.002	0.51 ± 0.21	0.55 ± 0.14	1.14 ± 0.28 p = 0.833
patient 3 Im.1 45°	0.976 ± 0.031	0.49 ± 0.14	0.63 ± 0.11	1.42 ± 0.56 p < 0.005
patient 3 Im.2 315°	0.784 ± 0.028	1.07 ± 0.28	-	-
patient 4 Im.1 348°	0.969 ± 0.005	0.22 ± 0.08	0.11 ± 0.09	0.57 ± 0.64 p = 0.009
patient 4 Im.2 78°	0.859 ± 0.032	0.85 ± 0.24	0.99 ± 0.11	1.24 ± 0.26 p = 0.021
patient 5 Im.1 250°	0.988 ± 0.014	0.30 ± 0.13	0.27 ± 0.13	0.89 ± 0.05 p = 0.517
patient 5 Im.2 160°	0.983 ± 0.017	0.03 ± 0.02	0.14 ± 0.03	6.52 ± 5.42 p < 0.005
patient 6 Im.1 320°	0.652 ± 0.019	0.11 ± 0.08	-	-
patient 6 Im.2 230°	0.975 ± 0.029	0.47 ± 0.05	0.45 ± 0.06	0.96 ± 0.03 p = 0.292
patient 7 Im.1 65°	0.884 ± 0.024	0.36 ± 0.19	0.31 ± 0.16	0.93 ± 0.28 p = 0.426
patient 7 Im.2 75°	0.985 ± 0.004	0.12 ± 0.02	0.11 ± 0.02	0.87 ± 0.06 p = 0.029

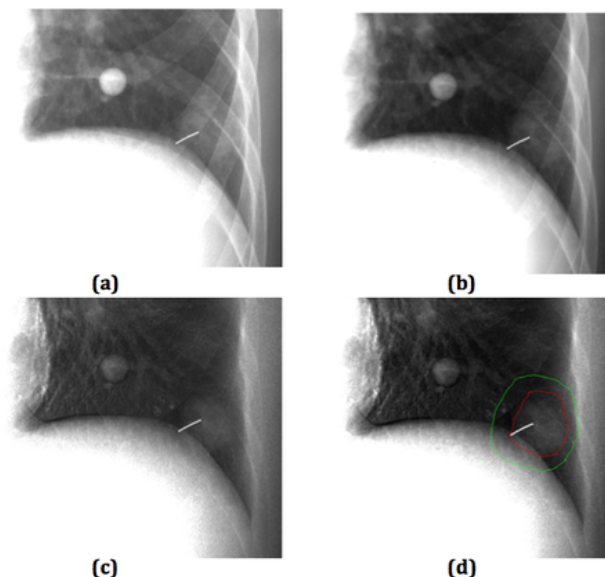


Fig. 1 A low-energy (a) and high-energy (b) image acquired at 160°, with the corresponding DE subtraction image without (c) and with (d) GTV and PTV contour, from a patient with a metastatic lesion in the right lower lobe.

SP080 - Other Radiation Oncology: Part 2

TRACK 04: RADIATION ONCOLOGY

SP080.1 - Estimation of the second cancer risk from adjuvant radiation therapy for stage I seminoma of the testis

Author(s): Michalis Mazonakis¹, Theocharris Berris¹, Charalambos Varveris², John Damilakis¹

¹Department Of Medical Physics, University of Crete, Heraklion/GREECE, ²Department Of Radiotherapy, University of Crete, Heraklion/GREECE

Purpose: To estimate the second cancer risk associated with the adjuvant radiation therapy for stage I seminoma of the testis.

Methods: The study population consisted of eleven patients with stage I testicular seminoma who underwent postoperative radiation therapy with a 6 MV photon beam. Three-dimensional conformal radiotherapy plans based on CT scans were generated for all patients. Two parallel-opposed anteroposterior and posteroanterior fields were used to deliver 20 Gy to the para-aortic lymph node region. The organ equivalent dose (OED) to stomach, colon, liver and pancreas, that were partly included within the treatment volume, was determined using differential dose-volume-histograms and a plateau dose-response model. Furthermore, a previously validated Monte Carlo model of a linear accelerator producing 6 MV X-rays was employed to calculate the radiation dose at sites excluded from the primarily irradiated area. Para-aortic irradiation to 20 Gy with standard treatment field sizes was simulated on a computational humanoid phantom representing an average adult man. Monte Carlo calculations were performed to determine the average radiation dose (Dav) received by each of the following out-of-field organs: brain, salivary glands, oral mucosa, thyroid, lung, esophagus, urinary bladder and prostate. The Dav and OED values together with organ-specific risk coefficients were used to estimate the excess absolute risk (EAR) of cancer induction at the age of 70 years due to radiotherapy of a typical 35-year-old patient.

Results: Monte Carlo simulations showed that the out-of-field organ dose from para-aortic irradiation varied from 0.004 Gy to 0.37 Gy. The mean OED value for stomach, colon, liver and pancreas, as derived by the patient study, was equal to 2.50 Gy, 1.88 Gy, 1.43 Gy and 5.60 Gy, respectively. The organ-specific EAR for developing second cancer at sites outside the treatment volume was (0.002-0.9) per 10000 persons per year. The corresponding risk range for the partially in-field organs was (2.5-10.6) per 10000 persons per year. The highest EAR value was found for stomach cancer.

Conclusions: The risk of out-field cancer after adjuvant radiotherapy for stage I seminoma of the testis is low. However, the above treatment may lead to an increased probability for carcinogenesis at sites exposed to primary radiation. This elevated risk should be taken into account during the follow-up of testicular cancer survivors.

SP080.2 - 3D Slicer Gel Dosimetry Analysis: Validation of the Calibration Process

Author(s): Kevin M. Alexander¹, Csaba Pinter², Jennifer Andrea², Gabor Fichtinger², L John Schreiner³

¹Department Of Physics, Engineering Physics And Astronomy, Queen's University, Kingston/ON/CANADA, ²School Of Computing, Queen's University, Kingston/ON/CANADA, ³Department Of Medical Physics, Cancer Centre of Southeastern Ontario, Kingston/ON/CANADA

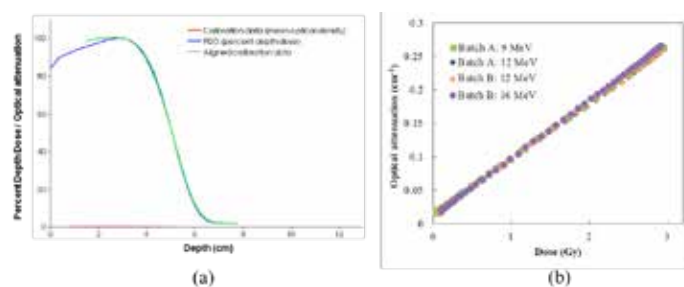
Advanced three-dimensional conformal radiation therapy tech-

niques have rapidly developed in recent years. The techniques generate dose distributions with steep dose gradients to cover the tumor and spare healthy tissue, and these deliveries need validation. Three-dimensional dosimetry tools, such as gel dosimeters, have been shown to be promising tools for measurement and verification of radiation dose deliveries, particularly during commissioning of new treatment techniques.

Gel dosimetry consists of three-dimensional chemical systems that quantify the effects of radiation-induced chemical changes in a gelatin matrix which can then be imaged using various systems, such as the Vista optical CT scanner (Modus Medical Devices, London, Canada). By its very 3D nature, gel dosimeters require extensive post-irradiation data processing. In our clinic, gel dosimeter analysis was traditionally performed using Matlab coupled with the Computational Environment for Radiotherapy Research and would take several hours to process and analyze data. To reduce analysis time and to produce a more robust analysis system, a gel dosimeter analysis workflow was developed using a custom extension in 3D Slicer (an open source and customizable computational tool used for image analysis and visualization). Gel dosimeter analysis using the extension now takes 5-10 minutes.

A major component of gel dosimetry analysis is the calibration relating the optical response of irradiated gel to dose. Here, we present a calibration method using measured depth dose data from well characterized electron beams compared to optical depth dose data in an imaged gel. Four 1L jars from two batches of Fricke gel dosimeter were made and irradiated with 6x6 cm² beams using three different beam energies. To validate the robustness of the calibration component of the 3D Slicer extension, the calibration gel jars were analyzed five times and the mean sensitivity of each of the gels was determined. Consistency of measurements for a single user examining the four gel irradiations was shown to have high reproducibility, with a relative standard deviation of 0.1%. To examine the effect of inter-user variability of the gel calibration process, the analysis was performed by three different users. The mean sensitivities determined by the three users had a maximum relative standard deviation of 0.6%.

Overall, the calibration step of the 3D Slicer Gel Dosimetry Extension makes gel dosimeter analysis more consistent and about 20 times faster than previous dose readout approaches.



(a) Ion chamber percent depth dose data (blue) and scaled and aligned gel dosimeter calibration data (green), as displayed in the extension's graphical user interface
(b) Mean calibration curves, averaged over five calibration trials, showing good agreement between all four calibration gels

SP080.3 - Whole body interactive 3D visualisation of both the benefits and risks of radiotherapy for common cancers: a tool to guide decision making

Author(s): David Edmunds, Ellen Donovan
Joint Department Of Physics, The Royal Marsden Hospital, Sutton/
UNITED KINGDOM

Purpose

More people who have had a common cancer are surviving. Radiotherapy is contributing to this success but it has long-term consequences. There is a complex relationship between the benefits of radiotherapy and the risks of adverse effects (e.g. cardiac damage or second cancer induction). These vary with many factors including disease stage, age at exposure to radiotherapy and radiation dose. The modern era of radiotherapy planning and delivery methods results in a wide variety of delivered dose to organs outside the treated region. Standard treatment planning systems calculate and display dose within the region of a planning scan. There is no tool describing doses beyond this region, or providing information on the benefits and risks of the radiotherapy based on plan specific doses and patient characteristics such as age.

We have developed the aRRESt (Radiotherapy Risk Evaluation System) program, which provides an interactive 3D visualisation of cardiac risks and second cancer risk estimates for radiosensitive organs throughout the body.

Method

A cross-platform graphical user interface (GUI) was developed using the C++ programming language, with 3D visualization and interaction provided by the Visualization Tool Kit (VTK) module. The GUI provides an indication of the lifetime risk of second cancer induction [1], and of major coronary event risk [2] for any treatment plan input. Dose cube and outlined regions of interest (ROI) are extracted from DICOM files exported from a commercial treatment planning system. Mean organ doses are used to estimate the lifetime/cardiac risks.

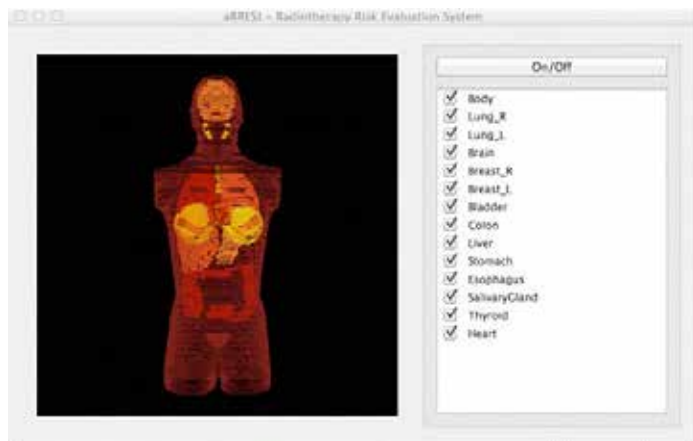


Figure 1

An image from the 3D interactive visualisation tool, which can be switched between dose and the risk of an adverse effect from radiotherapy for a selectable organ. The display shown is from a CT scan of an anthropomorphic phantom, extracted from the Pinnacle treatment planning system.

Conclusion

The aRRESt program provides a quick and convenient method of visualising the benefit-risk relationship for different radiotherapy treatment deliveries and patient characteristics. Currently based

on a generic body model, the ultimate aim is to use patient specific information. The tool will be used in combination with the standard treatment plan to assist decision making on a per-patient basis.

References

- [1] "Second Cancer Incidence Risk Estimates using BEIR VII Models for Standard and Complex External Beam Radiotherapy for Early Breast Cancer", Donovan et al., Med Phys, 2012.
- [2] "Risk of Ischemic Heart Disease in Women after Radiotherapy for Breast Cancer", Darby et al., N Engl J Med, 2013.

SP080.4 - A Software App for Radiotherapy with In-situ Dose-painting using high Z nanoparticles

Author(s): Mohammed Jermoumi, Altundal Yucel, Yao Hao, Gizem Cifter, Erno Sajo, Wilfred Ngwa
Department Of Physics And Applied Physics, Medical Physics Program, University of Massachusetts, Lowell/UNITED STATES OF AMERICA

The purpose of this work is to develop a user friendly and free-to-download application software that can be employed for modeling Radiotherapy with In-situ Dose-painting (RAID) using high-Z nanoparticles (HZNPs). The RAID APP is software program written in Matlab (Mathworks, Natick, MA, USA) based on deterministic code developed to simulate the space-time intra-tumor HZNPs bio-distribution within the tumor, and the corresponding dose enhancement in response to low dose rate (LDR) brachytherapy of I-125, Pd-102, Cs-131 and kilovoltage x-rays such as 50 keV and 100 keV. Through the graphical user interface (GUI) of the RAID APP, the user will be directed to different features to compute various parameters related to the dose enhancement and the biodistribution of NPs within high risk tumor sub-volumes. The software was developed as a tool for research purposes with potential for subsequent development to guide dose-painting treatment planning using radiosensitizers such as gold (Au) and platinum (Pt).

SP080.5 - Performing radiation therapy research using the open-source SlicerRT toolkit

Author(s): Csaba Pinter¹, Andras Lasso², An Wang³, Gregory C. Sharp⁴, Kevin M. Alexander⁵, David A. Jaffray⁶, Gabor Fichtinger²
¹School Of Computing, Queen's University, Kingston/CANADA, ²School of Computing, Queen's University, Kingston/CANADA, ³Radiation Medicine Program, Princess Margaret Cancer Centre, Toronto/CANADA, ⁴Radiation Oncology, Massachusetts General Hospital, Boston/UNITED STATES OF AMERICA, ⁵Department Of Physics, Engineering Physics And Astronomy, Queen's University, Kingston/CANADA, ⁶Techna Institute, University Health Network, Toronto/CANADA

Purpose: Radiation therapy (RT) is a common treatment option for a wide variety of cancer types. Although we have seen significant improvements in this technique over the past years, performing research in RT is limited to using either expensive, closed, proprietary applications or heterogeneous sets of open-source software packages with limited scope, reliability, and user support. Our SlicerRT toolkit aspires to overcome these limitations by providing an extensive set of RT research tools leveraging the advanced visualization and image analysis features of its base platform 3D Slicer (see <http://http://slicer.org>).

Methods: The SlicerRT toolkit (see <http://slicerrt.org>) comprises of a set of 3D Slicer extensions: SlicerRT core [1], Matlab Bridge, Multi-dimensional Data, and Gel Dosimetry. The SlicerRT core extension contains 26 modules, many of which provide common RT tools used in most RT research scenarios. Numerous core modules

employ the advanced algorithms provided by the Plastimatch library [2]. Matlab Bridge provides a convenient way for connecting the researchers' existing MATLAB algorithms to the SlicerRT ecosystem. Multi-dimensional Data offers a feature set for handling multi-dimensional datasets, such as longitudinal or 4D data. Finally, Gel Dosimetry [3] facilitates gel dosimetry analysis workflows through a streamlined, workflow-based end-user application. The toolkit is an open-source resource that is developed and maintained according to the highest standards in the industry, including flexible, maintainable architecture, automated testing, and the use of a software collaboration suite that enables accurate tracking of our efforts and plans.

Results: Four 3D Slicer extensions have been implemented, each of which can be downloaded from the 3D Slicer Extension Manager. Using these open-source software tools makes it possible to conduct cutting edge RT research without parallel development efforts. Essential RT tools are provided by SlicerRT core, augmented with the extensions Matlab Bridge and Multi-dimensional Data, supporting special use cases. Gel Dosimetry acts as a proof of concept for quick prototyping of advanced applications accommodating complex workflows. The user base of the toolkit is constantly expanding, with 30+ groups having adopted it so far. SlicerRT acts as a medium into which researchers can integrate their methods into, and which they can use to perform comparative validation, develop novel RT techniques, or transition advanced methods into routine clinical practice.

Future work: As SlicerRT has matured to contain most of the planned functions, our focus has shifted from feature development to usability and stability. Thus we propose to perform a complete overhaul of the current Contours mechanism to be more complete and more flexible. To enhance user experience, we plan to significantly improve our user documentation to make it as straightforward and helpful as possible. Also, although we have performed validation on core algorithms, it only covers a subset of the tools SlicerRT provides. It is also among our goals to validate the rest of the algorithms.

Acknowledgement: This work was in part funded by Cancer Care Ontario through Applied Cancer Research Unit and Research Chair in Cancer Imaging grants, and the Ontario Consortium for Adaptive Invention in Radiation Oncology (OCAIRO).

SP081 - Validation and Verification of Therapy Dose Delivery: Part 1

TRACK 05: DOSIMETRY AND RADIATION PROTECTION

SP081.1 - Validation of Eclipse Treatment planning system Commissioning using Octavius 4D

Author(s): Paul B. Ravindran¹, Aung Thuang²

¹Department Of Radiation Oncology, The Brunei Cancer Center, Brunei/BRUNEI, ²Radiation Oncology, Pinlon Hospital, Yangon/MAYANMAR

The accuracy of dose calculation in a treatment planning system mainly depends on the algorithm used for calculation, the beam data configured and the beam modelling in the treatment planning system. The Eclipse planning system uses the Analytical Anisotropic Algorithm (AAA) and the Acuros XB (AXB) for dose calculation and these have been extensively verified for its accuracy. The commissioning and quality assurance of a treatment planning system has been studied comprehensively ever since the computerised treatment planning system came in to use. Generally the validation of a TPS is limited to verification of point doses and dose profiles. The availability of the Octavius 4D enables a full 3D dose comparison.

Purpose: The purpose of this study was to validate the commissioning of Eclipse treatment system for photon beams of Clinac IX unit with Octavius 4D system that enables volumetric comparison of dose distribution.

Methods: Beam data configuration was performed on an Eclipse planning system (Version 13.0) for a Clinac IX dual energy linear accelerator with 6MV and 10 MV photon beams and six electron energies viz 6 MeV, 9MeV, 12 MeV, 15 MeV, 18 MeV and 22 MeV. The calculations for the validation were carried out with Analytical Anisotropic Algorithm (AAA) version 13 implemented in Eclipse planning system. Absolute point dose verifications were performed with 1D water phantom and 0.6 cc ion chamber supplied by PTW. The 729 detector array of the Octavius 4D system was used independently for 2D planar dose verification. The rotational unit of the Octavius 4D system with the inclinor and the 729 detector array was used for dose verification in 3D. Profile comparisons, 2D and 3D gamma analysis were performed to validate the Eclipse system for photon beam dose calculation.

Results: Good agreement was observed between the measured absolute point doses and the AAA calculated doses in water phantom. The agreement was within 2% and less than 1% at most points in the central axis. The 2D comparison of dose distributions pass rate for 3%/3mm gamma index criteria were 95% are above and the failed points were mostly in the penumbral region. The gamma analysis for 3D dose comparison also had pass rate of 96%-99% with 3%/3mm criteria for both 3D CRT and IMRT verifications.

Conclusions: The calculations performed by the Eclipse Treatment Planning system with the configured beam data and the Analytical Anisotropic Algorithm were accurate. The Octavius 4D system with the 729 detector array is a useful tool for comprehensive validation of the Treatment planning system for photon beams.

SP081.2 - Evaluation of Electron Beam Algorithm of Prowess Panther Planning System for Customized Electron Cutouts of different Sizes.

Author(s): Saadat Ali¹, Nauman Amjad², Basim Kakakhail³, Fayyaz Ahmad⁴, Areesha Zaman⁵, Sohail Murad¹, Kashif Islam¹, Raza Haid-er¹, Furqan Ali¹, Razzaq Aasia²

¹Medical Physics, Gujranwala Institute of Nuclear Medicine and Radiotherapy, Gujranwala/PAKISTAN, ²Medical Physics, Institute of Nuclear Medicine and Oncology, Lahore, Lahore/PAKISTAN, ³Department Of Physics And Applied Mathematics, Pakistan Institute of Engineering and Applied Sciences, Islamabad/PAKISTAN, ⁴Nuclear Medicine And Oncology, Director Medical Sciences, Islamabad/PAKISTAN, ⁵Medical Radiation Physics, institute of nuclear medicine and oncology lahore pakistan, lahore/PAKISTAN

Evaluation of Electron Beam Algorithm of Prowess Panther Planning System for Customized cutouts of Different Sizes

Abstract: In this comparative study electron beam dose calculation algorithm used in prowess panther TPS is evaluated. This is done by comparing PDDs and OPFs (Output Factors) of different cutout sizes with minimum field size dimension of 2 cm for electron energies of 6 MeV, 9 MeV, 12 MeV, 15 & 21 MeV. Cutouts are designed in TPS and then fabricated in mould room using lipowitz. The measurement of PDDs and OPFs are carried out by using CC01 and Omnipro-Accept software in 3D water phantom and Dose 1 electrometer. The OPFs are measured at D max of each energy and cutout size. The calculated PDDs and OPFs from Prowess Panther are compared. OPFs and PDDs comparison were made for both SSD 100 cm and SSD 110 cm. The R20 –R90 region of PDD is selected for comparison with an increment of 10 points. Data analysis is carried out by calculating mean difference and standard deviation for PDDs and percentage difference for OPFs between measured and treatment planning calculations.

The values of mean difference between calculated and measured PDDs at 100cm SSD are less than 2mm for 2cm diameter circle up to 12 MeV. Higher than 12 MeV the values of mean difference are greater than 3 mm. Similar results are obtained with squares and rectangles of different sizes like 2cm square and 9x2 rectangle and the mean difference is less than 2mm for 6MeV, it increases with increase in energy. For cutout sizes having large dimensions from 3cm the agreement is within 2mm irrespective of cutout shape size and applicator size. Overall trend shows that with increase in energy mean difference increases although increase is more prominent for 2cm circle at 21MeV as compared to squares and rectangles at same energy. For extended SSD 110cm, the mean difference of depth doses follow the same trend as in case of standard SSD 100cm. In case of higher energies the calculated results are lower in upper part of the curve from R90 to R60 while in lower part the calculated values are higher. Calculated and Measured OPFs are also compared. OPFs are in good agreement for fields greater than 4 cm. But for fields smaller than 4cm disagreement is more than acceptable limits. The Planning algorithm over estimate dose in case of small field sizes as compared to measured results.

Prowess panther accuracy depends on field size and energy and slightly depends on field shaping. Accuracy of prowess panther does not agree well for field size which has any dimension as small as 4 cm, especially for low energies. Additional correction factors must be applied on MUs calculated from Prowess panther for field sizes smaller than 4cm.

SP081.3 - Standard Measurements and MU Calibrations for Carbon Beam Therapy of SAGA-HIMAT

Author(s): Manabu Mizota, Takeshi Himukai, Yoshikazu Tsunashima, Hiroshi Sato, Mitsutaka Kanazawa, Masahiro Endo
Ion Beam Therapy Center, SAGA HIMAT Foundation, Tosu/JAPAN

Purpose

At SAGA-HIMAT(Saga Heavy Ion Medical Accelerator in Tosu) facility, we have started radiotherapy with carbon beam from the end of August 2013. The treated patient number reached up to 547 at the end of December 2014 and is steadily increasing.

In case of particle radiotherapy using passively modified beams, dose calibration measurements should have been executed prior to the treatment in order to determine the monitor unit(MU) for each therapeutic beam. Increase in the number of treatments leads to increase of MU measurements and consumption of the machine time for therapy including QA activities. We are preparing to introduce the MU calculation method in order to save machine time and avoid the errors from wrong measurement.

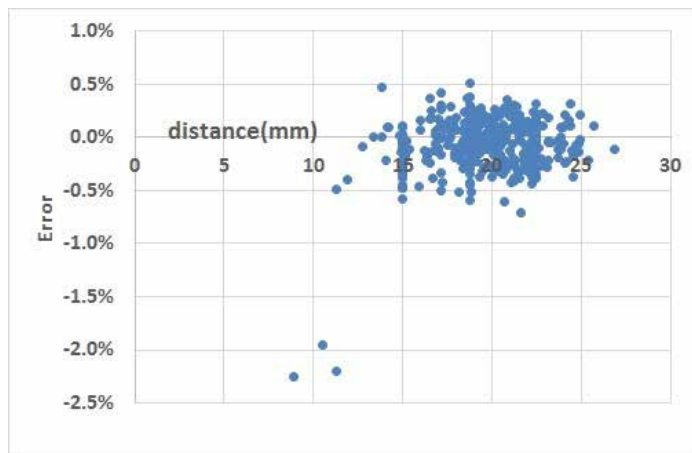
Methods

Routinely, a standard calibration measurement is repeated under the same condition at every port at each beam energy. We use beam energy of 400MeV/n and 290MeV/n for the correction of MU calibration in the corresponding energy. So we firstly checked its trend and the correlation among ports or among energies.

Secondly, we studied the applicability of MU calculation method which was developed at NIRS(National Institute of Radiological Sciences). In carbon beam dosimetry, MU depends primarily on the 3-dimensional field condition of broad beam method and secondarily on the aperture made by collimator. The aperture varies infinitely depending on the shape of target whereas the number of field conditions is limited. Precise field-size(aperture) effect calculation is done using kernel-beam model which is composed of two Gaussian functions.

Results

The good correlation between the two energies was obtained at each port. Also the MU calculation showed good agreement. The calculated values for MU have been compared with the measured ones used for therapy at beam energy of 400MeV/n in horizontal port of treatment room B. Figure shows the comparison results in vertically and the minimum distance between collimator and beam axis along horizontal axis. This calculation procedure reproduced successfully almost all the measured value within 0.5% accuracy, except for three case where the reference point is very near to a collimator edge. The discrepancy at these region seems to be due to the simplicity of the beam model.



Conclusion

The effectiveness of the MU calculation method was verified at SAGA-HIMAT. We are trying to put to practical use as soon as possible. Then the more efficient operation of the treatment beam would be possible.

SP081.4 - 3D “Bridge” Silicon Microdosimeter for RBE Studies in ¹²C Radiation Therapy

Author(s): Anatoly B. Rosenfeld¹, Linh T. Tran², Lachlan Chartier¹, Dale A. Prokopovich³, Susanna Guatelli¹, Marco Petasecca¹, Michael L.F. Lerch¹, Naruhiro Matsufuji⁴, Michael Jackson⁵

¹Centre For Medical Radiation Physics, University of Wollongong, Wollongong/AUSTRALIA, ²Centre For Medical Radiation Physics, University of Wollongong, Wollongong/NSW/AUSTRALIA, ³Institute Of Materials Engineering, Australian Nuclear Science and Technology Organisation, Sydney/NSW/AUSTRALIA, ⁴Medical Physics Research Program, National Institute of Radiological Science, Chiba/JAPAN, ⁵University of New South Wales, Sydney/AUSTRALIA

Radiotherapy using heavy ion beam such as Carbon-ion has the advantage of an enhanced dose distribution over conventional radiotherapy with X-rays due to the Bragg peak (BP) energy deposition profile. The Relative Biological Effectiveness (RBE) of a carbon-ion radiotherapy beam greatly depends on a depth of the target volume in the body and the nuclear fragmentation process that occurs in the BP or spread-out BP(SOBP) as well as neutrons. It is important to understand the RBE of the heavy ions in hadron therapy applications in order to deliver correct dose.

Microdosimetry is extremely useful technique, used for dosimetry in unknown mixed radiation fields typical of hadron therapy. Conventional detectors for microdosimetry consist of tissue equivalent proportional counters (TEPC) which have advantages of a spherical sensitive volume and tissue equivalency through use of a tissue equivalent gas. However, TEPC has several limitations such as high voltage operation, large size, which reduces spatial resolution and introduces wall effects, and an inability to simulate multiple cells.

A new silicon microdosimeter with 3D sensitive volumes (SVs) has been proposed to overcome the shortcomings of the conventional TEPC. The new microdosimeter is called “bridge” microdosimeter as it has thin Si bridges between the SVs to support the Al tracks over the SVs. The charge collection study of the new device and its application for RBE determination in ¹²C radiation therapy at the Heavy Ion Medical Accelerator in Chiba (HIMAC), Japan is presented.

Derived RBE₁₀ values based on the Microdosimetric Kinetic Model and SOI bridge microdosimetric spectra is presented in Fig.2. The RBE₁₀ values match very well with those obtained from the TEPC measurements. Due to the high spatial resolution of the microdosimeter, more detailed RBE₁₀ measurements were obtained at the end of the SOBP compared to the TEPC. It should be noted that the bridge microdosimeter measurements were done in a PMMA phantom while the TEPC measurements were carried out in water.

This work presented the first RBE₁₀ derivation in a ¹²C ion therapeutic beam using a high spatial resolution SOI microdosimeter and demonstrated a simple and fast method for Quality Assurance in charge particle therapy using silicon microdosimeter.

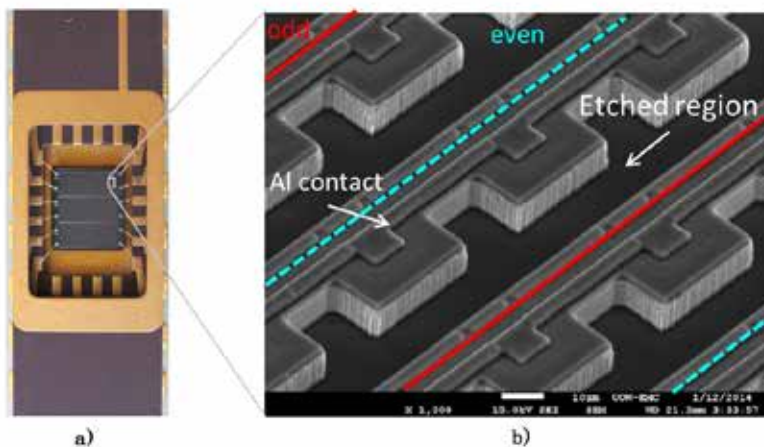


Fig. 1 a) A bridge microdosimeter mounted on a DIL package, b) a SEM image of arrays of SVs

Fig.1a shows the 3D bridge microdosimeter mounted on a dual-in-line (DIL) package and Fig.1b shows SEM image of arrays of SVs where the etched region outside the SVs was clearly visible. This new technology provided well-defined micron sized 3D SVs of similar dimensions to biological cells.

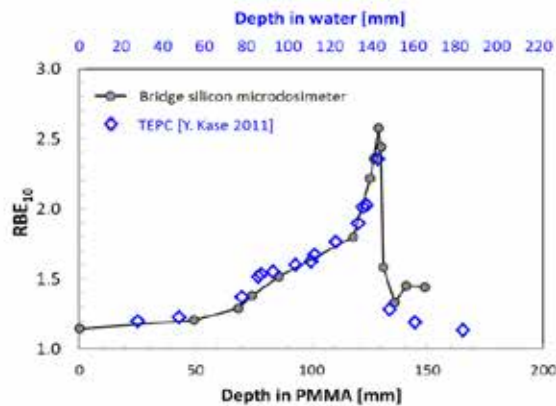


Fig. 2 Derived RBE₁₀ along the central axis of the ¹²C ion beam, obtained by SOI bridge microdosimeter and TEPC at NIRS [2]

SP081.5 - Characterization of a ZnSe(Te) inorganic scintillator for scintillation dosimetry applications

Author(s): Patricia Duguay-Drouin¹, Sam Beddar², Luc Beaulieu¹
¹Radio-oncologie Et Axe Oncologie Du Centre De Recherche Du Chu De Québec, CHU de Québec, Québec/CANADA, ²University of Texas MD Anderson Cancer Center, Houston/TX/UNITED STATES OF AMERICA

Purpose: The purpose of this work is to characterize a ZnSe(Te) inorganic scintillator for future application in scintillation dosimetry. This study will determine the usability of this scintillator within a multipoint scintillation detector system.

Methods: Different lengths of a ZnSe(Te) scintillator (MolTech GmbH) ranging from 0.5 to 3.0 mm were tested and optically coupled to a 15 m optical fiber (ESKA GH-4001). The photodetectors used in this study are a spectrometer (QE65Pro, Ocean Optics) and a photomultiplier tube (H10721, Hamamatsu). The detector was irradiated using an orthovoltage device (Xstrahl 200) at 120, 180 and 220 kVp, and a linear accelerator (Varian Clinac iX) at 6 and 23 MV for photons beams and at 6, 12 and 18 MeV for electrons beams. The energy, particle type, dose and dose rate dependencies were examined. Also, the attenuation within the scintillator was measured and its emission spectrum was characterized under various irradiation conditions.

Results: The scintillator demonstrates energy and particle type dependence for both the light production and spectral shape. The ZnSe(Te) measured spectrum ranges from 550 to 800 nm for beam energies listed above. For electron beams and MV photon beams, a component at 690 nm is added and the peak at 771 nm is shown to increase with energy (fig. 1). For a given energy, linear dose dependence is observed for all beams tested ($R^2 > 0.996$). Moreover, the scintillator exhibits no dose rate dependence for MV photons beams tested. However, at 120 kVp, a dose rate dependence obeying a power function ($R^2 = 0.998$) is observed (fig. 2).

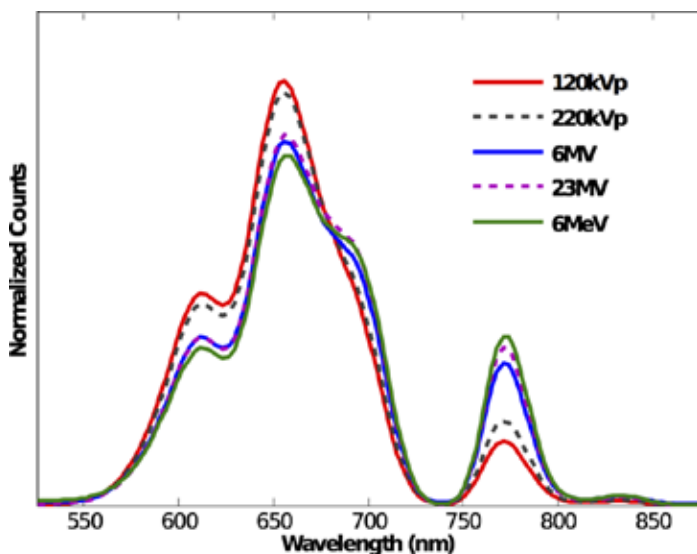


Figure 1: Spectra for different energy beams

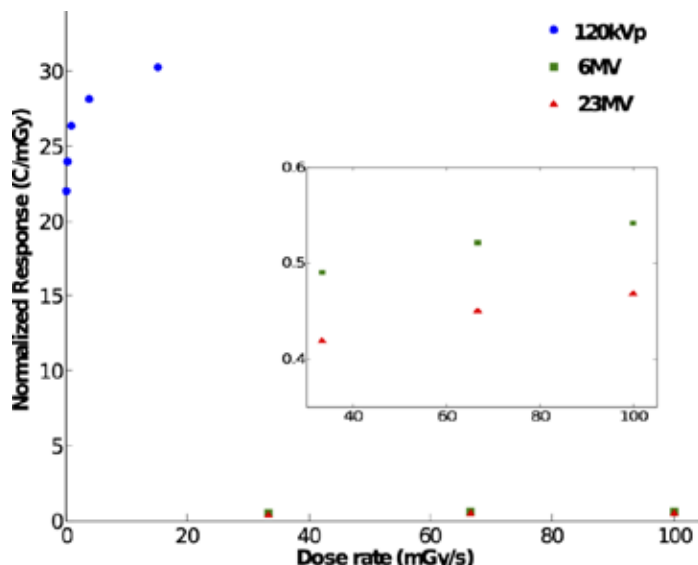


Figure 2: Dose rate dependence for 120kVp, 6MV and 23MV

Conclusion: The ZnSe(Te) inorganic scintillator has been characterized for dosimetry applications. When using this scintillator, one must take into account the dose rate, energy and particle type dependences. Despite these dependencies, this scintillator with a spectrum of higher wavelength remains a good candidate for multipoint applications.

SP081.6 - Determination of correction factors for the use of ionization chambers in the presence of magnetic fields

Author(s): Gabriel O. Sawakuchi, Geoffrey S. Ibbott, Michelle V.P. Mathis
 Radiation Physics, The University of Texas MD Anderson Cancer Center, Houston/UNITED STATES OF AMERICA

Various groups in Europe, North America and Australia are currently developing magnetic resonance imaging (MRI) guided radiotherapy technology by integrating an MRI scanner to a linac (MRI-linac). MRI-guided radiotherapy will provide exquisite images of soft-tissue with high temporal resolution to allow tracking tumor and organ motions in real-time. One of the challenges to implement MRI-linac technology in clinical practice is to calibrate the radiation output under the presence of a strong magnetic field (B-field). The addition of the permanent B-field from the MRI affects the response of ionization chambers (ICs) (Meijsing et al. 2009, *Phys. Med. Biol.* 54 2993-3002; Smit et al. 2013, *Phys. Med. Biol.* 58 5945-57; Reynolds et al. 2013, *Med. Phys.* 40 042102). In this work we show preliminary results of Monte Carlo (MC) calculations of beam quality correction factors under the presence of a B-field for various ICs. We used the Geant4 toolkit throughout this work. First we established the best set of parameters for the Geant4 condensed history algorithm so that the code passes the Fano test within 0.5% (Poon et al. 2005, *Phys. Med. Biol.* 50 681-94). Then, we used well-established methods from the literature (Muir and Rogers 2010, *Med. Phys.* 37 5939-50) to calculate k_Q values for several ICs in a SL25 6 MV beam without (k_Q) and with ($k_{QB}=1.5T$) the presence of a 1.5 T B-field. The maximum percentage difference between our k_Q values and TG-51 (McEwen et al. 2014, *Med. Phys.* 41 041501) results for a set of seven chambers was 1.4%, demonstrating that our MC model is adequate (Table 1). Our results in Table 1 show that $k_{QB}=1.5T$ values strongly depend on IC model/geometry and material composition of the ICs, i.e., for identical geometry but different collector and wall materials, $k_{QB}=1.5T$ values were different. For the set of ICs

investigated we observed corrections of up to 4.4% for the Exradin A19 chamber. Among the investigated chambers, the PTW 30011 presented the smallest correction factor (1.2%). Our future work will use a realistic energy spectrum of an MRI-linac unit (Atlantic, Elekta Inc.) to calculate $k_{QB=1.5T}$ values for selected ICs. Future work is also needed to validate calculated $k_{QB=1.5T}$ values against experimental data.

Table 1: kQ values calculated using Geant4 with and without the presence of a 1.5 T B-field. The B-field was perpendicular to the beam and perpendicular to the axis of the cylindrical ICs.

Chamber	Vol. (cm ³)	Collector	Shell	Guard	kQ (TG-51)	kQ (This work)	$k_Q^{B=1.5T}$
NE 2571	0.6	Al	Graphite	N/A	0.992±0.008	0.985±0.005	0.959±0.005
PTW 30010	0.6	Al	PMMA	Graphite	0.992±0.008	1.006±0.005	0.980±0.006
PTW 30011	0.6	Graphite	Graphite	Graphite	0.992±0.008	1.001±0.005	0.988±0.006
PTW 30012	0.6	Al	Graphite	Graphite	0.994±0.008	1.005±0.005	0.978±0.006
Exradin A1	0.053	C552	C552	C552	0.991±0.008	0.986±0.014	0.959±0.015
Exradin A1SL	0.053	C552	C552	C552	0.992±0.008	0.983±0.014	0.954±0.014
Exradin A19	0.622	C552	C552	C552	0.991±0.008	1.003±0.005	0.956±0.006

SP082 - Nonlinear Dynamic Analysis

TRACK 09: BIOSIGNAL PROCESSING

SP082.1 - Aging Process: Central Pressure Waveform Loss of Complexity

Author(s): Ricardo L. Armentano¹, Leandro J. Cymberknop², Walter E. Legnani¹, Manuel R. Alfonso², Franco M. Pessana³

¹School Of Advanced Studies In Engineering Sciences, National Technological University, Ciudad Autónoma de Buenos Aires/ARGENTINA, ²Buenos Aires Regional Faculty, National Technological University, Ciudad Autónoma de Buenos Aires/ARGENTINA, ³Faculty Of Engineering And Exact And Natural Sciences, Favaloro University, Ciudad Autónoma de Buenos Aires/ARGENTINA

Introduction: Aging is defined as the age-related decline in physiological function where arterial stiffening and hypertension constitute related disorders in the cardiovascular system. Age can be considered as one of the most powerful determinants of cardiovascular risk, usually been viewed as a chronological, unmodifiable and even untreatable factor. Arterial mechanical properties of the small vessels are known to be altered with advancing age (dilating and stiffening), leading to a rise in pulse pressure (PP). In this sense, central pulse pressure (cPP) has been more closely related to cardiovascular events than peripheral pulse pressure (pPP). From the point of view of chaos theory, multiscale and nonlinear complexity (structure and interactions of individual subsystems) appears to degrade with aging and disease. In our previous studies, waveform complexity of arterial pressure (AP) was related to stiffness variations as well as to the presence of wave reflection. Additionally, age related changes were also analyzed in cPP waveform. **Objective:** The aim of the present study was to evaluate changes in the waveform complexity of cPP as a result of the aging process. **Material and Methods:** Continuous, noninvasive blood pressure measurements were analyzed in 16 healthy subjects (8 young, 20-29 yr and 8 aged, 50-69 yr). Individuals with cardiovascular disease risk factors were excluded from the experiment. A generalized transfer function was used to obtain the cPP waveform from the pPP (measured by applanation tonometry) using a customized software (SphygmoCor, AtCor Medical, Sydney, Australia). Time series waveform complexity was assessed by means of fractal dimension (FD) calculation, based on the method provided by Higuchi. Statistical analysis was carried out using an unpaired Student's t-test. A value of $p < 0.05$ was considered statistically significant. **Results:** A significant decrease in FD values was obtained in cPP waveform for aged subjects (1.09 ± 0.02 to 1.04 ± 0.01), concomitant to a cPP increase. **Conclusion:** Considering previous studies, the loss of complexity has been hypothesized to be an indicator of the transition from normal aging to frailty. In the present work, loss of waveform complexity was observed as a consequence of the aging process in cPP. Arterial structural changes were reflected in FD variations, independently of the AP calibration, due to the space filling property and the fine structure of the waveform were analyzed. Further studies are necessary in order to determine if changes in waveform complexity can be utilized as a complementary factor of vascular aging.

SP082.2 - Changes in COP scaling behaviour in quiet stance after mTBI

Author(s): Coren Walters-Stewart, Andre Longtin, Heidi Sveistrup University of Ottawa, Ottawa/CANADA

The analysis of centre of pressure (COP) timeseries is well suited to the evaluation of balance control. Balance control is often interpreted as a physiological control system with coordinating sensory

inputs and muscle outputs. COP variables can provide clues about the controlling mechanisms affecting balance. Mild traumatic brain injury (mTBI) often results in functional impairments including balance impairments that seem to suggest altered signalling within the brain. It was hypothesized that the altered mechanisms affecting balance after mTBI might be reflected in altered scaling properties of COP. University football players ($n=74$) were tested at the beginning of the season as a baseline and were retested if they sustained an mTBI during the season ($n=6$, tested an average of 15.7 ± 7.2 days after injury). Players who did not sustain an mTBI were also retested at the end of the season for comparison ($n=17$). Each participant was asked to stand quietly with eyes closed for 90 seconds on a portable force platform. Scaling behaviour was determined by (1) classifying the timeseries using the beta estimate, (2) identifying how many scaling regions exist, and (3) calculating scaling estimates for each region. Data for mTBI and uninjured groups were compared to their own respective baselines. Results demonstrated that while typical scaling behaviour of COP timeseries were always the same—short-term persistence ($H_1 > 0.5$) and long-term anti-persistence ($H_2 < 0.5$)—the group who had sustained mTBIs demonstrated a significant change (between baseline and post-mTBI) toward less random short-term values in the mediolateral direction whereas the uninjured players did not (see Figure 1). While the overall ability to maintain balance is not altered, demonstrated by the unchanging long-term scaling behaviour and by the fact that no players were falling over, some subtle changes to how the COP is being controlled in balance do occur after an mTBI. This method of measuring changes to balance may be useful in determining whether or not players are being returned-to-play when still impaired in ways that may lead to re-injury.

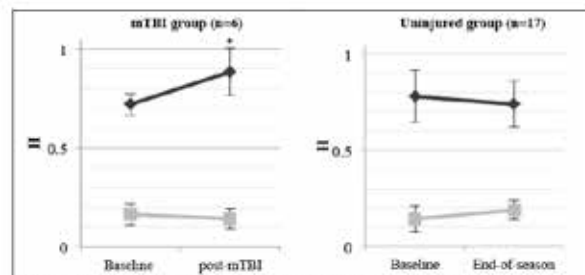


Figure 1 Comparison between testing sessions of the mTBI group (figure to the left) and the end-of-season group (figure to the right) showing the short-term (H_1 , \blacklozenge) and long-term (H_2 , \blacksquare) scaling parameters (mean + standard deviation). The asterisk(*) indicates a significant change ($p < 0.05$) from baseline of the short-term scaling parameter in the mTBI group. Only results for the mediolateral direction are shown.

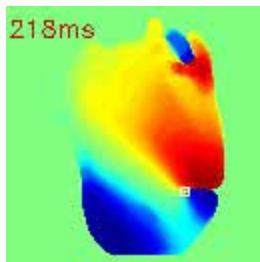
SP082.3 - Tracking algorithm of spiral wave core in a cardiac tissue using Hilbert transform and phase variance analysis

Author(s): Naoki Tomii¹, Masatoshi Yamazaki², Haruo Honjo², Ichiro Sakuma¹

¹The University of Tokyo, Tokyo/JAPAN, ²Nagoya university, Nagoya/JAPAN

Arrhythmia is a common and increasing disease, especially in developed countries. There are several treatment approaches toward arrhythmia such as anti-arrhythmic drug, radio frequency ablation and electrical stimulation. To investigate about mechanism of arrhythmia and improve efficacy of these treatments, optical mapping system has been used in many previous works. Optical mapping is a useful measurement system of cardiac excitation. This mapping system is mainly composed of isolated heart dyed with voltage sensitive dye, high brightness excitation light, and high speed camera. Because emitted spectrum of voltage sensitive dye changes with a change of transmembrane potential of each cardiac cell, we can measure the activation potential at each points and it's propagation as the change of fluorescence spectrum. Using this system, propagation of excitation in cardiac tissue can be measured in high speed (more than 1000 fps) and in high resolution (less than 0.05 mm / pixel).

Spiral wave propagation of excitation in a cardiac tissue (spiral reentry) is known to play key role to cause and sustain dangerous arrhythmia, such as tachycardia and fibrillation both in ventricular and atrium. It has been reported that stability of the center of spiral wave (spiral core) is related to the sustainability of spiral reentry. Thus detection and tracking of spiral core in optical mapping images is important to analyze spiral reentry. Bray et al. proposed phase analysis of spiral reentry using Hilbert transform. In this method, core of spiral is mathematically defined as “phase singularity point” around which the contour integration of phase value is 2π or -2π . However, applying this definition to detect the spiral core in optical mapping images is difficult because there are huge amount of surrounding counters in an image. In this work, we present novel detection algorithm of the core of spiral reentry in optical mapping images. Using angular dispersion of phase values in a bounding box, we detected high dispersion point as the core of spiral. We will report the accuracy of the detection and the computational cost of this algorithm.



SP082.4 - Mapping the Fractal Dimension of Arterial Pressure

Author(s): Leandro J. Cymberknop¹, Ricardo L. Armentano², Franco M. Pessana¹, Manuel R. Alfonso¹, Walter E. Legnani³

¹Buenos Aires Regional Faculty, National Technological University, Ciudad Autónoma de Buenos Aires/ARGENTINA, ²Faculty Of Engineering And Exact And Natural Sciences, Favaloro University, Ciudad Autónoma de Buenos Aires/ARGENTINA, ³School Of Advanced Studies In Engineering Sciences, National Technological University, Ciudad Autónoma de Buenos Aires/ARGENTINA

Introduction: The cardiovascular system is constituted by a complex network of vessels, where highly uniform hierarchical branching structures, that cover a wide range of diameter scales, are regulated by the anatomy and local flow requirements. In recent years, homeodynamic and holistic concepts such as fractal and nonlinear analyses were proposed to be helpful to study the complexity of physiological functions. In the systemic circulation, arteries bifurcate many times before they became capillaries where the scaling factor of vessel length, diameter and angle between two children branches is established at each level of recurrence. For these reason, this type of vascular system can be described using a fractal scaling principle. In this sense, it was observed that the basic pattern of blood distribution is also fractal, imposed both by the anatomy of the vascular tree and the local regulation of vascular tone. In our previous studies, arterial pressure time series (AP) waveform complexity changes were evaluated by means of a fractal dimension (FD) measure. To our knowledge, a holistic analysis of FD variations throughout the arterial network has not been previously reported. **Objective:** The aim of the present study was evaluate the variation of arterial pressure waveform complexity considering its anatomical location in the branching structure. **Material and Methods:** Continuous, AP measurements were obtained in the following sites: left ventricle and descending thoracic aorta (five male mongrel dogs, instrumented with solid-state implantable pressure sensors, Konigsbeg inc., Pasadena, USA) and carotid and femoral arteries (five male middle-aged subjects, without cardiovascular risks factors, evaluated by applanation tonometry, Millar Inc., Houston, USA). Due to experimental limitations, invasive (in animals) and non-

invasive (in humans) measuring methodologies were performed. Assessment of FD in AP time series waveforms was developed by applying Higuchi's method. Topological dimension was not considered in FD relative changes (ΔFD) calculation. Statistical analysis was carried out using the paired Student's t-test. A value of $p < 0.05$ was considered statistically significant. **Results:** A significant increase in ΔFD was observed at the thoracic aorta (higher complexity) in respect to ventricular pressure FD values ($+233.06 \pm 75.34\%$). On the other hand, femoral artery AP manifested a decrease in ΔFD (lower complexity) in comparison to the carotid site ($-56.51 \pm 13.62\%$). **Conclusion:** A holistic evaluation of AP waveform complexity in the arterial network was performed, where its FD changes were related to the vascular site. While the ventricular pressure time series was observed to be 'fractalized' at the aortic level (due to the waveform is more exposed to the multiple wave reflections), AP showed a loss of complexity at distant sites from the cardiac muscle, manifesting an 'unwrinkling' phenomenon.

SP082.5 - Moving detrended fluctuation analysis for inspecting time evolution of scale invariant structures in biomedical signals

Author(s): Hamidreza Saghir, Tom Chau, Azadeh Kushki Ibbme, University of Toronto, Toronto/CANADA

Detrended fluctuation analysis (DFA) is commonly used for characterizing the fractal structure of biomedical signals. One of the underlying assumptions of DFA is that the fractal structure is consistent [AK1] in time and can be characterized by a single scaling exponent. However, the scale invariant structures of multifractal signals are modulated in time and lead to the existence of a spectrum of scaling exponents. Conventionally, Multifractal analysis has been used to study the statistical distribution of a range of scaling exponents. However, these methodologies do not provide any information about the time evolution of scaling exponents.

This article introduces a new methodology based on DFA, called moving detrended fluctuation analysis (MDFA) for examining the evolving scale-invariant structure of a signal in time through phase-couplings between temporal scales. Instead of using non-overlapping time intervals as in conventional DFA, MDFA computes the root mean square of the detrended residuals in a moving window at each time scale, resulting in a time- and scale- dependent root-mean-square measure. The scaling exponent is then numerically calculated as the linear slope of the log-log plot of root mean squares versus scale at each time instant.

We used MDFA to inspect time evolution of scaling exponents in ECG signals during a movie-watching task as well as an anxiety-inducing task (Stroop Color-Word Interference task) in 33 participants ($n=33$, age: 12.5 ± 2.9 years, full-scale IQ: 112.9 ± 14.1 , 19 male [AK2]). The results show that the modulation of the local scaling structure was significantly influenced by condition (i.e. relaxed, stroop practice, anxious, $p=0.04$). This modulation was not significantly different for a white noise series of the same length. MDFA returns an average scaling exponent of 0.5 [AK3] for white noise which is consistent with the results of other methods. These results suggest that MDFA is a useful tool for inspecting the time evolution of scale-invariant structures in multi-fractal signals and should be further investigated.

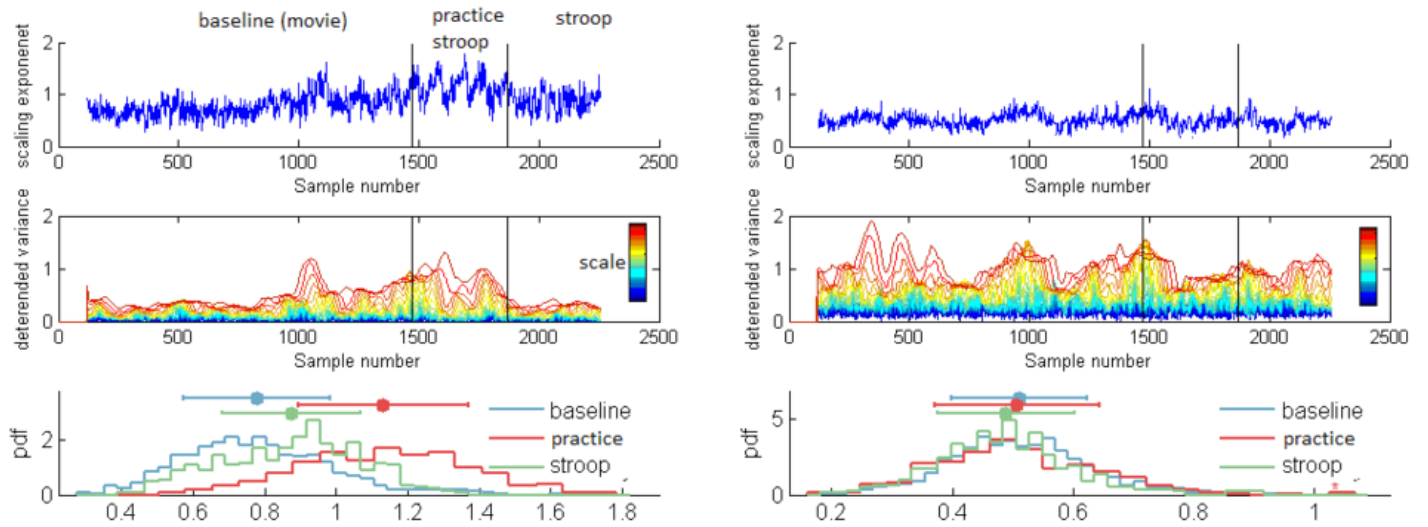


figure 1. Example of MDFA for one participant (left) compared to white noise (right). Top panel demonstrates the time modulation of scaling exponents. Middle panel shows the evolution of root mean square residuals across time and scales. Bottom panel shows the probability distribution of scaling exponents in anxious (stroop) and relaxed (baseline) conditions. (practice is a transitory state in which the participant practices the task a few times before starting the stroop task)

SP083 - Lower Limb Injury Assessment and Treatment & Prosthetics and Assistive Devices

TRACK 10: REHABILITATION MEDICINE, SPORTS MEDICINE, REHABILITATION ENGINEERING AND PROSTHETICS

SP083.1 - Design of a braking simulator for the assessment of lower limb fracture recovery

Author(s): Andrew O'Connell¹, Alvan Buckley¹, Andrew Furey¹, Maria Doyle², Amy Hsiao²

¹Faculty Of Medicine, Memorial University of Newfoundland, St. John's/CANADA, ²Mechanical Engineering, Memorial University of Newfoundland, St. John's/CANADA

"When can I drive?" is a question frequently asked of orthopedic surgeons following injury and surgery of the lower limb. Surgeons are left to make a difficult decision, as there are no specific guidelines on when patients should be cleared to drive, and there are significant discrepancies between mean recovery times for different procedures in the literature. Although there is no clear consensus between law enforcement, insurers, road authorities and the medical community, the decision as to whether an orthopedic patient can adequately brake an automobile following surgery is generally defaulted to the surgeon. Surgeons are faced with the dilemma of managing their duty to the patient, to the public, and the medicolegal risks involved with giving patients advice on when they can get back on the road. Studies suggest that a simulator may be useful in assessing braking capacity following surgery of the lower limb; however, they are currently not widely used by surgeons. Significant recurring issues exist with current or proposed simulators: (1) they generally cannot be used to assess trauma patients due to the need for baseline testing preoperatively, (2) limited data is available to demonstrate their ability to evaluate a patient's braking performance, (3) braking forces are not translated into stopping distances or indeed not considered at all, (4) and the devices are often not practical in an outpatient setting. In order to drive safely, one must be capable of stopping a vehicle in an emergency. Braking capacity depends on a host of patient variables including visual acuity, neurological function, musculoskeletal function, and the influence of drugs among others. Our intention is to develop a method to evaluate performance of the lower limb, specifically. This work presents the design of a simulation device that will provide surgeons with an objective assessment of their patient's braking performance in an outpatient clinic. This simulator will compare calculated total stopping distances after the appearance of an emergency stimulus with the total stopping distance recommended for specific driving speeds in the literature. Alternatively, this maximum stopping distances will be inferred using recommended brake reaction times and forces to provide a benchmark for the assessment of braking performance.

SP083.2 - Quantitative measurement of subtalar joint passive stiffness in children with cerebral palsy

Author(s): Wei Chen¹, Fang Pu¹, Yang Yang¹, Jie Yao¹, Li Z. Wang¹, Yu B. Fan²

¹Key Laboratory of Rehabilitation Technical Aids, Ministry of Civil Air, School of Biological Science and Medical Engineering, Beihang University, Beijing 100191, P. R. China, Beijing/CHINA, ²National Research Center for Rehabilitation Technical Aids, Beijing 100176, P.R. China, Beijing/CHINA

Subtalar joint (STJ) passive stiffness is critical to foot valgus defor-

mity for children. The aim of this study was to develop a STJ passive stiffness measuring device to obtain the STJ passive stiffness. The reliability of clinical measurements was used to assess the STJ passive stiffness in weight bearing between normal children and those with cerebral palsy (CP). Ten feet of five non-disabled children and ten feet of seven with CP taken of affected foot were collected to measure their STJ passive stiffness (6.5 ± 2.1 years vs 6.3 ± 1.9 years). The Intraclass Correlation Coefficient (ICC) was used to assess the reliability of the device for measuring STJ passive stiffness. Statistical analysis was conducted using one-way ANOVA to assess between-group differences. ICCs were 0.98 for inter-reliabilities STJ passive stiffness of CP group and 0.99 for control group. STJ passive stiffness can be used to quantitatively assess the progressive changes of foot valgus deformity. It is concluded that STJ passive stiffness is a reliable measurement due to its high repeatability.

SP083.3 - Differences in the parameters of impedance between knees with and without meniscal injury in female athletes

Author(s): Marysol Garcia-Pérez, Marco Balleza-Ordaz, Miguel Vargas-Luna, María Raquel Huerta-Franco
División De Ciencias E Ingenierías, Universidad de Guanajuato, León, Guanajuato/MEXICO

Introduction. The medical trials used to diagnostic these pathologies are the x-ray and MRI techniques. The x-ray reveals injuries in hard tissues (bones), while MRI evidences the injuries in soft tissues (meniscus and tendons). These kind of medical diagnosis techniques are expensive in most cases. Our research group propose the electrical bio-impedance (EBI) technique as an option to assess the knee condition.

Objective. The main objective of this research is to compare the impedance parameters between knees with and without meniscal injury in female athletes.

Materials and methods.

a) Volunteers. In this study participated 6 sportswomen (Age: 19.5 ± 0.8 years, BMI: 20.4 ± 3 kg/m²). Previously, all volunteers were assessed for meniscal problems comparing right and left knees by a sports medical professional staff. All volunteers had physical condition according to the parameters of the American College of Sports Medicine. Body composition were measured to all volunteers.

b) Procedure. The bio impedance parameters were assessed with a BIOPAC System (MP150), which injects an electrical current of 1 mA at different frequencies (12.5 kHz, 25 kHz, 50 kHz, 100 kHz).

In order to monitor the knee condition by bio-impedance, four electrodes were placed in each knee. All volunteers were asked to fully extend each leg in periods of 5 seconds to perform the test at 30 seconds.

c) Signal processing. All the data were analyzed using the Matlab software. The impedance data were analyzed and compared at different impedance frequencies. Subsequently, these results were correlated with the clinical findings made to all the volunteers.

d) Statistical analysis. The comparison of impedance parameters between knees with and without meniscal injures were made using a t-test for independent groups.

Results. All the volunteers had meniscal injure in the right knee; however there were not statistical differences when we compare the length of the lower pelvic limb the mean and standard deviation ($X \pm SD$), were: 91.9 ± 7.4 vs. 91.8 ± 7.0 , for right and left limbs ($t=0.02$, $p=0.98$). The mean and standard deviation of the bio impedance parameters were as follows: 48.9 ± 10.7 vs. 71.5 ± 19.1 . When we compare with a t-test we found significant differences between knees

with and without injure ($t=-3.58$, $p=0.002$), see figure 1.

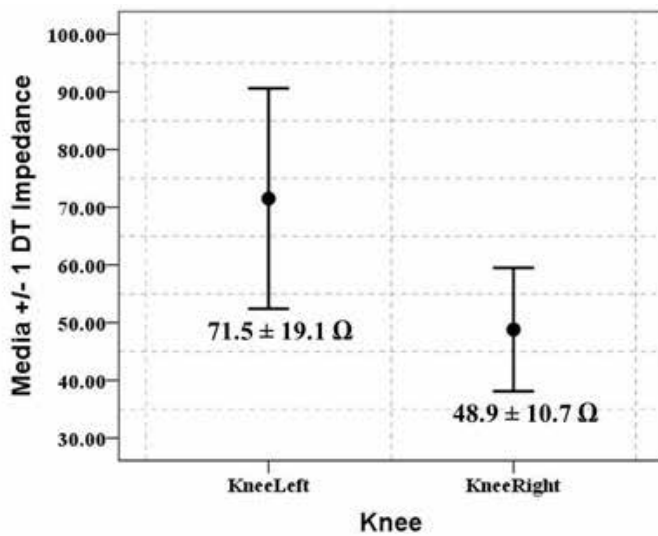


Fig 1. Differences in the mean and SD of impedance parameters of right and left knee with and without meniscal injures, $t=-3.58$, $p=0.002$.

Conclusions. In this study we demonstrated that the impedance technique could be a good option in order to monitor the knee condition.

SP083.4 - Development and evaluation of a mechanical stance controlled orthotic knee joint with stance flexion utilizing a timing based control strategy flexion

Author(s): Hankyu Lee¹, Matthew J. Leineweber², Jan Andrysek²

¹Institute Of Biomaterials And Biomedical Engineering, University of Toronto, Toronto/CANADA, ²Bloorview Research Institute, Holland Bloorview Kids Rehabilitation Hospital, Toronto/CANADA

Medical conditions such as spinal cord injury, spina bifida poliomyelitis and others can result in severe loss of lower limb muscle function and lead to impairments in mobility. For patients who have the potential to walk, orthotic treatments including knee-ankle-foot-orthosis are commonly used to address problems with knee instability. Recent advancements have led to the development of more sophisticated orthotic knees that restrict knee flexion during stance-phase while allowing articulation during the swing-phase. These stance-control orthotic knee joints stabilize the knee joint during the stance-phase of gait without restricting swing-phase flexion, thus achieving a more normal gait for individuals with quadriceps muscle weakness. However, there are inherent challenges in ensuring safe weight-bearing capabilities while allowing for maximum knee flexion during swing-phase over a range of walking speeds. **The work here presents a new type of stance control strategy and stance controller design employing a mechanical timing system, which was modelled using empirical data and functionally tested in a gait laboratory.**

Pilot clinical testing was performed on a prototype stance-control orthotic knee joint incorporating a novel timing system for controlling knee lock during swing- and stance-phase. Our timing-based control strategy was developed using empirical models of gait cycles at normal and fast walking speeds. Clinical feasibility of this approach was tested on a poliomyelitis patient using spatiotemporal, kinematic, and kinetic gait data captured using a standard motion capture system and floor-mounted force plates. Walking trials were performed with the orthotic in its unlocked functional mode, as well as

in a locked mode to represent traditional knee-ankle-foot-orthoses.

The results of these tests showed that our prototype design provided reliable knee stability while facilitating swing-phase flexion, for more normal knee joint kinematics in both the swing and stance phases. In particular 44 degrees of swing-phase flexion and 15 degrees of stance-phase flexion were achieved, compared to 5 degrees stance-flexion in the locked conditions. Our empirical stance-control model indicates that the timer can range from 0.572 to 0.963 seconds while allowing for successful operation for both normal and fast walking speeds. During clinical evaluation, all trials were completed with the subject being able to consistently unlock the knee during walking without incidence of instability when the knee would not unlock.

The stance control mechanism was effective for gait initiation, steady state walking and gait termination, however further testing is needed in-situ to assess other mobility conditions. Critical to the reliability and robustness of the proposed strategy, was the requirement of the chosen triggering conditions to be sufficiently independent of variations in walking speed. Our analysis shows that a large enough window exists for which a single timer duration would ensure the timely locking of the knee joint, to ensure both swing-phase initiation and proper locking throughout stance-phase. In addition to providing stance control and stance flexion, the knee joint design was significantly decreased size and weight from current stance-controlled orthotics.

SP084 - New Designing Ideas

TRACK 12: MEDICAL DEVICES

SP084.1 - Soprano - Nasogastric Tube Insertion Guide

Author(s): Karthik Kannan¹, Sum Kok Meng², Foad Kabinejadi-an³, Hwa Liang Leo¹

¹Department Of Biomedical Engineering, National University of Singapore, Singapore/SINGAPORE, ²Singapore General Hospital, singapore/SINGAPORE, ³Department Of Surgery, National University of Singapore, Singapore/SINGAPORE

Nasogastric Tubes (NGTs) are used for feeding and administering oral medication in patients with either impaired swallowing mechanisms or obstruction in the upper aero digestive tract that prevents oral feeding. They are inserted through the nose into the stomach and represent an important means of long-term feeding especially in patients with neurological diseases (e.g. strokes). In the US alone, 1.2 million NGTs are inserted yearly. NGT placement entails a significant risk of malpositioning that may result in death from aspiration of liquids into the lungs and expose healthcare institutions to significant medicolegal liability risks. Yet, current methods of confirming correct placement are not foolproof. Moreover ensuring proper placement consumes significant resources- e.g. Chest x-rays for confirmation, hospitalization for costly alternative endoscopic and radiological guided placement methods.

Our device, Soprano is coined on the concept of frugal engineering. With a simple, elegant and innovative solution, we addressed a clinical problem that demands immediate attention and possibly save numerous lives and millions of dollars. Our basic specifications were easy steerability and an accurate and reliable feedback mechanism to identify the correct placement of NGT in the esophagus. (1) Our device is a semi-rigid guide that has a specific elliptical cross-sectional profile that acts as a funnel through which the NGT can be passed through easily into the esophagus and thereby all the way into the stomach. (2) The guide has been specifically designed with an inherent curvature conforming to the anatomy of the nasopharynx area that enables easy steering. (3) Additionally, the guide provides an accurate audio feedback that works on the basis of our inherent inhalation and exhalation cycles. This produces an audio feedback should the guide be wrongly inserted into the trachea. However, no sound is produced if the guide is correctly inserted in the esophagus. Further research into human physiology and sound frequency produced within the esophagus would allow us to further improvise Soprano to accurately detect the frequency of sound produced when correctly placed in the esophagus, giving a positive signal instead of the current negative confirmation. (4) The NGT can then be passed through the guide and the guide later removed via a special slit and having a perforated guide. Soprano promises to be a simple, cost and time-effective solution that for both patients and healthcare professionals alike.

SP084.2 - High Output Impedance Current-Conveyor Oscillator for Electrical Bioimpedance Applications

Author(s): Pedro Bertemes-Filho¹, Volney C. Vincence¹, Dejan Krizaj²

¹Electrical Engineering, Universidade do Estado de Santa Catarina, Joinville/BRAZIL, ²Laboratory For Bioelectromagnetics, University of Ljubljana, Faculty of Electrical Engineering, Ljubljana/SLOVENIA

The objective of this work is to investigate the use of a current conveyor oscillator with current output for tissue excitation in a wide frequency range. It was implemented using a sinusoidal oscillator that provides an output current in a wide frequency range with a

maximum amplitude of 650 μ App. It uses a second generation class AB current conveyor developed with CMOS AMS-0.35 μ m technology and is configured in a Wien bridge structure. It has a low power oscillator supplied by ± 1.5 V with a consumption of approximately 400 μ W. The simulation results showed a frequency sweep between 1.04 to 1,230 kHz by using an integrated bank of capacitors. The maximum total harmonic distortion was 1.8% in the frequency range. The output impedance was bigger than 46 M Ω at lower frequencies but 2.4 M Ω at 1 MHz. The development of a low power current source without using an external voltage generator might be very attractive for measuring cell impedance at the electrode site and for designing battery powered bioimpedance systems.

SP084.3 - Healthcare Device for People Affected by Dementia

Author(s): Sara M. Velez, L V. Wilches
Mechatronics Engineering, Escuela de Ingeniería de Antioquia, Envigado/COLOMBIA

Dementia may be defined as a progressive disorder that affect cognitive abilities in a level enough to cause disability to face everyday life [1]. Around 44 million of people worldwide suffer Dementia and it is expected that this number will reach until 75 million to 2030. Almost 60% of them live in countries without high incomes and have a weak public health service. Although the term Dementia refers to a group of illness that can produce similar symptoms, the Alzheimer's disease is the main of them in terms of patients affected. The symptoms can be devastating because of they include a total memory loss and the lack of recognize familiar objects, remember and perform basic activities. In addition, changes in personality and the necessity of professional assistance affect not only the patients but also their families and friends [2, 3].

At least 25% of the hospitalized patients in clinical services have dementia, and many of these admissions could be prevented if their relatives provide a better support at home [4]. Although this condition implies a save of significant health resources, there are risks related to an inadequate healthcare of patients affected by Dementia outside of a hospital. In this way, the first problem to solve is their technical support.

Technical support can be defined as one device that aims to monitor, assist, prevent, or alleviate a disability without losses in the quality of life of the patients that require it. As a response of this necessity, it has developed a device to allow the technical support of the patients with Dementia, without direct vigilance from their caregivers. The device is a bracelet that reminds the users about his or her daily activities through easy recognition signals. A tracking system that uses sensors in limited areas provides information about the patient's location. In addition, a record system allow regulation of medicines, activities and other relevant information about patients in real time. This device provide autonomy and independence when the Dementia is in its early or middle stage.

The main features of this device are their low cost, easy construction and simple functioning compared to other options available in the market. These differences allow to extend its use in countries with emerging economies without significant investments. In addition, its use could help to relieve the saturation of health services and save resources in different medical assistance levels.

[1] Jagtap A. (2015) Biomarkers in Vascular Dementia. Biomarkers and Genomic Medicine. Elsevier Taiwan LLC. 11 – 001. Available from: <http://dx.doi.org/10.1016/j.bgm.2014.11.001> - (Accessed 30 January 2015)

[2] Karolinska, W. (2010) World Alzheimer Report 2010, The Global Economic Impact of Dementia. Alzheimer's Disease International

(ADI) Stockholm, Sweden. Available from: <http://www.alz.co.uk/research/files/WorldAlzheimerReport2010ExecutiveSummary.pdf> - (Accessed 07 January 2015)

[3] Prince, M. (2013) Policy Brief for Heads of Government, The Global Impact of Dementia 2013–2050. Alzheimer's Disease International, London – UK. Available from: <http://www.alz.co.uk/research/GloballmpactDementia2013.pdf> - (Accessed 07 January 2015)

[4] Healthcare at Home (2011) Understanding Out-of-Hospital Report 2011. Available from: http://www.hah.co.uk/sites/default/files/upload/files/HAH_Report_web.pdf - (Accessed 15 January 2015)

SP084.4 - Wide Field-of-View Fluorescence Imaging with Curved Sample Chamber for Point-of-Care CD4 Test

Author(s): Kyunghoon Kim, M. Mohiuddin K. Shourav, Subin Kim, Jung Kyung Kim
Kookmin University, Seoul/KOREA

It is a technical difficulty to acquire large field image under the complexity and cost restrictions of diagnostic and instant field research purpose. The goal of developing our wide field-of-view imaging system is to achieve tolerable resolution to detect fluorescently-labeled micron-sized particles or cells in the entire image field without the field curvature effect, while maintaining a cost-effective procedure and simple design. In order to obtain a large field image with a simple lens-based optical imaging system, we designed a curved sample chamber. We conducted a systematic study including optical simulations and experiments with a curved sample substrate to ensure a simple and practical design of the proposed system, aimed for a clearer and wider large field of view on a flat plane image sensor. In order to apply our system to point-of-care CD4 test, which can monitor HIV/AIDS disease progression by counting absolute number of CD4 T-cells in a known volume of the blood, the curved sample chambers were manufactured by an injection molding technique. The curved sample chamber reduces the field curvature and image distortion at acceptable level for the CD4 test without using a sophisticated optical elements. The optimal design has a field-of-view of 13 mm and a magnification factor of 0.54. The designed system enables us to image the objects at a spatial resolution $> 8 \mu\text{m}$ and it can be also used for dynamic measurements, such as microscale flow dynamics and micro-organism behavior, by time-lapse imaging and particle tracking methods. Potential applications include a point-of-care medical diagnosis as well as a rapid environment monitoring in field study.

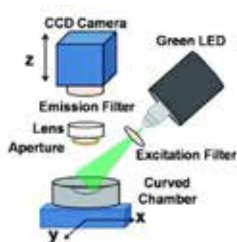


Fig. 1. Experimental setup for wide field-of-view fluorescence imaging with a curved sample chamber.

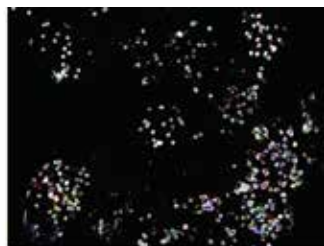


Fig. 2. Trajectories of fluorescent beads moving on the curved substrate (12 mm x 12 mm) incorporated in wide field-of-view fluorescence imaging system.

SP084.5 - Moisture effect on antibody longevity on paper substrate and the role of hydroxyl groups in the concept of "bio-compatible paper"

Author(s): Ziwei Huang, Junfei Tian, Wei Shen
Biopria, Chemical Engineering, Monash University, Clayton/AUSTRALIA

Paper is a bio-compatible alternative for different biological analyses. For example, paper-based blood grouping device is being developed based on the fact that antibody bioactivity can be maintained on substrates as ubiquitous as paper towel. The most common reasons for antibody bioactivity loss on paper due to a molecular change resulting from decreasing water content in the system. However, this is currently a mere hypothesis without any systematic study regarding the moisture effect on antibody longevity on a paper substrate. Additionally, the current paper-based biosensors have used different commercial products of paper, each containing different additives. Whether paper remains bio-compatible without any additives is also unknown. To answer these two questions, a systematic study of antibody longevity was performed with different paper substrates under different relative humidity (RH) environments. Three different kinds of paper were used: pure paper without any additives (30 gsm hardwood paper, PP), pure paper (30 gsm hardwood paper) with 2% of polyamideamine-epichlorohydrin (P-PAE), and commercial paper towel (PT). Our results show that antibodies quickly lose their bioactivity on PP when compared with PT, and a high RH environment accelerates antibody bioactivity loss on both PP and PT. This result suggests that paper without any additives is not bio-compatible and the antibody bioactivity lasts longer under a low RH environment. One significant difference between PP and PT is that the latter employs polymers to increase the wet strength of paper, where the polymer will block some of the hydroxyl groups on the paper surface. Indeed, research has shown that the amount of "free" hydroxyl groups in paper substrate increases under a high RH environment. Therefore, we hypothesize that antibody bioactivity loss is closely related to the amount of "free" hydroxyl groups on the substrate surface. Based on this theory, we used PAE to block partial hydroxyl groups of PP and made P-PAE to carry antibody longevity study under 100% RH. The result of this study has shown a significant increase in antibody longevity with P-PAE, which indicates that "free" hydroxyl groups on the substrate surface is essential in antibody longevity on paper. In conclusion, moisture decreases antibody longevity on paper substrates due to the increasing amount of "free" hydroxyl groups. More importantly, paper without any additives to block the "free" hydroxyl groups can hardly be bio-compatible regarding the antibody longevity. Blocking the hydroxyl groups on the solid substrates can improve the performance of many bio-sensors relying on the antibody bioactivity and further improve the prospects of future paper-based diagnostic devices.

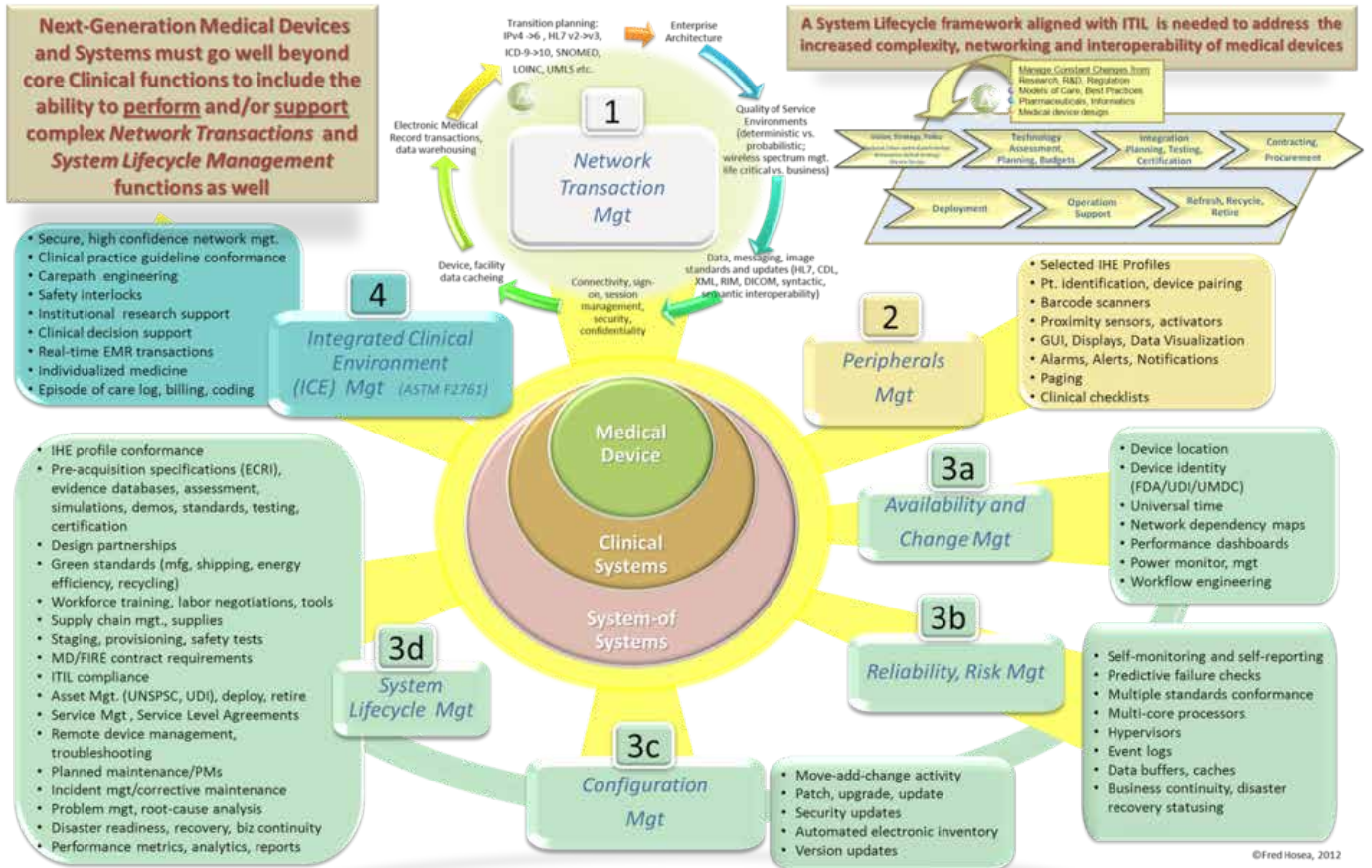
SP084.6 - An Interoperability Maturity Roadmap for Medical Device Design and Alignment with IT Systems

Author(s): Fred W. Hosea
Clinical Technology, Kaiser Permanente, Oakland/UNITED STATES OF AMERICA

Despite the existence of numerous standards bodies and professional associations, there are nevertheless very significant gaps between the ways that medical devices and IT systems are designed and integrated, resulting in problems of interoperability and integration that are expensive to resolve in the operational stage of the system lifecycle. The ITIL (Information Technology Infrastructure Library) model of process management is proposed as an essential bridging framework that will enable medical device and IT industries to work together at the design stage, to align their product roadmaps and create a more coherent staging of functionality over a 5-10 year period.

Interoperability Maturity Roadmap

A shared **Interoperability Maturity Roadmap** is essential to align stakeholders in the global re-engineering of medical devices, building upward from SMART DEVICES with semantic and syntactic capabilities, to achieve PRAGMATIC interoperability for workflows and service management



New technological capabilities (such as multi-core processors with hypervisors) are enabling medical devices to execute a much wider range of functions than has been historically possible. Next generation medical devices will be able to support or perform a wide range of process control functions and business functions that augment their value beyond the core clinical functions. “Intelligent” medical devices will be able to identify themselves on the network, support heightened security safeguards, do periodic self-tests and status reports, support remote diagnosis and repairs, issue predictive failure alerts, perform essential functions autonomously offline, enforce safety “guardrail” precautions against user error, and interface automatically with service and asset management processes to enable real-time updates, configuration management, and performance monitoring.

Four major stages of interoperability maturity are proposed, with specific functions assigned to each stage and sub-stage. (1) Network Transaction management, (2) Peripherals management, (3a) Availability and Change Mgt, (3b) Reliability, Risk Mgt, (3c) Configuration Mgt, (3d) System Lifecycle Mgt, (4) Integrated Clinical Environment (ICE, ASTM 2761). Key functions are identified that will enable more rigorous standardization of data and process models.

SP085 - Women in Medical Physics

TRACK 18: GENDER, SCIENCE AND TECHNOLOGY

SP085.1 - Women in medical physics: Current status Results from IOMP survey

Author(s): Virginia Tsapakis

Konstantopoulio General Hospital, Athens/GREECE

Introduction: The gender composition of medical physicist (MP) workforce around the world is principally unidentified. Acknowledging this issue, IOMP decided to perform a survey to investigate the percentage of women MPs in different countries as compared to total MPs. It was expected that the survey would provide information on gender imbalance, if it existed, and provide a basis for establishment of a subcommittee. Moreover, the results of the survey could provide an opportunity for countries as well as IOMP, for a more in-depth analysis and deliberate on further actions.

Materials and Methods: An online questionnaire was created, prepared as a Google Forms survey asking the country, the total number of MPs, the number of women MPs and finally the gender of the person providing the data. The questionnaire was sent to all 6 regional member organizations of IOMP and a major country, the USA. The regional organizations were asked to distribute it among national member organizations (NMOs) and even to non-IOMP member countries.

Results: Sixty-six countries responded to the survey. The results cover more than 3/4 of the MP manpower in the world. The total number of MPs was 17024, of which 28 % were women (4807). The median values of percentages of women were 21 % in the USA, 47 % in Europe, 35 % in Asia, 33 % in Africa and 24 % in Latin America. It was noted that a substantial number of European countries were far away from the target that the European Commission has set, that is 40 %. On the other hand, there were countries in other regions of the world such as the Middle East and Asia, in which women MPs outnumbered men MP. Interestingly enough, there were countries where only women MPs existed and all these were developing countries

Conclusion: This is the first international survey ever that investigated the gender situation on MPs around the world. Due to these very interesting findings, IOMP decided to perform a more in-depth study in the very near future.

SP085.2 - Is there a 'Leaky Pipeline' for Women in Clinical Medical Physics in Canada?

Author(s): Leigh Conroy¹, Elizabeth Watt¹, Wendy L. Smith²

¹Department Of Medical Physics, Tom Baker Cancer Centre, Calgary/AB/CANADA, ²Department Of Oncology, University of Calgary, Calgary/AB/CANADA

We examined the role of women in clinical medical physics in Canada through a representative career path. Gender data for centers affiliated with the Commission on Accreditation of Medical Physics Education Programs (CAMPEP)-accredited residencies and graduate programs were found through departmental websites and informal surveys. Historical certification data was obtained from the Canadian Organization of Medical Physicists (COMP).

Canadian medical physicists receive certification of competence through Canadian College of Physicists in Medicine (CCPM) examinations. Members (MCCPM) must have a minimum level of work experience and fellows (FCCPM) must have additional work experi-

ence and significant contributions in the field. A cross-sectional view of the proportion of women at each career stage is shown in Figure 1.



Fig. 1 Proportion of women in 2014 at each stage of a representative career. Female representation at the MCCPM level was comparable to graduate students; however there was decrease at the FCCPM level.

We hypothesized that the paucity of women with FCCPM certification could be due to the natural time delay between career stages. Figure 2 shows the historic trends of the number of CCPM members in total (members and fellows) and fellows separated by gender.

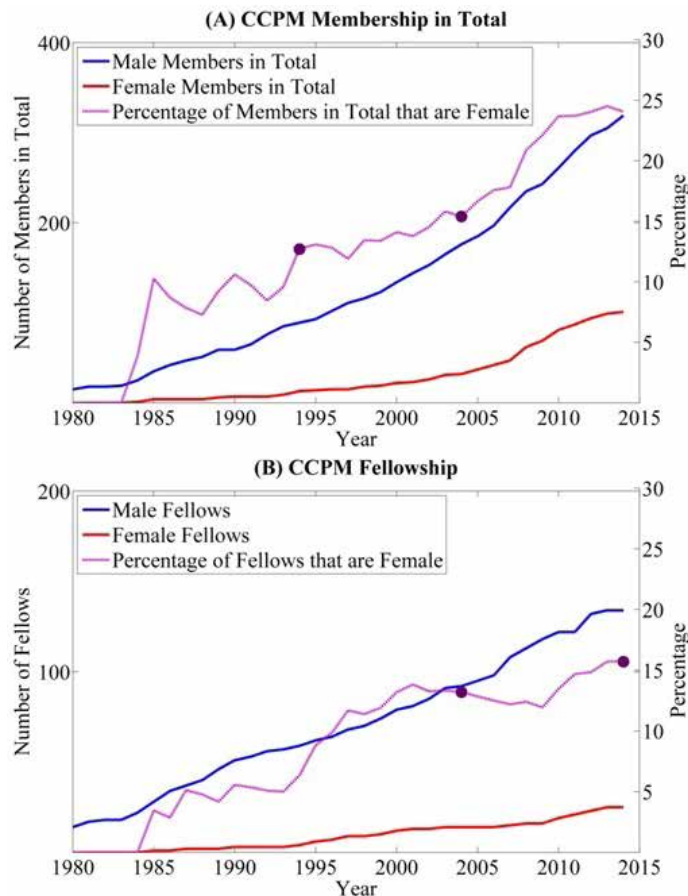


Fig. 2(A) CCPM members in total and (B) fellows. The purple dots demonstrate that in the past decade, the proportion of FCCPMs that are women has echoed the membership of the previous decade.

There were a lower proportion of women at the highest levels of clinical medical physics. Of the 41 identified CAMPEP-accredited director positions (clinical, residency, and graduate program directors), only 7 were held by women.

Overall, we found that women who choose to enter clinical medical physics remain and progress; however, there are comparatively

fewer women in leadership positions. This may change in time as the increasing number of women entering the field advance through their careers.

SP085.3 - Women in Medical field in Brazil: gender equality?

Author(s): Lidia V. De Sá, Simone K. Renha

Medical Physics Department, NATIONAL NUCLEAR ENERGY COMMISSION, RIO DE JANEIRO/BRAZIL

The women participation in the Brazilian workforce has increased greatly since 1970; however, it is still lower than men in many specialized professions. In 2013, for a population around 200 million people, the female birth rate was 49.3%. Despite that, at the age of vocational training (20 to 25 years old) this percentage reverses to 50.4%, reaching 53.8% for women older than 60 years, retirement age. In order to verify the presence of women in the medical field a study was carried out including physicians, nurses and medical physicists based on the Brazilian Health System and professionals associations records. The results showed that for physicians there is already gender equality among professionals, presenting an increase from 37% to 52% in ten years for female professionals. For nursing, approximately 80% are women, showing the predominance of this gender due mainly to the characteristics of "caretakers" of this profession. For medical physics area, the scenario is not the same. The country has a reasonable number of certified medical physicists (MP) in radiotherapy, 273, considering that there are 275 linear accelerators, 68 cobalt equipment, 88 high dose rate (HDR) and 61 low dose rate (LDR) brachytherapy devices in use. However, only 36% of these professionals are women. In nuclear medicine, there are in total only thirty certified MPs while only 30% of them are female with the appropriated skill to attend the demand that currently comprises 814 SPECTs, 110 PETs devices and more than 3000 therapy procedures. Diagnostic radiology presents an even more critical situation, with sixty nine certified MPs for a large number of devices, around 3648 CTs, 22052 X-rays, 4250 mammography units, among others practices, where only 36% are women. In conclusion it can be observed that the women representation in scientific and technical workforce is growing fast in the last decade. However, for medical physics field, the women representative in the medical physics area is not expressive and has not been increasing at the same rate of the others medical professionals. Significant efforts should be made on professional formation, emphasizing the female MP education.

SP085.4 - Women Biomedical Engineers as Consultants in Clinical Engineering Field in Latin American Countries: Case of Study

Author(s): Gabriela Jimenez Moyao, Carmen Rendon Isguerra, Sandra Galan, Claudia D.C. Cárdenas Alanís, Erendira Jimenez, Maria Fernanda Zumpano Romero, Stefany Penafort Flores, Paola Salgado Rodriguez, Pamela Lopez Uroza
Escala Biomedica, Mexico City/MEXICO

The Consultancy in the engineering field has been a common practice since many years ago; the Biomedical Engineering is not an exception; the multidisciplinary of the career gives the biomedical engineers a wider perspective in the clinical practice, infrastructure planning, management, logistics and engineering fields and the analytical results of this convergence promotes the problem solving and high accuracy advices. Women Biomedical Engineers in the consultancy field are a growing hired staff in Mexico and a specific case of study is a clinical engineering consultancy company in Mexico City with projects mostly in Mexico and Latin America, whose staff is mainly formed by women.

The objective of this article is to define the consultancy model inside and outside the company describing how the women inside the

company have been educated based on an inspirational leadership, mostly since the school by the company's founder experience about the clinical engineering field and the motivation to follow values such as truth and justice and also to develop skills such as leadership, effective communication, strategic thinking, innovation and creativity and a systematic improving of their technical knowledge in order to be creative in the problem solving in the consultancy field.

Furthermore, outside the company, describing the challenges women have faced during the consultancy work in the different work fields with different stakeholders such as Hospital Staff, Planning Hospitals Teams, Medical Equipment Vendors, how it has been faced and the solutions and the contribution of these experiences to positioning the company and the women staff members in a competitive mostly men labour field.

In the article there is reference to the interviewed women and also there are mentioned significant testimonies that confirm the hypothesis about the huge impact of the women consultancy work in the clinical engineering field within work teams in the healthcare sector. As a conclusion the experiences described suggest that the women biomedical engineers with leadership skills and good technical knowledge are valuable for the improvement of the healthcare sector and the impact is huge when the knowledge is share inside different organizations through the consultancy efforts.

SP086 - Biological Effects of Ionizing Radiation

TRACK 19: BIOPHYSICS AND MODELLING

SP086.1 - Sensitization of DNA to Ionizing Radiation by Platinum Chemotherapeutic Drugs

Author(s): Mohammad Rezaee¹, Darel Hunting², Leon Sanche²
¹Nuclear Medicine And Radiobiology, University of Sherbrooke, Sherbrooke/QC/CANADA, ²Département De Médecine Nucléaire Et Radiobiologie, Faculté De Médecine Et Des Sciences De La Santé, Université de Sherbrooke, Sherbrooke/CANADA

Concomitant chemoradiotherapy is a common treatment modality for various types of cancers, including upper aerodigestive tract, gastrointestinal, gynecological and genitourinary malignancies, and has improved patient survival. The most significant clinical rationale supporting the use of concurrent chemotherapy with radiation is the role of chemotherapeutic drugs as radiosensitizers. Among the anticancer drugs, platinum analogues are most commonly administered. Their radiosensitizing properties results essentially from their binding to nuclear DNA. Although several mechanisms such as increase in the radiation damage to DNA and inhibition of their repair have been proposed, the contribution and efficiency of the underlying molecular mechanisms of radiosensitization remain unknown. The present study investigates the relative efficiency of the platinum chemotherapeutic drugs (Pt-drugs) in the sensitization of DNA to the direct and indirect effects of ionizing radiation. In particular, it addresses the role of low-energy electrons (LEEs), hydrated electrons and hydroxyl radicals in the radiosensitization of DNA modified by Pt-drugs.

With respect to the direct effects of radiation, LEEs are found to be the main species responsible for the enhancement in DNA damage, particularly cluster damage including double-strand break (DSB) and interduplex cross-links. Irradiation with 10-eV electrons of a 3199-basepair plasmid DNA modified by an average of two Pt-drug adducts results in significant increases in the DSB formation by factors of 3.1, 2.5 and 2.4, respectively, for carboplatin, cisplatin and oxaliplatin relative to unmodified DNA (Table below). Irradiation of these samples with subexcitation-energy electrons (i.e., 0.5 eV) produces substantial number of DSB in the modified DNA, while no DSB is observed in the unmodified DNA. Since 0.5 eV is well below that energy required for the electronic excitation of organic molecules, dissociative electron attachment must be the main mechanism responsible for the formation of strand breaks in the presence of Pt-adducts. Our results also indicate that carboplatin and oxaliplatin have higher efficiency than cisplatin in the enhancement of radiation damage to DNA (Table below).

For the indirect effects of radiation, our results show that both hydroxyl radicals and hydrated electrons are responsible for the enhanced formation of damage in modified DNA. In the presence of Pt-adducts, hydroxyl radicals mainly contribute to the formation of single-strand break, while hydrated electrons are the main species responsible for the DSB formation.

In conclusion, Pt-drug modification is an extremely efficient means of enhancing the formation of DNA DSBs by both LEEs and hydrated electrons created by ionizing radiation.

DNA damage yield (10 ⁻⁸ /Gy/bp) for electron-irradiation of unmodified and Pt-modified DNA.								
Elec- trons	DSB-Formation				SSB-Formation			
	Pure-DNA	Cisplatin+DNA	Carboplatin+DNA	Oxaliplatin+DNA	Pure-DNA	Cisplatin+DNA	Carboplatin+DNA	Oxaliplatin+DNA
0.5-eV	---	4.4 ± 1.5	6.0 ± 2.3	7.4 ± 3.1	324.9±73.8	487.4 ± 74.5	701.5 ± 44.3	531.7 ± 59.1
10-eV	1.2±0.2	3.0 ± 0.2	3.7 ± 0.2	2.9 ± 0.2	78.7± 16.2	110.1 ± 15.8	120.4 ± 21.7	114.3 ± 26.3
10-keV	0.7±0.1	0.9 ± 0.1	1.2 ± 0.1	1.2 ± 0.1	145.3±23.6	152.2 ± 26.5	160.4 ± 18.6	151.4 ± 18.9

SP086.2 - Lymphoma and Choroidal Melanoma cells in the presence of gold nanoparticles: In-Vitro study**Author(s):** Somayeh Asad¹, Mehdi Vaez-Zadeh¹, Sahar Balaghali², Mostafa Olfat¹, Mozghan Rezaeai², Fatemeh Alikarami²¹Physics, K.N.Toosi University of Technology, Tehran/IRAN, ²Ophthalmic Research Center,, Shahid Beheshti University of Medical Sciences, Tehran/IRAN

The aim of this work is to investigate the effects of different sizes and concentrations of gold nanoparticles (GNPs) on the cell viability in both lymphoma and choroidal melanoma cells. To this end, GNPs were synthesized following the Fern's method in three sizes of 20, 40 and 60 nm. Both Melanoma and Lymphoma cells were grown in 6 (24-well) plates so that the first three plates containing Melanoma cells and the last three plates containing Lymphoma cells. In all six plates, the first five wells were coated with five different concentrations of GNPs and the sixth of them was assigned as control. For both Melanoma and Lymphoma cells, one plate was injected by GNPs with the diameter of 20 nm in five different concentrations of 200, 150, 100, 50 and 25 µg and two plates were injected by GNPs with the concentrations of 600, 400, 200, 100 and 50 in which the nanoparticles have a diameter of 40 nm in one of them and 60 nm in another. MTT method was used to assay the cell viability after incubating the cells for 48 hours at 37°C. Compared to the control, in all six plates the results show that both melanoma and lymphoma cells grown were decreased in the presence of nanoparticles. However, there was difference on cell growth between Melanoma-GNPs and Lymphoma-GNPs exposures in-vitro. For instance, at the concentration of 200 µg the present GNPs in Lymphoma cells showed strong decrease of cell viability, while, the viability decrease in melanoma cells was not very considerable. Choice of the size and concentration of GNPs to achieve the best results in ophthalmic brachytherapy are depend on the tumor. Considering the sensitive tissue which the eye is involved in, the dose to normal tissues in comparison with the resultant dose increase in the tumor is of utmost importance in investigation of GNPs effects on ophthalmic brachytherapy dosimetry which require In-Vivo study. Also, further *in vivo* cytotoxicity tests are required before high-concentration GNPs can be used for choroidal melanoma treatment.

SP086.3 - Multiple Code Comparisons of Proton Interactions in the Presence of Gold Nanoparticles in the Human Eye**Author(s):** Mohammad Faraz Samavat, Somayeh Asadi, Hanie Tavassoli, Mehdi Vaez-Zadeh, Shaghayegh Gaeeni
Physics, K.N.Toosi University of Technology, Tehran/IRAN

The main focus of the present study is to investigate dose enhancement effects in presence of gold nanoparticles (AuNPs) in proton delivery site of the ocular melanoma by the use of fixed pencil beam method associated with the Harvard ocular nozzle in a series of Monte Carlo simulations. Moreover, this paper also aims to present a comparison of the obtained results between the actual eye model, consisting of all sections of the eye and realistic compositions in the presence of AuNPs, and in the exact same organ, albeit in privation of the mentioned material. Previous Monte-Carlo simulations have strained to acquire the same results obtained through latest experiments that have considered dose enhancement effects of proton treatments with existence of AuNPs, but to no avail; thus, multiple simulation codes such as MCNP, GEANT4, and FLUKA have been taken into account to insure the least possible deviation from *in vivo* findings. Rigorous libraries and models have been used, and all physical processes involved have been accounted for; furthermore, for the sake of accuracy, the production of the most probable secondary particles due to interactions with matter has also been examined. Contribution to dose enhancement effects are due to stopping losses, coulomb interactions, and elastic and non-elastic collisions of proton itself, as well as from secondary particles that are produced in mentioned processes. The attempt of such

paper is to shed light on the endless possibilities of escalating the efficiency of medical endeavors through interdisciplinary methods which combine various aspects of science and technology to attain desired results.

SP086.4 - An in-vitro method for calibrating the gamma-H2AX DNA double strand break focus assay in blood lymphocytes for radionuclide therapy**Author(s):** Uta Eberlein¹, Harry Scherthan², Michel Peper², Maria Fernández¹, Michael Lassmann¹¹Department Of Nuclear Medicine, University Hospital of Würzburg, Würzburg/GERMANY, ²Bundeswehr Institute of Radiobiology, Munich/GERMANY

Objectives: Radiation-induced DNA Double strand breaks (DSBs) cause, in their vicinity, the phosphorylation of the histone H2AX (then called γ-H2AX) and the accumulation of the 53BP1 protein that binds to and signals damaged chromatin at a DSB site. This leads to the formation of microscopically visible nuclear foci containing both markers which thus mark radiation-induced DSBs. The aim of this study is to develop a method that allows generating a calibration curve for the DNA DSB focus assay in-vitro after internal irradiation with radionuclides. The samples should be exposed to radionuclides used in radionuclide therapy, nowadays also called molecular radiotherapy (MRT), simulating absorbed doses and dose-rates that are similar to the ones that have been observed in patients.

Therefore, we studied the induction of radiation-induced co-localizing γ-H2AX and 53BP1 foci in lymphocytes as surrogate markers for DSBs, and correlated the obtained foci per cell values with the *in-vitro* absorbed doses to the blood for the two most frequently used radionuclides in MRT (I-131 and Lu-177).

Methods: We investigated blood samples of 3 healthy blood-donors. 9 experiments were carried out (2 experiments with I-131 and 1 with Lu-177 for each volunteer). For each experiment we withdrew approximately 28ml of blood at different time-points. One sample without radioactivity was used to determine the individual background focus rate. Radionuclides of known activities were diluted with NaCl and mixed with whole blood (3.5ml) to result in radioactive blood samples with different nuclide concentrations to deliver absorbed doses rates between 5mGy/h and 100mGy/h. Each vial was incubated for 1h at 37°C on a roller-mixer to uniformly blend the samples during the exposure. Thereafter, white blood cells were recovered by density centrifugation and washed in PBS followed by fixation in 70% ethanol. Samples were subjected to two-colour immunofluorescence staining and the average frequencies of the radiation-induced colocalizing γ-H2AX and 53BP1 foci/nucleus were counted manually using a red/green double band pass filter on a fluorescence microscope by an experienced observer. From each blood sample an aliquot was recovered for determining the activity with a calibrated germanium detector. The average absorbed dose rates to the blood per nuclear disintegrations occurring in 1ml of blood were calculated for both isotopes using the radiation transport code MCNPXv2.71.

Results: Overall 55 blood samples were evaluated in a dose range between 6mGy and 95mGy. Only minor nuclide-specific, intra- and inter-subject deviations were observed. We obtained a linear relationship between the number of DSB-marking γ-H2AX and 53BP1 foci/nucleus and the absorbed dose to the blood ($R^2=0.92$) which agrees well with published values for external irradiation.

Conclusions: This *in-vitro* calibration method for the DNA double strand break focus assay will provide additional information for *in-vivo* measurements in patients after molecular radiotherapy and will further improve the absorbed dose to the blood calculation method.

SP086.5 - Dose enhancement during concomitant chemoradiotherapy using FDA approved concentrations of carboplatin and oxaliplatin nanoparticles

Author(s): Gizem Cifter¹, Yucel Altundal², Alexandre Detappe¹, Erno Sajo², Ross Berbeco¹, G. M. Makrigiorgos¹, Wilfred Ngwa¹
¹Department Of Radiation Oncology Division Of Medical Physics, Harvard Medical School Dana Farber Cancer Institute, Boston/ UNITED STATES OF AMERICA, ²Medical Physics, University of Massachusetts Lowell, Lowell/UNITED STATES OF AMERICA

Radiation boosting has been shown in a number of studies to be effective in the prevention of cancer recurrence. To further the effectiveness of this technique, we propose a new method of enhancing dose locally by administering nanoparticles of carboplatin (CaNPs) and oxaliplatin (ONPs) as adjuvants to brachytherapy and external beam therapy (EBRT). To investigate the efficacy of this method, dose enhancement calculations were carried out to calculate the energy deposited by photoelectrons and Auger electrons produced by low energy photons from either (EBRT) or brachytherapy sources with CaNPs and ONPs. Our results show a significant increase in the dose enhancement for various carboplatin and oxaliplatin concentrations up to their allowed FDA limits.

SP087 - Educational and Professional Activities: Part 2**PRESIDENTS CALL****SP087.1 - The potential role of IFMBE in improving the state of medical equipment in developing countries**

Author(s): Anna Worm¹, Andrei Linnenbank²
¹Tropical Health and Education Trust, London/UNITED KINGDOM, ²Electrical Engineering, Mathematics And Computer Science, Delft University of Technology, Delft/NETHERLANDS

In developing countries medical equipment is often non-functional. Well known reasons for that are donations of already broken equipment and lack of spare parts and consumables. It is to be expected that current state of the art medical equipment is even less suitable for donation, given the way they are designed to function under conditions that are hard to find in rural areas in low resource countries. The key to start solving these problems lies in improving technical education at all levels in these countries. This paper explores how the IFMBE can work together with several other institutions (WHO, local professional organizations, non-profit organizations, Ministries of Health and Education,...) to train and sustain a competent technical workforce that can do maintenance, repair, and design of biomedical equipment using locally available materials and knowledge.

SP087.2 - Biomedical Engineering Education through Outreach Programs in Hospitals

Author(s): Franco Simini¹, Fernando Leon Moloney¹, Jorge De Giobbe²

¹Núcleo De Ingeniería Biomédica, Universidad de la República, Montevideo/URUGUAY, ²Rio Negro, Hospital ASSE, Fray Bentos/URUGUAY

Health expenditure is a measure of the share of activity related to health care, both preventive and curative. Industrialized Countries spend around 10% of Gross Domestic Product (GDP) [1] with a high 17.9% for the USA. Middle income Countries, such as Uruguay, have lower figures, but growing as does the dissemination of medical actions in larger portions of the population. More hospitals are build and more equipment are installed every year. Traditional Engineering Education is slow at developing Biomedical Engineering (BME) Programs, because initial demand is scarce and because existing Electrical or Mechanical Engineers usually take over specific functions after some training by equipment providers. Uruguay has a 120 years old University but is only starting to train BME graduates. Job offers greatly exceed qualified staff available, which led us to suggest urgent training programs based on an Outreach Program in Hospitals (OPH), therefore at low cost.

OPH based BME training is build upon existing Electrical Engineering and Systems Engineering Programs, using courses of maths, physics, chemistry, software development, electrical engineering and management. Six optional courses are added, from electronic design to medical image processing and management (DICOM, PACS), electrical safety standards, medical terminology, physiology and anatomy.

A full year design project of a biomedical equipment is assigned to groups of three students, to both foster collaborative attitude and to obtain a functional solution to a clinical instrumentation problem.

Students are then assigned in their fourth University year to a full time six months intern-ship in a Secondary Level Hospitals, where

BME is non-existent. This is done within a University Outreach Program. As the only technological reference persons in the Hospital Director's office, BME students face a variety of maintenance, purchasing, staff training, safety measures enforcement, documentation and installation/removal of equipment. Every student is assigned a remote instructor who acts as a reference available on call or otherwise. The instructors are University teachers in capital city Montevideo, while students are in remote (100 Km to 600 Km) hospitals, where a basic "intern-ship" salary is paid, in addition to feeding/lodging on premises.

Results of this low budget, OPH based BME program are promising with first graduations expected June 2015. The main results are (1) self confidence and sense of responsibility acquired by student (2) its low cost and (3) the interest of BME firms for future employment.

From the Hospital Point of view, equipment documentation, staff safety instruction and maintenance purveyors relations are the benefits so far.

This model of integrated, easily implemented BME Program based on University Outreach has the potential to be considered in other settings in Latin America, the Caribbean and elsewhere, where quick BME staffing requirements must be met at low cost, helping to reduce Health Expenditure.

[1] <http://databank.worldbank.org/data/views/reports/metadataview.aspx>

SP087.3 - Clinical Engineer: a health professional to recognize Author(s):

Background

In latter years, Clinical Engineer's figure is taking on more and more importance in health technology management, due to his technical knowledge and capacity to interact with different fields professionals. Unfortunately, this situation does not reflect reality: in many low and medium income countries this figure does not exist and in many high income countries Clinical Engineer is not recognized as health professional, but very often compared as biomedical technician. Internationally Clinical Engineers, as subset of Biomedical Engineers, belong to Unit Group 2149 "Engineering Professionals Not Elsewhere Classified" under the International Standard Classification of Occupations produced by the International Labour Organization.

Objective

Clinical Engineers community is strictly collaborating with World Health Organization (WHO), in particular with Adriana Velazquez Berumen, Senior Adviser on Medical Devices, to recognize Clinical and Biomedical Engineer's figure worldwide.

The main aim is to stress the importance of Clinical Engineer in healthcare facilities. This work will be a chapter of Human Resources for Medical Devices, part of *WHO Medical device technical series*.

Methods

The approach used in this work analyses the main activities carried out by Clinical Engineer, in order to give awareness of all activities involving this figure. Therefore the analysis focuses on Clinical Engineer's role at national level, in particular within the Ministries of Health of different Countries. This analysis was possible through several statements by professionals who work at national level. Finally the analysis gives attention to Clinical Engineering's diffusion worldwide in the six WHO regions (*African Region, Region of Americas, Eastern Mediterranean Region, European Region, South-East Asia Region, Western Pacific Region*) through data from Clinical Engineering Societies around the world.

Conclusions

Clinical Engineer is without doubt a professional who needs to be recognized worldwide with more support. He is a fundamental resource in health technologies management and contributes both to healthcare organization and patient health.

SP087.4 - "Rehabilitation Engineering: Designing for Ability" - A summer outreach course for attracting talented high school students to the rehabilitation engineering field

Author(s): Vicki Komisar¹, Emily C. King², Eve Moore³, Sabah Hassan⁴, Aaron Marquis⁵, Justin Chee⁶, Rosalie H. Wang⁷, Sunita Mathur⁸, Tilak Dutta², Cesar Marquez-Chin⁵

¹Institute Of Biomaterials And Biomedical Engineering, University of Toronto, Toronto/CANADA, ²Department Of Mechanical And Industrial Engineering, University of Toronto, Toronto/CANADA, ³Handy-Metrics Corporation, Toronto/CANADA, ⁴Central Neighborhood House, Toronto/CANADA, ⁵Toronto Rehabilitation Institute - University Health Network, Toronto/CANADA, ⁶Rehabilitation Sciences Institute, University of Toronto, Toronto/CANADA, ⁷Department Of Occupational Sciences And Occupational Therapy, University of Toronto, Toronto/CANADA, ⁸Department Of Physical Therapy, University of Toronto, Toronto/CANADA

Motivation: We need to inspire talented students to pursue rehabilitation engineering, and develop the technologies that will help our aging population overcome disabilities and live fulfilling lives for as long as possible. Our team experiences a perennial challenge of attracting top-quality students to important yet often unglamorous facets of this field (e.g. supporting independent toileting for people with mobility challenges), partly because prospective students may not recognize these challenges, or see how they can be addressed through science and engineering. In response, we developed a week-long course in rehabilitation engineering for high-school students through the University of Toronto's "Da Vinci Engineering Enrichment Program", which we have led every summer since 2012.

Course structure: The course was designed provide students with memorable interactive experiences in a range of rehabilitation engineering applications. To discover accessibility challenges, students completed a "Built Environment Obstacle Course", where they navigated UoT while simulating mobility and vision deficits, then assessed how built environment features affected their experience. Students participated in hands-on demonstrations in Toronto Rehab's Challenging Environment Assessment Laboratories and Neural Engineering Lab to understand how engineering technologies are being applied to problems such as preserving hand dexterity in cold weather, and allowing people who are 'locked-in' to control their own environments. Guest speakers included engineers, clinicians and an entrepreneur who could communicate authentically to the students about the challenges, importance and rewards of developing and commercializing technologies to improve the lives of people with disabilities. The week culminated with a "Home-Care Design Challenge", focused on solving problems related to aging-in-place. These design problems were selected from real client case studies presented by a home-care field educator.

Student feedback: Students reported significant improvements in their understanding of key learning objectives (Figure 1). Students appreciated the Toronto Rehab visits, the diverse topics, the design challenges, and the instructional team's ability to make the content understandable, interactive, and relevant.

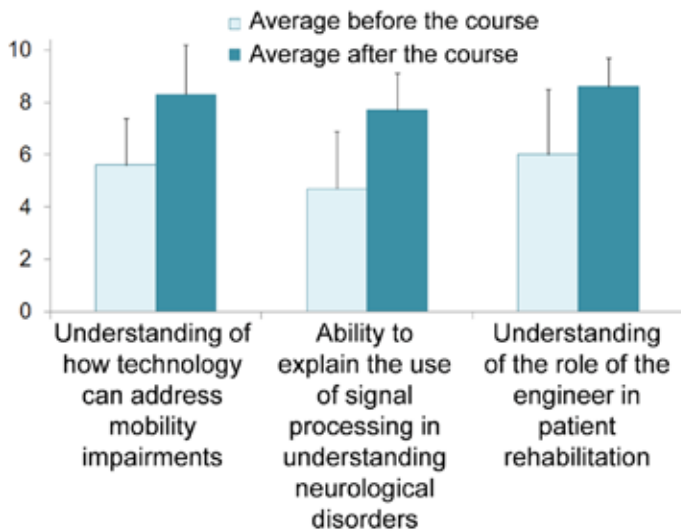


Figure 1: Mean student responses to learning objective questions before/after the 2013 course (scale of 1-10). 22/25 students responded.

Expected outcomes: All of the participating students gained an awareness of the problems faced by older adults and the societal importance of finding solutions. Those who pursue engineering will better understand their potential roles in rehabilitation engineering and the importance of including stakeholder perspectives. Conversely, those who pursue other medical disciplines will appreciate the importance of engineering in medicine and the potential for collaboration with engineers to advance their work.

SP087.5 - A Novel Approach to Train Biomedical Engineers in a Ugandan Setting

Author(s): Robert T. Ssekitooleko¹, Philippa N. Makobore²
¹Physiology, Makerere University, Kampala/UGANDA, ²Instrumentation Division, Uganda Industrial Research Institute, Kampala/UGANDA

Whereas many universities in the developed countries are now offering degrees in Biomedical Engineering or closely related subjects, Africa sees very few such programmes being offered. The Biomedical Engineering degree programme offered at Makerere University is seen to be the first of its kind in Sub-Saharan Africa. It has been running for less than three years with some other institutions in the country offering Diplomas.

The degree has been designed in such a way that student internship is an integrated part of the training where the students are actually graded for their performance. This was brought about to improve the awareness of the Biomedical Engineers and students in hospitals as well as companies where they were otherwise unknown. Internship posts have been secured in all government hospitals and many private hospitals and companies. Companies Such as SinoAfrica Uganda, Joint Medical Stores have continuously offered placements for the students. The students are given clear objectives with specific outcomes from each placement. They get a placement supervisor as well as an academic supervisor to monitor their progress.

The Uganda Industrial Research Institute (UIRI) has gone a step further in supporting the degree programme. They not only provide placements for the students but also offer dedicated training such as embedded systems and programming that students can take to improve their knowledge and skills.

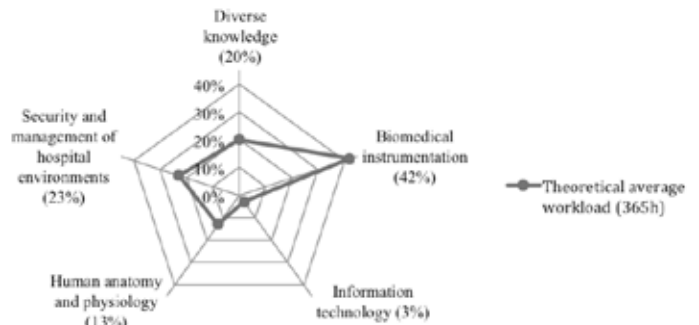
Such engagement with different organisations has helped students

not only to gain more confidence in the degree programme but to also identify potential jobs in a country where the field is just growing.

SP087.6 - A Health Information Technology Management Course for Brazilian Clinical Engineers

Author(s): Fernando O. Andrade, Saide Calil
 Department Of Biomedical Engineering (deb), State University of Campinas (UNICAMP), Campinas/BRAZIL

The excessive and inappropriate adoption of computerized technologies in the healthcare system have, greatly increased the occurrence of incidents, transforming these new resources into potential sources of risk. As manager of healthcare technologies, the clinical engineer (CE) should establish the necessary management measures to ensure the safety of patients and operators. This study aims to present a process to develop curriculum directives for a distance education course for professional specialization of CE, on risk management of health information technology (HIT). The method starts by evaluating the curricular training courses on clinical engineering in Brazil and identifying the areas of knowledge. It was analysed 160 disciplines from 11 training courses for CE in Brazil. The content of the disciplines were analyzed and classified into five categories presented below.



The process for developing the proposed curriculum was performed by structuring the types of knowledge needed for risk management on HIT obtained through the exploration and study of the environment in which these technologies are embedded. The exploration of the literature and specific standards to manage IT risks pointed out several incidents involving the use of HIT. It was also investigated the types of risks associated with the use of HIT, the professional characteristics of IT professionals and the necessary requirements to apply the standards for risk management on the healthcare system. This investigation has shown the kind of knowledge required by the CE professionals. The proposal curriculum to train clinical engineers for managing HIT are shown at Table 1.

N°	Module	Workload (h)
1	Introduction on health information systems	50
2	Medical IT-network	70
3	Usability, ergonomics and accessibility	30
4	Technology project management	30
5	Safety and risks of IT-network	70
6	Risk management	30
7	New technology in healthcare	50
8	Multidisciplinary and hospital infrastructure	30

The proposal here intended not only to upgrade the expertise of the clinical engineering professionals, but also aims to improve the inte-

gration and the teamwork with professionals in the field of information technology. The course is already in progress and currently has 63 students from different regions of Brazil.

SP087.7 - A Successful High School Science Mentorship Program: Students on the Beamlines at the Canadian Light Source

Author(s): Tracy Walker¹, Tomasz W. Wysokinski¹, Mark A. Webb¹, Ning Zhu¹, George Belev¹, Cécilia Barrette-Leduc², Katarina Stevanovic², Lylia Xiao², Sara Marrè², Shu Yi Zhai², Yu Xin Zhuang², Marie-Eve Brassard², Denise Miller¹

¹Bmit, Canadian Light Source Inc., Saskatoon/CANADA, ²Pensionnat Saint-Nom-de-Marie, Montreal/CANADA

Canada's only synchrotron is an extremely brilliant source of X-ray and infrared light for research in a multitude of disciplines. We also have a unique program that engages high school students in authentic science research experiences. The Students on the Beamlines (SotB) [1] program connects high school students from across Canada with scientists at the Canadian Light Source (CLS) for mentorship through an authentic science research experience. "Authentic" indicates that we facilitate a research project that is as close to what professional scientists do as a high school student is capable. These are not demonstration experiments. Students must design a project that builds on previous work (through literature review) and ask a scientific question that requires synchrotron techniques to address. The results of their experiment are expected to potentially produce novel information that is of interest to the scientific community. It is this negotiation between the goals of producing 'good science' and creating an 'educational and learning experience' that is part of what makes this program unique. Key to the program is that the students function as primary investigators. Their mentors facilitate, direct and advise the students, but the project belongs to them and they make the decisions.

of this presentation is to share our experience so the concept of student participation in mentored authentic science research can spread. In our case, using a synchrotron is the context and a hook to attract student participation. Any research context would work similarly.

1. <http://www.tandfonline.com/doi/abs/10.1080/08940886.2013.753778#.VPoStvnF98E>



The case study presented is one from Pensionnat Saint-Nom-de-Marie, a girls' school in Montreal, Canada. Honey bees in Canada are suffering significant winter death due to infestations of the *Nosema* fungus. It is known that the infestation deforms the digestive system of infected bees. Students used the Biomedical Imaging & Therapy (BMIT) beamline at CLS to collect x-ray projection and CT images of healthy and infected bees clearly showing the bees' digestive system.

More than 500 students have participated in SotB so far and report that the experience has had a profound impact on their view of research, careers in science and of scientists. Teachers are eager to involve their students because the program fits with current educational initiatives encouraging student engagement through the use of inquiry methods in the science classroom. Several other synchrotron research facilities are emulating the program. The point

SP088 - Computer Aided Diagnosis

TRACK 01: IMAGING

SP088.1 - Automatic Analysis of Plantar Foot Thermal Images in at-Risk Type II Diabetes by Using an Infrared Camera

Author(s): Luis Vilcahuaman¹, Rachid Harba², Raphael Canals², Martha Zequera³, Carlos Wilches³, M.T. Arista¹, L. Torres¹, H. Arbanil¹
¹Biomedical Engineering, PUCP, Lima/PERU, ²Prisme, University of Orleans, Orleans/France, ³Electronic Department, School Of Engineering, Pontificia Universidad Javeriana, Bogota/COLOMBIA

Temperature of the plantar foot surface is an important feature in type II diabetes as abnormal temperature variations can be an early sign of foot diseases. In this paper, automatic way to analyze these temperature variations is presented by using an infrared camera. A robust acquisition protocol is proposed and an image processing software is developed. Three types of analysis are performed. First, the mean plantar foot temperature of both feet results from a segmentation procedure based on the Chan and Vese active contour method. Second, the point-to-point absolute mean difference between the 2 feet is assessed by using a rigid registration method. Third, significant hyperthermia regions such that the point-to-point absolute difference is greater than 2.2°C are highlighted. All these measures are fully automatic and do not need manual intervention. 82 type II diabetic subjects in a pre-ulcerative state were recruited in the Dos de Mayo hospital (HNMD) in Lima, Peru. These persons were classified in two risk groups of developing an ulcer based on a medical exam: a medium risk group, and a high risk group. Results show that the mean temperature of the plantar foot surface is higher of 1°C in the high risk group compared to the medium risk group. The mean point-to-point absolute difference shows identical values in the 2 groups. Finally, 9 subjects out of the 82 ones show significant hyperthermia of one foot compared to the other (6 in the medium risk group and 3 in the high risk group). It is expected that the new opportunity to automatically analyze foot temperature in hospitals or in diabetic health centers will help in reducing foot ulcer occurrence for type II diabetic persons.

SP088.2 - Computer Assisted Diagnosis of Sclerotic Bone Lesions from Dual Energy CT

Author(s): Duc Fehr¹, Charles R. Schmitdlein¹, Sinchun Hwang², Joseph O. Deasy¹, Harini Veeraraghavan³

¹Memorial Sloan Kettering Cancer Center, New York/NY/UNITED STATES OF AMERICA, ²Radiology, Memorial Sloan Kettering Cancer Center, New York/NY/UNITED STATES OF AMERICA, ³Medical Physics, Memorial Sloan Kettering Cancer Center, New York/UNITED STATES OF AMERICA

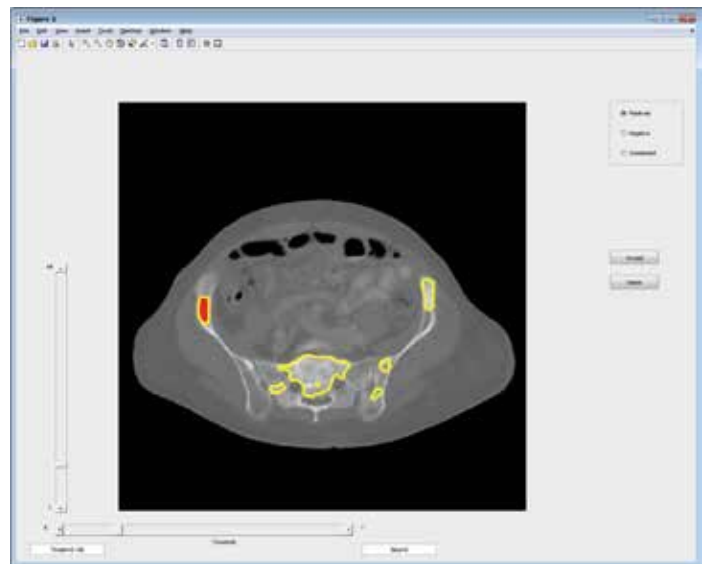
Purpose: To develop a computer assisted diagnosis (CAD) tool for the detection of sclerotic bone lesions in the pelvic region from dual energy computed tomography (DECT). Automatically identifying every single bone metastatic lesions from CT images is difficult owing to (a) large number of such lesions, and (b) very low contrast between the lesions and the marrow or bone.

Method: We developed a CAD tool that automatically detects sclerotic bone metastases from DECT images from the pelvic region. Our method consists of two stages. In the first stage, the bone and marrow regions are automatically segmented through a voxel-wise classification of the DECT image represented as a composition of multiple materials by using support vector machine classifier, followed by morphological smoothing. The appropriate material composition is determined through a learning using SVM that selects

the best material composition for segmenting the bone and marrow from the rest of the image. In the second stage, the contrast inside the bone and marrow regions are enhanced through bi-histogram equalization followed by mean shift clustering. Mean shift clustering groups voxels with similar intensities into single clusters. Finally, the segmented regions extracted from the mean shift clusters are scored by their shape. The following parameters including area, eccentricity, solidity, major axis, minor axis, perimeter, and the medial axis are used as constraints on the shape. Shape filtering prefers isolated regions that are solid, with small elongation and smaller size rather than highly elongated shapes (such as the bones). The shape filtering outputs potential sclerotic bone lesion regions, which can then be validated by a radiologist.

Results: We compared the candidate regions generated by our method with the ground truth regions manually identified by a radiologist. Our results agreed with the radiologist marked regions despite the presence of confounding metal artifacts and the low contrast between healthy bone and the lesions.

Conclusions: We developed a CAD tool that automatically detects sclerotic bone lesions in the pelvic areas from dual energy CT. The detected lesions using our approach highly similar to the radiologist identified regions despite the presence of confounding structures with similar intensities including the sclerotic lesions, healthy bone and metal artifacts.



SP088.3 - Mutual Information Based Template Matching Method for the Computer Aided Diagnosis of Alzheimer Disease

Author(s): Esra Polat, Albert Guvenis
 Institute Of Biomedical Engineering, Bogazici University, Istanbul/TURKEY

Background

Early and reliable detection of Alzheimer Disease (AD) from Positron Emission Tomography images using computerized methods is a desirable objective for the effective management of that disease. Several characteristics of the computer aided diagnostic system (CAD) are important for improving this process: (1) Taking advantage of the growing number of images in databases (2) Ability to search a database for similar cases (3) Robustness with respect to data acquisition and processing factors (4) Full automation. In particular the third and fourth requirements are important in view of the fact that many CAD systems require user intervention.

Purpose

Our goal was to develop a fully automated CAD system for detecting AD that can meet these requirements.

Method and Materials

We have used the Alzheimer's disease Neuroimaging Initiative (ADNI) database for this study. Images for each patient were co-registered in order to correct for patient motion and had voxel sizes of 160 x 160 x 96. Voxel size was 1.5x1.5x1.5 in mm. There was 397 PET images including 259 normal and 138 AD patients.

A similarity measure based on mutual information (MI) was used to determine the closest matches for a new case. A K-Nearest Neighbor algorithm based distance measure was used to decide if a new image was from a healthy or AD patient. A leave one out evaluation method was implemented. Evaluation results were computed using ROC analysis. All development was carried out in a Matlab environment.

Results

Initial ROC analysis resulted an area under the curve (AUC) equal to 0.744 ± 0.025 for this dataset. Much higher AUC values are expected for the nonlinearly registered images across patients. This is work in progress.

Conclusions

First results show that it is possible to discriminate between AD and healthy individuals by using template matching and mutual information as a similarity metric. Further studies are underway in order to improve these results by introducing nonlinear registration methods and by adjusting the image size and grey scale parameters used in the process. Robustness, adaptation ability to growing databases without having to retrain the system and case based reasoning possibilities will be some advantages of the new CAD system.

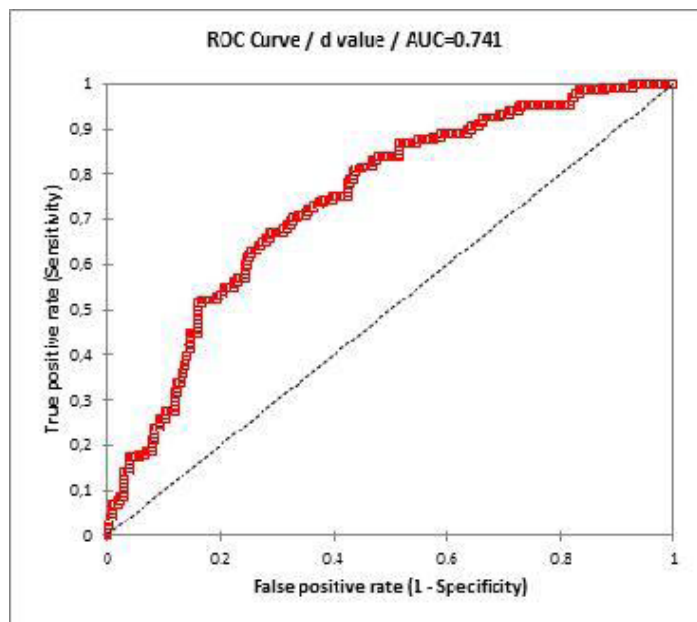


Figure 1 ROC Curve for the first database of images

SP088.4 - Development of an Anatomical Measurement and Data Analysis Tool Based on the Kinect Sensor for Physical Rehabilitation Applications.

Author(s): David A. Duarte-Dyck¹, Gerardo S. Romo-Cardenas², Alejandra Guillen-Peralta³, Lucas Callorda-Fedeczko³
¹School Of Engineering And Technology, Montemorelos University, Montemorelos/MEXICO, ²School Of Engineering, Montemorelos University, Montemorelos/MEXICO, ³School Of Health Sciences, Montemorelos University, Montemorelos/MEXICO

Cyber-physical systems (CPS), integrate computer systems and communication capabilities for the monitoring and control of physical systems through hardware and embedded systems. These consider methods and technologies whose scope have applications in medical and biological areas.

A particular case on the application of these systems, relates to the field of physical rehabilitation, where using the detection capabilities on environments and bodies in 3 dimensions by means of specific positioning devices, like the Kinect sensor developed by Microsoft. Many studies have reported efforts developed in this direction.

At the Biomedical Engineering Laboratory of the Montemorelos University, we have developed a system called "ETMASD" (Environment Track, Measurement and Analysis of Skeletal Data) which allows appropriate locate joints and measure distances between them, as well as the positioning of a subject in a tridimensional plane, all of this through the skeletal mapping system done with the Kinect on a MATLAB environment. A specific algorithm was developed in order to measure the caput-collum-diaphyseal angle, making this an alternative for the traditional x-rays, given the chance to use this development for both scientific and physical rehabilitation applications. This paper describes the progress made on the development of a computational application focused on the initial diagnostic evaluation of anatomical pathologies.

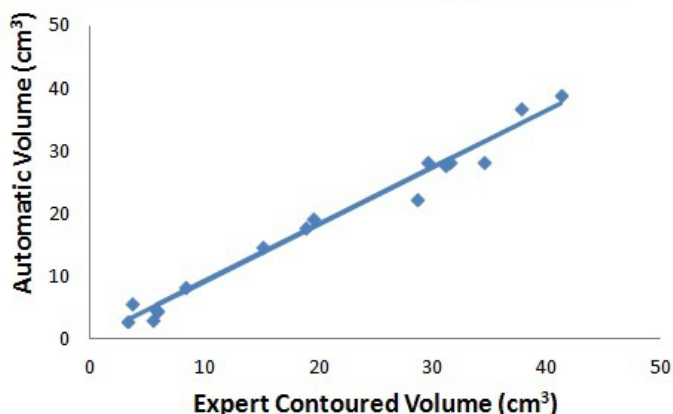
SP088.5 - Quantitative CT Assessment of Vertebral Fracture Severity

Author(s): Curtis Caldwell¹, Trinette Wright², Arjun Sahgal³, Cari Whyne⁴, Michael Hardisty⁴, Mikki Campbell⁵
¹Medical Imaging, Sunnybrook Health Sciences Centre, Toronto/CANADA, ²Physical Sciences, Sunnybrook Research Institute, Toronto/CANADA, ³Department Of Radiation Oncology, University of Toronto, Toronto/ON/CANADA, ⁴Orthopaedic Biomechanics Laboratory, Sunnybrook Research Institute, Toronto/CANADA, ⁵Radiation Therapy, Sunnybrook Health Sciences Centre, Toronto/CANADA

The intent of this work is to develop a simple semi-automated method of quantitatively assessing the severity of vertebral fractures based on imaging to assist in clinical management. Fractures may be relatively stable and asymptomatic, while others may be mechanically unstable leading to pain, neurological complications and progression. Severity may be assessed by a visual determination of the extent of vertebral volume and/or height reduction, yet such subjective assessments can be difficult and time consuming for even expert observers. In the absence of pre-fracture radiographs, visual estimation of changes may be subject to significant error. These subjectively determined imaging factors (vertebral volume, height reduction, etc.) are combined with other clinical factors into scoring systems (Genant, SINS, TLICS) that guide management. CT has been less commonly used to assess bone fracture due to its relatively high radiation dose. However, in some populations, such as patients with spinal metastasis being planned for treatment with radiation therapy, there is less concern for diagnostic CT dose levels. It is easier to assess changes in bone volume from a 3D imaging modality such as CT than with a 2D-x-ray approach. In this study, CT scans of 13 patients known to have spinal metastases and vertebral fractures were assessed; 3 of the 13 patients

also had imaging prior to fracture. An expert Radiation Therapist manually contoured the residual bone within the fractured vertebral body. A system based on Claron Technology Inc's "Spinemapper" application that automatically identifies vertebral levels and segments vertebral bodies, previously applied in unfractured vertebral bodies was extended to automatically contour the volume of each fractured vertebral body. The automatic method produced volumes highly correlated ($R^2=0.994$) with, but approximately 9% less than the expert contoured volumes. Using a curve fit to the volumes of adjacent "normal" vertebrae, the percentage change in volume in the fractured vertebra was estimated. Based on such curve fits, the estimated percentage volume loss ranged from 5% to 40% in the patient group studied. For the three subjects where both pre- and post-fracture CTs were available, the post-fracture assessment of predicted percentage volume loss matched the measured value based on pre- and post fracture data within 10%. This study demonstrates the viability and precision of this method to automate the analysis of fractured vertebral body volume and height reduction. These factors can then be incorporated into the scoring and management of patients with vertebral fractures.

Fractured Vertebral Body Volumes: Automatic vs Manual Segmentation



SP089 - Tissue Modelling

TRACK 03: BIOMECHANICS AND ARTIFICIAL ORGANS

SP089.1 - The protective effect of the eyelid on ocular injuries in blunt trauma

Author(s): Xiaoyu Liu¹, Lizhen Wang², Jing Ji², Yubo Fan³
¹School of Biological Science and Medical Engineering, Beihang University, Beijing/CHINA, ²School of Biological Science and Medical Engineering, Key Laboratory for Biomechanics and Mechanobiology of Ministry of Education, National Key Lab of Virtual Reality Technology, Beihang University, Beijing/CHINA, ³National Research Center for Rehabilitation Technical Aids, Beijing/CHINA

The instinctive blink reflex makes the eyelid close when a foreign body is approaching the eye. This study aimed to investigate the protective effect of eyelid on ocular injuries in blunt trauma. A finite element model of the eyelid model was created and was incorporated into a validated eye model. The process of a projectile impacting on a naked eye and an eyelid-covered eye were reproduced in dynamic simulation. Dynamic responses on the cornea and retina were performed to evaluate the risk of damage to the tissues. The simulation indicated that the eyelid significantly protected the cornea against damage from blunt impact, especially for a small-size projectile. This is because the eyelid distributes the local stress concentration to the whole ocular surface. However, the eyelid failed to provide the retina with an effective protection against damage in blunt trauma. This is because the retinal damage is a typical contre-coup injury, which is the result of shockwave propagation in the eyeball. In conclusion, the eyelid has different protective effects on ocular injuries caused by different injury mechanisms for eye closure.

SP089.2 - A Tale of Two Tendons: The Tradeoff between Strength and Fatigue Resistance

Author(s): Samuel P. Veres, Tyler W. Herod, Neil C. Chambers
 Saint Mary's University, Halifax/CANADA

Two predominant, functional classes of tendons exist: energy storing tendons and positional tendons. Energy storing tendons operate under much greater *in vivo* stresses than positional tendons, and are more prone to injury. Using a bovine forelimb model, we assessed the ultrastructural differences between superficial digital flexor (SDF, energy storing) and common digital extensor (CDE, positional) tendons. Scanning electron microscopy was used to study the ultrastructures of 4 SDF/CDE tendon pairs from 4 different animals at magnifications up to 90,000X. SDF tendons were found to have significantly smaller diameter collagen fibrils than CDE tendons (77.3 ± 26.6 vs. 134.9 ± 51.7 nm; $p < 0.0001$). The collagen fibrils in SDF tendons were often bundled together by a dense network of filamentous webbing that ran predominantly perpendicular to fibrils' longitudinal axis. Similar webbing was not observed in the CDE tendons. Hydrothermal isometric tension analysis of intermolecular collagen crosslinking, conducted using 7 SDF/CDE pairs from 7 different animals, showed that the energy storing SDF tendons had significantly more crosslinking (denaturation temperature: 65.2 ± 1.1 vs. $62.9 \pm 1.1^\circ\text{C}$; $p = 0.0003$), and significantly more thermally stable crosslinking (proportion of samples that survived the temperature ramp to 90°C : 85.7% vs. 0% ; $p = 0.0006$) than the paired, positional CDE tendons. Thermal assessment using differential scanning calorimetry confirmed SDF and CDE tendons to have markedly different collagen crosslinking. Samples from paired SDF and CDE tendons had significantly different onset temperature (64.2 ± 0.7 vs. $63.1 \pm 1.0^\circ\text{C}$; $p = 0.0035$), endotherm full-width-at-half-maximum

(1.6 ± 0.1 vs. $3.0 \pm 0.5^\circ\text{C}$; $p=0.0055$), and enthalpy of denaturation (34.0 ± 9.4 vs. 54.8 ± 12.7 J/g; $p=0.0349$). We related ultrastructural characteristics of the SDF and CDE tendons to their ability to resist rupture and fatigue damage. Samples from 4 SDF/CDE tendon pairs from 4 different animals were tested in tension until rupture. The positional CDE tendons were found to be both significantly stronger (37.6 ± 8.1 vs. 23.1 ± 7.7 MPa; $p=0.0038$) and tougher (14.3 ± 3.6 vs. 6.8 ± 3.4 MJ/m²; $p=0.0108$) than the paired energy storing SDF tendons. Ultrastructural examination of samples from the ruptured tendons showed that collagen fibrils from the CDE tendons underwent extensive plastic deformation during overload (discrete plasticity damage), while fibrils from the SDF tendons did not deform plastically. A second set of samples from the 4 SDF/CDE tendon pairs were subjected to 500 cycles of tensile loading to 30% of their ultimate stress, determined from the strengths of the matching ruptured samples. Samples from the cyclically loaded tendons were examined for fatigue damage using scanning electron microscopy. CDE tendons were found to readily accumulate nanoscale fatigue damage in the form of sharp folds that laterally traversed multiple fibrils, and longitudinally repeating kinks, characteristic of discrete plasticity damage. SDF tendons, on the other hand, were highly resistant to fatigue damage, showing no ultrastructural differences compared to the control tendons. It appears that tendons may suffer from a structure-function tradeoff: the ultrastructural characteristics required for strength optimization may result in poor fatigue quality, and vice-versa. Subsequent study of how energy storing and positional tendons develop may lead to novel therapies that can induce ultrastructural change in order to achieve target mechanical properties.

SP089.3 - Dynamic plantar pressure simulation integrated in case specific multibody gait simulations

Author(s): Wouter Aerts¹, Friedl De Groot², Zimi Sawacha³, Ilse Jonkers⁴, Jos Vander Sloten¹

¹Department Of Mechanical Engineering, Biomechanics Section, KU Leuven, Leuven/BELGIUM, ²Department Of Mechanical Engineering, Pma, KU Leuven, Leuven/BELGIUM, ³Department Of Information Engineering, University of Padova, Padova/ITALY, ⁴Department Of Kinesiology, KU Leuven, Leuven/BELGIUM

INTRODUCTION

Insoles and customized footwear are used to alter the plantar pressure (PP) distribution during gait. However, so far, it is not possible to predict the effect of these interventions on PP. This would undoubtedly enhance the customization process. The aim of this study is to evaluate a newly developed contact model, which allows to calculate dynamically the PP within a multibody gait simulation framework.

METHODS

Standard gait analysis was performed on 10 healthy subjects (mean age 62.2 ± 4.6 years, mean BMI 24.6 ± 2.2 kg/m²). The experimental setup included a 6 cameras BTS stereophotogrammetric system (60Hz), synchronized with 2 Bertec force plates (960Hz) and 2 PP systems (Imagortesi, 150Hz).

The PP simulation is performed during a moment-driven forward analysis using the experimental 3D kinematics and ground reaction forces in combination with a scaled generic musculoskeletal model as input in OpenSim. A scattered bed of spring-damper systems [1] was used as contact surface attached to the calcaneus of the model, which was obtained from a CT-scan of a healthy subject. An optimization procedure optimized the contact parameters and geometry position based on the experimental ground reaction force. The performance of the contact model is evaluated by comparing the simulated and measured peak pressure curves (fig. 1)

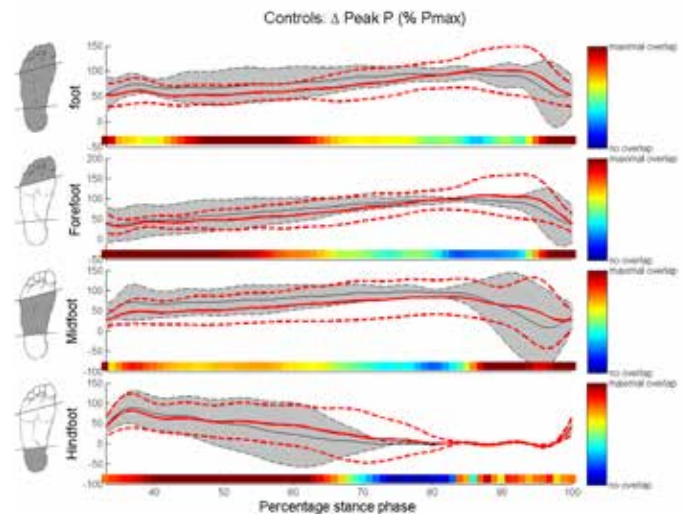


Figure 1: The plots show the measured (gray) and simulated (red) peak pressure curves for the 4 regions: whole foot, forefoot, midfoot and hindfoot, subdivided using anatomical masking [2]. The curves are averaged over the 10 subjects, with its nominal 95% bootstrap prediction bands [3]. The overlap between the bands is indicated by the colored bar, with blue representing no overlap and red maximal overlap.

RESULTS

A good agreement between simulated and measured peak pressure was found for all regions (see Fig. 1). In the first part of stance (30-60%) the overlap was nearly maximal, while around 80% of the gait cycle the overlap was lower. The hindfoot contact is prolonged during the simulation compared to the measurements.

DISCUSSION

The newly developed contact model showed a good performance in predicting the peak PP over time. With respect to finite element contact simulation, this contact model allows a continuous simulation of PP at a limited time. Due to its characteristics this contact model has potential to be used in the design of insoles and customized footwear.

REFERENCES

- [1] Sherman M.A. et al, *ProcediaUTAM*(2011) 2;p241-261
- [2] Giacomozzi C. et al, *Med.Biol.Eng.Comput*(2000), 38;p156-163
- [3] Lenhoff M.W. et al, *Gait&Posture*(1999) 9;p10-17

SP089.4 - 3D numerical investigation of the effects of altered mechanical loading during skeletal growth

Author(s): Kamel Madi¹, Peter D. Lee¹, Katherine A. Staines², Andrew A. Pitsillides², Andrew J. Bodey³, Brian K. Bay⁴
¹Manchester X-ray Imaging Facility, University of Manchester, Didcot, oxon/UNITED KINGDOM, ²The Royal Veterinary College, London/UNITED KINGDOM, ³I13-2 Branchline, Diamond Light Source, Didcot/UNITED KINGDOM, ⁴School Of Mechanical, Industrial & Manufacturing Engineering, Oregon State University, Corvallis/OR/UNITED STATES OF AMERICA

Purpose

Abnormal growth plate closure during endochondral ossification and subsequent deformity resulting from altered mechanical loading has key implications in the progression of joint deformities such as

varus and valgus. Despite several studies investigating changes in bone growth in response to mechanical loading [1], there is a lack of 4D data (3D with time) quantifying the relationships between the closure of the growth plate and the local micro-mechanical environment that the cells in the epiphyseal growth plate may experience. We aimed to combine X-ray computed tomography and computational modelling to investigate whether there is a correlation between the 3D high resolution images of growth plate cartilage topology, the octahedral shear stress (believed to promote endochondral ossification [2]) and the spatial localisation of the bridges.

Methods

Synchrotron-based micro-CT imaging of joints from a mouse strain (Str/ort) with natural susceptibility to OA and age-matched CBA (control) mice was performed at different stages of the disease on the Diamond-Manchester Branchline I13-2 (effective pixel size: 1.1 µm). Novel image processing methods were developed to map the location/density of the bridges onto the joint surface and to characterise the 3D topology of the growth plate cartilage. In parallel, 3D volumetric meshes of the entire tibia including the growth plate cartilage were generated from the tomographic images and finite element computations were carried out to simulate static compressive tests (sustained loading).

Results

Compared to control mice, the growth plate cartilage of late-OA joints is thicker with higher local curvature (Fig. 1), suggesting different remodelling and local stress state. Our first micro-FE computations in a late-OA joint revealed that the bridges seem to act as stress concentrators and are hence more likely to fracture under loading and/or to redistribute stresses within these particular vicinities of the growth plate cartilage.

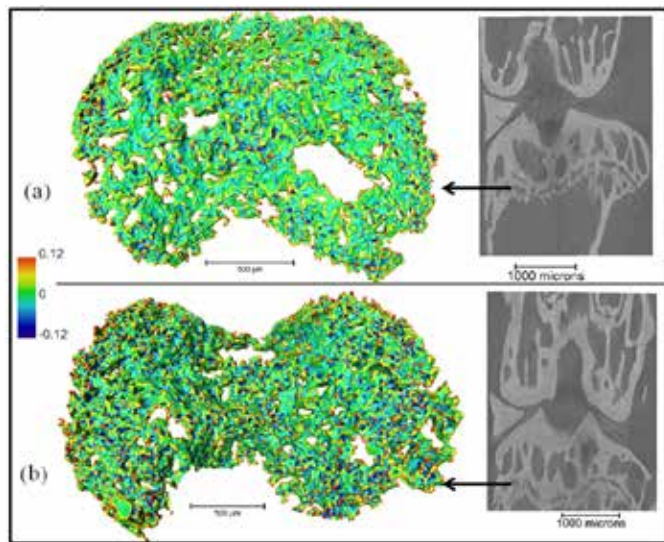


Fig. 1 Distribution of the local mean curvature in the growth plate cartilage of adult mice: (a) CBA mice (control, average thickness = 49 ± 17 µm, surface area-to-volume ratio = 0.146), (b) Str/ort mice (average thickness = 67 ± 24 µm, surface area-to-volume ratio = 0.101).

Conclusions

Our data reveal changes in the internal 3D topology of the growth plate cartilage in a model of spontaneous mouse osteoarthritis that could be linked for the first time to the micro-mechanical environment experienced by the growth plate during skeletal growth. Further investigation at earlier disease stages will reflect how these different topologies impact the stress and strain distributions and whether this may correlate with growth rate, greater bridge cluster-

ing found in late OA and the location of articular lesions that characterise osteoarthritis.

References

[1] Villemure L & Stokes IA, JBiomech 42(12):1793:1803 (2009)
 [2] Gao J, Williams JL, Roan E, Open J Biophys 4:13-21 (2014)

SP089.5 - Effects of changing small airway mechanics and inspiratory flow waveforms on pulmonary ventilation: a modeling study

Author(s): Tianya Liu¹, Yuxing Wang¹, Jian Ma¹, Deyu Li¹, Yubo Fan²
¹Key Laboratory For Biomechanics And Mechanobiology Of Ministry Of Education, International Research Center For Implantable And Interventional Medical Devices, School of Biological Science and Medical Engineering, Beihang University, Beijing/CHINA, ²National Research Center for Rehabilitation Technical Aids, Beijing/CHINA

Introduction and Objectives: For patients with chronic obstructive pulmonary disease (COPD), pathological changes of small airways can cause air trapping and lung overinflation, which can easily be aggravated during mechanical ventilation. Understanding the effects of small airways on pulmonary ventilation will be helpful in guiding mechanical ventilation for patients with COPD. Studies investigating pulmonary ventilation during mechanical ventilation did not address the behavior of small airways, especially the collapse of small airways. Therefore, the effects of small airways on pulmonary ventilation during mechanical ventilation were analyzed theoretically in this study.

Methods: A nonlinear model of breathing mechanics with two parallel alveolar compartments was developed. Each of the alveolar compartments was in series with a collapsible airway segment and a lower airway segment, whose parameters represented pathological changes in small airways of patients with COPD. Parameter values of small airways in one alveolar compartment were changed according to the pathology of COPD. Four inspiratory flow waveforms, including the constant, decelerating, accelerating and sinusoidal flow, were studied.

Results: Change in the collapsible airways resulted in more severe air trapping of the affected branch than change in the lower airways, but resulted in reduction in maldistribution of ventilation. The decelerating flow got the most even distribution of inspired gas and peak alveolar pressure regardless of changes in airway mechanics, but the patterns of inspiratory flow had little influence on air trapping.

Conclusion: The results suggest that the collapsible airways play an important role in air trapping and the lower airways have a large effect on ventilation distribution. In addition, the decelerating flow results in the most even distribution, indicating the decelerating flow is preferred during mechanical ventilation.

SP090 - QA Measurements for Therapy Dosimetry

TRACK 05: DOSIMETRY AND RADIATION PROTECTION

SP090.1 - Response Characteristics of a Large-Area Ion Chamber with Various Radiotherapy Beams

Author(s): Makan Farrokhkish¹, Andrew J. Jung², Yinkun Wang², Bern Norrlinger², Robert K. Heaton², Mohammad K. Islam²
¹Radiation Physics, Princess Margaret Cancer Centre, Toronto/ON/CANADA, ²Radiation Physics, Princess Margaret Hospital, Toronto/ON/CANADA

Introduction: Previously described Integral Quality Monitoring (IQM) system, utilizes a large area gradient ion chamber mounted at the collimator to measure the “dose-area-product” of field segments. The gradient in spatial response is created by a slope in separation between electrode plates. The system verifies the dose delivery by comparing the measured and predicted signals in real-time. Since the signal of the ion chamber is comprised of the beam fluence through the open aperture as well as the attenuated beams through collimating structures, it creates a new dosimetric paradigm in Radiation Therapy. This presentation describes several dosimetric performances of the IQM detector including the response variation with various field sizes, beam energies, dose rates, and spatial sensitivity of treatment fields in several Linear Accelerator (Linac) platforms.

Method: Dosimetric measurements were performed in Elekta Synergy (80 leaf-MLCi2) and Infinity (160 leaf-Agility), as well as Varian iX and TrueBeam (160 leaf- Millennium) Linacs. The beam energies across these platforms were 6, 10, 18 MV, 6 MV Flattening Filter Free (FFF) and 10 MV FFF. All the beams deliver 1 cGy/ MU for a 10 × 10 cm² field at a dmax-depth, with the source to detector distance of 100 cm. The chamber was mounted on the accessory tray of Elekta and the upper wedge tray of Varian Linac.

Results: The chamber signals, expressed in IQM Count, for a 10 × 10 cm² field with 6 MV beams were 1946 and 2259 Counts/MU for TrueBeam and Infinity respectively. The difference in counts can be attributed primarily to: (i) differences in the source to chamber distance (ii) differences in MLC and jaw transmission factors and the back-up jaw configuration. The field size factors for 6 MV beams, normalized to a 10 × 10 cm² field, ranged from 0.008 to 4.352 for TrueBeam and 0.023 to 3.941 for Infinity for fields ranging from 1 × 1 cm² and 20 × 20 cm² respectively. The relative energy response varies widely with field size, machine model, and beam filtration. A maximum difference in response for 10 MV, 18 MV, 6 MV FFF and 10 MV FFF beams, relative to 6 MV beams in corresponding Linac were found be 20.6, 23.4, 23.9, and 39.4 % for field sizes ranging from 1 × 1 cm² to 20 × 20 cm². When a 3 × 3 cm² field was shifted by 3.0 cm in the direction of increasing gradient, signal difference of up to 12 % and 10 % were observed for TrueBeam’s 10 and 6 MV beams respectively. For a 10 VM FFF beams however, no measurable difference in signal was observed for the same shift, due to the combined effect of chamber gradient and off-axis profile

Conclusion: Since the IQM Chamber intercepts the entire projected area defined by the primary jaws, the signal is comprised of the open beam and the attenuated beam through the MLC and jaws. A significant difference in some key dosimetric response is therefore expected across various beam energy, filtration and Linac models.

SP090.2 - Very small circular fields output factors: Comparison of MC calculations, EBT3 film and micro-diamond measurements

Author(s): Eyad A. Alhakeem¹, Sergei Zavgorodni²
¹Physics & Astronomy, University of Victoria, Victoria/CANADA, ²Medical Physics, BC Cancer Agency, Victoria/CANADA

The purpose of this work was to obtain output factors (OFs) of 6MV beam collimated by customized circular cones of 1.3 and 3.5 mm diameter at isocenter. We also compared OFs from these cones with OFs from BrainLab™ of 10, 12.5, 15 and 40 mm cones.

OFs were measured using GafChromic EBT3 films and micro-diamond detector. Detectors were placed isocentrically in a water phantom at 1.5 cm depth. Two sets of EBT3 measurements were extracted from different image resolutions as shown in Table 1. Micro-diamond detector was also used to measure cone OFs with detector axis orthogonal to the incident beam. BEAMnrc/DOSXYZnrc codes were used to calculate OFs and dose profiles in water with 1x1x1 mm³ voxels for the 10-40 mm cones and 0.1x0.1x0.1 mm³ voxels for the 1.3 and 3.5 mm cones, respectively.

Results for OFs (relative to 40 mm diameter cone) are shown in Table 1. Differences of 15.4% and 15.9% were found for cone 1.3 and 3.5, respectively. Maximum differences of up to 4.0%, 2.9% and 1.9% were found for cones 10, 12.5 and 15 mm, respectively. Scanning resolution of the films was critical for the two smallest fields and the differences between two EBT3 OF’s measurement set were 6.7% and 14.3% for cone 3.5 and 1.3, respectively.

In conclusion, differences in output factor were within 4% for cones with 10 mm diameter and greater. However, larger differences were observed for the 3.5 and 1.3 mm field sizes. Scanning resolution has significant effect on the output factor of the smallest cones in this work.

Table 1. Output factors measured and calculated for a range of circular cones. Statistical uncertainty of MC calculations was within ±2.5%.

Cone diameter (mm)	1.3†	3.5†	10	12.5	15	40
Diamond	-	0.687	0.878	0.931	0.960	1.000
EBT3 (1.8 mm pixel size)	0.132	0.586	0.909	0.953	0.961	1.000
EBT3 (0.13 mm pixel size)	0.154	0.628	0.910	0.958	0.965	1.000
MC (0.1 mm voxels)	0.137	0.605	0.874	0.931	0.978	1.000
% Diff = (OFmax-OFmin)/(OFmax+OFmin)/2	15.4	15.9	4.0	2.9	1.9	N/A

† In-house customized collimators with indicated nominal field size at isocenter.

SP090.3 - Investigation of pass rate variability in ArcCheck measurements

Author(s): Harald Keller¹, Albert Chen², Daniel Létoirneau²
¹Radiation Oncology, University of Toronto, Toronto/ON/CANADA, ²Radiation Medicine Program, Princess Margaret Cancer Centre, Toronto/ON/CANADA

Spine SBRT (stereotactic body radiation therapy) is an emergent radiation therapy treatment technique for bone metastasis in the spine. Such treatments are nowadays delivered using volumetric modulated arc therapy (VMAT). The ArcCheck detector (Sun Nuclear Corporation, Melbourne, FL) is part of the patient-specific QC process to routinely evaluate the ability to accurately deliver VMAT plans. It was found that the results of such ArcCheck measurements

for spine SBRT plans can vary widely from patient to patient, more so than for other treatment sites. The purpose of this work was to investigate potential sources of this variability in order to streamline the QC process for spine SBRT patients.

A set of 144 spine SBRT treatment plans published between July 2012 and May 2014 was available. All plans used a single 360 degree arc with isocenter in the spine. The vast majority of treatment plans were delivered on a single linac (Elekta Beam Modulator (TM)).

Absolute dose pass rates (ADPR) are the percentage of values (detectors) in a measured dose map (cylindrical surface within the ArcCheck phantom) that have passed a set of criteria, usually a 3% dose-difference and 2 mm distance-to-agreement criterion with respect to the calculated dose map obtained from the planning system (Pinnacle, Philips). The number of detectors participating in the comparison is set by a dose threshold (TH).

For this work, the pass rates and their variability were studied for several parameters associated with the measurement and analysis of the dose map: the TH threshold, sensitivity of the results to ArcCheck phantom (dose map) shifts, global and local gradients in the measured dose maps and the degree of beam modulation as assessed by the number of monitor units per delivered dose (MU/cGy) of the arc. For efficient analysis, an emulation of the pass rate algorithm was implemented in Matlab and validated against the commercial software (SNC patient, Sun Nuclear).

The ArcCheck results for the spine SBRT plan set showed a mean ADPR of 86% with a wide range between 60% and 98%. ADPR was largely constant for most patients as a function of TH, except for TH below 10% where most pass rates dropped significantly and increased variability within the set. As expected, ADPR decreased with applied dose map shift for most instances, but ADPR was not correlated to the degree of ADPR sensitivity to these dose map shifts. The within-set ADPR variability was almost independent of "flatness" of the dose map (quantified as the sum of the gradient taken over the dose map). Only for very flat dose maps with small gradients the ADPR was consistently above the set mean (around 90%). Degree of beam modulation had some correlation with ADPR (correlation coefficient 0.608) where higher/lower beam modulation resulted in lower/higher pass rates, respectively.

In summary, there is no known single parameter that is driving the variability of the ADPR. Multivariate analysis should be performed and parameters that influence the computation of the dose map need to be incorporated as well.

SP090.4 - Characterization and image quality evaluation for a clinical 2.5 MV in-line portal imaging beam

Author(s): Jeniffer Owen¹, Jose E. Villarreal-Barajas², Rao Khan², James Grafe²

¹Physics And Astronomy, University of Calgary, Calgary/AB/CANADA, ²Oncology, University of Calgary, Calgary/CANADA

Characterization and image quality evaluation for a clinical 2.5 MV in-line portal imaging beam

Recently, a 2.5 MV inline portal imaging beam has been made available on Varian TrueBeam™ Linacs. The aim of this work is to present our initial investigations of the 2.5 MV beam characterization and imaging quality assessment.

The 2.5 MV beam output was calibrated following the AAPM TG-51 procedure. The beam output has been stable over four months to within 1%. The PDD was measured with a CC13 chamber, a Markus chamber, and Gafchromic EBT3. The resulting depth of maximum dose, d_{max} , and PDD at 10 cm depth (%dd(10)) was measured to be 5.7 mm (51.7%), 6.1 mm (51.9%), and 5.1 mm (51.9%) for a 10x10

cm² field size at 100 cm SSD for the CC13, Markus and EBT3 film, respectively (Figure 1). The beam quality is slightly lower than that of a ⁶⁰Co beam; however we estimated a kQ value of 1.00 for output calibration purposes. Additionally, the measured HVL was 9.8 mm Cu (14.8 mm Cu for ⁶⁰Co), corresponding to an effective energy of approximately 550 keV. The relative entrance dose as measured with EBT3 films was 63%, compared to 23% for a 6 MV beam.

The image quality was assessed with the Standard Imaging Phantom QC-3. The estimated MTF for the MV-imaging system shows that 2.5 MV has better spatial resolution than the 6 MV beam (Figure 2). The 2.5 MV exhibited nearly three times higher surface dose than the 6 MV, however, for a separation of 20 cm, the 2.5 MV mid-separation dose is 78% of the 6 MV dose and the exit is only 58% of the 6 MV dose. Future work will focus on the clinical implementation and development of quality control protocols for this novel imaging beam modality.

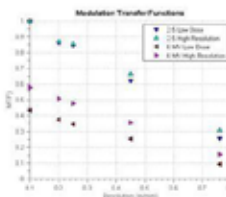


Figure 2. Normalized Modulation Transfer Functions (MTF) of both 2.5 MV and 6 MV portal imaging beams, calculated from the Standard Imaging QC3 phantom. The Low Dose mode delivers 1 MU for the 2.5 MV beam and 1.5 MU for the 6 MV beam and the High Resolution mode delivers 1.5 MU and 3 MU for 2.5 MV and 6 MV, respectively. The plots are normalized to the 2.5 MV Low Dose MTF for the 2.5 MV Low Dose and 6 MV Low Dose curves, and to the 2.5 MV High Resolution MTF for the 2.5 MV and 6 MV High Resolution curves.

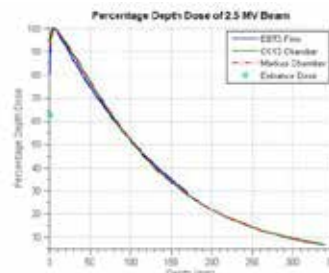


Figure 1. Percentage-depth dose plots of the 2.5 MV imaging beam measured with EBT3 Gafchromic film, a CC13 ion chamber, and a Markus ion chamber for a 10x10 cm² field at 100 SSD. The entrance dose was measured using EBT3 film placed perpendicularly to the beam on a solid water phantom.

SP090.5 - Usefulness of the commercialized EPID based dMLC QA tool for Elekta Agility MLC

Author(s): Samju Cho¹, Woonhoo Choi¹, Ho Lee¹, Kwangwoo Park¹, Jungil Lee¹, Jeongmin Yoon¹, Eungman Lee¹, Suk Lee², Sang Hoon Lee³, Juree Kim³, Jinho Choi⁴, Sangwook Lim⁵, Ki Chang Keum¹

¹Radiation Oncology, Yonsei University, Seoul/KOREA, ²Radiation Oncology, Korea University, Seoul/KOREA, ³Radiation Oncology, Catholic Kwandong University, Seoul/KOREA, ⁴Radiation Oncology, Gachon University, Seoul/KOREA, ⁵Radiation Oncology, Kosin University, Busan/KOREA

The dynamic intensity modulated radiation therapy (dIMRT) and volumetric modulated arc therapy (VMAT) requires accurate leaf position, leaf speed, gantry position and gantry speed while modulating the dose rate. The Elekta Agility linear accelerator (Elekta AB, Stockholm, Sweden) could be to meet these characteristic with

accurate leaf positioning and rapid leaf speed 3.5 cms^{-1} . Considering the time consuming procedures in dynamic MLC QA, dedicated EPID based dynamic MLC QA program was widely used. The purpose of this study is to monitor several month results of EPID based dMLC QA and is to establish the reference parameters and tolerance levels for each QA category. We commissioned ARTISCAN™ (AQUILAB, Lille, France) for four Agility MLCs and validated six category including calibration of image, dMLC dosimetry, static picket fence, VMAT picket fence, dose rate/gantry speed and MLC speed for dynamic MLC QA. We acquired 21 EPID images using vendor provided dynamic delivery MLC file and validated it as an analysis protocol (Figure 1).

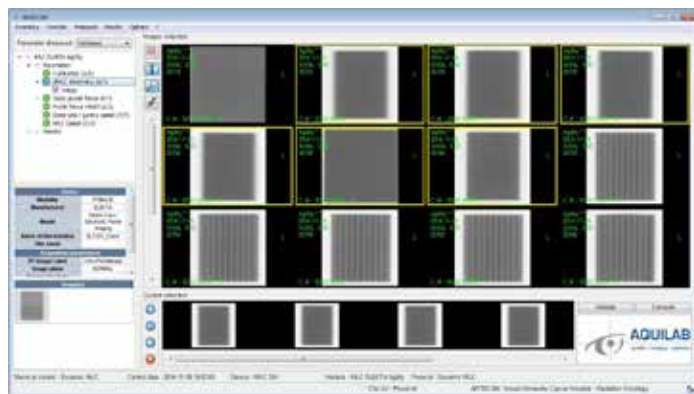


Figure1 Validated EPID images for dMLC QA

The acquisition of images and analysis of results took about 25 min. We performed dMLC QA using same dynamic delivery MLC file for 3 month in the 4 Agility linac MLC and averaged result parameters. These parameter values were established as our reference and tolerance level. We could figure out Agility MLC changing trend using ARTISCAN report tools after the parameters were validated. The EPID based dMLC QA program not only improve the QA procedures by reduce the time consuming process, but also guaranties the dosimetric accuracy of dIMRT and VMAT by verification of MLC/gantry position and speed.

Acknowledgements: This work was supported by the Radiation Safety Research Programs (1305033) through the Nuclear Safety and Security Commission.

SP090.6 - In-vivo and pre-treatment quality assurance software validation and verification

Author(s): Eleonora Vanzi¹, Luca Reversi², Giuliano Giani², Chiara Arilli¹, Pierluigi Bonomo³, Marta Casati¹, Antonella Compagnucci¹, Daniela Greto³, Livia Marrazzo¹, Silvia Scoccianti³, Stefania Pallotta², Marta Bucciolini², Cinzia Talamonti²

¹Sod Fisica Medica, Azienda Ospedaliera Universitaria Careggi, firenze/ITALY, ²Department Of Experimental And Clinical Biomedical Sciences, "mario Serio", University of Florence, Florence/ITALY, ³Sod Radioterapia, Azienda Ospedaliera Universitaria Careggi, Firenze/ITALY

The aim of this study is to test the accuracy of the dose calculation algorithm available in DosimetryCheck (DC, MathResolution®), a patient QA software for both pre-treatment QA and in vivo dose verification, that uses the EPID measured fluence of the treatment fields to reconstruct the dose distribution in the CT planning model of the patient.

First tests were performed on the IBA "I'mRT" phantom to assess DC performances in the steps of entrance fluence estimation and dose calculation both for pre-treatment and in-treatment measurements. The central insert was filled with three different materi-

als (air, bone and homogeneously with RW3) and different square field sizes (FS) were irradiated to evaluate the isocenter dose in the homogeneous phantom. The global accuracy was assessed by comparing OFs and PDDs evaluated with TPS with that reconstructed by DC.

Then, DC was run pre-treatment and in-vivo for 15 patients: 1) 7 IMRT prostate cases, 2) 3 abdominal VMAT cases, 3) 5 head VMAT cases. Gamma analysis (3%, 3mm) was used to compare measured with calculated dose distribution.

Isocenter dose was equal within 1.75% for pre-treatment and in-treatment measures and for all FS. Due to the use of a pencil beam algorithm, high OF and PDD differences (up to 64.2% and 110%, respectively) were found in the air filled phantom at small FS.

In patients, gamma passing rates evaluated on the whole treatment volume were above 98% and 94% for pre-treatment and in vivo prostate cases respectively; above 92% for both pre-treatment and in vivo abdominal VMAT patients, and above 89% and 73% for head VMAT patients.

In conclusion, DC is capable of successfully reconstruct the dose distribution in the patient from the EPID measured exit fluences, even if a more accurate algorithm is needed when low density regions are involved.

SP091 - Nanotechnology in Radiation Therapy and Imaging: Part 2

TRACK 05: DOSIMETRY AND RADIATION PROTECTION

SP091.1 - New Technologies in Cancer Research and Treatment

Author(s): Eva Bezak¹, Barry J. Allen², Ivan Kempson³

¹Medical Physics, Royal Adelaide Hospital, Adelaide/AUSTRALIA, ²Faculty Of Medicine, University of Western Sydney, Liverpool/NSW/AUSTRALIA, ³Ian Wark Research Institute, University of South Australia, Mawson Lakes/SA/AUSTRALIA

Learning Objectives:

1. To review the current status of targeted alpha-therapy and its role in treatment of metastatic cancer.
2. To gain understanding of mechanisms of gold nanoparticle radiosensitization.
3. To review future trends in novel systemic targeted and nanoparticle therapies.

Targeted Alpha-Therapy

Despite the latest technological advances in radiotherapy, cancer control is still challenging for several tumour sites. The survival rates for cancers, such as ovarian and pancreatic, have not changed over the decades. The solution to the problem lies in the change of focus: from local treatment to systemic therapy [1].

Radio-immunotherapy is one such approach where cancer cells are targeted by vectors labelled with a radioisotope. In a specific case of targeted alpha-therapy (TAT), a tumour-specific antibody/protein is radiolabelled with an alpha-emitting radionuclide, termed a radioimmunconjugate (RIC). This radioimmunconjugate attaches preferentially to tumour-specific antigens, and releases high-linear energy transfer (LET) α -particles of a few MeV kinetic energy. Alpha radiation has the shortest range and highest energy transfer (and correspondingly high radiobiological effectiveness), resulting in localized but significant ionization damage (e.g. to DNA). Alpha-emitting radioisotopes can be used to kill isolated cells, small cell clusters and to regress tumours [2]. The high-LET α -radiation produces increased rates of DNA double-strand breaks. The LET is $\sim 100\text{keV}/\mu\text{m}$, giving a higher probability of causing DSBs; ratio SSB/DSB ~ 20 compared with 60 for low-LET radiation.

Over the past 20 years the development of RICs has enabled TAT to progress from *in vitro* studies, through to pre-clinical *in vivo* experiments and clinical trials. The dose to normal tissues provides a limitation to the injected dose and to that received by the tumour. However, TAT can achieve cancer regression within the maximum tolerated dose (MTD) for normal tissues. TAT was originally thought to be an ideal therapy for leukaemia and micro-metastases, because the short radioisotope half-lives were sufficient to target blood-borne cancer cells. At present, studies and clinical trials of TAT for several cancers have been reported. Alpha-therapy is demonstrating efficacy in leukaemias and in glioblastomas, where results from intracavity administration are promising, with a 52-week median survival. The use of peptides for targeting GBM is also under investigation [3]. In phase-1 trials of intra-lesional and systemic therapy in metastatic melanoma patients, TAT was found to be safe and demonstrated some evidence of anti-tumour activity [4]. Consequently, in the clinical setting of small-volume disease, TAT may complement current anti-melanoma therapies.

However, for solid tumours the promise of TAT is greatly extended by the development of tumour antivascular alpha-therapy (TAVAT); i.e. killing of tumour capillary endothelial cells that results in disrupting of tumour capillary networks and shrinking tumours [5].

High-Z Nanoparticle Radiosensitization

High-Z nanoparticles (NPs) have been a topic of interest in medical research since 1950s. It has, however, only been in the last 20 years that the practical use of NPs for imaging and radiotherapy has been demonstrated [6]. It has been shown that the presence of gold (or other high-Z material) nanoparticles improves the cell-killing effect of radiation *in-vitro* and with *in-vivo* mouse models. High-Z nanoparticles are being used in human trials for sensitization of tumour in radiation therapy, yet the mechanisms of enhancement are still being investigated [7, 8].

In a specific case of gold, NPs generally have an individual diameter between 1nm-1 μm and are suspended in an aqueous solution. The high atomic number of gold relative to tissue means that when gold is introduced into a tumour, it acts as a contrast agent for imaging and it amplifies the biological damage in the case of external beam therapy. Cell death after radiotherapy occurs due to DNA damage induced by Reactive Oxygen Species (ROS). The ROS are generated from interactions of the incident radiation with atoms, emissions and scattering from those atoms, and subsequent interaction with oxygen based molecules. This process relies on emission of photo-electrons and Auger electrons, Compton Scattering, and Pair production.

Increasing localised dose deposition can improve therapeutic outcome, but needs to be done so that healthy tissues are not compromised by spurious dose deposition that nanoparticles may cause. It is very difficult to quantitatively analyse a statistically relevant number of individual cells for both nanoparticle content and biological markers. X-ray-Fluorescence (XRF) microscopy can be used to correlate nanoparticle content of individual cells with biological consequence to identify specific mechanisms of radiosensitization. This information is critical for understanding implications of such technologies as they move into human trials. XRF microscopy has only recently been able to rapidly image large area samples, and is uniquely available at the Australian Synchrotron [9]. This is a notable advance in the technique and is unique in the world. It can be used to quantify the mass of gold in each cell and hence deduce the number of nanoparticles. Subsequently, number of DNA breaks and Au content can be correlated to investigate the role of variables.

This lecture gives an overview of clinical results in an endeavor to recommend whether and how TAT and High-Z NPs can be integrated into the therapeutic armamentarium for cancer.

BJ Allen, E Bezak, LG Marcu, "Quo Vadis Radiotherapy?" BioMed Research International, doi:10.1155/2013/749203, 2013.

J Elgqvist, "Targeted alpha-therapy: part I". Curr Radiopharm, 4(3):176, 2011.

S. Kneifel, D. Cordier, et al., "Local targeting of malignant gliomas by diffusible peptidic vector 1,4,7,10-tetraazacyclododecane-1-glutaric acid-4,7,10-triacetic acid substance P," Clinical Cancer Research, 12(12):3843-3850, 2006.

BJ Allen, AA Singla, et al., "Analysis of patient survival in a Phase-I trial of systemic TAT for metastatic melanoma". Immunotherapy, 3(9):1041-1050, 2011.

BJ Allen, C Raja, et al., "Tumour anti-vascular alpha-therapy: a mechanism for the regression of solid tumours in metastatic cancer," Physics in Medicine and Biology, 52(13):L15-L19, 2007.

S McMahon et al., "Energy dependence of gold-nanoparticle radiosensitization in plasmid DNA," J. Phys. Chem. 115(41):20160-20167, 2011.

Nanobiotix sees “*Clinical Advance in Soft Tissue Sarcoma Pilot Trial with Lead Product*”, NBTXR3 [press release]. Nanobiotix, 2014.

L Maggiorella, G Barouch, et al. “*Nanoscale radiotherapy with hafnium-oxide nanoparticles*”. *Future Oncol.* **8**(9):1167-81, 2012;

T Liu, I Kempson, et al., “*Quantitative Synchrotron X-Ray-Fluorescence Study of the Penetration of Transferrin-Conjugated Gold-Nanoparticle inside Model Tumour Tissues*”. *Nanoscale* **6**(16):9774-9782, 2014.

SP091.2 - Enhanced uptake of gold nanoparticles coated with polyethylene glycol

Author(s): Charmaine Cruje, Devika B. Chithrani
Department Of Physics, Ryerson University, Toronto/ON/CANADA

Polyethylene glycol (PEG) has promoted the prospective cancer treatment applications of gold nanoparticles (GNPs). *In vivo* stealth of GNPs coated with PEG (PEG-GNPs) takes advantage of the enhanced permeability and retention effect in tumor environments, making them suitable for targeted treatment. Because PEG minimizes gold surface exposure, PEG-GNP interaction with ligands that mediate cancer cell uptake is lower than uncoated GNPs. Hence, the cellular uptake of PEG-GNPs is significantly lower than uncoated GNPs *in vitro*. As intracellular localization of GNPs maximizes its therapeutic enhancement, there is a need to improve the uptake of PEG-GNPs. To enhance uptake, a peptide sequence containing an integrin receptor binding site, or RGD, was conjugated with PEG-GNPs of varying core sizes. Spherical GNPs of diameters 14, 50 and 70 nm and a PEG chain length of 2 and 5 kDa were used to determine a preferred core size and chain length for uptake *in vitro* in HeLa and MDA-MB-231 cells. Results show that enhanced cancer cell uptake may be achieved with the peptide sequence used for all sizes of PEG-GNPs in HeLa cells. For MDA-MB-231 cells, higher cancer cell entry was observed less significantly and only for a size of 14 nm. Hence, improved cancer cell entry of PEG-GNPs into HeLa cells may be achieved with the use of an RGD peptide, while a different peptide sequence would have to be used for MDA-MB-231 cells.

SP091.3 - Nuclear targeting of gold nanoparticles for improved therapeutics

Author(s): Celina J. Yang, Devika B. Chithrani
Biomedical Physics, Ryerson University, Toronto/CANADA

The combining of nanotechnology and medicine is gaining more and more interest in the field of biomedical sciences. Gold nanoparticles (GNPs) have been extensively used in cancer research due to their ability to act as an anti-cancer drug carrier for chemotherapy and as a dose enhancer in radiotherapy. Most GNP research in the past involved a system where GNPs were in the cytoplasm of the cell as unmodified GNPs enter the cell through a receptor mediated endocytosis. However, it is predicted that therapy response can be further enhanced if GNPs can be effectively targeted into the nucleus. Nuclear targeting requires a modification to the GNPs to escape the regular endo-lyso pathway and target to the nucleus. An effective strategy for designing a GNP-peptide complex for targeting the nucleus will be presented. Two different sequences of peptides where conjugated onto GNPs. The role of one peptide enhanced the uptake into the cell, while the other induced nuclear delivery. With nuclear targeting, there is a possibility in producing additional low-energy secondary electrons in response to irradiation within the nucleus. This can cause more damage to the DNA. This research will establish a more successful NP-based platform for combining treatment modalities that can lead to a more effective approach in the treatment of cancer.

SP092 - Neural Signal Processing: Part 1

TRACK 11: NEUROENGINEERING, NEURAL SYSTEMS

SP092.1 - Delta-Modulated High Frequency Oscillations Linked to Pathological Brain in Female Mecp2-Deficient Mice

Author(s): Sinisa Colic¹, Min Lang², Rob Wither², Liang Zhang³, James H. Eubanks⁴, Berj L. Bardakjian⁵

¹Electrical And Computer Engineering, University of Toronto, Toronto/CANADA, ²Department Of Physiology, University of Toronto, Toronto/CANADA, ³Department Of Neurology, University of Toronto, Toronto/ON/CANADA, ⁴Department Of Surgery, University of Toronto, Toronto/CANADA, ⁵Institute Of Biomaterials And Biomedical Engineering, University of Toronto, Toronto/ON/CANADA

Mutations in the X-linked gene encoding methyl CpG-binding protein 2 (MeCP2) have been linked to a neurodevelopmental disorder known as Rett syndrome. Rett syndrome is predominantly found in females, occurring 1 in 10,000 live births. Among other impairments the clinical manifestation of Rett syndrome typically involves epileptic seizures, providing a unique genetic model of epilepsy. Mecp2-deficient mouse models recapitulating many of the deficits of Rett syndrome have been developed to examine the seizure-like activity from intracellular electroencephalogram (iEEG) recordings. The majority of the studies to date have focused their analyses on the low frequency oscillations (LFOs) associated with the epileptiform discharge rhythm occurring in the 6 – 10 Hz frequency range. However, some more recent studies on Mecp2-deficient mice have revealed the existence of high frequency oscillations (HFOs) in the frequency range 80 – 600 Hz and shown that these HFOs interact with the phase of the LFOs. HFOs are an important clinical biomarker for seizure-onset zone, often used by clinicians to determine resection areas in patients with intractable epilepsy. Furthermore, recent clinical studies are suggesting that by examining the LFO-HFO interactions it may be possible to achieve a more accurate identification of the epileptogenic zone which would potentially lead to more successful resection outcomes. In this study the coupling of HFOs to the phase of the LFOs was examined in female Mecp2-deficient mice before and after mecpc2 gene reactivation therapy. Our analyses show that the modulations could be subdivided into two distinct categories, coupling between the phase of the delta LFO (3 – 6 Hz) with the amplitude of the fast ripple HFO (400 – 600 Hz) and coupling between the phase of the theta LFO (6 – 10 Hz) with the amplitude of the fast ripple HFO (400 – 600 Hz). Examining the differences in modulation before and after mecpc2 gene reactivation revealed that the delta with fast ripple modulation was abolished, whereas the theta with fast ripple modulation diminished. This matches the findings of a recent clinical study showing that the modulation of the delta with the fast ripple was an indicator for epileptogenic onset zone, and when that region was resected it would lead to successful surgical outcome. As the mecpc2 gene is reactivated the animals show significant improvements suggesting that an interplay exists between the delta LFOs and the fast ripple HFOs leading to a pathological brain. Understanding this interaction could potentially be used as a biomarker for accurately identifying pathological seizure activity and potentially lead to better treatment outcomes.

Acknowledgement This work was supported by grants from the Natural Sciences and Engineering Research Council of Canada and from the Canadian Institutes of Health Research.

SPO92.2 - Contrast between Spectral and Connectivity Features for Electroencephalography based Authentication

Author(s): Chungmin Han¹, Sangkyong K. Kim¹, Heenam N. Yoon¹, Wonkyu K. Lee¹, Cheolsoo S. Park², Kokeun K. Kim³, Kwang Suk Park⁴

¹Interdisciplinary Program Of Bioengineering, Seoul National University, Seoul/KOREA, ²Department Of Computer Engineering, Kwangwoon University, Seoul/KOREA, ³Center for Cognition and Sociality, Institute for Basic Science, Seoul/KOREA, ⁴Department Of Biomedical Engineering, The College Of Medicine, Seoul National University, Seoul/KOREA

Biometrics using electroencephalography (EEG) have received attention as a strong security method and has been investigated by many researchers. Studies applied spectral and connectivity features to identify individuals. However, comparison of spectral and connectivity features are not yet conducted in the aspect of stability. In this paper, we present contrast between spectral and connectivity features for EEG based authentication with signals measured in different days. Spectral features are represented as power spectrum density (PSD) over 2-40Hz with 1Hz resolution provided from each channel. Connectivity features are presented as coherence (COH) of two channels combined, frequency range of 2-40Hz with 1Hz resolution. Total of 20 subjects participated and measured 32 channels of EEG for 10 seconds in eyes-closed resting state in three different days. We evaluated false authentication rate (FAR), false rejection rate (FRR) and half total error rate (HTER) as performance of authentication system designed: by using data measured in first day as train data (600 trials) and others as test data (1,173 trials). The similarity of data is measured using correlation modified Euclidean distance. During the decision making process, two values of threshold were set. The results were achieved with minimum of 10.45% HTER when using PSD, and 17.45% of HTER when using COH. It is well known that PSD features are relatively stable over time thus we post-analyzed coherence characteristics of EEG measured over three different days to evaluate stability. To assure stability, those that failed to reject ANOVA and highly correlated (over 0.8) were filtered in each subject in alpha band (8-13Hz) and composed coherence map for each participant. We concluded that considering both PSD and COH, feature filtering is necessary in order to guarantee efficient EEG based authentication.

SPO92.3 - EMG artifact removal using ICA-based dipole distribution from scalp EEG of epileptic patients

Author(s): Chunsheng Li¹, Daniel Jacobs¹, Trevor Hilton¹, Jose Martin Del Campo², Peter L. Carlen², Berj L. Bardakjian¹

¹Institute Of Biomaterials And Biomedical Engineering, University of Toronto, Toronto/CANADA, ²Toronto Western Hospital, Toronto/CANADA

Biomarkers used to guide the resection of the epileptogenic zone depend on proper placement of intracranial electrode sets, which in turn depend on analysis of scalp EEG. Under normal conditions, such signals are contaminated by muscle artifact. Neck, eye, face and mouth muscles are major sources of this artifact. Due to volume conduction, the artifact can be detected across the entire head. In this study, we introduce an artifact removal method based on component source analysis to identify the generator of the muscle artifact. The goal is to objectively identify the components which would otherwise require time-consuming manual inspection.

Methods:

The proposed method examines the dipole source distribution of the independent components (ICs) produced by independent component analysis (ICA) with respect to the underlying muscle anatomy, as well as their spectral characteristics. Firstly, dipole fitting method (DIPFIT) is used to reconstruct each IC's dipole in a four layer head

model. The head model is divided by seven regions based on the anatomical basis shown in Fig. 1.

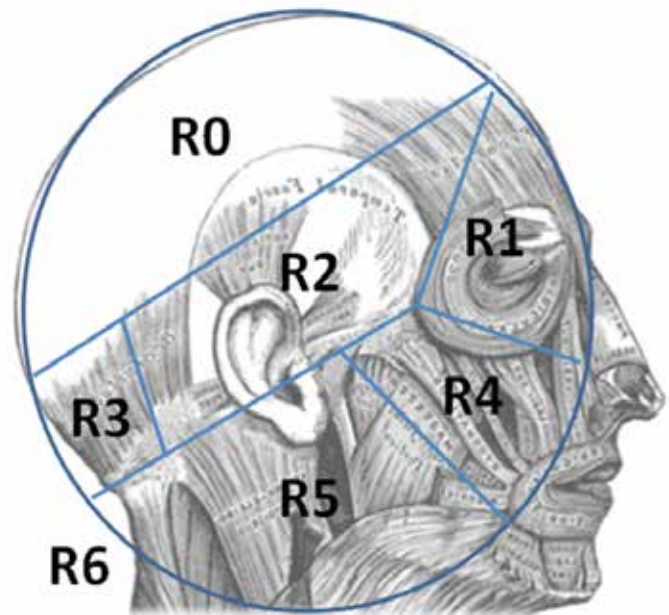


Fig.1 Sphere space partition, central region (R0), forehead (R1), temporal (R2), occipital (R3), mouth (R4), neck (R5) and outside regions (R6). (Adapted from Shackman et al. 2009).

Each dipole is assigned to one of the seven regions. Dipoles assigned to R0 are assumed to be EMG free since there are no muscle sources in that region. All other regions contain functionally independent EMG sources which can be identified by computing various spectral signatures. For example, the linear decrease of EEG power spectrum with linear increasing log frequency can be used in identification of an EMG component. Other signatures include peaks in frontalis activity around 25Hz, whereas temporalis generates a low peak around 20 Hz and broad plateau centered around 40-80 Hz (Goncharova et al. 2003). Scalp EEG for 4 patients with epilepsy from the Toronto Western Hospital was analyzed.

Results:

Combining the dipole distribution and spectral characteristics, artifactual ICs can be removed. Sources modeled from synchronous iEEG data are used to validate sources modeled from the artifact-removed EEG.

This work is supported by NSERC, CIHR, and China Scholarship Council.

SPO92.4 - Power based features of epileptic iEEG rhythms to demarcate brain regions for resection

Author(s): Joshua A. Dian¹, Yotin Chinvarun², Peter L. Carlen¹, Berj L. Bardakjian¹

¹University of Toronto, Toronto/CANADA, ²Phramongkutklao Hospital, Bangkok/THAILAND

Epilepsy impacts up to 1% of the populations and despite optimal care with anticonvulsant medications 33% of patients continue to suffer uncontrolled seizures. Resection surgery provides a subset of these patients an alternative treatment which promises seizure freedom; however, identification of regions suitable for resection remains a challenging problem and results in many patients not achieving meaningful improvement despite surgery.

Intracranial EEG (iEEG) data was obtained from grid electrodes (8x8 or 8x6) implanted in epilepsy patients in preparation for resection surgery. Recorded time series were filtered to remove line noise and differentially referenced resulting in 4x8 or 4x6 channel grids. Previous studies have identified low frequency oscillations (LFO) (<30 Hz) and their relationship with high frequency oscillations (HFO) (>80 Hz) as key markers in classifying ictal events and delineating the epileptogenic zone. In particular, our group has previously shown that amplitude modulation of the HFO activity by the delta rhythm can be used to delineate electrodes of interest for resection.

Here we investigate the use of computationally efficient power based features of the iEEG in order to identify target regions suitable for resection. Empirical mode decomposition (EMD) was used to extract rhythmic components of the iEEG which corresponded to both LFOs and HFOs. Power ratios computed on temporal windows of the extracted LFOs and HFOs formed the feature space. A support vector machine (SVM) classifier was trained/validated using the features extracted from Engel Class I patients and was subsequently used to identify grid electrodes suited for resection. Consistent with previous reports, classification accuracy was state dependent as the characteristic features varied at different phases of the ictal event. The classifier was further able to selectively mark electrodes that were consistent with good surgical outcomes (Engel Class I).

SPO92.5 - The alpha rhythm in a rodent model of epilepsy is enhanced when adenosine receptors are blocked

Author(s): Vanessa Breton, Peter Carlen, Berj L. Bardakjian
University of Toronto, Toronto/CANADA

There are observable spectral markers of seizures in the electroencephalograms and intracranial recordings of epileptic patients. A closer inspection of the pathological rhythms underlying these seizures may aid in the identification of certain neuronal and glial cell populations or synaptic networks involved in the transition through the seizure events. In epilepsy, it has been suggested that the ketogenic diet has a therapeutic effect on seizures by metabolically down-regulating the enzyme adenosine kinase thereby increasing ambient adenosine and activating the adenosine A1 receptor in the cortex. During seizures, it has been proposed that adenosine levels rise, which cause binding of this ligand pre- and post-synaptically to these A1 receptors, inhibiting the excitatory synaptic network and terminating seizures. Mice that have been kindled with pentylenetetrazol treatment experience generalized seizures and show an increase in the cell surface expression of the A1 receptor in many brain regions, including the somatosensory cortex. This finding validates the use of a mouse model of epilepsy in the study of the adenosinergic actions on seizures. What has yet to be identified is the direct effect of the adenosine-A1 receptor complex on the rhythms underlying these epileptic events. The purpose of this investigation is to first assess whether or not a common rodent cortical seizure model shows similar spectral features as clinical cases, and then whether or not there is a pathological frequency band that is restrained due to the presence of extracellular adenosine. Local field potentials were recorded from 500um thick coronal slices from layers 2 and 3 of the mouse somatosensory cortex. Omitting the magnesium in the extracellular artificial cerebral spinal fluid induced two forms of spontaneous field events: long duration seizure like activity and short duration bursts. The pathological oscillations underlying these bursting events were characterized by time-frequency spectral analysis using the continuous wavelet transform. The A1 receptor antagonist DPCPX was applied extracellularly at various concentrations. Dose dependent changes in the power of certain frequency bands were quantified. This model was shown to contain pathological rhythms in the delta (1-3Hz) and theta (4-8Hz) bands. It has been observed that although this antagonist does not significantly alter the duration of the long duration seizure like events, it does increase the total number of shorter duration bursts between

these events and selectively enhances the overall power of the alpha rhythm (9-14Hz) in a dose dependent manner. During the initial phase of the long duration seizure like events the power of the alpha rhythm was enhanced under DPCPX + low magnesium compared to similar intervals taken from seizure like events in the low magnesium model. The change in rhythms underlying subsequent phases of the long duration seizures and short duration bursts are currently being characterized.

SP093 - Health Technology Assessment and Cost Effective Technologies for Developing Countries and Usability and Human Factors Engineering for Medical Devices and System Design: Part 1

TRACK 16: CLINICAL ENGINEERING, CLINICAL PHYSICS, AND PATIENT SAFETY

SP093.1 - The maintenance needs of oxygen concentrators in low-resource settings and implications for technician training: Experience from The Gambia

Author(s): Beverly D. Bradley¹, Samantha Chow², Ebrima Nyassi³, David Peel⁴, Yu-Ling Cheng¹, Stephen R. Howie⁵

¹Centre For Global Engineering, University of Toronto, Toronto/CANADA, ²University of Toronto, Toronto/CANADA, ³Biomedical Engineering, Medical Research Council Unit The Gambia, Fajara/GAMBIA, ⁴Ashdown Consultants, Essex/UNITED KINGDOM, ⁵Child Survival, Medical Research Council Unit The Gambia, Fajara/GAMBIA

Oxygen is an essential medicine for treating pneumonia, the leading cause of death in children under five worldwide. Yet, providing a sufficient and reliable supply of oxygen is a major challenge for many health facilities in the developing world, particularly in paediatric care units. The cost-effectiveness of oxygen concentrators versus compressed gas cylinders as a source of oxygen in low-resource health facilities has been demonstrated. However, some maintenance and repairs are required to optimize their longevity. To date, evidence of their long-term functionality in the field has been scarce.

The Biomedical Engineering Department at the Medical Research Council Unit in The Gambia manages and maintains 27 oxygen concentrators at several sites across the country, and has kept electronic records of all repairs and preventive maintenance (PM) on these devices since 2006. Through a retrospective analysis of about 800 repair and PM records between 2006 and 2013, we found that the majority of concentrator repairs were low-cost and required a low technical experience level to complete. For example, the most common repairs were filter, battery or valve replacements, and faulty tubing - all were repairable for less than US\$10 each. Median cost of replacement parts per concentrator over the entire analysis period was US\$9.44 [interquartile range: US\$0, US\$63.40]. Seventy-one per cent of all parts replaced contributed only 7% (approximately US\$135) to the total amount spent on parts since 2006. More expensive and complex repairs were rare, and typically occurred after 2.5 years of operation. The concentrators had received an average of over three PM checks per year. Of the 27 concentrators introduced since 2006, 85% are still in service with a median age of over 6 years. We estimate that the useful lifespan of oxygen concentrators in low-resource settings could reasonably exceed 7 years provided a system is in place for repairs and preventive maintenance.

Additionally, we used these repair data for a skill-mapping analysis whereby we identified 31 basic biomedical engineering technician skills that would be sufficient for the repair of over 90% of observed oxygen concentrator failures. Most of the skills identified were drawn from the library of Biomedical Technician Assistant (BTA) skills developed by Duke University's Developing World Healthcare Technologies Lab and Engineering World Health (<http://library.ewh.org>). Each of these skills can be taught to a BTA in 2 hours. We used this skill-mapping analysis to propose an evidence-based training

curriculum specifically tailored to the maintenance of oxygen concentrators in low-resource settings.

This work has provided insight into on the broader support ecosystem required to manage and maintain oxygen concentrators and other low-complexity medical devices in low-resource settings. Specifically, some of the key elements for the successful use of oxygen concentrators in our Gambian setting have been: uniform and context-appropriate device selection; trained technicians and an established health technology management program; a system for routine preventive maintenance; and resources for and access to spare parts. With this support ecosystem in place, oxygen concentrators can be an appropriate and low-cost technology for supplying medical oxygen in low-resource settings.

SP093.2 - Global Medical Devices Pricing Survey

Author(s): Adriana Velazquez Berumen, Maria E. Moreno Carbajal, Olumurejiwa Fatunde, Yael A. Rodríguez-Guadarrama His/emp/pau/medical Devices, World Health Organization Headquarters, Geneva/SWITZERLAND

To guarantee equitable access to medical devices, reliable information must be available for policy-makers and procurers. Due to lack of information on medical devices pricing, Low and Middle-Income Countries (LMIC) face several disparities during the acquisition process; a public procurer in Latin America paid 300% more for the same device as a public sector organization in Europe. A few countries, such as Brazil, Japan, and Iran have made several efforts to provide reference information to procurers within their countries. However, the majority of countries have no such information available. Since health technology is an essential building block to achieving Universal Health Coverage, information transparency and pricing regulation should be treated as priorities by high-level health authorities.

Since 2011, the WHO Medical Devices Unit has begun to address the issue of pricing inequity by building an evidence base. Two studies have been completed by the Medical Devices Unit. The first study detailed price components throughout the supply chain as well as a breakdown of the operational costs generated by 7 selected medical devices (excluding medicines, drugs and vaccines). This study conducted a pilot survey that includes defined parameters to measure price components and operating costs of medical devices over a worldwide representative countries sample and industry sector. The second study provided a conceptual framework for financial access to medical devices. This work supported the pilot of Global Medical Devices Pricing Survey (GMDS), which was launched in 2013. For the GMDS, quantitative information on price components of 21 medical devices were collected from several stakeholders within the health sector, qualitative information on procurement, industry and trade were collected as well. Technologies, brands and models were selected through research and evaluation of the products used most commonly throughout the world.

Results from surveys derived from these studies shared a common dilemma: a lack of responses with comparable and useful information. In the first case, only 6 out of 24 countries had completed the survey. For the GMDS, only 15 organizations worldwide submitted responses. Most survey responders chose to report general information on industry, procurement, and trade, rather than medical devices price components. As a result, it is necessary to do an extensive review of the selected medical devices as well as the surveyed participants.

In order to improve global data collection for the forthcoming GMDS, WHO is taking into account the outcomes of the pilot of GMDS, the Global Atlas of Medical Devices (GAMD) 2013 and efforts made by other countries. This includes redefining qualitative information and reselection of medical devices to be included on the

forthcoming survey. To prevent the lack of responses, the survey will exclude industry stakeholders and will be addressed only to global funding organizations, international procurers and countries which have national level of procurement, private health providers and helpful information submitted in the GAMD 2013.

Availability of reliable information on medical devices pricing is the first step in the long path to achieve transparency and pricing regulation policy, possible solutions for disparities within the medical devices market for LIMC.

SP093.3 - Methodology to evaluate physical environment parameters in healthcare services

Author(s): Gustavo A. Elias¹, Saide Calil²

¹Department Of Electronics And Biomedical Engineering, CEFET-MG, Belo Horizonte/BRAZIL, ²Department Of Biomedical Engineering, Unicamp, Campinas/BRAZIL

The physical environment in hospitals should provide adequate conditions in terms of lighting, thermal comfort, air quality, noise level, and workplace. If such conditions are not appropriate, both workers and patients may be negatively affected. The main objective of this work is to develop a human factors and ergonomics based methodology to enable the evaluation of the physical environment in patient care areas. In order to do so, the methodology was developed according to six steps. First, literature research was performed to determine the parameters to be evaluated, which were, then, organized in six groups: work area, noise, lighting, environmental parameters, power outlets, and medical gas outlets. Second, three methods to evaluate the selected parameters were defined: measurement, observation, and written survey. In the third step two forms were created to aid in the parameters measurement and observations. The fourth step involved the development of a written survey in the form of a questionnaire to be applied to healthcare staff. The fifth step consisted of the creation of a method to process the collected data (measurements, observations, and written survey). Finally, in the sixth step, dashboards were developed to report the collected data. The methodology was applied in two intensive care units (ICU) of a public teaching hospital, generating two reports. The analysis of these reports showed that the temperature, relative humidity, and noise in some ICUs were not always in accordance with the established limits. Moreover, the fact that some workers were negatively affected by physical environment parameters such as noise, lighting, and temperature could be verified through survey answers. In addition, there were complaints regarding risk of slip, trip or fall; reflex, glare or shadows; annoying drafts, unpleasant odors, and air quality; as well as the number and positioning of power outlets and medical gas outlets. The methodology met its targets, having generated results that allowed the diagnosis of the effect of some environmental parameters on workers. In addition, the ICU clinical board used the study results in order to develop a campaign aiming at noise reduction.

SP093.4 - HB-HTA method for the evaluation of exclusive Medical Devices

Author(s): Paolo Lago, Ilaria Vallone, Antonio Scarso, Corrado Gemma, Cosimino Russo
Clinical Engineering Dept., San Matteo Hospital, Pavia/ITALY

Introduction:

The Hospital Based Health Technology Assessment (HB-HTA) method is applied to the purchasing process of exclusive and so called "irreplaceable" medical devices, to support the decision of hospital managers.

Objectives:

According to Lombardy region rules for transparency and anticorruption, our hospital adopted a standard procedure for the assessment of exclusive medical devices. It involves a panel of experts: clinical engineers, physicians and economists. Clinical Engineering Department collects informations and collaborates with healthcare professionals in order to write short reports about each technology for hospital decision makers.

Methods:

The evaluation method, according to HB-HTA approach, is focused on the most important aspects of the clinical use of the technology such as security, reliability and organization impact.

The standard procedure starts with the compilation of a form in which physicians describe the clinical needs related to a specific innovative medical device, then a scientific literature research and a market survey are carried on. From the data collected in the Italian Medical Devices Database (CND Classification) of the Ministry of Health, possible technical and clinical alternatives are evaluated and compared.

Conclusion:

The final aim of Medical Device assessment is a structured report for healthcare management. Quality informations make decisions more robust, consistent, transparent and verifiable in order to maximize the health gains for the patients and to minimize costs and resources, through a better purchasing method.

SP093.5 - Applying Heuristic Evaluation on Medical Devices User Manuals

Author(s): Fernando O. Andrade, Leonardo N. Novaes, Guilherme A. Wood, Saide Calil

Department Of Biomedical Engineering (deb), State University of Campinas (UNICAMP), Campinas/BRAZIL

Driven by the importance of user manuals as a complement to training courses on the operation of medical devices, the objective of this paper is to verify if the heuristic evaluation approach proposed by Zhang and co-authors is applicable to such manuals. After applying the method in the evaluation of a non-medical device user manual and finding some difficulties to interpret the original terms and definitions, we adapted some of the usability heuristics so they would be more directly related to manuals than to devices. The adapted heuristics were applied on the usability evaluation of a linear peristaltic infusion pump's user manual. Although no healthcare professionals were present in the evaluation team, heuristic violations associated to diverse usability heuristics were identified, including some classified as usability catastrophes (the ones which could lead to patient's harm). Even with adaptations, members of the team reported difficulties in focusing on the user manual when the current usability problems seemed to be on the medical device itself. Despite the difficulties, the evaluation provided enough data on the user manual problems to formulate some corrective recommendations for the device manufacturer. Additional studies are required to confirm if modifications to some of the original fourteen usability heuristics are really necessary and, if so, what adaptations would be most adequate.

SP094 - Biological Modelling

TRACK 19: BIOPHYSICS AND MODELLING

SP094.1 - Finite Element Analysis of Dynamics of Two Microbubbles Under Ultrasonic Field

Author(s): Xiao-Hui Qiu¹, Li Li Zhou¹, Yang Yang¹, Xiao-Jian Wang²
¹Information Engineering Institute, Gannan Medical University, Ganzhou/CHINA, ²Department of Chemotherapy, Ganzhou Tumor Hospital, Ganzhou, China, Ganzhou/CHINA

The finite element numerical model of the two microbubbles in the microvessel is built in our study. The model is solved by finite element analysis software. The pressure of observing point P (away from one of two microbubbles A 3 μm) is used to express the intensity of ultrasonic cavitation. The results show that the pressure on point P is higher than single microbubble case because of the aggravation of the cavitation effect, and with the increasing of the distance of two microbubbles, the effect of adjacent microbubble on point P decreases. These results lay the foundation of the research of the agent concentration effect on clinical diagnosis and treatment.

SP094.2 - The value of individual measurements for tumor control probability predictions in head and neck patients

Author(s): Iuliana Toma-Dasu¹, Mattias Hedman², Alexandru Dasu³
¹Medical Radiation Physics, Stockholm University and Karolinska Institutet, Stockholm/SWEDEN, ²Department Of Oncology, Karolinska University Hospital, Stockholm/SWEDEN, ³Department Of Radiation Physics, Linköping University Hospital, Linköping/SWEDEN

In the age of personalized cancer medicine, individual measurements of *in vitro* radiosensitivity and proliferation parameters have great potential for predicting treatment outcome. However, cellular radiosensitivity is quite heterogeneous and therefore concerns exist towards its impact on treatment predictions. It was therefore the purpose of this study to investigate this aspect. Individually-determined radiosensitivities and potential doubling times, as well as tumor volumes from 46 head-and-neck carcinomas treated with radiotherapy, were used to predict tumor control probabilities (TCP) under various biologically-relevant assumptions for heterogeneity in radiosensitivity. TCP predictions were then compared to clinical local control using a ROC curve analysis. The analysis showed that TCP calculated under the assumption of heterogeneous radiosensitivity have the same power of distinguishing between patients with or without local control as from single values for the radiobiological parameters (a sensitivity of 66% and a specificity of 80% for an area under the curve of 0.69). The only difference was in the discrimination criterion (TCP>93% for single parameters and TCP>65% for heterogeneous parameters), illustrating the difference in appearance of the TCP curve under the assumption of heterogeneity. Nevertheless, the results showed that individually determined radiobiological parameters could be quite effective towards predicting treatment outcome for individual patients.

SP094.3 - A Novel Technique for Measuring Electrical Permittivity of Biological Tissues at Low Frequencies (100 KHz or lower)

Author(s): Seyyed Hesabgar¹, Karen Lam¹, Ravi Menon², David Holdsworth², Abbas Samani³

¹Medical Biophysics, Western University, London/ON/CANADA, ²Robarts Research Institute, Western University, London/ON/CANADA, ³Electrical & Computer Engineering, Western University, London/ON/CANADA

Accurate measurement of electrical permittivity (EP) of biological tissues is highly important for a broad range of applications including ECT (Electrical Capacitance Tomography), EPT (Electrical Permittivity Tomography), bone health assessment (Meaney et al.), interaction of electromagnetic fields with biological tissues (Peyman et al.) and food quality classifications (Ngadi et al.). As such many researchers in the past three decades have conducted numerous measurements to obtain electrical properties of biological tissues but despite the fact that most of the researchers have traditionally used an open-ended coaxial cable and vector network analyzer (VNA) for their measurements, a robust and accurate method of measuring biological tissues EP especially at low frequencies has not been developed yet. It is noteworthy that, EP imaging at low frequencies has a good potential to provide valuable diagnostic information. Gabriel et al. indicated that the uncertainty and error percentage of using open-ended coaxial probe and VNA which has been applied in the past three decades as a conventional way of measuring biological tissues EP is quite significant at low frequencies. Computer simulation also indicates that the accuracy of EP measurement for ex-vivo biological samples from conventional procedure (using open-ended coaxial probe and VNA) depends highly on the size and thickness of the samples. This implies that an accurate and reliable measurement of biological tissues EP at low frequencies (100 KHz or lower) may not be achievable by using the conventional technique. In this work we introduce a novel and reliable technique which is capable of measuring the EP of biological tissues at low frequencies in an accurate and robust way. In this technique, we use a highly sensitive capacitive sensor we developed in our laboratory. This sensor consists of two plates that sandwich the tissue sample before its electrical excitation followed by highly precise measurement of the capacitance formed by the two plates and the sample. In order to estimate the sample's EP, an initial guess of the sample's permittivity along with its known geometry is fed into an inverse Finite-Element (FE) algorithm we developed for this estimation. This algorithm follows a non-linear optimization framework which changes the sample's permittivity in its FE model systematically until the capacitance obtained from the FE model matches the experimental capacitance. The last permittivity value is considered as the estimated permittivity of the tissue sample. The mentioned technique has been utilized to extract the EP from ten freshly excised bovine heart and bone samples. Our results indicate that the average EP of 571F/m and 22418 F/m at 32 KHz for the bone and heart samples which compare well with values reported in the literature. Also the standard deviation of 50.8 F/m and 1609.3 F/m for the mentioned samples are quite low, which suggest that the proposed technique is highly repeatable.

References:

Meaney et al., International Journal of Biomedical Imaging, V.2012, 10p.

Peyman et al., WHO Workshop on Dosimetry of RF Fields, Russia, 2005

Ngadi et Al., International Journal of Food Properties, 2010

Gabriel et al., Phys. Med. Biol. 51, 6033–46, 2006

SP095 - Biosignal Processing & Pulmonary & Respiratory

PRESIDENTS CALL

SP095.1 - Power Spectral Density Analysis of Tonic Electrodermal Activity for Sympathetic Arousal Assessment

Author(s): Hugo F. Posada-Quintero, Ki Chon
Biomedical Engineering, University of Connecticut, Storrs Mansfield/UNITED STATES OF AMERICA

Electrodermal activity (EDA) has become a promising technique for assessing sympathetic nervous system (SYM) arousal. Afferent neurons from the sympathetic axis of the autonomic nervous system innervate eccrine sweat glands, and their activity modulates conductance of an applied current. Sympathetic innervation of sweat glands is revealed in quantifiable fluctuations in skin conductance at the skin's surface, termed EDA. EDA comprises slow and more rapid transients. Tonic EDA states have been assessed using two main measures: skin conductance level (SCL) and nonspecific skin conductance responses (NS.SCRs). The aforementioned measures require manual scoring and human visual verification in the time domain which is cumbersome and often subjective. Hence, there is a need for quantitative signal processing techniques to assess the SYM arousal. To this end, we applied power spectral density (PSD) analysis to EDA signals in order to determine correlations between frequency-domain EDA index (0.045 to 0.15 Hz) and EDA measures in the time-domain (SCL and NS.SCRs). We employed the same range of frequency used for sympathetic assessment in heart rate variability analysis, which corresponds to low frequency (LF) index. We also tested the ability of those indices to discriminate between levels of sympathetic arousal. Sympathetic arousal was elicited using orthostatic stress (supine, standing and sitting positions). Seven subjects were recruited and 4 minutes of EDA signals were recorded for each position. Two minutes of clean signal (after one minute of starting recording and one minute after asking the subject to change position) were used for further processing. LF-EDA and SCL was weakly correlated ($r = 0.374$, $p = 0.055$); LF-EDA and NS.SCRs more correlated ($r = 0.545$, $p = 0.032$) than SCL. SCL and NS.SCR presented statistically significant differences between sitting and supine, but not between standing and sitting. However, LF-EDA showed statistically significant differences between the three positions. This shows a potential of PSD of EDA for assessing sympathetic arousal under orthostatic stress.

SP095.2 - Multivariate Analysis Classification Based on Multi-Channel EMG Multisite Microelectrode Recording, Principal Component Analysis, and Hierarchical Clustering

Author(s): Venkateshwarla R. Raju
Biomedical Eng & Neurology & Neurosurgery And, Nizam's Inst of Medical Sciences (NIMS) University & Hospital, HYDERABAD/INDIA

Hypothesis/Rationale The main HYPOTHESIS is that when a Writer's cramp (WC) subject writes with an abnormal posture, it is difficult to determine if that posture is because of the primary dystonic force or if a compensatory force (applied by the WC subject) has overcome the primary dystonic force and has resulted in that posture. One way to differentiate between those two would be to look at the mirror movements. Mirror movements (MMs) are seen in the right hand (RH) while writing with the left hand (LH). In case the primary dystonic force is resulting in the abnormal posture while writing with right hand, the MMs would be in the same direction i.e., they would be **concordant**. If a compensatory force (overcoming the primary dystonia) has resulted in the posture, this would be seen in

the MMs which would be in the opposite direction i.e., they would be **discordant**. We hypothesize that there is no EMG recognizable difference in MMs of concordant and discordant subjects. If the data reveal that there are significant differences in MMs of the two groups of subjects (as we expect it to be) our expectation that there is EMG recognizable difference between the groups is justified and the analysis can lead to (clinically) meaningful insight. This study showed significant quantifiable EMG differences in the signals seen while writing with the right and left hands between those writer's cramp subjects with concordant mirror movements (C group) versus those with discordant mirror movements (D group). These differences were robust and seen in every measure of dispersion, such as in the patterns of significance of f-values for ratios of variances. Cluster analysis and more sophisticated analyses using advanced multivariate techniques leading to effective data summarization and measures of dissimilarity between subjects as reflected in the signals recorded and consequent possible clustering among them, however, did not lead to any meaningful clinical conclusions. These analyses could possibly be applied to longitudinal follow-ups and correlations with a normal control population in future to better comprehend the WC-phenomenon. The work on muscle signals and their application in neurological disorders as well as disabilities of dexterous movement, such as writing and the results in a vast data regarding the functioning on the muscles certainly and gainfully utilized by the biomedical scientists for further modeling of EMG. **Background:** Prevalence-rate-of-generalized/focal dystonia according to various studies (Muller J and many other scientists) varies from 0.17 to 5 per 100,000 population and 3 to 732 per 100,000 populations (USA 30/(100,000), Europe 12, Germany 10, Italy 732, Norway 16, N. England 13, Serbia 14, Israel, China 3, Japan 6, Egypt 10). In a community based study from India, by Das et al., crude prevalence rate of primary dystonia was 53.91 per 100,000 population and that of focal dystonia varied according to type of dystonia. **Objective:** to develop a computational modeling- using the model to develop a new clinical experimental setup, to design and build a multi-channel EMG machine and attempt to differentiate between those with concordant (C) and discordant (D) MMs in WC, in order to establish that there is a quantifiable difference between these two groups.

SP095.3 - Blanket Fractal Dimension for Estimating Tidal Volume from the Smartphone Acquired Tracheal Sounds: Preliminary Results

Author(s): Natasa Reljin, Bersain Reyes, Ki Chon
Biomedical Engineering, University of Connecticut, Storrs/CT/UNITED STATES OF AMERICA

Tidal volume is one of the parameters used for monitoring respiratory activity. Various methods exist for measuring the tidal volume; however, all of them require the use of specialized equipment. Due to their attractive specifications and portability, smartphones are becoming more popular and suitable for measuring vital signs and health monitoring in nonclinical and everyday settings. In this paper, we propose the use of blanket fractal dimension (BFD) for estimating the tidal volume from a smartphone acquired tracheal sounds. Tracheal sounds, as part of respiratory sounds, are non-stationary and stochastic signals, and as such are suitable for fractal analysis. Blanket method creates a strip around the tracheal signal, thus closely following the changes within the signal. As the signal changes faster, the value of BFD becomes higher. In this study, we recorded tracheal sounds with an Android smartphone, while simultaneously we collected the respiratory inductance plethysmography signal via Respitrace system. Prior to every recording, the Respitrace signal was calibrated with a spirometry system, and the obtained calibration errors were less than 10 % (which is in accordance with the manufacturer's manual). Signals were collected from five ($N=5$) healthy and non-smoker volunteers. Each volunteer performed the experiment two times; first to obtain linear and

exponential fitting models, and then to fit new data onto the existing models. Thus, the total number of recordings was 10. The estimated volumes were compared to the true values, obtained with a Respiratory signal, which was considered as a reference. These reference volumes were limited to a range from 0.2 to 1 L, as it is the normal breathing range, and consequently, only the corresponding portions of tracheal sounds were used in analysis. Since Shannon entropy (SE) is frequently used as a feature in tracheal sounds' analyses, we also estimated the tidal volume from the same sounds by using SE. The evaluation of the performed estimation, using BFD and SE methods, was quantified by the normalized root-mean-squared error (NRMSE). The results show that the BFD outperformed the SE (at least twice smaller NRMSE was obtained during both days). The smallest NRMSE error of 15.877 ± 9.246 % (mean \pm standard deviation) was obtained with the BFD and exponential model. In addition, it was shown that the fitting curves calculated during the first day of experiments could be successfully used for at least one following day. These results indicate the possibility of obtaining a portable system for tidal volume estimation, which can be used for more than one day without the need to calculate fitting curves during every day's experiment.

SP095.4 - A Robust and Realistic Framework for Clinical Classification of Myocardial Infarction

Author(s): Yasin Yazıcı¹, Yasin Mamatjan²

¹Zirve University, Gaziantep/TURKEY, ²Mars Centre, Princess Margaret Cancer Center, Toronto/ON/CANADA

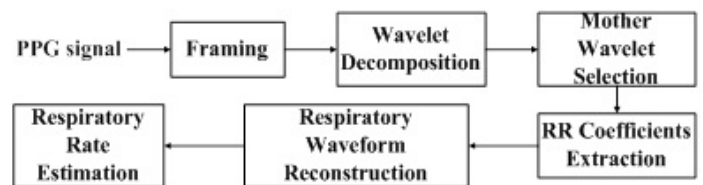
Early detection of Myocardial Infarction (MI) or heart attack is important to reduce mortality rate of cardiac diseases and automatically recognize them in order to help the diagnoses and eventually effective treatment of MI patients. Although various advanced algorithms have been published previously, there are a number of issues regarding reproducibility, public availability, clarity that even some of them 'over fitted' the classifier and performed biased pre-processing (feature selection) with all the data set to achieve high accuracy. We aim to create a robust and realistic framework for clinical classification of MI. To achieve this, firstly, we set the requirements for realistic clinical evaluation using predictive modelling and validation as well as proposed practical guidelines for reproducibility. Secondly, to detect MI efficiently and accurately, a novel approach based on Stacked Autoencoder (SAE) is used which has deeper representation power and also needs less pre-processing. We also give essential insight on why and how SAE works for different ECG data. Thirdly, we conducted systematic comparisons of the newly proposed SAE method and Continuous Wavelet Transform (CWT) based Linear Discriminant Analysis (LDA) using real ECG data set. Lastly, based on the predefined requirements, we reflected the clinical reality and corrected some other papers mistake while considering the realistic aspect of separating training and testing dataset to avoid 'over fitting' and biased feature selection and thus performed cross validation (with 2 level 10 fold cross validation). SAE always outperformed CWT based LDA approach. The accuracy of SAE is 87 % while the biased and 'over fitted' model produced an accuracy of over 99 % which is clinically unrealistic. We are improving SAE approach as it is new for ECG application, so there are more room for future improvement. The novel classification approach developed in this paper can reliably and efficiently provide useful information to clinicians and alert when state of the heart patient changes, could help clinicians realistic diagnoses and eventually effective treatment of cardiac patients.

SP095.5 - A Mother Wavelet Selection Algorithm for Respiratory Rate Estimation from Photoplethysmogram

Author(s): Dan Guo, Zhijian Li, Huijun Ding

Department Of Biomedical Engineering, School of Medicine, Shenzhen University, Shenzhen/CHINA

Photoplethysmogram (PPG) is known as a low-cost optical measure for detecting the blood volume changes. Recently, a new attempt at estimating respiratory rate (RR) from PPG signal becomes an active area. It can be implemented by different algorithms among of which wavelet based methods are commonly used with good performances achieved. In previous work, several popular mother wavelets, including db10, sym8, bior6.8, rbio6.8 and coif5, are compared and db10 exhibits the best performance on restoring the useful respiratory information from PPG signal. However, the study on the reason why different mother wavelets have different performances on RR estimation as well as how a suitable wavelet can be easily selected is insufficient. In order to explore this issue, a mother wavelet selection algorithm is proposed in this paper shown in the following figure.



In our approach, the input PPG signal is decomposed by six popular mother wavelets, namely db10, db12, sym8, bior6.8, rbio6.8 and coif5, and the results are compared in terms of the sum of decomposition coefficient magnitudes in every frame. The mother wavelet with maximum value is chosen to extract the wavelet coefficients containing RR information. By using the extracted coefficients, the reconstruction process is applied to form the respiratory waveform. In the experiments, the proposed algorithm is compared with the related six mother wavelets working separately. Two datasets are used, one of which has 21 PPG signal segments recorded by our PPG acquisition system and the other has 16 PPG signal segments randomly selected from the MIMIC database. Two evaluation tools, root mean squared normalized error (RMSNE) and Bland & Altman plot, are adopted. In RMSNE comparison between reference RR and estimated RR, the proposed algorithm obtains the minimum error rates of 2.37% and 1.4% on two datasets respectively. For Bland & Altman plot where smaller range between 95% limits of agreement indicates a better performance on RR estimation, the proposed algorithm obtains the minimum ranges of [-0.013, 0.011] Hz and [-0.003, 0.007] Hz on two datasets respectively. The above evaluation results demonstrate the better performance of the proposed algorithm. In addition, the finding reveals that the mother wavelet with a larger sum of coefficient magnitudes has a better performance on RR estimation from PPG signal which can be used as wavelet selection criteria in this area.

SP095.6 - Mathematical assessment of variability in respiratory airflow patterns

Author(s): Saravana K. Raman, Christopher Druzgalski

California State University Long Beach, Anaheim/CA/UNITED STATES OF AMERICA

Mathematical approach was used to study and determine unsteady respiratory airflow dynamics for inspiratory and expiratory breathing cycles and to analyze pulmonary data under different levels of ventilatory conditions. The work involved acquiring and processing of respiratory airflow patterns from healthy subjects under varying levels of induced obstruction. A set of mathematical equations based on the Fourier series model were developed to describe the airflow

patterns. Coefficients obtained from the Fourier series model were evaluated to obtain their ranges of values for different levels of ventilations. The goal to assess the airflow mechanics is approached by numerical modeling of the respiratory airflow network. Graphical methods were used to evaluate the goodness of fit and their statistics including the SSE, R-Square, Adj R-Sqr and RMSE. Basic statistical analysis which includes the mean and standard deviation for the airflow signals was obtained. In order to study the variability of airflow limitations, different size mouthpieces were used.

SP095.7 - Spectral Analysis of Respiratory and Cardiac Signals Using Doppler Radar

Author(s): Philip Tworzydło, Adrian D.C. Chan
Systems And Computer Engineering, Carleton University, Ottawa/CANADA

Inmate injuries and deaths remain a significant problem for correctional institutions, increasing the need for continuous monitoring of inmates. A Doppler radar device is investigated for use as a contactless method of vital sign monitoring (e.g., breathing and heart rate) in a single cell setting. The recorded radar signal is analysed in both the time domain, and in the frequency domain. The radar signal and its frequency spectrum is compared against the signals and frequency spectrums obtained from an electrocardiogram and a respiratory inductance plethysmography band. The breathing and heart rate estimates obtained from the radar match up with the estimates provided by the respiratory band and electrocardiogram. Results show that the radar device demonstrates good potential for contactless vital sign monitoring.

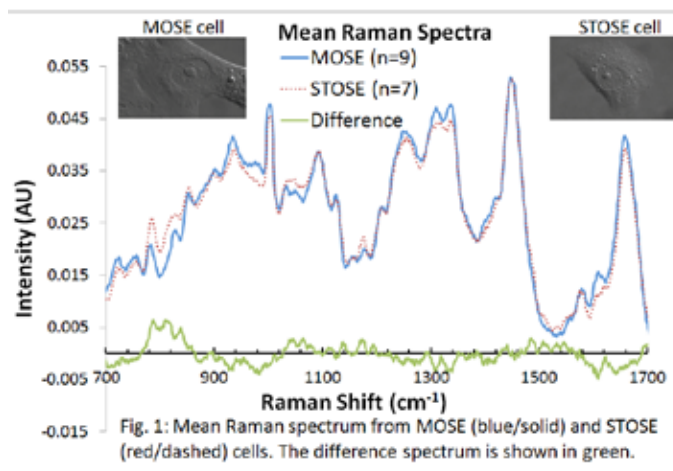
SP096 - Optical Imaging: Applications

TRACK 01: IMAGING

SP096.1 - Live-cell Raman microspectroscopy to differentiate between normal and malignant ovarian surface epithelial cells

Author(s): Santa Borel¹, Emil A. Prikryl², Nhung Vuong³, Barbara Vanderhyden³, Brian C. Wilson⁴, Sangeeta Murugkar²
¹Department Of Medical Biophysics, University of Toronto, Toronto/ON/CANADA, ²Department Of Physics, Carleton University, Ottawa/ON/CANADA, ³Department Of Cellular And Molecular Medicine, University of Ottawa, Ottawa/ON/CANADA, ⁴Ontario Cancer Institute, Toronto/ON/CANADA

Raman microspectroscopy (RMS) is a non-invasive, label-free optical technique that is based on the inelastic scattering of light by vibrating molecules. It provides a fingerprint of the common molecular bonds in specimens, including cells and tissues. This technique, in conjunction with multivariate statistical analysis methods, has been applied successfully for the label-free classification of living cells based on their molecular composition, which can be correlated to variations in protein, DNA/RNA, and lipid macromolecules. Here, RMS is applied to normal mouse ovarian surface epithelial (MOSE) cells, M0505, and spontaneously-transformed ovarian surface epithelial (STOSE) cells, which are derived from the MOSE cells and are a model for high-grade serous ovarian cancer. The Raman spectra collected from individual cells undergo initial preprocessing (background subtraction, normalization and noise reduction) to yield true Raman spectra representative of the cells for subsequent statistical analysis. The means of these spectra are shown for both types of cells in Fig. 1. Although the corresponding images (differential interference contrast microscopy) of the MOSE and STOSE cells shown in the inset appear identical, there are clear differences observed in the spectra that are attributed to differences in molecular concentrations. Using Principal Component Analysis (PCA) followed by Linear Discriminant Analysis (LDA), a clear separation of the cells into the two groups (MOSE and STOSE), with the exception of one outlier, is evident in the preliminary data shown in Fig. 2. The objective of this ongoing work is to characterize the spectral differences between the two cell types in order to correlate them with specific molecular or structural changes. The multivariate classification model constructed using such Raman spectra of MOSE and STOSE cells could thereby potentially be utilized for early detection of ovarian cancer.



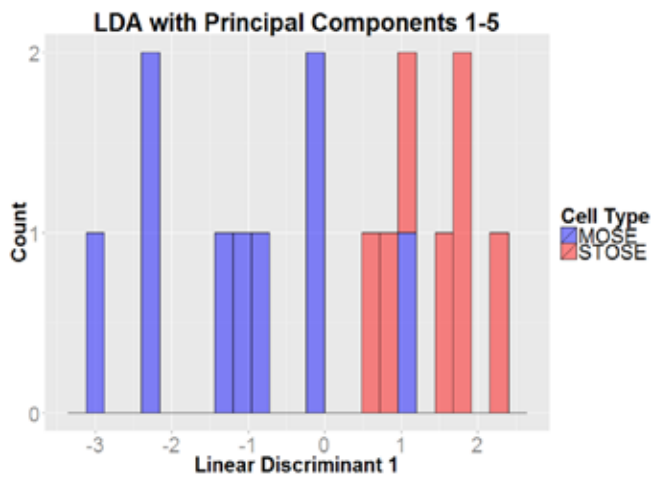


Fig. 2: Stacked histogram of the resulting values of the discriminant function for MOSE and STOSE cells.

SP096.2 - Quantitative image analysis of fluorescence endomicroscopy video sequences for mesenchymal stem cell tracking in regenerative lung treatment

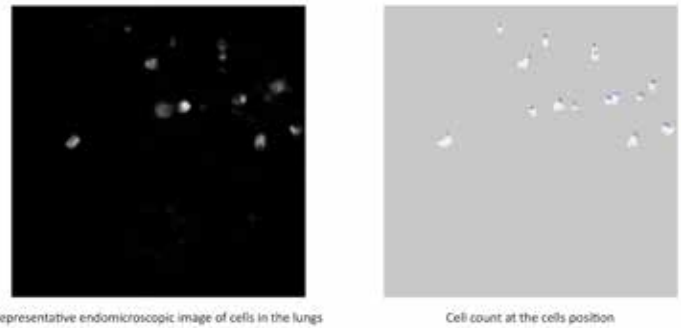
Author(s): Jessica R. Perez¹, Norma Ybarra², Frederic Chagnon³, Olivier Lesur³, Issam El Naqa¹

¹Biomedical Engineering/medical Physics, McGill University, Montreal/CANADA, ²Radiation Oncology, McGill University health center, Montreal/CANADA, ³Sherbrooke University, Sherbrooke/CANADA

Introduction: Fluorescence endomicroscopy is a powerful new minimally invasive tool that allows real-time visualization of fluorescently labeled cells within the lungs in clinical and preclinical models. In the context of regenerative medicine for lung damage, the objective of this project is to gain insight into the behaviour of mesenchymal stem cells (MSCs) in the lung of a rat model of lung injury post-radiotherapy. Interpretation and analysis of large video sequences is important to quantify the efficacy of such treatment under different experimental scenarios. In this work, we are proposing an image segmentation method to quantify the number of cells present in the field of view at each timepoint in the acquired endomicroscopy video sequence.

Materials and Methods: MSCs were labeled in culture with a membrane dye (DiD) prior to administration. MSCs were delivered endotracheally into the lung and followed by fluorescence endomicroscopic imaging. Images were acquired in the red channel (660 nm) through a tracheotomy procedure. We followed the rats for a week period and images were acquired on days 1, 2, 5 and 7. Regarding video sequence analysis, we treated each frame individually as a stand-alone image. We used a granulometry approach to determine the size of objects (cells) present in the image and performed morphological opening to detect them. Opening is a morphological operation that dilates then erodes the image with a selected structuring element, in this case a disk, in order to remove small erroneous objects and only select cells. A threshold was subsequently applied to the resulting image to select fluorescent cells over background and each detected object was counted.

Results: We were able to detect labeled MSCs in the lungs in vivo and followed them for a period of one week. At any given time point during the movie we were able to obtain an estimate of the corresponding number of cells present in the field of view. Figure 1 shows a representative endomicroscopy image with the resulting corresponding cell count of 15 cells. We compared this automated method to manual cell counting on a test set of 30 frames and achieved a good accuracy with a root-mean-squared error (RMSE) of 4 cells per frame.



Conclusion: We determined the feasibility of lung fluorescence endomicroscopy for tracking of MSCs in vivo and developed an automated image analysis method to quantify the number of cells in different experimental conditions.

SP096.3 - Shape-Based Diffuse Optical Tomography for Reconstruction of Photothermal Lesions in Prostate Focal Therapy

Author(s): Robert A. Weersink¹, Jie He², Sahil Chaudhary², Kenrick Mayo², Brian C. Wilson³

¹Radiation Oncology, University Health Network, Toronto/ON/CANADA, ²University of Toronto, Toronto/CANADA, ³Ontario Cancer Institute, Toronto/ON/CANADA

Near-infrared interstitial photothermal therapy is undergoing clinical trials as an alternative to watchful waiting or radical treatments for patients with low/intermediate-risk focal prostate cancer. MRI-based thermography is currently used to monitor target tumor destruction based on the measured tissue temperature and calculated thermal energy dose. This indirect method of imaging the treatment zone is used to assess if treatment fully covers the target volume while avoiding damage to adjacent normal tissues, particularly the rectal wall. As an alternative, we are developing transrectal diffuse optical tomography (TRDOT) to directly monitor the photothermal therapy by imaging the photocoagulation boundary based on changes in tissue optical scattering.

In this presentation, we describe the development of shape-based diffuse optical tomography as applied to the particular problem of monitoring the expanding photothermal lesion. Standard methods of diffuse optical tomography present an ill-posed inverse problem since the number of source-detector combinations is less than the variant parameters (optical properties within the volume). Hence, there are typically no unique solutions for standard DOT reconstructions. Current practice resolves this situation by imposing spatial or spectral constraints on the solutions.

In our clinical problem, the shape of the coagulated/treated tissue rather than the optical properties is of primary interest. We present a shape-based diffuse optical tomography solution in which shape parameters are used to set varying optical properties within the tissue volume. The shape is an ellipse symmetric about its short axis for a general lesion shape plus spherical harmonics to model small variations from the general ellipsoidal shape. The optical properties of the thermal lesion may vary, but with the assumption that these properties are invariant within the lesion shape.

The solution is applied to simulations of photothermal focal therapy, modelling a growing thermal lesion around a linear 10mm diffusing treatment fiber placed 10mm from the prostate wall. The modelled lesion grows in 1mm radius increments to a final radius of 9mm. Tissue scattering of the thermal lesion was set at 4X the scattering of the surrounding tissue, similar to measured tissue results. Axial and longitudinal source-detector configurations relative to the essentially elliptical thermal lesion were modelled.

The shape-based tomography successfully recovered the correct shape of the thermal lesion for lesion radii $>3\text{mm}$, with the error in the radius $<0.5\text{mm}$. Accuracy improved as the radius increased, equivalent to the lesion boundary approaching the prostate surface. Increasing noise added to the simulated data had little impact on the shape recovery: for lesions within 4mm of the prostate surface, radii error $<1\text{mm}$ up to 16% noise, for smaller lesions, ellipse radii error $<3\text{mm}$ when the noise was greater than 10%. Since the actual optical properties of the lesion may be difficult to recover, the robustness of the shape-based tomography to recover a correct solution when the reconstruction assumes different optical properties than the actual properties of the lesion was tested. Over a large range of optical properties, the shape parameters were recovered within $\pm 1\text{mm}$.

Shape-based DOT is a viable, accurate method of recovering thermal therapy treatment lesions.

SP096.4 - Transrectal diffuse optical tomography to monitor photocoagulation during interstitial photothermal therapy of focal prostate cancer

Author(s): Jie He¹, Robert A. Weersink², Israel Veilleux³, Brian C. Wilson¹

¹Department Of Medical Biophysics, University of Toronto, Toronto/CANADA, ²Radiation Oncology, University Health Network, Toronto/ON/CANADA, ³University Health Network, Toronto/CANADA

Near-infrared interstitial photothermal therapy is undergoing clinical trials as an alternative to watchful waiting or radical treatments for patients with low/intermediate-risk focal prostate cancer. Currently, MRI-based thermography is used to monitor thermal energy delivery and determine indirectly the completeness of the target tumor destruction while avoiding damage to adjacent normal tissues, particularly the rectal wall. As an alternative, transrectal diffuse optical tomography (TRDOT) is being developed to directly monitor the photothermal therapy by imaging the photocoagulation boundary based on the changes in tissue optical properties, particularly scattering. Numerical simulations of optical signals were performed using Nirfast to assess the sensitivity of changes in the optical signals to a growing coagulated lesion with higher optical scattering contrast to normal tissue, for varying light source-detector separations in both longitudinal and transverse imaging geometries. The simulations were validated experimentally in tissue-simulating phantoms using an existing continuous-wave TRDOT system. A MR compatible TRDOT applicator probe with a source-detector configuration that is capable of acquiring optical measurements and representative of the potential intended clinical use is assembled and used in these experiments. Phantom measurements and numerical simulations provide critical guidance for the optimum design of a further version of the transrectal applicator probe, in achieving maximum sensitivity to the presence of the coagulation boundary and, consequently, the highest accuracy in determining the boundary location relative to the rectal wall.

SP096.5 - The first in vivo, optical images of neuroblasts migrating away from the subventricular zone deep in mouse brain reveal two patterns of migration: implications for future therapeutic use

Author(s): Ben Kemp, Teresa A. Murray
Biomedical Engineering, Louisiana Tech University, Ruston/LA/
UNITED STATES OF AMERICA

Neural stem cells exist naturally in the adult brain in humans, mice and other animals. Their existence has sparked hope for treating neurodegenerative diseases, stroke and brain injury. In mammals, adult neural stem cells divide and begin differentiating in one of two bilateral germinal zones. One of these is the lateral subventricular

zone (SVZ). Partially differentiated cells exit the SVZ and migrate to other regions of the brain. When neural stem cells in the SVZ of mice begin to differentiate into neural precursor cells, or neuroblasts, they normally travel in clusters to the olfactory bulb. This pathway is called the rostral migratory stream. However, after a cortical injury, some of these migrating cells change course and migrate into the cortex. This has piqued interest in manipulating the mechanisms of neurogenesis to repair neural damage. Yet, what is known about neuroblast migration relies predominantly on brain slice studies. These studies have produced conflicting observations regarding mechanisms that drive proliferation and migration, and the rates of movement. To overcome the limitations and confounds inherent in slice preparations, an in vivo imaging system was created using a permanently implanted, optimized gradient index (GRIN) lens and multiphoton microscopy. The SVZ is in a subcortical region that is beyond the reach of standard multiphoton microscopy. The implanted lens overcomes this depth limitation. A preliminary longitudinal study was conducted using mice that express green fluorescent protein under the *dcx* promoter to label neuroblasts. This study is the first to produce images of neuroblasts migrating away from the SVZ in live mice. As expected, most neuroblasts traveled in clusters toward the rostral migratory stream. Surprisingly, a few neuroblasts did not travel with a cluster. These individual cells moved at markedly faster rates and frequently changed directions. In future studies, we will determine what factors influence the migratory path of these lone neuroblasts with the goal of redirecting large numbers of neuroblasts for future therapeutic uses.

SP097 - Quantitative Imaging: Part 2

TRACK 01: IMAGING

SP097.1 - Ischemia-time dependent CBF threshold for infarction determined in a porcine model of stroke using CT Perfusion and F-18 FFMZ PET imaging

Author(s): Eric A. Wright¹, Christopher D. D'Esterre², Laura Morrison³, Neil Cockburn³, Michael Kovacs⁴, Ting Yim Lee⁵

¹Robarts Research Institute, London/ON/CANADA, ²Department Of Radiology, Foothills Medical Center, Calgary/CANADA, ³Lawson Health Research Institute, London/ON/CANADA, ⁴Department Of Medical Imaging, Western University, London/ON/CANADA, ⁵Medical Biophysics, The University of Western Ontario, London/CANADA

Introduction: CT Perfusion (CTP) derived cerebral blood flow (CBF) has been proposed as the optimal parameter for delineating the infarct core prior to reperfusion (1), however lack of ischemia-time dependent CBF thresholds for infarction has been problematic. Previous CTP-CBF threshold derivation studies have been limited by uncertainties caused by infarct expansion, and DWI lesion reversibility (2). This study proposes a porcine model for determining ischemia-time dependent CBF thresholds for infarction using contemporaneous CTP and 18F-fluoroethylflumazenil (FFMZ) PET imaging, with the objective of deriving a CBF threshold for infarction after 3h of ischemia.

Methods: Cerebral ischemia was induced in the left hemisphere of 11 pigs by injecting endothelin-1 (ET-1) into the cortex through a burr hole in the skull. CTP scans were completed at baseline, 10, 30 then every then every 30 until 180min post ET-1 injection. If the CBF map at any time point showed reperfusion of the ischemic tissue then a second dose of ET-1 was administered. F-18 FFMZ was injected 2.5h after the first ET-1 injection and a 25min PET acquisition was started 25min post F-18 FFMZ injection. CBF maps from each CTP imaging time point were co-registered and a median CBF map was produced by taking the median value of each pixel. The median CBF maps, the PET images, average images from the baseline CTP study, and blood volume (BV) maps from the 10min post ET-1 CTP study were co-registered. ROIs were drawn over the cortex on the affected and contralateral side and superimposed onto all maps and images. Infarct pixels were identified on PET images as having signal less than the average minus 2 standard deviations from the contralateral ROI. Average images were used to segment out white matter within the affected side ROI by removing pixels with CT number less than 40HU. Blood vessel pixels were excluded if they had a BV greater than the average plus 2 standard deviations from the affected side ROI or if they had median CBF over 100mL100g⁻¹min⁻¹. The remaining infarct and non-infarct grey matter ROIs were superimposed onto the median CBF map and pixel values were imported into Matlab for logistic regression and ROC analysis. This process was repeated for each animal that developed infarction.

Results: 6 of the 11 animals developed infarction with an average infarct volume of 1.41±0.38cm³. The optimal operating points of the ROC curves corresponded to CBF values of 14.2, 11.8, 18.9, 13.4, 13.9, and 19mL100g⁻¹min⁻¹. The average of these 6 values was calculated to find a 3h ischemia-time CBF threshold for infarction of 15.2±1.2mL100g⁻¹min⁻¹.

Conclusions: The 3h ischemia-time infarction CBF threshold of 15.2mL100g⁻¹min⁻¹ agrees well with the threshold of 12mL100g⁻¹min⁻¹ derived in a previous study (3). The ET-1 stroke model has the potential to derive CBF thresholds for infarction at other ischemia times by varying the time between the ET-1 injection and the start of PET imaging.

References: 1) Kamalian et al. Stroke, 2011; 42:1923-1928. 2) Labeyrie et al. Stroke, 2012; 43:2986-2991. 3) Jones et al. J Neurosurg, 1981; 54:773-782.

SP097.2 - Characterization of scatter factors in thyroid studies using a pinhole collimator by Monte Carlo Simulation.

Author(s): Adlin Lopez Diaz¹, Sunay Rodriguez², Angelina Diaz², Aley Palau¹, Juan Miguel Martin¹

¹Nuclear Medicine, Hospital Hermanos Ameijeiras, La Habana/CUBA, ²Physical Research, CEADEN, Havana/CUBA

To study the scatter factors during I-131 thyroid scintigraphic studies with a pinhole collimator (5mm hole) was developed a Monte Carlo (MC) simulation using GAMOS code. First, to check the accuracy of the Monte Carlo model, simulated and measured data using a thyroid phantom were compared. The accuracy of the Monte Carlo model was verified by the good agreement between measured and simulated energy spectra and the maximum discrepancies of 2% in the counts/sec/MBq. Next, simulations to investigate scatter were performed for different tissue thickness between the thyroid and collimator (5-15mm). The image's scatter contribution was significant in the 5mm pinhole, being between 27-40%. On the basis of the separated scatter from direct count included in window energy spectra, a preliminary evaluation of multiple window energy correction methods was performed. For the simulated thyroid geometry with pinhole, the reduce inferior double energy window methods (15% on 364keV photopeak window) provides a reasonable correction for scatter. This study is the first approach; we recommend including real thyroid geometry with different thyroid depth-thickness and mass.

SP097.3 - Fluid Quantification Using Temporal Subtraction: Comparing Single to Dual-Energy Digital Chest Radiography

Author(s): Shailaja Sajja¹, Samuel Richard², Ali Ursani¹, Fatima Ursani¹, Megan Hickey³, David Fooks², Narinder Paul¹

¹Department Of Medical Imaging, toronto general hospital, toronto/ON/CANADA, ²Research And Innovation Labs, Carestream Health, rochester/NY/UNITED STATES OF AMERICA, ³Brock University, Saint Catherines/CANADA

Background: Accurate quantification of thoracic water content is integral to assessing patient health in many disease states. Computed tomography (CT) provides tissue characterization and quantification but is generally not available for critically ill patients. Portable chest radiography (CXR) is often the only imaging modality available to immobile patients; however, it has limited ability for estimating fluid content. Temporal subtraction (TS) provides temporally separated projections for quantifying differences in tissues over time, but performance is limited by image misregistration. Dual-energy (DE) CXR removes overlapping ribs and can reduce structures that are challenging to register. This research investigates the utility of portable TS-CXR and TS-DE-CXR for the detection and quantification of thoracic water.

Evaluation: Temporal subtraction of CXR images taken pre- and post-operation were used to determine change in fluid volume. The algorithm utilized the difference in x-ray attenuation signal between images to derive water thickness and to estimate the difference in water volume. 1-5 solid water blocks (40 ml each) were added (total volume of 200 ml) into the thoracic cavity of a static anthropomorphic chest phantom. CXR (120 kVp) and DE-CXR (60/120 kVp) were acquired after addition of each solid water block. A set of TS-CXR and TS-DE-CXR images were generated by subtracting the no-water image from the set of images with added water, from which volume estimates were derived. The experiment was repeated on a horizontally-moving phantom to simulate motion. Intensity-based rigid image registration was performed between pre- and post-op-

eration images followed by temporal subtraction. Image segmentation of the lung region was improved with TS-DE-CXR due to a clear demarcation between lung space and remaining thoracic region without the confounding impact of ribs. In addition, TS-DE-CXR had fewer misregistration artifacts resulting in improved registration performance and superior accuracy in estimation of water volume. The root mean squared error (RMSE) was 4.74 ml using TS-DE-CXR and 8.9 ml using TS-CXR. The range of error percentage was -7% to +2% with TS-DE-CXR and +6.3% to +16% with TS-CXR.

Discussion: TS-DE-CXR images are superior to TS-CXR images in providing accurate estimation of thoracic water volume. TS-DE-CXR has potential to enhance the diagnostic utility of DE-CXR for immobile patients.

Conclusions: TS-DE-CXR provides an accurate estimation of the volume of thoracic water. Further work will target validation of the TS-DE scheme on clinically acquired CXR images.

SP097.4 - Quantitative low-kVp CT angiography in carotid artery imaging

Author(s): Tingyu Mao¹, Meili Yang¹, Pengwei Wu¹, Gaofeng Wang¹, Xiangyang Tang², Hongjie Hu¹, Tianye Niu¹

¹Sir Run Run Shaw Hospital, Institute of Translational Medicine, Zhejiang University, Hangzhou/CHINA, ²Department of radiology, Emory University, Atlanta/GA/UNITED STATES OF AMERICA

Shading and streaking artifacts brought by beam hardening and photon starvation is commonly observed in low-kVp CT angiography (CTA) for carotid artery imaging. Image quality is thus significantly degraded and a faithful observation of carotid artery is impeded. In this paper, we propose a novel quantitative image postprocessing scheme to eliminate these artifacts. In shading correction, we follow general knowledge of the relatively uniform CT number distribution in one tissue component, and continuous and low-frequency shading artifact distribution in projection domain. Coarse image segmentation is first applied to construct an ideal template image where each structure is filled with the same CT number of that specific tissue. By forward projecting the difference between uncorrected CT image and the ideal template, we estimate the continuous and low-frequency shading error signal in projection domain using low-pass filtering. An error map is then reconstructed using standard filtered back-projection algorithm from the error signal and added to the original image to correct for the shading artifacts. To suppress the increased noise and streaking artifacts, we first perform a texture extraction to estimate the noise distribution in the image and then incorporate the estimated noise variation into a nonlocal filtering method. The proposed scheme is evaluated in carotid CTA scan using a dual-source CT at 80 kVp, in which the shading and streaking artifacts can be successfully corrected by reducing the CT number error from 246 HU to 63 HU and spatial non-uniformity by a factor of 2.2, respectively. In the volume rendering generated from the corrected CT images, the visualization of carotid artery is improved substantially and comparable to that generated from a CTA scan at 140-kVp. The proposed method is implemented directly on the CT image without access to the raw projection data and is thus attractive for clinical application in low-dose CTA.

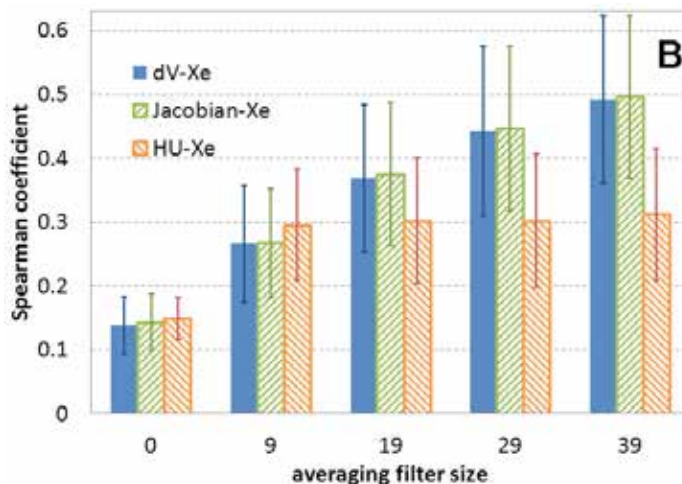
SP097.5 - Evaluation of the ΔV Ventilation Calculation Method Using In Vivo XeCT Ventilation Data

Author(s): Geoffrey G. Zhang¹, Kujtim Latifi¹, Kaifang Du², Joseph M. Reinhardt³, Gary E. Christensen³, Kai Ding⁴, Vladimir Feygelman¹, Eduardo G. Moros¹

¹Radiation Oncology, Moffitt Cancer Center, Tampa/UNITED STATES OF AMERICA, ²Human Oncology, University of Wisconsin School of Medicine and Public Health, Madison/WI/UNITED STATES OF AMERICA, ³Biomedical Engineering, University of Iowa, Iowa

City/IA/UNITED STATES OF AMERICA, ⁴Radiation Oncology, Johns Hopkins University, Baltimore/MD/UNITED STATES OF AMERICA

Ventilation distribution calculation using 4DCT and deformable image registration (DIR) has shown promising potential in several clinical applications. This study evaluated the direct geometric ventilation calculation method, namely the ΔV method in which the local volume change is calculated geometrically using a deformation transformation, with Xenon-enhanced CT (XeCT) ventilation data from four sheep as the gold standard. The results are also compared to two other published ventilation calculation methods, namely the Jacobian and the Hounsfield Unit (HU) methods. The Diffeomorphic Morphons (DM) method was applied as the deformable image deformation (DIR) technique, and it was evaluated using the 4DCT data of the sheep with manually delineated landmarks in the end-expiration and end-inspiration phases in this study. Spearman correlation coefficient (SCC) and Dice similarity coefficient (DSC) were used for evaluation and comparison. The average target registration error of the landmarks by the DM method was 1.9 ± 1.5 mm. The average SCC with one standard deviation was 0.49 ± 0.13 with a range between 0.36 and 0.67 between the XeCT and ΔV ventilation distributions; 0.50 ± 0.13 (range 0.37 - 0.67) between the XeCT and the Jacobian ventilation distributions, and 0.31 ± 0.10 (range 0.23 - 0.44) between the XeCT and the HU ventilation distributions. The average DSC value for upper 30% ventilation volumes between the XeCT and ΔV ventilation distributions was 0.82 ± 0.03 with a range between 0.79 and 0.86, while for the upper 50% volumes, it was 0.70 ± 0.05 (range 0.64 - 0.77). The average DSC results between XeCT and Jacobian ventilation distributions were the same while between XeCT and HU they were 0.64 ± 0.05 for the upper 50% ventilation volumes (range 0.60 - 0.70) and 0.79 ± 0.03 for the upper 30% ventilation volumes (range 0.75 - 0.82). High ventilation volumes in ventilation distributions generated from 4DCT data were more accurate compared to low ventilation volumes. Ventilation difference introduced by deformable image registration errors improved with smoothing. The following figure shows the SCC values between the XeCT and the ventilation calculated using the three algorithms versus smoothing.



In conclusion, ventilation distributions generated using ΔV-4DCT and deformable image registration are reasonably accurate and therefore potentially useful in clinical practice. This evaluation study and previous reports support the use of ventilation calculated using 4DCT in clinical applications in areas such as radiation treatment planning and pulmonary function assessment.

SP097.6 - Predicting Survival Outcomes of Post-Treatment Glioma Patients by Quantification of Viable Tumour Volume on CMET/FLT PET and MRI.

Author(s): Christopher Leatherday¹, Ros Francis², Andrew Campbell¹, Anna Nowak², Laurence Morandeau³, Michael Bynevelt⁴, Nelson Loh², Michael Mccarthy²

¹Medical Engineering And Physics, Royal Perth Hospital, Perth/WA/AUSTRALIA, ²Wa Pet Service, Sir Charles Gairdner Hospital, Perth/WA/AUSTRALIA, ³Medical Technology And Physics, Sir Charles Gairdner Hospital, Perth/WA/AUSTRALIA, ⁴Radiology, Sir Charles Gairdner Hospital, Perth/WA/AUSTRALIA

Aim: To compare the utility of tumour volumes selected using ¹¹C-Methionine (CMET), ¹⁸F-Thymidine (FLT) PET and Gadolinium (Gd) enhanced T1 MRI imaging in prediction of survival outcome in post-treatment glioma patients.

Method: 27 glioma patients (19 m, 8 f, mean age 56, age range 34-77) were given standard clinical treatment at Sir Charles Gairdner Hospital, Perth. After either 2 or 3 chemotherapy cycles, participants underwent PET/CT imaging with both CMET and FLT; the administered dose was adjusted for patient weight. A volumetric Gd enhanced T1 MRI was also acquired. All imaging was completed within 7 days.

For both PET tracers, background normalisation of the tumour was performed on a voxel-by-voxel basis using the uptake in the contralateral hemisphere. For CMET the tumour to normal (T/N) ratio was used. For FLT, due to low tracer uptake in normal tissues, the absolute difference in standardised uptake values (SUV) was taken.

A modality dependent 'viable tumour volume' was measured for each subject. Voxels with a T/N ratio exceeding 1.5 for CMET images and a SUV difference of 0.2 for FLT images were considered viable tumour. For MRI images, viable tumour volume was chosen by manually thresholding the Gd enhanced images.

ROC curve analysis was used to identify the optimal tumour volume threshold above which a subject's survival would be less than the median survival time (78 weeks) of the cohort for each modality. Survival time differences for subjects with volumes below and above the optimal values were examined using a log-rank test.

Results:

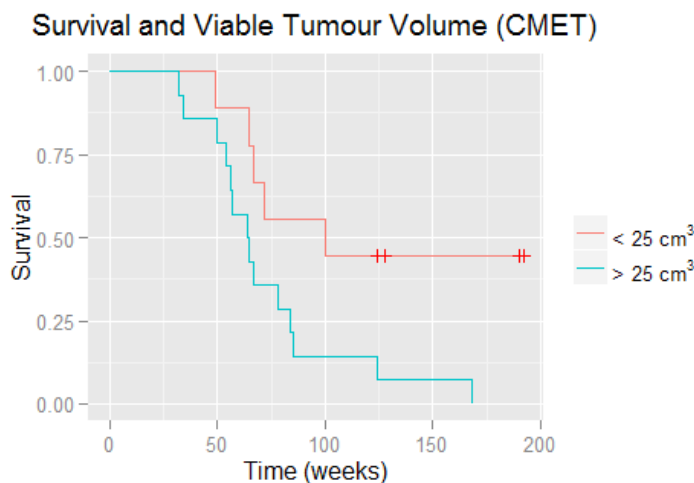


Fig 1: A Kaplan-Meier survival plot for CMET tumours above and below 25cm³.

The optimal tumour volume thresholds were 25 cm³, 42 cm³ and 20 cm³ for CMET, FLT and Gd-MRI respectively. There was a significant difference in survival time for tumour volumes above and below

these thresholds for CMET-PET (p=0.02), but not for FLT-PET or Gd-MRI.

Conclusion: CMET-PET defined viable tumour volumes may discriminate between high and low survival times in post treatment glioma. FLT-PET or Gd-MRI defined volumes do not appear to be predictive of survival time. Further analysis with more subjects is required to verify the utility of method.

References: ¹HERHOLZ, K., KRACHT, L. W. & HEISS, W. D. 2003. Monitoring the effect of chemotherapy in a mixed glioma by C-11-methionine PET. J Neuroimaging, 13, 269-71.

SP097.7 - A Novel Method for Lung's Air Volume Estimation in Exhalation and Inhalation Phases From CT Images

Author(s): Hadi Moghadas Dastjerdi¹, Mohammad Reza Ahmadzadeh¹, Elham Karami², Abbas Samani³, Ali Sadeghi-Naini⁴

¹Electrical And Computer Engineering, Isfahan University of Technology, Isfahan/IRAN, ²Imaging Research Laboratories, Robarts Research Institute, London, ON/CANADA, ³Medical Biophysics, Western University, London/CANADA, ⁴Medical Biophysics / Radiation Oncology, University of Toronto, Toronto/ON/CANADA

Lung's air volume measurement is of great importance in pulmonary function assessment. CT Image segmentation can be used effectively for lung volume measurement, especially for patients who are not fit for other diagnostic tests, leading to invaluable diagnostic information [1], [2]. Despite that advanced segmentation techniques have been developed over the last decades, thresholding remains effective for various clinical applications if implemented properly [3], [4]. A critical step in this method is finding and fine-tuning the threshold values. The proposed lung's air volume estimation algorithm with CT imaging benefits from the availability of image sequence over the respiration cycle to determine the threshold values based on the lung parenchyma biophysics. The algorithm considers three volumes of lung's air, soft-tissue, and background-air. The main concept is that these volumes vary in size and shape in the lung images acquired throughout the respiration cycle. Accordingly, as illustrated in Figure 1, an optimization framework was developed to find the optimal threshold values that minimize a cost function derived based on the principles of tissue incompressibility and air mass conservation throughout the respiration cycle. In general, image intensity of each voxel in a lung CT image is the intensity resultant of tissue and air within the voxel. The probability of having significant tissue fraction in the exhalation phase is higher than in its inhalation counterpart [5], [6]. As such, after determining the threshold values through optimization, the proposed method calculates the air volume by multiplying corresponding voxels number by voxels size and voxels fractional air volume coefficients (FAVCs). Preliminary results obtained from an *ex vivo* porcine lung study where the amount of inhaled air was recorded in each respiration phase shows that the air volume estimated using the proposed method is significantly more accurate when FAVCs are used in the air volume estimation.

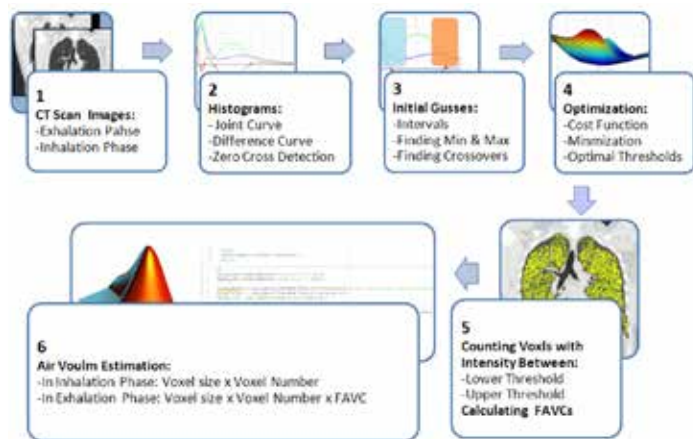


Figure 1: Block diagram of the proposed method.

- [1] J. D. Fleisch *et al.*, *Chest*, vol. 142, no. 2, pp. 506–10, Aug. 2012.
- [2] G. L. Ruppel, *Respir. Care*, vol. 57, no. 1, pp. 26–35; discussion 35–8, Jan. 2012.
- [3] A. Sadeghi Naini *et al.*, *IEEE Trans. Biomed. Eng.*, vol. 58, no. 1, pp. 152–8, Jan. 2011.
- [4] K. U. Juergens *et al.*, *Am. J. Roentgenol.*, vol. 190, no. 2, pp. 308–314, 2008.
- [5] J. Tomaszewski Jr. *et al.*, Springer New York, 2008, pp. 20–48.
- [6] E. Roan *et al.*, *Am. J. Physiol. Lung Cell. Mol. Physiol.*, vol. 301, no. 5, pp. L625–35, Nov. 2011.

SP097.8 - High-resolution micro-CT protocol for assessing lung ventilation and perfusion: image subtraction versus multi-energy analysis

Author(s): Pierre Deman¹, Samantha Tan¹, Davood Karimi², John Schipilow³, Rabab Ward², Nancy L. Ford¹

¹Oral Biological And Medical Sciences, University of British Columbia, Vancouver/BC/CANADA, ²Electrical And Computer Engineering, University of British Columbia, Vancouver/BC/CANADA, ³Centre For High-throughput Phenogenomics, University of British Columbia, Vancouver/BC/CANADA

Introduction:

Micro-CT allows full-organ, high-resolution imaging of airways and lung vasculature in rodents when using contrast agents. Advantages include linearity of the measured signal versus the concentration of the contrast agent and co-registration between scans with high resolution leading to a good accuracy. We propose to compare a multi-energy imaging protocol and an image subtraction method to estimate the concentration of two contrast agents at an acceptable x-ray dose level for longitudinal monitoring.

Methods:

Respiratory-gated micro-CT imaging (CT120, Gamma Medica) was performed on 6 rats. Each rat was anaesthetized with isoflurane (1.5–2% in O₂), intubated and mechanically ventilated. Low-energy images (50 kV, 63 mA, and 0.1 mm copper filtration) and high-energy images (120 kV, 40 mA, and 0.6 mm copper filtration) were obtained at baseline and post-injection of a vascular contrast agent (Binitio eXIA 160XL, 0.45 mL/ 100g). Rats were euthanized and ventilated with xenon while images were obtained with both the low- and high-energy protocols. The spectrum of each protocol was evaluated using HVL measurements and by simulation with the Spetkr freeware.

The dose deposited in air was estimated using a thimble ionization chamber at isocenter of the micro-CT scanner. We performed a histological study (H&E and movat staining) to ensure no damage to the lungs resulted from the x-ray dose received.

Images were reconstructed with 0.05 mm voxel spacing using a FBP algorithm. The concentration of both contrast agents was calculated based on multi-energy equations. To improve the accuracy of the concentration calculations, we tested different denoising methods (on projections and the reconstructed volume).

Results:

The dose of each low- and high-energy scan was estimated to be 96.5 mGy and 91.2 mGy respectively. An example of the concentration of contrast agent map is shown Figure 1. Analysis was performed on the H&E stained histological sections to quantify the percentage of inflamed area over the total area of the lung section and the number of white blood cells present.

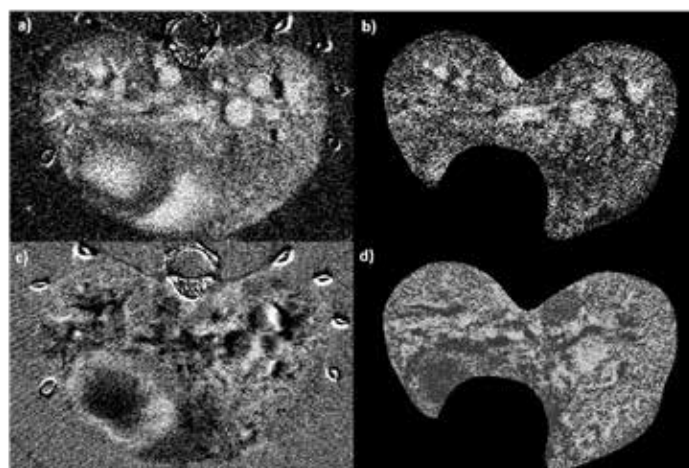


Figure 1: (a) Low-energy subtraction, iodine minus baseline. (b) Multi-energy after iodine injection. (c) Low-energy subtraction (iodine + xenon – iodine). (d) Multi-energy after iodine and xenon injection.

Conclusion:

High-resolution imaging of the vasculature and airways in rodents is achievable at low dose with contrast-enhanced micro-CT using subtraction methods. Because the K-Edges of the two most common CT contrast agents are very close, the multi-energy protocol was more difficult, and would benefit from advanced signal processing and reconstruction algorithms.

SP098 - Biomaterials and Regenerative Medicine

TRACK 02: BIOMATERIALS AND REGENERATIVE MEDICINE

SP098.1 - Finite Element Analysis Of Abdominal Aortic Aneurysms To Predict Risk Of Rupture - The Role Of The Thrombosis Thicknesses.

Author(s): [Omar Altwijri](#)

Department Of Biomedical Technology, King Saud University, Riyadh/SAUDI ARABIA

Abdominal aortic aneurysm (AAA) is a cardiovascular disease occurring when the aorta becomes weak and develops a balloon expansion in its wall. This balloon diameter can reach sizes up to 4 times the normal aortic diameter, with the diameter enlarging at rates of 0.2–1.0 cm/year. Ruptured aneurysm leads to death in 78% – 94% of diseased aortas [1]

Aneurysm rupture is a biomechanical event that occurs when the mechanical stresses in the wall of the aorta exceed the failure strength of the aortic tissue [2].

In medical practice, when the maximum diameter of AAA exceeds 5 cm it is considered at risk of rupture. Surgical repair is usually not considered until the diameter reaches at least 5 cm. However, it is frequently observed that AAAs with diameters less than 4 cm can rupture which raise the need of finding a more reliable method to assess rupture risk.

The role of the intraluminal thrombus (ILT) which exists in more than 75% of AAA was examined using variable thickness and material properties of the thrombus. The role of the ILT has been experimentally examined in number of studies [4; 5; 6].

ILT with variable thicknesses were used here to examine the effect of ILT on wall stresses compared with AAA without ILT.

SP098.2 - High-Frequency Ultrasonic Measurement of Ischemia and Revascularization in Mice with Ligated Femoral Arteries

Author(s): [Andrea N. Quiroz](#)¹, [Michaëlle A. Cadet](#)¹, [John A. Chapell](#)², [Paul Slezak](#)³, [Cyrill Slezak](#)⁴, [Timothy E. Doyle](#)⁴

¹Biology, Utah Valley University, Orem/UT/UNITED STATES OF AMERICA, ²Dentistry, University of Louisville, Louisville/KY/UNITED STATES OF AMERICA, ³Ludwig Boltzmann Institute for Experimental and Clinical Traumatology, Vienna/AUSTRIA, ⁴Physics, Utah Valley University, Orem/UT/UNITED STATES OF AMERICA

High-frequency ultrasound (10-100 MHz) is particularly sensitive to small vascular structures that are close in size to the ultrasound wavelength (15-150 mm). The ability to rapidly determine the degree of vascularization in small animals *in vivo* would provide a useful characterization tool for regenerative medicine. The objective of this study was to determine if direct ultrasonic measurements in the 10-100 MHz range could be used as a vascularization assay for small animals and tissue specimens. To accomplish this, a study was performed at the Ludwig Boltzmann Institute for Experimental and Clinical Traumatology (Vienna, Austria), where the femoral artery in one hind limb of each of sixteen mice was ligated and tested for eight days. Eight of the ligated limbs were treated with vascular endothelial growth factor (VEGF, “treated”) while the remaining eight ligated limbs were not treated (“untreated”). All of the ligated limbs were then allowed to grow ischemic. The unligated limbs were controls. Pitch-catch and pulse-echo measurements were acquired using a 50-MHz immersion transducer (Olympus NDT,

V358-SU), a high-frequency square-wave pulser/receiver (UTEX, UT340), and a 1-GHz digital oscilloscope (Agilent, DSOX3104A). The ultrasonic transducers were coupled to the limbs using glycerol, and triplicate waveforms were acquired from each limb every other day. The ultrasonic parameters analyzed were wave velocity and peak density. Peak density is the number of peaks and valleys in the ultrasonic spectrum between 20-80 MHz, and provides a measure of spectral complexity. In two hospital studies on breast cancer surgical margins, peak density was demonstrated to be sensitive to microstructural changes in tissue due to both benign and malignant processes. The mice were also evaluated with laser Doppler interferometry (LDI), multispectral optoacoustic tomography (MSOT), micro-CT (computed tomography), and histopathology. The results indicated that ultrasonic signals from untreated limbs displayed a steady decrease in wave velocity over the test period as compared to the treated limbs. Peak density displayed no trends for either untreated or treated limbs. The peak density results were consistent with the other evaluation methods, which primarily reveal changes in tissue microstructure and showed no significant differences between the untreated and treated limbs. In contrast, wave velocity is sensitive to the stiffness of the tissue, a material property that is not measured by the other methods. The decrease in wave velocity for the untreated limbs indicates a softening of the muscle tissue, possibly due to inflammation or edema, whereas the decrease and then return to normal for the treated limbs indicates recovery of the tissue. The high-frequency ultrasound may therefore have detected effects due to ischemia and revascularization that were hidden to LDI and histopathology (MSOT and micro-CT data have yet to be analyzed). The study results indicate that high-frequency ultrasound, in particular wave velocity measurements, may provide an added dimension to small animal imaging methods for detecting revascularization. The method is currently being expanded to include high-resolution imaging.

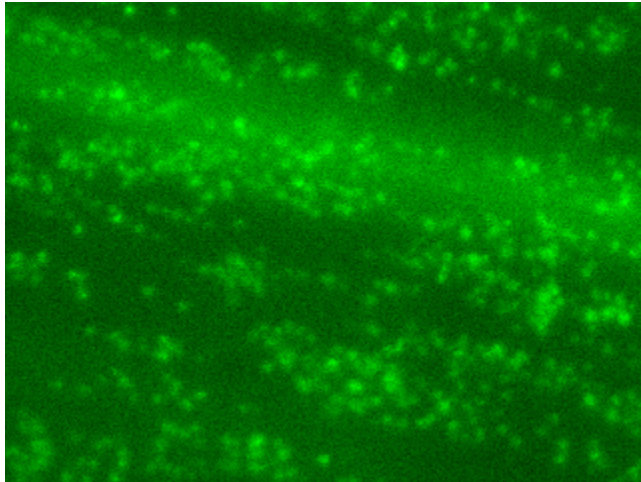
SP098.3 - Prevention of Thrombogenesis with a new Silane Based Adlayer on Commonly used Polymers in Medical Equipment Components

Author(s): [Kiril Fedorov](#), [Christophe Blaszykowski](#), [Sonia Sheikh](#), [Michael Thompson](#)

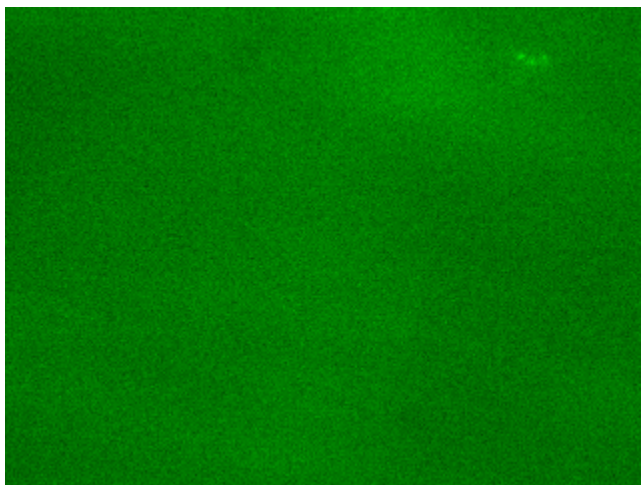
University of Toronto, Toronto/ON/CANADA

In the 21st century the medical field has majority of its equipment coming in contact with blood is manufactured from plastic polymers. This causes a major concern, where exposure may result in undesirable protein-material interactions that can potentially trigger deleterious biological processes such as thrombosis. To address this problem, we have developed an ultrathin antithrombogenic coating based on monoethylene glycol silane surface chemistry. The strategy is exemplified with several polymers including: polycarbonate and *poly (vinyl chloride)* -plastic polymers increasingly employed in the biomedical industry. The various straightforward steps of surface modification were characterized with X-ray photoelectron spectroscopy supplemented by contact angle goniometry. Anti-thrombogenicity was assessed after 2,5,10 and 60 min exposure to whole human blood dispensed at a shear rates of 300, 900, 1000 and 1500 s⁻¹. Remarkably, platelet adhesion, aggregation, and thrombus formation on the coated surface was greatly inhibited on all shear rates and both surfaces (>92% decrease in surface coverage) compared to the bare substrate and, most importantly, nearly nonexistent.

Unmodified Plastic



Coated Plastic



SP098.4 - Nature's Own "Smart" Biological Material to Inspire Next-Generation Biomaterials

Author(s): Joanna Ng¹, Lauren Kark¹, Renee Whan², Melissa Knothe Tate¹

¹The Graduate School Of Biomedical Engineering, The University of New South Wales, Sydney/AUSTRALIA, ²Biomedical Imaging Facility, The University of New South Wales, Sydney/AUSTRALIA

INTRODUCTION

The periosteal sheath that surrounds all non-articular surfaces of bones exhibits mechano-active and biologically responsive properties, hallmarks of a "smart" material. Due to the intimacy of structure: function relationships in nature, our approach was to capture the periosteum's three-dimensional (3D) spatial relationships. Using high-resolution imaging, we aim to correlate its composition and architecture with its prevailing function.

METHODS

Middiaphyseal transverse sections of the ovine femur, periosteum and surrounding tissue were imaged using a Leica SP5 II inverted multi-photon microscope tuned to 830nm (~100fs pulse). The second harmonic signal of collagen was collected using a 390-440nm band-pass filter and the elastin signal was collected using a 410-490nm emission-filter. A tiled image with a 63x1.3NA oil objective

was collected at the major and minor centroidal axes (CA) and within the tiled area, a high-resolution z-stack was acquired to quantify the 3D distribution of elastin and collagen.

RESULTS

The architecture of collagen fibers ranged from highly organized and parallel fibers at the periosteum, to loosely woven strands in muscle attachment sites, and then to irregular and thin fibers at the perimysium (Fig. 1). The elastin fibers were spring-like, short, and of irregular architecture and arrangement. Elastin fibers were also primarily abundant in the major centroidal axis, and formed a 3D mesh in the z-stack (Fig. 1).

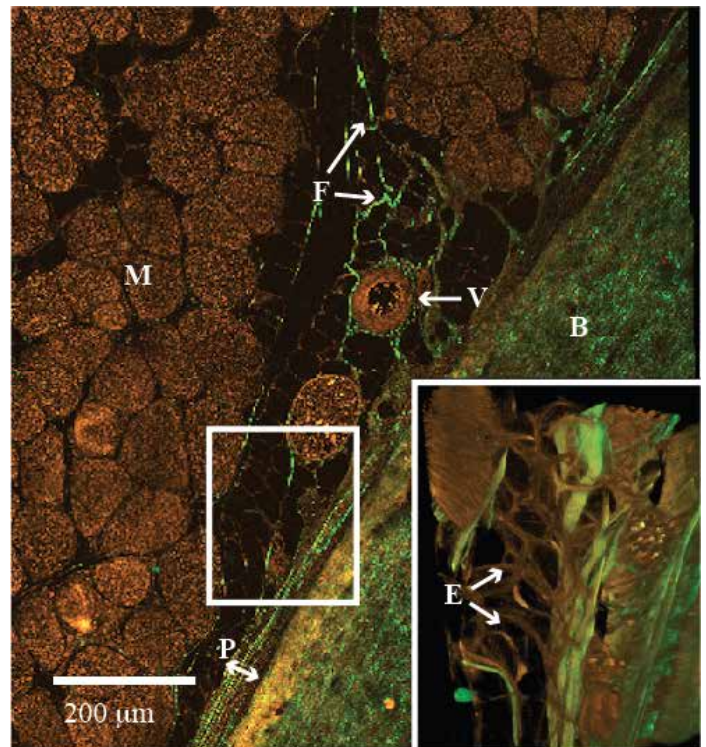


Figure 1. Tiled ROI of major CA showing the periosteum (P) to be illuminated under the collagen signal; elastin (E) abundant between the periosteum and muscle (M) shown in Z-stack insert; vessels (V) elastic and fascia exhibiting both collagen and elastin features.

DISCUSSION

Collagen fibers are mechanically robust, flexible and able to resist tensile loading. The network of fasciae, comprising of mostly wavy collagen fibres branching from the perimysium to the periosteum (Fig. 1), suggest that fascia may be mechanically significant in supporting tissue structures, e.g. preventing distension between the muscle and bone.

Since centroidal axes correlate within 5% of anatomical axes, variations in the arrangement and composition of elastic fibers can be associated with its function. Hence the abundance of elastin in the posterior major CA may be functionally associated with the prevalence of greater muscle bulk in its corresponding anatomical aspect.

CONCLUSIONS

Therefore, by harnessing the "smart" properties of nature's own biological materials and applying a bottom-up approach to engineering novel materials, we aim to facilitate the development and engineering of functional and biomimetic materials. First applications are ongoing for development of novel functional textiles to prevent and

treat lymphoedema as well as to provide an optimal interface (liner sleeve) for trans-tibial and femoral prostheses.

ACKNOWLEDGEMENTS

This project has been supported in part through the Paul Trainor and Promobilia Foundations.

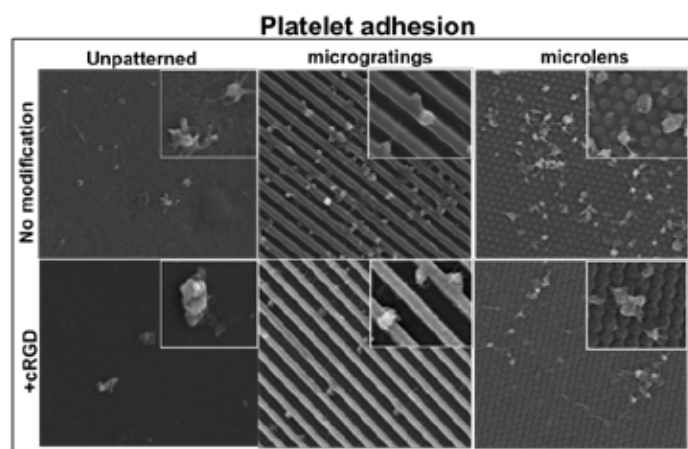
SP098.5 - Vascular endothelial cell adhesion and hemocompatibility of biochemically- and topographically-modified poly(vinyl alcohol)

Author(s): Marie F. Cutiungco¹, Deirdre E.J. Anderson², Monica T. Hinds², Evelyn K.F. Yim¹

¹Biomedical Engineering, National University of Singapore, Singapore/SINGAPORE, ²Biomedical Engineering, Oregon Health & Science University, Portland/UNITED STATES OF AMERICA

Currently available synthetic small diameter vascular grafts used for bypass or replacement of native arteries fail within the first 10 years. The lack of mechanical properties matching native arteries, thromboresistance and capacity to stimulate *in situ* endothelialization prevent the long-term application of small diameter vascular grafts. Thus, there is a critical need for new synthetic small diameter vascular grafts that can achieve compliance, hemocompatibility and endothelialization. Poly(vinyl alcohol) hydrogel (PVA) is an excellent candidate for vascular grafts due to its tunable mechanical properties, high water content and high tensile strength. Yet the bio-inertness of PVA must be addressed to improve endothelialization *in situ*. Both biochemical and topographical modifications have been used to stimulate specific vascular endothelial cell behaviours on synthetic materials by mimicking the physiological cellular niche. Thus, we hypothesize that the modification of PVA with both biochemical and topographical modifications can provide a hemocompatible micro-environment that stimulates endothelialization. PVA modified by the immobilization of fibronectin, RGDS peptide, and cyclic RGD (cRGD) peptide showed slight increase in the adhesion of human umbilical vein endothelial cells (HUVECs) while PVA modified with immobilized heparin showed significant decrease in the endothelial cell adhesion. The cRGD modified PVA did not exhibit any significant change in platelet adhesion, activation and morphology when compared with unmodified PVA in an *in vitro* hemocompatibility assays using LDH assay, microparticle release percentage and scanning electron microscopy, respectively. Using solvent casting, unmodified and cRGD-modified PVA were incorporated with micro-gratings or microlens topography. Combination of cRGD and micro-gratings or microlens topography on PVA showed significant increase in endothelial cell viability compared with unpatterned and unmodified PVA. Platelet adhesion on all PVA modified with microgratings was comparable with unpatterned and unmodified PVA. PVA with microlens topography significantly increased platelet adhesion, while PVA with both convex and cRGD modification showed no difference with unpatterned and unmodified PVA. Platelets also changed from the fibrous, activated phenotype on PVA with microgratings or microlens to round and less active phenotype on PVA with both cRGD and topography (Figure 1). The *in vitro* vascular endothelial cell adhesion tests and hemocompatibility tests demonstrated that modification of PVA with both biochemical and topographical cues may serve as an excellent surface for hemocompatible vascular grafts with enhanced endothelialization.

Figure 1. Platelet adhesion on PVA surfaces modified with cRGD and topography.



SP012.1 - Effects of PEMF on Neuroblastoma Cells Previously Exposed to Antidepressants

Author(s): Teodoro Cordova - Fraga

Ingeniería Física, Universidad de Guanajuato, León/MEXICO

PEMF on Neuroblastoma Cells Previously Exposed to Antidepressants

Teodoro Cordova-Fraga¹, Adolfo Toledo-Solano², Gloria Barbosa-Sabanero³, Lérica Liss Flores-Villavicencio², and Myrna Sabanero-López² ¹Departamento de Ingeniería Física - DCI, Universidad de Guanajuato campus León ²Departamento de Biología - DCNE, Universidad de Guanajuato campus Guanajuato. ³Departamento de Ciencias Médicas - DCM, Universidad de Guanajuato campus León

Interaction between magnetic field and living systems is inevitable; in fact, we are immersed in an ocean of magnetic field due to the magnetic field of the earth and the technology developments. Interaction between magnetic field and living systems is inevitable; in fact, we are immersed in an ocean of magnetic field due to the magnetic field of the earth and the technology developments, this one already have medical applications, currently, the pulsed electromagnetic fields (PEMF) are an alternative option for the treatment of some mental illness as the depression or schizophrenia. In order to have estimation of the side effects from PMF and drugs used for treat this kind of disorders. In this work, it is presented a comparison of the effects of imipramine, a drug for the treatment of depression, and the effects of PMF on cells from the line SHSY5Y, which provide us a representative model of neuronal tissue. The assays were done in both ways, the separately effects and the jointly effects. The imipramine at high dosage for a short period (120 mg/mL, for 20 min) shows cell damage on both, the morphology and the metabolism. Meanwhile, the PMF (50 Hz, 7 mT for 8 h) shows a cell proliferation and a decrease of their metabolism. The jointly assay indicates that the PMF balances the morphological negative effects from imipramine. In the long term these results can impact a therapy that may be more efficient. However, more research is needed in this area

SP012.2 - Porous bio-SiC ceramics from wood: approaching new medical implants

Author(s): Oleksandr Gryshkov¹, Nikolai Klyui², Volodymyr Temchenko², Vitalii Dubok³, Vitalii Kiselyov², Alexander Belyaev², Birgit Glasmacher¹

¹Leibniz University Hannover, Institute for Multiphase Processes, Hannover/GERMANY, ²V. Lashkaryov Institute Of Semiconductor Physics, National Academy of Science of Ukraine, Kyiv/UKRAINE, ³I. Frantsevich Institute For Problems Of Materials Science, National Academy of Science of Ukraine, Kyiv/UKRAINE

Introduction

Silicon carbide ceramics (SiC) are porous structures derived from different wood sources. The porosity and pore size of such ceramics may repeat the structure and porosity of specific bones in human body. Additional coating of SiC ceramics with hydroxyapatite (HA) and tricalcium phosphate (TCP) using a novel gas-detonation deposition method (GDD) could be advantageous with regard to bone replacement. This work investigates the porosity of SiC ceramics and explores the method to obtain bioactive surfaces.

Methods

Biomorphic porous SiC ceramics were synthesized using forced infiltration with liquid silicon of carbon matrices derived from different hardwood precursors (Hornbeam, Sapele, Tilia and Pear). This process involves impregnation of carbon matrices by silicon and synthesis of SiC ceramics. The porosity of SiC ceramics was analyzed based on 10 images taken using a Carl Zeiss Stereo Discovery.V12 microscope. The HA and TCP coatings were obtained utilizing the GDD method by transporting the powder using a detonation wave at high velocities [1]. The surface morphology of SiC ceramics and deposited coatings was characterized using a scanning electron microscope (SEM).

Results

The GDD method allowed obtaining high-adhesive and structurally perfect bioactive coatings onto SiC ceramics derived from different wood sources (Figure 1). The surface morphology of synthesized SiC ceramics was regular throughout the surface. The smallest pores were observed for SiC ceramics synthesized from Tilia ($27.2 \pm 10.1 \mu\text{m}$), whereas Sapele-derived ceramics yielded the pores with a mean size of $131.2 \pm 41.1 \mu\text{m}$. The calculated highest porosity was inherent to Hornbeam-derived SiC ceramics ($45.3 \pm 3.4\%$). Moreover, the porosity was greater for more dense SiC ceramics and was also dependent on mean pore size.

Acknowledgments

The authors acknowledge the exchange program with East European Countries funded by DAAD and are looking for further funding of the project.

References

- [1] Klyui NI, Temchenko VP, Gryshkov AP *et al.* (2011). *Functional Materials* 18(3): 285-292

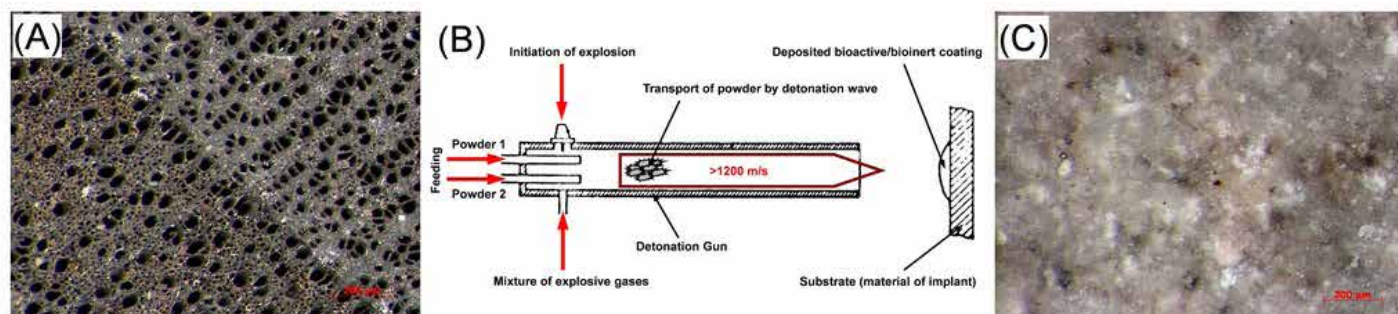


Figure 1. SiC ceramics synthesized from Tilia: surface morphology of ceramics (A) and HA coating (C) obtained by GDD method (B)

Conclusions and outlook

In this study, the bio-SiC ceramics synthesized from different wood precursors were characterized for surface morphology, porosity and pore size distribution; whereas the GDD method was used to generate bioactive HA and TCP coatings. The advantage of these ceramics is that the porosity and pore size can be optimized for different bones by varying the initial wood source. In turn, application of biocompatible and bioactive surfaces onto SiC ceramics could accelerate bone substitution.

SP099 - SPECIAL SESSION: Current situation of dosimetry in radiology and radiation protection

TRACK 05: DOSIMETRY AND RADIATION PROTECTION

SP099.1 - Current situation of dosimetry in radiology and radiation protection

Author(s): Madan M. Rehani¹, Harry Delis², Pablo Jimenez³, Joanna IZewska⁴

¹Radiology, Harvard Medical School, Massachusetts General Hospital, BOSTON/UNITED STATES OF AMERICA, ²International Atomic Energy Agency, Vienna/AUSTRIA, ³World Health Organization/Pan American Health Organization (PAHO), Washington/UNITED STATES OF AMERICA, ⁴Nuclear Sciences And Applications, International Atomic Energy Agency, Vienna/AUSTRIA

Radiation protection in medicine essentially poses dosimetry issues pertaining to patient dosimetry with some aspects of occupational dosimetry mainly relating to the lens of the eye. Dosimetric measurements in diagnostic radiology are required for the establishment and use of guidance levels, for the assessment of equipment performance and for comparative risk assessment. However, since radiology involves a diverse range of examination types, from simple projection radiography to advanced cross-sectional imaging, several dose quantities have been developed and have been well worked out by IAEA and ICRU. Further, data on the status of patient doses in different radiology procedures enable comparisons with diagnostic reference levels. The reference dose quantities have been well deciphered by the IAEA and ICRU. Some information about patient doses has become available through multi-national studies on patient doses to adults and children in CT, image guided interventional procedures (as relatively high dose procedures), as well as in mammography and conventional radiography of other organ systems. Image quality has been considered in some situations. Important findings include frequent lack of optimization in paediatric CT. There is a need for coordinated actions by different international organizations and professional bodies to improve optimization of protection which requires management of the radiation dose commensurate with the medical purpose. Particular to medical imaging, this equates to the lowest possible dose necessary to acquire diagnostic quality images. Regarding occupational radiation protection, cataract risk is important among staff in interventional suites. Currently there is near absence of monitoring of eye lens doses and actions are needed to develop and implement practical methods for eye lens dosimetry. This issue has attained greater significance granted the drastic reduction of the occupational eye lens dose limit from 150 mSv/year to 20 mSv/year, recommended by the International Commission on Radiological Protection (ICRP) and adopted in the new BSS. The IAEA has been working on promoting and supporting best practices in dosimetry, including traceability of measurements to the International System of Measurement, and strengthening the medical physics capacity throughout the world since the early sixties. As it represents one of the main resources for the medical physicists, and often, especially in developing countries, the only one, work is done in producing guidelines on dosimetry in diagnostic radiology, (Dosimetry code of Practice (TRS-457), Dosimetry for Paediatric Patients (HHS-24), Dosimetry of Wide beam CT (HHR-5)) to support dosimetry in the clinical environment. Therein exists a role for international organizations to promote and support actions on patient and staff dosimetry to improve both patient and occupational safety. This joint session will discuss modalities of cooperation. This joint session will address the current and future activities and areas for cooperation in the field.

SP100 - Dose Optimization: Focus on DRLs

TRACK 05: DOSIMETRY AND RADIATION PROTECTION

SP100.1 - A Contribution to the Establishment of Diagnostic Reference Levels in Computed Tomography in Brazil

Author(s): Lucas D.L. Narciso, Ana M. Marques Da Silva, Nathan W. Lima, Caroline M. Dartora
Faculdade De Física, PUCRS, Porto Alegre/BRAZIL

Diagnostic reference level is important to guarantee dose optimization, and can be defined nationally, regionally or locally, using dose descriptors, such as volumetric computed tomography (CT) dose index (CTDIvol, mGy) and dose-length product (DLP, mGy.cm). The aim of this work is to present the local DRL values for a CT department located in Porto Alegre, Brazil, intending to determine, in the future, national and regional DRL. For this purpose, retrospective data have been collected and analyzed, from head, chest and abdomen non-contrasted CT adult (>15 years old) and pediatric (<15 years old) exams. The DRL values have been compared to those described on previous national studies from UK, US, Germany and Switzerland. The results are shown in the following table. These values are similar to the DRLs from Germany, UK, US and Switzerland. The present study is the first of its kind to determine the DRL for scanners operating in the south region of Brazil. Similar studies in other regions of Brazil are necessary in order to establish a National Dose Reference Level.

Table 1 CT service DRLs values for head, chest and abdomen exams by age group.

<i>CT Centre DRLs</i>		
Age group	CTDIvol (mGy)	DLP (mGy.cm)
<i>Head</i>		
0-1	18	290
1-5	30	550
5-10	35	670
10-15	44	880
>15	50	950
<i>Chest</i>		
0-1	5	64
1-5	7	130
5-10	-	-
10-15	-	-
>15	10	350
<i>Abdomen</i>		
0-1	4	110
1-5	5	170
5-10	6	220
10-15	-	-
>15	12	380

SP100.2 - Canada's Computed Tomography (CT) Survey: Overview and Moving Toward Establishment of DRLs

Author(s): Graeme M. Wardlaw, Narine Martel
 Consumer And Clinical Radiation Protection Bureau, Health Canada, Ottawa/ON/CANADA

Increasing numbers of Computed Tomography (CT) scanners, examinations and CT's relatively higher patient dose (compared to planar x-ray) have resulted in increased focus on the modality, both in Canada and world-wide. The key pillars of safe imaging, justification and optimization, are becoming especially important to follow. It follows that as CT use increases; protocol optimization (reduction of patient dose while maintaining necessary image quality) is an ever crucial part in reducing patient dose. A widely endorsed and adopted method is the establishment of diagnostic reference levels (DRLs) – typically accepted as the 75th percentile of CTDIvol and/or DLP distributions for a given patient exam type/indication – which help identify protocols that may benefit from further investigation and any necessary dose reduction initiatives.

The establishment of DRLs requires a significant and representative pool of scanning practice data – Canada's National CT Survey collected data from 381 CT units across the country via distributed survey booklets (1 per CT unit) divided into four (4) sections: General CT information (e.g. Vendor/Model), Routine Protocols (as available), Individual Patient data (as applied) and limited CTDIvol measurements. The resultant electronic database includes a large cross-section of general vendor/model data, 2896 routine protocol samples (3494 sequences), 18 985 individual (actual) patient exam samples (24 280 sequences) and some CTDIvol measurements.

Table1: Common CT protocols (anatomical region) polled and clinical indications (not exhaustive) – Adults ≥ 19 yrs. and 70±20 kg, Pediatric ≤ 13 yrs. and < 50 kg.	
EXAM TYPE/ANATOMICAL REGION	CLINICAL INDICATION
Routine Head [Adult]	Headache, Cerebrovascular Accident (CVA), or Transient Ischemic Attack (TIA)
Chest [Adult]	Primary cancer, known/suspected metastasis or lung nodule follow-up
Abdomen, Pelvis [Adult]	Primary/metastatic work-up or abscess
Chest, Abdomen, Pelvis [Adult]	Lymphoma staging, follow-up or Trauma
Head [Pediatric]	Trauma, including non-accidental injury
Chest [Pediatric]	Detection of malignancy, Trauma
Abdomen [Pediatric]	Detection of malignancy, Trauma

The national survey database covers seven (7) common exam types (Table 1) and is a significant step toward establishment of national DRLs which will help support protocol optimization efforts. Of course, prior to calculation of any reference levels, applied data quality assurance is essential. In our experience, key issues had to be addressed: (i) booklet, patient and sequence numbering mistakes were vetted by an iterative algorithm to verify their accuracy and association (ii) CT vendor/model names were inconsistent, thus a standard convention was applied to facilitate future analysis (iii) incomplete patient mass, potentially limited DRL sample sizes. Implementation of iterative, logical algorithms allowed AP and LAT measurements to act as a surrogate, increasing representative sample numbers (iv) Other, incomplete exam descriptors (contrast/non, modulated/fixed etc.) presented potential issues, but similar iterative, logic algorithms were also applied to help “complete” samples. E.g. string based search/flag clarification.

Ultimately, the large national sample will provide DRLs, based upon dose metrics for 7 common CT examinations, supporting local optimization efforts and radiation protection of patients across Canada.

SP100.3 - Review UAE Dental Radiology Dosimetry Results for National DRLs Establishment

Author(s): Fatima S. Al Kaabi¹, Jamila S. Alsuwaidi², Jacek Janaczek¹, Alfán S. Al Ameri³, Sara M. Booz³, Wadha M. Alshamsi⁴
¹Medical Physics Department, Tawam Hospital, Abu Dhabi Health Services (SEHA), Al Ain/UNITED ARAB EMIRATES, ²Department Of Medical Education, Dubai Health Authority (DHA), Dubai/UNITED ARAB EMIRATES, ³Clinical Imaging Department, Mafraq Hospital, Abu Dhabi Health Services (SEHA), Abu Dhabi/UNITED ARAB EMIRATES, ⁴Radiology Department, Al Ain Hospital, Abu Dhabi Health Services (SEHA), Al Ain/UNITED ARAB EMIRATES

Establishment of the Diagnostic Reference Levels (DRLs) is required and essential for all radiology procedures including Dental Radiology. The objective of this study is to investigate pediatric and adult doses in different Dental Radiology modalities. It is also part of technical projects structured by the International Atomic Energy Agency (IAEA) to evaluate and monitor patient radiation doses. In UAE dental centers, 85% of dental radiology units in operation are digital systems. Total number of dental units involved in this survey is 122 Intra-Oral dental units and 16 Panoramic (OPG) dental units.

All of the dental radiology units evaluated in this survey are digital. For Intra-Oral units measurements, Multi-O-Meter electronic dosimeters are used. Quality control tests are applied for all dental units involved in this study. Multi-O-Meter (Dental Unfors) and CT Cylindrical Ionization Chamber are used for OPG measurements. Molar examination which is the longest exposure time used in dental procedures is selected. Patient Entrance Dose, HVL, Exposure time and kVp are measured for adult and pediatric. DRLs in this review study were based on the average and 3rd Quartile dose values. The 3rd Quartile of patient entrance doses of intra oral dental were 0.880 mGy and 0.704 mGy for adult and pediatric, respectively. For OPG, the 3rd Quartile doses were 5.09 mGy and 3.49 mGy for adult and pediatric, respectively.

The results of this review study are considered as initial UAE DRLs. These indicate that the dose level within the UAE are comparable to those published in the literature. It is required to expand our study to include further study for Cone Beam Dental CT. The study is in progress for further dose evaluation for digital intraoral and OPG units within the UAE.

SP100.4 - Should restrictions on the patients' behavior during the radiopharmaceuticals incorporation and after 99mTc bone scans be imposed?

Author(s): Josep M. Martí-Climent¹, Verónica Morán¹, Elena Prieto¹, Berta García-García², Lidia Sancho², Benigno Barbés¹, José A. Richter²
¹Radiofísica Y Protección Radiológica, Clínica Universidad de Navarra, Pamplona/SPAIN, ²Nuclear Medicine, Clínica Universidad de Navarra, Pamplona/SPAIN

The dose received by members of the public due to Nuclear Medicine patients is of great interest. However, little information is available on the radiation dose produced by said patients during the input of radiopharmaceuticals in diagnostic procedures. We have evaluated and compared the amount of dose produced by the patient during the radiopharmaceutical incorporation and after the diagnostic procedure.

Methods

After undergoing ^{99m}Tc -HDP bone examinations, 143 patients were studied. Dose rates [$\text{H}^*(10)$] were measured from the mid thorax after radiopharmaceutical injection and after bone scan with a Geiger dose-meter at 0.1, 0.5, and 1.0 m. A number of different scenarios were carried out during absorption period and after leaving the Department of Nuclear Medicine. A dose of 1 mSv/year was used upon which restrictions should be imposed. The results were evaluated using the 95th percentile.

Results

The injected activity [median (min-max)] was 744 (370-844) MBq while absorption time and time for imaging procedure were 160 (80-280) and 55 (25-117) minutes.

The median dose rates measured at the three distances were 112.4, 29.8 and 11.5 $\mu\text{Sv/h}$ after the ^{99m}Tc -HDP administration and 29.9, 9.8 and 4.3 $\mu\text{Sv/h}$ after the image scan.

The absorbed doses were:

Absorbed dose (μSv) (95th percentile) due to patient contact in different scenarios during the ^{99m}Tc -HDP incorporation			
Scenario		Delay 0 h	Delay 1 h
The escort	Incorporation time (0,5m)	108.2	---
Attending physician	5min @1m + 10min @0.5m + 5 min @0.1m	21.0	18.7
Coffee shop	30min @0.1m	82.5	73.5
Restaurant	1h @1.0m	39.5	35.2

Absorbed dose (μSv) (95th percentile) for different scenarios and delay of initial contact after leaving the hospital					
Scenario		Delay 0 h	Delay 1 h	Delay 2 h	Delay 3h
Public transport	1h @0.1 m	52.7	47.0	41.8	37.3
Private transport	1h @1.0m	7.9	7.5	6.3	5.6
Work place	8h @1.0m	---	38.9	34.7	30.9
Attending physician	5min @1m)+ 10min @0.5m + 5 min @0.1m	7.6	6.8	6.0	5.4
Coffee shop	30min @0.1m	27.1	24.2	21.5	19.1
Restaurant	1h @1.0m	15.0	13.4	11.9	10.6
Spouse/partner	6h @1m + 8h @0.1m	169.9	150.9	134.5	119.8

During an incorporation interval of 4 hours, the absorbed dose to which a subject could be exposed to due to contact with and injected patient in the waiting room would be 543, 134, and 52 μSv at a distance of 0.1, 0.5, and 1.0 m.

Conclusions

The people with higher doses are those who are in close contact with the patient (the escort and the spouse/partner). Nevertheless, the imposition of restrictions is not needed. However depending on

the workload of the physicians, some restrictions might be required. Furthermore, the dose received in the waiting room from an injected patient is comparable to a bone scan.

SP101 - Stimulation and Monitoring

TRACK 11: NEUROENGINEERING, NEURAL SYSTEMS

SP101.1 - Biological Targets of Seizure Therapy in Major Depressive Disorder using EEG Microstate Analysis

Author(s): Sravya Atluri¹, Willy Wong¹, Daniel M. Blumberger², Zafiris J. Daskalakis², Faranak Farzan²

¹Institute Of Biomaterials And Biomedical Engineering, University of Toronto, Toronto/CANADA, ²Centre for Addiction and Mental Health, Toronto/CANADA

Introduction: Understanding the exact mechanism of action of electroconvulsive therapy (ECT) can support the optimization of alternative treatments such as magnetic seizure therapy (MST) towards high efficacy and less side effects. Recent evidence suggests that major depressive disorder (MDD) may be associated with impaired brain functional connectivity and that ECT may achieve high efficacy in treatment-resistant MDD by normalizing abnormal neural connectivity. Resting-state EEG microstate analysis is one promising method that classifies global neural activity into discrete and short periods (80-120ms) of quasi-stable functional brain topographic maps (known as microstates) that change over time to represent dynamic states of global functional connectivity. **Methods:** For this study, pre- and post-treatment 60-channel resting state EEG data of 14 MDD patients (7 responders and 7 non-responders) receiving ECT and 13 MDD patients (3 responders and 10 non-responders) receiving MST were obtained from the Temerty Centre at the Centre for Addiction and Mental Health. The criterion for treatment response was a minimum of 50% improvement in the Hamilton Depression Rating Scale (HAM-D) score. Three main analyses were conducted with the data: (a) Spectral analysis was performed to determine whether previous findings of ECT-induced EEG slowing could be replicated. (b) Microstate analysis was performed to assess seizure therapy-related changes in the dynamic states of global functional connectivity. Four microstate classes were identified and four features were calculated for each class: (i) frequency of occurrence, (ii) transition time between each class, (iii) average duration and (iv) coverage time (fraction of total time covered by a class). (c) Finally, correlation analyses were performed to examine whether baseline microstate and power features could predict response (change in HAM-D score) to seizure therapy. **Results:** (a) Similar to previous findings, frontal delta (0.5-3.5Hz) and midline theta (4-7Hz) were found to be significantly larger in ECT responders than non-responders. However, this effect was not observed in MST treatment. (b) Also following ECT treatment (but not MST), the frequency of appearance of each microstate class was significantly lower in responders than non-responders ($p = 0.03$). The transition time between two consecutive microstate classes increased in responders but did not significantly change in non-responders ($p = 0.04$). The average duration of all four microstate classes were significantly longer for both responders and non-responders ($p = 0.001$). A change in HAM-D score was associated with an increased coverage time of class C ($r = 0.56$, $p = 0.03$) and a decreased coverage time of class A ($r = -0.62$, $p = 0.02$). (c) Lastly, the frequency of microstate class C pre-treatment was correlated with reduced response to ECT ($r = -0.61$, $p = 0.02$) and an increased response to MST ($r = 0.54$, $p = 0.05$). **Conclusion:** Preliminary results suggest that microstate features from resting-state EEG data may provide new and predictive information about the effect of seizure therapy in MDD and should be further explored with larger datasets.

SP101.2 - Magnetic Seizure Therapy for Treatment Resistant Depression: Insights from TMS-EEG Measures

Author(s): Yinming Sun¹, Faranak Farzan², Daniel M. Blumberger², Willy Wong¹, Zafiris J. Daskalakis²

¹Ibbme, University of Toronto, Toronto/ON/CANADA, ²Psychiatry, University of Toronto, Toronto/ON/CANADA

Magnetic seizure therapy (MST) is a potential therapeutic option for treatment resistant depression (TRD) that has shown comparable efficacy and less side effects relative to electroconvulsive therapy. Since cortical inhibition is abnormal in TRD patients, measures of inhibition from combined transcranial magnetic stimulation and EEG (TMS-EEG) may further the understanding of MST treatment and provide predictors of its treatment response. Thirty-three TRD patients were recruited in this TMS-EEG study. Before a course of MST treatment, responses from single pulse TMS over the motor cortex and dorsolateral prefrontal cortex (DLPFC) were recorded using EEG. The peak value of the TMS evoked potential near 100 ms (i.e. N100) was computed for each patient and correlated with changes in clinical measures of depression (Hamilton Depression Rating Scale, HDRS-24) and suicidality (Scale of Suicidal Ideation, SSI) collected before and after treatment. For DLPFC stimulation, the N100 value over the frontal electrodes was significantly correlated with a decrease in the HDRS-24 (max at F2, $R = -0.51$, $p = 0.006$) and SSI (max at F6, $R = -0.61$, $p = 0.001$) values. Moreover, when patients were grouped into responders and non-responders based on SSI change (responder: 50% or more decrease from baseline), the N100 value can predict the label with 80% sensitivity and 89% specificity. These results were not found for motor cortex stimulation. Correlation and classification results suggest that frontal N100 values resulting from TMS stimulation of the DLPFC can be a potential predictor of clinical response to MST treatment for resistant depression.

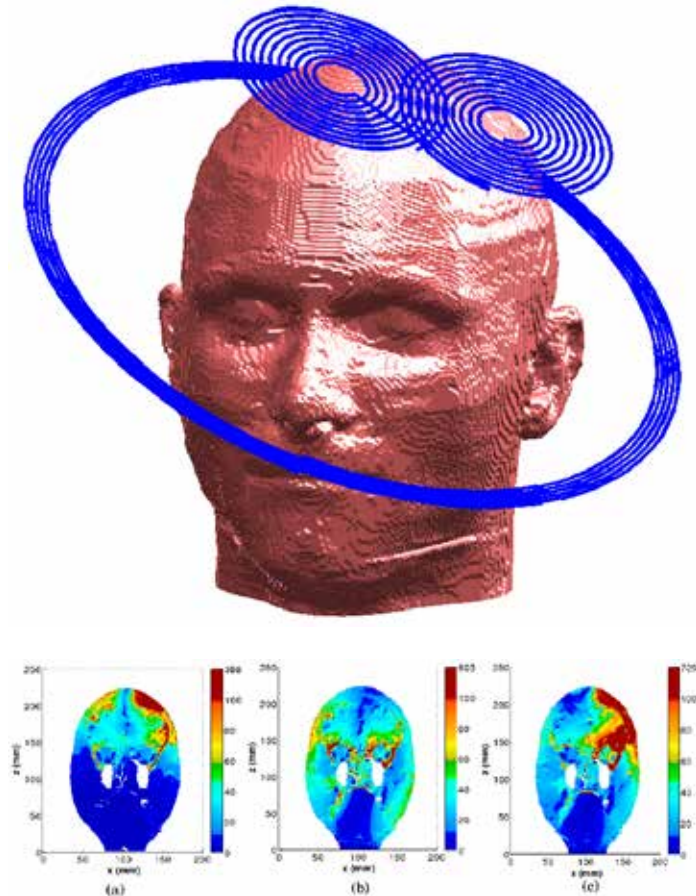
SP101.3 - Deep Transcranial Magnetic Stimulation Using Figure-of-Eight and Halo Coils

Author(s): Mai Lu¹, Shoogo Ueno²

¹Key Lab. Of Opt-electronic Technology And Intelligent Control Of Ministry Of Education, Lanzhou Jiaotong University, Lanzhou/CHINA, ²Department Of Applied Quantum Physics, Graduate School Of Engineering, Kyushu University, Fukuoka/JAPAN

Transcranial magnetic stimulation (TMS) is a technique for noninvasive stimulation of the human brain, which has become a major tool in brain research and, potentially, a promising treatment for various neuro-behavioral disorders. Recently, interests in stimulating deeper cortical, subcortical and limbic areas have arisen and have become an active research topic in TMS, because several studies show that activation of deeper prefrontal and limbic regions may increase the antidepressant effect. The Halo coil, a large circular coil being placed around the head was developed for deep transcranial magnetic stimulation (dTMS). It was shown that the Halo coil working with a typical round coil at the top of the head can increase the fields at depth in the brain. The present study was to study the field characteristics of a figure-of-eight coil (Fo8) which was placed at the left dorsolateral prefrontal cortex (DLPFC) working with a Halo coil which was parallelly placed with that of Fo8 coil (Fo8-Halo assembly) as shown in Fig. 1. The same pulse currents with amplitude of $I=5$ kA and working frequency 2381 Hz was fed into each of the coils. A 3D realistic human head model with 1 mm resolution has been employed in this study. We have calculated the magnetic fields, electric fields and current density in head tissues by using impedance method. Figs. 2(a)-(c) show the variation of induced electric field in the cross section of the head model at 80 mm slice (coronal) for Fo8, Halo and Fo8-Halo assembly coils, respectively. It was observed that the field intensity in deep brain regions have been improved by Fo8-Halo assembly coil. Results suggest that the conventional Fo8 coil can be applied for dTMS by working with a

Halo-coil for DLPPFC stimulation.



SP101.4 - Optogenetic Stimulation and Wireless Cortical Recording in Modulating Motor Plasticity and Performance of Free-Moving Rat

Author(s): Chun-Wei Wu, Cho-Han Hsieh, Jia-Jin J. Chen
Biomedical Engineering, National Cheng Kung University, Tainan/TAIWAN

Cortical theta burst stimulation (TBS) could modulate motor plasticity via long-term potentiation/depression (LTP/LTD)-like mechanisms and enhance motor performance, which makes TBS a potential non-invasive therapy for motor deficit diseases such as Parkinson's disease (PD). In our previous rodent study, we had demonstrated that long-term cortical electrical stimulation (CES)-TBS protocols were capable to regulate motor-evoked potentials (MEPs) and enhance motor performance in chronic PD rats. However, the immediate effect of CES-TBS on motor performance in awake, freely moving rat was constrained by wired electrode and stimulators. Since CES excited all types of neurons surrounding the electrode in cortex, it is difficult to differentiate the effect of TBS on specific neural circuit that responses to motor plasticity and performance. It is also known that LTP/LTD occurred dominantly at glutamatergic synapse. The aim of this study is to apply the cell type-specific optogenetic stimulation and wireless recording of local field potentials (LFPs) to reveal the functional roles of glutamatergic neuron in motor plasticity of freely moving rat.

CaMKII α promoter driven channelrhodopsin-2 (CaMKII α -ChR2) was expressed in glutamatergic pyramidal neuron in primary motor cortex (M1). Optogenetic stimulation was achieved using blue laser guided by optical fiber, which was connected by a rotary joint

to allow freely rotation. Then the fiber was connected to optical cannula implanted on skull. Optical cannula was homemade of a stainless tube containing a short segment of optical fiber inside. Both ends of the fiber were polished to minimize optical scattering when Laser was emitted into cortex. Stainless tube of the optical cannula was functioned as cerebral electrode to collect electrophysiological signal. Brain biopotentials were then amplified, band-pass filtered and converted to a frequency modulated radio-frequency (RF) signal sent by a small and light (2.7 g) wireless transmitter headstage connected to stainless tube. RF signals were transmitted to the host unit and was demodulated into analog signal and sampled by DAQ card. Optogenetic evoked potentials were analyzed and displayed using average calculation during and after optogenetic TBS treatment.

Our results showed that the local field potentials were recorded in high fidelity and responded well to the optical stimulation. The averaged MEPs amplitude were increased after optogenetic TBS treatment. The observations indicate that motor plasticity was modulated resulting from TBS on glutamatergic neurons in M1. However, there was no significant change in cortical excitability revealed from LFPs. In summary, our results suggested that LTP/LTD-like effects induced by cortical TBS treatment might be located at glutamatergic projections downstream of M1. The modulation of motor plasticity using cell type-specific optogenetic TBS scheme in M1 could be an efficient therapy scheme for neural disorders like PD via targeting specific neural circuit. Ongoing project is working toward the observation of animal behavior during and after optogenetic-TBS treatment of free-moving rat.

SP101.5 - Identification of calf muscles response to functional electrical stimulation as linear models

Author(s): Hossein Rouhani¹, Michael Same², Ya Q. Li², Kei Masani², Milos R. Popovic²

¹Lyndhurst Centre, Toronto Rehabilitation Institute - University Health Network, Toronto/CANADA, ²Institute Of Biomaterials And Biomedical Engineering, University of Toronto, Toronto/CANADA

Functional electrical stimulation (FES) is used to artificially induce contractions in paralyzed muscles as neuroprosthesis to substitute lost motor functions, in individuals with spinal cord injury or other neuromuscular impairments. The dynamic response of muscles to FES is an integral component of closed-loop controlled neuroprostheses such as neuroprostheses for standing balance. This study aimed at identifying the dynamic response of ankle muscles to FES in a standing posture with FES as an input and the exerted isometric ankle torque as an output using both first-order and critically-damped second-order models.

Thirteen healthy subjects participated in the experiment. Each subject stood on a standing frame with his/her extended knee and hip mechanically locked. The ankle plantarflexors and dorsiflexors were separately stimulated bilaterally through surface electrodes using a programmable functional electrical stimulator (Compex Motion II, Compex SA, CH). The subject's feet were fixed firmly to the foot-plates connected to a torque transducer (TS11-200, Durham Instruments, DE) that recorded the exerted isometric ankle torque. The stimulus waveform was rectangular with pulse frequency of 20Hz and pulse duration of 0.3msec. The pulse amplitude was modulated on sinusoids between 20mA and 60mA at frequencies of 0.07, 0.15, 0.3, 0.75, and 1.2Hz. The sinusoids of FES pulse amplitude and fitted to the generated ankle torque curve were considered as input and output, respectively. A Bode diagram was plotted based on the five obtained amplitude gains and phase lags between the input and output. The first-order and critically-damped second-order linear models were fitted to the diagrams and their parameters were estimated for each subject.

Correlation coefficient and RMS error between the experimental and fitted data were calculated to evaluate the fitting. Two-way ANOVA (factor1: first-order or second-order models, factor2: plantarflexors or dorsiflexors) revealed that both models were not significantly different in correlation coefficient and RMS error for both amplitude gain and phase lag ($p>0.6$) (Table 1). The inter-subject variability was expressed as CV ($=100 \times SD/mean$). The CV of the time constants obtained by the second-order model for plantarflexors (18.1%) was significantly smaller than the CV of the time constants obtained by the first-order model (79.9%) (F-test, $p<0.001$). Therefore, the time constant obtained by the critically-damped second-order model was more consistent among subjects for plantarflexors. This finding should be considered in the design of closed-loop controlled neuroprostheses when immediate torque generation is expected. In the future, the physiological interpretation and nonlinear components of this modeling should be further investigated.

Table 1. Results are presented as mean±SD (standard deviation) over the 13 subjects.		Plantar-flexors		Dorsi-flexors	
		1st order	2nd order	1st order	2nd order
		Correlation coefficient for fitting	Amplitude gain	0.92±0.14	0.90±0.19
Correlation coefficient for fitting	Phase lag	0.88±0.18	0.89±0.30	0.75±0.38	0.83±0.32
RMS error for fitting	Amplitude gain	0.21±0.29	0.20±0.21	0.14±0.14	0.13±0.15
RMS error for fitting	Phase lag	14.6±18.8	16.4±22.7	14.6±16.7	15.3±16.6
Estimated zero-frequency gain		2.90±1.04	2.75±0.98	0.67±0.36	0.64±0.35
Estimated time constant		0.26±0.21	0.11±0.02	0.19±0.11	0.09±0.03

is similar and accomplished. On the platform offered here, study on specific individual subject would be easy and practicable. Deep structures will be produced vectorial in the future work.

SP101.7 - Study on electric field in real head model induced by H-coil

Author(s): Huanhuan Cheng, Chen Zhao, Zhipeng Liu, Tao Yin
Institute Of Biomedical Engineering, Chinese Academy of Medical Sciences, Tianjin/CHINA

To study the distribution of induced electric field in human brain under the H-coil and to explore the deep character of H-coil, this paper builds a real head model with limbic system inside, and an H-coil model close to the real head model. The electric field distribution in scalp and limbic system induced by H-coil was calculated via finite element method and the results were compared with those of figure-of-eight coil. It is found that the deep field performance of H-coil was much better than figure-of-eight coil. Although the induced electric field by H-coil is not focusing on scalp, it can concentrate deeply on anterior cingulate cortex, which is an important part of limbic system. It provides a valid evidence for H-coil to stimulate deep brain structures.

SP101.6 - Establishment of Real Human Head Conductivity Model with Ventricular Structure used in TMS Simulation Study

Author(s): Chen Zhao, Huanhuan Cheng, Zhipeng Liu, Tao Yin
Institute Of Biomedical Engineering, Chinese Academy of Medical Sciences, Tianjin/CHINA

For accurate simulation studies on distribution of electromagnetic field induced by Tran-cranial Magnetic Stimulation, a real human head conductivity model with deep cerebral structure was reconstructed from MRI raw data, by using of MIMICS and ANSYS. This model reflects geometric structural information of Scalp, Skull, Cerebrospinal Fluid (CSF), Gray Matter, White Matter, Cerebellum, Ventricle and Eyeballs. The ventricular structure has relatively higher conductivity, whose effect on induced field could not be neglected. This paper mainly introduces the method to establish the ventricle part of the entire head model, which is used for ANSYS low-frequency magnetic simulation, while the way to generate other parts

SP102 - Clinical Information Systems and Decision Support

TRACK 13: INFORMATICS IN HEALTH CARE and PUBLIC HEALTH

SP102.1 - A Multi-Attribute Decision Theory Approach to Radiation Dose De-escalation in Oropharyngeal Cancer

Author(s): Wade P. Smith¹, Ahmad Aljadaan², John Gennari², Upen-dra Parvathaneni¹, Mark Phillips¹

¹Radiation Oncology, University of Washington Medical Center, Seattle/WA/UNITED STATES OF AMERICA, ²Biomedical Informatics And Medical Education, University of Washington, Seattle/WA/UNITED STATES OF AMERICA

BACKGROUND:

Debilitating late normal tissue toxicities such as xerostomia and dysphagia have long been an accepted part of radiotherapy treatment for oropharyngeal cancer. In addition to the physiological changes, both of these health states can induce serious social and emotional burdens. Recently, it has been found that HPV+ populations of oropharyngeal cancer patients survive longer after therapy. Radiation dose de-escalation is being explored as a method to reduce the toxicity for these patients [1].

De-escalation of therapy will result in cure and toxicity rates which are different from the current standard-of-care. This balance between the two is explored implicitly by clinical trials which are explicitly examining de-escalation of therapy. The currently accepted equilibrium did not evolve through a quantifiable methodology, nor do the current trials address the issue of determining the optimal operating point.

Methods:

We developed an outcome model for oropharyngeal cancer which combines cure rates and late toxicity effects into a single quality of life metric. We chose an Influence Diagram to model the decision process because it can incorporate probabilities from previous clinical trials, retrospective analysis, and the beliefs of experienced physicians. We used a Markov model to calculate Quality-Adjusted Life Years (QALYs) for outcomes.

We performed sensitivity analysis to determine the robustness of the model predictions to model parameters, see Fig. 1. In particular, the sensitivity of individual patient preferences was explored in the event that a single standard-of-care approach cannot be taken for this disease site.

RESULTS AND DISCUSSION:

In order to change clinical practice the QALYs for de-escalated therapy must be higher than for standard therapy. We delineated the outcomes of the trials which would and those which would not change clinical practice, within the boundaries of our sensitivity analysis. This type of model has broad applicability to other disease sites in radiotherapy and to clinical trials in medicine in general. Developing the clinical decision model up front could help design a trial that can provide the necessary information for changes in clinical practice.

References

[1] Masterson L, Moualed D, Liu W, et al., De-escalation treatment protocols for human papillomavirus-associated oropharyngeal

squamous cell carcinoma: A systematic review and meta-analysis of current clinical trials. *Eur J Cancer* 2014;50:2646-48.

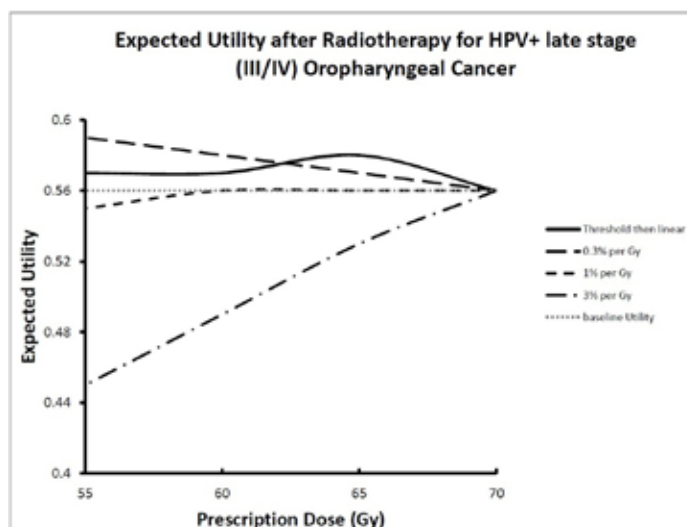


Fig 1. Expected Utility for four possible models for the variation of disease control rate as the prescription dose is reduced. The utility decreases as the disease control rates fall, and increases as toxicity rates fall.

SP102.2 - Large-scale data of basic patient and treatment characteristics significantly improve predictions for post-radiotherapy dyspnea

Author(s): Timo M. Deist¹, Arthur T.C. Jochems¹, Cary Oberije¹, Andre Dekker¹, Katrien Vandecasteele², Yolande Lievens², Johan Van Soest³, Philippe Lambin¹

¹Department Of Radiation Oncology (maastro Clinic), GROW - School for Oncology and Developmental Biology, Maastricht University Medical Center, Maastricht/NETHERLANDS, ²Radiation Oncology Department, University Hospital Ghent, Ghent/BELGIUM, ³Department Of Radiation Oncology (maastro), Maastricht University Medical Centre+, Maastricht/NETHERLANDS

Purpose

Dyspnea is a known side effect of lung radiotherapy. Personalized medicine approaches require reliable models predicting the patient-specific risk. As the number of events is limited, large datasets are needed for model building and these can be obtained by using data from routine clinical practice. This approach limits data to basic patient and treatment features with an increased likelihood for incompleteness and errors. We show that such models for post-treatment dyspnea enhance predictions even if solely based on basic data from clinical practice.

Materials/Methods

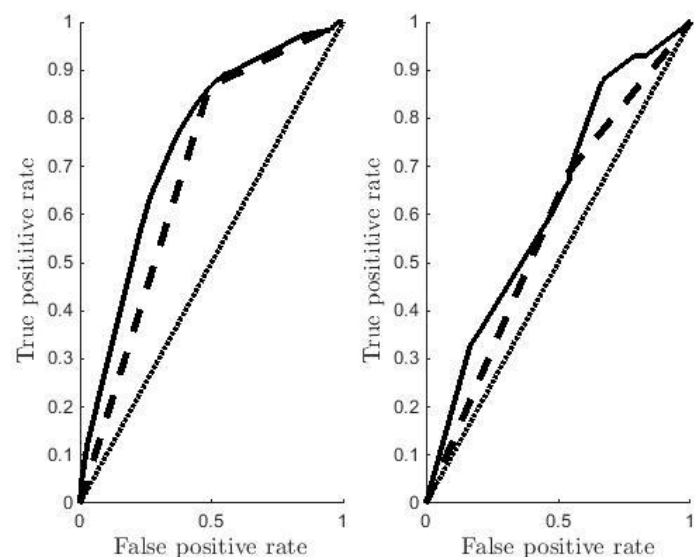
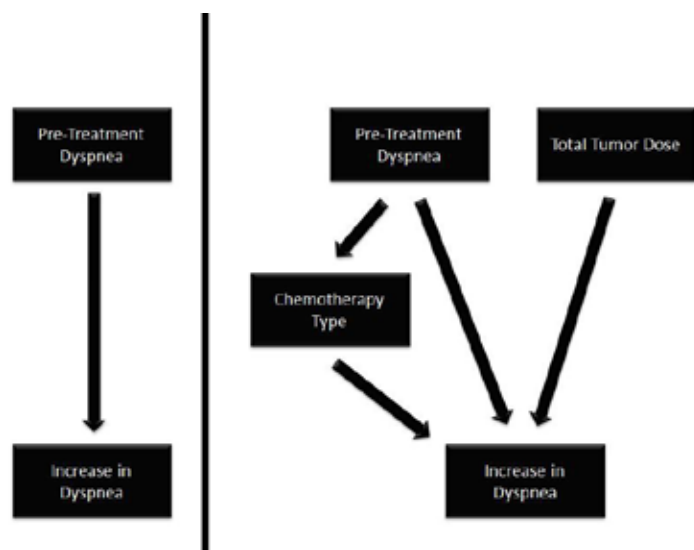
Clinical data were collected retrospectively (2008-2014) from MAASTRO Clinic, the Netherlands, consisting of dyspnea levels before and after radiotherapy, chemotherapy type, and total tumor dose during therapy. 1031 lung cancer patients with a pre-treatment dyspnea score below 2 (according to CTCv.3 or 4) were selected to ensure non-iatrogenic dyspnea did not bias the results. A validation set of 82 patients was provided by Ghent University Hospital, Belgium. A Bayesian Network was learned to predict an increase in the dyspnea score given pre-treatment dyspnea, chemotherapy type, and total planned radiation dose. For comparison, another estimator was constructed solely based on pre-treatment dyspnea which is known to carry high predictive value.

Results

The enhanced model and the estimation only using pre-treatment dyspnea have been cross-validated using 10 folds. The enhanced model outperforms the univariate estimation with an average AUC of 0.7319 versus 0.6852. The additional features yield a significantly different AUC (p-value<0.01, Wilcoxon signed-rank test). These findings are externally validated with the enhanced model increasing the AUC from 0.5740 to 0.6236.

Conclusions

Improvements in the prediction of worsened dyspnea after lung radiotherapy are achieved using only clinical patient and treatment data. This example provides additional evidence for the potential of prediction models based on clinical data to improve patient care and furthering the goal of personalized medicine.



SP102.3 - Substituting human MRI-observed tumor length with automated tumor length calculations for prediction model application

Author(s): Johan Van Soest¹, Jeroen Buijsen¹, Philippe Lambin¹, Vincenzo Valentini², Andre Dekker¹

¹Department Of Radiation Oncology (maastro), Maastricht University Medical Centre+, Maastricht/NETHERLANDS, ²Department Of Radiotherapy, Università Cattolica del Sacro Cuore, Rome/ITALY

Introduction

The development and use of prediction models in radiation oncology is emerging, especially in the context of individualized medicine. Although prediction models can indicate clinical outcomes, automated execution is a problem when information is only available as unstructured text (or missing). For example, van Stiphout et al. (PMID: 21176986) developed 3 prediction models to predict a pathologic complete response (pCR) in rectal cancer patients. In two out of three prediction models, tumor length (determined by radiologists on MRI scans) is used as a model variable, which needs to be manually extracted from free-text radiological reports. In this study, we attempted to find another measurement method for tumor size in already available data, and to measure its influence when applying it to the pre-treatment (clinical) pCR prediction model as a substitute for tumor length measured by a radiologist on MRI.

Methods

We used a dataset of 71 patients having a pre-treatment PET-CT scan and clinical radiotherapy gross tumor volume (cGTV) delineations available. For 41 of these patients the tumor length observed by a radiologist on an MRI was available. We used either this cGTV directly or a semi-automatic PET-threshold based GTV (tGTV) using 40% of the maximum of the standardized uptake value on the PET-CT scan. For both cGTV and tGTV, we calculated the volume, maximum Euclidian and axial distances (transversal perspective). Afterwards, we determined the correlation between MRI-observed tumor length and the computed metrics; using univariate regression analysis. Finally, we substituted the tumor length for the computed metrics in the clinical prediction model, and calculated the area under the receiver operating curve (AUC).

Results

Results of the correlation and substitution are shown in the table below. Based on this table, there is a significant correlation for the Z-axis, determined by a regression coefficient closest to 1 for both cGTV and tGTV. For the cGTV and tGTV, substituting the tumor length along the Z-axis resulted in a reasonable performance comparable to the original model (AUC 0.69 and 0.70), and resulted in a better performance for tGTV volume (AUC 0.78).

N=71	Correlation with MRI tumor length (N=41) Regression Coefficient (p-value)	Model substitution AUC
cGTV Euclidean distance	0.58 (1.75*10 ⁻⁴)	0.57
cGTV absolute max X-axis	0.36 (4.96*10 ⁻²)	0.57
cGTV absolute max Y-axis	-0.06 (6.91*10 ⁻¹)	0.67
cGTV absolute max Z-axis	1.01 (1.55*10 ⁻⁸)	0.69
cGTV volume	0.03 (3.48*10 ⁻⁴)	0.63
tGTV Euclidean distance	0.79 (1.03*10 ⁻⁴)	0.72
tGTV absolute max X-axis	1.23 (1.86*10 ⁻⁴)	0.71
tGTV absolute max Y-axis	0.59 (4.67*10 ⁻²)	0.69
tGTV absolute max Z-axis	0.92 (2.68*10 ⁻⁶)	0.70
tGTV volume	0.09 (2.66*10 ⁻⁴)	0.78

Conclusion

We have shown a correlation between the MRI-based tumor length and GTV-based distances; specifically for the Euclidian, Z-axis distance and volume. In general, the semi-automatic tGTV dimensions are better for substitution of the MRI-observed tumor length. Although the results are promising, this dataset is too small (N=71; positive events: 14) to make final conclusions and requires an external validation.

SP102.4 - An Artifact Detection Framework for Clinical Decision Support Systems

Author(s): Shermeen Nizami¹, James R. Green¹, Carolyn Mcgregor²
¹Systems And Computer Engineering, Carleton University, Ottawa/CANADA, ²University of Ontario Institute of Technology, Oshawa/CANADA

This research develops a standardized framework to integrate artifact detection (AD) in computerized Clinical Decision Support Systems (CDSS). Review of the state of the art has revealed a number of limitations currently preventing the widespread implementation of AD algorithms within CDSS. To address those limitations, this paper develops a novel component-based AD framework for integration in CDSS. The novelty of this research is the development of a Common Reference Model (CRM) with standard definitions for component interfaces. These definitions include common physiologic data attributes of: (1) type; (2) frequency; (3) length; and (4) Signal Quality Indicator.

SP102.5 - Design and implementation of an IT management system for a Medical Physics Department activity workflows.

Author(s): Leonello Servoli¹, Massimiliano Paolucci¹, Bruno Chiccucci¹, Roberto Di Lorenzo¹, Mariano Gattafoni², Mario Tiburzi², Alessandro Carnevale²
¹Istituto Nazionale di Fisica Nucleare, Sezione Perugia/ITALY, ²BTREE Srl, Foligno/ITALY

The everyday activities of a Medical Physics Department, either in a single Hospital or in a network of Hospital and Medical Institutions, are very complex and the management of the data flow coming from the different tasks, of the scheduled quality controls and maintenance

tasks is difficult and time consuming. There are currently no commercial products that tackle in a satisfactory manner the problem.

The aim of this work is to describe the design, implementation and operation of an Enterprise Resource Planning (ERP) and a Database Management System (DBMS) focused on managing the most important workflows of a Medical Physics Department.

The system requirements are based on the application of Italian national radiation protection and quality assurance regulations, guidelines and operating procedures and on the inputs of the Medical Physics Service of the AUSL Umbria 2 (Italy) comprising 8 Hospitals. The systems has been using a 3-tiers architecture, implemented via incremental releases: presentation, middleware and data level with a presentation layer using a user friendly Graphical User Interface (GUI).

The system prototype is capable of recording informations related to all the medical instruments and diagnostic equipments, their relevant characteristics, status and history. Is also capable of recording all the data coming from the quality controls and maintenance activities, digest them and produce the relevant legal and administrative reports.

Furthermore it has a dedicated section for Occupational Exposure to Ionizing Radiation, where several parts have been implemented, as radiological surveillance of working environment and individual worker, quality assurance program in diagnostic radiology.

The prototype system has been deployed by the AUSL Umbria 2 Medical Physics Department and used from 2013.

The most relevant results are the increased levels of data security, the optimization of scheduled tasks, implying a more efficient use of manpower, the homogeneity of the approach to the management of many different activities. Furthermore the incremental release model using a 3-tier architecture allows the development of a flexible as well as robust solution.

Therefore it is a system with a high degree of innovation, that could bring significant benefits to the work of medical physics staff and a model for future developments.

SP102.6 - Differential Feature Space in Mean Shift Clustering for Automated Melanoma Assessment

Author(s): Javier Eslava, Christopher Druzgalski
 Electrical Engineering, California State University Long Beach, Long Beach/CA/UNITED STATES OF AMERICA

Malignant melanoma is one of the most dangerous forms of skin cancer. However, an important aspect of this type of cancer is that, if detected early, it can be successfully treated. This characteristic makes automated early melanoma detection systems clinically desirable. Therefore, a novel technique for melanoma segmentation based in Mean Shift clustering methods along with a complete melanoma detection system were implemented. Mean Shift main benefit over other clustering techniques is that it does not need a known number of clusters, instead, a distance function and bandwidth value are defined affecting the number of clusters that are calculated.

Conducted studies which focused on diagnostic assessment consider two implementations of the Mean Shift algorithm; one that takes the color of the image as the feature space and another that uses the color and texture information to create a two-dimensional feature space. The segmentation algorithm was used with a database of 200 images including unaltered dermatological images and illumination corrected ones in order to study the effects of two

widely used illumination correction methods in the segmentation stage.

The first illumination correction technique was developed by making use of morphological operators, specifically the morphological closing. The second illumination correction technique was the algorithm known as Retinex. Performance measurements of the Mean Shift implementations were included with further comparisons of two existing segmentation techniques; image thresholding using Otsu's method and Gradient Vector Flow (GVF) Snakes. The classification results of using two different classifiers are also demonstrated as part of the complete melanoma detection system. The first classifier was based on Support Vector Machines (SVMs). The second classifier used linear discriminant analysis with various discriminant functions: linear, quadratic and mahalanobis distances.

This approach demonstrates enhanced classification capabilities of melanoma detection which can also be extended to other dermatologic applications.

SP102.7 - Fuzzy-state machine for Triage priority classifier in emergency room

Author(s): Agustin I. Cabrera Llanos¹, María G. Ramírez-Sotelo², Emmanuel S. Sánchez Velarde², Itzamná O. Rico-Asención², Nayely R. Budar-Alemán², Alejandro A. Sotelo-De Ávila², Rodrigo Sánchez-González²

¹Bioprocesos, Unidad Profesional Interdisciplinaria de Biotecnología - IPN, Distrito Federal/MEXICO, ²Bioprocesos, Unidad Profesional Interdisciplinaria de Biotecnología, Distrito Federal/MEXICO

In this paper, a fuzzy classifier stage of a patient in the emergency room is presented. This classifier is divided into 3 stages: data entry by staff health, the evaluation provided by the software and finally the creation of a report for electronic patient file. A clinical classification system called triage give us the severity and priority of the patient, taking into consideration parameters like consciousness, blood pressure, appearance, temperature, heart rate and respiratory rate, achieving an effective prevaluation. The program is designed for adult patients aged 18 to 40 years.

SP102.8 - An Australian mining boom: development of an Australian radiotherapy datamining network for rapid learning from clinical data to support improved clinical decisions

Author(s): David Thwaites¹, Lois Holloway², Michael Bailey³, M Samir Barakat¹, Martin Carolan⁴, Geoff Delaney², Matthew Field¹, Andre Dekker¹, Tim Lustberg¹, Andrew Miller², Johan Van Soest⁵, Shalini Vinod⁶, Sean Walsh¹

¹Institute Of Medical Physics, School Of Physics, University of Sydney, Camperdown, Sydney/AUSTRALIA, ²Department Of Radiation Oncology, Liverpool & Macarthur Cancer Therapy Centres and the Ingham Institute, Liverpool/NSW/AUSTRALIA, ³Medical Physics/medical Informatics, University of Wollongong, Wollongong/AUSTRALIA, ⁴Radiation Oncology, Illawarra Cancer Care Centre, Wollongong/AUSTRALIA, ⁵Department Of Radiation Oncology (maastro), Maastricht University Medical Centre+, Maastricht/NETHERLANDS, ⁶Department Of Radiation Oncology, Liverpool & Macarthur Cancer Therapy Centres, Liverpool/NSW/AUSTRALIA

Objective: Large amounts of data are routinely collected on radiotherapy patients, which can potentially provide additional clinical evidence to inform better clinical decisions. A collaborative project has begun between the MAASTRO clinic and a pilot network of Australian cancer centres, to validate and implement MAASTRO-developed prediction models (PMs) in Australian clinical practice and assess their impact on decisions for future patient treatment. Wider objectives include developing multi-institutional rapid learning, to enable PM evolution by incorporating more centres/data, using a

distributed learning approach of transporting the model to the data, rather than data out of the centres, thereby protecting data privacy.

Methods: Two initial stand-alone pilots were conducted: one on datasets for radically-treated Stage I-IIIb non-small cell lung cancer (NSCLC) patients in the Liverpool Hospital Cancer Centre and the second on radically-treated Stage I-IV larynx patient datasets in the Illawarra Cancer Care Centre, both Pinnacle+Mosaik users. Open-source rapid learning systems, using Semantic Web based tools, were installed, supporting collection of data, from the TPS and OIS databases, relating to the patients, diseases, treatments and recorded outcomes. The MAASTRO PMs were learned (on 'training cohorts') and validated against local datasets ('clinical cohorts'). Further lung studies are currently underway in three other hospitals (Eclipse+Aria and Pinnacle+Mosaik users).

Results: For the lung patients, of 419 datasets identified meeting the PM criteria, 159 had all required data to be eligible for inclusion in the clinical cohort. Some missing data were imputed using Bayesian methods, increasing eligible datasets to 225. The larynx data were relatively complete; 109/125 datasets identified had all data parameters recorded to be eligible for inclusion. For both pilots, the MAASTRO PMs successfully predicted better and worse prognosis groups, but showing some differences to the models, which reflected differences between the Dutch and Australian patient groups and practice. For example, the PM-predicted good prognosis lung group was differentiated from a combined medium/poor prognosis group (2-year overall survival, 69% vs. 27%, $p < 0.001$) in the Australian data. Stage was less able to identify prognostic groups; most good prognosis patients in this clinical cohort having higher stage disease. For larynx, the proportion of clinical cohort patients in the predicted poor/medium/good prognosis groups were 47%/42%/11%, compared to the training cohort defined as 25%/50%/25%. Thus the larynx model could classify different clinical cohort prognosis groups, but the good prognosis group was smaller, as the clinical cohort was older and had more advanced cancers, nodal spread and non-glottic cancers than the training cohort.

Conclusion: The technical infrastructure and the basic MAAS-TRO prediction models support the prognosis prediction of lung and larynx patients in Australian clinical cohorts, showing promise for support of future personalized treatment decisions, improved treatment quality and potential practice changes. The infrastructure is being extended: for an initial distributed learning pilot between multiple NSW centres; for expansion into more NSW centres, other states and linkage to trials databases; and for model parameters to include radiomics data. Data quality for routine patients is vital when creating a rapid learning infrastructure, to maximize the information's potential.

Collaborators: V. Ahern/R. Alvandi/M. Ebert/K. Foo/D. Fraser/A. George/A. Ghose/G. Goozee/S. Greenham/P. Greer/F. Hegi/J. Johnson/N. Kadaan/T. Kron/J. Lehmann/P. Lambin/J. Ludbrook/C. Oberije/D. Stirling/S. Yau.

SP103 - Health Technology Assessment and Cost Effective Technologies for Developing Countries and Usability and Human Factors Engineering for Medical Devices and System Design: Part 2

TRACK 16: CLINICAL ENGINEERING, CLINICAL PHYSICS, AND PATIENT SAFETY

SP103.1 - Novel Medical Device Procurement Tracking

Approach

Author(s): [Gleb Donin](#), Ilya Ivlev, Silvie Jeřábková, Jakub Vacek, Peter Kneppo

Department Of Biomedical Technology, Czech Technical University in Prague, Kladno/CZECH REPUBLIC

This paper presents approaches implemented in the medical device procurement tracking system in the Czech Republic. The System was created to enable the monitoring and assessment of procurement efficiency and to provide valid information to different stakeholders during future medical equipment purchases planning. Data collection process was proposed and implemented into practice. Several reports run on the grounds of a multi-criteria comparison based on comprehensive data model, which enable to analyse the procurement data and to formulate hypotheses relative to procurement efficiency. The multi-criteria approach is based on the valuation of the medical equipment procurements upon the set of criteria specified by the user, such as procurement terms and conditions, medical equipment price and technical specifications. The System developed allows users to compare purchase contracts with the purpose of identifying their weaknesses and planning future purchases.

SP103.2 - Influence of shifting patients with off-axis tumor for Tomotherapy

Author(s): [Yingjie Xu](#), Jianrong Dai, Zhihui Hu, Peng Huang, Pan Ma, Kuo Men, Ke Zhang, Minghui Li, Dawei Jin, Wenting Ren
Department Of Radiation Oncology, Cancer Institute & Hospital, Chinese Academy of Medical Sciences, Beijing/CHINA

Objectives:

For tomotherapy, it's common practice to set up a patient centrally no matter where a tumor is in his or her body. Here is to evaluate the influence of shifting the patient on plan quality and treatment time if the tumor is off the rotational axis of tomotherapy machine.

Methods:

15 patients with off-axis tumor were chosen for planning in tomotherapy planning system (Accuray Inc.). The off-axis distance ranged from 2 to 12cm. In one group of plans, all patients were shifted in the planning system to make the tumor center coincide to the machine's rotation axis (HiArt) while in the other group, all patients were not shifted. Except center position, all planning settings such as pitch, field width, and modulated factor were the same for two groups. Conformal index, homogeneity index and mean dose of normal tissue were compared in these two groups. So did the treatment time and monitor units.

Results:

The CI, HI and DNTmean were 0.84 ± 0.053 , 1.06 ± 0.023 , and 12.37 (quartile range 5.78) for the first group of plans (the plans with patients shifted), and were 0.84 ± 0.053 , 1.07 ± 0.027 , and 12.4 (quartile range 5.91) for the second group, respectively. There was no significance. But the treatment time was shorter for the first group, and the difference became larger with off-axis distance. So did the MUs. When the distance was more than 6 cm, the treatment time saving was over 10%. These changes were mainly caused by the machine's flattening filter free design.

Conclusion:

For patients with large off-axis tumor, treatment time and MUs can be reduced significantly if the patients are shifted so that the tumor center coincides to the machine's rotational axis.

SP103.3 - Smart pump user interface evaluation

Author(s): [Carlos A.B. Viviani](#)¹, Saide Calli²

¹Deb, UNICAMP, Campinas/BRAZIL, ²Department Of Biomedical Engineering, Unicamp, Campinas/BRAZIL

There are at least 73 infusion pump manufacturers registered with the Food and Drugs Administration (FDA).

Many events reported by the FDA occurred due to usability problems of medical devices, which are often related to lack of consistency in the interface. This may induce the user to error and consequently the occurrence of problems during the device operation.

To minimize such events, it is required a careful evaluation of the interface device and also its standardization.

Infusion pumps are always present in ECRI's reports as one of the devices that have the highest probability of risk to the patient.

The objective of this study is to verify the interfaces consistency of four infusion pumps developed by leading manufacturer in world market.

The methodology is structured in two stages. The first stage referred to the development of an appropriate set of criteria for comparing the interfaces of the smart infusion pumps. In the second stage, it was applied the developed criteria to the interfaces using the four pumps as a practical study

Evaluation results showed that there is no standardization for designing medical devices of the same type and category; in this case study the smart pumps. It also suggested that each manufacturer designs a device considering only aesthetic issues and does not maintain any consistency with other manufacturers and even with other models or different version devices.

This preliminary study provides us with evidence that this lack of consistency between the interfaces of these devices can lead to usability problems, and can lead untrained users to error. Additional studies are needed to further investigation and thereby demonstrate qualitatively results.

SP103.4 - Studying the human computer interface of a continuous monitoring software by approaching it from both directions**Author(s):** [Ying Ling Lin](#)¹, Anne-Marie Guerguerian², Patricia Trbovich¹¹Centre For Global Ehealth Innovation, University Health Network, Toronto/CANADA, ²University of Toronto, Toronto/CANADA

A software to manage the data from continuous monitoring has been implemented in paediatric intensive and cardiac critical care units of a large, tertiary hospital, in Canada, but in its current version has not been integrated in clinicians' work. In this study, we present two components of a proposed four-phase project which each approach the human-computer interface (HCI) from two directions. Established human factors methods will be employed: first, from the computer side using heuristics or "rules of thumb", frequently used in software design, and second, from the human-user side, using cognitive task analysis. These two phases aim to inform an optimized interface design eventually used to study the impact of this software on clinician decision-making within this complex socio-technical workplace.

Computer Side – Heuristic Analysis

In this phase, the interface was assessed using 14 heuristics, developed by leading experts in interface design and modified for medical devices. Three evaluators assessed the same version of the software for issues and their heuristic violations and severity. The first assessment was performed by a "double-specialist" with novice-level knowledge of both the clinical work and human factors; the second was performed by two domain experts each from clinical nursing and human factors fields.

In total, 68 usability issues were found; 23 were found in the first assessment, 45 were found in the second assessment, and 18 found in both assessments. These were associated with over 200 violations to the heuristics generally, of severity 2 (minor usability problem) or 3 (major usability problem). The most common types of heuristic violations were visibility, match, memory and error.

Human Side – Cognitive Task Analysis

Cognitive task analysis (CTA) is generally referred to as the set of methods used to identify the mental demands and cognitive skills needed to complete a task. Monitoring and decision-making in the technology intense environment of an ICU requires a high degree of staff expertise to carry out these cognitive tasks. A cognitive task analysis was used to understand how different clinicians in the ICU use the information at their disposal to make decisions regarding patient care. Physicians, nurses and respiratory therapists make decisions for a range of tasks required for continuous care. They obtain their information from disparate monitoring technologies and an understanding of their prioritized information sources is key to the design of software interfaces aimed at facilitating their access and integration of this information. We designed four simulated, paper-based, scenarios to aid the CTA.

By using tools from decades of knowledge of software interface design and from structured methods of understanding the work of clinicians, basic usability issues and tasks can be identified. Results from these two directions will inform the next phase of testing, a low-fidelity usability study, using true-to-work tasks and inherent software interface issues.

SP103.5 - Analysis and experimentation of plantar foot segmentation from thermographic digital images for preventive diagnosis of diabetic foot**Author(s):** [Carolina Rosado](#)¹, [Alex E. Dávila](#)², [Yahir Pandzic](#)², [Luis Vilcahuaman](#)¹, [Marko Alpiste](#)²¹Faculty Of Electronic Engineering, Pontifical Catholic University of Peru, Lima/PERU, ²Pontifical Catholic University of Peru, Lima/PERU

Plantar foot surface temperature is an important feature in type II diabetes as it is an early sign of foot ulcer. We have reviewed the scientific and technical foundations for the use of digital thermography of the sole of the foot as a prevention procedure to avoid foot ulceration. This project has progressed in the implementation of a new segmentation algorithm to analyze plantar foot temperature and its assessment by qualitative judgment. We have processed thermographic images of the feet. To achieve this we first proceeded to capture images from two soles of feet -surrounded or not by a foam block- and then to segment them using two different methods each of which include the iterative closest point (icp) Method: 1) fuzzy clustering modeling (FCM) and 2) growing seeds. Images properly segmented were judged by three observers who have estimated the quality of the contour tracing. Medians and quartile deviations are calculated to estimate the segmentation's quality. As a result, the quality contour tracing was less suitable when there was not a foam block surrounding the sole of foot while imaging was performed. Likewise, the segmentation using FCM was less suitable than the segmentation by growing seeds. Overall, these results suggest the possibility of avoid using foam block by optimizing the software with growing seed method which increase the comfort of patients and asepsis inside hospitals.

SP104 - Phantoms

TRACK 01: IMAGING

SP104.1 - Monte Carlo simulation of interventional cardiac scenarios using a newborn hybrid phantom and MCNPX code

Author(s): [Fernanda R. Cavalcante](#)¹, [Albérico B. Carvalho Júnior](#)², [William S. Santos](#)³, [Choonsik Lee](#)⁴

¹Departamento De Física, Universidade Federal de Sergipe, São Cristóvão/BRAZIL, ²Departamento De Física, Universidade Federal de Sergipe, Aracaju/BRAZIL, ³Instituto De Pesquisas Energéticas E Nucleares, Comissão Nacional de Energia Nuclear, São Paulo/BRAZIL, ⁴Division Of Cancer Epidemiology And Genetics, National Cancer Institute, Bethesda/UNITED STATES OF AMERICA

We developed exposure scenarios of pediatric interventional cardiology using a newborn hybrid phantom and the radiation transport code MCNPX. Six angiographic projections (AP, PA, LAO45, RAO45, LAO90 and RAO90) were simulated considering three X-ray energy spectra (60, 70 and 80 kVp), focus-skin distance (FSD) not less than 45 cm and a 7 x 7 cm² field size. Equivalent and effective doses were computed and normalized by kerma-area product (KAP) resulting the conversion coefficients HT/KAP and E/KAP. The results showed highest HT/KAP values in AP projection at 80 kVp. Increasing photon energy, average E/KAP values presented relative differences of 18% (60 to 70 kVp) and 15% (70 to 80 kVp). E/KAP values were compared with those published for mathematical newborn phantom. Results showed relative differences of 14% for AP projection (70 kVp) and 60% for lateral projections (60 kVp).

SP104.2 - Computed tomography of a beating heart: High resolution simulator for the assessment of motion artifacts during CT scan of the heart

Author(s): [Yair Zak](#)¹, [Vadim Beniagouev](#)¹, [Sarah Cohen](#)², [Dov Malonek](#)¹

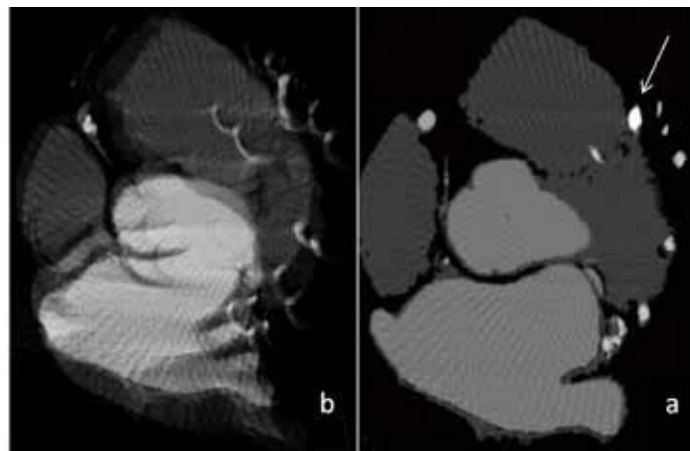
¹Medical Engineering, Ruppin Academic Center, Emek Hefer/ISRAEL, ²Glocal System, Philips Healthcare, Haifa/ISRAEL

Computerized tomography of internal organs is an important diagnostic tool for the clinician in spite the use of ionizing radiation with the potential for causing harmful deterministic and stochastic effects to the patients. CT angiography, that allows detecting and evaluating coronary heart disease, is a technological challenge as the image acquisition process is done while the heart is moving resulting in information loss. Fast acquisition and precise synchronization to cardiac motion are common techniques to reduce information loss, but they fail when irregular cardiac rhythm is encountered.

We have developed a computerized CT simulator to investigate the effect of irregularities in cardiac cycle during CT scan on the obtained image quality. The CT simulator utilizes high resolution computer phantom mimicking realistic cardiac motion with anatomically realistic heart and associated vasculature. Normal cardiac motion is generated using XCAT/HADES phantom generator with anatomical resolution exceeding 0.25mm. Irregular cardiac rhythm is controlled by a dedicated ECG simulator capable of generating normal and abnormal rhythms. The simulator allows simulation of prospective gating technique ("Step and shoot"). Various reconstruction algorithms have been incorporated in the simulator. Effects of geometry of the scanner, pixel size, gantry rotation speed and other physical parameters on image quality can be studied.

We showed the simulator's capabilities by the introduction of a small calcium block into a coronary artery of the beating heart phantom.

Its detectability was tested while changing the simulated heart rate variability. The calcium block was easily detectable in the reconstructed images when simulating acquisition during normal cardiac rhythm. When heart rate variability was increased to 10%, the coronary artery block was not detected in the reconstructed images.



We suggest that such computerized simulator have the potential to be used in future development of CT techniques, to investigate the effects of anatomy and motion on acquisition protocols and to customize imaging protocols for individual patients based on their measured heart rate variability.

SP104.3 - Development of Dynamic Anthropomorphic Heart Phantom for Computed tomography

Author(s): [Ali Ursani](#)¹, [Murray Rice](#)¹, [Shailaja Sajja](#)², [Fatima Ursani](#)², [Narinder Paul](#)³

¹Medical Engineering, University Health Network, Toronto/ON/CANADA, ²Department Of Medical Imaging, Toronto general hospital, Toronto/ON/CANADA, ³Medical Imaging, University Health Network, Toronto/CANADA

Background:

Currently available large detector CT scanners with high rotational speed and dual-source have demonstrated good diagnostic accuracy for coronary artery disease. However, the appearance of a coronary stenosis during computed tomographic coronary angiography (CTCA) does not always equate the actual blockage in the arteries. This discrepancy is due to calcified plaque can cause bloom artifact or similarly measured density of non-calcified plaque is strongly affected by partial volume artifact from adjacent densities including luminal contrast. Higher or irregular cardiac motions has significant role in producing these artifacts, hence multiple scans are required with different gating techniques. These limitations can be addressed by improvement in image reconstruction algorithms and acquisition techniques.

Method:

This project presents development of a realistic dynamic anthropomorphic heart phantom (DHAP), which can mimic any heart rhythm of patient while waiting in the holding area. The dynamic heart phantom driven in real time from the patient's ECG; then can be scanned in the CT to establish the best gating protocol suitable to current heart rhythms of the patient. Once the protocol is established the patient can be scanned only applying single gating technique; hence significant radiation dose can be reduced for these patients.

The phantom can also support research studies addressing the detection issues due to cardiac motion in space and time domains. Thus phantom can also serve as a useful tool in building new CTCA

reconstruction algorithms for improving image quality.

Specifications:

- *Fluid Pump* (piston type):

Capacity: 270 ml

HR: 50 to 125 BPM

Piston stroke (max) = 140 ml@120 bpm

- *Heart module* (Urethane rubber 30A/ 60HU@120kVp; wall thickness = 1cm):

Chambers: Two; LV & RV; 70ml each at relaxed state.

End-diastolic volume [EDV] = up to 130 ml (typical 120 ml)

End systolic volume [ESV] = down to 40 ml (typical 50 ml)

Arterial angular displacement around the axis = up to 2 cm

-*Software*:

NI LabVIEW Control Design and Simulation Module running on PC with the help of Quanser Q2-USB H.I.L control board. A pressure wave corresponding to the heart chamber movements is simulated and fed into the closed-loop PI position controller to drive the linear shaft of piston-pump.

Results:

Attached figure: Two trans-axial 0.5mm computed tomography images through the basal left ventricle (top right) and apical left ventricle (bottom right) show the presence of non-calcified plaque causing eccentric (top) and central (bottom) luminal stenosis.

Currently following studies are being carried out with the help of DAHP at UHN.

Study.1 -Optimal image reconstruction for detection and characterization of mixed coronary plaque during CTCA.

Study.2 -Influence of X-ray pulse duration on lung nodule sharpness during digital radiography in a dynamic anthropomorphic chest phantom.

SP104.4 - Development of a PET/MR/CT Compatible Tumour Motion Phantom

Author(s): John C. Patrick¹, Mohammad A. Tavallaei², Frank S.

Prato³, R T. Thompson³, Maria Drangova³, Stewart Gaede³
¹Physics And Engineering, London Regional Cancer Program, London/CANADA, ²Imaging Research Laboratories, Robarts Research Institute, London/ON/CANADA, ³Medical Biophysics, Western University Canada, London/ON/CANADA

The development of PET/CT scanners has improved staging for lung cancer, especially for nodal and distant metastatic sites. In the case of chest wall infiltration and mediastinal tumours, MRI is superior to PET/CT. PET and CT are acquired sequentially and thus motion in PET that is acquired over minutes cannot be corrected with the CT, which is acquired over several seconds. Siemens' hybrid PET/MRI acquires both modalities simultaneously, eliminating the impact of respiratory motion due to sequential scanning. This could have a major impact on respiratory-gated lung cancer radiotherapy. Before implementing PET/MRI for lung cancer radiotherapy clinically, the benefits of this novel imaging technique should be validated in an appropriate phantom. Therefore, the goal of this work is to demonstrate a PET/MR/CT compatible respiratory motion phantom that

can be used to understand and validate the impact of tumour motion on hybrid PET/MRI.

The phantom's main torso compartment has internal dimensions of 274.5mm long with an oval profile of 292mm by 240.5mm. The lung compartments have oval profiles with internal dimensions of 89mm by 125.5mm, by 274.5mm long. The spine compartment also has an oval profile with internal dimensions of 32.3mm by 23.6m, by 274.5mm long. The superior-end cap has two fill holes; one to fill the spine compartment and a larger one to fill the torso compartment. The inferior-end cap has two through holes to match the profiles of the lung compartments, which allow a spherical tumour compartment with a stem to be mounted to an MRI-compatible motion stage. This motion stage from Vital Biomedical Technologies can provide user-defined motion profiles to move the tumour (Figure 1A).

The 3.5cm diameter spherical tumour compartment was filled with saline and 17kBq/mL of F18 to mimic tumour uptake of FDG. The torso compartment was filled with saline and 4.27kBq/mL of F18 to mimic normal back ground uptake in a patient body. The motion stage was programmed to produce a repeating 4 second sinusoidal cycle of linear motion that was 2cm long in the superior/inferior direction. PET/MR images were acquired on a Siemens Biograph mMR via T1-VIBE sequence with simultaneous list-mode PET acquisition.

Figure 1B shows that the co-registration of the PET and MRI was achieved with no post-processing, despite the presence of motion.

The PET/MR/CT-compatible Tumour Motion Phantom can be used to generate accurate images of known geometries and reproducibly simulate respiration motion or user-defined motion profiles of a tumour.

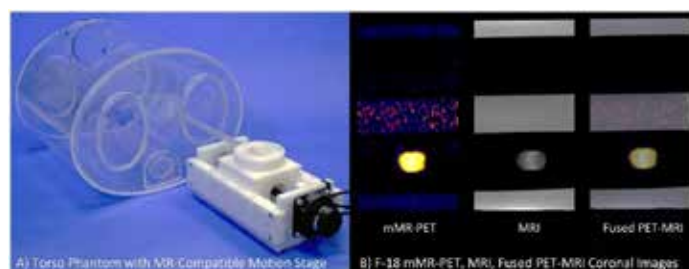


Figure 1. A) Completed Phantom with B) Non-gated images in mMR-PET, T1-VIBE MRI, and Fused PET-MRI of moving phantom filled with saline and F-18.

SP105 - MRI: Novel Approaches and Molecular Imaging & Applications

TRACK 01: IMAGING

SP105.1 - Advancing MRI for Non-invasive Physiological and Cellular Imaging

Author(s): Hai-Ling Margaret Cheng

Institute Of Biomaterials & Biomedical Engineering, University of Toronto, Toronto/ON/CANADA

Magnetic resonance imaging (MRI) is a non-invasive, high-resolution whole-body imaging modality for probing deep tissue structures without requiring exposure to ionizing radiation. The exquisite soft-tissue contrast MRI affords is unparalleled, thus firmly establishing its importance in clinical diagnostic imaging. MRI also has great potential for imaging events at the physiological, cellular, and molecular level. Although most of these efforts currently remain within the domain of pre-clinical research, advancing MRI beyond conventional anatomical imaging is key to opening new avenues for exploration.

In this talk, I will describe the efforts in our laboratory to advance MRI for physiological, cellular, and molecular imaging for eventual translation to humans. Our emphasis is on “quantitation”, meaning that we use imaging to “measure” biological events. This focus is critical to improving the way we detect disease, since early changes in cells and tissue function often occur long before physical abnormalities become apparent, and having the ability to detect and measure these changes is crucial to early diagnosis and intervention. It will also enable us to tackle emerging applications, such as tissue engineering, where the ability to track transplanted cells and determine their fate or to monitor tissue development *in vivo*, can be assessed realistically only inside a living subject. The technical capabilities we are developing will be described alongside their application to guiding tissue-engineering approaches for regeneration and to new concepts for cancer detection (Figure 1) and cardiovascular imaging (Figure 2).

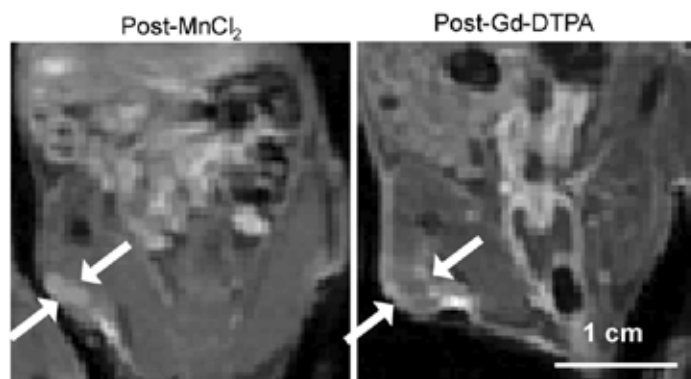


Figure 1. Early MRI detection of small primary MCF7 breast tumors in mice using Mn-enhanced cellular imaging at 3 Tesla.

From Alhamami M, Bayat Mokhtari R, Ganesh T, Tchouala Nofiele J, Yeger H, Cheng HL. Manganese-enhanced magnetic resonance imaging for early detection and characterization of breast cancers. *Mol Imaging*, 2014;13.

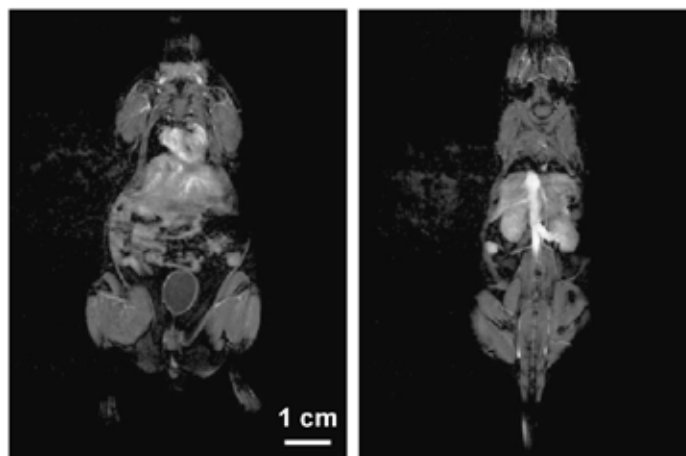


Figure 2. High-resolution MR angiography of mouse vasculature at 3 Tesla with long-circulating MRI contrast agents.

SP105.2 - Detection of Regional Radiation-Induced Lung Injury using Hyperpolarized ^{129}Xe Localized Magnetic Resonance Spectroscopy

Author(s): Brandon Zanette¹, Ozkan Doganay², Elaine Hegarty³, Giles E. Santyr⁴

¹Physiology And Experimental Medicine, The Hospital for Sick Children, Toronto/ON/CANADA, ²Department Of Medical Biophysics, University of Western Ontario, London/ON/CANADA, ³Robarts Research Institute, London/ON/CANADA, ⁴Department Of Medical Biophysics, University of Toronto, Toronto/ON/CANADA

Introduction: Radiation induced lung injury (RILI) remains one of the most important limitations of radiotherapy of the thorax. Magnetic Resonance Spectroscopy (MRS) using hyperpolarized ^{129}Xe may be useful for early detection of RILI by quantification of gas exchange between lung air spaces, lung tissue (T), and red blood cells (RBC)¹. Previous work using whole lung irradiation and ^{129}Xe MRS has shown detection of inflammatory changes associated with RILI (i.e. pneumonitis) as early as two weeks post-irradiation in rats². This work extends these methods to regional detection of RILI using localized MRS in a rat model involving irradiation of the right versus left lung.

Methods: Sprague Dawley rats were used following Western AUC-approved protocols. One cohort was irradiated with 18 Gy to the right thorax and incubated for two weeks, while the other cohort served as unirradiated controls. Localized ^{129}Xe spectra were obtained from an 8x8 matrix in the coronal plane and processed to yield total tissue signal (ST) and total RBC signal (SRBC) for the whole lung as well as each of the left and right lungs, similar to Thind et al.³ For each rat, whole lung and individual lung (right and left) SRBC/ST ratios were calculated, after which ratios of SRBC/ST between right and left lungs (R/L) were calculated. Afterwards, lungs were removed, fixed, sectioned and stained (H&E) for histology.

Results: Eight rats were analyzed (three irradiated, five unirradiated). R/L was significantly different between the two cohorts ($p = 0.009$) with mean values $0.91 (\pm 0.08)$ and $0.69 (\pm 0.07)$ for the unirradiated and irradiated cohorts respectively. The difference between SRBC/ST between the cohorts was less significant for the left lung ($p = 0.056$) compared to the right ($p = 0.019$), while whole lung comparison was intermediate ($p = 0.022$).

Discussion: These results confirm that regional RILI differences are detectable at two weeks using hyperpolarized ^{129}Xe localized MRS of rat lungs following single-lung irradiation of 18 Gy. The strong

difference between tissue and RBC signal seen in the right lung and left lung of the irradiated cohort suggests that both the tissue and blood pool are affected by the direct effects of radiation. The smaller but significant response of the unirradiated left lung in the irradiated cohort may indicate pneumonitis is present in the left lung with little vascular damage. We hypothesize that the right lung of the irradiated cohort may be exhibiting both pneumonitis (increasing ST) and vascular damage (decreasing SRBC), while the left only exhibits pneumonitis. This agrees with previous studies showing organ-wide pneumonitis to localized irradiation in a similar rat model³. In future, histological analysis may help support this hypothesis. SRBC/ST may be a useful biomarker for early, regional detection of RILI in humans as the technology becomes available clinically. Early detection of pneumonitis and vascular damage may allow for modification of treatment, mitigating the irreversible effects of RILI.

References: 1. Sakai et al., J Magn. Reson. B. (1996), 111:300-304. 2. Fox et al., Med. Phys. (2014), 41. 3. Thind et al., Radiother. Oncol. (2014), 110:317-322.

SP105.3 - Conjugate-Mapped Compressed Sensing: a technique to mitigate the side effects of compressed sensing on MTF

Author(s): Amr A. Heikal¹, Keith Wachowicz², B Gino Fallone³
¹Medical Physics, Cancer Centre of Southeastern Ontario, Kingston/CANADA, ²Medical Physics, Cross Cancer Institute, Edmonton/CANADA, ³Physics, University of Alberta, Edmonton/AB/CANADA

Purpose:

Compressed sensing (CS)¹ in MRI allows images to be generated with a dramatic reduction in acquired k-space data while retaining similar appearance to those conventionally acquired. However, it has been shown that CS can have a detrimental effect on the modulation transfer function (MTF) of chemical shift images.² The aim of this work is to quantitatively illustrate the impact of CS on 2D MRI, and to introduce a modified randomization and reconstruction algorithm (conjugate-mapped compressed sensing (CMaCS)).

Theory:

CMaCS exploits the conjugate symmetry property of the k-space representation of a zero-phased image which allows the unpaired k-space conjugate locations to be estimated prior to reconstruction. The resulting increase in k-space filling should translate to increased resolution of the CS reconstructions.

Materials and Methods:

A phantom with a fan array of alternating 2.9° acrylic wedges and fluid-filled voids was used to measure the MTF. The fans array allows for a square-wave input function (arc profile on fan structure) with continuous variation in spatial frequency (Fig. 1). A 2D T2-weighted turbo spin-echo sequence with a 1x1 mm² nominal resolution was used to scan the phantom on a 3T Philips Intera platform. The resulting k-space data was 3-times sub-sampled in the x-direction (phase-encode) with a randomized 1/r³ probability distribution for CS and CMaCS reconstruction. CS reconstruction was based on the method outlined by Lustig et al.¹, using a 2D wavelet sparsity constraint. The CMaCS modification constrained the 1/r³ randomization to avoid conjugate k-space replicas. Prior to conjugate-mapping, a zero-order phase correction was performed in k-space based on k_{0,0}. After reconstruction, arc profiles over a range of radii on the real, phase-corrected images were used to calculate the MTF in the x-direction at the corresponding spatial frequencies as discussed by Heikal et al.²

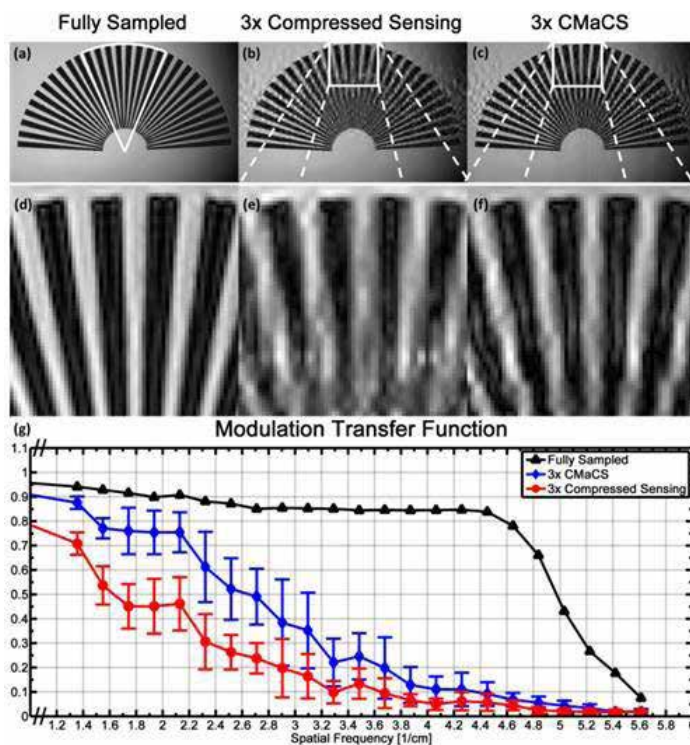


Figure 1: (a) The fully sampled image of the phantom showing the region-of-interest for calculating the MTF (white), (b) 3xCS reconstruction, (c) 3x CMaCS reconstruction, (d) close up of the top of the fully sampled image, (e) close up of the CS image, (f) close up of the CMaCS image, (g) MTFs of the 1 fully sampled image, 10 CS reconstructions and 10 CMaCS reconstructions.

Results and Conclusions:

Similar to results given by Heikal et al.², Fig. 1(g) shows that the spatial frequency response for the CS implementations was markedly lower than the fully sampled acquisition that they are intended to imitate (black plot). CMaCS (blue plot) provided a near two-fold increase in spatial frequency response compared to standard CS. However, due to potential B₀ field variations across the FOV, a zero-order phase correction may prove insufficient for robust CMaCS, requiring more complex phase-handling.

References:

1. M. Lustig, et al. Magn.Reson.Med. (2007).
2. A. A. Heikal, et al. Med.Phys. (2013).

Acknowledgements: Philips Medical Systems for technical support in this work.

SP105.4 - Gadolinium Labeled Glycosylated Nanomagnetic Particles as Metabolic Contrast Agents in Molecular Magnetic Resonance Imaging

Author(s): Sara -. Heydarnezhadi, Nader Riyahi-Alam, Soheila Haghgoo, Mehdi Khobi, Banafshe Nikfar, Ensieh Gorji, Behrouz Rafiei
 Tehran university of Medical Science, tehran/IRAN

Difficulties in the use, preparation, and cost of radioactively-labeled glycosylated compounds led us to this research and development study of a new gadolinium-labeled glucose compounds that do not

have a radioactive half-life or difficulties in its synthesis and utilization. Despite its good resolution, Magnetic Resonance Imaging (MRI) has low sensitivity, therefore, using MRI contrast agents, such as GD-DTPA (Magnevist) will improve tissue discrimination in MRI images.

The purpose of this study is the synthesis and physicochemical characterization of glycosylated gadolinium as metabolic contrast agent for molecular MRI (mMRI). In-vitro T1 relax-ivity measurement and signal intensity of the glycosylated compounds has been also performed in comparison with mag-nevist (GD-DTPA). Based on the structure of the 2-fluoro-2-deoxy-D-glucose molecule (FDG), first compound consisting of D-glucose con-jugated to a well-known chelator, diethylenetriamine penta-acetic acid (DTPA), was syntheside, labeled with Gd to achieve Gd-DTPA-DG, another comound consisting of gado-linium oxide-based nanoparticle coating of diethyleneglycol conjugated with D-glucose via N,N-carbon-ylidimidazole (CDI) mediate reaction, to achieve Gd-DEG-DG, and characterized by various analytical technique, utilizes dynamic light scattering (DLS) to determine the size distribution. The nanoparticle size and morphology were using high resolution transmission electron microscopy (HTEM). In our study, the Gd-DTPA-DG were well defined nanoparticle with size 40 nm in diameter TEM images. While Gd-DEG-DG were 10 nm. The mean hydrodynamic diameter of nanoparticles, as measured by DLS, were 300 nm and 70 nm for GD-DTPA-DG and GD-DEG-DG, respectively. The synthesized GD-DTPA-DG and GD-DEG-DG were shown higher relaxometry rates in vitro relative to magne-vist. GD-DEG-DG and GD-DTPA-DG demonstrated shorter T1 than GD-DTPA at the same conecetration.

SP105.5 - Hyperpolarized ^{129}Xe Magnetic Resonance Imaging of a Rat Model of Radiation-Induced Lung Injury Involving Single-Lung Radiation Therapy

Author(s): Ozkan Doganay¹, Elaine Hegarty², Rolf F. Schulte³, Charles Mckenzie⁴, Giles E. Santyr¹

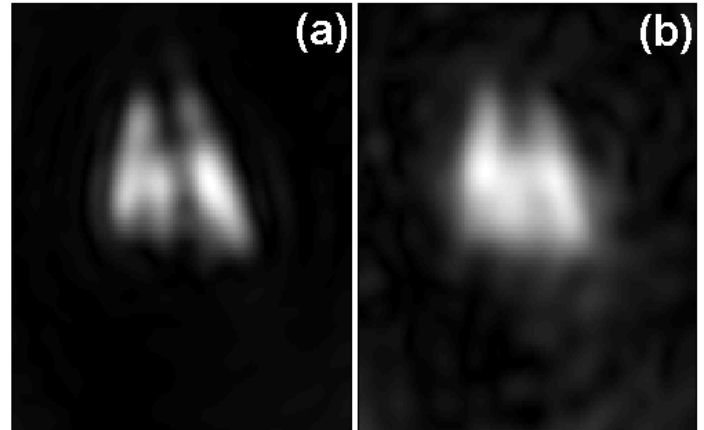
¹Medical Biophysics, Western University, London/CANADA, ²The Hospital for Sick Children, Toronto/ON/CANADA, ³GE Global Research, Munich/GERMANY, ⁴Robarts Research Institute, London/ON/CANADA

Radiation therapy is a common treatment for lung cancer, but is limited by radiation-induced lung injury (RILI)[1]. It has been previously shown that Magnetic Resonance Imaging (MRI) with hyperpolarized ^{129}Xe can detect changes in both lung tissue signal as well as exchange between gas and tissue (ie. pneumonitis) as early as two weeks following whole thorax irradiation in rats[2]. In this study, a novel MRI approach is developed for imaging of hyperpolarized ^{129}Xe both in the gas phase and dissolved in lung tissue. The method is applied to a rat model of RILI involving single-lung irradiation.

The right thorax of three Sprague Dawley rats were irradiated with a cobalt-60 irradiator (18Gy), following previously described methods[2]. Three rats served as non-irradiated controls. 2D coronal spiral IDEAL[3] images were acquired using a repetition time (TR) of 300ms. Following three wash-in breaths of hyperpolarized ^{129}Xe , IDEAL gas images and tissue images were acquired from the lungs within a breath-hold time of 6 seconds. Signal-to-noise ratios (SNR) of the averaged IDEAL gas images and the lung tissue images, for both the left lung (SGL, STL) and the right lung (SGR, STR) of both cohorts were calculated. To account for potential differences in ventilation and polarization, the lung tissue SNR values were normalized by respective gas SNR values for both left and right lungs (STL/SGL and STR/SGR). Following imaging, lungs were removed for histological examination.

Fig.1 shows coronal IDEAL gas (a) and tissue (b) images from a representative non-irradiated rat. STL/SGL and STR/SGR was strongly correlated with tissue area measured by histology ($R=0.75$), with a Pearson coefficient P -value=0.005 at $p<0.01$.

This study shows that MRI of hyperpolarized ^{129}Xe in the gas space and in the lung tissue is feasible, and can be used to detect increases in tissue signal in the lungs of irradiated rats as early as two weeks post-irradiation. An increase of approximately 50% in tissue signal was observed in the right lungs of the irradiated cohort compared to the unirradiated cohort corresponding to increases in tissue area (ie. pneumonitis) measured using histology. These methods should be readily translatable to human subjects given the growing availability of hyperpolarized gas technology in the clinic. Early detection of pneumonitis may allow adjustment to the radiotherapy plan and/or the application of alternate therapies to mitigate RILI.



References:[1] Santyr G. et al. NMR Biomed. 2014;27(12):1515-24. [2] Fox M.S. et al. Medical Physics 2014;41(7):072302.[3] Wiesinger F. et al.MRM2012,68(1):8-16.

SP105.6 - Ultra-short Echo Time (UTE) Magnetic Resonance Imaging of Cortical Bone: An Undersampled Acquisition Study

Author(s): Yanchun Zhu¹, Qun He², Jiang Du², Yaoqin Xie¹

¹Institution Of Biomedical And Health Engineering, Shenzhen Institutes of Advanced Technology, Chinese Academy of Sciences, Shenzhen/CHINA, ²Department Of Radiology, University of California, San Diego/UNITED STATES OF AMERICA

Purpose: Ultra-short echo time (UTE) sequences have shown great utility in visualizing short T2 tissues like cortical bone which shows little or no signal with conventional clinical magnetic resonance imaging (MRI) techniques. Several short T2 contrast mechanisms have been developed to enhance bone contrast by suppressing signals from surrounding long T2 tissues including muscle and fat. These contrast mechanisms may significantly prolong the acquisition times.

Methods: A series of UTE pulse sequences were implemented on a 3-T Signa TwinSpeed scanner (GE Healthcare Technologies, Milwaukee, WI, USA) with a maximum gradient performance of 40 mT/m and slew rate of 150 mT/m/ms. In this paper, UTE, dual echo UTE (dUTE), adiabatic inversion recovery prepared UTE (IR-UTE) and adiabatic inversion recovery prepared dual echo UTE (IR-dUTE) with different undersampling acquisition ratios were compared by measuring signal-to-noise ratios (SNRs), contrast-to-noise ratios (CNRs), signal distortion, contrast, image sharpness and streak artifact power. The feasibility of using undersampling acquisition in UTE approaches was demonstrated by imaging cortical bone in vitro and in vivo using the clinical 3T scanner.

Results: Results showed that UTE, dUTE, IR-UTE and IR-dUTE data acquisitions can be highly undersampled to save scan time, while providing images with limited undersampling artifact especially for IR-UTE and IR-dUTE acquisitions. Figure 1 shows the dUTE

undersampling images of distal tibia.

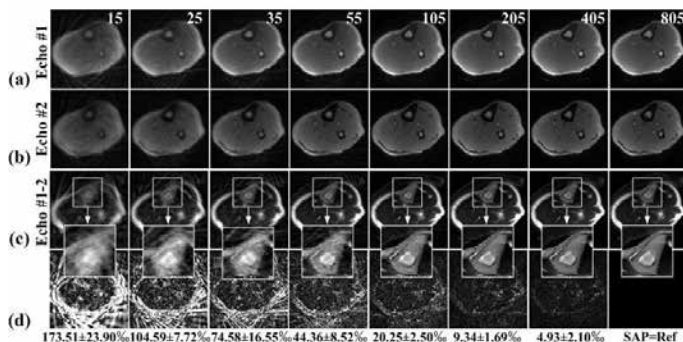


Figure 1: dUTE undersampling study of in-vivo distal tibia. dUTE images of a volunteer's distal tibia with different number of projections (15, 25, 35, 55, 105, 205, 405 and 805) are shown in the first row (a) for the first echo images and the second row (b) for the second echo images. Subtraction images between these two echoes are shown in the third row (c). Residual images in the fourth row (d) are used to show streak artifacts in subtraction images.

Conclusion: This study has shown that UTE imaging of cortical bone with highly undersampling acquisition (accelerating factor up to 23) is feasible when surrounding long T2 tissues are efficiently suppressed.

SP105.7 - Brain activation associated with working memory maintenance under anxiety-provoking distracter in patients with obsessive compulsive disorder

Author(s): Gwang-Won Kim¹, Jong-Chul Yang², Gwang-Woo Jeong¹
¹Radiology & Biomedical Engineering, Chonnam National University Medical School, Gwang-Ju/KOREA, ²Psychiatry, Chonbuk National University, Jeonju/KOREA

The purpose of this study was to discriminate the brain activation patterns associated with the anxiety-provoking distracter during the working memory (WM) maintenance for the human faces between patients with obsessive compulsive disorder (OCD) and healthy controls by using a function magnetic resonance imaging (fMRI).

Twelve patients with OCD (mean age = 31.3±7.4 years) and 12 healthy controls (mean age = 33.3±7.8 years) underwent the functional MRI on a 3.0 Tesla MR Scanner (Siemens Medical Solutions, Germany). The activation paradigm consisted of a string of “encoding - WM maintenance - distracter - retrieval.” In the encoding task, three different human faces sequentially appeared once on a quartile coordinate of a screen monitor. During the delay time following the encoding, the subjects were asked to maintain the WM for the encoded faces. Then, distracters were given to the subjects while maintaining the WM of the encoding step, in which the distracters consisted of an anxiety-provoking picture and a neutral picture. In the retrieval task, either of the face presented in the encoding task or a new face was presented. The brain activation mapping and the resulting qualification were processed by SPM8.

The average scores of perceived anxious emotion for anxiety-provoking picture were 7.8±1.4 and 7.7±1.4 in patients with OCD and healthy controls, respectively. The scores for the face recognition task with anxiety-provoking distracters were 67.8±9.1% and 68.3±11.9% in patients and healthy controls, respectively, while the scores for neutral distracters were 62.1±15.7% and 70.0±12.1%, respectively. The patients with OCD showed significantly decreased activities in the ventrolateral prefrontal cortex, superior parietal gyrus, middle temporal gyrus, and fusiform gyrus during the WM maintenance with the anxiety-provoking distracters as contrast to healthy controls, whereas the patients with OCD significantly increased

activities in the inferior temporal gyrus and median cingulate gyrus (p<0.001).

It is concluded that our findings provide an evidence for the differential brain activation patterns associated with anxiety-provoking distracter between patients with OCD and healthy controls during the delay interval of the WM task. This finding will be helpful to understand the neural mechanism related to general impairment of emotional function in patient with OCD.

SP105.8 - Fractional Anisotropy, Voxel Wise Morphometry and Resting State in Patients with Lateral Amyotrophic Sclerosis
Author(s): Maria M. Lopez-Titla, Salvador Gsrcía, Lourdes M. Martínez
 Imágenes Cerebrales, Instituto Nacional de Psiquiatría, México/ MEXICO

Introduction:

The Amyotrophic Lateral Sclerosis (ALS) is a degenerative disease that is characterized by the damage of the Upper Motor Neurons (UMN) and the Lower Motor Neurons (LMN). Many studies have found that motor areas are affected by this disease, being the main affected areas the corticospinal tract, the posterior limb of the internal capsule and the anterior and medial parts of the corpus callosum; other studies have also found a general decrement of the gray matter in all the brain. The ALS has a difficult prognosis because the symptoms can be misleading; therefore it is really important to find biomarkers that help us in the diagnosis of this disease and in improving its medical treatment.

The Magnetic Resonance Imaging (MRI) is a non invasive neuroimage method that offers information in vivo of the brain structures. This method counts with different advanced techniques which evaluates many parameters that could be used as biomarkers to identify distinct diseases or disorders.

Among the MRI advanced techniques are: a) The diffusion tensor imaging that can provide the Fractional Anisotropy (FA) index which takes values between 0 and 1 and it is used to evaluate the integrity of the white matter; b) The Voxel-wise morphometry that helps to quantify the volume and the amount of gray and white matter in the brain; c) The functional Magnetic Resonance Imaging (fMRI) based on the Blood Oxygen Level Dependent (BOLD), that is used to identify different brain areas that are activated during specific tasks and to infer the connectivity between different brain regions that may be interconnected, as it is shown in the resting state connectivity.

Methods:

A total of 16 voluntary subjects participated in this study, 8 patients with ALS (age 18-54) and 8 control subjects, age matched, without antecedents of neurologic or psychiatric disease. The images were acquired with a Philips magnetic resonance scanner, Ingenia 3.0 T with a 32 channel head coil. We acquired sagittal T13D-weighted images with spatial resolution of 1x1x1mm³, axial diffusion tensor images with 33 independent directions of diffusion and b of 1000 s /mm². Axial fMRI based on BOLD with echo planar images (EPI) technique, TR=2s and 150 dynamics. Axial T2FLAIR-weighted images were also acquired to identify intra cortical and supra cortical lesions. The software FSL v.2.0 was used for the analysis of the data.

Results:

The FA is decreased in the corticospinal tract in bilateral form and in the posterior limb of the internal capsule. The Voxel-wise Morphometry analysis shows a decrement of the volume of all the brain in patients with ALS. The motor network obtained by the resting state

images is affected in cerebellum in patients with ALS. In this study we tried to correlate these two different techniques of MRI to find biomarkers for a better diagnosis of the ALS even though it is important to mark that results are very dependent on the analysis method used, for that reason is very important to assure good reproducibility in the results.

SP106 - PR: Proton Therapy

TRACK 04: RADIATION ONCOLOGY

SP106.1 - Proton therapy – close to becoming mainstream

Author(s): [Thomas Bortfeld](#)

Massachusetts General Hospital and Harvard Medical School, Boston/UNITED STATES OF AMERICA

The number of patients treated with proton therapy is now well over 100,000. The field of proton therapy is growing at a remarkable and stable growth rate: the numbers double every ten years. To make this growth rate sustainable, and for proton therapy to become mainstream, we argue that two goals must be achieved: First, proton therapy must become cheaper and more compact. Secondly, we must be able to fully exploit the physical potential of proton therapy.

Many developments are underway to help with the first goal. Single room solutions and “compact” proton machines are becoming increasingly available. We will give an overview of the available options and report on our own experience with proton therapy retrofitted in a conventional treatment area. The biggest proton therapy component and one of the most expensive ones is the gantry. Based on an analysis of almost 5,000 patients treated with gantries in our center, we find that the vast majority of them could have been treated without the gantry. Developments of robotic patient positioning and immobilization, advanced in-room imaging solutions, as well as advances in pencil beam scanning delivery, will further reduce the need for a gantry.

The second goal requires the precise localization of the end of range of the proton beam in the patient. There are a number of developments underway to reduce range uncertainties. We will report on advances of measuring the proton range through the prompt gamma radiation produced by the proton beam in the patient. This will allow one to determine the proton range with millimeter precision in realtime.

SP106.2 - Monte Carlo-based Inverse Treatment Plan Optimization for Intensity Modulated Proton Therapy

Author(s): [Yongbao Li](#)¹, [Zhen Tian](#)², [Ting Song](#)², [Zhaoxia Wu](#)¹, [Yaqiang Liu](#)¹, [Steve B. Jiang](#)², [Xun Jia](#)²

¹Department Of Engineering Physics, Tsinghua University, Beijing/CHINA, ²Department Of Radiation Oncology, University of Texas Southwestern Medical Center, Dallas/UNITED STATES OF AMERICA

Intensity-modulated proton therapy (IMPT) can achieve a better dose distribution than passive scattering or uniform scanning. For IMPT optimization, Monte Carlo (MC) is desired for spots dose calculations because of the high accuracy in heterogeneous cases. Due to its capability of computing linear energy transfer (LET), MC-based IMPT planning is preferred in biological optimization scheme. However, MC simulation is too slow to be used for this purpose. Although GPU-based MC engine has been developed, the achieved efficiency is still not ideal. The purpose of this work is to develop a new scheme to include GPU-based MC into IMPT. The conventional approach for this purpose is simply using MC repeatedly for each spot dose calculations. However, this is not the optimal approach, because of the unnecessary computations on spots that turned out to have very small weights after IMPT optimization. Memory writing conflict also poses a challenge, if one sequentially compute dose at each spot. To solve these problems, we have developed a new MC-based IMPT plan optimization framework that iteratively

performs MC dose calculations and plan optimization. At each dose calculation step, the particles are sampled from different spots based on previously optimized spots intensity map with Metropolis sampling method. Simultaneous handling multiple spots also solves the memory writing conflict problem. We validated the proposed MC-based optimization schemes in one prostate case. It took 5-6 min of total computation time including both spots dose calculation and optimization with only one GPU card for the proposed method, whereas a conventional method naively using MC for spot dose calculations would be ~2-3 times slower.

SP106.3 - FoCa: a protontherapy treatment planning system written in object-oriented MATLAB

Author(s): Daniel Sanchez-Parcerisa, Alejandro Carabe
Radiation Oncology, Hospital of the University of Pennsylvania, Philadelphia/UNITED STATES OF AMERICA

Purpose: Monte Carlo transport codes are useful in protontherapy research as they provide accurate calculations, but at the cost of long calculation times. On the other hand, commercial treatment planning systems provide fast dose calculation but with limited access to the calculation engine behind them. To address these issues, we developed FoCa, an in-house treatment planning system, developed entirely in object-oriented MATLAB, which includes forward dose and LET calculation of proton radiotherapy plans in both active and passive modalities as well as a generic optimization suite for inverse treatment planning. **Methods:** Our approach was to provide the user with a set of classes dealing with the different aspects of a treatment planning system (CT importing, structure sets, dose kernel calculation, et cetera). We chose MATLAB for its fast prototyping capabilities, its speed at matrix calculations and its extensive geometry libraries. FoCa implements the proton-convolution-superposition algorithm for dose calculation and a similar pencil beam algorithm for analytical LET calculation. We included a user-friendly GUI for basic user interaction, as well as scripting capabilities for advanced operations. The inverse treatment planning framework is presented with an open architecture, not specific to any treatment mode or optimization algorithm, which allows researchers to work on their own optimization methods or therapy modalities. **Results:** We developed and tested the FoCa code. The validation results show a good agreement with the commissioning data, the 3D dose distributions based on patient-specific CT data calculated by a commercial treatment planning system, and 3D Monte Carlo calculations of dose and LET performed with Geant4. Finally, the inverse treatment planning suite was used to produce the first prototype of intensity-modulated, passive-scattered proton therapy, using 13 passive scattering proton fields and multi-leaf modulation to produce a concave dose distribution on a cylindrical solid water phantom without any field-specific compensator. **Conclusions:** We have demonstrated the validity and capabilities of the FoCa TPS in a wide range of setups. Its current and potential uses range from the fast calculation of any physical, radiobiological or clinical quantity in a patient CT geometry, to the development of new treatment modalities not yet available in commercial treatment planning systems. FoCa is currently available within our institution to a selected number of test users and it will be made available to the research community after all the necessary testing has been completed.

SP106.4 - Assessment of the limitations of the dose calculation algorithm of a commercially-available treatment planning system for proton pencil beam scanning

Author(s): Jessica E. Scholey, Liyong Lin, Christopher G. Ainsley
Department Of Radiation Oncology, The University of Pennsylvania, Philadelphia/PA/UNITED STATES OF AMERICA

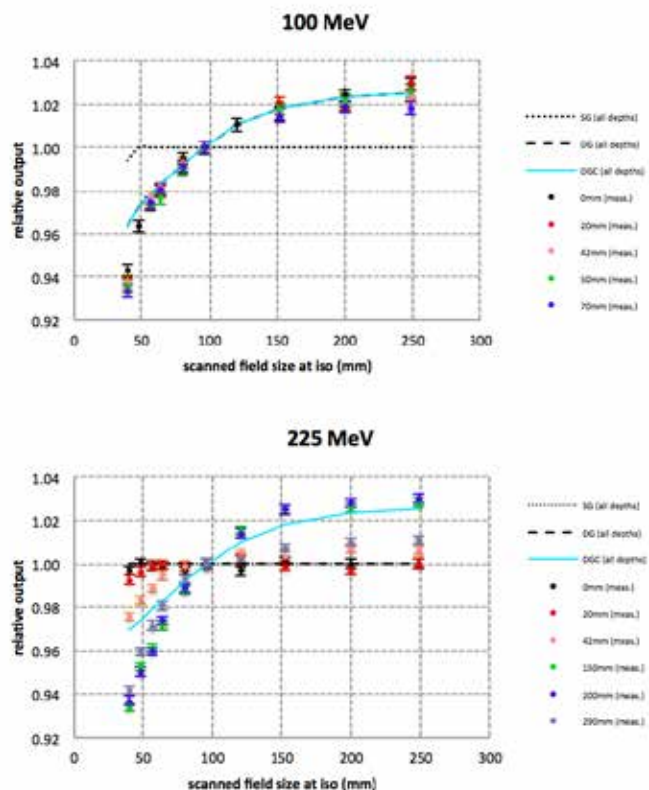
This study evaluates the accuracy and limitations of a commer-

cially-available treatment planning system's (TPS) dose calculation algorithm for proton pencil-beam scanning (PBS) and quantifies the sensitivity of the accuracy to the proton beam source modeling.

In-air fluence profiles of PBS spots were modeled in the TPS alternately as single- (SG) and double-Gaussian (DG) functions, based on fits to commissioning data. Uniform-fluence, single-energy-layer square fields of various sizes and energies were calculated with both beam models and delivered to water. Dose was measured at several depths (Figure 1). For lower energies (100-150 MeV), the DG model fits the measurements well at all depths, while the SG model does not. For higher energies (150-225MeV), both the SG and DG models fit the measurements well at shallow depths (< 4 cm), but not deeper, where dose contributions from proton-nuclear interactions become important, suggesting a limitation of the algorithm. The possibility of using, instead, a third model, based on double-Gaussian functions with parameters contrived to offset this inadequacy (DGC) was therefore investigated.

Eleven cuboid-dose-distribution-shaped fields with varying range/modulation and field size were subsequently generated in the TPS, using each of the three beam models described, and delivered to water. Dose was measured at the middle of the spread-out Bragg peak. Percent differences between calculated and measured doses (Table 1) were greatest for the SG model, increasing the smaller the field. The DG model showed improvements for all field sizes in shorter range beams, though the percent differences for smaller fields persisted in longer range beams. The DGC model was, however, able to predict the measurements to within 2% for all beams.

It can be concluded that while neither SG nor DG models, employed as intended, are ideally suited for routine clinical use, the TPS's DG model can be tuned judiciously to yield acceptable results.



cuboid plan (R = range, M = modulation, F = field size, all in cm)	% dose difference at mid-SOBP (TPS vs. measurement)		
	SG	DG	DGC
R12 M4 F4	7.1	1.5	1.4
R12 M4 F9.6	3.4	0.7	1.0
R12 M4 F20	1.9	1.9	1.9
R17 M9 F9.6	4.2	2.9	1.5
R22 M10 F4	6.5	5.3	0.7
R22 M10 F9.6	2.2	2.0	-0.5
R22 M10 F20	1.3	1.1	1.0
R27 M10 F9.6	1.0	1.1	-1.5
R32 M10 F4	6.3	6.1	0.5
R32 M10 F9.6	1.3	1.1	-1.3
R32 M10 F20	-0.4	-0.6	-0.5

SP106.5 - Impact of the microdosimetric spread on cell survival data analysis

Author(s): Gloria Bäckström¹, Fernanda Villegas-Navarro², Shirin A. Enger¹, Anders Ahnesjö²

¹McGill University, Montreal/CANADA, ²Uppsala University, Uppsala/SWEDEN

Purpose/Objective

The microscopic uncertainty of the energy imparted (microdosimetric spread, MDS) at the cellular/cell nuclei level due to the stochastic nature of ionizing radiation is normally not explicitly considered during parameterization of experimental survival fraction data. The magnitude of the MDS is higher for protons than for photons because of the known differences in track structures. The aim of this work is to present a method to quantify the impact of MDS on the biological radiation response. We estimate the effect on the α and β parameters of the linear quadratic (LQ) model used to describe experimentally obtained cell survival curves in different volumes sizes for various radiation qualities.

Materials and Methods

The Monte Carlo transport code LlonTrack was used to simulate event-by-event proton tracks in liquid water for the energies 0.91, 1.4, 1.72, 3.18, 3.59, and 4.97 MeV u^{-1} , as well as for a ⁶⁰Co source. The frequency distribution of specific energy for one track $f_1(z)$ and the dose dependent frequency distribution of specific energy $f(z,D)$ were calculated with in-house analysis codes for a range of spherical volume sizes typical of cell nuclei. Experimentally obtained survival curves intrinsically account for the MDS. When the specific energy z given by $f(z,D)$ is weighted with the LQ equation, $\exp[-(\alpha z + \beta z^2)]$, the α and β values based on D instead of z exclude the MDS variations and can be determined by fitting α and β to survival curves calculated from published α_{exp} and β_{exp} values. The RBE₁₀ at 10% survival with ⁶⁰Co as the reference radiation for the α_{exp} and β_{exp} was also factorized into a factor equal to the RBE for the fitted α and β values (RBE_{inh}), and a factor representing effects of the MDS (RBEMDS). RBEMDS for a tissue with variable cell nuclei sizes was calculated by weighting $f(z,D)$ with the size distributions presented by Poole *et al* [Submitted to *Med. Phys.* 2015] for healthy and tumor tissues.

Results

The $f(z,D)$ can be quite well represented by a narrow normal distribution for the lowest LET radiation (⁶⁰Co) even at small volumes, becoming wider and skewed towards lower specific energies with increasing particle LET. The relative MDS increases with decreasing dose and decreasing volume. The RBEMDS factor decreases with increase in LET and volume thereby reducing the RBE_{inh}. For a

heterogeneous size sample, the RBEMDS for healthy tissue reduces the RBE_{inh} the most when compared to the tumor tissue.

Conclusions

Our data suggests that the MDS in experimental data smears out the higher efficiency of the inherent RBE. The MDS component in a clinical scenario with an irradiated volume that consists of cells with different sizes might be smaller for tumor tissues than for healthy tissues due to the higher number of larger nucleus sizes in tumor tissues.

SP106.6 - Magnetically scanned-beam proton radiography using Micromegas detectors

Author(s): Derek Dolney¹, Godwin Mayers², Mitch Newcomer², Douglas Bollinger¹, Niral Desai², Robert Lustig¹, Kevin Teo¹, Richard Maughan¹, Timothy D. Solberg¹, Robert Hollebeek²

¹Radiation Oncology, University of Pennsylvania, Philadelphia/PA/ UNITED STATES OF AMERICA, ²Physics And Astronomy, University of Pennsylvania, Philadelphia/PA/UNITED STATES OF AMERICA

Purpose: While the energy of the therapeutic proton beams can be adjusted to penetrate to any given depth in water, range uncertainties arise in patients due in part to imprecise knowledge of the stopping power of protons in human tissues. Proton radiography is one approach to reduce the beam range uncertainty, thereby allowing for a reduction in treatment margins and dose escalation.

Methods: The authors have adapted a novel detector technology based on Micromesh Gaseous Structure ("Micromegas") for proton therapy beams and have demonstrated fine spatial and time resolution of magnetically scanned proton pencil beams, as well as wide dynamic range for dosimetry. In this work, proton radiographs were obtained using Micromegas 2D planes positioned downstream of solid water assemblies. The position-sensitive monitor chambers in the IBA proton delivery nozzle provide the beam entrance position.

Results: Radiography with Micromegas detectors and actively scanned beams provide spatial resolution of up to 300 μ m and water-equivalent thickness (WET) resolution as good as 0.02% (60 μ m out of 31 cm total thickness). Dose delivered to the patient by the proton radiography technique would be 2 cGy. The spatial resolution as a function of sample rate and number of delivered protons is found to be near the theoretical Cramer-Rao lower bound. Using the CR bound, we argue that the imaging dose could be further lowered to 1 mGy, and still achieve sub-mm spatial resolution, by relatively simple instrumentation and beam delivery modifications.

Conclusion: For proton radiography, high spatial and WET resolution can be achieved, with minimal additional dose to patient, by using magnetically scanned proton pencil beams and Micromegas detectors.

SP107 - Beam Delivery

TRACK 04: RADIATION ONCOLOGY

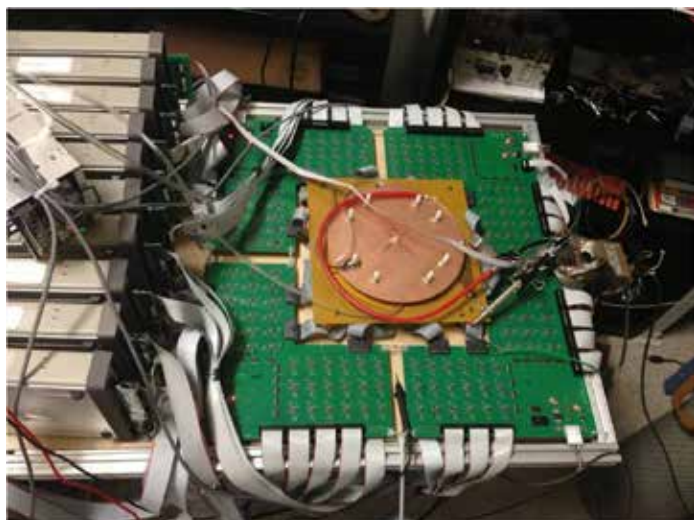


Figure 1: Prototype Micromegas-based system for proton radiography.



Figure 2: A radiography experiment in which the edge of a 1 mm piece of solid water on top of a 24 cm stack is imaged.

SP107.1 - A Quantitative Analysis of Teletherapy in Low Resource Settings: Cobalt or Linac?

Author(s): Rachel Mccarroll¹, Bassem Youssef¹, Beth Beadle¹, Maureen Bojador², Rex Cardan³, David Followill¹, Geoffrey Ibbott¹, Anuja Jhingran¹, Christoph Trauernicht⁴, Peter Balter¹, Laurence Court¹
¹University of Texas MD Anderson Cancer Center, Houston/UNITED STATES OF AMERICA, ²University of St. Tomas Hospital, Manila/PHILIPPINES, ³University of Alabama Birmingham, Birmingham/UNITED STATES OF AMERICA, ⁴Groote Schuur Hospital and University of Cape Town, Cape Town/SOUTH AFRICA

Purpose: There exists a deficit of more than 6,500 megavoltage teletherapy units worldwide, many in low resource-settings. Medical linear accelerators and cobalt units would address this need, and the tradeoffs between them have been compared qualitatively in the literature. Often discussed are dose rate, power infrastructure, and machine downtime all of which affect machine availability and treatment time. We have quantitatively addressed these topics and their effect on patient throughput (treatments/day).

Methods: Patient treatment time was calculated as the sum of patient set-up, beam-on, and mechanical motion time, with input data from clinical observation and electronic records (1000+ patients). The following treatment techniques were considered: linacs (conformal with MLC, Step-and-Shoot IMRT, Dynamic IMRT, and VMAT), and cobalt units (conformal therapy with and without MLC). Power data from The World Bank for 44 African countries were divided into three power scenarios based on frequency of outages. We assumed that cobalt units remain operable during outages using a backup generator. Machine downtime data was acquired from in-house records (linacs) or experienced users (cobalt).

Results: Low dose rates associated with cobalt units increase conformal treatment beam-on time between 0.6 and 2 minutes, depending on source activity. This represents between 14% and 28% of the total treatment time. Advanced modalities increase treatment time, particularly step-and-shoot IMRT which requires the most mechanical motion time, an average of 2.6 minutes (28% of total treatment time). VMAT and Dynamic IMRT treatments have shorter mechanical motion time (0.5 and 1 minutes, respectively) but longer beam on time (2 and 1.9 minutes, respectively). Patient throughput, under each of the seven treatment techniques and three outage scenarios, is shown below. In scenarios of “fewer” or “fewest” outages, the two machines are comparable when linac delivers conformal or VMAT treatments. If linac downtime is increased to account for availability of service parts and personnel, throughput is decreased by 6%, but conclusions remain unchanged. If a cobalt unit uses blocks instead of MLCs, throughput is reduced by 14-24% (1-3 block changes per fraction). Additionally, effects of machine utilization, IGRT usage, geographically specific cancer incidences (IARC data), fractionation schemes, and palliative or curative treatment goals were investigated.

Treatment Technique	Outage Scenario		
	Fewest	Fewer	Most
Linac Dynamic	1.5	1.5	1.5
Linac VMAT	1.5	1.5	1.5
Linac Conformal	1.5	1.5	1.5
Cobalt Conformal Year 1	1.5	1.5	1.5
Cobalt Conformal Year 2	1.5	1.5	1.5
Cobalt Conformal Year 3	1.5	1.5	1.5

Discussion: While additional aspects, including cost comparisons, dosimetric advantages, and personnel requirements remain to be addressed, this work establishes a framework for teletherapy implementation in low resources settings, and identifies power as the predominant influence on patient throughput.

SP107.2 - The study of Total Marrow Irradiation Based on Rotational Intensity-modulated techniques

Author(s): Shouping Xu¹, Chuanbin Xie², Baolin Qu², Wei Yu², Wei Xu², Xiaohu Cong², Xiangkun Dai²

¹Key Laboratory Of Particle & Radiation Imaging, Tsinghua University, Ministry of Education, Beijing/CHINA, ²Radiation Oncology, PLA General Hospital, Beijing/CHINA

Total body irradiation (TBI) is a special form of radiotherapy, generally as part of bone marrow conditioning regimens. Conventional TBI is difficult to achieve dose uniformity because of using the large field of simple technique. In recent years, tomotherapy technique has been used for TBI, due to delivering highly conformal and uniform target dose, and providing better normal structure avoidance. But this kind of technique isn't widely used for its expensive cost. Volumetric-modulated arc therapy (VMAT) could achieve rotational intensity modulation based on the traditional accelerator and may obtain the efficient and accurate treatment with the imaging-guided device. The purpose of this study is to compare the dosimetric characteristics and efficiency of RapidArc and Tomotherapy in total marrow irradiation (TMI) for hematologic malignancies in order to get the reference data for the choice of clinical application. Eight patient plans were retrospectively designed and analyzed for RapidArc and Tomotherapy. Total bone marrow was contoured as clinical target volume excluding the cubitus and hand part, then plus a 3.0mm margin as planning target volume. The prescription was 12Gy in 10 fractions. ArcCHECK system was used for dose verification, and the safety and accuracy of clinical delivery would be evaluated. The results of this study showed that the two techniques could well achieve the target coverage. The conformity indexes of RapidArc and Tomotherapy were 0.54 ± 0.05 vs 0.52 ± 0.07 ($p=0.45$), but Tomotherapy plans have a visible advantage over RapidArc plans in the dose uniformity of target. The homogeneity indexes were 0.19 ± 0.02 vs 0.13 ± 0.02 ($p=0.00$). Tomotherapy plans showed better in sparing of the critical organs apart from the whole brain, oral, parotid gland, the small intestine, rectum, and the maximum dose of lens of Tomotherapy plans was reduced by 41% comparing to RapidArc plans. The MUs and treatment delivery time of RapidArc and Tomotherapy were 2608MU/560s vs 12842MU/891s. The γ -analysis passing rates for head-neck, chest-abdomen, pelvic were $98.9\% \pm 1.9\%$, $98.4\% \pm 1.8\%$, $97.4\% \pm 2.1\%$ for RapidArc and $94.3\% \pm 1.5\%$, $96.5\% \pm 1.2\%$, $94.1\% \pm 1.9\%$ for Tomotherapy plans. This study shows that the two methods using RapidArc and Tomotherapy could achieve the acceptable dose of TMI, and the delivery efficiency of RapidArc was better than Tomotherapy. Two kinds of techniques are promising and can solve the clinic implementation of TMI.

SP107.3 - IMRT and VMAT comparison for a case of bilateral breast carcinoma

Author(s): Erick O. Montenegro¹, Juan F. Lucero¹, Rafael E. Lengua¹, Luis A. Linares¹, Milton E. Ixquiaco², Ricardo Contreras²
¹Medical Physics, HOPE International Radiotherapy Center, Guatemala/GUATEMALA, ²Physics, Universidad de San Carlos De Guatemala, Guatemala/GUATEMALA

Introduction: A comparison was made between IMRT and RapidArc (VMAT) plans for a patient with bilateral breast carcinoma involving supraclavicular lymph nodes and skin. The prescription dose is 50Gy (25 fractions, 2Gy each), one of our goals was to maintain the organs at risk (OAR's) as low as possible.

Objectives:

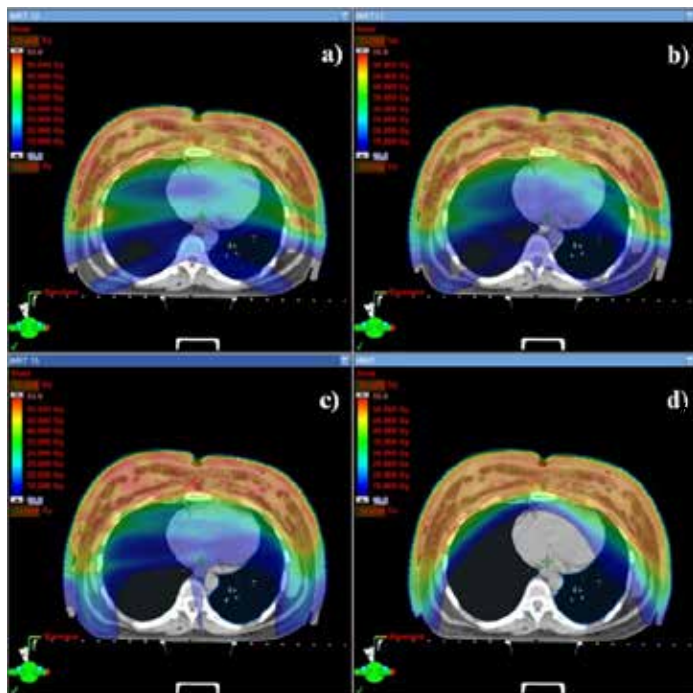
- Select the best suited treatment modality for the this case, taking into account the coverage to the PTV, the OAR's irradiation and the treatment delivery time.
- Evaluate the dosimetric parameters such as homogeneity, conformity index and monitor units.

Methodology: Four different treatment plans were created; three IMRT plans using 10, 11 and 16 fields and two full rotations VMAT.

All plans were optimized Eclipse (Ver.10.0) from Varian Medical Systems Inc. and delivered in a ClinacIX with Millenium Multileaf Collimator (120 MLC). The gamma evaluation was performed using the EPID AS500 and the ArcCheck from SunNuclear Corporation.

Results:

	IMRT 10	IMRT 11	IMRT 16	VMAT
DMinPTV	71.60%	74.60%	75.00%	83.80%
V20GyLung (L)	35.91%	31.12%	14.05%	16.60%
V20GyLung (R)	49.60%	43.00%	27.28%	16.72%
DMeanHeart	23.16 Gy	20.31 Gy	19.61 Gy	9.49 Gy
DMaxSpinal Cord	29.00 Gy	28.85 Gy	24.92 Gy	23.04 Gy
Homogeneity(D5% - D95%)	11.94	10.79	12.74	5.77
Conformity Index (V95% / VPTV)	1.04	1.04	1.01	1.04
Time(min)	14:55	16:05	22:30	3:57
Gamma Evaluation $\gamma < 1$ (EPID) $\Delta D=2\%$, $DTA=2mm$	95.71%	93.49%	93.09%	90.70%
Gamma Evaluation $\gamma < 1$ (ArcCheck)	81.85%	83.30%	64.60%	83.00%



1: Comparison of dose distributions.

Conclusions:

It was decided to treat the patient with the VMAT plan. It is observed that it presents better PTV coverage, but more importantly the OAR's receive less dose and it reduces drastically the treatment delivery time and the monitor units.

According to the gamma evaluation, all plans are equally reproducible.

References:

1. Giorgia Nicolini, **Simultaneous integrated boost radiotherapy for bilateral breast: a treatment planning and dosimetric comparison for volumetric modulated arc and fixed field intensity modulated therapy** *Radiation Oncology* 2009;4(27)
2. Low D A, **A technique for the quantitative evaluation of dose distribution.** *MedPhys*1998;25(5):656-661
3. Q.-R. Jackie Wu, **Quality of coverage: Conformity measures for stereotactic Radiosurgery** *MedPhys*,2003;4(4)

SP107.4 - Measuring the Location and Dynamics of the Beam Spot and Field Centre on a Therapy Linear Accelerator in X-Ray Mode

Author(s): Victoria C. Foss¹, Tyler S. Meyer², David P. Spencer²
¹Physics And Astronomy, University of Calgary, Calgary/CANADA, ²Medical Physics, Tom Baker Cancer Centre, Calgary/AB/CANADA

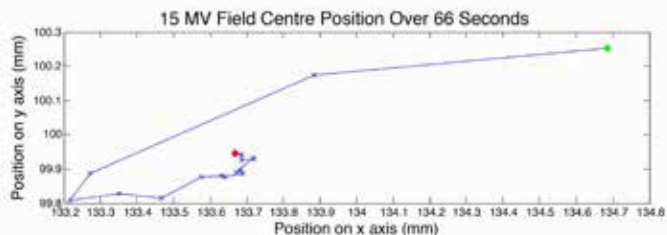
Introduction: On radiation therapy linacs the X-Ray source location, or beam spot, is critical to accurate treatment. Yet it is not measured. Instead, we accept that the vendors adjust symmetry and radiation-light field agreement. The beam spot will, therefore, be different for different photon energies. We set out to measure the location of the beam spot on a machine where the rad-light agreement was different for the 6 MV and 15 MV energies. We used images of the X-Ray projections of BBs at different source-to-object distances and 180° collimator rotations. We discovered that the beam spot actually moved during beam delivery. We believe this is due to the dynamic beam steering attempting to adjust beam parameters such as flatness and symmetry.

Methods: We mounted two 4 mm diameter Tungsten balls just off-axis on plastic trays in the upper wedge slot and in the cutout location of an electron cone. We took images at about 5 second intervals on a Varian Trilogy™ using an output rate of 100 MU/min in Service Mode on the linac and AM Maintenance High Quality mode on the aSi-1000 portal imager with a 4x4 cm field for both 90° and 270° collimator angles. We do not think the use of Service mode invalidated the use of our data for Clinical mode. Only the Collimator and Accessory interlocks were overridden. The images are analyzed using Doselab™.

Results: We observed that for 15X the field centre moved as much as 1.5 mm at the isocentre over the first 30 seconds of beam (see Figure), while our 6X beam moved about 1 mm. We also tested a stereotactic cone which showed field motion up to 0.3 mm at 6X and 0.6 mm at 15X. This motion made it difficult to measure the location of the beam spot, since two separate images were required to determine its location. Assuming that sequential runs showed the same pattern, we paired the images to show that the beam spot moved about 0.15 mm for 6X, settling about 0.14 mm from the rotational axis. For 15X it moved 0.4 mm, settling about 0.12 mm from the rotational axis.

Conclusions: This means that beam spot size measurements assuming the beam is static may be incorrect. SRS delivery may be af-

ected. Field symmetry and location will be time-dependent, so the QC time-scale should reflect clinical use. Investigations will continue on our other 8 linacs.



SP107.5 - Monte Carlo based optimization of flattening filters for a cobalt-60 total body irradiation unit

Author(s): Ingrid H. Lai¹, Chandra P. Joshi², Ling B. Xu³, L John Schreiner²

¹Department Of Physics, Engineering Physics & Astronomy, Queen's University, Kingston/ON/CANADA, ²Medical Physics Department, Cancer Centre of Southeastern Ontario, Kingston/ON/CANADA, ³Engineering, Best Theratronics, Ottawa/ON/CANADA

Introduction:

A dedicated total body irradiation (TBI) unit (GammaBeam 500, designated here as the GB-500) is being developed by Best Theratronics (Kanata, ON). It uses a cobalt-60 source with a fixed rectangular collimator and brass flattening filters to produce clinically useful fields at a source to treatment axis distance (SAD) of ~220cm. Different filters are required to maintain an appropriate constant dose rate (within 5% of ~20MU/min over the treatment length) as source decays and to accommodate local treatment protocols. The calculation of filter shapes using simple ray-tracing approximations is complicated by the large source size and broad beam geometry. In this work we compare measured beam profiles to Monte Carlo (MC) calculated profiles for the open beam and beams flattened by two prototype/testing filters. The validated MC simulations are then used to design alternate filters. The goal is to provide a design tool so that filters required for various clinical implementations of the GB-500 can be designed rigorously and not by trial and error.

Materials and Methods:

The dose profiles along the two axes of an open and two filtered fields (filter A, and a thicker filter B) of the GB-500 were measured with a Standard Imaging (Middleton, WI) A12 ion chamber at 10cm depth in the centre of a 30x30x27cm³ (small) solid water phantom placed at various positions. These profiles were then calculated using the EGSnrc MC code (National Research Council, Canada) set to the conditions of the GB-500. Doses were calculated at 10cm depth in a continuous 360x120x27cm³ (large) water phantom and in the same small phantom as used in measurements. Over 60 billion histories were run on a CPU cluster to achieve an estimated dose uncertainty of <0.8% in the clinically useful field.

Results and Conclusions:

Measured and MC calculated longitudinal profiles are shown in Figure 1. For both filters, the beam flatness over 200cm treatment length for measured doses is approximately 3%. The beam flatness for MC calculated doses is slightly better for filter B (5%) than for filter A (6%). MC calculated doses (in both the small and large phantom) differ from the measured doses (in the small phantom) by a maximum and average of around 4% and 1% respectively, for all open and flattened fields. The agreement shows that the MC simulation faithfully models the GB500. Additional results showing prediction for new filter designs will be presented.

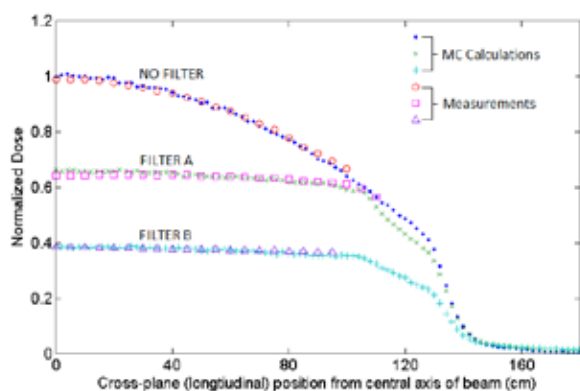


Figure 1: A comparison of MC calculated and measured dose profiles at 10 cm depth in water at SAD = 220 cm for open and filtered beams of the GB-500 TBI unit.

SP107.6 - Monte Carlo study for the design of a novel Gamma-Tomo SBRT system

Author(s): Grisel M. Mora¹, Omar Chibani², Ahmed Eldib², Jinseng Li², C.M Ma²

¹Institute Of Biophysics And Biomedical Engineering, University of Lisbon, Lisbon/PORTUGAL, ²Radiation Oncology, Fox Chase Cancer Center, Philadelphia/UNITED STATES OF AMERICA

Introduction: The ⁶⁰Co beam emerging from the Gamma-Tomo source assembly was simulated in a previous study [1] and the authors reported the spectra of particles reaching the plane immediately (1mm) before the collimation system entrance. In the present work, we simulate the ⁶⁰Co beam emerging from a novel Gamma-Tomo SBRT collimation system and calculate the output factors and dose rates for different source configurations and collimator sizes.

Methods: A Gamma Tomo system includes 13 ⁶⁰Co source capsules, source housing, a primary collimator and 4 different changeable collimators. The sources (6.22 mm of diameter) are located in 2 rows with different angles and distances to the longitudinal axis and the beams can be collimated to obtain four different circular field sizes at the isocenter (35 mm, 16 mm, 7mm, and 3.5mm). The BEAM-Monte Carlo [2] code is used to realistically model the collimation system geometry, including primary collimator and 4 different changeable collimators. The previously calculated phase space file [1] is used to transport particles throughout the collimation system to the patient plane for all of the changeable collimators of the Gama-Tomo System, and the respective phase space files of particles are stored at isocenter for each of the circular fields to be used as input of the GEPTS [3] to perform dose calculations. A newly designed geometry module is used to determine the dose distributions in a spherical polystyrene phantom with an 8cm radius centered at the isocenter.

Results: The characteristics of the particle spectra emerging from the collimation assembly are determined and the effect of the source-collimator position on the spectra reaching the isocenter found to be dependent on field size. We observed differences up to 5% between the energy spectra and fluence distributions calculated for different configurations of the source-collimator assembly. The effect of the source-collimator position is observed (up to 6%) on dose distributions calculated at isocenter and is dependent upon the size of the circular field.

Conclusions: The resulting data from the present study supports the machine design process and is valuable in building a well-represented source model for all sources to perform the dose calculations for all of the changeable collimators for this novel Gamma-Tomo system.

References:

- 1) G. Mora, O. Chibani, A. Eldib, J. Li, C. M. Ma. Monte Carlo Source Simulation for a novel Gamma-Tomo SBRT system. 2014 - AAPM abstract.
- 2) D.W.O. Rogers, B. A. Faddegon, G.X. Ding, C. M. Ma, J. Wei, and T. R. Mackie, BEAM: A Monte Carlo code to simulate radiotherapy treatment units. Med. Phys. 22, 1995.
- 3) O.Chibani, B.Moftah and C.M. Ma, On Monte Carlo modelling of megavoltage photon beams: A revisited study on the sensitivity of beam parameters, Med. Phys. 38, 2011.

SP107.7 - A dosimetric evaluation of flattening filter-free volumetric modulated arc therapy for postoperative treatment of cervical cancer

Author(s): Fuli Zhang

Radiation Oncology Department, The Military General Hospital of Beijing PLA, Beijing/CHINA

AIMS: To compare flattening filter free (FFF) beams and conventional flattening filter (FF) beams in volumetric modulated arc therapy (VMAT) of cervical cancer after surgery through a retrospective planning study. **MATERIALS AND Methods:** For a cohort of 15 patients, VMAT plans of FFF beams and normal flattened (FF) beams were designed. The prescribed dose was 45Gy/1.8Gy/25f, 95% of the planning target volume received this dose. Doses were computed with a commercially available TPS using Monte Carlo (MC) algorithm. Plans were compared according to dose-volume histogram (DVH) analysis in terms of PTV homogeneity and conformity indices (HI and CI) as well as OARs dose and volume parameters. **Results:** FFF-VMAT was similar as FF-VMAT in terms of CI, but inferior to the latter for HI. No statistically significant differences were observed between FFF-VMAT and FF-VMAT in terms of pelvic bone marrow, small bowel, bladder and rectum. **Conclusions:** For patients with cervical cancer after hysterectomy, the FFF beam achieved similar target and OARs dose distribution as the FF beam. Reduction of BOT in cervical cancer is beneficial.

SP108 - Patient and Occupational Dose Assessment

TRACK 05: DOSIMETRY AND RADIATION PROTECTION

SP108.1 - Radiation dose to patients from cardiac interventions performed using image intensifier, flat detector and novel flat detector systems

Author(s): Roshan S. Livingstone¹, Anna Varghese¹, Paul V. George²
¹Radiology, Christian Medical College, Vellore/INDIA, ²Cardiology, Christian Medical College, Vellore/INDIA

Background: Radiation dose to patients from interventional cardiology are of concern whether it is being performed using image intensifier (II) or flat detectors (FD). There are very few reports on achieving reduced doses using novel FD systems with advanced real-time image noise reduction algorithms and optimized acquisition chain. This study intends to compare radiation doses from cardiac interventions performed using II, FD and novel FD systems.

Design and Methods: Coronary angiography (CA) and single stent percutaneous transluminal coronary angioplasty (PTCA) were performed using Philips Integris H5000 II, Philips Xper FD10 and Philips Allura ClarityFD10 mono plane systems (Philips Healthcare, Netherlands). The novel FD - Allura clarityFD10 was equipped with real-time noise reduction algorithms and optimized acquisition chain for dose reduction. Dose area product (DAP) was measured using DAP meter available in all systems. During interventions, low dose protocol with 0.4mm Cu filter for fluoroscopy and 0.1mm Cu for cine runs were selected in all systems.

Results: Tables 1 and 2 show dose related information for CA and PTCA performed in II, FD and novel FD systems. During fluoroscopic screening, DAP values were similar in all systems. However, during cine runs, a reduction of the order of 60% and 30% in DAP was observed in novel FD when compared to II and FD respectively. A 20 – 50% reduction in the overall doses could be achieved with the use of novel FD systems during CA procedures following standard imaging protocol.

Conclusion: Though all systems utilised stringent dose reduction strategies involving heavy filtration; significant dose reduction without compromising diagnostic image quality was observed using novel FD systems involving real time image noise reduction algorithm.

Table 1: Radiation doses from CA different angiography systems

	Integris II	Xper FD10	Clarity FD10
n	28	39	140
Fuoro time(min)	3.96 (0.4 – 10.2)	2.11 (0.5 - 6.23)	3.24 (0.5 – 10.5)
cine runs	8.14 (5 – 13)	6.7 (4 – 10)	7 (4 – 14)
Fuoro DAP-Gycm2	5.53 ± 1.13 (0.6 – 15.4)	5.46 ± 3 (1.3 – 13.4)	5.53 ± 3.6 (0.9 – 16)
Cine DAPGycm2	22.18 ± 2.02 (11.4 – 57.2)	11.92 ± 4 (3.6 – 21.2)	8.44 ± 4.2 (1.5 – 28.2)
Total DAPGycm2	27.7 ± 2.49 (12.6 – 69)	17.4 ± 5.7 (6.6 – 28.8)	13.9 (4 – 37.6)

Table 2: Radiation doses from PTCA performed using different angiography systems

	Integris II	Xper FD10	Clarity FD10
n	18	12	43
Fuoro time(min)	11.57 (5 – 30)	8.7 (3.5 – 13.4)	10.8 (5 – 26.5)
cine runs	17.2 (8 – 31)	15 (9 – 20)	16.2 (7 – 27)
Fuoro DAPGycm2	17.88 ± 9 (6.9 – 39)	16.1 ± 8.9 (9.8 – 22.4)	17.2 ± 10 (6 – 39.5)
Cine DAPGycm2	30.79 ± 16 (9 – 66.2)	18 ± 11.8 (9.6 – 26.4)	16.5 ± 9 (5.4 – 31)
Total DAPGycm2	48.7 ± 25 (21.3 – 98)	34 ± 33 (18.6 – 40.6)	33.7 ± 18 (11.4 – 70.1)

SP108.2 - First National Occupational Radiation Dose Registry in Ministry of Health and its Validation: An Oman Experience

Author(s): Arun Kumar L S, Rashid Al-Hajri, K Jaseer, Saeed Al-Kalbani
 Medical Physics, Ministry of Health, Muscat/OMAN

In Ministry of Health (MOH), Oman; radiation is used for diagnosis, radiation therapy, bio-medical research and for the irradiation of blood & blood products. As per the IAEA Basic Safety Standards (2014), it is the responsibility of the employer to make arrangements for the assessment & recording of occupational exposures and for the workers' health surveillance. Not only that, the records of occupational exposure for each worker must be maintained during and after the worker's employment, at least until the worker attains the age of 75 years, and for not less than 30 years after cessation of the work. However, the current national radiation protection legislation

of Sultanate of Oman does not mandate the recording of occupational doses or a national dose registry. To overcome this problem in MOH, Oman; we developed the first National Occupational Radiation Dose Registry (NORDR) for its workers.

This in-house developed NORDR - Centralised Dose Recording System (CDRS) - for the management of personal monitoring of radiation workers, is having about 1500 radiation workers in about 145 health facilities. Each one of them is monitored by issuing a Thermo Luminescent Dosimeter (TLD) every month through the CDRS by tagging the serial number of each TL dosimeter with the unique MOH staff number of each worker by post for a wear period of one month. Some of the above locations are very remote - few thousand kilometers away from the capital city, Muscat. End of every month, the TLD's are collected back and processed for Hp(10) and Hp(3). Upon estimation and recording of doses, individual and institutional dose reports are sent to the health facilities. The cumulative annual dose report of each worker is also dispatched from the NORDR facility to each worker.

CDRS also records age, sex, category of staff, section and department of staff, duration of work with radiation, dose received prior to joining MOH, any episode of an overexposure or any suspected over exposure, annual and cumulative radiation dose of each radiation worker etc. If a worker uses more than one TL dosimeter such as for forehead, lens, ring right, ring left etc; each will be accounted and accordingly dose will be estimated according to the type & the corresponding dose report will be generated. Also, the same software will handle the individual dose(s) of each worker on a monthly, quarterly, half-yearly, yearly basis and the dose history for the entire period of radiation job. CDRS will also perform the dose analysis of an individual worker, a group of workers in an institution and all the radiation workers available in CDRS as a whole. If a worker exceeds the annual dose limit or investigation level, the CDRS will alert accordingly. The details of our in-house national occupational radiation dose registry - CDRS - will be further discussed during presentation. This dose registry can be emulated by other countries those who do not have a national dose registry for their radiation workers especially for those who are having relatively smaller number of radiation workers.

SP108.3 - Assessment of Patient and Staff Doses in Interventional Cerebral Angiography Using OSL

Author(s): Chryzel Angelica B. Gonzales

Center For Device Regulation, Radiation Health, And Research (cdrrhr), Department of Health (DOH) - Food and Drug Administration (FDA) Philippines, Manila City/PHILIPPINES

Assessment of Patient and Staff Doses in Interventional Cerebral Angiography Using OSL

Chryzel Angelica B. Gonzales, M.Sc.1,2 and Augusto A. Morales, Jr., D.Sc. 1,2.

¹The Graduate School, University of Santo Tomas, Manila, Philippines

²Center for Device Regulation, Radiation Health and Research, Food and Drug Administration, Department of Health, Manila, Philippines

Abstract— In interventional radiology (IR) procedures, radiation doses received by both patient and staff are relatively high. The objectives of the study are: (1) determine/measure entrance surface dose (ESD) to patient using nanoDot optically stimulated luminescence (OSL) dosimeter, (2) verify that patient doses do not exceed established international guidance levels set by IAEA and ICRP Report 103, as stated in the BSS, applied in the Philippines, (3) estimate the effective dose E to operator and using InLight OSL dosimeters, (4) estimate the annual effective dose E for the operator

and staff performing interventional cerebral angiography procedure, (5) determine who among the staff have training in radiation protection in interventional radiology/cardiology, and if so, if such training is applied in practice, and (6) verify that staff doses do not exceed established dose limits set by the IAEA and ICRP Report 103, as stated in the BSS, applied in the Philippines.

Clinical data and technical factors were gathered from interventional cerebral angiography procedures (4-vessel angiogram/6-vessel angiogram) performed at the University of Santo Tomas Hospital (USTH). It was found that none of the ESD values approach the dose thresholds for induced skin injuries (erythema or epilation). The estimated weighted annual dose for all the interventional medical workers is 5.9 mSv which is lower than the dose limit given by the IAEA and ICRP Report 103, as stated in the BSS. However, the primary operator has exceeded the investigation level of 30% of the annual dose limit of 20 mSv (13.44 mSv in the case of research badge #3). The computation of the annual dose for this study was based on a survey for the maximum number of IR procedures performed per year.

SP108.4 - A wireless personal dosimeter for Interventional Radiology medical personnel.

Author(s): Leonello Servoli¹, Massimiliano Paolucci², Maurizio Biasini³, Lucia Bissi³, Andrea Calandra³, Bruno Checcucci¹, Stefania Chiocchini³, Roberto Cicioni³, Elia Conti¹, Roberto Di Lorenzo², Anna C. Dipilato³, Stefania Fabiani⁴, Nevio Forini¹, Daniel Magalotti⁵, Agostino Maselli², Daniele Passeri³, Andrea Pentiricci⁶, Pisana Placidi³, Maurizio Scarpignato², Andrea Scorzoni³

¹Istituto Nazionale di Fisica Nucleare, Sezione Perugia/ITALY, ²AUSL Umbria 2, Foligno/ITALY, ³Università degli Studi di Perugia, Perugia/ITALY, ⁴Università degli Studi dell'Aquila, L'Aquila/ITALY, ⁵Università degli Studi di Modena e Reggio Emilia, Modena/ITALY, ⁶AUSL Umbria 1, Perugia/ITALY

A personal wireless active dosimeter prototype has been developed to be worn by medical staff during Interventional Radiology procedures to obtain real-time measurement of the dose-rate.

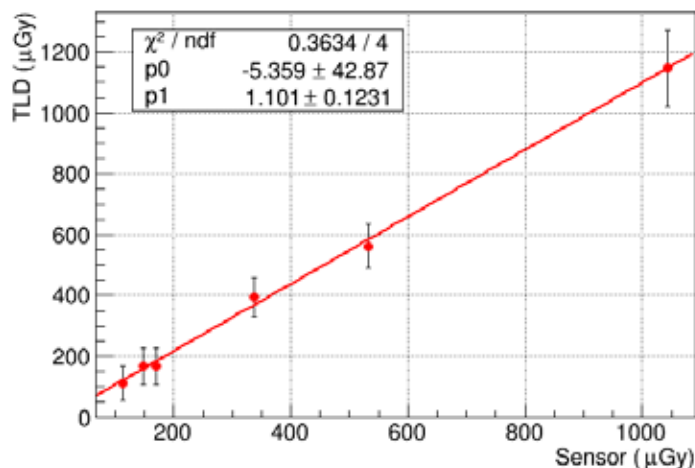
It has been tested both on phantom and during several different medical procedures. It is battery powered with an autonomy up to 8 hours.

The dose-rate measurement is performed at a frequency of 5 Hz, and transmitted to the receiving station with no dead time and a packet error rate less than 1%. Even this small information loss could be recovered with simple data handling strategies, transmitting the integrated dose at the end of each procedure.

The dose-rate measurement capability, using a certified X-ray beam facility, is linear up to 400 microGy/s, higher than the rate diffused by the most demanding procedures, while there is virtually no upper limit on the dose measurement linearity, as long as the battery is working, because the sensor element is reset after each measurement (> 1.5 Gy/h).

The sensitivity to diffused photon energy is below 10 keV.

The linearity of the response to an absorbed dose during medical procedures is shown in the following picture, where on the horizontal axis are reported the dose measured by the prototype and on the vertical axis the dose measured by the control dosimeter system (TLDs). Both systems have been calibrated simultaneously on the same certified X-ray beam.



A measurement precision between 5 and 10%, compared to reference dosimeters and dominated by their measurement uncertainty, has been obtained either on phantom than during actual medical procedures.

SP109 - Micro- and Nano-Dosimetry

TRACK 05: DOSIMETRY AND RADIATION PROTECTION

SP109.1 - Development of a Thick Gas Electron Multiplier Based Multi-element Microdosimetric Detector

Author(s): Zahra Anjomani¹, Andrei R. Hanu², Sahar Darvish-Molla¹, William V. Prestwich¹, Soo H. Byun¹

¹Medical Physics And Applied Radiation Sciences, McMaster University, Hamilton/CANADA, ²NASA Goddard Space Flight Center, Greenbelt/UNITED STATES OF AMERICA

A prototype multi-element gaseous microdosimetric detector using Thick Gas Electron Multipliers (THGEM) has been designed and constructed for monitoring mixed neutron-gamma radiation fields¹. The multi-element design was employed to increase the neutron detection efficiency²⁻³, particularly for weak radiation fields commonly encountered in radiation protection applications. Owing to the absence of wire electrodes, the THGEM multi-element detector offers flexible and convenient fabrication⁴. The prototype THGEM multi-element detector consists of alternating layers of tissue-equivalent plastic hexagons and each layer houses an array of cylindrical gas cavity elements with equal height and diameter. The fundamental signal and stability performance of the THGEM detector was tested using a ²⁴⁴Cm alpha source and the detector responses to various neutron fields are currently under comprehensive investigation using the ⁷Li(p,n) neutron source at the McMaster Tandatron accelerator. A preliminary result on the neutron microdosimetric and absorbed dose responses of the prototype detector will be presented in contrast to the responses of a commercial detector.

[1] Z. Anjomani, A.R. Hanu, W.V. Prestwich, S.H. Byun, Nucl. Instr. and Meth. in Phys. Res. A 757 (2014) 67.

[2] H.H. Rossi, Health Phys. 44 (1983) 403.

[3] P. Kliauga, H.H. Rossi, G. Johnson, Health Phys. 57 (1989) 631.

[4] G.M. Orchard, K. Chin, W.V. Prestwich, A.J. Waker, S.H. Byun, Nucl. Instr. and Meth. in Phys. Res. A 638 (2011) 122.

SP109.2 - Development of a 2-D THGEM Microdosimetric Detector

Author(s): Sahar Darvish-Molla¹, Andrei R. Hanu², Zahra Anjomani¹, William V. Prestwich¹, Soo H. Byun¹

¹Medical Physics And Applied Radiation Sciences, McMaster University, Hamilton/CANADA, ²NASA Goddard Space Flight Center, Greenbelt/UNITED STATES OF AMERICA

Inspired by our prototype Thick Gas Electron Multiplier (THGEM) detector [1,2], an advanced two-dimensional microdosimetric detector is currently under development at McMaster University. This detector aims to measure the spatial distributions of high and low linear energy transfer radiation doses simultaneously in mixed radiation fields, which will enable us to overcome the operational limitation of the classical tissue-equivalent proportional counters (TEPCs), particularly for high dose rate fields. Compared to the traditional TEPCs, wire electrodes were replaced by THGEM, which not only enhances the gas multiplication gain but also offers a flexible and convenient fabrication process for building two-dimensional detectors.

A prototype detector consists of an array of 3×3 gas cavities, equivalent to 9 TEPCs, each of which has a dimension of 5 mm diameter and length. By filling its sensitive volume with propane based tissue

equivalent gas, at a pressure of 167 torr, each detector simulates a spherical soft tissue of 2 μm in diameter. To process nine detector signals simultaneously, taking the overall cost, size and flexibility into account, we developed a multi-input digital pulse processing system using a modern microcontroller interfaced with an ADS807 12-bit sampling ADC with a sampling rate of 42 Msps. The prototype signal processor was tested using a NaI(Tl) detector and the test results have proven that it is faster than a traditional analogue system and a commercial digital system. Using the McMaster Tandemron $^7\text{Li}(p,n)$ accelerator neutron source, both signal performance as well as neutron dosimetric response of the detector have been extensively investigated. A preliminary test result will be presented.

SP109.3 - Quantum versus classical trajectory Monte Carlo simulations of low energy electron transport in condensed media

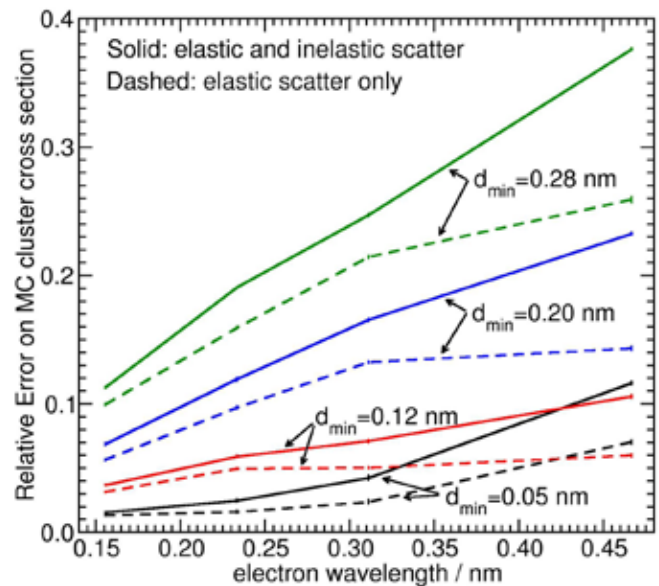
Author(s): Rowan Thomson¹, Iwan Kawrakow²

¹Physics, Carleton University, Ottawa/CANADA, ²ViewRay Inc, Cleveland/UNITED STATES OF AMERICA

Widely-used Monte Carlo simulations of electron transport neglect the quantum wave nature of electrons; however, quantum effects have the potential to be non-negligible at sub-1 keV energies. Low energy simulations are increasingly employed across medical physics and beyond to model the interactions of radiation with matter on sub-micron scales, e.g., interactions of electrons with DNA. This work compares quantum mechanical (QM) and classical trajectory Monte Carlo (MC) simulations for low energy electron transport.

A simplified model of electron scattering in small volumes (nanometre droplets) of condensed media, e.g. water, consisting of $> 10^3$ point scatterers (molecules) is developed. Adjustable model parameters include the number of scatterers, average and minimum distances between scatterers (d_{av} , d_{min}), cross sections for elastic and inelastic scattering, and droplet size and shape. QM calculations involve numerically solving $\sim 10^3$ coupled equations for the electron wavefield incident on each scatterer in a droplet. Results are averaged over $> 10^4$ droplets, each having different scatterer positions but with the same parameters. Average QM water droplet incoherent cross sections and scattering event densities are compared with MC results. A relative error (RE) on MC results is computed.

RE is highly sensitive to electron wavelength (energy), scatterer density, droplet shape and structure, and the presence of inelastic scatter. The figure shows the RE on droplet incoherent cross section plotted as a function of electron wavelength for water droplets (radius and length of 2.124 nm) with the realistic average scatterer spacing of $d_{av}=0.311$ nm for varying levels of structure (d_{min}) as well as with and without inelastic scatter (always with elastic scatter). As shown in the figure, it is generally found that RE increases considerably with increasing d_{min} , corresponding to more structured water (representative of water in the human body). Further, introducing inelastic scatter while maintaining the same elastic scattering cross section increases RE, suggesting that electron mean free path is a relevant length scale. It is also found that droplet cross section and relative error on MC results are sensitive to droplet size and shape, with considerable errors observed in changing droplet size and shape.



In condensed media, the quantum wave nature of electrons may be non-negligible for simulation of sub-1 keV transport. These results within a simplified model of electron transport in condensed media suggest that electron transport is strongly affected by the structure of the medium and that inelastic scatter does not necessarily improve agreement between QM and MC simulations.

SP109.4 - Investigation of the relations between absorbed dose to cellular targets and to bulk tissue for kilovoltage radiation using Monte Carlo simulations and cavity theory

Author(s): Patricia Oliver, Rowan Thomson

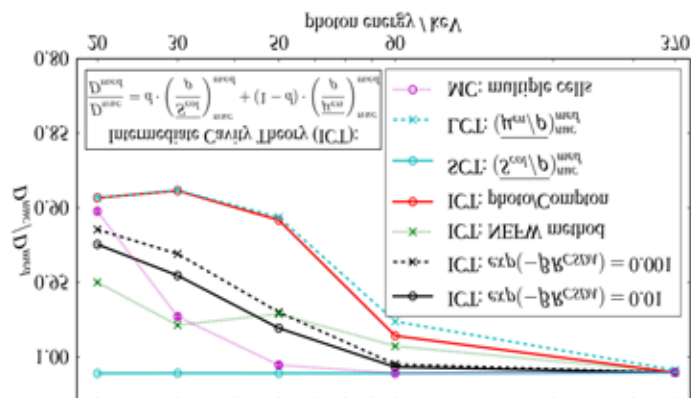
Physics, Carleton University, Ottawa/CANADA

Relationships between macroscopic (~ 1 mm) and microscopic (cellular) dose descriptors for incident photon energies between 20 and 370 keV are investigated using Monte Carlo (MC) simulations and cavity theory.

MC simulations of clusters of cells, single cells, and single nuclear cavities embedded in phantoms are carried out for various normal and cancerous tissues; cell (nucleus) radii range from 5 to 10 microns (2 to 9 microns). Results are compared to cavity theory predictions for the dose to a cavity of nuclear size and elemental composition embedded in a bulk tissue phantom (D_{nuc}), relative to the dose to the corresponding average bulk medium (D_{med}). Large (LCT), small (SCT), and various intermediate (ICT) cavity theory approaches are investigated. The ICT approach (see figure) is a weighted sum of SCT and LCT contributions (stopping power and energy absorption coefficient ratios, respectively). Approaches for computing the weighting parameter d include MC simulations determining the fraction of cavity dose due to electrons set in motion by photons interacting in the surrounding medium ('ICT: NEFW method') and others involving Burlin's approach (1969) where $d = (1 - \exp(-\beta L)) / \beta L$, with β given by $\exp(-\beta R_{CSDA}) = 0.01$ or $\exp(-\beta R_{CSDA}) = 0.001$ and L is the cavity's mean chord length, taking R_{CSDA} as the CSDA range corresponding to the most energetic electron or using a weighted sum of photoelectron and Compton electron components ('ICT:photo/Compton').

The ratio D_{nuc}/D_{med} varies considerably with tissue type, cell and nucleus size and elemental composition, and source energy. ICT predictions for D_{nuc}/D_{med} are highly sensitive to the method used to estimate the parameter d . The figure provides example results for

the dose ratio D_{nuc}/D_{med} for one cell model (cell and nucleus radii of 7.35 and 5 microns, respectively) in melanoma tissue; MC results give dose to the nucleus of the central cell in a multiple cell model. At low energies, LCT qualitatively predicts nuclear doses, whereas at energies above 50 keV, SCT predictions are reasonable. In general, over the range of energies and simulation geometries (tissues, cell types) considered, ICT with Burlin's approach ('ICT: $\exp(-\beta R_{CSDA})=0.01'$) provides the best estimate of D_{nuc}/D_{med} , resulting in an average discrepancy of 4%. However, no cavity theory method accurately predicts MC results over the entire range of energies and simulation geometries; thus, there is no general conversion method to obtain dose to the cellular nucleus from macroscopic dose descriptors. Further, neither dose to water nor dose to medium provides an accurate estimate of nuclear dose.



SP109.5 - Development of transmitted alpha particle microdosimetry using Timepix: Investigation of A549 lung carcinoma cells exposed to alpha particles irradiated from Ra-223

Author(s): Ruqaya Al Darwish¹, Alexander H. Staudacher², Eva Bezak¹

¹Department Of Medical Physics, Royal Adelaide Hospital, Adelaide/AUSTRALIA, ²Centre For Cancer Biology, Translational Oncology Laboratory, Adelaide/SA/AUSTRALIA

Aim

To investigate the survival of A549 human lung carcinoma cells when irradiated with α -particles.

To correlate the number of DNA double-strand breaks (DSBs) per cell with the number of transmitted α -particles from Ra-223.

Materials and Methods

A549 cells were seeded at 15,000 cells on transwell inserts (0.14 cm²). The transwell system consists of two compartments: a larger well containing an evaporated Ra-223 source and an insert with a 10 μ m thick polycarbonate membrane to which cells adhere.

The Timepix detector, Amsterdam Scientific Instruments, is a hybrid semiconductor pixel radiation detector. It consists of a pixelated silicon layer of 256 x 256 pixels (55 μ m² each) bump-bonded to a CMOS pixel readout chip. Experiment setup is shown in figure 1 (A). Transmitted α -particles were detected and imaged with respect to seeded cells (figure 1 (B)). The quantitative correlation between the distribution of α -particle hits and cell damage was investigated for 1-5 hours irradiation times.

To assess the cell radiation damage, unirradiated (controls) and irradiated cell monolayers were stained with the DNA DSB marker γ -H2AX (green staining) and cell nuclei were counterstained with DAPI (blue staining). The number of DNA DSBs per cells after irra-

diation as well as the total damaged cell count were determined.

Results

γ H2AX staining showed that the number of DNA DSBs was six-fold higher for 5 hour irradiated cells compared to controls. The incidence of 6 and more DSBs in an irradiated cell was 22 times higher compared to control cells. These numbers correspond to more than 5000 transmitted α -particles.

Conclusion

Timepix can be used effectively as a transmitted microdosimetry detector, providing high resolution images and excellent spatial resolution of detected α -particles. The relationship between the number of transmitted α -particles and the number of the DNA DSBs is being evaluated for us in targeted alpha therapy.

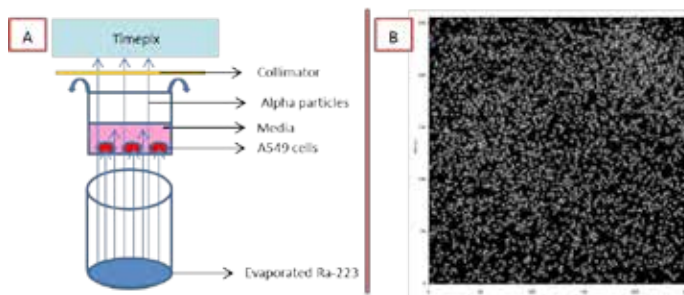


Figure1: A) Experimental setup: Timepix chip was mounted above the A549 monolayer with an evaporated Ra-223 α -source underneath. B) Detection of transmitted α -particles using Timepix.

SP110 - Surgical Navigation: Part 2

TRACK 07: SURGERY, COMPUTER AIDED SURGERY, MINIMAL INVASIVE INTERVENTIONS, ENDOSCOPY AND IMAGE-GUIDED THERAPY, MODELLING AND SIMULATION

SP110.1 - Optical Navigation in Functional Neurosurgery

Author(s): Karin Wårdell

Department of Biomedical Engineering, Linköping University, Linköping/SWEDEN

Learning objectives:

Understand the basic principle of blue-light fluorescence microscopy

Be able to present two different fluorescence methods used in neurosurgery

Give examples of intraoperative navigation options used during DBS-implantations

Optical Navigation in Functional Neurosurgery

During the last decade, the use of optical techniques for navigation during neurosurgery has increased. Neurosurgical microscopes, introduced already in the 1950^s, are today available with video recording and fluorescence imaging. Among these the blue-light setting is designed for visualization of malignant tumours by means of 5-aminolevulinic acid (ALA) [1]. In order to also quantify the fluorescence during tumour surgery, we have developed a hand-held optical probe adapted to the requirements of the operating room [2]. The performance of the probe-system has been compared with fluorescence microscopy and biopsies and the results show that it is superior in detecting weak fluorescence when using the recommended microscopy-dose of ALA (20mg/kg). By combining the blue-light microscope and the hand-held probe both an overview of the operational field as well as the point specific fluorescence can be visualized.

Laser Doppler perfusion monitoring (LDPM) and imaging (LDPI), and diffuse reflectance spectroscopy (DRS) are other optical techniques currently under assessment as navigation support during neurosurgery. DRS allows for extraction of information from tissue chromophores and thus makes estimations of for instance saturation tissue of oxygenation possible [3].

With LDPI the cortical blood perfusion can be visualized whereas high resolution detection of differences in blood flow and tissue greyness can be achieved by LDPM. This dual function has been applied as an intra-operative navigation tool in relation to stereotactic deep brain stimulation (DBS) implantation. Its performance has now been evaluated in more than 110 lead implantations, and typical "bar codes" for optical trajectories have been defined towards two common DBS-targets the subthalamic nucleus (STN) and the ventral intermediate nucleus (Vim) [4]. In addition, the forward-looking LDPM-probe has shown as a potential to prohibit bleedings, by indicating blood flow peaks at a 0.5mm resolution along pre-planned trajectories.

Optical techniques have already proven to be useful as navigation tools in neurosurgery. However, continuation of technical and methodological evaluations based on the clinical needs is necessary in parallel to translation into the neurosurgical demands and environments, both as stand-alone techniques, and methods based on multiparametric approaches for improving intraoperative navigation.

References

1. Stummer, W., et al., *Fluorescence-guided surgery with 5-aminolevulinic acid for resection of malignant glioma: a randomised controlled multicentre phase III trial*. *Lancet Oncol*, 2006. **7**(5): p. 392-401.
2. Richter, J.C., et al., *Fluorescence spectroscopy measurements in ultrasonic navigated resection of malignant brain tumors*. *Lasers Surg Med*, 2011. **43**(1): p. 8-14.
3. Johansson, J.D., et al., *Combined Diffuse Light Reflectance and Electrical Impedance Measurements as a Navigation Aid in Deep Brain Surgery*. *Stereotact Funct Neurosurg*, 2009. **87**(2): p. 105-113.
4. Wårdell, K., et al., *Relationship between laser Doppler signals and anatomy during deep brain stimulation electrode implantation toward the ventral intermediate nucleus and subthalamic nucleus*. *Neurosurgery*, 2013. **72**(2 Suppl Operative): p. ons127-40.

SP110.2 - Endoscopic Electro spray: A minimal invasive tool for physical targeted gene delivery

Author(s): David Hradetzky¹, Stephan Boehringer¹, Paulius Ruzgys², Prosper A. Fiave³, Karin F. Blaser¹, Thomas Geiser², Amiq Gazdhar³
¹Institute For Medical And Analytical Technologies, University of Applied Sciences and Arts Northwestern Switzerland (FHNW), School of Life Sciences, Muttenz/SWITZERLAND, ²Department For Pulmonary Medicine, University Hospital Bern, Bern/SWITZERLAND, ³Department Of Clinical Research, University of Bern, Bern/SWITZERLAND

Targeted gene or chemotherapeutic drug delivery offers a great potential for various diseases. In comparison to systemic delivery, side effects can be reduced and the quantity of delivered agent may increase. Also physical delivery is expected to reduce inflammatory and immunological reactions which often accompany targeted delivery utilizing viral vectors [1].

Physical localized delivery based on electro spray process, utilizes the bombardment of accelerated droplets containing the therapeutic molecule on targeted tissue, facilitating the entrance of the molecule into the cells. Electro spray process is based on Coulomb repulsion of charged particles, and to generate and accelerate the aerosol high electrical potential difference between a capillary and a counter electrode is required.

To transfer this method into clinical application single-port access instruments are needed providing the accelerating power and the fluid to the intraluminal region. The electrical field is applied by connecting the targeted tissue with ground potential, at the tip of the devices thus acting as counter electrode, while the high voltage is connected to the capillary axially placed within a working chamber. This configuration assures a predefined working distance and provides repeatable conditions of application.



Based on described concepts, different instruments were designed and realized (Figure 1). First standalone devices (Ø10mm, adjustable working distance 0-10mm, rigid, fabricated with additive manufacturing) for endoscope assisted application and second miniaturized

systems (\varnothing 2-3mm, flexible, fabricated from Polydimethylsiloxane) applicable through the working channel of a bronchoscope.

To check the feasibility of the electro spray devices for physical targeted gene delivery, the rigid device was tested in vitro (A549) for transfection of enhanced green fluorescent plasmid (eGFP, 50-500 μ g/ml), at different applied potentials (2.5-4.5kV, distance 3mm). The rigid and flexible devices were also tested in an ex-vivo scenario (cultivate explanted rat lung tissue). The fluorescence signal of eGFP was detected after 24hrs incubation at 37°C using fluorescence imaging. GFP after electro spray expression indicates the successful transfection.

Both, the rigid and the miniaturized flexible electro spray instrument successfully transfected the plasmid into the cells, proving the suitability of electro spray for physical targeted delivery and providing a feasible concept of rigid and flexible electro spray instruments for gene therapy in clinical application.

This work was supported by the School of Life Sciences of the University of Applied Sciences and Arts Northwestern Switzerland, the Department for Pulmonary Medicine at University Hospital of Bern and the Scientific Exchange Program NMS.CH.

[1] K. Hall, *et al.*, *Biochem J*, vol. 431, pp. 321-36, Oct 11 2010.

SP110.3 - Cone-Beam CT-Guided Fluorescence Tomography for Intraoperative 3D Imaging

Author(s): Michael Daly, Nidal Muhanna, Harley Chan, Brian C. Wilson, Jonathon Irish, David Jaffray
Princess Margaret Cancer Centre, Toronto/CANADA

A multi-modality intraoperative imaging system has been developed for hybrid cone-beam computed tomography (CBCT) and fluorescence diffuse optical tomography (FDOT). This translational research system is under investigation for clinical applications in head and neck surgery including oral cavity tumour resection, lymph node mapping, and free-flap perforator assessment. The fluorescence imaging system is configured for use with indocyanine green (ICG) using a collimated 760 nm laser diode and a 14-bit near infrared (NIR) camera. Freehand image collection in a non-contact geometry is achieved using a stereoscopic optical camera for real-time localization of the laser source and camera. Intraoperative CBCT images with sub-mm spatial resolution are acquired with a flat-panel C-Arm. FDOT is implemented using a finite element method for diffuse tissue optics (NIRFAST), with structural information from CBCT used directly in the optical reconstruction algorithm using Laplacian-type regularization ("soft priors"). The light rays from the laser source and camera pixels are geometrically projected onto the boundary elements of the tissue mesh using algorithms for ray-triangle intersection and camera lens distortion. Registration errors between real and projected boundary points are <2 mm for typical acquisition geometries. Surface flux is converted from CCD photon counts using free-space radiometry models and camera photon transport calibrations (e.g., filter transmittance, camera quantum gain, sensor noise). Pre-clinical studies using tissue phantoms and small animals are presented to characterize 3D imaging performance as a function of sub-surface fluorophore size, depth, and concentration. Experiments with ICG inclusions embedded in liquid phantoms demonstrate that the use of CBCT spatial priors improves the quantitative performance (<15% error, a reduction of 50% relative to no priors) in the tomographic reconstruction of fluorescence yield at depths <2 cm.

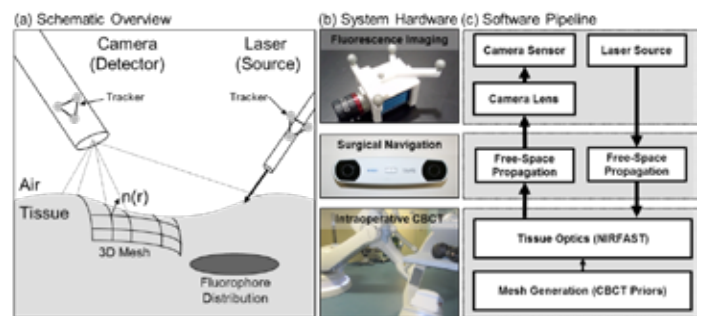


Figure 1. (a) Schematic of a surgical navigation system for CBCT-guided fluorescence tomography. Volumetric mesh segmentations are generated from intraoperative CBCT images. Laser source and camera detector positions relative to the tissue surface are obtained in real-time from an optical tracking system. (b) System hardware components include a NIR CCD camera (PCO Pixelfly USB) and lens (Edmund Optics), a stereoscopic optical tracking system (NDI Polarix Vicra), and a flat-panel cone-beam CT C-Arm (Siemens Zeego). (c) Software pipeline for non-contact fluorescence tomography. Registered fluorescence CCD images are used in a finite element diffuse optics model to generate 3D reconstructions of sub-surface fluorescence inclusions (e.g., tumours, lymph nodes, blood vessels) that are fused with intraoperative CBCT.

SP110.4 - An Optimal Motion Profile for a Wireless Endoscopic Capsule Robot

Author(s): Sina Mahmoudzadeh, Hamed Mojallali
Faculty Of Engineering, University of Guilan, Rasht/IRAN

Purpose: The inner parts of the GI track such as the small intestine are inaccessible using conventional methods. We propose an optimal model of motion profile for a wireless endoscopic capsule robot (capsubot) for obtaining diagnostic data from the GI track. Critical criteria such as the size and smoothness of the movement of the capsu bot are taken into consideration for the optimization process, making it possible to fabricate the capsu bot smaller in size, making it easier for the patient to swallow, and causing less discomfort during the procedure.

Methods: The legless capsu bot model used in this work mainly consists of two parts: the inner mass and the capsule body which would contain the diagnosing equipment. The inner mass can move back and forth inside the capsule body. By applying a force to the inner mass in the proper direction, the capsule body can be moved forward or backward. An optimization model was developed for the motion of the capsu bot which takes into account the limitations on the capsule body, such as shape, length and weight. The optimization model, uses non-linear optimization to minimize the power consumption and maximize the traversing distance given a limited battery source. Finally, a sensitivity analysis was performed to test the robustness of the proposed model to fabrication errors.

Results: The results showed 82% reduction in battery consumption for the movement of the capsu bot compared to the other work in the literature, which allows the capsu bot to be smaller than those in the literature. The results for simulation of the trajectory and the speed of the capsu bot showed a smooth movement of the capsu bot without any backward movement. Under the same conditions (same duration and available power for moving the capsu bot) the capsu bot moved a distance 89% longer than the best result of other work in the literature with the same power consumption. The sensitivity analysis results showed very low variability among the quality of movement of capsu bot and distance traversed under small variations in different parameters of the capsu bot such as size and length of the capsule body.

Conclusions: The results for the proposed model showed significant improvement in the motion of the capsbot and the required power. Since the dimensions of the battery could be decreased due to the reduced required power, the model can be used to fabricate a potentially smaller capsbot. This allows fabrication of a smaller capsbot that could be swallowed more easily by the patient causing less discomfort, or a better use of the capsule space for adding additional features such as drug delivery and biopsy equipment.

SP110.6 - Orthogonal IR System for Instrumental tracking in Minimally Invasive Spine Procedures for training using Wiimote Technology

Author(s): Juana E. Martínez, Daniel Lorias, Arturo Minor
Electrónica, CINVESTAV, México, D.F./MEXICO

In this paper we present a system for track the movements of the training instrumental in 3D space, using two infrared Cameras from two Nintendo Wii Remotes in order to evaluate the progress surgeons during the learning phase for making incisions and placement of screws in the spine throw minimally invasive procedures. The cameras are positioned orthogonally, and they detect the position of IR markers that are placed in the training instrumental.

SP110.7 - Use of a Patient-Specific Ventriculostomy Surgical Simulator to Develop a Model for Preoperative Risk Assessment Based on Measures of Anatomical Variation

Author(s): Ryan Armstrong, Roy Eagleson, Sandrine De Ribaupierre
University of Western Ontario, London/CANADA

Insertion of a ventricular catheter –an external ventricular drain – is a common neurosurgical procedure. Though considered a simple procedure and often performed by residents, catheters are inserted blindly, most often without image guidance, relying on the surgeon's spatial abilities and anatomical landmarking. The relatively high malplacement rates reported by some institutions reflect the difficulty. We used a virtual reality surgical simulator with patient-specific scenarios to examine the anatomical factors that influence user performance. Using objective metrics to quantify user performance and anatomical variations, we developed a model to predict malplacement risk based on measures of anatomical variation.

A diverse set of patient scenarios were created by segmenting the lateral and third ventricles from MR and CT images and incorporating the geometries into a custom ventriculostomy module within the NeuroTouch simulator. The simulator consists of a mannequin head with a pointing tool. Users are tasked to select a burr hole location and indicate the trajectory into the lateral ventricle. Metrics to evaluate user performance were devised to reflect clinical outcome using a single aggregate score. A model was constructed to estimate the difficulty of a given case based on the mean and variance of user performance. To examine the role of anatomical variations, we examined measures thought to influence performance, including ventricle volume, midline shift, Evan's ratio and maximal width of the anterior horn. One neurosurgical expert and seven residents were recruited for a user study and each performed the surgical task of burr hole and trajectory selection a number of times on various cases. We found that anatomical variation in the simulator had a significant impact on user performance. Correlation with performance was seen for all anatomical measures, although the strongest predictors of performance were ventricle volume, midline shift and anterior horn maximal width. By determining the difficulty of each case based on user performance, we were able to produce a model to predict risk of malplacement (based on targeting accuracy) using an optimized weighting of each anatomical variant measure considered.

Results provide the foundation for an objective model to predict surgical risk based on measures of anatomical variation. While image-guidance systems exist for such procedures, they are usually not used as they are often deemed impractical by the bed-side due to immobility and increased setup time. Determining the inherent risk of each case allows us to set guidelines for the use of guidance systems where there is a high chance of malplacement, which often results in complications. Additionally, identifying high-risk cases can help determine when use of simulated rehearsal using patient-specific simulators is an appropriate component of the preoperative process. This knowledge can also aid in the selection of appropriate training scenarios in development of a simulation curriculum. Ultimately, we aim to provide trainees with the knowledge and the tools to guide the preoperative planning process, improving patient outcomes.

SP111 - Cardiovascular

TRACK 12: MEDICAL DEVICES

SP111.1 - Ultrasound-induced heart rate decrease: Role of age in female rats

Author(s): Olivia C. Coiado, William D. O'Brien Jr.
 Bioacoustics Research Laboratory - Department Of Electrical And Computer Engineering, University of Illinois at Urbana-Champaign, Urbana/UNITED STATES OF AMERICA

Objective:

Use of ultrasound in therapy has been increasing and new techniques have been developed as, for instance, in cardiac diseases. Animal models for cardiovascular disease support the hypothesis that female sex and/or the sex hormone estrogen may contribute to the sexual dimorphism in the heart and to a better outcome of cardiac diseases in females. Aging is associated with reduced responsiveness of many hormone receptors. The goal was to investigate the age-dependent changes in the cardiac system in female rats exposed to pulsed ultrasound that may benefit therapeutically with heart rhythm abnormalities.

Methods:

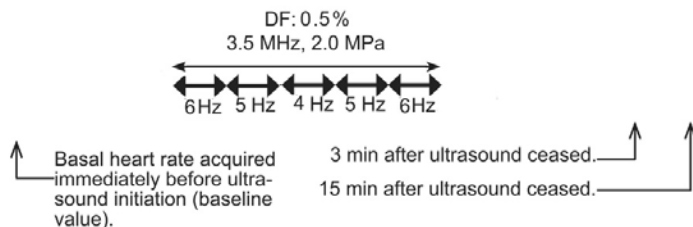
Transthoracic ultrasonic exposure experiments were divided into two female Sprague-Dawley rat groups (n=5 ea): Group 1: Five 3-mo-old 200-250-g rats and Group 2: Five 24-mo-old 250-400-g rats. The ultrasonic exposure protocol was the same for both groups: 3.5 MHz pulses of 2.0 MPa peak rarefactional pressure amplitude (equivalent to spatial peak intensities of 133 W/cm²), variable pulse repetition frequencies (6, 5, 4, 5, 6 Hz), 10-s each sequence (0.5% duty factor), see Figure. Cardiac conditions were evaluated before (at baseline) and at 3 and 15 min after ultrasonic exposure ceased (3 and 15 min results normalized to each rat's baseline values).

Results:

Group 1: at 3 and 15 min, respectively, the heart rate decreased 12% and 15%, and the cardiac output decreased 16% and 14%. Group 2: at 3 and 15 min, respectively, the heart rate decreased 12% and 15%, and the cardiac output increased 14% and 15%. There was no significant difference between the younger and older rats for the heart rate or for the cardiac output.

Conclusions:

Pulsed ultrasonic exposure caused similar decreases in the heart rate and cardiac output in the two rat-age groups, that is, there were no age-dependent differences in the cardiac system of young and old female rats stimulated by pulsed ultrasound. The results are promising for therapeutic application in cardiology as treatment for heart rhythm abnormalities in women of different ages. This work was supported by NIH R37EB002641.

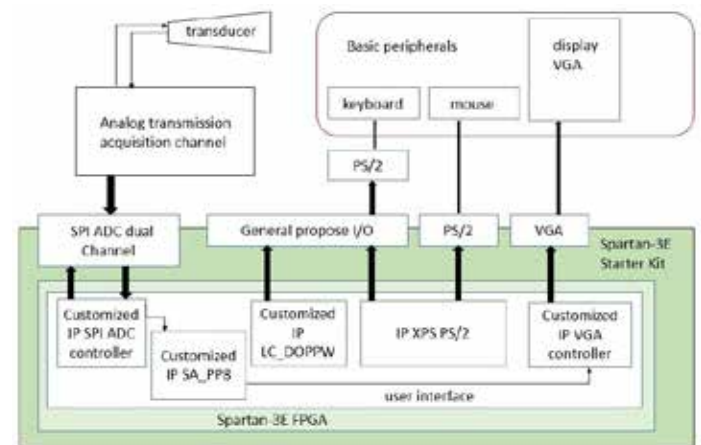


SP111.2 - Low cost pulsed wave Doppler ultrasound system for vascular studies

Author(s): Isabel Arnaiz
 Cebio, High Polytechnic Institute "José A. Echeverría", Havana/CUBA

Recently reports made by World Health Organization establish that vascular diseases are the leading cause of death by non-communicable diseases around the world. In Cuba, it is the second one. Doppler ultrasound technique is the main method for non-invasive high risk vascular diagnosis which convergent to cardiovascular diseases. Nowadays, commercialized Doppler ultrasound systems are expensive and overbroad to more than one technique. As possible solution for Cuba's Health Service, it is designed a spectral Doppler pulsed wave ultrasound system with user interface for visualizing the blood flow profile relative to Doppler shift spectrum. Data visualization occurs by RGB mode with 9 bits color depth, 8 bits for velocity resolution and 7.5 ms of time resolution. The visualization of the sonogram is at 130 frames/s. Digital processing and user interface are implemented on a Xilinx Spartan-3E FPGA. This low cost alternative for diagnosing vascular pathologies on superficial vessels helps to prevent and assist the high number of cases affected by vascular diseases in Cuba.

Keywords— vascular diseases, ultrasound, FPGA, low cost.



SP111.3 - Real-Time Three Degree-of-Freedom Measurement of Catheter Motion for Input to a Robotic Catheter Navigation System

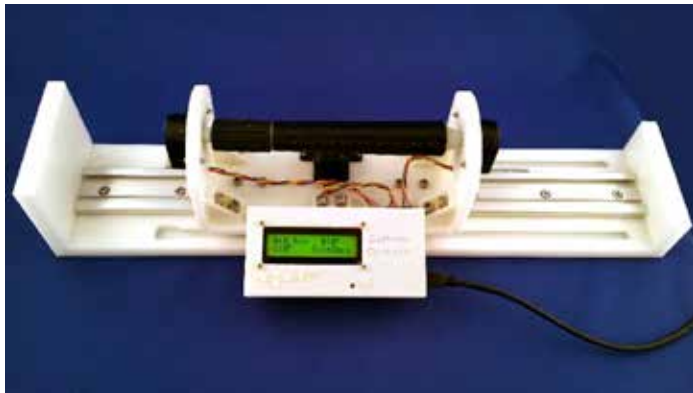
Author(s): Daniel Gelman, Michael K. Lavdas, Maria Drangova
 Robarts Research Institute, Western University, London/ON/CANADA

BACKGROUND: Commercial robotic catheter navigation systems (RCNS), used for many types of cardiac ablation therapy, enable the interventionalist to remotely manipulate a catheter's position. Typically, the interventionalist operates the robotic systems unnaturally with a provided user interface that is not instinctive, often including a joystick-based controller. Specialized training is required to operate these systems, which may lead to future dependence on this technology. An intuitive solution was previously developed to facilitate translation from conventional to robotic intervention [1]. This device detects axial and rotational changes of a master-side catheter and although inherent to the interventionalist, its use in contemporary RCNSs is limited because modern interventional catheters are steerable, permitting catheter tip deflection. To address this, we have developed a master-side input device that detects motion changes in all three positional degrees-of-freedom.

Methods: The input device enables direct manipulation of an ergonomic master-side catheter handle. A shell of a recycled steerable

catheter handle is rigidly attached to 3D-printed concentric inserts. Incremental optical rotary encoders are coupled to extended shafts of the inserts to detect motion changes in the rotational and tip deflection degrees-of-freedom. The catheter handle assembly is then mounted on a custom linear motion stage whereby a rack and pinion mechanism coupled to another encoder detects axial motion. A dedicated electronic system with a powerful microcontroller provides quadrature encoding and robotic motion scaling to enable higher levels of precision. A wireless module provides position streaming to a slave robot. The design of the input device provides a calculated axial resolution of 13 μm and both rotational and deflection resolution of 0.18°. The accuracy of the input device was evaluated using an optical tracking system. Five 30-second motion profiles were manually imposed on each degree-of-freedom. Position data provided by the embedded system and the tracking system, were then compared for their mean error.

Results: The input device, depicted in the image below, shown to have an absolute mean error in the axial direction to be 0.44 ± 0.33 mm, rotary direction to be $0.41 \pm 0.15^\circ$, and tip deflection to be $0.54 \pm 0.43^\circ$. The on-board embedded system enables reliable, high-speed data transmission for optimal master-slave robotic control and permits selectable motion scaling.



Conclusion: We have developed and evaluated an instinctive master-side input device that can be used with an RCNS to fully manipulate a slave-side steerable interventional catheter with high precision and dexterity.

[1] Y. Thakur et al., *SPIE*. (2007)

SP111.4 - Pulse Wave Velocity as a Function of Cuff Pressure – Extra Information About the Cardiovascular System

Author(s): Akos Jobbagy, Peter Nagy
Measurement And Information Systems, Budapest University of Technology and Economics, Budapest/HUNGARY

High blood pressure (BP) is one of the biggest global health risks. Non-invasive methods determine only the momentary value of systolic- and diastolic BP. Knowing arterial rigidity would provide cardiologists with invaluable extra information.

A Home Health Monitoring Device, HHMD, was developed at the Dept. Measurement and Information Systems, Budapest University of Technology and Economics. HHMD inflates and deflates the cuff slowly (6 mmHg/s) and records also ECG and photoplethysmographic signal (PPG) at both index fingertips. Among other parameters the pulse wave transit time, PWTT is calculated. Measured from a healthy senior person, Figure 1 shows a typical PWTT – cuff pressure (CP) curve. Occlusion with the cuff causes temporary alteration in the dynamic properties of the brachial artery. The alteration can be characterized by the change of PWTT.

Fig. 1.

The slope of the PWTT – CP curve is characteristic for the cardiovascular system. We determined the CP belonging to the steepest change. During inflation it is denoted by *dup*. PWTT was averaged for 8 s with CP=0 before (PWTTbefore) and after (PWTTafter) inflation and deflation. The ratio of the two PWTT values is $\Delta\text{TRatio} = \text{PWTT}_{\text{before}} / \text{PWTT}_{\text{after}}$.

170 were selected and analyzed from more than 1500 recordings taken from patients who underwent open-chest cardiac surgery and also from young- and senior healthy control persons. The results confirm that the PWTT – CP function provides extra information about the state of the brachial artery. Based on our research we suggest three parameters to quantify this information.

The difference between *dup* and DBP: For all the three tested group *dup* correlates with DBP. The difference is smallest for the young healthy group. Values for the senior healthy persons and for the patients are similar.

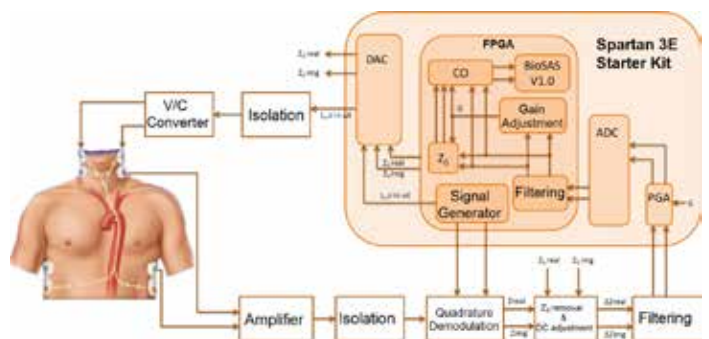
The change of PWTT: In most cases PWTT is greater after than before occlusion, thus $\Delta\text{T Ratio} < 1$. It can be interpreted that occlusion temporarily increases the elasticity of the brachial artery. For patients $\Delta\text{T Ratio}$ can exceed 1. The value of $\Delta\text{T Ratio}$ is an indicator of arterial rigidity; it correlates neither with SBP nor with DBP.

Slope of increase of PWTT during inflation: There is almost no difference among tested persons regarding the slope of increase of PWTT during inflation when CP exceeds *dup*. However, there are two patients who sometimes produced much higher values than the maximum of all other tests (6 s/mmHg). This indicates momentary increased rigidity of the arterial wall.

SP111.5 - Cardiac Output estimation through Impedance Cardiography using reconfigurable hardware.

Author(s): Leidy M. Alvero González
Bioengineering Department, High Polytechnic Institute Jose Antonio Echevarría, Havana/CUBA

Impedance Cardiography allows the noninvasive determination of cardiac output quickly and continuously. Cardiac output provides vital information for evaluating and analyzing the hemodynamic information in patients who are in critical medical conditions. A distribution of current-injection electrodes is used to sense changes to pulsed voltage changes that are proportional to the thorax bio-impedance.. The acquired signal combines basal impedance component with dynamic tissue components. It is the resulting product of an amplitude modulation with frequency components located on either side of the frequency component of the injection signal. A quadrature demodulation stage is used for translation to baseband of the signal in order to preserve amplitude and phase information. Digital signal processing is implemented on FPGA, allowing high flexibility during the research process.



SP111.6 - Microfluorimetry System Instrumentation for Ca2+-

Associated Fluorescence Imaging of Cardiomyocytes in Response to High Electric Fields

Author(s): Marcelo Zoccoler¹, Pedro X. Oliveira²

¹Faculty Of Electrical And Computing Engineering, University of Campinas, Campinas/BRAZIL, ²Center of Biomedical Engineering, University of Campinas, Campinas/BRAZIL

The defibrillation is the only effective therapy against ventricular fibrillation. Although a common clinical procedure, this technique also harms healthy cells by means of electroporation, possibly re-introducing arrhythmias. In order to study how myocytes respond to high electric fields (**E**), scientists commonly use fluorescent dyes in sophisticated and expensive microscopes. These devices produce high quality data, but they are sometimes financially unreachable. We have developed an artisanal microfluorimetry system employing some pieces from deactivated medical equipments. The system proved successful as we could generate quality fluorescence images of isolated adult rat cardiac myocytes loaded with Ca²⁺-associated fluorescent dye Fluo-3 and subjected to monophasic high intensity **E**. Cells with major axis parallel to **E** direction were selected. Using regions of interest (ROIs) analysis, we verified that fluorescence variations in ROIs facing the electrodes are bigger and asymmetric, with higher variations at the side towards the anode.

SP111.7 - A practical device to warn on impending syncopal episodes

Author(s): Michael Cheng¹, Venkatesh Thiruganasambandamoorthy², Hilmi R. Dajani³, Miodrag Bolic⁴

¹Biomedical Engineer, ottawa/ON/CANADA, ²Emergency Physician, Ottawa Hospital, ottawa/CANADA, ³School Of Electrical Engineering And Computer Science, University of Ottawa, Ottawa/ON/CANADA, ⁴School Of Electrical Engineering And Computer Science, University of Ottawa, N/CANADA

Syncope (fainting) can lead not only to serious personal injury but also can endanger public health such as when the sufferer is driving a car. An electronic monitoring device can help to minimize syncopal events due to cardiac rhythm changes. This kind of devices will greatly enhance the ability of the patient to take immediate action to safeguard personal and public health.

On the current consumer market, there are numerous heart rate monitoring devices catering for sports use with sophisticated software support; however such devices are not specific to individual patient's needs. On the other hand, ample devices are available to monitor and record various patient data to be analyzed by proprietary clinical software catered for physician use; but such devices are relatively expensive, sold only to physicians, and the data are interpreted "off line" (by the physician).

This paper proposes a simple device to be worn by sufferers of cardiac arrhythmia to provide online (instant) warning signals directly to the wearer on impending fainting. The sufferer could act immediately to stop physical activities, sit, lie down, or stop the car etc. and so help prevent potential injury to the sufferer or to others. The device concept is based on physiological findings that when

the time interval between successive heart beats (the RR interval) is

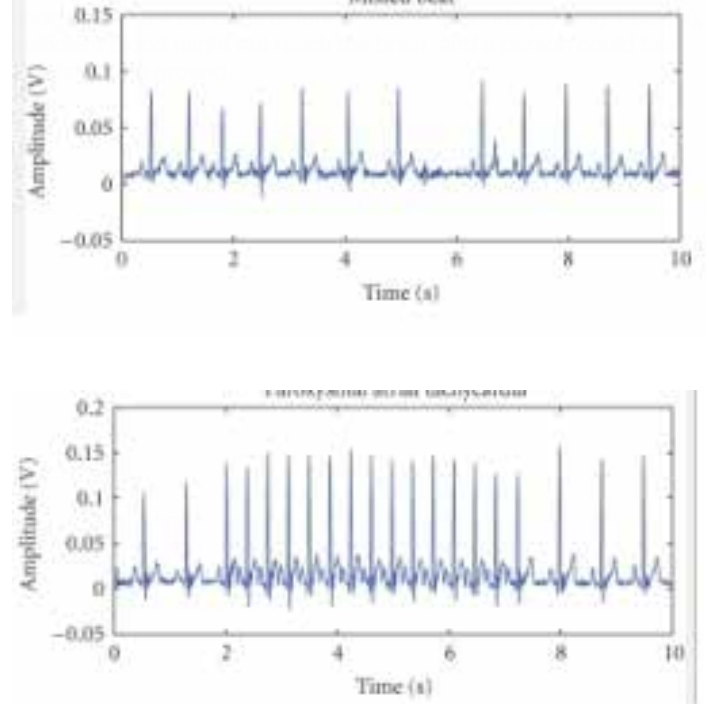


Fig 1 sample ECG strips on cardiac arrhythmia. The interval between consecutive QRS complex is the RR interval

Thus, the device measures each inter-heart beat intervals in real-time; then compare this interval with pre-set values (say 0.4, 2 seconds). If the RR interval is lower or greater than the set values, the device will immediately issue an alarm warning (audio/visual). The person should then stop any activity, sit or lie down to reduce the demand on body blood circulation and avoid a serious syncopal episode.

This device will resemble a watch to be worn on the wrist with electronic sensors. Initially, simple electronic circuitry and software are sufficient. If desired later, more sophisticated, intelligent software algorithm can be incorporated for a variety analyses such as blood pressure changes and types of cardiac arrhythmia.

SP111.8 - Robust Blood Pressure Monitoring in Atrial Fibrillation Patients

Author(s): Saif Ahmad¹, Izmail Batkin¹, Miodrag Bolic¹, Hilmi R. Dajani¹, Voicu Z. Groza¹, Sanjeev Chander²

¹University of Ottawa, Ottawa/CANADA, ²Ottawa Cardiovascular Centre, Ottawa/CANADA

Background Blood pressure (BP) is an important vital sign characterizing cardiovascular health. Therefore, hypertension/hypotension diagnosis and management through accurate monitoring is critical for reducing risk of life-threatening conditions like stroke. Automated non-invasive BP (NIBP) devices are increasingly recommended in clinical practice. However, these devices tend to be unreliable in patients with chronic conditions like atrial fibrillation (AF) and obesity [1] – resulting in inefficient BP management and hence increased risk [2]. Unreliability arises because NIBP monitors estimate BP by analyzing arterial pulses alone and these patients may present weak, erratic, and/or unpredictable arterial pulses. **Method/ Results** Health Parametrics Inc. (HPI), a University of Ottawa spinoff, is investigating novel technology for increasing the accuracy of automatic NIBP estimation. Briefly, we have developed a novel yet simple method for simultaneous acquisition of electrocardiogram

(ECG) and arterial pulse wave data within the automatic NIBP monitoring paradigm [3]. Algorithms analyze arterial pulses with the assistance of ECG data, which tends to be less affected by the above conditions, to improve BP estimation accuracy [4-5]. We recently conducted a pilot clinical investigation in which 13 patients with chronic conditions including AF and obesity were recruited. For each patient, in about 30 minutes, 6 BP measurements taken by our prototype were compared with 6 BP measurements taken by BpTRU, a commonly used clinical NIBP monitor (78 measurements/device for N=13). The average systolic and diastolic BP measured by our prototype were not significantly different (Student's t-test, $p > 0.05$). Moreover, standard deviation of systolic and diastolic BP measured by our prototype was lower than that of BpTRU in 10/13 (77%) and 9/13 (69%) of the patients respectively (Figure 1). **Conclusion** These initial results suggest that our technology has the potential to improve the accuracy and reliability of NIBP estimation in patients with chronic conditions – leading to improved BP monitoring/management and therefore reduced risk. **References** [1] T.S. Lamb et al., "Comparison of two oscillometric blood pressure monitors in subjects with atrial fibrillation," Clin. Invest. Med., 33, 2010. [2] J. Handler, "The Importance of Accurate Blood Pressure Measurement," Perm J., 13, 2009. [3] I. Batkin et al. "Apparatus And Method For ECG-Assisted Blood Pressure Measurement," US/UK/CAN Pat. Appl., 2012. [4] M. Forouzanfar et al., "Coefficient-Free Blood Pressure Estimation Based on Pulse Transit Time-Cuff Pressure Dependence," IEEE Trans. Biomed. Eng., 60, 2013. [5] S. Ahmad et al., "Electrocardiogram-Assisted Blood Pressure Estimation," IEEE Trans. Biomed. Eng., 59, 2012.

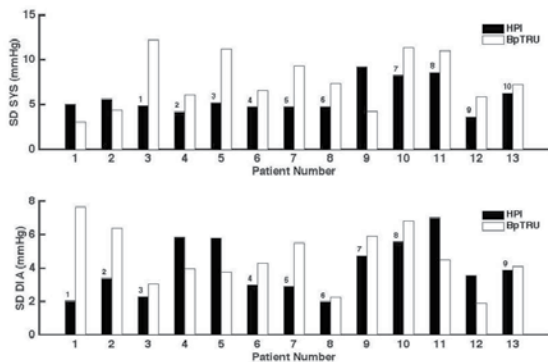


Figure 1: Standard deviation [SD] of systolic pressure (top panel) and diastolic pressure (bottom panel) for each patient as measured by HPI's prototype (black bars) and the BpTRU monitor (white bars). The numbers on top of the black bars indicate the number of patients for whom the SD of BP measured by HPI's prototype was lower than that of BpTRU – 10/13 (77%) patients for systolic and 9/13 (69%) patients for diastolic pressure.

SP112 - Instrumentation

TRACK 12: MEDICAL DEVICES

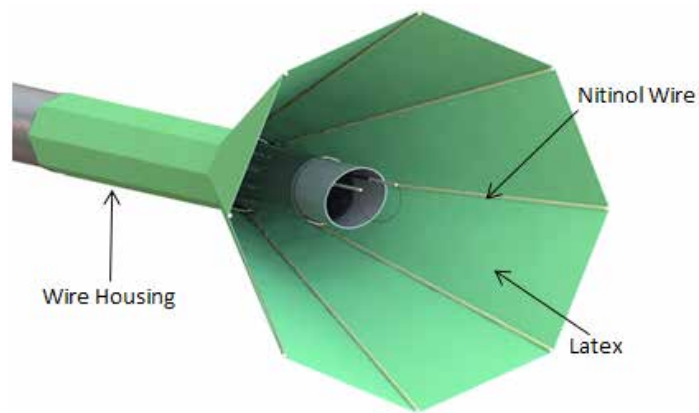
SP112.1 - Adaptation of Surgical Instruments for the Removal of Bladder Tumours

Author(s): Spencer C. Barnes¹, Duncan E.T. Shepherd¹, Daniel M. Espino¹, Richard Viney², Prashant Patel², Richard T. Bryan²
¹Mechanical Engineering, University of Birmingham, Birmingham/ UNITED KINGDOM, ²School Of Cancer Sciences, University of Birmingham, Birmingham/UNITED KINGDOM

Background: Transurethral resection of bladder tumour (TURBT) is the gold standard in non-muscle invasive bladder cancer removal. The tumours are removed piecemeal and this is thought to be a key reason for the high recurrence rate of up to 78% at 5 years.

Aims: A novel device has been designed to facilitate a decrease in this high recurrence rate by creating a sealed environment in which the surgeon can resect a tumour. This device aims to arrest the spread of cancer cells to the rest of the bladder wall.

Methods: Shape memory metal (Nitinol), 3D printing and latex have been used to create an actuating cone which can press against the bladder wall, surrounding the tumour. This design, in the open state, can be seen in figure 1 around a resectoscope, the device currently used for removing bladder tumours. Shape memory alloys (SMAs) such as Nitinol exhibit the property of solid phase change when heated and as such are able to move to a pre-trained shape. Nitinol wires were 'trained' at 550 °C in a steel jig at 30°. These wires were then sequentially placed in a 3D printed housing and soldered together in a series configuration. Subsequently, liquid latex was painted onto the wires using a mould, and allowed to dry. After being initially deformed to a closed state the device was then able to open when heated.



Testing: The device was actuated successfully using a 2.6 ampere 10 volt supply in liquid environments at 37 °C using custom made testing apparatus. Despite the extra heat loss due to the liquid environment the device was still able to open. The ability of the device to seal was also successfully tested with blue dye.

SP112.2 - A compact gantry based on pulse powered magnets for a laser-based proton radiotherapy

Author(s): Leonhard Karsch¹, Thomas Hermannsdörfer², Florian Kroll², Umar Masood¹, Michael Schürer¹, Jörg Pawelke¹
¹TU Dresden - OncoRay, Dresden/GERMANY, ²Helmholtz-Zentrum Dresden - Rossendorf, Dresden/GERMANY

Purpose: The new approach of particle acceleration by high intensity lasers may provide size and cost reduction for proton facilities. However, laser-driven proton beams are characterized by intense and short (few picoseconds) pulses with low repetition rates, high energy spread and large beam divergence. In addition to more compact accelerators due to the short acceleration length of few micrometers, also more compact beam transport systems are possible. The beam pulse structure enables more compact gantries by the use of pulse powered magnets without iron core, but much higher magnetic field strengths. Using pulsed magnets, the magnetic field is only generated for a short time period but still sufficient long for the transport of a proton pulse.

Method: First, a gantry was designed regarding laser accelerator specific requirements like a proton capturing element and an energy selection system. Secondly, prototypes for every type of pulsed magnets necessary for the gantry - solenoid, dipole and quadrupole - were designed and realized. Thirdly, these prototypes were experimentally characterized at a pulsed 10 MeV proton beam of a tandem accelerator. This beam is well defined in energy and intensity, the pulse duration is arbitrary adjustable down to 1 microsecond which is still longer than the pulse duration of laser driven beams. Therefore, it allows to test the ion optical behavior at low electrical risks, i.e. at reduced magnet current.

Result: A gantry for laser driven proton therapy was designed being much smaller than existing devices. A radius of 2.5 m and a length of 3 m is achieved by deploying high magnetic fields of up to 40 T inside the solenoid, up to 10 T inside the dipole and a magnetic field gradient of up to 300 T/m in the quadrupole. The achieved magnetic pulse durations with these prototypes are approximately 1 ms. The duration during which the field is constant is about 100 microseconds. Each of the individual magnets, as well as their combination to a pulsed beamline, show the expected ion optical properties like focussing and bending.

Outlook: After an adaption of the setup, further experiments at clinical relevant proton beam energies (up to 230 MeV) will follow. For this purpose, the proton beam from the conventional cyclotron at a facility in Dresden recently put into patient treatment, has been adapted to deliver pulsed beams to an experimental bunker. The work is supported by the german government BMBF (no. 03Z1N511).

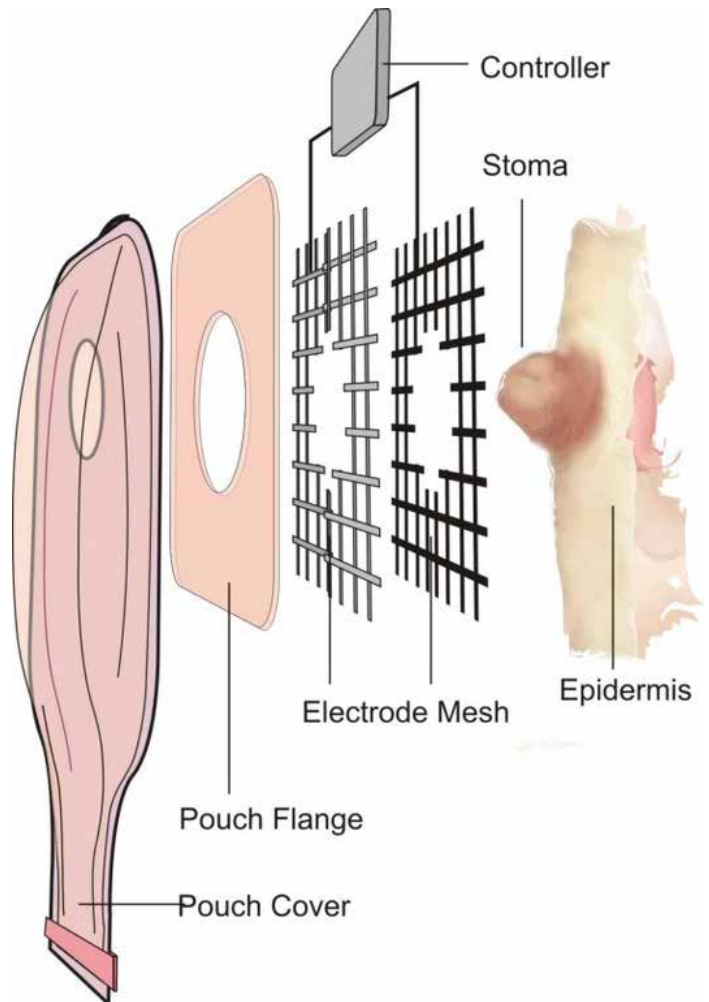
SP112.3 - Developing a pH Responsive Mesh as a Smart Skin Wafer in Ostomy Appliances

Author(s): Anna McIister, James Davis
 Nibec - Computing & Engineering, Ulster University, Newtownabbey/UNITED KINGDOM

Despite notable advancements in the management and treatment of ostomies over the past number of years, one problem still persists; peristomal skin complications (PSCs). The erosion of the skin directly underneath the skin wafer as a consequence of exposure to stoma fluid can lead to debilitating irritation and ulceration and is one of the most common post surgical complications. In the US alone, it is estimated that over one million patients deal with the routine of ostomy care, the majority of which will have, at some point, suffered from a PSC. Despite requisite pre and post-operative education for new patients, PSCs continue to be a perennial issue with incident rates ranging from 10-70%.

The present communication outlines progress towards the design of a smart wafer system that can actively monitor the skin condition

and respond accordingly to minimize the onset of irritation dermatitis. A conductive, mechanically flexible mesh incorporating poly-L-tryptophan is detailed and its modification to yield a pH sensitive diagnostic layer is outlined. The system has been characterized and its potential integration and application in stoma appliances is critically appraised.



SP112.4 - Development of a smart needle integrated with a micro-structured impedance sensor for the detection of breast cancer

Author(s): Niall T.P. Savage¹, Brian D. O'Donnell², Martin J. O'Sullivan³, Eric J. Moore¹
¹Life Science Interface, Tyndall National Institute, Cork/IRELAND, ²Department Of Anesthesia, Cork University Hospital, Cork/IRELAND, ³Department Of Surgery, Cork University Hospital, Cork/IRELAND

The aim of this research is to develop a novel medical device for the detection of breast cancer within the clinical setting. Breast cancer is the second most common cancer in women worldwide and the use of population-based screening programmes has increased the demand for more sensitive and specific detection tools to limit the number of patients being misdiagnosed or over-treated. This research will focus on the development of a minimally invasive diagnostic probe for the determination and localisation of cancerous tissue within the structure of the breast. Gold microelectrodes fabricated on a silicon substrate were developed in Tyndall National Institute and used to obtain electrical impedance recordings from *ex vivo* tissue samples of both animal and human origin. Functional prototype devices have been produced using both photolithogra-

phy and metal deposition processes to pattern the dual-electrode structures. The probes have been characterised using a series of techniques including CV and EIS. The prototype probes have been shown to be reproducibly manufactured and the electrochemical response of the electrodes has been very positive to date. A study of the electrical impedance response of animal tissues (beef, lamb and pork) has shown that a variety of tissues (fat, muscle and liver) can be discriminated using the prototype gold electrodes for the detection of discrete electrical responses. There are a number of potential uses for this device including improved biopsy localisation, cancer-free border determination during lumpectomy and the possibility of DCIS determination without invasive surgery. It is envisaged that this novel device would be used primarily as an adjunct to the gold-standard of x-ray mammography detection of breast cancer tumours during the routine screening process.

SP112.5 - Towards development of a wearable, miniaturized, bioartificial lung

Author(s): Esther C. Novosel¹, Joerg Schneider², Fabian Metzger², Annika Wenz³, Kirsten Borchers³, Markus Schandar³, Petra Kluger³, Brigitte Vollmar⁴, Peter Lelkes⁵, Georg Matheis²

¹Business Development, Novalung GmbH, Heilbronn/GERMANY, ²Novalung GmbH, Heilbronn/GERMANY, ³Cell Systems, Fraunhofer IGB, Stuttgart/GERMANY, ⁴Experimental Surgery, University of Rostock, Rostock/GERMANY, ⁵Bioengineering, Temple University, Philadelphia/PA/UNITED STATES OF AMERICA

Introduction

Chronic obstructive pulmonary disease is the 4th leading cause of death worldwide. Extracorporeal lung assist devices that promote oxygenation and /or CO₂ removal, like the Novalung interventional lung assist device (iLA[®]), can improve lung protection and increase quality of life [1]. As a drawback these systems limit patient mobility. In addition, longterm use is frequently accompanied by thromboembolic complications and device fouling due to inappropriate material characteristics of the blood contacting surfaces. Our goal is to develop the first wearable miniaturized lung assist device with improved surface properties [2].

Methods

We developed prototypes of new miniaturized hard- and software components, as well as a suitable carrying system. We also designed a new, disposable gasexchange unit with optimized geometry to minimize hemolysis and thrombogenicity. Hemolysis and gas exchange performance tests were carried out in vitro and validated in a porcine model.



Fig1: transformation of the iLA[®] to a longterm ambulatory lung assist device.

To improve the hemocompatibility of the gas exchange material Polymethylpentene (PMP), we seeded human dermal endothelial cells onto PMP hollow fibers, either coated with heparin/albumin, or covalently functionalized with heparin/RGD. Seeding efficiency and cell coverage were analyzed microscopically using live/dead staining and staining for van Willebrand factor.

Results

We successfully miniaturized all hardware components and developed a new design of the gas exchanger to improve blood distribution, while maintaining adequate gas exchange *in vitro* and *in vivo*. Following seeding of stacked PMP fiber mats, the endothelial cells formed a confluent monolayer on the fibers, which was preferentially retained for 5 days on the heparin/RGD coated fibers under both static and dynamic *in vitro* testing conditions in a new bioreactor system.

Conclusion

We successfully designed and implemented a miniaturized wearable lung assist device, which is currently being tested in a porcine model. Importantly the gas exchange property of the miniaturized device are adequate to provide significant respiratory support. Future studies will test these devices in a first in man trial.

References

1. "Protective and ultra-protective ventilation: using pumpless interventional lung assist (iLA)", Quintel et al. *Minerva Anesthesiol.* 77(5):537-44. 2011
2. "Artificial lung: progress and prototypes.", Zwischenberger et al. *Expert Rev Med Devices.* (4):485-97.2006

Acknowledgements

We acknowledge productive collaboration with our consortium partners from Imperial College London and the University of Florence and thank the EU for the financial support under the 7th framework program through the key action «medical technology for transplantation and bioartificial organs».

SP112.6 - Development of a Low Cost Spectrometer for Studies of Diffuse Reflectance with Dermatological Science and Applications

Author(s): Gerardo S. Romo-Cardenas, Sydney Dominguez-Dominguez, Rusbel Dominguez-Dominguez
School Of Engineering, Montemorelos University, Montemorelos/ MEXICO

From an optical perspective, skin with all its layers and surfaces are made from different tissues that have different or unique pattern of reflectance, which could help to differentiate normal or healthy tissues from those with a presence of any type of injury or pathology. The application of optical tool for the characterization of bio- tissues have gained importance due to its noninvasive nature.

In this work it is proposed to conduct a study to develop an inexpensive spectrometer and a light source of broad spectrum; as well as the protocol that would allow the exploration of diffuse reflectance of colloids with the intention of develop a tool that could be used to identify any type of pathology. In this paper, the preliminary results of the study, involving the development of the light source, a low-cost spectrometer and the measurement and analysis protocol to explore the feasibility of implementation in areas of biomedical science areas are discussed.

Beside the development of the system, agar and dyed gelatin tis-

sue phantoms were used in order to study the performance of the system.

Results show a good consistency in the performance of the developed spectrometer, in its capability to acquire the diffuse reflectance from the tissue samples. As well, as in accordance to the irradiated wavelength and the amount of dispersion induced in the tissue phantom. Still, results cannot be conclusive in order to determine significant differences that could lead to the application of this technology in health applications, it is expected to obtain a better specificity with future work.

SP112.7 - Correctness of bioimpedance data for body composition obtained by BIA approach in various external conditions

Author(s): Jan Hlubik¹, Lenka Lhotská¹, Jan Kříž²

¹Cybernetics, Czech Technical University, Prague/CZECH REPUBLIC, ²Department Of Physics, Faculty of Science University of Hradec Kralove, Hradec Kralove/CZECH REPUBLIC

This paper presents our ongoing research in a field of body composition obtained by body impedance analysis. In this work we were focused on changes in bioimpedance in dependence on change of measurement external conditions. This paper also deals with question if data obtained from this method are enough informative with ought any information about the performed measurement. We discovered that it is crucial to have information about the whole measurement procedure and that operator that is performing such measurement should know exact type of device that is used for measurements. Influence of specific conditions did not statistically changed results of calculated values. However in directly measured values resistance and reactance at high frequencies (250 kHz and 500 kHz) were found statistically significant changes ($P=0,05$) for highly conductive gel. Overall was concluded that external conditions that can be normally encountered at laboratories do not have effect on obtained values. However it is important to know which device was used so the set of used equations are comparable.

SP113 - Information Technologies in Healthcare Delivery and Management: Part 1

TRACK 14: INFORMATION TECHNOLOGIES IN HEALTHCARE DELIVERY AND MANAGEMENT

SP113.1 - Technologies for Patient Self-Care of Chronic Illness: Development and Evidence.

Author(s): Joseph A. Cafazzo

Centre For Global Ehealth Innovation, University Health Network, Toronto/CANADA

The global plight of chronic illness has affected healthcare systems around the world. The delivery of care for those who need it most is not sustainable without a re-evaluation of enabling patients and their informal caregivers with the ability to perform self-care. Technological innovation in this area is showing great promise with the advent of mobile devices and wearables, but is not without the challenges of design, implementation, and a lack of clinical evidence. The keynote will outline addressing these challenges and the emerging evidence that shows the untapped potential of patients when given the opportunity for self-care facilitated through technology.

SP113.2 - A mobile monitoring tool for the automatic activity recognition and its application for Parkinson's disease rehabilitation

Author(s): Jorge Cancela, Matteo Pastorino, Eugenio Moreno, Maria T. Arredondo Waldmeyer

Life Supporting Technologies, Universidad Politecnica de Madrid, Madrid/SPAIN

In order to perform a continuous monitoring of patients in their daily lives, it is the need to contextualize the collected data coming from the patients. In this sense, the identification of the Activities of the Daily Life (ADL) carried out by the subjects is essential to understand and to put in context other data linked to the monitoring disease itself. This work was aimed at using the accelerometers integrated in most of the current available smartphones to build an automatic activity recognizer based on the signal coming from this sort of sensors. The validation carried out showed the impact of the frequency sampling in the classifier performance as well as the impact in the battery usage. Finally, it suggested that the use of one second as sampling period is a fair trade-off between accuracy in the classification and power saving.

SP113.3 - My Patient: An Electronic Patient Information Management System

Author(s): Satish Jaywant¹, Qaiser Muhammad²

¹Uhn International Program, Princess Margaret Cancer Center/University Health Network, Kuwait City/KUWAIT, ²University Health Network, Toronto,Canada, Kuwait/KUWAIT

Princess Margaret Cancer Center/University Health Network (UHN), Toronto, was approached to improve cancer services over a period of five years at the Kuwait Cancer Control Center (KCCC), Kuwait. As an integral component of this project, a computerized appointment scheduling system was implemented to reduce patient wait times, improve patient satisfaction and efficiency. It also provided an opportunity for data collection, tracking and management of resources. For this purpose, an electronic patient management system called "My Patient" was developed that will allow users to

become familiar with the basic steps and processes of creating, accessing and updating patient records. UHN Kuwait Information Management/Information Technology teams performed the gap analysis and requirements for the KCCC outpatient department workflows. It then worked closely with KCCC clinicians to finalize the clinical engagement, project governance and implementation plan. An in-house outpatient department scheduling module for KCCC was built. The pilot was launched May 2014 for 2 months in the gastro-intestinal site and has now been implemented for Radiation Oncology.

The tasks and functions in My Patient cover four distinct areas:

Registration: Staff within the Medical Records Department has access to register patients, create new patient files and modify patient demographic information. Other users must contact Medical Records to have these functions performed.

Scheduling: This functionality is available within the outpatient departments to staff with appointment booking access. Any other My Patient users can only view schedules whereas booking, updating and cancelling appointments is limited to scheduling users only.

Laboratory Ordering: The cytology laboratory staff has access to the laboratory management tool for laboratory order entry, specimen number generation and specimen label printing.

Administrative: The supervisory staff within each department has administrative access to correct entry errors within their department.

Various safety and patient confidentiality features are in place in this tool. As an example, every staff member accessing My Patient for clinical or administrative purposes has a unique user name and password.

This presentation highlights the application of My Patient to Radiation Oncology.

SP113.4 - Hom-e-call – An enhanced fall detection system based on accelerometer and optical sensors applicable in domestic environment

Author(s): Daniel Wohlrab¹, Markus Heß², André Apitzsch², Mandy Langklotz³, Andreas Schwarzenberger¹, Sebastian Bilda², Henry Schulz³, Gangolf Hirtz², Jan Mehner¹

¹Professorship Of Microsystems And Biomedical Engineering, Technische Universität Chemnitz, Chemnitz/GERMANY, ²Professorship Of Digital Signal Processing And Circuit Technology, Technische Universität Chemnitz, Chemnitz/GERMANY, ³Professorship Of Sport Medicine And Sport Biology, Technische Universität Chemnitz, Chemnitz/GERMANY

A reliable detection of falls is an important challenge for applications of ambient assisted living. Especially for elderly people living autonomously at their home, such a system would help to treat possible injuries faster. Most of the currently used systems are only based on the analysis of the movement data recorded by a wearable device. In this study an automatic fall detection system is developed that can be installed in domestic environment. Based on an accelerometer fixed to the body and optical sensors mounted on the wall, the fusion unit analyses the actual posture of the patient and detects fall events. By means of simulated fall scenarios performed by young athletes, the overall system performance is tested. To identify the false alarm rate of the fall detection system elderly people have performed activities of daily living in a furnished test flat. The combined system approach can be used to improve conventional fall detection algorithms.

SP113.5 - An Algorithm Based on Voice Description of Meal for Insulin Dose Calculation to Compensate Food Intake

Author(s): Piotr Foltynski¹, Piotr Ladyzynski¹, Ewa Pankowska², Karolina Mazurczak², Karolina Migalska-Musial¹

¹Nalecz Institute of Biocybernetics and Biomedical Engineering, Polish Academy of Sciences, Warsaw/POLAND, ²Department of Pediatrics, The Institute of Mother and Child, Warsaw/POLAND

Diabetes may lead to serious complications when blood glucose levels are not maintained in save ranges. Proper insulin dosing is crucial in good metabolic control, however it is not easy for all patients. There are some computer applications supporting insulin bolus calculation based on the meal composition, but they may be difficult to use for some patients. Our team decided to developed a voice-driven system helping patients in calculation of the proper insulin dose for food intake compensation. The system consists of several software applications (on smartphone and MS Windows server) working with developed language dictionaries and with nutrient database. The speech recognition software was trained with sets of words from meal descriptions. The algorithm for transition from the text description is based on language dictionaries with variety of food item descriptions related to one product in nutrient database. The system calculates the number of insulin units for patients using insulin pen or delivery time and number of insulin units for patients with insulin pump. The algorithm for insulin dosage works not only on the basis of the amount of carbohydrates, but also takes into consideration protein and fat content in the meal. The system was successfully tested on the group of 34 subjects achieving 92.3% of correctly recognized food descriptions in the first try. The overall percentage of fails in recognition was 1.5%.

SP113.6 - Building neuroscientific evidence and best practices in active and healthy aging

Author(s): Panagiotis D. Bamidis

Medicine, Lab Of Medical Physics, Aristotle University of Thessaloniki, Thessaloniki/GREECE

Supporting the elderly by means of technology has recently taken the form of monitoring the elderly in an unobtrusive way. The latter is linked with the task of installing various devices inside the home as well as requesting the elders to wear specific garments (e.g. watches, bracelets etc) or being trained by means of cognitive and physical exercise games (serious gaming; exergaming). The latter forms a contemporary trend within the field of Active and Healthy Aging (AHA). Serious games for elderly healthcare provide a promising and novel way to promote the well-being of senior citizens. However, to fully understand the underlying mechanisms as well as to accumulate scientific evidence for such approaches, we argue that one needs carefully designed neuroscientific experiments, along the usual batteries of neuropsychological tests and subjective measures like quality of life questionnaires.

In the past 6 years we have been using a comprehensive protocol of EEG recordings pre- and post any game enriched intervention. This allows for a much stronger analysis of the effects but also a deeper understanding of the underlying neuroplasticity mechanisms. In this paper, we demonstrate how functional neuroimaging analysis of these dense EEG measurements can reveal brain sources/ areas responsible for the de-noising of the elderly brain after the intervention. What is more, functional connectivity network analysis can reveal a reorganisation of the default mode network due to combined physical and cognitive training. Our results refer to a wide pilot deployment involving more than 150 senior subjects over an intensive training protocol of 2 months.

Besides this, recent emergence of motion capture technology has enabled acceptable unobtrusiveness as well as other features of making the game challenging and seniors being motivated. A key

step towards this direction would require using emotional queues in the midst of the game-flow and within the gaming environment, so as to allow for suitable embodiment of real-time mental (cognitive and emotional), and physical data. To properly study the above, one needs ecologically valid but yet controlled set-up, in the form of home-like environments. We have designed and implemented such an Active and Healthy Aging Living Lab/e-home within our Assistive Technologies and Silver Science Lab to facilitate such simulation as well as experiments and recordings with real elderly users. A vast amount of "daily-living" data is therefore created. These are then analysed with intelligent methods enabling early symptom identification and allowing decision support for early disease diagnosis. Emphasis is given on interlinking robust scientific methods and tools of studying emotions, as well as, age-related cognitive decline within the gaming environment and in-game metrics.

ACKNOWLEDGMENTS

This work was funded by the Operational Program "Education and Lifelong Learning" of the Greek Ministry of Education and Religious Affairs, Culture and Sports (Project STHENOS, www.sthenos.gr, ref. number 2012ΣΕ24580284).

SP113.7 - Intelligent System for Identification of patients in Healthcare

Author(s): Alexandra Vasquez¹, Monica Huerta¹, Roger Clotet¹, Ricardo Gonzalez¹, Giovanni Sagbay², David Rivas³, Jose Pirrone Puma⁴

¹Networks And Applied Telematics Group, Universidad Simon Bolivar, Caracas/VENEZUELA, ²Electrónica, Universidad Politécnica Salesiana, cuenca/ECUADOR, ³Electronic, Universidad de las Fuerzas Armadas, Latacunga/ECUADOR, ⁴Esc. Ingenieria En Telecomunicaciones, Universidad Catolica Andres Bello (UCAB), Caracas/VENEZUELA

The Inadequate identification of patients in health care centers remains as a common problem that has brought incidents and adverse event to this kind of facilities. This work present a system design to deal with this situation. To develop this proposal different identification systems and patient monitoring systems in health centers was studied, and a comparative study was conducted between existing technologies to develop this proposal. The NFC technology was chosen to develop a system solution because of its availability in mobile phones, its feature of information security, speed, low cost and simplicity in data exchange. Confidentiality of the patient information is guaranteed through authentication profiles for system access and data security through SSL and HTTPS protocols. The purpose of the proposed system is to provide correct information transfer, keeping track on patients and facilitate control of them by the health care center staff, in order to minimize accidents and mistakes of identification and to improve the healthcare facilities' quality.

SP114 - Dosimetry and Radiation Protection

PRESIDENTS CALL

SP114.1 - Development of Object Simulator for Evaluation Periapical Radiographs

Author(s): Jadna M.S. Mendes¹, Elias S. Sales Junior², Cinthia M.M. Paschoal³, Cledison J. Cunha⁴, Lourdes M. Brasil⁵, Fernanda C.L. Ferreira¹

¹Federal University of South and Southeast of Pará,, Marabá/BRAZIL, ²Physics, Federal University of South and Southeast of Pará, Marabá/BRAZIL, ³Civil Engineering, State University of Vale do Acaarau, Sobral/BRAZIL, ⁴Physics, Federal University of Sergipe, São Cristovão/BRAZIL, ⁵University of Brasília, Brasília/BRAZIL

This study aimed to develop a dental phantom with cysts for evaluation of periapical radiographs that was tested in private dental offices in the city of Marabá, northern Brazil. Through some tests with the object simulator (phantom) were obtained 12 periapical radiographs (one in each of the offices visited) that waking up to the standards of Ordinance N°. 453 were visually evaluated by observing the physical parameters of exposure (kVp and mA), time revelation of the radiographic film, later the other radiographs were visually compared with C6 ray set as the default. Among the results, it was found that only two of the twelve rays cysts could not be viewed and, therefore, these two images were deemed unsuitable for accurate diagnosis in the 10 images the cysts could be displayed, however according the images have different qualities comparisons. In addition, it can be concluded that the performance of the phantom was highly satisfactory showing to be efficient for use in quality control testing of dental X-rays, the quality control of radiographs and continuing education of dental professionals for a price much more accessible.

SP114.2 - Impact Created by Medical Physicist from Regulatory Quality Assurance Controls in Developing Country

Author(s): Samba Richard Ndi¹, Simo Augustin²

¹Control And Inspection, National Radiation Protection Agency, Yaounde/CAMEROON, ²Directorat General, National Radiation Protection Agency, Yaounde/CAMEROON

Background: The use of Ionizing Radiation in medicine has been increasing rapidly over the years in Countries in general and Cameroon in particular. Individual occupational exposure and patient safety varies widely among those involved in medical care. There are certain medical procedures that might give substantial doses to medical staff, normal tissues of patients and the education of medical professionals in radiation protection and quality control issues are continuing problems. Regulatory bodies are mandated through laws and regulations to regulate all ionizing radiation sources as well as the protection of people and environment against ionizing radiation hazards.

Objectives: Improvement of regulatory framework by Medical Physics Quality Assurance Controls.

Methodology: National Radiation Protection Agency (NRPA) of Cameroon activities started with inventory program in 2009, which was completed in July 2010. Over 500 occupationally exposed workers were recorded with about 12 % being monitored 5% of quality assurance undertaken. There was no national dosimetry service provider, all were monitored from abroad. Regulatory Technical control started in 2011. A medical physicist was employed by NRPA in 2010 to coordinate Quality Control and dosimetry activities as

regulatory aspect. There were a lot of discrepancies recorded at the level of occupational monitoring and state of equipment to produce quality images. NRPA acquired dosimetric monitoring and quality control kits in 2010 and 2011 respectively. These are widely used in quality control, radiation protection and safety, offer a number of potential advantages for medical applications (diagnostic and radiation therapy).

Results: As of 2014, remarkable improvement has been noticed in the dose reduction of workers, patients and the quality of the machines used in then controlled medical facilities. In this, the results of occupational exposure from 2011 to 2014 is shown and the results of the quality control executed from 2011 and 2014 compared are illustrated in tables.

Recommendation: Recommendations are ditched out to competent authorities at various levels for the continuous improvement of quality assurance programme and occupational monitoring to safeguards radiation protection/safety culture.

Conclusions: Radiation Principles are being applied by using national and international standards for the benefits of both patients and workers in radiological practices. This can never be sustainable without the creation of the awareness of Medical Physicist policy and roles in developing countries.

SP114.3 - Evaluation of Dental X-rays equipment in Sobral-CE, Brazil

Author(s): F L. Meneses¹, Fernanda C.L. Ferreira², Cinthia M.M. Paschoal¹

¹Civil Engineering, State University of Vale do Acaraú, Sobral/BRAZIL, ²Federal University of South and Southeast of Pará, Marabá/BRAZIL

The ionizing radiation has important application in dental diagnosis. In Brazil, the National Ordinance No. 453/1998 of the Ministry of Health regulates the operation of medical and odontological diagnostic radiology services. However, the inspection of periapical dental X-ray equipment is not carried out by some Sanitary Surveillances. This study intended to determine the suitability to the ordinance of the dental offices of Sobral-CE, Northeast of Brazil, and to compare the results with literature data for other cities of Brazil. It was performed tests of radiation field and image quality, and it was applied questionnaires to the professionals. For the image quality test, it was used a dental phantom and the processing of the films was performed in the clinics and at the laboratory (standard). The questionnaire assessed physical parameters that interfere on the radiation protection and on the quality of images. The results show that the ordinance is not being properly followed and that it is necessary to inspect the periapical X-ray equipments. Moreover, in general, it is observed that dental professionals should have better training on ionizing radiation and on radiation protection.

SP114.4 - Effect of static magnetic field exposure on human blood electrolyte levels in vitro

Author(s): Pankaj Parashar¹, Kishore K. Deepak², Sneha Anand³, Ashok K. Mukhopadhyay⁴, Sudip K. Datta⁴, Jitendar K. Sharma⁵, Jyoti Kumar⁶, Raoji S. Shinde⁷, Mithilesh K. Pal⁸, Prabhat Arora⁵

¹Centre For Biomedical Engineering, Indian Institute of Technology Delhi, New Delhi/INDIA, ²Physiology, All India Institute of Medical Sciences Delhi, New Delhi/INDIA, ³Centre For Biomedical Engineering, Indian Institute of Technology, New Delhi/INDIA, ⁴Laboratory Medicine, All India Institute of Medical Sciences Delhi, New Delhi/INDIA, ⁵Healthcare Technology Division, and WHO Collaborating Center, National Health Systems Resource Center, Ministry of Health and Family Welfare, Government of India, New Delhi/INDIA, ⁶Instrument Design And Development Centre, Indian Institute

of Technology, New Delhi/INDIA, ⁷Accelerator Magnet Technology Division, Raja Ramanna Center for Advanced Technology, Indore/INDIA, ⁸Biomedical Engineering Unit, All India Institute of Medical Sciences Delhi, New Delhi/INDIA

This proposed paper presents a study of effect of strong static magnetic field (SMF) exposure on electrolytes in human blood in-vitro. There have been major concerns of safety from magnetic fields (static and dynamic magnetic fields) to life and their effects on physiology. It is noteworthy that magnetic fields are listed as 'Potentially carcinogenic' by W.H.O. There are evidences of SMF causing special sensations in humans and animals like bizarre behavior and magnetophosphenes, these are probably attributed to cell membrane property changes.

Magnetic therapy is a treatment modality being used since ages, the claimed mechanism of action being the presence of iron in the blood and the alteration in blood viscosity, which is mostly doubted by the modern science.

Here, the effect of SMF exposure on blood electrolytes was studied. A Case - Control study was carried out, collecting blood samples from healthy young volunteers. The samples were divided into 6 equal parts in 3 pairs of Case and Control, and exposed in vitro for 20 minutes to SMF strengths of 500 Gauss (G), 5000 Gauss and 1 Tesla respectively one after the other. Here case sample was exposed to 500G SMF generated by a coil electromagnet between 2 soft iron cores and the control samples shielded by placing in an iron box. After 20 minutes of exposure and shielding, both samples were estimated for electrolytes: K⁺, Ca⁺⁺ (ionic), Na⁺, Cl⁻ and pH by indirect Ion Selective Electrodes method on a Combiline[®] blood gas analyzer machine. The process was repeated for the other pairs of samples with cases on 5000G and 1 Tesla (1 Tesla = 10000 Gauss) SMF one after the other and shielding controls to match the effects of the time lapse. The data acquired was analyzed by applying paired T test on the case and control samples for each ion parameter at each SMF strengths exposed, the P value was taken to be significant at p<0.05. Here, no statistically significant changes in the ionic concentrations of the case and control samples were found. The results indicate that the SMF of 500 Gauss, 5000 Gauss and 1 Tesla did not result in any significant change in the electrolyte concentration in the samples, possibly inferring to no significant change in leakiness of the red blood cell (RBC) membrane

This study suggests that very strong SMF of up to 1 Tesla, as used in this experiment, do not affect the electrolytes and possibly the leakiness of the RBC membrane in vitro. In this study it was also found that the SMF of around 500 Gauss, the strength of the magneto-therapy magnets also did not show any change in electrolyte concentration, hence no change in membrane leakiness of the RBCs. This study, hence points towards the safety of the magnetic field exposure on the red blood cell membrane leakiness.

SP115 - CT Image Quality and Dose Optimization

TRACK 01: IMAGING

SP115.1 - Towards Image Quality Analysis of Small and Full Field of View Dental Cone Beam CT Systems

Author(s): Elias Cantarelli Hoffmann¹, Ana Maria Marques Da Silva², Dario F.G. Azevedo³
¹Núcleo De Pesquisa Em Imagens Médicas, PUCRS, Porto Alegre/BRAZIL, ²Faculdade De Física, PUCRS, PORTO ALEGRE/BRAZIL, ³Faculdade De Engenharia, PUCRS, PORTO ALEGRE/BRAZIL

Cone-beam CT (CBCT) systems have been used for dentomaxillofacial surgery applications. Different dental CBCT devices are being developed and released, with a wide variability of exposure parameters and fields of view. Although they have sufficient diagnostic quality, a quantitative analysis of image quality and radiation dose is required to enable their optimal use. The aim of this study was to develop and implement a feasible methodology for image quality analysis for different dental CBCT devices. The methodology was based on conventional CT quality control procedures and adapted to overcome the limitations of dental CBCT. A prototype phantom was specially designed to allow the acquisition of image quality parameters relevant to dental imaging. Equipments were divided into categories, related to their field of view: Small Field of View (SFOV) and Full Field of View (FFOV). The following image quality parameters were evaluated: uniformity, noise, contrast-to-noise ratio, CT number accuracy, artifacts, spatial resolution and geometric distortion. Applicability of the methodology was assessed using one SFOV and four FFOV CBCT devices. Results from preliminary analyses of the prototype phantom showed its potential for routine quality assurance on dental CBCT. Large differences in image quality performance were seen between the devices.

SP115.2 - Rapid non-invasive spatially varying HVL measurements for CT sources

Author(s): Matthew Randazzo, Mauro Tambasco
 Physics, San Diego State, San Diego/CA/UNITED STATES OF AMERICA

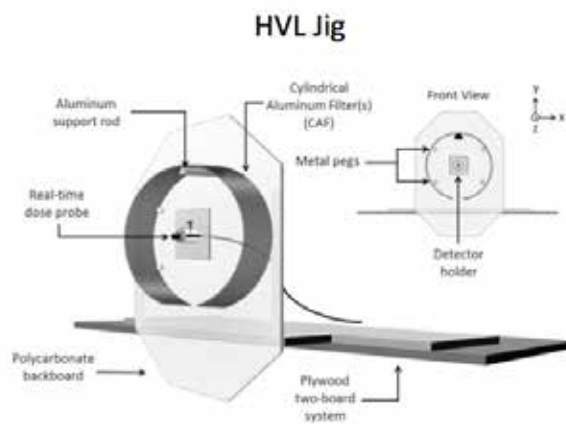
Purpose: A method is presented generate spatially varying half value layers (HVLs) that can be used to construct of computed tomography (CT) x-ray source models for CT dose computations.

Methods: To measure the spatially varying HVLs, we combined a cylindrical HVL measurement technique with the characterization of bowtie filter relative attenuation (COBRA) geometry. An apparatus (HVL-Jig) was fabricated to position a real-time dosimeter off-isocenter while surrounded by concentric cylindrical aluminum filters (CAFs). Data was acquired using axial CT protocols filters to investigate the energies of 80, 100, and 120 kVp on a single CT scanner (GE Optima CT580). In this geometry, each projection of the rotating x-ray tube is filtered by an identical amount of high-purity aluminum while the stationary detector records an air kerma rate versus time waveform. The CAFs were progressively nested to acquire exposure data at increasing filtrations to calculate the HVL. Using dose waveforms and scanner geometry, each timestamp was related to its corresponding fan angle. These measurements were validated against the more laborious conventional step-and-shoot approach.

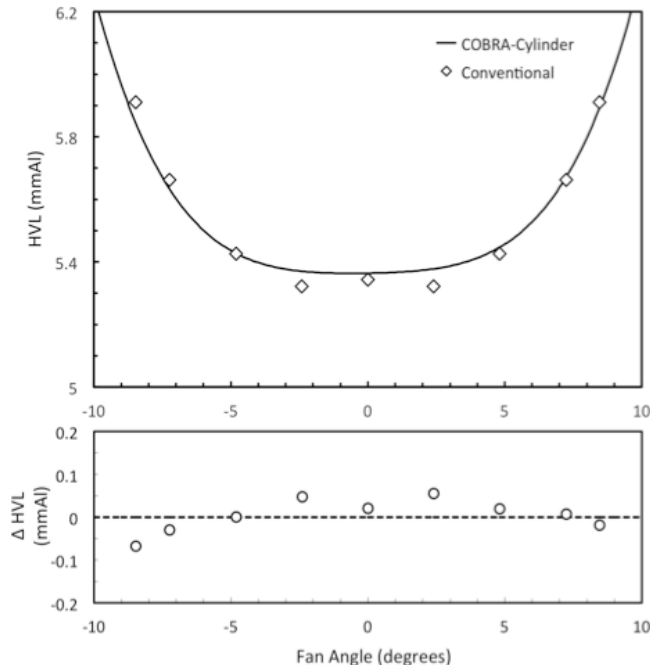
Results: At each energy, HVL data from the COBRA-cylinder technique was fit to a trendline and compared with the conventional approach. The average relative difference in HVL between the two

techniques was 1.3%. A systematic overestimation in HVL was observed due to scatter contamination, but by applying a 1% downward shift to all measurements, all differences lie within a 0.2 mm Al threshold needed to generate spectra for accurate Monte Carlo CT dose computations.

Conclusion: The rapid, accurate, and non-invasive approach described allows one to acquire the spatially varying fluence and HVL data using a single experimental setup and three scans. These measurements can be used to characterize the CT beam fluence and energy spectra along the BT filter direction, which can serve as input for CT dose computations.



80 kVp Off-Axis HVL Measurements



SP115.3 - Development of a CT protocol management system for automated review of CT scanner protocols

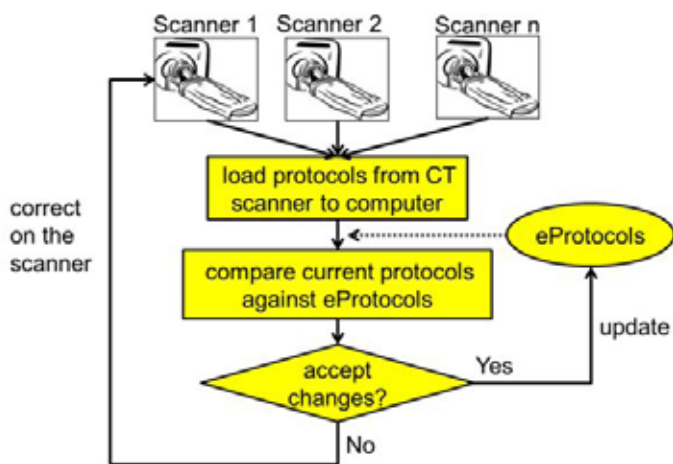
Author(s): Josh Grimes, Shuai Leng, Yi Zhang, Cynthia Mccollough
Mayo Clinic, Rochester/MN/UNITED STATES OF AMERICA

Protocol review is mandatory in some states and for ACR CT accreditation. The benefits of protocol review include a decreased risk of patient injury and increased consistency in CT image quality. There can be many CT protocols loaded on a scanner and continual protocol customization and optimization can make manual review of these protocols labor intensive, error prone and costly. The objective of this work was to develop software for automatic protocol review to help ensure the accuracy of protocols loaded on CT scanners.

The protocol management software was developed in MATLAB. The general workflow of the software is as follows. First, protocol files are copied from the CT scanner. Next, the scanner protocol files are compared to the corresponding eProtocols, which are the set of instructions that the technologists at our institution follow for CT examinations. All CT scanners of a given model are compared simultaneously with the eProtocols for that particular scanner type. Differences between the scanner protocol files and the eProtocols are flagged and this comparison is summarized in an excel spreadsheet. A lead technologist reviews the spreadsheet and decides whether the flagged protocol parameters are correct in the eProtocols or on the scanner. A list of these decisions is automatically created. Using this list, the technologist must update the eProtocol or correct the protocol on the scanner.

The software can be configured to run completely automatically by loading the protocol files off of the scanner and running the protocol monitoring software according to a predetermined schedule (e.g. daily or weekly). In this case, alerts can be automatically sent each time a discrepancy is found between the scanner protocol file and the eProtocol. Another useful application of the software is to run the program each time the scanner protocols are modified. This provides the user with immediate feedback about whether or not the protocols were set appropriately on the scanner.

An automated CT protocol management system is essential to ensure protocol accuracy and consistency. The protocol management software developed in this work can be applied to a wide range of practices with negligible impact on workflow.



SP115.4 - Evaluation of automatic exposure control systems in computed tomography

Author(s): Paulo R. Costa, Thamiris R. Reina, Denise Y. Nersissian
Nuclear Physics, Radiation Dosimetry and Medical Physics Group, Physics Institute, São Paulo/BRAZIL

Introduction: The greatest and relatively new advance in CT to lower the patient dose is the automatic exposure control (AEC) systems [1]. These systems modulate the dose distribution along the patient taking into account their size and tissue densities [2]. AEC-systems are complex and their functioning is not fully understood [3]. This work aims to evaluate the performance and susceptibilities of AEC-systems.

Methods: The approach was the extraction of tube current modulation (TCM) data from DICOM image sequences and analysis of the image noise of those images [4]. The TCM of each CT scanner provides the performance of the AEC-system. Dose measurements with the AEC-system ON and OFF were made to verify if the tube current was consistent regarding the dose distribution behavior.

Results and Discussion: Figure 1 shows the TCM, and the corresponding noise for a Philips Brilliance 16 longitudinal AEC mode, Z-DOM, and the longitudinal AEC mode with the DoseRight ACS option ON. This example shows that this option causes a great increase on tube current, with a lower image noise and it doubles the dose compared to Z-DOM with this option OFF and the image noise decreases about 25%.

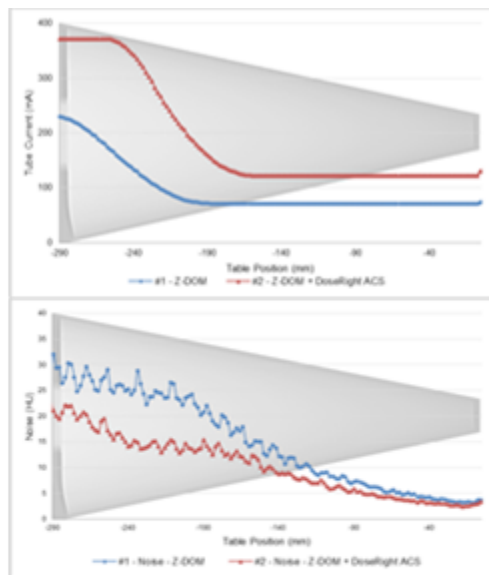


Figure 1 - Tube current modulation and correspondig image noise for the longitudinal AEC mode, Z-DOM, and the longitudinal AEC mode with the DoseRight AEC option ON. The blue line represents the Z-DOM and the red line represents the Z-DOM with DoseRight ACS option ON.

Conclusions: The results attained give rise to optimizations on the AEC-systems applications and, by consequence, decreases the patient dose without compromising the diagnostic image quality.

Acknowledgments: The authors thank FAPESP (project 2010/12237-7) and CNPq/FAPESP INCT Radiation Metrology in Medicine.

References:

1. Medicine and Health Care products Regulatory Agency, MHRA. CT scanner automatic exposure control systems. London: MHRA, 2005. (MHRA Report 05016)
2. Kalender, W.A. Computed Tomography. 3rd Ed.; Publicis Publishing, Erlangen, Germany, 2011.
3. MATSUBARA, K.; et al. American Journal of Radiology; v. 192: p. 862-865, Apr. 2009
4. SCAN HEADER. Available at: <http://www.medphys.it/down_scan_header.htm>. Accessed in: 29 May 2014

SP115.5 - Development of a Software for Image Quality Assessment in Computed Tomography using the Catphan500® Phantom

Author(s): Daniel V. Vieira, Paulo R. Costa, Denise Y. Nersissian
Departamento De Física Nuclear, Instituto de Física da Universidade de São Paulo, São Paulo/BRAZIL

Introduction: A software for image quality assessment in computed tomography (CT) was written using MatLab® language. This software intends to improve CT scanners quality control programs, evaluating quantitatively the Catphan500® images. The software can identify the images from each section of the phantom and calculate the physical quantities of interest in these images. This process is performed with minimal direct user interference.

Methods: The software was written in modules. The MTF module uses images of the beads of the Catphan section CTP528 and subtracts the background, obtaining the PSF. The MTF is calculated from the resulting PSF. Due to the system symmetry, the two-dimensional MTF can be averaged over the azimuthal angle to obtain a radial MTF, MTFrad, in function of the spatial frequency f_r . The uncertainty is also evaluated by averaging the MTFrad of multiple bead images.

The noise module uses images acquired from the section CTP486, and evaluates the noise and the NPS of the CT system. Noise is calculated taking the pixel mean and standard deviation in a central region of interest (ROI) and other four peripheral ROI's, as recommended by the Catphan user manual[i]. The two-dimensional NPS, NPS2D, in function of the spatial frequencies f_x and f_y is calculated by the method proposed by the ICRU Report n° 87[ii]. The NPS2D of multiple image pairs are then averaged to lower the uncertainty.

Results: Figure 1 illustrates the mean NPS2D and MTFrad calculated by the software, using 49 noise image pairs and 82 bead images respectively, selected from a set of 868 images in total. The images were acquired in a GE Discovery 690 PET/CT scanner. These results are consistent with previous qualitative results obtained from the quality control program implemented in the same equipment.

Figure 1: NPS2D (left) and radial MTFrad (right) of the GE Discovery scanner.

Conclusions: The preliminary results from the software agree with the expected from previous works. Without such software, the calculations of NPS and MTF is not always done, as it takes many hours; this software greatly reduces this time. Also it makes the analysis less subjective, more quantitative, and improves reproducibility.

Acknowledgements: The authors thank CNPq for financial support under project 131667/2014-9.

References

- [i] The Phantom Laboratory, 2006. *Catphan 500 and 600 manual*. (Salem, NY: The Phantom Laboratory).
- [ii] Oxford University Press, 2012. *ICRU Report n° 87 - Radiation Dose and Image Quality Assessment in Computed Tomography*. (Geneva, Switzerland: ICRU).

SP115.6 - Performance of attenuation-based dynamic CT beam-shaping filtration for elliptical subject geometries in dependence of fan- and projection-angle

Author(s): Stella Veloza¹, Hans-Ulrich Kauczor², Wolfram Stiller²
¹Department Of Physics, Universidad Nacional de Colombia, Bogota, D.C./COLOMBIA, ²Department Of Diagnostic And Interventional Radiology (dir), University Hospital Heidelberg, Heidelberg/GERMANY

Purpose: The computed tomography (CT) beam-shaping filter, also called bowtie filter, modulates X-ray beam intensity across the fan beam, compensating for decreasing absorption due to shorter X-ray path lengths through patient body periphery compared to its center. The effect of replacing static beam-shaping filter geometry currently used in commercially available CT systems by a novel filter geometry dynamically adapted to the attenuation of objects of elliptical cross-section during the image acquisition has been evaluated with regard to its potential for signal homogenization and radiation exposure reduction.

Methods and Materials: A theoretical model of a beam-shaping filter that dynamically adapts its attenuation profile to subjects of elliptical cross-section as a function of fan- and projection-angle has been developed. To achieve comparison, an accurate empirical model of a static large bowtie filter has been determined from Compton spectroscopy measurements of the X-ray spectra at different angular distance (0°-21°) from the central ray of the fan beam of a CT system for a tube potential of 120kVp by using a low energy Germanium detector. In order to calculate relative radiation exposure reduction achievable by replacing static with dynamic bowtie filtration in CT, spatial dose distributions in a homogeneous elliptical water phantom with a major axis of 32 cm and a minor axis of 25 cm were Monte-Carlo simulated with Geant4 for projections a.p. to lateral in steps of 15° (20 million of photons per projection) and exploiting phantom symmetry, total dose maps were calculated.

Results: Regarding signal homogenization the performance of dynamic adaptive beam-shaping filtration fully lives up to expectation in as much as the attenuation becomes constant throughout the complete FOV, i.e. independent of fan angle, for all projection angles. Compared to a CT acquisition with the static beam-shaping filter, a significant additional radiation exposure reduction of 15% can be achieved by using dynamically adapted beam-shaping filtration. Replacing static by dynamic filtration allows relative patient skin dose reductions of around 23% in the antero-posterior (a.p.) projection and 40% in the lateral projection.

Conclusions: The new dynamic adaptive beam-shaping filter concept allows to homogenize absorbed radiation dose distribution and has potential for saving additional absorbed radiation dose compared to static beam-shaping filtration currently used in CT. The results suggest that static beam-shaping filter geometry should be reevaluated in favor of a dynamic adaptive beam-shaping filtration concept such as developed and evaluated here in order to reduce patients' (skin) dose.

SP115.7 - A software tool for automated artifact detection in scans of the CT daily water phantom**Author(s):** Josh Grimes, Shuai Leng, Lifeng Yu, Cynthia Mccollough
Mayo Clinic, Rochester/MN/UNITED STATES OF AMERICA**Purpose:** The objective of this work was to develop a software tool for automated artifact detection in scans of the daily CT water phantom.**Methods:** The artifact detection algorithm developed in this work uses a uniformity map created from convolution of the water phantom image with a small region of interest (ROI). Non-uniformities in the image are detected by looking for connected objects with CT numbers outside of an acceptable range inside the uniformity map. A pilot study was conducted to test the artifact detection algorithm on water phantom images acquired on a Siemens Sensation 64. This pilot study was split into two phases. First, a training dataset consisting of one month of daily water phantom images was collected for tuning the parameters of the artifact detection algorithm. Parameters to tune included the size of the ROI used in the convolution to generate the uniformity map, an acceptable CT number range in an artifact free image, and the minimum size of a connected region to count as a non-uniformity. Histograms summarizing how often connected objects of varying sizes occur for different CT number ranges were used to tune the parameters of interest. In the second phase, the software was used to monitor daily water phantom images for five more months.**Results:** The training dataset revealed several important characteristics of the water phantom images. These characteristics included: a normal image (artifact-free) might not be uniform, there can be variation in "normal" non-uniformities between slices, and there are fluctuations in mean CT numbers from day-to-day as well as drift in average CT number over time. The artifact detection algorithm was modified to deal with these characteristics as follows. First, a normal image acquired on a previous date and known to be artifact-free is subtracted from the current water phantom image under investigation. This subtraction is performed slice-by-slice to deal with the variation observed between slices. Second, the average CT number of each water phantom image is subtracted from each pixel in the image to address the fluctuation in CT numbers from day-to-day. The histograms that were plotted to show the frequency of connected objects of various sizes with different settings for the acceptable CT number range demonstrated that a reasonable set of parameters for detecting artifacts was to classify a connected object as an artifact if it was larger than 200 pixels in size and had a CT number greater than +2 HU or less than -2 HU. Using these parameters for the second phase of the study, no artifacts were detected by the software over the five month period. No artifacts were reported by a technologist during this same period. When the software was used to analyze water phantom images with known artifacts from other scanners, these artifacts were correctly identified.**Conclusion:** A general method for detecting non-uniformities in water phantom images was developed. This software should not be used to replace the human observer, but can serve as an added daily check for scanner issues.**SP115.8 - Monte Carlo Simulation of X-ray Spectra in Computed Tomography Scanner using GATE****Author(s):** Mohammad Reza Ay, Samira Nezhaddehghani, Saeed Sarkar
Department Of Medical Physics & Biomedical Engineering, Tehran University of Medical Sciences, Tehran/IRAN**Introduction:** X-ray spectrum modeling has an important role in medical imaging and many of researchers are still trying to find a simple and accurate method for simulation of x-ray spectrum. Monte Carlo simulation is a powerful tool in prediction of the x-ray spec-

trum. In this study, the x-ray spectra of the computed tomography system simulated using GATE Monet Carlo code. After validation the effect of the anode angle, tube voltage and thickness of filter on x-ray spectrum was investigated by using of Monte Carlo (MC) simulation. The simulated results were compared with MCNP4C MC simulated x-ray spectra and the spectra calculated by IPEM report No.78.

Materials and Methods: The GATE and NCNP4C MC packages were used for accurate modeling of the x-ray tube. The geometry of the x-ray tube in both codes was implemented precisely the same. The tungsten target with 7 degree and focal spot size 1.2x1.2 mm² was simulated. The x-ray spectra simulated using various tube voltages and different anode and variable thickness of Copper filter. The IPEM report No.78 was used as a reference to compare with the results from simulation codes.**Results:** The changes in quality and quantity of the spectrum for four different tube voltages 60, 80, 100, and 120 kVp were investigated and the results indicated that by increasing the voltage, the average of spectrum reached to the higher energy level. The x-ray spectra simulated for 4 different anode angle 7, 9, 11, and 13 degree. The simulated spectrum by using GATE was compared with two spectra from MCNP4C and IPEM report No.78 and in general there was good agreement between the results.**Conclusion:** The effect of different variables on the spectrum was investigated. Good agreement between the simulated spectra by using GATE, MCNP4C and IPEM report No.78 were observed, although there are systematic differences between the simulated and reference spectra especially in the K-characteristic x-rays intensity. The results indicate that the GATE MC package is a useful tool for generating x-ray spectra of CT.

SP116 - Image Processing and Visualization: Part 2

TRACK 01: IMAGING

SP116.1 - Automated segmentation of whole-slide histology for vessel morphology comparison

Author(s): Yiwen Xu¹, J Geoffrey Pickering², Zengxuan Nong², Aaron D. Ward¹

¹Medical Biophysics, The University of Western Ontario, London/ON/CANADA, ²Robarts Research Institute, London/ON/CANADA

Introduction: Characteristics of microvasculature can be revealed by immunohistochemical tissue staining, but manual quantification of these characteristics on whole-slide images containing potentially hundreds of vessels on each is tedious and subject to operator variability. Conventionally, manual quantification is performed for selected regions of the whole tissue section where the regions may not be representative of the pathology. Major challenges to automated segmentation include the irregularity of staining of vessel walls and artefactual appearance of DAB stain on structures other than vessel walls. Our objective was to develop and validate a fully automated segmentation of the vascular smooth muscle layer on whole-section histology of normal and regenerated post-ischemia mouse hind limb microvasculature, stained for smooth muscle using 3,3'-diaminobenzidine (DAB) immunostain.

Methods: Our approach accounts for irregularity of vessel wall staining using colour deconvolution to isolate the DAB stain, and joining the morphological skeletons of the vessel wall fragments disjointed by inconsistent staining. Artefactual fragments were removed based on incoherence of neighbouring tissue in an accurate 3D histology reconstruction (Y Xu, SPIE Medical Imaging 2014). The vessel wall thickness, vessel density, area, and perimeter were quantified.

Results/Discussion: For segmentation validation, vessels were manually delineated and compared to the automated segmentation approach on a normal mouse, resulting in a Dice similarity coefficient of 0.84 (Figure 1). Differences in the vessel measurements observed between the normal and ischemic mice were concordant with the known effects of regeneration of vasculature in ischemic mice ($p < 0.05$, Table 1). Fully automatic and accurate measures of the vascular morphology are feasible with the automated segmentation of the vascular smooth muscle. With refinement and validation of this method on a larger data set, we aim to provide a valuable tool for scientists requiring high-throughput vascular segmentations and morphological measures for the analysis of vasculature for disease state comparisons.

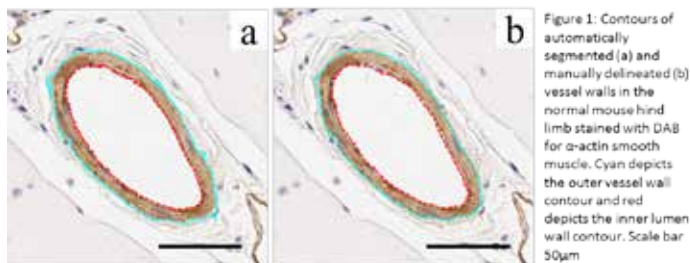


Figure 1: Contours of automatically segmented (a) and manually delineated (b) vessel walls in the normal mouse hind limb stained with DAB for α -actin smooth muscle. Cyan depicts the outer vessel wall contour and red depicts the inner lumen wall contour. Scale bar 50µm

Table 1: Automatic vessel smooth muscle morphological measures

	Area (μm^2)		Perimeter (μm)		Thickness (μm)					
	Median	IQR	Median	IQR	5th Percentile	50th Percentile	95th Percentile			
Normal 1 (n = 2198)	27.8	69.3	19.7	22.0	0.6	0.8	1.4	1.6	2.7	2.7
Normal 2 (n = 2568)	23.1	58.8	20.8	21.1	0.5	0.6	1.3	1.4	2.5	2.4
Post ischemic (n = 3808)	31.1	82.8	19.1	24.6	0.7	0.8	1.6	1.6	2.8	2.7

SP116.2 - Using Gamma Maps of Anatomy to Highlight Changes in Anatomy During Image-Guided Adaptive Radiotherapy: Head and neck example

Author(s): Jeff Kempe¹, David Palma², Bryan Schaly¹, Jerry J. Battista²

¹Physics And Engineering, London Health Sciences Centre, London/ON/CANADA, ²Department Of Medical Biophysics, Western University, London/CANADA

In recent years, technology has allowed radiation therapy of increasing complexity to be delivered to cancer patients, with the goal of improving tumour control and reducing toxicity. In adaptive radiotherapy (ART), imaging information acquired during treatment is used to adjust the treatment plan if necessary. During treatment of head and neck cancer, anatomical changes (e.g., weight loss) may occur and patients are flagged for re-CT simulation if the changes are substantial. But, how do we know when to flag patients for treatment replanning? The goal of this abstract is to demonstrate a graphic tool to aid in assessing changes in patient anatomy using the gamma comparison.

In the past, gamma function calculations have been used for quality assurance of the dose delivered to phantoms by the treatment machine compared with the planned computed dose. We propose using this function to highlight changes in patient anatomy, instead of dose, as a tool (an alarm) to aid the therapist and oncologist in deciding whether to flag the patient for re-CT simulation. Implementing this function in 3-D is computationally intensive; but, recent advances in graphics processing units (GPUs), and associated software, have greatly accelerated this calculation. With GPU hardware (costing under \$1,000) the gamma function comparing two full-size 3-D CT data sets (512x512x60) can be calculated in one minute. This result could be displayed at the treatment console to determine if a treatment adjustment merits consideration. We will demonstrate a sample application of this approach to head and neck cancer.



Figure 1: Gamma function on pairs of CBCT data sets of the head and neck region. ΔHU : 30 (absolute) Δr : 5 mm

SP116.3 - Improvement of Ventricle Volumetric Calculation and Visualization in Cardiac MRI**Author(s):** Yarish Brijmohan¹, Naren Ramchander², Stanley Mneney¹, William I.D. Rae³¹Electronic Engineering, University of Kwa-Zulu Natal, Durban/SOUTH AFRICA, ²Electronic Engineering, eThekweni Municipality, Durban/SOUTH AFRICA, ³Medical Physics, University of the Free State, Bloemfontein/SOUTH AFRICA

Magnetic resonance imaging (MRI) is widely used in medical care services to perform visualisation of the human heart in order to assist in the diagnosis of several cardiovascular diseases. The severity of these disease states is often diagnosed and evaluated by analysing the blood volumes and flow rates within the ventricles. An accurate segmentation of the left and right ventricle from MRIs, at the end diastolic and end systolic cardiac phases, is the first step required for the volumetric calculations. Simpson's rule for measuring volumes is currently the most commonly used method in the literature, in which the volume at a particular cardiac phase is obtained by multiplying the segmented area by the slice thickness per slice and performing a summation over all slices. This method results in volumetric errors for imaging performed with large (non-isotropic) slice thickness. In this paper, methods of surface modelling are introduced to interpolate the volume between slices, providing a smooth surface visualisation of the ventricles. Furthermore, by using segmentation information from three orthogonal MRI views, improvements in the visualisation and volume calculation is formulated.

SP116.4 - Inter-operator variability of 3D prostate magnetic resonance image segmentation using manual and semi-automatic approaches**Author(s):** Maysam Shahedi¹, Derek W. Cool², Cesare Romagnoli², Glenn Bauman³, Matthew Bastian-Jordan², Eli Gibson⁴, George Rodrigues¹, Belal Ahmad³, Michael Lock¹, Aaron Fenster⁵, Aaron D. Ward⁶¹London Regional Cancer Program, London/ON/CANADA, ²Department Of Medical Imaging, The University of Western Ontario, London/ON/CANADA, ³Department Of Oncology, The University of Western Ontario, London/ON/CANADA, ⁴Graduate Program In Biomedical Engineering, The University of Western Ontario, London/ON/CANADA, ⁵Imaging Research Laboratories, Robarts Research Institute, London/CANADA, ⁶Department Of Medical Biophysics, The University of Western Ontario, London/CANADA**Purpose:** To measure accuracy and inter-operator variability of a semi-automatic prostate segmentation method for T2-weighted endorectal magnetic resonance (MR) imaging.

Materials and Methods: MR images from 42 prostate cancer patients were acquired. Manual border delineation was performed by one observer on all the images and by two other observers on a subset of 10 images. Simultaneous truth and performance level estimation (STAPLE) segmentation was calculated from all three segmentations. Our algorithm calculated inter-subject prostate shape and local boundary appearance similarity during its training phase. To initiate the segmentation, the operator indicated the anteroposterior prostate orientation and selected the prostate centre on the most-superior, mid-gland, and the most-inferior slices. These inputs were used to identify candidate prostate boundary points using learned appearance characteristics, which were regularized according to learned prostate shape information to produce the final segmentation. On all subjects, we evaluated our method against the manual reference segmentations using complementary boundary-, region- and volume-based metrics: mean absolute distance (MAD), Dice similarity coefficient (DSC), recall rate, precision rate, and volume difference (ΔV). On 10 cases, we measured the inter-operator variability of manual segmentation by comparing the reference segmentations to the STAPLE segmentation, and conducted a multi-operator study to measure inter-operator variability of the semi-automatic algorithm.

Results: Table 1 shows our results on our 42 subjects with a single operator. Table 2 compares the consistency of manual and semi-automatic segmentations on 10 cases. The variability of all of the metrics resulting from the semi-automatic segmentation was reduced, compared to the manual segmentation.

Conclusions: We observed substantial inter-operator variability in manual segmentation and reduced variability in semi-automatic segmentation. In studies evaluating prostate segmentation algorithm accuracy using a single-operator reference standard, it is important to consider the measured errors in the context of inter-operator manual segmentation variability.

Table 1: Accuracy and variability for semiautomatic segmentation: mean ± standard deviation of MAD, DSC, recall, precision, and ΔV for different regions of interest.

Region of interest	MAD (mm)	DSC (%)	Recall (%)	Precision (%)	ΔV (cm3)
Whole gland	2.0±0.5	82±4	77±9	88±6	-4.6±7.2
Mid-gland (1/3)	1.6±0.5	90±3	90±7	91±6	-0.1±2.0
Apex (1/3)	2.0±0.7	79±6	82±14	80±13	0.1±3.3
Base (1/3)	2.6±0.8	73±10	61±14	93±6	-4.5±3.7

Table 2: Consistency of manual and semi-automatic segmentation: average of means (average of standard deviations) of the metrics across three manual and three semi-automatic segmentations by three expert operators. (N: number of images, reference: STAPLE segmentation).

Segmentation Method	N	Region of interest	MAD (mm)	DSC(%)	Recall(%)	Precision(%)	ΔV(cm3)
Manual	10	Whole gland	1.3(1.6)	90(11)	88(19)	94(6)	3.9(10.1)
		Mid-gland	0.8(0.9)	95(5)	93(10)	97(2)	0.8(2.1)
		Apex	1.4(1.8)	86(15)	85(24)	93(8)	1.4(3.3)
		Base	1.6(1.9)	86(14)	86(22)	91(11)	1.6(4.8)
Semi-automatic	10	Whole gland	1.9(0.3)	80(4)	75(7)	88(3)	-3.2(2.9)
		Mid-gland	1.5(0.3)	90(2)	90(3)	91(2)	0.2(0.7)
		Apex	1.8(0.4)	82(4)	87(8)	80(8)	0.8(1.2)
		Base	2.7(0.5)	68(7)	57(12)	93(6)	-4.2(2.5)

SP116.5 - Derivation of Residual Noise of Filtered Poisson and Gaussian Series

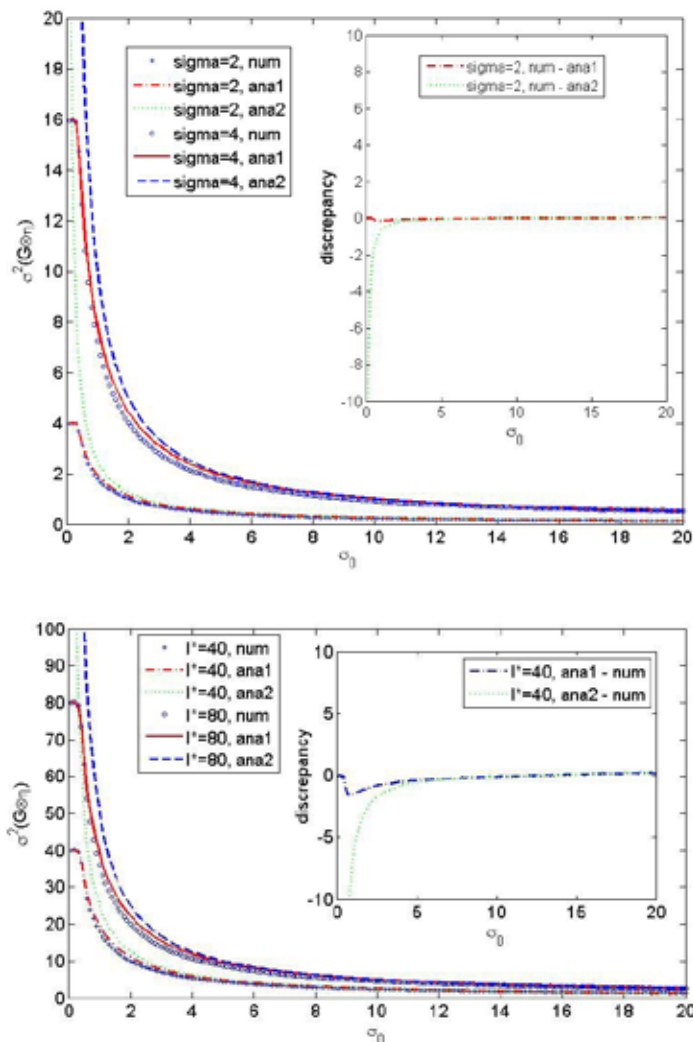
Author(s): Weiguang Yao¹, Jonathan B. Farr²

¹St. Jude Children’s Research Hospital, Memphis/UNITED STATES OF AMERICA, ²St. Jude Children’s Research Hospital, Memphis/ TN/UNITED STATES OF AMERICA

Residual noise analysis is useful in designing optimal filters for noise reduction. To begin we derived the variance of residual noise σ^2 , from Poisson filter and Gaussian series after filtered by a Gaussian filter. For Poisson series, we have $\sigma^2 = \sqrt{(2\pi)} I^* / (4\sigma_0)$, and for Gaussian series, $\sigma^2 = \sqrt{(2\pi)} \sigma^2 / (4\sigma_0)$, where I^* is the noiseless signal in the Poisson series, σ and σ_0 are the standard deviations of the Gaussian series and the Gaussian filter, respectively.

The figures below compare the analytically derived σ^2 , noted as «ana2» in the legends, with the numerically simulated ones, noted as «num». The first figure is for Gaussian noise sequences η , with standard deviations 2 and 4, respectively, and the second figure is for Poisson noise sequences $I^* + \eta$ with noiseless $I^*=40$ and 80 respectively. The discrepancy is mainly due to pixelation of the Gaussian filter. For example, when $4\sigma_0 / \sqrt{(2\pi)} < 1$, the shape of the pixelated filter used in numerical simulations is very different from the bell shape Gaussian. If one uses the shape of the pixelated filter in the analytical derivation, the results, noted by “ana1” were much improved.

By utilizing these results, we designed an optimal filter with the aim of minimizing the local noise-to-signal ratio in a Poisson series with $I^* = 40 + A \sin(kx)$, which can represent the change of contrast and resolution of an image with A and k , respectively. Given A and k , the optimal standard deviation in the Gaussian filter was analytically obtained, and excellently agreed with that from numerical simulations. See our full paper for the details, Thus the analytical form of the variance of residual noise can be utilized to design filters and determine the optimal values of the filter parameters.



SP116.6 - Fast Registration of Intraoperative Ultrasound and Preoperative MR Images Based on Calibrations of 2D and 3D Ultrasound Probes

Author(s): Fang Chen, Ruizhi Liao, Hongen Liao
Biomedical Engineering, School of Medicine, Tsinghua University, China, Beijing/CHINA

During the intraoperative-ultrasound-guided intervention, ultrasound (US) is often registered with other high-quality preoperative images like computed tomography (CT) or magnetic resonance (MR) to improve the navigation accuracy. However, real-time registration is difficult to achieve due to the difference of image modality and dimensionality. To solve this problem, we apply preoperative 3D US image collected with a 3D calibrated probe to simplify 2D US and 3D MR image registration into two easy-achieved steps: 2D-3D US intra-modal registration and 3D US 3D MR pre-operative registration. To achieve fast intraoperative 2D US and preoperative 3D US registration, we take advantage of effective 2D and 3D US probes' calibration results and get a near optimal registration transform. Then intraoperatively we just need to do an automatic local adjustment, which will make real-time registration become possible. To achieve effective calibrations, we design an improved calibration phantom and propose a warm-start iterative closest points (ICP) method.

SP116.7 - Development of digital subtraction angiography for coronary artery without motion artifacts enabling read-time processing

Author(s): Megumi Yamamoto, Yasuhiko Okura
Clinical Radiology, Hiroshima International University, Higashihiroshima/JAPAN

Purpose: The purpose of this study is to develop a new method of digital subtraction angiography (DSA) for coronary artery reducing motion artifacts caused by heart beat and by the periodic motion in the lung field.

Methods: In this study, the mask image is produced by the density difference image. That is made by subtracting plain mask image from contrast-enhanced live image. Our approach employed fluctuation of pixel value at the same position. First, the pixel value for the mask image is selected from the plain mask image, when the density difference value is larger than a threshold level. The search area for the maximum pixel value was selected from two volume areas using the value of the standard deviation (SD) for each pixel from the previous 14 image frames. Next, when the SD value in the 14 frames was greater than a threshold level, the search area of the maximum value was set 1 pixel x 1 pixel x 14 frames. Otherwise, 32 pixels x 32 pixels x 7 frames was selected as the search area mentioned above. Finally, the pixel value in mask image was selected from either volume area. To evaluate images obtained by our method, we used standard deviation of total pixel values in subtraction image sequences as an objective evaluation method. In addition, subjective evaluation was carried out. Cardiologists evaluated the degree of motion artifacts using score (1 to 5: 1 is the most deteriorated by artifacts). Twenty coronary arteriograms with various occlusion severities in vessels were used. We employed the PC (CPU: 2.4GHz, 4 GB memory) to produce DSA image process by our method.

Results: As results of objective evaluation, standard deviations of total pixel value of subtraction images were 33% lower than that of normal DSA, in 20 cases of coronary arteriogram. In subjective evaluation, average score of motion artifacts was 4.2 whereas 2.6 for normal DSA images. These results showed that the motion artifacts were extremely decreased by our method. Coronary artery and carotid artery and vein were clearly enhanced. The calculation time to produce one subtraction image by our method was 0.085 sec/image. This result shows this method will be able to use in a real-time in the clinical situation.

Conclusions: In conclusion, we proposed this new method where using standard deviation of pixel value and searching the highest value in the volume area. The results showed that the motion artifacts were extremely decreased and will be able to use in a real-time. Coronary artery, carotid artery and vein were clearly enhanced. This method would be very helpful for the diagnosis of angiography with motion.

SP116.8 - Real-time measurement of cardiomyocyte contraction and calcium transients using fast image processing algorithms

Author(s): Vratislav Čmiel, Jan Odstrčilík, Marina Ronzhina, Ivo Provazník
International Clinical Research Center - Center Of Biomedical Engineering, St. Anne's University Hospital Brno, Brno/CZECH REPUBLIC

An improved technique for recording of contraction of heart cells simultaneously with recording of calcium transients by fluorescence method is introduced. The technique aims to quantify contractions under conditions including low image quality caused by reduced transmitted light. The proposed methods allow more accurate detection, lower error rate using the up-to-date image processing, and automation of the process comparing to recent approaches.

The technique is compared with direct optical measurement method using processing of two-dimensional digital images of the cardiac cell. The technique is improved to be fast enough to be included in the system for real-time measurements.

SP117 - Treatment Planning - Knowledge Based

TRACK 04: RADIATION ONCOLOGY

SP117.1 - Next Generation Radiotherapy Treatment Planning: Current Status and Future Prospects

Author(s): [Steve Jiang](#)

Radiation Oncology, University of Texas Southwestern Medical Center, Dallas/TX/UNITED STATES OF AMERICA

Treatment planning is one of the most important links on the chain of cancer radiotherapy. The current treatment planning systems have the following issues.

First, there exists a large variation in plan quality, depending on who develops the plan, for which attending radiation oncologist, at which institution, and using what planning system, etc. This is particularly a big problem for resource-limited regions and institutions.

Second, the current treatment planning procedure is very inefficient, usually taking one week or longer, partially due to the iterations between the planner and the radiation oncologist that are often required to reach the acceptable plan quality. There is an urgent need to greatly improve the treatment planning efficiency and thus to reduce the waiting time for patients with cancer, - a frightening disease, from both clinical and psychological points of view.

Third, the current treatment planning practice is costly, not only due to the wasting of the clinical staff's, especially radiation oncologists', costly time, but also due to the expenses associated with the purchase, installation, commissioning, maintenance, and upgrade of the planning workstations, as well as with the setting up and maintenance of the dedicated data centers for patient data storage.

Forth, the current distributed treatment planning practice makes it difficult for cross institution collaboration, experience sharing, data sharing and mining and multi-institution clinical trials.

All these problems need to be resolved during the development of the next generation treatment planning systems. In this presentation, we will review and discuss various technologies that have been or are being developed for various aspects of next generation treatment planning, including automatic segmentation, knowledge-based automatic plan optimization, interactive plan tuning, personalized plan quality control, and efficient plan quality assurance, etc.

SP117.2 - Overlap-Guided Fixed-Patient Support Positioning for Cranial SRT

Author(s): [Robert L. Macdonald](#)¹, [Christopher G. Thomas](#)²

¹Physics And Atmospheric Sciences, Dalhousie University, Halifax/NS/CANADA, ²Medical Physics, Nova Scotia Cancer Centre, Halifax/CANADA

Purpose: To investigate potential dosimetric improvements by optimizing fixed-couch rotation position for cranial stereotactic radiotherapy (SRT)

Methods: The current convention at the Nova Scotia Cancer Centre (NSCC) for planning of cranial stereotactic radiotherapy (SRT) with volumetric modulated arc therapy (VMAT) is a fixed-couch approach in which each individual arc is at a static patient treatment couch position. Three to four arcs are typically used in a plan, and for each of these arcs, the couch is positioned 45° apart, with one arc at

couch rotation 0°. In some cranial SRT cases, the planning target volume (PTV) is in very close proximity to vital organs-at-risk (OARs), and these cases require additional modification of patient treatment couch position due to this anatomical arrangement. Using six previously delivered cranial stereotactic radiotherapy plans for acoustic neuromas treated at the NSCC, we have redesigned the treatment arrangement to find the optimal couch rotation position based on the reduction of overlap between OARs and PTV. Maintaining the arc lengths from the delivered treatment, the couch position was determined based on a cost function analysis of accumulation of overlap score from an equation developed by Yang *et al*[2] and refined by MacDonald *et al*[1]. The algorithm incorporates factors for depth of OARs and PTV volumes and radiation dose sensitivities of each OAR.

Results: In a six patient population with application of this optimization technique, maximum and mean doses to the OARs were reduced by approximately $35.48\% \pm 5.38\%$ and $36.60\% \pm 4.68\%$ respectively, as compared to the original delivered plans. In addition, PTV coverage was maintained during optimization. The average homogeneity index [3] was 7.53 ± 1.46 for conventional plans and 4.89 ± 0.38 . The conformity number [4] was 0.76 ± 0.05 for conventional plans and 0.76 ± 0.05 for optimized plans.

Conclusion: The reduction in OAR doses is a substantial improvement in plan quality. The modification of the existing delivery technique with guidance from a PTV-OAR overlap cost-function analysis technique can yield significant dosimetric improvements with no increase to delivery or planning time. This technology is immediately implementable on any linear accelerator capable of basic stereotactic radiotherapy.

References

1. MacDonald, R. Lee, Thomas, Christopher G, "Dynamic Trajectory-Based Couch Motion for Improvement of Radiation Therapy Trajectories in Cranial SRT" Medical Physics (Publication accepted and pending)
2. Yang, Yingli et al. "Choreographing Couch and Collimator in Volumetric Modulated Arc Therapy." International Journal of Radiation Oncology, Biology, Physics 80, no. 4 (July 15, 2011).
3. Oliver, Mike. et al "A Treatment Planning Study Comparing Whole Breast Radiation Therapy against Conformal, IMRT and Tomotherapy for Accelerated Partial Breast Irradiation." *Radiotherapy and Oncology: Journal of the European Society for Therapeutic Radiology and Oncology* 82, no. 3 (March 2007).
4. Van't Riet et al. "A conformation number to quantify the degree of conformality in brachytherapy and external beam irradiation: Application to the prostate." *International Journal of Radiation Oncology Biology Physics* 37, no. 3 (February 1, 1997).

SP117.3 - Automated Dose Map Prediction Through Radiomics and Regression on the Patient Manifold

Author(s): Chris McIntosh, Thomas G. Purdie
Princess Margaret Cancer Centre, Toronto/CANADA

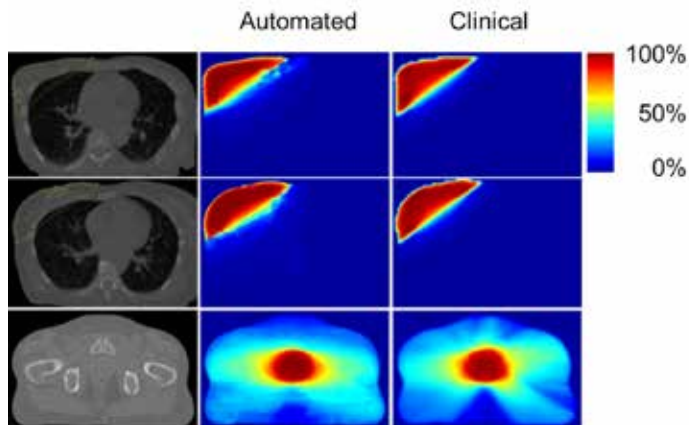
Technical innovations in RT have improved the quality of RT plans at the cost of increased complexity. Therefore, automated planning methods have been suggested to improve the highly manual, iterative and complex RT planning process. To date, treatment planning has focused on optimizing volume-based objectives (e.g. <30% of the right lung volume should receive <50% of the prescribed radiation dose) which are derived from a template and manually adjusted at each planning iteration or selected from a database in the case of automated planning approaches. These objectives neglect fundamental spatial information and only represent surrogates

of the actual clinical treatment intent with the resulting RT plans limited in their capacity to tailor dose for each patient. We propose a paradigm shift in automated RT planning. By explicitly modelling the relationship between patient anatomy and radiation dose, this research is the first to generate automated RT plans that directly specify the spatial distribution of the radiation dose to the patient.

Our method uses a novel machine learning (i.e. customized regression) algorithm based on thousands of previous RT plans deemed to be of high quality, to learn relationships and patterns in the data (i.e. how radiomic features describing patient organ/target appearance and geometry correlate with radiation dose to ensure a clinically acceptable RT plan). For a new patient, the algorithm computes relevant radiomic features, to be correlated with features in the database. Machine learning uses the radiomic features to predict a probabilistic dose for each voxel in the image, based on features at both the voxel and whole image level.

Our preliminary results have focused on three distinct RT treatment sites using intensity modulated RT (IMRT) and volumetric modulated arc therapy (VMAT): whole breast (tangent IMRT), breast cavity (non-coplanar IMRT), and prostate bed (VMAT). We used 336 training patients, 143 testing patients, and measured automated planning accuracy via Gamma analysis comparison with each patient's clinically delivered treatment plan. Our overall accuracy rates were 88.2%, 74.9%, and 86.1% respectively, with 50.6%, 20.0%, and 25.7% having a Gamma over 90%. An example image is shown below with fully automated planning results from two breast cavity, and one prostate bed plan.

Our method will enhance the existing RT process by reducing RT planning times, promoting simplification and standardization, and improving the quality of personalized RT. The research will realize a novel clinically implementable framework and provide a training knowledge base for RT.



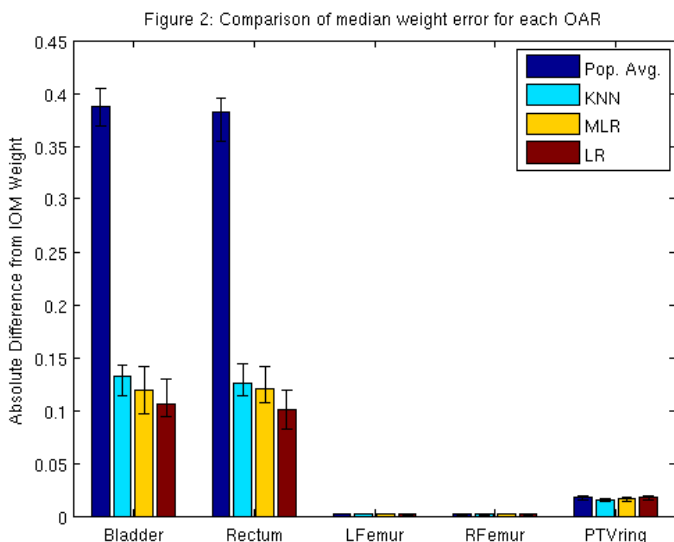
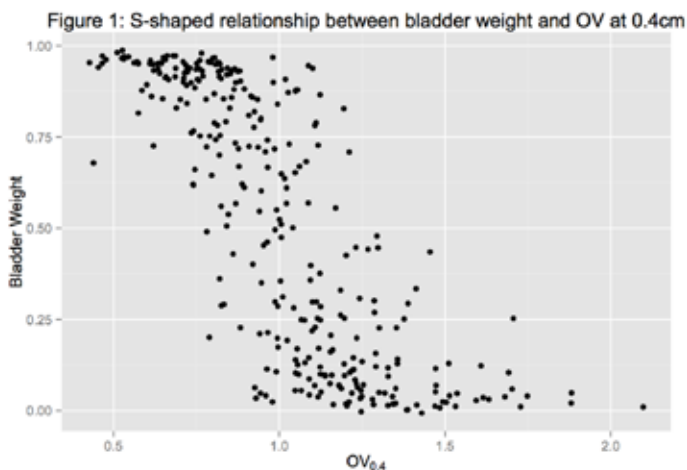
SP117.5 - Models for Predicting Objective Function Weights in Prostate Cancer IMRT

Author(s): Justin J. Boutilier¹, Taewoo Lee¹, Tim Craig², Michael B. Sharpe², Timothy C.Y. Chan¹

¹Mechanical And Industrial Engineering, University of Toronto, Toronto/CANADA, ²The Princess Margaret Cancer Centre, Toronto/CANADA

Purpose: To develop and evaluate the clinical applicability of advanced machine learning models that simultaneously predict multiple optimization objective function weights from patient geometry for intensity-modulated radiation therapy (IMRT) of prostate cancer. **Methods:** A previously developed inverse optimization method (IOM) was applied retrospectively to determine optimal objective function weights for 315 treated patients. We used

an overlap volume ratio (OV) of bladder and rectum for different PTV expansions and overlap volume histogram slopes as explanatory variables that quantify patient geometry. Using the optimal weights as ground truth, we trained and applied three prediction models: logistic regression (LR), multinomial logistic regression (MLR), and weighted K-nearest neighbor (KNN). The population average of the optimal objective function weights was also calculated. **Results:** The OV at 0.4 cm feature was found to be the most predictive of the objective function weights (Figure 1). We observed comparable performance (i.e., no statistically significant difference) between LR, MLR, and KNN methodologies, with LR appearing to perform the best. All three machine learning models outperformed the population average by a statistically significant amount over a range of clinical metrics including bladder/rectum V53Gy, bladder/rectum V70Gy, and dose to the bladder, rectum, CTV, and PTV. When comparing the weights directly, the LR model predicted bladder and rectum weights that had, on average, a 73% and 74% relative improvement over the population average weights, respectively (Figure 2). The treatment plans resulting from the LR weights had, on average, a rectum V70Gy that was 35% closer to the clinical plan and a bladder V70Gy that was 29% closer, compared to the population average weights. **Conclusion:** We demonstrated that the KNN and MLR weight prediction methodologies perform comparably to the LR model and can produce clinical quality treatment plans by simultaneously predicting multiple weights that capture trade-offs associated with sparing multiple OARs.



SP118 - Diagnostic Radiology: Dosimetry and Quality Control

TRACK 05: DOSIMETRY AND RADIATION PROTECTION

SP118.1 - Measuring absorbed-dose to cardiac implantable electronic device using OSL.

Author(s): Étienne Létourneau
Radio-oncologie, Centre intégré de cancérologie de Laval, Laval/CANADA

Purpose/Objectives

The American Association of Physicists in Medicine (AAPM) Task Group 34 and more recently 203 raised the issue about the management of radiation oncology patients with a cardiac pacemaker or an implantable cardioverter-defibrillator (ICD). Clear guidance about dose limits are given in these reference works. However, most dose levels reported in the literature and used clinically to evaluate the absorbed-dose are based on calculated values and not on direct measurements. In this study, direct measurements using optically stimulated luminescent (OSL) detectors placed directly inside a pacemaker were performed for planning CT scan, positioning CBCT scan and external beam radiation therapy treatment in order to compare with the planned dose.

Materials/Methods

Output measurements of the CT scan at 140 kVp and of the CBCT X-ray tube were performed at 100 kVp and 120 kVp. Measurements were based on the AAPM Task Group 61 protocol using a Farmer-type ionization chamber calibrated for the corresponding beam quality. Once the outputs were determined at the reference point, the correlation between OSL's number of counts and the resultant dose was achieved for both imaging methods. Then, an OSL dosimeter was placed inside a Biotronik pacemaker in the electronic section. Several measurements were performed placing the pacemaker recovered with bolus on an anthropomorphic phantom. Using different scanning parameters and protocols, a clinically relevant overview could be achieved.

Results

Direct exposition of the pacemaker could give a maximum reading of 4 cGy for a CT scan acquisition and 3 cGy for a CBCT scan acquisition with our in-house protocols.

Conclusions

Knowing the measured absorbed-dose to the cardiac implantable electronic device (CIED) from our different planning and positioning imaging protocols, adequate classification of risk group of patients with (CIED) could be done. Therefore, dosimetric decisions regarding the planning can be performed under a sounder basis.

SP118.2 - Organ dose estimation in computed tomography based on Monte Carlo simulation

Author(s): Camille Adrien¹, Cindy Le Loirec¹, Juan Carlos Garcia-Hernandez¹, Serge Dreuil², Jean-Marc Bordy¹
¹Dm2i, CEA, List, Gif-sur-Yvette/France, ²Service De Physique Médicale, Gustave Roussy, Villejuif/France

Due to the significant rise of computed tomography (CT) exams in the past few years and the increase of the collective dose due to medical exams, dose estimation in CT imaging has become a

major public health issue. However, in clinical practice, dose is still estimated by empirical index such as CT air kerma indices and air kerma-length product. Protocols can hardly be optimised with such information. On this basis, we decided to develop an organ dose estimator providing dosimetric information for DICOM patient images and/or numerical standard phantoms. In this paper, developments and validations of the Monte Carlo (MC) dose simulator are mainly discussed. A MC tool, based on the 2006 release of the PENELOPE code, has been adapted to enable CT exams simulations in a voxelized numerical phantom mimicking the human anatomy.

For that purpose, the GE Lightspeed VCT 64 CT tube was modelled by adapting the method proposed by Turner *et al* (Med. Phys. 36: 2154-2164). First of all, equivalent spectra were determined for 100 kVp and 120 kVp by using experimental half-value layers (HVL). Measurements were performed in static mode with a CdTe detector associated with a method developed by the French national laboratory of metrology for ionizing radiations (LNHB) to achieve experimental spectra (X-ray Spectrometry 43(5): 298-304) and validate the tube model. Equivalent bowtie filter shapes were then established by using dosimetric profiles. Furthermore, axial and helical rotations of the X-ray tube were implemented in the MC tool. To improve the efficiency of the simulation, two variance reduction techniques were used: a circular and a translational splitting. The splitting algorithms allow a uniform particle distribution along the gantry path to simulate the continuous gantry motion in a discrete way. To validate the calculation, simulated sinograms are compared with the expected ones and the particle distribution along the gantry path is checked.

First validations were then performed in homogeneous conditions using a home-made phantom and the well-known CTDI phantoms. Comparisons between measured and simulated values are in good agreement with less than 10% deviation for several cases. Then, validations were performed in CIRS ATOM anthropomorphic phantoms using both optically stimulated luminescence dosimeters for point doses and XR-QA Gafchromic® films for relative dose maps. Last results are very encouraging with less than 20% deviation for punctual doses.

Organ Doses for several acquisition parameters into the ICRP male and female phantoms (ICRP, 2009. Adult Reference Computational Phantoms. ICRP Publication 110. Ann. ICRP 39 (2)) should soon be provided by the simulator in order to build a dosimetric data base which could be used in clinical practice.

SP118.3 - Comparative study of Average Glandular Doses of three different digital mammography units in three Ministry of Health Hospitals in Oman: An analysis

Author(s): Arun Kumar L S, Rashid Al-Hajri, Saeed Al-Kalbani
Medical Physics, Ministry of Health, Muscat/OMAN

Breast cancer accounts about 12% of all new cancers worldwide (WHO, World Cancer Report 2014) and this is about 25 % in the Sultanate of Oman (2013) which is also the highest among all cancers in Oman. Breast screening by mammography can reduce mortality by about 25% and hence we follow a comprehensive radiation acceptance & quality assurance protocol for the testing of mammographic units installed in ministry of health (MOH), before handing over for routine patient care work. Of the many radiation parameters measured, the average glandular doses (AGD) of three different digital mammographic units from three manufacturers installed in three different hospitals was analysed in this study so as to make sure that the mammographic units meet WHO/IAEA standards as the Sultanate does not have currently a national protocol for acceptance of mammographic units.

The Average Glandular Dose (AGD) of three different digital mammo units was estimated by using a 4.5 cm polymethyl methacrylate (PMMA) phantom along with a calibrated 3.0 cc mammo ion

chamber. Of the three mammo units, the first two had identical x-ray spectral features - W/Rh, Mo/Mo & Mo/Rh where as the third unit had W/Rh & W/Ag spectrum. The phantom used is assumed to have a glandularity of 50:50. The Entrance Surface Air Kerma (ESAK) and half value layer (HVL) of the beam was measured by the mammo chamber. The paddle is made in contact with the ion chamber and arranged the phantom & chamber side by side such that ESAK is measured without backscatter. From the measured ESAK and HVL values, AGD was estimated as per the European Guidelines (2003) by the formalism of Dance *et. al.* (2000 and 2009). i.e., $AGD = Kgc$ where K is the ESAK without backscatter and g , c & s are correction factors. The phantom was compressed to the same breast thickness in all the three hospitals so that compressed breast thickness remained the same. ESAK and HVL for all available spectral qualities were measured in the three units and AGD's were estimated for each spectral quality.

Also, AGD's were estimated for phantom thicknesses of 3cm, 6cm and 8cm in the three units for the above spectral qualities. The results showed that AGD's increased with the increase in thickness as expected. The system/mammo unit estimated/displayed entrance surface dose & organ dose (AGD) were noted and compared with the measured values of ESAK & the estimated values of AGD of the corresponding setting. Of the three hospitals, the estimated AGD's were quite comparable in two hospitals where as the third hospital shown a variation of about 18% from the other two. However, in all the three hospitals, AGD's were within the recommended value of 3 mGy for each projection.

Surveys shown that mammo units operating at optimal parameters have increased detection rates for smaller lesions with optimal dose to the breast. A well performed QA programme in mammography will yield good quality mammograms which in turn delivers an optimal dose to the patients undergoing mammographic investigations.

SP118.4 - First Data on Quality Control Test done in Diagnostic X-ray facility at Major Public Hospitals in Kathmandu Valley, Nepal.

Author(s): Kanchan P. Adhikari, Navagan Ghimire, Prakash D. Gautam, Tirthraj Adhikari
Department Of Clinical Oncology, National Academy of Medical Sciences, Bir Hospital, Kathmandu/NEPAL

One of the most important goals of good medical practice in the use of X-ray is to diagnose the disease and its extent to minimize an adverse effect. During any action taken in diagnostic X-ray, there is an important issue of quality of the image and dose to the patient. Hence, regular practice of quality control in diagnostic X-ray is essential to provide a good quality images and less hazard to the patients and its checking on regular basis enhances the appropriate diagnosis with minimum side effects.

The quality control tests were carried out at thirteen X-ray units at seven different government hospitals in Kathmandu valley. The parameter like kV, kVp, dose, dose rate, HVL and mAs were measured with the acceptance limits. In this study, beam alignment test, radiation leakage test and focal spot test were also done.

During the study, we found that there is not any established proper method for the installment of diagnostic X-ray equipment and acceptance testing procedure in Nepal. Actions were not taken to improve the old X-ray machine and for restoring it to a proper working condition. The study shows that the need for quality assurance of diagnostic X-ray to be taken to avert detrimental effects to patients and staffs. Radiographers should provide sufficient training to ensure proper condition of X-ray machine. Radiation regulation now is essential for such programs to be introduced. Any program to manage patient dose in radiology should provide a high priority in the country like Nepal. Dose given in diagnostic X-ray should be

compared with standard reference level on regular basis to identify the condition of the X-ray. Institute must introduce a mandatory system for acceptance test of X-ray when installed and regular quality control program.

Keywords— X-ray, acceptance test, quality control, radiation regulation

SP118.5 - Estimation of dose distributions in mammography into a tissue equivalent phantom

Author(s): Josilene C. Santos¹, Alessandra Tomal², Tania A.C. Furquim¹, Paulo R. Costa¹

¹Radiation Dosimetry And Medical Physics Group, Physics Institute, University of São Paulo, São Paulo/BRAZIL, ²Physics Institute Gleb Wataghin, State University of Campinas, Campinas/BRAZIL

Mammography is the most important method to detect premature breast cancer. However, there is a risk of inducing cancer by the exposure to radiation in this kind of examination. In this way, it is important to know the dose distribution in typical techniques used in mammography procedures. The aim of this work was to estimate the dose distributions in different positions parallel to the image plan and different depths of a tissue equivalent phantom using LiF thermoluminescent dosimeters (TLD).

LiF TLDs pellets were positioned at 5 positions on the xy plan (Figure 1) on a BR12 phantom (CIRS, model E14) at different depths. The set was irradiated in a GE Senographe DS System for a maximum field size. The dosimeters were irradiated using Mo/Mo anode/filter combination, 100 mAs, and different X-ray tube voltages (25, 28, 30 and 32 kVp). A fixed X-ray tube voltage (28 kVp), 100 mAs, was also used with different anode/filter combinations (Mo/Mo, Mo/Rh and Rh/Rh). A similar set of TL dosimeters were calibrated using mammographic X-ray beam qualities RQR-M 2 and RQR-M 4 in an accredited SSDL. The TL signal was read on a TL/OSL reader (Risφ, model DA-20). Dose distributions in different xy positions and depths of the phantom were estimated.

Dose variation in the y direction was more significant than in the x direction. It were observed variations up to 8% and 28.2% in x and y directions respectively. For the tube voltage 28 kVp, the maximum dose in the phantom surface in the y-axis was 16(1) mGy for Mo/Mo, and 15.0 (9) mGy for Mo/Rh and 12.8(6) for Rh/Rh.

The dose variation obtained is probably due to the non-uniformity of the field. The maximum dose value calculated corresponds to a position that is next to the chest wall in a compressed breast. This occurs due to the Heel effect.

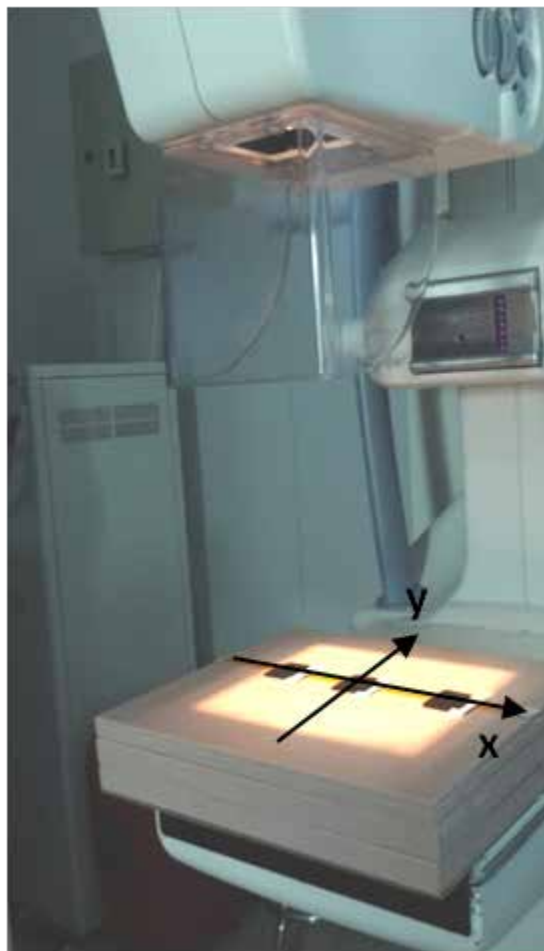


Figure 1: – TLDs positioning scheme in a phantom BR12 for irradiation in a GE mammography system

SP118.7 - Radiation Dose Assessment for Retrospectively ECG-Gated Coronary Computed Tomography Angiography (CCTA) Examination

Author(s): T S Tuan Muda¹, C H Yeong¹, Sock Keow Tan¹, Kwan Hoong Ng¹, Yang Faridah Abdul Aziz¹, Zhonghua Sun²

¹Biomedical Imaging Department, University of Malaya, Kuala Lumpur/MALAYSIA, ²Discipline Of Medical Imaging, department Of Imaging And Applied Physics, Curtin University of Technology, Perth/AUSTRALIA

Purpose:

Coronary computed tomography angiography (CCTA) has been recognised as a reliable diagnostic technique for the assessment of coronary artery disease since the introduction of 64-slice CT. However the radiation dose received by the patients from CCTA is still high compared to other examinations, thus raising concerns in the medical field. This study aimed to assess the entrance skin dose (ESD) and organ absorbed dose measured in both patients and phantom during retrospectively ECG-gated CCTA examination.

Methods:

ESD for 30 patients (15 males, 15 females, 58±10 year-old) who underwent CCTA using a dual-source CT scanner (Siemens Definition DS, Germany) were measured at selected radiosensitive organ regions (eye lens, thyroid, breast, heart and reproductive system)

using optically stimulated luminescence dosimeters (OSLD). The measurement was extended to organ absorbed dose in an anthropomorphic phantom (Atom702G, CIRS, Virginia) with OSLD placed within the respective organs. Effective dose was then calculated using the CT Expo V2.3.1 software (Hannover, Germany).

Results:

The ESD measured on both male and female patients are presented in Figure 1. Figure 2 shows the absorbed dose measured within the selected organs of the ATOM phantom. The effective doses calculated from the CT Expo software showed that female patients received significantly higher effective dose than the male patients (14.70 ± 4.35 vs. 10.40 ± 5.94 mSv; $p < 0.05$). The ESD of the breasts was about 8-9 times higher than the ESD reported from a typical mammogram of a breast of 5 cm compressed thickness.

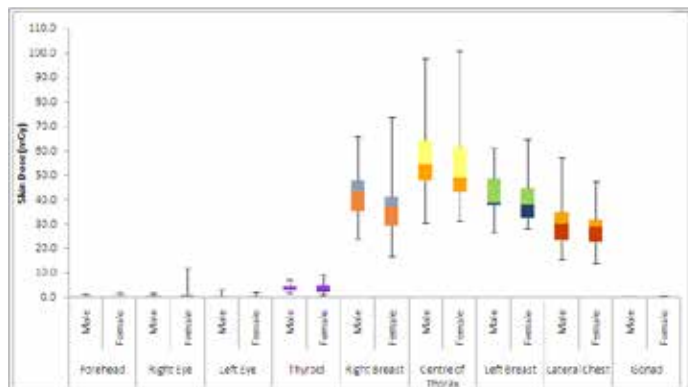


Figure 1: Entrance skin dose (mGy) measured on selected radiosensitive organ regions on the male and female patients.

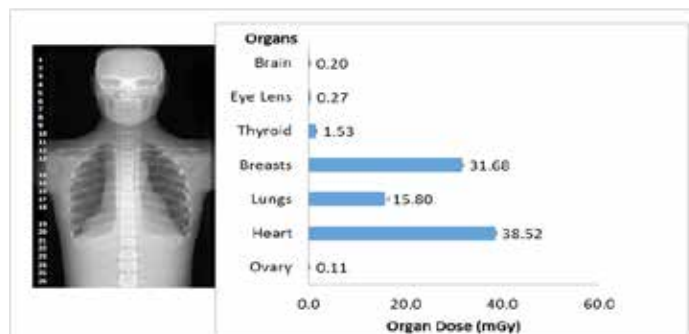


Figure 2: Absorbed dose (mGy) measured within the selected organs of the ATOM phantom.

Conclusion:

Due to the high radiation dose delivered to the patients, serious attention should be given to CCTA examination for dose reduction. Optimisation of the CCTA protocols should be carried out to minimise radiation dose to the patients.

Acknowledgment:

This work is supported by the HIR Grant (UM.C/625/1/HIR/MOHE/MED/36)

SP119 - Dose Surveys in CT and Interventional Radiology

TRACK 05: DOSIMETRY AND RADIATION PROTECTION

SP119.1 - CT Dose Optimization: First Results from a Province-Wide Program in Quebec

Author(s): Manon Rouleau¹, Moulay Ali Nassiri¹, Philippe Després²
¹Centre d'expertise clinique en radioprotection (CECR), CHUS, Sherbrooke/CANADA, ²Département De Physique, De Génie Physique Et D'optique, Université Laval, Québec/QC/CANADA

Purpose: Many studies have shown a statistically significant increase of life-time risk of radiation-induced cancer from CT examinations. In this context, the province of Quebec has created and mandated the Center for clinical expertise in radiation safety (CECR) to proceed with a province-wide tour of CT installations in order to: i) evaluate the technical and functional performances of CT devices, ii) initiate a dose optimization process in CT scanning protocols and iii) support and guide the local team of technologists, radiologists and managers with regards to dose reduction strategies in CT.

Methods: To achieve these objectives, the CECR coordinates a tour of the province's 180 CT installations. The tour consists in two-day visits to CT centers by a team of medical physicists and technologists in medical imaging (TIMs). The first day of the visit is dedicated to CT performance evaluation by medical physicists and to clinical CT image inspection by TIMs. The former includes tests related to HU numbers, collimator aperture and CTDI accuracy while the latter verifies scan range compliance with protocols and dose levels for recent studies of the head, chest and abdomen. On the second day, observations by the CECR experts are presented to the local team along with recommendations on radiation safety good practices and potential improvements of CT protocols with regards to the dose. Upon consent from a local radiologist, optimized CT protocols were used for patients scheduled on day two. Prompt feedback on optimized images by the radiologist allowed fine-tuning of the protocols with the experts on site. Then, in the next month, images acquired with optimized protocols were scored with a qualification form and sent back to CECR for compilation.

Results: Since 2011, the CECR has evaluated 110 CT devices, 60% of which are 64-slice scanners. Local protocols were modified in 64%, 80% and 70% of the time for adult head, thorax and abdomen-pelvis respectively. The average dose reduction obtained with these optimized protocols was 18%, 24% and 20% for adult head, thorax and abdomen-pelvis respectively. The general recommendations often made by the CECR experts were: 1) the implementation of low-dose protocols for the follow-up of pulmonary nodules and for renal calculi, 2) the compliance to the prescribed scan range as defined by local practice guides, 3) the adequate positioning of patients, and 4) the use of bismuth shielding to reduce the dose to superficial radiosensitive organs, such as the breast, lens of the eye, and thyroid.

Conclusion: The approach used by CECR to optimize CT protocols takes into account the performances of CT devices as well as current modulation and iterative reconstruction when available. It is based on the active participation of all stakeholders in the process: radiologists, biomedical engineers, TIMs and managers. The clinical requirements as expressed by radiologists remain at the core of the optimization process. This approach, based on support and guidance as oppose to formal inspection, is very well accepted and led to significant dose reductions.

SP119.2 - CT overexposure as a consequence of scan length**Author(s):** Mohamed K. Badawy¹, Michael Galea², Kam S. Mong¹, Paul L. U¹¹Medical Physics, Austin Health, Heidelberg/AUSTRALIA, ²Radiology, Austin Health, Heidelberg/AUSTRALIA**Background**

The diagnostic benefits of CT scans with appropriate clinical reasoning far outweigh the potential radiation risks and this has seen an increased number of CTs ordered yearly in Australia. In saying that, effort must be made to lower radiation dose to the patients to ensure that the risk is kept as low as reasonably achievable.

A simple method of dose optimization is ensuring the correct scan length is chosen for the corresponding scan type, i.e. imaging only the anatomy that is required and nothing more. Initially, a scout image is obtained to ensure the patient is set up correctly for their scan. Adjustments to scan lengths based on anatomical landmarks and radiologist protocol should be made on the scout image before executing the CT scan on the patient.

Aim

This study aims to quantify the increased effective dose as scan length were chosen that deviated from standard protocol.

Methods

This study was performed using Monte Carlo software and a mathematical phantom to represent real patient data. The software package used in this study was CT-Expo V2.2. The software was validated by comparing the calculated CTDI_{vol} and DLP to the CT-_{DI}vol and DLP given on the CT scanner.

A reference scan was obtained for each scan protocol and the scan parameters, including kV, mA, rotation time, collimation width, table feed and slice thickness, were entered into CT-Expo to calculate the effective dose. The reference scan was acquired using CTU-41 CT Torso Phantom and the correct scan length for each simulation was based on the anatomical landmarks suggested by ARPANSA in the National DRL survey user guide.

The scanned region was then increased by 0.5 cm either side of the standard protocol and the effective dose increase was recorded.

Results

The results of this study show that for scans with a high CTDI_{vol} the patient is exposed to an extra 1 mSv within 6 cm of overscan. Protocols that investigated large scan areas may not see a significant relative dose reduction, however radiation exposure should be kept as low as reasonably achievable

Conclusions

The main emphasis of CT dose optimisation has been focused on new scanner technologies, however the operator can still play a key role in reducing patient dose. Ensuring the correct scan length is chosen by the radiologist and selected by the radiographer can potentially reduce the effective dose of each scan by up to 2 mSv. High dose protocols, such as head and spine, can benefit significantly in dose reduction with more stringent adherence to the anatomical region to be imaged.

SP119.3 - Regional survey of pediatric patient doses from CT examinations in Tehran, Iran**Author(s):** Hamid R. Khosravi¹, D Chettle¹, Leila Sadri², Saeed Setayeshi², Khadijeh Asnaashari³, Hossein Khosravi⁴, Mehran Midia⁵¹Medical Physics, McMaster University, Hamilton/ON/CANADA, ²Nuclear Engineering, Amir Kabir university of Technology, Tehran/IRAN, ³Allied Medicine, Tehran University of Medical Sciences, Tehran/IRAN, ⁴Medical Physics, Tarbiat Modares University, Tehran/IRAN, ⁵McMaster University, Hamilton/ON/CANADA

Objectives: To establish regional diagnostic reference levels (RDRLs) for typical paediatric CT examinations in Tehran, Iran and compare them with established international data. In addition, the aim was to develop a method of analyzing local scan parameters for further optimization.

Methods: The dose assessment was performed in terms of weighted CT dose index (CTDI_w) and dose length product (DLP) for head, sinus, chest, abdomen and pelvis CT examinations using standard methods. CTDI were measured in a polymethyl methacrylate (PMMA) Head and Body phantoms. RDRLs were derived from mean survey values for different age categories in 19 CT facilities in Tehran, Iran.

Results: The mean range of CTDI_w for all age categories were 41.77-53.04, 24.37-26.55, 12.45-13.48 and 13.18-18.25 for Brain, Sinus, Chest and Abdomen-pelvis, respectively. Related DLPs were 325.5-495, 181.5-222.7, 143.2-250.6 and 198.5-488.4, respectively.

Conclusion: Many hospitals were incorporating adult scanning parameters for children, resulting in very high effective doses. The great variations of CTDI_w and DLP observed among hospitals and relatively high values of DLP in some centers are evidence that radiation doses of Paediatric patients from CT examinations need to be optimized.

SP119.4 - Dose Reduction Efforts in PET/CT: the Quebec Experience**Author(s):** Moulay Ali Nassiri¹, Manon Rouleau¹, Philippe Després²
¹Centre d'expertise clinique en radioprotection (CECR), CHUS, Sherbrooke/CANADA, ²Département De Physique, De Génie Physique Et D'optique, Université Laval, Québec/QC/CANADA

Problematic and objective: The province of Quebec (Canada) has 15 publicly funded PET/CT center for a population of 8.2 million. This relatively large per capita ratio makes PET an accessible technology that significantly contributes to the collective radiation dose of medical origin in the province. In this context, the province of Quebec has created and mandated the Center for clinical expertise in radiation safety (CECR) to proceed with a province-wide tour of PET/CT installations with the objective of establishing good radiation protection practices for patients and caregivers.

Methods: The CECR first conducted a province-wide survey to establish a snapshot of the current practice in 2014. This survey was followed by on-site visits by a team composed of a medical physicist, a nuclear medicine technologist and a CT imaging technologist. The 2-day visit consisted, on day 1, in 1) quality controls and performance evaluation of the CT, PET and dose calibrator, 2) verification that the procedures used to perform the PET/CT studies (preparation and execution) are defined and observed. Furthermore, 15 whole-body and 4 high-resolution (fine CT slice thickness) head and neck 18F-FDG PET/CT studies were analyzed. Specifically, the signal to noise ratio (SNR) for both PET and CT images were obtained for the liver (whole-body studies) while the CTDI, the DLP, the injected activity and the injection/acquisition interval were retrieved from images or their DICOM header. The team also verified all aspects of radiation protection practices in the visited center.

On day 2, the team presented their observations to the local team of technologists, physicians and managers and made recommendations for improving the radiation protection practices. For adult studies, the amount of 18F-FDG recommended was based on both EANM guidelines for tumor imaging and on the Japanese guidelines. The measured performance of the PET system was also taken into account for the determination of the optimal injected dose. With the approval of local physicians, PET/CT studies scheduled for the second day were performed using the proposed protocols. Prompt feedback from the physician on image quality allowed the CECR expert to fine-tune the protocol parameters in order to reach optimal quality with the minimal dose.

Results: Survey results showed that PET examinations vary considerably across centers, with dose varying from 8 to 30 mSv for 18F-FDG whole-body protocols, which account for 99% of all PET studies. Recurring visit recommendations for adult protocols include: 1) using automatic tube current modulation for CT, resulting typically in 20% dose savings, 2) reducing the tube current by 20% for high-resolution head and neck CT protocols, 3) reducing by 30% the amount of injected activity, 4) complying with the prescribed injection/acquisition interval.

Conclusion: The approach used by CECR to optimize PET/CT protocols takes into account the performances of devices and EANM/Japanese guidelines. It is based on the active participation of all stakeholders in the process: nuclear medicine physicians, biomedical engineers, technologists and managers. This approach, based on support and guidance as oppose to formal inspection, is very well accepted and led to significant dose reductions.

SP119.5 - Assessment of high cumulative patient doses of repetitive CT examinations

Author(s): [Cecile R. Jeukens](#), Roald S. Schnerr, Sandra Niesen, Joachim E. Wildberger, Marco Das
Maastricht University Medical Centre+, Maastricht/NETHERLANDS

Purpose

In daily routine patients often undergo multiple CT examinations within a short time frame, which may lead to a high radiation exposure. Our purpose was to evaluate patients who received a cumulative effective dose of more than 100 mSv within one year with repeat CT examinations.

Methods and Materials

15,000 consecutive CT examinations were systematically analyzed using dedicated dose monitoring software (Radimetrics™, Bayer Healthcare) within the time period 08/2013-08/2014. The effective dose (according to ICRP 103) is calculated from the technical and dose related parameters retrieved from the CT scanners, using an incorporated Monte Carlo module. All patients with a cumulative effective dose above 100 mSv were identified. Besides patient specific parameters (sex, age, weight), patients were analyzed with respect to cumulative effective dose, number of CT scans and scan series, dose per CT scan, time interval of the scans, clinical scan indications and anatomical scan regions.

Results

A small fraction (0.27%) of forty-one patients were identified (63% male, mean age 62, range 24-83, mean weight 82 kg). These patients received 347 CTs in total. The median of the received number of CTs was 7.0 (range 3-20) with 3.5 series per scan within a time frame of 166 days (median; range 8-320). Median cumulative effective dose was 117 mSv (range 100-301). A positive correlation was found between the number of CTs and the received effective dose (Figure 1). Most frequent scan indications were: oncology, abdomi-

nal imaging for abscess and drainage as well as complications after surgery. The most frequently selected scan region was the abdomen (n=150) with a median effective dose of 11 mSv (range 2.5-49), followed by combined thorax/abdomen protocols (n=39, median 17 mSv, range 6.4-57).

Conclusion:

Very high cumulative doses (>100mSv) only occur in a fraction of patients..As clinical indications justify each examination and the average radiation dose per scan was acceptable, these cumulative doses may represent common clinical practice in severely ill patients.

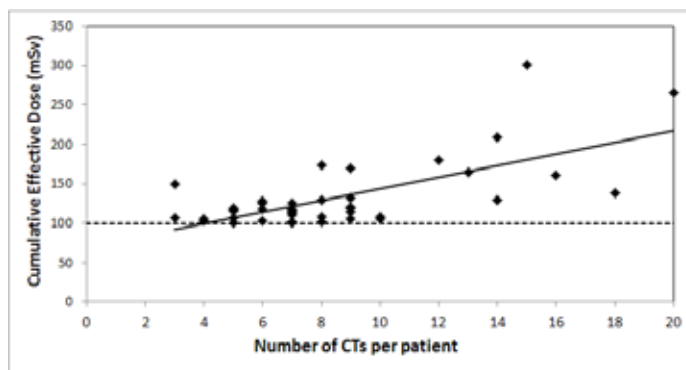


Figure 1 The cumulative effective dose per patient as a function of the number of CTs a patient received. The solid line indicates a linear fit ($R^2 = 0.46$), the dashed line the 100 mSv inclusion criterium.

SP119.6 - IAEA survey of pediatric computed tomography practice in Pakistan procedures and protocols (2005-2015)

Author(s): [Areesha Zaman](#)
Medical Physics, institution of nuclear medicine and oncology lahore INMOL, LAHORE/PAKISTAN

TITLE IAEA survey of pediatric computed tomography practice in Pakistan procedures and protocols.(2005-2015)

Objective: To survey procedures and protocols in pediatric computed tomography (CT) in Pakistan.2005-2015

Methods: Under a project of the International Atomic Energy Agency, 45 CT facilities throughout the country responded to a survey of CT technology, exposure parameters, CT protocols and doses.

Results: Modern MDCT systems are available in 70 % of the facilities surveyed, dedicated pediatric CT protocols available in 90% . However Specific CT protocols for certain age groups were unavailable in around 50 % of the facilities. Indication-based protocols were used in 40 % of facilities. Estimates of radiation dose using CTDI or DLP from standard CT protocols demonstrated wide variation up to a factor of 100. CTDIvol values for the head and chest were between two and five times those for an adult at some sites. Sedation was frequently reported and use of shielding and immobilization was not in routine use. Records of exposure factors were kept at 10 % of sites.

Conclusion: This survey demonstrates significant potential for improvement in CT practice and protocol use for children in less resourced sites .Dose estimates for young children varied widely. it provides critical baseline data for ongoing quality improvement efforts by the IAEA.and PNRA Pakistan regulatory authority for reduction in pediatric doses.

SP119.7 - Occupational Dose Measurement in an Interventional Radiology Facility in Jakarta

Author(s): Lukmanda Evan Lubis, Nur Aida, Nurdina G. Pratiwi, Kristina Tri Wigati, Supriyanto Ardjo Pawiro, Djarwani Soeharso Soejoko
 Department Of Physics, Faculty Of Mathematics And Natural Sciences, University of Indonesia, Depok/INDONESIA

The increasing use of ionizing radiation for diagnostic aims increases the alert on radiation protection. Whereas high standard and awareness are typically possessed by workers on Diagnostic Radiology facilities, personnel of Interventional Radiology departments are of higher need of attention. The works in Interventional Radiology the procedures are done with a long time fluoroscopy and the personnel being inside the imaging room. Two studies were performed on occupational dose measurement in Cardiac Interventional Radiology. The first study was done by measuring exposure levels on working staffs during a single interventional procedure, with the efficacy of available shielding being evaluated also. Second study was carried on by measuring scattered dose levels in various positions during a range of varied cardiac interventional procedures. On the whole, resulting remarks served as an input for the workers on the feasibility of their equipment, and scattered radiation during Cardiac Interventional Radiology procedures.

SP119.8 - Evaluation of the Comparative Effectiveness of Various Jurisdictional Computed Tomography Radiation Dose Reduction Models

Author(s): Anne Li¹, Mark Fan², Anthony Easty²
¹Institute Of Biomaterials And Biomedical Engineering, University of Toronto, Toronto/ON/CANADA, ²Humanera, Techna Research Institute, University Health Network, Toronto/CANADA

Background: High reliance on computed tomography (CT) worldwide results in high levels of radiation exposure to patients, which translates into increased cancer risks. Efforts to manage radiation dose are progressing, but the approach has not been standardized. It was, therefore, the aim of this study to systematically assess and compare jurisdictional policies that have been developed to optimize CT radiation dose.

Methods: Six jurisdictions (British Columbia, Ontario, Texas, California, Germany, Ireland) that contain institutions with dose tracking systems were selected to account for several possible approaches to radiation dose management. Each policy was reviewed and indexed for recurring themes. Five themes (technical requirements, operating requirements, radiation safety committee/quality assurance programs, radiation dose reporting, diagnostic reference levels) emerged. An assessment instrument was formulated by identifying 3 domains of related constructs (executability, comprehensiveness, rigor) that would negate common knowledge translation barriers. Two reviewers performed independent policy evaluations using the assessment framework until inter-rater reliability was judged to be sufficient ($\kappa < 0.75$). Inter-rater reliability was calculated using Weighted Cohen's kappa. Final scores were achieved through consensus once κ was satisfactory. Statistical analyses were performed using Pearson correlations.

Results: Two rounds of independent evaluations were necessary to achieve sufficient inter-rater reliability. Inter-rater reliability was high ($\kappa=0.830$) for the assessments after discussion occurred to clarify the definition and application of the domains. Final domain and theme scores for each jurisdiction are presented in Table 1. There was strong positive correlation for the domains, but not themes.

Conclusions: The assessment instrument may be useful for relative comparisons of knowledge translation potential in regulatory policies. Positive correlations between the domains suggest that carry-over effects may be present if policymakers focus intensively on developing any one domain. The evaluations revealed that precise accreditation standards (such as those in British Columbia and California) exhibited the most executable, comprehensive and rigorous model for managing radiation dose. California's efforts in mandating CT facility accreditation and dose reporting achieved the highest score overall (51 out of 72). Ireland and Germany achieved comparable scores, despite developing different interpretations of the same regulatory framework (Euratom's Directive 97/43) that resulted in varying approaches to dose management. The framework can be further enhanced to account for these critical differences. Our goal is to improve patient safety globally, by encouraging translatable jurisdictional models for radiation dose management. Further evaluations will need to validate the relationship between jurisdictional policies and radiation dose reduction over time.

Table 1: Final Domain and theme scores for each jurisdiction						
Domain	British Columbia	Ontario	California	Texas	Germany	Ireland
Exeuctability	15	5	17	11	11	10
Comprehensiveness	16	2	17	10	10	10
Rigor	13	4	17	9	13	12
Theme						
Technical Req.	11	4	10	6	4	4
Operational Req.	10	2	10	6	7	7
Radiation safety committee/ Quality assurance programs	11	0	10	9	5	6
Radiation dose reporting	9	5	12	4	7	6
Diagnostic Reference Levels	3	0	9	5	11	9
Aggregate	44	11	51	30	34	32

SP120 - Biomedical Diagnosis & Prediction

TRACK 09: BIOSIGNAL PROCESSING

SP120.1 - Desaturation event characteristics and mortality risk in severe sleep apnea

Author(s): Antti Kulkas¹, Anu Muraja-Murro², Timo Leppänen², Pekka Tiihonen², Esa Mervaala³, Juha Töyräs²

¹Clinical Neurophysiology, Seinäjoki Central Hospital, Seinäjoki/FINLAND, ²Clinical Neurophysiology, Kuopio University Hospital, Kuopio/FINLAND, ³Institute Of Clinical Medicine, Faculty Of Health Sciences, University of Eastern Finland, Kuopio/FINLAND

Obstructive sleep apnea (OSA) is a public health problem with severe health consequences. The current OSA severity estimation is based on the average number of breathing cessation and desaturation events per hour of sleep, neglecting the individual event characteristics. The aim of the current study was to evaluate desaturation event morphology in deceased and matched control patients with severe OSA.

12 deceased and 12 AHI, age, BMI and follow-up time matched alive control patients with severe OSA were analyzed. Desaturation event durations, depths, and areas of the deceased and alive control patients were compared. Also the effect of different baseline level selection in the desaturation depth analysis was investigated.

Patient demographics, apnea-hypopnea-index (AHI) and oxygen-desaturation-index (ODI) did not differ statistically significantly between the groups. The average oxygen saturation levels were statistically significantly lower 89.8% vs. 93.2% ($p=0.002$) in the deceased patients compared to the alive controls. The median desaturation event duration 31.8s vs. 25.9s ($p=0.017$), depth 15.0% vs. 9.5% ($p=0.006$) and area 349.9s% vs. 201.4s% ($p<0.001$) were statistically significantly greater in the deceased patients compared to the alive control patients when using 100% saturation as baseline level for desaturation events. When the first point before desaturation onset was used as baseline no statistically significant differences ($p=0.089$) were found between the deceased and alive control patients in desaturation depths. Based on quantitative inspection of the distributions of individual desaturation event characteristics the desaturation events were more severe in the deceased group.

Patients with similar AHI and ODI can have different individual desaturation event characteristics. Selection of the baseline for desaturation event depth analysis can affect the estimation of the event severity. The analysis of the individual desaturation event characteristics can provide supplementary information on the severity estimation of OSA and support the individual mortality risk estimation in severe OSA patients.

SP120.2 - Static Posturography of Elderly Fallers and Non-Fallers with Eyes Open and Closed

Author(s): Jennifer Howcroft¹, Jonathan Kofman², Edward D. Lemaire³, William E. McIlroy⁴

¹Department Of Systems Design Engineering, University of Waterloo, Waterloo/ON/CANADA, ²Systems Design Engineering, University of Waterloo, Waterloo/ON/CANADA, ³Crrd, The Ottawa Hospital Research Institute, Ottawa/CANADA, ⁴Department Of Kinesiology, University of Waterloo, Waterloo/ON/CANADA

Static posturography can be used to assess postural balance, which is important for activities of daily living. For older adults, poor postural balance can indicate increased fall risk. This study investigated eyes open and eyes closed static posturography assessments of 100

elderly participants (≥ 65 years) in two-foot stance. Twenty-four of these people had fallen in the previous six months. Range in anterior-posterior (AP) and medial-lateral (ML) motion; center of pressure (CoP) root mean square distance from mean; AP, ML, and resultant CoP velocity; and percent body weight on left and right feet were calculated from Wii Balance Board vertical force data. All AP measures and resultant CoP velocity were significantly greater with eyes closed than eyes open for fallers and non-fallers. ML CoP velocity was significantly greater with eyes closed than open for fallers. The largest percent increase from eyes open to eyes closed was for AP velocity, followed by 2D velocity for both fallers and non-fallers. Therefore, AP-based center of pressure-derived posturography measures appear to be sensitive to changes in postural control due to elimination of visual input. Significant differences were not found between fallers and non-fallers.

SP120.3 - Quantitative analysis of ventricular ectopic beats evaluated from short-term recordings of heart rate variability before imminent tachyarrhythmia

Author(s): Marisol Martinez-Alanis, Claudia Lerma
Departamento De Instrumentación Electromecánica, Instituto Nacional de Cardiología Ignacio Chávez, Mexico City/MEXICO

Background: Several analysis of heart rate variability (HRV) data recorded with implantable cardioverter defibrillators (ICDs) have been proposed as predictors of ventricular tachyarrhythmia (tachycardia VT, or fibrillation VF). Most analysis are based on normal-to-normal sinus beat (NN) intervals or the effect of premature ventricular complexes (PVCs) upon the sinus rate. This work is based on the analysis of PVCs features in relation to NN intervals (called heartprint), which has several risk markers of fatal or near-fatal arrhythmias obtained from long-term recordings (over 70,000 beats).

Objective: The aim was to compare PVCs characteristics with the heartprint before a sustained tachyarrhythmia (VT/VF) versus control in time series from short-term HRV recordings (about 1,000 beats).

Methods: Data was obtained from the Spontaneous Ventricular Tachyarrhythmia Database (<http://www.physionet.org/physiobank/database/mvtdb/>), which contains 135 pairs of short-term RR interval time series recorded by ICDs in 78 subjects. RR intervals from PVCs were identified with an adaptive filtering algorithm (available: <http://tocsy.agnld.uni-potsdam.de/>). Heartprint indexes included the coupling interval (CI, the RR interval between each PVC and its preceding sinus beat) and the number of intervening sinus beats between two PVCs (NIB). Mean and standard deviation (SD) of NN intervals and CI were estimated for each time series, as well as the most frequent value of NIB (NIB score), which quantifies the prevalence of repeating forms of PVCs. According to the mean heart rate (HR) during the last minute before VT/VF, the recordings were classified into two groups depending on whether the HR was faster or slower than 90 beats per minute (bpm). Since most indexes had no normal distribution, median values were compared using Wilcoxon signed-rank test (VT/VF versus control) or Mann-Whitney U-test (HR \geq 90 bpm versus HR<90 bpm).

Results: Table 1 shows that for the group with accelerated HR (HR \geq 90 bpm), several indexes were different before VT/VF (faster HR, more ectopy, shorter and more fixed CI) versus control. In contrast, the group with HR<90 bpm had similar indexes before VT/VF versus control. Although the group with HR<90 bpm was characterized with faster HR and shorter CI than the group with HR \geq 90 bpm, both groups had similar ectopy.

Conclusions: Several quantitative characteristics of PVCs evaluated with the heartprint method in short-time HRV series obtained from ICDs are potential markers of imminent tachyarrhythmia (VT/VF). The interaction between accelerated HR and high ectopy (previously known risk factors of tachyarrhythmia) should be considered in future evaluation of CI indexes as risk indicators for VT/VF.

Table 1. Results shown as median (percentile 25 – percentile 75).

	HR \geq 90 bpm (N=82)		HR<90 bpm (N=53)	
	Before VT/VF	Control	Before VT/VF	Control
Mean NN (ms)	645(565–674)*	755(696–883)	842(742–920)&	834(768–939)&
SDNN (ms)	52(35–85)	51(28–79)	48(34–68)	40(27–68)
PVCs/hour	182(36–509)*	92(10–424)	150(44–330)	52(16–238)
Mean CI (ms)	464(405–527)*	558(490–624)	592(545–633)&	603(536–648)&
Mean CI/Mean NN	0.770(0.708–0.823)	0.723(0.667–0.796)	0.711(0.652–0.771)&	0.723(0.668–0.789)
SDCI (ms)	55(39–69)*	60(42–72)	73(56–84)&	57(37–99)
Snib	13(4–29)	6(2–26)	7(3–22)	4(1–15)

*p<0.05 (before VT/VF versus control) &p<0.05 (HR \geq 90 bpm versus HR<90 bpm)

SP120.4 - An evaluation of Arterial Stiffness Index in Relation to the State of the Cardiovascular System

Author(s): Jan Havlík¹, Jakub David², Jan Dvořák³, Lenka Lhotská⁴
¹Faculty Of Electrical Engineering, Czech Technical University in Prague, Prague /CZECH REPUBLIC, ²Faculty Of Electrical Engineering, Czech Technical University in Prague, Prague /CZECH REPUBLIC, ³Faculty Of Electrical Engineering, Czech Technical University in Prague, Prague/CZECH REPUBLIC, ⁴Cybernetics, Czech Technical University, Prague/CZECH REPUBLIC

The study deals with an evaluation of correlation between an Arterial Stiffness Index and a state of the cardiovascular system. The main goal of the research is to show whether the ASI is an appropriate parameter for CVS state classification. The statistical evaluation of the dependency of the ASI on the CVS state and other parameters has been done using the linear regression analysis and the t-test of mean values. The ASI has been correlated with the age of the patient, the blood pressure (low/normal/high), the mean arterial pressure and the presence both of the cardiovascular diseases and diabetes mellitus. For the evaluation the signal database which consists of signals from more than 90 persons in wide age range (from 20 to 94 years) has been used. It has been proved that the ASI depends on the age of the patient, on the MAP and on the presence both of the cardiovascular diseases and diabetes mellitus in the study. Only the correlation between the ASI and blood pressure (low/normal/high) has not been directly proved. Although the results are statistically significant, the study shows the limitations of ASI as a CVS status marker. The ASI is a suitable parameter for primary screening, but it should be complemented by additional parameters for increased reliability.

SP120.5 - Investigating a Novel Non-invasive Measure to Assess the Upper Airway Narrowing during Sleep

Author(s): Ying Xuan Zhi¹, Elma Zola², Milos Popovic³, Azadeh Yadollahi¹

¹Institute Of Biomaterials And Biomedical Engineering, University of Toronto, Toronto/CANADA, ²Ryerson University, Toronto/CANADA, ³Toronto Rehabilitation Institute, University Health Network, Toronto/CANADA

Introduction: Previous studies from our team have shown that upper airway (UA) narrowing during sleep could increase its resistance. Increased UA resistance and the associated inspiratory flow limitation are important means of assessing both the cause and the consequences of breathing disorders during sleep. While gold standard assessment of the UA resistance requires invasive measurement of pharyngeal pressure, previous studies have shown that the

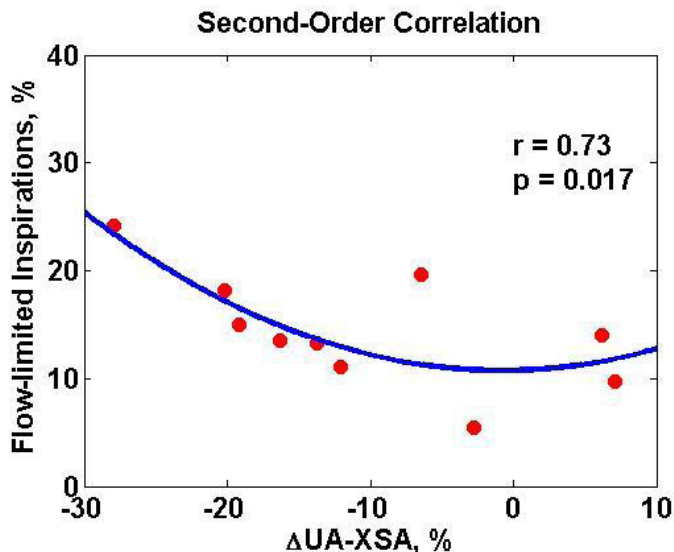
contour of nasal airflow could be used as a non-invasive technique to detect increased UA resistance during sleep. However, these studies have not investigated whether the non-invasive estimation of the UA resistance is associated with physiological variations such as the narrowing in UA cross-sectional area (UA-XSA). The objective of this study is to evaluate the sensitivity of the non-invasive measures of the UA resistance to estimate the changes in the UA-XSA during sleep.

Methods: Subjects attended a regular sleep study in our sleep laboratory. The nasal airflow was collected non-invasively using a nasal cannula. The sleep apnea severity was assessed by the apnea-hypopnea index (AHI). Before and after sleep, UA-XSA was measured by acoustic pharyngometry. For each inspiration, different temporal features such as the number and location of peaks and the plateau in the airflow contour were extracted. Those features were used to manually annotate the inspirations, which correspond to severe flow limitation in the UA and increased UA resistance. The correlation between changes in UA-XSA due to sleep and the percentage of the flow-limited breaths were examined.

Results: 10 non-obese men, age 31.8 \pm 26.7 years and AHI of 41.4 \pm 12 completed the protocol. After sleep, UA narrowed by -11.87 \pm 10.38% (P<0.001). From each subjects, 244 \pm 80 episodes of inspiratory airflow signal were randomly selected from their stage 2 of sleep, and annotated by two experts with consistent agreement. We found that there was a second-order significant correlation between the narrowing in UA-XSA and the percentage of flow-limited inspirations (r=0.73, p=0.017).

Conclusions: Our results show that non-invasive assessment of the UA resistance, obtained by measuring the contour of nasal airflow, can be used as a sensitive measure to assess the severity of UA narrowing during sleep.

Acknowledgement: This study was supported by Toronto Rehabilitation Institute and the University of Toronto.



SP120.6 - Establishing a New Biomarker to Determine Patients at Increased Risk of Developing Obstructive Sleep Apnea Due To Fluid Overloading

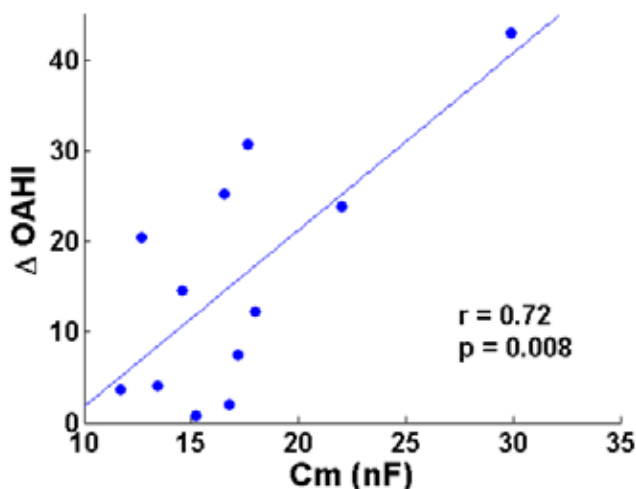
Author(s): Milos R. Popovic, [Bojan Gavrilovic](#), Azadeh Yadollahi
Toronto Rehabilitation Institute - University Health Network, Toronto/
ON/CANADA

Introduction: Obstructive sleep apnea (OSA) is common in 10% of adults and is characterized by repetitive collapse of the pharynx. OSA prevalence increases in fluid retaining patients such as those with heart or renal failure. It is shown that OSA severity worsens with overnight fluid accumulation in the neck. The objective of this study is to develop a new biomarker to assess fluid accumulation in the neck which can be used to determine patients at high risk of developing OSA due to fluid overload.

Methods: This study was part of a double cross-over study to investigate the effects of experimentally induced fluid overloading during sleep on OSA severity. During the control arm saline was infused at a minimal rate to keep the vein open, while during the intervention approximately 2L of saline was infused intravenously during sleep. OSA severity was assessed using polysomnography to estimate obstructive apnea-hypopnea index (OAH). Before and after sleep, neck fluid volume was measured using bioelectrical impedance at 50kHz. For each subject, resistance and reactance was extracted from the impedance measurements. Neck impedance can be modeled as a resistor (extracellular fluid, RE) in parallel with a capacitor (cell membrane, Cm) and resistor (intracellular fluid, Ri). Increase in intracellular fluid could swell the cell and increase Cm. The recorded reactance and resistance from bioimpedance measurements can be expressed in terms of Ri, RE, Cm, $\omega(2\pi f)$ and τ ($Cm[Ri+Ro]$). Assuming that $\omega^2 \times \tau^2 \ll 1$, the recorded resistance and reactance can be simplified to $R = Ro$, and $Xc = -\omega Cm Ro^2$, respectively. Using these relations, the bioimpedance recording of neck can be used to estimate Cm, which could represent the intracellular fluid of the neck.

Results: Subjects who had an increase in OAH from the control to saline infusion arm were investigated. 12 non-obese men, age 44 ± 13 , with OAH 18 ± 23 were included. Our results show that subjects with a larger Cm before sleep during the control arm had a larger increase in OAH from control to intervention ($P=0.008$). This indicates that those with a larger estimated capacitance and intracellular fluid were more susceptible to the adverse effects of fluid overload on OSA severity.

Conclusion: These promising results demonstrate that non-invasive measurements of bioimpedance can be used to develop a novel biomarker to assess patients at high risk of fluid overloading and developing OSA.



SP121 - Deep Brain Stimulation

TRACK 11: NEUROENGINEERING, NEURAL SYSTEMS

SP121.1 - A 16-bit High-Voltage Digital Charge-Control Electrical Stimulator

Author(s): Soheil Mottaghi¹, Richard Pinnell¹, Ulrich G. Hofmann²
¹Neuro Surgery, Neuro Electronics Systems, University Hospital Freiburg, Freiburg/GERMANY, ²Neuro Surgery, neuro Electronic Systems, University Hospital Freiburg, Freiburg/GERMANY

Research on the effects of electrical stimulation, needs an accurate system able to generate any arbitrary waveforms with different frequencies and interphase delays. Some applications such as Deep Brain Stimulation (DBS) turn to smaller electrodes resulting in higher impedances, causing obstacles to deploy the same amount of charge to the tissue. In this paper a 16-bit digital charge-control current stimulator is presented which can produce up to $\pm 35V$ output swing voltages. Platinum flexible electrodes have been used to compare the performance of the developed with two commercial stimulators.

SP121.2 - A method for side effect analysis based on electric field simulations for intraoperative test stimulation in deep brain stimulation surgery

Author(s): Daniela Pison¹, Fabiola Alonso², Karin Wårdell², Ashesh Shah¹, Jérôme Coste³, Jean-Jacques Lemaire³, Erik Schkommodau¹, Simone Hemm-Ode¹

¹Institute For Medical And Analytical Technologies, School of Life Sciences, Muttenz/SWITZERLAND, ²Department Of Biomedical Engineering, Linköping University, Linköping/SWEDEN, ³Image-guided Clinical Neurosciences And Connectomics (ea 7282, Centre Hospitalier Universitaire de Clermont-Ferrand, Clermont-Ferrand/FRANCE

Despite an increasing use of deep brain stimulation (DBS) the fundamental mechanisms underlying therapeutic and adverse effects remain largely unknown. The simulations of electric entities are increasingly used to evaluate stimulation effects. So far no group has considered such simulations combined with a side effect analysis of data obtained during intraoperative test stimulations. The aim of the present paper is to introduce a method allowing patient-specific electric field simulations for stimulation amplitudes inducing side effects during DBS-surgery.

Two female patients presenting essential tremor, both bilaterally implanted in the ventral intermediate nucleus (VIM) region (Clermont-Ferrand University Hospital, France) were included in the study. Intraoperative test stimulations were performed on central and posterior trajectories in each hemisphere. At each position, in addition to the evaluation of the therapeutic effects, side effects such as pyramidal symptoms and paresthesia without localization indicator or paresthesia with localization indicated by the patient (in the hand or in the fingers) were noted. The anatomical structures such as VIM and its neighbors were preoperatively manually outlined using the iPlan software (Brainlab, Feldkirchen, Germany) according to spontaneous MRI contrasts [1]. The so identified structures were exported via a specifically designed interface (VVLink, Brainlab, Feldkirchen, Germany). Whenever side effects occurred the inducing stimulation amplitude was chosen for electric field simulations. A finite element method [2] was applied to calculate the electric field distribution. Conductivity values were deduced from the patient's T1 weighted MRI. An isofield level of 0.2V/mm was chosen and the

points of the isosurface were exported. They were visualized together with the extracted anatomical structures and the trajectories. The different structures presented inside the volume defined by the isofield level and their appearances were determined. Combinations of structures always appearing together for a specific side effect were identified.

For both patients, eight electric field simulations were performed. A first analysis showed that pyramidal effects appear when parts of the ventro-oral nucleus (VO) and the VIM were present inside the isosurface. The ventrocaudal lateral nucleus (VCL), the ventrocaudal medial nucleus (VCM) and the VIM were among the identified structures in hand paresthesia (VCL, VIM), finger paresthesia (VCL, VCM, VIM) and paresthesia with location not formally identified by the patient (VCM, VIM).

The application of our method to two patients has shown its feasibility. Our results are consistent with anatomical knowledge that stimulation of VCL and VCM induce paraesthesia in the body and the face respectively. Nevertheless, more patient data have to be analysed to draw any conclusions. The present method will allow an optimised data exploration compared to existing methods only taking into account the anatomical position of the center of the measurement electrode.

References

[1] Lemaire JJ et al. MRI anatomical mapping and direct stereotactic targeting in the subthalamic region: functional and anatomical correspondence in Parkinson's disease *Int J CARS* 2007 2 75–85

[2] Wårdell K et al.. Deep Brain Stimulation of the Pallidum Internum for Gilles de la Tourette Syndrome: A Patient-Specific Model-Based Simulation Study of the Electric Field. *Neuromodulation*, 2014. doi: 10.1111/ner.12248

SP121.3 - Comparison of Three Deep Brain Stimulation Lead Designs under Voltage and Current Modes

Author(s): Fabiola Alonso, Malcolm A. Latorre, Karin Wårdell
 Department Of Biomedical Engineering, Linköping University, Linköping/SWEDEN

Since the introduction of deep brain stimulation (DBS) the technique has been dominated by Medtronic systems. In recent years, new DBS systems have become available for patients, and some are in clinical trials. The present study aims to evaluate three DBS leads operated in either voltage or current mode. 3D finite element method (FEM) models were built in combination with a neuron model for this purpose. The axon diameter was set to $D = 5 \mu m$ and simulations performed in both voltage (0.5-5 V) and current (0.5-5 mA) mode. The evaluation was achieved based on the distance from the lead for neural activation and the electric field (EF) extension at 0.1 V/mm. The results showed that the neural activation distance agrees well between the leads with an activation distance difference less than 0.5 mm. The shape of the field at the 0.1 V/mm isopotential surface in 3D is mostly spherical in shape around the activated section of the steering lead.

SP121.4 - Effect of closed-loop and open-loop deep brain stimulation on chronic seizures control

Author(s): Muhammad T. Salam¹, Roman Genov², Jose Luis Perez Velazquez³

¹Electrical Engineering, University of Toronto, Toronto/CANADA, ²Electrical Engineering, University of Toronto, Toronto/ON/CANADA, ³Neuroscience & Mental Health Programme And Division Of Neurology, Hospital for Sick Children, Toronto/ON/CANADA

Objective: To investigate the effects of closed-loop and open-loop neurostimulation of the hippocampus on the suppression of spontaneous seizures in a rodent model of epilepsy. **Method:** Chronic seizures in ten rats were induced by intraperitoneal kainic acid injection. Two bipolar electrodes were implanted into the CA1 regions of both hippocampi. The electrodes were connected to the custom-built programmable therapeutic neuromodulation device that can trigger an electrical stimulation either in a periodic manner or upon detection of the intracerebral electroencephalographic (icEEG) seizure onset. This device has a microchip consisting of a 265-channel icEEG recording system and a 64-channel stimulator, and a programmable seizure detector built in a field-programmable gate array (FPGA). This device was used to evaluate seizure suppression efficacy in the epileptic rats for 240 days (5760 hours). For this purpose, all rats were randomly divided into two groups: the non-stimulation and the stimulation group. The non-stimulation group did not receive stimulation; whereas the treatment group received closed-loop stimulation and later, open-loop stimulation. **Result:** The non-stimulation and stimulation groups had a similar seizure frequency baseline, average 5 seizures per day, but the closed-loop stimulation reduced seizure frequency by 90% and the open loop stimulation reduced by 17% in the stimulation group. **Significance:** In this study, this closed-loop stimulation strategy proved superior to the open-loop stimulation in the seizure suppression using the optimal number of stimulations. Therefore, an effective alternative to the open-loop neurostimulator is the closed-loop neurostimulator, in which the involvement of the deep brain stimulation is minimal. Such a system would be able to sense the upcoming seizure in real time, and deliver the proper stimulation. The new era of deep brain stimulation strategies based on closed-loop paradigms may be able to target different pathological aspects of brain activity for the treatment of various neurological disorders.

SP121.5 - Clinical validation of a precise tremor assessment system to aid deep brain stimulation parameter optimisation

Author(s): Thushara Perera¹, Shivanthan A.C. Yohanandan², Mary Jones³, Richard Peppard³, Wesley Thevathasan¹, Andrew H. Evans⁴, Joy L. Tan¹, Colette M. Mckay¹, Hugh J. Mcdermott¹

¹Neurobionics, Bionics Institute, East Melbourne/AUSTRALIA, ²Electrical And Electronic Engineering, The University of Melbourne, Melbourne/AUSTRALIA, ³Department Of Neurology, St Vincent's Hospital, Melbourne/AUSTRALIA, ⁴Department Of Neurology, The Royal Melbourne Hospital, Melbourne/AUSTRALIA

Introduction

Deep brain stimulation (DBS) is an established therapy for Parkinson's disease and Essential Tremor. Yet finding the most efficacious stimulation amplitude, pulse duration and frequency is difficult due to the numerous parameter permutations. The therapeutic outcomes are measured using a variety of clinical assessments including subjective rating scales. These measures lack sufficient sensitivity to inform DBS parameter optimisation, thus justifying our aim to develop a more precise and objective measure.

Methods

The Tremor Biomechanics Analysis Laboratory (TREMBAL) system, developed at the Bionics Institute, provides real-time tremor severity measurements for clinicians using an electromagnetic motion

tracker (Ascension, Vermont, US) to acquire absolute displacements and rotations of the tremulous body part. TREMBAL automatically computes tremor amplitude, velocity, peak frequency and peak power spectral density (PSD) for both translational and rotational components of motion.

We placed two sensors on each hand at the proximal phalanges of the middle fingers and approximately 5 cm above the olecranon of the elbows to measure proximal and distal tremors of nine participants with existing DBS therapy. Four trials were performed where DBS level was systematically reduced from 100% (clinically optimal level) to 75%, 50% and finally 0% (DBS off). In each trial, after waiting 12 minutes for adaptation, the participant held their hands outstretched for 10 seconds and performed the finger-nose exercise. These were video recorded and presented to three blinded experts (W.T., A.H.E., J.L.T.) for clinical rating using the Bain Tremor Rating Scale. Linear regression analysis between the average expert tremor ratings and computed tremor metrics were used to validate TREMBAL. Pearson's correlations were also performed to confirm any associations.

Results

Sixty-four clinical ratings were included in the analysis. One patient was excluded because they presented with dystonia. Results were deemed significant if $p < 0.0063$ (Bonferroni correction for multiple comparisons). Objective measures of translational amplitude and velocity had the strongest ability to predict clinical ratings (table 1).

Motion Type	Metric	R ²	SE	r	p
Translation	Amplitude	0.81	0.53	0.90	<0.001
	Velocity	0.81	8.34	0.90	<0.001
	Frequency	0.32	0.09	0.56	<0.001
	PSD	0.71	0.22	0.84	<0.001
Rotation	Amplitude	0.34	0.27	0.59	<0.001
	Velocity	0.34	5.15	0.58	<0.001
	Frequency	0.20	0.09	0.45	<0.001
	PSD	0.20	0.01	0.44	<0.001

Table 1. The coefficient of determination (R²) and standard error (SE) indicated the goodness-of-fit of the linear regression between clinical ratings and TREMBAL metrics for distal tremor of the worst affected hand. Pearson's correlations indicated strength (r) and statistical significance (p) of the association. PSD = Power Spectral Density.

Discussion

Tremor frequency and PSD in addition to all angular measures showed weaker agreement with clinical ratings. We believe that clinicians rely mostly on displacement and speed to assess tremor severity thus accounting for the high concordance with translational TREMBAL data. Further work will aim to determine the test-retest reliability of the system and the optimal combination of metrics to reduce TREMBAL's output to a single measure based on machine learning algorithms.

Acknowledgements

Colonial Foundation and the Victorian Government Operational Infrastructure Support Program.

SP121.6 - The Role of Microelectrode Recording (MER) in STN DBS Electrode Implantation**Author(s):** Venkateshwarla R. Raju¹, Rukmini M. Kandadai²¹Biomedical Eng & Neurology & Neurosurgery And, Nizam's Inst of Medical Sciences (NIMS) University & Hospital, HYDERABAD/INDIA, ²Neurology, Nizam's Inst of Medical Sciences, Hyderabad/INDIA

The purpose of this paper is to study the correlation of microelectrode recording with the final tract chosen during bilateral STN DBS performed at a specialized centre in South India. Deep brain stimulation (DBS) of bilateral subthalamic nuclei (STN) is an efficient method of rehabilitation in subjects (diseased conditions—patients) with advanced idiopathic Parkinson disease (PD). Accurate targeting of STN neurons and placement of microelectrodes are paramount importance for optimal results after STN-DBS. Stereotactic assessment, intra-operative microelectrode recording and intra-operative stimulation effects have all been used in targeting, albeit the individual role of each modality is still not known. Microelectrode recordings (MER) of STN were detected in a mean of 3.5 ± 1.1 channels on right hemisphere and 3.6 ± 1.04 on left hemisphere. Final channel selected were most commonly central seen in 42.3% followed by anterior in 33.7%. Concordance of final tract with the channel having the highest recording was 58.7%, with the channel showing maximum depth of recording was 48% and with either was 64%. Absence of any recording in the final tract chosen was seen in 6.52%, in these subjects the tract was chosen based on stimulation results. The depths of microelectrodes were detected by MER in 75.6%. Thus, MER is useful to detect—confirm the tract in which DBS electrodes are placed and is most useful in determining the depth of electrodes placement but has to be taken in consideration with effects seen on macro-stimulation.

SP121.7 - Effectiveness of Micro-Electrode-Recording(MER) in Determining Subthalamic-Nuclei Deep Brain Stimulation (STN-DBS) Lead Position in PD Conditions**Author(s):** Venkateshwarla R. Raju, Praveen P. Ankathi

Biomedical Eng & Neurology & Neurosurgery And, Nizam's Inst of Medical Sciences (NIMS) University & Hospital, HYDERABAD/INDIA

Objectives: To study the effectiveness of microelectrode-recording in determining final tract for placing DBS-electrode during bilateral-STN-DBS

Background: Deep-brain-stimulation of bilateral subthalamic-nuclei is an effective mode-of-therapy in subjects with idiopathic Parkinson's-diseased-conditions(PDpatients). Accurate targeting and placement of microelectrodes are paramount importance for optimal results after STN-DBS. Stereotactic-assessment, intra-operative microelectrode-recording and intra-operative stimulation effects have all been used in targeting, though the individual role of each modality is still unknown.

Methods: 52PDsubjects were included in the study. Subjects with advanced PD of >5 years with good response to levodopa and H and Y score of <4 with normal cognition were eligible for surgery. Functional_Surgery was planned using a CRW frame with an MRI protocol using Framelink software with5channels. Microelectrode recording was performed in all subjects extending from 10mm above target to 10mm below STN. Final target-selection was based on the effects and side effects of macrostimulation and confirmed by post op MRI.

Results: 52PDsubjects with_their mean_age_of 58.1 ± 9.1 years, mean_disease_duration of 8.8 ± 3.64 years were included. Prior to implantation, mean-UPDRS-score in 'off' state was 52.7 ± 10.6 and in 'on' state was 13.4 ± 5.0 . STN microelectrode recordings were detected in a mean of 3.5 ± 1.1 channels on right-hemisphere and 3.6 ± 1.04 on left-hemisphere. Final channel selected were most com-

monly central seen in 42.3% followed by anterior in 33.7%. Concordance of final track with the channel having highest recording was 58.7%, with the channel showing maximum-depth-of-recording was 48% and with either was 64%. Absence-of-any-recording in the final tract chosen was seen in 6.52%, in these subjects the tract was chosen based on stimulation results. The depth of microelectrodes was identified by microelectrode recording in 75.6%.

Conclusion: Microelectrode-recording(MER) is useful to identify and confirm the tract in which DBS electrodes are placed and is most-useful in determining depth-of-electrodes placement but has to be taken in consideration with-effects seen on macrostimulation.

SP122 - Bioinformatics

TRACK 15: BIOINFORMATICS

SP122.1 - Machine learning for bioinformatics in the face of class imbalance

Author(s):

Many pattern classification challenges of interest to bioinformatics involve the prediction of rare events. Examples include prediction of true protein-protein interactions among the millions of potential protein pairs within the human proteome, differentiating the few thousand true microRNAs from the millions of pseudo-miRNA sequences in the human genome, and identifying rare post-translational modification sites characterized only by degenerate sequence motifs. To create effective bioinformatics classifiers in the presence of severe class imbalance requires careful application of appropriate techniques during both the training and evaluation phases of system development. This talk will discuss a number of these techniques and include illustrative examples from recent studies conducted in our lab.

SP122.2 - Bioinformatics-based identification of osteoarthritis-associated genes in synovial tissues

Author(s): Yi-Jiang Song¹, Guiling Li², Li Yang¹

¹Key Laboratory Of Biorheological Science And Technology, Ministry Of Education, Bioengineering College, Chongqing University, Chongqing/CHINA, ²Institute Of Genomic Medicine, Wenzhou Medical University, Wenzhou/CHINA

Objective

Osteoarthritis (OA) is a highly prevalent chronic degenerative joint disease. Piling evidence has shown that primary OA is closely associated with aberrant genetic components. The current study aims to identify genes that are associated with OA in synovial tissues, and to further predict the biological pathways in which they may be involved, as well as their expressional microRNA (miRNA) regulators.

Methods

We applied both data mining and microarray analysis in this study to identify genes that differentially express (fold-change > 2, *p*-value < 0.05) in synovial tissues between OA and the control patients. To further study the biological roles of these differentially expressed genes (DEGs), they were analyzed using DAVID. In addition, TargetScan was used to predict the conserved miRNAs that target the interested genes.

Results

The microarray data series were first downloaded from GEO, and then analyzed to obtain OA-related gene expression profile. We have identified 2,602 and 1,556 DEGs from series GSE29746 and GSE55235, respectively. The subsequent gene function annotation revealed that a number of pathways in which the DEGs may be involved, including cytokine-cytokine receptor interaction, MAPK signaling pathway, Hematopoietic cell lineage and cell adhesion molecules, might be associated with OA pathogenesis. Among them, 5 DEGs may be the potential molecular targets of OA (Table 1). MiRNAs have been reported to regulate genes expression in joint disease. So conserved miRNAs that target these genes were also predicted. However, the biological functions of these genes in OA, as well as their regulation by miRNAs, need further elucidation.

Conclusion

We have studied the expression of genes between OA and healthy controls, and identified a number of DEGs that may be putative molecular signatures of OA. miRNA regulators of five distinct DEGs were also predicted. *TIPARP* may be targeted by miR-221/222. And we found that *TIPARP* expression was significantly reduced in OA patients. Taken together with the fact that miR-221/222 is significantly over-expressed in rheumatoid arthritis synovial fibroblasts, *TIPARP* may play a role in OA pathogenesis via negative regulation by miR-221/222. The newly identified dysregulated genes and their miRNA regulators in OA may act as genetic markers for OA diagnosis and treatment in the future.

Table 1: miRNA regulators and GO functional annotation of five putative osteoarthritis-associated genes

Gene1	miRNA2	GOTERM_BP_FAT3	GOTERM_MF_FAT4
ADH1C	miR-3978/1273e/1290	ethanol metabolic process	transcription regulator activity, ion binding
ETS2	miR-33ab	skeletal system development, regulation of transcription	DNA binding, transcription regulator activity
RORA	miR-302abcde/372/373/520be/520acd-3p	positive regulation of biosynthetic process, regulation of transcription	DNA binding, transcription regulator activity, ion binding
STXBP6	miR-133ab	vesicle-mediated transport	
TIPARP	miR-221/222	skeletal system development, cell surface receptor linked signal transduction	ion binding

1 fold-change > 2, false discovery rate-adjusted *p*-value < 0.05; 2 Predicted conserved miRNA regulators; 3 GO Biological Process term; 4 GO Molecular Function term

SP122.3 - Dynamic Epistasis Analysis

Author(s): Aseel Awdeh, Theodore Perkins
University of Ottawa, Ottawa/CANADA

Identifying regulatory relationships between genes is a central and challenging problem in the field of genetics. One classical approach is epistasis analysis (Avery & Wasserman, Trends in Genetics, 1992). Broadly speaking, epistasis between a pair of genes in a pathway, X and Y, happens when the phenotypic consequence of deleting genes X and Y is “unexpected” based on the results of deleting each gene individually. By following the rules of epistasis, one can sometimes infer which of X or Y is upstream of the other, and whether the relationship between them is activating or repressing. However, different pathway structures can result in identical phenotypes upon gene deletion. Thus, it is not always possible to infer the relationship between X and Y.

We propose *dynamic epistasis analysis*, which extends the classical approach by assuming that we can drive the pathway with a time-varying input signal. Intuitively, the time-varying input may help us discriminate between alternative pathway structures that are otherwise indiscriminable—for instance, because of how quickly the signal propagates to the phenotypic output, or because of transient changes in the output. Moreover, the approach is feasible in practice, because robotic flow cytometry and microfluidics devices make it relatively easy to interrogate cells with time-varying signals such as drug dosages or nutrient concentrations. Here, however, we report on a theoretical investigation of the limits and benefits of dynamic epistasis analysis.

First, we computationally enumerated all possible acyclic network topologies on two genes X and Y, which regulate the state of a third “output” gene Z, and which are themselves influenced by an “input” signal S. (Epistasis analysis is generally restricted to studying feedforward pathways, hence the limitation to acyclic networks. However, we impose no other limitations.) We adopted a discrete-time Boolean model for all variables, S, X, Y and Z. When there is a regulatory link between a pair of variables, we assumed it can be activating or repressing. When a variable takes input from more than one other variable, we assume it adopts either the AND or the OR of its inputs (or their negations, in the case of repressive links). We found a total of 4608 possible networks that differ either by structure or regulatory functions. We then studied how many of those could be uniquely identified based on classic epistasis analysis, which looks at Z under different knockout conditions and static signal states $S=0$ or $S=1$, and dynamic epistasis analysis, which looks at Z under different knockout conditions and arbitrary time-varying S. We found that no network had unique patterns of phenotype Z in the classical approach, whereas 7.3% do under dynamic epistasis. If we allow gene knock-ins, which force X or Y to be on, classical epistasis can still only identify 0.7% of pathways, whereas dynamic epistasis identifies 19.4%. Thus, we conclude that dynamic information is potentially a very powerful addition to epistasis analysis.

SP122.4 - Transcription factor binding in an expanded epigenetic alphabet

Author(s): Coby Viner¹, James Johnson², Charles E. Grant³, William S. Noble⁴, Timothy L. Bailey², Michael M. Hoffman⁵

¹Department Of Computer Science, University of Toronto, Toronto/ON/CANADA, ²Institute For Molecular Bioscience, University of Queensland, Brisbane/QLD/AUSTRALIA, ³Department Of Genome Sciences, University of Washington, Seattle/WA/UNITED STATES OF AMERICA, ⁴Department Of Genome Sciences, University of Washington, Seattle/UNITED STATES OF AMERICA, ⁵Princess Margaret Cancer Centre, Toronto/ON/CANADA

Many transcription factors (TFs) initiate transcription only in specific sequence contexts, providing the means for sequence specificity

of transcriptional control. A four-letter DNA alphabet only partially describes the possible diversity of nucleobases a TF might encounter. Cytosine is often present in the modified forms 5-methylcytosine (5mC), 5-hydroxymethylcytosine (5hmC), 5-formylcytosine (5fC), and 5-carboxylcytosine (5caC). TFs have been shown to distinguish unmodified from modified bases. Modification-sensitive TFs provide a mechanism by which widespread changes in DNA methylation and hydroxymethylation found in many cancers can dramatically shift active gene expression programs.

To understand the effect of modified nucleobases on gene regulation, we developed methods to discover motifs and identify TF binding sites in DNA with covalent modifications. Our models expand the standard A/C/G/T alphabet, adding m (5mC), h (5hmC), f (5fC), and c (5caC). We adapted the well-established position weight matrix (PWM) formulation of TF binding affinity to this expanded alphabet.

We engineered several tools for expanded-alphabet sequence and PWMs. We developed a program, Cytomod, to create the sequence using data from bisulfite sequencing. Cytomod decides between multiple modifications at a single position using a configurable evidence model. We also developed new versions of MEME (Multiple EM for Motif Elicitation) and FIMO (Find Individual Motif Occurrences) that enable de novo discovery of modification-sensitive motifs and identification of modification-sensitive binding sites.

We created an expanded-alphabet genome sequence using mouse embryonic stem cell data, and identified cis-regulatory modules that we believe are active only in the presence of cytosine modifications. We found new binding sites for known methylation-sensitive TFs, such as Klf4 and the c-Jun/c-Fos heterodimer. Using ChIP-seq data on TF binding locations, we discovered novel expanded-alphabet motifs.

SP122.5 - Identification of Molecular Phenotypes in Lung Cancer by Integrating Radiomics and Genomics

Author(s): Patrick Grossmann¹, Olya Grove², Nehme El-Hachem³, Chintan Parmar¹, Emmanuel Rios-Velazquez¹, Ralph T.H. Leijenaar⁴, Benjamin Haibe-Kains⁵, Philippe Lambin⁶, Robert J. Gillies², Hugo J.W.L. Aerts⁷

¹Radiation Oncology, Dana-Farber Cancer Institute, Harvard Medical School, Boston/UNITED STATES OF AMERICA, ²Cancer Imaging And Metabolism, H. Lee Moffitt Cancer Center and Research Institute, Tampa/UNITED STATES OF AMERICA, ³Institut de recherches cliniques de Montreal, Montreal/CANADA, ⁴Radiation Oncology (maasro), Research Institute GROW, Maastricht/NETHERLANDS, ⁵Princess Margaret Cancer Centre, University Health Network, Toronto/CANADA, ⁶MAASTRO Clinic, Maastricht/NETHERLANDS, ⁷Radiology, Brigham and Women's Hospital, Harvard Medical School, Boston/UNITED STATES OF AMERICA

Medical imaging can visualize phenotypic characteristics of human cancers non-invasively. Radiomics is the process of converting images to mineable data and can provide a comprehensive quantification of tumor phenotype non-invasively by applying image feature extraction algorithms. Radiomic data have been suggested to be associated with clinical outcomes, however the biological basis of these associations is unknown. We therefore analyzed two independent lung cancer cohorts (one North American discovery cohort and one European validation cohort) totaling 351 patients, for whom diagnostic computed tomography (CT) scans, gene-expression microarrays, and clinical data were available. The tumor phenotype was characterized based on 636 radiomic features describing tumor intensity, texture, shape and size (Figure 1). We performed an integrative analysis by developing association modules of coherently expressed radiomic features and molecular pathways. We identified thirteen independently validated radiomic-pathway association modules ($P < 0.05$), the most prominent of which were associated

with the immune system, p53 pathway, and other pathways involved in cell cycle regulation (Figure 2A). Eleven modules were significantly associated with clinical factors ($P < 0.05$, Figure 2B). We further observed strong predictive power for pathway activation status; the areas under the receiver operating characteristic curves (AUCs) of the strongest predictions of every module ranged from 0.62 ($P = 0.03$) to 0.72 ($P < 1E-6$). In addition, combining radiomic data with clinical factors and genomic information resulted in consistent increases in power to predict overall survival in the validation dataset (concordance index max 0.73, $P < 1E-9$). In conclusion, we show that radiomic approaches permit a non-invasive assessment of molecular and clinical characteristics of tumors, and therefore have the potential to support clinical decision-making and advance therapeutic strategies using routinely acquired, standard-of-care imaging data.

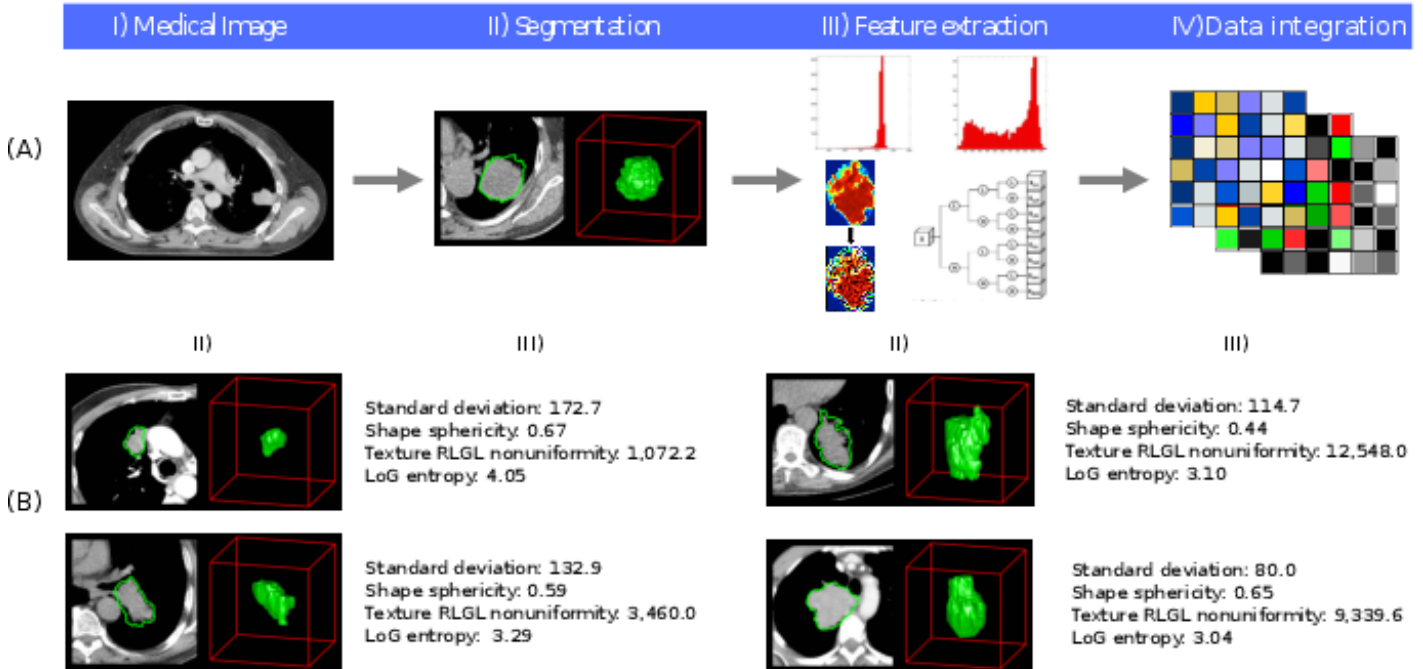
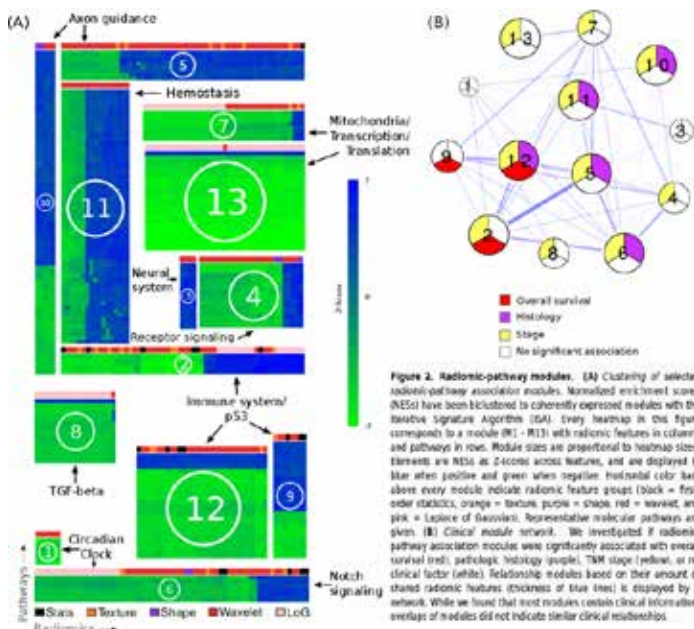


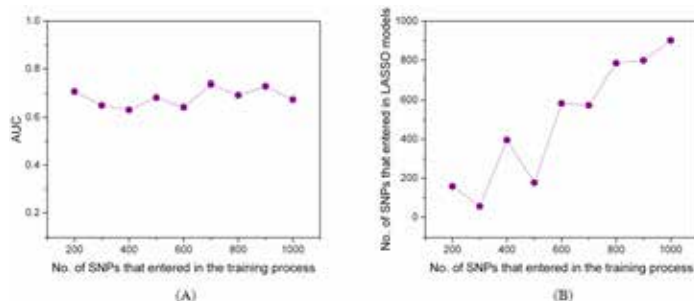
Figure 1. Radiomic strategy. (A) Workflow of extracting radiomic features: I) A lung tumor is scanned in multiple slices. II) Next, the tumor is delineated in every slice and validated by an experienced oncologist. This allows to create a 3D representation of the tumor outlining strong phenotypic differences in tumors of different patients. III) Radiomic features are extracted from these 3D images, and IV) integrated with genomic and clinical data. (B) Representative examples of lung cancer tumors. Visual differences in tumor shape and texture between patients can be objectively defined by radiomically defined features such as standard deviation of voxel intensity values ("How dispersed are the intensities?"), sphericity of the tumor ("How compact is the tumor?"), non-uniformity of texture run-length gray-levels (RLGL) ("How heterogeneous is the tumor?"), and entropy of voxel intensities after applying a Laplacian of Gaussian (LoG) filter ("How uncertain are the intensities?").



SP122.6 - A machine learning method to build multi-SNP predictive models of clinical radiosensitivity**Author(s):** Jung Hun Oh¹, Sarah Kerns², Harry Ostrer³, Barry Rosenstein⁴, Joseph O. Deasy¹¹Memorial Sloan Kettering Cancer Center, New York/NY/UNITED STATES OF AMERICA, ²University of Rochester Medical Center, Rochester/NY/UNITED STATES OF AMERICA, ³Albert Einstein College of Medicine, New York/NY/UNITED STATES OF AMERICA, ⁴Mount Sinai School of Medicine, New York/NY/UNITED STATES OF AMERICA**Purpose:** Genome-wide association studies (GWAS) have become a vital method to identify single nucleotide polymorphisms (SNPs) associated with common complex diseases. Many current GWAS analyses have used single-SNP models by individual association test. However, these methods suffer from multiple-testing correction due to a large number of SNPs being evaluated, which may cause some potentially important SNPs to fail to achieve genome-wide significance. Moreover, single-SNP models do not take into account correlations or interactions among significant SNPs.**Materials/Methods:** To overcome these weaknesses of the single-SNP approaches, we propose a machine learning-based multi-SNP model for predicting radiation-induced late rectal bleeding toxicity in prostate cancer patients. Our method consists of the supervised principal component analysis (SPCA) and least absolute shrinkage and selection operator (LASSO). Using SPCA, many irrelevant SNPs are filtered out and redundant SNPs are further removed via sparse regression models in the LASSO process.

In this radiosensitivity study, 365 prostate cancer patients who received radiotherapy were analyzed. For these patients, germline DNA extracted from lymphocytes was genotyped using the Affymetrix genome wide array (v6.0). To build a predictive model, we coded the status of rectal bleeding as 0 (grade 0 or 1; n=291) or 1 (grade 2+; n=74) using the Radiation Therapy Oncology Group (RTOG) late radiation morbidity scoring schema.

For an unbiased assessment, the dataset was split once and for all into two groups: a training dataset (2/3 of samples) and a validation dataset (1/3 of samples). In the modelling process, only the training dataset was used and the validation dataset was used to validate final predictive models.

Results: With the training dataset, univariate analysis was performed using Chi-square test. Based on the p-value, with an increasing number of top ranked SNPs (from 200 to 1000 SNPs), the model building process was conducted. Figure (A) shows the best AUC results obtained using the validation dataset with a different number of SNPs that were fed into the model building process. Figure (B) shows the number of SNPs that entered into the LASSO models after irrelevant and redundant SNPs were removed. When 700 SNPs were input into the model, an AUC of 0.74 was obtained with 573 SNPs that entered into the LASSO models.**Conclusions:** Our proposed machine learning-based method was used to build a predictive model of late rectal bleeding toxicity for prostate cancer patients. We demonstrated that the proposed method has the potential to improve the prediction power in GWAS.**SP122.7 - Updated Free Energy Parameters Increase MicroRNA Prediction Performance****Author(s):** Robert J. Peace¹, James R. Green²¹Systems And Computer Engineering, Carleton University, Ottawa/CANADA, ²Department Of Systems & Computer Engineering, Carleton University, Ottawa ON/CANADAMost *de novo* microRNA prediction tools rely on RNA structure prediction as a pre-screening step – only those sequences that exhibit miRNA-like hairpin structures are considered as putative miRNAs. However, little attention has been paid to the quality of this pre-screening step. This prescreening may unduly limit the sensitivity of the miRNA prediction method. We here demonstrate that leveraging recent advances in RNA structure prediction results in significant increases in overall miRNA prediction recall and precision.

SP123 - Patient Safety, Medical Errors and Adverse Events Prevention Related to Health Technologies

TRACK 16: CLINICAL ENGINEERING, CLINICAL PHYSICS, AND PATIENT SAFETY

SP123.1 - Incident reporting and learning systems improving quality and safety in radiation oncology

Author(s): *Mary Coffey*

Radiation Therapy, Trinity College Dublin, Dublin/IRELAND

The publication of a number of fatal incidents in radiotherapy globally has led to an increased emphasis on openness and transparency and underpins the importance of reporting and learning from minor incidents and near misses in the prevention of further major incidents. Incidents and near incidents are a fact of life and cannot be eliminated completely, what is important is to learn from these and to share that learning with the wider radiotherapy community.

Reporting as part of the cycle of investigation, analysis, feedback and learning is one method of improving the safety of radiotherapy. Reporting can be mandatory or voluntary, internal or external depending on the requirements of the individual country. In the last decades a number of initiatives at country or professional organization level have resulted in the development of comprehensive reporting systems. One of the most recent systems to be put in place, the RO-ILS, was launched at ASTRO in 2014. Canada are currently piloting a national system, the ASN in France, the United Kingdom and The Netherlands have well established national systems and two voluntary international systems are in place: the Radiation Oncology Safety Information System (ROSIS) and the International Atomic Energy System: Safety in Radiation Oncology (SAFRON).

The Radiation Oncology Safety Information System (ROSIS) was established in 2001 and went live online in 2004. The IAEA Safety in Radiation Oncology (SAFRON) went live in December 2012. ROSIS and SAFRON share information with each other and SAFRON is currently developing further links with other national systems. In 2013/14 as part of a project supported by Varian and Elekta the taxonomy of ROSIS was revised to be consistent, as far as possible, with SAFRON, the AAPM system and RO-ILS.

The European Society for Radiotherapy and Oncology has established a Risk Management Committee with reporting and learning in the context of the recent European legislation a key focus.

SP123.2 - Applying an Evidence-based Approach to Managing Alarm Safety: A University Health Network Case Study

Author(s): *Anne Li¹*, Dave Gretzinger²

¹Institute Of Biomaterials And Biomedical Engineering, University of Toronto, Toronto/ON/CANADA, ²Department Of Medical Engineering, University Health Network and Mount Sinai Hospital, Toronto/ON/CANADA

Background: High reliance on medical technologies to perform a myriad of tasks, ranging from surveillance to delivery of therapies, in modern medicine has resulted in excessive number of alarms on clinical units. This translates into an increased risk of alarm fatigue amongst caregivers, lowered quality of care and interrupted patient recovery. Technologies (such as alarm communication management systems and smart algorithms) have been developed to address alarm safety, but there are inherent limitations to every technology. It was, therefore, the aim of this case study to develop an evidence-

based approach to alarm safety management that can be applied across clinical units.

Methodology: Two intensive care units, a Level 3 (Medical Surgical Neurological Intensive Care Unit (MSNICU)) and a Level 2, at the Toronto Western Hospital were investigated. A recommended alarms management program by the ECRI Institute was modified to include only steps that were applicable to the investigational units and their associated workplace cultures. A multi-disciplinary team consisting of clinical engineers, nursing educators, and allied health professionals assembled bi-weekly to steer the direction of this initiative. Observations in the clinical units, nursing alarm surveys for MSNICU staff and review of incident reports from April 2012 to September 2014 were used to determine the areas of greatest vulnerability and establish priorities. Recurring themes in the textual data were indexed and refined.

Discussion: Thematic analysis revealed that alarm safety concerns centered around three themes of related constructs (alarm noise, alarm desensitization and alarm workflow). However, the relative contribution of each theme to alarm concerns varied due to differences in workflow and patient population. A universal management option, therefore, does not exist. The negative impact of continuous noise on patient recovery was unanimous amongst the surveyed nurses. High number of false positive and/or clinically irrelevant alarms resulted in caregiver apathy and desensitization, which caused true monitor events to be neglected. Non-standardized workflows (such as procedure for coverage of breaks and physiological parameter adjustments) also contributed to alarm safety issues.

Conclusions: Observations revealed that institution-wide procedural changes, such as mandatory physiological parameter adjustments and implementation of a standardized procedure to temporarily pause alarms when continuous monitoring is not required, may reduce excessive noise and false positive alarms. Frustrations often arose due to incomplete knowledge of the medical technologies. Information sessions and easily accessible answers to frequently asked questions (FAQ) could lessen this aspect of concern. Cultural changes are anticipated to provide a good first step to alarm safety management, however, qualitative data alone is insufficient to drive alarm safety initiatives. Since there is no "one size fits all" solution, future studies will require analysis of alarm data (number per bed, type and duration) to identify high-priority areas per clinical unit. Alarm data collection systems provide a safe process to monitor and evaluate the effectiveness of interventions. Sustainable improvements in alarm safety will require long-term commitment from all levels of institution.

SP123.3 - Using infusion pump logs to recreate a patient safety event: considerations for smart pump improvement

Author(s): *Andrew Ibey¹*, Derek Andrews², Barb Ferreira³

¹Biomedical Engineering, Providence Healthcare, Vancouver/CAN-ADA, ²Pharmacy, Vancouver Coastal Health, Vancouver/BC/CANADA, ³Acute & Chronic Health, Vancouver Coastal Health, Vancouver/BC/CANADA

The authors describe the reconstruction of a unique event involving a nurse's response to an error with an infusion pump in a critical care environment, and subsequent learning opportunity. The authors propose further considerations for smart pump improvement.

A 75-year-old male patient presented in July 2013 to a major teaching hospital with a massive gastrointestinal bleed and myocardial infarction, and was admitted to the intensive care unit. Although in tenuous health, the patient's condition stabilized with multiple infusion lines providing life-sustaining medication. At some point during the patient's care, the pump alarmed a "Communication Error" message. The nurse attempted to clear the alarm but the pump

appeared unresponsive. She disconnected the module to reprogram the pump, causing an interruption in the DOPamine infusion. This caused the patient's blood pressure to plunge, resulting in a cardiac arrest. The pump was subsequently quarantined and sent to Biomedical Engineering for analysis.

The smart pump was a modular infusion pump with one central PC unit (PCU) and up to four large volume pump modules. Pump logs and the server database were mined and discovered that three PCUs and eight modules were connected to the patient at the time of the error. All equipment was functional and operated within the manufacturer's specification. The inter-unit interface connecting the PCU and module infusing DOPamine had corrosion and white "fluff" on the contacts, which is believed to be the cause of the "communication error".

During the investigation, the manufacturer explained that the pump's fail safe mechanism is to continue to infuse the drug at the prescribed rate during a "communication error" message. The pump gave no explicit instructions to resolve the issue, and resolution was not intuitive. Learning yielded a nursing practice alert to clarify how a nurse should resolve a "communication error".

The authors believe that infusion pump logs are not designed with any forethought as to how they will be used in an incident investigation. Pump logs are awkward and the data extracted is often heavily coded and not easily interpretable in plain English. Vendor software lacks meaningful tools to easily analyze the data, leaving the investigator to make sense of raw data.

Modern smart pump technology does not operate as a patient focused system. Instead, each PCU operates independently, lacking the ability to allow soft warnings or hard stops for a combination of contraindicated drugs (e.g. additive, potentiation or antagonistic) in the drug library that are infusing on separate channels of a PCU. Similarly, if 2 or more PCUs are connected to the patient, none of the PCUs know what is being infused on the other PCU channels. Pumps should be able to be daisy chained together so that they can communicate and record information as a cohesive system *per patient*.

Smart pumps have succeeded mitigating bedside medication errors. Secondary uses for incident investigations and multiple pumps to operate as a cohesive system on a patient should be considered for future enhancements.

SP123.4 - Developing an information retrieval engine for medical devices' vigilance reports

Author(s): Charalampos Tsimpas¹, Athanasios Anastasiou¹, Maria Haritou², Dimitrios Koutsouris¹, [Nicolas Pallikarakis](#)³

¹School Of Electrical & Computer Eng., National Technical University of Athens, ATHENS/GREECE, ²Biomedical Engineering Lab., Institute of Communication and Computer Systems, ZOGRAFOU, ATHENS/GREECE, ³Biomedical Engineering Unit, University of Patras, Rio-Patras/GREECE

Objectives: Patient safety is a fundamental cornerstone of care and a critical component of healthcare systems. To create a safer environment, it is necessary to provide effective and efficient medical device (MD) vigilance information. The traditional approach, based only on user reports of adverse incidents, has been proven inadequate today.

Approach: In this work we describe our experience on the development of the EIPAS NLP engine, an information retrieval module in the context of the EIPAS project aiming at developing an innovative cross validation vigilance platform for medical devices. EIPAS NLP engine is mainly focused on retrieving information from direct sources such as vigilance reporting databases (VRDs). In other words, it

is constructed with the goal of providing structured data related to medical devices' adverse events, by extracting the appropriate information from semi-structured vigilance reports. Although the input data (vigilance reports) is raw, we considered it as semi-structured as it follows the structure defined by the definition of the report. More specifically the vigilance reports contain sections of descriptions related to medical devices malfunctions, as well as detailed information of the recalling process.

Method: The proposed engine is organized in three basic phases: the phase of preprocessing and parsing, the phase of entity extraction and the phase of ontology population. The phase of *preprocessing and parsing* is responsible for recognizing and separating the interesting section of the vigilance report related to the medical devices. The phase of *entity extraction* is the core process of our approach. During this stage, the entities of interest from each vigilance report are extracted. In our case, terms of interest among others include the manufacturer, model, serial number, etc. The phase of *ontology population* includes the mapping of the previous phase outputs into ontology individuals.

Results & Conclusion: For evaluating purposes we fed the NLP engine with 30 reports (in html format) from FDA which were also manually annotated. In order to test our NLP engine we examine two aspects. Firstly, we assess the efficiency of preprocessing and parsing and its capacity to dissociate the areas of the report which are related to product description (PD), code description (CD), reason description (RD) and recalling firm description (RFD). The second examined aspect is the ability to extract the entities Manufacturer, Model, Serial, Product Metric (PM) and Product Amount (PA) from the respective sections.

Based on the results, it is expected that the proposed engine through the design, development and implementation of modern ICT tools, will create a prototype system, which will provide critical, on time and customized information to health care institutions with regard to MD adverse events.

Acknowledgements: The presented work was carried out in the framework of the project "EIPAS", funded under the THALES programme, co-financed by the European Union (European Social Fund-ESF) and Greek national funds through the Ministry of Education, Lifelong Learning and Religious Affairs and the Operational Program "Education and Lifelong Learning" of the National Strategic Reference Framework (NSRF).

SP123.5 - Efficient, all-in-one, Monte Carlo simulations of transit EPID cine-mode dose distributions for patient-specific VMAT quality assurance

Author(s): [Shiqin Su](#)¹, Parmveer Atwal¹, Julio Lobo², I Antoniu Popescu¹

¹Medical Physics, British Columbia Cancer Agency, Vancouver/CANADA, ²Electrical And Computer Engineering, The University of British Columbia, Vancouver/CANADA

Introduction: The purpose of this study is to present a novel tool within the BEAMnrc/DOSXYZnrc environment for Monte Carlo (MC) simulations of transit EPID dose. During a standard DOSXYZnrc simulation, each particle history is tracked using a randomly sampled time-like variable (i.e. MU index ranging from 0 to 1), but the temporal information is discarded during dose deposition, producing a cumulative distribution. This means that if we wish to determine dose distribution as a function of time, separate simulations would have to be run for each interval of interest. Consequently, it is clinically unfeasible to perform MC simulations of transit EPID cine-mode acquisition for a VMAT plan delivered to a patient. To overcome this limitation we developed a method capable of providing these transit EPID distributions, per control point, or over any user-defined time interval, in a single simulation.

Methods: We modified DOSXYZnrc (version V4-2.4.0) to optionally output a 4D IAEA phase space during a source 20 simulation, in order to collect particles exiting the patient during a VMAT treatment. This phase space can be used for further synchronized simulations of EPID dose using the MU index associated with each particle. We have also modified DOSXYZnrc to output a new file in which this time-like variable is binned in a user-defined manner (e.g. consistent with the EPID cine-mode acquisition), and associated with each bin is the amount and location of energy deposited by particles whose MU indices fall within that bin.

Results: Evaluation of the new technique was done with an anthropomorphic phantom for a 2-arc head-and-neck VMAT plan. Comparison of the EPID cine-mode images with the corresponding MC calculated distributions, via the Gamma metric (3%, 3mm), showed greater than 96% agreement (see Figure). Total simulation times were not increased and the time-integrated dose was identical to that from a standard 3ddose file.

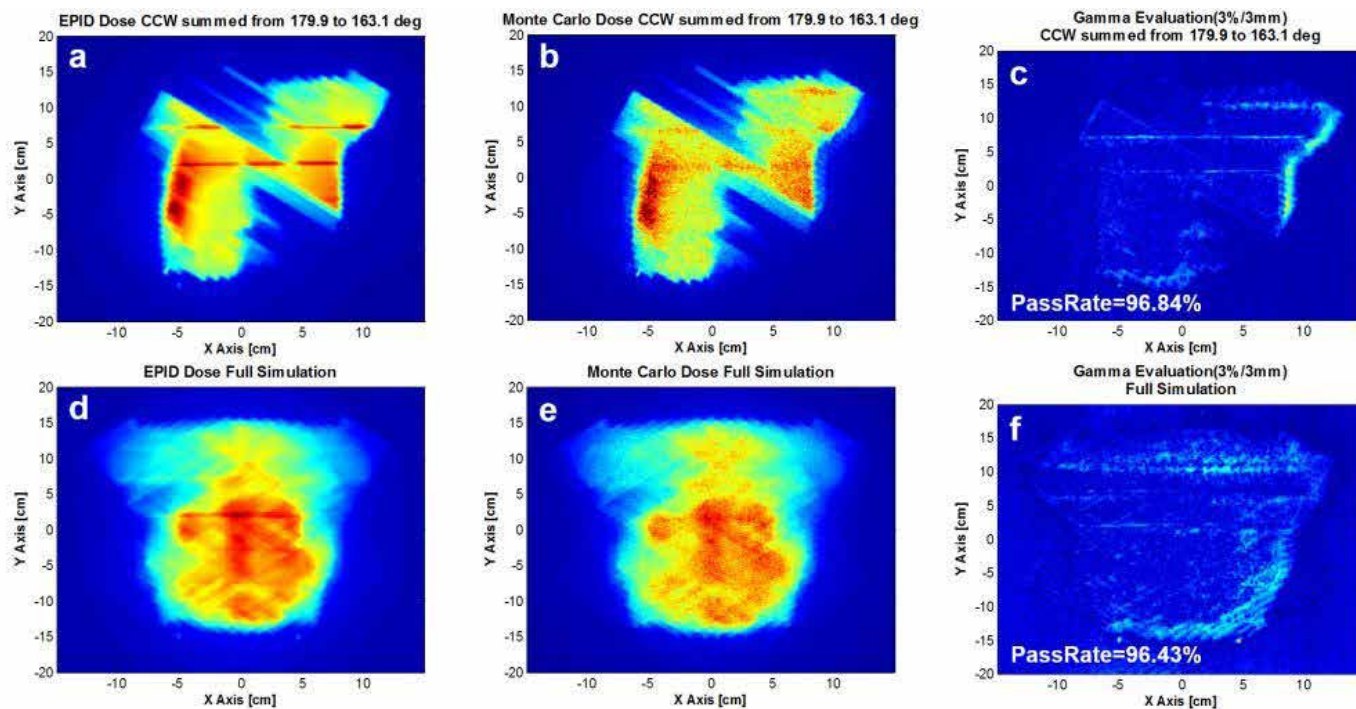


Figure. EPID dose images (a, d) compared with MC distributions (b, e), using 3%/3mm Gamma metric (c, f). Upper row corresponds to a segment of one arc; bottom row corresponds to full treatment (2 arcs).

Conclusions: Our method allows for comparisons of the 4D MC phase space EPID prediction with the actual EPID data acquired with the patient on treatment. This technique also allows for creation of a dose rate map within a phantom or patient. We demonstrated the feasibility of including transit EPID cine-mode MC simulations as part of a comprehensive patient-specific VMAT quality assurance process.

SP123.6 - Development of an interactive training tool to help reduce error rate associated with shared infusion volume management tasks

Author(s): Kyle Tsang¹, Patricia Trbovich², Sonia Pinkney³

¹Institute Of Biomaterials And Biomedical Engineering, University of Toronto, Toronto/CANADA, ²Humanera, University Health Network, Toronto/ON/CANADA, ³Centre For Global Ehealth Innovation, University Health Network, Toronto/CANADA

Background Medication administration errors in a hospital pose a serious threat to patients. Several types of medical technologies (e.g. smart pumps, alarms) have been introduced into the hospital environment, yet despite their numerous benefits, preventable medication administration errors still exist. Analysis reveals that inadequate training is a primary reason for these preventable errors. In the context of intravenous (IV) infusion systems, a clinician's training is mainly associated with the specifics of "how" to use certain equipment, but a fundamental understanding regarding IV infusion principles (e.g. hydrostatic pressure) is often missing. In particular, the concept of shared infusion volume, which refers to the common volume shared by 2 or more infusions in the IV tubing between the patient's vein and the point of medication delivery, is often incorrectly accounted for, which can result in unpredictable and hard to detect medication errors (e.g. delays in therapy, medication incompatibilities). Nurses often do not understand nor consider the presence of shared infusion volume in their practice and there are currently no explicit training methods to address this issue. This research aims to design and test an interactive training tool (ITT), in the form of a computer based e-learning module, to help improve a clinician's ability to deal with shared infusion volume management.

Objective The purpose of this research is to understand the different mental processes (e.g. decision making) associated with shared infusion volume using a cognitive task analysis method. Once a critical decision model is formed, the knowledge gained will be applied to the refinement of an ITT. This ITT will help train nurses to better understand multiple IV infusions by supporting the cognitive processes required and removing identified barriers associated with shared infusion volume.

Design A cognitive task analysis method consisting of semi-structured interviews with experienced clinicians will help determine the cognitive processes (e.g. specific critical cues) required to successfully manage the problem of shared infusion volume. Based on the processes discovered, an ITT will be refined, which will focus on improving the performance of IV infusion tasks. An experimental study using nurse participants from intensive care units will then be conducted. The number of errors in the high-fidelity simulated critical care environment will help assess the effectiveness of the newly developed ITT compared to a baseline condition of no training.

Conclusions It is expected that the use of an ITT can help reduce the error rate related to medication administration when dealing with multiple IV infusions. When designing an ITT for a complex task (e.g. shared infusion volume management), it is important to perform a suitable cognitive task analysis method to better understand the mental processes associated with the procedure. It is expected that a well-designed ITT that encompasses a proper knowledge framework can better train critical care nurses to effectively tackle complex medication administration tasks by making the invisible features of shared infusion volume visible. Improving patient safety by reducing the number of preventable human-related errors through ITTs may potentially reduce the number of preventable adverse events related to IV infusions.

SP124 - Medical Physics in Developing Countries

TRACK 17: EDUCATIONAL AND PROFESSIONAL ACTIVITIES

SP124.1 - Medical Physics Training Resources for Developing Countries

Author(s): [Muthana Al-Ghazi](#)

Radiation Oncology, University of California, Irvine, Orange/UNITED STATES OF AMERICA

Purpose: To outline resources available to developing countries for the training of medical physicists

Background: Cancer incidence in developing countries is rising with dearth of resources to combat it. In recent years, there has been a concerted effort on the part of national and international organizations (e.g. IAEA) to provide a framework and resources including complex radiotherapy technologies to address the problem. An important component of this effort is provision of trained personnel. Medical physicists play a leading role in the safe implementation of modern radiation treatment planning and delivery technologies and establishment of cancer care programs..

Methods: The advent of the World Wide Web, internet and social media make possible the use of these media to devise training resources aimed at developing educational and training programs for medical physicists in developing countries with little or no cost. The information is already available. What is required is guidance to colleagues in developing countries to harness these resources in a structured manner. The resources include, by way of example:

American Association of Physicists in Medicine (AAPM) resources such as task group reports, medical physics graduate and residency program structures, standards of practice, international educational portal and partner-in-physics (PIP) membership category

International atomic Energy Agency (IAEA) web-based resources

These do not require special access requirements and are globally available. There are many others based on UK, Canada, European medical physics organizations.

A key component is guidance by an experienced physicist based in a developed country who is specifically interested in education and development of the profession in developing countries to establish contact with a counterpart(s) in developing countries and work with them to tailor the available resources to their specific needs. This will generate interest in the country(ies) concerned and initiate awareness amongst authorities once the advantages of the effort are realized. This communication will develop and lead to the establishment of national medical organizations in developing countries which can then become IOMP members and access the full advantages of IOMP membership.

Results: Based on the author's experience, the approach described above led to the promotion and establishment of several national medical physics organizations in developing countries. All started from a single encounter.

Summary: Modern communication methods based on the availability of the internet can assist in promoting the field of medical physics and the training of medical physicists in developing countries who will contribute to the safe implementation of radiation treatment planning and delivery. This contributes positively to the global effort of combating cancer.

SP124.2 - Medical Physics in Indonesia: Current Status and Plans

Author(s): Djarwani Soeharso Soejoko, Supriyanto Ardjo Pawiro, Lukmanda Evan Lubis
Department Of Physics, Faculty Of Mathematics And Natural Sciences, University of Indonesia, Depok/INDONESIA

Since the nation-wide introduction of medical physics profession in 1980s, Indonesia continuously seeks a way to improve physics services in clinical environments in response to the rapidly-enhancing devices coming into use. It begun with efforts to primarily enhance educational aspect, to be followed by the work of making equipment and legal instruments available. Major hold-back is caused by inadequate number of master-degree holders in medical physics due to limited number of universities offering relevant degrees. Physics Department, Faculty of Mathematics and Natural Sciences, University of Indonesia has started to contribute on Medical Physics enhancement since 1998. Since then, nation-wide developments and changes has taken place involving our department, with more efforts to approach international standard still in place. This paper serves to share Indonesia's Medical Physics status and plans of enhancements.

SP124.3 - Surveying Trends in Radiation Oncology Medical Physics in the Asia Pacific Region

Author(s): Tomas Kron¹, Kwan Hong Ng²

¹Physical Sciences, Peter MacCallum Cancer Center, Melbourne/AUSTRALIA, ²Department Of Biomedical Imaging, University of Malaya, Kuala Lumpur/MALAYSIA

Aim

Medical Physicists are important contributors to patient care in radiation oncology. However, their work is often less visible than that of clinicians or allied health staff which could affect their status as members of the health care team. It is the objective of our study to assess and track the work load, working conditions and professional recognition of radiation oncology medical physicists (ROMPs) in the Asia Pacific Region over time.

Methods

Since 2008 we have been conducting surveys on profession and practice of ROMPs in the Asia Pacific Region. A structured questionnaire was mailed in 2008, 2011 and 2014 to approximately 20 senior medical physicists representing 23 countries. The questionnaire covers 7 themes: 1. Education and training, 2. Staffing, 3. Typical tasks, 4. Professional organisations, 5. Resources, 6. Research and teaching, and 7. Job satisfaction.

Results

Across all three surveys the response rate was >90% with the replies representing practice affecting more than half of the world's population. The expectation of ROMP qualifications has not changed much over the years and typically requires a master degree and between 1 and 3 years of clinical experience. This is in line with the policy documents of IOMP; however, formal professional certification is only available in a small number of countries. Compared to 2008, the number of medical physicists in many countries has doubled. However, the number of experienced ROMPs compared to the overall workforce is still small in particular in low and middle income countries. The increase in staff is matched by a similar increase in the number of treatment units over the years. Furthermore, the number of countries using complex techniques (IMRT, IGRT) or installing high end equipment (tomotherapy, robotic linear accelerators) is increasing.

A trend towards increasing quality assurance activities over treat-

ment planning can be observed and most ROMPs are required to work overtime, usually not fully remunerated. The number of ROMPs who find time for research is still small and typically only 10% or less of the workforce have academic appointments, even if more are required to teach other professions. Resource availability has only improved marginally; however, better opportunities exist now than 6 years ago as nearly all medical physicists have access to the internet. Overall, ROMPs still feel generally overworked and the professional recognition, while varying widely, appears to be improving slightly.

Conclusion

Radiation Oncology Medical Physics practice has not changed significantly over the last 6 years in the Asia Pacific Region. However, both the number of physicists and the number and complexity of treatment techniques and technologies have increased dramatically. It is important to increase our effort now to improve the quality of the workforce and its professional recognition.

Acknowledgement: We would like to acknowledge the support of our colleagues in the Asia Pacific Region.

SP124.4 - The Status of Medical Physics in Iraq

Author(s): Muthana Al-Ghazi

Radiation Oncology, University of California, Irvine, Orange/UNITED STATES OF AMERICA

Purpose: To provide an overview of the status of medical physics in Iraq

Background: Iraq is a Middle Eastern country with a population of approximately 30 million It has a history of excellent educational and healthcare systems in the Middle East. In the past three decades these suffered greatly due to wars, sanctions and civil strife. Despite these challenges, steps are being taken to advance the field of medical physics concurrent with developments in cancer care and attention that is being directed towards establishment of modern radiotherapy facilities where medical physicists play a critical role.

Medical Physics Practice: Most medical physicists are graduates of main stream academic physics programs and receive on the job training upon employment. There is one university that offers graduate medical physics studies at M.Sc./Ph.D. levels. Courses in radiation dosimetry, medical imaging, anatomy and physiology, radiobiology and radiation safety are included in the curriculum. This program has been re-structured recently to follow modern recommendations (e.g. AAPM report #197). This development is a result of improved communication between educators in Iraq and their counterparts in the West.

Professional Activities and Organization: The Iraqi Medical Physics Society (IMPS) was established in 2010. It has the usual structure (constitution and officers). It is a member organization of IOMP through the Middle East Federation of Organizations of Medical Physics (MEFOMP), the latter being the regional chapter of IOMP. IMPS has 40 members.

The majority of IMPS members are employed in cancer hospitals. There are three such hospitals in the capital and one each in 6 of the major provinces. The physicists' main responsibilities are in radiotherapy physics. Some collaborate with biomedical engineers in diagnostic imaging departments. There is a national radiation protection agency that monitors radiation safety in the country. The major cancer hospital in Baghdad has 70 oncology beds and serves as the Oncology teaching hospital for the University of Baghdad. This hospital takes advantage of the radiotherapy quality assurance program offered by the IAEA through the latter's TLD service for monitoring linear accelerators' output.

Discussion: There are 11 megavoltage units, 9 treatment planning systems, 9 CT-simulators and one Gammaknife, with another 10 linear accelerators planned, along with associated imaging and treatment planning systems. In the past 7 years, radiotherapy practice has advanced to include 3DCRT. One center has started using IMRT, with others expecting to follow. While these are encouraging developments, recent surveys indicate that only one third of the population has access to cancer care. This is because of shortage of centers within reach of majority of the population and travel challenges in a war zone.

Cancer incidence in the country is higher than that in developed countries and most patients present with advanced disease making their outcome poorer than their counterparts in the developed world.

Summary: Medical physics in Iraq is developing in the right direction by establishing a medical physics society, modernizing educational programs and acquiring new technologies to establish imaging and cancer treatment programs befitting modern clinical practices. Detailed numerical data will be presented.

SP124.5 - Evaluation and Adaptation of Medical Physics Practicum for Nicaraguan Students at a Canadian Cancer Centre

Author(s): Sarah Quirk¹, Jose E. Villarreal-Barajas², Coline Dirkse³, Alana Hudson¹

¹Medical Physics, Tom Baker Cancer Centre, Calgary/CANADA, ²Physics And Astronomy, University of Calgary, Calgary/AB/CANADA, ³Oncology, Tom Baker Cancer Centre, Calgary/AB/CANADA

On-the-job training is paramount to success in any career and must be particularly rigorous in medical professions. Unfortunately, practicum or residency-type clinical opportunities for medical physicists from low-income countries are in short supply, often requiring new graduates to transition to clinical work without the necessary knowledge, exposure, and experience. Inadequate training programs can lead to sub-optimal and even unsafe treatment conditions. This is especially true in cases where countries are preparing to transition to more modern radiation therapy technologies, and local knowledge from more senior medical physicists is limited. In order to help bridge this gap in practical training, our cancer centre in Canada hosted two medical physics students from Nicaragua in a three-month practicum towards the end of their studies. The practicum had students rotate through clinical and QA areas including simulation, treatment planning, treatment delivery, HDR brachytherapy, radiation safety, and nuclear medicine. The primary goal of this practicum was to provide fundamental medical physics knowledge and hands-on experience for treatment techniques currently used in Nicaragua (simulator, Cobalt RT, simple treatment planning and delivery). The other major goal was to provide exposure to linac-based treatments in preparation for the purchase of a new linac in the Nicaraguan clinic in the upcoming years.

Benchmarking [Brown et al., 2014, IAEA, 2007] has been previously highlighted as a top priority for implementing new technologies in low-income countries. A similar concept was applied to this practicum. Upon arrival, the students were asked to give presentations on their educational background, and their expectations for the practicum, and details about cancer treatment in Nicaragua. A short written survey was also implemented to assess these factors and their basic medical physics knowledge. These written and oral evaluations allowed us to evaluate both the level of education and previous training, and English language proficiency. The evaluations were crucial in personalizing the training to meet their specific needs. Benchmarking surveys/quizzes were given before each rotation. Based on the student responses, appropriate learning objectives were then set. Students were re-evaluated again after each rotation to determine if the learning objectives were met. Any shortcomings

were noted and added to the schedule. At the end of each rotation, the students were given feedback evaluations in order to address both individual concerns and interests that could be added to the final month of the schedule. Ideally, the practicum would get a final evaluation in one year once the students have spent time practicing medical physics in Nicaragua.

We are using this practicum hosting experience as a guide to determine 'what works best' and the feasibility of hosting more students in the future at our centre, and at other Canadian centres.

In addition to evaluating the practicum on a functional level, we also looked at it from a staffing and resource level by tracking the amount of dedicated time spent with the Nicaraguan students by medical physicists and clinical staff. In this way we can provide detailed information to other institutions interested in supporting this type of program.

SP124.6 - Coordination of AAPM Educational Courses for Developing Countries with Major International and Regional Organizations of Medical Physicists

Author(s): Eugene P. Lief

Radiation Oncology, White Plains Hospital, Pelham/NY/UNITED STATES OF AMERICA

American Association of Physicists in Medicine (AAPM) has had an active program of arranging two educational courses a year in developing countries since 1992. Typically, AAPM reimburses travel expenses for five AAPM members who volunteer their time for teaching practical topics in diagnostic and therapy medical physics for physicists from developing countries.

As a result of joint meetings of AAPM, IOMP, and EFOMP officials in 2013, these educational courses are now organized in close collaboration with International Organization for Medical Physics (IOMP), International Atomic Energy Agency (IAEA), and regional Medical Physics organizations, such as EFOMP, ALFIM, and others.

While choosing a place, time, and topic of such an education event, it is extremely important to avoid duplication of efforts by excluding regions that recently had a benefit of a similar educational course conducted by IAEA, IOMP, EFOMP, ESTRO, ALFIM, or some other international or regional organization.

A recent example was a course in Radiation Therapy organized in Estonia last year. The course was developed in the framework of AAPM International Scientific Exchange Programs Committee (ISEP) and IOMP on 16-20th of June 2014 in the capital of Estonia-Tallinn. The course was endorsed by EFOMP and IAEA. These agencies also provided financial assistance and sponsored some participants and speakers bringing the total number of lecturers to 10.

The meeting was attended by 62 clinical physicists and 10 company representatives. Third of participants were from the Baltic States (Estonia, Latvia, Lithuania), another third from the former Commonwealth of Independent States countries (Russia, Ukraine, Belarus, Azerbaijan, Kazakhstan), and the remaining third - from other Eastern European countries (Poland, Romania, Serbia, Montenegro, Croatia, Czech Republic, Slovenia, Bulgaria, etc.). Altogether, the participants represented 25 countries. By all measures, the course was a success and was highly evaluated by the attendees.

Conclusion: To be really efficient, future educational efforts in developing countries should be organized in close coordination and collaboration with the major international and regional organizations.

SP125 - Technology Enhanced Education

TRACK 17: EDUCATIONAL AND PROFESSIONAL ACTIVITIES

SP125.1 - e-Learning in Medical Physics – pioneering and future trends

Author(s): [Slavik Tabakov](#)

Medical Engineering And Physics, King's College London, London/ UNITED KINGDOM

Medical Physics was one of the first professions in the world to develop its own original e-learning materials. The projects EMERALD and EMIT (1994-2004) developed extensive e-Learning materials – training tasks, image databases (including 4000+ images), simulations, and one of the first e-learning web sites (www.emerald2.eu). Further, the project EMITEL (2005-2013) developed the first e-Encyclopaedia of Medical Physics (3100+ articles) with Multilingual Dictionary of terms (translated in 29 languages) – both major reference materials for the profession (www.emitel2.eu). These materials are used by thousands of colleagues all over the world. The success and impact of Medical Physics e-learning through these projects was recognised with the first educational award of the European Union – the Leonardo da Vinci Award.

The projects, initially including specialists from UK, Sweden, Italy, Portugal, Ireland, France, Czech Republic and Bulgaria, expanded rapidly through EFOMP and IOMP to include more than 320 senior colleagues from 36 countries. The unique experience of the profession led to further expansion through other e-Learning projects and web sites delivering quick educational and professional information to the whole medical physics community.

This development was extremely useful for a dynamic profession like medical physics, characterised by constant development of new methods/equipment and their implementation in medicine. Our experience and surveys showed strong involvement in e-learning development of all different sub-fields of the profession. At the same time we noticed an increased ratio of the time of development to the time of use of e-learning simulations, (mainly due to change of software versions). The web sites above ([emerald2](http://www.emerald2.eu) and [emitel2](http://www.emitel2.eu)) were specifically coded for the purpose, what assures their long uninterrupted life. Their platforms are now available to be used for additional e-learning materials and IOMP is now forming Task Groups to update and expand the existing ones.

In parallel with the above development, we are witnessing expansion of Virtual Learning Environment (VLE) platforms in all Universities – a cost-effective way to supply students with lecture notes and Power Point handouts, as well as handling assessments. These platforms (especially useful for distance education) could further deliver specific “tailor-made” e-learning content, what will increase the effectiveness of the learning process.

In our opinion medical physics, one of the first professions to pioneer e-learning, should concentrate on rapid development of specific e-learning materials, synchronised with the introduction of new methods and equipment. IOMP and its large Regional Organisations include highly experienced specialists, who have all capacity to do this. Such development will significantly increase the speed of delivery of new information to the users. The new IOMP Journal Medical Physics International could facilitate this dissemination. The development of e-learning and its current trends will be described in the presentation (available also in an e-book to be launched at the Congress).

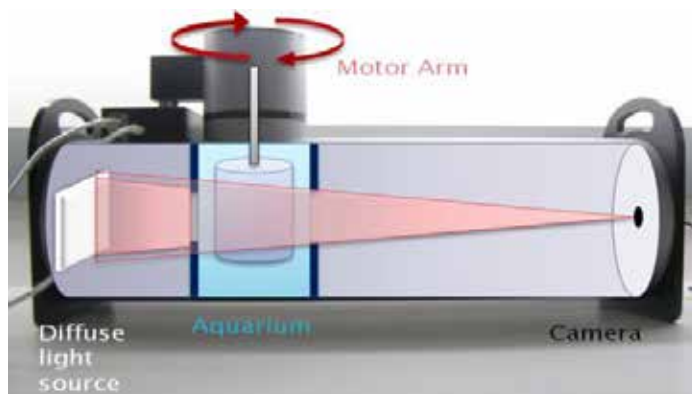
SP125.2 - A Desk-Top Optical Scanner for Teaching the Principles of Computed Tomography (CT)

Author(s): Jerry J. Battista¹, [Linada Kaci](#)², Kurtis H. Dekker¹, Arvand Barghi², Colin Versnick², Michael Peng², John Miller³, Jennifer Dietrich³, Kevin J. Jordan²

¹Department Of Medical Biophysics, Western University, London/CANADA, ²Physics And Engineering, London Regional Cancer Program, London/ON/CANADA, ³Modus Medical Devices, London, Ontario/ON/CANADA

Medical imaging is widely used for diagnostic and treatment guidance purposes. Students are often faced with difficulties in understanding the concepts of computed tomography (CT) image reconstruction because of the lack of practical demonstrations while learning these concepts. DeskCAT™ is an optical CT system (<http://www.deskcat.com/>) that has been introduced at 40 universities as a very effective tool for teaching the principles of CT. It is a safe device for classroom or lab demos since it uses visible light instead of x-rays, allowing interactive real-time teaching.

The system offers a dozen lab exercises that introduce different concepts such as: exploring 3D medical imaging by localizing fiducial markers, measuring linearity by scanning materials with known optical attenuation coefficients, assessing spatial resolution by plotting the contrast profiles of line pairs in a phantom, exploring Fourier methods to calculate the Modulation Transfer Function (MTF) and learning the importance of contrast-to-noise ratio in the context of low-dose imaging. More advanced labs also explore artifacts caused by incorrect, incomplete, or inconsistent projections and cone-beam scattering effects, emission CT (SPECT) with attenuation corrections, and Dual Energy CT to discriminate structures according to their absorption at different imaging energies. Artifacts occurring due to organ motion or beam hardening are also observed. Iterative reconstruction is tested as a means of dose and artifact reduction. This presentation will highlight the learning objectives of several of these labs and show sample images and plotted results obtained by DeskCAT™ students.



SP125.3 - Medical Physics e-Encyclopaedia and Multilingual Dictionary – Upgrade and New Developments

Author(s): [Slavik Tabakov](#)¹, Perry Sprawls², Franco Milano³, Sven-Erik Strand⁴, Cornelius Lewis⁵, Magdalena Stoeva⁶, Asen Cvetkov⁶, Vassilka Tabakova¹, John Damilakis⁷

¹Medical Engineering And Physics, King's College London, London/UNITED KINGDOM, ²IOMP, Atlanta/UNITED STATES OF AMERICA, ³Medical Physics, University of Florence, Florence/ITALY, ⁴Medical Physics, University of Lund, Lund/SWEDEN, ⁵Medical Eng And Physics, King's College Hospital, London/UNITED KINGDOM, ⁶Medical Imaging Dept., Medical University - Plovdiv, Plovdiv/BULGARIA, ⁷Department Of Medical Physics, University of Crete, Heraklion/GREECE

Since its launch at the World Congress in Munich (2009) the EMITEL on-line Encyclopaedia of Medical Physics and Multilingual Dictionary of terms established itself as a very useful reference source for the profession. About 5.3 million searches have been made for its 5 years of existence with approximately of 800 unique users per week. Two more languages were added during this period, thus making the Dictionary with 29 languages in total. The image below shows the number of unique EMITEL users per week for the last 5 years

EMITEL (www.emitel2.eu) includes about 3100 articles with over 2000 illustrations (with volume about 2100 pages). All these were developed by 7 teams working in parallel (Diagnostic Radiology; Magnetic Resonance; Nuclear Medicine; Radiation Protection; Radiotherapy; Ultrasound; General terms). The overall number of colleagues working on the Encyclopaedia included more than 120 senior specialists, while the 29 groups of translators included another 200+ colleagues). During 2013 it was published on paper by CRC Press. On the next year the EMITEL was prepared to go under IOMP – the largest international medical physics organisation, who will care for its future updates.

A Group was formed under the IOMP Education and Training Committee to deal with the first upgrade including Gerard Boyle, Paola Bregant, Asen Cvetkov, John Damilakis, Mario De Denaro, Charles Deehan, Antonio De Stefano, Peter Dunscombe, Geoffrey Ibbott, Lefteris Livieratos, Renata Longo, Renato Padovani, Magdalena Stoeva, Vassilka Tabakova, Sameer Tipins, Slavik Tabakov.

The first task of the group will be to expand the Thesaurus with new terms (methods, equipment, etc). After this, in parallel with the development of the encyclopaedic entries, the Dictionary will be updated. In fact the Dictionary updates were already initiated. The upgrading process uses the existing EMITEL guides, thus providing all new additions similar to the existing materials. Before upload all new materials will be reviewed by members of the EMITEL Editorial Team (S.Tabakov, P.Sprawls, M.Lewis, A.Simmons, S.Keevil, F.Stahlberg, S-E.Strand, B-A.Jonson, M.Peterson, C.Lewis, P.Smith, J.Thurston, F.Milano, I-L.Lamm, C.Deehan, J.Chick, D.Goss, T.Janson, G.Taylor, W.Hendee). The Upgrade Group will continue to expand aiming to have the first updates ready by the WC2015.



SP125.4 - Physics for Medical Students: Technology Enhanced Teaching from the Dipole to the Vectorcardiogram**Author(s):** Robert Arnold, Ernst Hofer

Institute Of Biophysics, Medical University Graz, Graz/AUSTRIA

Teaching Biophysics of the electrocardiogram (ECG) to first-year medical students is challenging. In research, the origin of cardiac field potentials has been explored in detail with computer simulation programs. Such programs allow ECGs to be computed at any given site of the body with almost arbitrary resolution and complexity. However, in the first year, medical students cannot take advantage of such detailed knowledge as they lack the necessary background in physics, physiology and cardiology. Therefore, the goal of our first semester course is to establish the relevant fundamental laws of physics, apply them in simple qualitative and semi-quantitative models, and explain the origin of the ECG and vectorcardiogram (VCG).

Our course follows a sequence of teaching steps and themes, leading from the electrical dipole to the VCG. Starting with Coulomb's law, we consider the electric field and potential caused by electric dipoles. We then demonstrate the projection of a dipole vector on to given axes and its reconstruction by back-projection. We introduce the principle of superposition, and use it to explain how a depolarization wavefront generates a dipole-like field, which is represented as the instantaneous heart vector. Students are shown how the spread of excitation can be represented as a sequence of heart vectors describing a vector loop. The relationship of ECG and VCG is demonstrated by an animation of projection and back-projection of the vector loop on standard limb leads I, II and III. Finally, students record their own ECG and VCG and perform exercises demonstrating the role of signal filtering, noise detection and measurement of ECG intervals.

Students are provided with a set of template slides, which are completed during the lecture by the teacher using an interactive pen display in overlay mode. Students can finish their notes on their own tablet or on printed handouts. Animations and interactive simulation tools (Java, Physlets, Flash), both developed in-house and acquired from free and commercial sources, are embedded in the course material. These interactive resources provide the simplest possible models of the physical effects relevant to understanding the VCG.

For practical experiments we developed a 2D-conductor apparatus with a rotatable dipole, whose angle is set by the teacher but remains hidden to the students. Field potential measurements are performed around the hidden dipole using polar, Cartesian and cardiac lead axes. This allows the students to identify the angle of the hidden dipole vector and to verify the law of projection.

Commercially available ECG recorders are closed systems. We therefore developed hardware and software for an open system ECG-VCG recorder, where two arbitrary lead signals can be recorded simultaneously using a standard laptop computer. Students can introduce power-interference noise, experiment with different lead systems, analyze the power spectrum of the ECG, test the impact of various digital filters on noise and on the waveform, and display the vector loop of the subject. With these diverse teaching technologies and methods, we constructed a robust framework for teaching the origin of VCG from simple physical laws.

SP125.5 - matRad: a multimodality open source treatment planning toolkit**Author(s):** Eduardo A. Cisternas¹, Andrea Mariani², Peter Ziegenhein³, Oliver Jäkel⁴, Mark Bangert¹

¹Department Of Medical Physics In Radiation Oncology, German Cancer Research Center, Heidelberg/GERMANY, ²Centro Nazionale di Adroterapia Oncologica, Pavia/ITALY, ³Joint Department Of Physics At The Institute Of Cancer Research And The Royal Marsden Nhs Foundation Trust, London, Uk, The Institute of Cancer Research, London/UNITED KINGDOM, ⁴Heidelberg Ion-Beam Therapy Center (HIT), Heidelberg/GERMANY

We present matRad, an open source software for three-dimensional radiation treatment planning supporting intensity-modulated photon, proton, and carbon ion therapy. matRad is entirely written in MATLAB; it is developed for educational and research purposes. The code features high modularity and consequently flexibility. At the same time, matRad allows for an efficient workflow considering realistic patient cases. It comprises descriptive visualizations of the underlying physical aspects. Besides the source code itself, matRad also includes example patient data and appropriate base data for photon, proton, and carbon ion irradiation.

Starting from a segmented patient CT, the toolkit features a set of individual functions modeling the entire treatment planning workflow based on well-established algorithms. The main modules are:

Dose calculation: For photons, matRad uses a singular value decomposed pencil beam algorithm. For particles, matRad uses a pencil beam algorithm facilitating a single Gaussian to approximate the lateral dose profile. Base data for the dose calculation algorithms is obtained during measurements at the German Cancer Research Center (photons), analytical computation (protons), and Monte Carlo simulations (carbon ions).

Ray tracing: All modalities facilitate an exact three-dimensional ray tracing algorithm for the computation of radiological distances.

Fluence optimization: Fluence optimization is performed with pre-computed dose influence data through the minimization of a piece-wise quadratic objective function.

Sequencing: For photon IMRT, matRad includes a multileaf collimator sequencing algorithm to translate the continuously optimized fluence weights into deliverable segments.

Visualization: The result of matRad's treatment planning workflow can be visualized via dose volume histograms and two-dimensional dose distributions.

Using a voxel resolution of $3 \times 3 \times 2.5 \text{ mm}^3$ and a bixel resolution (spot distance) of $5 \times 5 \text{ mm}^2$, we achieve computation times of 60-100s (60-400s) for realistic patient cases including photon (particle) dose calculation and fluence optimization. Memory consumption ranges between 0.2GB and 2.2GB. Figure 1 shows an example photon dose distribution from our benchmarking experiments using AAPM's TG119 phantom.

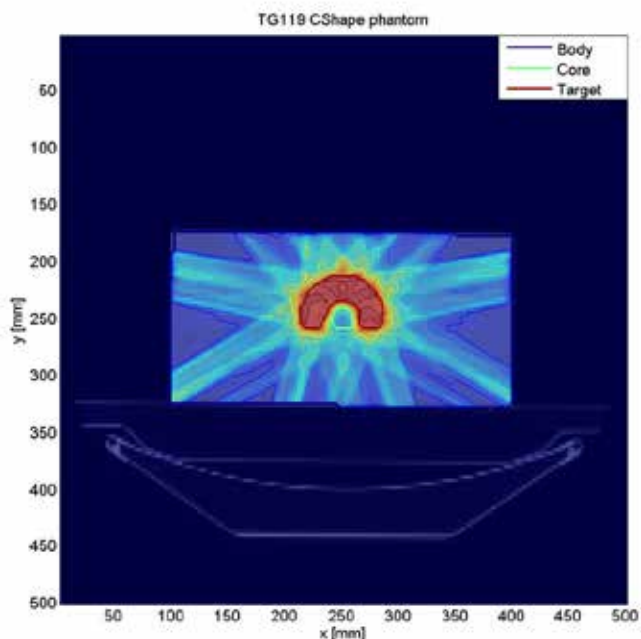


Figure 1: Transversal dose distribution of a photon treatment plan applying nine equi-distant coplanar fields on AAPM's TG119 phantom.

matRad is the first open source toolkit supporting treatment planning for intensity-modulated photon, proton, and carbon ion therapy. Both the computational and dosimetric results encourage a future use of matRad in an educational and scientific setting. A first beta release of matRad is available at <http://e0404.github.io/matRad/>

This work has been supported by the DFG coordinated research program SFB/Transregio 125 Cognition-Guided Surgery.

SP125.6 - Creation of a model for online education of clinical engineering and management of medical technologies to reach professionals worldwide.

Author(s): Maria E. Moreno Carbajal¹, Marco A. De Roman Mello²
¹Education, CLINICAL AND BIOMEDICAL ENGINEERING INSTITUTE, PUEBLA/MEXICO, ²Biomedical Engineering Department, MEXICAN GENERAL HOSPITAL, MEXICO CITY/MEXICO

The Institute of Clinical and Biomedical Engineering, SC (ICYB), was created at the end of 2012, to meet the needs of training and updating professionals involved with the performance of : assessment, installation, maintenance, and replacement of medical devices; processes better known as clinical engineering and management of health technologies.

Due to the need of Mexico and Latin American countries to train professionals in order to perform management in benefit of better decision making regarding health technologies, a survey was developed and launched to identify the real need as well as an effective online education model. The survey conducted to the development of an e-learning model that permits the interaction of both experts and professional students from different regions of the world. After almost 3 years of the beginning of the institute, most of our expert teachers are heads of departments in hospitals at Mexico, Canada and Colombia.

Up to date, we have trained 126 chief engineers of biomedical engineering departments. The method of education we use has reported good results and can be taken as a model for developing similar projects in other developing countries.

SP125.7 - Develop of a Mixed, Haptic and Virtual System to Simulate Radiographic Images

Author(s): Guillermo E. Avendaño¹, P Pizarro²
¹Escuela De Ingeniería Biomédica, Universidad de Valparaíso, Valparaíso/CHILE, ²BIORAD LIMITED, Valparaíso/CHILE

It has been conceived, designed and built a system, simulator of conventional equipment x-ray made to work on technique called *two-points* ie selecting values of kVp and mAs, with the aim of teaching professionals who must make radiographic pictures of patient, such as Medical Technologist, Biomedical Engineers and others to obtain correct images without the need for an actual equipment emitting X-ray, the system consists of similar technical devices to real in terms Hardware and software, suitable for generating images of different quality depending on the parameters selected and the student learns without generating radiation or spend consumables, advantages that allow manufacture and market a highly innovative system, safe and friendly with environmental.



Fig. 1 Console Fig. 2 125 KV / 30 mAS Fig. 3 90 KV / 20 mAS

SP126 - Computational Biology & Hemodynamics

TRACK 19: BIOPHYSICS AND MODELLING

SP126.1 - Evaluation of Decomposition Analysis on Multi-Models for Digital Volume Pulse Signal

Author(s): Sheng-Cheng Huang¹, Hao-Yu Jan¹, Wen-Chen Lin¹, Cheng-Lun Tsai², Kang-Ping Lin¹
¹Department Of Electrical Engineering, Chung-Yuan University, Taoyuan/TAIWAN, ²Department Of Biomedical Engineering, Chung-Yuan University, Taoyuan/TAIWAN

Photoplethysmography (PPG) is an important technique to evaluate and monitor vascular health. Pulse Decomposition Analysis is (PDA) a method widely used to analyze DVP waveform in physiology and hemodynamics. There are several different models used to decompose DVP wave, but there is no common model. This research intends to investigate and evaluate some efficient models for decomposition analysis of digital volume pulse wave signal. The multi-Gaussian models and Gamma-Gaussian complex models are used in this study. Each model is evaluated by residual analysis. In this paper, four multi-Gaussians models and four Gamma-Gaussian Complex models have comparatively good results.

SP126.2 - Discordant alternans in a one-dimensional cable of ischemic heart tissue.

Author(s): Yunuen A. Cervantes Espinosa, Jorge H. Arce Rincón
 Science Faculty, Physics Department, National Autonomous University of Mexico, Mexico city/MEXICO

T-wave alternans are related to discordant alternans in the cellular action potential. T-wave alternans have been associated with block in the propagation, induction of reentry and to ventricular arrhythmias.

The hypothesis of this study is that discordant alternans could be initiated during ischemia in a simulated one-dimensional cable of ischemic heart tissue stimulated at fixed frequency.

The ventricular tissue of the cable was simulated with the Luo Rudy 1 [Circ.Res. 68, 1501-1526 (1991)] ionic model, the effect of ischemia was model by raising the external potassium ion concentration $[K^+]_o$ in the whole strand. $[K^+]_o$ increases from 5 up to 12 mM. To search for the discordant alternans, the stimulation frequency in the cable varied. Meaning that for every $[K^+]_o$, there is a fixed stimulation frequency. Several cable lengths were studied from 10 to 4 cm.

We found that discordant alternans appear at high pacing frequencies during ischemia. In fact, there is a range of $[K^+]_o$ in which discordant alternans are initiated, depending on the cable length. The larger the cable length, the window to initiate the discordant alternans is wider. These cases are presented in a bifurcation diagram.

The discordant alternans formed in the cable of ischemic heart tissue present one or multiply nodes, and in some cases block in the conduction was observed.

SP126.3 - A Novel Biomechanical Model of the Left Ventricle for Cardiac Contraction Force Reconstruction Applications

Author(s): Seyyed Mohammad Hassan Haddad¹, Maria Drangova², James A. White³, Abbas Samani⁴
¹Graduate Program In Biomedical Engineering, Western University, London/ON/CANADA, ²Imaging Research Laboratories, Robarts Research Institute (RRI), London/ON/CANADA, ³Libin Cardiovascular Institute Of Alberta, University of Calgary, Calgary/AB/CANADA, ⁴Medical Biophysics, Western University, London/ON/CANADA

Accurate regional viability assessment of the myocardium is critical for assessing reversibility of ischemic injuries. While viability assessment of cardiac tissue can be achieved through a number of imaging techniques, none of them provide information pertaining directly to the tissue mechanical efficiency. A major constraint with some imaging modalities is that their data cannot be interpreted easily, leading to diagnosis uncertainty. As such, we are developing a technique for imaging myocardial contraction forces. This technique involves a reconstruction method which inputs the myocardial displacement data acquired using imaging techniques and outputs the myofibers contraction forces through an optimization procedure. This forward model must be run iteratively within the optimization algorithm to determine the contraction forces. Hence, a computationally cost-effective cardiac mechanics model is required which was developed in our laboratory.

In typical myocardial mechanical models, hyperelasticity, anisotropy, and active response of the cardiac tissue leads to intricate nonlinear Finite Element (FE) formulations which are not fully incorporated in commercial FE solvers. As such, custom-developed FE solvers are required which are cumbersome to develop, and may have sub-optimal performance and convergence issues. Moreover, these models cannot be easily adapted for simulating diverse cardiac pathological conditions as appropriately altered passive and active tissue responses are necessary for modeling the pathological tissue portion. To tackle these issues, we propose a new left ventricle (LV) mechanical model which considers all cardiac mechanics aspects, including cardiac anisotropy, hyperelasticity, and active fiber's contraction forces. The novelty of the model lies in modelling of the myofibers and their contraction forces. This model treats the myocardial tissue as a composite material including a background tissue through which microscopic reinforcement bars are distributed. These bars simulate the fibers within the myocardial tissue whereas their orientations are in accordance with the fibrous cardiac anatomy, leading to a self-contained anisotropic model. As a result of applying contraction forces to the bars while blood pressure is applied to the LV endocardial surface, LV contraction occurs. This model can be developed using many off-the-shelf commercial FE solvers and it does not require custom-developed solver. Hence, the proposed model is optimized to be less time-consuming and less prone to divergence. Our model was applied to normal and infarcted LV and demonstrated. Figure 1 shows stress distribution through the infarcted LV which indicates higher stresses at the infarcted region similar to what is reported in the literature frequently.

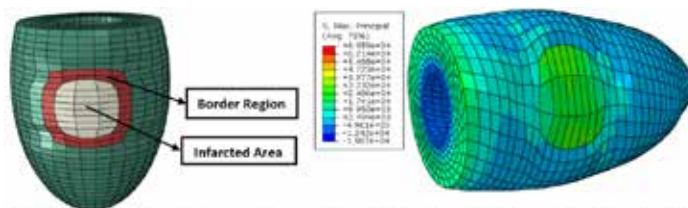


Figure 1a. Infarcted *in silico* LV model constructed using finite elements.

Figure 1b. Maximum principle stress field of the infarcted LV model at the instance when the bars' active stresses reach their maximum value.

SP126.4 - A simulative model approach of cardiopulmonary interaction**Author(s):** Chuong Ngo¹, Berno Misgeld², Steffen Leonhardt², Robert Schlözer², Thomas Vollmer³, Stefan Winter³¹Rwth Aachen University, Chair of Medical Information Technology, Aachen/GERMANY, ²Chair Of Medical Information Technology, RWTH Aachen University, Aachen/GERMANY, ³Philips Research, Aachen/GERMANY

We introduce a new sophisticated model of the cardiopulmonary system. The model consists of the heart, circulation and respiration systems with emphasis on the cardiopulmonary interaction. Heart and lungs are anatomically and physically coupled through the intra-thoracic pressure since they are both located in the same chest cavity. A novel extended lung model with emphasis on the pleural dynamics was developed. Interactions with the cardiovascular system were modeled using the pleural pressure. This model was implemented in MATLAB Simscape using electrical equivalent circuits. Simulation results for spontaneous breathing show a high agreement with physiological knowledge. Hence, the model could be used to explain many observed phenomena in the physiology.

SP126.5 - The Development of SIM to Characterize Blood Volumetric Flow Rate and Hemodynamics in Human Coronary Arteries**Author(s):** Iyad Fayssal, Fadl Moukalled

American University of Beirut, Beirut/LEBANON

The genesis and progression of heart diseases are primarily originated from hemodynamic disorders. Among the important hemodynamic parameters to estimate is the blood volume flow rate in coronary arteries. Knowing how the volumetric flow rate is related to geometric and physiologic parameters is challenging. The end product of this paper is a Seven Input Model (SIM) developed to characterize blood volume flow rate in human coronary arteries which can be translated into clinical applications. Several mathematical relations were established relating all primary hemodynamic (pressure and velocity), geometric, and boundary parameters to the volume flow rate. An equation for predicting blood volumetric flow rate was first developed for arterial segments of uniform cross section by solving the set of continuity and momentum equations in cylindrical coordinates. The governing equations were coupled with a total pressure formulation at the inlet and a dynamic pressure-flow lumped model at the outlet to capture in-vivo coronary hemodynamics. The model was then generalized for an artery of variable cross section area and for arteries with low to medium stenosis severities. Two different algorithms were also developed to solve the set of developed equations; (1) a numerical algorithm following Gauss-Seidel method with successive iterative forward and backward substitution; and (2) an alternative analytical approach where an equation of blood volume flow rate was obtained and related to all model parameters, including geometry, inlet and outlet boundary parameters, blood density and viscosity, and normal shear stress at inlet. In the analytical approach, the blood flow rate is directly computed from a single developed model (SIM); local pressure and velocity distributions are then directly obtained. The performance of the developed models and algorithms were tested on (i) an artery with uniform cross section; (ii) an artery of variable cross section; and (iii) an artery with low severity symmetrical stenosis. Predictions were then compared with a full CFD 3D model for validation purposes. An excellent agreement was achieved.

SP126.6 - Determination of Bergman's Minimal Model parameters for diabetic mice treated with *Ibervillea sonorae***Author(s):** Agustin I. Cabrera Llanos, María G. Ramírez-Sotelo, Emmanuel Sánchez-Velarde, Nayely R. Budar-Alemán, Alejandro A. Sotelo-De Ávila, Itzamná O. Rico-Asención, Rodrigo Sánchez-González

Bioprocesos, Unidad Profesional Interdisciplinaria de Biotecnología - IPN, Distrito Federal/MEXICO

This article shows the estimation of Bergman's Minimal Model parameters for glucose-insulin interaction in three stages: evolution of the concentration of insulin, evolution of glucose and glucose/insulin interaction itself. First, the dynamics of glucose measured in healthy mice treated with extracts of *Ibervillea sonorae* root in a range of 100-400 mg/kg; likewise, for mice previously induced with diabetes mellitus type 2 values are determined. The different parameter values obtained are compared showing how they influence the dynamics of Bergman's Model. The values of the glucose/insulin interaction were obtained *in vivo* by blood samples of the mice every hour. The evolution and variability of the estimate are shown in graphical form; also the estimation error is quantified by performance curves, which were associated to the energy that is implied in the difference between the values of the parameters obtained and the data obtained in the kinematics of the mice. The results indicate the estimated level reached, where the upper value of the performance curve was 3.0128, while the lower was 0.1978, with standard error values between 1.55% and 10.47%

SP126.7 - Investigation of flow and turbulence in carotid artery models of varying compliance using particle image velocimetry**Author(s):** Amanda Dicarlo

Physics And Astronomy, University of Western Ontario, London/CANADA

Atherosclerosis in the carotid artery is one of the main risk factors for stroke. Arterial compliance, a measure of the elasticity of blood vessels, is a common indicator of vascular disease and is known to decrease in association with other stroke risk factors, including age, diabetes, and hypertension. Decreased local compliance leads to changes in the flow and pressure waveforms and corresponding changes in the velocity field. Resulting hemodynamic parameters, such as shear stress and turbulence, play a primary role in the process of plaque and clot formation. While it is difficult to accurately extract complex in vivo blood flow structures using clinical techniques, in vitro experimental models can be used to mimic physiological flow systems. Particle image velocimetry (PIV) is an established optical technique for measuring velocity fields with high temporal and spatial resolution that can be applied to study specific aspects of the flow system when used in controlled test models. The aim of this work was to analyze the effect of compliance on carotid artery flow patterns and turbulence intensity experimentally within carotid artery phantoms using PIV. This was accomplished using a custom in vitro flow facility. Two types of polydimethylsiloxane (PDMS) phantoms were used to study compliance, a thin-walled vessel or rigid block phantom model, with identical vessel geometry, 50% eccentric stenosis of the internal carotid artery. Phantoms were perfused using a computer controlled pump to generate a physiologically realistic pulsatile flow rate waveform. A custom blood-mimicking fluid with matching refractive index serves to minimize distortion and model the dynamic viscosity and density of human blood. Downstream flow resistors create a physiological 60:30 flow division at the bifurcation. PIV data were collected using a commercial stereoscopic PIV system (LaVision Inc). Turbulence intensity (TI) was calculated from central plane velocity maps as a metric for quantifying flow disturbances. Slightly higher overall velocity magnitude was observed in a more rigid phantom model compared to the geometrically-matched compliant version, with maximum jet internal carotid artery velocities reaching 1.98 m/s compared with 1.90 m/s.

A stiffer vessel wall resulted in increased maximum average turbulence intensities, 0.41 ± 0.02 m/s in compliant models and 0.48 ± 0.03 m/s in rigid phantom models. The rigid vessel region of maximum turbulence also occurred more proximal to the bifurcation apex (i.e. more upstream). Mean TI over a downstream region of interest at the location of maximum TI was seen to drop off slower with cardiac cycle phase in rigid models suggesting a higher cumulative exposure to disturbed flow over time due to reduced compliance.

SP127 - Informatics In Health Care And Public Health / Biosensor, Nanotechnology, Biomems And Biophotonics

PRESIDENTS CALL

SP127.1 - A study on the leading cause of immunisation schedule fall up defaulting and early child hood malnutrition sicknesses in developing countries (uganda in particular) rural areas/villages

Author(s): [Waigonda Saad](#)

Physiology, MAKERERE UNIVERSITY, kampala/UGANDA

Uganda is one of the countries that make up east Africa. It's one of the developing countries in the world, one of the countries on this globe that has been affected by immunizable diseases and child hood malnutrition every year. A study to assess the causes of the rampant immunization schedule fall up defaulting by mothers and early child hood malnutrition in developing countries rural areas was conducted in ten districts of Uganda, (Kampala, Jinja, Wakiso, Kaliro, Iganga, Mayuge, Bugiri, Namutumba, Namayingo, and Kamuli districts) for a period of 12 months. The target population were all babies aged one year who had completed polio, DPT1, DPT2, DPT3 AND Measles vaccinations by one year. A total of 1000 babies were collectively seen. While immunization services were easily available at every health centre from health centre's one to hospital settings and free of charge, a total of 902 (90.2%) babies had not completed their immunization as scheduled and a total of 780 (78%) babies had been affected by malnutrition. A total of 805 (80.5%) mothers had lost their babies immunization cards by one year and so couldn't recall when their babies were to be taken back for fall up vaccinations. 15% of the mothers couldn't find any reason for immunizing their babies since they looked healthy from day one. I proposed to design a phone application which will keep tracking all registered babies milestones and keep reminding mothers on the next immunization dates of their babies through sending short messages on to their phones two days before as well keep sending mothers nutrition information of their babies per milestone reached.

SP127.2 - From Smart Phones to Smart Health

Author(s): [Melannie Pin](#)¹, [J Huang](#)¹, [Diego Zelaya](#)¹, [Julio Cruz](#)¹, [Ronald Alvarado](#)¹, [Ricardo Silva](#)²

¹Ciencias Médicas, Universidad de Guayaquil, Guayaquil/Ecuador, ²Senescyt, Guayaquil/Ecuador

All progress in Telemedicine we have opened new destinations so far only dreamed, allowing use Smartphones as valuable tools for continuous monitoring, recordkeeping, medical alerts, prevention and prediction of various diseases related to our master pump, the human heart. And these devices can do all this without our assistance and in parallel with our recreational, household and daily work. Therefore smart phones are paving the road for smart health. We present the possibilities of smart phone based smart health for cardiovascular patients and our particular approach to this field.

SP127.3 - Diagnostic Data: a Manifesto

Author(s): [Peter Pennefather](#)¹, [West Suhanic](#)²

¹Leslie Dan Faculty Of Pharmacy, University of Toronto, Toronto/CANADA, ²gDial Inc, Toronto/ON/CANADA

Diagnostic data is the fuel that drives medical information systems by enabling independent input variables to be related to dependent

outcome variables within models of care in ways that can guide medical decision making. By definition, diagnostic data-sets are assembled with specific purposes in mind. The ISO definition of quality is: "the degree to which a set of inherent characteristics fulfills requirements". Therefore the quality of that data, and of that data's ability to fulfill requirements, is dependent of the quality of the documentation concerning data generation. We propose as self-evident therefore that for diagnostic value-sets entered into medical information systems to become diagnostic data-sets, then those value-sets must include not only the measured values but also other values that are needed to verify data-quality. The process generating all of those values must be the product of a well documented, replicable and qualified process and must be accompanied by documentation and values that can assist independent evaluators to understand precisely how those value-sets were produced. Our manifesto is that it is the co-location of all values needed to evaluate data quality in addition to those needed to specify value relationships that transforms value-sets into data-sets. This implies that the documentation informing evaluators of why the value-set is a data-set is also in the same data-envelope as the name/value pairs proscribed by that documentation. A complete diagnostic record therefore is one where all steps that led to the generation of the data-set are described and registered in sufficient detail so that those trained in the art can: i) judge the likelihood that each step in the process is within known boundaries of reasonableness, relevance, and reliability, ii) plan how to replicate the process and attempt to acquire similar values and iii) assess the validity of the values. For diagnostic values-sets to be considered diagnostic data-sets, a capacity to support those three steps is both necessary and sufficient. This leads to simplifications of the data-quality management process and flexibility in interpreting the data. For example data-sets entered into medical information systems can support data-analysis, an inferential process aimed at estimating newly derived values from previously recorded data. As with the original data, such data transformations need to be sufficiently documented so as to allow those transformations to be replicated. By meeting that condition the derived value-set can be considered a part of the original diagnostic data-set. Indeed there is no need to distinguish between primary or secondary data or even data and metadata as their meaning should be clear. There is only data. For information systems used to guarantee the quality of medical decision making, there should only be classes of data and not-data. We will describe a diagnostic data-recording method that allow this diagnostic-data manifesto to be respected (see <http://www.google.com/patents/US20140122491>).

SP127.4 - Comparative analysis of co-expression networks reveals molecular changes during the cancer progression

Author(s): Pegah Khosravi¹, Vahid H. Gazestani², Brian Law³, Gary D. Bader⁴, Mehdi Sadeghi⁵

¹School Of Biological Sciences, Institute for research in fundamental sciences, Tehran/IRAN, ²Institute of Parasitology, McGill University, Montreal/QC/CANADA, ³Department Of Computer Science, The Donnelly Centre, University of Toronto, toronto/CANADA, ⁴The Donnelly Centre, University of Toronto, toronto/CANADA, ⁵National Institute of Genetic Engineering and Biotechnology, Tehran/IRAN

Prostate cancer is a serious genetic disease known to be one of the most widespread cancers in men, yet the molecular changes that drive its progression are not fully understood. The availability of high-throughput gene expression data has led to the development of various computational methods for the identification of key processes involved.

In this paper, we show that constructing stage-specific co-expression networks provides a powerful alternative strategy for understanding molecular changes that occur during prostate cancer. In our approach, we constructed independent networks from each cancerous stage using a derivative of current state-of-art reverse

engineering approaches. We next highlighted crucial pathways and Gene Ontology (GO) involved in the prostate cancer. We showed that such perturbations in these networks, and the regulatory factors through which they operate, can be efficiently detected by analyzing each network individually and also in comparison with each other.

Using this novel approach, our results led to the detection of 49 critical pathways and GOs related to prostate cancer, many of which were previously shown to be involved in this cancer.

Correct inference of the processes and master regulators that mediate molecular changes during cancer progression is one of the major challenges in cancer genomics. In this paper, we used a network-based approach to this problem. Application of our approach to prostate cancer data has led to the re-establishment of previous knowledge about this cancer, as well as prediction of many other relevant processes and regulators.

SP127.5 - Copper Meshed Carbon Black PDMS Electrode for Underwater ECG Monitoring

Author(s): Justin Bales

Biomedical Engineering, University of Connecticut, Storrs, CT/ UNITED STATES OF AMERICA

The traditional method to obtain an electrocardiogram (ECG) in an underwater environment requires the industry standard silver/silver chloride (Ag/AgCl) electrodes to be completely insulated and adhered to the skin with a form of chemical water proof adhesive. However, this can lead, to severe skin irritation with prolonged use and damage to the surrounding area of skin when the covering is removed. To alleviate these discomforts, we developed hydrophobic copper-meshed carbon black/poly-dimethyl siloxane (CB/PDMS) dry bio-potential electrodes that are non-irritating, re-usable, in addition these electrodes do not require wetting, or hydrogel, making them compatible for long term application in more extreme environments. To evaluate the performance of the novel electrodes, we tested them alongside the other various commercially available electrodes (Polar[®] textile, silver coated textile, and carbon rubber electrodes) as well as our previous CB/PDMS design without the embedded copper meshed wire under a submerged use-case scenario.

We found that only the meshed CB/PDMS electrodes provided high-fidelity ECG signal morphologies without any amplitude degradation when collecting ECG data in a freshwater scenario. In fact, based on preliminary data from 5 subjects, the meshed CB/PDMS electrodes provided ECG signal amplification during. The textile electrodes did not fare well as there was significant ECG signal amplitude reduction. Both carbon rubber and non-meshed CB/PDMS electrodes performance in immersed conditions fared better than textile-based electrodes, however, they too had significant ECG signal amplitude reduction.

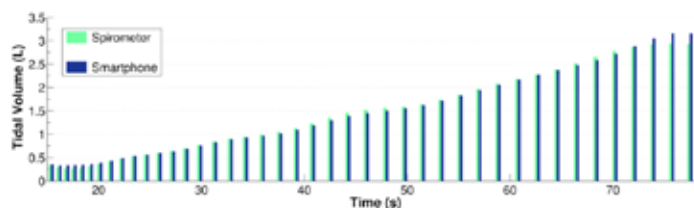
ECG signal amplitude reduction in water immersion holds a particular significance due to the fact that with body movements, the ECG waveform's morphologies may not be easily discernible due to motion artifacts. By being able to record an corrupted signal the newly developed meshed CB/PDMS electrodes have the potential to be used for a wide variety of application in a various environments where collecting the fine features of a bio-impedance measurement such as an ECG is critical.

SP127.6 - Smartphone-based Monitoring of Tidal Volume and Respiratory Rate

Author(s): Bersain Reyes¹, Natasa Reljin¹, Youngsun Kong², Yuny-oung Nam², Ki Chon¹

¹Biomedical Engineering, University of Connecticut, Storrs/CT/ UNITED STATES OF AMERICA, ²Department Of Computer Science And Engineering, Soonchunhyang University, Asan/KOREA

A breathing monitor should provide information about the frequency of breathing (respiratory rate, RR) and about the depth of breathing (tidal volume, VT). Clinical devices exist for such tasks, e.g. spirometry or inductance plethysmography, but the need for a portable, accessible to the general population, and low-cost monitoring device still remains. This study employs an optical approach coupled with an algorithm implemented directly on a smartphone for non-contact estimation of both RR and VT. The algorithm tracks chest wall displacements via the smartphone's frontal camera and provides a chest movement signal from which the two aforementioned breathing status parameters are estimated. Spirometer-based volume signal was regarded as reference and was simultaneously recorded while the volunteers ($N=8$) were breathing at VT ranging from 0.3 to 3 L. The Empirical Mode Decomposition was used to detrend the spirometer and smartphone signals. Regarding the RR estimation, a time-frequency analysis based on the smoothed pseudo Wigner-Ville distribution was employed. The smartphone-based RR estimates showed a strong linear relationship with the corresponding reference values from spirometry ($r^2=0.999 \pm 3.85 \times 10^{-5}$, mean \pm SD) with a root-mean-square error (RMSE) of 0.338 ± 0.043 bpm. Bland-Altman analysis showed a statistically significant bias of -0.014 bpm, and 95% limits of agreement of -0.675 to 0.647 bpm. Regarding the VT estimation, the relationship between the peak-to-peak amplitude of the smartphone-acquired chest movement signal and the VT from spirometry was analyzed and a strong linear relationship between both quantities was found ($r^2=0.974 \pm 0.016$). Therefore, a calibration was performed on a subject-by-subject basis with half of the data randomly selected to obtain the model parameters via least squares linear regression, while the remaining half of the data was used to test the computed model. No statistically significant bias was found (bias= 0.006 , $p=0.46$), the RMSE was 0.219 ± 0.137 L, and the 95% limits of agreement were -0.253 to 0.265 L on the test data set. An example of the VT estimates is shown in Figure 1. Given these results, we foresee the possibility of developing a portable and inexpensive monitor which provides information about both frequency and depth of breathing, when calibrated on an individual basis, and that could be available outside the research and clinical settings due to the increasing ubiquity of smartphones.

**SP128 - Multimodality Imaging****TRACK 01: IMAGING****SP128.1 - Localizing cortical motor representation:****A comparative study between navigated transcranial magnetic stimulation, BOLD contrast and arterial spin labeling fMRI**

Author(s): Elisa Kallioniemi¹, Minna Pitkänen², Mervi Könönen³, Ritva Vanninen³, Petro Julkunen¹

¹Department Of Applied Physics, University of Eastern Finland, Kuopio/FINLAND, ²Department Of Neuroscience And Biomedical Engineering, Aalto University, Espoo/FINLAND, ³Department Of Clinical Radiology, Kuopio University Hospital, Kuopio/FINLAND

Introduction and aim of the study

Localizing the cortical motor representations accurately is important in clinical applications as brain tumours and traumas, such as stroke may relocate, expand or reduce the representation to abnormal locations [1, 2]. In this study, we used navigated transcranial magnetic stimulation (nTMS) for mapping motor representation areas through excitatory motor evoked potential (MEP) and inhibitory silent period (SP) responses, as well as BOLD contrast fMRI and pseudo-continuous arterial spin labelling (ASL) fMRI. Considering that both fMRI and nTMS are widely used in clinical practise to locate the motor cortex, the aim of the study was to evaluate the consistency of those methods.

Methods

Ten healthy right-handed volunteers participated in the study (5 females, age range 21-32 years). Block design fMRIs were scanned with a 3T Philips Achieva MR scanner by using finger wiggling as the motor task. nTMS was performed by first roughly mapping the cortical representation of the first dorsal interosseous and determining the resting motor threshold (rMT) and silent period threshold (SPT) [3]. This was followed by the actual mapping with a stimulation intensity of 110% of rMT in MEP mapping and 120% of SPT in SP mapping. In all the measurements, both hemispheres were studied in random order. The statistical analyses of fMRI local maxima and nTMS center of gravities (CoGs) were done in MNI space using a linear mixed model with Sidak post-hoc test (significance-level at $p = 0.05$).

Results

In lateral-medial direction, there were no differences between the methods ($F=1.32$, $p=0.277$) but representations were more lateral on the left hemisphere ($F=4.13$, $p=0.046$). Furthermore, there was a significant interaction between method and hemisphere ($F=3.11$, $p=0.033$).

In anterior-posterior direction, there was a significant difference between the methods ($F=6.78$, $p<0.001$). There was no difference between nTMS MEP and nTMS SP representations, but they together differed from ASL ($p<0.025$). No difference was found with nTMS and BOLD contrast ($p>0.751$), but ASL and BOLD differed ($p<0.001$). Hemisphere had no influence on the representations ($F=1.22$, $p=0.274$). On average, the Euclidian distance between nTMS and BOLD representations was 7.4 ± 0.8 mm and nTMS and ASL 7.2 ± 1.5 mm.

Discussion and conclusion

Statistically, BOLD contrast fMRI was slightly more consistent with nTMS than ASL, as ASL local maxima seemed to be more posterior than BOLD and therefore possibly having stronger sensory compo-

ment. However, the Euclidian distances of BOLD and ASL to nTMS were in the same range. In conclusion, all the methods agreed well generally, but demonstrated somewhat systematic differences. The relevance of those differences should be evaluated in the future in the applied clinical setting.

References

Liepert, J., et al. *Restor Neurol Neurosci* 2004;22:269–277.

Fandino, J., et al. *J. Neurosurg* 1999;91:238–250.

Kallioniemi E, et al. *Clin Neurophysiol* 2014;125:2247–2252.

SP128.2 - Evaluation of probable dementia with Lewy bodies using ^{123}I -IMP brain perfusion SPECT, ^{123}I -MIBG myocardial SPECT and voxel-based MRI morphometry

Author(s): Naoki Kodama¹, Yasuhiro Kawase², Hiroshi Takeuchi¹

¹Department Of Healthcare Informatics, Takasaki University of Health and Welfare, Takasaki/JAPAN, ²Kawase Neurology Clinic, Sanjo/JAPAN

Dementia with Lewy bodies (DLB) is the second most common cause of degenerative dementia after Alzheimer's disease. Approximately, 20% of elderly Japanese manifest DLB. The main symptoms of DLB are visual hallucinations, fluctuating cognitive impairment and parkinsonism. Current imaging modalities for DLB are magnetic resonance imaging (MRI), computed tomography (CT), single photon emission computed tomography (SPECT), and positron emission tomography (PET). We evaluated the diagnostic usefulness of studies with statistical methods in ^{123}I -IMP brain perfusion SPECT, cardiac sympathetic nerve function by ^{123}I -MIBG, and voxel-based MRI morphometry for patients with probable DLB.

Twenty-six patients with probable DLB (16 male, 10 female; mean age \pm SD, 80.7 \pm 5.7 y; range, 74–90 y) was enrolled this study. Three-dimensional stereotactic surface projections (3D-SSP) were used to analyze the results of ^{123}I -IMP SPECT. For ^{123}I -MIBG imaging, we calculated early and delayed heart-to-mediastinum (H/M) uptake ratios. Whole brain T1 weighted three dimensional magnetization prepared rapid acquired echo MPRAGE turbo flash sagittal sequence (slice thickness 1mm) was acquired using a 1.5T Siemens Magnetom Avanto MR imaging system. Using a free software program, the voxel-based specific regional analysis system for Alzheimer's disease (VSRAD) based statistical parametric mapping 8 plus DARTEL.

Qualitative analysis using 3D-SSP demonstrated occipital hypoperfusion in 22 patients (84.6%). Twenty-five patients (96.2%) had decreased cardiac MIBG uptake in the delayed images. Fourteen patients (53.8%) showed z-score of VSRAD exceeded 2.0. We found reduced gray matter in midportion of the middle and inferior temporal gyrus, amygdala, rectal gyrus, and sylvian vallecula in DLB.

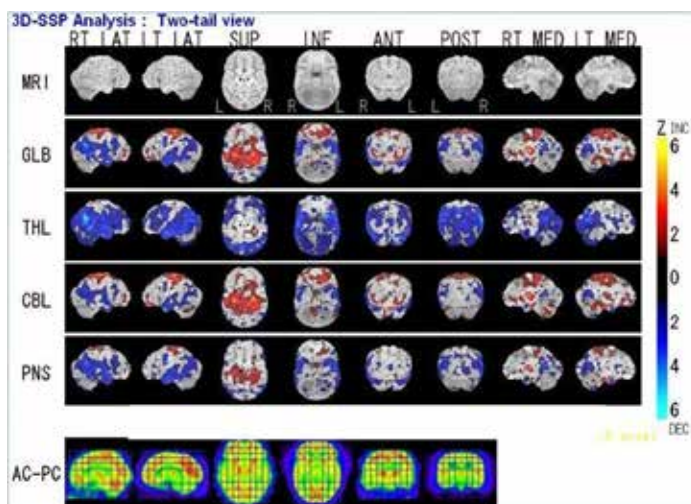


Figure 1 ^{123}I -IMP SPECT

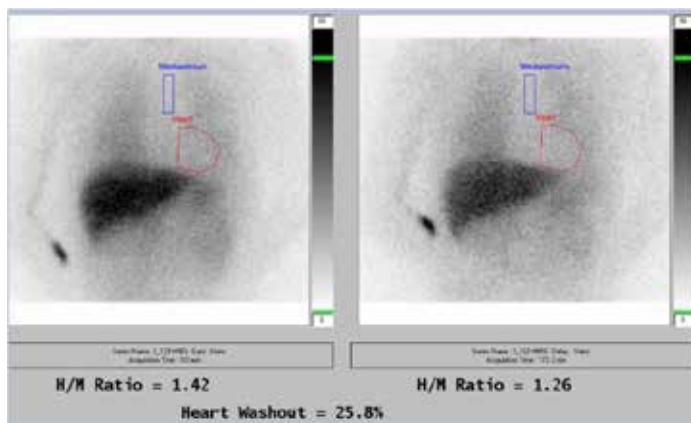


Figure 2 ^{123}I -MIBG SPECT

These results suggest that cardiac sympathetic nerve function with ^{123}I -MIBG would be useful supporting diagnostic inpatients with DLB. Furthermore, degree of midportion of the middle and inferior temporal gyrus, amygdala, rectal gyrus, and sylvian vallecula atrophy may be a useful imaging biomarker.

SP128.3 - Targeted all-organic nanovesicles for multimodal PET/CT and optical fluorescence assessment of lymphatic disseminations in gynaecologic cancers: A radio-pharmaceutical kit to prepare parenteral injections for a "first-in-woman" clinical study.

Author(s): Michael S. Valic¹, Wenlei Jiang², Marcus Q. Bernardini³, Gang Zheng⁴

¹Institute Of Biomaterials And Biomedical Engineering, University of Toronto, Toronto/ON/CANADA, ²Techna Institute For The Advancement Of Technology For Health, University Health Network, Toronto/ON/CANADA, ³Division Of Gynecologic Oncology, Princess Margaret Hospital/University Health Network, Toronto/CANADA, ⁴Department Of Medical Biophysics, University of Toronto, Toronto/CANADA

Motivation: Metastatic tumour spread through the lymphatic vessels and regional lymph nodes (LNs) occurs with a predictable pattern and prevalence in women with gynaecologic cancers (GCs). It has been an outstanding goal in the treatment of GCs to develop a robust diagnostic tool that can guide patient selection for whom lymphadenectomy—that is, the surgical assessment of regional pelvic and para-aortic LN-basins for disease—is indicated. Recent approaches using either optical dyes or radiographic tracers for

lymphatic and sentinel lymph node (SLN) mapping have yielded mixed clinical results (e.g., low sensitivity and specificity) in GC patients. Lacking in these approaches are mechanisms for resolving microscopic extra-uterine and lymphatic disseminations either pre- or, preferably, intra-operatively in order to accurately identify LNs positive for metastatic disease.

Problem Statement: To address this and other issues, we have developed an intravenously administered lymphotropic multimodal contrast agent as a sensitive imaging tool of LN metastasis in GCs. We have previously described an all-organic unilamellar nanovesicle (Porphysome) with intrinsically activatable biophotonic properties. In addition to being biodegradable and biocompatible, Porphysomes can directly and stably chelate radioactive copper-64 (^{64}Cu) to serve as a highly accurate and non-invasive PET/CT imaging tool. ^{64}Cu -Porphysomes functionalized with targeting ligand peptide-folate have been experimentally validated for measurable tumour-specific accumulation lasting 48 hours in primary ovarian cancer xenografts overexpressing folate receptor. We hypothesize that optimising for nanovesicle physiochemical properties including size, surface charge, and targeting ligand, we can anticipate the performance of ^{64}Cu -radiolabelled Porphysome nanovesicles as selective lymphotropic agents for LNs burdened with metastatic disease in pre-clinical tumour models with reproducible lymphatic dissemination.

Methodology: Porphysome nanovesicles are prepared with pyropheophorbide-lipid, cholesterol, and 1,2-distearoyl-*sn*-glycero-3-phosphoethanolamine-N-[methoxy(polyethylene glycol)-2000] (DSPE-mPEG-2000) in molar ratios 55/40/5, respectively. For folate receptor targeting, 1 mol/mol % peptide-folate conjugated DSPE-PEG-2000-Folate was subrogated into the above formulation. Various sized unilamellar Porphysomes were formed following conventional liposomal preparation. To investigate the lymphotropic performance of optimally sized Porphysomes, four preclinical models of reproducible lymphatic tumour dissemination were developed: a VX2 endometrial carcinoma model with pelvic and retro-peritoneal LN metastasis in rabbits, an intra-prostatic MAT-Ly-Lu tumour and a subcutaneous intra-footpad hyperplasia models in rats, and an intra-uterine VEGF-C overexpressing tumour model with augmented lymphangiogenesis in mice.

Results: Radio-pharmaceutical Porphysome kits are manufactured in accordance with good manufacturing practices (GMP); specifically, suitable pharmacopeial grade materials were used throughout manufacture and each production batch is subjected to quality control assays typical of pharmacopeial standards for non-sterile pharmaceutical compounding (e.g., pH, sterility, bacterial endotoxins, etc.) before release. One-step radiolabelling of Porphysome kits with copper-64 prepared parenteral quality injections with high radiochemical purity (> 98%) and specific activity of approximately 2,800 Ci/ μmol per nanovesicle. The sensitivity, specificity, and accuracy of optimally sized ^{64}Cu -Porphysome kits for malignant LNs was quantified for both imaging modalities and correlated with histopathology in our preclinical models.

Implication: Our ^{64}Cu -Porphysomes will permit the synchronous, non-invasive evaluation of GCs for (1) the extent of metastatic tumour spread and LN dissemination by PET/CT (i.e., pre-operative staging), followed by (2) intra-operative fluorescent imaging to detect cancerous LNs in real-time for image-guided lymphadenectomy.

SP128.4 - Generation of 4-Class Attenuation Map for MRI Based Attenuation Correction of PET Data in the Head Area Using a Novel Combination of STE/DIXON-MRI and FCM Clustering

Author(s): Parisa Khateri¹, Hamid Saligheh Rad¹, Amir Homayoun Jafari², Anahita Fathi¹, Afshin Akbarzadeh¹, Mohsen Shojae Moghadam³, Arvin Aryan⁴, Pardis Ghafarian⁵, Mohammad Reza Ay¹

¹Research Center For Molecular And Cellular Imaging, Institute for Advanced Medical Technologies, Tehran/IRAN, ²Research Center For Biomedical And Robotics Technology, Institute for Advanced Medical Technologies, Tehran/IRAN, ³Mri Imaging Center, Payambar Hospital, Tehran/IRAN, ⁴Imaging Center, Imam Khomeini Hospital Complex, Tehran/IRAN, ⁵Chronic Respiratory Diseases Research Center, National Research Institute Of Tuberculosis And Lung Diseases (nritld), Shahid Beheshti University of Medical Sciences, tehran/IRAN

Purpose: Despite remarkable advances in positron emission tomography (PET), the effect of photon attenuation still remains unsolved. The act of attenuation correction based on magnetic resonance imaging (MRI) is a challenging issue, since distinguishing between air and bone in adjacent areas is not possible in conventional MRI. In this study, a novel combination of short echo-time (STE) MRI and a dedicated image segmentation method is proposed to derive bone tissue. A four-class attenuation map (μ -map) is proposed based on STE/Dixon-MRI for attenuation correction of positron emission tomography (PET) data of head.

Methods: 5 normal volunteers underwent MRI and CT scans. Two consecutive MRI pulse sequences; STE technique, (echo-time, 1.1 msec; repetition time, 12 msec; voxel size, 1.2x1.2x2 mm³; acquisition time, 462 sec), and Dixon technique for fat and water decomposition (echo-time 1, 2.38 ms; echo-time 2, 4.76 msec; repetition time, 12 msec; voxel size, 1.2x1.2x2 mm³; acquisition time, 462 sec) were applied. Therefore, 3 MRI data sets for each volunteer were available: STE images (from STE technique), in-phase and out-of-phase images (from Dixon technique).

A four-class μ -map including cortical bone, soft tissue, fat tissue, and air regions was derived from MR images. The image analysis protocol was mainly performed by an in-house-developed software written in MATLAB (The MathWorks, Inc.). Steps for this generation of μ -map are illustrated in Figure 1. Tissue attenuation coefficients were calculated using ICRU 44 report.

To assess MRI-based μ -maps, ultra-low dose CT (ULDCT) data were acquired. After registration CT with MRI, CT-based μ -maps were generated. Quantitative assessment was applied to evaluate the MRI-based μ -maps in comparison to CT-based μ -maps. The values of sensitivity, specificity and accuracy were calculated performing a voxel-by-voxel comparison between segmentation results. To assess correlation between MR-based and CT-based μ -maps, joint histogram was plotted and correlation coefficient was calculated.

Results: The voxel-by-voxel comparison of the MRI-based and CT-based segmentation results showed that values of accuracy and specificity were more than 95% for classes of cortical bone, soft tissue and air region. The average value of sensitivity was calculated 75% for cortical bone and more than 90% for other classes. Evaluation of correlation between MRI and CT results yielded an overall correlation coefficient of 0.98 and 0.97 for integrated μ -maps over 15 slices.

Conclusions: Results indicate that STE/Dixon-MRI data in combination with FCM-based segmentation yields precise MR-based μ -maps for PET attenuation correction in hybrid PET/MRI systems.

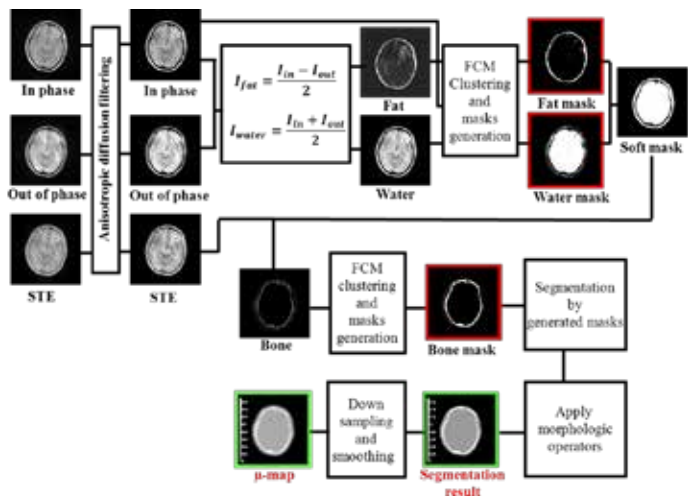


Figure 1. Generation of MR-based μ -maps

SP128.5 - A new low field MRI/gamma detector hybrid system.

Author(s): Andrea Abril¹, Luis Agulles-Pedros²

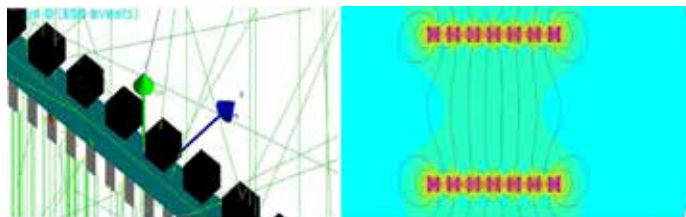
¹Physics, Universidad Nacional de Colombia, Bogotá/COLOMBIA, ²Physics, Universidad Nacional de Colombia, Bogotá/COLOMBIA

The hybrid systems like MRI/PET and MRI/gamma camera, offer advantages, combining the resolution and contrast capability of MRI with the better contrast of nuclear techniques. This work presents, the design of a low field NMR system made up of permanent magnets compatible with a γ radiation detector. The γ detector is based on gel dosimetry. This gel undergoes a T2 relaxation time dependence with the dose. The design is performed using the software fme for estimation of the magnetic field, and geant4 for the physical process involved in radiation detection and effect of magnetic field.

Low field MRI (lfMRI) is, in one hand, a cheaper and versatile alternative to high field MRI. On the other hand, high field MRI is not easily compatible with other techniques that involve radio frequencies and ferromagnetic materials.

The homogeneity in magnetic field is achieved with an array of NbFeB magnets in a linear configuration with a separation between the magnets, minimizing the effect of Compton back scattering compared with a no-spacing linear configuration. The final magnetic field in the homogeneous zone is ca. mT.

The radiation detector used in this work is a Gel, which is the innovative part. The radiation detectors are expensive and need an electronic set-up, which can interfere with the NMR process or viceversa.



Geant4 and fme simulation of the hybrid system.

In our hybrid proposal, although the gel detector do not have spatial resolution, it is possible to obtain a dose profile as a function of the x-axis position by using a collimator array. We present two different

methods of collimation. The first one uses sheets of lead, and the other one uses the magnets of the lfMRI array as collimator, taking advantage of the high density and atomic mass of its components.

As a result, the system described allows a complete integrated radiation detector within the lfNMR system. Finally we present the better configuration for a hybrid system capable of obtain a 1D image, MRI and gamma dose, simultaneously.

SP129 - Image Quality Assessment (Mammography and Other)

TRACK 01: IMAGING

SP129.1 - Kilovoltage-CBCT of a Linear Accelerator as a relative imaging device of a spiral CT scanner - dosimetric results

Author(s): James K. Annkah¹, Ivan Rosenberg², Naina Hindocha², Syed A. Moinuddin³, Kate Ricketts¹, Abiodun Adeyemi⁴, Gary Royle¹
¹Department Of Medical Physics & Biomedical Engineering, University College London, London/UNITED KINGDOM, ²Radiotherapy Physics Department, University College Hospital, London/UNITED KINGDOM, ³Radiography Department, UCLH, London/UNITED KINGDOM, ⁴Radiotherapy Physics Department, Royal Berkshire Hospital, Reading/UNITED KINGDOM

Title: kV-CBCT of a Linear Accelerator as a relative imaging device of a spiral CT scanner - dosimetric **results**

Purpose: Many African countries are in the process of replacing Co-60 equipment with linacs as part of upgrading radiotherapy centers. The purpose of this work is to investigate kV-CBCT of state-of-the-art linacs as a relative imaging device of a spiral CT scanner, which may be useful in radiotherapy centers in developing countries, and evaluate the dosimetric accuracy of a simple method of HU-ED calibration on the Truebeam.

Problem Statement: Radiation oncology in developing countries is hindered by numerous factors including availability and choice of equipment. Currently, sub-Saharan Africa depends on Co-60 in most cancer centers, with standard equipment in a typical state-funded radiotherapy center being Co-60, CT scanner, TPS and other dosimetric equipment. However, with the combination of the modern equipment and techniques, cancer care in Africa can see an exponential rise with higher survival rates.

Due to maintenance and service costs, CT scanners frequently breakdown so RT centers rely on external CT scanners operated by individuals for commercial purposes. Clinical images are acquired and eventually sent to the radiotherapy centers for treatment planning. Since each CT scanner has its own calibration curve, it is nearly impossible for the TPS to have all the individual HU-RED calibrations of the commercially available CT scanners. Treatment plans from such CT scanners may therefore be prone to dosimetric errors. CBCT has been reported to provide accurate dosimetric results where they have been used directly to perform treatment plans. Therefore, a simple method to obtain accurate dosimetric results can be useful in radiotherapy centers in developing countries in the event of replanning or the breakdown of a CT. This may be considered as an alternative to relying on commercial CT scanners if dosimetric accuracy is established.

Method: HU-ED calibrations were performed without a bowtie filter. Images for treatment planning were acquired on GE Light Speed CT scanner at 120 kV, 220 mA and 2.5 mm slice thickness. Another set was acquired using the Truebeam using at half fan beam mode using clinical parameters. IMRT plans were produced on the Eclipse TPS using both set of images while all dosimetric calculations were based on the HU-RED calibration curve of the CT scanner. The results were evaluated, considering HU accuracy, geometric and dosimetric accuracies of the Truebeam.

Results & Conclusion:

Previous results using sophisticated correction methods produced results of $\pm 3\%$ of the prescribed doses. This simple approach pro-

duced $\pm 5\%$ of the prescribed doses, but can also produce results with better accuracies. Further modifications to the setup and calibration can improve dose accuracy, and this can be advantageous in situations where the TPS software has limited features.

SP129.2 - Overall performance, image quality and dose in CR mammography systems operating in the Mexico public health sector

Author(s): María-Ester Brandan¹, Cesar Ruiz-Trejo¹, Juna Carlos Cruz-Hernandez¹, Naxi Cansino¹, Lizbeth Ayala-Dominguez¹, Adriana Moreno-Ramirez², Jaime Aeberto Rodriguez-Lopez², Mario Gomez-Zepeda², Margarita Chevalier³

¹Instituto De Física, Universidad Nacional Autónoma de México UNAM, Mexico City/MEXICO, ²Centro Nacional De Equidad De Genero Y Salud Reproductiva (cnegrs), Secretaría de Salud, Mexico City/MEXICO, ³Fisica Medica, Facultad De Medicina, Universidad Complutense de Madrid, Madrid/SPAIN

Breast cancer is the first cause of cancer death in Mexican women. Approximately, 20 million women are 40 years old or older; annually, 20,444 new cases (35.4 per 100,000 women) and 5,584 deaths (17.2 per 100,000 women older than 25) are due to this disease. Breast cancer prevention, diagnostics, treatment, control and monitoring is regulated by National-Official-Regulation NOM-041 that recommends a mammogram every 2 years for women 40-69 y.o. NOM-229 establishes technical requirements for mammography equipment. Compliance with these regulations is controlled and monitored by COFEPRIS, a Ministry of Health (SS) commission.

About 2 million mammographic screening studies are performed annually in public services. Public services own 754 mammography units, 351 of these belong to SS. Three technologies are employed: screen/film (33% of SS units), digital flat-panel-detectors-DR (26%) and computed-radiography-CR (41%). An independent 2014 study for 65 CR systems in central Mexico reported that only 6% of services met NOM-041 standards, 79% produced images with artifacts and non-uniformities, and 42% met the minimum score of ACR phantom.

This study, collaboration with CNEGSR-SS, has focused on CR systems operated by SS institutions. The goal was to evaluate overall performance, image quality and dose in 15 CR systems which perform approximately 64,000 studies yearly. 40 evaluation tests, including use of CDMAM phantom and MTF evaluation, were applied in services located in 8 States.

Quality control procedures were those suggested by IAEA QA Programme for Digital-Mammography, Spanish Protocol for Quality Control in Diagnostic Radiology and Spanish Protocol for Quality Control in Digital-Mammography, and those in NOM-229 and -041.

The evaluation was grouped into 7 areas: Electromechanical performance, automatic exposure control, radiation yield, beam quality, dose, image quality and monitor visualization conditions. Systems were combinations of various mammography units with Carestream, Konica or Fujifilm CR plates. Within a month after the evaluation, services received a report with results, description of deficiencies, and strong recommendations to solve problems immediately.

Severe failures in the equipment performance, and general non-compliance with Mexican regulations and international recommendations were found. Percentage of systems complying with recommendations for representative tests were: Mammography unit mechanical evaluation (50%), compression force (64%); AEC thickness compensation (0%); mean-glandular-dose (57%); quantum noise dominance in images (9%); plate homogeneity (0%); spatial resolution (38%); visualization of CDMAM 0.1 mm object (8%); absence of artifacts (0%). 50% of centers had 5 MP interpretation monitors and 30% of rooms presented appropriate visualization

conditions. On the positive side, 100% of systems showed appropriate half-value-layers, linearity of yield with mAs, and linear (in terms of $\ln(\text{ESAK})$) detector response function. Some positive changes happened after sending the reports: 3 mammography units were replaced, one high-resolution monitor was purchased and conditions in two interpretation rooms were improved. On Dec-2014, after these results, SS informed that CR systems will no longer be purchased for the CNEGSR-Breast Cancer Program, promoting migration to DR systems. It is hoped that this collaboration might result into needed actions, particularly, NOM-229 update.

We thank J Márquez, MJ Villagómez-Casimiro, A Álvarez-Luquin, and grants IAEA RC17683 and PAPIIT-UNAM-IN105813.

SP129.3 - A Catphan attachment for three dimensional measurements of the modulation transfer function

Author(s): Balazs J. Nyiri, Elsayed S.M. Ali
 Medical Physics Department, The Ottawa Hospital Cancer Centre, Ottawa/CANADA

Commercial image quality phantoms (e.g., Catphan) suffer from two limitations related to the modulation transfer function (MTF). First, the phantoms are suitable for determining the cutoff frequency only, not the full MTF shape. Second, the potential directional dependence of the MTF is ignored, making the quantification of directional blur difficult. In this study, these two limitations are addressed by proposing a Catphan attachment for 3D measurements of the full MTF shape (figure 1). Example results are shown for the Elekta XVI CBCT system. Cylindrical coordinates are chosen because MTF directional dependence is likely along these coordinates – e.g., lag/ghosting blurs the image along the rotating scan direction, thus affecting the azimuthal MTF. The cyclic pattern in each dimension consists of ten groups of line pairs with frequencies from 1.00 to 4.55 lp/cm in increments of ≈ 0.4 lp/cm. This frequency range is chosen to capture the sloping portion of the MTF for the XVI system. All lines are 5 mm long and 3 mm deep, and the centers of the line groups in the three coordinates are 36° apart and 5 cm off-center. The MTF is extracted using Fourier analysis of the line profiles along the cyclic patterns to determine the amplitude at the principal frequency. Figure 2 shows example results for the XVI system. For a given set of scan parameters, the longitudinal MTF is superior to the other two directions, and the radial MTF is better than the azimuthal MTF at higher frequencies (ghosting/lag could be a factor). For a given mAs per scan, reducing the scan time from 2 to 1 minute leads to deterioration of the longitudinal MTF and to improvement in the azimuthal MTF. In conclusion, the proposed 3D MTF attachment can be a useful tool to evaluate the overall performance of imaging systems.

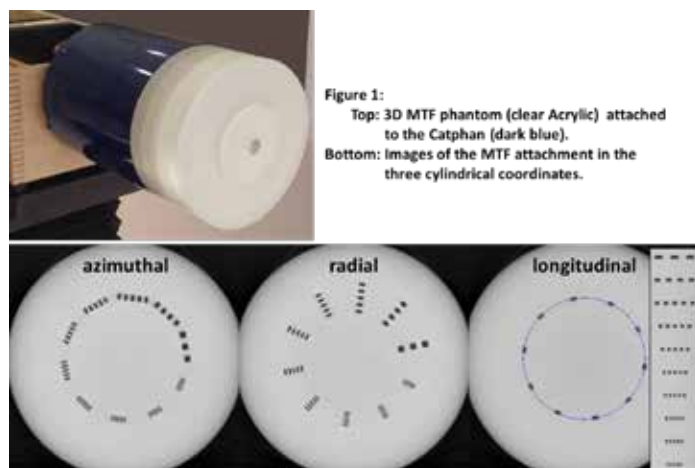


Figure 1: Top: 3D MTF phantom (clear Acrylic) attached to the Catphan (dark blue). Bottom: Images of the MTF attachment in the three cylindrical coordinates.

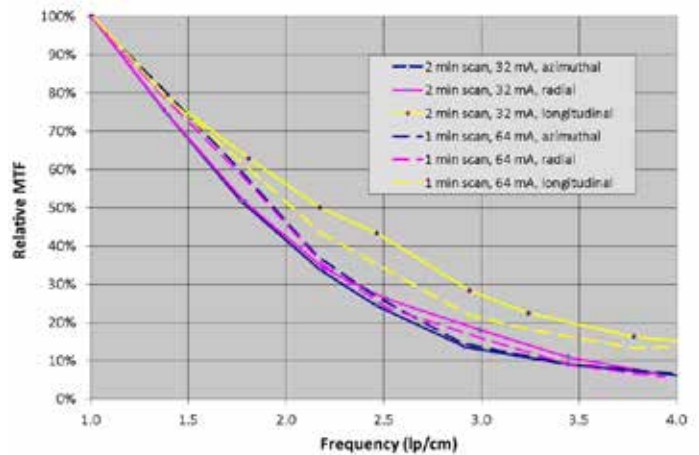


Figure 2: Relative MTF for scans with the following parameters: 120 kVp, bowtie filter, medium FOV, 40 ms per pulse, clockwise, high resolution reconstruction

SP129.4 - Sensitometric analyses of screen-film systems for mammography exams in Brazil

Author(s): Luis Magalhaes
 Universidade do Estado do Rio de Janeiro - UERJ, Rio de Janeiro/ BRAZIL

A determination of the sensitometric parameters of screen-film systems to evaluate their qualities was performed. The quality control of the automatic film processor was carried out to ensure a high level of efficiency. Based on ISO 9236-3, the following potentials were applied on the X-ray tubes: 25 kV, 28 kV, 30 kV and 35 kV. Four different mammography films from different manufacturers with and without screens were tested for curve shape, speed and average gradient. The results indicated that film 1 exhibited better contrast, film 3 demonstrated the highest energy dependence, and film 4 presented the largest base+fog density. None of the four mammographic films tested achieved satisfactory results in all parameters analyzed. Improvements in the manufacturing process for these films must be completed to avoid losses in the image quality.

SP129.5 - New Line Contrast Figure of Merit for image quality assessment

Author(s): Aris Dermitzakis, Anastasia Daskalaki, Kristina Bliznakova, Nicolas Pallikarakis
 Biomedical Technology Unit, Dept. Of Medical Physics, University of Patras, Patras/GREECE

A novel Figure of Merit (FoM) is presented which is based on analysis of data extracted from line profiles within the image. This FoM is referred as Line Contrast (LC). In order to evaluate its performance, the proposed FoM along with Contrast to Noise Ratio (CNR), are applied in a simulated phase contrast image and the resulting figures are compared. Phase contrast image is created using the XRAYImagingSimulator an in-house developed software platform for x-ray imaging simulation. A semi-cylindrical phantom especially designed for phase contrast applications that contains materials mimicking the refractive properties (indexes) of breast tissues was used. Images were produced at 20 keV with source to isocenter distance (SID) 23m and object to detector distance (ODD) 400mm and pixel size of $5\mu\text{m}$. Results from the application of both FoMs shows that LC comes into full accordance with visual assessment and that it overpass the traditionally used CNR, especially in the ability of detecting the edge enhancement due to phase contrast, of the different structures within the image. The edge detection features make it optimal for phase contrast investigation where the effect on the edge enhancement is of utmost importance.

SP129.6 - Assessment of Photostimulable Storage Phosphor Imaging Plates Quality in Computed Radiography

Author(s): Bárbara Q. Friedrich¹, Ana Maria Marques Da Silva¹, Renata M. Luz², Jéssica V. Real², Alexandre S. Capaverde²
¹Núcleo De Pesquisa Em Imagens Médicas, PUCRS, Porto Alegre/ BRAZIL, ²Hospital São Lucas, PUCRS, Porto Alegre/BRAZIL

Image quality of Computed Radiography (CR) systems has been studied, but there have been little effort to evaluate the physical performance of the photostimulable phosphor imaging plates (IPs). Due to their reusability, they are subjected to normal wear and tear from scratches, scuffs, cracks, and contamination with dust and dirt, which may interfere with the production of an appropriate diagnostic image. Some manufacturers discard the IPs only based on the number of exposures. However, this parameter is insufficient to evaluate their quality and lifetime indications. The aim of this study is to investigate quantitative and qualitative quality control (QC) procedures which can assure the IPs quality in CR systems, providing evidences of the lost of diagnostic quality. Two groups of Fujifilm HR-BD IPs were investigated: four plates were in use and four plates had been discarded. The IPs were stimulated using phantoms (PMMA, aluminium sheets and a mammographic phantom) in Mammomat 3000 Siemens mammography equipment, and scanned by Fuji FCR system, model Profect CS Plus. The QC procedures evaluated were: signal-to-noise ratio (SNR); contrast noise ratio (CNR); contrast; ghost effect; uniformity; visual analysis of the image; and integrity. The results indicated that the ghost effect, integrity and uniformity QC tests give evidences to evaluate CR imaging plates' degradation.

SP130 - Treatment Planning**TRACK 04: RADIATION ONCOLOGY****SP130.1 - Comprehensive Dosimetric Planning Comparison for Early Stage Non-Small Cell Lung Cancer with SABR: Fixed-Beam IMRT versus VMAT versus Tomotherapy**

Author(s): Ilma Xhaferllari, Stewart Gaede
 Department Of Medical Biophysics, Western University, London/ ON/CANADA

Introduction: Volumetric modulated arc therapy (VMAT) is emerging as leading technology in treating early-stage non-small cell lung cancer (NSCLC) with Stereotactic Ablative Radiotherapy (SABR) due to its efficiency. However there are other various techniques available to deliver IMRT: fixed-beam, and helical Tomotherapy (HT). TrueBeam™ linear accelerators (Varian Medical Systems, Palo Alto, USA) allows for fixed-beam and VMAT techniques to be executed using flattening filter free beams, achieving dose rates up to 2400 MU/min, significantly reducing treatment times. The purpose of this study is to provide an extensive dosimetric comparison among the IMRT techniques previously mentioned for treating early-stage NSCLC with SABR.

Methods: Ten early-stage NSCLC patients were retrospectively optimized using three fixed-beam techniques with 9-11 beams (high and low modulation step-and-shoot (SS-IMRT), and sliding-window (SW-IMRT)), two VMAT techniques using two partial arcs (SmartArc (SA-VMAT) and RapidArc (RA-VMAT)), and three HT fan beam widths (1 cm, 2.5 cm, and 5 cm); accounting for 80 plans total. SS-IMRT and SA-VMAT, HT plans, and, SW-IMRT and RA-VMAT were optimized using Pinnacle v9.1, Tomoplan v.3.1.1, and Eclipse (Acuros XB 11.3 dose calculation algorithm), respectively. All plans met target coverage and critical organ constraints according to the SABR-COMET protocol.

Dose-volume histogram statistics, dose conformity, and treatment delivery efficiency variables were analyzed. To determine statistical significance, the Shapiro-Wilk test checked for normality. For normal distributions, ANOVA and Tukey post-hoc tests were performed; otherwise, Kruskal-Wallis followed by a Mann-Whitney test were performed (significance defined as p-value <0.05).

Results: Conformality index, ratio of the volume of 80% and 50% isodose to the planning target volume (CI80%, CI50%), significantly increased with HT-5cm compared to all other modalities, with RA&SA-VMAT being the most conformal. The percent volume of contralateral lung receiving 5 Gy or more (V5GyC) significantly increased in all HT plans (p=0.002) and mean lung dose significantly increased in the HT-5cm plan (p=0.002). In both scenarios, RA&SA-VMAT achieved the lowest values.

When RA&SA-VMAT were grouped and compared to SS-IMRT; the maximum dose to the bronchus (p=.011) and heart (p=.005) significantly increased, whereas, all lung parameters expect lung covered by 10 Gy or more (V10Gy), and the maximum dose to cord significantly reduced with RA&SA-VMAT. When comparing RA&SA-VMAT, CI80%, CI50% and D2cm were significantly reduced with the RA plan, whereas V10Gy and total monitor units significantly increased.

Estimated treatment time significantly increased amongst HT (p<0.001), 13.2±1.8, 8.3±5.2, and 6.4±4.1 minutes for HT-1cm, HT-2.5cm and HT-5cm respectively, and fixed-beam IMRT plans (p<0.001), 2.5±0.3, 3.0±0.5, and 4.4±1.4 minutes for SS-IMRT low and high modulation, and SW-IMRT respectively, compared to both, RA&SA-VMAT, 2.0±0.3, and 1.9±0.2 minutes respectively. However,

there was not a significant difference between RA vs. SA-VMAT ($p=.393$).

Conclusion: RA&SA-VMAT outperformed HT in all parameters measures and statistical difference was observed in ten parameters, none of which showed VMAT to be inferior. Despite an increase in dose to the heart and bronchus, this study shows that VMAT is dosimetrically advantageous in treating early-stage NSCLC with SBRT compared to fixed-beam IMRT, while providing significantly shorter treatment times than any other modality studied.

SP130.2 - Development and Validation of an Open Source Tool for Determining Planning Target Volume Margins in Intracranial Stereotactic Radiotherapy

Author(s): Winnie Li, Tim Craig, An Wang, Young-Bin Cho, Tara Rosewall, Kristy Brock, David Jaffray
Radiation Medicine Program, Princess Margaret Cancer Centre, Toronto/CANADA

Purpose/Objective(s): Awareness of inter- and intra-fraction uncertainties is increasingly important in the era of stereotactic radiotherapy (SRT); their incorporation into the planning target volume (PTV) margin (MPTV) is essential to ensure prescribed dose to the target. The purpose of this work is to develop a method to formulate MPTV for Gamma Knife (GK) intracranial SRT to manage geometric uncertainties.

Materials/Methods: The Margin Calculator was developed in open-source software to determine patient-specific MPTV. The tool was initially validated against van Herk's (MvH) formula using a synthetic sphere and stochastic simulations for a range of systematic and random uncertainties over several fractionation schedules. Under ethics approval, 10 GK intracranial stereotactic radiosurgery targets and dose distributions underwent stochastic simulations for systematic and random uncertainties ranging from 0 – 1.5 mm and 4 fractionation schedules (1, 3, 5, 10). Simulation of MPTV expansion in the calculator was performed through dose distribution image scaling. Incremental MPTV expansions were performed until cumulative dose population histograms reached a goal of 90% population receiving a near-minimum dose of 95%. The performance of image scaling as a method of MPTV expansion was validated through comparison of the automatic scaled plans on the required MPTV versus manually generated replans for 22 cases in the treatment planning system. The new dose distribution was imported back into the *Margin Calculator*, and simulations repeated using the original target volume (i.e. no MPTV added), the new dose distribution (i.e. including the MPTV), specified fractionation schedule, and original set of systematic and random uncertainties. If the MPTV-Initial satisfies the coverage criteria with the prescribed dose, additional MPTV (MPTV-Additional) required should be minimal.

Results: Phantom sphere validation results showed strong agreement between the MvH-predicted and calculator generated MPTV ($R^2=0.965$). 640 MPTV were generated for 10 intracranial targets over 4 fractionation schedules. A 73% agreement within ± 1 mm between calculated to MvH-predicted MPTV was observed, showing larger (80%) margins were required with the MvH approach. Lower fractionation and irregularly shaped targets required larger MPTV. Compared to manual replans, the automatically scaled plans required an additional 0.2 mm MPTV-Additional in 81% (18/22) of the cases; all targets required < 1 mm additional MPTV-Additional to ensure dosimetric coverage.

Conclusion: A process for a *Margin Calculator* has been developed and validated. This open-source tool accounts for patient-specific target size, target contour, dose specifications, geometric uncertainties, fractionation schedules and treatment goals, and is useful for deriving evidence-based MPTV for intracranial GK-SRT.

SP130.3 - Dosimetric impact of accurately delineating of the left anterior descending artery in photon and proton radiotherapy

Author(s): Janid Blanco Kiely¹, Benjamin M. White¹, Sabina Vennarini², Andrea Dimofte¹, Lillie Lin¹, Gary Freedman¹, Stefan Both¹
¹Radiation Oncology, University of Pennsylvania, Philadelphia/ UNITED STATES OF AMERICA, ²L'unità Operativa Di Protonterapia, Azienda Provinciale per i Servizi Sanitari, Trento/ITALY

Purpose: The purpose of this study was to quantify the dosimetric impact of motion on the dose delivered to the left anterior descending artery (LAD) in deep inspiration breath hold (DIBH) CT using proton uniform scattering (US), pencil beam scanning (PBS) and 3D conformal photon radiotherapy (3DCRT). Because dose volume histogram (DVH) indicators based on whole heart dose do not consistently predict radiation-induced risk for myocardial infarction, dose to the LAD itself has been suggested as a better indicator of radiation-induced cardiac toxicity. Routine radiotherapy treatment planning clinical imaging protocols do not compensate for heart motion, introducing a source of uncertainty in contouring and in reported dose to the LAD. Ultimately, a method that quantifies the dosimetric impact of motion could improve the LAD's dose estimate.

Materials and Methods: Ten consecutive patients with left breast cancer received a routine clinical DIBH CT where cardiac motion was not accounted for during patient simulation. An expert radiologist contoured the LAD in the routine DIBH CT. Using an unsharp filter, the LAD's uncompensated motion blurring in the DIBH CT images was extracted from the contoured LAD to create a corrected LAD volume. Treatment plans were created using proton (US and PBS) and photon (3DCRT) planning techniques. In order to be consistent with literature, the maximum and mean dose to the LAD were used as DVH endpoints. The relative dosimetric impact of using a corrected LAD volume on the LAD DVH indicators was determined by quantifying the relationship between the DVH indicators, which were calculated from the corrected versus the uncorrected LAD volume.

Results: Using a corrected LAD volume for calculation of the maximum dose LAD DVH indicator reduced its reported value by 2% (3DCRT), 4% (US), and 25% (PBS). The maximum absolute dose reduction was greatest for the 3DCRT plans, where the corrected LAD volume reduced the maximum dose by 87.5 ± 117.4 cGy. Proton plans had a smaller difference: US and PBS plans had a LAD maximum dose reduction of 35.8 ± 55.4 cGy and 16.3 ± 17.0 cGy respectively. The corrected LAD volume had the dosimetric impact of increasing the mean LAD dose for each treatment modality by 25% (3DCRT), 61% (US), and 35% (PBS). The greatest overall mean dose increase was found in the 3DCRT plans, where the average mean LAD dose increase was 167.9 ± 163.9 cGy. Both the US and PBS plans had less average mean dose difference (1.9 ± 3.8 cGy and 0.4 ± 1.3 cGy, respectively).

Conclusion: Uncompensated coronary motion in DIBH CT might reduce the accuracy of the LAD DVH indicators for all photon and proton modalities. Therefore, overestimating LAD volume could potentially be the source of inconsistencies within dose and radiation-induced cardiac toxicity correlations reported in the literature. These findings may be more clinically relevant for photon therapy, since photon therapy tends to deliver higher LAD doses relative to proton modalities (proton modalities are already associated with low LAD doses with or without motion correction).

SP130.4 - Objective function surrogates for iterative beam angle selection

Author(s): Mark Bangert¹, Jan Unkelbach²

¹Division Of Medical Physics In Radiation Oncology, German Cancer Research Center DKFZ, Heidelberg/GERMANY, ²Radiation Oncology, Massachusetts General Hospital, Boston/UNITED STATES OF AMERICA

Optimized non-coplanar beam ensembles may yield substantial improvements of radiation therapy treatment plan quality. However, beam angle selection (BAS) is a non-trivial process and automated beam ensemble optimization is not supported by most commercial treatment planning systems, in part due to the lack of efficient algorithms.

We focus on iterative BAS, where a beam ensemble is sequentially constructed: the basis for BAS during iteration n is a treatment plan containing $n-1$ fixed beams. To select the n th beam, each remaining beam from a discrete set of candidate beams is added one-by-one to the current beam ensemble and the fluence map optimization (FMO) problem is solved. The beam that yields the lowest objective function value is selected.

In this work we investigate two alternative methods relying on objective function surrogates to score candidate beams in order to make iterative BAS computationally more efficient: Conventional iterative BAS is compared to (1) an approach where the FMO problem is not solved to optimality but stopped after five iterations of a gradient based algorithm and (2) an approach where candidate beams are scored based on a projected gradient of the FMO problem in the first iteration.

In a treatment planning study including one pancreas, one prostate, and one intracranial case, it is observed that both iterative BAS methods using objective function surrogates yield similar plan quality compared to naïve iterative BAS with regard to the resulting the objective function values (see figure 1) and DVHs (see paper). At the same time, the surrogates enable reductions in computation time by a factor of 50-100 making them highly attractive for clinical application.

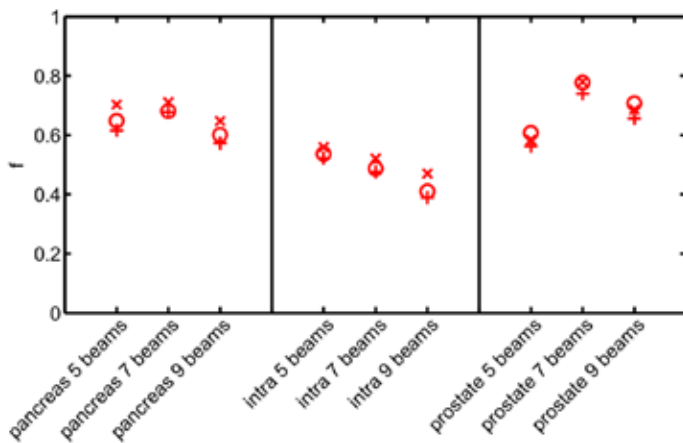


Figure 1: Normalized objective function value vs. number of beams for the three investigated cases for iterative BAS using the objective function value after a full FMO (plus signs), the objective function value after five FMO iterations (circles), and the initial projected gradient (crosses). 1 corresponds to the objective function value of a coplanar equi-spaced beam ensemble with the same number of beams; 0 corresponds to the objective function value of an unattainable benchmark IMRT plan that uses all candidate beams.

SP130.5 - A preliminary study on the effect of modulated photon radiotherapy (XMRT) optimization for prostate cancer treatment planning

Author(s): Philip McGeachy¹, Jose E. Villarreal-Barajas¹, Yuriy Zinchenko², Pooyan Shirvani², Rao Khan¹

¹Medical Physics, Tom Baker Cancer Centre, Calgary/CANADA, ²Mathematics And Statistics, University of Calgary, Calgary/CANADA

This preliminary work compared a new optimization technique, modulated photon radiotherapy (XMRT), with intensity modulated radiotherapy (IMRT) in a treatment planning study on a cohort of eight prostate cancer patients. XMRT differs from IMRT in that it allows the typically fixed beam energy to act as a variable such that the optimizer finds a dose distribution by simultaneously optimizing photon beamlet fluence and energy. Plans were comprised of a seven-coplanar beam arrangement, with IMRT restricted to 6 MV while XMRT used 6 and 18 MV beams. Both IMRT and XMRT optimization was based on a linear programming model with partial-volume constraints implemented through the conditional variable at risk (cVaR) approach. A dose-volume histogram for one of the patients is given in figure 1. XMRT and IMRT provided similar coverage to 95% of the target (PTV) with the prescribed dose (78 Gy), however XMRT improved the homogeneity index (HI) (Table 1). XMRT was able to reduce the dose to a greater extent ($p < 0.05$) for the rectum, bladder, and femoral heads, particularly in the low-dose region (≤ 40 Gy). Further, XMRT provided an improvement in the high dose-region of the bladder with a lower near maximum dose, D2%, Bladder, and reduced volume receiving at least 80 Gy, V80, Bladder ($p < 0.05$). Although there was a statistically significant decrease in certain dosimetric parameters for healthy organs using XMRT, whether or not this has a clinical impact has yet to be determined and is a point of interest for future investigations. Further, neutron dose needs to be considered for XMRT and the possible ramifications on the risk of secondary cancers.

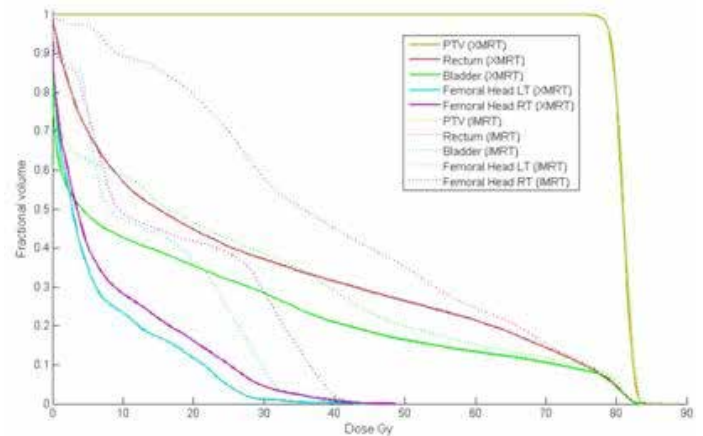


Fig 1. Dose-volume histogram for XMRT (solid) and IMRT (dashed) solutions for a prostate patient.

Table 1. XMRT and IMRT results for cohort of eight patients, presented as the mean \pm standard deviation.

	XMRT	IMRT	p-value
V95,PTV	95.6 \pm 3.2	95.8 \pm 2.5	0.4
D2,PTV	83.6 \pm 0.3	85.7 \pm 2.0	0.003
HI	0.108 \pm 0.05	0.136 \pm 0.06	\ll 0.05
V20,Rectum	69.7 \pm 13.9	82.6 \pm 7.0	0.007
D2,Bladder	81.9 \pm 0.4	83.0 \pm 0.8	0.001
V80,Bladder	8.7 \pm 3.1	10.3 \pm 3.5	\ll 0.05
V40,Bladder	34.0 \pm 11.0	38.7 \pm 9.6	0.03
V20,Bladder	46.1 \pm 13.0	51.3 \pm 10.2	0.07
V20,FemHeadLT	33.7 \pm 18.0	48.8 \pm 12.0	0.1
V20,FemHeadRT	31.0 \pm 18.3	50.5 \pm 9.0	0.05

The preliminary, unoptimized implementation finds the most similar plan in less than 7 minutes when choosing from 5 plans, and it is anticipated that increasing the number of plans will result in only a small relative increase in computation time. The estimated computation time for 10 comparison studies is less than 10 minutes, which is acceptable for this use case. This system, while currently set up for five studies, can easily be extended to hundreds or thousands of studies with little effort if other patients' plans are also included. The decrease in time required to perform this computation when using the cloud decreases the time to the point where it would be reasonable to perform this computation clinically. This will lead to a reduction in the time required to create a new optimized radiation plan for the same patient.

SP130.6 - Measuring radiation treatment plan similarity in the cloud

Author(s): Jennifer Andrea, Csaba Pinter, Gabor Fichtinger
School Of Computing, Queen's University, Kingston/ON/CANADA

Measuring radiation treatment plan similarity in the cloud

J. Andrea, C. Pinter and G. Fichtinger

Laboratory for Percutaneous Surgery, School of Computing,
Queen's University, Kingston, ON, Canada

Radiation therapy is a form of cancer treatment in which carefully designed plans are used to direct treatment over multiple occasions (fractions). Creating radiation plans is quite laborious, so it is not feasible to manually create a plan for each fraction to maintain treatment quality. We propose to use a database of plans to find the most similar anatomy, based on which a suitable daily plan might be automatically created, thus reducing staff time. However, the computation for finding the most similar plan is long and computationally intensive, which presents an obstacle to performing the procedure clinically. We present a method for finding the most similar plan using cloud resources to reduce computation time. Using the cloud to perform the comparison computation enables each comparison between the daily study and an assigned study from the database to be computed in parallel.

The similarity analysis computation was performed on Amazon Web Services (AWS) Elastic Cloud Compute instances, using 3D Slicer and SlicerRT. 3D Slicer (www.slicer.org) is an open source platform for medical image analysis and visualization and SlicerRT (www.SlicerRT.org) is a radiation therapy research extension for 3D Slicer. The AWS Simple Storage Service and Simple Queue Service were also used, for storage of the studies and messaging between the local computer and the instances, respectively. The similarity of the studies were evaluated by computing the Dice coefficient for pairs of matching contoured structures from each study. As contouring is a time-consuming process, contour comparison was used as a proof-of-concept for using the cloud and SlicerRT together to find the most similar plan. In the future, the similarity measure of raw anatomical data will be used for comparison instead.

The system was tested on simulation data created by applying random deformation fields to an existing phantom radiation plan. The system was evaluated both in terms of accuracy and in terms of time. Five different studies were presented to the system as the daily study, and the system returned the correct result in each case.

SP131 - Quality Assurance: Part 3

TRACK 04: RADIATION ONCOLOGY

SP131.1 - Sensitivity of Helical Tomotherapy and Elekta Agility VMAT dose distributions to multileaf collimator motion uncertainties for breast radiation treatment with extensive nodal irradiation

Author(s): Jason Belec, [Eric Vandervoort](#)
 Medical Physics, Ottawa Hospital Cancer Center, Ottawa/CANADA

Purpose: Breast radiation therapy treatments including extensive nodal irradiation require additional photon intensity modulation to properly spare normal tissues such as the heart and the lungs. In this work, we use Monte Carlo dose calculation methods to quantify the sensitivity of those treatments to uncertainties in the motion of multileaf collimator (MLC) for treatment delivered using Helical Tomotherapy (HT) and Elekta Agility VMAT (EA-VMAT).

Materials and Methods: Treatment plans for 10 patients were generated using TomoTherapy Planning 5.0 and Elekta Monaco 3.1 treatment planning systems. Monte Carlo simulations were performed with a modified version of the BEAMnrc/DOSXYZnrc codes. Errors in the MLC motion were introduced in the treatment plans and the impact on the dose distribution was assessed by comparing the dose with and without the errors.

Results: Figure 1 shows an example of dose volume histograms for HT and EA-VMAT. The EA-VMAT plans were optimized using a 5 mm minimum leaf gap soft constraint to achieve similar treatment plan quality as with HT. The sensitivity of the EA-VMAT mean target dose was 3.0% per mm of error in the leaf gap size (0.5 mm error in the position of each leaf). The sensitivity of the HT mean target dose was 0.5% per ms of error in the opening time of each leaf. The sensitivity of the target dose to single leaf error was also investigated for HT. The maximum dose change to a point in the target due to a 5 ms opening time error in one leaf is between 0.4% and 0.7% depending on the leaf. An ongoing investigation is currently extracting similar information for EA-VMAT.

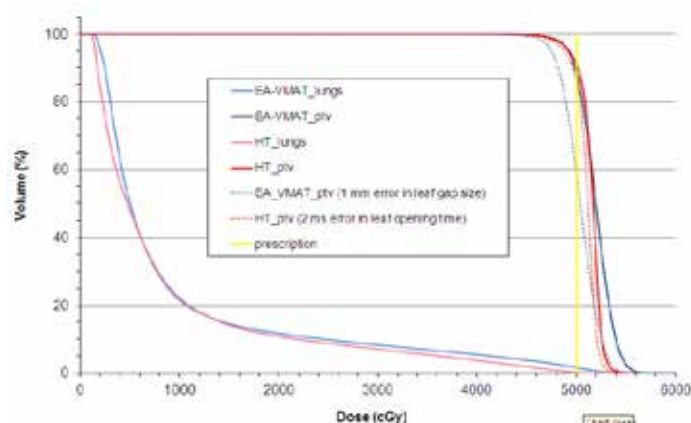


Figure 1. Example of cumulative dose volume histograms of planning target volume (ptv) and lungs for a breast treatment with extensive nodal irradiation. Dotted lines also show the impact of introducing errors of 2 ms in the leaf opening time (HT) and errors of 1 mm in the leaf gap size (EA-VMAT).

Conclusion: Breast radiation therapy treatments including extensive nodal irradiation require additional photon intensity modulation to properly spare normal tissues such as the heart and the lungs. Results show that it is possible to achieve similar treatment plan quality with EA-VMAT as with HT. The sensitivity of the EA-VMAT mean target dose to MLC position uncertainties is 3.0% per mm of

error in the leaf gap size (0.5 mm error in the position of each leaf). The sensitivity of the HT mean target dose to MLC position uncertainties is 0.5% per ms of error in the opening time of each leaf.

SP131.2 - Use of Varian Trajectory Log Files for Patient Specific Quality Control of TrueBeam VMAT FFF Treatment Deliveries with Portal Dosimetry and Eclipse

Author(s): [Michael Fan](#), Francois Deblois, Jonathan Thebaut
 Radiation Oncology, Jewish General Hospital, Montreal/QC/CANADA

Purpose:

Varian Portal Dosimetry System (PDS) (Varian Medical System) is an integrated tool for dosimetric quality control (QC) of flattened beams. However, flattening filter free (FFF) beams are not yet supported in PDS. In this work, we propose a workaround to (1) analyze FFF beam deliveries in PDS and (2) visualize treatment delivery discrepancies within Varian Eclipse treatment planning system (ETPS) by using the Varian TrueBeam trajectory log files.

Method and Material:

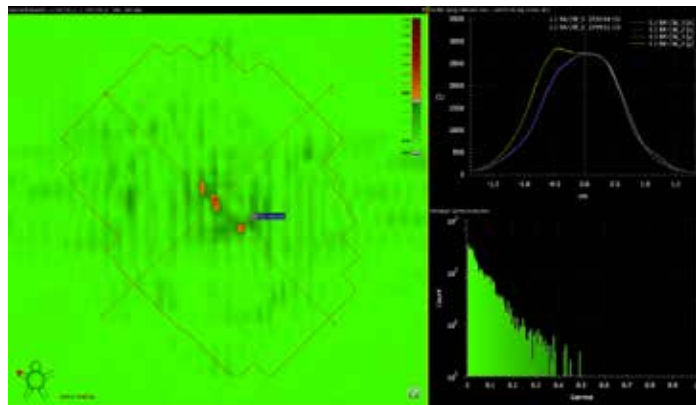
Five brain stereotactic radiosurgery plans were optimized with ETPS using a volumetric modulated arc delivery (VMAT) technique for 6 MV FFF beam on TrueBeam. Treatment verification plans were validated in a phantom by taking a point dose measurement with a Farmer-type ionization chamber (IC) and with a Gafchromic EBT3 film (Ashland Inc.). The trajectory log-files (version 1.5) were generated for every treatment and QC plan delivered. The log-files contain cumulative monitor units (MU) delivered, leaf positions, gantry positions, and other machine parameters sampled every 20 ms. We developed a user-friendly web application to parse log-files and automatically generate corresponding DICOM-RT reconstructed plans (DRP). The DRPs were imported into the ETPS and the dose distribution was recalculated on both the original QC and patient CTs using the delivered MUs. The planned mean dose to the IC was compared to the measured dose and the DRP dose. Gamma map analysis was performed between (1) the planned photon fluence (PFF) and the film measurement and (2) the PFF and DRP dose. The latter was analyzed in PDS by converting the DICOM dose files (PFF and DRP) to a format readable by PDS. Treatment delivery discrepancies on planning objectives were analyzed by comparing dose-volume histogram metrics between the original plan and the DRP.

Results:

The point dose differences between ETPS and IC and between ETPS and DRP were $1.6 \pm 1.5\%$ and $0.17 \pm 0.08\%$ respectively. The percentage of pixels passing fluence map gamma analysis between ETPS and film was $99.0 \pm 0.7\%$ (3%/3 mm) and between ETPS and DRP (FIG1) was $99.8 \pm 0.2\%$ (0.5%/0.5 mm). Across all analyzed plans, ETPS and DRP showed an average difference of $0.56 \pm 0.33\%$ for $V[10 \text{ Gy}]$ to brain excluding PTV and an average difference of $0.22 \pm 0.15\%$ for $V[100\% \text{ of prescription}]$ to PTV.

Conclusion:

This work demonstrates the successful use of TrueBeam trajectory log-files with a user-friendly web application to reconstruct the delivered dose in ETPS for patient specific QC.



SP131.3 - Machine Learning Facilitates Failure Mode Analysis and Virtual QA for IMRT

Author(s): Gilmer Valdes, Ryan Scheurmann, Chun-Yu Hung, Marc Bellerive, Arthur Olszanski, Timothy D. Solberg
 Radiation Oncology, University of Pennsylvania, Philadelphia/UNITED STATES OF AMERICA

Purpose: To develop metrics that describe the deliverability of IMRT plans and use them for a priori prediction of IMRT QA results.

Methods: 498 IMRT plans from multiple treatment sites were planned in Eclipse version XI and delivered using a dynamic sliding window technique on two linac platforms (Clinac iX and TrueBeam, Varian Medical Systems, Palo Alto, CA). Using 2% dose / 2mm distance tolerances with local normalization, 38 plans failed the 90 % gamma criterion. Four failure modes were identified: MLC leafs’ transmission, leaf end leakage, jaws’ transmission and the tongue and groove effect. 23 different metrics were defined to characterize these failure modes. Geometrical features as well as those features weighted by the monitor units were included. Machine Learning Algorithms (MLA) were developed to analyze the data. A two-leaf decision tree with information gain maximization was used for each feature to determine thresholds that result in maximizing the probability of identifying failing plans. Features were ranked according to T- test, Kolmogorov-Smirnov Test and the information gain in 2 leaf decision trees. Additionally, a RUSBoost algorithm with oversampling was developed to predict the virtual passing results of each plan. All the statistical analysis was performed using Matlab R 2014a.

Results: All features analyzed were significantly different in the plans that failed compared to the plans that passed QA at a 5% confident interval for all the tests performed, and the weighted geometrical features were determined to be highly significant. Thresholds resulting in a substantial increase of the probability of plans failing QA were determined. The most important feature for each failure mode, and accompanying threshold, are shown in Table 1. The weighted average ratio of MLC to jaw aperture (WAveRatio) was the most important feature overall. Plans with a WAveRatio smaller than 0.1090 were approximately 37 times more likely to fail. The modulation factor, which relates to different failure modes, was also an important feature in that plans exceeding a value of 6.86 were approximately 19 times more likely to fail. Finally, a cross-validated decision tree ensemble resulted in correctly classifying 87% percent of failing plans and 88% of passing plans.

Conclusion: Passing rates of IMRT plans can be described by weighted geometrical features. Different thresholds for these features can be used to improve the plan deliverability. MLA can play a key role in planning and QA, particularly for adaptive strategies, which may require QA to follow clinical delivery.

Failure Mode:	MLC leafs’ transmission	Leaf end leakage	Jaws’ transmission	Tongue and Groove effect
Features:	Weighted average ratio of MLC to jaw aperture	Fraction of Monitor Units delivered through leaf gaps smaller than 2mm	Weighted fraction of area receiving out-of-field radiation	Weighted average perimeter
Threshold:	<0.11	>0.21	> 0 .01	> 45.05 mm
Increased probability of plans failing:	37.02	9.13	5.86	5.29

Table 1. Failure Modes, features and their respective thresholds.

SP131.4 - Dosimetric analysis of respiratory-gated RapidArc with varying gating window times

Author(s): Ju Young Song
 Radiation Oncology, Chonnam National University Hwasun Hospital, Hwasun-Eup/KOREA

The volumetric modulated arc therapy (VMAT) which modulates beam intensity with the variation of a dose rate, a gantry speed and a multi-leaf collimator (MLC) positioning in each rotation angle can also use the respiratory gated method for the treatment of moving lesions. The gated VMAT method is inherently can make a dosimetric inaccuracy due to the uncertainty of gantry position during the stop and go motion of the heavy gantry. In this study, the dosimetric inaccuracy in a gated VMAT was reviewed with the analysis of measured dose distribution according to the variation of beam-on time period. The linear accelerator used in this study was Novalis Tx (Varian, USA) and total 10 VMAT plans for the treatment liver cancer were prepared. The used gate system was RPM-gating system (Varian, USA) and the Dynamic Platform Model 008PL (CIRS Inc., USA), which can simulate respiratory motion, was used to set up the beam-on time. Two different delivery quality assurance (DQA) plans for VMAT plans were created. One is the portal dosimetry method which use EPID (electronic portal imaging device) measurements and the other is the measurement of dose distribution using 2-dimensional diode detector array, MapCHECK2 (Sun nuclear, USA). The respiratory period was set to 4 sec and the DQA for gated VMAT was performed with the two different beam-on time sets, 1 sec and 2 sec. The matching rate in absolute dose mode was calculated by the gamma evaluation method for the gamma index, a 3% dose difference, 3 mm distance to agreement with 10% dose threshold. The calculated matching rates in each DQA measurement are shown in Table 1. The average matching rates of portal dosimetry analysis were 98.72% in the no gating treatment, 94.91% in the gating with 1 sec beam-on time and 98.23% in the gating with 2 sec beam-on time. The average matching rates of MapCHECK2 analysis were 97.80% in the no gating treatment, 95.38% in the gating with 1 sec beam-on time and 97.50% in the gating with 2 sec beam-on time. The dosimetric error was increased as beam-on time became shorter, which made more stop and go motion during a gated VMAT process. The results showed that a gated VMAT is proper to the patients who can sustain longer exhalation phase time, which enables longer beam-on time and less stop and go motion.

Table 1. The calculated matching rates in each DQA process for a gated VMAT

Patient	Portal Dosimetry			MapCHECK2 with MapPHAN		
	No Gating	Gating(1sec)	Gating(2sec)	No Gating	Gating(1sec)	Gating(2sec)
A	96.5%	95.2%	95.6%	99.5%	97.1%	99.0%
B	98.8%	95.4%	98.2%	98.3%	96.5%	98.2%
C	98.5%	94.6%	98.3%	97.5%	95.4%	97.4%
D	99.0%	91.7%	98.8%	97.7%	96.7%	98.1%
E	99.1%	93.0%	98.5%	97.2%	95.4%	97.8%
F	98.8%	95.3%	98.3%	96.9%	93.1%	96.5%
G	99.2%	95.5%	98.7%	98.6%	95.7%	98.2%
H	99.4%	96.6%	99.0%	96.5%	93.4%	96.0%
I	99.1%	94.4%	98.8%	98.5%	95.5%	97.5%
J	98.8%	97.4%	98.1%	97.3%	95.0%	96.3%

SP131.5 - Current status of dose-tracking using an integrated commercial system

Author(s): Stina Svensson¹, Mehrsima Abdoli², Jan-Jakob Sonke², Björn Hårdemark¹

¹RaySearch Laboratories, Stockholm/SWEDEN, ²Department Of Radiation Oncology, The Netherlands Cancer Institute, Amsterdam/NETHERLANDS

We have investigated the current status of dose tracking using an integrated commercial system (RayStation v4.7, Raysearch Laboratories). Ten patients treated for head and neck squamous cell carcinoma with dual arc VMAT plans were retrospectively dose-tracked based on daily acquired cone-beam CTs (CBCTs).

For each fraction, the following (automatic) steps were performed:

1. establishment of a frame-of-reference (rigid) registration between planning CT (pCT) and CBCT based on the treatment position alignment,
2. establishment of CBCT values to density table using a bulk density approach,
3. segmentation of external contour,
4. propagation of support ROIs from planning CT (pCT) to CBCT based on the treatment position alignment,
5. dose computation on CBCT by moving the beam setup according to the treatment position alignment and using the density table,
6. deformable image registration (DIR) between pCT and CBCT,
7. contour propagation of relevant organs-at-risk from pCT to CBCT for evaluation using the DIR, and
8. deformation of the dose computed on CBCT in step 5 to pCT geometry using the DIR for subsequent dose accumulation.

For the first fraction, all steps were done manually in RayStation. Thereafter, the remaining fractions were processed using a script.

The external contour was visually inspected by browsing through the CBCT in the transversal plane. In all cases but one, where the input threshold was adjusted manually, the automatic algorithm was judged to perform well.

For 6% of the fractions, the DIR algorithm did not succeed in creating an invertible deformation vector field using the default settings. In those cases, a volume of interest (VOI) excluding the shoulder region was defined and used as input to the DIR algorithm.

For DIR, the ANACONDA algorithm was used. It has shown to perform well in comparison with state-of-the-art methods for thoracic 4DCT data as well as being an improvement with respect to rigid registration for CT / CBCT DIR (Weistrand, Svensson, Med Phys, 2015). ANACONDA was run without using contour guidance as no contours were initially defined on the CBCTs. All DIRs, together with propagated contours, were qualitatively validated by visual comparison to rigid registration in a side-by-side view. Contours on pCT and CBCT were shown overlaid. In all cases, the DIR and propagated contours were satisfactory.

Average processing time for one fraction using scripting was 53 seconds on a machine running Windows 8.1 (64-bit) operating system with 32GB RAM, one Intel Xeon E5-2697 (12 cores) CPU and two AMD FirePro D700 GPUs. Both DIR and dose computation use GPU acceleration. Estimated time spent on visual inspection of external contour, propagated contours and DIR was around one minute. VOI creation and DIR recomputation took around two minutes for the fractions mentioned above.

To summarize, we have shown that retrospective dose-tracking can be done in an integrated commercial system. The process can be efficiently implemented using scripting. Some manual interaction is still required (6-10%) for initialization and occasional adjustment in segmentation and DIR.

References

Weistrand, Svensson. The ANACONDA algorithm for deformable image registration in radiotherapy, Med Phys, 42(1):40-53, 2015

SP131.6 - Enabling Continuous Quality Improvement in a Rapidly Changing Clinical Environment through a Multi-Year Multi-Centre IMRT QC Program: 3 Year Experience

Author(s): Andrea Mcniven, David A. Jaffray, Daniel Létourneau
Radiation Medicine Program, Princess Margaret Cancer Centre, Toronto/ON/CANADA

Introduction: Several different audit or credentialing programs have been created in multiple jurisdictions to assess radiotherapy planning and/or delivery performance using a variety of methodologies. The Collaborative Quality Assurance (CQA) Program is unique in that it was created as a multi-year program to assess site-specific planning and delivery quality through on-site visits that also incorporate diagnostic tests. Quantitative results for phantom positioning accuracy and MLC calibration from Year 3 is reported as well as the cumulative experience.

Methods and Materials: Fourteen independent radiotherapy centres have participated in the CQA Program. The yearly test includes a clinically realistic site-specific planning exercise (Year 1: head and neck, Year 2: prostate, Year 3: spine SBRT), and an on-site visit. The site visits include phantom imaging (diode array), dose calculation and dose delivery. The measurement portion of the visit includes delivery of the centre’s own plans (IMRT or VMAT), re-delivery of plans from previous visits and diagnostic tests. Diagnostic components include a vendor/MLC-specific IMRT plan created by the CQA program and quantitative analysis of phantom positioning accuracy and MLC calibration (introduced year 2 and 3 respectively). Measured to planned dose agreement is analyzed using both 3%/3mm criteria with gamma analysis and 3%/2mm criteria with composite analysis.

Results: 41 site visits completed to date, 14 in Year 3, including measurement of 17 spine SBRT plans (15 VMAT and 2 IMRT), re-delivery of 11 H&N and 6 prostate plans, and 3 new H&N plans and 6 new prostate plans. There has been a rapid adoption of VMAT delivery during the 3-year course of the program as only 3 of the 15 H&N plans in Year 1 were VMAT. Year 3 visits included 9 difference combinations of treatment planning system (4) and linac/MLC (5), and over 3 years the site visits have included 14 difference combinations. For the Year 3 spine SBRT plans, the percentage pass rate ranged from 97.3 – 100% for 3%/3mm gamma analysis and 89.4-100% for 3%/2mm composite analysis. Phantom positioning was good (all translational errors <2 mm) and was found to have no correlation with dosimetric results. Tighter tolerances are being investigated for correlation with MLC calibration. MLC calibration was quantified on 15 different linacs using portal imaging with all leaves (assessed at 5 different positions) within 2 mm of nominal position, and average impact on field size was < 1mm for 14/15 linacs. Overall, no significant change in performance was observed over three years for a single treatment site, however, on a single-centre basis, improvements up to 10% (3%/2mm criteria) were observed and can be linked to changes in planning technique and infrastructure.

Conclusion: The CQA Program has been established as a unique multi-year IMRT QA program incorporating diagnostic tools that can enable continuous quality improvement through feedback to the participants. Achievable performance levels have been identified as targets and the repeat visit model can highlight changes in IMRT planning and delivery performance and assess the impact of clinical practice changes, technology implementation or infrastructure change.

SP131.7 - A new approach to spatial gradient signal encoding for external beam radiotherapy delivery verification

Author(s): Robert K. Heaton¹, Xun Lin², Bern Norrlinger³, David Jaffray¹, Mohammad K. Islam¹
¹Radiation Oncology, University of Toronto, Toronto/ON/CANA-

DA, ²Institute Of Biomaterials And Biomedical Engineering, University of Toronto, Toronto/ON/CANADA, ³Radiation Physics, Princess Margaret Cancer Centre, Toronto/CANADA

Introduction: A spatially encoding dose-area product transmission chamber provides an effective method to monitor the delivery of external beam radiotherapy. Previous designs achieved spatial signal encoding by introducing a sloped separation between electrodes. The wedge shaped collection volume generates a linearly varying signal which depends on the position of the field on the chamber. In this study, we report on a chamber design to achieve a spatial gradient from a uniform electrode separation while providing measurements from complementary spatial gradients.

Methods: A spatial gradient is achieved by replacing the uniform area collecting electrode with an interleaved conducting comb pattern etched into an insulating substrate. The gradient is achieved by changing the width of the tines in the comb linearly with position, while the complementary interleaved pattern varies in the reversed pattern. In this configuration, a constant electrode plate spacing of 0.5 cm was used between polarizing and collection electrodes, with each measurement comprised of signals from each of the two combs.

Investigations of this chamber configuration used collection patterns etched into a PCB circuit board and a fluorine doped TiO₂ coating on a glass substrate, with a pair of complimentary tines occupying a width spanning 0.5 cm with a maximum widths varying from 0.05 to 0.45 cm over a length of 23 cm and 26 cm on PCB and glass, respectively. Field sizes on the order of 1 to 6 cm² were investigated, with the chamber moved through the beam to sample chamber positional response.

Results: Measurements for small fields performed at different positions along the gradient of the chamber show the expected positional dependence behavior, with complementary combs exhibiting a mirrored positional response. An example of the gradient response is shown in Figure 1. Simple calculations of the expected gradient yield a value of 0.067 cm⁻¹, which compares favourably to the measured gradient of 0.056 cm⁻¹ in the linear gradient range.

Conclusions: This study demonstrates the feasibility of using an interleaved comb collection electrode in a parallel plate chamber geometry to achieve spatial encoding for radiotherapy treatment monitoring. Comparable signal behavior was achieved for both the PCB and glass based substrates. Future work will focus on optimizing the design of chamber for clinical use.

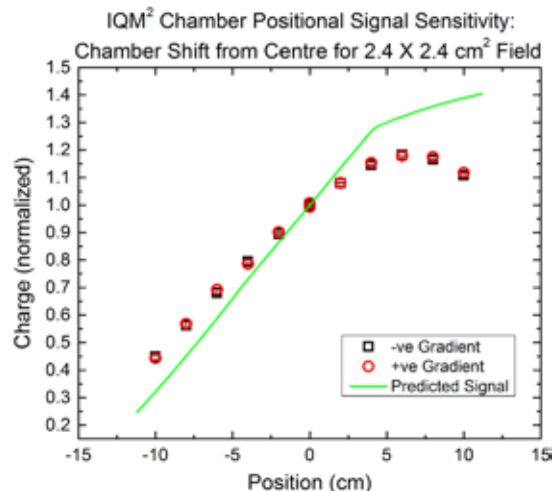


Figure 1: Detector signal as a function of position along the gradient direction. Note that the negative gradient has been reflected in position for ease of comparison.

SP132 - Guidelines and Radiation Protection Reference Levels for Patients and Personnel

TRACK 05: DOSIMETRY AND RADIATION PROTECTION

SP132.1 - Implementation of the new BSS including radiation safety culture in medicine

Author(s): M.M. Rehani¹, O. Holmberg², P. Jimenez³

¹Radiology, Harvard Medical School, Massachusetts General Hospital, Boston/MA/UNITED STATES OF AMERICA, ²Radiation Protection of Patient sUnit, IAEA, VIENNA/AUSTRIA, ³World Health Organization/Pan American Health Organization (PAHO), WASHINGTON/DC/UNITED STATES OF AMERICA

The International Basic Safety Standards for Protection against Ionizing Radiation and for the Safety of Radiation Sources, commonly known as BSS, provide a robust framework of safety requirements for medical exposures that can serve as a powerful tool for countries to strengthen radiation safety regulations and for medical physicists to strengthen their position and professional involvement. The new BSS have been jointly sponsored by 8 intergovernmental organizations, including the WHO, and published by the IAEA in 2014. The medical physicist (MP) as defined in the BSS is: "A health professional with specialist education and training in the concepts and techniques of applying physics in medicine and competent to practice independently in one or more of the subfields (specialties) of medical physics". This definition is very important as it categorizes the MP as a health professional. Previously the requirements for MPs were stringent primarily for radiotherapy; now, they have expanded as well for other areas like high dose procedures in radiology, image guided interventional radiology and nuclear medicine. The words medical physics/physicist occur more than 20 times in new BSS as many requirements and responsibilities have been assigned to the MP. Further there is clear assignment of responsibility to the Radiation Protection Officer (RPO) as pertains to oversight of the application of regulatory requirements, particularly insofar as radiation protection of workers and members of the public rather than patient protection. In some facilities, the MP can have additional responsibility as RPO whereas the inverse is not applicable. Promotion and maintenance of safety culture are requirements in the new BSS and MPs have an inherent role in its implementation, in fostering commitment and creating a common understanding, in providing means for implementation at the level of individuals and teams, and in practicing and encouraging dually inquisitive and learning attitudes. The presentation, while reviewing actions on implementation taken by IOMP, IAEA and WHO, will invite feedback and suggestions on implementation in different countries.

SP133 - Validation and Verification of Therapy Dose Delivery: Part 2

TRACK 05: DOSIMETRY AND RADIATION PROTECTION

SP133.1 - Dosimetric Comparison of 3DCRT, IMRT and VMAT for Spine Radiotherapy based on Secondary Cancer Risk

Author(s): J Rehman¹, J Ashraf¹, M Isa¹, M Afzal¹, G Ibbott², [James Chow](#)³

¹Islamia University of Bahawalpur, Bahawalpur/PAKISTAN, ²UT MD Anderson Cancer Center, Houston/UNITED STATES OF AMERICA, ³Princess Margaret Cancer Center, Toronto/CANADA

This study evaluated the secondary cancer risk after 3D-conformal radiotherapy (3DCRT), intensity modulated radiotherapy (IMRT) and volumetric modulated arc therapy (VMAT) for spine. Computed tomography image set of a RPC spine anthropomorphic phantom was exported to the Pinnacle³ treatment planning system. Radiation treatment plans for spine were created using the four-field 3DCRT, seven-field IMRT and dual-arc VMAT techniques. The mean and maximum doses (Table 1), dose-volume histograms and volumes receiving more than 2 Gy and 4 Gy of organs-at-risk (OARs) (Table 2) were calculated and compared. The lifetime risk for secondary cancers was estimated according to NCRP Report 116. Quality Assurances of IMRT and VMAT were performed using the Arc-CHECK method with gamma index criteria set to 3%/3mm. For our dosimetric comparisons, planning target volume coverages were found to be 90.5 %, 91.4 % and 95.9 %, for 3DCRT, IMRT and VMAT, respectively. VMAT was found to deliver the lowest maximum dose to esophagus (3.22 Gy), bone (6.48 Gy), heart (1.69 Gy), spinal cord (5.15 Gy) and the whole lung (4.52 Gy). Volumes of esophagus receiving more than 4 Gy were 0% for VMAT, 37.56% for IMRT and up to 43.76% for 3DCRT. The estimated risk for secondary cancer in the respective OAR is considerably lower in VMAT compared to other techniques. Results of maximum doses and volumes of OARs suggest that the risk of secondary cancer induction for spine in VMAT is lower than in IMRT and 3DCRT, whereas VMAT has the best target coverage.

Table 1: Maximum and mean doses of OARs.

Organs-at-Risk	3DCRT		IMRT		VMAT	
	Mean dose (Gy)	Max Dose (Gy)	Mean dose (Gy)	Max Dose (Gy)	Mean dose (Gy)	Max Dose (Gy)
Esophagus	3.20	6.58	2.38	6.50	0.84	3.22
Bone	2.17	6.17	2.07	6.86	0.98	6.48
Heart	2.96	5.17	1.26	2.77	0.71	1.69
Spinal Cord	3.29	5.96	2.88	6.45	0.88	5.15
Lung	1.08	6.44	0.49	6.28	0.52	4.52

Table 2: OARs receiving doses greater than 2 and 4 Gy.

Organs-at-Risk	3DCRT		IMRT		VMAT	
	%Val>2Gy	%Val>4Gy	%Val>2Gy	%Val>4Gy	%Val>2Gy	%Val>4Gy
Esophagus	52.87	43.57	43.26	37.56	7.4	0.0
Bone	47.28	25.24	37.9	32.57	17.36	7.85
Heart	83.12	2.59	7.92	0	0	0.0
Spinal Cord	74.56	50.55	57.78	48.27	6.75	0.0
Lung	22.57	5.71	5.96	0.5	3.87	0.05

SP133.2 - Validation of VMAT FSRT calculated doses using a multi-configurational phantom

Author(s): Michel Lalonde¹, Kevin M. Alexander², Tim Olding³, Tim Owen¹, Andrew Kerr¹

¹Cancer Centre Of Southeastern Ontario (ccseo), Kingston General Hospital, Kingston/ON/CANADA, ²Department Of Physics, Engineering Physics And Astronomy, Queen’s University, Kingston/ON/CANADA, ³Department Of Oncology, Queen’s University, Kingston/ON/CANADA

Introduction

Volumetric modulated arc therapy (VMAT) allows for a simultaneous integrated boost (SIB) technique to be employed for the delivery of brain fractionated stereotactic radiation therapy (FSRT). The goal of this study is to validate VMAT FSRT plans by comparing calculated doses against measured doses using a variety of dosimeters in a multi-configurational phantom.

Methods

VMAT FSRT plans were prepared using Eclipse treatment planning (Varian) and delivered with a Truebeam linac (Varian) onto an acrylic multi-configurational phantom (Fig. 1) that allows gel (Fricke-xylene orange), film (EBT3 Gafchromic), or ion chamber (Capintec PR-05P 0.07 cm³) dose measurements. In each plan, an 18 cm diameter spherical structure was contoured to mimic the whole brain within the phantom. Additionally, four spherical boost PTV structures ranging in diameter from 3-20 mm were contoured and positioned in a diamond pattern in the coronal mid-plane of the phantom (100 cm SAD). An SIB VMAT plan comprising two 6 MV coplanar full arcs was then optimized (AAA v10.0.25) to deliver 200 cGy/fraction to the whole brain structure and 400 cGy/fraction to each boost PTV. The plan was normalized to ensure that 95% of each boost PTV volume was covered by 400 cGy. Dose profiles were generated to compare calculated and measured dose. Gamma analysis was also performed for both film (2D) and gel (3D) dosimeters.

Results/Conclusion

Dose profile comparisons for certain boost PTV sizes are shown in Fig. 2. Ion chamber point dose measurement (at isocentre) agreed within 1% of the calculated dose. Measured peak boost PTV doses agreed with calculated doses to within 3.1% and 4.9% for gel and film respectively. Both 2D and 3D gamma analyses (3%/3 mm) showed greater than 95% agreement with calculated dose distributions. Film and gel dose profiles successfully characterized the full shape and gradients of the calculated profiles.

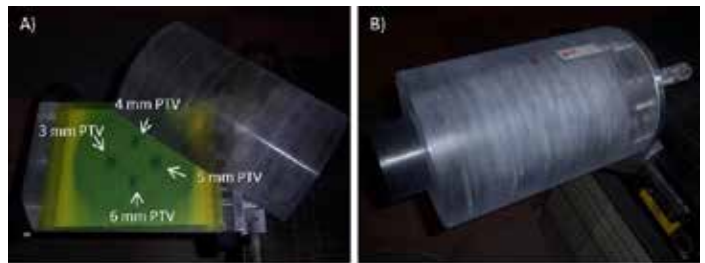


Fig. 1: Multi-configurational cylindrical phantom in two configurations: a) for film: overhead view with post-irradiation film at coronal mid-plane with top half removed, and b) for gel: lateral view of phantom with gel jar insert. The phantom is made of acrylic, measures 20.4 cm diameter by 30 cm length and is supported over the end of the linac couch. The third configuration for a point ion chamber is not shown.

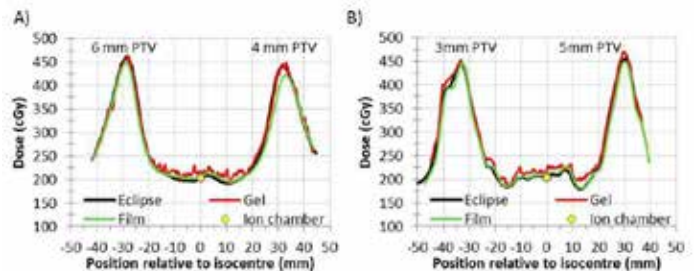


Fig. 2: Dose profiles through the isocentre in the coronal mid-plane of the phantom in the a) crossplane and b) inplane direction at 100 cm SAD. The PTV sizes for the corresponding dose peaks are labeled.

SP133.3 - Dosimetric verification for tangential breast irradiation in commercial treatment planning system using indigenous female wax torso.

Author(s): Kamlesh R. Passi, V.Saran Raj, Konthoujam Manimala Devi, Ishu Sharma, Naveen Kanda, Sandhya Sood
Department Of Radiation Oncology, Mohan dai oswal hospital, Ludhiana/INDIA

Dosimetric verification for tangential breast irradiation in commercial treatment planning system using indigenous female wax torso.

Kamlesh Rani Passi, Saran raj, Konthoujam Manimala, Ishu Sharma, Naveen Kanda, Sandhya sood.

Mohan Dai Oswal Hospital Department of radiation Oncology, Ludhiana (Punjab), INDIA.

Introduction:

Accuracy of Clarkson algorithm employed in a commercial 3D TPS was evaluated for conditions simulating tangential breast treatment. A breast phantom was fabricated from machineable wax to examine the accuracy of tangential breast irradiation. This Paper specifically describes the use of unique self-designed wax breast phantom to validate the accuracy of three-dimensional dose calculations performed by Xio- CMS planning system for breast tangential irradiation. Steven et al⁽¹⁾ has done a related study using anthropomorphic breast phantom .In our study the accuracy of dose calculations has been verified using 0.6cc ionization chamber. The treatment plans has been generated using the combined 6 and 15 MV photon beams and field in field technique. Measured doses have been compared to those calculated from the treatment planning system and found to be in good agreement with previously published results. Our results indicates that the inexpensive wax phantom can be used for verification in absence of expensive anthropomorphic breast phantom which may be of great help for verification of 3D breast plans in developing countries.

Material and Method:

A Wax phantom of size {33(l)*34(w)*29(h)} cm³ was fabricated in the departmental mould room. An important consideration in the design of the phantom was the reproduction of a geometry that could realistically duplicate the female torso in treatment position was taken care. The ion chamber was positioned 4.5 cm below from the surface of the breast phantom. The medial, lateral, superior, and inferior field borders previously marked on the phantom, were delineated with fiducial marker. CT images of the phantom with 0.6cc chamber were taken with 3-mm slice thickness. The images were imported to Cms Xio TPS for planning via Focal system after contouring. A phantom plan was created taking the calculation point at centre of chamber cavity volume by superimposing each patient plan in the indigenous breast phantom. 20 patients were taken for this study & Measurements were performed using a 0.6cc ionization chamber.

Result and Discussion:

Comparison was made between measured and calculated dose. We got good results for maximum number of patients within 1.5% and few patients above 3%. The dose-calculation verification measurements performed in this study utilizing a indigenous phantom clearly demonstrate absolute homogenous dose calculation accuracy even in case of tangential irradiation of the breast.

Conclusion:

A measurement of dose in the phantom shows good agreement in variety of treatment field configurations. This confirmed the utility of an indigenous breast phantom as a tool to assess accuracy of 3D tangential breast dose measurements for photon dose calculation.

References:

1. *Verification of the accuracy of 3D calculations of breast dose during tangential irradiation: measurements in a breast phantom. JOURNAL OF APPLIED CLINICAL MEDICAL PHYSICS, VOLUME 2, NUMBER 2, SPRING 2001.* Steven M. Kirsner,* Kari L. Prado,# Ramesh C. Tailor,\$ and Jose A Bencomo

SP133.4 - Dosimetric comparison of IMRT versus RapidArc (VMAT) optimization in whole breast irradiation of early stage breast cancer

Author(s): Nader Moshiri Sedeh

Physics, Florida Atlantic University, BOCA RATON/UNITED STATES OF AMERICA

Dosimetric comparison of IMRT versus RapidArc (VMAT) optimization in whole breast irradiation of early stage breast cancer

1. Florida Atlantic University, Department of Physics, Boca Raton, FL, 33431

2. South Florida Radiation Oncology, Boca Raton, FL, 33431

3. South Florida Radiation Oncology, Jupiter, FL, 33458

Purpose: The purpose of this study is to compare the dose-volumetric results of intensity modulated radiation therapy (IMRT) with RapidArc (RA Varian Medical Systems, Palo Alto, CA) for whole breast irradiation.

Methods: 25 patients previously treated for whole left breast (either RapidArc plan or IMRT) were the subjects of this planning study. Eclipse v 11.0.47 was used to make all retrospective plans using the same contours, energy, machine and normalization. Prescription dose to the planning target volume was 5000 Gy in 25 fractions. All

plans were normalized such that 100% covered 95% of planning target volume (PTV).

Results: V10, V20 and Dmean Gy of left lung significantly differed between the two plans (p-value <0.0001, =0.0473 and <0.0001 respectively), but V30 Gy did not (p-value 0.463). V25, D33 and Dmean Gy of heart significantly differed between the two plans (p-value =0.034, <0.0001 and 0.01 respectively), but V10 Gy did not (p-value 0.058). V5 of both right breast and right lung significantly differed between the two plans (p-value <0.0007 and =0.0112, respectively). Also Dmean of both right breast and right lung significantly differed between the two plans (p-value <0.0001 for both). The mean conformity index did not significantly differ, p-value 0.142. There was a significant difference between the mean MUs of the two plans as well, p-value <0.0001.

Conclusion: The dose-volumetric results of IMRT vs RA were different for most of the constraints although all plans were made within the threshold values recommended by RTOGs. Mean doses to left lung, heart, right lung and right breast were significantly different in RA than IMRT plans. It's been said that RA is more efficient/faster in the treatment delivery than IMRT in terms of total monitor units used, but in this study the results did not prove that. In fact, since both plans have the same mean of conformity index, based on what was observed in this study IMRT is not only faster but also safer regarding not irradiating the organs at risk.

[1]Email: nmoshiri@fau.edu

Cell: +1 561 318 1659

SP134 - Biosignal Sensing and Body Sensor Networks

TRACK 08: BIOSENSOR, NANOTECHNOLOGY, BIOMEMS AND BIOPHOTONICS

SP134.1 - Impedance and comfort of dry multipin electrodes for electroencephalography

Author(s): Patrique Fiedler¹, Richard Mühle¹, Stefan Griebel², Carlos Fonseca³, Filipe Vaz⁴, Lena Zentner², Frank Zanow⁵, Jens Hauelsen¹

¹Institute Of Biomedical Engineering And Informatics, Ilmenau University of Technology, Ilmenau/GERMANY, ²Mechanism Technology Group, Ilmenau University of Technology, Ilmenau/GERMANY, ³Departamento De Engenharia Metalurgica E De Materiais, Faculdade de Engenharia, Universidade do Porto, Porto/PORTUGAL, ⁴Departamento De Física, Universidade do Minho, Guimarães/PORTUGAL, ⁵Eemagine Medical Imaging Solutions GmbH, Berlin/GERMANY

Dry-contact electrodes allow for rapid, preparation-free EEG acquisition and new applications of brain signal analysis. However, dry electrodes require reproducible and stable electrode-skin contact to provide signal qualities comparable to conventional wet electrodes. Our recently introduced dry multipin electrodes comprise 30 pins on a flat baseplate. A non-conductive Polyurethane substrate is subsequently coated with a conductive Ag/AgCl film. Our earlier studies proved this design to enable hair layer penetration and a stable contact as long as sufficient contact force is applied.

In this study we focused on the influence of contact force and substrate flexibility (shore hardness) on the electrode-skin impedance on a hairless frontal position (Fpz) and a hairy temporal position (T4). The study was performed with 10 volunteers of similar age and different gender and hair length. An analogue force sensor and a custom-made electrode adduction and fixation mechanism allowed for reproducible variation of the adduction force between approx. 0.25 to 4 N. Furthermore, we tested shore A98, 90, 80, and 70 substrates. Positioning of the electrodes was performed manually. The evaluation of wearing comfort was performed using a scale 1-10 wherein 1 is absolute comfort while 10 is maximum pain. Impedance and force were recorded simultaneously. Comfort evaluation was performed prior and after each measurement.

The mean interfacial impedance for shore A98 electrodes decreased on average from 67 kOhm at 1 N to 36 kOhm at 2N, 30 kOhm at 3N, and 26 kOhm at 4 N at the frontal position. Furthermore, the standard deviation decreased from 34 kOhm to 20 kOhm, 16 kOhm, and 14 kOhm, respectively. Mean impedances on the hairy temporal positions decreased similar from 79 kOhm at 1N down to 21 kOhm at 4 N with standard deviations of 200 kOhm and 11 kOhm, respectively. A similar trend was visible for the other shore values. However, Shore A80 and A70 electrodes showed increased standard deviation and required higher contact pressure. The wearing comfort was best up to 1 N while it started to decrease to 1.2, 1.7 and 2.1 at 2, 3 and 4 N, respectively.

In summary, a shore hardness of A98 or 90 in combination with contact forces between approx. 2 and 3 N reliably provide sufficiently low and reproducible impedances while avoiding extensive pressure and thus maintaining wearing comfort. This information provides the base for designing future cap or helmet systems enabling comfortable, reliable rapid dry EEG acquisition.

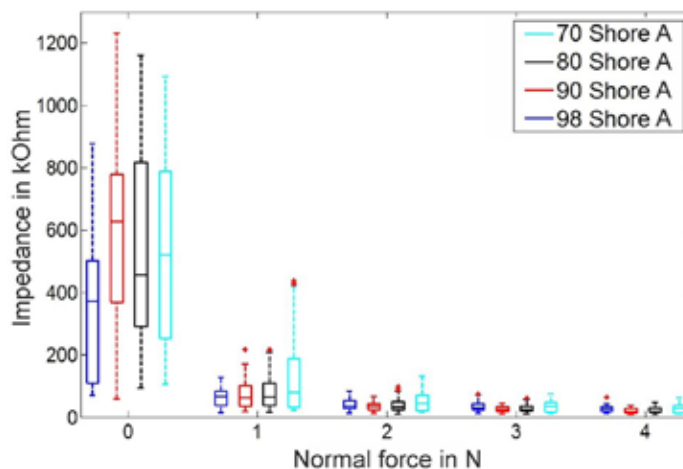


Figure 1: Relationship between impedance and adduction force applied to Multipin electrodes of different Shore A hardness

SP134.2 - Wearable Gait Analysis using Vision-aided Inertial Sensor Fusion

Author(s): Eric Ma, Milos Popovic, Kei Masani
Toronto Rehabilitation Institute, University Health Network, Toronto/CANADA

Gait analysis is useful in characterizing impaired gait in patients with various neuromusculoskeletal disorders. Contemporary gait analysis is conducted in a laboratory setting, typically consisting of numerous optical cameras and force plates. However, this setup is restricted to a constrained and artificial testing environment, which may lead to unnatural movements that poorly represent real-world human gait. In recent years, it has been demonstrated that the wearable inertial measurement units (IMU)—composed of accelerometers, gyroscopes, and magnetometers—can be an alternative for gait analysis in natural and ambulatory environments. IMU is capable of estimating the position and orientation of the human body during walking by integrating from acceleration and angular velocity. However, they are prone to unbounded drift due to the integration operation. Additionally, the relative positions of multiple IMUs cannot be accurately estimated using IMUs alone. These limitations prohibit the estimation of the global COP, which is an important gait parameter for the evaluation of postural stability and requires the knowledge of the relative positions of the feet. In this study, we introduced a solution to constrain the integration drift and to obtain the relative position of IMUs using vision-aided inertial sensor fusion.

We proposed a shoe-mounted system composed of two 9-axis IMUs, an IR camera, and a pair of instrumented shoes. Foot orientations and 3D foot travel trajectories were estimated using the IMUs, enhanced using zero-velocity updates and maximum spatial separation constraints. Using the camera on one foot and a four-point LED frame on the other foot, the relative position between the two feet was obtained using a pose estimation algorithm from computer vision. The inertial and vision measurements were sensor fused using an Extended Kalman Filter to minimize the errors in the 3D foot position outputs. The in-shoe COP of each foot was estimated using the instrumented shoes. Knowledge of the 3D foot positions was fused with the in-shoe COP to calculate the global COP. The proposed system estimated the 3D foot trajectories and the global COP. Based on these, the system was capable of estimating for key gait parameters such as step length, stride length, gait phases, and COP excursion. The validation of this system was performed against gait laboratory results for standing and walking tasks.

The proposed system is the first wearable system that provides

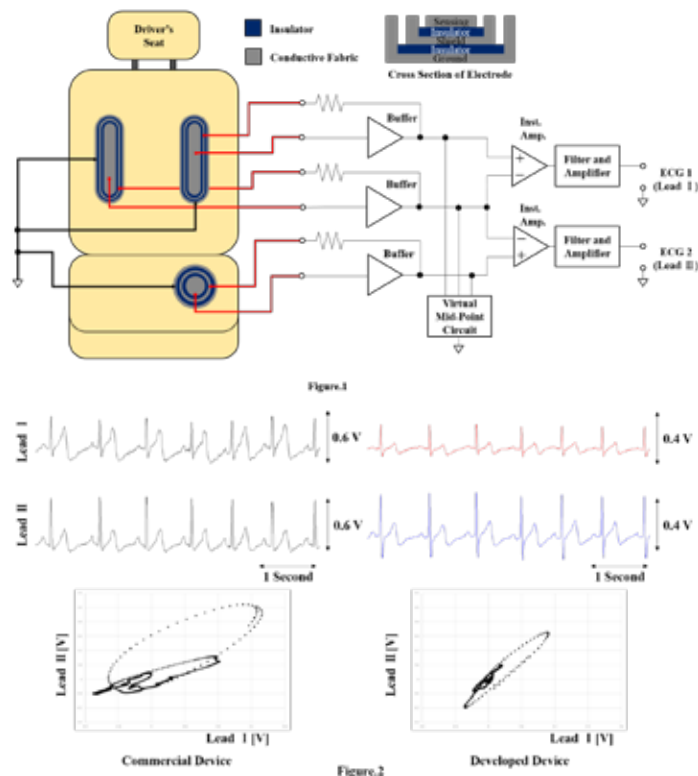
the estimation of global COP during gait. It provides a portable and unobtrusive method of performing lower-limb gait analysis in unconstrained and ambulatory environments, and it may enable new and practical applications in areas of clinical gait evaluation, long-term monitoring, rehabilitation, and sports performance.

SP134.3 - Two-Vector Capacitive Electrocardiogram Measurement Using Three Fabric Electrodes for Automobile Application

Author(s): Shunsuke Takayama, Akinori Ueno
Electrical And Electric Engineering, Tokyo Denki University, Tokyo/JAPAN

With a view to applying to driver's sensing, we propose a method for measuring two-vector capacitive electrocardiogram (cECG) from three electrodes placed on a driver's seat. The proposed method consists of three techniques of electrode arrangement, circuit grounding and an electrode configuration. The proposed electrode arrangement (see Fig.1) enables detection of biopotentials corresponding to limb lead I, II and III. Also, it has a feature that can keep steady electrode coupling. As shown in Fig.1, two of electrodes were horizontally placed on the right and left side of backrest, and another is placed beneath driver's left breech. Consequently, three electrodes form a triangle similar to Einthoven's triangle. The introduced circuit grounding technique is so called virtual middle point. All of three electrodes were used as exploring electrode and connected indirectly to the middle point. Two-vector cECG corresponding to lead I and II can be measured without any ground electrode. This technique has a tolerance to individual vectorcardiographic difference. Fig.2 shows measured two-vector cECG while subject is sitting on the driver's seat. The employed electrode configuration is composed of fivefold layers of sensing layer, shielding layer, ground layer and insulating layers (see Fig.1). It is reported to have a tolerant with movement artifact. [1]

[1] Y.Fukuyama, R.Suzuki, S.Takayama, A.Ueno, "Multi-layered Fabric Electrode for Movement Artifact Reduction in Capacitive ECG Measurement" IEEE EMBS Osaka, Japan, 3-7 July, 2013, pp.555-558.



SP134.5 - Detection of REM Behaviour Disorder Based on Low-Power Compressive Sensing of EMG

Author(s): Jeevan K. Pant¹, Mehrnaz Shokrollahi², Sridhar Krishnan¹
¹Department Of Electrical And Computer Engineering, Ryerson University, Toronto/CANADA, ²Department Of Computer Science, University of Toronto, Toronto/CANADA

Background:

Rapid eye movement (REM)-behaviour disorder (RBD) can be detected by using electromyogram (EMG) signals measured from the chin of the subject. Portable sensors attached to the chin and equipped with wireless transmission capability can be effective for the acquisition of such EMG signals. For durable operation, such sensors are desired to be power efficient. We study a low-power sensing framework based on compressive sensing (CS) for detection of RBD. This framework involves application of the CS technique based on sparse random projection matrix, and application of the CS reconstruction algorithms based on promoting temporal correlation. Classification algorithm used is based on nonnegative matrix factorization followed by kernel-based sparse representation.

Method:

The database contained several EMG signals recorded during the period of REM from the persons suffering from the RBD disorder and from those not suffering from it. Each record contained two signals obtained using two sensors placed on the left and right sides of the chin. CS was applied on the difference of the left-chin and right-chin signals with four values of the compression ratio (CR), namely, . Reconstruction of the difference signal was carried out by using the -RLS, -RLS, and BSBL-BO algorithms. The classification algorithm was used to classify whether the reconstructed difference signal corresponded to the RBD disorder or not.

Results & Conclusion:

Fig.1(a) shows classification accuracy (CA) averaged over total 10 realizations of the CS measurement matrix, and Fig.1(b) shows variance of CA over the same 10 realizations. As can be seen, approximately 72% average CA of RBD can be attained by applying CS with a compression ratio of 90%. By realizing a CS-based wireless sensor with a CR of 90%, its power consumption can be significantly reduced. Yet, 72% classification performance can be acceptable in various applications, including the one requiring rough estimation of the risk of happening RBD.

Variance of CA for -RLS algorithm is the smallest relative to that for the other algorithms. Thus, the -RLS algorithm offers the most stable classification performance.

Hence, the CS-based RBD classification system can be useful for the development of low-power CS-based sensor for a stable detection of RBD.

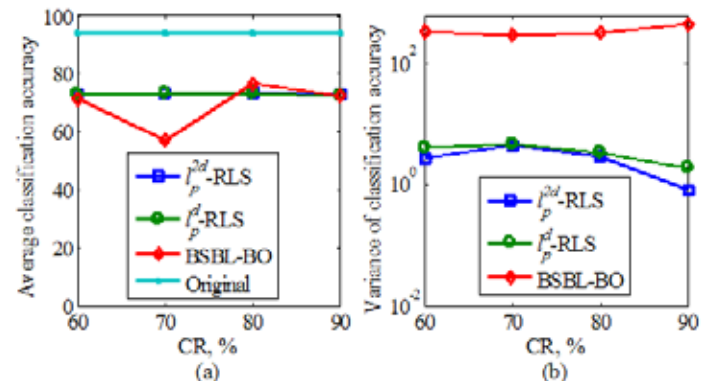


Fig. 1: (a) Average classification accuracy, (b) Variance of classification accuracy.

SP134.6 - Externally applied pressure on the skin electrode impedance

Author(s): Bahareh Taji¹, Adrian D.C. Chan², Shervin Shirmohammadi³

¹University of Ottawa, Ottawa/CANADA, ²Carleton University, Ottawa/CANADA, ³Engineering, University of Ottawa, Ottawa/ON/CANADA

The objective of this abstract is to introduce the effects of externally applied pressure on the skin-electrode impedance for electrodes such as standard Ag/AgCl and orbit electrodes. This issue is of interest because it is one of the factors that affect the quality of signal collected from that electrode. Skin-electrode impedance is modeled as an electrical circuit including a resistor (R_s) in series with a parallel resistor (R_d) and capacitor (C_d). Skin-electrode impedance is measured by an impedance interface device and a frequency response analyzer.

Pressure is applied with a regular Omron blood pressure cuff. Experiments are done in several trials to verify electrodes behaviour under pressure and their tendency to keep the changes due to applied pressure. Measurement procedure steps are as follows:

- a. Two electrodes were placed on the subject's right bicep at a 7 cm distance from each other and connected to the measurement devices.
- b. The Omron cuff was wrapped around subject's bicep on top of the electrodes.
- c. The pressure was set to 0 mmHg or 30 mmHg appropriate for the trial (Table 1).
- d. Wait for 1 minute.
- e. The impedance was measured.
- f. Repeat, starting from step c, until all trials are completed.

Table 1 Cuff pressure per trials

Trial	T1	T2	T3	T4	T5	T6	T7	T8	T9	T10	T11
Cuff pressure (mmHg)	0	30	0	30	0	30	0	30	0	0	0

Results show that skin-electrode impedance of orbital electrodes decreases as pressure increases and after some trials they tend to keep the changes and vary less and less when pressure is applied and removed, whereas Ag/AgCl electrodes variation due to pressure are small and negligible.

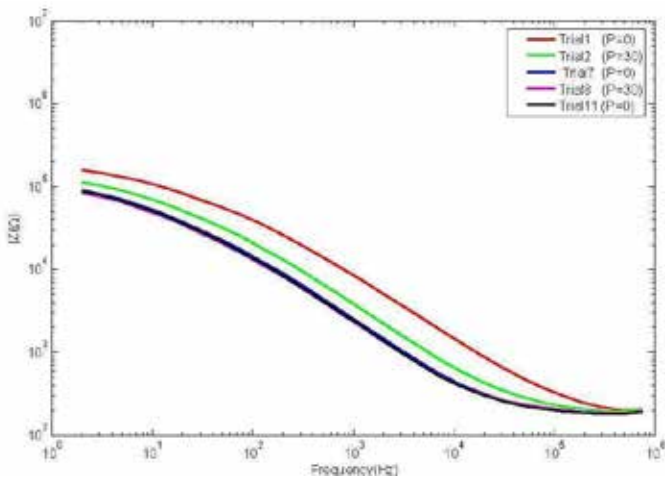


Figure 1 Skin-electrode impedance of Orbital electrodes

SP135 - Neural Signal Processing: Part 2

TRACK 11: NEUROENGINEERING, NEURAL SYSTEMS

SP135.1 - Epileptogenic zone estimation by localizing the generators of delta and high-frequency rhythms extracted from human scalp EEG

Author(s): Daniel Jacobs¹, Chunsheng Li¹, Trevor Hilton¹, Yotin Chinvarun², Jose Martin Del Campo³, Peter Carlen³, Berj L. Bardakjian¹
¹Institute Of Biomaterials And Biomedical Engineering, University of Toronto, Toronto/CANADA, ²Phramongkutklao Hospital, Bangkok/THAILAND, ³Toronto Western Hospital, Toronto/CANADA

Up to 20 million people globally might develop drug-resistant epilepsy and may become candidates for surgical intervention. However, 40% of patients who undergo surgery to remove seizure onset zones (SOZs) do not achieve long-term seizure freedom. This may be because the SOZs identified by electroencephalography (EEG) do not completely represent the epileptogenic zone (EZ). Correct identification of the EZ remains a challenge. Our lab has identified that EEG rhythms with delta and high frequency oscillations (HFO), recorded intracranially from subdural electrode grids (SEGs) placed in patients suffering from epilepsy, contain novel markers for the seizure onset zone. This work hypothesizes that these rhythms may be isolated from scalp EEG, whereupon their generators can be approximately localized to an intracranial location. This would facilitate the placement of intracranial electrodes to more completely identify the EZ.

The patient data used to compare rhythm localization between scalp and intracranial EEG was recorded from 4 patients with epilepsy at the Toronto Western Hospital, Toronto, Canada. The patient data used to validate the rhythm localization method consists of intracranial EEG recorded from 7 patients with epilepsy at the Phramongkutklao Hospital, Bangkok, Thailand.

Methods: Electrical noise and all harmonics are removed via notch filtering. Rhythmic decomposition of individual scalp EEG traces is performed by ensemble empirical mode decomposition (EEMD). This permits isolation of the rhythms of interest. Artifact within the selected rhythms is distinguished by analysing components produced by independent component analysis (ICA): blink components can be manually distinguished, and other artifactual components are identified by the Multiple Artifact Rejection Algorithm (MARA) plugin within the EEGLAB toolbox. These artifact components are removed, and the remaining rhythmic components are reconstructed to their original scalp distribution. Localization of the generators of this distributed rhythmic activity is performed using standardized low-resolution brain electromagnetic tomography (sLORETA).

Results: Preliminary investigations indicate that the generators of particular rhythms can be localized to intracranial regions with the following properties: (a) They coincided with placement of intracranial SEGs in patients as determined by the neurologists, and (b) the patients were seizure free (Engel class I) after surgery. As such, this technique may serve as a useful tool in the placement of SEGs.

The authors would like to acknowledge financial support from NSERC and CIHR.

SP135.2 - Automated Alzheimer's Disease Diagnosis Using a Portable 7-Channel Electroencephalography Device

Author(s): Raymundo Cassani, Tiago H. Falk
INRS-EMT, Montreal/QC/CANADA

The world elderly population is growing at its fastest rate ever; by 2050, 2 billion people will be aged over 60. For many individuals, age-related diseases cause cognitive decline and eventually limited functional capacity. Across North America, Alzheimer's disease (AD) has become the fifth leading cause of death in persons aged over 65 years. In order to tackle these problems, the WHO, together with Alzheimer's Disease International, have called on governments to implement national dementia plans to improve early diagnosis. In response to this call, several new biomarkers have been found based on expensive equipment, such as SPECT and fMRI. Such equipment, however, is scarce in low- and middle-income countries, as is the availability of trained medical personnel to operate them. Recent projections, on the other hand, suggest that by 2050, 71% of all people with dementia will live in low- or middle-income countries, thus it is crucial that lower-cost solutions be found.

Recently, the authors have proposed a new feature extracted from electroencephalography (EEG) that showed to discriminate healthy elderly patients from patients with AD with over 90% accuracy [1-3]. The proposed features characterize the cross-frequency coupling of EEG amplitude modulations, as detailed in [3]. These previously obtained results, however, relied on 20+ channel EEG systems, which can cost in the order of several tens of thousands of dollars. In this paper, we explore the use of a lower-cost solution, namely the use of the 7-channel portable COGNISION™ system (Neuronetrix, USA). Data was collected across seven centers in the USA during a clinical trial led by Neuronetrix [4]. Eighty-three healthy participants (age: 73 ± 7 years; education: 15 ± 3 years; 49 female) and 93 patients with mild-AD (age: 76 ± 7 years; education: 14 ± 3 years; 49 female) were recruited and performed a 30-minute ERP test followed by a 3-minute resting (eyes-open) period.

Here, fourteen cross-frequency amplitude modulation features were extracted, for each of the seven electrodes, from the 3-minute resting period. Features were extracted after automated EEG artifact removal [1]. A Kruskal-Wallis test with Dunn-Sidak posthoc correction was performed to test the discriminative power of the features. Of the 14 extracted features, six were found to provide significant difference between the two groups across the seven tested electrode sites. Features that resulted in superior separation between the two classes related to beta-theta, alpha-delta, and alpha-theta amplitude modulation couplings. These features coincide with those found with higher-density EEG systems, thus show their importance for AD diagnosis. Such findings suggest that AD risk assessment may be done *in-situ* not only in some of the poorest countries in the world, but also in remote or rural regions of developed countries that have with limited access to qualified medical personnel. In such cases, remote patient monitoring could play a key role.

References

- [1] R. Cassani et al, *Frontiers Aging Neuroscience*, 6(55), March 2014.
- [2] F. Fraga et al, *PLoS ONE*, 8(8): e72240, August 2013.
- [3] T. Falk et al, *EURASIP Journal Advances Signal Processing*, 2012, ID:192.
- [4] Clinicaltrials.gov ID: NCT00938665.

SP135.3 - Transient Propagation of Information Among Cultured Hippocampal Cell Assemblies in a Two-Chamber MEMs Device

Author(s): Bruce C. Wheeler¹, Gregory J. Brewer², Thomas Demarse¹

¹Biomedical Engineering, University of Florida, Gainesville/UNITED STATES OF AMERICA, ²Biomedical Engineering, University of California at Irvine, Irvine/CA/UNITED STATES OF AMERICA

Transiently active neuronal cell assemblies are thought to underlie many operations within the brain and provide the basis for a number of complex cognitive processes. Perhaps one of the most well known structures is that of the hippocampus. Using advanced MEMs technologies combined with multi-electrode electrophysiological recording (shown in Figure 1), we created a two-chamber system in which cell populations from distinct regions of the hippocampus are co-cultured and communicate via axon growth through micro-scale tunnels connecting each chamber including DG(dentate gyrus)-CA3, DG-DG, and CA3-CA3. In a prior report we verified the cell composition and specificity unique to each region using genetic (PCR) analysis and provide evidence for directional connectivity between DG and CA3 that recapitulates the feed-forward nature of the hippocampus.

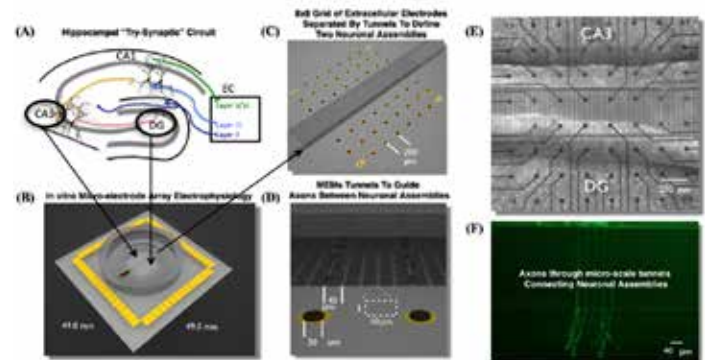


Figure 1. A MEMs device for the study of cell-assembly activation and transmission of information in an *in vitro* pair-wise model of the Hippocampal Tri-Synaptic loop (Panel A). Neurons from each region are cultured on a multi electrode array (B) containing a two-chamber PDMS device (C-E) that connect each population via axons through the tunnels (F).

Each region became spontaneously active with the emergence of population-wide neuronal oscillations in the form of rapid bursts of neural activity that appeared to propagate from region to region. This ensemble of activity in each region was then analyzed to detect the presence and activation of cell-assemblies within these oscillations and measure any communication that might occur between assemblies within and between each region. An average of 4.4 ± 0.1 cell assemblies per region were detected during each 5 min recording. Each assembly was composed of an average of 9.6 ± 0.3 member neurons with 2.2 ± 0.1 of those neurons belonging to more than one assembly. We also found that the anatomically correct pairing of DG with CA3 resulted in DG and CA3 regions with more cell-assemblies and differences in the number of neurons within each assembly compared to DG-DG and CA3-CA3 alone. The average duration of each activation of an assembly was for 60 ± 2 ms during bursts. Cell Assemblies were also persistent recurring 177 ± 7 times during each recording. Finally we show that neurons that are members of cell-assemblies activated during each burst event in DG-CA3 communicate across regions with greater fidelity compared to the other groups.

SP135.4 - Investigating the Cortical Dominance in the Pre-Motor Potential during Unilateral Voluntary Task

Author(s): Raquel S. Branco, Paulo José G. Da Silva, Maurício Cagy, Antonio F.C. Infantesi

Lapis - Signal Proc Lab, Biomedical Engineering Program - COPPE - UFRJ, Rio de Janeiro/BRAZIL

The Bereitschaftspotential (BP), a negative-slope electroencephalographic (EEG) activity that precedes voluntary movement, is related to the neuronal motor planning and postural control strategies. Generally, this pre-motor potential is generated 2s prior to onset-movement, with predominance over the contralateral motor cortex area. In this study, the influence of cortical dominance was investigated using the BP from 26 healthy subjects (17 right-handed). Motor task consisted of self-paced unilateral shoulder flexion carried out in orthostatic posture with eyes open (in order to minimize alpha activity). During this task, EEG (C3: right shoulder cortical response; C4: the left one), EMG of the anterior deltoid muscle and accelerometer signal (positioned on the styloid process of the radius) were acquired simultaneously. A set of 100 unilateral movements (50 for each shoulder) and 50 bilateral movements (used as distracter stimuli) were carried out in random order and distributed into five blocks. An inter-block interval of 3min (subjects resting seated) was used to avoid EEG habituation and muscle fatigue. The BP was estimated by coherent averaging artifact-free EEG epochs, synchronized by the onset-movement detected by the accelerometer. Figure 1a depicts, for a right-handed volunteer, the BP and its PMM (movement-monitoring potential), in which it is noticeable higher slopes and PMM amplitude in the dominant cortex (C3: right shoulder) compared to those of the non-dominant (C4: left shoulder). Besides, the PMM occurred previously for dominant cortex. Similar results was observed for left-handed volunteer (Figure 1b). These findings could suggest that the motor planning is related to cortical dominance and therefore the ability to perform the task with the dominant limb. Nevertheless, for all subjects, independently on the laterality, the Wilcoxon sign-rank test suggested no difference ($p=0.38$) between the slopes (and also the PMM amplitudes) for dominant and non-dominant cortices. Moreover, no difference was observed (Wilcoxon $p=0.58$) in the PMM time occurrences. Besides, regardless the dominant cortex, no difference was observed between right and left-handed volunteers (Wilcoxon-Mann-Whitney, $p=0.16$). These findings are maybe explained by the inter-subjects variability to plan and perform the motor task. Alternatively, independent on the laterality of the subjects, they indicate no influence of the dominant cortex in the pre-motor potential during unilateral self-paced shoulder tasks.

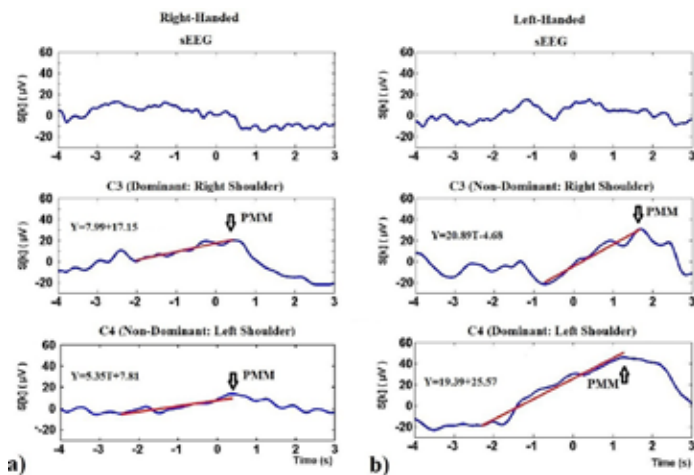


Figure 1. Coherent average of the spontaneous EEG and task (C3: right shoulder; C4: left shoulder): a) right-handed volunteer (#14); b) left-handed volunteer (#3). The regression line (red) estimated from the minimum of BP (between -2500 and -700ms) and PMM.

SP135.5 - A New Dynamic Virtual Stimulation Protocol to Evoke M-VEP and Linear Vection during Orthostatic Posture Control

Author(s): Paulo José G. Da Silva, Maurício Cagy, Antonio F.C. Infantesi

Lapis - Signal Proc Lab, Biomedical Engineering Program - COPPE - UFRJ, Rio de Janeiro/BRAZIL

Cortical processing of visual motion and self-motion sensation has been related to the perception-action cycle during postural control protocol. The dynamic virtual reality stimulation (DS) was employed to investigate postural control response using the motion-related visual evoked potential (M-VEP) and linear vection. The multi-channel electroencephalogram (EEG) and the center-of-pressure (COP) displacement signals were acquired simultaneously during stabilometric test with DS scenes interspersed by 10s of static scene (SS). The trials from 29 healthy volunteers were performed in orthostatic position on a force platform observing a virtual scene ($1.72 \times 1.16m$) projected 1m ahead and centered at the vision line (visual angle: $\theta_l = 81.4^\circ$ and $\theta_v = 60.2^\circ$). The scenario was moved randomly in forward (DSF) or backward direction (DSB), during 250 ms (velocity: 2m/s), so that the furniture was expanded or reduced, while the chess-board floor, walls and ceiling were moved in parallel direction. For each DS, the luminance varied 2 cd/m². Such dynamic effect was employed to generate an optical flow as a tunnel pattern. Thus, DSF increases optical flow up to the periphery of the visual field. Otherwise, DSB, optical flow decreases. For each subject, the M-VEP was estimated by coherent averaging up to 50 artifact-free EEG epochs, synchronized by the onset of DS. Similar procedure was applied for the COP signal. Figure 1 depicts the grand-averaged M-VEPs (N2 peak dominance) and the COP displacement response due to vection. The running t-test ($\alpha = 0.05$) suggested that there is difference between DSF and DSB M-VEPs 600 ms after DS onset, with an increasing time delay from occipital to central derivations (gray area, Figure 1a). Moreover, considering no significant change in COP displacement just preceding DS (ANOVA, $p > 0.8$), the DS induced COP displacements in the same direction of the exhibiting scene (Figure 1b, $p < 0.001$). Therefore, vection is dependent on the DS direction, mainly during DSF, for which the linear vection varies from 72% to 90% (Figure 1c). These findings suggest that the cognitive, planning and motor processing to control balance depends on the DS direction and hence indicate the potential applications of this dynamic virtual protocol in postural control studies.

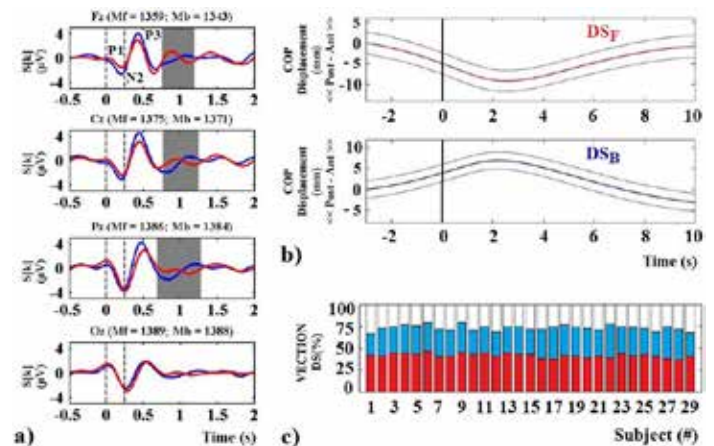


Fig. 1 Grand-averaged: a) M-VEP from DSF (red) and DSB (blue). Vertical dashed lines indicate DS (250ms). In gray, time interval where the waveforms differs (running t-test, $p < 0.05$); b) COP displacement; c) amount of vection.

SP135.6 - Assessment of Bilateral SSEP Signals Enhancement following Transectional Spinal Cord Injury Using Linear Modeling

Author(s): Hasan Mir¹, Hasan Al-Nashash¹, Thow Thow Xin Yuan², Jukka Kortelainen², Soo Min Chua², Janani Manivannan², Astrid Astrid², Angelo H. Ali³

¹Bme, American University of Sharjah, singapore/SINGAPORE, ²Sinapse, National University of Singapore, Singapore/SINGAPORE, ³Orthopedic Surgery And Biomedical Engineering, National University of Singapore, Singapore/SINGAPORE

Introduction: Partial or complete loss of sensory and motor function between the brain and peripheral nerves is a likely consequence of spinal cord injury. However, it has been reported that a certain degree of plasticity in the central nervous system may result in functional recovery. Somatosensory evoked potentials (SSEP) have been used extensively in assessing the functional integrity of spinal cord pathways by examining the reduction or increase in signal amplitude and time latency. In this study, we use linear modeling coefficient values to quantify the degree of relationship between contralateral forelimb SSEPs recordings. Preliminary results demonstrate the effectiveness of this method in quantifying the level of similarity between SSEP signals obtained from different limbs.

Protocol: The SSEPs were recorded from 4 epidural screw electrodes implanted to the cranium of 22 rats. The electrodes were located at the specific somatosensory cortex areas of hindlimbs and forelimbs. Dental cement was applied to fix the electrodes to the cranium. Four different types of spinal cord transection injuries were produced, located at either the T8 or T10 of the rat spinal cord: (i) left-hemisection at T8, (ii) right-hemisection at T10 (iii) left T8 and right T10 hemisection and (iv) full transection at T8. SSEPs were recorded from a cohort of 20 animals with 5 animals in each injury type. The SSEP recordings were recorded day 4, 7, 14, and 21 post-injury. The evoked potentials were generated by stimulating the left and right Tibial nerves of the hindlimbs and Median nerves of the forelimbs, one limb at a time, with a pair of stainless steel sub-dermal needle electrodes. The stimulation of each limb was carried out using 150 consecutive current pulses with amplitude of 3.5 mA and a duration of 200 μ sec delivered at a frequency of 0.5 Hz. During the stimulation, the SSEPs were recorded with a sampling frequency of 4882 Hz.

Method: The post-injury SSEP signals were modeled as a transformation of the baseline signal. The transformation was assumed to generate from a finite-impulse response (FIR) filter with a sparse set of delays. The solution of the filter coefficients were combined into a single metric, termed the H-index, in order to reflect the level of injury,

Results: Figure shows the H-Index obtained after modeling the SSEP signals recorded from the left cortex (corresponding to RF) after stimulating the RF. The SSEP signals recorded on Days 4 and 7 from the right cortex (corresponding to LF). The x-axis shows the rat number increasing with the level of injury. It is observed that the H index increases with injury level depicting an increased degree of correspondence between signals recorded from left and right sides of the cortex.

SP136 - Brain, Head/Neck, Spine: Part 1**TRACK 12: MEDICAL DEVICES****SP136.1 - Photopolymerization device for minimally invasive implants: application to nucleus pulposus replacement**

Author(s): Andreas Schmockler¹, Azadeh Khoushabi², Pierre-Etienne Bourban³, Dominique Pioletti², Christophe Moser¹

¹Microengineering Institute, Ecole Polytechnique Fédérale de Lausanne, Lausanne/SWITZERLAND, ²Institute Of Bioengineering, Ecole Polytechnique Fédérale de Lausanne, Lausanne/SWITZERLAND, ³Laboratory Of Polymer And Composite Technology, Institute Of Materials, Swiss Federal Institute of Technology, Lausanne/SWITZERLAND

Photopolymerization is a common tool to harden materials initially in a liquid state. A surgeon can directly trigger the solidification of a dental implant or a bone or tissue filler. Traditionally, photopolymerization has been used mainly in dentistry. Over the last decade advances in material development including a wide range of biocompatible gel- and cement-systems open up a new avenue for in-situ photopolymerization for musculoskeletal, cardiovascular or neurosurgical applications.

However, at the device level, surgical and endoscopic probes need to be developed to deliver the liquid photopolymer, harden it by light and to monitor that the hardened material has the appropriate property. Here we present a miniaturized light probe where a photoactive material can be 1) mixed, pressurized and injected 2) photopolymerized or photoactivated and 3) monitored during the chemical reaction. The device enables surgeries to be conducted through a hole smaller than 1 mm in diameter. Beside basic injection mechanics, the tool consists of an optical fiber guiding the light required for photopolymerization and also for chemical analysis. Using fluorescence spectroscopy, the current state of the photopolymerization is inferred and monitored in real time.

Biocompatible and highly tunable Poly-Ethylene-Glycol (PEG) based hydrogels were used as injected material. The device was tested on a model for intervertebral disc replacement and hydrogels were successfully implanted into a bovine caudal model. These in-situ photopolymerized implants were evaluated at the tissue level (tissue integration and mechanical properties), at the cellular level (biocompatibility and cytotoxicity) and ergonomic level (sterilization procedure and feasibility study) and thus seem to be a promising alternative to traditionally used tissue and bone fillers.

Currently further promising applications are under investigation. The results will be presented at WC2015.

SP136.2 - Design and Technical Evaluation of an Implantable Passive Sensor for Minimally Invasive Wireless Intracranial Pressure Monitoring

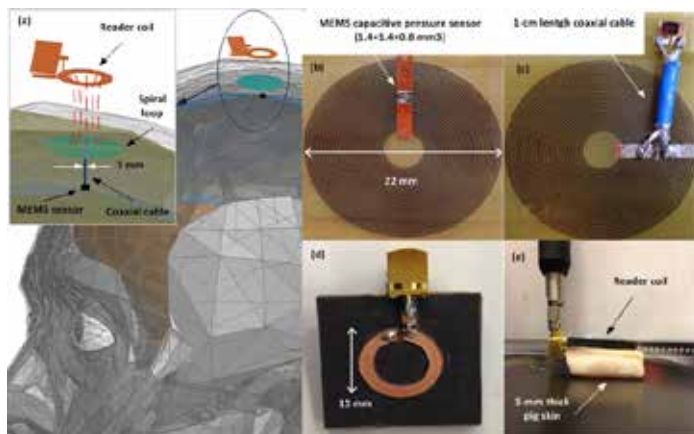
Author(s): Mohammadhossein Behfar, Elham Moradi, Lauri Sydänheimo, Toni Björninen, Leena Ukkonen
Electronics And Communications Engineering, Tampere University of Technology, Tampere/FINLAND

Elevated Intracranial pressure (ICP) is characterized as neurological problem mainly caused as a consequence of traumatic brain injuries (TBI) and cerebrospinal fluid (CSF) circulation disorders. Early detection of increasing ICP is of great importance in management of TBI. The main complications with the existing methods are the risk of infection and hemorrhage due to catheter insertion into the intracranial cavity. To address this issue, battery powered implant-

able wireless ICP measurement devices were proposed. The main drawback of this kind of devices is the increased size of the implants and limited lifetime. Therefore, passive (battery less) implantable sensors are attractive for minimally invasive ICP monitoring.

In this research, we designed and evaluated an implantable passive sensor for continuous wireless subdural ICP monitoring. The sensor consists of a 30-turn spiral loop in parallel with a mm-size (1.4x1.4x0.8 mm³) microelectromechanical systems (MEMS) capacitive pressure sensor forming an LC tank (Fig. 1b). The sensor is made on an ultra-thin (50 μm) flexible polyimide substrate making it minimally invasive for implantation. The pressure sensor is wirelessly interrogated through the near field inductive link between the implantable sensor and an on-body reader coil. The on-body reader coil is connected to a capacitor to form an LC circuit. The two LC tanks form a simple and efficient telemetric system communicating through strong magnetic coupling. Consequently, ICP variation can be detected through: 1) change in the resonance frequency of the implantable sensor, 2) variations of the magnitude and phase angle of the reader coil's input impedance.

The effect of human skin on the wireless operation was simulated by placing a 5-mm thick pig skin between the sensor and the reader coil (Fig. 1e). The sensor was designed so that the spiral loop is implanted under the skin and the pressure sensor is placed into the subdural space (Fig. 1a). The spiral loop and the pressure sensor are connected through a coaxial cable with the length of 1 cm (Fig. 1c). In order to evaluate effects of the cable on the sensitivity of the pressure readout, we conducted two sets of experiment with and without the cable. The results show that the cable only reduces the sensor's sensitivity toward the resonance frequency variation and does not affect the sensitivity toward the magnitude and phase angle variations. Evaluation of the sensor proved the capability of highly linear pressure measurement ranging from 0 to 70 mmHg at 5-mmHg intervals.



SP136.3 - Investigating the Feasibility of EVestG Assessment for Screening Concussion

Author(s): Abdelbaset Suleiman¹, Brian Lithgow², Behzad Mansouri³, Zahra Moussavi²
¹Biomedical Engineering, University Of Manitoba, Winnipeg/CANADA, ²Electrical And Computer Engineering, University Of Manitoba, Winnipeg/MB/CANADA, ³Internal Medicine (neurology), University Of Manitoba, Winnipeg/MB/CANADA

In this project we evaluated a new technology, Electrovestibulography (EvestG™) that holds the potential to objectively, quickly and cost-effectively measure both the severity of concussion and quantitatively measure recovery from concussion. EVestG signals

are recorded painlessly and non-invasively from the external ear in response to a vestibular stimulus; they are the brainstem sensory oto-acoustic signals modulated by the vestibular response. When concussed, people commonly experience balance (vestibular) problems, dizziness, confusion and memory loss. Considering the well-known bidirectional anatomical links of the vestibular system, it is expected that the EVestG signals will change after a concussion.

In this study, we investigated the relationship between characteristic features of the extracted field potentials (FPs) of EVestG signal in people with side-impact concussion in comparison to those of control subjects. Our study included 10 side-impact concussed individuals (4 Right side-impact and 6 left side-impact) and 10 age and gender matched healthy individuals as control subjects. We analyzed the EVestG signals recorded during side tilt motion. The results show that the difference between the left and right FP width, is significantly (P<0.05) different between two groups. Figure 1 shows the left-right difference in the area (bounded by the baseline and the action potential (AP) point) of the normalized FPs extracted from acceleration and deceleration phases of the EVestG signals during the side tilt. The features show a clear asymmetry between the left and right side vestibular responses for the concussed but not control group. In 3 out of the 4 right side-impact patients, the FP in the right side was narrower than the left side. In 5 out of the 6 left side impact patients, the FP in the left side was narrower than the right side.

The results of this study is encouraging on the use of EVestG analysis for monitoring the effects of concussion.

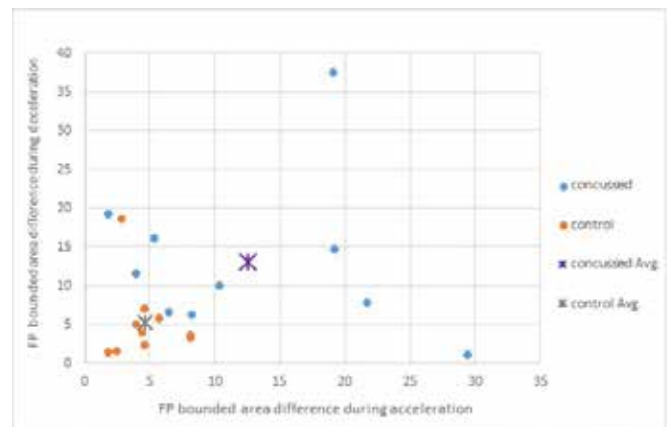


Figure 1: Control vs. Side concussed patients (n=1010) after subtracting the area (bounded between the baseline and the AP point) in right side from the left side during acceleration and deceleration phases of side tilt.

SP136.4 - Transcranial Direct Current Stimulation of the Rat Medial Prefrontal Cortex: Antidepressant Effects and Regional Brain Changes

Author(s): Francis R. Bambico, Jose N. Nobrega
 Centre For Research Imaging, Centre for Addiction and Mental Health, Toronto/CANADA

Transcranial direct current stimulation (tDCS) is a neuromodulation procedure that employs weak DC to stimulate brain regions non-invasively. Its basic design has been investigated for psychiatric disorders, such as melancholic depression, as far back as the early 19th century (Parent, *Can J Neuro Sci* 2004). It has recently regained attention and has been demonstrated to produce some benefits in cognitive performance and psychiatric symptoms (Mondino et al., *Biol Psychiatry* 2014). However its precise therapeutic mechanisms remain unknown. We therefore developed a rat model of tDCS and tested effects in the forced swim test (FST), novelty-suppressed feeding test (NSFT) and elevated plus maze test (EPMT), all of which

predict antidepressant/anti-anxiety activity. We targeted the medial prefrontal cortex (mPFC) because clinical and animal studies have shown antidepressant effects of mPFC deep brain stimulation (DBS) (Hamani and Nobrega, *Eur J Neurosci* 2010). We devised a current generator that delivered low power current (0.1 mA) onto a conducting cathodal metal plate (1.5±0.25 x 2.5±0.25mm) fixed on the skull surface over the mPFC (AP+4.7 to +2.2mm; Paxinos and Watson, *The Rat Brain in Stereotaxic Coordinates* 2005). The anodic end was connected to a stainless steel screw lodged behind the cerebellum (AP+18). Animals received sham (n=6) or tDCS (n=6) twice on day 1 and once on day 2 (30 min before behavioural testing). In the FST, stimulated animals exhibited significantly lower (56.16%) immobility episodes ($p<0.05$), which was not a result of non-specific motor activation, and therefore suggests an antidepressant-like activity. Indeed, motor activity was increased only during stimulation, and not immediately after cessation of stimulation or 5-6 hours after the last stimulation. A non-significant increase in anxiety-like behaviour was observed in tDCS animals in the NSFT and EPMT. Post-mortem brain analyses using in situ hybridization imaging of the immediate early gene *zif268*, a marker of cell activation, revealed lasting significant increases in neural activity almost exclusively within the target regions. In particular, there was an increase ($p<0.01$) in the cingulate (Cg), prefrontal (PrL) and orbital (Or), as well as in the insular cortex (Ins) and claustrum (Cl), as indicated in the figure. Together, these data suggest that tDCS can be effectively modeled in the rat, yielding highly selective patterns of brain activation. Furthermore, mPFC tDCS shows antidepressant-like properties, which can further be investigated as a potential non-invasive alternative for mPFC DBS.

SP137 - SPECIAL SESSION: Building Medical Physics Capacity in Developing Countries

TRACK 17: EDUCATIONAL AND PROFESSIONAL ACTIVITIES

SP137.2 - Implementing Training Modules of the Emerald Program in Brazil

Author(s): Ricardo A. Terini¹, Paulo R. Costa², Slavik Tabakov³, Elisabeth M. Yoshimura², Denise Y. Nersissian²

¹Depto. De Física, Pontifícia Universidade Católica de São Paulo, São Paulo/BRAZIL, ²Departamento De Física Nuclear, Instituto de Física da Universidade de São Paulo, São Paulo/BRAZIL, ³Medical Engineering And Physics, King's College London, London/UNITED KINGDOM

Introduction: The Leonardo EU project for European Medical Radiation Learning Development (EMERALD) (www.emerald2.eu/cd/Emerald2/), a Consortium of Universities and Hospitals from many countries, developed three training modules in medical radiation physics: X-ray Diagnostic Radiology, Nuclear Medicine and Radiotherapy. The modules are for the training of graduated university students in Medical Physics (MP) or related disciplines, their tutors, as well as other Hospital employees. The Institute of Physics of the University of São Paulo, Brazil, and the King's College of London established a research cooperation program to conduct the translation to Portuguese language, adaptation and update of the X-Ray Diagnostic Radiology training module of the Emerald Program. The Emerald teaching material in X-Ray Diagnostic Radiology is divided in ten topics covering the basics of Diagnostic Radiology, Quality Control and Radiation Protection.

Methodology: The referred work, besides the translation of the texts into Portuguese, comprised the review of the previously produced material. During the review process, it was decided to update some of the training tasks and add more information related to current topics, such as digital X-ray imaging modalities, multi-slice computed tomography and tomosynthesis. These new additions will also be available in English. The translated or composed texts have been submitted to a cross-reviewing process by the co-authors in order to standardize the language. Moreover, national radiological protection recommendations were included to assist the users of the teaching material with the Brazilian rules of radiation safety and quality control in X-ray medical applications. A Workshop was held in São Paulo in March 2014, to diffuse and discuss a preliminary version of the Brazilian modules, named Emerald-BR. During this meeting, part of the material was submitted to a validation and also to a practical assessment process by means of a critical analysis by experts in Medical Physics education (Fig. 1).

Results and Discussion: Finally, a pilot implementation has been organized and scheduled in order to do the last adjustments before making the material available to other users in Portuguese language. Further assessment and feedback procedures were planned in both London and São Paulo, aiming to evaluate and disseminate the final product (*Med. Phys. Int. J.*, v. 2(1), p. 18-21, 2014). Emerald-BR will certainly contribute to the offer of organized training programs in the country (and in Latin America) to the growing number of young physicists starting in Medical Physics area each year in the region.



Fig. 1 Participants of the Workshop for diffusion of the Emerald-BR project in São Paulo .

the residents was employed by the hospitals where they did their residency. Two residents worked for a company providing radiology equipment testing services, three worked for the national regulatory agency for radiation facilities, one worked for another hospital, one taught undergraduate physics, and one was supported by her parents.

Assistance from the IAEA in the form of experts sent to give lectures and to undertake assessment of the residents during and at the end of the residency training were invaluable, especially because none of the supervisors had had previous experience in a structured on-the-job training program.

Three ROMP residents successfully completed the program. Seven out of eight DRMP residents successfully completed the program.

Important lessons have been learned from the pilot. Solutions for the problems encountered have been proposed.

SP137.3 - Pilot Implementation In The Philippines Of Structured Medical Physics Residency Programs Using The Iaea Training Guides For The Clinical Training Of Medical Physicists

Author(s): Agnette D.P. Peralta¹, Lilian V. Rodriguez², Joyce N. Melchor¹

¹Department Of Health, Center for Device Regulation, Radiation Health, and Research, Food and Drug Administration, Manila/PHILIPPINES, ²Radiotherapy Department, Jose R. Reyes Memorial Medical Center, Manila/PHILIPPINES

The Philippines piloted the implementation of the structured medical physics residency training programs in radiation oncology medical physics (ROMP) from 2009 to 2012 and in diagnostic radiology medical physics (DRMP) from 2010 to 2013. The pilot programs were undertaken under the Regional Cooperation Agreement project RAS 6/0/38 “Strengthening Medical Physics through Education and Training” of the International Atomic Energy Agency (IAEA). Used as the training guides were the IAEA publications “Clinical Training of Medical Physicists Specializing in Radiation Oncology” and “Clinical Training of Medical Physicists Specializing in Diagnostic Radiology”.

The full support of the Department of Health (DOH) was essential to the project. The national project coordinator (APPeralta), the national program coordinator for ROMP (LVRodriguez), and the national program coordinator for DRMP (JNMelchor) all came from the DOH. A National Steering Committee (NSC) was created for each program. Represented in the NSC for ROMP were the Center for Device Regulation, Radiation Health, and Research (CDRRHR) of the Food and Drug Administration of the DOH, the Philippine Nuclear Research Institute, the Philippine Organization of Medical Physicists, the Philippine Association for Radiation Protection, the Philippine Radiation Oncology Society, and one of the training hospitals. For the DRMP NSC, the Philippine College of Radiology was the medical specialty society represented. These assignments were all covered by Department Orders issued by the Secretary of Health.

For the ROMP pilot, the original number of five participating hospitals was reduced to four. All the hospitals were private hospitals. For DRMP, the original number of participating hospitals (one private and three government) was maintained.

Not all the residents were actually employed by the hospitals. For ROMP, one of the four residents was teaching undergraduate physics to support himself during his residency. For DRMP, none of

SP138 - Biosensor, Nanotechnology, Biomems And Biophotonics / New Technologies In Cancer Research And Treatment

SP138.1 - Measurement of the Received Power in a Realistic Intrabody Communication Scenario

Author(s): [Zeljka Lucev Vasic](#), Igor Krois, Mario Cifrek
Faculty Of Electrical Engineering And Computing, University of Zagreb, Zagreb/CROATIA

In intrabody communication (IBC) the human body is an integral part of the signal transmission channel. Previously, we have measured transmission characteristics of the IBC channel in the frequency range from 100 kHz to 100 MHz using the same network analyzer as the transmitter and the receiver, galvanically decoupled from the IBC channel by two balun transformers. In this paper, a proprietary battery-powered transmitter and battery-powered spectrum analyzer mimicking the receiver are connected directly to the test subject. The received signal power is measured for four electrode configurations (transmitter A - receiver A (AA), transmitter A - receiver B (AB), transmitter B - receiver A (BA), and transmitter B - receiver B (BB)) and eight transmitter-receiver distances along both arms. The results agree qualitatively with the transmission characteristics of the IBC channel. It was also noticed that, especially for some electrode configurations, a standing wave occurs between a transmitter and a receiver along the human body.

SP138.2 - Focused ultrasound-triggered release of Sorafenib from temperature sensitive liposomes for treating renal cell carcinoma

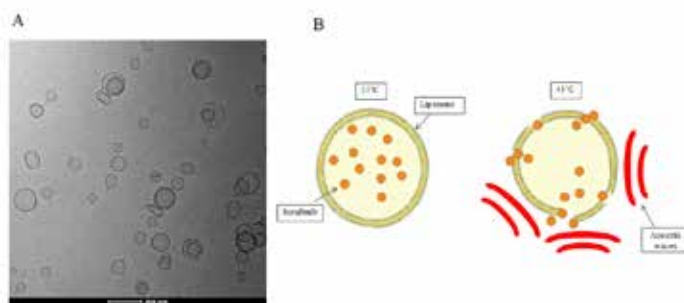
Author(s): [Hakm Murad](#)¹, Caleb Abshire², Jaspreet Arora³, James Liu², Vijay John³, Benajamin Lee², Damir Khismatullin¹
¹Biomedical Engineering, Tulane University, New Orleans/LA/ UNITED STATES OF AMERICA, ²Surgery, Tulane School of Medicine, New Orleans/LA/UNITED STATES OF AMERICA, ³Chemical Engineering, Tulane University, New Orleans/LA/UNITED STATES OF AMERICA

Specific Aims: High-intensity focused ultrasound (HIFU) emerges as a powerful technology for noninvasive or minimally invasive non-ionizing treatment of cancer. HIFU deposits a large amount of acoustic energy at the focal region within the target tissue (i.e., tumor), causing tissue heating and necrosis. Limited research has been performed applying focused ultrasound, alone or in combination with other therapeutic modalities, to renal cell carcinoma. The aim of this study was to explore focused ultrasound as an adjuvant to chemotherapy; particularly as a method to thermally trigger the release of drug from Sorafenib-encapsulated liposomes into cancer cells.

Research Methodology: Liposomes were fabricated using Dipalmitoylphosphatidylcholine, L- α -Phosphatidylcholinehydrogenated Soy and Cholesterol at a molar ratio of 70:20:10 using the thin film hydration protocol. Liposomes were formulated with addition of Rhodamine B or D-282 for uptake visualization and encapsulated Sorafenib for the treatment arm. The liposomes were characterized for their particle size, surface morphology and the percentage of drug entrapment. Fluorescent liposomes were used to study their uptake in an *in-vitro* model. A suspension of RCC 7860 human renal cancer cells (100 μ l, 2.7 million cells/ml) was placed in a 0.2 ml thin-wall PCR tube to mimic dense tumor aggregation. Cell pellets were then inoculated with Sorafenib alone or Sorafenib loaded liposomes and treated with focused ultrasound for 90 seconds. The

focused ultrasound signal was generated by a 1.1MHz transducer at an acoustic output power of 2.73W to ensure the temperature rise to 43°C. This temperature is above the transition temperature of the heat sensitive liposomes and triggers the rapid release of Sorafenib. The viability of the cells was measured by the MTT assay at 2, 24, and 72 hours post-treatment.

Results: Liposomes were similar in their surface morphology. The mean particle size was 150 ± 12.33 nm, and their zeta potential was -2.55 ± 3.21 mV. Sorafenib encapsulated liposomes demonstrated $101.2 \pm 1.3\%$ entrapment efficiency based on UV spectrometry. Fluorescent and confocal microscopy consistently confirmed particle uptake by the cells. According to the MTT assay, cellular death rates were 2.8%, 3.0%, and 7.4 % for Sorafenib alone, Sorafenib loaded liposomes, and Sorafenib loaded liposomes with HIFU 24hr post-treatment. Cellular death rates increased to 4.5% for Sorafenib alone, 7.2% for Sorafenib loaded liposomes alone, and 52% for Sorafenib loaded liposomes with HIFU 72hr post-treatment. Thus, focused ultrasound triggered liposomes show significant promise as a feasible strategy for chemotherapy.



A) TEM imaging of the Sorafenib loaded heat sensitive liposomes. Average size of liposomes are 150nm. The cancer cells uptake liposomes through endocytosis.
B) Schematic showing the drug Sorafenib encapsulated by the heat sensitive liposomes. The intense acoustic waves caused by the HIFU exceeds the glass transition temperature of liposomes causing the release of drug into cell.

SP138.3 - Synthesis and Characterization of SPION Functionalized third Generation dendrimers Conjugated by Gold Nanoparticles and Folic acid for Targeted Breast Cancer Laser Hyperthermia: An Invitro-assay

Author(s): [Mohammad Khosroshahi](#)¹, Maryam Tajabadi², Shahin Bonakdar³, Vahid Asgari³
¹Biomedical Engineering, Amirkabir University of Technology, Tehran/IRAN, ²Amirkabir University of Technology, Tehran/IRAN, ³Pasture Institute, Tehran/IRAN

Abstract- In this study, 9 nm superparamagnetic iron oxide nanoparticles (SPION) were functionalized by polyamidoamine (PAMAM) dendrimer. Magnetodendrimer samples were conjugated by gold nanoparticles (Au-NPs) using two reducing agents of sodium borohydride and hydrazine sulfate. Presynthesized 10-nm Au-NP were used to evaluate the efficiency of conjugation method. Laser Induced Fluorescence Spectroscopy (LIF) of these materials showed that the nanocomposite and magnetodendrimer have the fluorescence properties covering the whole range of visible spectrum. For targeting and the biocompatibility, the synthesized materials were conjugated by folic acid molecules. Laser-induced hyperthermia using Au-NPs was performed. The samples were characterized using X-ray diffractometry (XRD), transmission electron microscopy (TEM), Fourier transform infrared (FTIR) spectroscopy, UV-Visible spectroscopy, and fluorescent spectroscopy. Two cell lines of breast cancer, i.e. MCF 7 and MDA MB 231, were chosen for cytotoxicity evaluation of the synthesized nanostructures. The Results indicated a high biocompatibility of nanoparticles (up to 50 μ g/mL).

SP138.4 - FIB/SEM Characterization of Microcavity Surface Plasmon Resonance Biosensors**Author(s):** Nazanin Mosavian

Physics, Indiana University, Bloomington/IN/UNITED STATES OF AMERICA

A miniature, integrable surface plasmon biosensor using a dielectric sub-micron diameter core utilizes a noble metal spherical shell structured with a subwavelength nanoaperture believed to excite stationary surface-plasmon-resonances at the biosensor's surface. The sub-micron cavity enhances the measurement sensitivity of bonding molecules to the sensor surface. Visible range spectroscopy is used to study the wavelength shift as bio-molecules absorb/desorb at its surface. The microcavity surface plasmon resonance sensors (MSPRS) were used to analyse conformational changes of bound biomolecules as the oxidation state changes. Present work uses Scanning Electron Microscopy (SEM) and Focused Ion Beam (FIB) to study the characteristics of MSPRS using a novel fabrication technique.

SP138.5 - The current status of Microbeam Radiation Therapy at the ESRF and future perspectives**Author(s):** Elke T. Brauer-Krisch

Experiments Division, ESRF, Grenoble Cedex /FRANCE

Background: Microbeam Radiation Therapy (MRT) uses a spatially fractionated filtered white X-ray beam from a high energy wiggler Synchrotron Source (energies 50-350keV) with extremely high dose rates (up to about 20kGy/s). The typical planar beam width in an array is 25-100 μ m with 100-400 μ m wide spaces between beams. Such beams are very well tolerated by the tissue, even the high "peak" doses delivered in the path of the microbeams, when respecting a dose prescription in the "valley" that corresponds to a dose used of conventional Radiation Therapy (RT) converted to a single exposure. The superior tumor control when compared to that realized by conventional RT is achieved by differential effects of MRT on the normal tissue vasculature versus the tumor vasculature.

Materials and Methods: The MRT technique has been technically set up, tested and successfully applied during the last 20 years on various tumor models. Presently, the project is mature enough to be used for the treatment of spontaneous tumors in pets. Unified efforts from several teams with very different expertise now permit Microbeam Radiation Therapy in animal patients with a high degree of safety, in pursuit of the ultimate goal of clinical applications in humans.

Results: The MRT trials for animal pets as tumor patients required substantial work for developing, upgrading and progressively implementing instrumentation, dosimetry protocol, as well as the crucial patient safety systems. Progress on the homogenous dose measurements using ionisation chambers and Alanine dosimetry as well as the comparison of high resolution dosimeters with the dose calculations based on a novel tumor planning system will be summarized. A general overview on the different achievements will be presented as well as a vision for possible human trials.

SP139 - Optical Imaging: Methods**TRACK 01: IMAGING****SP139.1 - Toward super-resolution imaging of proton radiation-induced DNA double-strand breaks for characterization of γ -H2AX foci clusters****Author(s):** Arash Darafsheh, Consuelo Guardiola, Jarod C. Finlay, Alejandro Carabe, Timothy D. Solberg

Radiation Oncology, University of Pennsylvania, Philadelphia/PA/UNITED STATES OF AMERICA

Repair kinetics assays can be used to characterize the sensitivity to radiation for patients that require radiotherapy as a treatment option. γ -H2AX foci assays have been recognized as one of the most powerful techniques to characterize the repair kinetics properties of radiation induced damage to DNA. The interests in these assays are the rate at which radiation-induced foci disappear, which is presumably related to the rate of DNA damage repair; and the foci size, which is related to the clustering complexity of the DNA damage. Both aspects are interconnected by the fact that larger foci take longer time to disappear, meaning that the larger the clustering the slower the repair rate. Therefore, it is important to understand both aspects in order to understand repair kinetics effects, especially after radiotherapy with particles high linear energy transfer (LET), such as protons. Due to much higher damage density in the DNA in the case of irradiation by protons compared with the case of irradiation by particles with low LET, using high-resolution microscopy to enhance the imaging resolution for γ -H2AX foci characterization is desirable.

Foci counting and size measurement is usually performed by optical microscopy, however, the far-field spatial resolution of any standard lens-based optical microscope is limited by the wavelength of imaging light (λ) and by the numerical aperture (NA) of the lens system due to diffraction of light waves. A variety of imaging techniques have been developed in the past to overcome the diffraction-limit in optical microscopy; most of these techniques, however, have complex design and high economic cost, and require scanning across the specimen that increases the acquisition time.

In this work, we investigated a novel simple super-resolution imaging technique for application in γ -H2AX foci characterization. We fabricated super-resolution microscope coverslips composed of barium titanate glass microspheres (Diameters \sim 30-150 μ m and refractive index \sim 1.9-2.1), fixed in a polydimethylsiloxane (PDMS) elastomer layer, to collect high spatial frequency harmonics present in the optical near-field of the object and transmit them to the far-field with magnification providing high imaging resolution. When the super-resolution coverslip is placed over the specimen, each microsphere forms a magnified virtual image underneath the specimen's surface that is simply captured by the objective lens.

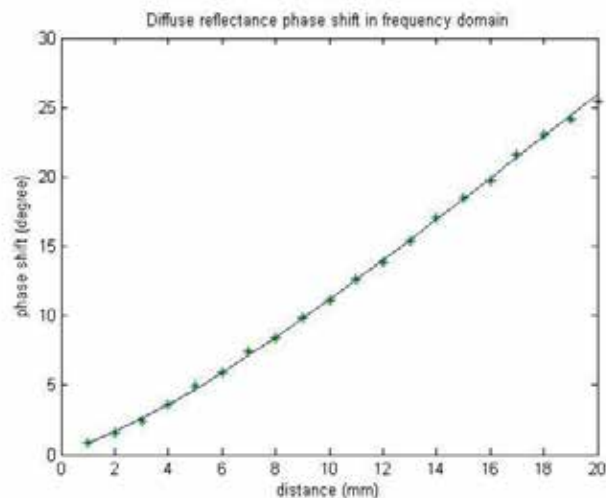
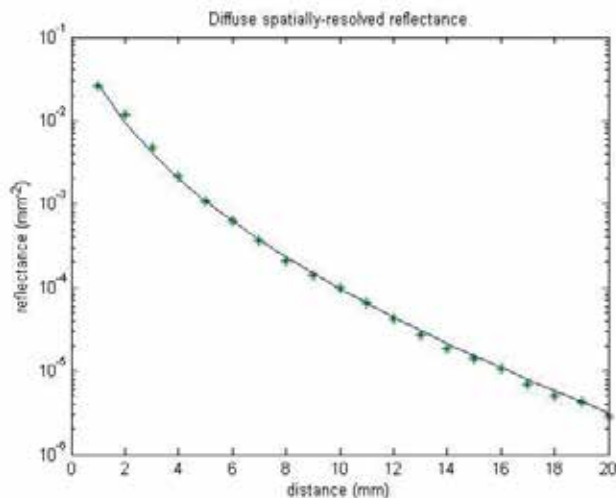
We used microsphere-assisted imaging technique for the observation of double-strand DNA breaks, manifested as foci using an immunofluorescence treatment, in U87 glioblastoma cells irradiated by proton beams. Our results indicate magnification and resolution advantages of microsphere-assisted super-resolution imaging over conventional fluorescent microscopy. Our imaging method is a promising candidate in developing various applications in biomedical imaging and nanophotonics.

SP139.2 - Solution of radiative transport equation in turbid layered media in spatial and frequency domains

Author(s): Heping Xu

Cape Breton Cancer Centre, Sydney/CANADA

Study of light transport in turbid media has many applications in bio-medical imaging and therapeutic research. Although approximate diffusion solution is widely used to circumvent difficulties in exactly solving for the radiative transfer equation, seeking exact solution is still interesting biomedical optics community as it not only serves as a bench mark for Monte Carlo (MC) simulation, but also well describes light transport in the region when diffusion theory fails (in high absorption region). This abstract obtains exact solutions for two layered media in spatial and frequency domains. Monte Carlo method has been employed to verify the obtained solution. The turbid medium consists of a top layer with the absorption and scattering coefficients 0.02/mm and 1.3/mm, and a bottom layer with the absorption and scattering coefficients 0.01/mm and 1.2/mm. The thickness of the first layer was 2.0 mm. The second layer is much thicker than that of the first one and can be considered as semi-infinite. The refractive index of the medium was 1.4. Anisotropic factor in Hengyey-Greestein phase function is 0.9. The source beam was incident perpendicularly on the top layer with no lateral dimension. Exact solution of RTE was obtained through the method of rotated reference frame (MRRF) as demonstrated in previous literatures. In this method, all quantities were expanded in terms of the spherical harmonics which was defined in a coordinate system, whose z axis coincided with the direction of the wave vector k . The solutions can be expressed with eigenvalues and eigenvectors of a series of infinitely-dimensional matrices in an analytical form. In practice, sufficiently accurate solutions were obtained through truncating those matrices to finite dimensions. Spatially-resolved reflectance, photon density waves at 100MHz modulating frequency (amplitude and phase shift) were calculated using the exact solution and were successfully verified by Monte Carlo methods.



SP139.3 - Development of a hybrid optical-gamma camera: A new innovation in bedside molecular imaging

Author(s): Aik Hao Ng¹, Sarah L. Bugby², Loyal K. Jambi², Mohammed S. Alqahtani², Patricia E. Blackshaw¹, Paul S. Morgan³, John E. Lees², Alan C. Perkins³

¹Radiological And Imaging Sciences, School Of Medicine, University of Nottingham, Nottingham/UNITED KINGDOM, ²Space Research Centre, University of Leicester, Leicester/UNITED KINGDOM, ³Medical Physics And Clinical Engineering, Nottingham University Hospitals NHS Trust, Nottingham/UNITED KINGDOM

Introduction:

A novel prototype compact hybrid optical-gamma camera has been developed through collaboration between the Space Research Centre at the University of Leicester and Medical Physics at the University of Nottingham. This system offers high resolution gamma imaging together with real-time optical imaging for use at the patient bedside or in the operating theatre. This presentation describes the innovative design characteristics and the first results of use in the clinical setting.

Material and Methods:

The camera comprises of a CsI(Tl) columnar scintillator coupled to a charge-coupled device (CCD), a tungsten pinhole collimator and an optical camera. Both optical and gamma cameras are co-aligned to allow accurate fusion of images. The camera can be mounted on a trolley with flexible articulated arm for hand free use. A qualitative user survey was carried out to obtain feedback for optimising ergonomic factors for use of the camera and trolley system in the clinical environment. A sentinel node phantom was fabricated using polymethyl methacrylate (PMMA) to validate the performance of the camera for sentinel node localisation in the presence of high activity at the injection site.

12-20 MBq sources of Tc-99m were used to simulate radioactivity at the injection site and lymph nodes with the node-to-injection site activity ratios of between 1:100 and 10:100. These were placed at different separations and depths to simulate the uptake at different anatomical sites in the body.

The first patient studies using the hybrid camera were carried out in the Nuclear Medicine Clinic at Queen's Medical Centre, Nottingham.

Results:

The system spatial resolution, system sensitivity and energy resolu-

tion of the camera system with 0.5 mm diameter pinhole collimator was 1.28 mm (@ 13 mm), 214 cps/MBq (@ 3 mm) and 58 % (full width half maximum at 141 keV) respectively. Phantom simulations revealed that the camera system could detect low-activity in nodes up to the depth of 45 mm from the phantom surface by visual examination of images. Overall the user feedback indicated satisfactory design of the bedside trolley system and influenced the final design of the camera head casing, mounting and arm assembly. The initial patient studies included bone, lymphatic, and lacrimal drainage investigations. These showed that the hybrid images provided good evidence of localisation of radiotracer distribution with reference to the visible anatomical features, thus aiding the diagnostic utility.

Conclusion:

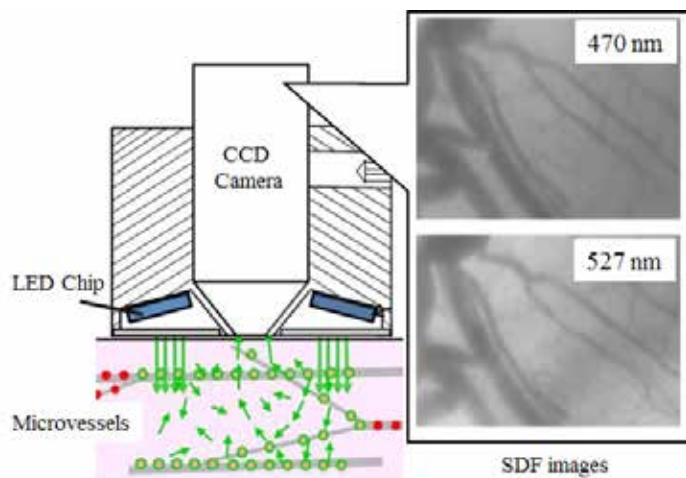
A novel hybrid optical-gamma camera system has been developed, characterised and the first studies performed in the clinical environment. This system would be ideally suited to use in operating theatre for procedures such as sentinel node detection and tumour localisation. This system offers potential for use with the new generation of hybrid fluorescent-radionuclide tracers currently under development.

SP139.4 - Sidestream Dark-Field Oximetry with Multicolor LEDs

Author(s): Tomohiro Kurata¹, Zhenguang Li¹, Shigeto Oda², Hiroshi Kawahira³, Takashi Ohnishi³, Hideaki Haneishi³
¹Graduate School Of Engineering, Chiba University, Chiba/JAPAN, ²Graduate School Of Medicine, Chiba University, Chiba/JAPAN, ³Center For Frontier Medical Engineering, Chiba University, Chiba/JAPAN

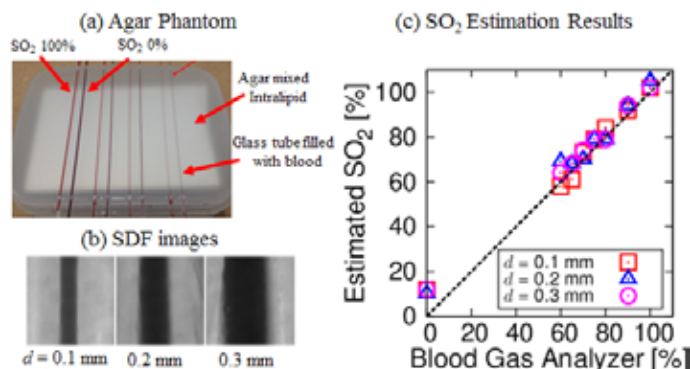
We investigate the possibility of oxygen saturation (SO₂) estimation from images obtained by the sidestream dark-field (SDF) technique. The SDF technique is a noninvasive optical technique allowing direct visualization of microvessels near tissue surfaces.

To advance the capability of the SDF technique, we develop an image-based oximetry method with the SDF technique (SDF oximetry) with LED illumination sources. This method is based on the Lambert-Beer's law with dual-wavelength illumination. For establishing the method, we developed a trial SDF device used multicolor light-emitting diodes (LEDs) (peak wavelengths: 470 and 527 nm) to obtain two-band images. Figure 1 shows the configuration of our trial device and microvessel images.



In this study, we propose a SDF oximetry method with the trial device and report evaluation results of the validity of the method. As an approach to verify the method, we performed both a Monte Carlo photon propagation simulation and experiments with a phantom and *in vivo* small intestine of a pig. In the phantom experiment, we

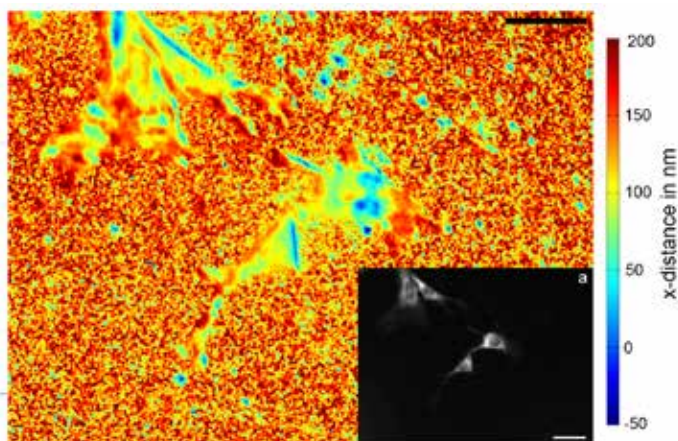
tested the proposed method with a phantom made of agar and 10% Intralipid. In order to simulate vessels, glass tubes filled with bovine blood were embedded just below the surface of the phantom. Figure 2 shows the phantom, the SDF images, and SO₂ estimation results with different internal-diameter tubes. From the results, we found that there was strong correspondence between estimated SO₂ values and measured values by a blood gas analyzer. This result suggested the validity of the proposed SDF oximetry method. Moreover, we estimated SO₂ of microvessels near the surface of the small intestine of a pig. Although the validation of the experiment is still under study, the results of the validation and computer simulation will be presented at the conference.



SP139.5 - Development of Polymer Substrates for Waveguide Evanescent Field Fluorescence Microscopy

Author(s): Rony Sharon¹, Frederik Fleissner², Silvia Mittler²
¹Biomedical Engineering, the university of western ontario, London, ON/CANADA, ²Physics And Astronomy, The university of western ontario, London, ON/CANADA

False color representation of a dye distance map with four osteoblasts. The inset represents an overexposed Waveguide Evanescent Field Fluorescent (WEFF) Microscopy image of the same field of view. Osteoblasts appear at dye/plasma membrane distances between ~ 75 to 110 nm. Dye locations very close to the surface, adhesion areas, are labeled blue. Both scale bars represent 50 μm. The color bar shows a range from - 50 nm to 200 nm. One pixel is equal to (0.266 μm)².



WEFF Microscopy was developed recently to image ultra thin films (quality control) and to investigate adhesions of cells to substrates and to produce quantitative distance maps of the plasma membrane to the substrate.

A key component in WEFF microscopy is the glass substrate optical

device containing a planar waveguide and an optical coupling grating.

Previous work has shown a better growth of cells on polymer substrates. Therefore, the objective of this study is the development and fabrication of polymer based substrates with similar characteristics to existing glass substrates.

Polymethylmethacrylate (PMMA) substrates were fabricated by hot embossing a coupling grating from a master silicon mold, and subsequent spin coating of OrmoCore, a photoresist, or alternatively polystyrene serving as waveguides. The master mold was fabricated by spin coating Shipley 1805 photoresist on a silicon wafer followed by laser interference lithography implementing the grating pattern. Photoresist gratings were developed and oxygen plasma cleaned before performing reactive ion etching to embed the structure within the silicon.

The correlation between the embossed substrate and the silicon mold grating constant was examined with scanning electron microscopy: taking the variations of temperature, the time and process pressure into consideration. The results determined a set of parameters for PMMA substrate fabrication, and demonstrated that the same quality of coupling gratings can be achieved as seen in existing glass substrates. The next step is the fabrication of optical quality polymer waveguides on top of the PMMA substrate to start imaging fixed and living cells.

WEFF microscopy could have many applications, especially in the field of tissue engineering, cellular biology and implant development. Paving the road for mass production of WEFF substrates and to foster WEFF microscopy, spreading it among optical microscopy users which will be able to upgrade their existing microscopes to a surface sensitive tool and extend research capabilities without major modifications, is the driving force and importance of this work.

SP139.6 - Higher-Order Structural Investigation of Mammalian Septins by Super-Resolution Fluorescence Microscopy

Author(s): Adriano Vissa¹, Maximiliano A. Giuliani², Theodore Pham³, William S. Trimble³, Peter K. Kim³, Christopher M. Yip²

¹Institute Of Biomaterials And Biomedical Engineering, University of Toronto, Toronto/CANADA, ²Institute of Biomaterials & Biomedical Engineering (IBBME), Toronto/ON/CANADA, ³Cell Biology, Hospital for sick children, Toronto/CANADA

Septins belong to a family of GTP-binding structural proteins that are thought to have various functions in mammalian cells including acting as scaffolds for protein recruitment, forming diffusion barriers, and participating in cytokinesis. Defects in Septin organization have been linked to hereditary neuralgic amyotrophy and several types of cancers. During interphase, these heterooligomeric complexes colocalize with F-actin stress fibers and have been shown to stabilize their formation through direct interaction with non-muscle myosin II. However during cytokinesis septin complexes maintain NM II association and form characteristic higher order ring structures at the midbody scaffold to facilitate cell division. The structural versatility of septins is likely directly related to their many roles yet the organizational motifs by which oligomeric building blocks form filaments and higher order structures has not been elucidated in mammalian cells. In addition, their intricate spatial relationship with F-actin and myosin is of great interest in understanding the formation of stable cytoskeletal stress fibers. To address these questions, we used the sub-diffraction imaging technique dSTORM (Direct Stochastic Optical Reconstruction Microscopy), one of several recently developed methods of super-resolution microscopy. Also known as nanoscopy, it has revolutionized the optical study of proteins and cellular processes by achieving resolution below 20 nm, and its implementation is at the crossroads of cell biology, biomedical engineering and computer science. We report two-colour dSTORM imaging of Septin2/Septin9 in filament and ring structures and

characterization of their periodic structural contribution in human fibroblast cells using AlexaFluor 647 and ATTO 532 on a custom-built combinatorial microscopy platform. To gain insight into septins' role in nanoscale cytoskeletal protein organization, an array of two colour superresolution imaging was carried out on combinations of septin proteins, F-actin and non-muscle myosin II isoforms A and B and discrete nanoscale spatial arrangements were characterized.

SP140 - Special Treatment Techniques: Part 1

TRACK 04: RADIATION ONCOLOGY

SP140.1 - Credentialing of radiotherapy centres in Australasia for a phase III clinical trial on SABR

Author(s): Tomas Kron¹, Brent Chesson², Nick Hardcastle¹, Natalie Clements¹, Mark Burns², Melissa Crain³, David Ball⁴

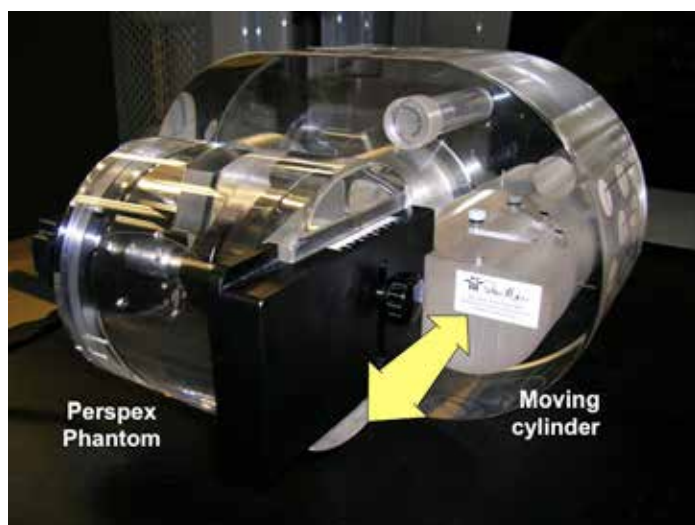
¹Physical Sciences, Peter MacCallum Cancer Center, Melbourne/AUSTRALIA, ²Radiation Therapy, Peter MacCallum Cancer Centre, East Melbourne/AUSTRALIA, ³Quality Assurance, Trans Tasman Radiation Oncology Group, Newcastle/AUSTRALIA, ⁴Department Of Radiation Oncology, Peter MacCallum Cancer Center, Melbourne/VIC/AUSTRALIA

Aim

Stereotactic Ablative Body Radiotherapy (SABR) is a relatively new treatment modality that utilises image guidance, motion management and many small often non-coplanar radiation beams to deliver high biological doses of ionising radiation in very few fractions. A randomised phase III clinical trial comparing SABR with conventional radiotherapy for early stage lung cancer in peripheral location is running in Australia and New Zealand under the auspices of the Trans Tasman Radiation Oncology Group (TROG). As SABR technology at the commencement of the trial was new to most participating centres a credentialing program was developed for centres wishing to join the trial.

Methods

The credentialing program was developed using a prospective risk management approach. Key elements include the ability to create a plan that meets all dosimetric constraints, the dose calculation in the presence of inhomogeneities and the management of motion. Participating centres were asked to develop treatment plans for two test cases made available in DICOM format, and inhomogeneity corrections and dose delivery was assessed during a site visit using a phantom with moving inserts as shown in figure 1.



Results

Site visits were conducted in 20 radiotherapy facilities. All centres were able to produce acceptable plans for both test cases using 54Gy in 3 fractions, or for lesions close to the chest wall, 48Gy in 4 fractions. The tests with lung and air inhomogeneities confirmed

known shortcomings of the AAA algorithm for dose calculation behind the inhomogeneity. The dose was assessed in the phantom using an ionisation chamber and radiochromic film both in a stationary and moving cylinder as shown in figure 1 (sinusoidal motion, 1cm amplitude, 4s period). These measurements including at least one non-coplanar beam, confirmed in an end-to-end test that all participating centres were able to treat a lesion with the required accuracy. The site visit took 3 hours of linac time and was well received by participating staff proving to be a useful step in the process of developing a SABR program.

Conclusion

The credentialing process based around a site visit documented that participating centres were able to deliver dose to a phantom as required in the trial protocol. It also gave an opportunity to provide education about the trial and discuss technical issues such as 4D CT, small field dosimetry and patient immobilisation with staff in participating centres.

Acknowledgement: We would like to acknowledge the financial support of the study through Cancer Australia

SP140.2 - LED-optimized SBRT for Peripheral Early Stage Lung Cancer: A technique to reduce lung dose and potentially allow for re-irradiation

Author(s): Brandon Disher, George Hajdok, Stuart Gaede, Alexander Louie, Jerry J. Battista

London Regional Cancer Program, London Health Science Center, London/CANADA

Introduction

Stereotactic Body Radiation Therapy (SBRT) is a treatment option for early stage lung cancer. Initial reports suggest local control rates comparable to surgery (87.2%, 3 years). 1 Survivors are at risk of developing a second primary lung cancer (SPLC) at a rate of approximately 3% per year.² Patients with recurrent disease or SPLC may benefit from a second course of SBRT, but normal lung dose may limit retreatment. Recently, we developed LED-optimized SBRT (LED-SBRT),³ which exploits lateral electron disequilibrium (LED) to produce steep dose gradients at the tumor/lung interface. Here, we demonstrate that LED-SBRT can potentially reduce normal lung dose to avoid possible toxicity from re-irradiation.

Methods

Ten early stage lung cancer patients, with peripherally located disease, were retrospectively selected at random. Time-averaged 4-Dimensional CT image sets were acquired with a Philips 16-slice helical CT scanner. For each patient, two treatment plans (Pinnacle³ TPS) were created for comparison: 1) a 6MV 225° VMAT plan (control), and 2) a 6MV 180° arc LED-SBRT plan (field size $\approx 2 \times 2$ cm²). An internal target volume (ITV) was created to account for tumor motion due to breathing. Two planning target volumes (PTV) were created: PTV_{VMAT} = ITV + 5mm, and PTV_{LED} = ITV + 2mm. A reduced margin was used for PTV_{LED} to accommodate a smaller field size. Plans were generated using the collapsed-cone convolution algorithm, and dose was normalized such that 95% of the PTV received at least the prescription dose (i.e. 54Gy/3fractions or 60Gy/8fractions).

Results

The LED-SBRT plan created a steeper dose gradient at the tumor/lung interface (see Figure 1), which reduced normal lung dose. For example, the average percent reduction [(LED-SBRT - VMAT)/VMAT x 100%] in the mean lung dose, V₅, and V₂₀ were 27.4+/-11.9%, 25.0+/-8.5%, and 35.1+/-11.9%, respectively, averaged over all pa-

tients. On the contrary, the PTV hot spot and mean dose increased on average by 86.4 +/- 32.5% and 45.1 +/- 11.9%, respectively.

Conclusions

LED-SBRT can be used to reduce normal lung dose, and may allow for retreatment of small peripheral early stage lung lesions. As this technique relies on small field sizes (< 3x3 cm²) and reduced target margins, advanced forms of image-guidance, gating, and/or tracking must be implemented for tumor targeting. Furthermore, only those algorithms that model electron transport must be used to ensure dose accuracy in regions of severe LED. With these precautions, LED-optimized lung re-irradiation could prove to be clinically viable for re-treatment situations.

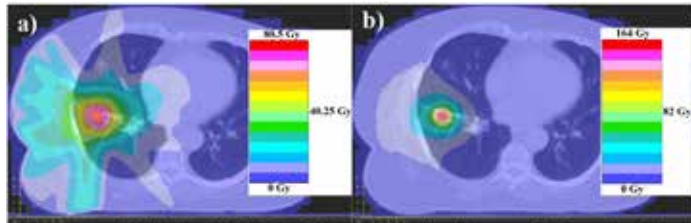


Figure 1 a) and b) display the VMAT and LED-SBRT dose distributions overlaid on patient 10's CT anatomy (prescription dose = 60Gy in 8 fractions). Comparing Fig. 1 a) and b), LED-SBRT creates steeper dose gradients at the tumour/lung boundary compared to the conventional VMAT plan. This effect can be exploited to greatly increase the tumour hot spot, while reducing normal lung dose.

References

1. Timmerman R et al., JAMA. 2010 Mar 17;303(11):1070-6.
2. Jaklitsch MT et al. J Thorac Cardiovasc Surg. 2012;144:33-8.
3. Disber B et al., Phys Med Biol. 2013 Oct 7;58(19):6641-62.

SP140.3 - Delivery of VMAT treatments with nonstandard SAD using dynamic trajectories

Author(s): Joel Mullins¹, Krum Asiev², Francois Deblois², Jan Seuntjens¹, Alasdair Syme³

¹Department Of Physics, McGill University, Montreal/CANADA, ²Medical Physics Unit, Department Of Oncology, McGill University, Montreal/CANADA, ³Radiation Oncology Department, Jewish General Hospital, Montreal/CANADA

Introduction: The Varian TrueBeam™ offers an optional research mode that permits dynamic control over many of its radiation and mechanical systems. Translational couch motion can be programmed in synchrony with gantry rotation to emulate treatment at either shortened or extended SADs. Shortened SADs offer the benefit of an increased dose rate and better dose conformity to the target volume due to the decreased leaf projection size, while extended SADs allow for increased field sizes and can obviate the need for field junctions (for example in cranio-spinal irradiation).

Materials and Methods: Water tank measurements were used to commission an 85 cm SAD and a 120 cm SAD beam model in the Varian Eclipse™ treatment planning system. For each beam model, reference dosimetry (AAPM TG-51) and beam validation tests (IAEA TRS 430) were performed. A total of 9 VMAT treatment plans were generated (four at 85 cm SAD, five at 120 cm SAD) and exported from Eclipse™ to DICOM-RT plan files. A software routine was developed in Python using the pydicom library (v0.9.8) to convert the plans into an .xml-formatted file for delivery with the TrueBeam™ research mode. To emulate nonstandard SAD delivery on a conventional SAD linear accelerator, translational couch motion was added to move the treatment couch in a circular trajectory as a function of the gantry and couch rotation angles, and the MLC leaf and jaw positions were scaled by the ratio of conventional to nonstandard SAD. Ionization chamber and Gafchromic EBT3 film measurements were used to record point dose and planar dose distributions for comparison with corresponding dose calculations in Eclipse™. MATLAB software was written to generate gamma index comparisons with

the Eclipse-exported dose planes.

Results: The beam models for both 85 cm SAD and 120 cm SAD agreed with measurement to within 1% for in-field profiles and PDDs beyond dmax for all field sizes. For profiles in penumbra and out-of-field regions, agreement was mostly within 5%, with some exceptions reaching up to 10%. Validation measurements indicated good agreement between measurement and Eclipse™ calculation. Ionization chamber measurements for the treatment plans at 85 cm SAD yielded an average agreement of -3.9±2.0%; Eclipse™ underestimated the measured dose in all cases. With 120 cm SAD, the average agreement for four of the five plans was -0.33±0.55%, with an outlier measurement of -7.4% for ionization chamber positioned in a steep dose gradient area. Ignoring out-of-field regions, the film gamma index pass rates for all treatment plans at both SADs were above 90%.

Conclusion: Dynamic couch trajectories were used to emulate nonstandard SAD delivery on the Varian TrueBeam™ STx with VMAT treatment plans, yielding good agreement between Eclipse™ treatment planning system dose calculations and both ionization chamber and film measurements. Discrepancies included a systematic underestimation of the delivered dose compared to measurement at 85 cm SAD, and poor agreement for one measurement located in a high dose gradient region at 120 cm SAD, but relative dose distributions showed good agreement as evidenced by the gamma index analysis of film measurements.

SP140.4 - Cone-Beam CT assessment of inter-fraction and intra-fraction motions during lung stereotactic body radiotherapy with and without abdominal compression

Author(s): Mengying Zhang¹, Runqing Jiang², Lixin Zhan²

¹Medical Science, University of Western Ontario, London/ON/CANADA, ²Medical Physics, Grand River Regional Cancer Centre, Kitchener/ON/CANADA

Purpose/Objective(s): The purpose of this study is to assess the effect of abdominal compression on the inter-fraction and intra-fraction variations for lung stereotactic body radiotherapy (SBRT) using cone-beam computed tomography (CBCT).

Materials/Methods: Sixty-nine lung stereotactic body radiation therapy patients were investigated in this study. The patients were separated into two groups, one with abdominal compression, and the other without abdominal compression. Seven to nine conformal beams were used for SBRT treatment plans. The prescriptions doses were 50 Gy in 5 fractions or 48 Gy in 4 fractions. At each treatment, two CBCTs were performed before and during the treatment. Set-up errors were measured on the first CBCT, which were recorded as inter-fraction variation. Tumor movements during treatment were measured by the second CBCT during treatment, which were recorded as intra-fraction variation.

Results: For intra-fraction variation, the shifts ≥ 3 mm for “abdominal compression” group were 12.0% in AP direction, 4.6% in SI direction, 5.0% in LR direction, corresponding to 17.3% in AP direction, 21.2% in SI direction and 11.5% in LR direction respectively, for the group “without abdominal compression”. For inter-fraction variation, The shifts ≥ 5 mm for “abdominal compression” group were 22.8% in AP direction, 22.8% in SI direction, 24.9% in LR direction, corresponding to 15.4% in AP direction, 48.1% in SI direction and 15.4% in LR direction, respectively for the group “without abdominal compression”. Abdominal compression reduced breathing organ motion during SBRT lung treatment in all three directions. However, setup error was just reduced significantly in SI direction for abdominal compression group. There is a slightly increase for setup error in AP and LR direction for abdominal group. Both inter-fraction and intra-fraction variations had been greatly reduced in SI direction after abdominal compression was applied.

Conclusion: Abdominal compression reduced the amplitude of intra-fraction lung breathing motion in all directions during lung SBRT treatment. However, the use of abdominal compression seemed to increase the inter-fraction variation in AP and LR directions although the inter-fraction variation in SI direction was reduced significantly. Therefore, target matching is required to localize the inter-fraction variation.

SP140.5 - Initial experience in establishing frameless intra-cranial stereotactic radiosurgery program with Varian TrueBeam STx, 6DoF couch and VisionRT motion control system

Author(s): Sergei Zavgorodni¹, Isabelle Gagne¹, Will Ansbacher¹, Derek M. Wells¹, Tony Mestrovic¹, Quinn Matthews¹, Tracy Mitchell², Isabelle Vallieres²

¹Medical Physics, BC Cancer Agency, Victoria/CANADA, ²Radiation Oncology, BC Cancer Agency, Victoria/CANADA

Implementation of a stereotactic radiosurgery (SRS) program requires linac and TPS commissioning, selecting planning and delivery techniques, "end-to-end" treatment delivery verifications for clinically appropriate treatment scenarios, establishing planning and imaging protocols (including planning CT and MRI, pre-treatment position verification and image-based intra-fraction monitoring). The program must also include SRS-specific daily and monthly QA procedures (on top of regular machine QA) as well as pre-treatment patient dose verification.

Commissioning of the TrueBeam STx linac and Eclipse TPS was performed keeping in mind its intended use for both intra- and extra-cranial treatments; therefore the beam model was tuned to cover small as well as medium VMAT/IMRT fields. Micro-diamond detector was used in beam data collection in the range of field sizes from 1x1cm² to 22x40 cm².

Conformal, conformal arc, IMRT and VMAT techniques were evaluated, and VMAT was the method of choice for the majority of cases due to its versatility and capability of combining steep dose fall-off with fast delivery. We anticipate mostly using co-planar treatments with 6MV and 10MV-FFF beams and simultaneous dose delivery to multiple targets.

End-to-end target localization and dosimetry tests were performed using a customized anthropomorphic head phantom with imbedded tungsten bead and an insert for the detector. Treatment plans for localization tests were created with the isocentre of circular conformal fields positioned on the bead. CBCT imaging was used for moving the phantom to treatment position. Portal images were then taken for each field, and offset of the beam axis from the bead was measured. For dose verification the center of calculated dose distributions was positioned at the measurement point of micro-diamond detector, and measured dose was compared to TPS calculation. QFix S-Frame Aqualast (3.2mm thick) head immobilization mask is also being evaluated for intra-fraction motion control by acquiring CBCT images pre and post treatment from CNS patients enrolled in this study.

For patient-specific dosimetry QA we intend to use in-house EPID-based 3D dose calculations as well as Monte Carlo calculated dose, reconstructed from trajectory files. Isocal calibration that confirms the congruence of imaging and treatment isocentres will be performed pre-treatment.

Anticipated work-flow of the SRS treatments involves patient CT and MR imaging, treatment planning, patient-specific QA, pre-treatment daily SRS-specific machine QA. During treatment CBCT images will be used to move the patient to the treatment position and to verify the move. Optical image will be captured by VisionRT system (not installed yet) immediately after verification CBCT and will be used to insure no motion during treatment. Once the treatment completed,

trajectory log files will be saved for dose reconstruction.

So far results for the mask immobilization intra-fraction were acquired for 3 patients and showed a mean intra-fraction motion of 0.7mm and a maximum of 1.1mm. Localization tests confirmed the beam axis to be within 0.5 mm from the bead target. Dosimetry verification tests showed good agreement (within 2%) of planned and measured dose for targets of 10 mm diameter and larger. For smaller targets the measured dose exceeded the plan by as much as 11%.

SP141 - Development of New Methods in Therapy Dosimetry: Part 3

TRACK 05: DOSIMETRY AND RADIATION PROTECTION

SP141.1 - Theoretical description of the saturation correction of ionization chambers in pulsed fields with arbitrary repetition rate

Author(s): Leonhard Karsch

TU Dresden - OncoRay, Dresden/GERMANY

Purpose: Gas-filled ionization chambers are the most important radiation detectors in radiotherapy. The recombination of radiation induced charge carriers causes an incomplete charge collection resulting in a reduced dose measurement value. A quantitative description and correction of the recombination effects exists for two cases, for continuous radiation exposure and for pulsed radiation fields with short single pulses, i.e. pulses of vanishing pulse duration and low repetition rate, so that the pulses do not affect each other. These two cases result in different dependencies of the collection efficiency on the chamber voltage which allows their experimental and theoretical differentiation. This work gives a new description for pulsed beams with arbitrary pulse rate, for which the prerequisites of the two existing descriptions are not fulfilled. Furthermore, an extension of the validity of the two existing cases is investigated.

Method: The process of charge collection and recombination between two pulses was described for a plane-parallel ionization chamber with a differential equation system. This differential equation system was solved by assuming simplified charge distributions and calculating the first terms of series expansion at recombination. The resulting complex formula for the correction term was simplified for easier handling and discussion.

Result: A formula describing the collection efficiency of plane parallel ionization chambers in pulsed fields with arbitrary pulse rate was developed which allows calculating the exact amount of recombination. This new formula contains the two existing descriptions for exposure by single pulses and continuous irradiation as limiting cases. By comparing the dependency of the new formula with the different dependencies on chamber voltage for the two existing cases, it was possible to determine the pulse rate range for which each of the three descriptions is applicable.

Discussion: As long as the time between two pulses is lower than one third of the collection time of the chamber, the collection efficiency can be very well described by the description for a continuous exposure. The description for single pulse irradiation is only valid if the repetition rate is less than 1.2 times the inverse collection time. Even if the calculation is done for plane parallel chambers, the derived formula and results should also be applicable for cylindrical ionization chambers by introducing an effective electrode gap.

The work is supported by the German government BMBF (no. 03Z1N511).

SP141.2 - Performance characteristics of Gafchromic EBT3 film in therapeutic electron beams and its practical application as an in-vivo dosimeter in the clinic.

Author(s): Amanda Barry, Lynda Fennell, Alan Pembroke, Eimear O'Neill

Radiotherapy, UPMC Whitfield Cancer Centre, Waterford/IRELAND

Purpose:

To assess the dosimetric properties of self-developing Gafchromic® EBT3 film in therapeutic electron beams with a view to assessing its suitability as an in-vivo dosimeter for electron beam radiotherapy.

Background:

Self-developing EBT2 film has been used by our organisation for in-vivo dosimetry in electron beam radiotherapy. [1] In 2012, a new generation of self-developing Gafchromic® film namely EBT3, became available providing the same practical solution as EBT2 for in-vivo dosimetry in electron beams. The suitability of EBT3 film for in-vivo dosimetry is due largely to the simplicity and flexibility with which films can be prepared and analysed. As it is practically water equivalent with a thickness of 0.28 mm, it does not give rise to the large perturbation effects that are typically associated with the use of electron diodes. Compared to EBT2 film, EBT3 has the added advantage of having a symmetrical composition which eliminates both side orientation dependence and Newton's rings.[2]

Methods:

EBT3 film calibrations were performed under reference conditions using two electron beam energies. MapCheck® was used with an EPSON V750 Pro scanner to generate calibration curves and read films under different test conditions.

Post-exposure developing time, dose-rate dependence, MU linearity, inter- and intra-film reproducibility, film orientation and position on the scanner and effects of repeated scanning were measured for films irradiated in a 9 MeV beam. The film's energy dependence was assessed in electron beams ranging from 6 to 18 MeV.

Minitab® was used to perform a statistical analysis to determine: (1) the variability in the EBT3 films dose response under the different test conditions; (2) the statistical significance of differences in the dose response of films irradiated with electron energies in the range 6-18 MeV using two calibration energies; and (3) the absolute dose measured using an ion chamber.

Results:

Initial results show that for a particular batch of film, there is no significant difference in recorded dose between individual sheets. Within one sheet of film, there is a maximum variation of 5%. Placing films on the scanner's central axis eliminates scanner inhomogeneities. Films scanned in the up orientation showed no difference to those scanned in the down orientation. However, rotating films by 90° reduced the recorded dose by up to 17%. The calibration energy did not affect the film dose response for any given electron beam energy. However, the films appeared to show a weak energy dependence.

Conclusions:

From our results, we conclude that EBT3 film may be suitable for in-vivo dosimetry in therapeutic electron beams providing the correct tolerance levels are applied.

REFERENCES:

[1] A. Barry, C. Marshall, A. Pembroke and E. O'Neill, *Physica Medica*, 28(4), 338 (2012)

[2] Gafchromic_EBT3.pdf at <http://perlamar.ie>

SP141.3 - Photon and electron spectra inside small field detectors for narrow and broad 6 MV photon beams**Author(s):** Hamza Benmakhlouf¹, Pedro Andreo²¹Department Of Medical Physics, Karolinska University Hospital, Stockholm/SWEDEN, ²Department Of Physics, Medical Radiation Physics, Stockholm University, Stockholm/SWEDEN

To investigate differences in detector response with respect to field size and detector type, photon and electron fluence spectra were calculated inside eleven small field detectors and in a small volume of water in narrow (0.5cm x 0.5cm) and broad (10cm x 10cm) Varian Clinac 6 MV photon beams. The usercode PenEasy, based on the PENELOPE MC system, was used to simulate three ionization chambers (IBA-CC01, PTW-T31016, PTW-T31018), two diamond detectors (PTW-T60003 and PTW-T60019), and six silicon diodes (IBA-EFD, IBA-PFD, IBA-SFD, PTW-T60016, PTW-T60017, PTW-T60018). This work follows the calculations in Benmakhlouf *et al.* 2014 *Med Phys*. This compilation of detectors include air and liquid ion chambers, natural and synthetic diamond detectors, shielded and unshielded silicon diodes of different sizes, all of interest for small field dosimetry.

Peaks in the photon spectra were found in all silicon diodes at energies between 22 keV and 26 keV due to characteristic x-rays emitted from some detector components surrounding the active detector volume. An additional very large peak was found (for both fields) in the shielded IBA PFD diode due to the emission of characteristic x-rays from the dense shielding material surrounding the diode. The photon fluence spectra inside the detectors for both field sizes were in general similar to the photon fluence spectra in water except for the shielded silicon diodes (in the case of the broad beam as expected) where the shielding causes a significant reduction of the fluence at low energies. The electron fluence spectra inside the ion chambers and diamond detectors were close to that in water whereas large differences between the detector spectra and water spectra (up to 50% difference) were found; the difference increased with decreasing field size due to lack of charged particle equilibrium.

The MC-calculated doses for both field sizes were compared to analytically determined collision kerma and restricted cema using the scored fluence spectra. The collision kerma was always larger than the MC-dose for the narrow beam due to lack of lateral charged particle equilibrium whereas the restricted cema (based on a common cutoff value of 15 keV for all detectors) was smaller and larger than the MC-dose (within $\pm 2\%$) depending on the detector type and field size. The differences increased with decreasing field size.

SP141.4 - Real Time Dose Reconstruction in MV Photon Therapy using a 2D solid state detector array.**Author(s):** Ziyad A. Alrowaili¹, Michael L.F. Lerch¹, Martin Carolan², Marco Petasecca¹, Peter Metcalfe¹, Anatoly B. Rosenfeld¹¹Centre For Medical Radiation Physics, School Of Physics, Faculty Of Engineering, university of Wollongong, Wollongong/NSW/AUSTRALIA, ²Radiation Oncology, Illawarra Cancer Care Centre, Wollongong/AUSTRALIA

Introduction: Real time verification of the dose delivered during the patient treatment is important step for quality assurance in IMRT and VMAT. We have developed such a system based on a solid state transmission 2D detector array called "Magic Plate".

Purpose: We study the performance characteristics of the MP system operated in Transmission Mode(MPTM). Of particular interest is to quantitatively demonstrate direct dose reconstruction for different field sizes in a phantom based on the response of the MPTM.

Methods and Materials: The MPTM was positioned in the block tray of a linac so that the central detector of the array lies on the central axis of the radiation beam. The response of the central MPTM diode was compared with depth dose distribution along the central beam axis in a phantom for field sizes ranging from 5x5 cm² - 40x40 cm² to determine a conversion factor from measured diode response to dose in the phantom, which is independent of the field size. The same conversion factor is used for all diodes in the 2D array to reconstruct the dose along rays projected from the source through each detector and into the phantom, at any depth of interest.

Results: The optimum(i.e. independent of field size) response-to-dose conversion factor for the central diode of MPTM was found at a depth of 1mm in the phantom. Figure 1(a) shows a comparison of the measured and reconstructed dose profiles in the phantom for several field sizes. Figure 1(b) demonstrates that for all detector in-field elements in the 2D array and all field sizes that the 2D reconstructed and measured doses in a phantom at depth of Dmax agree to within $\pm 2.48\%$ (2 SD). Both in and out of field PDD change is less than 1% with the MP in place.

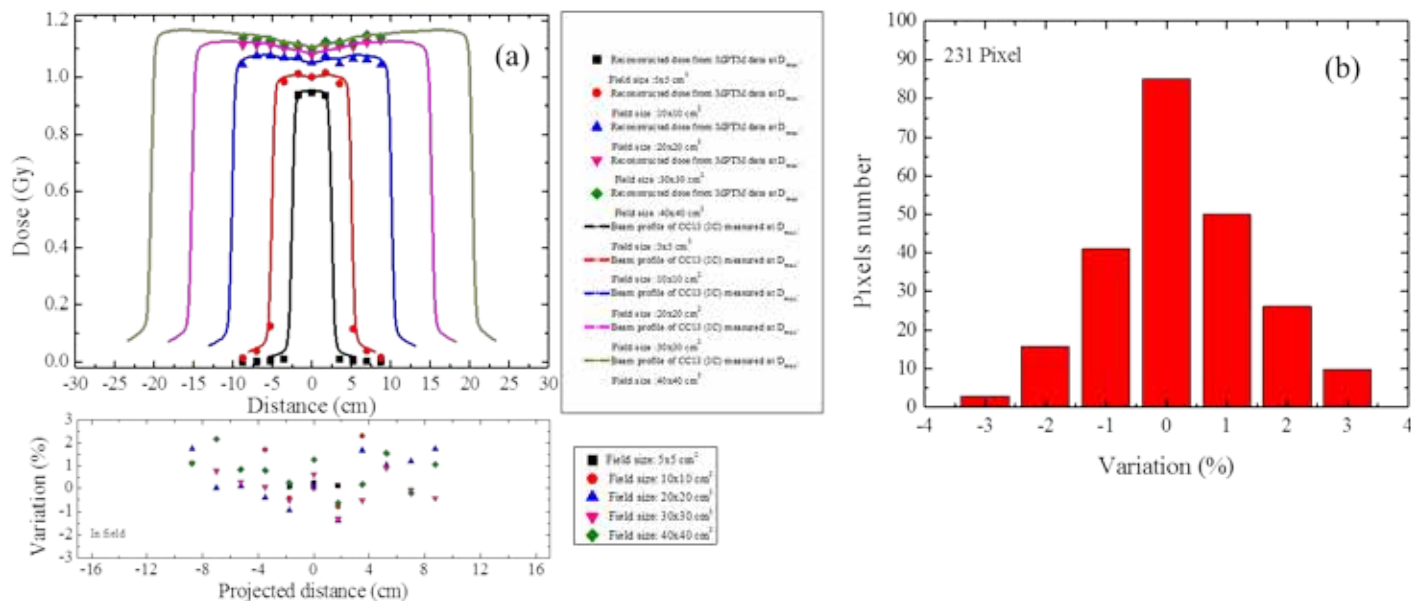


Figure 1. (a) 6MV beam dose profiles measured with CC13 IC in comparison with those reconstructed from MPTM response dose at depth of D_{max} for diodes along the central row (row 6 of 11 rows). (b) Frequency histogram of the variation between measured and reconstructed dose at depth of D_{max} for all in-field points and field sizes tested.

Conclusions: A 2D MP detector array in a transmission mode provides negligible beam perturbation and is an exciting potential candidate for real-time, 2D and 3D dose reconstruction. The success of this work is an exciting development toward real time QA during radiotherapy treatment.

SP141.5 - Energy Correction factor for Plane Parallel ion-chamber and its Use in Clinical photon Beam Dosimetry

Author(s): Konthoujam Manimala Devi¹, Arun S. Oinam², Kamlesh R. Passi¹, Suresh C. Sharma²

¹Department Of Radiation Oncology, Mohan dai oswal hospital, Ludhiana/INDIA, ²Department Of Radiotherapy, post graduate institute of medical education and research, Chandigarh/INDIA

Purpose:

Plane Parallel ion-chambers are recommended as reference dosimetry for photon beam measurements. In dosimetry protocols, experimental values of energy correction factor available for a particular chamber can compare with theoretical calculation considering perturbation factors. However, for Plane parallel chamber, energy correction factor are not available as they are not recommended for photon beam due to the relatively large uncertainty in the wall perturbation factor. Bragg-Gray theory and Spencer-Attix water/air stopping-power ratios, sw,air , of beam qualities Q and Q_0 , are employed in this study to investigate the energy correction factors for plane parallel chambers considering the perturbation factor of the specific chamber in high energy photon beams.

Material and Method:

Water phantom RFA-300, Exradin A19 farmer chamber, PPC-40 Roos, and Standard imaging Max 4000 electrometer were used. Using TRS-398 and Spencer Attix data available in TRS-277 protocol, values of perturbation factor are calculated with high statistical precision for Plane parallel chamber for both 6 and 15 MV photon beams. The dependence of perturbation factor on the beam quality are also studied.

Result and Discussion:

The variations of beam quality index for “PPC-40Roos” from “Exradin A19” were very much lesser as 0.0026 (or 0.39%) and 0.0022 (or 0.29%) for 6 and 15 MV respectively. This result indicates that the responses of both the chambers are within acceptable limit of 1%. Energy correction factors “ K_{QQ_0} ” for PPC-40Roos which was determined theoretically and experimentally shows that the variation between theoretical and experimental for PPC-40 Roos was very much less as 0.5% and 0.08% for 6 and 15 MV respectively. Variation of 0.5% and 0.09% of absorbed dose was observed for 6 & 15 MV respectively between theoretical and experiment values of

PPC-40. However, there was no variation in absorbed dose between the experimental value of PPC-40Roos and Exradin A19.

Conclusion:

The appropriate selection of the reference point of plane parallel chamber is an important issue. If it is accounted correctly then P_{dis} would be almost independent of depth. With precise calculation of perturbation factor, energy correction factors of PPC-40 for higher beam energy can be determined theoretically and compared with experimental value, obtained a good result which is within 0.5%. So, PPC-40 Roos can be recommended for dosimetry of high energy photon beams after considering specific chamber perturbation factor.

SP142 - Light Ion Radiotherapy

TRACK 06: NEW TECHNOLOGIES IN CANCER RESEARCH AND TREATMENT

SP142.1 - Proton Minibeam Radiation Therapy (pMBRT): implementation at a clinical center

Author(s): Cécile Peucelle¹, Catherine Nauraye², Annalisa Patriarca², Eric Hierso², Nathalie Fournier-Bidoz², Immaculada Martínez-Rovira¹, Yolanda Prezado¹

¹Laboratoire D'imagerie Et Modélisation En Neurobiologie Et Cancérologie, Centre National de la Recherche Scientifique (CNRS), ORSAY/FRANCE, ²Centre De Protonthérapie D'orsay, Institut Curie, ORSAY/FRANCE

Purpose

The more selective energy deposition of protons in depth is advantageous compared to photons to preserve normal tissues. Nevertheless, an even better tissue sparing might be possible in proton therapy if combined with the well-established tissue preservation of spatially fractionated submillimetric beams. This sparing effect has been observed in studies performed with synchrotron minibeam radiotherapy (MBRT) [1,2].

The innovative approach proposed here, called pMBRT, was shown to provide favourable dose distributions in Monte Carlo studies [3]. The dose profiles in normal tissue consist in peaks and valleys, while the tumour receives a (quasi)-homogenous dose distribution [3]. The goal of this study was to verify the technological feasibility of creating minibeam in a clinical environment and to evaluate their dosimetric aspects.

Material and methods

The implementation of pMBRT was carried out at the ICPO. To generate minibeam patterns, collimators with micromillimetric line apertures were manufactured. Gafchromic EBT3 films were irradiated in water phantoms by an array of 100 MeV protons (700 μm -wide) minibeam. Depth dose distributions and lateral dose profiles were studied. Relevant dosimetric parameters in spatially fractionated techniques, namely peak and valley doses and their ratio (PVDR) [4], were assessed. Beam penumbras and output factors were also evaluated.

Results

The technical implementation met pMBRT dosimetric specifications. A spatial fractionation of the dose was obtained in normal tissues (PVDR up to 7) while a quasi-homogeneous dose distribution was reached at the Bragg peak location (see figure 1), in agreement with theoretical predictions [3]. The reduced penumbras (600-1100 μm) in healthy tissue make pMBRT a good candidate for radiosurgery applications.

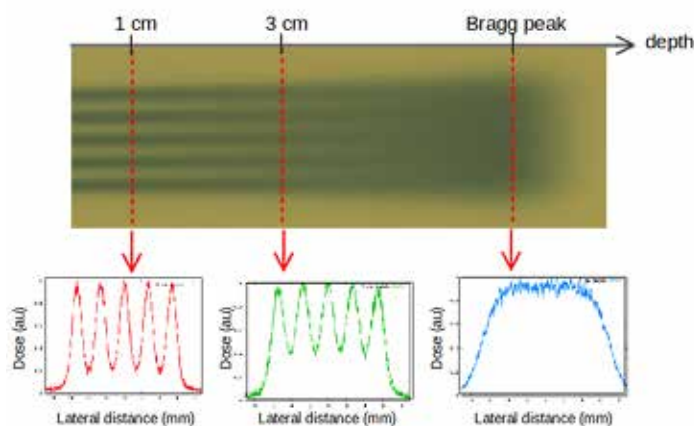


Figure 1: Gafchromic film, irradiated longitudinally, showing a spatial fractionation in normal tissues and a (quasi)-homogeneous dose distribution at the Bragg peak position.

Conclusion

This study experimentally proves the technical feasibility of pMBRT at a clinical center. The first experimental dosimetry measurements were successfully performed despite the extreme irradiation conditions. The PVDR values obtained showed the potential of this approach, which might conduct to a reduction of the normal tissue complication probability. Animal irradiation experiments are planned to confirm the normal tissue sparing capability of pMBRT.

References

- [1] P. Deman et al., *Int. J. Radiat. Oncol. Biol. Phys.*, 82 (2012)
- [2] Y. Prezado et al., *J. Synchrotron Radiat.* 19, 60–65 (2012)
- [3] Y. Prezado et al., *Med. Phys.* 40 (3) (2013).
- [4] F. A. Dilmanian et al., *J. Neuro-Oncol.* 4, 26-38 (2002).

SP142.2 - Hadron minibeam radiation therapy: feasibility study at Heidelberg Ion Therapy Center

Author(s): Immaculada Martínez-Rovira¹, Iurii Sorokin², Stephan Brons³, O Kovalchuk², V Iakovenko², M Campbell⁴, X Llopart⁴, S Pospisil⁵, V Pugatch², Yolanda Prezado¹

¹Laboratoire D'imagerie Et Modélisation En Neurobiologie Et Cancérologie, Centre National de la Recherche Scientifique (CNRS), ORSAY/France, ²Kiev Institute for Nuclear Research, Kiev/UKRAINE, ³Heidelberg Ion Beam Therapy Center (HIT), Heidelberg/GERMANY, ⁴CERN, Geneva/SWITZERLAND, ⁵Institute of Experimental Applied Physics (IEAP), Prague/CZECH REPUBLIC

Introduction and Purpose

Despite recent advancements in radiotherapy and radiosurgery, significant limitations remain. Although hadrontherapy, being in clinical use for more than 15 years, has shown remarkable effectiveness, it still could benefit from a lower impact on non-targeted tissues to allow its administration at higher doses. This is the reason why we propose a new approach called hadron minibeam radiation therapy (hadron MBRT). The technique is based on the well established tissue-sparing effect of arrays of parallel, thin or small beams, observed in studies performed with synchrotron radiation [1-2]. In parallel, significant tumor growth delay was observed in highly aggressive tumors by using interlaced irradiations [1-3]. Hadron MBRT combines the advantages of MBRT with the high

dose conformability and the remarkable biological effectiveness of hadrontherapy. This novel strategy might guarantee tissue recovery and reduce the side effects of radiation in healthy tissues. The main goal of this study was to explore this new approach from dosimetric point of view and to verify its technical feasibility at a clinical center (Heidelberg Ion Therapy Center, Germany). In particular, carbon and oxygen minibeam were studied.

Materials and Methods

Carbon and oxygen minibeam were generated through a tungsten multislit collimator with line apertures of 700 μm -wide separated by 3600 μm . Several beam spots were used to cover a given irradiation field size ($1 \times 1 \text{ cm}^2$) and a spread out Bragg peak (SOBP) region of 5 cm at 8 cm-depth in water. Radiochromic films (EBT3) were placed at several depths in a solid-water slab phantom to evaluate dose distributions. Quenching effects of these films were also assessed and results were accordingly corrected. Metal Microstrip and Micropixel (TimePix) detectors were explored for beam distribution measurements [4].

As a figure of merit, the ratio between the central dose of one minibeam (peak dose) and the dose in the middle of two consecutive beams (valley dose) was evaluated. This magnitude, named peak-to-valley dose ratio (PVDR), is a very relevant magnitude in such spatially fractionated techniques [5].

Results

The measured lateral dose profiles in carbon and oxygen MBRT consisted in a pattern of peaks and valleys, which prove the technical feasibility of this approach. This first dosimetric study showed PVDR values around 10-20 in the first centimeters of the phantom. PVDR values progressively decrease up to around 5 at 8-cm-depth. These PVDR values are in the order of the ones obtained in x-rays MBRT, for which biological effectiveness has already been proven. Finally, Metal Microstrip and Micropixel (TimePix) detectors have demonstrated excellent performance measuring PVDR values, in agreement with radiochromic films.

Conclusions

This is the first exploratory study that experimentally proves the technical feasibility of hadron MBRT at a clinical center. The PVDR values obtained showed the potential of this radiotherapy approach, which might allow to reduce side effects in the healthy tissues. Animal experiments are warranted.

References

- [1] Dilmanian, *Proc.Natl.Acad.Sci.USA.* 103 (2006).
- [2] Deman, *Int.J.Radiat.Oncol.Biol.Phys.* 82 (2012).
- [3] Prezado, *J.Synchrotron.Radiat.* 19 (2012).
- [4] Pugatch, *Nucl.Instr.Meth.A* 581 (2007).
- [5] Dilmanian, *Neuro.Oncol.* 4 (2002).

SP142.3 - Acoustic Range Verification of Proton Beams: Simulation Assessment of the Challenges of Clinical Application**Author(s):** Kevin C. Jones¹, Chandra M. Sehgal², Stephen Avery¹¹Department Of Radiation Oncology, University of Pennsylvania, Philadelphia/UNITED STATES OF AMERICA, ²Department Of Radiology, University of Pennsylvania, Philadelphia/UNITED STATES OF AMERICA

For radiation treatment of cancer, proton therapy efficacy is limited by range uncertainty. The ability of protons to deliver substantial dose at the Bragg peak is a benefit that improves localization, but it also magnifies the risk of range uncertainty; over- or undershooting the target drastically changes the delivered dose. *In-vivo* proton range monitoring has the potential to eliminate range uncertainty and the associated risks. The measurement of sound waves generated by proton beams (protoacoustics), is an undeveloped technique with potential for *in-vivo* range verification. Similar to thermoacoustics, protoacoustic emissions are generated because the energy deposited by pulsed proton beams is converted into heat, which causes expansion and emission of pressure waves.

Previous work has established the viability of protoacoustic range verification under ideal conditions. Simulations with 5 mm diameter, 1 μ s proton beams have shown that protoacoustic measurements can determine the Bragg peak position to 1 mm accuracy. Previous experiments with fast, <1 μ s rise-time proton pulses have measured the acoustic signals. Simulations and experiments under non-ideal, common clinical conditions are still lacking. Here, through Green's function based numerical simulations of 5 mm diameter pencil beams, we assess the challenges to translating protoacoustics into the clinic, where proton currents are often limited to nanoamperes and proton pulse rise-times are in the 10's of microseconds.

Based on the simulation results, the protoacoustic signal amplitude is linearly proportional to the current and weakly dependent on the rise-time. A current of 300 nA is expected to generate ~0.1 Pa, which is at a level that is measurable with commercially available detectors. As the rise-time increases from 1 to 40 μ s, the pressure amplitude drops by 20%. The most significant observed effect of increasing rise-time is a broadening of the protoacoustic signal, which decreases the time-of-flight range-verification accuracy from 1 mm (1 μ s rise-time) to greater than 1 cm (40 μ s rise-time). For a homogeneous medium irradiated with 5 mm diameter beams, the simulated signals have frequency spectra centered at 80 kHz (1 μ s rise-time) and 5 kHz (40 μ s rise-time). Although clinical proton beam characteristics limit the protoacoustic amplitude, simulations predict that protoacoustic signals are detectable under clinical conditions. Long proton pulse rise-times degrade the accuracy of range calculations based on simple time-of-flight calculations, suggesting that multiple measurements or comparisons to modeling are necessary to improve accuracy.

SP142.4 - Radiochromic Film Based Dose Calibration and Monitoring for Radiobiological Experiments using Low Energy Proton Beams**Author(s):** Belal Mofteh¹, Saad Aldelajjan¹, Mamoun Shehadeh¹, Faisal Alzorkany¹, Ghazi Alsbeih¹, Jan Seuntjens², Slobodan Devic³
¹Biomedical Physics, King Faisal Specialist Hospital and Research Center, Riyadh/SAUDI ARABIA, ²Medical Physics Unit, McGill University, Montreal/CANADA, ³McGill University, Montreal/CANADA**Purpose**

Low energy proton beams could be of potential interest for radiation treatments of shallow lesions (intra-operative radiotherapy, melanomas, non-cancerous skin diseases) due to expected higher relative biological effectiveness (RBE) and sharp fall off behind clinical target. Output measurements for MTT assay were performed using the EBT3 model GafChromic™ film based reference dosimetry system.

Methods

Figure 1.a represents experimental setup used to measure depth dose curve (Fig.1.b) and beam output with a calibrated PTW Markus ion chamber. To improve stability of irradiations (26.5 MeV protons originating from CS30 cyclotron) an aluminum cylinder was added in front of the beam exit serving as a timed shutter. Measured signal was corrected by monitor chamber reading and subsequently scaled by ratio of stopping powers for water and air at given depth, while the effective depth of measurements was scaled by ratio of CSDA ranges water to air. Output was measured at 3 mm depth in the middle of the plateau ahead of the Bragg peak where PDD was normalized. Following the TRS398 reference dosimetry protocol for proton beams, output was measured in water in terms of Gy/nC where nC is reading of the monitor chamber. Once the output of the beam was known, we calibrated EBT3 film model for doses of up to 35 Gy (Fig.1.c). For MTT assay, attached breast cell cultures (MCF-7, MCF-12, MDA-MB-231) in 96-well plates were irradiated by horizontal beam (Fig.1.d). Behind the plate, piece of film was placed to monitor dose distribution during each experiment.

Results

For each irradiated 96-well plate, a dose image was reconstructed (Fig.1.e) and then scaled by the measured PDD data. Natural Gaussian shape of the beam was used to obtain multiple dose points within the same plate from a single exposure. Dose values per wells were used to construct the survival curve (Fig.1.f). The average RBE of proton beam compared to x-ray at the ID50 (50% inhibitory dose) was 1.22 (SD = 0.05) which was statistically higher (P = 0.02) than the 1.1 commonly used in standard clinical proton therapy.

Conclusions

Radiochromic film-based dose monitoring system that can be used for MTT radiobiology assays with a low energy proton beam was described. Having a sharp dose fall-off behind the Bragg peak, a high dose rate proton beam originating from a production cyclotron could further allow for dose escalation protocols in the case of superficial lesions. This work was supported by NSTIP 11-BIO1428-20.

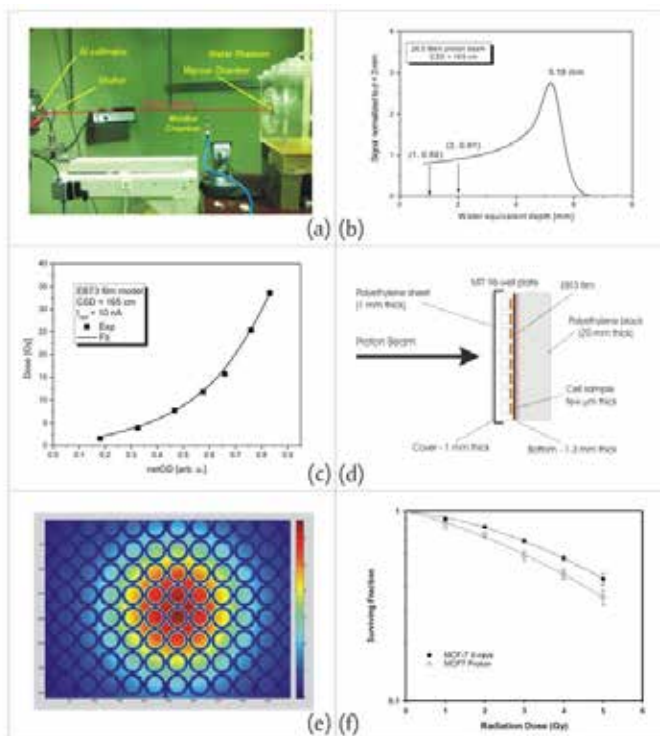


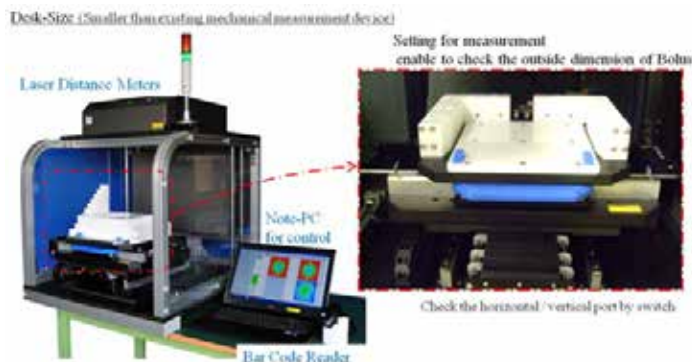
Figure 1: Dose Calibration for Radiobiological Experiments with Low Energy Proton Beams: a) experimental setup used for dosimetry measurements; b) PDD curve measured using Markus parallel-plate chamber; c) calibration curve for EBT3 model GafChromic™ film using red color channel of scanned tiff images; d) experimental setup during MTT assay irradiations; e) dose map measured with EBT3 GafChromic™ film model during MTT assay; f) comparison of survival fractions for MCF-7 breast cancer cells irradiated with 320 kVp photons and 26.5 MeV proton beam.

SP142.5 - Development of 3D measurement device dedicated for range-compensator QA

Author(s): Shigekazu Fukuda¹, Eriko Urakabe¹, Kiyohiro Yamada²
¹Research Center For Charged Particle Therapy, National Institute of Radiological Sciences, Chiba/JAPAN, ²Accelerator Engineering Corporation, Chiba/JAPAN

Purpose

In light ion therapy including carbon beam therapy, the broad-beam method is used to irradiate beams to the tumor conformally. The broaden beams are cut to the shape of the target tumor projected in the beam's eye view by a patient collimator or multileaf collimator (MLC). To adjust the range of the beams to the target in the depth a range-compensator is used. The range-compensator is a block that has an engraved depression in the shape of the target tumor. [1] Though it is desirable to check the 3D shape of the range-compensator compared to the planned shape at all points, over 2000 points, in terms of QA/QC, only the limited points, 30-40 points, are usually checked by the contact length measurement sensor device (CLMSD). To verify all points automatically in a short time, the 3D measurement device (3DMD) dedicated for range-compensators QA has been developed.



Methods

The 3DMD has a XY-stage with high precision and a range-compensator is attached to the XY-stage. Two CCD laser displacement sensors were employed to measure the height of each point of the range-compensator by detecting reflected laser. We verified some range-compensators.

Results

Due to the shape there were some points which cannot be measured, but the ratio of the number of the unmeasured points to that of all points was less than 1%. The precision of the measurements by the 3DMD was within less than 0.1 mm, and the concave positions were verified as acceptable. It took less than 20 minutes to measure and verify the all points of the large patient compensator such as 20 cm x 20 cm x 15 cm.

Conclusion

After further commissioning of the 3DMD, we plan to use this device to check the range-compensators routinely.

References

[1] "Recent Innovations in Carbon-Ion Radiotherapy", S. Minohara, S. Fukuda, and et.al., J. Radiat. Res., 51, 385-392 (2010)

SP143 - Radiotherapy and Guidance

TRACK 07: SURGERY, COMPUTER AIDED SURGERY, MINIMAL INVASIVE INTERVENTIONS, ENDOSCOPY AND IMAGE-GUIDED THERAPY, MODELLING AND SIMULATION

SP143.1 - Sliced Mary: a deformable phantom for the validation of set-up based on surface imaging in radiotherapy treatments

Author(s): [Stefania Pallotta](#)¹, Serenella Russo², Marco Esposito², Livia Marrazzo³, Cinzia Talamonti¹, Pierluigi Bonomo³, Fabiola Paia³, Lorenzo Livi⁴, Cristina Svensson⁵

¹Department Of Experimental And Clinical Biomedical Sciences, University of Florence, Florence/ITALY, ²Azienda Sanitaria di Firenze, Florence/ITALY, ³AOU Careggi, Florence/ITALY, ⁴Department Of Experimental And Clinical Biomedical Sciences, University of Florence, Florence/ITALY, ⁵C-RAD Positioning AB, Uppsala/SWEDEN

Ionizing radiation is generally used to check patient setup in radiotherapy treatments but data concerning patient position can also be derived using surface imaging (SI) systems. The absence of additional radiation exposure and the execution rapidity make this approach particularly interesting. The main drawback of these techniques consists in the worse accuracy caused by the deformation of external body surfaces. As deformable image registration algorithms could potentially solve this problem, some SI developers have included elastic deformation tools in their software. In this work a deformable phantom, suitable for SI acquisition, and with internal tissue contrast for both kilovoltage (kV) and megavoltage (MV) imaging modalities has been developed to evaluate deformable image registration algorithms. The phantom consists in 33 slices of expanded polystyrene slabs shaped thus to simulate part of a female body. Anatomical details, simulating ribs and spinal cord, together with internal targets are included in thorax and abdominal parts. Two mammalian prosthesis and two objects, simulating arms, were fixed to the phantom which was finally covered with a white Lycra tissue. Independent and realistic head rotation, arms flexion as well as body torsion around a longitudinal axis and bending around lateral and vertical axes can be achieved. A preliminary test to assess the deformable phantom usability was performed. The elastic registration algorithm implemented in C-RAD Catalyst software was tested by applying to the phantom different head and arm rotations and comparing SI and portal imaging (PI) registration results.

SP143.2 - Evaluation of ion chamber response in high dose per pulse electron beams of IORT accelerator using EGSnrc Monte Carlo code

Author(s): [Mostafa Robotjazi](#)¹, Seied Rabi Mahdavi², Abbas Takavar¹
¹Medical Physics, Tehran University of Medical Sciences, Tehran/IRAN, ²Medical Physics, Iran University of Medical Sciences, Tehran/IRAN

Introduction: The use of high dose per pulse electron beams produced by mobile dedicated linacs for intraoperative radiotherapy (IORT) has been increasing in recent years. The dosimetry of such beams requires particular care when performed by ionization chambers. A delicate aspect in this respect is the determination of the factor, k_s , that corrects for ion recombination in the irradiated chamber. There are some methods and studies in evaluation of k_s for the purpose of application in IORT fields. One of the standard methods in dosimetry is the Monte Carlo (MC) simulation. In this study, we evaluated the response of parallel plate chamber response in high dose per pulse electron beams of dedicated IORT linac using MC simulation.

Material and Methods: The following MC calculations are performed with the EGSnrc user codes. The BEAMnrc code was used for linac head modeling and DOSRZnrc was used for tuning of the relative and absolute dosimetry. In evaluation of relative dosimetry gamma-index was used. The criteria for this purpose was selected 2% (Dose Difference) and 2mm (Distance To Agreement). In the tuning of the virtual linac for absolute dosimetry, we used the fact that linac was tuned to deliver the 1 cGy/MU in the depth of maximum dose (D_{max}). The dose of the monitor chamber of the linac was used as a normalization point and application of MU in dose calculations. The geometry of ion chamber in water phantom and dose in sensitive volume of the chamber was simulated using CAVITY_CPP code. The correction factors of chamber such as P_{cav} , P_{wall} , and absolute dose in D_{max} was calculated in this code. Finally, the absolute dose value using this code was compared by experimental data.

Results: There was good agreement between experimental and simulated relative dosimetries. More than of 95% of gamma values were passed in evaluation of relative dose comparisons. The experimental measurements using ion chamber were performed in D_{max} . The correction factors of chambers (K_{qq0} , K_{tp} , K_{pol}) was done using IAEA-TRS398. The K_{sat} in experimental measurements were performed by Laitano method. The chamber response in experimental measurements was 0.994 cGy/MU whereas the simulated value for chamber without and with applying the K_{wall} and K_{cav} was 0.9374297($\pm 0.21\%$) and 0.993072951($\pm 0.3\%$) cGy/MU, respectively. The discrepancy between the measured and experimental response of chamber was about 0.09%.

Conclusion: One of the uncertainty sources in high dose per pulse electron beams in dedicated IORT linac is determination of K_{sat} . In this study, we showed that the response of parallel plate chamber using mentioned correction factors has a good response in high dose per pulse electron beams of dedicated IORT linacs.

SP143.3 - Compared QA of APEX Radiosurgery System using ARCHECK Phantom in Dynamic Conformal Arc System and VMAT System

Author(s): [Jae Hyuk Seo](#)¹, Hun Joo Shin², Shin-Wook Kim², Choong-Il Lee¹, Mina Yu¹, Se-Cheol Yoon¹, Tae-Suk Suh³, Young Nam Kang⁴

¹Radiation Oncology, The Catholic University of Korea Bucheon St. Mary's Hospital, Bucheon-si, Gyeonggi-do/KOREA, ²Department Of Radiation Oncology, Incheon St. Mary's Hospital, College of Medicine, The Catholic University of Korea, Incheon/KOREA, ³Department Of Biomedical Engineering, College Of Medicine, The Catholic University of Korea, Seoul/KOREA, ⁴Department Of Radiation Oncology, Seoul St. Mary's Hospital, College of Medicine, The Catholic University of Korea, Seoul/KOREA

PURPOSE

In this study, we estimated the accuracy and usefulness of APEX system for the radiosurgery with the use of the ArcCHECK phantom in dynamic conformal arc therapy (DCAT) and volumetric modulated arc therapy (VMAT) system.

MATERIAL AND METHOD

We used the ArcCHECK phantom and APEX system. When APEX system which is mounted to the gantry is rotating, we compared DCAT and VMAT System. MONACO (ver. 3.3) was utilized as a radiation treatment planning system (RTPs). APEX system has the micro multi leaf collimator (mMLC) with leaf thickness of 2.5 mm. INFINITY Tx Machine was used. We performed two different techniques for the comparison. One is DCAT plan and the other is VMAT plan. In order to evaluate the APEX system, 3D gamma analyses were conducted using 3% / 3 mm and 2% / 2 mm criteria.

RESULTS

The difference between the DCAT and VMAT plans was found to be less than 3%. Also, the 3D assessment showed a significant difference between the DCAT and VMAT (both gamma pass rate of above 98% with 3% / 3 mm criteria, both gamma pass rate of above 95% with 2% / 2 mm criteria).

CONCLUSIONS

DCAT plan can not modulate the intensity of radiation while the gantry is rotating. And mMLC shape and gantry rotating speed is fixed at the each control point. However, VMAT plan can modulate the intensity of radiation through the optimized mMLC shape and gantry rotating speed. Therefore, our results show that the VMAT plan is superior to the DCAT plan. we conclude that APEX system should adapt the VMAT system for the accurate radiosurgery.

SP143.4 - Head and Neck CT/CBCT Deformable Registration for Image-guided Accurate Radiotherapy System ARTS-IGRT

Author(s): Qian Wu¹, Ruifen Cao¹, Jing Jia¹, Liqin Hu¹, Xi Pei²

¹Key Laboratory of Neutronics and Radiation Safety, Institute of Nuclear Energy Safety Technology, Chinese Academy of Sciences, Heifei/CHINA, ²Key Laboratory of Neutronics and Radiation Safety, Institute of Nuclear Energy Safety Technology, Chinese Academy of Sciences, Heifei/CHINA

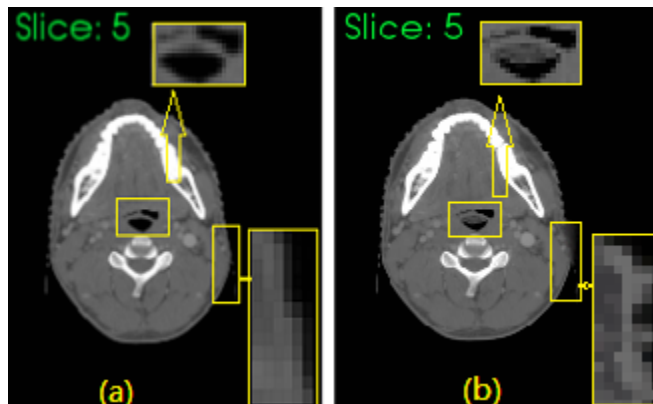
Objective: Deformable image registration (DIR) between the planning CT and the daily cone-beam CT (CBCT) played a key component in image-guided radiation therapy (IGRT). The traditional DIR algorithms, such as Demons, failed in CT/CBCT image registration due to CBCT worse image quality and intensity inaccuracy. The purpose of this work was to develop a CT/CBCT DIR method for ARTS-IGRT prototype system and implementation GPU in CUDA programming environment. **Methods:** Our algorithm tried to correct CBCT intensity value in the processing of symmetric Demons registration. CBCT intensity value was corrected based on that of the corresponding CT, because of the relative better image quality and more accurate intensity value of CT. The algorithm was carried on as follows: (1) CT and CBCT images were split into several disjoint tissues by intensity histogram matching, image label was assigned to voxel according to the intensity value and spatial neighboring voxels. (2) The deformation field was calculated by the displacement field formula of symmetric force Demons. (3) CBCT intensity value was corrected voxel by voxel. There didn't exist a global intensity correspondence in light of all voxels of CT and CBCT. We firstly modeled the intensity correspondence by linear polynomial model; and further interpolated the intensity values where the voxel pairs were at the same tissue to estimate those of voxel pairs consisting of different tissue type, because over-correction will appear for different tissue type voxel pairs. (4) CBCT was rescaled and a new deformation field was calculated with the corrected CBCT and the deformed CT, then returned to (3) for the next iteration.

Results: Registration tools were tested for head-neck images. From the result of symmetric Demons algorithm, we can find that anatomical structures in the deformed CT were significantly distorted due to CBCT intensity inconsistency, especially in those regions with severe scatter artifacts. Our algorithm yielded undistorted deformed CT that matched well with corrected CBCT. The performance was also quantitatively evaluated by normalized mutual information (NMI), the average NMI increased to 0.68 ± 0.02 and the computational time decreased to 50 seconds for the image size of $256 \times 256 \times 49$.

Conclusions: We implemented an effective intensity correction based CT/ CBCT DIR method. CT/ CBCT was considered as mono-modality image after CBCT intensity correcting and the corrected CBCT with better image quality could be used for radiotherapy such

as inter-fractional setup error correction and replanning.

Keywords: Image registration; Demons algorithm; Cone-beam CT; Intensity Correction; Image guided radiotherapy



SP144 - EMG/MMG**TRACK 09: BIOSIGNAL PROCESSING****SP144.1 - Estimation of dorsiflexion torque from a mechanomyogram using a Kalman filter**

Author(s): Takanori Uchiyama, Shunichi Otsuka
Applied Physics And Physico-informatics, Keio University, Yokohama/JAPAN

A mechanomyogram (MMG) is a vibration detected on a skin surface with a displacement sensor or an acceleration sensor. Measuring an MMG is easier than measuring dorsiflexion torque because sensors are simply fixed on the skin's surface. The measurement technique does not require the restriction of human motion. An MMG is a signal that reflects mechanical properties of muscle and subcutaneous tissue. We assume that an MMG contains a signal from muscle contraction as a low-frequency component and noise from subcutaneous tissue as a high frequency component. We propose a method for estimating dorsiflexion torque from the mechanomyogram smoothed by using a Kalman filter. Six healthy male subjects participated in the experiments. A subject sat on a chair, and his thigh and leg were immobilized with nylon belts. His foot was fixed on the equipment to measure the dorsiflexion torque during isometric contraction. First, the dorsiflexion torque was measured by applying a transcutaneous electrical stimulation to the common peroneal nerve with Ag-AgCl surface electrodes. The system from the electrical stimulation to the dorsiflexion torque was identified by the singular value decomposition method, and the system, control, output, and feed-forward matrices of the state-space equations were calculated. Then, a Kalman filter was constructed using the matrices. Second, the subject was instructed to perform a task while tracking a target dorsiflexion torque displayed on a screen in front of the subject. The torque was approximately 50% of the maximum voluntary contraction. The onset and duration of the contraction were random. The MMG of the tibialis anterior muscle was measured with a laser displacement meter. The neural action potential was measured for 60 s with the Ag-AgCl electrodes, which were used as stimulation electrodes in the first experiment. The EMG of the tibialis anterior muscle was also measured to compare the proposed method to the conventional method of using the root mean square of the full-wave rectified EMG (EMGrms). The signals were sampled at 2,000 Hz and stored on a PC. The MMG was smoothed with a Kalman filter constructed by the matrices of the state-space equations of the dorsiflexion torque. Here, the neural action potential was used as an input signal to the system. We regarded the smoothed MMG as the extracted dorsiflexion torque from the MMG. The time course and frequency response of the extracted torque and the EMGrms were compared to those of the observed dorsiflexion torque. The observed torque was approximated well by the extracted torque as compared to the EMGrms in both the time and frequency domains for all six subjects. In conclusion, a noble method of extracting the dorsiflexion torque from the MMGs was proposed in this study. The method provided a better approximation of the dorsiflexion torque as compared to the conventional method that uses EMGrms.

SP144.2 - Upper-Limb Force Modeling using Rotated Ensembles with Fast Orthogonal Search on High-Density Electromyography

Author(s): Gregg Johns¹, Evelyn Morin², Keyvan Hashtrudi-Zaad³
¹Electrical & Computer Engineering, Queen's University, Kingston/CANADA, ²Electrical & Computer Engineering, Queen's University, Kingston/ON/CANADA, ³Electrical And Computer Engineering, Queen's University, Kingston/CANADA

Robust estimation of net limb forces has a plethora of important applications. However, the most reliable methods are invasive and are not feasible in most cases. The use of surface electromyography (EMG) for estimating muscle forces is non-invasive, and generally unobtrusive. However, many physiological and non-physiological factors limit the precision of these methods. The rich spatiotemporal information collected from high-density surface EMG (HD-EMG) grids has been used to mitigate the problem; however, the instability of electrode-skin contact for these systems creates outlying channels, which may lead to substantial error. We build non-linear predictors on rotated ensembles, which when aggregated provide robust and highly accurate (RMSE<2.6%) estimation of the force induced at the wrist under isometric contractions.

SP144.3 - MMG detection of intentional movement in the presence of dyskinetic movements

Author(s): Marcela Correa Villada¹, Tom Chau²
¹University of Toronto, Toronto/ON/CANADA, ²Bloorview Research Institute, Toronto/CANADA

Cerebral palsy (CP) is a permanent disorder that affects an individual's development of movement and posture and is characterized by the presence of variable involuntary movement that may affect the individual's desire to communicate and interact with their surroundings. Assistive technologies may enable these individuals to perform functional activities such as communication (Tai, Blain, and Chau 2008, 204-219).

One of the access pathways commonly used for assistive technologies is muscle activity. Muscle activity can reflect the condition of muscles as well as reveal the underlying user intention. While EMG is widely used in many fields for the study of muscle activity, the mechanomyogram (MMG) is gaining popularity in biomedical engineering applications. MMG is a technique used to study the mechanical activity of muscles which arises from the lateral oscillation of muscle fibers during active voluntary contraction (Posatskiy and Chau 2012, 320-324; Uchiyama and Miyazaki 2013, 461-464; Islam et al. 2013; Kim et al. 2008, 33-42; Orizio 1993, 201-243; Jaskólska et al. 2007, 336-347).

This research intends to answer the following question:

In what ways can information about muscle contractions be combined to enhance the detection of intention amid dyskinetic movements beyond that achievable by conventional agonist-based detection?

This study has two main objectives: first, to detect the contribution of task muscles in a reaching movement in children with DCP, and second, to combine information from a group of task muscles to enhance the detection of movement intention

We are recruiting a control group of typically developing children and a group of children and youth with dyskinetic cerebral palsy between the ages of 8 and 18. MMG signals are simultaneously recorded using a tri-axial accelerometer placed on the surface of the skin of 6 muscles (flexor, extensor, biceps, triceps, anterior deltoid and pectoralis major) involved in the reaching and drawing task. Participants are asked to perform horizontal and vertical lines on a tablet for a period of 25 minutes. The signal has been processed by wavelet analysis decomposition and denoising in order to filter out gross motor movement. The mother wavelet used for this analysis is Daubechies 10. Preliminary data collected from participants has shown that Singular spectrum analysis (SSA) is a promising noise reduction technique to determine muscle contraction, onset time of contraction, and offset time of contraction.

In order to achieve objective 2, we will develop a model to predict movements with varying number of MMG inputs. Possible mod-

els will include an artificial neural network with time series inputs (Specht 1990, 344-353). We will compare the predictability of a movement while changing the number of MMG signals used for input data.

Children and youth with physical disabilities could benefit from the use of MMG as an access technology system. However, there is not enough research on the adequate use of MMG on children with dyskinetic cerebral palsy. This project aims to evaluate the information from task muscle contractions during a reaching task in order to enhance the detection of intentional muscle activity in the presence of dyskinetic movements.

SP144.4 - Dynamic Noise Reduction in Accelerometer-based Mechanomyography during Pediatric Gait

Author(s): Katherine Plewa¹, Tom Chau²

¹Institute of Biomaterials and Biomedical Engineering, University of Toronto, Toronto/CANADA, ²Bloorview Research Institute, Toronto/CANADA

Neurological lesions result in a loss of motor and sensory function needed to effectively produce complex movements. The patient's adaptability to these dysfunctions depends on their substitution for missing afferent information; therefore, measuring impaired muscles during gait may provide a pathway for redefining that functional movement. Mechanomyography (MMG) is a method for measuring muscle activity, contraction timing, and providing biofeedback [1]. However, research in MMG has been limited to simple contractions because the muscle signal is lost within motion artifacts from gross limb movements during dynamic activities [1].

Improving the signal-to-noise ratio of MMG is important because of the overlapping frequency content of both motion artifact and useful muscle information[1]. Although microphone and coupled transducers have been suggested for measuring MMG in dynamic environments [2, 3], this study will focus on improving accelerometer-based MMG by developing noise reduction and feature extraction techniques that have been previously utilized [4, 5]. Wavelet based methods have been successful in de-noising and detecting muscle contractions; however, they have not been implemented in dynamic environments. Therefore, the main objective of this study is to optimize accelerometer-based MMG during gait.

MMG data will be collected from 100 healthy pediatric participants (ages 8-18) during self-paced gait using tri-axial accelerometers. MMG will be measured at four muscle locations (i.e., tibialis anterior, medial gastrocnemius, vastus lateralis, and biceps femoris). Electromyography (EMG) data will be simultaneously collected from the same muscles and used to validate MMG muscle activity. Once the sensors have been attached, participants will be asked to walk at their typical pace around a track for 15-minutes. MMG and EMG data will be bandpass filtered, then wavelet-based denoising will be applied to the MMG signals to isolate muscle activity. Feature extraction algorithms will then be applied to identify muscle contractions. We will further use this MMG data to characterize the sequence of coordinated muscle activations and derive stride intervals for fractal analysis. Initial results indicate that wavelet-based denoising is a promising method for isolating muscle signals from noising MMG signals, and singular spectrum analysis has been successful at identifying bursts of muscle activity. We hope that by improving MMG noise reduction methods in dynamic activities, we can utilize MMG for fractal analysis of gait and as a biofeedback tool in gait rehabilitation settings.

References:

1. Madeleine, P., et al., *Effects of electromyographic and mechanomyographic biofeedback on upper trapezius muscle activity during standardized computer work*. 2006. **49**(10): p. 921-933.

2. Posatskiy, A. and T. Chau, *Design and evaluation of a novel microphone-based mechanomyography sensor with cylindrical and conical acoustic chambers*. 2012. **34**(8): p. 1184-1190.

3. Silva, J. and T. Chau, *Coupled microphone-accelerometer sensor pair for dynamic noise reduction in MMG signal recording*. 2003. **39**(21): p. 1496-1498.

4. Alves, N. and T. Chau, *Automatic detection of muscle activity from mechanomyogram signals: a comparison of amplitude and wavelet-based methods*. 2010. **31**(4): p. 461.

5. Vaisman, L., J. Zariffa, and M.R. Popovic, *Application of singular spectrum-based change-point analysis to EMG-onset detection*. 2010. **20**(4): p. 750-760.

SP144.5 - EMG-EMG Coherence in Multisite Writer's Cramp Waveforms - A Study with Advanced Multi-Channel EMG System

Author(s): Venkateshwarla R. Raju¹, Roopam R. Borgohain²

¹Biomedical Eng & Neurology & Neurosurgery And, Nizam's Inst of Medical Sciences (NIMS) University & Hospital, HYDERABAD/INDIA, ²Neurology, Nizam's Inst of Medical Sciences, Hyderabad/INDIA

We setup a multichannel EMG amplifier for capturing signals with special reference to Writer's cramp (WC) from the subject having input impedance greater than 100MegOhm(MΩ). Using the setup we gathered EMG-EMG data signals from WC subjects (diseased conditions) hand muscles: ECR and ECU, FCR and FCU, followed by fifth muscle using a set-of-five innocuous micro-wire-electrodes (50μ) in each-subject. We then assessed coherence and conducted chi-square (χ^2) tests on these data in eight subjects of concordant(C) group and 4 subjects of discordant (D) group of right-hand-writing-signal (RHWS) and in left-hand-writing-signal (LHWS) studied. We compared the difference between flexor-aspect-of-forearm and extensor-aspect-of-intrinsic hand-muscles. This showed significant-coherence in both concordant and discordant groups of WC mirror-movements (MMs) in mirror-Dystonia. These observations suggest that the nature of EMG-EMG coherence in dystonic WC may be constrained by the descending-motor-systems, both in terms of their anatomical-distribution and their frequency-characteristics. In our computation, coherence showed symmetry along the diagonals in graphs. We thus state that, this study showed significant quantifiable EMG differences in the signals/waveforms seen while writing with the right and left hands between those WC subjects with concordant MMs (C group) versus those with discordant MMs (D group).

SP144.6 - An Exploration of the Erector Spinae Muscle for Knee Exoskeleton Control

Author(s): Denis D. Rodriguez, Ana Cecilia Villa Parra, Teodiano Freire Bastos

Post-graduate Program In Electrical Engineering, UFES, VITORIA/ BRAZIL

Lumbar erector spinae muscle has been little explored for knee exoskeleton control through sEMG signals, which could improve the onset and offset of motion. In this study, a simultaneous sEMG record was obtained in three movements routine (knee extension-flexion, stand-up from seated position and seat-down from up position) from five trunk levels, and five muscles of the leg. sEMG signals were smoothed to obtain the envelope through the captured sample entropy method, which can be used to detect the onset/offset through an adaptive threshold value.

The onset/offset related to knee motion was obtained on trunk muscles, during knee extension-flexion, stand-up and sit-down activities, which is suitable for knee exoskeleton control.

SP145 - Developing Tools for Successful Aging: Independent Mobility & Visual Impairment

TRACK 10: REHABILITATION MEDICINE, SPORTS MEDICINE, REHABILITATION ENGINEERING AND PROSTHETICS

SP145.1 - Aging Successfully at Home: Research and Development to Address the Biggest Challenges Older Adults Face

Author(s): Tilak Dutta

Idapt, Toronto Rehab Institute, Toronto/ON/CANADA

Learning Objectives:

1. To support older adults living in their homes we need to find better ways to prevent falls while encouraging safe mobility and preventing injury in caregivers. We can do this through the development of new products and policy changes.
2. Researchers need to stay involved with the product ideas they develop to ensure they get on the market. The passion and vision behind a disruptive product can be lost if intellectual property is transferred to a centralized technology transfer office.
3. The use of simulators allows for efficient and safe iterative testing of new products/policy changes.

Abstract:

Older adults often do not have the tools they need to age successfully in their own homes. Our team develops products and policies to overcome the biggest barriers to growing older in place.

Our team includes clinicians (OTs, PTs, nurses), technical experts (industrial designers, machinists, engineers) as well as trainees. We work closely with commercial partners and policy makers throughout the development process to ensure products/policies get taken up quickly.

We use a series of simulators to safely evaluate products with target users in challenging conditions ranging from a cold, snowy winter day to cramped home to a patient's room in a hospital. Three projects will be described that demonstrate our development process:

1. It is difficult for consumers to assess the performance of footwear - most marketing information available to consumers is misleading. We have developed a method for accurately measuring footwear slip resistance by having participants walk on ice and snow covered surfaces to determine the maximum angle that each type of footwear can achieve (Figure 1).
2. Development of the MoveEasy Pole System (Figure 2): An affordable, modular system of pressure-fit vertical grab poles and clip-on horizontal rails. The MoveEasy system can be easily installed using pressure-fit poles in areas where the user needs support without permanently modifying the home (no screws or nails are needed).
3. Caregiver back injury prevention with a novel patient lifting tool called SlingSertter (Figure 3) that removes the need to turn/log-roll patients when inserting a sling under them. This device makes using a patient lift effortless even with very large bariatric patients.



Figure 1. WinterLab being used to test footwear slip resistance on ice.



Figure 2. HomeLab being used to test the MoveEasy Kit.



Figure 3. SlingSertter being tested in CareLab.

SP145.2 - The effect of age and previous exposure to slippery surface on gait adaptation

Author(s): Sharon Ravindran¹, Yue Li², Adam Katchky², Tilak Dutta², Geoff Fernie³

¹Engineering Science, University of Toronto, Toronto/CANADA, ²Technology Lab, Toronto Rehab, Toronto/ON/CANADA, ³Surgery, University of Toronto, Toronto/CANADA

Introduction

Falls are a leading cause of injury in Canada [1]. Many falls result from slipping on ice [2]. Humans adapt their gait when exposed repeatedly to a postural challenge or in anticipation of a slippery surface to prevent injury [3]. It is unclear whether individuals will continue to employ gait adaptations when moving from a slippery to a non-slippery surface. This study examines the gait adaptations of both young and older adults after walking on ice to understand the preventative strategies adopted.

Methods

Twelve younger adults (7 females-5 males;19-34 years) and twelve older adults (8 females-4 males;65-78 years) participated in this experiment. Harnessed participants walked along surfaces made of concrete (baseline surface) and wet ice, both 4m by 0.5m. Reflective markers on the footwear and pelvis were used to quantify kinematics using motion capture system before and after walking on a wet-icy surface. All participants wore the same winter boots and walked at a preferred self-selected pace. All variables were analyzed with a mixed model repeated measures ANOVA, with significance defined as $p < 0.05$.

Results

Younger participants demonstrated significant decrease in adaptive gait changes in floor foot angle (FFA) and anterior-posterior distance from the pelvis to the heel (PHAP) at heel contact, and step time between both baseline surfaces (Table 1). Age was not found to have a significant effect on the change of any of the gait parameters. A decreased FFA is often associated with hazardous slips, indicating a flatter foot was preserved after walking on a slippery surface[4]. Younger participants shifted their centre of mass anteriorly (indicated by reduced PHAP) thereby adopting a more conservative gait strategy [5] and possibly a mechanism to prevent backward falls.

Variable	Younger Population (n=12)				Older Population (n=12)			
	Before Wet Ice Surface		After Wet Ice Surface		Before Wet Ice Surface		After Wet Ice Surface	
	Mean	SD	Mean	SD	Mean	SD	Mean	SD
D_Piv_Heel (m)	0.38	0.02	0.35*	0.04	0.38	0.05	0.37	0.05
FFA (°)	27.9	4.8	25.2*	6.2	25.4	4.9	23.9	6.1
T_step (s)	0.38	0.03	0.37*	0.03	0.38	0.04	0.37	0.04

Table 1: Data was collected in Winter Lab in the Challenging Environment Assessment Laboratory at Toronto Rehab. Twelve younger (Y) participants (7 females, 5 males, age: 24.6 ± 4.8, weight: 67.6 ± 13.2 kg) and twelve older (O) participants (8 females, 4 males, age: 71.5 ± 5.0, weight 65.1 ± 13.8 kg) participated in this experiment. D_Piv_Heel represents the anterior-posterior distance from the pelvis to the heel in meters (m) at heel contact (HC). FFA represents the floor foot angle at HC, measured in degrees (°). T_step is the amount of time taken to complete one step, measured in seconds (s). (*) indicates a $p < 0.05$ between the baseline conditions before and after the wet ice surface.

Discussion & Conclusion

Younger participants showed adapted gait strategies after walking on a slippery surface, demonstrating the preservation of adaptations when walking on a non-slippery surface. Age was not found to be a significant factor; only young adults altered their gait to prepare for future surfaces. The alteration was small but statistically significant. Further research is required to investigate whether this conserved gait strategy represents a large enough modification to be beneficial in preventing future falls and moreover, understanding the implica-

tions for the lack of gait adaptation by older adults.

References

- [1]Seniors' Falls in Canada, PHAC, 2014
- [2]Courtney et al, Int.J.Ergon., 44:1118-1137
- [3]Cham et al, J.Gait & Posture, 15:159-171
- [4] Moyer et al, J.Ergonomics, 49(4):324-343
- [5]Chou et al, J.Gait & Posture, 33(3):406-411

SP145.3 - An intelligent rollator for people with mobility impairment

Author(s): Olof Lindahl¹, Tomas Bäcklund¹, Marcus Karlsson¹, Thomas Hellström², Peter Hohnloser², Anna Brändal³, Xiaolei Hu⁴, Per Wester³

¹Radiation Sciences/biomedical Engineering, Umeå University, Umeå/SWEDEN, ²Computing Sciences, Umeå University, Umeå/SWEDEN, ³Public Health And Clinical Sciences, Umeå University, Umeå/SWEDEN, ⁴Community Medicine And Rehabilitation, Umeå University, Umeå/SWEDEN

Assistive technology for the mobility impaired includes canes, wheelchairs and walkers. The walker is a very common mobility device and is used by approximately 0.7 percent of the population according to statistics for US in the mid 1990's. Corresponding statistics for Sweden show almost 4 percent in 2003. More than 47,000 accidents related to falls associated with walkers and canes occurred in the US 2009. Apart from direct costs related to the accidents, increased and safer usage of walkers may delay transition of the elderly people to nursing homes considerably. Hence, technical improvements of walkers can lead to large cost savings for society, in addition to greater convenience and safety for the users. Possible improvements include support for collision avoidance, automatic braking, navigational support, and additional functionality like automatic parking. Navigating walkers in small passages and doorways are regarded as particularly problematic.

We describe the development of an automated walking aid, an intelligent rollator (IRO). While walkers strictly do not have wheels, and rollators do, the two words are often used interchangeably. We refer to IRO as a rollator, while other walking aids most often are referred to as walkers. IRO functionality for indoor and outdoor use includes detection and avoidance of corners, doorposts, furniture and other obstacles. The IRO rollator is a retrofit on a commercial four-wheeled rollator. The added equipment comprises rollators (Rebel and Carl-Oscar, Human Care), an embedded computer (Arduino Mega 2560), two electrically controlled solenoid brakes (Multicomp MCSMT-3257L 12STD), rotation hall sensors on the wheels (Allegro Microsystems A3423) and a series of IR-distance sensors (Sharp GP2Y0A02). The sensors are used to detect obstacles and direction of motion, and brakes are used to influence the direction of motion. The distance reported by each distance sensor is compared in the computer to the nominal distance determined from reflection against a surface (wall or floor). A shorter distance indicates presence of an obstacle such as a wall or piece of furniture. Negative obstacles such as curbs and holes in the ground cause the distance to be longer than normal and can be detected in a similar fashion. The information from the sensors is used to control the brakes and thereby affect the direction of motion. A detected obstacle to the left causes activation of the right brake, causing the rollator to turn away from the obstacle if and when the user continues to push the rollator forward. This passive control mechanism leads to safer usage. Detection of an obstacle straight in front of the rollator will activate both brakes such that the rollator rather stops than turns. The design also includes a novel approach to detect and prevent sideway drift that may occur both indoors and outdoors. Our approach to use a

commercially available rollator as base, and low cost components with low power consumption is believed to enable an affordable and useful product for the health care market. Preliminary testing on healthy subjects and patients with stroke in a controlled indoor and outdoor environment shows promising results.

SP145.4 - Rehabilitation Engineering: A review of current teaching tools ad project based learning

Author(s): Anastosis Kessarisi¹, Prdrag Pesikan², Charanjit Bambra³
¹Biomedical Engineering Technology, Centennial College, Toronto/CANADA, ²Biomedical Engineering Technology, Centennia College, Toronto/CANADA, ³Biomedical Engineering Technology, Cetennial College, Toronto/ON/CANADA

Many of Ontario colleges are developing an applied research capacity to participate in industrially relevant R&D activities. The key drivers for Canadian biomedical industry are the aging population, managed care/cost containment, and miniaturization of devices and equipment. Taking into account that only a few formal academic rehabilitation training programs exist in Ontario, rehabilitation engineering was identified as a key area for potential expansion. While “learning by doing” is a popular mantra at many engineering schools, many experts agree that it needs to be formally reinforced through project based learning (PBL). Tools exist for teaching biomechanics and robotics and these have resulted in “Lego Mindstorms” and means for teaching hepatics. A project based educational paradigm is currently being used to design assistive rehabilitation devices (Roach et al., IEEE Pulse 51). A review of currently available teaching tools, and our experience with the project based education in rehabilitationengineering, will be presented.

SP145.5 - Effects of sloped icy surface on older adults’ gait in a simulated winter environment

Author(s): Yue Li¹, Sharon Ravindran¹, Adam Katchky¹, Tilak Dutta², Geoff Fernie²
¹Technology Lab, Toronto Rehab Institute - UHN, Toronto/ON/CANADA, ²University of Toronto, Toronto/ON/CANADA

Introduction

Falls and fall-related injuries among older adults are a significant and growing public health concern. Fall-related injuries among older adults are associated with adverse weather events[1].Slips and falls occur more frequently while walking up and down slopes[2]. However, older adults’ balance and gait on icy slopes have not been examined. This study investigates how older adults alter their gait on icy slopes.

Methods

This study was conducted in WinterLab (Challenging Environment Assessment Laboratories). The ice walkway was 4m long by 0.5m wide and 7 incline angles were tested (-7.1°,-4.8°,-2.9°, 0°, +2.9°, +4.8°, and +7.1°). A positive angle denotes walking uphill, negative angle denotes walking downhill. All 12 able-bodied older adult participants (65-78 years; 4 male, 8 female) wore the same type of winter boots and walked at their preferred self-selected pace. Step length, step width, step speed and cadence were calculated using an motion capture system (Motion Analysis) tracking reflective markers placed on participants’ footwear. All data were analyzed across 7 slope angles with a mixed model repeated measures ANOVA (p < 0.05).

Results & Discussion

During uphill walking on the icy surface, as the angle of incline was increased, older participants increased their step width and

decreased their cadence, step length and walking speed (Figure 1) to avoid a slip[3]. However, during downhill walking, when the incline angle increased to 7.1°, older adults increased their cadence significantly but did not change their walking speed. Moyer et al.[4] showed that hazardous slips were associated with greater step lengths and decreased cadence, and that walking with increased cadence was beneficial when anticipating a slippery floor [5]. Older participants appeared to intuitively increase their cadence and step width while decreasing step length, in order to negotiate the most slippery condition (downhill at 7.1°).

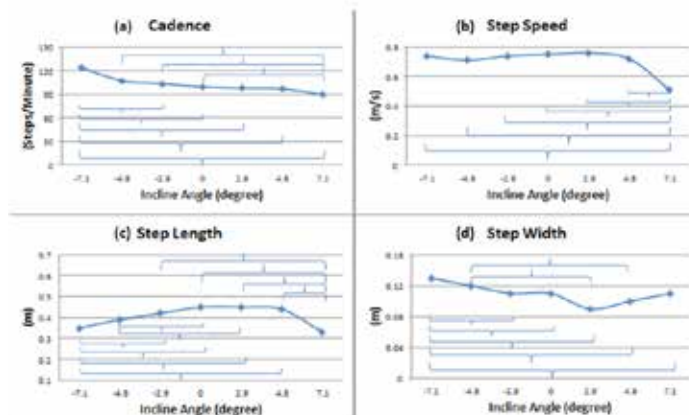


Figure 1: Effect of incline angle on gait parameters: (a) Cadence, (b) Step speed, (c) Step length, (d) Step width. — denoting significant difference between incline angles.

Conclusion

Spatiotemporal kinematic data were measured and analyzed for 12 able-bodied older adults walking on level, up and downhill slopes. A similar data set has not been previously reported for a cohort on this range of inclines on an icy surface. When walking on the sloped icy surface, older adults adopted different strategies for uphill and downhill walking. Additional research is needed to determine if this gait speed control strategy is effective for reducing slip events.

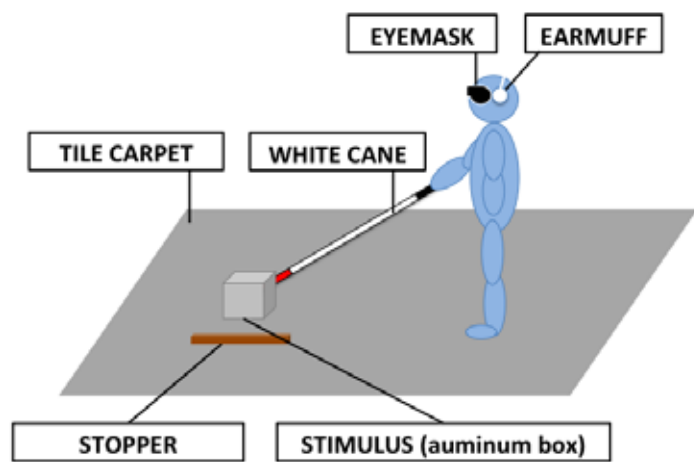
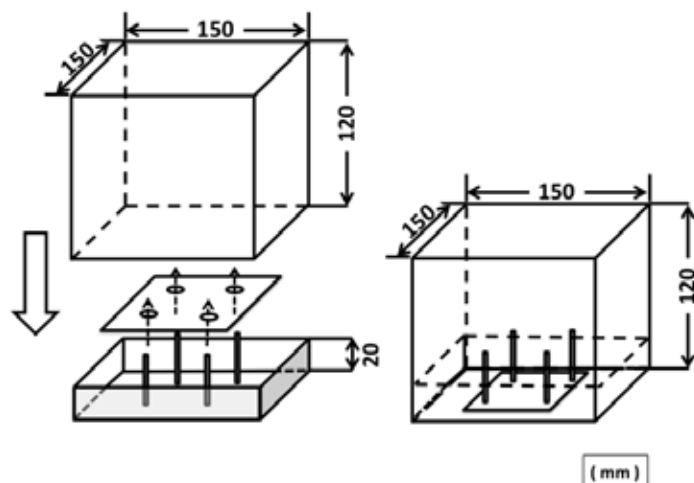
- [1]Mondor et al, Age Ageing 199(2014).
- [2]Gao and Abeysekera, Ergonomics 47:573–598(2004).
- [3]Chang et al, Gait&Posture(2015).
- [4]Moyer et al, 49:329–343(2006).
- [5]Chambers et al, IIE Trans. Occup. Ergon. Hum. Factors 1:166–175(2013).

SP145.6 - Judging Weight of an Object by a White Cane

Author(s): Kiyohiko Nunokawa¹, Kouki Doi², Manabu Chikai³, Shu-ichi Ino³
¹School Of Human And Social Sciences, Tokyo International University, Kawagoe/JAPAN, ²National Institute of Special Needs Education, Yokosuka/JAPAN, ³National Institute of Advanced Industrial Science and Technology, Tsukuba/JAPAN

The purpose of this study is to collect basic knowledge to develop an operation method that improves the accuracy of a white cane target recognition. The primary purpose of using a white cane is to be able to detect street conditions and obstacles based on the reverberations and tactile information that is gathered from the tip. But some users reported being able to differentiate between specific kinds of materials and objects. Allowing the recognition of target attributes through the contact of a white cane is an important function. In training courses for the visually impaired, three methods

are taught for holding a white cane: 1) stretch the index finger across the flat face of the grip and lightly hold the grip with the thumb and other three fingers, 2) hold the grip like a pen or pencil, and 3) press the thumb on the flat face of the grip and hold the grip with the four fingers. Different methods can be selected based on the circumstances. In this study, to understand a weight perception using white canes, we compared using a hand pushing and using a white cane without accompanying auditory information. And to examine the influence of a manner to grasp a white cane on object's weight perception, we compared the three methods for holding a white cane. Participants were sighted university students. They gave magnitude estimates for six weights that changed by 100g from 500g to 1,000g. Results indicated that using a white cane produced higher sensitivity level than using a hand. Therefore, using a white cane enhances the information of object's weight. And the difference of sensitivity for weight perception was caused by manner to grasp the white cane.



SP145.7 - The Effect of Sub chronic Low Dose of DDVP and Sodium Azide on some Bone Biochemical Indices of Albino Rats
Author(s): Patrick U. Agbasi
 Prosthetics And Orthotics, FEDERAL UNIVERSITY OF TECHNOLOGY OWERRI NIGERIA, OWERRI/NIGERIA

Background: The frequent use of organophosphorous insecticides in our everyday life especially in our houses, offices and even against pests to preserve foods and agricultural products especially

in the third world and sodium azide (a herbicide) extensive use in the farms have necessitated this study. **Purpose:** This research is designed to investigate the effect of low dose DDVP (dichlorvos) and sodium azide co-administration on some bone biochemical parameters (calcium and phosphate) of Albino rats bearing in mind the rising cases of chronic arthritis and deformities. **Method:** Seven groups of five rats each were used for the study. Group A was used as control and received no chemical treatment, groups B and C were injected with 1% and 3% LD50 of sodium azide respectively, while groups D and E received 1% and 3% LD50 of DDVP respectively. Equally, group F received combined doses of 1% LD50 of DDVP and 1% LD50 of Sodium azide while group G received 3% LD50 of DDVP and 3% of LD50 Sodium azide. The chemicals were administered at alternate days for twenty one days. At the end of twenty one days study period, the animals were anesthetized with chloroform and blood were aspirated through cardiac puncture into empty clean 5ml containers and then allowed to clot. The serum were then separated and frozen before calcium and phosphate estimations were carried out. **Results:** The two dose levels of sodium azide did not produce any significant effect on calcium and phosphate levels where as 3% DDVP did. The calcium and phosphate values of group G (3% LD50 of DDVP and 3% LD50 of Sodium azide) produced significant increase when compared to control and also dose dependently increased compared to group F.

Conclusion: Co- administration of DDVP and sodium azide produced significant increase in calcium and phosphate values in rats in sub chronic administration.

The effect low dose DDVP and Sodium azide on the calcium and phosphate values Albino rats

Group	Calcium	Phosphate
Group A Control	2.08±0.08	3.58±0.09
Group B (1% sodium azide)	2.08±0.16	3.54±0.06
Group C (3% sodium azide)	2.2±0.15	3.6±0.12
Group D (1% DDVP)	2.24±0.11*	3.58±0.083
Group E (3% DDVP)	2.8±0.02*	3.64±0.11*
Group F (1% DDVP & 1% sodium azide)	2.22±0.15*	3.6±0.07
Group G (3% DDVP & 3% sodium azide)	2.44±0.11*#	3.64±0.11*

Results expressed as mean ± SEM

*= Statistically significant compared to control

#= Statistically significant compared to group E

P ≤ 0.05

SP146 - MSK**TRACK 12: MEDICAL DEVICES****SP146.1 - Development of Personalized Tourniquet Systems Using a New Technique for Measuring Limb Occlusion Pressure**

Author(s): James Mcewen¹, Bassam Masri², Brian Day², Alastair Younger²

¹Electrical And Computer Engineering, University of British Columbia, Vancouver/CANADA, ²Department Of Orthopaedics, University of British Columbia, Vancouver/BC/CANADA

A new technique has been developed to facilitate safer personalized tourniquet systems for surgery, using a unique dual-purpose tourniquet cuff that enables automatic measurement of tourniquet Limb Occlusion Pressure (LOP), while overcoming limitations inherent in manual and automatic techniques of LOP measurement. A study was performed to determine the accuracy of this new technique compared to LOP measured using a gold standard Doppler ultrasound technique. 252 pairs of LOP measurements were taken from upper and lower limbs of 143 surgical patients, enrolled from three different surgical clinics, using the new technique and the Doppler technique. LOP difference was defined as new technique reading minus Doppler technique reading. The mean LOP difference (new-Doppler) \pm SD mmHg was $+0.56 \pm 11.73$ for all limbs (252 limbs), $+0.99 \pm 7.79$ for upper limbs (134 upper), and $+0.08 \pm 15.03$ for lower limbs (118 lower). Additional analysis was performed to further improve the performance of the new technique by noise detection and by development of rules allowing identification and removal of outlier data prior to completion of each LOP measurement. In this study, the additional analysis removed 3/252 pairs of LOP measurements and reduced the SD: mean LOP difference (new-Doppler) \pm SD mmHg was improved to $+0.30 \pm 10.31$ for all limbs (249 limbs), $+0.99 \pm 7.79$ for upper limbs (134 upper), and -0.50 ± 12.62 for lower limbs (115 lower). We conclude that the new technique of LOP measurement has surgically acceptable accuracy comparable to LOP measurement by Doppler ultrasound. Additionally, the new technique may facilitate adoption of safer personalized tourniquet systems by incorporating inherent advancements over manual and automatic techniques of LOP measurement, including: elimination of a distal LOP sensor; reduced procedural complexity and surgical time; related improvements in the rate of success of LOP determination; and reduced direct and indirect costs.

SP146.2 - Vertebral Metrics – development of a third and improved prototype

Author(s): Ana Teresa Gabriel¹, Cláudia Quaresma², Mário Secca³, Pedro Vieira¹

¹Physics, Faculty of Sciences and Technology New University of Lisbon, Caparica/PORTUGAL, ²Physics, LIBPhys-UNL, Faculty of Sciences and Technology New University of Lisbon, Caparica/PORTUGAL, ³Ressonância Magnética, Caselas/PORTUGAL

Back pain is among the most common health problems worldwide and is the leading cause of activity limitations. A forehand identification of people affected by spinal disorders is extremely important because early and specific interventions may be applied. Methods currently available to assess spinal curvatures include several types of diagnostic imaging, however, the most frequently used techniques are not radiation free and, for that reason, its application should be avoided. Vertebral Metrics is a non-invasive system that was designed to study the biomechanical changes of the spine. Through the identification of the tridimensional position of the vertex

of the spinal processes it is able to provide a 3D reconstruction of the spinal column, in the standing position. Studies with the two previous prototypes indicated that the equipment is reliable and has sufficient accuracy for the global evaluation of the spinal column, however, the required time for data collection is too long. Because of that the further development of the system has become necessary. The required steps to develop a new prototype are presented in this work. Before each scan a fluorescent dye will be used to identify the spinal processes above the skin. During a complete scan, the improved device will move upwards while is recording a video of the back. Once finished the video recording, image processing algorithms will be applied to recognize the fluorescent marks in the skin. The stereo vision method will be used to determine the spatial position of each mark. Preliminary tests were performed using a skin phantom. Fluorescent points became clearly visible in the binarized images. The determined position of each point is very close to reality. In addition, pictures of the skin were collected and binarized. The perfectly identification of the fluorescent marker in the images is a huge success for the development of equipment..



Figure 1 Scheme of Vertebral Metrics.

SP146.3 - Does low-intensity pulsed ultrasound stimulation effectively promote bone fracture repair? An overview

Author(s): Orlando Rey R. Rúa

Física Industrial Y Bioingeniería, Instituto de Cibernética, Matemática y Física, La Habana/CUBA

This work is an overview of evidences to evaluate the effectiveness of low-intensity pulsed ultrasound (LIPUS) stimulation to promote bone fracture repair. A search of MEDLIN, LILACS and Google Scholar was performed using the keywords 'low-intensity ultrasound' and 'bone fracture', limited to English and Spanish languages up to December 2014. Clinical eligible studies were randomised and quasi-randomised trials (RCTs) that considered skeletally mature patients with any kind of fractures. Also, special attention was dedicated to the results reported in previous reviews and meta-analyses conducted in the issue, resulting finally 19 trials for our analyses. Furthermore, LIPUS physical mechanisms of action that can be paralleled to an improvement of bone healing and the associated biological responses were reviewed. It was found that the efficacy of LIPUS to enhance fracture healing is reported controversially in several RCTs, showing substantial heterogeneity in the related outcomes. In addition, there was not appreciated a consensus concerning how to evaluate the efficacy of LIPUS therapy regarding to important outcomes for the patient. Therefore, the impact of this physical intervention in the medical management of bone fracture is relatively limited nowadays. But, frequently insufficient attention has been devoted to the ultrasound beam profile and its characteristic parameters that finally determine the local ultrasonic cellular or tissue stimulation, in a context that besides consider the biomechanical model utilized to validate the therapy, even for a process of fracture healing consistent for all fractured bones. Despite, when the healing criterion was a radiological and/or a clinical healing of the fracture, LIPUS significantly shorten the time to the radiological union for acute fractures undergoing non-operative treatment and acute fractures of the upper limb, the clinical and radiological healing of non-operative treated distal radius fractures and the treatment time in tibial distraction osteogenesis. On the other hand, physical mechanism of action of LIPUS and its mechanotransduction pathways are not well understood, basically by the intrinsic complexity of the biological tissue and the number of cells that respond to the mechanical stimulus in a complex cellular-molecular network of signally pathways. Yet, some of the reported LIPUS induced effects are a higher cellular membrane permeability; *in vitro* increase of collagen synthesis in human fibroblast; augmentation of intracellular concentration of calcium; stimulation to IGF, TGF- β , VEGF and PDGF-AB growth factors; elevation of levels of PGE2; increment of the vascularity at the fracture site; enhancement to osteogenic activity in human periosteal cells; promotion to osteogenic differentiation of human bone marrow stromal cells. **Conclusion:** further randomized controlled trials of high methodological quality are needed to investigate LIPUS effectiveness to improve bone fracture repair using a multidisciplinary approach, considering important healing outcomes for the patient.

SP146.4 - Electrical Stimulation of the Calf Muscle to Reduce Seated Leg Fluid Accumulation and Subsequent Rostral Fluid Shift While Supine

Author(s): Daniel Vena, Milos R. Popovic, Azadeh Yadollahi

Institute Of Biomaterials And Biomedical Engineering, University of Toronto, Toronto/ON/CANADA

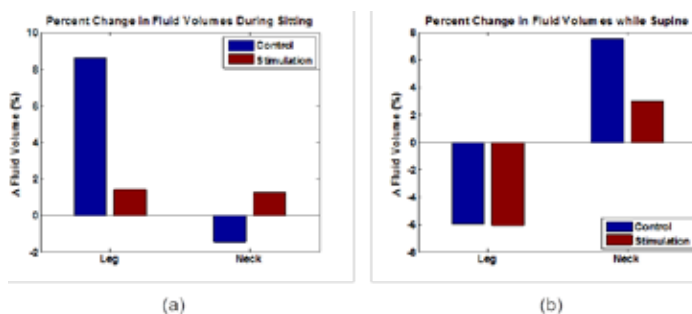
Introduction: A sedentary lifestyle or prolonged sitting could enhance the effects of gravity to increase fluid accumulation in the legs during the day. Upon lying supine, fluid shifts rostrally from the legs and accumulates in the neck. Fluid accumulation in the neck is a risk factor for increases in the upper airway narrowing and resistance during sleep. Therefore, reducing leg fluid accumulation during the day could be an effective method for reducing neck edema when

lying supine and protecting against the partial or complete collapse of the upper airway. The objective of this study is to test the efficacy of electrical stimulation (ES) of the calf muscle pump on reducing daytime leg fluid accumulation and the subsequent rostral fluid shift upon lying supine.

Method: The study is a randomized, single-blind double cross-over protocol in which participants sit for two and a half hours and receive either active ES or sham ES (control). Following the seated period, participants lie supine for one hour. After one week, participants crossed-over to the other study arm. Fluid is estimated by measuring bioelectrical impedance in the dominant leg and neck simultaneously and continuously throughout the seated and supine periods.

Results: Two men (age 49 and 63) have completed the protocol to date. Results demonstrate that ES substantially reduces fluid accumulation in the legs, where mean increases in leg fluid were 8.4% (75 ml) with sham ES and only 1.6% (13 ml) with active ES (Figure 1a). Upon lying supine, the amount of fluid leaving the legs was similar, however less fluid shifted into the neck, where mean increases in neck fluid were 7.5% (19.7 ml) with sham ES, and only 3% (8 ml) with active ES (Figure 1b).

Conclusion: Our preliminary results demonstrate ES as an effective means of reducing fluid accumulation in the legs while seated and subsequent rostral fluid shift into the neck when lying supine. Future work is focused on investigating the effects of this reduced leg fluid accumulation and subsequent rostral fluid shift on respiratory pathologies such as sleep apnea.



Funding: Ontario Graduate Scholarship; Mitacs Accelerate PhD Fellowship; Health Care, Technology and Place Fellowship

SP146.5 - Surgical process analysis identifies lack of connectivity between sequential fluoroscopic 2D alignment as a critical impediment in femoral intramedullary nailing

Author(s): Hamid Ebrahimi¹, Albert Yee¹, Cari Whyne²

¹University of Toronto, Toronto/CANADA, ²University of Toronto, toronto/CANADA

The current standard of care in lower extremity long bone fracture stabilization is closed intramedullary (IM) nailing. The surgical protocol associated with this surgery is well defined. Yet, challenges arise that impede the surgical workflow, add operative time and radiation exposure (to patients and medical staff), and lead to frustration in the operating room. Clear description and analysis of a surgical process can expose challenging steps and activities that can facilitate surgical workflow optimization, guide surgical technology development, improve surgical planning, and enhance surgical training and education. To date, a number of studies have presented methodologies to model individual surgical process models or to develop generic surgical process models. Comparisons between surgical process models have also been studied with respect to procedure parameters such as operating time, number of activities, etc., to evaluate the impact of surgeon experience or to understand

differences in terms of sequentiality of activities during surgeries. However, implementation of identified surgical models to optimize the surgical process has received little attention. Hence, the aim of this study was to map the IM nailing process, identify surgical challenges that impede the surgical process and elucidate their underlying causes.

This study consisted of semi-structured interviews and surgical observations. Eight surgeons from community (three) and teaching hospitals (five) were interviewed to identify the IM nailing surgical procedure, surgical challenges, and their use of adapted surgical techniques. During the eight IM nailing surgeries, information on the surgical procedure was grouped into activities (physical tasks), steps (sequence of activities) and phases (major events) to represent different levels of granularity in the surgical process. In steps identified as challenging or when barriers were encountered, individual activities were analyzed to elucidate underlying causes.

Seventy-five percent of surgeons identified reduction as the most challenging step of IM nailing, consistent with the surgical observations. The greatest challenges were manipulation of fracture fragments for realignment and identifying their 3D orientation using 2D x-ray images (where fragments aligned in one plane were misaligned out of plane). Adapted manipulation techniques used universal chucks with T-handles, mallets, wraps or Shanz screws. In one unsuccessful case the fracture was opened to allow realignment. The entry point step was identified as most difficult by 25% of surgeons, due to challenges in access and 3D K-wire orientation. Adapted techniques aimed to alter patient positioning (torso abduction and/or knee adduction) or eliminate the need for a straight access line through use of an awl. Lateral positing was suggested to facilitate entry point access in obese or muscular patients.

In both the reduction and entry point steps identified as challenging by IM nailing surgical process analysis, 3D alignment was the critical barrier. Utilization of repeated 2D fluoroscopy without connectivity between sequential images to guide reorientation was a consistent impediment to 3D entry point guidewire positioning and femoral fragment realignment. These findings have important implications toward guiding technological improvements and competency based surgical training.

SP147 - Information Technologies in Healthcare Delivery and Management: Part 2

TRACK 14: INFORMATION TECHNOLOGIES IN HEALTHCARE DELIVERY AND MANAGEMENT

SP147.1 - The Electronic Medical Record: Can it be integrated with Treatment Delivery and Management?

Author(s):

In the United States (and other venues), there have been numerous efforts to promote an integrated Electronic Medical Record (EMR), one that will incorporate all (or at least key) aspects of the patient's history (medical and social), diagnostic examinations, treatments, results, and follow-ups. The Meaningful Use (MU) program has as one of its goals to provide improved clinical decision support (CDS) to healthcare providers. The reality is that current EMR systems function more as data repositories, providing much improved access to clinical information, but not making the leap to true clinical decision support. There are many impediments to closing this gap, including the reticence of most EMR manufacturers to enter the realm of treatment delivery, which would likely result in significant changes in their FDA risk classification. This has been shown in Radiation and Medical Oncology Information Systems, some of the earliest EMR systems to be fully integrated into the treatment process, but not connected to ambulatory EMR systems due to the differences in FDA classification.

SP147.2 - AIM Quality Assurance Program Development for CT X-Ray Systems

Author(s): [Douglas J. Mctaggart](#)

Medical Engineering, University Health Network, Princess Margaret Cancer Centre, Toronto/CANADA

The University Health Network purchased Toshiba Aquilion CT X-ray systems that offer improved diagnostic image quality. It is clinically important to maintain good image quality on these systems. The problem that was addressed was how to develop and implement a comprehensive CT image quality assurance program at the University Health Network.

Important image quality parameters were identified using X-ray system specifications. An appropriate image quality test phantom was selected and evaluated using measured results. This topic deals with the technical problem of how to develop and implement an x-ray image quality assurance program for the Toshiba Aquilion CT systems at the University Health Network. This is a significant project because the outcome will assist both the technical and clinical staff to monitor and maintain the stability of the image quality of the CT system. Optimal image quality is essential for the clinical staff to view patient anatomy and perform an accurate diagnosis of the patient's condition. The project will deal with the selection of an image quality phantom, establishing baseline data derived from the phantom and storing the data for future reference. An important objective is to provide a user friendly interface for viewing the image quality data. Since the scope of the project deals with CT scanners across five hospitals, the process must be clear and concise to all clinical users of the image quality program. It was decided that the best way to implement a program like this was to develop a website interface to allow all clinical users to access the image quality data on the available desktop computers. This presented the problem of setting up a dedicated image quality server and creating software that will satisfy the needs of the image quality assurance program.

Another challenge of the project was to develop a quality assurance program that will satisfy the corporate vision of the University Health Network. This vision is concerned with achieving global impact. The work done in this report will be relevant to Canadian standards and incorporate global standards as well. These standards were used for build a formal AIM CT Accreditation Program. This internal UHN CT Accreditation program was developed to satisfy the needs for a standardized annual testing of CT dose and image quality parameters.

A comprehensive quality assurance program was then developed and implemented. The program was used to baseline existing system parameters and record variations in image quality. The AIM server provided an ideal centralized interface to store and display CT image quality data, CT Accreditation reports and CT clinical protocols. It is recommended that a CT image quality program be used at other hospitals to maintain and improve system performance and clinical protocol standards.

SP147.3 - Evaluation of Improved Automatic Speech Recognition Prototype for Estonian Language in Radiology Domain

Author(s): Andrus Paats¹, Tanel Alumäe², Einar Meister², Ivo Fridolin¹
¹Department Of Biomedical Engineering, Technomedicum, Tallinn University of Technology, Tallinn/ESTONIA, ²Laboratory Of Phonetics And Speech Technology, Institute Of Cybernetics, Tallinn University of Technology, Tallinn/ESTONIA

The aim of this study was to determine the dictation error rates in finalized radiology reports generated with a new automatic speech recognition (ASR) technology prototype for the Estonian language. Apart a preliminary attempt, no Estonian language based ASR systems exist currently in radiology. Lack of a mother-language supported ASR system for under-resourced and agglutinative languages could be one reason. The scientists from Tallinn University of Technology in collaboration with radiologists from North-Estonian Medical Centre (NEMC), Tallinn, Estonia, took a step closer towards an ASR application in radiology for Estonian language by performing a study using Estonian based models.

The training of language model was performed in two steps. Firstly, for training a language model, 177 659 real radiology reports from different imaging modalities were used including 77 067 x-ray, 30 929 ultrasound, 28 825 computed tomography, 14 815 mammography, 12 082 endoscopic, 8 792 magnetic resonance tomography, 3 950 radiology consultation and 1 199 angiographic reports. Manually normalized versions of 1299 randomly selected reports were created to standardize the report corpus. The ASR prototype, incorporating the trained language and acoustic models, was tested in Radiology Department, North Estonia Medical Centre, Tallinn, Estonia, by 17 radiologists (11 female and 6 male). In total, 261 reports were dictated, including 13 x-ray, 12 ultrasound, 119 computed tomography, 37 mammography, 12 endoscopic, 66 magnetic resonance tomography, and 2 angiographic reports. Word error rates (WER) and report error rates (RER) were calculated for each speaker and modality.

In second phase, the model was improved by taking account the errors from the first test. Moreover, applying of deep neural network based acoustic model and adapting acoustic and language model based on dictated speech, an enhanced ASR prototype was achieved. Additionally, 500 000 real radiology reports from different imaging modalities were included into model training.

In the first ASR prototype, total WER over all material was 18.4% and total RER 93.1%, not sufficient for clinical practice. Live experiments with the ASR prototype showed differences between the users depending on their experience and speech characteristics. An improved ASR prototype was applied onto dictated records resulting total WER 5.0%, which is acceptable for real clinical use. In summary, the ASR prototype for Estonian language in radiology domain was the first time successfully applied and assessed in

routine clinical practice. User feedback based automatic correction of language model is planned to implement into next ASR prototype.

SP147.4 - Usability engineering approach towards secure open networks in the integrated operating room of the future

Author(s): Klaus Radermacher, Armin Janss
 Chair Of Medical Engineering, RWTH Aachen University, Aachen/GERMANY

Nowadays, the number of technical systems in the operating room increases constantly. Besides improving the therapeutic quality, these changes may also lead to new human-induced risks for patients, therapists and third parties. In particular, within intra-operative activities requiring a safe and fast operation, surgeons and nurses rely on sophisticated and efficient solutions in terms of Human-Machine-Interfaces in order to perform their tasks effectively, efficiently and reliably [1]. Therefore, proprietary integrated workstations with a central user interface cockpit have been provided for the operating theatre in recent years. Risk management as well as usability validation have to be provided by the integrating manufacturer. However, these “monolithic” solutions limit the flexibility of the operators and users regarding interoperability and integration of independent innovative devices in these integrated OR solutions. Against this background, the project OR.NET – Secure Dynamic Networking in Surgery and Clinic – funded by the Federal Ministry of Education and Research (2012-2015; overall budget 18,5 M€; www.or.net.org) is a national flagship project involving more than 50 partners from the fields of research, industry, clinical operators and standardization. The main objective of the OR.NET project is to develop the technological as well as legal and operational basis for an open platform and standards for the modular dynamic integration of medical devices and IT systems into the future operating room and its clinical environment. Regarding the aspect of usability engineering, open modular integration, a modular definition of workflows, contexts of use as well as device configuration scenarios seems to be mandatory. Whereas modular standardization on an abstract application specific level limits flexibility to a certain extend, it enables risk management and usability control of modular networks. In this context, we develop a concept of Medical Device Profiles (technical specifications) including Medical Devices User Interface Profiles (MDUIP) representing specifications of human resources required for the interaction with the specific device and related process-dependent medical device functionality for the modular design of a central user interface in the integrated operating room. The use of standardized MDUI Profiles will allow the manufacturers to integrate their medical devices, respectively the provided functions in the OR.NET network, without disclosing the risk analysis and related confidential know-how or proprietary information- and without explicit knowledge on the final configuration of the device set-up and combination in the integrated OR. The MDUI Profiles will allow both, an automated optimized selection and composition of various user interfaces, and implicitly an optimal design of a central GUI with respect to the criteria of usability and an integrated human risk analysis in terms of Human-Machine Interaction. The concept has been evaluated for neurosurgery. The overall OR.NET concept and the evaluation of the MDUIP approach for the integration of an ultrasound dissector and an OR microscope in a neurosurgical test scenario (navigated spinal decompression) will be presented.

[1] A. Janß, W. Lauer, F. Chuembou Pekam, and K. Radermacher. Using new model-based techniques for the user interface design of medical devices and systems. *Human Centered Design of E-Health Technologies: Concepts, Methods and Applications*. Hershey, PA, pages 234–251, 2011.

SP147.5 - Whiteboard ESB: Next Generation Data and Workflow Management for Radiation Oncology

Author(s): John Wolfgang¹, Harold Beunk², Hanne Kooy¹

¹Radiation Oncology, Massachusetts General Hospital, Boston/ UNITED STATES OF AMERICA, ²Healthcare, ICT Automatisering, Eindhoven/NETHERLANDS

Introduction

The practice of Radiation Oncology has evolved into a data dependent operation involving a diverse set of specialized subsystems whose interactions in the clinical environment require careful management. While much effort has been applied to the quality and efficiency of the operations themselves (e.g. dose calculation, delivery, image fusion, segmentation), the interoperability and data management of these systems has been of a secondary concern.

This work introduces a electronic service bus to improve data and workflow management infrastructure for the evolving radiotherapy clinic, we refer to as the MGH Radiation Oncology Whiteboard. Using a web-based architecture to maximize access, ideas such as data immutability, data availability and data-driven workflow management are directly addressed. This new system has been designed using DICOM 2nd Generation models, and implements IHE-RO standards in order to ensure interoperability between the multiple subsystems encountered in a radiotherapy clinic.

Methods

The intent of this system is to support 'best-of-class' technologies in a multiple vendor environment rather than reliance upon a single monolithic software implementation. In this implementation, all systems interact with a central patient context constructed from interactions with the service applications tasked with patient care operations.

Such a system allows for direct workflow management, where activities are orchestrated by a centralized workflow logic management system. Given the patient state from all proceeding states, the system is able to automate the next steps in the patient workflow sequence. Ideally this system shall integrate all clinical subsystems, including but not limited to; CT simulation, intake, PACS, treatment planning, treatment QA, image fusion and segmentation and treatment delivery.

Workflow management is implemented using the DICOM UPS pull model, where subsystems, corresponding to desired activities, are provided with worklists. These worklists defined and orchestrated by the workflow management system, define the tasks to be performed along with the corresponding data needed to accomplish this task. Extending the functionality, the system may then automate much of the information access requirements of the task, pushing the appropriate data as referenced by the patient model to the appropriate subsystem and initializing the task itself.

This design allows for the proactive design of clinically "safe" workflow models where the underlying workflow business logic may be interrogated to identify hazardous workflow operations. These clinical behaviors may then be mitigated before clinical implementation occurs.

Treatment session management is provided as a service in this architecture, where the IHE-RO IPDW (Integrated Position and Delivery Workflow) model is applied to a proton treatment facility. The system introduces management of imaging, registration, positioning and treatment activities, requiring a return from the positioning and delivery system a report regarding the performed procedures.

Conclusion

This system introduces a careful redesign of information system architecture for the radiation oncology clinic. Motivation for this change comes from risk abatement due to unmanaged clinical subsystems and ad-hoc practice behaviors from care givers. By providing clinical workflow management, we aim to focus the clinician on patient care decision operations and automate the information gathering tasks, maximizing the strengths inherent in an electronic information environment.

SP148 - Medical Devices / Surgery, Computer Aided Surgery, Minimal Invasive Interventions, Endoscopy And Image-Guided Therapy, Modeling And Simulation

PRESIDENTS CALL

SP148.1 - Oncometer

Author(s): Priyajit Ghosh

Electronics And Communication Engineering, asansol engineering college,india, durgapur/INDIA

Cell culture is a process by which cells are grown under controlled conditions. Using artificial cell cultured medium/growth medium we wish to artificially culture different types of cells in the body. Apart from common salts, amino acids, sugars, vitamins and organic nutrients that are required, we also require catalysts which promote cell division. The artificial cultural medium will be contained in a specifically designed piezoelectric container. A piezoelectric container is a normal artificial cultural container but it will be connected to a piezoelectric crystal in one of its sides. As the cells in the cultural medium grows, the inner compartment gets filled. It applies pressure on the piezoelectric crystal which is measured using a sensitive device. We wish to use this mechanism on cancerous cells. Unlike normal cells, cancerous cells have different properties. Cancerous cells would not exhibit the property of contact inhibition and if the growth nutrients and catalysts in the cultural medium are sufficient, the cells would grow enough to exert more pressure on the crystal and therefore a high voltage would be generated.

Using the above results, we aim to build a simple device based on simple mechanisms which can detect cancer cells. The device will basically contain 2 compartments as shown in figure below---As shown above, the first compartment has a piezoelectric crystal on its boundary, the second one consists of an artificial cultural medium. A common movable wall in between will separate the 2 compartments. One side of the wall will have a protruding flat hammer head pointing towards the piezoelectric crystal at the boundary of the device.

When the cell sample will be given into compartment 2, cells would start dividing. However, normal cells on account of their property of contact inhibition, would stop dividing after sometime without exerting sufficient pressure to move the inner wall.

If the sample contains cancer cells, they would continue to divide and in sometime would create a mass of cells large enough to start exerting pressure on the inner wall. After sometime, the inner wall would move towards compartment 1 and strike the piezoelectric crystal. The crystal would generate voltage from the sudden pressure and the voltage output would be recorded. Sufficient experiments would be conducted to see the value of voltages, as well as time range of producing the voltage. Also, it will be taken care if practically normal cells produce miniscule voltages, but then we would also note the differences of voltages produced. The voltage value would be recorded using a special circuit so that the output can be checked anytime who is using the device.

We wish to create a portable, home using cancer testing device.

SP148.2 - Ways to outreach medical devices in low resource countries (LRC)

Author(s): K Siddique Rabbani

Biomedical Physics & Technology, University of Dhaka, Dhaka/BANGLADESH

ECG and X-ray machines were invented more than one hundred years back, still almost 80% of global population living in the LRCs does not get benefits of these devices. We can easily visualise the situation with more modern equipment. This failure pains us as scientists or engineers. Some factors for this failure, particularly in medical devices, are: i) design and manufacture only in the developed countries of the world, ii) long periods of patent protection allows some people or group to monopolise, leading to technology disparity and the consequent economic disparity, which in turn caused unaffordability of medical devices in LRCs, iii) engineering education in LRCs not geared to design of devices. Because of manufacture in a remote developed country, the problems faced with the current medical devices in an LRC are, i) the procurement cost is very high, ii) the devices are not user friendly to people in different LRCs as they have different cultures and languages, iii) the devices do not suit local power line abnormalities and weather conditions resulting in premature failure, iv) the devices are not repairable in many instances. The last factor happens because of a) remoteness of manufacturer, b) unavailability and/or high price of spares, c) lack of manpower with adequate technological know-how and d) tendency of manufacturers to keep technology secret, which has increased in recent times with the advent of microcontroller based equipment where software can easily be kept hidden. Again one important point often unnoticed is that the technology innovator in an LRC has also to be the entrepreneur for commercial manufacture. In fact this happened during the industrial revolution in Europe which led to industries that can support R&D for manufacture of new products now. Unfortunately no industrial revolution happened in the LRCs and such R&D based industries do not exist.

Therefore, the single major solution to the unacceptable situation hinted above is empowering persons with engineering background in all LRCs in the design, manufacture and marketing of medical devices. With this aim we have recently initiated a 'Centre for Technology Equalisation (CTE)' in Bangladesh under a registered society. At CTE we are planning to organise a workshop where electronics engineers from the LRCs will be trained in the design, development and commercial manufacture of a computerised ECG machine that we have developed indigenously and which has performed well for more than a year of field trial. What WHO, UN and other world bodies can do is to provide support to such local initiatives for technology development and dissemination, which may have different characters in different countries depending on local situations and conditions. Based on the results of such initiatives, the better ideas and models can then be promoted in other LRCs through special educational, training and other supportive programmes.

SP148.3 - South African - Swedish effort on pre-hospital diagnostics of stroke and traumatic injuries

Author(s): Mikael Persson

Signals And Systems, Chalmers University of Technology, Gothenburg/SWEDEN

Global health faces a number of unprecedented challenges that cannot be approached effectively from the perspective of a single discipline or a single country. During the last century many countries in the western world has undergone a transition in the spectrum of diseases away from communicable diseases towards chronic diseases often depending on considerable resources from society. The one billion people living in the world's poorest countries have yet to make this transition and the burden of disease, which is already extremely high, is set to escalate.

Stroke care represents one of these major global unmet challenges of the global health care system. The human cost of stroke is horrific. Out of the 15 million people that suffer a stroke each year, 5 million die and another 5 million are permanently disabled. Among stroke survivors, 20% have serious remaining dysfunctions. A much larger proportion has less conspicuous, dysfunctions, which still seriously affect quality of life for the patient and relatives. In the western world, stroke is placed third among reasons for acute death, and first among reasons for neurological dysfunction, resulting in most days of hospital nursing and therefore the most costly disease within western world health care. In the developing world statistics are more uncertain. In South Africa, stroke was found to be the fourth most common cause of death, accounting for 6% of all deaths in 2000.

The purpose of the present project is to start the path towards implementation, of cost efficient, easy to use, diagnostic tools for stroke in the sub-Saharan Africa, where there are very limited resources in terms of medical personnel, hospitals and diagnostic devices. We have developed and tested a new diagnostics system for stroke intended for the around 200,000 ambulances and the 17 million yearly stroke patients, around the world. For the society this product will help reducing the large cost of stroke and traumatic brain injuries. While of uttermost importance for the western world, less developed countries may come to benefit even more due to the potentially low cost and easy handling of the technology used.

SP148.4 - A portable multi-frequency impedance measuring device for biodynamic analysis

Author(s): Takao Nakamura¹, Toshimasa Kusuhara¹, Yoshitake Yamamoto²

¹Graduate School Of Health Sciences, Okayama University, Okayama/JAPAN, ²Okayama University, Okayama/JAPAN

[Introduction]

We have proposed a biodynamic analysis method using bioelectrical impedance[1]. We developed a system to measure the frequency characteristics of bioelectrical impedances that have high time resolution[2]. The frequency characteristics obey the "Cole-Cole circular arc law," characterized by four impedance parameters: Z_0 , Z_{∞} , f_m and β . Using the developed measuring system, we showed that the movements of the forearm and throwing motions in baseball were easily distinguished by the impedance parameters of the frequency characteristics[3, 4]. However, this system requires a wave generator driven by AC power, a high-speed A/D converter, and a desktop computer. Therefore, the system is large and has low portability, thus it is difficult to use the system in outdoor environments. In this paper, we propose a portable multi-frequency impedance measuring device.

[Materials and Methods]

The four-electrodes technique is used in the proposed device for the measurement of human body impedance. This device consists of five oscillators whose frequencies are 4, 10, 20, 40, and 100 kHz; a differential amplifier; analog switches for synchronous rectification; and low-pass filters. The voltage signal obtained by adding sine waves of the five frequencies is converted to constant current (RMS value: 250 μ A). The current flows to the human body via two current electrodes and the voltage in the measured body part is detected using two potential electrodes and the detected differential voltage is amplified. The amplified signal is rectified for each frequency using analog switches and low-pass filters (cutoff frequency: 25 Hz). The output signals of this device are resistance R and reactance X , for each of the five frequencies. This device is powered by USB mobile phone battery.

[Results and Discussions]

The measurement range of the device is 0–80 Ω . The errors in resistance and reactance were less than $\pm 1\%$ and $\pm 2\%$, respectively. The impedance parameters are calculated from the five sets of resistance and reactance with a numerical optimization. For example, in a conventional system, when 200 sets of the impedance parameters every second need to be measured, the sampling frequency and data acquisition rate must be 2 MHz and 800 kS/s. In contrast, in the proposed device, a sampling frequency of 200 Hz and a data acquisition rate of 2 kS/s is sufficient.

[Conclusion]

The proposed multi-frequency impedance measuring device is sufficiently accurate for measuring bioelectrical impedance parameters. Further, it requires no external oscillator or high-speed A/D converter, and it is powered by a USB mobile phone battery. Therefore, the proposed device is easy to use, portable, and well suited for outdoor use. A future study will further develop the use of impedance parameters in biodynamic analysis.

[Acknowledgement]

This work was supported by JSPS KAKENHI (Grant-in-Aid for Challenging Exploratory Research) Grant Number 26560352.

[References]

1. Nakamura T, Yamamoto Y, Tsuji H, Yamamoto T (1992) Med Biol Eng Comput 30:465-473
2. Nakamura T, Kusuhara T, Yamamoto Y (2006) Proc SPIE 6357:63571s1-63571s5
3. Nakamura T, Kusuhara T, Yamamoto Y (2007) IFMBE Proc 17:122-125
4. Nakamura T, Kusuhara T, Yamamoto Y (2013) J Phys Conf Series 434 12070: 1-4

SP148.5 - A Study of the Challenges of Donating Medical Equipment to Developing Countries

Author(s): Bill Gentles¹, Beverly D. Bradley², Shahrzad Mirzazadeh¹
¹International Outreach Committee, CMBES, Toronto/ON/CANADA, ²Centre For Global Engineering, University of Toronto, Toronto/CANADA

Previous studies conducted in the United States and Europe have shown that as much as 70% of medical equipment that is donated to low-income countries is never put into use in these countries [1]. As a result an unnecessary burden is created, and many of the recipients' equipment needs remain unresolved. In this study, funded by the International Development Research Centre in Canada, we are examining the practices of Canadian organizations that donate equipment to developing countries. In addition, we plan to trace the path of shipments of donated equipment from their point of origin, to their ultimate destination. The goal is to better understand why so many organizations are still making inappropriate donations despite the existence of well-publicized guidelines promoting donation best practices [1]. To achieve the goals of the study, we are building on partnerships with the biomedical engineering community in Ghana, including their recently established Biomedical Engineering Association.

To date we have identified about 70 Canadian organizations that donate medical equipment and supplies to developing countries. We have contacted these organizations and asked them to answer a survey questionnaire; we received 43 survey responses. Based

on these responses, we approached the most active organizations and asked if we could visit their facilities and interview key staff so that we could better understand their processes. We have visited 12 of these facilities, and conducted telephone interviews with an additional 5 facilities.

We have also hired a research assistant in Ghana to collaborate with us and track down the ultimate destination of some of the shipments of donated equipment from Canada to Ghana. By doing this we hope to gain a better understanding of which shipments had the highest success rate in meeting the needs of the recipients, and what type of planning process was involved in preparing these shipments.

Through the survey, interviews, and shipment tracking, we intend to develop a number of case studies or 'stories of unsuccessful donations' in which we trace the path of a donation from the well-intentioned donor, through the hazards of international shipping and customs brokers, to the final destination – often in the hands of an unsatisfied recipient. We plan to use these case studies to promote as widely as possible a better understanding of the pitfalls of medical equipment donations, and educate Canadian donor organizations on best practices and the causes of unsuccessful donations.

In our presentation at the World Congress, we will present a summary of what we have learned to date, as well as future plans to continue this work. We also hope to make contact with recipients of donated equipment from developing countries other than Ghana, so that we can expand our study in the future.

[1] "Medical device donations: considerations for solicitation and provision. (WHO Medical device technical series)," World Health Organization, Geneva, 2011. Accessed: March 10, 2014. Available at: http://whqlibdoc.who.int/publications/2011/9789241501408_eng.pdf?ua=1.

SP148.6 - The Clinicopathologic Characters and Activity Survey of Sudden Death of Infant in a Depressed Economy: South-Eastern Nigeria Experience.

Author(s): Gideon I. Ndubuka¹, Kenneth Ngwogu², Kenneth I. Nkuma-Udah¹, Chuks I. Kamanu³, Tobias I.N. Ezejiofor⁴, Samuel C. Iwujii¹

¹Biomedical Technology, Federal University of Technology, Owerri, Nigeria, Owerri/NIGERIA, ²Chemical Pathology, Abia State University, Aba/NIGERIA, ³Obstetric And Gynaecology, Abia State University Teaching Hospital, Aba/NIGERIA, ⁴Biotechnology, Federal University of Technology, Owerri, Owerri/NIGERIA

Sudden death of infant (SDI) is among the clinical conditions called sudden infant death syndrome (SIDS) referred to as death situation in which all clinical causative factors play apparent and hideous roles within an hour of unexpected death of infant within one year of age. To ascertain SDI at ABSUTH, a 6 year study of all infant death cases in record books were searched and two types of questionnaires added. Medical officers and hospital staff involved in infant healthcare were 343, and 1400 mothers contacted were of age ranges 18-40 years. Causes of SDI were respiratory failure 107, RTA 4, circulatory failure 25, alimentary distress 103, trauma and domestic accident 10, and cardiac failure 70 cases. Highest Frequency of occurrence in the years was observed in 1999 and gave 104. Commonest clinical characters were anaemic heart failure, child neglect and abuse, drug toxicity, haemorrhage, and vagal inhibition. The rapidity with which SDI occurred in 25.2% of 107 respiratory failures was within 10 seconds to 5 minutes, and to 232 cases was within 24 minutes of hospitalization. Common clinical symptoms were mild to high fever, intermittent coughing and vomiting, malnourished body, respiratory distress, and apnea while 77.1% full term birth cases had body weight of 2100 to 2500g. Child neglect and abandonment were evident in 49.3% mothers of lean economies. SDI peak was from 5th to 8th months, at which

periods 112 female and 168 male infants were wean to death by 280 mothers. Yearly highest incidence of SDI is 1999.

SP149 - Iterative Reconstruction

TRACK 01: IMAGING

SP149.1 - Preliminary study on reduction of cartoon artifact in the iteratively reconstructed images from sparse projection views

Author(s): Sunhee Wi, Sajid Abbas, Seungryong Cho
Korea Advanced Institute of Science and Technology, Daejeon/KO-REA

OBJECTIVES In this study, we developed an approach that can help reducing cartoon artifact in the reconstructed images from sparse projection views. Sparse-view CT has been actively investigated as a viable option for low-dose CT, and compressive-sensing-inspired image reconstruction frameworks have been developed accordingly. One of the problems in such algorithms is the over-smoothing in the reconstructed images often called the cartoon artifact. Sparsity of the transformed image is maximized during the iterative image reconstruction steps from the insufficiently sampled data, which helps preserve the edge information but may cause such an over-smoothing. The cartoon artifact not only degrades accuracy of the reconstructed images but also may confuse the clinician's interpretation. In this study, we analyzed the noise statistics of the reconstructed images and performed a preliminary study to reduce cartoon artifact.

METHODS Projection-Onto-Convex-Sets (POCS)-based Total-Variation (TV) minimization algorithm was employed for image reconstruction from sparse-view projection data set. We separated the noise image using a conventionally reconstructed image from full-views and examined the noise statistics. A random number generation following the investigated noise statistics was realized from Pearson type-4 Distribution and was added to the image pixel values during iterations. The frequency and amplitude of the added noise were empirically determined. We considered a case of using 25% sparse projection views compared to the full-view case, and applied the proposed method. The XCAT numerical phantom was used for simulating a male patient with his heart containing iodine.

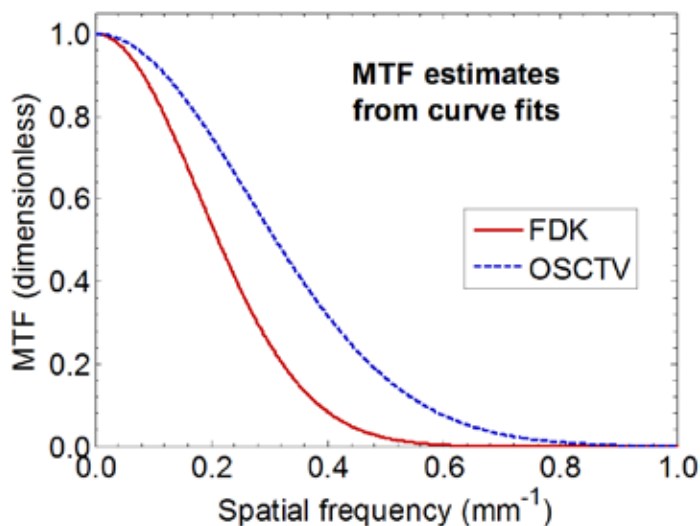
RESULTS Kurtosis of the conventionally reconstructed images from full-views was relatively lower than POCS-TV reconstructed images from sparse-views. Accordingly, the textures of the two reconstructed images were different. Based on the findings in the noise statistics, the parameters in our noise addition module were determined. The reconstructed images using our proposed method visually appeared more similar to the conventionally reconstructed images, and the SSIM value has increased up to near 0.9. In other words, the cartoon artifact was much reduced in the narrow window setting.

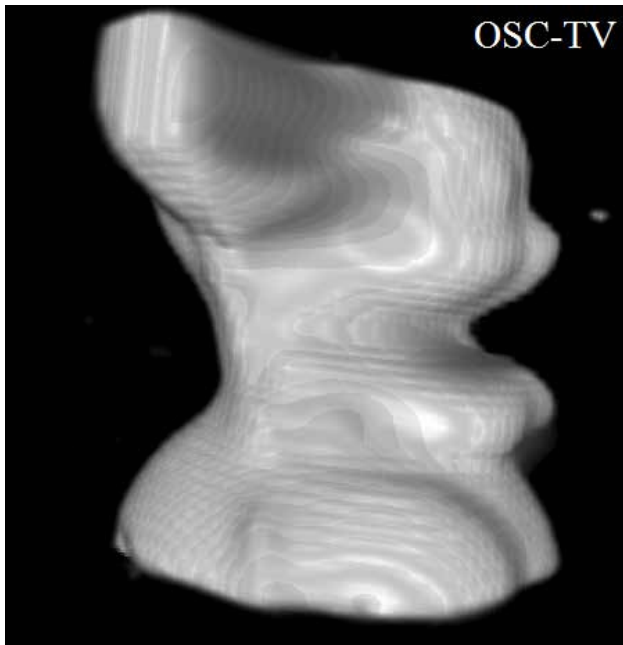
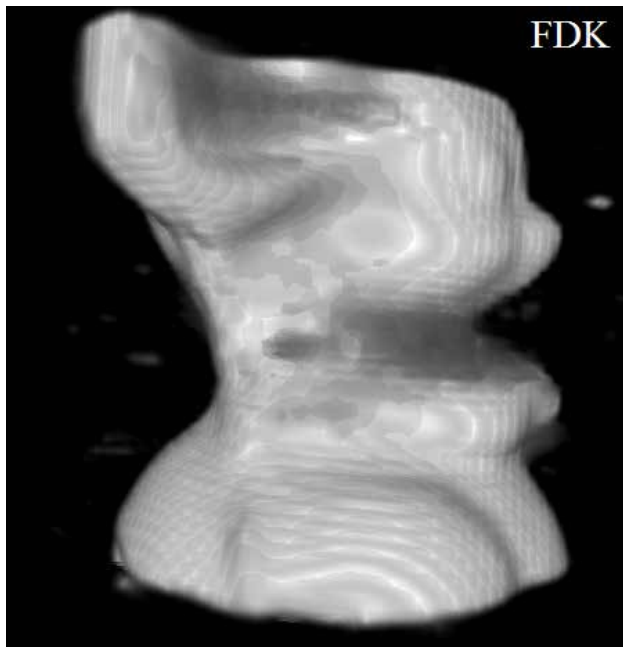
CONCLUSIONS Reconstructed images using POCS-TV algorithm have shown severe cartoon artifacts in the reconstructed images from sparse-view data. The cartoon artifact reduction method was proposed to convert noise texture from a cartoon-like noise to a salt-and-pepper noise. Our preliminary study showed that the proposed method maintains the image quality and reduces cartoon artifacts in the reconstructed images. Although more investigation is necessary to optimize the condition of proposed method, the cartoon artifact reduction method seems to be potentially useful for clinical applications of low-dose CT.

SP149.2 - Evaluation of the OSC-TV Reconstruction Algorithm for Optical Cone-Beam Computed Tomography

Author(s): Dmitri Matenine¹, Yves Goussard², Philippe Després³
¹Département De Physique, De Génie Physique Et D'optique, Université Laval, Québec/QC/CANADA, ²Département De Génie électrique / Institut De Génie Biomédical, École Polytechnique de Montréal, Montréal/QC/CANADA, ³Département De Radio-oncologie, CHU de Québec, Québec/QC/CANADA

This paper evaluates an iterative reconstruction technique, the OSC-TV regularized maximum-likelihood algorithm, in the field of optical cone-beam computed tomography (CT). This imaging modality is commonly used in gel-based three-dimensional (3D) dosimetry for external beam radiotherapy. It is conjectured that model-based iterative reconstruction may improve optical CT image quality and encourage a wider use of this modality in clinical dosimetry. The OSC-TV algorithm was evaluated using experimental data from a commercially available optical cone-beam CT system, and the resulting images were compared with those obtained via filtered backprojection. Physical phantoms were scanned with the goal of evaluating the modulation transfer function, reconstruction precision and accuracy. Reconstruction artifacts were studied as well. The OSC-TV algorithm yielded images of improved quality compared to the filtered backprojections, thanks to a model-based simulation of the photon attenuation process. It was shown to improve spatial resolution, reduce noise and improve accuracy and precision of linear attenuation coefficients' estimation. In addition, image artifacts due to acquisition process and total signal loss were corrected. Overall, this study demonstrates that OSC-TV represents a valuable alternative to filtered backprojection for optical cone-beam CT





contains cylindrical contrast targets with contrast levels of 0.3%, 0.5% and 1% and diameters ranging from 2 - 15 mm. The module contains a supra-slice set of contrast targets arranged in an outer circumference and a sub-slice set of targets arranged in an inner circumference.

The phantom was scanned at 120 kVp over a CTDIvol range of 1.3 – 19 mGy on 4 different scanners. Images were reconstructed using FBP and the iterative algorithms available on each scanner. We used the following scanners (iterative algorithms): GE DiscoveryCT750HD (ASIR™ and VEO™); Siemens Somatom Definition AS+ (SAFIRE™); Toshiba Aquilion64 (AIDR3D™); and Philips Ingenuity iCT256 (iDose™). In total, 328 images were acquired.

Four experienced clinical physicists scored the visibility of the low contrast structures using the 1% nominal contrast supra-slice targets on a 6 MP Coronis Fusion Barco display. 82 images were selected for double rating to check inter and intra-observer reliability. Rater reliability was analyzed using the 'irr' package in the R statistical program using two-way intra-class correlation models. We used the Student's t-test to compare average image scores for different scanners/algorithms.

Results and Discussion

The internal reliability of the rater scores was determined, using the Cronbach's alpha with a value of 0.97. Using the two-way fixed effects model, the inter-rater coefficient was 0.87 while the intra-rater coefficient was 0.93, signifying good agreement and consistency between raters, respectively.

The mean rater scores over the entire dose range on all four CT scanners are as shown. (a) GE Discovery CT750HD: 6.6 ± 1.1 , 6.9 ± 1.1 , 7.5 ± 1.1 , 8.2 ± 1.2 , 7.6 ± 1.2 , 8.4 ± 1.2 , and 7.1 ± 1.3 for FBP, ASIR20, ASIR40, ASIR60, ASIR80, ASIR100 and VEO respectively; (b) Siemens Somatom Definition AS+: 4.9 ± 0.7 , 5.2 ± 0.7 , 5.9 ± 0.6 and 7.6 ± 0.9 for FBP, SAFIRE-L1, SAFIRE-L3 and SAFIRE-L5 respectively; (c) Toshiba Aquilion64: 3.8 ± 0.8 , 4.6 ± 1.0 , 4.4 ± 0.8 and 5.1 ± 1.1 for FBP, AIDR3D-mild, AIDR-3Dstandard and AIDR3D-strong respectively; (d) Philips Ingenuity iCT256: 4.6 ± 0.8 , 4.9 ± 0.8 , 5.4 ± 0.9 , and 5.8 ± 0.8 for FBP, iDose⁴-L1, iDose⁴-L4 and iDose⁴-L6 respectively.

The results showed that, generally, the highest levels of iterative reconstruction gave the highest mean score at all doses for the scanners investigated. The differences in the mean rating scores using iterative reconstructions are statistically significant ($P < 0.05$) for SAFIREL3 – SAFIREL5, ASIR40 – ASIR100 and all AIDR3D algorithms with respect to FBP, using the average inter-rater scores. In contrast however, the results obtained for ASIR20, VEO, SAFIRE-L1 and all iDose⁴ algorithms were not significantly different ($P > 0.05$) with respect to FBP.

Conclusion

Our results show that higher levels of the iterative reconstruction algorithms outperform FBP on GE, Toshiba and Siemens scanners. Lower levels of iterative reconstruction algorithms produce similar results to FBP on the GE and Philips scanners.

SP149.3 - Subjective low contrast performance of four CT scanners with iterative reconstruction

Author(s): Azeez Omotayo¹, Idris Elbakri²

¹Medical Physics, CancerCare Manitoba, Winnipeg/MB/CANADA, ²Medical Physics, CancerCare Manitoba, Winnipeg/CANADA

Subjective low contrast performance of four CT scanners with iterative reconstruction algorithms

Introduction

We assessed the subjective detectability of low contrast structures inside a commonly used quality control phantom for CT using modern CT scanners with iterative algorithms.

Method and Materials

We used the Catphan500 phantom low contrast module which

SP149.5 - Sparse-view image reconstruction with compressed sensing and its application in low dose CT myocardial perfusion imaging**Author(s):** Esmail Enjilela¹, Ting-Yim Lee¹, Jiang Hsieh², Kelley Branch³, Robb Glenny⁴, Aaron So¹¹Imaging Research Laboratories, Robarts Research Institute, London, ON/CANADA, ²CT Engineering, GE Healthcare, Greater Milwaukee Area/UNITED STATES OF AMERICA, ³Division of Cardiology, University of Washington Medical Center, Seattle/UNITED STATES OF AMERICA, ⁴Division of Pulmonary and Critical Care Medicine, University of Washington, Seattle/UNITED STATES OF AMERICA

Computed tomography (CT) perfusion is a process by which perfusion to an organ is measured by CT images. This technique requires repetitive scanning together with injection of contrast agent resulting in high radiation dose (~5 to 20 mSv). We have developed a low x-ray dose method for quantitative CT perfusion imaging. It relies on reconstructing dynamic contrast-enhanced (DCE) CT images from sparsely sampled x-ray projections using a compressed sensing (CS) based algorithm. The feasibility of this approach is demonstrated in the myocardial perfusion imaging of a pig. For this purpose, we performed prospectively ECG triggered dynamic CT imaging on a 70 kg farm pig at 140 kV and 80 mA (28 mAs) with a GE Healthcare (GE) CT750 HD scanner with contrast injection (0.7 mgI/kg) at 3 ml/s. DCE images were then reconstructed from all (984) and one-third (328) of available projection views with filtered backprojection (FBP) and CS respectively. Myocardial perfusion (MP) maps from five consecutive 5 mm slices of the porcine heart generated with CT Perfusion (GE) using CS image sets were compared with those from full view FBP reconstruction and also with microsphere MP measurements. Compared with full view FBP MP measurements, CS maps had biases of -0.01 mL/min/g (95% CI -0.05 – 0.03). When measurements from CS MP maps were compared against ex-vivo fluorescent microspheres technique, the mean bias was -0.12 mL/min/g (95% CI -0.26 – 0.03). This animal study demonstrated that the proposed sparse view coupled with CS image reconstruction is able to generate MP maps with one-third of projection views (sparse-views) required in the conventional FBP technique, resulting in 66.67% reduction in radiation dose.

SP149.6 - Feasibility study for 3D cone-beam computed tomography reconstruction with few projection data using MLEM algorithm with total variation minimization**Author(s):** Dong Hoon Lee¹, Ye Seul Kim², Sung Hoon Choi², Haeng Hwa Lee², Hee Joung Kim²¹Department Of Radiation Convergence Engineering, college Of Health Science, Yonsei university, Wonju/KOREA, ²Department Of Radiological Science And Research Institute Of Health Science, Yonsei University, Wonju/KOREA

Since, the CBCT (cone-beam computed tomography) was developed in 1967, it has been widely used in medical field. The CBCT has relatively simple geometry and less time consuming characteristics to obtain three-dimensional volume data. On the other hand, the major disadvantage of CBCT system is higher radiation exposure to the patient. Thus, it is necessary to apply proper reconstruction method to reduce patient dose.

In this study, simulated sparse projection data was obtained by GATE (Geant4 application for tomography emission) v6.0 simulation tool and those two dimensional projections were reconstructed by MLEM (maximum-likelihood expectation-maximization) algorithm. The total variation minimized image processing method was applied to improve the image quality. The images were evaluated by CNR and FWHM. Furthermore, absorbed dose in simulated phantom was evaluated by GATE v6.0 dose actor.

The images reconstructed by MLEM algorithm and total variation minimized method result in high image quality despite of sparse of projection. Especially image obtained by 60 projections showed comparable image quality with that from 360 projections.

In conclusion, sparse-projection reconstruction with MLEM and total variation minimization is a useful approach to reduce radiation dose with maintaining quality of reconstructed images.

SP149.7 - A weighted stochastic gradient descent algorithm for image reconstruction in 3D computed tomography**Author(s):** Davood Karimi¹, Rabab Ward¹, Nancy L. Ford²¹Electrical And Computer Engineering, University of British Columbia, Vancouver/CANADA, ²Oral Biological And Medical Sciences, University of British Columbia, Vancouver/BC/CANADA

We present and evaluate an algorithm for image reconstruction from a small number of projections in 3D x-ray computed tomography (CT). The proposed algorithm is similar to the class of projected gradient methods. Because each iteration of these algorithms for large 3D CT reconstruction is very computationally demanding, our goal is to devise an algorithm with fast convergence. To achieve this goal, in the proposed algorithm the gradient descent for reducing the measurement misfit term is carried out using a stochastic gradient descent iteration and the gradient directions are weighted using weights suggested by parallel coordinate descent. To further improve the speed of the algorithm, at each iteration we minimize the cost function on the subspace spanned by the direction of the current projected gradient and several previous update directions. We apply the proposed algorithm on simulated and real cone-beam projections and compare it with a well-known accelerated projected gradient algorithm, Monotone Fast Iterative Shrinkage-Thresholding Algorithm (MFISTA). Evaluations show that the rate of convergence of the proposed algorithm is superior to that of MFISTA.

SP149.8 - Investigation of sparse-angle view in cone beam computed tomography (CBCT) reconstruction algorithm using a sinogram interpolaton method**Author(s):** Dohyeon Kim¹, Su-Jin Park², Byungdu Jo², Hyemi Kim², Hee Joung Kim¹¹Department Of Radiation Convergence Engineering, College Of Health Science, Yonsei University, Wonju/KOREA, ²Department Of Radiological Science, College Of Health Science, Yonsei University, Wonju/KOREA

Several methods for reducing patient dose have been widely studied in computed tomography (CT). The radiation exposure dose for patient can be decreased with sparse-angle view reconstruction in CT. In sparse-angle view reconstruction, limited projection images are taken around the object and these are incomplete projection data for obtaining the complete sinogram data. A sinogram interpolation method is the one of solutions to reconstruct the image in sparse-angle view. In this study, we applied a linear sinogram interpolation method in cone-beam computed tomography (CBCT) reconstruction. We simulated the CBCT system with the MATLAB R2012a program to obtain projection data and reconstruct images using three-dimensional version of the Shepp-Logan phantom. Root mean square error (RMSE) was measured in a sinogram interpolation method and normal Feldkamp-Davis-Kress (FDK) reconstruction. The lower RMSE factor means the reconstruction image was similar to the original image. In conclusion, our results demonstrated that the sinogram interpolation method can minimize the error with original image compared with normal FDK reconstruction.

SP150 - X-Ray Phase Contrast & Scatter Imaging

TRACK 01: IMAGING

SP150.1 - Reducing signal extraction artefacts for x-ray scatter imaging with multiple pencil beams

Author(s): Paul C. Johns, Joseph W.S. Carter
Physics, Carleton University, Ottawa/CANADA

X-ray scatter imaging is a novel radiologic technology which delivers increased soft tissue contrast. Multiple pencil beams are scanned over the object. The scatter image is built by extracting the low-angle scatter cross section integrated along each primary beam from the captured dataset of overlapping scatter patterns. The resulting image is much more sensitive to tissue composition than are conventional projection images which are based on the primary linear attenuation coefficient. In our work, a Maximum Likelihood-Expectation Maximization (ML-EM) iterative algorithm is used to disentangle the scatter patterns.[1]

Artefacts can arise from the signal disentanglement. E.g., when a bright scatter signal is adjacent to a dim signal, the algorithm generates ghosts of the signal from one pencil beam location to another. We investigate the reasons for this and possible improvements to the signal extraction algorithm. We used two categories of data: (i) experimental phantom data acquired previously at the Canadian Light Source synchrotron using five 33.2 keV beams of area ~ 0.6 mm² located approximately in a plane, and (ii) simulated data from a Matlab model, with scatter selectable to be from beams passing through muscle, fat, bone, and/or a minimally-scattering object such as air. Attenuation of the Laue scatter ring patterns can be selected to be azimuthally symmetric, or asymmetric, about the pencil beams. The scatter pattern data were input to the ML-EM algorithm and the sensitivity to the inputs studied. Furthermore, we modified the algorithm to segment the Laue rings in radial sectors.

Our results confirm that the ML-EM algorithm performs best when adjacent beams have comparable Laue ring intensity. For example, the algorithm is better at separating signals from two beams that passed through muscle and fat, than for two beams passing through muscle and bone, because of the greater attenuation for the latter. The cause of the ghosting artefact is established to be a fundamental limitation of ML-EM. In the first few iterations, low-spatial-frequency scatter signals are subdivided equally and assigned to multiple beam locations, swamping small signals. The global optimization minimum rectifies the problem, but ML-EM's approach to the global minimum is unacceptably slow, requiring over 10,000 iterations. Azimuthal segmentation of the scatter patterns allows a closer fit to the measured scatter data but still does not reach the global minimum. We have increased the ML-EM convergence rate. In the algorithm, the ratio of measured to estimated scatter patterns is computed and used to correct the next update. By scaling the difference from unity by a factor of 2.0 every three iterations, the resulting rms difference between the estimated and measured scatter patterns can be reduced, for example, from 2.66% at the 16th iteration to 2.02%. The global minimum however is still not reached in reasonable time. We are also investigating the use of the primary pencil beam information from adjacent beams. Spatial interpolation of these data can give approximate transmission factors with which to correct the recorded scatter data for spatially-dependent attenuation.

[1] Landheer & Johns, Rev. Sci. Instrum. 83(9), 095114, 7 pp. (2012).

SP150.2 - Live animal phase contrast x-ray velocimetry of the lungs: Optimising imaging speed for synchrotron and lab source imaging

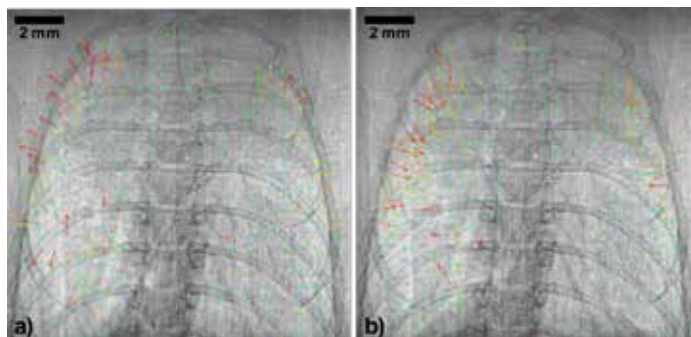
Author(s): Rhiannon P. Murrie¹, Kaye S. Morgan¹, Andreas Fouras², David M. Paganin¹

¹School Of Physics, Monash University, Clayton/VIC/AUSTRALIA, ²Division Of Biological Engineering, Monash University, Clayton/VIC/AUSTRALIA

Lung diseases such as lung cancer, asthma, emphysema and cystic fibrosis affect all ages of the world's population. One of the key difficulties in accurately diagnosing, monitoring and treating these lung diseases has been our inability to image the dynamics and detail of the lungs and airways whilst they are breathing. In particular, this limits the availability of regional information that can provide the most sensitive measure of changes in lung function.

X-ray phase contrast (XPCI) imaging allows us to image the lungs in high resolution by exploiting the difference in refractive indices between tissue and air. When imaged with x-rays of sufficient spatial coherence, refraction from the tissue/air interfaces result in high quality edge-enhanced airway images. Phase contrast imaging of the many alveoli of the lungs produces a characteristic speckle pattern (Kitchen *et al.*, 2004). By combining XPCI with an engineering technique used to track the motion and flow of fluids, known as velocimetry, we can study the motion of the speckle pattern to reveal the local motion of the lungs and the flow of air through the lungs and airways (Dubsky *et al.*, 2012, Fouras *et al.*, 2012). This technique, dubbed x-ray velocimetry (XV), improves our ability to find small areas of disease under natural ventilation conditions. This allows for earlier and more accurate diagnosis of disease and allows us to expand research into treatment development and improvement through direct, real-time, high-resolution visualisation of lung dynamics.

X-ray velocimetry has, up until now, been primarily performed using a synchrotron x-ray source. As we move towards more accessible and cost-effective laboratory-based set-ups, this project investigates the optimal imaging speed to capture the lung motion in-vivo in small animals using XV. This optimisation balances the noise inherent in a short exposure with the motion blur that results from a long exposure, over a range of velocities. Results from both a synchrotron and laboratory source will be compared and considered via both simulation and experimental data.



References:

- Kitchen *et al.*, 2004, *Phys. Med. Biol.* **49**, 4335-4348.
 Dubsky *et al.*, 2012, *J. R. Soc. Interface* **9**, 2213-2224
 Fouras *et al.*, 2012, *Ann. Biomed. Eng.* **40**, 1160-1169

SP150.3 - X-ray Phase-Contrast imaging: from mammography to breast tomography using synchrotron radiation

Author(s): Renata Longo¹, Fulvia Arfelli¹, Ronaldo Bellazzini², Ubaldo Bottigli³, Alessandro Brez², Francesco Brun⁴, Antonio Brunetti⁵, Pasquale Delogu⁶, Francesca Di Lillo⁷, Diego Dreossi⁸, Viviana Fanti⁹, Christian Fedon¹, Bruno Golosio⁵, Nico Lanconelli¹⁰, Giovanni Mettievier⁷, Massimo Minuti², Piernicola Oliva⁵, Graziella Pili¹¹, Michele Pinchera², Luigi Rigon¹, Paolo Russo⁷, Paquale L. De Ruvo¹², Antonio Sarno⁷, Gloria Spandre², Giuliana Tromba⁸, Alessandro Vincenzi¹³
¹Dept Of Trieste, University of Trieste & INFN, Trieste/ITALY, ²INFN Pisa & PiXirad Imaging Counters srl, Pisa/ITALY, ³University of Siena & INFN, Siena/ITALY, ⁴Department Of Engineering And Architecture, University of Trieste, Trieste/ITALY, ⁵Università degli Studi di Sassari & INFN, Sassari/ITALY, ⁶University of Pisa & INFN, Pisa/ITALY, ⁷Dipartimento Di Fisica, Università di Napoli Federico II & INFN, Napoli/ITALY, ⁸Elettra-Sincrotrone Trieste S.C.p.A, Basovizza, Trieste/ITALY, ⁹Department Of Physics, Università di Cagliari & INFN, Cagliari/ITALY, ¹⁰Department Of Physics And Astronomy, University of Bologna & INFN, BOLOGNA/ITALY, ¹¹Università di Cagliari, Cagliari/ITALY, ¹²INFN Pisa, Pisa/ITALY, ¹³PiXirad Imaging Counters srl, Pisa/ITALY

In addition to absorption-based x-ray imaging, over the last two decades other techniques devoted to exploit the wave nature of x-rays were developed to enhance visibility of details and increase image contrast. These methods are called Phase-Contrast imaging (PCi) techniques and were developed in order to obtain high contrast and high spatial resolution images of biological samples. The first clinical study based on a PCi technique was performed at the SYRMEP beamline (Synchrotron Radiation for Medical Physics) of ELETTRA, the Italian synchrotron facility; the free space propagation approach was applied. The clinical study was based on 71 female patients that underwent digital mammography at hospital and, due to questionable or suspicious breast abnormalities not clarified at UltraSonography, underwent phase contrast mammography with synchrotron radiation (MSR). The study shows that Phase-Contrast allows improving the image quality and increases significantly the diagnostic performance of MSR in comparison with digital mammography: difference between methods in the area under the ROC curve is 0.2 ($P < 0.001$). The mean glandular doses (MGD) delivered during MSR exams are, on the average, 42% lower than the ones delivered during DM exams, due to the properties of synchrotron radiation. Moreover the use of monochromatic beam, in the energy range 18-22 keV, allowed the direct measurement of the breast linear attenuation coefficients for each patient.

The new clinical project in breast imaging at the SYRMEP beamline, concerns breast tomography and it is carried out by the SYRMA-CT collaboration, an interdisciplinary team supported by INFN, ELETTRA and the Trieste University Hospital. The SYRMEP mammography facility will be deeply modified to allow the acquisition of tomographic images, and the dosimetric and safety system will be upgraded too. A complete Monte Carlo simulation code has been developed and tested for dose evaluation and exam optimization. The detector selected for this application is PIXIRAD-8: a CdTe detector working in single photon counting mode. The active area is 25x2.5 cm², the pixel size is 60 micrometers in hexagonal arrangement, the frame rate is 14 frame/s and the pixel rate capability is 5 10⁵ counts/pixel/s.

The aim is to acquire tomographic images of the breast delivering MGDs in the range 4-20 mGy. The beam energy will be in the range 38-40 keV, the upper limit is determined by the beam available at the SYRMEP beamline. To obtain high quality images at a clinical acceptable delivered dose new image reconstruction approaches will be explored, in order to reduce the number of necessary projections: simultaneous algebraic reconstruction tomography (SART) and equally sloped tomography (EST) approaches are under investigation. Moreover phase retrieval algorithms will be applied to the projection before the tomographic reconstruction in order to

increase the image contrast.

In the present communication the results of the Phase-Contrast mammography clinical study will be summarized, in terms of image quality, delivered dose and linear attenuation measurements, the SYRMA-CT project will be presented and the preliminary Phase-Contrast CT images obtained at ELETTRA in clinical compatible condition will be discussed.

SP150.4 - 4 Years of X-ray Imaging at 05B1-1 Beamline at BMIT

Author(s): George Belev¹, Denise Miller¹, Nazanin Samadi², Mark A. Webb¹, Tomasz W. Wysokinski¹, Ning Zhu¹, L. D. Chapman², David M.L. Cooper²
¹Bmit, Canadian Light Source Inc., Saskatoon/CANADA, ²Anatomy And Cell Biology, University of Saskatchewan, Saskatoon/SK/CANADA

The BioMedical Imaging and Therapy (BMIT) facility located at the Canadian Light Source, provides synchrotron-specific imaging and radiation therapy capabilities [1-5]. There are two separate endstations used for experiments, Bending Magnet beamline described here and Insertion Device beamline that started general user program in 2015.

The bending magnet beamline 05B1-1 was used to acquire first image in December 2008 and was officially opened for general user program in 2011. This endstation is designed for imaging and therapy research primarily in animals ranging in size from insects to mice to small dogs and cats, as well as tissue specimens including plants.



Fig. 1 3D Model of the BM Beamline components [3].

Core research programs include human and animal reproduction, cancer imaging and therapy, spinal cord injury and repair, cardiovascular and lung imaging and disease, bone and cartilage growth and deterioration, mammography, developmental biology, gene expression research as well as the introduction of new imaging methods.

The monochromatic spectral range spans 15-40 keV, and the beam is more than 200 mm wide in the experimental hutch. Several different focal plane detectors (cameras) are available with resolutions ranging from 2 μm to 200 μm.

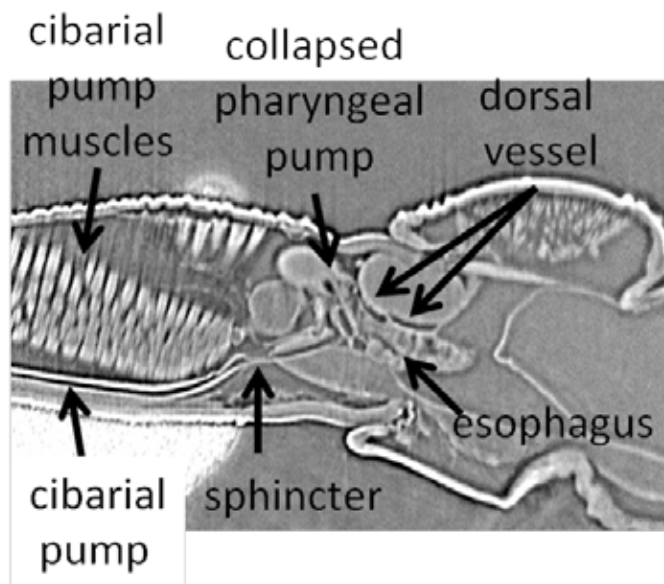


Fig. 2 Example of the high resolution CT scan collected on 05B1-1 endstation: Cross section view of a CT scan of the blood-feeding insect *Rhodnius prolixus*, the vector of Chagas' disease. Courtesy of Juan Janowski.

References:

- [1] L. Dean Chapman, CLSI Document No. 26.2.1.1 Rev. 0.A, 2007.
- [2] L. Dean Chapman, CLSI Document No. 26.2.1.2 Rev. 0, 2006.
- [3] Tomasz W. Wysokinski, et.al. NIM A: 582 (2007) 73-76.
- [4] Tomasz W. Wysokinski, et.al. J. Phys: Conf. Ser. 425, (2013) 07.
- [5] Tomasz W. Wysokinski, et.al. NIM A: 775 (2015) 1-4.

SP150.5 - An energy dispersive bent Laue monochromator for K-edge subtraction imaging

Author(s): Nazanin Samadi¹, Ying Zhu², Mercedes Martinson³, Basseyy Basseyy³, George Belev⁴, L. D. Chapman⁵
¹Bimedical Engineering, University of Saskatchewan, Saskatoon/CANADA, ²Mccaig Inst For Bone And Joint Health, University of Calgary, Calgary/CANADA, ³Physics And Engineering Physics, University of Saskatchewan, Saskatoon/CANADA, ⁴Bmit, Canadian Light Source Inc., Saskatoon/CANADA, ⁵Anatomy And Cell Biology, University of Saskatchewan, Saskatoon/SK/CANADA

K-Edge Subtraction (KES) is a powerful synchrotron imaging method that allows the quantifiable determination of a contrast element (i.e. iodine) and matrix material (usually represented as water) in both projection imaging and computed tomography. A bent Laue monochromator is typically employed to prepare imaging beams above and below the contrast element K-edge which focus at the subject location and subsequently diverge onto a detector. Conventional KES prepares the two beams by utilizing a splitter that blocks approximately 1/3 of the vertical beam size to prevent "edge crossing" energies beyond the monochromator (Figure 1).

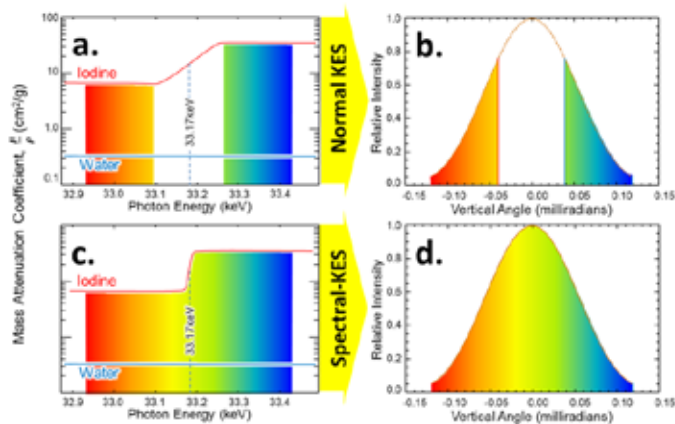
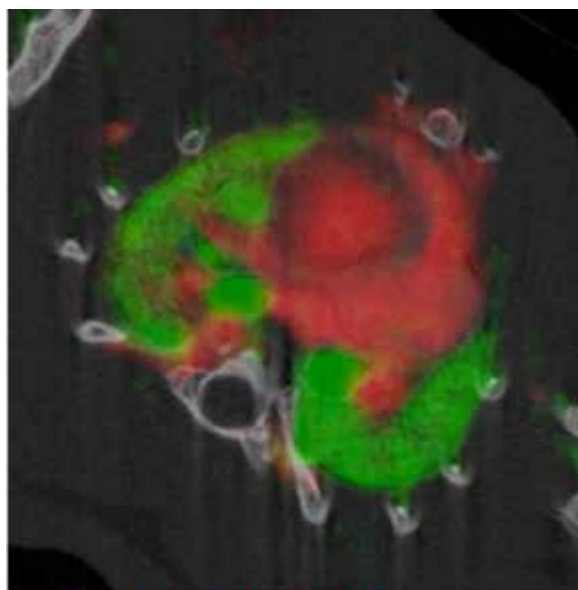


Figure 1. Iodine absorption edge (a & c) and vertical synchrotron beam profile (b & d) for a conventional bent Laue system (a & b) and Spectral-KES (c & d). Note that fully 1/3 of the beam in the conventional system is removed to avoid edge crossing energies which is not the case for Spectral-KES.

A bent Laue monochromator has been developed that has very good focal and energy dispersive properties for KES. Approximately 5% of the vertical beam profile is involved in "edge crossing" energies (Figure 1c,d), thus no splitter is employed. The combination of good spatial resolution, energy dispersive properties, flux and a unique approach to data analysis make this system nearly ideal for KES.



Red – Iodine Green – Xenon Grey – Water
 Figure 2. composite image of rat thorax showing iodine in the heart and xenon in the lungs. Image courtesy of Prof. Nancy Ford & Dr. Pierre Deman, UBC

Details of the monochromator will be discussed, especially the focal and energy dispersive properties. Example images (i.e. Figure 2) of the beam and the object images will be presented as well.

SP150.6 - An incoherent implementation of x-ray phase contrast imaging and tomography that maintains high sensitivity at low delivered doses

Author(s): Alessandro Olivo, Charlotte Hagen, Paul C. Diemoz, Fabio A. Vittoria, Gibril Kallon, Anna Zamir, Dario Basta, Thomas P. Millard, Marco Endrizzi
 Medical Physics And Biomedical Engineering, University College London, London/UNITED KINGDOM

X-ray phase contrast imaging (XPCI) has been one of the hottest topics in x-ray research over the last two decades, because of its potential to revolutionize diagnostic radiology and other medical applications of x-rays. Indeed, its ability to improve diagnostic potential in mammography is currently being demonstrated by the in vivo work on human patients underway at the Trieste synchrotron in Italy.

However, translation into everyday clinical use has proven very difficult, to the extent that part of the community is starting to doubt this will ever happen.

We argue that the main reason for the above lies in the fact that all implementations of XPCI proposed so far have been based on coherent approaches. While some of these are very promising, the need for source coherence prevented them from being usable in clinical practice, at least until a new generation of sources will become available that can simultaneously provide high x-ray flux and high coherence. Whenever incoherent sources have been employed, devices have been introduced to artificially increase their coherence (e.g. crystals or gratings). This resulted in a significant reduction of the x-ray flux, leading to excessive exposure time, as well as delivered dose whenever these devices are positioned after the sample.

This talk will present a solution based on a completely incoherent approach to XPCI, centred on the adaptation (through apertured masks) of the “edge-illumination” principle to polychromatic and divergent x-ray beams generated by conventional sources. This talk will show that:

- 1) The method is completely incoherent, but this notwithstanding provides a phase sensitivity equal to that of other coherent approaches while using unfiltered and uncollimated focal spots of up to 100 micron (compatible with e.g. current mammography sources). We will show that the coherence length is much smaller than both the size of the apertures in the used masks and the separation between them, and explain how phase sensitivity is measured. Based on recent experiments performed with energy-resolved detectors, we will also show that the method is completely achromatic.
- 2) In planar imaging, the delivered dose is lower or equal than in e.g. conventional mammographic examinations, and in CT it is well below the limits imposed by e.g. small-animal imaging.
- 3) The technique is highly flexible and can be easily adapted to tomosynthesis, microscopy and micro-CT, etc, and that “dark-field” (sometimes referred to as “ultra-small angle scattering”) images are also readily achievable, still within clinically acceptable dose limits.

After the technical excursus outlined above, we will show examples from recent applications in medicine and biology, including in mammography, imaging of cartilage and joints, use of new contrast agents and monitoring of regenerative medicine processes. Finally, we will provide an outlook on future technical developments of the method, which include options for “single-shot” retrieval of attenuation, phase-contrast and dark-field images, as well as strategies to reduce the exposure time (currently ~10s for planar imaging) and the overall dimensions of the imaging system, scale up the field of view, completely automatize the alignment.

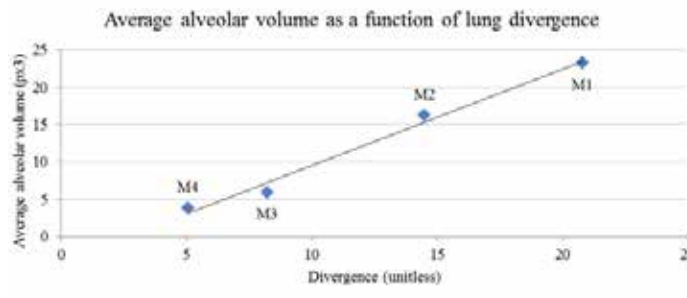
SP150.7 - Indirect measurement of average alveolar size using dynamic phase-contrast imaging

Author(s): Mercedes Martinson¹, Rob Lewis², Andreas Fouras³, Megan Wallace⁴, Melissa Siew⁴, Stuart Hooper⁵, Paul Babyn⁶
¹Physics And Engineering Physics, University of Saskatchewan, Saskatoon/CANADA, ²Biomedical Engineering, University of Saskatchewan, Saskatoon/SK/CANADA, ³Division Of Biological Engineering, Monash University, Clayton/VIC/AUSTRALIA, ⁴The Ritchie Centre, MIMR-PHI Institute of Medical Research, Clayton/VIC/AUSTRALIA, ⁵Department Of Obstetrics And Gynaecology, Monash University, Clayton/VIC/AUSTRALIA, ⁶Medical Imaging, University of Saskatchewan, Saskatoon/SK/CANADA

For some lung diseases, assessment of alveolar dimension could add critical information to inform patient care and disease progression. However, current clinical imaging techniques, such as computed tomography, lack the resolution required to measure these small structures in patients. While the gold standard imaging modality for measuring alveoli is micro-CT, this technique is not possible in clinical use due to the size of the patients and the radiation dose. An alternative imaging modality is phase-based contrast imaging, which would deliver a lower dose to patients and increase the size limit. Phase contrast X-ray imaging has previously been combined with particle image velocimetry (PIV) to measure lung motion, another indicator of lung disease. Thus it was hypothesized that average alveolar size could also be measured indirectly using PIV. In the work reported here, we show that average alveolar size shows a high correlation to the mathematical divergence of the velocity vector field that results from the speckle pattern produced by phase imaging of mouse lungs. This correlation is linear with $p < 0.006$. If this correlation holds in human lungs, it could potentially be calibrated to indirectly measure average alveolar size in human patients using some of the grating-based phase-contrast imaging methods that are showing great promise in clinical use.

PCXI and μ -CT Results:

Mouse identifier	Age	Average Divergence	Average Alveolar Dimension (px3)
M1	3 weeks	20.8	23.25
M2	3 weeks	14.5	16.19
M3	8 weeks	8.22	5.95
M4	8 weeks	5.06	3.83



SP151 - Cardio Mechanics & Organs

TRACK 03: BIOMECHANICS AND ARTIFICIAL ORGANS

SP151.1 - Biomechanics and artificial organs

Author(s): Alexandros Repanas, Marc Mueller, Fedaa Al Halabi, Oleksandr Gryshkov, Michael Bode, Holger Zernetsch, [Birgit Glasmacher](#)
Leibniz University Hannover, Institute for Multiphase Processes, Hannover/GERMANY

Introduction

Tissue engineering is an interdisciplinary field that combines the principles of engineering and life sciences with the goal of restoration, repair or replacement of tissues and their functions. Bridging the gap between isolated cells and functioning tissue, the scaffolds become an instructive extracellular microenvironment that actively guides cells both locally and in time towards tissue formation and regeneration. Additionally, the mechanical properties and the microstructure of the scaffolds play an important role to cell proliferation, differentiation and eventually regeneration of the damage tissue site. Electrospinning is a technique for the production of ultrafine polymer fibers from polymer melts or polymer solutions through electrostatic interaction¹. It is most often used as scaffold material in tissue engineering applications due to its similarity to the filamentous microenvironment in native tissues. This similarity often promotes a more positive cell response to the generated fibers than to the bulk material alone. Moreover, this method is also suitable to generate alginate 3D gel-structures for immunoisolation and cryopreservation². Here, we describe the production of aligned fibers with different 3D structures such as mats and tubes, the incorporation of bioactive substances and their biomechanical evaluation.

Materials & methods

Different kinds of biodegradable polymers of natural and synthetic origin (polycaprolactone, poly-L-lactide acid, polyethylene glycol, chitosan etc) that have been approved for biomedical applications were dissolved inside organic solvents (chloroform, acetone, ethanol etc) at adequate concentrations for electrospinning. Single jet or/and coaxial jet electrospinning was used to create fibers gathered on the surface of collectors with different geometry (rectangular, rotating mandrel, tubular etc). Morphology of the fibrous scaffolds was examined by scanning electron microscopy (SEM) having previously been sputter-coated with gold. Uniaxial mechanical tests were performed with an electroforce tensile testing instrument by BOSE®, equipped with a 200 N load cell and a static tensile testing instrument by INSTRON®, equipped with a 500 N load cell. Young's modulus was calculated from the linear phase of the stress-strain plot. Strain and stress at failure and at maximum load were calculated and analyzed.

Results and Discussion

Scaffold design via electrospinning resulted in versatile scaffolds made out of various polymers that exhibited different macroscopic and microscopic structures, various pore sizes and porosities. From aligned fibers that could be used in nerve tissue engineering, tubular scaffolds for vascular grafts and coaxially electrospun membranes with encapsulated pharmaceuticals, artificial scaffolds were created to fit the need of various applications. The mechanical properties of the scaffolds were in line with the need for each case, comparable with natural tissues. Electrospun scaffolds showed to address both controlled release and structural cues with adequate pore sizes and resulting porosity enabling cell proliferation.

Acknowledgments

The authors would like to thank the German Research Foundation (DFG) for the financial support of these studies within SFB 599 and EXC 62/1.

References

- [1] Szentivanyi A. *et al.* Advanced Drug Delivery Reviews 2011;63:209–220
- [2] Gryshkov O. *et al.* Materials Science and Engineering: C 2014;36:77–83

SP151.2 - The Continuous Flow Total Artificial Heart in Clinical Practice

Author(s): [David Macku](#)

Department Of Cybernetics, Czech Technical University in Prague, Prague/CZECH REPUBLIC

My minireview describes an inventive medical device for the replacement of pulsatile circulation by pulseless circulation for patients awaiting heart transplantation. The Continuous flow total artificial heart (CFTAH) is a device consisting of two continuous ventricular assist devices that produce pulseless flow into both systemic and pulmonary circulation. Its utilization is not yet widespread. The Continuous flow total artificial heart has only been implanted in humans three times as an off-label use of a ventricular assist device. All three men have been supported by chronic pulseless flow. The issue of chronic pulseless vs. chronic pulsatile blood flow and its effects on organs and tissue perfusion has been debated in medical and biomedical scientific journals for decades. There are many animal studies, views of many scientists and many hypotheses, but no clear answer to the basic question: will a person be able live a quality life with pulseless flow for months and years?

SP151.3 - Power Control Range of Operation for the Left Ventricular Assist Device in Bridge-to-Recovery Treatment

Author(s): [Marwan A. Simaan](#)¹, George Faragallah¹, Yu Wang²

¹University of Central Florida, Orlando/FL/UNITED STATES OF AMERICA, ²University of Louisville, Louisville/KY/UNITED STATES OF AMERICA

Left Ventricular Assist Devices (LVADs) are mechanical pumps that may be used as an alternative to drug therapy for patients with congestive heart failure. These rotary pumps are implanted in patients to provide an alternative path for blood flow from the left ventricle to the aorta that supplements the natural blood flow through the aortic valve. Although the LVAD is used largely for bridge-to-transplantation or destination therapy treatments, in recent years considerable interest has been devoted to using the LVAD as a bridge-to-recovery device. This type of treatment is typically intended for patients whose heart condition may improve as a result of a limited time LVAD support. Candidates for this type of treatment may be weaned from the LVAD when their hemodynamic and physiological changes indicate recovery of the heart muscle.

The amount of blood flow supplied by the LVAD depends on the rotational speed of the pump which is controlled by the electric power supplied to the pump motor from the LVAD battery pack. Current LVAD technology allows for the option of operating the pump only at a fixed power setting. This means that the power controller cannot react to any changes in the activity level of the patient by automatically adjusting the supplied power. The next generation LVADs however, will be equipped with controllers that have this capability. The purpose of this paper is to address the important engineering challenge of determining the *range of operation* available to the

power controller within which it can: (1) automatically adjust the power so that the resulting total blood flow meets the physiological demand of the patient; and (2) promote recovery by maintaining normal operation of the aortic valve. Using a mathematical model we have shown that if this power is increased beyond a certain *critical value* the aortic valve will close permanently due to the inability of the left ventricle to retain enough volume that can build pressure high enough to open the valve and let the blood flow through it. Permanent closure of the aortic valve may cause complications such as valve fusion or stenosis, stagnation of blood flow and/or thrombus formation, all of which may be harmful to the patient by delaying or preventing the recovery of the heart muscle. In this paper we investigate the effect of the power provided to the LVAD pump on the ability of the aortic valve to open and close regularly during the cardiac cycle hence avoiding all of the above mentioned complications. We derive a relationship between the *critical value* of power that causes the aortic valve to permanently close and the patient's level of activity. We show that independent of the degree of severity of the heart condition, this *critical value* is directly related to the patient's level of activity and that the more active the patient, the larger the *range of operation* available to the LVAD power controller. This means that increased activity reduces the possibility of exceeding the *critical value* and consequently increases the chance of faster recovery.

SP151.4 - An quantitative estimation method of peripheral perfusion by using a CCD camera during rotary blood pump support

Author(s): Yasuyuki Shiraishi, Kyosuke Sano, Shota Watanabe, Tomoyuki Yambe
Medical Engineering & Cardiology, IDAC, Tohoku University, Sendai/JAPAN

The rotary blood pump support for ventricular circulatory assistance has become a standard procedure as the bridge use or the destination therapy for the surgical treatment of severe heart failure in recent years. While the outcome of the long term support by the rotary blood pumps in the patients is excellent compared with the heart transplantation, the optimal driving condition of each pump still remains to be seen. It is anticipated that the pulsatile flow can be generated by the interaction between the native heart function and the pump which is to be contributing to maintain the peripheral perfusion. One of the definitive condition of the revolution number in each pump is to investigate the aortic valve opening during the systole for providing the native heart contractile function. Recently, a pulse detection technology by using CCD cameras has been represented for the diagnostic purpose of patients' hemodynamics. We also have applied and develop the noninvasive evaluation method for the investigation of peripheral perfusion during the rotary blood pump support in order to examine the pulsatile effects of the pump characteristics on peripheral organs. In this study, the brightness of color components derived from the CCD camera (NEX-FS100JK, Sony, Japan) under the different blood density conditions was examined in vitro by using an originally designed peripheral model made of open-foamed polyurethane sponge at the density of $1.7 \times 10^{-2} \text{ g/cm}^3$. After the static characteristic tests, the peripheral perfusion at a goat face was evaluated under the left ventricular assist condition using the centrifugal blood pump (Evaheart, SunMedical, Japan). The animal study was performed with the left ventricular assist using an adult healthy Saanen goat under the normal anesthesia using 2 % isoflurane with remifentanyl. All the animal experimental procedure was investigated and allowed by the Animal Experiment Committee in Tohoku University.

The results were as follows: In the static model study, the relationship between the brightness and the blood density in the sponge model was calculated. It was indicated that the brightness value calculated under the green color LED lighting condition was elevated by around 30 % by the increase of sponge density by 3 %. In the

animal experiment, the peripheral perfusion could be obtained as the synchronous pulsation with the cardiac beats under the rotary blood pump support. The pulsatility calculated from the goat's face perfusion indicated that the elimination of pulse might be caused by the increase of the revolution number of the pump. Consequently, the pulsation by the noninvasive CCD detection could be evaluated as the changes in peripheral blood flow based on these data.

SP151.5 - Mathematical Modeling of Left Ventricle Stroke Work Following Transcatheter Aortic Valve Replacement Associated With Paravalvular Leaks

Author(s): Azadeh Saeedi¹, Abdelghani Djebbari², Zahra Keshavarz-Motamed³, N Dahdah⁴, Lyes Kadem¹

¹Mechanical And Industrial Engineering, Concordia University, Montreal/QC/CANADA, ²Department Of Electronics, University of Tlemcen, Tlemcen/ALGERIA, ³Laval University, Quebec/QC/CANADA, ⁴Sainte-Justine Hospital, Montreal/CANADA

Objectives The objective of this study was to develop a lumped parameter model to evaluate the effect of paravalvular leaks (PVL) following transcatheter aortic valve replacement (TAVR) on the total load supported by the left ventricle (LV).

Background A significant number of elderly patients with severe symptomatic aortic stenosis are denied surgical aortic valve replacement due to its high operative risk. TAVR has recently emerged as an alternative solution for high-risk inoperable patients with aortic stenosis. However, TAVR is often associated with paravalvular leaks (PVL). PVL leads to left ventricular volume overload and increased stroke work of the left ventricle. Under such conditions it is difficult to evaluate the net benefit from TAVR since the benefit from the increase in valve area is damped by the presence of PVLs.

Methods A mathematical model was developed based solely on non-invasive data allowed for the description of the interaction between effective orifice area (EOA), PVL and the left ventricle work (LVW) pre and post-TAVR. The model was used to simulate different configurations in terms of valve areas and valve regurgitation/PVLs before and after TAVR. The following conditions were investigated: 1) Before TAVR: severe aortic stenosis with EOAs of 0.56 cm², 0.66 cm² and 0.76 cm² with no, mild, moderate and severe aortic regurgitation; 2) After TAVR: EOAs of 1.37 cm², 1.61 cm² and 1.90 cm² with no, mild, moderate and severe aortic regurgitation paravalvular leaks. For each case, LV stroke work has been computed as well as the net reduction/increase in LV stroke work as a result of TAVR.

Results and Conclusion The model was able to reproduce physiological waveforms found in patients with aortic stenosis and regurgitation. The results show that in several configurations, TAVR did not lead to a significant reduction in LV stroke work because of the presence of PVLs.

Defining a new parameter for evaluating TAVR success, as the ratio of the actual reduction in LV stroke work to the ideal reduction expected in the absence of PVLs, showed that in only 53% of cases TAVR was successful (>75% efficiency) in reducing LV stroke work. In 19% of cases the efficiency of TAVR was between 50-75%, in 18% of cases the efficiency of TAVR was between 0-50% and in 10% of cases TAVR led even to an increase in LV stroke work because the benefit of increasing EOA was damped by the negative impact of PVLs. In conclusion, TAVR is an effective option to reduce the left ventricle overload in high risk patients with severe AS. However, this is only true in the absence or mild paravalvular leaks. Severe or moderate paravalvular leaks significantly limit the benefit of TAVR and might even lead to an increase in the left ventricle overload.

SP151.6 - Criteria to study Heart Failure derived from ESPVR

Author(s): Rachad M. Shoucri

Mathematics And Computer Science, royal military college of canada, Kingston/ON/CANADA

The problem of heart failure with normal or preserved ejection fraction (HFpEF) has been the object of extensive studies. In a series of studies by the author, basic relations were derived between the ejection fraction (EF) of the left ventricle and the parameters describing the end-systolic pressure-volume relation (ESPVR), represented by the line d3Vdm in Fig. 1 (left).

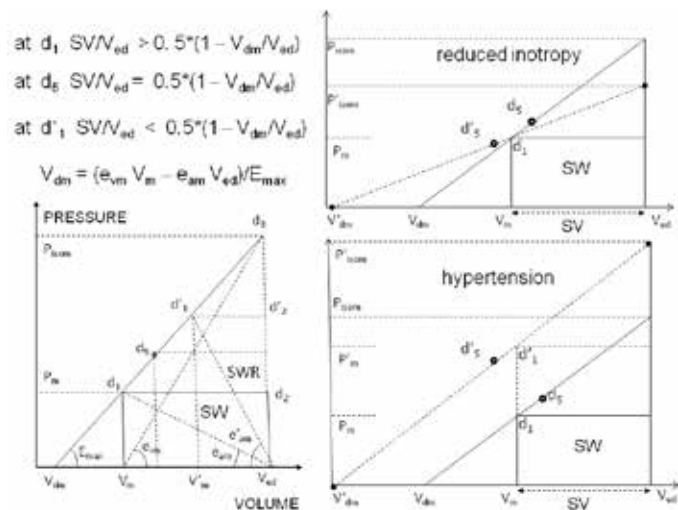


Figure 1: (left) The ESPVR is represented by the line d3Vdm with midpoint d5 and slope Emax. The pressure-volume relation is represented by the loop Vedd2d1Vm in a normal ejecting contraction. P_{isom} is the peak active pressure of the myocardium. (right) Normal physiological case with d1 below mid-point d5 (solid line); abnormal case with reduced contractility with d1 above midpoint d'5 (dotted line, top); abnormal case of hypertension with d'1 above midpoint d'5 (dotted line, bottom); notice that the three cases have the same EF = SV/Ved.

The ventricular pressure P_m is assumed constant during the ejection phase, d1 is the corresponding point on the ESPVR. One can distinguish three states for the operation of the left ventricle:

- a) Normal physiological state, with d1 below d5 on the line d3Vdm. In this case we have stroke volume SV > (Ved - Vdm)/2, with slopes ratio Emax/eam » 2 and P_{isom}/P_m » 3. This case corresponds also to maximum efficiency for oxygen consumption by the myocardium.
- b) Mildly depressed state, with d1 and d5 nearly coinciding. In this case we have SV » (Ved - Vdm)/2, with Emax/eam » 1 and P_{isom}/P_m » 2. Notice from Fig. 1 that when d1 moves on the line d3Vdm, the stroke work SW reaches its maximum value SW_x when d1 coincides with the mid-point d5. SWR = SW_x - SW is the stroke work reserve.
- c) Severely depressed state, with d1 above d5 on the line d3Vdm. In this case we have SV < (Ved - Vdm)/2, with Emax/eam < 1 and P_{isom}/P_m < 2 (see Fig. 1, right side).

In cases (b) and (c) an increase in P_m causes a decrease in SW, resulting in cardiac insufficiency. These results are confirmed by a wide variety of clinical data taken from the medical literature and give new insight and better understanding of the mechanics of left ventricular contraction.

SP151.7 - Fluid Dynamics of Transcatheter Aortic Valve Associated with Paravalvular Leak

Author(s): Azadeh Saeedi¹, Zahra Keshavarz-Motamed², Philippe Pibarot², Lyes Kadem¹

¹Mechanical And Industrial Engineering, Concordia University, Montreal/QC/CANADA, ²Laval University, Quebec/QC/CANADA

Objectives The objective of this study is to investigate, using three dimensional numerical simulations, the effect of paravalvular leak on the diastolic flow-field characteristics following transcatheter aortic valve replacement.

Background Transcatheter Aortic Valve Replacement (TAVR) has emerged as the preferred therapeutic intervention for inoperable patients with severe symptomatic aortic stenosis and as an alternative option in high surgical risk individuals. However, one of the major TAVR related complications is Paravalvular Leak (PVL). PVL leads to left ventricular volume overload and increased stroke work of the left ventricle. Despite its clinical significance, only few studies addressed specifically the hemodynamic effects of paravalvular leaks after TAVR.

Methods Three dimensional simulations using finite volume method were performed on an Edwards SAPIEN 26 mm transcatheter aortic valve. PVL was modeled by creating three different orifices (with the area of 1 mm², 4 mm² and 20 mm² respectively) at the level of the aortic root. The diastolic velocity waveform applied at the inlet of the model was obtained from in vivo phase contrast magnetic resonance imaging measurements performed in a patient with PVL. The model was used to investigate flow characteristics (velocity and secondary flow) and wall shear stress (WSS) on both aortic and ventricle sides in the presence of PVLs.

Results and Conclusion Three high speed jets were generated through the regurgitant orifices. The velocity of the jets rapidly increased during early diastole to reach a maximum velocity. At the peak of diastolic regurgitant flow, peak velocities were 4.13 m/s for the 20 mm² orifice, 3.18 m/s for the 4 mm² orifice and 2.33 m/s for the 1 mm² orifice. In the aortic side, the asymmetrical flow caused by PVL leads to elevated WSS, up to 3.05 Pa, around the coaptation area of the leaflets. In addition, high localized WSS exist even on the left ventricular side close to the location of the regurgitant orifice of 4 mm². We conclude that paravalvular leak following transcatheter aortic valve replacement leads to significant disruption in blood flow both upstream and downstream of the implanted valve. The abnormal flow is characterized by high speed jets, small and large scale coherent structures and markedly elevated shear stresses on both sides of the implanted aortic leaflets especially on the left ventricular side. Such unfavorable flow configuration may promote a more rapid degeneration of the transcatheter valve leaflets.

SP152 - Special Treatment Techniques: Part 2

TRACK 04: RADIATION ONCOLOGY

SP152.1 - Optimal timing in concomitant chemoradiation therapy of colorectal tumors in nude mouse treated with Cisplatin and Lipoplatin™

Author(s): Thititip Tippyamontri¹, Rami Kotb², Benoit Paquette¹, Leon Sanche¹

¹Nuclear Medicine And Radiobiology, University of Sherbrooke, Sherbrooke/QC/CANADA, ²Systemic Therapy, BC Cancer Agency's Vancouver Island Centre, Victoria/BC/CANADA

Background: Cisplatin is a chemotherapeutic agent, which under certain conditions can become a radiosensitizer. Cisplatin given concurrently with radiation enhance cell death by several mechanisms, including the inhibition of radiation-induced DNA damage repair and the induction of additional DNA damage or modification of radiation induced DNA damage. In recent fundamental investigations on cisplatin-DNA complexes, it was found that DNA damage induced by the low-energy secondary electrons, produced by ionizing radiation, was considerably increased when cisplatin was bound to DNA. This finding implies that the highest concomitant effect should be achieved, when the amount of cisplatin binding to DNA is highest.

Materials and Methods: Using an animal model of colorectal cancer, we determined the platinum window of maximum radiosensitisation and synergism, defined by studying the pharmacokinetics and time-dependent intracellular distribution of cisplatin and Lipoplatin™, the encapsulated form of cisplatin recently proposed to overcome its toxicity. In nude mice, bearing HCT116 human colorectal carcinoma treated with cisplatin or Lipoplatin™, the platinum accumulation in blood, serum, different normal tissues, tumor and different tumor cell compartments was measured by inductively coupled plasma mass spectrometry. Radiation treatment (15 Gy) was given 4, 24, and 48 h after drug administration and was correlated to the amount of platinum-DNA adducts in the cancer cells. The resulting tumor growth delay was reported and correlated to apoptosis analysis.

Results: The optimal treatment and highest apoptosis were observed when radiation was given at 4 h or 48 h after drug injection. These times correspond to the times of maximal platinum binding to tumor DNA. An enhancement factor (ratio of group treated by combined treatment compared to chemotherapy alone) of 13.00 was obtained with Lipoplatin™, and 4.09 for cisplatin when tumor irradiation was performed 48 h after drug administration.

Conclusion: The most efficient combination treatment with radiation and cisplatin or Lipoplatin™ was observed when the amount of cisplatin binding to DNA is highest. These results improve our understanding of the mechanisms of platinum-induced radiosensitization and should have significant impact on the design of more efficient treatment protocols.

SP152.2 - Grid therapy: impact of radiobiological models on calculation of therapeutic ratio

Author(s): Somayeh Gholami¹, Hassan Ali Nedaie², Ali S. Meigooni³, Francesco Longo⁴

¹Department Of Medical Physics And Biomedical Engineering, Tehran University of Medical Sciences, Tehran/IRAN, ²Radiotherapy Oncology Department, Cancer Research Centre, Cancer Institute, Tehran University of Medical Sciences, Tehran/IRAN, ³Comprehensive Cancer Centers of Nevada, Las Vegas/NV/UNITED STATES OF AMERICA, ⁴Department Of Physics, University of Trieste and INFN, Trieste/ITALY

Grid therapy, also known as Spatially fractionated radiation therapy, is a novel technique that has been introduced for treatment of patients with advanced bulky tumors. Several investigators have used linear quadratic radiobiological model to demonstrate the therapeutic advantages of the Grid therapy. Despite the success of the linear quadratic (LQ) model, for evaluation of the limitation of the Grid therapy with such large doses per fraction still there are challenges that need to be met. In this study we have applied both LQ and MLQ radiobiological models to calculate therapeutic ratio (TR) of spatially fractionated radiation therapy. This evaluation is performed using Monte Carlo simulation.

In this study the Geant4 (version 9.6.p02) is used to simulate the photon spectrum of a 6 MV x-ray beam emitted by a Varian2100C linear accelerator, based on vendor detailed information. Percentage depth dose (PDD) and dose profile of 6MV photon beam were obtained at 5cm depth for 10x10 cm² open radiation field size in a water phantom. To verify Monte Carlo simulation calculations, these results were compared with the experimental measured data by a calibrated PTW 31010, 0.125 cc Semiflex chamber. The Grid block with hole-diameter of 1cm and a center-to-center distance of 1.8 cm at the isocenter was also simulated.

Therapeutic ratios of tumors with different histology (Melanoma, Squamous cell carcinoma (SCC), Adenocarcinoma and Sarcoma) have been calculated using both radiobiological models. Survival fraction of tumors at 2 Gy dose (SF2) and tumors cell lines radiobiological parameters were extracted from published data. In addition, various maximum doses are used to evaluate relationship between maximum dose and therapeutic ratio. Table 1 shows results for predicting TR at the different prescribed doses using LQ and MLQ models. The difference between the two models is less than 5% for the TR calculations.

Tumor	SF2	TR (LQ Modell)			TR (MLQ Model)		
		10 Gy	20 Gy	30 Gy	10 Gy	20 Gy	30 Gy
Melanoma	0.485	1.22	1.37	1.55	1.27	1.42	1.56
SCC	0.483	1.21	1.37	1.54	1.28	1.44	1.60
Adeno.Ca	0.43	1.12	1.23	1.36	1.18	1.30	1.40
Sarcoma	0.42	1.10	1.21	1.33	1.15	1.25	1.32

Equivalent uniform dose (EUD) for all prescribed doses for both models has a value between 2.19 Gy and 3.87 Gy.

In this study, we have provided a dosimetric simulation and assessed the therapeutic ratio of four different types of tumor cells based on two LQ and MLQ radiobiological models for different doses. The results indicate that using radiobiological models that are more appropriate for high dose per fraction would not change the theoretical prediction of spatially fractionated radiotherapy. This is because the value of equivalent uniform dose (EUD) in Grid therapy is in the range that LQ model is valid.

SP152.3 - Will CyberKnife M6™ Multileaf collimator offer advantages over IRIS™ collimator in prostate SBRT?

Author(s): Vindu Kathriarachchi¹, Charles Shang², Theodora Leventouri¹, Georgios Kalantzis¹

¹Physics, Florida Atlantic University, BOCA RATON/UNITED STATES OF AMERICA, ²Radiation Oncology, Lynn Cancer Institute, Boca Raton Regional Hospital, BOCA RATON/UNITED STATES OF AMERICA

Purpose: CyberKnife M6™ InCise™ Multileaf collimator (MLC) has become a new modality in practice. Its ability of forming irregularly shaped beamlets offers a potential for more efficient dose optimization and treatment delivery in comparison with that by IRIS™ dodecagon beams. This study is focused on quantification of such time-saving ability in prostate SBRT with comparable dosimetry plans.

Methods: Eight prostate cancer patients were planned in MultiPlan™5.1.2 respectively utilizing IRIS and MLC for 36.25 Gy in 5 fractions. PTV was outlined for treating prostate only. All plans were evaluated by dose conformity index (CI), homogeneity index (HI), new conformity index (nCI) and PTV coverage. In addition, maximum doses at the bladder and rectum, calculated treatment time per fraction and planned MUs were also compared and tested for significance with the Wilcoxon test.

Results: In both IRIS and MLC plan groups, PTV Dmax was scaled to 115% while the HI was maintained at 1.15. The mean V100 was 95.42% for IRIS, and 95.36% for MLC (p=0.48); mean CI: 1.08 vs. 1.05 (p=0.09); and mean nCI: 1.13 vs. 1.11 (p=0.11). Between the groups, the differences of Dmax for the bladder and rectum were found insignificant (p=0.4). Changing from IRIS to MLC, the average treatment time per fraction was reduced by 35% (43.5 ± 2.6 min vs. 28.3 ± 1.6 min, p<0.01) and the planned MU's were decreased by 40% (50318 ± 8976 vs. 30286 ± 2211, p<0.01).

Conclusions: This investigation demonstrated the ability of CyberKnife M6™ to produce prostate SBRT plans equivalent to those using IRIS in terms of target coverage, and dose sparing of critical structures. However, a significant 35% reduction in treatment time and 40% reduction in number of MUs were achieved by replacing IRIS with MLC without dosimetric compromise in planning quality.

SP152.4 - Retrospective analysis of treatment margins for stereotactic ablative lung cancer treatments based on 4D CBCT

Author(s): Sheeba Thengumpallil¹, Jean-François Germond¹, Nicolas Péguret², Jean Bourhis², François Bochud¹, Raphaël Moeckli¹

¹Institute Of Radiation Physics, CHUV, Lausanne/SWITZERLAND, ²Radio-oncology Department, CHUV, Lausanne/SWITZERLAND

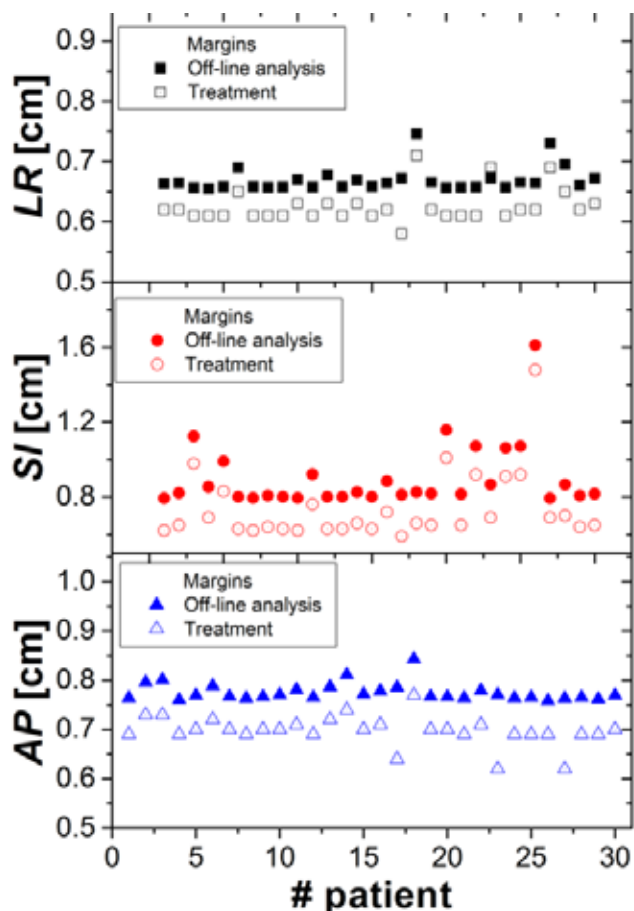
Purpose/Objective: The objective of this study was to evaluate treatment margins defined after the 4D CBCT off-line analysis and compare them with literature.

Materials/Methods: Thirty stereo-ablative T1-T2 N0 M0 lung cancer patients were analyzed (with a total of 229 fractions). All patients were treated in frameless and free breathing conditions. The treatment margins were defined according to van Herk recipe on Mid-Ventilation phase. The treatment margins before 4D CBCT off-line analysis were defined using the systematic and random components taken from literature (Sonke et al. IJROBP 2009). For each patient, we assessed the tumor motion amplitude and the intra-fraction variability from 4D CBCT images realized for tumor positioning (baseline shift), for couch correction verification and for intra-fraction motion (three 4D CBCT were performed for each fraction). From these data, we derived the resulting systematic and random errors for our patient cohort, leading to related margins for each patient.

Results: A summary of systematic and random errors are shown in the Table. When comparing the treatment margins applied to the patients (data from literature) and the margins retrospectively calculated from our patient cohort we observed that the margins applied to the patients should have been slightly larger (~1 mm 3D vector) (see Figure).

Conclusions: Tumor localization accuracy and intra-fraction motion uncertainties were assessed in our patient cohort by analyzing 4D CBCT images performed during each treatment fraction. We found that slightly larger margins should have been applied to our patients. According to the probabilistic approach of the van Herk recipe, a difference in the PTV margins as small as 1mm (3D vector) should not lead to a difference in tumor local control. However, the consequences of these differences should be evaluated in a dosimetric point of view in order to confirm that assumption. This is the object of an ongoing study.

SYSTEMATIC ERRORS				
		LR [cm]	AP [cm]	SI [cm]
Off-line analysis	<i>localisation</i>	0.09	0.15	0.12
Treatment		0.08	0.09	0.08
Off-line analysis	<i>delineation</i>	0.2	0.2	0.2
Treatment		0.2	0.2	0.2
Off-line analysis	<i>intrafx</i>	0.03	0.07	0.12
Treatment		0.12	0.18	0.12
RANDOM ERRORS				
Off-line analysis	<i>localisation</i>	0.20	0.22	0.25
Treatment		0.11	0.14	0.11
Off-line analysis	<i>intrafx</i>	0.14	0.15	0.22
Treatment		0.13	0.18	0.15
Off-line analysis	<i>tumour motion</i>	0.36 x A (LR)	0.36 x A (AP)	0.36 x A (SI)
Treatment		0.36 x A (LR)	0.36 x A (AP)	0.36 x A (SI)



SP152.5 - Using surgical clips in the tracking of liver tumors applied to CyberKnife SBRT treatments

Author(s): Leonie Petitclerc, Karim Boudam, Jean-Francois Carrier
Radiation Oncology, CHUM, Montreal/QC/CANADA

Radiotherapy is still considered as a last resort treatment in liver cancer cases, when the patient’s condition doesn’t allow for more conventional treatment options. However, the same health factors that prevent the use of these methods also affect the risks associated with radiotherapy and further reduce the spectrum of treatment options that are available.

At the CHUM, liver tumors are treated using the CyberKnife system aided by the implantation of gold seeds as markers for tracking. However, some patients’ liver condition doesn’t permit the inser-

tion of those markers. In these cases, we are left with the need for some other way to visualize the movements of the tumor during treatment. Surgical clips, which are already present in the liver of the patient, will then be used as surrogates to monitor the movement of the tumor. These clips have very different physical and radiological properties from gold seed markers and therefore their use needs to be investigated further to assess their relevance as markers and to optimize their use in the clinical context.

We have evaluated the in-treatment images taken at the CyberKnife for previous patient cases and using an anthropomorphic phantom for a more general outlook. It was then measured that, to maximize the contrast between the clips and the surrounding tissue, it is best to use both high kV and mA settings on the imager, as can be seen on figure 1. The capability of the CyberKnife’s algorithm to detect and track the clips was evaluated by comparing the calculated and real positions of the clips in the treatment images. The ensuing error on the position could then be analyzed and compared with the corresponding error in the case of gold seed markers and the recommended margins of error for radiotherapy treatments. This displacement was also assessed experimentally by using a moving phantom with inserted clips. The margin of error and any blurring effects on the expected dosimetric treatment map were measured using dosimetric film.

This research allows us to draw conclusions as to the utility of surgical clips in tracking liver tumors. Using our conclusions as well as those found in literature, we were able to make recommendations for good clinical guidelines for treating liver tumors using surgical clips as radiological markers for tracking.

SP152.6 - A Novel Couch-Gantry Trajectory Based Stereotactic Treatment Method

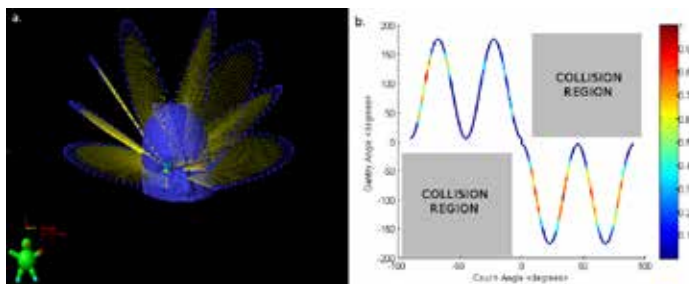
Author(s): Byron Wilson¹, Karl Otto², Ermias Gete¹
¹Medical Physics, BC Cancer Agency, Vancouver/CANADA, ²Physics And Astronomy, University of British Columbia, Vancouver/BC/CANADA

Introduction

We propose an inverse planning solution for trajectory-based stereotactic (SRS) treatments of small lesions in the brain with a c-arm linac. The beam trajectory is formed by simultaneously rotating the linac gantry and the treatment couch, thus enabling a wide selection of beam angles in a time efficient manner. Dose is optimized by dynamically varying the dose rate and the MLC leaf positions along the beam trajectory.

Methods

The trajectory-based inverse planning algorithm we propose is based on the VMAT technique developed by Karl Otto. The pre-defined beam trajectory (Figure1) is formed by rotating the patient couch through 180° while the gantry produces a series of 6 to 8 partial arcs of +/-170° each. This trajectory allows delivery from a wide array of directions while the couch is constrained to move at a slow and constant angular velocity, thus ensuring patient comfort. Dose rate and MLC leaf positions are modulated.



An optimized beam intensity pattern is formed along this trajectory (figure1b), while the MLC aperture changes continuously. The optimization adds controls points using the progressive sampling algorithm and varies each control points' MLC positions and dose rates with stochastic perturbations, keeping only the perturbations that lower the cost function. Since the default trajectory samples the entire phase-space, unwanted portions of the trajectory are removed by dose rate modulation. MLC aperture optimization is used mainly for target conformity. Therefore, our method emphasises beam weight perturbation and we are able to speed up the optimization by adding momentum to beam weight perturbations.

We have tested our method on two cranial cases (acoustic neuroma (plan1) and brain mets (plan2)) that were previously treated with SRS using non-coplanar dynamic conformal arcs. Treatment plans were generated and compared to the original conformal plans. These plans were successfully delivered on the TrueBeam Linac using the Developer Mode.

Results

For plan1, there was a reduction of the mean dose to the organs at risk (OAR): brainstem (17%) and optic tract (51%). For plan2, dose to OARs were comparable to the original plan and were maintained at less than 2% of the prescription dose. Conformity to the PTV improved for both plans. Delivery time for a 15Gy fraction at the isocenter was approximately 6 minutes.

Conclusion

The method proposed will be achievable on current conventional linacs once concurrent couch and gantry motion are enabled. This technique produces high quality, reproducible and efficient treatment plans for SRS patients.

SP153 - Quality Assurance: Part 4

TRACK 04: RADIATION ONCOLOGY

SP153.1 - Comparison of AAA and CCC Algorithms for H&N RapidArc pre-patient treatment QA

Author(s): Thuso M. Ramaloko¹, John K. Bhengu²
¹Medical Physics, Addington Hospital, Durban/SOUTH AFRICA, ²Medical Physics, Inkosi Albert Luthuli Central Hospital, Durban/SOUTH AFRICA

Objectives: Because adherence to quality assurance (QA) is important to patient safety, moving from gamma passing criteria to patient DVH-based QA won't be a bad idea. The aim of the study was to evaluate OAR dose difference for H&N between COMPASS and Eclipse.

Materials and Method: The

Eclipse TPS, COMPASS software, 30 H&N RapidArc patient's plans, 5 Prostate RapidArc patients' plans, Delta-4, MatrixX and Varian trilog Linac were used. All 35 plans were computed with eclipse TPS using 2.5 Arcs, 2.5mm grid size, 1.8-2Gy per fraction for 28-33 fractions and field size ranged from 5cm² to 12cm². The computed dose fluence(s) were measured with MatrixX and Compass software dose reconstruction was carried out using 2.5mm grid size. The maximum dose (D2%) as per ICRU-83 recommendations was used for comparison between Eclipse and Compass. The prostate plans were primarily used for checking field size dosimetric effect between the two systems.

Results and discussion: Table 1 summarizes the head and neck plans comparison between the Eclipse TPS and the COMPASS verification software for different organs.

	Maximum dose difference ($D_{2\%}$)											
	Mean \pm 1 δ (%)											
	PTV	GTV	L Lens	R Lens	O Chiasm	S Chord	Pituitary	B Stem	R O Nerve	LO Nerve	R Parotid	L Parotid
Volume												
Mean	-1.9	-2.0	16.8	11.4	2.3	-3.1	15.2	1.9	4.7	-6.1	-9.1	-6.7
STDEV	0.7	0.3	6.5	6.3	1.3	2.7	8.1	0.9	1.2	5.0	5.6	5.1

Table 1: Summary of H&N plans maximum dose difference between the COMPASS and Eclipse

Table 2 summarizes the Prostate plans comparison between the Eclipse TPS and the COMPASS.

	Maximum dose difference ($D_{2\%}$)					
	Mean \pm 1 δ (%)					
	PTV	GTV	Rectum	Bladder	LF head	R F Head
Volume						
Mean	-1.6	-1.9	-1.3	-1.1	4.1	3.1
STDEV	0.8	0.5	0.9	0.4	2.4	2.6

Table 2: Summary of Prostate plans maximum dose difference between the COMPASS and Eclipse

The Delta-4 gamma index are 97.9 \pm 1.4% and 97.9 \pm 2.2% for H&N and prostate plans respectively, and Compass gamma index are 97.0 \pm 1.1% and 97.2 \pm 2.1% for H&N and prostate plans respectively.

Conclusion: The results were in agreement with Oncologist’s quantec protocol and Physicists total dose gamma index criteria. The small volumes displayed high dose difference and were documented. The baseline values were established.

SP153.2 - Tuning treatment planning system model parameters for accurate VMAT dose calculation using conformal arc plans
Author(s): Orest Ostapiak
 Medical Physics, Juravinski Cancer Centre, Hamilton/CANADA

Machine models parameters within a treatment planning system (TPS) must be carefully tuned in order to accurately calculate dose due to VMAT plans. This is best achieved by comparing the results of calculations with those of measurements for VMAT plans that: deliver reproducibly; yield relatively homogeneous dose distributions; and, are sensitive to model parameters such as those characterizing the MLC. In Pinnacle version 9.2, creating deliverable VMAT plans requires first commissioning a candidate model, then running an optimization to generate a set of VMAT control points. These control points may have irregular shapes which complicate the analysis of discrepancies between calculated and measured dose.

The purpose of this work is to present a method for creating simple VMAT-like plans in a TPS that can be used to test and fine-tune MLC model parameters.

Plans were designed to irradiate a cylindrical phantom containing an ion chamber aligned along its central axis. A single voxel at the central axis in each slice comprised the target region of interest. Four conformal arcs beams spanning successive 45 degree sectors irradiated the target with a margin. Margins were tailored to create MLC slit fields of 1, 5 or 10 mm width. Each arc is created with the isocentre shifted 2 cm toward the mid-arc incident direction in order to force the MLC slit to sweep across the field. Control points were defined every 2 degrees of gantry arc. The isocentre for each arc was then centered on the ion chamber using the same control points. Each arc delivers a narrow slit field that sweeps across the ion chamber as the gantry rotates. Since

each arc is opposed, the dose varies by less than \pm 1.5% within 1 cm of the ion chamber cavity centre.

Doses measured using each of two chambers (A16 and PR06) agreed to within about 1% for all slit widths delivered by a single machine. Dose variation between two machines was 1, 2 and 5% corresponding to slit widths of 10, 5 and 1 mm respectively. Our clinical Eclipse model computes doses that are between 4 and 24% low compared to measurement. Adjusting the dynamic leaf gap from 0.08 mm to 1.6 mm brings computed doses within 3% of those measured. In Pinnacle, setting the MLC leaf tip radius to 12 cm and using the machine’s leaf offset table yields computed doses that are between 2.5 and 13.8% low compared to measurement. Increasing the leaf tip radius to 1000cm and setting all leaf offsets to -0.08 mm (to match the Eclipse dynamic leaf gap) yields calculated results that are within 1.2% of the measured values.

Plans that mimic VMAT delivery may be created within a TPS using standard forward planning techniques. While not clinically relevant, these plans are useful for model tuning since the calculated dose is sensitive to small adjustments in MLC model parameters but robust with respect to delivery and measurement.

SP153.3 - Prostate brachytherapy with Oncentra Seeds: Intra-operative planning and delivery software validation assisted by an FMEA

Author(s): Renee X. Larouche, Yannick Hervieux, Dominic Béliveau-Nadeau, Jean-Francois Carrier, Daniel Taussky, Guila Delouya
Radio-oncologie, CHUM - Hôpital Notre-Dame, Montreal/CANADA

Introduction: For the past 9 years, our center has been treating patients with prostate cancer with permanent seed implant prostate brachytherapy. This has been done using a Nucletron intra-operative planning and delivery system (FIRST™). We have now changed to a new Elekta Brachytherapy software (Oncentra® Seeds 4.2 (OCSe)). The goal of this study was to validate the new software for clinical use. Published guidelines from the AAPM and CPQR as well as a Failure Mode and Effect Analysis (FMEA) were used to review software and process.

Methods: We reviewed and implemented applicable guidelines from TG-43, TG-53, TG-56, TG-59, TG-64, TG-128 and TG-137. We also followed CPQR standard for Low Dose Rate Permanent Seed Brachytherapy. In total, over 60 tests were done to validate the new software. A FMEA was also performed.

Results: Using the tests, we identified weaknesses in the software:

- Discrepancy between software indication of ultrasound (US) imaging plane and the actual US imaging plane due to latency of the US image stream;
- Contour displacement when switching between modes;
- Line source dosimetry at 0 and 5° does not meet accuracy criteria;
- Poor robustness to system crashes. Over 10 min required to reboot system;
- The system does not force acknowledgement of error messages;

Some of these weaknesses were due to connectivity issues with third party equipment (US scanner). Following communication with the vendor, some issues were addressed through workarounds. The FMEA (see Table 1) lead to discussions with the vendor regarding workflow. In order to make our institution's process more robust and less vulnerable to failures, planning system settings were customized to our needs.

Table 1 : Top 5 Failure modes identified during the FMEA

Step	Failure modes	S	F	D	C I
4	Accidental needle update	5	5	2	50
4	Error in needle position due to frozen US image	4	5	2	40
4	Mismatch between re-constructed needle and software needle "cartoon" used for positioning	4	2	4	32
2	Wrong US scanning parameters	5	2	2	20
3	Plan transfer not possible due to empty needles	4	5	1	20

Over twenty-five patients have now been treated using OCSe. Issues not identified during the pre-clinical testing were encountered, most notably surrounding corrections for prostate motion. Our process was reviewed and adapted taking into account these issues.

Our learning curve has been very quick. Time required to complete an implant is now comparable to that achieved through years of optimizing our process with the previous Nucletron system.

Conclusion: Based on data gathered so far, our results show that the extensive testing done before clinical implementation was valuable. These tests served to identify problems in the software and improve our process. Proper software validation in the context of the whole clinical process is very important and strongly recommended in assuring quality treatments.

SP153.4 - Investigation of predictive parameters for pre-treatment measurement pass rates in hypo-fractionated volumetric arc therapy (HF-VMAT) plans of single brain metastasis

Author(s): Young K. Lee¹, Matt Wronski², Anthony Kim², Mark Ruschlin²

¹Department Of Radiation Oncology, University of Toronto, Toronto/ON/CANADA, ²Department Of Medical Physics, Sunnybrook Health Sciences Centre, Odette Cancer Centre, Toronto/CANADA

Purpose: HF-VMAT planning for brain metastases can be complicated, as these cases often involve small treatment volumes (planning target volumes (PTV)<25cm³) in close proximity to critical organs-at-risk (OAR). Pre-treatment dosimetric verification for such cases often yields sub-optimal pass rates. The purpose of the present study was to investigate the combined effects of OAR-to-PTV distance, as well as the differential between OAR tolerance dose and PTV prescription dose, in predicting what measurement pass rate is achievable.

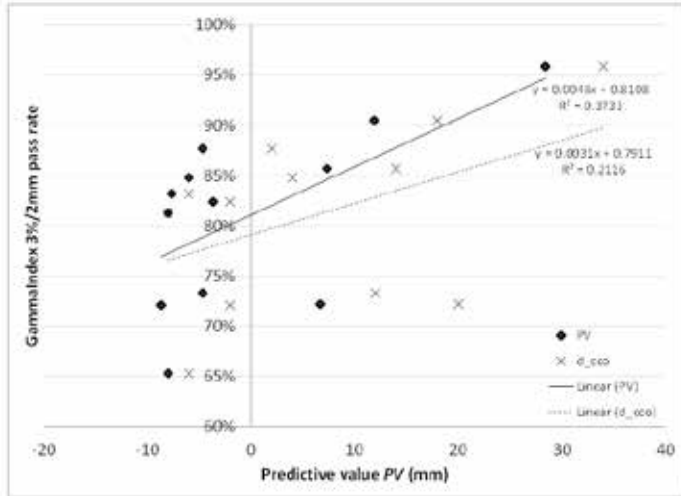
Methods: Twelve single lesion brain HF-VMAT cases were planned using Pinnacle v9.2 with 6MV Elekta Agility (Crawley, UK). The prescription doses ranged from 25 to 35 Gy in 5 fractions. All plans were recalculated and measured using an ArcCHECK diode phantom (SunNuclear Corporation, Melbourne, USA) employing Gamma analysis with criterion set at dose agreement of 3% and distance agreement at 2 mm. The predictive value, *PV*, investigated in the present study was as follows:

$$PV = dcco - (\delta D/G)$$

delta_D is the difference in dose between the prescription dose and dose-limiting OAR dose in Gy, *G* is the nominal dose gradient (150 and 400 cGy/mm for in-plane and out-of-plane of PTV, respectively), and *dcco* is the distance calculated using overlap-volume-histogram to the closest critical OAR in mm, where negative *dcco* indicates overlap between the expanded PTV and OAR. Smaller or increasingly negative values of *PV* were expected to predict increasingly modulated plans and hence lower measurement pass rates.

Results: Median (range) of PTV was 11.5 (4.1 - 24.7) cm³. The closest critical OAR observed in 8/12 cases was brainstem and for 10/12 cases the OAR was in the same plane as the PTV. Figure 1 shows the *dcco* and *PV* plotted against the ArcCHECK measurement pass rates. *PV*<10 mm show pass rates of <90% for Gamma analysis with the criterion set at 3%/2mm. A stronger correlation was observed between *PV* and pass rates than *dcco* and pass rates.

Figure 1. $d_{50\%}$ and predictive value (PV) calculated and plotted against measurement Gamma Index pass rate of 3%/2mm.



Discussion: We show a relationship between PV and pre-treatment verification pass rate. Though the PV was calculated using a small dataset, it can be used to predict if a complicated VMAT plan may be required at the planning stage. This may allow the planner to decide if another planning methodology can be used to avoid pre-treatment verification failures that can cause problems in the planning process.

SP153.5 - Inter-centre comparison of dose delivery accuracy for six different linac-planning system combinations for SBRT lung cancer treatment using FFF beams.

Author(s): David Thwaites¹, Sam Blake¹, Prabhjot Juneja¹, Jonathan Sykes¹, Michael Bailey², Jeff Barber³, Regina Bromley⁴, Gwi Cho⁵, Shrikant Deshpande⁶, Sandra Fisher⁷, Joerg Lehmann¹, Carsten Brink⁸, Christian Hansen⁹

¹Institute Of Medical Physics, School Of Physics, University of Sydney, Sydney/AUSTRALIA, ²Radiation Oncology, Illawarra Cancer Care Centre, Wollongong/AUSTRALIA, ³Radiation Oncology, Nepean Cancer Care Centre, Penrith/AUSTRALIA, ⁴Radiation Oncology, Northern Sydney Cancer Centre, Sydney/AUSTRALIA, ⁵Radiation Oncology, Chris O'Brien Lifehouse at RPAH, Sydney/AUSTRALIA, ⁶Radiation Oncology, Liverpool Hospital, Liverpool/AUSTRALIA, ⁷Radiation Oncology, Prince of Wales Hospital, Sydney/AUSTRALIA, ⁸Institute Of Clinical Research, University of Southern Denmark, Odense/DENMARK, ⁹Laboratory Of Radiation Physics, Odense University Hospital, Odense/DENMARK

Purpose: Flattening filter free (FFF) beams are being rapidly adopted for stereotactic body radiotherapy (SBRT). Compared to conventional flattened beams (FF), they have higher dose rates, lower lateral beam hardening changes, lower leakage and lower out-of-field doses. Together these provide the potential to improve treatment plans. Elekta and Varian have implemented FFF beams using different energy definitions and have different MLC designs; both of which might influence the achievable plan quality. In addition the MLC segmentation, IMRT optimisation and dose calculation engines employed in the various treatment planning systems (TPSs) may influence performance. This multi-centre, multi-system study compared plans and delivery accuracy of FFF lung SBRT treatments across six different linac/TPS combinations.

Materials and Methods: Ten lung patient cases were provided to seven different radiotherapy centres for SBRT planning with FF and FFF beams. Linac/TPS combinations included are: Varian-Eclipse, Varian-Pinnacle, Novalis/Varian-Eclipse, Elekta-Pinnacle, Elekta-Monaco and Tomotherapy-Tomoplan. The planning protocol

was common for all. Prescribed minimum doses were 48Gy/4fr for tumours located <1.5cm from the thorax wall, 50Gy/5fr for those within 2cm of the main bronchial tree and 54Gy/3fr elsewhere in the lung. 180°-200° VMAT arcs were used for all standard linac plans, avoiding the contra lateral lung. Relevant DVH metrics were tested for significant differences, using a paired two-sided Wilcoxon-signed rank test and 5% significance. Plans were delivered to a Sun Nuclear ArcCheck phantom, where planned and measured doses were compared using a 3%/3 mm gamma analysis with a 10% threshold, and global normalisation. Beam on times were recorded.

Results: In the preliminary analysis, high quality dose plans and good delivery accuracy were observed for all the linac-TPS combinations across these ten plans. Mean gamma pass rates of 98.1% (FF) and 97.4% (FFF) were observed (Table 1). For Elekta-Pinnacle, FFF plans have lower pass rates than FF plans, but the relative calibration of the ArcCheck phantom (performed in low dose rates) may be a factor in this and is being investigated. FFF plan MU are higher in Varian/Novalis-Eclipse, but not for Elekta -Pinnacle. Eclipse generally used more MU than Pinnacle. Beam-on times are significantly reduced, with largest gains observed for Elekta-Pinnacle.

Conclusions: FFF beams produce acceptable plan quality and high dose delivery accuracy for SBRT lung treatments, across a range of linac-TPS combinations and representative tumour positions. Each combination has specific issues, which indicate further investigation possibilities. The TomoTherapy-Hi Art combination data is still to be fully evaluated.

TABLE 1	FF	FFF			
All	mean	SD	mean	SD	p
Beam on [sec]	303	77	131	59	<0.001
MU	2912	732	3022	763	0.009
Pass rate [3%,3mm]	98.0	2.1	97.4	1.7	0.007
Elekta-Pinnacle					
Beam on [sec]	312	72	109	25	<0.001
MU	2783	653	2796	598	0.60
Pass rate [3%,3mm]	98.9	1.9	97.7	1.6	0.001
Varian/Novalis-Eclipse					
Beam on [sec]	306	79	175	59	<0.001
MU	3040	799	3249	855	0.005
Pass rate [3%,3mm]	97.6	1.8	97.3	2.0	0.27

SP153.6 - A pilot study investigating the impact of treatment delivery uncertainties for lung SABR using step and shoot IMRT and VMAT

Author(s): Samuel J. Blake¹, Sankar Arumugam², Lois Holloway², Shalini Vinod³, Cesar Ochoa³, Penny Phan³, David Thwaites¹

¹Institute Of Medical Physics, School Of Physics, The University of Sydney, Sydney/NSW/AUSTRALIA, ²Department Of Radiation Oncology, Liverpool & Macarthur Cancer Therapy Centres and the Ingham Institute, Liverpool/NSW/AUSTRALIA, ³Department Of Radiation Oncology, Liverpool & Macarthur Cancer Therapy Centres, Liverpool/NSW/AUSTRALIA

Purpose

Advanced RT techniques require conservative approaches to planning, e.g. safety margins added to target volumes and the level of

QA performed. This is partly due to a lack of detailed knowledge about the uncertainties involved in treatment delivery. The optimization and application of advanced techniques would benefit from a better understanding of such uncertainties and their impact on treatment effectiveness. This study investigates how delivery uncertainties affect target coverage for step-and-shoot IMRT (sslMRT) and VMAT in SABR patient treatment plans.

Methods

6 MV sslMRT and VMAT reference plans for three lung SABR patient datasets were created using the Pinnacle³ TPS (version 9.8) for an Elekta Synergy linac. Copies of these plans were modified using in-house code to generate a series of systematic 'error-introduced' plans, where the values of three beam delivery parameters were altered across all control points for each plan (gantry angle, collimator angle and MLC leaf positions). Gantry and collimator angles were changed from their reference values by +/- 1 or 2 degrees; MLC leaf positions by shifting each leaf from its reference position by +/- 1 or 2 mm. Error-introduced plans were read back into Pinnacle and dose calculations were performed on the reference patient anatomy. Target DVH metrics, including the volumes of PTV receiving 95% and 100% of the prescribed dose (VPTV95 and VPTV100, respectively) and the 50%, 100% and 105% isodose volumes (V50, V100 and V105, respectively) were extracted from each plan. The conformity index, high dose (105%) and low dose (50%) spillage were also quantified. Percentage differences between values for the error-introduced plans and their respective reference plan were calculated to quantify the impact of varying each delivery parameter. Results were compared between the sslMRT and VMAT plans to consider dependencies on delivery technique.

Results

For all DVH metrics considered, increasing the magnitude of the introduced error generally resulted in larger percent deviations from reference plan results. The VPTV95 and VPTV100 consistently decreased with increasing magnitude of MLC leaf shift. A maximum decrease in VPTV100 of approximately 5% was observed for MLC shifts of 2 mm in both the sslMRT and VMAT plans. Collimator and gantry angle variations typically resulted in VPTV95 and VPTV100 deviations of <1%. Of the DVH metrics investigated, high dose spillage was the most sensitive to introduced errors for both treatment techniques. When collectively considering all beam delivery parameters investigated in this study, high dose spillage increased on average by between 12 and 27% for the sslMRT and VMAT plans, respectively.

Conclusion

The impact of treatment delivery uncertainties on sslMRT and VMAT patient dose distributions was investigated with an initial pilot cohort of lung SABR plans. Target coverage was typically compromised more by changes in MLC leaf positions than gantry or collimator angle. Of the DVH metrics and delivery parameters considered, high dose spillage was the most sensitive to treatment delivery uncertainties. The study is being extended to a wider set of plans with the aim of quantifying site- and technique-specific treatment delivery uncertainties in advanced RT techniques.

SP153.7 - Adaptive patient dose assessment using daily 3D cone beam CTs and Monte Carlo simulations

Author(s): Nevin Mcvicar¹, Parmveer Atwal¹, Julio Lobo², I Antoniu Popescu³

¹Medical Physics, BC Cancer Agency - Vancouver Cancer Centre, Vancouver/CANADA, ²Electrical And Computer Engineering, The University of British Columbia, Vancouver/CANADA, ³Physics And Astronomy, The University of British Columbia, Vancouver/CANADA

Introduction: Modern radiation therapy (RT) techniques, including IMRT and VMAT, provide very conformal dose distributions enabling high doses to be delivered to tumors. These complex delivery schemes require sophisticated quality assurance (QA) procedures to confirm accurate plan delivery. This study presents a novel workflow to assess daily dose distributions using patient position information from pre-treatment on-board imaging (OBI) cone beam computed tomography (CBCT) and Monte Carlo (MC) based dose predictions.

Methods: A clinical dataset from a patient with prostate cancer who received RT at our clinic was used. This patient was prescribed 7800 cGy/39 fx to be delivered using VMAT. A planning CT (PlanCT) was acquired 15 days prior to treatment. Critical structures and target volumes were contoured onto PlanCT and a VMAT plan was developed. A kV CBCT was acquired before each fraction. All image and contour registrations were performed automatically with the MIM software suite (MIM Software Inc, OH). The PlanCT was registered to daily CBCTs, using a deformable image registration (DIR), generating new data sets (planCTDEFORMED). Upper and lower regions of planCT were added to planCTDEFORMED to create planCTFINAL (**Figure 1**) to minimize truncation effects caused by the smaller CBCT volume. Dose distributions on PlanCT and PlanCTFINAL were calculated using the MC codes BEAMnrc/DOSXYZnrc.

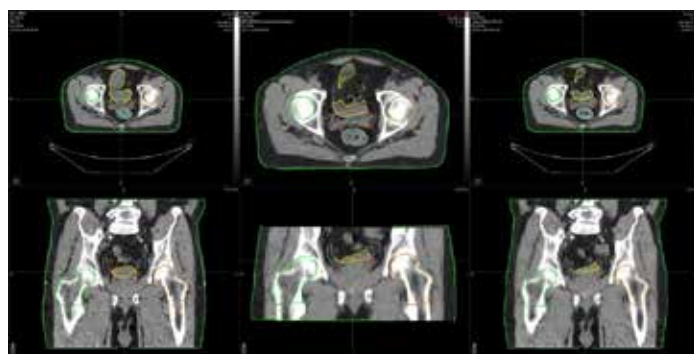


Figure 1. Axial (*top*) and sagittal (*bottom*) views of the PlanCT (*left*) and PlanCT_{DEFORMED} (*center*). The composite image of PlanCT and PlanCT_{DEFORMED} produced PlanCT_{FINAL} (*right*).

Results: Dose volume parameters for the planning target volume (PTV), bladder, rectum, pelvis and both femoral heads are compared in **Table 1**.

Table 1. Differences in dose volume parameter calculated with MC using PlanCT and PlanCT for one daily treatment

Plan	Structures	Dmean (%)	Dmax (%)	V95% (%)
	PTV	98.9	103.7	97.7
	Bladder	53.6	102.0	11.6
PlanCT	Rectum	49.8	101.8	8.3
	L Fem Head	19.6	42.1	1.0
	R Fem Head	16.6	46.3	0.5
	PTV	95.3	103.5	65.5
PlanCTFinal	Bladder	48.1	96.1	1.5
(one fraction)	Rectum	58.3	103.5	22.8
	L Fem Head	20.3	45.8	2.7
	R Fem Head	14.9	39.3	0.0

Discussion: Significant differences in dose volume parameters are calculated when using daily CBCTs. Note the large difference in V95% due to inter-fraction prostate movement. Preliminary results highlight the need for more sophisticated QA procedures, including adaptive dose accumulation over the entire course of treatment. This technique is intended to complement daily *in vivo* dosimetry using EPID-based techniques.

SP154 - Developments in Radiation Protection

TRACK 05: DOSIMETRY AND RADIATION PROTECTION

SP154.1 - Out-of-field radiation dose to critical organs due to radiotherapy for testicular seminoma with modified dog-leg fields: is there a risk for stochastic effects?

Author(s): Michalis Mazonakis¹, Theocharris Berris¹, Efrossyni Lyrarakis², John Damilakis¹

¹Department Of Medical Physics, University of Crete, Heraklion/GREECE, ²Department Of Radiotherapy, University Hospital of Heraklion, Heraklion/GREECE

Purpose: Modern radiotherapy of stage II seminoma involves the use of modified dog-leg fields with reduced dimensions compared to conventional portals. The objectives of this study were to (a) calculate the out-of-field dose to critical organs from irradiation with modified dog-leg fields using a Monte Carlo approach and (b) estimate the associated risk for stochastic effects.

Methods: The Monte Carlo N-particle transport code was used to simulate the head of a linear accelerator generating 6 MV X-rays. The model was validated against in-field dose measurements performed on a water tank and out-of-field thermoluminescent measurements generated on a humanoid phantom. A mathematical phantom representing a typical adult patient was implemented into the Monte Carlo environment. Radiotherapy was simulated with a pair of anteroposterior and posteroanterior modified dog-leg fields covering the para-aortic and ipsilateral iliac lymph nodes. Radiation dose calculations were made for all critical organs that defined by the ICRP publication 103 and located outside the simulated treatment fields. The calculated organ doses were combined with the appropriate risk factors to estimate the probability for developing secondary malignancies and heritable effects.

Results: The measured and calculated in-field radiation doses were in an excellent agreement with a difference of less than 2 %. A small mean difference of 9.6 ± 5.3 % was also found between out-of-field Monte Carlo dose calculations and experimental measurements. Simulated radiotherapy with modified dog-leg fields delivering 30 Gy to the tumor site resulted in an out-of-field organ dose range of 31.4-830.1 mGy. For a testicular cancer patient subjected to radiotherapy at the age of 30 years, the radiation doses received by non-targeted organs may increase the lifetime risk for second cancer development up to 2.2 %. The risk for heritable effects in future generations was estimated to be 0.2 %.

Conclusions: Radiotherapy with modified dog-leg fields may result in a relatively increased risk for second cancer induction. The probability for developing hereditary disorders is low compared to the natural incidence of these effects.

SP154.2 - Peripheral photon dose in organs

Author(s): Beatriz Sanchez Nieto¹, Rodrigo El Far², Leticia Irazola³, José A. Terrón⁴, Francisco Sanchez-Doblado³

¹Instituto De Física, Pontificia Universidad Católica de Chile, Santiago/CHILE, ²Centro De Cáncer, Pontificia Universidad Católica de Chile, Santiago/CHILE, ³Fisiología Médica Y Biofísica, Facultad Medicina, University of Seville, Sevilla/SPAIN, ⁴Servicio De Radiofísica, Hospital Universitario Virgen Macarena, SEVILLA/SPAIN

There are an increasing number of RT patients who survive for periods comparable/larger than the latent period of a second cancer.

Additionally, new techniques provide a better dose conformation at the cost of higher doses in organs outside the treatment field. That makes mandatory to compare the benefits (TCP) and the risks (NTCP and second cancer risks SCR) of the patient exposure. And yet, in spite of the treatment planning systems (TPS) providing accurate calculations of the dose delivered to the target, organs placed at a distance are not considered. Consequently, TPS only generate information regarding tumour control and radiation toxicity of neighbouring organs. The lack of algorithms to estimate equivalent dose to peripheral organs, together with uncertainties on risk factors, make the estimation of SCR not trivial.

Equivalent dose in organs can be calculated as the sum of equivalent doses for each radiation quality. We proposed a methodology to estimate equivalent neutron dose in organs for RT treatments ($E > 10\text{MV}$) [1, 2] and developed an algorithm to calculate photon doses (to be submitted) for conformal radiotherapy -3DCRT- and IMRT [3].

The aim was to propound a methodology to calculate the mean absorbed photon dose in peripheral organs for individuals from a point-based algorithm requiring steadily available patient parameters.

Organs' lengths for individuals are calculated by using a scale factor (patient's/Cristy phantom's lengths). It is assumed that the mean organ photon dose is the integral of doses along the organ as follows:

$$Dose_{organ,y} = \frac{1}{L_{organ}} \int_{x_{organ}}^{x_{organ}+L_{organ}} Dose(\epsilon, f, z, x') dx'$$

L is the organ length and X the distance from the most cranial point to isocenter. Our model [3] established an expression for point dose calculation as the sum of the transmission and leakage (constant) and a second exponential term depending on the distance to a virtual scattering source (calculated from the isocenter depth $-z$ and x'). The fitting parameters, obtained for 3DCRT treatments, were modified to account for other treatment efficiencies (ϵ = prescription dose/ MU) and field sizes, both relatives to 3DCRT. This algorithm was built into Matlab through a Graphical User Interface and was validated [4] and used for calculations on how moving from 3DCRT to IMRT may result in an increase in peripheral organ doses [5].

From equivalent dose in organs, SCR estimations can be made for comparison to epidemiological data on induced RT cancer rates.

[1] Phys.Med.Biol. 57, 2012

[2] Med.Phys. 42, 2015

[3] Med.Phys. 41(6), 2014

[4] ESTRO, 2015

[5] EFOMP, 2014

SP154.3 - Gamma Radiation Dose-Response Relationship of Human Thyroid Follicular Cells

Author(s): Shyamal R. Chakraborty¹, Arun K. Deb¹, Md. M. Uddin², Md. M. Rahman³

¹Department Of Physics, University of Chittagong, Chittagong/ BANGLADESH, ²Department Of Radiotherapy, Chittagong Medical College and Hospital, Chittagong/ BANGLADESH, ³Department Of Radiotherapy, Sylhet M A G Osmani Medical College Hospital, Sylhet/ BANGLADESH

Introduction: Thyroid gland is sensitive to gamma irradiation. Thyroid follicular cells produce the hormones T3 (triiodothyronine) and T4 (tetraiodothyronine or thyroxine) which play vital role in our lives. During radiotherapy (Co-60 teletherapy) in head-neck region, patients' thyroid gland is exposed to high level gamma irradiation. The exact dose on thyroid depends upon the tumor site, stage and overall total radiotherapy dose.

Aim of the work: In this research, an attempt had been made to find the relationship between gamma radiation dose to thyroid gland and the consequent response of its follicular cells.

Methodology: A total of one hundred and eighty head-neck cancerous patients of Chittagong Medical College hospital and Sylhet MAG Osmani Medical College Hospital who had to be treated with radiotherapy (⁶⁰Co) were selected in the present research. The patients' hormones T3, T4 and TSH (Thyroid Stimulating Hormone or thyrotropin) had been measured six times for each patient. The measurement times of which were before the beginning of their radiotherapy course, immediately after the radiotherapy, six weeks after the radiotherapy, twelve weeks after the radiotherapy, six months after the radiotherapy and finally twelve months after the radiotherapy for individual patients.

Results and Discussion: Thyroid follicular cells' response had been estimated by the percent of decrease in secretion of hormones T3 and T4 in spite of increased secretion of TSH by the pituitary gland. Graphs had been plotted by keeping the dose to thyroid (from 0 to 66 Gy) of patients (due to head-neck cancer) as abscissa and the percent of reduction of T3 and T4 hormones after one year of completion of radiotherapy as ordinate. For T3 hormone, the most fitted graph had been found to be an exponential one satisfying the equation, $y = y_0 + Ae^{-x/b}$ where, y_0 , A and b are constants. The analyses had been done by the software OriginPro 7.5. For the T4 hormone, similar graph and equation had been found with slightly different parameters. For TSH, the corresponding relation had been found to be somewhat linear. No significant response had been observed unto twelve weeks after the completion of radiotherapy. At six months after the completion of radiotherapy, significant change in hormone levels had been observed. However at one year after the completion of radiotherapy course, drastic change in hormone levels had been observed. The more the level of exposure to thyroid, the more reduction in hormone T3 and T4 levels had been observed. For the exposure level of 66 Gy, graphs had also been plotted to find the role of time in the manifestation of radiation-response (reduction in the levels of T3 and T4) of thyroid follicular cells. Linear relations had been observed for T3 and T4 and for that 365 days time period.

SP154.5 - Aligning the ALARA principle with FFF treatment modalities

Author(s): Stephen Sawchuk, Craig Lewis
Physics And Engineering, London Regional Cancer Program/ Western University, London/ ON/ CANADA

The recent popularity of flattening filter free (FFF) treatment beams featuring high dose rates has created some new radiation safety considerations. The softer FFF beams are less penetrating than their counterpart flattened beams (FF) of the same nominal energies. Thus in replacing FF treatment units the existing shielding is usually

adequate.¹ However, higher dose rates available for FFF beams can present radiation safety issues depending on workload, existing shielding, and occupancy factors. We report such a case for our first Varian TrueBeam linac. Ultimately, the ALARA principle is used to justify the modification of shielding to reduce the instantaneous dose rate (IDR)² beyond one primary barrier.

A Varian TrueBeam featuring four energy modes of 6-MV and 10-MV with FF and FFF was to replace its decommissioned predecessor, a Varian 21EX 6MV and 10 MV accelerator. The shielding design and previous radiation survey for the existing treatment bunker was analyzed to assess radiation safety for the new unit, focusing on beam quality, elevated dose rates, and an increased workload. This led to modifications of one existing primary barrier to reduce the IDR. The calculated IDR beyond this barrier for the FFF quality beam at the highest dose rate was 41 mSv / h, above the threshold for a controlled area at 25 mSv / h.¹⁻³ Thus extra shielding was required because of the increase in the dose rate from 6 Gy / minute to 24 Gy / minute at 100-cm SAD, not because of beam quality for the 10MV FFF beam.

A lead wall approximately 1 TVL thick covering this projected field plus margin was constructed at the primary barrier. Radiation survey results using an ion chamber survey meter yielded 28 mSv / h and 7.7 mSv / h for the unmodified and modified barriers respectively. Corresponding calculations were 41 mSv / h and 5.7 mSv / h.

The room beyond the modified primary barrier is an adjacent treatment bunker and thus already a controlled area with the appropriate posting of radiation warning signage. Because the IDR without barrier modification was high, it was reasonable to reduce the exposure for that room by adding the shielding. Thus we used the ALARA principle to further protect our staff.

We have modified a primary barrier for a treatment unit with a FFF beam with high dose rate capabilities. The ALARA principle was used to justify reducing the exposure to further protect staff. The increased exposure was due to the increase in maximum dose rate even though the FFF beams are softer and less penetrating. Hypothetically, situations can arise from a combination of workload, occupancy factors, and existing shielding that not only could cause increases in IDRs, but also the annual equivalent doses. Thus care should be taken in shielding design to deal with the high dose rates.

References:

Phys. Med. Biol. **54** (2009) 1265–1273. S F Kry *et al.*

NCRP REPORT No. 151.(2005)

<http://laws-lois.justice.gc.ca/eng/regulations/SOR-2000-203/page-7.html#docCont>

SP155 - Characterization of Detector Systems for Therapy Dosimetry: Part 3

TRACK 05: DOSIMETRY AND RADIATION PROTECTION

SP155.1 - Ferrous - methylthymol blue - gelatin gel dosimeter with improved auto-oxidation stability

Author(s): Kalin I. Penev, Kibret Mequanint

Chemical And Biochemical Engineering, University of Western Ontario, London/CANADA

The ferrous sulfate – methylthymol blue – gelatin (FMG) dosimeter is a recently-developed modification of conventional ferrous xylenol orange – gelatin (FXG) dosimeter that allows optical scanning with red light (615 – 635 nm), as opposed to amber light (580 – 590 nm). Scanning at the higher wavelength is beneficial as: optical scatter in the gelatin matrix decreases, and these wavelengths can be used for other optical dosimeters, allowing for simpler scanner design. It has previously been shown that the dose sensitivity and diffusion for both FMG and FXG are similar due to equivalency of the signal generation processes. Radiation-induced oxidation of ferrous iron (Fe^{2+}) in the acidified gel produces ferric iron (Fe^{3+}) in proportion to the delivered dose; and an intensely-coloured complex is formed between Fe^{3+} and either xylenol orange (XO) or methylthymol blue (MTB). Unfortunately both gels are prone to autoxidation. We propose decreasing the auto-oxidation in FMG gels by adding phenanthroline-type ligands.

In preliminary experiments 5-nitro-1,10-phenanthroline (Nn) and bathophenanthroline disulfonic acid (BD) were tested as stabilizing agents for Fe^{2+} with MTB in sulfuric acid (SA) solutions at 25 to 40 mM SA. Heating at 72 °C for one hour was used in lieu of a longitudinal study of autoxidation. Relative to Nn, the addition of BD led to higher optical density and, unexpectedly, lower autoxidation protection. Therefore, Nn was selected for the follow-up in-gel tests. The gels were prepared with 5% (w/v) gelatin, 25 or 35 mM SA, 0.1 mM Fe^{2+} , 0.1 mM MTB or XO and 0 or 0.3 mM Nn. Table 1 presents a subset of the results, given as the optical density (OD) at the respective wavelength of maximum absorbance (λ_{max}) for each composition. Generally, FMG gels exhibited slightly higher autoxidation than the corresponding FXG gels, and the dose response ($\Delta(\text{OD})/\text{Gy}$) dropped with addition of Nn. At least one gel composition (in bold) had a very stable, low background optical density and adequate dose response. Unfortunately the diffusion coefficient was relatively high but addition of glyoxal (5 mM) decreased the diffusion by 10% without significantly affecting the sensitivity and stability (results not shown). In our opinion this FMG composition provides a viable alternative to FXG gels dosimetry.

Table 1. Properties of select set of gels

[SA], mM	Dye	λ_{max} , nm	Nn	Bckg. OD (day1)	Bckg. OD (day21)	$\Delta(OD)/Gy$ (day1)	$\Delta(OD)/Gy$ (day21)	Diff. coeff., mm ² /h
25	MTB	585	-	0.062	0.545	0.067	0.074	0.43
25	MTB	585	+	0.072	0.126	0.0080	0.0067	1.05
35	MTB	585	-	0.051	0.220	0.073	0.076	0.52
35	MTB	585	+	0.068	0.167	0.026	0.027	0.70
35	XO	620	-	0.047	0.302	0.067	n.d.	0.56
35	XO	620	+	0.105	0.179	0.027	n.d.	0.60

SP155.2 - The dosimetric property of TLD2000 thermoluminescent dosimeter

Author(s): Nan Zhao, Ruijie Yang, Junjie Wang
Radiation Oncology, Peking University Third Hospital, Beijing/CHINA

Purpose: To study the dosimetric properties of TLD2000 thermoluminescent dosimeter (TLD), including repeatability, linearity of dose response, energy response and dose rate effect.

Materials and Methods: 1300 TLD2000 TLDs were read out after exposure to a dose of 1 mGy of 65 keV x-ray, then were sorted out to have the same sensitivity within $\pm 3.0\%$. TLDs were irradiated to a dose of 120 MU using 6 MV x-ray then irradiated to the same dose after 24 h. TLDs were irradiated by two ¹²⁵I seeds with the same activity for 24 h, and the interval time was 24 h, to study the repeatability of TLDs for 6 MV x-ray and ¹²⁵I seed. TLDs were irradiated to different doses using ¹³⁷Cs (662 keV γ -ray), ¹²⁵I seed and 6 MV x-ray, to study the dose response of the TLDs. TLDs were irradiated to a dose of 1 mGy using ¹³⁷Cs, 48 keV, 65 keV, 83 keV, 118 keV and 250 keV x-rays, to study the energy response of the TLDs. TLDs were irradiated to a dose of 120 MU using 6 MV x-ray with different dose rates of 37 MU/min, 75 MU/min, 150 MU/min, 300 MU/min and 600 MU/min; TLDs were irradiated to the same dose using three ¹²⁵I seeds with different activities of 0.739 mCi, 0.675 mCi and 0.559 mCi, and the irradiated time were 24 h, 26h 17 min and 31 h 48 min, respectively, to study the dose rate effect of TLDs for 6 MV x-ray and ¹²⁵I seed.

Results: 350 TLD2000 TLDs were selected with the sensitivity within $\pm 3.0\%$. The maximum deviations of the repeatability were 2.7% and 4.0% for 6 MV x-ray and ¹²⁵I seed, respectively. The dose response of TLDs for ¹³⁷Cs and ¹²⁵I seed were linear. For 6 MV x-ray, the linear response range were 0.74 Gy-10.0 Gy, beyond 10.0 Gy the dose response became supralinear but proportional to the absorbed dose to TLD. The energy response for 48 keV, 65 keV, 83 keV, 118 keV and 250 keV x-rays, relative to the energy response of ¹³⁷Cs, were 1.25, 1.08, 0.99, 0.91 and 0.96, respectively. There were no dose rate effects in the dose rate range of 37 MU/min to 600 MU/min for 6 MV x-ray and 0.66 cGy/h to 0.87 cGy/h for ¹²⁵I seed.

Conclusions: TLD2000 TLD has good repeatability and linear dose response for ¹³⁷Cs, ¹²⁵I seed and 6 MV x-ray without dose rate effect, but the dose response is energy dependent.

SP155.3 - Application of 2D thermoluminescent dosimetry in QA test of Cyberknife

Author(s): Renata Kopec¹, Krzysztof Slosarek², Jan Gajewski¹, Aleksandra Grzadziel², Maciej Budzanowski¹
¹Institute of Nuclear Physics, Kraków/POLAND, ²Center of Oncology – Memorial Institute, Gliwice/POLAND

A measurement of thermoluminescence consists of increasing of temperature of TL material in a controlled way with simultaneous measurement of emitted light. Measurements of light intensity were up to now based on thermoluminescent (TLD) detectors and were realized almost entirely with use of photomultipliers (PM). In 2005 new specially prepared planar thermoluminescent (TL) reader with CCD camera was developed at the Institute of Nuclear Physics of the Polish Academy of Sciences (IFJ) Kraków, Poland. The ultrasensitive 12-bit monochromatic CCD camera was applied instead of PM. The results from that system are 2-D images of TL lighting. The new system has found a few practical applications. Two-dimensional (2-D) thermoluminescence (TL) dosimetry system was developed and tested by evaluating 2-D dose distributions around radioactive sources for different purposes e.g.: radiotherapy, radiology (1) and individual dosimetry (2). In this work additionally the results of studies on the two-dimensional technique based on the 2D planar foils to Cyberknife QA test are presented. Comparison between results from standard Gafchromic films and TL foils are also presented. To analysis of images gamma index method is applied.

(1) R. Kopec, L. Novák, E. Carinou, I. Clairand, J. Dabin, H. Datz, C. De Angelis, J. Farah, C. Huet, Ž. Knežević, H. Järvinen, M. Majer, F. Malchair, A. Negri, S. Haruz Waschitz, T. Siiskonen, A. Szumska, A. Trianni, F. Vanhavere, Intercomparison of Gafchromic™ films, TL detectors and TL foils for the measurements of skin dose in interventional radiology Radiation Measurements, 71 (2014) 282-286

(2) R. Kopec, M. Budzanowski, P. Olko, P. Pawlik, Quantitative analysis of TLD static and dynamic radiation exposure, Radiat. Meas., 45, (2010) 713-715

SP155.4 - Towards Optical CT scanning of radiochromic 3D dosimeters in mismatched refractive index solutions

Author(s): Kurtis H. Dekker, Jerry J. Battista, Kevin J. Jordan
Department of Medical Biophysics, Western University, London/ON/CANADA

Introduction: The radiochromic plastic dosimeter, PRESAGE® (Heuris Inc., USA), shows promise for 3D radiation dosimetry using optical CT readout, as it offers good optical quality, has linear dose response[1], and is commercially available. Unfortunately, difficulty using oil-based refractive index matching solutions limits widespread clinical use. If lower-viscosity, water-based solutions could instead be used in the optical CT aquarium, this practical barrier could be overcome. Such liquids have a lower refractive index than

PRESAGE[®], causing ray-bending and incomplete sampling in CT projections. Computer simulation studies[2], [3], however, show that iterative reconstruction could allow accurate reconstruction of a subvolume of the dosimeter, if the paths of rays through the sample are known. In this study, we present a method to measure ray paths using fiducial marker tracking, along with early results from intentionally mismatched-index scanning using a laser CT system.

Methods: For a fan-beam CT scan of a cylindrical object, with projections about 360°, the fiducial will occlude a given light ray twice. Assuming the rotation angle at each occlusion is known, the path of each ray can be calculated using the cylinder's radius. Using a custom built scanning-laser CT system with a large area detector[4], we scanned a uniform solution phantom made of a transparent teflon cylindrical vessel in an aquarium with a matched refractive index. Inside this vessel, liquid with refractive index 6% higher was used. Since Snell's law of refraction depends on the *ratio* of indices, this experiment simulates the case of a PRESAGE[®] dosimeter scanned in 60% (by weight) glycerol in water, which we found to be sufficiently low in viscosity for optical CT. The fiducial method was used to measure ray paths in order to re-sort the sinogram into parallel beam geometry, and a basic SIRT[5] algorithm was used for image reconstruction.

Results: The reconstruction shows uniformity within 3% for 84% of the radius, beyond which incomplete radial sampling leads to inaccurate values. The reconstructed attenuation coefficient of $0.342 \pm 0.004 \text{ cm}^{-1}$ within this region agreed with a central-axis measurement of $0.34 \pm 0.02 \text{ cm}^{-1}$ using the known phantom diameter.

Conclusions: With 6% refractive index mismatching, approximately 85% of the radius of a uniform object was reconstructed within 3% accuracy. This suggests that it should be possible to scan the PRESAGE[®] solid dosimeter in a 60% glycerol solution and accurately reconstruct the dose map within 85% of the radius. In future work we will image PRESAGE[®] samples with deposited dose distributions to determine if this approach enables practical clinical dosimetry.

References:

- [1] P. Y. Guo, J. A. Adamovics, and M. Oldham, *Med. Phys.*, vol. 33, no. 5, pp. 1338–1345, 2006.
- [2] S. J. Doran and D. N. B. Yatigammana, *Phys. Med. Biol.*, vol. 57, no. 3, pp. 665–683, 2012.
- [3] L. Rankine and M. Oldham, *Med. Phys.*, vol. 40, no. 5, p. 051701, 2013.
- [4] K. Jordan, D. Turnbull, and J. Battista, *J. Phys. Conf. Ser.*, vol. 444, p. 012062, 2013.
- [5] P. Gilbert, *J. Theor. Biol.*, vol. 36, no. 1, pp. 105–117, 1972.

SP155.5 - Development of a Novel Linear Energy Transfer Detector Using Doped Plastic Scintillators and Monte Carlo Simulation

Author(s): Humza Nusrat¹, Geordi Pang², Syed Bilal Ahmad³, Brian Keller⁴, Arman Sarfehnia⁴

¹Department Of Physics, Ryerson University, Toronto/CANADA, ²Imaging Research, Sunnybrook Health Sciences Centre, Department Of Medical Biophysics, University of Toronto, Toronto/CANADA, ³Physical Sciences, Sunnybrook Research Institute, Toronto/CANADA, ⁴Department Of Radiation Oncology, University of Toronto, Toronto/CANADA

In radiotherapy, absorbed dose is a common quantity used to measure the amount of delivered radiation; however, dose is not a good

indicator of actual biological damage. Linear energy transfer (LET) is the energy deposited per unit length along a charged particle's pathway; studies have shown that LET correlates well with relative biological effectiveness. This research seeks to design and develop a portable, clinically-suitable LET detector. According to Birks' law, light output of plastic scintillators is stopping power dependent. This dependency can be varied through doping by various high Z elements.

By measuring light output signals of differently doped plastic scintillators at a given point (represented by column vector \mathbf{S} , where each row corresponds to a different scintillator material), fluence of charged particles of a given LET (represented by column vector ϕ , where each row corresponds to different LET bins) can be unfolded by $\mathbf{S}=\mathbf{R}\cdot\phi$, where \mathbf{R} is system response matrix. Hence, the higher the resolution of LET fluence required (i.e. increased rows of matrix ϕ), the higher the number of distinct scintillating materials that must be used. Moreover, ϕ can only be solved if \mathbf{R} is invertible, and the unicity of ϕ is given by the rank of matrix \mathbf{R} .

Monte Carlo GEANT4.10.1 was used to determine optimal doping of polyvinyltoluene (base scintillator) to ensure distinctness of detector response, and invertibility of \mathbf{R} . Various dopant materials (W, Pb, Mo) at several concentrations (1%, 10%) were simulated, FIG 1A. Preliminary results show doping with 1%Pb caused energy deposited to increase by 8.8%+/-0.07%; for 10%Pb this increased to 41.5%+/-0.07%.

GEANT4 was also used to evaluate \mathbf{R} ; each row represents a differently doped scintillator, each column corresponds to different electron LET. \mathbf{R} was further corrected for signal loss in various connections used to transfer light from scintillator to PMT (i.e. housing, fiber). This was done experimentally using an integrating sphere and calculating the ratio of light transfer in presence/absence of connection assembly (FIG 1B).

Experimental setup shown schematically in FIG 1C was used to measure light output from scintillating materials. In-house code was written to integrate the PMT signal over time. Initial measurements were done using commercially available undoped polyvinyltoluene scintillator and a 1%Pb-doped scintillator.

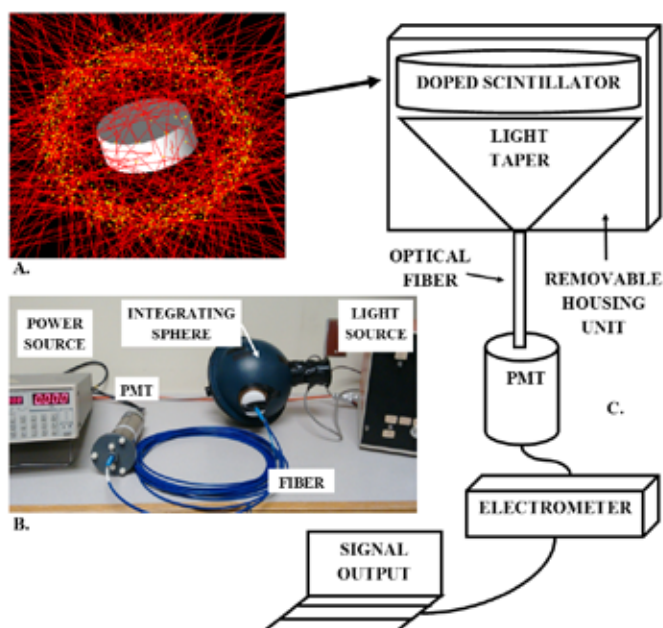


Figure 1: A. Sphere of isotropic mono-energetic electron sources simulated to determine scintillation response of each uniquely doped scintillator to electrons of given LET; **B.** Setup used to correct **R** for signal loss; **C.** Experimental Setup.

SP155.6 - Reduction of residual signal in LiF:Mg, Cu, P thermoluminescent material.

Author(s): Vinod K. Nelson

Medical Physics, Liverpool & MacArthur Cancer Therapy Centres, Campbelltown/AUSTRALIA

Purpose: LiF: Mg, Ti (TLD-100) is a well-established material for medical dosimetry over the past forty years since its development in the 1960s due to its tissue equivalence, negligible fading over lengthy periods, reasonable radiation sensitivity and relatively low minimum radiation detection level. However recently LiF: Mg, Cu, P has become a popular TL dosimeter in routine applications of personal, environmental and clinical dosimetry due to its the high sensitivity, almost flat energy response, linear dose response, and the shorter annealing procedures. The main drawback of the LiF: Mg, Cu, P based dosimetry is the significant residual signal due to the presence of a high temperature peak in the temperature range of approximately 270°C - 300°C. Considerable effort has been invested in the development of a LiF: Mg, Cu, P material with a greatly reduced residual signal. However, the integrated processes of sintering and microstructure development in a crystalline compound remain complex even after many years of research. The purpose of this work was to explore the possibility of using a low heating rate and longer TL signal integration time to reduce the residual signal in LiF: Mg, Cu, P (TLD100-H) dosimetry material.

Materials and Methods: TLD100-H material in the form of chips of thicknesses 0.9 mm (thick) and 0.4 mm (thin) were used. The chips were annealed at 240°C for 10 minute after each irradiation and prior to next use. Irradiation was carried out in a solid water phantom at 5 cm depth using 6 MV x-rays. A dose of 0.5Gy was delivered for each irradiation. Three readout cycles were tested, and repeat readouts were carried out immediately after the first readout, using the same parameters. The three heating rates used were 15°C / sec, 10°C/ sec, 5°C/sec and 1°C / sec. The signal was integration time was 30 sec, 60 sec, 60 sec and 300 sec, respectively. The residual signal was calculated as a ratio of first readout TL signal over the second readout TL signal.

Results: The mean residual signal for thick TLD chips was 6.1% and that from thin TLD chips was 7.5% when the heating rate was 15°C/sec. When the heating rate was reduced to 5°C/sec, the mean residual signal for thick TLD chips was 1.9 %. For thin chips the residual signal was negligible (<0.1%) when the heating rate was 7 °C/sec. At the heating rate of 1°C/sec, the residual signal was practically removed and was less than the background noise of the TLD reader.

Conclusions: The present study shows that a slow heating rate reduces the residual signal in TLD100H dosimeters. The effect is more pronounced in thinner TLD chips. When low dose measurements are performed using TLD100-H material, thin chips with a heating rate of 7°C/sec should be used. A heating rate of 1°C/sec would be ideal for 0.9 mm thick TLD100-H chips; however a heating rate of between 1 and 5 °C/sec would achieve a good balance between low residual signal and a practical overall readout time.

SP155.7 - Application of dose gels in HDR brachytherapy

Author(s): Diana Adliene¹, Karolis Jakstas², Neringa Vaiciunaite¹, Jurgita Laurikaitiene³, Reda Cerapaitė-Trusinskiene⁴

¹Physics Department, Kaunas University of Technology, Kaunas/LITHUANIA, ²Oncology Clinic, Republican Siauliai Hospital, Siauliai/LITHUANIA, ³Centre Of Mathematics, Physics And Information Technology, Aleksandras Stulginskis University, Kaunas/LITHUANIA, ⁴Physics, Mathematics And Biophysics Department, Lithuanian University of Health Sciences, Kaunas/LITHUANIA

Normoxic gels are frequently used in clinical praxis for dose assessment or 3D dose imaging in radiotherapy due to their relative simple manufacturing process, well expressed radiation induced modification of physical properties and well defined spatial shape of the polymerized gel part in the irradiated volume. Normoxic polyacrylamide (nPAG) gels were irradiated in high dose rate (HDR) after loading brachytherapy system MicroSelectron v2 with ¹⁹²Ir source. The source was inserted into 6 Fr catheter which was fixed at the axial position of the gel filled beaker during gel preparation phase. Varying composition and manufacturing process conditions free standing polymerized gel shapes were produced around a catheter as polymerization center. Dose and dose rate related properties of the free standing polymerized gel shapes were evaluated using Raman spectroscopy and were compared to those of in the gel volume located polymerized gel regions of usual nPAG gels. Analysis of the obtained results is provided and possibility to pre-assess special dose distribution in the prescribed irradiation target using these free standing polymerized gels is discussed.

SP155.8 - Practical 3D QA for Radiation Therapy Based on High-Resolution Laser CT of Reusable Radiochromic Polymer-Gel Dosimeters in Dedicated Phantoms

Author(s): Marek Maryanski¹, Liyong Lin², Ali Kassae², James Kraus², Stephen Avery²

¹MGS Research Inc., Madison/CT/UNITED STATES OF AMERICA, ²University of Pennsylvania, Philadelphia/UNITED STATES OF AMERICA

Current quality assurance measurements are not sufficient to detect fine structure errors from complex plans. Treatment delivery methods are becoming more complex with higher doses and fewer fractions. A high resolution technique is needed to account for the subtle errors which combine resulting in a treatment plan which is ultimately inaccurate. Presently water phantoms are used for measuring and determining the dose distribution of radiation produced by a particle beam or photon radiation beam. The standard dosimetry system is comprised of: a water tank, an ionization/diode detector positioned in a fixed position and software used to control the motion of detector and analyze data. It is not possible to use the water tank system for advanced delivery techniques such as Arc Therapy or IMRT. Due to the point-by-point measuring concept this system cannot quantify the effect of modulated beams. 2D detectors such Matrixx or Mapcheck are used for quality assurance measurements but are limited to measuring one plane at a time. This information is adequate for QA test, but with the advancement of treatment planning techniques and treatment machines that deliver highly conformal dose; it's impossible for a 2D detector to capture all the subtleties in the treatment plan. The promise of the clinical benefits of intensity modulated particle therapy (IMPT), for example, will only be achieved by having adequate 3D dosimetry and QA tools. Clinical 3D dosimetry will be critical in keeping pace with the rapid advancements in present day technology.

Our system offers reusable dosimeters which we have demonstrated the feasibility of the signal decay correction and the response signal decay rate; that ranges from hours to days depending on the formulation. The VOLQA™ software is capable of image reconstruction, DICOM import, 3D registration using orthogonal projections,

dose calibration, comparison of measured plans vs calculated plans and automatic generation of the QA summary table. The workflow from end of laser CT scan to QA report is 30 minutes with a dosimetric precision/accuracy of 99.5%/99.0%. There is no quenching effect for proton beams. The system has demonstrated excellent agreement (measurement vs plan) with gamma passing rate above 95% at 2mm/2% acceptance level down to the 50% isodose line. Isotropic spatial resolution ranges from 0.25 to 1 mm with a FOV up to 23 cm. The cost per QA is approximately \$50-\$100.

A practical 3D QA for modern radiation therapy has been developed and tested for clinical QA applications. High resolution and dosimetric accuracy is combined with minimum time required on the part of physics staff. Widespread use in both radiosurgery and particle therapy QA is anticipated. This system has the potential to improve quality assurance of radiation therapy treatment of cancer and other diseases by the introduction of fast, accurate, high-resolution, three-dimensional dosimetry based on laser CT of soft-tissue-equivalent polymer dosimeters whose local optical density changes in proportion to local dose. The new technology could potentially be used in acceptance and commissioning testing for all existing treatment modalities.

SP156 - Patient-Specific Modeling and Simulation in Surgery

TRACK 07: SURGERY, COMPUTER AIDED SURGERY, MINIMAL INVASIVE INTERVENTIONS, ENDOSCOPY AND IMAGE-GUIDED THERAPY, MODELLING AND SIMULATION

SP156.1 - A Technique for Prostate Registration by Finite Element Modeling

Author(s): Jianfei Liu¹, Fangsen Cui¹, Zhuangjian Liu¹, Jimin Liu²

¹Engineering Mechanics, Institute of High Performance Computing, A*STAR, Singapore/SINGAPORE, ²Quantitative Image Processing Group, Singapore Biomedical Imaging Consortium, A*STAR, Singapore/SINGAPORE

Magnetic resonance imaging (MRI) targeted and transrectal ultrasound (TRUS) guided needle biopsy is currently the clinical standard routine for diagnosis of prostate cancer. The prostate under TRUS procedure possesses different orientation and shape from its presentation in MRI procedure. Therefore, registration of suspicious tumor sites identified in the MRI images to that of TRUS images is an essential process to ascertain the needling targets during the TRUS procedure. In this paper, an effective technique is proposed to directly transform the prostate geometries from MRI volume to TRUS volume, based on finite element (FE) method and biomechanical models. Both the procedure and the accuracy of this registration method were studied through 2D transformation of prostate axial cross-section. The overall target errors can be reduced to less than 1 mm even for a large deformed prostate.

SP156.2 - Modeling study of neo-aortic root for arterial switch operation: a structural finite element analysis

Author(s): Aike Qiao¹, Zhaoyong Gu¹, Youlian Pan¹, Rongxi Jia¹, Nianguo Dong²

¹Beijing University of Technology, Beijing/CHINA, ²Huazhong University of Science and Technology, Wuhan/CHINA

In order to investigate the influence of sinotubular junction and sinus diameter on the aortic valve closure, numerical simulations were performed. Models of neo-aortic root for arterial switch operation to the patient with complete transposition of the great arteries were established. The 3-dimensional geometry of a reference aortic valve model A, with the aortic annulus diameter (DAA)=9.70mm, the diameters of sinotubular junction (DSTJ)=9.70mm and the sinus diameter (DS)=12.30mm, was built. Then the DSTJ and DS were modified to create four geometric models with different dimensions, named as B(DSTJ=11.60, DS=12.30), C(DSTJ=7.76, DS=12.30), D(DSTJ=9.70, DS=14.76), and E(DSTJ=9.70, DS=9.84). The mechanical behavior of the aortic root on the closing diastolic phase was simulated. The performance of the aortic leaflets was assessed in terms of stress of neo-aortic root, change of the aortic annulus diameter as well as leaflet contact force during closing phase. The reference model A showed a maximum leaflet stress of 96.29kPa. For models B and C, leaflet contact forces are respectively increased by 43.33% and decreased by 10.00% with the sinotubular junction diameter respectively increased by 1.2 times and decreased by 0.8 times compared with reference model A. Compared with model A, leaflet contact forces in models D and E are respectively increased by 6.67% and decreased by 23.33% with sinus diameter respectively increased by 1.2 times and decreased by 0.8 times. It is evident that increasing the sinotubular junction and sinus diameter within a range of 20% can increase the maximum stress and the leaflet contact force for aortic root and vice versa. It may be the reason why neo-aortic valve insufficiency occurs after a long period of time for patients with arterial switch operation.

SP156.3 - Preoperative in silico analysis of atherosclerotic calcification vulnerability in carotid artery stenting using Finite Element Analysis by considering Agatston score

Author(s): Sadegh Riyahi Alam¹, Umberto Morbiducci¹, Hiroyuki Katano², Kiyoko Yokoyama³, Shady Ali¹, Alberto Audenino¹, Filippo Molinari⁴

¹Mechanical And Aerospace Engineering, Politecnico di Torino, Turin/ITALY, ²Department Of Neurosurgery, Graduate School Of Medical Sciences, Nagoya City University, Nagoya/JAPAN, ³Graduate School Of Design And Architecture, Nagoya City University, Nagoya/JAPAN, ⁴Electronics And Telecommunications, Politecnico di Torino, Turin/ITALY

The role of calcification inside fibroatheroma during carotid artery stenting operation is controversial. Cardiologists face a major problem of “plaque vulnerability” during the placement of both balloon and stent, with stiff plaques containing advanced calcifications that break the arterial wall or give rise to unstable thromboembolic stroke. The aim of this work is to evaluate the role of calcification (in terms of material and mechanical properties) in plaque vulnerability and wall rupture and to find plaque maximum resistance before breaking. Image-based models of carotid artery stenting were used and Finite Element Analysis (FEA) was performed to simulate the impact of balloon and stent expansion in the presence of calcified plaques. In detail, a nonlinear static structural analysis was performed on 20 patients acquired using *in vivo* MDCT angiography. The Agatston Calcium score was obtained for each patient and subject-specific local Elastic Modulus was calculated. The *in silico* results showed that by imposing maximum ultimate external load of 1.2MPa and 4.2MPa on balloon and stent respectively, average ultimate stress of 55.7±41.2kPa and 171±41.2kPa as well as average Plaque Wall Stress of 19.03±16.05kPa and 64.3±63.3kPa were obtained on calcifications, respectively. Elastic and plastic strain average values of 0.03±0.02 and 0.006±0.01, respectively, were obtained on the calcified plaques after stent expansions. These average data are in good agreement with results obtained by other research groups relative to the values of compressive Elastic Modulus of atherosclerotic plaques and its ultimate stress, strain values after performing carotid artery stenting. Even if our findings are markedly influenced by local geometry and plaque shape, this study enriches the literature in pre-operative prediction of ultimate mechanical parameters in stenting operation to prevent rupture before balloon/stent expansion.

SP156.4 - Biomechanical modeling for foot inversion

Author(s): Junchao Guo¹, Cheng-Fei Du¹, Li Z. Wang¹, Yu B. Fan^{*2}

¹Key Laboratory for Biomechanics and Mechanobiology of Ministry of Education, School of Biological Science and Medical Engineering, Beihang University, Beijing/CHINA, ²National Research Center for Rehabilitation Technical Aids, Beijing 100176, P.R. China, Beijing/CHINA

Foot inversion was the most common injury of lower limb injury, it seriously affected the foot balance and posture control during standing and walking. The purpose of this study was to describe the rationality of biomechanical modeling for foot inversion. Plantar pressure measurements and foot roentgenogram had been reported. However, direct measurement of the internal tissues stress was difficult. A three-dimensional finite element model of foot inversion was developed to investigate the region of foot inversion injury. Compared with normal foot, the results showed that subtalar joint region was mainly weight-bearing region. Peak von Mises stress of the internal bones was transferred to the lateral longitudinal arch. The simulation in this study would provide the suggestion of therapeutic planning to foot inversion.

SP156.5 - Deformation Method and 3D Modeling of the female body to simulate Core Biopsy procedure

Author(s): Maria Tereza D. Melo, Vinicius P. Da Silva Corrêa, Vladimir F. Nogueira, Victor Hugo L. Goncalves, Henrik D-Oark R. Costa, Lourdes M. Brasil, Jairo Simão S. Melo, Beatriz A. Rodrigues University of Brasília-UnB at Gama-FGA, Brasilia/BRAZIL

Core biopsy is an invasive surgical procedure that collects the tissue samples to be evaluated by an expert. The withdrawal of samples is performed with large-caliber needles, attached to a special pistol. It is a technique conducted by an imaging equipment to guide the procedure. Usually consists of ultrasound guided core needle biopsy or stereotactic mammography.

This procedure can be used in the investigation of various diseases and through it, you can identify precise information on the nature of the injury or the degree of impairment of the tissue for diseases. For breast cancer, the results with the biopsy are essential to set an appropriate treatment, and may this be a surgical intervention or not. Thereby, it is guaranteed greater effectiveness in the final results.

Thus, the simulation modeling of surgery and examination has an elastic deformation behavior of human skin through the puncture. It is used physical and mathematical methods to describe computationally this imputed deformation on the skin in a mammary biopsy procedure. Thus, the deformation of Infinite Elements is characterized and justified for such a technique. The method chosen features complex structures with a greater realism, which is ideal for the representation of the breast. And to improve the results obtained on deformation, it is used Fuzzy Logic for the interpretation of the output data.

With the aim of providing the medical students and other health professionals greater dexterity in performing breast biopsy, it was developed the project: 3D Anatomical Atlas Applied to Mama, in order to develop a learning environment using virtual reality precepts. The project is divided into five modules: three-dimensional (3D) modeling, ontological modeling, development of an Intelligent Tutor System (ITS), deformation and pathology. This paper presents the 3D modeling in conjunction with the deformation. The 3D modeling is responsible for creating 3D structures of the female body and its internal composition being used in virtual simulation of surgical procedure Core Biopsy, illustrated by Fig. 1. Thus, professionals can train your skills and, at the same time, using the modeling tools to make them more didactic, so that a student can assimilate the precepts.

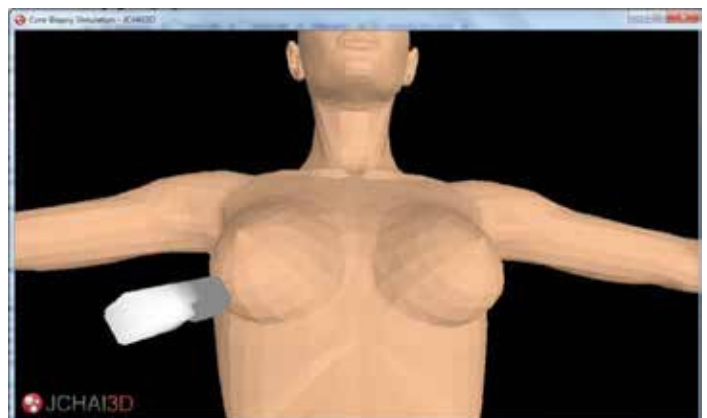


Fig. 1. The simulation of Core Biopsy procedure

SP156.6 - Effects of Band Position on Hemodynamics of Pulmonary Artery: A Numerical Study of Patient-specific Virtual Procedure

Author(s): [Jin Long Liu](#), Wei Min Zhang, Qin Yan, Hai Fa Hong, Jin Fen Liu
 Department of Cardiothoracic Surgery, Shanghai Children’s Medical Center, Shanghai Jiao Tong University School of Medicine, Shanghai/CHINA

Hemodynamics of pulmonary artery flow after different strategies of pulmonary banding (PAB) was not well understood. By using computer-aided design (CAD), three PAB models were devised and numerical study was done by computational fluid dynamics (CFD). The results indicated that whirling flow was formed in all the PAB models, which is more significant in that with proximal PAB, leading to unbalanced perfusion of lungs. While in distal PAB models, the flow disturbance is relatively mild and unbalanced flow to left pulmonary artery has decreased. Integrated CAD and CFD study can be applied to predict and optimize the surgical outcomes of PAB.

SP156.7 - Experimentally validated Biomechanical Model of in vivo Lung under EBRT considering Diaphragm motion hysteresis

Author(s): [Elham Karami](#)¹, Stewart Gaede², Ting-Yim Lee³, Abbas Samani⁴
¹Medical Biophysics, Western University, London/CANADA, ²Department Of Oncology, Western University, London/CANADA, ³Imaging Research Laboratories, Robarts Research Institute, London, ON/CANADA, ⁴Electrical & Computer Engineering, Western University, London/ON/CANADA

Lung cancer is by far the most common cause of cancer death in both men and women. Both small-cell and non-small cell lung cancers are frequently treated with radiation therapy, which is often combined with chemotherapy, surgery or both. However, External Beam Radiation Therapy (EBRT) may lack desirable dosimetric accuracy because of respiration induced tumor motion. Recently, biomechanical modeling of the respiratory system has become a popular approach for tumor motion prediction and compensation. This approach requires reasonably accurate data pertaining to lung geometry, thoracic pressure variation, diaphragm position and tissue biomechanical properties in order to predict tumor motion. However, given the pleural pressure nonuniformity on the lung’s surface and contact between the lung, diaphragm and heart, modeling the lung loading is cumbersome. A simple approach frequently used in lung models applies uniform negative pressure on the lung’s surface at the end exhalation phase to simulate the inhalation phase [1,2,3]. The negative pressure’s magnitude is obtained either from reported pressure-volume curves in the literature or from 4D CT data. Other approaches include modeling the thoracic pressure and diaphragm motion separately [4,5].

To our knowledge, none of the existing lung biomechanical models account for respiratory cycle hysteresis. The lung hysteresis results from surfactant action during inhalation and tissue recoiling during exhalation. In this paper, we present preliminary results obtained from lung 4D CT image processing which indicate that the human diaphragm motion’s hysteretic nature. This hysteresis further contributes to the lung hysteresis. To track the diaphragm motion, 22 points located on its surface were tracked in a set of 4D CT images using Free Form Deformable registration. The displacement values in the superior-inferior direction were normalized between 0 and 1 for all the points. The average curve depicted in Figure 1 indicates that the diaphragm motion has similar pattern to the lung compliance curve. These results suggest that, to achieve desirable accuracy with lung biomechanical modeling, this strong diaphragm motion hysteresis should be considered. This was done by modifying the model we presented in [4], leading to significant improve-

ment in tumor motion prediction.

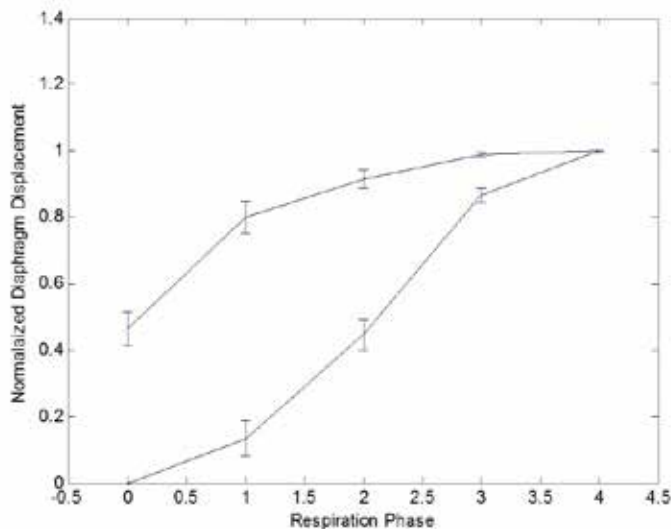


Figure 1 : Normalized Diaphragm displacement versus respiratory phase

- [1] Werner, et al. Med. Phys. 36, 1500-1511 (2009).
- [2] Zhang, et al. Med. Phys. 31, 2412-2415 (2004).
- [3] Eom, et al. Lect. Notes Comput. Sci. 5762 LNCS, 348-355 (2009).
- [4] Karami, et al. Accepted for presentation at SPIE Medical Imaging (2015).
- [5] Fuerst, et al. IEEE Trans. Med. Imaging, (2014).

SP157 - Biochips and Blood Analysis

TRACK 08: BIOSENSOR, NANOTECHNOLOGY, BIOMEMS AND BIOPHOTONICS

SP157.1 - On-chip blood Plasma separation using vacuum-assisted micropumping for point-of-care application

Author(s): Linfeng Xu, Kwang W. Oh

Electrical Engineering, SUNY at Buffalo, Buffalo/NY/UNITED STATES OF AMERICA

SMALL (Sensors and MicroActuators Learning Lab), Department of Electrical Engineering, University at Buffalo, The State University of New York (SUNY at Buffalo), Buffalo, New York 14260,

Introduction: To become useful diagnostics tools in global mobile health point-of-care (POC) settings, a disposable biosensor will require further improvement by integration of sample preparation, which has been troublesome due to incorporation of external active valves and pumps [1]. Our approach aims to simplify the on-chip blood plasma separation required to perform specific sensing of biomolecules, all without compromising biosensor functionality. Without any of the requirements of sophisticated equipment or dilution techniques, we could extract the plasma from the whole blood, which is suitable for point-of-care applications. This talk will cover a selected example in the emerging POC applications, such as hemolysis-free on-chip blood plasma separation by using a simple hand-held power-free vacuum-assisted pumping method.

PRINCIPLE/DESIGN: Pneumatic chambers, A and B, are neighbouring with the separation chamber and the dead-end ring channel, respectively, which are physically disconnected each other through a thin air-permeable PDMS wall (separation chamber/PDMS wall/pneumatic chamber A and ring channel/PDMS wall/pneumatic chamber B). Each pneumatic chamber is connected to a hand-held syringe. By pulling the plunger of the hand-held syringe, a vacuum will be generated inside the pneumatic chambers (due to the volume change from 2 μ L to 2 mL). This will indirectly withdraw the blood sample in the separation chamber through the air-permeable PDMS wall. Flow rates can be tuned by adjusting the PDMS wall thickness and overlap area between the pneumatic chamber and the separation chamber. Meanwhile, by gravity, blood cells will sediment at the bottom of the separation chamber therefore plasma could be separated from the whole blood. Moreover, phaseguides are employed at the bottom of the separation chambers (1) to prevent air trapping inside the separation chamber and (2) to increase the plasma separation efficiency by avoiding the slide of blood cells that are already sediment down.

EXPERIMENTS/Results: The secret is to indirectly and slowly pump the whole blood into a dead-end chamber/channel embedded with smart microstructures (e.g., phaseguides in order to both enhance the separation efficiency and reduce the separation time) by well-controlled air-diffusion through the thin PDMS wall, due to the syringe-generated pressure difference (atmosphere in the dead-end chamber/channel vs. vacuum in the pneumatic chamber/syringe). This allows fast sedimentation of blood cells and thereby filter-free and hemolysis-free plasma separation. Through the experiments, we found the followings: (1) Pinning time due to the phaseguides was in inverse proportion to the separation efficiency. By adjusting the design parameters of the neck structure in the phaseguides, pinning time could be reduced. (2) The ratio between the height of the phaseguides and the separation chamber was proportional to the separation efficiency. (3) Flow rates were also in an inverse relationship to the separation efficiency. Similar results were also verified by a set of straight channels.

Conclusion: We have investigated a simple hand-held power-free vacuum-assisted pumping method, its application for hemolysis-free on-chip blood plasma separation, and the key parameters that would affect the separation efficiency. The present device is expected to be an effective tool for blood separation, especially for point-of-care applications.

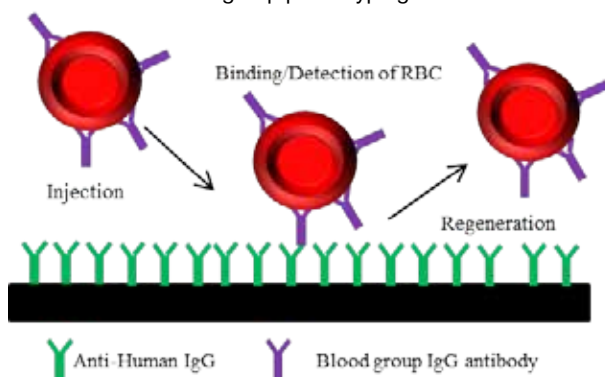
1. Maiwenn Kersaudy-Kerhoas and Elodie Sollier, "Micro-scale blood plasma separation: from acoustophoresis to egg-beaters," Lab Chip, 13, 3323-3346, DOI: 10.1039/C3LC50432H, 2013

SP157.2 - Multi-Functional Platform for Blood Group Phenotyping using Surface Plasmon Resonance

Author(s): Whui Lyn Then¹, Marie-Isobel Aguilar², Gil Garnier¹

¹Chemical Engineering, Bioresource Processing Research Institute of Australia (BioPRIA), Monash University, Melbourne/VIC/AUSTRALIA, ²Biochemistry, Monash University, Melbourne, Melbourne/VIC/AUSTRALIA

Accurate and reliable phenotyping of blood groups is of the utmost importance prior to transfusion. Mismatching of incompatible donor and patient blood types could potentially lead to a haemolytic transfusion reaction, which can be fatal. Currently, there are many well established blood typing methods available, such as the column agglutination test (CAT), however methods quantifying these antibody-antigen interactions are limited. This is particularly important to identify and characterize weak interactions between weak subgroup variants, which are often difficult to determine by the naked eye and have the potential to be overlooked. The biosensing system, BIAcore, relies on surface plasmon resonance (SPR) detection to quantify interactions between biomolecules. Previous studies have shown the use of SPR for blood group antigen detection and antibody detection; however, these methods showed poor regeneration and loss of functionality after a single use due to the inability to fully desorb bound material. Each chip (~AUD200) was also limited to a single blood group. A fully regenerable, multi-functional platform for quantitative blood group phenotyping via SPR detection can be achieved by covalently immobilizing an antibody, anti-human IgG, to the chip surface. Anti-human IgG is able to recognize and bind to the Fc region of human IgG antibodies for detection. The surface can therefore be used as an interchangeable platform capable of quantifying the blood group phenotyping interactions between RBCs and IgG antibodies. Much like the Indirect Antiglobulin Test (IAT) used to detect blood groups using IgG antibodies with the CAT, the blood group IgG antibody is incubated with RBCs, and the cells become sensitized, which allows them to bind to the anti-human IgG on the chip surface. This test has potential to quantitatively detect any blood group with a corresponding IgG antibody. A clear distinction between positive and negative results has been achieved using anti-D IgG and reagent red cells, as well as complete regeneration of the anti-human IgG surface. Very little degradation, if any, of the immobilized surface has been observed after over 100 regenerations. Consecutive testing of different blood types has also been successful, allowing multiple blood groups to be detected using a single chip. This multi-functional platform presents potential for quantifying antibody-antigen interactions for blood group phenotyping.



SP157.3 - Harmonic generation microscopy investigation of human pathological samples for automated cancer determination

Author(s): Richard Cisek¹, Danielle Tokarz², Ahmad Golaraei³, Serguei Krouglov³, Carolyn Niu⁴, Shingo Sakashita⁴, Ming-Sound Tsao⁴, Sylvia Asa⁵, Brian C. Wilson⁴, Virginijus Barzda³

¹Chemical And Physical Sciences, University of Toronto, Mississauga/ON/CANADA, ²Wellman Center For Photomedicine, Massachusetts General Hospital, Harvard Medical School, Boston/MA/UNITED STATES OF AMERICA, ³Chemical And Physical Sciences, University of Toronto, Mississauga/CANADA, ⁴Princess Margaret Cancer Centre, University Health Network, Toronto/ON/CANADA, ⁵Toronto General Hospital, University Health Network, Toronto/ON/CANADA

Nonlinear harmonic generation microscopy was used to investigate human pathological samples revealing quantitative differences between tumor and non-tumor regions in the extracellular matrix of several tissues including breast, lung, pancreas and thyroid. During tumor initiation and progression, alterations to the structure of collagen inside the extracellular matrix of different tissues can occur, which can be used for developing new biomarkers in cancer diagnosis. Second harmonic generation (SHG) is a spectroscopic nonlinear optical signal that is sensitive to changes in the ultrastructure of collagen, such as the organization of collagen into fibers, and the distribution of collagen fibers within a femto-liter laser focal volume, and therefore, SHG can be used as a biomarker for cancer diagnosis. The novel technique, polarization-in, polarization-out (PIPO) SHG microscopy was utilized, which is an accurate way to extract the second-order nonlinear optical susceptibility ratio component, $\chi^{(2)}_{zzz}/\chi^{(2)}_{zxx}$, which is related to the ultrastructure of collagen at each pixel. The PIPO SHG technique requires measuring the SHG intensity at each pixel of the image, at different orientations of the linear polarization of outgoing SHG as a function of the linear polarization orientation of the incident laser radiation. A MATLAB based fitting routine is used to deduce $\chi^{(2)}_{zzz}/\chi^{(2)}_{zxx}$ from the PIPO SHG image stacks, producing a color-coded map consisting of the $\chi^{(2)}_{zzz}/\chi^{(2)}_{zxx}$ value at each pixel. Additionally, the average orientation of the fibers is also deduced at each pixel of the image revealing long range collagen organization in the tissue. The $\chi^{(2)}_{zzz}/\chi^{(2)}_{zxx}$ maps reveal areas of altered collagen structure within tissue sections, and are independent of collagen concentration. Statistically-significant differences in $\chi^{(2)}_{zzz}/\chi^{(2)}_{zxx}$ were found between tumor and non-tumor tissues, which varied from organ to organ. Therefore, PIPO SHG microscopy has the potential to be used as a high throughput pathological sample pre-diagnosis system, aiding pathologists in cancer diagnostics. Additionally, PIPO SHG microscopy could also visualize and characterize the structure of collagen *in vivo* without staining which may aid in the study of collagen-related biological processes such as wound repair.

SP157.4 - Protein Patterning: An investigation on the use of different protein deposition techniques and parameters to transfer proteins onto various surfaces.

Author(s): Kathryn Clancy¹, Dan V. Nicolau²

¹Biomedical Engineering, McGill University, Montreal/QC/CANADA, ²Bioengineering, McGill University, Montreal/QC/CANADA

Protein microarrays are used to develop tools in various research areas including drug discovery, diagnosis, and protein-ligand interaction analysis. Their efficacy depends on a well-defined pattern of immobilized proteins that have retained their bioactivity. Protein microarrays are most commonly made via pin or inkjet printing that can lead to spots having uneven protein adsorption within the spotted area. Although automated, these processes have been shown to lead to inaccurate readings. Alternative techniques exist, including microcontact printing (μ CP) with a poly(dimethylsiloxane) (PDMS) stamp that produces protein patterns on surfaces, while maintaining bioactivity for a wide range of proteins.

In previous work we have qualitatively compared the distribution of deposited proteins via pin printing versus μ CP with both flat and pyramid-shaped posts. Here we propose to quantitatively compare these two methods, in addition with inkjet printing, to produce an even fluorescent signal within a defined area. Variation of the protein solution and surface properties, in addition to the deposition method, will also be studied with respect to fluorescent signal production.

Investigation into the experimental parameters used in protein patterning to produce an even protein adsorption pattern will enable reliable assay readings by increasing the signal to noise ratio in printed protein microarrays.

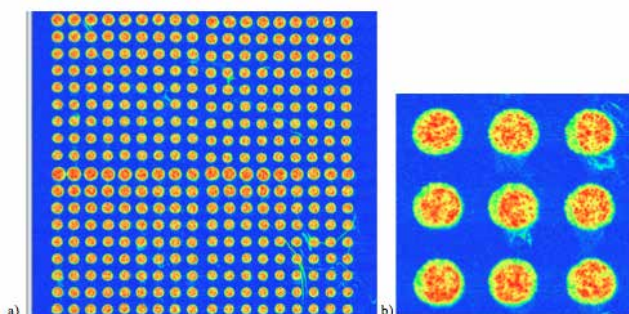


Figure 1 | a) Fluorescent images of fluorophore conjugated IgG solution (6.25 μ g/ml) deposited via pin printing onto a 3-(aminopropyl)-triethoxy silane glass slide with a contact angle of 61.58°, and b) 100% zoomed in image

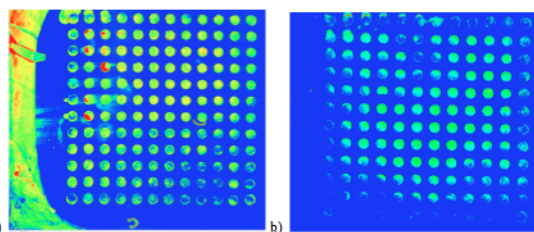


Figure 2 | Fluorescent images of fluorophore conjugated IgG, with a) 25 μ g/ml and b) 10 μ g/ml solutions deposited via μ CP with flat stamps onto a 3-(aminopropyl)-triethoxy silane glass slide with a contact angle of 76.83°.

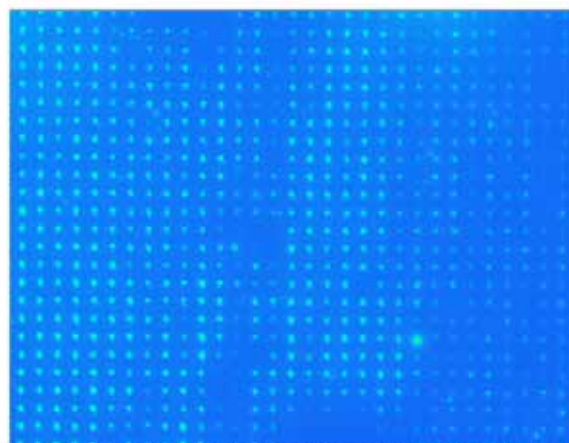


Figure 3 | Fluorescent image at 60X magnification of 10 μ g/ml fluorophore conjugated IgG microarray deposited via μ CP with a pyramid stamp onto an alcohol cleaned glass slide with a contact angle of 76.60°.

SP158 - Educational Activities and Training in Medical Physics

TRACK 17: EDUCATIONAL AND PROFESSIONAL ACTIVITIES

SP158.1 - Medical Physics Residencies-101: The What's, Where's, and How's

Author(s): Jeff Frimeth
Xspect Inc., Toronto/CANADA

Medical Physics residencies serve as an excellent bridge between putting together the didactic knowledge obtained from a graduate program with practical experience in a Medical Physics sub-specialty. Most residency programs are within the Radiation Therapy sub-specialty, although Diagnostic Imaging-based residencies are slowly starting to become more prevalent over recent years. Residency programs prepare one to take a board examination in order to become a Qualified Medical Physicist. The boards which an individual can apply to are the Canadian College of Physicists in Medicine (CCPM) and the American Board of Radiology (ABR). Residencies can be accredited by the Commission on Accreditation of Medical Physics Educational Programs (CAMPEP) body, but this is not essential. Since CAMPEP states minimum requirements to be met in order to ensure adequate coverage of residency program content, there is a continual push for an increase in the number of CAMPEP-accredited residencies. CAMPEP also accredits Medical Physics graduate programs. Enrolling in an accredited graduate program ensures that the individual graduating obtains a minimum standard of didactic knowledge, which will serve him/her for successful completion of a residency program. This talk will serve to inform the individual of how to prepare for applying to a residency program, what one may expect from a residency program, and where one can apply to residency programs. Participants will also be exposed to how one can prepare for taking a board examination, as well as the general scheme of how the board examinations are administered. CAMPEP requirements for residency and graduate programs will also be introduced.

SP158.2 - Education and Clinical Training of Medical Physics in Thailand

Author(s): Anchali Krisanachinda¹, Malulee Tantawiroon², Nisa Chawapun³, Puangpen Tangboonduangjit⁴, Nuntawat Udee⁵
¹Department Of Radiology, Faculty of Medicine Chulalongkorn University, Bangkok/THAILAND, ²Department Of Radiology, Faculty of Medicine Siriraj Hospital Mahidol University, Bangkok/THAILAND, ³Department Of Radiology, Faculty of Medicine, Chiang Mai University, Chiang Mai/THAILAND, ⁴Department Of Radiology, Faculty of Medicine, Mahidol University, Bangkok/THAILAND, ⁵Department Of Radiological Technology, Faculty of Allied Health Sciences, Naresuan University, Phitsanulok/THAILAND

There are 5 education programs for medical physics in Thailand. The first was started in 1972 at Ramathibodi Hospital, Mahidol University. Followed In 1990, the M.S. in Radiological Science program was started at Siriraj hospital, Mahidol University. Then in 2001, the second medical physics program was established at Chiang Mai University. The M.Sc. program in Medical Imaging was started at Faculty of Medicine Chulalongkorn University in 2002. The fifth program has been started at Naresuan University, Phitsanulok in 2014. The major problem in medical physics was the shortage of clinically qualified medical physicists. The situation was improved when IAEA started clinical training for radiation oncology medical physics (ROMP) in 2005, diagnostic radiology medical physics (DRMP) in 2009 and nuclear medicine medical physics (NMMP) in 2010.

Objective: To report the education and clinical training of medical physicists in Thailand with the cooperation of Thai Medical Physicist Society (TMPs), the International Atomic Energy Agency (IAEA) and Chulalongkorn University.

Method: All educational programs are two- year program of the didactic lecture, laboratory, on-the- job training, clinical practice and research. The clinical training using IAEA training guides, self assessment, progress report, external visit and external assessment by IAEA experts were obtained under the Regional Cooperative Agreement (RCA) for Asian and Pacific Region. Thai Medical Physicist Society is processing on licensing for qualified clinical medical physicist after the document submission to the committee of Ministry of Public Health.

Results and Conclusions: Even though the number of the medical physicists graduated from all programs is over 300, the lack of qualified medical physicists is still the problem. The success of the ROMP, DRMP and NMMP serves the needs at major university hospitals and the cancer centers. The clinical training was officially accepted by Chulalongkorn University for the Higher Graduate Diploma of Clinical Sciences Program in Medical Physics and started in 2011. The final medical physics education program of Ph.D. in Medical Physics will be started at Chulalongkorn University in August 2015. This program should support the need for medical physicist position in the university.

SP158.3 - Radiation Protection in Medical Imaging and Radiation Oncology

Author(s): Magdalena Stoeva¹, Richard Vetter², Kin-Yin Cheung³, Renate Czarwinski⁴, Francesca MCGowan⁵
¹Medical Imaging Dept., Medical University - Plovdiv, Plovdiv/BULGARIA, ²Mayo Clinic, Rochester/MN/UNITED STATES OF AMERICA, ³Medical Physics & Research, Hong Kong Sanatorium & Hospital, Happy Valley/HONG KONG, ⁴International Radiation Protection Association, Berlin/GERMANY, ⁵CRC Press, Taylor & Francis Group, London/UNITED KINGDOM

Radiation protection is one of the leading and fastest developing areas of medical physics and society as evidenced by the emphasis hospitals and medical organizations are placing on radiation protection culture. The interdisciplinary nature of radiation protection makes it a key discipline in ensuring safety of the public.

Safety and quality assurance in the use of radiation in medicine aims to reduce unnecessary radiation risks while maximizing the benefit. Improvements in quality and safety in radiation medicine require a strong radiation safety culture. To better achieve the goal of strengthening radiation safety in healthcare and better protection of the patients from excessive or unnecessary radiation exposure, a concerted effort by all the role players together with the radiologists, referring practitioners, technologists, professional organizations, international bodies and regulators is essentially needed.

The International Organization for Medical Physics (IOMP) and the International Radiation Protection Association (IRPA) have worked together to produce a book on Radiation Protection in Medical Imaging and Radiation Oncology, intended for use both in countries that have well developed medical and health physics disciplines and in developing countries.

The International Organization for Medical Physics (IOMP) represents over 18,000 medical physicists worldwide and 81 adhering national member organizations. The mission of IOMP is to advance medical physics practice worldwide by disseminating scientific and technical information, fostering the educational and professional development of medical physicists, and promoting the highest quality medical services for patients.

The International Radiation Protection Association (IRPA) represents some 18,000 members from 50 associate societies representing 63 countries. IRPA's vision is to be recognized by its members, stakeholders and the public as the international voice of the radiation protection profession in the enhancement of radiation protection culture and practice worldwide

Awareness of the need for emphasis on radiation protection contributes significantly to the safety of healthcare providers, patients, and the public. Contributions are most evident in facility design, in monitoring of personnel and the patient care environment, and in development of procedures and practices for proper handling and limitation of radiation exposure. Medical health physicists are often challenged to maximize protection of personnel while minimizing the cost of resources necessary to keep radiation doses ALARA. Advances in medical health physics will continue to be based on evidence gathered through basic and applied research. Periodic review of the evidence will help medical health physicists to focus on the issues and to advance the science.

The book *Radiation Protection in Medical Imaging and Radiation Oncology*, focuses on the professional, operational, and regulatory aspects of radiation protection covering virtually all regions of the world. The theoretical background is complemented by detailed practical sections and professional discussions by the world's leading medical and health physics professionals. Information is well organized into discreet chapters from basic protection to advanced imaging and treatment modalities. This book is a valuable source of information for the medical physicist and related specialties targeting a reading level of MSc and above.

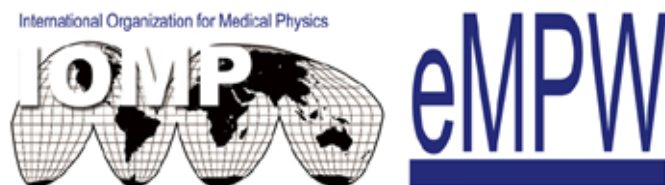
SP158.4 - It's a Medical Physics World! Presenting the Official Bulletin of the International Organization for Medical Physics

Author(s): Magdalena Stoeva¹, Virginia Tsapakis², Kin-Yin Cheung³, Slavik Tabakov⁴, Ibrahim Duhaini⁵, Madan Rehani⁶, Anchali Kri-sanachinda⁷

¹Medical Imaging Dept., Medical University - Plovdiv, Plovdiv/BUL-GARIA, ²Konstantopoulio General Hospital, Athens/GREECE, ³IOMP - Medical Physics World, York/UNITED KINGDOM, ⁴Medical Engineering And Physics, King's College London, RS/UNITED KINGDOM, ⁵Radiation Oncology, Rafik Hariri University Hospital, Beirut/LEBANON, ⁶Harvard Medical School and Massachusetts General Hospital, Boston/UNITED STATES OF AMERICA, ⁷Department Of Radiology, Faculty of Medicine Chulalongkorn University, Bangkok/THAILAND

Medical Physics World (MPW) has been the official bulletin of the International Organization for Medical Physics for over 30 years. The first issue of the bulletin was published in 1982 presenting a challenge to the IOMP and the medical physics societies around the world: "... to make 'Medical Physics World' worthy of its title".

Ever since then the IOMP's leading professionals have chaired and contributed to the development of MPW.



Medical Physics World Editors 1982-2015

Prof. Lawrence H. Lanzl

Prof. Colin Orton

Richard L. Maughan

Dr. Bhudatt R. Paliwal

Dr. Azam Niroomand-Rad

Dr. E. Ishmael Parsai

Dr. Virginia Tsapaki

The last several years mark a great progress in Medical Physics World. The new style and layout introduced in 2012 increased the interest towards MPW not only among our professional society, but also among corporate members and professionals from other disciplines. MPW is now regularly distributed on all major professional events – AAPM meetings, RPM, ICMP, many regional events.

Medical Physics World has always been in-line with IOMP's initiatives and hot topics. Besides providing the regular organizational reports, we have actively supported some of the IOMP's most successful activities – IOMP's 50th anniversary, the foundation of the Medical Physics International Journal (MPI), the International Day of Medical Physics (IDMP) and the formation of the IOMP Women subcommittee (IOMP-W).

During this 3-year period we successfully conducted a dissemination campaign that resulted in MPW's wide recognition among world's leading institutions. The journal is now regularly delivered to the European Congress of Radiology (ECR), the UNESCO International Center for Theoretical Physics (ICTP) and to the US Library of Congress.

The latest achievement of MPW's editorial team is including Medical Physics World in the International Standard Serial Number registrar.

With all the contemporary technology our world turned into an electronic world, so did Medical Physics World. We often call it eMPW now, but we are still devoted to the very first promise "... to make 'Medical Physics World' worthy of its title".

SP158.5 - The new IOMP Professional Journal - Medical Physics International - first results

Author(s): Slavik Tabakov¹, Perry Sprawls²

¹Medical Engineering And Physics, King's College London, RS/UNITED KINGDOM, ²IOMP, Atlanta/UNITED STATES OF AMERICA

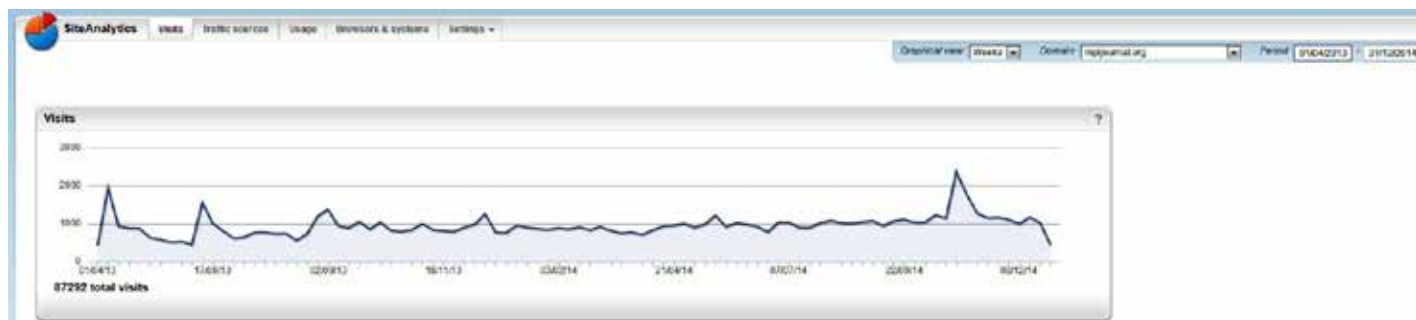
The medical physics profession is served by a collection of outstanding journals, each distinguished by its content, method of publication, geographic coverage, and organizational affiliation. The new IOMP journal, *Medical Physics International (MPI)*, joined this group in 2013, filling a specific niche, not as a competitor, but as an active supporter and collaborator with the other journals. MPI is the official journal of the International Organization of Medical Physics (IOMP) and is with fully open access on Internet (www.mpjournal.org), providing information at no cost to the global medical physics community. The mission of MPI is to publish articles that contribute to medical physics education, professional development, communication about international medical physics activities, and to preserve the history and heritage of the profession. The Journal is peer reviewed and publishes also approved abstracts from Medical Physics Conferences.

A distinguishing feature of *Medical Physics International* is that it does not publish manuscripts reporting on research and development. For these we recommend the other established Journals as: *Physics in Medicine and Biology* (the first journal to be designated as an official journal of IOMP in 1969), *Medical Physics*, *Journal of Applied Clinical Medical Physics* (the AAPM journals), *Physica Medica* (the European Journal of Medical Physics) and other regional

and national medical physics journals that provide such publication opportunities.

Currently MPI has 4 issues published, which include 260 pages with original papers on education and professional issues, history of the profession, new innovations from the medical physics industry, tutorials and abstracts of PhD theses. Additionally MPI has published 840 pages of approved abstracts from the International Medical Physics Conference ICMP2013 (Brighton, UK) and the International Conference on Radiation Protection in Medicine 2014 (Varna, Bulgaria).

The results are very encouraging - from its first issue MPI Journal has a steady number of about 1000 readers per week (see the statistics attached here). Its web site is designed in a way to allow both download of individual papers and whole PDF issues. Many papers have hundreds of downloads, what is a clear reflection of the need of such a Journal.



SP158.6 - Two First Years of Reuniting, Engaging and Discovering: The Canadian Conference for Undergraduate Women in Physics

Author(s): Madison Rilling¹, Marie-Joël Bergeron-Savard¹, Marie-Eve Boulanger¹, Émilie Cloutier¹, Amélie Dumont¹, Chloé Gaudreau¹, Marie-Pier Labonté¹, Jasmine Poirier¹, Carmelle Robert², Brigitte Vachon³

¹Département De Physique, De Génie Physique Et D'optique, Université Laval, Quebec City/QC/CANADA, ²Centre de Recherche en Astrophysique du Québec, Quebec City/QC/CANADA, ³Department Of Physics, McGill University, Montreal/QC/CANADA

A first *Conference for Undergraduate Women in Physics* was hosted by the University of Southern California in 2006. A few years later, six regional conferences were being held simultaneously and annually throughout the United States [1]. Inspired by this successful model centrally coordinated by the American Physical Society, McGill University hosted a first *Canadian Conference for Undergraduate Women in Physics (CCUWiP)* in January 2014, with 54 participants from Ontario and Quebec universities [2]. On 9-11 January 2015, a second, bilingual edition of the CCUWiP was hosted by Université Laval, which welcomed 75 undergraduate students from Eastern Canadian universities [3]. The goal of the CCUWiP is to give undergraduate women studying in a physics-related field the opportunity to experience a professional conference and discover a variety of career paths in academia, industry and health sectors. Moreover, this conference encourages the development of a national network of women in physics and promotes the accomplishments and leadership of women in STEM (Science, Technology, Engineering and Mathematics) fields. In light of having organized the two first Canadian editions, the organizational details involved in providing a student-accessible conference and the typical program of a CCUWiP will be introduced. We will describe the importance of the CCUWiP as a training and career development experience for women at the undergraduate, graduate and professional levels. As a student initiative sponsored by the Canadian Organization of Medical Physicists, the methods of promoting graduate studies, research

and careers in medical physics will be highlighted. Finally, based on its success and the growing interest in this conference, we will discuss the future of *Canadian Conferences for Undergraduate Women in Physics* and the potential and efforts in making the CCUWiP an official, annual event.



References:

- [1] <http://www.aps.org/programs/women/workshops/cuwip.cfm>
- [2] <http://www.physics.mcgill.ca/ccuwp14/>
- [3] <http://craq-astro.ca/CCUWiP/>

SP158.7 - Students' perspective on studying online at Heidelberg University, Germany (UHD)

Author(s): Marcel Schaefer¹, Simone Barthold-Beß¹, Jürgen Debus², Lena Gebauer-Hötzel¹, Ina Niedermaier¹, Oliver Jäkel¹, Wolfgang Schlegel¹

¹Dept. Of Medical Physics In Radiation Oncology, German Cancer Research Center (DKFZ) Heidelberg, Germany, Heidelberg/GERMANY, ²Department Of Radiation Oncology And Radiation Therapy, Heidelberg University Hospital, Heidelberg/GERMANY

Purpose: UHD established two postgraduate MSc programs in Medical Physics. In 2010 the English speaking Master Online “Advanced Physical Methods in Radiotherapy” (APMR) started as first distance learning online program at UHD comprising three mandatory attendance phases (duration from 4-14 days) in Germany during the two years of study. Furthermore, since 2012 the International Master “Clinical Medical Physics” (CMP) is on offer in cooperation with Pontificia Universidad Catolica de Chile (PUC). CMP combines two on-site semesters in Chile taught in Spanish by PUC with a third online semester held in English by UHD. The students terminate their studies with a Master Thesis, written either at PUC or UHD.

After five years' experience in online teaching and learning we would like to present a first result of undertaken evaluations emphasizing on the importance of an ideal curriculum design for postgraduate students working in Medical Physics.

Material and Methods: The CMP program is designed for students from Latin America and it introduces the basics (such as Anatomy and Physiology or Physics of Radiation and Dosimetry) and advanced topics in Medical Physics (such as IMRT or IGRT) to students at the beginning of their professional career. In contrast the APMR program is dedicated to students with a clear background and professional experience in Medical Physics. Thus, it only concentrates on advanced topics such as IMRT, IGRT, Ion Therapy or Advanced Dosimetry and Quality Assurance to educate professionals from all over the world.

The modules of each program adopt the so called “blended learning approach”, a combination of online and on-site learning settings. Interactive synchronous online sessions, recorded video lectures and problem based discussions make effective use of emergent internet technologies for its learning objects while offering opportunities to practice skill and network with peers and teachers in hands-on attendance phases at modern radiotherapy facilities in Heidelberg for APMR students and in Chile for CMP participants.

At the end of each semester the students are asked to join formative anonymous online surveys as part of the evaluation system of UHD. Furthermore, during each attendance phase the students have feedback sessions with the program coordinators in order to discuss the last online modules without teachers. This allows students to give positive or even negative feedback in a private and secure setting.

Results: The qualitatively and quantitatively reviewed results of the surveys and the intensive face-to-face discussions represent the students' perspective of the e-learning approaches of both programs and allow us to deepen our understanding of special needs of professionals in the field of Medical Physics. The students reported their satisfaction about the curriculum design in the frame of a permanent supervision by both the teaching and coordinating team.

Conclusion: In conclusion both discussions and survey results helped us to improve our curriculum design. Our continuous modifications seem to be the key for our low drop outs during the last 4-5 years.

SP158.8 - Launching of the ASEAN College of Medical Physics

Author(s): Kwan Hoong Ng¹, Agnette Perio Peralta², Anchali Kri-sananchinda³, Djarwani S Soejoko⁴, James Cheow Lei Lee⁵, Nguyen Tan Chau⁶, Freddy Haryanto⁷, Supriyanto Ardjo Pawiro⁴, Chai Hong Yeong¹, Norial Jamal⁸, Marlon Raul Z Tecson⁹, Sakborey Chhom¹⁰

¹Department Of Biomedical Imaging, Faculty Of Medicine, University of Malaya, Kuala Lumpur/MALAYSIA, ²Center For Device Regulation, Radiation Health, And Research, Food And Drug Administration, Department of Health, Manila/PHILIPPINES, ³Department Of Radiology, Chulalongkorn University, Bangkok/THAILAND, ⁴Physics Department, University of Indonesia, Jakarta/INDONESIA, ⁵Division Of Radiation Oncology, National Cancer Centre, Singapore/SINGAPORE, ⁶Unit Of Pet-ct & Cyclotron, Cho Ray Hospital, Ho Chi Minh City/VIET NAM, ⁷Department Of Physics, Institut Teknologi Bandung, Bandung/INDONESIA, ⁸Planning And International Relation Division, Malaysia Nuclear Agency, Bangi/MALAYSIA, ⁹Medical Physics and Health Physics Services, Inc, Manila/PHILIPPINES, ¹⁰National Cancer Centre, Calmette Hospital, Phnom Penh/CAMBODIA

Medical physics is rapidly advancing in the world and the situation is the same in South East Asia. There is an acute need for both qualified and experienced medical physicists to work in hospitals throughout the region.

The Association of Southeast Asian Nations commonly known as ASEAN is a geo-political and economic organization of 10 countries located in Southeast Asia, which was formed on August 8, 1967. The member countries are Brunei, Cambodia, Indonesia, Laos, Malaysia, Myanmar, Philippines, Singapore, Thailand and Vietnam. The motto of ASEAN is “One Vision, One Identity, One Community”. Its aims include the acceleration of economic growth, social progress, cultural development among its members, and the promotion of regional peace.

The spirit of ASEAN resonates in the South East Asian Federation of Organizations for Medical Physics (SEAFOMP). The idea of setting up an organization for Southeast Asian medical physics societies was first mooted in 1996. During the International Organization of Medical Physics (IOMP) World Congress at Nice, the formation of SEAFOMP was endorsed by member countries and it was officially accepted as a regional chapter of the IOMP at the Chicago World Congress in 2000. SEAFOMP congresses have been held regularly since its inception and these congresses have stimulated much growth and progress in medical physics in the region.

After a long gestation period, another regional entity, the ASEAN College of Medical Physics, was born in October 2014 at the 12th Southeast Asian Congress of Medical Physics held in Ho Chi Minh City. The founding president of the College is Professor Kwan-Hoong Ng, president-emeritus of SEAFOMP. The secretariat is located in Indonesia.

The vision is to make the ASEAN College of Medical Physics (ACOMP) the premier education and training centre for medical physics in the ASEAN region. To achieve the vision, members will galvanise their talents to develop sustainable activities, and will take advantage of information and communications technologies to achieve their goals.

Some future activities being planned include schools on Monte Carlo simulation, advanced radiation dosimetry, radiation emergency and disaster management, non-ionizing radiation protection, and a project on radiation dosimetric intercomparison.

Finally, official recognition is being sought from international organizations such as the International Organization for Medical Physics (IOMP) and the International Atomic Energy Agency (IAEA). Endorsement and support from these bodies will be an added impetus to the success of the ACOMP.

SP159 - Transport and Physiological Modelling

TRACK 19: BIOPHYSICS AND MODELLING

SP159.1 - Dwarfing Big Data for Oncology Applications: Necessity and Possibilities

Author(s): [Issam El Naqa](#)

Oncology, McGill University, Montreal/QC/CANADA

Learning Objectives:

- 1) Review of big data applications in radiotherapy.
- 2) Side effects of integrative approaches
- 3) Statistical machine learning and decision theory

Title:

Dwarfing Big Data for Oncology Applications: Necessity and Possibilities

Abstract:

Radiotherapy is a natural resource of big data in terms of large volume, wide variety, fast velocity, and qualitative veracity. A typical radiotherapy treatment scenario can generate a large pool of information that is comprised of patient demographics, radiation dosimetry, multimodality imaging features, and biological markers over a treatment period that can span several weeks. This data constitutes a unique interface between clinical, physical, and biological data interactions. Efforts using commercial and in-house tools are carried out to facilitate data aggregation, sharing, and varying analytics in a secure environment. However, the classical p (variables) \gg n (samples) inference problem of statistical learning is challenged in the Big data realm and this is particularly true for oncology applications where p -omics is witnessing exponential growth while the number of cancer incidences has generally plateaued over the past 5-years leading to a quasi-linear growth in samples per patient. Within the Big data paradigm, this kind of phenomenon may yield undesirable effects such as echo chamber anomalies, Yule-Simpson reversal paradox, or misleading ghost analytics. In this presentation, we will discuss these effects as they pertain to radiotherapy and engage small thinking methodologies to counter these effects ranging from classical statistical techniques to modern machine learning approaches. We will particularly discuss the potential and application of semi-supervised learning methods to big data in radiotherapy, in which the data is partially labeled and the techniques occupy some middle ground between supervised learning (all the data are labeled) and unsupervised learning (data is unlabeled) approaches. We will contrast the application of these methods with other big data analytics as promising approaches for radiotherapy outcome prediction and decision support.

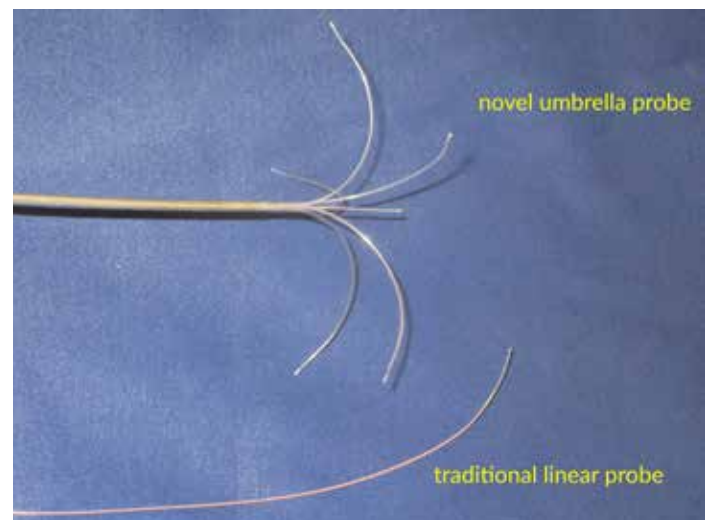
SP159.2 - Improved temperature monitoring and treatment planning for loco-regional hyperthermia treatments of Non-Muscle Invasive Bladder Cancer (NMIBC)

Author(s): [Gerben Schooneveldt](#)¹, Henry P. Kok¹, E.D. Geijssen¹, Fasco Van Ommen¹, Akke Bakker¹, Mattias Westendarp Zanartu², Jean J.M.C.H. De La Rosette², Maarten C.C.M. Hulshof¹, Theo M. De Reijke², Johannes Crezee¹

¹Radiotherapy, Academisch Medisch Centrum, AMSTERDAM/NETHERLANDS, ²Urology, Academisch Medisch Centrum, AMSTERDAM/NETHERLANDS

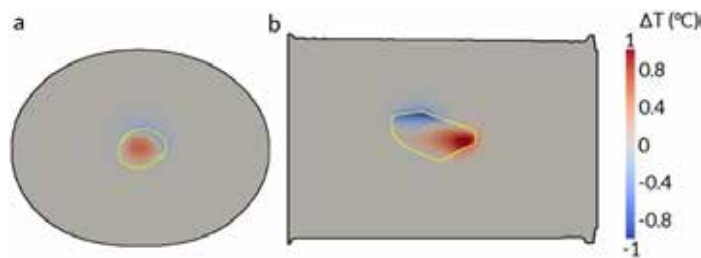
Introduction— Hyperthermia is a cancer treatment that increases the effectiveness of radiotherapy or chemotherapy by heating the tumor area to 41–43°C. Recently, a multi-center phase III randomized clinical trial comparing adjuvant treatment of NMIBC using Mitomycin C with and without loco-regional hyperthermia has started. This invites careful consideration of the bladder as a treatment site. Optimal treatment and quality control requires reliable thermometry and accurate hyperthermia treatment planning. This study aims to improve the current standard in both areas.

Materials and methods— We developed a novel multi-sensor ‘umbrella probe’ with five thermocouple probes to measure the bladder wall temperature, and a central probe measuring in the bladder center (Fig.1). We extended our treatment planning system with a fluid model computing the convective heat flow within the bladder. The umbrella probe was tested using phantom experiments comparing temperature measurements on the interior and exterior of a porcine bladder placed in tissue equivalent gel, and heated to reach a 4°C temperature rise. The experiments were simulated using both the new convective model and the standard treatment planning system.



Results— The umbrella probe temperature measurements at the interior bladder wall were comparable to temperatures measured on the bladder exterior but differed 0.5°C from temperatures in the bladder center.

The temperature distributions computed by the convective model and by the current treatment planning system showed good agreement within the phantom's gel regions; temperature differences between the models exceeded $\pm 1^\circ\text{C}$ inside the fluid and in neighboring tissue regions, *i.e.* the bladder wall (Fig.2).



Conclusions— The umbrella probe reliably measures the clinically relevant bladder wall temperature. The convective model is a marked improvement over the current treatment planning system in the region of interest. Explicit modeling of fluids is particularly important when the bladder or its direct vicinity are part of the hyperthermia treatment target area.

SP159.3 - A Full 3D CFD Model Coupled with an Outflow Lumped Boundary and Inflow Total Pressure Formulation to Estimate Human Cardiac Perfusion

Author(s): lyad Fayssal, Fadl Moukalled, Samir Alam, Robert Habib, Hussain Ismaeel
American University of Beirut, Beirut/LEBANON

There is discordance between the anatomic severities of the coronary narrowing and their corresponding functional significance, i.e. how much this narrowing is truly causing ischemia in the downstream perfused cardiac tissue bed. Fractional flow reserve (FFR) is among the physiological parameters invasively measured to assess the hemodynamic significance of a stenosis during maximal hyperemia with values ≤ 0.8 indicating vessel at risk for ischemia. Recently, noninvasive prediction of FFR was shown to be possible from noninvasive comprehensive predictive techniques involving computational fluid dynamics (CFD). In this work, a boundary condition formulation is suggested and coupled with a full 3D CFD model to estimate cardiac perfusion. The modeling process starts by truncating the domain of interest at a specific location and separating it from the vascular beds. A lumped dynamic model is considered and coupled to the 3D domain outlet boundary to account for the downstream effects from the vascular bed resulting from truncating the 3D domain. A generalized algorithm is established to handle the dynamic model at the outflow boundary to avoid/damp spurious numerical reflections. On the other hand, the inlet section of the domain is modeled with a total, rather than static, pressure formulation. The developed inflow and outflow boundary formulations coupled to the 3D CFD model allow characterizing the myocardial perfusion of the modeled vessel (i.e. determine the % loss in blood volume flow rate in stenosed arteries). The method is tested on idealized healthy and stenosed arterial branches and single segments under rest and hyperemic conditions. Results have revealed promising indications towards translating the developed methodology into clinical practice.

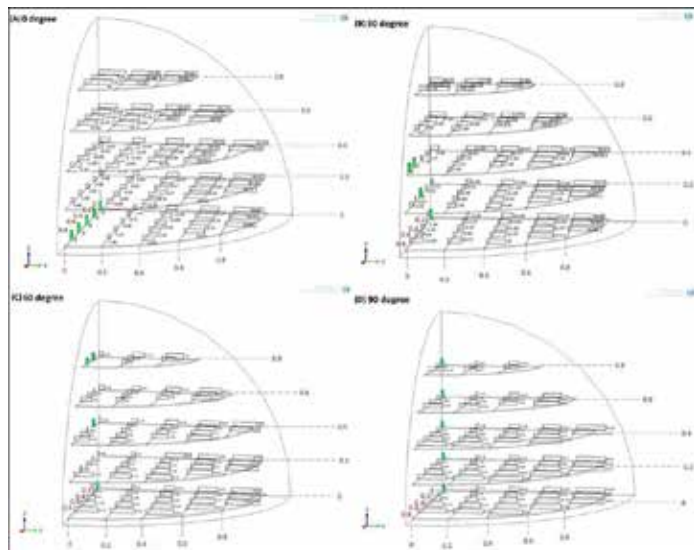
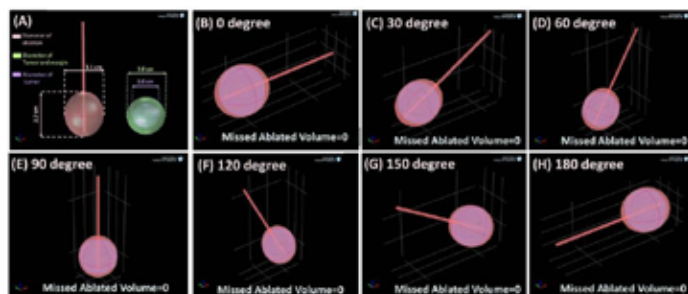
SP159.4 - Simulation Model of Image-Guided Percutaneous Thermal Ablation in the Assessment of Optimal Approach for Complete Tumour Ablation

Author(s): Sogol Givehchi, Basri Johan Jeet Abdullah, Chai Hong Yeong
Department Of Biomedical Imaging And University Of Malaya Research Imaging Centre, Faculty Of Medicine, University of Malaya, Kuala Lumpur/MALAYSIA

Purpose: To develop a 3D simulation for imaged-guided percutaneous thermal ablation of the liver tumours based on a geometrical model to investigate the ablation versus tumour volumes with varying needle position and angulations.

Materials and Methods: This study was carried out using Finite Element Analysis software (Comsol Multiphysics 4.3, COMSOL Inc, USA) to simulate a spherical tumour of 2 cm diameter and a radiofrequency ablation (RFA) needle from the Cool-tip RFA system (Covidien, Massachusetts, USA). Clinical margin of 0.5 cm surrounding the tumour was applied. Common points of intersection of axial, sagittal and coronal planes within the tumour volume were assigned as target sites for needle tip placement. The RFA needle was modeled to pass through the target sites with different angles before advancing it to the edge of the tumour margin. The target sites and the angles of needle insertion were considered as optimal approach if no missed ablation volume was observed within the tumour and its clinical margins.

Result: According to the simulation results, the target site at the epicenter of the tumour was identified as optimal location for needle tip placement despite any variations in needle angulations (Figure 1). Hence, identifying the epicenter of the tumour on the central slice of the axial images is essential for increasing the success rate of complete tumour ablation. Despite the epicenter, complete ablations are also possible by placing the needle tips at several sites as shown in Figure 2.



Conclusion: Complete ablation of the tumour can be constantly achieved by passing the needle through the epicenter of the tumour before advancing it to the edge of the tumour margin, regardless of the angles of the needle insertion. As the needle trajectory deviated from the epicenter, the risk of incomplete ablation increased with increasing angles of insertion.

SP160 - Neuroengineering, Neural Systems / Biophysics And Modelling

PRESIDENTS CALL

SP160.1 - From “Fracking” and “Macrovoids” to the Onset of Cancer Metastasis: A Mechano-Metabolomics Model of a Plausible Fluid-Solid Network Instability in Tumors

Author(s): Sai S. Prakash

Chemical & Biomolecular Engineering, Brady Urological Institute, Johns Hopkins University and Medicine, Pikesville-Baltimore/MD/ UNITED STATES OF AMERICA

Based on analogy and inductive reasoning, we postulate that a malignant tumor (carcinoma) grows in size until the “de-percolation” threshold of its encapsulating basement membrane (BM) which undergoes proteolysis during oncogenesis. Typically, BMs are composed of tri-continuous hydrogel networks of collagen-IV, laminin, and interstitial fluid, with connector proteins such as nidogens, and perlecan. The aforementioned threshold is determined by the mechanochemical state of the tumor-membrane complex vis-à-vis its microenvironment and, herein, conjectured to synchronize with the tensile yielding/rupture of the BM. Thereupon, peripheral cells of the tumor undergo epithelial-to-mesenchymal transitions (EMT), becoming motile, and migratory.

We test this postulate by formulating a mathematical model based on continuum fluid-solid mechanics, diffusion, and cell bioenergetics theories. This approach may be characterized as “mechano-metabolomics” modeling at the continuum scale and complements genomic, and proteomic approaches. In this model, a prototypical, viscous tumor spheroid grows radially, consuming metabolic nutrients (viz., glucose, oxygen, and lactate) while being constrained by an elastic BM ca. 0.5-2 microns-thick, and a network of linkages of cell adhesion molecules (CAMs), chiefly cadherins and integrins. A fundamental schema “induced” from geology and polymer physics is the fluid-solid mechanical network instability observed in rock formations during hydraulic fracturing (fracking) and during formation of synthetic asymmetric membranes (vis-à-vis large voids), respectively. Polymer physics also furnishes scaling concepts to develop equations of state for cells, and concepts describing cell and tissue rheology via gel poroelasticity theory. Besides, critical perspectives from other recent developments, viz., homeorhetic tumor pressures, mechanotransduction, and symbiotic glucose-lactate metabolism observed in cancer cells, are incorporated, to base the framework on well-grounded physicochemical principles in abiological and/or microbial systems. The nonlinear model is computationally analyzed via Comsol Multiphysics®.

The theoretical simulations (“*in silico* experiments”) lucidly support the *a priori* conjecture and are consistent with biological observations of oncogenesis *in vivo*, and physicochemical measurements *in vitro*. Computed stress-strain fields in the tumor microenvironment suggest that proteolyzed BMs, quantified by decreased elastic moduli, participate in aberrant tumor growth dynamics and likely undergo tensile rupture and stress localization-induced cellular detachments, initiating EMTs, and metastasis. Subsequent crack-tip stresses may also shift strains on CAMs from compressive to tensile, suggesting mechanotransduced conformational switches, such as from non-invasive, adherent E-cadherins to invasive N-cadherin phenotypes.

The model also provides a rationale to detect metastatic potential of tumors via a convenient diagnostic imaging tool such as positron emission tomography (PET). PET locates abnormally-high glucose uptake rates in cells and tissues, which are related to the mechani-

cal field evolution of the tumor microenvironment, and thereby, the likelihood of BM rupture. Complementarily, newer techniques that characterize tissue elasticity such as elastography may also be applied in concert with the developed framework.

A major conclusion of this research is that a hallmark of cancer may be a measurable, microscale “physical event” in contrast to nanoscale genomic or proteomic events. Besides proteolysis as a “proximal cause” to rupture, other cancer phenotypes such as higher proliferation rates, softer cells, fractality, etc., can also be incorporated into the model. Experimentation is required to verify the postulate.

SP160.2 - Surface electromyography in quantifying Parkinson’s disease and its treatment with deep brain stimulation

Author(s): Saara M. Rissanen¹, Zhe Li², Markku Kankaanpää³, Jian Wang⁴, Olavi Airaksinen², Pasi A. Karjalainen¹

¹Department Of Applied Physics, University of Eastern Finland, Kuopio/FINLAND, ²Department Of Physical Medicine And Rehabilitation, Kuopio University Hospital, Kuopio/FINLAND, ³Department Of Physical Medicine And Rehabilitation, Tampere University Hospital, Tampere/FINLAND, ⁴Department Of Physical Education, Zhejiang University, Hangzhou/CHINA

Parkinson’s disease (PD) is a progressive neurodegenerative disorder that affects millions of people worldwide. The disease cannot be cured but the motor symptoms can be relieved with medication or with deep brain stimulation (DBS). However, there is a lack of objective and quantitative methods for monitoring PD and the efficacy of its treatment. Finding these objective methods is a global challenge.

Surface electromyography (EMG) and a principal component (PC)-based monitoring method was used here for quantifying PD-characteristic features in the EMG signals. The aim was to find the most effective combination of EMG signal features for characterizing PD and its treatment with DBS. It was quantified, if the EMG signals of PD patients change into more similar with the signals of healthy subjects with DBS.

Two groups of PD patients (9 patients with DBS ON and OFF, and 22 patients with medication OFF) and one group of healthy subjects (13 age-matched subjects) were measured during isometric contraction of biceps brachii (BB) muscles and during elbow flexion-extension movements. Surface EMGs were recorded from BB muscles. Several parameters were calculated from the EMG signals. The following parameters worked best in discriminating between healthy controls and PD patients: recurrence rate, correlation dimension, sample kurtosis and crossing rate variable of EMG during isometric contraction, and EMG burst frequency, sample kurtosis and recurrence rate of EMG during extension movements. These variables were chosen to form feature vectors for each subject in the PC-based monitoring method. The analysis revealed clear differences in the EMG features between healthy controls and PD patients (see Fig. 1), and also between DBS OFF and ON. In eight out of nine patients, the surface EMG features changed into more similar with the features of healthy controls when the stimulator was switched on.

The results showed that surface EMG is capable of characterizing patients with PD and effects of DBS treatment. Surface EMG is therefore a potential method for monitoring PD and its treatment efficacy objectively and quantitatively.

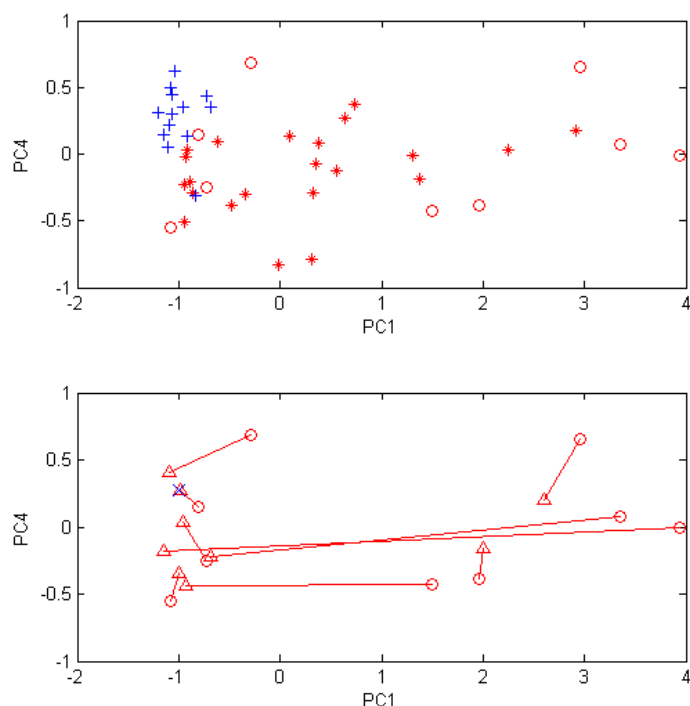


Fig. 1. PCs of 13 healthy controls (+), 22 PD patients with medication OFF (*), and 9 PD patients with DBS OFF (o) in the top figure. The PCs of the 9 PD patients with DBS OFF (o) and ON (Δ) in the bottom figure. The DBS OFF- and ON-states are connected with a line and the center of healthy controls is marked with a cross (x) in the bottom figure.

SP160.3 - A Decade of Experience with Intraoperative Micro-electrode Recording in Determining the Subthalamic Nuclei (STN) Deep Brain Stimulation – Lead Positions in 260 Parkinson Diseased Conditions in South India – A Retrospective Study

Author(s): Venkateshwarla R. Raju

Biomedical Eng & Neurology & Neurosurgery And, Nizam's Inst of Medical Sciences (NIMS) University & Hospital, HYDERABAD/INDIA

To study the correlation of microelectrode recording with final tract chosen during bilateral STN DBS performed at a specialized centre in South India in 260 Parkinson's disease (PD) Subjects (patients in disease states). In Parkinson's disease there is a decreased dopaminergic output from the substantia-nigra, which changes the firing patterns of many neurons of nuclei (the nucleus). One of the consequences is an increased firing from the neurons of subthalamic nucleus (STN) which by stimulating to the neurons of globus-pallidus interna (GPi) causes inhibition of thalamus and cortex causing slowing of voluntary movements. The STN is an almond shaped nuclei located in the midbrain, ventral to the thalamus, and bordered by zona incerta cerebral peduncle, medial lemniscus, SNpr,pc, red nucleus, etc. The simplistic view was supported by the fact that high-frequency current delivered to STN or GPi neurons or other neurons of basal ganglia (BG) which caused their inhibition improved indication of symptoms. It is now known that there is a significant change in the firing pattern and a reorganization of the entire basal ganglia with DBS. A retrospective study was carried out at a tertiary care NIMS - AP State University Super-specialized Hospital with a dedicated movement disorder unit from south India. 260 subjects (patients) with diagnosis of PD as per United Kingdom Parkinson disease society brain bank criteria were included. All the subjects were willing to undergo the procedure and fulfilled the following criteria to be eligible for STN-DBS, i.e., they had a disease

duration of more than 12 years, good response to levodopa, able to walk independently in drug 'on' state and had normal cognition. All the PD subjects who were wheel chair or bed bound, had dementia or severe psychiatric disturbances were excluded. Surgery was performed in all by a qualified neurosurgeon. Stereotactic targets were acquired employing a specialized system with a specially designed stereotactic CRW frame which has a luminant MR localizer to directly target points within the STN of brain. The targeting was performed according to Lozano's Technique – 2mm sections are taken parallel to the plane of anterior commissure –posterior commissure line and at the level with maximum volume of red nucleus, STN is targeted at 3mm lateral to the antero-lateral border of red nucleus. The MER itself is not a complete tool to clearly discriminate the optimal target as the line of the DBS lead may not correspond to the axis of the STN. Further the impedance of the microelectrode may vary as they may be influenced by the brain tissue and may not show a clear recording. However, MER definitely confirms the clear position of the electrodes and bolsters the confidence of the neurosurgeons that they are in the target. Further, the availability of MER recording results in a vast data in connection with the functioning on th neurons situated deep in the brain and may help in unraveling the mysteries of the brain. From our experience, we say that MER facilitates selection of the final electrode location in STN DBS.

SP160.4 - Vortex of the Magnetic Field on the Growth Rate of Escherichia Coli

Author(s): Teodoro Cordova - Fraga

Ingeniería Física, Universidad de Guanajuato, León/MEXICO

Vortex of the Magnetic Field on the Growth Rate of Escherichia Coli

J.C. Martínez: Academy of Mechatronics & Biotechnology Laboratory, Instituto Politecnico Nacional-UPIIG, Mineral de valenciana 200 Puerto interior 36275, Silao de la Victoria, GTO, Mexico., jcmartinez@ipn.mx

T. Cordova: Department of Physical & Engineering-DCI, Universidad de Guanajuato campus Leon Loma del Bosque N. 103, Lomas del Campestre, 37150 Leon, GTO, Mexico. theo@fisica.ugto.mx

P. Villegas: Biotechnology Laboratory, Instituto Politecnico Nacional-UPIIG, Mineral de valenciana 200 Puerto interior 36275, Silao de la Victoria, GTO, Mexico., movipa93@gmail.com

O. Díaz: Biotechnology Laboratory, Instituto Politecnico Nacional-UPIIG, Mineral de valenciana 200 Puerto interior 36275, Silao de la Victoria, GTO, Mexico., oscarimed@gmail.com

M. Vargas: Department of Physical & Engineering-DCI, Universidad de Guanajuato campus Leon Loma del Bosque N. 103, Lomas del Campestre, 37150 Leon, GTO, Mexico. mvargas@fisica.ugto.mx

A. E. Reyes: Biotechnology Laboratory, Instituto Politecnico Nacional-UPIIG, Mineral de valenciana 200 Puerto interior 36275, Silao de la Victoria, GTO, Mexico., areyes@ipn.mx

G. Basurto: Department of Natural Sciences-DCNI- Unidad Cuajimalpa, Universidad Autonoma Metropolitana Av.Vasco de Quiroga 4871, Santa Fe Cuajimalpa, 05300 Cuajimalpa de Morelos, México, D.F. normandox@hotmail.com

Corresponding Author: J.C. Martinez, Mineral de valenciana 200 Puerto interior 36275, Silao de la Victoria, GTO, Mexico. Telephone: +52 55 57296000 Extension 81301, jcmartinez@ipn.mx

Microorganisms are widely used in large-scale production of industrial items; therefore the bacterial growth is a key point in this technology development. In this study it is shown a non-chemical

growth acceleration system by the stimulation of magnetic field vortex on *Escherichia coli* (ATCC 9637). It was used a magnetic field intensity from 1.13 to 4.13 mT, it was applied for 6 h, in cycles with five different frequencies: 100, 800, 1500, 2450 and 2500 Hz, in the sinusoidal signal, the sample was a temperature of 37 °C and 150 rpm constant stirring. The results shown that magnetic stimulation has a proliferative effect when the effect when the stimulus is continuous comparing with either intermittent or un-stimulated samples. Growth of *Escherichia coli* (*E. coli*) could be altered under magnetic field induces effects. *E. coli*, so these cultures exhibited higher changes in its viability compared to unexposed cells. The increase in rates of microbial growth can accelerate some of the fermentative processes in the food industry, or allow greater obtaining of biomass of producer strains of molecules high biotechnological value as biopolymers, biopharmaceuticals and nanomaterials of biomedical use.

SP160.5 - Electro Magnetic Therapy and Laser in the Chronic Pain Of The Woman.

Author(s): Manuel E. Zuniga

Private, INTEGRAL MEDICAL CENTER, GUAYAQUIL/ECUADOR

Introduction: The medical Physics is the application of the physics to the medicine. It is a branch of the multidisciplinary physics. It applies the physical foundations in many therapeutic techniques. Luis Galvani in the century XVIII, scientist and Italian doctor discovered that the muscles and nervous cells were able to produce electricity. In the century XIX he developed himself to electromagnetism based on the relation electricity and human body, being developed thus new contributions to the treatment. These knowledge gave origin to new scientific areas like bio-electromagnetism. German scientific Helmholtz, was the first to demonstrate the electromagnetic action. In the Europe of century XVI, Paracelso used magnets to deal with a variety diseases. Two centuries later Mesmer became famous by treating many disorders with magnets.

OBJECTIVES: To apply the electromagnetic therapy for the chronic pain in the woman. To relieve the pain instantly. To suppress all chronic gynecological such as the pelvic inflammation, pain breasts, headache and others. To offer to well-being and satisfaction in the woman in few minutes.

Methods: Reviewing a meticulous clinical history for the pain. Determining that an organic cause does not exist. Making a careful and detailed physical examination. Determining the cause the pain. Evaluating the scale of pain. Applying the electromagnetic therapy related to laser. Applying (I10 N80) the suitable electrodes, at a frequency of 80 Hz in one weekly session of 2 minutes and for 5 weeks time. Obtaining of pressed magnetic fields and application of laser in the painful zone.

Results: In more than 20 years of treatment with electro-magnetic therapy and laser, the result for the population of patients was highly satisfactory with 90 % success. We have treated with patient with diagnosis of inflammatory pelvic disease and chronic pain, patients with mastalgia, migraine, fibromialgia, etc., all with excellent results. Patients of all ages that goes from 20 up to 80 years old. With this treatment of electro-magnetic therapy we stimulate the own body with the production of substances with analgesic effect, like the endorphins and others.

Conclusions: We conclude with the high effectiveness of the electro-magnetic therapy and laser. The therapeutic answer was outstanding and highly satisfactory. Valuing the subjective answer as much as the objective one. Comparing the therapeutic result of the pain before the electro-magnetic therapy and later of its implementation, the suspension of the pain was excellent after. The electro-magnetic therapy is an alternative medicine practice that implies the use of magnetic fields on the human body.

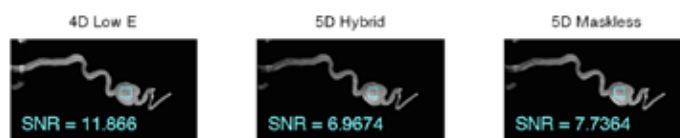
SP161 - Angiography / X-ray Imaging

TRACK 01: IMAGING

SP161.1 - 5D DSA Using Dual Energy Acquisition

Author(s): Gabe Shaughnessy, Charles Mistretta, David Dunkerley, Jordan Slagowski, Michael Speidel
Department Of Medical Physics, University of Wisconsin, Madison/ WI/UNITED STATES OF AMERICA

Traditional DSA techniques require the acquisition of mask and fill projections at a single energy. Acquisitions at two energies offer discrimination between materials, allowing a reduction in artifacts associated with misregistration of moving tissue/air interfaces, e.g. bowel gas. We are investigating the application of dual energy projection acquisition to time-resolved volumetric DSA (4D DSA). In the method termed "5D Hybrid DSA", dual-energy projections are acquired from both mask and fill rotations. We utilize a material decomposition algorithm separating high and low kV projections into two basis material projections of Iodine, which include bone, and soft tissue. This method serves to isolate the vasculature before being fed into the 4D reconstruction algorithms. The iodine basis images derived from a fill rotation employing fast-kV switching may provide enough data suitable for DSA reconstruction in a variety of applications. Therefore, we propose a "5D Maskless DSA" method which would allow lower total breath hold requirements compared to the usual mask plus fill approach. In a study in a dynamic aneurism phantom it was found that, when care is taken to remove residual bone and soft tissue signal in the iodine basis projections, a maskless dual energy method can provide time-attenuation curves that agree with conventional low energy 4D DSA to within 9% (RMSD). In the Figure, we present the MIPs of a time frame from the 5D DSA reconstructions along with the conventional 4D DSA from the low energy data for comparison. The SNR from the maskless and hybrid methods are competitive with the low energy 4D DSA.



SP161.2 - Investigation of Rhenium-Doped Microsphere-Based Contrast Agents for Diagnostic X-Ray Imaging

Author(s): José Carlos De La Vega¹, Bradford Gill², Katayoun Saatchi¹, Urs O. Häfeli¹

¹Faculty Of Pharmaceutical Sciences, The University of British Columbia (UBC), Vancouver/BC/CANADA, ²Radiation Oncology, BC Cancer Research Centre, Vancouver/BC/CANADA

The administration of iodine-based X-ray contrast agents (XCA) is the gold standard to enhance the contrast of blood vessels and soft tissues in computed tomography (CT). Nonetheless, large and repeated doses are required and severe adverse effects, such as contrast media induced nephrotoxicity and anaphylactoid reactions, occur at an incidence of 3 and 15% with low- and high-osmolality formulations, respectively. The objective of this study was to overcome these limitations by developing microspheres doped with a radiopaque element, like rhenium. These microspheres could potentially be used to appraise the biodistribution and kinetic degradation of polymeric drug delivery systems.

Since there is a positive correlation between the atomic number and

SP161.5 - Use of Conventional Regional DXA Scans for Estimating Whole Body Composition

Author(s): Mohammad Reza Salamat¹, Amir Hossein Salamat², Mahdi Asgari¹

¹Medical Physics And Biomedical Engineering, Isfahan University Of Medical Sciences, Isfahan/IRAN, ²Isfahan Osteoporosis Diagnosis Center, Isfahan/IRAN

BACKGROUND:

Using soft-tissue composition in conventional regional dual-energy X-ray absorptiometry (DXA) scans of the spine and hip to predict whole body composition (whole-body fat mass, whole-body lean mass and trunk-fat mass) instead of a whole body DXA scan.

Methods:

We identified 143 adult patients who underwent DXA evaluation of the whole body. Anthropometric indices were also measured. Data-sets were split randomly into two parts; the derivation set including a sample of 100 subjects, and the validation set including a sample of 43 subjects. Multiple regression analysis with the backward stepwise elimination procedure was used for the derivation set and the estimates were then compared with the actual measurements from the whole-body scans for the validation set. The R^2 (adjusted coefficient of multiple determination) and SSE (error sum of squares) criteria were applied to compare regression models.

Results:

Using multiple linear regression analyses, the best equation for predicting whole-body fat mass ($R^2 = 0.945$) included gender, height, weight, waist circumference (WC), spine fat fraction and hip fat fraction; the best equation for predicting whole-body lean mass ($R^2 = 0.970$) included gender, weight, WC, spine fat fraction and hip fat fraction; and the best equation for predicting trunk-fat mass ($R^2 = 0.944$) included gender, weight, spine fat fraction and hip fat fraction.

Conclusion:

The results of this study show that regional DXA scans of the spine and hip can be used to accurately predict body composition.

imaging at the Biomedical Imaging and Therapy beamline at the Canadian Light Source. Using the 311 reflection from a 511 silicon crystal wafer bent to a radius of 95 cm, the system prepares a 0.5 mm wide focused polychromatic x-ray beam with a spectral range of 27 keV to 43 keV, covering both the iodine and barium K-edges of 33.17 keV and 37.44 keV, respectively. As an example use, test objects with iodine and barium (common contrast agents used in clinical imaging) along with water and bone were imaged and successfully extracted independent quantifiable images of these four materials. The biomedical imaging system is presented with emphasis on the polychromator used to prepare the imaging beam.

SP161.6 - Multiple Energy Synchrotron Biomedical Imaging System- Preliminary Results

Author(s): Basseyy Basseyy¹, Mercedes Martinson¹, Nazanin Samadi², George Belev³, Cahit Karanfil⁴, Dean Chapman⁵

¹Physics And Engineering Physics, University of Saskatchewan, Saskatoon/CANADA, ²Bimedical Engineering, University of Saskatchewan, Saskatoon/CANADA, ³Experimental Facilities Division, Canadian Light Source Inc., Saskatoon/SK/CANADA, ⁴Physics, Muğla Sıtkı Koçman University, Muğla, Turkey, Kötekli-Muğla/TURKEY, ⁵Anatomy & Cell Biology, University of Saskatchewan, Saskatoon/CANADA

The drive to improve and expand the amount of information extracted from various imaging modalities has led to the use of multiple (usually two) x-ray photon energies in computed tomography clinical systems. With the use of a single photon energy, the ability to differentiate soft from hard tissues is a problem which multiple energy imaging can solve. The continuous spectrum available from synchrotron light facilities provides a nearly an ideal source for multiple energy imaging. For living biological subjects a multiple energy system that can extract multiple endogenous or induced contrast materials as well as water and bone images would be ideal. A novel bent Laue single crystal monochromator that has a wide angularly dispersed energy range (polychromator) has been developed to explore the use of multiple energies simultaneously for biomedical

SP162 - Ultrasound and OCT: Applications

TRACK 01: IMAGING

SP162.1 - Endoluminal Ultrasound Biomicroscopy for in vivo detection of caustic esophagitis in rats

Author(s): Rodrigo D.M. Gomes¹, Rossana C. Soletti², João C. Machado³

¹Post-graduation Program In Surgical Sciences/department Of Surgery, Federal University of Rio de Janeiro, Rio de Janeiro/BRAZIL, ²Pharmacy Unit, Centro Universitário Estadual da Zona Oeste, Rio de Janeiro/BRAZIL, ³Biomedical Engineering Program/coppe, Federal University of Rio de Janeiro, Rio de Janeiro/BRAZIL

Introduction: the ingestion of caustic substances constitutes a serious public health problem and a pediatric emergency that can lead to serious sequelae. The majority of these accidents occur in the home environment where children ingest cleaning products. Among adults, the caustic ingestion is usually intentional and related to suicide. The most serious complication in the short term following caustic consumption is the esophagus perforation, which can lead to mediastinitis and death. Therefore, a diagnostic technique to evaluate the damage to the esophagus wall is important and endoscopy is primarily employed. Nevertheless, it is a technique that does not provide visualization across the esophagus wall. Recently, a high frequency (40 MHz) minimally invasive imaging ultrasound technique, named endoluminal ultrasound biomicroscopy (eUBM), was implemented to diagnosis small animal digestive diseases. The eUBM has been used successfully in longitudinal studies to follow-up the growth and differentiation of colon tumors, or even in the diagnostic evaluation of inflammatory lesions in the digestive tract, of small animal models. So far, reports related to the use of eUBM in the evaluation of inflammatory and neoplastic diseases in rat esophagus has not been found.

Objective: to explore the use of eUBM as diagnostic technique at the acute phase of esophageal caustic lesions in rats.

Methods: eight Wistar rats were used and distributed into groups I (injured esophagus) and S (sham), of four rats in each. The animals in group-I received sodium hydroxide (NaOH) at 20%, to cause caustic injury, through a catheter inserted into the distal esophagus while those in group-S received saline. Twenty-four hours after caustic burn induction, the animals in group-I were examined simultaneously through endoscopy and eUBM. Prior to esophagus inspection, the animals were anesthetized with intraperitoneal administration of ketamine (50 mg/kg) and xilazine (5 mg/kg) and thereafter accommodated on an intubating rat platform and intubated. The eUBM system contained an ultrasound mini-probe catheter that rotated 360° around its axis, providing cross-sectional ultrasound images of the esophagus wall. The ultrasound mini-probe was inserted into the accessory channel of a flexible choledochoscope (2.5 mm outer diameter), allowing simultaneous acquisition of endoscopic and eUBM images. During the procedure, the esophagus was irrigated with saline, injected through a flush port on the mini-probe catheter that acted as the ultrasound coupling medium between the transducer and the esophagus wall. After inspection, the esophagus was removed for histological examination.

Results: eUBM images of all animals of group-I presented erosions and ulcers, which had correspondence with histological and endoscopic findings. Additionally, eUBM revealed thickened wall and ulcers reaching up to the esophagus muscle layer, which was not possible to observe from endoscopy. For the animals in group-S, eUBM revealed the esophagus wall without any change, with intact layers.

Conclusion: eUBM is an imaging method able to accurately assess the acute inflammatory lesions caused by caustic agents in the esophagus of rats.

SP162.2 - To tap or not to tap: A comparison of cranial 3D to 2D ultrasound in extremely preterm neonates with post-hemorrhagic ventricle dilation to predict the necessity of interventional ventricular tap

Author(s): Jessica Kishimoto¹, Walter Romano², David S.C. Lee², Sandrine De Ribaupierre², Aaron Fenster¹

¹First Floor Imaging, Robarts Research Institute, London/CANADA, ²Western University, London/CANADA

Introduction

Preterm babies are at risk of post-hemorrhagic ventricle dilation (PHVD), which has been linked to brain injury and morbidities such as poor motor coordination and cerebral palsy. PHVD is currently monitored with 2D cranial ultrasound (US), though no consensus has been determined for when interventional surgical therapy is required. Patients with rapid PHVD will require interventions known as 'taps' to remove excess cerebral spinal fluid from the ventricles to prevent further brain injury through excess intracranial pressure. Ventricle volumes (VV) derived from 3D US will be able to distinguish neonates with rapidly increasing VV versus those with stable ventricles.

Methods

The novel 3D US system used in this study has been previously validated in the laboratory through phantom experiments as well as in an *in vivo* study. Neonates with PHVD were enrolled into the present study after informed parental consent following a protocol approved by the REB. Clinical 2D US and 3D US images were acquired within 10 minutes of each other 1-2 times per week throughout the patient's stay in the Neonatal Intensive Care Unit (usually 2-4 months) and analyzed offline. Linear estimates of the ventricles' size (Levene's index (LI), anterior horn width (AHW), third ventricle width (3rd w), and thalamo-occipital distance (TOD)) were measured on the 2D images by a collaborating radiologist. Ventricle volume (VV) was measured from 3D US images by a trained observer and reviewed by a collaborating clinician. Changes in the measurements between subsequent image sets were recorded for each patient.

Results

162 imaging sets were collected from 19 very preterm neonates with PHVD. Strong correlations were found between VV and AHW, 3rd w, and TOD ($R^2 > 0.71-0.78$), while moderate correlations were found between VV and LI ($R^2 = 0.60$). No strong correlations were found between changes in ventricle volume and changes in 2D US measurements ($R^2 < 0.50$). The rate of change in 3D US VV were significant different ($p < 0.001$) between infants requiring an intervention and infants with spontaneously resolved PHVD. No such sig. difference was found using 2D US derived measurements.

Figure 1 a) coronal 2D US image depicting linear measurements used in the study b) segmented 3D US image of a neonate with PHVD

Discussion/Conclusion

While 2D US measurements are reasonable estimates of VV, changes in the measurements are not good indicators of changes in VV. As such, clinicians cannot reliably use changes in 2D US based measurements to determine if a patient has dilating ventricles. This could lead to neonates experiencing dangerous increases in intracranial pressure to have a delay in treatment until more symptoms emerge causing further brain injury. 3D US VV enables better, more

confident monitoring of progressive ventricular enlargement, and seems to predict which patients could require interventional therapy, though a study on a larger cohort would be required to confirm.

SP162.3 - Endoleak and Thrombus Characterization with Dynamic Elastography after Endoleak Embolization following Aneurysm Endovascular Repair

Author(s): Antony Bertrand-Grenier, Fatemeh Zehtabi, Claude Kauffmann, Guy Cloutier, Sophie Lerouge, Gilles Soulez
Centre De Recherche Du Centre Hospitalier De L'université De Montréal, Université de Montréal, Montréal/CANADA

PURPOSE

Supersonic Shear Wave Imaging (SSWI) can be used to measure the tissue elasticity in real-time. Our goal is to characterize the mechanical properties of abdominal aortic aneurysm (AAA) after endovascular aneurysm repair (EVAR) in a canine model (endoleaks, thrombus, walls) and compare the results with CT-Scan, Doppler Ultrasound (DUS) and pathologic findings.

METHODS AND MATERIALS

EVAR was done with creation of type I endoleak in 18 aneurysms created in 9 dogs (common iliacs arteries). Two embolization gels, Chitosan (Chi) or Chitosan-Sodium-Tetradecyl-Sulfate (Chi-STS) were injected in the sac to seal the endoleak and promote healing. SSI and Doppler Ultrasound were performed at baseline (implantation, 1-week, 1-month, 3-months) whereas angiography and CT-scan were performed at sacrifice. Macroscopic and histopathological analyses were processed to identify and segment five different regions of interest (ROIs): endoleak, fresh or organized thrombus, Chi or Chi-STS. Elasticity modulus values were compared in these ROIs.

RESULTS

At sacrifice, 10 aneurysms had endoleaks, 9 had fresh thrombus, 15 had organized thrombus and 3 were completely sealed. At 3 months, elasticity modulus (in kPa) of 0.1 ± 0.2 , 9.2 ± 3.5 , 47.3 ± 25.7 , 55.9 ± 21.7 and 69.6 ± 29.0 were respectively found in endoleak, fresh and organized thrombus, Chi and Chi-STS regions. Elasticity values of endoleak and fresh thrombus areas were significantly lower than organized thrombus, Chi and Chi-STS areas ($p < 0.001$). Elasticity values of fresh thrombus ranged between 3 and 19 kPa (8.7 ± 3.6 kPa) at 1-week and 30.2 ± 13.8 kPa at 3-months indicating that SSI can evaluate thrombus maturation. Aneurysm with fresh thrombus did not shrink as fast as aneurysm with only organized thrombus.

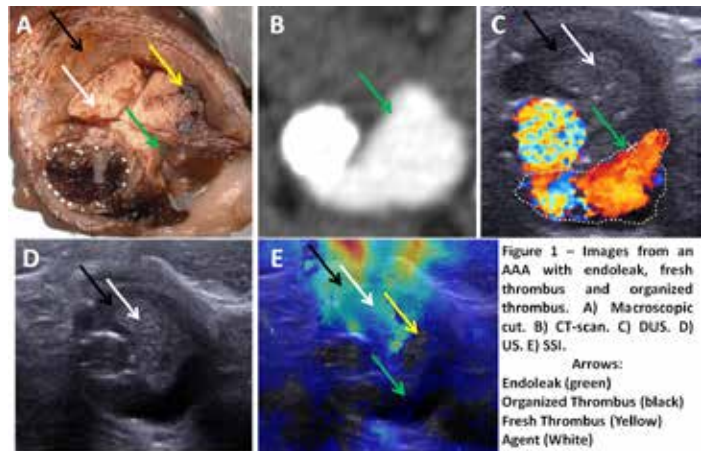
CONCLUSION

The results show that SSWI was able to characterize thrombus organization, embolization agents and healing over time after endoleak embolization following EVAR. The next objective is to evaluate in clinical study the feasibility and efficacy of this approach.

CLINICAL RELEVANCE/APPLICATION, NEW OR BREAKTHROUGH WORK TO BE PRESENTED

1. The Supersonic ShearWave Imaging was able to detect endoleak in real-time.
2. This technic has the potential to characterize thrombus organization within the aneurysm sac and in particular fresh thrombus which is associated with endoleak and endotension. The SSWI was able to distinguish fresh thrombus that cannot be detected on CT-scan (actual gold-standard).
3. The SSI can complement conventional DUS in post-EVAR surveil-

lance since the same machine can be used for both examinations. It could reduce the cost, the exposition to ionizing radiation and nephrotoxic contrast agents of surveillance CT-Scan follow up of AAA after EVAR.



SP162.4 - Detecting lipid-rich artery plaque using a handheld photoacoustic imaging device

Author(s): Susumu Hirano¹, Tsuyoshi Shiina¹, Takeshi Namita¹, Kengo Kondo², Makoto Yamakawa³

¹Graduate School Of Medicine, Human Health Sciences, Kyoto University, Kyoto/JAPAN, ²Center For The Promotion Of Interdisciplinary Education And Research, Kyoto University, Kyoto/JAPAN, ³Advanced Biomedical Engineering Research Unit, Kyoto University, Kyoto/JAPAN

Objectives: Carotid atherosclerotic plaque rupture is a cause of brain infarction. To prevent plaque rupture, it is important to detect the lipid-rich vulnerable plaque. However, it is not easy to evaluate such plaque by conventional medical imaging. Photoacoustic imaging is investigated as a novel modality of visualizing the difference of tissue characteristics. We have developed a handheld photoacoustic imaging device and tried to evaluate the possibility to detect lipid-rich artery plaque with it in phantom experiments.

Methods: Carotid artery plaque was modeled by injecting beef fat into a bovine aortic wall. The bovine aorta was submerged in saline. Light of a pulse-laser source is conducted to the measurement cross section of the ultrasound probe by holding a bundle of optical fibers close to the probe. Light at wavelengths of 800-1400nm was irradiated. The photoacoustic signal distribution was measured as photoacoustic images.

Results : In photoacoustic images at wavelengths where lipid absorbs light highly, strong photoacoustic signals were observed from the boundary between fat and the vessel wall. Figure 1 presents the spectrum of photoacoustic signals from the boundary. Although peak wavelengths subtly differ between the above spectra and the absorption spectrum of lipid, the shapes of the spectra are similar. At wavelengths of 1240-1300nm where the lipid spectrum shape differs, the similarity between the photoacoustic spectra and the absorption spectra was evaluated by calculating the correlation coefficient. As shown in Fig. 2, there is high correlation at the boundary between fat and the vessel wall.

Conclusion: The possibility of detecting lipid-rich plaque was confirmed based on an analysis of the photoacoustic spectrum. For future work, there are some issues to consider, such as experiments using more realistic models considering blood, its flow, and subcutaneous tissue; optimization of irradiated light intensity; selection of appropriate wavelength; and signal processing to improve SNR.

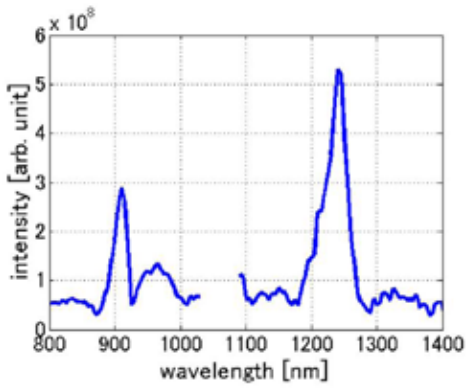
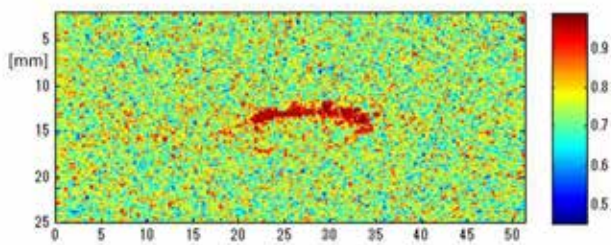
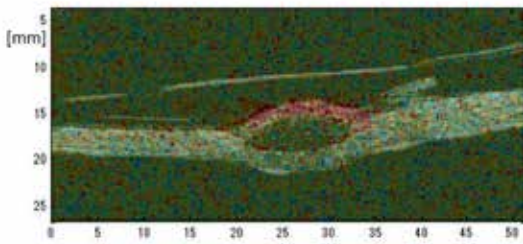


Fig.1 A spectrum of photoacoustic signals observed from boundary between fat and the vessel wall



(a) Distribution of correlation coefficient between absorption spectra of lipid and spectra of photoacoustic signals



(b) Superimposition of detected lipid-rich area on B-mode image

Fig. 2 A result of phantom experiment

SP162.5 - Intersex differences in posterior eye chamber by spectral optical coherent tomography

Author(s): Karina Maciejewska, Iwona Pajonk, Zofia Drzazga
 Medical Physics, A Chelkowski Institute of Physics, University of Silesia, Katowice/POLAND

Optical coherent tomography (OCT) is a modern, non-invasive interferometric imaging technique. In our research, it was used to scan retina in young, healthy group of students in order to investigate the intersex differences in the structures of retina layers and its elements. 24 healthy eyes with normal vision were examined using SOCT Copernicus HR device. SOCT scans were conducted for a fovea of retina and in region of optic disc with the use of 3D, Asterix and Circle modes. In general, 120 measurements were performed. In obtained scans, the distance between RPE (retina pigment epithelium) and choroid was smaller in women than in men group, what seems to be the reason of a thinner retina in women. Analysis of optic disc revealed significantly higher rim area in women group than in men, but a little lower cup/disc ratio. These findings may be of a great importance in diagnosis glaucoma and other eye diseases when comparing intersex results.

SP162.6 - Longitudinal Analysis of 3D Pre-Term Neonatal Ventricle Ultrasound Images

Author(s): Wu Qiu, Jing Yuan, Jessica Kishimoto, Sandrine De Ribaupierre, Aaron Fenster
 Robarts Research Institute, University of Western Ontario, London/CANADA

Intraventricular hemorrhage (IVH) is a major cause of brain injury in preterm neonates. Measuring ventricular dilatation or shrinkage quantitatively is an important step in monitoring patients and evaluating treatment options. 3D ultrasound (US) has been developed to monitor ventricle volume as a biomarker for ventricular dilatation and deformation. Ventricle volume as a global indicator, however, it does not allow for the precise analysis of local ventricular changes, which could affect specific white matter bundles, such as in the motor or visual cortex, and could be linked to specific neurological problems often seen in this patient population later in life. In this work, we report a spatial-temporal nonlinear registration approach, which is applied to analyze the detailed local changes of the ventricles of preterm neonates with IVH from 3D US images. In particular, we employ a novel sequential convex/dual optimization to efficiently extract the optimal spatial-temporal deformation, which simultaneously optimizes the sequence of 3D deformation fields. The experiments with four patients with 4 time-point images for each patient showed that the proposed spatial-temporal registration approach accurately and efficiently recovered the longitudinal deformation of the ventricles from 3D US images, generating a Dice similarity coefficient (DSC) of $81.0\% \pm 2.2\%$, a the mean absolute surface distance (MAD) of 0.5 ± 0.5 mm and a maximum absolute surface distance (MAXD) of 3.0 ± 2.1 mm by comparing the registered follow-up image with corresponding baseline image. The obtained results suggests that the proposed approach may be potentially used to analyze the change pattern of cerebral ventricles of IVH patients, their response to different treatment options, and to elucidate the deficiencies that a patient will have later in life.

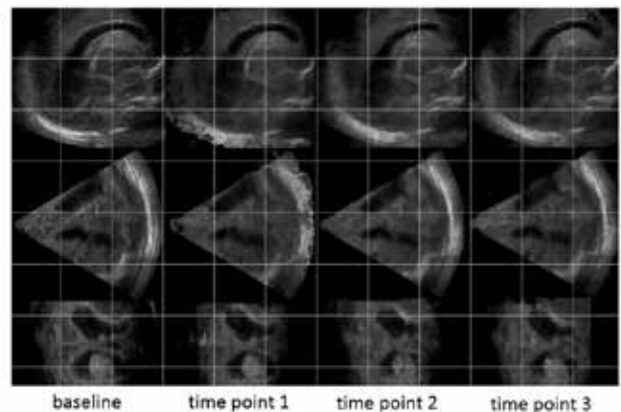


Figure 1. An example of registration results of 3D ventricle US images of an IVH neonate. 1 - 4 columns: baseline, registered images at time points 1-3. The first - third row: sagittal, coronal, and transversal view.

Table 1. Registration results of 4 patient images (4 time points each patient) in terms of DSC, MAD, and MAXD (p1-p4: patient ID), represented as the mean \pm standard deviation.

		p1	p2	p3	p4	All
DSC (%)	Rigid	65.2 ± 2.5	71.3 ± 4.5	67.5 ± 2.8	63.5 ± 3.3	66.9 ± 4.2
	Non-rigid	79.2 ± 1.5	83.6 ± 1.8	82.5 ± 2.5	78.6 ± 2.0	81.0 ± 2.2
MAD (mm)	Rigid	1.2 ± 0.8	0.9 ± 0.7	1.1 ± 1.0	1.3 ± 1.2	1.1 ± 1.2
	Non-rigid	0.6 ± 0.3	0.5 ± 0.2	0.4 ± 0.5	0.6 ± 0.7	0.5 ± 0.5
MAXD (mm)	Rigid	7.5 ± 3.5	5.2 ± 4.5	8.0 ± 5.2	6.5 ± 3.8	6.8 ± 4.5
	Non-rigid	3.2 ± 1.5	2.5 ± 2.0	3.0 ± 2.1	3.4 ± 1.8	3.0 ± 2.1

SP162.7 - Breast Invasive Ductal Carcinoma Assessed by Conventional Ultrasound and Contrast-Enhanced Ultrasound in Different T-Stages

Author(s): Yanchun Zhu¹, Zhiyuan Wang², Yaoqin Xie¹
¹Institution Of Biomedical And Health Engineering, Shenzhen Institutes Of Advanced Technology, Chinese Academy of Sciences, Shenzhen/CHINA, ²Department Of Ultrasound, Hunan Cancer Hospital, Changsha/CHINA

BACKGROUND: Accurate assessment of tumor size is necessary when selecting patients for breast-conserving surgery. There was little evidence of an association between conventional Ultrasound (US) and Contrast-enhanced US (CEUS) in predicting T stage of Breast Invasive Ductal Carcinoma (BIDC).

OBJECTIVE: The purpose of this study was to explore the value of CEUS in measuring the size and predicting T stage of BIDC.

Methods: Conventional US and CEUS were performed before pathology examinations by using a Siemens-Acuson S2000 scanner. One hundred and six patients confirmed with nodules of BIDC were included in the study. Person's correlations, linear regression and Wilcoxon signed-rank test were used to evaluate the relationship between two methods.

Results: Among 106 nodules, there were 16 nodules in T1 stage, 71 nodules in T2 stage and 19 nodules in T3 stage. The results show that CEUS consistently enlarge tumor size measurement: the width differences were 3.11±1.34mm, 3.91±1.78mm and 3.16±2.56mm for T1, T2 and T3 stages, respectively; and depth differences were 1.96±1.13mm, 2.47±1.19mm and 2.34±1.77mm for T1, T2 and T3 stages, respectively. As shown in Figure 1, significant correlations were observed between size measurements of US and CEUS (width measurement: $r = 0.908$, $r = 0.925$ and $r = 0.927$ for T1, T2 and T3 stages respectively; depth measurement: $r = 0.959$, $r = 0.971$ and $r = 0.976$ for T1, T2 and T3 stages respectively; all $P < 0.001$). Linear regression models similar among different T stages.

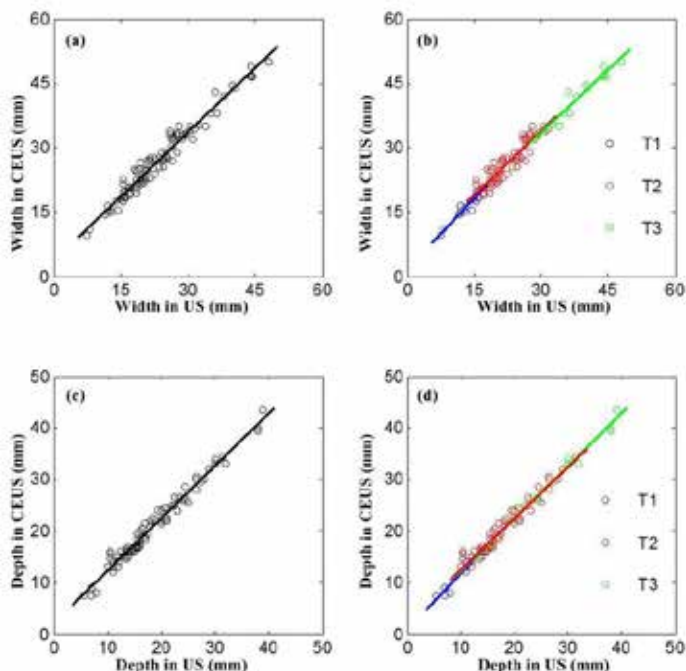


Figure 1. Comparison of CEUS and US measurements of all subjects and subjects with different T-stages.

Conclusions: In conclusion, this study suggests that larger size measured by CEUS than US. CEUS is a useful method for measuring the size and predicting the T stage of BIDC.

SP162.8 - Comparison of ultrasound systems in scoliosis measurement

Author(s): Maggie Hess¹, Daniel Borschneck², Gabor Fichtinger³, Tamas Ungi¹
¹School Of Computing, Queen's University, Kingston/CANADA, ²School Of Medicine, Queen's University, Kingston/CANADA, ³School of Computing, Queen's University, Kingston/ON/CANADA

Introduction:

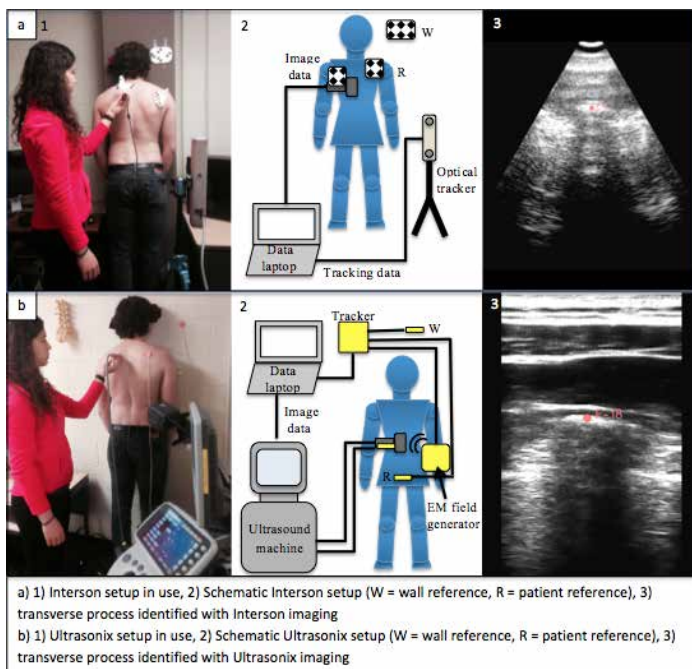
Idiopathic scoliosis is the most frequent spinal deformation presenting as a spatial deviation from the medial vertebral line. It is diagnosed in early adolescence and monitored until adulthood when surgical correction may happen. Patients are monitored by X-ray imaging every 3-6 months, exposing them to aggregating ionizing radiation, which increases the risk of cancer. Tracked three-dimensional ultrasound imaging allows for risk-free and accurate measurement of spinal curvature (Ungi et al. Ultrasound Med Biol, 2014). In this work, we compared the utility of inexpensive portable ultrasound with more expensive stationary ultrasound in spinal curvature measurement.

Methods:

An open-source tracked ultrasound based scoliosis measurement platform (Ungi et al. Ultrasound Med Biol, 2014) was utilised. This system is based on the SlicerIGT (www.SlicerIGT.org) open source environment that allows for seamless swapping among tracking devices and ultrasound scanners without requiring any programming or engineering development work. Two configurations of this system (Figure 1a) were compared: Interson USB ultrasound (Interson Corp, Pleasanton, CA, USA) with optical MicronTracker Hx60 (Claron Technology Inc., Toronto, ON, Canada); and Sonix Touch (Ultrasonix, Richmond, BC, Canada) with electromagnetic Ascension M180 (Ascension, Milton, VT, USA). In both configurations, a reference marker was attached to the patient and to the wall to compensate for gross body motion during ultrasound scanning. The intrinsic accuracy of SlicerIGT with both optically and electromagnetically tracked ultrasound was previously analyzed (Lasso IEEE TBME, 2014). This work focused on ultrasound image utility. Three human volunteers were scanned downward from the 7th cervical vertebra along the thoracic and lumbar regions. Two physicians experienced in spine ultrasound evaluated the visibility and clarity of the tip of transverse process, the anatomical feature that is necessary for curvature measurement.

Results and Conclusions:

For both physicians, in all patients and in all vertebrae, the transverse process tip (N=102) was clearly visible with both Interson and Ultrasonix, without failure. In the hands of these two experienced physicians, the Interson and Ultrasonix scanners were functionally identical for the purpose of scoliosis measurement. The Interson scanner costs only \$3,500. The optical and electromagnetic trackers cost about the same. The complete system with Interson, Micron tracker and laptop computer easily fits into a backpack. Altogether this configuration offers a highly portable, inexpensive and risk-free solution for ultrasound-based scoliosis monitoring and it may also open the way for scoliosis screening and be adopted in chiropractic care.



SP163 - Primary Dosimetry Standards

TRACK 05: DOSIMETRY AND RADIATION PROTECTION

SP163.1 - Candidate Technologies for Next-Generation Dosimetry Standards

Author(s): [Ronald Tosh](#)

Radiation Physics Division, NIST, Gaithersburg/MD/UNITED STATES OF AMERICA

Primary standard instruments are broadly understood to be capable of realizing the unit of a physical quantity directly, according to its definition from basic physical principles, and because of their fundamental role in the calibration chain ideally possess the highest attainable accuracy and precision permitted by the state of the art. Because of its highly complex interactions with matter, however, ionizing radiation poses special challenges for its metrology and for the establishment of primary standards in which the measurand and the resulting units of measurement can be readily abstracted from the target material and physical attributes of the radiation source. This poses certain difficulties for advancing the state of the art in the quest for candidate technologies on which to base next-generation primary standards.

The extent to which this situation has inhibited the migration of technological advances from allied fields into radiation metrology may be difficult to ascertain, but is suggested by the resemblance of present-day water calorimeters to the earliest prototypes, developed decades ago, in which radiation-induced temperature rise is measured with thermistor probes sealed in a glass vessel. Heat transfer and scattering perturbations attributable to these components are well understood, however even when correction factors are readily obtainable the resulting instrument is still limited for use at fixed depth in static, flat radiation fields.

Remote detection of temperature rise by use of light or ultrasound is well established in non-destructive testing, but its use here, to detect the temperature field in an irradiated volume would seem to offer distinct advantages for the dosimetry of certain nonstandard beams and, more generally, for spatial mapping of dose distributions within matter. At NIST, both ultrasonic and optical techniques have been developed and exploited for high precision thermometry of water for purposes of radiotherapy-level dosimetry. In the case of ultrasound, work proceeds along two general lines, development of an imaging array for obtaining dose distributions in water and specialized studies with fewer transducers investigating detection limits and strategies for recovering faint signals. Parallel work using lasers in place of the ultrasound has yielded therapy-level dose measurements in both water and PMMA, and, via the use of sensitive interferometric techniques, shows considerable promise for exceeding the thermal sensitivity achievable with existing calorimetry systems.

Realization of an imaging calorimeter based on light or ultrasound remains a distant goal, however, with many technical hurdles yet to overcome, and thus work also continues on ways to adapt and improve thermistor-based systems for new primary standards for radiotherapy beams, and, most recently, for CT beams. A prototype calorimeter with thermistor beads embedded in a polystyrene core has been used in a HDPE phantom subjected to therapy-level radiation from a clinical accelerator and diagnostic-level radiation from a CT imaging system. With further refinements, the anticipated instrument would provide a calorimetry response to dose spanning over 3 orders of magnitude for beam energies ranging from keV to MeV, potentially making the system a portable "universal" primary reference standard that only requires electrical calibration of the thermistors.

SP163.2 - Absorbed dose to water measurements in a clinical carbon ion beam using water calorimetry**Author(s):** Julia-Maria Osinga¹, Steffen Greilich², Oliver Jäkel³, Ulrike Ankerhold¹, Achim Krauss¹¹Department Of Dosimetry For Radiation Therapy And Diagnostic Radiology, Physikalisch-Technische Bundesanstalt (PTB), Braunschweig/GERMANY, ²Division Of Medical Physics In Radiation Oncology, German Cancer Research Center (DKFZ), Heidelberg/GERMANY, ³Heidelberg Ion-Beam Therapy Center (HIT), Heidelberg/GERMANY

Introduction: Until now, dosimetry of heavy ions with ionization chambers has not reached the same level of accuracy as dosimetry of conventional high-energy photons. The standard uncertainty associated with carbon ion dosimetry is about a factor of 3 higher as compared to high-energy photons [1]. This is mainly caused by the limited knowledge of the so-called $k_{Q,Q0}$ factor, which corrects for the different response of the ionization chamber to the actual user beam quality Q (here: ^{12}C) compared to the reference beam quality $Q0$ (here: ^{60}Co). A significant discrepancy between fluence- and ionization-based dose measurements in carbon ion beams was shown in a previous study [2], which could indicate an inaccurate $k_{Q,Q0}$ factor. The $k_{Q,Q0}$ factor is, up to now, determined by calculations based on cavity theory and Monte-Carlo transport simulations and asks for experimental verification. This can be done by use of a primary standard for absorbed dose to water that allows for a direct calibration of the chamber in the user beam quality Q . Therefore, a project was initiated to perform absolute absorbed dose to water measurements in carbon ion beams by water calorimetry [3] to determine the $k_{Q,Q0}$ factor with a lower standard uncertainty.

Materials and Methods: The water calorimeter measurements at HIT had to be adjusted to the specific conditions, namely (1) the irradiation with a pulsed beam using the raster-scan method and (2) the off-isocenter position of the calorimeter. Therefore, a number of investigations were required prior to the calorimetric measurements to determine and optimize the beam parameters at the measurement position complying with the following requirements: Firstly, the irradiation time needs to be as short as possible to minimize heat conduction effects occurring during the calorimetric measurements. At the same time, a homogenous and reproducible dose distribution is necessary to achieve a low standard uncertainty in the subsequent calorimetric measurements. To perform the corresponding investigations, a water-equivalent slab phantom was designed to mimic the real measurement condition of the calorimeter offering high flexibility in measurement set-ups. Based on the optimal beam parameters found, a series of measurements (>100) with the water calorimeter and two Farmer-type ionization chambers were performed in the entrance channel of a 430 MeV/u carbon ion beam.

Results: Current results of the calorimetric and ionometric measurements performed over a time period of 6 months, including the experimental determination of associated correction factors as well as calculations of the induced heat transport effects for the water calorimeter, will be presented. Further, a preliminary estimation of the currently investigated $k_{Q,Q0}$ factor for both ionization chambers will be given.

Conclusion: We investigated optimized irradiation conditions enabling accurate calorimetric measurements in a scanned carbon ion beam. The latest results indicate that the experimental determination of the corresponding $k_{Q,Q0}$ factor for ionization chambers with a relative standard uncertainty below 1 % is achievable.

Literature

[1] International atomic energy agency, Technical Reports Series 398, 2000.

[2] Osinga, J.-M. *et al*, Radiat Prot Dosimetry 161(1-4):387-92, 2014.

[3] Krauss, A. and Kapsch R.-P., Phys. Med. Biol. 59:4227–4246, 2014.

SP163.3 - Results from the on-going key comparison BIPM.RI(I)-K6 : What have we learned ?**Author(s):** Susanne Picard, David T. Burns
BIPM, Sevres cedex/FRANCE**Results from the on-going key comparison BIPM.RI(I)-K6 : What have we learned ?**Susanne Picard¹ and David Burns²

Bureau International de Poids et Mesures

Pavillon de Breteuil – 92312 Sèvres cedex - France

The BIPM is presently carrying out a series of comparisons of absorbed dose to water, D_w , in accelerator beams of National Metrology Institutes. For this purpose, the BIPM developed a primary standard graphite calorimeter [1, 2] designed to be transported to the institutes for measurements in accelerator photon beams. The aim is to validate national primary standards by determining their degree of equivalence, published in the BIPM online key comparison database [3].

The BIPM standard has been successfully transported to the NRC (Canada), PTB (Germany), NIST (USA), LNE-LNHB (France), ARPANSA (Australia) and the NPL (UK), where comparisons in the accelerator photon beams of each institute have been carried out, as well as with the VSL (Netherlands) [5 – 12]. Future comparisons are planned, notably for the NMIJ (Japan), NIM (China), KRISS (Korea), ENEA (Italy), METAS (Switzerland) and the MKEH (Hungary).

A closer study of the first comparisons in this series is made. Monte Carlo calculations have been carried out for 17 different beam qualities allowing the prediction of Monte Carlo coefficients for future comparisons. Accumulated calorimeter measurement data serve as a basis for quality control, and may give an indication of spectral dependence. Accumulated ionometric and calorimetric data have also been used for a determination of W_{air} (the mean energy required to create an ion pair in dry air) and I_g (the mean excitation energy for graphite) for these beams [13]. The degrees of equivalence are discussed and the results are compared to other comparisons made for the same quantity.

The authors are grateful to their colleagues at the NRC, PTB, NIST, LNE-LNHB, ARPANSA, NPL and the VSL for their participation.

References[1] Picard S, Burns D T, Roger P 2009 *Rapport BIPM-2009/01* (Sèvres: Bureau International des Poids et Mesures)[2] Picard S, Burns D T, Roger P 2010 International Symposium on Standards, Applications and Quality Assurance in Medical Radiation Dosimetry *in Standards, Applications and Quality Assurance in Medical Radiation Dosimetry (IDOS)*, 2011, vol. 1 55–65, Proceedings Series – International Atomic Energy Agency 2011[3] Key Comparison BIPM.RI(I)-K6 / BIPM Key Comparison Database <http://kcdb.bipm.org/>[4] Salvat F, Fernandez-Varea J M, Sempau J 2009 *NEA No. 6416 Workshop Proc. (Barcelona, Spain 30 June – 3 July 2008)* (Paris: NEA/OECD)[5] *Metrologia* 47 2010 *Tech. Suppl.* 06025[6] *Metrologia* 48 2011 *Tech. Suppl.* 06020

- [7] *Metrologia* 50 2013 *Tech. Suppl.* 06004
- [8] *Metrologia* 50 2013 *Tech. Suppl.* 06015
- [9] *Metrologia* 51 2014 *Tech. Suppl.* 06006
- [10] BIPM.RI(I)-K6 2013 NPL, United Kingdom / BIPM, in preparation.
- [11] BIPM.RI(I)-K6 2014 NPL, United Kingdom / BIPM, in preparation.
- [12] BIPM.RI(I)-K6 2014 VSL, Netherlands / BIPM, in preparation.

SP163.4 - Absorbed dose-to-water primary standard and traceability system for radiotherapy in China

Author(s): Kun Wang, Sunjin Jin, Jian Zhang
National Institute of Metrology, Beijing/CHINA

The absorbed dose-to-water was measured both by ionization and calorimetry method at radiotherapy dose levels in China. A graphite ionization chamber, based on the cavity theory and combined with Monte Carlo simulation, was developed to measure absorbed dose to water for Co-60 gamma radiation. With Townsend compensation method to achieve ionization current measurement, using EGSnrc package for graphite cavity ionization chamber to simulate water perturbation parameter, measured the ion recombination and radial inhomogeneity correction factor, the combined standard uncertainty to measure absorbed dose to water for Co-60 was 0.37%.

The standard based on a water calorimeter is designed to operate in Co-60 and megavoltage photon beams from a linear accelerator. The water calorimeter operated at 4 °C to eliminate the problems associated with convection in water phantoms at room temperature. A low-noise temperature measurement circuit was able to resolve temperature differences at the μK level. With the bath and Peltier cooling system, the temperature of water phantom is stable at (4 ± 0.0001) °C. Using the cylindrical sealed glass vessel and bead thermistor of 10 k Ω , in the H₂-saturated high pure water system, the resistance was measured by Wheatstone AC bridge. After calibrating thermistor and bridge separately, absorbed dose to water is absolutely measured with the combined standard uncertainty of 0.38%.

NIM participate in the comparison organized by Asia-Pacific Regional Metrology Programme (APMP), the differences with the reference value in APMP.RI (I)-K4 comparison was 0.04%, NIM finally had the ability for the traceability of absorbed dose to water.

The primary standard of water absorbed dose for photon radiation from 4 MV to 25 MV will be established and achieve the traceability of water absorbed dose for radiation therapy. This new standard will significantly reduce the uncertainty of ion chamber calibrations for Chinese radiotherapy centers and open up new areas of research for the NIM.

SP163.5 - Design of an MRI-compatible water calorimeter for use in an integrated MRI-Linac and Gamma-Knife

Author(s): Niloufar Entezari¹, Davis Ly², James Renaud³, Arman Sarfehnia⁴

¹Department Of Physics, Ryerson University, TORONTO/ON/CANADA, ²Department Of Engineering, University of Waterloo, Waterloo/ON/CANADA, ³Medical Physics Unit, McGill University, Montréal/CANADA, ⁴Department Of Radiation Oncology, University of Toronto, Toronto/CANADA

Purpose: The aim of this work is to present numerical design and optimization of a portable water calorimeter appropriate for dual use in an integrated MRI-linac and Gamma-Knife®, based on the

concept of 4°C stagnant water calorimetry. In calorimetry, dose to water (D_w) is measured based on the principle that energy absorbed in a sensitive volume is completely converted to temperature rise (ΔT) using specific heat capacity of medium $c_{P,D} = c_P \Delta T / k_{ht}$, where k_{ht} is heat transfer correction and compensates for heat gain or loss at point of measurement due to conductive and convective effects.

Methodology: The calorimeter dimensions, constrained by the size of an MRI-linac bore and Gamma-Knife collimator ring, were numerically optimized to maximize thermal stability. Several materials were investigated to be used for the calorimeter body, and thermal insulation.

A comprehensive numerical optimization study of four different calorimeter designs was undertaken using a commercial finite element method software package by accurately modeling heat transport inside a given geometry (FIG 1). For each design, thermal stability of system in presence of minor ambient thermal fluctuations was evaluated.

To study the effects of possible coolant temperature fluctuations (circulating in calorimeter to keep it at 4°C), several simulations were performed in which the temperature of coolant was kept either constant, slowly increasing, or fluctuating at a given frequency. The long term drift (48h) was simulated, and k_{ht} due to seven consecutive irradiation runs by a high energy beam was calculated.

Results and Conclusions: The calorimeter was designed to be used in upright position in MRI-linac with the radiation beam incident from the top, while it is rotated 90 degrees for use in Gamma-Knife. In the latter case, its semi-spherical end is placed at the isocenter of Gamma-Knife collimator ring, providing a constant depth of measurement for every incident beam angle.

Due to MRI-compatibility requirements, the calorimeter is to be rapid prototyped/built entirely out of plastic. Among all insulation materials tested, solid state aerogel-based insulation resulted in highest performance and thermal stability.

k_{ht} was found to be 1.002 ± 0.014 , 0.984 ± 0.013 , 0.986 ± 0.029 , 1.002 ± 0.013 ($k=1$) for designs in FIG1a-d respectively. The design in Fig.1d was chosen for prototyping, as it demonstrated the greatest long term stability (0.36 $\mu\text{K/hr}$).

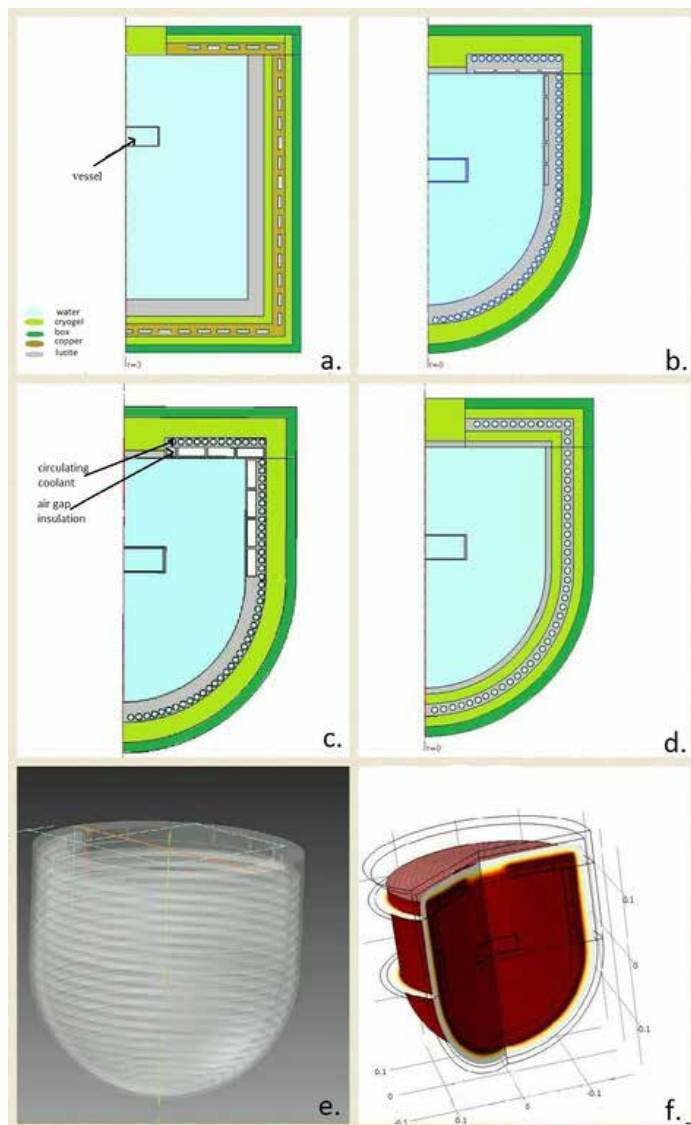


Fig. 1: Four calorimeter designs investigated in this work (a to d); A rendering of coolant passageway inside the calorimeter wall (e). Simulated temperature distribution inside calorimeter design depicted in FIG1(c) following 48 hours drift (f).

SP163.6 - On the practical use of calorimetry for routine absolute dosimetry in the radiotherapy clinic

Author(s): James Renaud¹, Arman Sarfehnia², Jan Seuntjens¹

¹Medical Physics Unit, McGill University, Montréal/CANADA, ²Department Of Medical Physics, Sunnybrook Health Sciences Centre, Toronto/ON/CANADA

Purpose: The aim of this work is to describe the construction, development, and modes of operation of a small-scale graphite calorimeter probe (GPC) conceived for use as an absolute dosimeter in the radiotherapy clinic (Patent No. PCT/CA2013/000523).

Similar in size and shape to a 0.6 cm³ cylindrical ionization chamber, the GPC has been designed to help meet the clinical need for accurate reference dosimetry in nonstandard radiation fields.

Materials and Methods: Based on a numerically optimized design obtained in previous work (Fig. 1), a functioning prototype with embedded active thermal control capable of quasi-adiabatic and isothermal operation was constructed in-house.

In quasi-adiabatic mode, the radiation-induced temperature rise is measured in the sensitive volume (*i.e.* the core) while the outermost portion of the device is thermally stabilized by a software-based temperature controller. In isothermal mode, the entire device is subject to active thermal control and the quantity of interest in the electrical power necessary to maintain a stable temperature while irradiated.

An experimental characterization of the GPC repeatability, linearity, and dose rate dependence while operated in quasi-adiabatic mode was carried out in a water-equivalent phantom, under reference conditions, in a 6 MV photon field. Similarly, a characterization study of the GPC's isothermal mode was conducted by simulating radiation fields of various dose rate (0.5 – 11.8 Gy/min) and duration (10 – 180 s) by means of electrical power dissipation.

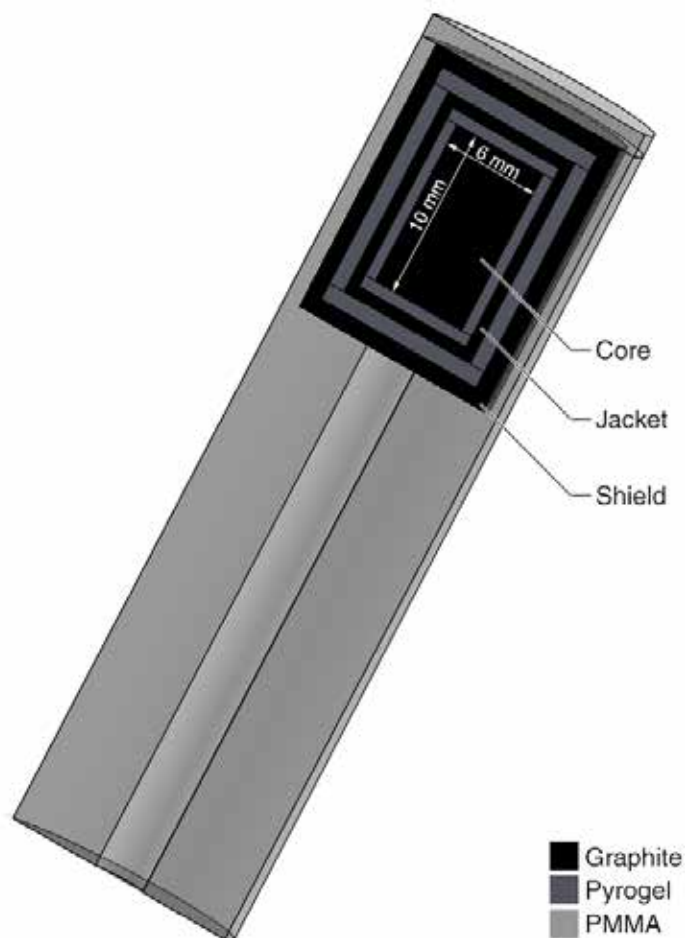


Fig 1. An isometric cutaway view of the GPC

Results: For the quasi-adiabatic mode, a repeatability of 0.4% was established ($n = 64$), linearity was characterized by an adjusted R^2 value of 0.9996 ($n = 40$), and no statistically-significant dose rate dependence was observed.

For isothermal mode, differences between expected and actual GPC response ranged between 0.3 - 1.4%, and in general, agreement was superior for longer irradiations with dose rates greater than 2 Gy/min.

Discussion and Conclusions: This proof of concept points to the feasibility of operating the GPC in both quasi-adiabatic and isothermal mode for the purpose of absolute clinical dosimetry. As expected from a calorimeter, the GPC is characterized experi-

mentally (quasi-adiabatic) and through simulation (isothermal) by a strong linear response and relative dose rate independence.

Plans to experimentally verifying the isothermal mode of operation by showing self-consistency between the two modes are underway. Further comparison against other reference class dosimeters in standard and non-standard fields are to follow.

SP164 - Adaptive Radiation Therapy (ART)

TRACK 06: NEW TECHNOLOGIES IN CANCER RESEARCH AND TREATMENT

SP164.1 - Real-time dose reconstruction for adaptive radiation therapy

Author(s): [Martin F. Fast](#), Cornelis Philippus Kamerling, Peter Ziegenhein, James L. Bedford, Simeon Nill, Uwe Oelfke
Joint Department Of Physics, The Institute of Cancer Research and The Royal Marsden NHS Foundation Trust, London/UNITED KINGDOM

Currently dose reconstruction can only be conducted after the treatment fraction due to its computational cost and missing real-time data interfaces. In future, real-time treatment interventions such as dynamic multi-leaf collimator (dMLC) tracking will require on-line dose reconstruction to ensure target coverage and organ-at-risk (OAR) sparing.

To facilitate this study, we have implemented on-line dose reconstruction by connecting our software for delivery & tracking (DynaTrack) and for dose calculation & planning (DynaPlan) through a TCP/IP network. DynaTrack is interfaced to our research Elekta Synergy linac/Agility MLC and controls treatment delivery and dMLC tracking via a real-time tracking interface. Actual MLC apertures and (simulated) target positions are reported to DynaPlan every 40 ms and 20 ms respectively. DynaPlan then relies on a set of pre-calculated dose influence matrices (D_{ij}) with $5 \times 5 \text{ mm}^2$ bixel resolution generated in research RayStation using its singular value decomposed pencil beam algorithm to calculate the actually delivered dose. To investigate the impact of dMLC deliveries on dose distributions, we generated two plans in Pinnacle: a lung patient (RTOG 1021, 54 Gy, 3 Fx, 15-beam, PTV 34 cm^3) and a prostate patient (RTOG 0938, 36.25 Gy, 5 Fx, 7-beam, PTV 104 cm^3). The dose was accumulated onto a voxel resolution of $1.95 \times 1.95 \times 3 \text{ mm}^3$ (lung) and $2.3 \times 2.3 \times 1.5 \text{ mm}^3$ (prostate). Three treatment scenarios were evaluated: a static delivery (no motion, no tracking), a conventional delivery (motion, no tracking), and an adaptive delivery (motion, tracking). Two motion trajectories were used to propagate the PTV contour within the planning CT (assuming static OARs).

We successfully implemented truly on-line dose reconstruction for experimental treatment deliveries on a linac. The dose reconstruction was updated at 25 Hz and took $\leq 30 \text{ ms}$ (prostate) and $\leq 20 \text{ ms}$ (lung) per MLC aperture. D_{ij} data of up to 1 GB per beam segment was handled at a memory throughput of $\leq 43 \text{ GB/s}$ on a single workstation computer. The reconstructed dose distributions (see table) highlight the fact that target dose can be safely recovered using dMLC tracking for these patients and motion conditions.

Lung tracking		Planning target volume (PTV) [Gy*]				Lung [%]
		D _{mean}	D95	D5	HI**	
No motion	Static	68.7	54	79.1	0.36	4.6
Sinusoidal	Conventional	65.9	50.7	77.6	0.4	4.6
	Adaptive	68.5	53.7	78.7	0.36	4.4
Baseline-Shift	Conventional	67	49.9	78.6	0.42	4.6
	Adaptive	68.6	55.1	78.8	0.34	4.5

Prostate tracking		PTV [Gy*]				Rectum [Gy*]
		D _{mean}	D98	D2	HI**	
No motion	Static	37.23	35.95	38.06	0.057	35.29
Erratic	Conventional	37.15	35.55	38.21	0.071	35.29
	Adaptive	37.12	35.1	38.19	0.083	35.25
High frequency	Conventional	36.48	34.4	37.53	0.085	35.27
	Adaptive	36.85	35.61	37.74	0.058	35.23

Sinusoidal: 1d motion in SI direction; period 4 s & peak-to-peak amplitude 15 mm. Baseline-Shift, Erratic & High-frequency characterise real patient 3d trajectories.

* Dose values are normalised so that the static D95 dose coincides with the RTOG prescription.

** HI = (D_{high} - D_{low})/D50. D50 results are not shown.

Real-time dose reconstruction is technologically feasible without compromising on resolution or accuracy. This is an important milestone towards the implementation of on-line replanning for adaptive radiation therapy and dose-guided dMLC deliveries. Future work will assess the impact of the motion model on the dose and use collapsed-cone Dij data for lung patients.

Disclaimer: Thanks to Elekta (research agreement on tracking) and RaySearch (support of Dij export).

SP164.2 - Evaluation of unified intensity-modulated arc therapy (UIMAT) for the treatment of head-and-neck cancer

Author(s): Michael Macfarlane¹, Douglas Hoover², Eugene Wong³, Jerry J. Battista², Nancy Read⁴, David Palma¹, Varagur Venkatesan⁴, Alex Hammond⁴, Jeff Z. Chen⁴

¹Department Of Medical Biophysics, Western University, London/CANADA, ²Department Of Oncology, Western University, London/CANADA, ³Department Of Physics & Astronomy, Western University, London/CANADA, ⁴London Regional Cancer Program, London Health Science Center, London/ON/CANADA

Purpose: Recently our group developed a unified intensity-modulated arc therapy (UIMAT) technique which combines IMRT and VMAT optimization and delivery in a single arc [1]. In this current study, we evaluated the potential benefit of UIMAT for the radiation therapy of complex head-and-neck cancers.

Method: A retrospective planning study was performed on 20 head-and-neck cases (13 treated clinically with VMAT and 7 with IMRT). These cases were re-planned using our UIMAT technique and the results were compared with the clinically delivered plans. Plans were assessed in terms of target coverage, target conformity, and sparing of organs at risk. The feasibility of plan delivery was verified with an ArcCheck phantom and a Varian TrueBeam linear accelerator operating in clinical mode.

Results: When compare to VMAT or IMRT alone, UIMAT plans maintained target coverage and conformity while significantly reducing the mean doses to organs at risk. This trend is summarized in Table 1. A comparison of dose-volume histograms between VMAT and UIMAT plans is also shown in Figure 1. In addition to its dosimetric advantage, UIMAT plans can be delivered with the same level of efficiency as VMAT.

Conclusion: Compared with IMRT or VMAT alone, UIMAT appears to offer dosimetric advantages for the radiation therapy of head-and-neck cancers.

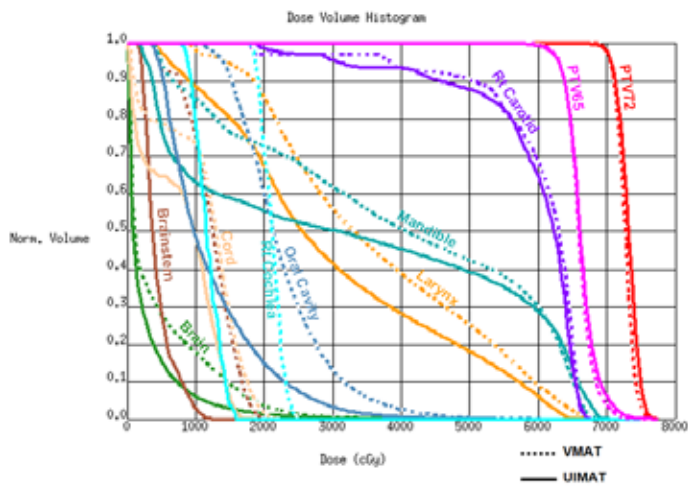
References:

[1]. D. Hoover, M. MacFarlane, E. Wong, J. Battista, J. Chen, Feasibility of a unified approach to intensity-modulated radiation therapy and volume-modulated arc therapy optimization and delivery. *Med. Phys.* **42**, 726 (2015)

Table 1: Comparison of average dose-volume parameters between clinical (VMAT or IMRT) and UIMAT plans. The mean PTV dose and dose to 95% of the PTV volume (D95) is represented as a percentage of the prescription dose. All p-values were calculated using a paired, one-tailed t-test.

		Planning Target Volume			Oral	Lt.	Rt.	Larynx	Cord	Brainstem	Lt.	Rt.
		Conformity Index	Mean (Gy)	D95 (%)	Cavity	Parotid	Parotid				Cochlea	Cochlea
					Mean (Gy)	Mean (Gy)	Mean (Gy)				Max (Gy)	Max (Gy)
Average	Clinical	0.57	103.2	98.1	25.1	24.9	25.9	32.5	33.3	29.4	18.4	15.9
	UIMAT	0.57	103.2	98.3	22.8	23.3	23.5	30.9	31.6	24.8	14.5	10.9
% Difference		0%	0%	+0.2%	-9.1%	-6.4%	-9.1%	-4.8%	-5.3%	-15.7%	-21.1%	-31.0%
p-value		0.283	0.291	0.189	< 0.001	0.001	< 0.001	0.002	0.011	< 0.001	< 0.001	< 0.001

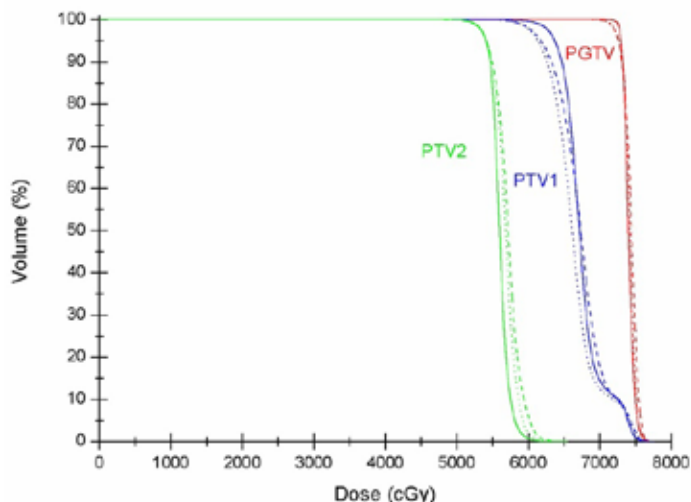
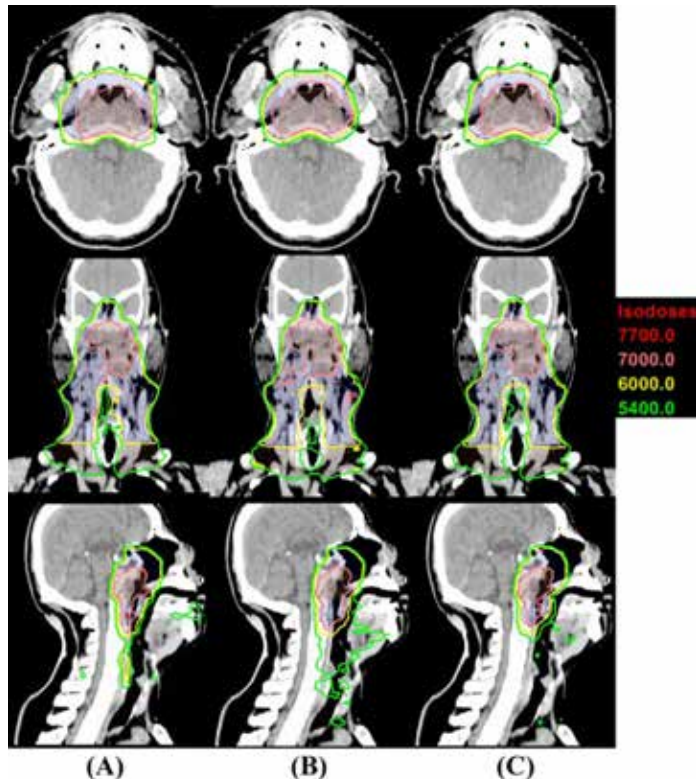
Figure 1: Comparison of dose-volume histogram between VMAT and UIMAT.



SP164.3 - A Hybrid IMRT/VMAT Technique for the Treatment of Nasopharyngeal Cancer

Author(s): Nan Zhao, Ruijie Yang, Yuliang Jiang, Suqing Tian, Fuxin Guo, Junjie Wang
Radiation Oncology, Peking University Third Hospital, Beijing/CHINA

Purpose: This study is to investigate a Hybrid IMRT/VMAT technique which combines intensity modulated radiation therapy (IMRT) and volumetric modulated arc therapy (VMAT) for the treatment of nasopharyngeal cancer (NPC). **Methods:** 2 full arcs VMAT (2ARC-VMAT), 9-field IMRT (9F-IMRT) and Hybrid IMRT/VMAT plans were created for 10 patients with NPC. The Hybrid IMRT/VMAT plans were combination of 1 full arc VMAT (Hybrid-VMAT) and 7-field IMRT (Hybrid-IMRT). The dose distribution of planning target volume (PTV) and organs at risk (OARs) for Hybrid IMRT/VMAT was compared with 9F-IMRT and 2ARC-VMAT. The monitor units (MUs) and treatment delivery time were also evaluated. **Results:** For PTV70 and PTV59.4, the Hybrid IMRT/VMAT technique significantly improved target dose conformity compared with 9F-IMRT (0.62 vs 0.47, $p=0.01$; 0.64 vs 0.58, $p=0.01$) and 2ARC-VMAT (0.62 vs 0.43, $p=0.00$; 0.64 vs 0.60, $p=0.01$). For PTV54, the Hybrid IMRT/VMAT technique improved target dose conformity compared with 9F-IMRT (0.69 vs 0.63; $p=0.00$). The near maximum dose (D2%) and mean dose of mandible in Hybrid IMRT/VMAT were 5.2% ($p=0.00$) and 4.2% ($p=0.03$) lower than 9F-IMRT plans, respectively. The mean dose of TMJ, temporal lobe and unspecified tissue for Hybrid plans were 12.8% ($p=0.00$), 11.4% ($p=0.01$) and 4.0% ($p=0.02$) lower than 9F-IMRT plans, respectively. The V30 of right and left parotids for Hybrid plans and VMAT plans were 34.7% vs 35.7% ($p=1.00$) and 36.1% vs 37.1% ($p=1.00$), respectively. The mean dose of TMJ, D2% of mandible for Hybrid plans and 2ARC-VMAT plans were 37.4 Gy vs 39.3 Gy ($p=0.34$) and 63.7 Gy vs 64.7 Gy ($p=0.06$), respectively. **Conclusions:** Hybrid IMRT/VMAT technique can be a viable radiotherapy technique with better plan quality.



SP164.4 - Interactive real time adaptation of IMRT treatment plans

Author(s): Cornelis Philippus Kamerling¹, Katrin Welsch¹, Peter Ziegenhein¹, Simeon Nill¹, Jamie McClelland², Uwe Oelfke¹
¹Joint Department Of Physics, The Institute of Cancer Research and The Royal Marsden NHS Foundation Trust, London/UNITED KINGDOM, ²Centre For Medical Image Computing, Dept. Of Medical Physics And Bioengineering, University College London, London/UNITED KINGDOM

Recently we introduced a software platform for IMRT treatment planning based on a sequence of local dose adaptations. These are facilitated by direct interaction of the planner with the graphical representation of the patient dose in a real-time feedback loop. Here we report on an extension of this interactive dose shaping (IDS) software for adaptive radiotherapy based on daily cone beam CTs (CBCTs).

The developed workflow consists of five essential components as indicated in figure 1. All related algorithms are integrated with our research TPS Dynaplan and optimized for speed to comply with the interactive planning paradigm. To facilitate deformable image registration (1a), the NiftyReg (UCL, London, UK) package was integrated.

As an example for the performance of the implemented workflow we report its application for a prostate patient aiming to re-establish the initially planned dose (based on planning CT) on a new patient geometry observed on a CBCT in fraction 5. The center-of-mass shift from PTV and rectum were 5.3 and 4.4mm respectively, mainly in posterior direction. The PTV dose prescription was 67Gy. Dose quality indicators were evaluated for (i) initial plan on initial geometry, (ii) initial plan on new geometry, (iii) adapted plan on new geometry and are reported in table 1. The recovered target dose indicates a successful restoration of the initially planned dose. The slightly higher rectum dose is the result of the decreased distance between PTV and rectum. The computations were performed on a low-end Intel i7 desktop PC with an image processing runtime of 2min, dominated by image registration (1a) with 84s. IDS recovery (5a) took 5s.

This work provides a first proof of concept study for the integration of an ART therapy workflow into an IDS TPS. Further validation aiming to optimize the image processing parameters and IDS recovery performance is in progress.

Table 1

Scenario	PTV			Rectum			
	D _{95%} [Gy]	D _{5%} [Gy]	D _{1%} [Gy]	V _{5%} [%]	V _{10%} [%]	V _{30%} [%]	V _{40%} [%]
I Initial plan on initial geometry	67.0	63.2	69.7	11.4	4.0	0.1	0.0
II Initial plan on new geometry	66.0	57.3	69.6	3.8	0.0	0.0	0.0
III adapted plan on new geometry	67.2	62.9	70.9	14.6	4.9	0.9	0.0

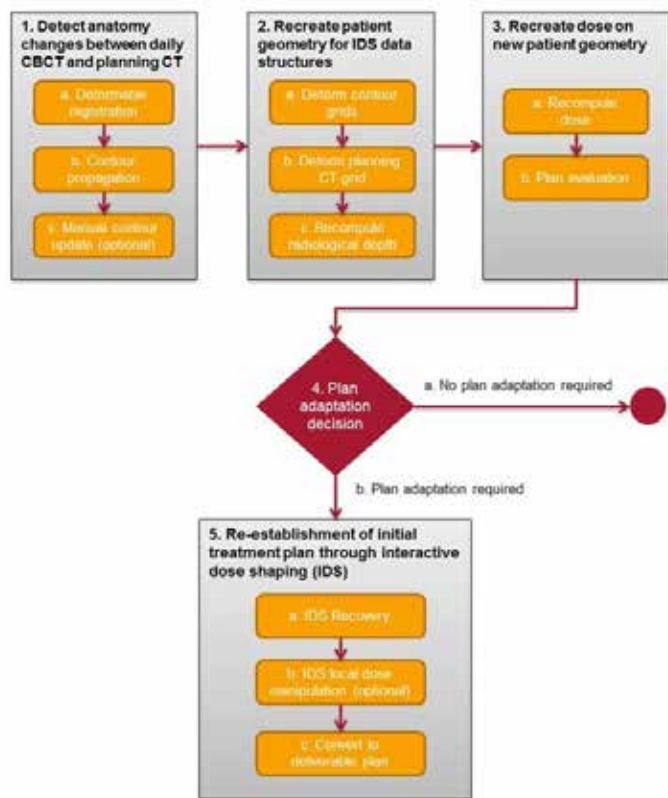


Figure 1: The flowchart summarizes the proposed adaptive radiation therapy workflow for interactive dose shaping.

SP164.5 - A Hybrid IMRT/VMAT technique for the treatment of non-small cell lung cancer

Author(s): Nan Zhao, Ruijie Yang, Junjie Wang, Xile Zhang
Radiation Oncology, Peking University Third Hospital, Beijing/CHINA

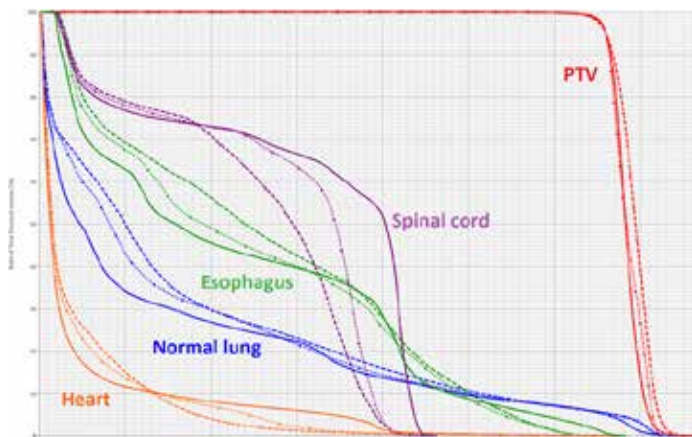
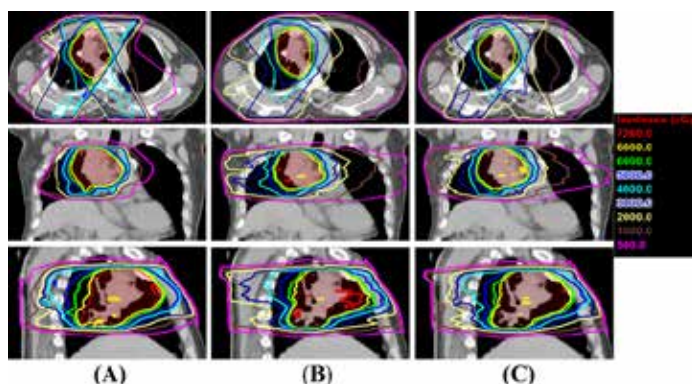
Purpose: To investigate a Hybrid IMRT/VMAT technique which combines intensity modulated radiation therapy (IMRT) and volumetric modulated arc therapy (VMAT) for the treatment of non-small cell lung cancer (NSCLC).

Methods and Materials: 2 partial arcs VMAT, 5-field IMRT and Hybrid IMRT/VMAT plans were created for 15 patients with NSCLC. The Hybrid IMRT/VMAT plans were combination of 2 partial arcs VMAT and 5-field IMRT. The dose distribution of planning target volume (PTV) and organs at risk (OARs) for Hybrid IMRT/VMAT was compared with IMRT and VMAT. The monitor units (MUs) and treatment delivery time were also evaluated.

Results: Hybrid IMRT/VMAT significantly improved the target conformity and homogeneity compared with IMRT and VMAT. The V30 of normal lung for hybrid plans was significantly lower than IMRT plans (17.7% vs 18.7%; p<0.05) and VMAT plans (17.7% vs 18.4%; p<0.05). The V5, V10, V30 and mean lung dose (MLD) of normal lung for hybrid plans were 5.1%, 7.7%, 3.8% and 3.9% lower than those for VMAT plans, respectively (p<0.05). The maximum dose of spinal cord for hybrid plans was 5.6 Gy lower than that for IMRT plans (p<0.05). The dose received by esophagus and heart for

hybrid plans were significantly lower than those for IMRT plans. The mean delivery time of IMRT, VMAT and hybrid plans were 280 s, 114 s, and 327 s, respectively. The mean MUs needed for IMRT, VMAT and hybrid plans were 933, 512, and 737, respectively.

Conclusions: The Hybrid IMRT/VMAT technique significantly improved the target conformity and homogeneity compared with IMRT and VMAT. It reduced V5, V10, V30 and MLD of normal lung compared with VMAT, and protected the OARs better with fewer MUs compared with IMRT. Hybrid IMRT/VMAT technique can be a viable radiotherapy technique with better plan quality.



SP164.6 - Offline adaptive VMAT - feasibility study using planning CT deformed electron density mapping on daily CBCT to estimate parotid dose volume relationship.

Author(s): Ayyalusamy Anantharaman¹, Vellian Subramani², V.S Subramanian¹, Gandhi Arun³, Shanmugam Thirumalai Swamy³, Murugesan Kathirvel³, Ilamurugu Arivarasan³
¹Research And Development Centre, Bharathiar University, Coimbatore/INDIA, ²Radiation Oncology, All India Institute of Medical Sciences, New Delhi/INDIA, ³YASHODA HOSPITAL, HYDERABAD/INDIA

Aim:

To evaluate the parotid dose volume relationship in offline Adaptive Volumetric Modulated Arc therapy by using deformable mapping of planning CT electron density values on daily CBCTs.

Methods and Materials:

Daily CBCTs were acquired for 10 head and neck patients undergoing rapid arc treatments. The Smart Adapt system was used to

deform the planning CT to the daily CBCTs, obtaining the anatomical information of the day with the electron density values of the planning CT. The deformed contours were checked for any discrepancies and Rapid Arc plans were calculated with fixed MUs on the deformed CTs. Based on the calculated plans, a cumulative DVH was generated and the variation in the parotid volume and the delivered mean doses of parotids were analyzed.

Results:

There was shrinkage of parotid volumes during the course of the treatment. In this study, the observed maximum, minimum and mean parotid volume reduction were 52%, 13% & 29% respectively. The mean dose of parotids varied from -3.6% to 17% from the planned doses. The parotid volume and dose variation for 10 patients are shown in the table below. It was observed that for parotids closer to high dose regions a small volume shrinkage causes a remarkable increase in mean dose due to more of the parotid volume inside the high dose region. Whereas for parotids closer to low risk nodal regions, there is no significant change in mean dose even for a volume shrinkage of 30%. Parotid mean doses were less than the planned doses for two patients due to shrinkage along cranio-caudal direction also.

PATIENT	VOLUME (%)		MEAN DOSE (%)	
	LEFT	RIGHT	LEFT	RIGHT
1	52	44	17.1	7.4
2	30	14	0.5	4.6
3	31	41	7.5	7.3
4	13	15	4.8	-2.8
5	18	25	13.9	0.8
6	29	32	-3.6	9.8
7	27	25	1.2	9.1
8	19	15	6.7	5.2
9	23	35	8.1	10.3
10	21	18	6.3	2.5

PAROTIDS VOLUME DOSE COMPARISON

Conclusion:

The results from the study showed that it is clinically feasible to estimate the parotid shrinkage and the delivered dose - volume relationship in VMAT using planning CT electron density mapping on daily CBCTs.

SP164.7 - Plan Optimization for a Lung Patient on a Parallel Linac-MR System

Author(s): Daniel Tamagi, Brad Warkentin, Amir Keyvanloo, B Gino Fallone, G. Colin Field
 Medical Physics, Cross Cancer Institute, Edmonton/CANADA

Purpose: In a hybrid Linac-MR system, the magnetic field of the MRI produces a Lorentz force on charged particles that affects dose deposition. The resulting effects on patient dose distributions are expected to be most significant in low density regions such as lung, where the mean free paths of electrons and positrons are longer. This study uses a simplified (three-beam) Stereotactic Body Radiation Therapy treatment plan for a lung patient to investigate the importance of these dosimetric perturbations in the fluence optimization and dose calculation stages of the treatment planning process.

Methods: Modified versions of the EGSnrc Monte Carlo codes

BEAMnrc and DOSXYZnrc were used to generate patient-specific beamlets in 1) the absence of a magnetic field, and 2) in the presence of a magnetic field (either 0.56T or 1.5T) oriented parallel to the beam. These beamlets were imported into a research version of the RayStation TPS (RaySearch Laboratories, Sweden), and were used: 1) to perform “forward” dose calculations of unmodulated beams, and 2) to optimize fluence patterns for modulated beams. Forward calculations using the kernels for 0T, 0.56T and 1.5T were performed for MLC shaped fields and were compared to determine the dosimetric effects of the magnetic field. The RayStation fluence optimization software was used to determine fluence patterns for each of the 3 fields to achieve clinical goals. MATLAB code was written to compare these optimized fluence patterns as a function of magnetic field strength. A forward calculation was performed for these optimized fluence patterns and the resulting dose distributions were compared for the 3 magnetic fields.

Results: As a function of magnetic field strength, fewer Monitor Units (max % differences of -0.9% for 0.56T, and -2.4% for 1.5T compared to 0T) were required to achieve equivalent target coverage, due to the confinement of scattered electrons by the magnetic field. We also observed more lung sparing (Mean dose of 0.8% less for 0.56T, and 9.5% less for 1.5T compared to 0T) as a function of magnetic field strength due to the scattered electron confinement, and the reduced MU's. With identical optimization objectives, percent differences for fluence elements were within +-5% between the 0T and 0.56T optimizations, but were as large as 60% for some elements between the 0T and 1.5T. We found that optimizing the fluence without the magnetic field being considered resulted in worse target coverage (D5 % differences of 0.2% and 2.6% for 0.56T and 1.5T respectively compared to 0T). This effect is clinically negligible for the 0.56T case, but was more significant at 1.5T.

Conclusion: Our study suggests that modeling the magnetic field during fluence optimization and during the forward dose calculation is significant at 1.5T, but is clinically negligible at 0.56T. Our study also indicated that equivalent target coverage (compared to a conventional linac) can be achieved with better sparing of lung if the magnetic field is modeled during forward planning and fluence optimization. These results are for a lung patient with a simplified 3 beam treatment plan. More investigation is needed.

SP165 - EEG**TRACK 09: BIOSIGNAL PROCESSING****SP165.1 - A Fully Unsupervised Clustering on Adaptively Segmented Long-term EEG Data**

Author(s): Vaclav Gerla¹, Elizaveta A. Saifutdinova¹, Vaclav Kremen¹, Michal Huptych¹, Vladimir Krajca², Lenka Lhotska¹

¹Department Of Cybernetics, Czech Technical University in Prague, Prague/CZECH REPUBLIC, ²Department Of Biomedical Technology, Czech Technical University in Prague, Kladno/CZECH REPUBLIC

Several new procedures for efficient processing of long-term EEG recordings has been validated on long-term comatose EEG data. The proposed solution is based on the use of cluster analysis over a set of various features derived from adaptively segmented EEG data. Special attention was given to utilization of clinically relevant information from multichannel EEG data. Methods for validation of the cluster analysis results were implemented and tested. Suggested algorithms speeds up a subsequent evaluation of the data and simplify a tedious and time-consuming work of neurologists or sleep technicians, making the evaluation more objective, and represent results in an understandable form.

SP165.2 - A Real-Time Clustered MUSIC algorithm for the localization of synchronous MEG/EEG source activity

Author(s): Christoph Dinh¹, Matti S. Hämäläinen², Daniel Baumgarten¹, Jens Haueisen³

¹Institute Of Biomedical Engineering And Informatics, Technische Universität Ilmenau, Ilmenau/GERMANY, ²Athinoula A. Martinos Center For Biomedical Imaging, Massachusetts General Hospital - Massachusetts Institute of Technology - Harvard Medical School, Charlestown/MA/UNITED STATES OF AMERICA, ³Biomagnetic Center, Clinic For Neurology, Jena University Hospital, Jena/GERMANY

Magnetoencephalography (MEG) and Electroencephalography (EEG) provide millisecond temporal resolution and are thus ideally suited for real-time monitoring of brain activity. Among various inverse algorithms mapping sensor space measures to sources in the brain, spatio-temporal dipole fitting methods such as MUSIC (Multiple Signal Classification) and RAP-MUSIC (Recursively Applied and Projected MUSIC) have demonstrated superior ability in the localization of a restricted number of independent sources. However, these methods are computationally extensive and commonly applied for offline data analysis subsequent to the measurement.

We propose a novel Real-Time Clustered MUSIC algorithm (RTC-MUSIC) that makes use of the advantages of the well-established MUSIC algorithm but can be applied to real-time data streams during the measurement. For this purpose, regional cortical activity is represented by a small number of dipoles based on a cortical atlas and a k-means algorithm, thus considerably reducing the size of the gain matrix. The computation of the subspace correlations between dipole pairs is highly parallelized. Moreover, performance optimization is achieved by employing Powell's Conjugate Gradient Method [26] as the search algorithm to find the best dipole source combination without performing a brute-force calculation of all dipole correlations.

Our results show that the gain matrix clustering improves the condition of the underlying inverse problem. In addition, the reduction of the gain matrix to the most representative dipoles considerably reduces the computational effort. Performance optimization in RTC-

MUSIC yields a further reduction of the required calculation steps by approximately 50 % for the same number of dipoles, sensors and independent sources, respectively, compared to the MUSIC algorithm. Moreover, the number of computational steps is exponentially decreasing with the number of parallel cores employed for the calculation.

Applying our novel RTC-MUSIC algorithm to single trial MEG data from an auditory task reveals similar localization precision compared to the original MUSIC algorithm. The real-time performance of our algorithm was confirmed in measurements with the Elekta Neuromag® MEG system.

We conclude that our novel RTC-MUSIC algorithm with gain matrix clustering allows for real-time localization of correlated sources of neuronal activity. It copes with the low SNR of single trial data and considerably reduces the computational time compared to MUSIC.

SP165.3 - Spatial harmonics for compressive sensing in electroencephalography

Author(s): Uwe Graichen¹, Christina Salchow¹, Daniel Strohmeier¹, Patrique Fiedler¹, Roland Eichardt¹, Jens Haueisen²

¹Institute Of Biomedical Engineering And Informatics, TU Ilmenau, Ilmenau/GERMANY, ²Institute Of Biomedical Engineering And Informatics, Ilmenau University of Technology, Ilmenau/GERMANY

Magnetoencephalography (MEG) and electroencephalography (EEG) provide information on brain function with a high temporal resolution. Recent developments in EEG allow for ubiquitous recording using dry electrodes. However, multichannel dry electrodes still suffer from higher channel dropouts compared to standard wet EEG.

We propose a new technique for interpolating EEG channels based on compressive sensing (CS). The complete signal is reconstructed from an incomplete set of measurements via convex programming. An adapted, convex optimization problem was designed to solve the interpolation problem. EEG is neither sparse in the canonical basis in the original time domain nor sparse in transformed time domains. Therefore, current CS algorithms cannot achieve good recovery quality. Consequently, we propose compressive sensing in the spatial domain. We use our recent spatial harmonic analysis (SPHARA) to decompose measured data obtained with a dry 97-channel EEG cap. SPHARA is based on the Eigenanalysis of the discrete Laplace-Beltrami operator defined on a triangular mesh. It allows a spatial Fourier analysis of the spatial potential distribution of EEG data. Pattern reversal visual evoked potentials (VEP) were measured using the dry electrode cap and a commercial amplifier (RefaExt, ANT B.V., Enschede, The Netherlands) for four healthy male volunteers. Channel dropouts were simulated for an increasing number of channels: 5, 10, 15, 20, 25, 30, 40 and 50%. Both, randomly chosen channels and channel patches were considered.

Our proposed method is able to interpolate randomly chosen dropout channels up to 50% of the total number of channels. Channel patches could be interpolated for dropout channels up to 20% of the total number of channels. Figure 1 shows two examples of reconstructed VEPs of one volunteer after 20% channel dropout for a frontal and an occipital patch. The SPHARA based interpolation was compared to k-Nearest Neighbors (kNN) and a spherical spline interpolation. Spherical spline interpolation performed significantly worse to kNN and SPHARA for randomly chosen channels and channel patches. kNN performed similar to SPHARA for randomly chosen channels but worse for larger channel patches.

In conclusion, we proposed a new compressive sensing technique for the interpolation of missing EEG channels. Moreover, this interpolation approach allows transformations between different EEG montages.

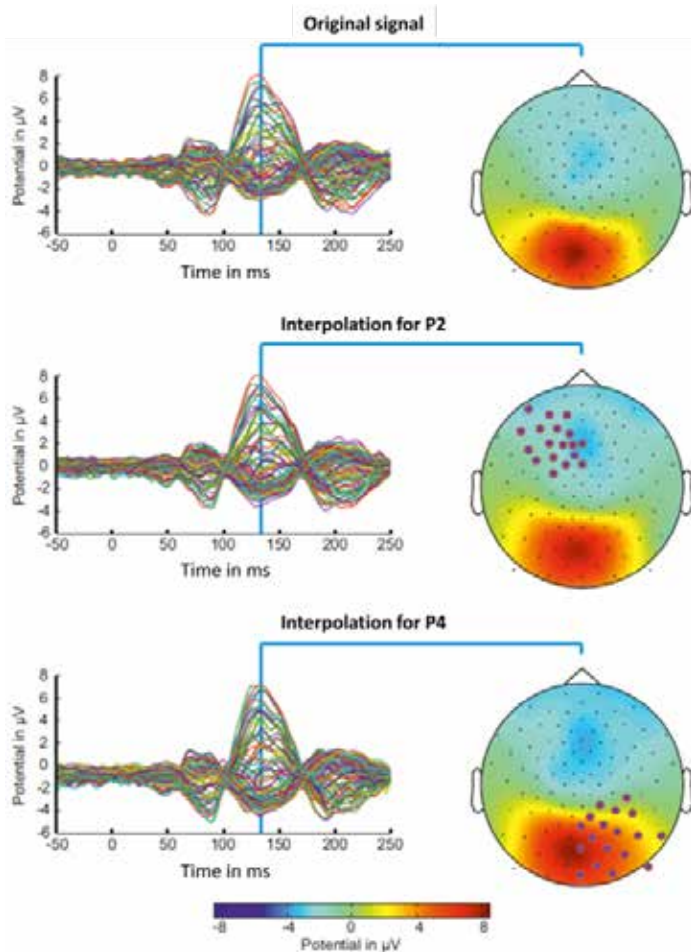


Figure 1: Original VEP signal (top row), SPHARA interpolation of frontal patch (P2) of 20% dropout channels (middle row), and SPHARA interpolation of occipital patch (P4) of 20% dropout channels (bottom row). The position of the dropout channels is indicated by violet filled circles.

SP165.4 - An Evaluation of Performance for an Independent SSVEP-BCI Based on Compression Sensing System

Author(s): Teodiano Bastos-Filho¹, Richard Godinez-Tello², Sridhar Krishnan³, Jeevan K. Pant⁴, Sandra M. Torres-Muller²

¹Electrical Engineering, Federal University of Espirito Santo, Vitoria/BRAZIL, ²Electrical Engineering, Federal University of Espirito Santo, Vitoria/BRAZIL, ³Ryerson University, Toronto/CANADA, ⁴Department Of Electrical And Computer Engineering, Ryerson University, Toronto/CANADA

Background:

This paper compares performance of two popular feature extraction methods, namely, multivariate synchronization index (MSI) and canonical correlation analysis (CCA) methods, for their use in a compressive sensing (CS)-based Steady-State Visual Evoked Potential (SSVEP) brain-computer interface (SSVEP-BCI) system. A person with severe motor disability would focus his/her visual attention on a bilateral visual stimulus generated on a computer screen. Meanwhile, the SSVEP-BCI system can be applied by performing various signal processing operations including EEG signal acquisition, application of CS, EEG signal reconstruction, feature extraction, and visual stimulus-frequency recognition. The MSI and CCA methods can be used to estimate respective features from the signals reconstructed using a CS algorithm. Simulation results indicate that the classification performance offered by the MSI method for the signals

reconstructed using a CS algorithm, with compression ratio (CR) of up to 75%, remains at par with that for the original uncompressed signals. Whereas, the classification performance offered by the CCA method is reduced after the application of CS. Therefore, the MSI method can be more suitable for designing CS-based low-power wireless sensors for the acquisition of EEG signals in the SSVEP-BCI systems.

Method:

Five male subjects (29.8 ± 2.17 years) participated in this study. Initially, signals from three occipital channels (O1, O2 and Oz) were extracted. Signals were compressed using CS with CR of 75%. Compressed signals were reconstructed using the -RLS, -RLS, and BSBL-BO algorithms. In the pre-processing stage, the data were segmented and windowed with window lengths (WL) of 1 s and 4 s, each one with an overlap of 50%. Then, the Common Average Reference (CAR) and band-pass filter in the range 3-60 Hz were applied. The CCA and MSI methods were applied independently, and the classification performance was evaluated.

Results and Conclusion:

The comparison of performance (mean and standard deviation) was tested in 50 repetitions of reconstructed Electroencephalographic (EEG) signals averaged for 5 subjects and different windows length. Finally, these results were also compared with the original EEG signals. From the results, we can see that generally the higher the window length of the data, the higher is the precision. As it can be noticed for all cases tested, the MSI technique surpassed that of CCA. The results regarding the reconstructed signals were slightly closer to the original signal: $\approx 72\%$ (WL = 1 s) and $\approx 85\%$ (WL = 4s). The three reconstruction algorithms showed results very similar to each other. For the proposed system, the MSI method can offer acceptable performance for high CR. The proposed system offers faithful detection performance and is suitable for the design of low-power wearable wireless electrodes. By using the stimulus frequency based on the MSI method, it is demonstrated that the proposed system can offer acceptable performance for a high CR compared to CCA technique. Consequently, the power-consumption in wireless EEG can be significantly reduced.

SP165.5 - Multi-way based Source Localization of Multichannel EEG signals Exploiting Hilbert-Huang Transform

Author(s): Saeed Pouryazdian, Soosan Beheshti, Sridhar Krishnan Electrical And Computer Engineering, Ryerson Univeristy, Toronto/CANADA

Background: Electroencephalogram (EEG) non-invasively measures the electrical potential at the scalp arising primarily from synchronous neuronal activity of the brain cells. EEG is high-dimensional and it is known that the processing of information by the brain is reflected in dynamical changes of the electrical activity in time, frequency, and space. Study of brain's physiological, mental and functional abnormalities requires methods that can describe these variation of EEG signals in time and frequency and space in a localized and quantitative way. Localization of the electrical activity of brain has been an active area of research known as EEG source localization. **Methodology:** EEG source localization is an ill-posed problem which in case of matrix (two-way) analysis forces us to add specific constraints, which may not be physiologically meaningful. Multi-way (tensor) analysis, on the other hand, is desirable in a sense that it's unique under mild condition and no such constraints are required. Parallel Factor Analysis (PARAFAC) is a well-known and common multi-way model in high-dimensional data modeling context. Temporal, Spatial and Spectral information of the multichannel EEG are used here to generate a three-way Time-Frequency-Space EEG tensor. The required Time-Frequency (TF) plane for generation of EEG tensor is provided through TF representation of each

EEG channel. Continuous Wavelet Transform (CWT) is conventionally used in literature which suffers from the lack of ability to exactly localize a single oscillatory event in time and frequency contemporarily. Motivated by the high-resolution capability of Hilbert-Huang Transform (HHT) in both temporal and spectral domain and its data dependent and adaptive nature, here we use HHT for TF representation. HHT consists of a combination of Empirical Mode Decomposition (EMD) and Hilbert Transform (HT). EMD is a fully data-driven technique for decomposing a non-stationary time series into a set of oscillatory and spectrally localized components called Intrinsic Mode Functions (IMFs). HT of the extracted IMFs, that reveals the non-stationarity of a signal through the computation of the instantaneous frequency and the instantaneous amplitude, is the second step of HHT. Furthermore, EMD-based TF representation enables us to embed the detrending of EEG signals by simply removing the corresponding IMFs. Results and **Conclusion:** Events in EEG can be uniquely characterized by a set of temporal, spectral and spatial signatures which their outer product makes a rank-one tensor. In a PARAFAC model, the observed EEG tensor is decomposed as a linear combination of rank-one tensors, each of them corresponding to an EEG event. Simulation results show that multi-way analysis of EEG greatly improve separation and localization of overlapping events in EEG and furthermore, the extracted signatures using PARAFAC decomposition of HHT-based EEG tensor, exploiting the merits of HHT, are more localized compared to CWT-based tensor analysis by having a higher Gini Index, which is used for measuring the sparsity and the concentration of energy in a signal. Removal of low frequency trends in EEG signal is essential and failure to do so can result in masking of the event of interest. Detrending of EEG is effectively embedded in HHT-based multi-way analysis.

SP166 - NeuroProstheses

TRACK 11: NEUROENGINEERING, NEURAL SYSTEMS

SP166.1 - Enhanced Transcutaneous Electrical Nerve Stimulation (eTENS): A Novel Method of Achieving Posterior Tibial Nerve Stimulation Therapy for Overactive Bladder

Author(s): [Paul Yoo](#)

Institute Of Biomaterials And Biomedical Engineering, University of Toronto, Toronto/CANADA

Overactive bladder (OAB) is characterized by symptoms of urinary urgency, frequency, and incontinence that can significantly affect quality of life. Posterior tibial nerve stimulation (PTNS) is an emerging therapy for OAB, where clinical efficacy has been shown as comparable to drugs and sacral nerve stimulation. PTNS therapy is delivered as periodic (e.g., weekly) stimulation sessions that result in improved bladder symptoms over a period of 12 weeks. While early studies attempted to use conventional transcutaneous electrical nerve stimulation (TENS) for providing OAB therapy, percutaneous stimulation using needle electrodes was subsequently found to provide significantly greater therapeutic effects. Despite the improved therapeutic outcomes however, percutaneous stimulation requires a trained clinician to deliver therapy and also entails repeated visits to the clinic. Furthermore, recent PTNS trials identify long-term compliance to therapy as a significant limiting factor for patients (i.e., annual drop-out rate > 12 %).

As a potential solution, we present a novel method of electrically stimulating peripheral nerves. Called enhanced transcutaneous electrical nerve stimulation (eTENS), this method achieves neural activation by coupling a conventional TENS electrode with an electrically-passive element placed in close proximity to the target nerve. Using computational software (Comsol Multiphysics + Matlab), we implemented the eTENS system in a model of the rat posterior tibial nerve (PTN). The electrically passive element was modeled as a nerve cuff placed around the PTN trunk; while the TENS electrode was depicted as a monopolar electrode located on the skin surface. The level of neural activation achieved by current passing through the TENS electrode was quantitatively approximated by the activating function, i.e., the second spatial difference of the extracellular potential along myelinated PTN fibers (diameter = 10 μm).

The results of our computational simulations showed that neural excitability by surface stimulation – as predicted by the activating function – increased significantly when the target nerve was instrumented with an electrically-passive implant (e.g., nerve cuff). When compared to the case with “no implant”, our model predicted that the eTENS system can achieve activating function values that were up to 6.4 times greater. These results, in turn, suggest that electrical activation of a target nerve can be achieved with stimulation amplitudes 0.15 times lower than that required by conventional TENS. Our computational model further shows that this enhancement in neural excitability depends on several key factors: physical dimensions and conductivity of the passive implant, depth of the target nerve from the skin surface, and relative alignment of the passive implant with the surface electrode.

The results of our computational study support the idea of enhancing the effectiveness of TENS by coupling the stimulus with an electrically-passive element. We have characterized the role of individual model parameters with respect to neural excitability, and have thereby identified key design parameters critical for testing the eTENS system in vivo. Further long-term implant studies are required for clinical translation in OAB patients.

SP166.2 - Decreasing Upper Extremity Demands During Sitting Pivot Transfers for Individuals with Spinal Cord Injury by Utilizing Functional Electrical Stimulation

Author(s): Stephanie N. Bailey¹, Scott W. Slivka², Lisa M. Lombardo¹, Kevin M. Foglyano¹, Ronald J. Triolo³

¹Motion Study Laboratory, Louis Stokes Cleveland Department of Veterans Affairs Medical Center, Cleveland/UNITED STATES OF AMERICA, ²Department Of Physical Therapy, Cleveland State University, Cleveland/UNITED STATES OF AMERICA, ³Departments Of Orthopaedics And Biomedical Engineering, Case Western Reserve University, Cleveland/UNITED STATES OF AMERICA

INTRODUCTION

The sitting pivot transfer (SPT) is a functional task performed by individuals with spinal cord injuries (SCI) that requires quick, intense forces on the upper extremities (UEs). Performed an average of 15-20 times/day [1], this repetitive task could be a contributing factor to the prevalence of secondary shoulder pathologies that develop in this population. Implanted functional electrical stimulation (FES) systems have been utilized in individuals with SCI to improve mobility, however, have not been evaluated in the ability to improve SPTs by reducing the demand to the UEs.

METHODS

A single subject performed SPTs between a standard wheelchair (WC) and modified chair, placing one hand on the WC armrest and the other on the seat of the chair, similar to the work of Desroches et al [2]. Using a Vicon MX system (Oxford UK) at 100 Hz, kinetics were recorded using an in-chair force plate, one in the floor, and a load cell attached to the armrest of the WC (AMTI, Watertown MA). Trials were randomized between two conditions: volitional and with stimulation to both quadriceps. The quasi-static peak and average moments were calculated about both shoulder joints during the lift pivot phase of SPTs. Paired t-tests (p<0.05) were performed to determine if there was a difference between stimulation conditions.

RESULTS AND DISCUSSION

There were many significant (p<0.05) decreases in average and peak moment about both shoulders when using stimulation (Table 1), which shows that both the leading and trailing limb can benefit from this transfer technique.

Table 1: Decreased Moments during SPT when using Stimulation compared to Volitional						
	Average Moment (Nm)			Peak Moment (Nm)		
	Mean	StDev	p-value	Mean	StDev	p-value
WC to Chair (n=6)						
Leading UE (L)	17.77	5.00	0.014	30.47	9.96	0.038
Trailing UE (R)	18.70	4.86	0.009	12.97	4.68	0.064
Chair to WC (n=12)						
Leading UE (R)	26.84	3.44	<0.001	33.25	3.31	<0.001
Trailing UE (L)	23.76	3.51	<0.001	28.00	7.04	0.007

Future research should focus on an improved set up that is able to detect moment during each phase of the SPT as well as including additional participants with various levels of paralysis to validate findings.

CONCLUSIONS

Utilizing FES in the lower extremities during SPTs has potential to decrease the moment about the shoulder joint bilaterally by shifting a portion of the weight-bearing to the lower extremities.

REFERENCES

- Gagnon D, et al. Biomechanics of sitting pivot transfers among individuals with a spinal cord injury: a review of the current knowledge. *Top Spinal Cord Inj Rehabil*, **15(2)**, 33-58, 2009.
- Desroches M, et al. Development of an automated method to detect sitting pivot transfer phases using biomechanical variables: toward a standardized method. *J. NeuroEngineering Rehabil*, **9:7**, 2012.

ACKNOWLEDGEMENTS

Funding by Merit Review #RX-001204 from the Rehabilitation R&D Service of the US Department of Veterans Affairs.

SP166.3 - Design of Orthotic Mechanisms to Control Stand-to-Sit Maneuver for Individuals with Paraplegia

Author(s): Sarah R. Chang¹, Mark J. Nandor², Kevin M. Foglyano³, Maria Lesieutre², Rudi Kobetic³, Ronald J. Triolo³

¹Department Of Biomedical Engineering, Case Western Reserve University, Cleveland/UNITED STATES OF AMERICA, ²Department Of Mechanical Engineering, Case Western Reserve University, Cleveland/UNITED STATES OF AMERICA, ³Motion Study Laboratory, Louis Stokes Cleveland Department of Veterans Affairs Medical Center, Cleveland/UNITED STATES OF AMERICA

Individuals with paraplegia can use functional neuromuscular stimulation (FNS) to accomplish sit-to-stand, standing, and stand-to-sit maneuvers. Stand-to-sit (STS) requires eccentric contractions or lengthening of the active quadriceps muscle. However, eccentric contractions are not well controlled with FNS due to a lack of feedback to the extensor muscles during the maneuver. STS using only FNS results in large impact forces at initial contact with the seating surface, high accelerations at the impact, high knee angular velocities, and a heavy reliance on the upper limbs [1]. In this study, we design and evaluate two different orthotic approaches for controlling the stand-to-sit transition.

A hydraulic hip-knee coupling mechanism was designed to lock, unlock, or couple the ipsilateral hip and knee motion of a hip-knee ankle orthosis. Fluid flow is directed between cylinders at the hip and knee joints, where hip flexion causes the hip cylinder rod to extend and move fluid into the rod side of the knee cylinder, forcing the knee cylinder to retract. The blind sides of the cylinders are connected to move fluid from the knee cylinder blind side into the hip cylinder blind side during movement. A mechanical transmission is used to convert the retraction of the knee cylinder rod to a knee flexion moment. Since the ipsilateral hip and knee will be coupled, individuals with paraplegia can control their hip angle via the upper limbs and thereby control their knee angle.

A hydraulic knee damping mechanism was designed to lock, unlock, or damp knee motion for a hip-knee ankle orthosis. Fluid flow is modulated between rod and blind sides of the knee cylinder through a proportional valve. When the proportional valve is fully closed, the knee cylinder is unable to move and locks the knee. When the proportional valve is partially open, the knee cylinder provides a damping force to help slow the knee angular velocity during knee flexion of STS.

Both mechanisms are undergoing bench testing to ensure safety of the device before clinical evaluation in able-bodied volunteers and

subjects with paraplegia. The hip-knee coupling mechanism provides a consistent 1:1 coupling ratio, where one degree of hip flexion results in one degree of knee flexion. The 1:1 ratio will achieve hip-knee angle relationships as seen in able-bodied STS maneuvers and provide a way to better control the STS for individuals with paraplegia. The damping created by the proportional valve mechanism is in the process of being characterized in bench testing. The mechanisms will be implemented in STS maneuvers for recipients of implanted neuroprostheses with spinal cord injury to quantify the extent to which the mechanisms assist in reducing the impact force on the seating surface and in controlling the STS maneuver.

This work was supported by Grant B0608-R and W81X-WH-13-1-0099 from the Department of Veterans Affairs and Department of Defense, and S.R. Chang was supported by training grant 5T32AR007505-28 to Case Western Reserve University.

[1] Chang SR, et al. *J Rehabil Res Dev. In Press.*

SP166.4 - Improved Peripheral Nerve Recording with a Small Form-Factor Nerve Cuff Electrode: A Computational Study

Author(s): Parisa Sabetian, Paul Yoo
University of Toronto, Toronto/CANADA

Electrical nerve stimulation has been successfully used to treat a wide range of neurological disorders (e.g., epilepsy, obstructive sleep apnea) by surgical implantation of nerve cuff electrodes. However, very limited progress has been made in the using these electrodes as part of closed-loop controlled neuroprosthetic systems. The current literature indicates that poor signal-to-noise ratio (SNR) of the recorded neural signal as one of the primary limitations of using nerve electrodes to measure peripheral nerve activity. To this end, we investigated the feasibility of improving signal fidelity by optimizing the design of a small form-factor, bipolar nerve cuff electrode.

A computer model – which combined the use of finite element software (Comsol Multiphysics) and Matlab – was implemented to simulate single fiber action potentials (SFAP) recorded by either a pseudo-tripolar or bipolar nerve cuff electrode. Our simulations showed that the inter-electrode distance (hence, the total length of the nerve electrode) significantly affects the peak-to-peak value (Vpp) of the simulated SFAP. The pseudo-tripolar electrode showed a 17.5-fold increase in Vpp as the cuff length was increased from 7mm to 33mm; whereas the bipolar configuration resulted in a 2-fold increase as the cuff length increased from 7mm to 20mm. Interestingly, at nerve cuff lengths below 13 mm, the Vpp of the SFAP recorded by the bipolar electrode was larger than that of the pseudo-tripolar electrode. Our model also revealed that the edge length (distance between the outer electrode contact and the edge of the insulating nerve cuff) had a significantly greater effect on the Vpp of SFAPs recorded from bipolar electrodes than that with a pseudo-tripolar electrode: 80% vs. 1% increases, respectively. Furthermore, simulations involving external noise sources and electrically-shielded nerve cuff electrodes showed dramatic (up to 99%) increases in the SNR of the recorded neural activity.

Concomitant experiments in 12 anesthetized rats confirmed our computational study. By recording stimulation-evoked compound nerve action potentials (CNAPs) from the sciatic nerve, we compared the Vpp value of the CNAP obtained from 3 electrode configurations: pseudo-tripolar (cuff length = 11 mm), bipolar (type A, inter-electrode distance=7 mm), and bipolar (type B, inter-electrode distance=3 mm). The type A (bipolar) electrode yielded the largest Vpp signal, which was 18% and 29% greater than pseudo-tripolar and type B electrodes, respectively. In 5 experiments, we also showed that electrically shielding the nerve electrode with a highly conductive material significantly increased the SNR by up to 65%.

The preliminary results of this study suggest that modifications to conventional nerve cuff electrodes can have significant effects on the fidelity of recorded neural signals. Both computational and experimental data suggest that design variable such as the edge length, inter-electrode distance and the presence of external shielding markedly improve the SNR. Further work is needed to test these ideas under more realistic conditions, such as spontaneous neural activity in either acute or long-term implant studies.

SP166.5 - Effect of stimulation on non-erect postures with a standing neuroprosthesis

Author(s): Brooke Odle¹, Musa L. Audu¹, Raviraj Nataraj², Ronald J. Triolo¹

¹Biomedical Engineering, Case Western Reserve University, Cleveland/UNITED STATES OF AMERICA, ²Orthopaedics, Case Western Reserve University, Cleveland/UNITED STATES OF AMERICA

Neuroprostheses can enable individuals with spinal cord injury stand erect from otherwise seated positions in the wheelchair [1]. To prevent collapse, current systems stiffen the lower extremities through continuous supramaximal activation of the knee, hip and trunk extensors. This approach does not allow for modulation of stimulation to enable users assume other than erect postures except by pulling or pushing against the continuously activated muscles with the arms. We hypothesized that appropriate changes in stimulation to ankle and hip muscles would decrease upper extremity effort exerted on a support device with changing posture. Preliminary experiments were performed to determine effects of altering stimulation on standing postures for one recipient of an implanted neuroprosthesis with motor and sensory complete paraplegia.

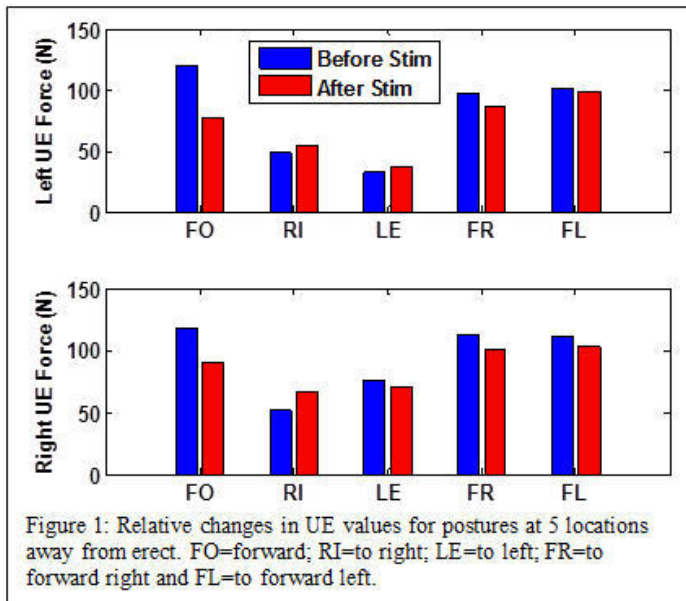
The limits of the postures achievable with upper extremity effort on a walker were defined with constant stimulation as the subject leaned as far as possible from erect in five different directions: forward, left, right, and diagonal (forward-right and forward-left) while center of pressure (CoP) at the extreme leaning positions were recorded. A subject-specific musculoskeletal model was used to generate optimal muscle activations required to maintain postures at the five extreme positions using inverse dynamics. Muscle activations were scaled to the threshold and saturation level pulse-widths (PWs) for each of the stimulated muscles. With real-time visual feedback, subject later adjusted her standing posture to move her CoP from erect to each of the 5 locations from the first experiment. After stabilizing at the new posture, stimulus levels were adjusted to coincide with the optimal values for the new CoP location as computed from inverse dynamics while the UE forces exerted on the instrumented walker were measured.

UE effort reduced by about 30% between left and right in the fore-aft direction and between 5%-10% in the diagonal directions (Figure 1). A relative increase (mean 20% between left and right UEs) was noted for movements to extreme left/right directions. The preliminary results indicate the potential for reducing UE forces (especially toward the forward direction) when optimal stimulus levels are applied. Future experiments will involve repeated trials on additional subjects. The ability to vary stimulus levels would enable users of standing neuroprostheses to vary their postures in a task-dependent manner to undertake activities of daily living which would otherwise be impossible from an erect posture.

Funding: NINDS Grant: R01NS040547.

References:

Triolo R.J et al, *Arch Phys Med & Rehab.* 1996, 7(11), 1119-1128, 1996.



SP166.6 - Automatic Detection of Destabilizing Wheelchair Conditions for Modulating Actions of Neuroprostheses to Maintain Seated Posture

Author(s): Anna Crawford¹, Musa L. Audu¹, Ronald J. Triolo²
¹Louis Stokes VA Medical Center, Cleveland/UNITED STATES OF AMERICA, ²Department Of Orthopaedics, Case Western Reserve University, Cleveland/UNITED STATES OF AMERICA

The number of wheelchairs users and thus wheelchair related accidents in the United States is growing. There are an estimated 100,000 wheelchair related accidents a year in the United States, primarily resulting from tips and falls¹. Constant stimulation of the otherwise paralyzed core hip and trunk muscles can stabilize seated posture and return users to and maintain erect sitting positions in response to applied disturbances^{2,3}. The goal of this study is to automatically predict and detect potentially destabilizing conditions encountered by wheelchair users to control the actions of a neuroprosthesis to prevent falls and improve manual propulsion efficiency by appropriately modulating stimulation. Wireless inertial measurement units consisting of tri-axial acceleration and gyroscopic sensors⁴ were applied above the right caster of the wheelchair frame and on the sternum of 4 individuals with low cervical to low thoracic spinal cord injuries. Subjects propelled over level ground, ascended and descended 5 and 10 degree ramps, negotiated sharp turns and simulated rough terrain consisting of closely spaced and loosely spaced rumble strips, and completed simulated collisions such as sudden stops and a curb drop. A Vicon motion capture system acquired signals from the wireless sensors and tracked the position of both the wheelchair and user for use as a gold standard for detecting the each event and classifying each maneuver. Sensor data were exported and processed in Matlab. Mean and standard deviations of features including individual components and resultant magnitudes of the accelerometer and goniometer signals at the onset and during, and the steady state propulsion leading up to or following each event were calculated for each trial. Distinctly different signatures of feature values were observed for each event which could be incorporated into a generalized classifier for discrete event detection. For example, the gyroscopic data in forward and lateral directions and the component of acceleration in the anterior-posterior direction as well as the resultant acceleration were most sensitive to discriminating sudden stops from other states. Construction and verification of a wireless inertial measurement based wheelchair event classifier to control a neuroprosthesis to modulate stimulation in an appropriate manner to maintain seated stability and optimal performance is ongoing.

REFERENCES

[1] Xiang, H., et al. *Injury Prevention* 12:8-11. Feb. 2006.
 [2] Triolo, Ronald J., et al. *Archives of Physical Medicine & Rehab*, 94(9):1766-75, 2013 and 94(10):1997-2005, 2013
 [3] Murphy, Julie O., et al. *Journal of Rehab Research & Development*, 51(5):747-760, 2014.
 [4] Foglyano, Kevin M., et al. *33rd Annual International Conference of the IEEE EMBS*. Boston, Ma. Aug 30-Sept. 3, 2011.

FUNDING SOURCES

Rehabilitation R&D Service of the US Department of Veterans Affairs Merit Review I01RX001204 and Spinal Cord Research Program of the US Dept of Defense Grant SC090230.

SP166.7 - Selecting Upper Extremity Command Signals to Modulate Electrical Stimulation of Trunk Muscles during Manual Wheelchair Propulsion

Author(s): Kyle P. Tepe¹, Stephanie N. Bailey², Ronald J. Triolo²
¹Biomedical Engineering, Case Western Reserve University, Cleveland/OH/UNITED STATES OF AMERICA, ²Motion Study Laboratory, Louis Stokes Cleveland Department of Veterans Affairs Medical Center, Cleveland/UNITED STATES OF AMERICA

Introduction

Manual wheelchair propulsion (MWCP) is known to be mechanically inefficient. Shoulder pain is frequently reported by manual wheelchair users after paralysis due to spinal cord injury (SCI)¹. Neuroprostheses employing functional neuromuscular stimulation (FNS) can reactivate paralyzed muscles controlling the pelvis and torso while sitting². Low-level constant stimulation to stiffen the hips and trunk can improve mechanics of MWCP over level surfaces and at comfortable speeds³. We hypothesize that synchronizing activation of the hip and trunk flexor and extensor muscles with the MWCP cycle is necessary to improve efficiency in more challenge tasks like ramps and sprints. This study evaluated the suitability of upper extremity (UE) electromyographic (EMG) activity as a command signal to appropriately time stimulation with the stroke cycle.

Methods

A 38-year-old female with a T3 SCI (AIS A) was instructed to push her own wheelchair while on a treadmill in a V-Gait virtual reality environment (Motek Medical, Amsterdam, the Netherlands). Wireless EMG (Delsys, Natick MA) from eight bilateral UE muscles was acquired synchronously with pushrim kinetics (SmartWheel, OutFront, Mesa AZ). Threshold-based detection of total pushrim force was used to define individual MWCP cycles and distinguish contact (push) from recovery phases⁴. At least 50 MWCP cycles were obtained at self-selected, fast (+20%) and slow (-20%) speeds. EMG data during individual propulsion cycles were obtained using synchronized SmartWheel data, normalized in length, and averaged across all cycles.

Muscles were qualitatively classified as contact or recovery phase muscles based on their activity over the cycle. Signal strength was quantified by calculating the statistical range of each ensemble average for each condition. Relative timing of the strongest and most consistent signals with respect to contact and recovery phase transitions were considered optimal candidates for command sources for an implanted neuroprosthesis.

Results

Right pectoralis major and right posterior deltoid muscles exhibited the largest statistical ranges and were best correlated with contact and recovery phases, respectively, for all propulsion conditions. Performance of a classification algorithm using this combination of muscles to detect contact and recovery states of wheelchair propulsion is currently being quantified in preparation for clinical testing of an EMG-based neuroprosthesis control system to modulate stimulation appropriately with the propulsion cycle and determine its effect on MWCP efficiency during challenging real-world conditions.

References

- 1: Mercer, Jennifer L., et al. "Shoulder joint kinetics and pathology in manual wheelchair users." *Clinical Biomechanics* 21.8 (2006): 781-789.
- 2: Triolo, Ronald J., et al. "Effects of Stimulating Hip and Trunk Muscles on Seated Stability, Posture, and Reach After Spinal Cord Injury." *Archives of physical medicine and rehabilitation* 94.10 (2013).
- 3: Triolo, Ronald J., et al. "Effects of intramuscular trunk stimulation on manual wheelchair propulsion mechanics in 6 subjects with spinal cord injury." *Archives of physical medicine and rehabilitation* 94.10 (2013): 1997-2005.
- 4: Kwarcia, Andrew M., et al. "Redefining the manual wheelchair stroke cycle: identification and impact of nonpropulsive pushrim contact." *Archives of physical medicine and rehabilitation* 90.1 (2009): 20-26.

SP167 - GI and GU

TRACK 12: MEDICAL DEVICES

SP167.1 - Medical Devices

Author(s): [Aaron Fenster](#)

Imaging Research, Robarts Research Institute, London/ON/CANADA

The continuous advances in technology and software, as well as their widespread use in diagnosis and treatment has provided new and transformative capabilities to physicians. The past 3 decades have witnessed revolutionary advances with the development and optimization of PET, CT, MRI and ultrasound imaging for diagnosis of a wide range of diseases. The next few decades are likely to bring advanced technologies to surgical and minimally invasive interventional methods to treat diseases. Advanced robotic systems have already had an important impact on surgical procedures as demonstrated by the da Vinci robotic system. While advanced tools and visualization software are continuing to be developed for robotic aided open surgical systems, many innovations are still required for image-guided minimally-invasive (i.e., percutaneous) interventional systems.

Many researches and companies have been focusing on developing a variety of novel robotic, navigation, guidance and visualization systems to be used for specific surgical/interventional indications. For example, revolutionary systems have been developed to be MR compatible (i.e., operate within or near an MR scanner), allowing accurate, precise and reliable minimally invasive MR-guided interventions such as prostate biopsy and therapy. Other systems have been developed that use 3D ultrasound fused with MR or CT images to guide biopsy and interventional tools. This approach makes use of the high quality images provided by MR and CT for identification of the targets together with the real-time ultrasound guidance of the interventional tools into the body. Examples of this type of systems include 3D ultrasound with MR fusion to guide prostate biopsy, as well as 3D ultrasound fused with CT images to guided focal ablation of liver tumors using radio-frequency or microwave energy delivery systems.

Innovations in robotics/mechatronics coupled to advanced software tools have resulted in complex and crowded surgical and therapy rooms. Thus, innovators have been developing a variety of virtual-reality guidance and navigation technologies making use of optical and electro-magnetics navigation systems. These systems are being developed and used in neuro-surgery as well as for focal liver tumor ablation. In addition, manipulation of tools and the complex set of images has required innovation in non-touch control as viewing and manipulating of tools and image display through use of a mechanical device such as a mouse, keyboard or touchscreen are problematic, requiring the physician to break the sterile field during surgery. Additionally, the surgeon's hands are likely covered in bodily fluids, which could interfere with use of these devices. Thus, gesture-based systems allowing 3D control through real-time high-content virtual reality navigation would permit complex functions to be controlled without touching mechanical devices.

Clearly, we are in the middle of possibly the next revolution for medical imaging devices, which promise to integrate robotics, advanced software, virtual reality navigation with a variety of therapy/surgical tools. In this paper, we will focus on a survey of image-guided surgical/interventional medical devices and the potential direction this field will take over the next decade.

Learning Objectives:

- 1) Challenges facing developers of image-guided intervention devices
- 2) Current state of medical devices used in image-guided intervention.
- 3) Opportunities for development of new and transformative medical devices used in image-guided intervention.

SP167.2 - Dielectric Properties of Urine for Diabetes Mellitus and Chronic Kidney Disease between 0.2 GHz and 50 GHz

Author(s): Hua Nong Ting¹, Peck Shen Mun¹, Teng Aik Ong², Yip Boon Chong³, Kwan Hong Ng⁴
¹Department Of Biomedical Engineering, University of Malaya, Kuala Lumpur/MALAYSIA, ²Department Of Surgery, University of Malaya, Kuala Lumpur/MALAYSIA, ³Damansara Specialist Hospital, Petaling Jaya/MALAYSIA, ⁴Department Of Biomedical Imaging, University of Malaya, Kuala Lumpur/MALAYSIA

This paper investigates the dielectric properties of urine among normal subjects, subjects with diabetes mellitus (DM) and subjects with chronic kidney disease (CKD) at microwave frequency between 0.2 GHz and 50 GHz. The measurements were conducted using open-ended coaxial probe at room temperature (25°C), 30°C and human body temperature (37°C). Statistical significant differences in dielectric properties were observed across temperatures among normal, DM and CKD subjects. Significant differences were reported across subject groups at 25°C, 30°C and 37°C respectively.

SP167.3 - Intraoperative Bioelectrical Impedance Measurement for Assisting Segmental Renal Artery Clamping Partial Nephrectomy

Author(s): Jun Du¹, Yu Dai², Qing Yang¹, Jianxun Zhang²
¹Tianjin Medical University Cancer Institute and Hospital, Tianjin/CHINA, ²Institute of Robotics and Automatic Information System, Nankai University, Tianjin/CHINA

Critical procedures of segmental renal artery clamping partial nephrectomy (SACPN) includes segmental renal artery (SA) discrimination and ischemic area identification. Due to limitations of intraoperative ultrasonography, novel technique to facilitate SACPN is being needed. The aim of this paper is to explore whether intraoperative bioelectrical impedance spectroscopy (EIS) assessment could facilitate SACPN. Five domestic pigs were included in present study. The noninvasive electrical impedance sensor we developed consists of two stainless steel spherical electrodes, which are used to measure impedance spectra over the frequency range of 200 kHz to 5 MHz. EIS of renal artery and renal vein were assessed. After SA clamping, EIS of ischemic area, nonischemic area and ischemic-nonischemic boundary of kidney were examined. In porcine model, EIS of renal artery is significantly higher than renal vein ($p < 0.05$). After SA clamping, EIS of ischemic area was significantly higher than nonischemic area ($p < 0.05$). In addition, EIS of ischemic-nonischemic boundary was between that of ischemic and nonischemic area. The experimental results proved that the intraoperative EIS assessment could possibly facilitate SACPN through SA discrimination and renal ischemic area identification.

SP167.4 - Renal Volume Estimation by Ultrasound Parallel Scanning for Polycystic Kidney Disease Follow-up

Author(s): Franco Simini¹, Mauro Sitrin¹, Esteban Arrua¹, Diego Tobal², Luciana Urruty¹, Oscar Noboa²
¹Núcleo De Ingeniería Biomédica, Universidad de la República, Montevideo/URUGUAY, ²Nephrology Department, Universidad de la República, Montevideo/URUGUAY

Renal size provides information for the diagnosis and prognosis of kidney diseases. Volume measurement is usually based on ellipsoid calculations derived from Ultrasound (US) imaging. Complex pathologies such as Polycystic Kidney Disease (PKD) require images obtained with contrast media or ionising radiations (X Rays), not suitable due to toxicity and radiation effects. We have developed NEFROVOL, a low cost, noninvasive solution to reconstruct renal structure and to estimate its volume, using parallel US scans (Figure 1)

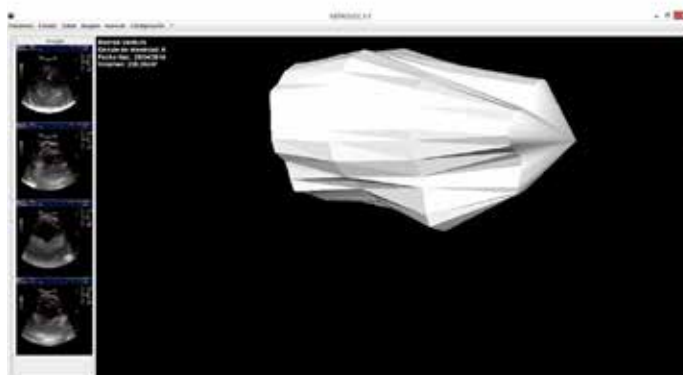


Figure 1: 3D reconstruction of a sweet potato. Four US scans are shown at the left and a view of the solid in the centre.

Parallel and equidistant kidney sections are obtained using a cutaneous Grid. The set of 4 to 8 scans are processed by the Volumetric Pixel Method (VPM) after each kidney layer was obtained with the Layered Convex Hull Method (LCHM), keeping both the precision of the VPM and the speed of LCHM.

Table 1 Test of NEFROVOL measuring KIDNEYS of volunteers

Patient	Cuts	Dimensions	Real	NEFROVOL	Difference %
1	3	10.74x4.99x6.56	184.08	138.05	-25
2	3	9.30x4.56x6.41	129.85	164.01	21
3	4	11.84x5.04x5.49	171.39	172.76	1
4	3	10.35x3.73x5.50	111.18	109.0	-2

Tests on geometric solids, fruit and patients yield estimates within 13%, 17% and 25% of the real volume, respectively. The volume of normal kidneys can be measured by conventional ellipsoidal formula and agrees with NEFROVOL calculation in patients 3 and 4. Transplanted patient 1 and volunteer patient 2 show larger differences: up to 25% of the volume.

NEFROVOL generates standard electronic medical record documents (single measurement or trend), and is compatible with 3D printing by generating STL files.

NEFROVOL addresses the problem of 3D reconstruction of organs from US scanner images, adding the estimation of volume for follow up purposes. Despite the low precision, NEFROVOL can be of used to monitor kidney volume increase, which is the goal of the research. Better precision will be addressed by including intermediate parallel scans.

SP167.5 - Can Removal of Middle Molecular Uremic Retention Solutes be Estimated by UV-absorbance Measurements in Spent Dialysate?

Author(s): Kai Lauri¹, Merike Luman², Jana Holmar¹, Ruth Tomson¹, Sigrid Kalle¹, Jürgen Arund¹, Fredrik Uhlin³, Ivo Fridolin¹

¹Department Of Biomedical Engineering, Technomedicum, Tallinn University of Technology, Tallinn/ESTONIA, ²Centre Of Nephrology, North-Estonian Medical Centre, Tallinn/ESTONIA, ³Department Of Nephrology, University Hospital, Linköping, Linköping/SWEDEN

The objectives of this study were: (1) to compare removal of the middle molecular (MM) and small uremic retention solutes; (2) to investigate if MM removal can be assessed by UV-absorbance at the wavelength of 297 nm during various dialysis treatment modalities. Seven uremic patients, four females and three males, mean age 58.1±8.7 years, were included into the study during 28 chronic hemodialysis sessions. A parameter, reduction ratio (RR) in percentage, was calculated for a small uremic retention solute urea, for a MM retention solute beta2-microglobulin (B2M), and for UV-absorbance at the wavelength of 297 during different dialysis modalities: conventional hemodialysis (HD), high flux hemodialysis (HF-HD), and postdilutional online hemodiafiltration (HDF) with different parameter settings. Achieved results were compared regarding mean values and SD, and by systematic and standard errors (BIAS±SE). It was found that RR is similar for small and MM uremic retention solutes in case of dialysis modality with the highest convective transport, HDF (78.9±8.1% for urea and 78.1±6.8% for B2M, N=7). Moreover, RR of small uremic retention solutes can be estimated with sufficient accuracy by UV-absorbance at 297 nm in the spent dialysate for all modalities (BIAS±SE: 1.7±4.0%, N=28), and for MM uremic retention solutes only for HDF (BIAS±SE: 1.1±7.1%, N=7). The results should be confirmed by appropriate kinetic modeling in the next studies.

Keywords— Middle molecules, uremic toxins, beta2-microglobulin, uremic retention solutes, urea, dialysis, UV-absorbance.

SP167.6 - Discrimination of prostate tissue with a combination of Raman spectroscopy and tactile resonance technology

Author(s): Olof Lindahl¹, Morgan Nyberg², Ville Jalkanen³, Kerstin Ramser¹, Börje Ljungberg⁴, Anders Bergh⁵

¹Centre For Biomedical Engineering And Physics, Umeå University, Umeå/SWEDEN, ²Engineering Sciences And Mathematics, Luleå University of Technology, Luleå/SWEDEN, ³Applied Physics And Electronics, Umeå University, Umeå/SWEDEN, ⁴Surgical And Perioperative Sciences, Urology And Andrology, Umeå University, Umeå/SWEDEN, ⁵Medical Bioscience, Pathology, Umeå University, Umeå/SWEDEN

Prostate cancer (PCa) is the most common cancer in men in Europe with 416 700 new cases reported in 2012 and in the USA with an estimate of 233 000 new cases for 2014. The most prevalent curative treatment for PCa is radical prostatectomy (RP). In Europe, RP made up 59 % of the curative treatments in 2000 and in the USA about 70 000 men were offered RP in 2003. The standard procedure after RP is to examine the resected prostate histologically. One important examination is the evaluation of tumour cells in the surgical and the anatomical margins (PSM) since there is an increased risk of PCa recurrence if tumour cells are found at the surgical margin. A new dual-modality probe has been developed for prostate cancer detection by us. The probe combines two methods, a tactile resonance sensor that measures the tissue stiffness modality, and Raman spectroscopy, that measures the molecular content. Together the two methods are the basis for the dual-modality probe and a hypothesized method intended for detecting PSM during radical prostatectomy. The idea is that the surgical margin, i.e. the surface, of the prostate is to be scanned to locate stiffer areas using the stiffness modality of the combined instrument. Harder nodules are an indication of tumour presence but also of stiff benign structures,

such as prostate stones. The Raman spectroscopy modality would then be applied at these locations to discern the boundaries between cancerous and non-cancerous stiff tissue.

The aim of this study was to evaluate the ability of the combined probe to discriminate different tissue types in fresh human prostate slices *ex vivo*.

The results from four human prostates show that the tactile resonance modality was able to discriminate significantly between two different tissue types: soft epithelial tissue and stiff stroma ($p < 0.05$). The Raman spectra exhibited a strong fluorescent background at the current experimental settings. However, stroma could be discriminated from epithelia by integrating the value of the spectral background. Combining both parameters resulted in 100% sensitivity and 91% specificity.

We conclude that the results indicates that the two modalities together increase the sensitivity and specificity and are promising for further development of an instrument and method for discriminating prostate tissues and thus also cancer that is the final goal.

SP167.7 - Appropriate Medical Devices for Low Resource Settings: Electronically Controlled Gravity-Feed Intravenous Infusion Set

Author(s): Philippa N. Makobore¹, Paul Niyitanga¹, Simon Ssekitoleko¹, Robert Ssekitoleko², Peter Rolfe³

¹Instrumentation Division, Uganda Industrial Research Institute, Kampala/UGANDA, ²Ugandan Maternal and Newborn Hub, Kampala/UGANDA, ³School Of Electrical Engineering And Automation, Harbin Institute of Technology, Harbin/CHINA

ABSTRACT

Background

Despite an improvement in the reduction of the Infant Mortality Rate (IMR), 45/1000 as of 2012 down from 54/1000 in 2009, Uganda continues to lag far behind target for achieving the Millennium Development Goals. Children continue to die from preventable diseases such as pneumonia and diarrhoea which contribute to nearly 40% of the IMR. The majority of neonates and infants with pneumonia, diarrhoea and malaria often present in advanced disease stages; hence requiring intravenous fluid and/or drug delivery. Unfortunately, existing infusion sets are not tailored to the needs and resources of Uganda. Medical equipment surveys in Low and Middle Income Countries (LMICs) show that equipment needed for neonatal and infant care are imported and in short supply largely due to high cost. It is also invariably poorly maintained, and is often rendered non-functional or potentially hazardous by users. Furthermore, electrically operated devices are usually unable to withstand prevailing intermittent power supply.

Method

The Electronically Controlled Gravity-Feed Intravenous (ECGI) Infusion Set has been designed to overcome the deficiencies of existing intravenous therapy systems by providing an easy to use, cost effective plug-on intravenous administration monitoring and control system. Additional features will include occlusion detection, high and low drip rate alarm settings and visual readout of the drip rate all provided for on a microcontroller platform. The power supply will be characterized by a hybrid battery charging bed (solar and electrical mains). Implementation will be executed using Proteus software, preliminary prototyping with bread boards and finally Printed Circuit Board (PCB) development.

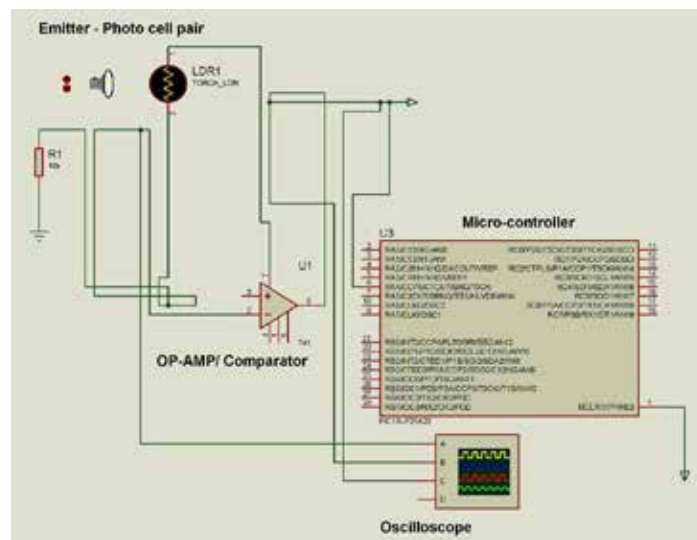
Results

Design and simulation of the sensing/monitoring hardware circuit has been completed in Proteus simulation software with desirable waveforms displayed on the oscilloscope in the illustration below.

This circuit has been implemented on a bread board and output results are within 5% error when compared with the simulation results. Interference due to noise and ambient light are apparent in the breadboard circuit. We anticipate a smaller error margin once implemented on a PCB. The control module has also been simulated in Proteus and is yet to be implemented on a bread board and subsequently PCB.

Conclusions

Pending designs include simulation of the user interface display hardware circuit in Proteus and incorporation of LCD function coding and testing. We will also identify a charge management Integrated Circuit (IC) for the rechargeable batteries to build the power supply system.



SP168 - Health Challenges in Resource-Poor Nations

TRACK 12: MEDICAL DEVICES

SP168.2 - Challenges of introducing health technologies to low resource settings in global framework: a case study at WHO

Author(s): Cai Long, Adriana Velazquez Berumen, Daniela Rodriguez Rodriguez
Essential Medicines And Health Products Department, World Health Organization, Geneva/SWITZERLAND

Asphyxia, defined as the failure to initiate and sustain breath at birth, is responsible for a quarter all neonatal deaths (around 700,000)¹. Effective neonatal resuscitation, immediate care including thorough drying, suction and stimulation after assessment, and positive-pressure ventilation can prevent a large number of these neonatal deaths.^{2,3}

The United Nations Commission on Life-Saving Commodities for Women and Children (UNCLSC) aims to increase access to life-saving commodities for people in low resource settings. In collaboration with UNICEF, United States Agency for International Development (USAID), PATH and Clinton Health Access Initiatives (CHA), WHO has worked on developing technical specifications for neonatal resuscitation commodities, including neonatal resuscitation bag with masks, suction machine, single use and reusable suction bulb. These technical specifications provide a technical baseline for any policy-maker, manager, procurement officer, manufacturer or non-governmental agency in low resource settings to access affordable, safe and good quality neonatal resuscitation devices.

For neonatal resuscitation bag with masks, which ventilate newborns with positive air pressure, three major technical specifications were specified: bag size, pressure relief valve maximum pressure and face mask size. Unexpected challenges and barriers were faced and solved in this process, including:

- Discrepancies among existing standards and professional association guidelines.
- Lack of international standards for certain technical specifications for life-saving essential health technologies.
- Lack of information and research for life-saving essential health technologies.
- Making unbiased optimal recommendations in a smaller market with limited vendors
- Other challenges: logistics, procurement, disinfection, decommissioning and overall safe use of neonatal resuscitation devices in low resource setting countries.

Multi-stakeholder tactics were used to solve the challenges in the process of documenting WHO technical specifications:

- Collaborate with international associations, NGOs.
- Consult within institution experts and external experts.
- Gather feedback and comments from users' perspective.
- Review current market status quo.
- Literature review.

· Encourage research on simple, essential lifesaving health technologies.

Technical specifications were identified and submitted for further global expert review. In the future, in order to increase access to life-saving health technologies for the world's most vulnerable people, WHO, regulatory bodies and NGOs should encourage greater attention on essential health technologies needed in low resource settings.

References

1. Wall S N, Lee A C C, Niermeyer S, et al. Neonatal resuscitation in low-resource settings: what, who, and how to overcome challenges to scale up International Journal of Gynecology & Obstetrics, 2009, 107: S47-S64.
2. Guidelines on basic newborn resuscitation, World Health Organization, 2012
3. Knippenberg, Rudolf, et al. Systematic scaling up of neonatal care in countries. The Lancet 365.9464 (2005): 1087-1098.

SP168.3 - Portable microwave based stroke and trauma diagnostics

Author(s): Mikael Persson¹, Mikael Elam², Andreas Fhager¹, Stefan Candefjord¹

¹Signals And Systems, Chalmers University of Technology, Gothenburg/SWEDEN, ²Dept. Of Clinical Neurophysiolog, Sahlgrenska Academy, Inst of Neuroscience and Physiology, Gothenburg/SWEDEN

Worldwide, about 17 million people suffer a stroke each year. The human cost is horrific. Out of the sufferers 5 million die and another 5 million are permanently disabled. Among stroke survivors, 20% have serious remaining dysfunctions. A much larger proportion has less conspicuous, dysfunctions, which still seriously affect quality of life for the patient and relatives. The European yearly cost (2010) has been estimated to 64.1 billion € for the around 800 000 stroke patients.

Here we present different brain diagnostic devices based on microwave technology and the associated proof of principle measurements that show that the systems can differentiate hemorrhagic from ischemic stroke in acute stroke patients, as well differentiate hemorrhagic patients from healthy volunteers. The system was based on microwave scattering measurements with an antenna system worn on the head. Measurement data were analyzed with a machine-learning algorithm that is based on training using data from patients with a known condition. CT images were used as reference. The detection methodology was evaluated with the leave-one-out validation method combined with a Monte Carlo based bootstrap step.

The clinical motivation for this project is that ischemic stroke patients may receive acute thrombolytic treatment at hospitals, dramatically reducing or abolishing symptoms. A microwave system is suitable for pre-hospital use, and therefore has the potential to allow significantly earlier diagnosis and treatment than today.

The relative simplicity and potentially small size of a microwave-based diagnostic system underlines a specific aim of the project which to start the path towards implementation, in the sub-Saharan Africa, where there are very limited resources in terms of medical personnel, hospitals and medical devices, that can be used by ambulance personnel, at the scene of incident, for instance at the patients home, or at the local hospital.

Our microwave-based systems have the advantage of being com-

pletely safe and without side effects since the power levels used are only a fraction of what is transmitted by a mobile phone. This also allow the systems to operate in continuous mode as a monitoring devices. The systems also have the potential of becoming quite cost effective as the component costs are driven down by the considerably larger telecom industry.

SP168.4 - Bending the cost curve: Towards a \$1000 diagnostic X-ray imager for scalable and sustainable healthcare

Author(s): Karim S Karim, Sina Ghanbarzadeh
Electrical And Computer Engineering, University of Waterloo, Waterloo/CANADA

Cost, quality and accessibility are major barriers to disease detection globally. For an easily communicable disease like tuberculosis, diagnostic or screening tests based on sputum, blood and urine analysis have slow response, are difficult to administer in remote locations, and have relatively high transportation and storage costs. Medical-grade state-of-the-art digital x-ray imaging systems are versatile in disease detection, faster, incorporate teleradiology for remote diagnosis, but are prohibitively expensive making them affordable only by major hospitals or labs that are located mostly in urban centers with high patient volumes. Here, a value priced, high quality, digital x-ray imaging system could address many global health issues by enabling fast, accessible and inexpensive early detection of curable diseases including tuberculosis especially in rural, remote or under-populated areas.

In this research, we propose a path to achieving an inexpensive, high quality, digital X-ray system by focusing on the X-ray imager, a component that can reach 50% of the manufacturing cost of an imaging system. High manufacturing costs today are largely a function of small production volumes and various specialized fabrication processes. Our approach leverages two technologies developed in-house that leverage existing manufacturing infrastructure because they are fully compatible with older generation amorphous and poly-silicon TFT display manufacturing lines: the first is a low dark current, high quantum efficiency optical radiation sensor that rivals state-of-the-art amorphous silicon pin photodiodes and the other an amplified pixel circuit having a straightforward offset and gain correction scheme that yields higher signal-to-noise ratio than state-of-the-art passive pixels. When our sensor and pixel circuit technologies are integrated, the result is a high performance, low manufacturing cost diagnostic X-ray imager that can help achieve sustainable healthcare globally.

SP168.5 - Creating a Continental Network of Healthcare Innovation Centers: Collaborating across National Boundaries to design Devices and Best Practices

Author(s): Fred W. Hosea
Clinical Technology, Kaiser Permanente, Oakland/UNITED STATES OF AMERICA

Managing the lifecycle challenges of healthcare systems exceeds the current capacities of any country in the world, and the difficulties are only growing. Central problems are: -Unprecedented technical complexity -Demand for universal services and new service lines -Interdependence of systems -Global economic slowdown, without likelihood of recovering previous growth rates -Velocity of change -Obsolete, inadequate infrastructures -Fragmentary market mechanisms and perverse incentives -Political and economic interests that preserve a dysfunctional status quo -Obsolete professional and organizational structures -Disjointed incrementalism -Demographic pressures that exceed current and future capacity -Predicted impacts of climate change: migration of populations, infectious diseases; and economic refugees to unprepared locations A new age of integrated innovation is essential to achieve the possibilities of Health for All.

-New forms of collaboration and interdisciplinary knowledge are necessary. -Innovation must be re-defined to include innovations that effectively integrate established technologies, instead of creating a relentless treadmill of expensive high-tech point solutions that often promise more than they deliver. -National innovation centers will serve as hemispheric resources in their areas of investigation and best practices (e.g., telemedicine, tropical diseases, disaster management), and will serve as consultation centers to all other countries in the network, providing expertise oriented along the entire lifecycle of successful innovation.



We envision innovation that leverages collective resources more effectively to achieve a higher adoption rate of appropriate and interoperable technologies with less wastage of resources, less planned obsolescence, more universal coverage, lower cost, and a more rational staging of medical infrastructures as economies and service models mature.

COLLABORATIVE DESIGN FORUMS to engage key stakeholders at the trans-national level of strategy and planning

NON-PROFIT INTER-SECTORAL ALLIANCES to solve core technology challenges (e.g., The Continua Alliance)

STRATIFIED INNOVATION GOALS to re-target manufacturing, facilities and workforces more equitably to low and medium resource markets, with more local production.

STRATEGIC CONSULTATIONS with regional alliances across Ministries of Health to develop and align mid- to long-term infrastructure plans and capital budgets, within regional and multi-national planning and purchasing frameworks

COORDINATED ACADEMIC PARTNERSHIPS COORDINATED to cultivate sustained, multi-disciplinary research and professional development programs aimed at integrated healthcare planning

REGIONAL/CONTINENTAL NETWORKS OF INNOVATION CENTERS to distribute the enormous workload of innovation design, assessment, testing and planning

“DESIGN FOR CASCADE” – design of higher-cost systems for staged re-use in low-resource locations

Adoption of a COMMON INTEROPERABILITY MATURITY roadmap that enables co-evolution of medical devices with IT systems and clinical treatment practices.

SP168.6 - Towards a WHO List of Priority Medical Devices for Cancer Care, targeting low and middle income countries

Author(s): M. Mikhail Lette, A. Velazquez Berumen, G. Jimenez Moyao, A. Migliore, D. Rodriguez Rodriguez; HIS/EMP/PAU/Medical Devices, World Health Organization Headquarters, Geneva/SWITZERLAND

Cancer mortality disproportionately affects low and middle income countries’ populations; 70% of global deaths attributable to cancer occur in low and middle income countries. In view of an alarming trend of increased incidence and prevalence of NCDs (non-communicable diseases) and their disproportionate adverse effects upon low and middle income populations, the WHO Medical Devices team has embarked upon a promising new project to develop a Priority Medical Devices List for Cancer Care, to target low and middle income countries, in the goal of better empowering countries to develop or improve cancer healthcare capacities. During this incipient few-year endeavor, the entire spectrum of devices needed for the continuum of cancer care - screening, diagnostics, and treatment (both curative and palliative) - will be analyzed and compiled for six types of cancer: cervical, breast, prostate, lung, colorectal, and leukemia. Collaboration is being invited. Project progress is presented.

First, an extensive review of evidence-based clinical guidelines was performed to select ones which comprise the continuum of diagnostics and care and are aligned with current clinical knowledge benchmarks (with guideline database updated at regular intervals). Guidelines were chosen from several world regions and current implementation and relevance of them in low and middle income settings will continue to be assessed. Based upon guidelines, matrices of clinical interventions were developed and stratified for each type of cancer. This provided a basis to generate an extensive database of medical devices per intervention via the following algorithm: Condition\Stage of Care\Intervention\Steps of the Procedure\Procedure\Device Category\Device Code\Name(s) of the Medical Device\Description\Level of Care.

Nomenclature of interventions was compared against and harmonized with the ICHI (International Classification of Health Interventions). Likewise interventions were segregated by level of care and the associated health care facility:

- Community level health post
- Health center (outpatient care)
- District or general hospital
- National or specialized referral hospital

This project also seeks to provide a concise clinical background and staging overview for each disease in question, to research epidemiologic data on global burden of disease, to define countries to involve in this project, and eventually to conduct in-country workshops and case studies.

Further work will include inter-agency cooperation (with other UN organizations) and with professional organizations (e.g. NGOs, collaborating centres, professional societies, academic institutions). Experts and expert groups will be sought to form relevant committees willing to contribute to this project in their respective areas of expertise, to verify the interventions and priority medical devices, and eventually to validate and support implementation of the lists.

This project has been undertaken courtesy of a grant from OFID (the OPEC Fund for International Development, Uniting against Poverty).

The ultimate goal is to have available information on technologies that are required to diagnose and treat cancer patients in low and middle income countries.

SP169 - Self Engagement, Patient Empowerment and mHealth

TRACK 13: INFORMATICS IN HEALTH CARE and PUBLIC HEALTH

SP169.1 - Empowering patients through information technologies

Author(s): Eleni Kaldoudi

School Of Medicine, Democritus University of Thrace, Alexandroupoli/GREECE

Patient empowerment is about enabling the patients to be involved in managing disease and adopting and sustaining health promoting behaviors. Patient empowerment, although a popular concept, is rather ill defined. This lecture aims to elucidate the different meanings and perceptions, together with misconceptions, that surround this construct, and to discuss how patient empowerment relates to current medical methodologies, such as evidence based medicine, and other societal and organizational factors. Furthermore, the lecture will provide an overview of how information and communication technologies are employed to empower patients, with emphasis in chronic patients with comorbidities.

The discussion will first address the “who”. This includes an overview of common health problems that call for empowered patients, the types of patients that normally engage in empowering interventions and the specifics of the stakeholders who design and support such interventions.

Then we will look at the “how”. The discussion here will focus on an overview of the diverse approaches and services that have been deployed to empower patients. This will also include the span of various technologies used and, where applicable, their measured induced outcome for the patient and the health care process.

Although the “who” and “how” of patient empowerment can rather easily be discerned from a literature research, the “what” is rather more elusive. The concept of patient empowerment has emerged as a new paradigm that can help improve medical outcomes while lowering costs of treatment by facilitating self-directed behavior change. Patient empowerment has gained even more popularity since the 1990’s, due to the emergent of eHealth and its focus on putting the patient in the centre of the interest. Current literature provides systematic reviews of the area, and shows that well defined areas (or dimensions) have eventually emerged in the field: *education, engagement, and control*. Despite such findings, current research lacks of a structured approach towards patient empowerment. In an attempt to shed more light onto the process of empowering patients, this lecture will discuss a newly proposed holistic model of patient empowerment as a cognitive process, where we acknowledge three levels of increasing complexity and importance: *awareness, participation, and control*.

The lecture will conclude with a proof of concept example of using this approach to develop and evaluate empowerment services for the comorbid cardiorenal patient or the patient at risk of this condition. Open issues and challenges will be presented for discussion with the audience.

SP169.2 - Distributed learning: developing a predictive model for dyspnea in lung cancer patients based on data from multiple hospitals

Author(s): Arthur T.C. Jochems, Andre Dekker, Philippe Lambin, Johan Van Soest

Radiotherapy, Maastric Clinic, Maastricht/NETHERLANDS

Purpose/Objective

Predictive models play a major role in enabling personalized medicine. Predictive models require patient data to be trained successfully. One of the major hurdles in enabling personalized medicine is obtaining sufficient patient data to feed into predictive models. Combining data originating from multiple hospitals is difficult because of ethical, legal and administrative issues. In order to avoid these issues a distributed learning approach can be used. In this approach, the model training application is sent to the hospitals. The model learns from the data in each individual hospital without the data leaving the hospital. After training, the models are sent back to a central location where they are combined into one fully trained model.

In this work, we show that it is possible to use the distributed learning approach to train a Bayesian network model on patient data originating from multiple hospitals. The model predicts dyspnea, which is a common side effect after radiotherapy treatment of lung cancer.

Material/methods

Clinical data from 170 lung cancer patients, treated with curative intent with chemoradiation (CRT) or radiotherapy (RT) alone were collected and stored in 3 different medical institutes (123 patients at Maastric, 14 at Jessa and 33 at Liege). A Bayesian network model was developed to predict dyspnea (\geq Grade 2 according to the CTCv3.0). The model used gender, WHO performance status, age and overall treatment time to make predictions. Training of the model was based on data originating from two out of the three centers. The data of the remaining center was used for validation. The model was trained and validated 3 times each time using data from two different centers as the training set. The three trained models were combined by taking the average of the learned conditional probability tables. The model’s performance was expressed as the Area Under the Curve (AUC) of the Receiver Operating Characteristic (ROC). The maximum value of the AUC is 1.0; indicating a perfect prediction model. A value of 0.5 indicates that patients are correctly classified in 50% of the cases, e.g., as good as chance.

Results

Thirty-four patients (27%), 6 patients (42%) and 13 patients (39%) developed dyspnea in the Maastric, Jessa and Liege datasets respectively. The AUC of the model that was trained on data from Maastric and Jessa and validated on data from Liege was 0.66 (95%CI, 0.63–0.78). The AUC of the model that was trained on data from Maastric and Liege and validated on data from Jessa was 0.63 (95%CI, 0.49–0.72). The AUC of the model that was trained on data from Jessa and Liege and validated on data from Maastric was 0.56 (95%CI, 0.48–0.59).

Conclusion

Using a distributed learning approach, we have successfully trained and validated a Bayesian network model for dyspnea prediction in lung cancer patients on data from multiple hospitals. Future work will involve using a larger number of hospitals and higher numbers of patient data to train better predictive models using the distributed learning approach.

SP169.3 - User Centered Design to incorporate predictive models for Type 2 Diabetes screening and management into professional decision support tools: preliminary results.

Author(s): Giuseppe Fico

Life Supporting Technologies, Universidad Politécnica de Madrid, Madrid/SPAIN

Type 2 Diabetes screening and risk stratification tools could benefit from the incorporation of predictive systems based on computer modelling. The adoption of User Centered Design techniques is fundamental in order to integrate these systems in an effective and successful way. The work presented in this paper describe the methodologies used in the context of a multidisciplinary research project and provides an overview of the preliminary results.

SP169.4 - Quantifying Bipolar Disorder for Technology-Assisted Self-Management

Author(s): James D. Amor¹, Martina Svobodova², Ian Jones², Christopher James¹

¹School Of Engineering, University of Warwick, Coventry/UNITED KINGDOM, ²National Centre For Mental Health, Institute Of Psychological Medicine And Clinical Neurosciences, Cardiff University, Cardiff/UNITED KINGDOM

Bipolar Disorder (BD) is a serious mental health condition that is characterized by recurring affective episodes, interspersed with periods of remission. Current treatment for BD focuses on pharmacological and therapeutic techniques to control the condition. In addition to this, a significant number of people with BD adopt self-management techniques in order to help maintain a stable life pattern and control their condition. There are two significant drawbacks to current self-management in that current systems tend to be paper based and reliant on user self-insight, which is frequently lost in the run up to an affective episode. These two shortcomings can be addressed with a technology-enabled solution. Through the use of specific sensors and an electronic mood diary, the important indicators of relapse in BD can be monitored and users alerted to potential indicators of relapse in a timely manner so that they can take appropriate action.

This paper presents work that has been carried out in the development of the Auto-Motive system on the quantification of indicator metrics in BD for use in a technology-enabled self-management system. We present the methodology and results from a series of focus groups that have been carried out with users and professionals to identify the important indicators in BD and the way in which the can be quantified for use in a decision support system.

Results from the focus groups are in line with the literature and professional insight and point to sleep (hours of sleep and sleep quality), physical activity, time at home and at work and medication compliance as being particularly important indicators to quantify and use in the Auto-Motive system.

SP169.5 - Hippocratic Protocol Design to Improve Security and Privacy in Healthcare Applications for NFC Smartphone

Author(s): Jose Pirrone Puma¹, Monica Huerta²

¹Esc. Ingeniería En Telecomunicaciones, Universidad Católica Andrés Bello (UCAB), Caracas/VENEZUELA, ²Universidad Politécnica Salesiana, Cuenca/ECUADOR

Today the evolution of electronics technologies had created a lot of intelligent personnel devices, like calculators, GPS, and Smartphone for example. These terminal have lowers prices than terminals used before and are fully programmable that's why are beginning to use in all sectors for implement mobile services.

Healthcare sector is not outside of this development and some experiences have been done, using not only its connectivity but also an identification technology named NFC. This result in a series of new problems, which are being studied. One of the main problems for the use of these technologies is the maintenance of privacy and security in management of patient information when using Smartphone as a mobile terminal to read data. In previous years, there have been lot of work in these areas for the health sector, for privacy and authentication,.

NFC is an evolution of Radio Frequency Identification technology (RFID), specifically contactless smart cards, and interconnection technologies. Operates in the frequency band of 13.56 MHz, with very low power levels, which means that devices must be close (less than 10 cms.) to exchange data.

Hippocratic Databases fit the Hippocratic Oath, which makes doctors upon graduation. Its use has been gaining popularity due to privacy requirements appeared in new legislation on health of some countries, e.g. United States and arises as a need for implementing privacy in today's social networks.

Transferring the Hippocratic Database concept to design a specialized protocol for the health sector, would result requirements like Verification of the purposes of data Exchange, Authentication, Data Integrity, Encryption and modes of operation for transmitting, receiving and control, which allow the user to implement accessibility and verify the above.

A family of standards ISO 11073 *Personnel Health Device Communication*, define a communication scheme between personal health devices and an external computer. ISO standard 11073_20601 describes a common communications infrastructure, independent of the underlying transport infrastructure data due to logical connection procedure based on Agent Manager relation, and can be used to implement this protocol.

A scheme of the proposed Health Hippocratic Protocol (H²P) is shown. It is composed for two states and five procedures. The use of this protocol improves the design of health applications that use Smartphone and the use of Hippocratic Databases in healthcare sector. Given its structure, the protocol can withstand attacks of man in the middle, impersonation and unauthorized data seamlessly, as the authentication process with the Checking permissions task guarantee security. The objective is to present a protocol that includes Hippocratic principles in its structure to improve security and privacy on personnel devices that use these technologies in the healthcare sector.

The design of a Hippocratic Health Protocol, based on a standard, for use in Smartphone with NFC will improve security and privacy in personnel healthcare applications, but more work is necessary because the design of the database that permits the implementation of Hippocratic considerations is not a simple work.

SP169.6 - Extracting Intention from Web Queries- Application in eHealth Personalization

Author(s): George Drosatos¹, Avi Arampatzis², Eleni Kaldoudi¹

¹School Of Medicine, Democritus University of Thrace, Alexandroupoli/GREECE, ²Department Of Electrical And Computer Engineering, Democritus University of Thrace, Xanthi/GREECE

Personalizing healthcare applications requires capturing patient specific information, including medical history, health status, and mental aspects such as behaviors, intentions, and attitudes. This paper presents a privacy-friendly system to deduce patient intentions that can be used to personalized eHealth applications. In the proposed approach patient intention is deduced from web query logs via query categorization techniques. The architecture assumes

a user application which conceals the user's queries from the central system, while only relevant intentions are disclosed. The paper presents a prototype implementation of the proposed architecture to extract intentions for personalizing empowerment services for the cardiorenal patient. Emphasis is placed on identifying intentions related to travel, diet and physical exercise, as these play an important role for the daily management of cardiorenal disease.

SP170 - Information Technologies in Healthcare Delivery and Management: Part 3

TRACK 14: INFORMATION TECHNOLOGIES IN HEALTHCARE DELIVERY AND MANAGEMENT

SP170.1 - Wireless equipment localization for medical environments

Author(s): Daniel Laqua¹, Paul Fritzsche¹, Sven Niemöller¹, Peter Husar¹, Vincenz Busch², Michael Nass³, Jörg Pospiech⁴, Kutaiba Saleh⁵, Rudi Jäger⁵, Martin Specht⁵

¹Biosignal Processing Group, Technische Universität Ilmenau, Ilmenau/GERMANY, ²CE-SYS Engineering GmbH, Ilmenau/GERMANY, ³CE-LAB GmbH, Ilmenau/GERMANY, ⁴AVT GmbH, Ilmenau/GERMANY, ⁵Jena University Hospital, Jena/GERMANY

Searching for medical equipment in hospitals produces high costs. However, it is necessary to check each medical device periodically. Wireless systems in a medical environment must comply with the legal limits for electromagnetic interference (EMI). This work presents a tagging system for real time localization of tagged equipment respecting that some medical devices are very sensitive for EMI. Therefore, every room is equipped with a base station and a star-shaped 2.4 GHz wireless network topology, which conforms with the latest legislative requirements for the EC and US market. Considering that, the device tags consist of a compact IEEE 802.15.4 ZigBit transceiver module with an adapted and extended stack. Furthermore, the device tags are equipped with sensors for detecting manipulation and motion. The base stations are connected to the server via wired TCP/IP network with Power over Ethernet (PoE), which reduces the radio traffic and considerably simplifies communication. Virtual floor plans in the dashboard software visualize the actual positions of the medical devices. The user is able to locate either a single device by its name or a list of all devices in a ward. Using two AAA batteries the device tags have an operation time of 24 months, wherein they can be in motion for 7.75 percent. The web-based dashboard software grants the medical staff an easy access via computer or mobile device. In addition, the dashboard is able to access the SAP database of the hospital for detailed information about the medical device.

SP170.2 - Exploring Approaches to Optimise the Estimation of Preterm Birth Using Machine Learning Techniques

Author(s): Monique Frize¹, Daphne Ong¹, Jeff Gilchrist¹, Hasmik Martirosyan¹, Erika Bariciak²

¹Systems And Computer Engineering, Carleton University, Ottawa/CANADA, ²Neonatology, Children's Hospital of Eastern Ontario, Ottawa/CANADA

In past work, our research group obtained a number of high quality databases of newborns and mothers in order to develop models to predict premature birth before 23 weeks gestation, using only data collected from pregnant mothers. Unfortunately, the most accurate test currently used is the fetal fibronectin, which is invasive, expensive, and is done some weeks later in the pregnancy. Our initial development succeeded in matching the accuracy of the fetal fibronectin test using data from the PRAMS (Pregnancy Risk Assessment Monitoring System) database with an accuracy of 66% sensitivity (true positive cases) and 85% specificity (true negative cases). [Catley et al, 2006]

Recent work has concentrated on exploring a number of machine learning techniques such as decision trees (DTs) and artificial neural

networks (ANNs) and the addition of new databases to optimise the performance of the models we develop to predict preterm birth (PTB). One approach is to use decision trees with the 5-by-2 cross validation method to help select the most important features to use with our ANN tool. The methodology consists of separating cases involving preterm versus full term babies, and then randomly creating ten different train and test sets to perform the prediction with decision trees. Our previous work focused on selecting the variables that had the best compromise between sensitivity and specificity when used to generate the single DT model and incorporating them as features to build an ANN model for PTB. [Frize and Yu, 2010] We are now assessing the average variable usage across all ten DT models and by eliminating the variables that have limited usage, we hope to improve the classification of preterm cases when using these variables to build the final ANN model. This new ANN was developed using the FANN (Fast Artificial Neural Network) Library as a base, on which we built many enhancements that we were using in previous work. [Frize et al. 2013] Moreover, the use of a new database collected on all newborns in Ontario (BORN= Better Outcome Registry and Network) will enable our team to determine which variables in both the PRAMS and BORN databases can optimise the classification of PTB. Preliminary results are encouraging.

Catley C, Frize M, Walker CR, Petriu DC. (2006) "Predicting high-risk preterm birth using artificial neural networks." *IEEE Transactions of Information Technology in Biomedicine*. Special section mining biomedical data. Vol 10 (3): 540-549.

Frize M, Yu N. (2010) "Estimating Pre-Term Birth Using a Hybrid Pattern Classification System." *Proc. MEDICON2010*, Chalkidiki Greece, May: 893-896.

Frize M, Barciak E, Gilchrist J. (2013) "PPADS: Physician-Parent Decision-Support for Neonatal Intensive Care." *Proc. Medinfo 2013*. Copenhagen, Denmark, August: 23-27.

SP170.3 - Smartwatch App as the Chest Compression Depth Feedback Device

Author(s): Yujin Jeong, Youngjoon Chee, Yeongtak Song, Kyo-In Koo
School Of Electrical Engineering, University of Ulsan, Ulsan/KOREA

For the high quality CPR (Cardio-Pulmonary Resuscitation), the feedback devices to show chest compression depth are used to ensure the compression depth to be over 51 mm, which is one of key factors of the 2010 American Heart Association (AHA) guidelines for adults. We propose the smartwatch based app as the chest compression depth feedback device and evaluated its accuracy. The accelerometer which is inside the smartwatch makes the signal during chest compression and the real time signal processing techniques are used to estimate the compression depth. Through the manikin study, the estimation error was 3.2 mm in average which can be acceptable for its usage. With the smartwatch app as the feedback device, the rescuer can perform the chest compression without the inconvenience of gripping the device and the visual interference with hands.

SP170.4 - Diagnosis of the corporal movement in Parkinson's Disease using Kinect Sensors

Author(s): Raquel Torres¹, Monica Huerta², Roger Clotet¹, Ricardo Gonzalez¹, Jose Pirrone Puma¹, Mayra Erazo³, Giovanni Sagbay⁴
¹Network And Applied Telematics Group, Universidad Simón Bolívar, Caracas/VENEZUELA, ²Prometeo Project Researcher (SENESCYT, Quito/ECUADOR, ³Electrónica, Universidad de las Fuerzas Armadas ESPE, Iatacunga/ECUADOR, ⁴Electrónica, Universidad Politécnica Salesiana, Cuenca/ECUADOR

This paper presents an approach to capture of the human movement and posture with a Kinect Sensor, in order to assist physicians in the Parkinson's Diagnosis. The Kinect Sensor allow to measure displacements in the motionless posture that can be interpreted as increments of tremors intensity. This paper presents an approach to capture of the human movement and posture with a Kinect Sensor, in order to assist physicians in the Parkinson's Diagnosis. The Kinect Sensor allow to measure displacements in the motionless posture that can be interpreted as increments of tremors intensity.

SP170.5 - A System to Support Regional Screening Programs to Identify School-age Children at Risk of Neurodevelopmental Disorders.

Author(s): Elsa Santos Febles¹, Vivian Reigosa-Crespo², Klaudia Garcia-Liashenko¹, Adan Echemendia-Montero¹, Gabriel Pujols-Fariñas¹, Enrique Plasencia-Montero³, Aymée Alvarez-Rivero², Eduardo Eimil-Suarez⁴

¹Software Development, Cuban Neuroscience Center, Havana/CUBA, ²Developmental Cognitive Neuroscience Department, Cuban Neuroscience Center, Havana/CUBA, ³Cuban Neuroscience Molecular Biology Department, Cuban Neuroscience Center, HAVANA/CUBA, ⁴Speech And Hearing Sciences Department, Cuban Neuroscience Center, Havana/CUBA

This paper describes a system to support regional screening programs to identify school-age children (6 to 12 years old) that are at risk of a neurodevelopmental disorders. The screening method is based on research carried out at the Cuban Neuroscience Center. The system is a combination of an Android application for a Tablet and a Web application. The Android app enables easy and quick exploration of learning and behavior disorders, hearing impairment, parental care and certain clinical health parameters. All the information is provided by teacher reports or direct measuring on the child. The Web application manages the screening program and organizes it by geographical regions, allowing adaptations to the local educational system. The user's access is role-based and depends on the job function and the regions assigned to the user. The Web application was developed using the PHP framework Symfony2 and stores data using a relational MySQL database. The data exchange between both applications is implemented via download and upload XML file, thereby allowing the Android app to work offline in order to use it in sites with limited communication infrastructures. The system can gather, store, access and analyze data to aid in decision-making. The system will clarify the need of referral for early intervention services and/or other evaluations. It will also enable longitudinal follow-up neurodevelopmental studies in large samples of children.

SP170.6 - Support platform to decision making in research and technological development in public health: a brazilian scenario approach.

Author(s): Carlos E. Rocha, Yuri P. Marca
Carlos Chagas Institute, Oswaldo Cruz Foundation, Curitiba/BRAZIL

The area of biosciences has promoted significant changes in national competence linked to innovation in health care by creating scientific favorable for the construction of public policies on ST & I, has also been presented as a strategic dimension of prominence in the training of human resources within areas of future patients, as well as the installation and consolidation of organizations linked to the process of Research, Development and Innovation.

Thus, the activities biotechnological processes require more accurate and consistent decision-making and consider the variables inherent in the organizational environment itself Institutions of Science and Technology. This position paper analyses the current state of affairs concerning the Brazilian health industry in strategic sectors.

A brief overview of the most critical infectious diseases and the associated technologies available for their diagnosis is given, pointing out research and development opportunities for the national industry for the health sector. Therefore Decision making in the process of implementation of projects of Research and Development in Health is an important activity in Brazil, since the amount of proposed projects is incompatible with the financial resources. An estimate to ensure the success of the proposal is something that would facilitate the manager's work.

For this, it was developed an application in the programming language C++ that serves as support for the manager in decision making, where it makes the evaluation of the proposed project based on some modeling variables. Moreover, the use of this software can make it more robust and over time more effective for determining the estimated success of a proposal.

Finally, current challenges and perspectives concerning national policies for the brazilian health sector are discussed.

SP171 - Clinical Engineering / Physics, Patient Safety & Imaging

PRESIDENTS CALL

SP171.1 - Properties Evaluation of Gd2O3-DEG as New Contrast Agent Nanomagnetic Particles Comparing to Gd-DTPA in MRI

Author(s): Banafsheh Nikfar¹, [Nader Riahi-Alam](#)¹, Soheila Haghgoo², Ensiyeh Gorji², Hosein Ghenaati³, Behrooz Rafiei³, Sara - Heydarnezhadi¹, Mohammad Khosroshahi⁴

¹Tehran University Of Medical Sciences (tums), Medical Physics & Biomedical Engineering Department, tehran/IRAN, ²Ministry Of Health, Tehran, Food & Drug Laboratory Research Center, tehran/IRAN, ³Tehran University Of Medical Sciences (tums), Medical Imaging Center of Imam Khomeini Hospital, tehran/IRAN, ⁴Laser And Nanobiophotonics Lab., Biomaterial Group, Faculty Of Biomedical Engineering, Amirkabir University of Technology, Tehran/IRAN

Magnetic resonance imaging (MRI) is widely used for imaging purposes. However, the sensitivity and intrinsic contrast of the MRI is low. In order to improve the quality of images Gd-DTPA (commercial Magnevist) is normally. Because of some limitations of low molecular weight of gadolinium chelates, nanoparticles gadolinium based contrast agents are proposed. In this study, we synthesized Gd-DTPA and compared its effects with Gd2O3-DEG nanoparticles. The samples were prepared at concentrations of 0.3, 0.6, 0.9 and 1.2 mM respectively by adding 1.5 ml deionized water. The corresponding Gd2O3-DEG nanoparticles diameter was measured about 80 nm. An in vitro study was performed using a 1.5 T scanner with standard spin echo protocol. Clearly, the signal amplitudes in both cases were increased with the Gd concentration at constant relaxation time. Also, a linear relation between signal intensity and longitudinal relaxation rate (R1) was observed with a correlation coefficient close to 1. The values of 4.30 and 14.27 (s⁻¹.mM⁻¹) were achieved for Gd-DTPA and Gd2O3-DEG nanoparticles special relaxivity, respectively.

SP171.2 - Imaging the Schlemm's Canal using an ultrahigh resolution spectral-domain optical coherence tomography working at 1.3 micrometer center wavelength

Author(s): [Masreshaw D. Bayleyegn](#)

Center Of Biomedical Engineering, Addis Ababa Institute of Technology, Addis Ababa/ETHIOPIA

We present an ultrahigh resolution spectral-domain optical coherence tomography imaging system that uses a broadband superluminescent diode light source emitting at a center wavelength of 1.3 micrometer. The light source consists of two spectrally shifted superluminescent diodes that are coupled together into a single mode fiber. The effective emission power spectrum has a full width at half maximum of 200 nm and the source output power reaches up to 10 mW. The imaging system has an axial resolution of 3.9 micrometer in air (< 3.0 micrometer in biological tissue), and a lateral resolution of 6.5 micrometer. The sensitivity and the maximum line rate are 95 dB and 46 kHz, respectively. Images of an infrared viewing card and a cornea from human eye suffering from glaucoma showing Schlemm's canal are presented to illustrate the performance of the system.

SP171.3 - Technology Trayjectory Hybrid Tomography by Positron Emissions

Author(s): Victor Malvaez

Management Of Technology, CIECAS IPN, Mexico/MEXICO

This work studies, by means of the technological surveillance, the origin and evolution of the hybrid tomography by positron emission, commonly known as PET-CT. This tomographic technique is currently used in the medical diagnosis of patients with tumors or neoplasias, and its efficient use in Mexico could reduce costs and increase the opportunities for more people to have access to advanced medical technologies. To this end it is necessary to make them known, together with the fields of actual and potential applications. The main providers of this technology and their core competences are detected by means of patent analysis, as well as their technological profiles, advances and future developments. Patent analysis is carried out by consulting data bases as USPTO, EPO, JPO and WIPO. The technological surveillance was accomplished with the help of the International Classification of Patents (ICP) protocol, which allows the identification of the technological fields that are related to PET-CT. Future trends in the technology and possible evolution of equipment and radioactive marker prices are also found.

SP171.4 - Myocardial perfusion imaging by low-dose CT

Author(s): Sabeel Molloy, Benjamin Ziemer, Logan Hubbard, Jerry Lipinsky, Bahman Sadeghi, Hanna Javan, Elliott Groves
Radiological Sciences, University of California, Irvine/UNITED STATES OF AMERICA

Coronary heart disease remains widely prevalent and is the leading cause of mortality and morbidity in the world. It is well established that the extent of coronary artery disease and left ventricular dysfunction are predictive of future cardiac events. Several clinical trials have demonstrated that mortality and morbidity can be reduced when medical and surgical interventions are applied to selected subsets of patients stratified according to coronary anatomy and left ventricular function. Coronary CT angiography is a well-established, non-invasive imaging modality for the detection and exclusion of atherosclerosis. However, coronary CT angiography cannot accurately determine whether an intermediate severity stenosis is flow limiting that requires additional functional testing, which increases the radiation dose and cost to the patient. Furthermore, international guidelines recommend the functional assessment of stenosis severity prior to revascularization. A CT perfusion technique would provide valuable functional information, in addition to the anatomical data obtained from CT angiography. As a result, many dynamic CT perfusion techniques have been developed to provide functional assessment of coronary artery disease; however, widespread clinical implementation of such techniques has been hampered by the fact that these techniques deliver a high radiation dose. Hence, there is a need for a low-dose CT perfusion technique for noninvasive functional assessment of coronary artery disease. It is possible to measure myocardial perfusion using a low-dose first-pass analysis (FPA) technique. This technique relies on conservation of mass by making measurements in an arterial tree perfusion bed before contrast exits through the venous system. Implementation of this technique using CT requires fast, whole-heart scanning combined with ECG-gating. Therefore, the FPA technique was implemented with a prospective ECG-gated protocol using a 320-slice CT scanner. This technique can measure myocardial perfusion using a minimum of two volume scans, which can substantially reduce radiation dose as compared with existing dynamic perfusion techniques. The study was carried out in anesthetized, closed-chest swine using angioplasty balloon catheters to produce partial occlusion. After segmentation of the myocardium and extraction of the coronary arterial trees, perfusion measurements were made using the FPA technique. The perfusion measurements were validated using colored microspheres as the

reference gold standard. The perfusion measurements using FPA (PFPA) and colored microspheres (PMic) were related by PFPA = $0.97\text{PMic} + 0.12 \text{ mL/min/g}$ ($r^2=0.92$). The results show that CT perfusion measurements have excellent correlation with microsphere perfusion measurements. In conclusion, the results indicate that accurate CT perfusion can be made with a substantial reduction in radiation dose as compared with existing dynamic CT perfusion techniques. Therefore, CT can potentially be used for both anatomical and physiological assessment of coronary artery disease.

SP171.5 - Renal Dynamic Phantom for Use in SPECT

Author(s): Divanizia D.N. Souza¹, Fernanda C.L. Ferreira²

¹Phyisics, Federal University of Sergipe, São Cristóvão/BRAZIL, ²Federal University of South and Southeast of Pará., Marabá/ BRAZIL

Renal Dynamic Phantom for Use in SPECT

M. A. Dullius^{1,2}, M. Fonseca², M. Botelho², F. C. L. Ferreira.² and D. Souza,²

¹Universidade Federal da Fronteira Sul, Campus Cerro Largo-RS, Brazil

²Universidade Federal de Sergipe, São Cristóvão-SE, Brazil

Quality control of nuclear medicine is performed through the use of phantoms during the processes necessary for consummation of quality control tests. Ideally, a specific phantom is employed for each type of procedure. Dynamic renal scintigraphy using DTPA (diethylenetriamine pentaacetic acid) is labeled with technetium-99m. This renal radiopharmaceutical tracer allows evaluation of the dynamics of renal blood flow and its symmetry, the topography and morphology of the kidneys, and the passage of the radiopharmaceutical through the urinary tract to the bladder until arrival. The objective of this study was to develop and evaluate the performance of a renal dynamic phantom, for use in SPECT. An adult human kidney was used for making the mold, ensuring phantom geometry. It was used alginate for the manufacture of the shaped form of the kidneys. Following preparation, the acrylic kidney was connected to the top of each kidney with one injection pump connected to a reservoir. To perform the flow, the phantom is controlled with injection pumps. The electrical system controls how long each pump is in operation. Changes of the operating time of the pump at different flow rates imply elimination of the radioisotope, allowing it obtain various forms of disposal. The renal dynamic phantom was constructed of acrylic and included injection pumps to simulate renal dynamics in scintigraphy with ^{99m}Tc-DTPA. This phantom was scanned with a dynamic protocol and compared with clinical data. Using this phantom it is possible to acquire similar renal images as in clinical scintigraphy, including the response of the imaging system to the form of a renogram with normal renal scintigraphic appearance. Moreover, it is expected to perform intercomparisons between different renograms scintillation cameras and nuclear medicine clinics. Therefore, the dynamic renal phantoms can be very effective for use in the quality control of renal scintigraphy and image processing systems.

Keywords— Dymimic phantom, nuclear medicine, quality control.

Renal Dynamic Phantom for Use in SPECT

SP171.6 - Physics Plan Checking Practices

Author(s): Gordon Chan¹, Lee Chin², Harald Keller³, Keith Nakonechny⁴, Cathy Neath⁵, Greg Salomons⁶

¹Medical Physics, Juravinski Cancer Centre, Hamilton/ON/CANADA, ²Odette Cancer Centre, Toronto, Canada, Toronto/CANADA, ³Radiation Medicine Program, Princess Margaret Cancer Centre, Toronto/ON/CANADA, ⁴Simcoe Muskoka Regional Cancer Centre, Barrie/CANADA, ⁵Medical Physics Department, R.S. McLaughlin Durham Regional Cancer Centre, Oshawa/ON/CANADA, ⁶Cancer Centre of Southeastern Ontario, Kingston General Hospital, Kingston/CANADA

The physics treatment plan / chart check has been shown to be a critical factor in ensuring safe high-quality radiation therapy. However, there is very little publicly available documentation on plan checking. Anecdotal evidence suggests that the practice of plan checking is highly variable even among physicists within the same centre. In order to ensure a high and uniform quality in treatment plans it is imperative that the process be standardized and documented.

In order to determine the current practice in regards to physics treatment plan checking, the Medical Physics Community of Practice Working Group in Ontario conducted a survey of the medical physics departments at all cancer centres in Ontario. The survey was intended to cover all aspects of the physics checking, including which elements of a patient’s plan are being checked by the physicist, what level of documentation is being performed with the checking, and where in the planning to treatment process the physics plan checking is being performed. The survey was designed to have the physicists at each centre (typically 5-6) complete the survey together as a group and provide a single response from their centre. Answers to the questions were designed to reflect the variability in practice within a centre.

We will present the results from this survey such as the responses shown in Figure 1 below. Initial survey results suggest that often the plans are accepted as is even though they could be improved upon. Comments accompanying the question indicated that the time between a physicist receiving the plan for review and the patient’s scheduled appointment, was a big factor in deciding whether to accept a sub-optimal plan or not.

The process of completing the survey also provided direct benefits to the participating centres. Initial feedback suggests that the dialogue which was generated was beneficial to the participating physicists and will hopefully increase the consistency and quality of the plan checking process in those centres. Hopefully, the dialogue generated by publishing the results of the survey will have an equally beneficial effect. It is anticipated that the results of this survey will lead to new guidelines for physics involvement in patient plan QA.

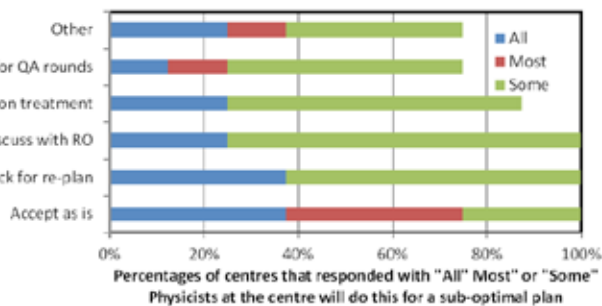


Figure 1. Responses to the question: What is done with a sub-optimal plan that meets the prescribed goals? The responses indicate the proportion of physicists who will take a certain action for a sub-optimal plan. Multiple selections were allowed.

SP171.7 - Commissioning of a Flattening Filter Free

Author(s): Satya Ranjan Saha

Medical, Tradevision Limited, dhaka/BANGLADESH

Commissioning of a Flattening Filter Free (FFF) using an Anisotropic Analytical Algorithm (AAA)

Satya Ranjan Saha ¹, Mohammad Amran Hossain ², Md Safiqul Islam ³

Aim: To compare the dosimetric parameters of the flattened and flattening filter free (FFF) beam and to validate the beam data using anisotropic analytical algorithm (AAA).

Materials and Methods: All the dosimetric data’s (i.e. depth dose profiles, profile curves, output factors, penumbra etc.) required for the beam modeling of AAA were acquired using the Blue Phantom RFA for 6MV, 6FFF, 10MV & 10FFF. Progressive resolution Optimizer and Dose Volume Optimizer algorithm for VMAT and IMRT were also configured in the beam model. Beam modeling of the AAA were compared with the measured datasets.

Results: Due to the higher and lower energy component in 6FFF and 10FFF the surface doses are 10 to 15% higher compared to flattened 6MV and 10MV beams. FFF beam has a lower mean energy compared to the flattened beam and the beam quality index were 6MV 0.667, 6FFF 0.629, 10MV 0.74 and 10FFF 0.695 respectively. Gamma evaluation with 2% dose and 2mm distance criteria for the Open Beam, IMRT and VMAT plans were also performed and found a good agreement between the modeled and measured data.

Conclusion: We have successfully modeled the AAA algorithm for the flattened and FFF beams and achieved a good agreement with the calculated and measured value.

Corresponding Author: Satya Ranjan Saha

Name of institution: United Hospital, Dhaka, Bangladesh; Dept. of Radiotherapy

Email: satya.saha@tradevision.com.bd

Machine: Truebeam by Varian Medical Systems AG

SP171.8 - Effects of 24 hour Wakefulness on Tilt Based Targeting Tasks

Author(s): Jeffrey Bolkhovskiy¹, Ki Chon², Michael Qin³

¹Biomedical Engineering, University of Connecticut, Storrs/UNITED STATES OF AMERICA, ²University of Connecticut, Storrs, CT/CT/ UNITED STATES OF AMERICA, ³Naval Submarine and Medical Research Laboratory, Groton/UNITED STATES OF AMERICA

This study investigated the effects of short term sleep deprivation while using a tilt-based control device. Accuracy and various performance parameters of subjects using tilt based devices to perform target acquisition tasks were monitored over a period of 24 hours to assess the susceptibility of performance to acute sleep deprivation. Performance was analyzed by means of the principles of Fitts’ law using movement time, throughput, and time intercept as measurements. All task sessions were analyzed using movement time and difficulty correlation to determine that the tasks completed by all participants did in fact adhere to Fitts’ law with an average R² of 0.99 and a standard deviation of 0.01. Accuracy was examined by looking at movement error, movement variability, and number of target reentries. These accuracy statistics were derived by comparing the subject paths for acquiring targets to the ideal paths within the task. Ten volunteers completed sets of two sets of learning tasks and then completed a set of tasks every two hours up to a time at which the subject had been awake for a consecutive 24 hours. Each

set of tasks included 240 trials over a 20 minute period in which the subject controlled a ball, with a movement gain of 25 and a size of 20 pixels (px) in order to hit a target that varied in size (40 px, 60px, 100px), distance from the start point (125 px, 250px), and location (8 cardinal directions). The control of the ball was derived using a combination of the tilt of the device and the gain. It was found that over the period of 24 hours of wakefulness there was no reliable change in movement time ($p = 0.52$), average throughput ($p = 0.135$) or average intercept ($p = 0.09$). The correlation between each of these measurements and time was -0.33, 0.39, and 0.52 respectively. It was also determined that the accuracy measurements of movement variability ($p = 0.39$), movement error ($p = 0.07$), and movement reentries ($p = 0.72$) did not change significantly over the trial period. The correlation of the three statistics over time were 0.18, 0.10 and 0.07 respectively. It was found that this particular task was not significantly affected by acute sleep deprivation over a period of 24 hours. This control setup displayed as robust in task performance and accuracy with increase wakefulness. Possible reasons for this type of result include a limited range of difficulty displayed in the task as well as lack of vigilance required to complete this task. These additions would be valuable to examine for future experiments.

This work was sponsored by the Office of Naval Research.

SP172 - Mammography and Tomosynthesis

TRACK 01: IMAGING

SP172.1 - Evaluation of automatic exposure control in digital mammography

Author(s): Alessandra Tomal¹, Tania A.C. Furquim², Nestor Barros²
¹Departamento De Física Aplicada, Universidade Estadual de Campinas, Campinas/BRAZIL, ²Universidade de São Paulo, São Paulo/BRAZIL

Digital mammography has been largely employed in several screening programs for detection of breast cancer. In this technique, the exposure technique is usually chosen by the automatic exposure control (AEC) in order to optimize the relation between the absorbed dose and the image quality.

In this work, we compare the contrast-to-noise ratio (CNR) and the average glandular dose (Dg) obtained for different x-ray spectra in order to evaluate the exposure techniques provided by the AEC. The study was performed in a Senographe DS equipment (GE Medical Systems) using CIRS breast phantom with different thicknesses and compositions: 4 cm – 50% glandular (model 010B), 5 cm – 30% glandular (model 010A) and 6 cm – 20% glandular (model 010C). All AEC modes available were studied: standard, contrast and dose. Additionally, using the manual exposure mode, all the different anode/filter combinations selectable on the systems (Mo/Mo, Mo/Rh and Rh/Rh) were evaluated for all tube voltages settings available. The results of CNR and Dg were combined in a Figure of Merit ($FOM = CNR^2/Dg$) in order to study the optimal x-ray spectra for each thickness.

The results obtained using the AEC mode showed that the exposure techniques selected for the 4 cm thick phantom is the combination Mo/Rh at 27 kV, while the Rh/Rh combination at 29 kV was selected for both 5 and 6 cm phantoms. All AEC modes selects the same techniques, while the mAs values chosen by the AEC-dose mode are up to 37% and 102% greater than for the AEC-standard and AEC-contrast, respectively. The variation in relative noise (σ/p) with pixel values (p) was adjusted to an allometric function ($\sigma/p = kp^{-n}$) and an n value equal to 0.27 was obtained, which indicates the presence of a non-neglect structural noise. Results of the FOM indicated that the optimal spectrum for the 4 cm phantom is the Mo/Rh combination at tube voltage between 28-30 kV. For the thicker phantoms, the Rh/Rh at tube voltage between 26-28 kV showed the best performance in terms of dose saving or image quality improvement. The results obtained indicate that x-ray spectra with energies lower than those selected by the AEC mode should be used in this system, which differs of the most energetic x-ray spectra obtained in previous works. This result can be related to the high contribution of the structural noise in the detection system evaluated. Finally, our results show that the optimization studies are system dependent, instead universal, and the exposure techniques selected by the AEC should be revisited. Besides, the determination of the optimal exposure parameters also should take into account the major components for noise in image. Thus, further studies regarding optimization of mammographic techniques could evaluate other image quality parameters (i.e., image contrast and DQE) and/or include the determination of the optimal mAs.

SP172.2 - Comparing the use of force-standardized and pressure-standardized mammographic compression protocols in an Asian context

Author(s): Kwan Hoong Ng¹, Susie Lau¹, Yang Faridah Abdul Aziz¹, Ralph Highnam², Ariane Chan²

¹Department Of Biomedical Imaging, Faculty Of Medicine, University of Malaya, Kuala Lumpur/MALAYSIA, ²Volpara Solutions Limited, Wellington/NEW ZEALAND

Background: Mammographic compression is used for optimizing image quality and reducing radiation dose. Excessive compression can cause pain and discomfort to women. Current force-based compression guidelines have largely been optimized for western women and do not take breast size into account. Thus, Asian women are subjected to protocols that might not be suitable for them. Previous studies using a 10 kPa pressure-standardized protocol significantly reduced pain without compromising apparent image quality and radiation dose.

Purpose: To investigate mammographic compression practice at our center, by analyzing the variability of compression parameters between and within women in terms of both force and pressure.

Materials and Methods: We processed 18,436 digital mammograms (CC and MLO views) from 4,609 women aged 40-80 years using VolparaAnalytics and VolparaDensity to assess compression force (CF), compression pressure (CP), compressed breast thickness (CBT), breast volume (BV), volumetric breast density (VBD) and mean glandular dose (MGD) as a function of contact area (CA). Standard deviation and Wilcoxon test were used to assess variability and statistical significance between and within women, respectively.

Results: CFs were significantly different for CC (10.8 ± 2.9 daN) and MLO (13.2 ± 2.9 daN) views ($p < 0.001$). Similarly, CPs were also significantly different for CC (21.5 ± 11.5 kPa) and MLO (13.3 ± 4.9 kPa) views ($p < 0.001$). CBTs were significantly different between CC and MLO views (5.1 ± 1.0 cm and 5.7 ± 1.3 cm, respectively; $p < 0.001$). Lastly, CA was significantly different between CC (0.6 ± 0.4 dm²) and MLO (1.1 ± 0.4 dm²) views ($p < 0.001$). Compression parameters including CF, CP, CBT and CA for CC and MLO views were highly variable between and within women, as indicated by the large standard deviations and Wilcoxon test. Figure 1(a)-(f) shows the relationships of CF, CP, CBT, BV, VBD and MGD versus CA. Based on our median CA (0.8 dm²) and the proposed 10 kPa pressure-standardized protocol, the corresponding CF should be about 8.0 daN (Figure 1(a)). In comparison, our women population was subjected to about 50% higher (12.0 daN) force.

Conclusion: We observed compression parameters were highly variable between and within women. Based on the suggested CP standardized at 10 kPa, we estimated the CF should be approximately 50% lower than our current practice. We will investigate the impact of the pressure-standardized protocol on image quality and radiation dose in Asian women (who generally have smaller breasts) that is of great interest.

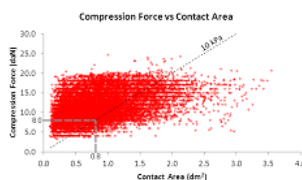


Figure 1(a). Compression force as a function of contact area.

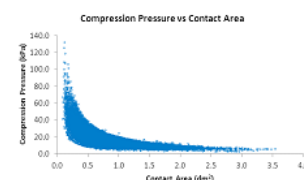


Figure 1(b). Compression pressure as a function of contact area.

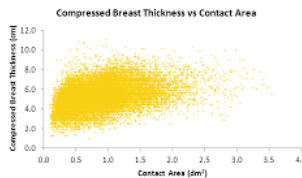


Figure 1(c). Compressed breast thickness as a function of contact area.

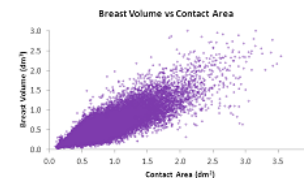


Figure 1(d). Breast volume as a function of contact area.

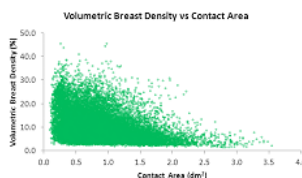


Figure 1(e). Volumetric breast density as a function of contact area.

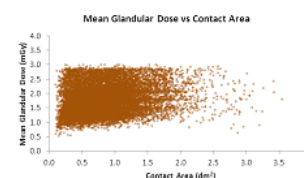


Figure 1(f). Mean glandular dose as a function of contact area.

SP172.3 - Radiation dose of step-and-shoot digital breast tomosynthesis using an anti-scatter grid compared to full field digital mammography in a clinical population

Author(s): Cecile R. Jeukens¹, Leonie E. Paulis¹, Ramona W. Bouwman², Ulrich C. Lalji¹, Nicky N. Gelissen¹, Joachim E. Wildberger¹, Marc B. Lobbes³

¹Maastricht University Medical Centre+, Maastricht/NETHERLANDS, ²Dutch Reference Center for Screening, Nijmegen/NETHERLANDS, ³GROW School for Oncology and Developmental Biology, Maastricht/NETHERLANDS

Background

Digital breast tomosynthesis (DBT) has emerged as a promising breast imaging modality able to improve breast cancer detection, while reducing the number of false-positive findings, which is of particular interest in breast cancer screening programs. To develop into a widely applicable breast cancer detection tool, the radiation exposure of a DBT examination should be kept as low as possible, without compromising the examination's diagnostic accuracy

Purpose

Our study aim was to assess the radiation dose of a new commercially available DBT system (Senographe Essential with a SenoClaire DBT add-on, GE Healthcare) in comparison to full field digital mammography (FFDM) in a clinical setting.

Methods and Materials

To allow a direct comparison, only patients with complementary FFDM and DBT exams on the same system were included ($n=204$ patients with $n=236$ exams). The requirement for obtaining informed consent was waived by the local ethics committee. Entrance surface air kerma (ESAK) and average glandular dose (AGD) were calculated, according to the method described in the European guidelines¹. For this, the Xray tube output and half value layer were measured for a range of spectra using an ionization chamber dosimeter (Radcal). Patient-related data and additional parameters, e.g. target/filter-material, tube voltage, tube load and breast thickness were retrieved

from the DICOM meta-data.

Results

The mean patient age was 55 ± 13 years (range 30-85), the mean compressed breast thickness was 55 ± 13 mm for DBT and 58 ± 13 mm for FFDM. The AGD values increase with increasing compressed breast thickness (Figure 1). The mean AGD for a single view DBT and FFDM exposure were 1.49 ± 0.36 mGy and 1.62 ± 0.55 mGy, respectively, which is a small but statistically significant difference (Wilcoxon matched-pair signed-rank test, $p < 0.001$). Subanalysis where patients are categorized according to breast thickness, revealed that only for breast thickness categories >50 mm the AGD of DBT was significantly lower than the AGD for FFDM, indicating that the dose reduction is most pronounced in thicker breasts.

Conclusion

On average, the radiation dose of a single view DBT exposure is comparable to a single view FFDM. For patients with thicker breast, the radiation dose of DBT is found to be slightly lower than FFDM.

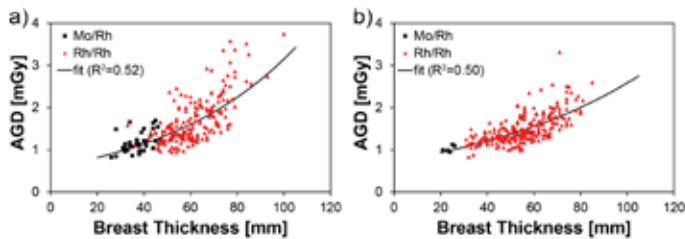


Figure 1 AGD values as a function of breast thickness for single view acquisitions for a) FFDM and b) DBT.

¹European Guidelines for Quality Assurance in Breast Cancer Screening and Diagnosis. 4thed. 2006

SP172.4 - Absorbed dose in PMMA and Equivalent Breast Phantom in a Digital Breast Tomosynthesis system: Monte Carlo Assessment

Author(s): Luis Magalhaes

Universidade do Estado do Rio de Janeiro - UERJ, Rio de Janeiro/ BRAZIL

Digital breast tomosynthesis (DBT) is a screening and diagnostic modality that acquires images of the breast at multiple angles during a short scan. The Selenia Dimensions (Hologic, Bedford, Mass) DBT system can perform both full-field digital mammography and DBT. The system acquires 15 projections over a 15° angular range (from -7.5° to $+7.5^\circ$). The estimation of breast dose is an important part of mammographic quality control for x-ray mammography. Nevertheless, there are presently no standard protocols for dosimetry of breast imaging in 3D. The purpose of this work was to assess the absorbed dose by projection angle in slabs of polymethyl methacrylate (PMMA) and breast equivalent thickness using the Monte Carlo code MCNPX and typical x-ray energy range (25, 28, 31, 34, 37 and 40 kVp) recommended for breast tomosynthesis. Absorbed dose is a nearly linear function of glandularity, independently of x-ray spectra and decrease with increased PMMA thickness. Taking into account 45 mm thick PMMA and 53 mm thick equivalent breast, the difference in absorbed dose by projection angle has been up to 1.33%, 3.83% e 10.98% for x-ray energies of 25, 28 and 40 kVp, respectively. Normalized glandular dose (DgN) values may be used directly to measure the glandular dose in DBT quality control procedures.

SP173 - Ultrasound and OCT: Methods

TRACK 01: IMAGING

SP173.1 - A comparison study on shear wave velocity estimation of thin layered media using shear wave imaging

Author(s): Jun Keun Jang¹, Kengo Kondo², Makoto Yamakawa³, Tsuyoshi Shiina¹

¹Graduate School Of Medicine, Human Health Sciences, Kyoto University, Kyoto/JAPAN, ²Center For The Promotion Of Interdisciplinary Education And Research, Kyoto University, Kyoto/JAPAN, ³Advanced Biomedical Engineering Research Unit, Kyoto University, Kyoto/JAPAN

Shear wave imaging allows noninvasive and quantitative evaluation of mechanical properties of human tissues. Generally, shear wave velocity (CS) can be estimated using lateral time-of-flight method (LTOFM) if a medium is unbounded. Thereafter, Young's modulus (E) is calculated directly from the estimated CS, i.e. $E=3\rho CS^2$ where ρ denotes density. However, shear waves propagating through a thin layered medium are influenced by strong dispersion effects. Recently, Lamb wave based method (LWBM) has been proposed to overcome this limitation. In this study, the two methods were compared to validate the effectiveness of LWBM by performing a finite element (FE) analysis and a phantom experiment for thin layered media.

Figure 1 shows the results of the FE analysis using PZFlex[®] for a thin layered model (thickness=1mm). The perpendicularly applied pressure generated shear waves propagating in the transverse direction. After obtaining axial velocity data from the FE analysis, CS was estimated using the two methods. CS_MEAN in (b) was not equal to CT in (a) and showed a non-uniform distribution, although the model was assumed to be homogeneous. On the contrary, LWBM precisely estimated CS in (c) by fitting the FE result with the theoretical curve of leaky Lamb waves.

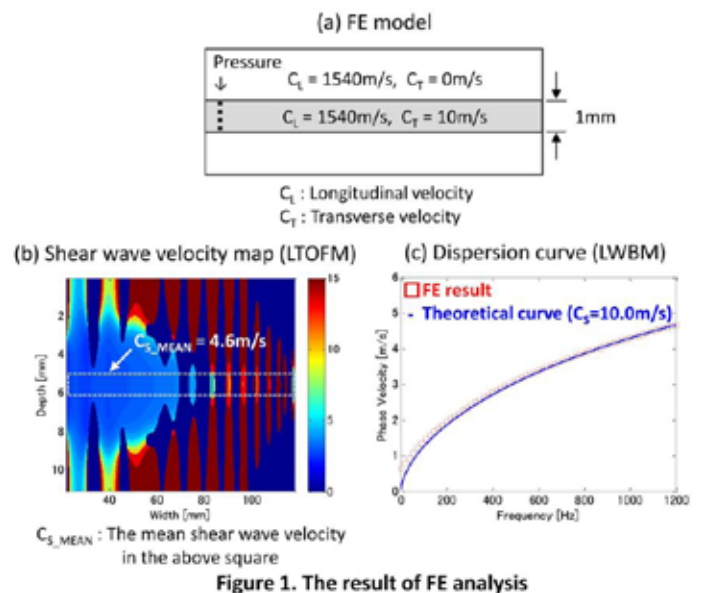


Figure 2 illustrates the results of a thin layered phantom (thickness=1.9mm). To obtain axial velocity, a 2D autocorrelator was employed to ultrasound in-phase quadrature data acquired with Aixplorer[®] and a 7.5MHz linear probe. There was a considerable discrepancy between CS_MEAN in (b) and the previously measured CS (=5.6m/s) of a bulk sample of 1.5% agar phantom. As for LWBM,

no significant difference in C_s was shown between the layered phantom and the bulk phantom.

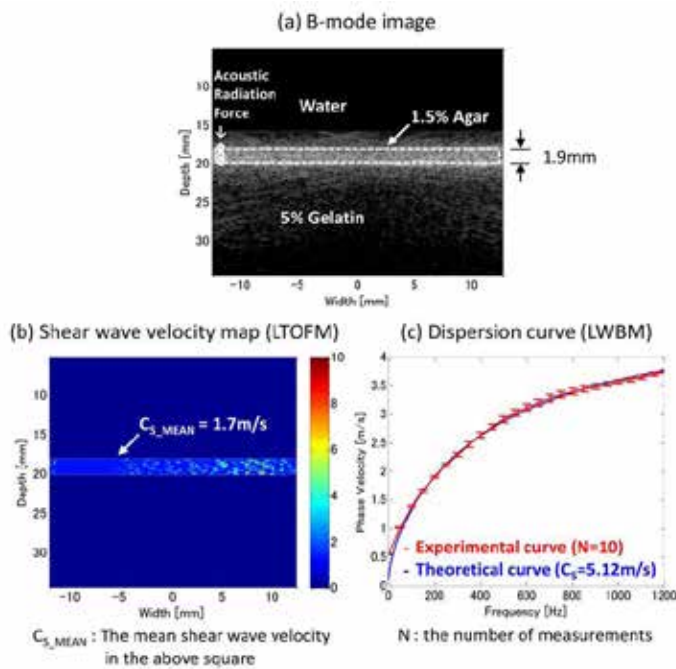


Figure 2. The result of phantom experiment

In conclusion, we showed that LWBM can be applied to accurately estimate shear wave velocity for thin layered media, while LTOFM is suitable only for unbounded media.

SP173.2 - Temperature Dependence of Nonlinear Acoustic Harmonics in Water: Measurement and Simulation

Author(s): Borna Maraghechi, Michael C. Kolios, Jahan Tavakkoli Physics, Ryerson University, Toronto/CANADA

Thermal therapeutic applications of ultrasound consist of hyperthermia and thermal ablation which are both clinically approved. In ultrasound hyperthermia, the tissue temperature increases up to 45°C through exposing it to a therapeutic ultrasound beam in order to destroy cancer cells or to sensitize them to radiotherapy or chemotherapy. A temperature monitoring technique is required to control and guide the heating during the thermal therapy.

In this study, the temperature dependence of the harmonics generated by nonlinear ultrasound beam propagation in water at a transmitting fundamental frequency of 13 MHz has been investigated both experimentally and through simulations.

The experiments were performed using a wide-band high-frequency single-element circular focused ultrasound transducer (f-number 2.1). Acoustic harmonics were generated by transmitting 15-cycle pulses at 13 MHz with focal positive peak pressures of approximately 1.3 MPa in water. The acoustic pressure signals were measured by a calibrated needle hydrophone placed at the focal point of the transducer. Water temperature was uniformly increased from 26°C to 46°C in increments of 5°C. The pressure amplitudes of the fundamental frequency (p_1), and its harmonics (second (p_2), third (p_3), fourth (p_4), fifth (p_5) and sixth (p_6)) generated by nonlinear ultrasound propagation were obtained by calculating the frequency spectrum of the measured acoustic pressure signals.

Nonlinear ultrasound beam simulations were performed using a time-domain numerical solution of a modified Khoklov-Zabolotskaya-Kuznetsov (KZK) nonlinear wave equation in which the

temperature dependence of the medium parameters were included. Nonlinear propagation of a 15-cycle pulse at 13 MHz in water with the source pressure amplitude of 0.1 MPa from the same transducer geometry used in the experiment was simulated. This source pressure amplitude was used in simulation in order to get the same degree of nonlinear waveform distortion as to what obtained in experiment at the focus when the water was at the baseline temperature of 26°C. The changes in the p_1 , p_2 , p_3 , p_4 , p_5 and p_6 values at the focus were analysed as the water temperature increased from 26°C to 46°C.

The experimental results show that due to the temperature elevation the p_1 , p_2 , p_3 , p_4 , p_5 and p_6 values increased by 2.5%±2%, 14%±7%, 18%±5%, 30%±12%, 34%±7% and 63%±15%, respectively compared to their initial value at 26°C. The results obtained from the KZK nonlinear simulations show that the p_1 , p_2 , p_3 , p_4 , p_5 and p_6 values changed by 0%, 1.6%, 3.3%, 5%, 7%, 9% as the temperature was raised from 26°C to 46°C. The simulation and experimental results show similar trend in the temperature dependence of the harmonics generated in water. However, the magnitude of the changes is lower for the simulation results and the source of the difference is currently under investigation.

The results indicate that the nonlinear harmonics generated in water from a 13-MHz transmit pulse are temperature dependent and their temperature sensitivity increases with the harmonic number. Therefore, the nonlinear harmonics generated from high-frequency ultrasound beams could potentially be used for ultrasound-based thermometry.

SP173.3 - 3D trans-rectal ultrasound for high-dose-rate prostate brachytherapy: a comparison of sagittally-reconstructed 3D image volumes with sagittally-assisted axial image sets

Author(s): William T. Hrinivich¹, Douglas Hoover², Kathleen Surry², David D'Souza², Aaron Fenster³, Eugene Wong⁴

¹Department Of Medical Biophysics, Western University, London/CANADA, ²Department Of Oncology, Western University, London/CANADA, ³Imaging Research Laboratories, Robarts Research Institute, London/ON/CANADA, ⁴London Regional Cancer Program, London Health Science Center, London/CANADA

Background: High-dose-rate brachytherapy (HDR-BT) is a prostate cancer treatment option where hollow applicators are inserted into the gland through the perineum. Dose is delivered by indexing a high-activity source to dwell positions within the applicators based on the relative positions of applicators, the prostate, and nearby organs. Conventional HDR-BT imaging involves indexing a trans-rectal ultrasound (TRUS) probe in the superior/inferior (S/I) direction, typically in 5-mm intervals, using the axial crystal to produce an image set for planning. These axial images have limited spatial resolution in the applicator insertion direction (S/I), so the sagittal crystal is used to identify applicator tips, which are transferred to the axial image set through a manual registration of the axial images and live sagittal view, adding a potential source of uncertainty. Correct localization of applicators is critical for accurate dosimetry. A sagittally reconstructed 3D-TRUS image volume with high S/I spatial resolution could eliminate the need to identify applicator tips on separate images, potentially mitigating errors in applicator tip position.

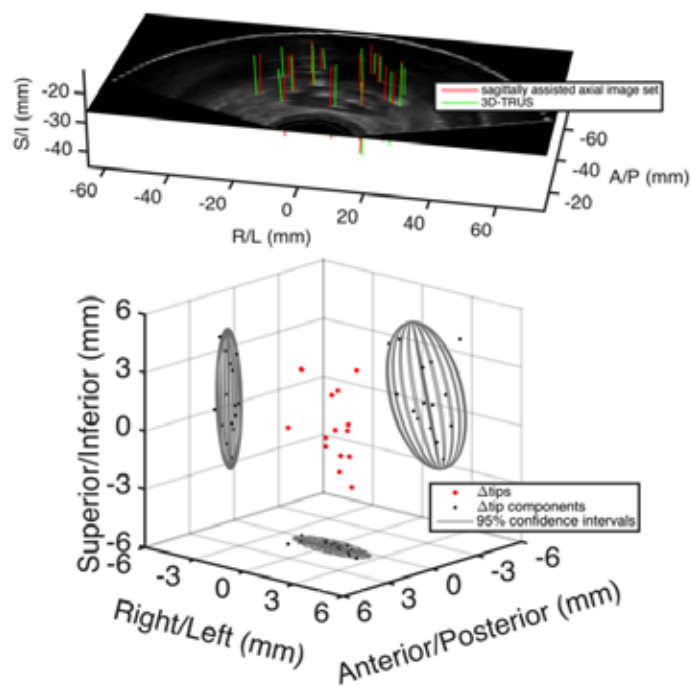
Purpose: To compare applicators localized on 3D-TRUS to those localized on sagittally assisted axial image sets, and to assess the dosimetric impact of these differences.

Methods: Our lab previously developed a mechatronic device for image-guided trans-perineal needle insertions enabling sagittally reconstructed 3D-TRUS. The device has recently been used for both axial image and 3D-TRUS acquisition. A patient underwent HDR-BT using a sagittally assisted axial image set. A 3D-TRUS image volume was acquired prior to the axial images, enabling rigid image

alignment using anatomical landmarks. Applicators were then localized on 3D-TRUS, and dwell positions were compared with those determined intra-operatively. Planned dwell times were transferred to the 3D-TRUS-localized dwell positions and changes in relevant dosimetric parameters were assessed.

Results: Mean \pm SD differences in Right/Left, Anterior/Posterior, and Superior/Inferior applicator tip positions were 0.2 ± 1.1 mm, 0.3 ± 0.4 mm and 0.3 ± 1.8 mm respectively. The 3D-TRUS dwell positions resulted in reductions in prostate V100% from 97.1% to 95.5%, urethra D10% from 116.8% to 112.0%, and rectum D0.5cc from 64.4% to 63.5%.

Conclusions: Applicator localization with 3D-TRUS has the advantage of eliminating a source of uncertainty relative to sagittally assisted axial image sets. Differences in dwell positions were largest in the applicator insertion (S/I) direction. For this patient, spatial differences had little effect on dosimetric parameters. We will report on-going analysis of a larger patient cohort comparing 3D-TRUS with sagittally assisted axial image sets for HDR-BT.



SP173.4 - Understanding lung ultrasound artifacts using a phantom lung model

Author(s): Justine Shuhui Loh¹, Robin O. Cleveland², Andrew P. Walden³

¹Accident And Emergency Department, John Radcliffe Hospital, Oxford/UNITED KINGDOM, ²Old Campus Road Research Building, Institute of Biomedical Engineering, Oxford/UNITED KINGDOM, ³Royal Berkshire Hospital, Intensive Care Unit, Reading/UNITED KINGDOM

Background: Fluid resuscitation as part of the early goal-directed therapy in sepsis is recommended. A conservative fluid strategy is associated with reduced risk of pulmonary oedema, highlighting the importance of limiting fluid therapy in patients at risk of pulmonary oedema. Ultrasound has been used to assess this. Diseased lungs have better ultrasound penetration and resolution, producing ultrasound artefacts known as B-lines. There is an association between

these B-lines and lung water volume. However, there is limited study in classifying and quantifying B-line artefacts as a function of lung water volume.

Objective: To recreate A-line and B-line ultrasound artifacts using a phantom lung model, and determine factors influencing changes in these artifacts, and the possibility of quantifying these changes.

Method: A phantom lung model was created from melted gel wax, which was solidified in a phantom holder over 12 hours, and placed on a layer of cling film wrapped over an air-filled plastic container. 10 μ L and 200 μ L pipette tips, and 0.5mL tube were embedded in the phantom model. Using a linear probe, the A-line and B-line artifacts were obtained from scanning the phantom model. Factors assessed were the different phantom thickness, different phantom surfaces, ultrasound frequency, location of meshed gel wax and weight of meshed gel wax. Data collected and analysed were based on the number of A-lines, distance between each A-line, and the average length of B-lines.

Results: Scanning empty pipette tips and tube created A-lines. B-lines were created by scanning pipette tips and tube filled with liquid (i.e. water, Gelofusin, and plasma) and semisolid (i.e. meshed gel wax) materials. **The A-lines** - The thickness of phantom model is directly proportional to the distance between A-lines, but inversely proportional to the number of A-lines. The ultrasound frequency is inversely proportional to the intensity of A-lines. There was no difference in the A-lines between the flat and semicurved surface phantom, or the different pipette tips and tube sizes. **The B-lines** - The B-lines in pipette tips filled with water showed broader distance between each B'-lines compared to pipette tips filled with meshed gel wax. The ultrasound frequency was inversely proportional to the intensity and average length of B-line. The average length of B-lines appears to increase with increasing meshed gel wax weight, although not in a progressive manner. The distance between each B'-lines appears to be shorter in water-filled and plasma-filled compared to Gelofusin-filled tubes. There was no difference in the B-line between the different pipette tips and tube sizes. There was no relationship between the average length of B-lines and the location of meshed gel wax within the pipette tips (i.e. distance between ultrasound probe and meshed gel wax).

Conclusion: We managed to recreate A-line and B-line artifacts using this model. Increasing volume of substance was associated with ultrasound artifacts changes, confirming a potential role for ultrasound use in quantifying volume. Although there were factors with good association to ultrasound artifacts demonstrated, there were several limitations identified. Further improvement to the phantom model design is required for more accurate study.

SP173.5 - Accuracy of Tissue Elasticity Measurement using Shear Wave Ultrasound Elastography: A Comparative Phantom Study

Author(s): Chu En Ting¹, Chai Hong Yeong², Kwan Hoong Ng², Basri Johan Jeet Abdullah¹, Huong En Ting¹

¹Department Of Biomedical Imaging, Faculty Of Medicine, University of Malaya, Kuala Lumpur/MALAYSIA, ²University Of Malaya, University of Malaya Research Imaging Center, Kuala Lumpur/MALAYSIA

Introduction:

There is a strong correlation between tissue elasticity (Young's modulus) and pathological state. The information of tissue elasticity superimposed to any anatomical image provides great diagnostic value, hence improving treatment outcome. Shear wave elastography (SWE) is a relatively new imaging technique using ultrafast ultrasound to measure tissue elasticity. Though studies have reported the reliability, specificity and reproducibility of SWE in elasticity quantification, the accuracy of elasticity measurements compared

to a gold standard has not been reported.

Aims and Objectives:

The objectives of this study were to verify the accuracy of tissue elasticity measured using SWE compared to the gold standard (electromechanical microtester) and to investigate several factors (size, depth and overlapping inclusions) that might affect the accuracy of SWE measurement.

Methods and Materials:

A tissue-mimicking phantom with acoustic and shear elasticity properties similar to the human breast was developed using animal hide gelatine. Elasticity values of inclusions embedded in the phantom were manipulated by varying the amount of its gelatine content. Each inclusion was made in pair, one for *in vivo* measurement using a commercial SWE scanner (Aix-plorer, SuperSonic Imagine, France) and the other for destructive *in vitro* measurement with the microtester (Model 5848, Instron Co, USA). The measurements using both methods were compared statistically using the paired-sample t-test with 95% confidence interval. To investigate the possible factors affecting SWE measurements, the phantom was also designed to encompass inclusions with varying diameters and elasticity values, embedded at different depths in the phantom. The diameters of the inclusions were varied using pairs of hemispherical moulds with sizes ranging from 17 to 30 mm. SWE measurements were obtained for each inclusion.

Results and Discussion:

Despite a strong linear correlation, a statistically significant difference ($p < 0.05$) was found between the elasticity values measured using SWE and the gold standard, whereby the SWE overestimated the elasticity by a mean of 22.79 ± 15.00 kPa. This overestimation might be due to artefacts caused by wave interferences between the elasticity boundaries. Shear wave reflection at boundaries could cause either constructive or destructive interference, depending both on boundary conditions and the incoming wave, consequently causing underestimation or overestimation of the actual elasticity values. Due to shear wave reflection, an increase in contrast between elasticity boundaries was also shown to reduce reproducibility of consistent measurements. A spatio-temporal directional filter has been suggested as a means to reduce the artefacts in the reconstructed shear modulus map. Size and depth of inclusions did not affect SWE measurements; however the depth of shear wave detection was limited to 8 cm from the surface.

Conclusion:

Elastography plays a significant role in clinical diagnosis by providing useful structural and pathological information on soft tissues. This study shows that the elasticity values derived from commercial SWE system were consistently higher than the gold standard, which is likely due to wave interference at the elasticity boundary. In order for SWE to be incorporated into clinical diagnostic practice, it is vital to identify a solution to overcome these artefacts.

SP174 - Motion Management: Part 2

TRACK 04: RADIATION ONCOLOGY

SP174.1 - Assessment of lung dose in patients undergoing deep inspiration breath hold for left sided breast cancer

Author(s): Peta Lonski¹, David Jolly¹, Shankar Siva², David Ball², Boon Chua³, Damien Phillips⁴, Maria Portillo⁴, Steven David², Amanda Phillips⁴, Tomas Kron¹

¹Physical Sciences, Peter MacCallum Cancer Center, Melbourne/AUSTRALIA, ²Department Of Radiation Oncology, Peter MacCallum Cancer Center, Melbourne/VIC/AUSTRALIA, ³Sir Peter MacCallum Department Of Oncology, University of Melbourne, Melbourne/VIC/AUSTRALIA, ⁴Radiation Therapy Services, Peter MacCallum Cancer Center, Melbourne/AUSTRALIA

Aim: Deep inspiration breath hold (DIBH) is being used to reduce cardiac dose in patients undergoing radiotherapy for left sided breast cancer. Due to chest wall expansion there is concern that the amount of lung in the high dose region could increase. We aimed to evaluate this in a cohort of patients from a prospective trial who had both a free breathing (FB) and DIBH CT scan for planning comparison purposes.

Methods: Ten consecutive left sided breast cancer patients were enrolled in this study. Each patient underwent a FB and a DIBH CT scan in treatment position on an elevated breast board using a Philips Brilliance wide bore 16 slice CT scanner. Plans were created using 6 MV x-rays to treat the whole breast volume as marked clinically. A field in field tangential technique was used. Plans were created in Varian Eclipse version 11 using the Anisotropic Analytical Algorithm (AAA version 11.0.31). The volumes of lung receiving 5, 20 and 30 Gy (V5, V20 and V30 respectively) were assessed on the FB and DIBH scans. Lung DVH data was analysed in terms of both absolute and relative lung volumes.

Results: There was an average increase in absolute volume of lung receiving 5, 20 and 30 Gy in DIBH compared to FB. However, assessment of the same DVH parameters in terms of relative volume of lung showed an average decrease in DIBH. The difference in V5, V20 and V30 between DIBH and FB (positive values indicate a higher dose in DIBH) are shown in the table in terms of absolute and relative lung volumes.

	DIBH - FB: absolute lung volume (cc)		DIBH - FB: relative lung volume (%)	
	mean	standard deviation	mean	standard deviation
V5	+ 203	167	- 0.2	4.1
V20	+ 91	103	- 0.7	2.7
V30	+ 87	99	- 0.6	2.5

Conclusion: DIBH resulted in an increase in the absolute volume of lung present within the target region but paradoxically reduced the evaluated DVH parameters in terms of dose to relative lung volume. Lung DVH data therefore requires careful evaluation when assessing the dosimetric consequences to lung in patients undergoing DIBH. Comparative evaluation of the clinical consequences of absolute versus relative irradiated lung volume in DIBH is warranted.

SP174.2 - Evaluation of 4D dose accumulation in CyberKnife and IMRT treatments

Author(s): Vincent Cousineau Daoust¹, Emily Heath², Jean-Francois Carrier¹, Stephane Bedwani³

¹Radio-oncology, CHUM/Notre-Dame Hospital - Université de Montréal, Montréal/CANADA, ²Physics, Carleton University, Ottawa/CANADA, ³Radio-oncologie, CHUM- Notre-Dame hospital, Montréal/CANADA

Pulmonary cancer is the main cause of death amongst all cancers in Canada with a prognosis of about 15% survival rate in 5 years. The efficiency of radiotherapy treatments is lower when high displacements of the tumors are observed, mostly caused by intrafraction respiratory motion. Advanced techniques such as radiosurgery and intensity-modulated radiotherapy treatments (IMRT) are expected to provide better clinical results by delivering higher radiation doses to the tumor while sparing the surrounding healthy lung tissues. The goal of this project is to perform 4D Monte Carlo dose recalculations to assess the dosimetric impact of moving tumors in CyberKnife and IMRT treatments using dose accumulation in deforming anatomies. Scripts developed in-house were used to model both situations and to compare the Monte Carlo dose distributions with those obtained with standard clinical plans. Deformation fields are obtained from 4D CT data set and a deformable image registration (DIR) algorithm which allows a voxel-to-voxel correspondence between each respiratory phase (Figure 1). The DIR is computed by the Advanced Normalization Tools (ANTs) software and is mostly based on diffeomorphisms. A modified version of DOSXYZnrc from EGSnrc software, defDOSXYZnrc, is used to transport radiation through non-linear geometries.

Current results are mostly centered toward the validation of defDOSXYZnrc with DOSXYZnrc. Theoretical affine deformations were applied to a virtual phantom and the dose distributions for both algorithms were compared using the gamma test and the Kawrakow-Fippel (KF) method. The gamma index for the two distributions is 96.7% for the 1%/1mm criterion and the KF method showed that no significant systematic differences exists between the two algorithms. A set of tools was created to link together dose calculation and DIR softwares, and also to provide the user a simple dose analysis environment. Data from patients who underwent CyberKnife or IMRT treatments with lung tumors moving at least 5 mm is used for the dose comparison.

SP174.3 - Application of RADPOS System for Dose and Position Quality Assurance of 4D CyberKnife Treatments

Author(s): Raanan Marants¹, Eric Vandervoort², Joanna Cygler³

¹Physics, Carleton University, Ottawa/ON/CANADA, ²Medical Physics, The Ottawa Hospital Cancer Centre, Ottawa/ON/CANADA, ³Radiology, University of Ottawa, Ottawa/ON/CANADA

Introduction

The CyberKnife robotic radiosurgery system uses Synchrony respiratory motion compensation. This complex dose delivery system needs independent performance verification to assure safe patient treatments.

In this work, we use the RADPOS 4D dosimetry system to verify CyberKnife's motion tracking and delivered dose. RADPOS motion measurements are compared with internal metal fiducials and external LED optical markers log files. Dose measurements are compared with GAFCHROMIC film and treatment planning system (TPS) calculations.

Methods

RADPOS and EBT3 GAFCHROMIC films were calibrated using an ion chamber in Solid Water (5 cm depth, 80 cm source-detector distance, 60 mm cone). A CT based treatment plan was created for a Solid Water breast phantom containing fiducials and the RADPOS detector. Dose calculations were performed using the MultiPlan TPS, Monte Carlo (MC) and ray tracing (RT) algorithms on static phantom only. Before treatment, film was inserted inside the breast phantom adjacent to the RADPOS detector. The breast phantom and LED markers were positioned on the chest platform of a Quasar Respiratory Motion Phantom. Position logging began for RADPOS and Synchrony, Quasar motion started, and irradiation commenced. A coordinate alignment algorithm was implemented, allowing all position tracking modalities to be compared within the fiducial coordinate system.

Results

Position

After LED and RADPOS position data are aligned to the fiducial coordinate system (average difference < 0.01 mm in any direction), the standard deviation of the differences between LED and RADPOS position measurements was 0.33, 0.39, and 0.56 mm along the left/right, superior/inferior, and anterior/posterior directions, respectively.

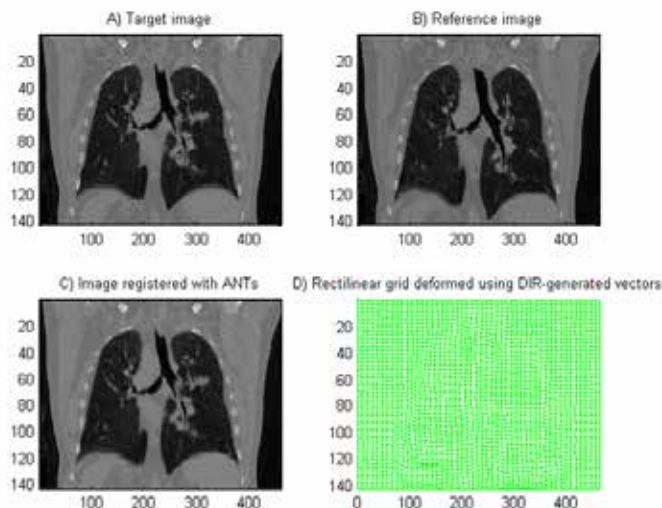


Figure 1 - A) A respiratory phase from a 4D CT scan is defined as a target image. B) Another respiratory phase is defined as a reference image C) which will be deformed toward the target image using DIR algorithm. D) Vectors obtained from the DIR are used to deform the grid geometry. Dose is computed in the deformed geometry using defDOSXYZnrc and then mapped back to a rectilinear grid [back to the reference image].

Dose

TPS		Measured									
RT Dose (cGy)	MC Dose (cGy)	Phantom	RADPOS Dose (cGy)	% diff (RAD-POS/RT)	% diff (RAD-POS/MC)	Film Dose (cGy)	% diff (Film/RT)	% diff (Film/MC)	% diff (RAD-POS/Film)	γ-index, 3%/1 mm (RT)	γ-index, 3%/1 mm (MC)
146.7	145.3±1.0%	Static	147.2±1.3%	0.3%	1.3%	147.5±1.9%	0.5%	1.5%	-0.2%	97.2	96.7
		Dynamic	149.6±1.2%	2.0%	2.9%	145.3±1.8%	-1.0%	0.0%	3.0%	97.3	97.0

Discussion

Position

LED positions were sampled approximately 2.5 times as frequently as RADPOS positions. Also, during coordinate system alignment, the user synchronizes semi-automatically two motion signals in time. These temporal uncertainties were dealt with as follows:

$$\sigma_t = \sqrt{(\sigma_{t,LED})^2 + (\sigma_{t,RADPOS})^2} = \sqrt{[(1/2 \times dt_{LED})^2 + (1/2 \times dt_{RADPOS})^2]} = 53.6 \text{ ms}$$

This lead to a positional uncertainty of 0.02, 0.04, and 0.19 mm along the left/right, superior/inferior, and anterior/posterior directions, respectively.

Dose

The MC and RT TPS dose values were very similar because both calculations were done for primarily homogeneous, unit-density material. RADPOS dose readings made during dynamic treatment were slightly higher than all other dose values, but still fell within two standard deviations of experimental uncertainties. Average gamma results were greater than 96% for both MC and RT dose calculation algorithms, as well as for dynamic and static treatments.

Conclusions

Our work demonstrates that RADPOS is a useful tool for independent QA of CyberKnife treatment with Synchrony respiratory compensation.

SP174.4 - Derivation of the probabilistic treatment margin for two targets with correlated motion

Author(s): Simon Van Kranen, Jan-Jakob Sonke, Marcel Van Herk
Radiation Oncology, The Netherlands Cancer Institute, Amsterdam/
NETHERLANDS

Introduction

Margin recipes are widely used to derive PTV margins from random and systematic errors. Here we address a common situation with unknown solution: a margin that jointly covers two targets with correlated motion. E.g., primary tumor and lymph node targets in lung cancer are known to move somewhat correlated.

Material and methods

We assume two targets moving in 3D with a normal distribution with random / systematic error vectors σ and Σ . For simplicity we assume the following type of correlation: each vector component of target 1 correlates with the corresponding component of target 2 with the same and known correlation, r . Finally, we assume that the margin for systematic errors can be expressed as $\alpha \Sigma$, where α is function of r . Because the margin for **random errors** is derived from the local target motion relative to the dose distribution, correlation has no influence, and the margin remains unchanged, e.g., 0.7σ simplified. The margin for **systematic errors** needs to achieve an acceptable probability that both targets are covered together. For a single target, 90% probability is reached with $\alpha = 2.5$. For two

targets with uncorrelated motion, α needs to be 2.8 to achieve 90% joint probability for both targets (0.95^2). To finally derive the appropriate margin given correlation r , we need to establish the correlation R of the dichotomous (i.e. 0 or 1) variables $V1 < \alpha \Sigma 1$, and $V2 < \alpha \Sigma 2$, where V is the error vector length of a target. The probability, P , that $V1 < \alpha \Sigma 1$ and $V2 < \alpha \Sigma 2$ is given by $P = p^2 + p(1-p)R$ {equation 1}, where p is the probability of this condition for each target independently. In this study continuous correlation r and dichotomous correlation R are linked using a simulation for a practical range of α .

Results

We first obtain R from r , then p from R , and finally α from p . Our simulations show that for this type of correlation, R fits r^4 well for $2.5 < \alpha < 3.2$. The appropriate p given correlation R is a solution of eq. 1 for $P=0.9$. Finally, α is found as the inverse of the cumulative chi-square distribution with three degrees of freedom at p (e.g., 2.5 for $p=0.9$). The combined equations are approximately linear with $z = 1-R$, or $z = 1-r^4$. The simplified margin recipe is given by $M = 0.7\sigma + (2.5 + 0.3z)\Sigma$, which assures with 90% probability that 2 targets are within the 95% isodose line.

Conclusions

Based on an empirical relation between a continuous and a dichotomous correlation, a practical margin recipe for two targets with correlated motion was derived. This margin formula is generic, except that z depends on the type of correlation. Because the dichotomous

correlation R is much smaller than the underlying continuous correlation, $r < 0.5$ can be treated as uncorrelated. The introduced formalism opens up the way to derive analytical margin recipes for an arbitrary number of targets with correlated motion.

SP174.5 - How Truthful Is the 4D Dose Calculation?

Author(s): Gang Liu¹, Di Yan², Hong Quan¹

¹School Of Physics And Technology, Wuhan University, Wuhan/CHINA, ²Radiation Oncology, Beaumont Health System, Royal Oak/MI/UNITED STATES OF AMERICA

Purpose:“4D dose” can be constructed using patient respiratory-correlated 4D CT image. However, patient respiratory-induced target/organ motion is most likely heterogeneous between breathing periods. Therefore, it is questionable if the 4D dose represents the “true dose” obtained from the entire breathing motion during the CT scanning. In this study, 4D CT scanning was simulated and used in the 4D dose calculation. The dose discrepancy between the “4D dose” and the “true dose” was evaluated and correlated to the heterogeneity of respiratory-induced motion pattern.

Method& Material: Computer simulation was performed using simulated and measured free breathing curves to generate a 4D target and an adjacent normal organ motion CT images. Two 4D dose distributions in the target and organ were constructed. The first one, named the 4D dose (D1), was calculated by tracking the point displacements in the target or organ manifested on the 4D CT images and including the physical density changes in the phase CTs, meanwhile the second one, named the true dose (D2), constructed based on the point displacements and density changes along the whole breathing motion curve. Treatment dose was generated using 6 co-planer beams aimed to the target center without using target margin. Dose discrepancy between D1 and D2 was calculated using different breathing curves with either non-uniform excursion or heterogeneous breathing period. The correlation between breathing pattern variation and dose discrepancy in the target and organ adjacent to target was determined and evaluated.

Result: The dose discrepancy in both the target and adjacent organ is highly correlated to the variation of breathing-induced target motion excursion and period. The maximum dose discrepancy in the target was on average 5% ($\pm 2.7\%$ of one SD) to 8% ($\pm 7.3\%$) with the standard deviation of the motion excursion variation from 1mm to 4mm, meanwhile 6% ($\pm 3.7\%$) to 12% ($\pm 8\%$) with the standard deviation of the motion period variation from 0.3 sec to 0.7 sec. For the adjacent normal organ, the dose discrepancy was larger, especially for the motion period variation. When both variations appeared, the dose discrepancy could be $>12\%$ ($\pm 8.3\%$) for the target, and $>16\%$ ($\pm 11.5\%$) for the adjacent organ, meanwhile 10.6% ($\pm 9.8\%$) of the target volume and 21.8% ($\pm 15.8\%$) of the organ volume had dose discrepancy bigger than 5%.

Conclusion: The 4D dose constructed using 4D CT image can have large discrepancy when patient respiratory-induced target/organ motion has a heterogeneous pattern. However, this dose discrepancy can be estimated for treatment planning evaluation using the measured breathing curve during the 4D CT scanning.

SP175 - Treatment Planning - Biology & Fractionation

TRACK 04: RADIATION ONCOLOGY

SP175.1 - Adaptive radiotherapy for bladder cancer using deformable image registration of empty and full bladder

Author(s): Prabhjot Juneja¹, Hannah Caine², Peter Hunt², Jeremy T. Booth¹, David Thwaites¹, James O'Toole², Anen Vestergaard³, Jesper Kallehauge³, Andrew Kneebone², Thomas Eade²

¹Institute Of Medical Physics, School Of Physics, University of Sydney, Sydney/NSW/AUSTRALIA, ²Northern Sydney Cancer Centre, Royal North Shore Hospital, Sydney/NSW/AUSTRALIA, ³Department Of Medical Physics, Aarhus University Hospital, Aarhus/DENMARK

A common objective of various adaptive radiotherapy (ART) strategies for bladder cancer is to reduce irradiation of normal tissue, thereby reduce the risk of radiation induced toxicity, and maintain or improve the target coverage. Bladder radiotherapy, typically involves generous margins (up to 20 mm) for bladder planning target volume (PTV).

The goal of this retrospective study is to define, evaluate and optimize new patient-specific anisotropic PTVs (a-PTVs) using deformable image registration (DIR) between empty and full bladder computed tomography (CT) scans. This will provide an ART that incorporates the extreme deformations of the bladder, and is applicable from the first day of treatment.

Deformation vector fields (DVF), measured from the deformable image registration between empty and full bladder CTs, were scaled and constrained to construct the a-PTVs. For each patient, four a-PTVs were constructed such that a-PTV1 was the largest and a-PTV4 was the smallest. All the a-PTVs were defined such that they covered at least the bladder volume plus 5 mm margin. These a-PTVs were retrospectively evaluated and compared to the current clinical standard (conv-PTV), with 10 mm uniform margins, using 5 bladder cancer patients and a total of 100 fractions.

It was found that the smaller a-PTV, a-PTV4 and a-PTV3, were appropriate in 87% of the fractions, while a-PTV2 and a-PTV1 were required in 12% of the fractions respectively. The use of the a-PTVs reduced the PTV volume by 32% (28-36%) as compared to conv-PTV.

In conclusion, the results of this pilot study indicate that the use of a-PTVs could result in substantial decrease in the course averaged planning target volume. This reduction in the PTV is likely to decrease the radiation related toxicity and benefit bladder cancer patients. Currently, more patients are being investigated to strengthen these findings, and also dosimetric analysis is underway.

SP175.2 - Dosimetric and clinical benefits of conformal radiotherapy combined plus volumetric modulated arc therapy in the treatment of non-small cell lung cancer

Author(s): Xiance Jin, Congying Xie

Radiation Therapy And Chemotherapy, The 1st Affiliated Hospital of Wenzhou Medical University, Wenzhou/CHINA

Background Radiation pneumonitis (RP) is one of the most common dose-limiting toxicities in conformal radiotherapy (CRT) and has a considerable impact on patient's morbidity and mortality for lung cancer patients. Intensity-modulated radiotherapy (IMRT) and volumetric modulated arc therapy (VMAT) have been applied in the

treatment of lung cancer in an intent to spare the normal lung tissue and escalate dose to target. However, the use of IMRT and VMAT have been limited due to low dose dosimetric considerations. The purpose of this manuscript is to investigate the dosimetric and clinical benefits of a technique by combining conformal radiotherapy (CRT) plus VMAT in the treatment of non-small cell lung cancer (NSCLC). **Materials and methods** There were 200 NSCLC patients analyzed retrospectively and treated by CRT, CRT plus VMAT, and full course of VMAT, respectively. Matches were chosen based on stage, PTV size, tumor location, age, and gender. CRT scheme was planned with two parallel opposed, antero-posterior and postero-anterior (APPA) beams for 36 Gy, then followed by off-cord conformal beams for 24 Gy at 2 Gy per fraction. CRT plus VMAT was planned with initial CRT APPA beams for 36 Gy, then followed by a single-arc VMAT plan for 24 Gy. The full course VMAT plan was 60 Gy over 30 fractions with a single arc. Dosimetric differences, RP rates and their correlation were investigated. **Results** The number of patients analyzed in CRT, CRT plus VMAT and full course of VMAT were 42, 28, and 53, respectively. The V93 and V95 (percent volume covered by isodose line) of PTV were improved from $95.7\% \pm 2.2\%$ and $94.5\% \pm 2.4\%$ in CRT to $97.9\% \pm 4.6\%$, $98.3\% \pm 3.2\%$ and $96.3\% \pm 5.8\%$, $97.1\% \pm 4.1\%$ in CRT plus VMAT and full course of VMAT, respectively. CRT plus VMAT improved the PTV coverage compared with CRT in a cost of higher spinal cord maximum dose ($p=0.02$), larger lung volume receiving 5 Gy (V5, $p=0.02$) and mean lung dose (MLD) ($p=0.04$), and decreased the low dose lung volumes compared with VMAT. The RP rates were 26%, 39% and 49% for CRT, CRT plus VMAT and VMAT, respectively. V5 was significantly associated with RP and had a threshold of 60% and 65% for CRT plus VMAT and VMAT, respectively, to limit the RP rate $<30\%$. The median three-year overall survival were 17.5, 23.2, 24.5 months for CRT, CRT plus VMAT and VMAT, respectively, without significant difference ($p=0.29$). **Conclusions:** CRT plus VMAT is a promising with increased target coverage compared with CRT and reduced low dose lung volume and RP compared with full course of VMAT in the treatment of NSCLC. V5 was significantly associated with RP and with a predicted threshold of 60% and 65% for CRT plus VMAT and VMAT, respectively, to limit the RP rate $<30\%$. The interplay effect of chemotherapy with CRT plus VMAT on RP needs further study. Clinical trials with large population are needed to further verify the benefits of CRT plus VMAT in the treatment of NSCLC.

SP175.3 - Non-uniform spatiotemporal fractionation schemes in photon radiotherapy

Author(s): Jan Unkelbach

Radiation Oncology, Massachusetts General Hospital, Boston/MA/ UNITED STATES OF AMERICA

Fractionation decisions in radiotherapy face the tradeoff between increasing the number of fractions to spare normal tissues, and increasing the total dose to achieve the same level of tumor control. In that regard, the ideal treatment would fractionate in normal tissues while simultaneously hypofractionating in the tumor. Interestingly, this is possible to a limited degree by delivering distinct dose distributions in different fractions. The dose distributions have to be designed such that similar doses are delivered to normal tissues while delivering high single fraction doses to parts of the tumor. In this paper, proof-of-concept is provided that this concept may lead to an improved therapeutic ratio for rotation therapy treatments using conventional photon beams. An idealized model of a large tumor treated in two fractions is considered. Fractionation effects are modeled via the biologically equivalent dose model. It is shown that the optimal treatment delivers the dose to the center of the tumor in a single fraction, while the second fraction delivers dose only to the rim of the tumor. The approach may potentially be interesting for large tumors embedded in a dose-limiting organ treated with stereotactic regimens.

SP175.4 - Compressed Sensing-Based LDR Brachytherapy Inverse Treatment Planning with Biological Models

Author(s): Christian V. Guthier¹, Katharina P. Aschenbrenner¹, Frederik Wenz², Juergen W. Hesser¹

¹Experimental Radiation Oncology, Medical Faculty Mannheim, Heidelberg University, Mannheim/GERMANY, ²Radiation Oncology, Medical Faculty Mannheim, Heidelberg University, University Medical Centre, Mannheim/GERMANY

New compressed sensing-based planning algorithms allow for fast computations of optimal planning results in low-dose-rate (LDR) brachytherapy. This enables to integrate complex models in the planning process. In this paper, we develop a new strategy for including a biological model on tumor control probability (TCP) and normal tissue complication probability (NTCP) into the objective function for plan optimization. These models were tested on clinical prostate cancer cases for their effects on the planning results relative to standard physical dose constraints for planning as reference. Interestingly, with weighting treatment risks, we observe plans using biological models assign more dose to the urethra since it is less radiation sensitive than the rectum whereby the latter is spared in order to reduce side effects. At the same time, the overall TCP is comparable. We conclude that the standard plan quality evaluation based on physical dose alone does not easily allow correctly assessing treatment risks. Hence, biological models for LDR brachytherapy treatment planning are a promising approach for an optimal management of treatment outcomes of brachytherapy.

SP175.5 - Investigation of Dosimetric and Biological Differences between Flattened and Unflattened Beams from the TrueBeam System

Author(s): Yue Yan¹, Kaifang Du², Daniel Saenz¹, Michael Bassetti², Bhudatt Paliwal¹, Paul Harari²

¹Medical Physics, University of Wisconsin Madison, Madison/UNITED STATES OF AMERICA, ²Human Oncology, University of Wisconsin School of Medicine and Public Health, Madison/WI/UNITED STATES OF AMERICA

Purpose/Objective(s): To investigate the dosimetric and biological differences between flattened and unflattened beam plans using different anatomic cancer sites.

Materials/Methods: Flattened and unflattened beams of the TrueBeam system were commissioned on the Eclipse treatment planning system (TPS). Beam energies were chosen to be 6 MV and 10 MV. Fourteen clinical cancer cases were used to simulate the clinical treatment. Static intensity modulated radiation therapy (IMRT) and volumetric modulated arc therapy (VMAT) were used to deliver the dose. Based on the dose-volume-histogram (DVH), biological effective dose (BED), equivalent uniform dose (EUD), tumor control probability (TCP) and normal tissue complication probability (NTCP) were calculated to evaluate the biological effectiveness of the treatment plan. In-house developed Matlab code was used to statistically analyze the results. Direct comparisons were made to study the dosimetric and biological differences between the flattened and the unflattened beams for both energies.

Results: Nearly the same target coverage was obtained by the unflattened beam compared with the flattened beam for all cancer cases. For organ-at-risk (OAR) with high radiation sensitivity but received low dose (e.g. lens of the eye), the unflattened beam had up to 38% mean dose reduction and 34% maximum dose reduction compared with the flattened beam, leading to 85% reduction in the NTCP value. For OARs which were closer to the treatment field and had larger dose (e.g. brainstem), the unflattened beam had up to 14% reduction in the mean dose, 10% reduction in the maximum dose and 55% reduction in the NTCP value.

Conclusion: The clinical data indicated that the unflattened beam

could provide similar target coverage as the flattened beam in all 4 types of cancer. Improved dose sparing effect was obtained by the unflattened beam, leading to lower NTCP value in general. Significant dose sparing effect of the unflattened beam was observed for the head and neck cancers with large field size (about 16x20 cm²). The maximum dose rate of the unflattened beam may not always be achievable for large treatment field size (e.g. 20x20 cm²) due to the speed limitation of the multileaf collimator (MLC).

SP176 - Characterization of Detector Systems for Therapy Dosimetry: Part 4

TRACK 05: DOSIMETRY AND RADIATION PROTECTION

SP176.1 - Evaluation of surface dose distributions using ferrous benzoic xylenol orange translucent PVA cryogel radiochromic dosimeters

Author(s): Molham Eyadeh, Marcin Wierzbicki, Kevin Diamond
McMaster University and Juravinski Cancer Centre, Hamilton/
CANADA

Purpose

The purpose of this study is to evaluate the ability of a radiosensitive bolus material to monitor the surface dose distribution. Poly-(vinyl alcohol) cryogels (PVA-C) are flexible and can be fit snugly against skin over large, curved regions, where it may be challenging to achieve the same coverage with film or TLDs. We propose a method to use ferrous benzoic xylenol orange (FBX) in translucent PVA-C in place of bolus to perform *in vivo* dosimetry in regions where surface dose is important.

Materials and Methods

In this study, a series of open fields with gantry angles ranging from 0° to 90° were delivered to a radiochromic bolus and film stack on the surface of a polystyrene phantom. These measurements established the relationship between surface dose (estimated using Gafchromic EBT-2 film) and the dose measured in a 5 mm thick piece of radiochromic bolus. This calibration was then applied to clinical head and neck IMRT treatment plans that were delivered to a RANDO phantom. Radiochromic bolus was added electronically to the CT scan of the RANDO phantom to approximate the conditions of the actual patient treatments. The radiochromic bolus was imaged pre- and post-irradiation using a charge coupled device (CCD) camera, illuminated using a uniform, red LED array. All radiation treatment plans were developed using Pinnacle 9.2.

Results

The ratio between surface dose and the dose measured in the radiochromic bolus increased with increasing gantry angle, ranging from 0.745 ± 0.005 at 0° to 0.890 ± 0.017 at 67.5°. The average ratio of 0.799 ± 0.009 was used as the calibration factor. The calibration factor was applied to the radiochromic bolus dose measurements of the IMRT treatments delivered to the RANDO phantom. A gamma comparison between the radiochromic bolus and film was performed, using 3%/3mm criteria and a 10% threshold. The pass rate ranged from 95.1% to 97.7%.

Conclusion

A comparison of film and FBX-PVA translucent cryogel suggests that the radiochromic bolus provides an accurate estimate of surface dose using a simple correction factor. It may be possible to improve agreement using a more complex, angle dependent correction scheme, but this may over-complicate the dose estimation process.

SP176.2 - Suitability of Diodes for Point Dose Measurements in IMRT/VMAT Beams**Author(s):** Tanya Kairn¹, Salma Ibrahim², Emma Inness², Scott Crowe³, Jamie Trapp⁴¹Physics, Genesis CancerCare Queensland, Auchenflower/QLD/AUSTRALIA, ²Radiation Oncology, Princess Alexandra Hospital, Woolloongabba/QLD/AUSTRALIA, ³Radiation Oncology, Royal Brisbane and Women's Hospital, Herston/QLD/AUSTRALIA, ⁴Science And Engineering Faculty, Queensland University of Technology, Brisbane/AUSTRALIA

Recent advances in diode dosimetry analysis techniques, and resulting improvements in the accuracy of diode measurements of small field dose, have led to renewed interest in the use of diodes to measure point doses in modulated radiation fields. This study investigated one potential source of inaccuracy for diode measurements in modulated beams; the effect of diode housing asymmetry on measurement results.

Point dose measurements in modulated beams are used to augment dose plane measurements, for both system commissioning and treatment verification, and small-volume dosimeters have the potential to minimise volume averaging across dose gradients. For this reason, diodes are an attractive option for the measurement of intensity modulated radiotherapy (IMRT) and volumetric modulated arc therapy (VMAT) point doses. However, use a non-water-equivalent (silicon) active volume with a variable field size dependence, which is often embedded in epoxy resin and surrounded by high-density shielding and electrical contacts. The longitudinal asymmetry of cylindrical diode construction is expected to lead to inaccurate or unpredictable results when the diode positioned parallel to the beam (usually horizontally) in a solid phantom, for IMRT/VMAT point dose measurements.

In this study, the possible effects of diode housing asymmetry on the measurement of steep dose gradients were evaluated by measuring beam profiles, for a 5x5 cm² static field, with three cylindrical diodes and two commonly used ionisation chambers, with each dosimeter positioned in a 3D scanning water tank with its stem perpendicular to the beam axis (horizontal) and parallel to the direction of scanning. The resulting profiles were used to compare the penumbræ measured with the diode stem pointing into (equivalent to a "stem-first" setup) and out of the field (equivalent to a "stem-last" setup) in order to evaluate the effects of dosimeter alignment and thereby identify the effects of dosimeter asymmetry.

Small but noticeable differences between the penumbræ measured in the stem-first and stem-last directions, for all five dosimeters used in this study. The different orientations resulted in differences of up to 0.2 mm in the measured 20-80% penumbra widths and differences of up to 0.4 mm in the off-axis position of the 90% isodose. These differences, which are smaller than previously reported for older model dosimeters, were apparent in the profile results for both diodes and small-volume ionisation chambers.

As an extension to this study, the practical use of all five dosimeters was exemplified by measuring point doses in IMRT test beams. These measurements showed good agreement (within 2%) between the diodes and the small volume ionisation chamber, with all of these dosimeters being able to identify a region 3% under-dosage which was not identified by a larger volume (6 mm diameter) ionisation chamber.

This study does not attempt to resolve the issue of diode over-response to the small beam segments delivered during modulated treatments, however the results of this work should help to remove some of the barriers to the use of diodes for modulated radiotherapy dosimetry in the future.

SP176.3 - Development of a boron distribution monitor using prompt gamma-rays for boron neutron capture therapy**Author(s):** Hiroki Tanaka, Yoshinori Sakurai, Takushi Takata, Minoru Suzuki, Shinichiro Masunaga, Akira Maruhashi, Koji Ono
Radiation Life Science And Radiation Medical Science, Kyoto University Research Reactor Institute, Osaka/JAPAN

At Kyoto University Research Reactor Institute, over 500 clinical studies of Boron Neutron Capture Therapy (BNCT) have been performed as of January 2015 using research reactor. On the other hand, clinical trials using accelerator-based epithermal neutron source were started on December 2012. The information of neutron and boron concentration is needed to perform BNCT. Boron concentration is measured by prompt gamma-ray analysis or an Inductively Coupled Plasma (ICP). Blood sample containing with boron is taken before the irradiation. During the irradiation, boron concentration is keeping by using the method of continuous injection of boron compound. However, the real-time information of not only neutron flux but boron concentration is needed to perform the precise dose estimation. We already developed the real-time neutron flux monitor using tiny scintillator combination with the quartz fiber. It is necessary to develop a monitor of boron distribution during the irradiation. In this presentation, we report the developed real-time boron distribution monitor using the information of prompt gamma-rays.

During the BNCT irradiation, prompt gamma-rays with the energy of 478 keV are emitted by the reaction between thermal neutron and boron-10. Boron concentration can be estimated using the measured counts of prompt gamma-rays and thermal neutron flux. We developed the system for measuring prompt gamma-rays using 8x8 Gd3Al2Ga3O12 (Ce:GAGG) scintillator array combination with multi-anode photomultiplier. Ce:GAGG scintillator was manufactured by FURUKAWA Corporation LTD. This scintillator has the characteristics such as higher light output, shorter decay time, better energy resolution compared with BGO scintillator that is usually used for the imaging of gamma-rays. Each scintillator with the size of 5mm x 5mm x 10mm³ is isolated with the light reflector. Scintillator array is coupled with multi-anode photomultiplier of H8500C. Each readout signal of photomultiplier is shaped and amplified by multi-channel amplifier and converted to digital signal to obtain energy spectrum of prompt gamma-rays. The gamma-ray collimator is set in front of detection head. This system is surrounded by lead and LiF to shield back ground gamma-rays and thermal neutrons, respectively. Performance test using ¹³⁷Cs gamma-ray source was performed. It was confirmed that gamma-rays of 662 keV was measured at each readout channel with the energy resolution of less than 12%. The gamma-ray image from ¹³⁷Cs source was measured by using the region of interest around 662 keV of energy spectrum for each scintillator. It was shown that this system was able to detect the image of prompt gamma-ray emitted from the reaction between thermal neutron and boron-10. In the future, this system will be applied to BNCT irradiation field to detect boron distribution.

SP176.4 - Study of potential effects of a strong magnetic field on radiation dosimeters (TLD, OSLD, EBT3 film, PRESAGE)**Author(s):** Zhifei Wen¹, Michelle V.P. Mathis¹, Gabriel O. Sawakuchi², David Flint², Ramesh Tailor², Geoffrey S. Ibbott¹, Sam Beddar¹
¹Radiation Physics, The University of Texas MD Anderson Cancer Center, Houston/UNITED STATES OF AMERICA, ²Radiation Physics, MD Anderson Cancer Center, Houston/UNITED STATES OF AMERICA

Introduction: Accurate dosimetry in the presence of a strong magnetic field (B) is essential to the use of a magnetic resonance image-guided linear accelerator (MRI-linac) system. In particular, it is important to characterize the response of dosimeters in a B field to determine which types of dosimeters may be used for beam quality assurance and in-vivo dosimetry in a MRI-linac system. In

this study, four types of radiation dosimeters were investigated, including thermoluminescent dosimeters (TLDs), optically stimulated luminescence detectors (OSLDs), EBT3 radiochromic films, and PRESAGE® dosimeters.

Method: All four types of dosimeters were separated into two categories which were either exposed or not exposed (control) to a strong B field. In each category a group of dosimeters was irradiated with a dose of 0, 2, 4, or 6 Gy. In the first part of the experiment, dosimeters were exposed to a B field inside a small animal MR scanner in a B field slightly greater than 2.5 T for at least 1 hour pre-irradiation and at least 1 hour post-irradiation. Results were compared with irradiated control groups without exposure to a B field. In the second part of the study, dosimeters were irradiated inside an MR-linac prototype where the B field was 1.5 T, and the control groups were irradiated with a conventional Linac without a B field.

Results: For dosimeters exposed to a B field before and after irradiation, small difference (<2%) was observed in comparison to the control groups for all four types of dosimeters. For dosimeters with simultaneous exposure to a B field and radiation, OSLDs had the best agreement with the control groups (~1%). For TLDs and films, the agreement was about 5%, which was within experiment uncertainty (~6%). However, larger disagreement in PRESAGE dosimeters was observed (10-12%).

Conclusion: Exposure to a strong B field before and after irradiation does not appear to change the dosimetric properties of TLDs, OSLDs, EBT3 films or PRESAGE dosimeters. With simultaneous exposure to both the B field and radiation, TLDs, OSLDs, and films seem not significantly affected by the B field within the experimental uncertainty (6%). The cause of disagreement in PRESAGE dosimeter data has not been fully determined. Further study is ongoing to test reproducibility and reduce experiment uncertainty.

SP177 - Radiation Shielding - Design and Outcomes

TRACK 05: DOSIMETRY AND RADIATION PROTECTION

SP177.1 - Simple expression of x-ray doses below 1 MeV grazing incident on shields of concrete and iron backed by lead

Author(s): Nobuteru Nariyama

Light Source And Optics Division, Japan Synchrotron Radiation Research Institute, Hyogo/JAPAN

For an x-ray beam, metal pipes are sometimes used to transport the beam, in which the scattering x-rays are grazing incident on the inner surface of the pipe. Moreover, for targets in medical accelerator facilities, a thick shield is necessary near the target; however, far from the source, a thinner shield is sufficient. For such a tapered shield, the x-rays can be incident on the thin part at a small angle. With increasing incident angle, the contribution of almost vertically scattered x-rays will be dominant owing to the shortest travelling path in the shield, as shown in Fig. 1. In this study, the doses for broad x-rays grazing incident on slabs of concrete and iron backed by lead were calculated using Monte Carlo codes.

The results showed that the dose transmission in concrete can be expressed as $D = D_0 e^{-\mu' t}$ at $\cos \theta = 0.01$ and 0.1 between 0.2 and 1 MeV as shown in Fig. 2; D_0 is the assumed source strength at the scattering point, and t is the shield thickness. The parameter μ' was found to be almost equal to the attenuation coefficient for the nearly vertically scattered x-rays. The values of D_0 were dependent on θ . For iron backed by lead between 0.08 and 1 MeV when θ was 88° , the attenuation slope gradually changed and converged to the rate corresponding to the energies of the nearly vertically scattered x-rays in lead. The same experiment was also performed for a stainless steel pipe wrapped with lead slabs of $0-2$ mm thickness and white narrow x-rays with a peak energy of 0.09 MeV incident at 85° . The results reproduced the doses predicted by the Monte Carlo calculations.

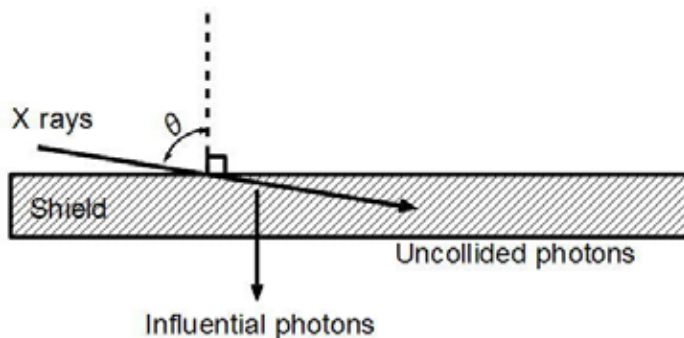


Fig. 1 Grazing incident x-rays on the shield

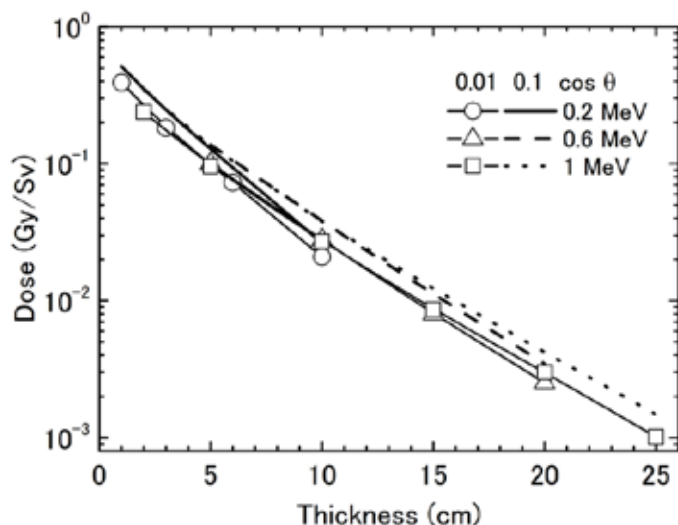


Fig.2 Dose transmission in concrete

SP177.2 - Evaluation of conversion coefficients from Air Kerma to Ambient Dose Equivalent for secondary barriers in diagnostic radiological facilities

Author(s): Paulo R. Costa¹, Alejandro H..L. Gonzales²
¹Nuclear Physics, Radiation Dosimetry and Medical Physics Group, Physics Institute, São Paulo/BRAZIL, ²Radiation Dosimetry and Medical Physics Group, Physics Institute, University of São Paulo, São Paulo, Brazil, São Paulo/BRAZIL

Introduction: The ambient dose equivalent operational quantity is used in many countries for planning purposes of the physical barriers in a radiographic installation. Therefore, it is important to use a conversion coefficient, which turns this dosimetric quantity into a recommended operational quantity [1]. Brazilian regulation establishes that a conversion coefficient (1.14 Sv/Gy) must be used in area monitoring.

Methods: An experimental method was developed for measurement of secondary spectra using a spectroscopic system with CdTe detector [2] and an 1800 cm³ ionization chamber. The thoracic region of an anthropomorphic phantom, RANDO[®] Man, was used as a scatter region. The voltages used began 40 kV up to 150 kV in displacements of 10 kV, the scattering angles were 30°, 60°, 90° 120° and 150° with respect to the axis of the primary beam. The mean conversion coefficients are calculated using the equation [3]:

$$\bar{C}_k = \frac{\int_0^{E_{max}} C_k(E) \cdot \Phi(E) \cdot E \cdot \left(\frac{\mu_{en}(E)}{\rho}\right)_{ar} \cdot \exp(-\mu(E) \cdot x) \cdot dE}{\int_0^{E_{max}} \Phi(E) \cdot E \cdot \left(\frac{\mu_{en}(E)}{\rho}\right)_{ar} \cdot \exp(-\mu(E) \cdot x) \cdot dE}$$

Results and Discussion: The Figure 1 shows the mean conversion coefficient as a function of the mean energy of the spectra for secondary beams scattered in angles of 30°, 60°, 90°, 120° and 150° degrees. The blue line corresponds to the constant value of 1.14 Sv/Gy.

Conclusions: In a typical example of radiometric survey, the estimated ambient dose equivalent using the conversion coefficient calculated from the evaluated spectra, is 40% higher compared to the value obtained using the coefficient recommended in Brazil.

Acknowledgments: The authors thank FAPESP for financial sup-

port under project 2010/12237-7 and CNPq/FAPESP INCT Rad Metrology in Medicine.

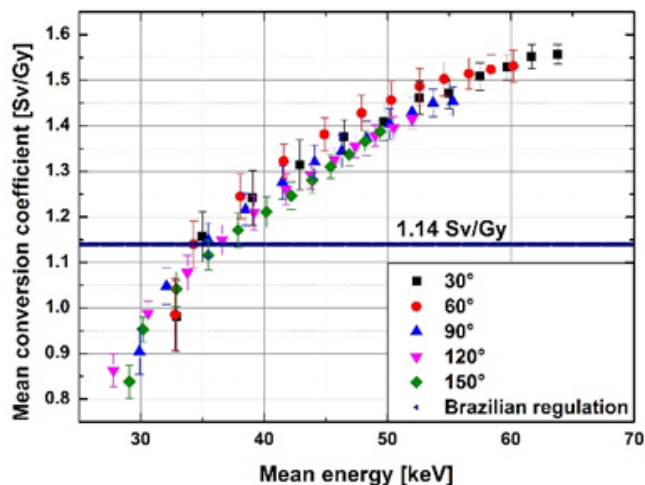


Figure 1 - Mean conversion coefficient as a function of the mean energy of the spectra for secondary beams scattered in angles of 30°, 60°, 90°, 120° and 150° degrees. The blue line corresponds to the constant value of 1.14 Sv/Gy

References:

- 1 WAGNER, S. R.; et al.. *Radiation Protection Dosimetry*, v. 12, n.2, p 231-235, 1985
- 2 TOMAL, A. et al.. *Appl. Rad. Isot.*, 2015 (in press)
- 3 KHARRATI, H.; ZARRAD, B. et al. *Medical Physics*, v. 31, n.2, p 277-284, 2004

SP177.3 - Shielding photon beams to account for adjacent, underground building of a radiation therapy facility

Author(s): Dario E. Sanz
 Radiation Therapy, Fundación Escuela de Medicina Nuclear, Mendoza/ARGENTINA

Introduction

Adjacent buildings may impose not obvious conditions to shield the floor of radiotherapy treatment rooms. Even when a full occupation is considered in lateral places, potential underground, adjacent sites can be of concern due to oblique transmission through the floor.

Method

We consider a barrier wall (primary or secondary), buried underground to a certain depth *H*, without a concrete slab floor (figure 1). With the same use and occupation factors of the points P1 and any P2, the line *p* will be sufficiently protected when the broad beam transmission factor corresponding to the path length between the source and P2 is less or equal to that of *T*, which in turn accounts for any possible position of the source. The variation of the distance from the source to the points on *p* is neglected, a fact that makes

the model analytically tractable and conservative.

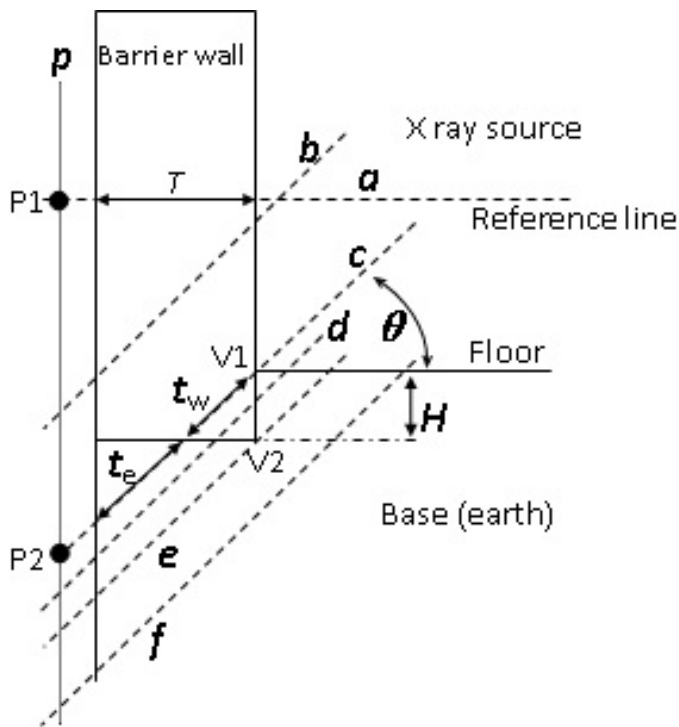


Figure 1: Shielding barrier of material w and thickness T . The lines a , b , c , d , e and f represent different ray trajectories. t_w and t_e represents the wall and earth thickness traversed by the line c .

Let define the scaling factor from the first tenth value layers: $f_w, e = TVL_w / TVL_e$.

If $f_w, e \geq 1/2$ (standard density wall) then the transmission factor corresponding to the line c passing through vertex $V1$ is greater than those of other parallel lines. The same holds for the line e if $f_w, e < 1/2$ (high density wall). Interestingly, a compact expression was obtained:

$$H_{max}/T = \sin^3 \theta_{max} / (1 - \cos^3 \theta_{max}) \text{ for } f_w, e \geq 1/2 \text{ and}$$

$$H_{max}/T = \sin^3 \theta_{max} / \cos^3 \theta_{max} \text{ for } f_w, e < 1/2,$$

where $\cos^3 \theta_{max} = f_w, e$ and H_{max} is the maximum wall depth necessary to shield the line p for any ray trajectory and the given beam energy.

Results

For earth and ordinary concrete (1.5 and 2.35 g/cm^3) we have $f_w, e = 0.638$, $\theta_{max} = 30.6^\circ$ and $H_{max}/T = 0.364$ for any beam energy and type of barrier. In case of high density walls, deeper wall penetration is needed.

Conclusions

The critical angles θ_{max} are compatible with typical source positions. The effect of distance has little effect on the accuracy, i.e. it is of the order of $\cos^2 \theta_{max}$.

Unless there is a basement under the floor, a full concrete slab is not necessary to shield nearby underground areas. Similar, compact expressions were obtained when bending the wall inwards a certain horizontal length to shield the floor in laminated, primary barriers.

In these cases, the approach can also be extended to account for groundshine radiation in a nearby floor.

SP177.4 - Vectorization of the time-dependent Boltzmann transport equation for photon beams: applications in radiation shielding

Author(s): Agustin C. Cobos¹, Ana L. Poma², Guillermo D. Alvarez³, Dario E. Sanz³

¹CONICET, Mendoza/ARGENTINA, ²FAMAF, Cordoba/ARGENTINA, ³Radiation Therapy, Fundación Escuela de Medicina Nuclear, Mendoza/ARGENTINA

Purpose

We introduce a method to evaluate the steady state solution of the angular photon flux after numerical evolution with the time-dependent Boltzmann transport equation (TE). The Penelope Monte Carlo (MC) method was used to test the convergence and accuracy for different time, energy, direction and spatial mesh sizes. Benchmarking was performed by calculation of radiation transmission in primary barriers of radiotherapy treatment rooms for different wall materials, beam energies and angles of incidence. Laminated barriers were simulated to assess the effect that different positions of a lead layer within a concrete slab has on the overall transmission factor and beam energy spectra.

Formalism

We applied our model on a semi-infinite slab, yet preserving the main phase space data details. The TE was converted into a system of ordinary differential equations by integration over a number of spatial mesh intervals, keeping only the temporal derivative. A weighted diamond difference scheme was used to ensure positive solutions. Flux vectorization in angle and energy was carried out using discrete ordinates and the multi-group approach, respectively. The system was expressed as $d\Phi(t)/cdt = \mathbf{A}\Phi(t) + \mathbf{b}$, where Φ is the vectorized flux, c is the speed of the particles, \mathbf{A} is a time independent, square matrix that contains physical and numerical parameters like cross sections and spatial mesh sizes. The vector \mathbf{b} accounts for the boundary conditions.

We found that under proper numerical conditions the matrix \mathbf{A} is strictly diagonally dominant by columns. As such, it is non singular and the steady state can be calculated from $\Phi(t \rightarrow \infty) = -\mathbf{A}^{-1}\mathbf{b}$. Also, all the elements of \mathbf{b} are non negative and the matrix $-\mathbf{A}$ is a non singular, M matrix. As such, all the elements of its inverse are non negative. Thus, the former product always yields positive values.

Jacobi and Gauss Seidel methods can be used by discretization of the time variable in intervals Δt . For a spatial mesh size Δz , the former properties of \mathbf{A} and numerical convergence are attained if $\Delta z^{-1} + \sum T < (c\Delta t)^{-1}$, where $\sum T$ is the maximum total, macroscopic cross section for the given mesh size and energy spectrum under consideration.

Results and conclusions

Numerical simulations agreed well with MC simulations and published data of transmission factors for different barriers and incident beam angles were accurately predicted. Interestingly, it was found that the position of a lead layer within a concrete slab significantly affects the overall transmission factor of the laminated barrier when irradiated with Co^{60} beams. We note that beam softening in the concrete part improves the lead absorption capability when placed in the distal part of the shield. This could be relevant when lead is used to increase the shielding of a Co^{60} high dose rate brachytherapy room.

Spatial integration and matricial theoretical treatment of the transport equation allowed for the numerical conditions for convergence,

positivity and speed of the approach, without the need of explicit construction of the matrix **A**.

Despite the algorithm was tested for a 1D geometry, the concept could be extended to 2D and 3D situations.

SP177.5 - The use of FLUKA Monte Code in the re-design of radiotherapy mazes with the use of lead cladding of a few mm thickness

Author(s): Ihsan A.M. Al-Affan¹, Richard P. Hugtenburg¹, Simon Evans²

¹College Of Medicine, Swansea University, Swansea/UNITED KINGDOM, ²Department Of Medical Physics And Clinical Engineering, Singleton Hospital, S/UNITED KINGDOM

Abstract

A novel proposal of covering part or the whole of the maze concrete walls with a few mm of lead will be presented. The findings have direct implications for new designs of mazes for radiotherapy rooms and can help with upgrades, especially when space is limited [1]. Covering part or all of the maze walls with lead was studied in situations where extending the maze length or changing its shape would be not possible because of space restriction.

FLUKA

Monte Carlo simulations were used to examine the reduction of the dose from scattered photons at the maze entrance of radiotherapy room facilities. A pilot study at Singleton Hospital in Swansea, UK, has pioneered the use of lead sheets of various thicknesses to absorb scattered low energy photons in the maze of radiotherapy room. The Figure shows the new shape of the maze incorporating this feature. The FLUKA computations have shown that there was a noticeable reduction in the dose when lead sheet of a 2 mm thickness was added to certain walls and floor in the maze (Table). One explanation for this finding is that the reduction was due to the strong effect of the photoelectric interaction of the lead, in effect trapping the back scattered photons. The results showed that adding 1 to 4 mm lead to walls and floor of the maze reduced the dose at the maze entrance by up to 90%. However, certain walls contributed more than others for the dose reduction. The floor was found to contribute about 8% in the dose reduction when it was covered with 2 mm lead. Other scenarios were simulated where the reduction was most cost effective. By comparing the dose reduction from the FLUKA calculations with measurements it is concluded that FLUKA Monte Carlo Code was found a very useful tool for maze design, supporting modifications that offer better access for patient and machine maintenance without sacrificing radiation protection.

[1] Al-Affan I A M, Hugtenburg R, P, Bari D S, Saleh W, M, Piliero M, Evans S, Al-Hasan M, Al-Zughul B, Al-Kharouf S and Ghaith, A, 2015, Dose reduction of scattered photons from concrete walls lined with lead: implications for improvement in design of megavoltage radiation therapy facility mazes. *Medical Physics*, **42** 606-714.

Table.

Calculations of dose at the maze entrance using FLUKA code for scattering photons from concrete walls with 2mm lead (4 maze walls and floor).

Photon Energy MeV	Fluka dose (Gy/ photon) concrete only	Fluka dose (Gy/ photon) 2mm lead + concrete	Ratio	Dose Reduction Factor %
0.5	6.83E-22±12%	4.61E-23±23%	0.07	93
1	1.11E-21±12%	8.00E-23±27%	0.07	93
3	1.27E-21±18%	1.2E-22±27%	0.1	90
7	1.37E-21±9%	4.98E-22±36%	0.36	64
10	1.53E-21±6%	1.47E-21±13%	0.96	4

SP178 - Neuroimaging, Neuronavigation and Neurological Disorders

TRACK 11: NEUROENGINEERING, NEURAL SYSTEMS

SP178.1 - Characterization of Single Units in Human Neocortical Slices Maintained In Vitro

Author(s): [Sara Mahallati](#)¹, Joshua A. Dian², Milos R. Popovic², Taufik Valiante³

¹Rehabilitation Engineering Lab, Toronto Rehabilitation Institute, University Health Network, Toronto/ON/CANADA, ²Institute Of Biomaterials And Biomedical Engineering, University of Toronto, Toronto/CANADA, ³Division Of Fundamental Neurobiology, Toronto Western Hospital Research Institute, Toronto/CANADA

A fundamental challenge in understanding mechanisms behind functional and pathologic states of the brain is to describe the functional and effective connectivity within the brain. This knowledge is a key step towards developing neuromodulatory strategies to control cortical circuits in the treatment or prevention of neurological disorders. In humans large scale functional networks obtained from electroencephalography, intracranial EEG, or functional magnetic resonance imaging cannot describe cortical processing at the microcircuit level, the result being that to date this aspect of human neocortex remains largely unexplored. A high throughput approach is required to elucidate connectivity principles between different neuron phenotypes in the human brain and link cellular activities to physiological signatures such as cortical rhythms and how these rhythms modulate cognition and behavior.

We have recently described that human cortical tissue, which is maintained in vitro, can be induced to generate coordinated population activity (oscillations) similar to those observed in vivo. Both narrow and broad band power increases were observed with narrowband activity being dominated by theta oscillations and which modulated high gamma (broadband) activity. Theta oscillations were coherent between cortical laminae with deep layer theta leading superficial layer activity. By further exploring the cellular basis of these findings, we have described laminar specific cellular specializations: deep layer putative pyramidal neurons have features that promote theta generation in deep layers (h-current, higher input resistance).

To extend these results, and investigate large scale cellular activities in the human cortex, we have performed *in vitro* multi-electrode array recording. Data were obtained from 500 μm thick temporal neocortical slices (tangential to pia) using a submerged 64-channel multi electrode array (MEA) system USB-MEA60 (Multi Channel 151 Systems, Germany) on a TiN array with inter electrode spacing of 200 μm . The data was acquired at 25 KHz and then split into local field potential (LFP; 1-300 Hz) and multiunit activity (MUA; 300-3000 Hz) using band pass filters. Individual spikes were detected in the MUA time series using a negative threshold defined to be 4 times the average background noise level. Slices were ultimately processed histologically to localize the electrodes and confirm the units' depth in the cortical laminae. Unit activity was characterized during a 10 minutes baseline period, during bath application of 50 nM kainate (10-15 min), and then addition of 50 μM of carbachol - condition during which we have observed theta oscillations.

This protocol induced theta oscillations and gamma activity observed as increases in spectral power in LFP signals. Preliminary analyses on MUA signals revealed that we can sort units into narrow-spiking and broad spiking units, and these units display distinct patterns in their inter-spike intervals, which appears to be layer specific. Overall our results suggest that there are laminar specific specializations at the cellular level that may underlie the coherent

theta oscillations observed between superficial and deep laminae.

SP178.2 - Astrocytes enhance neuronal long term potentiation in a biophysical model of epilepsy

Author(s): [Vasily Grigorovsky](#), Berj L. Bardakjian

Institute Of Biomaterials And Biomedical Engineering, University of Toronto, Toronto/ON/CANADA

While originally astrocytes have been thought to only act as support to neurons, recent studies have implicated them in multiple active roles. In particular they have been shown to be able to moderate and alter neuronal firing patterns both in normal and epileptic conditions. Astrocytes can perform this using several mechanisms, including potassium clearance from the extracellular space as well as through the formation of tripartite synapse with both pre- and post-synaptic terminals. It has been shown that astrocytes exhibit impaired potassium clearance in epileptic models, which leads to hyperexcitable conditions in the network. Additionally, astrocytes react to glutamate release into the synaptic cleft triggering a signalling pathway that culminates in the increase of intracellular calcium concentration in postsynaptic neurons. In addition to being involved in the hyperexcitability of epileptic networks, intracellular calcium increase is also key in long term potentiation (LTP) of neuronal connections which is mediated both through NMDA-receptor channels and via the formation of new AMPA channels. Coincidentally, ripple high frequency oscillations (HFO; ~ 100 Hz) which have been experimentally shown to invoke LTP under normal conditions, have also been suggested as one of the potential biomarkers for epilepsy in patients. Despite these findings and general interest in the deeper insight into the biophysiological mechanisms behind epileptic seizures, computational modelling efforts have been focused more on complex neural networks without the significant inclusion of astrocytes.

Methods

In this study we introduce a computational model of CA3 region of hippocampus, consisting of a network of an astrocyte and a pyramidal cell with a feedback inhibitory interneuron. We use it to investigate the effects of astrocytic ion homeostasis moderation and calcium dynamics on long term potentiation as one of the factors in the onset and cessation of seizure like events. In addition to phenomenological feature assessment, frequency analysis is used to determine frequency dynamics during long term potentiation and depression.

Results

Preliminary results of the model show that astrocytes respond to seizure-like conditions with (a) increased calcium release, (b) reduced rates of potassium clearance mechanisms, and (c) enhancement of long term potentiation of pyramidal cell-interneuron connection following 100 Hz stimulation of the pyramidal cell.

SP178.3 - Influence of the 'sympathetic slump' on biomechanics of the sympathetic trunk

Author(s): [Liesbeth Van Hauwermeiren](#), Laura Bekaert, Tom Van Hoof

Basic Medical Sciences, Ghent University, Ghent/BELGIUM

Introduction

Several sources show a correlation between altered peripheral nerve biomechanics and disturbed nerve function. Some clinical studies suggest that mechanical strain on the sympathetic trunk (ST), a small autonomous nerve bundle in front of the spine, could play a role in chronic disorders like sympathetically maintained pain. A clinical test, the 'sympathetic slump', consisting of full spinal

flexion combined with contralateral lateral flexion and rotation in a long sitting position, was proposed to maximally lengthen the ST and thus evoke symptoms. However, biomechanical data is lacking. Investigation of the ST is challenging both through dissection and medical imaging due to its position, size and numerous side branches.

Therefore, the aim of this study is to develop a technique to visualize and quantify ST motion in the sympathetic slump position.

Methods

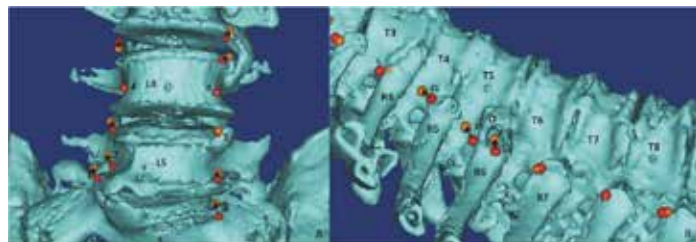
The ST's of a cadaver specimen were dissected from an anterolateral angle, until there was sufficient visualization for bilateral insertion of 30 metal markers without detaching the ST from its environment. CT scans were performed in supine position, neutral long sitting position, and sympathetic slump position to the left and right. A second supine CT scan was used to assess possible marker migration. Markers and vertebrae were segmented and 3D-rendered. Displacement of markers from the neutral to each experimental position were calculated and adjusted for vertebral movement using custom Matlab code. Furthermore, inter marker distances between adjacent markers (along a mathematical spline curve drawn between the markers to approximate the course of the ST) were calculated for each position to measure ST changes in length. Only marker movements larger than the combined errors of segmentation, registration and marker migration were taken into account (4.22mm for long sitting position, 4.51mm for slump positions and 2.18mm for inter marker distances).

Results

Overall, marker movement and inter marker movement were consistent. Only the lower lumbar markers showed significant cranial movement in both sympathetic slump positions (fig1.A), and significant movement was noted around two osteophytes during contralateral sympathetic slump (fig1.B). The traditional slump showed no significant movement of the ST.

Conclusion

Despite the limitations in motion quantification (strain could not be calculated since only markers and not the entire nerve structure was visualized), the results of this study suggest that the sympathetic slump inflicts most ST movement in the lower lumbar region and around structural pathological changes like osteophytes. Larger datasets could confirm these findings and further increase insight into ST biomechanics.



SP178.4 - Superparamagnetic Nanoparticles for Epilepsy Detection

Author(s): Maysam Pedram¹, Amir Shamloo², Aria Alasti², Ebrahim Ghafar-Zadeh¹

¹Dept. Of Electrical Engineering And Computer Science, York University, Toronto/ON/CANADA, ²Sharif University of Technology, Tehran/IRAN

Epilepsy is the most common neurological disorder that is known with uncontrolled seizure. Around 30% of patients with epilepsy

resist to all forms of medical treatments and therefore, the removal of epileptic tissue is the only solution to get these patients free from chronic seizures. The precise detection of an epileptic zone is the key to its treatment. In this paper, we propose a method of epilepsy detection using brain magnetic field. The application of superparamagnetic nanoparticles (SPMNs) as nanoprobe for the detection of the epileptic area inside the brain is investigated in this new research approach. The aggregation of nanoparticles in the weak magnetic field of epileptic brain is modeled using potential energy minimization technique. The results prove the aggregation of nanoparticles influenced by weak magnetic field in the range of pT.

SP178.5 - Automatic detection of epileptic seizures in scalp EEG

Author(s): Yasser Pérez

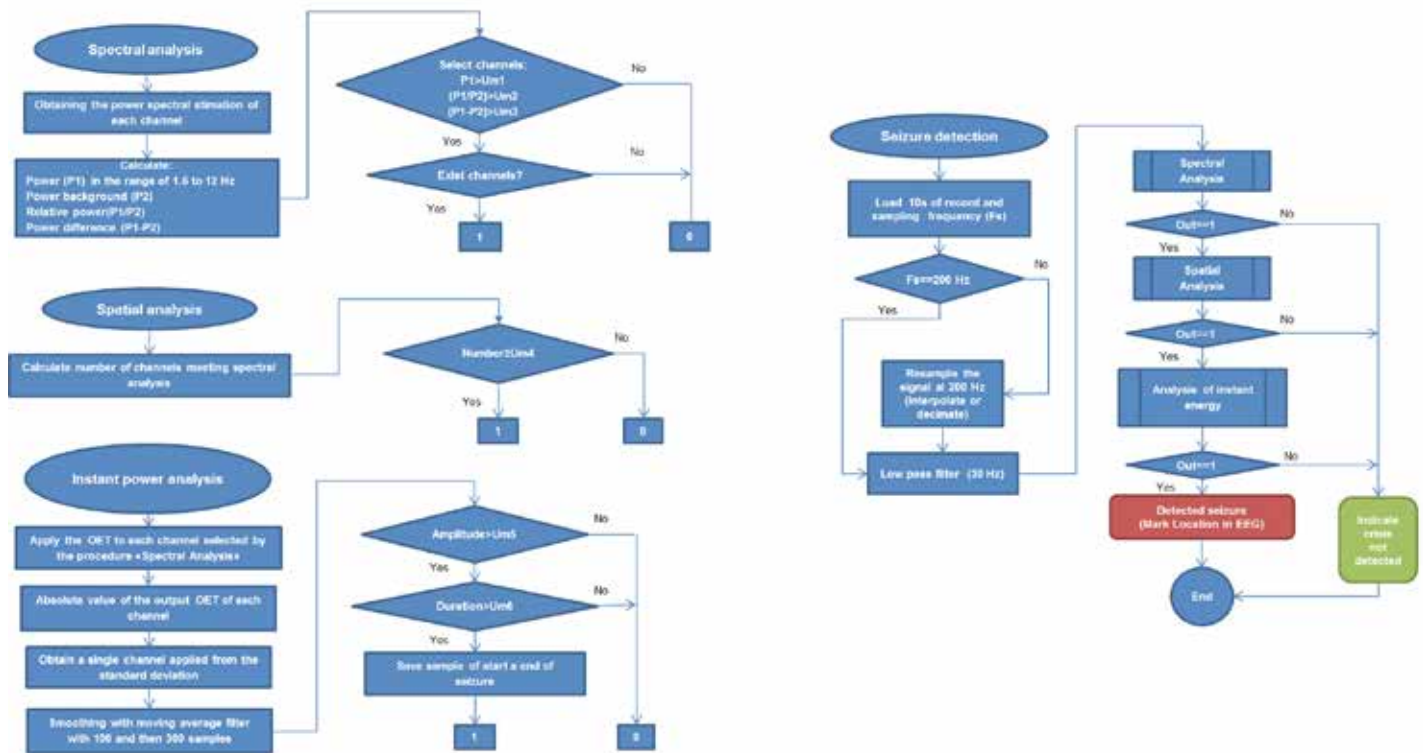
Bioengineering, Polytechnic José Antonio Echeverría, Havana/ CUBA

The study and clinical diagnosis of epilepsy is performed by a specialist with years of experience through simple visual inspection of the EEG record with the aim of identifying areas where seizures that characterize this condition occur. However, given the variability of the morphology of epileptic seizures and their similarity to other events as various artifacts, alpha spindles and paroxysmal activity detection work is hindered greatly. In addition, long-term records, due to the volume of information, the time used specialist study is considerable. For this reason the automatic detection of epileptic seizures has become a vital tool for the specialist.

This research proposed design and development of an algorithm for automatic detection of epileptic seizures by using simple statistics measurements, the Teager Energy Operator and power spectral analysis techniques for features extraction from a data set of reference seizure events. The database used for this project belongs to Cuba Neuroscience Center (CNEURO) it contains non-invasive EEG recordings of 20 patients of both sexes, aged between 4 and 37 years, of which 15 had may generalized seizures and 5 partial seizures, further data were recorded in the various states of wakefulness and sleep. EEG signals were acquired using the equipment MEDICID 5 at a sampling frequency of 200 Hz and an A / D converter of 16 bits. For the record signal an array of 19 electrodes with international Positioning System 10-20 and referential mount was used. The implementation of the algorithm was performed in the MATLAB tool, and then scored as a result of quantitative evaluation of the sensitivity of 94.5% and a selectivity of 87.6%.

The results of the quantitative evaluation of the algorithm show that could be used as a tool to support the specialized medical staff.

Seizure Detection Algorithm



SP178.6 - Beta/Theta Neurofeedback Training Effects in Physical Balance of Healthy People

Author(s): Wenya Nan¹, Xiaoting Qu¹, Limin Yang¹, Feng Wan¹, Yong Hu², Pedro Mou¹, Pui-In Mak¹, Peng Un Mak¹, Mang I Vai¹, Agostinho Rosa³

¹University of Macau, Macau/CHINA, ²University of Hong Kong, Hong Kong/CHINA, ³University of Lisbon, Lisbon/PORTUGAL

This study aimed to investigate beta/theta ratio (BTR) neurofeedback training (NFT) effects in physical balance of healthy individuals. Thirty-one healthy volunteers were randomly assigned to NFT group (n=15) and non-NFT control group (n=16). The NFT group completed 25 sessions in consecutive five days with five sessions per day. Before and after NFT, physical balance was measured by Wii Balance Board (WBB). The non-NFT control group only performed the physical balance test on the first day and the fifth day without any training. The results showed no significant improvement in physical balance in the NFT group compared to the non-NFT control group. The reason of the failure will be further studied in our future work.

SP178.7 - Potential Benefits in Comparing the Neural Control Networks Studies Between the Oculomotor and Cardiac Pacing Systems

Author(s): Alireza Ghahari¹, Michael Cheng²
¹University of Connecticut, Mansfield/CT/UNITED STATES OF AMERICA, ²Biomedical Engineer, ottawa/ON/CANADA

Clinical evidence has reported cases of acquired ocular motor apraxia after aortic surgery [1]. This paper draws attentions to potential insights gained by comparing neural control network studies between the oculomotor and cardiac pacing systems.

Both authors independently did original research on the oculomotor system, but no experience in the cardiac pacing system. In view

of the rapidly increasing health problems of cardiac arrhythmia particularly among aging populations, we report our findings in the oculomotor system and suggest implications for the cardiac pacing system. It is not unusual for the biological systems to share common mechanisms for their operations.

In 1974, Cheng, Outerbridge performed inter-saccadic interval analysis of nystagmus eye movements of vestibular and optokinetic [2] origins. Optokinetic nystagmus from healthy human subjects were recorded at different intensity levels elicited by different speeds of the optokinetic stimulus. The time intervals between the onset of consecutive saccadic components, which appear random, were analyzed statistically. Resulting interval histograms showed multimodal form in which the higher order modes were approximately integral multiples of the basic mode. Now, the inter heart beat intervals (RR intervals) during cardiac arrhythmia appears also to be random, and if the histograms of the RR intervals also exhibit multi-modal behavior, it would imply that during heart-beat pauses in some “sick sinus syndrome”, there is high probability that ensuing pauses between hear beats could suddenly take on twice or three times as long, thus greatly raising the risks of syncopal episodes.

Recently, Ghahari, Enderle used advanced computational modeling to demonstrate an integrative systems approach to address the challenges involved in the implementation of the saccade dynamics from the local neural circuit computations in the midbrain [3]. A biophysically-realistic neural network model was developed to examine the saccade dynamics. To explore the synaptic network function and characteristics in post-saccade oscillations, computational neural modeling of the glissades was investigated as a deficiency in the oculomotor control mechanism. In conclusion, comparison of the glissades with normal saccades confirmed that glissades were observed because of anomalies in saccade neuronal programming. They theorized that such deficits are due to unplanned post-inhibitory rebound burst firing in the antagonist motoneurons, as a coordi-

nation error in returning to tonic firing rates.

The brainstem has neural sites in the medulla oblongata responsible for controlling heart rates. Potential research are: First, explore more evidence to answer a vital question: "could glissades in eye movement be compared with the sick sinus syndrome of cardiac arrhythmia?" Second, search details on neuroconnectivity structure and underlying neural control processes important for driving the cardiac sinus pacemaker. The answers are hoped to have far-reaching proportions in benefiting patients dealing with arrhythmia disturbances.

References

R.D. Yee and V.A. Purvin, "Acquired Ocular Motor Apraxia After Aortic Surgery", *Trans Am Ophthalmol Soc* / vol105, pp152-159, 2007,

Cheng M, Outerbridge JS "inter-saccadic interval analysis of optokinetic nystagmus" *Vision Research*, 14:1053-1058, 1974

A. Ghahari and J. Enderle, *Models of Horizontal Eye Movements: Part3, A neuron and muscle based linear saccade model*, Morgan & Claypool Publishers, San Rafael, CA, 2014, 158pp

SP179 - Brain, Head/Neck, Spine: Part 2

TRACK 12: MEDICAL DEVICES

SP179.1 - Acceptance Test of the first Hospital Cyclotron for Production of PET tracers in Iran

Author(s): Pardis Ghafarian¹, Seyedeh Masoumeh Khamesi¹, Mohammadrasa Golrokh Nodehi¹, Mohammad Reza Ay²

¹Chronic Respiratory Diseases Research Center, National Research Institute Of Tuberculosis And Lung Diseases (nritld), Shahid Beheshti University of Medical Sciences, tehran/IRAN, ²Research Center For Molecular And Cellular Imaging, Tehran University of Medical Sciences, Tehran/IRAN

Introduction: The first fixed-energy hospital isochronous cyclotron (GE PETtrace 700) installed in Masih Daneshvari hospital can accelerate the negative hydrogen ions (H^-) up to 9.6 MeV energy. This cyclotron equipped with six targets for production of the most common radioisotopes used for PET/CT scanners. It is well known that the acceptance tests should be done by physicist when a cyclotron installed in order to measure the performance claimed by manufacturer. This study reports the results of acceptance tests in our GE PETtrace 700 after installation for all targets.

Material and methods. Production of ^{18}F is done using the fluorine-18 silver body target with 1.7 ml volume by bombardment of enriched ^{18}O -water in 120 minutes irradiation time and using 50 μA target current and high-pressurized helium. Whereas by bombardment of ^{16}O -water with 35 μA target current, the $^{13}N-NH_3$ is produced after 25 minutes. The $^{13}N-NH_3$ target consists of a silver container with 0.8 ml volume which over pressure methane is used to the target for direct production of $^{13}N-NH_3$. Production of $^{11}C-^{11}CO_2$ is performed by the gaseous target with aluminum target body and volume of 23 ml. The $^{11}C-^{11}CO_2$ is produced by the bombardment of Nitrogen-14 using 30 μA target current in 30 minutes. After bombardment the activities were transferred to the dispenser unit and measured by dose calibrator separately (ATOMLAB 500).

Results: The yield performance of 2858.32, 138.15 and 1047.5 mCi has been observed for ^{18}F , $^{13}N-^{13}NH_3$ and $^{11}C-^{11}CO_2$ after 120, 25 and 30 minutes irradiation time with target current 50, 35 and 30 μA respectively. It is clear that product yield that measured in factory were 2500, 75 and 900 mCi, respectively using the mentioned standard situation.

Conclusion: during our acceptance test, the measured yield for all tracers was higher than the value reported by manufacturer

SP179.2 - HiFEM - An Integrated Approach for Human Centered Risk Management for Medical Devices

Author(s): Armin Janss¹, Klaus Radermacher²

¹Chair Of Medical Engineering, RWTH Aachen University, Aachen/GERMANY, ²Chair Of Medical Engineering, RWTH Aachen, Aachen/GERMANY

The implementation of appropriate processes for risk management and usability engineering are mandatory for the approval and application of medical devices (s. ISO 14971:2006 & IEC 62366:2007). As the complexity and speed of development of medical devices is increasing together with the incidents of human error in medicine [1-3], more sophisticated tools for interlinking usability engineering and risk management, i.e. human error risk analysis and human risk control respectively seem to be mandatory. The HiFEM methodology and the corresponding software tool mAIXuse developed in our lab, supports medical device manufacturers and developers by a

model based human risk analysis approach. Based on a two-folded approach, HiFEM provides a task-type-sensitive modelling structure with integrated temporal relations based on [4] combined with a subsequent analysis of critical resources allocation and related potential errors adopted from and related error taxonomies. The approach can be used in an early developmental stage as well as for product validation. In a comparative study the HiFEM method outperformed a classical process-FMEA related the detection of critical errors of a surgical planning and navigation systems. These positive results have been confirmed in further applications. Moreover, we implemented a new method for systematic human risk control (mAIxcontrol) as part of the HiFEM methodology. Accessing information from the method's knowledge base enables the operator to detect the most suitable countermeasures for a respective risk. 41 approved generic countermeasure principles have been indexed as a resulting combination of root causes and failures in a matrix. The methodology has been tested in comparison to a conventional approach as well. Evaluation of the matrix and the reassessment of the risk priority numbers by a blind expert demonstrate a substantial benefit of the new mAIxcontrol method vs. classical methods. Concerning the number of appropriate counter measures for risk control, the mAIxcontrol method shows predominance compared to classical brainstorming approach, although the required time for application of the method is slightly higher than for brainstorming. Evaluation showed, that the use of the method requires a certain learning curve. The test subjects needed a learning time of more or less 15 minutes before a working routine had been adopted. This presumes a learning effect that increases time efficiency for experienced users.

References

[1] Rau, G., Radermacher, K., Thull, B., & v. Pichler, C. (1996). Aspects of Ergonomic System Design Applied to Medical Worksystems. In Taylor, R.H. (Eds.), Computer-integrated surgery: technology and clinical applications. MIT Press, 203-221.

[2] Radermacher, K., Zimolong, A., Stockheim, M., & Rau G. (2004). Analysing reliability of surgical planning and navigation systems. In Lemke, H.U., & Vannier, M.W. (Eds.), International Congress Series 1268, 824-829.

[3] Schmitt, R. H., Rauchenberger, J., Radermacher, K., Lauer, W., & Janß, A. (2009). Neue Wege für das Risikomanagement bei der Entwicklung risikosensitiver Produkte am Beispiel der Medizintechnik. In FQS (Eds.) FQS-DGQ Band 88-04, Beuth Verlag.

[4] Paternò, F., Mancini, C., & Meniconi, S. (1997). ConcurTaskTrees: A Diagrammatic Notation for Specifying Task Models. Proc. of IFIP Int. Conf. on Human-Computer Interaction Interact '97 Sydney, Chapman & Hall, London, 362-369.

SP179.3 - Ultrasonic Microscanning for Digital Dental Impressioning

Author(s): Thorsten Vollborn¹, Daniel Habor¹, Fabrice Chuembou Pekam¹, Juliana Marotti², Joachim Tinschert², Stefan Wolfart², Stefan Heger¹, Klaus Radermacher¹

¹Chair Of Medical Engineering, RWTH Aachen, Aachen/GERMANY, ²Department Of Prosthodontics And Biomaterials, University Hospital Aachen, Aachen/GERMANY

Introduction

Silicone based impression-taking of prepared teeth is well-established but potentially less reliable, error-prone and inefficient for computer aided design and manufacturing (CAD/CAM) of dental prosthetics. Intraoral optical scanners have been introduced to increase efficiency of CAM but no breakthrough occurred so far. An accurate impression of the tooth preparation is highly important for

the final fit of the prosthesis. Therefore, retraction cords or electro-surgery are commonly used to invasively uncover subgingival margins prior to the impression. These methods may lead to inflammation or permanent damage of the gum. In addition, bleeding from inflamed gingiva, saliva, air bubbles or other particles can decrease the accuracy outcome of both the conventional and optical impression. Digitizing a gingiva-covered margin is an infeasible task due to the fact that optical waves can hardly penetrate gingival tissue.

Concept

High frequency ultrasound (HFUS) has been recently introduced as an alternative to optical scanning [1]. HFUS is less sensitive against oral fluids and in principal able to penetrate gingiva non-invasively. Although HFUS-systems have been introduced in other medical fields, none of them suits the challenging requirements and high accuracy demands for dental impressioning. Hence, our goals are to develop a new ultrasonic technology, which is able to scan supra- and subgingival dental hard- as well as soft-tissue structures and to integrate it into the CAD/CAM-process for dental restorations. Whereas in case of optical digitization the dentist usually has to wait until bleeding and swelling subside, an HFUS-based impression can be performed within the same session.

Results

We conceived a miniaturized device based on HFUS-technology and a coupling adapter for impedance matching during intraoral application [1]. Therefore, we have integrated a HFUS transducer (>50 MHz) into an intraoral scanner in order to achieve the necessary spatial resolution for impressioning. A multi-axis kinematic has been developed and successfully tested for accurate positioning of the HFUS-probe. In-vitro surveys using comparable transducers have already proved the applicability of the concept [2]. In a recent study Marotti et al. show a potentially good fitting accuracy of metallic copings for single tooth crowns planned with HFUS-Scans [3].

Discussion and Conclusion

Ultrasound-based impressions have been able to compete with optical systems concerning the accuracy and the final fit. Subsequent to the completion of the technical development the evaluation of the presented system in clinical surveys remains.

References

[1] Vollborn T, Habor D, Chuembou Pekam F, Heger S, Marotti J, Reich S, Wolfart S, Tinschert J, Radermacher K. Soft Tissue-preserving Computer-aided Impression: A Novel Concept using Ultrasonic 3D-Scanning. Int J Comput Dent, 2014; 17:277-296

[2] Chuembou Pekam F, Marotti J, Wolfart S, Tinschert J, Radermacher K, Heger S. High-Frequency Ultrasound as an Option for Scanning of Prepared Teeth: An in Vitro Study. Ultrasound in Medicine & Biology, 2015; 41:309-316

[3] Marotti J, Heger S, Tinschert J, Kirsten A, Wolfart S. Ultrasound as a New Technology for Dental-Scanning. J Dent Res, 2013; 92:541

SP179.4 - A study on prefrontal blood flow in patients with moderate dementia and severe dementia using near -infra-redinfrared

Author(s): Shingo Takahashi¹, Naoki Kodama²

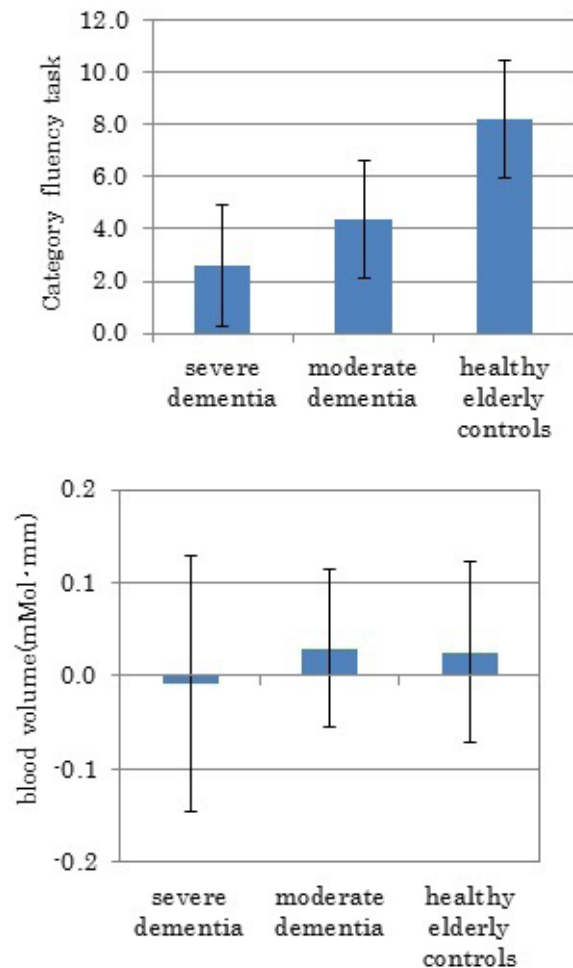
¹Department Of Healthcare Informatics, Takasaki University of health and welfare, takasaki/JAPAN, ²Department Of Healthcare Informatics, Takasaki University of Health and Welfare, Takasaki/JAPAN

Recently, near-infrared spectroscopy (NIRS) is one of the most im-

portant measurement tools of brain function. In this study we have used a NIRS to examine the prefrontal blood volume of the brain by performing a category fluency task function test to determine with severe dementia and moderate dementia, health elderly controls if this method can be used to determination for severity of dementia. Recently, NIRS is one of the most important measurement tools of brain function. In this study we have used a NIRS to examine the prefrontal blood volume of the brain by performing a category fluency task function test to determine with severe dementia and moderate dementia, health elderly controls if this method can be used to determination for severity of dementia.

We examined 30 patients with severe dementia (age 83.7 ± 6.6 , 7 male, 23 female, MMSE:1-14) and 20 moderate dementia (age 82.7 ± 7.1 , 5 male, 15 female, MMSE:15-23), 16 health elderly controls (age 80.5 ± 4.6 , 2 males, 14 females, MMSE:24-30). Activation with the subtasks starts at 0, 15 and 45 second in the category fluency task, 45 and 75 second subtasks again.

The average number of category fluency task is shown in Fig.1. Severe dementia patients achieved an average score of 2.7 ± 2.3 in the category fluency task. On the other hand, moderate dementia achieved score of 4.4 ± 2.3 , health elderly controls score were 8.2 ± 2.2 . Figure.2 shows increase volume of prefrontal blood in Fp1. Our results have shown that health elderly controls show an increase in the blood volume during the category fluency task while those with severe dementia patients did not show any relevant increase of blood volume while performing the same task.



The results obtained suggest that category fluency tasks and near-infrared spectroscopy may be useful to determination for severity of dementia.

SP180 - Information Technologies in Healthcare Delivery and Management: Part 4

TRACK 14: INFORMATION TECHNOLOGIES IN HEALTHCARE DELIVERY AND MANAGEMENT

SP180.1 - Increasing efficiency of data transfer in WBANs

Author(s): Luka Celic, Ratko Magjarevic

Department Of Electronic Systems And Information Processing, University of Zagreb Faculty of Electrical Engineering and Computing, Zagreb/CROATIA

Due to aging of the society and subsequent increase of incidence of chronic diseases, use of wireless technologies in patients monitoring had large growth in latest years. After initial relatively simple point to point telemetry applications, today there is a large number of wireless devices for patients' physiological data monitoring, mobility tracking and exercising evaluation etc. These new applications are due to development of low power and inexpensive wireless communication technologies and they are mainly realized as a wireless body area network (WBAN). In health care today there is a need for more complex patient monitoring with trend predictions which cause increasing quantities of data for their transfer from the patient, but also increase current consumption drawn from the battery. It is crucial to obtain high efficiency of all segments in WBAN communication, so the device can maintain reduced battery size and keep continuance. For user acceptance, it is crucial to make the wireless sensor nodes of the WBAN sensor node inconspicuous, enabling that they do not interfere with measurements. In this paper we present a solution for direct database access from microcontrollers in WBANs, which is power and code efficient. It provides standard powerful way of using microcontroller based WBANs with classic SQL database. This reduce development time and lower power consumption.

SP180.2 - Decision support system for no common emergency in a big city with intelligent routing algorithm and attention quality parameters evaluation.

Author(s): Lupe N. Toscano¹, M.J.F De Oliveira²

¹Ingeniería Electrica Y Electrónica, Universidad Nacional de Ingeniería, Lima/PERU, ²Universidade Federal do Rio de Janeiro, Rio de Janeiro/BRAZIL

The latest news on no common emergencies or disasters occurred in the world show us the necessity to develop tools in order to support a rapid and efficient response. The arrival time and the first attention to the patient in the emergency place is the golden time of the response. The objective of this paper is to support decisions in a disaster for a big city focus on decrease arrival time and improve attention quality in the place of the emergency. It is important to notice that the model is for a no common emergency like earthquake, flood, tsunami or terrorism and specific when we don't know what is happening on the route of the emergency and the scope of the tragedy so for the first reaction. The first instants of the response have been modelated to have two important details, the routing of the emergency vehicle and the primary attention in the place of the emergency. A specific routing algorithm for states of not common emergency was developed. The algorithm has been implemented in language C, having being defined two interactive knowledge bases for the information network and an intelligent search with a specific heuristic for no common emergency. Besides, a discreet event simulation model is used to support decisions of the rescue teams

on the place of the emergency. This model is a good tool to be implemented inside the rescue vehicles in order to support rescues, it could be used without capacitation time if the rescues manage interactive computers tools. Finally we can conclude that rescues could use this tool for the first reaction to the emergency and this gold time could be supported.

[1] L. N. P. Toscano and M. J. F. de Oliveira, "An Intelligent Routing Algorithm for Emergency Cases". In "World Congress on Medical Physics and Biomedical Engineering". 2012. Beijing – China.

[2] De OLIVEIRA, M. J. F. ; TEIXEIRA, A. P. ; MORAES, R. S. . A collaborative platform for Hospital Admission. In: ORAHS 2013, 2013, Istanbul. Proceedings of the ORAHS 2013 conference. Istanbul: Koç University, 2013.

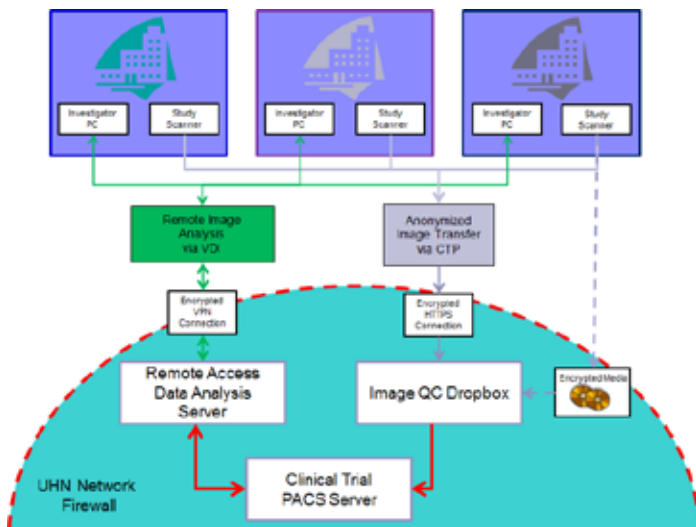
SP180.3 - Development of a Multi-Center Clinical Trial Data Archiving and Analysis Platform

Author(s): Brandon Driscoll¹, Ivan Yeung², Catherine Coolens², Gavin Disney², Igor Svistoun², David Jaffray²

¹Techna Institute, University Health Network, Toronto/ON/CAN-ADA, ²Radiation Medicine Program, Princess Margaret Cancer Center, Toronto/ON/CANADA

Quality results from multi-center clinical trials require consistent and robust trial protocols capable of quantifying or eliminating differences across participating institutions. The vision of the Quantitative Imaging for Personalized Cancer Medicine (QIPCM) program is to provide end to end testing and analysis support for clinical trials to achieve improved consistency and reliability in clinical trial data.

Methods: The QIPCM clinical trial data archiving and analysis platform consists of a customizable image anonymizer and secure transport pipeline (RSNAs Clinical Trial Processor, CTP), a dedicated remote analysis platform, and a dedicated server for the archival and storage of medical images.



The anonymized images received from the remote sites are held in a secure drop box where there are subjected to a quality assurance check. This check ensures both that no patient health information remains and that the image set is complete before it is then subsequently forwarded to the clinical trial PACS at which point trial based permission controls are enforced. The images can then be analyzed either by QIPCMs dedicated team of imaging experts or remotely by the trial investigators.

In addition to the platform infrastructure, a set of customized image analysis tools has been developed which are available for use on the

remote analysis workstations. These tools range from quantitative functional imaging tools for 4D kinetic modeling of dynamic contrast enhanced-CT and MR and hypoxic fraction analysis in PET; to simple 1D RECIST. Alternatively remote users can choose to utilize their own custom applications on the virtual environment while still making use of the central data storage and powerful remote analysis servers.

Results: The QIPCM team has established infrastructure and support services to sustain an ever growing number of multi-center clinical trials. The platform currently serves 15 internal and 6 multi-center clinical trials spanning 9 hospitals and imaging centers in Canada and the United States, with more trials to be added over the upcoming months. The image store currently holds in excess 1.8 million individual tomographic slices comprising more than 510 individual imaging studies from over 145 patients. The QIPCM team has also provided PET QA services for 3 different multi-center trials at 10 different sites across North America.

Conclusions: The current QIPCM platform is a fully functional commercial system with robust backup, storage and processing capacity. Within the next two months a further 50 TB of storage and 2 more high powered computational servers will further enhance performance.

SP180.4 - Global Health Catalyst: A systematic Space-time compression platform for catalyzing global health collaborations in Radiation Oncology

Author(s): Michele Moreau¹, Wilfred Ngwa²

¹University of Massachusetts, Lowell/UNITED STATES OF AMERICA, ²Radiation Oncology, Dana Farber/Harvard Cancer Center, Boston/UNITED STATES OF AMERICA

The benefits of global health collaborations in cancer Care, Research and Education (CaRE), are already well established, and there is growing consensus that our ability to address the growing global burden of cancer will increasingly depend on concerted international collaborations. Such collaborations could benefit from a major recent upsurge of interest in radiation oncology global health highlighted in recent Red Journal articles. However, appurtenant to this upsurge, a common issue evident at global health summits, seminars, or symposia is that SPACE-TIME is a major barrier to many who really want to participate/collaborate in global health CaRE. Given the increasing disproportionate global burden of disease in Low and Middle Income countries (reported in the recent World Health Organization report), there is growing urgency for strategies that can reduce this space-time barrier, make it easier for people to collaborate. Systematic Space-time compression represents one such strategy. Here space-time compression refers to the use of advanced Information and Communication Technologies (ICTs) that condense or elide spatial and temporal distances. In this work a catalogue of ICTs for space-time compression to enhance global health collaborations in Radiation Oncology (RadOnc) including Medical Physics is presented. A new platform, Global Health Catalyst, being developed at Harvard Medical School to integrate these ICTs for concerted high impact global health CaRE collaborations is presented. Preliminary projections show that this systematic approach could convert the huge upsurge in global health interest into coordinated high impact global health collaborations in RadOnc CaRE, and enhance the effectiveness of other global health initiatives. Figure 1 highlights some of these ICTs for Radiation Oncology Global health integrated in the Global Health Catalyst platform.

POSTER ABSTRACTS

PS01 - TRACK 01: IMAGING

PS01.001 - A discontinuity artefact at the isocenter of on-board CBCT images

Author(s): Elsayed S.M. Ali¹, Paul C. Johns², Balazs J. Nyiri¹

¹Medical Physics Department, The Ottawa Hospital Cancer Centre, Ottawa/CANADA, ²Physics Department, Carleton University, Ottawa/CANADA

In our recent investigation [Ali *et al* PMB **60** 1461 (2015)], rotational artefacts in the Elekta XVI cone beam computed tomography system were identified and corrected for. However, a residual discontinuity artefact remained at the isocenter. It was dependent on the scan direction but only slightly on its speed. In the present study, we have identified the cause of this discontinuity artefact. A 1-cm air gap is introduced between the two halves of a 30-cm diameter Solid Water phantom to accentuate the artefact, which is manifested as fading stripes in the scan direction (figure 1a,b). The artefact remains when the phantom is rotated to place the gap at an arbitrary angle relative to the horizontal. As the gap thickness is increased, a semi-circular dark streak appears around the isocenter. In the sinograms (figure 1c,d), the artefact does not follow a sinusoidal path; instead, it is a fading remnant of the gap at a fixed detector location. This indicates that the artefact is caused by detector lag due to the incomplete readout of the flat-panel imager, which leads to ghost signals after high intensity irradiation. The lag blurs the edges by a few pixels, which leads to the discontinuity at the isocenter (figure 2). Analysis of the sinogram profiles (figure 1c,d) shows that the lag decay can be described by a double exponential, which agrees with the literature. The variation of the lag with the mA yields different decay time constants. Previous studies have characterized and/or corrected for the radial increase and the azimuthal decrease of the lag, but have not identified the presence of a discontinuity at the isocenter as a manifestation of detector lag.

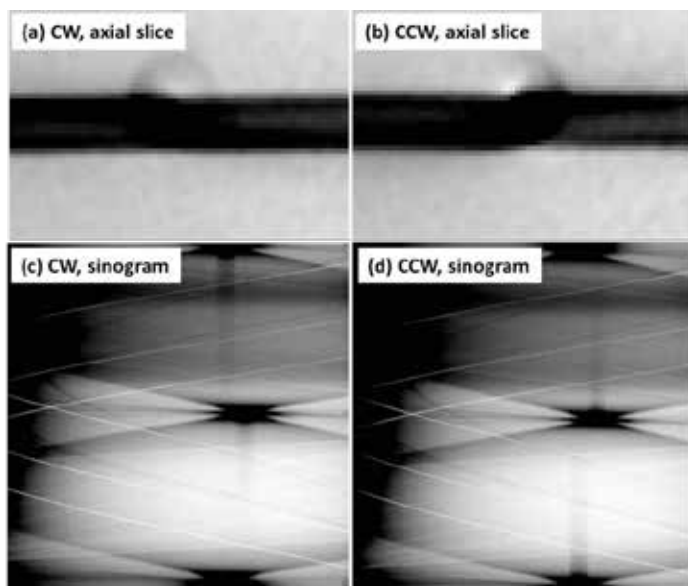


Figure 1: (a,b) Discontinuity artefact at the isocenter for clockwise (CW) and counterclockwise (CCW) scans. (c,d) Lag effect, demonstrated as a fading remnant of the gap at a fixed detector location. Time is flowing downwards in the CW sinogram and upwards in the CCW sinogram.

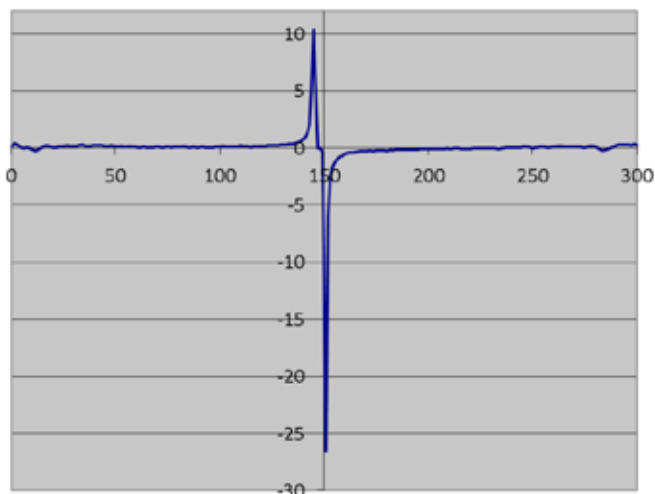


Figure 2: A vertical profile from the difference of the sinograms, CW minus CCW. The abscissa is the index of the projections. The ordinate is the pixel value in thousands. The discontinuity is around the projections that pass through the air gap.

PS01.002 - Correction of Metal Artefacts Induced from Pacemaker and ICD Leads in CT-Based Attenuation Correction of Cardiac SPECT data

Author(s): Mohammad Reza Ay¹, Zahra Etemadi², Ahmad Bitarafan-Rajabi³, Hadi Malek³, Navid Zeraatkar², Pardis Ghafarian⁴

¹Department Of Medical Physics & Biomedical Engineering, Tehran University of Medical Sciences, Tehran/IRAN, ²Research Center For Molecular And Cellular Imaging, Tehran University of Medical Sciences, Tehran/IRAN, ³Cardiovascular Interventional Research Center, Department of Nuclear Medicine, Rajaei Cardiovascular, Medical, and Research Center, Iran University of Medical Sciences, Tehran, Iran., ⁴Pet/ct And Cyclotron Center, Masih Daneshvari Hospital, Shahid Beheshti University of Medical Sciences, tehran/IRAN

Objective: In CT-based attenuation correction (CTAC) of myocardial perfusion SPECT data, the metallic artefacts due to pacemaker and ICD leads attached to the myocardial wall can induce overestimation or underestimation of activity in some segments of the myocardium. In the present study, the impact of the application of metal artefact reduction (MAR) algorithm for generation of artifact free attenuation map (μ -maps) during CTAC process of SPECT data was assessed and quantified.

Methods: A cardiac phantom with the capability of inserting pacemaker and ICD leads was used. The CTAC was performed using the μ -maps without and with MAR. The volume-of-interest (VOI)-based quantitative comparison was performed between the actual activity and the activity concentration in the SPECT images, and also attenuation-corrected (AC) SPECT images without and with MAR. In addition to the phantom study, the SPECT data of 5 patients with ICD and 4 patients with pacemaker were used for clinical validation and quantification.

Results: The findings show that after applying the MAR, relative error can reduce about 4% and 6% on overestimated segments and about 2% and 2% on underestimated segments in the images of the phantom with pacemaker and ICD, respectively. In clinical evaluation, the Bland-Altman plots show no significant difference between two reconstructed SPECT images on overestimated segments for the patients with pacemaker and ICD.

Conclusion: Although the study shows improvement in SPECT image quantification and generated μ -maps after correction of metallic artifacts, it has no effect on the clinical interpretation of cardiac images corrected for attenuation with and without artifactual μ -maps.

It should be noted that due to low spatial resolution of SPECT images and considering the CT-based attenuation correction process which smoothes the CT images, the impact of metallic leads in SPECT images that corrected for attenuation using artifactual CT images is not clinically significant.

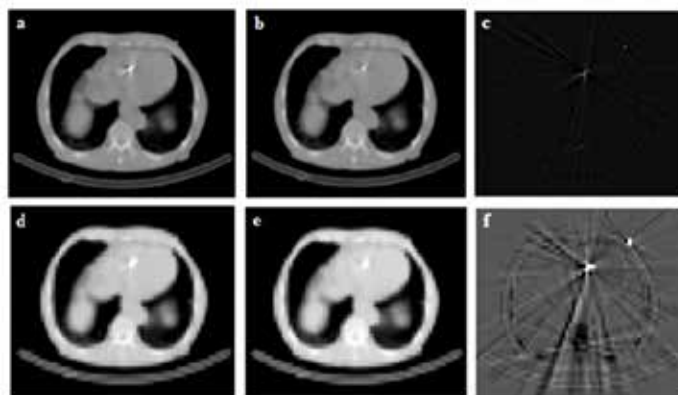


Figure 1. Typical CT image in a patient with a ICD lead: (a) artefactual CT image, (b) corrected CT image with MAR, (c) difference image between a and b, (d) μ -map of artefactual CT image, (e) μ -map of corrected CT image with MAR, (f) difference image between d and e.

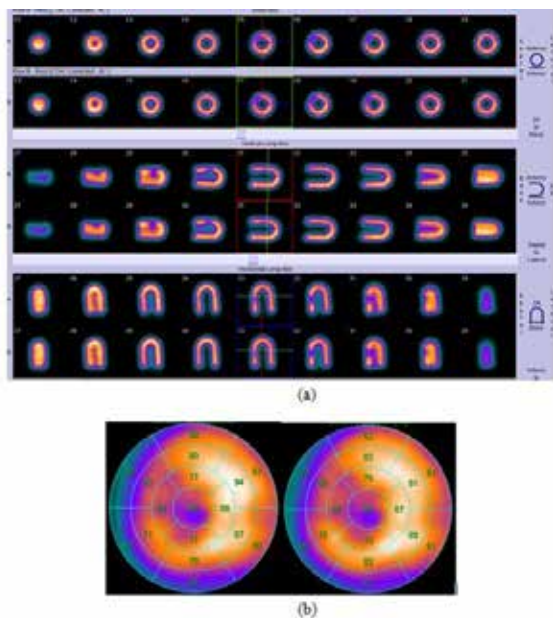


Figure 2 (a) The reconstructed SPECT images of a typical patient with ICD lead reoriented on typical short axis, vertical, and horizontal long axis with the ICD lead without MAR (top row) and with MAR (bottom row). (b) Bull's eye view of the attenuation-corrected SPECT images without (left) and with (right) MAR obtained using QPS software.

PS01.003 - Anthropomorphic Phantom of the Pancreas for Scintillation Camera Tests

Author(s): Halaine C.M. Silva¹, Fernanda C.L. Ferreira², Lourdes M. Brasil¹, Glécia V.D.S. Luz¹, Leandro X. Cardoso²
¹University of Brasilia at Gama, Brasília/BRAZIL, ²Federal University of South and Southeast of Pará,, Marabá/BRAZIL

It is well known that several medical procedures involving the use of ionizing radiation has made the radiation physics indispensable in modern medicine. The nuclear medicine, for example, is a medical specialty that uses the known radiopharmaceuticals. The radiopharmaceuticals, also known as radioactive tracers, have radionuclides associated with drugs in their composition and are administered

to the patient for diagnosis and treatment of various diseases. For diagnostic purposes, particularly, it is important that the images reveal, more accurately possible, the relevant details of any present anomaly. Therefore, to ensure the quality of the equipment used in nuclear medicine services, it is important that quality control tests be performed frequently. In this context, organizations such as the International Atomic Energy Agency (IAEA) recommend periodic testing of quality control of scintillation cameras. However, it is unacceptable that such tests be performed directly on patients, since the use of ionizing radiation can damage your health. In this regard, the use of physical and anthropomorphic phantoms becomes indispensable for quality control tests be performed more safely and efficiently. Therefore, the objective of this work was the development of the phantom of the pancreas for quality control optimization in scintillation cameras, and hence obtaining images more reliable for diagnosis in addition to controlling the dose of the radiation is used in efficiently to the quality and definition in image processing. The studies performed showed that the anthropomorphic phantom of the pancreas can be used to optimize image acquisition devices, in particular for spatial resolution tests. Besides the nuclear medicine test equipment, it is important to mention that the simulations with phantom of the pancreas can contribute to the continuing education of professionals in nuclear medicine, improving its ability in the identification of cold nodules and/or hot nodules.

PS01.004 - Comparing two image processing techniques, Wavelet and Segmentation by threshold, for detecting microcalcifications in an image mammographic.

Author(s): Rubens V. Souza Sales¹, Lourdes M. Brasil², Fatima Elpidio¹, Janice Lamas¹
¹Gama, University of Brasilia (UnB), Gama-DF/BRAZIL, ²Fga, UnB, Brasília/BRAZIL

According to the, World Cancer Research Fund, breast cancer is currently the second most common cancer in women worldwide. Many breast cancers are characterized by the presence of calcifications which are calcium accumulation in breast regions, which can be benign or malignant. Among the calcifications stand out microcalcifications, are generally smaller than five millimeters, these are more suspicious of malignancy making early diagnosis essential.

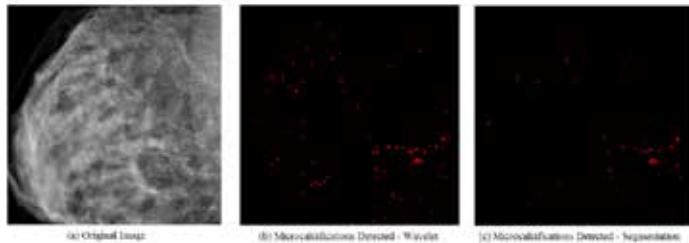
Due to the size, microcalcifications are more difficult to detect directly in an image of mammography, requiring image processing techniques, to assist the health professionals in the diagnosis. The techniques used for comparison in the detection of microcalcifications are: one based on Transformed Wavelet and another in segmentation by threshold.

Prior to the comparison, it is necessary to perform the detection of microcalcifications using each technique separately from the same image. In Figure 1.a has the original image of mammogram used in both techniques for microcalcifications detection. After the implementation of the two techniques, we can compare the results of both based on the number and position of the detected microcalcifications. The platform and language for development of algorithms is the Software Matlab, while that mammography images used are provided by Radiology Clinic Janice Lamas of Brasilia, Brazil.

In the wavelet technique, the image is decomposed into three directions (horizontal, vertical and diagonal), and the sum of these produces the resulting decomposition, it performed using two levels of decomposition and the Haar mother wavelet. After the decomposition occurs thresholding and binarization. In segmentation, an initial thresholding is used to define the points of interest, the dilatation of these points is then performed, and then the image are thresholded and binarized to indicate the detected microcalcifications. For your hit rating and detection performance, is needed help of specialist.

The Figure 1.b shows the microcalcifications detected using wavelet

technique, while Figure 1.c shows the detected microcalcifications using a technique segmentation by threshold. Note that by Wavelets could be detected more calcifications compared with segmentation (2.1 times more). This shows the advantage of using wavelet due to the fact that we can work on multiresolution for different frequencies. The Segmentation there is more information losses in steps thresholding and dilation. The main challenges of this work was to detect efficiently and reliably microcalcifications, set values for thresholds which often are not in the medical literature.



PS01.005 - Measuring red blood cell velocity in capillary using video and image processing

Author(s): Siwa Suwanmanee¹, Pedro Cabrales², Surapong Chatpun¹

¹Institute Of Biomedical Engineering, Faculty Of Medicine, Prince of Songkla University, Hatyai, Songkhla/THAILAND, ²Bioengineering, University of California, San Diego, La Jolla/CA/UNITED STATES OF AMERICA

Microvascular blood flow velocity is important in physiological health monitoring and it is essential in oxygen supply, nutrient transportation and waste removal. Blood flow is relevant to the occurrence of many diseases such as Raynaud’s phenomenon, diabetes, hypertension, sepsis and cardiac diseases. Red blood cells (RBCs) velocity can represent microvascular blood flow. In capillaries, it is an important parameter in clinical hemorheology and microcirculation. For both in vitro and in vivo studies, RBCs velocity can be determined by using video image processing. Therefore, this study aimed to determine RBCs velocity from the videos recorded. The capillary blood flow videos were recorded from an animal dorsal skin window chamber model. The computer algorithm was developed to estimate the RBCs velocity. The proposed algorithm applied a digital image processing method to provide quantitative assessment of video signal to determine RBCs velocity. There were four steps to perform image processing of video images: i) image improvement, ii) image binarization, iii) image segmentation and iv) RBCs centroid estimation. In order to estimate the velocity of RBCs, it can be calculated by using the moving distance of centroid of RBCs between frames. Each frame was stored and used to calculate the RBCs velocity by dividing the frame rate of the video. Moreover, to make this algorithm more useful and efficient, the graphic user interface (GUI) was developed and tested. The final outcome of this study provided the in-house software for the velocity of RBCs in a capillary.

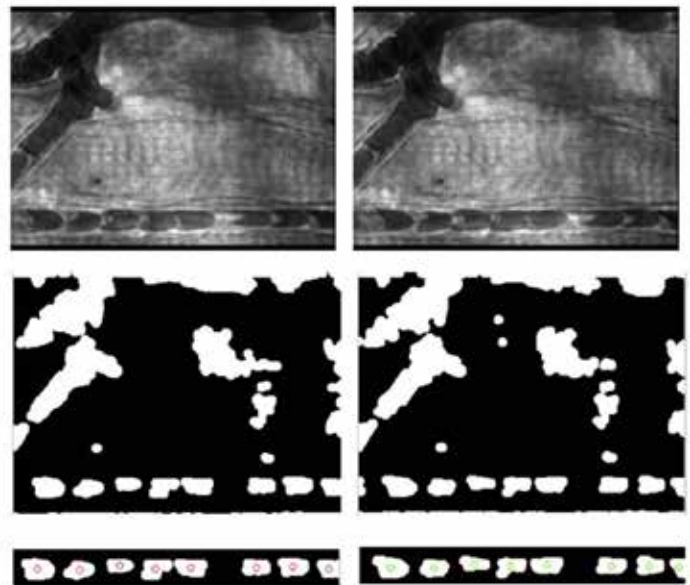


Figure Steps to determine RBCs centroids from capillary blood flow video images: (a) and (b) image improvement of image frames #195 and #196; (c) and (d) image binarization; (e) and (f) image segmentation and RBCs centroids estimation.

PS01.006 - Development of a Quantitative PET QA Procedure for Multi-Center Clinical Trials

Author(s): Brandon Driscoll¹, Ivan Yeung², Doug Vines³, Harald Keller³

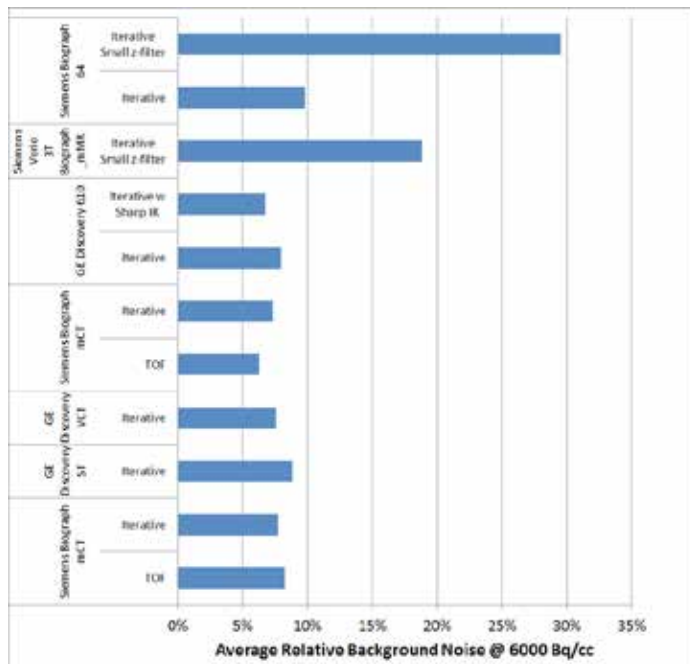
¹Techna Institute, University Health Network, Toronto/ON/CANADA, ²Dept Of Radiation Oncology, University of Toronto, Toronto/ON/CANADA, ³Radiation Physics, Princess Margaret Cancer Center, Toronto/CANADA

Purpose: To develop an inter-institutional PET QA procedure especially tailored to the increasing requirement for quantitative (as opposed to qualitative) image analysis. Such a QA procedure should allow for harmonization of image acquisition and reconstruction such that images can be pooled across institutions.

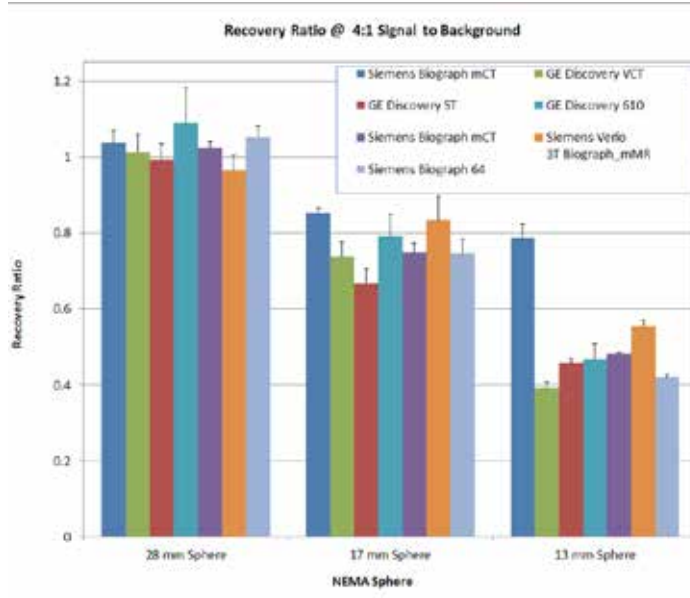
Methods: The PET QA procedure utilizes the NEMA IEC Body Phantom which contains a set of 6 spheres and a torso shaped background reservoir. The phantom is filled at two background levels (2:1 and 4:1) and imaged three times at each level. Well counter readings from the signal and background compartments are collected for absolute quantification. The sites were each asked to select the protocol they would utilize for a full body PET scan with a time per bed position of 5 minutes.

At this stage, 7 different scanners have been tested across 4 institutions. For each scanner a number of quantitative measures were analyzed such as dose calibrator to well counter cross-calibration, absolute agreement with well counter, recovery ratios, and background noise levels.

Results: The protocols utilized by individual sites varied considerably in terms of reconstruction and image acquisition parameters. Two PET scanners had Time-of-Flight acquisition capability contributing to the variability.



The relative average background noise at 6000 Bq/cc activity level was 9.6% with a substantial variation between the scanners (7.6-18.9%).



Variations of the recovery ratio were equally severe especially for the smaller spheres. The average recovery ratio for the 13mm sphere was 0.51 with relative standard deviation of 26%.

Conclusions: There is a large variation in noise and sensitivity of the PET images across the different institutions. Some PET metrics such as tumour hypoxic fraction rely on local quantification of image noise and are therefore especially prone to variations. Reliability of such metrics for multi-center clinical trials requires harmonization of PET image acquisition and reconstruction.

PS01.007 - Unwrapping highly wrapped phase using Nonlinear Multi-Echo phase unwrapping

Author(s): Chemseddine Fatnassi¹, Rachid Boucenna¹, Habib Zaidi²

¹Radio-oncology Department, Hirslanden, Lausanne/SWITZERLAND, ²Department Of Nuclear Medicine And Molecular Imaging, Geneva University Hospital, Geneva/SWITZERLAND

Introduction: The unwrapping problem has been a major topic of research for more than a decade. A variety of algorithms have been proposed to overcome this problem, although a correct solution is by no means guaranteed, and many of the proposed approaches are time-consuming. In this work, we propose a simple and fast method, which combines conventional temporal unwrapping with the nonlinear phase model to unwrap multi-echo data (nonlinear multi-echo (NME) unwrapping). The approach was tested on simulated and *in vivo* brain data acquired from 10 subjects at 3 Tesla. The accuracy of the proposed method was evaluated against 2D and 3D spatial unwrapping methods and also against conventional temporal unwrapping.

Materials and Methods: The proposed method to unwrap highly wrapped phase NME requires a minimum of 2 echoes. The first echo is acquired with an echo time TE smaller than the maximum velocity encoding. Therefore, the echo difference between the two acquisitions TE can be selected on the basis of knowledge of the typical range of the field map B0 values encountered at the field strength in question to avoid unintentional phase wrapping. The second echo is acquired at long echo time TE (>20ms) to get a high wrapped phase. In the presence of large susceptibility artifacts, the linear assumption of the phase evolution is broken. To overcome this problem, we propose a model to account for this nonlinearity using a 1D random walk theory when the images are acquired at long TE. Finally, we combine the nonlinear approach to describe the temporal phase evolution and the conventional temporal phase unwrapping to correct for high phase aliasing. To assess the accuracy of our approach in presence of high phase wraps at long echo time; we used simulated wrapped phase with different wraps complexity and different noise levels. *In vivo* MRI scans were performed on a 3T Magnetom Trio (Siemens Healthcare, Erlangen, Germany). Data were acquired with a 3D bi-polar multi gradient echo sequence. NME was compared with 2D conventional Matlab unwrapping, 2D and 3D spatial phase-unwrapping.

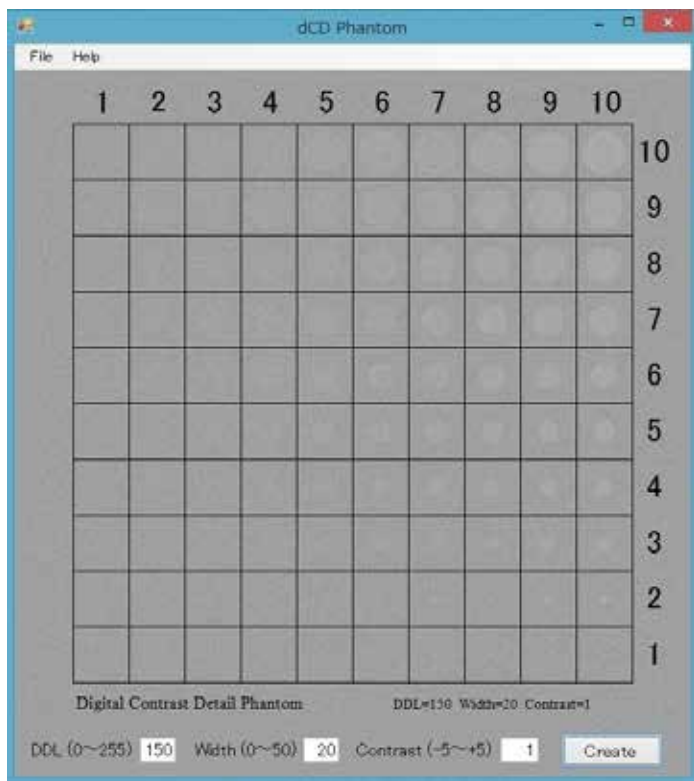
Results and Discussion: Both simulated and *in vivo* results showed that NME provides a good phase unwrapping with high accuracy (>90%) in the presence of high phase topography complexity and noise level, which reflects the real image quality at long echo time TE. Therefore, 2D, 3D spatial unwrapping and conventional temporal unwrapping present some limitations especially when phase wraps complexity and noise level are high. NME requires 2 echoes acquired at different TE; the method removes with success phase wraps occur near brain edges and paranasal sinus where the field gradient inhomogeneity is large. NME accounts for the nonlinear phase model which reduces significantly regions over-unwrapped with the conventional temporal unwrapping.

Conclusion: In this work, we proposed a simple and fast method to unwrap highly wrapped phase; the method combines conventional temporal unwrapping and nonlinear phase model to overcome phase aliasing even in the presence of high field gradient artifacts.

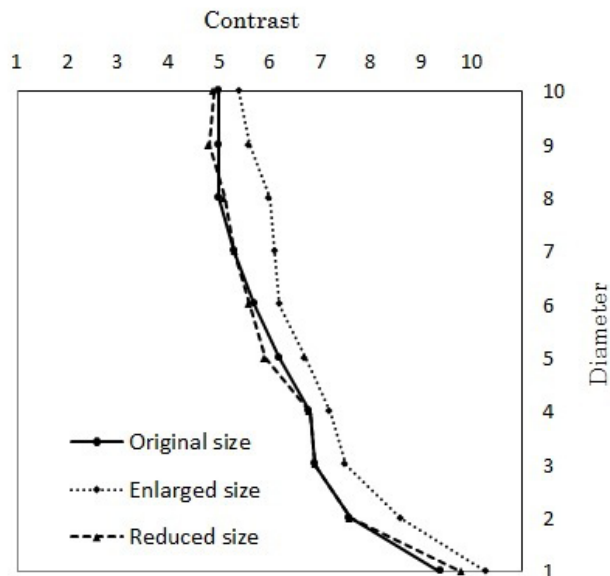
PS01.008 - Investigation of optimal display size for viewing MRI images using a digital contrast-detail phantom

Author(s): Hideki Fujita, Nao Kuwahata, Hiroyuki Hattori, Hiroshi Kinoshita, Haruyuki Fukuda
Radiation Oncology, Osaka Saiseikai Nakatsu Hospital, Osaka/JAPAN

In this study, we clarified the relationship between the display size of MRI images and observer performance using a digital contrast-detail (d-CD) phantom. The d-CD phantom was developed using Microsoft Visual Basic 2010 Express (Figure 1). It had a 512 × 512 matrix in size and a total of 100 holes, whose diameter increased stepwise from 4 to 40 pixels with a 4-pixel interval in the vertical direction; the contrast varied stepwise in the horizontal direction. The digital driving level (DDL) of the background, the width of the DDL, and the contrast were adjustable. These parameters were determined on the basis of the actual T1-weighted magnetic resonance (MR) images of the brain. In this study, the DDL, width, and contrast were set to 85, 20, and 1, respectively. The observer performance study was performed for three different display sizes (30 cm × 30 cm as the enlarged size, 13 cm × 13 cm as the original size, and 7 cm × 7 cm as the reduced size) using a 2-megapixel color liquid crystal display monitor and the results were analyzed using the Friedman and Wilcoxon statistical tests. The observer performance for the original display ($P < 0.01$) and the reduced display sizes ($P < 0.01$) was superior to that for the enlarged size, whereas there was no significant difference between the original display and reduced display sizes ($P = 0.7$) (Figure 2). Evaluation with the digital phantom simulating MR imaging also revealed that the original and reduced display sizes were superior to the enlarged display size in observer performance. The d-CD phantom enables a short-term evaluation of observer performance and is useful in analyzing the relationship between display size and observer performance.



The appearance of the developed d-CD phantom.



Contrast-detail curves for the visual evaluation.

PS01.009 - Investigation of presampled MTF using a slit device with slightly wider aperture

Author(s): Yasuyuki Kawaji¹, Tatsuhiro Gotanda¹, Tetsunori Shimonno¹, Shinichi J. Nakayama¹, Miki Hisamoto¹, Sae Matsumoto², Ayato Misago², Rumi Gotanda³

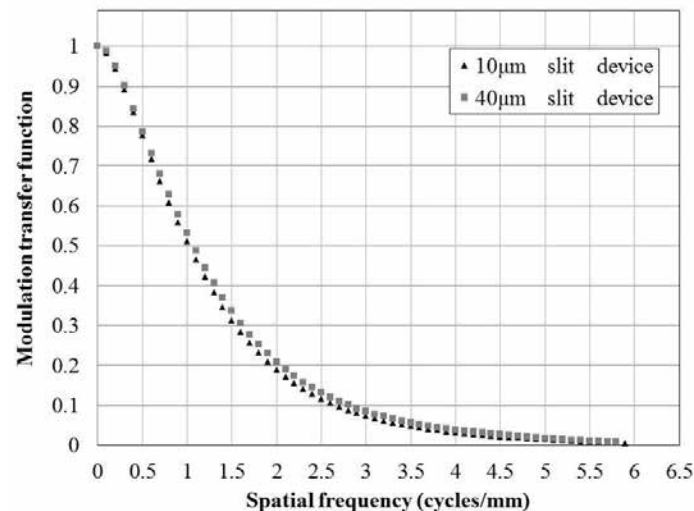
¹Department Of Radiological Science, Faculty Of Health Sciences, Junshin Gakuen University, Fukuoka/JAPAN, ²Department Of Radiological Science, Faculty Of Health Sciences, Junshin Gakuen University, fukuoka/JAPAN, ³Department Of Radiological Sciences, Ibaraki Prefectural University of Health Sciences, Inashiki-gun, Ibaraki/JAPAN

The resolution properties of an imaging system are commonly described by its modulation transfer function. The slit and edge methods are the two most commonly used and accepted techniques for measuring the MTF. The use of a slit requires very precise fabrication and alignment of the device in the radiation beam, a high radiation exposure to allow sufficient transmission through the narrow slit (aperture 10 μm). We took notice of the slit aperture and a new slit device with slightly wider aperture (40 μm) was made for the improvement of the conventional slit device. The aim of this work was to show the properties such as the X-ray tube loading, the alignment and the MTF using the new slit device with slightly wider aperture. Imaging plates in the CR system were employed in this measurement.

The use of the 40 μm aperture slit device can decrease one-fourth of the X-ray tube loading compared to the conventional device (Table 1). The use of the 40 μm aperture slit device can improve the alignment for the slit device rotation and the incidence X-ray offset. The MTF using the 40 μm aperture slit device is higher than that using the conventional device (Fig. 1). The maximum difference was 0.025 (at 1.3 cycles/mm). The exposure condition of the 40 mm aperture slit device is near to clinical conditions and the MTF indicates the resolution property under clinical conditions.

Our results showed that the use of 40 μm aperture slit device allows easy acquisition of a slit image on the detector without precise alignment and ensures an appropriate MTF for the CR system under near-clinical exposure conditions.

	(((10 μm slit	(((40 μm slit
74 kV	(((1008 mAs	(((252 mAs



PS01.010 - 3D Tumor delineation in Positron Emission Tomography reconstructed images restored by the use of Lucy Richardson blind deconvolution method

Author(s): Alpaslan Koc, Albert Guvenis
 Institute Of Biomedical Engineering, Bogazici University, Istanbul/TURKEY

Background Positron Emission Tomography (PET) can give the metabolically active tumor volumes necessary for radiotherapy planning and the therapeutic management of cancer patients. However, the automated edge finding algorithms and the partial volume effect due to the limited resolution of the camera can be a challenge. **Purpose** To evaluate the gain obtained in tumor volume estimation by making use of the image restoration Lucy-Richardson blind deconvolution method for 3D active contour based delineation strategies. **Method and Materials** Three 3D active contour methods have been used for delineation: Active contour with 50% threshold, active contour with edge attraction, and active contour with clustering. We have used a set of simulated 3D [18F]FDG PET oncology images including spheres of diameters 37, 28, 22, 17, 13 and 10 mm in a NEMA cylindrical phantom which were reconstructed using a 3D filtered backprojection algorithm. Data were obtained from the NCI database. The images were deconvolved by using the Lucy-Richardson blind deconvolution method. The deconvolution parameters were adjusted for best accuracy. The number of iterations was set to 7. **Results** First results showed that none of the three 3D active contour methods showed a consistently better accuracy for all spheres. The errors increased with smaller spheres. Significant improvements were obtained for all three delineation algorithms for the first four largest spheres between by deblurring the images. The improvements ranged between 98% and 25%. **Conclusion** The accuracy of 3D Active Contour delineation of tumors for estimating metabolically active tumor volumes is higher when images are deblurred with the Lucy-Richardson blind deconvolution. Work is underway for improving the accuracy of delineation of the smaller spheres.

PS01.011 - Different options for stimulation intensity in mapping cortical motor area in navigated transcranial magnetic stimulation

Author(s): Petro Julkunen, Elisa Kallioniemi
 Department Of Clinical Neurophysiology, Kuopio University Hospital, Kuopio/FINLAND

Background: Navigated transcranial magnetic stimulation (nTMS) is a modern technique used for mapping cortical motor areas in presurgical planning and stereotactic radiosurgery. One of its drawbacks is that it is sensitive to the selection of an appropriate stimulation intensity (SI) used in the procedure. Too low SI does not produce responses with good confidence and too high SI cannot perform focal stimulation. The SIs are determined based on resting motor threshold (rMT) prior to mapping. Commonly suprathreshold SI of 110% or 120% of rMT is used. Intuitively, a method able to determine an SI for the mapping procedure should be based on the lowest possible SI that maximizes the occurrence rate of motor responses. This can be accomplished via the use of the upper motor threshold (UT) determined with Mills-Nithi method [1] as it assumes 100% occurrence rate instead of the 50% assumed by the rMT [2].

Methods: 9 right-handed volunteers (6 males, age 24–61 years) were studied. The primary motor cortex on the left hemisphere was mapped for the extent of cortical area producing motor evoked potentials (MEPs) in three resting hand muscles using controlled suprathreshold stimulation intensity of 110% and 120% of the rMT as well as using UT. Stimulus locations and corresponding responses were used to evaluate the size of the excitable cortical motor area [3].

Results: UT was higher than 110%rMT ($p=0.026$) and lower than 120% of rMT ($p=0.011$). The representation sizes followed a similar trend. Comparison of size variations between the subjects revealed that the range of the resulting motor representation sizes was lowest with UT, while the size with UT and 110% rMT were significantly smaller compared to 120%rMT (Figure). The representation size determined with UT demonstrated best inter-subject repeatability based on confidence interval width with 2.0cm², while the confidence interval width of 2.2cm² and 2.8cm² were observed with 110% and 120% rMT, respectively.

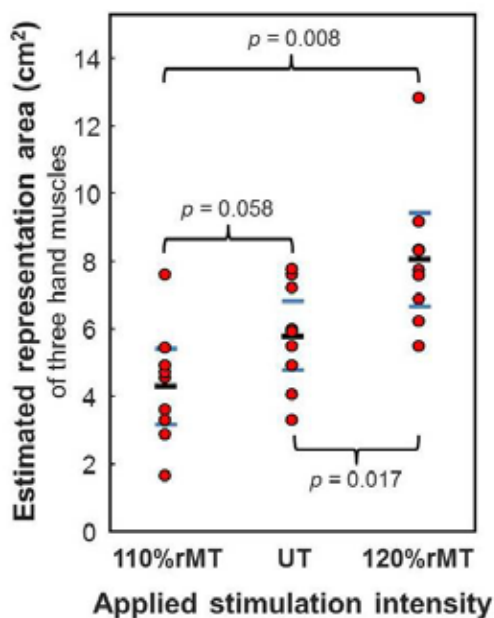


Figure: Estimates of motor cortical muscle representation area of three hand muscles determined for all subjects applying three stimulation intensities. The red dots represent area of each individual subject. The blue lines represent the 95% confidence intervals and black line indicates the mean. Non-parametric paired-samples comparisons are indicated.

Conclusions: The highest repeatability in representation size was observed with UT as compared to the commonly used 110% and 120% rMT SIs. Then the UT appears as an appropriate choice to be used with motor mapping applications to outline functional motor areas on the cortex when using rTMS in presurgical applications and radiosurgery planning to base the mapping SI to UT.

References:

- [1] Mills KR and Nithi KA, Muscle Nerve 1997;20:570–6
- [2] Awiszus F, Suppl Clin Neurophysiol 2003;56:13–23
- [3] Julkunen P, J Neurosci Methods 2014;232:125–33

PS01.012 - Software Breast Phantom for Phase Contrast Imaging Applications

Author(s): Anastasia Daskalaki, Kristina Bliznakova, Nicolas Palikarakis

Biomedical Technology Unit, Dept. Of Medical Physics, University of Patras, Patras/GREECE

Breast cancer is the most common cancer in women worldwide. Although mammographic screening techniques have considerably reduced breast cancer mortality, the rate of missed lesions and false positives remain crucial. Phase Contrast Imaging is an emerging technique based on X-ray phase change arising from diffraction and refraction effects that take place at the boundaries of different refractive materials, producing images with strong edge enhancement. There are no phantoms for phase contrast breast imaging applications available today. The goal of this work is to develop a software phantom that mimics the refractive properties (indexes) of breast tissues, specialized for phase contrast applications. Such a phantom will enable simulated image quality evaluations and dose analysis in the case of phase contrast imaging. For this reason 17 different compounds were investigated in order to find the optimum materials to represent fibroglandular tissue, adipose tissue, skin,

lymph, microcalcifications and breast masses for an energy range between 18keV and 40keV. A comparison of the δ values between these breast tissues and the mimicking materials has been calculated according to the equation $\delta_{Diff} = (|\delta_{BT} - \delta_M| / \delta_{BT}) * 100$. Where δ_{BT} represents the refractive index of the breast tissue and δ_M the refractive index of the mimicking material. The *XRAYImagingSimulator*, an in-house developed software platform used for novel investigations in x-ray imaging, has been used for image acquisition. Simulation modules have been adapted to analytically simulate physical interactions taking place in Phase Contrast imaging based on Fresnel-Kirchoff diffraction theory. A breast like semi-cylindrical phantom of 18mm radius and 45mm thickness filled with polystyrene as background material has been modeled. In this background five cuboids of nylon, polyethylene, paraffin wax, polystyrene and silicone gel, two spheres of water of 1mm and 2mm radius and two clusters of Al of 0.098mm and 0.115mm respectively were inserted. Subsequently, x-ray planar images were produced with coherent radiation emerging from a point monochromatic source in both Phase Contrast and Absorption mode. The two images of the phantom were obtained at 20keV, with SID 23m and ODD 400mm and 5 μ m resolution. The two planar images were compared in terms of contrast and edge enhancement using four different line profiles. Results from the evaluation of the line profiles showed an important edge enhancement of the details embedded in the phantom. Especially for the adjacent materials polyethylene and paraffin wax that cannot be differentiated in the absorption mode, phase contrast image was able to clearly reveal their borders. Simulation images acquired show a significant edge improvement when the phase contrast effect was taken into account. For further investigation we are planning to verify the presenting results with synchrotron experimental data.

PS01.013 - Actions for Implementation Program of Image Quality of Mammography

Author(s): Rianne B. Venancio¹, Leticia S. Oliveira¹, Ana Cláudia Patrocínio², Rodolfo D.S. Ribeiro¹, Cecilia L. Debs³

¹College Of Electrical Engineering, Federal University of Uberlandia, Uberlandia/BRAZIL, ²Laboratory Of Biomedical Engineering, Federal University of Uberlândia, Uberlândia/BRAZIL, ³Institute Of Radiology - College Of Medicine, University of Sao Paulo, Sao Paulo/BRAZIL

Globally were established many quality programs that have proven effective in early detection of the breast cancer. In Brazil was instituted, by the Department of Health, the ordinance 531/2012 that establish the basic guidelines for the implementation of the National Program for Quality in Mammography (PNQM) to ensure the quality of digital mammography exams. But in November 2013 it was updated by the ordinance n°2898 added which the role of public and private agencies to fulfillment this ordinance, not adding any technique process. This work has the aims to implement the ordinance 531/2012 with a principal focus on training and periodic retraining of health professionals. As methodology was proposed a set of actions for hospitals and clinics regularize the conditions imposed by the law, always seeking quality mammographic images. The result was the creation of seminars and specific courses for radiologists and radiology technician, with the aim to resolve such failures always prioritizing the quality in the image digital mammography. Other tender, for comply the ordinance, is the establish a committee that will go assess the insertion of PNQM, regularly sending reports to health authorities regarding the implementation of the program and regiment and still taking providences in case of non-compliance with the quality criteria.

PS01.014 - Evaluating Techniques of Transformation Intensity for Contrast Enhancement in Mammographic Images

Author(s): Ana Cláudia Patrocínio¹, Raquel J.P.D. Lima¹, Michele F. Angelo²

¹Faculty Of Electrical Engineering, Federal University of Uberlândia, Uberlândia/BRAZIL, ²Department Of Technology, State University of Feira de Santana, Feira de Santana/BRAZIL

Mammography has a high sensitivity, but the interpretation of the images may be affected by factors such as the density breast and the limitations of mammography equipment. Thus, it is of great importance the use of image pre-processing techniques to enhance contrast and consequently the present structures in the image are interpreted correctly. This work is dedicated to the study of the performance of intensity transformation techniques for contrast enhancement of mammographic structures. Initially, five different techniques (logarithmic, exponential, gamma, sigmoid and stretching linear function) were applied in regions of interest containing microcalcifications. Subsequently, the signal/noise ratio and the contrast/noise ratio of the images were calculated to evaluate the performance of the techniques. According to the results, the sigmoid function presented the better performance.

PS01.015 - Influence of Contrast Enhancement to Breast Density Classification by Using Sigmoid Function

Author(s): Michele F. Angelo¹, Pedro Cunha Carneiro², Talita C. Granado², Ana Cláudia Patrocínio²

¹Department Of Technology, State University of Feira de Santana, Feira de Santana/BRAZIL, ²Faculty Of Electrical Engineering, Federal University of Uberlândia, Uberlândia/BRAZIL

The classification of breast density is very subjective even for the experts, the categories 2 and 3, in many cases are confused. Thus, the objective of this study is to evaluate the influence of the sigmoid function in the density classification of images with lesions by using texture attributes. It was used 28 images with lesion, 19 belong to the category 2 (P2 - partially fat) and 9 to category 3 (P3 - dense). The sigmoid function was implemented and applied to all images to contrast windowing. A set of 14 Haralick descriptors were implemented. After the attributes extraction step it used the clustering technique K-Means to classify the category images of breast density 2 and 3. Seven of the 14 Haralick descriptors (energy/uniformity, contrast, variance/homogeneity, average sum, variance of the sum, entropy difference and maximum correlation coefficient) showed higher success rate when used images processed with sigmoid function. However, five attributes (correlation, entropy sum, difference variance, correlation information measured 1 and 2) presented classification results below those that results by using the original images, and two attributes (inverse difference moment and entropy) obtained the same results, for classification of both images (images with sigmoid function and original images). The attributes combination used to classify images with sigmoid function were better and the combination that had the best classification accuracy rate was the contrast and variance attributes. The use of the sigmoid function directly influenced the results of classification in the categories 2 and 3, however, when it was used by only one attribute in the classification, not all attributes showed great correct response rates, as happened to the results obtained using attributes combination.

PS01.016 - Evaluation of the difficulties of the learning process of mammographic readings

Author(s): Pedro Cunha Carneiro¹, Letícia Oliveira Mamere², Ana Cláudia Patrocínio¹

¹Laboratory Of Biomedical Engineering, Federal University of Uberlândia, Uberlândia/BRAZIL, ²Faculty Of Medicine, Federal University of Uberlândia, Uberlândia/BRAZIL

Breast cancer is the second most frequent type of cancer in the world, being the most common among Brazilian women. Thus, the best way to prevent from such disease is by having mammographic exams regularly. However, the mammographic report does not depend exclusively on the analysis of the physiological factors of the visualized structures and the technical characteristics of the image acquisition and storage system, but also on the interpretation of the images by the specialist. The aim of this paper is to identify and evaluate the parameters used to elaborate the mammographic reports which show a higher level of difficulty from the quantification of mistakes of the residents when reporting mammographic exams.

On this paper, 346 mammographic images were analyzed by radiology residents using a questionnaire elaborated on a previous work and it is based on BI-RADS™ to characterize the mammographic lesions found. The collected and analyzed data are: the positive and negative cases of the BI-RADS™ classification, the pattern of density and complexity of the image, the capacity of identifying nodules, calcifications of the vascular/parallel type, calcification of benign aspect and axillar and intramammary lymph nodes. In order to broaden the evaluation of the results some statistical methods were used, such as: sensitivity (Se), specificity (Sp), Kappa coefficient (K) and area under ROC curve (AUC).

Later, these reports were compared to the reports provided by the staff (specialized physicians), aiming at identifying the level of difficulty of the radiology residents in reporting mammographic exams. Out of the 321 negative reports defined by the staff, the residents matched 292 of them (91%). On the 25 positive cases defined by the staff, the residents matched 13 of them. Regarding the level of complexity of the lesions, the highest percentage of mistakes is found in cases considered of very high complexity. Table 1 presents a summary of the results obtained to each one of the parameters evaluated.

Table 1. Results obtained

Collected data	Se (%)	Sp (%)	AUC	Kappa
(+) and (-) BI-RADS™ Reports	68	95.6	0.852	0.57
Presence of nodules	74	99.3	0.89	0.79
Presence of vascular calcifications	84	99.6	0.931	0.88
Presence of calcifications of benign aspect	92.2	96.3	0.951	0.89
Presence of axillar lymph nodes	92	98	0.959	0.91
Presence of intramammary lymph nodes	91	98.7	0.959	0.88
(+) and (-) BI-RADS™ Reports	68	95.6	0.852	0.57
Presence of nodules	74	99.3	0.89	0.79

This study made it possible to identify which is the pattern of breast that presents the highest difficulty in being analyzed by the residents. It was noticed that the detection of positive reports was a failed process, suggesting the little familiarity of the residents to the malign lesions. The results highlight the necessity to implement a training method which provides the resident with a better learning method when characterizing mammographic lesions, favoring the early detection of breast cancer.

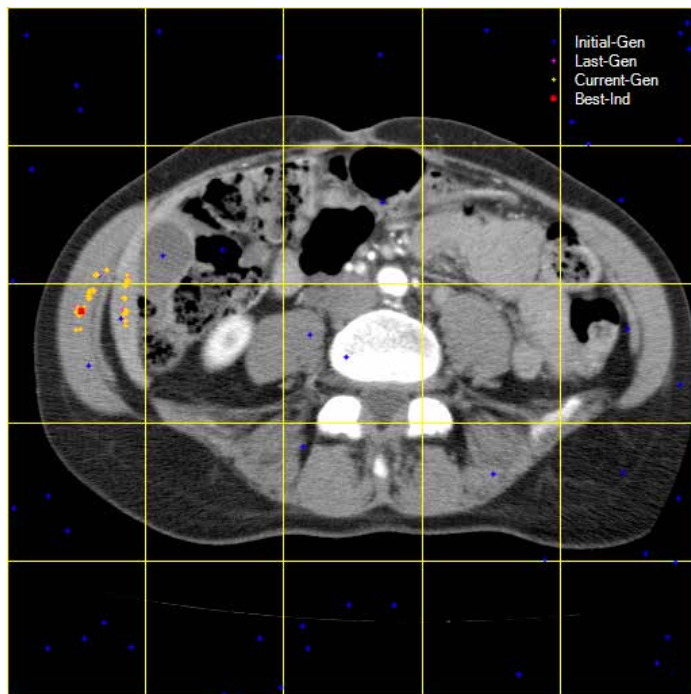
PS01.017 - Non-deterministic optimization using Differential Evolution algorithm to launch seeds for liver segmentation in MDCT

Author(s): Ricardo L. Thomaz¹, Rogério Anastácio¹, Tulio A.A. Macedo², Ana Cláudia Patrocínio¹, Alcimar B. Soares¹
¹Faculty Of Electrical Engineering, Federal University of Uberlândia, Uberlândia/BRAZIL, ²Faculty Of Medicine, Federal University of Uberlândia, Uberlândia/BRAZIL

The automatic segmentation of liver in Multi Detector Computed Tomography (MDCT) is considered a complex task due to the similarity and proximity of the liver with other soft tissues. Although some techniques already achieve good results, their deterministic characteristic might prevent the feasibility of the algorithm in complex situations. Thus, this paper purpose the use of Differential Evolution (DE) as a non-deterministic evolutionary algorithm in order to optimize the launching of seeds for region growing segmentation algorithms. In order to achieve this goal, a fitness function, based on intensity, contrast, morphology and localization features of the liver, along with a full exam analysis methodology were developed. Ten MDCT exams were then submitted to the method, resulting in 7 exams with at least 85% of correctly seeded liver, as shown in the table below.

Non-deterministic seed launching results					
Exams [#]	Slices [#]	Seeded [#]	False-Negative	False-Positive	Correctly Seeded
1	118	072	0.00%	39.83%	60.17%
2	376	158	0.26%	02.92%	96.82%
3	210	163	5.24%	00.00%	94.76%
4	366	172	0.55%	02.73%	96.72%
5	611	386	0.00%	38.29%	61.71%
6	385	385	0.00%	63.64%	36.36%
7	521	191	1.15%	00.00%	98.85%
8	501	260	0.20%	12.57%	87.23%
9	476	193	1.47%	00.00%	98.53%
10	094	067	7.44%	00.00%	92.56%
Total	3658	2047	1.63%	15.99%	82.37%

However, some exams presented high false-positive seeding due to the complexity of the images, such as the proximity of abdominal muscles near the end of the liver, as depicted in Fig. 1. In conclusion, the purposed use of DE has shown promising results on launching seeds inside the liver on MDCT images.



PS01.018 - Influence of ROI pattern on segmentation in lung lesions

Author(s): Marcelo L.N. Franco¹, Lara M. Nunes², Ana Paula P. Froner³, Ana M. Marques Da Silva³, Ana Cláudia Patrocínio¹
¹Laboratory Of Biomedical Engineering / Faculty Of Electrical Engineering, Federal University of Uberlândia, Uberlândia/BRAZIL, ²Biomedical Engineering Department / Faculty Of Electrical And Computer Engineering, State University of Campinas, Campinas/BRAZIL, ³Graduate Program Of Electrical Engineering, Pontifical Catholic University, Porto Alegre/BRAZIL

The early diagnosis of lung cancer is critical in determining the chances of recovery and survival of patients. Sometimes the differences between malignant and benign tissues can be imperceptible to not trained human eyes, thus, a good diagnosis depends on radiologists ability.

Because of these facts, CAD systems have been designed to get features of lesions in digital images to report the probability of malignancy nodule. An important step of developing these systems is the nodule image segmentation. If segmentation does not provide satisfactory results, the descriptors used cannot describe the real features of lung tissue.

Considering the significance of segmentation step, this project aims to compare the results obtained by two segmentation algorithms: the first one consists basically in a selection of rectangular region of interest (ROI) followed by Otsu segmentation technique and the other added an elliptical ROI after applying Otsu technique, eliminating possible structures adjacent of lesion.

The images used in this project are from 22 CT exams (5088 slices) acquired at São Lucas Hospital (PCU-RS), all containing radiological report. All exams were analyzed to determine the extent of each lesion, reducing the number of images to be processed.

Then, the ROI was selected by 2 mouse clicks on the image: each one at one vertex of main diagonal of the desired rectangular region (ROI_r). Afterward, the one-threshold Otsu method was applied, segmenting the lesion. Finally, the elliptical region (ROI_e) is created

based on ROI_R shape and the location to cut the ROI is replicated for all slices on the even exam.

A planar morphological transformation with disc structuring element is applied on the image to define the extent of the lesion and all structure which had associated pixels less of 25% of all white pixels in the segmented image were eliminated.

On the segmented image, 11 geometric features have been extracted: area, perimeter, compactness, irregularity and 1 to 7 invariant moments of HU.

The difference between the two ways of ROI selection is shown by Fig. 1: on the left, there's a neighbor tissue segmented as part of lesion and on the right the lesion was completely separated from neighbor structures. Some of the descriptors showed statistical differences between measures made from nodules segmented with or without an elliptical ROI.

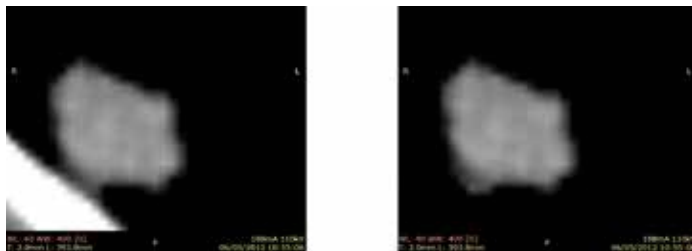


Fig. 1 Example of segmentation with ROI_R on the left and on the right the respective segmentation with ROI_E

PS01.019 - Comparison between Elliptical and Squared ROI to Launch an Automatic Seed to Region Growing Algorithm on Hepatic Segmentation using CT images

Author(s): Rogério Anastácio¹, Ricardo L. Thomaz¹, Cecília R. Moraes¹, Giulia C.M. Almeida¹, Taissa O. Ferreira¹, Murilo R. Cândido², Tulio A.A. Macedo³, Ana Cláudia Patrocínio¹

¹Faculty Of Electrical Engineering, Federal University of Uberlândia, Uberlândia/BRAZIL, ²Faculty Of Mathematics, Federal University of Uberlândia, Uberlândia/BRAZIL, ³Faculty Of Medicine, Federal University of Uberlândia, Uberlândia/BRAZIL

Early detection of liver cancer increases the survival rate by 60-70% in five years. As part of CAD development for the liver, two automatic seed selection techniques (for automatic liver segmentation using region growing technique) are compared, using the calculation of Mean Squared Error (MSE), to analyze which one has the lowest error when compared with manual segmentation.

It was used 2631 liver computer tomography slices, the first step is make the preprocess of these slices, that were submitted in the windowing CT and after it is applied a mean filter with the gamma transformation.

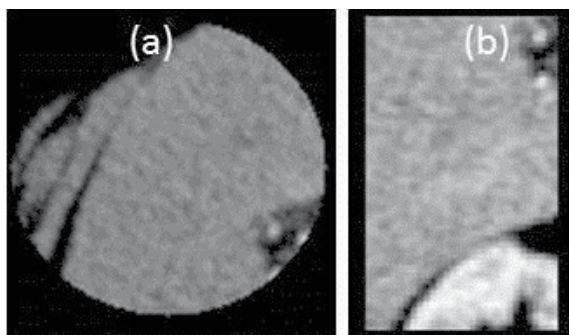


Figure 1 – ROI by two techniques: (a) SLEA, (b) SLSA.

The first technique defines the Seed Launch on Elliptical Area (SLEA), Figure 1(a), for find the seed point, and the second technique defines the Seed Launch into Square Area (SLSA), Figure 1(b), for find the seed point.

And the seed points that were found with each one of these techniques are used to perform the liver segmentation with the region growing algorithm, and from the liver segmented is performed the entire exam volume and the MSE calculation for each technique, and these results compared with the manual segmentation.

Thus the results of this process are in the Table 1, then the average liver volume measured manually was of 1,369.99cm³, and with SLEA technique the average liver volume measured automatically was of 1.625,62cm³ and the average MSE was of 65.49±94.12cm³, and for the SLSA technique the average liver volume measured automatically was of 1,643.23cm³ and the average MSE was of 181.48±281.39cm³. The smallest MSE SLEA was of 2.04cm³ and the bigger was of 391.82cm³, and for the SLSA the smallest MSE was of 2.122cm³ and the bigger was of 1,110.82cm³. It was observed that both techniques have the average volume similar, but the SLEA technique has the smallest values and averages of the MSE.

Table 1 – Volumes and MSE of exams, in cubic centimeter (cm³).

Exam	Man. Segmentation		Automatic Segmentation			
	Volume	MSE	Group 1 (SLEA) Volume	Group 1 (SLEA) MSE	Group 2 (SLSA) Volume	Group 2 (SLSA) MSE
1	1,093.81		1,625.62	65.49	1,643.23	181.48
2	755.643		867.421	2.035	845.559	2.122
3	728.407		927.565	2.955	1,008.156	87.399
4	958.481		1,333.415	10.473	1,362.426	21.742
5	1,484.484		1,309.368	18.719	1,379.553	105.531
6	1,489.596		2,069.978	14.327	2,027.966	19.431
7	616.924		689.947	55.281	760.939	70.669
8	837.183		1,008.276	9.388	798.242	14.812
9	409.374		397.421	160.165	298.048	211.108
10	1,239.312		1,911.426	86.276	1,936.030	86.706
11	2,523.733		1,895.641	391.815	1,468.828	511.517
12	1,772.447		2,112.223	24.174	2,366.901	490.359
13	2,101.525		3,101.390	70.700	3,629.204	1,110.824
14	1,184.060		1,945.443	39.687	1,787.874	42.199
15	1,844.455		2,635.397	40.464	2,586.204	40.085
16	2,880.524		2,749.024	104.056	2,665.452	122.850
Mean	1,369.998		1,625.621	65.487	1,643.229	181.484
+ SD	+ 681.11		+ 770.06	+ 94.12	+ 838.58	+ 281.39

PS01.020 - Gd-based Nanoparticles Mediated Magnetic Field Enhancement Inside Homogenous Tissue: Simulation using Finite Element Method

Author(s): Sahar Rezaei¹, Nader Riyahi-Alama¹, Mohsen Ostovari²

¹Medical Physics And Biomedical Engineering Department, Tehran University of Medical Science, Tehran/IRAN, ²Medical Physics Department, Ahvaz Jundishapur University of Medical Science, Ahvaz, Iran, Tehran/IRAN

Tumor detection in the early stages is of utmost importance in cancer diagnosis and treatment. Magnetic resonance molecular imaging (MRMI) is a considerable medical imaging method to distinguish normal cells from cancerous cells initiating metastasis. Current MRI contrast agents are required to prevent adverse chemical activity in the body. Therefore, in conventional form of Gd-DTPA due to their relatively large size and coverage can be used only in extracellular spaces. Meanwhile, nanoparticles, because of their small size relative to the body cells, are capable of intrusion inside the cells. These materials can be used for molecular imaging; Gd based paramagnetic nanoparticles are the most widely used agents. In this paper, variation in external magnetic field as a result of using Gd-based nanoparticles in homogenous tissue was investigated with finite element method. To this end, simulations have been carried out in the presence of Gd nanoparticles and without them. This study indicated that magnitude of external magnetic field increases due to the presence of nanoparticles, and we compared the results with Vibrating Sample Magnetometer (VSM) results. In addition, Gd nanoparticles showed sigmoidal (superparamagnetic) behavior in both data set of simulation and VSM, applicable to normal cell uptake and so tumor cell tracking for cancer detection.

PS01.022 - Linear tomosynthesis with flat-panel detector for image guided radiation therapy**Author(s):** Dong-Su Kim¹, Tae Ho Kim¹, Seong-Hee Kang¹, Kyeong-Hyeon Kim¹, Min-Seok Cho¹, Siyong Kim², Tae-Suk Suh¹¹Biomedical Engineering And Research Institute Of Biomedical Engineering, College Of Medicine, The Catholic University of Korea, Seoul/KOREA, ²Radiation Oncology, College Of Medicine, Virginia Commonwealth University, Richmond/UNITED STATES OF AMERICA

In this study, we propose a novel imaging technique using linear tomosynthesis with flat-panel detector that can produce tomographic images at arbitrary anterior-posterior depth position for image guided radiation therapy. To verify the usefulness of the imaging performance, we performed systematic simulation studies for simple linear movement of a couch with digital phantoms in several layers along the coronal direction. Projections were acquired at specific position through the calculated proper shift amounts for particular or multi-focal level imaging. The linear tomosynthesis images were reconstructed by shift-and-add (SAA) method. Furthermore, to increase blurring effect of out-focal objects in the image, we investigated a subsidiary technique that used sections of extra detector pixels along the anatomical axis. According to our preliminary results, a designed specific coronal plane was well focused with good image sharpness and multi-focal image layers were realized with the proposed method. We have also derived the thicknesses of the focused image layer as functions of the number of pixels used in focal or out-focal section of the pixel array. Our results showed that defined plane-of-interests were well focused with image sharpness and the position of image layer center was adjusted precisely with proper shift amounts in the linear motion tomosynthesis. We expect that the proposed method will be very useful for accurate localization with less dose than other imaging modality such as cone-beam computed tomography.

PS01.023 - Evaluation of image quality and dose for digital breast tomosynthesis (DBT) using a semi-analytical model**Author(s):** Alessandra Tomai¹, Martin E. Poletti²¹Departamento De Física Aplicada, Universidade Estadual de Campinas, Campinas/BRAZIL, ²Universidade de São Paulo, Ribeirão Preto/BRAZIL

Digital breast tomosynthesis (DBT) is a 3-D imaging technique that has higher sensitivity and specificity, compared to mammography, for early diagnostic of breast cancer, with a similar radiation dose. The risks associated with the DBT examination is evaluated with respect to the mean glandular dose (MGD), determined from air kerma measurements and specific normalized glandular dose factors. The image quality can be evaluated by means of the contrast-to noise ratio (CNR) and artifact spread function (ASF) In this work, we describe semi-analytical models, which were developed to study the MGD, CNR and ASF in DBT, by determining the deposited energy in single and double interactions and the intensity of transmitted radiation. The semi-analytical model was used to study the dependence of these quantities with different projection angle, different breast thicknesses and glandularities. The anode/filter combinations evaluated were: Mo/Mo, Mo/Rh and Rh/Rh, and a W anode combined with K-edge filters (Zr, Mo, Nb, Ru, Rh, Pd, Ag, Cd, In and Sn), for tube potential between 23 and 35 kV. Results demonstrate that the normalized glandular dose decreases up to 25%, as the projection angle increases, being this decrease most pronounced for thicker and denser breasts. A decreasing in the CNR and ASF values was observed as the angular range decreases. Besides, it was observed variations up to 70% on the MGD and CNR with the x-ray spectra and breast characteristics (composition and thickness). The ASF is almost independent on the x-ray spectra. Finally, it was verified that the semi-analytical models developed in this work provided results of image quality and dose parameters in DBT in a fast and simple way, with a good agreement with those or by MC simulation (discrepancies lower than 10%).

PS01.024 - Optimization of acquisition parameters of the test of an overall SPECT/CT system performance.**Author(s):** Piotr Tulik¹, Monika Tomaszuk², Paulina Wojcik¹, Alicja Hubalewska-Dydejczyk³, Anna Sowa-Staszczak²¹Institute Of Metrology And Biomedical Engineering, Warsaw University of Technology, Faculty of Mechatronics, Warsaw/POLAND, ²Nuclear Medicine Unit, Department Of Endocrinology, University Hospital in Krakow, Krakow/POLAND, ³Department Of Endocrinology, Jagiellonian University Medical College, Krakow/POLAND

An overall SPECT/CT system performance test provides the most comprehensive information about a long term stability of a uniformity and resolution of gamma camera installed in a clinic, but its conducting is time consuming. The recommended frequency of the test and manner of its implementation varies between different countries and nuclear medicine departments. Different acquisition parameters for this purpose are proposed by NEAM, IAEA report #6 and AAPM report #22. The question arises how to get an image with the best quality, in the least amount of time. Is it possible to decrease the time needed for an overall SPECT/CT system performance test execution and in consequence being able to perform it more often in the clinic, but not to compromise with the requirements of recommendations on the quality of the observed image? The purpose of this study was to present the process of optimizing of acquisition parameters of an overall SPECT/CT system performance test, which could be implemented in each nuclear medicine department.

All measurements were performed with the use of Symbia T16 SPECT/CT (2010, Siemens). The Jaszczak SPECT phantom with cold spheres provided for high-resolution gamma cameras filled with 740MBq of ^{99m}Tc was used.

The influence of the duration of a single projection (10, 15, 20, 25, 30, 45, versus 60 sec per projection), the number of projection (64, 96 versus 128 projections in a full 360-degree rotation) and the size of acquisition matrix (64x64 versus 128x128) on the quality of the resulting image were analyzed. The scans for each combination of the parameters were performed three times with two exceptions. The study with 30 sec per projection, 128 projections and 128x128 matrix were chosen to be a reference (in accordance with IAEA recommendations and additionally a standard protocol for clinical applications in the Department). All images were subjected to visual evaluation (uniformity and spatial resolution) by 2 experienced medical physicists. Quantitative evaluation of image contrast was performed with the use of Mann-Whitney nonparametric test. Each SPECT image was evaluated with and without attenuation correction, but always with scatter correction.

The proposed process of an evaluation of the parameters that are crucial for the image quality in nuclear medicine gave a possibility to identify the optimal acquisition parameters for considered test. Image, indistinguishable from proposed reference, but acquired in the half of time (decrease from 32 min for 16 min, respectively), was obtained with the following parameters: 30 sec per projection, 64 projections and 128x128 matrix size, with the use of attenuation correction. Reduction of the duration of a single projection, and especially the size of the matrix, or lack of AC, deteriorated image quality. An increase of the duration of a single projection over 30 sec did not bring a significant improvement of image quality, but increased the duration of the test.

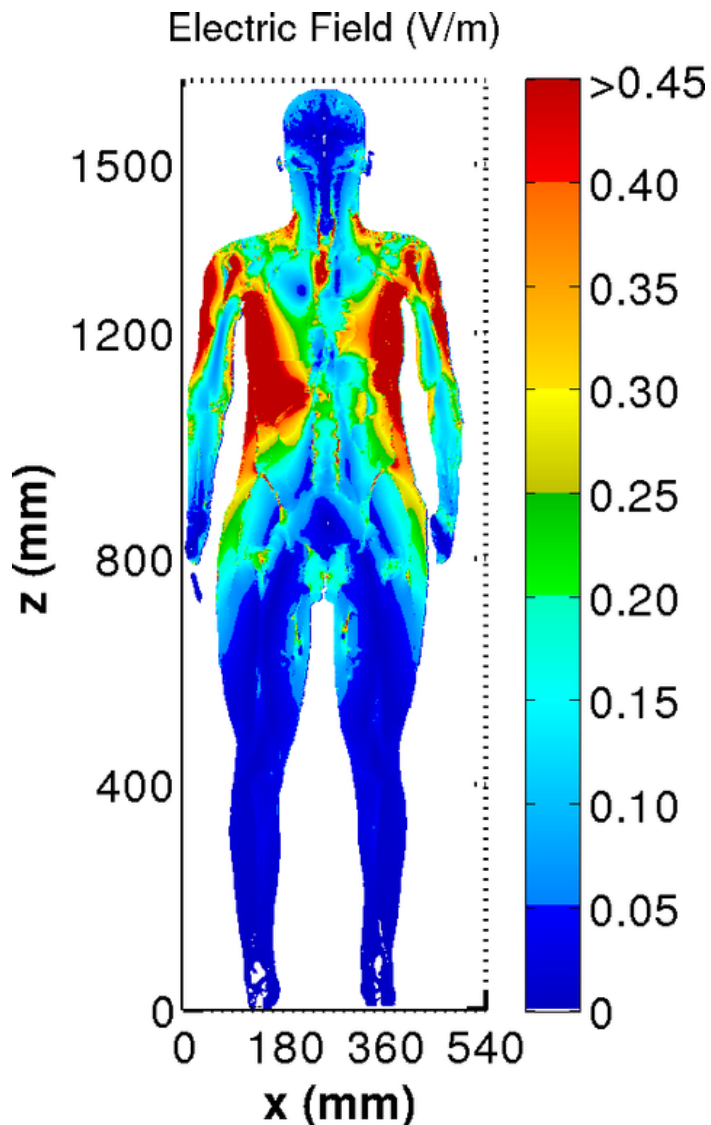
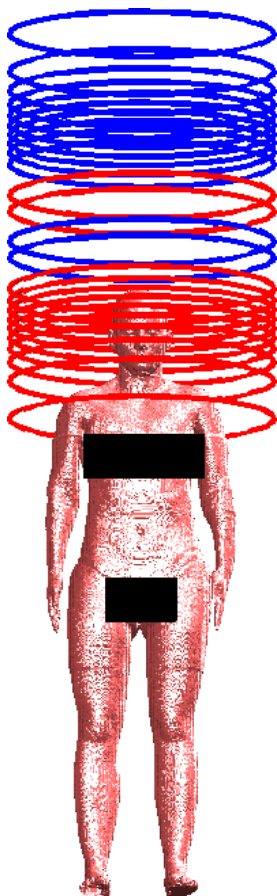
The methodology of optimization of acquisition parameters for an overall SPECT/CT system performance test has been presented for Symbia T16 SPECT/CT system in terms of time of a single acquisition and quality of acquired images.

PS01.025 - Dosimetric Analysis of Patient to a Z-Gradient Coil in Head Magnetic Resonance Imaging

Author(s): Mai Lu¹, Shoogo Ueno²

¹Key Lab. Of Opt-electronic Technology And Intelligent Control Of Ministry Of Education, Lanzhou Jiaotong University, Lanzhou/CHINA, ²Department Of Applied Quantum Physics, Graduate School Of Engineering, Kyushu University, Fukuoka/JAPAN

In magnetic resonance imaging (MRI), magnetic field gradient coils are commonly switched at low frequency of around 1 kHz or so. Time-varied gradient magnetic fields may stimulate nerves and muscles by inducing electric fields and currents in patients, which may potentially cause health problem. The International Commission on Non-Ionizing Radiation Protection (ICNIRP) has set international guidelines for limiting the exposure. For the working frequency of 1 kHz, the ICNIRP guidelines define the reference level (RL) as 80 μ T, and the basic restriction in both CNS and body tissues as 0.4 V/m. The guidelines require that the basic restrictions are not exceeded at any time. In this study, a 3D human body model i.e. the patient as shown in Fig.1 was placed in a z-gradient coil for simulating the head MRI exam. A realistic cylindrical z-gradient coil with 24 circular rings has been numerically designed. The time variation of the applied magnetic field causes induced electric fields in the body through Faraday's induction mechanism, and can be calculated by the impedance method. The electrical properties are modeled using the 4-Cole-Cole method and can be obtained by fitting to experimental measurements. The induced electric fields in all CNS tissues have been averaged over a volume of 2mm x 2mm x 2mm, and the 99th percentile value of the averaged field strength were compared with the ICNIRP basic restrictions. Fig. 2 shows the typical slice of the induced electric fields within the coronal plane. The spatially averaged magnetic flux density was found to be approximately 9.49 times the ICNIRP reference level, and the maximum value of the induced electric fields in CNS was found to be 5.95 times the ICNIRP basic restriction.



PS01.026 - A Novel Optical System for Contrast Enhancement in Histological Plates to Be Processed Digitally

Author(s): Rubiel Vargas-Canas¹, Jorge Cortez¹, Jairo A. Vasquez-Lopez²

¹Physics, Universidad del Cauca, Popayan/COLOMBIA, ²Morphological Sciences, Universidad del Cauca, Popayan/COLOMBIA

For many decades, visualization of histological samples was performed using a contrast media (stain) in order to visually enhance relevant details of tissue structures that characterize a histological tissue. However, so far, there is no perfect dye or staining technique that allows visualization of all relevant details in a histological preparation because it depends on the type of dye and chemical affinity with tissue. Additionally, chromatic changes such as low contrast resolution or excess dye in the tissue are presented as a result of the misuse of the staining technique. On the other hand, nowadays, histological images can be digitally processed to obtain a variety of information, including: classifying textures, glands segmentation and identification, and nuclei and cell counting. Nevertheless, in order to perform digital processing in an efficient manner and to obtain reliable results, images must have high quality and meet certain conditions, such as uniform colouring and a good difference in contrast.

In this paper, a novel methodology to improve visualization of histological samples is presented. It uses previously calculated colour

lighting to illuminate the sample. Colour is calculated using feature lighting and a physical-mathematical model based on RGB and HSI colour spaces; this lighting differs from the white light conventionally used in optical microscopes. Because of the aim is to increase contrast in the area of interest, this development is based on the complementary colour theory, which states the following: "Each colour which allowed the painters' primaries (red, yellow, blue) to be arranged opposite their complementary colours (e.g. red opposite green), as a way of denoting that each complementary would enhance the other's effect through optical contrast. ", or expressed in other words, complementary colours enhance contrast to maximum each other, which is ultimately what we want to observe in a histological preparation.

The proposed technique was tested subjectively and quantitatively, first, by measuring intra- and inter-observer variations after observing morphological patterns by the histologist and pathologists, second, quantitative assessment of histological image after segmenting areas of essential interest for establishing diagnosis more objectively. With the development of the proposed digital optical system, contrast, within different areas of interest in a tissue sample, both visually and through computer vision techniques, is automatically increased, so digital images can be processed more comfortably. The implementation of this technique will reduce time and cost of examinations such as tissue biopsies, facilitate diagnostic evaluation by pathologists and will reduce the waste of histological material; which will end in to benefit the most important person in the process of health care: the patient.

PS01.027 - Pixel-based dynamic contrast-enhanced CT study with low temporal resolution

Author(s): Sun Mo Kim¹, Michael Milosevic², Masoom A. Haid-er³, Ivan Yeung⁴, David Jaffray¹

¹Radiation Physics, Princess Margaret Cancer Centre, Toronto/ON/CANADA, ²Radiation Medicine Program, Princess Margaret Cancer Centre, Toronto/ON/CANADA, ³Medical Imaging, Sunnybrook Health Sciences Centre, Toronto/ON/CANADA, ⁴Radiation Physics, Princess Margaret Cancer Centre, Toronto/CANADA

Purpose: In dynamic contrast enhanced CT (DCE-CT) study, a CT scanning with high temporal resolution is necessary to obtain accurate kinetic parameter values, but such scanning scheme substantially increases the radiation dose to the patient. A method of principal component analysis (PCA) filtering combined with the arterial input function (AIF) estimation technique is proposed to reduce patient radiation dose, while maintaining high accuracy of kinetic parameter estimates in a pixel-by-pixel analysis of DCE-CT data acquired at a low scanning frequency.

Methods: With the coarsely sampled AIF of a patient, an AIF in high temporal resolution can be generated by using the previously published technique which uses the orthonormal bases of the arterial impulse responses (AIR) extracted from a cohort of 34 patients with cervical cancer. In addition, principal component analysis (PCA) filtering was applied to the tissue curves of all the pixels in a region of interest to increase their signal to noise ratios (SNR). The proposed method was applied to each DCE-CT data set of a cohort of 14 patients at varying levels of down sampling schemes between intervals from 2 to 15 s. Subsequently, the kinetic analyses using the modified Tofts' model and singular value decomposition (SVD) method were performed for each of the down-sampling schemes. The results were compared with analyses done with the measured data in high temporal resolution (i.e. original scanning frequency) as the reference.

Results: The results of kinetic analyses using the proposed method compared with down sampling alone showed that the method is superior in maintaining the accuracy in the quantitative histo-

gram parameters of volume transfer constant (standard deviation (SD), 98th percentile, and range), blood volume fraction (mean, SD, 98th percentile, and range), and blood flow (mean and median) for longer sampling intervals between 10 and 15 s. The preliminary results suggest that the method is able to support the longer scanning intervals at a cost of 8.4%–20.5% loss in accuracy of the histogram parameters for volume transfer constant and 6.9%–18.2% for blood volume fraction, and 5.9%–8.7% for blood flow.

Conclusion: The radiation dose to patient during a DCE-CT study can be reduced by up to a factor of 15 with the proposed method of PCA filtering combined with the AIF estimation technique. The results indicate that the method is useful for pixel-by-pixel kinetic analysis of DCE-CT data for patients with cervical cancer.

PS01.028 - Method for restoring CT images obtained at low doses.

Author(s): David Adame Brooks¹, Rafael A. Miller-Clemente¹, Marlen Perez-Diaz²

¹Group Of Radiation Medical Physics, Biofísica Médica, Santiago de Cuba/CUBA, ²Study Center On Electronic And Information Technologies, Universidad Central "Marta Abreu" de las Villas, Santa clara/ CUBA

The advent of computed tomography (CT) has revolutionized diagnostic radiology. Since its inception in the seventies, its use has grown rapidly and has become the technique of choice for a wide range of indications, due to the timely and reliable diagnostic information it provides. However, despite clear evidence that CT provides valuable information for the diagnosis and treatment of the patient, there is a potential risk for the use of ionizing radiation. The benefit of an accurate diagnosis and timely justifies the use of this technique. Despite this, it's important to reduce radiation doses particularly in children and young patients that if they are exposed to these multiple times radiation during their lives may accumulate a significant dose of ionizing radiation, which in turn could lead to an increased risk. In TC, there is a compromise between image quality and dose of ionizing radiation. The problem is that by reducing the radiation dose in CT, the amount of noise in the images is increased. This is because the scanner detectors are fewer photons, which decreases the signal to noise ratio. As consequence, the noise can hide anatomical detail and decrease the detection of lesions with low contrasts. At very low doses, can also exacerbate undesirable effects on images, such as artifacts. To reduce the noise in images have been proposed different algorithms and mathematical methods. Among these are algorithms that directly filtered X-ray projections or reconstructed images. Process the reconstructed images instead of the projections has practical advantages: the images are available to any user, the methods are applicable to any type of scanner regardless of the manufacturer and usually do not demand high performance computing capacity. We proposes a method , which takes as a basis the bilateral filter theory with some changes to improve efficiency and add a component, the separation in frequency bands; to combine the images of high and low frequency after being filtered by the bilateral filter. In our case we use three filter functions most used in the image processing in the domain of the frequencies, the ideal, Butterworth and Gaussian filter, also add the use of an edge operator to improve contrast and highlight the edges of the anatomical structures. Our preliminary results suggest that it is possible to reduce the noise in at least one 30 to 50%. The studies with mathematical observers revealed that our method can decrease the noise of images and even guarantee a diagnostic quality suitable for the diagnosis that could result in the reduction of the dose of radiation.

PS02 - TRACK 02: BIOMATERIALS AND REGENERATIVE MEDICINE

PS02.001 - Chitosan: A Chitinous Biopolymer For The Treatment Of Crude Oil Polluted Water

Author(s): Eillen E.C. Agoha, C Atowa, Fatima Okafor, C.A. Ozodigwe
Food Sciences And Technology, Abia State University, Uturu,, Uturu/NIGERIA

The level of crude oil pollution of Taabaa village stream in Ogoni, Rivers State, Nigeria and the effectiveness of snail shells waste chitosan in the treatment of crude oil polluted water were investigated. Triplicate samples of crude oil polluted water were treated with varying concentrations (0.1, 0.2 and 0.3mg/L) of chitosan. Results indicated that untreated crude oil polluted water samples had a brown colour, hydrocarbon taste and odour and a high turbidity value of 17.00 units Hazen. The water also contained high levels of lead (0.10mg/L), arsenic (0.34mg/L), and iron (0.84mg/L), and had a total plate count of 310CFU/mL, coliform count of 150CFU/mL and *E. coli* count of 25CFU/mL. Chitosan treated water sample was clear, colourless, tasteless and odourless with a 100% reduction in turbidity. Chitosan treatment at 0.1, 0.2 and 0.3mg/L concentrations produced 80 and 90% reductions in lead and reduced the arsenic content from 0.34mg/L to 0.04mg/L. Similarly, chitosan treatment produced

100% reduction in *E. coli*, while the total plate and coliform counts were reduced to WHO acceptable levels. The results showed that the Taabaa village stream was highly contaminated with crude oil and also indicated the potential use of chitosan in the treatment of crude oil polluted water

PS02.002 - Temperature of ice formation affects integrity of alginate 3D constructs after cryopreservation

Author(s): Oleksandr Gryshkov, Lothar Lauterboeck, Nicola S. Hofmann, Birgit Glasmacher
Leibniz University Hannover, Institute for Multiphase Processes, Hannover/GERMANY

Introduction

Cryopreservation is the one available method for long-term preservation of rare cell types. Application of alginate encapsulation may improve cell viability by protecting the encapsulated cells from the ice re-crystallization and osmotic stresses upon freezing and thawing. This work explores the effect of the temperature of extra-cellular ice formation on the integrity of alginate beads.

Methods

The alginate beads with a diameter of 300 μm were generated using the high voltage encapsulation method [1]. After encapsulation and cross-linking for 15 min or 45 min, the alginate beads were re-suspended in cold culture medium (0.5 ml, 4°C). The double-concentrated cryomedium containing 5/10/15/20% (v/v) dimethyl sulfoxide and 20% (v/v) fetal bovine serum was added (0.5 ml) and the beads were equilibrated at 4°C on ice for 15 min or 45 min. Afterwards, the sample was transferred onto a quartz dish, covered with a cover slip and placed into the Linkam cryostage (FDSC 196, Linkam, UK). The following protocol with no active control over the temperature of ice formation was used: cooling rate -1 K/min from 4°C to -20°C, equilibration at -20°C for 5 min with further thawing from -20°C to 4°C with 100 K/min.

Results

The cryomicroscopy results showed that the application of 2.5%, 5%, 7.5% and 10% DMSO with pre-freezing DMSO loading intervals (15 min, 45 min) influenced differently the integrity of alginate beads post-thawing (Figure 1). The temperature of ice formation also affected the integrity of the alginate beads after thawing. The formation and further growth of specific ice crystals at higher temperatures (-12.8°C) caused mechanical rupture of alginate beads. In addition, the temperature of spontaneous ice formation varied from -12.8°C to -19.2°C.

Figure 1. Analysis of freezing/thawing of alginate beads via cryomicroscopy for 10% (v/v) DMSO and 15 min of pre-freeze loading interval. Scale bar is 100 μm .

Conclusions and outlook

In this study it was found that the temperature of ice formation is one of the main factors affecting integrity of alginate beads after thawing. Further work will be performed to study the effect of ice formation temperature on the encapsulated cells functionalities after thawing.

Acknowledgments

This work is in part supported by the German Research Foundation (DFG) through a scholarship of the cluster of excellence REBIRTH (EXC 62/1)

References

[1] O. Gryshkov *et al.* (2014). Encapsulating non-human primate multipotent stromal cells in alginate via high voltage for cell-based therapies and cryopreservation. *PLoS One* 9, e107911.

PS02.003 - Influence of proteins on magnesium in vitro degradation

Author(s): Ana Silva¹, Florian Evertz¹, Sara Knigge¹, Muhammad I. Rahim², Peter P. Mueller², Hans J. Maier³, Birgit Glasmacher¹
¹Leibniz University Hannover, Institute for Multiphase Processes, Hannover/GERMANY, ²Helmholtz Centre For Infection Research, Helmholtz Centre for Infection Research, Braunschweig/GERMANY, ³Leibniz University Hannover, Institute of Material Science, Garbsen/GERMANY

Introduction

Magnesium is studied as a biomaterial for nonpermanent biomedical implants. Our study is focused on magnesium *in vitro* degradation. Extensive *in vitro* experiments in a simulated physiological environment have been carried out to investigate the influence of proteins on the degradation rate in order to create a protein coating that prevents the fast initial corrosion and decreases the whole corrosion rate during the implantation period, which is the major problem of the use of magnesium and its alloys as biomedical implants.

Methods

Pure magnesium samples and samples of pure magnesium coated with bovine serum albumin were analyzed. In our experiments we used porcine plasma and a simulated body fluid (r-SBF) as corrosion fluids, to test the influence of proteins. Thus, we want to be able to compare the results with the *in vivo* experiments. The *in vitro* degradation studies were done in static conditions and therefore the samples were immersed in each model fluid in 6-well-plates and placed in the incubator in a 5% CO₂ atmosphere at a temperature of 37°C. The magnesium concentration released in the fluid test during the experiment was measured photometrically and the pH was

controlled regularly. The mass loss was also calculated and for that the samples were treated with chromic acid, following the ASTM-Standard G1-03 protocol, in order to remove the oxide layer and weighted after that. SEM/EDX-Analyses were also performed.

Results

Our results show that the degradation rate depends directly on the composition of the fluid which is used we revealed that the coating and the addition of proteins have a significant influence on the degradation rate. An increase on magnesium concentration can be seen in all cases for the initial days. However, a lower initial corrosion has been observed for the coated samples, either in plasma and r-SBF.

Conclusion

The value of the degradation rate for pure magnesium in plasma is much lower than in SBF's. However in the case of the r-SBF when the samples are coated with proteins the degradation rate decreases. These studies show a slower and decreased degradation of magnesium coated samples, leading to a positive influence from proteins on corrosion prevention.

Acknowledgements

This work is supported by funding from the Collaborative Research Center (SFB 599) of the German Research Foundation (DFG).

PS02.004 - Electrospinning of vascular prostheses with anti-kinking properties

Author(s): Michael Bode, Marc Mueller, Holger Zernetsch, [Birgit Glasmacher](#)

Leibniz University Hannover, Institute for Multiphase Processes, Hannover/GERMANY

Introduction

One of the major challenges in developing appropriate vascular substitutes is to produce a graft that adapts to the biological and mechanical conditions at the graft site. One approach is the use of electrospun grafts pre-seeded with autologous cells using methods of tissue engineering. When transplanted in a graft site with high deformation, stiffness of the graft leads to kinking which may result in vascular obliteration. The aim of this study was to develop an electrospun vascular graft consisting of biodegradable polymers which additionally possesses a high flexibility to avoid kinking.

Methods

In order to improve the bendability of the grafts, various collectors with different geometries were structured using six different patterns (30°, 60°, 90°, 120° V-thread, knuckle thread and acme thread). Subsequently, the grafts were examined with regard to fiber deposition, mechanical strength and bendability.

Results

It was shown that using a collector structured with a V-shaped thread (flank angle of 120°) leads to a homogenous and reproducible fiber deposition. The results of the tensile tests were comparable to the unstructured reference sample, proving the first observation. Studies on bendability were performed using a custom made flow-bending test setup. It was shown that the flow through the V-shaped grafts reduced to less than 45 % of the reference value even after bending the graft to an angle of 140° (Figure 1). Compared to this, the flow through an unstructured graft reduced to more than 50% after bending to an angle of 55°.

Conclusion

The presented data, which were obtained with the developed flow-bending test setup demonstrate the need for optimizing the bendability of the commonly used electrospun vascular grafts. In this regard a macroscopic v-shaped engineered collector seems to be a promising method to overcome the issue of graft kinking.

Figure 1 Comparison of two samples with different surface structures. Unstructured reference sample at 40° bending (A). Pleated sample with 120° V-thread at 90° bending (B).

Acknowledgments

This work was partially supported by the the Graduate Academy of Leibniz University Hannover.

PS02.005 - Electrospinning of polycaprolactone/chitosan polymeric fibrous membranes as scaffolds for cardiovascular tissue engineering applications

Author(s): Alexandros Repanas, Fedaa Al Halabi, Marc Mueller, Holger Zernetsch, [Birgit Glasmacher](#)
Leibniz University Hannover, Institute for Multiphase Processes, Hannover/GERMANY

Introduction

Cardiovascular diseases only in the USA account for more than 30% of all deaths with costs exceeding 300 billion dollars, according to the 2013 American Heart Association report [1]. While heart transplantation is the only cure for end-stage heart failure there is need for new strategies to develop materials that can support cell repopulation and functionality recovery. Electrospinning is a facile and cost-effective technique that can produce biocompatible structures to serve as extracellular matrix (ECM)-like scaffolds where cells can be seeded and proliferate eventually forming a hybrid bio-artificial tissue [2]. Fibrous mats, tubes and more complex 3D shapes can be successfully engineered not only to induce cell proliferation but also to release in a controllable manner biomolecules (e.g. proteins, growth factors) that can further support tissue formation [3].

Materials & methods

Polycaprolactone (PCL) and chitosan (CS) were dissolved in 99,8 % 2,2,2-Trifluoroethanol (TFE) at concentrations of 190 mg/ml and 10 mg/ml respectively. The solution was stirred at room temperature for 24 hours. Electrospinning was performed at a custom made apparatus with flow rate of 4 mL/h and electrical field of 1 kV/cm. Morphology of the fibrous scaffolds was examined by scanning electron microscopy (SEM) having previously been sputter-coated with gold. Cyclic sinusoidal uniaxial mechanical tests were performed with an electroforce tensile testing instrument by BOSE, equipped with a 200 N load cell. Rectangular, 15x10 mm strips were cut and tested at 0-20% strain, 1 cycle/sec, RT, dry conditions. Young's modulus was calculated from the linear phase of the stress-strain plot and hysteresis ratio from the area between the loading and unloading steps of each cycle. Static water contact angle experiments were performed to study the physical behavior of the fibers' surface. Chemical characterization including Fourier-Transformed Infrared Spectroscopy (FTIR) and X-rays diffraction (XRD) was carried out in order to determine the physicochemical state of the polymers in the fibers.

Results and Discussion

Structural and morphological analysis indicated that the created fibers have a smooth, "spaghetti-like" shape with an average diameter of $1.098 \pm 0.52 \mu\text{m}$ and random orientation. The average value of Young's modulus was $10 \pm 5 \text{ MPa}$ and the hysteresis ratio 0.35

± 0.07 revealing the viscoelastic nature of the fibers. The surface of the fiber-mats can be considered relatively hydrophilic as the static water contact angle was $70 \pm 5^\circ$. FTIR and XRD data lead to the conclusion that PCL and CS interact in the blend, possibly forming non-covalent bonds with PCL being in a semi-crystalline state and CS in an amorphous form in the fibers.

Acknowledgments

This study was granted by the DFG EXC 62/1 grant via the German Research Foundation (DFG).

References

- [1] Go A.S. et al. *Circulation* 2013;127:143-152
- [2] Szentivanyi A. et al. *International Journal of Artificial Organs* 2011;34(10):986–997
- [3] Szentivanyi A. et al. *Advanced Drug Delivery Reviews* 2011;63:209–220

PS02.006 - Coaxial electrospinning of piezoelectric PVDF/PCL scaffolds for nerve regeneration

Author(s): Fedaa Al Halabi, Alexandros Repanas, Sara Knigge, Birgit Glasmacher
Leibniz University Hannover, Institute for Multiphase Processes, Hannover/GERMANY

Introduction

In neural tissue engineering piezoelectric polymers are being investigated as potential scaffolds for supporting nerve regeneration processes. A promising material is Polyvinylidene fluoride (PVDF) because of its proven biocompatibility and piezoelectric properties, which can possibly stimulate cell ingrowth with its electrical activity upon mechanical deformation [1]. This work reports the coaxial electrospinning of Polyvinylidene fluoride (PVDF) and Polycaprolactone (PCL) core/sheath nanofiber mats in order to enhance the mechanical and physical properties of the PVDF fibers.

Experimental methods

Coaxial electrospun scaffolds were produced from PVDF 20% dissolved in N,N-dimethylformamide and acetone (4:1) as a core and PCL 170 mg/ml dissolved in Tetrafluoroethylene as a sheath. In the electrospinning process flow rates of 0.5 ml/h for the core and 1 ml/h for the sheath and voltages of 22 kV were applied to produce defined fibers. The structures of the PVDF/PCL scaffolds were observed and analyzed with SEM to determine their morphology and fiber diameter. The mechanical properties of the scaffolds were tested using a tensile testing machine (BOSE-Electroforce-LM1-Test-Bench). To determine the configuration of the core/sheath structure in the coaxially electrospun scaffolds and their piezoelectric properties the scaffolds were compared with untreated/raw PVDF pellets with respect to the presence of the nonpolar α -phase and piezoelectric polar β -phase by using FTIR and DSC. The contact angles of the scaffolds surfaces were measured using deionized water. Subsequently All results were analyzed and evaluated comparing with single-jet electrospun PVDF scaffolds.

Results

Coaxial electrospun PVDF/PCL Scaffolds exhibited a higher tensile strength of 1.9 MPa and strain at break of 130 % as compared with the maximum tensile strength of the single-jet electrospun scaffolds of 138 kPa with 75 % elongation at break. The PCL layer increases the hydrophilic property of the coaxial PVDF/PCL scaffolds, which could enhance the adhesion and proliferation of the neural cells on

the scaffolds. Similar to single-jet Electrospinning of PVDF scaffolds, the coaxial PVDF/PCL scaffolds resulted in a polar β -phase formation, which is relevant for the piezoelectric effect, and showed a β -phase adsorption ratio of 53% at 841 and 1277 cm^{-1} in the FTIR-spectrum.

Conclusion

This study shows the ability to produce coaxial nanofibers of PVDF and PCL with better mechanical and physical properties. The FTIR and DSC results demonstrate the piezoelectric effect of the coaxial PVDF/PCL scaffolds. Next steps will be carrying out in vitro and in vivo experiments to evaluate the cytotoxicity of the coaxial scaffolds and to investigate the neural cells culturing on the piezoelectric PVDF/PCL scaffolds.

Acknowledgements

This work is supported by the Collaborative Research Center (SFB 599) of the German Research Foundation (DFG). We gratefully acknowledge the benefit derived from the stimulating discussion with Prof. Dr. med. vet. Kirsten Haastert-Talini from the Hannover Medical School and Prof. Dr. Ir. Willem Wolkers from the Institute for Multiphase Processes, Leibniz University Hannover.

References

- [1] F. AL Halabi, P. Behrens, and B. Glasmacher, "Application of electrospun piezoelectric PVDF scaffolds for nerve regeneration", *Proceedings of the 48th annual conference of the German Society for Biomedical Engineering*, 2014, pp. 193-197, doi: 10.1515/bmt-2014-4566

PS02.007 - Bio rapid prototyping project: Evaluation of spheroid formation for cells construct

Author(s): Takeshi Shimoto¹, Satoru Ikebe², Atsushi Ishikawa², Hidehiko Higaki², Shizuka Akieda³, Koichi Nakayama⁴, Shuichi Matsuda⁵, Hiromasa Miura⁶, Yukihide Iwamoto⁷

¹Fukuoka Institute of Technology, Fukuoka/JAPAN, ²Kyushu Sangyo University, Fukuoka/JAPAN, ³Cyfuse Biomedical K.K, Tokyo/JAPAN, ⁴Saga University, Saga/JAPAN, ⁵Kyoto University, Kyoto/JAPAN, ⁶Ehime University, Ehime/JAPAN, ⁷Kyushu University, Fukuoka/JAPAN

In the field of regenerative medicine, 3-D tissue engineering, which intends to regenerate lost tissues and organs, is mainly focused. Formation of a 3-D construct outside the body has already been attempted by using combination of three elements, cells, growth factors or genes, and scaffold. We have already established a technique to make a 3-D construct only with cells. However, these constructs are usually made by skilled technicians who are familiar with cells, reagents, and cells culture methods. Therefore, we are developing a cell processing robot for regenerative medicine.

Cells construct is made by spheroid-culturing the cells and neatly arrange the spheroids. Therefore, quality of spheroids is important. The spheroids are manufactured by dispensing cell turbid liquid into a special multiwell plate. If there is a difference in the number of cells when dispensing the cells turbid liquid, spheroids in different sizes are generated. Moreover, spheroids are not generated if the number of cells is extremely small, and if large, spheroids in distorted shapes are generated. Therefore, this study was aimed to evaluate spheroids formation.

In this study, operations was performed by non-skilled technician and skilled technician. We used MSC (Mesenchymal Stem Cell) harvested from a Japanese white rabbit. Cultures of MSC were carried out on the culture dishes ($\Phi 150$ mm, H25 mm, FALCON). Upon reaching the required number of cells, they were dispensed into the

special multiwell plate for forming spheroids can generate 96 spheroids per plate. Cell number of a spheroids was set at 2×10^4 , 3×10^4 , 4×10^4 , 5×10^4 , 6×10^4 and 7×10^4 , were taken by the camera every 24 hours. We analyzed the quantitative evaluation, i.e., area, diameter and degree of circularity, with the images of spheroid.

The result of the experiment was that there are difference in the spheroids created by non-skilled technician and skilled technician. The handwork was conducted by a skilled technician and there was no failure in the spheroid generation. However, when it was conducted by a non-skilled technician, sometimes resulted in failure. This case could have happened because the cells were exposed to the external air for a long time or the pipettes were erroneously operated and resulted in the occurrence of contamination, death cells, or no uniform works. Incidentally, the size of spheroids formed by the number of cells was different. In particular, it was found that there is a range of cell number to form spheroids with high degree of circularity. Therefore, by adjusting the number of cells, it may be possible to control the size of the spheroids.

We are performing the development of a spheroid building system. In spheroid exfoliation by pipetting or stirring of cells turbid liquid, it is necessary to reconstruct the motions of skilled technicians with specialist knowledge and technique so as not to damage the cells. Therefore, by the system reproduces techniques of the skilled technicians, we can obtain the spheroids uniformity, and can adjust the size of the spheroids.

PS02.008 - Scaffold Prototype for Heart Valve Tissue Engineering: Design and Material Analyses

Author(s): Marcia M.O. Simbara, Ronny C. Carbonari, Sônia M. Malmonge
Biomedical Engineering, Universidade Federal do ABC, Santo Andre/BRAZIL

Cardiac valves are specialized structures that ensure unidirectional flow through the heart. The aortic valve is the most frequently diseased and substituted. The current alternatives have reached a satisfactory level, but they still have their limitations, the most relevant one being the inability to remodel and grow, a critical problem especially for pediatric patients. Tissue engineering is expected to be the ultimate solution to this, for it creates viable structures. The aim of this work is to propose a scaffold prototype for heart valve tissue engineering using bioresorbable polymers and analyze its design and materials through computational analyses. The scaffold design was based on existent biological valves and a 3D model was built using SolidWorks 2008. Poly(3-hydroxybutyrate-co-valerate) (P3HBV), poly(L-lactic acid) (PLLA) and poly(ϵ -caprolactone) (PCL) were submitted to tensile tests in order to obtain their mechanical properties. The data collected was used to perform the computational simulation using ANSYS. The parts of the prototype were built using compression molding and airbrushing techniques. Results show that the designed geometry and the materials chosen allow the scaffold to withstand the stresses which they are subjected to. Also, the techniques chosen were indeed adequate for the manufacturing of the prototype, resulting in a very resistant structure. Some adjustments can and will be made in order to optimize mechanical behavior, but generally the scaffold seems to be adequate for heart valve tissue engineering.

PS02.009 - Unidirectionally-frozen silk/gelatin scaffolds for cardiac tissue engineering

Author(s): Maria Christine T. Asuncion, James Cho-Hong Goh, Siew-Lok Toh
Biomedical Engineering, National University of Singapore, Singapore/SINGAPORE

On a global scale, cardiovascular diseases (CVDs) remain to be the leading cause of death. Not only a pathological problem for the patient, CVDs are also an economic burden due to the prescribed maintenance medication and resulting decrease in physical productivity of the patients. One of the most common CVDs is the narrowing of the coronary artery that leads to ischaemia and tissue necrosis. Due to the heart's limited capacity to regenerate, heart transplants have long been the gold standard if a full functional restoration of the organ is desired. However, organ donor shortage and transplant rejection remain as challenges faced by heart transplants, making a tissue engineering strategy a more promising alternative. In this study, unidirectional freezing was achieved using a custom mold, and together with freeze-drying to fabricate a silk fibroin/gelatin-based scaffold with an aligned structure in an effort to mimic the natural anisotropy of cardiac tissue. Silk fibroin was chosen for its biocompatibility, biodegradability, low immunogenicity and good mechanical strength. Gelatin was added to enhance cell attachment to the scaffold. Scaffold morphology transitioned from an isotropic structure to an aligned structure as the freezing temperature was decreased, whereas pore morphology transitioned from an elliptical shape to a lamellar shape. Average pore size for the aligned scaffolds decreased as the freezing temperature decreased. All scaffolds exhibited a high degree of swelling with magnitudes of 656-700%. Cell viability and attachment was also investigated. The application of the aligned silk/gelatin scaffold as a cardiac patch is the objective of future studies. Although unidirectional freezing has been explored in previous investigations, its application as a cardiac patch has received little attention as of yet. It is hypothesized that the structural anisotropy of the scaffold will help promote differentiation of stem cells into a cardiomyogenic lineage without further external stimuli.

PS02.010 - Engineering Mesenchymal Stromal Cells (MSCs) to be More Immuno-evasive by Altering Cell Culture Conditions

Author(s): Shashank Bhatt¹, Armand Keating², Sowmya Viswanathan¹

¹Cell Therapy Program - Dmoh, University Health Network, Toronto/CANADA, ²Dmoh, University Health Network, Toronto/ON/CANADA

We demonstrate that by minimally altering culture conditions for adult human bone marrow (BM) mesenchymal stromal cells (MSCs) to serum-free, cytokine-supplemented, non-adherent conditions, we can change the expression of adhesion molecules and human leucocyte antigens (HLA-ABC). This change is not accompanied by any other phenotypic changes; cells maintain the expression of minimal MSC cell surface antigens (CD90 (99.9%), CD105 (98%), CD73 (99.9%), CD14 (0.2%), HLA-DR (0.1%), CD34 (0.1%) and retain their ability to undergo trilineage differentiation. However, these cells show a decrease in HLA-ABC expression (d7: 47%, vs 99.9% d14: 10.4% vs 95.9%, and d21: 3.8% vs 90%), vascular cell adhesion protein-1 (VCAM-1) expression (d7: 14.6% vs 95.2%, d14: 1.4% vs 88% , and d21: 0.1% vs 80%) and Intercellular adhesion molecule-1 (ICAM-1) expression (d7: 13% vs 78.2%, d14: 0.5% vs 70%, and d21: 2.6% vs 62.3%). A standard ⁵¹Cr cytotoxicity assay showed that MSCs cultured in suspension, under serum-free, cytokine-supplemented conditions had reduced susceptibility to cytotoxicity from NK-92, a permanent allogeneic NK cell line under clinical investigation for treating hematopoietic malignancies (9.08% \pm 1.86% killing vs. 59.17% \pm 3.66% killing at a 40:1 NK-92:MSC ratio). Cytotoxicity at lower effector-to-target ratios (20:1, 10:1, and 5:1) was effectively 0% (SD <2%) for MSCs grown in altered conditions, compared to

approximately 30% (SD <3%) for traditional, adherent-grown MSCs. In vivo experiments in an acute inflammatory (lipopolysaccharide (LPS) paw edema) murine model are ongoing to examine effects on modified homing and anti-inflammatory properties when MSCs are grown in altered, suspension cultures vs. traditional cultures. We conclude that by subtly changing culture conditions we can alter adhesion molecules and HLA-ABC expression, which in turn affects immunoevasion, homing and migration of MSCs, equipping the cells for potentially more potent therapeutic effects in treating immune-related disorders.

PS02.011 - Novel zwitterionic polypeptides for improving resistance to non-specific protein adsorption

Author(s): Xiaojuan Wang¹, Kemei Shi¹, Hanqing Gu²

¹Pain Management Center, The Second Hospital of Tianjin Medical University, Tianjin/CHINA, ²Tianjin Institute Of Urology, Tianjin Medical University, Tianjin/CHINA

In the past three decades, because of the potential applications in biomedical fields, numerous biomaterials have been widely studied, such as medical implants, drug delivery carriers, and biosensors. Protein adsorption is the first response from human body to foreign materials exposed to physical environment. However, non-specific protein adsorption often induces biological incompatibility, thus, it's very urgent to explore new surface modification of different materials in medicine. Herein, we developed a good candidate coating material, zwitterionic dimethyl aminopropyl amine-grafted poly (α , β -L-aspartic acid)s (DMAP-PASP), by performing the aminolysis of poly (succinimide) (PSI) with different amount of a cationic monomer dimethyl aminopropyl amine, followed by hydrolysis of the residual PSI.

The modified polypeptide derivatives composed of certain negatively carboxylic acid and positively charged aminopropyl amine, and this is why DMAP-PASP could be considered as random zwitterionic copolymers. The ¹H NMR spectrums were used to demonstrate the ratio of successful conjugated cationic units. A novel turbidity and zeta potential measurements were used to study the dilute solution behaviors of DMAP-PASP under different pH values. Each of the synthesized zwitterionic copolymer exhibited an isoelectric point (IEP) and showed opposite charges below and above the IEP. Compared to our previously reported zwitterionic polypeptide derivative, synthesized by amidation of Poly (α , β -L-aspartic acid) with L-histidine methyl ester, this synthesis route is more convenient and the number of dimethyl aminopropyl amine functionalitie could be controlled in a quantitative way. Therefore, the isoelectric point of the zwitterionic polypeptides could be easily tuned from pH 3.8 to 9.5.

There the fibrinogen, a blood protein resulting in the blood coagulation cascade, was used as a model protein. Therefore the zwitterionic polymer with an IEP of 5.3 was firstly pre-coated on the positive silica surface NH₂-SWs for the purpose of evaluating its protein-resistant characteristics. The amount of protein adsorbed to each sample was quantized and compared with those on the NH₂-SWs without polymer modification. In compared with the unmodified surface, fibrinogen protein adsorption on surfaces was eliminated effectively by DMAP-PASP polymer film. Furthermore, the anti-biofouling behavior through electrostatic interactions was affected by the surface charge density, which means in a dose-dependent manner.

Due to the good biodegradability and superior anti-protein-fouling property, this series of pH-responsive zwitterionic polypeptides are promising candidates for serving as an anti-biofouling material for in vivo applications, including medical implants, drug delivery carriers, and biosensors.

This work was funded by the National Natural Science Foundation

of China (51303133) and Research Foundation of Tianjin Medical University (2013KYQ03)

PS02.012 - Study on preparation and mechanical properties of polyurethane foam with negative Poisson's ratio

Author(s): Lizhen Wang¹, Yifan Liu², Yubo Fan³

¹School Of Biological Science And Medical Engineering, Beihang University, Beijing/CHINA, ²School Of Biological Science And Medical Engineering, Key Laboratory For Biomechanics And Mechanobiology Of Ministry Of Education, National Key Lab Of Virtual Reality Technology, Beijing, China, Beihang University, Beijing/CHINA, ³National Research Center for Rehabilitation Technical Aids, Beijing/CHINA

Auxetic foam was a new kind of material which exhibit negative Poisson's ratio effect. It has a wide application prospect. However, auxetic foam would gradually expand to its original volume with time increasing, and the negative Poisson's ratio effect will disappear. The practical use of the auxetic foam has been limited, and it becomes an urgent problem to be solved before its application. The preparation conditions and the recovery ability of auxetic foam, the 60 ppi open cell polyurethane (PU) foam was used as the parent material. The PU foams were compressed in three dimensions and been heat treated at setting temperatures. After cooling down, the auxetic foams were made. In this study, all samples were set with the same radial compression ratio, but three different axial compression ratios. During the heat treatment process, the setting temperatures were 140°C, 150°C and 160°C respectively. It was found that the setting temperature in the condition of this study should be heated until 150°C to obtain the re-entrant structure.

PS02.013 - Proliferation of cardiomyocytes in neonatal, furture implication in heart regeneration

Author(s): Lincai Ye¹, Lishen Qiu², Haibo Zhang², Huiwen Chen², Chuan Jiang¹, Haifa Hong¹, Jinfen Liu¹

¹Pediatric Congenital Heart Disease Institute, Shanghai Children's Medical Center, Shanghai/CHINA, ²Department Of Thoracic And Cardiovascular Surgery, Shanghai Children's Medical Center, Shanghai/CHINA

Background- Human heart is a limited-mitotic organ that responds to injury with limited cell renewal. In young infants, study of the regenerative capacity of cardiomyocytes may provide an important approach for heart regeneration.

Methods and results- Human right atrial specimens were obtained during routine surgery for ventricle septal defect(VSD) and were divided into two groups: Young infant group (age, 1-3 months) and Old infant group (age, 4-6 months). Results showed that Ki67 is expressed in proliferating cardiac myocytes, and that the number of Ki67-positive cells in young infant group is significantly higher than old group. The Notch pathway was found to regulate cardiomyocyte proliferation and apoptosis during development. Current data showed that NICD expression is significantly higher in young age group and NICD was mainly expressed in cardiomyocyte nuclei.

Conclusions- Proliferating cardiac myocytes are more abundant in the young infant period (<3 months) and the Notch pathway is conserved in humans. Further understanding of their proliferative ability at different ages may provide novel therapeutic targets that can be used to enhance cardiovascular regenerative capacity.

PS02.014 - Synergetic effects of released ions from CaO-MgO-SiO₂-based multiphase bioceramics on osteogenic proliferation and differentiation

Author(s): Meng J. Zhang, Xian C. Chen, Xi M. Pu, Xiao M. Liao, Zhong B. Huang, Guang F. Yin
College of Materials Science and Engineering, Sichuan University, chengdu/CHINA

Bioceramics have great potential for bone regeneration and tissue engineering applications. A novel CaO-MgO-SiO₂-based multiphase glass-ceramic, composed of akermanite (Ca₂MgSi₂O₇), wollastonite (CaSiO₃), and dicalcium silicate (Ca₂SiO₄) crystalline phases, was designed and synthesized by sol-gel method. As reported, this glass-ceramic could induce the formation of bonelike-CHA layer when soaked in simulated body fluid (SBF), and obviously promote cell proliferation and differentiation of human osteoblasts. Further research confirmed that the ionic products released from this CaO-MgO-SiO₂-based ceramic played an important role in the modulation of cell proliferation and differentiation. In this research, the synergistic effects of its released ions (calcium ions, magnesium ions, and silicic acid radical ions, simply marked as Ca, Mg, and Si ions) on MG63 cell behaviors and their effective ion concentrations were systematically and thoroughly investigated. Original extract was prepared according to International Standard Organization (ISO/EN 10993-5), and then times diluted into 1/2, 1/4, 1/8, 1/16, and 1/160. The corresponding concentrations of Ca, Mg, and Si ions in different diluted extracts were detected by inductively coupled plasma optical emission spectroscopy (ICP-OES), and the diluted extracts were used for cellular experiments. All the results showed that released ions from CaO-MgO-SiO₂-based bioceramic could stimulate cell proliferation and osteogenic differentiation of MG63 cells at certain concentrations. Such effects were concentration-dependent, and 1/4 diluted extract (Ca 104.69 ppm, Mg 13.13 ppm, Si 33.36 ppm) was the most significant. Moreover, even 1/160 diluted extract also stimulated osteogenic proliferation and differentiation, which might be caused by additional trace amounts of Si ions (Si 0.92 ppm). It is suggested that trace amounts of Si ions could work accompanied with certain concentrations of Ca and Mg ions. Above results inferred that synergetic Ca, Mg, and Si ions played an important role in osteogenic proliferation and differentiation. However, results of MTT and FCM revealed that 1/2 diluted extract (Ca 119.15 ppm, Mg 10.99 ppm, Si 45.08 ppm) slightly inhibited MG63 proliferation by hindering the transition of cell cycle from G₁ to S phase in the first day. This phenomenon indicated that excessive concentration of Ca and Si ions could result in inhibiting effect on cell proliferation, and with the presence of Mg ions, the effective combination concentrations of Ca and Si ions can not exceed 119.15 and 45.08 ppm, respectively. In general, synergistic effect of various ions is crucial for cell proliferation and differentiation. To merely investigate the ion concentration range of single ion would be of lesser significance, because the beneficial ion concentrations with the existence of various ions are certainly not as the same as that with single ion. This research displayed the synergistic effects of Ca, Mg, and Si ions on the regulation of osteogenic proliferation and differentiation, and investigated the effective concentrations of Ca and Si ions released from bioceramics with the presence of Mg ions. It would be the basis to investigate the biological function of these bioceramics, and would be of great importance to design CaO-MgO-SiO₂-based bioceramics applied as bone tissue engineering scaffolds.

of biodegradable potential medical implant alloy Mg₂Ca result from rapid solidification with four cooling rates by using the generalized nonlocal model pseudopotential (GNMP) theory. Results indicate that cooling rate plays important role in the formation of icosahedron local structure, the lower the cooling rate, the more icosahedron micro-cluster forms in the system. It is also found that cooling rate is also have important effects on the glass transition, the higher the cooling rate, the higher the temperature the glass transition happens at.

PS02.015 - Cooling Rate Effects on the Microstructure Evolutions of Biodegradable Mg₂Ca Potential Medical Implant Alloy

Author(s): Li Li Zhou, Yang Yang, Xiao Hui Qiu, You Lin Peng
Department Of Information Engineering, Gannan Medical University, Ganzhou/CHINA

The molecular dynamics simulation calculations have been performed to investigate the cooling rate effects on the microstructure evolutions

PS03 - TRACK 03: BIOMECHANICS AND ARTIFICIAL ORGANS

PS03.001 - Musculoskeletal and Finite Element Simulation of Archery

Author(s): Yahia M. Al-Smadi

Mechanical Engineering, Texas A&M University - Kingsville, Kingsville/UNITED STATES OF AMERICA

In practice the behavior of the Bow-Arrow-Archer system termed ‘interior ballistics’ and the arrow in flight termed ‘exterior ballistics’ are complicated. In order to understand the mechanics of archery computer models are required. The musculoskeletal simulation is becoming a popular method in the research field of biomechanics to estimate muscle activity from body motion. The objective of this study is to conduct biomechanical simulation for a musculoskeletal of archery. This simulation aims to find the movement patterns in several working postures, stress induced on muscles and the amount of elongation of different muscles responsible for performing archery.

The work presented discusses the anatomical body arrangements and conducts biomechanically correct simulation. A design of experiment technique was utilized to find the optimum parameters such as muscle effort, angle, stress, strain etc to eliminate excessive stresses on glenohumeral, sternoclavicular & cromioclavicular joints. Initially a three dimensional model of bow and arrow is generated in Solidworks. Next stage of the experiment was performing musculoskeletal simulation using AnyBody software using “Any-script” language which is similar like other existing programming languages. During this simulation of archery, all the programming codes were taken care thoroughly to reduce errors.

The anatomy of the shoulder is unique – it has a relatively shallow socket which results in amazing

flexibility and range of motion to the glenohumeral joint which is unparalleled elsewhere in the body. The dynamic forces and stress of arm shoulder using lagrangian mechanics approach which is verified using simulation in AnyBody software. The stresses found in the deltoid, trapezius and biceps and tricep muscles are analyzed along with the range of elongation is shown in Figure 1

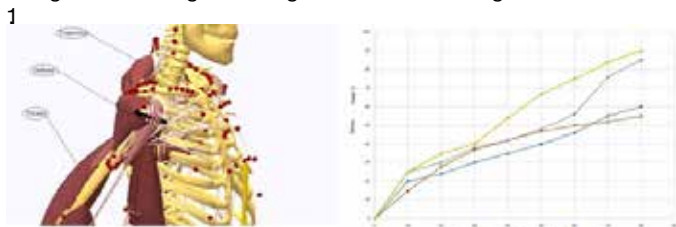


Figure1: AnyBody Simulation and Stress vs Elongation

By simulating the model one can analyze the causes for most common shoulder pain observed in archer. For each analysis, the system stores the maximum stress of muscle at any point of the movement. The simulation estimates the optimum parameters to eliminate stress overloading on the muscles and investigates muscle efforts and joint forces depending on postures.

PS03.002 - Dysfunction Screening in Experimental Arteriovenous Grafts for Hemodialysis Using Inflow and Outflow Hemodynamic Game Analysis

Author(s): Wei-Ling Chen¹, Chung-Dann Kan², Chia-Hung Lin³

¹Department Of Engineering And Maintenance, Kaohsiung Veterans General Hospital, Kaohsiung/TAIWAN, ²Department Of Surgery, National Cheng Kung University Hospital, Taiana/TAIWAN, ³Department Of Electrical Engineering, Kao-Yuan University,, Kaohsiung City/TAIWAN

This study proposes inflow and outflow hemo-dynamic game analysis for early evaluation of the risk of arteriovenous access dysfunction during hemodialysis (HD) treatment. In physical examinations, inflow and outflow pressure drops and the resistive (Rsc) index reflects pulsatile flow and changes in flow volume resulting from changes in pressure, in terms of the degree of stenosis (DOS). Using static differential pressure sensors, the measured pressure drop is used to estimate the injection velocities and Res indexes through an in vitro access in on-line analysis. A less parameterized cooperative game (CG) based decision-making model is then utilized to evaluate the risk of an access dysfunction. As a simulator of the cardiovascular system and hemodialysis circulation system, the findings indicate that the proposed measurement method and decision-making model can be used in practical examinations during HD treatment.

PS03.003 - The Effects of Limb Dominance, Sex, and Gait Speed on Multisegment Foot Kinematics During Gait

Author(s): Victoria Chester¹, Usha Kuruganti¹, Jeffrey Grant²

¹Kinesiology, university of new brunswick, fredericton/CANADA, ²Kinesiology, University of New Brunswick, Fredericton/CANADA

While the foot plays a critical role in support and propulsion during gait, multisegment foot research is still in its infancy. Most gait research has modeled the foot as a single rigid segment consisting of two rotational degrees of freedom. With advances in motion capture technology, there has been a recent increase in the number of studies using multisegment mechanical models. These models divide the foot into multiple compartments or segments allowing the relative motion between segments to be measured (e.g. forefoot vs hindfoot). Currently, we know little about the factors that may affect multisegment foot motion. Therefore, the purpose of the present study was to examine the effects of speed, gender, and limb dominance on multisegment foot kinematics during gait. Such studies will lead to an improved understanding of foot mechanics in typical and atypical gait.

Twenty-one adults (11 female, 12 male) aged 18 to 28 years were recruited to participate in the study (age = 23.0±2.6 years; height = 1.73±0.1 m; weight = 72.1±10.1 kg). Participants were asked to perform gait trials at 5 different walking speeds. A 12-camera Vicon T160 motion capture system (Oxford Metrics Group, Oxford, UK), sampling at 100 Hz, was used to track the three-dimensional trajectories of 34 reflective markers placed on the participant. The rigid body model consisted of five segments: 1) the shank, 2) the total foot (single rigid segment), 3) the calcaneus, 4) the midfoot, and 5) the forefoot. The hallux and metatarsal bones were modeled as line segments for the computation of planar angles. Euler angle data was analyzed using custom software created in Matlab (Mathworks, Inc). A MANOVA and post hoc analyses were used in SPSS to test for significant differences in maximum joint angles between sex and dominant and non-dominant limbs across the 5 walking speeds.

No significant differences (p>0.05) in mean maximum joint angle data were found between limbs and sex during gait. Significant differences (p < 0.002) in the mean values of temporal-spatial variables between speed groups were found for stride length, toe-off, percentage of time spent in single leg stance, and cadence. Significant differences (p < 0.002) in mean maximum joint angle data

were found in the sagittal plane only. Changes in speed altered the angular kinematics of the calcaneus vs tibia, midfoot vs calcaneus, and forefoot vs calcaneus. In addition, planar angles of the hallux, metatarsals, and medial longitudinal arch also varied with speed.

Similar to the results of simple foot models, the results of this work suggest that walking speed has an effect on multisegment foot kinematics. The relative angles between foot subsegments changed as a function of gait speed. The midfoot segment, which is often ignored in multisegment studies, showed significant changes in angular data with respect to the calcaneus. Therefore, multisegment foot studies of clinical populations should use speed-matched control data for comparative purposes. This would facilitate the identification of pathological gait from speed-mediated effects. Future studies will examine the effects of walking speed on multisegment foot kinematics in varying age groups.

PS03.004 - Investigation of transfibular locking plate to treat open extra-articular distal tibia fractures

Author(s): Ryan Normore¹, Helena Greene¹, Allison Delong¹, Andrew Furey², Amy Hsiao³, Stephanie Atkinson¹

¹Faculty Of Medicine, Memorial University of Newfoundland, St. John's/NL/CANADA, ²Faculty Of Medicine, Memorial University of Newfoundland, St. John's/CANADA, ³Mechanical Engineering, Memorial University of Newfoundland, St. John's/CANADA

The current surgical treatments for extra-articular distal tibia fractures have significant limitations; therefore the structural stability of a novel trans-fibular method of fixation was investigated. The fracture site was secured using a locking plate attached to the lateral side of the fibula by threaded locking screws projecting through the fibula and securing into the tibia. Synthetic sawbone specimens, that have been shown to behave similar to human bone, were chosen for this initial construct testing because of their anatomic consistency. The specimens have had osteotomies to simulate distal tibia fractures and have undergone trans-fibular fixation. The specimens were then tested using a hydraulic load frame under three different axial loading conditions; linear loading to 700N, cyclic loading of 700N for 10,000 cycles, and a specimen load to failure. Failure was defined as vertical displacement of the fracture site greater than 5mm or an angular displacement greater than 5°. Vertical displacement, applied load, and angular displacement of the specimen were recorded and a preliminary analysis was completed, including a comparison of the stability of this novel construct with that of previously investigated method of fixation.

PS03.005 - Kinematic analysis after total hip arthroplasty during weight-bearing activities

Author(s): Satoru Ikebe¹, Hidehiko Higaki¹, Yoshitaka Shiraishi², Takeshi Shimoto³, Yoshitaka Nakanishi⁴, Daisuke Hara⁵, Satoshi Hamai⁵, Yasuharu Nakashima⁵, Yukihide Iwamoto⁵

¹Kyushu Sangyo University, Fukuoka/JAPAN, ²Ehime University, Ehime/JAPAN, ³Fukuoka Institute of Technology, Fukuoka/JAPAN, ⁴Kumamoto University, Kumamoto/JAPAN, ⁵Kyushu University, Fukuoka/JAPAN

The hip joint has a wide range of motion. It achieves various daily activities. In the field of biomechanics, kinematic analysis of the hip osteoarthritis (OA) and total hip arthroplasty (THA) is important. Motion capture system has been widely used as kinematic analysis *in vivo*. However, external markers attached to the skin would be affected by soft tissue artifact with substantial errors. There is 2D-3D registration method as the kinematic analysis technique of high accuracy. There are reported of kinematic analysis technique of the natural knee and artificial knee joint using window analysis technique and single plane X-ray images. This study was aimed to analyze weight-bearing activities before and after THA. It was

confirmed to be utility of this technique by kinematic analysis during squatting and chair-rising.

In this report, the subject was one female before and after THA. Kinematic analysis at pelvis after THA was used image correlation between X-ray images and the computational simulating image. The image matching of the cup and stem was matched shape of implant in X-ray images and simulating image of 3D shape data. The accuracy of this analysis method is within 0.28 mm and 0.30 degree. We evaluated the hip joint, femoral and pelvic rotational motion. The rotational motion of the hip joint evaluates the relative motion of the femur for the pelvis, and femoral and pelvic rotational motion evaluates the tilt of the each bone for the vertical plane.

In flexion angle of the hip joint during squatting, difference between normal hip and a subject was about 23.3-32.0 degree at initial position. In femoral flexion angle during squatting, we confirmed difference of about 15.3-21.0 degree between normal hip and a subject. The posterior tilt of pelvis at a subject (16.9 degree at OA, 17.2 degree at THA) was larger than that of normal hip (10.0 degree) during squatting. In flexion angle of hip joint during chair-rising, we confirmed difference of about 6.0-12.7 degrees between normal hip and a subject. In femoral flexion angle during chair-rising, difference between normal hip and a subject was about 1.7-7.0 degrees at initial position. The posterior tilt of pelvis at a subject (16.0 degree at OA, 3.4 degree at THA) was larger than that of normal hip (9.1 degree) during chair-rising. The OA was limited range of motion in hip joints. And, range of motion became widely after THA. The pelvic posterior tilt at the OA permitted high-flexion of the femur.

In this report, we analyzed movement of the normal, OA and THA hip joints during squatting and chair-rising. The results of the study demonstrated that limited range of motion in OA hip joints was compensated by pelvic tilt. The limited range of motion in OA hip joint was become widely by THA. From these results, we were able to analyze movement of the hip joint *in vivo* using window analysis technique.

PS03.006 - Estimation of Compressive and Shear Forces on Lumbar Spine during Lifting by Wii Balance Board

Author(s): Hieyong Jeong¹, Kenji Yamada¹, Soichiro Watanabe², Moe Yokoyama¹, Michiko Kido³, Taishin Nomura⁴, Yuko Ohno³

¹Robotics & Design For Innovative Healthcare, Graduate School of Medicine, Osaka University, Suita/JAPAN, ²Konoike Institute Of Technology, KONOIKE Transport CO., LTD., Osaka/JAPAN, ³Division Of Health Sciences, Graduate School of Medicine, Osaka University, Suita/JAPAN, ⁴Mechanical Science And Bioengineering, Graduate School of Engineering Science, Osaka University, toyonaka/JAPAN

[Background]

Compressive and shear forces on lumbar spine are recognized as a risk factor for low back pain. Previous studies of forces have shown how injurious stresses on the low back can be predicted by such biomechanical models of the torso during the early phases of designing materials handling tasks in industry, but there are little studies on posture analysis with measurement of combined center of mass between a worker and an object during lifting under realistic field conditions.

[Purpose]

The purpose of this study is to propose the evaluating method to estimate compressive and shear forces on lumbar spine during lifting by using the Wii Balance Board under realistic field conditions.

[Methods]

The Wii Balance Board is able to measure both the position and

weight of combined center of mass between a worker and an object, and also to estimate trunk kinematics through two-degree-of-freedom link model. The proposed method is to calculate compressive and shear forces on lumbar spine during lifting with measured results of the position and weight of combined center of mass and estimated results of trunk kinematics. To compare with the conventional method, we let the center of balance of posture in the conventional method correspond with the center of pressure in the Wii Balance Board. The system for estimating is portable and inexpensive because the system is composed of the Wii Balance Board and the laptop computer.

[Results]

Through comparison, we found that results of proposed method were familiar with results of conventional method during bending forward or unbending backward, however, there was the difference between two estimated results just before bending forward or unbending backward. We considered that this came from the difference between the measurement and the assumption for combined center of mass.

[Conclusions]

We propose the evaluating method to estimate compressive and shear forces on lumbar spine by using the Wii Balance Board under realistic field conditions, and our method shows the effectiveness through comparison with results of conventional method. Additionally, the proposed method shows the possibility to be used to let participants know whether the current own lifting posture is proper or not in order to prevent workers in industry from worsening low back pain under realistic field conditions.

PS03.007 - A biomechanical evaluation of a novel pedicle screw-based interspinous device used to stabilize the lumbar spine

Author(s): Yu-Shu Lai¹, Hsin-Chang Chen², Chi-Wei Chou¹, Cheng-Kung Cheng¹

¹Orthopaedic Device Research Center, National Yang-Ming University, Taipei/TAIWAN, ²Orthopaedic Department, Taipei City Hospital, Heping Fuyou Branch, Taipei/TAIWAN

Interspinous spacers alters the load to be transferred through the spinous process instead of anterior column and the consequent fractures of the spinous process would be raised for patients with poor bone quality. In order to reduce the risk of spinous process failure, this study developed a novel pedicle screw-based supporting system with an "M" geometry, which was designed to overcome the previous disadvantages from spinal fusion, artificial disc replacement, and traditional interspinous devices.

The first part of this study was to evaluate the mechanical strength of the novel device by using a material testing machine (MTS Bionix 370.02). Six sets of titanium alloy-made devices were tested with a fixator referred to ASTM F2624 and ASTM 2790. The second part was to design a spine simulator for evaluating the range of motion in porcine lumbar spines (Fig. 1). Total of 24 sets of spine were tested (6 intact, 6 L3-L4 implanted with the new devices, 6 L3-L4 implanted with X-Stop, and 6 L3-L4 implanted with the posterior fixation).

The results of mechanical strength showed that there was no failure occurred in the new devices under the maximal loading of 15 Nm in the backward bending test. The new device group demonstrated a similar range of motion in forward bending (0.3°) and lateral bending (2.3°) compared to the X-Stop group and a higher of that compared to the posterior fixation group. As for backward bending, the new device was proved to possess a higher stiffness compared to X-Stop and posterior fixation.

In conclusion, the novel interspinous device has enough mechanical strength, and it constraint the spinal extension to avoid nerve root/spinal cord compression, unconstrained spinal flexion, and the lowered influence on adjacent levels.

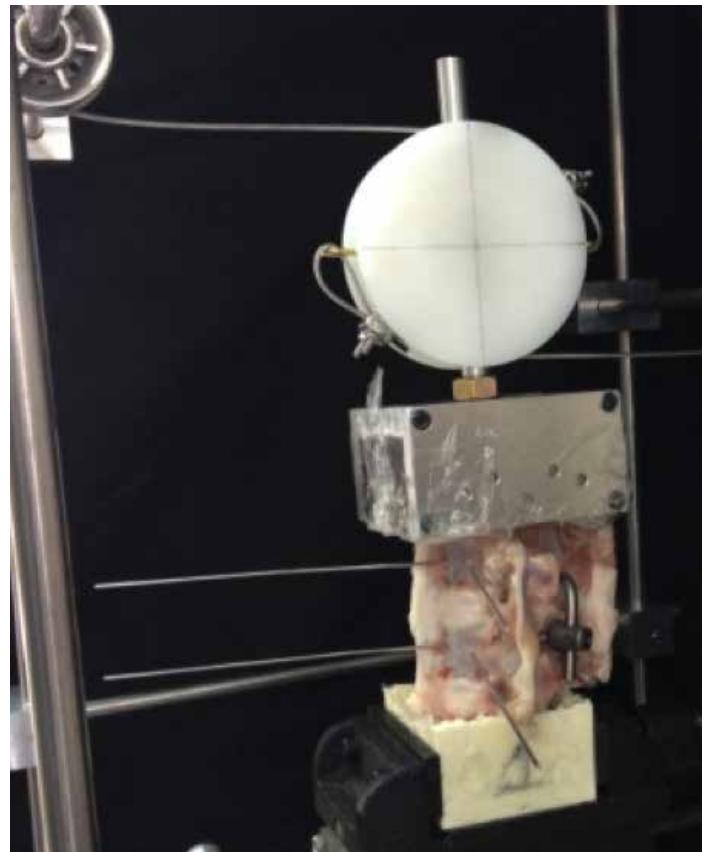


Figure 1

PS03.008 - Hematological, Biochemical, and End-organ effects of the CH-VAD in Ovine Model

Author(s): Changyan Lin

Biomedical Engineering, Beijing Anzhen Hospital, Capital Medical University, Beijing/CHINA

Background The CH-VAD is an implantable, fully magnetically suspended ventricular assist device developed by CH Biomedical Corporation for full cardiac support. This study was performed to evaluate the short-term (35 days) hematological, biochemical, and end-organ effects of the CH-VAD left ventricular assist device (LVAD) in a sheep model trial. Methods Six sheep underwent CH-VAD implantation without the use of cardiopulmonary bypass. The pump inflow was inserted into the left ventricle and the outflow graft was anastomosed to the descending aorta. Data on pump function and the health condition of the animals, including hematologic and biochemical tests, were collected during the study period. When each study was determined to termination, the sheep were humanely euthanized and the end organs were examined macroscopically and histopathologically. Hemolysis was evaluated based on the amount of free hemoglobin in the plasma. Results Except for one device that stopped operation on the 25th postoperative day because of thrombus formation, the planned date of termination (35 days) was reached in all the animals without complication and device failure. Gross examination of the pump interiors, inflow and outflow, and of the arterial anastomosis sites showed no signifi-

cant abnormalities. Hematologic and biochemical test results were within normal limits during the study period. Elevations observed in the levels of white blood cell count, and decreases in hematocrit, hemoglobin, and red blood cell count were of short duration, these parameters returned to normal within 20 days of surgery. Serum urea nitrogen, creatinine, SGPT(ALT), SGOT(AST), and lactate dehydrogenase levels showed transient increases within the first five days of surgery. Other biochemical parameters were within normal limits. Macroscopic and histopathologic examinations of the explanted organs revealed no evidence of ischemia or infarction associated with the device implantation, except for small foci of infarction in the kidneys of two sheep. The free hemoglobin level in plasma peaked at 9.5 mg/dL on the fifth postoperative day. Conclusions Hematological, biochemical, and end-organ functions were not adversely affected by short-term CH-VAD system.

PS03.009 - Novel Low-Profile External Fixator with Simple Locking Mechanism Compared with Commercial Available External Device Could Provide Better Stability in Multicycle Dynamic Loadings

Author(s): Kun-Jhih Lin¹, Chih-Hui Chen², Wen-Chuan Chen¹, Hung-Wen Wei¹, Jue-Ying Li¹, Cheng-Lun Tsai³, Kang-Ping Lin¹
¹Technology Translation Center For Medical Device, Chung Yuan Christian University, Taoyuan/TAIWAN, ²Department Of Orthopaedic Surgery, Taichung Veterans General Hospital, Taichung/TAIWAN, ³Department Of Biomedical Engineering, Chung Yuan Christian University, Taoyuan/TAIWAN

Recently, the standard locking compression plate (LCP) as an external fixator was introduced and coined the term supercutaneous plating. However, there are some limitations of LCP external fixation, such as limited screw holes available and insufficient strength compared with traditional fixator. We developed a LCP-like large plate to provide more screw numbers and higher strength to withstand the force during walking. Conceptually, the novel plate fixator was based on a tibial locking plate (A Plus Biotechnology Co., Ltd., New Taipei City, Taiwan) which acts for internal fracture fixation. The plate fixator is featured as thinner, wider and proximally arced shape, and can be positioned close to the skin (Fig. 1).



Fig. 1. Model of a novel plate external fixation with simulated tibia fragments apart.

We performed a repetitive loading test (200N to 200N, 1Hz, 50,000) (N=5) for the novel plate external fixator and compared with a commercialized traditional external fixator (Synthes GmbH, Oberdorf, Switzerland). The plate was fixed on polyacetal cylinder models simulating tibia with a 20 mm gap. Axial displacement of the bone fragment was recorded during testing. Statistical analysis was performed using t-test with significance set at P<0.05.

No specimen failure was found for the two fixators after 50,000 dynamic loading cycles. The novel fixator had smaller displacement than that of the Synthes fixator despite no significant difference was seen (Table 1).

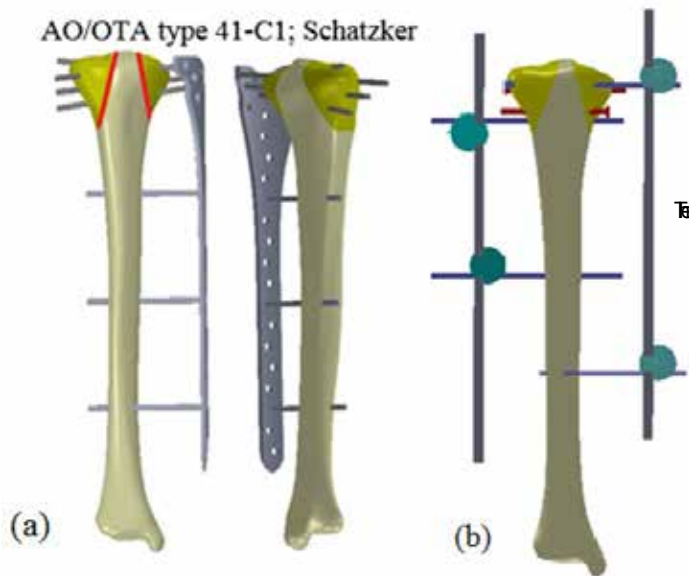
Table 1. Bone fragment movements from experimental measurements			
Displacement (mm): mean±standard deviation	Novel fixator	Synthes fixator	P value
Tensile	1.54±0.13	2.21±0.22	0.48
Compressed	0.66±0.05	0.83±0.11	0.55
Total	2.2±0.26	3.03±0.18	0.15

This dynamic load analysis revealed lesser fragment movement in the novel fixation. Additionally, the plate fixator was developed with low profile which is easily concealed under regular clothing and much less tendency for the frame to strike the contralateral lower leg in swing phase during ambulation. More importantly, this study demonstrated better stability in the novel fixator than traditional external fixator. The LCP-like large plate is demonstrated the ability of fragment stability. We expected this improvement may reduce the nonunion rate noted in the LCP application.

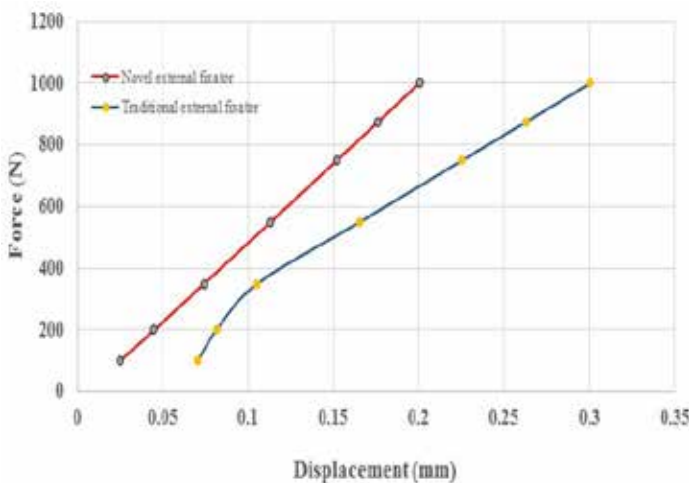
PS03.010 - A simple external fixation technique for treating bicondylar tibial plateau fracture: a finite element study

Author(s): Wen-Chen Lin¹, Kun-Jhih Lin¹, Chih-Hui Chen², Bo-Hao Li³, Jue-Ying Li¹, Wen-Chuan Chen¹, Hung-Wen Wei¹, Cheng-Lun Tsai³, Sheng-Cheng Huang¹, Kang-Ping Lin¹
¹Technology Translation Center For Medical Device, Chung Yuan Christian University, Taoyuan/TAIWAN, ²Department Of Orthopaedic Surgery, Taichung Veterans General Hospital, Taichung/TAIWAN, ³Department Of Biomedical Engineering, Chung Yuan Christian University, Taoyuan/TAIWAN

Bicondylar tibial plateau fractures are difficult to treat with a high complication rate due to difficulties in achieving stable fixation. External fixation methods such as monolateral external fixator, circular external fixators, or a hybrid between a monolateral and a circular external fixator are considered to be good mechanical methods of stabilising these complex fractures. However, main disadvantages of these traditional external fixators are bulky and cumbersome for the patient during daily activities. Therefore, we developed a simple low-profile external device to overcome these drawbacks. This novel external device is characterized as arced shape proximally and multi-directional screw insertion trajectory to enhance fixation stability of fracture. This study aimed to investigate the biomechanical performance of the novel device and to compare with commercialized traditional external fixator. Finite element method was employed to carry out all biomechanical analyses. Three CAD models of a normal tibia bone, the simple low-profile external device, and a traditional monolateral external fixator were reconstructed (Fig 1). Bicondylar tibia plateau fracture was simulated according to AO classification (AO/OTA type 41-C1; Schatzker type-V). A 1000N axial compression load was applied to the tibial plateau with fully fixed distal end of the tibia. Maximum von Mises stress on bone, screws, and fixators were calculated. The construct stiffness of both groups were calculated also.



results showed that the maximum von Mises stress on implants was much lower than the yielding strength of the material for both groups. The construct stiffness of the novel device (4992.5 N/mm) was 49.8% higher than the traditional external device (3333.3 N/mm) (Fig 2). This study demonstrated that the fixation strength of the novel external device was higher than the traditional monolateral fixator. Clinical evaluation for the novel device is still necessary to further verify its usefulness.



sensitivity, wide dynamic range and sharp frequency selectivity of our hearing.

Unfortunately, however, OHCs are vulnerable to noise exposure, ototoxic acid, aging and so on. Previous studies have shown that exposure to intense noise causes functional loss of OHCs from the innermost row (i.e., close to the modiolus) to the outermost row (i.e., close to the cochlear wall). On the contrary, by other traumatic stimuli such as ototoxic acid, aging and ischemia, such loss of OHCs has been reported to occur from the outermost row toward the innermost row. However, how the cochlear amplification changes when coordinated movement of OHCs is impaired remains unclear. Since the OC is vulnerable and sound-induced displacement amplitude of the OC is quite tiny, measurement of the dynamic behavior of the OC is difficult. Analysis using finite element method (FEM) is thus helpful.

In the present study, therefore, a finite element (FE) model of the gerbil cochlea, which takes the motility of OHCs into account, was developed based on our previous FE model. Using this model, changes in the displacement amplitude of the BM due to the functional loss of OHCs in one, two or all three rows were investigated and the effects of incoordination of the three rows of OHCs on cochlear amplification were estimated. Results showed that the displacement amplitude of the BM significantly decreased when either the innermost row or the outermost row of OHCs lost its function, suggesting that all three rows of OHCs are required for cochlear amplification.

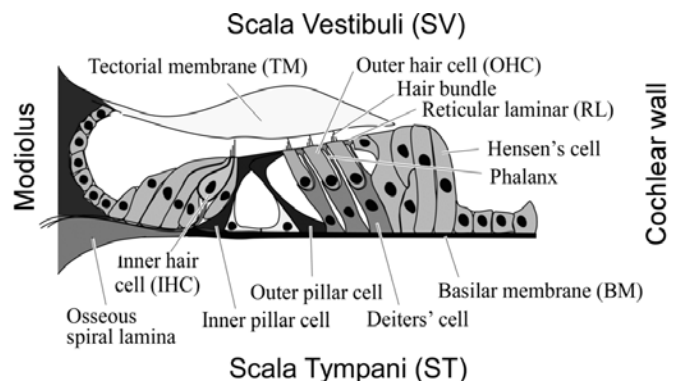


Fig. 1. Schematic of structure of the OC. The OC contains two types of sensory cells, i.e., the inner hair cells (IHCs) and the outer hair cells (OHCs), and the supporting cells. The tectorial membrane (TM) is an extracellular matrix and covers the OC.

PS03.011 - Numerical analysis of the elaborate sound amplification mechanism of the mammalian inner ear

Author(s): Michio Murakoshi¹, Hiroshi Wada²

¹Department Of Mechanical Engineering, Kagoshima University, Kagoshima/JAPAN, ²Department Of Intelligent Information System, Tohoku Bunka Gakuen University, Sendai/JAPAN

Sounds are converted to the mechanical vibration by the tympanic membrane and this vibration is transmitted to the basilar membrane (BM) and the sensory organ of hearing named organ of Corti (OC) in the cochlea. The OC consists of one row of inner hair cells (IHCs), three rows of outer hair cells (OHCs) and other supporting cells, as shown in Fig. 1.

The process known as cochlear amplification is realized by coordinated movement of the OHCs in response to changes in their membrane potential. In this process, the displacement amplitude of the BM is thought to be increased, thereby leading to the high

PS04 - TRACK 04: RADIATION ONCOLOGY**PS04.001 - Image-Guided Intra-arterial Delivery of Yttrium-90 Radioactive Microspheres for the Treatment of Liver Tumors**

Author(s): Muthana Al-Ghazi¹, Varun Sehgal¹, Suhong Yu¹, Garrett Green¹, Glenn Samford², Jeffrey Kuo¹, Dayantha Fernando², David Imagawa³

¹Radiation Oncology, University of California, Irvine, Orange/UNITED STATES OF AMERICA, ²Radiological Science, University of California, Irvine, Orange/CA/UNITED STATES OF AMERICA, ³Surgery, University of California, Irvine, Orange/CA/UNITED STATES OF AMERICA

Purpose: To outline the use of yttrium-90 (Y-90) for the treatment of liver tumors.

Background: Y-90 is a β^- emitter with an energy of 2.28 MeV. It decays to Zr-90 with a half-life of 64 hours. It is produced from the decay of Sr-90; the latter in turn is produced by chemical high-purity separation from strontium-90, a fission product of uranium in nuclear reactors. The short range of the emitted β^- makes Y-90 ideal for irradiation of tumors at very short range.

Liver tumors arise as either primary tumors (e.g. hepatocellular carcinoma) or as metastases resulting from e.g. colorectal primaries. In the simplest form, these tumors destroy the local vasculature of the liver. As such, delivery of Y-90 coated microspheres through liver vessels will terminate at the tumor site enabling very high doses to be delivered locally.

Methods: Healthy liver tissue gets its blood supply from the portal vein. The hepatic artery supplies blood to the tumor. Therefore, delivery of a "radioactive drug" through the hepatic artery will lead to the site of the tumor leaving healthy liver tissue and its blood supply unaffected. A catheter is inserted intrafemorally under fluoroscopic image guidance to reach the site of the tumor via the hepatic artery. This intervention is performed under local anesthesia. In the meantime the descending gastric artery is coiled to prevent Y-90 microspheres from escaping to the gastrointestinal tract and causing untoward toxicity. The required Y-90 activity to deliver a dose in the range 100 – 150 Gy to the tumor site is calculated using a multi-compartmental model that takes into consideration (a) liver volume, (b) body surface area, (c) tumor burden expressed as a percentage of liver volume and (d) the "lung shunt", the latter is the amount of the circulation from the liver to the lung. Patients with lung shunt equal or greater 10% are not candidates for this procedure due to unacceptable pulmonary toxicity.

Results: This method of image-guided brachytherapy enables safe delivery of doses in the range 100 – 150 Gy to the tumor site with minimal normal tissue toxicity due to the short range of the emitted β^- particles, taking advantage of the destruction of the vasculature by the tumor and the nature of the hepatic blood circulation. There appears to be a favorable dose response associated with this minimally invasive procedure for patients who are not surgical candidates and have exhausted other treatment options.

Conclusion: Y-90 radioactive microspheres can be safely used to deliver doses in excess of 100 Gy locally to liver tumors with minimum toxicity taking advantage of the low energy (2.28 MeV) of the emitted β^- particles and the nature of the hepatic blood circulation. This advantage along with the short half-life of this isotope enables this minimally invasive procedure to be performed as a same day surgery. Preliminary evidence suggests a favorable dose response at this dose range

PS04.002 - Commissioning of an ASi EPID for patient specific IMRT QA.

Author(s): David N. Alonso Fernández¹, Rodolfo Alfonso¹, Eduardo Larrinaga², Jose L. Alonso Samper², Rogelio Diaz Moreno²

¹Nuclear Engineering, High Institute for Applied Technologies and Sciences (InSTEC), Havana/CUBA, ²Department Of Radiotherapy, Institute of Oncology and Radiobiology, Havana/CUBA

The use of the Electronic Portal Image Device (EPID) in an Elekta Linac for patient-specific Intensity Modulated Radiotherapy (IMRT) Quality Assurance (QA) is assessed and validated. A linac Elekta was used, with IMRT step&shoot capability using Multileaf Collimator (MLC). An EPID image calibration was performed for a 6MV photon beam and a 10x10cm² field size. The EPID effective water scattering depth (d_{eff}) was assessed through the measurement of its response versus the field size variation; and compared to the output factor scatter at different depths calculated from Radiotherapy Treatment Planning System (RTPS) Elekta XiO data. A correction matrix was created from a 24x24cm² field profile padded with radial symmetry.

The EPID d_{eff} found was close to 5cm. Dose profiles and dose maps were calculated to d_{eff} with the RTPS using a collapsed beam arrangement. Also they were measured with the bidimensional (2D) ion chamber array PTW Seven29 Octavius sandwiched in PTW RW-2946 slabs for validation purpose. Point measurements with an ion chamber PTW M30013 Farmer type were carried out also. The dose maps and profiles were compared to the processed EPID images for simple cases (i.e. open fields and wedged fields) and more complex cases (Head and Neck IMRT clinical cases).

The EPID obtained dose maps were compared with the RTPS calculated dose maps and the measured with the 2D-array. Comparison was performed using the PTW VeriSoft v5.1 software. Results showed that approximately 90% of all points passed using a 3% dose/4mm Distance to Agreement (DTA) for the gamma analysis for both methods.

PS04.003 - Status of Radiotherapy Treatment in Lebanon

Author(s): Ibrahim Duhaini¹, Antar Aly²

¹Radiation Oncology, Rafik Hariri University Hospital, Beirut/LEBANON, ²Hamad Medical corporation, Doha/QATAR

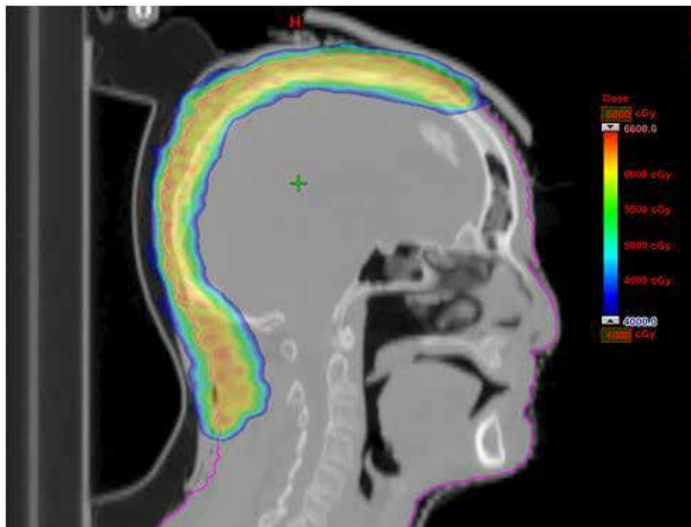
Abstract:

Lebanon is located in the heart of the Middle East Region with a population of 4.5 million and is considered one of the best places of Medical Hot Spot destination that attracts many of the neighboring Arab countries to seek medical treatment. This is due to the fact of the highly skilled medical professionals and advanced health infrastructure in the country. Radiotherapy started in the early 70's with Cobalt Machines and has developed tremendously through the years to include the highly technological and advanced Linac Systems. Now, there are 10 Hospitals that offer Radiotherapy Treatment with 14 Linacs equipped with the state of the art technology using 3-D Conformal, IMRT, Stereotactic Radiosurgery, IGRT and other modalities. In this presentation, an overview of the current cancer treatment in these 10 hospitals will be revealed. Detailed information will be unwrapped for the newly opened Radiotherapy Center at Nabih Berry Governmental University Hospital (NBGUH) in South Lebanon, which covers one third of the Lebanese population in that region.

PS04.004 - Verification of VMAT Arc Radiation Therapy Technique for Full Scalp Treatment

Author(s): Cynthia Araujo, Islam Mohamed, Claude Lapointe, Dawn Gillund, Kristine Mcgee
 Radiation Therapy, BC Cancer Agency - Southern Interior, Kelowna/ CANADA

A VMAT arc technique was designed to treat the full scalp for a patient with angiosarcoma of the scalp to a dose of 6000cGy in 25 fractions.



The CT of the entire head was acquired with the patient in supine treatment position with a 0.5 cm thick custom bolus-cap on the top and back of the head, an immobilization shell, and additional bolus attached to the shell.

A VMAT plan to be treated on a Varian True Beam LINAC was optimized in Eclipse using the photon dose AAA calculation version 11. Two full arcs with couch at 0° and collimator at +/- 10° where used along with two partial arcs with couch at 270° and collimator at 90°. The treatment was optimized to cover the skin, and a PTV margin, while sparing the underlying brain and limiting the dose to the optic apparatus and lacrimal glands. The dose to the brain was limited so that V20Gy, V30Gy and V40Gy were 710, 390 and 193 cm³ respectively. The mean dose to the brain was 2385 cGy.

On the 2nd treatment day, 13 TLDs were positioned on the patient's scalp. The TLDs were spaced 2cm apart, 9 along the midline sagittal plane, and 4 along an axial plane. The dose measured by the TLDs was compared to the treatment planning calculation and it showed an excellent agreement. The mean difference between the measured and calculated dose was 1% with a standard deviation of 4%.

TABLE 1: Results of the TLD dose measurements compared to the treatment planning calculation for 13 positions spaced 2 cm apart on the patient's scalp.

	Treatment Planning (cGy)	TLD Dose (cGy)	Difference
Mean	245	247	1%
Standard Deviation	5	9	4%
Minimum	236	231	-6%
Maximum	253	259	7%

PS04.006 - Uncertainty evaluation of radiation treatment with DIBH for left-sided breast cancer using MV cine imaging

Author(s): Jae Beom Bae, Byung Chul Cho, Kyoung Jun Yoon, Young Eun Choi, Su Ssan Kim, Seung Do Ahn, Sang Wook Lee, Jung Won Kwak
 Radiation Oncology, Asan Medical Center, Seoul/KOREA

Purpose/Objective: Deep inspiration breath-hold (DIBH) technique has been utilized to reduce the radiation exposure of heart for left-sided breast cancer patients during radiotherapy. Obtaining MV x-ray cine images during beam delivery, we evaluated the inter- and intra-fractional variations of breast cancer treatment with DIBH technique.

Materials/Methods: For five left-sided breast cancer patients treated with DIBH technique, about 15000 cine images (7.5 frame/sec) in 209 fractions were acquired by Electronic Portal Image Device (aSi1000, Varian). The acquired DICOM image files were converted into ASCII format using ImageJ (Java image processing program, NIH). The ASCII files were imported into ROOT (Data Analysis Framework, CERN) to generate the 2D maps of local standard deviations (LSTD) calculated with each pixel and 4 neighboring pixel values. The edges of organs could be easily extracted by selecting local maximums in the 2D LSTD map. As the projected profiles from the ROI regions of the 2D LSTD maps were taken into account for fast processing, the local maximum points in the projected profiles were interpreted as the relative positions of heart boundary, chest wall, and skin from the edge of MLC. The cine images of the medial and lateral fields for each fraction were separately accumulated to obtain the representative positions in each fraction.

Results: The inter- and intra-fractional variations of each organ during DIBH breast radiotherapies for 5 breast cancer cases were evaluated using the 15000 cine images. The averages of inter-fractional variations about the skin, chest wall, and heart for 5 cases were 0.37 cm, 0.31 cm, and 0.33 cm. The averages of intra-fractional variations of the skin and chest wall positions were measured to be about 1/10 of inter-fractional variations. The results showed that inter-fractional variations were much bigger than the intra-fractional values except of the position of heart edge. For the position of heart edge, the intra-fractional variation was measured to be about the same level to the inter-fractional variation.

Conclusion: MV cine imaging was assessed as an appropriate tools to evaluate the intra- and inter-fractional variations of DIBH breast cancer treatments. The inter-fractional variations for the skin, chest wall, and heart positions were all about 3~4 mm, which were quite reasonable in patient setup with skin marks. The skin level guidance with RPM system and the cooperation of patients seemed to result in much smaller intra-fractional variation than inter-fractional variances. The cardiac motion caused the intra-fractional variation of the anterior-left edge of heart was similar to the inter-fractional variation. For the robust conclusion, the analysis with the bigger statistics is in progress.

PS04.007 - Evaluation of the Applicability of Pinpoint ion chamber for Dosimetric Quality Assurance of SRS

Author(s): Jong Geun Baek¹, Hyun Soo Jang¹, Yong Hee Lee², Eng Chan Kim², Young Kee Oh³, Sung Kyu Kim⁴
¹Radiation Oncology, Dongguk University Gyeongju Hospital, Gyeongju/KOREA, ²Physics, Yeungnam University, Gyeongsan/KOREA, ³Department Of Radiation Oncology, Keimyung University Dongsan Medical Center, Daegu/KOREA, ⁴Department Of Radiation Oncology, Yeungnam University College of Medicine, Daegu/KOREA

A number of investigators demonstrated that Pinpoint chamber is not suitable for dosimetry in small field because the effect of finite detector size led to large volume averaging problems in regions of

high dose gradient. However, Pinpoint chambers still have been used for the measurement of absolute dose in dosimetric quality assurance (QA) of stereotactic radiosurgery (SRS). The aim of the present study was to evaluate the applicability of Pinpoint ion chamber for the measurement of small photon beams in dosimetric QA under the actual SRS treatment circumstances.

A total 23 cases of SRS plans were used for the verification and the diameters of the target volumes were divided into two groups, the diameter of <10 mm (10 cases) and of ≥10 mm (13cases). The PTW 31014 Pinpoint chamber was used to measure the absolute dose of small beams in SRS treatment and the chamber has an active volume of 0.015 cm³. To compare the dosimetric uncertainties for Pinpoint chamber, the PTW 60003 natural diamond detector was used as a reference dosimeter. A custom-made cylindrical acrylic phantom (15 cm diameter, 15 cm length) was designed for measurement. The noncoplanar arc plan was created to deliver a prescription dose (15-25 Gy) to 80% of the maximum dose of the target in a single fraction and then the calculated plan was projected on the CT images of the phantom as inserted each detector for verification planning. All irradiations were performed using a Varian Clinac IX 6MV equipped with a micro-multileaf-collimator designed by BrainLAB. The acceptability criteria of the dose difference at our institution is less than 3%.

The dosimetric uncertainty was represented as a percentage dose difference between planned and measured. For Pinpoint chamber in the target diameters of <10 mm, the maximum dose difference was 4.85%, the mean ± standard deviation (SD) discrepancy was 2.82±1.41%, and the number of the dosimetric uncertainty of >3% was 4 of 10 cases. For diamond detector in the same diameters, the values were 2.70% and 1.51±0.74% and all measured discrepancies were <3%. Statistical analysis indicates that the dosimetric uncertainties for Pinpoint chamber in the target diameters of <10 mm were significantly different from the uncertainties for diamond detector (p<0.05). On the other hand, the maximum difference was 1.56% and mean ± SD discrepancy was 0.81±0.44% for Pinpoint chamber in the target diameters of ≥10 mm and the values were 1.79% and 1.09±0.41% for the diamond detector. The correlations between the dosimetric uncertainties and the all target diameters in our study by determining the R2 regression coefficient. A highly significant but moderate correlation was observed for Pinpoint chamber (R2=0.483, p<0.001), whereas the weak correlation was observed for diamond detector (R2=0.053, p=0.230). Based on the results of this study, Pinpoint chamber is unsuitable for the measurement of the absolute dose of SRS field designed by the target diameters of <10 mm, whereas the chamber can provide reliable and acceptable data for verifying the SRS fields created by the diameter of ≥10 mm.

PS04.008 - Development of a VARIAN 600 C/D Linear Accelerator model using MCNPX 2.6 Monte Carlo code.

Author(s): Jorge L. Batista Cancino, Clarysson A. Mello Da Silva, Rômulo Verdolin De Sousa, Claubia Pereira
Departamento De Engenharia Nuclear, Universidade Federal de Minas Gerais, Belo Horizonte/BRAZIL

In radiotherapy treatment planning, tools that improve the accuracy of patient dosimetry are valuable. The Ministry of Health of Brazil has near of 240 linear accelerators in the radiotherapy service. VARIAN is the main distribution company in the country and more than 60% are linear accelerators of low-energy (4-6 MeV). In this research work, a simple and useful model was developed for VARIAN 600 C/D linear accelerator using MCNPX 2.6 Monte Carlo (MC) code. The essential components of VARIAN 600 C/D head was simulated for 6 MeV electron beam using MCNPX 2.6 MC code. In this study is considered a monoenergetic electron beam of 6 MeV as a source.

Photons generated by Bremsstrahlung in tungsten target are transported too. Percentage depth doses (PDD) and beam profiles were calculated for different field sizes. The MC calculated results were compared against measurement and good agreement was obtained. The comparison between MC calculations and measurement of PDD showed less than 5% of error for build up region. Also, there was a high coherence in beam profiles comparison. In the flat region was less than 3% of error and near to 10% difference was seen for penumbra region. In conclusion, our study showed acceptable results according to the reference criteria. The developed model will optimize the patient dosimetry in radiotherapy treatment planning.

PS04.009 - A Comparison of Dosimetric Characteristic Between Integrated and Cine Acquisition Modes of a-Si EPID

Author(s): Omemh Bawazeer¹, Siva Sarasanandarajah¹, Sisira Herath², Tomas Kron², Shu Hui Hsu³, Pradip Deb¹

¹School Of Medical Radiation, RMIT University, Melbourne/AUSTRALIA, ²Radiation Oncology, Peter MacCallum Cancer Centre, Melbourne/AUSTRALIA, ³Radiation Oncology, Montefiore Medical Centre, New York City/UNITED STATES OF AMERICA

Electronic Portal Imaging Device (EPID) is currently used for the dosimetry purpose. There are two acquisition modes, integrated and cine mode [1]. The aim of this study is to compare the dosimetric characteristic between both acquisition modes. The a-Si 500 EPID that attached to Varian Synergy linear accelerator was used in this study. The comparison included the response of EPID to dose, reproducibility, field size dependence, ghosting effect, dose rate and multi-leaf collimator effect. In addition, the ionization chamber response under the identical setup was acquired to assess the dosimetric characteristic of EPID response with two acquisition modes. All acquired images were analysed using MATLAB programme. The preliminary results of comparison between acquisition modes for dose response and field size dependent represent in Figure 1 and Figure 2. The results indicated that the differences between two modes is because the difference in the pixel value range for each mode, however both modes have a comparable response to dose. In each mode, the ratio between following points is varied with the increasing MU. For example the ratio between 100 to 200 MU for integrated mode is slightly different from the ratio between 200 to 300 MU. In contrast, this ratio for integrated and cine mode is equal. In clinical application, even both acquisition mode has a relatively similar response, each mode required individual calibration factor for dosimetry purpose due to the difference in the range of pixel value intensity for each mode.

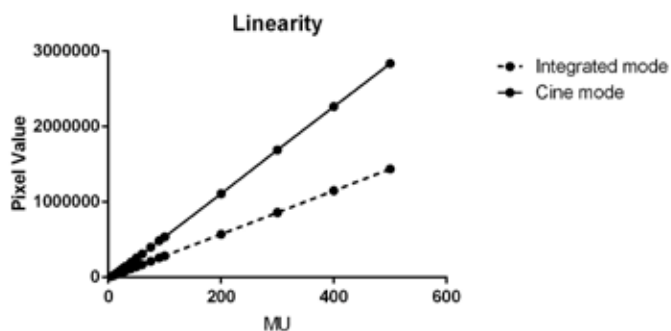


Figure 1: Response of a-Si EPID in both acquisition modes as a function of MU, error bars are too small to see.

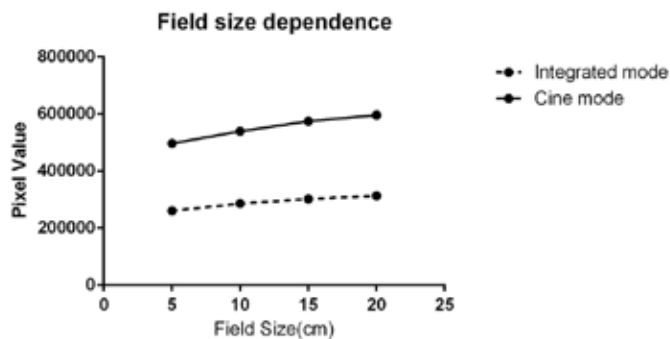


Figure 2: Response of a-Si EPID in both acquisition modes as a function of field size.

Reference:

- Greer, P.B. and P. Vial, *EPID dosimetry, Proceedings of SSD*. 2011. p. 129-144.

PS04.010 - Predicting clinical outcomes in locally-advanced non-small cell lung cancer using machine learning focusing on tumor and node imaging features

Author(s): Heyse Li¹, Nathan Becker², Srinivas Raman³, Timothy C.Y. Chan⁴, Jean-Pierre Bissonnette³

¹Department Of Mechanical And Industrial Engineering, University of Toronto, Toronto/ON/CANADA, ²Radiation Oncology, UHN Princess Margaret Cancer Center, Toronto/ON/CANADA, ³Radiation Oncology, UHN Princess Margaret Cancer Center, Toronto/CANADA, ⁴Mechanical And Industrial Engineering, University of Toronto, Toronto/CANADA

There is evidence that computed tomography (CT) and positron emission tomography (PET) imaging metrics are prognostic and predictive in non-small cell lung cancer (NSCLC) treatment outcomes. We investigated the use of image features extracted from the radiotherapy target volumes to predict relapse in a cohort of NSCLC patients undergoing chemoradiation treatment (CRT). A prospective cohort of 25 patients with locally-advanced NSCLC underwent PET/CT imaging for radiation planning. Thirty-seven image features were derived from the CT-defined volumes and standard uptake values (SUV) of the PET image, for both the tumor and nodal target regions. The machine learning methods of logistic regression and repeated stratified five-fold cross-validation (CV) were used to predict local and overall relapse at two years of follow up. We selected features through an exhaustive search over all combinations of single- and two-feature classifiers. Classifiers were evaluated on their Matthew's correlation coefficient (MCC) after CV.

For local relapse, the best classifier had a mean CV MCC of 0.42. The classifier was composed of two features: (1) the volume of tumor having an SUV greater than the 95th percentile of the SUV distribution and (2) the volume of the whole tumor based on the CT scan. For overall relapse, the best classifier had a mean CV MCC of 0.51. The classifier was composed of two features: (1) the volume of tumor having an SUV greater than half of the 95th percentile SUV and (2) the volume of the nodes having an SUV greater than half of the maximum SUV.

Adding node-specific SUV information to the classifier improved the ability to predict overall relapse two years following treatment in our cohort of NSCLC patients. Also two-feature classifiers outperformed single-feature classifiers in predicting both local and overall relapse.

S04.011 - Risk estimate of second primary cancers after breast radiotherapy

Author(s): Eva Bezak¹, Alexandre Santos², Loredana Marcu³

¹School Of Physical Sciences, University of Adelaide, Adelaide/SA/AUSTRALIA, ²Medical Physics, Royal Adelaide Hospital, Adelaide/AUSTRALIA, ³University of Oradea, Oradea/ROMANIA

Purpose: Induction of second primary cancers (SPCs) after breast radiotherapy (RT) has been known for some time and organs such as the lungs and the oesophagus have been identified as common sites for SPC formation¹. At present, breast cancer patients can be treated with a number of RT techniques that may have different morbidity risks. As a result, the current study investigated the risk of secondary carcinogenesis associated with particular radiotherapy techniques for breast cancer; these included 3DCRT whole breast, segmented breast, partial breast and mammosite brachytherapy.

Method: Seven breast cancer patients had all major organs contoured by a radiation oncologist on their planning CT images. Whole breast, segmented breast, accelerated partial breast irradiation (APBI) and mammosite boost treatment plans were generated for each patient using Pinnacle3 v 9.2 treatment planning system. Whole and segmented breast techniques used two tangential wedged fields; where the segmented techniques consisted of more MLC defined segments. Prescribed dose of 2 Gy for 25 fractions was used for calculations. APBI treatments were planned based on the Trans-Tasman Radiation Oncology Group (TROG) "trefoil" technique, using three non-coplanar fields. 6 MV photon beam was used for all treatment plans with a prescribed dose of 3.85 Gy for 10 fractions. Mammosite treatments consisted of a brachytherapy balloon (~35 mm diameter) inserted into the tumour bed inside a breast. Ir-192 source was positioned in the centre of the balloon to deliver the dose of 3.5 Gy for 10 fractions. Differential dose volume histograms were generated for a number of critical structures: bladder, brain and CNS, breast, colon, liver, lung, mouth and pharynx, oesophageous, ovary, salivary gland, small intestine, stomach, and uterus.

The lifetime attributed risk (LAR) of cancer induction was then estimated using the BEIR VII² and Schneider et. al³ excess absolute risk models and calculated dose volume histograms for the above organs.

Results: The sites with the highest LAR estimates were the ipsilateral and contralateral lungs, and contralateral breast for all treatment techniques. For all sites, the LAR estimates for the segmented breast and mammosite treatments were lower than those for the whole breast and APBI treatments. For right sided target volumes the liver also resulted in high LAR estimates, with all techniques having a LAR greater than 20 per 10,000 PY, except for mammosite with a mean LAR estimate of 13.2 per 10,000 PY, as calculated by the full model³. For left sided target volumes the stomach also resulted in high LAR estimates, with both whole breast and APBI having a LAR greater than 20 per 10,000 PY, and mammosite the lowest with a LAR of 8.3 per 10,000 PY, calculated by the full model³.

Conclusions: Whole breast, segmented breast, APBI and mammosite treatment plans were generated for seven breast cancer patients, and the DVHs were used to estimate the risk of secondary primary cancer induction. As expected from reported clinical studies; the lungs and contralateral breast showed high LAR estimates. Results show that mammosite technique results in the lowest risk estimate for SPC induction.

PS04.012 - A beam angle optimization technique for proton pencil beam scanning treatment planning of lower pelvic targets

Author(s): Janid Blanco Kiely, Benjamin M. White, Stefan Both
Radiation Oncology, University of Pennsylvania, Philadelphia/UNITED STATES OF AMERICA

Purpose: For deep seated targets in the lower pelvis, the highly conformal nature of proton therapy offers advantages in sparing organs at risk (OARs) located in the beam's path. A sharp distal penumbra effectively removes dose beyond the distal edge, completely sparing the OARs located beyond the distal edge. However, OARs located proximal to the beam's distal edge may receive significant dose. Selection of an optimal proton pencil beam scanning (PBS) beam angle has the potential to reduce the magnitude of dose to OARs by minimizing the integral dose. This would ensure target coverage and minimize the number of treatment beams. The purpose of this work is to investigate if a single optimal proton PBS beam angle could be quantitatively determined for lower pelvic targets.

Methods: This study employed a cohort of ten consecutively enrolled patients with high risk rectal cancer. The clinical target volume (CTV) was delineated by an attending radiation oncologist. Three plans were created for each patient where each plan had a single beam oriented in the left lateral, right lateral, and posterior directions. For each of the three beam angles, a ray-tracing approach was used to calculate the values of optimization metrics. The optimization process was based on two objectives; path length and HU homogeneity. The goal was to minimize the path length of the proton PBS beam from the patient surface to the distal edge of the CTV, relative to the entry point, while simultaneously minimizing HU inhomogeneity along the path length. The path length of a ray was calculated as a straight-line Euclidean distance from the surface of the skin to the distal edge of the CTV. HU homogeneity, which is to say inter-ray HU variation, was quantitatively defined as the standard deviation of the average intra-ray HU intensity distribution of the several hundred beamlets which comprise one beam. Both metrics were assessed for normalcy with a Kolmogorov-Smirnov test (KS test) where the criteria for a normal distribution classification was $p < 0.05$.

Results: The KS test demonstrated that the distribution of path lengths were normally distributed in each beam angle. The average p-value was 0.03 ± 0.01 . 87.1% of the HU intensity distribution along individual rays was found to be normal where the average 90th percentile p-value was 0.04 ± 0.01 . Over the entire cohort, the beam angle with the shortest mean path length was the posterior beam at an average of 132.7 ± 18.1 mm compared to the lateral beams at average of 232.7 ± 25.4 mm. The lateral beams had less HU intensity variation on average at 31.7 ± 4.9 HU compared to an average of 36.0 ± 4.5 HU for the posterior beam. Though lateral beams had less HU intensity variation than the posterior beam, the difference in HU intensity variation was much less than the difference between path lengths. Numerically, the posterior beam's shorter path length resulted in its classification as the optimal beam angle.

Conclusion: A posterior PBS beam angle was found to be optimal for lower pelvis targets through an optimization approach that minimized the average path length and HU variation along multiple rays.

PS04.013 - Neutron-Photon mixed field dosimetry by TLD700 glow curve analysis and its implementation in dose monitoring for Boron Neutron Capture Therapy (BNCT) treatments

Author(s): Esteban F. Boggio, Pablo Andres, Juan Longhino
Reactor And Radiation Physics - Bariloche Atomic Center, Atomic Energy National Commission, San Carlos de Bariloche/ARGENTINA

Introduction. BNCT is a cancerous cells selective, non-conventional radiotherapy modality to treat malignant tumors such as glioblastoma, melanoma and recurrent head and neck cancer. It consists of

a two-step procedure: first, the patient is injected with a tumor localizing drug containing a non-radioactive isotope (Boron-10) with high slow neutron capture cross-section. In a second step, the patient is irradiated with neutrons, which are absorbed by the Boron-10 agent with the subsequently nuclear reaction $B-10(n,\alpha)Li-7$, thereby resulting in dose at cellular level due to the resulting high-LET particles. The neutron fields suitable for BNCT are characterized by high neutron fluxes and low gamma dose. Determination of each component is not an easy task, especially when the volume of measurement is quite small or inaccessible for a miniature ionization chamber. A method of measuring the photon and slow neutron doses (mainly by N-14 and B-10) from the glow curve (GC) analysis of a single 7LiF thermoluminescence detector is evaluated. This method was suggested by the group headed by Dra. Grazia Gambarini and used in the TAPIRO Research Reactor (Casaccia, Italy) and in the TRIGA MarkII of LENA Reactor (Pavia, Italy).

Material and Methods. The dosimeters used were TLD-600 (6LiF :Mg,Ti with 95.6% 6Li) and TLD-700 (7LiF :Mg,Ti with 99.9% 7LiF) from Harshaw. Photon dose measurement using the GC analysis method with TLD-700 in mixed fields requires the relation of the two main peaks of a TLD-600 GC shape obtained from an exposition to the same neutron field, and a photon calibrated GC with TLD700. The requirements for slow neutron dose measurements are similar. In order to properly apply the GC analysis method at the RA-6 Research Reactor BNCT facility, measurements were carried out in a standard water phantom, fully characterized on the BNCT beam by conventional techniques (activation detectors and paired ionization chambers technique). Next, the method was implemented in whole body dose monitoring of a patient undergoing a BNCT treatment, using a BoMAB (Bottle Manikin Absorption) phantom, with representative measuring points of critical organs. Finally, mice phantoms were constructed and irradiated in the BNCT beam using an experimental setup specifically designed for biological models experimentation. TLD-700 and activation detectors were implemented to compare with the Monte Carlo (MCNP) calculation model results, in order to evaluate the method performance.

Results. Implementation results and methodology evaluation are satisfactory.

Conclusions. The potential of GC analysis method to estimate both photon and slow neutron dose by using a single TLD-700 is shown, resulting in a dosimetric tool of great value. Using this method, whole body dosimetry results simple and precise, in contrast with the traditional method being used. Experimental validation for Monte Carlo (MCNP) calculation models of little animal irradiation setups were carried out successfully, especially when ionization chambers cannot be used because of instrument dimensions.

PS04.014 - Boron Neutron Capture Therapy (BNCT) neutron beam at RA-6 reactor: Quality Assurance and Quality Control

Author(s): Esteban F. Boggio¹, Juan Longhino¹, Mariana Casal², Diana Feld³

¹Reactor And Radiation Physics - Bariloche Atomic Center, Atomic Energy National Commission, San Carlos de Bariloche/ARGENTINA, ²Constituyentes Atomic Center, Atomic Energy National Commission, Buenos Aires/ARGENTINA, ³Ezeiza Atomic Center, Atomic Energy National Commission, Buenos Aires/ARGENTINA

Introduction. BNCT is a cancerous cells selective, non-conventional radiotherapy modality to treat malignant tumors such as glioblastoma, melanoma and recurrent head and neck cancer. It consists of a two-step procedure: first, the patient is injected with a tumor localizing drug containing a non-radioactive isotope (Boron-10) with high slow neutron capture cross-section. In a second step, the patient is irradiated with neutrons, which are absorbed by the Boron-10 agent

with the subsequently nuclear reaction B-10(n, α)Li-7, thereby resulting in dose at cellular level due to the resulting high-LET particles. The Argentine clinical facility for superficial tumors treatment is located at the RA-6 Research Reactor (Bariloche Atomic Center). The neutron beam is defined as hyperthermal, designed as a combination of high thermal and epithermal neutron intensities, in order to provide a maximum of thermal neutron fluency at 1 cm depth. The clinical treatments were initiated in October 2003, having successfully completed 10 irradiations in 7 patients of cutaneous melanoma in extremities until 2007. In 2007, the highly-enriched fuel of the RA-6 reactor was replaced by the new low-enrichment uranium, which included a power upgrade and the reconfiguration of the core. This was the opportunity to improve the BNCT facility, mainly in terms of irradiation room size and beam port, protruding its end. Furthermore, the neutron beam was improved in specific irradiation parameters, such as an extended uniformity of the irradiation field.

Material and Method. The neutron beam and facility design process required the complete structural description for the calculation model in Monte Carlo (MCNP5). At the end of this process, the construction was executed, being completed in 2011. In order to ensure the new BNCT beam output, a Quality Assurance (QA) process was initiated by means of calculation model experimental validation. Usual activation techniques were employed to obtain thermal, epithermal and fast neutron fluxes, both with beam free-in-air and into standard water phantom. Gamma and fast neutron doses were measured in both configurations implementing the paired ionization chambers method, using tissue-equivalent and graphite miniature chambers. All measurements were carried out over the axial, parallel and transverse axis to the beam. A few modifications were performed to ensure essential parameters of the beam, and the full characterization was done and reported. Finally, the Quality Control (QC) protocol was developed and became effective before the restart of the clinical trials.

Results. QA process and its results will be shown in detail. Main beam parameters were compared and ensured with other techniques that have been implemented in the dosimetric characterization process.

Conclusions. Nowadays, under rigorous quality indicators, the Argentine BNCT Project is in conditions to restart the clinical trials in the short term.

PS04.015 - Improved Pareto navigation using a plan database with segmented plans

Author(s): Rasmus Bokrantz¹, Katrin Teichert², David Craft³
¹Department Of Research, RaySearch Laboratories, Stockholm/SWEDEN, ²Department Of Optimization, Fraunhofer Institute for Industrial Mathematics, Kaiserslautern/GERMANY, ³Department Of Radiation Oncology, Massachusetts General Hospital, Boston/MA/UNITED STATES OF AMERICA

Background

Pareto surface navigation is a form of decision support for intensity-modulated radiation therapy that allows planners to browse through a space of possible dose distributions. This technique relies on interpolation of a number of pre-calculated plans' doses. The standard for step-and-shoot delivery is to represent Pareto surfaces by a database of fluence optimized plans. Such a representation inevitably leads to perturbations of the navigated dose when it is converted to a deliverable plan, because non-restricted fluence modulation is an idealization that cannot be matched in practice. The aim of the present work is to minimize the presence of conversion errors. To this end, we investigate navigation with respect to segmented plans, i.e., plans that take the physical limitations of the delivery system into account.

Materials

Navigation with segmented plans was assessed with respect to two head and neck cases obtained from Massachusetts General Hospital. The cases were selected because conversion errors had been a difficulty during the preparation of the clinical plan.

For comparative purposes, separate Pareto surfaces were generated with non-segmented (i.e., fluence-optimized) and segmented plans. Navigation was simulated by sampling 100 random points per surface. The associated navigated doses were converted to deliverable plans.

The magnitude of dose and dose-volume histogram (DVH) errors for organs at risk were quantified in terms of overdosage relative to the navigated dose: the error for a point that was nominally planned to receive 10 Gy but that received 11 Gy after the conversion is 1 Gy. Dose errors within targets were quantified analogously, but with underdosage also taken into account. All experiments were performed in RayStation v4.7 (RaySearch Laboratories).

Results

Figure 1 summarizes the collected error measures for one of the patients, which are representative also for the second patient. With segmented plans, the dose error in percent of the prescription was within 1.4% on average and within 6.8% at the 98th percentile level for all structures. The corresponding figures for the DVH errors are 0.9% and 3.3%. About a factor 2-3 larger errors were observed with non-segmented plans: the averages and 98th percentiles of the dose errors were up to 3.5% and 15.9%, respectively, and up to 2.6% and 9.4% with respect to DVH. The smaller errors indicate that a representation with segmented plans has the potential to provide more informed and streamlined planning.

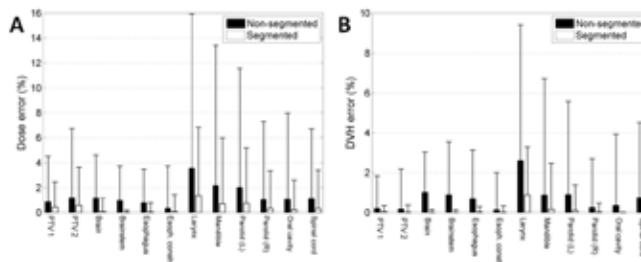


Figure 1: Averages (bars) and 98th percentiles (whiskers) of the dose (A) and DVH errors (B).

PS04.016 - Automated measurement of dwell and tandem position in ring HDR applicators

Author(s): Bruno Carozza, Fabiola Vallejo
 Radio-oncologie, Centre intégré de cancérologie de Laval, Laval/QC/CANADA

Accuracy and efficacy in measuring in house dwell and tandem positions in ring applicators is very important due to steep dose gradients encountered in HDR brachytherapy.

It is suggested that measuring those offsets should take place when commissioning/replacing a ring applicator and after every source change. For each applicator, the reproducibility of these positions must also be considered.

Previous work has failed to address the inter/intra-observer variability of measurements as well as the time required to commission a ring applicator.

This work describes a new approach to determine dwell and tandem positions for ring applicators in which the ring is imaged and its dwell and tandem positions automatically measured in the ring applicator coordinate system.

An image analysis computer algorithm was developed for this. It uses edge detection techniques and Hough transform for circle and ellipse detection to process axial and sagittal CT scouts of the ring applicator for each dwell position.

The algorithm performs the measurement of hundreds of dwell positions in seconds with an uncertainty below 0.2mm (CT Scout with up to 0.6mm pixel spacing) which allows us to speed up the ring applicator commissioning process along with removing inter/intra-observer variability.

Our results showed that source dwells and tandem within Elekta's HDR CT/MR ring applicators can deviate from expected (Elekta's) positions by up to 4 millimeters. These results reinforce the importance of developing an in house technique to accurately measure dwell and tandem positions.

PS04.017 - eMU Whisperer: An application for assessing patient surface topology and its impact on monitor units in electron beam therapy.

Author(s): Paule M. Charland¹, Baochang Liu¹, Shane L. Lawrence², Natascha H. Van Lieshout³

¹Medical Physics, Grand River Hospital, Kitchener/ON/CANADA, ²Department Of Physics, University of Waterloo, Waterloo/ON/CANADA, ³Electrical And Computer Engineering, University of Waterloo, Waterloo/ON/CANADA

Standard quality assurance protocols of patient specific radiation treatment plans require that monitor units (MUs) be verified with an independent mean. While Monte Carlo methods for electron beam treatment planning have opened up a new era where we anticipate reasonable dose accuracy in complex irradiation geometry and media composition, an independent (MU) verification is still to be performed to evaluate, within tolerance, if the Monte Carlo predicted MUs could be endorsed. The intent is to flag suspicious dose calculation that would warrant further investigation. These independent methods to verify MUs are normally based on simpler calculations consisting of empirical multiplicative functions with shortcomings such that flat geometry and straight beam incidence have to be assumed. The decoupled functions nevertheless provide insightful values. In a logical extension of current methodology for routine independent MU check, we have exploited the multiplicative property to define a correction factor, CF_{topo} , to account for topology effects. It is defined as the ratio of the dose output on the central axis at a nominal depth of maximum dose (d_{max}) of a given surface topology relative to the dose to a flat phantom, for the same irradiation conditions.

We have characterized CF_{topo} for a variety of phantoms on a True-Beam linac (Varian). Phantoms were constructed of different rounded masses of tissue equivalent material superposed to solid water slabs to create different surface topologies where the beams are incident. Point dose measurements were performed with a Markus-type ionization chamber inserted into one of the solid water slabs on the central axis at nominal d_{max} for a constant source-surface-distance of 100 cm. Energies under consideration were 6, 9, 12, 16 and 20 MeV and cone sizes ranged from 6 cm x 6 cm to 25 cm x 25 cm. It was found that the magnitude of CF_{topo} could drop as low as around 80%, the lowest energies 6, 9 and 12 MeV being generally the most impacted.

This motivated the development of a methodology to provide CF_{topo} from any arbitrary surface topology for our routine patient-specific plan quality assurance. We have developed the application "eMU Whisperer" in Matlab (MathWorks) which takes as input the three-dimensional patient surface topology based on the external body contour according to the CT image exported from the Eclipse treatment planning system (Varian). A cropped area in the beam's-eye-view, function of the range of the electron energy under consideration

is used by the application to analyze and quantify the topology. A function for a given energy, previously determined from the aforementioned measurements, is used to map the topology parameter to the corresponding CF_{topo} .

The propounded methodology has been carried out on different clinical cases. The "eMU Whisperer" application provided CF_{topo} to help reconcile MUs. Data showed the marked impact of topology change, which if unaccounted for would lead to an unintended dosage. Detailed user evaluation demonstrates the strengths, limitations and practical value of the proposed quality assurance method.

PS04.018 - Beam modeling of the flattening filter-free beams for VMAT SBRT using the collapsed cone convolution superposition algorithm

Author(s): Samju Cho¹, Woonhoon Choi¹, Ho Lee¹, Kwangwoo Park¹, Jungil Lee¹, Jeongmin Yoon¹, Eungman Lee¹, Suk Lee², Sang Hoon Lee³, Juree Kim³, Jinho Choi⁴, Sangwook Lim⁵, Ki Chang Keum¹
¹Radiation Oncology, Yonsei University, Seoul/KOREA, ²Radiation Oncology, Korea University, Seoul/KOREA, ³Radiation Oncology, Catholic Kwandong University, Seoul/KOREA, ⁴Radiation Oncology, Gachon University, Seoul/KOREA, ⁵Radiation Oncology, Kosin University College of Medicine, Busan/KOREA

Flattening filter-free(FFF) megavoltage beam has a highly forward peaked beam profile, increased dose rate from 1200 MU/min up to 2400 MU/min, less variation of off-axis beam hardening, less photon head scatter and less leakage outside of beam. In SBRT, high dose rate reduce the delivery time with benefit inpatient discomfort and with potential limitation of intra-fraction motion. The volumetric modulated arc therapy(VMAT) technique with FFF megavoltage beam have recently started to be used in the SBRT. The aim of this study is to create accurate FFF megavoltage beam model with the collapsed cone convolution superposition (CCCS) dose calculation algorithm for VMAT SBRT implementation.

The beam data sets of off-axis profiles, depth dose and relative output factor for photon 6 and 10 MV were measured in a PTW MP3 water phantom with a source to surface distance of 90 cm SSD. The off-axis profiles and depth dose were acquired with LA 48 linear chamber array at dose rate 300 MU/min from 1x1 up to 30x30 cm². The relative output factors were measured with the Farmer chamber for field size 10x10 cm² and larger, and the 0.004 mm³microDiamond detector for less than 10x10 cm² field size. Absolute calibration was performed according to IAEA TG 398 with 0.6 cm³ Farmer chamber using dose rate 1000 MU/min. Extra audit for output verification was carried out using OSLD with IORC Houston. The beam models were evaluated by making point dose measurement using cheese phantom and verifications of dose distribution using Sun Nuclear ArcCheck phantom with 3 mm/3% Gamma criteria.

The verification of CCCS beam modeling results showed that the point dose measurements were within 3% agreement between computed dose data and cheese phantom measured dose data. The ArcCheck phantom evaluation results were well within the accepted clinical tolerance level. Our results show that beam modeling of CCCS algorithm could provide reliable FFF beam model for the VMAT SMRT treatment.

No	Energy	Dose @Ray (cGy)	Dose @ ArcCheck (cGy)	Dose @ 3DVH	Gamma (3mm/3%)	3DVH (3mm/3%)
1	6MV	1403.000	1386.848	-1.15%	92.40%	97.7%
2	6MV	1407.000	1405.213	-0.13%	97.30%	96.8%
3	6MV	1555.000	1520.735	-2.20%	94.40%	99.3%
4	6MV	1503.000	1505.051	0.14%	90.4%	99.5%
5	10MV	1631.000	1620.996	-0.61%	98.90%	97.4%
6	10MV	1612.000	1620.996	0.56%	99.30%	95.9%
7	10MV	1795.000	1773.428	-1.20%	98.00%	98.4%
8	10MV	1621.000	1620.996	0.00%	98.9%	97.3%

PS04.019 - Dependence of Collimator Angle on Prostate VMAT: A Treatment Planning Study
Author(s): M Isa¹, J Rehman¹, M Afzal¹, James Chow²
¹Islamia University of Bahawalpur, Bahawalpur/PAKISTAN, ²Princess Margaret Cancer Center, Toronto/CANADA

This study investigated the dose-volume dependences of planning target volume (PTV) and organs-at-risk (OARs) on prostate volumetric modulated arc therapy (VMAT), when the collimator angle is varied. Single-arc VMAT plans at different collimator angles (0°, 15°, 30°, 45°, 60°, 75° and 90°) were created systematically based on a Harold pelvis phantom and the 6 MV photon beams. The conformity index (CI), homogeneity index (HI), gradient index (GI), machine monitor units (MUs), dose-volume histogram and mean and maximum dose of the PTV were calculated and analyzed (Table 1). The dose-volume histogram and mean and maximum doses of OARs such as bladder, rectum and femoral heads for different collimator angles were determined from the plans (Table 2). From our dosimetric results, there was no significant difference, according to the planned dose-volume evaluation criteria, found in the VMAT optimizations for all studied collimator angles. However, a higher CI (0.53) and lower HI (0.064) resulted from the 45° collimator angle. The 15° collimator angle provided a lower value of HI similar to the 45° angle while collimator angles of 75° and 90° were found to be good for rectum sparing. In addition, collimator angles of 75° and 30° worked well for sparing the right and left femur. The PTV dose coverage for each plan was comparatively independent of the collimator angle. The dosimetric results in this study provide support and guidance in the collimator angle selection for prostate VMAT to improve the PTV coverage and OARs sparing.

Table 1: Dosimetric results of PTV for different collimator angles.

Collimator angles	0°	15°	30°	45°	60°	75°	90°
D _{95%} (Gy)	72.41	72.59	72.40	72.60	72.40	72.61	72.73
D _{5%} (Gy)	78.44	78.44	78.79	78.55	78.96	78.86	78.40
D _{2%} (Gy)	73.47	73.50	73.38	73.63	73.34	73.71	73.58
D _{max} (Gy)	79.40	79.24	79.89	79.87	79.62	80.41	79.40
D _{mean} (Gy)	76.20	76.25	76.28	76.38	76.24	76.42	75.96
CI	0.49	0.51	0.51	0.53	0.48	0.52	0.37
HI	0.06	0.064	0.07	0.064	0.073	0.065	0.066
GI	7.9	7.6	4.97	5.5	5.7	5.4	9.4
MUs	351	352	365	356	362	364	366

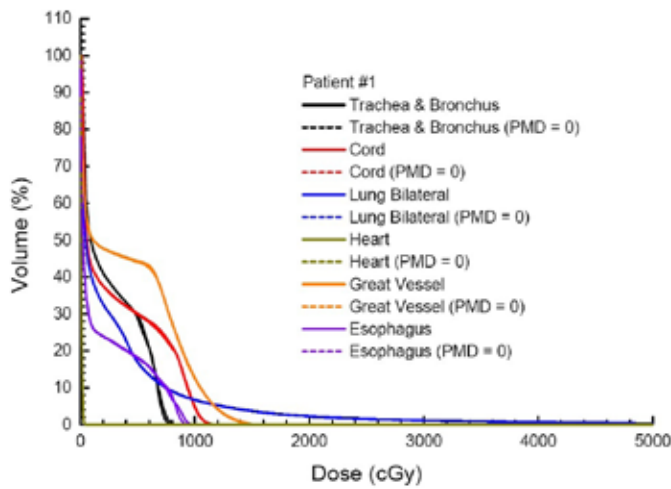
Table 2: Dose-volume criteria, mean and maximum doses.

Collimator angles	0°	15°	30°	45°	60°	75°	90°
Rectum							
D _{max} (Gy)	53.69	53.56	52.59	53.62	52.05	53.61	52.29
D _{5%} (Gy)	79.13	79.09	79.77	79.87	79.62	79.92	79.12
D _{2%} (Gy)	50.29	50.09	49.66	49.97	49.17	50.07	50.35
D _{mean} (Gy)	58.33	58.39	58.07	59.14	58.93	58.66	59.25
V _{100%} (%)	36.26	36.26	36.22	36.26	36.19	36.26	35.64
V _{125%} (%)	35.43	35.96	33.07	35.3	31.69	34.76	31.67
Bladder							
D _{max} (Gy)	53.08	52.47	51.59	51.99	52.37	52.49	50.69
D _{5%} (Gy)	78.73	78.58	79.36	78.24	79.47	78.96	78.63
D _{2%} (Gy)	50.40	49.33	49.31	48.92	48.69	50.59	50.00
D _{mean} (Gy)	69.02	68.74	68.93	69.15	68.41	69.46	70.16
V _{100%} (%)	59.84	59.69	58.12	59.53	59.84	57.31	54.40
V _{125%} (%)	54.24	55.48	51.22	50.43	52.56	40.51	44.43
Left Femur							
D _{max} (Gy)	16.06	16.20	15.19	18.06	16.12	20.34	17.75
D _{5%} (Gy)	31.63	32.42	37.46	34.42	35.17	37.32	45.89
D _{2%} (Gy)	27.13	28.32	29.27	29.86	30.03	32.50	35.54
V _{100%} (%)	105.66	108.19	105.07	114.8	103.8	112.8	99.5
V _{125%} (%)	95.65	91.40	69.20	100.98	75.18	107.64	80.02
Right Femur							
D _{max} (Gy)	17.32	17.34	16.33	14.92	15.14	14.33	22.73
D _{5%} (Gy)	37.06	39.05	40.62	40.08	40.80	43.55	54.14
D _{2%} (Gy)	31.04	32.14	28.88	31.17	31.31	32.27	39.74
V _{100%} (%)	108.68	111.12	107.56	100.17	102.69	95.87	117.4
V _{125%} (%)	98.96	98.16	87.20	65.57	67.53	56.94	111.7

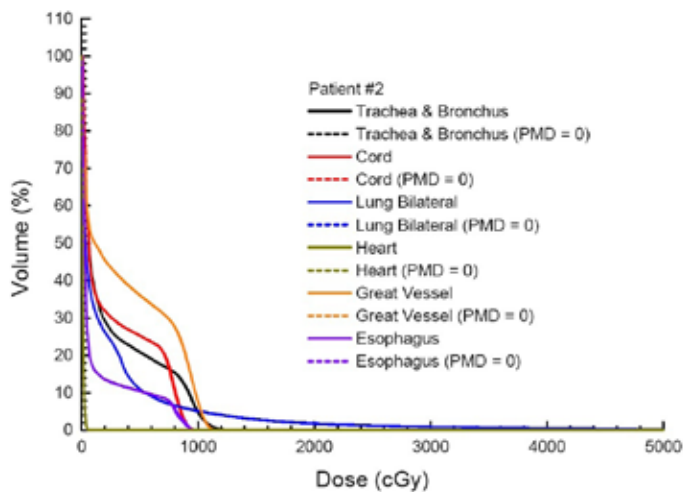
PS04.020 - Dosimetry of Pacemaker in VMAT for Lung SBRT

Author(s): James Chow¹, R Jiang²
¹Princess Margaret Cancer Center, Toronto/CANADA, ²Grand River Regional Cancer Center, Kitchener/CANADA

This study investigated the possibility to include the pacemaker in volumetric modulated arc therapy (VMAT) plan optimization for lung stereotactic body radiotherapy (SBRT) to reduce the pacemaker dose. Moreover, dose distributions of the planning target volume (PTV) and organs-at-risk (OARs) with and without lowering the pacemaker dose in VMAT plans were compared with the PTV close to and far away from the pacemaker. Patients with PTVs in their left and right lung were selected in lung SBRT. VMAT plans with pacemaker regarded as an OAR or not in the plan optimization were created. Dose-volume histograms (DVHs) of PTVs and OARs were determined and compared. Our results of VMAT plans (Figure 1(a): left lung and 1(b): right lung) showed that no significant deviation of dose-volume criteria of OAR was found, whether the pacemaker was or was not regarded as an OAR. This demonstrated that it is possible to achieve an acceptable PTV coverage by lowering the pacemaker dose in the VMAT plan, though larger dose-volume deviation of PTV can be found when it is closer to the pacemaker. In addition, DVH deviations for OARs were not significant when the pacemaker was regarded as an OAR in the plan. We also found that the dosimetric change is sensitive to OARs namely, trachea, bronchus, esophagus and cord when the pacemaker was included in the plan optimization. We concluded that it is possible to reduce the pacemaker dose by including it as an OAR in the VMAT plan for lung SBRT. This is especially important for patient depending seriously on the pacemaker, as VMAT beams for SBRT are directly on the device with a very high dose per fraction.



(a)



(b)

Fig. 1 DVHs of OARs for Patient (a) #1 and (b) #2 with (solid line) and without (broken line) lowering the pacemaker dose.

PS04.021 - Determination of ion chamber correction factors for small composite fields used by the CyberKnife radiosurgery system

Author(s): Eric J. Christiansen¹, Bryan R. Muir², Jason Belec³, Eric Vandervoort³

¹Medical Physics Unit, McGill University, Montreal/QC/CANADA, ²Measurement Science And Standards, National Research Council, Ottawa/CANADA, ³Medical Physics, Ottawa Hospital Cancer Center, Ottawa/CANADA

Purpose: A dosimetry formalism has been proposed to determine ionization chamber correction factors (CFs) for small and non-standard fields. Small field ionization chamber CFs have been shown to depend on off-axis position and source-to-axis distance (SAD). In this study, CFs were calculated using the EGSnrc user code egs_chamber for six composite fields delivered by the CyberKnife system with varying SAD and off-axis position.

Methods: Percentage depth dose (PDD) curves and output factors (OFs) for CyberKnife's largest (60 mm) and three smallest collimators (5 mm, 7.5 mm, and 10 mm) were measured with an Exradin A16

microchamber. A model of the CyberKnife G4 head was created in BEAMnrc with initial electron energy and spatial distribution tuned by matching measured PDDs and OFs to simulations performed in egs_chamber with detector response effects modelled based on manufacturer specifications.

This beam model was used to calculate dose-to-detector (D_{det}) to dose-to-water (D_w) CFs for the A16 in six different composite fields (5 isocentric, one non-isocentric) using the 5 mm collimator. The first three used all the standard beams employed by CyberKnife for skull lesions (average SAD= 800 mm), while the last three used a set of beams optimized for the treatment of trigeminal neuralgia (TN) (average SAD=700 mm). The point of intersection of the beams varied between different fields using the same beam set. The final field was a non-isocentric optimized clinical TN plan, where detector off-axis position varied between beams.

Results: Calculated and measured PDDs for the 60 mm collimator are in good agreement (root mean square deviation=1.1%) after tuning the electron energy. Figure 1 shows measured OFs and calculated D_{det} ratios used to select the beam's spatial distribution. The D_{det} to D_w CFs for the skull lesion fields were calculated to be 1.2464 ± 0.0023 , 1.2391 ± 0.0022 , and 1.2598 ± 0.0024 . The CFs for the isocentric TN fields were calculated to be 1.2565 ± 0.0021 , and 1.2495 ± 0.0021 ; the CF for the non-isocentric field was 1.2103 ± 0.0028 .

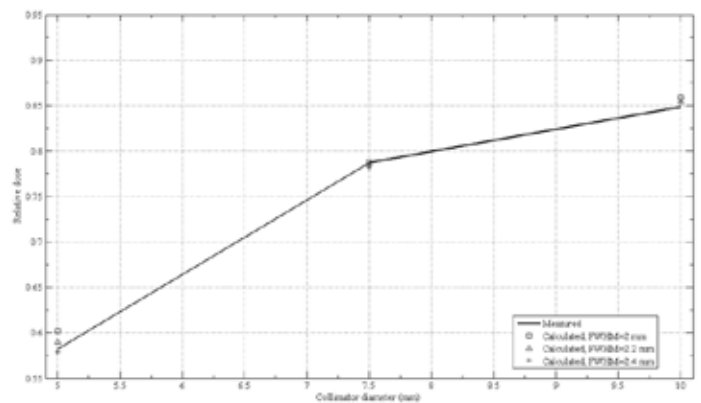


Figure 1. Comparison between measured and calculated OFs. The OFs were calculated with an electron energy of 6.7 MeV and varying full width at half maximum (FWHM).

Conclusions: CFs for the skull lesion fields varied by no more than 2% as a function of the location of the point of intersection of the beams. For "isocentric" TN fields, they varied by no more than 1%. If the non-isocentric field is included, the variation increases to 4%, demonstrating that a clinically-optimized plan requires larger CFs.

PS04.022 - One-year review of a real-time, ultrasound-based, single-fraction prostate HDR program – the Halifax experience

Author(s): Krista Chytky-Praznik¹, Amanda Cherpak¹, David Bowes², Nikhilesh Patil³, Mammo Yewondwossen¹

¹Medical Physics, QEII Health Sciences Centre, Halifax/NS/CANADA, ²Radiation Oncology, QEII Health Sciences Centre, Halifax/NS/CANADA, ³Radiation Oncology, Dalhousie University, Halifax/NS/CANADA

Introduction: The QEII Health Sciences Centre began a high-dose-rate prostate brachytherapy program in March 2014. As of January 2015, 25 prostate cancer patients have been treated under general anaesthetic using the real-time Oncentra Prostate (v. 4.2) treatment planning system (Elekta), with ultrasound imaging (BK Medical).

Materials and Methods: Two radiation oncologists and three physicists have been trained in the procedure. The patients were prescribed 15 Gy in a single fraction to the entire prostate (dose constraints listed in Table 1). The planning method for the first 10 cases involved 1) obtaining initial US image set 2) detailed contouring of the prostate, urethra and rectum 3) choosing virtual catheter positions 4) pre-plan dose optimization (using DVHO algorithm) 5) catheter insertion 6) catheter tip reconstruction 7) final imaging 8) final contouring 9) catheter reconstruction and catheter free length measurement and 10) final dose optimization. By the 11th patient, this planning flow was redesigned by replacing the first six steps with four: 1) obtaining initial US image set 2) choosing catheter positions 3) simultaneous needle insertion and preliminary contouring of prostate, urethra and rectum and 4) needle tip reconstruction. The remaining steps follow in the same order as the original planning method.

Results: Average treatment time (US probe insertion until the start of treatment delivery) was 177 ± 24 min (114 min – 216 min). Eliminating pre-planning steps for later patients increased efficiency of the treatment, with an improvement in average treatment time from 193 min for the first five patients to 155 min for the last five patients. The average prostate volume treated was 32.4 ± 9.4 cc (21.2 cc - 58.0 cc) with the average number of needles used equal to 15.1 ± 1.4 (11 – 17). A standard template for needle placement was not used, however general guidelines have been developed and are consistently followed. Prostate coverage for all patients was met, with an average V100% = 96.44% and a V90% = 99.35%, as were the constraints for the urethra and rectum (see Table 1). Comparing the dose constraints achieved for the first five patients and the last five patients, prostate coverage was consistent, but the quality of the plans improved by the last five patients (achieved lower V150% and V200% values).

Conclusion: Careful commissioning and practice runs of the procedure aided in a successful start to the program which has evolved and been refined over the initial 12 months.

	All patients	First 5	Last 5
Prostate: V100% (goal: 95-99%)	96.44%	96.28%	96.19%
Prostate: V90% (goal: 99-100%)	99.35%	99.15%	99.38%
Prostate: V150% (goal: <35%)	36.05%	39.95%	33.91%
Prostate: V200% (goal: <11%)	11.77%	14.47%	9.77%
Urethra: D10% (goal: <118%)	113.81%	114.61%	113.03%
Rectum: V80% (goal: < 0.5 cc)	0.281	0.245	0.321

Table 1: Summary of dose constraints and average results over all patients, the first five patients and the last five patients.

PS04.023 - Retrospective evaluation of visually monitored deep inspiration breath hold for breast cancer patients using edge detection

Author(s): Leigh Conroy¹, Rosanna Yeung², Sarah Quirk¹, Tien Phan², Wendy L. Smith²

¹Department Of Medical Physics, Tom Baker Cancer Centre, Calgary/AB/CANADA, ²Department Of Oncology, University of Calgary, Calgary/AB/CANADA

Purpose: Deep inspiration breath hold (DIBH) can reduce cardiac dose during left-sided breast cancer radiotherapy. This study uses cine imaging with edge detection to evaluate a visually-monitored DIBH technique (VM-DIBH).

Methods: Cine images were acquired weekly during the medial tangent field of patients treated with VM-DIBH. Edge detection was used to identify the field borders and chest wall edges in digitally reconstructed radiographs (DRRs) and cine images of 15 patients. The distance between the field border and chest wall was measured at the center of the field and used as a surrogate for patient position during breath hold. Setup uncertainties were found by comparing DRR measurements to the first cine image measurement for each fraction. Intra-beam motion during individual breath holds was assessed by comparing the first cine image measurement to all subsequent cine image measurements for each fraction.

Results: The mean setup uncertainty (M) was 1.2 mm; random (σ) and systematic (Σ) setup errors were both 2.0 mm. The chest wall position was within 5 mm of the DRR position in 92% of cine images. Intra-beam motion was within +/- 2 mm in 98% of images, and was slightly skewed in the posterior direction, indicating that patients tend to relax or exhale during breath holds.

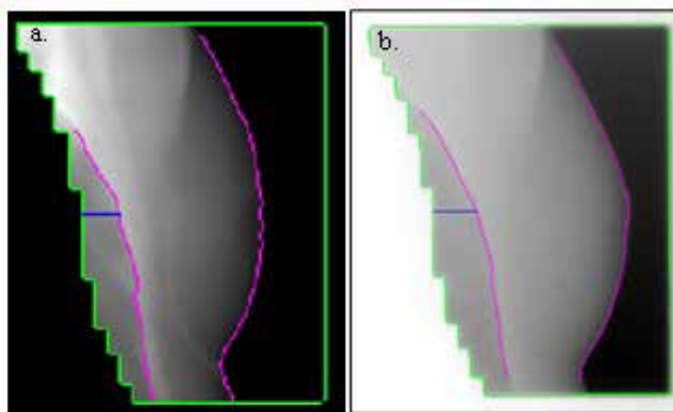


Fig. 1 Chest wall edge detection of field borders (green), chest wall (pink) and chest wall position measurement (blue) for a DRR (a) and cine image (b).

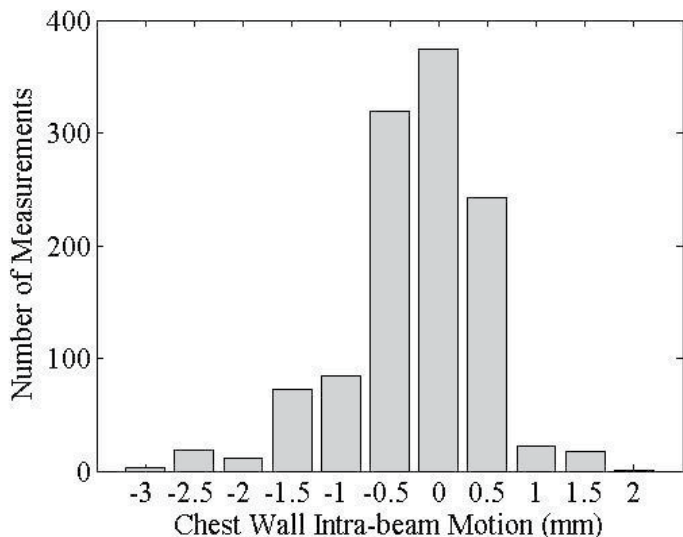


Fig. 2 Intra-beam chest wall motion for all cine images.

Conclusion: Edge detection of field borders and the chest wall in cine images and DRRs was successfully used to evaluate inter-fraction and intra-beam uncertainties for a VM-DIBH technique. Setup uncertainties and chest wall position measurements indicated adequate breath hold setup reproducibility for the majority of patients. Intra-beam motion measurements showed excellent stability of breath hold during treatment.

PS04.024 - DECT Tissue Characterisation and Artefact Suppression Method for Improved Dose Calculations in Brachytherapy Treatments.

Author(s): Nicolas Cote, Stephane Bedwani, Jean-Francois Carrier
Radio-oncologie, CHUM- Notre-Dame hospital, Montreal/QC/
CANADA

Doses in brachytherapy, for many years now, have been evaluated using the TG-43 formalism which make use of standard equations determined from a full water based medium. However, the accuracy of these calculations, particularly in Low Dose Rate (LDR) brachytherapy, are misleading, as they are highly dependent on inter-seed attenuation and patient tissue heterogeneities due to its low energy range (20-30 keV). This Monte Carlo study allows the evaluation of the dose distribution in individual cases by encompassing patient specific tissue information with a voxel by voxel determination of the effective atomic number (EAN) and electron density (ED). Using a dual energy computed tomography (DECT), these physical parameters can be extracted using the stoichiometric calibration method. The DECT is also be used to minimize the presence of metallic artifact contributed by sealed radioactive sources containing materials of high atomic number. This new technique is quick and simple as it uses a mixture of both distinct energy scans. The concept behind the suppression is manipulating the differences in Hounsfield Units (HU) variations between different structures in order to find an image describing the artifacts alone. Thereafter, the initial image can be treated from metallic artifacts by subtracting it from the latter (Figure 1). The dose calculations have been accomplished using BrachyDose from the EGSnrc series. Using this software, variations in the dose have been analyzed from inter-seed attenuation and show differences ranging roughly 5.8% to 6.2% in the dose at 90 % of the target volume (D_{90}). Also, with the stoichiometric method, the extraction of ED and EAN, using DECT suppressed artifact images, allows for a voxel-to-voxel tissue characterization depicting a better reality of patient anatomy. This would in consequence be integrated in the Monte Carlo simulation to analyze further variations from TG-43

formalism. Results currently suggest an increase in dose variations when considering these heterogeneities compared to inter-seed attenuation. Henceforth, this study would help bolster the recommendations in brachytherapy dose calculations suggested by the TG-186 report as it implements techniques that reach beyond the TG-43 formalism.

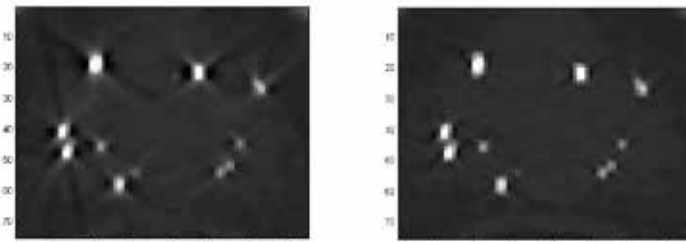


Figure 1. A CT scan (left image) treated with the DECT artifact suppression method (right).

PS04.025 - Radiotherapy Planning using CEER and CADPLAN in a Prostate Cancer Patient

Author(s): Juan Alberto L. Cruz¹, Maíra Mariana C. Uchôa², Diego S. Dolci¹, Ernando S. Ferreira¹, Wilfredo G. Infante³
¹Department Of Physics, State University of Feira de Santana, FEIRA DE SANTANA/BRAZIL, ²Radiotherapy Section, Hospital Aristides Maltez, Salvador/BRAZIL, ³Department Of Atomic Molecular And Nuclear Physics, University of Granada, Granada/SPAIN

The authors accurately reproduced 3D conformal radiotherapy treatment plan beamlet and patient configurations using Computational Environment for Radiotherapy Research (CERR) and CADPlan treatment planning system (Varian Medical Systems, Palo Alto, CA). These planning were carried out with seven radiation fields of X-ray using a Therac-20 Neptune linac. All fields were calculated with a source surface distance of 100 cm, symmetric collimators in the X-axis and asymmetric in the Y-axis, and with a total field of 12 x 10.5 cm². The nominal energy was 18 MV except for a one field, which was chosen 6 MV. The initial parameters to perform the calculation were complemented with the inclination angles of the couch and gantry. Were used a set of Computerized Tomography images obtained of an anonymous patient with prostate cancer diagnosed and indication for radiotherapy (the prescribed dose was 58.5 Gy). Iso-dose contours maps, normal tissue complication probability (NTCP), and dose-volume histograms (DVHs), are shown and discussed. The results show that on the gross tumour volume (GTV), there is 99 % of its volume receiving 56.67 Gy. It is observed that approximately the GTV receive the prescribed dose. The PTVHD and PTVLD that includes the GTV with margins also show high probabilities of receiving the prescribed dose. The risk organs, bladder and rectum has a probability of 68 % and 89 % of its volume to receive an equivalent dose of 27 Gy and 36.76 Gy, respectively. Comparing the planning results obtained from two codes, it is observed that both are consistent with the established standards. The results shown that the CERR is appropriate to be used in clinical treatment planning.

PS04.026 - Impact of increasing irradiation time on the treatment of prostate cancers

Author(s): Alexandru Dasu¹, Iuliana Toma-Dasu²
¹Department Of Radiation Physics, Linköping University Hospital, Linköping/SWEDEN, ²Medical Radiation Physics, Stockholm University and Karolinska Institutet, Stockholm/SWEDEN

This study aimed to investigate the expected impact of intrafraction repair during increasing irradiation times for the treatment of prostate cancers. Lengthy sessions are indeed expected for some

advanced irradiation techniques capable to deliver the large fractional doses required by the increased fractionation sensitivity of the prostates. For this purpose, clinically-derived parameters characterizing repair rates and dose response curves for prostate tumors have been used to calculate the expected loss of effectiveness when increasing the irradiation time. The results have shown that treatment sessions lasting more than about 20 to 40 minutes could reduce the probability of biochemical control of prostate tumors by more than 20 to 30 percentage points. These results are in agreement with some observed clinical results and therefore they suggest that treatment durations in prostate radiation therapy should be carefully recorded in order to explicitly account for intrafraction repair, especially when irradiation techniques make use of multiple beams and imaging sessions. Failure to do so might overestimate the expected effectiveness of the treatment and could lead to disappointing clinical results precisely from the demanding treatment modalities expected to increase the therapeutic gain in prostate radiotherapy.

PS04.027 - Hemi-body Electron irradiation: Development and Verification of this new technique

Author(s): Panagiotis G. Delinikolas, Kalliopi Platoni, Vasilios Koulioulas, Georgios Patatoukas, Maria Dilvoi, Efstathios Efstathopoulos
2nd Department Of Radiology, Radiotherapy Unit, Attikon Hospital, medical School, National University of Athens, Greece, Chaidari -Athens/GREECE

Purpose

Half body (or Hemi body) electron irradiation aims to deal with cases of surficial skin tumors with more symptomatic density on upper or lower body (upper and lower HBI techniques). Like Total Skin Electrons Beam Technique (TSEB), the spectrum of using HBI includes various deceases such as Kaposi's sarcoma and T-Cell Lymphoma plus its product diseases. As today half body irradiation techniques are using photons (x radiation produced from linacs or γ radiation produced by Cobalt Units) mainly for bone metastatic cancers, the need of introducing electron beams for skin tumors was raised. The purpose of the following study is to introduce a new electron HBI technique, implementing dosimetry and standards protocol in accordance with TRS 398 (IAEA). The evaluation of the results is according to AAPM's Report No.23 and IEAE's Review of radiation Oncology Physics: A handbook for teachers and students.

Materials and Methods

A linear accelerator of the radiotherapy division of Attikon Hospital (Athens Greece), used to produce electron beams, a custom crafted chamber (used for TSEB in "Attikon" hospital) and an additional and adjustable (for Upper and Lower HBI taking patient's height into consideration) Pb shielding placed before patient are used for this new treatment. Custom standing technique is used both for lower and upper body cases. Parameters and characteristics of the beam which are measured and evaluated are: PDD on treatment plane and 2 dimensions profile of single beam (fig. 2) for both upper and lower regions, surficial and in reference depth absorbed dose in plain phantom and human like phantom. The above resulted in a calculation of the monitor units need for the delivery of the prescribed dose.

Results

The results are different especially close to the points of high dose spikes, to those extracted for the TSEB techniques driving to different homogeny of dose distribution on upper or lower extremities optimized for different metrical characteristics of patients and their clinical cases.

Conclusion

Electron HBI technique delivers the prescribed dose in the portion of the skin which needs treatment. This will minimize the dose delivered to healthy skin and allow us to handle each case differently and provide more choices for each individual.

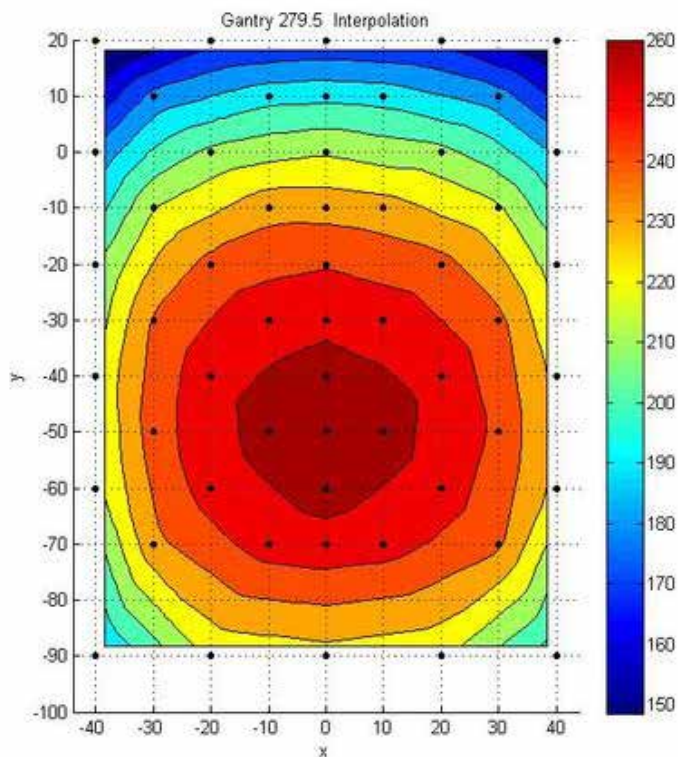


Figure 2 – 2 Dimensional Beam profile on treatment plane

PS04.028 - Deformable image registration and automatic contouring using Cone-Beam CT imaging: A study of volume statistics and similarity measures

Author(s): Olivier Fillion¹, Luc Gingras², Louis Archambault²
¹Centre De Recherche Sur Le Cancer, Universite Laval, Quebec/QC/CANADA, ²Departement De Radio-oncologie, Hotel-Dieu de Quebec - CHU de Quebec, Quebec/QC/CANADA

Volume statistics and similarity measures provide useful tools for an image-guided adaptive radiotherapy protocol to evaluate the need for re-planning during treatment. The aim of this study is to assess the accuracy of such indices when calculated on contours generated by a deformable image registration algorithm and an automatic contouring tool compared to manual references.

The study was done using the OnQ rts software (Oncology Systems Limited, Shrewsbury, UK). This software includes modules to register and/or recontour image series and evaluate the automatic contours it generates. Two methods are tested to generate contours during treatment: (1) registering the planning CT onto daily CBCTs and applying the deformation map to the planning CT structures to create an adaptive plan; (2) using the automatic atlas-based contouring tool directly on the daily CBCTs. These 2 sets of deformed structures are then compared against the same 240 structures manually contoured by a physician on daily CBCTs. The 240 reference CBCT structures with the 25 reference CT structures define the ground truth for volume statistics such as Δ Volume and Dice index.

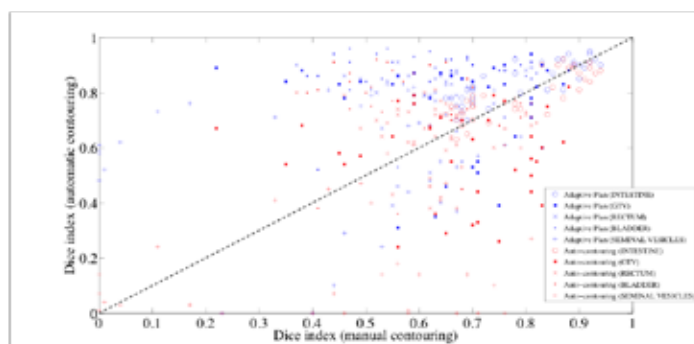


Figure 1. Dice index for structures generated by automatic contouring (Adaptive planning and Auto-contouring) with respect to the expected Dice index as given by the manually contoured structures (Intestine, GTV, Rectum, Bladder and Seminal vesicles) on the reference CT and CBCT. The dashed line $y = x$ indicates a perfect registration, where manual Dice index = automatic Dice index.

Results in Figure 1 show the adaptive planning tends to over-estimate the Dice index for many organs, thus generating not as large a deformation as required. Figure 2 shows the ratio of Dice indexes tends to diverge from 1 if the structure shrinks during treatment. Such deformations, especially for the bladder and independent of the method, would wrongly indicate the organ had not moved or deformed during the treatment.

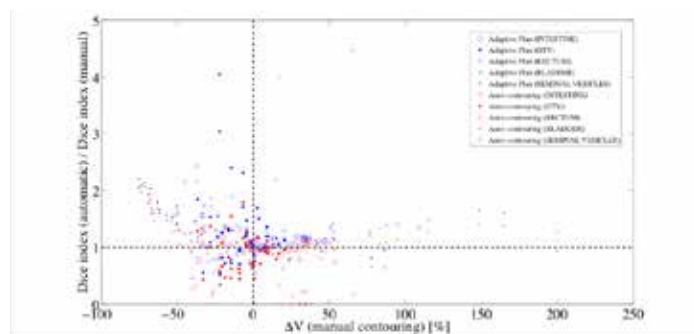


Figure 2. Ratio of the automatic contouring Dice index (Adaptive planning and Auto-contouring) on the manual contouring Dice index given by the reference CT and CBCT structures (Intestine, GTV, Rectum, Bladder and Seminal vesicles) with respect to the variation in volume of the structures between the reference CT and the reference CBCT. The vertical dashed line at $x = 0$ indicates no variation in volume between the reference CBCT structure and the reference CT structure. The horizontal dashed line at $y = 1$ corresponds to a perfect registration, where manual Dice index = automatic Dice index.

To conclude, automatic contouring on CBCTs depends on the organ, the method and the deformation. Looking at Dice indexes, organs such as the intestines show good agreement with manual contours, but the variability is larger for the seminal vesicles. Ultimately, the decision to re-plan treatments could be based on thresholds for selected indices and organs.

PS04.029 - Acceptance Modulated Radiation Intensity and Enhanced Dynamic Wedge using 2D Ion Chamber Array

Author(s): Oscar J. Garcia Contreras¹, Luis D. Casas²
¹Unidad De Cancerologia, Hospital Universitario de Neiva, Neiva/COLOMBIA, ²Radiotherapy Service, Oncologist from Occident Foundation, Pereira/COLOMBIA

Dynamic techniques for dose delivering used in external radiotherapy such as modulated radiation intensity (IMRT) and enhanced dynamic wedges (EDW) tend to be used with more frequency due to the benefits in terms of higher treatment dose to the tumor while preserving the exposure of healthy tissues and reduction in treat-

ment times needed in wedged beam techniques, respectively. In seeking to ensure accuracy in dose delivery in dynamic techniques are several the measurement methods and systems developed. One of the factors of interest to medical physicists who daily use these techniques in the clinic routine is the quick and easy configuration of measurement systems and analysis to carry out QA tests. This paper presents the results of tests of acceptance for Intensity Modulated Radiation Therapy and Enhanced Dynamic Wedge Commissioning made on a Varian iX with 6 and 10 MV energies using a 2D array ionization chamber Octavius2D. This paper presents the results of acceptance tests for IMRT and EDW commissioning made on a 6 and 10 MV Varian iX using a 2D array Octavius2D PTW ionization chamber. Acceptance factors considered were: absolute dose delivery, reproducibility and exactitude fluence patterns, dose profile and QA of specific patient. The results obtained show a good accordance with the field parameters having higher acceptance percentages to 90% in all realized tests.

PS04.030 - Dose Calculation in Gynecological Brachytherapy using Monte Carlo simulation for intracavitary treatment of Cervical Cancer

Author(s): Oscar J. Garcia Contreras¹, Luis F. Cristancho Mejia²
¹Unidad De Cancerologia, Hospital Universitario de Neiva, Neiva/COLOMBIA, ²Physics Department, National University of Colombia, Bogota/COLOMBIA

Intracavitary brachytherapy with high dose rate (HDR) is nowadays one of the complementary specialities for the treatment of cervical cancer. This work presents results of an application for the deposited dose calculation in brachytherapy treatments for cervical cancer using distributed tools in the GAMOS and Geant4, aimed at studying the effects on dose distribution considering the variation of tissue inhomogeneities and decay characteristics for an mHDR-v1 Nucletron Classic source. The anatomy of the patient is included in the developed Monte Carlo simulation using CT images of a typical HDR brachytherapy for cervical cancer treatment defining a voxel grid which contains the composition and density information due to body tissues, extracted from CT images, and converted to material voxels through the CT Number characteristic curve. The results obtained are in agreement with values reported by the planning system used, showing a difference possibly due to overestimation due to AAPM Task Group No. 43 formalism, the effect due to variation in tissue and the noise contained in the image.

PS04.031 - An inverse treatment planning module for Gamma Knife Perfexion™ using 3D Slicer

Author(s): Kimia Ghobadi¹, Yago Oliveira², Kevin Wang³, Dionne Aleman⁴, David Jaffray⁵
¹Techna Institute, University Health Network, Toronto/ON/CAN-ADA, ²Computer Science, University of Toronto, Toronto/CAN-ADA, ³Radiation Oncology, Princess Margaret Cancer Centre, Toronto/CANADA, ⁴Mechanical And Industrial Engineering, University of Toronto, Toronto/ON/CANADA, ⁵Radiation Medicine Program, Princess Margaret Cancer Center, Toronto/ON/CANADA

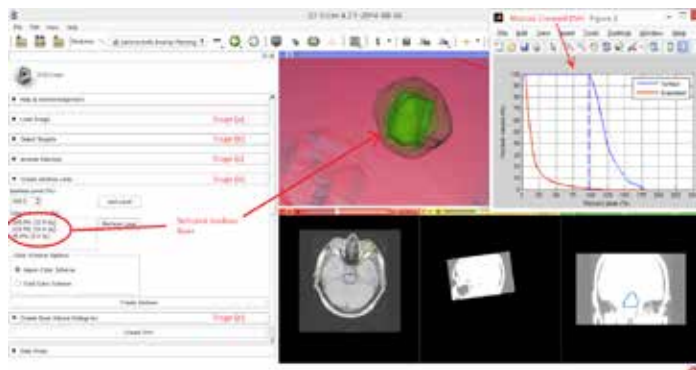
We developed an inverse treatment planning module for Leksell Gamma Knife Perfexion™ using 3D Slicer as the interface. Perfexion™ is a cobalt-60 system that delivers stereotactic radiosurgery treatments for head-and-neck tumours. Inverse treatment planning for Perfexion™ has been previously shown to produce quality treatment plans [1], however, a medium to easily use and test the inverse plans does not exist. Our module provides a layout that simplifies input/output format and the result illustration process for any Perfexion™ inverse treatment planning algorithm that is written in MATLAB.

The Gamma Knife Perfexion Inverse Treatment Planning (GK-Inverse-

Plan) module is developed in Python and MATLAB using 3D Slicer (v4.3.1 r23560) and its SlicerRT (v0.14.5) and MatlabBridge (v0.11.0.) extensions. GK-InversePlan provides the inverse planning optimization algorithm with inputs, such as, tumour volumes, organs-at-risk (OARs), and clinical prescriptions and guidelines. It also captures and illustrates the outputs including dose-volume matrices and final shots.

The GK-InversePlan module is divided into five stages of (a) Load Image, (b) Select Target, (c) Inverse Planning, (d) Isodose Illustration, and (e) Dose-Volume Histogram (DVH) Illustration (Figure 1). In Stage (a), the user can load DICOM formatted images, as well as other data including target volumes, OARs, and other organs of interest, which are all typically contoured previously in Perfexion™'s treatment planning environment (GammaPlan). Once the images and the organs are imported, the user will be prompted to Stage (b) where the target volume(s), their prescription dose, and other clinical guidelines can be specified. In Stage (c), the inverse treatment planning algorithm is performed by calling the optimization model from MATLAB. Any MATLAB figures, interfaces, and scripts that are contained in the inverse plan algorithm will be shown to the user at this point. Once the inverse treatment plan is obtained, the user can use Stages (d) and (e) to illustrate the isodose lines and DVH graphs, respectively.

GK-InversePlan is a module in 3D Slicer that provides a platform for integrating MATLAB-written inverse treatment planning tools for Perfexion™ with clinical visual interface and easy input and output access. Figure 1 depicts a snapshot of GK-InversePlan and a conformal plan [1] (Paddick CI of 0.83) for a synthetic acoustic neuroma on a sample MRI image, and shows the obtained DVH graph and isodose volumes.



[1] Ghobadi, Ghaffari, Aleman, Jaffray, Ruschin. *Automated treatment planning for a dedicated multi-source intra-cranial radiosurgery treatment unit using projected gradient and grassfire algorithms*, Medical Physics, 39(6):3134-3142, 2012.

PS04.032 - Bladder and rectum DVH prediction: a statistical approach for prostate treatment

Author(s): Frédéric Girard, Martin Hinse
 Département De Radio-oncologie, Centre intégré de cancérologie de Laval, Laval/CANADA

Purpose: To predict bladder and rectum DVH values for prostate treatment based on the intersection of these structures with the PTV.

Methods: DVH values for the rectum (V50, V60, V65, V70 and V75) and the bladder (V40, V65, V70 and V75) were extracted from prostate and post-operative prostatic bed treatment plan. All the planification process of these plans from the contouring of OAR and target volume to the VMAT inverse planning technique was performed using a standard procedure. For convenience, all plans

are optimized at the total treatment dose and then scaled down to the specific plan dose. Correlation of each DVH value with relative volume of bladder and rectum that are within the PTV or an 18 mm expansion of the PTV was verified using multi-linear regression. The correlation with a parameter was judged significant if the p value is inferior to 0.05. In order to improve the correlation of the regressions with the parameters, treatment plans were divided in three categories that shared common target morphology: treatment of the prostate with or without seminal vesicles (N = 191, 2 Gy per fraction, prostate receives 78 Gy, seminal vesicles receive 54 Gy); treatment of the prostate that included both seminal vesicles and the lymph nodes (N = 37, 2 Gy per fraction, lymph nodes receive 44 Gy); and post-operative prostatic bed treatment (N = 62, total dose of 66 Gy in 33 fractions). Post-operative prostatic bed treatments that included lymph nodes were removed from the analysis due to the small sample size. Outliers were removed from each distribution.

Results: DVH values that are close to the total treatment dose showed the best correlation with the intersection of bladder and rectal volume with the PTV and only marginally or not at all with the intersection of the expanded PTV. The overall regression models showed better results with tighter confidence intervals than the ones for low dose values. This is to be expected since the highest isodoses are tailored almost perfectly around the PTV. Correlation with the PTV intersection decrease gradually as the DVH dose values get further away from the total dose and the correlation with the expanded PTV intersection because more significant. Rectum V50 and bladder V40 showed the poorest correlation which suggest that there is a great variability in the optimization of these parameters due to the patient morphology and/or planner decision. The use of the statistical models in clinical practice is in the early stage but we can already see an improvement in planification time and overall better rectum and bladder sparing.

Conclusion: Building a statistical model of bladder and rectum DVH values against intersection of these structures with the PTV provides a simple mean to predict the DVH outcome of future plan, to prevent planification error and to guide beginning dosimetrist.

PS04.033 - Retrospective evaluation of applicator localization for HDR cervix brachytherapy – A comparison of MR versus CT

Author(s): Lisa Glass¹, Daron Owen², Daxa Patel², Aaron Vandermeer², Cathy Neath²

¹Department Of Radiation Oncology, University of Toronto, Toronto/ON/CANADA, ²Medical Physics Department, R.S. McLaughlin Durham Regional Cancer Centre, Oshawa/ON/CANADA

The international standard for treating cervix cancer with brachytherapy is 3D volume-based planning. Currently at the Durham Regional Cancer Centre (DRCC; Oshawa, Canada) CT and MR imaging are acquired and fused for each fraction. The MR image is used to aid target contouring and the applicator is reconstructed on the CT dataset using an applicator model provided in our brachytherapy planning software.

Although MR-only planning would reduce patient transfers, thereby lowering the risk of applicator motion or uterine perforation, a limiting factor is the inferior visibility of the applicator in MR versus CT imaging. **In this retrospective study, applicator placement with MR versus CT imaging using the applicator model is compared.** In order to assess the relative applicator position in a single coordinate system, the applicator is contoured on the CT image set and copied to the fused MR image set. The applicator model is then placed on the MR image set first using the CT applicator contour, and then using the MR image only. Fifteen cervix cancer brachytherapy treatments at the DRCC were evaluated.

As demonstrated in Figure 1, the source dwell positions vary by an average of 1.3 ± 0.5 mm in the ring and 1.0 ± 0.3 mm in the tandem,

when comparing CT to MR. Furthermore, we investigate the dose equivalency between CT and MR-based applicator model placement. As shown in Table 1, there is no significant difference in D90 to the CTV and in D2cc to the OARs between CT and MR, varying on average by less than 3%. Other dose indicators and individual treatment DVHs also support the conclusion that doses to target volumes and OARs are comparable between applicator model placement on CT versus MR image sets.

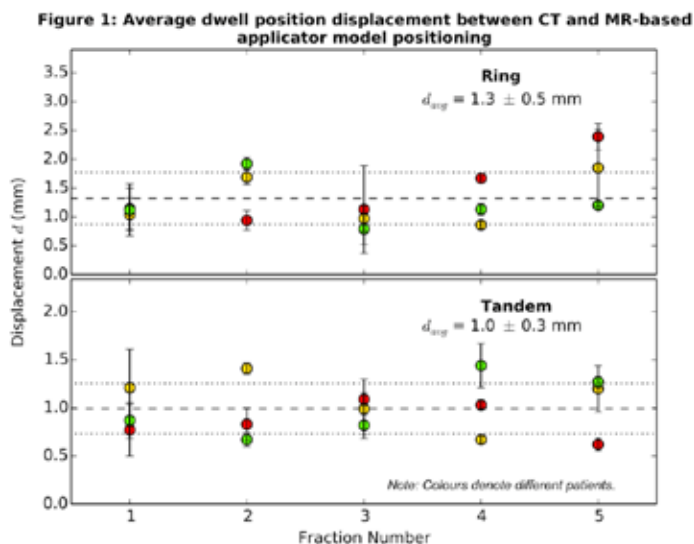


Table 1: Dose difference in MR-based applicator model placement compared to placement on CT

	$\Delta(D90)$
CTV	$-0.5 \pm 1.8 \%$
	$\Delta(D2cc)$
Bladder	$+0.6 \pm 2.6 \%$
Rectum	$0.0 \pm 2.7 \%$
Sigmoid	$-0.2 \pm 2.4 \%$

PS04.034 - A general source model for clinical linac heads in photon mode

Author(s): Wilfredo González, Marta Anguiano, Antonio M. Lallena
 Department Of Atomic Physics, Molecular And Nuclear, University of Granada, Granada/SPAIN

In this work a general source model has been developed to describe clinical linac heads when operating in photon mode. Six different linacs (three operating at 6 MV, one at 15 MV and two at 18 MV) have been studied. The construction of the model as well as its validation have been carried out on the base of the virtual linac approach in which the complete linac geometries have been simulated with the

Monte Carlo code PENELOPE. The model includes a primary and a secondary sources for photons and two sources for electron contamination whose geometrical characteristics are determined from a set of simulated fluence distributions in air. The energy distributions are obtained from the Monte Carlo energy distributions, for photons of the photons moving along the beam axis, and for electrons of electrons below the flattening filter. To verify the model, output factors, percentage depth doses and transverse profiles in water obtained from a calculation performed with the complete geometry are compared to those found with the source model. A reasonable agreement is obtained in all cases analyzed.

PS04.035 - Measurement of the beam quality TPR 20,10 of small radiotherapy fields: Comparison of experimental measurements and Monte Carlo simulations

Author(s): Eduardo A. González-Villa, Jose M. Larraga-Gutierrez
 Laboratorio De Física Médica, Instituto Nacional de Neurología y Neurocirugía, México city/MEXICO

Purpose. To measure the beam quality of small radiotherapy fields by using several detectors commonly used in small beam dosimetry and to verify the accuracy of these measurements by means of Monte Carlo simulations.

Material and Methods. The detectors employed in this work were a PTW-Farmer ionization chamber (to measure TPR 20,10 in reference conditions), PTW-31014, and PTW-60019 (PTW-Freiburg, Germany), and IBA-CC01 and IBA-SFD (IBA-Dosimetry, Germany). The experimental measurements were performed in a water scanning phantom MP3-XS (PTW-Freiburg, Germany). The irradiation of the detectors was carried out with a Novalis (BrainLAB, Germany) linear accelerator operating in x-ray mode at 6 MV with an exposition rate of 480 UM/min. The reading instrument used was a PTW UNIDO-Swebline electrometer. TPR 20,10 was determined as the ratio of doses at 20 and 10 cm in a parallel beam with a source to axis distance of 100 cm. The data were acquired for conventional field sizes of 10 x 10, 5 x 5, and unconventional field sizes of 3 x 3, 2 x 2 and 1 x 1 cm. The DOSRZnrc code was used for Monte Carlo simulations of photon transport through the linear accelerator and for the calculation of absorbed dose in water. Phase spaces data were used to calculate dose profiles in water for the conventional and unconventional field size (José Lárraga, Phys. Med. Biol. 60 905, 2015).

Results. For the PTW-31014 TPR 20,10's differences between Monte Carlo Simulation were 0.2 to 5.5%. For the IBA CC-01 were 0.2 to 4.0%. For the IBA-SFD were 0.2 to 2.3%, and for the synthetic diamond PTW-60019 were 0.2 to 2.3%. The uncertainty measurements for conventional fields were 0.1% and for the unconventional small fields were 0.2%. The major difference that was taken into the field 10 x 10 cm was in SFD IBA-Dosimetry, and for the field 1 x 1 cm was in PinPoint PTW-31014.

Conclusions. The best matches between Monte Carlo and measured detectors TPR 20,10 were the stereotactic field diode and the synthetic diamond detector. The high deviation present in the measurement of beam quality of small radiotherapy beams may be related to the partial volume averaging. Further research in needed to establish if this results may be applied to small beam corrections factor determination for small beams.

PS04.036 - The Effect of Assessment Criteria on Inter-rater Variability in the Evaluation of Skin Reactions following Breast Cancer Radiation Therapy

Author(s): Riya Goyal¹, Alexander Blood¹, Louis Potters², Ajay Kapur¹

¹Hofstra North Shore LIJ School of Medicine, Hempstead/UNITED STATES OF AMERICA, ²North Shore LIJ Cancer Institute, Lake

Success/UNITED STATES OF AMERICA

Purpose: Although the Common Terminology Criteria for Adverse Events (CTCAE) grading scales are utilized to assess adverse reactions to radiation therapy, few studies have investigated their reliability. In our previously reported image-based retrospective study, variability between caregivers (radiation oncologists, nurses) in assessing skin reactions in breast cancer radiation therapy using this scale was found to fall within a “moderate” range of concordance (Fleiss kappa score 0.43) per the Landis-Koch criteria. In this work, the potential impact of specific toxicity assessment terms documented by raters in our previous study on overall scale reliability was evaluated.

Methods: In an institutional-review board approved retrospective study, clinical notes documented by 8 caregivers were interpreted to assess how discordances among grades of skin lesions following radiation therapy potentially related to the use of freehand terms to describe the adverse events. 25 terms commonly used in the commentary were identified and categorized into those that were and were not outlined in the CTCAE scale. The percentage incidence and free marginal kappa scores for each term was calculated.

Results: The free marginal kappa scores for the terms stated in the CTCAE scale ranged from 0.333 to 0.565, suggesting a fair-to-moderate level of concordance between grades given by caregivers who used such terms. Certain terms not included within the CTCAE scale such as “hyperpigmentation” exhibited a higher rate of incidence (80%) and concordance (free marginal kappa score of .512) than those included explicitly in the scale.

Conclusion: The low kappa scores associated with terms in the CTCAE scale suggest variability in caregivers’ interpretation of assessment criteria. Revision of the wording of the scales may be needed to make definitions unambiguous and ensure a reliable grading scheme. The high frequency and kappa scores of terms including “hyperpigmentation” suggests revisions may also require inclusion of new clinical toxicity assessment criteria.

PS04.037 - Two-dimensional probability density function presenting the pre-treatment variability of the rectal wall integrating the variability of the motion of the rectum and the rectal wall thickness

Author(s): Grigor N. Grigorov, Johnson Darko, Ernest K. Osei
 Medical Physics Department, Grand River Hospital, Kitchener/
 CANADA

Taking into account inter-fraction changes in anatomy and rectal content, it can be assumed that the position of the rectum (Rm) and the thickness of the rectal wall (tw) could be different for each fraction. This may cause a disagreement between the planned and the delivered dose map to the rectum. Probability density functions ($PDFm$) describing the organ motion uncertainties of the rectum have been reported by many authors. We further propose a probability density function describing the changes in the rectal wall thickness ($PDFtw$) and hence introduce a two-dimensional function $PDFm&tw$, incorporating the variability of Rm and tw using their $PDFm$ and $PDFtw$, respectively. Our model is based on the histogram of the average tw of 587 randomly selected prostate patients. The average tw values were calculated in a treatment planning system based on the rectal structure contours drawn in the planning dataset using the initial planning CT scan of the patient. The new $PDFtw$ was established as a mixture of a three-mode distribution with specific mean value, standard deviation and weight, namely, for full (3.31, 1.82 and 77.1%), partially full (7.7, 0.809 and 15.2%) and empty state of the rectum (10.27, 0.906 and 9.4%), respectively. The $PDFm&tw$ function was introduced as a product-mixture model of the two functions $PDFm$ and $PDFtw$ and it has been

graphically and mathematically reviewed. The *product-mixture* is an original model presenting the pre-treatment variability of the rectal wall.

Figure 1a Figure 1b

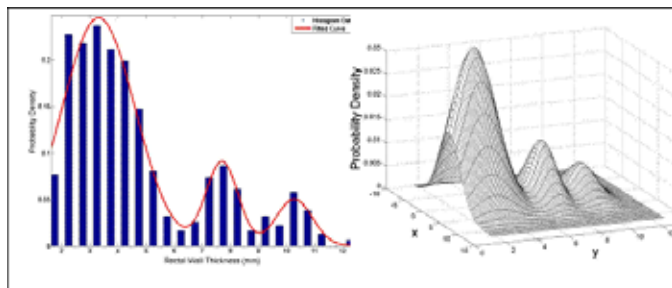


Figure 1a. Normalized histogram data with a fitted three-mode Gaussian curve.

Figure 1b. Anterior–posterior direction. A *Product-Mixture* model of the multivariate probability density function $PDFm&tw$ which includes both the motion of the rectum (axis X [mm]) and the rectal wall thickness variability (axis Y [mm])

PS04.038 - Unbiased Assessment of Detail Detectability in Image Guided Radiation Therapy

Author(s): Victor A. Gurvich¹, Lester L. Greer², George Davydenko³
¹Government Contractor In Radiology Clinic, Fort Belvoir Community Hospital, Fort Belvoir/VA/UNITED STATES OF AMERICA, ²Fort Belvoir Community Hospital, Fort Belvoir/VA/UNITED STATES OF AMERICA, ³Society of Euro-American Medical Physicists, Alexandria/UNITED STATES OF AMERICA

The accuracy of delineation of targets and organs at risk during radiation therapy treatment planning as well as precise verification and localization for image guided beam delivery considerably depends on detectability of small and low contrast details. The assessment of detail detectability with Las Vegas phantom, Leeds test objects and some other standard test tools recommended by vendors is very subjective because of fixed disposition of test elements known to an observer. On the other hand, physical parameters of the image obtained with instrumental tools often do not adequately reflect its clinical quality. The proposed method allows fast, simple and unbiased evaluation of detectability using standard phantoms and special StatPhan software.

An observer should estimate the likelihood of pathology simulator presence in the image of selected phantom areas. Then the results of the estimation are compared with real locations of the simulators. The number of selected areas and locations of test elements can be changed so that they are not known to the observer beforehand. StatPhan software calculates sensitivity, specificity and accuracy of test elements detection, signal-to-noise ratio, areas under receiver operating curves that define overall decision performance, and the factor of observer’s tendency to overestimation or misses. For our experiments we used Las Vegas phantom, Leeds test objects, ALVIM statistical phantoms with pathology simulators in aluminum, tissue and bone equivalent materials, aluminum step-wedge with holes of different diameter, and Catphan phantom for computer tomography. The detail detectability was measured for CT simulators, electronic portal image devices with 6 MV and 16 MV photon beams, and for on-board imager system in radiographic and cone beam CT modes. The smallest test elements (pathology simulators) distinguished with $Pdet \geq 0.9$ was assumed as a measure of image quality.

In all experiments we selected at least 10 areas with identical test elements and equal amount of areas with and without simulators when the accuracy had the most meaningful value. Low contrast resolution of Phillips Big Bore CT simulator and Varian On-Board Imager in cone beam mode was defined as detectability of supra-slice cylinders with 1% and 0.5 % contrast, for 100 kV at the X-ray tube, narrow window width (100 or less) and appropriate window level, so that low contrast disks were distinguished as well as possible. Cylinders of 3.0 mm, 1% contrast and 6 mm, 0.5% were detected in CT-sim images. The results for CBCT systems were 6.0 mm cylinders with 1% contrast and 9 mm, 0.5%. In images taken in On-Board imager radiographic mode 16 Leeds test disks and holes with diameter 1.1 mm in aluminum, 1.2 mm in bone and 1.4 mm in tissue equivalent material respectively were distinguished. Data for contrast-detail curves were obtained with aluminum step-wedge phantom.

The suggested method and StatPhan software were used for unbiased rapid statistical evaluation of therapeutic image quality using phantoms with fixed disposition of test elements and can be helpful for acceptance testing, establishment of QA base line, maintenance of excellent image quality, teaching and training of physicians and technical staff.

PS04.039 - Assessing radiation protection of members living close to patients with implanted ^{125}I seeds in prostate

Author(s): Takashi Hanada¹, Atsunori Yorozu², Sachiko Shinya², Shiro Saito³, Toshio Ohashi¹, Naoyuki Shigematsu¹

¹Department Of Radiology, Keio University School of Medicine, Tokyo/JAPAN, ²Department Of Radiology, Tokyo Medical Center, National Hospital Organization, Tokyo/JAPAN, ³Department Of Urology, Tokyo Medical Center, National Hospital Organization, Tokyo/JAPAN

Purpose/Objective(s): Permanent seed implant treatment using ^{125}I is currently a common procedure for localized prostate cancer. For using the isotopes, we are frequently asked for more detailed information regarding the true exposure rates and associated risk that patients pose to the members living close to patients. However, there are few data for specific measurements situations, or considering lifestyle habits. In this study, a direct measurement was performed to determine the expected lifetime exposure from the patient with ^{125}I seed brachytherapy prostate implant to members living close to patients.

Materials/Methods: Measurements were obtained from 25 consecutive unselected patients at Tokyo Medical Center, Japan. After a permanent brachytherapy implant with ^{125}I seeds, patients and their member living close to patients were provided radiation monitors to measure direct radiation exposure at lifestyle. Each patient and their members were given a monitors to hang it on the neck, continuously, 24 hours a day. Monitors were returned approximately 1 week after the started day of measurements, and lifetime exposure were calculated based on the reading from the dosimeters. In addition, same measurements were performed after approximately 4 weeks after the first measurement for correctness verification of exposure monitoring.

Results: Based on dosimeter readings, the calculated mean lifetime dose to members living close to patients was 0.19 mSv (range, 0.02-0.54). There were no correlations between the calculated mean lifetime dose from patients of 7.61 mSv (range, 0.45-20.44) and their members. The average of calculated mean lifetime dose of second/first measurement ratio was 1.05 (range, 0.44-3.18) for patients. Results for the members, on the other hand, were 1.82 (range, 0.21-7.04). Radiation exposure to the members were differ in two measurements term, even when measured under the same conditions. That is to say, spending time the members contact with patients were not always the same in a day, leading to the non-

negligible uncertainty of occupancy factors, used in calculating the lifetime dose.

Conclusions: There were no correlations between the measured radiation dose from patients and their members. However, radiation exposure to members living close to patients receiving a permanent prostate brachytherapy implant with radioactive ^{125}I is very low and well below the limits recommended by the general guideline.

PS04.040 - Improvement of MV planar image by elimination of Compton scattered photons and re-projection as primary photons

Author(s): Masatsugu Hariu, Atsushi Myojoyama, Hidetoshi Saitoh
Radiological Sciences, Tokyo Metropolitan University, Tokyo/JAPAN

Introduction

For the IGRT technique of the radiation therapy, a MV planar image is acquired with an electronic portal imaging device (EPID). And displacement of patient position will be adjusted by image registration between the MV planar image and a reference image that digitally reconstructed from 3D X-CT image. Arbitrary structures, e.g. bone, soft tissue and lung, on the MV planar image are guide for image registration, therefore high image quality is required. However, density distribution of the MV planar image is deteriorated because of Compton scattered photons.

Purpose

To compute information of Compton scattered photons impinged on the EPID aiming to real time processing, an original Monte Carlo (MC) was coded. Then energy spectrum distribution of scattered photons was acquired using the MC code. Improvement of image density was attempted by eliminating contribution of scattered photons from the MV planar image and re-projecting as primary photons from Compton interaction point.

Method

The original MC code and the image-processing program were coded with the integral development environment Qt 5.0. This MC code can simulate Compton interaction within voxels that reconstructed from 3D X-CT image. Mean absorbed dose by scattered photons (D_s), primary photons (D_p) and total photons (D_t) to the EPID were estimated using energy and fluence and mass energy absorption coefficient of the EPID. It is assumed that the pixel value (P) of the EPID is proportional to absorbed dose (D) of $\text{Gd}_2\text{O}_2\text{S:Tb}$ scintillator. In order to process the image excluding scattered photons (P_s), the image by scattered photons (P_s) was subtracted from the raw MV planar image (P_t). The P_s image was processed by multiplying the P_t and the ratio of D_p/D_t . To improve image density of arbitrary structure, which is guide for image registration, scattered photons were back projected to interaction point and re-projected as primary photons on the assumption that Compton scatter did not take place. The image by primary photons (P_p) was processed by multiplying the P_s and the ratio of D_p/D_s . Finally, corrected image density (P_c) was processed by adding P_s and P_p .

Result and Conclusion

A chest phantom was modeled in this study. As a result of bone-weighted image, it was obvious that P_c image was easier to distinguish the spinous process of vertebra, the intervertebral disks and the ribs than the P_t image. Additionally, by the soft tissue-weighted image, the bone structure was suppressed and Bronchi were observed clearly. Consequently, usability of proposed image density processing was clarified.

PS04.041 - Determination of exit fluence by MCNP4 code for IMRT treatment fields and its validation with a conventional EPID system

Author(s): Benjamin Hernandez Reyes, Modesto A. Sosa Aquino
Physical Engineering, University of Guanajuato campus Leon, Leon/ MEXICO

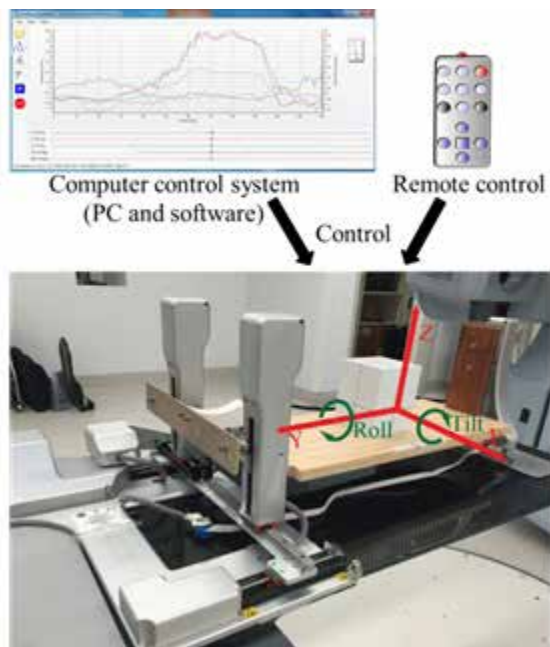
Dosimetry in intensity modulated radiotherapy (IMRT) is a fundamental process in quality control assurance. The electronic portal imaging devices (EPID) are widely used in IMRT dosimetry to measure the fluence of a radiation field and compare with the expected value calculated by a prediction algorithm. The objective of this work was to determine by Monte Carlo simulation the exit fluence of a treated patient with IMRT fields using MCNP4 code for a Varian linear accelerator Clinac iX model and then validate the simulation with fluences measures in the Varian aS1000 EPID system. Portal dosimetry configuration was previously performed by measuring output factors and dose calculation kernel. Comparisons between the simulated and the measured were made with a gamma evaluation (acceptance criterion $\Delta D=3\%$ and $\Delta r=2$ mm), finding that over 95% of the points fall within the acceptance criteria. Verification with radiochromic film was also evaluated, also found correspondence >95% of the points evaluated between the simulated and measured. This work will assist in the implementation of 3D *in-vivo* IMRT dosimetry.

PS04.042 - Accuracy in simulating tumor translation and rotation: Commissioning a motion platform, Hexamotion for tumor motion management QA

Author(s): Chen-Yu Huang¹, Jeremy T. Booth², Jin A. Ng¹, Adam Rice², Paul Keall¹

¹Radiation Physics Laboratory, Sydney Medical School, The University of Sydney, Camperdown/AUSTRALIA, ²Northern Sydney Cancer Centre, Royal North Shore Hospital, Sydney/AUSTRALIA

Purpose: The success of gating and tumor tracking requires rigorous QA and validation to meet the goal of better coverage of the target and sparing of organs at risk. The Hexamotion 5 degree-of-freedom (DoF, 3 DoF translation and 2 DoF rotation) programmable motion platform uniquely uses the patient specific tumor motion trajectory and reproduces it in 5 dimensions (Fig 1). The purpose of this study is to commission the Hexamotion that to be served as an end-to-end tumor motion tracking or gating system QA device.



Methods: Three Calypso electromagnetic transponders were fixed to Hexamotion to record its real-time position. Range, velocity, acceleration were measured for each of the 5 DoF. Representative lung patient tumor motion trajectories were selected and input into the Hexamotion to measure the dynamic accuracy. The tolerances for all tests are that both the mean and standard deviation of the difference between the programmed trajectory and the measured data are <0.5 mm as the accuracy of tumor motion detection and adaptation methods reach submillimeter accuracy.

Results: Hexamotion's range, velocity and acceleration are adequate to reproduce prostate and lung tumor motion during treatment (Table 1). Hexamotion demonstrated a high mechanical accuracy of 0.5 mm. In the dynamic accuracy test, the mean and standard deviation differences between the input lung trajectory and Calypso measured continuous position are less than 0.5 mm. Hexamotion has been used in our center to perform QA for the tumor motion detection system - Kilovoltage Intrafraction Monitoring (KIM) and the tumor motion tracking system - Dynamic MLC tracking.

Table 1. Hexamotion range, velocity and acceleration meet the requirement of reproducing tumor motion.

	Range (mm or deg)	Velocity (mm or deg/s)	Acceleration (mm or deg/s ²)
X (LR)	-43 ~ 43	-30 ~ 30	Up to 100
Y (SI)	-43 ~ 43	-30 ~ 31	Up to 100
Z (AP)	-40 ~ 41	-37.5 ~ 22	Up to 100
Tilt	-3.5 ~ 8	-7 ~ 7.5	Up to 100
Roll	-11 ~ 11	-10.5 ~ 10	Up to 100

Conclusion: The Hexamotion platform is capable of reproducing individual patient-specific tumor trajectories with a high degree of accuracy. It can be served for end-to-end tumor motion management systems QA device including 4DCT imaging, monitoring, gating and tracking.

PS04.043 - Dosimetric impact of the Acuros XB Algorithm for 25 lung SABR patients treated using the TrueBeam FFF 6MV

Author(s): Derek Hyde¹, Tony Teke¹, Matthew Schmid²

¹Medical Physics, BC Cancer Agency - Centre for the Southern Interior, Kelowna/BC/CANADA, ²Medical Physics, BC Cancer Agency - Southern Interior, Kelowna/BC/CANADA

Purpose:

Stereotactic Ablative Radiotherapy (SABR) requires the delivery of a high biologically effective dose in only a few fractions. The Varian Truebeam has optional Flattening Filter Free (FFF) modes which greatly increase the dose rate and reduce treatment times. We previously commissioned the 6MV FFF beam (1400 MU/min) in Eclipse using Varian's Analytical Anisotropic Algorithm (AAA), but have recently commissioned the Acuros XB algorithm (AXB). To examine the clinical significance of the new algorithm, we have retrospectively recalculated the dose distributions for the 25 patients that we have already treated.

Methods:

The standard commissioning data was acquired for Varian's AAA and AXB beam models, and then MLC-defined fields were acquired for verification. Measurements were completed with the IBA Blue Phantom, using the CC13 and CC01 ion chambers and PTW diode. Heterogeneous dose calculations were then independently verified

using Monte Carlo Simulations and Gafchromic film (EBT3, Ashland), confirming that the heterogeneous dose calculations were improved with the AXB algorithm. We have treated 25 lung patients, in which we used 4D-CT to define an ITV, added a 5mm expansion for the PTV, and then forward-planned on the fast-helical image, using a 3D conformal, non-coplanar technique to deliver 48 Gy (covering 95% of the PTV) in 4 fractions. The original MU from the AAA plan was used to calculate the 'dose to medium' as well as 'the dose to water', using the new AXB algorithm. Finally, both AXB plans were rescaled to the volume-based prescription, as per clinical practice.

Results:

When the dose distribution was recalculated with same MU for the dose to water, the difference of the PTVmean (avg=1.1%) was statistically significant (P=0.02). Neither the difference of the PTVmin (avg=-1.0%) nor the difference of the PTVmax (avg=0.13%) were statistically significant.

When the AXB dose to medium was calculated (with the same MU), the difference of the PTVmean remained similar (avg=1.1%), but the difference of the PTVmin (avg=-1.3%) became significant (P=0.04) and although the difference of the PTVmax increased (avg=0.97%), it was still not significant. It should be noted that the maximum differences for the PTVmin, PTVmax and PTV mean were -10.1%, 5.6% and 4.9% respectively.

When the AXB dose calculations were renormalized with the standard prescription of 48Gy covering 95% of the PTV, on average there was almost no affect on the calculated dose to water, but some effect on the calculated dose to medium. The maximum differences for the PTVmin, PTVmax and PTV mean were -5.2%, 16.2% and 4.3% respectively, for the dose to medium.

Conclusions:

The PTVmin is typically lower with the AXB calculation. Consequently, any volume based prescription will tend to increase the PTVmean as well as the PTVmax. Although the average differences for this patient set were only about 1%, individual patients illustrated the potential for much greater differences.

PS04.044 - Dynamic resource allocation: Investigating ways to distribute resources in a patient cohort based on plan quality

Author(s): Elin Hynning

Department Of Research, RaySearch Laboratories, Stockholm/SWEDEN

Radiation therapy is a resource intensive type of treatment and resources are always limited. This study aims at investigating ways to dynamically allocate resources among a cohort of patients. The idea is to take into account the plan quality that can be achieved for the individual patients with regard to the considered resource when allocating the resources.

A cohort of 13 prostate patients has been investigated, and the considered resource is the delivery time for a treatment fraction. The delivery time for a treatment fraction was represented as the number of beams used in the treatment plan. For each patient, six SMLC plans were automatically generated, with 5, 7, 9, 11, 13 and 15 beams respectively. All plans were required to fulfill a set of clinical goals and moreover to achieve as low average dose to the rectum as possible. The average dose to the rectum was used as the measure of plan quality. The available treatment time for all patients in the cohort was 91 beams, i.e. all patients in the cohort could receive a plan with seven beams. Three different schemes to allocate the available resources were considered; equal distribution, minimax distribution and population average distribution. In the equal distribution, all patients received a plan with seven beams. In the minimax distribution,

resources were allocated to improve the plan quality for the patients with the worst plan quality. In the population average distribution, resources were allocated to achieve the best average plan quality for the cohort.

The resulting allocations of treatment time stemming from the different allocation schemes are shown in table 1.

Patient	Equal	Minimax		Population average	
	Average dose rectum	Beams	Average dose rectum	Beams	Average dose rectum
1	23.14	5	28.62	5	28.62
2	37.57	9	29.03	9	29.03
3	37.90	9	32.27	9	32.27
4	29.13	7	29.13	7	29.13
5	27.44	7	27.44	7	27.44
6	28.22	7	28.22	7	28.22
7	26.20	5	35.02	7	26.20
8	37.57	9	34.01	5	41.02
9	31.10	7	31.10	7	31.10
10	24.90	7	24.90	7	24.90
11	26.37	7	26.37	7	26.37
12	20.47	5	26.62	7	20.47
13	33.12	7	33.12	7	33.12
Average	29.47		29.68		29.06

Neither the minimax distribution nor the population average distribution allocate more than nine beams to any patient in the cohort. Thus, adding more than nine beams does not make significantly better plans for any patient in the cohort.

The minimax distribution and population average distribution lead to different resource allocations between the patients in the cohort. As expected, the population average distribution lowers the population average compared to the equal distribution, and the minimax distribution improves the plan quality to the three patients with the worst plan quality in the equal distribution. Even though no distribution dominates any other distribution in both worst case and population average measures, the results show that if there exists an objective on population basis apart from giving all patients the same resources, then dynamic resource allocation should be considered.

PS04.045 - Physical plan evaluation of Head and Neck Cancer at Square Hospital, Bangladesh.

Author(s): Md. Anwarul Islam¹, Md.Mahmudul Hasan¹, Golam Abu Zakaria²

¹Department Of Oncology & Radiotherapy Centre, Square Hospitals Ltd, Dhaka/BANGLADESH, ²Dept. Of Medical Radiation Physics, Academic Teaching Hospital Of The University Of Cologne, Gummersbach Hospital, Colongn/GERMANY

Purpose: To compare the physical parameters of Three Dimensional Conformal Radiotherapy (3DCRT) with Intensity Modulated Radiotherapy (IMRT) for Head & Neck cancer and the dose profiles of primary tumors, electively treated organ (Lymph node) and Organ at Risk (OARs).

Materials and Methods: From January 2010 to October 2014, total 473 patients were diagnoses with head and neck cancer in Square

Hospitals Ltd. Among those patients, five (5) patients treated with 3DCRT and five (5) with IMRT technique have been selected randomly for this study. All the 3DCRT and IMRT plans were done using ECLIPSE (version 8.6) treatment planning system of VARIAN Medical System. All the cases were immobilized with Head & Neck thermoplastic mask and scanned at 3.75 mm slice width with GE Light Speed CT simulator. For each case of 3DCRT (66 Gy) and IMRT (70 Gy), target volume for primary lesions and electively treated regions (50 Gy) were contoured respectively. In this study, parotid gland, spinal cord and mandible have been contoured as OARs. The beam direction of 3DCRT plans were selected laterally parallel opposed with wedge and Field in Field (FiF) technique either co-planar or non co-planar to avoid shoulder. The beam weights were adjusted in order to minimize tumors dose inhomogeneity. The beam arrangements of IMRT plans were nine and seven equispaced non-opposed coplanar beams. The same dose volume constraints were used for all IMRT plannings during inverse optimization. The physical parameters, Target Coverage (TC), Conformity Index (CI), Conformation Number (CN), Lesion Under dose Factor (LUF), Healthy Tissue Over dose Factor (HTOF), Homogeneity Index (HI) and DVHs have been calculated for each treatment plan. The 100% is the perfect TC coverage, whereas if the 95% isodose covers all of the clinical and pathologic target volume, treatment is considered to comply with the protocol. A CI equal to 1 corresponds to ideal conformation. The CN ranges from 0 to 1, where 1 is the optimal conformity and value close to 0 indicates less conformal plan. The lower the values of LUF and HTOF, the higher is the conformal plan. Smaller values of HI correspond to more homogeneity and 0 corresponds to absolute homogeneity. According to the RTOG and QUANTEC guideline, mean and maximum doses (1cc and 1%) have been considered for Organ at Risk (OARs) dose evaluation.

Results: The mean values for 3DCRT and IMRT were 95.07 and 95.33 for TC, 0.466 and 0.895 for CI, 0.441 and 0.795 for CN, 0.045 and 0.028 for LUF, 1.115 and 0.100 for HTOF and 0.145 and 0.085 for HI respectively. The mean dose for parotid glands were 47.28 and 23.80, maximum dose for spinal cord 43.78 and 39.63 for mandible 64.20 and 59.17 Gy correspondingly for 3DCRT and IMRT.

Conclusion: IMRT is superior to 3DCRT in dose delivery and critical structure sparing for the treatment of Head & Neck cancer. The primary tumor can get higher equivalent dose by IMRT techniques.

PS04.046 - IAEA multicentre study of the methodology for advanced dosimetry audit: single IMRT field dose delivery

Author(s): Barbara Bencsik, Paulina Grochowska, Joanna Iżewska Nuclear Sciences And Applications, International Atomic Energy Agency, Vienna/AUSTRIA

New auditing methodology for national dosimetry audit networks is under development within an IAEA co-ordinated research project (CRP): "Development of Quality Audits for Advanced Technology in Radiotherapy Dose Delivery". It consists of four steps: (1) verification of TPS calculation of small beam output factors, (2) film dosimetry audit of MLC positional performance, (3) film audit of single clinical IMRT field dose delivery and (4) 'end-to-end' dosimetry audit (imaging, planning, dose delivery) for multiple field IMRT techniques. The current work refers to part 3 of this CRP. The purpose is to verify the audit methodology for checking the delivery of an IMRT treatment field by comparing the relative dose distributions delivered to the film and that calculated by the treatment planning system.

Sixteen research groups from 14 countries were involved in this multicentre study. Each group received a set of instructions, datasheets and a sheet of radiochromic EBT3 film from the IAEA. The participants were asked to choose a highly modulated single treatment field from a typical inverse planned IMRT head and neck treatment plan and then deliver it to the EBT3 film placed at depth in a solid

phantom. Upon receipt of the irradiated films by the IAEA Dosimetry Laboratory, a comparison was performed between the TPS calculated and the measured film dose distributions using gamma analysis tool (FilmQA Pro™, Ashland). The gamma acceptance criterion of 3%/3mm over all pixels values exceeding 20% of the maximum dose was adopted, with 90% of pixels passing the criterion. Agreement of the profiles through the maximum dose region was also checked with the criteria of 7% of the maximum dose for low gradient regions and 4 mm position error for high gradient regions.

The results are obtained for 8 different accelerator models, 6 MLC models, 4 different TPSs and 8 dose calculation algorithms. All participants achieved the minimum passing level of 90% with the actual passing rate between 95.4% and 100%. The average result of gamma analysis for Varian machines was 99.0% (12 participants) and for Elekta machines 97.7% (4 participants). Comparison of dose profiles showed that the largest differences occur in the high dose gradient regions, where precise positioning of the MLC leaves has the greatest impact on the accurate dose delivery; 4 mm error in such regions can bring more than 20% difference in the dose.

The methodology of this audit has been examined through a multicentre study and proven to work well. The study was performed smoothly; instructions and datasheets appeared to be clear and straightforward to follow. As the EBT 3 films are easy to damage in transport, it is important to handle them carefully and pack properly for mailing. The results show good agreement between the planned and the measured dose distributions, with all participants having achieved satisfactory results. The analysis criteria adopted for this study have been confirmed for future use by national dosimetry audit networks in countries participating in the CRP.

PS04.047 - Electron Density Measurements of Metallic Implants with Cobalt-60 Computed Tomography

Author(s): Christopher Jechel¹, Greg Salomons², L John Schreiner²
¹Physics, Engineering Physics & Astronomy, Queen's University, Kingston/ON/CANADA, ²Department Of Medical Physics, Cancer Centre of Southeastern Ontario, Kingston/ON/CANADA

Introduction: The photon starvation and beam-hardening artifacts produced by high density and atomic number objects in kilovoltage CT images are a well known phenomenon in radiation therapy planning. Metal artifacts can obscure anatomy and impact dose calculation accuracy as the quantitative information in CT images is used to provide a map of relative electron density (RED) within the patient's body. Further calculation perturbations arise when the range of allowed CT values is constrained to 12 bits. In this work we investigate the importance of these effects in treatment planning.
Methods: Our group has developed a benchtop cone-beam CT system to investigate the potential for patient alignment on a cobalt-60 teletherapy unit. The high energy (~1.25 MeV) and nearly monoenergetic gamma ray spectrum of cobalt-60 reduces metal-induced artifacts, suggesting cobalt-60 CT (CoCT) may be useful for evaluating RED information derived from kVCT images acquired in the presence of metal objects. Images of metal rods of varied RED and atomic number within water phantoms were gathered via CoCT and conventional kVCT including images reconstructed using a commercial metal artifact reduction algorithm. To demonstrate the importance of accurate electron density information, large field (6MV, 25x25cm²) dose profiles were measured with an ion chamber in a water phantom containing metal rods and compared to treatment planning system calculations based on kVCT and CoCT images. **Results/Conclusions:** Converting images from CT number to RED and comparing with known electron density distributions shows that the starburst artifacts surrounding the metal rods in kVCT are absent from CoCT (Figure 1a-b). In kVCT images, pixels above a threshold electron density are assigned the same CT number, the maximum of the allowed range. This leads to an

ambiguous condition where different high density materials cannot be differentiated in kVCT images (Figure 1c). Reduced artifacts in regions surrounding metal objects and the lack of a limit on CT number range enable a more faithful representation of electron density information with CoCT. Compared to ion chamber measurements at a point downstream of a titanium rod, calculations based on kVCT and CoCT images differed from measurements by -12.7% and 3.2%, respectively. This result is likely attributable to the treatment planning system's assumption that threshold value kVCT pixels are approximately equivalent to stainless steel, a 76% overestimate of the true electron density of titanium. CoCT imaging enables the evaluation of metal artifact perturbations in planning CT and work assessing vendor correction algorithms is underway.

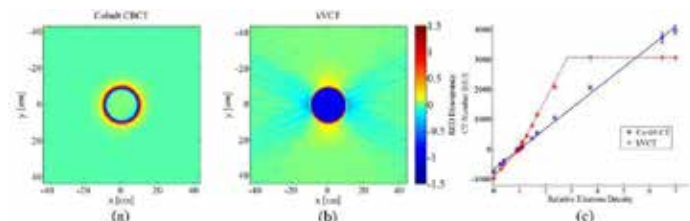


Figure 1: Discrepancies between measured and true electron density distributions (normalized to that of water) surrounding a titanium (relative electron density=3.73) cylinder for (a) cobalt-60 CT and (b) conventional kVCT. RED-CT number data is shown in (c) for Co-60 CT and kVCT scanners demonstrating how the limited CT number range in kVCT images obscures the difference between high density materials.

PS04.048 - A Systematic Analysis Of The Error Sources Within The CyberKnife M6 Daily AQA Test

Author(s): Kevin T. Jordan, Alan Mayville, Tewfik Bichay
Lacks Cancer Center -- Radiation Oncology, Mercy Health Grand Rapids, Grand Rapids/UNITED STATES OF AMERICA

Objectives: To determine and critically analyze the sources of error within the daily Automatic Quality Assurance (AQA) test used on the CyberKnife M6 system.

Methods: A systematic analysis of the inherent uncertainties involved in the CyberKnife M6 AQA test was conducted to quantify the uncertainty in each of the components making up the AQA process. The identified components included the robot positional uncertainty, film scanning precision, film response and the kV imaging system. A range of 10-20 repeat measurements were carried out for each of these identified components. A modified Winston-Lutz test with orthogonal images was carried out using GAFchromic EBT3 film. The exposure was by a dedicated AQA plan within Accuray's Multiplan Software. The images were scanned on an Epson 10000XL film scanner. The SRS profiler QA device was used to determine the robot positional accuracy and repeatability.

Results: The total film AQA uncertainty using IRIS and FIXED cone was found to be 0.349 and 0.339 millimeters ($\pm 3SD$) respectively. The Epson 10000XL flatbed scanner was used to scan RGB pixel intensity. The scanner uncertainty was very small; repeat measurements of the same film suggested a scanner precision of 0.015-0.025 millimeters ($\pm 3SD$). The act of repositioning a film contributed a small uncertainty of 0.0008-0.0014 millimeters ($\pm 3SD$). The largest uncertainty was due to the imaging system. The kV imaging system Fiducial tracking algorithm uncertainty was 0.150 millimeters ($\pm 3SD$), while the 6D skull algorithm was 0.300 millimeters ($\pm 3SD$). The SRS Profiler suggested a robot precision uncertainty of 0.1 mm or less.

Conclusion: The total AQA uncertainty appears to be largely due to the kV imaging system. These results suggest an uncertainty of less than 0.1 mm for the film, film scanner, and robot components of the AQA test. The kV imaging system uncertainty could reach 0.3 mm and is the main source of uncertainty. This information explains greatest weakness in daily CyberKnife QA and may be useful in establishing realistic expectations of daily AQA results.

PS04.049 - The Use of Boron Neutron Capture Therapy in the Treatment of Cancer Tumours in the Czech Republic

Author(s): Veronika Burianova¹, Lubomir Sklenka², Ivana Jurickova¹
¹Department Of Biomedical Technology, Czech Technical University in Prague, Faculty of Biomedical Engineering, Kladno/CZECH REPUBLIC, ²Department Of Nuclear Reactors, Czech Technical University in Prague, Faculty of Nuclear Sciences and Physical Engineering, Prague/CZECH REPUBLIC

Boron neutron capture therapy is an experimental method of the treatment of malignant tumors of today. The study first gives a comprehensive overview of the state of the art both in the Czech Republic and abroad. It describes a low power research nuclear reactor which will be utilized as the radiation source used in the therapy. The feasibility study introduces the project proposal and the approximate cost of the facility construction. The feasibility study further quantifies the reactor's operating cost and summarizes the cost of treatment with neutron capture therapy. Based on the market analysis, the marketing strategy and the marketing mix are devised. The professions needed for the facility operation are defined. The study assesses the project's impact on the environment, presents the risk analysis and sensitivity analysis. Boron neutron capture therapy has a great potential to become a successful therapy in the treatment of some types of malignant tumors under certain conditions in the future.

PS04.050 - Partial Arc Breast Boost

Author(s): Tania Karan¹, Daria Comsa¹, Woodrow Wells², Erin Barnett¹

¹Medical Physics, Stronach Regional Cancer Centre, Newmarket/ON/CANADA, ²Radiation Oncology, Princess Margaret Cancer Centre, Toronto/ON/CANADA

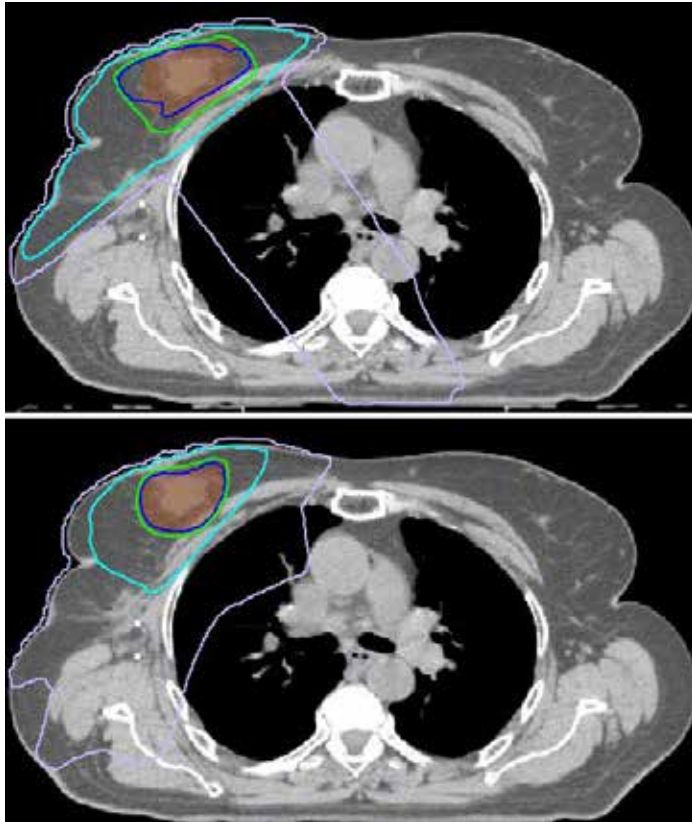
Adjuvant radiotherapy to the excised tumour bed following radiotherapy of the entire breast is routinely used to reduce risk of local recurrence in select patients. Boost treatments are generally delivered via conformal radiation therapy (CRT) with 2-3 fields, making use of tangential geometry. This study explores volumetric modulated arc therapy (VMAT) as an alternative to conventional CRT. A modulated partial arc was planned, spanning the angles between the tangential fields used in the initial phase of treatment to the entire breast.

The plans of 15 previously treated patients (7 left-sided, 7 right-sided, one bilateral) were retrospectively re-planned in *Pinnacle* (Philips, v9.0). The left-sided patients were all CT simulated in a breath hold position using the *active breathing control* system. The average volume of the tumour cavity was 19 cc (range: 4-57cc). A class solution for beam geometry and optimization objectives of the arc plans was achieved, and plan comparison was based on coverage of the tumour bed by 95% of the prescription (950 cGy) and doses to the pertinent organs at risk. All plans were normalized to achieve target coverage equivalent to or better than the original plans. Robustness of the two techniques was evaluated by simulating breast contour changes in *Pinnacle*.

The arc plans achieved significant improvements in dose conformity, as exemplified in **Figure 1**. Doses to 10 cc of heart increased in the arc plans, while the volume of ipsilateral lung receiving >2 Gy did not show a consistent trend. The maximum point dose to skin (a 3mm thick rind contracted from the external contour) increased, particularly in superficial targets, however the maximum dose to 10cc of skin decreased. The low-dose exposure to the contralateral breast in the arc plans was controlled with a medial optimization structure and was equivalent with the CRT technique. The overall maximum point dose was higher in the arc plans, however the volume receiving 105% of the prescribed dose did not vary monotonically when compared with CRT plans. Arc plans were equivalent

or superior in retaining target coverage following breast contour changes when compared with conformal plans. Based on the performance of arc plans in this small cohort of patients, an investigation involving a larger retrospective dataset is warranted.

Figure 1. Comparison of a conformal (above) and arc (below) breast boost plan. Target is shown in brown colourwash, along with the 100% (blue), 95% (green), 50% (cyan) and 10% (violet) isodoses



by time when the values obtained before and after breathing were compared ($p < 0.05$); 30% and 40% of the duty cycle, respectively, was determined to be the most effective, and the corresponding phases were 3060% (duty cycle, 30%; $p < 0.05$) and 3070% (duty cycle, 40%; $p < 0.05$).

Conclusions: Respiratory regularity was significantly improved with the use of the RPM with our visible guiding system; therefore, it would help improve the accuracy and efficiency of RGRT.

PS04.052 - Dosimetric Verifications of the Output Factors in the Small Field less than 3 cm² using the Gafchromic EBT2 films and the Various Detectors

Author(s): Se An Oh, Sung Kyu Kim, Ji Woon Yea
Radiation Oncology, Yeungnam University Medical Center, Daegu/ KOREA

The small field dosimetry is very important in modern radiotherapy because it has been frequently used to treat the tumor with high dose hypo-fractionated radiotherapy or high dose single fraction stereotactic radiosurgery (SRS) with small size target. But, the dosimetry of a small field ($< 3 \times 3 \text{ cm}^2$) has been great challenges in radiotherapy. Small field dosimetry is difficult because of (a) a lack of lateral electronic equilibrium, (b) steep dose gradients, and (c) partial blocking of the source. The objectives of this study were to measure and verify with the various detectors the output factors in a small field ($< 3 \text{ cm}^2$) for the 6 MV photon beams.

Output factors were measured using the CC13, CC01, EDGE detector, thermoluminescence dosimeters (TLDs), and Gafchromic EBT2 films at the sizes of field such as 0.5×0.5 , 1×1 , 2×2 , 3×3 , 5×5 , and $10 \times 10 \text{ cm}^2$. The differences in the output factors with the various detectors increased with decreasing field size.

Our study demonstrates that the dosimetry for a small photon beam ($< 3 \times 3 \text{ cm}^2$) should use CC01 or EDGE detectors with a small active volume. And also, Output factors with the EDGE detectors in a small field ($< 3 \times 3 \text{ cm}^2$) coincided well with the Gafchromic EBT2 films.

PS04.051 - Determination of the optimal phase for respiratory gated radiotherapy from statistical analysis using a visible guidance system

Author(s): Se An Oh, Sung Kyu Kim, Ji Woon Yea
Radiation Oncology, Yeungnam University Medical Center, Daegu/ KOREA

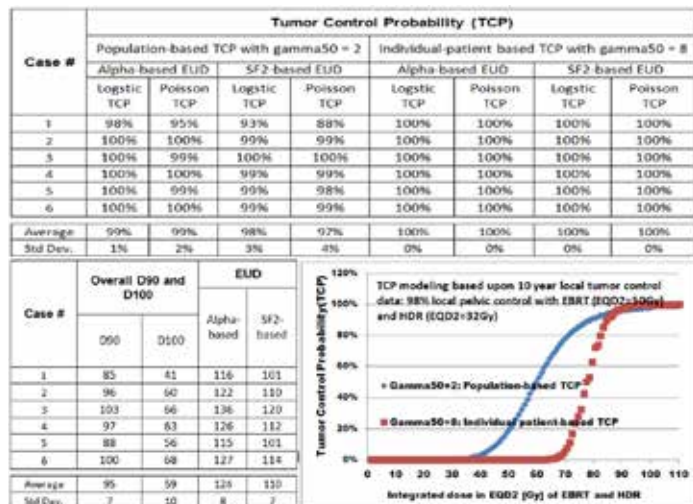
Purpose: Respiratory gated radiation therapy (RGRT) is used to minimize the radiation dose to normal tissue in lung cancer patients. Determination of the optimal point in the respiratory phase of a patient is important in RGRT but it is not easy. The goal of the present study was to see if a visible guiding system is helpful in determining the optimal phase in respiratory gated therapy.

Materials and methods: The breathing signals of 23 lung cancer patients were recorded with a Real-time Position Management (RPM) respiratory gating system (Varian, USA). The patients underwent breathing training with our visible guiding system, after which their breathing signals were recorded during 5 min of free breathing and 5 min of guided breathing. The breathing signals recorded between 3 and 5 min before and after training were compared. We performed statistical analysis of the breathing signals to find the optimal duty cycle in guided breathing for RGRT.

Results: The breathing signals aided by the visible guiding system had more regular cycles over time and smaller variations in the positions of the marker block than the free breathing signals. Of the 23 lung cancer patients, 19 showed statistically significant differences

PS04.053 - Methodology to Evaluate Combined EBRT and HDR Brachytherapy for Cervical Cancer using Equivalent Uniform Dose (EUD) and Tumor Control Probability (TCP)

Author(s): Yusung Kim, Cassandra S. Basak, Christopher J. Mart, Sarah M. Mcguire, Wenqing Sun, Sudershan Bhatia
 Radiation Oncology, University of Iowa, Iowa City/UNITED STATES OF AMERICA



Purpose: In order to predict tumor control for patients receiving both external beam radiotherapy (EBRT) and high-dose-rate (HDR) brachytherapy, we present a methodology of evaluating overall radiobiological parameters of equivalent uniform dose (EUD) and tumor control probability (TCP). The current tumor coverage metric is D90 for HDR cervical cancer by assuming the shape of DVH is reasonably same. EUD, accounting for whole DVH has potential as an additional plan quality evaluation tool.

Methods & Materials: A total of 6 biopsy proven cervical cancer patients with FIGO stage I were retrospectively analyzed. All patients received EBRT (45Gy with 1.8 Gy/fx) and Point-A based HDR plans (7Gy x 4fx or 5.5Gy x 5fx). Two patients received a parametrial boost (5.4 or 9Gy). The EBRT and HDR dose maps were converted into equivalent dose in 2Gy fraction (EQD2) dose maps with alpha/beta = 10 using an in-house tool. EUD values were measured from EQD2-DVHs using two different formulae: 1) Using alpha value = 0.15 and 2) Using survival fraction in 2 Gy (SF2) = 0.48. TCP values were calculated using Logistic and Poisson TCP models. The positional input parameters (D50) of TCP for stage I cervical cancer were modeled from long-term clinical data: D90 = 59 Gy and 75.7 Gy with gamma50 = 2 and 8, respectively.

Results: It was feasible to estimate the predicted TCP of the combined EBRT and HDR plans by combining differential EQD2-DVHs. The predicted TCP values for 6 patients were recorded as 100% when using the individual-patient based TCP (gamma50 = 8), and ranged from 88 – 100 % with the population-based TCP (gamma50 = 2). The TCP values were robust with respect to the two different TCP models with correlation coefficients of 0.99 – 1.0. EUD values were on average 124 ± 8 Gy and 110 ± 7 Gy using alpha-based and SF2-based formulae, respectively, with a correlation coefficient of 0.98. All EUD values were recorded as higher than their corresponding D90 values.

Conclusion: It was feasible to estimate the predicted TCP and overall EUD of combined EBRT and HDR plans by combining differential EQD2-DVHs. TCP values were robust regardless of Logistic or Poisson model.

Figure. Upper panel: TCP values calculated from the combined EUD

values of EBRT and HDR. Lower left: The combined EUD values compared with combined D90 and D100 values. Lower right: TCP models with gamma50 = 2 and 8.

PS04.054 - International Multi-Institutional Bench Mark Study on Dosimetric and Volumetric Modulation using Helical Tomotherapy Treatment Planning for Malignant Pleural Mesothelioma Tumors

Author(s): Allen Movahed, André Haraldsson, Claire Footitt, Milton Xavier Vargas Verdesoto, Thuy Lau, Thomas Lacornerie, Sharon Qi, X, Somsak Wanwilairat, Hew Choon Soong, Dale Matson, Dirk Verellen, Koen Tournel, Osama Hassad, Christine Higby, Belal Mofteh, Antoine Wagner, Tommy Knöös
 Radiation Oncology, Pomona Valley Medical Center, Pomona/UNITED STATES OF AMERICA

Purpose:

To determine the most desirable and achievable target dose and organ at risk (OAR) sparing using helical Tomotherapy planning system for mesothelioma treatment plans.

Introduction:

Mesothelioma is an incurable cancer involving the lining of the lung. Treatment options currently available are chemotherapy and external radiotherapy. Tomotherapy’s ability to treat unusually shaped tumors, particularly those wrapped around sensitive normal tissues (e.g.lung), enables higher doses of radiation to be delivered to the target while sparing the normal lung. This, in theory, should improve the treatment’s effectiveness.

Materials and methods:

Academic and clinical participants (from US, Canada, France, Sweden, Belgium, Malaysia Thailand, Mexico and Saudi Arabia) were given CT images and structure sets of a patient having mesothelioma with mediastinal nodes. The planning target volume (PTV) was created using margins of 3 mm inner and 1cm outer and was prescribed a dose of 54Gy to 95% of the volume. Each of participants was asked to create a helical Tomotherapy IMRT plan following same planning guidelines. They were given the goal of either (1) keeping the prescribed dose to the targets while reducing the dose to the OARs or (2) escalating the target dose while maintaining the original level of healthy tissue sparing.

Results:

The resulting treatment plans in primary lesion and nodal mass varied in coverage (95-98.7%) with PTV V54Gy (90.5-96.1%) with Max dose of (57.73-63.46 Gy). Conformality index were (0.950-1.730) and homogeneity index varied from (1.087-1.217) among the participating Tomotherapy centers. The most variable OAR constraint was mean total lung dose (16.4 -98.15%). Other OAR constraints varied less; total lung V5Gy (28.4-58.5%), total lung V20Gy (15.6-33.21%), contralateral lung V5Gy (0.87-39.45%) and heart V45Gy (20.7-28.9%). A range of planning parameters were used; pitch (0.22- 0.43) and delivered modulation factor of (1.143-2.084), and treatment time of (302.1 – 778.2seconds). The reviewers’ ranking assessment (Ranking in Groups: 1 = Good, 2 = Above Average, 3 = Average, 4 = Poor) varied with 3/9 treatment plans rated Good (rank = 1) in at least one category by at least one reviewer. The overall rankings revealed that a plan with balanced trade-off among all planning objectives was preferred by most participants and reviewers.

Conclusion:

Helical Tomotherapy is a promising technique in the multimodal-ity treatment of malignant pleural mesothelioma. Based on many

studies on the comparison of 3DCRT, IMRT and TomoTherapy, it is has been recommended that helical TomoTherapy provide better target coverage and sparing of OARs. Other studies found low doses to the contralateral lung to be limiting. This was not the case in our study, with TomoTherapy we found the dose to contralateral lung be as low as $V5Gy=0.87\%$. A pitch value of 0.287 or 0.43 and a delivered modulation factor of above 1.7 will be beneficial consideration in planning.

Acknowledgments: The authors would like to thank Nader Jafari, Paul Niedzielski, Etienne Lessard (Accuray Inc,USA) for their continued support and involvement in this project.

PS04.055 - Factors predicting of local relapse in irradiated patients with breast cancer: A Syrian Cohort study

Author(s): Moussa Krayem

Medical Physics Department, Al Bairouni University Hospital, Damascus/SYRIA

Background: Breast cancer is the most common cause of cancer death in women. Better understanding of cell biology and behavior may lead to improvement of disease control and prolongation of both disease free and overall survival rate.

Objective: The study is aiming to determining the factors implicated in local relapse in breast cancer patients treated with radiotherapy on chest wall.

Materials and Methods: The study is retrospective one, where we collected data from 2440 Syrian women with breast cancer during the period between 2007 to 2012 at Al Bairouni University Hospital, Damascus. Syria.

Results and Discussion: Among the 2440 patients, 1213 patients experienced local relapse with median period of 14 months. Factors associated with local relapse were: Tumor volume (P. Value 0.002),lymph\ vascular invasion (P. Value 0.005), quadrectomy (P. Value 0.0004) and Her-2 positive status (P. Value 0.0001). Patients with total mastectomy, small tumor volume and estrogen, receptors positive did not correlated with local relapse. Data showed that the most of our locally relapsed patients presented with locally advanced disease and big tumor volume which correlates with high rates of lymph\ vascular invasion, the thing can clarify the tendency for local relapse in this group of patients.

Conclusion: Our results showed that big tumor volume, lymph vascular invasion and Her-2 status are the main factors correlated with local relapse after radiotherapy irrespective of the dose and method of radiotherapy.

PS04.056 - Automated Routine Quality Assurance of VMAT

Author(s): Bryce Cyr¹, Michael Lamey², Grace Zeng-Harpell²

¹Department Of Physics, University of Victoria, Victoria/CANADA, ²Medical Physics, Trillium Health Partners, Mississauga/CANADA

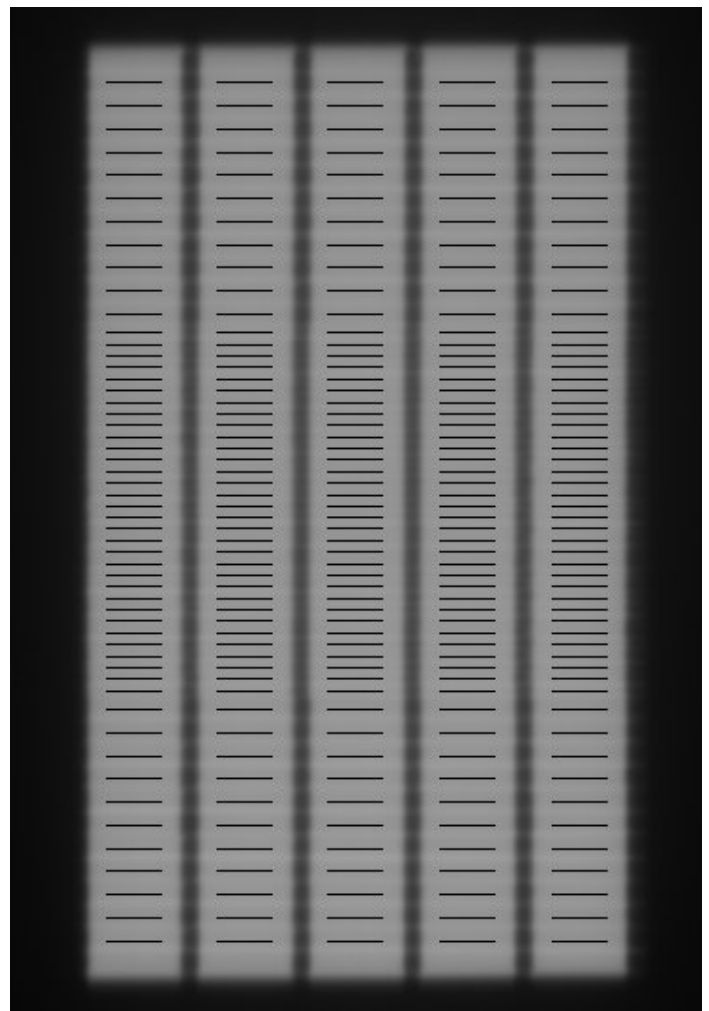
Purpose: The purpose of the work was to develop a standardized picket fence equivalent for Volumetric Modulated Arc Therapy (VMAT) QA, and to automate the analysis method such that the tests can be performed in routine fashion.

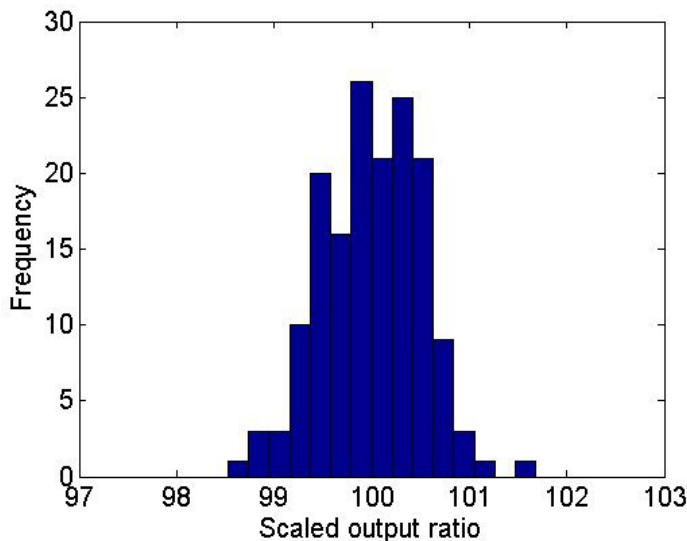
Materials & Methods: An in-house software program was developed using Matlab to automatically analyze delivery to a portal imager using VMAT with varying MLC speed, dose rate and gantry speed. The testing was separated into two cases: the first in which the dose rate and gantry speed are varied and the second in which the MLC speed is varied. For each case two files were delivered: (1)

a dynamic field in which MLCs and gantry moved and (2) a static open field in which the MLCs were retracted and the gantry was stationary. A ratio of the two fields was taken in order to remove field non-uniformities (i.e. horns). The software analyzed the completely irradiated area on the portal imager.

Results: An example of a delivered MLC speed file is shown in Figure 1. The analysis was separated into two regions (the 2.5mm & 5mm MLC widths) due to higher leakage in the 2.5mm region. The image intensity ratio in the 2.5mm MLC region, between the VMAT delivered field and the open field, is shown in Figure 2. The average of the image intensity ratio was scaled to 100 for ease of visibility. The data collected over a six month time frame illustrate that the spread in image intensity ratio is less than 2.5% in all delivered cases. Approximately 95% of the points are within 1.5% of the mean image intensity ratio.

Conclusion: The work herein illustrates that automated VMAT delivery analysis can be performed in a routine fashion while generating reproducible results. The results can be tracked and obtained quickly after delivery.





PS04.057 - Evaluation of the clinical usefulness of modulated Arc treatment

Author(s): Young Kyu Lee, Young Nam Kang
 Department Of Radiation Oncology, Seoul St. Mary's Hospital, College of Medicine, The Catholic University of Korea, Seoul/KOREA

To compare the dosimetric performance of three different arc treatment techniques; modulated arc (m-ARC), tomotherapy, volumetric modulated arc therapy (RapidArc, RA). The purpose of this study is to evaluate the clinical usefulness of mARC treatment techniques. The mArc treatment was selected patients with non-small cell lung cancer (NSCLC) for clinical usefulness of mARC. In order to do this, a study to find the most suitable plan condition of mARC treatment was performed and the usefulness was evaluated by comparing it with the other Arc treatment plans such as Tomotherapy and RapidArc. Three different arc treatments were performed on patients with NSCLC. In the case of mARC, to compare the dosimetric performance of three different main factors— An photon energies (6MV or 10MV), and segment number per each spacing angle were considered. The treatment plans produced using the three different techniques were compared based on the following parameters: conformity index (CI), homogeneity index (HI), target coverage, dose in the OARs, monitor units (MU), treatment time and the normal tissue complication probability (NTCP). As a result, the best dosimetric performance of mARC was observed with the main factors of 10MV photon energy and the spacing angle 6 degree, 59 segments. The target coverage was similar in three different treatment techniques. The RapidArc produced the best dose homogeneity index. However, the conformity index for RapidArc was 1.51 and 1.63 with an absolute difference of 1.07 and 1.52 than tomotherapy, 1.1 and 1.116 lower than mARC. The mARC produced the lowest V20. However, RapidArc produced the best mean lung dose. Both mARC and RapidArc plans had a shorter treatment time, compared with tomotherapy, with a relative fast of 62% and 77% in treatment time. As a result, this study has shown satisfactory result about the clinical usefulness of mARC plans.

PS04.058 - A comparison of linac-based IMRT with helical tomotherapy for craniospinal irradiation

Author(s): Cindy Tam¹, Alex Karotki², Anthony Kim², Young K. Lee¹, Arjun Sahgal¹

¹Department Of Radiation Oncology, University of Toronto, Toronto/ON/CANADA, ²Department Of Medical Physics, Sunnybrook Health Sciences Centre, Odette Cancer Centre, Toronto/ON/CANADA

Purpose: To determine if a linac-based intensity-modulated radiation therapy (IMRT) technique is comparable to helical tomotherapy (HT) for the treatment of craniospinal volumes in terms of planned dose to the planning target volume (PTV) and organs at risk (OARs).

Methods and Materials: A retrospective planning study was performed on 11 patients (3 female, 8 male) who received treatment at this center in the past. The IMRT plans consisted of three sets of beams (with each set having a separate isocenter) - five cranial, three upper spine, and three lower spine fields - and were inverse-planned using Pinnacle³ (v.9.2, Philips). Helical tomotherapy plans were generated with the TomoTherapy Hi-Art (v.4.0.4) planning system. All patients were prescribed 36 Gy in 20 fractions, and plans were optimized to achieve similar goals across both platforms, namely 95% volume coverage of both the brain and spinal PTVs, and reduced dose to all OARs. We compared the performance of each technique through dose-volume histogram (DVH) statistical parameters, mean and maximum doses, and conformity index, testing for significance using the Wilcoxon signed-rank test at a level of $p < 0.05$.

Results: We find that multi-isocentric IMRT generally produces comparable plans to those of HT in terms of PTV coverage and homogeneity. We find that D_{max} to the optic nerves, optic chiasm, lenses and eyes and D_{mean} to the heart are equivalent in our patient sample. Slight differences are noticeable in the larger organs. The volume of lung receiving low dose is less for IMRT (average $V_{5Gy} = 27.9\%$) than HT ($V_{5Gy} = 37.2\%$, $p < 0.005$), while the opposite is true for higher doses ($V_{10Gy} = 11.4\%$ for IMRT vs. 9.1% for HT, $p < 0.005$; $V_{20Gy} = 3.1\%$ for IMRT vs. 1.8% for HT, $p < 0.001$); this is perhaps unsurprising considering the three chosen IMRT spinal beam directions compared to the possible 360° field delivery of HT. Similarly, a decreased low-dose wash to the whole body from the linac-based IMRT is reflected in its ability to spare kidney dose, resulting in a lower mean dose and volume exposed to low dose (average $D_{mean} = 3.2$ Gy for IMRT vs. 4.4 Gy for HT, $p < 0.005$; $V_{5Gy} = 15.9\%$ for IMRT vs. 26.1% for HT, $p < 0.02$). Further differences we observed were a marginally higher mean dose to the parotids and esophagus, as well as higher D_{max} to the esophagus in the IMRT plans.

Conclusions: Based on our 11 patient sample set, the linac-based multi-isocentric IMRT treatment technique is able to produce comparable plans to helical tomotherapy in patients receiving craniospinal irradiation, with only minor tradeoffs in plan quality. This technique may provide an attractive alternative at treatment centers looking for a more conformal and homogeneous approach than conventional methods (ie. cranial lateral parallel opposed pairs with spinal posterior junctioned fields) but without access to HT.

PS04.059 - A Hardware-Accelerated Software Platform for Adaptive Radiation Therapy

Author(s): Seyoun Park¹, William Plishker², Adam Robinson¹, George Zaki², Raj Shekhar², Todd Mcnutt¹, Harry Quon¹, John Wong¹, Junghoon Lee¹

¹Radiation Oncology And Molecular Radiation Sciences, Johns Hopkins University, Baltimore/UNITED STATES OF AMERICA, ²IGI Technologies Inc., College Park/UNITED STATES OF AMERICA

A critical requirement of successful adaptive radiotherapy (ART) is the knowledge of anatomical changes as well as actual dose delivered to the patient during the course of treatment. While cone-beam CT (CBCT) is typically used to minimize the patient setup error and monitor daily anatomical changes, its poor image quality impedes accurate segmentation of the target structures and the dose computation. We developed an integrated ART software platform that combines fast and accurate image registration, segmentation, and dose computation/accumulation methods. The developed platform automatically links patient images, radiotherapy plan, beam and do-

symetric parameters, and daily treatment information, thus providing and efficient ART workflow. Furthermore, to improve the accuracy of deformable image registration (DIR) between the planning CT and daily CBCTs, we iteratively correct CBCT intensities by matching local intensity histograms in conjunction with the DIR process. We tested our DIR method on six head and neck (HN) cancer cases, producing improved registration quality. Our method produced overall NMI of 0.663 and NCC of 0.987, outperforming conventional methods by 3.8% and 1.9%, respectively. The overall ART process has been validated on two HN cancer cases, showing differences between the planned and the actually delivered dose values. Both DIR and dose computation modules are accelerated by GPUs, and the computation time for DIR and dose computation at each fraction is ~1min.



Fig. 1 Conceptual architecture and application GUI

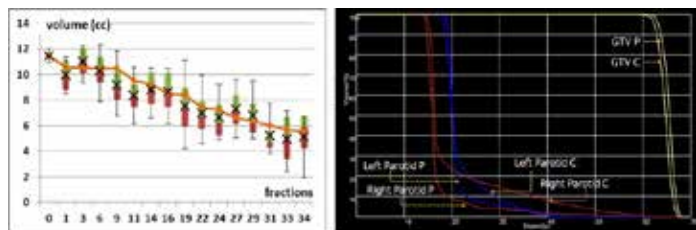


Fig. 2 Tumor volume change and DVH comparison

PS04.060 - Predicting the Impact of Surgery on Quality of Life and Risk Management in Patients Afflicted with Glioblastoma Multiforme

Author(s): Luca Y. Li¹, David G. Gobbi², Jacob C. Easaw³, Yves P. Starreveld⁴

¹Biomedical Engineering, University of Calgary, Calgary/AB/CANADA, ²Calgary Image Processing and Analysis Centre, Calgary/AB/CANADA, ³Tom Baker Cancer Centre, Calgary/AB/CANADA, ⁴Hotchkiss Brain Institute, Calgary/AB/CANADA

Introduction:

Glioblastoma multiforme (GBM) tumors are the most common brain malignancy with an average prognosis of 12-18 months with treatment. Surgical reduction of tumor volume by 78% or more increases patient life expectancy, and can be further extended by adjuvant radio/chemotherapy. However, the effect of treatment on patient Quality of Life (QOL) remains unknown. This study investigates: 1) the impact of more aggressive surgery on patient function, and 2) the utility of a tumor assessment score (TAS) to optimize treatment options by using tumor location and size to predict if the patient is healthy enough for adjuvant therapy. We hypothesize that: 1) there is a threshold between 78% and 98% resection where survival time will continue to increase but functional performance score will start to decrease, 2) a lower TAS based on anatomical location of tumour will reliably predict a lower post-operative functional score.

Methods:

Approximately 90 patients with GBM have gadolinium enhanced and non-enhanced T1 MR images taken pre- and post-surgery. Image pairs are registered and subtracted to highlight active tumor

tissue and have their volume measured to calculate the extent of resection (EOR) (Figure 1). Patient QOL is measured with the Karnofsky Performance Scale (KPS) score. The TAS has a value between 1 and 10 based on: 1) which lobes the tumor infiltrates, 2) left vs. right hemisphere, and 3) the volume of tumor within each region. The impact of surgery looks at the relationship between EOR and post-surgical KPS. The predictive ability of TAS is determined by how closely it can estimate post-surgical KPS.

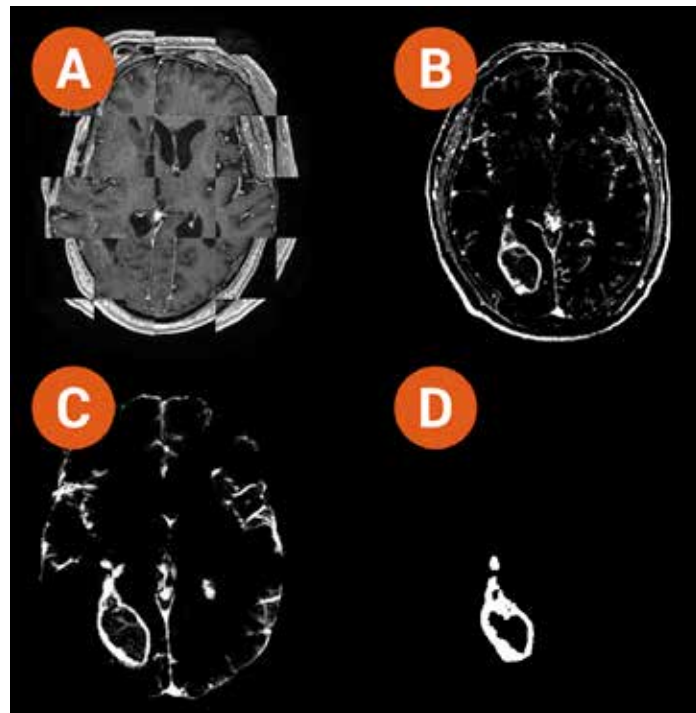


Figure 1: Tumour segmentation pipeline. (A) Registration of gadolinium contrast enhanced and non-enhanced axial T1 images. (B) Subtraction of the image pair highlights active tumour tissue. (C) Brain extraction removes skull and erosion reduces blood vessel connectivity. (D) Floodfill algorithm segments the tumour and provides a volume measurement.

Preliminary Results:

14 test patients were run with an EOR of 87.2%±5.9% for gross-total resection (GTR) patients, and 63.8%±29.5% for sub-total resection (STR) patients. KPS was slightly higher (p over 0.05) in STR (81±8) than GTR (75±14), supporting our first aim.

Conclusions:

Preliminary findings indicate that the pipeline can successfully segment the tumor for EOR calculation, and volumetric measurement of TAS.

PS04.061 - A memetic algorithm for body gamma knife stereotactic radiotherapy treatment planning

Author(s): Bin Liang¹, Bo Liu¹, Fugen Zhou¹, Bin Guo¹, Xuanang Xu¹, Jingbo Kang², Jianguo Li², Wei Liu²

¹Image Processing Center, Beihang University, Beijing/CHINA, ²Department Of Radiation Oncology, Naval General Hospital of PLA, Beijing/CHINA

Abstract—Body gamma knife stereotactic radiotherapy (SBRT) is an effective treatment for non-small-cell lung cancer (NSCLC). Treatment planning is both tedious and time-consuming due to its complexity. In order to address this issue, we present a memetic

optimization algorithm for body gamma knife SBRT treatment planning. Different from currently available methods, the memetic approach performs the optimization on relative dosimetric distribution, which results in an enlarged search space. Taking advantage of the prior knowledge about the interaction between the focuses, a heuristic initialization strategy and a set of genetic operators are developed. During optimization, the most time consuming part is accelerated by graphic processing unit (GPU). Three typical targets arising from real patient data are used to test the efficiency of this approach. Experimental results demonstrate that the memetic optimization could generate a feasible treatment plan quickly (94.6 sec for the largest case).

PS04.062 - Gamma evaluation of dose distributions from newly developed dosimetry system for helical tomotherapy

Author(s): Sangwook Lim, [Sangwook Lim](#), Sun Young Ma
Radiation Oncology, Kosin University College of Medicine, Busan/
KOREA

To see the reliability of the newly developed dosimetry system using phosphor screen for arc therapy such as helical tomotherapy. The cylindrical water phantom was fabricated with the rounded phosphor screen emitting the visible light, that is phosphorescence during the exposure. Three types of virtual targets were defined, one is a small rounded target, another is C-shaped target, and the other is multiple targets. All the targets were to be irradiated at 10 Gy respectively by tomotherapy. Every frame captured from the camera was integrated and the doses were calculated in pixel by pixel. The dose distributions from the phosphorescence images were compared with the calculated dose distribution from the TPS. The discrepancies were evaluated as gamma index for each treatment. The curve for dose rate versus pixel value was not saturated until 900 MU/min. The dosimetry system with the phosphor screen and the camera is respected to be useful to verify the dose distribution of the tomotherapy if the linearity correction of the phosphor screen improved.

Acknowledgements: This research was supported by Basic Science Research Program through the National Research Foundation of Korea (NRF) funded by the Ministry of Education, Science and Technology (2010-0013701 and 2013R1A1A2012013)

PS04.063 - Suitability of a Light Transparent and Electrically Conductive Glass Plate for Construction of a Beam Monitor for Radiation Therapy

Author(s): [Xun Lin](#)¹, Robert K. Heaton², Bern Norrlinger², Mohamad K. Islam²

¹Institute Of Biomaterials And Biomedical Engineering, University of Toronto, Toronto/ON/CANADA, ²Radiation Physics, Princess Margaret Cancer Centre, Toronto/CANADA

Introduction: Due to increasing complexities in radiation therapy technology and associated processes, several real-time independent beam monitoring systems have recently been proposed to minimize treatment errors. Proposed systems utilize a large area detector system or ion chamber mounted after the final beam forming collimator on medical linear accelerators. Some of these devices block light fields, disrupting workflow as therapists are required to remove and re-install the dosimetry device before and after patient setup. In this presentation we describe the suitability of electrically conductive and light-transparent glass plates for use as electrodes in a large area ion chamber

Method: Plates' suitability was assessed based on four properties: (1) surface electrical conductivity (2) light intensity attenuation (3) light field boundary deviations due to refraction (4) stability to radiation exposure.

A commercially available 30x30 cm² conductive glass plate from Sigma Aldrich (Oakville, Canada) was investigated. The plates are 2 mm thick Soda-Lime Glass, coated with 0.5 microns thick conductive layer of Fluorine-doped Tin Oxide (FTO).

Glass surface conductivity was measured and a prototype parallel plate Ion Chamber was created using 2 such plates and tested in radiation for functionality. Light attenuation caused by the prototype was measured using the light probe accessory from the Xi system manufactured by RaySafe (Billdal, Sweden). Light field deviation was calculated using Snell's law; incident angle needed for 1 mm deviation was determined for red and green light, and experimentally confirmed with red and green lasers. Finally, plates' effect on the light field's usability and impact on equipment and patient setup in clinical settings was evaluated by an independent observer using eQA – a commercially available light field and radiation congruence validation tool by Modus Medical (London, Canada) – with and without the prototype. Exposure history is documented and periodic inspections performed to assess radiation damage.

Results: Glass surface resistance was measured to be 51.2 Ω from corner to corner. Basic performance of the prototype was satisfactory. Light field intensity from a Varian linear accelerator was reduced by 35.6% with the 2-plate prototype. According to Snell's Law a 2 mm glass plate causes 1 mm deviation in ray-line with incident angles of 61.3° and 58.6° for red and green light respectively. Experimental results confirmed calculated values. The boundary of a 40x40 cm² light field makes 15° incident angle with the prototype when mounted at the collimator; therefore only 0.74 mm deviation in field size is expected. Field congruence value comparison measured by eQA with and without the prototype also showed no measurable changes to 24x24 cm² light field. No structural changes were observed after testing sessions where the prototype was exposed to radiation doses exceeding 1000 MU.

Conclusions: A commercially available electrically conductive glass plates was found to be suitable for construction of a transmission area ion chamber. The deviation in light-field boundary was found to be negligible. The reduction in light field intensity with 2 glass plates did not limit the usability.

PS04.064 - Objective assessment of skin erythema caused by radiotherapy

Author(s): [Hiroaki Matsubara](#)¹, Naruhiko Matsufuji¹, Hiroshi Tsuji¹, Naoyoshi Yamamoto¹, Kumiko Karasawa¹, Mio Nakajima¹, Wataru Takahashi², Masataka Karube¹

¹National Institute of Radiological Sciences, Chiba/JAPAN, ²The University of Tokyo Hospital, Tokyo/JAPAN

Skin toxicity of normal-tissue is unavoidable side effect in external-beam radiation therapy. Degree of skin toxicity has been visually categorized into discrete grades with having uncertainty owing to subjective evaluation by physicians. Skin dose irradiated in treatment is controlled for skin condition not to get worse than being erythema. This indicates that radiation-induced skin toxicity can be represented by degree of skin erythema. Skin erythema is caused by expansion of capillaries because of increase of blood flow, hemoglobin, owing to biological response for repair. The present study focuses on such physiological response in order to continuously assess skin toxicity.

Two kinds of non-invasive techniques to detect hemoglobin quantities have been developed. One is a Doppler laser flowmeter, which measures reflectance and wavelength-modulation of laser light scattered by skin. It detects skin blood flow in absolute value. The other is skin color pigments decomposition on digital image using independent component analysis (ICA) which is one of multivariate statistics methods. It decomposes a full-color skin image into color tones of hemoglobin, melanin, and others in relative value. Com-

bined analysis of these techniques is expected to provide skin blood flow distribution in a skin image.

Six patients who had carbon beam therapy on lung cancer were treated. Prescription dose of 50 GyE were irradiated from four ports in one day. Photography and skin blood flow measurement were done at 3 h, 1 and 3 month(s) later since the irradiation for study of time series. A conventional compact digital camera was used, but special instruments and lightning condition were not prepared. A fast fixed-point algorithm was employed for ICA. Skin colors were successfully decomposed as shown in Fig. 1.

The results obtained are that relationship between skin dose and blood flow and relationship between skin blood flow and pixel values in hemoglobin image have been observed with their correlation coefficients being larger than 0.9. It was shown that skin toxicity can be represented by change of skin blood flow which is objective quantity. Because the present study quantitatively connects pixel values in hemoglobin image with skin dose, it would be promising to predict skin condition after irradiation in advance by making use of artificial synthesized image processing.

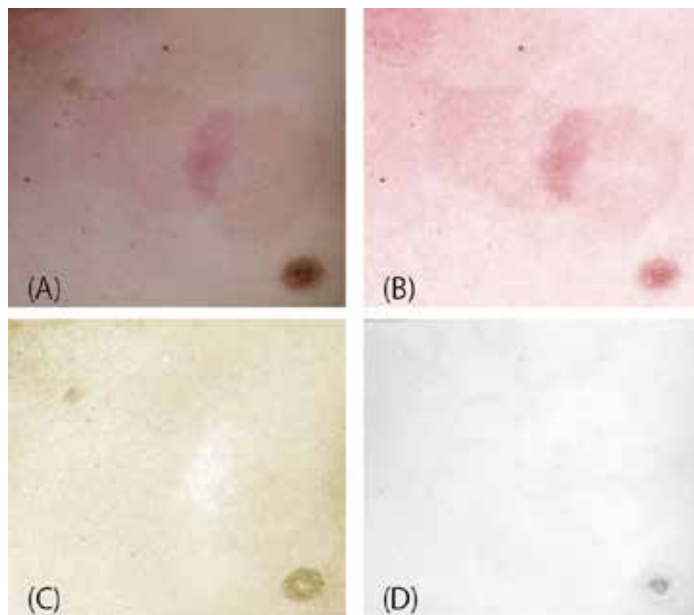


Fig. 1 Typical example of the color decomposition on a skin image which represents two-ports-irradiation erythema. An original image is (A). Color tones of hemoglobin, melanin, and others are (B), (C) and (D), respectively.

PS04.065 - Nasopharyngeal carcinoma tumor response to induction chemotherapy followed by concurrent chemo-radiotherapy: A volumetric magnetic resonance imaging study

Author(s): Nevin Movicar¹, Joshua Giambattista², Benjamin Maas², Cheryl Ho³, Monty Martin⁴, Eric Berthelet²

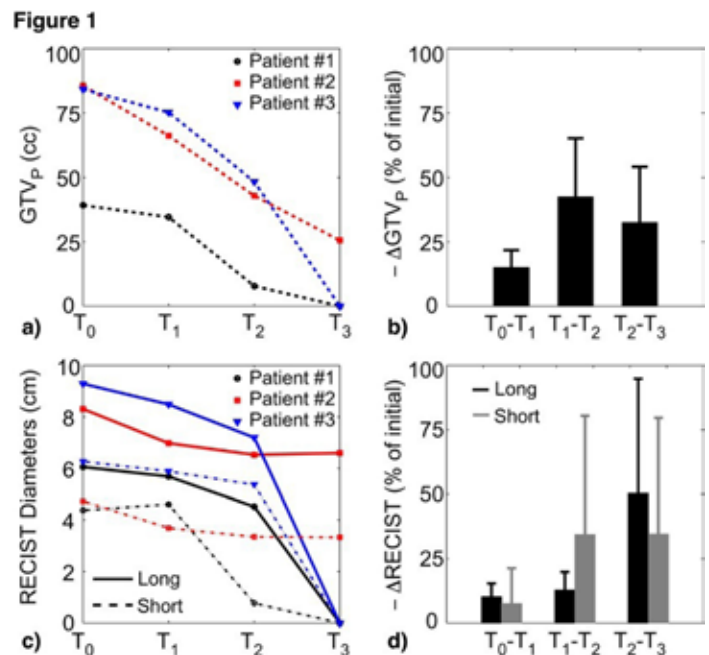
¹Medical Physics, BC Cancer Agency - Vancouver Cancer Centre, Vancouver/CANADA, ²Radiation Oncology, BC Cancer Agency - Vancouver Cancer Centre, Vancouver/CANADA, ³Medical Oncology, BC Cancer Agency, Vancouver/CANADA, ⁴Diagnostic Imaging, BC Cancer Agency - Vancouver Cancer Centre, Vancouver/CANADA

Purpose: Sequential induction chemotherapy followed by concurrent chemo-radiotherapy is currently under investigation for treatment of locally advanced nasopharyngeal carcinoma (NPC). Using magnetic resonance imaging (MRI), we have assessed tumor response at various stages of treatment for NPC patients prescribed with induction and concurrent chemo-radiotherapy. This study represents the first detailed volumetric analysis of primary gross tumor

volumes (GTV_P) in sequential treatment of NPC.

Methods: Fourteen locally advanced stage III-IV NPC patients who received treatment within the British Columbia Cancer Agency between 2011 and 2014 were used for this study. The induction phase included two cycles of gemcitabine combined with cisplatin. The concurrent phase included 5-7 cycles of cisplatin with radiation therapy delivered using volumetric modulated arc therapy (VMAT). All patients received a total dose of 70 Gy over 35 daily fractions given five days per week. All patients received three MRIs at specific stages of treatment (T₀: before treatment, T₁: after induction phase and T₃: three months after concurrent phase). A subset of three patients also received an MRI approximately mid-way through concurrent phase (T₂). GTV_P and RECIST long (RL) and short (RS) diameters were calculated based on MRIs acquired at 1.5 Tesla using a gadolinium-enhanced fat-saturation T₁ weighted spin-echo pulse sequence. GTV_P were contoured in each MRI. Mean values are reported ± one standard deviation.

Results: In this preliminary analysis, we report on the subset of 3 patients who underwent 4 sequential MRIs. Before treatment, the mean GTV_P was 69.6 ± 26.4 cc and the mean RL and RS diameters were 7.9±1.7 cm and 5.1±1.0 cm respectively. GTV_P and RECIST diameters measured at each stage of treatment are shown for the in Figures 1a,c respectively. Figure 1b,d displays the average change in GTV_P and RECIST diameters (as a percent of initial values calculated at T₀) between each treatment phase with error bars equal to one standard deviation (N=3).



Discussion: Preliminary results indicate that two cycles of induction chemotherapy consistently reduced GTV_P (15.1±6.7%) as well as RECIST diameters (long: 10.2±5.1%, short: 7.6±13.7%). NPC is very radiosensitive and tumor sizes reduced significantly throughout concurrent chemo-radiotherapy (~75%). RECIST diameters were more variable than GTV_P measurements and were not accurate indicators of GTV_P. NPC tumors are often irregular shapes making RECIST diameters not ideal markers of NPC tumor size. Analysis of the entire NPC patient dataset and quantification of tumor response during induction phase is ongoing.

PS04.066 - Volumetric Modulated Arc Therapy of Pancreatic Cancer: Dosimetric Advantages as Compared to 3D Conformal Radiation Treatment

Author(s): Xiangyang Mei¹, Tim Olding², Andrew Kerr³

¹Medical Physics, Cancer Centre of Southeastern Ontario at Kingston General Hospital, Kingston/CANADA, ²Department Of Oncology, Queen's University, Kingston/ON/CANADA, ³Oncology, Queen's University, Kingston/ON/CANADA

Volumetric modulated arc therapy (VMAT) has been gaining wider adoption in radiation treatment of various cancer sites, and some recent studies have shown benefits of VMAT to the treatment of pancreatic cancer. This study is to show dosimetric advantages of VMAT with our planning strategies when compared to 3D conformal radiation therapy (3D-CRT) of pancreatic cancer.

The VMAT planning was performed retrospectively on 8 selected pancreatic cancer patients treated using a 3D-CRT technique. The 3D-CRT plans used mostly 4-fields (except one case of 5-fields) with 15 MV photon beams, and the beams arranged to maximally avoid left and/or right kidneys, while keeping sufficient dose coverage to PTV. Dynamic wedges were used for dose inhomogeneity compensation in cases of oblique beam arrangements. Both VMAT and 3D-CRT plans were planned using the Eclipse treatment planning system v.10 for delivery on a Varian Clinac iX/Trilogy linear accelerators (Varian Medical System, Palo Alto, CA, USA). The prescription dose was 4500 cGy in 25 fractions for all cases. The VMAT optimization objectives were designed to achieve maximal sparing to organs at risks, including left and right kidneys, liver and spinal canal with very strong weighting on both left and right kidneys, while ensuring sufficient dose coverage to CTV and PTV. Double arcs of two full rotations (one from 181° to 179°, and the other from 179° to 181°) with 6 MV photon beams were used for all VMAT plans. The PTV volume of these patients was 736 ± 213 cm³. The VMAT plans were normalized such that 99.5% PTV volume is covered by at least 95% of prescription dose (i.e. D99.5% =4275 cGy).

The plan evaluation comparisons between VMAT and 3D-CRT are shown in Table 1. From these results we show that, with our planning objectives, VMAT plans can achieve significantly better dose sparing to both kidneys and liver with lower V20 Gy and/or V30 Gy, lower max spinal canal dose, and better dose conformity to PTV than 3D-CRT plans.

Table 1 Plan evaluation comparisons between VMAT and 3D-CRT plans

Volume	Dose parameter	3D-CRT	VMAT
CTV	*D99.5%(cGy)	4379±38	4492±29
	Mean dose(cGy)	4545±19	4595±21
PTV	*D99.5%(cGy)	4212±22	4275±0
	Mean dose(cGy)	4518±23	4568±19
	**Conformity number	0.72±0.04	0.91±0.02
Right-Kidney	***V20Gy	32.4%±20.6%	7.7%±7.8%
	Mean dose(Gy)	15.1±7.1	10.9±3.1
Left-Kidney	V20Gy	23.2%±9.4%	10.2%±5.5%
	Mean dose(Gy)	12.3±3.4	11.6±2.6
Liver	V30Gy	11.2%±10.2%	8.3%±7.5%
	V20Gy	28.9%±14.6%	21.5%±13.5%
	Mean dose(Gy)	12.2±5.0	11.5±4.2
Spinal canal	Max dose(Gy)	33.1±6.3	27.7±7.4
	Mean dose(Gy)	12.2±5.0	11.5±2.4

* D99.5% means the minimum dose that covers 99.5% of the volume.

** Conformity number was calculated as the ratio between PTV and the 95% iso-dose volume.

*** V20 Gy means the fraction of the specified volume that receives at least 20 Gy of dose.

PS04.067 - Application of ExacTrack BrainLab system for Choroidal melanoma treatments using Stereotactic Radiotherapy and a not invasive immobilization system

Author(s): Artur F. Menezes¹, Delano V. Batista¹, Lucia H. Bardella¹, Aluisio J. Castro¹, Ademir X. Da Silva², Felipe E. Erlich¹

¹Medical Physic, Centro de Oncologia Rede D'Or, Rio de Janeiro/BRAZIL, ²Programa De Engenharia Nuclear, Universidade Federal do Rio de Janeiro, Rio de Janeiro/BRAZIL

Ocular melanoma is an aggressive skin cancer with metastatic behavior that can lead to death¹. External beam radiation therapy is an option to treat medium size lesions (2.5 - 10 mm) not eligible for brachytherapy (tumors close to the optical disk)².

The best results are only achieved if the position of the patient's eye during the computed tomography simulation (CT) can be reproduced during delivery of the radiation dose³. Jaywant et. al³ developed an elaborated system for treatment of ocular melanomas, comprising of an attachment systems, miniature camera, light emitting diode (LED) and image processing software. Although a high degree of sophistication, these systems are possibly associated with a high cost. In this regard, we describe an alternative methodology provide a low cost system that enables correct positioning and fixation of the eye.

Patients were immobilized with BrainLAB's frameless thermoplastic mask. Eye movement was monitored with a camera mounted on a free end of a plastic rod, and the other end was rigidly fixed in the mask. A cavity in the mask was performed at the level of the treated eye, so the images could be viewed from outside the treatment

and CT rooms. To fix the patient's eye, we used a LED, next to the camera, and the patient was instructed to keep their eyes fixed on the bright spot to keep the eyeball static during the CT scans and the treatment delivery. The planning was carried out using a dose prescription of 50 Gy over 5 fractions, usually with 9 radiation fields.

References

- [1] Predrag Jovanovic, Marija Mihajlovic, Jasmina Djordjevic-Jocic, Slobodan Vlajkovic, Sonja Cekic, Vladisav Stefanovic. Ocular melanoma: an overview of the current status. *Int. J. Clin. Exp. Pathol.* 2013;6(7):1230-1244.
- [2] J. A. Shields, C. L. Shields, and L. A. Donoso, "Management of posterior uveal melanoma," *Surv. Ophthalmol.* **36**, 161–195 (1991).
- [3] S. M. Jaywant, E. K. Osei, and S. Ladak. Stereotactic radiotherapy in the treatment of ocular melanoma: A noninvasive eye fixation aid and tracking system. *Journal of Applied Clinical Medical Physics*, Volume 4, Number 2, Springer 2003.

PS04.068 - Dosimetric evaluation of deliverable and navigated Pareto optimal plans generated with Multi-Criteria Optimization

Author(s): Archonteia Kyroudi¹, Sarah Ghandour², Marc Pachoud², Oscar Matzinger², Kristoffer Petersson¹, Mahmut Ozsahin³, Jean Bourhis³, François Bochud¹, Raphaël Moeckli¹
¹Institute Of Radiation Physics, CHUV, Lausanne/SWITZERLAND, ²Radio-oncology Department, Riviera-Chablais Hospital, Vevey/SWITZERLAND, ³Radio-oncology Department, CHUV, Lausanne/SWITZERLAND

Multi-Criteria Optimization (MCO) is an optimization technique providing decision makers (radio-oncologist and medical physicist) with a wide range of clinical choices. It can help unfold the trade-offs involved in the treatment planning problem. MCO generates a set of fluence based Pareto optimal plans, for which no criterion can be improved without deteriorating another. This allows for continuous real time navigation among these optimal solutions. The solution selected by decision makers in the navigation step is converted to a deliverable dose distribution after a second optimization step, which includes direct machine parameter optimization and a final dose calculation. As a consequence, the final deliverable plan might not represent the clinical choices made during the navigation. The purpose of our study was to address this concern by exploring the dosimetric differences between navigated and deliverable plans.

Navigated and deliverable VMAT plans for five prostate and five lung cancer cases were created with RayStation TPS (RaySearch AB, Stockholm, Sweden). Two-dimensional Pareto fronts were created, representing the trade-off between PTV under-dosage vs. healthy tissue sparing. PTV under-dosage was evaluated through the volume of PTV receiving less than 95% of the prescribed dose, while healthy tissue sparing was evaluated through the $D_{50\%}$ parameter for rectum and V_{5Gy} for lung-PTV volume. In order to minimize the effect of the other parameters involved in the treatment planning problem we introduced optimization constraints on all other OARs, which ensured minimal dosimetric variations for these structures.

The Pareto front evaluation (see examples in Fig. 1) demonstrated a disagreement for the trade-off parameters between navigated and final deliverable plans for eight of our ten cases. For two prostate cases the deliverable Pareto fronts were improved compared to the navigated ones. For the other prostate cases the disagreement proved more random. In all lung cases, the deliverable plans deteriorated compared to the navigated ones, i.e. the PTV under-dosage increased (up to 17 %). Our results show that the final deliverable plan quality may be substantially different than that of the navigated plan selected by clinical decision makers, particularly for small

target volumes in lung.

Real time navigation on a wide range of treatment plans offer more and potentially better options during clinical decision making. However, dosimetric differences between navigated and deliverable plans due to the two-step approach may limit the practical use of MCO.

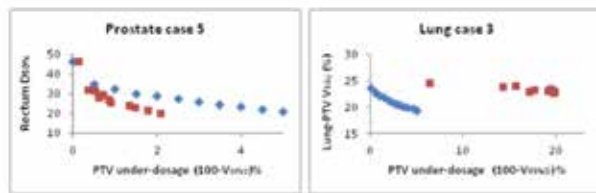


Figure 1: Example of navigated (points in blue) and deliverable (points in red) Pareto fronts for a prostate and a lung cancer case.

PS04.069 - 2D and 3D Approximate Entropy Algorithms for On-line Quantification of Threshold Structure Content in Large Radiotherapy Image Data

Author(s): Christopher J. Moore, Phillip Sharrock, Thomas Marchant
 Christie Medical Physics & Engineering, The Christie NHS Foundation Trust, Manchester/UNITED KINGDOM

Expert interrogation (EI) remains the 'gold-standard' in many medical applications, excelling at identifying occult abnormality and disease, particularly under threshold conditions where noise dominates a region of interest. Sophisticated regularity metrics have only been developed to help clinicians identify threshold structural changes in 1D data streams, e.g. approximate entropy ($ApEn_{1D}$) for physiological monitoring. This in the knowledge that the order in which the data appears, not just its variability, can indicate clinically significant perturbations [1].

Today, very large image data streams almost intractable to EI are commonplace. 3D data volumes are fast becoming 4D with the proliferation of dynamic scanning in both diagnostic and therapeutic imaging settings c.f. X-ray fan-beam and cone-beam CT (FB/CBCT). Hitherto, the $ApEn_{1D}$ algorithm has not been formally developed for routine use with higher dimensional data, though iterated deployment of 1D calculation [2] and promising pilot work towards an approach for differentiating cell and clinical images has been reported by the authors [3,4].

The purpose of this work is to show that it is feasible to rapidly compute a statistical measure of pattern regularity associated with all image points and their immediate surroundings, which is self-calibrating to represent simplistic through to random structural content. This is a first step towards understanding EI 'threshold working' in medical imaging in general, and manual radiotherapy structure delineation in particular, from an evidence based viewpoint with an associated single metric.

This paper formally presents approximate entropy algorithms in 2D and 3D forms ($ApEn_{2D/3D}$) for imaging. The concept of spatial divergence in the context of considering nearest neighbour pixel lattices is introduced as fundamental to the development of these algorithms. Observations of the mechanics of EI during interactive image interrogation are also shown to be consistent with this approach.

Pilot software to calculate $ApEn_{3D}$ for 3D image data was written using the scientific programming language IDL (ITT VIS, Boulder, CO). The time taken to compute $ApEn_{3D}$ for each of the 512x512 voxels in a single CT slice image was approximately 3 minutes using a PC with 3GHz CPU (note that the calculation operates in 3D, hence a

block of adjacent slices is processed to compute ApEn values for the block's central slice). Optimised recoding in C reduces this to 10 seconds, making on-line use feasible. Still faster implementation using an Intel Xeon Phi card's MIC architecture is current work in progress.

For illustration the new $ApEn_{2D/3D}$ algorithms are applied to FBCT and CBCT volume image data sets acquired for image-guided radiotherapy patients. Significant differences in the ApEn distribution between the two modalities are revealed, visually and quantitatively, reflecting the scatter-induced decreased uniformity and increased noise in CBCT.

[1] Moore, Manickam & Slevin, *Biomed Signal Proc & Ctrl*, 1 (2) pp. 113-119, 2006.

[2] Cullen, Saleem, Swindell, Burt & Moore, *Biomed Signal Proc & Ctrl*, 2010; 5;1;32-36.

[3] Marchant, Murphy, Madden & Moore, *Procs IEEE Intl Conf Image Proc*, Brussels, Belgium, 2011

[4] Marchant & Moore, 11th ESTRO Conf 2011, *Radioth & Oncol*, Abstr 99 (S1), ppS457, 2011.

PS04.070 - Dosimetric effects of seed positioning uncertainties in ophthalmic plaque brachytherapy

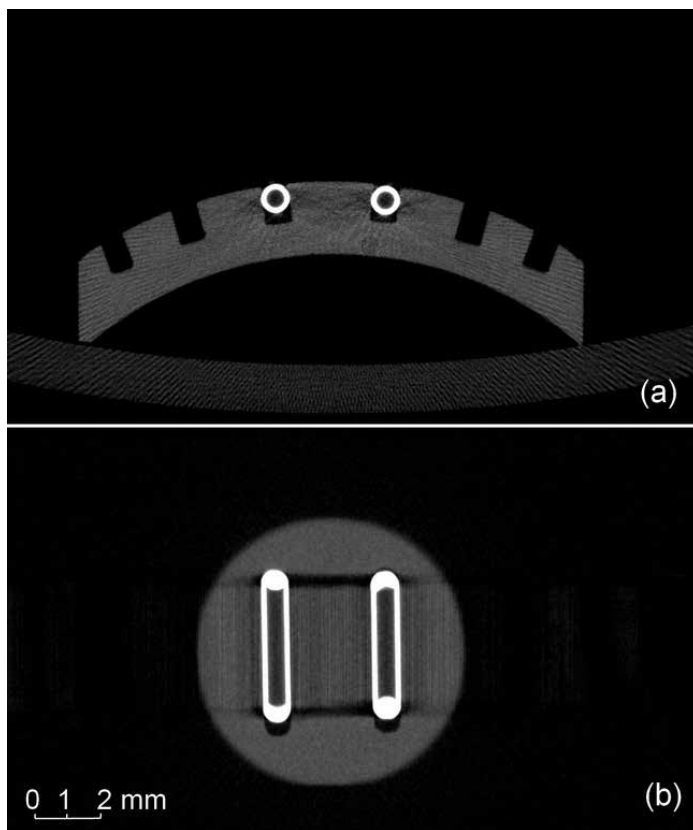
Author(s): [Hali Morrison](#), Geetha Menon, Hans-Sonke Jans, Ron Sloboda
Medical Physics, Cross Cancer Institute, Edmonton/CANADA

Uveal melanoma affects approximately 3000 people each year in North America, many of whom are then treated with plaque brachytherapy, now a commonly used alternative to enucleation. One significant challenge in plaque brachytherapy dosimetry is the presence of very sharp dose gradients due to short treatment distances, making even small shifts in depth result in large changes in dose. Uncertainties associated with seed positioning were examined using two approaches: (i) by comparing EBT3 GafChromic film dose measurements and Plaque Simulator ophthalmic brachytherapy treatment planning software calculated doses; and (ii) by measuring seed positions in a COMS plaque insert using microCT scanning.

Film pieces were placed at depths of 6 mm and 12.3 mm within two 24.6 mm diameter spherical PMMA phantoms. The films within the phantoms were then irradiated with both 16 mm COMS and Eye Physics Super9 (model #930) brachytherapy plaques, each of which contained two centrally loaded IsoAid Advantage I-125 model IA1-125A seeds with an average activity of 8.0 mCi. The irradiations were performed in a water tank to provide full backscatter conditions, and a minimum dose of 6.5 Gy was delivered to the centre of each piece of film. The film dose measurements were compared to calculated doses using Plaque Simulator v5.7.3 software, with dosimetry parameters for the IsoAid I-125 seed in PMMA to account for the non-water material of the phantoms.

The CAX calculated doses at depths of 6 mm and 12.3 mm differed from the equivalent ones measured using film by 8-16%. The differences in dose could be accounted for by an average shift in depth of 0.5 mm for both the 16 mm COMS and Super9 plaques. For the COMS plaque, this change in depth is at least partially associated with seed placement in the Silastic insert as the seed slots have a depth 0.45 mm greater than the seed diameter. To measure precise positions of the seeds within the 16 mm COMS Silastic insert, high resolution CT images were obtained using a Siemens Inveon micro-PET/CT hybrid scanner with the insert loaded with IsoAid I-125 seed shells (no silver core was in the Ti shells to reduce metal artifacts in the CT images), as seen in Figure 1.

These results highlight the impact of the steep dose gradients present in ophthalmic plaque brachytherapy as well as the importance of precise and careful assembly of the plaques for patient treatment.



PS04.071 - A Method for Evaluating Deformable Dose Accumulation in RayStation

Author(s): [Joanne Moseley](#)¹, [Biu Chan](#)², [Jean-Pierre Bissonette](#)²
¹Radiation Medicine Program, Princess Margaret Cancer Centre, Toronto/CANADA, ²Radiation Medicine Program, Princess Margaret Cancer Centre, Toronto/ON/CANADA

Purpose: To develop a method for evaluating the effect of various shrinkage rates on dose accumulation in the head and neck using a commercial treatment planning system (TPS).

Material/Methods: A biomechanical finite element based deformation software (MORFEUS) was used to register the planning CT and final fraction CT of a head and neck radiotherapy patient with large tumour shrinkage, thus generating a known deformation field. The deformation field was multiplied by fractions of the total deformation ranging from 10% to 100% to generate three series of target images (5 each) with varying amounts and rates of shrinkage. These images were imported into a commercial TPS (RayStation v4.4.100, Raysearch, Stockholm) and deformable image registration was performed using a hybrid algorithm (i.e., based on image intensity and contours). Dose was accumulated over 5 equidistant fractions in the following schemes: Shallow-Steep (10%-20%-30%-60%-100%), Linear (20%-40%-60%-80%-100%), and Steep-Shallow (10%-50%-80%-90%-100%). The dose statistics for the accumulated dose was compared with the planned dose using D_{99} for targets and D_{max} for organs at risk.

Results: The difference in dose statistics accumulated over 5 fractions for each of the three image sets is shown in Figure 2. For this particular disease presentation, the effect on dose difference is

greater the earlier the changes appear in treatment.

Conclusion: A set of images was generated with a known deformation field and linear changes between them. Images such as these can be used to evaluate the effect different magnitudes and rates of change have on accumulated dose.

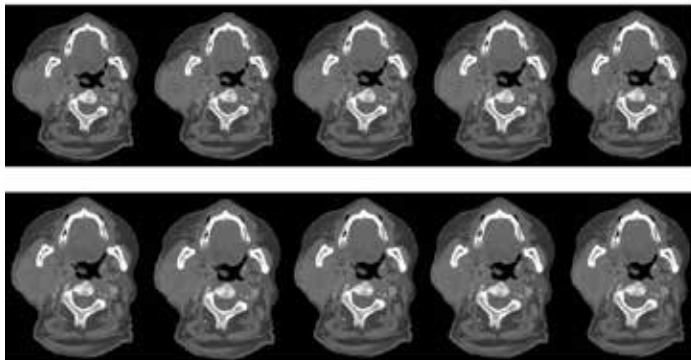


Fig. 1: Images deformed using MORFEUS, ranging from 10% of total deformation (upper left) to 100% of deformation (lower right).

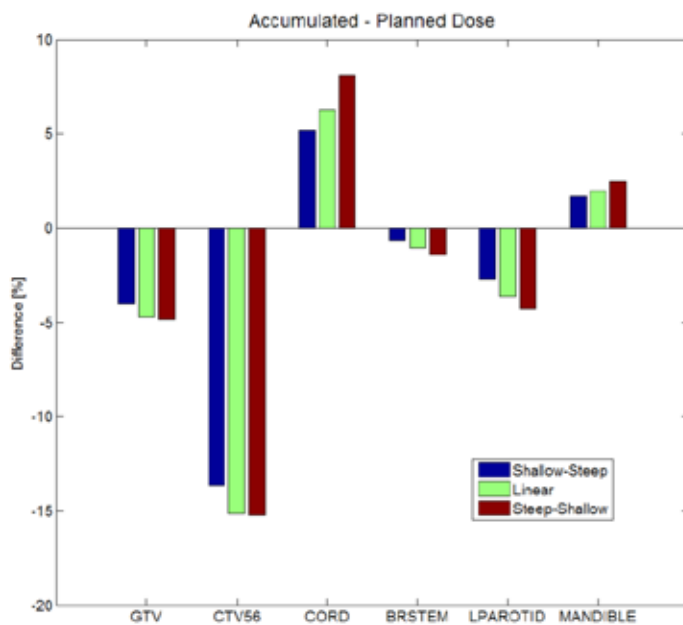


Fig. 2: The percentage difference between accumulated and planned dose over five fractions. D99 is compared for GTV and CTV, and D_{max} is compared for the organs at risk.

PS04.072 - Dosimetric comparison between 3D CRT, full Arc and Partial Arc Vmat techniques in the management of locally advanced lung Cancer using External Beam Radiation Therapy (EBRT).

Author(s): Samir Mouatassim¹, Omar El Alami¹, Latifa Mesbah²
¹Radiotherapy, Centre d'Oncologie Nakhil, Rabat/MOROCCO, ²Oncology, Moulay Youssef Hospital, Rabat/MOROCCO

BACKGROUND

The purpose of this study is to compare the planning target volume (PTV) coverage and sparing to organs at risk (OARs) achieved when using volumetric modulated arc therapy (VMAT) with Full Arc (FA),

Vmat with Partial Arc (PA) or static 3D Conformal Radiation Therapy treatment for locally advanced lung tumors.

MATERIALS AND METHOD

3D CRT and Vmat planning were done applying the 3A algorithm and the Vmat optimization module implemented on Eclipse workstations (v. 11 from Varian).

The treatment machine consists of a Varian high energy linac Silhouette with a 120 Multileaf collimator, on-board imaging (OBI) system including CBCT feature, IMRT and RapidArc capabilities.

Six patients with locally advanced NSCLC tumor were treated either by using 3D Conformal Radiation Therapy or Vmat (RapidArc) technique. Dose to Organs At Risk (OARs); such as the spinal cord, heart, esophagus, brachial plexus and lung were determined by performing and optimizing a 3D CRT plan and compared to those obtained with VMAT plans (FA Vmat and PA Vmat). All the Vmat plans were generated using the same dose constraints and planning objectives compiled from a systematic literature.

RESULTS

The VMAT plans delivered a significantly lower dose to the spinal cord, to brachial plexus, to lung and heart than do the 3D CRT plans. In addition, they show more optimal PTV coverage with better Conformity Index (CI) and more homogenous dose in the target. In contrast, the 3D CRT plans are obviously more efficient in dose delivery and the volumes of low dose are less important than those generated with Vmat plans.

The results demonstrate that using VMAT instead of static 3D CRT offers improvements in OARs sparing without detriment to PTV coverage. While both methods can result in conformal plans, the VMAT plans were found to conform more ideally to the target volume.

The PA Vmat plans show better OARs sparing and decrease of low dose to surrounding normal tissue compared to FA Vmat plans while both are leading to comparable PTV coverage, conformity and dose homogeneity.

PS04.073 - Dosimetric and clinical considerations for implementing CBCT based adaptive planning using RayStation
Author(s): Bongile Mzenda, Rochelle Hiscock, Angela Wells
 Auckland Radiation Oncology, Auckland/NEW ZEALAND

Introduction

This study reports on the implementation of a CBCT (Elekta XVI) adaptive replanning technique for pelvis, chest and H&N treatments at our centre.

Method

Density tables for use in replanning were compared between the bulk density correction method for the RayStation TPS (Fig1a) and user-defined density tables derived from Catphan and Gammex 467 phantoms (Fig1b). These were applied to Rando phantom plans as well as patients having no contour changes to determine their dosimetric accuracy.

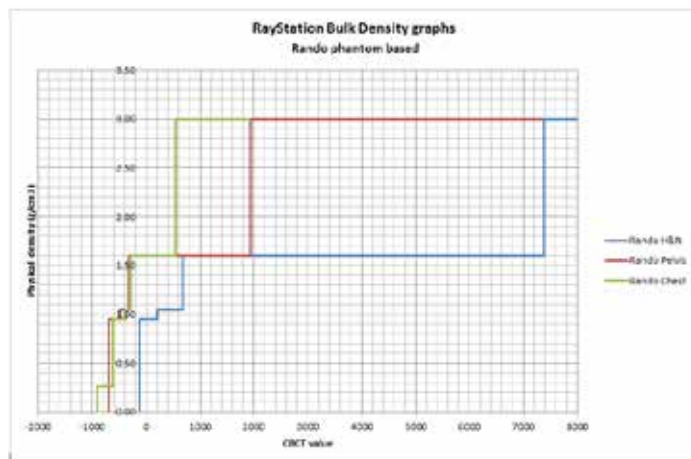


Figure 1a. Typical bulk density from RayStation TPS for Rando phantom sites

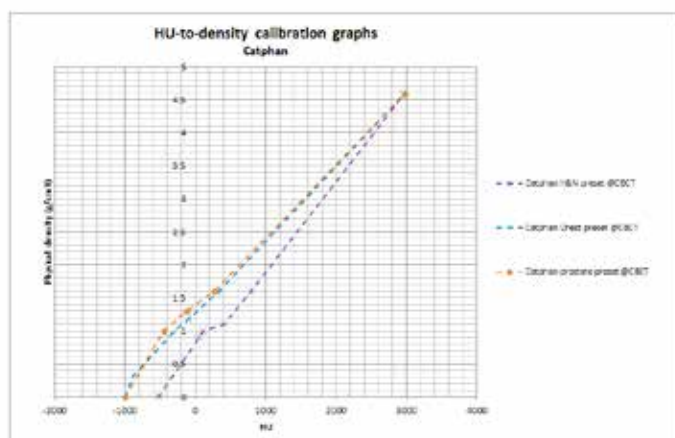


Figure 1b. Typical user derived densities for Rando phantom sites

For XVI adaptive planning additional presets were created for sufficient image quality and patient field of view.

In the clinical implementation for 10 patients who required replanning as a result of weight changes the CBCT method was compared to the repeat CT planning. Contouring was performed on both the repeat CTs and the CBCT images by the Radiation Oncologists and new plans generated. Contour comparisons of the CBCT generated volumes against the CT volumes were performed. Plan dosimetric metrics reviews and quantitative checks of gamma indices (3%/3mm and 2%/2mm) of the new plans were performed.

Results

For the pelvis region the bulk density method was found to be more consistent and accurate in real patients than the user-defined density table which gave higher discrepancy for the Rando phantom. For H&N and chest/thorax region the user defined density table consistently resulted in closer dosimetric agreement to the expected for phantom and real test patients. Good agreement was seen in the comparison between the plan metrics from repeat CT and computations on the CBCT datasets.

Conclusion

The implementation of CBCT plan adaptation for efficient clinical workflows requires critical assessment of the uncertainties due to imaging, density corrections and contour propagation on the resulting treatment plans.

PS04.074 - A Statistical Study based on comparison between two treatment planning systems while exporting RT structure set

Author(s): Richa Sharma¹, Kamlesh R. Passi², Konthoujam M. Devi², Sandhya Sood²

¹Department Of Radiotherapy, Delhi State Cancer Institute, Delhi/INDIA, ²Department Of Radiotherapy, Mohan Dai Oswal Hospital, Ludhiana/INDIA

Introduction: An RT structure set (RTSS) comprises of delineated target and OARs drawn on DICOM images by radiation oncologist. In a big radiation therapy department having many treatment planning systems (TPSs) and a huge patient load, it is a common practice to maximize the throughput by contouring on any available TPS irrespective of the TPS where actual planning is to be done. But when an RTSS is drawn on one TPS and is exported to other, volume of contoured structures gets modified. The objective of this study is to analyse such changes in volume on statistical basis in case of IMRT patients.

Material and Methods: In this study we have used two TPSs – CMS-Xio (v4.7) and Oncentra (v1.0). Thirty patients were selected from each TPS. RTSS volumes given by original TPS (on which RTSS was drawn) were recorded. After which all patient's DICOM images along with RTSS were sent to other TPS. Then, RTSS volumes given by new TPS were also noted down. These volumes were categorized organ wise. Thereafter, these *original volumes* and *altered volumes* were compared on the basis of percentage variation analyses. Moreover, range, measure of central tendency and absolute dispersion of percentage variation were determined for each category. Subsequently, *scatter diagrams* were plotted for each of the category, keeping originally drawn volumes on X-axis and altered volumes on Y-axis. Relationship between these volumes was estimated from respective approximating curve via least square fitting. With the help of such regression curve of Y on X, value of altered volume corresponding to a given original volume can be estimated. Measure of scatter about regression curve had also been found for each category. Total variation of altered volume, including explained variation and unexplained variation was also found for each categories and hence *coefficient of determination* and *coefficient of correlation* were determined. Further, this sample correlation coefficient r was used for estimating the value of *theoretical population correlation coefficient ρ* at 95% and 99% confidence level for each category on the basis of sampling theory of correlation.

Results and Discussion: High percentage variations had been estimated for small volume structures. Contours which had been drawn originally on Oncentra and CMS-Xio were found to have altered volumes greater than and less than originally drawn volumes respectively. But a few exceptions had also been noticed for both TPSs. In most of the cases nearly perfect linear correlation between volumes had been observed, except for a few cases like lens, indicating to the fact that the total variation of altered volumes in these cases comprise of a significant part of unexplained variation. Application of sampling theory of correlation further revealed that there is no linear correlation between original (drawn on CMS-Xio) and altered volumes for optic nerve.

In summary, it may be concluded that change in volume of RT structures on export between different TPSs may or may not be significant in other disease sites but is particularly important in case of brain and head and neck patients.

PS04.075 - The Characteristics and Implementation of XR-RV3 Gafchromic Film for Radiotherapy Dosimetry

Author(s): Supriyanto Ardjo Pawiro¹, Aditya Fergawan¹, Pamungkas Hudigomo¹, Sugiyantari Soegijono², Andreas Nainggolan³, Djarwani Soeharso Soejoko¹

¹Department Of Physics, Faculty Of Mathematics And Natural Sciences, University of Indonesia, Depok/INDONESIA, ²Department Of Radiotherapy, Persahabatan Hospital, Jakarta/INDONESIA, ³Department Of Radiotherapy, MRCCC Siloam Hospitals, Jakarta/INDONESIA

The purpose of this study is to compare the dosimetry characterization of XR-RV3 to EBT2 gafchromic film and also to implement both films in order to verify the dose of radiotherapy on IMRT and VMAT. The film response of each energies (foton 6 MV, 10 MV and Cobalt-60) was measured over the dose levels from 50 cGy to 10 Gy. Each film piece was scanned using EPSON Perfection V700 flat-bed scanner, 48-bit color, 75 dpi spatial resolution. The data were analyzed using FilmQA Pro for each images with ROI size 3 x 3 cm². Furthermore, the evaluation of targeted dose is determined by putting films of Gafchromic XR-RV3 and EBT2 on Rando Alderson slab phantom to simulate prostate cancer. The experiment was performed with Varian Clinac Trilogy, Inc. Two cases of IMRT and VMAT plans were made using Eclipse TPS ver. 10. Exposed Gafchromic films was scanned using Epson Perfection V700 into (.TIF) format in 720dpi and RGB 48 bit was analyzed by using in-house algorithm and FilmQA pro. The comparison between EBT2 and XR-RV3 Gafchromic films were used to obtain average dose in the form of histogram curve. From this study, the result revealed that there was no significant difference in characteristics response between XR-RV3 and EBT2 film with standard deviation of ±3%. The energy dependence of XR-RV3 and EBT2 film was found to be relatively small within measurement uncertainties ±1%. The dependence of XR-RV3 film side orientation is negligibly small with the standard deviation of 0.2. On the other hand, the percentage of errors in the case of verification of prostate cancer toward the planned dose were -4.85% in EBT2 Gafchromic films and -1.94% in the XR-RV3 Gafchromic films on IMRT technique, whereas for VMAT were -4.48% on EBT2 Gafchromic films and -7.47% on XR-RV3 Gafchromic films.

PS04.076 - Weighted comprehensive score evaluation of CBCT image guided positioning accuracy in lung cancer radiation treatment

Author(s): Yinglin Peng, Songran Liu, Botian Huang, Dandan Zhang, Wenzhao Sun, Hui Liu, Xiaowu Deng
Radiation Oncology, Sun Yat-Sen University Cancer Center, Guangzhou/CHINA

Background and Objective: Cone-beam computed tomography (CBCT) has been widely used in radiation treatment positioning as so called image guided radiation therapy (IGRT) technique. It is impossible to correct all local position error by doing global IGRT positioning since deformation always happens in the patient and the positioning shifts relies on the image registration technique used in the image guidance. This study evaluated and analyzed the regional accuracy of CBCT guided positioning used different image registration strategy with a comprehensive scoring method to provide a reasonable guidance for clinic application of cancer IGRT.

Materials and Methods: Planning CT and CBCT images acquired during the first radiation treatment positioning of 15 lung cancer cases were studied, registered with different image registration algorithms (bony and gray registration) and different registration area (target-only, ipsilateral structure and body). The CBCT target volume (GTV_{CBCT}) coverage by planning target volume (PTV_{CT}), the dice similarity coefficient (DSC) between the planning CT target volume (GTV_{CT}) and GTV_{CBCT}, the volume of organ at risk on planning CT (OAR_{CT}) and on CBCT (OAR_{CBCT}), and the position deviation of

the GTV geometric center were compared. A weighted comprehensive scoring function was used to evaluate the positioning correction. The comprehensive registration factors (CRF) was defined as following, while the CRF values 100 meant all specific structures registered 100%.

$$CRF = F_{GTV} \times F_{OAR} \times \dots \times F_{OAR} \times [DSC_{GTV} \times w_{GTV} + \sum_i (DSC_{OAR_i} \times w_i)]$$

Results: For the tested lung cases, the bony registration had less accuracy in almost all evaluated specifications, especially when registered the target only. The coverage ratio of PTV_{CT} to GTV_{CBCT} of bony and gray registration in the three groups of registering target only, ipsilateral structure, body were 66%±35% and 97%±8% (P=0.005), 98 %±5% and 99 %±2%(P=0.034), 98%±4% and 98%±4% (P=0.478), respectively. Using gray registration to register the ipsilateral structure had the best result, with the DSC of GTV and OARs of 0.86±0.10 (GTV), 0.71 ±0.10 (Esophagus), 0.76±0.10 (Spinal cord), 0.89±0.05 (Heart), and the deviation of GTV center of 2.5mm±1.6mm, meanwhile the CRF was 55.28 ±40.59.

Conclusions: CBCT guided positioning is able to ensure that the GTV covered by PTV, which is the first goal of IGRT, when suitable image registration strategy is applied. Using gray registration and registering the ipsilateral structure is recommend for CBCT guided lung cancer radiation treatment positioning. The weighted comprehensive scoring is helpful for evaluating the image registration of IGRT.

PS04.077 - MCNP Simulation of Leksell Gamma Knife Using Disk Sources for Different Phantom Materials

Author(s): Ma. Vanessa Francheska P. Perianes, Doreen Alexis F. Villanueva, Jade D. Trono
Physics, De La Salle University, Manila/PHILIPPINES

Leksell Gamma Knife (LGK) uses 201 Co-60 sources whose radiation intersects at the isocenter. The relative dose at the isocenter was verified using MCNP simulation. This study was divided into two simulations. Simulation A includes the simulation of 201-point sources to verify the location of the sources and the direction of the particles towards the center of a 160 mm water phantom. Simulation B includes the simulation of the 201-disk sources on the water phantom and water phantom with 1 cm thick shell made of Plastic Water. The diameter of the disk source used in the simulation corresponds to the diameter of the outer aperture of the full geometry collimator system for 4, 8, 14 and 18 mm. In order to produce a relative dose distribution, scoring bins were placed at the x-, y- and z-axes of the phantom. *F8 tally was used to convert the energy deposited into the scoring bins in MeV into dose in rad. Simple physics treatment was observed in the simulation. The relative dose distributions obtained in the simulation were compared. The results verified that the region of the highest dose was at the center of the phantom. The results of Water Phantom were compared with the results of Water Phantom with 1 cm thick Plastic Water shell (Figure 1 and Figure 2). There were no significant differences found between Simulation A and Simulation B. The lateral distribution of the dose along the z-axis increases as the diameter of the disk increases. In conclusion, the use of disk sources provides a simpler method in the simulation and obtaining a relative dose distribution instead of using the full geometry collimator system of the LGK.

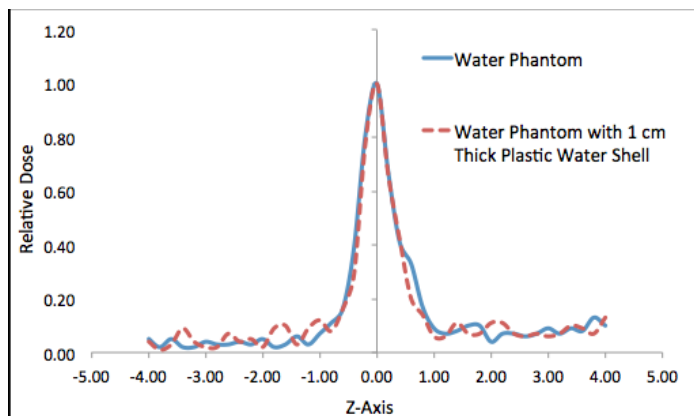


Figure 1 Relative Dose Comparison for 18 mm disk source

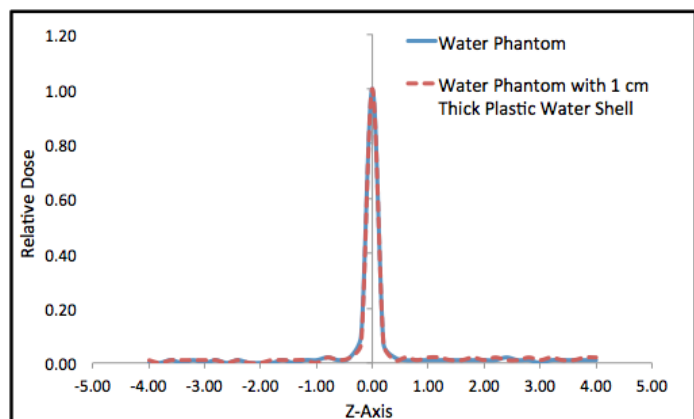


Figure 2 Relative Dose Comparison for 4 mm disk source

PS04.078 - Dosimetric comparison between RAPIDARC and 3DCRT planning in extremity soft tissue sarcoma

Author(s): Yannick Poirier¹, David Sasaki¹, Darlene Courtney², Mohamed Akra³

¹Medical Physics, CancerCare Manitoba, Winnipeg/CANADA, ²Treatment Planning, CancerCare Manitoba, Winnipeg/CANADA, ³Radiation Oncology, CancerCare Manitoba, Winnipeg/CANADA

Introduction: Soft-tissue sarcomas presenting in extremities are usually treated with neo-adjuvant radiation therapy prior to limb-preserving surgery. These sites often present with large planning target volumes (PTVs) that are challenging to treat as they can envelop weight-bearing bone (e.g. femur). Limiting the dose to bone and skin reduces the risk of fracture and lymphedema or delayed post-surgery wound healing, respectively, but is difficult to achieve using traditional 3-D conformal radiation therapy (3D-CRT). As part of our institution's efforts to join the incoming SRC-6 clinical trial, we investigated the ability of RAPIDARC volumetric modulated arc therapy (VMAT) to improve coverage and spare organs at risk (OARs) compared to 3D-CRT plans, and investigated the sensitivity of VMAT plan quality to arc parameters.

Materials and Methods: VMAT plans were generated for five extremity sarcoma patients previously treated with 3D-CRT in our institution. The PTV average longitudinal length was 20.6 ± 6.8 cm with a range of 10.1–30.8 cm. The sites were planned using two partial arcs designed to avoid irradiation through the contralateral extremity or the rest of the body. Complimentary collimator angles (e.g. $30^\circ/330^\circ$) were used to maximize optimization flexibility. Patients with PTV longitudinal length >20 cm were planned using a four arc technique to avoid large segments of open fields. First, the

original two arcs were duplicated. Then, the size of each field was decreased to a maximum of 20 cm such that the PTV was partially covered by two arcs overlapping near the middle of the PTV for each collimator angle. We assessed the sensitivity of VMAT plan quality to collimator angles by generating alternate plans with varying collimator angles from $(0^\circ/0^\circ)$ to $(90^\circ/270^\circ)$ in increments of 15° . A standard prescription of 50 Gy in 25 fractions was used for every plan.

Plan quality was assessed using objectives from the SRC-6 protocol: namely, $CTV V_{95\%Rx} = 100\%$, $PTV V_{95\%Rx} > 95\%$, $V_{110\%Rx} < 10\%$, infield-skin and longitudinal skin strip $V_{20Gy} < 50\%$, and in-field bone $V_{50Gy} < 50\%$.

Results: The generated VMAT plans satisfied all planning objectives for each patient. When renormalized to offer similar coverage, the VMAT plans outperformed the clinical 3D-CRT in dose homogeneity and OAR sparing. On average, $PTV V_{110\%Rx}$ was $5\% \pm 5\%$ higher in 3DCRT plans compared to VMAT. While bone V_{50Gy} was only $3\% \pm 1\%$ lower in VMAT plans compared to 3DCRT, VMAT offered much superior skin sparing by $10\% \pm 16\%$ for total skin V_{20Gy} and $59\% \pm 11\%$ for skin strip V_{20Gy} respectively.

VMAT plan quality was insensitive to collimator variation, as metrics showed variations of $<1\%$ for coverage and $\pm 3\%$ for OARs except for the extreme $(0^\circ/0^\circ)$ or $(90^\circ/270^\circ)$ cases.

Conclusions: A VMAT planning method was devised and validated for the treatment of extremity soft-tissue sarcoma. Collimator angle had minimal impact on the quality of the plan. Long (>20 cm) PTV volumes were successfully planned using a four-arc single-isocentre technique. VMAT plans were able to spare more of the circumference of the skin compared to 3DCRT.

PS04.079 - Cerebral Functional Alterations Before and After Intensity-Modulated Radiation Therapy in Patients with Nasopharyngeal Carcinoma

Author(s): Wenting Ren¹, Kai Wang¹, Peng Huang¹, Junjie Miao¹, Yuan Tian¹, Pan Ma¹, Jiayun Chen¹, Feng Ye², Han Ouyang², Jianrong Dai¹

¹Department Of Radiation Oncology, Cancer Institute & Hospital, Chinese Academy of Medical Sciences, Beijing/CHINA, ²Department Of Radiology, Cancer Institute & Hospital, Chinese Academy of Medical Sciences, Beijing/CHINA

Purpose: Nasopharyngeal carcinoma (NPC) is sensitive to Radiation therapy (RT). However, NPC patients received RT always suffered from the cognitive impairment, which happens from the early time of RT without visible cerebral necrosis [1]. It is still unclear whether and where the brain function are affected in patients with NPC right after the RT. Thus, the study aims to explore the brain functional alterations before and one day after RT in patients with NPC by using resting-state functional MRI.

Methods: Sixteen NPC patients and sixteen age, sex, height, weight, handedness and years of education matched normal controls were recruited in this study. All the patients were treated with intensity-modulated RT with a prescribed dose of 70-74Gy. Resting-state functional MRI scanning (Discovery MR750, General Electric, Milwaukee, USA) and neurocognitive tests including Montreal cognitive assessment (MoCA), Auditory verbal learning test (AVLT), Self-rating depression scale (SDS), Self-rating anxiety scale (SAS), Social function activity survey scale (FAQ) were administered individually to each patient 1 day before initiation of RT and 1 day after completion of RT. The normal controls were also required the same MRI scanning and the neurocognitive tests after they were recruited. Amplitude of low-frequency (0.01–0.8 Hz) fluctuations (ALFF) during resting-state functional studies, which is thought to reflect spontaneous neural activity [2], were calculated by DPARSF software package (<http://www.restfmri.net>) to characterize regional

cerebral function. Paired T test was used to compare the cerebral functional alterations and neurocognitive tests scores before and after intensity-modulated radiation therapy in NPC patients while independent T test was used to compare the alterations between patients and controls before intensity-modulated radiation therapy. Significance was set at $P=0.05$, corrected by AlphaSim program.

Results: Compared with the patients before and after RT, decreased ALFF were observed in right cerebrum including temporal gyrus, limbic lobe, hippocampal gyrus, fusiform gyrus, inferior frontal gyrus and cerebellum while increased ALFF in left cerebrum including occipital gyrus, middle temporal gyrus, fusiform gyrus, both sides medial and superior frontal gyrus. However, these brain regions were not observed significant changes when compared with the normal controls before RT. There was no significant results of neurocognitive tests scores.

Conclusions: Our findings firstly demonstrated that the function of cerebellum, temporal gyrus, hippocampal gyrus, occipital gyrus and frontal gyrus were altered right after the RT, suggesting the function of cerebrum is sensitive to RT which could explain the cognitive deficits in NPC patients after RT. Thus, efforts should be made to protect the cerebral function by reduce the radiation dose and irradiated volume of functional regions without compromising the coverage of target volume. There were no significant results of cognitive tests may be due to the observe time was too short after RT, long-term follow-up would be needed. Our study also proposed that functional MRI could be used as a potential method to monitor the effect of RT on cerebral function.

1. Hsiao K-Y, et al., *International Journal of Radiation Oncology* Biology* Physics*, 2010,77:722-726.

2. Cordes D, et al., *Am J Neuroradiol*, 2001, 22: 1326-33.

PS04.080 - A Study of Accuracy from Varian Portal Dosimetry for VMAT Patient Specific QA using Monte Carlo

Author(s): Mohamad F. Rhani¹, Freddy Haryanto², I G. Dirgayussa², Sitti Yani², Idam Arif², Shaun P. Baggarley¹

¹Department Of Radiation Oncology, National University Cancer Institute Singapore, Singapore/SINGAPORE, ²Department Of Physics, Institut Teknologi Bandung, Bandung/INDONESIA

Purpose: A study of VMAT portal dose acquisition based on comparison of patient specific QA of clinical VMAT plan with Varian Portal Dosimetry and Monte Carlo simulation using BEAMnrc is performed.

Methods: In our study, 29 cases of VMAT plan for patient specific QA are verified by Varian Portal Dosimetry. For this verification, treatment planning system (Eclipse) calculates the portal dose predicted image for each case and to be compared with the image produced by portal imager. To evaluate the result of verifications for every VMAT plan, gamma analysis of 95%(3%/3mm) is used as passing rate criteria. For this study, measurements are done by extending the portal imager to Source to Detector Distance of 140 cm. Monte Carlo Simulation will be performed for two cases which one has the poorest gamma analysis and the other has the best gamma analysis. For simulation, the linac head model for Varian C-series equipped with MillenniumMLC120 is implemented.

Results: From 29 VMAT cases, 27 cases have passing rate criteria range between 97.1% and 100%. Of all these good passing rate criteria is independent of treatment site. Only two cases have passing rate criteria of 92.1% and 94.4%. Interestingly, these two cases belong to the same treatment site of brain. From the verifications result, one case with the passing rate criteria of 100% will be compared with the result from the Monte Carlo simulation. The comparison of measurement and simulation will be presented in the

meeting. As well as the comparison will be done for the case that has 92.1% of passing rate criteria.

Conclusion: This study shows that the verification process in general has good passing rate criteria regardless of the treatment site, except for brain. The Monte Carlo simulation can be used for justification of the verification which has the poorest passing rate criteria.

PS04.081 - A study on improvement method of dose distribution using bolus in boron neutron capture therapy for head and neck tumors

Author(s): Yoshinori Sakurai, Hiroki Tanaka, Takushi Takata, Nozomi Fujimoto, Natsuko Kondo, Yosuke Nakagawa, Tsubasa Watanabe, Masaru Narabayashi, Yuko Kinashi, Shinichiro Masunaga, Minoru Suzuki, Koji Ono, Akira Maruhashi
Kyoto University Research Reactor Institute, Osaka/JAPAN

Purpose: In boron neutron capture therapy (BNCT) for head and neck tumors, the irradiation is extremely difficult and the irradiation time becomes often long, when the target volume is in oropharynx and/or hypopharynx. The first reason is the positional reason that it is hard to fix the oropharynx and hypopharynx parts by the ideal posture for a collimator aperture. The second reason is the geometric reason that the thermal neutrons generated near the target volume is easy to leak out from the volume. Therefore, we are studying to develop the irradiation methods that the leak-out of thermal neutron is prevented and the dose rate distribution at the target volume and its surroundings is improved. The mount of bolus on neck is studied as one of the methods. This bolus works not only as neutron moderator, but also as neutron scatterer. The effectiveness of this method is introduced, based on the data for the BNCT studies for head and neck tumors, which are carried out at Heavy Water Neutron Irradiation Facility (HWNIF) installed in Kyoto University Reactor (KUR).

Methods: A dose estimation system for BNCT, named "Simulation Environment for Radiotherapy Applications (SERA)", was used in the simulation for dose distribution. The comparison was performed between the actual dose-estimation result for without bolus and the result for using the bolus, in the BNCT studies for oropharynx and hypopharynx. The estimation was performed not only for the merits in the improvement of thermal neutron distribution, tumor dose rate etc., but also for the demerits in the increase of the mucosal and skin dose rates, etc..

Results and Discussion: For one of the BNCT studies, it was confirmed that the dose rate was increased almost at 15% near the tumor part by mounting the bolus on the neck. In the while, the mucosal dose rate was increased almost at 15% and the skin dose rate was increased almost at 50%. The reason for the increase of the mucosal dose rate in the same level for the tumor dose rate is that the tumor and the mucosa are contiguous in this study. For the increase of the skin dose rate, the increase of 50% is acceptable because the mucosal peak dose is set to the tolerant dose for the criteria in this study. It is resulted that the irradiation time is shortened by 87%.

Conclusion: The effectiveness of this method using bolus was confirmed for some of the BNCT studies for head and neck tumors which are carried out at KUR-HWNIF. It is planned to confirm for the other BNCT studies, in order to find the proper condition that the effectiveness of this method can be effectively used.

PS04.082 - Peripheral neutron dose estimation: comparison between experimental measurements and TPS estimation

Author(s): Leticia Irazola¹, Monica Ortiz-Seidel², Maria Trinitat Garcia-Hernandez³, José A. Terrón¹, Beatriz Sanchez Nieto⁴, Roberto Bedogni⁵, Francisco Sanchez-Doblado¹

¹Fisiologia Medica Y Biofisica, Facultad Medicina, University of

Seville, Sevilla/SPAIN, ²Servicio De Radiofísica, Hospital Universitario Virgen Macarena, SEVILLA/SPAIN, ³Servicio De Radioterapia Eresa, Hospital General de Valencia, Valencia/SPAIN, ⁴Instituto De Física, Pontificia Universidad Católica de Chile, Santiago/CHILE, ⁵Is-tituto Nazionale Di Fisica Nucleare, Laboratori Nazionali di Frascati, Frascati RM/ITALY

Introduction

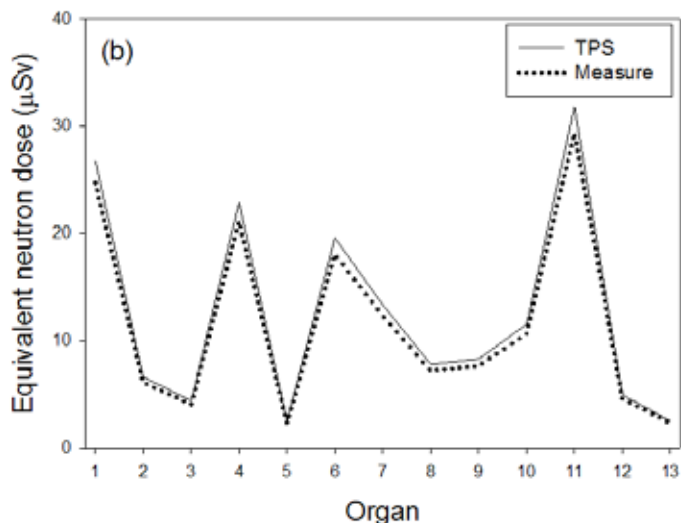
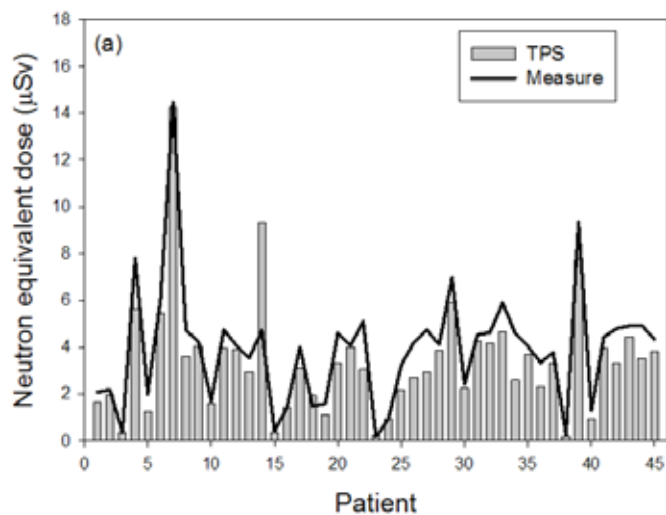
A newly TPS algorithm, implemented in Pinnacle³, has been developed for peripheral neutron dose estimation for radiotherapy patients. The script gives doses in several organs according to gender, treatment location and delivered high energy monitor units based on a previously facility characterization [1] following the procedure described in [2].

Material and Method

In order to validate these estimations, doses for a total of 119 patients were calculated with Pinnacle³ TPS script, and compared to the experimental measurements with the new Thermal Neutron Digital Detector (TNRD) [3]. The patients studied cover a wide range of pathologies for three different linacs (Siemens Primus, Siemens Oncor and Varian Truebeam) in 5 facilities from two institutions.

Results

As example, Fig.a shows peripheral neutron doses calculated by the TPS (grey bars) and measured (continuous line) for the thyroid in one of the Primus 15 MV linac, for a cohort of 45 patients. In addition, Fig.b shows organ neutron doses (1:thyroid, 2:oesophagus, 3:lung, 4:stomach, 5:liver, 6:colon, 7:bladder, 8:skin, 9:bone, 10:marrow,11:remainder,12:breast, 13:ovary) for a rectum treatment in Varian TrueBeam linac. TPS estimations are represented by the continuous line while measurements are in dashed line.



Conclusions

The implementation of the peripheral neutron dose calculation script in Pinnacle³ TPS has shown as an appropriate tool for peripheral neutron dose calculations. It is able to estimate peripheral neutron doses by terms of patient parameters and thus give an idea of peripheral neutron doses when choosing patient treatment strategy.

References

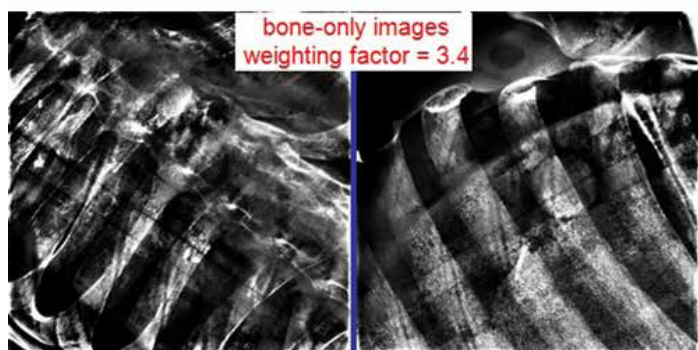
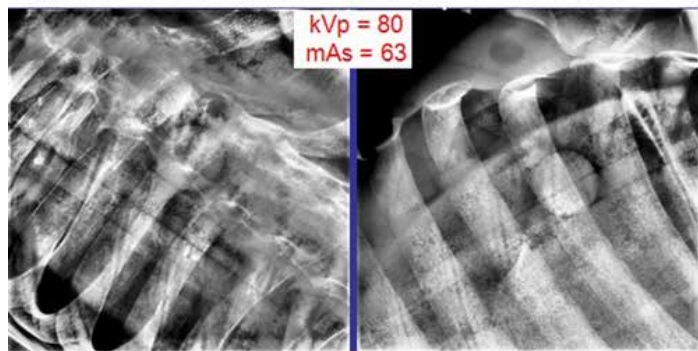
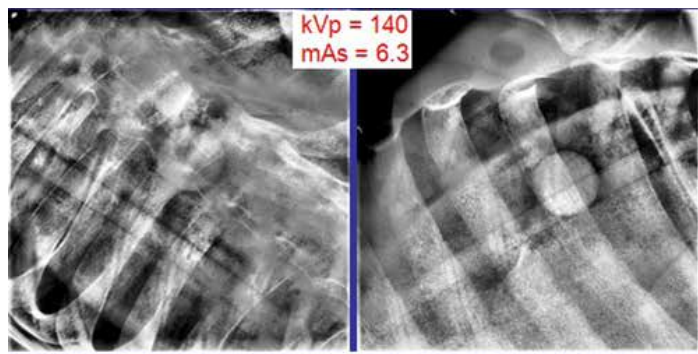
- [1] Med Phys (2015);42(1):276-281
- [2] Radiother and Oncol (2013);107:234-241
- [3] Med Phys (2014);41:112105:1-5

PS04.083 - Dual Energy X-ray Stereoscopic Image Guidance for Spine SBRT

Author(s): Mike Sattarivand, Wesley Bowman, James Robar
 Department Of Medical Physics, Cancer Care Nova Scotia, Halifax/CANADA

Image guidance is a key requirement for stereotactic body radiation therapy (SBRT) of spine to achieve a high accuracy in target positioning. Although cone beam computed tomography (CBCT) maybe used to acquire 3 dimensional volumetric imaging for target positioning, its acquisition is slow and it requires treatment interruption. Therefore, stereoscopic image guidance may be used which offers a faster image acquisition, finer resolution, and lower dose than CBCT. However, since stereoscopic imaging is based on projection imaging, soft tissue overlap on vertebral body may compromise its utility for spine SBRT, especially in large patients. The objective of this work is to investigate the feasibility of dual energy stereoscopic imaging to remove “anatomical noise” and create bone-only images for spine SBRT. An ExacTrac stereoscopic imaging system on a clinical linac was used to image an anthropomorphic Rando phantom with a 2.5 cm sphere (soft-tissue-equivalent) implanted in its lung (Figure 1). Tube voltage for low-energy and high-energy were chosen in the ranges of 40–80 kVp and 90–140 kVp respectively. A corresponding mAs was chosen in 6.3–63 range for each kVp to acquire high quality images without saturating the detectors. Weighting factors for log subtraction were chosen by trial and error. Imaging dose at isocenter from one X-ray tube was also measured for each available kVp using a calibrated dosimeter. Preliminary results showed that the best bone-only image could be obtained using a combination of 80 kVp and 140 kVp energies with a corresponding weighting factor of 3.4 (Figure 2). The corresponding dose

for 80 and 140 kVp were 8.61 and 27.07 microGy/mAs respectively. Our results demonstrate the feasibility of dual energy stereoscopic imaging to create bone-only images that could be applied to spine SBRT. An optimal dose allowance between the low-energy and high-energy images needs to be established.



PS04.084 - Comparison between our EPID-IMRT-QA tool and commercial phantom based QA tools

Author(s): Otto Sauer, Simone Fink
Department Of Radiation Oncology, University of Würzburg, Würzburg/GERMANY

Purpose: Different commercial solutions have been developed to take the increasing complexity of IMRT treatment plans into account and to provide a good relation between delivery errors of the calculated plans and the measured parameters. In our clinic we developed an IMRT quality assurance dosimetry tool based on the EPID attached to our LINACs. We compared the efficiency and accuracy of the patient specific plan QA between our EPID QA tool and two phantom-based commercial IMRT QA solutions.

Material and Methods: Elekta Synergy LINACs with 6 MV, 10 MV and 18 MV photons with an Agility MLC were used to perform the measurements. The EPID attached to these LINACs is the iView-GT™ being the standard aSi-EPID with 1024 x 1024 pixels of size 0.4 x 0.4 mm². This corresponds to a pixel size of 0.25 x 0.25 mm² in the plane of the isocenter. For the calculation of the dose distribution we used Pinnacle 9.8. Processing of the EPID measurement signals was done with in-house developed software based on MATLAB (MathWorks Inc.). For the calibration of the EPID measurement grey scale values to dose, we use the quotient of the output in water in 5cm depth to the EPID signal, free in air, for quadratic homogeneous fields. For the Gamma Analysis we used Verisoft 6.0 and compared the calculated planar dose distributions to the EPID measurements. Reference values were achieved with the ionization chamber array OCTAVIUS Detector 729 by PTW, which has 27 x 27 ionization chambers with a size of (0.5 cm)³ and a distance center-to-center of 1.0 cm. To test our procedure we also measured exemplary fields with intentionally introduced errors.

The phantom based QA tools were the ArcCheck by SunNuclear and OCTAVIUS 4D by PTW. Phantom QA data were evaluated following our standard clinical protocol.

Results: The plan evaluation of our QA tool showed good agreement with the dose distribution calculated by the planning system and the one measured with the ionization chamber array. Due to the high resolution of the pixel array, the stricter 2%/2mm gamma criterion could be used for comparison of the EPID measurement data and the calculated planar dose distributions. The 2%/2mm gamma evaluation with the reference values achieved with the OCTAVIUS Detector 729 turned out to be not meaningful due to the low resolution of the chamber array.

The outcome of the ArcCheck QA showed good accordance with those of the EPID QA with both the 3%/3mm and the 2%/2mm gamma evaluation. The analysis of the OCTAVIUS 4D, restricted to the 3%/3mm criterion also showed comparable results. All systems were able to detect the intentionally introduced errors in dependence of the magnitude of the alterations.

Conclusion: We developed an EPID QA tool suitable for efficient step-and-shoot IMRT plan QA. The comparison with the commercial systems showed good agreement. As we can use the advantage of the high spatial resolution of the EPID, our QA tool provides a benefit particularly for the analysis of highly modulated IMRT plans.

PS04.085 - Dosimetric assessment of a novel metal artifact reduction tool (iMAR)

Author(s): Esther Bär¹, Andrea Schwahofer², Stefan Kuchenbecker³, Peter Haering¹, Oliver Jäkel¹
¹Medical Physics In Radiation Oncology, German Cancer Research Center (DKFZ), Heidelberg/GERMANY, ²Vivantes Klinikum Neukölln, Berlin/GERMANY, ³Medical Physics In Radiology, German Cancer Research Center (DKFZ), Heidelberg/GERMANY

Purpose: Metal artifacts in CT images can cause relevant errors in

dose calculation. Algorithms developed to reduce these artifacts could improve these images but also introduce a bias in tissues surrounding metallic implants. The purpose of this study is to validate a pre-commercial metal artifact reduction tool for radiotherapy treatment planning.

Methods: The performance of the iterative Metal Artifact Reduction (iMAR) algorithm developed by Siemens Healthcare is evaluated on a test platform. A calibration phantom constituted of tissue-equivalent plastics is used to estimate the image bias from artifact correction. Patient CT data with metal implants (5 dental fillings, 1 bilateral hip) are reconstructed using the weighted filtered back projection (WFBP) and corrected using the iMAR algorithm. Radiotherapy treatment plans are calculated and compared on corrected and uncorrected images using the collapsed cone convolution (CCC) dose algorithm implemented in RayStation (RaySearch).

Results: Phantom scans show that iMAR reproduces HU for tissue equivalent substitutes in 3.6 cm² circular ROIs within ± 25 HU. The effect of this HU difference on megavoltage photon dose calculation is shown to be within ± 1 % dose error. Comparing patient plans from corrected and uncorrected images, dose differences of up to 5 % are discovered in PTV and OARs, depending on the treatment site.

Conclusion: The iMAR algorithm shows good performance in correcting metal artifacts in the context of radiotherapy. The technique reduces dose errors significantly while keeping calculated doses in the surrounding tissues within a clinically acceptable level in comparison to ground truth. Future work could aim at the improvement of benchmark methods for a clinical environment (e.g., the development of a specific test phantom).

PS04.086 - An Image quality and dose comparison between Varian OBI and Elekta XVI CBCT systems.

Author(s): [Amani Shaaer](#), Konrad Leszczynski, Shuying Wan, Michael Oliver
Medical Physics, Northeast cancer centre, sudbury/CANADA

Purpose: As image-guided radiotherapy (IGRT) becomes common practice in radiation treatment, its overall quality and performance, such as image quality and amount of dose delivered, need to be assessed. In this study, we investigated the image quality and dose of cone-beam computed tomography (CBCT) of two imaging systems commonly used in radiotherapy: Varian On-Board Imager (OBI) and Elekta X-ray Volumetric Imager (XVI).

Materials and Methods: Our investigation involved two units of Varian OBI and two units of Elekta XVI. For CBCT imaging quality, several quality tests were performed, including high contrast resolution, Hounsfield Unit (HU) accuracy, low contrast sensitivity, and image uniformity. All imaging tests were carried out using a Catphan 500 phantom (model: CTP 504) and current clinical imaging protocols provided with both systems. The reconstructed images were analyzed using Osirix software v.5.8.2. The CBCT dose was estimated using standard CT dose index (CTDI). CTDI was measured by using a head and a body phantom, in which a 3 cm³ ion chamber was inserted. Measurements were taken under several imaging protocols.

Results: Regarding CBCT image quality, OBI revealed better high contrast resolution and HU accuracy when using head and pelvis protocols. CBCT dose measurements demonstrated that the XVI used lower doses for both head and body protocols than OBI did, which explained the observed differences in image quality. For the standard-dose head protocol, for example, OBI (#1) delivered 5.74 mGy, while XVI (#1) used 0.93 mGy dose for the same protocol. In addition, the head protocols in both systems delivered lower doses compared to body protocols to minimize the exposure of superficial organs located at the anterior part of the head to the radiation.

This is because both systems used a half-rotation scan for head and neck protocols (200°). In head and neck protocols of the OBI units, the anterior part of the head received only one-quarter of the maximum dose measured (posterior region), while for the XVI units, the ratio was one-third.

Conclusions: The Varian OBI and Elekta XVI were evaluated by performing image quality and dose measurements for four clinical protocols: head and neck, pelvis, prostate, and thorax. Based on the results, both systems are suitable for performing image-guided radiotherapy on a regular basis.

PS04.087 - An open-source treatment planning system for research in particle therapy: Implementation and dosimetric evaluation

Author(s): Maxime B.J. Desplanques¹, An Wang², Justin Phillips³, Gueorgui Gueorguiev³, Yang-Kyun Park³, Andras Lasso⁴, Csaba Pinter⁴, David Jaffray², Gabor Fichtinger⁴, [Gregory C. Sharp](#)³, Guido Baroni¹

¹Politecnico di Milano, Milano/ITALY, ²University of Western Ontario, Toronto/ON/CANADA, ³Massachusetts General Hospital, Boston/UNITED STATES OF AMERICA, ⁴Queen's University, Kingston/ON/CANADA

The number of particle therapy centers substantially increased during recent years, yet it remains a very costly technique in terms of both facility and equipment. Commercial Treatment Planning Systems (TPS) are no exception and are often unaffordable for research groups. We introduce an open-source TPS aimed toward eliminating this economic barrier, and give global momentum to research in the radiotherapy community.

Our TPS is designed for passive scattering proton treatments, and is implemented based as part of the SlicerRt toolkit [1], which is an extension for the 3D Slicer medical image analysis and visualization tool [2]. It supports a large number of image types, including DICOM CT/MR/RT-images and the most widely supported image file formats. The interface was developed as a 3D Slicer Qt loadable module, and a pencil beam dose calculation engine was implemented in the open-source image computation software Plastimatch [3].

The dose calculation engine uses a differential approach for estimating Coulomb scattering along the beamlet pathway. Three different geometric approaches are used for pencil selection and summation. Computation results were compared with Monte Carlo simulations. The dose response of these algorithms show equivalent results to published literature in homogeneous conditions and better results for lateral scattering in heterogeneous media or air-gaps for the 10-250MeV energy range. These satisfying results allow a user to build accurate proton dosimetry of real, clinical cases like prostate or head & neck treatment plans. Regarding the calculation speed, our algorithms are approximately equivalent to commercial TPSs, and can calculate a dose volume for a multi-beams plan in few minutes.

The majority of the expected, user-friendly tools available in the commercial TPSs are also included in this open-source software: definition of a plan with multiple beams; automatic creation of a collimator fitting the beam aperture to the target shape; automatic construction of a range compensator in Lucite material; energy selection to create a spread out Bragg peak; selection of target proximal and distal limits; and margin calculations. The system also includes the possibility to visualize the Digital Reconstructed Radiograph, set a dose normalization point, or even customize the geometrical description of the beam line for a determined particle therapy center, including selection of the source and collimator positions and the source size.

We put forward our open-source TPS as a concrete solution for

research groups in the particle therapy field and confide that our efforts will contribute to the worldwide application of particle therapy. This software is continually in development and regularly improved with new tools.

[1] C. Pinter et al. "SlicerRT: Radiation therapy research toolkit for 3D Slicer". *Medical physics* 39(10): 6332-6338 (2012).

[2] S. Pieper, M. Halle, and R. Kikinis, "3D SLICER". Proceedings of the 1st IEEE International Symposium on Biomedical Imaging: From Nano to Macro (Brigham and Women's Hospital, Boston, MA) pp. 632-635. (2004).

[3] G.C. Sharp et al. "Plastimatch: An open source software suite for radiotherapy image processing", Proceedings of the XVth International Conference on the Use of Computers in Radiotherapy (ICCR) (Amsterdam, the Netherlands) (2010).

PS04.088 - GMM guided automated Level Set algorithm for PET image segmentation

Author(s): Chiara D. Soffientini¹, Elisabetta De Bernardi², Giuseppe Baselli¹, Issam El Naqa³

¹Deib, Politecnico di Milano, Milan/ITALY, ²University of Milano-Bicocca, Monza/ITALY, ³McGill University, Montreal/CANADA

AIM. Positron Emission Tomography (PET) is nowadays one of the main imaging modalities used in oncology field. The accuracy in lesions borders identification has a key role since it may affect diagnosis, treatment planning and consequently patient outcome. Ideally, segmentation algorithm should be accurate and automatic as much as possible, avoiding to obtain user dependent contours. Many efforts have been spent facing the problem in many different ways. Level Set (LS) algorithms are a well established methods for object contouring where an initial function evolves until convergence of a predefined cost function. One of the drawback of this method is the necessity to properly set the values of parameters that weight and balance internal and external forces used to shrink or dilate the estimated boundaries until convergence. The basic idea of the present work is to develop a segmentation algorithm based on LS formulation where the best values for the weighting parameters are iteratively estimated using information from a clustering algorithm based on Gaussian Mixture Model (GMM).

MATERIALS AND METHODS. The proposed algorithm (LSGMM) starts with the initialization of the LS function using the segmentation performed after two iterations of the GMM based algorithm. Then the LS function is updated as indicated by the minimization of the Mumford-Shah functional. The LS parameters iteratively updated in the proposed algorithm are the ones weighting the internal and external object homogeneity and the one weighting their balance. Every 10 iterations of LS, weighting parameters are then updated on the basis of equations formulated as Gibbs functionals, using hard or fuzzy classification performed with GMM algorithm. Basically, updating equations use information derived by a clustering method to correctly tune the LS parameters. Finally, as LS method, LSGMM performs the object boundaries identification evaluating the sign of the converged LS function. The proposed method was tested on simulated data divided into three categories: homogeneous and heterogeneous lesions, and lesions with low background contrast and/or near high uptake object that can be misinterpreted. Comparisons were performed among LSGMM, LS with manually tuned parameters, Black's and Schaefer's thresholding methods.

RESULTS. Applying LSGMM, segmentations of homogeneous and heterogeneous lesions were comparable to the ones obtained with manually tuned LS, with Dice indexes higher than 0.85 and errors in estimated volumes lower than 2% as mean value. LS parameters could increase or decrease independently in order to converge to the optimal ones. LSGMM was also able to overcome performances

of Black's and Schaefer's algorithms.

CONCLUSIONS. A completely automated LS based algorithm was presented and promising results were shown. Further evaluations will be done in order to assess robustness of the method and its applicability to multimodal data.

PS04.089 - Impact of the magnitude of MLC radiation leakage in IMRT treatment planning

Author(s): Jaziel Soto-Muñoz, Jose M. Larraga-Gutierrez
Medical Physics, Instituto Nacional de Neurología y Neurocirugía, Mexico City/MEXICO

Purpose: To assess the impact of the magnitude of the radiation leakage (RL) through the multileaf collimator (MLC) system on dose calculation for intensity modulated radiation therapy (IMRT) treatment planning. Previous works have demonstrated that the inclusion of RL on IMRT treatment planning is mandatory, in order to avoid dosimetric errors in treatment delivery up to 11% relative to the isocenter dose (Jin Sheng Li, *Med. Phys.* 2010). However, up to date there aren't studies about the impact on IMRT of different values of RL that may be originated by wrong measurements or MLC deterioration.

Material and Methods. Different values of RL (0.1, 0.5, 1.0, 1.5 and 2%) were used to simulate in the treatment planning system (TPS) wrong measurements and/or MLC deterioration of a m3-mMLC (BrainLab, Germany) with a 6 MV photon beam. The RL values were used to create TPS beam profiles, one for each RL value, in the TPS iPlan RT 4.1 (BrainLab, Germany) for dose calculation. A set of 5 IMRT patients were chosen randomly from our centre database, and a RL value of 1% was assumed to be the MLC true RL in order to set a reference beam profile. The 5 IMRT patients were re-optimized and the dose distributions were re-calculated and exported for posterior analysis by using each of the beam profiles (resulting in 4 re-optimizations per IMRT patient). After re-optimization, the monitor units (MU) were fixed and only the dose distribution was re-calculated and exported for each re-optimization by using the reference beam profile (RL=1.0%). The resulting dose distributions were compared by calculating the differences between the calculated dose distribution of the re-optimized and the referenced plans. The differences were normalized to the prescription dose that was set to 2.0 Gy/fraction. On the other hand, the dose volume histograms for each re-optimization were exported and compared by using the following metrics: dose maximum, coverage, homogeneity index and conformity index.

Results. The comparison of the dose distribution showed differences up to 4% using the profile with RL=2%. This difference may reflect an overall absolute dose difference of 2.4 Gy for an standard 30 fraction treatment. The spatial location of this differences were found in the normal tissue. The DVH analysis showed differences from 7 to 20% in the maximum dose to organs at risk, differences up to 2% in coverage, 25% in conformity index, and 2% in homogeneity index.

Conclusions. The present results suggest that an accurate measurement and/or frequently verification of TL factor is needed, since small differences (up to +/- 1%) in the RL value produce a difference up to 4% for the TPS and the MLC system used in this work. The above result may compromise the allowed uncertainty in radiation therapy of 5%.

PS04.090 - Modelling multi-leaf collimator defocusing and focal spot partial shielding for TomoTherapy and Elekta accelerators using Monte Carlo methods

Author(s): Jason Belec, Ryan Studinski

Medical Physics, Ottawa Hospital Cancer Center, Ottawa/ON/CANADA

Purpose: TomoTherapy and Elekta SynergyS/Agility accelerators include multi-leaf collimator (MLC) with defocused leaf sides with respect to the beam focal spot to minimize interleaf radiation leakage. We used Monte Carlo simulations and measurements to model MLC defocusing and quantify the impact on the dose distributions.

Materials and Methods: Monte Carlo simulations were performed with a modified version of the BEAMnrc/DOSXYZnrc codes. Measurements were done with films (EBT2), diodes (SFD) and ionization chambers (A1SL). The TomoTherapy MLC model was focused at a point located 2 mm above the target. The Elekta MLC model was rotated by 0.5 degrees around the crossplane axis and translated by 2.2 mm. Fine tuning of parameters were performed using different types of measurements such as transmission, tongue-groove and small off-axis fields.

Results: Figure 1 and Figure 2 show that tomotherapy simulations are modelling well (2%/1mm) small off-axis field and tongue-groove measurements. Figure 3 shows a similar example of tongue-groove measurements for the Elekta SynergyS accelerator.

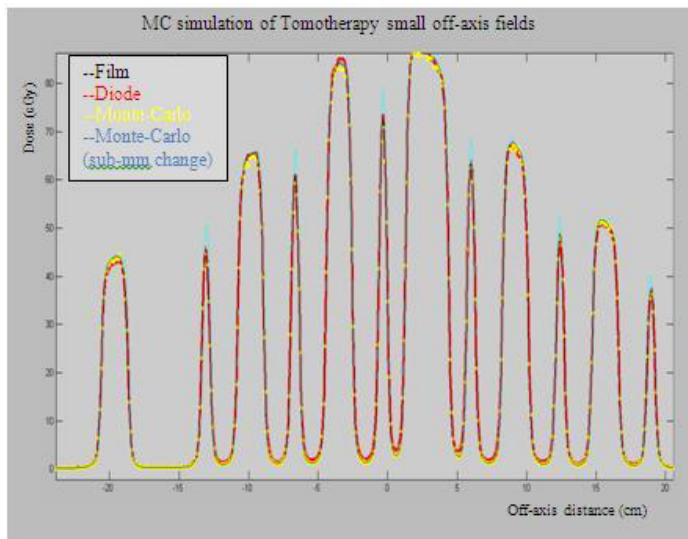


Figure 1 MC simulation of a modulated Tomotherapy field. The couch and the gantry are static and the field contains openings of different sizes (1 leaf, 2 leaves, 3 leaves) at various off-centered positions. Film measurements (normalized with ionization chamber reading in the largest open section of the field) are shown in black, SFD diode measurements are shown in red and Monte Carlo simulations are shown in yellow. The blue line is included to illustrate the impact on the Monte Carlo simulation of sub-mm changes in the MLC geometry parameters.

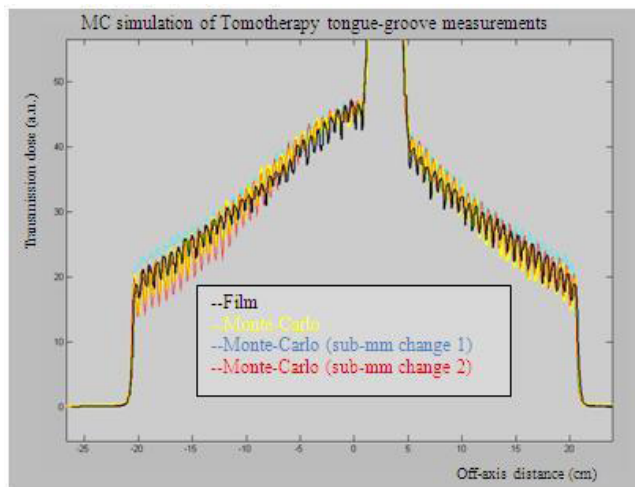


Figure 2 The Tomotherapy tongue & groove dose is obtained by summing the dose measured or calculated for two opposing fields having respectively odd and even leaves opened. Film measurements (normalized with ionization chamber reading in the small open section of the field) are shown in black and Monte Carlo simulations are shown in yellow. The blue line and the red line are included to illustrate the impact on the Monte Carlo simulation of sub-mm changes in the MLC geometry parameters.

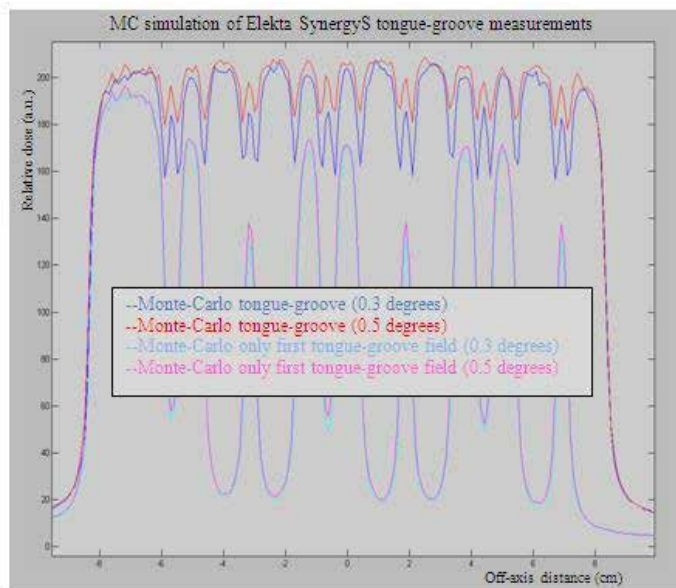


Figure 3 Monte Carlo simulation of tongue and groove dose for the Elekta SynergyS treatment unit. The tongue & groove dose is obtained by summing the dose calculated for a given set of open leaves and the dose calculated with the opposite field (leaves that were closed are opened and vice versa). The blue line is for an MLC rotation of 0.5 degree and the red line is for an MLC rotation of 0.3 degrees. Only one of the added profiles is shown in light blue and pink (one for each MLC rotation).

Conclusion: Modeling accurately MLC defocusing is important because it can have a significant impact on interleaf leakage (> 1%), field size (>0.5 mm) and off-axis small field output factors (>5%) due to partial focal spot shielding.

PS04.091 - Can Image-Guided Intensity Modulated Brachytherapy delivery be better than IMRT and classical brachytherapy methods for cervical cancer: A Dosimetric analysis

Author(s): Vellaiyan Subramani, D.N. Sharma, Sharma Seema, G.K. Rath, Pathy Sushmita, Chander Subhash

Radiotherapy, All India Institute of Medical Sciences(AIIMS), New Delhi/INDIA

Objective: To evaluate the dosimetric superiority of intensity modulated brachytherapy(IMBT) based on inverse planning simulated annealing optimization method with external beam intensity modulated

radiotherapy optimization and brachytherapy classical optimization methods in patients of cervical carcinoma.

Materials and Methods: Ten patient of cervical cancer who have already undergone interstitial HDR brachytherapy with MUPIT template, were selected for this study. The target volume was drawn and the target volume was in the range of 285.49 cm³ to 83.49 cm³. The planning was performed in PLATO-3D-planning system for HDR Ir-192 interstitial brachytherapy treatment. The actual treatment was carried out according to the catheter based plan using graphical optimization and considered as “conventional brachy plan” for comparison. The target based plans were made for dose point optimization(DPO), geometric optimization(GO), Inverse planning simulated annealing (IPSA) optimization techniques. The same target and OARs were transferred to Eclipse 3D planning system for external beam intensity modulated radiotherapy (IMRT) planning. The prescription dose was 10Gy to the target. All plans were evaluated using following dosimetric indices: volume receiving 90%(V₉₀), 95%(V₉₅), 100%(V₁₀₀), 150%(V₁₅₀) and 200%(V₂₀₀) of prescription dose and coverage index(CI), conformity index (COIN), dose non-uniformity ratio (DNR), homogeneity index (HI) and external volume index (EI) for target. For OARs, dose received by volume of 1cm³ (D_{1cc}), 2cm³ (D_{2cc}), 5cm³ (D_{5cc}) and also volume received by 50% and 75% of prescription dose (V₅₀) and (V₇₅) were evaluated for both bladder and rectum. The statistical analysis was done using paired t-test and a p-value <0.05 was considered significant.

Results: Percentage difference was calculated with respect to conventional brachy plan optimization. The maximum difference in V₉₅ was 16.8%, 18.1%, and 33.6% in DPO, GO, and IPSA respectively and it was statistically significant between conventional versus IPSA (p<0.001). Maximum difference in COIN was 58.1% for IPSA (p<0.0001) with conventional plan. The differences in DNR, EI, HI between classical optimizations and inverse optimizations were significant (p<0.0001). Maximum differences for IPSA in D_{5cc} was 30.7% and 33.9% and in V₇₅ the difference of 47.8% and 51.8% for both rectum and bladder respectively (p<0.001). In comparison between IMBT versus IMRT, the percentage difference was calculated with respect to brachy plan. The maximum difference in V₉₅ between IMBT and IMRT plans was 20.1% and it was statistically significant (p<0.001) with IMBT. The similar difference in CIION was 3.8% and it was not significant. In OAR dose comparison, the maximum differences between IMBT and IMRT in V₅₀ and V₇₅ were not statistically significant for both bladder and rectum

Conclusion: The IPSA resulted in improved dose conformity and homogeneity and reduced dose to OAR compared to classical brachytherapy optimization techniques. It has also been observed that the conventional brachy plan resulted in improved target coverage compared to IMRT technique. But, the target dose conformity was greatly improved with IMRT. As for OAR dose, IMRT technique resulted in reduced dose as compared to conventional brachy plan. The differences between IMBT and IMRT, in terms of target dose conformity and homogeneity and dose to OAR were not statically significant.

PS04.092 - Analysis on Volumetric and Dosimetric accuracy of Maximum-Intensity Projections based 4DCT for stereotactic body Radiotherapy

Author(s): Vellaiyan Subramani, Singh Megha, Sharma Seema, Chander Subhash
Radiotherapy, All India Institute of Medical Sciences(AIIMS), New Delhi/INDIA

Purpose: To compare and evaluate volumetric and dosimetric accuracy of 4DCT for stereotactic body radiotherapy between free breathing and maximum-intensity projection (MIP) imaging.

Method and Materials: Three lung cancer patients who had under-

gone the treatment of stereotactic body radiotherapy and QUASAR respiratory motion phantom were used in this study. The Philips 85cm Big-bore brilliance 16-slice CT scanner with bellow-belt system was used to generate the 4DCT data sets. The planning CT was done in free breathing (FB) conditions for treatment verification purpose. The patient 4DCT was obtained and its amplitude of motion parameters was used to acquire 4DCT data of moving phantom. Each patient had 13 different 4DCT sets. All these images were imported into the 3D-RTP system. Treatment planning was made using ADAC Pinnacle 8.0 system for Synergy-S linear accelerator for both phantom and patients for conformal stereotactic body radiotherapy. The treatment planning was made such as 0%-plan, 10%-plan, 20%-plan 30%-plan 40%-plan 50%-plan 60%-plan 70%-plan 80%-plan, and 90%-plan, AvgiP-plan, MIP-plan and FB-plan for both phantom and patients for comparison.

Results: In the phantom study, the percent of volume differences were found to be 55%, 35%, 74% between FB vs MIP for GTV, OAR-1 and OAR-2 respectively. In the patient study, the percent of volume differences were found to be 38% for GTV and 74%, for the spinal cord between FB vs MIP, respectively. All dosimetric variations between FB vs Avg-iP CT based plans were found to be 10-19.2% for target and OAR for both phantom and patients studies.

Conclusion: The volumetric and dosimetric variations between free-breathing and MIP images for both phantom and patient targets and organs-at-risk were significant. The free-breathing CT was underestimated the volumes compared to MIP images. The effect of motion becomes important for accurate dose planning in stereotactic body radiotherapy.

PS04.093 - 2D/3D registration for compensation of patient positioning error in Korea Heavy Ion Medical Accelerator Center **Author(s):** Min Joo Kim¹, Woong Cho², Won Gyun Jung³, Tae-Suk Suh¹

¹Dept. of Biomedical Engineering Research Institute of Biomedical Engineering The Catholic Univ. of Korea, Seoul/KOREA, ²Department Of Radiation Oncology, Seoul National University Hospital, Seoul/KOREA, ³Division Of Korea Heavy-ion Medical Accelerator, Korea Institute of Radiological and Medical Science, Seoul/KOREA

This research has proposed to develop the validation tool for compensation of patient positioning error using 2D/3D and 3D/3D image registration. For 2D/3D registration, digitally reconstructed radiography (DRR) and three-dimensional computed tomography (3D CT) image was applied. The ray casting algorithm is the most straightforward method to generate DRR. We adopted the traditional ray casting method which finds intersections of a ray with all objects, voxels of the 3D CT volume in the scene. Similarity between extracted DRR and orthogonal image was measured by using normalized mutual information method. Two orthogonal image was acquired from Cyber-knife system from anterior-posterior (AP) view and right lateral (RL) view. 3D CT and two orthogonal image of an anthropomorphic phantom and head and neck cancer patient were applied in this study. For 3D/3D registration, planning CT and in-room CT image was applied. After registration, translation and rotation factor was calculated to set 6 dimensionally movable couch. Registration accuracy with average errors of 2.12 mm ± 0.50 mm for transformation and 1.23° ± 0.40° for rotation using an anthropomorphic Alderson-Rando phantom has been acquired in 2D/3D registration. Also, registration accuracy with average errors of 0.90 mm ± 0.30 mm for transformation and 1.00° ± 0.2° for rotation using CT image sets has been acquired. We demonstrated that this validation tool could compensate the patient positioning error. Also, this research could be fundamental research step to compensate patient positioning error in first Korea heavy ion medical accelerator treatment center.

PS04.094 - Cardiac movement in deep inspiration breath-hold for left-breast cancer radiotherapy

Author(s): Seu-Ran Lee¹, Min Joo Kim¹, Jae-Hong Jung², Tae-Suk Suh¹

¹Dept. of Biomedical Engineering Research Institute of Biomedical Engineering The Catholic Univ. of Korea, Seoul/KOREA, ²Department Of Radiation Oncology, Soonchunhyang University Hospital, Bucheon/KOREA

Most of breast cancer patient has suffered from unnecessary radiation exposure to heart, lung. Low radiation dose to the heart could lead to the worsening of pre-existing cardiovascular lesions caused by radiation. The objective of this study was to determine cardiac displacement by comparing the CT data and cardiac radiation exposure levels during Deep Inspiration Breath Hold (DIBH) and free breathing (FB). Treatment planning was performed on the computed tomography (CT) datasets of 10 patients who had received lumpectomy treatments. Heart, lung and both breasts were outlined. The prescribed dose was 50 Gy divided into 28 fractions. Displacement of heart was measured by calculating the distance between center of heart and left breast. Radiation dose to heart, minimum, maximum and mean dose to heart were calculated. Mann-Whitney U test was used for the statistical analysis of each evaluation index, and significance was set at an adjusted value of ≤ 0.05 . The DIBH technique could help to reduce the risk of radiation dose-induced cardiac toxicity because the heart moved as far as 8.98 mm from the left breast with this technique; additionally, the cardiac motion in the LR direction varied between the DIBH CT and FB CT datasets (maximum, 7.9 mm), and the DIBH technique was found to reduce the delivered dose to the heart by a maximum of 3670 cGy, compared with FB. The DIBH technique could be used in an actual treatment room for a few minutes and could effectively reduce the cardiac dose.

PS04.095 - Dosimetric evaluation according to patient set-up errors using biophysical indices in whole breast irradiation

Author(s): Seu-Ran Lee¹, Min Joo Kim¹, So-Hyun Park², Ji-Yeon Park³, Min-Young Lee¹, Tae-Suk Suh¹

¹Biomedical Engineering, The Catholic University of Korea, Seoul/KOREA, ²Department Of Radiation Oncology, Uijeongbu St. Mary's Hospital, College of Medicine, The Catholic University of Korea, Uijeongbu-si, Gyeonggi-do, Seoul/KOREA, ³Department Of Pediatrics And Molecular Imaging Program At Stanford, Stanford University, Stanford/UNITED STATES OF AMERICA

Purpose: The dose-related effects of patient setup errors on biophysical indices were evaluated for conventional wedge (CW) and field-in-field (FIF) whole breast irradiation techniques.

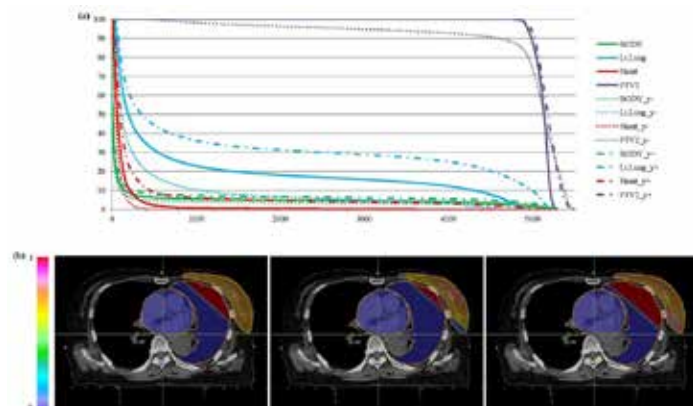
Methods: The treatment plans for 10 patients receiving whole left breast irradiation were retrospectively selected. Radiobiological and physical effects caused by dose variations were evaluated by shifting the isocenters and gantry angles of the treatment plans. Dose-volume histograms of the planning target volume (PTV), heart, and lungs were generated, and conformity index (CI), homogeneity index (HI), tumor control probability (TCP), and normal tissue complication probability (NTCP) were determined.

Results: For "isocenter shift plan" with posterior direction, the D_{95} of the PTV decreased by approximately 15% and the TCP of the PTV decreased by approximately 50% for the FIF technique and by 40% for the CW; however, the NTCPs of the lungs and heart increased by about 13% and 1%, respectively, for both techniques. Increasing the gantry angle decreased the TCPs of the PTV by 24.4% (CW) and by 34% (FIF). The NTCPs for the two techniques differed by only 3%. In case of CW, the CIs and HIs were much higher than that of the FIF in all cases. It had a significant difference between two techniques ($p < 0.01$). According to our results, however, the FIF had more

sensitive response by set up errors rather than CW in bio-physical aspects.

Conclusions: The radiobiological-based analysis can detect significant dosimetric errors then, can provide a practical patient quality assurance method to guide the radiobiological and physical effects.

Figure 1. The physical and radiobiological results of isocenter shifts for a breast cancer patient (a) Dose volume histogram (DVH), (b) Tumor control probability (TCP) and normal tissue complication probability (NTCP) mapping of computed tomography (CT) images of the principal structures. The field-in-field technique was used. The origin, negative y direction, and positive y direction are shown in order.



PS04.096 - Comparison of proton boron fusion therapy with boron neutron capture therapy

Author(s): Joo-Young Jung, Do-Kun Yoon, Han-Back Shin, Moo-Sub Kim, Tae-Suk Suh

Biomedical Engineering, The catholic university of korea, Seoul/KOREA

Proton boron fusion therapy (PBFT) is based on the treatment using characteristic of alpha particle. Because the PBFT is similar to the boron neutron capture therapy (BNCT) technique, the verification of feasibility of PBFT can be possible by the comparison of some performances of the BNCT. The verification and analysis were progressed by the Monte Carlo simulation code. Basically, the virtual water phantom including boron uptake region (tumor region) was simulated for the verification. The proton beam passed through the water phantom. The alpha particles were generated from reaction point between proton and boron particle. The variation of the alpha particle was observed from the percent depth dose (PDD) of proton beam. Also, the dramatic effectiveness of alpha particle by the PBFT was confirmed by the comparison. The utility of PBFT was verified using the simulation. It has sufficient worth of usage of radiation therapy.

PS04.097 - Verification for prompt gamma ray imaging during proton boron fusion therapy: A Monte Carlo study

Author(s): Han-Back Shin, Joo-Young Jung, Tae-Suk Suh, Do-Kun Yoon, Moo-Sub Kim

Biomedical Engineering Research Institute Of Biomedical Engineering, The Catholic University of Korea College of Medicine, korea/KOREA

Purpose: The purpose of this study is to verify the three dimensional single photon emission computed tomography (SPECT) image using prompt gamma ray originated from proton boron fusion therapy (PBFT).

Methods: The imaging system during PBFT was simulated to acquire the reconstructed image of prompt gamma ray by using Monte Carlo simulation (MCNPX). We acquired the percentage depth dose (PDD) of the proton in the water phantom, energy spectrum of the prompt gamma ray and tomographic image. In order to verify the reconstructed image, the image profile and receiver operation characteristic (ROC) curve were analyzed.

Results: The PDD in the BUR shows higher efficiency than conventional proton therapy on the tumor region. The area under curve (AUC) of ROC values were acquired from results.

Conclusion: We confirmed that the prompt gamma ray image was successfully deducted, and results of quantitative image analysis show good agreement with the original pattern of the BUR.

PS04.098 - Feasibility study of flattening filter free beam for stereotactic ablative radiotherapy of localized prostate cancer patients

Author(s): Jin-Beom Chung¹, Jae-Sung Kim¹, Jeong-Woo Lee², Sang-Won Kang³, Tae-Suk Suh³
¹Radiation Oncology, Seoul National University Bundang Hospital, Seongnam/KOREA, ²Department Of Radiation Oncology, Konkuk University Medical Center, Seoul/KOREA, ³Biomedical Engineering, The Catholic University of Korea, Seoul/KOREA

The study was to evaluate the feasibility of flattening filter free (FFF) beam in stereotactic ablative body radiotherapy (SABR) planning for treatment of clinically localized prostate cancer using an endorectal balloon. Fifteen patients were enrolled for this study. Prostate SABR plans using volumetric modulated arc therapy (VMAT) with 2 full arcs were optimized in the Eclipse treatment planning system (TPS) using TrueBeam linear accelerator with high-definition multileaf collimator. All plans were prescribed with 42.7 Gy in 7 fractions of 6.1 Gy each. For each case, four SABR plans were computed with two FF beams and two FFF beams of 6 MV and 10 MV. All dose distributions were calculated with Acuros XB (AXB, version 11). For all plans, the cumulative dose-volume histograms (DVH) for the planning target volume (PTV) and organs at risk (OARs) were analyzed. Technical parameters, such as total Monitor units (MUs) and treatment delivery time, were also recorded and accessed. A pretreatment quality assurance (QA) using I'matrixx system and cubic phantom were performed to verify treatment delivery and the Gamma analysis was used to quantify the agreement between calculations and measurements. Differences in DVH for the PTV and OARs between plans with FFF and FF beams were statistically insignificant while remarkable reduced for treatment delivery time. All pretreatment plans were verified acceptable agreement. This study confirmed that prostate SABR with FFF beam provide the treatment efficiency relative to those with FF beam, and the strategy is associated with high dose conformity to prostate and decreased intra-fraction movements because of the shorter treatment delivery time. Future studies are necessary to assess clinical outcome and toxicity.

PS04.099 - The evaluation of radiobiological and physical impacts based on multi-modality images using in-house software

Author(s): Seu-Ran Lee¹, Ji-Yeon Park², Min Joo Kim¹, Tae-Suk Suh¹
¹Biomedical Engineering, The Catholic University of Korea, Seoul/KOREA, ²Department Of Pediatrics And Molecular Imaging Program At Stanford, Stanford University, Stanford/UNITED STATES OF AMERICA

Purpose: To develop an enhanced treatment plan evaluation tool based on multi modality imaging which incorporates physiological and radiobiological parameters

Methods: A software system was developed using MATLAB

v.7.10.0499 (The Mathworks, Inc., Natick, MA). The plan evaluation tool was enabled for users to provide physiological and radiobiological plan comparison and evaluation based on multi modality imaging. It incorporated to visualize 3D images after importing of various images such as computed tomography (CT), magnetic resonance image (MRI), and positron emitted tomography (PET). Dicom-RT files (dose, structure) exported from radiation treatment planning system also represented the input to the software. The differences of planning target volume (PTV) and organs at risk (OAR) contours and volumes depending on images were displayed with respect to the isocenter using the 3D coordinates of structure files. Further, the dose difference and gamma value (for reference Daniel Low's study) also were suggested in which cross section using this program. Finally, it can represent dose volume histogram (DVH) and calculate the normal tissue complication possibility (NTCP) and tumor control possibility (TCP) based on the equivalent uniform dose (EUD) referred to Niemierko's study. Three cases of treatment sites like head and neck, brain and lung were selected to verify the functions provided by this software.

Results: The results of plan evaluation can be compared more intuitively and easily depending on plan based images for using this program. To test the program this study showed the results of three cases that there were the improvement of planning using multi modality images rather than only CT images.

Conclusions: The application of plan evaluation can help the user choose more biologically optimal treatment plans and potentially predict treatment outcome more accurately.

Figure 1. CT and MR images and 3D contouring of brain case

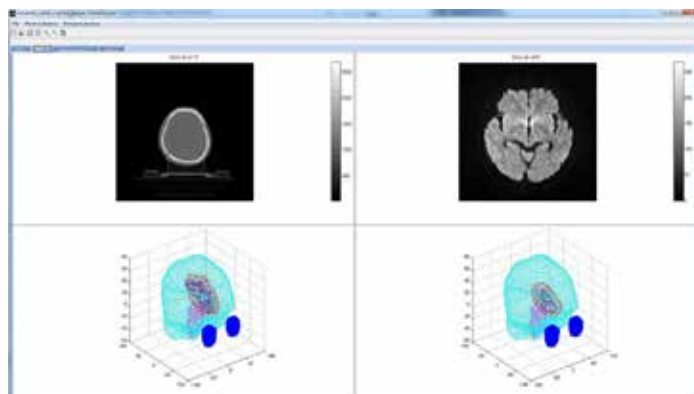
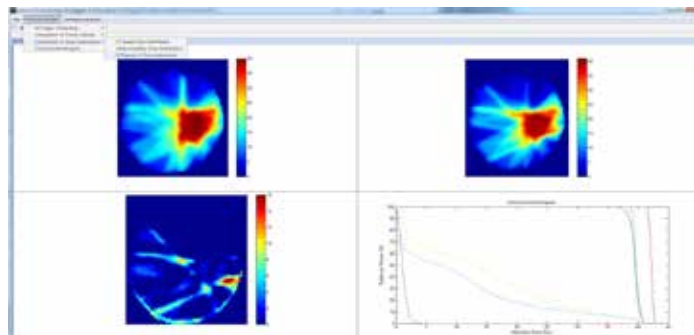


Figure 2. Analysis of dose distribution and DVH



PS04.100 - Comparison of Conventional 3D Static Planning and 4D Planning using Dose Warping Technique for Liver SBRT**Author(s):** Seong-Hee Kang¹, Siyong Kim², Tae Ho Kim¹, Dong-Su Kim¹, Min-Seok Cho¹, Kyeong-Hyeon Kim¹, Tae-Suk Suh¹¹Department Of Biomedical Engineering, Research Institute Of Biomedical Engineering, College Of Medicine, The Catholic Univ. of Korea, seoul/KOREA, ²Radiation Oncology, College Of Medicine, Virginia Commonwealth University, Richmond/UNITED STATES OF AMERICA

Currently, SBRT has been widely used to deliver highly conformal dose to target while sparing normal tissue. So, SBRT need accurate target delineation, dose calculation and motion management techniques such as breath-hold or abdominal compressor. In spite of the benefits about these techniques, there are still deformation and movement which could lead to reduce the probability for tumor control, imprecise prediction of normal tissue complication. This study aims to evaluate the dosimetric difference between four-dimensional planning using dose warping technique (4D dose) and conventional 3D static planning (3D dose) in liver stereotactic body radiotherapy (SBRT). Five patients who had previously treated liver SBRT were included in this study. The average prescription dose and the fraction size was 40 Gy and 8 Gy. Four-dimensional computed tomography (4DCT) images with 10 phases for all patients were acquired on multi-slice CT scanner (Siemens, Somatom definition). Treatment planning and delineation was done on 100% exhalation phase image. Target volume was generated according to the clinical protocol. The internal target volume (ITV) was defined as the sum of GTV at end exhalation and end inhalation phases, and a PTV was defined by adding 5mm margin to ITV. 3D dose calculation was performed using end-exhalation phase as a reference image. And then, the same planning information were copied to the other phases. 4D dose was accumulated using intensity-based deformable image registration (DIR) algorithm (Horn and Schunck optical flow) in DIRART. The target and normal organs dose were evaluated with the 4D dose and compared with those from 3D dose. The dose difference between 3D dose and 4D dose were analyzed from dose-volume histogram (DVH) and Index of achievement (IOA) which assesses how close the planned dose distribution is to be the planned one. The average difference of Dmean, Dmax, Dmin, EUD, and IOA was 0.6 %, 0.9 %, 1.6 %, 2.1 %, and 1.1 %. These results illustrate that there is no significant difference in PTV. The average difference of Dmean, Dmax, EUD, and BED was decrease by 3, 1, 5, and 4% in normal liver. however, in duodenum, it was decrease 16, 19, 16, and 21%, respectively. In case 2, we could find significant difference in duodenum which located close to PTV. Although the 3D dose calculation considered the moving target coverage, significant differences of various dosimetric parameters between 4D and 3D dose were observed in normal organs. In contrast, there was no significant difference for PTV. 4D dose which can consider dosimetric effect of respiratory motion has a possibility to predict the more accurate delivered dose to target and normal organs and improve treatment accuracy.

PS04.101 - Monte Carlo Design and Simulation of a Grid-type Multi-layer Pixel Collimator for Radiotherapy: Feasibility Study**Author(s):** Do-Kun Yoon, Joo-Young Jung, Han-Back Shin, Moo-Sub Kim, Tae-Suk Suh

College Of Medicine, Department Of Biomedical Engineering, The Catholic University of Korea, Seoul/KOREA

Purpose: In order to confirm the possibility of field application of a different type collimator with a multi-leaf collimator (MLC), we constructed a grid-type multi-layer pixel collimator (GTPC) by using a Monte Carlo n-particle simulation (MCNPX).

Methods: In this research, a number of factors related to the performance of the GTPC were evaluated using simulated output

data of a basic MLC model. A layer was comprised of a 1024-pixel collimator (5.0 × 5.0 mm²) which could operate individually as a grid-type collimator (32 × 32). A 30-layer collimator was constructed for a specific portal form to pass radiation through the opening and closing of each pixel cover. The radiation attenuation level and the leakage were compared between the GTPC modality simulation and MLC modeling (tungsten, 17.50 g/cm³, 5.0 × 70.0 × 160.0 mm³) currently used for a radiation field. Comparisons of the portal imaging, the lateral dose profile from a virtual water phantom, the dependence of the performance on the increase in the number of layers, the radiation intensity modulation verification, and the geometric error between the GTPC and the MLC were done using the MCNPX simulation data.

Results: From the simulation data, the intensity modulation of the GTPC showed a faster response than the MLC's (29.6%). In addition, the agreement between the doses that should be delivered to the target region was measured as 97.0%, and the GTPC system had an error below 0.01%, which is identical to that of MLC.

Conclusions: A Monte Carlo simulation of the GTPC could be useful for verification of application possibilities. Because the line artifact is caused by the grid frame and the folded cover, a lineal dose transfer type is chosen for the operation of this system. However, the result of GTPC's performance showed that the methods of effective intensity modulation and the specific geometric beam shaping differed with the MLC modality.

PS04.102 - Feasibility study of patient alignment method using tactile array sensors**Author(s):** Tae Ho Kim¹, Seong-Hee Kang¹, Dong-Su Kim¹, Min-Seok Cho¹, Kyeong-Hyeon Kim¹, Siyong Kim², Tae-Suk Suh¹¹Biomedical Engineering, Research Institute Of Biomedical Engineering, The Catholic University of Korea College of Medicine, Seoul/KOREA, ²Radiation Oncology, College Of Medicine, Virginia Commonwealth University, Richmond/VA/UNITED STATES OF AMERICA

Ideal alignment method based on the external anatomical surface of the patient could consider an entire region of interest. However, optical camera-based systems cannot blindly monitor such areas, like the patient's back position, for example. Furthermore, it is impossible to collect enough information to correct the associated deformation error. The study aim is to propose a new patient alignment method using the tactile array sensors that can measure the distributed pressure profiles along the contacting surface. The TactArray system includes one sensor, a signal conditioning device (USB drive/interface electronics, power supply, and cables), and a pc. The tactile array sensor was placed between the patient's back and the treatment couch, and the deformation at different locations on the patient's back was evaluated. Three healthy male volunteers were enrolled in this study and pressure profile distributions (PPD) were obtained with and without immobilization. After the initial pretreatment setup using the laser alignment system, the PPD of the patient's back was acquired. The results were obtained at four different times and included a reference PPD dataset. The contact area and the center-of-pressure value were also acquired based on the PPD data for a more elaborate quantitative data analysis. To evaluate the clinical feasibility of the proposed alignment method for reducing the deformation error, we implemented a real-time self-correction procedure. Despite the initial alignment, we confirmed that PPD variation existed in both cases of the volunteer studies (with and without the use of the immobilization tool). Additionally, we confirmed that the contact area and center-of-pressure varied in both cases, and this variation was observed in all three volunteers. Based on the proposed alignment method and the real-time self-correction procedure, the deformation error was significantly reduced. Through the proposed alignment method, it is possible to account for the

limitation of the camera-based system and to improve the accuracy of the external surface-based patient setup.

PS04.103 - Analysis of motion-induced dose errors according to the tumor motion in helical tomotherapy

Author(s): Min-Seok Cho, Tae Ho Kim, Seong-Hee Kang, Tae-Suk Suh, Dong-Su Kim, Kyeong-Hyeon Kim
Department Of Biomedical Engineering, And Research Institute Of Biomedical Engineering, The Catholic University of Korea, Seoul/KOREA

Motion-induced dose errors caused by tumor motion, couch motion, and gantry rotation can be observed in helical tomotherapy. The purpose of this work is to analyze motion-induced dose errors according to the change of the tumor motion amplitude, period, baseline drift and phase shift. Gafchromatic EBT2TM film (Ashland Inc., Covington KY) was used to acquire the static dose to make a total dose distribution. Slightly irregular tumor motion was simulated by 10% variations in the tumor motion parameters of amplitude, period, and baseline. Large irregular tumor motion was simulated by 40% variations. In addition, in order to account for the effects of phase shift on the total dose distribution, the initial phase of a tumor motion when the beam delivery started was divided into end-inspiration, mid-expiration, end-expiration, and mid-inspiration. The total dose distribution was determined by integrating the static dose on the different part of tumor due to tumor motion and couch motion. A position versus time curve was used to analyze the cause of motion-induced dose error. The larger variation of tumor motion parameters, the larger the motion-induced dose error that was generated. The larger variation of tumor motion parameters, the larger difference of total dose distributions according to the initial phase of a tumor motion was observed. Additionally, larger difference of total dose distribution was observed in the baseline drift case than tumor motion amplitude case and period case. These motion-induced dose errors can be reduced by using abdominal compression and respiratory training. This study could help to understand the impacts of tumor motion parameters and the initial phase of a tumor motion on the total dose distribution.

PS04.104 - Drift correction techniques in the tracking of lung tumor motion

Author(s): Peng T. Teo¹, Kaiming Guo¹, Nadia Alayoubi¹, Katherine Kehler¹, Stephen Pistorius²
¹Physics And Astronomy, University of Manitoba, Winnipeg/CANADA, ²Medical Physics, CancerCare Manitoba, Winnipeg/CANADA

This work compares three methods of tracking lung tumor motion using an optical flow algorithm to analyze portal images. An earlier approach used sequential image pairs (CU) to track the motion. Errors in the position of the tumor were found to accumulate when patient traces were used and two new approaches were introduced. The first method re-calibrates the position of the tumor at the end-of-exhale (EoE) of each breathing cycle. This was done by computing the position directly between the new image and the previous reference image. The new image at the EoE is then assigned as the new reference frame, a process called reference shifting (RFSF). Between two EoE, sequential tracking was employed. The second approach derives the position of the tumor in each frame by applying the optical flow computation directly between each image and a reference image. However, since tracking is limited to a finite range (i.e. threshold), new reference images were required when the tumor exceeds a set distance from the reference position, a process called threshold shifting (THSF). Direct comparison of the position in subsequent images was made with respect to the new reference image. A 3D tumor prototype was fabricated using 3D printing techniques and seven patient traces were evaluated. Average position errors of

-0.01 ± 0.65 mm, -0.10 ± 0.42 mm and -0.14 ± 0.25 were obtained for the CU, RFSF and THSF methods respectively.

PS04.105 - Application and Parametric Studies of a Sliding Window Neural Network for Respiratory Motion Predictions of Lung Cancer Patients

Author(s): Peng T. Teo¹, Neil Bruce², Stephen Pistorius¹
¹Physics And Astronomy, University of Manitoba, Winnipeg/CANADA, ²Computer Science, University of Manitoba, Winnipeg/MB/CANADA

In real-time adaptive image-guided radiotherapy (IGRT), the beam delivery position is changed to follow the tumor motion. Most systems cannot respond instantaneously, and compensation for system lag is required. Typically, future tumor positions are predicted based on the respiratory motion tracked from an external surrogate. In the current work, a sliding window of time series data taken from the respiratory cycle is input into a neural network to predict a future position. The finite past history of the respiratory position is used to train the model. A nonlinear autoregressive neural network with exogenous inputs was used to simultaneously predict future positions. Patient data from the Respiratory Trace Generator (RTG) [1] was used for the training, validation and testing of the model.

Parametric studies involving the number of input nodes (length of sliding window), number of hidden nodes and prediction horizon were performed. Tradeoffs between under-learning, training rate and over-learning were identified. While training error decreases as the number of hidden nodes increases, the validation error increases beyond 20 nodes. Large errors occur during transitions between inhale and exhale as well as when the prediction horizon increases.

PS04.106 - VMAT delivery through couch tops: an illustration of loss of dose coverage for prostate plans

Author(s): Daria Comsa¹, Monique Van Prooijen², Mohammad K. Islam², Robert K. Heaton³

¹Medical Physics, Stronach Regional Cancer Centre, Newmarket/ON/CANADA, ²Radiation Physics, Princess Margaret Cancer Centre, Toronto/CANADA, ³Radiation Oncology, University of Toronto, Toronto/ON/CANADA

Introduction: Complex radiation therapy treatments are designed using computer algorithms which rely on specific dosimetric inputs. Optimization will be continued until all dosimetric criteria are met or otherwise accepted. Such optimization typically takes place on data sets that exclude the treatment couch top, yielding plans that do not reflect reality. We investigated what ignoring the couch top means dosimetrically for five full arc VMAT prostate plans.

Method: Four different couch tops were considered: iBeam evo, Sinmed Mastercouch, Varian flatpanel and Varian unipanel with t-bar support. Each of the Varian couch tops was considered with support bars in and out. Plans were selected based on range in target size and planning complexity. The starting point in each case was a previously accepted clinical case planned without a couch top. Couch tops were added in succession while maintaining the original beams. Parameters characterizing the dose distribution were assessed for each combination, including our standard clinical evaluation criteria. Prescription isodose line shifts were measured on 5 slices, at 3 posterior and 1 each lateral and anterior locations.

Results: For a prescribed dose of 78 Gy, the CTV V78Gy decreased from 0.2 – 40%, while the PTV V74.1Gy decreased from 0.6 – 9%. The greatest loss of dose occurred at the 105% dose level within the CTV.

Conclusion: CTV and PTV coverage reductions observed in this

study show that introducing couch information at the planning stage would produce a different plan than without couch information. These differences significantly exceed plan objectives and assessment criteria. This implies that either the current planning goals for these techniques are overly precise, resulting in little patient benefit gain from time invested in fine tuning a plan, or that planning which includes a model of the treatment couch is required to achieve the precision of dose delivery specified by the clinician.

PS04.107 - Edge Detection for Automated Biological Tumor Volume Definition Based on FDG-PET/CT-fused Imaging: An Agar Phantom study

Author(s):

Purpose: Fused positron emission and computed tomography (PET/CT) images have an important role in external beam radiotherapy (RT), especially for target volume delineation. For contouring on PET/CT images, the source-background algorithm is currently the used method, but its sensitivity to partial volume effects may produce inaccuracies when applied on small lesions. The goal of this research was to develop a computational algorithm based on the Canny's edge detection tool for processing PET/CT images. **Materials and Methods:** The software was implemented using the data analysis framework ROOT and the Grassroots DiCoM GDCM libraries (CERN, Geneva, Switzerland). First, a pre-processing Gaussian smoothing was applied to these images. Then directional derivatives and gradients were computed on the basis of multivariate calculation tools. Upon completion of this process, the boundaries of uptake regions having cylindrical shape within an Agar phantom were automatically sought by searching for the gradient magnitude and laplacian upper a pre-defined gradient threshold. **Results:** The mean diameters calculated by using the developed software have differences below 3% respect to the measured value (69 mm) for all the gradient thresholds between 15% and 55%. The diameters delimited with the source-background algorithm are different to the measured value and only are similar when a source-background threshold of 35% is defined. **Conclusion:** Images from the gradient magnitude and Laplacian of counts for the Agar Phantom with 18F-FDG PET-CT, are associated with diffusion processes explained by the Fick laws. According to the obtained results, methods of delimitation of tumors with 18F-FDG PET-CT are still useful, even in the presence of diffusive phenomena.

PS04.108 - Comparison between HybridARC and sliding windows IMRT for Spine SBRT tumor

Author(s): [Daniel Venencia](#), Nestor Vacca, Edgardo Garrigó, Lucas Caussa
Fisica Medica, Instituto de Radioterapia - Fundacion Marie Curie, Cordoba/ARGENTINA

Introduction

Spine SBRT treatments require high radiation dose to the PTV, located very close to organs at risk (OAR) like spinal cord, esophagus, kidneys and lung with very low tolerance doses compared to the prescribed tumor dose. The treatment requires high precision and treatment time should be as low as possible due to the patient condition. The objective of this work is to compare HybridARC (HA) with sliding windows IMRT (dMLC) treatment modality

Method and Materials

A 6MV photon beam with 1000MU/min dose rate (SRS beam) produced by a Novalis TX (Varian/BrainLAB) equipped with HD MLC was used. The treatment planning system used was iPlan v4.5.3 (BrainLAB). Treatment plans comparison was done for 5 patients.

Dose prescription was 27Gy to in 3 fractions; all plans were equally normalized keeping OARs within dose tolerances. HybridARC plans were created using 1 arc plus 3 (HA3), 5 (HA5) and 8 (HA8) fixed IMRT fields. HybridARC plans used arc aperture optimization and IMRT inverse planning (OAR high modality). Between 60-40% of the prescribed dose was given by the arc. Treatment with dMLC used 15 fixed gantry angle beams. Treatment times, monitor units (MU), conformity index (CI), V50% and V20% was used for plans comparisons.

Results

Assuming dMLC IMRT treatment plans as reference, the treatment time was reduced by -14.6% with HA8, -8.6% with HA5 and -23% with HA3. Increasing arc dose proportion in HA (arc MU > 2000) requires 2 or more arcs which increments treatment time. Using 1000MU/min HA3 and HA5 exhibits beam hold off for fixed IMRT fields which in some cases need to be split in 2 segments. MU varied +4% with HA8, +3.7% with HA5 and -5% with HA3. CI increased +5% with HA8, +23% with HA5 and +37% with HA3. V50% increased +5% with HA8, +43% with HA5 and +62% with HA3. V20% increased +13.2% with HA8, +7.6% with HA5 and +1% with HA3. OARs doses were keep within tolerances in all plans. Patient specific QA for all modalities shows more than 90% of the pixel with $g < 1$ with 3%/3mm pass criteria and high dose threshold of 30%.

Conclusion

HybridARC using an SRS beam for spine SBRT with 8 fix IMRT gantry angle shows a treatment time reduction, comparable MU and similar dose conformation to dMLC IMRT. HybridARC with 5 or 3 fix IMRT fields produce undesirable beam hold off, worse dose conformation and increments the total volume with 50% of the prescribed dose.

PS04.109 - real time dynamic prostate brachytherapy dose calculations using permanent i125 implants: technical description and preliminary experience

Author(s): Edgardo Garrigó, Maria J. Almada, Yaqueline Schworer, Daniel Venencia
Fisica Medica, Instituto de Radioterapia - Fundacion Marie Curie, Cordoba/ARGENTINA

INTRODUCTION: Low dose rate (LDR) prostate brachytherapy is an accepted treatment option for low risk prostate cancer patients. However, differences in prostate spatial location, volume and gland deformation between the images acquisition and later on during the implant procedure could carry to an incorrect dosimetry. The aim of this work is reporting on our treatment technique based on interactive real-time dynamic intra-operative dose calculation and to determine dosimetry differences

METHODS: Images from base to apex are obtained using a motorized stepper connected to the ultrasound and planning system. Physician draws the volumes Prostate, Uretra, Rectum, Bladder, and when is necessary a Boost volume. Then, we implant the peripheral needles and capture them by the planning system in the true position. We finish the plan with central needles. Once definitive needle positions have been captured, dosimetry is performed intra-operatively and the physician approves the corresponding isodoses on real time. Each array of seeds are corrected in accordance with actual implanted seeds. This allows real-time intraoperative dosimetric analysis, allowing for correction of under-dosed zones during implantation in an interactive dynamic way. In this work we selected 10 plans and we compare the plans with real needles position (RNP) against the same plans without regard to needles position modifications (WRNP).

RESULTS: We began our LDR prostate brachytherapy program on

2012. We have treated 73 patients, all patients were treated with our real time dynamic intra-operative planning system. A median of 165.5Gy-165.5Gy for D90, of 53.6%-54.3% for V150, 97.2%-96.5% for V100 and 0.0% – 1.7% for Uretra V200 and 1.0cc – 1.1cc for Rectum V100. Was calculated for RNP plan and WRNP plan respectively.

CONCLUSION: Real-time intra-operative planning was successfully implemented in our Institution. It avoids the possible implant quality and dose delivery disadvantages by improving the accuracy of seed placement on real time. The main advantage is the urethral protection which is translated in lower rates of acute and chronic GU morbidity

PS04.110 - Design of a simple device for end to end test of IGRT system using ExacTrac

Author(s): Daniel Venencia, Maria J. Almada, Yaqueline Schworer, Luis C. Medina, Edgardo Garrigó
Fisica Medica, Instituto de Radioterapia - Fundacion Marie Curie, Cordoba/ARGENTINA

Introduction

The ExacTrac system (BrainLAB) for image-guidance radiotherapy (IGRT) uses an infrared pre-positioning system and two RX oblique images for patient positioning based on bones or implanted fiducial. The accuracy of this system depends on the quality of the images, image transfer between TAC-TPS-ExacTrac, volume definition, isocenter calibration and mechanical precision of the treatment machine. Quality control of this complex network requires a phantom capable of verifying each of the stages.

The aim of this study is to design and test a simple phantom sufficient to verify end-to-end process of this IGRT using ExacTrac.

MATERIALS and METHODS

A rectangular acrylic phantom of 30 cm long, 30 cm wide and 6 cm high was designed. It has a cylindrical acrylic insert of 3 cm diameter with spherical endings in their borders, one constructed of plastic (PE) with different density and at the opposite border a lead sphere (PbE) of 2mm diameter in the center of the corresponding circumference. On the surface of the phantom baseplate with infrared markers are placed for CT. CT images of 2.5mm thickness are acquired with the cylindrical inserted in the PE side. CT images are sent to the TPS (iPlan v4.5.3) where the spherical volume of PE is drawn. Considering this volume as target an anterior field is located where the coordinate of the isocenter is the center of mass (CM) of the PE. Plan is exported to ExacTrac and isocenter coordinate matching is verified. ExacTrac system is calibrated using BrainLAB infrared and RX calibration phantoms. The phantom is placed on the treatment couch with the cylinder inserted in the PbE side with infrared markers used for treatment. Phantom prepositioning is performed guided by the spheres according to the movements indicated in ExacTrac screen. Then X-ray oblique images are obtained and the displacement of the radiological isocenter of ExacTrac to the center of the lead sphere is recorded. Using a 2x2cm² beam from the Linac portals images with ANT and LAT incidence are obtained. Images are analyzed and PbE displacements are determined relative to the center of the radiological field using RIT v5.3 software or ARIA off line review software. Primus linear accelerator (Siemens) and Novalis TX (BrainLAB / Varian) equipped with ExacTrac system were used to test the phantom.

Results

Density difference between acrylic insert and PE allowed adequate delineation. The coordinate of the treatment field, based on CM of PE, match with the center of the sphere. ExacTrac X-ray images showed an overlap of the radiological isocenter with the PbE projec-

tion image (error <1mm) in both treatment machines. The radiological displacement of the PBE with the center of the Linac field was less than 1mm for both machines. The duration of the end-to-end test with this device was less than 3 hours.

Conclusions

The designed phantom is economical and practical for End-to-End QA of ExacTrac IGRT system. Its construction is simple, easy positioning and its use allows a quantitative or qualitative correlation between displacement and errors obtained.

PS04.111 - Study on the use of an in-house device to consider the motion effects on absorbed dose determination and measurements using different calculation algorithms in lung SBRT cases

Author(s): Victor A. Villamares-Vargas¹, Mariana Hernández-Bojórquez², Héctor J. Uriarte-Rivera³, Jorge O. Hernández-Oviedo², Eugenio Torres-García¹

¹Facultad De Medicina Area De Posgrado, Universidad Autónoma del Estado de México, Toluca/MEXICO, ²Radioterapia Y Radiocirugía, Centro Médico ABC - Centro de Cáncer, México, D.F./MEXICO, ³Departamento De Física, Instituto Politécnico Nacional - Escuela Superior de Física y Matemáticas, México, D.F./MEXICO

One of the challenges in radiation therapy consists in the administration of treatments for tumors that are susceptible to modify their position due to the respiratory cycle, as occurs in those located in the pulmonary or abdominal areas. There are different tomography simulation devices available which take into account the movements of the patient anatomy due to respiration cycles, known as *4DCT*. The *4DCT* scans are used to provide accurate representations of the motion effects, through datasets such as the maximum, minimum and mean projections. These can be useful for determining the contours of lung or liver tumors, which are modified by motion, as well as those of the surrounding organs at risk and healthy tissue. Therefore, the absorbed dose delivery considering these movements is possible. Also, a reduction of the target volume margins reduces the risk of complications due to the surrounding healthy tissue irradiation.

A movable platform was built to simulate one direction movement of an anthropomorphic thorax phantom in order to perform quality assurance (QA) processes for treatment planning using *4DCT*. In this work the performance of this device is examined to run some QA tests for lung stereotactic body radiation therapy, taking into account the breathing movement of the patient. The verifications which compose the QA process are made in typical treatments of 50 Gy in 5 sessions using different planning systems such as: *iPlan RT Dose* and *Eclipse*, using three different algorithms for the calculation of the absorbed dose: *Analytical Anisotropic Algorithm*, *Pencil Beam* and *Monte Carlo*. To measure the absorbed dose a *QUASARTM Multi-Purpose Body Phantom* thorax is used with in-house manufactured cavities that allow the access of a *SemiFlex*, *MicroLion* and *PinPoint* ionization chambers. In addition, a separate set of inserts was designed to use *radiochromic film sheets*. The values of the absorbed dose calculated by the three algorithms are compared with the measurements obtained from the actually delivered absorbed dose on the radiation detectors. With the above, the precision of these algorithms can be quantified considering the implicit respiratory movement.

PS04.112 - In-vivo skin dose evaluation for Pd-103 permanent breast radiotherapy implants

Author(s): Ronald E. Beals¹, Elizabeth Watt², Tyler Meyer³, Jose E. Villarreal-Barajas⁴

¹Physics And Astronomy, University of Calgary, Calgary/CANADA, ²Tom Baker Cancer Centre, Calgary/CANADA, ³Oncology, University of Calgary, Calgary/CANADA, ⁴Oncology, University of Calgary, Calgary/AB/CANADA

Permanent breast seed implant (PBSI) using permanent seed LDR breast brachytherapy was pioneered in Toronto with the first procedure completed in 2004. In late 2013, our centre started a PBSI program using Pd-103 seeds. This study presents our preliminary results of the *in-vivo* skin dose evaluation on a cohort of six PBSI patients. All patients were forward planned using CT images where the physician defined a PTV as a 1 cm expansion of the CTV trimmed to the skin and chest wall. The implant plans were designed to cover at least 90% of the PTV by the prescribed dose of 90 Gy. The planned dose to the skin was limited to a maximum of 81 Gy. Given the limitations of the water based (TG-43) dose calculation algorithm used by the treatment planning system and its potential under-estimation of the dose to the skin, an *in-vivo* skin dose evaluation was performed using radiochromic dye film dosimetry (EBT3). The EBT3 films strips used for the skin dose evaluations were positioned in contact with the skin of the patients at the central axis of the implant. The patient films dose integration period varied from 3.25 hours to 47 hours (see Table 1). These films were scanned in order to obtain their associated net optical density (net O.D.). The net O.D. was used to estimate the skin dose using a 100 kV_p calibration (Figure 1). The validity of the calibration was verified using two Pd-103 point doses from a well controlled EBT3 irradiation experiment. The two highest skin doses measured correlated with observed skin reactions in the corresponding patients. More research is needed to assess the clinical significance of the measured skin doses and their role in the development of an effective metric for the relevant skin dose in PBSI.

ID	net O.D.	Exp.time/h	Max. dose/Gy	Max. total dose / Gy
1	0.3490	47	4.710	61.3±4.3
2	0.0540	3.67	0.428	68.8±8.3
3	0.0423	5.0	0.324	38.3±7.3
4	0.0240	3.0	0.172	33.8±6.4
5	0.0293	3.75	0.215	33.8±7.1
6	0.0209	3.25	0.147	26.7±6.7

Table 1. Net optical density obtained by scanning the exposed films (red channel), patient film time exposure in hours, absorbed dose to water estimates for the corresponding exposure, and maximum total dose estimate obtained by integration based on the maximum dose in the patient film. The dose uncertainty in the maximum total dose column is derived from the variation (k=2) observed in the net O.D. derivation of the 5 x 5 mm² area used to score the maximum dose in the patient films.

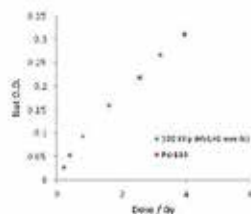


Figure 1. EBT3 film calibration using a 100 kV_p (HVL=3 mm Al) orthovoltage x ray clinical beam and two verification Pd-103 doses (2.55 and 3.95 Gy). The Pd-103 doses were estimated based on a measured activity and using the TG-43 formalism with a Monte Carlo based correction to obtain the dose to water in acrylic (PMMA). The Pd-103 dose estimates derived from the measured net O.D. are within 5% of the expected doses derived using a 100 kV_p x ray beam calibration.

PS04.113 - Dosimetric Variations in Permanent Breast Seed Implant (PBSI) Evaluated at Different Arm Positions using Deformable Image Registration

Author(s): Elizabeth Watt¹, Siraj Husain², Karen Long¹, Michael Sia², Derek Brown³, Tyler Meyer⁴

¹Tom Baker Cancer Centre, Calgary/CANADA, ²Oncology, University of Calgary, Calgary/CANADA, ³Radiation Medicine And Applied Sciences, University of California, San Diego, La Jolla/UNITED STATES OF AMERICA, ⁴Physics & Astronomy, University of Calgary, Calgary/CANADA

Purpose: Permanent Breast Seed Implant (PBSI) is a novel method of treating early-stage breast cancer. It is a one-day, outpatient procedure in which radioactive Pd-103 seeds are surgically implanted in and around the seroma following breast-conserving surgery. The planning for PBSI is done with the patient’s ipsilateral arm raised; however, changes in implant geometry can be expected due to healing and anatomical motion as the patient resumes her daily activities. The purpose of this study is to quantify the effect of arm position on postplan dosimetry.

Methods: Thirteen patients treated at the Tom Baker Cancer Centre in Calgary, Alberta were included in this study. All of these patients underwent two post-implant CT scans on the day of implant. One scan was taken with the patient’s ipsilateral arm raised above the head, recreating the position of the planning scan, while the other was taken with both arms down beside the body in a relaxed position. Postplans on both scans were completed using MIM Symphony™ (MIM Software, Cleveland OH). The pre-implant planning scan was deformably registered to the post-implant scan to deform the seroma contour and other relevant contours to the post-implant scan. An evaluation PTV, with a 0.5 cm margin to the seroma, was generated after deformation. Statistical analysis was performed using a paired, two-tailed t-test, and an alpha value of 0.05 was used for statistical significance.

Results: A summary of the dosimetric parameters for the target volumes and nearby structures for both arm positions is shown in Table 1.

Table 1: Comparison of Dosimetric Parameters for Ipsilateral Arm Up and Down

Parameter	Arm Up	Arm Down	p-value
CTV [%] V100	90.7 (70.9–100.0)	93.9 (79.7–100.0)	0.08
PTV [%] V90	83.7 (66.6–99.4)	86.0 (68.7–99.1)	0.17
V100	80.0 (60.8–97.9)	82.6 (65.3–98.0)	0.17
V150	58.8 (29.9–79.3)	61.2 (35.9–84.5)	0.21
V200	34.7 (15.9–54.5)	38.7 (18.9–61.5)	< 0.01
Skin [cc] V80	1.6 (0.0–6.2)	1.7 (0.0–7.8)	0.59
V90	1.2 (0.0–5.2)	1.3 (0.0–5.4)	0.52
Lung [cc] V20Gy	1.6 (0.0–5.2)	0.2 (0.0–1.4)	0.01
Heart* [cc] V20Gy	0.04 (0.00–0.30)	0.00 (0.00–0.02)	0.30
V40Gy	0.00	0.00	--

Notes: Values are mean (range).

*Only left-sided patients were analyzed for these parameters. Discussion and **Conclusions:** Results on thirteen patients thus far indicate that the implant becomes significantly hotter with the arm down (indicated by the increase in V200); however the increase exhibited when using a 1 cm PTV margin did not reach significance. Lung dose significantly improved in the arm down position. Change in seroma volume between the arm up and arm down scan (mean: -1.1%; range: -18.3% to 7.8%) is an influencing factor in dosimetric differences. Further investigation is necessary to also determine the effect of shape and seroma position. Seroma volume may change over time due to swelling and resolution (healing); future work will involve analysis of dosimetry on eight week post-implant CT scans to ensure that volume changes on the day 0 post-implant scan due to edema is not skewing the dosimetric results.

PS04.114 - Minimum Planning Target Volume Coverage Necessary for the Delivery of the Prescribed Dose in Lung Radiotherapy

Author(s): Madison Murdoch¹, Marcin Wierzbicki²

¹McMaster University, Niagara Falls, Ontario/CANADA, ²Juravinski Cancer Centre, Hamilton/ON/CANADA

Minimum Planning Target Volume Coverage Necessary for the Delivery of the Prescribed Dose in Lung Radiotherapy

Intensity Modulated Radiation Therapy (IMRT) has been used in lung cancer treatment to deliver dose distributions with steep gradients and exquisite target volume conformality. While many benefits of IMRT exist, significant challenges are involved when unpredictable intrafractional movement is combined with the highly optimized nature of IMRT. The National Cancer Institute (NCI) Guidelines for the Use of IMRT state that there is potential for significant dosimetric consequences if the target volume moves while treatment is being administered. Thus, lung IMRT is especially challenging due to breathing motion. Furthermore, tissue density differences at the lung-tumor interface contribute to disagreements between the

administered and planned doses. It is believed that inhomogeneities allow for a relatively large amount of the planning target volume (PTV) to be left without coverage and the target will still receive the prescribed dose during treatment. For example, the Radiation Therapy Oncology Group (RTOG) 0617 study requires that 95% of the PTV is to be covered by 93% of the prescription dose during planning. The study assumed this planning goal was sufficient in ensuring coverage during treatment, although it is unclear if this was achieved due to target motion and the dosimetric effects of inhomogeneities.

This study aimed to establish an IMRT lung planning goal that ensures 99% of the internal target volume (ITV) is covered by 95% of the prescribed dose during treatment. Ten previously generated IMRT plans were compiled for analysis. Each plan was renormalized such that 95% of the PTV is covered by increasingly higher doses, ranging from 93 to 97% of the prescription. For each plan, multiple target movements were simulated by shifting the isocentre of the beams within a range previously measured for this patient population and recomputing the dose. Finally, the coverage of the ITV obtained during simulated treatment was established using dose-volume histograms for each planning goal. Advantage of certain planning goals versus others was established by comparing the number of simulated movements causing inadequate coverage of the ITV.

Kruskal-Wallis analysis showed that none of the studied planning goals was significantly different from another based on the number of times the ITV was not covered by 95% of the prescribed dose. In other words, the RTOG 0617 planning goal of 95% of the PTV covered by 93% of the prescription achieves the same result as the goal where 95% of the PTV is covered by 97% of the prescription. The complete data suggested that coverage failure may decrease with increasing coverage but the current study did not show the decrease was significant. We are currently applying the RTOG 0617 planning goal clinically and will repeat this analysis with additional patient data to ensure optimal delivery of lung IMRT at our institution.

PS04.115 - A modified methodology to accurately validate CT number constancy for proton therapy

Author(s): Richard Y. Wu¹, Amy Y. Liu², Kazumichi Suzuki², Michael Gillin², Ron Zhu²

¹Radiation Physics, M.D. Anderson Cancer Ctr, Houston/TX/UNITED STATES OF AMERICA, ²Radiation Physics, M.D. Anderson Cancer Ctr, Houston/UNITED STATES OF AMERICA

A modified methodology to accurately validate CT number constancy for proton therapy

Purpose

In proton therapy, the CT number is calibrated to convert proton stopping power ratio (SPR) and the calibration factor is entered into a treatment planning system. Since CT number vs. SPR is a nonlinear curve throughout the range of clinical interest, the current CT number quality assurance (QA) method is not adequate to test CT# accuracy/constancy for the entire human tissue range. We developed a method that will establish the criteria of the CT number variations which provide the desired percentage variation of the baseline values of SPR

Method

We began with a CT number vs SPR curve established in the Eclipse planning system for a designated proton CT scanner (Fig. 1). We separated the CT number vs. SPR curve into 3 sections representing lung, soft tissue, and bone tissue ranges and fit each section with a polynomial curve. When a given +/- 1% change occurs in the

SPR, the corresponding CT number change can be calculated by applying the polynomial equation from each section.

Result

Table 1 illustrates the calculated CT number change as a result of +/-1% changes of SPR for each entry point. These values are used in the annual CT number QA testing to validate that each entry value is consistent with the original calibration.

Conclusion

We have established a simple and quantitative method for CT number annual constancy testing through the scanner's entire clinical range.

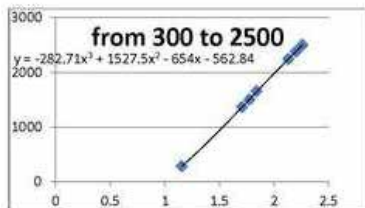
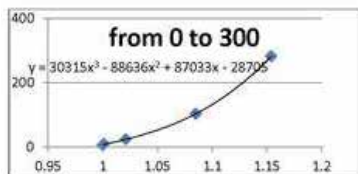
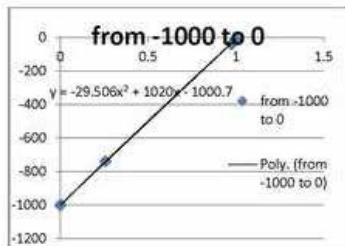


Fig.1
CT number vs. SPR curve are separated into 3 sections representing lung, soft tissue, and bone tissue ranges and each section is fit with a polynomial curve

CT#	SP	+1%SP	-1%SP	+/- HU	Measurement inserts HU	Derived QA HU limit
y	x					
-1000	0.001	0.00101	0.00099	0.0	-681.2	8.9
-739	0.258	0.26058	0.25542	5.2	-528.1	13.1
-38.6	0.975	0.98475	0.96525	18.8	-79.8	25.3
-7.1	0.999	1.00899	0.98901	19.2	-30.1	26.6
6.5	1	1.01	0.99	14.2	11.2	27.7
10	1.001	1.01101	0.99099	14.3	8.8	27.7
23.9	1.021	1.03121	1.01079	17.3	97.4	30.1
103.3	1.085	1.09585	1.07415	38.2	237.1	33.9
282.3	1.154	1.16554	1.14246	82.6	245.4	34.1
1365.6	1.707	1.72407	1.68993	71.3	1230.8	60.2

Table 1 Derived QA HU for each entry point from polynomial equations

PS04.116 - Development of a real-time portable applicator monitoring system for gynecologic intracavitary brachytherapy
Author(s): Christian Bauer, Reinhard Beichel, Yusung Kim, Timothy Waldron, Wenqing Sun, Sudershan Bhatia, Junyi Xia
 Radiation Oncology, University of Iowa, Iowa City/UNITED STATES OF AMERICA

Purpose

To develop a real-time applicator position monitoring system (RAPS) for intracavitary brachytherapy.

Materials and Methods

Applicator displacement during brachytherapy can produce suboptimal dosimetric effects, especially in 3D image-guided brachytherapy, which requires high accuracy applicator localization. 2D X-ray imaging devices, such as C-arm, are routinely used for measuring applicator displacement, however, they deliver extra radiation dose to patients and lack the capability of continuous applicator monitoring. The RAPS was developed for continuous applicator position monitoring without any radiation dose. The RAPS consists of two custom-designed tracking targets with infrared reflective markers and a calibrated infrared stereo-camera setup. The RAPS can measure in real-time the applicator movement by computing the relative displacement between the two tracking targets, which are attached to the applicator and the patient. Both 3D printed tracking targets were custom designed for optimal tracking performance and to be easily attached to the Varian Tandem and Ovoid applicator. A phantom study was conducted to compare RAPS' measurements with known displacements from a high accuracy positioning stage (0.03mm accuracy) in the range of +/-25 mm.

Results

The RAPS achieved 120 frames per second using a laptop with Intel Core 2 dual CPU. At a camera-to-marker distance of 50 cm, the mean difference between RAPS' measurements and the positioning stage was 0.068 mm with a standard deviation (STD) of 0.044 mm in superior-inferior direction, 0.013 mm with a STD of 0.015 mm in lateral direction, and 0.061 mm with a STD of 0.024 mm in anterior-posterior direction.

Conclusions

This work demonstrates the feasibility of RAPS to detect applicator motion in real-time. An accuracy of 0.1mm was achieved in the phantom study.

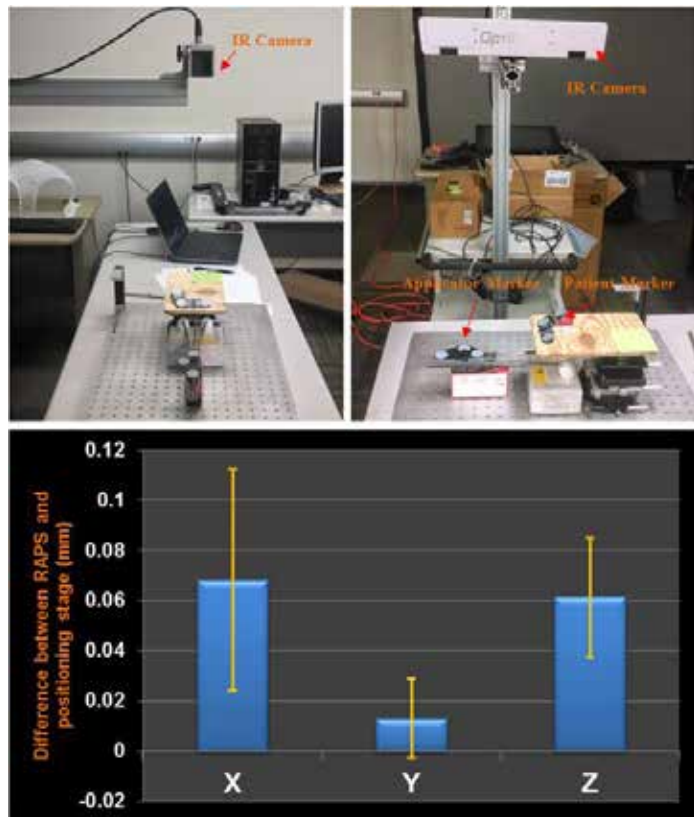


Figure 1. RAPS consists of two custom design infrared markers, an infrared camera, and a control laptop. The phantom study indicated that RAPS can achieve a mean accuracy of 0.07 mm in superior-inferior direction, 0.013 mm in lateral direction, and 0.06 mm in anterior-posterior direction.

PS04.117 - Quality Assurance of the Radiotherapy Workflow Integrating a Dedicated Wide-bore 3T MRI Simulator

Author(s): Aitang Xing, Gary Liney, Lois Holloway, Sankar Arumugam, Robba Rai, Ewa Juresic, Gary Goozee
Cancer Therapy Centre, Liverpool Hospital, Sydney/NSW/AUSTRALIA

Introduction: A MRI scanner dedicated for radiotherapy planning (also known as MRI simulator) was installed and integrated into our clinical workflow in June, 2013 [1]. There are international protocols regarding quality assurance of MRI for diagnostic performance [2], but there is lack of guidelines with regard to its integration in a radiotherapy workflow. The purpose of this study was to establish a QA program for quality control of an MRI-integrated radiotherapy workflow implemented in our centre.

Materials and methods: All scanning was performed on a dedicated wide bore 3.0 Tesla MRI scanner (Siemens Skyra) with radiotherapy accessories including a flat table top with integrated RF coil and external localization lasers for setting up patients at the same position as during treatment. The MRI simulator is integrated into our clinical workflow in following way: patient is first scanned on a Philip

4D CT simulator in the treatment position, and then scanned in this position on the MRI simulator which is in the next room. The CT and MRI image are sent to the treatment planning system (Pinnacle version 9.8). The MRI is initially auto-registered with CT images using a mutual information algorithm and then manually adjusted by the radiotherapist (RT) and oncologist. Once the MRI images are registered with CT images, the oncologists delineate the target and organs at risk on MRI images and transfer the contours to CT images. In order to provide a quality assurance of the whole workflow, a cylindrical phantom routinely used for checking laser alignment was employed. The phantom has a base for levelling the phantom and external marks for phantom setup. The QA procedure using phantom is exactly same as the patient workflow. The phantom was scanned using CT head-neck protocol and then setup on MRI by aligning its external marks with localisation lasers and scanned using bore coils and a standard SE sequence (TE=30ms, TR=3410ms). Both CT and MRI images are sent to Pinnacle for co-registration as described previously and the translation and rotation parameters were recorded. This procedure was repeated for a period of eight days.

Results and discussion: The averaged translation parameters in all three directions were less than 1.2mm, whereas the rotation is less than 0.3 degrees. Especially along z direction, on average, there is no rotation and less than 1mm translation along x direction. The standard deviation of translation and rotational parameters are less than 0.45, indicating that the MRI-integrated workflow is consistent and highly reproducible. It is recommended that the QA procedure be performed quarterly or in the event of MRI scanner maintenance and repair.

Conclusion: A phantom-based QA program for checking the consistency of MRI-integrated radiotherapy workflow was implemented in our centre. The QA procedure can be adopted by other centres.

References: [1] Xing A, Liney G, Holloway L, Arumugam s, Juresic E, Cassapi L and Goozee G. Commissioning and acceptance of a dedicated 3T MRI simulator for radiotherapy treatment planning. ESTRO33 (2014), Vienna, Austria.

[2] Devic S. MRI simulator for radiotherapy treatment planning. Med. Phys (2012): 6701.

PS04.118 - Evaluation of deformable accumulated parotid doses using different registration algorithms in adaptive head and neck radiotherapy

Author(s): Shouping Xu¹, Bo Liu², Haixia Liu³, Hanshun Gong³, Baolin Qu³, Lin Ma³, Fugen Zhou²

¹Key Laboratory Of Particle & Radiation Imaging, Tsinghua University, Ministry of Education, Beijing/CHINA, ²Beihang University, Beijing/CHINA, ³Radiation Oncology, PLA General Hospital, Beijing/CHINA

Purpose: Three deformable image registration (DIR) algorithms are utilized to perform deformable dose accumulation for head and neck tomotherapy treatment, and the differences of the accumulated doses are evaluated. **Material and methods:** Daily MVCT data for 10 patients with pathologically proven nasopharyngeal cancers were analyzed. The data were acquired using tomotherapy (TomoTherapy, Accuray) at the PLA General Hospital. The prescription dose to the primary target was 70Gy in 33 fractions. The contours of parotid glands on daily MVCTs were obtained by populating these contours from planning CTs to the daily CTs via rigid-body registration using the Adaptive plan software (Adaptive Plan, TomoTherapy) and were edited manually if necessary. The fractionated dose of parotids will be re-calculated. Three DIR methods (B-spline, Diffeomorphic Demons and MIMvista) were used to propagate parotid structures from planning CTs to the daily CTs and accumulate fractionated dose on the planning CTs. The mean accumulated doses of

parotids were quantitatively compared and the uncertainties of the propagated parotid contours were evaluated using Dice similarity index (DSI). **Results:** For 10 patient plans, the mean parotid volume ($19.19 \pm 10.23 \text{ cm}^3$) at the last fraction was significantly smaller than those ($29.44 \pm 13.32 \text{ cm}^3, p < 0.0001$) at the first fraction. The planned mean dose of the ipsilateral parotids ($32.42 \pm 3.13 \text{ Gy}$) was slightly higher than those of the contralateral parotids ($31.38 \pm 3.19 \text{ Gy}$). The difference between the accumulated mean doses of the ipsilateral parotids in the B-spline, Demons and MIMvista deformation algorithms ($36.40 \pm 5.78 \text{ Gy}$, $34.08 \pm 6.72 \text{ Gy}$ and $33.72 \pm 2.63 \text{ Gy}$) were statistically significant (B-spline vs Demons, $P < 0.0001$, B-spline vs MIMvista, $p = 0.002$). And The difference between those of the contralateral parotids in the B-spline, Demons and MIMvista deformation algorithms ($34.08 \pm 4.82 \text{ Gy}$, $32.42 \pm 4.80 \text{ Gy}$ and $33.92 \pm 4.65 \text{ Gy}$) were also significant (B-spline vs Demons, $p = 0.009$, B-spline vs MIMvista, $p = 0.074$). For the DSI analysis, the scores of B-spline, Demons and MIMvista DIRs were 0.90, 0.89 and 0.76. **Conclusion:** Shrinkage of parotid volumes results in the dose increase to the parotid glands in adaptive head and neck radiotherapy. The accumulated doses of parotids show significant difference using the different DIR algorithms between kVCT and MVCT. Therefore, the volume-based criterion (i.e. DSI) as a quantitative evaluation of registration accuracy is essential besides the visual assessment by the treating physician.

PS04.119 - Optimization of brain metastases radiotherapy with TomoHDA

Author(s): Slav Yartsev

London Regional Cancer Program, London/CANADA

Introduction. Simultaneous in-field boost (SIB) approach has been shown advantageous for dose distribution in axial plain in radiation treatment with prescription of 60 Gy to brain metastases, aka gross tumor volume (GTV), and 30 Gy to the rest of the brain in 10 fractions [1]. However, in the case of tomotherapy system with static jaws, a penumbra of the order of fan beam width is present in superior-inferior (SI) direction both for the whole brain (WB) and GTV regions. Recently, the idea of movable jaws by Gladwish et al. [2] has been realized in the commercially available TomoHDA system. This innovation allowed for drastic reduction of the SI penumbra for the WB, but not for the SIB region. We explore a possibility to take full advantage of dynamic jaws on TomoHDA for brain metastases and whole brain radiotherapy.

Methods. A challenging case of the GTV close (9 mm) to the right optic nerve was planned using SIB approach with static and dynamic jaws. Also, two non-SIB treatment plans were generated: 1) WB planning target volume was prescribed to 30 Gy in 10 fractions with 5 cm fan beam/dynamic jaws and the GTV was planned to 20 Gy in 10 fractions; 2) another plan with 2.5 cm fan beam/dynamic with planned irradiation of only the GTV with 60 Gy minus the dose to the GTV from the first plan. Planned maximum doses to the optic nerve and chiasm obtained in SIB and two-phase approach were compared.

Results.

Table 1. Values of selected parameters for the whole brain (WB) planning target volume, GTV, and optic nerve (ON) planned with SIB method using static and dynamic jaws, compared to sequential radiotherapy option with different field sizes.

Plans	SIB	SIB	WB only	GTV only	GTV + WB
Fields	2.5 cm	2.5 cm	5 cm	2.5 cm	5 cm+2.5 cm
Jaws	static	dynamic	dynamic	dynamic	dynamic
WB, D_{mean}	32 Gy	32.5 Gy	29.4 Gy	3.8 Gy	33.2 Gy
GTV, D_{mean}	61.2 Gy	62 Gy	20.1 Gy	39.4 Gy	59.6 Gy
Chiasm, D_{max}	36.9 Gy	39 Gy	25 Gy	7.7 Gy	< 32.8 Gy
ON, D_{max}	41.1 Gy	40.7 Gy	23.6 Gy	9.9 Gy	< 33.5 Gy
Beam-on time	8.4 min	8.8 min	3.9 min	3.1 min	7 min

Conclusions. The proposed sequential radiotherapy of brain metastases and whole brain on TomoHDA allows for using dynamic jaws benefit in full. It saves beam-on time and provides improved dose distribution in superior-inferior direction compared to simultaneous in-field boost with static beam. This method can be applied for other disease sites.

References.

[1] Bauman G, Yartsev S, Fisher B, Kron T, Laperriere N, Heydarian M, J. Van Dyk. Simultaneous in-field boost with helical tomotherapy for patients with 1 to 3 brain metastases. *Am J Clin Oncol* 2007;30: 38-44. [2] Gladwish A, Kron T, McNiven A, Bauman G, Van Dyk J. Asymmetric fan beams (AFB) for improvement of the craniocaudal dose distribution in helical tomotherapy delivery. *Med Phys*. 2004;31:2443-8.

PS04.120 - A Rapid Learning Approach for the Knowledge Modeling of Radiation Therapy Plan

Author(s): Lulin Yuan¹, Yaorong Ge², Fangfang Yin¹, Q Jackie Wu¹

¹Department Of Radiation Oncology, Duke University Medical Center, Durham/NC/UNITED STATES OF AMERICA, ²Department Of Software And Information Systems, University of North Carolina at Charlotte, Charlotte/NC/UNITED STATES OF AMERICA

Purpose: The purpose of this study is to implement a rapid learning method to train the knowledge models to predict the organ-at-risk (OAR) dose sparing in radiation therapy (RT) based on an array of patient anatomical features. We also aim to establish the evaluation criteria and a solid validation to ensure an accurate and efficient learning process.

Method and Material: The knowledge models to predict OAR dose sparing have been shown to be useful tools to guide RT planning. A rapid learning approach is utilized to train the knowledge models in this study. A total of 100 clinical cancer cases in the pelvic region were retrospectively analyzed. Among them, 40 cases are low-to-intermediate risk prostate cases (Type I), 20 are high-risk prostate cases with lymph node irradiation (Type II), 40 are anorectal cancer cases (Type III). Starting from a base model for type I cases, increasing number of cases with more complex planning-target-volume (PTV)-OAR anatomies (type II and type III) were continuously added into the training case pool. The studentized residual and the leverage values are calculated as evaluation criteria at each step. The studentized residual quantify how much the new case deviates from the previous model. The leverage measures the distance of the new case in the feature space to the distribution of the other cases and it is used to differentiate if a large residue is due to plan quality variation or because the new case is an isolated case in the feature space. Cases in the former category are excluded from model training.

The efficiency and accuracy of the learning method was quantified by the learning curve. It describes the longitudinal improvement of model accuracies with increasing number of training cases. In order

to reduce the effect of cross-sectional data variation to the learning curve, the modeling accuracies were obtained by a repeated random splitting cross validation method. The gEUD in the bladder and rectum are compared between the model predictions and actual values for the validation cases. The Median of the Absolute value of their Differences (MAD) are calculated for the validation cases.

Results: The MAD of the predicted OAR gEUD in all three types of cases gradually decreases when increasing number of training cases are added in training. The MAD of the bladder and rectum gEUD in both type II and III validation cases reaches a stable value of 2.1% to 3.5% of prescription dose when 12 type II or type III are added in training in addition to the 30 type I cases, and they are comparable with the MAD value of 2.0% to 3.4% when all cases are used in training in a batch mode.

Conclusion: The rapid learning approach is able to learn knowledge models for multiple cancer types in the pelvic region with comparable accuracy to the batch training method and with improved efficiency. This approach will facilitate the implementation the knowledge based radiation therapy planning in clinics.

PS04.121 - Plan comparison and delivery verification for intracranial stereotactic treatments using Varian TrueBeam STx linac

Author(s): Sergei Zavgorodni
Medical Physics, BC Cancer Agency, Victoria/CANADA

Modern stereotactic brain treatments are getting away from using rigid frame based head fixation systems and mostly rely on pre-treatment and intra-treatment imaging for patient setup and motion control. Circular cones are also getting obsolete and being commonly replaced by high definition multileaf collimators (HD MLCs) that allow using advanced treatment techniques producing more conformal dose distributions. With the aim to minimize potential intra-fraction motion treatment planning includes delivery time as one of considerations. Objective of this work was to evaluate different treatment techniques that utilize HD MLCs from the perspective of treatment plan quality, delivery time, and dosimetric accuracy achievable for different target sizes.

Treatment plans were produced using 7-field static conformal, conformal arc, 7-field IMRT, 2-arc VMAT, and 4-arc VMAT techniques with 6 MV and 10MV-FFF beams. In 4-arc VMAT plans two arcs were coplanar and another two were planned for 45 and 315 degree couch angles. The plans were produced and calculated using Eclipse AAA for the anthropomorphic head phantom that had an insert for micro-diamond detector for the dose measurements. The phantom also had a tungsten bead imbedded for beam position verification. The targets were outlined around the detector position as ellipsoids of 5, 8, 10, 15, 25 mm "effective diameter", and there where one to three targets per a plan. Plans were produced for treating all targets with a single isocentre. The plan quality was evaluated by using dose volume histograms for the target and surrounding artificial shells that allowed simple evaluation of the dose fall-off. Plans were delivered and the dose measured using micro-diamond detector. The setup was guided by CBCT and its accuracy was evaluated by comparing planned and treatment positions of the tungsten bead. If the plan had multiple targets, the dose in only one of them was measured.

VMAT produced the plans comparable to IMRT and superior to conformal techniques. Non-coplanar plans were more conformal, but the difference was deemed not significant. Plans that used 6MV beams were slightly more conformal than those produced by 10MV-FFF. However the latter, being four-fold faster to deliver are still attractive clinical option.

When treated using regular (4DoF) couch the phantom "roll" rotation

had to be set accurately as it was not possible to compensate for this rotational misalignment through available couch movements. Remaining positional error could then be as much as 3 mm compared to 0.5mm when roll rotation was set correctly. 6DoF couch was able to accurately compensate translations and rotations of the phantom and position it within 0.5mm of the plan. For all techniques the dose agreement within 2% was found for the targets of 10mm diameter and larger. For smaller targets the measured dose exceeded the plan by as much as 11%. IMRT and VMAT plans had similar delivery times when delivered in "automated" mode. Conformal plans were about 50% faster to deliver due to nearly twice less monitor units.

PS04.122 - A method to convert cone-beam computed tomography (CBCT) image for dose calculation and the phantom evaluation

Author(s): Guangshun Zhang, Shaomin Huang, Dandan Zhang, Xiaowu Deng, Cui Chen
Radiation Oncology, Sun Yat-Sen University Cancer Center, Guangzhou/CHINA

Background and Objective: Cone-beam computed tomography (CBCT) image is widely used for image guided radiation therapy (IGRT) and has the potentiality to support adaptive radiation therapy (ART). However, uncorrected CBCT images can not be used for re-planning dose calculation due to the larger scatters and artifacts in the Hounsfield unit (HU). Co-relationship between Fan-beam computed tomography (FBCT) and CBCT images was established and used to convert the CBCT image for dose calculation in this study. The results was simulated and verified with an anthropomorphic phantom for IMRT treatment plan computation, compared with the original FBCT based plan.

Method and material: Using a self-compiled software based on a fitting function, by registering the FBCT and CBCT image sets of an anatomical head simulated phantom, the CBCT images was converted to get an approximately corrected data sets as CBCT_{cv} for dose calculation. The precision of CBCT_{cv}-based dose calculation was then tested and validated, by comparing the iso-dose distribution and dose volume histogram (DVH) of planning target volume (PTV) and organs at risk (OARs) with the FBCT-based computation using an IMRT plan. Gamma comparison in different criteria between CBCT_{cv}- and FBCT-based plans was provided as well.

Results: The gamma comparison between CBCT_{cv}- and FBCT-based dose computations showed that the pass-rates of (1%, 1mm), (2%, 2mm) and (3%, 3mm) criteria were 71.28%, 97.55% and 99.72%. In the two results of the CBCT_{cv}- and FBCT based plan calculation, the differences in the mean dose, near minimum dose (D98%), near maximum dose (D2%) and V95% of the PGTV were 1.02%, 1.58%, 0.78% and 0.06%, separately; the near maximum dose (D2%) discrepancies of brain stem and spinal cord were 0.43% and 1.61%; deviation in the D50% of the left and right parotids were 0.89% and 0.88, separately. Fig 1 showed the DVH differences for the main structures.

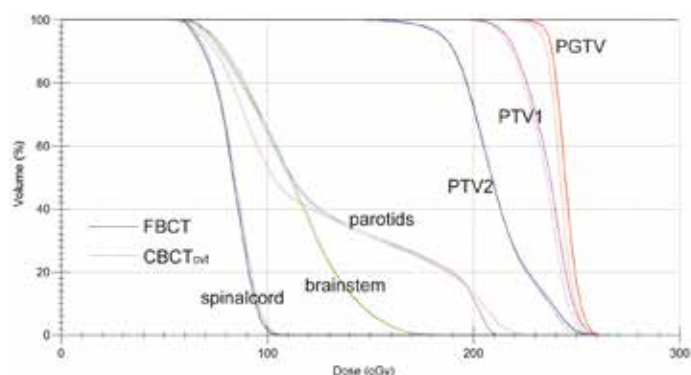


Fig. 1 DVH difference of the main concerned structures between the CBCTcv- and FBCT-based plan calculation.

Conclusions: We established an relatively simple method to approximately correct and convert the CBCT image for feasible use of radiation treatment dose calculation, by fitting the HU values of FBCT. In the validation test using anthropomorphic phantom, the maximum discrepancy in DVH between the converted CBCT- and FBCT-based plan was less than 2%.

PS04.123 - Thermoluminescent dosimetry of the model BT-125-1 ^{125}I interstitial brachytherapy seed

Author(s): Nan Zhao, Ruijie Yang, Junjie Wang
Radiation Oncology, Peking University Third Hospital, Beijing/CHINA

Purpose: To study the dosimetric parameters of dose rate constant, radial dose functions and anisotropy functions for the model BT-125-1 ^{125}I seed with thermoluminescent dosimeters.

Materials and Methods: The preliminary experiment is to study repeatability, linearity of dose response, dose rate effect and energy response of the thermoluminescent dosimeters (TLD). The seed was placed perpendicularly in the center of the PMMA phantom, and 12 TLDs were placed parallel to the source long axis at radial distance of 1 cm with 30° increments, to study the dose rate constant of the model BT-125-1 ^{125}I seed; the TLDs were placed at radial distances of 0.5, 0.7, 1.0 to 10.0 cm with a 0.5 cm increment and a 5° step, to study the radial dose functions of the model BT-125-1 ^{125}I seed. The seed was placed horizontally in the center of the PMMA phantom, and the TLDs were placed vertically to the longitudinal axis of the seed at radial distances of 0.5, 1, 1.5, 2, 3 to 7 cm with a 1 cm increment, and polar angles in 20° increments at the radial distance of 0.5 cm, while polar angles in 10° increments at the other radial distances, to study the anisotropy functions of the model BT-125-1 ^{125}I seed.

Results: For the model BT-125-1 ^{125}I seed, the maximum deviation of repeatability for TLDs was 4.0%. The TLDs had linear dose response without dose rate effect, but the dose response is energy dependent. The dose rate constant, radial dose functions and anisotropy functions were similar to the model 6711 ^{125}I presented in the TG43 U1 report.

Conclusions: The thermoluminescent dosimetry presented the dose rate constant, radial dose functions and anisotropy functions of the model BT-125-1 ^{125}I seed which were similar to those of model 6711 ^{125}I seed presented in the TG43U1 report.

PS04.124 - Phantom-based evaluations of two binning algorithms for four-dimensional CT reconstruction in lung cancer radiation therapy

Author(s): Fuli Zhang, Yd Wang
Radiation Oncology Department, The Military General Hospital of Beijing PLA, Beijing/CHINA

Objective: The purpose of this study was to evaluate the performance of the phase-binning algorithm and amplitude-binning algorithm. **Methods:** Quasar phantom data were used for evaluation. A phantom of known geometry was mounted on a four-dimensional (4D) motion platform programmed with twelve respiratory waves (twelve lung patients trajectories) and scanned with a Philips Brilliance Big bore 16-slice CT simulator. 4DCT images were reconstructed using both phase- and amplitude-binning algorithms. ITV (internal target volume, ITV) volumes of the phase- and amplitude-binned image sets was compared by evaluation of shape and volume distortions. **Results:** The phantom experiments illustrated that, as expected, maximum inhalation occurred at the 0% amplitude and maximum exhalation occurred at the 50% amplitude of the amplitude-binned 4DCT image sets. The amplitude-binned algorithm rendered smaller ITV than the phase-binning algorithm. **Conclusions:** the amplitude-binning algorithm for 4DCT reconstruction may have a potential advantage in reducing the margin and protecting normal lung tissue from unnecessary irradiation

PS05 - TRACK 05: DOSIMETRY AND RADIATION PROTECTION

PS05.005 - Dose analysis for paediatric patients under cardiac catheterization at Hamad General Hospital in Qatar.

A.E.Aly, H.A. Al-Saloos, H.M. Al Naemi
Hamad Medical Corporation, Qatar

Author(s): Antar Aly

Hamad Medical corporation, Doha/QATAR

Abstract

The risks associated with radiation exposure are higher in children compared adults. The use of fluoroscopy in common pediatric examinations such as left and right heart (L&R), patent ductus arteriosus (PDA), atrial septal defect (ASD), pericardial tap, patent truncus arteriosus (PTA) are the common procedures for paediatric undergoing cardiac catheterization requires accurate determination of the associated effective dose. In this study the results of an analysis of doses recorded for 198 paediatric patients for the last 2 years 2013 and 2014 carried out on pediatric patients.

Materials and Methods

One X-ray fluoroscopy machine from Hamad Medical Corporation (HMC) in Hamad General Hospital in the state of Qatar performing interventional Cardiology procedures used in this study. Database includes patient age, gender, procedure type and fluoroscopy time; Kerma Area Product (KAP) and Cumulative dose data were recorded for 198 patients. The average paediatric age, weight, and height were 3.03 year, 13.8 kg and 88.4 cm respectively. Peak voltage was 60.8kVp – 80 kVp .

Results and discussion.

Figure 1 and table 1 illustrate the common cardiac catheterization procedures for paediatric patients. The average KAP ± SD of cardiac catheterization was 956.7 ± 1278.23 cGy × cm². The average fluoroscopic time ± SD was 11.83 ± 9.7 minutes for children . The Cumulative Dose Interventional Reference point (CD_IRP) was 113.4± 45.4 mGy. Body weight is an effective indicator of KAP for cardiac catheterization procedures in children as shown in **figure 2**. It's clear in figure 3 also good correlation between KAP/BW and KAP (R²= 0.7) for the paediatric patients less than or equal 6 years of age .

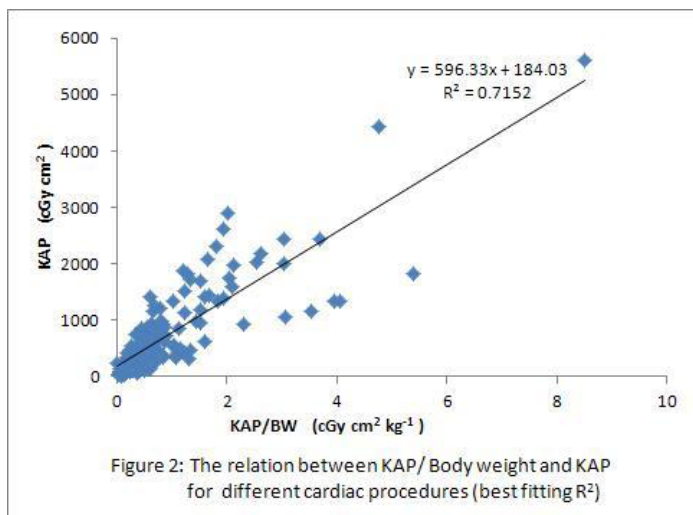
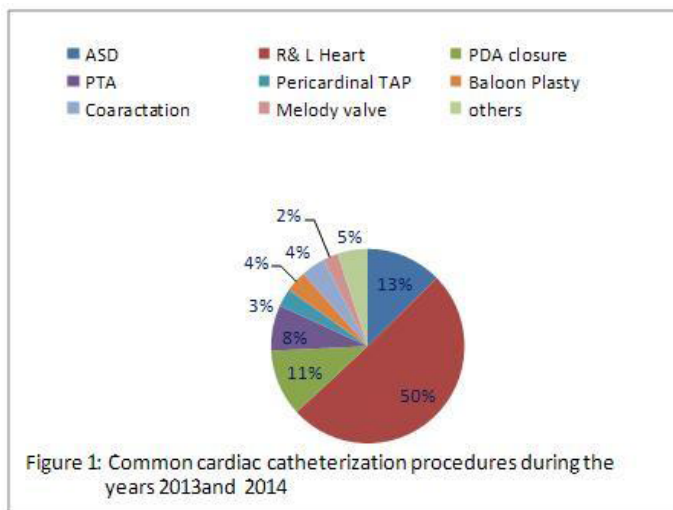


Figure 2: The relation between KAP/ Body weight and KAP for different cardiac procedures (best fitting R²)

Table 1: Mean Kerma area product, Mean fluoroscopy time and Mean CD_IRP for different procedure .

Heart disease	No. of patients (n=198)	Mean fluoroscopy time (min.)	Mean KAP/W (cGy×cm ² xkg ⁻¹)	Mean CD mGy
ASD	25	18.5	864.2	88.8
R&L heart	100	17.86	925.17	118.1
PTA	15	11.2	815	113.6
Balloon	7	8.1	67	73
PDA	22	4.41	308.8	40.2

PS05.006 - In vivo dosimetry implementation with diodes at the National Radiotherapy Center of the Korle-Bu Teaching Hospital, Ghana

Author(s): Vivian Della Atuwu-Ampoh¹, Cyril Schandorf², Samuel N.A. Tagoe³, Eric K. Addison⁴

¹Medical Physics, School of Nuclear and Allied Health Sciences, University of Ghana Atomic Ghana, Accra/GHANA, ²School Of Nuclear And Allied Sciences, University of Ghana - Atomic Campus, Accra/GHANA, ³National Centre For Radiotherapy And Nuclear Medicine, Korle-Bu Teaching Hospital, Accra/GHANA, ⁴Oncology Directorate, Komfo Anokye Teaching Hospital, Kumasi/GHANA

Protocol for in vivo dosimetry using silicon diodes in radiotherapy department of the Korle-Bu Teaching Hospital is implemented. The diodes were calibrated using IAEA standards (TRS 389); correction factors were determined with solid water phantom and then implemented on patients.

The phantom studies conducted established that the mean deviation (Δ± σ, %) between the measured and expected entrance doses was (0.34 ± 1.8%). Almost all were within ±5% as recommended by international standards .

The sites of measurement included; pelvis (n=60), head & neck (n=13), breast (n=48) and other cases (n=13) with corresponding mean deviations of 1.92± 4.05%, 0.15 ± 4.0%, 0.12 ± 4.20% and 1.66 ± 3.23% respectively.

Results obtained from patient measurements were comparable to works published in the literature. An overall mean deviation of 1.02%±4.1% was observed (n=134). The percentage of measurement (N %) for which the deviation was within the 5% tolerance was 79.85%. About 3.73% of the total deviations were beyond 7%.

However, two actions levels were adopted for this study as 5% and 7% for simple and tangential fields respectively in line with similar studies using diodes in Poland.

The few major deviations that were however recorded can be attributed to sources of errors (wrong beam parameters) such as depth, wedges and the inability to precisely position the dosimeter in blocked and wedged fields.

There is more room for reduction of uncertainties associated with the measurement protocol by carefully limiting or avoiding all the errors

PS05.007 - Assessment of radiation dose due to radio frequency emitted from medical high voltage modules

Author(s): Mosa Moradi¹, Alireza Kamali Asl¹, Mohammad Reza Ay²
¹Radiation Medicine, Shahid Beheshti University, tehran/IRAN, ²Department Of Medical Physics & Biomedical Engineering, Tehran University of Medical Sciences, Tehran/IRAN

Public and occupational exposure of electromagnetic fields due to the growing trend of electronic devices may cause adverse effects on human health. The effects of radiofrequency (RF) radiation absorption on human health can be expressed as high temperature and thermal effects on body tissue. But it also lead to cancer in the body, especially the in head and nervous system. In this study, the dose resulting from the high voltage power supply (HVPS) that has built for the Single Photon Emission Computed Tomography (SPECT) system has been measured. Also, risks arising from the waves, according to a report by International Commission on Non Ionizing Radiation Protection (ICNIRP), to every organ of the body is defined by the beam and electromagnetic radiation from this electronic device on the human was investigated. In this study, the dose of high voltage module in switching mode at different frequencies using a scintillation detector was measured. Results showed that the maximum personal dose over 15 min working of mentioned HVPS don't exceed from 0.31 μ SV/h (With aluminum shield). So, according to other sources of radiation, continuous working time of the system should not be more than 10 hours. Finally, a characteristic curve for secure working with modules at different frequencies been has reported. The RF input signal to the body for maximum penetration depth (δ) and specific electromagnetic energy absorption rate (SAR) of biological tissue can be obtained for each tissue.

PS05.008 - Software Assisted Skin Dose Calculation in Fluoroscopically Guided Interventional Procedures

Author(s): Mohamed K. Badawy¹, Daniel Carrion²
¹Medical Sciences, RMIT, Bundoora/AUSTRALIA, ²Independent, Melbourne/AUSTRALIA

Background

Patients undergoing fluoroscopically guided interventional procedures are subjected to ionising radiation which may lead to radiation injury. In order to predict the likelihood of radiation induced injury following a procedure a skin radiation dose estimation method must be employed. In order to achieve an accurate skin dose estimation from current monitoring methods, many factors must be taken into consideration and corrected for mathematically.

Objective

This presentation aims to instruct the audience how to calculate skin dose following a fluoroscopically guided procedure automatically by using the data provided in Digital Imaging and Communications in Medicine (DICOM) file headers and a simple Java program.

Methods

Using a Java program the audience is instructed in automating skin dose calculations for patients undergoing interventional procedures. This method relies heavily on manufacturer provided information found in the headers of DICOM files. The dcm4che project Java libraries are used in the Java program to interrogate this information from the DICOM files when calculating skin dose. This method is validated using direct measuring techniques to determine entrance skin dose which is then compared to values calculated by the program.

Results

The Java program is successfully used to calculate entrance skin dose following fluoroscopically guided procedures. However, there are many limitations that must be taken into considerations should this method be employed clinically. Validation of the program following corrections made for each unit provide accuracy to within 10%.

Conclusion

A Java program can be set up to automatically calculate the entrance skin dose from DICOM files following an interventional procedure. If limitations are taken into consideration this method proves accurate to within 10%.

PS05.009 - Current Statuses of a-Si EPID Dosimetry: An Application for Dose Verification in Standard Radiotherapy Techniques

Author(s): Omeh Bawazeer¹, Siva Sarasanandarajah¹, Sisira Herath², Tomas Kron², Pradip Deb¹
¹School Of Medical Radiation, RMIT University, Melbourne/AUSTRALIA, ²Radiation Oncology, Peter MacCallum Cancer Centre, Melbourne/AUSTRALIA

As radiotherapy becomes more complicated, a required of dose verification is strongly recommended. Electronic portal imaging device (EPID) is a promising detector to use with the dose verification of radiotherapy technique. This is due to its advantages compared to other detectors, such as a high spatial resolution, large imaging area, and real-time acquisition and less setup time. Therefore, the implementation of EPID for dosimetry purpose in clinical practice has currently received a great attention with the increasing the need of dose verification [1, 2]. The purpose of this study is to firstly list the commercially available solutions for EPID dosimetry. Secondly offer the solutions that used to improve the performance accuracy of EPID dosimetry. Thirdly summarize clinical or proposed approaches based on EPID dosimetry for different radiotherapy techniques. The previous publications demonstrated a variety of reliable and accurate dose verification methods used based on EPID for intensity modulated radiotherapy (IMRT) while the dose verification with volumetric modulated arc therapy (VMAT) and stereotactic ablative body radiotherapy (SABR) is still under development [3-5], see Figure 1. However, further efforts are needed to optimize the time required for verification procedure based on EPID. Also, further research is required to study the possibility of replaced pre-treatment verification with in vivo verification. This may have the benefit of reduced workloads in clinical practice.

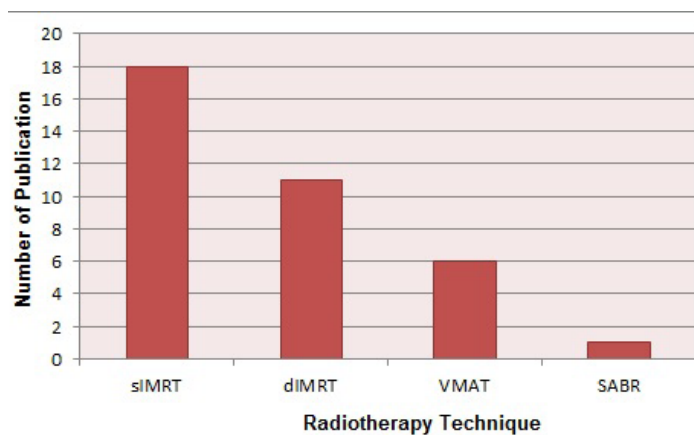


Figure 1: The current statuses of a-Si EPID in dose verification

Selected reference:

1. van Elmpt, W., et al., *A literature review of electronic portal imaging for radiotherapy dosimetry*. *Radiother Oncol*, 2008. **88**(3): p. 289-309.
2. Greer, P.B. and P. Vial, *EPID dosimetry*, in *Concepts and trends in medical radiation dosimetry: Proceedings of SSD Summer School*. 2011, AIP Publishing. p. 129-144.
3. Sabet, M., et al., *Transit dosimetry in dynamic IMRT with an a-Si EPID*. *Medical & biological engineering & computing*, 2014: p. 1-10.
4. Wendling, M., et al., *In aqua vivo EPID dosimetry*. *Med. Phys*, 2012. **39**(1): p. 367-377.
5. van Elmpt, W., et al., *3D dose delivery verification using repeated cone-beam imaging and EPID dosimetry for stereotactic body radiotherapy of non-small cell lung cancer*. *Radiother Oncol*, 2010. **94**(2): p. 188-194.

PS05.010 - Nanodosimetry of protons in the Bragg peak region based on ionisation cross sections of DNA constituents

Author(s): Daniel Bennett, Benedikt Rudek, Mingjie Wang, Marion Bug, Gerhard Hilgers, Hans Rabus
 Fundamentals Of Dosimetry, Physikalisch-Technische Bundesanstalt (PTB), Braunschweig/GERMANY

The spatial distribution of energy deposited at the micro- and nanometre scale plays a crucial role in the radiobiological effectiveness of different radiation qualities [1]. Realistic numerical simulation of this distribution is fundamental to nanodosimetry and can be obtained using dedicated Monte Carlo track structure codes. Experimental nanodosimetry also benefits from these computer simulations, particularly for checking the detector response in a well characterised field and geometry. However, these track structure simulations rely heavily upon theoretical and measured interaction cross section data. Due to the absence of a complete set of ionisation cross sections for DNA in the literature, it is common practice in track structure simulations to use liquid water as a substitute for biological material.

Conducted within the framework of the European Metrology Research Program, the research project "BioQuaRT" [2] aims to develop a track structure simulation code based on a multi-scale approach and on interaction cross sections of DNA components. To achieve this aim, this work focuses on the measurement of double differential cross sections for the ionisation of pyrimidine, tetrahydrofuran and trimethylphosphate by protons with energies in the Bragg peak region. The first molecule represents two of the DNA

bases, and the other two molecules represent the sugar and the phosphate residue of the DNA backbone. The experiments were carried out in our group's 150 keV ion accelerator. An electrostatic hemispherical electron spectrometer was used to detect the secondary electrons emitted at angles between 15° and 135° relative to the ion beam direction.

These ionisation interaction cross sections of DNA constituents are in the process of being evaluated and integrated into the multi-scale track structure code to obtain nanodosimetric quantities in biological matter and to benchmark the performance of nanodosimeters. Results will be presented at the conference.

References

- [1] D. Brenner and J. Ward, *Int J Radiat Biol*. 61, 737-748 (1992)
- [2] Project web site: <http://www.ptb.de/emrp/bioquart.html>

Acknowledgements: The EMRP is jointly funded by the participating countries within EURAMET and the European Union.

PS05.011 - Micronuclei assessment of Selenium and Vitamin E radioprotective effects in human lymphocytes

Author(s): Vahid Changizi, Aram Rostami
 Technology Of Radiology And Radiotherapy, Tehran University of Medical Sciences, Tehran/IRAN

Intoduction

Critical macromolecules such as DNA are in exposure to damage of free radicals that induced from interaction of ionizing radiation with biological systems. selenium and vitamin E are natural compounds that have been shown to be a direct free radical scavenger. The aim of this study was to investigate the in vivo/in vitro radioprotective effect of selenium and vitamin E against genotoxicity induced by 6MV x-ray irradiation in human cultured blood lymphocytes.

Methods:

Five volunteers received selenium and vitamin E. Their peripheral blood samples were collected before and 1, 2 and 3 hours after taking selenium and vitamin E. The samples were exposed to 2Gy of 6MV x-ray, and then were cultured with mutagenic stimulation to determine the chromosomal aberration with micronucleus assay on cytokinesis-blocked binucleated cells.

Result:

The lymphocytes in the blood samples collected at 1 hr after ingestion selenium and vitamin E, exposed in vitro to x-rays exhibited a significant decrease in the incidence of micronuclei, compared with control group at 0 hr. The maximum protection and decrease in the frequency of micronuclei(50%) was observed at 1 hr after administration of selenium and vitamin E.

Conclusion:

Selenium and vitamin E could be as radioprotector substances and may reduce genetic damage caused by x-ray irradiation.

PS05.012 - The Organ and Skin Dose Distribution in Total Body Irradiation

Author(s): Jeongmin Yoon, Jungil Lee, Ho Lee, Samju Cho, Eungman Lee, Woonhoon Choi
Radiation Oncology, Yonsei University Health System, Seoul/KOREA

Purpose:

To achieve uniform dose distribution is the most important in total body irradiation. The aim of this work is to verify the organ dose distribution and skin dose distribution using OSLD within $\pm 10\%$ of the prescribed dose.

Materials and Methods:

An Adult male phantom (CIRS, Model 701, Φ 14mm hole placement for nanoDot) was irradiated bilateral total body technique. We placed optically stimulated luminescence detectors (OSLDs) inside the adult male phantom to measure the dose at brain, neck, lung, abdomen, pelvis and thigh. At the same time we placed OSLDs on adult male phantom to obtain skin dose during bilateral irradiation. The phantom was set at 410cm of source-axis distance (SAD) and irradiated with field size $164 \times 164 \text{ cm}^2$ ($40 \times 40 \text{ cm}^2$ at SAD 100cm) which covered the entire phantom with 10MV x-ray (Agility, Elekta Ltd, Crawley, UK). The prescription dose is 150cGy per fraction. We used aluminum compensators to adjust the thickness of tissue deficit easily.

Results:

From the OSLDs measurements, we obtained inside dose of phantom at the various anatomical regions. The differences from the prescription dose were shown: 0.8% (brain), 8.9% (neck), -2.64% (lung), +6% (abdomen), 0.78% (pelvis), -1.13% (thigh). We also checked the skin dose at the same organ plate positions: -8.5% (brain), -2.1% (neck), -0.9% (lung), 0.4% (abdomen), -4.3% (pelvis), 0% (thigh). All of the measured points showed within $\pm 10\%$ of the prescribed dose. As the results, we could achieve the homogeneous dose distribution of organ and skin during total body irradiation.

Conclusions:

The OSLDs results showed not only the organ homogeneous dose distribution but also skin uniform dose distribution during total body irradiation

Key words:

Total body irradiation, Organ and skin dosimetry, OSLD, Adult male phantom

PS05.013 - Comparison of 6MeV and 9MeV Electron Beams for Total Skin Irradiation

Author(s): Ricardo Contreras, Erick O. Montenegro, Erick E. Hernandez, Juan F. Lucero, Luis G. Garcia, Rafael E. Lengua, Luis A. Linares
Medical Physics, HOPE International Radiotherapy Center, Guatemala/GUATEMALA

The total skin irradiation (TSI) is used to treat the Cutaneous T cell Lymphoma. The objective is to radiate superficially (3 to 5mm of depth) and evenly the entire patient's skin. The prescription dose is 36Gy in 1Gy daily fractions, 4 times a week. Protections for the eyes, gonads, nails and lips must be constructed.

The present work presents the comparison of two electrons beams (6 MeV and 9 MeV) generated by a Varian Clinac iX.

The Stanford technique was used. The distance calculated from the source to the patient was 3.90m.

Materials:

Varian Clinac iX linear accelerator, patient positioning platform, acrylic scattering screen (10mm thickness), IBA I'mRT phantom, PTW UNIDOS E electrometer, plane parallel ionization chamber PTW ROOS, PTW RW3 solid water phantom, GAFCHROMIC EBT3, EPSON PERFECTION V700.

Methods:

When using the Stanford technique, it's necessary to have a region of about 1.80m, depending on the patient's height, in which the field flatness is guaranteed to be below $\pm 10\%$ of variation. Because of the adaptors provided by the manufacturer, the field size was $36 \times 36 \text{ cm}$ for the 9MeV and $34 \times 34 \text{ cm}$ for the 6MeV beam. Since a single radiation field does not provide the desired flatness. It is indispensable to use two complementary fields that contribute 50% each and assure the desired flatness. The angle needed is calculated finding the 50% of a single irradiation field. The dose profile was measured using the gantry angles found, and it was below $\pm 10\%$ of variation for both energies.

Using the RW3 at treatment distance, the ionization chamber, the ionization-depth curve was found, from where the dose output was calculated.

Six different patient positions are used to complete a total irradiation, using three each day. These positions were simulated on the IBA phantom to obtain the dose distribution on a plane.

Results:

Measure	6 MeV	9 MeV
R100	3 mm	9 mm
R90	6 mm	14 mm
R80	8 mm	17 mm
R50	11 mm	22 mm
R10	15 mm	25 mm
Output	0.0635 cGy/MU	0.3911 cGy/MU
Gantry Angle	17.5°	15°
Treatment Time	3.5 min	48 min

Conclusion:

The best suited energy for the case is 6 MeV although the output is much smaller, translating to a longer treatment time.

References:

- AAPM Report 23; Total skin electron therapy: Technique and dosimetry.
- M.E.R Poli; Dose Measurements in the Treatment of Mycosis Fungoides with Total Skin Irradiation using a 4MeV Electron Beam
- S. Lloyd Morris; Results of a 5-Week Schedule of Modern Total Skin Electron Beam Radiation Therapy
- Eric P. Reynard; Rotational total skin electron irradiation with a linear accelerator

PS05.014 - Analysis of Informal Commerce Sunglasses using Spectroscopy**Author(s):** Juan Alberto L. Cruz, Tertuliano T. Neto, Ernando S. Ferreira

Department Of Physics, State University of Feira de Santana, FEIRA DE SANTANA/BRAZIL

Despite a growing of literature on the adverse biological effects of ultraviolet radiation on eyes and skin, a considerable number of persons follow buy sunglasses in informal commerce establishments, for photoprotection of the eye exposure at the ultraviolet radiation in sunlight. The main goal of this work was to perform experiments to verify if the sunglasses lenses with their filters types provide or not protection against ultraviolet radiation (280 – 380nm), in agreement with the specification of the European British Standard norm EN1836:2005, EN 1836. The experimental setup is basically composed by radiation sources (60 W white light and mercury lamps), which passes through the sunglasses lenses, and transmitted electromagnetic radiation is collected and guided by a optic fibre of 1 mm of diameter and 1 m of length connected to a spectrometer USB4000 from Ocean Optics. Then the spectrometer is coupled to a computer through which the measurements are controlled and analyzed using the Spectra Suite software. The spectrometer were configured to performed, transmission spectroscopy, to evaluate the lenses filtering power to ultraviolet radiation of 21 sunglasses pairs (42 lenses) commercialized in informal establishments of Feira de Santa city, in Bahia, Brazil. The results from the transmittance experiments in the visible, all lenses of the sunglasses were classified in categories according to requirements of the Standard norm mentioned above. From the analyze of the results obtained in the transmittance experiments with the UV radiation, 04 sunglasses of 21 (19,04%) were considered no conforms because they allow the passage of ultraviolet radiation between 280 and 380 nm, and could produce adverse biological effects on eyes in accordance with the standards.

PS05.015 - Dosimetric Evaluation Of Lung Dose Using Indigenously Developed Respiratory motion phantom**Author(s):** G Dheva Shantha Kumari¹, Shanmugam Senthilkumar²
¹P.g. Dept. Of Physics, Fathima College, Madurai/INDIA, ²Radiotherapy, Govt. Rajaji Hospital & Madurai Medical College, Madurai/INDIA**Introduction**

Respiration induced organ motion is one of the major uncertainties in lung cancer radiotherapy, which may cause clinically significant targeting errors and greatly degrade the effectiveness of conformal radiotherapy. Motion of the tumor due to respiration during the radiation treatment process is difficult to manage. Without managing the respiratory motion, the critical organs may receive high radiation dose with decreasing target dose. Intrafraction motion is an issue that is becoming increasingly important in the era of IMRT. Intrafraction motion can be caused by the respiratory, skeletal, muscular, cardiac and gastrointestinal systems. The main aim of the present study was to evaluate the lung dose in the presence of respiratory movement and absence of movement in lung and also compare the dosimetric difference using indigenously developed Respiratory Gating Platform.

Material and Methods

Respiratory motion platform (RPM) was designed indigenously and constructed for testing the targeting accuracy of the lung tumor in respiratory condition. It consists of acrylic Chest Wall Platform, 2 DC motors, 4 IR sensors, speed controller circuit, 2 LEDs and 2 moving rods. The essential component of the device is a movable platform mounted to a base using precision linear bearings. The base and platform are made of clear, 15mm thick polycarbonate plastic. The

platform is driven along a linear trajectory using a motor controller that drives a stepper motor attached to the Bi-slide assembly. The targeting accuracy of the respiratory tracking system was evaluated with varied amplitude of skin motion, respiratory rate and tumor distance. The device was designed to be able to simulate the gross anatomical anterior posterior motion attributable to respiration-induced motion of the lung. Depending on the particular application, an appropriate phantom would be placed on the platform. Speed of motion is controlled by Control knob. This parameter controls the period, or how fast one breath cycle in seconds takes place. This value can be adjusted in 1/2 second intervals between 2 and 6 seconds.

Results:

The RMP was used to measure the 20 lung tumor patients with treatment planning system (TPS) calculated dose in both the respiratory and non respiratory condition. We have found 3% dose difference between the TPS calculated dose and measured value with the help of RMP in respiratory and non respiratory condition. So, for lung cancer radiotherapy treatment, respiratory motion has to be taken for better dose delivery to the lung tumor.

PS05.016 - Activation of Medical Linear Accelerators**Author(s):** Adam C. Dodd

Accelerators, Canadian Nuclear Safety Commission, Ottawa/CANADA

Purpose: Radioactivity is induced in medical linear accelerators (linacs) operating at high energies for extended periods of time through photoneutron reactions and subsequent neutron capture. The disposal of linacs is a potential health hazard especially for workers engaged in recycling the tungsten parts. New gamma spectroscopy data and recent experimental data on neutron production in combination with published Monte Carlo results have enabled a general analysis of the longer lived radioactivity induced in linacs.

Methods: A mechanically cooled high purity germanium detector placed at isocentre was used to identify the gamma emitting isotopes for a Truebeam STX. Self absorption correction factors are derived from the data by a differential absorption analysis. Neutron production data in combination with Monte Carlo results are used to determine the activities of pure beta and electron capture radioisotopes.

Results: The principal activities with half-lives longer than 1 day are W-181, W-185, Co-57, Co-60 & Mn-54. Results are presented for Elekta, Siemens and Varian models as a function of beam energy, workload and operating lifetime. The length of time activated components from a decommissioned linac should be kept before they can safely be disposed of is presented for Elekta, Siemens and Varian models.

PS05.017 - Assessment of Patient Dose in Selected Non-Cardiac Interventional Fluoroscopy Procedures Using OSL Dosimeters**Author(s):** Isabel A. Elona

Center For Device Regulation, Radiation Health, And Research, Department of Health - FDA, Manila/PHILIPPINES

In recent years, interventional procedures have composed a major part in diagnostic radiology and increasingly replaced many surgical procedures. Despite its advantages, the utilization of ionizing radiation for diagnosis delivers radiation doses which present risk to the patient. The fundamental principles of radiation protection call for exposures to patients that are As Low as Reasonably Achievable (ALARA). The purpose of this study was to assess the level of radiation from selected non-cardiac interventional fluoroscopy proce-

dures at the University of Santo Tomas Hospital, Cardiac Catheterization Laboratory. Radiation dose measurements, using Optically Stimulated Luminescence Dosimeters (OSLD) were performed on 4 patients on femoral angiogram and hepatic embolization. The results showed that interventional procedure such as embolization of the liver may exceed the threshold value for deterministic effects.

PS05.018 - Measurement of Photon and Neutron Dose Distribution in Cyclotron Bunker During F18 and N13 Production

Author(s): Pardis Ghafarian¹, Seyedeh Masoumeh Khamesi¹, Mohammadrasa Golrokh Nodehi¹, Mohammad Reza Ay²

¹Chronic Respiratory Diseases Research Center, National Research Institute Of Tuberculosis And Lung Diseases (nritld), Shahid Beheshti University of Medical Sciences, tehran/IRAN, ²Department Of Medical Physics & Biomedical Engineering, Tehran University of Medical Sciences, Tehran/IRAN

Introduction: Self-shield hospital cyclotrons have been received a considerable attention due to have compact size and no necessity for concrete bunker. It is well known that during the bombardment of target in cyclotrons, neutron and gamma flux are produced. However, the activation caused by neutron interaction has considerable radiological hazard in cyclotron components. For safety purpose, measuring of neutron and photon dose rate in the area close to the shield are mandatory. In this investigation we measured the neutron and photon dose rate during 18F and 13N productions in different distance from radiation shield of GE PET Trace 700 the self shield cyclotron that recently installed in Masih Daneshvari hospital.

Material and methods: Dose rate measurement were done by neutron dosimeter (LB 6411) and Geiger Mueller dosimeter (BNS-92) during the operation of the cyclotron using different target current at various distance (from 0.5 to 2.5 meter) of self-shield cyclotron in step of 0.5 meter around the cyclotron. All measurements were done at the floor level and also the height of one meter (target position).

Results: With increasing target current from 30 to 35μA at the distance of 0.5 meter at the gap between left and right doors, the gamma dose rate varies from 8.9 to 10.7 μSv/h and decreasing neutron dose rate were obtained from 10 to 5.2 μSv/h with increasing distance from 0.5 to 2.5 meter at the height of one meter, during the F-18 production. Whereas the gamma dose rate increases from 2.86 to 8.6 μSv/h at the distance of 0.5 meter from cyclotron during N-13 production with increasing of operation current from 30 to 35μA. at 2.5 meter far from cyclotron at the interface of left and right doors this quantity reduced to 2 μSv/h at 35μA target current.

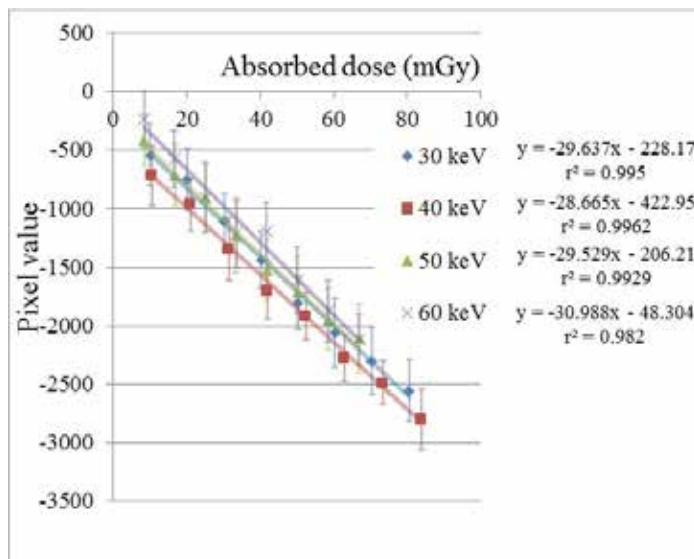
Conclusion: the low level of neutron and gamma dose rate outside the self-shield of cyclotron indicated that the polyethylene and concrete component used in GE PET Trace 700 cyclotron can produce nearly safe condition for entire the cyclotron bunker.

PS05.019 - Energy response of the GAFCHROMIC EBT3 in diagnosis range

Author(s): Tatsuhiko Gotanda¹, Toshizo Katsuda², Rumi Gotanda³, Tadao Kuwano⁴, Takuya Akagawa⁵, Nobuyoshi Tanki⁶, Akihiko Tabuchi⁷, Tetsunori Shimonoi⁸, Yasuyuki Kawaji⁹, Tadimitsu Ideguchi¹

¹Department Of Radiological Science, Faculty Of Health Sciences, Junshin Gakuen University, Fukuoka/JAPAN, ²Department Of Human Relation, Tokai Gakuin University, Kakamigahara/JAPAN, ³Department Of Radiological Sciences, Ibaraki Prefectural University of Health Sciences, Inashiki-gun, Ibaraki/JAPAN, ⁴Osaka Center for Cancer and Cardiovascular Diseases Prevention, Osaka/JAPAN, ⁵Department Of Radiological Technology, Tokushima Red Cross Hospital, Tokushima/JAPAN, ⁶Center For Life Science Technologies, RIKEN, Kobe/JAPAN, ⁷Kawasaki Medical School Kawasaki Hospital, Okayama/JAPAN

Although GAFCHROMIC EBT3 (EBT3) as a radiochromic film shows only slight energy dependency errors in comparison with other radiochromic films, the influence of energy dependence in the diagnosis energy range (less than 100 keV) is larger in the high energy range (over 100 keV). Based on this characteristic, adaptation of the EBT3 dosimetry in the diagnosis range was investigated. The energy response of the EBT3 in the diagnosis range at 30, 40, 50, 60 keV was measured using the density-absorbed dose calibration curve of the absorbed dose versus film density for the EBT3. Various data (degree of leaning, coefficient of determination) of each effective energy were compared. The density - absorbed dose calibration curves were linearly correlated in each of the effective energies. There was an energy dependent error of approximately 0.2 % from 30 to 60 keV (Fig. 1). As a result, it can be seen that the EBT3 is available in the diagnosis energy range. However, the influence of the non-uniformity error caused by the repeatability of the scan method must be considered because EBT3 distortion has a serious influence on measurement precision.



PS05.020 - Estimation of In Vivo Dosimetry Accuracy with Dose-Volume Histogram

Author(s): Victor A. Gurvich¹, John M. Pacyniak¹, Delnora Erickson²

¹Government Contractor In Radiology Clinic, Fort Belvoir Community Hospital, Fort Belvoir/UNITED STATES OF AMERICA, ²Radiation Oncology, Fort Belvoir Community Hospital, Fort Belvoir/UNITED STATES OF AMERICA

In vivo dosimetry is widely used for verification of the absolute dose received by patient during radiation treatment delivery. The difference between measured dose and calculated at the same point with treatment planning system (TPS) often exceed 5% and depends on patient's setup variation, organ movement and dose gradient in the point of measurement. The purpose of this study is the estimation of uncertainties and dose accuracy measured with small dosimeters like TLD, OSLD or MOSFET during radiation treatment delivery.

Our novel method for dosimetry measurements takes into consideration distance-to-agreement between measured and calculated points. However, instead of gamma index used as QA criteria in IMRT we apply a dose-volume histogram (DVH) for the area of assumed infra- and inter-fraction movement of measurement point. This area called a region of measurement (ROM) includes all most probable measurement points and can be contoured with TPS tools as organ at risk. Both cumulative and differential DVHs can be used for the analysis of in vivo dosimetry accuracy in the established acceptable dose interval. In our experiments we scanned an anthro-

pometric phantom with Philips Brilliance Big Bore CT simulator and established measurement points in three regions: head & neck, chest, and pelvis. Then 3D conformal treatment plans for head and lung areas and IMRT plans for prostate were created. The prescribed dose for targets was 200 cGy per fraction.

The radiation dose was measured in given points using OSLD and MOSFET dosimeters. Analyzing the DVH we defined the acceptable dose interval from D80 to D20. These intervals (and measured doses) were 184.6 – 210.4 (measured 191.1) cGy for the head and neck plan, 83.7 – 92.7 (87.1) cGy for lung, 73.6 – 89.3 (74.3) cGy for prostate IMRT and 62.0 – 86.4 (64.0) cGy for prostate rapid arc plan. The length of dose intervals depended on the treatment site, location of measurement point, size of ROM, and type of treatment plan. In all studies the measured doses fell into the given acceptance interval, thereby validating the novel method as a way to perform real-time dosimetry.

The proposed method allows estimating the accuracy of delivered dose taking into account the displacement of the measurement point. It applies flexible and justified acceptance criteria. It is possible to define the limits of dose deviation during a treatment planning process. The influence of distance and direction of the measurement point displacement as well as ROM heterogeneity on dosimetric accuracy can be quantitatively analyzed.

PS05.021 - Evaluation of the dosimetric properties of water equivalent microDiamond detector in high energy photon beam.

Author(s): Hyun Do Huh¹, Chang Yeol Lee¹, Woo Chul Kim¹, Young Hoon Ji², Hun Jeong Kim¹, Sang Hoon Lee³, Chul Kee Min⁴, Kum Bae Kim², Gwang Hwan Jo⁵, Dong Oh Shin⁶, Seong Hoon Kim⁷
¹Radiation Oncology, Inha University Hospital, Incheon/KOREA, ²Research Institute of Radiological and Medical Sciences, Korea Institute of Radiological and Medical, Seoul/KOREA, ³Department of Radiation Oncology, College of Medicine, Kwandong University, Gangdeung, Seoul/KOREA, ⁴Department of Radiation Oncology, College of Medicine, Soonchunhyang University, Cheonan/KOREA, ⁵Department of Radiation Oncology, College of Medicine, Soonchunhyang University, Boocheon/KOREA, ⁶Department of Radiation Oncology, College of Medicine, Kyunghee University, Seoul/KOREA, ⁷Department of Radiation Oncology, College of Medicine, Hanyang University, Seoul/KOREA

The aim of this study was to evaluate the characteristic of a water equivalent synthetic diamond detector (PTW 60019 microDiamond, Germany) for the small field dosimetry in high energy photon beam. We have obtained data in cyberknife 6 MV photon beams of six different collimator size (from 5mm to 30 mm). Data were included dose linearity, dose rate dependence, output factors (OF), percent depth doses (PDD) and off center ratio (OCR). The results were compared to those of pinpoint ionization chamber, Old diamond detector, microLion liquid ionization chamber and diode detector. The dose linearity results for the microDiamond detector showed good linearly proportional to dose. The microDiamond detector showed little dose rate dependency throughout the range of 100~600 MU/min, while microLion liquid ionization chamber showed a significant discrepancy of approximately 5.8%. The OF measured with microDiamond detector agreed within 3.8% with those measured with diode. PDD curves measured with silicon diode and diamond detector agreed well for all the field sizes. In particular, slightly sharper penumbras are obtained by the microdiamond detector, indicating a good spatial resolution. The results obtained confirm that the new PTW 60019 microDiamond detector is suitable candidate for application in small radiation field dosimetry. In future, we are evaluating using the Monte Carlo method in high energy photon beam.

PS05.022 - From simple to advanced dosimetry audits in radiotherapy: IAEA coordinated research

Author(s): Joanna IZewska, Pranabes Bera, Paulina Grochowska, Barbara Bencsik, Ahmed MeghziFene
 Nuclear Sciences And Applications, International Atomic Energy Agency, Vienna/AUSTRIA

A series of four coordinated research projects (CRPs) were conducted by the IAEA in 1995-2015 focusing on development of national quality audit programmes for radiotherapy dosimetry in low and middle income countries. The first CRP started with remote audits of beam output in reference conditions using thermoluminescent dosimetry (TLD). The audit programme was then extended through the second CRP to include dose audits in non-reference conditions for high energy photon and electron beams. The third CRP, concluded in 2012, has expanded the dosimetry audit tools to more complex techniques used for cancer treatment. New methodology has been developed and tested for dose audits of irregular fields shaped with multileaf collimators (MLC), dose in the presence of heterogeneities and 2D profiles of small photon MLC shaped fields. This audit programme was based on TLDs and radiochromic films and used specially designed phantoms. The current CRP, initiated in 2013, focusses on dosimetry audits for more advanced technology in radiotherapy dose delivery. Auditing methodology has been developed for remote verification of calculation of small beam output factors by treatment planning systems (TPS), film audit of MLC positional performance for intensity modulated radiotherapy (IMRT), film audit of single clinical IMRT field dose delivery and 'end-to-end' dosimetry audit (imaging, planning, dose delivery) for multiple field IMRT techniques using TLDs and radiochromic films. This approach of gradually increasing the audit programme complexity was adopted to learn from experience of previous audit steps and to apply consistently the methods for development, testing and analysis of results for subsequent audit steps.

The IAEA Dosimetry Laboratory has participated in the experimental part of the CRPs, developed new phantoms and conducted multi-centre pilot studies to test the newly developed methodologies. Following such studies, the CRP participants adopt the methodology and organize trial audit runs with local radiotherapy centres in their countries. In addition, the IAEA contributes to strengthening QA of national audit networks by exchanging dosimeters with national dosimetry laboratories. Through the link with the IAEA Dosimetry Laboratory, the national networks closely cooperate at the consecutive stages of developing the dosimetry audit methodology locally and by carrying out cross-measurements. In this way the national audit systems are interlinked to ensure that international and national radiotherapy dosimetry audit networks are working to the consistent levels and standards.

Overall, the IAEA has supported the establishment of several national audit groups for radiotherapy dosimetry and assisted in the development of methodology for a range of dosimetry audit levels, from basic to advanced. The scope of the dosimetry parameters included in subsequent audits corresponds to the evolving complexity of radiotherapy as more advanced technologies are becoming increasingly used for cancer treatment across the world.

Acknowledgments: D. Followill, S. Kry, D. Thwaites, J. Povall, D. Georg, W. Lechner, M. Tenhunen, M. Tomsej.

PS05.023 - Noise reduction of radiochromic film: median filter processing of subtraction image

Author(s): Toshizo Katsuda¹, Rumi Gotanda², Tatsuhiro Gotanda³, Takuya Akagawa⁴, Nobuyoshi Tanki⁵, Tadao Kuwano⁶, Kouichi Yabunaka⁷

¹Department Of Human Relation, Tokai Gakuin University, Kakamigahara/JAPAN, ²Department Of Radiological Sciences, Ibaraki Prefectural University of Health Sciences, Ibaraki/JAPAN, ³Department Of Radiological Science, Faculty Of Health Sciences, Junshin Gakuen University, Fukuoka/JAPAN, ⁴Department Of Radiological Technology, Tokushima Red Cross Hospital, Tokushima/JAPAN, ⁵Center For Life Science Technologies, RIKEN, Kobe/JAPAN, ⁶Graduate School Of Health Sciences, Okayama University, Okayama/JAPAN, ⁷Graduate School Of Medicine, Tokyo University, Bunkyo-ku/JAPAN

Pre-ultraviolet rays exposure is a useful method to reduce non-uniformity error of radiochromic films. However, dust and scratch noises such as spike noise disturb precise measurement. To reduce these noises, median filter processing is applied for pre-subtraction and subtraction images.

To reduce non-uniformity error of the thickness unevenness of Gafchromic EBT film, ultraviolet rays were exposed to correct data. There were three kinds of images obtained: first ultraviolet exposure image, second ultraviolet exposure image and the subtraction image of both. Median filter processing was performed on all these images. Eleven kinds of median filter radius factors (0.0 to 5.0) were applied using image analysis software. Data and graphs were then estimated.

The maximum pixels value of dust was 229 on the second ultraviolet exposure image of film 3. After median filter pre-processing, the pixel value of the noises were similar to the minimum value. A 2.0-radius median filter is a useful factor for processing.

Noise reduction that affected data of estimated images may be applied to measure radiation doses on a variety of radiochromic films. Ultraviolet exposure and subtraction method with median filter processing enable precise measurement and high spatial resolution dose distribution.

PS05.024 - Proposed Guidelines for Image Quality in Chest PA X-Ray Examinations in Bangladesh

Author(s): Shahed Khan

UCL, Twickenham/UNITED KINGDOM

Abstract— The common practice for chest PA examinations in Bangladesh employ low kV imaging. This practice involves low-contrast images and requires much larger radiation doses than those associated with higher beam energy. Thus, we propose a model relating the change of Entrance Surface Dose (ESD) in response to changes in beam energy, in accordance with European standards for diagnostic radiographic chest imaging to find the optimal ESD corresponding to values of kVp used in Bangladeshi hospitals.

Results show that in order to maintain the standards of Quality for Diagnostic Radiographic Image every 10kVp increase in beam energy must be followed by a decrease of 8/6 in ESD that corresponds to a reduction of 15% in the equivalent dose. Hence, the range of optimal ESD accounting for the kVps practiced for chest PA examinations is 5.6-10 mGy, which represents a factor of 35 above the recommended ESD.

Finally we investigate the effect of Body Mass Index (BMI) on optimal ESD for overweighted Bangladeshi patients. We find that, for each additional 1kg, the ESD must increase 18% in order to maintain standards for chest PA x-ray image.

PS05.025 - Evaluation of inhomogeneity correction using monte carlo simulation in stereotactic body radiation therapy (SBRT)

Author(s): Ji Na Kim¹, Hun Joo Shin², Hong Seok Jang³, Young Nam Kang³

¹Department Of Biomedical Engineering, College of Medicine, The Catholic University of Korea, Seoul/KOREA, ²Department Of Radiation Oncology, Incheon St. Mary's Hospital, College of Medicine, The Catholic University of Korea, Incheon/KOREA, ³Department Of Radiation Oncology, Seoul St. Mary's Hospital, College of Medicine, The Catholic University of Korea, Seoul/KOREA

Stereotactic Body Radiation Therapy (SBRT) requires high accuracy in order to protect surrounding normal tissue and destroy the tumor. The dosimetric behavior of the small beams used in SBRT in the presence of low-density inhomogeneities is critical for accurate dose optimization. In inhomogeneity materials for the lung, dose correction is not applied with the values calculated by applying the difference in calculation of the difference told that more than 30% are reported. Significant differences in dose calculation were made to compensate for heterogeneous material. However, the evaluation of dose calculation in molding the slope has not been accomplished. Integrated high-dose molding of slopes for dose calculation accuracy is critical. In this study, molding equipment for SBRT was acquired, including heterogeneous material, to evaluate the accuracy of dose calculation. The accuracy of treatment planning and measurement data, which applied the inhomogeneity correction factor made comparison with result of monte carlo simulation. To measure and evaluate the effects of heterogeneous medium, an inhomogeneity correction phantom is required. Inhomogeneity Correction Phantom (ICP) is able to insert the inhomogeneity materials, which have 12 types in each different electron density. Also it is able to adapt the EBT film and 0.125 cc ion chamber for measurement of dose distribution and point dose. In comparison with monte carlo simulation, the average difference applied the inhomogeneity correction factor was 1.63% and 10.05% in each plan and film measurement data, respectively. In addition, the average difference in dose distribution was 10.09% for each measurement film. The average difference of point dose was 0.43% and 2.09% in each plan and measurement data, respectively. In conclusion, if the inhomogeneity correction factor was not applied in small field, a greater difference in measurement data was observed. In SBRT using small field, it needs to precisely identify the correct inhomogeneity correction factor.

PS05.026 - Dosimetric effect of low dose 4D CT by a commercial iterative reconstruction on dose calculation in radiation treatment planning: A phantom study

Author(s): Hee Jung Kim, Ah Ram Chang, Sung Yong Park
Soonchunhyang University Hospital, Seoul/KOREA

We investigated the HU and dose difference due to the use of CT images acquired with the reduced imaging dose by using a commercial iterative reconstruction technique (iDose, Philips). The phantom with various density materials from 0.2 g/cc to 1.53 g/cc was scanned by the Philips Big Bore CT, using two energies (90 and 120 kV) and four currents (50, 100, 200 and 400 mAs). The CT images were reconstructed with and without iDose with level 5. As the density is higher, the use of iDose increased the mean HU that the maximum change of mean HU was 109 HU in 1.53 g/cc bone core material at 90 kV. At the same energy, the HU with reducing mAs showed a difference less than 27 HU. The 4D CT of lung phantom (CIRS) was scanned with two different exposures of 598 mAs without iDose and 163 mAs with iDose. We performed 2D and VMAT spine planning and 3D CRT and VMAT lung planning based on the 50% phase of CT with and without iDose reconstruction. The difference of mean dose was within 1% in all plans. Therefore, this dose reduction technique in big bore CT is applicable to the radiotherapy

treatment planning. If the high density material is included, it should be used with a caution for the dose calculation in the treatment planning because the HU difference due to the iDose is greater as the density is higher.

PS05.027 - An Evaluation of the Use Factor for CyberKnife using Clinical Data

Author(s): Yu Ra Cho¹, Dong Han Lee¹, Yong Min Lee¹, Mun Kyu Park¹, Han Yeong Lee², Ung Kyu Chang¹

¹Korean Institute of Radiological & Medical Sciences, Seoul/KO-REA, ²HanBeamTec, Seongnam-si/KOREA

In order to reduce the regulation limit of integral dose of CyberKnife to below 10%, presently the international guideline standard of the CyberKnife use factor is 0.05(%), which is very small compared to 5~40(% of conventional radiation therapy, and this shows that the shielding standard of CyberKnife is very strict. In this study, based on the clinical data of patients who had received CyberKnife treatment, tried to examine the adequacy of the existing shielding guideline. 60 patients among approx. 220 who had received CyberKnife (ver. 9.5, Accuray, Sunnyvale, USA) treatment from February 2013 to May 2014 were selected and for intracranial and body, two groups of 30 patients were classified into skull tracking and spine tracking mode. After extracting the specific trajectory of the robot on the beam data of each patient, the direction of the beam towards the shielding wall by using the origin (ver. 9.1, OriginLab, USA) program was reproduced in three dimensions. And many beams examined in each direction were set as one zone, and then MU of formed beams was analyzed. And in order to estimate shielding workload and IMRT factor, prescription dose and total MU were analyzed at the same time. Intracranial patients received an average of 1.9 fractions with 12 Gy per fraction prescribed at the 80.2% isodose line, using 147.2 beams and 1,8163 MU. Body patients received an average of 3.63 fractions with 9.5 Gy per fraction prescribed at the 77.6% isodose line, using 166.6 beams and 4,7942 MU. The most used collimator size was 7.5~35 mm, and fixed and Iris collimators of 1~4 types of size were used. In intracranial and body treatments, 82% of the total beams were distributed being directed towards the floor, and there were few beams directed towards the ceiling. And 18% of the beams were directed towards the surrounding walls and for body no beams were directed to the right side wall from the position of couch. It could be confirmed that more beams were spread on the walls in intracranial than body, and as a result of analyzing MU of each beam, it could be observed that more 'hot zone' were produced in intracranial than body. Because use factor and IMRT factor recommended by the CyberKnife shielding guideline are small and large respectively, more barriers are required for shielding of CyberKnife treatment rooms, which leads to spatial in-efficiency and cost increase in hospitals. Thus, if the use factor analyzed in this study based on the clinical data is considered in designing treatment rooms, more reasonable treatment room designing may be possible.

PS05.028 - Lung Dose Estimation for a Total Body Computed Tomography Protocol

Author(s): Juliana C. Martins, Denise Y. Nersissian, Paulo R. Costa
Radiation Dosimetry And Medical Physics Group, Physics Institute, University of São Paulo, São Paulo/BRAZIL

Introduction: Computed Tomography (CT) procedures are important diagnostic tools. It is estimated that CT accounts for over 13% of all diagnostic examinations, contributing for approximately 30% of the collective dose in the United States. In Germany, CT represents 7% of total X-Ray examinations, with contribution of 60% for collective effective dose. This work studies a methodology to estimate lung doses on an adult anthropomorphic phantom (The

Phantom Laboratory, Salem, USA), undergoing total body CT using Lithium-Fluorite (LiF) thermoluminescent dosimeters (TLD).

Methods: LiF TLDs were introduced inside the holes of the phantom, in nine slices, correspondent to lung position (Figure 1). Fourteen groups of five dosimeters were allocated in dosimeter-holders designed for this purpose. The phantom was irradiated in a PET/CT scanner (Discovery PET/CT 690, GE Healthcare). After performing double scan projection radiographs (SPR) (anteroposterior and lateral), the phantom was irradiated using a total-body protocol. TLD data were read by TL/OSL reader Risø (DTU Nutech, Inc., Roskilde, Denmark) and these results converted to "counts" by a routine implemented with the Software Origin 8.5.1 (OriginLab Co., MA, USA). These counts were corrected to a calibration curve, for radiation quality RQT 9. Mean absorbed dose, D , for the lung were calculated using equation (1)

$$D = \sum_i f_i \cdot D_i \quad (1)$$

where f_i is the fraction of the total lung mass in phantom slice D_i and is the average dose to the organ in slice.



Figure 1– Adult anthropomorphic phantom positioned inside the gantry (above); positions of the dosimeter-holders (in green) inside slice 15 (below).

Results and Discussion: The lung dose value obtained was (44.4 ± 1.5) mGy, with $0.148 \text{ mGy} \cdot \text{mAs}^{-1}$. This value is considered reasonable when compared to similar studies. The doses due to both SPR are accounted in this estimation, which could explain this larger absorbed dose values.

Conclusions: This work shows a methodology to estimate lung doses to adult anthropomorphic phantom due to CT exams. The methodology will be extended to other organs of interest and other protocols in the course of time, and also adapted to a pediatric anthropomorphic phantoms.

SP05.029 - Verification of axial dose distributions with radiochromic films for a translational Total Body Irradiation technique

Author(s): Bozidar Casar, Ignasi Mendez, David Cugura
Institute of Oncology Ljubljana, Ljubljana/SLOVENIA

Purpose:

Radiochromic films were used to validate dosimetrically a translational Total Body Irradiation (TBI) technique. The main objective was to analyze the homogeneity of the dose distribution in the axial plane for the thoracic and pelvic regions. Additionally, the surface dose was studied for two different positions of the PMMA beam spoiler.

Methods and materials:

Two phantoms were used: CIRS Thorax (Model 0002LFC, Computerized Imaging Reference Systems Inc. Norfolk, VA) and CIRS Pelvis (Model 002PRA). They were irradiated according to a translational TBI technique [1] in supine and prone positions, and with a 1 cm PMMA spoiler situated 15 cm and 125 cm above the phantom surface. For each irradiation, two 8 in. x 10 in. EBT3 Gafchromic films (Ashland Inc., Wayne, NJ) were used to measure the dose distribution in the phantom. Doses were calculated using Radiochromic.com v1.7 (<http://radiochromic.com>) [2].

Results:

The homogeneity index (HI), calculated as D_5/D_{95} , was 1.16 and 1.23 for the pelvis and thorax phantom, respectively. This was mainly due to the shape of the phantoms, which become thinner in the lateral direction, producing doses up to 20% higher in the laterals than in the midline. Considering only a segment of the dose plane of 6cm around the midline (3cm on each side), the HI was 1.03 and 1.07 for the pelvis and thorax phantom, respectively, exhibiting higher dose homogeneity in the anteroposterior axis. When the spoiler was situated 15 cm above the phantom surface, the skin dose in the midline was 94% of D_{max} . When it was 125 cm above the phantom, the same isodose was achieved at a depth of 6 mm.

Conclusions:

It was concluded that a 1 cm thick PMMA beam spoiler, situated 15 cm above the phantom, raises the surface dose to an acceptable level. Near the midline, this TBI technique delivers a dose homogeneity in the anteroposterior axis well within the common limits of +/- 10% relative to the prescription dose. For thinner regions, higher doses up to 25% relative to the prescription dose were considered admissible with the present technique.

References:

- [1] B.Casar, I.Vojvodic, V.Robar, U.Smrđel and I.Mendez, "New system for TBI with translation method at the Institute of Oncology Ljubljana", IFMBE Proceedings WC 2009, Vol 25, 996-997. (Springer, Munich, Germany, 2009)
[2] I. Mendez, P. Peterlin, R. Hudej, A. Strojnik, and B. Casar, "On multichannel film dosimetry with channel-independent perturbations," *Med. Phys.* 41, 011705 (2014).

PS05.030 - Experimental assessment of out-of-field dose components in high-energy electron beams used in external-beam radiotherapy

Author(s): Mohamad Mohamad Alabdoaburas¹, Jean Pierre Mège², Jean Chavaudra², Atilla Veres³, Florent De Vathaire², Dimitri Lefkopoulos², Ibrahima Diallo²

¹University of Paris-Sud(11), Orsay/France, ²Medical Physics, Gustave Roussy, Villejuif Cedex/France, ³Equal-Estro laboratory, Villejuif Cedex/France

Purpose/objective:

The higher survival rate of radiotherapy patients entails a growing concern on late effects associated to peripheral doses. The purpose of this work is to evaluate experimentally the peripheral dose outside applicators at the patient level, in different high-energy electron beams used in external-beam-radiotherapy.

Methods and materials:

Commissioning was performed for 6,9,12 and 18 MeV electron beams on three different linear accelerators equipped with three different types of applicators. For each beam energy, measurements were performed, in a water phantom, at different depths, with applicator sizes varying from 6 x 6 cm² to 20 x 20 cm², for off-axis distances from 5cm to 65cm outward. Thermoluminescent dosimeters (TLD-700) powder measurements were compared to EBT3 films measurements and plane-parallel ionization chamber NACP measurements. Measurements at 10 cm without applicator were made and were compared to the same measurements with applicator.

Results:

Whatever the field size and energy beam, a peak dose spot appeared about at 12.5 cm from the field edge for the Siemens applicators. For Siemens Primus with an applicator size of 10 x 10 cm², this peak reaches 2.3%, 1%, 0.9% and 1.3% of the maximum central axis dose (D_{max}) for 6,9,12 and 18MeV electron beams, respectively, doubled for 6 x 6 cm², field size. For Siemens Oncor, with the above applicator size, this peak dose reaches 0.8%, 1%, 1.4% and 1.5% of D_{max} for 6,9,12 and 14 MeV, respectively, increased when applicator size increased. In contrast for Varian 2300C/D, the doses at 12.5 cm from field edge are 0.3%, 0.5%, 0.6% and 1.1% of D_{max} for 6, 9, 12 and 18MeV, respectively, increased with increasing of applicator size. No peak dose spot is evidenced for Varian applicator. Measurements made at 10cm depth show that, depending on beam energy, applicator size, collimator size, and out-of-field distance, the peripheral dose represents 0.01% to 1% of D_{max} . Peripheral dose, for the measurements made at 10cm depth without applicator, was of 55% less than peripheral dose for the same measurements with applicator.

Conclusion:

In certain circumstances the peripheral doses from electron beams may be comparable to values reported for photon beams. Our results should be considered in the optimization of treatment planning and also in studies exploring RT long term effects.

PS05.031 - Dosimetric study for a set iodine-125 seeds using radiochromic films in solid water plates

Author(s): Arnaldo P. Mourao Filho¹, Lucas C. Tomaz², Suely E. Grynberg³

¹Nehos, CEFET-MG, Belo Horizonte/BRAZIL, ²Centro de desenvolvimento da Tecnologia Nuclear, Belo Horizonte/BRAZIL, ³Centro de Desenvolvimento da Tecnologia Nuclear, Belo Horizonte/BRAZIL

Brachytherapy seeds are frequently used in cancer treatment. A set of four iodine-125 seeds, model 6711 produced by Amersham Health, were used in this work. These seeds are ranked among the top choices when it comes to the treatment of prostate cancer. These sources emit X and gamma photons with an average energy of 28 keV and a half-life of 59.4 days. The dosimetric characteristics for a seed were obtained taking into account the recommendations of TG-43 protocol, developed by the AAPM (American Association of Physicists in Medicine). To realize the experiment three plates of Standard Grade Solid Water, model 457 Gammex were used. One solid water plate was machined for accommodate the seed set and radiochromic films were used on the machined plate and under

another solid water plate to recorder the radiation dose. The set of seeds was placed in a configuration trying to simulate an arrangement which may occur in vivo during treatment. The machined plate were placed between the other two for better reliability in measurements. The films were irradiated by an equivalent X-ray beam using the reference radiation RQR 3 IEC (International Electrotechnical Commission) with different doses (0.5 to 1.0 Gy) to obtain the calibration curve in the dose region measured. After validation of the methodology, the study of the interaction between the radiation fields of the set of seeds became possible and the survey of isodose curves of these setting was conducted.

PS05.032 - Evaluation of bismuth shielding use in cervical spine CT scans

Author(s): Arnaldo P. Mourao Filho, Carolina Aleme Nehos, Centro Federal de Educação Tecnológica de Minas Gerais, Belo Horizonte/BRAZIL

Computed tomography (CT) is one of the imaging techniques most commonly used for invasive assessments of internal structures of the human body. However, the radiation exposure of patients can cause damages to their health. This study aims to evaluate changes in image quality in scans of the cervical spine CT, when using bismuth shield to reduce the radiation dose deposited in the thyroid. In a multislice GE Bright Speed CT scanner with 32 channels were done two scans of the neck region, in order to generate diagnostic images of the cervical spine of an Alderson Rando male phantom. The scans were performed with the standard hospital protocol for cervical spine evaluation. The first scan using the thyroid bismuth shielding on the front neck region, and the second without it. Punctual radiation doses in organs (thyroid, breasts, lenses and spinal cord) was recorded using thermoluminescent dosimeters and the image quality control parameters were observed using the image J software. The use of bismuth shielding resulted in a reduction of 26% in the thyroid dose, while generated a small degradation in the axial images obtained, mainly in the frontal structures, closer to the surface where was the bismuth shielding. Thus, the use of bismuth shielding improved the diagnostic process allowing for dose reduction without compromising the diagnostic quality imaging of the skeletal structures of the neck.

PS05.033 - Scanning irradiation of microbeam x-rays in ionization chambers as micro-scale dose analysis tool

Author(s): Nobuteru Nariyama¹, Keiji Umetani²
¹Light Source And Optics Division, Japan Synchrotron Radiation Research Institute, Hyogo/JAPAN, ²Research And Utilization Division, Japan Synchrotron Radiation Research Institute, Hyogo/JAPAN

Microbeam x-rays have been used extensively in various applications, with further applications in the medical field being highly anticipated. For the realization of clinical applications, high spatial-resolution dosimetry is necessary. GafChromic films HD-810 have long been used for microbeam dose distribution; if another dosimeter is available, the use of these films for this purpose will be fully examined.

Ionization chambers are widely used as absolute dosimeters. The sensitive volume is surrounded by resin, so that the step-by-step scanning microbeam irradiation near the sensitive volume/resin interface was expected to enable the measurement of micro-scale dose distribution in the resin. Figure 1(a) shows the energy deposition in the sensitive volume of the Advanced Markus chamber calculated using a Monte Carlo (MC) code as a function of the incident microbeam position on the side of the chamber along the direction of electric force. Around the edge of the PMMA electrode, the right hand shoulder curves were almost in agreement with the dose distribution in the PMMA phantom calculated using the MC code [1].

An experiment was carried out at the BL28B2 beamline of SPring-8. A 25-mm-wide microbeam of x-rays was scanned at 6-mm intervals in the chamber. Figure 1(b) shows the resulting energy deposition curves compared with results at a 1-mm depth in the PMMA phantom measured using a GafChromic film [1] at a probably slightly different alignment condition.

[1] N. Nariyama, et al. Appl. Radiat. Isot. 67, 155 (2009).

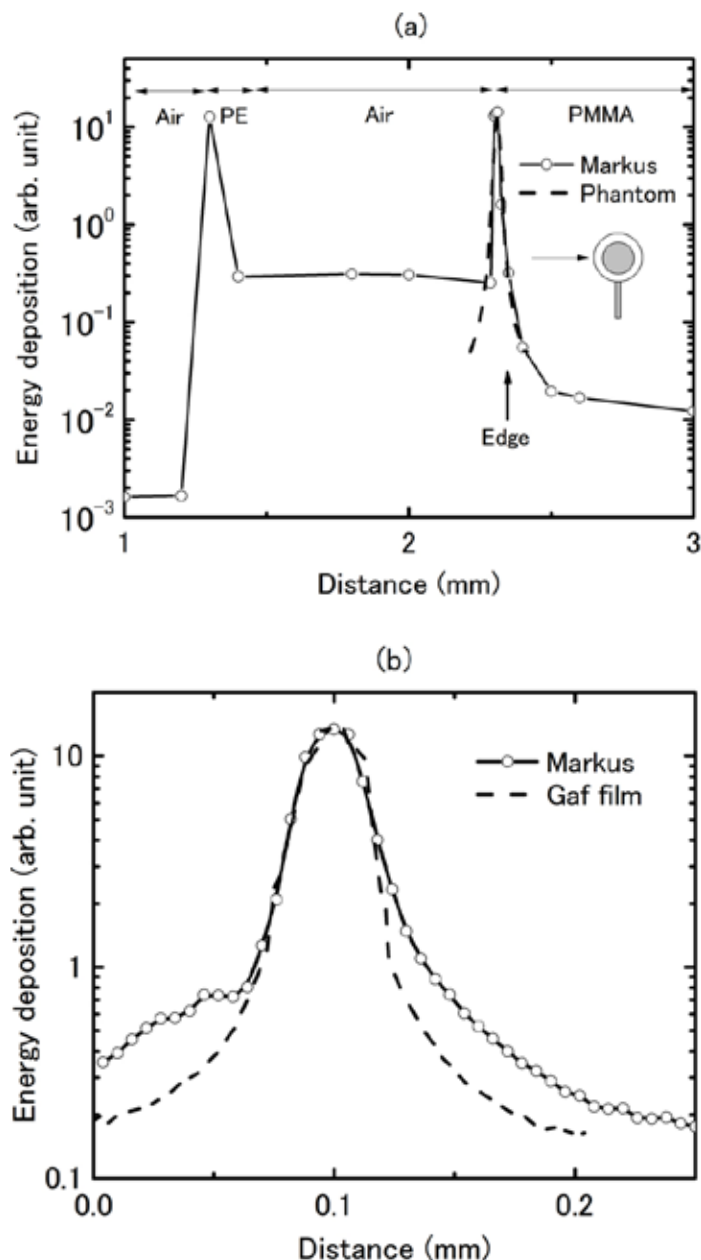


Fig. 1 a) calculated and b) measured energy depositions in the sensitive volume of the Advanced Markus chamber compared with phantom doses calculated using the MC code and measured using GafChromic films, which are fitted to the peaks for the Advanced Markus chamber, respectively.

PS05.034 - Dosimetric verification of the scatter integration algorithm of MIRS**treatment planning system for photon dose calculations**

Author(s): Mansoureh Sadat Nabavi¹, Hassan Ali Nedaie¹, Rasa Golrokh², Mansour Naderi¹, Bahram Andalib³, Saeedeh Sakhaee³
¹Radiotherapy Oncology Department, Cancer Research Centre, Cancer Institute, Tehran University of Medical Sciences, Tehran/IRAN, ²Dr.Masih Daneshvari Hospital, Tehran/IRAN, ³Karaj Radiotherapy Centre, Karaj/IRAN

Background and purpose: Dosimetric quality control methods by IAEA for treatment planning systems, were tested for scatter integration algorithm. The purpose of this study was to find out the extent of the deviation between planned and delivered dose in different fields and photon energies in homogeneous and heterogeneous media.

Materials and methods: The methodology was based on a semi-anthropomorphic 002LFC CIRS Thorax phantom. The computed tomography (CT) images of mentioned phantom with 2mm slice thickness were transferred to the examined TPS (MIRS treatment planning system) and seven different plans according to IAEA task report (TEC-DOC 1583) were designed. Experimental measurements by a farmer type chamber 0.6cc (PTW 30010 ion chamber) at 13 points carried out at 6, 10 and 18 nominal photon energies.

Results: A total of 21 clinical test case datasets for different energies were produced. In most of cases in homogeneous media, the results were in agreement with predefined criteria. The amount of variations in heterogeneous area increases with the beam energy and decreases with the depth increasing.

Conclusion: Large deviations exist in wedge fields and heterogeneities especially in lung. In homogeneous media and using open fields the scatter integration algorithm results are reliable.

PS05.035 - Characterisation of EPSONV700 flatbed scanner for EBT3 Gafchromic film dosimetry.

Author(s): Vinod K. Nelson

Medical Physics, Liverpool & MacArthur Cancer Therapy Centres, Campbelltown/AUSTRALIA

Purpose: When a flatbed type scanner, not specifically made for radiotherapy dosimetry, is used to acquire Gafchromic film dosimetry data, error can occur in the measured pixel value. These errors result from the position dependent response of the scanner, the variation in thickness of the active layer in Gaf film which occurs during the manufacturing process, rotation of the film dosimeters and the scattered photons entering the film dosimeter scanning area. The purpose of this work is to determine the magnitude of these errors and propose methods to correct for these errors.

Methods and Materials: To determine the positional dependent response of the flatbed scanner two types of tests were carried out. In the first test one whole unirradiated film was scanned. Average pixel value measured with the region of interest (ROI) covering whole film. Orthogonal profiles at five locations, covering the whole film were performed and average pixel value for each location was calculated. In the second test, the scanning area was divided into 12 equally spaced regions. A 2 cm² piece of unirradiated film was placed in each position and scans were performed for each location. To determine the effect of film rotation, one 2 cm² piece of film was irradiated to 1Gy dose. Scans were performed with the film at 0°, 22.5°, 45°, 67.5° and 90° rotations and change in the average pixel value and standard deviation was compared. The scanner was operated with SilverFast (LaserSoft Imaging) software, in transparency mode, with colour correction disabled. To reduce noise due to random fluctuations of the light signal, 3 scans were performed as a 48 bit non compressed TIF images. The central 1 cm² region of each square

was averaged to obtain the response (pixel value) corresponding to the delivered dose, using ImageJ software.

Results: The average pixel value for the whole film was 42093 ± 263 (0.6%) and for the 12 equally spaced areas of the scanned film, average pixel value was 42092 ± 275 (0.7%). For the 12 positions on the scanning area, the variation in the pixel value was 0.7% (41642 ± 297). The variation in pixel value for the five orthogonal profile measured different locations was close to ± 0.5% except for the left vertical region of the film. The variation in pixel value with film rotation ranged from -1% at 22.5° to -5% at 90° rotation, with respect to 0° rotation.

Conclusion: The ESPON V700 is a suitable scanner for EBT3 Gafchromic film dosimetry. The variation in pixel value of EBT3 film scanned using EPSONV700 scanner is negligible except in the extreme left and top of the scanned area. Placing the film dosimeters in the central part of the scanning area and using a template with cut outs for placing film dosimeters orthogonally will further reduce the errors due to film detector non-uniformity, scanner response, rotation of film dosimeter and the scattered light photons.

PS05.036 - Nanodosimetric parameters obtained using the Monte Carlo codes PARTRAC, PTra and Geant4-DNA: a comparison study

Author(s): Ana Belchior¹, Carmen Villagrasa², Heidi Nettelbeck³, Marion Bug³, Reinhard W. Schulte⁴, Werner Friedland⁵, Hans Rabus³
¹Associação do Instituto Superior Técnico para a Investigação e Desenvolvimento, Lisboa/PORTUGAL, ²Institut de Radioprotection et de Sûreté Nucléaire (IRSN), Fontenay-aux-Roses/FRANCE, ³Fundamentals Of Dosimetry, Physikalisch-Technische Bundesanstalt (PTB), Braunschweig/GERMANY, ⁴Radiation Research Laboratories, Loma Linda University, Loma Linda/UNITED STATES OF AMERICA, ⁵German Research Center For Environmental Health, Helmholtz Zentrum München, Neuherberg/GERMANY

The nanoscopic pattern of ionising radiation, called track structure, is a crucial tool for estimating nanodosimetric quantities that are not directly measurable in biological tissues. This work compares nanodosimetric parameters of track structure (NPTS) obtained with the Monte Carlo track structure codes PARTRAC [1], PTra [2] and Geant4-DNA [3].

In order to calculate the NPTS, two simplified target geometries were used: a liquid-water cylinder of 2.3 nm diameter and 3.4 nm length, representing a 10-base-pair DNA segment; and a liquid water cylinder of 6 nm diameter and 10 nm length, representing a nucleosome. For the comparison study of the three codes the following particle type and energies were used: electrons with energies ranging from 20 eV to 1000 eV, protons with energies between 3 MeV and 10 MeV; and alpha particles with incident energies of 8 MeV, 10 MeV and 20 MeV. The radiation field was simulated as a monoenergetic pencil beam incident on the surface of the liquid water cylinders at half their height. The ion beam energies were matched to those used for cell irradiations performed at the PTB ion microbeam facility as part of the BioQuaRT project [4].

In nanodosimetry, the physical features of charged particles passing or penetrating a given target volume at a given distance are described by the probability distribution of the number of ionisations occurring within the volume. This probability distribution, which characterises the radiation quality Q associated with the particle track, also depends on the geometry and orientation of the target volume. This work compares the probability distributions and their statistical moments, such as the mean ionisation cluster size $M_i(Q)$, obtained for all three codes. In general, the results show a good agreement between the codes for all particle types and energies, except for electrons below 150 eV, where results obtained with PTra deviate from those obtained with PARTRAC and Geant4-DNA.

This work has been funded by the EMRP Researcher Excellence Grant SIB06-REG3. The EMRP is jointly funded by the EMRP participating countries within EURAMET and the European Union.

References

- [1] W. Friedland et al., Mutat. Res. 711, 28-40 (2011)
- [2] B. Grosswendt, Radiat. Prot. Dosim. 110, 789-799 (2004)
- [3] S. Incerti et al., Med. Phys. 37, 4692-4708 (2010)
- [4] Project web site: <http://www.ptb.de/emrp/bioquart.html>

PS05.037 - A method to reduce the patient's eye lens dose during cerebral angiography procedures

Author(s): Mohammad Javad Safari, Kwan Hoong Ng, Jeannie Hsiu Ding Wong, Khairul Azmi Bin Abd Kadir
Biomedical Imaging, University of Malaya, Kuala Lumpur/MALAYSIA

Purpose: To propose a radiation protector layer to reduce the radiation dose to the patient's eye lens during cerebral angiography procedures.

Materials and methods: The radiation protector layer was fabricated using VytaFlex 40 polyurethane rubber, with thickness and CT number of 1.8 cm and 89.0 HU, respectively.

The radiation dose received at the left eye and left eyelid for an aneurysm procedure were measured using an adult female anthropomorphic phantom and Gafchromic XR-RV3 film [Fig. 1]. The procedure was repeated with and without using the protector layer and effects of this layer on the fluoroscopic image and Automatic Brightness Control (ABC) exposure parameters were studied.

Result: The protective layer reduced the dose to the left eyelid by 31% and to the left eye lens by 16.7%. The protector layer is radio-lucent under DSA, but it can be seen in fluoroscopy images [Figure 1(b& c)]. However, the protector does not affect the ABC exposure parameters and does not perturb and interfere with the treatment procedure.

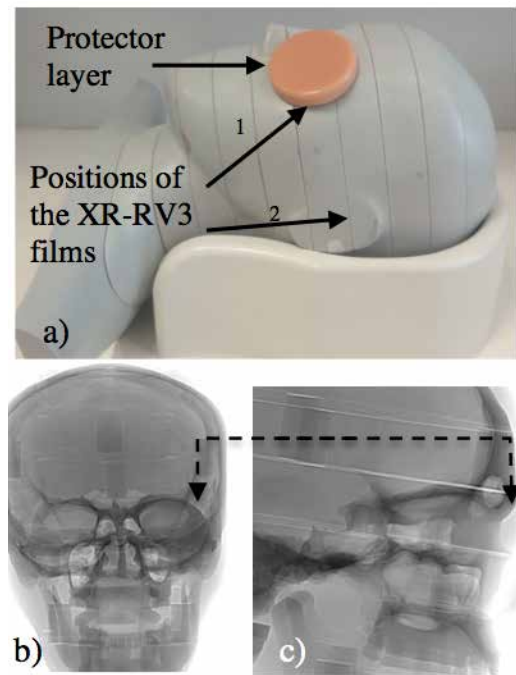


Figure 1a) The positions of the protector layer and radiochromic film, 1: underneath the protector layer and 2: sandwiched between the phantom's slabs. Effect of protector layer on fluoroscopic image from (b) frontal and (c) lateral tube

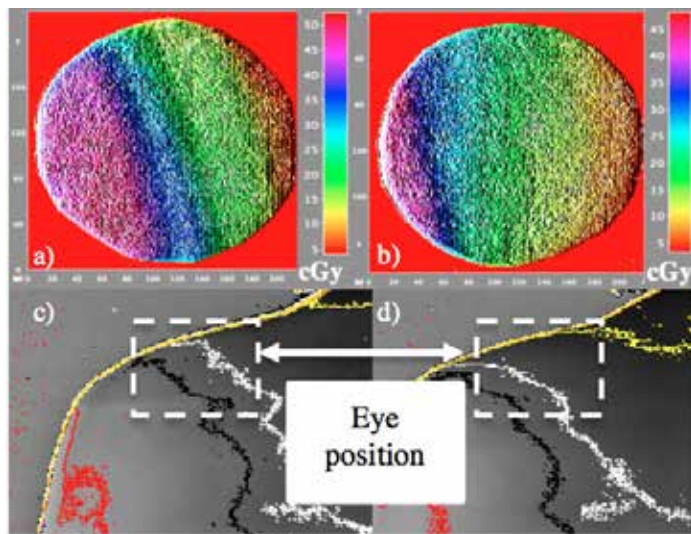


Figure 2 shows the effect of the radiation protector layer on dose level at left eyelid position, (a) without and (b) with protector, and dose distribution over the patient's head, (c) without and (d) with protector, during an randomly selected aneurysm procedure.

Conclusion: The eye lens protector layer reduces the patient's eye lens dose during cerebral angiography procedure by attenuating the primary x-ray beam from the lateral tube.

PS05.038 - Bremsstrahlung generating and shielding by the source of the beta ray.

Author(s): Hiroki Ohtani, Takeshi Shima
Tokyo Metropolitan University, Tokyo/JAPAN

⁹⁰Sr which generates a beta ray is contained in the radioactive material contained in the contaminated water generated according to the accident of the nuclear power plant. A beta ray generates bremsstrahlung by an interaction with a shield wall. In this case, there is radiation exposure to the worker of the contaminated water tank circumference. The purpose of this research shields the beta ray from ⁹⁰Sr with a lead or iron, and detects generating of bremsstrahlung. It presumes that the bremsstrahlung is of beta ray origin, and the validity of a shield with an acrylics board is verified.

The beta ray generated from seal ⁹⁰Sr was measured using the GM survey meter. The acrylics board was put in between the source of a beta ray, and the survey meter, and the beta ray shield ratio of the acrylics board was measured. To the beta ray generated from Sr-90, it shielded with Pb board of 1.0 mm, and Fe board of 1.6 mm, and bremsstrahlung generated from there was measured. The effect of the acrylics board was verified.

As a beta ray shield of an acrylics board, the beta ray shield ratio of thickness 2.0 mm was 98.1 %. The increases in the discrete value of bremsstrahlung origin were 1.5 % of a 1.0 mm Pb board, and 3.6 % of the 1.6 mm Fe board. Furthermore, the discrete value decreased in the case where an acrylics board is added. The shield of a beta ray with an acrylics board is effective, and it was suggested that generating of bremsstrahlung of beta ray origin can be suppressed by using an acrylics board.

PS05.039 - Angular dependence of absorption spectrum of Gafchromic EBT2 film

Author(s): Soah Park¹, Sei-Kwon Kang¹, Kwang-Ho Cheong¹, Taejin Hwang¹, Jai-Woong Yoon¹, Taejin Han¹, Haeyoung Kim¹, Me-Yeon Lee¹, Kyoungju Kim¹, Hoonsik Bae¹, Seung Jae Oh², Yong-Min Huh², Jin-Suck Suh²

¹Radiation Oncology, Hallym University College of Medicine, Seoul/KOREA, ²College Of Medicine, Yonsei University, Seoul/KOREA

It is important to study absorption spectrum in film dosimetry because the spectral absorbance of the film relates to the film's total absorption dose. We investigated the absorption spectra of Gafchromic EBT2 film with various rotational angles in a visible wavelength band. The film was irradiated with 6 MV photon beams and a total dose of 300 cGy. Absorption spectra were taken under different rotational angles after 24 h irradiation and we fitted the spectra using Lorentzian functions. There were two dominant absorption peaks at approximately 586 nm (green) and 634 nm (red). The measured spectrum was decomposed 542 nm, 558 nm, 578 nm, 586 nm, 626 nm, 634 nm, and 641 nm. The maximum total area of the red band absorption spectrum was at 45° (225°) and the minimum at 90° (270°). As the angle of rotation changed, the intensity and integrated area of the blue and green peaks also changed with 180° period, with minima at 90° and 270°, and maxima at 0° and 180°, although the overall absorbance is very low. The spectral peak wavelengths remained constant within ± 1.2 nm for all angles. There was no hysteresis of absorption spectrum of the film; spectra taken at 0° and 360° were substantially the same and showed similar behavior for all rotational angles. The change of absorbance with rotational angle of the film affected the dosimetric properties, resulting in rotational variations of film dosimetry in each red-green-blue channel.

PS05.040 - Patient dose audit in mammography

Author(s): Ana R. Roda¹, Maria Carmo Lopes², Maria Carmen Sousa², Grisel M. Paula³

¹Medical Physics, IPOCFG,EPE, coimbra/PORTUGAL, ²Medical Physics, IPOCFG,EPE, Coimbra/PORTUGAL, ³Fcul, Institute of Biophysics and Biomedical Engineering, Lisbon/PORTUGAL

This study presents the results of a patient dose audit performed in the period Dec 2013 to Feb 2014 on a full field digital mammography unit GE Senographe DS, to: evaluate conformance with the European diagnostic reference levels (DRL's); provide the physician with an estimate of the effective doses involved in bilateral mammography examinations; and, evaluate if displayed dose indicators (Entrance skin exposure (ESE) and average glandular dose (AGD)) can give direct information, relevante for patient dose assessment. According with the Portuguese legislation for medical radiological exposures [Decree-law n° 180/2002] we applied the diagnostic reference level concept in mammography examinations, estimating the average entrance surface dose (ESD) for a sample of 10 standard breasts, and compared it with the European DRL - ESD of the 3rd quartil of a broad dose survey distribution. To assess the patient radiation doses involved we estimated the average dose to the glandular tissue within breast (AGD) since it is the glandular tissue that is believed to be the most sensitive to radiation induced carcinogenesis, and optionally converted it into effective dose for comparison with other diagnostic radiology exams. Half-value layer (HVL) and radiation output data obtained from quality control (according with EFOMP Mammo Protocol 2014) were used for the entrance surface dose (ESD) and average glandular dose (AGD) assessments using the appropriate conversion factors [IAEA (2007), Dance (2000), Dance (2009)]. AGD and effective doses for bilateral mammography were obtained for a range of breast thickness intervals using Dance tables and ICRP 103 breast tissue weighting factor 0.12. The percentage of glandularity was determined using the qualitative method described by Byng (1994). The results were: ESD = 5.8 mGy for cranio caudal

(CC) and ESD = 6.1 mGy for medio lateral oblique (MLO) projections. These results are considerably below the European DRL's (10 mGy). Average effective doses for a bilateral mammography for each compressed breast thickness interval results were: E = 0.28 mSv for small breasts (34.5 \pm 4.5mm); For medium breasts we considered 3 compressed thickness intervals E = 0.35 mSv (44.5 \pm 4.5mm); E = 0.33 mSv (54.5 \pm 4.5mm); E = 0.45 mSv (64.5 \pm 4.5mm); E = 0.61 mSv for large breasts (74.5 \pm 4.5mm) and E = 0.69 mSv for very large breasts (84.5 \pm 4.5mm). In general, larger compressed breast thickness is associated with a higher AGD and patient effective dose. No correlation was found between AGD shown on the GE Senographe DS display and calculated AGD, but high correlation was found between the displayed entrance skin exposure (ESE) and entrance skin air kerma (ESAK) measurements the average conversion coefficient with 2 σ confidence level being (1.01 \pm 0.05). This results suggests we can use displayed ESE for dose assessments. The annual system conversion factor (CF) measurement (factor used by the system to convert brightness to dose for all AOP-related calculations) and HVL measurement (measures HVL and Output) are essential for dose optimization and patient dose calculations with Senographe DS.

PS05.041 - Experience in implementing a dosimetric registry in an oncological facility of a developing country

Author(s): Sandra L. Rocha Nava¹, Yolanda Villaseñor Navarro², Erick Benitez¹, Hector Galvan², Erika Ramirez Lopez¹
¹Biomedical Engineering, Instituto Nacional de Cancerologia, Mexico DF/MEXICO, ²Radiology Department, Instituto Nacional de Cancerologia, Mexico DF/MEXICO

Diagnostic Radiology and Nuclear Medicine studies are an effective tool especially in an oncology facilities where are needed for the diagnostic and also to know the treatment response.

Radiation and radiation dose reduction are at the top of the list of controversial topics in medical imaging today. The risks associated with the use of ionizing radiation in diagnostic imaging include cancer, burns and other injuries.

It is known that the main contribution to cumulative dose is for CT scans (49%), but represents a minus percentage (16%) by type of procedures. However in an Oncology Hospital of Mexico the CT's scans and PET-CT represent more than 30% of the total studies. In this country currently there aren't a national policy of registry or collection of dosimetric data.

We have identified several patients with more than 20 CT scans in 24 months or patients with several PET-CT in a small time. That is why in 2014 began the implementation of a registry dose for dosimetric data collection. Unfortunately even when all the radiological equipment are digital direct, some of them had not installed the ionization chamber. When was required data information to the service providers, they didn't know the topic.

A CT scanner was installed in 2011 and was not acquired the license DICOM RDSR. But a second CT was acquired in 2014 and the provider didn't know the license required. Also the PACS system has not the ability to receive DICOM RDSR and there are no plans to integrate or upgrade for registry dose data.

To choose the system to collect the dose data we did some market research and found that one of the commercial systems offered great logging capabilities of different modalities. However, this system is not available for the reference country.

That was why we decided to implement the Radiance system, which allowed us to start the dosimetry data collection of 4 CTs, finding information that allowed us to start internal political request for radiological studies.

PS05.042 - Effects of irradiation with low and high doses using in vivo rats: analysis of trace elements in blood using SR-TXRF

Author(s): Carla L. Mota¹, Arissa Pickler¹, Andrea Mantuano², Camila Salata³, Delson Braz¹, Liebert P. Nogueira², Samara Machado², Regina C. Barroso², Carlos Eduardo De Almeida²

¹Nuclear Engineering Program, UFRJ, RIO DE JANEIRO/BRAZIL, ²UERJ, Rio de Janeiro/BRAZIL, ³CNEN, Rio de Janeiro/BRAZIL

Both natural and man-made sources of ionizing radiation contribute to human exposure and consequently pose a possible risk to human health. While natural background radiation is unavoidable, the increased medical use of radiation, e.g. X-ray and CT scans for diagnosis, inevitably increases the public's health risk concerns over exposure of low doses of ionizing radiation. The effect of low-dose radiation on cells and tissues is a public health concern, because the human population is exposed to low-dose ionizing radiation coming from a variety of sources, such as cosmic rays, soil radioactivity, environmental contaminations, and various medical procedures. And the effect of high dose radiation can cause more severe damage, by radiotherapy treatment or nuclear accidents such as Chernobyl in 1986 and the Fukushima Daiichi Nuclear Power Plant in 2011. Exposure to ionizing radiation may cause various types of cell damage, and the type of damage is different from low to high doses of radiation. Although the damaging health effects of exposure to high doses of radiation are well documented, more work needs to be done to establish a biologic signature for exposure to low dose. Previous studies have shown that exposure to low radiation dose reduces cell killing compared with a single dose of high radiation dose. There is great interest in the identification of biological markers for exposure to ionizing radiation for the detection of people exposed to high or low radiation dose, which could be in risk to develop late side effects of this exposition. To our knowledge, until now there is no such a convenient biomarker. Our purpose is to use an animal model, with Wistar rats, to analyze the peripheral blood after low and high doses of ionizing radiation. In this work were used male Wistar rats ($n = 15$), three months old, weighing approximately 260g, will be kept in appropriate cages with 4 animals each, on a 12-h light/dark cycle with food and water provided ad libitum. The animals will be divided into three groups, five animals each: control (were not irradiated), LD (received 0.1Gy total body irradiation) and HD (received 2Gy total body irradiation). The study protocol was approved by the local ethical council (No. CEUA/010/2012). The aim is to quantify the trace elements contained in the blood, and compare the results between three groups (control, LD and HD). The obtained results will help to identify the differences in the elements concentrations among the analyzed groups, and it can be associated with the received radiation doses. These results are important to better identify individuals with potentially lethal exposures and providing appropriate therapy (eg, supportive care, growth factors, transfusions, antibiotics). The obtained results help to identify the differences in the elements concentrations among the analyzed groups, and it can be associated with the received radiation doses.

PS05.043 - Effects of cable extension and photon irradiation on TNRD neutron detector in radiotherapy

Author(s): Leticia Irazola¹, José A. Terrón², Beatriz Sanchez Nieto³, Roberto Bedogni⁴, Faustino Gómez⁵, Francisco Sanchez-Doblado¹

¹Fisiologia Medica Y Biofisica, Facultad Medicina, University of Seville, Sevilla/SPAIN, ²Servicio De Radiofísica, Hospital Universitario Virgen Macarena, SEVILLA/SPAIN, ³Instituto De Física, Pontificia Universidad Católica de Chile, Santiago/CHILE, ⁴Istituto Nazionale Di Fisica Nucleare, Laboratori Nazionali di Frascati, Frascati RM/ ITALY, ⁵Fisica De Particulas, Facultad de Fisica, Universidad de Santiago, Santiago de Compostela/SPAIN

Introduction

A new thermal neutron detector (*TNRD*), developed for nuclear

research, has shown to be effective for clinical use in peripheral neutron dose estimation, either in patient and 'in-phantom' measurements [1]. This work shows some difficulties when adapting *TNRD* to radiotherapy environments, mainly due to the fact that it has shown structural limitations. Two problems have been studied: (1) the influence of cable lengthening, necessary to be operative in a radiotherapy environment and (2) cable irradiation during the measurements. As we are measuring very small signals, we have to take into account not only these two facts but also the quality of the materials and connectors used.

Material and Method

Original cable length of *TNRD* detectors was 0.8 m but an extension to a 2.4 m (5.4 m for the reference detector [1]) cable was found to be necessary to reach all the anthropomorphic phantom measuring points from the electronic box. Cable lengthening influence (having special care in the implementation and quality of the components) and its linearity response, were evaluated under a 10x10 cm² squared field in 15 MV (SSD=100 cm). The influence of the unavoidable cable irradiation [2], was evaluated by series of 300 MU measurements in 4 consecutive fields, with and without cable irradiation (ranging from 10 to 65.6 cm of cable irradiated).

All the measurements were performed in a 15 MV Siemens Primus linac, with detectors inserted in the middle of 8 cm of polyethylene.

Results

Mean loss of signal of (-0.09±0.08) % per meter of cable, has been obtained for the six detectors when measuring with extension cables with respect to the original setup. A good linearity response with the new configuration, was observed ($R^2=1$) for all detectors in the range 100-4000 MU.

Table shows *TNRD* signal in 15 MV, difference in readings between irradiation and no-irradiation of the cable, and the percentage that represents this difference with respect to total values.

Field size (cm ²)	Total signal (V·s)	Irradiation- No Irradiation (V·s)	Relative Deviation (%)
10x10	74.17	-0.60	-0.63
20x10	81.49	-0.76	-0.70
30x10	87.30	-1.22	-1.19
40x10	87.68	-1.20	-1.09

Conclusions

Our experiences showed both, the substantial necessity of using extended cables and the impossibility of measuring in anthropomorphic phantom points without cable irradiation. Measurements are now possible with the proposed improved setup here detailed, taking special care on cables and connections quality. Cable extension has a negligible contribution. Cable irradiation could reach a variation up to 1.2%. Thus, the irradiation of the cables should be considered in order to minimize its influence during the measurements.

References

[1]Med Phys (2014)41:112105:1-5

[2]Med Dosim 25(3):121-126

PS05.044 - Thermoluminescence dosimetry (TLD) for *in vivo* dosimetry in radiation therapy with high single doses

Author(s): Andrea Schwahofer¹, Christin Glowka², Wolfgang Schlegel²

¹Radiation Therapy, Vivantes Clinic Neukoelln, Berlin/GERMANY, ²Medical Physics In Radiation Therapy, German Cancer Research Center, Heidelberg/GERMANY

Purpose: The aim of this work was to find an extrapolation model to describe the non-linearity of thermoluminescence (TL) dosimeters and to measure single high absolute doses *in vivo* in rat tissue as accurately as possible.

Materials and Methods: For dose-to-water calibrated TL phosphors (rod shaped LiF detectors), the supralinearity of high doses up to 70 Gy was determined using a self-developed calibration phantom. Dose values between 0.1 and 70 Gy were measured incrementally and the measurements were repeated three times. Supralinear behavior of TL phosphors generally follows the correlation $D_{TL} = f(D_{irr})$, whereas D_{TL} is the measured TL output and D_{irr} is the irradiated dose. The mathematical model is then used to perform a first trial of *in vivo* dosimetry in animals with TL-Detectors. For this trial, male rats were transplanted with a syngeneic prostate tumor (Dunning R3327-HI) at the right hind limb. The TL-Detectors were embedded in a commercially available shrink-on tube to avoid surface contamination of the detectors with substances of any kind e.g. dust, blood. Four detectors were placed via 3 mm long incisions subcutaneously around the tumor volume (Fig. 1b) of six male rats. Dose levels of 30, 50 and 70 Gy were chosen referring to former dose-response experiments with this tumor model.

Results: The resulting progression of supralinearity needed to be split in three regions regarding to the TL output. Following sections were specified: 1) linear relation for $D_{TL} = 0...2$ Gy, 2) square root fit for $D_{TL} = 2...55$ Gy and 3) cubic polynomial fit function for $D_{TL} = 55...70$ Gy (Fig. 1a). The resulting models fit the measured data points with an average error of ± 2.6 %. Measured values in the rats for irradiations with 30 (50 and 70 Gy) were determined between 29.5 and 32.5 Gy (50.1 and 53.1 Gy / 69.8 and 73.5 Gy, respectively). It was even possible to define dose gradients at the field edge due to the position of the TL detector according to the position of the tumor volume.

Conclusion: The trial was a novel method of *in vivo* dose measurement and produced convincing results with very high accuracy. Thus the experiments of this study are an important step for *in vivo* dosimetry. As a future project, the phosphors might be implanted already at an early stage of tumor growth in order to achieve more representative dose values in the center of the tumor volume.

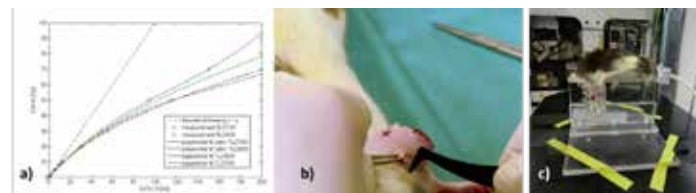


Fig. 2: a) determined supralinearity of the TL phosphors at the linear accelerator with 6MV photons, b) TL detector placed into a skin pocket around the tumor and c) experimental setup of the tumor irradiation at the linear accelerator

PS05.045 - Study of the response of ionization chambers in photon beams for off-axis point dose

Author(s): Tetsunori Shimono¹, Yasuyuki Kawaji¹, Kousuke Matsubara², Tatsuhiro Gotanda¹, Hiroshi Okuda³, Rumi Gotanda⁴

¹Department Of Radiological Science, Faculty Of Health Sciences, Junshin Gakuen University, Fukuoka/JAPAN, ²Department Of Quantum Medical Technology, Faculty Of Health Sciences Department Of Radiology, Faculty Of Medicine, Kanazawa University, Ishikawa/JAPAN, ³Department Of Radiology, Hoshigaoka Medical Center, Osaka/JAPAN, ⁴Department Of Radiological Sciences, Ibaraki Prefectural University of Health Sciences, Inashiki-gun, Ibaraki/JAPAN

Numerous challenges associated with small-field dosimetry compared with standard dosimetry, primarily because of the different irradiation conditions than that of the standard case. These challenges include concerns regarding reliability in the fields of small-field stereotactic radiotherapy and radiosurgery with respect to radiation detection. Furthermore, the use of intensity modulated radiotherapy (IMRT) has increased for the treatment of difficultly situated carcinomas. Therefore, while employing IMRT, measurements should include small fields as well as off-axis measurements. In this study, we investigated the response of small-volume ionization chambers and Farmer-type chambers for dose profile measurements at different measurement depths. We found that the response of the ionization chamber decreased at maximum dose depth when moving from the central axis to the 15 cm off-axis position. Until now, only a 0.1 cm³-volume ionization chamber has been investigated. The Farmer-type ionization chamber investigated herein behaved similarly to the small-volume ionization chamber. The response of for Farmer-type ionization chamber decreased by 3.1% and 3.5% for the 4 and 14 MV beams, respectively. Furthermore, the response both Farmer-type ionization chamber and small-volume ionization chamber increased with decreasing nominal photon energy. This under response could be the result of the variation of the wall correction factor.

PS05.046 - Analysis of gamma evaluation according to low-dose threshold on VMAT QA

Author(s): Ji-Hye Song¹, Min Joo Kim¹, So-Hyun Park², Seu-Ran Lee¹, Min-Young Lee¹, Dong-Su Lee², Tae-Suk Suh¹

¹Department Of Biomedical Engineering, And Research Institute Of Biomedical Engineering, The Catholic University of Korea, College of Medicine, Seoul/KOREA, ²Department Of Radiation Oncology, Uijeongbu St. Mary's Hospital, College of Medicine, The Catholic University of Korea, Uijeongbu-si, Gyeonggi-do, Seoul/KOREA

The American Association of Physicists in Medicine task group-119 (TG-119) recommends applying 10% of the low-dose threshold for gamma evaluation to restrict low-dose region. However, TG-119 didn't present clinical data to quantitatively demonstrate the impact of the low-dose threshold on the gamma index. Therefore, we performed a gamma evaluation with various low-dose thresholds in the range of 0% to 15% according to both global and local normalization and different acceptance criteria (3%/3 mm, 2%/2 mm, and 1%/1 mm). A total of 30 treatment plans—10 head and neck (H&N), 10 brain, and 10 prostate cancer cases—were selected from the Varian Eclipse treatment planning system (TPS) retrospectively. For the gamma evaluation, a calculated portal image was acquired through a verification plan process in the Eclipse TPS, and a measured portal image was obtained using an electronic portal imaging device. Then, the gamma evaluation was performed using Portal Dosimetry software. As a result, for the global normalization, the gamma passing rate (%GP) decreased as the low-dose threshold increased, and all cases of low-dose thresholds exhibited an acceptable %GP above 95% for both the 3%/3 mm and 2%/2 mm criteria. On the other hand, for local normalization, the %GP with 10% of low dose threshold increased by 18.64% and 17.45% compared with

the 0% of low dose threshold in brain case for 1%/1 mm and 2%/2 mm criteria, respectively. Even in 3%/3 mm acceptance criteria, the %GP increased by up to 9.22%. In conclusion, we suggest applying the 2%/2 mm criteria, which are more stringent criteria than those of 3%/3 mm, for the global gamma evaluation because it exhibits a tolerable passing rate for all low-dose thresholds. In contrast, local gamma analysis should be used for a lower dose threshold level below 10% to acquire more precise test results, despite the TG-119 recommendation, because it may provide an overestimated %GP by excessively excluding the dose discrepancy of the low-dose region.

PS05.047 - Dosimetric accuracy of Acuros XB dose calculation algorithm on an air cavity for EBT3 Gafchromic film

Author(s): Sang-Won Kang¹, Jin-Beom Chung², Jeong-Woo Lee³, Ji-Yeon Park⁴, Tae-Suk Suh¹

¹Biomedical Engineering, The Catholic Univ. of Korea, Seoul/KOREA, ²Radiation Oncology, Seoul National University Bundang Hospital, Seongnam/KOREA, ³Department Of Radiation Oncology, Konkuk University Medical Center, Seoul/KOREA, ⁴Department Of Pediatrics And Molecular Imaging Program At Stanford, Stanford University, Stanford/UNITED STATES OF AMERICA

Purpose: This study was to verify the dosimetric accuracy of Acuros XB (AXB) dose calculation algorithm on an air cavity for a single radiation field using EBT3 Gafchromic film.

Methods: A rectangular slab phantom containing an air cavity was made especially for this study. The phantom with and without the Gafchromic EBT3 films was scanned using Philips Big-bore CT scanner. The digital imaging and communications in medicine CT datasets of scanned the phantom were then transferred to the Eclipse treatment planning system. The central axis doses were calculated by anisotropic analytical algorithm (AAA) and AXB using a single field of 6 MV flattening filter-free beam from TrueBeam linear accelerator. In phantom, we used various field sizes from 2 × 2 cm² to 5 × 5 cm². The dose profiles were generated at the depth of 4.5, 5.5, 6.5 and 7.5 cm, including the presence of an air cavity. All measurements for film dosimetry were performed under the same condition of the calculation with film.

Results: With film in the slab phantom, CADs for AXB and AAA overestimated -5.55% and 131.60%, compared to those of measurements. However, differences of CADs without film were -27.72% and 144.20%. The CAD differences between AXB and AAA reduced with increasing field size and increased relative to the depth increment. The AXB dose calculation in an air cavity showed more agreement than AAA. Also the root means square error (RMSE) value of dose profiles for AXB were within 10%, while those of AAA were more difference than 30%.

Conclusions: In this study, we confirmed that inclusion of film within an air cavity has affected on dose calculation with both algorithms. Our experimental phantom study demonstrated that the AXB is significantly more accurate for dose calculation in the region of an air cavity when compared with AAA. Therefore, we recommend the use of AXB instead of AAA for avoiding inaccurate dose calculation, especially on the clinical cases including air cavity.

PS05.048 - Evaluation of Dosimetric Effects on Metal Artifact: Comparison of Dose

Distributions Affected by Patient Teeth and Implants

Author(s): Min-Young Lee¹, Jeong-Woo Lee², Ji-Yeon Park³, Hye-Jin Park⁴, Sang-Won Kang¹, Tae-Suk Suh¹

¹Department Of Biomedical Engineering, Research Institute of Biomedical Engineering, Seoul/KOREA, ²Department Of Radiation Oncology, Konkuk University Medical Center, Seoul/KOREA, ³Department Of Pediatrics And Molecular Imaging Program At Stanford, Stanford University, Stanford/UNITED STATES OF AMERICA, ⁴Department Of Radiation Oncology, Ajou University School of Medicine, Suwon/KOREA

Purpose: Implant-supported dentures seem particularly appropriate for the predicament of becoming edentulous and cancer patients are no exceptions. Metal artifacts generated by dental implants cause dose discrepancy in head-and-neck cancer cases due to the inaccurate predicted doses. To verify the theoretical analysis of the metal artifact, streak artifact and dark artifact, and also critical analysis of dosimetric effect which cause by dental implants in CT images of head and neck cancer patients with the patient teeth and implants inserted humanoid phantom. **Methods:** The phantom comprises cylinder which is shaped to simulate the anatomical structures of a human head and neck. Through applying various clinical cases, made phantom which is closely allied to human. Developed phantom can verify two classes: (i) dose measurement when patient closed mouth (ii) dose measurement when patient opened mouth. RapidArc plans of 4 cases were created in the Eclipse planning system. Total dose of 2000cGy in 10 fractions is prescribed to the whole planning target volume (PTV) using 6MV photon beams. Acuros XB (AXB) advanced dose calculation algorithm, Analytical Anisotropic Algorithm (AAA) and progressive resolution optimizer were used in dose optimization and calculation. **Results:** In closed and opened mouth phantom, because dark artifacts formed extensively around the metal implants, dose variation was relatively higher than that of streak artifacts. As the PTV was delineated on the dark regions or large streak artifact regions, maximum 7% dose error and average 3% difference was observed. The averaged minimum dose to the PTV predicted by AAA was about 5% higher and OARs doses are also 5% higher compared to AXB. **Conclusion:** AXB was found to have better dose predictions than AAA and at the tissue interfaces where backscatter occurs. Therefore, AXB is more appropriate to use for dose predictions, especially when low-density heterogeneities are involved.

PS05.049 - Advancement of Dedicated Phantom to demonstrate Dosimetric Effect of Metal Artifact in Head and Neck Cancer

Author(s): Min-Young Lee¹, Jeong-Woo Lee², Tae-Suk Suh¹, Ji-Yeon Park³, Hye-Jin Park⁴

¹Department Of Biomedical Engineering, Research Institute of Biomedical Engineering, Seoul/KOREA, ²Department Of Radiation Oncology, Konkuk University Medical Center, Seoul/KOREA, ³Department Of Pediatrics And Molecular Imaging Program At Stanford, Stanford University, Stanford/UNITED STATES OF AMERICA, ⁴Department Of Radiation Oncology, Ajou University School of Medicine, Suwon/KOREA

Purpose: Implant-supported dentures seem particularly appropriate for the predicament of becoming edentulous and cancer patients are no exceptions. The purpose of this study is to verify the clinical dosimetric effects of metal artifact in clinical cases by developing a realistic head and neck phantom.

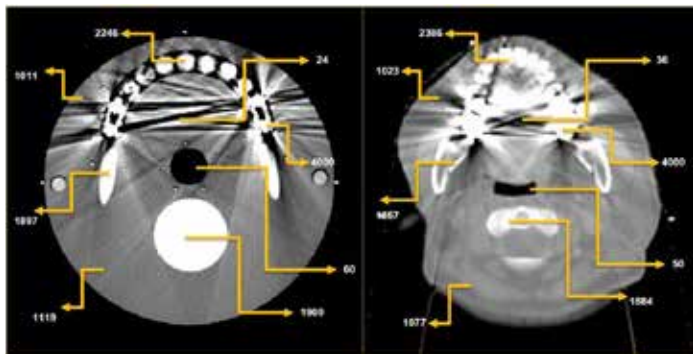
Materials and Methods: The phantom comprises cylinder which is shaped to simulate the anatomical structures of a human head and neck. Through applying various clinical cases, Fig.1, phantom is closely allied to human. Developed phantom can verify two classes:

(i) closed mouth (ii) opened mouth. Also, the inserted patient tooth can trade places. The phantom was made to enable film to be set-up between two slabs to compare the dosimetric impact and variation of dose distributions. Furthermore, mid-slabs of phantom contain few cylindroid holes for Radio-Photoluminescence Glass Dosimeter (RPLGD), same spots in opened and closed phantoms, where cause the streak and dark artifacts for the dose verification.

Results: The accuracy of dose calculations is essential to the quality of the radiotherapy treatment planning and tumor response. As after scanning the phantom, in closed and opened mouth phantom, because dark artifacts formed extensively around the metal implants, dose variation was relatively higher than that of streak artifacts. The phantom was capable of producing realistic head and neck metal artifact imaging data from which imaging devices and techniques can be evaluated.

Conclusions: The phantom provides a unique and useful tool in head and neck dosimetry research. It can be used in the development of new imaging instrumentation, image acquisition strategies, and image processing and reconstruction methods.

Figure1,



PS05.050 - Accuracy of radionuclide generation simulation using Antisymmetrized Molecular Dynamics (AMD)

Author(s): Masaaki Takashina¹, Yusuke Sakurai¹, Kouta Fukunaga², Masao Matsumoto¹, Masahiko Koizumi¹, Akira Ono³
¹Graduate School Of Medicine, Osaka University, Suita, Osaka/JAPAN, ²Division Of Health Sciences, Osaka University, Osaka/JAPAN, ³Graduate School Of Science, Tohoku University, Sendai/JAPAN

1. Introduction

During particle therapy, radionuclides are produced in patient bodies and equipment. In the view point of utilizing them for the beam on-line PET, radiation protection, etc., it is important to understand the phenomena induced by therapeutic particle beams, and simulation is essential as well as measurements. Although Quantum Molecular Dynamics (QMD) is frequently adopted in simulation as the model for nuclear reactions, they do not entirely reproduce experimental data. In this study, we focus on Antisymmetrized Molecular Dynamics (AMD), which is thought to have more theoretical validity than QMD, and investigate its accuracy comparing with QMD.

2. Materials and Methods

We use the AMD code developed by Ono¹). The QMD calculation is performed with PHITS²). AMD and QMD describe the dynamical processes of nuclear reactions. The resultant fragments may be in excited states, and decay with the statistical process, which is described by a generalized evaporation model (GEM)³). The GEM calculation after QMD is done as a sequence of the PHITS calculation. For GEM after AMD, we use the same code as in PHITS.

We investigate ¹²C induced nuclear reactions at E/A=20 MeV - 400

MeV. As the target nuclei, we consider ¹²C, ¹⁶O and ⁴⁰Ca. The calculated results are compared with experimental data.

3. Results and Discussion

Fig.1 is an example of the results, which shows the mass distribution of the fragments produced in the ¹²C+¹²C reaction at E/A=400 MeV. The open diamonds (triangles) represent the results of AMD (QMD) followed by GEM. AMD is found to give comparable results with QMD. In particular, they both give the cross sections of ⁷Be and ¹¹C close to the experimental data⁴) (solid circles). On the other hand, for the neutron cross section, AMD is better than QMD.

4. Conclusion

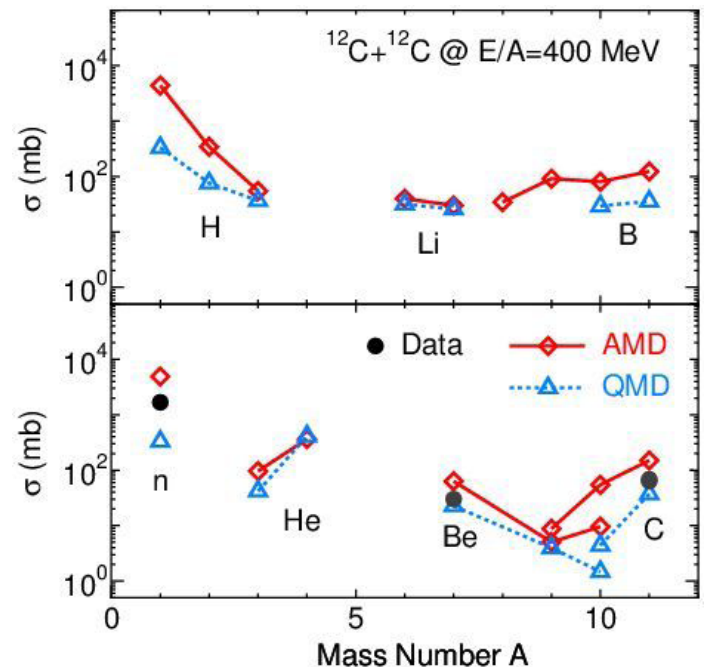
Since AMD and QMD show the similar results of cross sections, we cannot determine which model is better for ¹²C+¹²C reaction. For the ⁴⁰Ca target case, the difference is noticeable, but there exist too few appropriate data. In order to make simulation more accurate, more data are strongly desired.

Acknowledgements:

This work was supported by JSPS Core-to-Core Program (No.23003) and KAKENHI (No. 23791419).

References

- 1) A. Ono et al., Phys. Rev. Lett. 68 (1992) 2898.
- 2) T. Sato et al., J. Nucl. Sci. Technol. 50 (2013) 913.
- 3) S. Furihata, Nucl. Instr. Meth. B 171 (2000) 251.
- 4) H. Yashima et al., Rad. Ac. 91 (2003) 689.



PS05.051 - Accurate small field dosimetry requires systematic consistent approaches to measurement, modelling and data reporting.

Author(s): Gavin Cranmer-Sargison¹, Paul Charles², Jamie Trapp³, David Thwaites⁴

¹Medical Physics, Saskatchewan Cancer Agency, Saskatoon/CANADA, ²Radiation Oncology, Princess Alexandra Hospital, Brisbane/AUSTRALIA, ³Science And Engineering Faculty, Queensland University of Technology, Brisbane/AUSTRALIA, ⁴Institute Of Medical Physics, School Of Physics, University of Sydney, Camperdown, Sydney/AUSTRALIA

Small field dosimetry is clearly recognized as difficult, increasingly

so as the size reduces, yet consistent data is necessary for accuracy in clinical use, for applications of small fields themselves and also as components of more complex beams. However, the overall reported data in the literature contains relatively large inconsistencies. To consider how to resolve these differences and how to improve the practical approaches and associated uncertainties requires careful standardised measurements, validated Monte-Carlo (MC)-based correction factors and possible new thinking on detectors. In addition it requires clear understanding of what the parameters reported truly describe and clear reporting of data, where values should be correlated to actual delivered dosimetric field size, and not to nominal or set field size, to enable careful comparison between linacs. For very small field sizes, greater attention is required to the experimental measurement and reporting methods, requiring clear guidelines for what is a 'very small field size' and for when such more detailed methods are needed.

A range of measurements and MC modelling studies have been reported by our joint collaborative groups. Based on these methods and results, data and recommendations have been published on:

- commissioning/fine-tuning MC models for small field sizes; and the interplay between modelling and measurements to achieve this;
- modelling-based correction factors for a range of shielded and unshielded diodes for 6MV beams; - what constitutes a 'very small field size' (essentially fields smaller than 1.5 cm in size for 6 MV), based on the different effects as field size gets smaller and their consequences for uncertainties; - measurement methods necessary to control uncertainties at these smaller field sizes (essentially measuring beam profiles at the same time as output factor, to ensure good alignment, but also to measure the actual dosimetric field sizes; - reporting of output factors for consistent comparison and applications; ie reporting against an effective field size taking into account measured dosimetric field sizes; and not just against nominal field size, in order to reduce the variations in reported data and allow interpolation between reported tabulated data eg on correction factors; - observations on detector design and modelling for possible 'correction-free' small detectors (eg scintillators, but also modified standard detectors such as diodes).

The approaches to each of these areas and the practical use of the data must be systematic and consistent. The above sets of work and recommendations provide coherent approaches, which are inter-linked. As national (eg AAPM) and international (eg IAEA) bodies develop protocols for small field dosimetry, it is critical that clear inter-dependent measurement and modelling based methods and data are recommended to improve the consistency and uncertainties involved and to provide the best accuracy possible in these increasingly clinically-used conditions.

PS05.052 - Determination of Radon/Thoron Concentrations in Some Iraqi Building Materials By Using CR -39

Author(s): Abdulredha S. Younis¹, Nada Tawfiq²
¹Physiology Department, Hawler Medical University, Erbil/IRAQ, ²Al-Nahrain University, Baghdad/IRAQ

Common building materials used for construction of houses, which are considered as major source of radon / thoron gases in indoor environment such as cement, gypsum, sand, and bricks. Samples of these materials had been collected from different factories distributed at different Iraqi areas in Baghdad, south, and in the west. The determinations of radon/thoron concentrations have been studied by using sealed can technique and CR-39 track detectors were irradiation for 30 days in a closed can. Standardization of irradiation effects for the same period on CR-39 detectors has been done on samples of known alpha particles emitters' concentration, which are adopted by the International Atomic Energy Agency (IAEA). Radon/Thoron concentrations have been found to be varying from

minimum value of 119.7 ± 2.6 Bq/m³ for Lime sample to a maximum value of 309 ± 8.6 Bq/m³ for Ordinary black cement. These results show that Iraqi building materials constituents contains low concentrations of background Radon / thoron natural sources of radiation.

PS05.053 - Evaluation of Scattered Dose Reduction in Interventional Radiology Using Lead-Free Protection Sheets

Author(s): Khamizah Taharim¹, Chai Hong Yeong¹, Kwan Hong Ng¹, Basri Johan Jeet Abdullah², Chu En Ting¹

¹Department Of Biomedical Imaging, Faculty Of Medicine, University of Malaya, Kuala Lumpur/MALAYSIA, ²University Of Malaya, University of Malaya Research Imaging Center, Kuala Lumpur/MALAYSIA

Introduction

Occupational radiation dose in interventional radiology (IR) has become a concern due to increasing complexity of the procedures and fluoroscopic time. A lead-free (primarily Bi-83 and Sb-51) protection drape has been introduced to absorb scattered radiation by 50 to 95% at 90 kVp during IR procedures. To ensure the safety of medical personnel working with radiation, it is imperative that the efficacy of protection equipment meets the required standards.

Aims and Objectives

This research aimed to establish the physical characteristics and assess the efficacy of the protection drape (RadPad, Worldwide Innovations & Technologies, USA) in reducing scattered dose to the personnel, in comparison to a typical lead shield.

Methods

The physical characteristics of RadPad (Orange with a claimed 90% attenuation and Yellow with 75%) were assessed by establishing its attenuating and backscattering properties and its dose reduction profile. The percentage attenuation was measured using two calibrated semiconductor detectors, each placed before and after the protection drape, which was placed on a phantom and exposed at varying X-ray energies. Backscatter properties of RadPad were studied by measuring the entrance surface air kerma on a phantom, with and without the RadPad drape in place. An increase in reading when RadPad is in use would indicate backscattered radiation. RadPad's dose reduction profile was established by analysing exposed radiochromic films partially covered by the protective drape. Additionally, the films were sandwiched between sheets of 2cm thick Perspex phantom to simulate dose distribution at different depths within the patient body. RadPad's efficacy in dose reduction was further assessed through scattered radiation dose mapping during a simulated fluoroscopy-guided procedure, in which phantoms were used to simulate a radiologist and a patient. RadPad was placed over the patient phantom and exposure was made using routine fluoroscopy settings. Dose readings were obtained at varying heights on the radiologist phantom (brain, thyroid chest level) and at different positioning of the phantom in the fluoroscopy suite.

Results and Conclusion

RadPad significantly reduces scattered radiation dose to staff during prolonged fluoroscopy-guided procedure. RadPad Orange (90% attenuation) shows similar attenuation to 0.25 mm lead-equivalent shield at 90 kVp. However, empirical results show deviation from manufacturer specifications (85.8% and 71.6% for Orange and Yellow instead of 90% and 75% at 90 kVp respectively). Backscattered radiation was detected when RadPad was placed over the phantom, indicating possible increase in patient skin dose. 0.25 mm lead-equivalent produces higher backscatter radiation compared to RadPad, suggesting that RadPad is advantageous in reducing patient skin dose. RadPad has potential as additional radiation shielding, however its lower linear attenuation coefficient compared to lead suggests that it would not be an ideal replacement for lead as the primary personal radiation protection for medical staff.

PS05.054 - Dosimetric validation of Volumetric Modulated Arc Therapy (VMAT) in an upgraded Clinac 2100CD using AAPM TG-119 bench mark plans for Flattening Filter Free(FFF) photon beam

Author(s): S. Ashokkumar^{1,2}, K.M. Ganesh^{1,3}, K. Ramalingam^{1,2}, K. Karthikeyan^{1,2}, N. Jagadeeshkumar², V.S. Subramanian^{1,2}; ¹Bharathiar University, Research and Development Center, Coimbatore/INDIA, ²Department of Radiation Oncology, Yashoda Hospital, Secunderabad/INDIA, ³Department of Radiation Physics, Kidwai Memorial Institute of Oncology, Bangalore/INDIA

Introduction: Recently in our center we have upgraded our Varian Clinac 2100CD linear accelerator machine with 6MV Flattening Filter Free (FFF) beam. Even though the dosimetric characteristics of FFF beam have been reported both in experimental and Monte Carlo studies, the application of FFF beams in planning and delivery is complicated.

Aim of this study is to validate the commissioning of upgraded 6MV FFF beam dosimetrically using AAPM-TG-119 bench-mark plans for VMAT and to compare with IMRT plan data for both FF and FFF beams.

Material and Methods: AAPM TG-119 proposes a set of test clinical cases for testing the accuracy IMRT planning and delivery system. For these test cases, we generated two treatment plans. The first plan was done using 7-9 IMRT fields and a second plan utilizing one- or two-arc VMAT. Dose optimization and calculations were performed using 6MV FF & FFF photons in EclipseTPS. Dose prescription and planning objectives were set according to the TG-119 goals and plans were scored based on planning objectives. Treatment plans were compared using dose coverage, conformity index (CI) for reference dose and homogeneity index (HI D5–D95). Point doses were measured at points recommended using ion chamber CC13. Planner Dosimetry was done using Imatrix with Multicube and

gamma evaluation was done using omnipro IMRT software with the criteria of 3% DD and 3 mm DTA.

Results and Discussion: VMAT dose distributions were comparable to IMRT plans. Our planning results were matched TG-119 planning results as shown in figure 1. conformity indices were ranged from 1.02–1.18. The point dose results were within 2% of planned dose values. All gamma evaluation results show gamma less than one for more than 95% data points.

There was a average reduction in treatment time using FFF beam as compare to FF beams for sliding window IMRT. In case of VMAT the reduction in treatment time was not significant as the dose per fraction was low and the gantry speed cannot be increased beyond 4.8°/ sec.

Conclusion: The result from the study shows that FFF beam upgraded in Clinac 2100CD satisfies AAPM-TG-119 for the given bench mark plans. They are also helpful to gain confidence in new modalities like FFF based VMAT and to test its capabilities at preclinical implementation stage. Interestingly the study deduced that sliding window IMRT using 6MV FFF beam shows 40% reduction in the treatment time as compared to conventional 6MV FF.

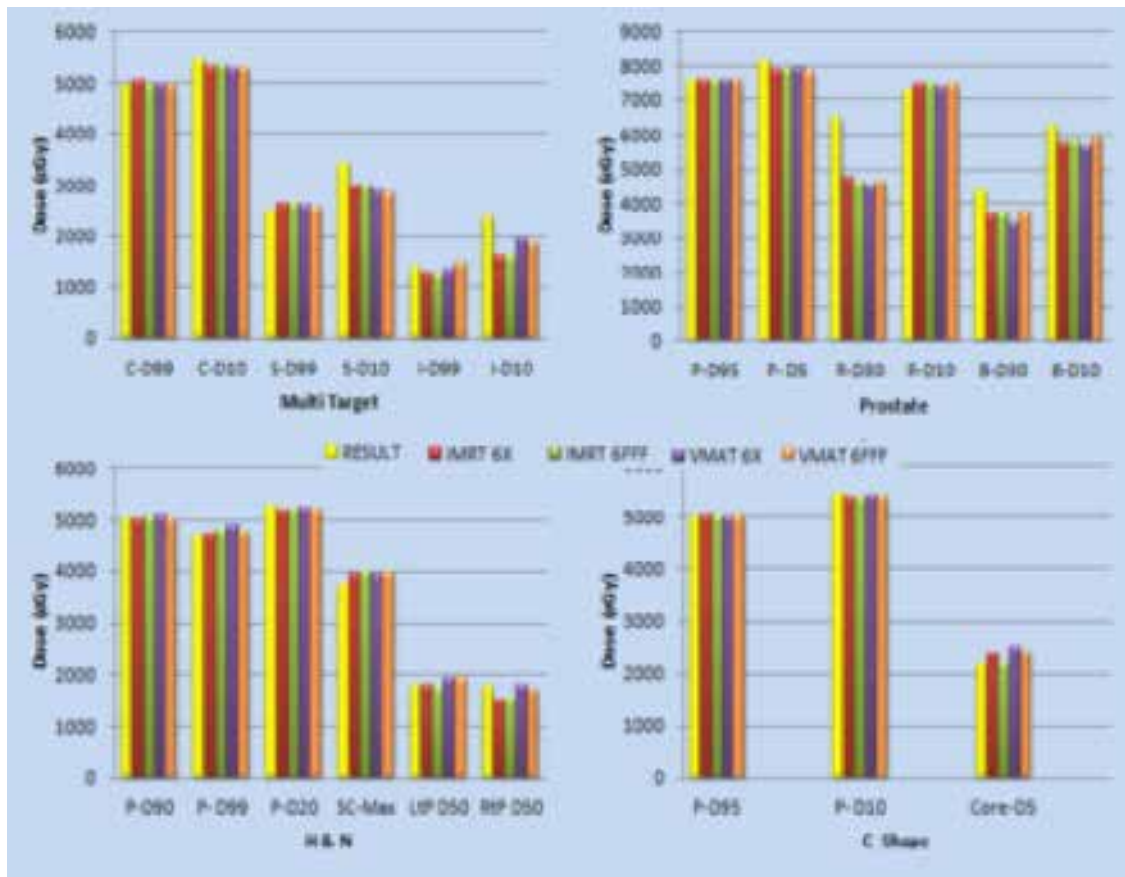


Figure.1-Results achieved for-TG-119cases.

PS05.055 - Study on Ion-recombination effect of 6MV Flattening Filter Free beam at isocenter and tray-level configuration using various detectors

Author(s): K. Ramalingam^{1,2}, S. Senthil Kumar^{1,3}, S. Ashokkumar^{1,2}, K. Karthikeyan^{1,2}, N. Jagadeeshkumar^{2,4}, S. Subramaniam^{1,2}; ¹Bharathiar University, Research and Development Center, Coimbatore/INDIA, ²Department of Radiation Oncology, Yashoda Hospital, Secunderabad/INDIA, ³Radiation Oncology, Madurai Medical College and Rajaji Govt Hospital, Madurai/INDIA, ⁴School of Advanced Science, Vellore Institute of Technology, Vellore/INDIA

Introduction: In high energy linac, removal of flattening filter from the path of the beam produces unflat-beam, with increased dose-rate (1400 MU/min for 6MV FFF beam and 2400 MU/min for 10MV FFF beam). The recombination of ions formed by separate ionizing particle tracks is dependent on the density of ionizing particles i.e., Dose-rate. This effect depends on the chamber geometry and applied polarizing voltage (IAEA-TRS398).

VMAT employs dose-rate modulation with Gantry angle, but during Patient specific QA, point dose and 2D-Planar dosimetry calibration is done with a fixed constant dose-rate.

Recently vendors are coming up with 3D-online verification methods using (Transmission) detectors placed near tray-level of the gantry. For 6MV-FFF, the dose-rate at tray-level (SDD=62cm) is 3750MU/min.

The aim of this work, is to study the ion-recombination factor(k_s) of 6MV-FFF beam at central-axis and off-axis of the beam using different volume chambers, with available dose-rates and also to study ion recombination effect near tray-level configuration.

Material and Methods: Measurements were performed on Vari-anTM Clinac 2100CD capable of delivering VMAT. Recently, we have upgraded the Clinac to deliver 6MV FFF beam with a maximum dose-rate of 1400MU/min. Different volume ion chambers FC65G, CC13, PPC05 and A14 with different electrode separation were used for measurement.

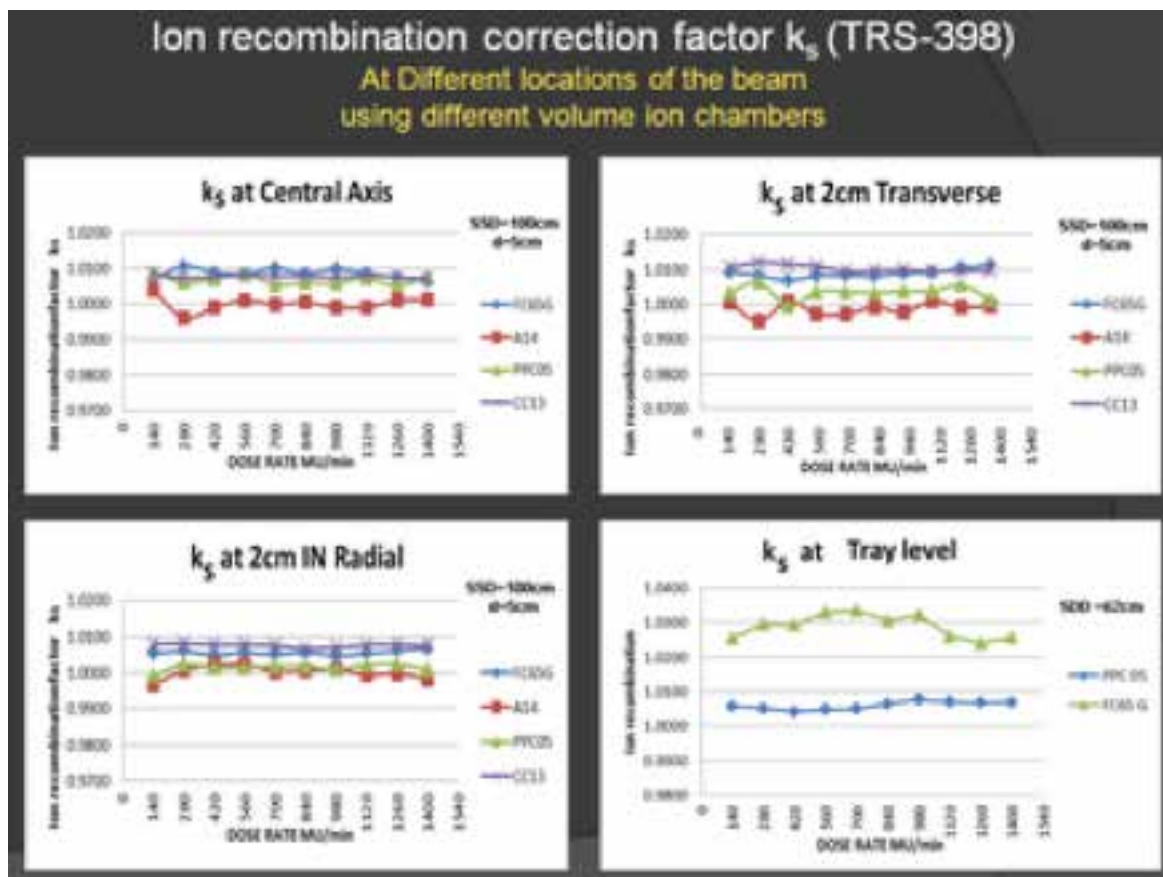
For a field size of 10x10cm², SSD=100cm and depth 5cm, k_s was measured at central-axis and 2cm off-axis for different available dose-rates. To simulate tray-level configuration k_s was measured using PPC05 and FC65G chambers with a build up of 2 cm. k_s was calculated using two-voltage method for +300V&+150V and analysed.

Results and Discussion: Ion recombination(k_s) was increasing with increase in chamber volume. But for a particular chamber, it was less significant for variations in nominal dose-rate, Figure 1.

At Central-axis the average k_s for FC65G (rcav=3.1mm,0.65cc) was 1.0086±0.0014 (1SD) and for CC13 (rcav=3.0mm,0.13cc) was 1.0091±0.0014 (1SD), which was closely comparable. It shows that k_s depends not only on chamber volume but also on electrode separation (rcav).

At Tray-level configuration, the average k_s was 1.029±0.0034(1SD) for FC65G (rcav=3.1mm) and 1.0060±0.0011(1SD) for PPC05 (2mm electrode spacing). However the k_s was less significant for variations with nominal dose-rate.

Conclusion: For 6MV-FFF VMAT-QA, small volume chambers can be used for verification without correcting for k_s in both CAX and off-axis. For Tray-level measurements, small volume chambers with electrode separation <2mm can be used without correcting for k_s . However, at tray-level, Ion-recombination effect should be accounted for when electrode separation is >2mm.



PS06 - TRACK 06: NEW TECHNOLOGIES IN CANCER RESEARCH AND TREATMENT

SP06.001 - GEANT4 versus MCNP5: Monte-Carlo ophthalmic brachytherapy dosimetry in the presence of gold nanoparticles for ^{125}I and ^{103}Pd

Author(s): Shervin Vahidian, Mohammad Vahidian, Somayeh Asadi, Mehdi Vaez-Zadeh

Physics, K.N.Toosi University of Technology, tehran/IRAN

The emphasis of the present work is to compare the effect of gold nanoparticles (AuNps) on healthy human ocular tissues in ophthalmic brachytherapy dosimetry, between water and eye phantoms by utilization of the two most noteworthy Monte-Carlo codes of GEANT4 and MCNP5. The intended study was based upon a simulated model of the human eye consisting different parts such as Lens, Cornea, retina, Choroid, Sclera, skull bone, Anterior Chamber and a melanoma tumor which was latticed to house AuNps required for the dosimetry comparisons of two uniquely defined radionuclides of ^{125}I and ^{103}Pd . The effects of the presence of AuNps on the absorbed dose by the tumor have been taken into account using both Monte-Carlo codes mentioned above; furthermore, the aberrations in dose calculations of the simple eye phantom and the realistic eye model were also an element of consideration. The importance of such evaluations on various compositions that are most common in Monte Carlo studies could prove to be rewarding, especially in presence of external anomalies such as AuNPs. With respect to the numerous distinctions between codes themselves, it is always fruitful to compare multiple of these programs with one another; hence, a rigorous inspection of the results has been executed, and dissimilarities have been highlighted for better understanding of the advantages and deficiencies of both codes. All in all, it is best stated that interdisciplinary methods of combining diverse therapeutic applications have gained much ground in our current era, and serve to significantly increase efficiency of cures worldwide.

SP06.002 - Clinical Implementation of an Elekta HexaPOD evo RT Couchtop with kV Cone beam Image Guided Radiation Therapy

Author(s): Lourdes M. Garcia, Cathy Neath
Medical Physics, Durham Regional Cancer Centre, Lakeridge Health, Oshawa/ON/CANADA

Image guidance is indispensable in modern radiation therapy, allowing fast and precise correction of misalignments thereby improving the efficiency and accuracy of the patient setup and treatment. The HexaPOD evo RT couchtop is a robotic couch with 6° of freedom, which allows automatic and remote correction of discrepancies between the pre-treatment and reference images. This work details the commissioning and post clinical implementation daily QA results of the HexaPOD installed on two linacs within our centre.

Commissioning of the HexaPOD and iGUIDE 2.0 tracking systems was performed by applying known translations and rotations of the Pentaguide phantom, acquiring and registering a CBCT (XVI 4.5), applying the shifts and evaluating residual error. The rotational accuracy of the 3D-CBCT is a limiting factor in the accuracy of the patient position. This was assessed using the EMMA phantom (SIEMENS) which has 12 localization beads at the 3, 6, 9, and 12 o'clock position in 3 planes, -9.5cm , 0 and $+9.5\text{cm}$. The daily QA assurance program established incorporates the Pentaguide mounted on the Tilt Plate (Modus Medical Devices Inc.) with known rotations (1.25° , 0.7° and 1.0°) and translations. A localization scan is performed, registered, shifts applied, and a verification scan is acquired to assess the residual rotation.

Results of the daily QA (Dec 2014-Jan 2015) residual rotation and

translation for both HexaPOD systems are illustrated in Table 1 and Figure 1. The average residual rotation is $0.05^\circ \pm 0.19^\circ$, and translation $0.00 \pm 0.01\text{cm}$, over all directions and both systems. The residual rotation is limited by the accuracy of the CBCT reconstruction found to be up to 0.4° as assessed with the Emma phantom.

The Elekta HexaPOD robotic couchtop is operating within the manufacturer specifications. However, when used in combination with our current XVI imaging system, larger uncertainties are present.

PS06.003 - Ex-vivo experimental study with a new cluster-type microwave ablation antenna

Author(s): Qun Nan, Xiaohui Nie
College of Life Science and Bio-engineering, Beijing University of Technology, Beijing/CHINA

Microwave ablation which has the advantages of minimally invasive and high-efficiency was more and more used into a number of areas such as cancer treatment. when the tumor diameter is less than 3cm the ablation effect is ideal, but for larger tumors it must be a higher ablation time and a higher power which can result in the reduction of the antenna performance, so the uncertainty of curative effect enhanced. Therefore the study uses in ex-vivo bovine liver to explore the performance of a new cluster-type microwave antenna which has three microwave ablation needles. The temperature distribution and 60°C isotherm which can decide the scope of the effective ablation were explored. The study carries out with net power of 40W , 60W ; ablation time was 5min , 10min , 15min , respectively. For the power of 40W , the maximum temperature, area, volume, diameter and longitudinal diameter was 88.812°C , 9.0511cm^2 , 7.917cm^3 , 2.902cm , 3.830cm , respectively with the ablation time 5min while 99.184°C , 19.043cm^2 , 50.936cm^3 , 3.794cm , 5.835cm , respectively with the ablation time 10min and 106.094°C , 25.627cm^2 , 81.655cm^3 , 4.612cm , 6.719cm , respectively with the ablation time 15min . For the power of 60W , the maximum temperature, area, volume, diameter and longitudinal diameter was 100.047°C , 25.372cm^2 , 80.345cm^3 , 5.343cm , 6.908cm , respectively with the ablation time 5min while 108.863°C , 42.216cm^2 , 185.716cm^3 , 6.319cm , 8.102cm , respectively with the ablation time 10min and 110.219°C , 49.803cm^2 , 244.965cm^3 , 7.228cm , 8.720cm , respectively with the ablation time 15min . The 60°C isotherm was ellipsoid-like. Under the same power, the 60°C isotherm increase with ablation time and at the same time, the 60°C isotherm increase with power, too. This study may make an important support for the development and clinical application of the antenna.

PS06.004 - Bio Magnetic Nano Particles (BMNPs) used for cancer treatment via Hyperthermia method

Author(s): Amirsadegh Rezazadeh Nochehdehi, Minoosadri, Ali Moahmmadzadeh
Biomaterials Engineering, Materials and Biomaterials Research center (MBMRC), Tehran/IRAN

Magnetic nano particles for various applications in the medical field such as Separation, Immunoassay, Drug delivery, Magnetic Resonance Imaging and Hyperthermia has been developed by many researchers. Therefore, the use of magnetic nano particles for the treatment of various cancers by using heat therapy is a rapidly growing and growing. In contrast, one of the main challenges facing researchers, optimization of properties and mechanism of biological effects induced Hyperthermia to control and minimize it. The purpose of this paper is to investigate, develop and identify different types of bio magnetic nano particles (BMNPs) in the diagnosis and treatment of cancer that has a new approach to the introduction of heat therapy (Hyperthermia) in the treatment of cancer as an alternative to radiotherapy and chemotherapy. Because of the use these nano particles directly in humans and animals, is very

important to evaluation of physical and bio-compatibility properties according to International Standard (ISO 10993) that in this article we have tried to be fully addressed. After studies done on previous research, it was found that the use of basic iron and cobalt nano particles with a bio-compatible coatings of polymer and ceramic compounds are the best option for medical applications. Furthermore, the need for fundamental and applied research in this area was further emphasized.

PS06.005 - GATE Monte Carlo Simulation for Dual Head LINAC Modeling

Author(s): Seungwoo Park, Han Kyeol Song, Su Chul Han, Haijo Jung, Kum Bae Kim, Young Hoon Ji
 Korea Institute of Radiological and Medical Sciences, SEOUL/KO-REA

Introduction

In this study, we purposed a new LINAC system which had dual head to reduce irradiation time for tumor treatment. In order to design the dual head LINAC, 6 MV photon beam was simulated and evaluated quantitatively with GATE Monte Carlo code as a preliminary study.

Materials & Methods

The LINAC head was designed with VARIAN manufacturer’s information. 6 MV photons were generated from the head and the photons irradiated to a water phantom for beam evaluation. GATE simulation was segmented by two stages, the one was to generate X-ray spectrum and the other one was for irradiation X-ray to the water phantom.

Results

The dual head irradiation was compared to single head irradiation in terms of the deposited energy which corresponded to treatment time. At single head simulation, the head was fixed along longitudinal axis direction. Whereas in dual head simulation the one head was placed at same position with the single head case but the other head was rotated along transversal axis direction. Fig 1-2 showed the deposited dose at box and sphere phantom, respectively. The efficiency was calculated that deposited dose from dual heads was divided by the dose from single head. At all conditions, dual heads showed higher treatment efficiency. Efficiency was increased about 40 to 60%.

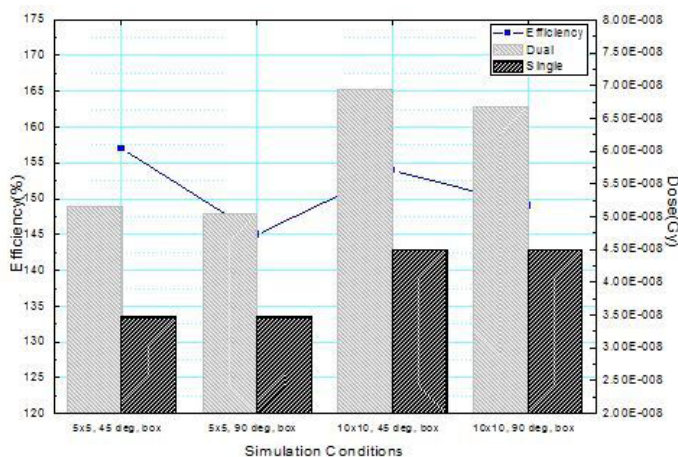


Figure 1. Comparison of the deposited dose and its efficiency at box phantom

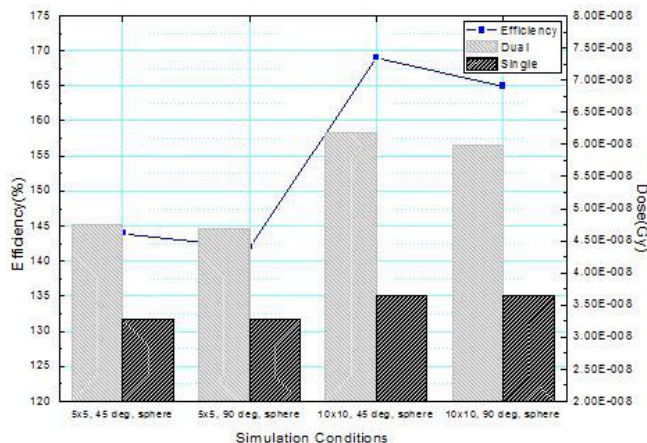


Figure 2. Comparison of the deposited dose and its efficiency at sphere phantom

Conclusions
 From the result, the dual head system had a higher dose deposition than a single head system. The dual head system will contribute to the real radiotherapy. However, the treatment planning system for dual head LINAC and dosimetry method are not established yet. The result was that measured deposited dose within the whole phantom size. Therefore, the planning method has to be defined and estimated. The real dual head LINAC system is being built and the specific research will be conducted on with the dual head system.

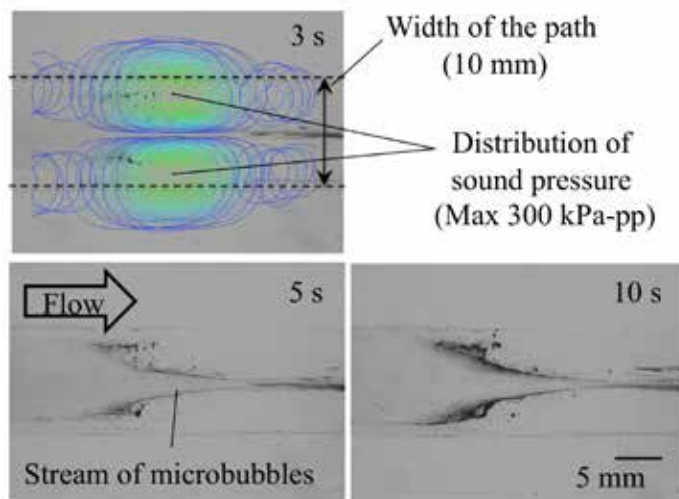
PS06.006 - Active control of microbubbles in flow using position and phase variations in three-dimensional acoustic field

Author(s): Kohji Masuda, Shinya Miyazawa, Toi Sawaguchi, Naoto Hosaka, Takashi Mochizuki
 Tokyo Univ. of Agriculture and Technology, Koganei/JAPAN

Though many experiments using effective combination of ultrasound and microbubbles for medical treatment, e.g., thermal therapy and drug delivery, have been reported, because injected microbubbles disperse in the human body, there are the following two major problems; low concentration of microbubbles in the target area, and risk of side effects due to unwanted microbubbles. To enhance local concentration of microbubbles, we have reported our attempts for active control of microbubbles by acoustic radiation forces, which were active path selection, aggregation formation, and trapping in flow. Since 2013 we have produced three-dimensional acoustic field of continuous wave to produce three-dimensional acoustic force using a matrix array transducer. In this presentation, we introduce our attempts for active control of microbubbles in flow using position and phase variations in three-dimensional acoustic field.

The flat array transducer has 64 elements on the aperture of 23.9 x 23.9 mm² with the resonance frequency of 1 MHz. A flow path was fixedly floated from the bottom of a water tank filled with water. Also we prepared the suspension of microbubbles with an average diameter of 0.5 μm, which were produced from poly(ethylene glycol)-modified liposomes and perfluoropropane gas.

We have produced time-shared acoustic fields including the pairs of two focal points. Figure shows the successive images of the observation area after injection of microbubbles suspension (concentration of 0.05 mg lipid/ml) with flow velocity of 30 mm/s, where the maximum sound pressure was 300 kPa-pp and the positions of two peaks were moved periodically along the direction of flow. The inner shape of the path was with the thickness of 2 mm and the width of 10 mm. In the first frame, contour lines were superimposed to indicate the magnitude of sound pressure. Stream-line of microbubbles was clearly confirmed in the middle of the two focal points, which indicates that most microbubbles were induced between them.



Here we have to mention that the phase difference between the two focal points in the figure was opposite phase. On the other hand, in case of in-phase between the two points, most microbubbles were trapped in the middle of the path because two points were merged to form greater acoustic field. From this result acoustic force can be produced from the sound source to not only a propelling direction but also an attractive direction by position and phase variations in three-dimensional acoustic field.

PS06.007 - Adaptive radiation therapy of pancreatic cancer patients treated using Tomotherapy: Validation of dose accumulation algorithms using deformable image registration in SlicerRT

Author(s): Eric Vorauer¹, Peggy Le¹, Mithunan Modchalingam¹, Daniel Glick¹, Hans Chung¹, Lee Chin²

¹Sunnybrook Health Sciences Centre, Toronto/CANADA, ²University of Toronto, Department of Radiation Oncology, Toronto/CANADA

Introduction

Pancreatic cancer is one of the leading causes of cancer death in Canada. Radiation therapy treatments for pancreatic cancer at the Odette Cancer Centre typically consists of 54 Gy administered over 30 fractions. Due to the long treatment course, the patient’s anatomy can shift away from what was used to create the original treatment plan. This interfractional variation can occur due to organ motion, weight loss or a change in the tumour volume. Using the Planned Adaptive™ module from Tomotherapy, planning contours can be rigidly fused to a daily IGRT MVCT image to determine the actual daily dose to the target and surrounding organs at risk and assess the potential dosimetric risk due to such anatomical changes. However, the Planned Adaptive module currently lacks the ability to account for non-rigid changes in organ motion. Deformable image registration has the potential to account for daily deformations by performing a voxel by voxel mapping of the planning contours to the daily IGRT image. Previously, we optimized and validated a DIR algorithm to perform non-rigid deformable image registration of contours between planning KVCT and daily MVCT images using the radiation therapy research toolkit, SlicerRT. In the current work, we verify the accuracy of the developed DIR algorithm for daily dose accumulation and dose volume histogram assessment for targets and organs at risk.

Methods

Deformable image registration was performed on the first and last daily MVCT images acquired from the Tomotherapy unit of a patient undergoing treatment for pancreatic cancer. Two methods were performed to validate the potential of the DIR algorithm for dose

accumulation.

In the “forwards” registration approach, planning contours are deformed onto the daily image containing on a “daily” dose calculated using the original treatment plan. In the “inverse” registration, the dose from the daily image is deformed onto the planning image containing the contours. Both registration directions use the same registration parameters, and in both cases, dose volume histograms are created after deformation. Dose volume histograms of the forwards and inverse methods will be compared using a DVH acceptance agreement criterion. In addition, V20 of the kidneys, V30 of the liver and max cord dose will be analyzed.

Preliminary Results

Initial results of the average DVH acceptance agreement from 5 patients are shown in Table 1.

Table 1. DVH acceptance agreement average for first and last fractions from 5 patients. Criterion is 1% dose and 1% volume.

First Fraction Organ	DVH Acceptance (%)	Last Fraction Organ	DVH Acceptance (%)
GTV	98.3	GTV	97.9
Spinal Cord	83.3	Spinal Cord	83.1
Liver	76.4	Liver	50.0
Right Kidney	83.1	Right Kidney	82.3
Left Kidney	86.1	Left Kidney	78.8

PS07 - TRACK 07: SURGERY, COMPUTER AIDED SURGERY, MINIMAL INVASIVE INTERVENTIONS, ENDOSCOPY AND IMAGE-GUIDED THERAPY, MODELLING AND SIMULATION

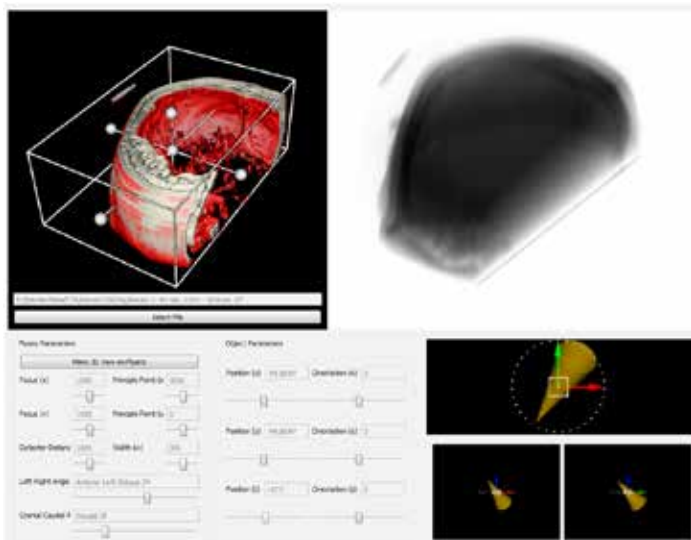
PS07.001 - Predictive Fluoroscopy: Minimizing Radiation Dose in Planning Endovascular Therapy for Intracranial Aneurysms

Author(s): John S.H. Baxter¹, Peter Johnson², Elvis C.S. Chen¹, Terry M. Peters¹

¹Imaging, Robarts Research Institute, London/CANADA, ²University Hospital, London/CANADA

Introduction: Intracranial aneurysms are vascular abnormalities thought to be the effect of localized weakness in the arterial wall. [1] These often appear as vascular outpouching which have significant risk of rupture causing subarachnoid haemorrhage with mortality rates ranging from 50% to 80% [2]. Endovascular procedures are often used, requiring some form of guidance. The standard-of-care is to employ pre-operative CT and CTA for detecting the aneurysm, followed by peri-operative rotational angiography to determine C-arm fluoroscopic working angles for use during the intervention. Determining the working angle is complex, requiring the interventionalist to reason about the orientation and geometry of the aneurysm and surrounding vasculature with many confounding factors making automatic working angle selection problematic. The imaging involved in this workflow also involves significant radiation dose to the patient, which is of major concern.

Objective: Our objective is to develop a peri-interventional system for the selection of fluoroscopic angles for endovascular procedures without the use of peri-operative rotational angiography, resulting in a lower radiation dose to the patient.



Methods: We first co-register the CT and CTA, treating their coordinate systems as synonymous. The CT is then registered into a physical co-ordinate space using two peri-operative fluoroscopic views. Our interface uses a custom direct volume rendering [3] class to render the CTA. This view is replicated by 'predictive' fluoroscopy derived from the CT with the closest feasible C-arm angles. Once an adequate visualization is chosen, these angles can be programmed into the C-arm prior to the intervention. In total, this system eliminates the necessity of rotational angiography, thus simplifying workflow and mitigating radiation dose.

Future Work: Phantom experiments and retrospective studies using human data will be performed. These studies will determine if the registration accuracy is sufficient and that selected working angles

on CTA are not significantly different from those selected using rotational angiography. Additional work in human factors will be used to characterize how users interact with this system, guiding further improvements.

References: [1] Hashimoto et al., *Neurol Res*, 2006;28:372-380. [2] Wiebers et al., *Lancet*, 2003;362:323-326. [3] Baxter et al., *SPIE Medical Imaging*, 2011

PS07.002 - Automatically Better Segmentation

Author(s): John S.H. Baxter, Terry M. Peters
Imaging, Robarts Research Institute, London/CANADA

Introduction: Image segmentation is a fundamental procedure in many medical image analysis and modelling applications. Recently, advanced in convex optimization such as discrete graph-cuts and continuous max-flow algorithms have allowed for complex image segmentation procedures to be expressed in terms of a series of weighted convex functions, the sum of which can be readily and globally optimized. However, such an optimization-based segmentation framework suffers from one major drawback: the increasing number and inter-relatedness of weighting parameters[1]. Parameter selection algorithms exist for segmentation problems with a low number of degrees-of-freedom[1] or for discrete (non-probabilistic) segmentation[2], but there has yet to be proposed a framework for parameter selection in segmentation problems founded in variation optimization, such as continuous max-flow.

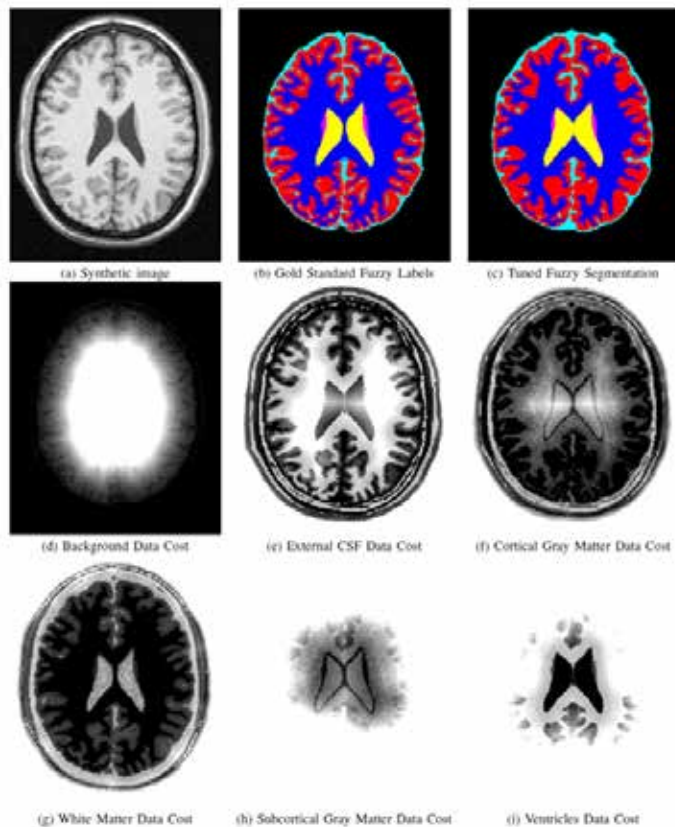
Methods: This approach is supervised meaning that a gold standard segmentation is provided to the algorithm which then finds the weighting parameters that imply the global optimality of the gold standard in terms of unweighted functionals also provided. The algorithm maintains an estimate of the set of these weights and iteratively generates competing max-flow-optimal segmentations. To ensure the gold standard has a lower energy than these competing segmentations, linear inequalities are created which further refine the estimate.

```

Compute  $E_D(u^G)$ ,  $E_S(u^G)$ , and  $E_D(u^*(\infty))$ 
Set  $P_{-1} \leftarrow \emptyset$ ,  $P_0 = \{\alpha \mid \alpha \geq 0, \alpha \in C(u^*(\infty))\}$ ,  $t \leftarrow 0$ 
while  $P_t/P_{t-1} \neq \emptyset$  do
     $Q \leftarrow$  the vertices of  $P_t$ 
     $M \leftarrow \text{mean}(Q)$ 
    if  $M$  is  $\geq \epsilon$  away from any prior evaluated  $\alpha$  then
         $u' \leftarrow$  output of solver with parameters  $M$ 
        Update  $P_{t+1} \leftarrow P_{t+1} \cap C(u')$ 
    else
        Remove any of  $P_{t-1}$ 's vertices from  $Q$ 
        Set  $P_{t+1} \leftarrow P_t$ 
        for  $\forall \alpha' \in Q$  do
             $u' \leftarrow$  output of solver with parameters  $\alpha'$ 
            Update  $P_{t+1} \leftarrow P_{t+1} \cap C(u')$ 
        end for
    end if
    Set  $t \leftarrow t + 1$ 
end while
Return  $P_t$ 
    
```

Results: The algorithm shown was proven to be mathematically correct. For empirical validation, the BrainWeb[3] MRI simulator was used with realistic functionals.[4] After four iterations, the algorithm

found the closest possible max-flow-optimal segmentation to the gold standard with only 2% of voxels mislabelled compared to 5% from thresholding. This algorithm is a low-cost, automatic method for improving segmentation, readily incorporated into any variational optimization-based segmentation framework used in modelling or simulation.



References: [1]McIntosh & Hamarneh, *Advances in Visual Computing*, 2009;1079-1088. [2]Szummer et al., *ECCV*, 2008;582-595. [3] Cocosco et al., *NeuroImage*, 1997. [4]van der Lijn et al., *NeuroImage*, 2008;43.4:708-720.

PS07.003 - Utilizing stream feature in GPU Monte Carlo Code to simulate photon Radiotherapy

Author(s): Yakub A. Bayhaqi¹, Supriyanto Ardjo Pawiro¹, Heru Suhartanto²

¹Department Of Physics, Faculty Of Mathematics And Natural Science, University of Indonesia, Depok/INDONESIA, ²Faculty Of Computer Science, University of Indonesia, Depok/INDONESIA

Introduction: The development of Monte Carlo algorithm is still being conducted, including the use of computational methods in parallel on a GPU that in some computer applications can provide increased efficiency significantly. As one of the latest development in the use of computing in the Monte Carlo method has been carried out in a package called gDPM been done by Xun Jia with basic DPM algorithms previously developed in 2011. This gDPM package has been known to accelerate computing DPM package prior to 69.1 ~ 87.2 times with the accuracy of more than 97% were observed at an NVIDIA Tesla C2050 GPU against a CPU 2.27GHz Intel Xeon processors. Meanwhile, the current GPU devices can do more advanced utilization in parallelization such as streaming and dynamic parallelism. Thus, further development of gDPM still needs to be done to decrease time of Monte Carlo Simulation.

Method and Materials: The package uses ionizing particle in-

teraction simulation scheme that divides the process into several separate kernel to simulate the interaction between electrons and photons. Each thread of the GPU is responsible for the simulation of a particle, either primary or secondary. This simulation separation of electrons and photons can increase the computation time because of transition when the GPU must change kernel electrons to photons and vice versa, respectively and repeatedly. The streaming feature on the GPU allows two different kernel runs in a single program, so the merger between the simulated photons and electrons can be done. Therefore, the purposed streaming method were tested by using the NVIDIA GTX TITAN BLACK GPU which supports streaming. The gDPM code were also modified to be run in the final CUDA version.

Result and Discussion: Theoretically, the use of stream to solve two or more kernels in the GPU program can reduce computing time with a speedup of up to 1.33x. The sequence between photon and electron were then turn into a concurrent process which gives a more flexible transition. The result of streamed code is almost significant to the original code in accuracy. A maximum of 8.67% estimated dose discrepancy compared to ion chamber measurement were achieved in simulating a 6 MV photon beam in homogenous water phantom with 1 billion of particle history. While, the original gDPM code has a maximum discrepancy of 6.34% estimated dose. The simulation were done within 2.37x faster than the original code. In addition, a simulation of an IMRT Head and Neck cancer patient example from the original gDPM code, were also been done to take account of the code optimization and accuracy in heterogeneous material. A maximum of 1.92% discrepancy in estimated dose compared to the original code were achieved with 1.83x of speedup.

Conclusion: This study shows that it is still possible to accelerate again in the computation time Monte Carlo along with the development of computing technology. The GPU stream feature slightly increase the efficiency of gDPM code. Although, there should be more investigation due to the accuracy because of the randomness in Monte Carlo method.

PS07.004 - The influence of two different drug infusion profiles on the pharmacodynamics model performance

Author(s): Ana L. Ferreira¹, Catarina S. Nunes², Joaquim Gabriel³, Pedro Amorim⁴

¹Faculdade de Engenharia da Universidade do Porto, Porto/PORTUGAL, ²Universidade Aberta, Departamento de Ciências e Tecnologia, Delegação do Porto, Porto/PORTUGAL, ³Inegi, Faculdade de Engenharia da Universidade do Porto, Porto/PORTUGAL, ⁴Centro De Investigação Clínica Em Anestesiologia, Serviço de Anestesiologia, Centro Hospitalar do Porto, Porto/PORTUGAL

To model the effect of anesthetic drugs on the Bispectral Index (BIS) of the EEG is of great importance for a reliable predictive response model during surgery. In this study, the impact of using two different drug infusion profiles in a pharmacodynamics interaction model was studied and the methods were compared with respect to their performance. Clinical data of 22 patients were considered. The interaction model was optimized per patient using nonlinear least squares during the induction of anesthesia, and tested for prediction abilities of test patients. In the optimization phase, all models could follow the BIS trend with errors not significantly different from zero. In the test data the choice of drug infusion profile proved to have a significant impact, showing that the performance is greatly influenced by the interaction. Results also show a time delay between the BIS signal and the Modeled BIS in both groups. This delay corresponds to a delay in the dynamics of the patient and could be related to the delay in BIS processing time. This work is an important step to predict the effect of anesthetic drugs.

PS07.005 - Force Modeling of MRI-Compatible Robot for Pediatric Bone Biopsy

Author(s): Peyman Shokrollahi¹, Elnaz Shokrollahi², James Drake³, Andrew Goldenberg²

¹Biomaterial And Biomedical Engineering, University of Toronto, Toronto/CANADA, ²Mechanical And Industrial Engineering, University of Toronto, Toronto/ON/CANADA, ³Division Of Neurosurgery, Hospital for Sick Children, Toronto/CANADA

Purpose

Prediction of forces is pivotal to the success of skull/bone drilling in stereotactic neurological operations and orthopedic surgery [1]. A general mechanical model of this process that would help developing methods of avoiding bone trauma does not exist [2]. Uncontrolled forces can cause bone tissue trauma due to drill-bit breakage, drill breakthrough, and excessive heat generation [3]. Furthermore, controlling the applied force is more complicated inside a magnetic resonance imaging (MRI) system due to the existence of large static and gradient magnetic fields. A model considering the nonlinearities of drilling mechanics as well as the MRI effects is required to determine the optimal design and parameters.

Methods

To perform innocuous pediatric bone biopsy in the MRI, our goal is to model the applied force generated by an ultrasonic actuator and transferred by the biopsy hollow-drill to the bone, while observing MRI effects on the force. Therefore, the initial force was measured outside the MRI to evaluate the range and bandwidth (BW) of the force by implementing the system (Figure 1). The drilling force was applied on the epiphysis, metaphysis, and diaphysis of hen and swine femurs utilizing a bone biopsy drill and a cordless power drill.

Results and Discussion

The penetration force was in the range of 60-80 N for the hen and 80-100 N for the swine, producing a sinusoidal shape with the biopsy drill. However, a step-shape signal was achieved with a force lowered by 20 N when the power drill was used (Figure 2). The BWs of the signals were calculated using the Fourier transform; a maximum BW of 15 Hz was achieved for manual drilling of the swine bone and a minimum BW of 5 Hz for the power drilling of the hen bone. In conclusion, the model is valuable for controlling MRI-compatible bone-drilling tools.

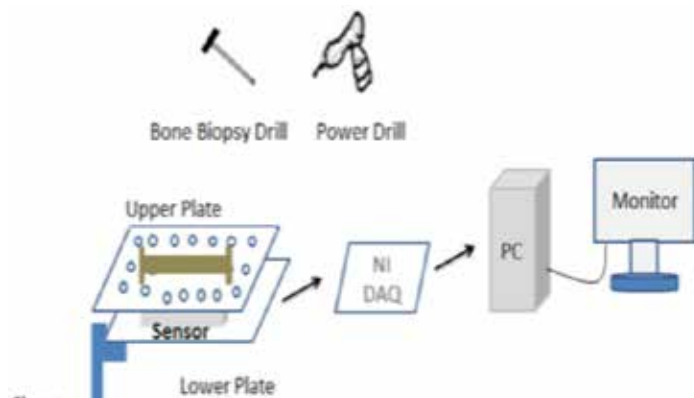


Figure 1: Bone Drilling System

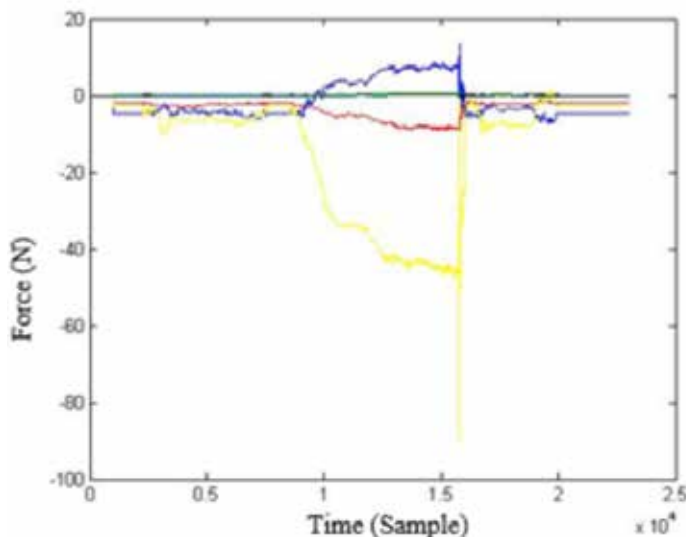


Figure 2: Applied force on hen bone using power drill

PS07.006 - Comparing the Effects of Three MRI RF Sequences on Ultrasonic Motors

Author(s): Peyman Shokrollahi¹, James M. Drake², Andrew A. Goldenberg³

¹Biomaterial And Biomedical Engineering, University of Toronto, Toronto/CANADA, ²Division Of Neurosurgery, Hospital for Sick Children, Toronto/CANADA, ³Mechanical And Industrial Engineering, University of Toronto, Toronto/ON/CANADA

Obtaining accurate force and kinesthetic information produced by actuators is necessary for the success of robot-assistive surgical operations. Access to such information is not readily possible in MR environments due to the effects of giant static and gradient magnetic fields. The goal of this study is to quantify the effects of MRI on the behavior of ultrasonic motors (USMs), while performing bone biopsies on pediatric surgery. In this study, the effects of three sequences (FFE, balanced FFE, and ultra-fast spin echo, SSH-TSE) were considered on the torque generated by a USM, transferred as an axial force by our implemented robot and measured by our developed force feedback system. Different sequences show different effects on the generated axial force while the motor rotates in different directions

PS07.007 - Robotic positioning system of ultrasound transducer for ultrasonic therapy

Author(s): Shinya Onogi¹, Kaoru Natsume², Takashi Mochizuki², Makoto Hashizume³, Kohji Masuda²

¹Center For Advanced Medical Innovation, Kyushu University, Fukuoka/JAPAN, ²Graduate School Of Bio-applications And Systems Engineering, Tokyo University of Agriculture and Technology, Tokyo/JAPAN, ³Faculty Of Medical Science, Kyushu University, Fukuoka/JAPAN

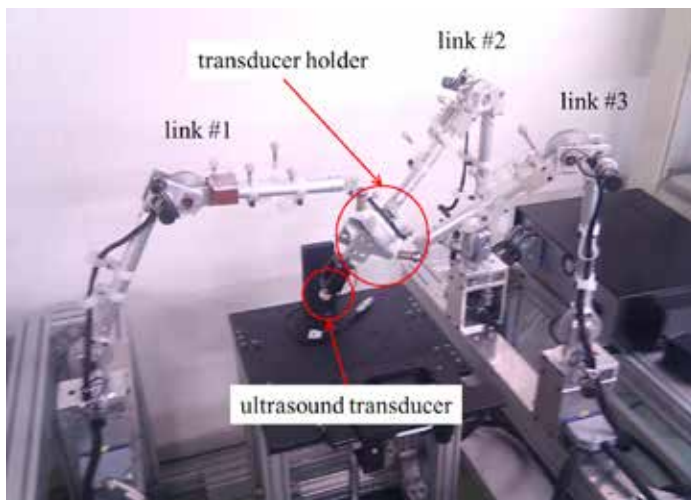
Microbubbles are widely used as contrast agents for ultrasound diagnosis. Moreover, microbubbles can also be used for therapeutic purpose; e.g. the heat amplification of high-intensity focused ultrasound ablation or carriers of acoustic targeted drug/gene delivery. However, injected microbubbles in a blood vessel are diffused throughout the whole body; therefore, the efficiency is limited. To address the issue, we have proposed microbubble delivery technique by using acoustic forces of ultrasound, and confirmed microbubbles can be controlled in an artificial blood vessel. To apply the technique in vivo, navigation and robotic system are required

to position ultrasound filed passing through target bifurcations of blood vessel network. In this study, we propose a robotic system for a microbubble delivery technique. The system feasibility was validated.

The system consists of a parallel link robot (Fig. 1) for positioning of a ultrasound transducer, an optical tracking device, in-house navigation software, and an ultrasound imaging device with a phased array 3D probe. To validate the system feasibility, we performed positioning accuracy validation by emitting ultrasound to a hydrophone in an agar phantom, and microbubble induction tests by using artificial blood vessel. Regarding the first experiment, the hydrophone was potted in the agar phantom and the position was measured by the tracking device. Under the guidance of the navigation, ultrasound was emitted to the hydrophone by the robot. The measured sound pressure was compared with the emitted ultrasound. Regarding the second experiment, a Y-shape artificial vessel (1 in and 2 out) was prepared and its Doppler volume was acquired by the 3D ultrasound. As pre-processing, bifurcations of the blood vessel network were extracted by the navigation software. To induce microbubbles into an intended path, the transducer position was controlled by the robot using the bifurcation position. Next, concentration of microbubbles was injected in the vessel, then ultrasound was emitted for induction of microbubbles. In the experiment, microbubbles behavior was observed by a microscope.

In the positioning accuracy validation, the system can position the transducer by 1 mm errors. Also, measured ultrasound pressure was 62.6 % of input pressure. The result includes attenuation. In the microbubble induction test, induced microbubbles were observed.

In this study, we developed and validated the robotic system with the ultrasound navigation for ultrasonic microbubble delivery technique in order to achieve less invasive therapy. We confirmed that ultrasound is surely emitted to a target position and microbubbles are induced by the system.



PS08 - TRACK 08: BIOSENSOR, NANOTECHNOLOGY, BIOMEMS AND BIOPHOTONICS

PS08.002 - Novel Optical Method to Determine Glass Transition Temperature of Polymers

Author(s): Yao-Xiong Huang, Jiang He

Department Of Biomedical Engineering, Ji Nan University, Guang Zhou/CHINA

A novel optical method is proposed for the determination of polymer glass transition temperature (T_g) by monitoring the refractive index variation of polymer microspheres with temperature using our method of microsphere imaging. It was demonstrated that the present method can eliminate most thermal lag and has sensitivity about six fold higher than the conventional method in T_g determination. So the determined T_g is more accurate and less change with heating rate than that obtained with conventional methods. The most attractive character of our method is that it can simultaneously determine the T_g of several polymers in an experiment, thus greatly saving time and heating energy. The method is not only applicable for polymer microspheres, but also for the materials with arbitrary shapes, therefore, it is expected to be broadly applied to different fundamental researches and practical applications of polymers.

PS08.003 - The Comparison of Temporal Change between Typically Developing Children and Children with ADHD in Rotational Motion Speed of Arms

Author(s): Miki Kaneko

Graduate School Of Systems Life Sciences, Kyushu University, Fukuoka/JAPAN

When medical doctors diagnose participants with ADHD, they evaluate soft neurological signs (SNS) from their motion by a visual observation. Rotational motion of arms (Pronation and supination) is one of SNS. The participant bends elbow to 90 degrees, and rotates the palm and the back of hands. These methods are hoped to be quantitatively established. In previous our study, we developed quantitative and simple evaluation system of pronation and supination using small wireless hybrid sensors. Our system was consisted of acceleration and angular velocity sensors and a notebook computer. We could obtain different features between typically developing children and children with ADHD by our system. In this paper, we compared temporal change of rotational motion speed between typically developing children (TDC) and children with ADHD in order to find features of pronates and supinates at full speed. Firstly, we separated 4 phases in measurement time and calculate FFT peak frequency in each phase. Measurement time is 10 seconds. Sampling frequency is 100 Hz. Subjects are 203 typically developing children and 40 children with ADHD aged from 7 to 12. From this result, we could obtain the different features between 2 groups (TDC and children with ADHD). The rotational motion speed of TDC decreased with time. In rotational speed of children with ADHD, variations were observed in each phase. From these result, rotational motion speed of children with ADHD is not stable compared to TDC. In TDC, the speed of rotational increased as they grew older.

PS09 - TRACK 09: BIOSIGNAL PROCESSING**PS09.001 - Sensitivity of heart rate variability indices for artificially simulated data**

Author(s): Aleksandr A. Fedotov, [Anna S. Alulova](#)
Lasers And Bioengineering Systems, Samara State Aerospace University, Samara/RUSSIAN FEDERATION

In modern cardiac practice methods for the analysis of heart-rate variability (HRV) are implemented to forecast the detection of different pathologies of the cardiovascular system. The heart rate is an important physiological index, which reflects processes of autonomic, neurohumoral, and central regulation in the cardiovascular system and throughout the entire human organism. In order to form diagnostic HRV indices mathematical analysis for the variability of durations of beat-to-beat intervals, defined as the time interval between two consecutive fiducial points of the biosignals like ECG signal or pulse wave are applied.

The application of modern mathematical methods of processing non-stationary and quasi-periodic data, such as Rescaled range analysis, Detrended fluctuation analysis, Rectified phase signal averaging, for analysis of heart rate variability (HRV) was considered. The mathematical models for simulating artificial cardiac beat-to-beat intervals that take into account the presence of various noise processes were created. The state model of the cardiovascular system based on analysis of self-similarity of heart rate was developed. The theoretical sensitivity of HRV indices to the change of the state of the cardiovascular system for the artificially simulated data was estimated.

The following HRV indices will be described and analyzed in details:

- 1) Statistical Index *RMSSD*: the square root of the mean of the squares of the successive differences between adjacent beat-to-beat intervals.
- 2) Spectral ratio LF/HF – the ratio of the spectral power density of beat-to-beat intervals at low frequency range (LF) (from 0.04 Hz to 0.15 Hz) to the spectral power at high frequency range HF (from 0.15 Hz to 0.4 Hz).
- 3) Hurst exponent *H*, calculated by the normalized range method (R/S analysis), characterize the ratio of the strength of the trend to the level of the noise.
- 4) The coefficient of fluctuations α , determined by Detrended Fluctuation Analysis (DFA). The DFA method enables to study the structure of different processes, including non-stationary processes, from the point of view of statistical self-similarity.
- 5) Acceleration capacity (AC) and deceleration capacity (DC) of heart rate. These coefficients are non-linear and determine the intensity of the quasi-periodic trends in heart rate and calculated by phase-rectified signal averaging method.

PS09.002 - The Smoothness of a signal as a new feature in Signal Averaged Electrocardiogram that can be used in cardiac electrophysiology diagnosis.

Author(s): Peyman Sheikhzadeh¹, Negisa Seyyedi²
¹Medical Physics And Engineering Department, Tehran University of medical science, tehran/IRAN, ²Medical Informatics Department, Shahid Beheshti university of medical science, Tehran/IRAN

Introduction:

Sudden cardiac death is the most common cause of death in the world. Myocardial infarction (MI) and ventricular arrhythmias caused

by MIs are among the main factors of sudden cardiac deaths. Accurate recognition, discrimination and prognosis of myocardial infarction and ventricular arrhythmias will be able to reduce the mortality. Several ECG-based methods such as Signal Averaged Electrocardiogram (SAECG) have been proposed, however signal analysis and extraction of new features is being investigated.

Methods and materials:

The signals of orthogonal leads from 120 cases containing healthy subjects and myocardial infarction with and without the history of ventricular tachycardia (VT) and fibrillation (VF) were filtered, denoised and averaged following their selection from PTB diagnostic database. After the calculation of vector magnitude, final signal smoothness was obtained which is the smoothness magnitude of the curve in SAECG. In order to measure the smoothness of function $y(t)$ over an interval $[0, n]$, the sum over square of second derivative of $y(t)$ was used, where t is the number of samples (time) and $y(t)$ is the signal amplitude (voltage). To obtain comparable criteria, the acquired values were normalized to the maximum peak in all cases. Finally, the new feature has been evaluated using T-test and Mann-Whitney U statistical analysis for the two groups of MI patients and healthy controls and MI Patients with and without ventricular arrhythmias (VT&VF), respectively.

Results:

Statistical comparisons of 50 MI patients and 50 healthy controls using T-Test analysis indicated that the signal smoothness in MI patients valued more than healthy people (0.2 ± 0.12 vs. 0.12 ± 0.03 , P-value < 0.001). Also, the area under the ROC curve for this feature was obtained 0.725. In addition, statistical comparisons of 50 MI Patients and 20 MI+VT/VF using Mann-Whitney U analysis showed that the value of signal smoothness in MI+VT/VF was much more than MI patients without any ventricular arrhythmias (0.3 ± 0.22 vs. 0.19 ± 0.11 , P-value = 0.208 (P < 0.05)).

Conclusion:

In this study, we proposed a new feature and index called curve smoothness in SAECG to differentiate MI patients from healthy controls. The feature represented good results to distinguish MI patients with and without ventricular arrhythmias so it can be very effective in prognosis of these arrhythmias. Evaluation of other cardiac signals using this new feature may hopefully leads to the valuable results in cardiac electrophysiology studies.

PS09.003 - Comparison of the Three Filter Algorithms for Detection of Electrically-Evoked Short-Latency Responses in Retinal Ganglion Cells.

Author(s): Myounghwan Choi¹, Jungyeol Ahn², Sungjin Oh³, Kilhwa Pi³, Youngjoon Chee¹, Hyoungho Ko⁴, Dongil Cho³, Yongsook Goo², Kyo-In Koo¹

¹Department Of Biomedical Engineering, University of Ulsan, Ulsan/KOREA, ²Department Of Physiology, Chungbuk National University School of Medicine, Cheongju/KOREA, ³School Of Electrical Engineering And Computer Science, Seoul National University, Seoul/KOREA, ⁴Department Of Electronics Engineering, Chungnam National University, Daejeon/KOREA

When retinal ganglion cells are stimulated *ex vivo* by electrical current, short latency responses (within 30 ms) and long latency responses (over 30 ms) are evoked. The short-latency response is suspected to be originated from the direct electrical stimulation. For optimal stimulation protocol of retinal prosthesis, this short-latency response is getting important more and more. In this paper, we compared and evaluated performance of the three algorithms for the short-latency spike detection; suppression of artifacts by local polynomial approximation (SALPA), moving average filter

(MAF), and forward-reverse filter (FR filter). The SALPA and the FR filter showed better detection performance comparing with the MAF algorithm.

PS09.004 - Photoacoustic Speckle and Spectral analysis of Vasculature Trees

Author(s): Muhammad N. Fadhel, Michael C. Kolios
Physics, Ryerson University, Toronto/CANADA

This paper discusses the use of ultrasound tissue characterization methods to photoacoustic (PA) data to differentiate between tissues with different vasculature structures. The dominant source responsible for ultrasound scattering in soft tissues (including tumors) is not well known in pulse echo ultrasound. PA imaging is based on the detection of ultrasound waves generated by optical absorption. Since the hemoglobin in blood dominates the absorption of light in soft tissues (at particular laser wavelengths), the PA signal is dominated by the contribution of the vasculature. Organized and chaotic vasculature trees were simulated using a fractal model to represent normal and tumor vasculature, respectively. The generated PA signals from these vascular were simulated through the solution of the photoacoustic wave equation using the Green's function approach. Ultrasound resolution PA signals generated were detected by simulating a 256 element transducer with a 10-50 MHz bandwidth. Reconstructed images were acquired using a delay and sum method. Image analysis was performed by fitting the image probability density functions (PDF) of Rayleigh, Nakagami (NG), and Generalized Gamma (GG) distributions to the histogram of the reconstructed images. The speckle sizes of the reconstructed PA images were calculated using autocovariance. Spectrum analysis of the ultrasound frequency components of the photoacoustic signals was performed by linear regression analysis of the power spectrums of the radiofrequency (RF) data, as done in conventional ultrasound tissue characterisation. The results suggest that the Rayleigh, NG distributions, and the power spectrum regression analysis can be used to differentiate between the simulated normal and tumor vasculatures. The changes in these parameters correlate to a higher density of tumor vasculatures than normal vasculatures.

PS09.005 - The algorithm for the diagnosis of ventricular tachycardias from electrocardiogram

Author(s): Martin Holub, Martina Šrutová, Vaclav Kremen, Lenka Lhotska
Department Of Cybernetics, Czech Technical University in Prague, Prague/CZECH REPUBLIC

Ventricular tachycardias (VT), fibrillations (VF) and flutters (FL) are heart rate disturbances ranked among life threatening arrhythmias. We designed and tested an algorithm for automated detection of VT, VF, and FL events from Holter ECG data. The algorithm is based on the detection in a frequency domain, which is supported by the detection in a time domain. The algorithm was tested using ECG signals including VT, VF, and FL taken from AHA and MIT-BIH databases. Overall performance of the algorithm was sensitivity 80.9% and positive predictivity 66.8% (whole data set). The results show a discrimination of VT, VF, and FL from the normal sinus rhythm and its discrimination from the noise. The importance to reach high sensitivity is reflected in the detection. The algorithm achieved a very high resistance to the power line interference and random noise. It provided very good results, in particular with well-balanced ratio between sensitivity and positive predictivity.

PS09.006 - Modelling of Platelet and White Blood Cell in Dengue Patients using Bioelectrical Impedance Analysis technique

Author(s): Fatimah Ibrahim¹, Nurhidayah Mohd Paiz¹, Saadah Sulaiman², Sharifah Faridah Syed Omar³
¹Biomedical Engineering, University Malaya, Kuala Lumpur/MALAY-

SIA, ²KPJ Damansara Specialist Hospital, Petaling Jaya/MALAY-SIA, ³Medicine, University Malaya, Kuala Lumpur/MALAYSIA

Abstract This paper presents a modelling for predicting white blood cell (WBC) and platelet (PLT) in dengue patients by using bioimpedance analysis (BIA) technique. Analysis was done using multiple regression analysis to find predictive equations for WBC and PLT. All BIA parameters, patient's symptoms and demographic data were investigated to find best predictors. In this analysis, best predictors are phase angle (PA), extracellular mass (ECM), total body water (TBW), dizziness, myalgia and petechial rash to predict WBC. For PLT, best predictors are resistance (RES), ratio of extracellular water to intracellular water (ERI), vomiting and epigastric pain. However, PLT and WBC modelling are able to predict 18.4% and 24.9%, respectively. **METHODS** Dengue database was obtained from Ibrahim, F. 2005. 210 adult patients aged 12 years and above, admitted in Hospital Universiti Kebangsaan Malaysia (HUKM) with confirmed dengue infection were prospectively studied. Before BIA measurement, patients were asked to refrain from eating and drinking at least 4 hours. Data collected were in the form of patient's clinical and epidemiological data, including fever onset, symptoms, signs, physical examination, blood results and BIA measurements. For BIA measurement, patient was asked to lie supine and two sets of electrodes were placed on hand and foot at right-hand side. As patients admitted at different stages of illness, data collected was based on day of defervescence, where the fever subsided below 37.5°C. Day 0 was used to represent defervescence day. Thus, PLT and WBC modelling was evaluated on fever day 0 as most patients' condition worsen and deteriorate suddenly. The statistical data analysis was done using simple linear regression and multiple linear regression tests to predict significant predictors for both models, using SPSS software. **RESULTS** From analysis done, resistance (RES) and ratio of extracellular water to intracellular water (ERI) were found as significant predictors for WBC. The adjusted R2 was around 1.8%. Gastric and vomit were also the significant predictors as well and when added to the model, the adjusted R2 improved to 18.4%. Hence the model can be written as follow: $PLT = 47.468 + 7.806(RES) + 11.145(ERI) - 25.588(vomit) - 18.574(gastric)$ Multiple regression analysis was used to find the best predictors for modelling WBC. As dizziness, myalgia and petechial rash were also found as significant predictors, they explained 15.9% of the WBC's variation. When PA, ECM and TBW were added into the model, adjusted R2 was around 24.9%. Hence the model can be written as follow: $WBC = 6.774 - 0.115(PA) - 0.090(ECM) + 0.115(TBW) + 1.227(dizziness) + 0.612(myalgia) - 1.771(petechial\ rash)$ **CONCLUSION** Future work is to improve the PLT and WBC modelling using BIA technique by increasing the number of samples and using an advanced artificial intelligence method. **REFERENCE** Ibrahim, F. Prognosis of Dengue Fever and Dengue Haemorrhagic Fever using Bioelectrical Impedance, PhD Thesis, Faculty of Electrical Engineering, July 2005, 1-398 **ACKNOWLEDGMENTS** We would like to thank University of Malaya High Impact Research Grant UM-MOHE UM.C/625/1/HIR/MOHE/05 from Ministry of Higher Education Malaysia and University of Malaya Research Grant (UMRG: RP009A-13AET) for supporting our research.

PS09.007 - Combination of Multiple Signal Processing Techniques for Multi-class Motor Imagery Detection using Mu Rhythm

Author(s): Rina Kojima, Masaki Kyoso, Yuichi Shimatani
The Graduate School Of Engineering, Tokyo City University, Tokyo/JAPAN

BCI (Brain-Computer Interface) can be classified into two types, that is, input type to send information to the brain and output type using reversal direction of information. We focused on the output type because it is a technology capable of controlling the external equipment at will and processes the measured brain signals in the

computer. Especially, noninvasive motor imagery based brain-computer interface (BCI) is an appropriate solution for upper limb stroke rehabilitation. However, in multi-class brain activity detection with scalp EEG, robustness against background EEG are required for practical use. We proposed the combined application of signal processing techniques such like independent component analysis (ICA), coherent analysis and so on to solve the problems. These are the techniques to separate and enhance each signal source with multi-channel mixed source signal. In this study, multi-channel scalp EEG signals recorded during hand and leg movements were used for the evaluations and the analysis. Figure 1 is an example of the measured mu rhythms from four electrodes with hand movement in 2-5 seconds. In mu rhythm, the amplitude is reduced while movement including pre-movements and recovery after movements however it must be processed with some techniques for applications because this phenomenon is unstable. This study also tried to apply the signal processing techniques to improve it. Multi-channel scalp EEG signal measurement was performed with four electrodes placed on the primary motor area along central sulcus. Slides for instructions were used to notify the timing of movements the subject. EEG signals measured from primary motor area were analyzed by ICA. Then the signals in which event-related desynchronizations were found were compared with the original signals. The results by using ICA show that the components with and without desynchronizations were separated. The results on the rate of amplitude degradation from event-related desynchronization show that ICA could enhance event-related desynchronization by separating background scalp EEG component. For further improvement, additional signal analysis is in progress. Techniques which can enhance the phenomena induced by the different motions such like coherent analysis have been applied to the ICA output.

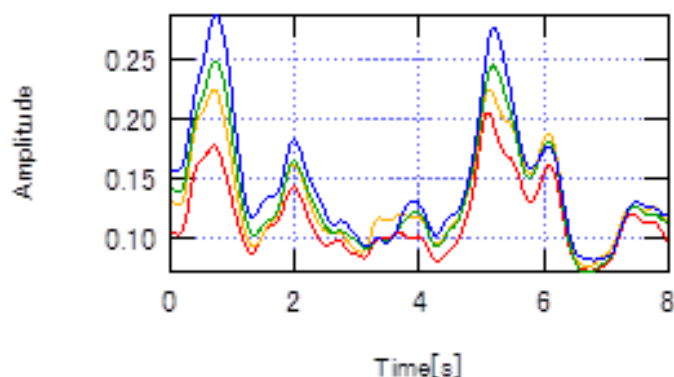


Figure 1 EEG amplitude

PS09.008 - The comparison of severity assessment methods of kinetic tremor in Parkinson's disease using wearable sensors

Author(s): Hong Ji Lee¹, Han Byul Kim¹, Hyo Seon Jeon¹, Sang Kyong Kim¹, Woong Woo Lee², Hye Young Park², Chae Won Shin², Beom Seok Jeon², Kwang Suk Park¹

¹Seoul National University, Seoul/KOREA, ²Seoul National University Hospital, Seoul/KOREA

Tremor is involuntary and rhythmical shaking movement of a body part and one of symptoms in Parkinson's disease (PD). Gold standard method for PD's tremor assessment is the Unified Parkinson's Disease Rating Scale (UPDRS). Because UPDRS is based on visual observation, tremor severities are subjectively rated depending on clinical expertise. Several studies have reported objective tremor assessment methods using accelerometers, EMG, and actigraphy.

They focus on rest and postural tremors that are rated relatively accurate because of steady state. However, although kinetic tremor, especially finger-to-nose test, includes several tremor factors such as intention tremor (goal-directed movement), action tremor (voluntary movement), and postural tremor (stretch forward and stay at target), there have rarely been researches about finger-to-nose test. Especially, kinetic tremor is difficult to assess by visual observation because of movement of a body part.

This study was approved by the Institutional Review Board of Seoul National University Hospital (IRB No. D-1407-011-590). 31 patients with PD participated in the kinetic tremor examination. All patients provided written informed consent prior to study participation. The number of patients was 9, 10, 7, and 5 according to mean UPDRS 0, 1, 2, and 3, separately.

Our device integrated tri-accelerometers and tri-gyroscopes ($\pm 8\text{ g}$ and $\pm 2000\text{ dps}$) was attached on the patient's index finger. Patients moved slowly their finger from their nose to the target repetitively. The sampling rate was 125 Hz. Measured accelerometer and gyroscope signals were scaled and integrated. Then, root mean square and peak power were calculated as features. The average UPDRS of two clinicians was used as standard.

Two filtering methods for removing voluntary movement during finger-to-nose were compared. The movement velocity considerably depends on patients. First, fixed frequency filter, 1 Hz or 2 Hz high-pass-filter that did not affect tremor frequency band (3-12 Hz), was used. Second, adaptive filter, Multivariate Empirical Mode Decomposition (MEMD), was utilized. The signals were expressed by the sum of the intrinsic mode functions in tremor frequency band. Moreover, two classifiers, linear Support Vector Machine (SVM) and Hidden Markov Model (HMM), were compared, because kinetic tremor is time dependent signal. Features were extracted from 3 s moving window with 1.5 s overlapping for HMM. Leave-one-out Cross-validation was used for performance evaluation.

Tremor severities were estimated as 0, 1, 2, or 3 by combination results of accelerometers and gyroscopes. When using fixed frequency filter to remove voluntary movement, the accuracy of tremor severity estimation showed 64.5% on SVM. However, the performances from MEMD filter increased to 83.9% on SVM. Moreover, the results from HMM had 93.5% accuracy that was higher than 83.9% accuracy from SVM.

Therefore, adaptive filter was suitable for removing background noise and voluntary movement during kinetic tremor and HMM classifier fits for time dependent tremor signals. Tremor severities are objectively and accurately assessed through this methods on rest and postural tremors as well as kinetic tremor.

ACKNOWLEDGMENT: This study was supported by a grant of the Korean Health Technology R&D Project, Ministry of Health & Welfare, Republic of Korea (No. HI13C0455).

PS09.009 - Unobstructive blinking detection wearable device utilizing transparent conductive ITO film for smartphone users to prevent of computer vision syndrome

Author(s): Jeong Su Lee, Kwang Suk Park
Seoul National University, Seoul/KOREA

About 90% of the people who spend three hours or more a day at a visual display unit device such as a computer screen or a television were affected computer vision syndrome (CVS), according to the National Institute of Occupational Safety and Health. CVS is resulting from focusing the eyes on visual display terminal for protracted periods of time. It includes some symptoms such as headaches, blurred vision, and dry eye. Recently, the risk of the syndrome has been boosted by the prevalence of smartphone. Decreasing of

frequency of blinking might cause dry eye. Conventional method of blinking is electrooculography (EOG) which requires direct electrical contact between the skin and Ag/AgCl electrodes via conductive gel. However, using of such electrodes is not adequate since it would cause skin irritation. Alternative methods which are image-processing approaches available for use with a video camera. However, these require the user's face to be within the angle of the video camera at a fixed distance. To resolve the lingering shortcomings of these alternative approaches, we propose a blink detection system based on a non-direct electrical contact electrodes which are capacitively coupled electrodes. We developed unobstructive blink rate detection wearable device which is glasses utilizing transparent conductive films. The films were attached to the lens of conventional glasses and able to measure eye blink while not blocking field of vision. When a user blinks the eye, significant positive peak was detected through the pair of films and acquired signal was transmitted to a computer. 4 Healthy subjects who were no symptom of dry eye were participated in this study to validate proposed system. Blinking rate was measured at rest state, during playing a smartphone game and searching the internet with smartphone for 5 minutes respectively. We counted the number of blinking at different task. According to the result, we found that the device didn't miss any blinking signals in comparison to reference EOG signal. We also found that blinking rate is decreased by up to 50% when the subjects using their smartphone in comparison with resting state. We expect that the proposed device with visual or auditory feedback when the rate of blinking is below certain threshold is able to prevent dry eye when smartphone users are using their smartphone.

PS09.010 - A Simple, CO₂-Based Method to Reconstruct the Molar Mass of the Dried Respiratory Gas within a New Double-Tracer Single Breath Washout

Author(s): Johannes Port, Christoph Joppek, Joachim H. Nagel
Institute of Biomedical Engineering, Stuttgart/GERMANY

A new single breath washout (SBW) using sulfur hexafluoride and helium as tracers has been proposed, which offers a considerable potential for the early detection of obstructive airway diseases like cystic fibroses (CF), chronic obstructive pulmonary diseases (COPD) and asthma (AS). After normal breathing of medical air, just one single breath of the double-tracer gas (DTG) that has the same molar mass (MM) as medical air, is necessary, a major advantage especially for elderly and very young patients since the measuring time is very short and only normal tidal breaths are required.

For the diagnosis, the expiration phase just after inspiration of the DTG is of interest. The respiratory flow and the carbon dioxide concentration (CO₂) of the undried gas, as well as the MM of the gas dried in a nafion tube, are measured. Specific parameters could be determined from the difference between the MM-signals with and without DTG. However, during this phase the MM without DTG is unknown and first needs to be reconstructed from the values of the MM- and the CO₂-signals measured without DTG. From these data, the first 25% but not more than 5s and the last 500ms are deleted. This precludes artifacts resulting from insufficient sealing of the mouth piece at the beginning of the measurement, and the rise time of a spike, which occurs at the inspiration of the DTG. Additionally, we use a 2nd order Bessel low pass filter with a cutoff frequency of 3Hz for the CO₂-signal to adapt its shape to that of the MM-signal, which due to dispersion effects within the nafion tube is low pass filtered.

With the results, the ordinary least squares regression method is applied to determine the slope and intercept values needed for the prediction of the MM-signal from the CO₂-signal. To compensate for the time delay between the MM- and the CO₂-signals, which are measured at different sites, we apply the regression method for different time shifts between both signals. The time shift, at which the

predicted and measured MM values yield the lowest mean square error, is taken to synchronize the signals.

This reconstruction method has been applied to the independent datasets of 92 adult subjects and 60 school-aged children. The adult group included 35 healthy (HA), 19 COPD, 13 CF, and 25 AS subjects, among the school-aged children, there have been 18 HA, 21 CF, and 21 AS children. The reconstruction proved independent from the health status, and the mean coefficients of determination calculated over all adult and school-aged subjects, and over the datasets separated by their health status yield values very close to 1 with standard deviations close to zero. Thus, the proposed reconstruction method fulfills all requirements to become the standard method of choice within the DTG-SBW, since it is simple and has a high reliability and reproducibility. Using a standard reconstruction method avoids variability within the datasets coming from different methods, and it makes the datasets comparable among each other.

PS09.011 - Mirror Movements in Writer's Cramp—A Study with Multi-Channel EMG

Author(s): Venkateshwarla R. Raju

Biomedical Eng & Neurology & Neurosurgery And, Nizam's Inst of Medical Sciences (NIMS) University & Hospital, HYDERABAD/INDIA

The purpose of present investigation is to design and fabricate multichannel EMG to differentiate between those with concordant(C) and discordant(D) mirror movements(MMs) in Writer's cramp (WC), in order to establish that there is a quantifiable difference between these two groups.

This study was conducted at Nizam's Institute of Medical Sciences (NIMS) a tertiary-care-centre in Hyderabad(India). A suitable multi-channel EMG was designed—fabricated (with an input impedance of 200Mega Ω to record digitized EMG signals simultaneously with a set of five, innocuous microelectrodes 50 μ). The basic signal data consisted of EMG-signals gathered from 5 muscles of RH, when subject (patient) first wrote with RH and then, with LH i.e., right-hand-writing-signal(RHWS) and left-hand-writing-signal(LHWS). Duration of signal-recording was 10 seconds, with 3kHz-Sampling-frequency, giving 30,000 readings for each-muscle. The study showed significant quantifiable EMG differences in the signals seen while writing with R and L hands between those WC-subjects with concordant MMs(C-group) versus those with discordant MMs(D-group). This was mainly seen in the measures-of-dispersion of signal(standard-dispersion), variances and their-ratio(F-ratio). These were statistically significantly different between two groups(C-and-D), and pattern-of-differences were consistent with the hypothesis that the D-group had a compensatory-force which overcame the dystonic-force resulting in the final abnormal-posture. This was seen in the form of larger-variances and standard-differences in the RHWS in D-group as compared to C-group, as the dystonic and compensatory-forces both contribute to the instability. These differences were robust and seen in every measure-of-dispersion, such as in the patterns of significance of f-values for ratios of variances. Cluster and more sophisticated-analyses using advanced-multivariate-techniques leading to effective data summarization and measures of dissimilarity between subjects as reflected in the signals recorded and consequent possible clustering among them, however, did not lead to any meaningful clinical conclusions. These analyses could possibly be applied to longitudinal follow-ups and correlations with a normal control population in future to better comprehend WC phenomena.

PS10 - TRACK 10: REHABILITATION MEDICINE, SPORTS MEDICINE, REHABILITATION ENGINEERING AND PROSTHETICS

PS10.001 - Human Knee Simulation Using CMAC ANN

Author(s): Roberto A. Lima, Lourdes M. Brasil, Vera R.F.D.S. Marães, João P. Martins Fga, UnB, Brasília/BRAZIL

This paper aims to show the use of a CMAC (Cerebellar Model Articulation Control), a kind of ANN (Artificial Neural Network). The CMAC is based on cerebellum of mammals, but despite this characteristic, actually, what promotes its use, is its very fast operation, which makes it suitable for adaptive control in real time. This type of control is needed, for example, to control an active transfemoral prosthesis. Simulation of knee angular velocities, based on collected data from the contralateral knee, is presented. The simulation is available as open source software.

PS10.002 - Development of New Method to Create In-school Tactile Maps for Visually Impaired Children

Author(s): Kouki Doi¹, Takahiro Nishimura¹, Masaru Kawano¹, Yumi Umehara², Harumi Matsumori², Hiroshi Fujimoto³, Mayumi Sawada¹, Yoshihiro Tanaka¹, Takeshi Kaneko¹, Katsuhiko Kanamori¹, Masumi Takei⁴

¹National Institute of Special Needs Education, Yokosuka/JAPAN, ²Graduate School Of Human Sciences, Waseda University, Tokorozawa-shi, Saitama/JAPAN, ³Waseda University, Tokorozawa/JAPAN, ⁴Gunma Prefectural School for the Blind, Maebashi/JAPAN

Adequate information support for visually impaired children and adults is necessary. In particular, there is a demand for information support tools that ensure students with visual impairment have access to necessary information in public facilities (e.g., schools). Teachers and visually impaired students at schools for the blind require tactile maps that allow the students to grasp the arrangement of school facilities and classrooms. On the other hand, because much time is needed to read and comprehend tactile maps, audio information support is also required. In this study, we established a method for creating in-school tactile maps (trial version) that can allow visually impaired students at schools for the blind to grasp the arrangement of school facilities and classrooms. In particular, we developed a device to create Braille and tactile maps using ultraviolet curable resin ink (Figures 1), and created tactile maps (trial version) with high tactility. We also improved the usability of a voice-reading interface (pen type) that allows visually impaired students to obtain audio information from tactile maps (Figures 2). Moreover, instead of using a stand-alone model for the pen-shaped interface, we placed voice-reading data on a network server, which allowed voice outputs of registered data from terminal units such as tablets. Therefore, it became easy to update the voice data. In addition, we conducted interviews with teachers in the field of education for the blind and visually impaired students to research the usability of in-school tactile maps. Their comments showed that almost all of the teachers and students who participated in this research found our proposed in-school tactile maps highly usable. This study led to the proposal of a method for creating in-school tactile maps that allow visually impaired students to grasp the arrangement of school facilities and classrooms.

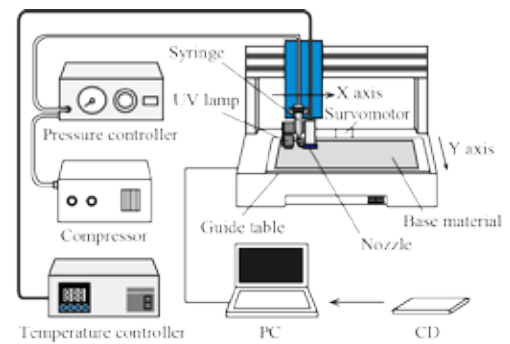


Fig.1 Device to create Braille and tactile maps using ultraviolet curable resin ink.



(a) In-school tactile map (b) Voice-reading interface (pen type)

Fig.2 In-school tactile map for visually impaired children and voice-reading interface.

PS10.003 - Experimental Study on Usability Evaluation of a Hydraulic Jack Lever

Author(s): Atsushi Sugama¹, Takahiro Nishimura², Kouki Doi², Shigenobu Shimada³, Manabu Chikai⁴, Kiyohiko Nunokawa⁵, Shuichi Ino⁴
¹National Institute of Occupational Safety and Health, Japan, ²Kiyose/JAPAN, ³National Institute of Special Needs Education, Yokosuka/JAPAN, ⁴Tokyo Metropolitan Industrial Technology Research Institute, Sumida/JAPAN, ⁵National Institute of Advanced Industrial Science and Technology, Tsukuba/JAPAN, ⁶Tokyo International University, Kawagoe/JAPAN

Hydraulic jacks can be used to rescue drivers trapped inside vehicles during car accidents or victims trapped under debris during earthquakes. However, firefighters using hydraulic jacks have indicated that they apply excessive workloads on the body. Therefore, the workload on the body should be reduced and their usability should be improved. The purpose of this study is to evaluate the physical load during lever operation of existing jacks and to determine the appropriate posture for lever operation, as an initial research step.

As an experimental task, subjects squatted to the side of a jack and operated the lever up and down with one hand. We used Blackhawk Automotive Porto-Power hydraulic cylinders for the hydraulic jacks. There were three experimental conditions consisting of squatting positions relative to the jack lever. The three conditions are as follows: a near condition (side1), a far condition (side2), and a front condition (front), as shown in Figure 1. The operating speeds were one second each for lifting and lowering the lever, and each trial was performed in 30 s. A Motion Capture System and floor reaction force sensor were used to measure operating postures and floor reaction force, as shown in Figure 2. In order to evaluate muscle loads, surface EMG sensors were used. For subjective evaluation, interview surveys during operation were investigated in 50 stages from 1 (extremely light) to 50 (maximal exertion).

From the results of the experiment, we found that the near condition experienced fewer loads than the far and front conditions. The

results of the EMG showed muscles such as deltoid, biceps, and triceps are active. In addition, erector spinae muscles are believed to be also active in maintaining a squatting posture. Since the lever requires repeated operation, it is necessary to reduce the muscle loads.

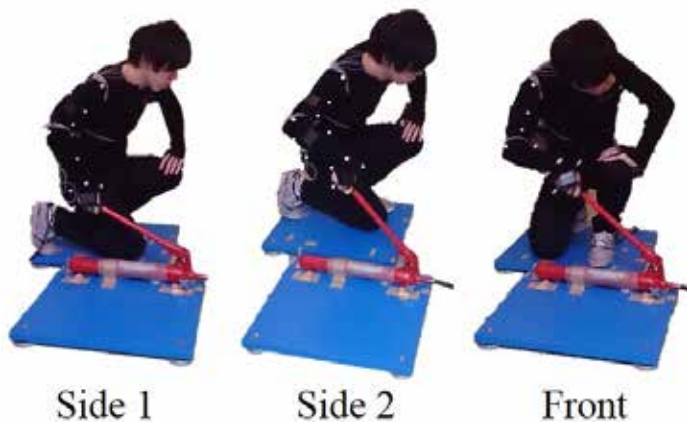


Fig.1 Experimental conditions

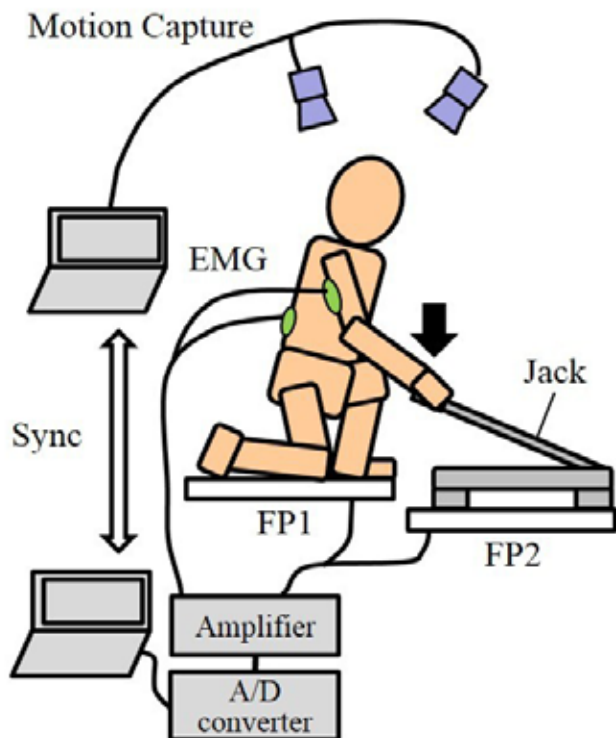


Fig.2 Measurement system

PS10.004 - Neuromuscular Reconnection Methodology By Cap Sense Absorption And Diffusion Signal

Author(s): Ricardo Jaramillo Diaz¹, Luis J. Martinez¹, Hermann Dávila Torres²

¹Coordinacion De Biomedica, Universidad ECCI, Bogotá/COLOMBIA, ²Bogotá D.c, Universidad ECCI, Bogotá D.C/COLOMBIA

According to statistics from the World Health Organization (WHO), approximately 250,000 to 500,000 people suffer from different types of spinal cord injury every year, therefore making the need for neuromuscular rehabilitation a global goal which seeks to continually improve the ability to return as much quality of life as possible to these patients. Spinal cord injuries type Asia A and type Asia B are potentially risky due to the possible development of secondary pathologies, therefore treatments should aim to regain communication from the sensorimotor cortex to isolated areas as promptly possible. Early treatment of spinal cord injuries by reconnecting the injured, isolated areas to the sensorimotor cortex prevents the development of secondary conditions that diminish quality of life for the patients. Systems such as brain computer interface (BCI) recover the motor signal generated from the brain but under current applications the signal is used to generate motion of a robotic prosthetic, without use of the muscles thus leading to muscle atrophy in the muscular system. World news about cell transplantation of olfactory mucosa to completely regenerate the human spinal cord provides an optimistic treatment option but the time between neurological reconnection, mobility and sensitivity is too long causing the process to be more aggravating for the patient. Pathway afferent and efferent signals can be reconnected to the generated signal by the respective cortex when the original signal is captured by CapSense and processed as resistance, inductance and analyzed as a nerve branch which is induced by hydrogel and characterized electromagnetically with ion doping. Potential somatosensory stimulus on the skin is captured by CapSense which manipulates a matrix of amplified mobile phone which activates various functions via cutaneous stimuli. Current technology changed for medical purposes provides emulation for some organic functions for medical treatments that are effective to complete rehabilitation.

PS10.005 - The Development of an Isokinetic Adapter for Prosthesis Users

Author(s): Usha Kuruganti¹, Victoria Chester², Sarah Hamza³

¹Faculty Of Kinesiology, University of New Brunswick, Fredericton/CANADA, ²Kinesiology, University of New Brunswick, Fredericton/NB/CANADA, ³Mechanical Engineering, University of New Brunswick, Fredericton/CANADA

Upper limb amputations can have a significant impact on daily function and affect the quality of life of an individual. There have been significant advances in the materials used to build prosthetic devices resulting in lighter and stronger artificial limbs; however, users have indicated that improved function and control strategies are desirable to become more in line with able-bodied limb function. Quantitative clinical assessment has been challenging due to the complexity of the muscle physiology of those with amputations. In addition, most clinical research has focused on studying isometric (stationary) limb movements. In order to develop more robust systems, it is critical to study muscle mechanics of those with amputations under dynamic (moving) movements. One method of safely examining dynamic movements is the use of isokinetic dynamometers. These machines allow measurement of upper and lower extremity isokinetic movements at controlled angular velocities while ensuring no stress is placed on the individual (even if the participant is unable to move the lever arm). For able-bodied participants, this does not present a problem. However, there is currently no commercially available isokinetic dynamometer adapter for prosthesis users. The purpose of this project was to develop an adapter that can be used by those with amputations to safely and effectively operate the

dynamometer.

There were three stages to the development of this new tool: prototype development, refinement and testing. During the prototype development stage an isokinetic dynamometer (Cybex) was examined to determine the method of attachment. From this a preliminary design was created. Refinements to the first prototype were then completed including attaching a mechanism to allow the user to change the elbow angle to improve the robustness of the device. Modifications were also required to allow the device to mould to the shape of the residual limb of a prosthesis user. The device was also lined to ensure safety and comfort of the user. Finally, the prototype adapter was tested for comfort on a willing below elbow amputee. The subject was asked to fit the adapter on his existing prosthetic with the end attachment removed, as well as to wear it without the prosthetic. The test subject showed no discomfort with either protocol. The tool that was developed connects to the arm of the dynamometer and is adjustable for different prosthesis users.

There are few devices available to evaluate functional ability of upper limb amputees. While there are measures such as hand held dynamometry and myometry as well as ambulatory accelerometry techniques, all other methods of measuring strength are questionnaire based and require observation of the patient (DASH, ADL). The ability to use an assistive device attached to the Cybex opens up many possibilities to measure strength from those with amputations. It may also help to develop strength training programs using this type of equipment. Future work will involve a clinical trial of the device with prosthetic users to determine the device's viability as well as comparing strength between prosthetic and non-prosthetic users.

PS10.006 - High Density Electromyography (EMG) for Improved Prosthesis Control

Author(s): Usha Kuruganti¹, Victoria Chester¹, Yves Losier², Craig Prime³

¹Faculty Of Kinesiology, University of New Brunswick, Fredericton/CANADA, ²Mechanical Engineering, University of New Brunswick, Fredericton/CANADA, ³Faculty Of Kinesiology, University of New Brunswick, Fredericton/NB/CANADA

Pattern recognition-based controllers have the potential to significantly improve myoelectric control systems for prosthesis control by increasing the number of controllable movements. These systems use pattern classifiers to analyze electromyography (EMG) signals and classify the movement produced based on predetermined settings. The effectiveness of the classifier is measured by its classification accuracy. Recently, high-density EMG (HDEMG) systems have allowed for non-invasive collection of myoelectric signals from many closely spaced electrodes. The data obtained can be examined through the use of 'colour maps,' which provide a visual indication of the distribution and intensity of muscle activation. The relationship between pattern classification accuracy and HDEMG based colour maps is unknown, however understanding this relationship may help to better understand muscle activation patterns with applications in prosthesis development as well as imaging muscle activity in rehabilitation (e.g. in stroke or sport injury). Thus, the purpose of this work was to examine four different hand movements to determine repeatability as well as the relationship between classification accuracy and colour map patterns.

A HDEMG system was used to evaluate four different hand movements (hand open, hand closed, pronation, and supination) at a self-selected medium contraction level. Twenty able-bodied individuals (mean age = 31.6 ± 12.0 years, 9 females and 11 males) participated in this study. Sixty-four channels of EMG were collected from electrodes placed in an 8 by 8 grid formation over the forearm region. The areas on the forearm that experienced muscle activity

during given movements were illustrated in topographical (colour) maps for each trial. Pattern recognition was performed to determine how well each contraction could be distinguished using a Linear Discriminate Analysis (LDA) classifier. The colour maps were visually inspected to determine any changes in intensity (amplitude) and pattern repeatability between trials. Pattern classification accuracies were computed for all movements (Table 1). Visual examination of each colour map suggests that both pattern and intensity changes differ in relation to classification accuracy with those with higher classification accuracy having more consistent colour maps. However, a mathematical relationship between classification accuracy and colour map changes is yet to be established.

These results suggest that classification accuracy differ according to both pattern and intensity changes, however the exact relationship remains elusive. Understanding this connection may help to provide better understanding of muscle activity for improved prosthetic control as well as develop new imaging techniques for those with reduced muscle activation due to injury or disability.

Table 1: Classification accuracies for hand open (HO), hand closed (HC), pronation (PR) and supination (SP). All values are %.

	HO	HC	PR	SP
Mean Pattern Classification Accuracy	87.9 ± 14.5	95.7 ± 11.1	86.4 ± 17.1	92.2 ± 13.6

PS10.007 - Influence of Spaces between Tactile Dot Patterns and Raised Boundary Line on Tactile Guide Map Line Perceptibility

Author(s): Harumi Matsumori¹, Kouki Doi², Hiroshi Fujimoto³

¹Graduate School Of Human Sciences, Waseda University, Tokorozawa-shi, Saitama/JAPAN, ²National Institute of Special Needs Education, Yokosuka/JAPAN, ³Waseda University, Tokorozawa/JAPAN

Tactile guide maps are well-known information support tools for visually impaired persons. In particular, tactile guide maps have long been used in schools for the blind. In a tactile guide map, area information is expressed using tactile dot patterns and raised boundary lines. Maps designers must place spaces between these tactile dot patterns and raised boundary lines so that users can easily discriminate the lines (Figure 1). However, there is a lack of quantitative data on the perceptibility of tactile guide map lines.

In this study, we investigated the influence of the spaces between the tactile dot patterns and raised boundary lines on the perceptibility of the lines. We developed test pieces with seven different dot distances for dot patterns and five different space distances. The participants included 20 younger sighted persons and 20 older sighted persons as tactile guide map beginners. The participants were asked to determine the direction of a line, which could be horizontal, vertical, diagonally left, or diagonally right (Figure 2). Based on the results, we found that lines were highly discriminable when the distance between the dot patterns and lines was greater than 5 mm (Figure 3). This knowledge will be helpful for maps designers.

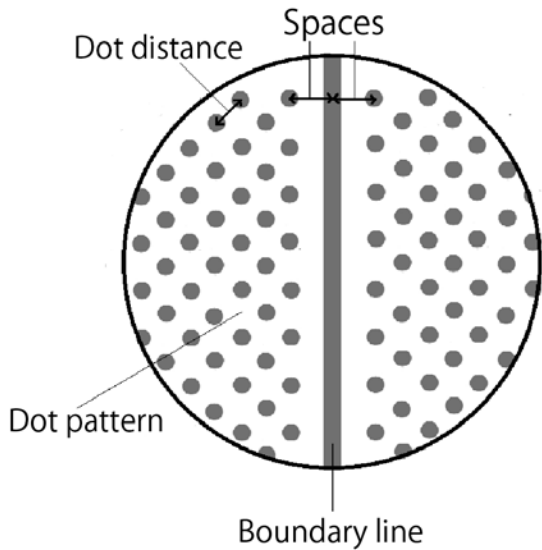


Figure 1. Test piece used in this experiment.

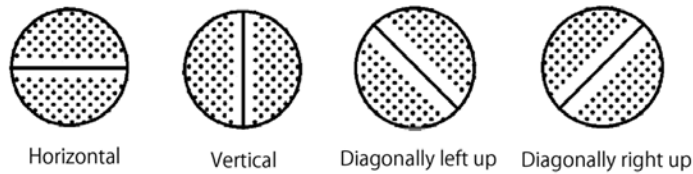


Figure 2. Direction of the boundary lines.

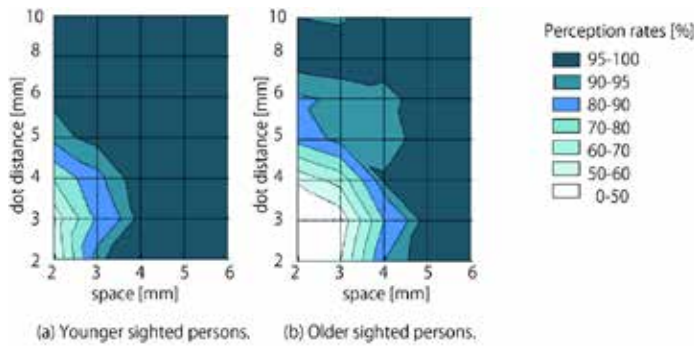


Figure 3. Results of perception rates.

PS10.008 - Influence of Dot Distances on Discrimination of Dot Patterns in Tactile Guide Maps

Author(s): Harumi Matsumori¹, Kouki Doi², Hiroshi Fujimoto³
¹Graduate School Of Human Sciences, Waseda University, Tokorozawa-shi, Saitama/JAPAN, ²National Institute of Special Needs Education, Yokosuka/JAPAN, ³Waseda University, Tokorozawa/JAPAN

Recently, many tactile guide maps have been installed at various public facilities. Designers have used raised dot patterns to display drawings on a tactile guide map. However, there is a lack of quantitative data on the discrimination of raised dot patterns for the design of easily understandable tactile maps. In this study, we investigated the influence of dot distances on the discrimination of the dot patterns used in tactile guide maps by conducting an experiment to find highly discriminable dot pattern combinations by comparing pairs of dot patterns (Figures 1 and 2). A total of 10 visually impaired persons (expert users) and 14 sighted persons (beginner users) par-

ticipated in this experiment. The results showed that combinations of dot patterns with larger differences in the distances between dots had higher discriminability (Figure 3). When the differences were the same, the combinations with larger dot distances had lower discriminability. Dot patterns with differences between dot distances greater than 5 mm were highly discriminable for sighted persons, whereas those with differences greater than 4 mm were highly discriminable for visually impaired persons. This knowledge will be helpful in discussions among map makers on how to design tactile guide maps.



Figure 1. Experimental picture during touching test pieces.

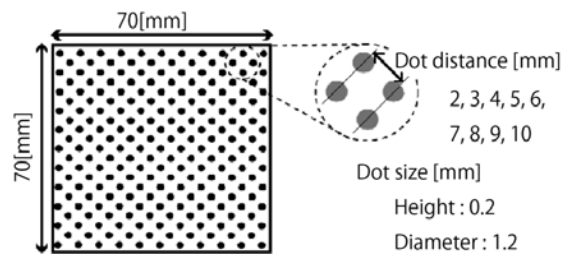


Figure 2. Test piece used in this experiment.

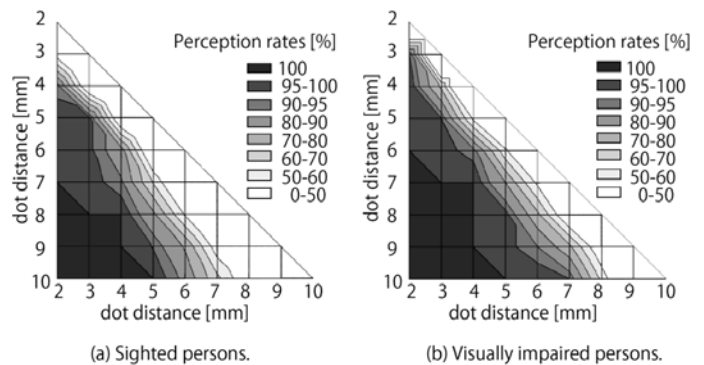


Figure 3. Results of perception rates.

PS10.009 - Statistical Evaluation of Objectivisation of Rehabilitation Process

Author(s): Iva Novotná¹, Michaela Tomanová², Lenka Lhotská¹
¹Cybernetics, Czech Technical University, Prague/CZECH REPUBLIC, ²Czech Technical University, Prague/CZECH REPUBLIC

Aim of the research described in this paper is to find the most objective and least stressful measurement and successive evaluation of the rehabilitation process based on the comparison of effectiveness of the treatment before and after application of a special rehabilitation INFINITY Method. As basic requirements we defined non-invasiveness, lower time demand, patient comfort, possibility of

comparison of temporal development and ease of examination for the medical professionals. We focused on well-known basic plantographic and posturographic parameters. Furthermore, we focused on patient's subjective pain recorded by visual analogue scale (VAS) before and after treatment. Data were collected from patients hospitalized in the Rehabilitation Centre Brandýs nad Orlicí. Three studies containing 33, 100 and 331 patients were used. Student's T-test and Wilcoxon signed-rank test were applied for statistical analysis. Majority of measured patients (60.6 %) showed an improvement in all relevant parameters, in the first study. According to VAS, relieve of pain came in 91 % of patients. The difference in the efficacy of therapy with INIFINITY Method and without is almost 20 % ($p < 0.001$) according to VAS. We evaluated statistically significant differences between the parameters measured in four standing positions in the third study. The overall results imply that in all four standing positions two parameters were statistically significant ($p < 0.05$). Therefore, experiments proved suitability of the proposed methodology. We succeeded in identification of the most informative parameters relevant to the course of the rehabilitation process. In this paper we will focus on statistical evaluation of the measured parameters and will discuss the reached results.

PS10.010 - Satisfactory Vibrating Conditions of Latissimus Dorsi Tendon to Induce Illusory Horizontal Shoulder Flexion

Author(s): Yumi Umesawa¹, Kouki Doi², Hiroshi Fujimoto¹
¹Human Science, Waseda University, Tokorozawa/JAPAN, ²National Institute of Special Needs Education, Yokosuka/JAPAN

Motor images of the human body can easily deteriorate – for example, due to quadriplegia or the fracture of a bone. In this study, we focused on the illusion of kinesthesia to develop practical applications that can be used for training or to enhance motor images. However, basic knowledge regarding the presence of illusions and vibrating conditions is lacking. In this study, we investigated satisfactory vibrating conditions for inducing illusory horizontal shoulder flexion and conducted an experiment to examine the satisfactory vibrating conditions. The participants in this study were 20 young people. The experimental factors were the vibration frequencies of 30, 50, 70, 90, 110, and 130 Hz. We subjectively assessed the presence or absence of an illusion and its vividness on a five-point scale. At the same time, we measured the perceptual time it took for an illusion to appear and the maximum illusory angle. The results showed that when the vibration frequency conditions were within 70–110 Hz, the occurrence rate of the illusion was 98% (Figure 1). In particular, when the vibration frequency condition was 110 Hz, the vividness of the illusion and the maximum illusory angle reached maximum (Figure 2). It took approximately 7 s for an illusion to appear, regardless of the vibration frequency conditions. Under these stimulation conditions, we found that horizontal shoulder flexion can be easily produced. Based on this knowledge, we plan to develop an interface device that will only provide kinesthetic sensations without the actual motion. This device could potentially be used in the rehabilitation and education fields for training on motor images.

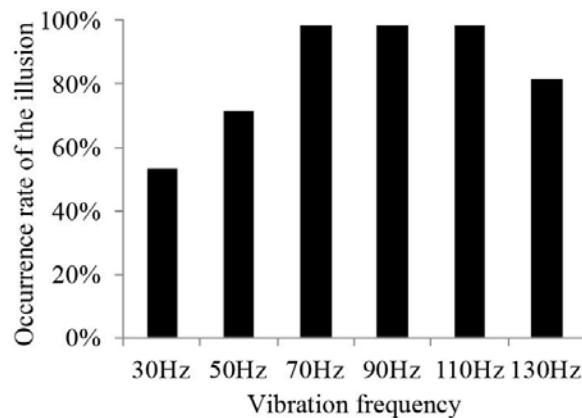


Figure1. Occurrence rate of the illusion

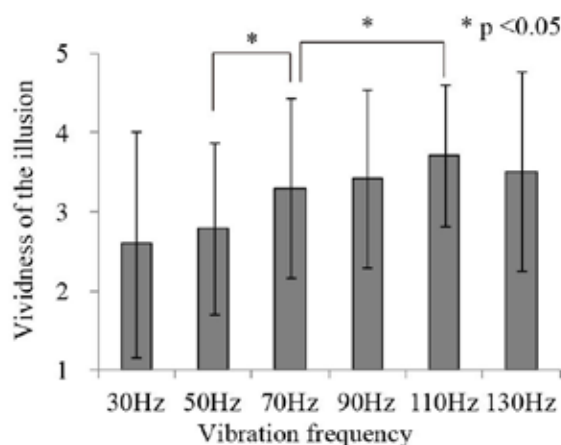


Figure2. Vividness of the illusion

PS10.011 - Satisfactory Vibrating Conditions of Extensor Digitorum Tendon to Induce Illusory Finger Flexion

Author(s): Yumi Umesawa¹, Kouki Doi², Hiroshi Fujimoto¹
¹Human Science, Waseda University, Tokorozawa/JAPAN, ²National Institute of Special Needs Education, Yokosuka/JAPAN

Motor images of the human body can easily deteriorate – for example, due to quadriplegia or the fracture of a bone. In particular, because a high level of dexterity is needed for finger movement, this movement is the most difficult to recover during rehabilitation. We focused on the finger movement illusion of kinesthesia to develop practical applications that can be used for training or to enhance motor images of high-dexterity behaviour with finger movement. However, basic knowledge regarding the presence of finger movement illusions and vibrating conditions is lacking. We investigated the satisfactory vibrating conditions for inducing illusory finger flexion. In this study, we conducted an experiment to examine these conditions for the metacarpophalangeal joint of the index finger. The participants in this study were five young people. The experimental factors were the vibration frequencies of 50, 70, 90, 110, 130, 150, 170, and 190 Hz. We subjectively assessed the presence or absence of an illusion and its vividness on a five-point scale. At the same time, we measured the perceptual time it took for an illusion to appear and the maximum angle of the Illusory finger flexion. The results showed that when the vibration frequency conditions were within 50–130 Hz, the occurrence rate of the illusion was 100% (Figure 1). In particular, when the vibration frequency condition was 90 Hz, the maximum angle of the Illusory finger flexion reached

maximum (Figure 2). It took approximately 4.8 s for an illusion to appear at 90 Hz. Under these stimulation conditions, we found that finger flexion can be easily produced. Based on this knowledge, we plan to induce a kinesthetic illusion of high-dexterity behaviour – for example, a grip or a pinch. This could potentially be used in the rehabilitation and education fields for training on the motor images of finger movement.

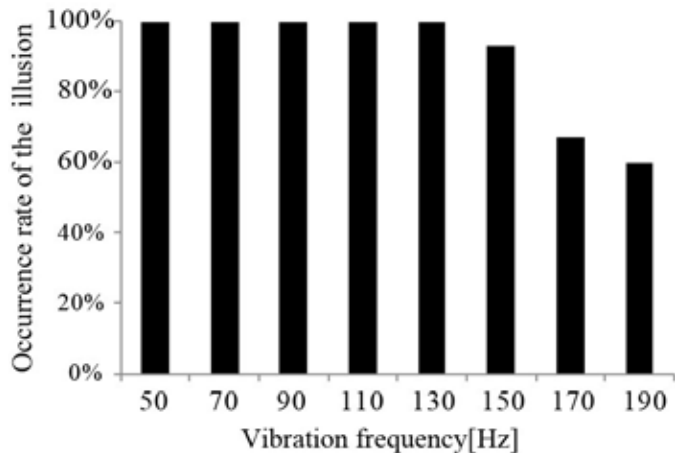


Figure1. Occurrence rate of the illusion

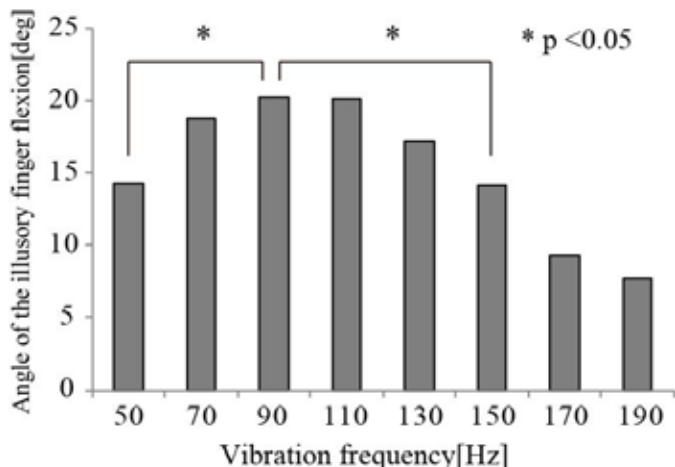


Figure2. Angle of the illusory finger flexion

PS10.012 - Prefrontal Brain Activity of Goal Keeper when Penalty Kick

Author(s): Taishi Kurioka¹, Miho Asano², Masayuki Nambu³, Masaki Yoshida¹

¹Department Of Physical Therapy, Osaka Electro-Communication University, Shijonawate/JAPAN, ²Open University of Japan, Chiba/JAPAN, ³Healthcare(System Institute, Seika/JAPAN

Penalty kick is the special play which influences a result of the game in the football. A goalkeeper should react to the ball instantaneously at the penalty kick, we estimated that the state of the reaction is different in a trained football player and an inexperienced person. Therefore, we got a hypothesis from which a cerebral reaction may be different by the trained football player and an inexperienced person. To inspect this hypothesis, we measured prefrontal activity of the trained and inexperienced subjects when they watch the video of penalty kick, using NIRS. Subjects were 12 years old to 25 years old. Four of them were trained football player and others were

inexperienced people.

In this study, we measured the cerebral blood flows of voluntary subjects when they watch the scene of the penalty kick, using a Near Infra-Red Spectroscopy (NIRS), because we focused on the prefrontal activity. We ordered subjects to sit down on the chair placed in front of the LCD monitor and watch the video. We also ordered subjects to concentrate to the scene of the video. Fig.1 shows the results of blood flow of the prefrontal area of inexperienced people when the kicker kicked the ball. Fig.2 shows that of trained football player. As the result of the experiment, we found that specific region of prefrontal area reacts strongly in a trained football player. Therefore, we suggest that prefrontal activity will be an index for state of training in the football.

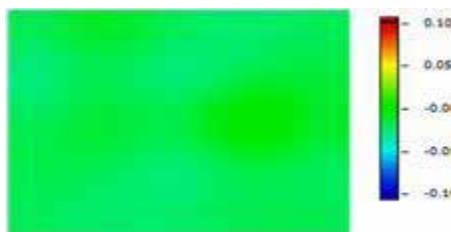


Fig.1 Blood flow of the prefrontal area of inexperienced people

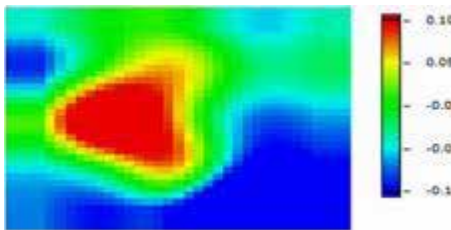


Fig.2 Blood flow of the prefrontal area of trained football player

PS10.013 - Effect of the moderate high pressure circumstances to metabolism

Author(s): Masaki Yoshida¹, Miho Asano²

¹Department Of Physical Therapy, Osaka Electro-Communication University, Shijonawate/JAPAN, ²Open University of Japan, Chiba/JAPAN

The high pressure air capsule was developed for the purpose of medical treatment. Recently, this capsule is attracted the attention of an effect of health, and is used for the conditioning or for the anti-aging. However, some peoples have a pain in an ear for high pressure. We can hope that many people are easily available by lowering the air pressure. Therefore we considered whether the same effect could expect moderate high pressure in this research. We made a moderate high pressure chamber (MHPC). The air pressure in MHPC is set 120 hPa higher than outside air pressure. In addition, the carbon dioxide density in the chamber increases in the carbon dioxide included in the expiration of the person, but is regulated not to exceed 5,000ppm. 13 subjects (20 - 40 years old, 3 females and 10 males) participated in this study. The subject stayed in the chamber for 60 minutes. We measured blood partial pressure of oxygen and carbon dioxide of the subject. Furthermore, we measured the basal metabolism before and after MHPC treatment. Fig. 1 shows the change of blood partial pressure of oxygen and carbon dioxide of the subject in the chamber. Blood partial pressures of oxygen increase rapidly just after a start, but gradually decrease afterwards. The blood carbon dioxide partial pressure rises from 30 minutes later. The basal metabolism at the end significantly increased in comparison with that at the start (see Fig.2). Other items did not have the meaningful change. It became clear to affect the human being in the moderate high pressure circumstances. For a physi-

ological index, the basal metabolism was most greatly affected. It is suggested that this is caused by change of the blood carbon dioxide partial pressure.

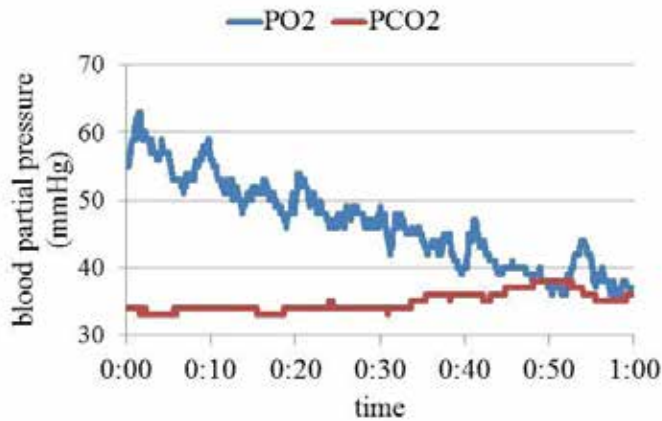


Fig. 1 Blood partial pressure of oxygen carbon dioxide

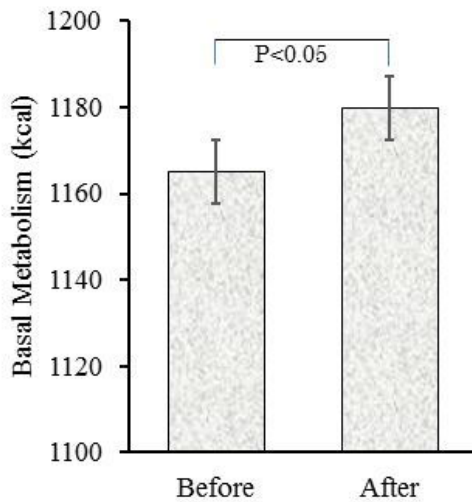


Fig.2 Basal metabolism

PS11 - TRACK 11: NEUROENGINEERING, NEURAL SYSTEMS

PS11.001 - Objective Evaluation of Likes and Dislikes by Prefrontal Blood Flows

Author(s): Miho Asano¹, Masayuki Nambu², Masaki Yoshida³, Yasuhiro Kawahara¹

¹Open University of Japan, Chiba/JAPAN, ²Healthcare System Institute, Seika/JAPAN, ³Department Of Physical Therapy, Osaka Electro-Communication University, Shijonawate/JAPAN

It is difficult to know the emotion of likes and dislikes. Questionnaire is the only method to know likes and dislikes, and has low reliability because it is not objective evaluation method. In this paper, we reported about a technique to distinguish the likes and dislikes objectively by measuring prefrontal blood flows, because emotions were based on prefrontal activity. We show images of selected solid colors which were red, blue, orange, indigo, yellow, purple, green, black, and white, and we measured the blood flows of the subject, using near infra-red spectroscopy (NIRS). In addition, we asked subjects about likes and dislikes with the color by the order after the experiment. The result of an experiment shown in fig.1. By the way, artifacts based on the body motion or change of the blood pressure are included the signal of the NIRS which is shown in fig. 1. Therefore, we obtained the approximation of the artifact using polynomial approximation algorithm. Then we subtract the approximation from the original signal. As the result of the subtraction, we confirmed the artifact was reduced as shown in fig.2. As the result of the experiment, the level of the oxyhemoglobin when the subject answered "I don't like" was relatively high, compared with the level of the oxyhemoglobin when the subject answered "I like". We consider that undesirable stimulus is more impressed than desirable stimulus. Furthermore, we consider that we will distinguish that likes and dislikes by measuring the cerebral blood flows in the future.

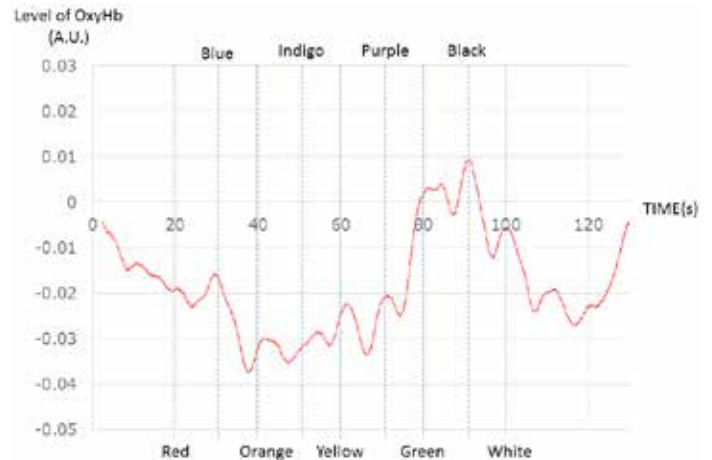


fig. 1

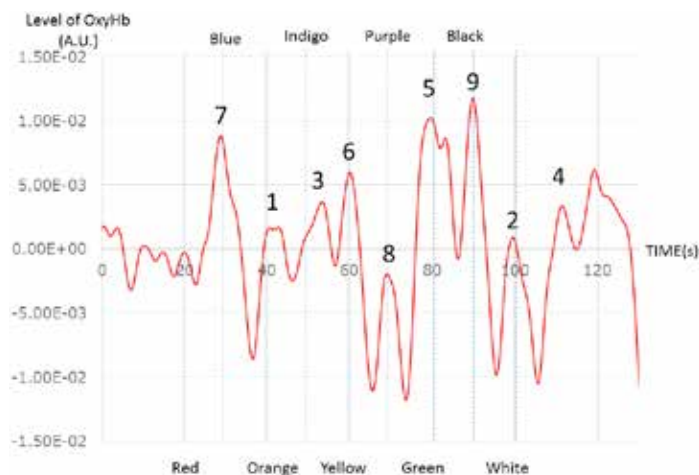


fig. 2

(Numbers of the graph show the order of likes and dislikes)

PS11.002 - Robotic Wheelchair Commanded by People with Disabilities Using Low/High-Frequency SSVEP-based BCI

Author(s): Teodiano Bastos-Filho

Electrical Engineering, Federal University of Espirito Santo, Vitoria/BRAZIL

Brain-Computer Interfaces (BCIs) are systems developed to improve the daily life of people with disabilities. Nevertheless, this assistive technology is yet far away from the patients' home and the BCI should adapt to the requirements of the user. This paper presents a practical BCI based on Steady-State Visual Evoked Potentials (SSVEP) currently being used by people with disabilities. The BCI was applied to navigate a wheelchair at two ranges of SSVEP frequency, increasing the possibilities of its application. Two stimulation systems were used: checkerboards flickering at low-frequency range and LED flickering at high-frequency range. Five volunteers with disabilities tested the SSVEP-based BCI. They attempted to command the wheelchair in order to accomplish four different navigation tasks. Then, the volunteers answered a questionnaire about their comfort and performance. Average accuracy detections of 54% and 51% were achieved at low- and high-frequency stimulation, respectively. Volunteers reported lesser visual tiredness when high-frequency LED stimuli were used. The flexible BCI system here developed showed that people with disabilities could operate a robotic wheelchair using visual stimuli in two ranges of frequency. Moreover, preliminary results indicated that visual stimuli flickering at high frequency were more comfortable than low frequency stimuli.

PS11.003 - Quantifying and overcoming the effect of distractions on cognitive load and brain-computer interface (BCI) performance: Implications for real-world BCI use and cognitive neuroscience

Author(s): Zahra Emami

Holland-Bloorview Kids Rehabilitation Hospital, Toronto/CANADA

Brain-computer interfaces (BCIs) are a revolutionary technology enlisting the neural activity, or cognitive capacity, of its user in order to operate a certain device or application. Since BCIs do not require any motor input, the technology has significant applications for individuals with severely impaired motor control, such as those with amyotrophic lateral sclerosis or locked-in syndrome. BCIs have been largely examined in the lab setting and under controlled conditions, however, the ultimate target for its use lies in real-world situations such as homes and clinics, which are often rife with distractions. Distractions can cause an enhanced burden on the cognitive

processes of BCI users through an increased expenditure of cognitive resources, which are already largely occupied by the BCI task at hand. Distractions can therefore potentially limit the resources available for BCI control, and in turn jeopardize BCI performance. The purpose of this proposed study is twofold. This study will look to determine the effect and extent of distractions on cognitive load and to compare this to the effect on BCI task performance. The study will also look to examine whether or not performance can be enhanced in the presence of distractions through techniques that reduce cognitive load. These techniques include emphasizing the BCI task visual interface or repeating the BCI task signaling stimuli in order to redirect attention from the distraction back to the BCI task. Following BCI neurofeedback training, 10 able-bodied participants will be enlisted to undergo a motor-imagery based EEG-BCI protocol in conditions of no distraction, visual distraction, and cognitive-load reducing techniques in the presence of distraction. Cognitive load will be determined via objective measures such as the Youden Index and EEG alpha band pattern, and subjective measures such as the NASA-TLX, and will be compared to measures of BCI performance for each condition. It is expected that optimal BCI performance will be attained in the no-distraction condition where cognitive load is relatively low, while the presence of task-irrelevant visual distractions will increase cognitive load and cause a decreased BCI performance. Redirection of attention to the BCI task stimuli, through emphasis or repetition, is expected to attenuate cognitive load and rescue BCI performance. The findings of the proposed study is expected to demonstrate the impact of task-irrelevant information on cognitive resources, its consequent influence on BCI performance, and will emphasize the potential importance of considering the effect of cognitive load on BCI systems, especially in real-world environments. With accounting for uncontrolled environmental factors, BCI systems can be robustified such that its translation from the lab to the home, or where the end-users are likely to use the technology, will be more effective.

PS11.004 - How Mental Strategy Affects Beta/Theta Neurofeedback Training

Author(s): Xiaoting Qu¹, Limin Yang¹, Qi Tang¹, Wenya Nan¹, Janir Nuno Da Cruz¹, Feng Wan¹, Pedro Antonio Mou¹, Pui-In Mak¹, Peng Un Mak¹, Mang I Vai¹, Yong Hu², Agostinho Rosa³

¹University of Macau, Macau/MACAU, ²University of HongKong, HongKong/HONG KONG, ³University of Lisbon, Lisbon/PORTUGAL

Neurofeedback training (NFT) has been proven to have positive effects for human cognitive performance enhancement and to be a potential non-pharmacological supportive treatment for many neurological and psychiatric disorders. The mental strategies the participants use during the NFT are a determinant feature in a successful NFT. However, most existing studies focus on either the training protocols or the training effects. Therefore, this study investigates the mental strategy effects during beta/theta ratio based NFT and attempts to find an efficient method to analyze the mental strategies that can be used to improve the success rate in NFT researches. Objective beta/theta ratio value scores and qualitative mental strategy classification were used for analysis. The results showed that no specific mental strategy is more significantly useful for NFT under this protocol but the strategies that required more attention performed better, which is consistent with the findings in previous NFT studies.

PS11.005 - Stimulation to Basal Ganglia and the Efficiency of Microminiaturized Electrode Recording (MER) to Quantify STN Neurons with Deep Brain Stimulator (DBS)— the Lead Point in Parkinson Diseased Conditions

Author(s): Venkateshwarla R. Raju

Biomedical Eng & Neurology & Neurosurgery And, Nizam's Inst of Medical Sciences (NIMS) University & Hospital, HYDERABAD/INDIA

Deep brain stimulation (DBS) of bilateral subthalamic nuclei (STN) is an efficient method of rehabilitation in subjects with advanced idiopathic Parkinson disease (PD). Accurate targeting of STN neurons and placement of microelectrodes are paramount importance for optimal results after STN-DBS. Stereo tactic assessment, intra-operative microelectrode recording and intra-operative stimulation effects have all been used in targeting, albeit the individual role of each modality is still not known. Microelectrode recordings of STN were detected in a mean of 3.5 ± 1.1 channels on right hemisphere and 3.6 ± 1.04 on left hemisphere.. Final channel selected were most commonly central seen in 42.3% followed by anterior in 33.7%. Concordance of final tract with the channel having the highest recording was 58.7%, with the channel showing maximum depth of recording was 48% and with either was 64%. Absence of any recording in the final tract chosen was seen in 6.52%, in these subjects the tract was chosen based on stimulation results. The depths of microelectrodes were detected by microelectrode recording in 75.6%. Microelectrode recording is useful to identify and confirm the tract in which DBS electrodes are placed and is most useful in determining the depth of electrodes placement but has to be taken in consideration with effects seen on macro-stimulation.

quences by interventions realized by medicines and its side effects or adverse, nutrition or therapy. The secondary purpose is to perceive where can be made interventions for to mitigate the causes of the disease for the next generations.

PS11.006 - SCHIZOPHRENIA: Interaction between factors

Author(s): Bernadete M. Voichcoski¹, Vicente Machado Neto²

¹Electronic Engineering, Technological Federal University of Parana, Curitiba-PR/BRAZIL, ²Electronica, Technological Federal University of Parana, Curitiba PR/BRAZIL

Background

Schizophrenia is an endogenous and multifactorial disease that causes for the person that suffers, disconnections with reality, difficulties at real facts processing, difficulties of cognition and memorization, disorders on social, affective and personal life. The disease is classified in six types and the causes are related with each brain area that is damaged. Like the disease is multifactor, is difficult to the doctor to view patient history as a whole. The panoramic view about the disease for each patient and the relations with and between them, the aim of this work, allows to the doctor perceives the patient by globalized and correlated form and no segmented, since the disease happens with the interaction the various factors together.

Methods

The research about possible causes and hypotheses for disease was raised through articles published on the fifteen years last and positioned at Block Diagram, according with main factors of the disease and relations between them.

Results

It was found six main factors of the disease: Genetic, Physical, Metabolism, Nutrition, Psychic and Environment. All the points studied can be positioned into this six main factors and it was possible to realize the relations between them.

Conclusions

The main purpose is to allow to the doctor perceive the patient by globalized form and facilitate the treatment preventing the conse-

PS12 - TRACK 12: MEDICAL DEVICES

PS12.001 - Challenges and opportunities in home-based monitoring of cardiac dynamics

Author(s): Yashodhan Athavale, Sridhar Krishnan
Electrical & Computer Engineering, Ryerson University, Toronto/ON/CANADA

Advances in sensor and data acquisition technologies, Big Data, rising health care costs, public awareness of improving the quality of life, has spurred a boom in wearable “health-tech” in the smart device market. Tele-monitoring of cardiac dynamics (or ECG analysis) using smart devices is becoming a popular choice as it helps the consumer in maintaining daily fitness, food intake, and also helps cardiac patients in proper treatment such as medicine intake times, relaxation or activity break times, or even calling the nearest health care facility in case of emergency. Although these devices give the user a nice graphical output about the cardiac state, their signal analysis is still challengeable with regards to device capability and the significance of clinical data [1, 2, 6].

Our survey indicates that clinical ECG exceeds the smart-device ECG, in terms of signal quality, low artifacts and information content [1-6]. Despite their reliability, hospital-based cardiac monitoring tools are cumbersome and don't support transfer to a home-based ECG monitoring environment [2]. Although some currently available devices (such as smart watches, wrist bands etc.) are capable of monitoring cardiac health, their analysis is quite limited and may not be helpful from a clinical perspective [6]. Meaning, the signals acquired through these devices may depict only a portion of the entire heart's dynamics, and cannot be interpreted into meaningful information by the consumer. Hence their usage is still questionable without the ground truth from clinicians [6]. Such type of unsupervised data acquisition and pattern recognition systems could also question the type of ECG data collected, its format, the storing methods, privacy and confidentiality of consumers. These wearable devices may be a lifestyle improvement choice for the underserved healthy population, but they may not be useful for subjects who have a tendency for severe cardiac disorders. Analysis of bio-signals such as ECG requires an algorithm which can extensively perform artifact removal, feature extraction, pattern recognition and highly optimized for processing hardware in terms of power and area requirements. Recommendations of a reliable and practical home-based ECG monitoring include the following specifications: [i] user friendly [1,2], [ii] compact and wireless hardware design, [iii] non-invasive and comfortable to use sensors, [iv] standardized data acquisition and security, [v] user understandable informed decision and output, [vi] provision for data synchronization with local healthcare provider, [vii] reliable signal quality, [viii] low power and memory consumption, [ix] low data processing time, and [x] cost effectiveness.

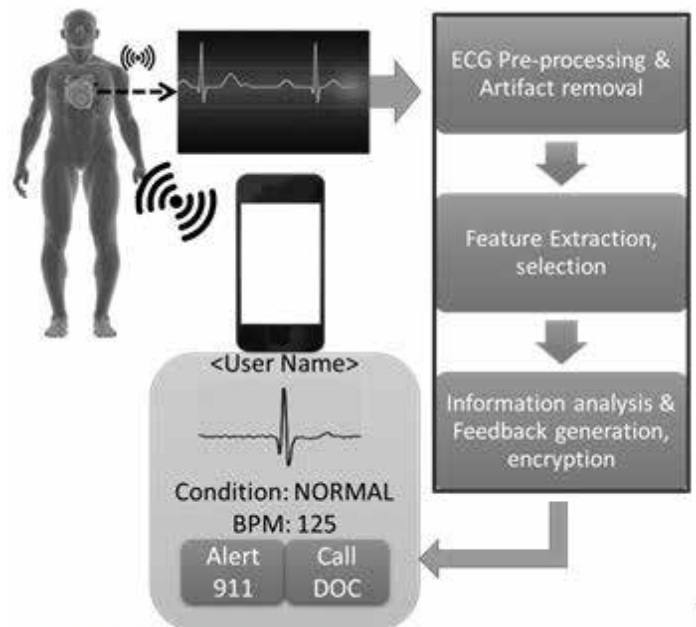


Figure 1. Design of a practical ECG Tele-monitoring System

PS12.002 - Application of Support Vector Machines in Intelligent Monitoring of Cardiovascular Health on a Mobile Device

Author(s): Omar Boursalie¹, Thomas E. Doyle², Reza Samavi³
¹School Of Biomedical Engineering, McMaster University, Hamilton/CANADA, ²School Of Biomedical Engineering, Electrical And Computer Engineering, McMaster University, Hamilton/CANADA, ³Computing And Software, McMaster University, Hamilton/CANADA

Cardiovascular Disease (CVD) is the leading cause of death in the developed world. There are many risk factors and early treatment through pharmacotherapy and lifestyle changes can reduce the severity of CVD. Due to this, patients at risk for CVD are closely monitored. Current monitoring techniques include periodic visits to the doctor, which causes stress on the healthcare system. Increasingly, mobile devices with unobtrusive sensors are providing patients with information regarding their own health. However they provide an abundance of data that patients and health care professionals do not use. In the case of wearable devices this has contributed to the low long-term usage of such devices.

Recent work has focused on the use of a support vector machines (SVM) for analyzing medical data. SVM is a flexible algorithm that can learn from data rather than following an explicit program. In a previous study, a SVM was developed for continuous monitoring of a patient's electrocardiogram (ECG) in real time. However this SVM was used for the comparison of a single variable and did not consider the wide variety of factors that contribute to CVD. Another study developed a multi-variable SVM algorithm that was used to monitor the effectiveness of drugs in diabetes patients in a smart-phone device. It depended on user input and analyzed multiple factors however it did not make use of the data collected automatically by smartphone devices. A similar CVD device has also not been developed to analyze multiple factors on a mobile platform.

The focus of this project would be a SVM-based program that will be used on smartphones to monitor the vitals of a patient with CVD. The device will obtain input data for a SVM algorithm through sensors and electronic health records (EHR). Sensors will be used to monitor the patient's real-time vitals. EHR provide information regarding the patient's basic information (gender, age, sex etc), medical history and demographics. Together, these sources of data will provide the SVM a comprehensive overview of the patient's health.

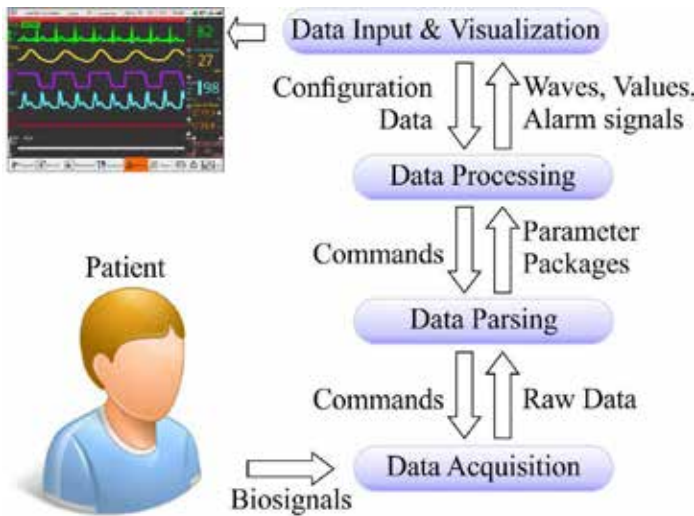
A SVM is a supervised, classification algorithm which is trained using known data provided from clinical databases. The algorithm is ideal for studying CVD because it can create solutions to complex problems where it is impractical or impossible to program a solution directly. The algorithm will be trained to monitor an individual patient's condition. The SVM will be able to identify and present only the relevant data to health care professionals and patients.

The SVMs will be evaluated by determining its accuracy in analyzing new data. It will improve on current monitoring systems because the SVM will allow for the integration of a wide range of factors and can be adapted for individual patients. The patient would be an active contributor in the management of their own disease. This will reduce stress on the healthcare system by informing health care professionals about serious cases and can be used in preventative medicine. The factors can then be further analyzed to determine if pharmacotherapy or lifestyle changes are necessary.

PS12.003 - Design and Implementation of the Software for Multi-parameter Patient's Monitor

Author(s): Maite Cañizares, Alberto R. Rodríguez, Gemma Rodríguez, Daniel Jiménez, Hector Torres, Daniel A. Romero, Miguel Portieles, Miguel Gómez, René González-Fernández
Digital Medical Technologies, Havana/CUBA

Features of design and implementation of the preliminary version of the main software for a multiparameter patient's monitor are presented. Alarm Control Subsystem is highlighted. The design fulfills requirements of standards for monitoring systems. The software was designed with multi-layer architecture conformed by four layers.



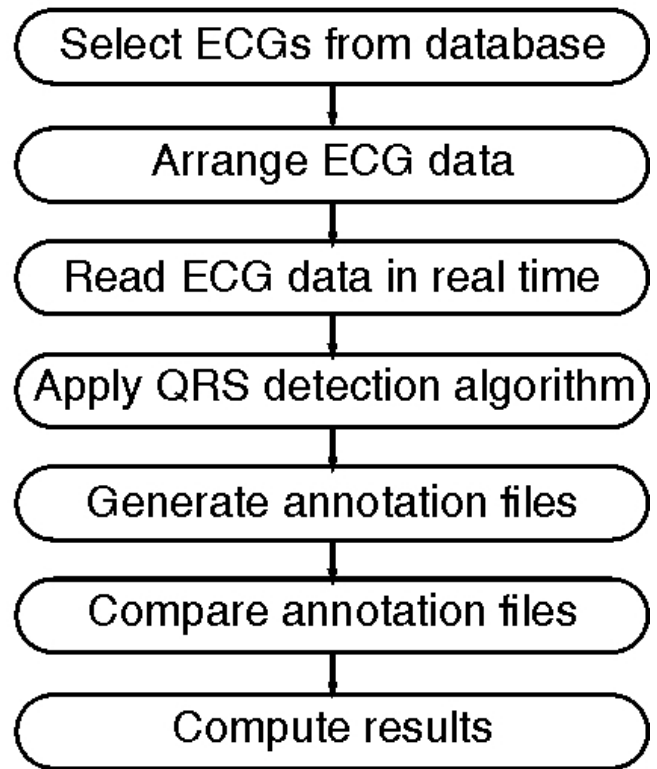
Functions for acquiring, processing and visualization of signals and values are connected but, at the same time, are independent. Software was implemented using Qt environment tools like multi-thread, object oriented programming and signals-slots. It provide to the doctors and nurse with different configuration options like setting variable limits and customize the performing of visual and sound alarm notifications. The software was implemented to be used on a monitoring device with a main board based on ARM-9 microprocessor. Using multi-layer architecture it is possible to verify each subsystem independently and to make more easy update and maintenance tasks. Monitoring and operational performance of the monitor reached expected results.

PS12.004 - Strategy and Tools for Validation of QRS Detection Algorithms in Real Time ECG Monitors

Author(s): Maite Cañizares, Alberto R. Rodríguez, René González-Fernández
Digital Medical Technologies, Havana/CUBA

Tools designed to help during the validation of algorithms for QRS detection included in real time patient monitors is presented. Validation of these algorithms is a requisite established in the international standards.

Steps of the strategy followed during validation process were described. First of all, an appropriated set of ECG signals must be selected from ECG databases recommended in the standards. The second step consists of arrange the ECG signals in the appropriated format (sample rate, data structure), according to the system where the detection algorithms must be validated. Patient monitor program must be able of reading ECG signals from files. Next step is to apply the QRS detection algorithm to all data read from the files and generate the annotations files with database annotation files format. Finally both annotations files must be compared for calculating sensibility and specificity of the algorithm.



Steps for validation of QRS detection algorithms in real time.

The proposed strategy was tested using a patient monitor based on ARM-9 and Linux architecture which acquires until three ECG channels with a sample rate of 250 Hz. For validation were re-sampled 50 ECG signals from the MIT-BIH Arrhythmia Database. Running a "Test Mode" option the program acquired signals in real time from re-sampled files. The functions of QRS detection algorithm were included in an external library that later could be included in another

similar application. Annotation files were created for each re-sampled signal. A Qt application was developed with visual interface for review signals and comparison of annotation files. This program implements functions for creation of re-sample ECG signals files and for generation and comparison of annotations files. The strategy defines the steps for validation of algorithms for ECG analysis in real time systems.

The created application has a friendly interface for viewing and analyzing validation results generated for algorithms used in real time system or those used offline.

PS12.005 - Basic Study on Variability of Measured Data from Touch Test Using Semmes-Weinstein Monofilaments

Author(s): Manabu Chikai¹, Emi Ozawa², Noriyo Takahashi³, Shuichi Ino¹

¹National Institute Advanced Industrial Science and Technology, Tsukuba/JAPAN, ²Showa Inan General Hospital, Komagane/JAPAN, ³Tokuyukai Rehabilitation Clinic, Toyonaka/JAPAN

The aim of our research was to develop new equipment for easily and noninvasively diagnosing diabetic peripheral neuropathy (DPN). The International Diabetes Federation (IDF) reported that 387 million people have diabetes. Diabetes is associated with life-threatening health risks. One of these risks is DPN, which causes hypoesthesia in a patient's toes. The early and easy detection of DPN in a clinic is the hope of diabetic patients and medical staff. Several methods are used for DPN screening tests. One of these is a touch test using a device with nylon Semmes-Weinstein monofilaments (SWMs) embedded in a plastic handle. A low pushing force is applied at the handle to bow the filaments. A member of the medical staff presses the filaments at nearly a 90° angle against the patient's hand or foot until they bow. A previous study reported that the SWMs did not generate the same values on repeated tasks. However, it was uncertain whether the variability of the measured data was caused by the mechanical property of the nylon fiber or the operator's hand motion. In this study, we elucidated the variability of the SWM test data.

We carried out two experiments on (1) the effect of the number of compressions on the buckling force of the SWMs and (2) the effect of the human operator variability using the SWMs. This study used 5.07/10g SWMs. In experiment 1, the SWMs were pressed using an X-axis positioning stage. We measured the buckling force of the SWMs using a force sensor. The stage moving speed was 10 mm/s. In experiment 2, the SWMs were operated by individual participants. Ten participants (6 men and 4 women) ranging in age from 20 to 60 years (mean age 42 years) were recruited. We measured their hand motion using an optical motion capture system, and measured the buckling force of the SWMs using a force sensor.

Based on the experimental results, the average buckling force of the first compression was 8.2 g, and it was 7.5 g after ten successive trials. The average force of all the compressions was 7.7 ± 0.3 g. The average hand motion velocity for all the participants and the average buckling force were 0.23 ± 0.1 m/s and 7.5 ± 0.6 g, respectively. Thus, the hand motion during the SWM tests varied by participant. Therefore, the SWM test results varied from both the effect of repeated tests and the effect of the operator's hand motion. In other words, an SWM test needs to consider the number of test cycles, and manual training needs to be developed for the medical staff.

We elucidated the variability problem of sensory testing using SMWs. The buckling force of the SWMs was decreased through numerous test trials, and the hand motion varied by participant. In future work, we will find a solution to the variability of the SWM test results and develop a new testing system for tactile sensibility for DPN screening.

PS12.006 - Design and construction of temperature and humidity control channel for a bacteriological incubator

Author(s): Carlos R. Duharte¹, Ibrain Ceballo², Carmen Busoch¹, Angel Regueiro¹

¹Centro De Bioingenieria (cebio), (CUJAE) Instituto Superior Politécnico Jose Antonio Echeverría, La Habana/CUBA, ²Centro Nacional de Electromedicina, La Habana/CUBA

During the study and research of microbial growth in biological samples, it is essential to have an incubation station. This incubator permits to control the temperature and humidity for an adequate characterization of the different stages of growth of microorganisms, especially pathogens. This paper supports the development of new methods for rapid detection of these microorganisms, not only applicable to industrial biological samples (food, raw materials, etc.) but also to clinical samples (urine, blood, etc.).

The paper discusses the design and characterization of a lab incubator prototype to support studies of Microbiology, particularly for research phase of bacterial growth in biological samples through integrating optical methods (photo stimulation and turbidimetry) and bioimpedance measurements. The basic stages of electrical design and operation are described as well as the control program (software) developed based on these of microcontroller AT89C51. Furthermore, the results of simulation and experimentation of the proposed design are shown for measurement channels of the variables of interest (temperature and humidity), in which high linearity and adequate strength from the selection of system components was obtained.

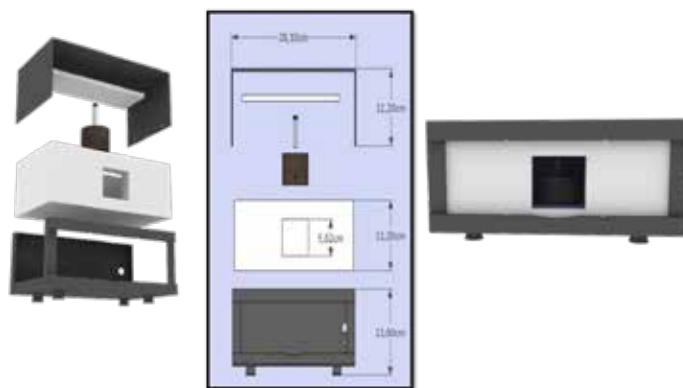


Figure 1. Mechanic design of incubator

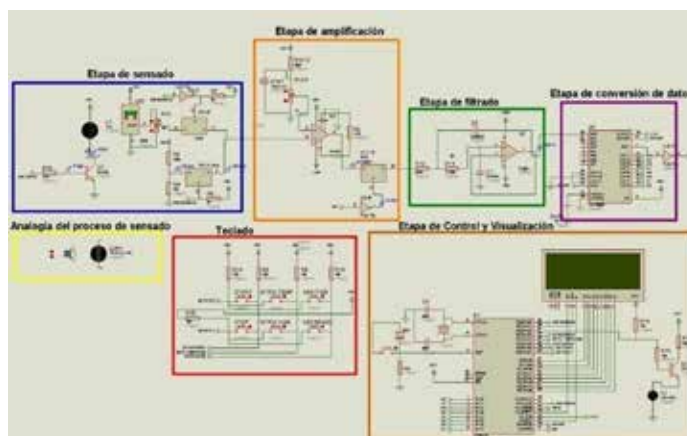


Figura 2. Diagram of the design of channel of temperature sensing and regulation.

PS12.007 - High-Reliability Nerve Stimulator For Aiding Regional Anesthesia Procedures

Author(s): Carlos A. Ferrí, Antônio A.F. Quevedo
Biomedical Engineering, UNICAMP, Campinas/BRAZIL

In the last decades, the use of nerve stimulators in nerve blockade anesthesia procedures has shown benefits to patients, since it allows a better location of the nerve plexus, leading to correct positioning of the needle through which the anesthetic is applied. However, many of the nerve stimulators available in the market for this purpose do not comply with minimum recommended features and specifications for a good stimulator. This can lead to risks to the patient. This study aims to develop an equipment that meets all the characteristics for a successful blockade. We developed a high-quality and high-precision device using embedded digital and analog electronics for accurate control for all stimulation parameters. The system consists of modules for generation and overall control of the current pulse, the patient interface, and communication interface with a personal computer. The results show that the proposed system fits into suggested specifications for a good neurostimulator to be used for nerve location during regional anesthesia procedures.

PS12.008 - A study of pressure-volume characteristics of the cuff for hemodynamic parameters measurement

Author(s): Jan Dvořák, Martin Tuček, Jan Havlík
Faculty Of Electrical Engineering, Czech Technical University in Prague, Prague/CZECH REPUBLIC

This contribution deals with the pressure-volume characteristics of the cuffs used for blood pressure measurement. The linearity of characteristics is a very important factor for the accurate conversion from volume change to pressure change. Several cuffs were tested during the study, including new cuffs, old cuffs, cuffs with different sizes, volumes and clamping systems. Results of the measurement in the range between minimal diastolic to maximal systolic pressure have been statistically evaluated.

PS12.009 - Format for National Inventory of the Genomic Technology

Author(s): Beatriz Hernandez
Medical Infrastructure, Vitalmex, Distrito Federal/MEXICO

Introduction: The scientific research in health is an important activity for development of the countries. In Mexico there are many Universities, private and public Institutions and companies that work in different research project. However this institutions needs money for buy laboratory equipment, solutions, materials and payroll.

In the last decade medicine genomic has had a big impact in medicine around the world, many countries have been spending many money for obtain infrastructure and laboratory devices for the different projects, but is necessary to make more efficient the existing technology. Mexico is a country that need improve the health. Mexico has priority in resolve the principal health problems that affect at the population, so research in medicine genomic is necessary for this goal.

For this is important have a national inventory where the scientific can obtain information about the kind of technology, conditions, specifications and location. The reserved information is very common in research it is a factor that not has permitted know about the different resources that each Institution have.

Objective: identify the information necessary that allow do one national inventory and know where is the laboratory devices, their specifications and which are their operational conditions. Looking for an more generation of collaborative agreements to decrease

spending on technology.

Material and methods: The first step was to identify the different Institutions and universities private and public as well as companies that do research or service in medicine genomic, also the different lines that medicine genomic has been developing, the kind of technology that use each Institution and their general technical specifications. Other action was to identify for each research line the kind of technology necessary and their importance in the different research.

An important point was know technical information, cost, sales level with the manufactures of genomic technology.

After we create a database and their contacts, we analyzed the information and we create a format for identify exactly that kind of technology have each Institutions. For this was necessary create indicators for determine that level of impact of each technology and focus the information only to technology with high impact.

At the same time we analyzed the variables of census that did SNIICyT (National system of information of science infrastructure and technology in Mexico), this information is only for government institutions.

Finally we used tools of market research for identify the variables for integrated in the inventory format.

Result: we create a format in paper and digital which can be used in the national inventory of genomic technology, applicable to private and public organizations as well as different kind of Institutions academic and not academic.

Conclusions: Is necessary have a reliable inventory that help to scientists and managers of genomics technology to generate collaborative project that make more efficient the resources, increasing the number of research that will impact in the public health.

PS12.010 - Development of the bedridden person support system using Kinect.

Author(s): Kouhei Ichimura, Kazushige Magatani
Tokai University, hiratsukashi kanagawa/JAPAN

The purpose of this study is to support the bedridden and physically handicapped persons who live independently. It is not so easy for them to control home environments, home appliances and to communicate with family or nursing care staffs. Therefore, some supports are necessary for them. Our objective is to solve these problems. We developed a home environments and home appliance control system using Kinect. And then this system was tested and the results of experiment were assessed.

Fig.1 shows the system overview. The system consists of the control interface, a personal computer and control objects. In our system, the control interface consists of sensors which are used for hand motion recognition and the display which indicate the application menu for operation. A control interface senses hand and finger motion and recognize these motions (raising a hand, grasp and release). Recognized results are used to operate the system. And this interface is also used to show the control applications on the display. Our system is constructed as the interactive system, and simple operations for the bedridden and physically handicapped user are realized.

We used Kinect which is a kind of infrared ray sensing system to detect hand motions. OpenNI2 and NiTE2 were also used as software developing libraries in our system. The skeleton detection that is supported by these libraries cannot use for the user who lays on the bed. So, the gesture applications which is provided by NiTE2 were

used in order to track hand motions. In our system, electric devices which support a user are controlled by a personal computer using a programmable infrared ray remote control interface. In other words pre-programmed infrared ray code according as objective is sent to the target device. In this paper, target devices are lighting equipment, a television and an air conditioner.

Our developed system was tested with some normal subject and results of the experiment were evaluated. In this experiment, all subjects laid on the bed and tried to control our system. As results, most of subjects were able to control our developed system perfectly. However, motion tracking of some subject's hand was reset forcibly. It was difficult for these subjects to make the system recognize his opened hand. From these results, we think if this problem will be improved our support system will be useful for the bedridden and physically handicapped persons.

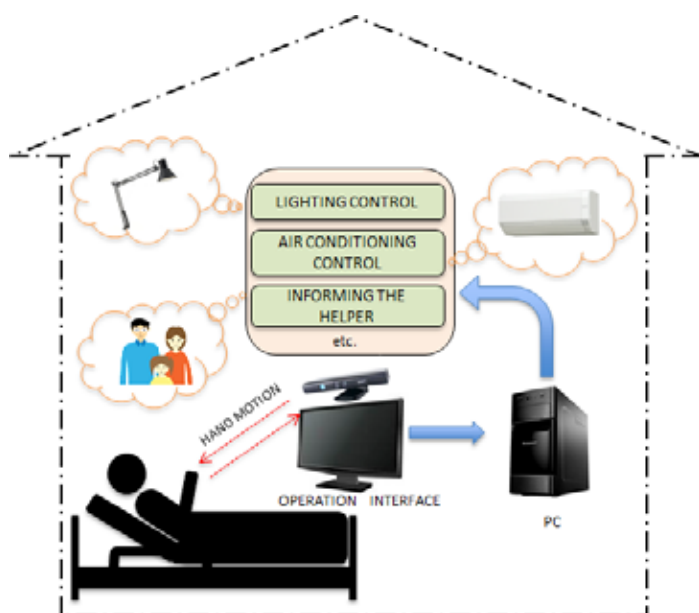


Fig.1 system overview

PS12.011 - Quantitative sensory testing using lateral skin stretch at the foot for simple screening of diabetic neuropathy

Author(s): Shuichi Ino¹, Manabu Chikai¹, Noriyo Takahashi², Tadasuke Ohnishi³, Kouki Doi⁴, Kiyohiko Nunokawa⁵

¹National Institute of Advanced Industrial Science and Technology, Tsukuba/JAPAN, ²Tokuyukai Rehabilitation Clinic, Toyonaka/JAPAN, ³Showa Inan General Hospital, Komagane/JAPAN, ⁴National Institute of Special Needs Education, Yokosuka/JAPAN, ⁵Tokyo International University, Kawagoe/JAPAN

Objective: Changes in food behavior and lifestyle have resulted in a considerable increase in the incidence of diabetes. Many people with diabetes have reduced quality of life because of diabetes-associated complications, which include neuropathy, retinopathy, and nephropathy. About half of the people with diabetes in the world, however, are unaware of their condition. One of the healthcare challenges is how to best implement screening, educational, and treatment programs for the prevention of diabetes. Conventional noninvasive diagnostic techniques for diabetic neuropathy have several problems, including the accuracy of a quantitative estimation, durability, and the time of testing. Therefore, the aim of this study was to develop simple point-of-care equipment to quantify plantar tactile sensibility for early diagnosis and tracking of peripheral neuropathy caused by diabetes.

Methods: We focused on reducing the tactile sensation at the

peripheral regions such as the foot and hand, which is a common symptom in patients with diabetic neuropathy and appears at a relatively early stage of disease. The tactile stimulation of our testing method is adopted for lateral skin stretches, which is more sensitive than perpendicular skin indentations. A new system of quantitative sensory testing for screening of diabetic neuropathy consists of a plantar tactile stimulation platform with a small moving contactor to stretch the skin tangentially, a response switch for each tactile stimulus, a motor control box, and a personal computer for psychophysical data processing. Seven healthy adults (3 women and 4 men; mean \pm SD age, 39.6 ± 8.6 years) and one patient (woman, aged 77 years) in the early stage of diabetes were examined to measure the absolute detection thresholds of the lateral skin stretch on the plantar surface using the system of quantitative sensory testing. The stretch stimulations were applied to five different sites (the first toe, fifth toe, first metatarsal head, fifth metatarsal head, and heel) of the right foot. The skin hardness of the plantar sites was measured using a durometer.

Results: The absolute detection thresholds of the lateral skin stretch at the foot ranged from approximately 10 to 30 μ m for healthy subjects. The thresholds at the fifth toe and first metatarsal head were higher than those at the other plantar sites ($p < 0.01$). The tactile sensitivity of each site mainly improved as the stretch speed increased. Significant difference in threshold value was observed between the healthy adults and the patients with early-stage diabetes ($p < 0.001$). Meanwhile, relatively weak correlations were found between the detection threshold and skin hardness at the foot sole.

Conclusion: The present study demonstrates that the detection threshold (μ m-order resolution) of the lateral skin stretch was highly sensitive in comparison with a two-point discrimination threshold (mm-order resolution) that was well known in sensory testing. The experimental results also suggest that our testing method based on the plantar sensation elicited by a lateral skin stretch may be a simple, noninvasive method for the quantitative screening of diabetic neuropathy.

PS12.012 - A development of the robot hand for the disability which include sensory feedback.

Author(s): Tomohiro Iwaki, Kazushige Magatani
Tokai University, kanagawa-ken/JAPAN

SEMG is an electrical signal associated with the activation of the muscle. Various artificial hands and robot hands which act according to SEMG patterns have been experimentally developed. Most of them can grasp and release an object according to the instruction from generated SEMG. However, most of them cannot feedback grasping power to the operator. Therefore, it is difficult to grasp an object using correct power in most systems. If an operator can feel grasping condition, more accurate operation will be enabled.

So, our objective of this study development of the feedback system which can defects grasping power of the artificial hand or robot hand and feedback this power to the operator as air pressure to the finger. Our developed system consists of two parts. One is the robot hand (the artificial hand) which acts some hand motions according to generated forearm SEMG pattern. The other is the grasping power feedback system which defect grasping power and feedback this condition to the operator.

In the robot hand system, 48 channel forearm SEMG are measured and analyzed. Motion of the robot hand was controlled according to analyzed result. And we also suppose that muscle power is proportional to the amplitude of SEMG. If analyzed result of hand motion is grasping, grasping power is calculated using SEMG amplitude, and grasping power of the robot hand is also controlled using this result.

In our robot hand, pressure sensors are set on the hand surface and

we can measure real grasping power. The grasping power feedback system consists of these pressure sensor, a micro-processor, a syringe and an air pressure display. The piston of a syringe is driven by a stepping motor which is controlled by a micro-processor. A rubber balloon which is connected with output of the syringe displays grasping power to operator's finger by change of air pressure. A block diagram of this system is shown in Fig.1.

The developed grasping feedback system was tested with some normal subjects and characteristics of this system were evaluated. In the experiment, all subject could feel the grasping condition of a robot hand. However, it became clear that there is some time delay in the response of the feedback system. From the experimental results, we think that if these problems are improved, our system will be useful system for the amputee.

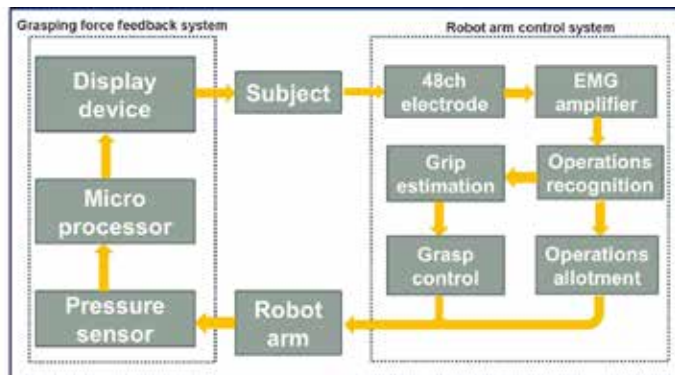


Fig.1 A block diagram of the system

PS12.013 - Motor cortical excitability enhanced by paired-pulse transcranial magnetic stimulation with biphasic pulse-form

Author(s): Petro Julkunen¹, Gustaf Järnefelt², Petri Savolainen², Jarmo Laine², Jari Karhu²

¹Department Of Clinical Neurophysiology, Kuopio University Hospital, Kuopio/FINLAND, ²Nexstim Plc, Helsinki/FINLAND

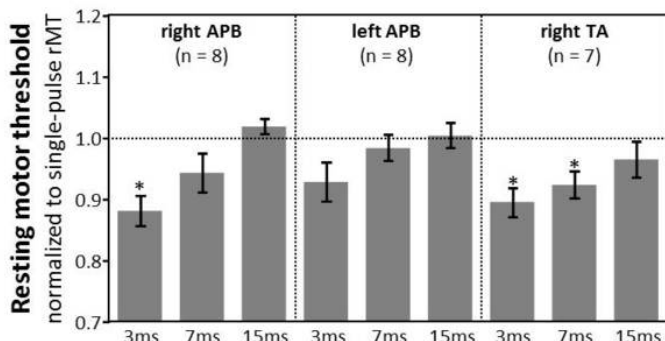
Introduction: Motor threshold is a commonly used measure of corticospinal excitability in transcranial magnetic stimulation (TMS) determined by stimulating the primary motor cortex. Conventionally, the immediate excitability of the motor cortex has been modulated by the use of paired-pulse TMS using monophasic pulses with and inter-stimulus interval (ISI) of 1.5-200ms. Monophasic pulses are more easily produced by the stimulator as compared to biphasic pulses, which instead are more energy-efficient. The problem with the biphasic pulse-form to produce biphasic pulses has been the low recovery-rate of the stimulator. However, provided that this problem can be overcome, it would be possible to produce same excitability modulation with biphasic pulses as with monophasic pulses, but with better energy-efficiency and with lower stimulus intensities, meaning that maximum stimulator output could be greater. This would make the biphasic paired-pulse paradigms better applicable in patients with reduced cortical excitability.

Materials and Methods: Nexstim Plc produced a prototype stimulator for biphasic paired-pulses, effect of which was studied in 8 healthy volunteers. Resting motor thresholds (rMTs) were determined from the subjects using single-pulse paradigm from the right and left hand abductor pollicis brevis muscles, and the right tibialis anterior muscle by targeting neuronavigated TMS to the corresponding targets on the motor cortex, mapped prior to rMT measurement. Then, 20 single-pulse motor evoked potentials (MEPs) were gathered at an intensity of 110% of rMT. Subsequently, rMTs and MEPs were measured using 3 paired-pulse setups (ISI = 3ms, 7ms or 15ms) from all muscles in randomized order. In the paired-pulses, the stimulus

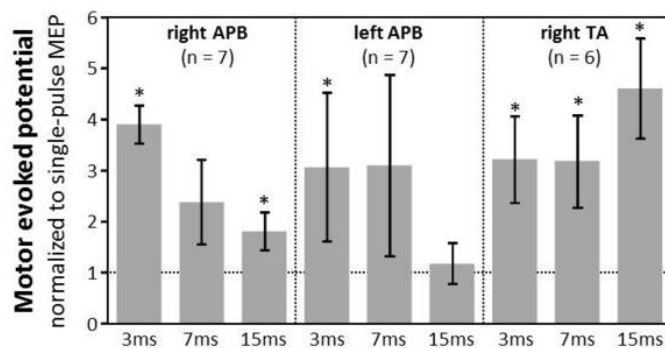
intensity of the second pulse was 80% of the first pulse intensity.

Results and Discussion: We found that the ISI had a significant effect on the rMTs, meaning that rMTs were lower than the corresponding single-pulse rMTs and MEPs with biphasic paired-pulses were also higher than with single-pulses (Figure). The effect was emphasized at 3ms ISI.

Our findings suggest that the application of biphasic paired-pulses is possible and the potential applications are not limited similarly to monophasic pulses. For instance, paired-pulse stimulation with biphasic pulse-form could potentially be applied in repetitive TMS, in order to enhance therapy effects.



A) Inter-stimulus interval



B) Inter-stimulus interval

Figure: A) Normalized resting motor thresholds (mean ± SEM) at different ISIs. B) Normalized motor evoked potentials (mean ± SEM) at different ISIs.

*p<0.05 compared to single-pulse TMS (non-parametric test).

PS12.014 - Quality management systems for medical devices in the production of hospital beds

Author(s): Ivana Jurickova, Vit Prindis

Department Of Biomedical Technology, Czech Technical University in Prague, Faculty of Biomedical Engineering, Kladno/CZECH REPUBLIC

Quality management systems becomes in recent years an integral part of the corporate structure. Almost every successful company at the world has established some kind of quality management system. This study describe the situation in the field of quality management systems used in serial production, especially in health care and in the company Linet spol. s r.o., one of the biggest manufacturers of medical equipment, specializes with manufacturing of hospital beds. Basis of this study are based on the analysis of the current situation in the world, domestic field and in the company itself. Based at the results was found recommendations for the next development of a quality system that ensures the growth of production with high-quality products at Linet spol. s r.o.

PS12.015 - Value of information analysis for use in health technology assessment

Author(s): Ivana Jurickova, Jiri Havlik

Department Of Biomedical Technology, Czech Technical University in Prague, Faculty of Biomedical Engineering, Kladno/CZECH REPUBLIC

Nowadays every decision is, less or more, associated with uncertainty. In everyday life we are intuitively trying to reduce this uncertainty by collecting new information, e.g. reading newspapers or watching TV. In health technology assessment, where we should consider besides health effects also safety, technical parameters, economic impacts etc., we can do it in more sophisticated and specific ways - through the specialized literature, consultation with experts certain decision problems or collection of new evidence in additional research. Theoretically, we can do this over and over until we have enough evidence to confirm our decision. Practically, facing limited resources, mostly financial, we have to find balance between information gathering and our resources and here we can use value of information analysis.

PS12.016 - Development of a Software Tool for Quick Re-entrainment of the Circadian Pacemaker

Author(s): Omid Ranjbar Pouya¹, Ehsan Shams², Zahra Kazem-Moussavi¹

¹Biomedical Engineering, University of Manitoba, Winnipeg/MB/CANADA, ²John Buhler Research Centre, Winnipeg/MB/CANADA

According to the Stat Canada, over a million people per month take trans-oceanic flights from Canada to overseas countries and vice versa .In all of travels exceeding five time zones , the misalignment of circadian phase, known as “jet lag”, can cause health problems for the travelers . Other than frequent travelers , as of 2006 there were approximately 1.5 million Canadians, excluding US residents, living abroad who suffer from jet lag whenever they travel to their motherland. The adverse effects of jet lag impair the judgment of business people and politicians, compromise the performance of athletes, and pose a threat to public safety as it degrades performance and operational readiness of deployed military personnel. However, despite several studies suggesting protocols for designing interventions that facilitate re-entrainment to a shifted sleep-wake schedule, there is yet no standard scheduled light therapy protocol. Furthermore, although light seems to be the main stimulus to the circadian system, but the combined effect of it with other stimulants, such as melatonin pills, has not received enough attention. In this paper, we have distilled a common denominator in the literature for the response of the circadian system to light and melatonin pills and have developed a software tool that can recommend optimal timing for light exposure/avoidance as well as taking melatonin pills to compensate for the loss of alertness. The produced schedule is based on returning the time of minimum body temperature, known as Tmin, into its correct location in the sleep cycle. Contrary to the most of available solutions, our software took into account individual circadian-phase differences by using Horne-Ostberg Morningness/Eveningness Questionnaire (MEQ) to quantify the differences and use them in calculating Tmin. This questionnaire consists of nineteen four-choice questions that can be optionally answered by user. Moreover, in the proposed software the average duration of the light exposure in each day can be estimated by user which affects the amplitude of phase shift. The produce schedule for re-entrainment is developed in both form of graphic output and simple text instructions(not shown here).The figure of the software and its produced schedule is provided below for better illustration:

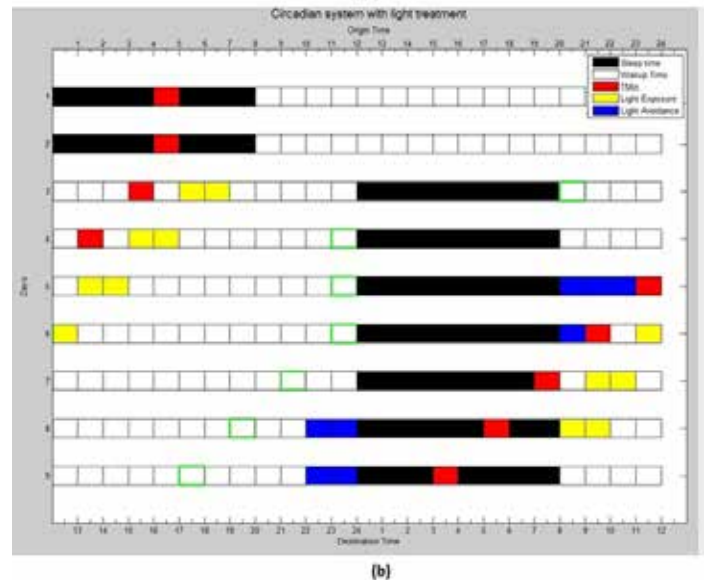


Figure 1: (a).User interface of the software. (b).Sample schedule for a passenger who travels 12 time zones to East . The green boxes show suggested times for taking melatonin pills.

PS12.017 - Which one is better in detecting the speed and quantity of intravenous infusion in the hospital, transmissive or reflective optical method?

Author(s): Hyun-Woo Lee¹, Jaeyeong Park², Jinhan Lee², Hyun Hee Bang², Chul-Woo Park¹, Sanghyun Joung¹, Kwangja Hur³, Kyoung Yong Park⁴, Ilhyung Park⁵

¹Medical Device and Robot Institute of Park, Daegu/KOREA, ²Division Of Biomedical Science, Kyungpook National University, Daegu/KOREA, ³Kyungpook National University Hospital, Daegu/KOREA, ⁴Korea Institute of Industrial Technology, Ansan/KOREA, ⁵Department Of Orthopedic Surgery, Kyungpook National University, Daegu/KOREA

We developed an infusion monitoring system using a reflective optical sensor which can detect the infusion speed and quantity. The system detect infusion drips and calculate the amount of intravenous fluid left. We use both reflective and transmissive optical sensor to detect the infusion drips, and compare the results.

Intravenous (IV) therapy is one of common treatment in the hospital for medication delivery, blood transfusion and chemotherapy. IV therapy primarily employ a drip chamber to prevent air embolism. Based on the individual prescription, the speed of IV infusion should be adjusted by medical staffs. Medical staffs observe the number of drips in the drip chamber and manually adjust the speed using a regulator. Furthermore, regular monitoring is required during IV therapy to prevent malfunction such as embolism, back flow and fluid overload. Thus, medical staffs need to frequently check the IV therapy and the patient’s status. To overcome these inconveniences, a new system

that automatically detects the infusion speed and quantity is required. Several researches to automatically monitor the IV therapy have been conducted using weight measurement, capacitance, or optical methods. The optical method is using a sensor attached to the drip chamber to detect infusion drips and calculate the infusion speed. The optical method can detect abnormal status such as blockage and fluid overflow. Regardless types of solution bags, the optical method is compatible because sensors are attached to the drip chamber. Figure1 (a) shows conventional transmissive method to detect drips in the chamber. Since the detection range of transmissive method varies depending on the angle of the drip chamber and the deviation of the output sensitivity, we suggest reflective method (figure1 (b)).

Two experiments were performed using the infusion set. We compare the performance between the transmissive and the reflective optical sensor. First, the drip detection rate was compared depending on each position angles using both transmissive and reflective methods. Second, the error rate of drip detection of the transmissive and reflective methods was respectively measured under the same condition.

In both experiments, the drip detection rate was significantly improved when using the reflective method. The reflective sensor showed a low error rate of less than 11%, in comparison up to 65% error rate of the transmissive sensor.

In this study, the reflective optical sensor was much more reliable than the conventional transmissive optical sensor.

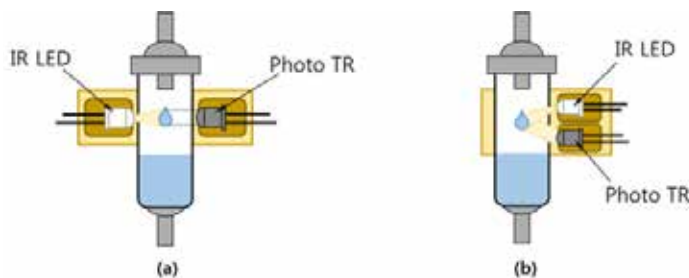


Figure1 Concepts of optical sensors; (a) conventional transmissive method, (b) suggested reflective method

PS12.018 - The effect of stented valve oversizing on hemodynamic flow in the diseased right atrium

Author(s): Munirah Ismail¹, Foad Kabinejadian², Hwa Liang Leo³, Karthik Kannan¹

¹Biomedical Engineering, National University of Singapore, Singapore/SINGAPORE, ²Department Of Surgery, National University of Singapore, Singapore/SINGAPORE, ³Department Of Biomedical Engineering, National University of Singapore, Singapore/SINGAPORE

Tricuspid regurgitation (TR) occurs in many individuals and is usually considered mild but severe TR is life-threatening. Even so, many patients with severe TR are denied of the replacement valve surgery because their old age or co-morbidities put them at high risk for conventional open heart surgery. With the advent of transcatheter technology, it is now possible to deliver the valve to the desired location without the need for open heart surgery. However, so far, there has been no commercially available transcatheter tricuspid valve. This may be because of the complex tricuspid valve anatomy and lack of an anchorage zone. Thus, the next best anchorage zone is the vena cava. Placing the valves in the superior and inferior vena cava will prevent the back flow of blood into the venous structures and possibly reverse peripheral edema and ascites which are caused by the elevated venous pressure. The hemodynamic characteristics of these valves are tested in a mock circulatory system

(MCS) which emulates the physiological pressure and flow conditions in the cardiovascular system. The sizes of the valves implanted onto the vena cava also affect the flow. In this study, we analysed how valves of different sizes affected the flow patterns as well as the magnitude of the velocity. Particle image velocimetry is used to study the flow characteristics in the MCS.

PS12.019 - Device trial to improve blood flow rate with controlled pressure for blood flow at venous side in single needle dialysis

Author(s): Yasuyuki Miwa, Kawabe Manabu, Takashi Kano, Yoshihisa Yamashita
School Of Biomedical Engineering, Faculty Of Health And Medical Care, Saitama Medical University, hidaka,saitama/JAPAN

Single needle dialysis can be performed using only one needle. However, because blood is both removed and returned with only one needle, the dialysis effect is less than when two needles are used. If the blood return time can be reduced when using controlled pressure for blood flow at venous side in the single needle method, improved blood flow rate and dialysis rate can be expected over time. In conventional single needle dialysis, air is compressed in a vein air capture chamber. Therefore, it isn't possible to actively control the return time. In the present study, we used air pistons run by solenoid in an attempt to reduce return time and to safely improve the efficiency of single needle dialysis. To design and test a device to improve blood flow rate in single needle dialysis and to compare the device with previous methods. The conventional method uses the force of compressed air within the air capture chamber to return blood. This method reduces pressure in the second half of blood return, which further reduces the amount of blood returned. The present device prevents the reduction in pressure using the solenoid. The blood in the vein air capture chamber is constantly pressured by the solenoid. This makes it possible to prevent a reduction in the sent blood flow rate. Results, the present device, when compared with conventional methods, significantly increases blood flow rate. The present device, although simple, can reduce blood return time and increase blood flow rate. Indicate that this device can be anticipated to improve dialysis efficiency.

PS12.020 - An Embedded Software Solution for Rest ECG Devices

Author(s): Gisela Montes De Oca, Maite Cañizares, René González-Fernández
ICID-Digital Medical Technologies, Havana/CUBA

This paper discusses the design and implementation of a software solution to be used in the development of digital electrocardiographs. These electrocardiographs acquire simultaneously the standard 12-lead electrocardiogram, display the waveforms (ECG) on a high-resolution graphic display and print the ECG with several formats. The software also performs measurements and diagnostic interpretation. ECGs and their associated information are stored on a database. The information can be transmitted to any informatics systems like HIS and expert consulting opinion systems which help physician on actions to take with the patient being treated. Software solutions were developed by using the Integrated Development Environment (IDE) Qt Creator and the cross-platform Qt library. The design and programming process employed object programming techniques developing classes to encapsulate all the functions used by the system. The hardware solution used the processing board CID 300-9, based on the S3C2440 microprocessor with ARM9 architecture and Linux operating system.. The technical parameters of the equipment and software were assessed according to the requirements of the IEC 60601-2-25 standard, with satisfactory results.

PS12.021 - Development of innovative gas phase sterilization technology for nucleolytic degradation**Author(s):** Toshihiko Okazaki¹, Yasushi Suzuki²¹Aro Advanced Medical Center, Kyushu University Hospital, Fukuoka city/JAPAN, ²Sealive, Niihama-city/JAPAN

With the worldwide major trends of next generation medical technology development, such as regenerative medicine and gene therapy, it is getting urgent need to establish and improve advanced aseptic (germ and virus-free) manufacturing environments of fabrication plant for quality assurance of the products. But there still remain critical problems with conventional sterilization method due to its limited spectrum, environmental pollution, health impairment and such, especially at present, there is no available decisive decomposition method for nucleic acid.

Recently we have developed innovative technology as the catalytic reaction type mixed gas generating system using methanol as a raw material, (Biovector, pat.no.5463378), and its remarkable efficacy of sterilization effect, as well as nucleic acid decomposition will be reported.

The Biovector system consists of a mixed biogas generator, a small experimental chamber and a scrub exhaust device for detoxification equipped with catalyst detoxification apparatus. The system enables to make continuous monitoring of inside temperature and humidity as well as the hydrogen concentration and other biogas elements.

We investigated sterilization effect of Biovector by biological indicators (BI) of both *Bacillus. atropheus* and *Geobacillus. stearothermophilus* (RAVEN Co.), and determination was evaluated according to Food and Drug Administration Guidance for Industry and Japanese Pharmacopoeia sterility testing. For evaluation of nucleolytic degradation efficacy of Biovector, DNA samples were purified from HeLa cell lines, and fragmented DNA was analyzed by real time PCR method and Bioanalyzer (Agilent Technologies) system for sizing and quantitation.

By the Biovector gas exposure for 5 minutes at 50 °C, the complete eradication effect was observed in all of BI applied in the amount from 106 to 108, which resulted in achievement of sterile assurance level (SAL) of 10⁻⁶. Also in the evaluation of nucleolytic degradation ability, the complete degradation effect of DNA into 10 or less base pairs was elucidated by the time of exposure for 15 minutes at 37°C of Biovector gas under the condition of both moist and dry of up to 10ug of DNA. It also revealed the ability of Biovector are temperature dependent (50>45>37°C).

Taken together, in this study, newly developed Biovector gaseous sterilization system revealed its remarkable sterility and nucleolytic degradation ability, which could not be attained in the conventional method so far. Biovector will be highly useful for improving aseptic environment and public health preventing pandemic risk for pathogenic organisms, moreover the future clinical applications such as endoscopic sterilization equipment and automated cell processing system.

PS12.022 - Ultrasound Modular Platform: a general purpose open architecture system for medical imaging research**Author(s):** Haroldo J. Onisto¹, Santiago Rodriguez¹, Glauber E. Sapia¹, Rodrigo G. Borges¹, Iliezer Tamagno¹, Eduardo T. Costa², José E. Bertuzzo¹¹Eldorado Research Institute, Campinas/BRAZIL, ²Biomedical Engineering Department, University of Campinas, Campinas/BRAZIL

Introduction: A demand signaled by the Brazilian Ministry of Health has led to the development of an Ultrasound Modular Platform which aims to medical imaging research. It was conducted in a partnership between top Brazilian universities, led by the University of Campinas jointly with Eldorado Research Institute, a top Brazilian center in IT and innovation engineering. In this paper we present the achievements and experiences gained in this recent development.

Methodology: Our platform is a real-time processing machine, designed with robust, versatile and flexible hardware architecture of 64 physically independent channels, expandable to 128. It is based on analog front-end circuits for the excitation of transducers in transmission mode and initial signal conditioning of received echoes. The core signal processing is left to reprogrammable integrated circuits, Digital Signal Processor (DSP) and Field-Programmable Gate Arrays (FPGAs), composing the digital back-end system.

The architecture consists of two identical 32-channel analog transmission boards and one 64-channel analog reception board along with four digital boards based on Virtex-6 FPGA. The digital boards are arranged so that one of them controls the two beamforming transmission boards and the reception board. An extra board is used to connect the DSP. The backplane integrates connectors for two probes and delivers signals from the power supply to the entire complex. A Personal Computer (PC) accounts for user interface, medical applications and image display.

The firmware architecture was designed to work as a mechanism of a data-flow machine. Thus, to develop algorithms for beamforming in addition to image and signal processing, we adopted the Model-driven Engineering approach using MATLAB to initially model their blocks and then to automatically generate Verilog/VHDL and C/C++ codes. This allowed rapid proofs of concept and reduced project costs.

The equipment works by setting a protocol (e.g. cardiac exam) using proper PC-based user interface, initializing medical application software. The protocol generates a service request to the hardware control, a role played by DSP. The DSP acts as a manager, first receiving settings from the PC and determining the beamforming parameters that is sent to the FPGAs. After receiving the pre-processed signals from FPGAs, the DSP performs image processing and delivers them back to the PC to be displayed on the screen.

At this stage, the developed system is able to generate B-mode and M-mode ultrasound imaging, with a module for Doppler imaging (Color and Power Doppler). The system accepts ECG signals for proper coupling to cardiac applications. Although being able to work in faster modes, it was decided to run the platform achieving at least 30 frames per second. The several university groups working on the platform are developing special modules as add on applications such as elastography, coded excitation, breast cancer detection and others.

Conclusion: Preliminary results have shown that the developed platform can be employed as a useful and low cost medical ultrasound system with great potential to test and innovate on medical (and non-medical) ultrasound imaging techniques.

PS12.023 - Design and Preliminary Validation of a Dual Mechanical-Anthropomorphic Breast Phantom with Inclusions**Author(s):** James Antaki, Molly Blank, Shigeto Ono
Biomedical Engineering, Carnegie Mellon University, Pittsburgh/
UNITED STATES OF AMERICA

Tissue phantoms can be categorized into two broad categories: anthropomorphic phantoms used for imaging calibration of structures, and mechanical or optical phantoms for validating tissue characteristics such as stiffness or acoustic attenuation. Both structural and mechanical features of lesions are useful in a complete clinical diagnosis of breast cancer, yet no phantom exists that can accurately depict anatomy and elasticity. Recent developments in ultrasound elastography have increased the need for more mechanically realistic phantom models since the pathology of a breast mass often correlates with mechanical stiffness. This work describes design and preliminary validation of representative benign and malignant masses in a dual structural and mechanical breast phantom.

Polyvinyl alcohol (PVA) cryogels are widely accepted as an accurate mechanical tissue analog and will be used to simulate both the bulk fatty, fibroglandular tissues of the breast and pathological inclusions. PVA cryogels exhibit wide ranges of elasticity and are tunable based on different preparation methods; predominantly varying the number of freeze-thaw cycles and concentration of PVA in the cryogel solution. Dynamic mechanical compression testing is conducted to validate the protocol to achieve elastic modulus values from literature comparable to that of fibroadenoma and invasive lobular carcinoma. The representative benign fibroadenoma is characterized by well-defined boundaries, and the malignant invasive lobular carcinoma has a speculated shape integrated into the surrounding tissues. The key contribution of this design is the shape of both the benign and malignant pathologies; derived from physician-annotated patient MRI images. A 3D mesh of the inclusions are exported into Solidworks and 3D printed into a thermoplastic polyester mold. Unlike existing phantoms, the breast phantom described combines anthropomorphic and mechanically validated inclusions to facilitate the development of diagnostic imaging devices and techniques.

PS12.024 - Evaluation and Analysis of the Results of a prototype Medical Device Vigilance System (MEDEVIPAS)

Author(s): Kalliroi Stavrianou¹, Zhivko Bliznakov¹, Athanasios Anastasiou², Nicolas Pallikarakis¹

¹Biomedical Engineering Unit, University of Patras, Rio-Patras/GREECE, ²School Of Electrical & Computer Eng., National Technical University of Athens, ATHENS/GREECE

Biomedical Technology has contributed decisively to the impressive progress of modern healthcare over the last half century and at the same time medical devices play a vital role in the delivery of high quality healthcare. Although recent technological advancements have led to much more reliable and safer Medical Devices (MDs) unfortunately the potential risk of failure on medical devices and the associated adverse incidents cannot be neglected. In fact, adverse incidents, due to MDs, have recently increased in absolute terms, because of the exponential increase in the number of devices used nowadays. Therefore, MD recalls by manufacturers contribute to the safe function of the devices, in order to avoid incidents that could lead to injuries and deaths.

In terms of technology, in order to create a safer environment, providing rapid and accurate information on adverse events, is necessary to avoid their repetition. The traditional approach of MD Vigilance based only on official user reports of adverse incidents has been proven inadequate today. A modern approach to the problem is based on the introduction of additional means, such as data mining, extraction, standardization and codification of the information, from different direct and indirect sources worldwide, and its systematic classification and archiving in dedicated databases. The aim is to timely extract the information on potentially hazardous MDs and make it available where appropriate.

Process evaluation involves collecting and analyzing information about a program's activities, characteristics, and outcomes and consequently yields the information needed to make adjustments to strategy implementation in order to strengthen effectiveness. Particularly, the system evaluation process performed included both data verification/validation and software evaluation. In some cases, the results were cross-checked using specific multiple approaches, assets and different dedicated techniques. The procedure for data processing included the determination, transformation, modelling and codification of the data in order to highlight relevant information, as well as to support decision making and conclusions.

To demonstrate and objectively assess the quality and usability of the design, questionnaire of the vigilance system has been created and filled-in by users and reviewers. Moreover an analysis of the

databases has been conducted aiming to provide a comprehensive interpretation of the results of this investigation. Additionally, various methods and techniques have been used to identify specific characteristics of the MDs failures and, based on that, forecast trends in areas requiring special attention were investigated. In conclusion, it has been demonstrated that MEDEVIPAS System could be a very effective tool for world-wide use advancing MD vigilance.

Acknowledgment: *This research has been co-financed by the European Union (European Social Fund – ESF) and Greek national funds through the Operational Program “Education and Lifelong Learning” of the National Strategic Reference Framework (NSRF) - Research Funding Program: Thalis. Investing in knowledge society through the European Social Fund.*

PS12.025 - Medical Device Development - Risk Management

Author(s): Mayur Patel, Mark Humphries

Cambridge Technology Centre, PA Consulting Group, Melbourn/UNITED KINGDOM

Risk Management is critical, and challenging to implement pragmatically during early phase development.

Pragmatic, compliant Risk Management currently challenges many medical device manufacturers in hospitals and start-up companies. The harmonized risk management of medical devices standard, ISO 14971:2012, gives presumption to conformity to some aspects of the Medical Devices Directive (MDD) along with other harmonized standards. ISO 14971:2012 is a process standard that establishes the requirements for risk management to determine the safety of a medical device. The challenge for developers is to determine how best to implement the standards during the ‘proof-of-concept’ as at this point of development it is not clear if the device is feasible in terms of technology and market-need.

A further challenge is to consider how to maximize investments in prototypes when the appropriate risk management approach has not been followed from the start.

I have come across many sophisticated prototype medical devices requiring regulatory approvals in hospitals and industry. Challenges arise when a prototype device is further developed and is to be approved in the absence of Risk Management documents relevant to the initial stages. Whilst undesirable, if the safety and efficacy of the device can be assured then a carefully structured and planned retrospective risk management file may be accepted for ISO 14971:2012 submission. The approach will still involve following all processes described in the standard but in a different perspective. It will require a carefully prepared risk management plan to address the risks that were not addressed in the prototype development stage.

Putting in place the right risk management processes and tools, is important for your development, and knowing how to use them correctly is critical.

The gap analysis above may be based around FTA, FMEA or FMECA depending on the status of prototype development. The scoring in the analysis plays an important role in identifying risks within the system. Many manufacturers are uncertain as to how best to construct their risk matrix tables – what is an acceptable risk? Whether to use qualitative or quantitative scoring for probability scores? Whether to use ‘detectability’ or ‘P1-and-P2’ scoring? [Here, the probability score P1 is a likelihood of failure occurring and P2 is likelihood of this failure resulting in harm] Such decisions are important as they have significant impacts on safety and compliance with the standard. To clarify the differences, consider a motor analogy - if a car braking system fails and the car is designed to detect the failure, then the ‘detectability’ score is high which would reduce the overall risk score significantly (but would not necessarily

reduce the potential for harm). If P2 score is used for the failure then the score will not reduce until the car system is designed to not only detect but also prevent harm.

Even after deciding the scoring mechanism, the next challenge is how to score the severity of the failure. Where should we set the score in the analysis – is it correct to use the worst case or the most likely?

PS12.026 - Analysis of the terminology to name medical devices used in Intensive Care Units - ICUs

Author(s): Pamela T. Ribeiro¹, José A. Ferreira Filho², Mariangela Araujo¹

¹Human Factors Laboratory Federal University of Itajuba, Itajuba/BRAZIL, ²Institute Of Systems Engineering And Information Technology, Federal University of Itajubá, Itajubá/BRAZIL

The purpose of the proposed study is to analyze the terminology of medical products used in Intensive Care Units - ICUs in Brazil, focusing on their morphological and semantic aspects. The research aims to understand the terminology used on this particular branch of medicine, with emphasis on the following specific objectives:

- a. Raising the names of medical products used in ICUs with the help of experts in the field;
- b. Searching variants of the selected terms;
- c. Observing the existence of synonyms and the coordination relations between terms;
- d. Describing the morphological and semantic behavior of the terms found.

For this research, it was first studied the theories regarding terminology, lexicography and word formation. After this step, we started collecting the terms relating to medical products used in ICUs in documents issued by the governmental regulator agency - ANVISA. Through documents called “Resolutions of the Board of Directors – RDC”, ANVISA adopts procedures and determines behaviors for all groups and institutions involved with the issue at hand. In the case of this study, we used as a reference specifically the Resolution of the Board of Directors RDC number 7, of 24 February 2010, which details the minimum requirements for Intensive Care Units operation. In a meeting with specialists, we concluded that we would use as corpora for this research the manuals of equipment manufacturers, since it is through them that the first contact between medical technologies and users is established.

The analysis of the manuals was made through Terminus, a software developed by the IULATERM Group, Institut Universitari of Applied Linguistics at Universitat Pompeu Fabra – Barcelona – ES. After validation of the terms that referred to medical devices by the specialists, were selected five of the 34 terms that name the medical products for a preliminary study.

From the analysis of selected terms and all its variants, we proposed conceptual relationships based on examples from the manual and, we notice complex relationships between the terms and an expressive number of syntagmatic formations.

PS12.027 - Determination of Breath Acetone in 298 Type 2 Diabetic Patients using a Ringdown Breath Acetone Analyzer

Author(s): Meixiu Sun, Zhuying Chen, Xiaomeng Zhao, Zhennan Wang, Yuan Yuan, Chenyu Jiang, Yingxin Li, Chuji Wang
Institute Of Biomedical Engineering, Chinese Academy of Medical Sciences, Tianjin/CHINA

Breath analysis is a promising new technique for noninvasive disease diagnosis and metabolic status monitoring by testing exhaled breath components. The detection of exhaled nitric oxide has been used as a tool in support of asthma diagnosis for some years. Breath acetone has long been known as a biomarker for diabetes. However the results from published data by far have been inconclusive regarding whether breath acetone is a reliable index of diabetic control. Huge variations exist among the results of different studies because there has been no “best-practice method” for breath-acetone measurements as a result of technical problems of sampling and analysis. Over 90 % of diabetic patients have Type 2 diabetes (T2D). In this work, a near-real-time on-line breath-acetone analyzer based on cavity ringdown spectroscopy was developed and used for breath-acetone measurement of 298 T2D subjects and 42 healthy subjects, one of the largest numbers of T2D subjects ever used in a single study. Four breath samples were taken from each subject under each of four different conditions: fasting, 2 h post-breakfast, 2 h post-lunch, and 2 h post-dinner. Simultaneous blood glucose (BG) levels were also measured using a standard diabetic-management blood-glucose meter. For the 298 T2D subjects, their exhaled breath acetone concentrations ranged from 0.1 to 19.8 ppm; four different ranges of breath acetone concentration, 0.1–19.8, 0.1–7.1, 0.1–10.9, and 0.1–10.6 ppm, were obtained for the subjects under the four different conditions, respectively. For the 42 healthy subjects, their breath acetone concentration ranged from 0.1 to 2.6 ppm; four different ranges of breath acetone concentration, 0.3–2.6, 0.1–2.6, 0.1–1.7, and 0.3–1.6 ppm, were obtained for the four different conditions. The mean breath acetone concentration of the 298 T2D subjects was determined to be 1.5 ± 1.3 ppm, which was 1.5 times that of 1.0 ± 0.6 ppm for the 42 healthy subjects. No correlation was found between the breath acetone concentration and the blood glucose level of the T2D subjects and the healthy volunteers. This study using a relatively large number of subjects provides new data regarding breath acetone in diabetes (Type 1 diabetes and T2D) and suggests that an elevated mean breath acetone concentration exists in T2D. However it arguably still too early to draw a general conclusion on the use of breath acetone as a reliable substitute of BG for diabetes diagnostics and screening on the basis of the currently limited data. The relationships between breath acetone level and BG level and other bioinformatic variables need to be further investigated with a large number of subjects (e.g. thousands) by use of a high-data-throughput real-time online analytical technique.

PS12.028 - A study of the differences between uncompressed sound source and compressed sound source gives EEG of human

Author(s): Takashi Suzuki¹, Kazushige Magatani²

¹Tokai University, Yokohama/JAPAN, ²Tokai University, Kanagawa-ken/JAPAN

In recent years, the way of sell music has changed CD into digital distribution. Mp3 is the representative of compressed sound source in online music distribution service.

Mp3 formatted sound quality is inferior as compared with CD-DA formatted sound quality, because mp3 has less information as compared to pre-compressed data. The objective of this study is by analyzing EEG to determine if people can recognize such difference as differences in sound.

In the experiment, one subject (Healthy adult, Male, Age: 22 years

old) were studied. A 16 channel EEG amplifier which is developed in our laboratory is used in the experiment. To play sound sources, we used SE-200PCI which is a sound card for PC manufactured by Onkyo Corporation, and SRS-2050A which is a headphone manufactured by STAX Ltd. "Waltz for Debby" by Bill Evans was used as music source in the experiment.

Four sound sources (LPCM, MP3 64kbps and 128kbps and 256kbps) were played sequentially. After the subject listened to each sound source for 60 seconds, sampling of EEG was carried out for 20.48seconds. (Sampling frequency: 1 kHz, Quantization bit rate: 16) We repeated this process 5 times.

Sampling data were added 5 times synchronously. Then obtained data were applied Fourier transformation.

Fig.1 and Fig.2 shows one of the results of experiments. Differences between LPCM and MP3 graphs were confirmable in Cz, F3, F4, T3, T4. In LPCM graphs, power spectral periodically increased and decreased at delta wave (0.5Hz~4Hz), otherwise, in MP3 graphs, power spectral periodically inhomogeneous increased and decreased at delta wave.

The results suggest that sound source format differences affected EEG that is come of higher cognitive function than auditory area, because differenced area were not exclusive to T3 and T4

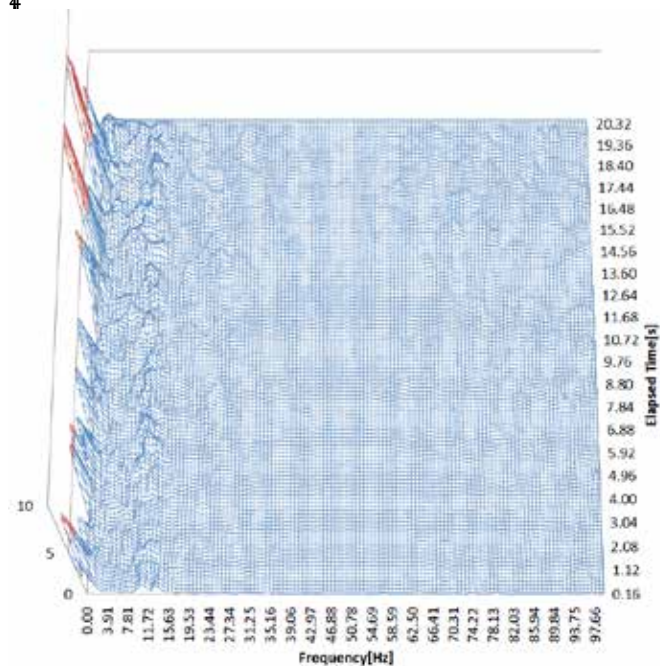


Fig.1. EEG(F4, MP3 64kbps)

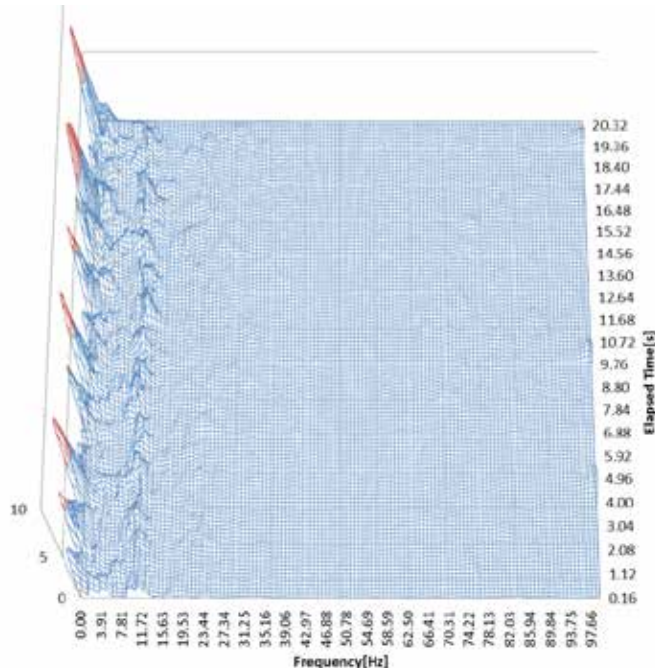


Fig.2. EEG(F4, LPCM)

PS12.029 - Evaluation of the interface pressure characteristics over a temperature regulating air-mattress under different surgical positions

Author(s): Eric Tam¹, Jieling Liu¹, Cindy Yip², Yu F. Chow²
¹Interdisciplinary Division Of Biomedical Engineering, The Hong Kong Polytechnic University, Hong Kong/CHINA, ²Department Of Anaesthesiology & Ot Services, Queen Elizabeth Hospital, Hong Kong/CHINA

Introduction

Intraoperative acquired pressure ulcers (IAPU) are deep tissue injury resulted from prolonged tissue compression during anesthesia. There exists clinical evidence showing that the onset of IAPU was associated with hypothermia during surgery. To maintain body core temperature, warm blankets are commonly used on the operating table. Recently, a temperature regulating air-mattress (Warmcloud, KanMed, Sweden) was introduced as an efficient patient warming system with pressure ulcer prevention. However, there are few scientific reports about the effectiveness of using Warmcloud to reduce the interfacial pressure generated during different surgical positions.

Methodology

Ten healthy volunteers (5 males, 5 females, average age 23, BMI: 22.3±5) participated in this study. Four surgical positions: supine, lateral, prone and lithotomy were evaluated at various inflation pressures of the Warmcloud system. Interface pressure was measured using a capacitive sensor mattress device (Xsensor, Canada). During the experiment, the temperature setting of the Warmcloud was set to 36°C. The average pressure, contact area, percentage of area below 33mmHg and peak pressure over bony prominences and other anatomical locations at risk of pressure ulcers were recorded. Comparisons of interfacial pressures were made between use and without use of the Warmcloud mattress on the operating table.

Results

Comparing to the operating table, contact area over the body-support interface with Warmcloud is significantly larger (p<0.05), varied

between 7 to 87% in the 4 surgical positions. The area of contact that experienced below capillary closing pressure also increased significantly (between 6-15%) when Warmcloud is in use. In terms of average pressure over the entire support surface, Warmcloud only provided significant pressure reduction during supine lying. For peak pressure loadings, different anatomical sites are involved. For supine, peak pressure was found at the scapula and the heels. Compared with lying on the operating table, use of Warmcloud significantly reduced the peak pressure by 53% and 70% at the sacrum and the heels respectively. In lateral position, while the majority (n=8) had reduction of peak pressure underneath the axilla, two subjects experienced pressure increase during the use of Warmcloud. In lithotomy position, Warmcloud significantly reduced the peak pressure at the sacrum. For prone position, peak pressure at the anterior iliac spines, chest and knees varied between use and without use of Warmcloud. Furthermore, our data also showed that the recommended pressure for inflating the Warmcloud mattress may not give the best pressure reduction outcome.

Discussion

This study revealed that the Warmcloud mattress can significantly reduce the average and peak interface pressure during supine and lithotomy positions. In lateral posture, we found that gel pad used underneath the axilla may introduce unwanted high pressure loadings at the interface which could be detrimental. For prone position, as chest pad is usually used during surgery, usage of Warmcloud may not be effective. Furthermore, we also found that the recommended inflation pressure for the Warmcloud system based on patient's BMI may not give the best pressure relief characteristics. For best protection to patients, pressure measurement of the body support interface on the operating table needs to be carefully considered.

PS12.030 - Continuous cuff-less estimation of systolic blood pressure from pulse wave transit time measured in a chair

Author(s): Toshiyo Tamura¹, Zunyi Tang¹, Masaki Sekine¹, Masaki Yoshida¹, Wenxi Chen²

¹Biomedical Engineering, Osaka Electro-Communication University, Neyagawa/JAPAN, ²Aizu University, Aizu-Wakamatsu/JAPAN

Introduction: To control blood pressure, especially hypertension, long-term monitoring of blood pressure at home can be effective and reliable compared with regular monitoring in a physician's office. This requires the development of more convenient blood pressure monitors to replace cuff-type sphygmomanometers. In this work, we propose a new method of non-invasive continuous cuff-less estimation of systolic blood pressure (BP) at home from pulse transit time.

Principle:

The cuff-less BP monitor estimates the BP by pulse wave transit time (PWTT). Generally, if BP is higher, the PWTT is faster. The PWTT is obtained from the R wave of the ECG and the peak of the first derivative of the PPG signal. Although the blood flow and PWTT depend not only on BP but also stiffness and tonus, PWTT is primarily related to BP.

Systolic blood pressure is estimated with the following equation¹⁾

$$P_e = P_b - 2 / (\gamma T_b) \cdot \Delta T$$

where P_b is the based blood pressure level, T_b is the PWTT corresponding to the pressure, ΔT is the change in PWTT, and γ is the peripheral resistance.

Method: The cuff-less BP monitor consists of three fabric electrodes

attached on both arms of a chair: a plus electrode for ECG installed on one side and a minus electrode and grand electrode for ECG are installed on the other arm. A PPG sensor is also installed on one arm. From ECG and PPG signals, we estimated BP. Seven healthy subjects aged 20-65 years participated in the experiments. Subjects sat in the armed chair and touched the electrodes and PPG sensor. Subjects also attached a continuous blood pressure monitor (Finometer; Finapres Medical Systems Corp.).

To evaluate the method, the continuous blood pressure monitor was used as a reference. The simultaneous recordings of the continuous blood pressure and the cuff-less BP monitor were monitored. The deviations and RMSE of the errors were calculated.

Results: Preliminary experiments showed that the errors in most results were under 10% compared with the reference. The deviations and RMSE of most results were not above 10 and the error ratios of most results were also below 10%.

Discussion: We attempted to estimate systolic BP from PWTT. The results were promising. We are satisfied with the current evaluation stage but more precise monitoring is needed to replace cuff-type sphygmomanometers and for predicting diseases related to high BP.

References

Chen W, et al., 'Continuous estimation of systolic blood pressure using the pulse arrival time and intermittent calibration', *Med. Biol. Eng. Comput.*, vol. 38, no. 5, pp. 569-574, 2000.

PS12.031 - A development of the pressure distribution display which is used in robot hand for the disability

Author(s): Kenya Tanaka¹, Kazusige Magatani²

¹University, hiratakashi kanagawa/JAPAN, ²TOKAI University, hiratakashi kanagawa/JAPAN

We are now investigating about a robot hand control system for the amputee which is controlled by SEMG. From previous studies, it became clear that a robot hand can be controlled by SEMG which is measured from a forearm. And we also developed the robot hand control system which could measure grasping power and feedback this power to an operator. In this system, a pressure sensor for one point was used for feedback system. For this reason, our previous system could not feedback the pressure distribution on the hand surface to the operator. It is thought that if the pressure distribution of the grasping object is known, the operator will be able to know the detail of the object. So, our objective of his study is a development of the sensor which can measure pressures of multi-point.

The pressure-sensitive conductive rubber is used in order to construct a multi-point pressure sensor. In this rubber, conductive material is uniformly spread. Thus, the resistance value of this rubber changes according to the stress that is given to the rubber. A construction of the sensor is shown in Fig.1 In our developed sensor, 25mm square pressure-sensitive conductive rubber sheet was used as a sensing material. As shown in this figure, 4 conductive lines are set on each row and column. And the rubber sheet is set between these lines. This sensor can sense pressure each 16 lattice points as conductive value. In our sensor, the sensing point is changed by analog switch driven a microprocessor.

A developed sensor was set on a robot hand and tested using aluminum object. Grasping power of the robot was set from 0.8 to 3.3 kg, and the response of a developed sensor was measured. From the experiment, following results become clear. 1) The sensitivity of all sensors are almost equal. 2) There are small crosstalk at each sensing point. However, these crosstalk of each point are almost equal. From these experimental results, we have

concluded that our developed sensor will be useful for the multiple sensing of the distributed pressure.

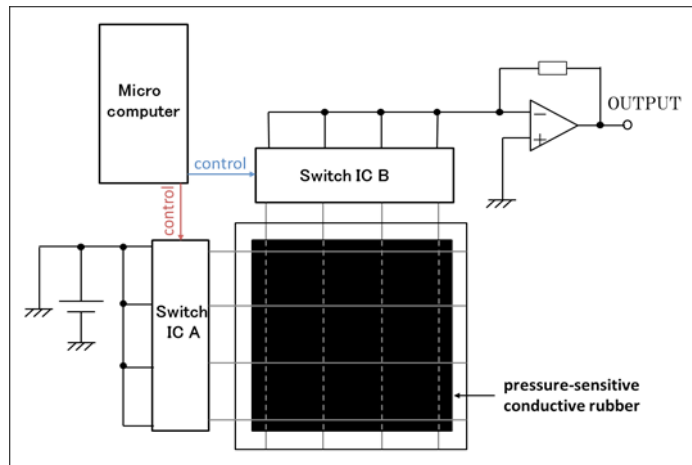


Fig1. construction of sensor

PS12.032 - Prototype Development Generating Vacuum for Treating Chronic Wounds Negative Pressure Level Laboratory

Author(s): Edison Vazquez-Gordillo¹, Gerardo S. Romo-Cardenas¹, Alejandra Guillen-Peralta², Raul De La Rocha-Encizo¹
¹School Of Engineering, Montemorelos University, Montemorelos/MEXICO, ²School Of Health Sciences, Montemorelos University, Montemorelos/MEXICO

At present time, the medical care is being referred not only to treatment of a diagnosis disease itself, but also their complications and variations that could become chronic and therefore more devastating. With the known increase in overall life expectancy, we know that we are facing a whole different types of diseases. A case of these chronic wounds; which is a condition that has generated a very high cost both in financial perspective, and the health complications that such diseases generate. Negative pressure therapy is a procedure that has caught the attention of health professionals due to its effectiveness. But for many of them still remains unknown the biochemical process behind this therapy. On the other hand, is a process becomes costing up to \$ 40,000. As only a small percentage of the population or health systems that could afford to use a system of this type in order to treat a condition of chronic wound. For this project a methodology that involves the development of a negative pressure prototype for chronic wounds is proposed. The scope of this paper is to analyze the variables involved in the negative pressure system in order to generate models of fluids and colloids for the study of the variables that are in the process of healing of chronic wounds. This with the intention of support research and development in the area of devices negative pressure therapy inexpensive that could expand the range of use and users.

PS12.033 - Tunable Irradiation System for Corneal Collagen Cross-linking

Author(s): Victor A.C. Lincoln¹, Sidney J. Faria E Sousa², Liliene Ventura³

¹Electrical Engineering, Universidade de Sao Paulo, Sao Carlos/SP/BRAZIL, ²Ophthalmology - Fmrp, Universidade de Sao Paulo, Ribeirão Preto SP/BRAZIL, ³Electrical Engineering - Eesc, Universidade de Sao Paulo, Sao Carlos SP/BRAZIL

An optical arrangement has been set up for spectroscopically measure the transmittance of UVA light through 10 human preserved corneas of over 400 μ m thickness during the corneal collagen cross-linking procedure under the current procedure protocol for

early stage keratoconus treatment. To enhance absorption of UV radiation, Riboflavin solution (0.1% and 400 mOsm) was applied prior to and during exposure. The UVA beam - 365nm \pm 5nm at 3mW/cm² \pm 0.003mW/cm² - was focused directly onto the corneal stroma. To enhance absorption of UV radiation, Riboflavin solution (0.1% and 400 mOsm) was applied prior to and during exposure. To enhance absorption of UV radiation, Riboflavin solution (0.1% and 400 mOsm) was applied prior to and during exposure. The UVA beam - 365nm \pm 5nm at 3mW/cm² \pm 0.003mW/cm² - was focused directly onto the corneal stroma. Our studies on the UVA transmittance of the cornea during the cornea collagen cross-linking have shown that without Riboflavin, there is a 61.6% transmittance of UVA light toward the endothelium and at the very end of the treatment it decays to 12.6%. However, the transmittance differs in each of the stage of the treatment. In our experiments, the average transmittance in terms of energy during the 30 minutes irradiation procedure fluctuated from 0.67 to 0.38mW/cm².(figure 1). These results indicate different levels of UV transmittance during treatment and lead to the development of new technologies and consequently new protocol considering using tunable UVA irradiation system and delivering different doses at each stage of the treatment, therefore to minimize irradiation time, reducing treatment time consumption

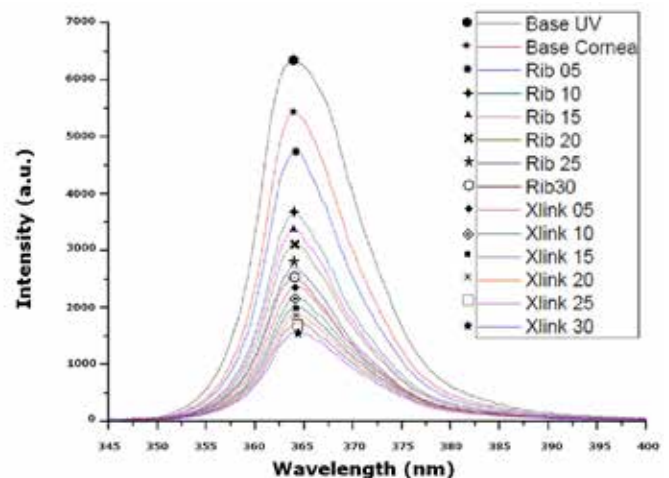


Figure 1: Transmission spectrum of a human cornea with CCT = 571mm during the collagen cross-linking procedure. (Base UV= Baseline; Base Cornea = cornea without epithelium and no application of Riboflavin; Rib = 1 drop of Riboflavin application; Xlink = Riboflavin + UVA irradiation; the numbers following the Ribs and Xlinks indicate the time interval in minutes that an event has been performed during the procedure).

PS12.034 - Electromagnetic high-hydrous gel phantom at a low-frequency band -Improvement in the electrical characteristics by using a carbon microcoil and investigation of its mechanism-

Author(s): Takahiko Yamamoto, Kohji Koshiji
 Department Of Electrical Engineering, Faculty Of Science And Technology, Tokyo University of Science, Noda/JAPAN

This paper presents an improvement in the electrical properties of a high-hydrous gel phantom by adding a carbon microcoil (CMC). A mechanism to improve the relative permittivity by the addition of the CMC is introduced. The CMC functions as an inductance at a certain frequency range. Adding a CMC to the conventional phantom is useful in improving the electrical characteristics at a frequency range of 10 MHz to 30 MHz, thereby increasing the relative permittivity.

PS12.035 - Examination of Bisphenol A Elution Concentration in Dialyzers

Author(s): Yoshihisa Yamashita¹, Ayako Yamashita², Isao Tsukamoto³, Yasuyuki Miwa¹, Hidetomo Nakamoto⁴, Hiromichi Suzuki⁵
¹Faculty Of Health And Medical Care(school Of Biomedical Engineering, Saitama Medical University, Hidaka-shi Saitama/JAPAN, ²Wakaba Internal Medical Clinic, Tsurugasima/JAPAN, ³International Medical Center(department Of Medical Engineering, Saitama Medical University, Hidaka/JAPAN, ⁴Department Of General Internal Medicine, Saitama Medical University, Irumagun Moroyama/JAPAN, ⁵Department Of Nephrology, Saitama Medical University, Irumagun Moroyama/JAPAN

[Objective]

Bisphenol A (BPA)—a chemical substance with an endocrine disruption effect—is contained in polycarbonates used in membranes, housing, constituents, etc. of dialyzers, and exposure of dialysis patients is unavoidable. We measured and examined the BPA elution concentration in various membranes used for hemodialysis therapy and dialyzers with various sterilization **methods**: here we report the results.

[Method]

RENAK PS-1.6 (AC sterilization, g-ray sterilization, and non-sterilization), APS-15SA, TS-1.6U, FDY-150GW, KF-15C, NV-1.6U, PES-15Eaeco, PES-15Saeco, VPS-15HA, PN-140, and NF-1.6H were the target dialyzers. For wet-type products, 1 ml of filling fluid was sampled first, then the blood side was cleaned using 1 L of purified water for 5 min at 200 ml/min, and 1 ml of the cleaning fluid remaining in each of the dialyzers was sampled for measurement. Portions of the hollow fiber and the housing were cut out and immersed in purified water at 70°C for 1 hr. A 1 ml aliquot of this immersion fluid was used to measure the BPA elution concentration from the constituent. High Sensitivity BPA ELISA Kit (Tokiwa Chemical Industries Co., Ltd.) was used as the measurement method.

[Results]

The BPA concentration of the filling fluid was the highest for NF-1.6H, and was equal to or less than the detection sensitivity for APS-15SA. The BPA concentration after cleaning was 0.86 µg/L for FDY-150GW: the highest value reported. The BPA concentrations of the filling fluids for RENAKPS1.6 with the AC sterilization, the g-ray sterilization, and the non-sterilization were 0.18 µg/L, 0.18 µg/L, and 0.28 µg/L, respectively. The BPA concentrations after cleaning were 0.18 µg/L, 0.14 µg/L, and 0.13 µg/L, respectively. Thus, different sterilization methods did not lead to noticeable differences in results. The BPA elution concentration from the constituent was the highest for FDY-150GW for both hollow fiber and housing.

[Conclusion]

The BPA elution concentration in dialyzers was the highest for FDY-150GW after cleaning, and a different sterilization method in RENA PS-1.6 did not lead to different results. BPA was detected in both membrane materials and the dialyzer constituents. It is important to minimize the amount of eluted BPA by improving the cleaning effect on BPA while suppressing the elution of BPA.

PS12.036 - Automation of a Dispersive Raman Spectrometer Using LabVIEW Aiming In Vivo Diagnosis of Skin Cancer

Author(s): Landulfo Silveira, Giovanni M. Schettino, Marcos T.T. Pacheco, Renato A. Zangaro
 Biomedical Engineering Institute, Universidade Camilo Castelo Branco, São José dos Campos/BRAZIL

The development of optical techniques for minimally or non-

invasive diagnosis of human tumors, and consequent discrimination between malignant, benign and normal tissues, can lead to rapid tumor diagnosis *in situ* with high sensitivity and specificity. Integrated optical systems that perform automated collection of spectra and provide diagnostic information *in vivo* in real time is a challenge for modern medicine. This work aimed to automate the spectra collection of a dispersive Raman spectrometer for use in *in vivo* experiments of skin cancer diagnosis. The routine of data collection, storage, pre-processing and processing of spectral data was developed within the Scientific Imaging Toolkit (Roper Scientific) under the computational environment LabVIEW (National Instruments), which has virtual instruments to control the excitation parameters (laser power), spectrometer (exposure time, number of accumulations), pre-processing signals (cosmic rays filtering, removal of fluorescence background and normalization) and spectral analysis (spectral models based on PCA and tissue biochemistry) in real time. The “RamanLife” routine allowed the use of the Raman spectrometer in procedures for skin tumors removal, with the estimation of the relative amount of basal compounds that constitute the biological tissues, such as lipids, phospholipids, proteins, amino acids, nucleic acids among others, is obtained during the collection of spectra. This provided reliable diagnostic information useful to differentiate between neoplastic, benign and normal tissues, offering the possibility of routine use in clinical diagnosis and in supporting histopathological evaluation for neoplastic skin lesions *in vivo* in real-time, avoiding unnecessary incisional biopsies and thus enabling assessments in large population groups.

PS12.037 - Effectiveness of Ozone-Liquid Mass Transfer aiming Ozone Therapy

Author(s): Henrique C. Carvalho, Milene S. Melo, Leandro P. Alves, Carlos J.D. Lima, Landulfo Silveira, Renato A. Zangaro
 Biomedical Engineering Institute, UNICASTELO, São José dos Campos/BRAZIL

The effectiveness of ozone therapy depends on the efficiency of the mass transfer phenomenon between gas-liquid phases. Many variables are involved in this process, whose techniques aiming biological applications require constant optimization. This study aimed to compare ozone-water mass transfer held by a Venturi and a Bubble Diffuser. The results show that the turbulence associated with increased liquid velocity in the Venturi is capable of generating ozone concentration of up to 6 times higher than Bubble Diffuser, or 0.87 mg/L in 20 minutes to the Venturi, and 0.15 mg/L for Bubble Diffuser. The use of Venturi in mass transfer processes in gas-liquid phase can promote the application of ozone therapy in biological systems, since turbulent processes do not damage the fluids involved in this process.

PS12.038 - Impedance plethysmograph based on reconfigurable hardware for the study of superficial vessels

Author(s): Laura L. Castro
 Dept. Bioengineering, Higher Polytechnic Institute Jose Antonio Echeverria, Havana/CUBA

Impedance Plethysmography (IPG) is a simple, low cost and non-invasive method to research and assess circulatory and vascular diseases in humans. An important feature of this method is that the volume changes of the blood flow in different organs or body parts can be detected. This paper aims to develop, simulate and implement a bioimpedance measurement system for the characterization of blood flow in surface vessels. Howland's scheme is implemented for current injection. Quadrature demodulation of bioimpedance signal is used to preserve both amplitude and phase information. The bioimpedance signal processing and a user interface based only in FPGA and basic peripherals (monitor, keyboard and mouse) linking

is achieved within the FPGA.

The implementation of this technique on reconfigurable hardware is a considerable advantage for the development and updating of design, allowing design flexibility and real-time processing due to parallelism offered by FPGA. The user interface greatly reduces system cost as it allows visualization and control of bioimpedance signal without using a computer.

PS12.039 - The study for bioelectric properties of tissue and organ measured by electrical impedance

Author(s): Toshiaki Nagakura¹, Kouya Watanabe¹, Yoshio Yasumura², Michiko Kido³, Moe Yokoyama³, Kenji Yamada³, Yuko Ohno³
¹Department Of Biomedical Engineering, Osaka Electro-Communication University, Shijonawate City Osaka Prefecture/JAPAN, ²Dpartment Of Cardiology, National Hospital Organization Osaka National Hospital, Osaka City/JAPAN, ³Division Of Health Sciences, Graduate School Of Medicine, Osaka University, Suita City Osaka Prefecture/JAPAN

About 60% of weight of the human exist as various solutions with water. And the dissolved substance concentration and localization in the solution are controlled severely. Each concentration is an important parameter for diagnosis and treatment, but there is very few continuous quantitative measurement method. From the physiologic point of view ion concentration and components of the biotissue are different, electrical specification is different. Though this is well known, and also the electrical measurement has the advantage that continuous measurement is possible, there are not developed the clinically useful measurement system. Therefore we tried to study the system for clinical application to measure a living body electrically. We applied the alternating voltage (5[Vpp]) of the level not to cause macro-shock to a living body and measured a frequency characteristic of frequency 0 - 20[MHz]. We measured the electrical specification (impedance and phase) change such as solutions of an electrolyte and the protein which there was to a living body. The impedance of most material in tissue including the liquid decreases to from 0 - 1MHz approximately monotonically. On the other hand, we found that it had quantitative tendency even if we injected electrolytic solution and a protein solution into biotissue. Moreover, with the measurement under various conditions, we measured the variance condition of the electrical specification in different kind of tissue and organ.

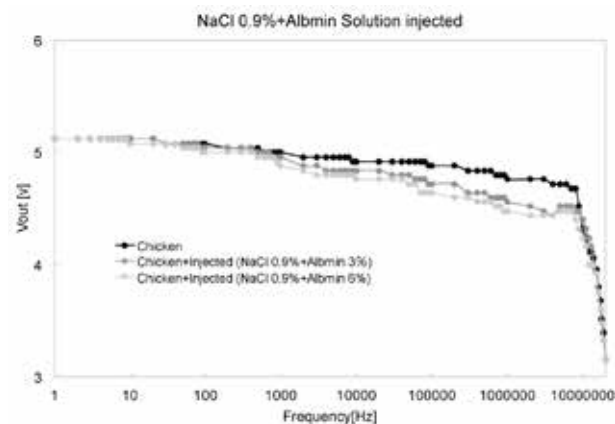


Figure 1 The relationship between the impedance of chicken muscle and concentration of solution. We were able to lead a difference and the tendency of the electrical characteristics in tissue and organ by this study. We could estimate that the solute and solvent transfer of an organ which having electric specificity of living body. We improve these results to be able to do clinical application.

PS13 - TRACK 13: INFORMATICS IN HEALTH CARE AND PUBLIC HEALTH

PS13.001 - A Method for Parental Engaged Consent in the Perpetual Secondary Usage of Health Big Data

Author(s): Yvonne Choi¹, Carolyn Mcgregor¹, Jennifer Heath²
¹University of Ontario Institute of Technology, Oshawa/CANADA, ²University of Wollongong, Wollongong/AUSTRALIA

Introduction

Knowledge discovery from the analysis of Big Data has contributed to significant breakthroughs in health care. However, personal health information is typically sensitive and identifiable thus presenting unique ethical and legal challenges when used for secondary research purposes. Our case study context, due to our recent research is Neonatal Intensive Care as the data that is generated by monitoring devices, generates a Big Data problem. In the case of neonatal research, parental engagement within the consent process is often required. Increased engagement with parents in ongoing studies requires a multileveled consent process that can be changed over time. Therefore it is important that the consent model respects their preferences and allows them to modify such preferences whenever possible and at their convenience over time.

Artemis is a platform for concurrent multipatient, multidagnosis, and multistream Big Data analysis for clinical management and research that uses continuous physiological data streams. The Artemis platform is composed of five components consisting of the: data acquisition, online analysis, knowledge extraction and the redeployment components. Currently, the Artemis platform does not support flexible consent over time. The primary and secondary usage of physiological data collected by the Artemis platform has already contributed to new clinical discoveries related to conditions, specific to the neonatal population.

Our research focuses on engagement of the parental community who have or have had an infant in the NICU with the use of a flexible consent model which will provide researchers with the ability to integrate the patient selection process with the data mining component of the research study.

Objective

In this work we extend the current Artemis knowledge discovery component. These extensions to the current consent model will support parental preferences regarding the consent and use of their infant's physiological data over time.

Methods

To address the research aims, new tables were defined within the Artemis database model to enable parental consent. The extensions not only enable this consent to be more explicitly tied with the data, but enable the consent to be changed over time or have parents engaged regularly for consent based on their chosen degree of consent through a web based portal.

Results

The extensions to the knowledge discovery component support parental engagement in the secondary use of their child's data through a continuum of secondary use of data retrospective studies. The architecture is currently being tested as part of our research into Apnoea of Prematurity.

Conclusions

Parents are surrogate decision makers for their infant. A flexible con-

sent model will be beneficial to various stakeholders including the parental community and researchers. Engaging parents or patients empowers them in the research process and enables their consent preferences to be respected. For researchers it is a platform that allows them to maintain continuous contact with the parental community thus maintaining a pool of potential research participants for them to contact for future recruitment purposes in addition to assisting with the results dissemination process to interested parents upon completion of the study.

PS13.002 - RENEM – Brazilian National List of Equipment and Materials

Author(s): Murilo Contó¹, Clarice Petramale², Erlon C. Dengo², Marcio L. Borsio²

¹Health Technologies Management And Incorporation, Ministry of Health of Brazil, Brasilia/BRAZIL, ²Health Technologies Management And Incorporation, Ministry of Health os Brazil, Brasilia/BRAZIL

To ensure the actions of the Brazilian Unified Health System (SUS) can be achieved with universality, integrality and gratuitous, the Ministry of Health (MoH) provides investment programs for institutions to acquire equipment and materials for the operation of its services. As the budget is always limited, the MoH implemented a methodology to make improvements in their processes of adoption and investment, divided into four fronts: (1)-Adoption of a National List of Equipment and Materials (RENEM); (2)-Regulatory processes for incorporation and management of RENEM; (3)-Creation a bench of prices; and, (4)-Automation of investment analysis. RENEM was adopted after systematic standardization of nomenclatures culminating in the preparation of equipment combos distributed according to the complexity of healthcare environments, eliminating issues of requests not according to their profile service. A computerized system was developed to manage the structure of RENEM and the entire process of investment analysis, streamlining routines and paper elimination. Regulating incorporation of RENEM items established the minimum requirements of scientific evidence and deadlines for decision making. A cooperation program was created to capture economic and technic information and a function was introduced into the system that provides the technical features of the equipment in multiple choices. Each technical feature has a monetary value associated that represents the impact on the final price. Thus, the system performs a dynamic price setting which automatically adjusts to the selected specification. A tool that performs the historical search of the quantity and value of equipment financed by state, city and institution allowed the creation of ABC curves and Pareto analysis, identifying the key items of RENEM that require further attention. As a main result, the number of investments approved in 2014 was almost four times higher than the previous year with significant improvement in projects quality.

PS13.003 - Becoming of Ubiquitous Sensors for Ubiquitous Healthcare

Author(s): Sergo A. Dadunashvili

Electrical Engineering And Elctronics, Georgian Technical University, Tbilisi/GEORGIA

Ubiquitous healthcare has become one of the prominent areas of research in order to address the challenges encountered in healthcare environment. Ubiquitous healthcare requires networks of intelligent sensor nodes that could be deployed “anywhere, anytime, by anyone and anything” and is a permanent part of the human presence. Management of systemic diseases via technology based ubiquitous patient monitoring services has been widely proposed as a viable option for economizing healthcare resources, and providing efficient, quality healthcare.

Ubiquitous sensors, devices and networks are paving the way towards a smart world in which computational intelligence is apply at all levels of the physical environment to provide reliable and relevant services to patients. This ubiquitous intelligence will change the computing landscape and environment around the patient, because it will enable new breeds of applications and systems to be developed and the realm of computing possibilities will be significantly extended. By enhancing everyday objects with intelligence, many tasks and processes could be simplified. The physical spaces where patients interact like the homes and hospitals could become more efficient, safer and more enjoyable. Ubiquitous computing, or pervasive computing, uses these many “smart things” to create smart environments, services and applications.

The Internet of Things is a new concept for telecommunication development. The Ubiquitous sensor Network is one of the general components of Internet of Things. A smart thing can be endowed with different levels of intelligence, and may be context-aware, active, interactive, reactive, proactive, adaptive, automated, sentient, perceptual, cognitive, autonomic and/or thinking. Research on ubiquitous intelligence is an emerging research field covering healthcare needs. A series of challenges exist to move from the current level of computing services in healthcare to the smart world of adaptive and intelligent services.

PS13.004 - Design and Implementation of an Application for ECG processing in Mobile Phones

Author(s): René González-Fernández, Margarita Mulet-Cartaya
Division Of Medical Devices, Central Institute of Digital Research, Havana/CUBA

The aim of this paper is to discuss the main features implemented in an Android application for ECG processing. The software was designed to use a mobile phone, connected to a battery-powered ECG device, as a signal acquisition layer in a Telemedicine platform oriented to implement several health services such as arrhythmia follow-up and remote pacemaker evaluation. The ECG device should be able to acquire and transmit, via Bluetooth, a bipolar ECG lead; the transmission time can be set previously. A friendly user interface was implemented for data entry and to display signals and result: all input data is validated according with its type and length. Error handling is focused on ensuring data reliability and the proper application functioning. The Android application receives the ECG data according to a simple protocol defined by the authors. Each data block is composed by a header byte, signal samples, electrode status and pacemaker spike identification. When a complete ECG strip is received, the electrocardiographic signal is filtered using a FIR moving average filter. QRS complexes are detected and classified, as premature or not, RR intervals are measured and heart rate is computed. An auxiliary function based on the Teager Energy Operator was combined with two thresholds to detect QRS complexes. The same function was applied to identify P wave regions previous to each QRS complex detected. P wave were delineated combining baseline estimation, a baseline-correction algorithm and heuristic rules. ECG strips are classified as arrhythmic or not taking in count the quantity of premature QRS complexes. A SQL database was designed to store patient general data, each ECG strip with the signal processing results and the data and time when the strip was captured. All these information is uploading to a web site using GSM/GPRS network and HTTP protocol. Also, all the data is store in a database implemented in the phone; this feature allows downloading that information into a personal computer when connectivity facilities are not available. The software was programming in Java language using Eclipse SDK and SQLite database engine.

The proposed software has been tested with five models of Android mobile phones, running Android operation system version 2.3 or higher. The user interface was rated as excellent by users involved

in testing process. Errors were not reported in Bluetooth communications when the distance between the ECG device and the phone was less than ten meters. QRS complex detection algorithm was tested with MIT-BIH database and the QRS detection sensitivity was 99.24%; false positives were not identified. P waves coupled to QRS complexes were studied in fifteen ECGs of the same database; sensitivity was 92.48%. It could be considered as a good performance, but the test has to be complete with the complete database.

The developed software seems a powerful tool to convert a mobile phone, combined with the appropriated ECG device, in a medical device for several Telecardiology services.

PS13.005 - A Telemedicine System to follow-up the Evolution of Chronic Diseases in the Community

Author(s): René González-Fernández, Margarita Mulet-Cartaya, Juan D. Lopez-Cardona, Alejandro Lopez-Reyes, Rolando Lopez-Creagh, Rolando Lopez-Rodriguez, Hector Torres, Eyglis Ledesma-Valdes

Division Of Medical Devices, Central Institute of Digital Research, Havana/CUBA

A system was designed to follow-up three chronic diseases: cardiac arrhythmia, hypertension and diabetes mellitus. Patient evolution can be studied daily without hospitalization and the objectives are:

- To document the evolution of the studied chronic diseases.
- To correct medical treatment as soon as it is necessary.
- To avoid inconvenience to patients because of the frequent visit to the hospital.

Patients are registered in the system during their first visit to the physician; they are trained to make the appropriated test at home to get the necessary measurements. The medical devices will be: a commercial blood pressure device, a commercial glucometer and a one-channel ECG device designed by the authors of this paper. If glucose and blood pressure device have Bluetooth capability, data is wireless transmitted. When this feature is not available, values are entered manually using a friendly interface implemented in the mobile telephonic terminal. Two alternatives are available for that terminal: an Android mobile telephone running an application developed by the authors and a specific telephonic terminal designed by the authors too. The physiologic data is processed, when it is necessary, in the mobile telephonic terminal and the results are uploaded to a website. A web application stores the uploaded information in a SQL database. Physicians log in the web application to study their patients; specific graphic tools were developed to help this analysis. This operation mode allows medical treatment can be adjusted as soon as it is necessary and medical care is improved. The following algorithms were implemented in Java and C languages for ECG processing: a FIR moving average filter to minimize noise presence; QRS complex detection and classification based on an energy collector combined with two thresholds and heuristic rules; heart rate measuring and ectopic beat rate measuring. Two prototypes of the ECG device and one of the mobile telephonic terminal were manufactured; plastic cases and print circuit boards for that prototypes were designed using CAD-CAM tools. The first version of the Android application and the web application were ended. The ECG device was evaluated according to the IEC 60601-2-47 standard with good results in all tests. The Bluetooth communication was tested with 600 one-minute simulated ECG strips without errors; received signal were identical to those originally transmitted and never data transmission was aborted because of fatal errors. ECG processing algorithms were evaluated with twelve thirty-minute ECG strips from the MIT-BIH arrhythmia database; the sensitivity in QRS complex detection was 98.77% and no false positives were identified.

PS13.006 - Developing an Appropriate and Affordable Expert System for Medical Diagnosis (ESMD) in Developing Countries

Author(s): Kenneth I. Nkuma-Udah¹, Gloria A. Chukwudebe², Josiah Ahaiwe³, Kennedy O. Ejeta¹, Gideon I. Ndubuka¹

¹Department Of Biomedical Technology, Federal University of Technology, Owerri, Nigeria, Owerri/NIGERIA, ²Department Of Electrical/electronic Engineering, Federal University of Technology, Owerri, Owerri/NIGERIA, ³Department Of Information Management Technology, Federal University of Technology, Owerri, Owerri/NIGERIA

Bringing intelligent healthcare informatics to bear on the dual problems of reducing healthcare costs and improving quality and outcomes is a challenge even in countries with a reasonably developed technology infrastructure. In the developing countries, like Nigeria, introduction of intelligent healthcare informatics then becomes constrained by considerations not only of *affordability* but also of *appropriateness* of the innovation. This research sets out to develop an appropriate and affordable expert system for medical diagnosis ESMD in developing countries. ESMD is designed to enable clinicians to identify diseases and describe methods of treatment to be carried out taking into account the user capability. The ESMD was designed using the C Language Integrated Production System (CLIPS). CLIPS is rule-based expert system tool, which means that knowledge is represented in rules, based on experience. ESMD shell has four modules: the user interface, the explanation system, the inference engine and the knowledge base editor. The knowledge base of ESMD was organized among several clinical signs, symptoms and features associated to drug therapy. The prototype of the ESMD was ready for use after nine months. The system does many random questions in order to enable clinicians make diagnosis and suggest therapy. The system is user-friendly and presented good time-response to give therapy advice. The knowledge base is editable and can be used to generate personal configuration based on population characteristics.

PS13.007 - Assessment of Mobile Health Applications

Author(s): Mary Marinou, [Nicolas Pallikarakis](#), Kallirroi Stavrianou
Biomedical Engineering Unit, University of Patras, Rio-Patras/
GREECE

During the last years, the usage of smartphones has rapidly infiltrated a plethora of daily functions. The health related applications which can carry out both simple functions such as recording vital signs or more complicated such as operating as computer-aided diagnosis systems, are amongst the most popular. In 2014 more than 100.000 mobile health applications (mHealth apps) have been found in the "medical" and "health and fitness" categories. It is estimated that in 2015 mHealth apps will be used by more than 500 million users worldwide, in which consumers, patients and healthcare professionals are included. This rapid development of mHealth apps revealed the need for their evaluation, assessment and regulatory compliance. This need is imposed by their particular nature, since lack of quality and specificity, or misuse of the information provided, may compromise user's health status, as well as security and privacy of the personal health data issues which are also of primary importance. The FDA and the European Commission of the EU are the only official authorities which developed regulations for apps that are classified as medical devices. Additionally various evaluation standards have been published by the private sector along with end-user assessment methods which have been also proposed.

It is expected that in the following years the adoption of the mHealth applications usage will improve the quality of the patients' lives and will promote the importance of prevention, user education and public awareness. It may also help to reduce the cost of healthcare, while increasing the frequency of interaction between patients and doctors and generally to greatly contribute to ameliorate Healthcare. Therefore it is necessary to develop a framework of adaptive

evaluation and assessment, along with a well balanced regulatory system, especially in cases where an external part is attached to the smartphone that could be considered as a medical device. In this work, it is presented how mHealth apps may in some example-cases replace medical devices and in which parameters their evaluation should rely on. Applications vary from simple devices such as a simple thermometer to more complex ones like an ophthalmoscope. Applications which do not require the attachment of an additional device or sensor, are also examined such as sharing medical images or supporting management of a chronic disease, like diabetes. Concluding, the need of an evaluation framework for mHealth apps is investigated, and among the basic elements of this analysis is confidentiality, security issues, the importance of usability of mHealth apps, as well as measurements' accuracy.

PS13.008 - An Investigation into using Pulse Rate Variability to Predict Clinical Events

Author(s): Usman Raza¹, David Maslove², Evelyn Morin¹, Karen Rudie¹

¹Department Of Electrical & Computer Engineering, Queen's University, Kingston/ON/CANADA, ²Kingston General Hospital, Kingston/ON/CANADA

Heart rate variability (HRV) describes the natural variation in time intervals between heartbeats, and is usually measured using R-R (peak to peak) times from the electrocardiogram (ECG). Reductions in HRV have been shown to correlate with cardiac events such as myocardial infarction and sudden cardiac death, as well as other critical illnesses such as sepsis. While ECG is the traditional method of collecting peak-to-peak data, it is expensive, cumbersome to use, and does not lend itself to ambulatory use.

It has been shown that pulse rate variability (PRV) is a sufficiently accurate estimator of HRV and can be calculated using photoplethysmography (PPG) [Schafer and Vagedes, International Journal of Cardiology, 2013]. Photoplethysmography uses two light emitting diodes, one red and one in the IR spectrum, and a light sensor to measure pulse oximetry, which can in turn be used to measure PRV. Devices that perform pulse oximetry are cheap, portable, and ubiquitous in clinical settings.

The aim of this work is to develop a prognostic system that can be used in hospital settings as a data-enabled early warning system. Using a stream of patient PRV data the system will be able to predict clinical events and alert a rapid response critical care team earlier than traditional methods. The system will be composed of two main components, the prediction software and a wireless pulse oximeter.

The prediction software will utilize a supervised training algorithm to develop a model using HRV metrics and clinical data. The large-scale incidence of PRV and HRV events will be determined using data stored in the MIMIC II database that contains clinical records and a matched set of multiple physiological signals for 2,809 ICU patients. A subset of the ICU patients that experience specific clinical events (Set A) will be identified and the PPG data in the associated waveforms will be used to calculate HRV metrics.

The algorithm will use a subset of Set A as a training sample and identify features that are highly correlated to the specific clinical events identified earlier. Once a feature-set has been determined, the remainder of Set A will be used to see whether the correlated features discovered in the training subset are also correlated in the testing subset. Iterative adjustments to the feature set and algorithm will take place until the prediction accuracy meets a satisfactory level. Once the system is accurately able to predict clinical events, it will be reconfigured to work with a live stream of clinical data collected across all 33 beds in the Kingston General Hospital ICU.

Concurrent to the development of the predictive system is the proto-

typing of an inexpensive and robust pulse oximeter that can transmit data over Bluetooth and Wi-Fi and be deployed to all admitted patients at a hospital. The current prototype can wirelessly transmit pulse oximetry data to an online database in "real-time" (~ 3 second delay). Future work on the module aims to reduce its size and power consumption and create an interface between it and the proposed predictive system.

PS13.009 - A simple device producing electrolyzed water for home care

Author(s): Koichi Umimoto

Biomedical Engineering, Osaka Electro-Communication University, Osaka/JAPAN

The prevention of opportunistic infection for the elderly is important in home care. When water containing sodium chloride is electrolyzed with an electrolytic cell having two chambers of equal volume, strongly acidic electrolyzed water with strong bactericidal ability due to the available chlorine (AC) is generated on the anode side. Weakly to slightly acidic electrolyzed water (WSAcEW, pH 4.0 to 6.5) is physiological pH and is suitable for biological applications. For producing WSAcEW simply and at a low cost, the present device was made of an asymmetric structure having a large anode chamber and a small cathode chamber. As a result, the pH and AC concentration of conventional electrolytic device were 2.3 and 27 ppm and this water was strongly acidic water, however, those of present electrolytic device were 4.0 and 31 ppm, respectively. WSAcEW was obtained directly by this experimental device and this water showed a strong bactericidal activity against bacteria. This device is useful for producing WSAcEW as a disinfectant to employ at home care, since it returns to ordinary water after use.

PS13.010 - Developing predictive models using retrospective study of liver cancer patients treated with radiation therapy.

Author(s): Jason R. Vickress¹, Michael Lock², Eugene Wong², Rob Barnett³, Slav Yartsev²

¹Medical Biophysics, Western University, London/CANADA, ²Western University, London/ON/CANADA, ³London Regional Cancer Program, London/ON/CANADA

Introduction: Radiation therapy is one of the primary treatments for cancer logistically providing an accumulation of information specific to each individual patient's treatment. A patient's electronic record in radiation therapy includes demographic data, diagnostic images, CT simulations, radiation planning and delivery parameters and verification imaging describing the patient's cancer treatment in great detail. Our goal is to harness this vast supply of treatment data along with outcome information in order to tailor radiotherapy treatments for future patients.

Methods: Selected radiation therapy planning parameters and outcome information were gathered for 118 patients treated for liver metastases at London Regional Cancer Program between 2004 and 2010. Planning and treatment information was available through an in-house designed system. Outcome information including patient survival, disease recurrence and blood work was collected prospectively. Multivariate Cox proportionality hazard ratio calculations were performed using SPSS version 22 (IBM) across combinations of all parameters in predicting the patient survival and disease recurrence. Patients were stratified into risk groups based on their hazard ratios of the most predictive parameters. All Kaplan-Meier curves were plotted and log rank tests of significance were performed for the patients separated by the median hazard ratio value.

Results: The most significant predictive parameters are presented in Table 1 for different numbers of covariates. Improvements of predictive power characterized by p-value were observed through

the increase in significance and mean values of Kaplan-Meir curve separation for each outcome individually. The minimum number of two covariates required for optimum prediction of specific outcome was determined. Mean differences between Kaplan-Meir curves for survival were 7, 10, 11.5, and 17.5 months if 1, 2, 3, and 4 covariates (Bilirubin, Serum Albumin, BED and GTV), respectively, were considered.

Conclusions: Multivariate modeling predictions obtained on the data for 118 patients provide physicians with quantitative parameters for more reliable interpretation of the implications and foreseen outcomes for patients receiving radiation therapy based on their proposed treatment and patient’s medical history. A larger patient cohort study will be performed to check the robustness of model predictions.

Table 1. Significance (p-values < 0.05 in bold) of predictions for Liver cancer treatment outcomes and mean separation (in days) between Kaplan-Meir curves when using up to 4 covariates. (Dose/fx = dose per fraction, #fx = number of fractions, BED = biological effective dose, GTV = gross tumor volume, Vx = liver volume receiving > x Gy)

Covariates	Survival	Recurrence		
		anywhere	in-field	out-field
1	Bilirubin	Dose/fx	BED	V30
2	Serum Albumin	V24	# fx	BED
3	BED	Bilirubin	Dose/ fx	n/a
4	GTV	n/a	n/a	n/a
Significance				
1	0.207	0.08	0.083	0.06
1+2	0.008	0.006	0.046	0.017
1+2+3	0	0	0	n/a
1+2+3+4	0	n/a	n/a	n/a
Mean separation (in months)				
1	7	8	10.5	12.5
1+2	10	11.5	14	15.5
1+2+3	11.5	14	23.5	n/a
1+2+3+4	17.5	n/a	n/a	n/a

for people to have the screening test. They are frequent supply of concrete knowledge on the screening tests and the condition of cancer, continuous and life-related motivation to the behavior for the screening test and forming the system available for people to have the test.

PS13.011 - A Study on the Problems for People to have Colorectal Cancer Screening Tests in Japan(-From the Results of Interviews for 30 Adults-

Author(s): Naoko Fujiwara¹, Miki Inagaki², Kenyu Yamamoto³, Misao Yoneda⁴, Masami Azuma⁵

¹Faculty Of Health Sciences, Naragakuen University, Nara/JAPAN, ²Baika Women’s University, Ibaraki/JAPAN, ³Osaka Center for Cancer and Cardiovascular Disease Prevention, osaka/JAPAN, ⁴Suzuka University of Medical Science, Mie/JAPAN, ⁵Osaka Kyoiku University (Honorary Professor), toyonaka/JAPAN

In late years, colorectal cancer fatalities and morbidity are increasing together and the rate for people to have colorectal cancer screening tests is regrettably sluggish in Japan. For future decrease in the mortality of colorectal cancer, we performed interviews for Japanese citizens about the factors influencing their behaviors to have colorectal cancer screening tests.

The contents of interviews were organized to four categories with 7-17 subcategories. These results suggest several important factors

PS14 - TRACK 14: INFORMATION TECHNOLOGIES IN HEALTHCARE DELIVERY AND MANAGEMENT

PS14.001 - DermApp: an application for Android mobile devices for reception and transmission of skin images

Author(s): Fabiana Garranchán¹, Samuel Ortega¹, Iván Escalona¹, Mayerith Torreyes²

¹Ingeniería En Telecomunicaciones, Universidad Católica Andrés Bello, Caracas/VENEZUELA, ²Dermatología, Hospital Militar Carlos Arvelo, Caracas/VENEZUELA

Unlike general practitioners, pediatricians and obstetrician-gynecologists, dermatologists are highly localized in large public hospitals or private clinics, which limit the possibilities to distant patients for care. Telemedicine is then useful for querying skin diseases.

DermApp is an application for Android mobile devices that covers the basic needs of specialists in the field of dermatology for better diagnosis, storing, transmitting and receiving skin images in any place where the doctor is present. DermApp allows a remote medical assistant to use a dermatoscope to capture images of skin lesions and select the most representative for transmission to a backup server that in turn sends the images to the dermatologist's mobile device.

A dermatoscope is a surface manual microscope widely used by dermatologists to visualize the pigmented structures in epidermis and dermal-epidermal junction for different skin phototypes. The phototype is the set of characteristics that determine whether a skin tan or not to sun exposure and the extent to which it does.

The used dermatoscope, DermLite II Red Hybrid m, has patented technology that combines non-polarized illumination with polarized light, with or without skin contact. This device offers high light output thanks to its 24 LED and a large 25mm lens.

To determine parameters for image quality, a survey was run to nine dermatologists in which images captured with mobile devices having different resolutions were presented. The minimum acceptable resolution was 3 MP. They also felt that the application had better functionality within the skin phototype III (darker white) which corresponds to a considerable percentage of the Venezuelan population.

From the evaluation of different mobile devices existing in the market we decided to use a smartphone with Android open OS for the facilities and other utilities in terms of programming offered by this operating system environment. In addition, we used a JPEG format because besides being compatible with most existing mobile devices on the market, it allows the transfer of files over a range of acceptable time without affecting markedly the image quality.

A VPN and SSH protocol were used to connect the mobile device with a backup server. Files were transferred with FileZilla program through the TCP protocol.

PS14.002 - Use of mobile devices for prevention in youngsters of risk factors common to chronic noncommunicable diseases

Author(s): Franxis Castañeda¹, Fiana Rodriguez¹, Iván Escalona¹, María S. Tapia², Luisa Angelucci³

¹Ingeniería En Telecomunicaciones, Universidad Católica Andrés Bello, Caracas/VENEZUELA, ²Inst. Ciencia Y Tecnología De Alimentos, Universidad Central de Venezuela, Caracas/VENEZUELA, ³Centro Inv. Y Formación Humanística, Universidad Católica Andrés Bello, Caracas/VENEZUELA

Promoting behaviors and healthy lifestyles is today one of the most used mechanism for the prevention of chronic non-communicable

diseases such as cancer, diabetes and CVD, which are leading causes of mortality in Venezuela (66%) and the world.

The application of telemedicine in the field of health education provided for the prevention of these diseases through the use of advanced technologies that help disseminate information about common risk factors and unhealthy diets, physical inactivity, stress, consumption of tobacco and alcohol.

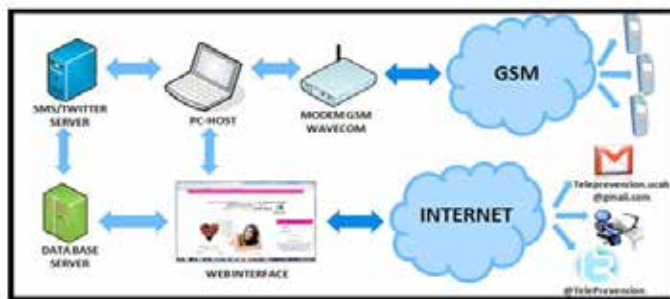
Promoting healthy behaviors through a telemedicine preventive system is sought by the use of mobile devices, based primarily on the technology of instant messaging (SMS) or social network Twitter widely used by youngsters in Venezuela and a query system via email.

Mobile phones and social networks are popular among the population. According to CONATEL (National Telecommunications Commission of Venezuela) 27 billion SMS text messages (1000 per capita) were sent in 2012. According to Semiocast (France) Venezuela was the 12th country on Twitter accounts and 6th in activity in 2012. Both media can be exploited to disseminate information about healthy behaviors and preventive factors of chronic non-communicable diseases.

The management system for instant messaging SMS and Twitter is implemented by a server to the database, a desktop application and a website. Text messages on physical activity or nutrition, prepared by students advised by psychologists, are sent to each of the mobile phones of youngsters through a modem connected to the GSM network. These youngsters can then use the system to consult psychologists and nutritionists.

Preliminary work was supported by a survey: randomly selected students were asked about their beliefs and attitudes to the risk factors of chronic non-communicable diseases and implementation of a platform for dissemination are measured content on healthy lifestyles. They were also asked about the preferred methods of communication (email, SMS, presentations, advertising) and most used social networks (Facebook, Twitter, Google+, LinkedIn, Instagram, MySpace or other) which can be used for the prevention of chronic non-communicable diseases.

The system is safe, accessible and easy to use and can be extended to different areas for the dissemination of information.



PS14.003 - Telemedicine in the Universidad Católica Andrés Bello (UCAB), Venezuela: an academic experience

Author(s): Iván Escalona¹, Jose Pirrone Puma², Mardemis Gutierrez¹

¹Ingeniería En Telecomunicaciones, Universidad Católica Andrés Bello, Caracas/VENEZUELA, ²Esc. Ingeniería En Telecomunicaciones, Universidad Católica Andrés Bello (UCAB), Caracas/VENEZUELA

Universidad Católica Andrés Bello (UCAB) is the oldest private university in Venezuela (1954). The School of Telecommunications En-

gineering started its academic activities in October 2001, pioneered Venezuela in this discipline with its own profile, which emerged in cooperation with Universitat Politècnica de Catalunya (UPC), Spain. In some autonomous public universities, Telecommunications often is a specialty in the program of Electrical Engineering.

The program requirements include a one-year special project in addition to regular and complementary courses. Based on the experience made since 1998 in the Group of Medical Physics, Faculty of Sciences of Universidad Central de Venezuela (UCV), one of the authors (IE) suggested the possibility of developing some special projects in telecommunications applications to the area of health. Unlike UCV, UCAB does not have a medical school, but a health center that provides outpatient medical care in various clinical specialties as part of social work at the University.

The first project started in October 2005, the second one in March 2006. In August 2006 there was a meeting Ministry of Health - Universities to establish a "Pilot project for sustainable development of the National Telehealth Network" which contemplated five subprojects to be executed in three years: Connectivity, Standards, Medical Informatics, Tele-specialties and Tele-education. Although the national project ultimately was not implemented our School maintained the development of one-year special grade works in the area of Telemedicine.

The interest for this area quantified in 164 students in nine years, which is almost 20% of 900 graduates. These works developed two lines of investigation: Telematics and Connectivity. Telematics projects have addressed issues in areas such as Imaging, Medical Informatics and use of mobile devices with open OS for Endocrinology, Dermatology, Cardiology, Spirometry and Remote Monitoring. Connectivity Projects took place mainly in non-urban care centers in counties of various states in Venezuela, sometimes in cooperation with the Medical Informatics Center (CIM), Faculty of Medicine of UCV. Fifty-nine students have also completed short internships at the Medical Informatics Center (CIM).

In October 2008, a new sixteen-week course, Topics in Telemedicine, incorporated as an elective course in the Telecommunications Engineering program. This course is primarily a seminar and also has a five-week workshop on Introduction to Tele-radiology that involves students with programs that allow viewing of medical images, image transfer between two terminals and access them via web. Another workshop with mobile devices to capture and transfer bio-signals will be included soon.

Telemedicine has been an important experience for inter-institutional and interdisciplinary activity and in just over nine years has opened a line of applied activity in addition to the more usual lines in the telecommunications area framed in Communications Technology, Electronics and Informatics.

The main objective of our Telemedicine Group has therefore been the contribution to social welfare by implementing telecommunications networks to support medical research activities and its applications to health and the use of mobile devices. Some results have been presented in eleven national and five international events (including WCOMPBE 2009 and 2012).

PS14.004 - Passage from analog to digital in radiodiagnostic processes

Author(s): Giulia G. Marchesi¹, Paola Freda²

¹3 B srl, Settimo Torinese/ITALY, ²S.c. Ingegneria Clinica, AOU Città della Salute e della Scienza di Torino, Torino/ITALY

The use of information technology in the medical field is becoming more and more popular, and healthcare companies recognize the

benefits deriving from it and are converting themselves to digitized workflows over paper, both for economic reasons and to simplify the work of operators (administrative, clinical, health ...). Among the various analog-digital conversions, the Ris/Pacs is one of the most interesting for its complexity. Digitizing an entire radiology department requires a very careful analysis phase, in order to model workflows with adequate accuracy. Modeling workflows is of fundamental importance, as there must be absolute correspondence between model and reality. Several steps are needed before completing the final project and it is very important to satisfy all the specific requirements of the health care company in order to increase productivity and efficiency. The current computer systems allow to implement ambitious projects, however guidelines and regulations have to be respected. It is clear that the state of art about analog-digital conversion rules are several from the technical point of view, but lacking for quality management. The present study aims to analyze all the aspects related to the passage of analog-digital radiology department, carefully assessing and detailing every aspect of the whole project.

PS16 - TRACK 16: CLINICAL ENGINEERING, CLINICAL PHYSICS, AND PATIENT SAFETY

PS16.001 - Increasing the health value per dollar spent: How Human Factors can help inform procurement of healthcare technology

Author(s): Sandra Ahedo¹, Laura Herrero², Ana Casado³, Lourdes Escobar⁴, Jose Carlos Manuel Palazuelos⁵, Elena Rojo⁶, Andrea Cassano-Piche⁷, Patricia Trbovich⁸

¹Innovation Department, IDIVAL Biomedical Research Institute, Santander/SPAIN, ²Innovation Department, IDIVAL Biomedical Research Institute, Santander/SPAIN, ³Material Resources, HUMV Valdecilla University Hospital, Santander/SPAIN, ⁴Management Nursing, HUMV Valdecilla University Hospital, Santander/SPAIN, ⁵Director Surgical Area, HvV Valdecilla Virtual Hospital, Santander/SPAIN, ⁶Teaching Department, HvV Valdecilla Virtual Hospital, Santander/SPAIN, ⁷Centre For Global Ehealth Innovation, University Health Network, Toronto/ON/CANADA, ⁸Ibbme, University of Toronto, Toronto/CANADA

Introduction: Use of technology systems is increasingly prevalent in healthcare and important in medical providers' efforts to promote quality health care delivery. Some healthcare organizations have already realized major gains through the implementation of multi-functional, interoperable healthcare technology systems. However, as with any well-meaning and innovative medical advance, these technologies bring both intended and unintended consequences to clinicians' work practices and patient safety. *The widespread implementation and adoption of healthcare technology has been limited by a lack of generalizable knowledge about what types of healthcare technologies and implementation methods will improve care.* In Healthcare the value per dollar spent in new technology is often of little value.

Inclusion of Human Factors (HF) in the procurement of healthcare technology is new to Spain. Through collaboration with HumanEra, Canadian experts in HF, Evaltec, a newly formed HF team, based at the Hospital Universitario Marques de Valdecilla, Spain, began to apply HF.

Objective: The aim of the present study is to describe a combination of human factors (HF) assessment techniques that were used to assess technologies and inform procurement, and implementation of a next generation device in a Spanish hospital.

Method: We present a case study in which two HF techniques (i.e. ethnographic field observations and heuristic evaluations) were used to inform the procurement of infusion pumps. Specifically, ethnographic field observations were conducted to study, in situ, use of the intravenous infusion pumps currently in use in the hospital to better understand the barriers and facilitators to the use of the device. Furthermore, heuristic evaluations were conducted to uncover design deficiencies of infusion pumps that are currently in use. This information was used to better understand users' needs and the system elements that must be in place prior to the procurement and implementation of the next generation pumps.

Results: The use of HF techniques provided a new lens with which to observe the healthcare system (i.e. technology, people and environment) and revealed several issues that had not previously been identified. Ethnographic field observations provided an understanding of institutions' current practices surrounding use of intravenous infusion technologies and barriers to the optimal use (e.g. lack of a match between the physician orders and drug libraries). Heuristic evaluations were effective for quickly identifying potential user interface design problems (e.g. clarity, consistency, and familiarity in the language and labeling used on the pump interface). Together, these results identified the importance and broad impact of both usability and safety issues and informed procurement requirements.

Conclusion: From this collaboration, the Evaltec team has realized the importance of applying Human Factors methods to the evaluation of medical devices. The knowledge gained from this experience will help ensure that the imminent procurement of the next generation of infusion pumps considers the user needs, reduces the waste of consumables, increases the efficient use of the pump, and increases the health value per dollar spent. The present study demonstrates how the application of HF can help inform the design of systems and ensure that unsafe devices are not introduced to healthcare facilities.

PS16.002 - Using Heuristic Analysis to support Usability Evaluation of a low risk medical device under development process

Author(s): Renata A.R. Custódio¹, Ana P.S.S. Almeida², João E. Côrrea³, Rodrigo M.A. Almeida⁴, Carlos H.P. Mello⁵, Egon L. Muller Jr²

¹Institute Of Mathematics And Computer Science, Federal University of Itajubá, Itajubá/BRAZIL, ²Institute Of Industrial Engineering, Federal University of Itajubá, Itajubá/BRAZIL, ³Institute Of Industrial Engineering, Federal University of Itajubá, Itajubá/MG/BRAZIL, ⁴Institute Of Systems Engineering And Information Technology, Federal University of Itajubá, Itajubá/BRAZIL

New technologies in the healthcare area have increased the possibilities to diagnose and treat the patients but also have added complexity and associated risks by use errors and users dissatisfaction during the use of complex machines. This paper deals with a new medical device under development in Brazil. The device is classified in the country as a low risk, but the device is intended to give comfort and to prevent futures problems to the patient under its use. The manufacture wants to evaluate the usability of the device to provide user satisfaction and efficient use of it. The heuristic analysis was the method chosen to evaluate the device, early as a prototype, in order to identify problems in the developing interface. The analysis was done by six specialists in Human Factor Engineering & Usability Lab in Federal University of Itajuba. We conclude that the heuristic evaluation was appropriate to evaluate the equipment in question, since helped identify relevant points that should be considered by the manufacturer to meet your customer and contribute with safety and efficiency in use.

PS16.003 - First Contact with Human Factors and Usability Evaluation in a Junior Research Project by a Biomedical Engineering Student

Author(s): Ana P.S.S. Almeida¹, Thais G. Andrade², Rodrigo M.A. Almeida¹, José A. Ferreira Filho¹

¹Iesti Lab Usabilidade E Fatores Humanos, Federal University of Itajuba, Itajuba/BRAZIL, ²Instituto Nacional De Telecomunicações, INATEL, Santa Rita do Sapucaí/BRAZIL

This study reports the experience of an undergraduate student enrolled at a junior research project in Human Factors Engineering (HFE) and Usability Evaluation of Medical Devices. The student was undergoing the third year of Biomedical Engineering, without any previous knowledge on HFE. The student was required made a literature review about the important concepts in the area first. The second part of the project consists on running a usability evaluation comparing two digital blood pressure monitors. A tutor, who is a human factors expert from another university, helped the student on setting up the methods, building the protocols and questionnaires.

In Brazil, Biomedical Engineering is a growing profession. The core curriculum of a Biomedical Engineer course is characterized by interdisciplinary. Although, it is uncommon to have disciplines related to HFE in undergraduate programs. HFE usually is taught as a small part of product development or in risk management related disciplines. This leads to biomedical engineering students with little knowledge on HFE, even with a high probability of working in the

development of medical devices in his career.

The junior research project was designed to give the student its first contact with HFE. It consists on comparing two digital blood pressure monitors, as if the student was required to choose and acquire one of them. Various HFE methods were presented and the student had to select the most appropriate ones. By understanding the basic functions of the equipment, with task analysis and cognitive walkthrough, the student developed protocols to perform the usability testing. There were two user groups of six participants, one for each device. Both groups had problems. The main issue was the difficulty of device installation and proper use, the clamp being one of the problems. Some of the functions, as memory, were also a source of problems. It is an important feature for patients who make a periodic pressure control, but it raised confusion on how to record and read the data, on both devices. The users pointed that they rather write down the values on a paper than using this function. The student found out that 83% of users ignored the instruction manual, even for the device that offered a quick guide. The instructions for use and the device labels were also conflicting. Another confusing point was the device alarms of high and low pressure, which caused misinterpretation.

Even though this was the first experience of the student performing the usability evaluations, she could raise a comprehensive list of considerations about the usability of the two products, with very interesting results. Unfortunately, the topic of HFE for medical devices is still unexplored in Brazil, even at academic environments for students training. With this research, the student could become aware of the importance of the issue, get to know HFE methods and applied them to the evaluation in real devices. The research also gave the student a better understanding on the importance of these topics in a product development.

PS16.004 - Non-Contact Measurement of Arterial Compliance (NCMAC)

Author(s): [Delran Anandkumar](#), Steve Greenwald, Ragu Prakash Ratnakumaran

Blizard Institute Of Cell And Molecular Science Pathology Group, Barts and the London School of Medicine and Dentistry, London/ UNITED KINGDOM

Introduction

Increased arterial wall stiffness (especially in the aorta) is implicated in cardiovascular disease (CVD). Pulse wave velocity (PWV) as a measure of arterial stiffness is a powerful prognostic indicator for CVD morbidity and mortality. However, current methods used to measure PWV require highly trained staff undertaking lengthy procedures to obtain reliable results, making PWV assessment unsuitable as a diagnostic tool. We propose a novel non-contact reflectance photoplethysmography (PPG) method (NCMAC) of measuring PWV with the aim of making PWV assessment more accessible and therefore suitable for routine screening in a primary care environment. The device is designed to detect the pulse wave in the intercostal arteries and relies on the assumption that the timing of the wave as it reaches superficial tissue near the ribs on the subject's back closely reflects that of the wave as it traverses the descending thoracic aorta. However, this study aimed to validate the NCMAC device against simultaneous measurements of carotid radial PWV using Doppler ultrasound to detect the pulse wave. The arm was chosen as a test location as the radial artery is larger and more superficial than the intercostal arteries.

Methods

We recruited 61 healthy volunteers (37 male, 24 female) between the ages of 18 and 30. Images of the medial aspect of the right forearm were captured by an infra-red camera (Eosens CL, Mikro-

tron, Unterschleissheim, Germany), for 30 seconds at a frame rate of 500Hz and analysed offline with custom Matlab software. This allowed the PPG signal to be extracted from individual or groups of pixels a known distance apart, from which the time delay and hence the PWV was calculated. The Doppler signals (MD2, Huntleigh Healthcare, Cardiff, UK) were recorded from the same arm shortly thereafter with the probes placed a known distance apart at the elbow and wrist.

Results

We found a weak but statistically non-significant correlation ($r = 0.045$, $p=0.73$) between NCMAC and Doppler PWVs. A Bland-Altman plot confirmed a lack of agreement between the methods, with a mean bias of -74.91m/s . Excluding NCMAC data clearly outside the normal physiological range (due to poor signal to noise ratio), gave a stronger and statistically significant correlation ($r=0.37$, $p=0.04$). The Bland-Altman plot confirmed the stronger relationship between the two methods with a mean bias of -6.978m/s . However, due to the wide limits of agreement we conclude that, in its current form, the NCMAC does not produce PWV estimates that are reliably and consistently close to their Doppler derived counterparts.

Conclusion

The NCMAC device failed in measuring PWV in the relatively simple vascular anatomy of the arm. The poor results may be attributed to limitations in sensitivity of the imaging process and the ability of the software to extract a pulsatile PPG signal. Future improvements in these areas will be directed at increasing the accuracy of the device. Initially, experimental investigations and numerical modelling should be focussed on the behaviour of light as it passes through the skin and underlying tissue and interactions with the pulsating blood vessels therein.

PS16.005 - Developing a Quantitative Performance Assurance Risk Classification Model within a Generalized Risk Scoring System

Author(s): [Vishvek Babbar](#)¹, [Agustina Krivoy](#)², [Petr Kresta](#)², [Michael Moore](#)², [Tidimogo Gaamangwe](#)²

¹Institute Of Biomaterials And Biomedical Engineering, University of Toronto, Toronto/CANADA, ²Clinical Engineering Program, Winnipeg Regional Health Authority, Winnipeg/CANADA

Risk classification is an essential process for various medical device management systems, e.g. performance assurance (PA). Several quantitative risk classification models have been developed but there is no standardized model because investigators may apply different rules to determine risk factors and risk categories. Most quantitative models also seem to assume that the distribution function for all the risk factors is the same. Therefore, the purpose of this work was to develop quantitative risk classification models within a generalized risk scoring system, taking into account the possible difference in the distribution functions. Example models, and applications are presented. The significance of the generalized system will be discussed.

Empirical rules were used to assign risk factor weights and risk category scores. The risk scores were applied to 134 devices randomly selected from the regional medical device inventory. Two models, linear and exponential, were developed to transform the assigned scores to actual risk scores. The actual risk scores were then normalized to a [0,1] range. After scoring, devices were assigned to either Low, Medium or High risk levels. The distribution of the inventory between risk levels was compared with the American Society of Healthcare Engineering (ASHE) distribution for similar devices.

Figure 1 shows that the inventory distribution between risk levels is model dependent. Comparison of this distribution with ASHE (Figure

2) shows that the exponential model seems to be in better agreement with ASHE system. The results suggest model difference in sensitivity between low and medium but relatively similar for high risk devices. The significance of the model differences on applications such as PA prioritization and setting completion targets will be discussed. The next step of combining risk level with retrospective factors, such as repair history and number of missed inspections, is being explored for refined inspection prioritization.

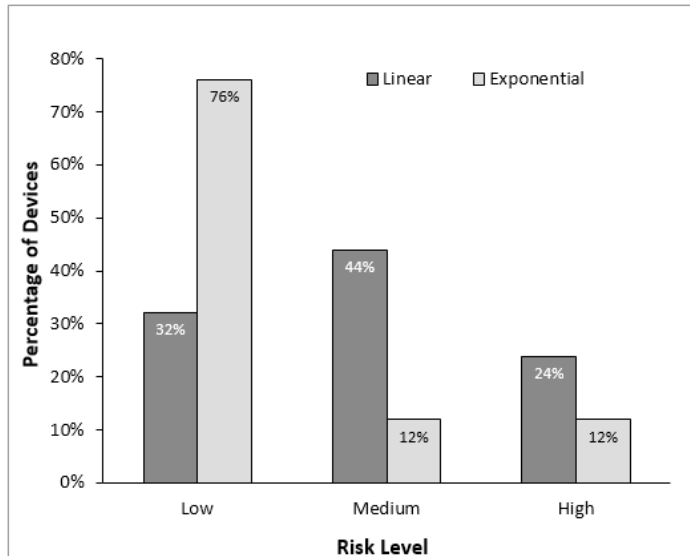


Figure 1. Percentage of devices assigned to each risk level based on the proposed models

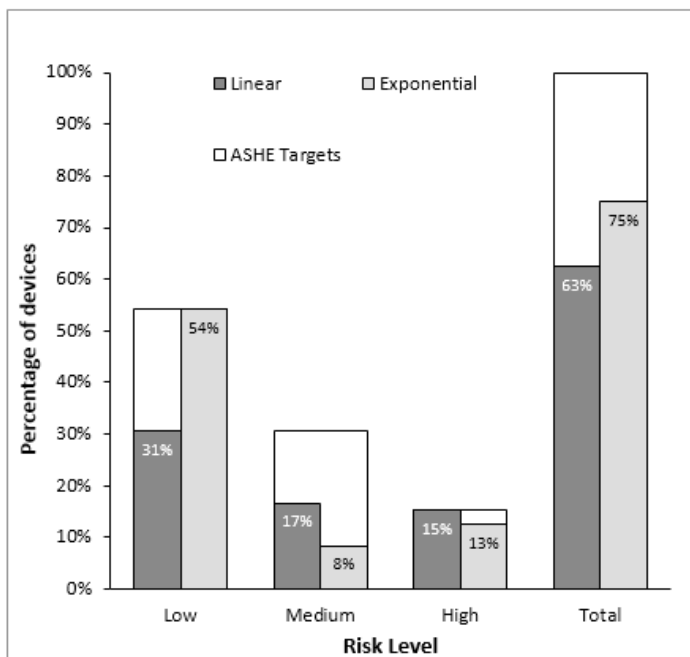


Figure 2. Out of the total number of devices common with ASHE, the percentage of devices with matching Risk level as well as the total matching percentage

PS16.006 - Project Management for Clinical Engineering – Considerations in the evaluation and acquisition of medical equipment for health services in Brazil

Author(s): Cleber S. Alves, Marília M.F. Gomes, Lourdes M. Brasil
 Post-graduate Program In Biomedical Engineering, University of Brasília, Gama/BRAZIL

The public health system in Brazil must provide the population, comprehensive care and with wide availability of resources. However, the actual conditions demonstrate that available resources are not sufficient to give full attention to required health. With regard to medical devices, it is observed that its acquisition is often done without adhesion to technical criteria aiming to support the technology throughout its life cycle. The project management processes enables the clinical engineer to join the assessment team of technology to be acquired proactively analyzing the acquisition of medical equipment throughout its life cycle. The research presented involved the search for articles that deal with the project management in state of the art applied to the evaluation of medical devices focused on the incorporation of these technologies in the health care environment, addressing an adapted model of the project management processes proposed by the Project Management Institute to the activities of clinical engineer.

PS16.007 - Human Factors for Health Technology Safety: A new book on incorporating Human Factors into the work of biomedical technology professionals

Author(s): Andrea Cassano-Piche¹, Patricia Trbovich², Melissa Griffin¹, Ying Ling Lin¹, Anthony Easty²
¹Centre For Global Ehealth Innovation, University Health Network, Toronto/CANADA, ²Ibbme, University of Toronto, Toronto/CANADA

In healthcare, adverse events involving medical technology failures have traditionally been the primary concern of biomedical technology professionals. In contrast, incidents involving the context of use (generally classified as “use errors”) have been left to clinical managers. Considering the high number of health technology-related adverse events caused by *use-error*, and the effectiveness of applying human factors principles to improve the design and safety of medical technologies, it follows that human factors methods should also be applied to technology development, evaluation, selection, implementation, training and the review of incidents, to support safe technology use.

While having a human factors professional as an integrated staff member of a healthcare facility is ideal, in reality, human factors professionals are not well established in this manner. Biomedical technology professionals, however, are well integrated within most healthcare facilities, routinely participating in evaluation, implementation, training and incident investigation related to health technologies. These responsibilities, when augmented by human factors methods, can improve the fit between a health technology and its context of use, which will lead to more effective, efficient, and safer use.

This presentation will introduce a new book, *Human Factors for Health Technology Safety*, aimed at providing biomedical technology and other professionals with the guidance required to integrate human factors methods into their tasks; acknowledging the familiar constraints of time and resources, and the complexity of the healthcare environment. The history of its development and structure of the document will be described and one or more case studies from the text will be shared to illustrate how the book can be used by biomedical technology professionals.

The text has been written based on what biomedical technology professionals know and do as core aspects of their profession. Each human factors principle and method is explained in the context of the biomedical technology professional’s core activities. Human fac-

tors methods are presented in sufficient detail so the depth and nuances of the discipline are not lost, but in an accessible manner so that non-human factors professionals do not become overwhelmed. Also, recognizing that biomedical technology professionals work in health care facilities world-wide, the book is written to be applicable and adaptable to audiences with varying levels of resources.

Other guidance documents about incorporating human factors into the design of new health technology exist, and are used widely by health technology manufacturers, but very little hands-on guidance exists about applying human factors methods in a healthcare setting. This book serves to bridge this gap and expand the practice of human factors in healthcare facilities, so that staff and patients can experience safer and more efficient healthcare.

Human Factors for Health Technology Safety was commissioned by the Clinical Engineering Division of the International Federation for Medical & Biological Engineering and was written by members of HumanEra. HumanEra's core focus is on the application of human factors methods and principles to improve healthcare safety, while taking into account health care technologies, practices, and environments of use.

PS16.008 - Politics, value and risk: a system to allocate medical equipment funding

Author(s): Peter Cook, Keith Ison
 Medical Physics Department, Guy's and St Thomas' Hospital, London/UNITED KINGDOM

Healthcare providers seek to provide the best possible patient care, using the most appropriate medical equipment. Yet there is never enough money to go round. How does an organisation get the most from the funding it has available? What guides its purchasing priorities between replacing old equipment, buying extra items or bringing in new technology?

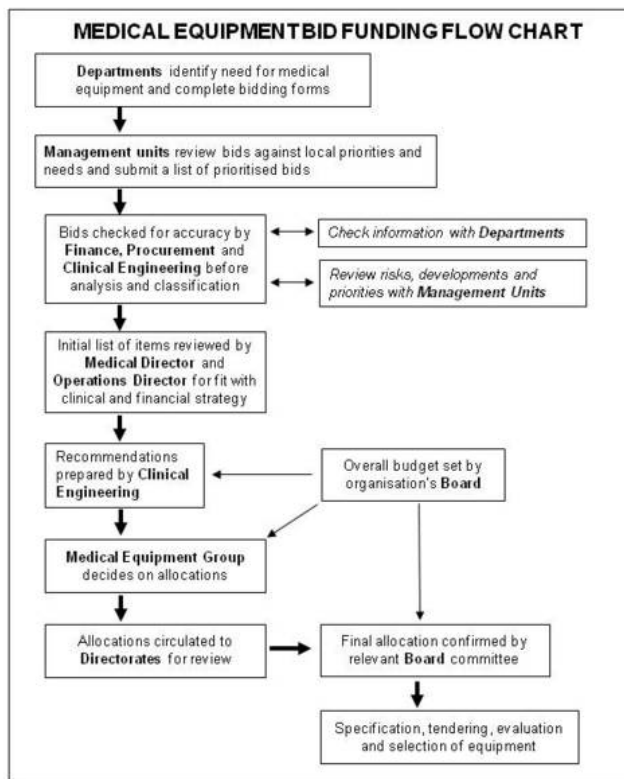
This poster presents a purchase prioritisation process which has been developed over 20 years and used at two large and one specialist hospital in London. This process encourages the active involvement of clinical departments, makes equipment requirements clearer and better coordinates purchasing. Although originally aimed at allocating funds to medical equipment costing over £5,000GBP, the process is easily scaleable. It supports the adoption of more elaborate systems needed to respond to economic and regulatory pressures in UK hospitals.

Important lessons learned in developing the process have included how to use risk alongside value for money in prioritisation; and the necessity of including 'soft' issues such as user preference and strategic and organisational impact alongside 'hard' measures such as return on investment and the degree of equipment standardisation.

Bids are collected from clinical departments before being checked and assessed. Purchase recommendations are drawn up, based on the relative risk of not getting equipment and/or the financial benefits of the investment and limited by available funding. These recommendations are considered by a group chaired by the hospital Medical Director that consists of several clinicians from different clinical disciplines, the senior operational manager and representatives from Finance, Estates, IT and Clinical Engineering. This group can adjust purchasing priorities in the light of clinical need and organisational strategy, with the outcome being formally approved by the relevant organisational Board committee.

A simplified flow diagram of the process is shown below. The process does not capture all bids, such as business cases for large infrastructure developments such as a new MR scanner. An amount of money is kept back each year as a contingency fund to replace

equipment which fails in year; the amount spent gives some indication on how well the bidding process prevents potential service disruption. Analysis of the outcome for over 10 years of data suggests any bias in the allocation of funds is small and feedback from clinical groups has been positive.



PS16.009 - Magnetic Resonance system configuration and editing tools

Author(s): Daniel C. Pizetta, Gustavo V. Lourenço, Danilo M.D.D. Da Silva, Edson L.G. Vidoto, Mateus J. Martins, Alberto Tannús
 Institute Of Physics Of Sao Carlos, University of Sao Paulo, Sao Carlos/BRAZIL

Magnetic Resonance (MR) technologies play a fundamental role in medical diagnosis systems and scientific research due to their powerful versatility and non destructive characteristics.

Current devices and methods require sophisticated tools not available for scientists who work with the equipment outside the manufacturer's realm. A limited number of studies, as ODIN (Object Oriented Development Interface for NMR) and DAMARIS (DARmstadt MAgnetic Resonance Instrument Software) has provided trials for meeting scientist's expectations.

This study describes tools for programming methods and MR systems. It includes a library – PyMR, an Application Programming Interface (API) and an Integrated Development Environment (IDE) with a graphical sequence editor.

The implementation of our system uses the state-of-the-art of computing technology and user's requirements. The structure includes PyMR, which acts as a front-end that generalizes its configuration and access. The API supplies the hardware-specific configuration and the IDE provides an easy way for the creation and management of MR sequences. The project was developed in Python along with PySide framework for the graphical user interface.

The environment is currently in use in our onsite system CIERMag spectrometer. Besides its feasibility and quality of code structure provided by code metrics, it can be easily adapted to different devices, such as receivers and transmitters.

A new and friendly way of programming MR equipment has been developed. It provides scientists with total freedom for developing their own MR method or instrumentation device.



PS16.010 - The Unintentional Irradiation of a Live Human Fetus During a CT Scan: a case study

Author(s): Jeff Frimeth¹, Eduardo Galiano-Riveros², Marcelo Godin³
¹Xspect Inc., Toronto/CANADA, ²Laurentian University, Sudbury/CANADA, ³Hospital del Cancer, Asuncion/PARAGUAY

Purpose: The purpose of this work was to calculate the dose accidentally absorbed by a live fetus during a diagnostic CT procedure to a pregnant patient, and to assess the likelihood that the premature termination of the pregnancy was radiation-induced.

Methods: A patient underwent a diagnostic CT procedure as part of her initial clinical work up for a FIGO stage II cervical cancer. At the time of imaging - and unbeknownst to the staff - the patient was found to be 12 weeks pregnant. Approximately two weeks later, the fetus became non-viable and was surgically removed. Following established institutional procedures, the case was referred to the Physics Department for further dosimetric evaluation to determine what role - if any - the fetal dose played in the premature termination of the pregnancy. The fetal dose was determined using Wagner's

CTDI Phantom Dose Reference Model method. The manufacturer's Abdomen Baby protocol was used to base the CTDIvol on, with appropriate corrections taking into account the actual scan parameters.

Results: Our estimated absorbed dose to the fetus was 19.3 mGy. Further, we estimate that the rotation of the fetus through an approximate 90° angle along the caudo-cephalic axis during imaging had no clinically relevant effect on the calculated absorbed dose.

Conclusions: The fetal dose was well below the consensus levels for negligible risk of abnormalities (50–150 mGy). At the time of exposure, the fetus was beyond the period of preimplantation; the most radiosensitive stage of pregnancy for a radiation-induced lethality. We conclude that the premature termination of this pregnancy is most unlikely to be of radiological etiology.

PS16.011 - Device reconditioning service for home-based assistance. How to choose the right approach.

Author(s): Roberta Chiarizia¹, Roberto Miniati², Ernesto Iadanza²
¹Clinical Engineering Department, ASUR Marche, ANCONA/ITALY, ²Department Of Information Engineering, University of Florence, Florence/ITALY

The home-based system's target is to give opportune responses to the problems which affect an increasing part of population. The aim of the service is to guarantee higher environmental performances and to maximize the effectiveness of these services. Starting from this, our experience was to show and suggest a method to deal with the difficulties on the management of a part of home-based service, called devices reconditioning service and identifying the best procedure to suite the needs. The critical elements and the different types of approach found, "in house" and "in outsourcing", in this health management system, were compared through Break Even Analysis. From an economical point of view this methodology points out which one, between the two presented management solutions, is the best according to collected data.

PS16.012 - Approach to the management of infusion systems in hospitals

Author(s): Roberta Chiarizia¹, Roberto Miniati², Ernesto Iadanza²
¹Clinical Engineering Department, ASUR Marche, ANCONA/ITALY, ²Department Of Information Engineering, University of Florence, Florence/ITALY

Drugs administration is the distinguishing feature of the infusion systems. They represent fundamental instruments in controlling clinical risk and in the improvement of the health care assistance. Using infusion systems allows the continuous drugs administration, resulting in the reduction of concentration fluctuation, and, keeping the appropriate speed infusion, is the way to guarantee the desired therapeutic effect. The study presented in this paper allowed us to analyze and describe some critical points in the management of infusion systems, volumetric and syringe pumps, inside a subarea of Azienda Unica Regionale Sanitaria delle Marche (ASUR Marche). Some management solutions have been suggested such as supplementary services, in order to keep the functional continuity of the medical units, ready-to-use extra devices and their traceability. These services would allow to have extra devices in case of breakdown or in emergency situations; extra devices would belong to the so called infusion library and their handling can be both free or with a penalty. In order to decide the proper quantity of infusion systems, from the one hand, and from the other assuring the full service of the available devices, a mathematical reasoning has been done using real data from medical units. In our view this would guarantee to the hospital to save money and to get the most from the devices. In the end we suggest for the introduction of the closed-circuits for

increasing the safety of the operator during the infusion of cancer therapy.

PS16.013 - A Basic Study on the Measurement of Electromagnetic Fields in a New University Hospital Building Before and After the Hospital Opened

Author(s): Kai Ishida¹, Ren Hosokawa², Tetsuo Endo³, Tomomi Fujioka³, Tetsushi Fujisaki⁴, Ryoji Yoshino⁴, Minoru Hirose²
¹Healthcare Informatics, Tokyo Healthcare University, Setagaya-ku/JAPAN, ²Medical Safety Engineering, Kitasato University, Sagami-hara/JAPAN, ³Building Technology Development, Taisei Corporation, Yokohama/JAPAN, ⁴Environmental Survey Office, Minato-ku/JAPAN

It is well-documented that establishing electromagnetic compatibility (EMC) is important for using medical equipment and communication devices in hospitals. To evaluate the basic electromagnetic environment, measurements should be conducted over 2 periods (before and after the opening of the hospital). We measured the electric field intensity induced by electromagnetic radiation in the broadcasting spectra coming from outside the hospital at 73 locations in our new hospital building in February 2014 (before any patients came into the hospital for the very first time) and August 2014 (6 months after the opening of the hospital). Frequency modulated radio signals, ultra-high frequency television signals, aeronautical radios, community wireless systems, and cellular phone system base stations were strongly detected at the windows of the upper floors. There was no great difference in measured levels between before and after the opening of the hospital. There were no cellular phone unit signals before the hospital opened its doors to patients, but were very strongly detected 6 months thereafter. In this study, the maximum electrical intensity was 0.28 V/m from cellular phone system base stations (2.1 GHz) observed on the south end of the 4th floor before the hospital first opened. This value was lower than the EMC marginal value of the general electronic medical equipment specified in IEC 60601-2-2 (3 V/m). Therefore, electromagnetic interference with medical equipment was extremely improbable in this situation. However, there were no cellular phone system base station signals in the elevator hall, in a portion of the corridor (located in the center of hospital), and in the hemodialysis unit. Measurements 6 months after the opening of the hospital revealed very strong cellular phone unit radio waves in the hospital. To promote greater EMC safety, the hospital should prepare countermeasures to improve these conditions, e.g., installing an interior cellular phone system base station.

PS16.014 - IAEA database of national dosimetry audit networks for radiotherapy

Author(s): Joanna Izewska, Paulina Grochowska, Ahmed Meghzi-fene
 Nuclear Sciences And Applications, International Atomic Energy Agency, Vienna/AUSTRIA

Recently, the IAEA has undertaken a task to review the coverage and operations of national and international dosimetry audit networks (DAN) for radiotherapy. The aim was to organize the global database describing the activities of dosimetry audit networks across the world. A dosimetry audit questionnaire has been designed including information on different aspects of the dosimetry audit, such as the audit framework and resources, its coverage and scope, the dosimetry system used and the mode of audit operation, i.e. remotely and through on-site visits. In 2010, 2011 and 2013, the IAEA questionnaire was circulated to numerous institutions known for having operated dosimetry audits for radiotherapy in their countries or internationally, including members of the IAEA/WHO Network of Secondary Standards Dosimetry Laboratories.

In response to the IAEA surveys, 54 institutions in 45 countries

confirm they operate dosimetry audit services for radiotherapy. The participation in audits is voluntary for a radiotherapy centre in 2/3 of responder countries and it is mandatory in the remaining. In general, audits are carried out regularly, with the frequency depending on the local circumstances; however, some organizations operate audits only by request. Most programmes verify megavoltage photon and electron beams, but some extend the audit scope to orthovoltage X rays, brachytherapy or radiosurgery. Few offer audits of tomotherapy and proton facilities. All organizations include the basic dose audit in the reference conditions in their programmes. Audits are also conducted for non-reference conditions, and for complex beam geometries, using semi- and/or anthropomorphic phantoms. Most clinical beams (85%) are checked through remote audits. Globally, approximately 2/3 of radiotherapy centres registered in the IAEA Directory of Radiotherapy Centres (DIRAC) have received some level of the dosimetry audit. However, better availability of the dosimetry audit is necessary for improving dosimetry practices in radiotherapy and for increasing safety of cancer patients undergoing radiation treatments.

The DAN database is located and maintained at the IAEA. The data from the 2010, 2011 and 2013 IAEA surveys were used to initially populate the database. When publicly available, this database can be used to provide information to international community on the availability of dosimetry audits in radiotherapy and the status of DAN activities across the world. At the same time, the information on participation in audits will be available to clinical trial organizations so that radiotherapy centres that are audited nationally and pass the national criteria are recognized as being competent to participate in international clinical trials as part of a global harmonization of clinical trial QA activities.

A concept for a DAN database was further developed to include a framework for international recognition system for national DANs activities. The introduction of such a system will be advantageous for comparing the auditing work between the various countries and regions, and to ensure that the national networks operate to the consistent internationally accepted standards and levels.

Acknowledgements: D. Followill, T. Kron, T. Knoos, C. Hurkmans, Y. Pynda.

PS16.015 - Telehealth - Achieving its Promise in 2015

Author(s): Thomas M. Judd
 Clinical Technology, Kaiser Permanente, Marietta/UNITED STATES OF AMERICA

Telehealth is achieving its promise in 2015. This will be demonstrated through three current case studies in which the presenter is participating:

1. US government HHS/HRSA study on evidence-based medical (EBM) tele-emergency care for rural locations
2. NGO EBM pilot for tele-neonatology between the national Childrens and OB Hospitals (and their key referral hospitals) based out of Skopje, Macedonia and Northside Hospital System Neonatology group in Atlanta, Georgia USA
3. NGO EBM tele-OB/Gyn and tele-neonatology as part of country-wide teaching and referral hospital development for Haiti; will bring together all parts of country as well as real-time e-consults with relevant specialists from all North America

The presentation will assess how clinical engineers can play a vital role in creating relevant solutions for use cases, partnering with other experts, such as these for and in developing countries.

PS16.016 - The New Japanese Guidelines for Use of Mobile Phones in Hospitals**Author(s):** Takashi Kano¹, Eisuke Hanada², Minoru Hirose³, Hidenao Atarashi⁴¹Saitama Medical University, Hidaka, Saitama/JAPAN, ²Saga University, Saga/JAPAN, ³Kitasato University, Kanagawa/JAPAN, ⁴The University of Tokyo Hospital, Tokyo/JAPAN

The new version of "Guidelines for Use of Mobile Phones and Other Devices in Hospitals" has been published by the Electromagnetic Compatibility Conference Japan (EMCC) in August, 2014.

The Japanese hospitals have been setting their own rules for using mobile phones at their facilities, taking into account the guidelines published in 1997 by EMCC and public manners in a comprehensive way.

In the meantime, we have seen drastic changes in pertinent circumstances, such as the penetration of mobile phones into daily life, the abolishment of second-generation mobile-phone services, and the improvement of medical electrical equipment for electromagnetic immunity.

These Guidelines have been created in consideration of the above circumstances through a review by experts, medical associations, wireless service providers, and relevant ministries and agencies in order to use mobile phones and other wireless communication devices more securely and safely in hospitals.

As mobile handsets (which hereinafter mean to include smartphones and tablets with a built-in cell-phone function) have become increasingly essential to daily life in recent years, it is desirable to allow the use of mobile handsets by patients and hospital visitors in hospitals to the extent possible for improvement of convenience and QOL for patients. On the other hand, while medical electrical equipment is required to have a certain level of immunity for electromagnetic fields, their operation may be affected by mobile handsets when they are used in close proximity. Another concern is public manners, such as sounds made during phone calls, of ringtones, of incoming mail tones, of operation, and of watching TV (hereinafter called "Calls"). Therefore, it is necessary to place certain restrictions on the use of mobile handsets in hospitals and establish proper rules for using them.

Since the kinds of medical electrical equipment, the need for using mobile handsets, and the need for consideration of others appear to differ greatly among specific areas in hospitals, they need to set area-specific rules. For the areas where the use of mobile handsets is allowed, they also need to set up the conditions for use (e.g., separations, precautions for use).

It's also necessary to set rules specifically targeted at hospital staff when hospitals establish rules for using mobile handsets at their facilities. Considering that the use of mobile handsets for medical practice contributes to the swift and optimum operation of medical services, the use thereof, including Calls, may be allowed in principle, on the condition that hospital staff is fully educated about the prevention of interference with medical electrical equipment.

By establishing rules for using mobile handsets by reference to these Guidelines, hospitals are more capable to properly manage and operate wireless communication devices in their facilities. To make wireless communication devices available more safely and securely along with further development of ICT for medical services, hospitals need to pay more attention to the management of the EMC environment by reference to these Guidelines.

The English version of "Guidelines for Use of Mobile Phones and Other Devices in Hospitals" has been published in EMCC URL (http://www.emcc-info.net/info/pubcom2/2608_5.pdf).

PS16.017 - Study on Medical Equipment Location Systems that use RFID Technology**Author(s):** Manabu Kawabe, Yasuyuki Miwa, Takashi Kano
School Of Biomedical Engineering, Faculty Of Health & Medical Care, Saitama Medical University, Saitama/JAPAN

(To protect the property of the hospital and periodically check medical equipment, it is important that the hospital staff can locate medical equipment used at various places in the hospital. Therefore, we have developed a location management system for medical equipment using RFID (Radio-Frequency Identification Device) technology (IT-Location.ME. Taisei Co., Ltd.). In this system, an antenna is installed in the doorway of the ward, and the RFID tag, attached to the medical equipment, makes its location known when passing by the antenna. The limit of this system is that it is difficult to identify the hospital room or treatment room in which the equipment is located even though the equipment is somewhere in the ward. To compensate for this limit, we have fabricated a handheld antenna to search and find the location of the medical equipment with the RFID tag attached. Furthermore, since the electric waves emitted from the RFID tag may be transmitted to the upper and lower floors, we have examined a method to shield the electric waves emitted from the RFID tag in order to prevent false detection. Since the system specialized in identifying the location, could not store basic information on the medical equipment and periodic maintenance log, we have linked the system with the database of the commercially available medical equipment management software.

(For the search of the medical equipment with the RFID tag attached, we have fabricated a directional phased array antenna consisting of two elements. Using this antenna, we have measured time to find the 10 infusion pumps attached with the RFID tags (lined up in a room in two lines with an interval of 2.1 m and a distance between lines of 9.0 m). In this measurement, six examiners could find the pump at an average search time of 45 ± 20 s and the probability of discovery was 93.4%. In addition, we have used a metallic knit fabric to prevent the false detection of the RFID tag in the upper and lower floors. By placing the fabric on a floor from which undesirable waves are transmitted, we could prevent the false detection of the RFID tag in the upper and lower floors. The linkage with the commercially available medical equipment management software was materialized by setting up a folder in a computer to share data between the databases of the medical equipment management software and the location management system and exchanging the information on the location of equipment and the basic information. This enables the medical staff to search the information provided by the location management system through the medical equipment management software, which is simply more accessible to the staff.

(In this study, we could solve the problems with the location management system we have developed, prevent the false detection of the RFID tag in the upper and lower floors, and link the system with the medical equipment management software currently used in the hospital. We believe that the usefulness of the location management system has been enhanced through this study.

PS16.018 - Development of a Regional Prioritization Process for Diagnostic Imaging Equipment Replacements**Author(s):** Rebecca Austman, Petr Kresta
Clinical Engineering, Ge 512, Health Sciences Centre, Winnipeg/CANADA

Prioritization of Diagnostic Imaging (DI) equipment for replacement in the Winnipeg Regional Health Authority (WRHA) is completed through a separate process than for other types of medical equipment. DI systems are first prioritized at the regional level, and then by a provincial committee against imaging systems throughout the province. Historically, the equipment prioritization approach within

WRHA has been through a largely qualitative and subjective voting process. As a result, the final prioritization depended on how well the manager of each site/program could sell their needs. Previous studies have developed various quantitative methods for prioritizing other types of medical equipment, but no known studies have developed a method targeted for DI equipment.

The purpose of this study was to develop a quantitative prioritization method by assigning points to selected criteria, or Prioritization Factors, that should be used when considering a piece of DI equipment for replacement. Based on a literature review, four Prioritization Factors were identified that were both relevant to DI equipment and easily obtainable: Remaining Useful Life, Support Status, Condition, and Clinical Capability. Each prioritization factor was assigned a weighted score (Table 1). Determining the relative weights for each of the factors involved input from managers from each of the DI sites, using a comparative process and involving some aspects of a previously established Analytical Hierarchy Process. Each Prioritization Factor had several categories within it (Table 1), from which the managers of the site/program had to select from on their request form. The form then automatically converted the selections into a corresponding score. The sum of the scores from the four Prioritization Factors was presented as the Priority Score. Other mitigating factors could also be written in the request justification, but were not assigned a score.

Table 1: Prioritization Factors Used with Corresponding Score Values

PRIORITIZATION FACTOR	CATEGORY	SCORE
Remaining Useful Life*	≤ 0 years	5
	0 < x ≤ 2 years	3
	2 < x ≤ 5 years	1
	x > 5 years	0
Service Support Status	Out of support	20
	Out of support but parts still available and/or supportable by a 3 rd party	15
	≤ 2 years until EOS date	10
	No known end of support (EOS) date; Or >2 years away	0
Condition	Poor	15
	Moderate	8
	Good	0
Clinical Capability	Lacks features/capabilities - high impact on patient care	10
	Lacks features/capabilities - moderate impact on patient care	6
	Lacks features/capabilities - low impact on patient care	2
	Meets all or nearly all clinical requirements	0

*Based on Canadian Association of Radiologists (CAR) guidelines, which incorporates both age and number of exams/year

This method was applied during this year's replacement prioritization exercise. The numerical scores acted as a guide to aid decision-making for the managers during the regional voting process, as well as for prioritizing the equipment within their sites. Overall, the feedback received from the users of the new system was positive, and it has been well accepted. It ensured that relevant factors such as age, condition, supportability, and capability were all considered when submitting the equipment requests, so that systems could be compared more objectively. Future work includes further refining the factors and scores based on the initial experience, as well as expanding this method to be used during the province-wide prioritization.

PS16.019 - Implantable Medical Devices: more Safety with Traceability and Surveillance

Author(s): Paolo Lago, Ilaria Vallone, Antonio Scarso, Corrado Gemma, Federica Cardellini
Clinical Engineering Dept., San Matteo Hospital, Pavia/ITALY

Background

Medical Devices (MD) market produces an annual turnover of about €100 billion in Europe: 70% is produced in Germany, France, United Kingdom, Italy and Spain. Small and medium enterprises cover

95% of MD field composed by 25 thousand industries. For these reasons, there is an increasing attention to this sector in Europe. European Directives 93/42/CEE, 90/385/CEE and 98/79/CE order the main rules for the MD commercialization in Member States. The European Database on Medical Devices (EUDAMED) was instituted by European Directive 98/79/CEE in order to strengthen supervision operations and to increase market transparency. In Italy, MD market is about €13.5 millions, with an annual growth rate of 4.7% in the period 2004-2012 and high innovation level. Italy is one of the few European Countries to create by law a MD List and to start a new data flow of MD consumption from healthcare facilities.

Objective

The aim of our work is to suggest some way to use these precious informations, already available through data flows, in order to obtain a traceability of Implantable Medical Devices. HTA analysis as well as better control on manufacturer warnings are possible too.

Methods

All official flow are analysed, identifying data and each database. Italian hospitals costs in MD are monitored through Consumption Flow. Different data flow connect patient data to implantable MD data.

In Lombardy Region, for example, the Patient Data Base is interfaced with the flow from the Hospital Discharge Forms. The implantable MD data are related to hospitalization codes. Therefore it is possible: a) to identify univocally the patient, tracing the National Insurance Number; b) to trace the whole clinic history after the implant; c) to carry out extremely detailed analyses.

Conclusions

Nowadays the major attention is about the economic and regulatory aspects of MD sector; for patient safety we correlate implantable MD with clinical events. This process could be useful for healthcare facilities (patient clinical issues and HTA) and for companies and competent authorities (post-market supervision and medical device surveillance).

PS16.020 - Using standard test methods to ensure quality and maximize supply of personal protective equipment in a time of global emergency response

Author(s): Ying Ling Lin¹, Adriana Velazquez Berumen², Yukiko Nakatani³

¹University of Toronto, Toronto/CANADA, ²His/emp/pau/medical Devices, World Health Organization Headquarters, Geneva/SWITZERLAND, ³Ministry of Health, Labour and Welfare, Tokyo/JAPAN

The rapid spread of 2014's Ebola outbreak, in West Africa, required a stable and adequate supply of personal protective equipment (PPE) to protect healthcare workers caring for patients with suspected or confirmed haemorrhagic fever. There quickly emerged an urgent need for off-the-shelf PPE traditionally destined for much different industrial applications to meet this health care service delivery demand. Clear and specific minimum standard performance criteria for each type of protective item had to be defined within a short period of time so that countries affected by Ebola infections could procure necessary PPE, put in place procedures and prepare staff to do their work in high risk environments. In the field, there was much variability in material performance and final item construction therefore, it was necessary to choose only the most relevant performance requirements and ensure an explicit minimum standard of quality, in order to simplify procurement of complex design PPE and to maximize its quantity from major manufacturers to priority countries. However, limited studies had been found to guide recommendations of these complex items and their combinations. Technical information was combined from industrial standards with practical input from clinical teams, field logisticians, global

procurement information and researchers of major manufacturers. These evolving minimum performance standards and combinations thereof, became more stringent as supply of products to priority countries stabilized. Also, the challenging combinations of performance criteria shaped the future design need for PPE items more suitable to current demands and preparation for future outbreaks. Indeed, the USA launched "Fighting Ebola: A Grand Challenge for Development. Fighting Ebola", a design competition to address, among other themes, the specific design issues of commercial PPE. The initiation and evolution of a small and highly technical component of a greater relief effort will be presented.

PS16.021 - Creation of a system for the coding of medical devices

Author(s): Mirko Dezi¹, Alessio Luschi², Ernesto Iadanza²

¹University of Florence, FIRENZE/ITALY, ²Department Of Information Engineering, University of Florence, Florence/ITALY

Medical devices have different nomenclatures for their classification. Some of the most significant nomenclatures are the Universal Medical Device Nomenclature System (UMDNS) and the Global Medical Device Nomenclature (GMDN) by the Emergency Care Research Institute (ECRI). In Italy the main are CIVAB and "Classificazione Nazionale Dispositivi Medici" (National Classification for Medical Devices – CND). The aim of this study is to create a system to automatically decode several device models from CIVAB to UMDNS code. All medical devices are coded with a table which is based on their definitions presented in these nomenclatures. The coding is lastly applied to a list of models of medical devices, developed by different companies.

PS16.022 - Establishment of Radiation Qualities for Radiodiagnosics in LCR/UERJ According to IEC 61267 and TRS 457

Author(s): Luis Magalhaes

Universidade do Estado do Rio de Janeiro - UERJ, Rio de Janeiro/ BRAZIL

The main goal of this work is to establish the radiation qualities of the Laboratório de Ciências Radiológicas (LCR) conventional X-ray equipment for calibrations in radiodiagnosics according to the recommendations of IEC 61267 and TRS 457. Tests were conducted to evaluate the homogeneity of the radiation field, high voltage applied to the X-ray tube, scattering, half-value layers (HVL) and homogeneity coefficients. The results obtained that characterize the radiation field, satisfy the conditions required by TRS 457. Invasive high voltage measures presented results compatible with the requirements of this standard. The HVL measures showed that for the first HVL the tolerance limits of IEC 61267, and the values for the homogeneity coefficients were within the limits established. The quality tests performed in this work were highly satisfactory in meeting the standard requirements. Thus, the main goal was achieved, and the methodology can be used by other similar X-ray systems.

PS16.023 - A Healthcare Facilities Qualitative and Multivariate Quantitative Assessment Methodology for Mongolia

Author(s): Claudio I. Meirovich¹, Adiya Bold²

¹Healthcare Facilities And Medical Equipment Planning, Meirovich Consulting, Madrid/SPAIN, ²Fourth Healthcare Sector Development Project, Ministry Of Health (fhdp), Ministry of Health of Mongolia, Ulaanbaatar/MONGOLIA

A qualitative analysis, multivariate analysis and a scoring system is proposed as the methodology to evaluate a healthcare infrastructure and technology city network. The methodology requires visiting each facility; interviewing the staff; completing an infrastructure

checklist; assessing each room including area measurements; making pictures of each room, all the installations and all the major infrastructure elements, making a full equipment inventory including the working conditions of the equipment; identifying the exact location of all the inpatient beds of each facility and writing an evaluation report. The collected information is then cleaned to do a multivariate analysis with "R". The assessment of each facility is focused on 4 areas (dimensions): infrastructure, installations, support services and equipment. A compound score is calculated using weights for each component that builds each dimension. The weights are defined by a group of experts. The resulting scores for each dimension of each facility are then evaluated and crosschecked with the pictures and the evaluation (qualitative) report. The level of confidence of the collected information is also rated. The proposed methodology was used to assess 33 healthcare facilities of Ulaanbaatar City in Mongolia: 9 specialized hospitals, 5 District Health Alliances, 6 district hospitals, 6 secondary general hospitals, 3 maternity hospitals and 4 Village Hospitals. The obtained results were used to prioritize new investments for the health sector over the next years. Further work is required in order to adjust the proposed methodology to better identify or classify a facility's conditions, adding more answer options and including more experts in the weight definition stage.

PS16.024 - Practice of HB-HTA on the Study of HIFU Technology for the Treatment of Prostate Cancer and Uterine Fibroma

Author(s): Roberto Miniati¹, Benjamin Latella², Francesco Frosini¹, Paolo Avezzano¹, Ernesto Iadanza¹, Fabrizio Dori¹

¹Information Engineering, University of Florence, Florence/ITALY, ²School Of Human Health, University of Florence, Florence/ITALY

The aim of the study has been the development of a Hospital Based – Health Technology Assessment, study directed to analyze the clinical, social and financial aspects derived from the use of the HIFU method for the treatment of prostate cancer and uterine fibroma in comparison with the traditional therapeutic approaches.

A systematic literature review was carried out inspecting the treatment of prostate cancer through the use of HIFU technology as well as its use for the treatment of uterine fibroma. At a later stage, clinical, social and financial indicators (gathered from EUnetHTA Core Model as well as from scientific literature) were defined and evaluated and a single benefit index was drawn in the end to have a rapid and direct comparison among the various treatment methods.

For the treatment of prostate cancer, HIFU reaches good results in the clinical setting obtaining 78% of negative biopsy results post-surgery and a 68% disease-free survival rate at 5 years. It also proves efficient in the social setting and equal to traditional surgeries. For the treatment of uterine fibroma, HIFU presents an improvement of post-surgery symptomology in 80% of cases, revealing a good clinical efficacy and showing particularly convenient in the patient quality of life.

Even though the traditional techniques represent the current gold standard, the initial results for the treatment of prostate cancer, exclusive to low risk of illness, and of uterine fibroma through the use of HIFU appear positive and, therefore, encouraging for the immediate future even though it remains fundamental to have greater availability of evidence especially in the long run.

PS16.025 - A Simulation Based Model for Planning Operating Theater Activity in Complex Hospitals: Case Study in Orthopedics

Author(s): Francesco Frosini¹, Roberto Miniati¹, Paolo Avezzano¹, Fabrizio Dori¹, Duccio Cocchi¹, Ernesto Iadanza¹, Sheila Belli², Maria Teresa Mechi³, Vega Ceccherini⁴, Andrea Belardinelli²

¹Information Engineering, University of Florence, Florence/ITALY

LY, ²Head Department, Florence Teaching Hospital, Florence/ITALY, ³Health Department, Florence Teaching Hospital, Florence/ITALY, ⁴School Of Hygiene And Preventive Medicine, University of Florence, Florence/ITALY

Operating theaters (OT) in hospitals represent some of the highest sources of economic expenditures since their high complexity in terms of technology equipment (integration of different complex devices and specific technical requirements), organization (multi-personnel area with complex patients flow) and usage (optimum planning between regular activity and emergency management). For the above reasons, it is essential to understand and plan the whole surgical path (patient and personnel) by avoiding foreseeable inefficiencies, delays and risks.

Hence, the aim of this study is fully modeling a generic orthopedics OT in order to support hospital decision makers in OT design and activity planning for both regular and emergency scenarios.

In order to do that and due to the complexity of the OT system, a simulation approach is fundamental for properly understanding the whole process and for clearly controlling and analyzing all the factors involved (surgical durations, types, working times and rooms availability, etc.). Discrete event models have been found reliable and accurate to simulate complex health systems (e.g. emergency management, beds management, logistic and assets estimation, etc.).

Finally, after selecting the most appropriate type of model, and using past surgical data and experts' opinions from the hospital for its development and implementation, a more precise and reliable clinical validation of the model is currently in progress, by concluding a data verification that needs a period of on-site data collection.

PS16.028 - Risk management tool in the application HFMEA in purge sector on the Material and Sterilization Centers.

Author(s): Sérgio S. Mühlen¹, Michele C.A. Sousa¹, Maria Isabel P. Freitas²

¹Biomedical Engineering Department, UNICAMP, .../BRAZIL, ²Nursing Department, UNICAMP, .../BRAZIL

Introduction: Material and Sterilization Centers in health care facilities should ensure the quality of medical instruments for safe patient care. For the sterilization process to be carried out properly, it is essential that the article to be sterilized is free from organic matter and some inorganic substances. If the activities of receiving, cleaning, rinsing and drying of surgical instruments, located in the Cleaning sector, are incomplete or inadequate for being performed quickly, they can compromise the cleanup. These failures may have diverse origins and they determine important factors to be identified for qualifying the work process. **Objective:** To assess critical points in processes and identify areas for improvement in the activities undertaken in the cleaning sector, Healthcare Failure Mode and Effect Analysis (HFMEA) technique was applied to the procedures performed in that sector. **Methods:** The HFMEA is a toll that provides a systematic evaluation of the critical points in processes by classifying them according to the severity of the potential effects of their failures and to their probability of occurrence, allowing the prioritization of the risks to be controlled. For its implementation a multidisciplinary team was formed, the process was mapped, the risk analysis was executed and the failure modes related to the process were evaluated. **Results:** 89 failure modes involving the cleaning and drying of instrumentation were found, and 262 potential causes associated with these failure modes were identified. Of this total, 131 potential causes (50 %) were selected and analyzed to propose measures and actions for improvement. A guide was prepared for to help implement the proposed improvement measures. **Conclusion:** The application of the HFMEA tool provided a diagnosis of the critical points of the process and resulted in the proposition of improve-

ment solutions that have been condensed into a guide action and measures that can aid the team managers of CME in incorporating safer routines in the execution of their activities and patient care.

PS16.029 - Generate health and wealth by innovation

Author(s): Mayur Patel, Mark Humphries

Cambridge Technology Centre, PA Consulting Group, Melbourne/UNITED KINGDOM

Innovation, health and wealth – hospitals have a unique capability in these three areas. Hospitals always strive to give the best health to patients, but innovation and wealth are often a lower priority, or lack the relevant infrastructure to carve out the aspects from clinicians and standard healthcare facilities. On a positive note, there are plenty of unexplored opportunities waiting to be exploited.

An ideal way for hospitals to adopt innovation and increase participation in research is to collaborate more with industry and universities. This arrangement can be used to exploit health and wealth in hospitals through Innovation.

“Innovation” is often interpreted as discovering a new technology or method and confused with invention. Innovation often results from the integration of known elements, directed towards a change in service, process, text, modification, development or research. Invention may not be required, rather benefits can occur from creatively redeploying our existing knowledge and assets in a new way to deliver the best healthcare services to patients, whilst meeting the wealth agenda at the same time. Such assets may not always reside within the same organisation and a more open approach, enabled through collaboration with the right set of organisations, can result in optimising the contributions from each party enabling innovative solutions to be created, and more importantly, deployed in relatively short timescales.

There are numerous ways to align health with wealth by first recognising, and then making use of existing assets and resources with hospitals. Some examples are:

- 1) Facilities re-use: There are plenty of sophisticated devices and services in hospitals that when not in use, could be used by device and drug manufacturers to carry out research, safety or performance testing. Imaging systems and clinical laboratories are such examples.
- 2) Collaboration with industry by providing consulting service: Clinicians, scientists, physicist and engineers working within the healthcare services are valuable resources for requirements definition, design and development of medical devices - Usability & human factors, Imaging systems and clinical laboratories, and Clinical Trials & investigations
- 3) Implementation of innovative **methods:** There are numerous services in the healthcare services that can be altered with minimal expenses which can result in greater savings and efficient functioning. Some examples are Medical equipment library, standardisation of medical devices in hospitals and effective management of medical device maintenance contracts.

Obvious questions that come to our mind are: how can hospitals generate more health & wealth by exploiting such resources? Why do such centres not exist or are not well known? How much more can hospitals innovate whilst not losing its core function to deliver

patient care?

The healthcare services require the right framework, expertise and skills to find & develop such opportunities. Medical Physics departments, being a centre of these facilities and having capabilities, provide a resource to identify initiatives to explore these opportunities.

PS16.030 - Validating and comparing Methods for testing Endothelial Function

Author(s): Ragu Prakash Ratnakumar, Steve Greenwald, Delran Anandkumar
Blizard Institute Of Cell And Molecular Science Pathology Group, Barts and the London School of Medicine and Dentistry, London/ UNITED KINGDOM

Background- Impaired endothelial function (EF) is strong predictor for the subsequent development of cardiovascular disease. Current EF testing involves using an expensive and technically difficult method known as Flow-mediated dilation (FMD). We are testing a simpler and more robust method known as the finger-tip endothelial function (FTEF) test, which measures the time difference between the arrival of the pulse at the middle finger of each hand (Δ PAT) before and after hyperaemic flow. As a preliminary validation of this new approach, we have compared the magnitude of the pulse arrival time difference with the maximum change in pulse wave velocity (measured in the radial and brachial arteries by Doppler ultrasound). We have also compared the time taken to return to baseline for the two methods and the area under the Δ PAT- or PWV- elapsed time curves.

Method- 48 healthy volunteers (31 male, 17 female) between the ages of 18 and 40 with no previous or current medical conditions were recruited. FTEF and the Doppler PWV measurements were performed simultaneously. Baseline data were recorded for 1 minute followed by hyperaemia induced in the left arm by 5-minute occlusion with a sphygmomanometer cuff. The response after cuff release was recorded for another 5 minutes.

Results- There was a statistically significant positive correlation when comparing relative/absolute difference in PWV against absolute difference in Δ PAT ($p=0.0168/p=0.0487$). A statistically significant positive correlation between the FTEF and Doppler PWV methods was observed when comparing time taken to return to baseline ($p=0.0264$). However, on average, Δ PAT returned to baseline significantly later than PWV ($P=0.0003$). A statistically significant correlation was also seen when comparing area under the magnitude time curve ($p=0.0187$).

Discussion- The FTEF test and Doppler PWV method of assessing EF demonstrated a correlated maximum effect, time course and area-under the magnitude time curve, thus we can assume the difference observed in Δ PAT is due to changes in brachial-radial PWV. FTEF proves to be a potentially simple and useful method for assessing EF. Comparison of FTEF with the gold standard (ultrasound FMD) is in progress to further validate the FTEF technique.

PS16.031 - Reliability Indicators in the Medical Equipment Management

Author(s): Camila S. Reis, William Castañeda, Renan Feltrin, Renato Garcia
Instituto De Engenharia Biomédica, Universidade Federal de Santa Catarina, Florianópolis/BRAZIL

This paper presents a study which uses reliability indicators for medical equipment management. There are considered corrective and preventive maintenance records to calculate the mean time between failures and the mean time to repair. The application of

this method, the maintenance records collected refer to anesthesia equipments used in operating rooms of five health care facilities in the public network of Santa Catarina state, Brazil. The analysis of the indicators was made according brands and date of installation of anesthesia equipments. The mean time between failures of the equipment under analysis is acceptable and was 16 months for brand A and 10 months for brand B. However, it was not possible to conclude whether the periodicity of preventive maintenance performed is being effective or not for the containment of failures. It is concluded that the analysis of indicators if not describes the operational context of use and may lead to a finding of reliability of precipitated brands, not being trusted to reality.

PS16.032 - Methodology for Safety Movement of Clinical Facilities Focused in Oncology

Author(s): Sandra L. Rocha Nava¹, Angel Herrera Gomez², Claudia Del Carmen Cárdenas Alanís³, Guadalupe D.J. Gutierrez Sánchez¹, Erika Ramirez Lopez¹

¹Biomedical Engineering, Instituto Nacional de Cancerología, Mexico DF/MEXICO, ²Medical Director, Instituto Nacional de Cancerología, Mexico DF/MEXICO, ³Escala Biomedica, Mexico City/MEXICO

The National Cancer Institute in Mexico City is the leader in critical cares on Oncology, it sets the policies and programs for the cancer control in all the country. For 40 years it was hold in a space of 1.5 hectares for its operation, and in 2011 the construction of a new facility began which provides more space and safety operations to patients, visitor and medical staff.

The transfer process of 10 clinical and diagnostic services to the new facility started in 2013. The Biomedical Engineering department implemented a process for time and motion, as well as risk analysis, to perform the movement with the least impact for patients and users, delaying the minimum diagnostic studies and treatment and the minimal effects in their activities.

The services in which this methodology was implemented were: Imaging, Nuclear Medicine, Clinical Laboratory, Pathology, Emergency, Operating Rooms, Intensive Care Unit, Recovery Room, Sterilization Facility and Inpatient Units.

Moving the Imaging and Nuclear Medicine departments represented the translation of approximately \$ 20 million dollars in medical equipment, among which stand out: 1 PET-CT, 1 SPECT-CT, 1 Gammacamera, 1 MRI 1.5 T, 1 Dual CT Scan, 1 Angiography System, 2 Digital Radiographic System and 1 Digital Fluoroscopy System, 4 Digital Mammographic and 1 Stereotactic System, 1 Digital Orthopantomograph, 1 Densitometer, 7 Ultrasound, 2 complete PACS-RIS systems with 15 diagnostic stations. The total time for transfer of both departments was 40 days and studies and services were not suspended or delayed for patients, with the exception of MRI and PET-CT, for which required support from neighboring hospitals to be done.

Clinical Laboratory moved eight laboratories: Hematology, Clinical Chemistry, Urinalysis, Bacterology, Tumor Markers, Molecular Biology, Coagulation and section sample distribution. The running time was 4 weeks.

The change in Clinical Pathology and its various services required 3 weeks for Cytopathology, Molecular Pathology, Immunohistochemistry, Histopathology and Inclusion.

In addition, eight Operating Rooms, 15 Recovery Rooms, 9 Intensive Care Rooms, 135 Inpatient beds and Sterilization facility were moved. For their flow operation and transcendence movement took place in two days each service with a strict control of the risks. All the movements were designed, documented and analyzed for a team of women biomedical engineers.

The implemented methodology allowed us to conduct the transfer of the above mentioned clinical, diagnostic and treatment services with minimal impact and control risks on patient care, considering services were not suspended or delayed, their safety was always verified, the safety for the users and the 643 medical equipment as well. No device was damaged or required major repair and working properly on hospital care and equipment

PS16.033 - Design of a remote use ECG with an Optical Communication System (FSO) for Telemedicine Applications

Author(s): Raul Rodriguez-Aleman, Yair Vazquez-Lopez, Gerardo S. Romo-Cardenas
School Of Engineering, Montemorelos University, Montemorelos/ MEXICO

This paper expose the current work in the development of an ECG of 12 derivations with the capability of connection through an optical communication system. Prior investigation shows that attention provided in the first minutes of a heart problem it's essential. The ECG signals are going to be transmitted into laser beam through the atmosphere to stablish communication between the ECG and the medical center, Capable to analyze the signals and give a proper diagnosis. There are a few challenges to this project; Multiplexing ECG signals into a laser Diode and effectively transmitting those signals through the atmosphere to a receptor.

This through an optical communication system which refers to the transmission of a laser beam modulated through the atmosphere to communicate between the scene to a medical center where a specialist doctor can analyze the ECG information, rate and blood pressure patient . Because the optical communication system are in recent exploration. Several techniques have not been investigated , capabilities and limitations in various scenarios and applications. An exploration of optical communication systems audio and video was performed to analyze their performance in the propagation in open space. Experiments were designed to simulate optical effects of transmission in the atmosphere by means of a base of gelatin, likewise absorption experiments and polarization of the beam is designed to better understand its operation , advantages and limitations of these communications systems. According to the Beer-Lambert law, the beam can be absorbed into the path to follow in the atmosphere having different effects on the propagation of the beam and the information is conveyed . Likewise the polarization effects generated in the intensity of the transmitted signal.

PS16.034 - Adverse events and death related to the use of the MRI equipment

Author(s): Ricardo A.M. Sá¹, Walter V. Mendes²
¹Gerência De Engenharia Clínica, SECRETARIA DE ESTADO DA SAÚDE DE GOIÁS - SESGO, GOIANIA/BRAZIL, ²Escola Nacional De Saúde Pública Sérgio Arouca, Fundação Oswaldo Cruz, Rio de Janeiro/BRAZIL

Objectives: The aim of this work was identify the occurrence of adverse events (AE) and the death related to the use of the MRI equipment informed in incident notification system.

Background: The World Health Organization (WHO) recommends that health care systems should be able to identify,report and recalls all incidentes, especially AE. A few authors have developed a generic system risk model to search and to analyse the root causes of AE. This system can be useful for identifying these causes and improve the protection of the health and safety of patients and users by disseminating information and to prevent the occurrence of AE.

Methods: MRI is “a diagnostic technique that uses a magnetic field and radio waves to produce a detailed image of the organs, tissues

and bones within body”. The AE notifications were collected from the Manufacturer and User Facility Device Experience Database (MAUDE). The AEs were classified based on Shepherd’s model (The Systems Risk Model). The concept of AE used in this study was “events that produce, or potentially may produce unexpected or unwanted outcomes that affect the safety of patients, users or others”.

Results: We found 1487 AE related to the MRI equipment in the last 10 years (period from 01/01/2004 to 12/31/2013), being 12 related to death, and 774 of them were related to injury, 295 reports were related to “malfunction”, 349 reports related to “others” and 51 reports related to “No Answer Provided”. We analyzed the 12 deaths occurred. Three cases were excluded because they are repeated. From the remaining 09 reports, 07 AEs were deaths of patients and 02 AEs were deaths of professional maintenance. The causes of deaths of patients were heart attack (03 cases), respiratory arrest due to disconnection or malfunction of the anesthesia machine (02 cases), collision with ferromagnetic objects (01 case) and diagnostic error (01 case). The causes of deaths to maintenance professionals were asphyxia (01 case) and collision with the magnet (01 case).

Conclusion: We think that Shepherd model is very useful to identify causes and assess the risks of AE surveyed. For future studies, we propose to use the Shepherd’s model to evaluate the AE related to the use of radiology equipment like digital x-ray and mammography.

References: Murff HJ, Patel VL, Hripcsak G, Bates DW. Detecting adverse events for patient safety research: a review of current methodologies. JAMIA 2003; 36:131-43.

ACCE – Health Technology Foundation. Impact of Clinical Alarms On Patient Safety. Plymouth Meeting, PA: ACCE, 2006.

Shepherd M. A Systems Approach to Medical Device Safety, In: J. Dyro, Ed.Clinical Engineering Handbook. New York, NY: Elsevier Academic Press 2004; 246-249.

Sá RAM, Mendes W. Assessment of adverse events (AE) related to the use of the Computed Tomography Equipment. Abstract accepted in ISQua 2012.

Sá RAM, Mendes W. Assessment Of Adverse Events Related To The Computed Tomography. Abstract accepted in HTAi 2012.

PS16.035 - Adverse events and injuries related to the use of the MRI equipment

Author(s): Ricardo A.M. Sá, Walter V. Mendes
Clinical Engineering, SECRETARIA DE ESTADO DA SAÚDE DE GOIÁS - SESGO, GOIANIA/BRAZIL

Background: The World Health Organization (WHO) recommends that health care systems should be able to identify, report and recalls all incidents, especially AE. A few authors have developed a generic system risk model to search and to analyze the root causes of AE.

Objectives: The aim of this work was identify the occurrence of adverse events (AE) and injuries related to the use of the magnetic resonance imaging (MRI) equipment informed in incident notification system and to classify them accordingly to their causes following the Shepherd’s model.

Methods: The AE notifications were collected from the Manufacturer and User Facility Device Experience Database (MAUDE). The AEs were classified based on Shepherd’s model (The Systems Risk Model - SRM). The concept of AE used in this study was “events that produce, or potentially may produce unexpected or unwanted outcomes that affect the safety of patients, users or others”.

Results: We analyzed 91 AEs related to injury occurred in the last year (period from 01/01/2014 to 12/31/2014). Three cases were excluded because they are repeated. From the remaining 88 cases, the study showed that 71 AEs were related to injuries in patients (80.7%), 11 AEs were related to injuries in MRI technicians (12.5%), 05 AEs were related to injuries in MRI professional maintenance (5.7%) and 01 EA was related only to damage of device (1.1%). The causes of injuries in patients were burn skin, the most frequent one (61 cases, 69.3%), collision with ferromagnetic objects (4 cases, 4.6%), and mechanical chock between patient and magnet (3 cases, 3.4%), and others (3 cases, 3.4%). The causes of injuries in MRI technicians were mechanical chock between operator and MRI table (7 cases, 8.0%), collision with ferromagnetic objects (3 cases, 3.4%) and fall of the technologist (1 case, 1.1%). The causes of injuries in MRI professional maintenance were collision with ferromagnetic objects (4 cases, 4.6%) and helium gas escape (1 case, 1.1%). Our work classified the AEs based on Shepherd's model, being the operator component the most frequent to the direct cause (46 cases, 52.3%) and all 46 cases were related to the education/training sub-component, the root cause. Of these AEs, 27 (30.7%) could not be analyzed because of the limited information provided in the MAUDE.

Conclusion: We think that Shepherd's model is very useful to identify causes and assess the risks of AE surveyed. For future studies, we propose to use this model to evaluate the AE related to the use of radiology equipment like digital x-ray and mammography.

References: ACCE – Health Technology Foundation. Impact of Clinical Alarms On Patient Safety. Plymouth Meeting, PA: ACCE, 2006.

Shepherd M. A Systems Approach to Medical Device Safety, In: J. Dyro, Ed. Clinical Engineering Handbook. New York, NY: Elsevier Academic Press 2004; 246-249.

Sá RAM, Mendes W. Assessment of adverse events (AE) related to the use of the Computed Tomography Equipment. Abstract accepted in ISQua 2012.

Sá RAM, Mendes W. Adverse Events And Death Related To The Use Of The Magnetic Resonance Equipment. Abstract accepted in ISQua 2014.

PS16.036 - Investigation on solar aging in sunglasses by developing of automated prototype for sun exposure of lenses

Author(s): Leonardo M. Gomes¹, Homero Schiabel², Liliiane Ventura¹
¹Electrical Engineering Department – Eesc, University of São Paulo, São Carlos/BRAZIL, ²Dept Of Electrical Engineering, University of São Paulo, São Carlos/BRAZIL

The first Brazilian standard for UV protection sunglasses, NBR15111, was drafted and published in 2003, hitherto a faithful copy (mirror) of European, BSEN1836 standard. From 2010 to 2013, the School of Engineering of São Carlos (USP) made contribution in the review and drafting of this standard and the main change so far is on the extension of the UV range analysis for protection of sunglasses, i.e. from 280 - 380nm to 280-400nm and the resistance to irradiation test increased from 25h to 50h. In previous studies, there are indications that ultraviolet protection degrades with use and exposure of sunglasses to natural ultraviolet radiation. Thus, this project aims to build a prototype for irradiating sunglasses lenses, where one of the spectacles will be submitted to the solar simulator; and the other to the prototype. This prototype consists of a box for protecting mechanical and electronic systems, an automatic lid and a laser cut acrylic panel, which houses 100 lenses arranged in the use position and which will be irradiated by the sun from sunrise until sunset. The lid opens automatically; the panel is ejected by a mechanical system from inside the box and should turn towards the sun, so

that the lens will always be irradiated from the front by the sun. The data about azimuthal angular position of the Sun for the city where the prototype is located is previously calculated and recorded on the memory of the prototype. Sensors will be installed to close the cover and protect the glasses of undesirable weather conditions and to determine the ultraviolet index to which the lenses are being subjected to. The exposure time and UV index will be recorded and automatic opening or closing the lid may also be interfered by a PC by online software. Previously to the lenses being placed on the panel, spectroscopy will be performed, in the range of 280nm - 2000nm, at 5 different positions imposed by the standard at 3 different temperatures: 230C; 50C; 350C; also polarization measurements of the lenses will be performed; as well as the flammability and resistance to impact tests. Just sunglasses in compliance with the standards will be subject of the study. All these tests will be performed over again after every 30 days of exposure. Figure 1 shows the prototype's mechanical design and how it should operate. Mechanical parts are being fabricated following the illustrated design.



PS16.037 - Integral clearance of medical rooms based on the type of medical treatment ensures a safe environment upon first use

Author(s): Casper Smit, Bärbel Van Den Berg
 Medische Technologie, Medisch Spectrum Twente, Enschede/
 NETHERLANDS

Aim

Patient and medical staff safety can only be guaranteed in a medical environment that is safe in terms of electricity, (ionizing/non-ionizing/thermal) radiation, liquids, gases and particles. The specifics of each type of medical treatment, e.g. invasiveness of treatment or nature of radiation, define which safety measures are required to provide a safe environment in a medical room. As all different types of safety measures have to act simultaneously, we propose an integral and multidisciplinary approach for acceptance testing of medical rooms.

Current situation

Our institute is building a new hospital. All new medical rooms have been built over a period of five years since the first sketches and initial determination of the requirements. For several rooms the intended types of medical treatment have changed during the construction period due to advancing methods of treatments or new medical equipment. Sometime these changes require additional safety measures. We also noticed that end users and supporting staff have an incomplete overview of aspects of newly constructed rooms that have to be validated. Additionally, responsibilities but also technical documentation of medical rooms are scattered among various officers and departments within the hospital. This lack of overview of all safety measures for each single room makes it impossible for the physician or head of department to take responsibility for a safe medical procedure upon first use. In order to ensure a safe environment upon first use, but also creating a solid base to handle future changes in types of medical treatment in a room, we have used an integral and multidisciplinary approach for acceptance testing of our newly built medical rooms.

New procedure

Our procedure to check the safety measures in medical rooms is based on the intended types of medical treatment, including the used medical equipment. The intended types of medical treatment (defined by answering questions such as “Is medical electrical equipment intended to be used in direct contact with the patient?”) must be agreed on by both the responsible physician and the head of the department in the initial phase of the construction period. During construction, changes in intended use are checked against the safety measures. After building the responsible officer (e.g. the radiation protection officer) must confirm that the safety measures taken in the room indeed match the intended use. The intended types of medical treatment and all checked safety measures are presented in one integral overview. Finally, the head of the department and the responsible physician share responsibility for final acceptance of the medical room based on the intended types of medical treatments.

Conclusions

Current methods for acceptance testing of medical rooms do not guarantee the safety of patients and staff. By introducing a procedure of integral and multidisciplinary acceptance testing of medical rooms based on the type of medical treatments, a safe environment upon first use is ensured. Our next steps will focus on the implementation of a change management procedure for medical rooms to guarantee the safety of a room during its life cycle.

PS16.038 - Real-Time Posture Classification and Correction based on a Neuro-Fuzzy Control System

Author(s): Leonardo P.D.V.M. Martins¹, Hugo Pereira¹, Bruno Ribeiro¹, Rui Almeida¹, Ana Teresa Gabriel², Cláudia Quaresma², Adelaide Ferreira¹, Pedro Vieira¹

¹Physics, Faculty of Sciences and Technology New University of Lisbon, Caparica/PORTUGAL, ²LIBPhys-UNL, Department of Physics, Faculty of Sciences and Technology New University of Lisbon, Caparica/PORTUGAL

Sitting position is one of the most common postures found in an office environments leading to long periods of time in that position. Assuming a poor posture in a sitting position during these long periods can even set this situation to worsen conditions, as this can lead to several health problems, namely back, shoulder and neck pain. To support the efforts in reducing such ailments, intelligent chairs are being developed in order to detect and correct poor sitting postures and alert the users to prolonged sitting behaviours. Here we describe the development of a chair prototype equipped with air bladders in the chair’s seat-pad and backrest, a pneumatic circuit composed of air and vacuum pumps to respectively inflate and deflate said bladders and piezoelectric gauge pressure sensor to measure the internal bladder pressure (Figure 1). The air bladders, which were previously manually manufactured, are now industrially assembled to improve reproducibility. We use a machine learning approach by using an Artificial Neural Network Algorithm (using 15 neurons, 1 hidden layer, tansig as the transfer function, and resilient backpropagation as the training function) to classify 12 standard sitting postures (Seated postures used in the experiments and their respective class label: seated upright, leaning forward, leaning back, leaning back with no lumbar support, leaning left, leaning right, right leg crossed, right leg crossed, leaning left, left leg crossed, left leg crossed, leaning right, left leg over right, right leg over left.) with an overall score of 81%. We optimized the classification to around 87% using Decision trees and the anthropometric information of the user, such as height and weight. Fuzzy Logic was introduced to the existing Algorithm by using as input the Centre of Pressure, the Posture Adoption Time and the Posture Output from the existing Neural Network Algorithm. This new Neuro-Fuzzy Algorithm now takes into ac-

count intermediate postures between the previous standard and the time period adopted in each posture, prompting the development of a Fuzzy Control System that inflates and deflates each bladder during a specific period of time according to the Fuzzy Output.

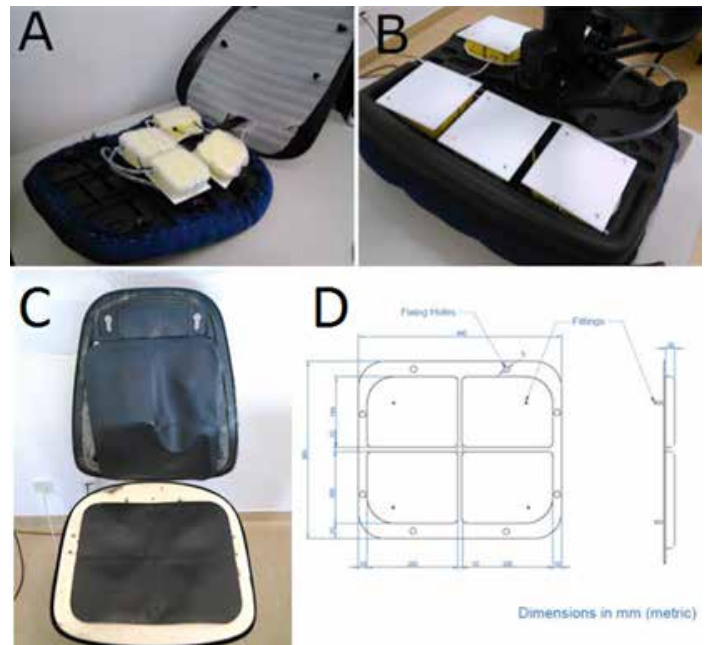


Figure 1: A – Placement of the pneumatic control modules in the back rest; B – Placement of the pneumatic control modules in the seat pad; C – Placement of the air bladders in the inside the padding of the chair. D – Industrial design of the air bladders from the second prototype

PS16.039 - Management of electromagnetic interferences in healthcare facilities - A Review

Author(s): Gnahoua Zoabli¹, Nabilath A. Akimey²

¹Biomedical Engineering, CSSS du Lac-des-Deux-Montagnes, St-Eustache/CANADA, ²Institute Of Biomedical Engineering, University of Montreal, Montreal/CANADA

Management of electromagnetic interference has become a major issue in Quebec hospitals. Several discussions on this issue have been held between managers of medical technologies departments. Some hospitals tend to allow more widespread use of wireless technologies while others continue to formally ban them. As a contribution, we present a review of literature on devices that may transmit frequencies that can interfere with medical devices, such as pagers, cordless phones, cell phones, tablets, portable radio transceivers, tracking devices, laptop computers, telecommunications antennas and medical equipment. Because of its wide availability, portability and accessibility, cell phone is the most popular wireless technology. The greatest distance of immunity known to date is 6 m, excluding the combination effect of the agglomeration of several electromagnetic sources in the same area. From our literature review it is safe to allow cell phones in a health facility if the usage is made out of a nursing unit, regardless of the vocation (critical or general Medicine) or outside of a diagnostic or medical department (medical imaging and laboratories). By cons, for medical imaging technologists carrying a pocket dosimeter (immunity of 38 cm), the use of cell phones might be banned while still carrying the dosimeter. The nuisance caused by cell phones, their need for regular disinfection by their owners and the protection of privacy should be considered by healthcare facilities in preparation of regulations, procedures or policies on health and safety at work. A subsequent study should

analyze electromagnetic interference of medical equipment between them. Hospitals that have already authorized the use of cell phones on the care units would benefit requiring phones with Flight mode enabled, pending the development of a Hospital mode that inhibits, in addition, sound recording, video camera and forces the phone ring mode to vibration.

PS16.040 - Hospital Mode Design in Smartphones and Tablets for Wireless Security in Healthcare Facilities

Author(s): Gnahoua Zoabli¹, Akimey A. Nabilath²

¹Biomedical Engineering, CSSS du Lac-des-Deux-Montagnes, St-Eustache/CANADA, ²Institute Of Biomedical Engineering, University of Montreal, Montreal/CANADA

Despite the presence of policies and procedures regarding the regulation of the use of wireless devices in hospitals, they are hard to make effective for employees, patients and visitors. Considering many concerns related to electromagnetic interferences and patient privacy, we suggest a more realistic approach based on the design of a Hospital Mode in smartphones and tablets. Hospital Mode manages electromagnetic interference, noise nuisance, protection of privacy, sound level and inhibits video camera and forces the phone ring mode to vibration in non-clinical area. A key aspect of Hospital mode resides on its ability to switch automatically the smartphone or tablet ON and OFF depending on the area of the hospital. We recommend a regulation towards smart building integrating dedicated frequencies bandwidth to manage Hospital Mode for any compliant wireless technology.

PS17 - TRACK 17: EDUCATIONAL AND PROFESSIONAL ACTIVITIES

PS17.001 - A discipline about Human Factors Engineering and Usability applied to Medical Devices for under graduation courses using Active Learning techniques

Author(s): Renata A.R. Custódio¹, Ana P.S.S. Almeida², Rodrigo M.A. Almeida³, José A. Ferreira Filho³, Alexandre C.B. Ramos¹
¹Institute Of Mathematics And Computer Science, Federal University of Itajubá, Itajubá/BRAZIL, ²Institute Of Industrial Engineering, Federal University of Itajubá, Itajubá/BRAZIL, ³Institute Of Systems Engineering And Information Technology, Federal University of Itajubá, Itajubá/BRAZIL

This paper proposes a new discipline with hybrid methodology mixing traditional approach and Project Based Learning, using some active learning techniques as peer instruction to teach Human Factors and Usability focused on Medical Devices. This course will be offered in Federal University of Itajuba for undergrad students in Computer Sciences, Information System, Computer Engineering, Control and Automation Engineering, Electronic Engineering and Industrial Engineering. The dynamics of the classes will be guided by working in teams of students and tutoring in the proposed Project Based Learning themes. Some formal lectures about specific concepts and methods throughout the development and analysis of the proposed problems will also be held. It is expected to have a greater conceptual gain with a higher engagement by students. To evaluate the student achievement, an assessment will be applied to the end of the course, targeting both the knowledge gain and the student's motivation.

PS17.002 - The medical equipment management inside the accreditation process: a comparison with the Brazilian accredited hospitals

Author(s): João E. Côrrea¹, Rodrigo M.A. Almeida², João B. Turrioni¹
¹Institute Of Industrial Engineering, Federal University of Itajubá, Itajubá/MG/BRAZIL, ²Institute Of Systems Engineering And Information Technology, Federal University of Itajubá, Itajubá/BRAZIL

This work aims to analyze the process of management of medical equipment in hospitals and compare the views of JCI, QMENTUM and ONA, a Brazilian accreditation model, on this topic. To the date these three accreditation models are the ones being used in Brazil. The survey results showed that for the Brazilian hospitals the accreditation model ONA becomes more efficient since it more in line with the reality of Brazilian hospitals.

PS17.003 - The Medical Physics M.Sc. program at the National University of Mexico:

Results and lessons learned after 100+ graduates

Author(s): María-Ester Brandan

Instituto De Física, Universidad Nacional Autónoma de México UNAM, Mexico City/MEXICO

The M.Sc. (Medical Physics) program at the National Autonomous University of Mexico (UNAM) is one of two in the country. After 17 years of activities, it has graduated more than 100 students who mostly work (60%) in clinical activities. A large fraction (26%) of the graduates is presently studying, or has already completed a Ph.D. in medical physics. 8% of our former students work in non-clinical activities related to medical physics. The academic program has been revised in 3 occasions (the original 1997 curriculum, and 2003 and 2009 revisions). Accumulated experience, increased available human resources, and recently published international recommendations for educating medical physicists have determined the curricu-

lar changes. The most visible operational changes have been higher entrance requirements and promotion of a more efficient use of the time during the thesis project execution. The main obstacle for a rapid graduation has always been the thesis completion. Thanks to various strategies, graduation time including the thesis defense, has decreased from almost 4 years at the start to 2.7 years now. The areas for the required thesis have always been relatively wide and continue to expand as medical and biological physics develop in the country. Former students who get a doctorate and join Mexican universities are having an impact in the development of new research groups. Currently, the UNAM Physical Sciences Graduate program considers establishing the medical and biological physics fields of knowledge as academic options within its Ph.D. in Physics.

PS17.004 - An Experience on the dosimetry of HDR Brachytherapy Treatment Planning of Cervical Carcinoma at BPKM Cancer Hospital, Nepal

Author(s): Surendra B. Chand

Radiation Oncology, BPKM cancer Hospital, Bharatpur/NEPAL

Propose: To identify the status of Brachytherapy planning by evaluating the bladder and rectum dose of cervical carcinoma patients those undergone HRD brachytherapy for six years.

Methods and materials: Fifteen hundreds and ten patients, from 2005 to 2010, were taken for this study. In total four thousands five hundreds and thirty treatment plans were done to complete all patients' treatment. The Fletcher Suit Delclos FSD types of applicators, orthogonal radiographs were used for dosimetry. Radio opaque dye and rectal probe is used to identify bladder and rectum location respectively.

Results: 1510 patients completed all three cycle of treatments. Maximum patients, 1055 (69.87%), have received bladder dose less than 4 gray per fraction. Less than five percent patients have received bladder dose more than 71 % of prescribed dose per fraction. Similarly; In case of rectum dose, total 1324 (87.68%) pts has received rectal dose less than 57 % per cycle. 1324 (87.68%) pts have received dose less than four gray per fraction.

Conclusions: Maximum patients were treated with bladder and rectal dose less than 60 Percentages of point A dose with satisfactory pear shape. Normal organ dose should minimise, however, it should not produce a significant reduction in disease control.

Keywords: HDR Brachytherapy, Remote after loading, ICRU38, cervical carcinoma patients.

PS17.005 - Health IT Education for Clinical Engineers

Author(s): Thomas M. Judd¹, Elliot B. Sloane²

¹Clinical Technology, Kaiser Permanente, Marietta/GA/UNITED STATES OF AMERICA, ²Executive Director, CHIRP, Blue Bell/PA/UNITED STATES OF AMERICA

Relevant Health IT education content and opportunities for Clinical Engineers (CE) and health technology management (HTM) leaders, both in developed and developing countries, will be explored through three case studies:

1. the US Veterans Administration (VA) HTM Health IT education program in 2015
2. a global program developed by ACCE and IFMBE-CED in 2015
3. Consultations for Ministry of Health Health IT in developing countries in 2014-2015

PS17.006 - Professional Development of Medical Physicists in Radiation Oncology for the Commonwealth of Independent States

Author(s): Valeriy A. Kostylev¹, Marina V. Kislyakova¹, Mikhail N. Ly-senko², Dmitriy V. Ulanov², Dmitriy V. Kostylev¹, Pavel V. Kazantsev¹ ¹Association of Medical Physicists in Russia, Moscow/RUSSIAN FEDERATION, ²State Atomic Energy Corporation "ROSATOM", Moscow/RUSSIAN FEDERATION

The need for the training and continuing professional development (CPD) of medical radiation physicists in Russia and CIS countries has dramatically increased lately due to the activation of the purchases of the state-of-the-art equipment and cutting-edge technologies for the modernization and reconstruction of radiation therapy departments. The efficiency of radiotherapy treatment for cancer patients and use of the state-of-the-art accelerator facilities highly depends on the qualification and number of medical physicists. There is currently an acute shortage of medical physicists in the CIS region. The qualitative professional training of medical physicists is the priority task in these countries. The fulfilment of this task has become possible due to the cooperation between the IAEA, Rosatom and Association of medical physicists in Russia (AMPR) who initiated and launched two IAEA Technical Cooperation (IAEA TC) Projects on Building Capacity for Medical Physics in Radiation Oncology for the Commonwealth of Independent States. The International Training Centre (ITC) of the Association of medical physicists in Russia based at the N.N. Blokhin Russian Cancer Research Centre is the main counterpart in the 2012-2015 IAEA TC Projects designed for the Russian-speaking medical physicists of the CIS countries to improve their knowledge and skills in the radiotherapy physics. The objective of the regional projects is to level differences in radiation oncology among CIS countries through education and training of medical physicists. ITC plays a key role in the implementation of the Projects by hosting trainees and executing training courses and practical sessions. During three years (2012-2014) of the IAEA TC projects 10 regional courses of 1-3 week duration were conducted. A 3-month group fellowship on practical aspects of medical radiation physics in radiotherapy was organized for 5 fellows from Kazakhstan, Kyrgyzstan, Moldova, Tajikistan and Uzbekistan. A total of 197 medical physicists were trained from 10 CIS Countries (Azerbaijan, Armenia, Belarus, Kazakhstan, Kyrgyzstan, Moldova, Russia, Tajikistan, Uzbekistan, Ukraine) and Lithuania. The table below shows the number of trainees from each country:

Country	Number of trainees
Azerbaijan	6
Armenia	6
Belarus	21
Kazakhstan	33
Kyrgyzstan	5
Moldova	9
Russia	67
Tajikistan	8
Uzbekistan	3
Ukraine	30
Lithuania	9
Total	197

PS17.007 - Assistive Technologies in Biomedical Engineering Education**Author(s):** Lenka Lhotska¹, Tatjana Welzer²¹Department Of Cybernetics, Czech Technical University in Prague, Prague /CZECH REPUBLIC, ²University of Maribor, Maribor/SLOVENIA

At present the need for interdisciplinary education supporting development and practical application of assistive technologies (AT) is continuously growing. It is given by development of demographic and age structure of the population and the need to ensure support and safety of elderly and handicapped people with increased health and other risks. Currently there is lack of graduates having interdisciplinary theoretical education in the fields of electronics and information and communication technologies and simultaneously focusing on the whole complex of practical needs of applications related to assistive technologies (AT). When we started developing courses in this area we realized that the closest and already established study program is Biomedical Engineering. The students get required courses in electronics, information and communication technologies and physiology. Thus we can relatively easily extend the curricula with new topics needed for managing the area of assistive technologies.

We are also well aware of the fact that the universities try to support education of students with special needs as much as possible. However, the requirements on support range from very simple tools up to very sophisticated systems. This area is not yet mapped very well and needs more elaborate review.

Although this area is very challenging it also offers opportunities for direct involvement of students with special needs into research projects focused on development of assistive technologies because they know the problems very well and as team members they can contribute to successful development of new more advanced tools, devices and systems.

Although it seems that all new technologies are somehow covered by existing courses in electronics, informatics, telecommunications, etc., we see and the practice proves it frequently that these courses are not properly interconnected. Nowadays we educate engineers specialized in electronics, or telecommunications, or informatics. But many of them are lacking the system view on an interdisciplinary problem. They often understand a narrow area very deeply but they do not see its connections to other neighboring fields that are necessary when developing a complex system.

In addition to purely technical courses there must be introduced courses that cover problems of handicapped people (for example their sensing limitations linked with necessity of having different computer or device interfaces, movement limitations – different design of equipment). The students must acquire knowledge about different types of handicaps and means how to compensate them. Further they must be educated in the design of tools and devices with respect to cognitive impairments, vision and hearing problems, supported communication, supported mobility; assessment and requirement analysis, and related topics. Another large area of interest is eAccessibility, namely improvement of access of handicapped people to electronic resources, including Internet. And last, but not least the legal, ethical and social issues must be considered since we are working with sensitive data similarly to medical domain.

In the paper we present examples of courses on AT and involvement of students and/or users with special needs.

PS17.008 - Future-Proofing Physics and Engineering in Medicine**Author(s):** Kwan Hoong Ng

Department Of Biomedical Imaging, Faculty Of Medicine, University of Malaya, Kuala Lumpur/MALAYSIA

Medical physicists and biomedical engineers have played a pivotal role in the development of new technologies that have revolutionized the way medicine is practised today. They have been transforming scientific advances in research laboratories to improving the quality of life for patients. Indeed innovations such as computed tomography, positron emission tomography, magnetic resonance imaging, linear accelerators, artificial hearts, robotic surgery and bionic limbs have collectively improved the medical outcomes for millions of people. The emergence of precision medicine exemplifies the potential of emerging science to improve patient outcomes and support efficient health delivery. The multi-disciplinary and cross disciplinary nature lends them an edge in research innovation. However, current emphasis tends to only enhance the specific skill development and competency at the expense of future roles and opportunities. This emphasis is largely driven by financial and political pressures for optimizing limited resources in health care. This has raised serious concern on the ability of the next generation to innovate and lead the development of new technologies. The use of nanoparticles to treat tumours, targeted radionuclide therapy, high-intensity focused ultrasound, electromagnetic wave ablation and image-guided surgery are just some areas challenging the old paradigm. We should venture into and explore non-traditional and blurred boundaries between various medical disciplines from diagnosis to treatment.

How do we future-proof the next generation? We must reform the existing curriculum by embracing contemporary sciences such as molecular biology, systems biology, nanotechnology, advanced materials, bioinformatics, spectroscopy, etc. We should encourage collaboration and interchange of ideas between medical and non-medical physicists; biomedical and non-biomedical engineers. The next-generation must be able to work or lead effectively as part of a collaborative multidisciplinary team. They should be able to participate in intelligent discussions with surgeons, neurologists, cardiologists, imaging specialists, pharmacologists, technologists, statisticians, computer scientists, spectroscopists and biologists to various extent. Furthermore, they must also engage with the public on their role in healthcare and research activities. With the right approach, the next generation will then look forward to making continued and significant contributions to the “new world” medicine. As it is, various global health challenges await the ingenuity, versatility and curiosity of medical physicists and biomedical engineers.

PS17.009 - Nuclear and Radiological Emergencies - First IAEA Training Course for Medical Physicists**Author(s):** Fridtjof Nuesslin¹, Ahmed Meghzi²¹Radiooncology, Technische Universität München, Munich/GERMANY, ²Dosimetry And Medical Radiation Physics, IAEA, Vienna/AUSTRIA

The role of the medical physicist in preparedness and response to nuclear and radiological emergencies (NRE) has been discussed at previous joint IOMP-IAEA-WHO workshops (WC-2012, ICMP-2013). There was broad agreement that by virtue of their academic education and clinical training Medical Physicists with their expertise in radiation protection (e.g. radiation dosimetry, dose measurement, etc.) may be an added value of the workforce dealing with NRE. Most current medical physics curricula include topics relevant for NRE, like radiation dosimetry, handling radioactive materials and assessment of exposure, instrumentation, radiation monitoring, shielding, etc. However, specific training is essential – particularly in countries with no adequate emergency preparedness infrastructure – to enable a clinical medical physicist to be fully prepared to

respond efficiently in an event of NRE, within a national or local emergency response plan. To improve preparedness of the clinical medical physicists for events of NRE and to set a standard for knowledge acquirement, the IAEA developed a specific training package for medical radiation physicists. The training package consists of 14 modules, which can be delivered through a one-week Workshop. Additionally to the above topics, the course program includes specific training on protection strategies, medical management, psycho-social effects, impacts on mental health and effective risk communication. The 1st Workshop to be held shortly after the WC2015 will be organized by the IAEA and hosted by the University of Fukushima, in co-operation with the National Institute of Radiological Science (NIRS). The purpose of the Workshop is to provide the participants with a good understanding of their potential complementary roles in NRE situations, and to prepare them to contribute effectively to support the response to an NRE situation as identified in emergency preparedness plans. This pilot Workshop will target trainers who have the potential to train other medical physicists in their countries as well as other health care professionals in the response to NRE situations. Replication of this Workshop in due time is expected in order to increase the number of medical physicists who will be fully prepared to support NRE worldwide.

PS17.010 - Academic Real Time Digital Medical Image Processing Environment

Author(s): Rodolfo D.S. Ribeiro, Rianne B. Venancio, Ana Cláudia Patrocínio
College Of Electrical Engineering, Federal University of Uberlândia, Uberlândia/BRAZIL

In this work we developed an academic tool for teaching Digital Medical Image Processing in a Graphical interface using functions developed in MatLab. This platform makes possible the visualization of histograms, Fourier Spectra and the image in real time, with their modifications occurring as long as the user alter the image. We included the following functions in the software: brightness control, contrast control, contrast enhancement, histogram equalization, image inverse, image normalization, exponential transformation, gradient filter, logarithmic filter, Sobel filter, sum with original image, arithmetic average, geometrical average, Gaussian filter, median, maximum, minimum. We also included some noise options: exponential noise, gama noise, Gaussian noise, ReyLeight noise, Pepper noise, Salt noise, pepper and salt noise, white noise. Another interesting possibility is the comparison between the processed image and its original version besides the histogram and Fourier Spectra. A threshold tool is available to create binary images from the processing image. This process is possible anytime in the processing flow. It is possible to visualize the entire processing flow in an action log and save the image, histogram or Fourier Spectra in commercial image formats, such as .jpg or .tif. In addition, both common format images and DICOM are available in the software. In digital image processing classes in Federal University of Uberlândia, professors are already using the tool to show how some image processing functions work, besides a student who is developing his final undergraduate thesis in Biomedical Engineering in our system.

PS17.011 - Detection of Eye Movement; possibility how to control world

Author(s): Lukas Peter, Iveta Neprasova, Martin Cerny
VSB - Technical University of Ostrava, Ostrava/CZECH REPUBLIC

Electrooculography is one way how to detect eye movement. Nowadays represents this method a possible compromise between the price and accuracy of equipment. Development of this method also benefits from the contemporary trend of miniaturization when electrode can be attached e.g. to the goggles. It is not necessary

to have the electrodes attached on your face. Hardware solution of electrooculography and visualization software is presented. Furthermore mathematical dependency output voltage on input eye movement is determined. This work also brings the electrooculography method and principles to the awareness of students.

PS17.013 - Career Progression for Medical Physicists

Author(s): William H. Round
Engineering, University of Waikato, Hamilton/NEW ZEALAND

Some clinical medical physicists are employed under negotiated national/state/ provincial employment awards or contracts. These may be specific to medical physicists, or they may cover other clinical scientific professions as well. These awards often inherently define a career path for the physicists. In most countries a career path is not defined in any way, and in some countries a medical physics is not even recognised as a profession despite it being listed as such by the International Labour Organization.

But most medical physicists are not under an employment award, so they do not have a recognized career path to follow. Awards often provide guidance as to how a medical physicist's career is progressing and they often define the level of responsibility and expertise required at each stage of the structure. This provides certainty to the physicists as to what they can achieve career-wise and what they must do to progress.

A survey of existing employment structures and awards for medical physicists was carried out in early 2014. In some cases these were found to be little more than pay scales, but in some cases the documents are very detailed and run to dozens of pages. The more detailed documents define multi-level career structures with the degree of responsibility expected at each level and what must be achieved to advance through from one level to the next being explicitly defined. The more detailed awards inherently define how a medical physicist's career should progress and to offer guidance to those who employ medical physicists as to how they can develop career structures that will enable their employees to optimise their career and performance.

A well-designed award will also define minimum education and training requirements, require employers to make provision for the physicists' continuing professional development, deal with issues that arise when a physicist leaves the workforce for a period of time and wishes to re-enter it, and encourage and provide for joint clinical and academic appointments.

While regional medical physics societies are professional and not industrial organizations, they should all have career progression policies in place to offer guidance to both clinical medical physicists and their employers to ensure that the members of the clinical physics workforce can develop to their full potential. This will lead to improved medical physics professional standards and improved health care delivery.

PS17.014 - IOMP-W – the International Organization for Medical Physics Women Subcommittee

Author(s): Magdalena Stoeva¹, Virginia Tsapakis², Simone Kodlovich³, Anchali Krisanachinda⁴, Nicole Ranger⁵, Teh Lin⁶, Amanda Cherpak⁷, Jamila Al Suwaidi⁸, Efi Koutsouveli⁹, Pola Platoni¹⁰

¹Medical Imaging Dept., Medical University - Plovdiv, Plovdiv/BULGARIA, ²Konstantopoulou General Hospital, Athens/GREECE, ³National Commission of Nuclear Energy, Rio de Janeiro/BRAZIL, ⁴Radiology, Faculty of Medicine Chulalongkorn University, Bangkok/THAILAND, ⁵c/o Landauer Inc, Glenwood/IL/UNITED STATES OF AMERICA, ⁶Fox Chase Cancer Center/Temple University, Philadelphia/PA/UNITED STATES OF AMERICA, ⁷Nova Scotia Cancer Cen-

tre, Halifax/NS/CANADA, ⁸Dubai Health Authority, Medical Education Department, Dubai/UNITED ARAB EMIRATES, ⁹Ygeia Hospital, Athens/GREECE, ¹⁰Attikon Hospital, Athens/GREECE

The International Organization for Medical Physics Women Subcommittee (IOMP-W) has been recently established to meet the demands of the women in our professional society for an official representation in the governing body.



The objective of IOMP-W is in compliance with the main IOMP mission and directives to advance medical physics practice worldwide by disseminating scientific and technical information, fostering the educational and professional development of medical physicists, and promoting the highest quality medical services for patients.

IOMP-W Functions:

Develop, implement and coordinate tasks and projects related to the role of females in medical physics scientific, educational and practical aspects.

To disseminate the experiences, good practice and learning within IOMP NMOs and other relevant accessible areas/across the globe.

Popularize the role of the women in medical physics and encourage female medical physicist to advance in the profession.

Organize international cooperation in medical physics and related specialties.

Provide regular status/progress updates to the IOMP on all tasks and projects related to the IOMP Female Group.

IOMP-W has currently focused on various dissemination activities to popularize the committee among the professional society. The major dissemination activities are directed toward the development of IOMP-W section under the main IOMP website, various advertising materials, participation in scientific and professional events, establishing and strengthening our relations with other organizations. Parallel to these dissemination activities IOMP-W took a leading role in a worldwide survey to assess the role of the women in the field of medical physics.

IOMP-W is also turning to the past to memorize and honor the women that contributed towards the development of Medical Physics. Special posters have been developed to present the work of Marie Curie, Irène Joliot-Curie, Goeppert-Mayer, Rosalyn S. Yalow, Harriet Brooks, Chien-Shiung Wu.

IOMP-W are planning to extend these activities to a larger scale to cover IOMP Regional societies and NMO's to popularize the role of women MP's and contribute towards the improvement of our profession worldwide.

PS17.015 - AAPM/IOMP Used Equipment Donation Program

Author(s): Mohammed K. Zaidi

Idaho State University, Houston/UNITED STATES OF AMERICA

The objective of the Used Equipment Donation Program (UEDP) of the American Association of Physicists in Medicine (AAPM) and the International Organization for Medical Physics (IOMP) is to help developing countries acquire used equipment in good working condition through donations of used equipment made through AAPM/IOMP. The UEDP insists that the used equipment donated is in good working condition and verifies as-far-as possible that it meets the need of the recipient developing country (DC). The guidance in the 'WHO Guidelines for Healthcare Equipment Donations' (WHO, 2000) is adhered to and relevant regulations are followed. Technical assistance is given, if need in installation or training is needed. The recipient pays for the handling and shipping and some financial help is available in special cases. UEDP reports are published in the IOMP publication Medical Physics World (MPW).

PS18 - TRACK 18: GENDER, SCIENCE AND TECHNOLOGY

PS18.001 - Bone density measurements in strontium-rich bone-mimicking phantoms using quantitative ultrasound

Author(s): Bisma Rizvi, Eric D. Silva, Jahan Tavakkoli, Ana Pejovic-Milic
Physics, Ryerson University, Toronto/CANADA

Objectives: Osteoporosis is a disease characterized by decreasing bone density and microarchitectural deterioration of bone tissue, which enhances bone fragility and fracture risk. Strontium renalate, is reported to promote bone formation and inhibit bone resorption, thus maintaining and increasing the bone mineral density (BMD) of osteoporotic individuals. Consumption of the strontium renalate for more than six months affects BMD scores, as assessed by dual energy X-ray absorptiometry (DEXA). Such DEXA-determined BMD scores often present a positive bias. Self-administration of strontium-based supplements, which is becoming prevalent, is expected to have the same impact on bone density measurements as strontium renalate.

The objectives of this work are: (1) to develop novel bone-mimicking phantoms containing different concentrations of strontium, and (2) to investigate the effect of bone strontium content on bone mineral density (BMD) obtained by a bench-top transmission-through quantitative ultrasound (QUS) system.

Materials and Methods: Preliminary investigation was performed using the bench-top QUS beam on a new generation of bone-mimicking phantoms composed of hydroxyapatite and gelatin in an airtight container with dimensions of 2.5x6.5x6.5 cm³. These bone-mimicking phantoms contained different concentrations of strontium and/or with a varying bone density. Using the bench-top QUS system, the broadband ultrasound attenuation (BUA) and speed of sound (SOS) of the phantoms were measured in an ultrasound frequency range of 0.5-1.3 MHz.

Results: Measurements using the bench-top QUS system showed a strong dependency of the BUA with the BMD ($p < 0.001$). On the other hand, dependency between the SOS and the BMD was not statistically significant ($p = 0.095$). Moreover, increasing bone strontium concentrations up to 3 mol% strontium showed no effect on the BUA ($p = 0.749$) or the SOS ($p = 0.862$) values measured in this study.

Conclusions: The results obtained in this study suggest that the QUS is a promising diagnostic tool capable of providing BMD scores independent of bone strontium content. This could be relevant in QUS evaluations using commercially available clinical systems in individuals who are being treated for osteoporosis using strontium-based drugs or through self-supplementation with various strontium compounds.

PS19 - TRACK 19: BIOPHYSICS AND MODELLING

PS19.001 - Numerical Modeling Of The Electrical Impedance Method Of Peripheral Veins Localization

Author(s): Mugeb B. Al-Harosh, Sergey I. Shchukin
Medical And Technical Information Technology, Bauman Moscow state technical university, moscow/RUSSIAN FEDERATION

Veins in biological tissue produce electrical impedance to the alternating current passes through it. Bio-impedance method based on measuring this electrical impedance value using an array of surface electrodes has the capability of detecting peripheral veins. This paper presents the theoretical and experimental studies, reflecting the possibility of impedance method of peripheral veins localization. Mathematical model has been proposed to calculate the resistivity anomalies of vein in soft tissues and reflects the electrical impedance characteristic, depending on the location of the electrode system and the vein. A system electrode has been designed to be attached to the body in order to measure the electrical impedance value. The data obtained will determine the capabilities of the method. Experimental studies confirm the adequacy of the proposed mathematical model

PS19.002 - Modeling current density maps in the heart

Author(s): Mohammadali Beheshti¹, Farbod H. Foomany¹, Karl Magtibay¹, Stephane Masse², David A. Jaffray³, Kumaraswamy Nanthakumar², Sridhar Krishnan¹, Karthi Umapathy¹
¹ryerson university, toronto/CANADA, ²Peter Munk Cardiac Centre, toronto general hospital, Toronto/ON/CANADA, ³Radiation Physics Department, princess margaret hospital, toronto/CANADA

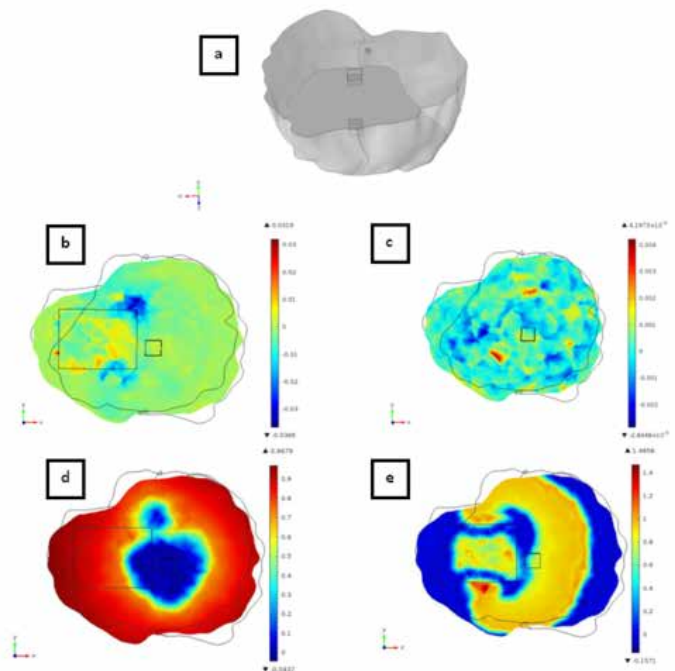
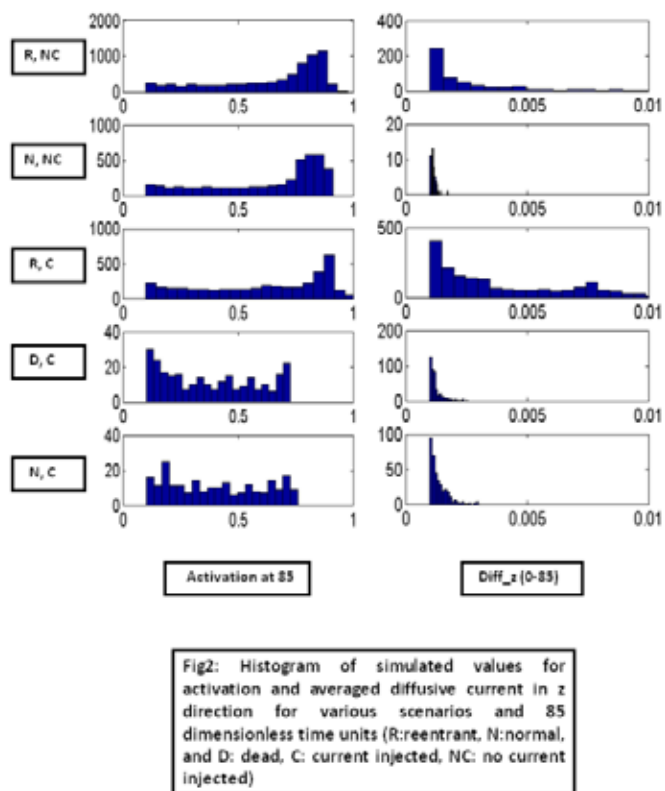


Fig1: a) Geometry of modeled heart, b) simulated diffusive current in z direction in a chosen slice for reentrant scenario, c) simulated diffusive current in z direction in a chosen slice for normal scenario, d) and e) simulated activation in the chosen slice at two different time steps for reentrant scenario (red represents active and dark blue represents cells at rest, the values are dimensionless based on Aliev-Panfilov model)



Background:

The electrophysiological state of the heart is known to vary in different heart conditions. However it is hard to measure electrical activity inside the heart tissue. Magnetic Resonance Imaging (MRI) based Current Density Imaging (CDI) is able to provide a three-dimensional map of current pathways inside the tissue. However due to the experimental setup and logistics issues it is difficult to perform CDI either in ex-vivo or in-vivo hearts. Therefore generating a model that simulates CDI maps for the purpose of studying cardiac electrical activity could improve the understanding of current distributions in various heart conditions.

Method:

The current density maps are simulated using Aliev-Panfilov electrophysiological model. The averaged diffusive current in the mathematical model is related to the current density and the diffusion tensor representing heart structure is extracted from Diffusion Tensor Imaging (DTI). A single source of excitation mimicking the Sinoatrial Node (small sphere in Fig1.a) is considered and two electrodes simulate the CDI electrodes (Fig 1.a). Three different heart conditions are considered for both cases of presence and absence of injected current. The condition “dead” (D) represents excitable cells while there is no natural excitation in the heart, “reentrant” (R) is created by blocking ion channels in a cubic area temporarily (Figs 1.b,d and e), and “normal” (N) in which there is natural excitation without any block.

Results & Conclusion:

Averaged diffusive current density patterns generated from the theoretical model shows the difference between states (Figs 1.b, and 1.c), Figs 1.d and 1.e show the activation maps at two time instances for reentrant scenario, the results are shown for a chosen slice. Histograms of the results (Fig 2) show the possibility of detecting various states using averaged diffusive current. This demonstrates high potential of CDI as a tool to study various heart states.

PS19.003 - Finite Element Modeling of Gelatin Phantom from Measured Impedance Spectra

Author(s): Douglas Dutra¹, Ana M.R. Pinto², Pedro Bertemes-Filho¹, Aleksander S. Paterno¹

¹Electrical Engineering, Universidade do Estado de Santa Catarina, Joinville/BRAZIL, ²INESC P&D Brazil, Santos/BRAZIL

Gelatin has been used as a phantom in different medical applications, as in electrical impedance spectroscopy. In this paper, the measured spectra of resistance and reactance of three gelatins with different concentrations of salt are presented. The Cole-Cole equation and the Debye model were used to fit the data by using a script written in MATLAB. The best set of these parameters offers the lower least mean square error when compared to the measured ones. The complex permittivity is then calculated as a function of frequency by using a software developed in finite element modeling (FEM), which solved the governing equations for the electrical field and potential. The measured and simulated data from FEM showed closer spectra than fitted one. It can be concluded that the FEM technique can be used to predict the impedance spectrum of gelatins as a tissue phantom. This might be a useful tool for modeling materials in biomedical, pharmaceutical and cosmetic applications.

PS19.004 - Prediction of radiation induced direct and indirect cellular damage using a novel ionisation spatial clustering algorithm

Author(s): Michael J.J. Douglass, Eva Bezak, Scott Penfold
Medical Physics, Royal Adelaide Hospital, Adelaide/SA/AUSTRALIA

Aim:

It is accepted that clusters of DNA DSBs lead to cell death rather than individual DSBs following irradiation. Consequently, the total number of ionisation events/DSBs does not directly correlate with cell survival. A novel clustering algorithm was developed in this work to group spatially correlated ionisation events from radiation tracks to predict DSB formation.

Methods:

The Monte Carlo particle interaction code RITRACKS was used to simulate ionisation track structures of various heavy ions and the corresponding production/diffusion of free radicals in water medium. A spatial clustering algorithm was developed based on a hierarchical clustering function in Matlab to group ionisation events into DSBs to predict radiation induced cell death. The definition of a DSB according to (Stewart,2001) is two or more ionisation events located on the DNA double helix within a distance of 20 base pairs (bp), corresponding to a distance of 6.8 nm. Using this DSB definition, an original ionisation clustering algorithm was applied to predict the formation of DSB clusters in a cell. It was also used to determine the relative contribution from direct and indirect radiation damage to DSB formation as a function of the LET and atomic number of the ion.

Results and Conclusions:

Figure 1 illustrates how the complexity of radiation induced DNA DSBs change with particle LET. While higher energy protons produce more ionisation events per track, the complexity of the radiation damages they produce is less compared to low energy protons.

Figure 2 shows the relative contribution from indirect radiation damage (% as compared with direct damages) with increasing particle LET. The indirect damage decreases exponentially with increasing LET. The indirect contribution from heavy ions can be as high as 70% for photons, 50% for carbon ions and 30% for iron ions in the LET range investigated.

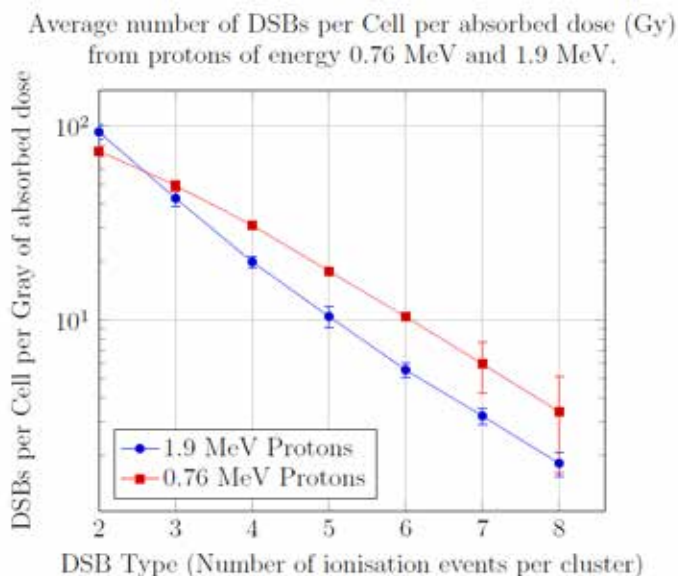


Figure 1.

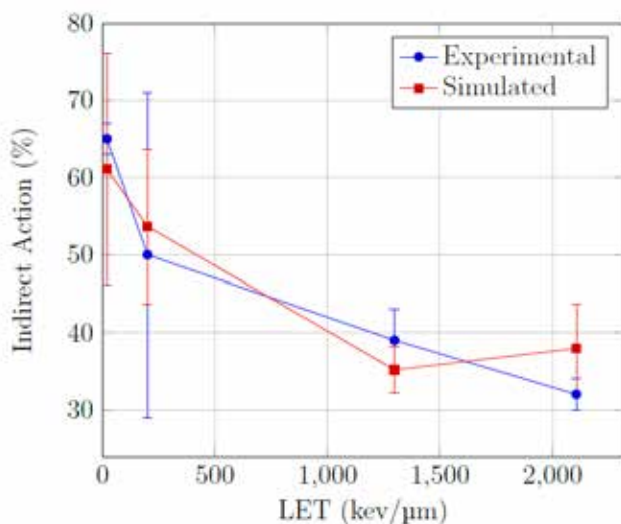


Figure 2.

PS19.005 - Research on Vibration of Cell Membrane of Plant Seed with Ultrasonic Excitation

Author(s): Hui Cao

School of Physics & Information Technology of Shaanxi Normal University, Xi'an/CHINA

Ultrasonic radiation for plant seed can enhance the permeability of cell membrane, which is mainly related to the mechanical effect of ultrasound. Enhancing the permeability of cell membrane improves the germination rate and production of plant seed. The shape of plant cell wall is approximately like ellipse and cell membrane as the boundary of cell is usually close to the cell wall. The elastic vibration induced by ultrasound is mainly the vibration of cell membrane from the perspective of structure and substance of cell wall and cell membrane, as cell wall can't vibrate elastically. Considering the complicated effect of cell wall and cytoplasm on the whole vibration system, it assumes that the effect can be ignored temporarily for simplifying calculation. So the cell membrane is studied as a single rectangular membrane and the frequency equation of cell

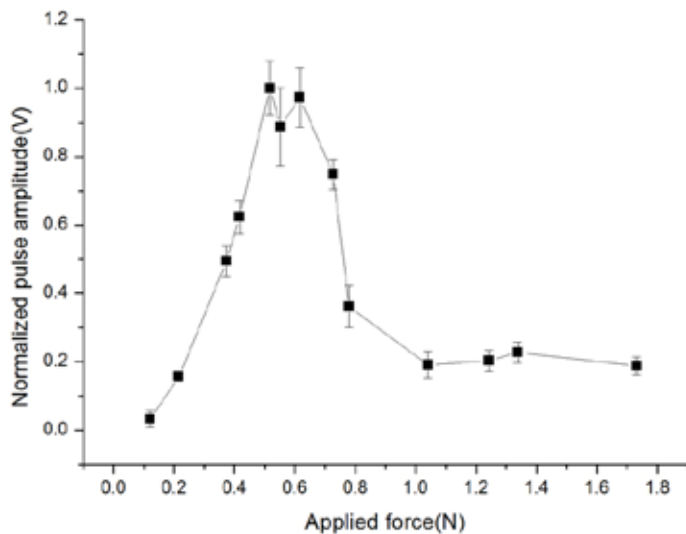
membrane under the ultrasonic excitation is obtained through the acoustical theory and biological knowledge. Provided that the cell membrane is a thin slice which is completely soft and has the same thickness. It further assumes that the cell membrane suffers uniform tension along any direction and the tension is so strong that the fluctuation of tension induced by the small deflection can be negligible in the course of vibration. Then according to the deduction of Ritz method, the vibration equation of cell membrane with ultrasonic excitation is obtained. The parameters included in the equation are the semi-major axis and semi-minor axis of ellipse, angular frequency, acceleration of gravity, surface tension and surface density. These parameters can be determined by experimental method, then the angular frequency is calculated through the equation and the resonance frequency is obtained. When the frequency of acoustic wave reaches the resonance frequency of cell membrane, it will make the cell membrane resonance and enhance the permeability of cell membrane. The vibration amplitude at this time is the largest, which makes ultrasonic energy enter the cell to the biggest extent and result in a series of biophysical effects. The conclusion of this paper is applied to the cells of gynostemma seeds and the theoretical value is found to coincide with the experiment value, thus confirming that this theoretical model has certain correctness.

PS19.006 - The Effect of Applied Force on Arterial Pulse with a New Flexible Pressure Sensor

Author(s): Wenxuan Dai¹, Ningqi Luo¹, Jing Liu¹, Xiaorong Ding¹, Ni Zhao¹, Yuanting Zhang²

¹Electronic Engineering, Chinese University of Hong Kong, Hong Kong/HONG KONG, ²Shenzhen Institute Of Advanced Technology, Chinese Academy of Science, Shenzhen/CHINA

Arterial pulse has always been considered as an important signal containing abundant information of human body. Thanks to the recent advancement of high sensitivity flexible pressure sensors, which are small, light-weighted and more adaptable to human skin, pulse signals can now be detected from radial or carotid artery over the skin unobtrusively and continuously. The flexible sensors can be worn on skin not only for the monitoring of health status but also for the possible early prediction of cardiovascular acute events in real time. One of the key issues regarding practical applications is to understand the interaction and adaptation of the sensors to human skin. In this work we used a resistive flexible pressure sensor made in our own research Lab to measure arterial radial pulse at wrist and studied the effects of external force applied over the flexible sensor on the measured arterial pulse signals. The signals were recorded from 10 healthy subjects under 13 increasing magnitudes of applied force (0.1-1.8N) with duration of 2 minutes for each trial. The following figure shows the normalized pulse amplitude (the amplitude of AC component of the detected arterial pulse signal) under different levels of applied force. It is observed from this study that 1) as applied force increased, the pulse amplitude of all subjects shared a same tendency-first increase and then decrease; 2) the force where the pulse amplitude reached its maxima varied among different subjects. Our experimental findings suggest that the effect of applied force should be carefully examined when applying the flexible device for physiological signal measurements. Based on this study, we are currently recruiting patients for a clinical trial and developing a model for the unobtrusive real time monitoring of the internal arterial pressure with the ultimate goal of predicting cardiovascular diseases at the early possible stage.



PS19.007 - The Art of Engineering Medicine: A New Fast Non-Invasive Method to Directly Assess Ischemia in Human Diseased Coronary Arteries

Author(s): [Iyad Fayssal](#), Fadl Moukalled, Samir Alam, Robert Habib, Hussain Ismaeel
American University of Beirut, Beirut/LEBANON

Fractional flow reserve (FFR) is a traditional indicatory index used to assess functional stenosis severity and determine whether a stenosis causes ischemia or not. Invasively measured FFR values ≤ 0.8 indicate that the downstream heart tissue perfused by this vessel is at risk for ischemia. Currently, measuring FFR is an invasive procedure that is expensive, time consuming, not widely available, and not without complications. Recently, comprehensive predictive techniques involving numerical methods have gained attention. In specific, the use of computational fluid dynamics (CFD) methodologies combined with patient specific data allows computing in-vivo FFR. However, these non-invasive methods are associated with high computational cost and require high performance computing technology. This study focuses on the development of new strategies to reduce computational run time of solution prediction. The first strategy is based on isolating the diseased artery and simulating it separately without implicitly integrating other arterial segments while retrieving the accuracy of in-vivo hemodynamic significance of the stenosis. Special treatment of boundary conditions at the truncated domain was done via an in-house developed methodology, allowing to directly estimating ischemia in the stenosed artery. The second strategy is based on replacing a full transient simulation by a steady state one performed under mean conditions. The value of the developed strategies lies in their potential to (i) replace the experimental method which is based on intrusive processes and (ii) be performed with low computational cost. The latter advantage can significantly impact the applicability of this method in clinical practice at large.

PS19.008 - Influence of the alteration of the flow topology during the abdominal aortic aneurysm growth.

Author(s): [Joly Florian](#), Gilles Soulez, Claude Kauffmann
Lcti, CRCHUM, Montréal/QC/CANADA

Introduction The Abdominal Aortic Aneurysm (AAA) is the 13th cause of death in the USA. Patient specific AAA growth prediction and rupture risk remains challenging but rests upon the sole measure of its maximal diameter. In order to update current diagnosis criteria, influence of the blood flow on growth mechanics should be taken into account. Knowledge of the patient geometry

and hemodynamics boundary conditions are required for a realistic numerical flow simulation. Flow can impact AAAs in several ways; here transient transport topology will be studied in the lumen. To correlate transport with morphological growth, simulations will be carried during the longitudinal study of patients with more than 4 follow-up CTA.

Methods Lumen and thrombus geometry extraction from all follow-up CTAs, volume computation and AAA growth estimation (i). Numerical simulation of the flow using FVM validated towards 4D MRI (ii). Simulation conditions: polyhedral mesh, Newtonian viscosity, transient mass flow inlet and 0D pressure outlet. Computation of the Finite Time Lyapunov Exponents (FTLE) of the flow (iii). The FTLE field is able to capture transport boundaries using data from a whole cardiac cycle.

Extraction and volume computation of enclosed stagnation zones and analysis of their progression over time, from AAA diagnosis to repair (iv).

Results Simulated flow topology showed a correspondence with MRI velocimetry experimental data. AAA lumen segmentation on seven patients over a cardiac pulse confirmed the hypothesis of a rigid wall condition on elderly patients. The transport study method allowed the isolation of stagnation zones from the circulating ones reproducibly. The volume of stagnation zones is highly correlated ($r=0.98$ and 0.93 , resp. red and green) with AAA growth while circulation zone's remains stable.

Discussion We present a numerical approach for the quantification of stagnation zones in AAAs. It takes into account the highly transient dynamics of the flow and offers a scalar Eulerian field representing a Lagrangian phenomenon. Stagnation zones are known for promoting the advection of shear-stress activated platelets to the wall leading to the apparition of ILT. More patients will be added to the study in order to better understand the relationship between transport, and AAA growth and thrombus formation. This could also give a better insight on the dynamics of the AAA growth, a step toward predicting!

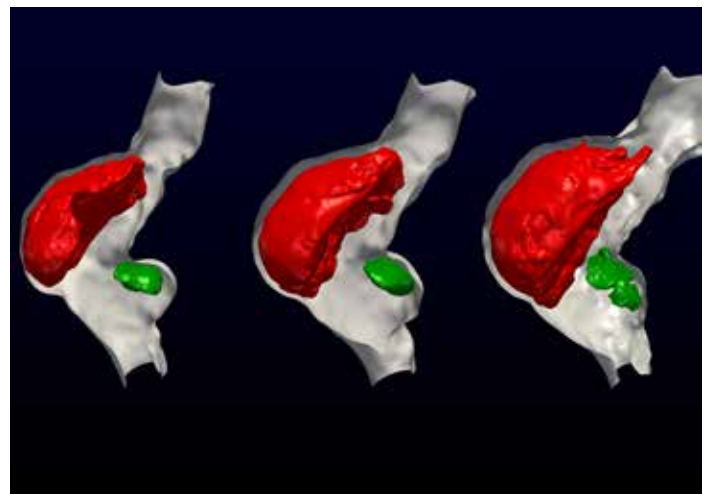


Figure: Example of the evolution over time (left to right: 2006, 2009 and 2012) and stagnation zones in a AAA. This patient presented two zones isolated in the flow.

PS19.009 - Using the DDST to Train and Test Anthropomorphic Robotic Children**Author(s):** Paul Frenger

A Working Hypothesis, Inc., Houston/TX/UNITED STATES OF AMERICA

Normal childhood growth and development (G&D) causes anxiety for parents, who want health care providers to examine their children, recording their progress against standards to facilitate early intervention if problems arise. The Denver Developmental Screening Test (DDST, 1967) can be utilized by doctors, nurses, teachers or other professionals with minimal G&D training. Along with its updated version (DDST II, 1992) it is the most widely used G&D measurement tool. The DDST was validated on normal children in Denver, Colorado, in the areas of gross motor, fine motor-adaptive, language and personal-social. Entries on the test sheets are organized by chronological age; i.e.: child “plays ball” at 10-12 months.

Recently, research into pediatric G&D led to models of robot-artificial intelligence (A.I.) that mimic child maturation processes. One example is the European iCub (2004-2010, Figure 1). The author’s ANNIE humanoid robot-A.I. (2000-present) predated iCub by four years. Regrettably, there is no standard training and evaluation methodology to uniformly compare techniques and outcomes between robots, or between the robot models and actual children. The author is attempting to fill this gap by using the DDST as a tool to accomplish these goals, with ANNIE the test subject.

ANNIE’s hardware and software have been described in detail at bioengineering and computer conferences, including CMBES. Its software relies on the Forth-language variant IEEE 1275-1994 (Open Firmware), a plug-and-play networking system. Its hardware includes analog artificial neuron circuits for its emotion engine and optical character recognition (OCR). The A.I. embeds a “subject-verb-object” format, compatible with DDST entries, in its schema-script system.

During training, modified DDST milestones in each of the four categories are input to the A.I. compiler. When ANNIE encounters objects not already known, (like “ball” or “raisin”) the compiler creates a blank database entry for each via Forth’s error-handling mechanisms. These unpopulated object entries are filled-in later as training progresses, including images taken from ANNIE’s machine vision eyes, sounds from its microphone-ears, and text from OCR and other sources.

During testing, each DDST challenge is presented to the robot (tests are input by keyboard rather than by ANNIE’s speech recognition system). The robot responds by attempting to demonstrate mastery of the test.

Result: with sufficient training, ANNIE performed every milestone except: walking, dressing, balancing, hopping- jumping (for which the robot is not yet equipped). The missing gross motor functions will be added in the future.



Figure 1: iCub plays ball (courtesy Wikimedia Commons).

PS19.010 - The new low-cost metaphase finder for biological dosimetry**Author(s):** Akira Furukawa

National Institute of Radiological Sciences, Chiba/JAPAN

Biological dosimetry is to estimate one’s dose by biological phenomena. Most popular and “gold standard” phenomenon is the appearance of dicentric chromosomes in one’s metaphase cells among white blood cells. Metaphase finder is a tool for biological dosimetry that finds metaphase cells on slide glasses. It consists of automated microscope, auto-focus system, X-Y stage, camera and computer. It does the image diagnosis of the microscopic images of the slide glasses, and displays the positions of metaphase cells. A metaphase finder is used for the personnel worked at Fukushima nuclear plant to know how much dose they irradiated.

The author and colleagues have already reported a low-cost metaphase finder system, using commercially-available products (1). Its software was application of mathematical morphology. But the system was a combination of multiple manufacturers and then it requires much knowledge and skill to the resellers and users. This system was more compact and less price than commercial products. The system would be another choice for resellers and users, but its speed was needed to faster.

Then, the author has collaborated with a software company to start new project to make another system. This system is using new special software is expected to be faster than non-custom made system. We used Nikon Eclipse Ni-E microscope with motorized X-Y stage, 4x objective lens and 1920 x 1024 pixels color camera for hardware. The software added the new function to compare the color of the image. The new system was also compact and low-price.

Now, the system was completed and we tested its speed. It was 13 minutes and 56 seconds per one slide, while capturing 1,333 images. We accomplished the aim of the project. The dicentric-dose curve will be shown in this presentation.

This research is supported by The Japan Science and Technology Agency.

(1) Akira Furukawa, Masako Minamihisamatsu, and Isamu Hayata: Low-cost metaphase finder system, Health Physics, Volume 98, Number 2, 2010.

PS19.011 - Concentrated photoactivation: focusing light through scattering

Author(s): Ana Teresa Gabriel¹, Jorge Machado¹, Ricardo Gomes², João Coelho³, Catarina Silva⁴, Catarina Reis⁴, José Paulo Santos¹, Pedro Vieira¹

¹LABPhys-UNL, Departamento de Física, Faculdade de Ciências e Tecnologia, Universidade Nova de Lisboa, Monte da Caparica/POR-TUGAL, ²Laboratório de Óptica Lasers e Sistemas, Faculdade de Ciências, Universidade de Lisboa, Lisboa/PORTUGAL, ³Instituto de Biofísica e Engenharia Biomédica, Faculdade de Ciências, Universidade de Lisboa, Lisboa/PORTUGAL, ⁴CBiOS - Centre for Research in Biosciences & Health Technologies, Universidade Lusófona,, Lisboa/PORTUGAL

Light has long been used in medicine; however, the high scattering of biological tissues always hindered its use. The aim of this work is the development of methodologies to focus light inside biological tissues. Geant4/GAMOS Monte Carlo platform was used to simulate the possibility of parameterize the time delay of multiple sources of external light, offset in time, as a function of the interest region position in order to create constructive interferences in a breast sample. A computational model was implemented and the platform was configured in order to perform these simulations. Preliminary results using a single light source were performed. It was concluded that scattering in adipose tissue is very high which is consistent with previous studies.

PS19.012 - Steered Molecular Dynamic Simulation Approaches for computing the Blood Brain Barrier (BBB) Diffusion Coefficient

Author(s): Maysam Pedram¹, Amir Shamloo¹, Aria Alasti¹, Ebrahim Ghafar Zadeh²

¹Sharif University of Technology, Tehran/IRAN, ²York University, Toronto/CANADA

In the recent years a great attention of research deals with different physical and biological aspects of the BBB structure, a robust shield that separates the blood and brain, a recent research held by the authors of this paper has focused on figuring out computing the diffusion coefficient of endothelial cell membrane. In this study, the major efforts have been concentrated on calculating a standardized measure for the amount of permeability and diffusion of this barrier. As a result, this work is dedicated to molecular dynamics (MD) simulation of calculating the interaction force between nano-particle and BBB membrane. data is recorded by using steered molecular dynamics simulation and crossing nano-particles with constant velocity for many times on both sides of the membrane. This data help to find diffusion coefficient in order it can convert the discrete medium simulation into continuum medium.

PS19.013 - The study of the relationship between the scatterer particle size of soft tissue in ultrasonic focal region and the frequency offset of backscattered signal

Author(s): Jianzhong Guo, Shuyu Lin, Hui Cao

School of Physics & Information Technology of Shaanxi Normal University, Xi'an/CHINA

The traditional B mode ultrasonic imaging equipment utilizes the information of amplitude envelope of ultrasonic backscattered RF signal to construct the soft tissue image, while other information such as frequency and phase is not fully utilized which is related to the microstructure of tissue. When the biological soft tissue have some pathological changes, its attenuation coefficient, elastic properties, particle size or concentration (the number of scatterers per unit volume) of ultrasonic feature scatterers will be changed accordingly. The power spectrum of ultrasonic backscattered RF signal of the soft tissue is related to the particle size, geometric shape, concen-

tration and elastic properties of ultrasonic feature scatterers.

Based on the ultrasound propagation property in biological soft tissues, it was studied that the relevance between the central frequency offset of ultrasonic backscattered RF signal and the particle size of ultrasonic feature scatterer. The interreaction of attenuation coefficient of tissue in the focal region of ultrasonic transducer, concentration of ultrasonic feature scatterer, as well as the central frequency, bandwidth and focusing properties of ultrasonic transducer on the central frequency offset was explored by means of the computer simulation.

Four experimental imitations with different particle sizes of scatterer were made, and the frequency characteristics of these fore types of ultrasonic backscattered signals were studied by the statistical signal process method. Experimental imitation was made by gelatin, glass bead, glycerin, distilled water, antiseptic and glutaraldehyde. The glass beads are special solid glass beads of 2#3#4# and 5# provided by Qinhuangdao QinHuang glass beads Co. LTD. Their average effective scatter radiuses are 36.25 mm, 47 mm, 55.25 mm and 64.25 mm, respectively.

The results of computer simulations reveal that the frequency shift of ultrasonic backscattered signal of soft tissues would increase with the particle size of ultrasonic feature scatterer increasing, and approximately shows a linear growth relationship. The frequency offsets is different with the different parameter of transducer such as the central frequency, bandwidth and focusing property, and the number concentration of ultrasonic feature scatterer and focusing property of transducer have not significant effect on the frequency offset.

The results of imitation experiments indicate that, with the increase of the effective scatter radius of ultrasonic feature scatterer, the central frequency of ultrasonic backscattered RF signals of experimental imitation would shift to the low frequency and is more and more close to the central frequency of ultrasonic exciting signal.

It can be concluded that the information of frequency and phase of ultrasonic backscattered RF echo signal may be used to study the microstructure characteristics of soft tissue and explore the application of ultrasonic diagnosis technology in the physiological pathology diagnosis of biological tissue.

PS19.014 - Dynamic Model for Shear Stress-Dependent NO and Purine Nucleotide Production from Endothelial Cells

Author(s): Patrick L. Kirby, Donald G. Buerk, Kenneth A. Barbee, Dov Jaron

School Of Biomedical Engineering And Health Sciences, Drexel University, Philadelphia/UNITED STATES OF AMERICA

We developed a dynamic mass transport model for a parallel-plate flow chamber apparatus that predicts concentrations of nitric oxide (NO) and purine nucleotides (ATP, ADP) produced by cultured endothelial cells (ECs). The flow chamber, which was designed and fabricated in our laboratory, permits real time *in vitro* measurements of NO produced by ECs at different levels of wall shear stress (τ_w) (Andrews et al., Nitric Oxide, 23(4):335-42, 2010). From steady-state NO measurements with bovine aortic ECs cultured in this chamber, Andrews et al. (2010) found that a hyperbolic function provided the best fit for the τ_w -dependent rate of NO production (R_{NO}).

$$R_{NO} = R_{\text{basal}} + R_{\text{max}} \left(\frac{\tau_w}{\tau_w + A} \right)$$

More recent studies with this flow chamber (Andrews et al., Cellular and Molecular Bioengineering, 7(4):510-20, 2014) investigated the role of τ_w -dependent release of ATP in modulating R_{NO} . In order to analyze data from these studies, we modified a previous model that characterizes the spatial distribution of NO in the chamber (Fadel

et al., *Annals of Biomedical Engineering*, 37(5):943-54, 2009). The modified model predicts how the net release rates and mass transport for NO, ATP, and ADP vary with changes in τ_w . Two previous models in the literature for ATP release and ADP formation were implemented. The first model (John and Barakat, *Annals of Biomedical Engineering*, 29(9):740-51, 2001) predicts a rapid rise in ATP and ADP to steady-state values within a few sec. The second model (Qin et al., *Biomechanics and Modeling in Mechanobiology*, 7(5):345-53, 2008) predicts a slower increase, reaching peak ATP and ADP values at different τ_w , followed by a slow decline in concentration, attributed to "receptor desensitization" (a reduction in the response with a longer stimulus).

Experimental data obtained after altering ATP and ADP concentrations with apyrase (Andrews et al., 2014) were analyzed to quantify changes in R_{NO} using this model. Apyrase is a calcium activated plasma membrane-bound enzyme that catalyzes the conversion of ATP to ADP, followed by conversion of ADP to AMP and inorganic phosphate. A reduction in τ_w -dependent R_{NO} was found when 1 Unit/mL apyrase was added to the media in the chamber, presumably due to lower ATP and ADP at the EC cell surface. The 2 ATP release models were used to predict effects of different isoenzymes of apyrase on ATP and ADP concentrations in the chamber, although the exact composition of apyrase used experimentally was uncertain. We explored different functional relationships to describe experimental changes in R_{NO} with τ_w due to changes in ATP and ADP. A reasonable fit was found with an apyrase isoform of Desiree which predicts the largest decrease in ATP and ADP. Further experimental data is required to validate the model and obtain better estimates for the model parameters. The dynamic model simulations provide a greater understanding of experimental results obtained with parallel-plate flow chambers and allows quantitative analysis of the relationship between τ_w , purine nucleotide concentrations, and NO produced by ECs.

PS19.015 - Mechanism of Phospholipase as a Potential Anti-Bacterial Drug Revealed by Nonlinear Spectroscopy

Author(s): Xiaolin Lu

School Of Biological Science And Medical Engineering, Southeast University, Southeast University, Nanjing/CHINA

Lipids play a fundamental role in diverse biological processes for energy storage, compartmentalization, and signaling, etc. In this respect, it is of great importance to understand the pathways and mechanisms of lipid metastasis triggered by phospholipase. Recently, it was found that the local enrichment of negatively charged lipids into biomembrane domains can lead to high activity of phospholipase A_2 (PLA₂), suggesting a potential anti-bacterial application of PLA₂ [1]. Here, we apply the 2nd-order nonlinear optical spectroscopy – sum frequency generation vibrational spectroscopy [2] to investigate the hydrolysis process of model lipid biomembranes catalyzed by PLA₂. Two types of phospholipases and two types of phospholipids were used including secretory human phospholipase A_2 type IIA (PLA₂-IIA), venom PLA₂, 1,2-dipalmitoyl-sn-glycero-3-phospho-(1'-rac-glycerol) (sodium salt) (DPPG, negatively charged) and 1,2-dipalmitoyl-sn-glycero-3-phosphocholine (DPPC, neutrally charged). Nonlinear spectroscopic results indicate, compared to PLA₂, PLA₂-IIA can strongly bind to the negatively charged DPPG biomembrane with certain specific orientation and trigger the fast hydrolysis process, confirming its anti-bacterial function.

[1] Leidy, C.; Linderoth, L.; Andresen, T. L.; Mouritsen, O. G.; Jorgensen, K.; Peters, G. H. *Biophys. J.* 2006, 90, 3165–3175.

[2] Shen, Y. R., *Nature* 1989, 337, 519–525.

PS19.016 - Cancer stem cells in a hierarchical model of tumour regrowth in five head and neck carcinomas

Author(s): Loredana G. Marcu¹, David Marcu², Sanda M. Filip²

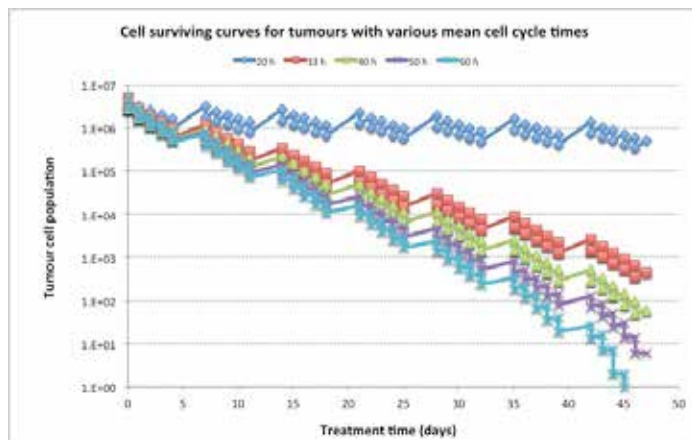
¹School Of Chemistry And Physics, University of Adelaide, Adelaide/SA/AUSTRALIA, ²Department Of Physics, University of Oradea, Oradea/ROMANIA

Introduction: Locally advanced head and neck carcinomas (HNC) are aggressive due to several tumour-related factors such as: hypoxia, elevated levels of the endothelial growth factor receptor and tumour repopulation during treatment. There is a growing body of evidence towards the existence of cancer stem cells (CSC), which represent a subpopulation of tumour cells that hold the ability to proliferate indefinitely, are tumorigenic and also more quiescent than non-cancer stem cells. Due to their ability to respond to triggers these cells are considered to be accountable for treatment resistance and failure, as well as tumour recurrence. However, there is insufficient quantitative information in the literature regarding the kinetics and behaviour of CSCs in order to assess their impact on tumour control. The aim of this work is to simulate the possible mechanisms behind CSC generation and contribution to tumour regrowth during treatment on five virtual HNC with different growth kinetic parameters.

Methods: A hierarchical model of HNC has been grown using probabilistic methods starting from one tumour-initiating cell. The model written in C++ has generated a virtual tumour of 10^7 cells having biologically real parameters. The radiation software module kills cells according to surviving fractions defined for each phase of the cycle. A fraction of 20% cells are recruited after irradiation as CSCs (which proliferate via symmetrical division) or non-CSCs (asymmetrical division). The fraction of CSCs is limited to 25% of total cells.

Results: The model has shown that tumours growing with different kinetic parameters (mean cell cycle time, volume doubling time) respond differently to conventional radiotherapy. Due to the repopulation ability of CSCs, tumours with shorter mean cycle times (20h – 40h) cannot be cured with 70Gy given in 2Gy/fraction, 5 days a week, over 7 weeks (see figure). A typical HNC with 33h mean cycle time would need an additional 26Gy, or a 6 day/week treatment to be cured, considering that the tumour is non-hypoxic. Tumours with mean cycle time of 20h exhibit a drastic resistance through repopulation, as the interfraction interval (24h) is larger than the time for cell division.

Conclusions: Differences in treatment response of various HNC models due to CSCs and their interplay with growth kinetics show the importance of CSC identification within the tumour. The need for accurate markers for CSC labelling is therefore imminent. Both quantitative and qualitative knowledge on CSC are needed to describe the resistant subpopulation and to design treatment regimens accordingly.



PS19.017 - Effects of interaction with electromagnetic field on cell culture of *Saccharomyces cerevisiae*

Author(s): Aracely Martínez, Julio C. Villagómez, Modesto A. Sosa-Aquino, Francisco A. Horta, Teodoro Córdova-Fraga
 Departamento De Ingeniería Física, División de Ciencias e Ingenierías, León/MEXICO

Saccharomyces cerevisiae has been regarded as a convenient target for investigating effects of electromagnetic fields, such as cell proliferation, given that it has wide applicability in industry. At the same time, the relationship between cell growth and form culture, could be an indicator of the conditions of their environment where it is growing. In this work, we studied the change in the rate of cell reproduction and changes in the pattern of growing of a cell culture of *Saccharomyces cerevisiae* when it's stimulated magnetically. The magnetic field used for stimulation was generated with a Rodin coil in the range of approximately 1 to 4 mT, at frequencies of 60, 100, 800, 1500 and 2450 Hz. The yeast was grown in liquid medium YPD, and stimulated for 8 hrs. For frequencies of 60 and 800 Hz the cell culture was a decrease in the rate of cell proliferation, relative to the control sample. The frequencies of 100 and 1500 shown an increase in the rate of cell proliferation, while the stimulated sample to 2450 didn't show a significant change. For the study about changes in the pattern of growth, it was performed a fractal analysis of the growing culture. Samples of *Saccharomyces cerevisiae* in YPD medium, was stimulated for 8 hours with the same Rodin coil at frequencies of 100, 800 and 1500 hz. The observation was performed by a microscope and the fractal dimension analysis was performed during the first two hours after stimulation. The box counting method was used for the determination of the fractal dimension. The results suggest that there are no changes in the pattern of crop growth.

PS19.018 - Obstructive and Sclerotic Disorders affecting Carotid Blood Flow to the Brain

Author(s): Onaizah Onaizah¹, Tamie L. Poepping², Mair Zamir³
¹Medical Biophysics, University of Western Ontario, London/CANADA, ²Physics And Astronomy, University of Western Ontario, London/ON/CANADA, ³Applied Mathematics, University of Western Ontario, London/ON/CANADA

Stroke remains one of the leading causes of death in North America. A large number of strokes are a direct result of carotid artery disease. Physiological and pathological changes in the carotid artery can result in obstructive and sclerotic disorders. The internal carotid artery (ICA), one of the branches of the common carotid artery (CCA), is a major route for blood supply to the brain. Thus, obstructive changes such as stenosis due to plaque development can impede blood supply to the brain. Sclerotic changes associated with the hardening of the artery result in changes to the pressure and flow relationship thus reducing blood supply to the brain.

An experimental in vitro flow loop was employed in combination with a lumped parameter (LP) model to study changes in blood supply to the brain as a result of obstructive or sclerotic disorders of the carotid artery. An LP model is an electrical analogue to the experimental in vitro flow loop, consisting of a pump supplied with an idealized carotid artery waveform. A family of carotid artery phantoms with varying compliances and stenosis severity were used. Simultaneous pressure and volumetric flow-rate waveforms were measured using flowmeters (EP620/625, Carolina Medical Inc.) and a pressure catheter (SPR 350S, Millar Inc.). The pressure waveform is as an input to the LP model to generate a predicted flow-rate waveform, which is then matched to the measured flow-rate waveform by varying the LP model parameters.

An LP model, specifically designed to match an in vitro flow loop, was validated and parameter values were extracted for five differ-

ent phantoms by matching waveforms. The increased resistance associated with the stenosis and the differences in the phantom compliances are shown in Fig. 1. Mean flow rates through the ICA were calculated using the experimentally measured flow-rate waveforms. Obstructive disease had minimal impact on mean flow-rate up to a certain threshold (70% stenosis) before it became significant ($p < 0.05$). A decrease in compliance on the other hand had a significant effect on mean ICA flow-rate ($p < 0.05$). While obstructive disease does not directly have a large impact on blood supply, it is still considered important due to its role in the development of thrombotic events.

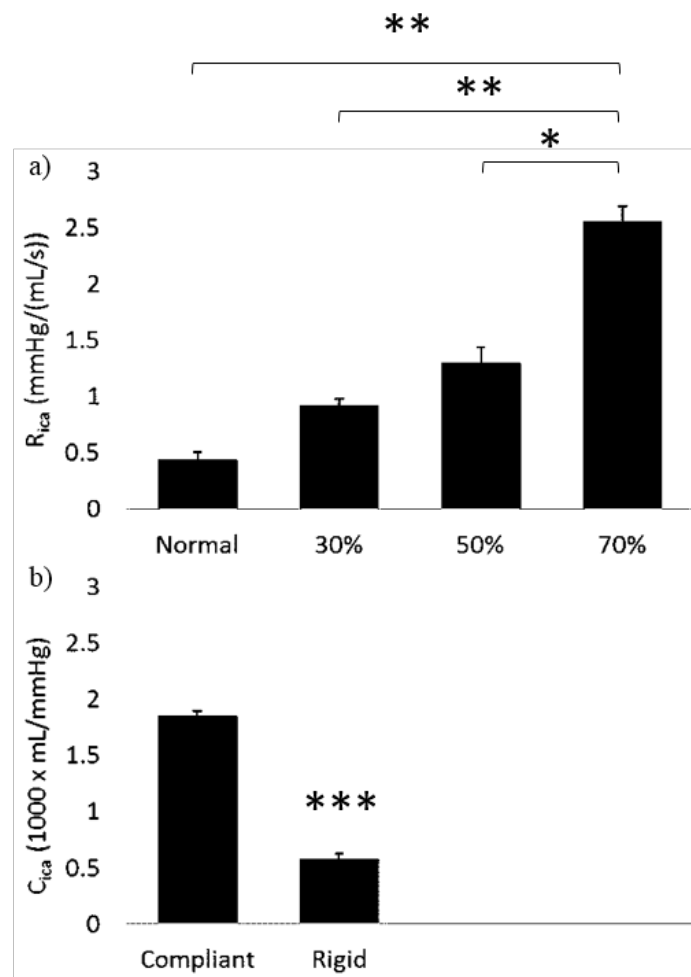


Fig. 1 The parameter values extracted from the LP model are shown: a) phantoms with increasing stenosis (R_{ica}), changes are significant (**, $p < 0.01$) for a severe (70%) stenosis, b) phantoms with decreasing compliance (C_{ica}), changes are significant (***, $p < 0.001$).

PS19.019 - Estimation of Tissue Temperature in Tumor Hyperthermia Using Ultrasonic Methods

Author(s): Xiao-Jian Wang¹, Xiao-Hui Qiu²
¹Department of Chemotherapy, Ganzhou Tumor Hospital, Ganzhou, China, Ganzhou/CHINA, ²Information Engineering Institute, Gannan Medical University, Ganzhou/CHINA

Estimation of tissue temperature in Tumor Hyperthermia is an extremely important assurance of therapeutic safety. In all kinds of measuring methods, ultrasonic nondestructive techniques are the safest and the most promising one. The main ultrasonic methods of temperature measurement are based on ultrasonic echo signal,

acoustic transmission signal, the characteristic parameters of ultrasonic image, theoretical model simulation and so on. The theories of various ultrasonic methods adopted for measuring tissue temperature are introduced in this paper with their application, limitation and research status analyzed respectively.

PS19.020 - Modeling of a Photosensitizer Distribution Relevant to Photodynamic Therapy of Malignant Non-Pigmented and Pigmented Tumors

Author(s): Marta Wasilewska-Radwanska¹, Zenon Matuszak²

¹Faculty Of Physics And Applied Computer Science, AGH University of Science and Technology, Faculty of Physics and Applied Computer Science, Krakow/POLAND, ²Medical Physics And Biophysics, AGH University of Science and Technology, Faculty of Physics and Applied Computer Science, Krakow/POLAND

Photodynamic therapy (PDT) is a branch of phototherapy and it is among many available methods used in clinical practice to treat cancer. PDT is approved procedure for treatment of many types of cancer such as esophageal, lung and skin cancer. Research investigation show that the PDT technique can also be effective against melanoma. Generally speaking, three crucial elements in the PDT must cooperate to cause therapeutic effect of PDT: photosensitizer (PS), oxygen (O_2) and light. The PDT's therapeutic effect depends on many factors involved in the PDT: accumulation of PS and oxygen availability in the treatment region, absorption of light by PS (activation) and efficiency of production of cytotoxic reactive oxygen species (ROS), mainly singlet oxygen (1O_2). The main mechanism of cell death occurs by photogenerated 1O_2 that attacks important parts of the cells (membranes) causing oxidative damages and cells death. To make the PDT a more effective treatment modality, an appropriate dosimetry is required. Two main factors must be controlled: PS accumulation within target tissue and optical penetration depth of light used (photon density). Because many of PS are fluorophores, monitoring PS fluorescence play significant role in localizing of PS and quantifying its concentration within tissue. The optical parameters of tissues (absorption and scattering properties) significantly influence both the intensity and shape of PS fluorescence, because the intensities of fluorescence excitation as well as emission light are modulated by the tissue. Additionally, melanin present in pigmented tumors strongly absorbs light, and it modifies both the propagation of excitation light and the resulting fluorescence emission. The goal of the present work is to model fluorescence measurements used for determining the PS concentration in non-pigmented and pigmented tissue. Monte Carlo (MC) method was used to simulate propagation of photons (exciting PS and emitting by PS) within tissue. The influence of melanin tissue concentration on distribution of the excitation and the emission light was estimated. Optical properties of tissue used in simulations are based on reported values for normal and pigmented skin. Computational model of skin consists of seven layers. The simulations were done for PS from porphyrin family since these compounds emit light at near 650 nm.

Spatial distribution of the fluorescence excitation and emission were simulated as functions of the tissues' optical properties. It was demonstrated that the model is able to predict the spatial distribution of the porphyrin type PS fluorescence excitation/emission pattern within skin and PS concentration. The results of MC simulations were compared with the experimental images of skin fluorescence textures.

CONTINUING EDUCATION

BMEE01 - GENERAL BME EDUCATION

BMEE01.1 - Biomaterials - Cell-Material Interactions: Biochemistry & Physics

Author(s): [Dennis E. Discher](#)

Molecular & Cell Biophysics Lab, University of Pennsylvania,
Philadelphia/PA/UNITED STATES OF AMERICA

Tissue cells and implants all interact with the innate immune system, especially phagocytes that try to 'eat' everything. However, 'Self' cells are spared, and it turns out that a polypeptide found on all cells marks cells (as well as engineered particles and surfaces as 'Self'), limiting their phagocytic interactions *in vitro* and *in vivo* [Rodriguez *Science* 2013]. If an injected cell thus survives and if it has stem-like properties, the tissue microenvironment can in principle influence its differentiation. We have focused on how matrix elasticity can direct stem cell lineage, recognizing that tissues can be very soft like fat and brain, or increasingly stiff like striated muscle and rigid like bone [Engler *Cell* 2006]. Stem cells feel and respond to such elasticity differences together with soluble factors [Discher *Science* 2009], and we now find such signaling propagates all the way into the nucleus, which adjusts its mechanics to tissue stresses but also feeds back on gene expression [Swift *Science* 2013]. What unifies these mechanisms of interest in immune recognition and in matrix-regulated stem cell differentiation is a convergence of decision-making pathways on cytoskeletal force generation.

P.L. Rodriguez, T. Harada, D.A. Christian, D.A. Pantano, R.K. Tsai, and D.E. Discher. Minimal 'Self' peptides that inhibit phagocytic clearance and enhance delivery of nanoparticles. *Science* 339: 971-975 (2013).

A. Engler, S. Sen, H.L. Sweeey, and D.E. Discher. Matrix elasticity directs stem cell lineage specification. *Cell* 126: 677-689 (2006).

J. Swift, I.L. Ivanovska, ... and D.E. Discher. Nuclear Lamin-A Scales with Tissue Stiffness and Enhances Matrix-directed Differentiation. *Science* 341: 1240104-1 to 15 (2013).

BMEE01.2 - Radiology 101: Intro to X-Ray tubes (manufacture & maintenance)

Author(s): [Phillip Bogolub](#), Cindy Friesen
xxx, xxx/UNITED KINGDOM

Dunlee presents, "X-Ray 101 & Working Together"

The presentation will begin with where X-ray tubes are used. This entails a brief overview of the different types of tubes.

We will then move onto what a tube does and what the outcome is.

The next section goes into detail of how an X-Ray and CT tube is made which includes the manufacturing process, the different varieties as well as the tube design itself.

We will show the anatomy of a tube and the various parts and what the specific functions of those parts are.

We will then go into the operation of the tube and what types of failures can be experienced.

We will also discuss why preventative maintenance and training is important.

We will conclude with questions and answer section.

BMEE02 - MEDICAL DEVICE DEVELOPMENT AND COMMERCIALIZATION

BMEE02.1 - Med-Tech Commercialization – A Research Hospital's Perspective

Author(s):

How do you define 'success' of your med-tech research? Seeing a commercialized product on the market available for use in patients around the world is arguably the most relevant, impactful and satisfying end-point for anyone in this field. However, the med-tech commercialization process is far from being a 'cookie-cutter' approach. What works in one field, falls short in others. What works at one institution, isn't optimal for others. What works for one technology, completely misses the mark for another. How one industry partner prefers to work, is not uniform across all partners. It is a dynamic environment requiring flexibility and optimization of the various factors. A research hospital's view on this exciting area will dive deep into the dynamics through a series of actual start-up and licensing examples demonstrating some of the approaches that have been implemented at the University Health Network, Toronto. A brief intellectual property primer will also be included to provide the attendee with a functional understanding of what is needed to succeed in some of the most common commercialization scenarios. How do you define 'success'?

BMEE03 - BIOINFORMATICS, TELEMEDICINE AND HOSPITAL INFORMATION SYSTEMS

BMEE03.1 - DICOM & PACS: Managing Digital Imaging Networks

Author(s): Marvin Mitchell
Healthcare, N/A, Barrie/CANADA

What does it really take to manage a Digital Network consisting of DICOM and PACS? The objective of my talk will answer this question. Many of you may have already been exposed to the words "DICOM" and "PACS". Although these words are normally used together, they are very different in achieving the goals they were designed for. Both technologies can exist together as well separate from each other.

Our conversation will begin with a short talk on the beginning, and continued evolution of "DICOM" and "PACS". We will have a look at Conformance Statements and how to effectively use them.

Our conversation will then continue with how to effectively manage a Digital Network containing both DICOM and PACS. Throughout my experience, I have had the pleasure in being a part of successful executions of Digital Network management and as well as being part of projects that had "lessons learned". The management of a DICOM and PACS Digital Network is continued work in progress that starts with Planning phase and ends with Decommissioning of the product. The topics we will explore to get a richer sense of what it takes to manage such Networks are:

- Planning and Integration
- Workflow considerations
- A typical DICOM and PACS Network
- People/Education
- Scalability
- Support Process
- Disaster Recovery
- Business Administration Challenges

BMEE04 - GENERAL BME EDUCATION

BMEE04.1 - Biomaterials - Polymer/Organic Coatings

Author(s): Min Wang
Department Of Mechanical Engineering, The University of Hong Kong, Hong Kong/CHINA

Many biomaterials currently in clinical use were originally developed for engineering applications and surface modification is thus needed for their biomedical applications. The biomaterials specifically designed and developed for certain medical application(s) may require another set of surface characteristics that are suitable for the material to be used in another clinical environment; or surface modification is required for enhancing the clinical performance of the biomaterial in its targeted application(s). What our body "sees" and deals with when an implant is placed in our body is the surface of the implant. Therefore, surface properties of materials or biomaterials are of paramount importance, which can determine the success or failure of a material for its intended biomedical applications. Different types of biomaterials – metals, polymers, ceramics and composites – are now used in various biomedical applications. As these substrates are drastically different from each other, different coatings and surface modification techniques are used for implantable metals, biopolymers, bioceramics and biomedical composites (porous composite scaffolds in particular in recent years). And coatings themselves can be polymeric, metallic, ceramic or even composite in nature. Polymer coatings are very attractive for the surface modification of biomaterials because they provide great versatility in chemical groups on the surface for controlling the cell-biomaterial interactions. They are relatively easy to form/produce, using simple techniques such as dip-coating or solvent casting. Coatings can also be made via chemical grafting of molecules onto the biomaterial surface. Techniques/structures such as self-assembled monolayers (SAMs) and layer-by-layer (LBL) assembly are extensively investigated in the biomedical field due to their distinctive advantages. For example, PEGylated SAMs are formed for controlling the surface interaction of biomaterials with proteins, and drugs are incorporated in LBL-formed polymer coatings for their controlled release *in vivo*. In the area of metal implants, NiTi shape memory alloys (SMAs) becomes a focus of research because they possess unique properties of shape memory and superelasticity. However, metals are bioinert and NiTi SMAs cause concerns over their long-term biocompatibility due to toxic ion release. Investigations have been performed to use the plasma immersion ion implantation and deposition technique to modify the NiTi SMA surface, yielding encouraging mechanical and biological results. For tissue regeneration, tissue engineering scaffolds play a crucial role but scaffold alone is not sufficient for regenerating functional body tissues. Growth factors are needed for prompting specific cell behaviors and functions. Additive manufacturing technologies such as selective laser sintering (SLS) may not be able to produce growth factor-incorporated scaffolds directly, but SLS-formed polymer scaffolds can be surface modified for incorporating growth factors for their controlled release later. One example is SLS-formed PHBV scaffolds with the surface modification of heparin onto which rhBMP-2 is incorporated. These advanced scaffolds have exhibited enhanced ability for bone tissue regeneration *in vivo*. This lecture will (1) briefly review clinical requirements (mainly surface requirements) for biomedical materials, (2) give an overview of coatings and surface modification techniques for different types of substrates, and (3) present and discuss the performance of some surface-modified biomaterials and indicate future trends.

BMEE05 - CLINICAL ENGINEERING/TECHNOLOGY MANAGEMENT

BMEE05.1 - Introduction to Medical Technology Management (Clinical Engineering Practice)

Author(s): Saide Calil¹, Anthony Chan²

¹Department Of Biomedical Engineering, Unicamp, Campinas/BRAZIL, ²Biomedical Engineering, British Columbia Institute of Technology, Burnaby/CANADA

The term “Management of Medical Technology” is widely used today but not many people really know its range. Some limit “Management” to maintenance services and consider only preventive maintenance and repair activities; some add other activities, such as technical training and quality control. The fact is many other activities can be added to “Medical Technology Management”, including risk management, cost assessment and control, equipment procurement, installation, discarding, and reporting to the hospital managers. The proposal here is to present and discuss:

1 – What activities are performed today by Clinical Engineers within what is called Management of Medical Technology?

2 – Which of these activities are really part of Management of Technology and which ones can be transferred to other subject such as; Financial Management

3 – Define what kind of knowledge is necessary for Technology Management to guide training courses on Clinical Engineering.

BMEE07 - BIOINFORMATICS, TELEMEDICINE AND HOSPITAL INFORMATION SYSTEMS

BMEE07.1 - E-medicine and Remote Medical Consultations

Author(s): [Gilad Epstein](#)

OTN (Ontario Telemedicine Network), Toronto/CANADA

Learning objectives

Overview of current Telemedicine programs

Trends in virtual care

Technology trends enabling new models of care

Telemedicine is growing in popularity and is moving from a pioneering stage into mainstream.

Innovative models of care leveraging technology are creating new opportunities in the healthcare industry.

In this session we will review the current state of Telemedicine in Ontario, and provide insights to future virtual care trends and the impact on patients and providers.

BMEE08 - GENERAL BME EDUCATION**BMEE08.1 - Biomechanics - Implant design****Author(s):** [Cheng-Kung Cheng](#)

Department Of Biomedical Engineering, National Yang Ming University, Taipei/TAIWAN

Biomechanics - Implant Design

In order to reasonably assure the implant's safety and effectiveness, the two major concerns of medical devices, computational models and biomechanical tests are conducted in the design phase. The computational models, including finite element model and kinematic model, are usually performed firstly because it is relative cost efficiency and easy to modify design parameters. In addition, using these models can quickly estimate the stress and strain distribution or kinematic performance of the implant. The biomechanical tests then take steps in to simulate the performance of implants under real-live mimic loading by following the ASTM and ISO standards. The research outcomes of the implants are essential for premarket approval.

Although most of the orthopedic implants were initially developed in Europe and North America, the substantial differences between Asian and Western population should be considered for implant designs nowadays. Not only the bone quality, size, and geometry differences but also the epidemiology of disease and lifestyle can greatly affect the design concept. For example, the high prevalence of avascular necrosis of femoral in Asia leads to total hip arthroplasty while osteoarthritis in Western is the top indication of total hip arthroplasty. Furthermore, demands of high flexion is much more important for Asian patients after total knee arthroplasty for achieving activities like prayers kneeling, cross-legged sitting, and Japanese proper sitting. Therefore, understanding the discrepancies among different populations is beneficial in unique implant design to the target market.

Customized implant has become another growing category of implant design with the development of novel technology, which resolves the difficulties of manufacturing in the past and lowers the cost of production. The revolutionary 3D printing with metal material has elevated implant design from prototyping to practical scenario.

BMEE09 - BIOINFORMATICS, TELEMEDICINE AND HOSPITAL INFORMATION SYSTEMS**BMEE09.1 - Medical Device Network Connectivity****Author(s):** [Ryan Forde](#)

Research And Development, Drager, Andover/UNITED STATES OF AMERICA

Medical device networks are becoming nearly ubiquitous in the developed world. These networks allow medical devices to share information with other devices, archive and store information for later access and warn caregivers about potentially hazardous situations before they occur. This talk will focus on patient monitoring networks and how they relate to hospital Information Technology networks and discuss some of the challenges of integrating the two. We will cover different communication technologies and when each might be used. Finally we will discuss some of the current efforts to create a standards landscape that will allow medical devices to interoperate and improve care for patients.

At the conclusion of the program, attendees will be able to:

- 1- Describe different communication protocols used by medical devices and explain what each might be used for.
- 2- Understand how patient monitoring networks can work with hospital IT networks and what some of the advantages, and challenges of connecting the two might be.
- 3- Understand the basic reasons why standardized medical device interoperability is important and how we might get there.

BMEE10 - GENERAL BME EDUCATION**BMEE10.1 - Multiscale Biomechanics in Deep Tissue Injury****Author(s):** Arthur F. Mak

Division Of Biomedical Engineering, The Chinese University of Hong Kong, Shatin/HONG KONG

LEARNING OBJECTIVES

- 1) Acquire a basic understanding of the problem of deep tissue pressure ulcers;
- 2) Review the recent literatures on in-vivo and in-vitro studies related to deep tissue injuries
- 3) Learn how computational biomechanics can be applied to study the formation of deep tissue injuries and their propagation to become clinical ulcers

ABSTRACT

Damages occur when cells and tissues are subject to excessive physical stresses. Such damage thresholds depend on the exposure duration of these physical forces. Deep tissue injury due to prolonged excessive skin/skeletal loadings can lead to clinical pressure ulcers, affecting millions of persons with physical disability. In this short course, we will review recent literatures on (1) the transmission of skin/skeletal loadings to muscle tissues around bony prominences, (2) how mechanical stresses at tissue level invoke cellular damages, (3) the involvements of the vascular and lymphatic systems, (4) the effects of post-ischemic oxidative reperfusion might affect the load-carrying capacity of the involved tissues and their sub-cellular and molecular mechanisms, and (5) how damages in the deep muscles can propagate towards the skin, resulting in a clinical through-thickness ulcer. Relevant In-vitro, in-vivo, and in-silico studies will be summarized.

BMEE11 - CLINICAL ENGINEERING/TECHNOLOGY MANAGEMENT / GENERAL BME EDUCATION**BMEE11.1 - Trends in Medical Device Certification and Improving Patient Safety through Evolving Standards****Author(s):** Dale Morgan

Certification & Test, CSA Group, Toronto/CANADA

The medical device chain consisting of development, manufacture, approvals, distribution/service and patient care use is generally considered to be governed by a highly regulated industry – presumably to assure safety, effectiveness and electrical compatibility for the care environments and infrastructures where the devices are used. Despite this, patient safety concerns and adverse events continue to occur and healthcare innovations have many hurdles before reaching the caregivers and patients. The regulatory processes for medical devices generally have 3 parts: Safety Technical File, Clinical Review (Licensing), and Quality Systems Registrations. Together these parts should be sufficient to ensure the aspects of safety and best practices are used in all phases of the medical device chain. These parts have also long been considered separate regulatory and compliance aspects involving different expertise, people and services.

Traditionally, the Safety Technical file is comprised primarily of electro-medical certification and test reports/certificates according to the use of recognized international and harmonized medical device standards (note- must include electrical code and other deviations in Canadian adopted Standards for Health Canada). The key electro-medical device standards are the IEC 60601 /ISO 80601 Family of Standards. Since the 2005 version of the 60601 standards (3rd edition) and recently the 2012 version (3.1 edition) there has been a remarkable evolution of scope and complexity. Focus has moved from inherent electrical safety (2nd edition) to a broader focus on Safety, Essential Performance, Risk Management, Software Life Cycle processes, Usability, Alarms, and new use environments such as Home Healthcare and Emergency Medical Services.

The application, knowledge and science of certification engineering and test for the evolving family of 60601 standards is now crossing the boundaries into the other 2 parts of the medical device regulatory processes – clinical and quality systems. All 3 processes have their separate requirements and roles in Regulatory approvals for sure. However, the trend is that a holistic approach in understanding all of the processes in the refinement and application of standards has the great ability to safely fast track innovation, advance safety and open global markets for med tech companies here and abroad.

A few of the substantial developments in the 60601 standards will be examined to illustrate the trend of evolving standards to improve safety and ultimately enabling better and safer patient care. For example, one of the most significant and challenging changes in 60601 standards is the use of the Risk Management process to facilitate rapid technology developments and clinical feature benefits. This is a knowledge area steeped in clinical applications and engineering, risk assessment, process design, and quality management.

Understanding these trends can enable healthcare and clinical engineering professionals to better gauge the safety and limitations that new medical technology will bring into their already sophisticated and evolving care environments.

BMEE11.2 - Quantitative Musculoskeletal Ultrasound

Author(s): Yong-Ping Zheng

Interdisciplinary Division Of Biomedical Engineering, The Hong Kong Polytechnic University, Hong Kong/CHINA

Learning Objectives:

1. To understand methods and applications of ultrasound elasticity measurement and imaging for musculoskeletal soft tissues
2. To understand what is sonomyography and its applications
3. To learn how to use 3D ultrasound imaging for musculoskeletal assessment, particularly for spinal deformity

This talk will introduce three different approaches for quantitative musculoskeletal assessment using ultrasound. Ultrasound imaging has been widely used for musculoskeletal tissue assessment, but mainly qualitatively and subjectively by operators. Only some simple parameters such as length and area may be obtained for static ultrasound images. Musculoskeletal ultrasound has been rapidly developed recently due to the reduced size and cost of ultrasound scanner, and a number of quantitative musculoskeletal ultrasound approaches have also been developed.

Elasticity and viscoelasticity of different musculoskeletal soft tissue plays a very important role in muscle contraction, motion, force transfer and load bearing. The change of elasticity may be associated with different diseases, such as osteoarthritis (cartilage tissues), spasticity and atrophy (muscle), diabetic foot (plantar tissue). Furthermore, muscle may changes its elasticity during contraction, making it a useful parameter to indicate muscle quality. Muscle elasticity cannot be measured but also imaged, thus it can be used to for diagnose some local tissue problems. In this study, different methods for the measurement and imaging of tissue elasticity will be introduced, including ultrasound indentation, acoustic radiation force impulse, supersonic shearwave imaging, etc. Applications for muscle, tendon, and articular cartilage assessment will be introduced.

The second quantitative musculoskeletal ultrasound method to be introduced is developed for muscle assessment, named as sonomyography (SMG), in relation to its counterpart electromyography (EMG). SMG is derived from real-time ultrasound images and represents the architectural changes of muscle during contraction. The architectural parameters include muscle thickness, cross-sectional area, pennation angle, fascicle length, etc. They are detected automatically from real-time ultrasound images continuously thus forming signals, which can then be used for muscle functional assessment as well as for control. In this talk, the development of this area will be introduced together with recent achievements by different groups.

3D ultrasound imaging has been commonly used for fetus assessment. The third topic is to introduce how to use 3D ultrasound imaging for quantitative musculoskeletal assessment, including how an 3D ultrasound image is form formed. The focus will be on the recent development of using 3D ultrasound for radiation-free assessment of spinal deformity, such as scoliosis. It has been demonstrated that 3D ultrasound is feasible to measure the spine curvature for scoliosis patient, including the lateral deformity as well as spinal rotation. 3D ultrasound imaging shows a promising future for scoliosis screening, monitoring for curve progression and assessment for treatment outcome. The potential applications of this new quantitative musculoskeletal ultrasound technique will be discussed.



Figure 1. Assessment of musculoskeletal tissue biomechanical properties using tissue ultrasound palpation sensor (TUPS).

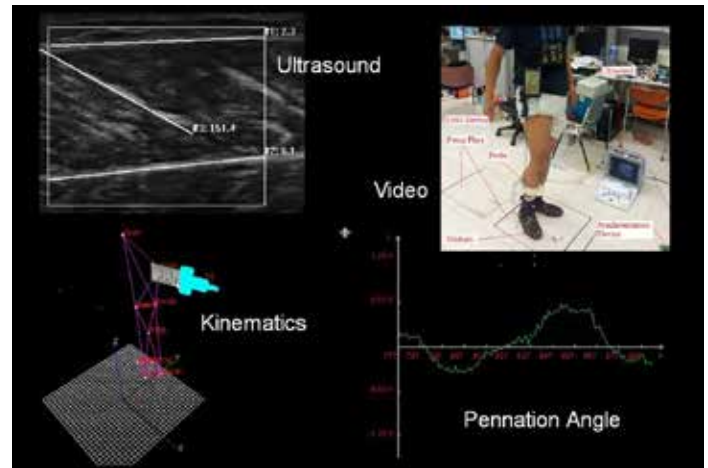


Figure 2. Compound motion analysis using conventional optical kinematic tracking method and sonomyography, which represents architectural change of muscle extracted from real-time ultrasound images during muscle contraction.



(a) (b) (c)

Figure 3. 3D ultrasound imaging for the measurement of spinal deformity for scoliosis patients. (a) Virtual 3D spine model formed using spinal bony landmarks detected on ultrasound images; (b) 3D ultrasound imaging system (Scolioscan) being used for assessing the spine of a body; (c) A coronal-view ultrasound images formed using the Scolioscan.

BMEE12 - CLINICAL ENGINEERING/TECHNOLOGY MANAGEMENT

BMEE12.1 - Clinical Engineers & Biomedical Engineering Technologists Certification - International Perspective

Author(s): Larry Boyce¹, Petr Kresta²

¹Clinical Technology Management, Sodexo Canada, Woodstock/CANADA, ²Clinical Engineering, Winnipeg Regional Health Authority, Winnipeg/CANADA

Certification of Biomedical Engineering Technologists and Clinical Engineers – International Perspectives

Abstract

The session addresses contemporary issues in the certification of clinical engineers and biomedical engineering technologists through presentations and panel discussion with audience participation.

The need for certification of Biomedical Engineering Technologists and Technicians (BMET) is examined after 33 years of operating the Canadian Board of Examiners under the International Certification Commission (ICC). In that time little has changed, certification remains voluntary while a license to cut hair is mandatory in the province of Ontario. Currently in Canada there is no law or regulation that prevents the “talented maintenance mechanic” from maintaining medical equipment. The fundamental question is, “Is the public protected?” The current Canadian process is reviewed in an attempt to determine if it is working well enough to ensure that the public is protected. Should BMET certification be voluntary or mandatory? What are other countries doing?

The dissolution of the International Certification Commission in favour of the newly formed AAMI Credentials Institute (ACI) eliminated the International component of certification. Why this happened, the impact on technologists and the future of certification is examined?

Certification in Clinical Engineering is examined in several jurisdictions globally including the United States, Canada, and China. Responsibility for the Certification in Clinical Engineer program in the US and Canada shifted recently from the Healthcare Technology Foundation to the American College of Clinical Engineering. The current structure and status of the Certification Program is reviewed. The emergence of new clinical engineering related certification programs sponsored by the AAMI Credentials Institute, is examined and their potential impact discussed.

Clinical Engineering Division of the International Federation for Medical and Biological Engineering (CED/IFMBE) has been working for several years on a project looking at developing an international umbrella under the CED/IFMBE for the programs of certification in clinical engineering (CCE). Since the latest International Standard Classification of Occupations of the International Labor Organization explicitly considers biomedical/clinical engineers (CE) as an integral part of the health work force, it stands to reason that formal career paths of CE should be demanding similar, if not the same, as career paths of other health professionals with commensurate duration and level of university education.

The objective of this paper is to present current project status and activities, together with the proposal for CCE from the CED/IFMBE perspective. The CED/IFMBE, in cooperation with other interested parties, advocates the regulation of the CE profession and is currently establishing the mechanisms and structures for the CCE. IFMBE should ask all national governments to adopt and follow this model.

Learning Objectives:

- 1) The attendee will be able to explain the need for certification of Biomedical Engineering Technologists (BMETs) and describe the basic steps involved to become certified in Canada.
- 2) The attendee will be able to explain the need for certification of clinical engineers (CEs) and describe the basic steps involved to become certified in the United States and Canada.
- 3) The attendee will be able to discuss the status of certification nationally and internationally.

BMEE13 - CLINICAL ENGINEERING

BMEE13.1 - Patient safety and Optimal Performance: A Holistic Framework for Medical Devices

Author(s): Michael Cheng¹, Saleh Altayyar², Hal Hilfi³, Julie Polisen⁴
¹Biomedical Engineering, ottawa/ON/CANADA, ²King Saud University, Riyadh/SAUDI ARABIA, ³Biomedical Engineering, Ottawa/ON/CANADA, ⁴Canadian Agency for Drugs and Technologies in Health, Ottawa/CANADA

The stated purpose of medical device regulations is to ensure the safety and performance of medical devices. However, many health care professionals and users of medical devices may not know the scope and limitations of medical device regulations; often they have unrealistic expectations about the device regulators' ability to protect public health. While literature and guidelines on medical devices abound, they were written in different contexts by different medical device groups employing diverse terminologies. For a policy-maker or a health care worker, the task of navigating and digesting enormous amount of information becomes very difficult.

This session will present a simple, three-stage framework summarizing three essential steps (regulation, contextualized assessment, operation management) and the key elements in each step to ensure the ultimate patient safety and optimal performance for any medical device. This three-stage framework, which also reflects World Health Assembly Resolution WHA60.29, is useful for medical device policy and management planning; it can serve as a common reference framework among stakeholders for education, communication, and collaboration. Its components can be linked to all levels of activities in the lifespan of a medical device. Guidance on how to execute these three steps is available in the worldwide literature; one can search for details without losing the "big-picture" relevance, and then choose the right tools appropriate to one's situation.

An insight from this framework is that, at present, medical device regulation, assessment, and management professionals tend to work in isolated groups; but the framework suggests a system with interconnecting components, through which there could be well-designed, functional interaction and collaborative activities among groups to enhance effective and efficient outcomes. Participants are encouraged to brainstorm on improving this situation.

At the conclusion of this presentation, attendees will be able to

1. know the unique difference between medical devices and drugs
2. clarify the differences between the general regulatory statement of "safety and Performance" and the ultimate healthcare objective of "patient safety and optimal performance" of medical devices
3. first do no harm.....identify the three essential steps to ensure patient safety with medical devices
4. expand the same three stages to include health technology assessment (HTA) and health technology acquisition and management (HTM) for optimal performance
5. know the basics of medical device regulations (HTR) and the essential elements for managing medical devices (HTM) (good management practices) in a healthcare facility
6. relate the widely available literature on medical devices to components of the big-picture holistic framework
7. use this simple three-stage as common framework to educate, communicate and collaborate with all stakeholders including the non-technical public as well as other healthcare professionals including the decision makers

8. hear the personal viewpoints on the importance of a holistic approach to medical device safety from the former Chair of the Asian Harmonization Working Party (<http://www.AHWP.info> , a medical device regulators' forum of 24 countries/economies in Asia, Africa and South America).

9. your turn: questions, comments, suggestions

10. take home challenges in enhancing the outcome of medical device utilization in your local environments.

BMEE14 - NEURAL & REHABILITATION ENGINEERING**BMEE14.1 - Neuro-robotics – Neurally Interfaced and Inspired Prosthesis****Author(s):**

Prosthesis technology, such as dexterous upper limb, has advanced greatly in sophistication. Not only are the motor mechanisms advanced, capable of extensive dexterous manipulation, but the more advanced prostheses also possessing sensors for feedback. However, controlling the prostheses remains a significant challenge. Here the need and the challenge is the neural interface, whether to the peripheral or the central nervous system, and deriving or providing the information for motor control and sensory feedback respectively. This talk will present the current state of the art of neural interface for dexterous upper limb prosthesis and how neural control may be achieved. Neural interface technology may be noninvasive or invasive, and utilizes micro to macro electrodes for signal acquisition, and decodes spiking information from neurons and cortical rhythms from brain surface or the scalp. Sophisticated decoding of neural population and signal processing of EEG and Electroco-ticogram can derive information needed to the control dexterous movement of the prosthesis. However, sensory information is not as readily relayed to the nerves or the brain and thus sensory prosthesis are not yet as advanced. Biologically inspired tactile sensors that take into consideration receptors and the nerve code may help achieve suitable sensory feedback via microstimulation of nerves or the brain of the amputee. Future research and development will be directed towards closing the loop, deriving cortical or peripheral nervous system information to control the prosthesis and return the sensory information to the subject. This vision of Neuro-robotics or Neuro-prosthesis calls for a chronically interface implanted or seamlessly integrated with the limb and the nervous system.

BMEE15 - CLINICAL ENGINEERING/TECHNOLOGY MANAGEMENT**BMEE15.1 - Introduction to Root Cause Analysis (RCA) and Failure Modes and Effects Analysis (FMEA) to Support Medication Safety Initiatives****Author(s):** Kim Streitenberger, Julie Greenall

N/a, Institute for Safe Medication Practices Canada, Toronto/CAN-ADA

Recently media attention has been focused on serious errors involving medications occurring in various healthcare settings. Often these reports express concern about lack of accountability of individual healthcare providers involved in these errors; however understanding the science of error helps us to realize that most errors are not related to individual competence but rather a complex interaction between the healthcare provider and numerous underlying system factors. This one-hour presentation will provide an overview of two structured analysis techniques, one prospective and one retrospective, that will assist individuals and organizations to improve their approach to safe medication management.

At the conclusion of this presentation, participants will understand:

the importance of incident analysis in organizational safety efforts

the impact of system factors on error potential in the medication use process

the need to apply human factors engineering principles in error analysis and system redesign

when to use retrospective analysis (root cause analysis) and prospective analysis (failure mode and effects analysis)

The Institute for Safe Medication Practices Canada (ISMP Canada) is an independent national not-for-profit organization committed to the advancement of medication safety in all healthcare settings. Our goal is the creation of safe and reliable systems for managing medications in all environments. For more information about ISMP Canada, please visit www.ismp-canada.org.

BMEE15.2 - Biomechanics - Computational Modeling and Analysis**Author(s):** Yubo Fan

School of Biological Science and Medical Engineering, Key Laboratory for Biomechanics and Mechanobiology of Ministry of Education, National Key Lab of Virtual Reality Technology, Beihang University, Beijing/CHINA

The learning objective is to understand:

(1) the basic concept of computational modeling and analysis in biomechanics,

(2) the applications of these computational methods,

(3) the development direction of the computational methods.

Biomechanical factors extensively participate the life activity of living organism. Mechanical environment involves the proliferation, differentiation and apoptosis of the cell, the growth and remodeling of the tissue, and the coordination of different physiological systems. Mechanical factors also play critical roles in the diseases and therapies. For example, wall shear stress participates the formation of atheromatous plaques; post-operative stress distribution affects the outcome of interventional surgery. The integration of biomechanics and microbiology has become the indispensable parts in the fields of physiology and medicine.

Computational simulation has been an important method for biomechanical investigation. Computational method can anticipate the irregular and complicated biological structure, predict and analyze the responses under extreme conditions. Despite that the simulations must follow by experimental validation and computational verification to ensure accuracy. We have conducted series of computational investigation in the areas of orthopedics, orthodontics, and injury prevention. These include:

(1) The protective mechanism of woodpecker's head for absorbing impacts was discovered. The special functions of beak and hyoid provided bionic insight in protective designs. (2) The finite element eyeball was simulated with an injury process, revealing the mechanism of amotio retinae. (3) Significant achievements on different orthopedic research and clinical application were also obtained, such as knee, cervical spine, wrist, fetal head, ankle, and osteoadaptation in space.

Computational technology has advanced the biomechanical researches in physiology and medicine. With the development of the computer technology and numerical algorithm, computational technology will continue to promote the interdisciplinary and multiscale studies in biomechanics and mechanobiology.

Acknowledgment

The present study was supported by grants from National Natural Science Foundation of China (NSFC 11421202, 11120101001), and National Science & Technology Pillar Program of China (2012BAI18B07, 2012BAI22B02).

BMEE16 - BME TECHNICAL/SERVICE COURSES

BMEE16.1 - Surgical Laser: Technology and Safety Issues

Author(s): Murray Greenwood

Biomedical Engineering, Trillium Health Partners, Mississauga/CANADA

With the recent updates to standards ANSI Z136.1 Safe Use of Lasers and CSA Z386-14 Safe Use of Lasers in Healthcare, the requirements for the administration of the hospitals' laser safety program will require updating.

At the conclusion of the program, attendees will be able to:

Apply the laser standards to various surgical active lasing mediums

Understand various safety challenges with different active lasing medium and their delivery systems

BMEE17 - MEDICAL DEVICE DEVELOPMENT AND COMMERCIALIZATION**BMEE17.1 - Technology Commercialization - Road Map and Precautions****Author(s):**

This lecture will discuss the process of technology commercialization and provide cautionary advice to entrepreneurial scientists and engineers in bioengineering and medical physics. Technology commercialization begins by making sure scientists and engineers are aware of the opportunities afforded by commercialization and the requirement to have the intellectual property (IP) properly secured. Disclosing an invention or a trade secret in a public talk invalidates IP rights. Industrial contracts must carefully spell out the IP rights. University technology transfer offices only file patents that have a high likelihood of licensing. Existing corporations typically license technology with high reward and low risk. Startup companies are left with higher risk technology. The startup process is fraught with difficulties related to lack of skill of founders, inadequate governmental and investment funding, poor choice of corporate partners, and affordable experienced management. Offering the right product at the right time with excellent development, operations, marketing, sales, and service are the key factors to the success of startup companies.

BMEE18 - GENERAL BME EDUCATION**BMEE18.1 - BioMEMS - Microsensors; Microactuators; Microfluidics; Micro-Total Analysis Systems (e.g., Genomics and Proteomics)****Author(s):** [David Weitz](#)

Physics & Seas, Harvard University, Cambridge/MA/UNITED STATES OF AMERICA

This talk will describe the use of drop-based microfluidics to perform very large numbers of experiments using small, picoliter-sized drops in an inert carrier fluid. This technology enables many new classes of experiments and applications. Both the underlying science and the applications will be described.

BMEE19 - BME TECHNICAL/SERVICE COURSES

BMEE19.1 - Rechargeable Batteries: Characteristics, Performance, and Maintenance

Author(s): Isidor Buchmann
Cadex, Richmond/CANADA

Topic As the reliance on the battery grows, so does the need for robust battery management standards and practices in healthcare. This is not happening uniformly and the *Association for the Advancement of Medical Instrumentation (AAMI)* rated battery management as one of the top 10 challenges for hospital's biomedical departments. An US FDA survey says that "up to 50% of issues in hospitals are related to the battery."

At a debriefing with the FDA at their Maryland HQ at which Mr. Buchmann participated, three shortcomings were identified with batteries in medical devices. Each of these will be discussed at the IUPESM World Congress, and are:

1. Deficiency in quality assurance in batteries by device manufacturers
2. Lack of understanding in battery system integration
3. Not knowing the end of battery life

Presentation Equipment manufacturers base the runtime of a device on a new battery, but this is a temporary state. Once rubber-stamped and approved by the authorities, the users are on their own. Little guidance is provided to assure continued performance and hints as to when to replace the battery.

A battery has a relatively short service life and will require several replacements during the life of the host device. Batteries are difficult to test and often escape the scrutiny of inspection. To assure reliability, a battery must be treated like any other serviceable part in a medical device.

When asking users of a battery-operated medical devices, "When should the battery be replaced?" no clear answers are given. Without a strategic management plan, a battery may stay in service too long, compromising reliability, but most are changed too early, increasing operational cost and stressing the environment.

Mr. Buchmann will give an overview of basic battery technology, discuss typical behaviors in healthcare, how their life can be optimized, pros and cons of a smart battery, when a battery should be replaced, and methods of analyzing batteries as part of maintenance systems.

Presenter Isidor Buchmann is the founder and CEO of Cadex Electronics Inc. and author of www.BatteryUniversity.com. For three decades, Buchmann has studied the behavior of rechargeable batteries in practical, everyday applications, has written award-winning articles including the best-selling book "Batteries in a Portable World," now in its third edition.

Company Cadex Electronics specializes in the design and manufacture of battery chargers and analyzers, as well as advanced rapid-test and monitoring systems. Sold in over 100 countries, Cadex products are known for their robust design, reliable service and long product life. During the 30 years of operations, Cadex has secured several patents in the field of battery diagnostics and monitoring.

Battery University www.BatteryUniversity.com is an education website that addresses strengths and limitations of batteries in the hands of the everyday user. The papers evaluate different battery types and offer the best choice for an application. The information

offers busy professionals a crash course on batteries; it helps engineers find a battery for a new product; students seeking answers for an academic project; and the everyday battery users wanting to prolong battery life.

BMEE20 - HUMAN FACTORS AND MEDICAL DEVICE SAFETY

BMEE20.1 - Clinical Alarms Management (incl. IHE Alarm Communication Mgt)

Author(s): Yadin David¹, Tobey Clark², Marjorie Funk³

¹Health Technology Foundation, Biomedical Engineering Consultants, LLC, Houston/TX/UNITED STATES OF AMERICA, ²Instrumentation & Technical Services, University of Vermont, Burlington/UNITED STATES OF AMERICA, ³School Of Nursing, Yale University, Orange/CT/UNITED STATES OF AMERICA

Background

The use of an instantaneous attention-getting feature, like an alarm, to improve management of a patient's health condition has been used for many years. Alarm systems, ranging from simple alerts to complex alarm systems, are found on many medical devices. Alarms are intended to protect patients, however, they also contribute to noise, error, and the phenomenon of "alarm fatigue", which can lead to adverse events.

Alarm fatigue results from staff being overwhelmed by a cacophony of non-actionable alarms, leading to a delayed response to the actionable alarms or to alarms being ignored or turned off. A high percentage of alarms are not actionable – they do not lead to changes in patient management.

Due to significant adverse events related to clinical alarms, the Healthcare Technology Foundation (HTF) began an initiative in 2004 to improve the management of alarms. A task force of clinical engineering professionals wrote a seminal white paper in 2007 summarizing the literature, adverse event data, and a national survey of 1,327 healthcare staff, which included observations and recommended improvements.

Between 2005 and 2009, the Food and Drug Administration received 566 reports of deaths related to alarms - over 100 deaths each year. The devices associated with the highest number of deaths were physiologic monitors and ventilators.

In 2011, the HTF administered a second national survey, to which 4,278 clinicians responded. The results of this survey were presented to the attendees at the 2011 AAMI Clinical Alarms Summit and distributed nationally. Little progress in alarm hazard reduction was found between the two surveys, with false alarms still comprising the most serious issue related to alarms. Almost 20% of the respondents reported that adverse events occurred in their hospital in the prior 2 years.

The ECRI Institute, an independent, non-profit health technology safety organization, identified alarm hazards as the #1 Health Technology Hazard for the past 4 years.

Effective January 1, 2014, the Joint Commission issued a National Patient Safety Goal (NPSG.06.01.01) requiring hospitals to establish alarm management as an organizational priority. Accordingly, organizations must design a systematic and coordinated approach to better manage this important safety issue. Policies, procedures, and education related to alarms will be required beginning in 2016.

Deliverables

This session will address quantitative and qualitative findings from the HTF alarm surveys. Results showed the impact of clinical alarms on patient safety, clinical perceptions of alarms, and alarm improvement efforts. Results of roundtables held at the 2015 AAMI annual meeting will be presented, along with current HTF activities, such as the development of an "Alarms 101" document for patients and families.

Care providers' views of the issues and best practices for meeting patient management goals and the Joint Commission NPSG.06.01.01 will be discussed, including a case study. Also, the development of unique educational tools, including online clinical alarms orientation and training, will be covered.

Objectives

1. Describe the problem of alarm fatigue and its impact on patient safety.

2. Identify effective strategies for alarm management.

3. Discuss attitudes and practices related to clinical alarms as revealed in the Healthcare Technology Foundation's national surveys.

BMEE21 - GENERAL BME EDUCATION**BMEE21.1 - Biomaterials - Cell-surface Interaction****Author(s):** Caroline Loy, Diego Mantovani

Lab Biomaterials And Bioengineering, Laval University, A/QC/CANADA

Cell-Materials Interactions for the Replacement and the Regeneration of Tissue and Organs**Caroline Loy and Diego Mantovani**

Canada Research Chair I for Biomaterials and Bioengineering for the Innovation in Surgery, Dept of Min-Met-Materials Engineering & Research Center, University Hospital Center, Laval University, Québec City, Canada

Over the last 50 years, biomaterials, prostheses and implants saved and prolonged the life of millions of humans around the globe. The main clinical complications for current biomaterials and artificial organs still reside in an interfacial mismatch between the synthetic surface and the natural living tissue surrounding it. Today, nanotechnology, nanomaterials and surface modifications provides a new insight to the current problem of biomaterial complications, and even allows us to envisage strategies for the organ shortage. Advanced tools and new paths towards the development of functional solutions for cardiovascular clinical applications are now available.

In this CE program, we are therefore proposing to present and discuss with English, French and Spanish speakers the past, present and future challenges of cell-material interactions. At the conclusion of this program, attendees will be able to:

Describe and discuss the principles of the host-response that any foreigner body generate when in contact with human cells and tissues;

Define and determine how to assess and predict in vitro the cell-materials interactions in the cardiac, vascular, neurological and orthopedic system, including those generated and the bone and blood interface;

Demistify the myth of the bionic man, and understand how diseased tissue and organs can be replaced, reconstructed or are envisaged to be regenerated.

BMEE21.2 - Biomaterials - Plasma Medicine**Author(s):** David B. Graves¹, Michael Keidar²

¹Chemical And Biomolecular Engineering, University of California at Berkeley, Berkeley, CA/CA/UNITED STATES OF AMERICA, ²The George Washington University, Washington/UNITED STATES OF AMERICA

A new field of cold atmospheric plasma (CAP) processing associated with biomedicine has emerged in the last 5-10 years. [1] CAP can be used to shrink tumors, promote wound healing and sterilization, and treat dermatological and dental disease, among other things. This presentation will focus on the role of reactive oxygen species (ROS) and reactive nitrogen species (RNS). ROS and RNS (or RONS), in addition to a suite of other radical and non-radical reactive species, are essential actors in an important sub-field of aerobic biology termed 'redox' (or oxidation-reduction) biology. Evidence will be presented that RONS generated by plasmas are probably responsible for much their observed therapeutic effects. [2,3]

At the conclusion of the CE program, attendees will be able to:

1- Describe and discuss the emerging field of cold atmospheric plasma biomedicine.

2- Understand some of the physical and chemical characteristics of the plasma sources as well as typical tools used by plasma scientists to measure and compute key quantities.

3- Recognize some of the emerging connections between reactive species in aerobic biology and the therapeutic mechanisms of CAP.

[1] M.G. Kong, et al., *New Journal of Physics*, **11**, article no. 115012, 2009.

[2] D.B. Graves, *Journal of Physics D-Applied Physics*, **45**(26), article no. 263001, 2012.

[3] D.B. Graves, *Clinical Plasma Medicine*, **2**, 38-49, 2014.

BMEE22 - GENERAL BME EDUCATION**BMEE22.1 - Biosensors and Signal Processing - Signal Analysis and Processing****Author(s):** [Sri Krishnan](#)Electrical And Computer Engineering, Ryerson University, Toronto/
CANADA**Abstract:**

In this talk the characteristics of biomedical (physiological) signals will be covered followed by the techniques and algorithms needed for processing, analysis and interpretation of these signals. Time-domain, frequency-domain, joint time and frequency domain, and sparse domain approaches will be covered in detail for applications related to body sounds' signals, ECG, EMG and gait rhythm.

Learning objectives:

- 1) design of biomedical signal analysis system
- 2) interpretation and quantification of biomedical signals for various applications related to health ICT and emerging mobile health applications
- 3) algorithms for processing of biomedical signals

BMEE22.2 - Cellular and Biomolecular Engineering - Nanoparticles in Diagnostic Therapy**Author(s):** [Mukesh Harisinghani](#)

Radiology, Massachusetts General Hospital, Boston/MA/UNITED STATES OF AMERICA

Magnetic nanoparticles have been used for imaging oncologic and immune disorders as they provide a means of assessing macrophage activity. conventional imaging in these areas is limited to anatomical depiction of abnormality, the use of magnetic nanoparticles provides the functional component and has been a poster child for bench to bedside application.

At the conclusion of the proposed program, attendees will be able to

1. Understand the mechanism by which magnetic nanoparticles provide functional information on MRI
2. Understand the clinical utility of imaging with nanoparticles and how it could profoundly influence patient care
3. Understand what some of the technical challenges are when imaging with magnetic nanoparticles

BMEE23 - CLINICAL ENGINEERING/TECHNOLOGY MANAGEMENT**BMEE23.1 - Clinical Engineering Standards of Practice – Canadian New Edition and Other Countries****Author(s):** Anthony Chan¹, [Bill Gentles](#)²¹Biomedical Engineering, British Columbia Institute of Technology, Burnaby/CANADA, ²Vice President, BT Medical Technology Consulting, Toronto/CANADA

Learning Objectives: At the conclusion of this session program, attendees will:

Understand the process of developing a Standard of Practice that is appropriate for their particular healthcare environment.

Understand the value of the discussions that take place during the development of a standard of practice.

Understand the main sections to include in a standard that is written to conform to ISO guidelines.

Understand how a standard of practice can be used as the basis of a peer review or accreditation process for Clinical Engineering services.

Abstract

Clinical engineering is one of several professional disciplines contributing to safe, effective and economical health care. The role and primary responsibility of a clinical engineering service is management of medical device technology, including adherence to recognized safety, quality, cost and efficiency standards.

The first Clinical Engineering Standards of Practice (CESOP) for Canada was published in 1998. The CESOP has since gone through 2 revisions, with the latest being published in 2014. Each revision was developed by a working group with broad representation from across the country. The working group for the 2014 revision met on a monthly basis for over a year, and produced 17 drafts before the final draft was presented to the membership for approval.

The CESOP is widely adopted by clinical engineering departments across Canada to establish scopes and practice; referenced by health care accreditation bodies; and used to formulate evaluation guidelines in peer review process.

Examples of standards of practice from other countries will be presented and compared to the Canadian standard.

BMEE23.2 - Emerging Medical Technologies - What to Expect, How to Prepare for it**Author(s):**

Medical technologies are evolving at a rapid pace. This change is significantly impacting how healthcare organizations and their technology managers should plan for, procure, support, and update their technologies. This presentation will review new and emerging technologies that are expected to have the most impact on the healthcare technology management profession. It will also discuss the operational and mindset changes that healthcare technology management professionals must make to best prepare for their emerging and future roles. This discussion will include a review of the processes used by ECRI to assess and make judgments about new and emerging technologies with commentary on how these processes can be applied at healthcare organizations.

At the conclusion of this program attendees will be able to:

1. Describe important new and emerging trends in healthcare technologies
2. Discuss key operational changes that healthcare technology management programs should be making to prepare for new and emerging medical technologies
3. Develop a methodology for evaluating and planning for new and emerging medical technologies

BMEE24 - MEDICAL DEVICE DEVELOPMENT AND COMMERCIALIZATION

BMEE24.1 - The Product Development Cycle

Author(s): [Lahav Gil](#)

Ceo, Kangaroo Group, Toronto/CANADA

Learning objectives:

1. Understand the nomenclature of medical devices product development and how it correlates with the (business) language of commercialization of a medtech company
2. Understand the key steps of development that a clinical technology goes through, from technology-transfer all the way to commercial grade, validated and approved medical device, based on the FDA recommendations for product realization
3. Understand how to assess and evaluate technology readiness, and where it currently is on the product development map

Abstract:

The presentation will provide a clear map and the milestones of medical devices product development starting with requirements gathering and product definition and ending with a validated medical device ready to ship. We will cover each step and explain the content of the inputs and outputs along the progress path.

Some of the topics that will be covered, amongst others are: Business justification, requirements gathering and needs assessment, stakeholders analysis and value drivers, feasibility studies, user feedback, system SPECs and architecture, different kinds of prototypes, alpha prototype, preproduction build, design controls, serial manufacturing, V&V, DHF, DMR, DHR, NPI, ISO 13485 QMS, traceability matrix, labeling, change controls

BMEE25 - CLINICAL ENGINEERING/TECHNOLOGY MANAGEMENT

BMEE25.1 - Clinical Engineering Best Practice and Bench-marking

Author(s): Binseng Wang

Quality & Regulatory Affairs, Sundance Enterprises, Inc., White Plains/UNITED STATES OF AMERICA

While debated for over 30 years, productivity and efficiency (cost) measurements and benchmarking continue to be a challenging topic for the clinical engineering (CE) community. At the core of this challenge is the lack of reliable indicators substantiated by actual data. An attempt was made to evaluate some traditional and newer indicators using data collected from two distinct sources in the USA, each with >150 hospitals. Results confirm early concerns that worked hours self-entered by CE staff are subject to misuse and, thus, should be avoided as a productivity benchmark. Likewise, the cost-of-service ratio (COSR) is easily manipulated and, thus, not reliable as an efficiency benchmark. In contrast, good statistical correlation was found for both staffing and cost data with several hospital indicators that are consistently collected for reimbursement and financial reporting purposes. Good correlation with CE department indicators was more difficult to find, apparently due to the lack of reliable records and consistent accounting of all CE resources and expenditures. While no single, easy to measure and understand indicators emerged as replacements for the worked-to-paid-hours ratio and COSR, it was possible to build multi-dimensional models for both productivity and cost efficiency. However, these models, while accurate, are not precise, so the results need to be interpreted carefully. Furthermore, anecdotal data obtained from other countries showed that there are substantial differences in both staffing and efficiency metrics, even though there are numerous similarities in technical metrics. In essence, benchmarking of staffing and cost can be good starting points for a more detailed analysis of the differences among organizations that could reveal substantive causes such as service scope and strategy, organizational characteristics and geographical challenges as well as opportunities for major productivity improvements and cost reductions.

BMEE26 - CLINICAL ENGINEERING

BMEE26.1 - Collaboration on Healthcare Technology Decision-Making

Author(s): Julie Polisena¹, Hal Hilfi², Michael Cheng³

¹Canadian Agency for Drugs and Technologies in Health, Ottawa/CANADA, ²Biomedical Engineering, Ottawa/ON/CANADA, ³xxx, xxx/UNITED KINGDOM

This education session will discuss two types of collaboration on healthcare technology decision making, both of which emphasize a multidisciplinary approach. Firstly, we will briefly describe a simple checklist that guides the routine assessment of any request for the purchase of medical devices in a healthcare facility. Secondly, we will outline the application of formal HTA (health technology assessment) to support informed decision making for new technologies, a large scale technology acquisition and/or complex technologies. We shall devote a major part of this presentation to describe the collaboration of hospital-based HTA network to support informed healthcare technology decision making.

HTA is a form of analysis on health technologies that provides decision makers with information on their clinical effectiveness, safety, cost-effectiveness, and encompasses patient preferences, and ethical, societal, organizational and other considerations. It is a principle component of the holistic framework, (presented yesterday) to enhance the optimal performance associated with the use of medical devices. More specifically, we will elaborate on how HTA in a network of healthcare providers can assist in making decisions on the purchase, use and discontinued use of medical devices in their institution. In addition, we describe how local HTA units can collaborate to facilitate information sharing, avoid unnecessary duplication of effort, and provide equal access to timely evidence-based information to decision makers. This network of HTA producers would allow their work to contribute fully to ensure the sustainability at all levels of healthcare.

Many jurisdictions continue to face hospital budget cuts that force them to look at innovative ways to address these shortfalls, while still managing health care technologies. HTA at the hospital and regional levels is gaining recognition and importance in many parts of Canada and Europe given its potential for greater impact on hospital policies and clinical practice by involving the end-users in the assessment and decision-making. More could be achieved through effective collaboration or networking to combine efforts and experiences.

At the end of this education session, attendees will be able to:

- 1- learn more details of the Stage 2 (assessment function) of the Holistic Framework for Medical Devices presented yesterday (11 June 2015)
- 2 appreciate how multidisciplinary collaborations in healthcare technology decision making are crucial in contributing to the safety, quality, and sustainability at all levels of healthcare.
- 3- use a checklist to guide routine assessment on simple requests for the purchase of medical devices in a healthcare facility
- 4 understand how HTA for more complex cases can enhance the optimal performance on the use of medical devices
- 5- understand how an HTA collaborating network can facilitate information sharing on purchasing, implementing, managing, and decommissioning of medical devices.

BMEF01 - GESTION EN GÉNIE BIOMÉDICAL/CLINIQUE

BMEF01.1 - Exemples de Donnes Pratiques en Génie Clinique et Indicateurs

Author(s): Mohcine El Garch

Groupe Biomédical Montérégie, Agence de la Santé et des Services Sociaux de la Montérégie, Brossard/QC/CANADA

Objectifs d'apprentissage: A l'issue de ce programme de la session, les participants pourront:

1. Comprendre les éléments requis pour mettre en place une démarche qualité dans un service de génie clinique.
2. Comprendre les éléments requis pour mettre en place une stratégie d'entretien des équipements médicaux
3. Identifier les éléments principaux d'une démarche de planification d'entretien préventif pour les équipements médicaux
4. Comprendre les éléments principaux d'un projet d'acquisition de technologie médicale
5. Identifier quelques indicateurs pertinents pour un service de génie clinique et les intégrer au sein d'un tableau de bord.

Exemples de bonnes pratiques en génie clinique et indicateurs

Le génie clinique est l'une des disciplines professionnelles qui contribuent à la sécurité et l'efficacité des systèmes de santé tout en contribuant à l'optimisation des coûts associés à l'utilisation des technologies. Le rôle et la responsabilité première d'un service de génie clinique est la gestion de la technologie des dispositifs médicaux, y compris le respect des normes de sécurité, de qualité, et les standards de gestion de coût et d'efficacité reconnus.

Cette session va présenter dans un premier temps les principaux éléments d'une démarche qualité pour un service de génie clinique. Cela nous permettra de constater que l'implantation d'une démarche qualité dans un service de génie biomédical ne constitue pas une fin en soi. C'est un outil pour améliorer l'efficacité de l'organisation d'un service de génie biomédical afin de répondre encore mieux aux attentes du personnel clinique, des patients et des administrateurs d'un établissement de santé. En utilisant les guides de pratiques reconnus dans le domaine du génie clinique, cette session présentera également des pistes pour revoir les principaux aspects de gestion des technologies de santé en hôpital tel que la stratégie d'entretien des équipements médicaux, la planification des entretiens préventifs des équipements, la gestion des projets d'acquisitions ou encore la mise en place d'indicateurs et de tableaux de bords.

ENGLISH

TITLE: Examples of standards of practices in clinical engineering, improvements and metrics - Exemples de bonnes pratiques en génie clinique, amélioration et indicateurs.

ABSTRACT: Clinical engineering is one of the professional disciplines that contribute to the safety and effectiveness of health systems and contribute to the optimization of costs associated with the use of technology. The role and primary responsibility of a clinical engineering department is the management of medical device technology, including compliance with safety standards, quality, and cost management recognized standards.

This session will present main elements of a quality system approach for clinical engineering departments. This will allow us to see that the implementation of a quality approach in a Clinical Engineering department is not an end in itself. It is a tool to improve the efficiency of the organization to better meet the needs of clinical

staff, patients and administrators of a health facility.

Using standard recognized practices in the field of clinical engineering, this session will also present ways to review key aspects of healthcare technology management in health technology such as maintenance strategy of medical equipment, planning of preventive maintenance equipment, management of acquisition projects or the development of performance metrics and dashboards.

Learning Objectives:

At the end of the program of the session, participants will:

1. Understand the elements required to implement a quality approach in a clinical engineering department.
2. Understand the elements required to implement a maintenance strategy of medical equipment
3. Identify the key elements of a preventive maintenance planning process for medical equipment
4. Understand the main elements of a medical technology procurement project
5. Identify some relevant indicators for clinical engineering services and integrate them within a dashboard.

BMEF02 - GESTION EN GÉNIE BIOMÉDICAL/CLINIQUE

BMEF02.1 - Clinical Engineering Standards of Practice – Normes de Pratique en Génie Clinique- Nouvelle Edition Canadienne en Français

Author(s): Mohcine El Garch¹, Bill Gentles²

¹Groupe Biomédical Montérégie, Agence de la Santé et des Services Sociaux de la Montérégie, Brossard/QC/CANADA, ²Vice President, BT Medical Technology Consulting, Toronto/CANADA

Le génie clinique est l'une des disciplines professionnelles qui contribuent à la sécurité et l'efficacité des systèmes de santé tout en contribuant à l'optimisation des coûts associés à l'utilisation des technologies. Le rôle et la responsabilité première d'un service de génie clinique est la gestion de la technologie des dispositifs médicaux, y compris le respect des normes de sécurité, de qualité, et les standards de gestion de coût et d'efficacité reconnus.

Le premier guide des pratiques en génie clinique (CESOP) pour le Canada a été publié en 1998. Le CESOP a depuis traversé deux révisions, la dernière ayant été publiée en 2014. Chaque révision a été développée par un groupe de travail avec une large représentation de partout au pays. Le groupe de travail pour la révision 2014 s'est rencontré sur une base mensuelle depuis plus d'un an, et a produit 17 avant-projets avant que le projet final soit présenté aux membres pour approbation.

Au cours de l'année 2015, le comité Bilingue du CMBES a entrepris la traduction du guide anglophone afin de pouvoir le partager avec la communauté en génie clinique francophone au Canada.

Le CESOP est largement adopté par les départements de génie clinique à travers le Canada pour établir les champs d'activité de la pratique professionnelle. Il est référencé par les organismes d'accréditation de soins de santé et il est également utilisé pour formuler les lignes directrices d'évaluation dans le processus d'examen des départements de génie clinique par les pairs.

Au cours de la session, des exemples de guides de pratiques d'autres pays seront présentés et comparés au référentiel canadien.

Objectifs d'apprentissage: A l'issue de ce programme de la session, les participants pourront:

1. Comprendre le processus d'élaboration d'un guide de pratiques qui est approprié pour leur environnement de soins de santé particulier.
2. Comprendre les principales sections du guide qui est rédigé en vue de se conformer aux lignes directrices de l'ISO.
3. Comprendre comment un guide de pratique peut être utilisée comme standard de base d'une revue du fonctionnement d'un service de génie clinique par les pairs ou dans le cadre d'un processus d'accréditation.

ENGLISH

Clinical engineering is one of the professional disciplines that contribute to the safety and effectiveness of health systems and contribute to the optimization of costs associated with the use of technology. The role and primary responsibility of a clinical engineering department is the management of medical device technology, including compliance with recognized safety standards, quality, and cost efficiency management standards.

The first Clinical Engineering Standards of Practices (CESOP) for Canada was published in 1998. The CESOP has since gone through two revisions, the latest having been published in 2014. Each revision

was developed by a working group with broad representation across the country.

During 2015, the Bilingual Committee CMBES undertook the translation of the English-speaking guide in order to share it with the francophone clinical engineering community in Canada.

The CESOP is widely adopted by clinical engineering departments across Canada to establish the scopes of professional practice. It is referenced by the health care accreditation bodies and it is also used to formulate the assessment guidelines in the review process for clinical engineering departments peer.

The session will be an introduction to the CESOP French translation with some comparison with examples of other countries standards of practices.

Learning Objectives: At the end of the program of the session, participants will:

1. Understand the process of developing a practical guide that is appropriate for their particular health care environment.
2. Understand the major sections of the guide that is written in order to comply with ISO guidelines.
3. Understand how practice guidelines can be used as standard based on a review of the functioning of a clinical engineering department peer or as part of an accreditation process.

BMEF03 - GESTION EN GÉNIE BIOMÉDICAL/CLINIQUE**BMEF03.1 - Impacts de la Technologie Médicale sur la Santé de la Mère et de l'Enfant****Author(s):** Gnahoua Zoabli¹, Akimey A. Nabilath²¹Biomedical Engineering, CSSS du Lac-des-Deux-Montagnes, St-Eustache/CANADA, ²Institute Of Biomedical Engineering, University of Montreal, Montreal/CANADA**Objectifs:**

1. Santé et sécurité au travail
2. Santé de la mère et du bébé
3. Outils pour se prémunir des effets néfastes de la technologie médicale sur l'humain
4. Prévention en milieu de travail pour les professionnels de la santé

Résumé:

L'environnement hospitalier comporte continuellement pour les employés différents risques selon la nature des tâches réalisées quotidiennement: proximité de patients infectés, exposition au bruit ambiant, exposition aux rayonnements ionisants, manipulation de produits chimiques ou biologiques, effort physique de manutention, risque d'éraflure ou de piqure accidentelle. Des mesures préventives et des directives appropriées permettent de minimiser ces divers risques et d'assurer aux employés des conditions de travail assez sécuritaires durant l'exercice de leur profession au sein de l'hôpital. Les dispositions mises en œuvre pour garantir une maternité sans danger ne sont pas appliquées de façon uniforme dans les établissements de santé, voire sur le même département. La présente formation est une mise à jour des connaissances qui a pour but de renseigner les professionnelles de la santé qui planifient d'être enceintes, qui le sont déjà, ou sont nouvellement mamans, sur les risques biologiques, chimiques et physiques induits par la proximité technologique ou les horaires de travail en milieu clinique. Des recommandations sont faites aux gestionnaires pour faciliter l'harmonisation des tâches et des congés connexes à la condition de grossesse ou d'allaitement chez la professionnelle exerçant en milieu clinique.

ENGLISH

Hospital environment has continuously presented different risks to the employees depending on the nature of the tasks performed daily: being close to infected patients, exposure to environmental noise or radiation, handling chemicals or biologicals, physical effort or ergonomics, risk of scratching or accidental needlestick injuries. Preventive measures and appropriate guidelines will minimize these various risks and ensure to employees fairly safe working conditions within the hospital. Procedures implemented to ensure safe motherhood at work are not applied consistently in health facilities or on the same department. This training is an update of knowledge which aims to inform health professionals who are planning to be pregnant, who already are, or are new moms. The risks studied here are related to biologicals, chemical and physical hazards induced by technological proximity or work shifts in clinical or medical areas. Recommendations are made to clinical and medical managers to facilitate the harmonization of tasks and optimize pregnancy or lactation leave conditions for female professionals working in a hospital.

Learning Objectives:

1. Occupational safety and health
2. Health of mother and baby

3. Tools to protect against adverse effects of medical technology on the human
4. Prevention workplace for healthcare professionals

BMEF04 - GESTION EN GÉNIE BIOMÉDICAL/CLINIQUE**BMEF04.1 - La Gestion de Projets et de Portefeuille de Projets en Technologies de la Santé****Author(s):** Mohcine El Garch

Groupe Biomédical Montérégie, Agence de la Santé et des Services Sociaux de la Montérégie, Brossard/QC/CANADA

L'objectif de ce cours est de donner des pistes de réflexion aux participants pour :

Définir la gestion de projet dans un contexte hospitalier

Réaliser la planification de leurs projets (petits ou grands)

Établir la charge de travail du ou des professionnels

Gérer la performance et les risques associés à un projet

Communiquer de façon efficace l'avancement des projets

Utiliser le logiciel MS Project pour réaliser la gestion d'un projet

Partager des projets et des ressources en mode multi-projets avec MS Project

La gestion de projets et de portefeuille de projets en technologies de la santé.

Les activités du service de génie biomédical dans un hôpital sont plus souvent qu'autrement réalisées en mode projet. Travaillant seul ou en équipe, le professionnel est souvent amené à développer des outils lui permettant de suivre ces activités. Que ce soit dans le cadre de petits projets ou de projet de grande envergure, la connaissance des méthodes de projets et des outils pratiques sont un incontournable.

Ce cours présente les éléments principaux de la gestion de projet en général, les enjeux, les risques et les outils à mettre en place pour mieux gérer ses projets. Des exemples de projets et de situations rencontrées spécifiquement dans le domaine du génie clinique seront présentés et des outils pour gérer les projets et les portefeuilles de projets seront également abordés.

ENGLISH

TITLE: Project management and program in health technology projects - La gestion de projet et de portefeuille de projet en technologies de la santé

ABSTRACT: The activities of the Clinical Engineering department at a hospital are more often than not carried out in project mode. When working alone or in teams, the clinical engineer needs to develop tools to monitor these project activities. Knowledge of standard practices and tools of project management are a necessity in the context of large-scale project or even with the small projects.

This course presents the main elements of project management, issues, risks and tools to put in place to better manage its projects. Examples of specific projects and situations encountered in the field of Clinical Engineering will be presented and tools to manage projects and program will be discussed.

Learning objectives:

The objective of this course is to give food for thought to the participants to:

- Define project management in a clinical engineering perspective;
- Plan their projects (whether small or large);
- Establish workload for clinical engineers;
- Manage the performance and risks associated with a project;

- Communicate effectively the progress of projects;
- Use MS Project to achieve the project management;
- Share projects and resources in multi-mode projects with MS Project

BMEF05 - GESTION EN GÉNIE BIOMÉDICAL/CLINIQUE**BMEF05.1 - Implantation du Guide des Bonnes Pratiques de L'ingénierie Biomédicale en Établissement de Santé****Author(s):** Fabienne Debiais¹, Christine Lafontaine²¹Génie Biomédical, Hôpital général juif, Montréal/CANADA, ²Génie Biomédical, Haelys, Terrebonne/QC/CANADA**Résumé:**

Cet atelier présentera le guide des bonnes pratiques de l'ingénierie biomédicale en établissement de santé et proposera une démarche d'implantation ainsi que des outils et méthodes pour y parvenir.

Cette session comportera un partage d'expériences variées provenant de plusieurs établissements de santé et faisant appel à diverses méthodologies (LEAN, ISO 9001...).

Objectif #1:

S'approprier le guide des bonnes pratiques de l'ingénierie biomédicale pour mieux le maîtriser et en tirer le maximum pour répondre aux exigences du milieu de la santé.

Objectif #2:

Découvrir différentes techniques de priorisation des bonnes pratiques de l'ingénierie biomédicale afin de maximiser l'impact des actions mises en oeuvre.

Objectif #3:

S'initier à des méthodes de gestion de la qualité (LEAN, ISO 9001) en découvrant des projets concrets réalisés en milieu hospitalier.

ENGLISH**TITLE: IMPLEMENTATION OF BIOMEDICAL ENGINEERING BEST PRACTICE GUIDE IN HEALTHCARE INSTITUTIONS**

ABSTRACT : This workshop will introduce the biomedical engineering best practice guide in healthcare institutions and will suggest an implementation process as well as tools and methods to achieve this. This session will include a sharing of varied experiences from several healthcare facilities and using various methodologies (Lean, ISO 9001 ...).

BMES01 - INTEROPERABILITY IN HEALTH TECHNOLOGY**BMES01.1 - Interoperability - Profiles - IHE****Author(s):** Vladimir Quintero

Universidad Simaon Bolivar, Barranquilla/COLOMBIA

Learning objectives

- 1- Why Interoperability is needed?
- 2- The role of IHE
- 3- Origin, purpose and use of Interoperability Profiles

ABSTRACT

The rapid advance of Information and Communications Technology, ICT, has produced, among other effects, the multiplication of data related to the health of a patient, data that is produced by the increasing amount of diagnosis, monitoring and treatment equipment available today to the medical science. Along with this development of technology-based data, models of care have evolved towards offering integrated services, often produced by different suppliers, with the consequent need for exchange and integration of clinical and financial information. Finally, the prioritization of patient-centered care has increased the number of actors, both users and producers of information in the processes of health care delivery.

The convergence of these three trends has exponentially increased the volume of data available for any patient, without simultaneously having developed a strategy to ensure that all such data, produced by different sources, can be seamlessly exchanged, integrated, processed, and used.

We have arrived to a paradoxical situation in which potential users of the information, like physicians, policymakers, researchers, and even the patients themselves, are surrounded by a sea of data, without being able to use it in an integrated and efficient way. What is needed is the implementation of interoperability between all those equipment, devices and systems.

According to HIMSS (Health Information Management Systems Society): in healthcare, interoperability is the Ability of different information technology systems and software applications to communicate, exchange data, and use the information that has been exchanged. Data exchange schema and standards should permit data to be shared across clinicians, lab, hospital, pharmacy, and patient regardless of the application or application vendor. Interoperability means the ability of health information systems to work together within and across organizational boundaries in order to advance the health status of, and the effective delivery of healthcare for, individuals and communities.

By the end of the 90's, the Radiology Society of North America, RSNA, the National Electric Manufacturer Association, NEMA and HIMSS came together to create a new organization to deal with this challenge of interoperability, the IHE: Integrating the Healthcare Enterprise.

IHE is an international initiative designed to encourage and promote the integration of medical devices and information systems that support the operation of modern health institutions. Its main objective is to ensure that in the care of patients, all required information for medical decisions is correct and available to healthcare professionals.

The strategy proposed by IHE articulates the needs of producers and users of equipment, devices and systems, from the viewpoint of Use Cases in which information exchange requirements are determined, and a solution that fits all participants needs is developed.

The methodology begins with the identification of priority situations of information exchange by users: Clinics and Hospitals, independent Doctors, research centers, etc. These requests are converted into use cases by a technical team of development engineers from major manufacturer of health equipment and systems in the world.

After identifying the particular characteristics of the exchange of information in each use case, they proceed to identify the most efficient standards for structuring this exchange (DICOM, HL7, ISO, IEEE, etc.) and with them they design and build a profile of interoperability, which is then published and implemented in equipment and systems by those producers who participated in its development, and finally tested under real conditions during the massive testing event: the Connectathon, held annually in various countries.

This scheme collaborative competition ensures that the solutions offered by the interoperability profiles, integrated into 'Technical Frameworks' which are also published free of cost, have the widest possible coverage and can facilitate the exchange of information between the maximum number of equipment and systems, regardless of their origin.

Production of IHE is structured in 14 'Domains' or thematic areas, to meet the different specialties and user needs. To date, the IHE has National Committees in 19 countries.

BMES02 - INTEROPERABILITY IN HEALTH TECHNOLOGY

BMES02.1 - Business Opportunities

Author(s): [Mario Castañeda](#)

Health Care Technology, Healthitek, San Rafael/CA/UNITED STATES OF AMERICA

The very existence of Health Care Technology departments, programs, and projects is at risk during times of organizational political and technical turmoil. Elections, reorganizations, austerity mandates, and disruptive technologies bring changes that impact the Health Care Technology leader. The leader's ability to demonstrate added value during organizational transitions is vital. Successful designing, delivering, and sustaining programs during turmoil can be itself transformational and in line with the changes.

Our approach recasts the problem into an opportunity for economic growth. Under uncertainty, one of the major challenges is to design a program that motivates other key stakeholders to provide support. We designed a successful program in Colombia and will describe the factors that made this possible: 1) adopting **the continuum of health model** as a foundational framework, 2) building a coalition of public, private, and academic organizations for support, and 3) developing and implementing a new facilitation model to distill the ideas of 40 participant thought leaders from local business, industry, health care, and academia.

Learning objectives

The participant will

- 1) Identify opportunities brought about by organizational change, turmoil, and disruptive technologies.
- 2) Learn from the success of the Colombian Case study how to apply success factors to solve their own challenges.
- 3) Learn about how to identify opportunities for business, academia, and government to obtain support of their leaders.

BMES03 - INTEROPERABILITY IN HEALTH TECHNOLOGY

BMES03.1 - Trends on IT and Health Technology

Author(s): Antono Hernandez

ACCE , GHIA USA, Potomac/UNITED STATES OF AMERICA

The healthcare sector has experienced fast evolution due to the convergence of information technologies and communications with the health technologies. We will present an overview of medical technology in healthcare facilities: standalone equipment, networks of medical devices (analog and digital), technology in public health servicing communities. Also, we will address the current trend in the use of mobile communication platforms for personal monitoring and auto management of health (people responsible for their own health). Parallel to this will be the evolution of epidemiological information systems, the clinical information systems and the information generated by mobile technologies. We will highlight some aspects of the integration and convergence of these technologies and the way they have impacted the workflow in healthcare facilities. This evolution brings benefits but also risks associated that are inherent to the use of technologies as well as some others made (intentionally or unintentionally) by the people. Also, this change of the healthcare delivery model gives more responsibility to the people in the management of their own health and well-being.

Topics include:

- The evolution and trend on healthcare technology
- The convergence of Health Technologies and Information and Communication Technologies

BMES03.2 - Healthcare Continuum

Author(s): Vladimir Quintero

Universidad Simon Bolivar, Barranquilla/COLOMBIA

Learning objectives

- 1- What is the Healthcare Continuum
- 2- Challenges and opportunities
- 3- Where Healthcrae Continuum and Interoperability meets

ABSTRACT

Traditional health delivery is structured to meet patients' specific and acute complications. It is focused on intervention and associated diagnoses. This system consolidates in the twentieth century in response to a large increase in demand for timely cure of diseases, especially infectious and viral. This business model requires companies able to make large investments in infrastructure and specialized equipment, as well as highly specialized personnel capable of performing complex surgeries. Therefore, it is a business that consumes a lot of resources (doctors, hospital beds, technology, medicine, etc.) contributing to increase the financial pressure on the health system. Besides being timely, it is a reactive health delivery to a patient's need. In this sense, offered products and services are a response to a specific complication in the patient's health. Therefore, consumers of products and health services that typically do not have such complications are not a target for companies in this business.

What is the necessary evolution of this way of delivering health given the significant changes in demand and environment? The need to provide a continuum of care to a population with further and further growing care needs is imposed. The aim of continuing care goes beyond the cure of a disease. It seeks to accompany the patient's or

consumer's health throughout his/her life. In the continuous delivery of health intervention still exists, but is limited to what is necessary, the population most in need. That is only a small part of a much more complex whole, where prevention, early disease detection and remote monitoring of patients play a key role. The consumer (and no sickness or hospital) is the center of this business. On the one hand, it supports the value chain by sending data on their health through proactive use of mobile or remote technology. On the other hand, the consumer is the key element of the proposed value chain, which seeks to provide a "complete solution" for health, promoting the establishment of lasting (and not one-time) relationships over time.

The main differences between the traditional value chain of health delivery and that of continuous healthcare delivery are reflected in the benefits of this new way of looking at health:

- Increased business opportunities
- Better health for patients
- Optimization of costs for companies and the system

This paradigm shift in the delivery of health services brings a significant multiplication of the actors involved, of the offered services, and of the corresponding integration mechanisms.

Finally, all that change must be supported by information, which now more than ever must be standardized to ensure "**the ability of different information technology systems and software applications to communicate, exchange data, and use the information that has been exchanged**" which corresponds exactly to the definition of interoperability.

JT01 - IMAGING**JT01.1 - SPECT and Gamma Camera State-Of-The-Art Technology and Current Research****Author(s):** R Glenn Wells

Physics, Carleton University, ottawa/CANADA

Dedicated cardiac SPECT cameras were recently introduced into the market. These cameras represent a significant departure from traditional Anger-camera designs. They employ novel collimators and acquisition strategies, large numbers of detectors, and solid-state cadmium-zinc-telluride detectors. These features produce a 4-8 fold increase in camera sensitivity which can be used to significantly improve image quality, reduce acquisition times or reduce patient radiation exposure. Some of these systems are also quasi-stationary, opening the door to exciting future applications in dynamic imaging. This presentation will describe the design features of the more popular dedicated cameras, the DSPECT system (Spectrum Dynamics) and the Discovery NM530c (GE Healthcare) and highlight how the new cameras achieve their improvements in sensitivity. As with any new technology, there is a learning curve associated with its use: familiar artifacts like those from attenuation have changed their appearance and prevalence, and new concerns arise such as image truncation due to a limited field of view. Therefore, I will also discuss some of these and other limitations and challenges inherent in the designs and some implications for their integration into a clinical environment. I will present some of the evidence supporting the use of these systems to reduce acquisition times and patient exposures. Finally, I will discuss the use of these cameras for dynamic imaging. Once solely in the domain of Positron Emission Tomography (PET), the improved sensitivity and temporal resolution of the new cameras make it possible to acquire dynamic cardiac SPECT studies with clinically practical protocols. This will allow measurement of absolute myocardial blood flow which PET studies have shown will improve diagnostic and prognostic accuracy over standard relative perfusion imaging. I will describe some of the research being done by my group and others to bring these novel capabilities to the clinic.

At the conclusion of the CE program, attendees will be able to

Understand the novel features of these dedicated cardiac cameras and how they provide improved performance.

Describe and discuss how these new cameras can be integrated into a clinical environment and how this may alter clinical protocols and workflow.

Describe some of the novel capabilities of the new cameras and potential for future applications.

JT01.2 - Magnetic Resonance Imaging State-Of-The-Art Technology and Current Research**Author(s):** Richard Frayne

Radiology And Clinical Neurosciences, University of Calgary, Calgary/AB/CANADA

Magnetic resonance (MR) imaging continues to be a rapidly changing field, with a clear connection between technologic innovation and clinical imaging enhancement. MR technology has been in near constant evolution since before the installation of the first clinical MR imaging units. The first clinical MR images in Canada were obtained in 1982; since this time advancements have been made in all facets of clinical MR imaging. These advances can be conveniently divided into hardware and software developments.

MR hardware has seen increases in main magnetic field strength, improvements in gradient performance, and tremendous advances

in imaging coil design. Today's leading edge clinical systems operate at 3 T (with some centers now exploring systems operating at 7 T and higher), with gradient performance often limited to established physiological safety limits, and adoption of flexible multi-channel (32 or more) receive coils and, most recently, multi-channel transmission. These developments have been used to increase signal-to-noise in acquired images, improve patient throughput, and maturation of a wide range of application-specific imaging coils.

MR software has arguably seen an even more explosive growth in both new approaches and applications. Most clinical MR scanners have research environments that can be accessed by user at vendors-approved research sites. This access has allowed software-based innovations to occur not only at vendor R&D facilities; but also at ever increasing rates at universities and academic medical centers. Advanced approaches include ongoing development of fast imaging approaches (that are often coupled with clever under-sampling schemes and matching image reconstruction strategies), artifact suppression strategies (*e.g.*, motion, fat), as well as new image contrast mechanisms. New MR applications have extended clinical MR imaging from purely anatomical/structural imaging to include the assessment of brain activation, diffusion, perfusion, relaxation rates, velocity and other functional/physiological parameters. Techniques are also under development to image molecular phenomena. An emerging concept, related to these new assessment methods, is the application of quantitative imaging techniques to patients.

At the conclusion of this presentation, participants will:

Understand the historical pattern of advances in MR imaging and their impact on clinical care.

Describe and discuss the relevance of state-of-the-art MR hardware advancements.

Describe and discuss the relevance of state-of-the-art in new MR software approaches and applications.

Have an enhanced appreciation of the relationship between technologic innovation and clinical imaging enhancement.

JT02 - PROCUREMENT AND EQUIPMENT SELECTION

JT02.1 - UNICEF's Approach to Medical Device Selection and Procurement for Low-Resource Settings

Author(s): Shauna Mullally¹, Ludo Scheerlinck²

¹Health Technology Centre, UNICEF Supply Division, Copenhagen/DENMARK, ²Health Technology Centre, Medical Devices Unit, UNICEF Supply Division, Copenhagen/DENMARK

UNICEF works in over 190 countries to promote the rights of children and is a major source of health, nutrition, education, water and sanitation and child protection supplies in low-resource settings. In 2013, for example, UNICEF procured \$2.8 billion worth of supplies for development programs and humanitarian emergencies in 130 different countries, of which approximately \$142 million was medical devices and kits for maternal, newborn and child health (MNCH).

The medical devices team within UNICEF's supply headquarters in Copenhagen leads the selection and procurement of 800 medical and clinical laboratory devices that form our standard product portfolio. Many are stored in our supply warehouse where kits are packed for rapid response during emergencies and to facilitate distribution to end users. In addition to our standard device portfolio, we supply personal protective equipment, assistive health technologies for children with disabilities, and vocational training products for healthcare workers for MNCH interventions.

Our procurement is guided by UN and public procurement rules that ensure clear segregation of duties for technical and contracting staff during the tendering process. Quality assurance is also a critical aspect of the process, and is managed by an in-house team that runs a test laboratory and audits manufacturers' quality systems. We have developed quality policies for in-vitro diagnostics and medical devices, and work with the World Health Organization (WHO) on pre-qualification of rapid diagnostics tests.

In addition to managing medical device procurement, we advise on supply chain management and health technology management in-country, beginning with needs assessments. We work closely with the WHO and other partners to foster product innovation, produce guidance for medical device selection in low-resource settings and harmonize specifications for essential supplies for MNCH. We also conduct fit for purpose evaluations and research on the markets of our essential, strategic devices.

Some examples of our current work include:

Strengthening MNCH services in the Democratic Republic of Congo through the supply of medical devices to equip 200 hospitals and 1,000 health centres nationwide

Leading two projects to foster innovation for child wheelchair solutions for use in emergencies and for improved acute respiratory infection diagnosis for children in their communities

Working with partners to evaluate new point of care HIV diagnostics in seven African countries

Working with the WHO and UN partners on a list of essential medical devices for MNCH services at different levels of care

Supplying a large percentage of the Ebola personal protective equipment to affected countries; developing technical specifications, leading an industry consultation and developing guidance

At the conclusion of the session, attendees will be able to:

Describe and discuss UNICEF's approach to device selection and procurement and incorporate some principles of the approach into their own work

Describe and discuss medical device selection and procurement challenges in low-resource settings and identify tools produced by UNICEF, the WHO and partners to address the challenges

Provide examples of UNICEF's current medical device projects and identify opportunities for collaboration with UNICEF on medical device innovation, selection and procurement and health systems strengthening work

JT02.2 - Equipment Donation and Disposal - Goodwill vs. Risk

Author(s): Mario Ramirez¹, Bill Gentles²

¹Medical Engineering, The Hospital for Sick Children, Toronto/CANADA, ²Vice President, BT Medical Technology Consulting, Toronto/CANADA

Learning Objectives: At the conclusion of this session program, attendees will:

Meet other participants who are involved in medical equipment donations and share contact information to promote further information sharing.

Understand the reasons for the failure of donated medical equipment in developing countries.

Understand the necessary 'best practices' related to people, processes, and metrics to most effectively donate medical equipment to developing countries

Understand the essential role of recipient organizations in improving the success rate of donations.

Abstract:

Previous studies conducted in the United States and Europe have shown that as much as 70% of medical equipment that is donated to low-income countries is never put into use in these countries[1]. As a result an unnecessary burden is created, and many of the recipients' equipment deficiencies remain unresolved.

Responses to natural disasters also generate a flood of donated medical equipment, which is often sent with a lack of understanding of what is really needed. A study of seven hospitals in Haiti found only 30 percent of the 115 pieces of medical equipment donated after the 2010 earthquake were working and 14 percent of the equipment could not be repaired. [2]

To address this ongoing problem, numerous articles and guidelines have been published. A recent guideline published in the UK includes a thorough examination of the reasons for the lack of success of medical equipment donations, and exhaustive recommendations to correct the problem. [3]

In this session we will review the current knowledge on the complexities of donating medical equipment to developing countries, and discuss possible approaches to improve the effectiveness of these donations.

[1] "Medical device donations: considerations for solicitation and provision. (WHO Medical device technical series)," World Health Organization, Geneva, 2011. Accessed: March 10, 2014. Available at: http://whqlibdoc.who.int/publications/2011/9789241501408_eng.pdf?ua=1

[2] Roger Dzwonczyk; Chris Rihall, "Medical equipment donations in Haiti: flaws in the donation process" Rev Panam Salud Publica vol.31 n.4 Washington Apr. 2012. Available at: http://www.scielosp.org/scielo.php?pid=S1020-49892012000400012&script=sci_arttext

[2] Adjabu, N., Bradley, B., Gentles, W., Mirzazadeh, S., "A Study Of

Medical Equipment Donations From Canada To Developing Countries” Presented at AHT2014, London, England, September 2014.

[3] Tropical Health Education Trust, “Medical Equipment Donations - Making it Work”, THET 2013, Available at: <http://www.thet.org/health-partnership-scheme/resources/publications-old/making-it-work-a-toolkit-for-medical-equipment-donations-to-low-resource-settings>

JT03 - IMAGING

JT03.1 - CT State-Of-The-Art Technology and Current Research Topics

Author(s): Ting-Yim Lee¹, Aaron So², Esmaeil Enjilela²

¹Imaging, Lawson Health Research Institute, London/ON/CANADA,

²Imaging Research Laboratories, Robarts Research Institute, London, ON/CANADA

Learning Objectives

1. State-of-art technology in CT - wide detector cone beam, iterative reconstruction, dual energy
2. Research applications of dual energy
3. Research applications of dynamic contrast enhanced scanning - perfusion imaging in stroke, cancer and heart attack

Abstract

The advent of slip ring, dual energy, cone beam acquisition with wide detector array and iterative image reconstruction have revolutionized the applications of CT in both the clinical and research arena since the 1990's. This presentation will discuss these different technological advancements and their implications in clinical and research applications. For clinical applications, examples will be drawn from dual energy material selective imaging, high resolution imaging and dose reduction. For research applications, perfusion imaging in stroke, cancer and heart attack and compressed sensing reconstruction for ultra-low dose perfusion imaging will be discussed.

JT03.2 - Review of PET State-Of-The-Art Technology and Current Research Topics, Including PET/CT and PET/MR

Author(s): Roger Lecomte

Sherbrooke Molecular Imaging Center, Research Center of CHUS (CRCHUS), Sherbrooke/CANADA

Positron emission tomography (PET) is a medical imaging modality using positron-emitting isotopes to investigate the fate of radio-labeled molecules in living organisms. By measuring the uptake, biodistribution and washout of the radiotracer, it is possible to obtain information about *in vivo* molecular processes involved in normal physiology, as well as in diseases such as cancer, neurological disorders, heart and cardiometabolic diseases. Major advances in PET technology have widened the range of applications of PET in both biomedical research and clinical diagnosis. Examples of these technological advances include very diverse and clever detector designs, sophisticated signal processing techniques, 3-dimensional imaging with iterative reconstruction algorithms, the introduction of time-of-flight measurement, and the combination of PET with X-ray computed tomography (CT) or magnetic resonance imaging (MRI). Whereas PET technology has made huge progress in the last decades, it has not reached its performance potential. This review will describe the basic principles, state-of-the-art technology and current developments of PET, including PET/CT and PET/MR dual-modality imaging. The overview will be concluded by detailing a few key research and clinical applications of PET imaging and by discussing some promising new ideas in the field.

At the conclusion of the CE program, attendees will be able to:

- 1- Describe and discuss PET imaging principles, technologies and applications used in diagnostic nuclear medicine and biomedical research.
- 2- Understand the underlying physical limitations and areas of potential advances of the PET imaging modality.

3- Explain the various advantages and limitations of different multi-modality imaging approaches.

JT04 - ETHICS

JT04.1 - Ethics for Biomedical Engineers and Medical Physicists Workshop

Author(s): Monique Frize¹, Jean-Pierre Bissonnette²

¹Systems And Computer Engineering, Carleton University, Ottawa/CANADA, ²Radiation Physics, Princess Margaret Cancer Centre, Toronto/CANADA

Learning objectives: (1) Become familiar with ethical theories, codes, and ethical decision-making; (2) learn the application process for obtaining ethics clearance for research projects; (3) explore various ethical dilemmas and how to deal with these.

Health professionals are concerned with a variety of questionable behavior and professional and ethical misconduct, especially when a patient's life is at stake. The workshop discusses the ethical decision-making process, including ethical theories and ethical codes, experimentation with humans and animals, clinical studies for prototype testing, and how to obtain ethics clearance for this type of research. The impact of technology and science on people, society, and the environment and means of minimizing harm are discussed. Ethics regarding gender and culture is also an important aspect to consider. For clinical practitioners, ethics regarding incident reporting, fairness, access to resources and skills, and educational practice are of concern. Ethics education and training is a must for anyone working in these two fields related to health care.

Format of the workshop :

The main ideas, concepts, and references will be presented (20 minutes). Groups of 4-5 persons will prepare an application to an Ethics Research Board for a research project of their choice; some ideas will be provided (30 minutes). Groups will review another group's application (20 minutes). Comments and ideas originating from participants will be collected and included in a report that follows the workshop (15 minutes). Although discussions will be conducted in English, groups preferring to submit their work in French will also be considered.

JT05 - LEADERSHIP**JT05.1 - What is Leadership? A Roundtable from Recognized Leaders**

Author(s): [David Jaffray¹](#), [Kin-Yin Cheung²](#), [Ratko Magjarevic³](#), [Tony Easty⁴](#), [Herbert Voigt⁵](#)

¹Ontario Cancer Institute / Princess Margaret Hospital, Toronto/CANADA, ²Medical Physics & Research Department, Hong Kong Sanatorium & Hospital, hong kong/HONG KONG, ³University of Zagreb Faculty of Electrical Engineering and Computing, Zagreb/CROATIA, ⁴University Health Network, Centre for Global eHealth Innovation, Toronto/CANADA, ⁵Biomedical Engineering, Boston University, Boston/UNITED STATES OF AMERICA

Leadership, and the dynamics of leadership, is one of the most complex topics in the workplace. Almost everyone has had the experience of being led by people they admired and respected and by people they did not. Since most leaders would prefer to be judged as belonging to the former group, it is useful to examine the attributes of a leader that engender admiration and respect and deconstruct them as a framework for us all to strive for.

In my opinion, very few people are natural leaders, and so for most of us, leadership takes work and effort. It is useful to regularly examine the ways in which we attempt to lead, to determine whether we are being effective. That said, what are some of the key attributes of effective leadership:

Know where you are going: It is hard for team members to follow you if you yourself haven't thought carefully about what you intend to achieve and how you intend to get there.

Communicate regularly: Most of us assume that those around us know more about our plans than they really do. It is easy to forget that key pieces of information have not been shared with team members, so try to make sure that this happens. It can be quite informal. It does not require endless memos and meetings.

Allow involvement and dissent: Not everyone agrees on how an issue should be tackled, and good leaders allow ideas to come forward from team members without fear of criticism or punishment. Ultimately, the leader may take the final decision on an approach, but the team is more likely to commit to it if it represents the collective talents and knowledge of the team. Good leaders should allow their ideas to be challenged and should be prepared to change if a team member proposes something better.

Provide support and encouragement: Sometimes things don't go well, and it is important for a leader to be open about what is happening since everyone usually knows anyway, but at the same time encourage the team to see a way forward and do the best that it can in the circumstances.

Avoid playing favourites and public humiliation: Every team member deserves to feel needed and valued. If the leader has clear favourites, everyone will see that and the team dynamic is affected. Public humiliation of a team member for poor performance may be tempting but should be avoided. Even if the other team members agree that their performance is poor, they will not enjoy seeing a colleague be humiliated, and will wonder when it will be their turn for such treatment.

Try to make it fun: It seems like a cliché to speak of work as fun. Most people work to earn a living, after all. However, many jobs can provide great satisfaction when something goes well and there is a good outcome, even if there is no direct reward for the team.

Learning Objectives:

Presentation of the above attributes will stimulate discussion among participants, and provide a framework for considering leadership.

Participants will have the opportunity to comment on whether they agree with this list or identify other attributes as more relevant to their experience.

At the end of the session, participants will be able to take this material, enhanced with their own experiences and insights, and apply it in their own work environments.

JT06 - LEADERSHIP

JT06.1 - Hosting and Organizing an International Meeting

Author(s):

For many professionals hosting an international meeting can elevate their career to a different level. Engagement in professional associations and organizations provides an excellent networking opportunity that helps support research and create general best practices.

Attending an international conference, one sometimes wonders what it takes to run an international conference yourself and what you need in place in order to do so. In this session we will be exploring

- How to attract/bid on a scientific/medical conference
- Creation of a bid team and the necessary committees
- Financial investments and liabilities
- Planning process and time commitment
- Stakeholders and team members of successful conferences

The session is designed to give a comprehensive overview of the process involved based on practical examples such as the IUPESM World Conference and other meetings.

A special focus will be given to financial concerns and how to mitigate the risk of a meeting by involving professional groups and setting the conference up properly in a legal and tax-accounting matter. Finally there will be time for specific questions.

Learning Objectives:

- How to successfully bid on hosting a professional conference
- Designing a Continuing education programme that delivers value
- Properly assess financial risk and overall planning and budgeting for a professional conference

JT06.2 - Social Media in Science and Medicine

Author(s): Parminder Basran

Medical Physics, BC Cancer Agency- Vancouver Island Centre, Victoria/CANADA

The use of websites and applications that enable users to create, share, and discuss content is not new to medical physicists and biomedical engineers, but how one might adopt modern social media tools and technology for these purposes may well be. In this session, we explore social media in science in medicine with a particular focus towards medical physicists and biomedical engineers. We will explore how modern social media tools might be used in clinical activities, as a tool for research, as an educational tool, and as a means of public outreach.

Key learning objectives of this presentation are:

1. To provide a brief description of key social media channels and technology relevant to the medical sciences;
2. To provide some examples of how social media may be used in clinical, research, education and outreach activities;
3. To explore personal and institutional privacy concerns when using social media in a professional setting.

JT07 - HUMAN FACTORS AND MEDICAL DEVICE SAFETY

JT07.1 - FMEA and Root Cause Analysis

Author(s): Eric Ford

Department Of Radiation Oncology, University of Washington, Seattle/WA/UNITED STATES OF AMERICA

Of the systematic tools available for improving the safety and quality of care in radiation therapy, two have proven particularly useful: Failure Mode Effects Analysis (FMEA) and Root-Cause Analysis (RCA). These two techniques offer complimentary methods for analyzing error pathways. FMEA provides a method of quantifying hazards before they occur, while RCA offers a means understanding the drivers of error through in-depth analysis of events that have already occurred. Recent data demonstrates that these two tools are most effective when used in combination with one another. This presentation will provide an overview of FMEA and RCA with reference to the concepts and methods established in AAPM Task-Group 100 (FMEA) and the RO-ILS: Radiation Oncology Incident Learning System in the US. A series of case studies will be included which illustrate the practical operational aspects of both FMEA and RCA.

At the conclusion of the CE program, attendees will be able to:

Describe the fundamental concepts behind FMEA and RCA

Understand in detail the methods used for each

Incorporate each tool into the quality management program of their own clinic

JT07.2 - Human Factors and Usability Assessment

Author(s): Patricia Trbovich

Institute Of Biomaterials And Biomedical Engineering, University of Toronto, Toronto/CANADA

Learning Objectives:

At the end of the session participants will:

1. Appreciate the importance of understanding systems issues and intrinsic human limitations in improving patient safety
2. Understand Rasmussen's model of migration to boundaries to explain the mechanism by which deviance occurs, stabilizes, regresses, or progresses to harm. This model assesses how accidents occur and helps to understand the human and system contributions to adverse events
3. Have a general understanding of usability assessment and key concepts that help protect against dangerous errors that could lead to patient injury
4. Understand the "Hierarchy of Effectiveness" in developing solutions to safety problems

Healthcare organizations depend on human beings to perform safety critical tasks in complex work environments. Consequently, it essential for these organizations to effectively address human factors and human performance considerations, to reliably achieve safe and successful outcomes. Human Factors (HF) is a discipline concerned with the study of how people interact physically and psychologically with products, tools, procedures, and processes. HF takes into account human capabilities, limitations, and characteristics and aims to make the environment function in a way that is safe and seems natural to people.

In this presentation, we will begin with a review of Human Factors and the relationship that exist between the high rate of preventable

adverse events in healthcare and the pace, and increase of new technology and approaches. We will discuss Rasmussen's model of risk management in a dynamic society, which addresses the dynamic aspects of safety, and consequently is well suited to understanding current conditions in modern healthcare delivery and the way conditions may lead to accidents. When errors involving medical devices occur, people typically blame the users rather than investigate broader systems factors that are likely contributing, such as a poorly designed interface

between the medical device and the user, or inadequate user training. We will discuss how usability assessment can help fulfill the need to understand how to better ensure that (a) medical devices are designed for optimum capability and ease of use, and (b) clinician training is thorough and effective. Finally, we will discuss the crucial role that healthcare professionals, including biomedical technology professionals, play in selecting the appropriate strategy to reduce and remedy medical error. It is often not obvious nor clear, which error prevention tool to use, even when system-based causes have been identified. We will discuss various error prevention tools and their respective effectiveness for creating lasting changes in the healthcare system.

JT08 - SCIENCE AND RESEARCH

JT08.1 - How to get Grants: Tips for Success

Author(s): [Aaron Fenster](#)

Imaging Research Laboratories, Robarts Research Institute, London/ON/CANADA

Success for obtaining a grant for research is getting increasingly more difficult as the number of applicants is rising and funds for research is not keeping pace. Thus, for research grants to be successful, they must be outstanding, or at the very least, nearly outstanding. While the current state for research funding appears to be highly intimidating, complex, and with challenges that are overwhelming, the steps to produce a successful grant are highly logical and follows a regular pattern. Never-the-less, the current research funding environment causes many research applicants to avoid starting their grant until it is too late to produce the level of the grant that would make it successful.

The current research funding in Canada is quite complex with funding sources that include Federal, Provincial, disease-based foundations and private sources (e.g., philanthropists). Grants can be written for funding to support operating costs of research, equipment, infrastructure and individuals' salaries. Details of the documents to be filled and submitted are usually different, requiring different types of information. However, the process for writing these grants follows the same steps: preparation, writing the grant, refinement, and submission of grant.

A successful grant writer would have these steps in mind and start their grant allowing sufficient time for each step. For example, while the most critical step is the *preparation step*, most researchers do not spend enough time or don't quite understand what is needed. Specifically, this step requires substantial investments in time to generate the "idea" that would be considered transformative and/or meeting an unmet need that would have a significant impact on their field (e.g., significant impact on diagnosis, treatment or understanding of a disease). Since the "idea" generation is critical to success, the grant writer must steer away from ideas that are just "interesting", "would be useful" or "somebody should do this". The "idea" must be of significant importance to the community or field that it would evoke the comments such as "I wish I thought of that" or "if the applicant can accomplish this task, it would change the way XXX would be done" or "if anyone in Canada (the world) can do this, this applicant has the best chance for accomplishing this goal". Clearly, evoking these type of comments and reviews are difficult to achieve, so the question is how to generate the "idea" that would evoke these types of comments.

In this paper, I will describe the process for writing a successful grant and the steps and timelines needed to achieve this. The information that will be provided is based on a personal experience of writing successful and unsuccessful grants over the past 30 years as well as the experience and discussions with the scientists at the Robarts Imaging Research Laboratories in London.

Learning Objectives:

- 1) Planning steps used to write a successful grant.
- 2) How to allocate sufficient time to write a successful grant.
- 3) What constitutes an "idea" that will be the basis of a successful grant and how to achieve this.

JT08.2 - How to Write and Review Research Articles**Author(s):** David Thwaites¹, David W.O. Rogers²¹Institute Of Medical Physics, School Of Physics, University of Sydney, Camperdown, Sydney/AUSTRALIA, ²Physics, Carleton University, Ottawa/CANADA**Learning objectives:**

1. To understand the basics of writing a scientific paper for submission to a peer-reviewed journal and the requirements of the journal.
2. To understand the importance of clear presentation of results for publication and how to achieve this.
3. To understand the reviewing process, to help in writing papers, as well as when/if invited to be a reviewer.

Publication of your work is necessary to move the research field forward, (and for your career!). Using our experience as authors, reviewers, editorial board members and editors, we summarize some observations on writing and reviewing scientific papers for a peer-reviewed journal.

i) *For writing and submitting a paper:* assuming the work is good as a starting point, the focus here is on what makes a clear paper. This is also likely to maximise the chance of it being acceptable. First, consider your main message and hence material selection and writing flow so that this is clear. Make the introduction relevant to where the work fits into the current state of related published research, going quickly from generalities to specifics. Even good well-presented work will not get into high-impact-factor journals unless it is clearly novel and/or significant. Methods should allow the work to be repeated; ask yourself if they are clear and complete. Explain acronyms. Results should clearly tie figures and tables to text. Conclusions should relate back to the key message and be verifiably supported by results. Discussion and conclusions should not just be re-stated results!

Ask a colleague, unconnected with the work, to read the 'final' draft paper and comment on clarity. If they can't understand it, neither will the referees! Re-read it yourself after a time gap. Check journal requirements and comply! Hastily prepared submissions are usually poorly prepared! Badly written papers, not complying with requirements and including mistakes, e.g. in references, give the impression that the work may also be poor. Work with experienced authors initially (e.g. supervisor). Look critically at papers you read and note what you think works well. New writers *can* learn good practice by example. Good luck!

ii) One area that needs really careful attention is the *clear presentation of results in tables, graphs and figures* and this is often not well done in submitted papers. Specific advice on this will be summarized.

iii) One potentially difficult issue regarding writing a paper is the question of '*Who should be an author?*' Various guidelines regarding this issue will be presented.

iv) *For reviewing papers* (important to think about for authors to help foresee potential issues that can be dealt with up front, as well as if invited to review), this **summary** will outline the review process at several major journals and discuss the role of the reviewer. The obvious central role is to ensure the scientific accuracy of the paper being reviewed and to ensure it properly situates the paper in the current state-of-the-art without becoming a review paper. It is also important to ensure the paper properly reports the results of others and to identify plagiarism if at all possible. The role is not to have the paper written the way the reviewer would write it, but to help the author make their paper clearer and unambiguous. The issue of a referee's potential conflict of interest will be addressed.

MPE01 - MEDICAL PHYSICS EDUCATION AND PROFESSIONAL ISSUES**MPE01.1 - Workforce Models for Medical Physicists****Author(s):** Julian Malicki

Medical Physics, Greater Poland Cancer Centre, Poznan/POLAND

Learning objectives

- To present the elements that make up a workforce model for medical physicists.
- To describe approaches to quantifying staffing levels.
- To show current trends in shifting duties from direct clinical obligation to a supervisory role with more safety-related tasks.

Given the ongoing changes in the field of medicine and physics, numerous factors must be considered in any analysis of the duties performed by medical physicists. For the last century, the main focus of their activity has long been on clinical work, along with research and, to a lesser extent, radiation protection and quality assurance. In recent decades, however, medical physicists have slowly become further removed from direct clinical responsibilities. This distancing first occurred in diagnostic radiology and it is now evident in radiotherapy.

Can a model be analytically derived and quantified?

A workforce model should be described both qualitatively and quantitatively; that is, the number of physicists needed, the types of activities required, and the time needed to perform these. To estimate the number of positions that need to be created, we could use a bottoms-up approach. However, such an approach tends to overestimate the number of physicists needed. Another approach is to survey the current situation, and to extrapolate from this to create a more economically-feasible model.

Clinical obligation

The rapid development of science has had a large impact on medical practice. More sophisticated equipment, such as modern CT or MRI scanner, does not require the presence of a physicist during the procedure nor for its interpretation. The only discipline in which medical physicists are still clinically active with duties for individual patients is radiotherapy. However, the emergence of new techniques require more time for quality assurance. This situation presents a challenge for medical physicists, who have had to give up part their of routine, easier clinical duties.

Interactions between various groups of staff

An important factor that influences the workforce model is how specific duties are allocated among the major staffing groups (physicians, medical physicists, and radiographers) involved in medical imaging and therapy. In countries with a shortage of medical doctors or physicists, more clinical duties are performed by radiographers (for example, ultrasound examinations, overseen by radiologists) and radiotherapy technologists (e.g., radiotherapy planning, supervised by physicists).

Research and teaching

The workforce model can vary if the institution carries out teaching and research activities along with clinical work. Clearly, physicists with teaching obligations cannot perform the same amount of clinical work as those who do not teach. However, there is no direct formula to calculate the proportion of clinical to teaching activity.

Quality

Quality control and assurance are becoming ever more important in light of the increasing complexity of modern devices that use ionizing radiation. In most large hospitals, a staff member is designated as the quality officer. Clinical audits are considered more effective than ISO 9001 audits, mostly because the auditing team is comprised of peers rather than administrative personnel. An emerging area is risk assessment, reporting and analysis of events. In the future, these obligations may take up a larger portion of the time available to medical physicists.

Radiation protection

Unlikely other medical disciplines, regulations on the safety of medical uses of ionizing radiation are stricter. In many countries, this increases the burden on medical physicists to contribute to radiation protection.

Conclusion

Guidelines and actual staffing levels create not one but a number of workforce models that describe how many posts are associated with different aspects of medical diagnostics and therapy.

The model is constantly changing, although the ongoing trend is towards a diminishing share of direct clinical work, with more emphasis on supervisory, safety-related, and quality control/assurance tasks with a commensurate decrease in medical physics research.

MPE01.2 - International Educational Standards: Can We Define a Common Medical Physics Curriculum?

Author(s): Raymond K. Wu¹, Colin G. Orton², Tomas Kron³, Ahmed Meghzifene⁴

¹Radiation Oncology & Cyberknife Department, University of Arizona Cancer Center, PHOENIX/UNITED STATES OF AMERICA, ²Radiation Oncology, Wayne State University, Grosse Pointe/UNITED STATES OF AMERICA, ³Physical Sciences, Peter MacCallum Cancer Center, Melbourne/AUSTRALIA, ⁴Dosimetry And Medical Radiation Physics, IAEA, Vienna/AUSTRIA

1. What are the common requirements to be considered a qualified clinical medical physicist
2. How do IOMP and IMPCB collaborate on maintaining and upholding the standards
3. Who are the stakeholders
4. When do we expect to reach the different milestones

Abstract

The IOMP in May 2012 approved two policy statements: The Medical Physicist: Role and Responsibilities, and Basic Requirements for Education and Training of Medical Physicists. Earlier, the International Medical Physics Certification Board (IMPCB) was established on May 23rd, 2010 after many years of discussions and planning. The Constituting Panel of the IMPCB asked the same question as the caption title and wrote into the Bylaws and the Model Certification Program the goals to establish requirements for general and medical physics education, and clinical training. The publication of the two IOMP policy statements helped IMPCB to move forward and enabled its Accreditation Committee to develop the requirements for certification and accreditation. In 2013 the International Atomic Energy Agency (IAEA) published the Human Health Series No 25 with the endorsement of IOMP. The comprehensive collection of international data and the publication point to the fact that it is possible to harmonize the roles and responsibilities of clinically engaged

medical physicists and the education and training requirements in many parts of the world. Further plans are being developed for collaborations between IMPCB and the IAEA to consider conducting special certification examinations for a group of medical physicists from regions not likely to create their own certification bodies in the near future. Recent initiatives of IOMP indicated the interest of collaborations between IOMP and IMPCB to work on medical physics certification matters. It has been proposed that the IOMP be assigned a special designation of Supporting Organization of IMPCB, with three members of the Board of Directors appointed by IOMP. In addition, the IMPCB is considering amending the Bylaws to reflect the leading role of IOMP. IMPCB will adopt the IOMP standards, and clarify that other certification models are acceptable. The IMPCB recognizes that there are national/regional variations to certification in medical physics based on differences in national/regional legislation and educational traditions, so it gives to national and regional certification bodies considerable freedom to decide on the manner in which a given organization seeking IMPCB accreditation conducts the certification process. However, minimum education and clinical training criteria as well as continuing education and professional development are required for all IMPCB certified medical physicists.

MPE03 - RADIATION THERAPY INVITED SPEAKER

MPE03.2 - In Vivo Dosimetry

Author(s): [Ben Mijnheer](#)

Department Of Radiation Oncology, The Netherlands Cancer Institute, Amsterdam/NETHERLANDS

The rationale for *in vivo* dosimetry (IVD) is to provide an accurate and independent verification of the overall treatment procedure. It is used to detect clinically relevant differences between planned and delivered dose, to record dose received by individual patients, and to fulfill legal requirements. It will enable the identification of potential errors in dose calculation, data transfer, dose delivery, patient setup, and changes in patient anatomy. The relation between IVD and other parts of the quality assurance (QA) process, such as the commissioning and QA of the treatment planning system and machine QA, will be elucidated.

After discussing briefly the main characteristics of the most commonly used (point) detector systems, the rapid development of EPIDs for 2-D, 3-D and even 4-D, patient dosimetry during advanced treatment techniques such as IMRT and VMAT, will be elucidated. The various ways of dose determination and dose reconstruction inside a patient will be reviewed. Methods to quantify differences between measured and predicted dose distributions will then be clarified, as well as tolerance and action levels when deviations are outside clinical criteria.

A number of examples will be given to illustrate the possibilities of different types of commercially available and in-house solutions of hard- and software used for IVD. Clinical experience of IVD during external beam radiotherapy showed that most errors were due to the properties of a specific plan, human errors in the clinic, and anatomical changes. These types of error can often not be traced by means of pre-treatment dose verification using phantom measurements or independent dose calculations. Anatomy changes and modification of patient setup can generally be observed by means of in-room imaging. However, 3D IVD can compliment IGRT because it quantifies the dosimetric effects of these variations. Follow up actions, including inspection of in-room imaging data, followed by phantom measurements and improvement of procedures, if required, will be discussed.

Specific problems related to the use of IVD during brachytherapy, such as the use of a detector with a small volume and a well-defined position with respect to patient anatomy and source configuration, will be elucidated. The role of IVD in proton and ion radiotherapy by measuring the decay of radiation-induced radionuclides will also be discussed.

Large scale introduction of IVD requires implementation of a fully automated process that is integrated in the clinical workflow. Several approaches yielding alerts without or with limited human intervention will be compared.

Finally recent developments and future approaches such as real-time IVD, enabling the linac to halt in case of serious delivery errors, time-resolved dose verification, and the use of IVD during adaptive radiotherapy techniques will be discussed.

Learning objectives

1. To elucidate the rationale and type of errors that can be detected with in vivo dosimetry
2. To describe the instrumentation and techniques applied for in vivo dosimetry
3. To review the current clinical experience and future developments of in vivo dosimetry

MPE04 - QUALITY AND SAFETY

MPE04.1 - Quality Framework: The Canadian Partnership for Quality Radiotherapy

Author(s): [Michael Milosevic](#)

Radiation Medicine Program, Princess Margaret Cancer Centre, Toronto/CANADA

Radiotherapy is an important curative and palliative treatment for cancer that is indicated in 40-50% of patients. Quality assurance plays a critical role in radiation treatment planning and delivery. Driven by an urgent need to harmonize radiation treatment quality and safety in Canada, the Canadian Partnership for Quality in Radiotherapy (CPQR) was established through collaboration with national professional associations involved in radiation treatment delivery. CPQR has focussed its efforts on the creation of guidelines to measure and support programmatic quality assurance, maintain high quality radiation treatment technologies, and support incident learning and management. CPQR has uniquely incorporated a patient perspective into all of its activities, and developed a national guideline to motivate patient engagement in radiation treatment quality and safety at the individual program level.

Moving forward, priority will be placed on incorporating key CPQR deliverables into national accreditation programs, defining pan-Canadian system performance metrics for radiation treatment quality and safety, and strengthening international collaboration to support global harmonization of best practice.

At the conclusion of this program, attendees will:

Understand the stakeholder engagement model used by CPQR to build a national program of radiation treatment quality and safety

Understand how key CPQR initiatives in programmatic quality assurance, equipment quality control and national incident learning have harmonized practice across Canada and improved system resilience

Be aware of opportunities to collaborate with CPQR to improve radiotherapy quality and safety, either at the level of individual treatment programs or on a regional or national scale

MPE04.2 - Radiation Oncology Practice Accreditation in the United States

Author(s): [Steven De Boer](#)

Radiation Medicine, Roswell Park Cancer Institute, Buffalo/NY/UNITED STATES OF AMERICA

Learning Objectives:

After attending this presentation the attendee should

1. Have an understanding of the accreditation process for Radiation Oncology facilities.
2. Know the importance of attaining practice accreditation.
3. Know the different regulatory requirements for practice accreditation.

Accreditation of a Radiation Oncology practice in the United States consists of the evaluation of an entire practice by an independent accrediting body, ensuring that it meets or exceeds guidelines.

The process varies between the different accrediting bodies, but commonly consists of ensuring that

- The policies and procedures are adequate and enforced.
 - There is acceptable quality of treatment prescriptions, design, and delivery.
 - The quality assurance of all equipment is in compliance with recognized standards.
 - The facility is in compliance with state and federal regulations.
 - There is appropriate review of patient status, progress and documentation.
- In most centers, obtaining practice accreditation is a voluntary process. However, many centers have chosen to obtain practice accreditation for many reasons. These include
- Improving the quality and safety of the medical practice.
 - Providing confidence in the quality and safety of current practice to administration, staff, peers and patients.
 - Providing a learning experience to the entire staff through the accreditation process.
 - Allow for marketing advantage for the practice.
 - Providing a legal confidence that appropriate measures are being taken to provide safe and quality treatment.
- Practice Accreditation is a valued service which has the goal of increasing treatment quality and patient safety.

MPE05 - COMPUTERIZED SYSTEMS

MPE05.1 - Database Rudiments and Clinical Use

Author(s): John Kildea

Medical Physics, McGill University Health Centre, Montreal/CANADA

Electronic databases are found everywhere in modern society, nowhere more so than in a radiotherapy department. However, few people understand how databases store data and even fewer are equipped with the tools to extract them. With just a little guidance it is possible to delve into any modern database and extract useful information. This workshop will cover the basics of database design and describe the tools available to extract useful data.

At the conclusion of the CE program, attendees will be able to:

- 1) Describe how a modern database is structured and how data is stored in relational tables
- 2) Download and install simple software to connect to a database
- 3) Write simple SQL queries.

MPE05.2 - Modern Radiotherapy Treatment Planning: Capabilities, Commissioning, and Clinical Use

Author(s): Benedick A. Fraass

Department Of Radiation Oncology, Cedars-Sinai Medical Center, Los Angeles/CA/UNITED STATES OF AMERICA

Learning Objectives:

1. Describe capabilities of modern radiation therapy treatment planning systems.
2. Summarize the clinical commissioning process and how that information can be used.
3. Illustrate ways to incorporate modern treatment planning methods into clinical use.

Modern radiation therapy treatment planning systems incorporate many advanced tools for planning, including automated segmentation (contouring), fusion of imaging datasets from multiple modalities, use of multileaf collimators, intensity modulated radiation therapy (IMRT) and volume modulated arc therapy (VMAT), image guided radiation therapy (IGRT) and advanced dose calculation algorithms. Appropriate clinical use of these advanced capabilities requires detailed and careful clinical commissioning of a multitude of functions and capabilities, followed by use of that commissioning information to educate planners, physicians, physicists about the proper use of those tools and algorithms. This presentation will summarize available modern radiotherapy treatment planning functionality, describe clinical commissioning of these complex systems, and make comments about ways to incorporate these capabilities into safe and effective clinical use.

MPE06 - IMAGING**MPE06.1 - 4D Imaging****Author(s):** Stewart Gaede

Physics And Engineering, London Regional Cancer Program, London/CANADA

At the conclusion of the CE program, attendees will be able to

1. Understand 4D-CT reconstruction methods.
2. Recognize motion artifacts in a 4D-CT dataset and understand methods to reduce them.
3. Determine how to implement 4D-CT clinically and how to address practical solutions to common problems, including management of irregular breathing patients and construction of the PTV for 4D-radiotherapy.

Four-dimensional computed tomography (4D-CT) imaging has become a staple for providing 3D dynamic anatomical information used in modern radiotherapy of tumours influenced by respiratory motion. A 4D-CT dataset is composed of a time series of 3D images at multiple phases of the patient's breathing cycle. This is accomplished by acquiring multiple projections of the same anatomical space under free breathing conditions and retrospectively binning either the projection data or sequentially acquired 2D axial slices according to a breathing trace that was acquired simultaneously. For projection binning, the CT scanner operates in low-pitch helical mode, where the pitch is related to the patient's breathing period. For image binning, the CT scanner operates in ciné mode, where time series of images are acquired over an entire breathing cycle at one fixed couch position then reacquired at sequential couch positions until the intended scan range is imaged. While 4D-CT scanning improves image quality compared to free-breathing 3D imaging, artifacts are still present, mostly due to irregular breathing patterns exhibited by many patients. As a result, sorting algorithms combine volumes from temporally misaligned respiratory phases into a single volume. Many methods have been proposed to improve 4D-CT sorting methods for irregular breathing patients, including phase tagging adjustment, respiratory trace manipulation, amplitude-based sorting methods, and non-linear image registration. Despite these improvements, motion artifacts can also be induced due to poor correlation between the motion of the internal anatomy and that of the respiratory surrogate. Retrospective binning of 4D-CT data in the absence of an external surrogate has been proposed and has shown to reduce motion artifacts. The resulting 4D-CT dataset can be used to define an envelope of the gross-tumour volume (GTV) for conventional free breathing treatment delivery or one or more phases can be chosen for respiratory-gated radiotherapy. In both scenarios, multiple methods have been proposed that utilize the 4D-CT dataset to construct the internal target volume (ITV), including manual delineation, auto-segmentation, or maximum intensity projection (MIP) generation via registration to the planning CT, which in itself can be a single 4D-CT phase, an average of the 4D-CT dataset, or ideally, the entire 4D-CT dataset. In the latter case, dose calculations are performed on each respiratory phase and through deformable registration the dose is summed over all phases. Although the advantages of 4D-CT imaging in modern radiotherapy of mobile tumours is clear, implementation into routine clinical practice is not necessarily straightforward. We are, therefore, proposing a CE program that is intended to address 4D-CT imaging technology, reconstruction methods, and practical solutions to common problems such as clinical implementation of 4D-CT, interpretation of 4D-CT for irregular breathing patients, construction of a planning target volume (PTV) for 4D-radiotherapy, and 4D-treatment planning considerations. Extension of 4D imaging to positron emission tomography (PET) and magnetic resonance imaging (MRI) will also be presented.

MPE06.2 - Dose from X-Ray Imaging Procedures**Author(s):** John M. Boone

Radiology Snd Biomedical Engineering, UC Davis, Sacramento/ UNITED STATES OF AMERICA

The learning objectives of this talk are to acquaint the attendees with:

- (1) the way in which radiation dose is estimated in radiography
- (2) the use of Monte Carlo methods for determining dose and dose distribution
- (3) Radiation dose assessment in computed tomography and several of the controversies associated with some dose metrics.

The estimation of x-ray dose is a basic requirement of a diagnostic medical physicist. In this presentation, x-ray dosimetry methods will be discussed for radiography, mammography, and computed tomography. For the projection imaging procedures, the entrance air kerma is used with conversion coefficients which are produced using Monte Carlo methods. In computed tomography, the entrance surface of the patient is ill-defined due to scanner rotation, and therefore the air kerma at isocenter of the scanner can be used. The acquisition of air kerma data at the scanner isocenter using various phantoms is also an important component of CT dosimetry, and these metrics include CTDI-100, CTDI-w, and CTDI-vol. In CT as with projection imaging modalities, Monte Carlo methods are used to generate coefficients useful for estimating radiation dose. While the dose methods used in radiography and mammography are relatively stable, there have been a number of important changes in the methodologies associated with CT dosimetry. These newer methods take into consideration both the size of the patient in the XY plane (using the size-specific dose estimate, SSDE, methodology), and the length of the scan in the z-dimension also has an impact on the radiation dose estimate. Recent activity with respect to dosimetry methods in computed tomography include AAPM task groups 111, 200, 204, and 220, as well as Report 87 from the International Commission on Radiation Units (ICRU). The general message from each of these reports will be discussed. In recent years, there has been a move to require dose reporting for some x-ray imaging procedures, especially computed tomography. The utility of fully automated CT dose reporting will also be demonstrated in this tutorial. While the use of effective dose as a metric has been used in certain circles of the radiology community, some of the pitfalls of effective dose as a dose metric will also be explored.

MPE07 - RADIATION SAFETY

MPE07.1 - What can IAEA do for the Clinical Medical Physicist?

Author(s): Joanna Izewska, Ahmed Meghzifene
Nuclear Sciences And Applications, International Atomic Energy Agency, Vienna/AUSTRIA

Learning objectives: (1) to learn about IAEA activities in dosimetry and medical radiation physics; (2) to get acquainted with IAEA educational material and training opportunities; (3) to learn about IAEA technical assistance for medical physicists.

Shortage of medical physicists, insufficient education and training opportunities, and lack of professional recognition exist in several countries. To address these issues the IAEA conducts systematic and comprehensive activities in support of medical radiation physics worldwide. They are related to education and training, scientific advice and guidance, research and development and also include technical services.

Recently, an IAEA report has been published that defines the roles and responsibilities of a clinically qualified medical physicist in radiotherapy, diagnostic radiology and nuclear medicine. The document, endorsed by IOMP and AAPM, also recommends minimum requirements for the academic education and clinical training, and for continuous professional development. It also addresses other topics of interest for the profession.

Three IAEA handbooks for teachers and students provide the basis for education of medical physicists initiating their university studies in radiotherapy, diagnostic radiology and nuclear medicine. These volumes are supplemented by a collection of slides prepared for all book chapters. The IAEA also developed training packages for clinical residents in medical physics. This teaching material has been adopted by many universities and hospital training centres worldwide. Multiple technical reports, guidance documents and advisory books are a useful resource for medical physicists in specific areas of their activities. 'Human Health Campus' website serves as an educational resource for professionals and students involved in radiation medicine.

For long time, the IAEA has maintained an interest in standardization and development of Codes of Practice (CoP) for dosimetry with several publications in the field. One important example is the TRS-398 CoP that is in use in most world regions. A new CoP for small radiotherapy fields is under preparation. There is also a long tradition of organizing conferences and symposia in dosimetry and medical radiation physics to foster the exchange of information among professionals and to highlight developments in the field.

Regional and national training courses, workshops and fellowships are available for medical physicists to upgrade their skills and practices. These activities lead to improvement of the professional status, enhance specialist capabilities and strengthen medical physicists' contributions to radiation medicine developments. Opportunities exist for participation in co-ordinated research efforts, with some projects leading to a doctoral degree.

The IAEA support to medical physics also includes technical assistance for implementing and reviewing QA programmes at hospitals. Traceable dosimetry calibration services are provided through the IAEA/WHO Network of SSDLs to promote accurate measurements of radiation doses. Dosimetry audits in radiotherapy and comprehensive clinical audits are offered by the IAEA to radiation medicine clinics. In particular, the IAEA/WHO postal dose audit service for radiotherapy dosimetry has been in operation for over 45 years and checked radiotherapy beam calibrations in 2000 hospitals in 130 countries.

To conclude, multiple IAEA projects are in operation at various

levels, which help in the development and growth of the medical physics profession worldwide.

MPE07.2 - Safety Learning and Safety Management to Prevent Radiotherapy Incidents

Author(s): Ola Holmberg
Radiation Protection Of Patients Unit, IAEA, Vienna/AUSTRIA

Radiation protection of patients must deal with the issues of not having dose limits, purposely exposing sensitive subgroups, and purposely using doses that could cause deterministic effects. While medical uses of ionizing radiation have been of tremendous value to the global population for nearly 120 years, it could be noted that radiation accidents involving medical uses have accounted for more deaths and early acute health effects than any other type of radiation accident, including accidents at nuclear facilities.

Safety reporting in radiotherapy can be mandatory or voluntary. There may be mandatory reporting to health authorities and/or radiation regulatory authorities in a single country, depending on the regulations in place. There are two types of events to consider in relation to mandatory safety reporting to the authorities. First, there are the recordable events that are errors that do not meet regulatory reporting requirements, but could indicate a gap in patient care. These are usually reviewed by the regulatory authority during an inspection or audit. The second type are the reportable events, or those events that have exceeded some threshold defined by a regulatory agency. The reported events should be focused on incidents with serious actual or potential outcomes, such as injury or death. Mandatory reporting should focus on these serious events in order to avoid obscuring the incidents that need to be investigated.

On the other hand, voluntary reporting systems are often confidential and focus on events and outcomes, instead of regulatory sanctions. They can capture "less serious" and near miss events with the purpose being to share knowledge on safety-related events and conditions and on lessons learned to improve the safety environment and patient outcomes. These reporting systems encourage institutions to focus on improvement of the safety environment; protect institutions from the legal system, handle information with confidentiality and allow for anonymous reporting of errors or circumstances that could lead to errors. An incident in another hospital can lead to identification of the hazard before a similar incident is realized locally. By collecting data from a large pool of events, better defined "lessons to learn" can be created that may improve patient safety.

The IAEA has developed a voluntary safety reporting system for radiotherapy. This is called Safety in Radiation Oncology (SAFRON). The system has incorporated data from other international, national and local reporting systems, and data directly from SAFRON participants, in order to make radiotherapy safety information more accessible. In addition, this database also provides links to publications of interest in the evaluation of incidents, lessons learned, and corrective actions. The system is designed to educate facilities about incidents and corrective actions.

In addition to looking at the characteristics of this system, such as severity scales and process steps, the seminar will also look at some other database elements forming the structure of safety reporting and learning systems in practice, such as safety barriers, causes and contributing factors. Additionally, practical operation of the system and dissemination of information will be discussed.

At the conclusion of the CE program, attendees will be able to

1. Understand differences in objectives and characteristics of mandatory and voluntary safety reporting in medical uses of ionizing radiation

2. Define and describe the different elements needed to form the structure of safety reporting and learning systems in practice, such as severity scales, process steps, causes and contributing factors
 3. Apply safety barriers (equipment or processes) to radiotherapy in practice, in order to strengthen safety and prevent unintended irradiation of patients

MPE07.3 - Equipment Standards and Performance Measurements for Radiotherapy Systems

Author(s): Jean M. Moran

Radiation Oncology, University of Michigan, Ann Arbor/MI/UNITED STATES OF AMERICA

Equipment standards continue to evolve with the increased complexity of treatment delivery systems. Guidance from the American Association of Physicists in Medicine (AAPM), such as that defined in Task Group 142, will be presented with respect to quality assurance (QA) standards and test frequency for linear accelerators. Mechanical, dosimetric and system safety checks will be described. In addition, Medical Physics Practice Guidelines are also becoming available from AAPM. These publicly available reports differ from Task Group reports and some impact radiotherapy system QA. The elements of the available guidelines will be presented. Finally, the evolving tools and techniques for performing QA will be discussed.

At the conclusion of the CE program, attendees will be able to

Describe the major elements of a radiotherapy system QA program

Learn about the different types of guidance available from the AAPM

Learn about evolving techniques and tools for performing QA measurements

MPE08 - QUALITY AND SAFETY

MPE08.1 - Quality Systems in Radiotherapy

Author(s): Mary Coffey

Radiation Therapy, Trinity College Dublin, Dublin/IRELAND

Quality and safety are inextricably linked in radiotherapy. This is clearly expressed in the European Society for Radiotherapy and Oncology (ESTRO) Vision statement 1.1: 'Optimal individualised patient care will be achieved by integrating new clinical and preclinical evidence from biology, molecular/functional imaging and the use of new systemic agents together with the delivery of high precision radiation therapy in a safety aware environment'.

In many instances the failures in radiotherapy, which have had catastrophic outcomes, are the result of system failures involving one or more steps in the radiotherapy process. Quality in radiotherapy is multifaceted and encompasses the full spectrum from referral to follow-up addressing both technical and clinical aspects: 'total quality management'.

Technical quality commences with the equipment purchase decision and subsequent commissioning procedures. Clinical quality commences with accurate diagnosis including staging and grading and review at a multidisciplinary meeting. These first stages can be influenced by a range of external factors and are often outside the direct control of the radiotherapy team. Comprehensive clinical audits, such as the IAEA QUATRO programme can identify problems within the process and, as such, can directly influence quality.

Following referral to radiotherapy the radiotherapy team has a responsibility to ensure that the treatment prescribed is the treatment that the patient receives. From a technical perspective assurance that the dose set is the dose delivered is controlled by practices such as daily output measurements, in vivo dosimetry and dose verification for procedures such as IMRT coupled with the routine quality assurance procedures.

Peer review is an important factor in ensuring clinical quality and can include peer-to-peer discussion, chart review prior to first treatment and peer review of volume delineation. A recent paper by Tol et al describes how different treatment planning protocols can lead to large differences in organ at risk (OAR) sparing and other publications previously have identified the importance of adherence to protocol in minimizing dose to the OARs.

Ensuring accurate treatment delivery requires care and attention to positioning and immobilisation. This includes correct selection of the immobilisation method, regular monitoring of equipment and verification of the treatment delivered.

Quality systems in radiotherapy must also include human factors and the impact of the rapid changes currently taking place in our discipline. "Change is creating new paths for failure and new demands on worker(s) ... revising their understanding of these paths is an important aspect of work on safety ... missing the side effects of change is the most common form of failure for organisations and individuals"

Learning Outcomes

To be able to discuss the spectrum of quality aspects in radiotherapy

To be able to describe the process of an external comprehensive clinical audit and its role in quality

To be able to review quality processes in their own department

MPE08.2 - Cost and Resource Management of Radiotherapy**Author(s):** Peter Dunscombe

Oncology, University of Calgary, Calgary/CANADA

The cost of health care in the 34 countries of the Organisation for Economic Cooperation and Development had been rising twice as fast as GDP up until 2009. The financial events of 2008 have tempered this growth with a third of OECD countries now reporting a decrease in per capita expenditure on health care over the period 2009-2011. Particularly as we continue to be beset with financial uncertainty, many over indebted countries and many more facing continuing negative growth, we can expect downward pressures on health care budgets to continue. Analyses suggest that the direct costs of cancer care to the health care system are around 5%. Societal costs of cancer including lost productivity and informal care actually exceed direct health care costs – a fact that we often lose sight of. However, considering the magnitude of the cancer problem, which can only increase with an aging population across the globe, cancer treatment still represents a relatively small part of the overall health care budget. And within the cancer treatment budget, radiotherapy represents less than 10%. Although the contribution of radiotherapy to overall direct health care budgets is small, <1%, we would be naïve in thinking that its relative financial insignificance will shield radiotherapy from the economic realities of today's world. In order to justify budgets and to maintain accessible, high quality radiotherapy for the benefit of the 50% of cancer patients for whom it is indicated we need to have a much better idea of the costs and benefits of this essential modality.

In this presentation we'll look at the economic data that support the contentions made above, search the literature for radiotherapy costing studies and examine a few relevant studies in more detail. The presentation will conclude with a brief overview of ESTRO's Health Economics in Radiation Oncology project.

At the conclusion of the CE program, attendees will be able to:

1. Identify sources of data on health care funding and its distribution.
2. Discuss the literature on radiotherapy costing studies.
3. Appreciate ESTRO's Health Economics in Radiation Oncology initiative.

MPE09 - RADIATION THERAPY**MPE09.1 - The Modern Physicist Tool Box: How to Choose Between Current Dosimeters****Author(s):****Learning Objectives**

To review the basic principles of radiation detector dosimetry

To review the dosimetry protocols for conventional and small radiation fields

To provide an overview and a suitability discussion of dosimeters for a particular clinical applications including conventional and small fields

Dosimetric accuracy remains of paramount importance in a context of image-guided radiation therapy using clinical protocols that increasingly make use of hypofractionation with high doses per fraction. Over the past decade radiation dosimetry has seen developments including novel radiation standards for absorbed dose to water, unprecedented accuracy in the determination of correction factors for detectors and new formalisms for dosimetry of small static and dynamic radiation fields. At the same time, manufacturers have brought new water-equivalent and perturbation-friendly detectors on the market. This presentation reviews some basic aspects of detector dosimetry, new detectors and their suitability for measuring absorbed dose in challenging dosimetric conditions.

MPE09.2 - Radiobiology Applications for Clinical Physicists: Isoeffective dose calculations; Hypofractionation; TCP/NTCP; Peripheral doses and secondary cancers**Author(s):** Michael Joiner

Department Of Oncology, Wayne State University, Detroit/MI/UNITED STATES OF AMERICA

The Linear-Quadratic (LQ) formulation deals specifically with the relationship between total dose and dose per fraction, and with interfraction interval using the Incomplete-Repair derivative model. The LQ description has been thoroughly tested in the clinical domain, but almost always in the "conventional" range of dose per fraction below 6 Gy. LQ is the simplest mathematical description of a non-linear relationship and though empirical in nature, it has nevertheless been subject to many attempts to connect with our understanding of how radiation injury is produced and repaired at the cell and molecular level. Yet any meaningful and clinically useful link in this respect has remained elusive. The relationship between total dose and overall treatment time is an even more complex relationship dependent on the different underlying radiobiology of different tissues even within the apparently same category of early-reacting or late-reacting tissues, distinguished by respectively a "high" or "low" ratio of α/β in the LQ equation. Overall time is therefore better handled independently of LQ.

A straightforward but untested hypothesis for the different α/β values for early- and late-reacting tissues, is that a naturally low α/β for a target cell population is smoothed out to a higher value as the sum of the responses of different proliferative subpopulations, and different phases of the cell cycle that these are in. This explanation could be applied to the responses of malignancies in the lung and head and neck, also adding in the additional response variation of cells at various levels of hypoxia in these sites. Of note is the connection between outcome of radiotherapy and HPV status in oropharyngeal cancers, which implies a possible difference in treatment strategy between these tumor subtypes and could also explain the high α/β of head and neck cancer overall as the sum of the responses of the different cancer subtypes (HPV + and -) which could

both have low α/β but different radiosensitivity. In some malignancies, notably prostate and breast, clinical data do indeed indicate a low α/β which might also reflect more uniformity in response perhaps more characteristic of lower proliferative or early-stage disease. This has resulted in new efforts to test hypofractionation which have also been enabled by better dose localization achievable with image-guided Volumetric Modulated Arc Therapy.

There is evidence that the LQ model becomes less reliable at doses per fraction < 1 Gy, due to possible low-dose hyper-radiosensitivity, and also at > 6 Gy per fraction for reasons not yet understood though increasing vascular damage and immunological/inflammatory effects occur at higher doses per fraction. It is axiomatic that LQ must indeed overestimate effect at very high doses per fraction because the effective D_0 would become unrealistically low. This makes the outcome of hypofractionated regimes less predictable: using LQ at high doses per fraction would be playing safe in predicting toxicity of hypofractionation, while overestimating the effect on the target malignancy, noting that possible hypoxia in a tumor could also limit the effectiveness of large dose fractions.

Learning Objectives

1. Understand that the simplest two-parameter LQ model is a utility for describing the relationship between total dose and dose per fraction for isoeffect
2. Know the dose range of 1-6 Gy per fraction over which using the LQ model can be most relied upon
3. Be aware of the underlying radiobiology which may explain responses at low or high dose per fraction to be inadequately predicted by LQ extrapolation of the response to 1-6 Gy per fraction

MPE10 - COMPUTERIZED SYSTEMS

MPE10.1 - Dose Computation Algorithms, Including Monte Carlo

Author(s): [Tommy Knoos](#)

Radiation Physics, Skane University Hospital and Lund University, Lund/SWEDEN

Learning Objectives for *Dose modelling in external photon beam radiotherapy*

Separation of beam modelling and dose engine

Classification of dose calculation engines

The role of measured data in model based

Modelling of absorbed dose to patients during external photon beam radiotherapy will be reviewed. This will include the modelling of the radiation source i.e. the linac head (beam modelling) and the various dose calculation algorithms applied within the patient (dose engine).

For the beam modelling, the different sources e.g. target, filters and collimators etc will be defined as well as their importance for the photon and electron fluence reaching the patient. The consequences of removing the flattening filter, which several vendors now have made commercially available, will also be shown.

The pros and cons regarding different dose engines ability to consider density changes within the patient will be covered (type a and b models). Engines covered are, for example, pencil-beam models, collapsed cone superposition/-convolution models and combinations of these, as well as a glimpse on Monte Carlo methods for radiotherapy. The different models possibility to calculate dose to medium (tissue) and/or water will be presented.

Finally, the role of commissioning data especially measurements in today's model based dose calculation will round of the lecture.

MPE10.2 - Treatment Planning Optimization: IMRT and VMAT

Author(s): [Jan Unkelbach](#)

Radiation Oncology, Massachusetts General Hospital, Boston/MA/ UNITED STATES OF AMERICA

Learning objectives:

Understand the concepts of fluence map optimization (FMO), leaf sequencing, and direct aperture optimization (DAO), which form the components used to assemble modern IMRT and VMAT planning algorithms.

Understand the formulation of VMAT planning as an optimization problem that aims to determine the trajectories of multi-leaf collimator leaves while the gantry rotates around the patient.

Understand the state-of-the-art in VMAT planning from an algorithmic perspective in the research literature and in commercial implementations.

Abstract:

Treatment planning for external beam radiotherapy is formulated as a large-scale mathematical optimization problem, which determines the machine parameters of the treatment device to achieve a desired dose distribution in the patient. Treatment plan optimization for intensity-modulated radiotherapy (IMRT) was historically developed as a two-step approach. In the first step, the fluence maps of incident beams are optimized; in the second step, a leaf sequencing

algorithm converts the fluence maps into a sequence of apertures that can be delivered using a multi-leaf collimator (MLC). These two steps, fluence map optimization (FMO) and sequencing, are still important components in modern treatment planning systems (TPS). However, advanced TPS adopt direct aperture optimization (DAO) methods, which aim at directly optimizing the shape and intensity of MLC openings. DAO methods partially overcome some of the drawbacks of the two-step approach, such as degradation of the FMO dose distribution during the sequencing step.

Over the past years, volumetric modulated arc therapy (VMAT) has found widespread clinical application. In VMAT delivery, the gantry continuously rotates around the patient while the treatment beam is on and delivers radiation, promising shorter delivery times compared to step-and-shoot IMRT. Many treatment planning studies have since compared VMAT and IMRT in terms of plan quality and delivery time. In contrast, publications on the mathematical optimization algorithms used in VMAT planning are scarce. VMAT planning ultimately aims at optimizing the trajectories of MLC leaves while the gantry rotates around the patient. Unlike FMO, this represents an inherently non-convex optimization problem. Most VMAT algorithms, including the commercial implementations, use the concepts of FMO, leaf sequencing, and DAO that were originally developed for IMRT, and adapt these methods to VMAT. VMAT implementations differ in the component they rely on the most and the exact implementation of each step.

The presentation will briefly review basic concepts in treatment plan optimization, but will subsequently focus on the state-of-the-art in IMRT and VMAT planning from an algorithmic perspective. Implementations in commercial systems are explained and approaches suggested in the research literature are presented.

MPE11 - RADIATION THERAPY

MPE11.1 - Linear Accelerator Technology

Author(s): Malcolm R. Mcewen

Measurement Science And Standards, National Research Council, Ottawa/ON/CANADA

Learning objectives:

Understand how an electron linear accelerator works to produce electron and photon beams.

Understand the commonalities between different manufacturers' machines and also the important differences.

Understand what is physically being controlled by the software running on the linac workstation.

Electron linear accelerators are the workhorses of today's radiation therapy clinics. This presentation will aim to take the covers off a modern linac and show the different components that are required to produce, accelerate and deliver the primary electron beam to the treatment head. Clinical users are often quite familiar with the treatment delivery 'end' of a linac (target, flattening filters, MLC, *etc*) so the focus of this presentation will be on the other parts of a linac, where perhaps the medical physicist has the least day-to-day experience – the electron gun, modulator, rf source, waveguide and bending magnets. The aim is to open up what has perhaps become a black (or more often, white) box. The presentation will trace the history of linac development since the 1950s to the present day and show that the modern machines of 2015 have more in common with those early accelerators than one might think.

The following systems will be dealt with in some detail:

rf sources/amplifiers (magnetron and klystron)

high-power modulator design

vacuum components

electron gun (diode and triode)

beam transport and bending magnets

The intention is to cover the designs from the major manufacturers of rotational gantry-based linear accelerators.

Although this session is aimed primarily at clinical medical physics involved in using linear accelerator technology it has been designed to be accessible to those without a highly technical understanding of linacs.

MPE11.2 - Reference Dosimetry and its Uncertainties

Author(s): David W.O. Rogers¹, Malcolm R. Mcewen²

¹Physics, Carleton University, Ottawa/CANADA, ²Measurement Science And Standards, National Research Council, Ottawa/ON/CANADA

Learning objectives

to understand the advances in photon beam reference dosimetry since 2000 (i.e., since publication of TRS-398 and TG-51).

to be aware of the implications for reference dosimetry when using FFF (flattening filter free) linac beams.

to understand the uncertainties in calculated values of kQ (= kQ_{Q0}).

to understand which ion chambers are suitable for reference dosimetry.

to be able to assess the various corrections needed (ion recombination, polarity, beam non-uniformity, etc).

to understand the uncertainties associated with reference dosimetry.

“Best Practice” reference dosimetry requires two components to obtain the calibration of an external beam radiation device:

1. Accurate input parameters (calibration coefficients, conversion factors), and
2. Accurate detector measurements in the radiation therapy clinic.

Calibration coefficients are determined by the primary, or secondary, standards laboratory and would be a presentation in themselves, so this session will look at conversion factors (e.g., k_Q factors, perturbation factors) and ion chamber measurements. Although the presentation will focus on the two most widely-used external beam protocols (IAEA TRS-398 and AAPM TG-51) the issues discussed will be applicable to other national protocols and codes of practice currently in use.

Part 1 – Conversion factors and beam quality specifiers.

Since 2000 there have been studies (mostly Monte Carlo) which demonstrated that the data used then for the various correction factors making up k_Q (P_{wall} , P_{repl} , P_{cel}) were individually wrong by up to 1%. Fortunately the calculated k_Q factors (k_{Q,Q_0} in TRS-398) only depend on ratios of these factors and the errors in k_Q were therefore somewhat less. One study showed that the $\%dd(10)_x$ and $TPR_{20,10}$ beam quality specifiers were equivalent for clinical beams with flattening filters. However, since then it has become common to use linacs without flattening filters and this leads to complications which will be discussed.

To overcome issues with the individual correction factors, it is possible to calculate k_Q values directly using Monte Carlo techniques with an uncertainty of 0.4% to 0.5%. When compared to measurements of k_Q for 26 different ion chamber models (with uncertainties of 0.3% for reference class chambers), the agreement was excellent, with χ^2/df values less than 1. The calculated values fall on smooth curves as a function of $\%dd(10)_x$ except for chambers with high-Z electrodes, which are not suitable for reference dosimetry for other reasons as well. The talk will present the experimental and calculated values to demonstrate each of the above statements.

Part 2 – uncertainty and the clinical medical physicist

As part of any measurement it is essential to estimate the uncertainty in the result obtained. Development of an uncertainty budget is not just a matter of obtaining a value; the steps followed to construct an uncertainty budget are, in fact, a process review that feeds directly into the quality documentation and procedures used by each institution.

This part of the session will examine the primary components of uncertainty in an absorbed dose to water measurement and describe how they depend on the user’s experimental method, the choice of chamber, *etc.* We deconstruct the basic measurement equations found in dosimetry protocols to understand what is required to obtain an accurate and precise determination of D_w . Issues that become apparent in doing this include the correct choice of ion chamber type, the errors that can arise from inadequate detector characterization, and the importance of understanding the performance of all systems that contribute to the final measurement.

Carrying out this analysis will demonstrate that the clinical medical

physicist is not simply someone following a recipe, but is actively involved in impacting the overall uncertainty in reference dose measurements.

MPE12 - COMPUTERIZED SYSTEMS**MPE12.1 - Image Registration****Author(s):** Michael Velec

Techna Institute, University Health Network, Toronto/ON/CANADA

Multiple imaging modalities are now commonly used to diagnose and classify disease. For radiation oncology in particular, tumor representations from several images need to be combined to define the treatment target and serial imaging is then used to guide therapy. Registration is the process by which the information in these images is combined into one model of the patient and exploited. Algorithms differ widely in how they function and therefore each have specific clinical scenarios where they are better suited. Recently deformable registration algorithms are being adopted for more advanced applications, adding further complexity to treatment processes. Understanding methods to assess if image registration is performing accurately, and techniques to apply when it is not, are essential to ensure that treatment accuracy is maintained.

At the conclusion of this session, attendees will be able to:

- 1) Describe fundamental components of image registration using common rigid and deformable algorithm examples
- 2) Understand quantitative and qualitative methods to perform validation and quality assurance for image registration
- 3) Discuss strategies to make tradeoffs between image registration limitations and clinical goals, using examples scenarios

MPE12.2 - Automated Segmentation of Images for Treatment Planning Purposes**Author(s):** Greg Sharp

Radiation Oncology, Massachusetts General Hospital, Boston/MA/UNITED STATES OF AMERICA

Automatic segmentation holds great promise for improving radiotherapy practice. Although it is primarily regarded as a method for increasing efficiency, automatic segmentation can also play a role in improving standardization and consistency. The application of segmentation to clinical research is also of interest, because it can easily scale up to large numbers of patients for retrospective studies. This CE session is intended to provide a gentle, but complete, introduction to the algorithms and expected performance of radiotherapy auto-contouring software.

The goals of the CE session are to provide understanding of

- Algorithms commonly used in automatic image segmentation software
- Methods for evaluating segmentation accuracy
- Expected segmentation accuracy for commonly segmented organs-at-risk

MPE13 - MEDICAL PHYSICS EDUCATION AND PROFESSIONAL ISSUES**MPE13.1 - Advocacy for Physicists and How to Deal with Government, Unions, Regulators, and Employers****Author(s):** Jerry J. Battista¹, Wayne Beckham²¹Medical Biophysics, Western University, London/CANADA, ²Medical Physics, BC Cancer Agency - Vancouver Island Centre, Victoria/BC/CANADA**Learning Objectives:**

To understand that a medical physics career evolves to the point of requiring administrative and negotiating skills

To recognize the need to interact with governments, regulators, unions, and employers

To understand the "hot buttons" in dealing with non-scientific interactions

Medical physicists are fortunate to enjoy a career with such wide diversity in activities but the priority of each activity changes over the course of a career. Early career is focused on acquiring necessary clinical skills in the safe administration of diagnostic or therapeutic medical procedures. If there is a concurrent university appointment, this also requires some level of activity in teaching and research, initially supported by internal grants and potentially growing to nationally peer-reviewed levels. In time, the physicist is assigned progressively more supervisory roles and significant administrative duties. Interactions with hospital administrators, legislative agencies at the provincial and federal levels, and employee unions expand. The role then requires an abrupt mental shift for scientists as discussions extend beyond having good data and logic. In dealing with hospital executives, a delicate balance of budget restraint, excellent patient services, and risk management must be struck. In dealing with government regulators, attention to procedural details and a population (macroscopic) perspective is needed for justifying acquisition and assuring safety compliance of all technology. In dealing with unions, fair play of the employee and relationship with the employer is the focus, under all foreseeable circumstances. Endless hours are expended in interpreting, applying or editing collective agreements for word precision describing "what if" scenarios such as displacement of employees by technological advances. In **summary**, medical physicists working in hospital environments must be prepared to advocate well beyond their core scientific know-how. A stronger background in budgeting, presentation of proposals and arguments at the lay level, understanding legislative language, and "big picture" viewpoints is needed. Without such preparation, future leadership of medical physics programs may be assigned to non-physicists.

MPE14 - RADIATION THERAPY

MPE14.1 - Radiotherapy Units: Cobalt-60 Units and Gamma Knife Units

Author(s): [Steven Goetsch](#)

Medical Physics, Dade Moeller Health Group, Solana Beach/CA/
UNITED STATES OF AMERICA

The original Leksell gamma unit was conceived and built in 1967. Since that time hundreds of such units have treated an estimated 1 million patients worldwide for brain tumors and other neurological diseases. In times of increasingly tight health care budgets single fraction Gamma Knife radiosurgery and 3 to 5 fraction stereotactic radiotherapy become increasingly attractive options for treatment of patients with intracranial disease. Over the last 48 years treatment times have become much shorter and treatment plans have become far more sophisticated. New radiotherapy units continue to be introduced to the U.S. healthcare system.

At the conclusion of the CE program, attendees will be able to:

Describe in detail how the Leksell Gamma Knife and other similar gamma radiosurgery (GSR) units work

Compare and contrast the methods and results of clinical applications of the gamma unit with those of competing technologies

Become familiar with new advances in GSR technology

MPE14.2 - Brachytherapy: Overview of State-Of-The-Art and New Developments

Author(s): [Nicole Nesvacil](#), [Christian Kirisits](#)

Department Of Radiation Oncology, Medical university of Vienna,
Vienna/AUSTRIA

The main learning objectives of this presentation are:

To get an overview of the uncertainty budget in modern 3D IGABT

To understand the correlation between dosimetric uncertainties and reporting of total treatment doses for different clinical sites and treatment schedules

To improve understanding of the consequences of uncertainties in the delivered dose for the usability of dose-response models in clinical decision making (definition of planning aims and decisions for/against use of IGABT vs IGBT without re-imaging before each irradiation, for individual patients)

Increasing availability of 3D image guided adaptive brachytherapy (IGABT) treatment techniques, allow us to tailor dose distributions for each individual patient to the specific anatomy and reduce risks of side effects, while increasing the dose to the tumour. However, individual dose plan optimization is always affected by dosimetric uncertainties that may lead to a difference between prescribed and delivered dose.

In this presentation we will review the most recent reports on uncertainties in brachytherapy and discuss the impact of different types of uncertainties on our understanding of dose-response analysis.

The sources of uncertainties can be of technological nature (source calibration, dose calculation and dose delivery), or due to the clinical workflow and anatomy of the patient (applicator movement, delineation uncertainties, anatomical changes (inter- or intra-fraction variations)). Recent reports highlight the magnitude of different types of uncertainties for different BT treatment sites (Tanderup et al. 2013, *Radiother Oncol* 107:1-5, Kirisits et al. 2014, *Radiother Oncol* 110:199-212, and references therein).

Uncertainties can be classified as systematic (e.g. source calibration) or random (e.g. interfraction variations). Recently, a lot of effort has been made to analyze dosimetric variations occurring due to anatomical changes, within and between different BT fractions for cervical cancer. For example, a multicenter study (Nesvacil et al. 2013, *Radiother Oncol* 107:20-25) revealed random intra- and inter-fraction uncertainties of the order of 10% for D_{90} of HR CTV and 20-30 % for D_{2cm^3} for organs at risk, for the physical dose of each BT fraction. In this case inter-/intra-fraction variations can be considered as the main contributors to the total uncertainty of the delivered BT doses. While dosimetric variations for the target appear to be dominated by contouring uncertainties, variations for OARs are also influenced by their changes in location and filling, as well as movements of the applicator and target in relation to the OARs.

In a hyperfractionated BT treatment protocol observed uncertainties of physical fraction dose will also lead to an accumulated uncertainty of the whole BT treatment dose (in EQD2) – which (including contributions from EBRT to the overall treatment) is used to analyze clinical dose-response relationships.

Comparison of examples for different types of uncertainties for various BT applications, tumour sites, OARs, and different treatment schedules, might help to define future goals and strategies to further increase precision in modern IGABT, and to better understand dose constraints for BT planning.

MPE15 - COMPUTERIZED SYSTEMS

made from “paperless” to fully implemented computerized TMS and EMR systems will be reviewed and evaluated.

MPE15.1 - Managing Respiratory Motion in Radiation Oncology

Author(s): [Paul Keall](#)

Radiation Physics Laboratory, University of Sydney, University of Sydney/AUSTRALIA

Learning objectives

1. Understand the clinical drivers for respiratory motion management in radiation oncology
2. Understand how respiratory motion management occurs at multiple stages of the patient treatment cycle
3. Understand the current status of respiratory motion management technology in radiation oncology

Presentation Description

One of the most exciting and dynamic areas of academic and clinical radiation oncology is the management of respiratory motion in radiation oncology. New technologies are being invented, innovations are occurring on existing technology and the growth of clinical data and findings is staggering.

Respiratory motion management in radiation oncology can be broadly classed into the four interconnecting areas where technology and the patient interact: (1) Imaging for treatment planning; (2) Treatment planning; (3) Pre-treatment imaging and (4) Treatment delivery.

In this talk the clinical drivers for respiratory motion management and associated technological development drivers will be described. Current clinical standards for the four broad respiratory management motion areas will be explained. Near and long term directions for respiratory motion management, including the interaction of respiratory motion management technologies with other emerging cancer imaging and treatment modalities will given.

MPE15.2 - RadOnc Treatment Management Systems and the Paperless Treatment Process

Author(s): [Benedick A. Fraass](#)

Department Of Radiation Oncology, Cedars-Sinai Medical Center, Los Angeles/CA/UNITED STATES OF AMERICA

Learning Objectives:

1. To describe differences between the traditional treatment process and the treatment process in a paperless environment.
2. To discuss the differences between paperless and truly electronic medical record and treatment management systems.
3. To discuss the issues involved in integrating quality assurance and safety concerns into our paperless and/or electronic treatment process.

Over the last decade, the radiation therapy planning and delivery process has morphed from a manual paper-chart-based process to one which is implemented with computerized treatment management systems (TMS) and electronic medical record (EMR) systems. The paperless process has numerous advantages over the older paper-based system as well as some disadvantages, especially when old techniques are carried over into the paperless environment. This presentation will discuss differences between traditional and paperless approaches and describe some of the quality assurance and safety concerns which must be properly handled in the new environment. The progress that the field of radiation oncology has

MPE16 - RADIATION THERAPY**MPE16.1 - Specialized Units: Tomotherapy and CyberKnife Systems****Author(s):** Martina Descovich¹, Robert J. Staton²¹Radiation Oncology, University of California San Francisco, San Francisco/UNITED STATES OF AMERICA, ²Radiation Oncology, UF Health Cancer Center - Orlando Health, Orlando/UNITED STATES OF AMERICA

The continual advances in radiation therapy technology lead to the development of specialized treatment units. The design and function of TomoTherapy & Cyberknife systems is significantly different than traditional medical linear accelerators. This session will provide an overview of the TomoTherapy and Cyberknife systems covering design and operation, available image guidance techniques, and quality assurance recommendations. Treatment workflow, clinical applications, and treatment planning techniques will also be discussed and compared.

Educational Objectives:

1. Understand the core concepts of Tomotherapy & Cyberknife treatment delivery.
2. Understand the image guidance options for Tomotherapy & Cyberknife machines.
3. Understand the QA procedures for Tomotherapy & Cyberknife.

MPE16.2 - Heavy Particle / Light Ion Therapy**Author(s):** Oliver Jäkel

Medical Physics In Radiation Oncology, German Cancer Research Center, Heidelberg/GERMANY

Proton beam radiotherapy celebrates its 60th birthday in 2015, but already 2 years after the first proton treatment in Berkeley, also helium was introduced for radiotherapy. Heavier ions like carbon, nitrogen, neon, silicon and argon have also been used for radiotherapy at Berkeley between 1977 and 1992.

After the Berkeley trials ended, the first clinical treatment facility started its operation in Chiba, Japan in 1994 with carbon ions. In Germany an experimental facility opened in 1997 and was the first facility to establish intensity modulated beam scanning for carbon ions. In the meantime five clinical centers are existing in Japan, four in Europe and two in China. One of the most advanced facilities opened in 2009 at Heidelberg University: it is the only facility with an isocentric scanning gantry for ions and also offers beams of helium and oxygen ions for pre-clinical research.

In the presentation the physics and radiobiological rationale for ion beam radiotherapy is outlined. Some current research topics in the field of medical physics will be highlighted and the status of ion beam therapy in the world as well as the current clinical evidence will be summarized.

At the conclusion of the CE program, attendees will be able to

- 1- Describe the physics and radiobiological rationale for using ion beams in radiotherapy
- 2- Describe how the physics of ions is connected to the biological effectiveness
- 3- Describe the most important research directions for ions and the existing clinical evidence for carbon ions

MPE17 - RADIATION THERAPY**MPE17.1 - Chemotherapy and its Influence on Radiotherapy: Basics for Clinical Physicists****Author(s):** Eva Bezak¹, Michael P. Brown²¹School Of Physical Sciences, University of Adelaide, Adelaide/SA/AUSTRALIA, ²Cancer Clinical Trials Unit, Royal Adelaide Hospital, Adelaide/AUSTRALIA

In this lecture the following learning objectives are aimed at:

1. To revise the role and basic principles of chemotherapy in cancer treatment.
2. To develop understanding of biological rationale for combined radiation and chemotherapy.
3. To review most common chemotherapy agents in current clinical use.

Cancer therapy of the last two decades has been marked by rapid development of combined therapies, especially of conventional chemotherapy (CHT) drugs with radiotherapy (RT).

While a complete understanding of biological mechanisms behind combined therapies is still being investigated, clinical trials have demonstrated improved survival for a number of cancers, including head and neck, stomach, oesophagus, lung, pancreas, colon, breast, glioblastoma multiforme and others. Some of the main chemotherapy agents are cisplatin, gemcitabine, tirapazamine (TPZ), temozolomide (TMZ) and 5-Fu (Fluorouracil) and analogues (1, 2).

The basic rationale for combined chemo/radio therapy lies in so-called spatial cooperation of the two modalities; with RT affecting the local tumour and systemic chemotherapy sterilizing the disseminated clonogenic cells (3). Additionally, the main objective is to enhance tumour response without enhancing normal tissue complications (the process known as radiosensitization). Chemotherapeutic agents target different physiological characteristics of the tumour, including hypoxia that is generally associated with tumour radioresistance. Other group of drugs (so-called radioprotectors) are used to reduce/mitigate normal tissue injury without compromising the tumour response (4).

The enhanced tumour response or radioprotection can be achieved with varying degrees of additivity, depending on the mechanisms of interaction of the drug and radiation and their interplay. Clinical data suggest that many of the enhanced tumour effects result from simple additivity; i.e. there is no direct interaction between the chemotherapy agent and radiation. Normal tissue protection, on the other hand, is often most pronounced when drugs are administered more closely to irradiation. The optimum scheduling and combinations are, however, still being investigated. Currently used scheduling has been in general developed from clinical trials and supported by modelling (1, 5).

The main/known mechanisms of interaction between drugs and radiation and the resultant additive and synergistic effects include: enhancement of DNA damage (i.e. change in the slope of the dose-response curve), formation of additional DNA adducts, interference with DNA repair processes (e.g. inhibition of repair of sublethal damage), enhancement of apoptosis, inhibition of proliferation, perturbation of cell kinetics (e.g. an increase of a number of cells in the sensitive cell cycle phase), hypoxic cell sensitization, inhibition of angiogenesis, and interference with signalling pathways.

The interaction between a chemotherapy agent and radiation is dose and time dependent, including drug dose and scheduling, time sequencing between drug and radiation delivery, radiation dose dose rate as well as fractionation schedule. There seems to be lesser

dependence on the tumour/tissue type.

References:

1. GD Wilson, SM Bentzen, PM Harari, Biologic basis for combining drugs with radiation. *Semin Radiat Oncol*. 2006 Jan;16(1):2-9.
2. F Al-Ejeh, MP Brown, Chapter 16: "Combined Modality Therapy: Relevance for Targeted Radionuclide Therapy", pages 220-235. In *Targeted Radionuclide Therapy*. Ed., Tod W. Speer. Lippincott, Williams & Wilkinson, Philadelphia, 2011.
3. GG Steel, Terminology in the description of drug-radiation interactions. *Int J Radiat Oncol Biol Phys*. 1979; 5:1145-1150.
4. KK FU Biological basis for the interaction of chemotherapeutic agents and radiation therapy; *Cancer (Impact Factor: 4.9)*. 06/1985; 55(9 Suppl):2123-30.
5. L Marcu, E Bezak and I Olver, Scheduling cisplatin and radiotherapy in the treatment of squamous cell carcinomas of the head and neck: a modelling approach, *Phys. Med. Biol.* 51 (2006) 3625-3637 doi:10.1088/0031-9155/51/15/002.

MPE17.2 - Models of Delivery of Radiation Therapy (Private, Public, BCCA/CCO, etc).

Author(s): Michael Sherar¹, Thomas Mcgowan²

¹Cancer Care Ontario, Toronto/ON/CANADA, ²Oncology, The Cancer Centre Bahamas & The Cancer Centre Eastern Caribbean, Nassau/BAHAMAS

Around the world, the mix of private and public delivery of radiation therapy services varies. The challenge for any model of payment for and provision of services is the assurance of and continual improvement of quality, including equitable access to services for the entire population. An examination of where the public and private sectors have been successful, and the challenges each type of model faces in different parts of the world is useful as we look to the problem of how to expand access to high quality radiation services globally.

Cancer Care Ontario (CCO) oversees the planning of and public payment for publically provided radiation therapy services in Ontario. There is no private involvement. Interestingly, the private sector did have a role in the evolution of Cancer Care Ontario to its current state. In the latter part of the last century long waiting lists in Ontario required sending 1,000 patients a year to the United States for care. A short term private sector contract (but using public hospital facilities) was put in place to eliminate out of country referrals, and bring the waiting list down. This wait times crisis was a key factor in changing CCO's role from being a provider to become a purchaser and quality improvement agency. Provision of services was reintegrated with local hospitals. Quality improvement according to provincial standards is driven as part of the Ontario Cancer Plan. Provincial and regional clinical leaders work with Regional Cancer Program Vice Presidents to drive quality improvement across all facilities. The benefits of a strong public provincial program including central capital planning and a population level approach are described as well as an analysis of some of the key challenges facing the Ontario system.

In contrast, The Bahamas provides an example of where the private sector played an essential role as it was able to provide the capital, and management expertise to build and operate a radiation facility in an environment where the government could not realistically afford to do so. Through a partnered care model, the private facility treats both public and private patients to the same standard, but provides radiation services to public patients at a reduced cost. This partnered care model is successful enough that the same private sector provider, at the request of the government of Antigua and

Barbuda, is building a similar facility to provide care for the population of The Eastern Caribbean.

The global problem of access to radiotherapy will be not solved through a single approach. We will need to learn from best practice in a variety of environments to tailor a solution to each environment.

Learning Objectives:

1. Understand the benefits and challenges of the both public and private payment and delivery models for radiation therapy.
2. Understand the challenges of improving global access to radiation therapy in the context of public, private or mixed payment and service delivery solutions.
3. Understand how the mix of public and private involvement in a radiation therapy delivery model can be dependent upon the local political and economic environment.

MPE18 - MEDICAL PHYSICS EDUCATION AND PROFESSIONAL ISSUES

MPE18.1 - Curriculum Design: How to Train the Next Generation of Physicists?

Author(s): John Damilakis

Medical Physics, UNIVERSITY OF CRETE, HERAKLION/GREECE

The International Organization for Medical Physics states in its Policy Statement No. 2 that 'Medical Physicists working as health professionals shall demonstrate competency in their discipline by obtaining the appropriate educational qualification and clinical competency training in one or more sub-fields of medical physics. Basic knowledge of the other sub-fields is also required. Medical Physicists practicing in hospital/clinical environments shall also participate in a continual professional development program'. Recommendations on the minimum levels of education and training for medical physicists are given in the same document. This lecture will present guidelines and recommendations developed by international organizations on the requirements for the education and training necessary for a physicist to become a clinically qualified medical physicist. These guidelines can be used for the development of the local curriculum for medical physicists.

An increasing number of higher education institutions have in recent years started to offer courses on Medical Physics. Moreover, Continuing Professional Development (CPD) for medical physicists is of great professional interest. CPD courses is an excellent way to ensure that Medical Physicists become knowledgeable about all current issues in their field and to provide the necessary knowledge, skills and competences for certified Medical Physicists to become Medical Physics Experts. However, external assessment of the quality of education or training provision is needed. Accreditation is the formal recognition that education and training on medical physics provided by an institution meets acceptable levels of quality. Accreditation should be based upon standards and guidelines. Requirements for accreditation of a training programme should take into account several aspects including facilities, staff, educational material and teaching methods.

EUTEMPE-RX is a European Commission (EC) funded project which aims to provide training opportunities to medical physicists in diagnostic and interventional radiology to become Medical Physics Experts i.e. to reach level 8 according to the European Qualification Framework (EQF). A network of excellent teaching centers in medical physics has been set up to develop a set of modules. The courses will achieve their learning objectives combining online with face-to-face teaching. More information about EUTEMPE-RX can be found at www.eutempe-rx.eu.

Learning Objectives

1. To present curricula for postgraduate education program on Medical Physics
2. To present guidelines and recommendations developed by international organizations on the requirements for the education and training necessary for a physicist to become a clinically qualified medical physicist
3. To discuss issues related to accreditation of the education and training in Medical Physics

MPE18.2 - Professional Standards and Certification of Qualified Individuals

Author(s): Matthew Schmid¹, Geoffrey Ibbott²

¹Medical Physics, BC Cancer Agency - Southern Interior, Kelowna/CANADA, ²Radiation Physics, UT MD Anderson Cancer Center, Houston/UNITED STATES OF AMERICA

Learning Objectives: 1. Understand the 4 underlying principles that form the basis for a certification program: a. Providing an examination process b. Providing a maintenance of certification (recertification) program c. Providing a public registry d. Providing a disciplinary process 2. Be familiar with the specifics of the CCPM and ABR certification processes (eligibility requirements, exam process) 3. Be familiar with the CCPM recertification process and the ABR maintenance of certification process **Abstract:** The Canadian College of Physicists in Medicine (CCPM) exists to protect the public by: (a) establishing standards of competence for those involved in the application of the physical sciences in the medical field in Canada. (b) identifying individuals who meet the established standards and maintaining a registry of these individuals. Similarly, the American Board of Radiology (ABR) has as its mission: To certify that our diplomates demonstrate the requisite knowledge, skill, and understanding of their disciplines to the benefit of patients. This talk will focus on how the CCPM and the ABR meet these objectives. By way of introduction, a brief description of the structure and governance of the CCPM and of the ABR will be presented. The core business of any certification organization is centered around its examination process. The eligibility requirements for membership in each board will be detailed, along with a description of the examination process. After initial certification has been obtained, both the CCPM and the ABR require that all members meet the requirements of an on-going maintenance of certification (recertification) program in order to maintain their certification status. The structure of the MOC programs will be presented. Members of the CCPM are required to comply with the Code of Ethics stated in the Regulations of the College, and this will be briefly discussed, along with a description of the disciplinary process in place to ensure member compliance with the Regulations of the College. The ABR is not a membership organization, but certification carries with it the expectation that the diplomate meet appropriate professional standards.

MPE19 - RADIATION THERAPY**MPE19.1 - Commissioning, Clinical Implementation and Quality Assurance for Stereotactic Body Radiation Therapy****Author(s):**

Stereotactic Body Radiotherapy (SBRT) has been applied clinically for over two decades. The accumulation of published technical and clinical studies currently available have offered insights into both the efficacy and special concerns associated with the delivery of SBRT to different sites. The safe and effective delivery of SBRT requires careful attention to many unique technical aspects, including dosimetry of small photon fields; management of respiratory motion; immobilization, localization and image guidance; accurate dose calculation; quality assurance; and understanding of normal tissue constraints to high dose irradiation. This session will provide an overview of these important technical considerations, guidance on safe and effective implementation in the main disease sites, and a survey of reported clinical outcomes.

At the conclusion of the CE program, attendees will be able to:

1. Describe key elements of initial SBRT equipment commissioning, patient-specific QA, and routine periodic machine performance QA;
2. Describe and discuss processes for small field dosimetry, and understand limitations in available algorithms for dose calculation;
3. Describe and discuss practical issues associated with patient immobilization, motion management, use of image guidance for accurate localization;
4. Describe and discuss standard treatment regimens and normal tissue dose constraints, to incorporate clinical and technical principles into their disease site-based programs of their own.

MPF01 - IMAGERIE**MPF01.1 - Tomodensitométrie: Les Nouveaux Développements et Avenues de Recherche****Author(s):** Philippe Després

Département De Physique, De Génie Physique Et D'optique, Université Laval, Québec/CANADA

Objectifs d'apprentissage

- 1) Apprécier l'évolution technologique de la tomodensitométrie depuis l'avènement des appareils multicoupes.
- 2) Comprendre les enjeux de radioprotection associés à la tomodensitométrie et reconnaître l'apport de diverses approches pour réduire la dose.
- 3) Découvrir de nouvelles applications en tomodensitométrie ainsi que les avenues de recherche actuelles, notamment en imagerie bi-énergie et en reconstructions tomographiques avancées.

La tomodensitométrie (TDM) n'a pas connu de bouleversements majeurs depuis l'avènement des appareils multicoupes et des acquisitions hélicoïdales. Cependant, cette technologie n'a pas cessé d'évoluer pour autant. L'évolution de la TDM au cours des dernières années sera abordée durant cette présentation selon différents points de vue: technologique, social et médical. D'un point de vue technologique, la TDM peut désormais compter sur une puissance de calcul numérique bonifiée, permettant l'exécution d'algorithmes de reconstruction plus performants en des temps raisonnables. Les processeurs graphiques (GPU) à architecture hautement parallèle, notamment, permettent aujourd'hui l'exécution rapide d'algorithmes itératifs où un modèle physique de détection est utilisé durant la reconstruction. Cette approche peut mener à des images de meilleure qualité acquises à des doses inférieures pour le patient. D'un point de vue social, le recours de plus en plus fréquent à la TDM et son accessibilité toujours grandissante ont soulevé des questions importantes en radioprotection. Les fabricants d'appareils TDM, bien conscients de ces enjeux, proposent aujourd'hui des technologies destinées à minimiser la dose au patient; celles-ci seront revues et discutées. D'un point de vue médicale, la TDM permet aujourd'hui davantage d'applications grâce à certaines innovations technologiques. Le cas de l'imagerie bi-énergie sera revu et discuté. Finalement, les avenues de recherche actuelles en TDM seront abordées, tant d'un point de vue technologique que médical.

ENGLISH

Computed Tomography: new developments and research avenues
 Learning objectives Appreciate the technical evolution of Computed Tomography (CT) since the advent of multislice devices. Understand the radiation safety challenges associated with CT and recognize the role of various approaches to reduce the dose to the patient. Discover new applications in CT as well as current research avenues, notably in dual-energy imaging and advanced tomographic reconstruction. Computed Tomography did not change significantly since the advent of multislice devices and helical acquisitions. However, this technology did not stop evolving altogether. The evolution of CT during the last few years will be reviewed from different points of view: technological, social and medical. From a technological perspective, CT can nowadays rely on unprecedented computing power, allowing the execution of advanced reconstruction algorithms in a reasonable time. Massively parallel Graphics Processing Units (GPUs), for instance, allow the use of complex physical models in iterative reconstruction. These approaches can yield better images acquired at lower patient exposures. From a public health perspective, the steadily increasing number of CT studies performed each year has drawn attention from the media and radiation safety authorities. CT manufacturers, well aware of this

situation, nowadays propose technologies aiming at reducing the radiation dose to the patient. These technologies will be reviewed and discussed. From a medical perspective, CT nowadays allow new applications thanks to technological developments. The case of dual-energy imaging will be reviewed and discussed. Finally, current research avenues in CT will be reviewed, from a technological as well as medical point of view.

MPF01.2 - Résonance Magnétique: les Nouveaux Développements et Avenues de Recherche

Author(s): Martin Lepage

Nuclear Medicine And Radiobiology, Université de Sherbrooke, Sherbrooke/QC/CANADA

The field of magnetic resonance imaging continues to develop both in terms of technological innovations and of novel clinical applications. Higher magnetic field strengths along with the development of accelerated acquisition methods have led to unforeseen applications because of previously unexploited contrast mechanisms. For example, the large susceptibility contrast available at fields of 3T and above has produced exquisite images of the human brain vasculature. Radio-frequency field inhomogeneity at high field was overcome by parallel transmission and this has led to the design of parallel excitation enabling faster image acquisition. Those are becoming useful in the clinical characterization of pathologies and may help tailor better treatment options. Meanwhile, combining information from multiple imaging modalities has the potential to refine the information extracted from images by highlighting the vascular and metabolic aspects of pathologies. This is expected to translate in improvements in diagnosis, treatment planning and therapy response.

At the conclusion of this presentation, attendees will be able to

Identify novel technological developments and novel contrasts in magnetic resonance imaging

Identify recent clinical application of magnetic resonance imaging

Identify where magnetic resonance imaging, alone or in combination with other imaging modalities, may further improve tissue characterization

MPF02 - SYSTÈMES INFORMATISÉS

MPF02.1 - Éléments de Base: Réseaux Informatiques, Serveurs, et Standards de Communication

Author(s): Stefan Michalowski

Radiation Oncology, CHUM, Montréal/QC/CANADA

Objectifs d'apprentissage

- 1) Comprendre l'environnement informatique dans le milieu médical, plus spécifiquement en radio-oncologie et radiologie.
- 2) Connaître les technologies de communication utilisées en radio-oncologie et radiologie.
- 3) Établir les liens entre les besoins cliniques et la technologie.

Résumé

Dans ce cours, les notions de base en informatique nécessaires aux physiciens médicaux opérant dans les secteurs de radio-oncologie et de radiologie seront expliquées. Ce cours, basé sur mon expérience de plus de 10 ans dans l'administration des systèmes d'information du département de radio-oncologique du CHUM, se découpe en trois sections: format de fichiers, communication, et infrastructure.

Dans la première section, en débutant par une explication des concepts de la numérisation, la compréhension des formats de fichier sera démystifiée. Utilisant ces nouvelles notions, le format de stockage des images médicales utilisé par DICOM sera expliqué. L'extension radiothérapie de DICOM (DICOM-RT) sera aussi détaillée. Par l'utilisation d'exemples pratiques, le cours touche les problèmes qui peuvent survenir lors de la manipulation et de l'échange de fichiers DICOM entre divers logiciels et systèmes afin de permettre aux participants de mieux comprendre et résoudre ces problèmes.

Dans la deuxième section, une explication de la réseautique standard (TCP/IP) sera abordée en plus des technologies de communication spécifique au milieu médicale tel que celles utilisées par DICOM et les standards couvert par l'organisme HL7. Une explication des concepts derrière la réseautique IP et des technologies de transport de donnée (Ethernet). Un des aspects très importants de la communication est la sécurité, surtout dans le contexte actuel. Les notions d'authentification et d'autorisation seront abordées. De plus, le chiffrement et les communications sécurisées seront expliqués. Ces notions vous permettront de comprendre la configuration des infrastructures réseautiques.

L'échange d'informations qui fait partie de la communication comporte des dangers qu'il faut surveiller, surtout lorsqu'on échange de l'information entre deux systèmes différents, que ce soit deux versions d'un logiciel ou deux logiciels différents. L'exportation et l'importation comporte des transformations qui peuvent modifier les données. Le cours couvrira ce sujet avec quelques exemples.

Finalement, la troisième section fera un survol des équipements et infrastructures nécessaires pour faire fonctionner les systèmes d'information radiologique (PACS) et radio-oncologique (ROIS). Cette section couvrira les concepts de base de donnée relationnelle en plus de se concentrer sur les infrastructures physiques nécessaires pour faire opérer les système d'information (serveur, SAN, RAID).

ENGLISH

Learning Objectives

- 1) Understand the information technology environment in the Health-care sector, more specifically in Radiation Therapy and Radiology.
- 2) Learn about the communication technologies used in Radiation Therapy and Radiology.

3) Establish the links between clinical needs and technology

Summary

In this presentation, the essential notions in IT necessary for Medical Physicists and Engineers operating in Radiation Therapy and Radiology will be explained. This presentation, based on my more than 10 years of experience in the management of CHUM's Radiation Oncology Information System, is composed of three sections: file formats, communication and infrastructure.

In the first section, through the introduction of the elements and concepts surrounding information digitisation, understanding of file formats will be demystified. Using these new notions, the image file format for DICOM will be explained. The Radiation Therapy extension to DICOM (DICOM-RT) will also be covered. Through the use of practical examples, the difficulties and issues that can arise when manipulating and transferring DICOM files between information systems and applications will be touched upon, this will allow participants to better understand and solve these issues.

In the second section, an explanation of the most common network technology (TCP/IP) will be discussed, in addition to the communication technologies specific to the Healthcare sectors such as those used by DICOM and the standards covered by the HL7 group. In more detail, the concepts of IP networking and transport technologies such as Ethernet will be explained.

As one of the most important aspects of communication is security, especially in today's context, the course will address this subject by covering the notions of authentication and authorisation. In addition, encryption and secured communications will be explained. All these notions should help participants understand the basics of configuring a safe network infrastructure.

There are important factors that have to be analysed when information is exchanged between two different systems, be it two different versions of the same software application or two different software applications. Because data can be modified by these exchanges, an information system manager has to understand these issues. Thus, this presentation will include a few examples of the dangers users are exposed to when exporting and/or importing data from one system to another.

Finally, the third section will overview the hardware and infrastructure required to run a Radiology Information System (RIS/PACS) and a Radiation Oncology Information System (ROIS). This section will cover database concepts as well as the technical details of the physical hardware to run such information systems (server, SAN, RAID).

MPF03 - RADIOTHÉRAPIE**MPF03.1 - Appareils Spécialisés: Tomotherapy, CyberKnife, Brainlab, Gamma Knife**

Author(s): Veronique Vallet

Ira, Centre hospitalier universitaire vaudois, Lausanne/SWITZERLAND

La radiothérapie 3D, par modulation d'intensité (IMRT) ou d'arc-thérapie volumétrique modulée (VMAT), font de plus en plus partie des techniques habituelles de traitement. En revanche, d'autres installations de traitement, comme la Tomothérapie, le CyberKnife, le Novalis (Brainlab) et le GammaKnife, sont des systèmes moins couramment utilisés dans la pratique clinique. Ces installations permettent des traitements hautement spécialisés et ont un véritable potentiel d'amélioration des traitements. Les spécificités de ces installations impliquent d'autres manières de préparer et de délivrer les traitements.

Les objectifs de ce cours sont les suivants:

1. Décrire ces installations et mettant l'accent sur les différences par rapport à des accélérateurs linéaires "conventionnels".
2. Montrer et décrire des plans de traitement typiques qui peuvent être obtenus avec ce type d'installations.
3. Décrire les avantages et les inconvénients de tels systèmes.

ENGLISH

3D conformal radiotherapy, intensity modulated radiotherapy (IMRT) or volumetric modulated arc therapy (VMAT), are increasingly used as standard treatment techniques. However, other treatment machine, such as TomoTherapy, CyberKnife, Novalis (Brainlab) and GammaKnife are less commonly used in clinical practice. These machines allow highly specialized treatment and have real potential to improve treatments quality. The specificities of these machines imply other ways to prepare and deliver treatments.

The objectives of this course are:

1. Describe the different treatment units focusing on their differences from "standard" linear accelerators
2. Show and describe typical treatment plans that can be achieved with this type of machines.
3. Describe the advantages and disadvantages of such systems.

MPF03.2 - Curiethérapie Guidée par l'image

Author(s): Luc Beaulieu

Radio-oncologie, CHU de Quebec, Quebec/CANADA

Objectifs d'apprentissages

- Identifier la ou les modalités d'imageries les plus appropriées selon le type de procédure de curiethérapie visé.
- Connaître les forces et les limitations des diverses modalités.
- Reconnaître les nouveaux besoins dans le cadre d'un programme de contrôle de la qualité.
- Identifier les nouvelles techniques d'imagerie pertinentes au domaine

La curiethérapie a connu une évolution importante grâce à l'apport de l'imagerie dans le processus de préparation (positionnement d'aiguilles, de cathéters et d'applicateurs) ainsi que dans celui de la planification des traitements. Dans ce dernier cas, le passage d'une planification de traitement 2D basée sur la localisation des cathéters

et applicateurs vers une planification 3D basée sur la délimitation de volumes cibles et des organes à protéger a profondément transformé la pratique clinique. Pour un site comme la prostate, l'utilisation de l'imagerie en temps réel pour le guidage de l'insertion d'aiguilles ou encore de cathéters a révolutionné la curiethérapie pour ce site pour en faire une procédure rapide, précise et efficace, au plus grand bénéfice des patients.

Cette présentation, faite dans le cadre d'une session de formation continue, fera un survol des modalités d'imagerie les plus courantes en curiethérapie, notamment la tomodensitométrie, l'imagerie par ultrasons, l'imagerie par résonance magnétique ainsi que la tomographie par émission de positron comme modalité de support. Les avantages et inconvénients de chacune de ces modalités seront présentés. La question des besoins supplémentaires en terme contrôle de la qualité de ces modalités pour assurer une planification de traitement optimale sera abordée.

Finalement quelques avancées en imagerie, telle que l'IRM multi-paramétrique, ayant de fortes probabilités d'influencer la pratique de la curiethérapie à court et moyen terme seront discutées.

MPF04 - LA FORMATION ET LE CHEMINEMENT DE CARRIÈRE DES PHYSIENS MÉDICAUX

MPF04.1 - Les Standards Professionnels et la Certification des Physiciens Médicaux

Author(s): Clément Arsenault

Medical Physics, Dr. Leon-Richard Oncology Centre, Moncton/
CANADA

Learning Objectives:

1. Understand the 4 underlying principles that form the basis for a certification program:
 - a. Providing an examination process
 - b. Providing a maintenance of certification (recertification) program
 - c. Providing a public registry
 - d. Providing a disciplinary process
2. Be familiar with the specifics of the CCPM certification process (eligibility requirements, exam process)
3. Be familiar with the CCPM recertification process

Abstract:

The Canadian College of Physicists in Medicine (CCPM) exists to protect the public by:

- (a) establishing standards of competence for those involved in the application of the physical sciences in the medical field in Canada.
- (b) identifying individuals who meet the established standards and maintaining a registry of these individuals.

This talk will focus on how the CCPM meets these objectives.

By way of introduction, a brief history of the CCPM will be presented, followed by a description of the current structure and governance of the CCPM.

The core business of any certification organization is centered around its examination process. The eligibility requirements for membership in the CCPM will be detailed, along with a description of the examination process.

After initial certification has been obtained, the CCPM requires that all members regularly demonstrate that they continue to meet certification requirements. The structure of the recertification program will be presented.

Members of the CCPM are required to comply with the Code of Ethics stated in the Regulations of the College, and this will be briefly discussed, along with a description of the disciplinary process in place to ensure member compliance with the Regulations of the College.

MPF05 - QUALITÉ ET SÉCURITÉ

MPF05.1 - Le Partenariat Canadien pour la Qualité en Radiothérapie

Author(s): Normand Frenière

Radio-oncologie, CSSSTR - CHAUR, Trois-Rivières/CANADA

Learning objectives:

- 1) Understand who the Canadian Partnership for Quality Radiotherapy is, its organizational structure and the opportunities to contribute
- 2) Be up-to-date with four priorities determined by CPQR which constitute the four main programs
- 3) Understand the process developed for the creation and revision of Technical quality control guidelines. Be up-to-date with guidelines published and those to come

Radiotherapy benefits to approximately 50% of cancer patients at some point in their cancer journey, either as curative treatment or to palliate symptoms. Currently, there are 42 radiotherapy programs across Canada. In 2010, national professional organizations involved in the delivery of radiation treatment in Canada founded the Canadian Partnership for Quality Radiotherapy (CPQR) with the objective to support the universal availability of high quality and safe radiotherapy for all Canadians. Professional organizations are: Canadian Association of Radiation Oncology (CARO), Canadian Organization of Medical Physicists (COMP) and Canadian Association of Medical Radiation Technologists (CAMRT). Strategic and financial support are provided by the Canadian Partnership Against Cancer (CPAC).

Four programs have been identified as offering the greatest potential to improve quality and safety and mitigate risk.

Quality assurance guidance and indicators

The intent of this program is to provide national guidance and indicators to motivate continuous quality improvement in a radiation treatment program. The published document outlines the overarching organizational structure and processes that are required to assure high quality and safe radiotherapy, along with key quality indicators for programmatic assessment.

In 2014, CPQR, CPAC and Accreditation Canada partnered to develop a Radiotherapy module for the Accreditation Canada's Qmentum program which uses a range of standards to focus on quality and safety. This module will adopt many of the indicators contained within CPQR's document and will help assure long-term sustainability of quality and safety measures in radiotherapy. Performance will be publicly reported to motivate utilization across Canada.

Technical quality control guidance

The intent of this program is to provide direction for assuring optimal performance of radiotherapy equipment in programs across Canada. Several guidelines are published and others are to come. A structured process was developed in the creation or revision of each guideline. It includes an expert review and revision, a broad community consultation to assure relevance and practicality, validations in real-world clinical environment, endorsement by the Quality Assurance Radiation Safety Advisory Committee of COMP, and a sustainability plan to assure continued relevance over time.

National reporting system

The intent of this program is to provide radiotherapy programs with a national reporting system which will provide a tool to report, track and analyze incidents from their own center and anonymously from other Canadian centers. Learning from near misses and incidents that occur during treatment planning and delivery is a key element of

quality assurance. CPQR is partnering with the Canadian Institute of Health Information (CIHI) on this project.

Patient satisfaction

The intent of this program is to establish an approach for measuring and reporting the patient experience in a meaningful way. A patient perspective will be integrated with each of the three other programs described above. In addition, new indicators of patient satisfaction and patient experience will be developed and incorporated into Qmentum program accreditation. We should not forget that the Patients and Canadian public are the ultimate beneficiaries of safe and effective radiation treatment.

MPF05.2 - L'ingénierie des facteurs humains

Author(s):

L'augmentation constante des possibilités technologiques entraîne une complexification de l'interaction avec les équipements et les logiciels utilisés en physique médicale et en génie biomédical. L'ingénierie des facteurs humains peut être mise à contribution pour réduire, et prévenir, cette complexification. Cette présentation décrira diverses méthodes, pratiques et normes pour y arriver. On illustrera le tout au moyen d'une étude de cas.

À la fin de cette présentation, vous serez en mesure de (d')

Décrire et discuter de moyens pour améliorer la performance et à réduire l'erreur humaines

Identifier des activités où il est possible d'intervenir pour réduire l'erreur humaine

Tenir compte de normes et de pratiques appropriées lors de la conception, l'achat ou la sélection d'équipement ou de logiciels

Abstract – English

Title: Human Factors Engineering

The constant increase in technological possibilities leads to a complexity of the interaction with the equipment and software used in medical physics and biomedical engineering. Human factors engineering can be used to reduce and prevent this complexification. This lecture will describe methods, practices and standards to achieve this. A case study will be presented to illustrate how to integrate those elements.

At the end of this lecture, you will be able to:

1. Describe and discuss means to improve human performance and reduce human error
2. Identify activities where it is possible to intervene to prevent human error
3. Consider appropriate standards and practices when designing, procuring or selecting equipment and software.

MPF06 - IMAGERIE**MPF06.1 - La Boîte à Outils du Physicien Moderne: Instruments de Contrôle de Qualité****Author(s):** Alain Gauvin

Medical Imaging, McGill University Health Center, Montréal/CANADA

La pratique du physicien œuvrant en imagerie médicale a beaucoup évolué au cours des dernières années. Ceci est évidemment en grande partie attribuable à l'évolution des technologies d'imagerie médicale, en particulier le passage au mode numérique. Certaines autres technologies ont aussi inauguré de nouvelles catégories dans l'instrumentation de mesure et de test, comme les dispositifs d'affichage. Toutefois, l'instrumentation de mesure a elle-même fait l'objet de changements substantiels. Il est donc utile de présenter l'appareillage de test utilisé dans la pratique contemporaine du physicien médical.

Une classification des tests sur la base du type de mesure est proposée. La construction de cette classification est effectuée de façon à se rapprocher de la quantité physique mesurée plutôt que de la composante de la chaîne d'imagerie faisant l'objet de la mesure. Cette façon regrouper les différentes mesures par type permet de bien faire ressortir les caractéristiques de l'instrumentation du physicien, et l'impact qu'ont ces caractéristiques sur les différentes mesures produites. Les situations où certaines caractéristiques des appareils de mesure ont un impact sur l'interprétation, voire la pertinence de certains tests sont discutées en détail. De plus, certains changements technologiques qui sont en cours sont aussi discutés, qu'il s'agisse de changement au niveau de l'appareillage de mesure, ou au niveau de la technologie de la chaîne d'imagerie faisant l'objet de cette mesure. De plus, il existe de nombreuses méthodes de mesures utilisant des objets de tous les jours pour mener à bien certains tests, souvent sans compromis au niveau de la qualité des mesures. Il est important d'identifier ces solutions de mesure simples et peu onéreuses en fonction de l'objectif recherché.

Finalement, les outils logiciels occupent un rôle croissant dans la pratique du physicien en imagerie médicale. Dans beaucoup de cas, il s'agit de méthodes d'appoint pour certains tests, par exemple en permettant l'analyse des valeurs obtenues. Dans d'autres cas, il s'agit plutôt de méthodes logicielles dont la portée est plus globale, comme pour la collecte, l'organisation ou la présentation des résultats du contrôle de la qualité. Finalement il devient de plus en plus important pour le physicien de disposer de visibilité sur certains aspects de la connectivité de l'appareil. En effet, certaines mesures obtenues par le physicien sont souvent présentées à l'opérateur et expédiées par l'appareil vers d'autres systèmes, par exemple le produit dose-aire. Puisqu'il était déjà important pour le physicien d'assurer le bon fonctionnement de tels dispositifs, la communication des mêmes résultats doit naturellement elle aussi être scrutée par le physicien, ce qui introduit une nouvelle classe d'outils logiciels.

En somme, l'appareillage utilisé par le physicien médical est typiquement très onéreux en acquisition, mais aussi en entretien. La compréhension du fonctionnement de cet appareillage doit être attentivement recoupée avec la finalité des différents tests effectués par le physicien afin que l'investissement engendre une valeur concomitante en termes de qualité et d'efficacité.

Au terme de cette session, les participants seront en mesure de

1- Comprendre la classification proposée pour les mesures effectuées par le physicien.

2- Comprendre le fonctionnement des différentes technologies utilisées pour chaque type de mesure de la classification, et certains enjeux découlant de ces technologies.

3. Connaître les outils logiciels employés par le physicien et la place croissante qu'ils occupent dans la pratique du physicien.

ENGLISH

The toolbox of contemporary medical physicists: quality control instruments.

The practice of medical physics in diagnostic radiology has evolved substantially in recent years. Obviously, this is largely due to changes in medical imaging technologies, in particular the transition to digital imaging. However, the development of some other new technologies has also led to the introduction of new categories of measurement and testing, for example display monitors. Moreover, the measuring instruments have themselves undergone substantial changes. Therefore, it is useful to present the test equipment used in the contemporary practice of medical physicists.

A classification based on the type of measurement is proposed. The construction of this classification is in contrast to an imaging system based approach, since the measurement of a given physical quantity can be required for many types of system. This in turn allows for a greater emphasis on the characteristics of measurement instruments, and on the impact that they have on the various types of use. In particular, some situations for which some of these characteristics have an impact of the interpretation, or even of the relevancy of some of the tests are described. In addition, some technological changes that are under way are also discussed, be it change in the measuring apparatus, or at the imaging chain technology. Furthermore, there are many methods of measurements using simple and inexpensive test objects to carry out certain tests, often with no compromise in the quality of the measurements. It is pertinent to identify these simple measurement solutions and their adequacy as a function of the survey objective.

Finally, software based tools occupy an increasingly important role in the practice of medical physicists. In some cases, these methods are used as an adjunct to some tests, for example for analyzing the values obtained. In other cases, they can be used for survey data collection and management. It is becoming more and more important for physicists to have some visibility on certain aspects of the connectivity of imaging systems. For example, some measurements obtained by the physicist are often also available to the operator and sent by the device to other systems, such as the dose-area product. Since it is important for the physicist to verify that imaging systems operate properly, the communication of the data pertaining to its operation must naturally also be verified by the physicist, which introduces a new class of software based tools in the physicist's toolbox.

In **summary**, the equipment used by the medical physicist is typically expensive to acquire and maintain. Understanding how this equipment operates allows for the physicists to maximize the quality and the efficiency of the survey.

After this session, participants will be able to

1- Understand the proposed classification for the measurements carried out by the physicist.

2. Understand how different measurement technologies are used and some of the issues arising from the use of these technologies.

3. Know the software tools used by the physicist and the growing position which they occupy in the practice of the medical physicist.

MPF06.2 - La Radiologie Interventionnelle, Incluant un Survol des Nouvelles Technologies et Approches

Author(s): Cécile Salvat, Jérémie Ragot, Annick Gotti, Antonella Jean-Pierre
Medical Physics, Paris Hospital, Paris/France

La radiologie interventionnelle est définie par un consensus d'experts français comme l'ensemble des actes médicaux invasifs diagnostiques et/ou thérapeutiques ainsi que les actes chirurgicaux utilisant des rayonnements ionisants à visée de guidage per-procédure, y compris le contrôle.

La radiologie interventionnelle se développe considérablement depuis quelques années. Les applications cliniques de plus en plus audacieuses se multiplient tant sur le plan des équipements vasculaires dédiés qu'au bloc opératoire sur des arceaux de bloc. Le nombre d'actes de radiologie interventionnelle à visée thérapeutique, le plus souvent possible en ambulatoire pour améliorer la prise en charge du patient, croît chaque année en France au détriment d'autres actes chirurgicaux souvent plus invasifs et plus lourds pour le patient.

Les domaines de la cancérologie, de la cardiologie, de la neuro-radiologie, de la pédiatrie, sans oublier les applications viscérales et ostéo-articulaires, tous sont concernés par les nombreuses innovations technologiques que proposent les constructeurs visant à améliorer la qualité de l'image. Les avancées technologiques concernent à la fois les matériels (capteurs, tubes, filtration...), les protocoles d'acquisition et les logiciels. Par conséquent, les procédures cliniques se réalisent avec des technologies de plus en plus complexes (acquisitions bi-plan, angiographie rotationnelle, roadmap 3D, acquisitions hybrides...) nécessitant des temps d'acquisition parfois très longs sous rayons X avec une formation des opérateurs de plus en plus pointue et évolutive. Les études en France constatent une augmentation globale de la dose patient en imagerie ces 10 dernières années et notamment dans le cadre des nouvelles approches thérapeutiques interventionnelles. Les accidents ou incidents en radiologie interventionnelle déclarés à l'Autorité de Sureté Nucléaire française ne représentent que 3 % des événements significatifs en radioprotection déclarés mais sont les plus graves enregistrés avec des effets déterministes importants chez le patient.

Nous présenterons les innovations technologiques proposées par les constructeurs ainsi que les paramètres qui sont à l'origine, en permanence, du compromis entre la dose et la qualité image nécessaire à l'élaboration du diagnostic et/ou des gestes thérapeutiques. Nous aborderons l'optimisation des protocoles et les outils de réduction de dose ainsi que l'arrivée récente sur le marché des DACS, logiciels de suivi et de cumul de dose patient dont le rôle est devenu incontournable.

Nous détaillerons le rôle essentiel que doit jouer le physicien médical, à l'interface entre les équipes médicales et les constructeurs, aidé par des outils désormais disponibles et de plus en plus performants, dans l'intérêt de la radioprotection du patient mais également des opérateurs.

MPF07 - RADIOTHÉRAPIE**MPF07.1 - Nouvelles Technologies et Approches en Curiethérapie**

Author(s): Luc Beaulieu

Radio-oncologie, CHU de Québec, Québec/CANADA

Objectifs d'apprentissages

- Identifier des problématiques clés de la pratique courante en curiethérapie qui bénéficieraient d'avancées technologiques.
- Identifier des technologies habilitantes.
- Saisir les bénéfices et les limitations des nouvelles technologies présentées.
- Extrapoler leurs utilisations pour de nouvelles approches de traitement

Cette présentation, faite dans le cadre d'une session de formation continue, veut porter un regard sur les sujets chauds de R&D en curiethérapie. Plusieurs avancées technologiques sont présentement considérées pour implémentation en curiethérapie. Ces avancées offrent des possibilités de changements significatifs à la façon dont seront planifiés ou traités les patients.

Pour cette présentation, cinq de ces avancées seront abordées. Première nous aborderons l'introduction de nouvelles méthodes de calcul de la dose et son impact sur la planification de traitement. Par la suite, nous brosserons un portrait des efforts liés à la conception de nouvelles sources et de nouveaux applicateurs qui pourraient permettre de nouvelles approches de traitements. Une nouvelle technologie pour le suivi en temps réel d'aiguilles, de cathéters et des applicateurs a été récemment proposée. Nous en regarderons à la fois l'impact et les limitations. Nous regarderons comment les technologies d'impression 3D pourraient personnaliser davantage les procédures de curiethérapie. Finalement, nous couvrirons la question de la robotique comme aide au médecin en curiethérapie interstitielle.

Pour chacune, nous allons aborder les problématiques physiques ou cliniques visées par leur introduction, les implications de leur utilisation ainsi des perspectives entre termes de modification possible par rapport à la pratique courante.

D'autres avancées, en particulier du côté de l'imagerie 3D et 4D, sont aussi d'importance, mais seront couvertes par d'autres présentations.

MPF07.2 - Protontherapy

Author(s): Alejandro Mazal¹, Farid Goudjil¹, Remi Dendale²

¹Physique Médicale, Institut Curie, Paris/France, ²Radiation Oncology, Institut Curie, Paris/France

Protontherapy is one of the most promising conformal approaches for radiation therapy and the number of operational facilities is increasing all over the world (around 40 centers in operation and more than 40 in preparation).

The rational of its use is based on physical properties of accelerated protons in media, in particular the dose deposition by ionization in depth with the shape of a peak (the Bragg peak). Adding different energies (energy modulation) produces a spread out Bragg peak (SOBP) to cover a target volume in depth with a homogeneous dose, but this also increases the entrance dose.

The main advantages of a proton beam compared to photons are the distal fall off and the lack of exit dose (reducing the integral dose to the patient), a homogeneous dose to the target, an homogeneous dose at the entrance path and a small penumbra at the entrance. There are some limits such as the skin dose, the uncertainty in the range, the large penumbra in depth (related to multiple scattering) and the neutron dose (related to nuclear interactions).

A clear evolution is seen in the technology, mainly in the accelerators (cyclotrons, synchrocyclotrons, synchrotrons, linacs and new approaches) as well as in gantries to propose compact and cheaper solutions, including single room approaches (as with electron-photons). Ancillary tools include specific solutions in treatment planning software, patient positioners, dosimetry and range verifiers devices. The present tendency is to use pencil beam scanning to treat with intensity modulated proton beams, in combination with conventional methods of image guided radiation therapy, management of organ movements and adaptive therapy.

Clinical protocols include well accepted but rather rare locations (uvea melanoma, base of skull chordomas and chondrosarcomas, pediatrics, radiosurgery for intracranial targets) and more common clinical sites including lung, breast and prostate, with a tendency to include all targets treated in radiation therapy with photons. There are also comparative studies with the use of heavier ions (e.g. Carbonne), which add radiobiological advantages to their physical specifications.

Research and development in the field include physical and engineering aspects (detectors, micro-beams, delivery systems, models and optimizations, robotics for positioning,...), radiation biology (equivalent doses, effects of dose rate, LET, neutrons, radiosensitizers...), and clinical research (combined treatments, hypofractionation, ...). The main limit to spread protontherapy today is the investment cost.

At the end of the CE program, attendees will be able to:

- 1- Describe the main physical interactions and dosimetric characteristics of clinical proton beams and define the existing technology and its evolution.
- 2- Understand the rationale for existing and upcoming clinical protocols
- 3- Have a scope of the research and development programs in the field.

MPF09 - IMAGERIE

MPF07.2 - Dosimétrie et Radioprotection en Radiologie

Author(s): [Sylvain Deschênes](#)

Medical Imaging, CHU Sainte-Justine, Montreal/CANADA

Objectifs pédagogiques:

1. Connaître les radiations ionisantes et mieux comprendre leurs effets.
2. Mieux connaître les risques reliés à la radiation ionisante.
3. Connaître les bonnes pratiques en matière de radioprotection en imagerie diagnostique et interventionnelle.

Abrégé:

Au cours des quinze dernières années, plusieurs publications ont traité des risques reliés aux radiations ionisantes lors d'examen de radiologie diagnostique et interventionnelle. Dans la même veine, des campagnes comme *Image Gently* et *Image Wisely* ont vu le jour afin de sensibiliser à cette réalité les institutions utilisant l'imagerie médicale. Or, de façon générale, les méthodes proposées afin d'évaluer quantitativement le risque associé à ce rayonnement s'accompagnent d'une certaine ambiguïté pour les niveaux de doses rencontrés en imagerie médicale. De plus, à l'heure d'une approche personnalisée de la médecine, cette estimation dosimétrique rencontre plusieurs embûches : indicateurs de dose non standardisés, passage vers une dose à l'organe complexe, etc.

Parallèlement, on voit apparaître plusieurs articles de loi, notamment aux États-Unis, qui obligeront prochainement les établissements de santé à tenir un registre des doses reçues par leurs patients. Dans cette foulée, plusieurs logiciels sont apparus dans les dernières années afin d'offrir la possibilité d'effectuer un tel suivi.

Dans cette présentation, nous tâcherons de mieux comprendre les effets de la radiation ionisante sur le corps humain. Par la suite, les différents indicateurs de dose rencontrés en imagerie médicale diagnostique et interventionnelle seront présentés. L'emphase sera mise sur les deux types d'examen les plus irradiants en radiologie : la tomographie assistée par ordinateur (CT-scan) et la radioscopie interventionnelle. Dans le cas du tomographe, les indicateurs proposés sont le Computed Tomography Dose Index (CTDI), le Size-Specific Dose Estimate (SSDE) et le Dose Length Product (DLP). La radioscopie, de son côté, présente la dose sous forme de produits dose-surface (Dose Area Product ou DAP) et de doses accumulées à la peau. Nous verrons comment ces différents indicateurs peuvent être utilisés pour évaluer une valeur personnalisée sous forme de dose aux organes et de dose effective. Nous verrons aussi comment ces métriques permettent de calculer les niveaux de référence diagnostiques (NRD) aidant à identifier les examens où la dose est potentiellement problématique, à optimiser les protocoles et à se comparer aux autres dans notre gestion de la dose. Des pistes de solution afin d'optimiser les procédures seront également présentées.

ENGLISH

Learning Objectives:

1. To understand the nature and effects of ionizing radiation.
2. To better understand the risks associated with ionizing radiation.
3. To learn good radioprotection practices in diagnostic and interventional imaging.

Abstract:

In the past fifteen years, there has been a growing interest for assessing the risks incurred by radiation exposure during diagnostic and interventional radiology procedures. As a result, campaigns such as *Image Gently* and *Image Wisely* have raised awareness regarding such issues. However, the information provided by radiological systems is oftentimes ambiguous, hindering the efforts to assess such risks. For example, in this age of personalized medicine, dose estimates have to address issues such as non-standardized dose indicators, the need for more accurate organ doses, etc.

Meanwhile, legislations have been or soon will be passed in North America regarding dose monitoring and reporting. For example, Bill 1237 is now enforced in California and it is a matter of time before such laws proliferate in many other states and countries. Accordingly, several software solutions are now offered to perform this monitoring.

In this talk, we will cover the nature of ionizing radiation and its effects on the human body. Then, we will introduce various dose indices describing patient's exposure for diagnostic and interventional imaging modalities. Emphasis will be placed on CT-scan and interventional radioscopy since they deliver substantial radiation to the patient. For CT-scan, the relationship between Computed Tomography Dose Index (CTDI), Size-Specific Dose Estimate (SSDE) and Dose Length Product (DLP) will be explored. For radioscopy, we will show how Dose-Area-Product (DAP) and cumulative entrance skin dose describe patient's irradiation.

We will finally see how these indices may be used to compute personalized dose reports where organ dose and effective dose are used to evaluate the risk for a specific patient. We will also see how computing Diagnostic Reference Levels (DRL) may help optimizing institutions protocols and identify exams where excessive dose has been delivered to a patient. Some tips will be provided to help minimize dose during procedures.

MPF08 - SYSTÈMES INFORMATISÉS/ QUALITÉ ET SÉCURITÉ**MPF08.1 - Algorithmes de Calcul de Dose, Incluant Monte Carlo****Author(s):** [Raphaël Moeckli](#)

Institute Of Radiation Physics, CHUV, Lausanne/SWITZERLAND

Les systèmes de planification jouent un rôle fondamental et central en radiothérapie. Le cœur du système est l'algorithme de calcul de la dose. L'algorithme de convolution/superposition est actuellement le plus utilisé, mais de nouveaux algorithmes, basés sur Monte Carlo ou sur les équations de transport, apparaissent progressivement sur le marché.

Les objectifs de ce cours sont les suivants:

1. Décrire les principaux composants des systèmes de planification.
2. Décrire les principaux algorithmes de calcul de la dose utilisés actuellement (convolution/superposition, Monte Carlo, équations de transport).
3. Décrire les avantages et les limitations des différents algorithmes.

MPF08.2 - Utilisation de la Maîtrise Statistique des Processus en Milieu Hospitalier**Author(s):** [Karine Herlevin \(Gérard\)](#), Vincent Marchesi, Océane Mougel, Isabelle Buchheit

Medical Physics Unit, Institut de Cancérologie de Lorraine, VAN-DOEUVRE-LES-NANCY Cedex/FRANCE

3 learning objectives:

1. Understand variability, its impact and behavior (differentiate random and special causes).
2. Describe the DMAICS method to introduce a SPC (Statistical Process Control) analysis.
3. Understand how to use control charts and performance indicators in the management of your department.

Quality indicators have been developed quite recently in health, compared to industry, but considerable progresses have been made. Indeed, we moved from an era where data was almost non-existent, to the current period where data has become abundant.

So, there is a need in health, to find a quality management method that can monitor quality indicators over time to facilitate a continuous and measurable improvement of quality.

One of the methods allowing this is the Statistical Process Control (SPC). SPC has made proves in industry and has been widely used since 1950 in Japan and since 1970 in the USA and in Europe. Concerning health, the first papers introducing SPC have appeared in 2005 and its use is still increasing. This method aims at controlling and improving the quality of a process through a statistical analysis, by using two main tools: performance indicators and control charts.

Performance indicators rate the ability of a process to produce data that are within predefined specifications, at a precise moment. So, performance indicators depend on the specifications that are often chosen empirically, based on practice and experience.

On the contrary, control charts monitor the results over time and do not take into account the specifications. They are only based on statistical rules. So, the aim of control charts is to monitor the process over time, by using statistical control limits that distinguish random (natural) variations (i.e values within the control limits)

from significant changes (special causes) that disturb the process. Thanks to the statistical control limits, the effects of special causes can be detected, and then actions can be undertaken to reduce or eliminate their effects. A process that is only subject to random causes of variation is statistically under control and thus statistically predictable.

In the presentation, we will develop a practical example of the use of SPC in the field of Radiotherapy. We will show how SPC can be used to monitor the IMRT (Intensity Modulation Radiation Therapy) pre-treatment quality controls and to make the dose delivery process under control. The aim is to increase the security of each patient's treatment while controlling the whole dose delivery process, without increasing time devoted to the analysis.

To conclude, SPC is a method that helps reducing the variability of a process, and thus decreasing the number of data out of specifications.

We are convinced that SPC should secure and improve quality of many processes in radiotherapy and in health in general. It could serve as a common language to evaluate processes' performance. Moreover, the ultimate goal of SPC is, considering a process is under control, to streamline the amount of quality control in a safe statistical environment by taking objective decisions to balance resources and quality.

MPF09 - IMAGERIE

MPF09.1 - TEP: Les Nouveaux Développements et Avenues de Recherche

Author(s): Roger Lecomte

Centre D'imagerie Moléculaire De Sherbrooke, Centre de recherche du CHUS (CRCHUS), Sherbrooke/CANADA

La tomographie d'émission par positrons (TEP) est une modalité d'imagerie médicale utilisant des isotopes émetteurs de positron pour suivre le devenir de molécules radiomarquées dans les organismes vivants. En mesurant la captation, la biodistribution et l'élimination du radiotracer, il est ainsi possible de tirer des informations sur les processus moléculaires *in vivo* aussi bien en condition physiologique normale que dans des états pathologiques comme le cancer, les désordres neurologiques et les maladies cardiovasculaires ou cardiométaboliques. Des avancées technologiques majeures ont permis d'élargir les domaines d'applications de l'imagerie TEP, que ce soit en recherche biomédicale ou pour le diagnostic clinique. Des exemples de ces avancées technologiques se retrouvent dans la multitude de concepts de détection et de techniques sophistiquées de traitement des signaux, en imagerie tridimensionnelle avec reconstruction tomographique itérative des images, l'introduction de la mesure du temps-de-vol, et la combinaison de l'imagerie TEP avec la tomodensitométrie par rayons-X (TDM) ou l'imagerie par résonance magnétique (IRM). Malgré d'énormes progrès au cours des dernières décennies, la technologie TEP n'a pas réalisé tout son potentiel. Cet aperçu passera en revue les principes de base de l'imagerie TEP, l'état actuel de la technologie et les développements en cours dans le domaine, incluant les réalisations en imagerie multimodale utilisant les approches TEP/TDM et TEP/IRM. En conclusion, nous discuterons quelques applications marquantes de l'imagerie TEP en recherche et en clinique et nous commenterons quelques nouvelles idées prometteuses offrant des perspectives intéressantes dans le domaine.

À la fin de ce programme d'éducation continue, les participants seront en mesure de :

- 1- Décrire et discuter les principes de l'imagerie TEP, les technologies et les applications utilisées en médecine nucléaire diagnostique et en recherche biomédicale.
- 2- Comprendre les limitations physiques sous-jacentes et les possibilités d'amélioration de la modalité d'imagerie TEP.
- 3- Expliquer les divers avantages et limitations des différentes approches d'imagerie multimodales.

MPF10 - RADIOTHÉRAPIE PT 1

MPF10.1 - La Radiothérapie Guidée par L'image, Incluant Doses et CQ

Author(s): Gregory Delpon¹, Myriam Ayadi-Zahra², Frédérique Lafay², Albert Lisbona¹

¹Medical Physics, Centre René Gauducheau, NANTES/
FRANCE, ²Radiotherapy Physics, Centre Léon Bérard, LYON/
FRANCE

Learning objectives:

- To define errors occurring during the treatment and their clinical impact
- To list the different technologies currently available for the IGRT and their specific QA / to define the concept of adaptive radiotherapy
- To discuss the dose delivered by the different devices

Abstract:

Radiotherapy consists in delivering ionizing radiation to the tumor while avoiding the surrounding normal tissue. Treatment efficacy is often limited by the resistance of tumors and the toxicity of healthy organs. Then prescription must represent a trade-off between risks and benefits. The dose-response curves for tumor control and normal tissue complications determine the therapeutic window that is the possibility of delivering a sufficient dose with an acceptable level of side-effects. The development of imaging modalities and treatment techniques aims at improving this therapeutic window. 3D and 4D imaging modalities allow to describe tumors and normal tissues and their motions. Intensity-modulated radiation therapy with static beams (IMRT) or arcs (VMAT), stereotactic body radiation therapy (SBRT) allow to deliver accurately highly conformal doses to the tumor and to spare a large volume of normal tissue. These developments that are changing the clinical practice are made possible thanks to the emergence of image-guided radiotherapy (IGRT).

IGRT is based on the acquisition of frequent in-room images during a course of radiotherapy. These images are used to verify the position of the target volume and/or the organs at risk with a higher frequency and a greater accuracy than portal images, more irradiating and of lower quality. IGRT integrates various imaging modalities that allow either direct visualization of the tumor by two-dimensional or three-dimensional images or indirect visualization of the tumor using surrogates such as implanted markers or bony structures. The anatomical data acquired during those imaging sessions lead to two types of decisions: the correction of the positioning and the modification of the treatment plan. After a rigid registration between planning images and in-room images, positioning of the tumor target can be corrected by moving the couch. This is done daily in radiotherapy departments. The treatment plan modification taking into account the anatomical deformations is more complex. It may impose one or more replanning during the course and requires the development and validation of tools not yet fully mature to date for clinical routine use. This is the concept of adaptive radiotherapy.

IGRT requires a close collaboration between physicians, technicians and physicists. Specific training should be put in place to help decision making when registering images. Depending on the therapeutic goal, the treatment site and the equipment, IGRT strategies may differ in terms of imaging modality and frequency. Each department should define its own protocols specifying the roles of each professional. The commissioning of the imaging systems should be performed by the physicists, whatever the modality (ionizing or non-ionizing, 2D or 3D, ...). In addition a quality control program should be implemented based on the international publications such as AAPM reports. The use of ionizing radiation devices raises the

problem of the additional dose delivered to patients. The dose due to in-room imaging sessions should be estimated by measurements or calculations to be reported. The management of this extra dose should be part of on site IGRT protocols.

IGRT offers new treatment opportunities such as toxicity reduction, dose escalation, hypofractionation, voxelization and adaptation. But the clinical implementation requires the staff to perfectly define the goals (positioning and/or replanning) and the roles.

MPF10.2 - Dosimétrie in Vivo

Author(s): Louis Archambault

Radio-oncologie, CHU de Quebec, Quebec/CANADA

Objectifs d'apprentissage: (1) décrire les différents outils permettant de faire de la dosimétrie in vivo; (2) identifier les champs d'application et les avantages potentiels de cette pratique; (3) se familiariser avec différentes approches pour faire l'implantation clinique d'une stratégie de mesure in vivo.

En radiothérapie, la dosimétrie in vivo est généralement définie comme la mesure de la dose de radiation faite au moment même où un patient reçoit une fraction de son traitement. L'attrait de la dosimétrie in vivo est grand, puisqu'elle est la seule manière de connaître réellement la dose de radiation administrée au patient. Toutefois, malgré cet avantage notable, ce type de mesure n'est toujours pas utilisé à grande échelle. Dans de nombreuses cliniques en Amérique du Nord, la dosimétrie in vivo n'est utilisée que marginalement ou pour des cas très particuliers. Des sondages ont démontré que l'apparente lourdeur clinique de la dosimétrie in vivo est un obstacle majeur à son adoption généralisée.

Dans un premier temps, nous ferons l'inventaire des différents détecteurs pouvant être utilisés pour faire la mesure de dose in vivo. Nous présenterons les forces et les faiblesses d'un grand nombre d'instruments, allant des appareils embarqués servant à faire la mesure de la dose à la sortie du patient (imageur portal) jusqu'aux appareils implantables directement au voisinage d'une tumeur ou d'un organe à risque. Nous porterons aussi une attention particulière à l'utilisation de ces instruments dans des conditions non standard telles que les mesures hors du champ primaire de radiation, les mesures de très faibles doses de radiation ou les mesures de patrons de dose fortement modulés. À moins que des précautions ne soient prises, la mesure dans des conditions non standard peut introduire une erreur systématique dans l'évaluation de la dose.

Deuxièmement, nous ferons un survol des champs d'application où la dosimétrie in vivo offre un grand potentiel tel que le contrôle de la qualité et le suivi des patients tout au long de leur traitement par imagerie portale; l'évaluation des doses reçues par des appareils cardiaques implantables (pacemakers) et la protection des organes à risque dans la radiothérapie hautement conforme. Nous discuterons aussi des avantages d'intégrer un programme de dosimétrie in vivo avec une approche de radiothérapie adaptative.

Finalement, dans un troisième temps, nous verrons comment il est possible d'implanter une stratégie de mesure in vivo tout en minimisant son impact négatif sur le flot des opérations cliniques. Nous passerons en revue des exemples de centres ayant implanté de telles stratégies et nous présenterons les rôles et responsabilités de chaque intervenant (physicien, technologue, etc.) ainsi que les besoins de formation. Nous discuterons aussi des outils logiciels et autres systèmes de bases de données nécessaires pour stocker et analyser l'information recueillie et garantir un suivi et une rétroaction efficace.

MPF11 - RADIOTHÉRAPIE PT 2**MPF11.1 - Stéréotaxie Extra-Crânienne: Techniques et CQ**

Author(s): Myriam Ayadi-Zahra, Guillaume Beldjoudi, Jean-Noel Badel, Claude Malet
Radiotherapy Physics, Centre Léon Bérard, LYON/FRANCE

Learning objectives:

- To list the different technologies currently available for SBRT
- To discuss about the crucial points in the implementation of SBRT(dose measurements, algorithm, ...) and the periodic QA to perform

Abstract:

Stereotactic Body Radiation Radiotherapy (SBRT) is rapidly expanding. This rising treatment strategy shows comparable clinical results with surgery concerning primitive tumors local control (Non-Small Cell Lung Cancer). SBRT can also significantly increase the overall survival of oligometastatic patients. This advanced technique classically delivers single or few fractionated large dose to tumors located in various sites of the body (thoracic, paraspinal, abdominal and pelvic sites). The treatment principle is based on the use of small size photon beams, providing high target conformity and narrow dose fall-off for better critical organs sparing. Consequently, this special treatment strategy requires a high level of accuracy, first, in the beam commissioning (dose measurements) and then, at each step of the treatment process, i.e simulation, treatment planning, delivery. The global uncertainty of the process must be kept as low as possible in order to keep clinical benefits without increasing the toxicity probability.

Key linac features that determine the SBRT feasibility are the beam collimation that allows a sharp beam penumbra and complex target management, and reliable image guidance. Various technologies can currently perform SBRT: conventional linac with appropriate image guidance, Tomotherapy™, Cyberknife™ and Vero™. In case of moving targets, additional systems exist to manage the patient breathing (breath hold, abdominal compression, Gating) in order to minimize the uncertainty due to target motion. Other solutions monitor the breathing patient combined with image guidance, and thus can allow a real time tumor tracking.

Imaging is crucial in SBRT because it helps to define the more precisely the target volume and position in the patient and it also guarantees the correct tumor targeting before and/or during the treatment delivery. Acquisitions parameters of the reference CT scan have to be optimized so that the best quality image is obtained (spatial resolution, contrast). 4D CT scan is necessary for all moving tumors as it gives the spatio-temporal position and deformation of the target. Multi-modality imaging, such as MRI, PET-CT and contrast-enhanced-CT, is mandatory too, to improve the tumor and critical organs delineation.

Concerning beam commissioning, critical aspect is the detector used for measurements. Caution must be paid to its resolution, volume and response considering the very small size beam. Performance of dose calculation algorithm is important especially in low density media because it can have a large impact on the isodose prescription. The periodic tests of Quality Assurance depend on the treatment delivery used for SBRT. For each new localisation to be validated, and regularly, End-to-End (E2E) tests are recommended. Many commercial E2E phantoms exist and help physicists to validate the overall workflow of the treatment.

The SBRT implementation in a clinic needs a robust educational program followed by all professionals involved in the patient treatment. These latter must refer to the recent published guidelines

(AAPM Task Group 101 report, etc...). In parallel, an "a priori" risks analysis should be done to refine the workflow and patient safety. Then, incidents have to be reported as part of an Experience Feedback Committee program.

MPF11.2 - La Radiothérapie Adaptative

Author(s): Bernard Lachance
Radio-oncologie, CHU de Québec, Québec/QC/CANADA

Objectifs d'apprentissage:

Acquérir une définition de la radiothérapie adaptative et comprendre les motivations justifiant son développement.

Connaitre les processus techniques ainsi que les divers éléments technologiques qui sont nécessaires au déploiement de la radiothérapie adaptative.

Apprendre les diverses stratégies d'adaptation du traitement de radiothérapie externe aux besoins spécifiques du patient.

La radiothérapie a connu de multiples développements technologiques au cours des deux dernières décennies. Ces développements ont conduit en premier lieu à une importante amélioration au niveau de la précision, de la rapidité ainsi que de la fiabilité des appareils de traitement. Deuxièmement, le grand avancement des capacités informatiques a permis le développement de logiciels toujours plus performants pour calculer et optimiser les distributions de dose dans le patient, pour gérer et faire circuler de grande quantités d'informations entre les divers systèmes et pour manipuler les images médicales. De plus, la planification des traitements de radiothérapie fait maintenant usage sur une base régulière de plusieurs modalités d'imagerie telle que la tomographie par émission de positron (TEP-CT) qui permettent aux radio-oncologues de définir les volumes cibles ainsi que les organes à risques (OAR) avec beaucoup de précision.

Ces avancées technologiques ont permis le développement de diverses formes de radiothérapie conformationnelle avec modulation d'intensité des faisceaux (RCMI). Les techniques de modulation d'intensité peuvent être divisées en deux grands groupes : les techniques utilisant des faisceaux stationnaires, appelées techniques « step and shoot » et « sliding window », et les techniques utilisant un déplacement continu de la source de rayonnement autour du patient selon un ou plusieurs arcs, appelées IMAT pour « intensity modulated arc therapy », VMAT pour « volumetric modulated arc therapy » ou tomothérapie sérielle ou hélicoïdale, selon la technologie employée.

Ces techniques de RCMI nous offrent la possibilité de conformer avec grande précision la distribution de la dose à des volumes cibles toujours mieux définis par les radio-oncologues à l'aide de multiples modalités d'imagerie. Un traitement plus conforme ouvre la porte à l'escalade de la dose dans l'objectif d'augmenter le contrôle local de la maladie. Toutefois, il existe divers facteurs limitant qui nous empêchent encore de tirer le plein potentiel de la RCMI à cibler avec précision les volumes du médecin. Par exemple, la position du patient n'est pas parfaitement reproductible d'une fraction à l'autre, il y a des mouvements des organes internes dus à la respiration ou au péristaltisme, il y a des changements au niveau du remplissage de la vessie et/ou du rectum, etc. Il s'agit là de facteurs reliés au patient, il y en a d'autres reliés à l'appareillage et à l'interprétation de l'anatomie. L'approche traditionnelle pour prendre en compte ces variations quotidiennes est d'adopter des marges de sécurité autour des volumes cibles définis par le radio-oncologue, ce qui conduit nécessairement à irradier plus de tissus sains.

L'idée de la radiothérapie adaptative a été introduite en réponse à

cette problématique des variations quotidiennes de la position du patient ainsi que de ses changements anatomiques. Les diverses stratégies d'adaptation visent à gérer le traitement d'un individu en identifiant et en quantifiant les variations propres au patient au cours de sa série de traitement et en utilisant ces informations pour optimiser le processus de planification et de délivrance du traitement. Toutes ces stratégies reposent sur l'utilisation d'une forme ou d'une autre d'imagerie embarquée, nous permettant d'obtenir des images planaires et/ou volumétriques du patient au moment même du traitement. C'est le développement récent de diverses technologies d'imagerie embarquée qui a rendu possible l'émergence de la thérapie adaptative.

Dans sa forme la plus simple, la thérapie adaptative se réduit à la radiothérapie guidée par l'image (IGRT : *image guided radiation therapy*) qui consiste au repositionnement quotidien du patient sans modification du plan initial. Des images planaires ou encore des images volumétriques sont comparées à des images de références acquises et/ou produites lors de la planification du traitement. Sur la base de cette comparaison, le patient est déplacé en translation et potentiellement aussi en rotation pour conformer sa position le plus possible à la position de planification.

En thérapie adaptative, on utilise l'information obtenue par l'imagerie embarquée pour modifier la planification initiale. Le processus d'adaptation peut-être relativement simple : modifier les marges de sécurité initiales après quelques observations et créer un second plan de traitement; ou encore très complexe : créer un nouveau plan en temps réel avant chaque fraction.

Un survol des diverses stratégies d'adaptation sera présenté. Les processus techniques impliqués ainsi que les outils technologiques nécessaires seront discutés. L'expérience du CHU de Québec dans le traitement adaptatif au niveau pelvien (traitement de l'adénocarcinome de la prostate et du cancer de la vessie) et au niveau de la sphère ORL sera en outre utilisée pour illustrer le propos.

MPS01 - RADIATION THERAPY

MPS01.1 - Radiobiology Applications for Clinicians - Isoeffective Dose Calculations, Hypofractionation, TCP/NTCP

Author(s): Beatriz Sánchez-Nieto

Instituto De Física, Pontificia Universidad Católica de Chile, Santiago/CHILE

Learning objectives:

To understand the relationship between dose and dose per fraction in the dose response curves of late- and acute- response tissues as well as for tumours.

To learn how to do isoeffective calculations in clinical practice

To learn the basic of commonly used TCP and NTCP biological models and how they can help in clinical decisions

ABSTRACT

Isoeffective dose calculations

It is well known that the biological effect of a given absorbed dose of ionizing radiation depends on how this is distributed over time. Moreover, the steepness of the isoeffective curves obtained for different combinations of total dose and fraction size strongly vary among different tissues [1]. The Linear Quadratic (LQ) model has been extensively used to quantify the relationship between total isoeffective dose and dose per fraction in fractionated radiotherapy [2]. And so, parameters such as BED, EQD2, TE, NTD have been used in order to allow comparisons between different treatment schemes or, for example, to predict the effect on tumours/normal tissues of changes in fractionation. These concepts have regained interest in the last years with the new radiotherapy techniques which allow a better sparing of normal tissues and so larger fraction sizes can be explored. From the point of view of isoeffective dose calculations, the current status of modified fractionation schemes (with the respect to the conventional 1.8-2Gy fraction size) will be revised (hypo-, hiper- and acceleration fractionation).

And yet, the problem is more complex. The inhomogeneous dose distributions usually delivered during radiotherapy, imply different fraction sizes for the different sub-volumes and consequently an inhomogeneous biological response throughout the irradiated volume (double-trouble effect) [3]. The above problem can be addressed by using BED distributions or, the more compact, Biologically Effective DVHs (BEDVHs). This approach is compulsory, for example, if external RT and brachytherapy techniques are going to be combined.

TCP/NTCP models

The end points which are truly relevant in radiotherapy are the probabilities of tumour control (TCP) and of toxicity of the normal tissues (NTCP). There are several reasons which justify why TCP and NTCP models are desirable [4]. The Marsden TCP model [3] and the Lyman model [5] will be presented as example of models which, correctly parameterized, reproduce the sigmoid shape of the dose-response curves. Clinical applications of those models will be also presented together with description of some freely available software (BIO-PLAN and BioSuit) [6,7].

References:

[1] Thames H. et al., IJROBP 8(2):219-226, 1982

[2] Fowler J. BJR 83:554-568, 2010

[3] Sánchez-Nieto B. and Nahum, A. IJROBP 44(2):369-380, 1999

[4] The handbook of radiotherapy, Rosenwald et al (eds.), 2007

[5] Lyman JT. Rad. Res 104, 1985

[6] Sánchez-Nieto B. and Nahum, A. Medical Dosimetry 25: 71-76, 2000

[7] Uzan J. and Nahum A. Br J Radiol 85(1017): 1279-1286, 2012

MPS02 - COMPUTERIZED SYSTEMS

MPS02.1 - Radiation Treatment Planning Systems and Dose Computation Algorithms (including Monte Carlo)

Author(s): Antonio Leal Plaza¹, Ana Ureba¹, Elisa Jiménez-Ortega¹, José Antonio Baeza¹, Rita Pereira Barbeiro¹, Sergio García-Gómez², Rafael Linares³, María Perucha³, Juan Carlos Mateos⁴, Santiago Velazquez⁴

¹Fisiología Médica Y Biofísica, University of Seville, Seville/ SPAIN, ²Hospital Univeristario Virgen de la Candelaria, Tenerife/ SPAIN, ³Servicio De Radiofísica, Hospital Infanta Luisa, Seville/ SPAIN, ⁴Servicio De Radiofísica, Hospital Universitario Virgen del Rocío, Seville/SPAIN

Learning objectives:

Discuss about the actual requirements for dose calculation for complex radiotherapy techniques.

Discuss the different dose calculation algorithms and Monte Carlo simulation, and how the latter is implemented in commercial treatment planning systems.

Presenting full Monte Carlo simulation as alternative for treatment planning.

Abstract:

Several studies show that a prescription dose deviation of 5% may compromise tumor response and morbidity. Although the accuracy of dose delivered to the patient depends on multiple factors involved in the radiation therapy process, it is considered that the criterion of acceptability for dose calculation algorithms ranges between 2% and 5% in dose. The dose calculation is performed with different degree of success by means of analytical algorithms such as convolution methods, collapsed cone, pencil-beam with corrections, convolution/superposition or anisotropic analytical algorithm. Apart from the electron beams, the dose distribution with photon beams can be calculated accurately enough in most of cases by means the planning system based on analytical algorithms. Nevertheless, when the radiotherapy techniques use a highly conformed radiation treatment, the media heterogeneities in the path of the photon beam has to be incorporated on the planning algorithm. For the pencil beam model, the necessary heterogeneity corrections are based on dose values calculated in a water equivalent material multiplied by a heterogeneity correction factor generated from an electron density matrix derived from a CT value matrix. It has been probed that the pencil-beam convolution algorithm does not work well in regions of electron disequilibrium, particularly when the field size is small. Other algorithms take into account satisfactorily the 3D scatter such as convolution/superposition, so the drawbacks linked to the heterogeneities in the patient are solved for most cases, although they present limited accuracy under certain circumstances due to several approximations used. Anisotropic analytical algorithm is a pencil-beam convolution/superposition algorithm which uses a multiple-source model to represent the beam and a patient scatter model represented by density scalable poly-energetic kernels. Regardless of the differences that have each other semi-analytical or analytical algorithms, all have in common the fact of having been tested with Monte Carlo (MC) simulations.

The dose calculation with MC is considered the most accurate technique today. MC has been used to validate these algorithms for complex techniques, such as intensity modulated radiotherapy (IMRT) where there is a significant amount of nonstandard conditions and where the beam modifiers play an important role in the characterization of the beams composing the modulated fields. Commercial companies have made efforts in the implementation of MC as alternative to analytical treatment planning systems. They try to maintain the MC advantages about the precision, while reducing

simulation time, but not always is easily to achieve the adequate compromise. For some radiotherapy plans or techniques, the level of approximation of the transport or the low number of sampling may end up making unjustified the implementation of MC.

The most complex techniques are being more and more frequent in the clinical practice. These techniques based on intensity modulation involve an important role of the beam modifiers. The contribution of scattered and transmission radiation from the collimators can represent a fraction of the dose in the organs at risk (OAR). In this scenario, MC could be an excellent tool in order to consider the particle transport and scattering, not only in the patient, but also along the linac head. Full MC (fMC) simulations, in addition to the dose calculation based on the physical heterogeneities in the patient, make possible to consider MLC transmission, scattering and secondary particles contributions in order to take into account the physical characteristics of the beam. Unfortunately, fMC based on an explicit radiation transport can be inefficient due to the time required to get a low statistical uncertainty.

The use of variance reduction techniques and parallel computing could overcome the problem of time consuming, whether it is performed also together with the implementation of algorithms along the optimization process which are especially appropriate to the characteristics of the MC simulation. The necessary number of histories to reach a precise dose distribution is related to the total number of voxels (dose points) defined in the CT patient and to the total number of incident beams (beamlets). A reduction of the number of beamlets and/or voxels will mean simplify the initial problem and will make possible to decrease the overall treatment planning time.

The approach of Direct Aperture Optimization (DAO) has been applied to both IMRT as well as VMAT with the main purpose of incorporating MLC properties directly into the optimization process. The reduction of involved geometries seems to be a convenient approach for the explicit transport by means of the MC simulation of the linac head.

On the other hand, it is also possible to reduce the size of the initial optimization problem by reducing the set of dose points. Usually, all the voxels composing the structures of interest are considered, since all of them are included when dose-volume constraints are implemented in the inverse planning optimization process. A selection could be done randomly or considering only those voxels directly involved in the complexity of the relative dose distribution, for example, the voxels in the intersection of PTV and a specific OAR. Linear functions and piecewise linear convex objectives and constraints can be solved with linear programming (LP). Optimization model can be written under LP formulation, in which each voxel can be identified in the objective function. If this voxel reduction is combined with few apertures the number of equations involved in a LP formulation can significantly reduce the computation time inherent to fMC in the optimization process. Furthermore, this formulation could make possible to take advantage of considering the problem at the voxel scale, what could be especially suitable for a dose painting approach to be applied according to functional and molecular information assessed by combined PET/CT imaging. It seems appropriate to make matching the more accurate dose calculation with the challenge of heterogeneous dose, as proposed with the application of dose painting, for both modalities by contour or by number.

MPS03 - RADIATION THERAPY

MPS03.1 - Protontherapy

Author(s): Alejandro Mazal¹, Farid Goudjil¹, Remi Dendale²

¹Physique Médicale, Institut Curie, Paris/France, ²Radiation Oncology, Institut Curie, Paris/France

Protontherapy is one of the most promising conformal approaches for radiation therapy and the number of operational facilities is increasing all over the world (around 40 centers en operation and more than 40 en preparation).

The rational of its use is based on physical properties of accelerated protons in media, in particular the dose deposition by ionization in depth with the shape of a peak (the Bragg peak). Adding different energies (energy modulation) produces a spread out Bragg peak (SOBP) to cover a target volume in depth with a homogeneous dose, but this also increases the entrance dose.

The main advantages of a proton beam compared to photons are the distal fall off and the lack of exit dose (reducing the integral dose to the patient), a homogeneous dose to the target, an homogeneous dose at the entrance path and a small penumbra at the entrance. There are some limits such as the skin dose, the uncertainty in the range, the large penumbra in depth (related to multiple scattering) and the neutron dose (related to nuclear interactions).

A clear evolution is seen in the technology, mainly in the accelerators (cyclotrons, synchrocyclotrons, synchrotrons, planes linacs and new approaches) as well as in gantries to propose compact and cheaper solutions, including single room approaches (as with electrons-photons). Ancillary tools include specific solutions in treatment planning software, patient positioners, dosimetry and range verifier devices. The present tendency is to use pencil beam scanning to treat with intensity modulated proton beams, in combination with conventional methods of image guided radiation therapy, management of organ movements and adaptive therapy.

Clinical protocols include well accepted but rather rare locations (uveal melanoma, base of skull chordomas and chondrosarcomas, pediatrics, radiosurgery for intracranial targets) and more common clinical sites including lung, breast and prostate, with a tendency to include all targets treated in radiation therapy with photons. There are also comparative studies with the use of heavier ions (e.g. Carbonne), which add radiobiological advantages to their physical specifications.

Research and development in the field include physical and engineering aspects (detectors, micro-beams, delivery systems, models and optimizations, robotics for positioning,...), radiation biology (equivalent doses, effects of dose rate, LET, neutrons, radiosensitizers...), and clinical research (combined treatments, hypofractionation, ...). The main limit to spread protontherapy today is the investment cost.

At the end of the CE program, attendees will be able to:

- 1- Describe the main physical interactions and dosimetric characteristics of clinical proton beams and define the existing technology and its evolution.
- 2- Understand the rational for existing and upcoming clinical protocols
- 3- Have a scope of the research and development programs in the field.

MPS03.2 - Nanoparticles and Radiotherapy**Author(s):** Yolanda Prezado

Imagerie Et Modelisation Pour La Neurobiologie Et La Cancerologie, CNRS, Orsay/France

Learning objectives of the lecture:

1. To provide an introduction to nanoparticles as radiosensitizers and its theoretical basis
2. To give an overview on the existent multi-disciplinary research on nanoparticles in radiotherapy
3. To understand the prospects for future studies and innovations and the potential for applications of nanoparticles in radiation therapy

Radiotherapy is one of the most important methods for cancer treatment. The major limitation to be able to deposit a tumoricidal dose is the deleterious side effects in the surrounding normal tissues. Therefore, the study of radiosensitizers has emerged as a persistent hotspot in radiation oncology as a means to enhance the biological effect of the deposited dose. Nanoparticles, especially noble metal nanoparticles (NPs), may be useful in enhancing the efficacy of radiotherapy because of their unique physical and chemical properties [1]. To date, several different NPs have been successfully applied as potential tumor-selective radiosensitizers in vitro and in vivo studies. Among them, the pioneer work of Hainfeld et al. [2] reached a factor 4 increase in one-year survival rate of mammary tumor-bearing mice injected with 1.9 nm gold nanoparticles prior to irradiation.

Understanding of the underlying nanoparticle-radiation interactions still demands further research, since there is a disconnect between the theoretically predicted increases in cell killing and experimentally observed results. Although Monte Carlo simulations of high-Z nanoparticles have demonstrated significant local dose enhancement in low energy photons of ^{192}Ir brachytherapy sources and also X-rays in kilovoltage range [3], some biological studies found comparable sensitization effects at kilovoltage and megavoltage X-ray energies [4]. Therefore, it was suggested that physical dose enhancement based on increased X-ray absorption could not be the main mechanism of sensitization.

In this lecture, an overview the existent, multi-discipline research on nanoparticles in radiotherapy, will be presented. The principles behind NP radiosensitization will be discussed. Special emphasis will be put to physics studies assessing the dose-enhancement effects and their limits. Relevant results of related in vitro and in vivo experiments will be reviewed. An outline of new combined strategies like theragnostics, that takes advantage of the ability of a nanoplat-form to ferry cargo- both therapeutic and imaging agents will be sketched. Other approaches like the use of magnetic NPs for hyperthermia plus RT or luminescent NPs for RT followed by photodynamic therapy will be briefly described. A reflection on the prospects for future studies and innovations and the potential for applications of nanoparticles in radiation therapy will conclude the lecture.

References

- [1] J. Conde et al. *J Drug Deliv* 2012 (2012) 751075.
- [2] J.F. Hainfeld et al. *Phys Med Biol* 49 (2004) N309-15.
- [3] S.X. Zhan et al. *Biomed Microdevices* 11 (2009) 925-93.
- [4] S. Jain et al. *Int J Radiat Oncol Biol Phys* 79 (2011) 531-9.

MPS04 - IMAGING**MPS04.1 - CT Basics****Author(s):** Caridad Borrás

School Of Medicine And Health Sciences, George Washington University, Washington/DC/UNITED STATES OF AMERICA

Learning objectives

Understand the processes involved in CT image formation

Become familiar with the definition and typical values of the parameters in CT image acquisition protocols

Learn the basics about CT image quality assessment and patient dosimetry

Abstract

The course will start describing the general principles of x-ray image formation. A historical review of early (1972) images of the EMI Mark I scanner will be presented. The processes involved in CT image formation, image acquisition (scanning), image reconstruction and display, will be explained. The characteristics of the x-ray generator and the x-ray tube, including common x-ray spectra used, and typical values of tube potential (kV) will be displayed. The CT number definition and the Hounsfield Scale of CT numbers will be presented. The different motions of the x-ray tube around the patient and the various components of the CT system: gantry, x-ray tube, patient table and detector array will be described. The historical evolution of the various generations of CT scanners with different types of detector arrays and their physical characteristics, including flat panel detectors, will be reviewed. Various detector configurations in multiple-row detector CT will be shown. The differences between sequential (axial) and helical scanning will be discussed. The concept of cone beam CT will be introduced. The process of image reconstruction using filtered back projection and iterative reconstruction algorithms, the number of views required to form an image, the role of antiscatter grids, the use of shaping (bow) filters and the need for x-ray tube z-axis oversampling in helical scanning will be examined. Common terms used in CT, such as pixel, voxel, matrix size, ray, view, reconstruction slice thickness, x-ray beam collimation, pitch, acquisition field of view and detector settings will be defined. The final CT imaging process which will be covered is the conversion of the digital data into a visible image represented by different shades of gray or brightness levels that can be displayed on a video monitor and controlled selecting the CT level, CT window width and display field of view (zoom). The images can then be recorded, stored and transmitted to a PACS system, as needed. CT image quality will be expressed by assessing the presence of artifacts and measuring spatial and contrast resolutions. The effect of kernels used to soften or sharpening an image will be illustrated. The impact on image quality of various acquisition, processing and displaying factors, collectively referred as CT protocols, can be assessed subjectively by discriminating geometric patterns embedded in phantoms, such as contrast-detail structures or bar line-pairs, or objectively, by measuring noise power spectra and modulation transfer functions. Although a full presentation on patient dosimetry is outside the remit of this lecture, basic CT dosimetry terms will be outlined: computed tomography dose index (CTDI), multiple scan average dose, volumetric computed dose index (CTDI_{vol}), dose length product, size specific dose estimate, and CT organ doses. Dose reduction techniques such as tube current modulation will be mentioned. The lecture will finish with a statement on health risk-benefits in CT scanning.

MPS05 - COMPUTERIZED SYSTEMS

MPS05.1 - Managing Respiratory Motion, Including 4D and Gating Techniques; QC

Author(s):

El manejo del movimiento respiratorio es de gran importancia en localizaciones de tórax y abdomen, siendo especialmente relevante en los tratamientos de SBRT de pulmón e hígado.

Existen diferentes sistemas para poder realizar estos tratamientos, desde los sistemas de compresión diafragmática con indicadores analógicos o digitales de la presión realizada al paciente, hasta los sistemas de respiración libre empleando marcadores fiduciales internos.

La adquisición de imágenes mediante TC se obtiene mediante respiración libre con métodos de Slow CT scan, Breath-hold CT o bien TC 4D. Estos últimos tienen dos métodos de adquisición de imágenes: sistemas prospectivos o sistemas retrospectivos.

Los métodos de irradiación pueden variar desde los que permiten realizar respiración libre y controlar el movimiento del tumor con CBCT 4D hasta los sistemas que emplean gating para realizar los tratamientos. Entre estos podemos diferenciar entre los que el paciente controla la respiración con un espirómetro y permiten la irradiación solamente en la fase de expiración y los que emplean sistemas de infrarrojos externos y marcadores internos. Estos sistemas disponen como método de IGRT radiografías estereoscópicas y se relaciona cada par de imágenes con una fase del ciclo respiratorio, de tal manera que se determina el movimiento del marcador (relacionado con el tumor, al estar en las proximidades de este) seleccionándose la fase del ciclo respiratorio donde el paciente se va a irradiar.

Los controles interfacción e intrafacción, es necesario en este tipo de tratamiento, es recomendable los CBCT de kilovoltaje para pulmón e hígado siendo aconsejable disponer de CBCT 4D. Los sistemas de radiografías estereoscópicas son favorables en SBRT siempre que se empleen marcadores internos, estos pueden ser bolas de oro o bien hilos de oro, [] ya que pueden permitir: correcciones en 6D, control intrafacción y una mayor rapidez en la adquisición de imágenes comparado con el CBCT.

Los sistemas de QC son imprescindibles en este tipo de técnicas, siendo muy variados en función del equipamiento empleado. Entre los procedimientos más relevantes podemos encontrar los siguientes: -expiración vs inspiración + expiración, localización del isocentro en un volumen blanco móvil, -correcta localización del isocentro independientemente de la fase del ciclo respiratorio elegida para tratamiento, -medida de dosis absorbida en irradiaciones con control respiratorio, medida de distribución de dosis absorbida en irradiaciones con control respiratorio.

1) Conocer los beneficios que aporta el control respiratorio en los tratamientos de radioterapia especialmente en los de SBRT. Entre ellos podríamos destacar la reducción de los márgenes entre GTV y PTV que trae como consecuencia la disminución de los tejidos sanos irradiados. También la necesidad de realizar el Tc de simulación con un control del ciclo respiratorio.

2) La exactitud con que deben ser administrados los tratamientos de SBRT mediante la IGRT y el control de la irradiación durante la irradiación. Para ello se deberán conocer los diferentes sistemas de irradiación: respiración libre, compresión diagramática, ABC y gating

3) Realizar el control de calidad del equipamiento empleado en el control respiratorio. Para ello se verán los diferentes sistemas para cada método de control respiratorio.

ENGLISH

Respiratory motion management has shown its importance at chest and abdomen radiotherapy treatments, being particularly relevant for lung and liver stereotactic body radiotherapy (SBRT) treatments. Several systems are available to consider respiratory motion, such as systems involving abdominal compression with analogic or digital pressure indicators or free breathing gating systems using internal fiducial markers.

Image acquisition with computed tomography (CT) can be performed through several solutions: slow scanning, breath-hold or prospective and retrospective 4D CT.

Irradiation techniques include free breathing and tumor motion control with 4D CBCT and gated treatments. Among them, it can be found techniques where patient controls breathing with a spirometer and irradiation is only allowed at exhalation phase. Or systems based on infrared external markers and internal fiducial markers. These systems use stereoscopic X-Ray as imaging system and each pair of images is related to a phase of the respiratory cycle, in such a way that the fiducial marker motion is defined (which is linked to the tumor, since it is located nearby) and therefore allowing the selection of the phase of the respiratory cycle for the irradiation.

Interfraction and intrafraction control is necessary. Kilovoltage (kV) cone-beam CT (CBCT) is highly recommended for lung and liver treatments and 4D CBCT would be an advantage. Stereoscopic X-ray imaging systems are also valid for SBRT if internal fiducial markers are used, such as gold seeds or cylinders, as they enable 6D corrections, intra-fraction control and a faster image acquisition compared to the CBCT system.

Quality assurance is extremely important at these techniques. Quality tests vary depending of the equipment. Among the most relevant we could highlight: exhalation vs exhalation + inhalation, isocenter localization at a moving target volume, correct isocenter localization, independent of the phase of the respiratory cycle chose for treatment, absorbed dose and dose distribution measurements when irradiation with breathing control.

Goals:

1 - Benefits of the respiratory control in radiotherapy treatments, mainly in SBRT. Among others, margin reduction between GTV and PTV with the consequence of a decrease in normal tissue irradiation. Also the need of a respiratory control during the simulation CT.

2 - SBRT treatments accuracy by means of IGRT and respiratory control. For that purpose all systems in respiratory control will be reviewed: Free breathing, Gating, ABC and diaphragmatic compression.

3 - Respiratory control equipment and Quality Assurance. Review of the different systems in respiratory control.

MPS05.2 - Computerized Systems Basics: Servers, Data Standards (DICOM, HL7), Virtual Machines, Portable Devices

Author(s): Armando Alaminos-Bouza

Development, Mevis Informática Medica - BRAZIL, São Paulo/BRAZIL

In the realm of medicine, Radiotherapy was a pioneer specialty in the use of computer technology, in particular for therapy planning. The first International Conference on the Use of Computers in Radiation Therapy (ICCR) took place in 1966 (Cambridge, UK). Since 1966, seventeen editions of ICCR took place, and the next, in London 2016, will celebrate the 50th anniversary of ICCR.

Today, several radiotherapy modalities are as entangled on computer infrastructure as with radiation treatment machines. This presentation will focus on a subset of the computerized framework on which modern radiotherapy depends, including hardware and software elements. Major breakthroughs in the computer industry with influence in radiotherapy will be mentioned, such as massive parallelization and portability. Two standards for handling, storing and transmitting digital medical information will be introduced: DICOM and HL7.

Learning objectives:

- 1 – Know the purpose and main modalities of the DICOM standard, in particular those supporting Radiotherapy workflow.
- 2 – Define the scope and purpose of HL7.
- 3 – Explain the role of informatics support infrastructure, such as servers, workstations, portable devices, networks, virtual machines, etc., in the context of the radiotherapy department.

MPS06 - COMPUTERIZED SYSTEMS

MPS06.1 - Optimization: IMRT and VMAT

Author(s): Antonio Leal Plaza¹, Rita Pereira Barbeiro¹, Ana Ureba¹, José Antonio Baeza¹, Elisa Jiménez-Ortega¹, Sergio García-Gómez², María Perucha³, Rafael Linares³, Juan Carlos Mateos⁴, Santiago Velazquez⁴

¹Fisiología Médica Y Biofísica, University of Seville, Seville/ SPAIN, ²Hospital Univeristario Virgen de la Candelaria, Tenerife/ SPAIN, ³Servicio De Radiofísica, Hospital Infanta Luisa, Seville/ SPAIN, ⁴Servicio De Radiofísica, Hospital Universitario Virgen del Rocío, Seville/SPAIN

Learning objectives:

Discuss the usual procedures for planning of treatments based on the intensity modulation radiotherapy treatments.

Estimate the different sources of uncertainty associated with IMRT and VMAT techniques.

Evaluate MC simulation as alternative for planning with the higher accurate as possible under an efficient way.

Abstract:

Recent technical developments and the ongoing pursuit to achieve an optimal dose distribution have led to the routinely use of modern techniques in the treatment of cancers, including intensity-modulated radiotherapy (IMRT). More recently, the interest in arc-based IMRT techniques (IMAT) is growing, in an attempt to overcome some of the limitations associated with conventional IMRT, such as increased treatment times and considerable rise in number of monitor units (MUs) delivered. These techniques involve delivering dose by means of a sequence of continuously evolving apertures with associated intensities as the gantry moves around the patient in one or more arcs. Additionally to the dynamic multileaf collimator (MLC) movement, the dose rate and gantry rotation speed may vary simultaneously during irradiation for volumetric modulated arc therapy (VMAT), as opposed to the original IMAT definition. VMAT has the theoretical potential to offer similar dose distributions in shorter treatment times compared with conventional static field IMRT, and is currently commercially available as either RapidArc™ (Varian Medical Systems, Palo Alto, CA) or VMAT™ (Elekta AB, Stockholm, Sweden).

It could be argued that the high complexity of VMAT presents a revolutionary treatment delivery, generating two different sources of uncertainty:

The classical issue linked to the dose calculation accuracy performed by commercial software. This is a dual problem concerning both, patient heterogeneities consideration and the beam modifiers contribution to the final dose.

The potential differences between the planned and delivered treatment, due to the discrete calculation of a continuous technique.

On the theoretical definition of VMAT presented by Otto, Monte Carlo was already proposed as an effective and necessary tool. Analytical algorithms cannot take into account the dose with the same accuracy as it is done with Monte Carlo. Moreover, the analytical algorithms are based on previous experimental measurements performed in different dosimetric conditions to those present in VMAT treatment. Consequently, MC has been used to validate these algorithms for techniques such as IMRT, where there is a significant amount of non-standard conditions and the beam modifiers play an important role in the characterization of the beams composing the modulated fields. The scenario for VMAT is similar to IMRT, and even more complex, due to the increment of parameters for the op-

timization process involved. The fundamental challenge of applying MC to solve these techniques is to enable the explicit consideration of all geometries implicated and perform the dose calculation in operating times for clinical practice. To this end, approaches based on parallel computing solutions are implemented in addition to the application of variance reduction techniques, allowing the use of Monte Carlo simulation in reasonable times. Apart from these points, radiotherapy techniques with many incidence beams, such as VMAT and dynamic IMRT approaches based on sliding windows, do not necessarily require a time longer for MC simulation than the time spent for simple treatments with fewer beams, while analytical algorithms take a longer time when increasing number of incidence beams. In these cases, a limited number of histories are required for each individual beam contribution, as it is the final dose due to the sum of all beams that should provide enough statistics. Nevertheless, MC never will be efficient enough, if we face the optimization problem in the same way as traditionally it has been done with the analytic algorithms.

In general, a reduction of the number of beamlets and/or voxels simplifies the initial problem and makes it possible to decrease the overall treatment planning time. Specific combination of mathematical algorithms along the optimization process will be discussed in order to establish the more appropriate set to the characteristics of the MC simulation. Actually, some of these approaches could be exported to the systems based on analytic dose calculation engines.

On the other hand, the accuracy assurance of the predicted dose distribution could be compromised by the possible differences between the discrete apertures proposed by the TPS and the finally delivered by the linac. If there are dramatic changes in the aperture shapes from one control point to the next, the linac can execute a different configuration to the parameters combination that was planned by the TPS. The mechanical limitations related to the relative speed between leaves and gantry and also the required changes in the dose-rate can generate these discrepancies. Therefore, the estimation of the patient dose based on information from the treatment delivery log files (e.g. MLC DynaLog files in Varian RapidArc), in which the MLC leaf and jaws positions, fractional MUs, and gantry angle are recorded, is essential for VMAT QA. In fact, it is necessary to know what is actually being performed by the linac during the VMAT treatment delivery.

Definitively, MC provides an adequate tool for the verification of the dose distribution within the patient geometry, allowing the verification of the dose calculated from the complex MLC apertures commonly used in the delivery of VMAT treatments. Furthermore, MC simulation of log files, recorded during treatment delivery, should be considered for a general VMAT QA able to cover both type of uncertainties commented above.

We will try to expose the essential characteristics that we believe the optimization algorithm has to fulfill to achieve a treatment planning system based on explicit MC simulation that could be used efficiently in the clinical routine.

We will also present an alternative VMAT QA system, based on an automated MC simulation of the explicit transport through the linac head and patient heterogeneities and experimental measurements with Gafchromic EBT3 film within a cylindrical phantom specifically developed to host the films rolled at different depth, available for a 3D and continuous dosimetric verification.

MPS06.2 - Automated Contouring

Author(s): Armando Alaminos-Bouza

Development, Mevis Informática Medica - BRAZIL, São Paulo/BRAZIL

Contour delineation remains one of the most time consuming process in Radiotherapy planning. Contouring depends on a computer vision technique called "image segmentation" that has continuously evolved since 1965. Image segmentation is commonly used to locate objects and boundaries. Automated methods for segmentation and contouring have the potential for significant time-saving in the planning process, being estimated in a range from 23 to 41 percent of the whole treatment planning. Several algorithms have been implemented for radiotherapy contouring including: gradient based, threshold based, atlas based, semi-automated (with human interaction), etc. There is no closed-form solution for the segmentation problem in general, so human expert inspection and correction is paramount. Today, automated contouring is an active field of research in Radiotherapy and major improvements are expected for the near future.

Learning objectives:

Identify the most common methods of automated contouring used in radiotherapy planning systems.

Indicate the accuracy and reliability of each method.

Propose methods for interactive contour correction.

MPS07 - RADIATION THERAPY**MPS07.1 - Image-Guided Radiotherapy, Including QC and Imaging Dose; Adaptative Radiotherapy****Author(s):** [Daniel Venencia](#)

Fisica Medica, Instituto de Radioterapia - Fundacion Marie Curie, Cordoba/ARGENTINA

Learning objectives

1. Understand the principles and challenges for image guidance radiation therapy (IGRT)
2. Understand issue related to IGRT commissioning, implementation in the routine clinical practice as well as quality assurance
3. Understand existing IGRT systems, specially room mounted kV x-ray systems

Delivery of conformal radiation dose to the target volume with conformal avoidance of critical structures requires a precise knowledge of the relationship between the patient's anatomy and treatment isocenter. Precise Radiotherapy allows us to reduce complications and improve the quality and likelihood of successful treatment. Uncertainties in Radiotherapy are associated with patient setup variation, internal organ movement and anatomical deformation. Image Guidance Radiotherapy (IGRT) gives us the possibility to reduce radiotherapy uncertainties improving the ability to setup patients on a daily basis and gives tools to detect anatomical changes which could require re-planning, Adaptive Radiation Therapy (ART). IGRT has become today, routine part of the modern Radiotherapy.

IGRT systems currently available allow us to get projection or volumetric imaging. Projection imaging used setup based on surrogates and includes conventional port films (films or CR), MV electronic portal imaging device (EPID), room mounted kV x-ray (ExacTrac, Cyberknife), ultrasound (BAT, Clarity) and active fiducial with GPS (Calypso). Volumetric imaging used setup based on GTV and includes CT/MRI on rail in the treatment room, MV spiral CT (Tomotherapy), kV CBCT (Elekta, Varian, BrainLAB) or MV CBCT (Siemens). IGRT systems use direct alignment (visualization of the target volume) or indirect alignment (bone and fiducial active or passive structures). The alignment method can be manual, automatic or point matching. IGRT strategies may involve an adjustment of the treatment parameters at the time of treatment (On-line) or the correction based on the accumulation of information (Off-line). Depending on the characteristics of IGRT system, its use would involve not deliver an additional dose to the patient, a low dose (< 1mSv) or medium (> 2mSv).

The use of IGRT requires a specific knowledge of the system and specific training for therapists, dosimetrists, radiation oncologists and medical physicists. IGRT systems require strict QC process. Problems associated with the system can lead to a global generation of systematic errors in the positioning. The coincidence between the treatment isocenter and reconstructed image isocenter is one of the most critical points. The image quality is related to clinical intervention.

This presentation will give an overview through all existing IGRT systems emphasizing on kV projection systems with radio opaque implanted fiducials. ART concept will be analyzed showing practical examples of application in head and neck IMRT.

MPS08 - MEDICAL PHYSICS EDUCATION AND PROFESSIONAL ISSUES**MPS08.1 - Curriculum Design: How to Train the Next Generation of Physicists?****Author(s):** [Maria-Ester Brandan](#)

Instituto De Fisica, Universidad Nacional Autónoma de México, Mexico City/MEXICO

Learning objectives:

1. Understand current recommendations for education + training of medical physicists.
2. Learn the situation of education + training of medical physicists in Latin America.
3. Be informed about the main difficulties faced by program organizers in Latin America to comply with recommendations, and strategies to cope with them.

Abstract:

Current recommendations for the formation of medical physicists describe the process as a "3-act" play. The first act is university education at the undergraduate level, in physics, engineering or another career with a strong content of physics. The second act is graduate-level education, typically a master degree in medical physics, aimed at teaching basic principles behind the main applications of physics in medicine. The last act is a formal clinical training. After these 3 steps, the interested individual has received the education and acquired the skills that make him/her a medical physicist qualified to work independently in the clinic.

This play is not easy to stage. In the last 15 years, Latin America has witnessed the creation of a relatively large number of university master programs --with different degrees of success-- and the number of graduated medical physicists increases steadily. However, clinical residencies are still missing in most of our countries.

The talk will present statistical information about programs and residencies, description of the academic curricula, identification of the problems faced to run programs and residencies, and general strategies devised to cope with local limitations and lack of resources.

MPS09 - RADIATION THERAPY

MPS09.1 - Peripheral Neutron and Photon Doses

Author(s): Francisco Sanchez-Doblado¹, José A. Terrón¹, Leticia Irazola¹, Beatriz Sánchez-Nieto²

¹Servicio De Radiofísica, Hospital Universitario Virgen Macarena, SEVILLA/SPAIN, ²Instituto De Física, Pontificia Universidad Católica de Chile, Santiago/CHILE

Learning objectives:

- Importance of peripheral dose in radiotherapy patients
- Dosimetrical problems for neutron and dose estimation
- Necessity of the introduction of a new parameter SCP (Second Cancer Probability), in addition to the TCP and NTCP, for a better clinical decision of the best treatment planning

Abstract

The comprehensive study in radiotherapy, of the dose estimation outside the target, is usually restricted to closely surrounding volumes. The dose affecting the rest of the body, currently known as peripheral dose, has rarely been considered in the clinical routine. This approach is mainly based on the argument of the risk-benefit ratio, applied to a patient with a “fatal” disease, such as cancer. However, in the last years, there has been a fast-growing concern about this unnecessary radiation dose. There are three main reasons that make this situation clear: a) the large size of the affected population; b) the great success rate, which guarantees a high life expectancy, allowing the appearance of long term side effects, including second cancer; and finally c) the new radiotherapy techniques, which increase the long time survival, but at the cost of larger volumes irradiated to low dose [1-2].



Figure 1. Experimental setup for patient organ neutron dose estimation in the treatment room. Detector location is marked in red.

Peripheral dose in conventional radiotherapy has two main components: leakage and scattered photons and neutron contamination. Photon dosimetry is well established whereas the neutron contribution to the peripheral dose is complex to determine. Our group has developed [3-8] photon and neutron peripheral dose models which are being implemented on a TPS. The equivalent dose to peripheral organs should be taken into consideration during planning selection and/or optimization.



Figure 2. Anthropomorphic phantom used to generate the equivalent neutron and photon dose estimation models.

The classical consideration of tumor control and normal tissue complication probabilities functions (TCP and NTCP) should be extended, as an extra complication term, which considers the secondary cancer probability (SCP) [9].

Therefore, an efficient use of MU is mandatory throughout the balance of potential long term benefits and side effects (organ toxicity and second cancer), together with the clinical judgment on illness prognosis and, consequently, life expectancy [10-12].

References

1. Phys Med Biol (2008)53:R193-R241
2. Lancet Oncol (2011)12:353-60
3. Phys Med Biol (2012)57:6167-6191
4. Radiother and Oncol (2013)107:234-241
5. Med Phys (2015)42:276-281
6. Med Phys (2014)41:231
7. Phys Medica (2014)30:e33.
8. Irazola *et al.*, “Peripheral neutron...” in this issue, WC2015
9. Radiother Oncol (2012)103:S576-S577
10. Radiother Oncol (2012)103:S576
11. IFMBE Proceedings 39, WC 2012:1735-1737
12. Med Phys (2012)39(6):3812

MPS10 - RADIATION THERAPY

MPS10.1 - The Modern Physicist Tool Box: How to Choose Between Current Dosimeters

Author(s): Faustino Gómez¹, Luis G. Brualla², Diego Miguel Gonzalez-Castaño¹

¹Riaidt, Radiation Physics Laboratory, Santiago de Compostela/SPAIN, ²Medical Physics, ERESA, Valencia/SPAIN

Current radiotherapy dosimetry toolbox for the medical physicist involves different technological embodiments of radiation detectors. This toolbox comprises old and new instruments such as:

1. Passive systems: film, alanine, TLD and gel dosimetry
2. Active systems:
 - 2.1. Point detectors: air filled ionization chambers, diode, diamond, scintillator detectors
 - 2.2. Multidetector systems: air and liquid filled ionization and silicon diode arrays
 - 2.3. Electronic portal imaging devices (EPID)

On the other hand, the development of radiotherapy modalities is growing steadily including nowadays those as IMRT, VMAT, FFF linacs, Radiosurgery, Gating, etc. The medical physicist is confronted with an increasing space and time modulation of the radiation fluence and high dose gradients to deal with the clinical goal of a better conformation of the dose distribution to the target volume.

Thus, the medical physicist must decide what dosimeters to use in the different phases of the clinical dosimetry process: modeling, commissioning, verification and quality assurance. It is very important in each situation to be conscious about the idoneity and limitations of the different dosimeters available: tissue equivalence, energy and dose rate dependence, detector size and volume averaging effect, sampling rate, repeatability, etc.

Some of the passive dosimetry tools, like radiochromic film exhibit excellent tissue equivalence and high resolution, although the dose uncertainty can be significant in some cases depending on the methodology and instrumentation employed.

In the case of point detectors for absolute and relative dosimetry, the family of air ionization chambers and silicon diodes has been enlarged recently with the new CVD diamond and organic scintillating detectors that provide tissue-equivalent composition and geometries adequate for small field and high dose-gradient dosimetry.

On the other hand the use of two dimensional dose distribution measuring arrays has become very common, because they offer a higher verification efficiency, since they can be used for a large number of immediate dose measurements in a single irradiation procedure. Current state-of-the-art detectors are also including 2D and 3D array measuring systems or assemblies of 2D systems that provide a 3D verification methodology. The dose fidelity of these detectors will be analyzed in terms of their response function and repeatability characteristics.

The use of point detectors require the choice of the adequate chamber geometry, materials and size. Their position in the radiation field has to be studied in order to provide a sufficiently homogeneous dose distribution to ensure measurement accuracy. Phantom selection in terms of geometry and materials is also a key factor for the adequate dosimetric verification. Eventually the use of EPID for dosimetry verification and treatment quality assurance is an complementary tool for the medical physicist.

This course is oriented to the description of the physical properties and main characteristics of current dosimeters to provide the necessary insight for their application. The talk will focus in the following

learning objectives:

- i) Radiation transport: physical constraints on dosimetry.
- ii) Characterization of the different technologies of active and passive dosimetry systems.
- iii) Implications of the use of array systems. Advantages and drawbacks.
- iv) Application of the dosimeter choice to the different dose verification situations.

All this concepts will be explained in a typical medical physics environment showing how to travel from theory to practice.

MPS11 - RADIATION THERAPY

MPS11.1 - Dosimetry Under Non-Reference Conditions

Author(s): Faustino Gómez¹, Araceli A. Gago², Juan Pardo Montero³
¹Física De Partículas, Facultad de Física, Universidad de Santiago, Santiago de Compostela/SPAIN, ²Instituto De Física, Pontificia Universidad Católica de Chile, Santiago de Chile/CHILE, ³Grupo De Imaxe Molecular, Instituto de Investigación Sanitaria (IDIS), Santiago de Compostela/SPAIN

Dosimetry under non-reference conditions

This course is oriented to the description of the problems arising from the use of small and composite fields in the clinical treatments and the need of reliable standard dosimetry procedures for their verification. The main learning objectives of the course are:

Explanation of the physical problems on small static field and composite dosimetry: energy response of the detector, beam hardening, charged particle equilibrium, field size definition and beam quality description.

New code of practice for standard non-reference conditions. Introduction and explanation of the new formalism: machine specific reference field (MSRF), plan class specific reference field (PSRF) and clinical fields.

The new CoP applied to the small static field dosimetry: factors to be considered and their determination and use.

The development of the standards of absorbed dose to water has led to Codes of Practice for dosimetry in reference conditions such as IAEA TRS398 or AAPM TG-51. The use of reference conditions was intended for the calibration of a broad beam in a close to charged particle equilibrium situation for conventional radiotherapy or clinical reference dosimetry. The development of new radiotherapy techniques has led to more frequent use of small and composite fields, such as those involved in Stereotactic Radiotherapy (SRT), Stereotactic Radiosurgery (SRS) or Intensity Modulated Radiation Therapy (IMRT). The proliferation of these narrow and composite fields has been boosted through the use of different multi-leaf collimator systems and new treatment delivery techniques. These developments have increased the complexity of clinical dosimetry and compromised the traceability to reference dosimetry based on conventional reference dosimetry protocols. There are two main reasons that affect the accuracy of dosimetric measurement in several of the new radiotherapy modalities:

CoP reference conditions can not be achieved in some of the new treatment machines.

In general terms, procedures for absorbed dose to water measurement in small and composite fields are not standardized.

Related to the first limitation in the realization of reference conditions, the new CoP approach is the definition of a reference field for each specific machine as close as possible to the standard conventional reference conditions. The correction factors for each chamber and specific reference field are tabulated in order to provide a standard dosimetric procedure. On the other hand, the determination of the beam quality has to be modified according to the achievable measurement conditions. The use of flattening filter free linacs imply the need of an extra correction factor to account for the difference in the beam quality correction respect to linacs that use a flattening filter. Additionally the ionization chamber volume-averaging effect may be taken into account with a proper convolution methodology. On the other hand, the new approach on composite field dosimetry imply the definition of PSRF (Planclass Specific Reference Field) with the purpose of reproducing the delivery features similar to those of clinical treatments. In this case a geometrically simple volume will

receive a homogeneous dose distribution. Different realizations of these PSRF have been already proposed in the literature for various treatment modalities. Substantial progress has been achieved in the last years, although this topic is still an important evolving subject for the international medical physics community.

MPS12 - IMAGING**MPS12.1 - PET State-of-the Art and Current Research Topics (Including CT-PET and CT-MRI)****Author(s):** Josep M. Martí-Climent

Radiofísica Y Protección Radiológica, Clínica Universidad de Navarra, Pamplona/SPAIN

Learning objectives:

- To understand the factors affecting the image quality and quantitation in PET
- To gain knowledge about the impact of the new PET developments in the quality of image.
- To understand the changes introduced in the PET detector technology due to the development of PET/MRI scanners.

Abstract:

Inorganic scintillator crystals are the detectors used with photomultiplier tubes (PMT) in positron emission tomography (PET). Bismuth germanate (BGO) has been widely used as scintillator. With the introduction of lutetium-orthosilicate (LSO) as scintillator, time-of-flight (TOF) information (allowing for the positron annihilation point to be localized accurately) has been incorporated to improve the image reconstruction. The development of the digital silicon photomultipliers (SiPMs), connecting each scintillator crystal to a single detector pixel, has improved the PET scanner performance.

Scanners without septa have allowed the use of a 3D acquisition, gaining sensitivity. The introduction of the iterative reconstruction methods, incorporating corrections such as scatter and attenuation in the modelling, instead of a direct correction of the projections or sinograms, have improved the image quality. Finally, with the point spread function (PSF) reconstruction algorithm, near-uniform spatial resolution can be achieved throughout the field of view.

PET image quality and quantitation are dependent of the reconstruction algorithms, including parameters used, and the corrections applied.

The disposition of a computer tomography (CT) scanner in tandem or in line with a PET scanner has led to the PET/CT scanner, providing accurately aligned of anatomical and functional images. CT images are used for attenuation correction of the PET data, eliminating the need of rotating radioactive ^{68}Ge sources around the patient and detection of the attenuated transmission signals. Conventional bed motion is stop and go, with overlapping bed positions due to the decrease in the axial sensitivity at the end of the field of view. The development of the continuous bed motion has improved protocols from bed planning protocols to organ specific examination protocols.

The combination of a magnetic resonance imaging (MRI) scanner with a PET scanner into a PET/MRI device has involved major modifications, especially in the PET detector technology. Different approaches have been proposed for the scanner configuration, including the two scanners mounted back-to-back to each other, similar to a PET/CT, a PET system within the MRI, and the two scanners mounted apart in the same or in a different room. Since the use of PMT in the magnetic field is excluded, scintillator detectors are coupled to position-sensitive avalanche photodiodes (APD) based detectors. In a PET/MRI scanner, tissue attenuation correction necessary for PET image reconstruction needs to be based on MR images. With that aim, different methods for attenuation correction have been developed.

MPS12.2 - 4D Imaging**Author(s):** Manuel Llorente Manso

Medical Physics, Centro Oncológico MD Anderson España, Madrid/SPAIN

Learning objectives:

- Present image modalities with 4D techniques.
- Explain different methods of acquisition and basic applications.
- Discuss artifacts affecting 4D images and ways to improve them.

Abstract:

Several medical image modalities are capable of producing three dimensional reconstructions. In the study of moving organs, such as heart and lung, 4D image modalities, that is, incorporating time as fourth dimension, have been developed in the recent years.

One example of the use of 4D medical images are the cardiac ultrasound (US) studies. Last generation US devices can create 3D images with a rate of 25 Hz, allowing a real time 4D vision, having a great impact on cardiac and hemodynamic studies.

Also 4D magnetic resonance imaging (MRI) has application on cardiac studies. MR can create planar images with a good spatial resolution in a very short time, that is, less than a heart beat. Several heart beats should be necessary to generate 3D reconstructions. Planes should be acquired in the same cardiac phase. Acquisition can be synchronized with ECG prospective or retrospectively. In the first case, point R in the ECG works as a trigger for image acquisition and resulting images correspond to the same point in the cardiac cycle. In the latter, images are acquired continuously along with the ECG curve and sorted afterwards. Result is a series of 3D images covering all the cycle.

Respiratory motion artifacts can be reduced by synchronizing acquisition with breathing cycle also. A respiration curve can be obtained using abdominal movement as a surrogate. Images are to be acquired only during a certain part of the respiratory cycle. Breathing phase can also be estimated using a navigator sequence: a fast sagittal sequence where diaphragm is easily found. System detects automatically diaphragm position and uses it as a trigger.

In 4D-CT cardiac studies, ECG is used as an external signal both in prospective and retrospective modes. In this kind of studies, acquisition time is short enough to be performed in one single breath hold, so breathing synchronization is not necessary.

4D-CT synchronized with breathing are of interest in Radiotherapy in the treatment of thoracic and abdominal tumors. In general, respiration curve is obtained from the abdomen movement and depending on the manufacturer images are acquired in prospective (ciné) or retrospective (helical) mode.

Cone beam CT images (CBCT) correlated with respiration are also of interest in Radiotherapy. Those images, taken on the treatment couch, help estimating tumor motion and position.

Also PET-CT images can be correlated with respiratory cycle, reducing motion artifacts. Such corrections can have an impact on patient diagnosis.

SPECIAL SESSIONS

SS06 - IOMP AWARDEES PRESENTATIONS

SS06.1 – IOMP Marie Sklodowska-Curie Award: A Brief History of X-Ray Therapy: Evolution, Convolution, and Revolution

Author(s): Colin G. Orton,
Ph.D., Professor Emeritus, Wayne State University, Detroit MI, USA

Evolution

X-ray therapy for the treatment of cancer evolved immediately after Roentgen's discovery of X rays in November, 1895: just two months later, Emil Grubbé treated a woman with breast cancer. It was not long after this, in 1899, that Stenbeck, in Sweden, delivered the 1st documented curative cancer treatment (basal cell carcinoma), using a grand total of 99 fractions! Why so many fractions? It was not because, as we learned much later, that treatments had to be fractionated in order to cure a cancer without exceeding normal tissue tolerance, but because outputs were so low and unpredictable. It was not until 1914, with the advent of the Coolidge hot-cathode X-ray tube, that high dose rates and controllable exposures became possible, and this sparked a debate on the need for fractionation, which was not resolved until 1932 when Coutard published his excellent results using fractionated radiotherapy. The Coolidge tube also sparked the evolution of X-ray machines of ever increasing energy in order to be able to treat deeper lesions, with energies rising to 1 MV by 1933. In the quest for even higher energies, new technologies were developed such as the Van de Graaff accelerator in 1937, the betatron in 1940, and the linear accelerator in 1953. The linear accelerator became the workhorse of radiotherapy by the end of the 1970s.

Convolution

Modern radiotherapy was sparked by three applications of computer technology in the 1980s and '90s: 3-D treatment planning, the use of computerized tomography in planning, and the advent of computer controlled linacs and multileaf collimators. Highly conformal radiotherapy became possible and this ultimately led to the development of IMRT, the CyberKnife, and Tomotherapy. At the same time, accurate targeting of treatments was evolving with real-time electronic portal, CT, PET and MRI imaging. The convolution of computerized delivery and sophisticated imaging is about to revolutionize radiotherapy.

Revolution

With the advent of flattening filter free linacs and the concomitant very high dose rates, combined with highly conformal treatments with tight margins and subsequent normal tissue sparing, the delivery of higher doses/fraction without excessive risk of complications is now possible. Such hypofractionation has been shown to be at least as effective as conventional fractionation for the treatment of several common cancers and, because it is so much more cost effective, it is likely to revolutionize radiotherapy within the next few years.

SS06.2 - IOMP Harold Johns Medal: The Importance of Teachers

Author(s): [William Hendee](#)

Distinguished Professor Emeritus of Radiology, Radiation Oncology, Biophysics, Community and Public Health, Medical College of Wisconsin, Milwaukee, WI USA

Receiving the Harold Johns medal from the International Organization of Medical Physics is a great honor that offers an opportunity to reflect on the importance of teachers in our professional and personal lives. We are all the product of dedicated teachers who provided guidance in the molding of our professional careers and personal characters. Were it not for these teachers, we would not be the physicists or persons that we are, and our lives would be decidedly different, as would the contributions we make to our profession and our families.

We can all think of individuals who have been instrumental in molding our personal and professional lives, many of whom were unaware they were doing so. In the same manner, each of us is a teacher of others, especially young medical physicists and biomedical engineers entering the discipline. We teach not only by what we say in the classroom, but also how we interact in the clinic, at meetings and in personal encounters both inside and outside the hospital. Teaching is more than what we say, although what we say is important. It is also how we conduct ourselves as professionals and as persons, and how we project ourselves as role models to those younger than ourselves.

Health care is experiencing momentous change around the world, especially in developed societies impacted by technologies, information systems and services that drive healthcare costs to unprecedented costs. Medical physicists work at the "sharp end" where these technologies, information systems and services impact directly on patients. In this position, physicists can influence how these developments are used in an effective and cost-efficient manner. But to fulfill this responsibility, younger physicists need senior leaders to serve as exemplars. Never in the history of medical physics has the need for devoted teachers been greater.

SS07.2 – IUPESM AWARDEES PRESENTATIONS

SS07.2.01 - IUPESM Award of Merit (Medical Physics): Cost-Effective Provision of Medical Physics and Medical Engineering Services in Healthcare

Author(s): Peter H S Smith
Aberdeen, UK

All healthcare services, in both developed and developing countries, are under increasing pressure. Growing use of technology is one of the factors involved and medical physics and engineering services are one just more cost pressure and therefore it is essential that these services are provided in the most cost-effective way.

A number of factors will be examined including organizational aspects, staffing and research and development. The author's experience of providing integrated engineering and physics services on a regional basis will be used to illustrate some of the issues, including the advantages and disadvantages of horizontally organized and integrated medical physics and engineering service.

The correct provision and deployment of professional, technical, administrative and other staff is essential and can raise difficulties: cultural, perceived job roles, professional barriers, supply and training. Should clinical engineers and physicists be involved in research? If so, who funds and what links to academic institutions are essential?

Manufactures of medical devices are a major influence on the deployment and maintenance of technology in healthcare and medical physicists and engineers can help ensure that appropriate technology is procured in accordance with defined needs and maintained in a cost-effective manner.

The contribution that can be provided by national, regional and international professional, governmental and UN organisations, to finding solutions to these issues will also be considered.

SS07.2.02 - IUPESM Award of Merit (Biomedical Engineering): Improvement of Health Care Quality by Medical and Biological Engineering (MBE) with the collaboration of Academia, Industry, the Government and the People

Author(s): Fumihiko Kajiya, M.D., Ph.D
Special Appointed Professor, Kawasaki College of Allied Health Professions

The American Institute for Medical and Biological Engineering (AIMBE) has highlighted nearly 30 medical technologies since the Hall of Fame began in 2005. In subsequent years new technologies were added as the key innovations of the 20th century until now. For example, artificial kidneys, X-ray, ECG, pacemakers, cardiopulmonary bypass, antibiotic production technology and defibrillators up to the 1960's, and since the 1990's genomic sequencing and micro-arrays, PET, image-guided surgery and optical coherence tomography (see AIMBE home page). Virtually, every person has benefitted from these key technical innovations in receiving better health care. For instance, more than 2 million people have hemodialysis treatment in the world (3 hundred thousand in Japan). However, the development of each technology doesn't progress in a straightforward way. As for artificial kidneys, it is well known that many crucial technological developments, such as dialysis-circuits, pumps, vascular access, anticoagulant measures and high performance membranes have been achieved. These are a result of fusion technology from many disciplines. Personally, I have been engaged as a co-chair (2004-13) in the Medical Engineering Technology and Industrial Technology (METIS) in Japan, i.e., Cooperative organization of academia, industry and government. The scope of METIS includes not only medical

devices but also science and engineering in health care. From my small experiences, I would like to emphasize the possible improvement of health care quality by future contributions of MBE in the interdisciplinary fusion with the collaboration of academia, industry, the government and the people.

To promote President Obama's Precision Medicine Initiative, cohort study of genome together with MBE, IT and other fields with the participation of the majority of people is very important. For MBE to walk along with society worldwide will be effective route to our goal.

SS08 - THE FUTURE OF CLINICAL ENGINEERING EDUCATION

SS08.1 - Clinical Education at University of Connecticut

Author(s): Frank R. Painter

Biomedical Engineering, University of Connecticut, Trumbull/UNITED STATES OF AMERICA

The clinical engineering graduate educational program at the University of Connecticut is in its 41st year. Dr. Joseph Bronzino started the program in 1973 at Trinity College and the Hartford Graduate Center in Connecticut, USA. In 1995 the program moved to the University of Connecticut. Dr. Bronzino retired in 2000 and Frank Painter assumed responsibility for the program under the guidance of Dr. John Enderle.

The program provides students with a two year clinical engineering internship experience as well as seven academic courses which focus on various aspects of clinical engineering. A successful student will graduate from UCONN with an MS BME degree.

There are 20-24 students in the program in most years. Each year 30-50 students apply for the CE internship program. Normally there are ten to twelve openings each year in the 17 participating internship locations. A few more students are selected to interview than the number of openings available. These candidates are then invited to come to the Southern New England area and in a four day period, as a group, they interview at all hospitals who have internship openings. In the interview the hospital's CE director and several of their staff, including the current interns, interview each candidate. During the end of the interviews the CE directors are asked to select their five preferred candidates and the candidates their five preferred hospital locations. A meeting of the directors is then held to match the choices and the candidates are informed of the outcome.

Starting in late August, the interns spend two full academic years in the program. They are required to work in the hospital 20 hours per week and spend an additional 10-15 hours per week in the hospital working on their class projects, homework, clinical observations, research, reading and studying. Additionally the students take the following clinical engineering focused course work over the four semester program. *Clinical Engineering Fundamentals* focuses on how a CE department is managed, *Engineering Problems in The Hospital* focuses on utility systems in the hospital which support medical equipment, *Human Error and Medical Device Accidents* focuses on managing the risks of healthcare technology, *Medical Instrumentation in the Hospital* focuses on high end medical systems, including imaging and therapy, *Clinical Systems Engineering* focuses on medical device integration and interoperability and *Clinical Rotations* focuses on observing clinician-technology-patient interface in the clinical environment.

The program is the result of a partnership between the hospitals and the University. The clinical engineering directors greatly contribute to the program a success. Each hospital signs a contract with the university and pays a yearly fee to finance the graduate student stipend and program administrative fees. Every hospital in the program has hired a program graduate and many have hired several.

The majority of the second year students receive multiple clinical engineering job offers before graduation. Most of the program graduates end up in a career working directly for hospitals. All of the remaining students work for companies either providing services or products to the healthcare technology community.

SS08.2 - The Future of Clinical Engineering Education in the Western Hemisphere: USA and Peru

Author(s): Thomas M. Judd¹, Luis Vilcahuaman², Rossana Rivas³, Herbert F. Voigt⁴

¹Clinical Technology, Kaiser Permanente, Marietta/UNITED STATES OF AMERICA, ²Health Technopole CENGETS PUCP, Pontifical Catholic University of Peru, Lima/PERU, ³School Of Public Health, Universidad Peruana Cayetano Heredia, Lima/PERU, ⁴Biomedical Engineering, Boston University, Boston/MA/UNITED STATES OF AMERICA

It is undeniable that engineers have played an important role in the delivery of modern health care. The boots on the clinical floors have been filled with BMETs, clinical engineers (CEs) and biomedical engineers (BMEs), the mix of which has been uniquely formulated in thousands of clinical environments globally. It is interesting that although educational opportunities to train BMETs are common, training of CEs at the undergraduate and graduate level is virtually non-existent in the Western Hemisphere.

In fact, there are only a few CE MS programs (some with no internship opportunities) and no CE Ph.D. programs in the western hemisphere. There is an urgent need to provide highly qualified, certified CEs at all levels, BMET, BS, MS and Ph.D. level. Many Universities that provide biomedical engineering undergraduate education do not offer clinical engineering internships, local or international, that are so important for training CEs. In addition, the clinical environments in developed countries offer very different challenges than those in developing countries. For certification purposes, this is likely to result in different weighting of the factors important in the various environments. This session will address the need for new clinical engineering programs at various educational levels to serve the current and future health system needs.

The CE profession is changing in ways that significantly impacts US and global healthcare. In addition to the historic CE medical device lifecycle management function (called health technology management or HTM), there is (1) the emerging integration of medical devices into electronic health records (also called Health IT or CE-IT), and (2) other key topics in which CEs help drive changes in clinical workflows at health organizations: planning, policies, acquisition, management, strategies, investments, risk, design of clinical environments and others. This is accomplished through the interoperability of devices and EHRs so that care everywhere (inpatient, clinic-based and mobile health) profoundly allows redesign of care delivery.

The profession needs practitioners with new skillsets - both for emerging graduates and people at all stages of their careers. These requirements are outlined in a White Paper by Sloane, Welsh, and Judd: *New Opportunities for BME/CE Health IT Education*, May 2014, (http://ceitcollaboration.org/docs/NewOpportunitiesBME_CE_Health_IT_Education.pdf). This session will address the pertinence and impacts of exploring more opportunities to grow Clinical Engineering Education in the U.S.A. and promote this specialty in developing countries and globally moving forward.

The Future of Clinical Engineering in the Western Hemisphere, which is a model for CE globally, will be addressed in oral presentations, followed by a Panel Discussion.

SS09 - INNOVATIVE BIOMEDICAL ENGINEERING RESEARCH IN ASIA

SS09.1 - Functionalized gold nanoparticles for point-of-care nucleic acid detection

Author(s): Thomas M.H. Lee

Interdisciplinary Division Of Biomedical Engineering, Hong Kong Polytechnic University, Kowloon/HONG KONG

Gold nanoparticles (AuNPs) have been extensively investigated for colorimetric detection of nucleic acid. This is enabled by the unique interparticle distance-dependent optical property of AuNPs. The solution color for monodispersed particles appears red (for widely used 13 nm AuNPs) but turns purple upon aggregation due to a red-shift in the surface plasmon resonance absorption band. Until now, all the reported platforms are not practical for point-of-care testing. To address this, our group developed a new platform by incorporating 11-mercaptopundecanoic acid-modified AuNPs (MUA-AuNPs) into loop-mediated isothermal amplification (LAMP). When added into the LAMP reaction mixture, MUA-AuNPs aggregated as a result of ion-templated chelation between the carboxyl groups and magnesium ion (Mg^{2+} , which plays an indispensable role in LAMP reaction as an enzyme cofactor). The solution color changed from red to purple. In the presence of a specific target DNA sequence, the LAMP reaction occurred and pyrophosphate ion ($P_2O_7^{4-}$) was generated as a reaction by-product. The chelated Mg^{2+} was then extracted by $P_2O_7^{4-}$, leading to the deaggregation/redispersion of the MUA-AuNPs and the solution color turned red. This new platform possesses all the ideal features for point-of-care testing, including simple preparation and operation, low cost, high sensitivity, and worry-free carryover contamination control.

SS09.2 - Hemodynamic function of Fontan circulation mechanical assistance in Fontan circulation animal experimental model

Author(s): Akihiro Yamada¹, Yasuyuki Shiraishi¹, Hidekazu Miura¹, Yusuke Tsuboko², Yasunori Taira², Masaaki Yamagishi³, Dai Homma⁴, Tomoyuki Yambe¹

¹Institute Of Development, Aging And Cancer, Tohoku University, Sendai/JAPAN, ²Graduate School Of Biomedical Engineering, Tohoku University, Sendai/JAPAN, ³Department Of Pediatric Cardiovascular Surgery, Kyoto Prefectural University of Medicine, Kyoto/JAPAN, ⁴Toki Corporation, Tokyo/JAPAN

Fontan procedure is selected the final palliative surgical operation in pediatric patients with serious congenital heart diseases. After Fontan procedure, there is non-pulsatile flow in the pulmonary circulation called Fontan circulation. We focused on the additional pulsatility in the Fontan circulation for the pulmonary flow assistance for congenital heart failure patients. In order to promote the pulsatility in the flow that infuses the lungs, we implemented an original mechanical contractile device which promotes flow pulsatility. Then we have been developing a circulatory support device with the function of peristaltic contraction for the promotion of an efficient assistance for Fontan circulation using shape memory alloy fibers. The structure of the device was a mechanically contraction from the outside of the extracardiac conduit. The device consisted the 16 units of the shape memory alloy actuators in parallel arrangement. In this study, we developed the animal experimental model for in vivo examination of the Fontan circulation assist device for the pre-clinical research. And also, we examined the hemodynamics function in the device driving by the animal experimental model. The animal experimental model was constructed in four adult goats (45.8±15.6 kg). The right heart bypass of inferior vena cava (IVC) to pulmonary artery (PA) was constructed by using extracardiac conduit (Dacron, D = 18mm, Boston Scientific Corporation, USA). The vascular tape was indwelling in IVC and right atrium (RA) anastomosis for clamping. And the left ventricular assist device (LVAD, Gyro Pump C1E3, Kyocera

Medical Corporation, Japan) was connected to the apex to reduce the left ventricular load. Rotational speed of the LVAD was set to 1400rpm. The right heart bypass circulation could be created by the IVC-RA clamping. IVC and PA pressure rose to 15mmHg during clamping. The device could be mounted easily to the conduit in the thoracic cavity. The pulsatile flow could be generated in the pulmonary circulation by the device contraction. In the faster peristaltic contractile speed, the device could be generated larger pulsatile flow waveform. The animal experimental model could be constructed to reproduce the hemodynamic of Fontan circulation by using LVAD. In our model, it was represented to steady flow in the bypass circulation. In the pulmonary circulation of the experimental model, the flow fluctuation was included by heart beat and respiratory variation. For the further investigation to more effective assistance, it is considered to require the control method including synchronization with the heart beat or respiration. We examined the function of the device in the animal experimental model. And it was indicated that the pulsatility by the device could be generated pulsatile flow in device implantation.

SS09.3 - Biomedical Engineering at the Nanoscale: the Inspiration We can Draw from Endogenous Systems Interactions to Design the Nano-Bio Interface

Author(s): James C.Y. Kah

Department Of Biomedical Engineering, National University of Singapore, singapore/SINGAPORE

Nanomedicine can be described as biomedical engineering on the nanoscale where we seek to apply intelligent design to tackle health challenges. The last decade has seen tremendous growth in this field as studies on the various applications of nanotechnology in medicine and biotechnology form a sizeable aspect of modern day research. Biomedical applications of these nanoparticles have been reported in four major areas, namely, drug delivery, disease diagnostics, imaging and therapeutic applications as an outcome of man's ingenious design on the nanoscale. Nature's intelligent design has also created a range of endogenous biomolecules that exist in the same size regime as nanoparticles. In biology, however, there are numerous examples of biomolecular systems that far surpass any man-made machine in terms of efficiency, precision, and complexity. Natural endogenous biomolecules such as DNA and proteins often self-assemble, or interact with other biomolecules in order to perform their naturally intended function. Most often, these interactions between biomolecules are useful, if not critical, to the survival of the organism. In a similar manner, nanoparticles also demonstrate a high propensity to interact with other biomolecules to form the nano-bio interface. Intelligent design of this nano-bio interface is therefore crucial to the functionality of nanoscale systems in biology. In this talk, I will show how we can draw inspiration from nature and design appropriate nano-bio interface formed from DNA, proteins and peptides to probe and control biology in at least four ways: (1) to enhance efficiency of protein translation *in vitro*; (2) tune cellular response; (3) to enable loading and trigger release of drugs; and (4) to develop a cost-effective and instantaneous biomolecular assay. I will also be sharing some of our current research that involves understanding and engineering the nano-bio interface in molecular and cell biology.

SS09.4 - High Frequency Ultrasound Elastography and its Biomedical Applications

Author(s): Chih-Chung Huang

Department Of Biomedical Engineering, National Cheng Kung University, Tainan/TAIWAN

It is well known that the mechanical properties of soft tissues, such as elasticity, viscosity, and mechanical impedance, change depending on the conditions of tissues, for instance disease and age, hence

the mechanical properties may give useful information in medical diagnosis. Several ultrasound elastographs have been proposed to measure the mechanical properties of tissue quantitatively, such as sonoelastographic image, shear wave image, and acoustic radiation force impulse image. However, the image resolutions of above elastographs are insufficient due to their operational ultrasound frequency. It remains difficult to estimate the mechanical properties of smaller organs and tissues using current elastographs. Therefore, the high frequency ultrasound elastographs based on acoustic radiation force impulse imaging and shear wave imaging were proposed in our Lab to assess the mechanical properties of some micro-structure tissues, such as cornea, plaque, and vessel wall. In cornea study, a 50 MHz high frequency acoustic radiation force impulse (ARFI) imaging system were built for mapping the hardness of cornea. A dual frequency ultrasonic transducer was designed for this objective. The outer 10 MHz element was used to push the fibers in cornea and the inner 50 MHz element was used to detect the displacement of cornea. The experiments were carried out using artificial porcine cornea and a new algorithm for high frequency ARFI imaging was established. In plaque study, a 40 MHz shear wave imaging system was built for measuring the elastic properties of blood clots. Furthermore, we applied our high frequency ARFI imaging and shear wave systems into intravascular ultrasound (IVUS). A concept of combining the high frequency ARFI and shear wave technology on IVUS for assessing the mechanical properties of thrombus and vessel was proposed in present study.

SS10 - IFMBE AWARDEES PRESENTATIONS

SS10.1 - IFMBE Otto Schmidt Award: Neuro-engineering for navigation, intervention and implementation in neurosurgery

Author(s): Karin Wårdell

Department of Biomedical Engineering, Linköping University, Sweden

Neurosurgery and neuro-intensive care are clinical areas in which highly specialized interventional, navigational and monitoring techniques are imperative for patient care and improved health in the society. The overall aim of our research is to develop and evaluate new methods and techniques for radical improvement of navigation, intervention and monitoring in neurosurgery. Topics of special interest are deep brain stimulation (DBS), optical techniques for intraoperative neuronavigation, brain microcirculation as well as the integration and translation of the new tools and methods for clinical use. In the DBS research we have developed a patient-specific modelling and simulation concept for investigation of the electric field around active DBS-contacts. This allows for visualization of the relative electric field changes in relation to the patient's anatomy by using MRI together with superimposed atlas structures. The simulation method has proven useful for clinical evaluations of movement and speech in Parkinson's disease and is now also introduced for new DBS-indications and brain targets. During the talk examples of both optical application in neurosurgery as well as projects related to DBS will be presented.

SS10.2 - IFMBE Vladimir Zworykin Award: Microfluidic Technologies for Disease Diagnosis, Therapeutics and Personalized Medicine

Author(s): Chwee Teck Lim

Provost's Chair Professor, Dept of Biomedical Engineering & Mechanobiology Institute, National University of Singapore

Our blood comprises ~5 billion cells in one cubic milliliter with red blood cells (RBCs) accounting for >99% of all cellular components suspended in protein-rich plasma. Besides blood constituents, pathogenic microorganisms or diseased cells can also be present in blood for certain diseases, which can present possible routes for disease detection, diagnosis and therapy. However, the presence of the large number of RBCs complicates removal of pathogens in blood as well as makes disease diagnosis such as detection of rare circulating tumour cells (CTCs) in blood of cancer patients extremely challenging. Here, we address these issues and demonstrate that physical biomarkers such as the unique size and deformability of diseased cells can be effectively used for their detection and separation from blood by using microfluidics. We do this by leveraging on the many inherent advantages of microfluidics such as high sensitivity and spatial resolution, short processing time and low device cost. We developed a suite of microfluidic biochips that exploit the principles of cell size/deformability based separation as well as inertial focusing to perform high throughput continuous detection and separation of diseased cells. These simple, efficient and cost-effective microfluidic platforms will be imperative in realizing point-of-care (POC) diagnostics and invaluable for many downstream clinical and biological applications as well as personalized treatment.

SS10.3 - IFMBE John A. Hopps Distinguished Service Award: Medical and Biological Engineering: Celebrating the Past, Envisioning the Future.

Author(s): Robert M. Nerem

Georgia Institute of Technology

Over the past half century engineers have made enormous contributions to both an increased understanding of biology and biological mechanisms and to improvements in clinical treatments. For these many contributions by engineers and physical scientists, there is much to celebrate. From the study of blood flow, to the role of hemodynamics in atherosclerosis and the role of the vascular endothelium, to the development of new medical devices, to regenerative medicine and stem cell technology, the contributions of the medical and biological engineering community have had a major impact. This includes everything from advances in pacemakers to continuing efforts to understand “the rules of life” that determine cell function. As one further envisions the future, although the application of engineering to the medical area will continue to be important, such new areas as energy, the environment, and food will be an expanded part of medical and biological engineering. Already we are seeing an industrialization of biology with the biomanufacturing of chemicals today becoming a significant element of the economy of the U.S. and there are efforts focused on creating biological machines, ones that might not even exist in nature. Over the past half century the International Federation of Medical and Biological Engineering (IFMBE) has had a major leadership role, and in the world of the future, IFMBE will have to evolve its role in order to provide the leadership necessary for the global community.

SS10.4 - IFMBE Laura M.C. Bassi Award: Machine learning in ultrasound imaging

Author(s): Professor Alison Noble OBE FREng,

Technikos Professor of Biomedical Engineering, Oxford University Department of Engineering Science, Director, Institute for Biomedical Engineering (IBME), President of the MICCAI Society

Machine learning approaches to biomedical image analysis are gaining popularity encouraged by successes in the sister field of computer vision and increasing availability of large clinical and biological image databases.

This talk will describe how we are applying machine learning in ultrasound image analysis, an area where quantification by traditional image analysis methods is very hard due to the wide range of data qualities met in real world applications.

A major application area of interest is “womb-to-cot” imaging – imaging in pregnancy and early life. I will describe progress towards developing machine learning based solutions for ultrasound-based biomarker estimation and quantification. These solutions are designed to be “accessible” – or easy to use – by a clinical end-user, and hence suitable for application in community care and to support healthcare delivery in the developing world.

SS11 - ICSU BIO-UNIONS CLUSTER SESSION

SS11.1 - The Role of IUPESM in the ICSU Bio-Unions Cluster

Author(s): Herbert F. Voigt

Biomedical Engineering, Boston University, Boston/UNITED STATES OF AMERICA

The Bio-Unions Cluster of the International Council for Science (ICSU) consists of 11 of the 32 International Scientific Unions that are Union-members of ICSU, of which the IUPESM (the International Union for Physical and Engineering Sciences in Medicine) www.iupesm.org/ is one. “The principal objective of IUPESM is to contribute to the advancement of physical and engineering sciences in medicine for the benefit and well-being of humanity.”

ICSU’s website states, “The International Council for Science (ICSU) is a non-governmental organisation with a global membership of national scientific bodies (121 Members, representing 141 countries) and International Scientific Unions (32 Members). ICSU’s mission is to strengthen international science for the benefit of society. To do this, ICSU mobilizes the knowledge and resources of the international science community to:

Identify and address major issues of importance to science and society.

Facilitate interaction amongst scientists across all disciplines and from all countries.

Promote the participation of all scientists—regardless of race, citizenship, language, political stance, or gender—in the international scientific endeavour.

Provide independent, authoritative advice to stimulate constructive dialogue between the scientific community and governments, civil society, and the private sector.”

The ICSU member unions fall into four clusters, one of which is the Bio-Unions Cluster. Since 2010, the Bio-Unions Cluster has been meeting among themselves to plan interdisciplinary activities, including:

a presence at each other’s congresses,

the joint sponsorship of meetings, and

joint sponsorship of teaching activities.

In 2013, the Bio-Unions Cluster met in Paris a day before the ICSU Unions meeting. At that meeting additional decisions were made. They decided:

- 1) To meet at least once a year.
- 2) To create a school that meets in conference facilities on a Greek island.
- 3) To consider supporting satellite conferences in conjunction with a World Congress of one of the ICSU members.
- 4) To organize a session(s) at one of the Bio-Union Cluster’s World Congress
- 5) To build into the Unions’ budget money to support the Bio-Union Cluster’s activities. (\$5,000 - \$10,000/year)

Our activities here today at IUPESM’s WC 2015 demonstrate a continuing commitment made by the Unions in the Bio-Unions Cluster to uphold these activities. But there are additional opportunities related to long-term programs that involve ICSU.

Two of ICSU's relatively new, long-term programs are: 1) Health and Wellbeing in the Urban Environment and 2) Future Earth (Global sustainability). IUPESM has resources and capacity to be helpful in both of these programs. For example, Future Earth, is a 10-year international research initiative "sponsored by the Science and Technology Alliance for Global Sustainability comprising the International Council for Science (ICSU), the International Social Science Council (ISSC), the Belmont Forum of funding agencies, the United Nations Educational, Scientific, and Cultural Organization (UNESCO), the United Nations Environment Programme (UNEP), the United Nations University (UNU), and the World Meteorological Organization" (Future Earth Website). Biology is essential to Future Earth and therefore the Bio-Unions Cluster must establish a role for itself in this complex activity.

SS11.2 - The International Council for Science (ICSU) Bio-Unions Cluster

Author(s): Nils Chr. Stenseth¹, Herbert F. Voigt²

¹Université Paris Sud Xi, IUBS, Orsay/France, ²Health Technopole CENGETS PUCP, Pontifical Catholic University of Peru, Lima/PERU

The Bio-Unions Cluster of the International Council for Science (ICSU) consists of 11 of the 32 International Scientific Unions that are Union members of ICSU. This session will be an introduction to some of the ICSU Unions making up the Bio-Unions Cluster. It will include speakers, primarily Officers, from several of the Unions within the Bio-Unions Cluster, who will address their Unions' Mission and their interactions with ICSU and other Unions within the Bio-Unions Cluster. The Session Chair is Nils Stenseth, Chair of ICSU Bio-Union Cluster and President, International Union of Biological Sciences (IUBS). Other speakers are: K.Y. Cheung, President-Elect, International Union for Physical and Engineering Sciences in Medicine (IUPESM); Elaine Faustman, Secretary General, International Union of Toxicology (IUTOX); Pingfan Rao, Past-President, International Union of Food Science and Technology (IUFoST); Walter Boron, Secretary General, International Union of Physiological Sciences (IUPS) and Herbert Voigt, President, International Union for Physical and Engineering Sciences in Medicine (IUPESM). The session will end with an open discussion regarding the future activities of the ICSU Bio-Unions Cluster.

Bio-Unions Cluster/ICSU

ICSU's website states, "The International Council for Science (ICSU) is a non-governmental organisation with a global membership of national scientific bodies (121 Members, representing 141 countries) and International Scientific Unions (32 Members). ICSU's mission is to strengthen international science for the benefit of society. To do this, ICSU mobilizes the knowledge and resources of the international science community to:

Identify and address major issues of importance to science and society.

Facilitate interaction amongst scientists across all disciplines and from all countries.

Promote the participation of all scientists—regardless of race, citizenship, language, political stance, or gender—in the international scientific endeavour.

Provide independent, authoritative advice to stimulate constructive dialogue between the scientific community and governments, civil society, and the private sector."

The ICSU member unions fall into four clusters, one of which is the Bio-Unions Cluster. Since 2010, the Bio-Unions Cluster has been meeting among themselves to plan interdisciplinary activities, including:

a presence at each other's congresses, the joint sponsorship of meetings, and joint sponsorship of teaching activities.

11 ICSU Unions in the Bio-Unions Cluster:

1. **IBRO (International Brain Research Organization)** www.ibro.info/ Pierre Magistretti, President pierre.magistretti@epfl.ch

2. **IUBS (International Union of Biological Sciences)** www.iubs.org/ Nils Chr. Stenseth, President n.c.stenseth@bio.uio.no

3. **IUFoST (International Union of Food Science and Technology)** www.iufost.org/

Rickey Yada, President lfs.dean@ubc.ca

4. **IUIS (International Union of Immunological Societies)** www.iuisonline.org/

Jorge Kalil, President jkalil@usp.br

5. **IUMS (International Union of Microbiological Societies)** www.iums.org/

Yuan Kun Lee, President micleeyk@nus.edu.sg

6. **IUNS (International Union of Nutritional Sciences)** www.iuns.org/

Anna Lartey, President aalartey@ug.edu.gh

7. **IUPAB (International Union for Pure and Applied Biophysics)** www.iupab.org/

Zi-He Rao, President raozh@xtal.tsinghua.edu.cn

8. **IUPESM (International Union for Physical and Engineering Sciences in Medicine)** www.iupesm.org/

Herbert F. Voigt, President hfv@bu.edu

9. **IUPHAR (International Union of Basic and Clinical Pharmacology)** www.iuphar.org/

S. J. Enna, President IUPHAR@kumc.edu

10. **IUPS (International Union of Physiological Sciences)** www.iups.org/

Denis Noble, President denis.noble@dpag.ox.ac.uk

11. **IUTOX (International Union of Toxicology)** www.iutox.org/

Herman Autrup, President ha@mil.au.dk

SS16 - ADDRESSING GLOBAL CHALLENGES

SS16.1 - Bioengineering in the 21st Century

Author(s): Robert M. Nerem

Mechanical Engineering, Georgia Institute of Technology, Atlanta/
GA/UNITED STATES OF AMERICA

Bioengineering in the 21st Century

Robert M. Nerem

Georgia Institute of Technology

In the last half century the field of bioengineering has evolved from its beginnings with the medical device industry to one that is much broader today and will be even broader as we move further into the 21st century. In this span of more than 50 years, there has been a technological revolution in healthcare and also an educational revolution. In the 1950s as the medical device industry began to develop, engineers at universities in the traditional fields began to apply their expertise to problems in medicine. With the advent of the biological revolution, however, what subsequently emerged is an engineering discipline based on the science of biology, i.e. bioengineering. As this new discipline has evolved, the medical device industry has expanded and continues to be important; however, there are major trends in public health that are influencing and will continue to influence the development of bioengineering. These include a shift from acute to chronic disease, an aging population, the disparities in healthcare, emerging and re-emerging diseases, and the escalation in healthcare costs. In this there will be a transformation of medicine and there will be a need for the development of new innovative technologies. These are technologies that reduce healthcare costs, also ones that allow for imaging at the molecular level, and in addition technologies that will drive science just as science drives technology. There also will continue to be a focus at the cell and molecular level and the application areas of regenerative medicine and stem cell technology. Here engineers can take the lead in developing new, innovative enabling technologies. This includes high-throughput screening techniques, improved culture and differentiation systems, and *in vitro* models engineered to be more physiologic. The last of these include organ-on-a-chip models and engineered *in vitro* tumor models that can lead to a better understanding of cancer. Finally, for cell-based biomanufacturing there is a need for further advances in scaleup, techniques for real-time monitoring, and for process automation. It is clear that the engineering approach with its quantitative, systems-based thinking can contribute much more to advancing medicine than it has to date. Engineering analysis can be used to identify the components of highly complex biological systems and provide an understanding of how these components work together. Furthermore, computational models will be increasingly important in our efforts to achieve a better understanding of complex biological systems. For all of these areas it is the bioengineers that will create the reality of the 21st century age of biotechnology.

SS16.2 - ICT for Prevention of Non-Communicable Diseases

Author(s): Niilo Saranummi

Health, VTT Technical Research Centre of Finland, Tampere/FINLAND

Non-communicable diseases (NCDs) – such as heart disease and stroke, cancer, diabetes, and chronic lung disease kill more people globally than infectious diseases and are responsible for about two-thirds of deaths worldwide. Six out of the seven most important risk factors for premature death (high blood pressure, high cholesterol, high Body Mass Index, inadequate fruit and vegetable intake, physical inactivity, and excessive alcohol consumption, smoking excluded) are related to diet and physical activity.

Our lifestyle choices combined with our social, built, and economic

environments influence the way our genes express in our dynamic phenotype and interactively contribute to health or disease. NCDs can to a large extent be prevented by following current health guidelines on diet, alcohol, physical activity, and smoking. Therefore, NCDs are often called lifestyle diseases.

Current thinking still views much of health promotion and prevention as relying on public health awareness campaigns to increase health literacy, education, feedback and support, as well policy and regulatory activities to decrease unhealthy behavior (e.g., regarding smoking, intoxicants, package labeling, and urban planning). Health statistics, however, show that the prevalence of NCDs is increasing around the world and that these efforts are only modestly effective in preventing disease and reducing the overall disease burden and health expenditure.

We need novel solutions to prevent disease and promote health, as well as to better manage NCDs while they occur. What is needed is an approach that *engages individuals* to manage their everyday health-related behaviors. Empowering people to manage their health and wellness and, if present, chronic diseases requires that two challenges are met.

The first is a disruption in the way health services are delivered and incentivized. The current illness-centered healthcare model needs to be replaced with a proactive health and wellness-centered model where people together with healthcare professionals manage their health and illness.

The second is to engage people to manage their health with innovative services and tools that people want to use and that provide them with the ability to respond wisely in health related situations. The new approach might be achieved with the following steps:

- Harness emerging mobile and ubiquitous digital technologies (sensors, mHealth apps, Internet of things (IoT), etc.) to collect comprehensive datasets on personal behavior in context while maintaining the required level of personal privacy and security;
- Liberate existing data; not just health or illness data but also data that are being already collected for various business purposes, such as loyalty cards in shopping for food and other items, credit cards telling a lot of our behavior, mobile phone use and location data etc.;
- Use data mining and systems modeling to build predictive models of personal behavior;
- Deploy these models combined with knowledge from systems medicine and behavior science to predict and anticipate personal behavior; and
- Provide users with personalized feedback at opportune moments that engages them to manage their health related behaviors.

SS19 - SOCIAL IMPLICATIONS OF TECHNOLOGY WORKSHOP (IN HONOR OF OUR FRIEND & COLLEAGUE; DR LODEWIJK BOS)

SS19.1 - "Realizing and Preserving Privacy and Security for Self in Interoperable Global Healthcare Venues"

Author(s): Robert Mathews

Office Of Scientific Inquiry & Applications, University of Hawai'i, Honolulu & Hilo/HI/UNITED STATES OF AMERICA

Canadians and Americans have both been steadfast advocates for personal privacy since the birth of the two nations on the North-American Continent. However, in the 21st Century, the rate of digital technology proliferation, the widening range of technology adoption, and uses, all without a sufficiently broad and systematic construal, or comprehension, has produced a decay of long evolving frameworks for civil liberties, and the desecrations of more founded personal privileges. Nowhere has this decay been more conspicuously grand more recently than in the area of Healthcare practices within the United States. Will it be possible to arrest this decay? Are the 'loss of privacy' expansions reversible? How can Globally Interoperable Healthcare Services ever be a reality at all, where Patient's personal safety and security cannot be properly assured?

SS19.2 - Social Implications of Technology

Author(s): Luis G. Kun

Private, Consultant, Vienna,/VA/UNITED STATES OF AMERICA

Wireless technologies and remote sensing when combined with social networks and geographical information systems are having a prominent role in the coordination, communication, planning, response and management to some of the most devastating disaster scenarios we have witnessed in the last few decades. On the other hand many issues we routinely experience with respect to solving health care or public health problems, such as medical errors, occur and are perpetuated because of our silos or stovepipes of information. The scientific community recognizes intimately that preparing for the provision of health care, and erecting our public health system of tomorrow, is not just a matter of converging heterogeneous technologies and science but of people and processes as well. As society prepares to shift the current systems into some where wellness and disease prevention will be the focus, society will face some major challenges. Many changes can affect positively medical and cost effective outcomes as well as the reduction and or elimination of medical errors and patient safety for example and yet privacy and security of personal medical information continue to be a major hurdle. Information Technology acting as a catalyst for change when combined with discovery and advances in research and development of new devices, and new drugs offers a multitude of avenues that were hard to imagine just a few decades ago. The convergence of science and technology open some doors of opportunity that may help diminish the polarization among the developed and underdeveloped nations. Society needs a systems approach and having a holistic view of the problem; to be able to see the whole and not just discrete pieces; and help determine, for example unintended consequences which are absent. Integration of multidisciplinary and interdisciplinary orientations and activities when trying to understand the problem and moving toward generating potential solutions are needed; yet present approaches are grossly insufficient in this respect. A new Global Health strategy where the public and private sectors work together will be presented as well as a wide range of opportunities that can start at the cellular, molecular and genetics levels and go as far as population health. A Global Economy that will be pushed to integrate surveillance and epidemiology for better protection against environmental threats and food borne diseases through the use of remote sensing data and a worldwide food enterprise architecture will also be discussed. The access to new

services such as home healthcare delivery and public health safety are generating a "new digital divide" discussion between those that have the means and those that don't. The current Internet Neutrality debate must incorporate these concepts in order to address new social challenges posed by the new technologies.

SS20 - EMBEDDED SENSOR SYSTEMS FOR HEALTH WORKSHOP

SS20.1 - Workshop on "Embedded Sensor systems for Health"

Author(s): Maria Lindén, Magnus Otterskog, Mobyen Uddin Ahmed, Ivan Tomasic, Elaine Åstrand, Arash Ghareh Baghi, Mats Björkman Mälardalen University, Västerås/SWEDEN

Demographic changes, where the expected lifetime of people is increasing and many suffer from not one but several chronic diseases, are challenging our healthcare system. There is a clear need for wearable and distributed health monitoring systems, allowing people to continue their normal activities independent of location; at home, at work or in hospital. Monitoring of changes and trends in health status can facilitate early intervention and prevent severe conditions to develop, and new technology enables simultaneous monitoring of multiple physiological parameters. Hence, this can prevent suffering for patients and also means large savings for society. Moving the point-of-care from hospitals to homes is a trend that will increase in the future. The recent development of embedded sensor systems, the rapid development in wireless technology, and the ability to include intelligence in small, embedded sensor systems are all key enablers to achieve ambient monitoring of health conditions. To successfully address these issues, holistic system approaches are necessary, including not only sensor and hardware expertise, but also software expertise. The current workshop will bring together experts in these areas, and will address the need and potential in using embedded sensor systems for monitoring of health conditions in home environments, including the use of Internet, Wi-Fi, and smart phones. A keypoint addressed will be the starting point from clinical needs, thus the involvement of clinical experts is essential throughout the whole development process. Also the user-friendliness of the systems is essential. If not easy to use, there will be a large resistance against using the systems. Topics to be addressed in the workshop are sensor system applications, signal processing, intelligent decision support, and infrastructure. Further, decision support distributed in the system will be included, together with safe and secure transport and storage of physiological data, to ensure personal integrity of the persons being monitored.

SS22 - IUPESM-HTTG WORKSHOP ON INNOVATIONS IN THE USE OF MOBILE DEVICES IN HEALTHCARE

SS22.1 - IUPESM-HTTG Workshop on "Innovations in the Use of Mobile Devices in Healthcare"

Author(s): Caridad Borrás¹, Kwan Hoong Ng², Yadin B. David³, K Siddique Rabbani⁴, Marlen Perez-Diaz⁵, Tobey Clark⁶, Colin G. Orton⁷

¹Health Technology Task Group, IUPESM, Washington/DC/UNITED STATES OF AMERICA, ²Biomedical Imaging Department, University of Malaya, Kuala Lumpur/MALAYSIA, ³Technology Management, Biomedical Engineering Consultants, LLC, Houston/UNITED STATES OF AMERICA, ⁴Biomedical Physics & Technology, University of Dhaka, Dhaka/BANGLADESH, ⁵Study Center On Electronic And Information Technologies, Universidad Central "Marta Abreu" de las Villas, Santa Clara/CUBA, ⁶Instrumentation & Technical Services, University of Vermont, Burlington/VT/UNITED STATES OF AMERICA, ⁷Radiation Oncology, Wayne State University, Grosse Pointe/MI/UNITED STATES OF AMERICA

Growing populations and shortages of healthcare workers paired with the explosive growth of mobile communications infrastructure over the last decade has sparked growing interest in the provision of health services through mobile and wireless technologies. This Workshop will address the use of mobile systems and devices such as smartphones, tablets, and laptops to address the unmet healthcare needs in rural/urban marginalized areas of the resource-limited regions of the world, where health conditions and vital signs data acquired from geriatric, pediatric and infirm patients have to be communicated in a timely manner to adequately trained and qualified caregivers. The Workshop will bring together experts to assess the clinical needs to be fulfilled, to review some innovative solutions that are ready to be implemented and to identify benefits from implementation of such mobile systems by overcoming barriers and matching patient needs with solutions. These experts will address and demonstrate new devices (hardware and software) that provide improved healthcare at the point-of-care, will review communication aspects and telemedicine (sending data to and from remote experts for consultation, diagnosis and prescription), and will discuss how to assure continuum of care and remote support to improve the utilization and maintenance of existing equipment.

Specific topics to be addressed include: The state of TeleHealth, TeleMedicine, and mHealth; implementation, barriers and policy issues in industrialized and resource-limited regions; telecommunications, interoperability, regulatory and legal issues; telemedicine challenges and opportunities; development of new mobile-centric hardware to detect health conditions; development of healthcare applications using facilities and functions available in modern mobile devices; quality of service assessment; and evaluation of maintenance and sustainability issues. Following the formal presentations, there will be an open discussion between the audience and the Workshop participants, from which final conclusions and recommendations will be drawn.

SS25 - CHALLENGES AND BENEFITS OF CLINICAL ENGINEERING PEER REVIEW

SS25.1 - Challenges and Benefits of Clinical Engineering Peer Review.

Author(s): Jean Ngoie¹, Michael J. Capuano²

¹Biomedical Engineering, Niagara Health System, St. Catharines/CANADA, ²Biomedical Technology, Hamilton Health Sciences, Hamilton/CANADA

Clinical engineering departments in Canada have the opportunity to be reviewed based on the CMBES Clinical Engineering Standards of Practice (CESOP). The process is designed to affirm well established programs, provide recognition of excellence in Clinical Engineering, and to provide programs with a baseline for improvement and knowledge exchange. The CMBES Peer Review Committee coordinates and approves all requests for review and assigns the reviewers (surveyors) to the requesting facility. Peer review requires the clinical engineering program to complete a pre-survey questionnaire and to provide information about the program including policies and procedures, organizational structure, explanation of processes, and demographics. A physical on-site visit is arranged lasting several days depending on the size of the organization and involves an equipment/work audit, interviews with staff and clients including senior management, tours of the facility, and review of department records. A summary report is provided after the review accompanied by a certificate of successful completion. This presentation will cover all of the above mentioned steps as well as past experiences and thoughts. Perspectives from the survey team and the reviewed will be presented including the benefits of Peer Review and the most challenging aspects of the process.

PLENARY SESSIONS

PL01 - WOMEN IN BIOMEDICAL ENGINEERING AND MEDICAL PHYSICS

PL01.1 - Engaging Women and Men for a Better Future Worldwide

Author(s): Monique Frize

Systems And Computer Engineering, Carleton University, Ottawa/ON/CANADA

From the three approaches suggested by Londa Schiebinger to harness the power of gender analysis, this part of the presentation deals with the first two: "Fixing the number of women" and "fixing the institutions". Women and men can generate and participate in activities that lead to an increased participation of women in biomedical engineering and medical physics. Evidence also exists, demonstrating that there are economic benefits and more complete solutions created by gender balanced design teams and an increased number of women in decision-making bodies such as corporate boards, management teams in industry, government, and universities. It is critical to collect sex disaggregated data on undergraduate post-secondary enrolments and graduations in science and engineering, as well as to understand the gender participation in the workplace in these fields. Examining the issues that limit women's participation at all levels is a first step, which can then be followed by the development and implementation of strategies that help eliminate gender bias and provide the necessary support for women to have a successful career in these fields.

PL01.2 - Gendered Innovations in Health & Technology

Author(s): Londa Schiebinger

Stanford University, Stanford/UNITED STATES OF AMERICA

How can we harness the power of gender analysis to discover new things? Schiebinger identified three major approaches to gender in science research, policy, and practice: 1) "Fix the Numbers of Women" focuses on increasing women's participation; 2) "Fix the Institutions" promotes gender equality in careers through structural change in research organizations; and 3) "Fix the Knowledge" or "gendered innovations" stimulates excellence in science and technology by integrating sex and gender analysis into research. This talk focuses on the third approach. Gendered Innovations: 1) develops state-of-the-art methods of sex and gender analysis for scientists and engineers; and 2) provides 24 case studies as concrete illustrations of how sex and gender analysis leads to new ideas and excellence in research. Several case studies will be discussed, including stem cells, assistive technologies for the elderly, and osteoporosis in men. All case studies can be found at: <http://genderinnovations.stanford.edu/>. To match the global reach of science and technology, this project was developed through a collaboration of over sixty experts from across the United States, Europe, and Canada (and has now extended to Asia). Gendered Innovations was funded by the National Science Foundation, the European Commission, and Stanford University.

PL03 - URBAN HEALTH AND FUTURE EARTH / GLOBAL HEALTH CHALLENGES

PL03.1 - The Changing Urban Environment and Health in a Future Earth

Author(s): Gordon Mcbean

Western University, London/ON/CANADA

Around our planet there have been increasing numbers of disasters due to floods, storms, earthquakes and other natural hazards. Although earthquakes are most horrific when they happen, climate-related events cause about three-quarters of all disasters and as the climate warms, these hazards are increasing. There is also the migration to people to major cities, often on coasts of the oceans or major rivers. The result is the intersection of the effects of the major issues of climate change, disaster risk reduction and sustainable development. In all cases we need to look to the future and take actions now to reduce losses in the future.

In 2015, nations will negotiate a revised framework on action on disaster risk reduction, a possible Paris-protocol on climate change and Sustainable Development Goals to be attained by all countries by 2030. The draft list of SDGs includes: end poverty and hunger; attain healthy life for all at all ages; secure water and sanitation; and build inclusive, safe and sustainable cities and human settlements. For the global science community, the challenge is providing the scientific basis for definitions and approaches, including how to achieve these goals and the criteria for measurement of progress.

This presentation will bring together these issues in the context of the new international research programs Future Earth: Research for Global Sustainability; Integrated Research on Disaster Risk; and Health and Wellbeing in the Changing Urban Environment: a Systems Analysis Approach; with a Canadian-funded project, Coastal Cities at Risk: Building Adaptive Capacity for Managing Climate Change in Coastal Megacities. The Future Earth program is adopting an approach to involve the stakeholder community in the research program from the beginning to co-design and co-produce the research based on the logic that this will make the research most directly relevant to societies needs to address these issues. The Coastal Cities research project is integrating across social-natural-economic-engineering and health sciences to develop a systems approach to quantifying urban resilience and then undertake "what if" experiments to identify the most effective approaches to improving resilience and reducing impacts, recognizing the complex interactions across these elements of society.

The International Council for Science is leading the Science and Technology Major Groups to input to these UN processes and will endeavour to bring these scientific principles to the negotiations. Working with UN agencies such as UNESCO, UNU and WMO, and non-governmental partners such as the Inter-Academy Medical Panel, the Council will continue in the coming decades to assert the importance of scientific bases for these international agreements and national actions. We need to have the full support of medical physicists and biomedical engineers engaged in supporting health care in diverse environments in order to achieve these societal objectives, consistent with the Council's Mission to strengthen international science for the benefit of society - all societies and all people.

PL03.2 - Global Health Challenges – Participating in the Health Revolution**Author(s):** [Mary Gospodarowicz](#)

Professor of Radiation Oncology, University of Toronto/CANADA. Medical Director, Princess Margaret Cancer Centre, and Regional Vice President, Cancer Care Ontario

The last century witnessed staggering increase in life expectancy, massive population growth, and steady migration out of extreme poverty. With this came the epidemiologic migration from acute life limiting illnesses to chronic or episodic illness and disability. The global healthcare industry has struggled to keep up with this change.

Cancer is an escalating health problem with 15 million new cases each year and this number is projected to grow to 24 million in the next 15 years. Cancer control requires a robust healthcare system capable of implementing a comprehensive cancer control plan from prevention through early detection, accurate diagnosis, effective treatment, and optimal support.

Fortunately the 21st century offers great promise for healthcare. Increasingly health is seen as a human right and investment in health as an economic necessity. Universal access to healthcare and the universal health coverage are on the global agenda. Recent increase in investment in healthcare such as seen in GAVI, Global Fund, PEP-FAR, and other programs is producing results faster than expected in some aspects of healthcare but the same level of investment is still to be applied to cancer.

The complexity and cost of cancer care calls for massive innovation to reduce the expected deaths and suffering. Rapid introduction and dissemination of new technologies (information, imaging, robotics, etc.) has potential for a huge humanitarian and economic benefit.

PL04 - EVIDENCE AND HEALTH INFORMATICS**PL04.1 - Academic Biomedical Informatics: Synergies and Challenges at the Interface with Industry****Author(s):** [Edward Shortliffe](#)

College Of Health Solutions, Arizona State University, Phoenix/ UNITED STATES OF AMERICA

Academic biomedical informatics has achieved great successes through research contributions and education of professional informaticians over several decades, now reflected in a thriving commercial marketplace for electronic health records and other informatics tools. That very success, coupled with changes in the ability of governments to support research at past levels, is forcing a reconsideration of the directions and emphases for faculty members in informatics academic units. In this presentation Dr. Shortliffe will discuss those forces and propose areas of emphasis that will strengthen the academic discipline as it continues to evolve. He will distinguish the roles of academic informaticians as practitioners of informatics, as researchers, and as educators. He will also stress the necessary synergies between academic informatics and the health information technology industry, arguing that both will be strengthened by more fertile relationships and joint efforts.

PL04.2 - Cognitive Challenges for Safe Human Computer Interaction**Author(s):** [Vimla Patel](#)

The New York Academy of Medicine and Columbia University, New York/UNITED STATES OF AMERICA

Given the complexities of modern medicine, delivery of safe and timely care is an ongoing and recognized challenge. Errors, misunderstandings, and inaccuracies—large and small—are routine occurrences in healthcare delivery. Health information technology (IT) has undoubtedly reduced the risk of serious injury for patients. However, its true potential for preventing medical errors remains only partially realized. Unfortunately, such systems may even give rise to hazards of their own. There is a growing recognition that many errors are attributable neither solely to lapses in human performance nor to flawed technology. Rather they develop as a product of the interaction between human beings and technology. In our view, errors are the product of cognitive activity in human adaptation to complex physical, social, and cultural environments. How well the design of health IT complements its intended setting and purpose is critically important for safe and effective performance. In this presentation, I will discuss the cognitive challenges we face in understanding human-computer interaction (HCI) that make the integration of computing and clinical practice a difficult task that, improperly addressed, can lead to threats to patient safety.